Proceedings of
Tailings and Mine Waste 2024

November 10–13, 2024, Colorado, USA

TAILINGS AND
MINE WASTE 2024



Volume 1

Editor
Joe Goodwill, Vancouver, BC, Canada

ORGANIZED BY



CIVIL AND ENVIRONMENTAL ENGINEERING
COLORADO STATE UNIVERSITY



C3 Alliance

Disclaimer

Any views and opinions expressed in the articles published in these proceedings are solely those of the authors and do not necessarily represent those of the University of Colorado State University (CSU), C3 Alliance Corp. (C3) or of the conference committees. The authors take full and exclusive responsibility for technical content and accuracy of the information published herein. This information is not intended nor implied to be a substitute for professional advice. CSU, C3, and the panel of editors are not responsible for any damage to property or persons that may occur as a result of the use of the information contained in this volume.

CONTENTS

Organizers xvi

Committees xvii

Technical Review Committee xix

Sponsors xxi

Exhibitors xxii

Preface xxiii

Message from the Chairs xxiv

Plenary Abstracts xxv

Chapter 1: Plenary Session Paper: What Could Tailings Facility Engineering Look Like in 2030? 1

What Could Tailings Facility Engineering Look Like in 2030? | Andy Small, Andrew Witte and Annika Bjelkevik 3

Chapter 2: Analysis 27

Numerical Simulation of Trigger Mechanisms of Static Liquefaction Applied to a Tailings Dam | Miguel A. Villalobos Bravo and Richard Witasse 29

TWIM Framework: A Digital Twin Approach for Strategic Dry Stacking Tailings Management | Cauê Stocchi Somensi, Douglas Deoclécio Tostes Firmo, Gustavo Marçal de Sousa, Alexandre Cristino Correa dos Santos and Lucio Schiavon Yamamoto 45

CPT Calibration Chamber Testing of Tailings Sand at High Confining Pressures | Matthew Haynes, Riccardo Fanni, David Reid and Kyle Smith 57

Interpretation of Pore Pressure Dissipation Test Results in Tailings | E. Rust and M. Rust 69

Estimation of Undrained Shear Strength Parameters from Laboratory Testing for Geotechnical Analysis: tff vs. qf | Masood Kafash, Thomas Barham, Lisa Yenne, Ranjiv Gupta and Georgia Lysay 83

A Critical Review of the Residual Pore Pressure Generation during Cyclic Loading | David Espinoza and Jenny Ramirez 95

Numerical Modeling Comparison of Large-strain Tailings Consolidation | Daniel Pham 107

Enhancing Data Management and Analysis for Mine Waste and Tailings Dam Design through Modern Data-Analytics Dashboards | Ela Talebi, Fariba Yavari and Kris Hojka 127

PLAXIS and CASM: Formulation, Implementation, and Verification │ Erick Rógenes, Ian Paes, Bruno Guimarães Delgado, Alessandra Gomes, Daniel Rocha Lanzieri, Felipe Cruz, Alomir Fávero Neto and Leandro Lima Rasmussen..... 137

A Comparison of Different Methods Used to Estimate the State Parameter to Assess the Static Liquefaction of Tailings │ Fahimeh Mahdavi Naftchali, Mathan V. Manmatharajan, Hamed Behzadipour and Michael Etezad 151

Silty Sand Tailings Saturation and its Influence on Interpreted CPTu Soil Behavior Type │ Andrew Burgin, Richard Dawson, Mauricio Pinheiro and Anelisa Vasconcelos 163

A New Implicit Kinetics Method to Estimate Shear Strength Mobilized in Liquefaction Flow Failures │ Jiarui Chen, Scott M. Olson, Soham Banerjee, Mandar M. Dewoolkar and Yves Dubief 173

Seismic Deformation Analyses of Germano Main Dam Part I: Calibration of PM4Sand Model for Sand Tailings using Field and Advanced Laboratory Test Data │ Pu Yang, Mehdi Qoreishi, Mauricio Pinheiro and Evan Hsiao 185

Seismic Deformation Analyses of Germano Main Dam Part II: Development of 2D FLAC Model and Sensitivity Studies Data │ Pu Yang, Mehdi Qoreishi, Mauricio Pinheiro and Evan Hsiao 197

Particle Size, Hydraulic Transportation, and In-line Mixing, from a Tailings In-Line Flocculation Perspective │ Raymond Guang and Trong Dang-Vu 209

Preliminary Design of the Tailings Cover System Using Numerical Modeling to Perform Sensitivity Analysis │ Bibhuti Panda, Rouzbeh Rasouli, Jason Chen and Anne-Marie Dagenais 223

The Evaluation of Nonlinear Dynamic Numerical Simulations of TSFs │ Michael James 237

Modeling of Embankment Scour Caused by a Tailings Pipeline Break and Potential Risk of Dam Breach │ Angus Rose, Mateus Nogueira and David Accadia 251

A Parameter Calibration Methodology for the Clay and Sand Model (CASM) Constitutive Model │ Alessandra Gomes, Erick Rógenes, Felipe Cruz, Paula Pais and Alomir Fávero Neto 265

Drained Laboratory Vane Shear Testing to Characterize Nonplastic Tailings │ Alvino Bezuidenhout and Luis A. Torres-Cruz 279

Modeling Assumptions and Implications during Closure Assessments on Legacy Tailings Facilities │ Benjamin Kramka, Erin Dunn, Lauren Meyer and Jason Cumbers 293

Enhancing the Safety of Tailings Dams: An Updated Approach in Fault Tree Analysis and Probabilities │ Geinfranco Villalta and Raquel Borja 305

Analysis of the Deformation and Cracking Mechanism of the Itabiruçu Dam – Case Study │ Paulo Cella, Carlos Santos, Felipe Neiva and Laura Rodríguez 323

Enhancing Pseudo 3D Seepage Modeling with Topographic Integration for Heap Leach Facilities │ I.J. Vega, A.G. Terlisky and M. Noël 339

Comparative Analysis of Vane Shear and Fall Cone Tests for Characterizing Oil Sands Tailings in the Sandy-fine Category │ Peter Kaheshi, G. Ward Wilson and Heather Kaminsky 351

Selection of the Seismic Coefficient in Pseudostatic Slope Stability Analyses of Tailings Dams | Jonathan Bray and Jorge Macedo 363

The Critical State Line Parameters of Iron Ore Tailings from Basic Laboratory Tests: Updated Insights with Additional Data | José Ccotohuanca and Daniel Klassen 379

Enhancing Tailings Dam Foundation Assessment: a SHANSEP Approach for a Brazilian Alluvium Soil | Carlos Besso, Sergio Capellão, Marcus Vinicius Lima Dias and Rodrigo Marinaro 393

Interpretation of Cyclic DSS Testing under Static Bias on Underflow Copper Tailings | Alfonso Cerna Diaz, Kevin Ritter and Jason Hilgers 409

Cyclic Response of Mine Tailings at Field and Laboratory Scales – Example Using a Novel Database | Cody Arnold and Jorge Macedo 423

Some Considerations on the Stability of Tailings Dams Subjected to Blasting Vibration | Ezra Coyle and Shayan Hashemi 433

Geotechnical Controls for Piles of Filtered Iron Ore Tailings | Danilo Eloi, Rodney Silva, Miguel Paganin, Letícia Cedro, Gricor Channakian, Felipe Bonucci, Mateus Leite and Adrielle Santos 441

2D and 3D Numerical Analyses of a Trial Embankment Construction over a Tailings Storage Facility | Alfonso Cerna Diaz, Lisa Yenne, Pooya Sheykhloo, Richard Davidson and Theo Gerritsen 453

Fabric Effects on the Onset of Static Liquefaction under Drained Conditions – Implications for Mine Tailings | Srinivas Vivek Bokkisa and Jorge Macedo 473

Numerical Modeling Evaluation of Consolidation Behavior of Saturated/Unsaturated Fluid Fine Tailings Consolidated Using the Applied Suction Method | Bereket Fisseha, G.Ward Wilson and Delwyn G. Fredlund 487

The Use of Waste Rock in Geotechnical Projects: the Challenge to Achieve the Geotechnical Parameters | Danilo Eloi, Miguel Paganin, Letícia Cedro, Rayssa Silva, Marina Ferreira, Gricor Channakian and Rodney Silva 505

Feijão Dam I 3D Numerical Simulation: A Comprehensive Approach, from Triggering to Dam Breach | Alfredo Arenas and Nicolas Pereira 517

The Use of Programming Language in GISTM Compliance for the Holden Mine | Summer Y. Sun and Phillip E. Crouse 531

Chapter 3: Application of GISTM 543

ALARP: Where are We Going and How Do We Get There? | Malcolm Barker, Chris Topham, Nick Glover and Manuel de Membrillera Ortuño 545

Conformance vs. Compliance: Contrasting the Voluntary GISTM to 9 years of Federal CCR Regulations | Lucas P. Carr, Steven F. Fecht and Nguyet Nguyen (Wit Win) 567

A Screening Approach for Preliminary ALARP Assessments of Societal Risks of Existing Tailings Dams | Chao Han and Wade Ludlow 585

Integrating Geometric Deposition and Hydrological Water Balance in Tailings Management: A Semi-Probabilistic Approach │ Paulo Victor S.A. De Castro, Miguel Palape, Roberto Cezar Rego Silva and João Marcus S.A. De Castro 601

Incorporating Lifespan Considerations into ALARP Decision-Making for TSFs: A Practical Methodology │ Ignacio A. Cueto, Osvaldo N. Ledesma and Franco Oboni 609

A Risk-Based Approach for Management of Change of Tailings Storage Facilities │ Bryan Bale, Shawn Gravel and Adam Chiorando 621

Global Climate Change due to Earth Cycles and Implications for GISTM Standards │ Kris Hojka and Fariba Yavari 633

Credible Failure Modes: Considerations for Assessment and Application │ Scott Martens and Angela Kupper 645

Practical Remedies to Improve the Defenses of Tailings Structures │ Jeremy Boswell, Anan Morshed, Thomas Kujawa and Meghan Barton 661

Update on GISTM Implementation at BHP – Lessons Learned on the Journey │ Chad LePoudre, Tenaya Brown, Justin Willis and Chris Sonntag 675

Meteorological Inputs to Tailings Storage Facility Assessments and Risk Assessments – Experience and Lessons Learned │ Bill Kappel, Doug Hultstrand and Andy Small 689

GISTM – Effective Implementation │ Lis Boczek, Richard Zayler and Gideon Steyl 711

A Case Study on ALARP for Safety Management of Tailings Storage Facilities │ Theo Gerritsen and Yi Zhu 721

Importance of Environmental Components in Assessing Risks under GISTM │ Karen Bechard, Heather Townsend and Rachel James 733

Maintaining Continuity – Lessons Learned from a TSF Incident Linked to Engineer Transitions │ George Afriyie, Jeremiah Williams, Rashida Umar and Ankomah Bosomtwi 745

Preventing Potential Consequences of a TSF Failure: Addressing the Other Side of the Risk Equation │ Susan Joyce and Keiran Doyle 753

Surveying the Landscape: Understanding Engineer of Record Challenges and Perceptions in the Brazilian Tailings Industry │ Luciano Souza, Luciana Praça, Matteus Hamade, Mauro dos Santos and Raika Silva 765

The Role of Engineer of Record – a Reflection of the Current State of Practice from an Australian Perspective │ Theo Gerritsen, Laura Fidel, Lis Boczek and Chris Hatton 779

Beyond HR: Embedding GISTM Principle 11 in Leadership for Transformative Tailings Management │ Johan du Toit and Fernando Damasio 791

Global Industry Standard on Tailings Management (GISTM) – Some Aspects of Implementation │ Marcelo Roberto Barbosa, Lucas Samuel Santos Brasil, Flavia Cruz Pereira, Denise Capanema and Marina Borges 803

Risk-based Planning of Monitoring Programs for TARPs │ Richard Sisson and Dirk van Zyl 813

Chapter 4: Breach and Inundation Estimates 827

Application of USACE LifeSim to the Feijão Dam B-1 Tailings Storage Facility Failure of January 25, 2019 | William Johnstone and Jesse Morrill-Winter 829

The Importance of Considering Dilute to Dry Tailings Rheology Formulations in Practical Tailings Dam Break Modeling | Reinaldo Garcia, Jacinto Artigas, Sergio Martinez, Pilar Garcia-Navarro, Javier Murillo, Nick Calero and Adolfo Correa 845

Dam Breach Analysis: A Methodology for Non-Newtonian Hazard Mapping and Fatality Rate Estimates | Mark Walden, Martin Rust, Nick Rocco, Sarah Melberg and Reinaldo Garcia 857

Multi-model Analyses of Tailings Impoundment Failure and Runout: Part III | Armin Saeedi, Mario Martinelli and Paul Simms 873

"Failing Forward" to Secure Oil Sands Tailings Impoundments against Catastrophic Failures: Preliminary Results | Armin Saeedi, Louai Alshafti, Xuexin Xia, Gonzalo Zambrano Narvaez, Nicholas Beier, Mario Martinelli and Paul Simms 885

Probability Distributions of Tailings Dam Breach Volumes by Failure Mode as Part of a Risk Screening-Level Tool | Stephanie Bale, Vincenzo Coia, Brad Russell and Daley Clohan 897

Volumes of Dam Material Mobilized by Erosion During Tailings Dam Failure Events | Daniel Adria, Violeta Martin and Heleman Wong 911

Estimation of Outflow Runout Distance in Tailings Dam Using an Artificial Intelligence Technique | Mohammad Rashidi, Sam Abbaszadeh and Jenisha Chhetri 929

Good Practices for the Elaboration of Hypothetical Dam Break Studies in Brazil | Caique Simões Renna Costa, Fernando Pereira Aguilar, Mônica Torres dos Santos Almeida and Vicente Mello 943

Good Practices for Hydraulic Safety for Mining Dams in Brazil | Fernando Pereira Aguilar, Manuelle Prado Cardoso Pereira and Vicente Mello 955

Chapter 5: Case Histories 965

Agnico Eagle LaRonde Filtered Tailings Project, Concept to Commissioning | Ajit Baruah and Paul de la Duarantaye 967

The Closure of the Germano Pit Tailings Storage Facility | Mauricio Pinheiro, Richard Dawson, Andrew Burgin, Mathieu Wacowich, Rogerio Torres, Jose Bernardo and Anelisa Vasconcelos 977

A Safe Approach to Assess the Trafficability of Tailings Beaches for Operation and Closure Construction Activities | Delakshan Inparajah, Gordon W. Pollock, Ahreum Lee, Anthony Faulder and Jason Chen 991

Long-term Performance of a Coarse-grained Monolayer Cover on a Pre-oxidized Mine Site | Karine Sylvain, Isabelle Demers, Thomas Pabst, Sophie Turcotte and Andréane Samson 1005

Geotechnical Failure of a Waste Rock and Heap Leach Facility at the Bellavista Gold Project | Terry Braun 1019

Tailings Disposal Management in Large Reservoirs – Case Study for Mirim Dam, Salobo Mine, Brazil │ Gustavo Belotto, Carlos Alex Alves Lima, Henrique Tropia Granja Guerzoni, João Paulo Rodrigues Costa, Felipe Campolina, Jefferson Oliveira and José Henrique Coelho Wanderley Costa 1033

Dam Safety Remediation Measures at the Aitik Tailings Management Facility, Northern Sweden │ Romain Girard and Joseph Quinn 1045

Tailings Pond Sedimentation Capacity: A Practical Approach │ Michael Louws, Karina Stapleton, Andrew Witte, Sam Nunoo and Faegheh Niyazi 1061

Key Parameters that Influence the Operation of Tailings Dry Stack Disposal, Considering Various International Practices │ Gino Vizcarra, Kathy Tehrani, Fernando Sgavioli, Thatyane Martins Gonçalves and Frank Pereira 1073

Characterization of Flocculated Fluid Fine Tailings Using On-line Microscopy │ Paul Mikula, Nan Wang, Adeola Bello-Hamilton and Randy Mikula 1083

Reducing Mine Closure Cost Risks by Employing Effective Construction Management Strategies │ Michael Nahir, Marie Rousseau and Geoff Karcher 1095

Proposal for Guidelines on Filtered Tailings Disposal: Detailing the Hypothetical Rupture Studies │ Elaine Soares, Waldemar Felitti, Fernando Aguilar, Alex Castro and Luiz Vilas Bôas 1111

The Use of an O-pile System for Foundation Seepage Control during Tailings Dam Construction: A Case Study │ Rui Couto and Siavash Farhangi 1123

Seismic Imaging Techniques in Mine Closure Planning: Case Studies Across Multiple Abandoned Mines │ Majid Mirzanejad, Zach Spence, Lincoln Steele, Will Levandowski and Dan O'Connell 1135

Tailings Risk Mitigations at Hudbay Flin Flon: Prioritization Approach and Implementation of Multiple Mitigation Measures │ Brad Russell, Trevor Ross, Matt Dugie, Matthew Schafer and Ed Carey 1149

Case Study of Optimizing Design by Performing Field Trials of a Filter Selection for a Rockfill Embankment │ Jason Hilgers, Thomas Barham, Julia Jarriel, Tiffiany Cromey, Robert Snow, Devinne Ramirez and Ranjiv Gupta 1163

Game-changing Technology for Large-scale Filtered Tailings │ Oliver Whatnall, Sam Caldwell, Stuart Wilson, Ricardo Santander and Juan Ccarita 1175

Characterizing Creep Behavior of a Fine-grained Zinc Pressure Leach Tailings │ Jade Chung, Adrian Wightman and Stephanie Alexander 1189

InSAR Study into Pre- and Post -Failure Deformations of the Jagersfontein Tailings Dam │ Divya Sekhar Vaka and Skevi Perdikou 1207

The Barriers to Widespread Adoption of Tailings Dewatering Technologies │ Ljiljana Josic, Ashley Verge and Kasra Majdanishabestari 1217

Monitoring Tailings Saturation at a TSF Using Tensiometers and Laboratory SWCC │ Mahmoud N. Hussien, Soumia El Mansouri, Vu Tran and Eric Cloutier 1231

A Framework to Determine Tailings Liquefaction – GISTM Conformance for the Holden Mine │ Mohammad Rashidi, Phillip E. Crouse and Summer Y. Sun 1241

Challenges and Mitigations to Bring a Historical Tailings Facility into Compliance with Modern Standards | Anthony Zhang and Chris Johns 1255

Chapter 6: Closure Issues 1267

Effect of Temperature on the Generation of Arsenic from Waste Rock from an Arctic Mine – A Laboratory Investigation | Elaura Seutin, Bruno Bussière, Benoît Plante and Vincent Boulanger-Martel 1269

Lessons Learned from Designing a Soil Cover System for a Tailings Storage Facility Exposed to an Arid Climate | Vincent Castonguay, Elissar Ozeir, Miguel Medina and Fannie Lessard 1281

Modeling Cover Systems for Tailings Facilities: Integrating Hydrus-1D and Python for Enhanced Seepage Prediction | Ariel Terlisky, Imanol Vega, Gastón Quaglia, Jonathon Doherty and Michel Noël 1293

The Vibro-consolidation Technique for Tailings Management and Dam Decommissioning Works | Gustavo Marçal de Sousa, Ana Torres, Felipe Moraes Russo and Lucio Schiavon Yamamoto 1307

Design, Construction, Monitoring and Numerical Modeling of Large-scale Field Trials: Assessing Cover Performance for Reclamation Method Selection | Karine Sylvain and Marie-Lin Breard Lanoix 1323

Kidston Hydro Electric Power: Re-purposing an Abandoned Mine | Malcolm Barker, Tony Ford and Peter Gaylard 1337

Enhancement of Tailings Properties by Cement Amendment for their Valorization in Cover Systems to Reclaim Active or Closed Tailings Storage Facilities | Audrey Jalce, Isabelle Demers, Benoît Plante, Thomas Genty, Eric Brouard, Marie-Pier Éthier, Sophie Turcotte and Marie-Andrée Guindon 1353

TRIM4Post-Mining: Geotechnical Input for Transition Information Modeling for Post-mining Landscapes | Gerald Verbeek and Gustavo Hamu 1367

Utilization of Novel Electrokinetic Geosynthetics for Stabilization of Ultra-fine Tailings | Nilan Jayasiri, Andy Fourie and Cristina Vulpe 1377

Enhanced Conceptualization of Reactive Filtered Tailings Oxidation Using a Reactive Transport Model | Katherine Raymond, Jared Robertson, Julie Zettl and Mike O'Kane 1391

Orphaned and Abandoned Mines in Manitoba: From Identifying Hazards to Achieving Closure | Mohammad Ahmeduzzaman, Dami Adedapo and Cory Graham 1407

Decharacterization of Tailings and Sediment Dams in Brazil – Hydrological and Hydraulic Aspects | Manuelle Prado Cardoso Pereira, Mônica Torres dos Santos de Almeida, Caique Simões Renna Costa, Helena Maria Campos Castro, Fernando Pereira Aguilar and Vicente Mello 1419

Checklist for Decharacterization of Mining Dams: Engineering and Environmental Aspects | Rafael Caetano Cardoso Boaventura, Murilo Damato, Gislene F.S.R. Fournier and Manoela C. A. Neves 1429

The Importance of Hydrogeological Models for Closure of Tailings Dams | Ana Carolina Neves and Waldemar Felitti 1439

Tailings Dam Decharacterization Projects: Proposal for Water Monitoring Plan | Ana Carolina Neves, Helen Simone Chiaranda, Bruno Resende Lopes and Rafael Gomes Oliveira 1451

Boodarie Tailings Storage Facility – Our Journey to Closure | Nathalia Revelo Mendez, Daniel Meunier, Darren Springer, Bria Whiter and Simon Harris 1465

Chapter 7: Design 1477

Lessons Learnt by Applying a Risk-based Approach to Tailings Storage Facilities | Peter Chapman, Scott Gover and Jordan Ribbons 1479

Evaluating the Stability of Upstream and Brittle Facilities – Case History Validation of the "Rules" | Michael Davies and John Lupo 1495

How to Design a Tailing's Dam Full Removal? Lessons Learned from a Case Study in Brazil | Benicio Junior, Claudio Rodrigues, Neil Singh and Luciano Souza 1507

Design of a Co-disposal Facility for Thickened Tailings and Potentially Acid-generating Waste Rock | Patrick Williamson and Wilson Muir 1521

A Study on the Possibilities, Constraints, and Motivation for Transitioning a Conventionally Designed TSF into a Full-scale Hydraulically Dewatered Stack Facility for Fine Residue Disposal in South Africa | N.W. Nxumalo, P. Newman and A. López 1533

The Relevance of Particle Crushing for the Design of Compacted Filtered Iron Ore Tailings Storage Facilities | João Paulo de Sousa Silva, Bruno Guimarães Delgado, Alexia Cindy Wagner, João Vítor de Azambuja Carvalho and Nilo Cesar Consoli.....1543

Iron Ore Tailings Dam De-Characterization: Evaluation of Key Parameters for Future Dry Stacking | Hugo Carlos Scheuermann Filho, Thatyane Martins Gonçalves, Nilo Cesar Consoli, Gino Vizcarra, Frank Pereira and Nilthson Noreña 1555

Lessons Learned in Applying the Observational Method to a Tailings Facility Constructed on a Soft Clay Foundation | Bryce Marcotte, Kyle Scale, Calvin Boese, Michael Andree, Travis Pastachak, Brent McFarlane and Jason Bell 1565

Compaction Sensitivity in Tailings Stack Infiltration Modeling: Unsaturated Properties Uncertainty Analysis | Letícia B. L. Garcia, Marcos A. Lemos Júnior and Guilherme J.C. Gomes 1577

Stay and Fight, or Flee? Assessing the Risks of Intervention Leading up to a Catastrophic Failure | Justin Willis 1589

Bayesian Networks Application and Analysis of Failure Mechanism and Triggers in Tailings Dams: A Case Study | Keith Mandisodza, David J. Williams and Chenming Zhang 1603

A Feed Forward Approach to Optimizing Oilsands Tailings Centrifuge Operation | Paul Mikula, Adeola Bello-Hamilton, Nan Wang, Jim Lorentz and Randy Mikula 1621

An Often-Overlooked Approach for Slope Stability of Tailings Dams Built Using Centerline and Downstream Construction | Jed D. Greenwood, Iván A. Contreras and Junhong Li 1633

Buttressing of Tailings Storage Facilities | Raquibul Alam and Ljiljana Josic 1645

Transportable Moisture Limit vs. Conveyability Testing | Christopher Olsen, Kenneth Rahal, Chris Braun and Skyler Pinnick 1661

Learning from Experience – Let's Get Real | Malcolm Barker 1679

Southeast Rock Disposal Site Tailings Co-disposal Facility | Ben Wickland, Don Parsons, Anthony Van Engelen and Scott Coombs 1695

Feasibility of Repurposing Wood Processing Waste as an Industrial Liner Material | Robyn Gaebel, Heidi Cossey, Ali Nasseri-Moghaddam and Kristin Salzsauler 1705

Operational Processes for Stacking Filtered Tailings – Itabira Case Study | Rodney Silva, Felipe Bonucci, Danilo Eloi, Miguel Paganin, Weslley Maciel, Jonas Guedes, Maira Drumond and Mateus Leite 1717

Performance Assessment of a Filtered Tailings Storage Facility Partially Built with Uncompacted Tailings | Edwin Sanchez and Denys Parra 1733

Next-Gen Tailings Waste Management: Transforming Life-Cycle Strategies | Lakshmin Bachu 1749

Chapter 8: Environment and Water 1763

Evaluation of Biogeochemical Processes for Weak Acid Dissociable Cyanide | Larissa Smith, Sandra Dworatzek, Jeff Roberts, Valerie Bertrand and Elizabeth Walsh 1765

Combining Approaches for Environmental Assessment of Tailings Ponds and Waste Piles in the Eastern Amazon | Silvio Ramos, Paula Ribeiro, Cecilio Caldeira, Wendel Pereira, Markus Gastauer and Pedro Souza-Filho 1775

Freeze-thaw Durability of Cemented Paste Backfill Containing Arsenic Trioxide Roaster Waste Dust | Caroline Alexon, Nicholas Beier, Amirhossein Mohammadi and Isabelle Demers 1787

Water Balance and Water Quality Predictions for the Cariboo Gold Project Filtered Tailings Facility | Adrian Moreau, Jiajia Zheng, Michelle Liew and Alex Fitzpatrick 1799

Development of a Calibrated Seepage Model to Predict Pore Pressure Reduction to Inform Tailings Storage Facility Closure Planning | W.E. Rouncivell, R.L.C. James and S. Lorentz 1813

Rapid Water Table Response to Transient Pressure Wave Generation in the Unsaturated Zone of Tailings Dams | Charné Theron and Simon A. Lorentz 1825

Geochemical Investigations toward a Groundwater Compliance Action Plan at the Moab UMTRA Project Site | Lisa Burgess, Keaton Belli, Chelsea Bokman, Jennifer Nyman, Liz Moran and Ken Pill 1837

Critical Seepage Analyses for Stability of Tailings Dams | Dobroslav Znidarcic, Gordan Gjerapic and David Rees Gillette 1849

Assessment of Silicate- and Catecholate-based Surface Treatment Performances to Limit the Mobilization of As from Low Sulfide Filtered Tailings | E. Lagae Capelle, L. Coudert, I. Demers, C. M. Neculita and G. Pépin 1861

The Internal and Interface Shear Strength of Geosynthetic Clay Liners for Mining Application | Andrew Jung and Reza Gorakhki 1873

Prediction of Pore Air and Water Pressure Propagation Induced by Extreme Rainfall in Tailings Dams | Simon A. Lorentz and Charné Theron 1883

Deportments of Magnesium and Silicon in a Two-part HCl-NaOH Leaching of Asbestos Tailings | Terry C. Cheng and Claude L. Morissette 1891

Evaluation of Best Available Technologies and Practices for Tailings Seepage Detection and Monitoring at Cobre Panamá | John H. Fortuna and Carlos Hubner Torres 1903

Standardizing Sediment Porewater Passive Samplers to Measure Metal Availability at Mine Sites | Florent Risacher, Jason Conder, Brent Pautler, Alex Sweett and Andrew Jackson 1925

Preliminary Assessment of the Environmental Impacts of Artisanal Gold Mining: The Case of the Kashozi Mining Site, South Kivu, DRC | Akonkwa Mudekuza Kepler, Alex Kalonji-Kabambi and Bwemere Ciribuka Grâce 1933

Implementation of Saturated and Unsaturated Seepage Analysis in a Polymetallic Tailings Storage Facility: A Case Study | Jose Alfredo Promotor, Sergio Hernández, Osvaldo Flores and Cesar Gallegos 1947

Challenges Faced in Developing Plans for Emergency Drinking Water Supply in the Context of Mining Dam Collapses | Josiani Esteves Cordova, Lucas França Carvalho Silveira, Yuri Abner Rocha Lebron, Gabriela Rodrigues Barroso, Fernanda Luiza Costa Lisboa and Vicente Alimento Júnior 1961

Chapter 9: Geotechnical Issues 1975

Exploration of Passive Desaturation of In-place Tailings Using Wicking Geosynthetics | Kendall Monley and Joseph Scalia IV 1977

Rate Effects in In-situ Testing in Hard Rock Mine Tailings and their Impact on the Estimation of Shear Strength Parameters | Mohammad Zarrabi, Estelle Nkamegue, Michael Demers-Bonin, Mohammad Kermani and Kendell Cator 1991

Geotechnical Challenges of Tailings Storage Facilities in Cold Regions | Morteza Esfehani 2003

Assessment of Flow Liquefaction Susceptibility of a Tailings Dry Stack Pile Using the State Parameter and Yield Stress Ratio Approach | Marcus Vinícius Lima Dias, Dieggo Santos, Mariela Silva, Gustavo Marçal de Sousa and Marília Freire 2015

Enhancing Soil and Tailings Characterization: Integration of Photonics Technology with Cone Penetration Testing | Iman Entezari, Dallas McGowan, Joseph Bindner, Joseph Glavina and Jason DeJong.....2027

Hydraulic Dewatered Stacking Demonstration – Approaching Operational Completion | Phil Newman, Mark Bruton, James Purrington, Alireza Nickman and Andrea López 2039

In-pond Mixing of Fine and Coarse Tailings – Results from a Commercial-scale Pilot in Canada's Oil Sands | Evan Davison, Lucas Hu, Bobby Hutchinson and Peter House 2053

Evaluating Iron Ore Tailings' Variability in an Upstream Dam For Dam Closure │ Thatyane Martins Gonçalves, Alexia Cindy Wagner, João Vítor de Azambuja Carvalho, Frank Pereira and Nilo Cesar Consoli 2067

Solar-Powered Electrokinetic Tailings Dewatering │ Ed Hanna and John Vandersleen 2079

Effect of In-situ Dewatering and Compaction of Copper Tailings Using Accelerated Mechanical Consolidation │ Oscar Santiago, William McAdam and Rafael Menezes ...2093

Influence of In-situ Soil Fabric on the Critical State of a Laminated Glaciolacustrine Silty Soil │ Morteza Mohamadi, Simon Dickinson, Chang-Gyun Jeong, Erinn Raison and Adrian Wightman 2107

Mechanical Behavior of Gold Mine Tailings Dried by Natural Dewatering │ Mayara Ferreira Rodrigues, Paula de Mello Martins and Jaime Pinheiro 2119

Analysis of Video Images Obtained during Cone Penetration Testing │ Gerald Verbeek, Gustavo Hamu and Oksana Khomiak 2131

Predicting Tailings Properties Using Hyperspectral Sensing and Machine Learning │ Joseph Bindner, Joseph Scalia IV, Christopher Bareither, Iman Entezari and Dallas McGowan 2143

Fundamental Properties of Filtered Tailings on Density-Moisture Curves │ Uddav Ghimire, Jackson S. Norbutas and Tejo V. Bheemasetti 2155

Multi-Test Approach to Determining Consolidation Parameters in Flocculated Tailings and Soft Soils │ Ehsan Eidi, Ken Dickson, Arazooben Patel, Louise Whitham, Morgan Tizzotti and Paul Simms 2167

Optimization of Operations Based on Monitoring and Construction Quality Assurance at Minera Peñasquito │ Christian Armstrong, Kenneth Rood, Eduardo Jose Garcia Romero and Patrick Mwamba 2179

How Many Triaxial Tests Do You Actually Need to Get a Critical State Line? │ Marcos Arroyo, Lluis Monforte and Stefano Collico 2191

Holden Mine Post Closure Monitoring – a Statistical Method for Developing Trigger Action Levels │ Summer Y. Sun, Ray Dorow, Paul Pellicer, Mohammad Rashidi and Phillip Crouse 2203

Shear Strength Characteristics and Joint Envelopes of Compacted Unsaturated Fine-grained Bauxite Residue │ Hua Tian, David J. Williams and Keith Mandisodza 2217

Measurement of Bingham Yield Stress and Plastic Viscosity of Tailings Slimes using an In-Situ Viscometer │ Dallas McGowan, Yasmin Byrne, Y. Simon Sun, Heather Kaminsky and Jason DeJong 2237

Mechanical Response of Plastic Fine Tailings under Constant Shear Drained Loading │ Luis Vergaray-Astupina and Jorge Macedo 2253

Development of Tailings-Specific Correlations for Estimating Fines Content from CPT Data Using Artificial Intelligence Method for the Holden Mine │ Mohammad Rashidi, Phillip E. Crouse and Summer Y. Sun 2263

Stacked Deposits of Filtered Fluid Fine Tailings Using Geotextile Tubes – Updates on Enhancing Chemical Stability │ Fernando Da Silva 2275

Spatial Variability Assessment of Mine Tailings | Luis Vergaray-Astupina and Jorge Macedo 2297

Tailings Characterization for Flow Liquefaction Evaluation at a Large Tailings Storage Facility by Advanced Laboratory Testing | Juan Carlos Ayes-Zamudio, Akhter Hossain and Tony Freiman 2309

Chapter 10: Monitoring and Risk Management 2321

Improving Tailings Deposition: A Drone and Satellite Survey Validation Framework for Enhanced Facility Management | John Thuysbaert, Joe Piccolo-Lawrance, Joseph Quinn and Romain Girard 2323

Risk Management for Access to Dams at Emergency Level Control: Control Levels (OMS Manual) and Safety Plan | Virginie Queiroz Rezende Pinto, Daniel Bernardes Raposo, Milena Fernandes Xavier Matos, Elias Silva de Sousa and Alexandre Cristino Correa dos Santos 2335

Passive Seismic and Interferometry Techniques in Dam Decharacterization Monitoring | Camilla Rodrigues, Marc Lambert and Ben Witten 2345

New Wireless Technology for Tailings Monitoring | Leonnardo Probst Simoes, Braulio Rodrigues, Sean Allen, Jake Lloyd, Vitor Almeida, Jhonimar Santos and Denis Rafael Valentim 2357

UPLOAD – ANALYSE – ACT: Artificial Intelligence-assisted Faster, Seamless, and Almost Real-time Tailings Dam Construction Quality Assurance is Knocking at our Doorstep | Anjan Kundu 2367

Vale Base Metals Modernization of Instrumentation Monitoring System for Dam Safety at Canada Tailings Storage Facilities | Wing-Keat (Wayne) Wong, Greg Puro and Lucas Lobato Ribeiro 2373

Assessing SAR, InSAR and Multispectral Optical Data for Mapping Supernatant Pond Evolution | Élyse Gaudreau, Ajinkya Koleshwar, Kenny Yue, Pablo Blanco, Riccardo Tortini and Giacomo Falorni 2383

The Application of a 3D Inclinometer in Monitoring the Performance of a TSF near an Active Mine Pit | Zhen Ran Yung, Qing Zhan, Stephen Darmawan and Rudy Moniaga 2397

Integration of Multi-Sensing Technologies for the Monitoring of Tailing Storage Facilities | Vincent Le Borgne, Adam Dulmage, Josh Sun, Evan Davison, Divya Sekha Vaka and Skevi Perdikou 2407

Integrated Analysis of Dam Surface Displacement Monitoring | Felipe Bolívar Domingos, Alessandra Mazon and Jefferson Barbosa 2419

Chapter 11: Site Investigation 2431

Enhancing Safety and Reducing Environmental Impact through Development of a Robotic Hybrid CPT Rig | David Slack, Roque Obusan, Yasmin Byrne, Dora de Melo and Jason DeJong 2433

Tailings Facility Surveying Leveraging Complementary Technologies | Veronique Nell and Andrea Krupa 2447

Potential of X-ray Micro-CT Imaging for Mine Tailings Deposit Characterization | Dharma Wijewickreme and Ana Valverde 2457

Influence of Density on Predicting Saturation in Filtered Tailings using an Electromagnetic Sensor | Garret M. Martin, Christopher A. Bareither and Joseph Scalia IV 2467

Testing of an Autonomous Rheometer for Optimized Tailings Thickeners Operation | Arno Talmon, Wiebe Boomsma, Bas Nieuwboer, Samir Rustamov, Menno Jaspers, Sven van Asperen and Miguel de Lucas Pardo 2485

Chapter 12: Author Index..... 2497

Author Index 2499

ORGANIZERS

Colorado State University

The Civil & Environmental Engineering Department (CEE) at Colorado State University is internationally recognized for world-class engineering research and education. Our faculty develop global solutions to address environmental issues including tailings and mine waste, wildfires, and other natural hazards compounded by climate change. Our faculty are pioneers in water research, from hydraulic design and stream restoration to stormwater treatment and wastewater monitoring. The department takes pride in over 150 years of history, dating back to the first department head, Elwood Mead, who oversaw the construction of Hoover Dam and was the namesake of Lake Mead. Beyond research, our faculty prioritize the preparation of future engineers and scholars by balancing rigorous coursework with dynamic and supportive instruction. The department hosts the ASCE Excellence in Civil Engineering Education (ExCEEd) workshop, helping engineering faculty across the U.S. and internationally become better teachers. The department offers two ABET-accredited Bachelor of Science degrees in civil engineering and environmental engineering, and a new construction engineering degree beginning fall 2025. CEE offers a Master of Science, a Master of Engineering, and a Ph.D. in civil engineering, as well as several certificates including a graduate certificate in tailings engineering.

For more information, visit the CSU website at https://www.colostate.edu/

C3 Alliance Corp.

At C3 Alliance Corp., our mission is to create stronger communities through innovative and inclusive solutions for resource development. We understand that the sharing of information and ideas is vital to gaining insights and developing relationships and that community members, business, and government representatives can all benefit from meeting to share stories and knowledge. C3's expert team of event planners specialize in providing project management, strategic knowledge and expertise for planning conferences and networking opportunities. We benefit from a vast network of professional contacts to organize exceptional events that connect people and knowledge across resources sectors, communities and government.

For more information, visit the C3 website at http://www.c3alliancecorp.ca/

COMMITTEES

Conference Leadership Committee

Chair – Christopher A. Bareither, Associate Professor, Civil & Environmental Engineering, Colorado State University

Co-Chair – Joseph Scalia IV, Associate Professor, Civil & Environmental Engineering, Colorado State University

Plenary Session Lead – Amanda Adams, Principal Engineer, Stantec

Plenary Session Lead – Jason Andrews, Senior Geotechnical Engineer, Senior Vice President, Engineering Analytics

Plenary Session Lead – Michael Henderson, Principal, Strata-Geo LLC

Plenary Session Lead – Kate Patterson, Tailings and Water Resources Engineer, Principal, Klohn Crippen Berger, Ltd.

Plenary Session Lead – Nicholas Rocco, Geotechnical Engineer, NewFields Mining Design & Technical Services

Plenary Session Lead – Ryan Shedivy, Assistant Vice President, Geological Engineer/ Mine Waste Mountain Team Leader, WSP USA Inc.

Short Course Technical Lead – Jason Hilgers, Associate Vice President, Geotechnical Engineer – Mining Group, AECOM

Social Events Coordinator – Sam Rivet, Senior Solutions Manager, MineBridge Software Inc.

Tradeshow Reception Lead – Shawn Steiner, Manager – USA West, ConeTec

Student Volunteer Coordinator – Emily Jagerhorn, Graduate Research Assistant, Civil & Environmental Engineering, Colorado State University

Organizing Committee

Marie-Josée Banwell, Business Development Manager, TRE Altamira Inc.

Dean B. Durkee, Sr. Consultant & Vice President, Gannett Fleming

Jason Cumbers, Principal Engineer, Stantec

Zach Fox, Senior Geotechnical Engineer, Knight Piésold Consulting

Robyn Gaebel, Senior Geotechnical Engineer, Geosyntec Consultants Inc.

Wes Herweynen, Senior Tailings Engineer, GHD

Ljiljana Josic, Sr. Director Tailings, Water and Geotechnical Engineering, AtkinsRealis

Andy Jung, Technical Manager, CETCO

Jean Kugel, Senior Engineer, BGC Engineering

Daryl Longwell, Principal Civil Engineer, Tetra Tech, Inc.

Linda Lorenzetti, Diemme Filtration

Dave Ludwick, Senior Civil Engineer, SRK Consulting Inc.

Ian McKechnie, Lead Product Manager, Hatch Ltd.

Doug Oliver, Principal Hydrogeologist, FloSolutions

Randal Osicki, Associate | Senior Geotechnical Engineer, Thurber Engineering Ltd.

Fab Pakizehkar, Veolia Water Technologies & Solutions

Omar Rodriguez, Design Engineer, Soletanche Bachy

Kurt J. Schimpke, Senior Geotechnical Engineer, Barr Engineering Co.

Teresa Speigl, Director Tailings, Crushed Leach, & Water, Freeport-McMoRan

Aaron Tomkins, Principal Geoscientist, GBG Group

Maythe Villavicencio, Marketing Manager, PhotoSat

Oliver Whatnall, VP, Americas, Jord International

Todd Wisdom, Director, Paterson & Cooke USA, Ltd.

Zygi Zurakowski, Principal Engineer, Water and Geotechnical Engineering, Newmont

Conference Secretariat

Sarah Weber, C3 Alliance Corp.

Melissa McRitchie, C3 Alliance Corp.

Meryl Nelson, C3 Alliance Corp.

Bronagh Furlong, C3 Alliance Corp.

Michaela Bub, C3 Alliance Corp.

Izzy Beard, C3 Alliance Corp.

TECHNICAL REVIEW COMMITTEE

The Organizing Committee expresses its appreciation and sincere gratitude to the following reviewers of the technical content, who helped to ensure the high quality of this publication.

Jason Hilgers, AECOM
Alfonso Cerna-Diaz, AECOM
Thomas Barham, AECOM
Lisa Yenne, AECOM
Bibhuti Panda, AECOM
Masood Kafash, AECOM
Caique Simões Renna Costa, AECOM
Rafael Boaventura, AECOM
Kevin Ritter, AECOM
Paula de Mello Martins, AngloGold Ashanti
Kurt Schimpke, Barr Engineering Company
Nathan Toohey, Barr Engineering Company
Dafar Obeidat, Barr Engineering Company
Jason Harvey, Barr Engineering Company
Andrea Lougheed, BGC Engineering
Chang-Gyun Jeong, BGC Engineering
Brad Russell, BGC Engineering
Jean Kugel, BGC Engineering
Mike Belfry, BGC Engineering Inc.
Renata Wood, BGC Engineering Inc.
Jack Seto, BGC Engineering Inc.
Caroline Bates, BGC Engineering Inc.
Tenaya Brown, BHP
Justin Willis, BHP
Andy Jung, CETCO
Mike Henderson, Colorado School of Mines
Marcos Lemos, Companhia Brasileira de Metalurgia e Mineração (CBMM)
Yasmin Byrne, ConeTec
Shawn Steiner, ConeTec, Inc
Robert Snow, D'Appolonia
Michael Davies, Davies Mining Consultancy
Francesco Kaswalder, Diemme Filtration srl
Morteza Esfehani, Director of Geotechnical Expertise, WSP Canada
Douglas Oliver, FloSolutions
Sebastian Torrealba, FloSolutions
Andrea Gehlhausen, FloSolutions USA Ltd.
Christopher Olsen, FLSmidth, USA
Emmanuel Orilogi, Freeport-McMoRan Inc.
Dean Durkee, Gannett Fleming
Mark Walden, NewFields Mining Design & Technical Services
Zygi Zurakowski, Newmont
Michael Shelbourn, Newmont
Brett Byler, Newmont
Kate Brand, Newmont
Hugh Davies, Newmont Corporation
Kristin Pouw, Newmont Corporation
Matt Treinen, Newmont Corporation
George Afriyie, Newmont Corporation
Hal Cooper, Okane Consultants
Todd Wisdom, Paterson & Cooke USA, Ltd
Niyayesh Khorshidi, PhD Student, [University of New Brunswick]
Oscar Santiago, Phibion
Veronique Nell, PhotoSat
Reinaldo Garcia, President
Zhen Ran Yung, Red Earth Engineering – A Geosyntec Company
Nicolas Pereira, Red Earth Engineering a Geosyntec Company
Bruno Bussiere, Research Institute on Mines and Environment (RIME), Université du Québec en Abitibi-Témiscamingue (UQAT)
Lucie Coudert, Research Institute on Mines and Environment (RIME), University of Quebec in Abitibi-Temiscamingue (UQAT)
Kim Morrison, Self-employed
Michael Etezad, Senior Principal Geotechnical Engineer
Terry Mandziak, SLR International Corp.
Lis Boczek, South32
Terry Braun, SRK Consulting
Simon Lorentz, SRK Consulting
Ignacio Cueto, SRK Consulting (Argentina) Inc.
Bryce Marcotte, SRK Consulting (Canada) Inc.
Dave Ludwick, SRK Consulting (U.S.)
Assaf Wunsch, SRK Consulting (U.S.)
Lukas Radmann, SRK Consulting (U.S.)
Clint Strachan, Stantec
Amanda Adams, Stantec Consulting Ltd.

Elizabeth Landowski, Gannett Fleming
Alex Walsh, Gannett Fleming
Divya Sekhar Vaka, GEOFEM
Luis Vergaray-Astupina, Georgia Institute of Technology
Robyn Gaebel, Geosyntec Consultants
Liz van Warmerdam, Geosyntec Consultants
Kristin Salzsauler, Geosyntec Consultants
Nathan Haws, Geosystems Analysis, Inc.
Jason Cumbers, Geotechnical engineer at Stantec
Eric Schlosser, GFNET
Anjan Kundu, GHD
Malcolm Barker, GHD
Wesley Herweynen, GHD
Vincent Le Borgne, GKM Consultants
Ian McKechnie, Hatch
Yuri Lebron, HSE&OR Office, Vale S.A.
Hua Tian, Hua Tian
Patrick Williamson, INTERA Inc
Oliver Whatnall, Jord International
Kate Patterson, Klohn Crippen Berger
Andrew Witte, Klohn Crippen Berger
Adrian Moreau, Klohn Crippen Berger
Luciano Souza, Klohn Crippen Berger
Jose Ccotohuanca, Klohn Crippen Berger
Rick Friedel, Klohn Crippen Berger
Jen Durocher, Klohn Crippen Berger
Zach Fox, Knight Piesold Consulting
Nicholas Sianta, Knight Piesold Consulting
Jeffrey Coffin, Knight Piesold Consulting
Peter Duvigneaud, Knight Piesold Consulting
Daniel Adria, Knight Piesold Ltd.
Joy Foley, Knight Piesold Ltd.
Tom Meuzelaar, Life Cycle Geo, LLC.
Jacob Waples, Life Cycle Geo, LLC.
Ajit Baruah, Metso
Sam Rivet, Muk3D
Terry Cheng, Natural Resources Canada
Nicholas Rocco, NewFields Mining Design & Technical Services
Kerry Magner, NewFields Mining Design & Technical Services
Martin Rust, NewFields Mining Design & Technical Services
Garret Martin, NewFields Mining Design & Technical Services
Mathieu Wacowich, Stantec Consulting Ltd.
Andrew Watson, Stantec Consulting Ltd.
Ernesto Ruiz Castro, Stantec Consulting Ltd.
Efrain Rondinel, Stantec Consulting Ltd.
Sara Fayek, Stantec Consulting Ltd.
Bereket Fisseha, Tetra Tech Canada
Daryl Longwell, Tetra Tech, Inc.
Brad Bijold, Tetra Tech, Inc.
Randal Osicki, Thurber Engineering Ltd.
Rob Charron, Thurber Engineering Ltd.
Jeremy Boswell, Thurber Engineering Ltd.
Ajinkya Koleshwar, TRE Altamira
Riccardo Tortini, TRE Altamira
Ezzeddine Khodja, Tunisian engineers order
Hugo Carlos Scheuermann Filho, Universidade Federal do Rio Grande do Sul (UFRGS)
Nilo Consoli, Universidade Federal do Rio Grande do Sul (UFRGS)
Alex Kalonji Kabambi, Universite Officielle Bukavu
Peter Kaheshi, University of Alberta
Uddav Ghimire, University of Arizona
Yuan Li, University of British Columbia
Jiarui Chen, University of California, Davis
Isabelle Demers, University of Quebec in Abitibi-Temiscamingue
Dr Luis Alberto Torres Cruz, University of the Witwatersrand
Gustavo Marçal, Vale
Gustavo Belotto, Vale S.A.
Gino Omar Calderon Vizcarra, Vale S.A.
Felipe Bolivar Domingos, Vale S.A.
Danilo Manata Eloi, VALE SA
Robert Stafford, Western GeoSystems
Juan Carlos Ayes-Zamudio, WSP
Daniel Pham, WSP
Negar Ghahramani, WSP
Ben Wickland, WSP Canada Inc
Mahmoud N. Hussien, WSP Canada Inc
Rui Couto, WSP Canada Inc.
Mohammad Zarrabi, WSP Canada Inc.
Ryan Shedivy, WSP USA Inc.
Christian Armstrong, WSP USA Inc.
Tanya Walkenbach, WSP USA Inc.
Beth Irish, WSP, UK

THE ORGANIZERS GRATEFULLY ACKNOWLEDGE THE FOLLOWING CONFERENCE SPONSORS AND EXHIBITORS:

SPONSORS

PATRON

FREEPORT
FOREMOST IN COPPER

PLATINUM

CONETEC
Geosyntec consultants
HATCH
Klohn Crippen Berger
srk 50 YEARS
wsp

GOLD

AECOM
AtkinsRéalis
BARR
GBGGROUP
BGC
CETCO
Diemme Filtration
A brand of Aqseptence Group
flo solutions
GHD
jord | VIPER
Knight Piésold CONSULTING
mk 3D
NewFields
Newmont
Paterson & Cooke
PhotoSat
SOLETANCHE BACHY
Stantec
TETRA TECH
THURBER
TRE ALTAMIRA
A CLS Group Company

SPECIAL EVENTS

RAMBOLL
SOMERSET INTERNATIONAL
Synthetex
Reinforcing infrastructure for good.
VIRIDIEN
VALE

SILVER

Teck

NETWORKING BREAK

INTERA

BRONZE

GANNETT FLEMING | TRANSYSTEMS
terraSoft

EXHIBITORS

AECOM
AGAT Laboratories
AtkinsRealis
Barr Engineering Co.
Beadedstream
BGC Engineering
Cambridge Insitu North America
Cascade Drilling L.P.
CETCO
ConeTec
Copperstone Technologies
Diemme Filtration
Engineering Analytics, Inc.
Enviro Integration Strategies Inc.
Esri
FloSolutions
Freeport-McMoRan
GBG Group
Geo Instruments
Geofem
GEOKON
Geosyntec Consultants
GF Piping Systems
GHD
Gregg Drilling, LLC
Hatch Ltd
HydraMetrix
HydroGEOPHYSICS, Inc.
Iconix Waterworks
Iko Coletanche USA Inc
Jord International
Keller
Klohn Crippen Berger, Ltd
Knight Piesold
LSI LASTEM s.r.l.
Menard Canada
MineBridge Software Inc.
Nanometrics
NewFields
Newmont
Nicholson Construction
NV5
Parsons
Paterson & Cooke USA, Ltd
PhotoSat
Roctest Ltd.
SkyGeo Inc.
SLR Consulting
Soilworks, LLC
Soletanche Bachy
Solmax
Somerset International
SRK Consulting Inc.
Stantec
Synthetex
Terra Insights
Terrasoft
Tetra Tech, Inc.
TRE Altamira Inc.
Veolia Water Technologies & Solutions
Viridien
Weir
WSP

Preface

The first conference in this series was on Uranium Mill Tailings Management in 1978, which was organized by Civil Engineering Department of Colorado State University, Fort Collins, Colorado. The organizing committee consisted of John Nelson, Thomas Shepherd, Steven Abt, Wayne Charlie, and John Welsh. The series of conferences on uranium mill tailings continued through 1985, and in 1984 and 1985, the conference title was expanded to Management of Uranium Mill Tailings, Low-level Waste and Hazardous Waste.

In 1986, the organizing committee, consisting of Steve Abt, John Nelson, Richard Wardwell, and Dirk van Zyl, changed the title and focus to Geotechnical and Geohydrological Aspects of Waste Management. Content informed the design and operation of waste disposal facilities. The same focus was maintained for the 1987 conference.

By 1988 the uranium market had declined, uranium mills had closed, and support for a symposium on uranium mill tailings, hazardous waste, or most any topic associated with mine waste had declined. Thus, the conference was not held from 1988 until 1994. In 1994, Colorado State University, the sponsor of the uranium mill tailings conferences, resuscitated the conference series as Tailings & Mine Waste, the title by which the series remains today. In 2004, attendance reduced leading to a negative financial situation for the conference and reluctance on part of Colorado State University to support the conference series; thus, the conference was not held from 2005 until 2008.

In late 2007 an organizational committee was established in Colorado through the support of several consulting engineering companies: Engineering Analytics, Golder, Knight Piésold, MWH Global, Robertson GeoConsultants, Inc., SRK Consulting, Inc. Tetra Tech, Inc. and URS Corporation. A stable financial basis was established for the conferences in Colorado. A partnership also was established between Colorado State University, University of British Columbia, and University of Alberta. The conference now rotates between the United States and Canada, whereby in even years Colorado State University hosts the conference and in odd years the conference rotates between University of British Columbia and University of Alberta.

Message from the Chairs

The Tailings & Mine Waste Conference is an industry-academia partnership that serves as a platform for professionals to network, share knowledge, debate, discuss lessons learned, and generally advance both the state-of-practice and state-of-art in tailings and mine waste management. Colorado State University is proud of the creation and continued success of this conference series. Over the past few years, the Colorado conference has continued to grow and was relocated to the Denver area to engage more working professionals. We hope that you enjoy this year's Conference at a new venue – the Westin in Westminster. We will be back to Westminster again in 2026, before (hopefully) celebrating the 50th Anniversary of the Conference back where it all began in 2028.

Although hosted by Colorado State University, conference planning and support would not be possible without the support of C3 Alliance, and all the industry sponsors. We would especially like to thank our Patron Sponsor, Freeport-McMoRan for their continued support, as well as ConeTec, Geosyntec, Hatch, Klohn Crippen Berger, SRK, and WSP for stepping forward as Platinum Sponsors. All revenue from the conference is used by Colorado State University to support graduate education and research in the area of tailings and mine waste. This attribute of the conference cannot be overstated. Our team has come together with a combined vision to host the world's leading technical conference in tailings and mine waste while supporting the growth of the next generation of professionals.

We thank the Organizing Committee, Conference Leadership Committee, Sponsors, Exhibitors, all the authors of the technical papers, and all Conference delegates for supporting the Conference. This Conference is for all of us.

Christopher Bareither and Joseph Scalia,

Chairs, Tailings and Mine Waste 2024

PLENARY ABSTRACTS

Plenary Session 1

A Corporate Look at Tailings Management – Lessons Learned

Moderators:
Jason Andrews & Michael Henderson

Speakers:
Tamara Johndrow
Jon Lapwood
Scott Martens
Jaime Awmack

Join us for the first plenary session of the 2024 Tailings and Mine Waste conference. The event will feature a welcome address by a representative of Freeport McMoRan, our Patron Sponsor, highlighting the 20-year evolution of tailings management. This session will also feature speakers from three mining companies discussing their tailings management journey. They will discuss lessons learned along the way and their outlook for future tailings management. The session will conclude with an interactive panel discussion with live questions form the audience.

Tamara Johndrow



Tamara Butler Johndrow is Director of Tailings, Crushed Leach, and Water at Freeport-McMoRan. She received her B.S. and M.S. in Civil Engineering and is a licensed Professional Engineer with 26 years of experience in water resources and geotechnical engineering, management and program development. She began her career as a consultant at Golder Associates (WSP) and Engineering & Hydrosystems (WSP Golder).

Ms. Johndrow joined Freeport-McMoRan in 2008, creating the Tailings, Crushed Leach, and Water team to support business critical areas of tailings storage facility, crushed leach stockpiles, and dam safety as well as water management across Freeport's portfolio. She has had responsibility for strategic planning, design, construction quality, operational support, inspection, review, governance processes and reporting, and due diligence for tailings storage facilities as well as for crushed leach stockpiles, levees, and water dams. Her current focus includes tailings & water governance, tailings innovation, and water management strategy.

Ms. Johndrow is a trusted advisor to Freeport-McMoRan executive leaders, and she represents the company in various external tailings research and management engagements. She currently chairs the International Council on Mining and Metals (ICMM) Tailings Management Working Group and the GeoStable Tailings Consortium Steering Committee.

Jon Lapwood
Principal Advisor Major Hazards, Group Technical Rio Tinto



Jon Lapwood is the Principal Advisor Major Hazards in Rio Tinto's Group Technical Major Hazards team. Jon is a geotechnical engineer with a broad range of experience in open pit mining operations, data integration and analysis, and the design, development and implementation of systems. He has a strong interest in geotechnical monitoring instrumentation, data, software and technologies and how these can be an integral part of effective risk management in dynamic mining environments.

Jon's current role includes the provision of technical guidance, technical support and undertaking second-line assurance activities. He is currently the project lead for the implementation of the Global Industry Standard on Tailings Management for Rio Tinto's diverse portfolio of tailings facilities, and is coordinating the implementation efforts across the business. Jon also leads a project which will combine geotechnical data with other technical and business information for enhanced understanding and improved oversight of Rio Tinto's major hazards.

Scott Martens
Director, Tailings, Tech Resources Limited



Scott Martens is the Director, Tailings at Teck Resources, providing corporate oversight of tailings governance and engineering at Teck's operating mines, development projects and legacy facilities across North and South America.

Scott has 29 years of geotechnical engineering experience, with 15 years in geotechnical consulting and 14 in geotechnical mining operations. He has a Bachelor of Civil Engineering degree from the University of British Columbia and a Master's degree in Geotechnical Engineering from the University of Alberta.

Scott is an Adjunct Professor of Geotechnical Engineering at the University of Alberta, a member of the independent review board for the tailings facilities at a gold mine, and is the Chair of the Mining Dams Committee for the Canadian Dam Association. Scott was a keynote speaker for TMW in 2021.

Jaime Awmack
VP, Operational Support, *Eldorado Gold*



Jaime Awmack is the VP, Operational Support at Eldorado Gold, where she works closely with site and technical teams to facilitate change at the operational level and drive continuous improvement globally. She is a professional mineral processing engineer with around 20 years' experience, and prior to joining Eldorado, she served as Process Manager at Newmont's Peñasquito mine in Mexico. Her current role ranges widely from tailings and heap leach stewardship to operational technology and asset management, and she's always looking to keep learning from the brilliant and fascinating people across this industry.

Moderator: Michael Henderson
Principal, Strata-Geo LLC



Michael Henderson has spent nearly all his plus 40-year career in the engineering and environmental aspects of managing mine waste, including tailings. Mr. Henderson's experience extends to projects in North America and overseas. Mr. Henderson has operations experience at several large mines, research experience at a National Laboratory where he conducted mine and energy research for the US Bureau of Mines and Department of Energy, and as a consulting engineer for the past several decades.

Mr. Henderson is a Professor in the Mining Engineering Department at the Colorado School of Mines and was the first Director of the Tailings Center, which is a multi-university/industry effort aimed at addressing the educational and research needs around tailings management. He is now a Director-at-Large, remaining fully engaged with the Tailings Center. He has taught professional development, undergraduate and graduate engineering courses on geotechnical issues, mine waste management, and risk assessment at Colorado School of Mines, Colorado State University and the University of Nevada.

Mr. Henderson is also a Principal with the firm of Strata Geo, where he is an Engineer of Record (EOR) on several large mining projects, an Independent Tailings Review Board Member (ITRB) for several mid-tier and large mining companies, and an advisor in establishing tailings stewardship and management programs for several mining companies. Mr. Henderson has authored dozens of papers on geo-environmental issues around mine waste, has contributed to three textbooks on the subject, and holds three patents on geophysical systems related to mine waste containment. Mr. Henderson has a B.S. in Civil Engineering from Colorado State University; an M.S. in Civil Engineering from the University of Pittsburgh; and a PhD (ABD) from the University of Nevada.

Moderator: Jason Andrews

Senior Geotechnical Engineer, Senior Vice President, Engineering Analytics



Mr. Andrews has experience in geotechnical engineering pertaining to mine site remediation, construction defect litigation, retaining wall design and repair, field investigations, and quality assurance and quality control oversight relating to geotechnical and environmental projects. He has served as a senior engineer and project manager for many mining design and reclamation projects, construction defect litigation projects, and civil engineering projects. His areas of experience include site investigation and characterization, feasibility investigations, engineering investigations, development of remediation alternatives, implementation of remedial design, and construction oversight. His areas of emphasis include slope stability analyses, expansive soils, collapsible soils, settlement analyses, and other aspects of geotechnical engineering. Mr. Andrews has performed geotechnical engineering and environmental investigations for forensic, mining, and public works projects in California, Colorado, Illinois, Nevada, New Mexico, Oregon, Washington State, Wyoming, and Peru.

Plenary Session 2

2030 and Beyond – Perspectives on Evolving Tailings Management

Moderators:
Amanda Adams & Martin Rust

Speakers:
Andrew Witte, KCB
Chris Sonntag, BHP
David Slack, ConeTec
Antonia Mihaylova, ICMM

Plenary Session Abstract: Tailings Facility Engineering – The Next Frontier

The future of tailings engineering is poised to embrace innovative technologies and methodologies to enhance sustainability and safety. Real time information management, advanced monitoring, predictive modeling and new deposition techniques aim to mitigate environmental impacts and ensure the integrity of structures, reflecting a shift towards more responsible and efficient industry practices. Tailings engineering continues to evolve, integrating new research and technologies to meet the challenges of modern mining operations and environmental stewardship. This session will explore the near-future through the presentation "What could Tailings Facility Engineering look like in 2030," presented by Andrew Witte, and speculate about the more remote future, through a panel discussion with diverse industry experts.

Panel Abstract: 2030 and Beyond – Perspectives on Evolving Tailings Management

The panel session will expand on the concepts presented by Witte et al. by engaging a number of diverse tailings management professionals. The panel will provide their perspectives of the 2030 vision of initiatives and advancements from owner, engineering, and other perspectives. Then, the panelists will explore even further into the future. They will discuss how we can build competency and capacity from the current shortage of qualified tailings professionals, how characterization of tailings and development of improved tools for characterization will change classical design approaches, and how a new vision for closure planning could emerge. The panel will be moderated, and opportunities for audience engagement will be available

Andrew Witte

Senior Geotechnical Engineer, Principal at Klohn Crippen Berger



Andrew is a Senior Geotechnical Engineer with over 20 years of consulting experience in geotechnical and water resources engineering on various mining, infrastructure, municipal, and industrial-related projects. Andrew's chief area of practice is the design, construction, safe operation and closure of earthfill and rockfill embankment dams within Canada and around the world; specifically, he is currently the lead engineer for several major cyclone sand tailings dams in British Columbia. Andrew also holds various design and review roles for numerous other proposed, operating, and closed tailings dams, each with their unique challenges.

Chris Sonntag



Chris graduated from the University of Saskatchewan with a BSc. In Civil Engineering and is the Manager Technical for BHPs Legacy Assets portfolio. He leads a team of Tailings, Groundwater and Geotechnical specialists who steward technical studies, support decisions and progress closure activities across approximately 20 mine sites in North America. Chris is active with tailings and mine workforce activities and currently chairs the SME Advanced Tailings Talent Attraction sub-Committee (ATTAC) and represents BHP on Industry Advisory Board for the Tailings Center.

David Slack



David is the Chief Operating Officer at ConeTec, where his passion for technological innovation and operational excellence drives his leadership in the geotechnical site investigation industry. With a degree in Mechanical Engineering from the University of British Columbia and nearly two decades of experience at ConeTec, David's progression from field technician to executive has provided him with both a robust technical foundation and a deep understanding of the industry. Prior to his current role, he served as Vice President and General Manager in Chile and Peru, where he was instrumental in expanding ConeTec's footprint across Latin America.

David believes in the immense potential of innovation and technology to address the pressing challenges of today. Within ConeTec, he is committed to fostering an environment that encourages innovation and technological advancement, strengthening the company's position as a leader in sustainable site investigations while also contributing to the advancement of industry standards and practices.

Antonia Mihaylova



Antonia Mihaylova is a Senior Manager at ICMM, leading the tailings management workstream and the Consolidated Mining Standard Initiative. Prior to ICMM, Antonia was at the International Union for Conservation of Nature (IUCN), where she headed the Director General's Office, serving as Special Adviser to the Director General. Prior to that, she managed the Global Tailings Review, the process that led to the development of the ICMM, UNEP and PRI-backed Global Industry Standard on Tailings Management (GISTM). She also served as a member of the International Advisory Panel convened by UNEP, the Church of England Pensions Board and the Council on Ethics of the Swedish National Pension Fund (on behalf of PRI) to support the establishment of a Global Tailings Management Institute. Antonia has spent several years at an international

development consultancy, working on World Bank and European Bank for Reconstruction and Development (EBRD)-funded mineral resource governance projects across Africa and Asia. In the early stages of her career, Antonia worked for an environmental NGO Global Greengrants Fund, supporting grassroots nature conservation initiatives. She holds a bachelor's in economics and politics; and a Master's in environmental policy from the London School of Economics (LSE).

Moderator: Amanda Adams



Amanda Adams, P.E, PMP, is a Principal Engineer at Stantec with 18 years of mining industry experience. Amanda currently serves as a member of Stantec's US Mining leadership team in the role of Business Center Operations Leader. She is a Colorado School of Mines Graduate with a B.S. In Geological Engineering. She has been employed at Stantec (through acquisition) since 2008. Her technical experience is primarily focused on the design of tailings storage facilities for mining clients. Her design experience has spanned all phases of project development from siting studies to pre-feasibility, feasibility, basic engineering, detailed design, construction, operation and closure. Amanda is a passionate advocate for diversity, equity and inclusion (DEI) in STEM fields. She is Past President of the Women in Mining (WIM) Denver Chapter and in 2024 received a Distinguished Service Award from WIM. She is a one of the founding members of the US Society on Dams (USSD) DEI Committee. Amanda is also involved in professional organizations to promote mining and tailings practices, including previously serving as the USSD Tailings Dams Committee Chair and she is the current Chair of the SME Tailings and Mine Waste committee.

Moderator: Martin Rust



Martin Rust, PhD, PrEng. is a Professional Civil Engineer with 24 years' experience primarily in the field of Geotechnical engineering. His experience includes various roles on some world class tailings and ash storage facilities mainly in Africa, and more recently in the Americas. He has served as Designer of Record (DoR), Engineer of Record (EoR) and member of the Independent Tailings Review Board (ITRB) on various sites. Martin has also conducted multiple Dam Safety Reviews (DSR). His experience includes design and construction quality assurance for large construction projects. He actively stays abreast of international best practices such as those published by GISTM, ICOLD, CDA and MAC.

Plenary Session 3

Are we getting distracted? How can we best use the GISTM as an effective path to risk reduction rather than it becoming a path to box-check auditing?

Moderator:
Ryan Shedivy
Speakers:
Mike Davies
Susan Joyce
Daniel Landers
Louise McNab

The International Council on Mining and Metals (ICMM), the United Nations Environment Programme (UNEP) and the Principles for Responsible Investment (PRI) co-convened a global tailings review (GTR) to establish the Global Industry Standard on Tailings Management on the 5th of August 2020.

The Global Industry Standard on Tailings Management strives to achieve the ultimate goal of zero harm to people and the environment with zero tolerance for human fatality. Underpinned by an integrated approach to tailings management, the Standard aims to prevent catastrophic failure and enhance the safety of mine tailings facilities across the globe. It embodies a step-change in terms of transparency, accountability and safeguarding the rights of project affected people. (GTR 2020)

Is the Global Industry Standard on Tailings Management effective at achieving its goals? Are we, as the tailings practitioner industry, getting distracted from these goals and in particular the ultimate goals and commitment to zero fatalities? How do we best use the GISTM as a path to risk reduction rather than having it become simply another path to auditing and consuming valuable time from the limited number of qualified tailings practitioners.

This plenary session will focus on these questions as we hear from four different perspectives followed by a moderated discussion based upon questions from those attending on how the industry can best achieve the GTR goals.

Susan Joyce: President, On Common Ground Consultants Inc.



Susan Joyce is a Social Performance Specialist with 30 years of experience working to achieve integrated decision-making and effective incorporation of non-engineering criteria in the management of mining operations, including management of tailings. She has worked extensively assisting companies, communities and financial institutions to manage social and human rights risks and to meet and exceed international standards. Her work includes development of effective on-the ground strategies for reducing risk to companies and communities and enhancing potential social value of mining activities. She served on the Expert Panel that developed GISTM and her current focus is on the effective integration of social performance into tailings management. She serves on an ITRB and provides technical support to others. Susan has a Professional Certificate of Tailings Management from the Australian Institute of Mining and Metallurgy and an MSc. in Development Sociology from Cornell University.

Dr. Michael Davies, P.Eng., P.Geo.



Dr. Davies is a Geotechnical/Geological Engineer, has spent his entire roughly 40-year career in the mining industry. Prior to founding his own consultancy in 2022, he was an Executive with Teck Resources. He also has official affiliations with several academic institutes. Prior to coming to Teck he spent over 25 years in consulting including projects and senior management. He has had a career-long involvement in industry groups and was the mining industry's advisor for the Global Industry Standard for Tailings Management (GISTM). He has worked on all stages of mining projects from advanced exploration through decommissioning and reclamation. He has direct experience with more than 100 tailings facilities and, while retired from full-time work, currently a member of several Independent Review Boards around the world.

Louise McNab

Group Principal Engineer: Tailings, Hydrology and Closure, at Gold Fields



Louise is a Group Principal Engineer: Tailings, Hydrology and Closure, at Gold Fields. With a global role, she oversees operational and technical support for 37 Tailings Storage Facilities across 5 continents.

Originally from Scotland, Louise earned her Master's in Civil Engineering from the University of Edinburgh. With over a decade of experience, she specializes in tailings management, design, operations, and closure, ensuring safety and sustainability in mining operations worldwide.

Daniel Landers
Vice President – Risk Engineer, Mining at Swiss Re



Daniel Landers is a Risk Engineer for a global insurance company, where he supports underwriting of the mining risk portfolio. He completes assessments for mining operations worldwide, analyzing risks that could generate insurable property losses, provides recommendations to insured clients on risk management, and supports the assessment of mining and energy construction projects. In this role he provides subject matter expertise on tailings facilities and assists in the development of underwriting guidelines related to the subject.

Prior to working in the insurance industry Mr. Landers held the role of corporate tailings manager for a senior gold mining company. He has held project engineering and execution roles at large engineering and gold mining companies, and his experience has included project permitting, design and construction delivery of mining dams, civil infrastructure and process facilities for projects in the USA, South America, and Africa. He is also involved in digital innovation and data analytics initiatives around risk assessment management and evaluates ways to improve the evaluation of man-made risks in mining, and specifically in the field of tailings operations and stewardship.

Moderator: Ryan Shedivy, PE
Assistant Vice President, Geotechnical Engineer, WSP USA Inc.



Ryan Shedivy is an Assistant Vice President, Geotechnical Engineer at WSP with experience leading interdisciplinary teams in the mining, power, and solid waste industries. His field, design and ranges from conceptual level design and cost estimation through permitting and issued for construction level design and bid package development in support of tailings, waste rock, heap leach, coal combustion residual, and landfill facilities. He is currently the EoR of three closed tailings facilities and deputy EoR of two active tailings facility.

Chapter One

What Could Tailings Facility Engineering Look Like in 2030?

TAILINGS AND
MINE WASTE 2024



What Could Tailings Facility Engineering Look Like in 2030?

Andy Small, Klohn Crippen Berger, Canada
Andrew Witte, Klohn Crippen Berger, Canada
Annika Bjelkevik, Tailings Consultants Scandinavia AB, Sweden

Abstract

Over the past five to ten years, there has been a surge in many different aspects of tailings facility engineering as the mining industry pays more attention to the importance of their tailings facilities as part of the overall success of their mining operations. This has been partly related to the Global Industry Standard on Tailings Management (GISTM) that was released in 2020, but is also due to other initiatives by several mining companies and organizations around the world that are committed to safe tailings facilities. There are major initiatives occurring on many fronts, including:

- Tailings technology and deposition strategies.
- Characterization of tailings and foundation soils, slope stability assessment (including deformation analyses), liquefaction predictions, dealing with high stresses, closure, filtered tailings, and so on.
- Closure strategies.
- Surveillance techniques.
- Competency building.
- Guidance documents that bolster the capabilities of the engineers working on tailings facilities.

This paper presents a summary of key issues that are currently confronting tailings facility engineers, owners, and regulators for each of the above topics. It describes initiatives that are currently underway or issues for which there are plans to address, and provides a vision for 2030. A survey of leaders in tailings facility engineering was conducted and the results of the survey are summarized in the paper.

Introduction

This paper envisions what tailings facility engineering could look like in 2030. Significant advances have been made in the field in recent years, and the pace of innovation is accelerating. The volume of tailings to be managed is also increasing, as mining operations are expected to increase production by about 3% per

year until at least 2030[1], while ore grades are decreasing (requiring more volume to be milled to realize a unit of each desired commodity).

Major focuses of this paper include improved tailings technology and deposition strategies, closure strategies, improved characterization methods for tailings and foundation soils, enhanced surveillance techniques, and the development of technical capacity and competency within the industry. Governance is a key aspect for safe tailings management that is also evolving, but is beyond the scope of this paper.

The authors have defined "tailings facility engineering" as covering the following areas of knowledge:

- tailings milling and processing,
- tailings storage facility design,
- closure design,
- geotechnical engineering,
- hydrogeological engineering,
- hydrotechnical engineering,
- geology,
- geochemistry,
- environmental protection,
- construction,
- operations,
- surveillance,
- risk assessment, and
- governance.

This paper continues with some context and discusses the method used to gather supporting information related to the key topics noted above. The paper presents the authors' understanding of these key topics summarized under the subheadings: Current Situation and Vision for 2030.

Context and why 2030?

Over the past five to ten years, there have been significant efforts to reduce the likelihood of catastrophic tailings failures through training, guidance documents, increased regulation, improved surveillance, etc. Increases in computing power have made complex analyses more efficient and have supported the use of artificial intelligence (AI).

Investors and insurance companies are paying close attention to the efforts to reduce risks associated with tailings storage facilities (TSFs). However, as these efforts drive the TSF risks to lower levels, a key challenge will be the demand for qualified people, as well as the demands on those qualified people. The demand for capable and experienced engineers of record (EoR), responsible tailings facility engineers/persons (RTFE/P), independent tailings review board (ITRB) members, and regulators is far greater than the supply, which is declining due to the age demographic of the people currently fulfilling

[1] This percentage is based on information from (i) Mining. Com: Copper production, price rebound on the horizon – report, July 2022; (ii) expertmarketresearch.com: Global precious metals market size, 2022; (iii) Canada Energy Regulator: Canada's energy future, raw bitumen production by type – evolving policies scenario, 2021, (iv) finance.yahoo.com: Investing in gold: Global gold mining market size is projected to grow at 3.5% CAGR, exceed $260 billion by 2030, September 2023.

these roles. The next ten years will see a significant reduction in the number of senior tailings facility engineers practicing, and there are not enough younger engineers available to backfill the current and expected demand.

The International Commission on Large Dams (ICOLD) has developed a world-wide registry of TSFs that has catalogued over 24,000 entries (Rana and Small, 2024). As noted above, the volume of tailings to be stored will increase by more than 3% per year over the next six years, which means more TSFs and larger TSFs.

Repurposing or expanding older TSFs to meet storage needs with the aim of reducing additional disturbance area, as well as upgrading those that were not built to today's standards will be undertaken, which pose significant technical challenges. For example, demonstrating the safety of existing TSFs, particularly those that employed classical upstream construction (i.e., upstream construction on unconsolidated fine tailings), is very complex. Furthermore, water conservation is becoming more important to operators and communities due to climate change and increasing regulation of the use of "clean water" and requirements on discharge of water to recipients.

From some perspectives, the year 2030 does not seem that far away, but, after reflecting on what has been accomplished in the past six years, the authors selected the year 2030 for this paper; six years from when this paper was prepared.

A number of guidance documents have been issued related to TSF safety. Table 1 shows that for the six-year period from 2011 to 2017, there were at least seven major guidance documents issued, whereas, for the following six years, 2018 to 2024, there were at least another nine (despite the industry navigating a global pandemic).

A major contribution to recent developments was Dr. Morgenstern's Victor de Mello lecture on performance-based risk-informed design (Morgenstern, 2018), which has influenced and impacted many of the guidance documents listed in Table 1 as well as regulations.

Additional key changes that have occurred over the past six years include:

- In 2018, there was significant trepidation associated with the EoR concept as a viable career path. Whereas in 2024, more young engineers see this as a career path (Prince and Boswell, 2023).
- In 2018, a limited number of dam safety surveillance programs had automation, but in 2024, there is extensive automation, remote monitoring, cameras, and monitoring centers.
- In 2018, AI was on the horizon, but in 2024, AI is being used to support complex surveillance data gathering and interpretation.

Table 1: Tailings dam safety guidance documents within the mining industry from 2011 to 2024

Year	Organization	Document title
2011	ICOLD	Bulletin 138: Improving Tailings Dam Safety
2011	ECCC	Guidelines for the Assessment of Alternatives for Mine Waste Disposal
2012	ANCOLD	Guidelines on Tailings Dams
2013	ICOLD	Bulletin 153: Sustainable Design and Post-Closure Performance of Tailings Dams
2014	CDA	Mining Dams Bulletin (Revised 2019)
2014	OSTDC	De-Licensing of Oilsands Tailings Dams
2011-2024	MAC	Updates to Guides on Management of Tailings Facilities and Developing OMS Manuals
2019	ICMM	Integrated Mine Closure: Good Practice Guide
2020	GTR	Global Industry Standard on Tailings Management (GISTM)
2021	ICMM	Tailings Management: Good Practice Guide
2021	CDA	Bulletin: Tailings Dam Breach Analysis
2021	ICOLD	Bulletin 181: Tailings Dam Design, Technology update
2022	SME	Tailings Management Handbook
2022	ICOLD	Bulletin 194: Tailings Dam Safety Guideline
2022	ACR	Assessment Tool for Landforms in the Oilsands
2011-2024	MAC	Updates to Guides on Management of Tailings Facilities and Developing OMS Manuals

ICOLD = International Commission on Large Dams, ECCC = Environment and Climate Change Canada ANCOLD = Australian Commission on Large Dams, CDA = Canadian Dam Association, OSTDC = Oil Sands Tailings Dam Committee, MAC = Mining Association of Canda, ICMM = International Council on Mining and Metals, GTR = Global Tailings Review, SME = Society for Mining, Metallurgy and Exploration, ACR = Alberta Chamber of Resources.

The authors believe that over the next six years, much can be done to maintain the momentum and to do more than just "continuous improvement." This paper explores additional initiatives and advancements in the next six years presented as a collective vision for 2030.

Method

To support the creation of a vision of what tailings facility engineering could look like in 2030, the authors reached out to colleagues and leaders in the tailings space around the world with a survey questionnaire to obtain a global perspective. An extensive questionnaire was issued to over 240 tailings practitioners covering the following topics:

1. Tailings technologies and deposition.
2. Closure strategies.
3. Characterization of tailings and foundation soils.

4. Surveillance of tailings facility performance.
5. Design approaches for slope stability assessment.
6. Guidance documents for tailings facility safety design.
7. Building competency and capacity.
8. Artificial Intelligence.

Over 60 people responded to the questionnaire (as of the end of May 2024) from 15 countries; the majority of the responses were from Canada and the United States. Presentations were given in Canada in May and June 2024 on the vision for tailings facility engineering in 2030 and additional input was obtained from the audience members from those presentations. The authors also consulted with several key people and organizations within different areas of tailings facility engineering.

This paper will also be presented at the ICOLD Symposium on Dams for People, Water and Environment and Development in India in September 2024 and at the Panamerican Conference on Soil Mechanics and Geotechnical Engineering in Chile in November 2024. The questionnaire results and an updated version of the paper will be available at the end of 2024 through the ICOLD committee on tailings dams and waste lagoons (Technical Committee L).

In this paper, the authors endeavored to summarize the results of the questionnaire and input from contributors. This paper was not prepared on behalf of ICOLD Committee L.

Building competency and capacity

Current situation

As noted above, there is, and will likely continue to be, a shortage of qualified engineers providing services for TSF safety and this topic was considered the most important by the respondents. Hence, this topic is presented first in this paper.

On the one hand, the field of tailings facility engineering is challenging, complex, interesting, and rewarding. It is no longer viewed as commodity engineering, and the professional contributions are viewed as being of value by mine owners and regulators. There are many training programs being offered by universities and technical associations. Consulting companies and mine owners are also providing in-house training.

On the other hand, with the growth in tailings, the limitations associated with how TSFs can be developed, and the higher expectations of regulators and stakeholders, the demands of tailings facility engineering will increase. Some universities are offering graduate degree programs in tailings engineering, but there is limited training at the undergraduate level and more master's level programs are needed.

Mining is not considered an attractive career opportunity to young people. Abenov et al. (2023) conducted a survey of people between the ages of 15 and 30 and asked if they would be interested in working in one of nine different sectors, including health care, financial services, construction, and mining. Mining ranked last among the nine sectors, with 70% of the respondents saying that they would not be interested in working in the mining sector. One possible reason for this is that there could be a disconnect between the value that mining provides and the perception of young people; that is, they do not realize that most of the conveniences and necessary infrastructure that they have comes from mining. These conveniences and infrastructure are taken for granted.

Vision for 2030

To help address the challenge of the human resources shortage, the authors recommend establishing the discipline of "Tailings Management Professional" (TMP) as a first step. In this context, tailings management includes the design, construction, operation, and closure of systems that are used to produce tailings and the facilities that are constructed to store tailings. This would include the following facilities:

- Conventional slurry, thickened, paste, filtered tailings.
- Co-mingled, co-disposed, co-deposited, and co-placed mineral residue (e.g., tailings and waste rock, fines and coarse discards, etc.).
- Containment facilities for sludge and sediment from process, water treatment plants, or runoff.

Ash lagoons for power-generating plants could also be covered here.

The TMP should have knowledge in the areas of knowledge listed above (in the Introduction) as tailings facility engineering, with a specialty in one or more of those knowledge areas and a general knowledge of the others.

ICOLD is forming a working group to develop the scope for the TMP discipline and will work with other organizations to define it. With this discipline defined, it will be possible to identify the TMP discipline as a distinct career path for young engineers, rather than, as so many do now, "just falling into tailings engineering."

Further, it will be possible to develop focused training that supports the development of TMPs. As noted above, there is a significant amount of training occurring, but there is not a comprehensive database that captures this training. Such a database is being developed by the Society for Mining Metallurgy and Exploration (SME), which will allow organizations to list the training they are providing. For example, Organization X may be planning to conduct slope stability training in Africa and can post that training to this database, indicating if it is in person and/or virtual. Then, engineers from around the world can search the database for slope stability training, find the one in Africa and determine if it meets their requirements.

With the discipline of TMP defined and a database offering current available training available, then a gap analysis can be done between what is required and what is currently being offered. Plans can then be developed to fill these gaps and provide additional opportunities to develop competency and capability.

One of the survey respondents recommended that graduate programs be developed to focus on the development of TMPs, but not have a significant research component. This program would be course-based and structured to run for one year. Because it would not have a research component, it would not be funded by research grants, which would require funding from industry to help support students who are interested in taking this program. Colorado State University and the University of Alberta are both considering this approach and plan to work with other universities to advance this concept.

As a result of discussions held with colleagues in the industry, the authors included the following question in the questionnaire: "Should there be an international certification program for tailings facility engineers?" There was a wide range of responses, from "Yes, this is important" to "No, this is not required." The reference to certification was not in the context of receiving a certificate after having completed a set of courses. Rather, it was intended to be a certification that is received after having also obtained experience from course work. There are some advantages to certification, but there are several challenges with establishing an internationally recognized certification program, which would require significant infrastructure to support. There was sufficient interest in this topic that ICOLD is creating a working group to explore the issue and provide a recommendation on whether such a certification is of value and, if so, then what such a program could look like. This would be done in concert with other key organizations to help decide whether certification should be pursued or not.

Given the disconnect between the perception of mining and the benefits of mining (and therefore tailings management), more work needs to be done by organizations such as ICMM, MAC, CIM, SME, etc. to educate young people about the benefits of mining to society and the value of being involved with responsible tailings management.

Tailings technologies and deposition

Current situation

The vast majority of existing TSFs worldwide employ conventional slurry-deposited tailings. Slurry deposition often results in loose, saturated deposits that are potentially prone to liquefaction.

Filtered tailings technology has evolved but the actual number of filtered tailings facilities is not quantified. The TSF registry that has been developed by ICOLD and the general consensus from the survey is that dewatered tailings operations (including high-density thickened, paste, and filtered tailings) make up less than 1% of existing tailings operations. The authors' experience, reinforced by the survey responses, is as follows:

- Filtered and paste tailings technology initially developed in the 1990s, but widespread application of this technology has been limited by economics, operational challenges at high throughputs, and technical challenges in wet climates.
- Combined management of tailings and waste rock (i.e., co-mingling, co-disposal, co-depositing, co-placement, etc.) is gaining traction in research trials but has not been fully proven at operational scale (Burden and Wilson, 2023).
- For new tailings facilities, the general approach to technology selection often involves performing a structured multi-criteria alternatives analysis of feasible sites, technologies, and strategies for tailings management (GISTM Requirement 3.2). However, this practice has not been widely adopted by the industry and is required by regulation in only a few jurisdictions, for example, British Columbia, Canada (Ministry of Energy, Mines, and Low Carbon Innovation, 2024).
- Water management is a key driver in tailings technology selection, with mines in arid climates opting to recover water in the process by dewatering to reduce evaporation losses, while mines in wetter climates tend towards conventional slurried tailings and managing surplus water via large supernatant ponds (MEND, 2017).
- Tailings geochemistry, including acid-generation potential, leads to a generally binary choice between wet or dry cover solutions, but there is a movement toward dry covers for closure with respect to risk (post-closure dam failure). Limited effort is put into designing tailings processing to reduce future risk, such as segregation of tailings into geochemically non-reactive and reactive streams and management of reactive streams in separate facilities. Tailings geochemistry is gaining much more importance in many mining districts, with a focus on source control.

Vision for 2030

The consensus among the survey respondents is that conventional slurried tailings will continue to be the norm for new tailings facilities in 2030. However, the selection of conventional tailings technology as the best available technology (BAT) for a site will need to be objectively demonstrated through tailings alternatives assessments (ECCC, 2011), supported by risk assessments to define design and operational controls. This position is based on a view that classical upstream construction methods will cease and be replaced by centerline construction, modified upstream construction (i.e., upstream construction that employs an engineered structural zone such as a compacted tailings beach) or downstream construction.

It is envisioned that filtered tailings will continue to gain popularity due to technological advances that allow scaling to throughputs of greater than 50,000 tonnes per day. However, filtered tailings will likely still represent a low percentage of future tailings facilities due to the high capital and operating costs, and the inability to match the scales of the world's increasingly high-throughput low-grade porphyry mineral

deposits. Rather, it is likely that filtered tailings may find a place as a feasible companion technology to support a primarily conventional operation, with the filtering process used to create dewatered tailings for use as a construction material for perimeter embankments, or to create smaller-scale deposits of reactive tailings concentrates that would be managed outside of a larger conventional facility. Such applications would benefit from guidance documents specific to filtered tailings with emphasis on hydrotechnical, geotechnical, and geochemical considerations, including surface water management, unsaturated strength, dust control, and seepage behavior. Some documents have been developed, but are not publicly available.

Multi-criteria alternatives analysis will move away from just focusing on the tailings facility and will include the overall mine plan that optimizes the mining operation, in concert with the tailings plan and closure plan. Factors such as water conservation and climate change will be given more prominence in these analyses.

Regardless of the tailings technology selection, we see tailings geochemistry taking a more active role in tailings-related decision-making due to increasing regulation of surface water and groundwater, and a perceived lack of appetite in the investment community for planned long-term water treatment in new mining propositions. The MAC tailings working group plans to update their *Tailings Guide* by 2026 to include more emphasis on geochemical failure modes in its guidance on risk and alternatives assessment.

Combined, the above vision for tailings technology selection requires the adjustment of classical financial models (e.g., net present value, NPV) to capture the true lifecycle cost or benefit of the tailings technology without discounting long-term costs to low present values. Although the world financial system is unlikely to make such a step-change by 2030, it is hoped that the momentum achieved by PRI and UNEP through the development of the GISTM will continue.

Closure strategies

Current situation

In 2024, there is no one global definition of "closure." ICOLD's Bulletin 194 (Preprint) – Tailings Dam Safety defined closure as: *A planned, final cessation of tailings disposal and the modification/engineering of the tailings dam with the objective of achieving long-term physical, chemical, ecological, and social stability, and a sustainable, environmentally appropriate after-use* (ICOLD, 2022). GISTM defines safe closure as: *A closed tailings facility that does not pose ongoing material risks to people or the environment which has been confirmed by an ITRB or senior independent technical reviewer and signed off by the Accountable Executive.* (GISTM, 2020).

The ICMM gap analysis of closure guidance documents for responsible closure (Slingerland and Hedley, 2023) differentiates "responsible closure" from "safe closure." The definitions of the two are:

- responsible closure means a final closed state where environmental, ecological, and social conditions are incorporated; and
- safe closure is a physically and chemically stable final closed state.

Because there is no consensus on the appropriate term at this time, the authors adopted the term "closure" for this paper, including all aspects of closure, i.e., both responsible and safe closure.

The survey responses indicated that the concept of TSF closure could encompass a broad range of considerations such as:

- long-term vision;
- alternative land use;
- environmental and social integration;
- regulatory compliance;
- limiting risk to humans and the environment by long-term physical, chemical, ecological, and social stability;
- principles related to ALARP (As Low as Reasonably Practicable); and
- limiting credible failure modes, i.e., elimination of potential failure modes or alternative ways to manage remaining risks/failure modes.

When it comes to care after closure, opinions on monitoring and maintenance differ. Some view safe or responsible closure as a state where no further human intervention is required, while others hold that, in some cases, there may be a need for ongoing monitoring and maintenance in perpetuity.

Many jurisdictions require closure plans and promote, or require, progressive closure at the permitting stage as well as financial guarantees for closure. Some jurisdictions require TSF closure plans as part of permitting conditions, prior to a mine starting or expanding. Efforts are being made by the industry to improve dialogue with stakeholders with respect to closure, but to gain the trust required for a constructive and transparent dialogue takes time.

At many facilities (particularly those that are not acid-generating), tailings deposition plans include reducing water volumes as the operation proceeds and, ultimately, the removal of impounded water after operations cease. Monitoring is planned to continue until the results show stabilized conditions, which in some jurisdictions are defined to be up to 30 years or so. Many companies are improving how they deal with closure, but implementation of today's ambitions varies across the industry.

The importance of tailings management and safe or responsible TSF closure is gaining recognition. Research initiatives are ongoing in several specialized fields of closure. Some mining companies have developed their own closure guidance documents.

Many mining companies use the economic principle of NPV to make decisions about whether to proceed with an operation or an option. NPV favors lower up-front capital and operating costs and encourages postponing costs and rehabilitation works, thus often creating significant liabilities at the end of a mining operation at a time when there is no revenue, or the mining company is not viable.

Vision for 2030 regarding TSF closure

Based on the results of the survey, the vision for 2030 when it comes to TSF closure is as follows:

- There will be a global definition of "closure." This will help to achieve consensus on closure strategies.
- There will be an engaged, open, and meaningful dialogue between all parties involved in TSF closure (i.e., mining companies, regulators and authorities, consultants, communities, NGOs, and other stakeholders) based on mutual trust and transparency.
- Global guidance documents and technical manuals will be developed that will provide guidance on goals to be achieved, closure criteria, acceptable levels of risk and the process of how to achieve closure, as well as an appropriate level and detail of closure cost estimates to reach a suitable accuracy to be relied upon.
- The knowledge and understanding of TSF closure will be improved and there will be improved acceptance of closure practices among all parties involved, including involvement and collaboration with academia.
- It will be acknowledged that the TSF owner will likely not be the future land user, and therefore will not be solely responsible for the closure vision. Therefore, all parties involved will take part in the process and take shared responsibility in determining the vision through a meaningful dialogue and process.
- TSF closure will be an adaptive process from first planning through design and operation to post-closure, where the design will include: a lifecycle perspective, processing methods to either limit tailings generation or produce benign tailings, integrated waste management (i.e. tailings, waste rock and possible other waste), long-term geotechnical aspects (including liquefaction, erosion etc.), geomorphological/landform design, chemical stability, water management (including surface water, acid rock drainage (ARD) etc.), climate change, and risk assessment and management.
- Large-scale trial areas will be used to test proposed closure designs.
- Financial models and systems will be developed for operating and new TSFs that support progressive closure, encompassing real costs and economic risks over time, and appropriate value will be paid to social benefits.

- All TSF operations will have integrated closure into operations, meaning operation is equal to preparing for closure, with the optimal goal being mining for closure, i.e., mining is done for two reasons: a) to extract a metal/mineral; and b) to create a new landscape/land use.
- There will be effective monitoring and maintenance systems available for closure monitoring and maintenance in perpetuity.
- TSFs will have a Reclamation Designer of Record (RDoR) who is responsible for closure design and progressive rehabilitation works over the life of the facility. The skill sets of an RDoR are different than the typical EoR. This framework may also include an Independent Reclamation Review Board (IRRB), like that of an ITRB but more multidisciplinary. Alternatively, the closure/reclamation discipline could be included in an ITRB.
- Third-party audits, covering technical, environmental, social and financial aspects, will be done for closure plans and closure for all TSFs.
- Responsibility for historical TSFs that have been abandoned by irresponsible operators will be allocated to bodies/parties with resources to properly close these (not just taxpayers) and there will be cost-effective strategies for closure of abandoned and historical TSFs.

Integrating the management of all waste materials produced, environmental sustainability, and economic development will be prime milestones in the circular economy (Das et al., 2024).

Many actions are required to achieve the vision for 2030. The following initiatives, underway or planned, will not fully address the requirements, but will make important contributions:

- The CDA Mining Dams Committee is developing closure guidelines and criteria for when a dam is no longer a dam and is developing guidance on risk-informed closure design.
- SME is developing a closure handbook that will provide comprehensive guidance, and details related to closure. Many of the topics identified above will be addressed in this handbook.
- MAC and ICMM are developing or updating their closure guidance.

The efforts by MAC, ICMM, SME, and CDA will be coordinated.

- The LDI[2] is developing detailed guidance on landform design.
- Ten mining companies have established the GeoStable Tailings Consortium[3] where large-scale closure field tests are run.

[2] The Landform Design Institute have a mission to make landform design routine in the mining industry by 2030 and focus on governance, leadership, and education in landform design.
[3] A consortium led by Newmont with Antamina, Barrick, BHP, Freeport McMoRan, Gold Fields, Teck, and Vale.

A change of the NPV financial model is required, but it is not clear at this time how the financial models can evolve to place more emphasis on low-risk closure solutions. This will require efforts by a number of stakeholders.

Despite current efforts, the challenges that are faced highlight the need for a comprehensive, transparent, interdisciplinary, and multifaceted approach to achieve closure of TSFs (safe or responsible). To design with the end in mind, building TSFs to final landform designs from the beginning and viewing closure costs as part of the lifecycle of TSFs is necessary. In support of this, flexibility and continuous update of closure plans are required to adjust for changes in mine planning and the development of good closure practices.

Characterization of tailings and foundation soils

Current situation

The geotechnical community has made great strides over the past century, refining site characterization tools that were introduced starting in the 1930s, such as the cone penetrometer (now with many add-ons) and the triaxial compression test (now the standard for critical state line [CSL] testing). These tools, and others, allow for detailed engineering characterization of soil elements both in-situ and in the laboratory. Fourie et al. (2022) provide a detailed account of the standard of practice for the characterization of mine tailings with detailed discussions on the applications of such tools. However, reliance on the tools alone, without appropriate consideration for geological and geomorphological processes, can lead to errors. Furthermore, lack of recognition of the fundamental mechanics of soil behavior (especially understanding of critical state soil mechanics [CSSM]) has contributed to the propagation of what Dr. Morgenstern termed "weak engineering" (Morgenstern, 2018).

Historically, budgeting to support extensive site characterization efforts for tailings facilities was constrained by short-term operational mindsets (e.g., focusing on characterizing only the minimum requirements for a single dam raise). These constraints have now been largely removed in most parts of the world by evolving Owners' commitments and regulatory requirements to develop an integrated knowledge base for the whole TSF (GISTM Principle 2), underpinned by a detailed site characterization model.

The consensus among the survey respondents is that most of the tools required for adequate site characterization are already available today (e.g., piezocone, shear vane, piston sampling, advanced laboratory testing, etc.), but the toolbox could be better organized, and the tools sharpened. Specific challenges are:

- Methods for establishing potential for liquefaction, especially in the absence of a significant earthquake triggering mechanism. There are indirect methods available with the CPT and

laboratory testing, but there is no direct method of discerning the in-situ void ratio of the tailings, which can be used to inform the liquefaction potential.

- Methods for discerning brittleness of tailings. As described in ICOLD preprint of Bulletin 194 (ICOLD, 2022), brittleness is a key aspect of discerning the risks associated with a TSF that has contractive and potentially liquefiable units in the dam and/or foundation. Methods for discerning brittleness are limited to laboratory testing, which has challenges with respect to sample quality and the extension of findings to field situations.
- Methods for assessing the post-liquefaction/large strain/residual strength of brittle materials.
- Methods for characterizing and understanding the behavior (for both strength and seepage) of unsaturated tailings are severely limited, and these will be essential for assessing and demonstrating that "safe/responsible closure" of tailings facilities can and has been achieved.
- Methods for understanding the evolution of geotechnical and hydrogeological properties of tailings (and mine wastes in general) in light of long-term geochemical weathering.

Vision for 2030

The vision for site characterization in 2030 is to fully embrace the principle of an interdisciplinary knowledge base for tailings management. This involves developing and regularly updating integrated site characterization models.

Site characterization should be treated as an iterative risk-informed process, in concert with the design process where conceptual models of the foundation, tailings embankments, and tailings deposition process are developed based on a geotechnical, geological, geomorphological, and hydrogeological understanding of the site and the tailings depositional scheme. Involving more engineering geologists in this activity would be beneficial. Once this is done, uncertainty (both geological and depositional) can be characterized and used to inform site investigation targets and methods; each drill hole or laboratory test should have a clear objective linked to reducing model uncertainty or facility risk.

Liquefaction characterization and unsaturated soil mechanics was a specific theme in the survey responses. Based on the survey results, the vision for 2030 includes:

- Characterization of liquefaction potential and post-liquefaction strength with the ability to accurately estimate in-situ void ratio is standardized and common practice in the industry.
- Characterization of brittleness is standardized and common practice in the industry.
- The impact of fabric/layering on tailings behavior is understood.
- Better methods for recovering "undisturbed" samples of fine and coarse tailings have been developed.

In addition, for large facilities, methods will be developed to characterize the soil between discrete investigation points.

Several university and industry groups are currently tackling these challenges through ongoing research and guidance initiatives. For example:

- The University of Western Australia (UWA) recently completed a round robin on CSL testing involving 15 independent laboratories around the world. The results indicated that the best reproducibility was obtained using end-of-test soil freezing to measure void ratio, which has been accepted as the industry standard (Reid et al., 2021).
- The University of Toronto (UoT) is researching the impact of partial drainage conditions on CPT penetration using calibration chamber testing, which indicates that the negative pore pressures observed in some tailings CPTs are indicative of dilative behavior (Lizhi et al., 2024).
- The ICOLD Bulletin 194 (2022) provides design guidance on soil brittleness and liquefaction potential with a flowchart on application of strength concepts (peak or residual) to factor of safety computation.
- Drilling contractors are adapting the nuclear and magnetic resonance technologies to in-situ tools for in-situ density (i.e., void ratio) and water content estimation.
- There is active research and development to incorporate pore pressure measurement on the electric vane shear test to overcome the uncertainty of drained conditions during vane shearing.

To continue moving forward, there is a need for innovation in non-destructive/non-invasive technologies that can provide screening level information or reduce uncertainty in conceptual site characterization models. This could take many forms, but emphasis should be placed on vadose zone geophysical surveying from the surface to estimate degree of saturation in tailings deposits, stacks, and cover systems.

To make this vision a reality, there also needs to be a focus on widespread sharing of common characterization data (e.g., adjacent operators in mining districts sharing data) and the formation of groups like the Canada's Oil Sands Innovation Alliance (COSIA) or the GeoStable Tailings Consortium to pool research funding and resources to develop solutions to common challenges.

Surveillance of tailings facility performance

Current situation regarding surveillance

The importance of surveillance of TSFs has become more apparent to mine owners; not only to provide information on the performance of the TSF and provide early warning of potential concerns, but to support the adoption of the performance-based design approach. There is widespread use of "point" measurements

(e.g., vibrating wire piezometers [VWPs], survey prisms, inclinometers, and seepage monitoring weirs) with automation of the instruments and data gathering becoming more the norm than the exception. However, the data management interfaces can be cumbersome and there are challenges with false positives in so-called "real time" data.

Cameras are in place for many dams. Monitoring centers are being established that have computer monitors showing the view of the TSF and the dams and the instrumentation results. Alert levels are set for the instrumentation that can trigger a response to preserve the safety of the TSF.

Drones, often equipped with survey capability, are commonly used to observe the TSFs, and INSAR[4] has proven to be an effective tool for monitoring features on a broader scale than "point" measurements.

Providers of surveillance methods have been at the cutting edge of developing new approaches and technologies, with many owners embracing these innovative techniques.

However, the surveillance methods are not necessarily linked to a comprehensive and realistic understanding of the potential failure modes, particularly for dams that have contractive elements in the structural body of the dam or foundation that can fail in a brittle manner. If the dam can fail by static liquefaction, then monitoring movements and pore water pressures to guard against static liquefaction may not provide adequate warning time in the event of a failure. Establishing trigger levels based on stability analyses alone can be misleading. Deformation models with appropriate constitutive models based on comprehensive field and laboratory testing programs can provide insight into the possible triggering mechanisms and a determination of whether an observational approach can be applied to this situation.

However, there have been instances of a "false confidence" being established that the surveillance will help to protect from failure in these circumstances. If a seismic event were to occur and cause a dam to fail by liquefaction, surveillance may be of little value other than to support the back analysis of the failure.

Internal erosion can occur at discrete points within a dam that are distant from where the instrumentation is established and cannot be discerned by point measurements.

Vision for 2030

By 2030, we anticipate the following to have been achieved:

- Surveillance programs will be targeted to address instability and internal erosion failure modes through the use of performance-based design to support slope stability assessment and seepage controls (refer to section above entitled "Current situation regarding surveillance"). Or it will have been demonstrated that surveillance cannot be effective to guard against those failure modes, that

[4] INSAR = Interferometric Synthetic Aperture Radar

the observational approach cannot be used, and additional controls need to be implemented to preserve the safety of the facility. ICOLD is developing a new Bulletin on surveillance that will address these items.

- Automation and data management interfaces will be improved to the point that the surveillance information can be directly integrated with engineering models to support calculations related to performance (e.g., deformations, factor of safety, seepage, etc.). AI will support the data acquisition and interpretation. Because of the massive amount of data that will be available, data scientists will be employed to assist with gathering and processing the data so that it can be interpreted effectively by engineers and operators. This will be led by service providers and data scientists.
- Methods of monitoring on a more areal extent will be commonplace. INSAR and drones are widely used, but other systems are evolving that can monitor performance over an aerial extent:
    - Fiber optic cable technologies can detect changes in temperature (which can provide indications of seepage), tension (to indicate deformations) and acoustic properties (to indicate changes in the material) and can be placed in critical positions of the dam section where seepage and deformations are expected and/or critical.
    - Permanent geo-electric monitoring of a dam and its foundation can be undertaken that can track the location of the phreatic surface over the length of a dam and identify areas where there may be concentrated seepage.
    - Deep penetrating radar and muon radiography from satellites can provide information on the internal configuration of a dam.

These initiatives are being advanced by service providers.

Design approaches

Current situation

With respect to slope stability assessment, limit equilibrium methods (LEMs) are the most commonly used tool, with conservative approaches adopted for dams that have contractive elements that are potentially liquefiable. However, there are a number of limitations with LEMs that need to be recognized when undertaking these analyses and establishing suitable targets for factor of safety (Krahn, 2001).

In 2018, Dr. Morgenstern (Morgenstern, 2018) advocated for the adoption of performance-based design for slope stability assessment that integrates a comprehensive understanding of the geotechnical conditions of the dam and foundation, performance information (deformations and pore water pressures), and deformation models to simulate the behavior of a TSF. Measurable performance objectives are established and as a TSF is constructed and performance information is obtained, the performance is

compared to the objectives and modifications made to the design, if necessary. “History matching” is done by updating the deformation model to match the performance information, which permits refinements to the understanding of the TSF and project future performance. Performance-based design has proven to be effective in cases in western Canada (Gelletta et al., 2023; Nguyen et al., 2022; Nguyen et al., 2023; Quinn et al., 2014) where water retaining dams built on pre-sheared clay shale have experienced significant deformation. Limit equilibrium analyses were not sufficient to represent the conditions and establish the potential for failure. Three-dimensional deformation analyses were able to demonstrate that the dam was safe and that the movements were tolerable.

For dams with contractive elements that are potentially liquefiable, case studies are being developed that show that the classical approaches for predicting liquefaction due to seismic events are possibly conservative. The use of deformation modeling, with appropriate constitutive relationships, may provide predictions of deformations that could occur as a result of a seismic event, rather than liquefaction (Kafash et al., 2021).

ICMM has provided training materials on performance-based design and CDA is also developing training materials.

LEM will still play an important role for stability analysis (when done properly and recognizing the associated limitations) and can be supplemented by performance-based design methods, particularly for complex geometries with multiple soil units.

Performance-based design can be extended to other facets of design such as flood control, seepage control, and internal erosion.

Risk informed design is an overarching philosophy that applies to all facets of design that account for the risks that are posed by a TSF. Because of the potentially significant losses to a mine owner and the downstream environment in the event of a TSF failure, ICMM recommends that extreme loading criteria be adopted for TSFs. The GISTM recommends that consideration be given to adopting extreme loading criteria. The GISTM states the following as Requirement 4.2:

> *A. Develop preliminary designs for the tailings facility with external loading design criteria consistent with both the consequence of failure classification selected based on current conditions and higher Consequence Classifications (including ‘Extreme’).*
>
> *B. Informed by the range of requirements defined by the preliminary designs, either:*
>
> 1. *Implement the design for the ‘Extreme’ Consequence Classification external loading criteria; or*
> 2. *Implement the design for the current Consequence Classification criteria, or a higher one, and demonstrate that the feasibility, at a proof-of-concept level, to upgrade to the design for the ‘Extreme’ classification criteria is maintained throughout the tailings facility lifecycle.*

Many owners have adopted this approach, but there are exceptions, particularly for TSFs that do not have life safety consequences.

Dam breach analyses are an important tool to understand the potential consequences associated with a TSF, and thus the risks. Significant progress has been made in the past five years on this topic, including the issuance of the Tailings Dam Breach Analysis Technical Bulletin by CDA in 2021 and the establishment of a consortium of universities in Canada to form CanBreach. The University of British Columbia, Queen's University, and Waterloo University formed CanBreach in 2019 with the goal of better understanding the tools and methods available to simulate a tailings dam breach. Part 1 of the research program was completed in 2023, and Part 2 is planned to commence in 2024. Part 1 advanced the understanding of the physical processes of a tailings dam breach and the outcome of a breach, as well as the computer models that are available to predict the extent of a breach. Part 2 will continue this work with further research on computer modeling, the released volumes of tailings, and the behavior of unsaturated tailings during a breach.

A key driver of TSF design can be the geochemical considerations, especially as they relate to closure and how the initial designs and operations need to account for this.

Vision for 2030

By 2030, we anticipate the following:

- Performance-based design for slope stability assessment will be a widely recognized and accepted approach.
- LEM analyses will still play an important role in design.
- Performance-based design for slope stability assessment and LEM will be viewed as complementary.
- Fully coupled deformation and seepage models will be able to achieve results closer to reality.
- The concepts of performance-based design will be extended to other facets of design as noted above.

For performance-based design for slope stability assessment to gain widespread acceptance, additional case studies need to be developed and presented in the literature with a critical view to the limitations associated with deformation modeling. Conferences and training sessions should convene targeted sessions related to performance-based design and how it can be integrated with LEMs.

A challenge that will limit the advancement of performance-based design is regulatory capacity; the ability of the regulators to understand performance-based design as opposed to simply meeting a factor of safety requirement.

With respect to dam breach analyses, the CanBreach consortium is initiating Part 2 of their research that will explore:

- Unsaturated soil behavior and how this should be considered in a tailings dam failure.
- Breach processes and how tailings dam breaches actually form, which will enable better predictions of failures associated with tailings dams that are buttressed with rockfill.
- Improved correlations between modeled failures and actual failures.

The geochemical aspects will be given greater prominence in the design in support of closure plans that will properly address these aspects and not simply result in pump and treat scenarios.

Guidance documents for tailings facility safety design

Current situation

As noted in Table 1, there are many guidance documents available to support the design of TSFs and some respondents to the questionnaire stated that there was sufficient guidance, i.e., "we should use what we have." However, there is a recognition that the state of practice for TSF engineering is evolving rapidly, and hence, several organizations are modifying their current guidance or developing new guidance related to TSF safety. These include:

- CDA – modifying the Mining Dams Bulletin that was issued in 2014 (revised in 2019) and the overarching dam safety guidance.
- MAC – modifying the tailings management guidance.
- United States Society of Dams (USSD) – developing a tailings dam safety guidance for the US.
- CDA and USSD – developing guidance for the EoR role and for risk informed decision making.
- SAICE (South Africa Institute of Consulting Engineers) – updating the Civil South Africa National Standard 10286 Mine Residue Code of Practice to be more aligned with GISTM.

A number of regulatory jurisdictions around the world have developed or updated their regulations related to TSF safety.

The questionnaire identified a number of gaps related to guidance, including:

- closure (see section above titled "Vision for 2030 regarding TSF closure");
- filtered tailings;
- methods for characterizing tailings and foundation soils; and
- spillway design.

Vision for 2030

As noted above, a tailings closure handbook is in progress by SME that is expected to be completed before 2030. Also, the LDI will have developed their guidance on landform design. The following additional guidance documents should also be available:

- Updates to the MAC tailings management guides.
- A document on filtered tailings that integrates the process and geotechnical aspects. This is to be led by representatives from industry who specialize in filtered tailings, supported by input from ICOLD and other organizations on the geotechnical aspects.
- A revised version of ICOLD Bulletin 194 that provides additional guidance on site characterization, hydrogeology and hydrology, spillways, undrained stability analyses, and brittleness.
- An ICOLD Bulletin on surveillance of tailings dams.

There will likely be additional guidance documents developed in addition to these.

Artificial intelligence

Current situation

Six years ago, AI was hardly discussed. Today, AI seems to be incorporated into our basic computer software (e.g., Microsoft Copilot). Regarding TSFs, AI is, in some cases, being used in surveillance activities to support the gathering and processing of large amounts of data. Discussion and research are ongoing regarding future possibilities and opportunities with AI. Some of the survey respondents are very interested and positive about AI, whereas others are more skeptical and negative and think AI is overhyped.

From the questionnaire there was a concern expressed with the increased computing power and AI as that might reduce emphasis on learning the fundamentals of tailings engineering. The authors agree that the use of AI does not replace the need for humans to understand how to do a task, but should be used as a means to improve efficiency of a task that the person already knows how to do well.

Vision for 2030

From the responses to the questionnaire there is no clear vision for 2030, and some emphasize a vision can only be for 2040 or beyond. However, the authors believe that by 2030 we will see AI used frequently within the industry and for TSFs within the following areas:

- Managing, processing and analyzing large data sets (weather, hydrology, monitoring – especially on-line monitoring) to identify trends and deviations to help in understanding the TSF performance.
- Integration of data sets such as mineralogy, geology, hydrology, and seismology to provide a more multifaceted picture of the TSF conditions.
- Pre-processing of data and prediction of operational aspects of tailings management to help in identifying potential risks and predicting future performance.

- Numerical modeling for stability and deformation analysis as well as breach inundation simulations.
- Enhanced adaptive management by monitoring real-time stability, identifying trends, anticipating risks, etc.
- Training programs and live guidance and support for operations.
- Reviewing literature and documents, summarizing information/reports, and reporting to standards/regulators.

Overall, while there is cautious optimism about AI's potential in tailings facility engineering, there is also a strong emphasis on the need for human oversight and the importance of integrating AI as a supportive tool rather than a replacement for expert judgment. However, AI could be part of the solution to the coming challenge of fielding enough TMPs to meet the growing demand.

To reach the vision for 2030 the industry will have to have an open mind towards AI and invest time and money in developing methods to use this potential tool that in many ways can improve, speed up and simplify data analysis, predictive modeling, numerical simulations, surveillance, and training, and enhance decision-making and risk management in TSF engineering. In addition, we cannot lose sight of the importance of understanding the fundamentals of tailings engineering and the role that models should play.

Conclusion

Through this work and while reviewing the provided information, the authors have been impressed by the overall developments and achievements in recent years and have been even more impressed by the anticipated and possible developments ahead to 2030. All the people who contributed to this work through the questionnaire, interviews, and discussions have shown a positive attitude to this work, and have displayed a general optimism regarding the changes and improvements on the horizon. The aim is to keep the momentum of improving tailings facility engineering and, with the support of ICOLD's Technical Committee L on Tailings Dams and Waste Lagoons and many other organizations, to work towards achieving the vision of what tailings facility engineering can look like in 2030.

We will publish a comprehensive summary at the end of 2024 of this work, including further input from this and coming presentations during the autumn.

References

Abenov, T., Franklin-Hensler, M., Grabbert, T. and Larrat, T. 2023. Has mining lost its luster? Why talent is moving elsewhere and how to bring them back. McKinsey & Company.

Burden, R. and Ward Wilson, G. 2023. Commingling of waste rock and tailings to improve "dry stack " performance: Design and evaluation of mixtures. *Minerals* 13(2): 295. https://doi.org/10.3390/min13020295

Das, A.P., van Hullebusch, E.D. and Akçil, A. 2024. *Sustainable Management of Mining Waste and Tailings – A Circular Economy Approach*. Routledge, Taylor & Francis Group.

Environment and Climate Change Canada (ECCC). 2011. Guidelines for assessment of mine waste disposal. Revised July 2013.

Fourie, A., Verdugo, R., Bjelkevik, M., Torres-Cruz, L.A. and Znidarcic, D. 2022. Geotechnics of mine tailings: A 2022 state of the art. In M. Rahman and M. Jaksa (eds), *ICSMGE 2022. Proceedings of the 20th International Conference on Soil Mechanics and Geotechnical Engineering.* Sydney, Australia: 121–183.

Gelleta, K., Nguyen , V., Mathison, K. and Henry, K. 2023. Incorporation of measured pore-water pressure readings from Gardiner Dam for 3D deformation modelling. *Proceedings of GeoSaskatoon Conference, 2023.*

GISTM. 2020. Global Industry Standard on Tailings Management. Global Tailings Review: International Council on Mining and Metals (ICMM), United Nations Environment Program (UNEP) and Principles for Responsible Investment (PRI). https://globaltailingsreview.org/global-industry-standard/

ICOLD. 2022. Bulletin Preprint 194 on Tailings Dam Safety. International Commission on Large Dams – Technical Committee L on Tailings Dams and Waste Lagoons. Accessed at https://www.icold-cigb.org/

Kafash, M.H., Cerna-Diaz, A., Cleason, J.J., Davidson, R. and Yenne, L. 2021. Seismic response of Kennecott tailings embankment to the M 5.7 Magna earthquake. *Proceedings of Tailings and Mine Waste Conference 2021*. Banff, Alberta, Canada.

Krahn, J. 2001. The 2001 R.M. Hardy Lecture: The limits of limit equilibrium analyses. *Can. Geotech J.* 40: 643–660.

Lizhi, Q., Zhao, H., Liu, W., Etezad, M., Sharp, J., Talesnick, M. and Ghafghazi, M. 2024. Calibration chamber testing on tailings for interpretation of partially drained CPT. *Proceedings of the 7th International Conference on Geotechnical and Geophysical Site Characterization*, Barcelona, 18–21 June 2024.

Madhusudhan, B.R. 2022. A review of cyclic simple shear test on soils: Challenges and new solutions. *International Journal of Advances in Engineering Sciences and Applied Mathematics* 14: 49–59. https://doi.org/10.1007/s12572-022-00321-4

Mine Environment Neutral Drainage (MEND) Program. 2017. Study of Tailings Management Technologies (2.50.1). October.

Ministry of Energy, Mines, and Low Carbon Innovation. 2024. Health, Safety and Reclamation Code for Mines in British Columbia. April.

Morgenstern, N.R. 2018. Geotechnical risk, regulation, and public policy. The Sixth Victor de Mello Lecture. *Soils and Rocks, São Paulo* 41(2): 107–129. DOI: 10.28927/SR.412107

Nguyen, V. Quinn, J., Gelletta, K., and Bertrand, D.G. 2022. Attaining model equivalence – calibrating material parameters for Gardiner Dam with 3D numerical modelling. *Proceedings of GeoCalgary Conference, 2022.*

Nguyen, V., Gelletta, K., Quinn, J., Bertrand, D.G., Mathison, K. and Henry, K. 2023. Investigating the Bearpaw shale shear plane response to reservoir loading at Gardiner dam.

Prince, M. and Boswell, J. 2023. The willingness of young engineers to assume the role of EOR for TSFs. *Proceedings of Tailings and Mine Waste, 2023,* Vancouver, Canada. https://doi.org/10.14288/1.0438104

Quinn, J., Chin, B., Pernito, M. and Scammel, J. 2014. Geotechnical assessment of the Alameda dam. *Proceedings of GeoRegina Conference, 2014.*

Rana, N. and Small A. 2024. Global registry of tailings storage facilities (v. 2024): overview and status update. 92nd ICOLD Annual Meeting & International Symposium on "Dams for People, Water, Environment and Development." – New Delhi, India.

Reid, D., Fourie, A., Ayala, J.L. et al. 2021. Results of a critical state line testing round robin programme. *Géotechnique* 71(7): 616–630. https://doi.org/10.1680/jgeot.19.P.373

Slingerland, N. and Hedley, R. 2023. Technical memorandum: tailings facility closure guidance gap assessment. Prepared for ICMM by WSP. Reference No. 23593840-001-TM-Rev0.

Chapter Two
Analysis



Numerical Simulation of Trigger Mechanisms of Static Liquefaction Applied to a Tailings Dam

Miguel A. Villalobos Bravo, Geocoba Projetos de Engenharia, Brazil
Richard Witasse, Seequent, The Netherlands

Abstract

Various possible triggering mechanisms of static flow liquefaction are well identified through a considerable body of data consisting of empirical observation of historical cases, and laboratory and field tests. In parallel, in computational soil mechanics, advanced numerical simulations and predictive models have also been developed to address the evaluation of soil liquefaction potential in engineering practice.

In this study, a back analysis of Dam I failure (Brumadinho, Brazil) is being considered to run a series of sensitivity analyses considering two potential triggers of liquefaction and investigate both their individual and combined contribution to the onset of static liquefaction.

The first mechanism is associated with a rising water table in the dam, which can be caused by intense rainfall and poor drainage conditions. More recently some efforts have been made in the field of computational analysis using models like NorSand to perform numerical simulations of the soil behavior observed in laboratory testing associated with this type of loading.

The second mechanism investigated was the effect of the fluid pressure used in drilling for instrument installation. The rapid increase in pore pressure could provoke a localized liquefied zone (loss of shear strength) at the bottom of the borehole that propagated generating a global collapse of the dam.

The results point out that a disturbance caused by the fluid overpressure of the borehole drilling was necessary to cause the collapse of the dam. However, the combined scenarios showed that the contribution of an infiltration that raised the water table increases significantly the chances of global instability.

This investigation also explored the application of constitutive models capable of reproducing this behavior. The two soil constitutive models considered, namely NorSand and Hardening Soil Small (HSS). They proved to be suitable for simulating the mechanism of static liquefaction analyzed, involving a rapid progression of instability throughout the model.

Introduction

Most flow-type slope failures are associated, to some degree, with an increase in pore pressure, the principal

causes of which are periods of intense rainfall, deficient drainage system and underground inflow, or even redistribution of pore water pressure from adjacent liquefied material (Morgenstern, 1994; Castro et al., 1992; Lade, 1993; Junaideen et al., 2010).

The mechanisms of a constant shear (CS) effective stress path, where decompression of the material (loss of mean effective stress) is caused by a slow buildup in pore water pressure, are often associated with a raising water table caused by intense rainfall, as well as surface and internal drainage conditions of the structure. Another related mechanism first investigated by Arroyo and Gens (2021) was the effect of the fluid pressure used in a drilling borehole, which provoked a localized liquefied zone at the bottom that generated a global collapse of the dam.

More recently some efforts were made in the computational analysis field to perform numerical simulations of this behavior observed in the laboratory, using critical state-based models like NorSand, and having to deal with theoretical aspects about work dissipation of stress dilatancy during yield in unloading, for which some idealization is required to define the yield surface (Jefferies and Been, 2015).

The case study of the present paper is the flow liquefaction failure of a tailings dam in Brazil. The geotechnical investigations for modeling these structures will be taken from well-documented available information in the public domain. The methodology of modeling was mainly based on the previous technical reports of Roberson et al. (2019) and Arroyo and Gens (2021).

After extensive investigations and the performance of many numerical simulations to back-analyze dam failure by Robertson et al. (2019) and Arroyo and Gens (2021), two main triggers emerged as more probable. One is increasing pore pressure due to rain infiltration, and the other is local liquefaction caused by the fluid pressure exerted while drilling a borehole, which was being conducted at the time of the dam collapse.

The PLAXIS FEA analyses proposed in this study include the simulation of the two more probable triggers separately, as well as their combined occurrences in both 2D and 3D simulations. Furthermore, with the aim of exploring the application of available and reliable constitutive models to reproduce the mechanisms that triggered static liquefaction of the dam with a rapid progression of instability throughout the structure, the constitutive soil models NorSand and Hardening Soil Small will be used.

Case study: numerical modelling of a tailings dam

The case study will be the flow liquefaction failure of a tailings dam in Brazil. The methodology of modeling was mainly based on the previous technical reports of Robertson et al. (2019) and Arroyo and Gens (2021).

Material properties

For the mechanical characterization of the tailings, two constitutive models were considered. First, the NorSand model (Jefferies, 1993), which is a critical state-based model that incorporates the state parameter that defines the plastic volumetric behavior of the material and can reproduce the softening behavior observed in loose saturated sandy and silt materials.

The other constitutive model considered in this study is the hardening soil with small-strain stiffness (HSS) model. According to Sottile et al. (2022), this model is based on the hardening soil model (HSM) but incorporates the xtress-dilatation formulation of the model family SaniSand (Li and Dafalias, 2000), which is more suitable for very loose materials.

Indeed, Benz (2007) implemented on the HSS model a dilatancy formulation based on the critical state soil mechanics framework, where the dilatancy is dependent on the state parameter. This formulation works with negative dilatancy angles characteristic of contractive material, making it possible to reproduce the peak strength and subsequent softening behavior of loose tailings in undrained conditions. This is a significant difference from the original hardening soil model, where a dilatancy cut-off of $\psi_m = 0$ is systematically considered even for negative values of ψ_m, consequently yielding too little plastic volumetric contraction, which is not representative of loose soil behavior.

The numerical model of the dam was based on the previous reports of Robertson et al. (2019), where the constitutive model used to simulate the liquefaction behavior of tailings was NorSand (Table 1). The parameter for the HSS model was calibrated against the stress-strain curves obtained with the NorSand set of parameters, following the methodology proposed by Sfriso et al. (2022), in the following sequence:

1. calibrate the model for drained behavior;
2. reduce parameters of elastoplastic rigidity in shear and compression to the minimum fair value;
3. increase the Poisson's ratio until obtaining the target maximum undrained resistance; and
4. increase the parameter *R* until the target residual resistance is obtained.

The adjusted stress-strain behavior is illustrated in Figure 1. The calibrated hardening soil small model parameters are presented in Table 1.

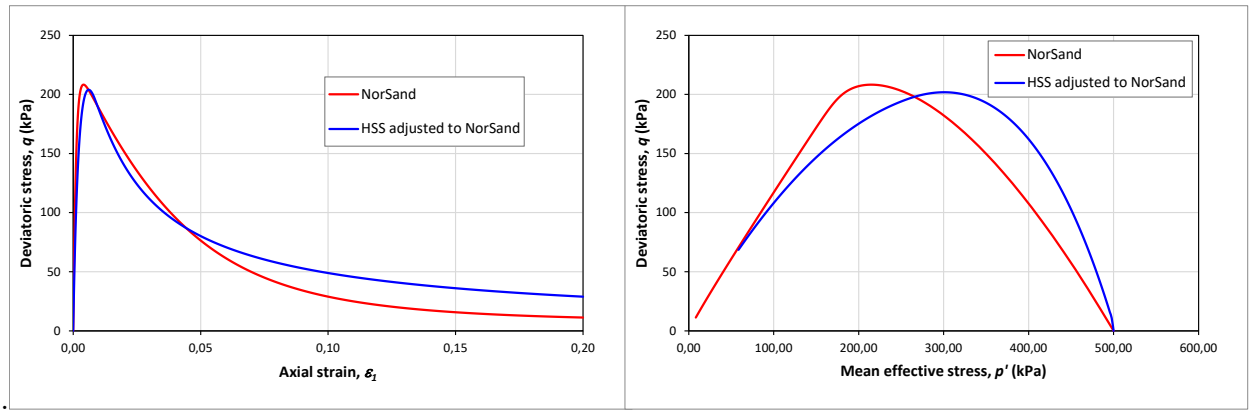


Figure 1 : Calibration of the HSS model parameters for and mean effective stress of 500 kPa

Table 1: Parameters for tailings. On the left, the NorSand model parameters (adapted from Robertson et al., 2019). On the right, the HSS model calibrated parameters

NorSand model parameters		
Parameter	**Unit**	**Value**
γ_{sat}	kN/m^3	27
γ_{unsat}	kN/m^3	27
G^{ref}	kN/m^2	100
P_{ref}	kN/m^2	300
n_G		1.0
ν		0.2
C_a		1.22
C_b		0.34
C_c		0.11
M_{tc}		1.38
N		0.27
χ_{tc}		6.0
H_0		160
H_ψ		1037
R		1.0
S		0.0
Ψ_0		0.14

Calibrated Hardening Soil Small (HSS) model parameters		
Parameter	**Unit**	**Value**
γ_{sat}	kN/m^3	27
γ_{unsat}	kN/m^3	27
E_{50}^{ref}	kN/m^2	10.0E3
E_{oed}^{ref}	kN/m^2	29.0E3
E_{ur}^{ref}	kN/m^2	190.0E3
ν_{ur}	-	0.2
power (m)	-	1.0
P_{ref}	kN/m^2	100
G_0^{ref}	kN/m^2	80.0E3
$\gamma_{0.7}$		0.2E-3
c'^{ref}	kN/m^2	1.0
ϕ'^{ref}	o	30
K_0^{cn}	-	0.6
R_f		1.0

The constitutive models and the parameters for the remaining materials (dike, foundation, etc.) considered in this study were adopted from Arroyo and Gens (2021).

Model construction

The numerical 2D plane strain model considered in this study is based on the critical section (cross-section 3) of the Arroyo and Gens (2021) report. The main characteristics of the adopted model included geometry, construction history, material parameters, hydraulic and hydrological conditions, and site activities.

Initially, a 2D plane strain analysis is performed, given that the type of failure observed developed simultaneously along a length of 300 m over the main face of the dam.

In the 2D cross-section, the localized zone induced by the borehole drilling (suspected to be one plausible cause of global dam failure) extends along the out-of-plane direction to the model (as a consequence of the plane strain assumption). Consequently, to obtain a more realistic simulation, it was deemed useful to also investigate the 3D effect of the localized liquefaction during the drilling of a borehole. The 3D model was developed following the criteria of Arroyo and Gens (2021), considering a 15 m slice extruded from the 2D model.

Figure 2 shows an analysis of the location on the plane and general arrangement of the critical section (cross-section 3 from Arroyo and Gens, 2021). The horizontal layers represent each phase of the dam construction, together with the raising dikes at every step of the dam-raising process.

The numerical model simulated 15 phases of raising and filling of the dam. A total of 30 numerical phases were necessary to reproduce the construction process of the dam plus the initial state phase, estimating the time based on the historical record of the structure over the 43 years of existence of the dam, as described by Robertson et al. (2019) and Arroyo and Gens (2021).

Following the numerical modeling process of Arroyo and Gens (2021), the first two phases establish the initial conditions of the foundation in terms of stress and pore pressure, adopting an initial stress ratio K_0=0.5 for the initial phase, and then using the flow boundary conditions to calculate the pore pressure distribution, considering relevant tailing ponds.

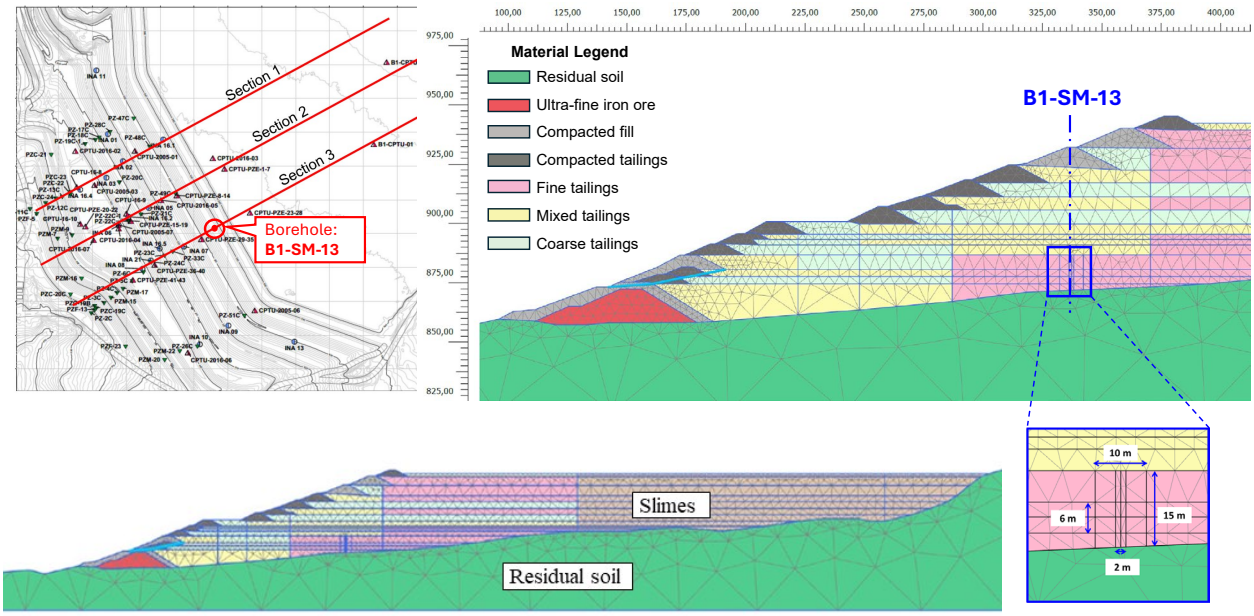


Figure 2: On the left is the location of cross-section 3; on the right is the 2D model of section 3 and material distribution of the dam and detailed location of borehole B1-SM-13; at the bottom is a general view of the 2D model. Adapted from Arroya and Gens (2021)

The final phase represents the inactive period of 912 days, after stopping tailings disposal, at elevation 942 m. During this phase only the ongoing consolidation process, along with the precipitation prescribed over the surface of the model, was considered.

Methodology for triggering static liquefaction

For this study, two potential liquefaction triggers were evaluated, performing simulations with effective stress conditions (and corresponding pore water pressure computed by mean of groundwater flow analysis), corresponding to the final state of the dam at the end of phase 30.

The first mechanism investigated was the elevation of the pore pressure within the dam due to precipitation (which was worthy of consideration, since the failure occurred during the rainy season). The other potential mechanism analyzed was associated with the drilling of borehole B1-SM-13 for the installation of a piezometer, which was happening at the time of the dam collapse. According to the technical registers gathered by Robertson et al. (2019) and Arroyo and Gens (2021), a coring technique with HQ-sized (i.e., 96 mm outer diameter) core and double barrel (wireline) was used. Also, the drilling of the borehole included a water recirculation system that involved the application of water overpressure with a total hydraulic head at least equal to the top of the borehole (~930 m). Arroyo and Gens (2021) ran numerical simulations of the conditions at the bottom of the borehole, demonstrating that liquefaction of tailings can be induced in a borehole with a combination of a fast trigger in terms of overpressure and low permeability developing in undrained conditions.

The two potential triggers were evaluated in different scenarios considering three different events of increased rainfall (1,095, 1,642, and 2,190 mm/year) and borehole overpressure independently, as well as in combination.

Section model of local liquefaction of borehole B1-SM-1

During the months prior to the dam failure, a series of drilling operations were undertaken to install complementary instrumentation. One of these boreholes, B1-SM-13, was being drilled when the failure occurred. The drilling of borehole B1-SM-13, where the overpressure of fluid used to cool the drilling bit is suspected to have caused localized liquefaction of loose, saturated tailings. It is therefore analyzed as a potential trigger for the instability.

The critical section under analysis (cross-section 3 of Arroyo and Gens, 2021) is very close to where the drilling of borehole B1-SM-13 took place, as shown in Figure 2. According to available records, borehole B1-SM-13 was initiated on January 21, 2019, and on the day before the failure, drilling had reportedly reached a depth of 65.5 meters below the ground elevation of approximately 930 meters, bringing it to a bottom elevation of approximately 863.5 meters.

All this detailed information about borehole B1-SM-13 was taken into account to develop a liquefaction trigger scenario, where the localized collapse at the bottom of the borehole was simulated by prescribing a small localized liquefied cluster (2 meters by 6 meters) around the tip of the borehole. The localized liquefaction region was modeled by assigning this small cluster at the bottom of the borehole (Figure 2) a liquefied residual strength of c_u = 10 kPa (and no friction angle). Calculations for this phase were performed under the assumption of undrained conditions, as instability progresses rapidly.

Numerical failure state in Plaxis (ΣM_{stage} multiplier)

In PLAXIS 2D, the changes to the geometry and loading configuration usually introduce changes in out-of-balance forces. These out-of-balance forces are stepwise applied to the finite element mesh (and of course subsequently balanced) using an automatic load-stepping procedure (Brinkgreve et al., 2022) until equilibrium is reached.

ΣM_{stage} is a multiplier that controls the staged construction process by monitoring the proportion of the out-of-balance force being equilibrated.

During a calculation phase, the multiplier ΣM_{stage} is increased from 0.0 to 1.0. As soon as ΣM_{stage} has reached the value of 1.0, the equilibrium is satisfied, the construction stage is completed, and the calculation phase is successfully terminated. If a staged construction calculation stops while ΣM_{stage} is still smaller than 1.0, the calculation cannot fully balance the introduced out-of-balance forces induced by the change of configuration compared to the previous phase, and the program will give an error message. The most likely reason in such a situation is that a failure mechanism has occurred. When failure of the soil body has occurred during the calculation, it is not possible to finish the construction stage and further calculations are meaningless, and therefore impossible in PLAXIS.

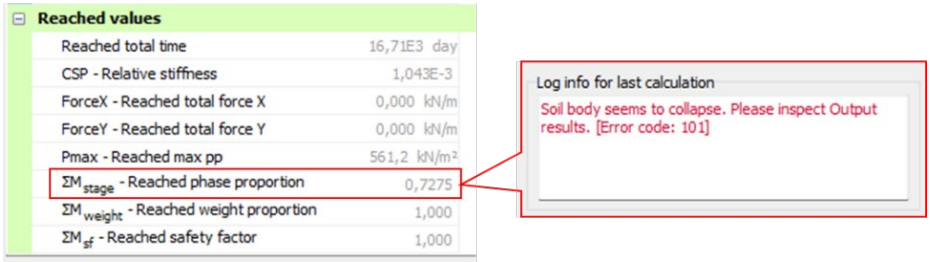


Figure 3: Plaxis results – phase calculation reached values and log information box

From the perspective of evaluating triggering mechanisms in our study, the ΣM_{stage} multiplier can be especially useful to determine the likelihood of reaching an unstable state for a given scenario. Knowing that a failure condition is established when a phase calculation finishes with ΣM_{stage} inferior to 1.0, the reached value indicates the proportion of the total loading or unloading that needs to be applied to result in the collapse of the body.

The patterns followed by the resulting values of the ΣM_{stage} multiplier for the series of combined scenarios analyzed will indicate whether static liquefaction is more likely to happen or not depending on the tendency (decreasing or increasing).

Results and discussions

In this chapter, a detailed examination of the numerical simulation results is presented. The evaluation is made over the critical section in 2D and 3D with contours in terms of effective stresses, pore pressure, displacements, and incremental shear strain.

Pre-failure stresses, displacements, and pore pressure

The stress state of the dam just before failure is derived by simulating the dam construction process according to historical records. Initiating the process by the construction of the starter dam on the foundation, every one of the 15 stages of raising and fill is simulated, considering the consolidation process the tailings underwent during the time of each phase.

The states of stress and pore pressure distributions are defined at the end of the last phase (phase 30), which corresponds to a period of 912 days (2.5 years) before failure, during which no further tailings were disposed on the dam. The construction phases were simulated with the calibrated HSS model for the tailings.

Figure 4 presents the contours of vertical and horizontal effective stress at the end of the last phase, representing the dam's state of stress field before collapse. Stresses increase with depth, accommodating to the geometry of the dam slope. Regions of maximum vertical and horizontal effective stresses are located at the base of the embankment below the crest, reaching values around 1,050 kPa and 650 kPa respectively.

Figure 5a shows the displacements that occurred over the last phase of the analysis, which simulates the last 2.5 years of the dam since it stopped operating in July 2016 until failure in early 2019. It indicates that the consolidation process continued for the last 2.5 years after the last loading of tailings was deposited at the storage facility.

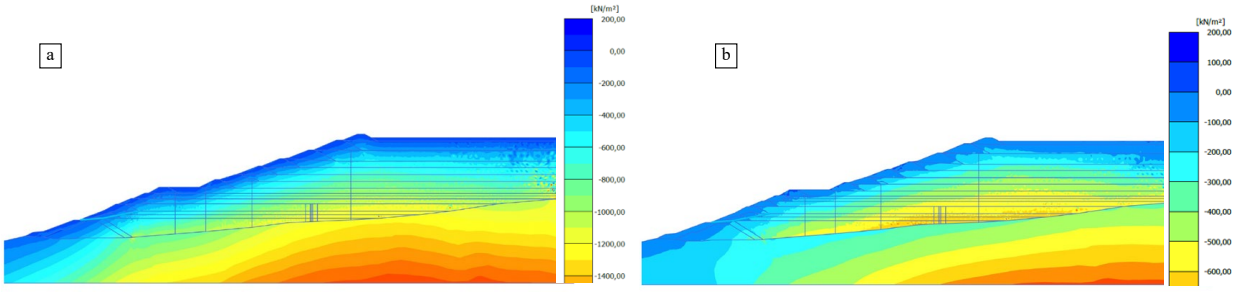


Figure 4: Contours of effective a) vertical and b) horizontal stress due to construction at the final stage before failure

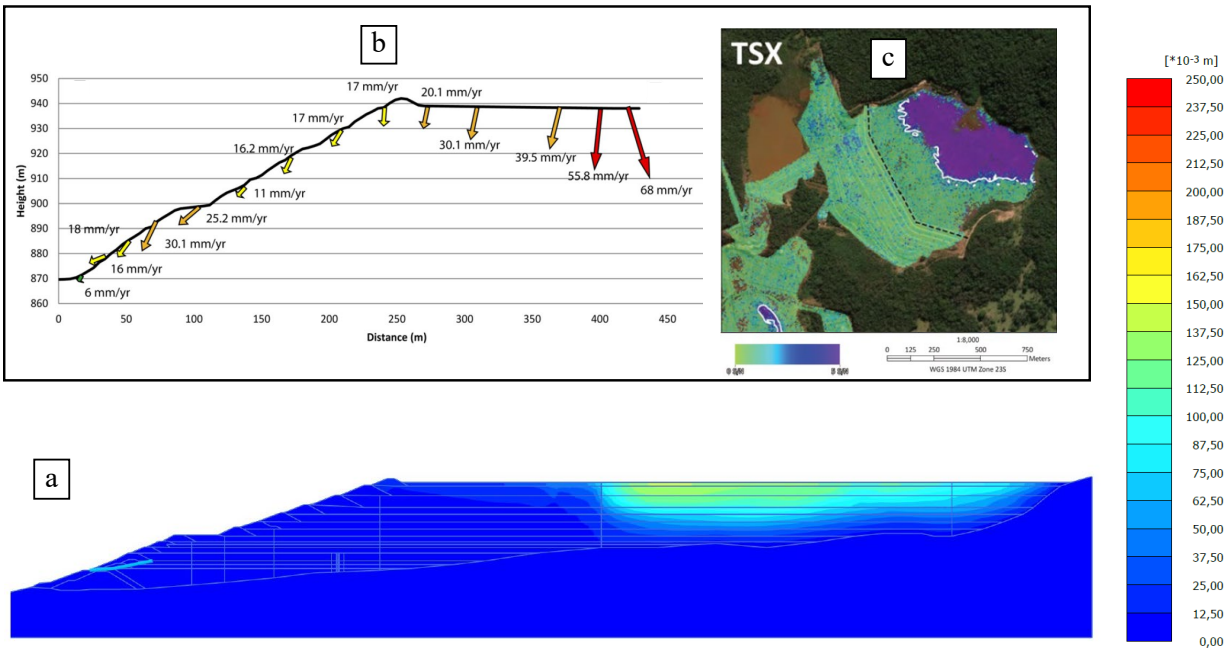


Figure 5: a) Calculated displacement in the last phase before failure, considering no precipitation, compared with b) the satellite measurements reported by Robertson et al. (2019) and c) the signal–to–noise ratio found by Holden et al. (2020)

The magnitude of the displacements found in the analysis, with values up to 150 mm, is consistent with the satellite measurements recovered and analyzed by Robertson et al. (2019). According to Robertson et al. (2019), larger vertical deformations, to a maximum of 140 mm/year, were detected in the tailing's impoundment. Since the settlements were mostly vertical and were well back from the crest, they were predominantly the result of ongoing settlement of the tailings due to long-term consolidation of the softer, finer tailings. This tendency of higher displacements toward the back of the storage facility is depicted by the satellite measurements in a cross- section (Figure 5b), showing deformation vectors obtained from InSAR TerraSAR-X-Sentinel-1 data by Robertson et al. (2019).

Satellite measurements presented by Robertson et al. (2019) in Figure 5b indicate a much lower rate of movement at the face of the dam. This is in contrast to the concentrated displacements at the rear of the dam, which resulted in our simulation (Figure 5a), showing minimal or very low displacements at the slope and near the crest region in the last phase. However, Holden et al. (2020) indicate that the settlements calculated at the crest and slope of the dam are highly affected by noise, presenting systematic estimates of the signal-to-noise ratio for their last-year average displacements (Figure 5c). The higher signal-to-noise ratio towards the back of the dam shown in Figure 5c is consistent with the calculated higher displacements in this same region (Figure 5a).

The field of pore pressure computed at the last phase of the dam, considering no contribution of infiltration due to rainfall and just before failure, is shown in Figure 6. These results are in good agreement

with the piezometric level registered in the last dam safety audit presented in 2018, according to Robertson et al. (2019), as well as with the simulation made by Arroyo and Gens (2021). Figure 6 also shows a comparison of the isoline at zero pore pressure, estimated by the instrument measurements of 2018 and the ones computed in this study (except perhaps for the starter dam).

In general, it can be observed that the zero pore pressure isoline is rather elevated within the dam, indicating that most of the tailings were saturated at the moment of failure, leaving just the upper part of the dam close to the crest in unsaturated conditions.

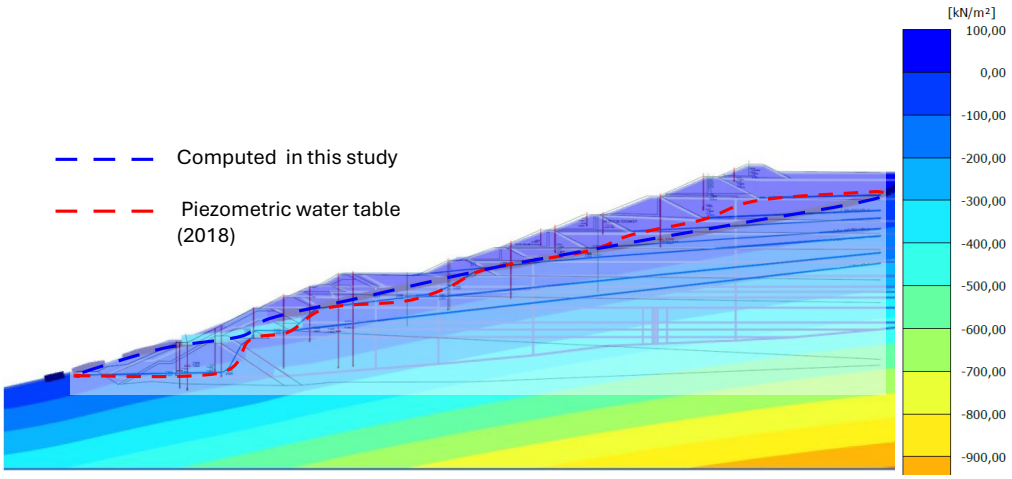


Figure 6: Comparison of zero pore pressure contours obtained in (1) this numerical simulation and (2) estimation from field testing and instrumentation

Analysis of potential liquefaction triggers

For this study, two potential liquefaction triggers were evaluated.

The first mechanism investigated was the elevation of the pore pressure within the dam due to precipitation. The progressive increase of pore pressure under a constant level of shear stress near a slope produces a loss of mean effective stress, represented in the stress space by a stress path moving horizontally in the direction of the failure envelope.

The other potential mechanism analyzed is associated with the drilling of borehole B1-SM-13 for the installation of a piezometer, which was happening at the time of the dam collapse.

These two potential triggers are investigated, including both their individual and combined contribution to the onset of static liquefaction.

Increased precipitation scenarios

The potential effects of increased precipitation were evaluated considering three magnitudes of rainfall (1,095, 1,642, and 2,190 mm/year). These values of precipitation were selected based on the average rainfall registered over the three years previous to the dam collapse. It was observed that the two highest values of

precipitation inflow simulated in the numerical model would correspond to a rate of infiltration that causes an almost complete saturation of the dam.

Comparing the pore pressure conditions simulated for the last phase before failure, the infiltration simulated by the highest precipitation rate indicates that 2,190 mm/year, as presented in Figure 7, caused a raising of the water table up to 15 m from the crest of the dam.

Figure 7 shows the contours of displacements in the final phase of analysis with the highest precipitation rate considered. The effect of increasing the precipitation rate is limited, with small movements appearing in a localized zone in the lower part of the dam slope. Overall, the increase of dam movements reaching a maximum value of 0.16 m, in relation to the scenario of no precipitation (Figure 5.3), is marginal.

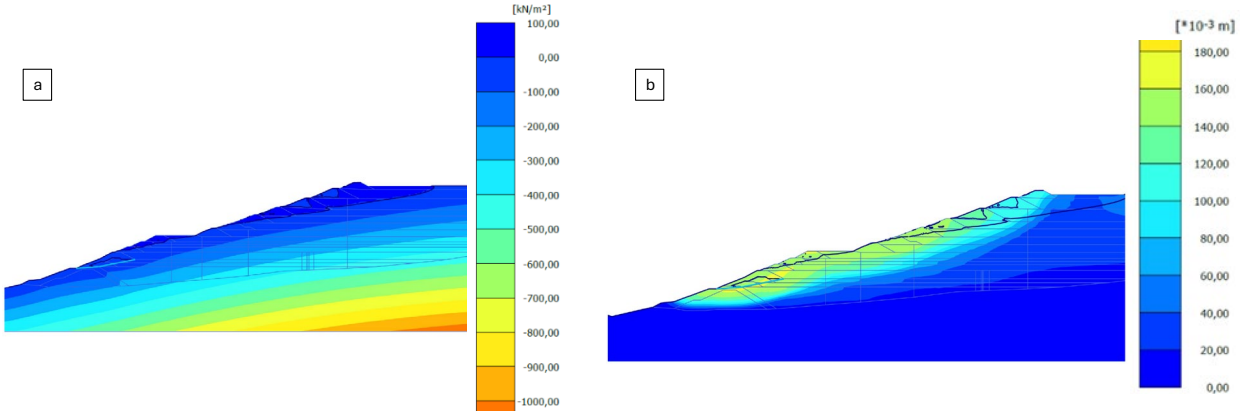


Figure 7: Contours of a) pore pressure and b) displacement during the final phase, with increased precipitation of 2,190 mm/year

Borehole local liquefaction scenario

The finite element model and associated numerical analysis strategy used for triggering static liquefaction have been described earlier in this paper. The localized liquefaction region is prescribed by a small cluster of 2 m × 6 m at the bottom of the borehole, to which a different material property set with only a liquefied residual strength of 10 kPa has been assigned. The calculation for this phase is done in undrained conditions, considering that instability progresses rapidly.

For these conditions, the simulation reached a global collapse state (as PLAXIS calculation stops with $\Sigma M_{stage}<1$) along the slope of the dam that propagates from the initial localized liquefaction region at the bottom of the borehole.

The simulated mechanism of the collapse using the NorSand constitutive model can be observed in Figures 8a, b, and c. Incremental displacements show the evolution of the movement at the time of failure. The incremental shear strains shown in Figure 8a give a clear representation of the failure surface, which propagates from the initial liquefied region at the bottom of the borehole.

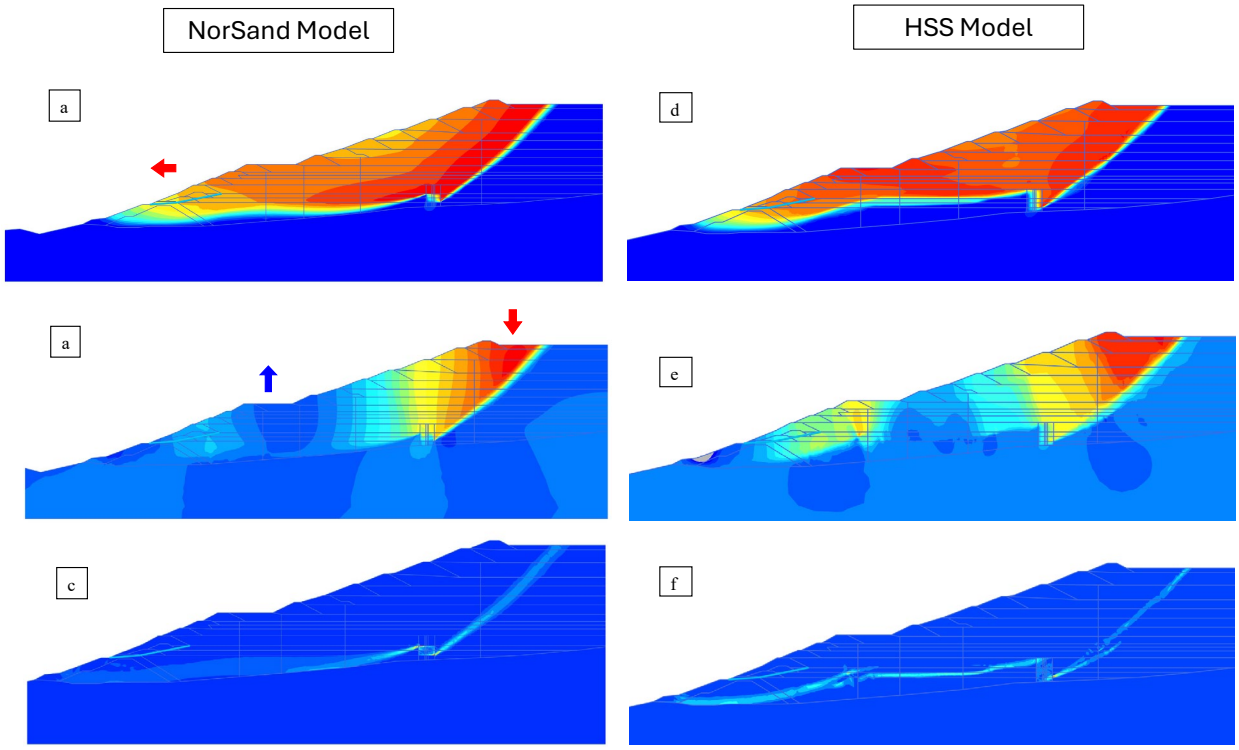


Figure 8: Liquefaction collapse using the NorSand and HSS constitutive model – a) and d) contours of incremental displacement; b) and e) contours of vertical incremental displacement; and c) and f) contours of incremental shear strains

Figure 8b shows the contours of incremental vertical displacement. The kinematic at the instant of collapse is clearly depicted with the rotation movement involving a downward displacement at the crest of the dam and a horizontal outwards bulging near the toe, consistent with the footage of the failure.

With the objective of evaluating the capability of the hardening soil small (HSS) model to simulate a mechanism of liquefaction collapse, the set of calibrated parameters (Table 1), was used to simulate the scenario of localized liquefaction at the borehole B1-SM-13.

Figures 8d, e, and f illustrate a remarkably similar pattern of instability simulated with the HSS model. The geometrical extension of the failure surface has a good correspondence to that obtained with the NorSand model simulation. Moreover, the kinematic analysis of the movement from the incremental displacements shown in Figures 8d and e also indicate the downward movement directions near the crest and bulging at the toe of the dam slope.

A plausible liquefaction trigger was found with the consideration of a localized liquefied zone at the borehole tip under pore water conditions encountered at the time of failure. As presented in Table 2, values for the loading parameter ΣM_{stage} closed to unity (roughly 0.9), indicating a clear but possibly limited likelihood of failure (especially as this corresponds to 2D analysis, for which endless propagation of the liquefied zone at borehole tip in the out-of-plane direction is implicitly being made).

Borehole local liquefaction and increased precipitation scenarios

Another set of sensitivity analyses was performed considering the combined effects of the borehole overpressure and increased precipitation with three levels of rainfall. The values of the loading parameter ΣM_{stage} for each intensity of rainfall and each constitutive model analyzed are presented in Table 2. The calculated values of the ΣM_{stage} parameter follow a pattern, with decreasing values as precipitation intensity increases. These results indicate that dam liquefaction likelihood increases, clearly demonstrating the influence of the infiltration process induced by rainfall (and the resulting increase in pore pressure).

Regarding the constitutive models employed, it is noteworthy that the calculated values of ΣM_{stage} for the HSS model were consistently slightly lower than those for NorSand. This suggests a more conservative tendency of the HSS model in predicting the onset of static liquefaction, showing a slightly higher probability of failure occurrence due to marginally lower ΣM_{stage} values.

Another relevant observation is that for a precipitation above 1,692 mm/year, where the infiltration simulated yields an almost complete saturation state of the dam body, the probability of failure occurrence remains approximately the same, as indicated by the low variation of the ΣM_{stage}.

Table 2: Loading parameter at failure phase, indicating reached proportion (ΣM_{stage})

Precipitation (mm/year)	ΣM_{stage} HSS model	ΣM_{stage} NorSand model
No infiltration scenario	0.874	0.905
1,045	0.728	0.735
1,692	0.514	0.673
2,190	0.539	0.698

3D-borehole local liquefaction analysis

Following the criteria used by Arroyo and Gens (2021), a 3D analysis of a slice of the dam was built to simulate a more realistic spatial extension of the disturbance produced by the drilling of a single borehole.

The 3D model was elaborated to represent a slice of the critical section over a width of 15 m, as was proposed by Arroyo and Gens (2021). Figure 9a shows the 3D, model including the material discretization used during the construction phases of the structure.

For the 3D model, the liquefied zone at the bottom of borehole B1-SM-13 was represented by a cluster of 2 m × 2m × 6 m, as depicted in Figure 9a, located at the center of the width of 15 m of the 3D slice.

The result of the 3D slice analysis, assuming a liquefied zone at the borehole B1-SM-13, is shown in Figure 9b. Global failure due to static liquefaction is obtained for this analysis as well, although the extension of the failure surface is slightly smaller compared to the one obtained with the 2D analysis.

Nevertheless, the kinematic of the movement is the same, showing a downward movement near the crest of the dam and an outward horizontal displacement at the toe of the unstable slope.

This may be taken as a different failure mechanism though, since this result shows an unstable mass restricted to the upper part of the slope, not corresponding to the footage of the propagation of liquefaction analyzed in detail during previous 2D analyses.

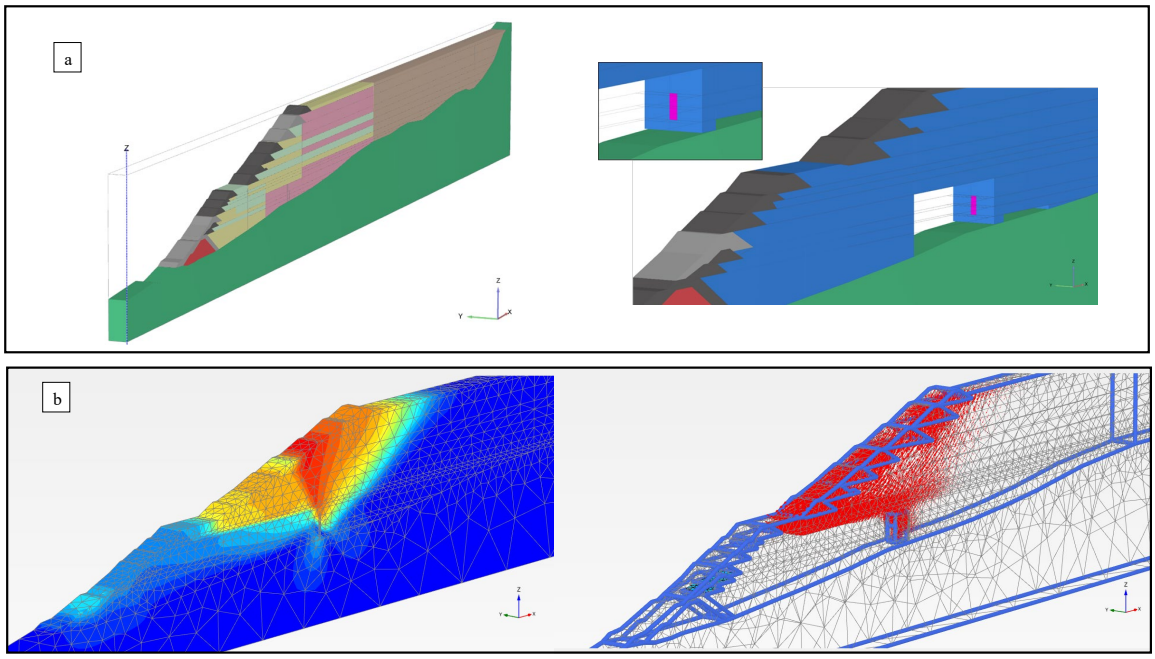


Figure 9: 3D model – a) slice over a width of 15 m and liquefied region at the bottom of borehole B1-SM-13. b) Contours of phase displacements and incremental displacement vectors

Conclusion

Simulation of the dam failure was conducted under varied conditions using both 2D and 3D numerical models to assess sensitivity and consistency in identifying possible triggers for liquefaction. Constitutive models, namely NorSand and HSS, were calibrated to replicate the same stress-strain behavior, proving to be effective in simulating the analyzed liquefaction mechanisms and in demonstrating a rapid progression of instability throughout the model.

Results from numerical simulations considering precipitation alone, even with a raised water table 15 m above the pre-failure elevation, did not exhibit signs of instability. This indicated that elevating the water table alone did not induce an unstable condition for the dam.

In the 2D analyses, considering a localized liquefaction zone in a borehole located on the main slope, the model exhibited a complete collapse with features consistent with the observed rapid failure and initial downward movement of the crest, followed by a horizontal downstream movement of the toe of the Dam.

Sensitivity analyses, considering the combined effects of the two triggers (water table elevation and borehole drilling), revealed an increased probability of occurrence. This was indicated by lower and below-1 ΣM_{stage} values.

The 3D analysis showed a similar collapse mechanism, although more restricted to the upper part of the slope, confirming the 2D initial evaluation and giving strong numerical evidence that the drilling of the borehole was a potential trigger of liquefaction.

Acknowledgements

Thanks to the Institute of Technology Vale and its dedicated staff for their unwavering support, provision of essential resources, and guidance that proved instrumental in the successful completion of this research endeavor.

References

Arroyo, M. and Gens, A. 2021. Computational analyses of Dam I failure at the Córrego de Feijão mine. Final Report for VALE S.A., August 2021. CIMNE International Center for Numerical Methods in Engineering.

Benz, T. 2007. Small-strain stiffness of soils and its numerical consequences. Ph.D. thesis, Universität Stuttgart.

Brinkgreve, R.B.J., Kumarswamy, S., Swolfs, F., Fonseca, N., Zalamea, W.M., Zampich, L. and Ragi-Manoj, N. 2022. PLAXIS 2022 user manual.

Castro, G., Seed, R.B., Keller, T.O. and Seed, H.B. 1992. Steady state strength analysis of the Lower San Fernando dam slide. *Proceedings of the 53rd Canadian Geotechnical Conference,* Montreal: 169–176.

Holden, D., Donegan, S. and Pon, A. 2020. Dam InSAR study: Analysis of TerraSARX, COSMO-SkyMed and Sentinel-1 images preceding the collapse. In *Proceedings of the 2020 International Symposium on Slope Stability in Open Pit Mining and Civil Engineering* (ed. Dight, P.M.): 293–306 (Australian Centre for Geomechanics, 2020).

Jefferies, M.G. 1993. Nor-Sand: a simple critical state model for sand. *Géotechnique* 43 (1): 91–103.

Jefferies, M.G. and K. Been. 2015. *Soil Liquefaction: A Critical State Approach*. Boca Raton, FL: CRC Press.

Junaideen, S.M., Tham, L.G., Law, K.T., Dai, F.C. and Lee, C.F. 2010. Behaviour of recompacted residual soils in a constant shear stress path. *Canadian Geotechnical Journal* 47(4): 648–661.

Lade, P.V. 1993. Initiation of static instability in the Nerlerk berm. *Canadian Geotechnical Journal* 30(6): 895–904.

Li, X. and Dafalias, Y. 2000. Dilatancy for cohesionless soils. *Géotechnique* 50(4): 449–460.

Morgenstern, N.R. 1994. Observations on the collapse of granular materials. The Kersten Lecture, 42nd Annual Geotechnical Engineering Conference, Minneapolis, Minnesota.

Robertson, P.K., de Melo, L., Williams, D.J. and Wilson, G.W. 2019. *Report of the Expert Panel on the Technical Causes of the Failure of Feijão Dam I.* Retrieved from http://www.b1technicalinvestigation.com/report.html.

Sfriso A., Sottile M. and Cobos D. 2022. *Análisis de vulnerabilidad a la licuación estática de presas de relaves*. XVII CGC. SRK Consulting.

Sottile M., Cueto I., Sfriso A., Ledesma O. and Lizcano A. 2022. Flow liquefaction triggering analyses of a tailings storage facility by means of a simplified numerical procedure. XX ICSMGE – *Proceedings of the 20th International Conference on Soil Mechanics and Geotechnical Engineering,* Sydney 2021.

TWIM Framework: A Digital Twin Approach for Strategic Dry Stacking Tailings Management

Cauê Stocchi Somensi, Geospace Digital Engineering/USP, Brazil
Douglas Deoclécio Tostes Firmo, Vale, Brazil
Gustavo Marçal de Sousa, Vale, Brazil
Alexandre Cristino Correa dos Santos, Vale, Brazil
Lucio Schiavon Yamamoto, Vale/USP, Brazil

Abstract

This paper introduces the TWIM (Tailings and Waste Interactive Management) Framework, a structured approach designed to enhance the management of dry stacking tailings operations through the integration of Digital Twin technology. The TWIM Framework leverages real-time monitoring, data analytics, and predictive modeling to address the complex challenges of tailings management. Developed as part of an Open Innovation initiative by Vale Company, and operationalized through the DSMS (Dry Stacking Management System) software, this framework provides comprehensive oversight and management capabilities. The paper shares key insights and lessons learned from the framework's implementation, highlighting its impact on improving operational efficiency, resource recovery, and environmental sustainability at Vale's "PDER Cianita" tailings facility in Brazil. The TWIM Framework and DSMS software represent a significant advancement in tailings management, promoting regulatory compliance and supporting sustainable mining practices. The findings suggest that this approach can be scaled and adapted to meet the specific needs of various operations within the mining industry.

Introduction

The primary aim of this paper is to introduce the TWIM (Tailings and Waste Interactive Management) Framework, a structured approach designed to enhance the management of dry stacking tailings operations. The framework leverages Digital Twin technology to integrate real-time monitoring, data analytics, and predictive modeling, addressing the complex challenges of tailings management. In addition to presenting the framework, this paper aims to share key insights and lessons learned from its implementation and operationalization as a cloud-based software solution.

The management of tailings and mining waste is a critical component in mitigating the environmental and operational challenges inherent in mining activities (Mining Association of Canada, 2021). Tailings, the by-product of ore processing, pose significant risks when stored in impoundments or upstream dams (Kossoff et al., 2014). Although the iron ore tailings dry stacking process is not new, recent structural failures of upstream tailings dams in Brazil have compelled many mining companies to adopt this method across various environments, processes, and waste types (Islam and Murakami, 2021).

Dry stacking tailings structures are designed for long-term operations involving repetitive tasks and the handling of massive material volumes, presenting unique management complexities. Current literature and market solutions reveal a significant gap in tools that can effectively integrate and organize technical documents, instrumentation data, and the management of processes and flows involved in tailings compaction. These critical elements must be compiled into a centralized and intuitive platform, capable of supporting at least a 6D model (3D Model + Schedule + Costs + "QAQC – Quality Assurance and Quality Control").

Digital Twin technology has emerged as a promising solution to these challenges by integrating real-time monitoring, data analytics, and simulation into a cohesive platform (Boje et al., 2020). This technology allows for the simulation of various scenarios, risk assessment, and process optimization, offering a comprehensive management tool that surpasses the capabilities of traditional methods. Although Digital Twin technology has been successfully applied in other industries such as manufacturing and urban planning, its application in tailings management is still in the early stages of development.

Current software solutions often fall short in managing the entire lifecycle of tailings operations, primarily serving as databases focused on storing data and documents without providing comprehensive oversight. There is a significant opportunity to advance these systems by integrating data collection, document management, real-time monitoring, and process optimization, thereby addressing the fragmented approach prevalent in existing practices. The increasing emphasis on regulatory compliance, particularly with standards such as the Global Industry Standard on Tailings Management (GISTM) (ICMM, 2020), highlights the urgent need for more integrated solutions. As the industry evolves, the adoption of advanced digital tools, such as Digital Twin technology, will be essential in enhancing the safety, efficiency, and sustainability of tailings management practices.

In 2021, in response to the adoption of dry stacking tailings in its tailings storage facilities (TSFs), Vale Company, in partnership with Mining Hub, launched an open innovation call to identify an integrated solution for managing the dry stacking tailings process. The sought-after solution was required to be based on the Building Information Modeling (BIM) concept and to offer an integrated environment for data management, while also enabling continuous improvement of the drained stacking processes.

Although BIM is a well-established design methodology in construction, primarily focused on creating and managing digital representations of buildings during the design phase (Egger et al., 2013), it falls short in addressing the ongoing operational needs of tailings facilities. BIM's design-centric approach lacks the flexibility and real-time data integration necessary for continuous monitoring and adaptive decision-making in dynamic environments like tailings management. In contrast, Digital Twin technology, introduced by Michael Grieves in 2002, offers significant potential for optimizing tailings management. By enabling real-time monitoring, simulation, and optimization, Digital Twins align operational processes with strategic objectives, ensuring software applications function effectively. Originally rooted in NASA's space programs, Digital Twin technology has gained momentum with advancements in IoT and 5G, becoming integral to Product Lifecycle Management (PLM) across various industries. As these technologies continue to evolve, Digital Twins are expected to play a crucial role in enhancing operational performance and problem-solving.

The TWIM (Tailings and Waste Interactive Management) Framework and its cloud-based software application, the DSMS (Dry Stacking Management System), were developed as part of an Open Innovation initiative led by Vale Company. Currently in their third year of development and implementation, these systems are being deployed at the "PDER Cianita" dry stacking tailings facility, which is part of the "Mina do Pico" mine managed by Vale Company in Minas Gerais, Brazil.

The TWIM Framework

The TWIM Framework was conceptualized and designed with the aim of establishing a robust foundation of best practices for managing the unique challenges of dry stacking construction methods. Rather than beginning with the creation of software tailored to specific user requirements, the framework was built on the principle that effective software emerges from strong methodologies and frameworks. In this approach, software development is an interpretation of the framework, remaining agnostic and guided by its structured principles. Frameworks like TWIM are essential tools that provide systematic structures for addressing complex problems across various fields, including scientific research, engineering, and project management (Kasser, 2019). They offer a flexible, overarching structure that ensures coherence and consistency across diverse practices, while also allowing for customization to meet specific needs.

The TWIM Framework is a structured approach designed to enhance the management and operational efficiency of dry stacking tailings operations in the mining industry. Central to this framework is the application of a systematic, target-driven Plan-Do-Check-Act (PDCA) cycle, which utilizes digital models within a controlled environment. This approach ensures continuous improvement by planning operational strategies, executing them, monitoring the outcomes, and making necessary adjustments to optimize tailings management processes. By integrating Digital Twin technology, the TWIM Framework brings together

real-time monitoring, data analytics, and predictive modeling to address the complex challenges of tailings management.

The framework is built on advanced management and optimization concepts that align with the principles of Industry 4.0, providing comprehensive operational oversight through continuous engineering data management, digital documentation, and precise control of stacking operations. Its primary focus is on enhancing the reliability, predictability, and auditability of tailings storage facilities, ensuring that all construction and operational processes are thoroughly documented and effectively managed. Key concepts underlying the TWIM Framework include:

- Engineering Data Management (EDM): Involves the systematic collection, storage, and analysis of engineering data, including geotechnical data, construction records, and instrumentation data;
- Digital Twin (DTs): Provides a virtual replica of the TSFs, enabling real-time monitoring, operational simulation, and forecasting;
- Cloud Computing: Offers scalable and secure data storage and processing capabilities, allowing real-time data access and collaboration among stakeholders, regardless of geographical location, thereby enhancing the overall efficiency and responsiveness;
- Geotechnical QA/QC: Implements a systematic approach to maintain geotechnical parameters, such as moisture, compaction degree, and layer thickness within specified values;
- Real-Time Instrumentation: Utilizes real-time data to monitor key indicators, automating alerts and notifications to the teams responsible for TSF management;
- Interactive Management: Emphasizes the importance of ongoing, real-time management of tailings operations, providing operational insights to ensure immediate responses to emerging issues;
- Regulatory Alignment: Ensures compliance with current regulatory standards, such as the Global Industry Standard on Tailings Management (GISTM);
- Strategic Goals (SGs): These are targets that align with company strategic goals and are incorporated in the design of solutions as KPI's that measure the adherence of operation and managing;
- Operation Cycle and Continuous Improvement: During the operational phase, continuous documentation, support, and methodological refinements are provided to enhance performance and ensure monitoring of critical components, enabling the system to adapt and improve continuously in response to operational needs.

Interactive management

The TWIM Framework is centered on interactive management, leveraging continuous versioning and digital twin models to create a dynamic, iterative process. This process ensures ongoing improvement in

tailings storage facility operations, while maintaining accurate, up-to-date "As-Is" documentation. The main cycle consists of operational ontologies, which act as parametric "recipes" that define the controlled constraints for simulating the operational environment. These ontologies are used to generate the Expected Digital Model (EDM), a 6D simulation of the tailings pile, offering valuable insights into resource demands. After planning and simulation, the execution phase begins, leading to the creation of the Realized Digital Model (RDM), where construction is continuously monitored to ensure it meets the desired parameters and requirements. All results are interactively collected during the Interactive Execution Management phase, reflecting real-time operations and providing key insights for management and ongoing improvements. This feedback loop informs the development of new ontology versions, driving a continuous cycle of enhancement and refinement.

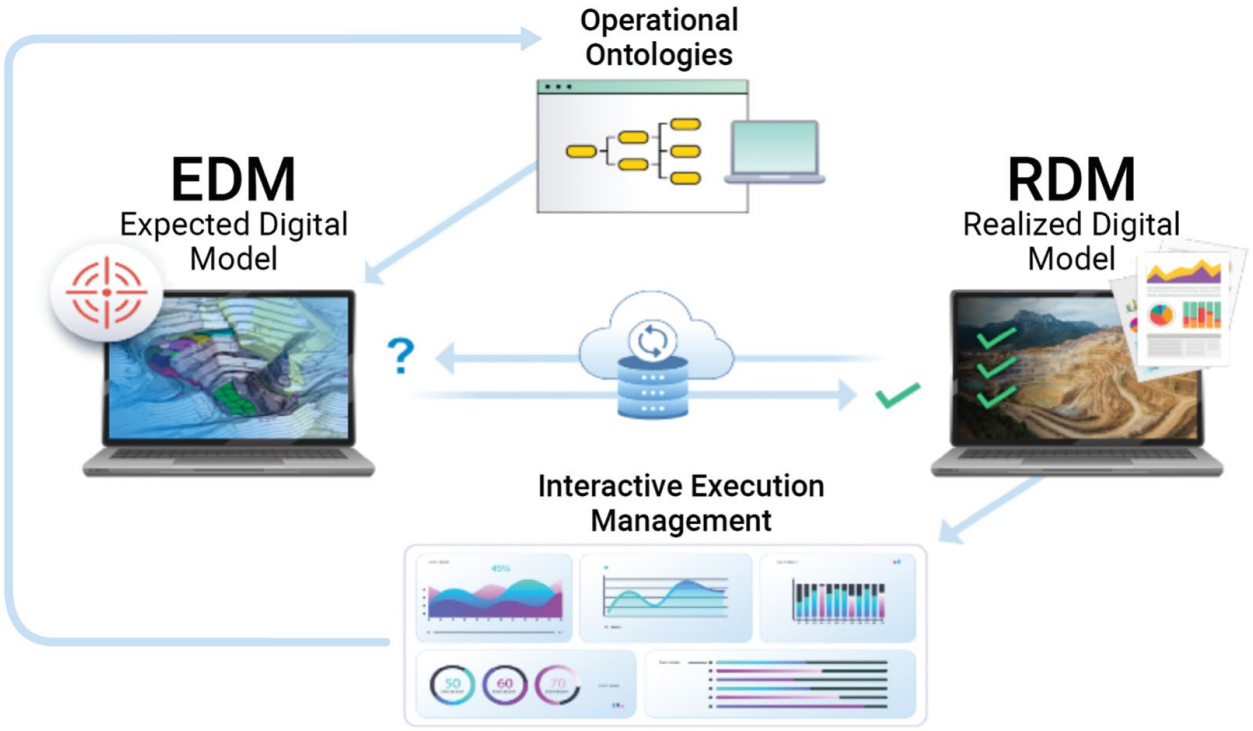


Figure 1: TWIM Framework continuous improvement cycle

The TWIM Framework enables the management of tailings stacking compaction operations, by means of a digital environment that guarantees the control of the five main pillars related to this type of structure: directory of documents produced, related to field and laboratory tests (routine tests for the approval of compacted layers and special tests for the verification of complete geotechnical parameters); control of geotechnical indicators that guarantee the quality of the filtered stacking operation process (e.g., material moisture, degree of compaction, layer thickness, etc.); visual control of the 5D model of the filtered tailings pile, based on continuous feeding of the model (continuous "as built"); control of the geotechnical

instrumentation to gauge the performance of the structure throughout its operation and useful life; and process control through the approval of activities present in the compaction flow of each layer.

The process of creating digital twins for tailings piles involves several steps. Initially, comprehensive data on the tailings pile's properties and behaviors are collected. This includes geotechnical data such as material moisture, degree of compaction, and layer thickness; operational data like stacking sequences and machinery used; and environmental data encompassing weather conditions and surrounding infrastructure. The aim is to gather detailed and accurate information to ensure the fidelity of the digital model. Once the data is collected, it is employed to develop a detailed multidimensional digital model of the tailings pile. This model represents the current state of the pile and serves as the basis for further simulations and analyses. By creating a precise digital representation, the model can be used to visualize the pile's structure and identify any potential issues that may arise.

A key feature of the digital twin is its integration of real-time data. Data input by humans, alongside sensor readings and other monitoring tools, continuously updates the digital model, ensuring it remains an accurate and dynamic representation of the physical tailings pile. This real-time or near real-time integration allows for ongoing monitoring and management, offering valuable insights into the current state of the pile and enabling predictions of future behaviors. The digital twins are then employed to simulate various management scenarios, helping to assess risks, optimize stacking processes, and forecast future conditions. By evaluating these scenarios, the most effective strategies for managing the tailings pile can be identified, ensuring both operational efficiency and safety.

Geotechnical stability simulations focus on evaluating the stability of tailings piles under various conditions, ensuring that management practices comply with regulatory standards. These simulations are crucial for identifying potential risks and developing strategies to mitigate them, thereby enhancing the overall stability of the pile. Equally important are environmental impact simulations, which assess the ecological consequences of tailings management practices. By analyzing different scenarios, these simulations help identify strategies to minimize adverse environmental effects, aligning management practices with environmental sustainability goals and reducing the overall environmental footprint of mining operations.

Currently, the framework requests the incorporation of rainfall simulations and runoff analysis, which are particularly critical for dry stacking operations in regions with significant rainfall. The dynamic geometry of the terrain in these operations changes rapidly over time, and without proper management, rainfall can reduce operational efficiency and necessitate the allocation of more space for ongoing tailings storage. By including these environmental factors in the simulations, the TWIM Framework can better anticipate and mitigate the effects of rainfall, ensuring that operations remain efficient and that the terrain is effectively managed.

Additionally, operational efficiency simulations aim to optimize the stacking processes, enhancing resource recovery and reducing operational costs. The parametric planning features automate the generation of Gantt charts for millions of individual items within the tailings management process. This advanced planning tool enhances resource allocation by providing a detailed and dynamic timeline of all operational activities. By simulating different stacking sequences and machinery usage, it is possible to identify the most efficient methods for managing the tailings pile. This leads to more sustainable and cost-effective operations, maximizing resource utilization and minimizing waste.

Ontologies and information organization

Ontologies play a central role in the TWIM Framework, organizing and structuring data to enhance the management of dry stacking operations. They consist of defined concepts and relationships that provide a standardized framework for data integration and analysis, ensuring data is interoperable and coherent across various domains. This enables effective structuring and querying of complex datasets, which is essential for comprehensive tailings management. Unlike simpler classification methods like taxonomies, ontologies offer a richer framework by capturing complex relationships such as part-whole and causal connections. This allows for more detailed modeling and deeper understanding of the data, which is critical for informed decision-making within the TWIM Framework.

In the TWIM Framework, ontologies integrate data across several key domains: the Physical Domain, which details the physical characteristics of tailings, including spatial dimensions and material properties; the Geotechnical Domain, capturing properties such as soil moisture, compaction levels, and stability indicators for precise management; the Management Domain, which integrates operational processes, documentation, and instrumentation data to ensure seamless management; and the Planning Domain, supporting scheduling, risk assessment, and long-term planning to optimize execution.

Adhering to the ISO/IEC 21838 standard ensures that the TWIM Framework's ontologies are compatible with high-standard data models, facilitating seamless information exchange. This alignment with international standards, combined with Digital Twin technology, makes the TWIM Framework a powerful tool for efficient and compliant tailings management..

Operationalization as a cloud-based application

This section highlights the key components of the DSMS software, developed to operationalize the TWIM Framework. The focus is on how the DSMS application translates the theoretical principles of the framework into practical tools for managing tailings storage facilities. The development process addressed significant challenges and provided solutions that ensure continuous, real-time management of tailings

operations, while maintaining technical and documentary quality. This digital tool enhances agility in controlling stacking activities, reflecting the practical outcomes of implementing the TWIM Framework.

The Ontology Editor (see Figure 2) within the DSMS application is a vital tool for managing the complex datasets associated with tailings storage facilities (TSFs). It provides a standardized framework for creating and managing operational ontologies, ensuring that all relevant data – such as physical characteristics, geotechnical properties, and operational parameters – are accurately represented and interconnected within the TWIM Framework. This standardization minimizes ambiguities, facilitates clearer communication among users and stakeholders, and maintains coherence across all digital twin models, leading to more effective data integration and analysis.

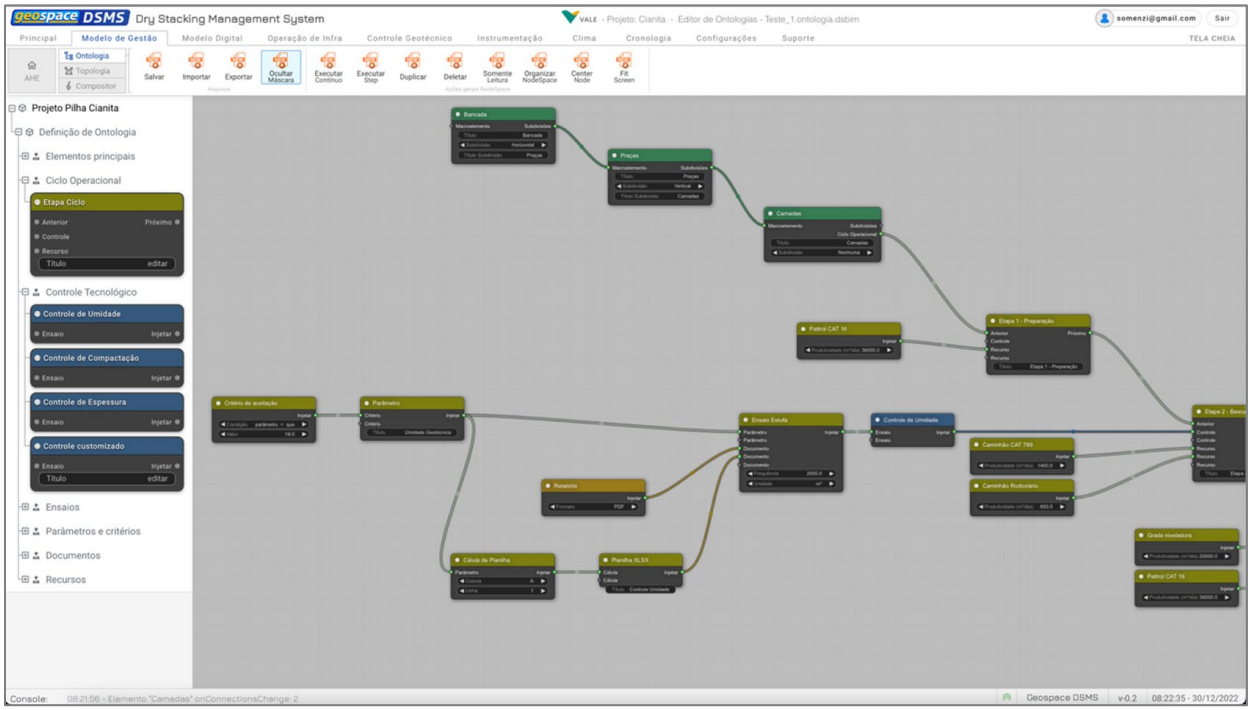


Figure 2: DSMS Ontology Editor

Additionally, the Ontology Editor enhances the DSMS's ability to integrate diverse data sources by offering a flexible yet structured approach to incorporating information from various origins. This capability is essential for comprehensive analysis and optimizing tailings management processes. By unifying data organization, standardization, and integration, the Ontology Editor supports better decision-making and improved operational performance, making it an indispensable component of the DSMS application.

In the DSMS application, parametric planning uses ontologies as a robust input mechanism to significantly improve the accuracy and efficiency of forecasting and scenario generation. Ontologies provide a detailed, standardized framework for capturing and representing knowledge across various

domains, such as physical, geotechnical, and operational data. This structured data forms the foundation for parametric planning, enabling the system to perform precise and comprehensive analyses. By integrating these complex datasets, the DSMS application ensures that all relevant factors are considered in the planning process.

Using ontologies as input, the DSMS application can forecast and generate multiple scenarios for tailings management. The system simulates various future conditions based on parameters like material properties, environmental changes, and operational strategies. These simulations allow stakeholders to understand potential outcomes and risks, leading to better-informed decision-making. The DSMS application then translates these scenarios into detailed Gantt charts, which visualize the timeline, sequence of activities, and resource allocation required for each potential outcome (see Figure 3). These Gantt charts provide clear, actionable plans that guide the steps necessary to achieve optimal results under varying conditions.

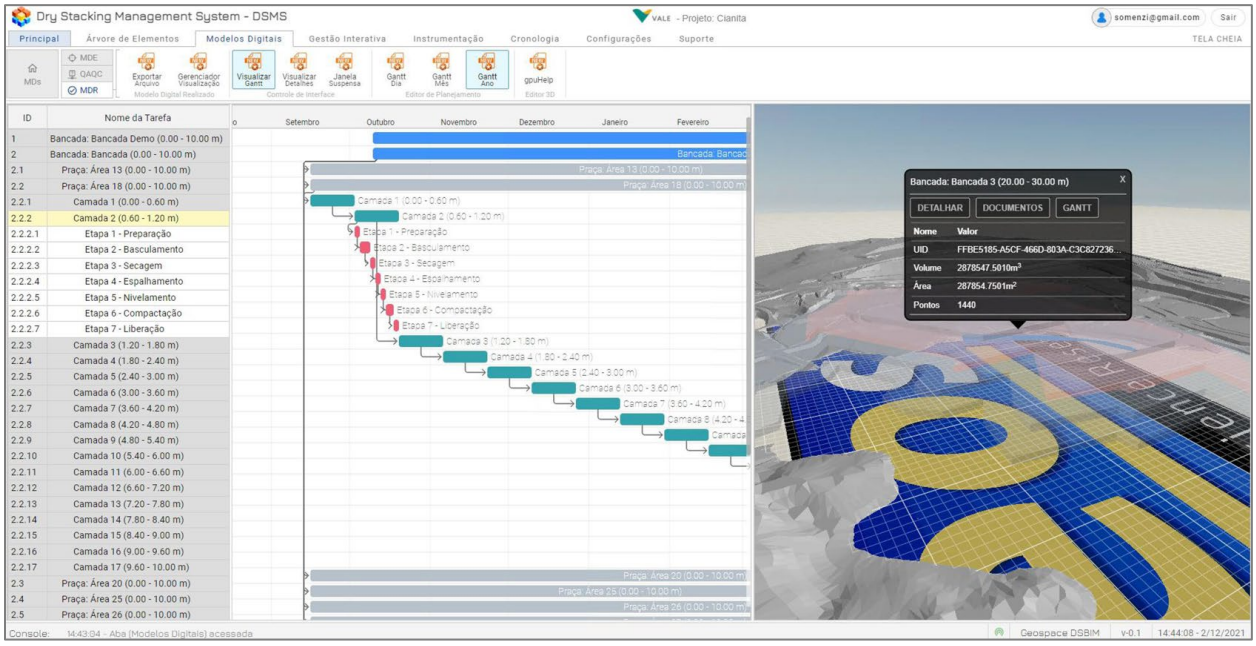


Figure 3: Parametric Gantt Simulator

By using parametric planning and ontologies, the DSMS application can generate distinct future scenarios to guide decision-making. For example, it creates a scenario of increase in material moisture due to predicted higher rainfall, necessitating adjustments in compaction processes and monitoring strategies. The Gantt chart for this scenario would detail the steps required to implement these changes, ensuring that the tailings storage facility remains stable and compliant with regulatory standards. In the second scenario, the system could predict a decrease in available workforce due to economic factors, requiring the

optimization of operational efficiency. The corresponding Gantt chart would outline a revised plan with reallocated resources and adjusted timelines to maintain productivity and safety.

Through the use of parametric planning, ontologies, and advanced forecasting, the DSMS application provides a powerful tool for managing tailings storage facilities. This approach allows for the creation of detailed, actionable plans that can adapt to varying future conditions, ensuring that operations remain efficient, compliant, and safe. Central to this functionality is the Registers Navigator (see Figure 4), an interface designed to enhance user interaction with digital models by offering an "explorer-like" structure. This intuitive navigation system allows users to organize and visualize 3D models, data, and documents within a unified interface. By enabling easy access to, and management of, all relevant information directly through the digital models, the Registers Navigator ensures that critical data is always at the user's fingertips, further streamlining the management and operational oversight of tailings storage facilities.

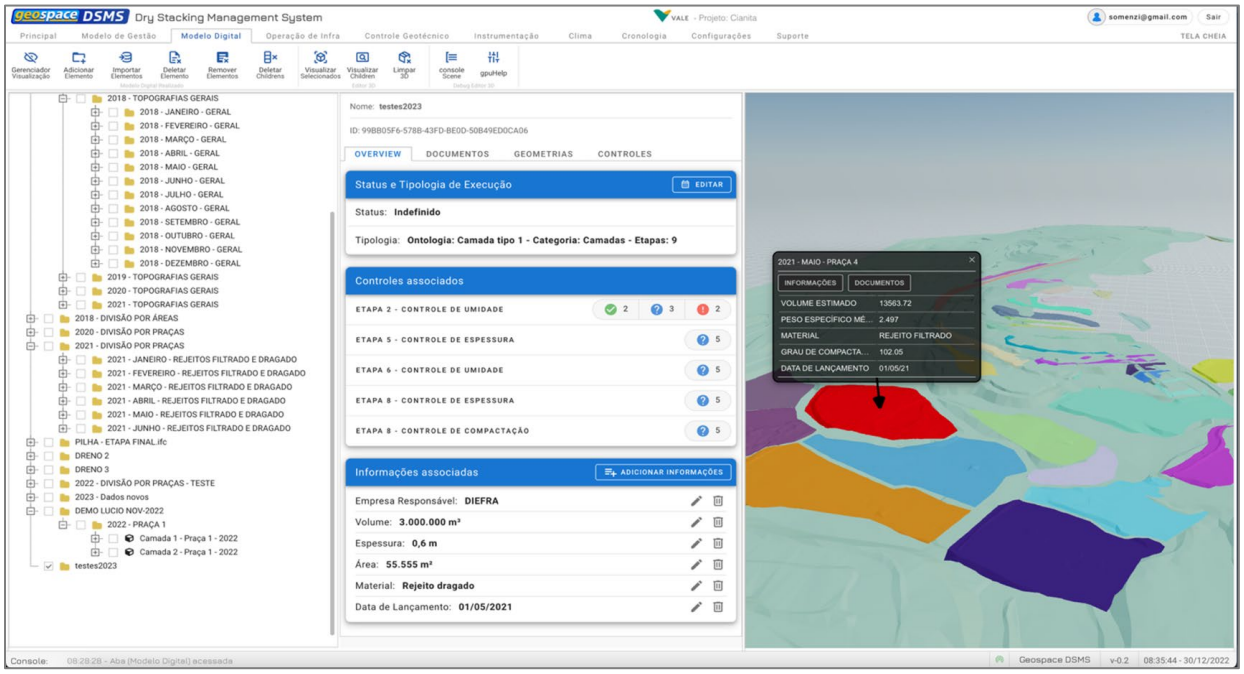


Figure 4: Registers Navigator interface in DSMS application

Conclusion

The TWIM Framework addresses critical challenges in managing dry stacking tailings by integrating Digital Twin technology, real-time monitoring, and predictive modeling. Initial deployment at Vale's tailings facility has shown promising improvements in both resource recovery and operational efficiency. The framework's development highlighted the importance of flexible software architecture and iterative testing, which were crucial in overcoming challenges like data integration and synchronization. As the framework continues to evolve, future efforts will focus on refining the software, expanding its use, and

ensuring it meets industry standards for safety and sustainability. The TWIM Framework provides a scalable, robust solution for the mining industry, enhancing the management of tailings storage facilities and supporting long-term operational success..

Acknowledgements

We sincerely thank Vale Company for their invaluable support and collaborate on, which were crucial to the development and application of the TWIM Framework. We also extend our gratitude to Geospace Digital Engineering Company for their technical expertise in developing DSMS Application.

References

Boje, C., Guerriero, A., Kubicki, S. and Rezgui, Y. 2020. Towards a semantic construction digital twin: directions for future research. *Automation in Construction* 114.

Egger, M., Hausknecht, K., Liebich, T. and Pryzybylo, J. 2013. *BIMLeitfaden für Deutschland. Information und Ratgeber.* Endbericht. ZukunftBAU.

Grieves, M. 2014. Digital twin: manufacturing excellence through virtual factory replication. Research paper.

ICMM. 2020. Global Industry Standard for Tailings Management, International Council on Mining and Metals. London.

Islam, K. and Murakami, S. 2021. Global-scale impact analysis of mine tailings dam failures: 1915–2020. *Global Environmental Change* 70: 102361.

ISO/IEC 21838-1:2020. Information technology – Top-level ontologies – Part 1: Requirements. International Organization for Standardization, Geneva, Switzerland, 2020.

Kasser, J.E. 2019. *Systems Engineering: A Systemic and Systematic Methodology for Solving Complex Problems*. CRC Press.

Kossoff, D., Dubbin, W.E., Alfredsson, M., Edwards, S.J., Macklin, M.G. and Hudson-Edwards, K.A. 2014. Mine tailings dams: Characteristics, failure, environmental impacts, and remediation. *Applied Geochemistry* 51: 229–245.

Mining Association of Canada (MAC). 2021. *A Guide to the Management of Tailings Facilities, Version 3.2*.

CPT Calibration Chamber Testing of Tailings Sand at High Confining Pressures

Matthew Haynes, WSP, Australia
Riccardo Fanni, WSP, Australia
David Reid, University of Western Australia, Australia
Kyle Smith, WSP, Australia

Abstract

The cone penetration test (CPT) is the leading tool to assess the in-situ state, strength, and liquefaction susceptibility of sandy soils and mine tailings. Much of the interpretation of CPT results is based on the historic databases of calibration chamber tests on sand and, increasingly, mine tailings. While these efforts have led to the current procedures to interpret CPT data, two factors relevant to CPT application and interpretation require consideration: (i) the available calibration chamber data is dominated by tests with consolidated mean effective stresses < 200 kPa; and (ii) tailings storage facilities (TSFs) are being constructed to heights such that in-situ stresses are far higher than those of the available calibration chamber test database.

While much of CPT interpretation is carried out in a dimensionless framework, there is clear evidence that, even across the range of stresses for which calibration chamber tests have been carried out, relationships between some forms of stress-normalized cone resistance and in-situ state are dependent on effective stress. This stress-dependence is not accounted for in some CPT interpretation techniques. However, industry standard cavity expansion techniques, such as the CPTwidget, attribute the stress-dependence to a variation in shear rigidity with effective stress. Additionally, at high stresses, other factors, such as the curvature of the critical state line (CSL) in an e-log(p') plane, are another possible source of stress-dependence. Guidance on CPTwidget modeling for materials with a curved CSL has not been developed, which leads to a variety of possible techniques to input semi-logarithmic CSL parameters.

A new calibration chamber and miniature CPT capable of testing soils consolidated up to 2,000 kPa was developed to test sands at stresses relevant to large TSFs. A tailings sand, referred to as residue sand, originating from the separation of fine and coarse bauxite residue, was tested. The CSL of the residue sand was observed to exhibit significant curvature. Calibration chamber tests were performed at mean effective stresses of 50 and 1,000 kPa to capture the effect of the CSL curvature over the range of in-situ stresses

within the TSF. The results of the calibration chamber testing were compared to numerical simulations at equivalent stresses using the CPTWidget. The results of the testing were used to create a CPT calibration specific to the residue sand, to infer in-situ state parameter from normalized tip resistance.

Introduction

Characterization of tailings is crucial for design analyses of tailings storage facilities (TSFs). A combination of in-situ and laboratory tests are used to estimate the strength of tailings. However, the in-situ strength of low plasticity silt and sand tailings can be difficult to infer through laboratory testing on intact specimens due to significant sampling disturbance. Therefore, in-situ tests such as the cone penetration test with pore pressure measurement (CPTu) are required to estimate the state parameter (Ψ) of these materials.

Current state of practice methods to estimate Ψ from normalized CPTu tip resistance (Q) have been developed by Been et al. (1988) and Been and Jefferies (1992) based on a database of calibration chamber testing. Tip resistance was normalized by Been and Jefferies according to Equation 1, where Q_p is the tip resistance (q_t) normalized by the mean total stress (p) and the mean effective stress (p'). Further, Equation 2 normalizes Q_p by the pore pressure ratio (B_q) and presents the relationship with Ψ and coefficients k and m. Finally, Shuttle and Cunning (2007) introduced Equation 3, which is the equation used in this paper.

$$Q_p = \frac{q_t - p}{p'} \quad \text{(Equation 1)}$$

$$q^* = \frac{Q_p}{1 - B_q} = k e^{-m\Psi} \quad \text{(Equation 2)}$$

$$Q_p(1 - B_q) + 1 = k e^{-m\Psi} \quad \text{(Equation 3)}$$

Shuttle and Jefferies (2016) introduced the cavity expansion model, CPTwidget, to provide an alternative to undertaking physical calibration chamber testing. The results of the CPTwidget were scaled using a cone factor (C_q) to match calibration chamber tests from the updated database used by Jefferies and Been (2015). This calibration chamber database is limited to a maximum p' of 457 kPa, with a mean and median of 109 and 75 kPa, respectively. However, the CPTwidget is frequently used for interpretation of CPTu data (Q vs. Ψ) for TSFs where the in-situ stresses far exceed that of the Jefferies and Been database that was used to develop the software (Oberle et al., 2020).

CPTwidget allows for calibration of Q vs. Ψ over a range of shear rigidity (I_r) values to capture the influence of I_r variation with effective stress. Variation of I_r is the only stress dependent relationship for drained simulations in the CPTwidget. However, another potential source of stress level bias is present for materials with a curved critical state line (CSL), where λ_e (ln of λ) changes with stress. Curved CSL inputs

have not been implemented in the CPTwidget, and guidance for inputting λ_e for materials with a curved CSL has not been provided by the authors.

This paper presents a comparison of small-scale calibration chamber testing using miniature CPT and CPTu cones at low and high effective stress. A sand with significant curvature of the CSL at high stresses was tested. Comparison to the CPTwidget simulations allowed for an assessment of the CPT inversion parameters and the stress level bias of the CPTwidget against the results of the calibration chamber tests.

Calibration chamber

Equipment

A small-scale calibration chamber, illustrated in Figure 1, was created, based on a triaxial testing apparatus.

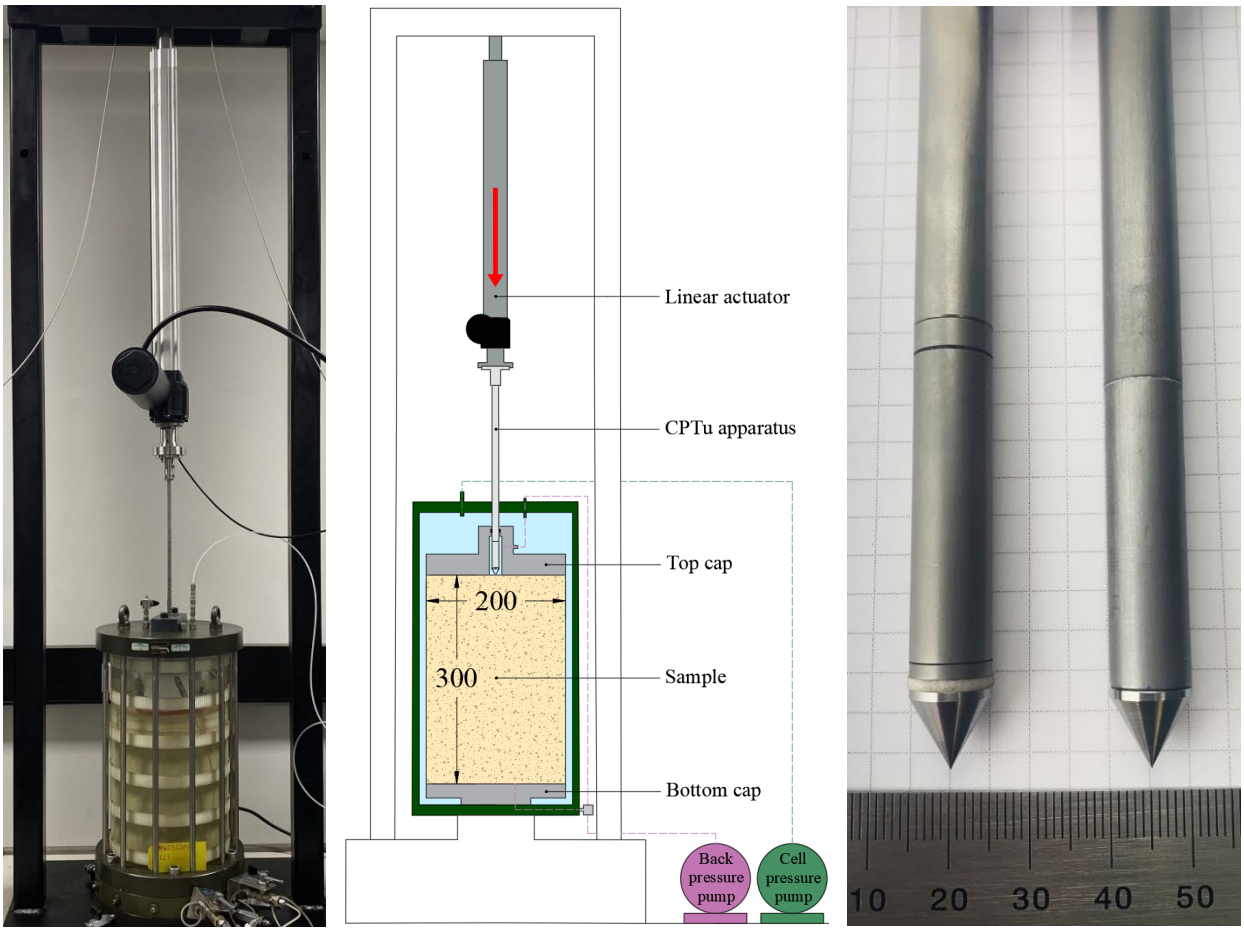


Figure 1: Miniature calibration chamber photograph (left), schematic (center), miniature CPTu and CPT apparatus (right)

The calibration chamber applies stress isotropically using cell pressure applied to the membrane and top cap. The steel bottom cap applies a fixed base restraint. Therefore, the boundary conditions are classified as BC4 (Been et al., 1986). The design of the testing apparatus was based on the design presented by Ayala

et al. (2020) and Damavandi-Monfared and Sadrekarimi (2015). Equipment from Haynes et al. (2024) was used with two modifications, as detailed below:

- 200 mm diameter stainless steel bottom cap modified with an external drainage port for connection to an access ring. The modification allowed for testing materials with corrosive pore fluid without damaging the aluminum triaxial cell.
- 400 mm stroke linear actuator, which replaced the triaxial loading frame. The linear actuator provided a larger stroke for cone penetration compared to the triaxial loading frame.

Additionally, the following equipment was used from the apparatus outlined by Haynes et al. (2024):

- 488 × 222 mm (internal height × diameter) triaxial cell with coupling to seal against the shaft of the CPTu apparatus.
- 2 × pressure/volume controllers to apply the cell and back pressures.
- 200 mm diameter top cap with a sealed opening for the shaft of the CPTu apparatus.
- 2 × 200 mm sintered-bronze porous stones for the top and bottom of the specimen. The top porous stone included an opening for the CPTu cone.
- 430 × 200 mm (height × diameter) latex membrane.
- 10 mm diameter miniature CPT and CPTu cones.

Both a miniature CPT and a miniature CPTu cone (refer to Figure 1) were used for testing. The CPT apparatus provided only a measurement of tip resistance, while the CPTu apparatus included a friction sleeve and pore pressure transducer. The miniature cones have an apex angle of 60° and are dimensionally consistent with the full-scale cones. Specifications of the CPT and CPTu apparatuses are provided in Table 1. The 30 MPa CPTu cone was limited to low stress tests (p' = 50 kPa) due to the tip loadcell capacity. The 100 MPa CPT cone was used for high stress tests (p' = 1,000 kPa). The 30 MPa CPTu cone was used for low stress tests due to the greater accuracy of the tip resistance load cell. The pore pressure (u_2) measurement also allowed estimation of drainage conditions at the penetration rate used.

Table 1: CPTu and CPT apparatus specifications

Parameter	CPTu	CPT
Tip resistance: q_t (MPa)	30	100
Frictional resistance: f_s (kPa)	1,000	N/A
Pore pressure: u_2 (kPa)	1,000	N/A

Specimen preparation

Specimens were prepared to a diameter of 200 mm and a height of 300 mm. The geometry of the specimens allowed for a 20:1 ratio of the specimen and cone diameter, as suggested by various studies (Bolton et al.,

1999; Gamez and Olson, 2022; Gui et al., 1998; Pournaghiazar et al., 2012). The specimen height of 300 mm allowed for penetration of the middle 100 mm, at a distance from the top and bottom boundaries which was greater than the distance from the horizontal boundaries.

Specimens were prepared using moist pluviation (MP), based on the method developed by Reid et al. (2024). This method was selected as pluviated specimens were shown to provide greater specimen uniformity compared to moist tamping (MT) (Haynes et al., 2024; Frost and Park, 2003). Dry or wet pluviation could not be used due to segregation of the specimens at low and high gravimetric water contents (GWC). To achieve a range of initial densities, a range of initial GWC and vibration frequencies were used for each test. This allowed for a range of Ψ to be achieved at the target consolidated p'. Due to the moisture in the specimen, pluviation through a funnel was not possible. Therefore, to place the soil in a controlled and evenly distributed manner, a 14 mm sieve was placed on top of the mold. The soil was then pushed through the sieve. This resulted in the pluviation height changing as more specimen was placed, which could have resulted in a denser to looser gradient from the bottom to the top of the specimen.

To confirm the specimen uniformity created by this technique, individually pluviated layers were placed in an acrylic column of similar dimensions to the calibration chamber specimens. The density of each layer was calculated after the specimen was pluviated. This check indicated that the specimen preparation technique used did not create a density gradient.

Procedure

A test procedure was developed based on the method used by Ayala et al. (2020). To estimate the change in void ratio (e) of the specimen during saturation and consolidation, a modified version of the cell calibration technique was adopted. End of test freezing was not used, owing to difficulties in freezing calibration chamber specimens due to the specimen size and cap arrangement. All tests using this procedure were back pressure saturated to 550 kPa. The test procedure is provided below:

1. Prepare a specimen using MP to the target density within a split mold. The specimen is sealed by the top and bottom caps and a latex membrane. During this stage, the cone is housed within a recess in the top cap.
2. Apply a suction of −50 kPa to the specimen and measure the height and circumference of the specimen at various locations.
3. Close the triaxial cell and fill it with water. The valves to the specimen are closed to maintain −50 kPa suction in the specimen.
4. Open the valves to the specimen and apply 0 kPa cell pressure and −50 kPa back pressure until a constant cell and back volume is achieved.
5. Increase the cell and back pressure in three steps:

a. 0 kPa cell and −20 kPa back pressure.
b. 30 kPa cell and −20 kPa back pressure.
c. 30 kPa cell and 15 kPa back pressure.

6. Flush the specimen by opening the top drainage line to atmospheric pressure, while applying a constant 30 kPa cell pressure and 15 kPa back pressure. After flushing, reconnect the top drainage line to the back pressure pump and reduce back pressure to 10 kPa.
7. Increase the cell and back pressure in 30 kPa increments, maintaining a maximum effective stress of 50 kPa. Achieve a constant cell and back pressure for each stage before going to the next stage. Repeat this process until reaching cell and back pressure values of 600 and 550 kPa, respectively.
8. Determine the B-value by increasing the cell pressure with valves to the top and bottom drainage lines closed.
9. Consolidate the specimen to the target effective stress by increasing the cell pressure in steps with a load increment of 1.
10. Test stage: insert the cone 240 mm into the specimen at a constant rate ≤ 1 mm/s, while maintaining a constant cell and back pressure.

Material properties

A bauxite tailings sand, referred to herein as residue sand, was tested. The residue sand was chosen due to its significantly curved CSL, with λ_e changing from 0.04 to 0.15 at p' of 50 and 1,000 kPa, respectively. The residue sand forms the embankment walls of an upstream raised TSF and is stored within the TSF at up to 50 m depth. Therefore, the in-situ vertical effective stress (σ_v') and p' are estimated to reach 1,000 and 700 kPa, respectively. The material properties are summarized in Table 2.

Table 2: Residue sand material parameters

Property	Value
Specific gravity: G_s (-)	3.37
Coefficient of uniformity: C_u (-)	3.78
D_{50} (mm)	0.425
Fines content (%)	4%
CSL: M_{tc} (-)	1.54
CSL power law: A (-)	1.19
CSL power law: B (-)	0.05
CSL power law: C (-)	0.70

The CSL of the residue sand was estimated based on six CID triaxial tests ranging from 30 to 550 kPa consolidated stresses. Four of the triaxial tests were performed using process liquor and two using demineralized water as pore fluids. This was done to assess if the pore fluid affected the CSL of the residue sand. The critical state points of the demineralized water tests tended towards the CSL derived using process liquor. The semi-logarithmic and power law CSL parameters are provided in Tables 2 and 3. Small strain shear modulus (G_{max}) and I_r were estimated from two bender element (BE) tests prepared to different initial densities. These results are presented in Figure 3.

Table 3: CPTwidget input parameters

Property (unit)	Value
State dilatancy: χ (-)	3.80
Volumetric coupling parameter: N (-)	0.29
Plastic hardening: H (-)	90-700Ψ
Poisson's ratio: ν (-)	0.20
CSL slope: λ_e (-)	0.04
CSL intercept: Γ (-)	1.32

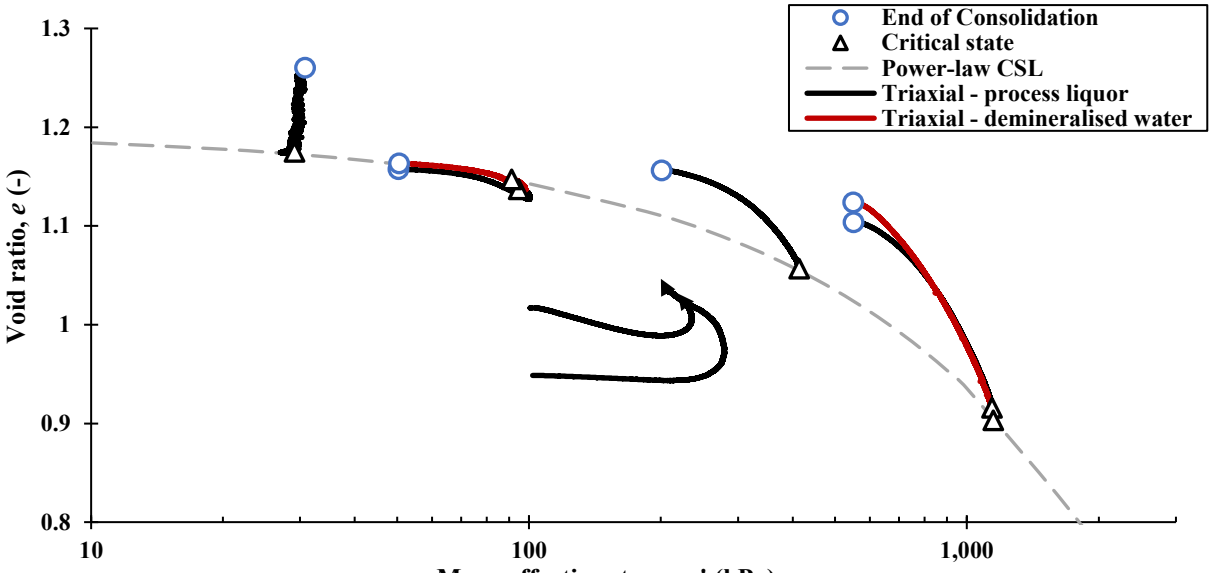


Figure 2: Residue sand CSL

Calibration chamber tests

Nine calibration chamber tests were performed, consisting of five tests at low stress (p' = 50 kPa) and four tests at high stress (p' = 1,000 kPa). All tests were performed under drained conditions during CPT and CPTu penetration. Specimens were prepared to a range of initial densities, resulting in a range of Ψ at the

target consolidated stress. Tests were performed using demineralized water as the pore fluid to avoid damaging the miniature CPT and CPTu apparatuses and to reduce the risk of leaks of large quantities of caustic liquor. This is not anticipated to affect the results of the tests, as the CSL of the residue sand was not affected by changing from process liquor to demineralized water.

Cavity expansion modeling

Spherical cavity expansion modeling was performed for comparison to the calibration chamber results using CPTwidget Version 2.5, developed by Shuttle (2019). Simulations were run for a range of Ψ at low and high stresses, equivalent to the stresses of the calibration chamber tests.

The constitutive soil model, NorSand, was used for the CPTwidget model (Jefferies, 1993). NorSand parameters were calibrated based on the results of two dense and six loose triaxial tests. Inputs for shear rigidity were estimated based on the BE tests presented in Figure 3. G_{max} was related to p' and e based on the equation (see Figure 3) proposed by Jefferies and Shuttle (2020) for calibration of NorSand. G was reduced by a factor of four from the BE result to allow for better calibration of NorSand. Use of similar reduction factors for this purpose was proposed by Shuttle and Jefferies (2016).

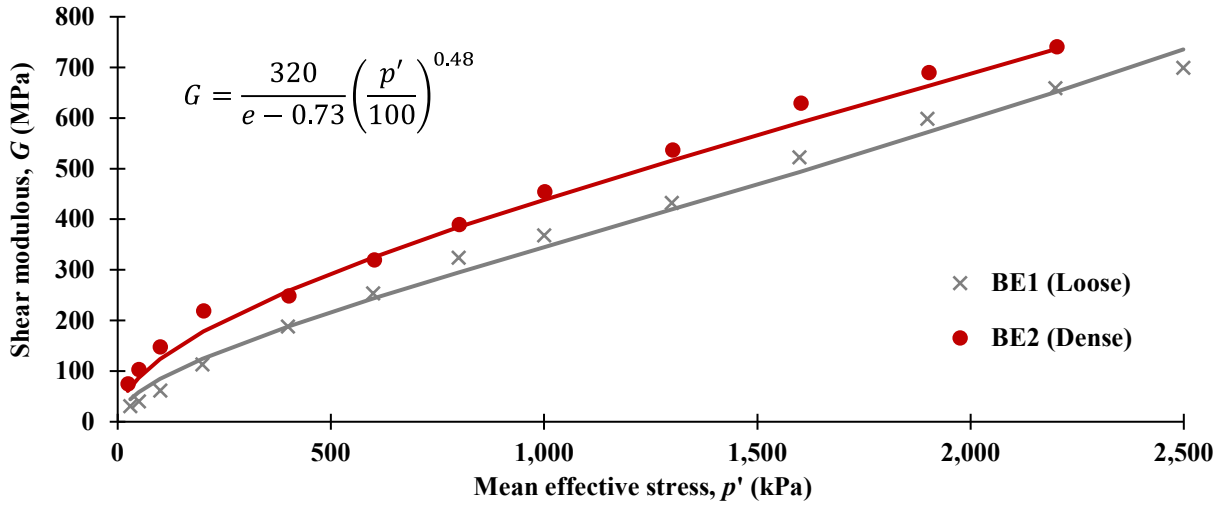


Figure 3: Bender element test results (G vs. p')

Inputs specific to the model are listed in Table 3. Semi-logarithmic CSL parameters (λ_e and Γ) were fit to the intermediate stress region of the CSL (Figure 2). A semi-logarithmic function does not fit well to the curved CSL at $p' > 200$ kPa.

Results

The results of the calibration chamber tests are presented in Figure 4, with trendlines fit to the low and high stress data using Equation 3. The tip resistance presented is the mean from the middle 100 mm of the

specimen. Error bars on the y-axis indicate the variability of tip resistance within the middle 100 mm of the specimen.

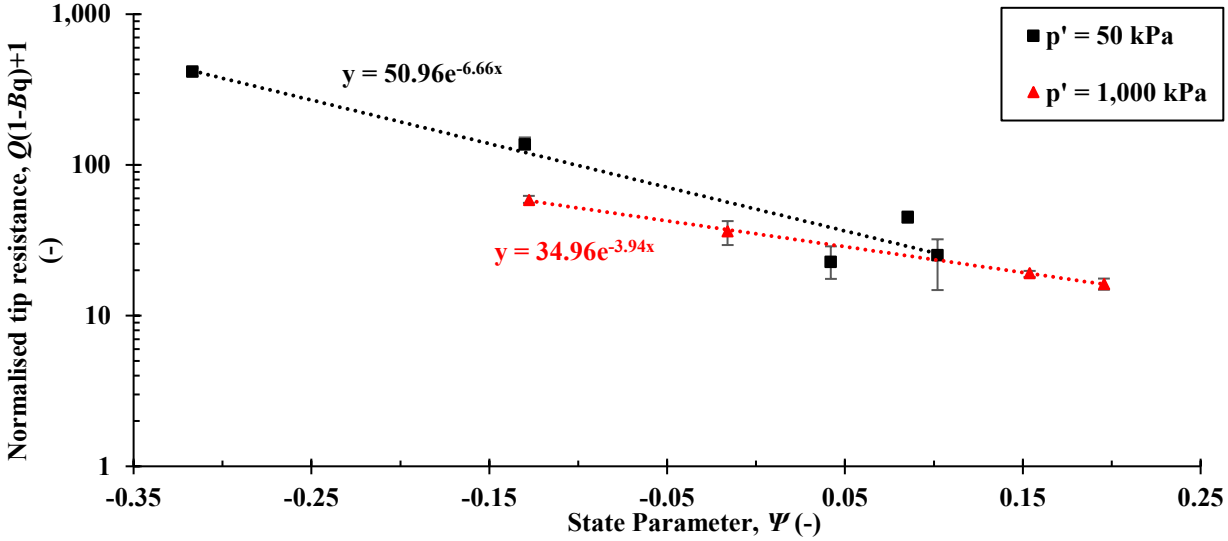


Figure 4: Calibration chamber results

The calibration chamber results at low and high stress show a linear semi-logarithmic trend consistent with the form of Equation 3. Based on the findings of Salgado et al. (1998) and Been et al. (1986), it is anticipated that the influence of boundary conditions would result in a reduction of $Q(1-B_q)+1$ at low Ψ. No significant reduction has been observed in the data.

The use of moist pluviation allowed for uniform loose specimens to be prepared and for several tests to be performed at a Ψ greater than the maximum Ψ in the Jefferies and Been (2015) database. Variability between tests and within each specimen was greater in specimens prepared to low initial densities, consistent with Haynes et al. (2024). Less variability was observed in high stress tests compared to low stress tests at equivalent Ψ. This may be due to the greater divergence of the normal consolidation line (NCL) and CSL at higher stresses, which allowed for high stress test specimens to achieve higher Ψ from higher initial densities.

Comparing the trendlines and inversion parameters, k and m, between high and low stress indicates a clear reduction of k and m with increased stress (Figure 4). This is consistent with stress level effects in the Jefferies and Been (2015) database, which are attributed to a reduction in I_r with increasing stress.

The results of CPTwidget modeling are plotted in Figure 5 for comparison to the calibration chamber result. The low stress CPTwidget simulation fits within the range of the calibration chamber data. However, the high stress CPTwidget result showed a significantly steeper trend (higher m) compared to the trend of the high stress calibration chamber data. Therefore, the stress level bias observed in the residue sand was larger than predicted by CPTwidget. This may be due to the effect of CSL curvature, which is not

incorporated into the CPTwidget result. This appears to be supported by the simulations of Martinelli and Pisano (2022).

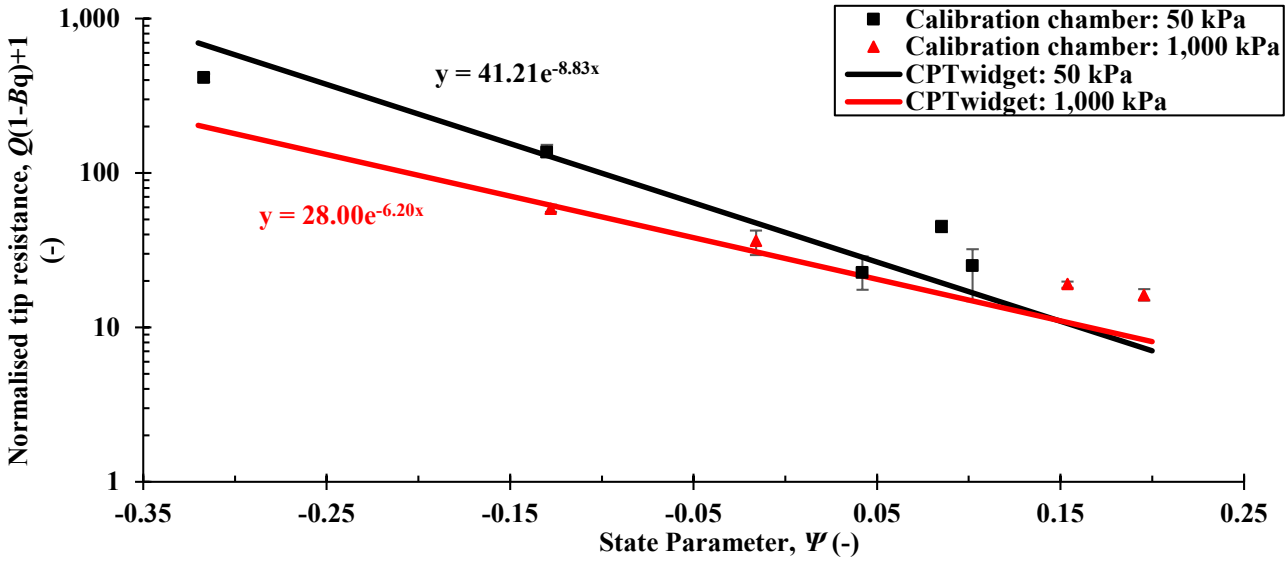


Figure 5: CPTwidget results compared to calibration chamber results

Conclusion

A series of calibration chamber tests were carried out on a residue sand under low and high consolidated effective stresses to assess the performance of the CPTwidget across a wide range of effective stresses in a material with a significantly curved CSL. This testing was carried out by incorporating modifications to a previously developed miniature calibration chamber system to enable higher stress testing. The following observations were provided by this work:

- Unique trendlines, with a linear semi-logarithmic form, were identified from the calibration chamber tests on residue sand at both low and high stresses.
- High stress calibration chamber tests showed a lower normalized cone resistance, with lower sensitivity to changes in Ψ (lower k and m values), compared to low stress tests.
- Comparison of calibration chamber results to the CPTwidget simulations showed a good fit at low effective stresses, but a poor fit at high effective stresses.
- Variances between the CPTwidget and calibration chamber result at high stress may be due to an additional source of stress level bias resulting from CSL curvature, which is not accounted for in the CPTwidget.

Acknowledgements

The authors are grateful for the ongoing support of WSP Australia, which provided financial support for

the research and calibration chamber equipment. Additionally, we acknowledge the contributions of personnel in the WSP Perth Laboratory and the University of Western Australia.

References

Ayala, J., A. Fourie and D. Reid. 2020. Cone penetration testing on silty tailings using a new small calibration chamber. *Géotechnique Letters* 10(4): 492–497. https://doi.org/10.1680/jgele.20.00037

Been, K., J.H.A. Crooks, D. E. Becker and M. G. Jefferies. 1986. The cone penetration test in sands: part 1, state parameter interpretation. Géotechnique 36(2):239–249. https://doi.org/10.1680/geot.1986.36.2.239

Been, K., J.H.A. Crooks and M.G. Jefferies. 1988. Interpretation of material state from the CPT in sands and clays. In *Penetration Testing in the UK*. London: Thomas Telford: 215–218. https://www.icevirtuallibrary.com/doi/abs/10.1680/ptituk.13773.0034

Been, K. and M.G. Jefferies. 1992. Towards systematic CPT interpretation. *Predictive Soil Mechanics: Proceedings of the Wroth Memorial Symposium*. London: Thomas Telford: 121–134. https://www.icevirtuallibrary.com/doi/abs/10.1680/psm.19164.0008

Bolton, M.D., M.W. Gui, J. Garnier, J.F. Corte, G. Bagge, J. Laue and R. Renzi. 1999. Centrifuge cone penetration tests in sand. *Géotechnique* 49(4): 543–552. https://doi.org/10.1680/geot.1999.49.4.543

Damavandi-Monfared, S. and A. Sadrekarimi. 2015. Development of a miniature cone penetrometer for calibration chamber testing. *Geotechnical Testing Journal* 38(6): 878–892. https://doi.org/10.1520/GTJ20150036

Frost, J.D. and J.Y. Park. 2003. A critical assessment of the moist tamping technique. *Geotechnical Testing Journal* 26(1): 57–70. https://doi.org/10.1520/GTJ11108J

Gamez, J.A. and S.M. Olson. 2022. Compressibility-based interpretation of cone penetrometer calibration chamber tests and corresponding boundary effects. *Geotechnical Testing Journal* 45(4): 778–796. https://doi.org/10.1520/GTJ20210129

Gui, M.W., M.D. Bolton, J. Garnier, J.F. Corte, G. Bagge, J. Laue and R. Renzi. 1998. Guidelines for cone penetration tests in sand. In T. Kimura, O. Kusakabe and J. Takemura (eds), *Proceedings of the International Conference on Centrifuge Modelling (Centrifuge '98)*, vol. 1. Tokyo. Rotterdam: A.A. Balkema: 155–160.

Haynes, M., D. Reid, R. Fanni and K. Smith. 2024. Development of a calibration chamber system for testing at high confining pressures. In M. Arroyo and A. Gens (eds), *Proceedings of the 7th International Conference on Geotechnical and Geophysical Site Characterization.* Barcelona: CIMNE: 2245–2252. https://doi.org/10.23967/isc.2024.120

Jefferies, M.G. 1993. NorSand: a simple critical state model for sand. *Géotechnique* 43(1): 91–103. https://doi.org/10.1680/geot.1993.43.1.91

Jefferies, M.G. and K. Been. 2015. *Soil Liquefaction: A Critical State Approach,* 2nd ed. Boca Raton (FL): CRC Press. https://doi.org/10.1201/b19114

Jefferies, M.G. and D. Shuttle. 2020. Critical state soil mechanics: notes. Vancouver Geotechnical Society. Accessed 9/7/2024 at: https://static1.squarespace.com/static/523c951be4b0728273e73d94/t/5fecc89dfc8ee327dda5f4da/1609353378093/CSSM-VGS+Course+Notes+rev9.pdf

Martinelli, M. and M. Pisano. 2022. Relating cone penetration resistance to sand state using the material point method. *Géotechnique Letters* 12(2): 131–138. https://doi.org/10.1680/jgele.21.00145

Oberle, B., D. Brereton and A. Mihaylova. 2020. Towards zero harm: a compendium of papers prepared for the Global Tailings Review. *Global Tailings Review*. Accessed 14/7/2024 at: https://globaltailingsreview.org/wp-content/uploads/2020/08/towards-zero-harm.pdf

Pournaghiazar, M., A.R. Russell and N. Khalili. 2012. Linking cone penetration resistances measured in calibration chambers and the field. *Géotechnique Letters* 2(2): 29–35. https://doi.org/10.1680/geolett.11.00040

Reid, D., R. Fanni and A. Fourie. 2024. A new method for producing uniform, loose, initially unsaturated specimens. *Géotechnique Letters*, ahead of print.

Salgado, R., J.K. Mitchell and M. Jamiolkowski. 1998. Calibration chamber size effects on penetration resistance in sand. *Journal of Geotechnical and Geoenvironmental Engineering* 124(9): 878–888. https://doi.org/10.1061/(ASCE)1090-0241(1998)124:9(878)

Shuttle, D. A. 2019. CPTwidget: a finite element program for soil-specific calibration of the CPT.

Shuttle, D.A. and Cunning, J. 2007. Liquefaction potential of silts from CPTu. *Canadian Geotechnical Journal* 44(1): 1–19. https://doi.org/10.1139/t06-086

Shuttle, D.A. and Jefferies, M.G. 2016. Determining silt state from CPTu. *Geotechnical Research* 3(2): 90–118. https://doi.org/10.1680/jgere.16.00008

Interpretation of Pore Pressure Dissipation Test Results in Tailings

E. Rust, Osimo, South Africa
M. Rust, NewFields, USA

Abstract

When a Piezocone is advanced through saturated soil (or tailings) it induces dynamic pore pressure. The dynamic pore pressure can be higher or lower than the ambient pore pressure in the soil depending on whether the soil is dilating or contracting due to disturbance by the cone. When the cone penetration is stopped or halted temporarily, the dynamic pore pressure dissipates until it reaches ambient pore pressure. Permeability and the coefficient of consolidation, notably in the horizontal direction, can in some cases be approximated from the rate of dissipation. In almost all cases the asymptotic value at the end of the dissipation test provides a direct measurement of the ambient pore pressure in the surrounding soil.

The purpose of this paper is to provide examples of typical pore pressure dissipation test results and discuss the reasons why these signatures exist.

Introduction

A Piezocone investigation on mine tailings is often carried out at a number of cross-sections where the stratigraphy of all the material in the tailings storage facility (TSF), as well as the foundation, is investigated and their engineering properties are determined, including the degree of saturation above the water table. Furthermore, from the dissipation tests alone the complete flow regime, including permeability, coefficient of consolidation, anisotropy in permeability, possible excess pore pressures and two-dimensional or three-dimensional flow-net, can be determined.

Dissipation test results in tailings are discussed in this paper, and a conceptual model of the dynamic pore pressure distribution during a dissipation test is introduced at the end of the paper.

A detailed pore pressure with depth profile

The frequency of dissipation tests depends on several factors; however, a controlling aspect is often the permeability of the tailings. Tailings properties can vary over a wide range due to their origin and/or the mineral extraction process employed. For the purposes of this discussion, it is sufficient to distinguish

between tailings that behave as a natural clay (including kimberlite, often iron ore, highly oxidized ore, alluvial tailings, and some others) and hard rock milled tailings that are predominantly fine sand and silt-sized. The clay-like tailings have low permeabilities and require long dissipation tests, while the hard rock tailings require shorter dissipation tests.

In high permeability tailings, as a rule of thumb, a dissipation test should be carried out every 2 m or 3 m. It is also recommended that the pore pressure be recorded continuously while the CPTu test is being carried out, even during a rod change that may only take a minute or so to produce an incomplete dissipation test. If it is possible to determine the ambient pore pressure every 2 m to 3 m, it may be possible to interpolate the pore pressure at all the short dissipations. This should allow for the determination of the time required to reach 50% of the dissipation (t_{50}) and maximize the information from the probe.

Tailings with a low permeability should be dealt with on a case-by-case basis. In some extremely low permeability tailings, the time required for dissipation of excess pore pressures could be several days, making it impractical to do as part of the probing campaign. In these cases, pore pressure dissipation tests are recorded until t_{50} is reached, as well as the installation of nested vibrating wire piezometers to provide a measurement of the ambient pore pressure is recommended.

An example of a detailed pore pressure profile with frequent pore pressure dissipation tests is shown in Figure 1. A dissipation test was recorded at each meter in this example. Some of the dissipations from this sounding are shown in Figure 2 (a to g). The black dots on the figure represent the ambient pressure at each dissipation and the black line that connects these dots represent the interpolated tendency of the pore pressure with depth. Below the water table the line will follow the rate pore pressure buildup.

If a dissipation test is carried out above the water table in unsaturated coarse (sandy) tailings the dissipation line will be horizontal and tend to be zero or slightly negative (-1 kPa to -2 kPa), for example Figure 2a. In this zone the layers of saturated fine tailings (slimes) will have a negative pore pressure due to the suction pressures generated by desiccation, for example the dissipations in Figures 2b and 2c. Figures 2d to 2g present typical dissipation tests below the water table.

This dynamic pore pressure profile will also assist in determining the degree of saturation above the water table (Rust, 2023). It is necessary for the design of the Piezocone to have a small fluid chamber so as to improve pore pressure response as well as data sampling at a higher frequency than generally used in industry to get such a detailed pore pressure response. The data frequency rate for this Piezocone is set at 5Hz (implying a reading every 4 mm), whereas the industry norm is generally to sample at depth increments of 25 mm. A positive ambient (static) pore pressure is rarely measured above the water table. Perched water tables and detectable wetting fronts are uncommon. All the dissipations contribute to a detailed understanding of the flow regime, especially when combined with adjacent profiles in a cross-section.

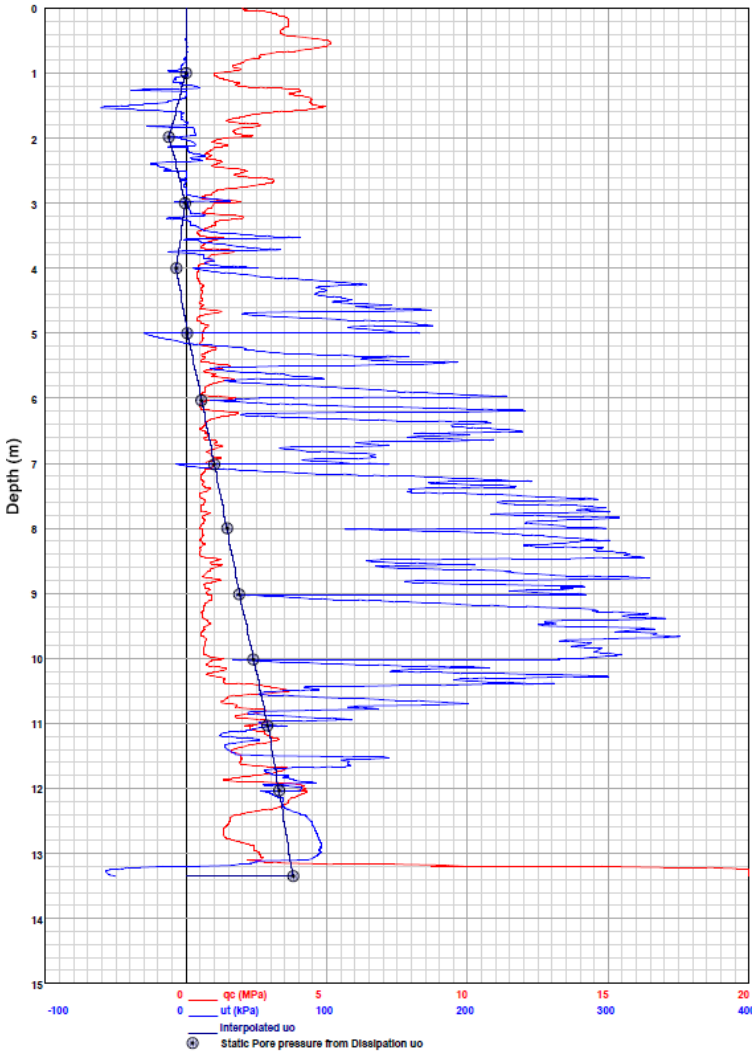
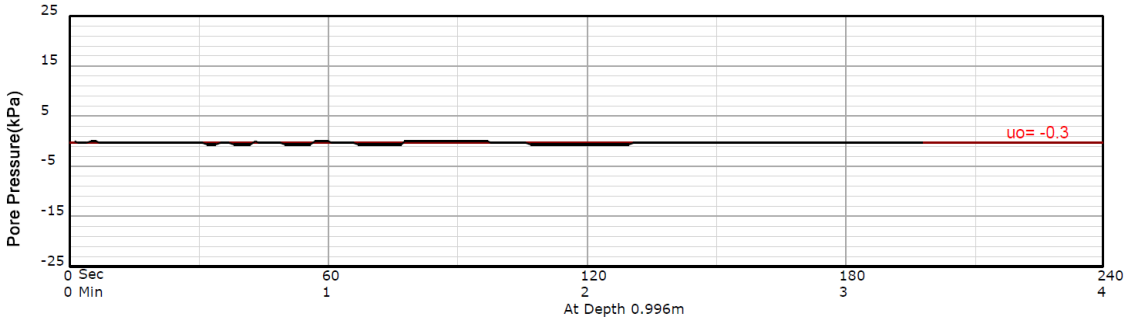
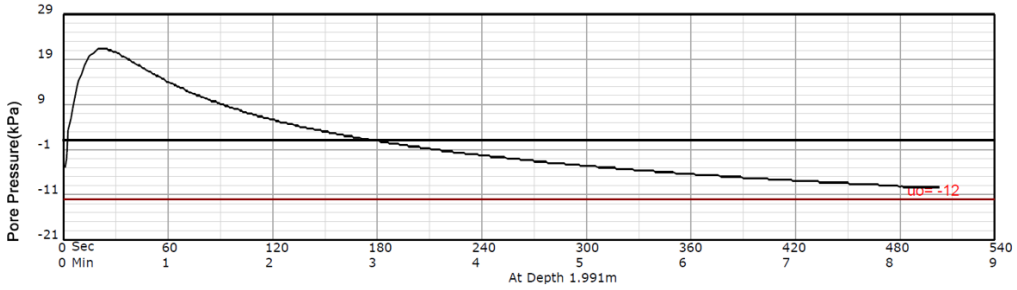


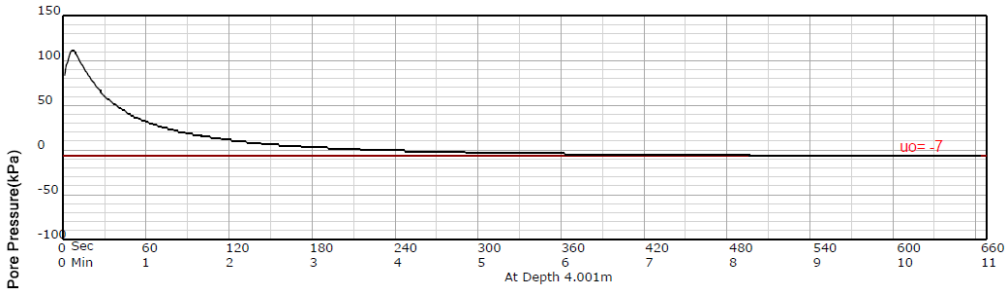
Figure 1: An example of a detailed pore pressure profile from a Piezocone sounding with the black dots indicating the ambient pore pressure from dissipation test results



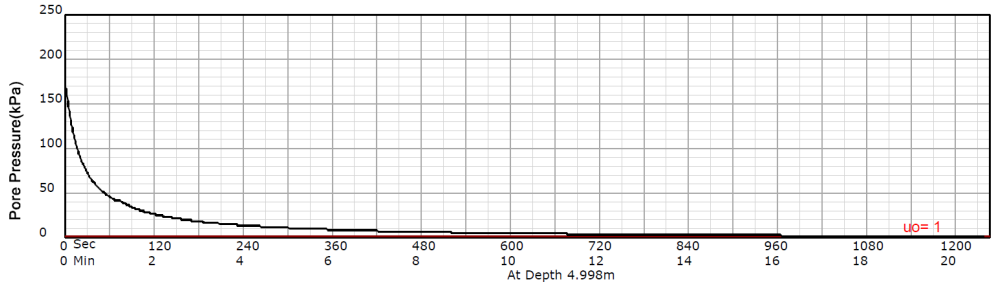
(a) Dissipation in unsaturated coarse (sandy) tailings. Pore pressure is usually 0 or slightly negative



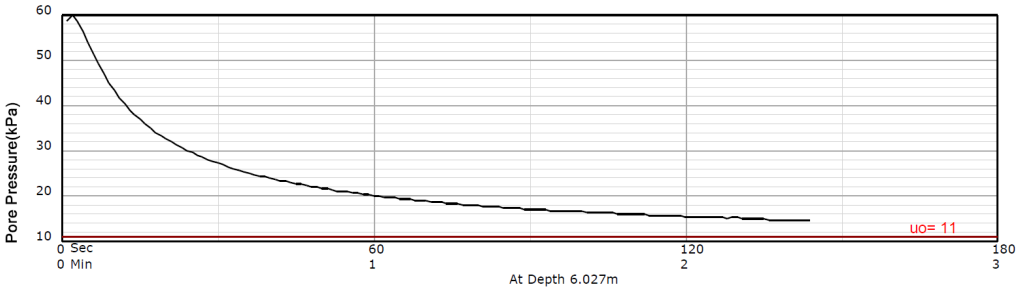
(b) Dissipation in a fully saturated desiccating fine tailings (slimes) layer above the water table with an ambient pore pressure of -12kPa



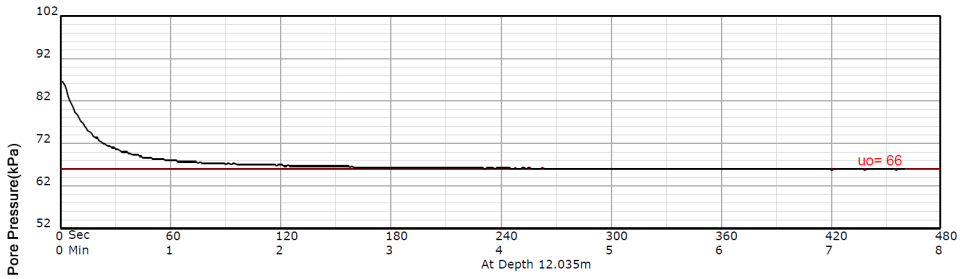
(c) Dissipation in the capillary zone



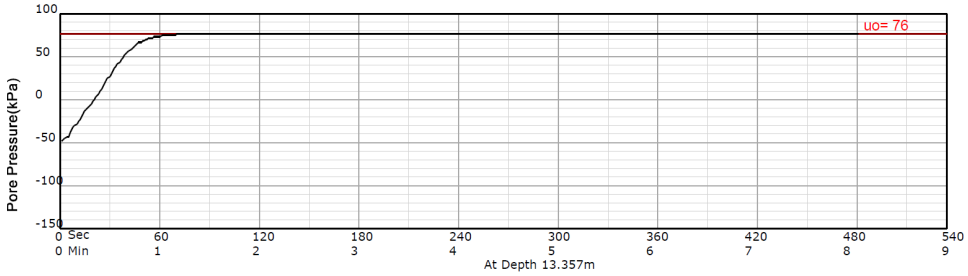
(d) Dissipation at the water table



(e) Short incomplete dissipation test below the water table



(f) Last dissipation in the tailings



(g) Dissipation in the underlying very stiff clay (decomposed shale)

Figure 2: Selected dissipation test results from the Piezocone result shown in Figure 1

Flow regime from a cross-section

Figure 3 shows a cross-section of the Merriespruit facility after the TSF failed on 22 February 1994 (in South Africa). The dissipation test results and trend lines connecting the dissipation test are shown on the cross-section. It provides detailed information on the phreatic regime in this TSF at the probed locations. It is important that all the dissipations are used, or at least all the dissipations below the water table, if the flow in the capillary fringe is going to be ignored.

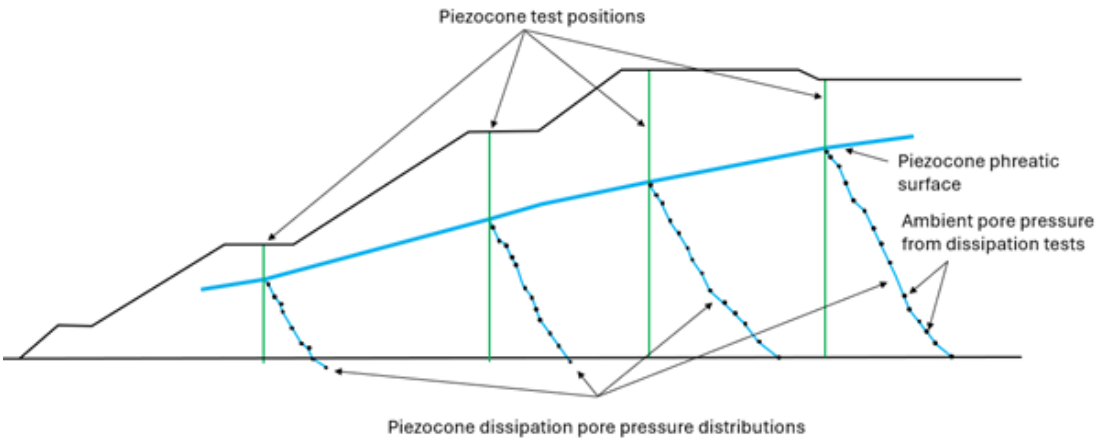


Figure 2: Cross-section of Merriespruit tailings facility showing the measured pore pressure distribution

The results from the dissipation tests can be used to develop a two-dimensional flow-net, and complex flow characteristics such as the anisotropy in permeability can be estimated by carrying out a detailed finite element flow analysis.

Shape of the dissipation test

A number of typical pore pressure dissipation responses or shapes are routinely found in tailings. Extensive research has been carried out on these dissipation tests and has been published by several researchers including Baligh and Levadoux (1980), Teh and Houlsby (1991), Rust (1996); Sully et al. (1998), Burns and Mayne, (1998) and Burns and Mayne,\ (2000). The shape of the dissipation test depends on the pore pressure generated during probing. This pressure is made up of the ambient (static) pore pressure, shear stress induced and normal stress induced pore pressure.

$$u = u_0 + \Delta u_{shear} + \Delta u_{normal}$$

$$u_e = \Delta u_{shear} + \Delta u_{normal}$$

Where u_e is the net induced excess pore pressure.

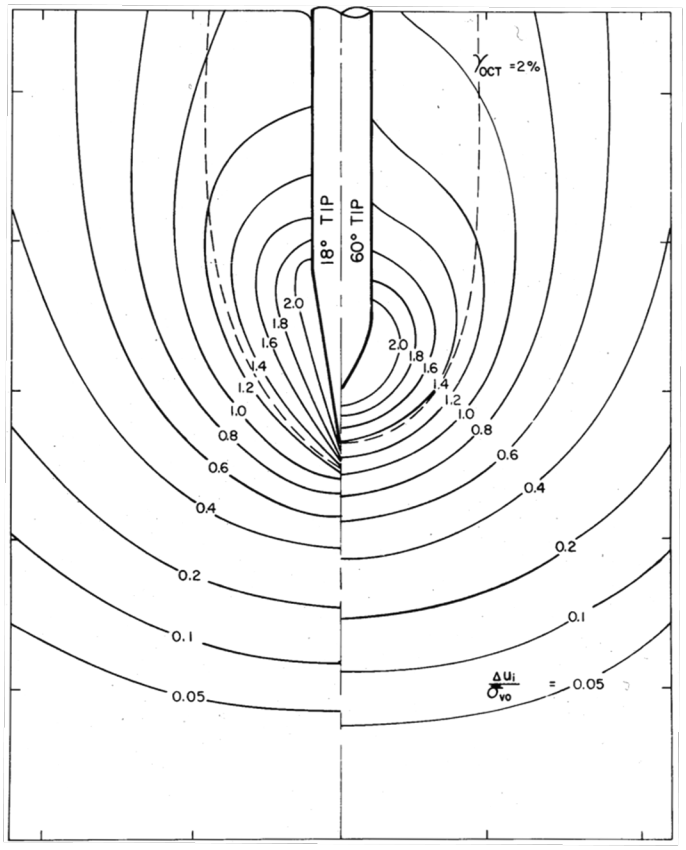


Figure 3: Predicted excess pore pressures during steady cone penetration in normally consolidated Boston Blue Clay (18° and 60° tips) (Baligh and Levadoux, 1980)

Figure 4 from Baligh et al. (1980) shows the induced excess pore pressure (u_e) determined using the strain path method. A normally consolidated multi parameter Boston Blue Clay model was used to derive the pore pressure distribution. The induced excess pore pressure is normalized with the initial total vertical stress.

The normally consolidated soil model shows a positive response in the net u_e (or u_i in the figure). Figure 5 from the same author shows the contribution of the shear induced excess pore pressure (Δu_{shear}).

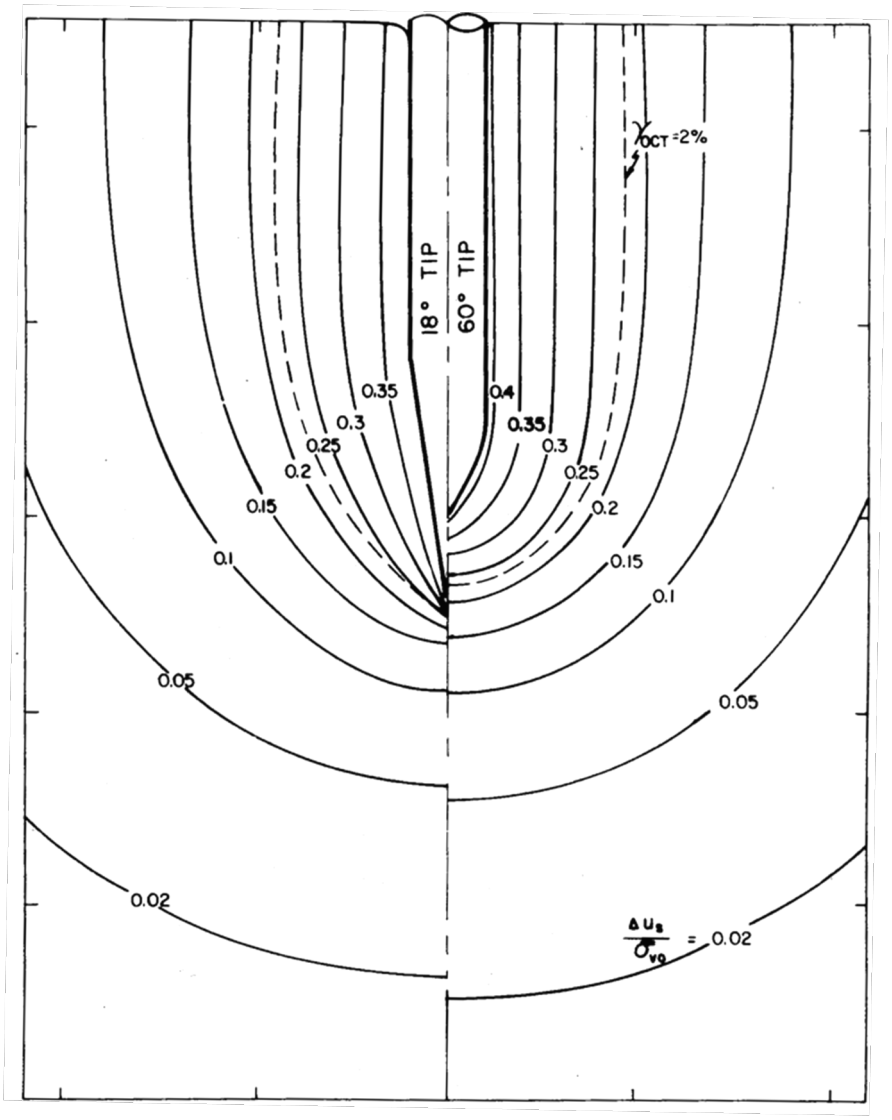


Figure 4: Predicted shear induced pore pressures during steady cone penetration in normally consolidated Boston Blue Clay (18° and 60° tips) (Baligh and Levadoux, 1980)

The pore pressures are positive because the soil model is for a normally consolidated soil. When comparing these two figures it is evident that the shear induced pore pressures are significantly less than

the total induced excess pore pressure and are limited to an area close to the probe. This distribution will produce a monotonic decaying dissipation with a clear t50 and u0 +, as per the example in Figure 6.

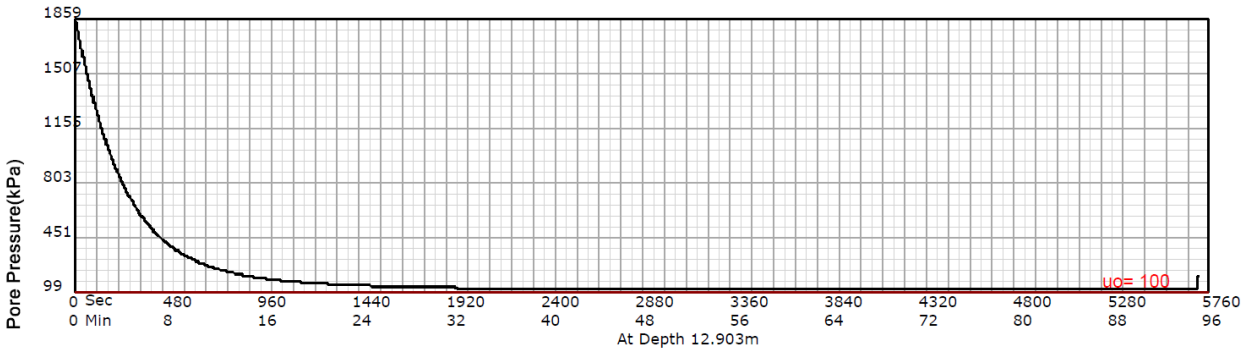


Figure 5: Monotonic decay of positive excess pore pressure in contractive tailings

However, a large proportion, if not the majority of dissipations in tailings, will display a different response. If the soil is over-consolidated, dilation may occur in the zone of high shear deformation close to the probe (Mayne, 2000). This will result in negative ushear pressures which will decrease pore pressure -close to the probe. This effect could be small, or it could dominate the entire dissipation regime and de-saturate the probe.

Dissipations with increasing dilation

Dissipation tests in tailings are commonly carried out in the layers of slimes (fine tailings). These layers tend to be slightly over-consolidated, mostly due to desiccation, and tend to dilate upon shearing. Therefore, one common type of pore pressure dissipation test result is an initial rising trend (increase in pore pressure) followed by subsequent decreasing pore pressure to an asymptotic value.

As the tendency to dilate increases, the shear induced negative pressure will increase and may dominate the dissipation test. Figures 7 to 10 show a sequence of pore pressure dissipation test results where shear induced dilation close to the cone has an increasingly larger effect on the pore pressure dissipation.

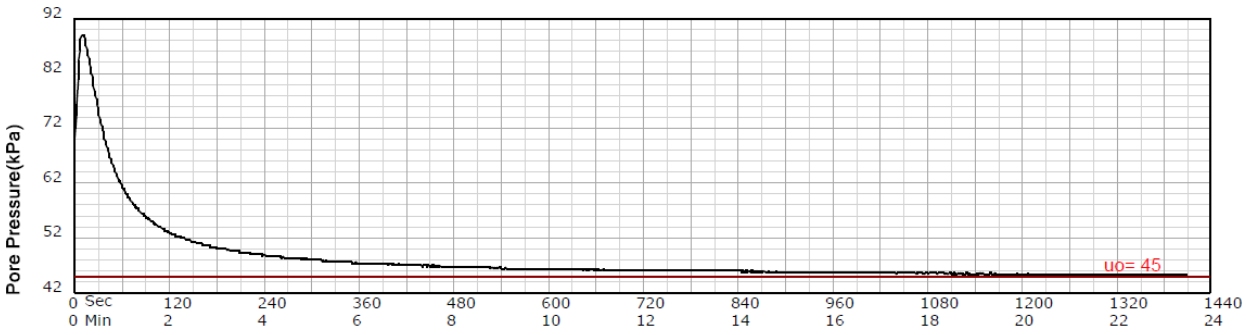


Figure 6: Dissipation test with moderate dilation

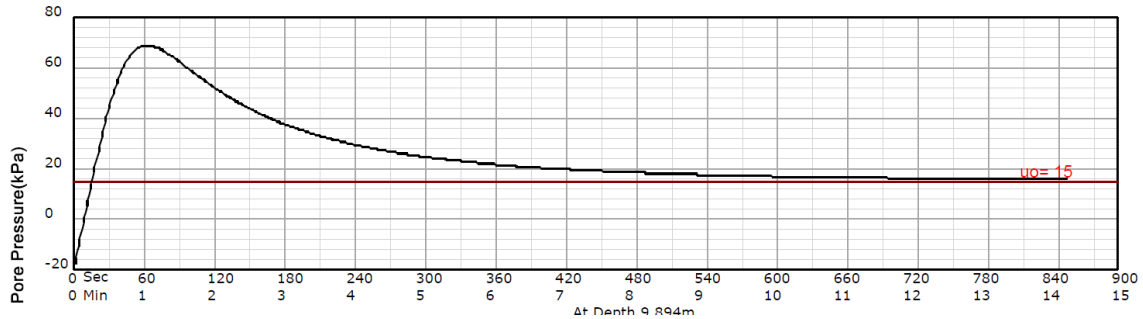


Figure 7: Dissipation test with dilation resulting in initial pore pressures less than ambient

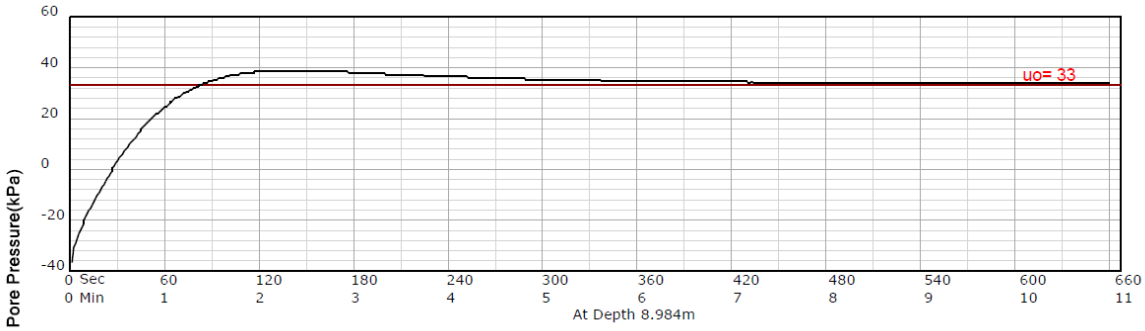


Figure 8: Dissipation test with shear induced dilation dominating the pore pressure dissipation showing only mild dissipation of positive excess pore pressures

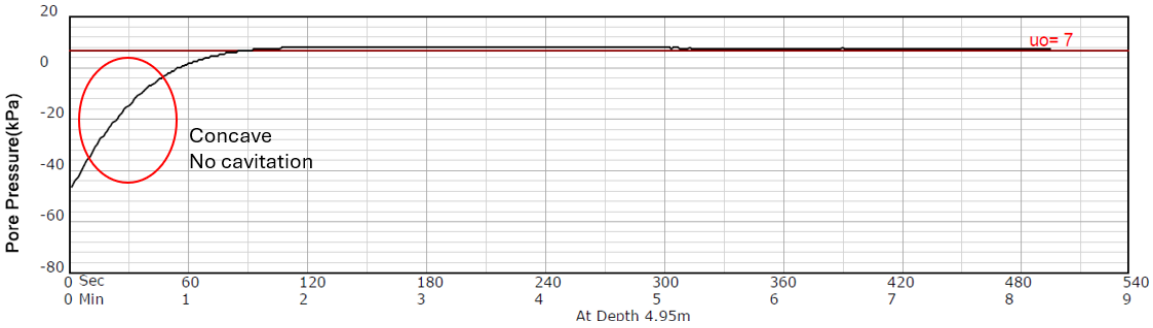
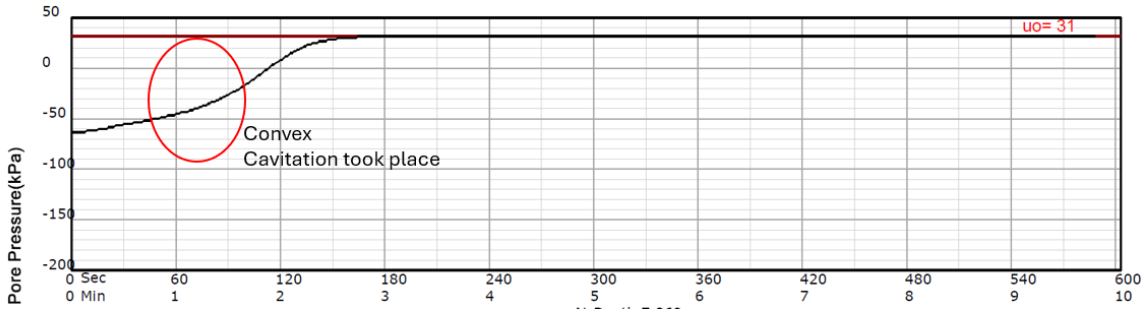


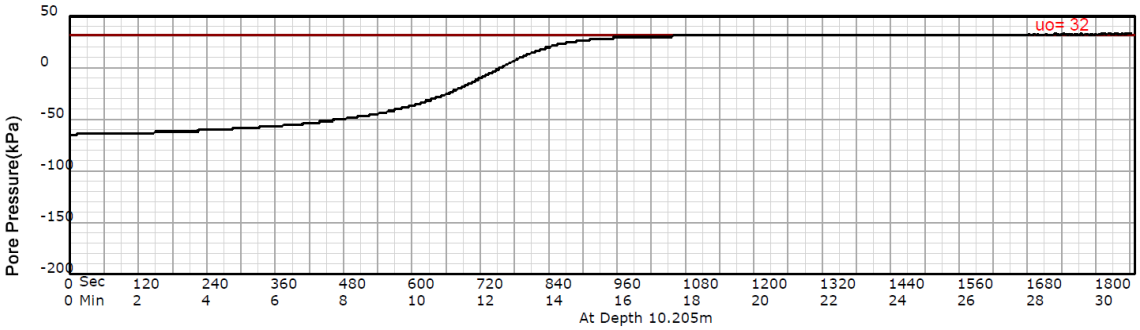
Figure 9: Dissipation test with shear induced dilation dominating the pore pressure dissipation with no dissipation of positive excess pore pressures evident

As the induced negative pressure gets larger (more negative) it may desaturate the probe through cavitation. The absolute maximum negative pressure recorded by the probe is equal to atmospheric pressure at the location of the site. At higher elevations (such as most of these examples done in South Africa at about 1,700 m above sea level) the atmospheric pressure is in the region of 80 kPa. For this reason, cavitation occurs at about -70 kPa to -80 kPa. In Figures 11a and b the measured pore pressure at the start of the dissipation test is -70kPa, indicating that cavitation had taken place. The cavitation occurred during probing, before the probe was stopped for the dissipation test. An example of this behavior is given in Rust

et al. (2022). Once the test commences, the pore pressure response is sluggish until the vapor bubbles reduce in size. Upon re-saturation, the excess pore pressure will dissipate, and the ambient pore pressure will be recorded (Figure 11a and b).



(a) Example of cavitation re-saturating in approximately 90 seconds



(b) Example of cavitation re-saturating in approximately 800 seconds

Figure 10: Two dissipation tests with shear induced dilation causing cavitation in the probe

Re-saturation of the probe results in a convex dissipation curve during the initial rising stage. This is highlighted by the red circle in Figure 11a. It can be noted from the dissipation test results of fully saturated tailings presented in Figures 7 to 10 that all the initial raising shapes are concave, as highlighted by the red circle in Figure 10. The shape of the initial rising stage can therefore be used to inform whether cavitation took place or not.

General model for dissipations in dilative tailings

The examples presented in the previous section were used to develop a model for the interpretation of dissipation test results. The model proposed in this paper is a conceptual model to illustrate the principles of Piezocone dissipation in a fully saturated material. There are two district zones, a dilative zone close to the probe where the soil is subjected predominantly to large shear strains, and a contractive zone further away, subjected to predominantly isotropic compression.

Figure 12 shows a horizontal line starting at the pore pressure transducer location and extending horizontally (radially) away from the probe. The variation in excess pore pressure response with radial distance from the probe is shown in the figure. The solid blue Lines 1 to 7 show the change in excess pore pressure response with time, with Line 1 the initial response and Line 7 following completion of most of the dissipation.

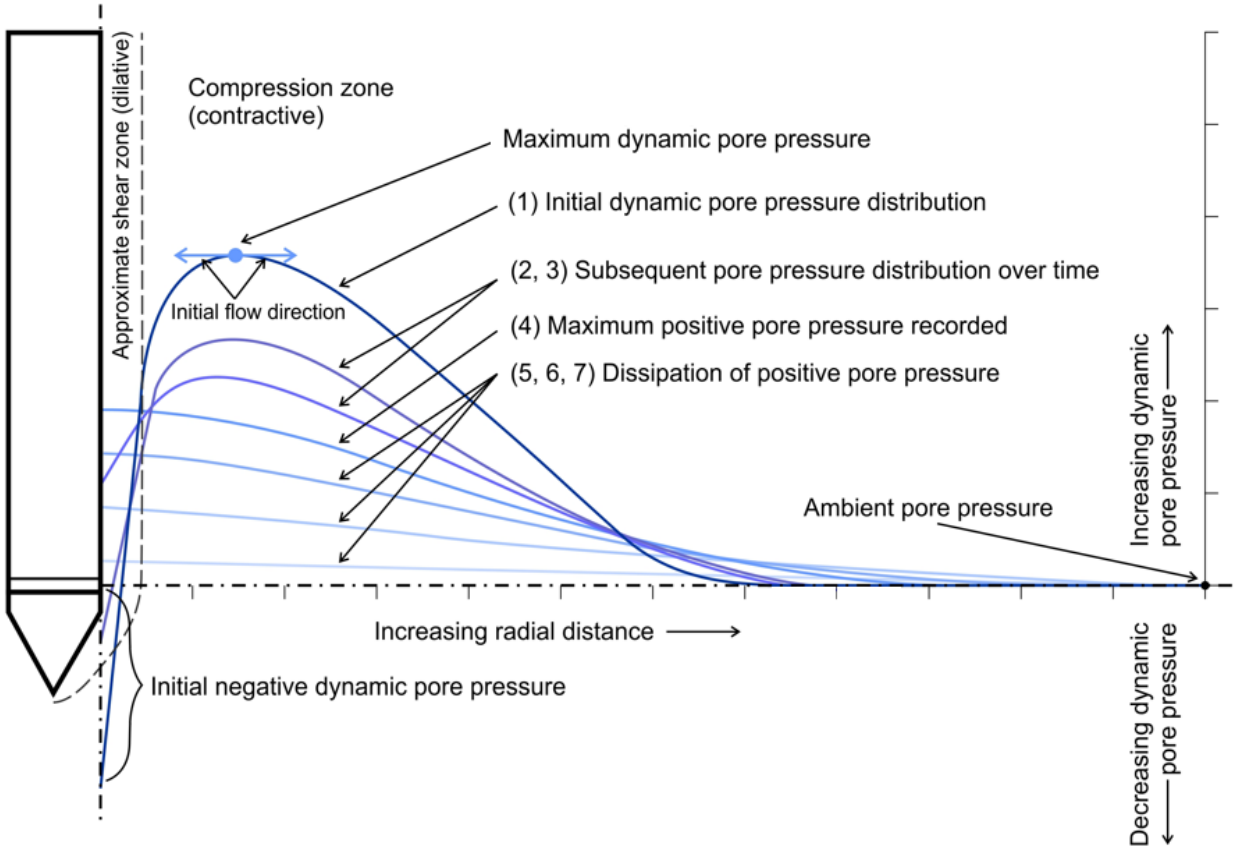


Figure 11: Excess pore pressure response developed in tailings that dilate in the shear zone and contract in the compression zone

The initial pore pressure response, depicted by Line 1, shows a negative excess pore pressure response due to dilation in the shear zone close to the cone and positive pore pressure response in the compression zone further away. A point of "Maximum dynamic pore pressure" and a point of "Initial negative dynamic pore pressure" can be noted. This large difference in pressure (on the same horizontal plane) over a short radial distance between these two points will cause a large gradient in hydraulic potential, or hydraulic gradient forcing flow towards the cone. At the same time there is a gradient from the "Maximum dynamic pore pressure" point to the "Ambient pore pressure" point at the edge of the zone of influence, as shown in the figure that will cause water to flow radially away from the probe as this pressure dissipates. As a result, the large negative pressure will dissipate relatively quickly when compared to the dissipation of the positive

pore pressure over a larger area (note that the upward dissipation in the result shown in Figure 8 is much steeper than the downward dissipation).

The initial negative pressure will dissipate (become more positive) until the maximum pore pressure is reached at the cone "Maximum positive pore pressure recorded," Line 4, which marks the end of the rising phase. Beyond this point, the dissipation will be radially away from the cone and the recorded pore pressure will reduce until the ambient pore pressure is recorded.

For the case of Monotonic dissipation tests, the shear zone will be contractive and the low pore pressure response close to the cone will be replaced by a positive pore pressure. A conceptual model of this case will only have lines similar to lines (4) to (7) in Figure 12.

Other pore pressure dissipation test results

The previous sections covered the classical pore pressure dissipation test results. However, a few cases remain that cannot be explained by the model presented. The first case deals with probing through relatively coarse tailings such as cyclone underflow that has a rapid rate of dissipation. The dynamic pore pressure may be zero (fully drained penetration) for the coarse tailings to a small response as the tailings becomes finer (say fine sand). If a dissipation test is carried out in this fine sand, it will have a very short dissipation (say 10 seconds with t50=1 second). Such a rapid dissipation test is not valid to determine the permeability since most of the generated excess pore pressure had dissipated during penetration. This raises the question of at what point is a dissipation test deemed to be valid? Several researchers have published on this topic, and they generally recommend a t50 of more than 30 seconds, with some recommending as much as 90 seconds. However, these rapid dissipation tests still provide a valid ambient pressure (see Figure 2a) and assist with the determination of the degree of saturation above the water table.

Another pore pressure trace occasionally found that cannot be explained by the mechanisms discussed involves the process of desaturation, or air entry, of layers of tailings above the water table (refer to Rust et al., 2022 for more detail). Saturated tailings layers often exist above the water table, and these are, in almost all cases, under negative pore pressure. When the negative pore pressure exceeds the air entry value of the tailings layer, air enters the voids between the tailings particles, displacing some of the pore water. The pore water pressure rapidly changes in these cases from the previously negative pore water pressure to atmospheric pressure. It is possible that disturbance by the cone could cause air entry or in some way damage the layer through micro fracturing or some other mechanism. An example of such a dissipation test is shown in Figure 13. In all such cases the pore pressure will revert to atmospheric pressure (or u=0).

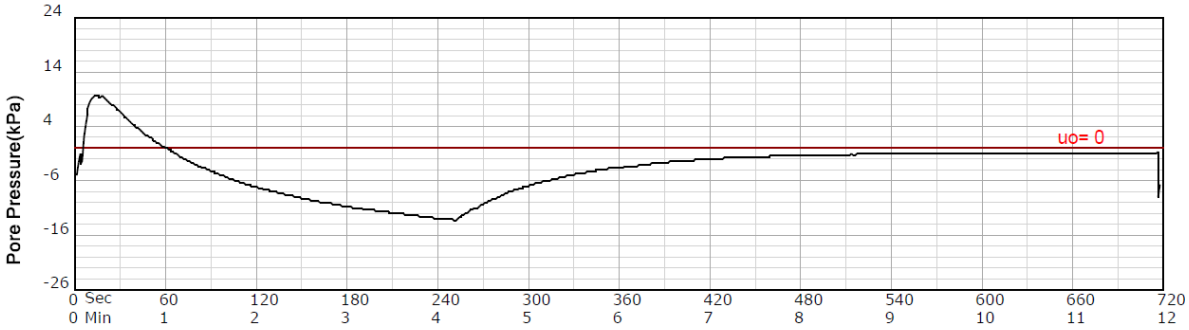


Figure 12: Initial classic dissipation test shape followed by air entry and pore pressure going to zero kpa

Conclusion

Dissipation tests in tailings have been presented to provide a variety of different characteristic shapes. These shapes depend on the soil characteristics. An improved understanding of the mechanisms causing the different characteristic shapes also improves the understanding of soil behavior.

If tailings are very loose and entirely contractive, only positive excess pore pressures are generated due to cone penetration. Denser tailings that dilate upon shearing induce some lower pore pressures in the shearing zone close to the cone. However, beyond the shear zone the tailing in pure compression may still contract and cause positive pore pressures. This interplay between negative and positive induced excess pore pressures can result in pore pressure dissipation test results that initially have low pore pressures that increase over time and subsequently decrease to ambient pore pressure. These features are apparent to a greater or lesser extent depending on the tailings state.

Detailed pore pressure distribution profiles in tailings facilities provide a wealth of information and these should be obtained and reviewed during the Piezocone investigation program. This requires a substantial number of complete pore pressure dissipation tests to be performed. The complete flow regime, including permeability, coefficient of consolidation, anisotropy in permeability, possible excess pore pressures, and two dimensional or three-dimensional flow-net can be determined from dissipation test results.

References

Baligh, M.M. and Levadoux, J.M. 1980. Pore pressure dissipation after cone penetration. *Research Report R80-11*, Order No. 662, Dept. of Civil Engineering, Massachusetts Institute of Technology, Cambridge, Mass., 367 pp.

Burns, S.E. and Mayne, PW. 1998. Monotonic and dilatory pore-pressure decay during piezocone tests in clay. *Can. Geotech. J.* 35: 1063–1073.

Burns, S.E. and Mayne, P.W. 2000. An approach to evaluation of field CPTU dissipation data in overconsolidated fine-grained soils: Discussion. *Can. Geotech. J.* 37: 1395–1397.

Rust, M., Rust, E. and Theron, M. 2022. Typical CPTu response and identification of probe desaturation in tailings. *Proceedings of Tailings and Mine Waste 2022*, Denver, Colorado, 149–160.

Rust, E. 1996. Interpretation of incomplete piezocone dissipation tests. PhD thesis. University of Surrey, UK.

Rust, E. and Rust, M. 2023. Determination of the degree of saturation above the water table from CPTu probing in tailings. *Tailings and Mine Waste 2023*, Vancouver Canada, 1429–1444.

Sully, J.P., Robertson, P.K., Campanella, R.G. and Woeller, D.G. 1998. Evaluation of field CPTu dissipation data in overconsolidated fine-grained soils. *Can. Geotech. J.*

Teh, C.I. and Houlsby, G.T. 1991. An analytical study of the come penetration test in clay. *Géotechnique* 41(1): 17–34.

Estimation of Undrained Shear Strength Parameters from Laboratory Testing for Geotechnical Analysis: t_{ff} vs. q_f

Masood Kafash, AECOM, USA
Thomas Barham, AECOM, USA
Lisa Yenne, AECOM, USA
Ranjiv Gupta, Freeport-McMoRan, Inc., USA
Georgia Lysay, Freeport-McMoRan, Inc., USA

Abstract

The use of laboratory testing in undrained shear strength ratio (USR) characterization of soils has been a critical factor, along with in-situ measurements, in the design of tailings and earth dams for many years. However, there are still discrepancies between geotechnical consultants and other subject matter experts on how to reduce laboratory results and apply them to the limit equilibrium method (LEM) slope stability and deformation analyses.

This paper provides an overview of approaches typically used in industry to estimate undrained shear strength parameters from laboratory tests and how these parameters are used in design. The paper will discuss various approaches used for the selection of undrained shear strength, such as q_f (top of Mohr circle) vs. t_{ff} (shear strength on failure plane at the time of failure), normalization of shear strength, incorporation of the effects of stress anisotropy, and how shear strengths are assigned in LEM software packages. This overview covers the information obtained from a literature review, and a survey performed by the authors of several consulting firms, and personal communication with selected faculty at North American universities.

This paper aims to help readers understand how the LEM slope stability factor of safety (FOS) can vary with the same set of laboratory tests depending on parameterization used in the analysis. Understanding the methods used for reducing laboratory tests and applying these in analysis can inform the decision-making process. The variability in results is demonstrated in this paper with an example where, for a given set of laboratory results, the reported FOS can vary by up to 16 percent, depending on how the data are reduced and applied in stability analyses.

Background

The authors use an anisotropic undrained shear strength characterization for limit equilibrium analyses in the program UTEXAS4 (Wright, 1999) and for deformation analyses in the programs FLAC (Itasca, 2012) and FLAC3D (Itasca, 2013). The anisotropic undrained characterization is generally developed using isotropically consolidated triaxial compression (CIU) testing to define shear strength for the active wedge and direct simple shear (DSS) testing for the horizontal and passive portions of the failure surface. The final shear strength characterization is guided by in-situ testing, case histories, and empirical correlations.

Undrained shear strength is typically assigned in geotechnical analysis programs using an undrained shear strength ratio (USR). The USR is commonly denoted as an $^{S_u}/_{p'}$ ratio where S_u is the undrained shear strength normalized to p' the effective consolidation stress. The authors found that most consultants use USR or $^{S_u}/_{p'}$ to denote an undrained strength ratio; however, there is inconsistency in the definitions of S_u and p' that ultimately affects reported FOS.

The authors use τ_{ff} for Su, where τ_{ff} is the shear stress on the theoretical failure plane at the time of failure. An alternate definition of S_u is q_f, which is based on the top of the Mohr Circle and can be defined in the terms τ_{ff}. The method of deriving τ_{ff} and q_f from CIU triaxial results is shown in Figure 1. In this paper, the notation USR or $^{S_u}/_{p'}$ will be used for undrained shear strength ratios defined as $^{\tau_{ff}}/_{\sigma'_{fc}}$. Where σ'_{fc} is the effective confining consolidation pressure before shearing, also shown in Figure 1.

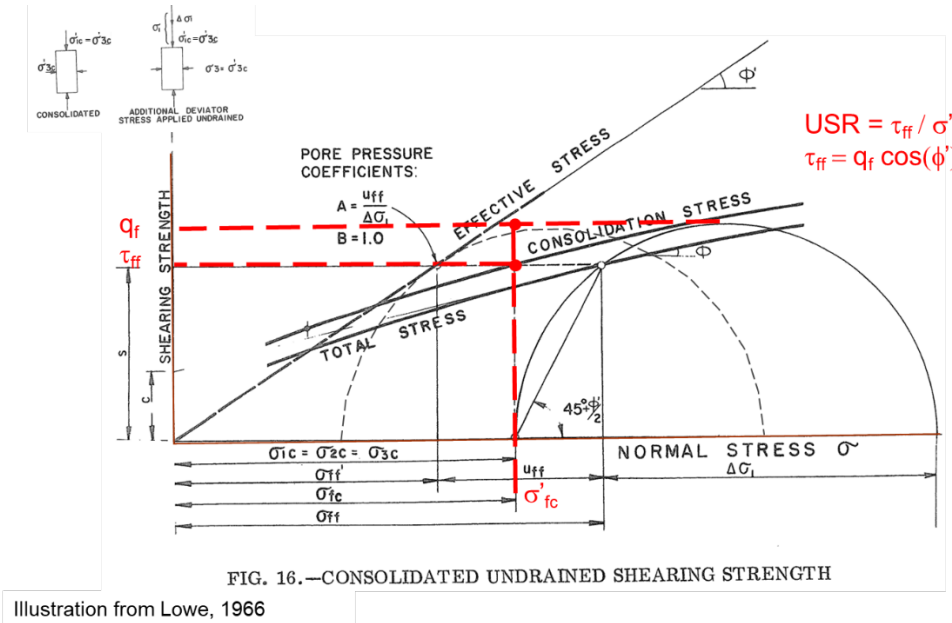


Figure 1: CIU undrained strength characterization

USR (τ_{ff}/σ'_{fc}) is similar to the s_u/σ'_{vc} defined in the SHANSEP procedure (Ladd and Foot, 1974) because the undrained shear strength is defined as a function of the effective consolidation stress before the load is applied. The initial SHANSEP process defined s_u as the top of the failure circle (q_f), consistent with Lambe and Whitman (1969). Later papers by Ladd (Ladd, 1991 and Ladd and DeGroot, 2004) recommended using the available shear strength on the "most realistic potential failure surface" when developing the undrained shear strength ratio from triaxial tests for use in limit equilibrium analyses (method of slices), when the base of the active wedge is inclined at angles other than 45 degrees from horizontal. Ladd defined the undrained strength as $c_u = \tau_{ff} = q_f \cos(\phi')$ in his 1986 Terzaghi lecture (Ladd, 1991). In Ladd and DeGroot's 2003 Casagrande lecture, they define $s_u = \tau_{ff} = q_f \cos(\phi')$ for undrained shear strength analysis in the method of slices (Ladd and DeGroot, 2004). Ladd and DeGroot (2004) acknowledge that many leading experts agree with Lambe and Whitman (1966) on the use of q_f for all undrained analyses.

Tailings materials are typically fine-grained soils that compress under increasing confining pressure and therefore should have effective confining pressure strength dependency and should be normalized. Shear strength is therefore normalized to the effective confining pressure (σ'_c). The effective confining pressure, σ'_c, is similar to the effective consolidation pressure on the failure plane, σ'_{fc}, in a sheared triaxial sample under isotropic conditions (CIU).

Many North American experts have adopted Ladd's approach for undrained shear strength assignment in undrained analysis; however, there are other opinions in industry supporting the use of q_f instead of τ_{ff}. Green and Marcuson (2014) provide a detailed discussion on this topic and present a clear understanding of the issues, particularly on the use of τ_{ff} with failure surfaces from effective stress analyses.

Consultants in support of using q_f argue that when a fully saturated soil is sheared under undrained conditions and the results are interpreted in terms of total stresses, it appears to behave as purely cohesive material (ϕ=0). The resistance under these conditions is actually based on the effective stresses mobilized at failure, but analyses in terms of total stresses are convenient because the shear induced pore pressures failure are not readily known and are implicitly accounted for in the undrained strength. This type of analysis is considered to provide the correct collapse load but probably not the correct kinematic mechanism. This has been used in practice for decades because of its convenience.

Ladd (1991) also discusses the difference between the undrained shear strength from a ϕ=0 analysis and the shear strength mobilized along a failure surface. Ladd observed that if adopting the latter shear strength in an undrained analysis is incorrect, it will generally be on the safe side by 10 to 15 percent.

To evaluate the effect of various approaches used for the selection of undrained shear strength, such as q_f (top of Mohr circle) vs. τ_{ff}(shear strength on failure plane at the time of failure), stress normalization

of shear strength, incorporation of the effects of stress anisotropy, and how shear strengths are assigned in analysis, the authors have surveyed several mining consulting firms approaches to undrained shear strength characterization and evaluated their impact on the limit equilibrium method (LEM) factor of safety (FOS) for a trial section.

Results of survey and potential implications review

AECOM, with support from Freeport-McMoRan, Inc. (Freeport), conducted a survey of five major geotechnical engineering consultants in 2024 to investigate the procedures commonly used for interpreting undrained shear strength from CIU tests. The survey questions included:

1. What is your company procedure for interpreting the undrained shear strength from isotropically consolidated undrained triaxial test (CIU test) for LEM Slope Stability analysis?
   a. Is it based on q_f or τ_{ff} as defined and depicted in the following figure (Figure 1)?
   b. What is your company procedure to incorporate the effect of stress anisotropy, such as CIU vs. CAU, when reducing the CIU data for use in stability analyses?
   c. What is the terminology your company uses for the undrained shear strength (i.e., Su/p', q_f/σ'_{vc}, q_f/σ'_{fc}, τ_{ff}/σ'_{vc}, τ_{ff}/σ'_{fc})?
2. What is your company procedure to incorporate the effect of structural anisotropy, such as weak bedding planes?
3. What is your company procedure to assign the undrained shear strength in stability analysis software packages? Is the shear strength for each slice calculated based on vertical effective stress or normal effective stress of each slide?

The results of the questionnaire are summarized in Table 1.

Table 1: Summary of surveyed consultants approach for undrained strength characterization

Source	q_f vs. t_{ff}	Common terminology	Assignment of shear strength on LE analysis	Stress anisotropy	Notes
Consultant # 1	t_{ff}	Su/p', t_{ff}/s'_{fc}	Normal stress	No additional reduction on CIU strength taken for anisotropic in-situ stresses	
Consultant # 2	q_f	S_u/p'_c for laboratory strengths, S_u/s'_{vc} for field strengths	Vertical stress	Mayne (1985) 13%	For critical situations, some CAU or DSS testing is done to inform judgement about the use of CIU
Consultant # 3	t_{ff}	S_u/p' for laboratory tests and interpretations, S_u/s'_{vc} for the analyses	Based on selected model	Laboratory based	Have used both q_f vs. t_{ff}
Consultant # 4	q_f	S_u/s'_{vc} or S_u/p'	Vertical stress	Laboratory based	
Consultant # 5	t_{ff}	S_u/p'	Both, project specific basis	Kulhawy and Mayne (1990)	

Table 1 highlights three key distinctions among industry approaches: the choice of undrained shear strength (i.e., q_f vs. τ_{ff}), consideration of stress anisotropy, and the strength normalization stress (vertical versus normal). Each of these factors is discussed briefly and their effects on calculated FOS are evaluated.

q_f versus τ_{ff}

Using the shear strength on the shear plane (τ_{ff}) versus the top of the Mohr circle (q_f) results in a reduction in shear strength given by $\tau_{ff} = q_f \cos(\phi')$. For tailings materials, typical friction angles (ϕ') range from 30 to 37 degrees, or a reduction on q_f of 13 to 20 percent. The impact of this strength reduction on FOS is highlighted with slope stability analyses using q_f and τ_{ff} strength selections in the active wedge portion of the failure surface. The results of this evaluation are summarized in Table 2 for Site 2, which had a friction angle of 34 degrees (17% difference in CIU strength from q_f to τ_{ff}).

Table 2: Summary of results for selected section and site

Site	CIU FOS τ_{ff}	CIU FOS q_f	Approx. % increase in FOS[1]
2	1.28	1.43	12

The authors performed similar analyses for eight cross-sections with various slope geometries and configurations. In summary, using q_f versus τ_{ff} increased the calculated FOS between 7 and 16 percent. Most of the sections (6 out of 8) increased less than 10 percent. The limited impact on FOS for these sections is attributed to the relatively small active (where CIU strength is assigned) versus horizontal and passive zones (where DSS strengths are applied). As the CIU portion of the failure surface is typically less than 50 percent, the impact on FOS between q_f and τ_{ff} is limited. Only two sections have more than a 10 percent increase on FOS. These sections have the biggest contribution from active (CIU strength assigned) on overall FOS.

Vertical stress versus normal stress

For non-cohesive soils such as tailings, the shear strength is typically dependent on in-situ stresses and incorporated using an USR. Assignment of shear strength parameters in limit equilibrium software packages varies based on the selected shear strength model (typically using either vertical (σ'_{vc}), or normal stress at the base of the slice (σ'_{fc}). Since vertical effective stress is typically closer to the maximum principal stress, this results in a higher shear strength for the same USR if vertical versus normal stress is used.

In an isotropically consolidated triaxial test, the confining pressures (σ'_1 and σ'_3) at the time of consolidation are equal such that the vertical consolidation stress (σ'_{vc}), the normal consolidation pressure on failure plane (σ'_{fc}), and maximum principal stresses are all equal. Therefore, for a CIU test, the same

normalization stress is used regardless of definitions, but in slope stability analyses depending on the angle at the base of the slice, σ'_{vc} and σ'_{fc} may not be equal. σ'_{fc} can be significantly less than σ'_{vc} if the failure plane is steep. Clearly, the impact of strength normalization is dependent on the shape of the failure surface. Table 3 provides an example of the effect of this variable on Site 2, discussed above. As shown in this table, assignment of shear strength properties based on vertical stresses is 5 to 13 percent, depending on what variables are compared.

Table 3: Effect of vertical stress or normal stress

Site	Selected sections	CIU FOS τ_{ff}		CIU FOS q_f		% Increase
		Assigned based on normal stress	Assigned based on vertical stress	Assigned based on normal stress	Assigned based on vertical stress	
2	Section E	1.28	1.34	1.43	1.45	5% (due to just normal stress vs. vertical stress) to 13% (due to τ_{ff} vs. q_f and vertical stress vs. normal stress)

Stress anisotropy

There are two types of anisotropy that are typically considered in shear strength selection; the structural anisotropy (due to the orientation of the failure plane related to bedding planes) and stress anisotropy (soil strength is a function of stress history, and stress paths). Structural anisotropy is typically addressed by conducting laboratory tests that match the anticipated mode of failure using CIU or DSS laboratory results. Incorporating stress history anisotropy (approximating the in-situ consolidation stresses) for tailings material is more challenging as horizontal in-situ stresses are typically unknown.

It is common practice to perform CIU (isotropic consolidation stress) tests instead of CAU (anisotropic consolidation stress), as they are easier and faster to set up and run. There are several published methods to convert CIU to approximate CAU strengths. Based on how stress anisotropy is accounted in the analysis, it results in a different FOS, as shown in Table 4 for Site 2.

Table 4: Effect of stress anisotropy

Site	Selected sections	No stress anisotropy	Kulhawy and Mayne (1990)/ Mayne (1985)[1]	% Decrease
CIU FOS τ_{ff}, Assigned based on normal stress				
2	Section E	1.28	1.25	3 (due to stress anisotropy)
CIU FOS q_f, Assigned based on vertical stress				
2	Section E	1.45	1.38	5 (due to stress anisotropy)

1) For site 2 fine tailings, Kulhaway and Mayne (1990) and Mayne (1985) result in similar Su/p' ratios

The authors conducted a limited laboratory testing program to quantify the effects of stress anisotropy and compare the laboratory test results to published methods to account for stress anisotropy when using CIU tests (Mayne, 1985; Wong et al., 1983). The laboratory testing program included five CAU and two CIU tests conducted on undisturbed Shelby tube samples of a uniform fine-grained low plasticity tailing material.

Table 5 summarizes the shear strength test results for the maximum principal stress ratio (PSR) failure criteria, shown in Figure 3, for three strength normalizations, and presents the CIU strengths converted to CAU using the methodology proposed by Wong et al. (1983) and Mayne (1985). The Mayne (1985) estimated strengths from the CIU tests are presented for both q_f and τ_{ff} . The following paragraphs discuss the observations from the test data. This discussion is grouped by the shear strength normalization to the vertical effective stress, and effective consolidation stress on the failure plane.

Table 5: Summary of test results from Site 2

Sample Depth (ft)	Test	σ'_{1c} (psi)	K_c	σ'_{fc} (psi)	Consol. Void Ratio	$\frac{T_{ff}}{\sigma'_{fc}}$	$\frac{q_f}{\sigma'_{vc}}$	$\frac{T_{ff}}{\sigma'_{vc}}$	$\frac{T_{ff}}{\sigma'_{fc}}$ Wong (1983) Estimate	$\frac{q_f}{\sigma'_{vc}}$ Mayne (1985) Estimate	$\frac{T_{ff}}{\sigma'_{vc}}$ Mayne (1985) Estimate
35–37	CAU	50	1.5	37	0.74	0.49	0.42	0.36	0.36	0.29	0.25
	CAU	50	2	30	0.71	0.54	0.39	0.33	0.44	0.29	0.25
	CAU	75	2	46	0.70	0.57	0.40	0.34	0.44	0.29	0.25
24–26	CIU'	50	1	50	0.70	0.29	0.34	0.29	–	–	–
80–82	CAU	85	2	52	0.81	0.46	0.33	0.28	0.44	0.28	0.24
	CAU	132	2	79	0.67	0.51	0.35	0.30	0.44	0.28	0.24
	CIU'	85	1	85	0.82	0.28	0.33	0.28	–	–	–

Figure 2 presents a summary of the test data shear strength (using max PSR failure criteria) normalized to the vertical effective stress versus Kc ($\sigma'_{1c}/\sigma'_{3c}$), along with the Mayne (1985) estimated anisotropic strength ratios for the CIU tests for both q_f and τ_{ff} . For each test, the consolidated vertical effective stress in psi is listed along with the consolidated void ratio. No apparent trend of strength ratio with Kc was observed when strength was normalized to σ'_{vc}. Note, the CIU strength when reduced to τ_{ff} is essentially equivalent to the strength reduction on q_f suggested by Mayne (1985) (~13%) for anisotropic conditions. All the anisotropic strength data points are essentially equal to or above the CIU strength and the Mayne (1985) anisotropic strength estimate using q_f.

Figure 3 presents the laboratory test data normalized to the effective consolidation stress on the failure plane (σ'_{fc}) along with the Wong et al. (1983) undrained shear strength estimates. The correlation is shown to be conservative when using the PSR failure criteria except for the purely contractive sample, which plots below the correlation but above the CIU′ (Kc=1) strength ratio.

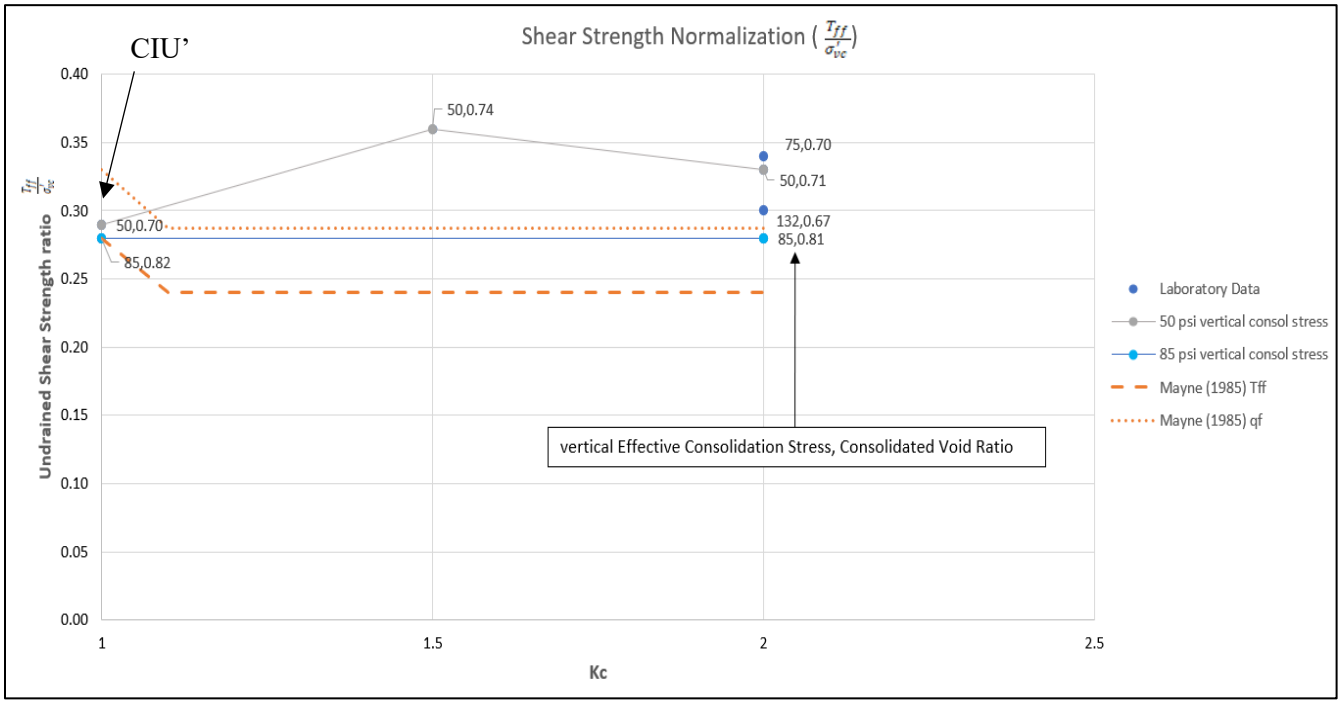


Figure 2: Laboratory data normalized to σ'_{vc} versus Mayne (1985) using Max PSR failure criteria. Lines drawn between similar σ'_{vc} to evaluate data trends

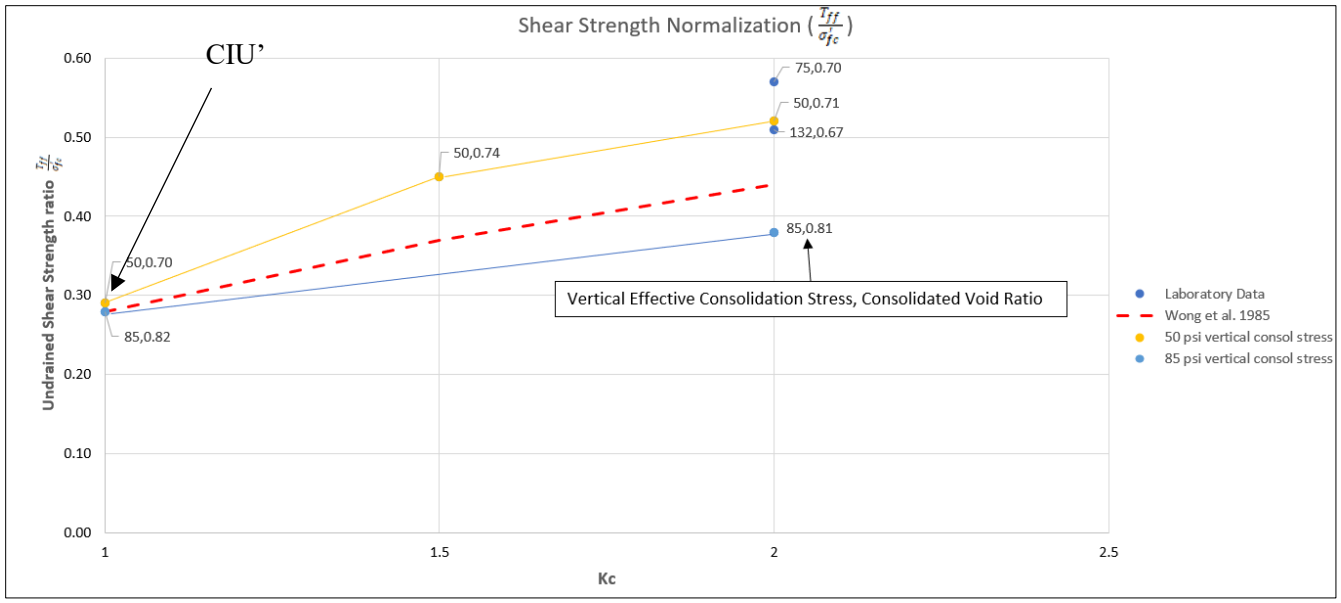


Figure 3: Laboratory data normalized to σ'_{fc} versus Wong et al. (1983) using max PSR failure criteria. Lines drawn between similar σ'_{fc} to evaluate data trends

The results of the laboratory testing program show that normalizing shear strength to either the vertical effective stress or the effective confining pressure on the failure plane are both reasonable options so long as the appropriate strength adjustments are taken, as suggested by Mayne (1985) and Wong et al. (1983), and the appropriate failure criteria is selected. The results also highlight that if τ_{ff} is used to reduce CIU test data, taking further reduction in strength (as suggested by Mayne) could compound conservatisms.

Summary of limit equilibrium analysis results

The author's survey asked five geotechnical engineering consultants about their practice for the selection of undrained shear strength from undrained triaxial testing (q_f vs. τ_{ff}), how strengths are normalized and input into the geotechnical model (effective vertical or normal stress), and how anisotropic consolidation is included in the strength assignment. Table 5 provides a summary of the results of the survey, and for one example, how the FOS is impacted by the approach selected. This small study highlighted that for the same set of laboratory results, the reported FOS for one section could vary by up to 16 percent, depending on how the data was reduced and applied in the LE stability analysis. Clearly the discrepancies in results can vary based on the actual problem being analyzed, based both on the factors discussed and other parameters involved in design that may have a higher impact on the calculated FOS. The designer needs to select the parameters and approach that best fit the project's level of uncertainty and risk.

Table 6: Summary of survey results and effect on FOS

Source	q_f vss t_{ff}	Common terminology	Assignment of shear strength on LE analysis	Stress anisotropy	Example of FOS:	% Change in comparison to Consultant #1
# 1	t_{ff}	Su/p', t_{ff} /s'$_{fc}$	Normal stress	No additional reduction on CIU strength taken for anisotropic in-situ stresses	1.28 (no stress anisotropy)	NA
# 2	q_f	Su/p'$_c$ for laboratory strengths, Su/s'$_{vc}$ for field strengths	Vertical stress	Mayne (1985) 13% drop from peak	1.38 (13% drop from stress anisotropy)	+8%
# 3	t_{ff}	Su/p' for laboratory tests and interpretations, Su/s'$_{vc}$ for the analyses	Based on selected model	Lab based	1.28 (assuming no stress Anisotropy, normal stress) 1.34 (assuming no stress Anisotropy, vertical stress)	0% +5%
# 4	q_f	Su/s'$_{vc}$ or Su/p'	Vertical stress	Lab based	1.45 (assuming no stress Anisotropy)	+13%
# 5	t_{ff}	Su/p'	Both, project specific basis	Kulhawy and Mayne (1990) $\left(\frac{Su}{\sigma'_{v0}}\right)_{CAUC} = 0.15 + 0.49\left(\frac{Su}{\sigma'_{v0}}\right)_{CIUC}$,	1.25 (K&M 1990 stress anisotropy and normal stress) 1.33 (K&M 1990 stress anisotropy and vertical stress)	-3% +4%

Conclusion

Laboratory testing is critical for understanding material behavior and for developing tailings shear strength characterization. Various methods have been proposed to reduce laboratory testing results, specifically triaxial testing, for application in geotechnical analyses. Each method has strong proponents, and no consensus in North America has been reached to set a standard of geotechnical practice. The survey results summarized in this paper highlight the differences in engineering practice among geotechnical engineering consultants and the impact of these discrepancies on the reported FOS for slope stability.

This study showed that for the same set of laboratory results, the reported FOS can vary by up to 16 percent, depending on how the data are reduced and applied in the analysis. This paper aims to help engineers, reviewers, and owners understand the impact of design parameter selection on FOS that should be factored in when developing recommendations from the slope stability analysis.

Recent failures of tailings embankments across the world have shown that precautionary limit equilibrium analyses alone are not sufficient for a robust design, considering their limitations and uncertainties as discussed above. It is recommended that designers consider this variability in design and

initiate a decision-making process that considers factors such as level of knowledge about the site, level of knowledge of material characterization, and performance of the structure, potentially enhancing the design through Performance-Based Design (Kafash et al., 2022).

Notation

CIU	isotropically consolidated-undrained shear test
CAU	anisotropically consolidated-undrained shear test
DSS	direct simple shear
K_c	ratio of horizontal to vertical consolidation stress
q	$0.5(\sigma'_v - \sigma'_h)$ or $0.5(\sigma'_1 - \sigma'_3)$
q_f	q at failure
Su	undrained shear strength
USA	undrained strength analysis
USR	undrained shear strength ratio
σ'_c	isotropic consolidation stress
σ'_{fc}	consolidation stress on failure plane
σ'_{ff}	effective stress on failure plane at failure
σ'_n	effective normal stress
σ'_v	vertical effective stress
σ'_{vc}	vertical consolidation stress
τ_{ff}	τ on failure plane a failure

References

Duncan, J.M., Wright, S.G. and Wong, K.S. 1990. Slope stability during rapid drawdown. *Proceedings of H. Bolton Seed Memorial Symposium* 2: 253–272.

Green, R.A. and Marcuson III, W.F. 2014. The φ = 0 concept: review of its theoretical basis and pragmatic issues with implementation. In *From Soil Behavior Fundamentals to Innovations in Geotechnical Engineering*. Geo-Congress 2014, Atlanta, Georgia: American Society of Civil Engineers: 308–321.

Kafash, M.H, Barham, T, Sheykhloo, P., Davidson R. and Yenne, L. Performance based design – how does performance based design work? *Proceedings of Tailings and Mine Waste,* 2022, Denver, CO.

Ladd, C.C. 1991. Stability evaluation during staged construction (22nd Terzaghi Lecture). *Journal of Geotechnical Engineering* 17(4): 540–615.

Ladd, C.C. and De Groot, D.J. 2004. Recommended practice for soft ground site characterization: Arthur Casagrande Lecture. *Proceedings of 12th Panamerican Conference on Soil Mechanics and Geotechnical Engineering*, Massachusetts Institute of Technology, Cambridge, MA.

Ladd, C.C. and Foot, R. 1974. New design procedure for stability of soft clays. *Journal of the Geotechnical Engineering Division* 100, GT7: 763–786.

Lambe, T.W. and Whitman, R.V. 1969. *Soil Mechanics*. New York: John Wiley & Sons.

Lowe, J. and Karafiath, L. 1960. Effect of anisotropic consolidation on the undrained shear strength of compacted clays. *Proceedings of the Research Conference on the Shear Strength of Cohesive Soils,* ASCE, Boulder, CO: 837–858.

Lowe, J. and Karafiath, L. 1967. Stability analysis of embankments. *Journal of Soil Mechanics and Foundation Division* 93(SM4): 1–33.

Mayne, P.W. 1985. Stress anisotropy effects on clay strength. *Journal of Geotechnical Engineering* 111(3): 356–366.

Wijewickreme, D., Dabeet, A. and Byrne, P. 2013. Some observations on the state of stress in the direct simple shear test using 3D discrete element analysis. *Geotechnical Testing Journal* 36(2): 20120066.

Wong, K.S., Duncan, J.M. and Seed, H.B. 1983. Comparisons of methods of rapid drawdown stability analysis, Report No. UCB/GT/82-05, Department of Civil Engineering, University of California, Berkeley, Dec., 1982, revised July, 1983.

Wright, S.G. 1999. UTEXAS4, A Computer Program for Slope Stability Calculations, Shinoak Software, Austin, Texas.

A Critical Review of the Residual Pore Pressure Generation during Cyclic Loading

David Espinoza, Geosyntec Consultants, USA
Jenny Ramirez, Geosyntec Consultants, USA

Abstract

Recent notable catastrophic failures of mine tailing containment structures, often followed by mudflows, have exposed tailings facility's vulnerability to slope instability. The physical characteristics and current understanding of these types of failures have led engineers to evaluate liquefaction as a critical failure mode. Since excess pore pressures and liquefaction are related, seismic liquefaction potential is typically evaluated in the laboratory under cyclic undrained conditions, where excess pore pressures are measured. In cyclic undrained triaxial tests, a fraction of the transient excess pore water pressures remains locked-in, resulting in residual excess pore water pressures that do not dissipate at the end of a stress (or strain) cycle. Residual pore pressure continues to gradually increase until the total pore water pressure equals the confining cell pressure, resulting in partial or complete liquefaction.

This paper presents a critical review of the mechanisms that trigger the generation of residual excess pore pressure in cyclic triaxial undrained tests on completion of loading cycles and postulates an alternative mechanism. This paper argues that residual pore water pressure is the result of the testing boundary conditions, which are not representative of the field conditions. Because of the large extent and the sheer number of tailing storage facilities worldwide, attaining a solid understanding of how excess pore pressure builds up is paramount to avoid unnecessary multimillion-dollar retrofits when less costly remedies would be more appropriate to reduce liquefaction potential to tolerable levels.

Introduction

When a mine tailing storage facility (TSF) fails, it often has catastrophic consequences (Zhu et al., 2024). These failures have led the mining industry to develop the Global Industry Standards on Tailings Management (ICMM, 2020), which suggests evaluating credible failure modes affecting TSFs and the extent of their impact. Because TSFs often store saturated loose materials, and subsequent raises of the TSF using the upstream method result in berm construction over saturated material, liquefaction is often

considered a credible failure mode. Liquefaction can be caused by rapid loading (e.g., earthquakes, rapid construction).

The earliest seismic-induced liquefaction research studies took place following the catastrophic liquefaction-induced failures of the 1964 Niigata and 1964 Alaska earthquakes and focused on saturated granular soils. Since then, to understand the mechanisms that trigger liquefaction, researchers have performed numerous laboratory tests using commercially available clean sands with well-known geotechnical properties (e.g., Lee and Seed, 1967; Castro, 1969; Shibata et al., 1972). In addition to sands, materials with yet higher permeability coefficients (e.g., gravels) have also been tested to study liquefaction (e.g., Evans and Seed, 1987; Nicholson et al., 1989). In all these tests, it was observed that a fraction of the transient excess pore water pressures (PWPs) remained locked-in in undrained triaxial cyclic tests and accumulated with each load cycle. Based on the results of these tests, researchers developed constitutive models describing how excess PWPs are generated in granular materials (e.g., Beaty and Byrne, 1998; Elgamal, et al., 2002; Chen and Arduino, 2021) to capture this feature observed in the laboratory, and then implemented these PWP-generation models in commercially available numerical codes. As the use of numerical codes for evaluation of liquefaction has become more widespread in engineering, the economic impact associated with model assumptions can be significant when designing new TSFs or retrofitting existing ones.

Pore pressure generation during rapid loading under drained conditions in the field

Before postulating the potential mechanism of the observed residual excess PWP generation in undrained cyclic triaxial tests, the authors present a qualitative description of how excess PWP develops in the field for a hypothetical saturated soil deposit in response to specific loading and boundary conditions (Figure 1). The transient nature of excess PWP can be attributed to two distinct mechanisms: (i) consolidation following load application that leads to a gradual decrease (dissipation) of PWPs over time; and (ii) the variation (increasing or decreasing) of applied loads themselves over time. To describe the transient nature of consolidation following instantaneous loading (q) of saturated soil deposits, Terzaghi developed the theoretical framework of the excess PWP (Δu) dissipation process based on force equilibrium and Darcy's law (Terzaghi, 1943). Figure 1a shows the consolidation model for a double drained boundary condition and the corresponding PWP isochrones at multiple times. As shown in Figure 1a, when a load increment is applied instantly, the entire load is transferred to the PWP (i.e., $\Delta u = q$) at the time of load application ($t = t_o$), before dissipation starts. On the contrary, the effective stress increment ($\Delta\sigma'$) is 0 at t_o and reaches q at the end of the consolidation process (t_f), at a rate that depends on soil permeability. Figure 1b illustrates the variation with time of PWP and the effective stresses $\Delta\sigma'$ for a given depth z (the dashed lines illustrate the expected paths for a typical consolidation process, that is, q is not removed).

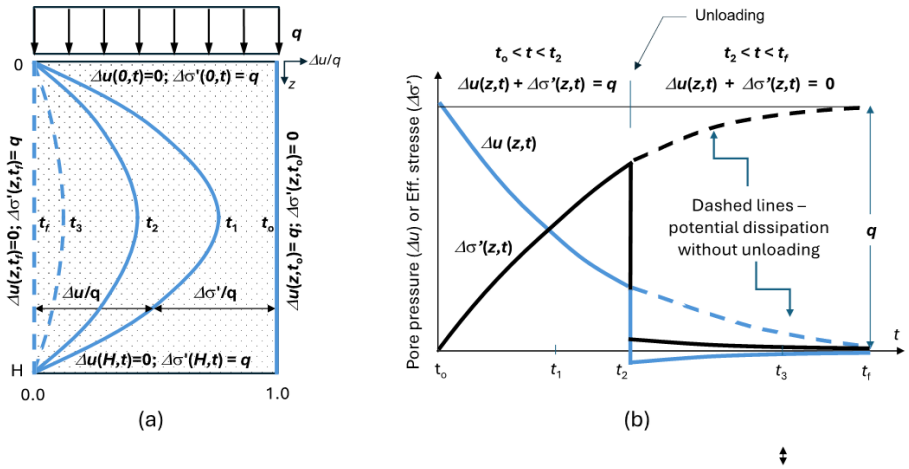


Figure 1: Excess PWP of a saturated soil layer following instantaneous loading and unloading: (a) PWP isochrones; (b) PWP dissipation with time at a given depth z after loading and unloading

In this hypothetical example, the excess PWP variation with time (t) due to changes in loading is clearly illustrated in Figure 1b (solid lines) when the layer is instantly loaded at $t = t_o$ ($\Delta u + \Delta\sigma' = q$) and instantly fully unloaded at $t = t_2$ ($\Delta u + \Delta\sigma' = 0$).[1] In both cases, equilibrium conditions are maintained. The instantaneous removal of q is used to facilitate the subsequent discussion because it avoids the commingling of the unloading and consolidation processes. Although the instantaneous loading and unloading illustrated in Figure 1b are extreme cases, they illustrate how excess PWPs are connected to load patterns and permeability (consolidation).

The study of excess PWP increase/decrease during one-dimensional consolidation due to intermittent cyclic rectangular loading/unloading has been analyzed using closed form solutions, numerical analysis and laboratory testing by multiple researchers (e.g., Wilson and Elgohary, 1974; Kim et al., 2021; Chai et al., 2022). The most salient feature of these studies is the fact that, independently of the soil permeability, pore pressures follow the loading/unloading patterns very closely. In other words, as illustrated in Figure 1b, an instantaneous load removal is followed by an instantaneous pore pressure reduction, that is, independent of permeability, PWPs instantly equilibrate with the new loading condition. If the soil was mostly gravel, negative PWP would not be generated and, therefore, PWP "dissipation" taking place upon unloading would not be observed either.

[1] Note that the figure shows realistically negative PWPs upon unloading, which dissipate towards zero as water flows back into the sample. In reality, trapped air within the voids may prevent full dissipation of negative pressures as samples may not be able to reach saturation. The negative PWPs are generated due to the tendency of soils to rebound, inducing volume expansion. The negative PWP magnitude will depend on suction characteristics of the soil matrix. Coarse particles generate smaller negative PWPs than finer particles.

To further illustrate the point, Figure 2 shows the excess PWP development with time in response to applying four equal loads instantaneously at different times to our hypothetical saturated soil deposit.

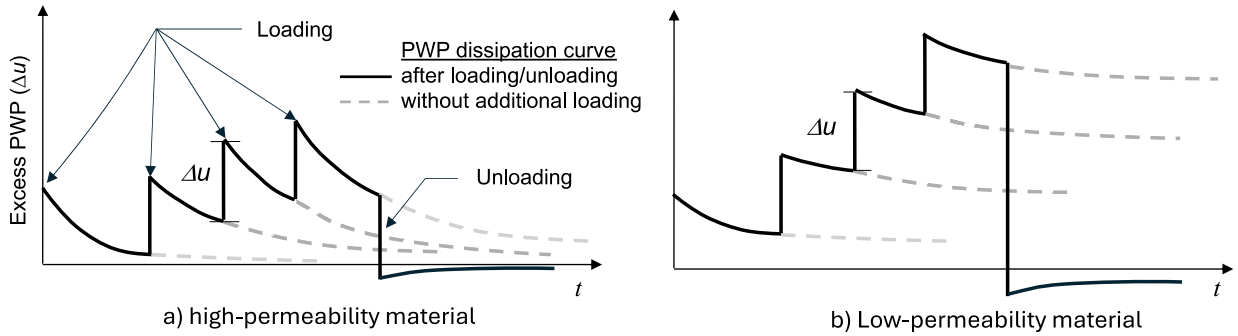


Figure 2: Schematic of PWP generation during incremental loading followed by instant unloading

As shown, each load generates an additional excess PWP (i.e., Δu) that is added to the remanent[2] excess PWP that has yet to dissipate, indicating that the previous applied loads have not been fully transferred to soil particles and the pore water is carrying a fraction of the applied stresses (Figure 2). In this hypothetical example, because the load is applied instantly, the magnitude of each increment of excess PWP (i.e., Δu) depends only on the magnitude of the applied loads regardless of the soil permeability. However, for the consolidation process, the remanent excess pore pressure at a given time will be higher for low-permeability soils than for high-permeability ones. If at any point during consolidation all the cumulative applied load is removed at once, the new equilibrium condition would require that the excess PWP be less than or equal to zero, regardless of the soil permeability at the time of load removal, and dissipating as water is drawn into the soil matrix (the total stress change would be zero throughout this process).

The magnitude of the accumulated excess PWP must be assessed to appropriately analyze the stability of earthen structures using effective stress (drained) or total stress (undrained) analyses. For slope stability calculations using effective stress analysis, the maximum excess PWP is an essential input parameter to calculate the critical failure surfaces. Although excess PWPs are not needed directly in stability calculations when a total stress analysis is used, they are needed to select representative stress paths to obtain appropriate undrained shear strength parameters.

Generation of residual pore water pressures in cyclic undrained tests

Typically, undrained laboratory tests are performed to mimic the condition of PWP build-up due to loads applied sufficiently rapidly that there is no time to dissipate the generated excess PWP. Excess PWPs

[2] The word remanent is synonymous of residual but it is purposely selected to avoid confusion with the term found in the literature to describe the residual PWP measured in undrained tests.

generated during undrained conditions should theoretically mimic the pattern of applied loads. As the load is gradually removed, the excess PWP should also approach zero (or become negative) to satisfy equilibrium conditions (i.e., change in total stresses equal to zero).

However, results from cyclic undrained triaxial tests show that when applied loads are momentarily at a zero load, a fraction of the excess PWP from the previous cycle remains. Figure 3 shows a typical PWP development due to applied cyclic stresses applied at 1 hertz (Hz). As shown by the black dots in this figure, the residual PWP increases with each cycle and gradually accumulates, reducing the confining stresses until eventually reaching failure (Shibata et al., 1972). Ishihara et al. (1975) attributed the generation of residual PWP measured in undrained triaxial tests of saturated sands to the development of irrecoverable plastic deformations during loading. Multiple researchers have reported similar results (e.g., Seed et al., 1976; Lee and Seed, 1967; Dobry et al., 1982; Sakai and Ochiai, 1986; Shoaei and Kassa, 1996; Tabata and Vucetic, 2010; Chen et al., 2019; Do et al., 2023).

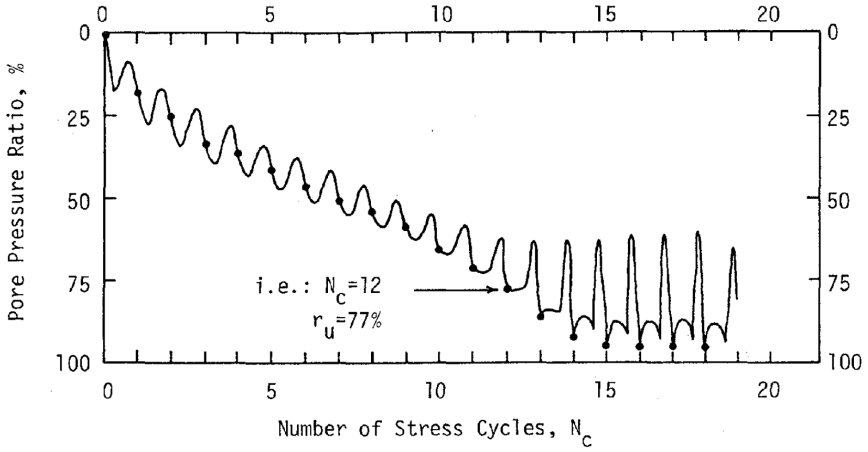


Figure 3: Residual PWP ration vs. number of cycles for 1 Hz load cycle (from Evans and Seed, 1987)

However, despite the reported results, it is hard to envision residual PWPs generating and accumulating in such highly permeable materials. To reiterate, in order to satisfy equilibrium conditions, excess pore pressures generated during undrained tests should theoretically track the applied loads (i.e., the PWP should be highest when the applied load is highest and then should be at zero or negative at the end of a load cycle). Because residual PWPs are detected at the end of a load cycle in granular materials, the origin and meaning of such pressures must be examined. Are they a real phenomenon (i.e., the result of plastic yielding during loading) or are they the result of the boundary conditions introduced by the test to simulate undrained conditions?

Because soil samples are the real-world representation of mathematical entities described by differential volumes elements with single values representing its state of stresses, it is implicitly assumed

that the stress field (including PWP) within the soil sample is homogeneous and that data collected on the sample periphery is representative of what exists inside it. On the contrary, excess PWP is not uniform within the sample. Despite its name, undrained testing conditions only means that the test is set up to prevent water draining out of the initial space delimited by the plates and the membrane encapsulating the soil sample. But, in order for contraction to occur during loading, pore water must flow out of the initial voids. A qualitative description of the water flow within a sample during undrained loading is shown in Figure 4.

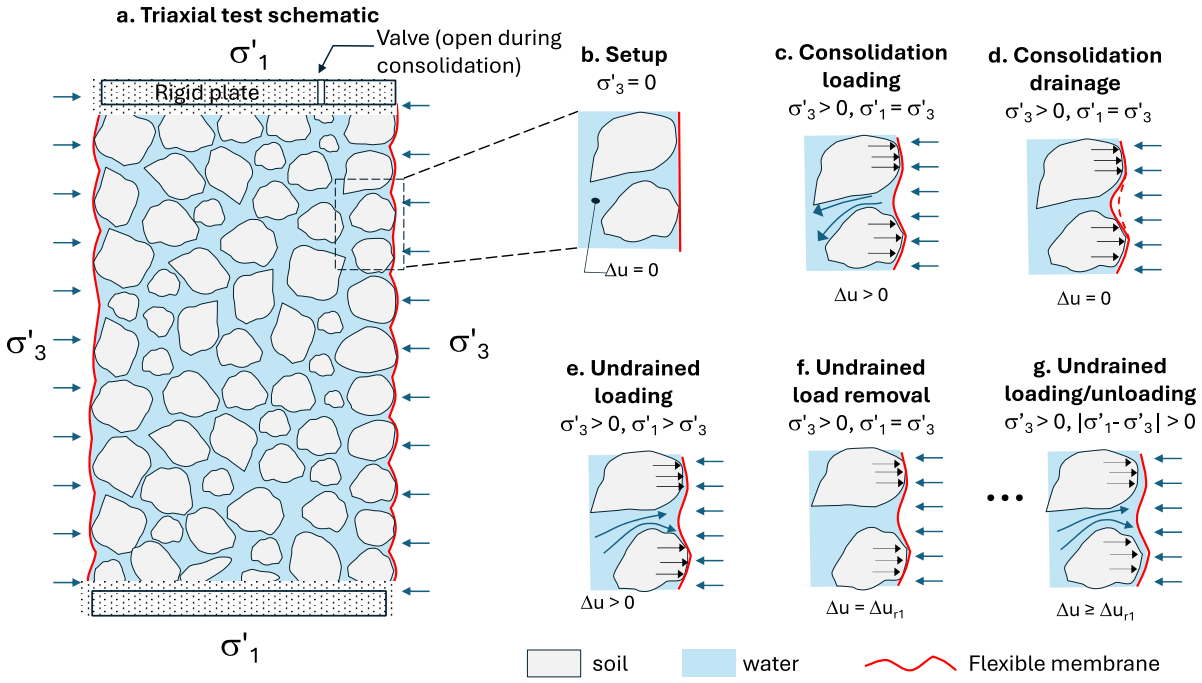


Figure 4: Schematic representation of the drainage process and residual PWP generation in triaxial tests

Similarly to the consolidation process described above, the boundary conditions imposed by the testing setup could induce a variation in the excess PWP within the sample ranging from a maximum at the sample axis to a minimum at the interface between the membrane and the soil (i.e., the boundaries) where it is zero at the beginning of the test (Figure 4a). Since the sample volume must remain constant to satisfy the undrained conditions, in contractive soils, pore water must flow from the center toward the interface, separating the soil from the membrane at some locations. As water relocates to the soil–membrane interface, a fraction of the confining cell pressure is transferred to the interstitial pore water rather than the soil particles.

The drainage process and PWP variation during the test are illustrated in Figure 4:

a. Saturated sample sketch.

b. Sample saturation begins; no excess PWP is generated.

c. Sample consolidation begins, application of a confining pressure generates excess PWP.

d. Sample consolidation continues, since valves are open, water drains out of the sample until excess PWP reduces to zero, sample is consolidated, soil/membrane contact area is maximized and 100% of cell pressure is applied to soil particles.

e. Undrained loading begins, valves are closed, excess PWP is generated, water flows towards soil/membrane/interface, contact area decreases, a fraction of cell pressure is applied to the sample water.

f. Removal of deviatoric load induces a reduction of excess PWP; since water at the interface cannot be pushed back into the sample, residual PWP (Δu_{r1}) begins to generate.

g. Residual PWP increases proportionally with additional loading/unloading cycles as the contact area between soil and membrane is reduced (i.e., the fraction of cell pressure applied directly to sample water is increased).

With increasing loading cycles (i.e., time), this fraction gradually increases until the residual PWP equals the confining pressure, which is the opposite of the consolidation process where the effective stresses gradually increases with time. Since soils are mostly inelastic, a reduction of voids during loading is typically larger than the increase in voids during unloading. Thus, in undrained tests of contractive soils, the amount of water trapped at the soil/membrane interface will increase with each load cycle, leading to the observed monotonic increase of residual excess PWP. The unique setup of the cyclic triaxial undrained test creates a variable boundary condition (i.e., decreasing confining effective pressure). The PWP at the interface is not 0 throughout the test as in the hypothetical example of the saturated layer above. As pore water flows toward the boundary (soil-membrane interface) during loading, PWP seeks equilibrium with the cell pressure.

Generation of residual pore water pressures in cyclic drained tests

Since an undrained test condition is only a representation of the extreme case of rapidly applied loads where consolidation does not affect the generated excess PWP, to complement the hypothesis that observed residual excess PWP is simply a result of the boundary conditions of undrained cyclic triaxial tests, the results of drained cyclic triaxial tests are discussed next. If residual PWPs in soils were indeed the results of plastic deformations during loading, such a phenomenon should not be limited to undrained tests. In drained conditions, the authors contend that PWPs should follow the same transient pattern of the applied loads, although at a reduced magnitude because a fraction of the PWPs would dissipate during loading as drainage takes place.

Chen et al. (2019) performed 12 strain-controlled cyclic-triaxial drained tests on Nanjing fine sand using (i) four relative densities (D_r) ranging from loose to dense sands; and (ii) three axial strains (ε_a). The soils were consolidated with a cell pressure of 100 kilopascals (kPa) and then the pressure remained constant throughout the tests. During the tests, excess PWP generated within specimens was dissipated by controlling back-pressure at a constant value of 400 kPa. Each test applied 250 cycles of axial strains with a sinusoidal wave shape characterized by a constant frequency of 1 Hz for a given strain amplitude. The results of four of the twelve tests are presented in Figure 5.

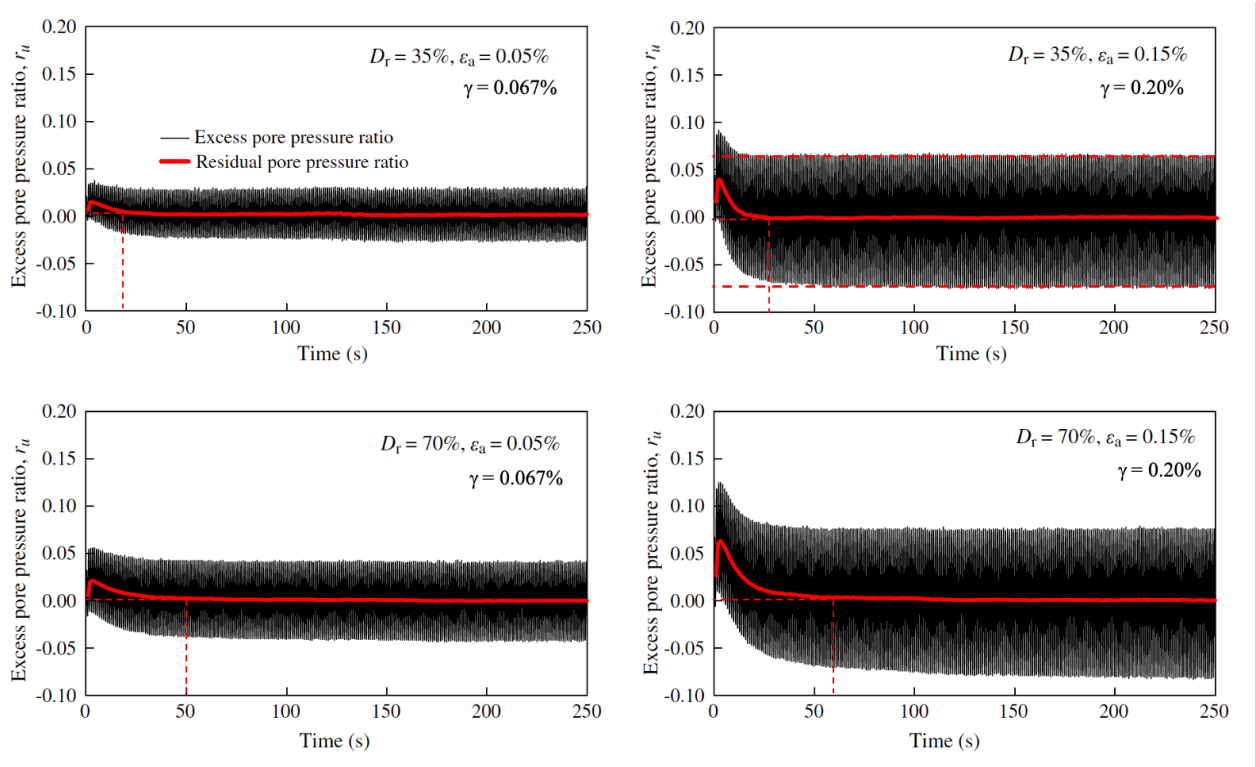


Figure 5: Pore water pressures during drained cyclic triaxial drained tests (Chen et al., 2019)

As shown in the figure, the maximum residual and transient PWPs in all tests initially increase but level off after a few cycles. This might be the result of delayed transducer measurements during unloading that may impact the accuracy of the initial readings when water flow within the soil sample is the largest. But after a few cycles and when the transducer readings become more stable, the transient excess PWP mimics the sinusoidal loading. As hypothesized, the resulting transient excess PWPs (black line) largely follow the sinusoidal shape of the axial loading, although at a fraction of the maximum applied axial load[3], whereas the residual excess PWP (red line) is zero except for the initial few cycles. The results indicate that drained cyclic tests on typical sands with loads applied at a frequency of 1 Hz are rapid enough to generate

[3] The axial loads were estimated from the plot of drained Young modulus as a function of vertical strain (Figure 8) reported by Chen et al (2019).

excess PWP that mimics the applied load. More importantly, for all practical purposes, the results indicate that no residual excess PWPs are generated. Since water is allowed to drain out of the sample, the tests boundary effect described in the previous section is not a factor that results in the artificial generation of "residual" PWP. In summary, since the generated residual PWP generated in undrained tests appears to be an artifact of the testing conditions, the validity of selecting undrained tests to perform stability analysis using total stresses in particular for liquefaction analysis is seriously questioned.

Conclusion

In this paper, the authors propose that the development of residual excess PWP observed in undrained cyclic triaxial tests is more likely a result of the test boundary conditions and the non-homogeneous conditions within the sample than the results of permanent plastic deformations. These deformations can only account for the difference in the amount of water expelled out and drawn into the sample. Considering the pore water flow that occurs in contractive samples during loading and unloading, the authors present a potential alternative mechanism that could explain why excess residual PWP is recorded during undrained tests.

Since the sample volume must remain constant, contraction (i.e., reduction in voids) can only occur if the membrane separates from the soil sample and the pore water expelled from the voids flows toward the space created at the soil/membrane interface. As water migrates toward this interface, a fraction of the confining cell pressure directly contacts the pore water through the membrane. As a result, the recorded residual excess PWP does not represent the process of liquefaction, but is simply a proxy for the fraction of the surface area that is no longer in contact with the soil particles.

It is also argued that if residual excess PWPs were indeed the results of plastic deformations during loading, they should not be limited to undrained tests; they should also manifest, at a reduced magnitude, in drained tests. Therefore, the authors presented the results of drained tests obtained for loading conditions similar to the undrained test. The results of drained triaxial tests support PWPs following the same transient pattern of the applied loads (i.e., PWPs mimic the shape of the applied loads). These results are in agreement with the theoretical and experimental results obtained in a one-dimensional consolidation test under cyclic loads (i.e., PWPs mimic the applied loads), which contest the wide-spread belief that it takes time for excess PWPs to equilibrate following removal of the load that generated such PWPs.

Although this paper focuses on the results of undrained cyclic triaxial tests, the influence of testing boundary conditions and pore water flow within the sample during testing should not be unique to these types of tests. Other popular cyclic tests may exhibit more or less pronounced effects on water flow to/from the membrane interface. Furthermore, the effect of boundary conditions is very likely an important issue in the interpretation of undrained monotonic triaxial tests where soils are typically tested to reach strains well over 20%. The authors recommend further research to investigate the potential boundary effects of cyclic

tests commonly used to evaluate liquefaction potential. Likewise, it is also recommended to evaluate potential modifications of existing testing apparatus to reduce/eliminate the described boundary effects.

Finally, the widespread use of undrained tests (monotonic and cyclic) to calibrate numerical codes to assess the liquefaction potential of existing and new TSFs makes the verification, implementation, and validation of accurate material constitutive models (e.g., PM4Sand, UBCSand, SANISAND) of upmost importance. Since most of these calibrations assume that residual excess PWPs generated in undrained cyclic tests are a naturally occurring phenomenon that should hold in the field, subsequent modeling using these assumptions will inexorably lead to developing fictitious PWPs that are the result of laboratory testing boundary conditions that do not replicate field conditions.

References

Beaty, M. and P.M. Byrne. 1998. An effective stress model for predicting liquefaction behavior of sand. *Geotechnical Earthquake Engineering and Soil Dynamics* 75: 766–777.

Castro, G. 1969. Liquefaction of sands. PhD Research Thesis, Harvard University.

Chai J.-C., S.-L. Shen, J. Wang, and M.D. Liu. 2022. Intermittent cyclic load induced 1D consolidation settlement, *Transportation Geotechnics* 36.

Chen, L. and P. Arduino. 2021. Implementation, verification, and validation of the PM4Sand Model in OpenSees. Pacific Earthquake Engineering Research Center, PEER Report No. 2021/02.

Chen G., D. Zhao, W. Chen and C.H. Juang. 2019. Excess pore-water pressure generation in cyclic undrained testing. *Journal of Geotechnical and Geoenvironmental Engineering* 145(7). DOI:10.1061/(ASCE)GT.1943-5606.0002057

Do, T.M., J. Laue, H. Mattsson and Q. 2023. Excess pore water pressure generation in fine granular materials under undrained cyclic triaxial loading. *International Journal of Geo-Engineering* 14:(8). https://doi.org/10.1186/s40703-023-00185-y

Dobry, R., R.S. Ladd, E.Y. Yodkel, R.M. Chung and D. Powell. 1982. Predictions of pore water pressure buildup and liquefaction of sands during earthquakes by the cyclic strain method. NBS Building Science Series, 138.

Elgamal A., Z. Yang, and E. Parra. 2002. Computational modeling of cyclic mobility and post-liquefaction site response. *Soil Dynamics and Earthquake Engineering* 22(4): 259–271.

Evans, M.D. and H.B. Seed. 1987. Undrained cyclic triaxial testing of gravels-the effect of membrane compliance. Earthquake Engineering Research Center. UCB/EERC-87/0B.

ICMM. 2020. Global Industry Standards on Tailings Management. Global Tailings Review.

Ishihara, K., F. Tatsuoka and S. Yasuda. 1975. Undrained deformation and liquefaction of sand under cyclic stresses. *Soils and Foundations* 15(1): 29–44.

Kim P, C.-U. Pak and H. Myong. 2021. Analytical solution for one-dimensional nonlinear consolidation of saturated double-layered soil subjected to cyclic loadings. *Journal of Engineering*. Nov. https://doi.org/10.1155/2021/5595232

Lee, K.L. and H. Bolton Seed. 1967. Drained strength characteristics of sands. *Journal of the Soil Mechanics and Foundations Division* 93(6): 117–141. https://doi.org/10.1061/JSFEAQ.0001048

Nicholson P.G., H. Bolton Seed and H. Anwar. 1989. Measurement and elimination of membrane compliance effects in undrained triaxial testing. Earthquake Engineering Research Center. UCB/EERC-89/10.

Shibata, T., H. Yukitomo and M. Miyoshi.1972. Liquefaction process of sand during cyclic loading. *Soils and Foundations* 12(1): 1–16.

Sakai, A. and H. Ochiai. 1986. Effects of initial static shear stress on the liquefaction of sand. Memoirs of the Faculty of Engineering. Kyushu University 46(1): 49–62.

Seed, H.B., I. Arango and K. Chan. 1976. Evaluation of soil liquefaction potential for level ground during earthquakes. Report prepared for the Nuclear Regulatory Commission.

Shoaei, Z. and K. Kassa. 1996. Mechanism of pore pressure generation due to the different direction of earthquake acceleration on saturated soil. *Transactions on the Built Environment* 20.

Tabata, K. and M. Vucetic. 2010. Threshold shear strain for cyclic degradation of three clays. *Proceedings of the Fifth International Conference on Recent Advances in Geotechnical Earthquake Engineering and Soil Dynamics.*

Terzaghi, K. 1943. *Theoretical Soil Mechanics*. New York: John Wiley & Sons.

Wilson, N.E. and M.M. Elgohary. 1974. Consolidation of soils under cyclic loading. *Canadian Geotechnical Journal* 11(3): 420–423.

Zhu, F., W. Zhang and A.M. Puzrin. 2024. The slip surface mechanism of delayed failure of the Brumadinho tailings dam in 2019. *Communications Earth & Environment* 5(33).

Numerical Modeling Comparison of Large-strain Tailings Consolidation

Daniel Pham, WSP, Australia

Abstract

Consolidation of mine tailings can take extended periods of time due to their high water content and relatively low permeability, which can affect the storage capacity of the tailings storage facilities (TSFs) during the Life of Mine (LoM), and the timeline to start their rehabilitation at closure. An understanding of the tailings consolidation behavior during TSF planning stages is therefore critical to achieve efficient and sustainable mine waste management during operations and prior to closure. This can be accomplished by a combination of laboratory testing and numerical modeling prior to the commencement of tailings deposition.

A numerical modeling comparison of large-strain tailings consolidation was undertaken with three software, Plaxis LE, FSConsol and MinTaCo, which are commonly used by tailings practitioners. The objectives of the study were to find the advantages and limitations for each software to assist with selecting the appropriate numerical modeling program corresponding to the project budget, complexity, anticipated effort, and outputs required. This paper presents a multicriteria assessment and a case study involving consolidation modeling undertaking on an in-pit tailings storage facility based on laboratory testing results using the software considered for both single and multiple filling scenarios, as well as with and without the effects of evaporation.

Introduction

Tailings have been generated in large volumes worldwide as byproducts of ore beneficiation from the process plants in the mine sites. Tailings are generally deposited in the form of slurry either on perimeter dykes constructed from their coarser fraction, i.e., waste rock above ground, or within the inactive open pits. These structures are called tailings storage facilities (TSFs). Settling and consolidation processes of mine tailings can take a long time, which reduces the storage capacity of the TSFs due to the conventional tailings characteristics of high water content and low hydraulic conductivity. As such, a combination of laboratory testing and numerical modeling is usually required prior to the commencement of tailings deposition to achieve effective planning and management during TSF operations and prior to closure.

Numerical modeling on tailings consolidation has evolved over the years, with multiple software available both commercially and for educational purposes, focusing on one-dimensional configuration. Each software has its own advantages, limitations, and functions, as well as variability in costs and model configurations. This study presents a comparison between three modeling software that have been used by tailings practitioners to model large-strain tailings consolidation, namely, Plaxis LE, FSConsol and MinTaCo.

It is acknowledged that there is other modeling software available on the market that can model large-strain consolidation such as Finite Strain Consolidation Analysis (FSCA), and the Norwegian Geotechnical Institute (NGI) approach to model tailings deposition and consolidation in FLAC. Due to access constraint to FSCA and the complexity of using FLAC, they have not been included in the scope of this study.

Background

Finite-strain consolidation

The consolidation of tailings can be broken down into three components:

1. Self-weight consolidation occurs following deposition and is the result of the settling of the tailings solid particles without additional loading.
2. Primary consolidation follows self-weight consolidation and is the result of the dissipation of pore-water pressure generated by an increase in vertical effective stress.
3. Secondary consolidation (or creep deformation) continues in the long term following primary consolidation and under a state of relatively constant stress. Note that secondary consolidation was not considered in the study presented herein due to its limited settlement magnitude in comparison to self-weight and primary consolidation.

During self-weight consolidation, tailings will undergo large deformations due to low effective stress and high void ratio in the early stage of tailings matrix (i.e., particle fabric) development. The hydraulic conductivity of tailings decreases as the density changes with increased thickness of the deposit during tailings deposition. Therefore, the conventional Terzaghi consolidation theory becomes invalid due to the inherent assumptions of infinitesimal strains and constant hydraulic conductivity. To capture the high nonlinearity due to initial large volume change at a high void ratio of tailings, a finite-strain consolidation theory for self-weight consolidation involving large-strain deformation must be adopted.

Numerical modeling software considered

Plaxis LE

Plaxis LE is a software for limit equilibrium slope stability analysis and finite element analysis of

groundwater seepage. Consolidation is a module within Plaxis LE that solves coupled hydro-mechanical processes that are available separately in the Groundwater and Stress software packages. The large-strain consolidation is modeled following the non-continuum mechanics in the Lagrangian coordinate system developed by Bonet (2008). The software has the capability to model both small-strain (constant soil properties) and large-strain (nonlinear soil properties) consolidation problems in both 1D and pseudo-3D (i.e., coupled 3D slurried tailings deposition scenario with the effects of saturated 1D columns) configurations. Note that the software was originally developed by SoilVision, a geotechnical engineering software provider that was acquired together with Plaxis by Bentley Systems in 2018.

FSConsol

FSConsol is a 1D consolidation program that uses the Finite Strain Consolidation Theory developed by Gibson et al. (1967) to determine the rate and magnitude of consolidation of soil slurries such as mine tailings, deltaic deposits, and other soft soils. The software can model a variety of consolidation problems ranging from a step-loaded laboratory consolidation test to a complex mine tailings pond scenario with varying filling rates, changing pond areas, and changing soil properties.

MinTaCo

MinTaCo is a 1D numerical modeling program developed by the University of Western Australia (UWA) in 1996. MinTaCo has the capability to incorporate the effects of drying on the conventional large-strain consolidation process (Seneviratne et al., 1996). It iteratively applies different suction values to the surface of the tailings to achieve a specific evaporation rate for the material. This iterative adjustment in suction continues until the layers reach the shrinkage limit density that is assessed by laboratory consolidation testing.

Multi criteria assessment

A basic multicriteria assessment (MCA) was conducted with the key criteria summarized in Table 1, while Table 2 presents a summary of the key advantages and disadvantages of the three software.

The main advantage of MinTaCo in comparison to the other two software is the ability to model unsaturated conditions such as the inclusion of evaporation during consolidation. Its major drawback is the lack of a functional graphical user interface (GUI), which can create many difficulties for first time users. Plaxis LE has the benefit of having the ability to do 3D modeling, which is more suitable for data visualization, and a well and fully developed GUI, which is more appealing to users.

Table 1: Summary of key outcomes from the multi criteria comparison

Criteria	Plaxis LE	FSConsol	MinTaCo
Ease of use	Advanced graphical user interface (GUI)	Basic GUI	No GUI available
Model configuration	1D and Pseudo-3D	1D	1D
Available license	Network	USB dongle	License is not required
Soil saturation conditions	Saturated only	Saturated only	Saturated & unsaturated

Table 2: Summary of advantages and limitations of each software considered

Software	Advantages	Limitations
Plaxis LE	Soil parameters required for constitutive models can be generated within the software using the "Apply fit" function. Multiple functions available for nonlinear compressibility. Ability to do pseudo-3D modeling in 3D based on aerial survey of site topography or using 3D models created in Plaxis Designer. GUI is easy to use and follow. The outputs are easy to process and understand with plots provided.	Only two settings for top and bottom boundary conditions regarding drainage: with and without drainage. There are no options available for other modeling scenarios such as decant pond at the top and partial drainage at the bottom. Stage settings during model set up can be time consuming and repetitive if significant numbers of stages are required. Results from deposition modeling using a 3D modeling software are required to inform the stages for 1D consolidation modeling.
FSConsol	Software is relatively easy to use with basic GUI. The outputs are relatively easy to process and understand with plots provided. Pond filling function adopting progressive filling based on various pond areas which can be considered as pseudo-3D. Ability to model creep deformation.	USB dongle is required to run the software. Soil parameters required for the compressibility and permeability functions need to be assessed separately using Excel. Inability to model unsaturated conditions. Outputs do not have flux rates of consolidated water at the top and bottom. Model solver can be unstable when dealing with more than one material.
MinTaCo	Ability to incorporate evaporation in consolidation modeling. Ability to consider multiple drainage conditions at the top and bottom. Output of the shear strength at the surface can be generated from the model. License is not required. Ability to set target height for deposition and consolidation, especially useful for multiple fillings.	Inability to model pseudo-3D. Soil parameters required for the compressibility and permeability functions need to be assessed separately using Excel. It takes longer for new users to be familiar with the software due to the lack of GUI. Outputs are not user-friendly. Plots are required to be drawn manually in Excel which requires significant effort and therefore is time-consuming. However, VBA can be used to automate this process, which requires programming skill. Results from deposition modeling using a 3D modeling software are required to inform the stages for 1D consolidation modeling.

Case study

Background

Consolidation modeling has been undertaken using the three software mentioned herein on an in-pit TSF (IPTSF) called De Grey pit that is located in Western Australia (WA) as a case study. De Grey is an inactive open pit and is part of the Shovelanna complex. The pits are located approximately 35 km east of Newman within the Pilbara region of Western Australia. The Hamersley Range and Fortescue Plains subregions (where the pits are located) are typified by an arid and tropical climate, with hot wet summers and cool dry winters. Average annual rainfall is typically 300 mm, most of which falls during the summer because of rain depressions and cyclones. Hot, dry, and sunny conditions in the Pilbara lead to an average annual evaporation rate of 3,200 mm.

Consolidation modeling

Design basis

De Grey and Swan pits have been identified as the candidates for a short-term tailings management solution, with tailings deposition planned to commence in mid-2026 when the process plant is commissioned. The tailings deposition strategy selected was two weekly rotated deposition cycles between the two pits to improve consolidation during the operational periods. Table 3 presents the design inputs and assumptions adopted in relation to the IPTSF operations for the deposition and consolidation modeling. Note that only the consolidation modeling for the De Grey pit is presented in this paper.

Table 3: Design basis of the IPTSF operations

Design Parameter	Design Input
Life of asset	Utilize full pit capacity.
Available capacity in pit	De Grey – 13.78 Mm^3 at maximum tailings elevation. Swan – 10.80 Mm^3 at maximum tailings elevation.
Commencement of tailings generation	1 August 2026 (FY27).
Tailings solids generated	5.89 Mtpa on average from FY27 to FY51
Deposition approach	Slurry deposition by spigots. Two deposition point locations adopted in Swan and De Grey pits.
Tailings deposition strategy	Multiple filling phases over the LoM and 2 weekly rotated deposition cycles between De Grey and Swan pits.
Representative tailings samples	Average Blend for the first three years of operations followed by High Dales during the LoM.
Beach slope	Assumed to be 0.5%, with no change in beach slope beneath the pond.
TSF decant pond depth throughout deposition	Minimum 1 m.

Laboratory testing

Multiple laboratory tests were conducted on the representative tailings samples to assess their classification and to characterize their consolidation behavior. A summary of the tests undertaken and their corresponding results that were considered to assist in establishing the model input parameters for consolidation is presented in Table 4.

Table 4: Summary of geotechnical laboratory test results for the representative tailings samples

Test	Parameters	Measurement for tailings samples prepared at 45% solids concentration	
		Average Blend	High Dales
Density bottle	Particle density (t/m^3)	3.99	4.02
e_0 beaker test	Solids concentration at e_0 (%)	49.4	47.1
	Initial void ratio e_0	4.09	4.52
	Dry density at e_0 (t/m^3)	0.78	0.73
Settling column with top drainage	Final settled dry density (t/m^3)	0.90	0.86
	Time to achieve final settled dry density (days)	20	19
Air drying test	Final air-dried density (t/m^3)	1.85	1.92
	Time to reach final air-dried density (days)	28	34
One-dimensional slurry consolidation	Pressure range tested (kPa)	10 to 1600	
	Void ratio, e	1.97 to 0.97	2.08 to 1.02
	Dry density (t/m^3)	1.34 to 2.03	1.31 to 1.99
	Hydraulic conductivity (m/s)	1.01×10^{-8} to 1.13×10^{-9}	5.4×10^{-9} to 9.17×10^{-10}
	Coefficient of consolidation ($m^2/year$)	4.5 to 170	5.2 to 82.9

Material input parameters

Plaxis LE and FSConsol

Tailings parameters for input to the model in Plaxis LE and FSConsol were estimated based on laboratory classification and consolidation testing of Average Blend and High Dales samples as summarized in the above section. They were used to establish the following:

- The relationship between void ratio and effective stress (fitted extended power function as presented in Figure 1)

Equation 1 (Average Blend): $e = 2.954(\sigma'_v + 0.11)^{-0.155}$ $(\sigma'_v \; in \; kPa)$

Equation 2 (High Dales): $e = 3.006(\sigma'_v + 0.051)^{-0.149}$ $(\sigma'_v \; in \; kPa)$

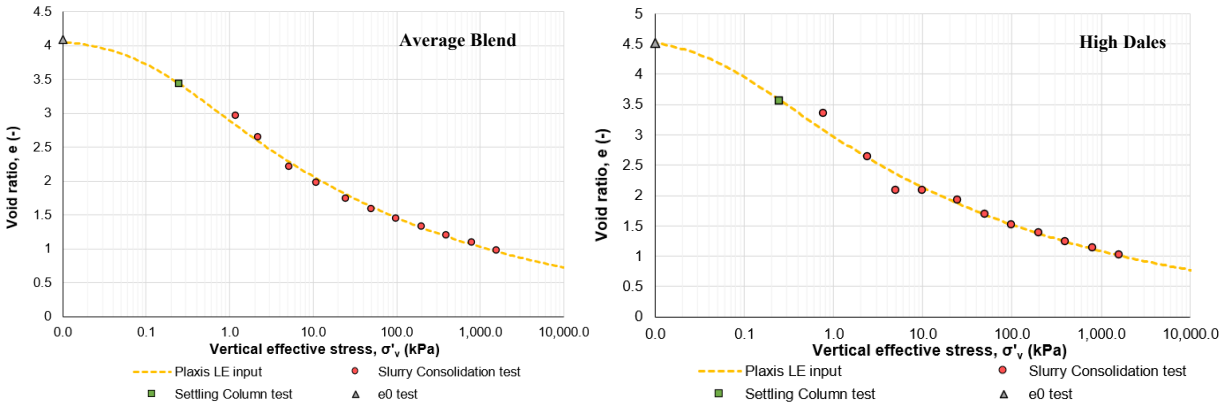


Figure 1: Functions adopted for void ratio (e) vs. vertical effective stress (σ'v)

- The relationship between permeability and void ratio (fitted power function as presented in Figure 2)

Equation 3 (Average Blend): $k_v = 1.0 \times 10^{-9}(e)^{3.047}$

Equation 4 (High Dales): $k_v = 9.0 \times 10^{-10}(e)^{2.806}$

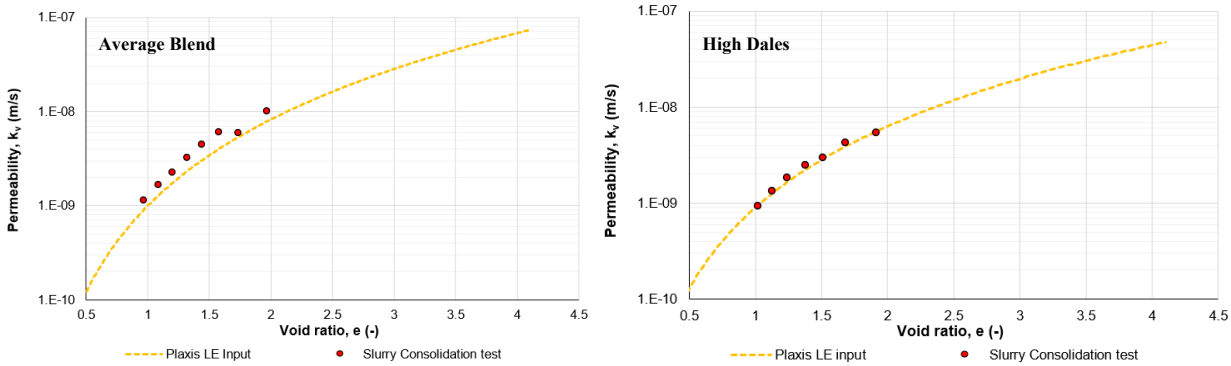


Figure 2: Functions adopted for permeability (kv) vs. void ratio (e)

Note that only Average Blend parameters were used in FSConsol due to the software being unstable when processing two tailings materials in the assessment.

MinTaCo

Tailings parameters for input to the model are summarized in Table 5. They were estimated based on laboratory classification and consolidation testing results of Average Blend and High Dales samples, as summarized in the Laboratory Testing Section.

Equation 5: $e = c(\sigma'_v)^d \ (\sigma'_v \ in \ kPa)$

Equation 6: $k_v = \frac{a(e)^b}{1+e} \ (k_v \ in \frac{m}{day})$

Table 5: Input parameters used to simulate Average Blend and High Dales tailings samples

Parameter		Tailings sample	
		Average Blend	High Dales
Specific gravity		3.99	4.02
Permeability constants	a*	2.16 × 10-4	1.56 × 10-4
	b*	3.6	3.55
Compressibility constants	c*	2.87	2.96
	d*	-0.148	-0.15
Void ratio at sedimentation		4.09	4.52
Shrinkage limit void ratio		1.16	1.09
Air entry suction at shrinkage limit (kPa)		430	890

Note: *estimated by curve fitting the consolidation test results

The shrinkage limit void ratios and the corresponding estimated air-entry suction values for both tailings samples are presented in Figure 3.

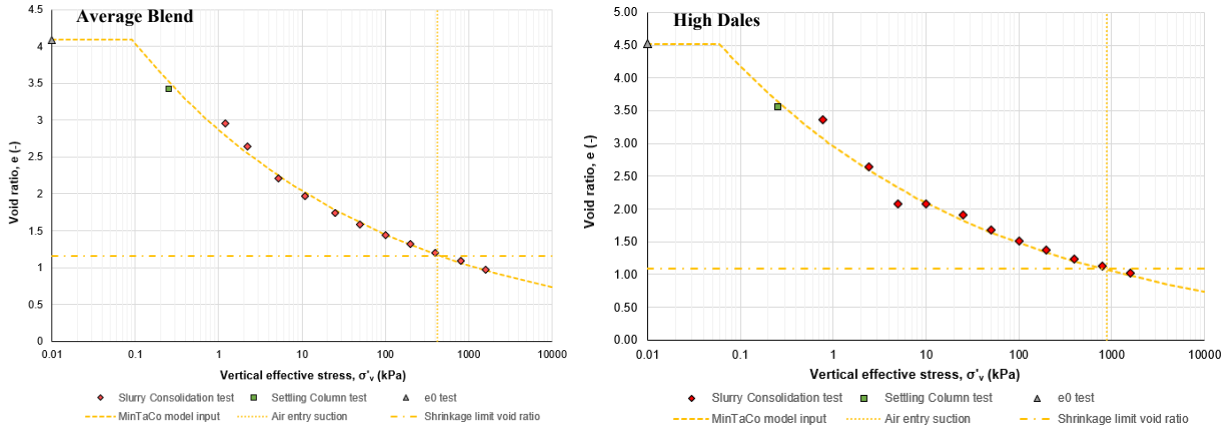


Figure 3: Laboratory test results and functions adopted for void ratio (e) vs. vertical effective stress (σ'v)

The relationship between void ratio and effective stress adopted in the models is presented in Figure 3, while Figure 4 shows the relationship between void ratio and hydraulic conductivity.

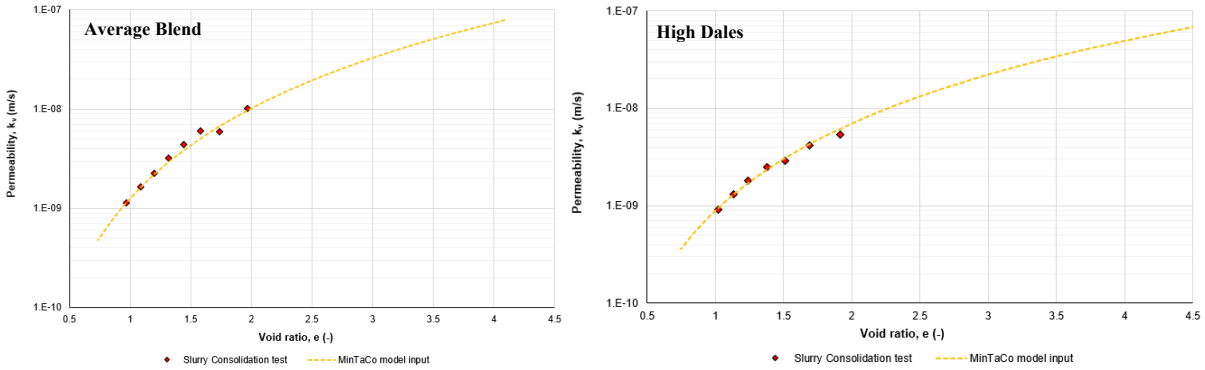


Figure 4: Laboratory test results and functions adopted for permeability (kv) vs. void ratio (e)

Modeling assumptions

The following inputs were incorporated and assumed in the models:

- A Poisson's Ratio of 0.3 is assumed for both Average Blend and High Dales tailings. This is considered appropriate for iron ore tailings as suggested by Priestley (2011).
- Decanting is operational at both pits during the deposition periods. A maximum pond depth of 1 m has been assumed to be developed within the depositional area.
- Freeboard requirements have been adopted in the consolidation modeling following the outcomes of overtopping assessment in conjunction with deposition modeling.
- An average annual lake evaporation rate of 5.9 mm/day (or 2.2 m/year) was adopted to simulate evaporation in the models. This is equivalent to a coefficient of conversion between A-Pan and the lake evaporation of 0.65. The data was extracted from SILO using Morton's shallow lake evaporation rates at the stations where the De Grey and Swan pits are located.
- Boundary conditions:
    - A conservative assumption of no flux at the lower boundary of the models (i.e., zero seepage with only upward drainage allowed).
    - Zero excess pore water pressure at the upper boundary to allow for water to drain at the surface. Tailings are assumed to remain fully saturated, which is representative of supernatant pond removal through decanting.
    - These boundary conditions are considered appropriate given the high rate of rise and low permeability of the tailings materials and pit base, as well as the likelihood that a supernatant pond will be allowed to form on the tailings surface.

Modeling results

1D modeling

Single filling phase

Consolidation modeling for the single filling was undertaken adopting the following scenarios and software: Plaxis LE, FSConsol, MinTaCo without evaporation and MinTaCo with evaporation.

The results are summarized in Table 6 and indicate the following:

- A storage life of 3.5 – 3.7 is achieved consistently in the scenario without evaporation using the three software. This is further illustrated in the output profiles in Appendix A.
- The incorporation of evaporation increases the storage life slightly to 3.9 years.
- The expected settlement within De Grey pit is approximately 55 – 58 m. Note that due to only one tailings sample being adopted for FSConsol, the results of settlement post deposition are not included for comparison purposes.

Table 6: Modeling results of De Grey pit for single filling phase

Parameters	Plaxis LE	FSConsol	MinTaCo (without evaporation)	MinTaCo (with evaporation)
Estimated storage life (years)	3.6	3.45	3.7	3.9
Total estimated settlement post-deposition (m)	55	N/A	54	58
Approximate time to reach 90% settlement from end of deposition (years)	47	N/A	44	44
Approximate tailings elevation at the end of settlement (RL m)	514	N/A	515	511
Average void ratio at the end of deposition	3.97	3.95	3.89	3.71
Average stored dry density at the end of deposition (t/m^3)	0.83	0.83	0.84	0.85

Multiple filling phases

Consolidation modeling for the multiple fillings was undertaken adopting the following scenarios and software: Plaxis LE (without evaporation) and MinTaCo (with evaporation).

An average tailings settlement magnitude of 5 m is assumed to be the target for tailings deposition restart following the fallow periods. Assessment in FSConsol was not included due to the maximum limit of 61 filling rates that can be inserted within the software, and the instability when handling more than one tailings material type.

The results are summarized in Table 7 and presented graphically in Figure 5. The results indicate the following:

- An overall storage life of ~9.4 years is anticipated to be achieved by incorporating evaporation in MinTaCo in comparison to ~5.2 years in Plaxis LE without evaporation, which is an increase of ~81% in storage life during operations.
- A reduction in total tailings settlement is anticipated when evaporation is considered, from 48 m to 39 m.
- MinTaCo takes longer to reach 90% settlement in approximately 80 years from FY51 in comparison to 51 years using Plaxis LE.

Table 7: Modeling results of De Grey pit for multiple filling phases

Parameters	MinTaCo	Plaxis LE
Estimated storage life at the end of the initial deposition phase (years)	3.9	3.6
Estimated total storage life at the end of the final deposition phase (years)	9.4	5.2
Total estimated settlement post-operations (m)	39	48
Settlement ratio (%)	37	46
Approximate time to reach 90% settlement from FY51 (years)	80	51
Approximate tailings elevation at the end of settlement (RL m)	525	516

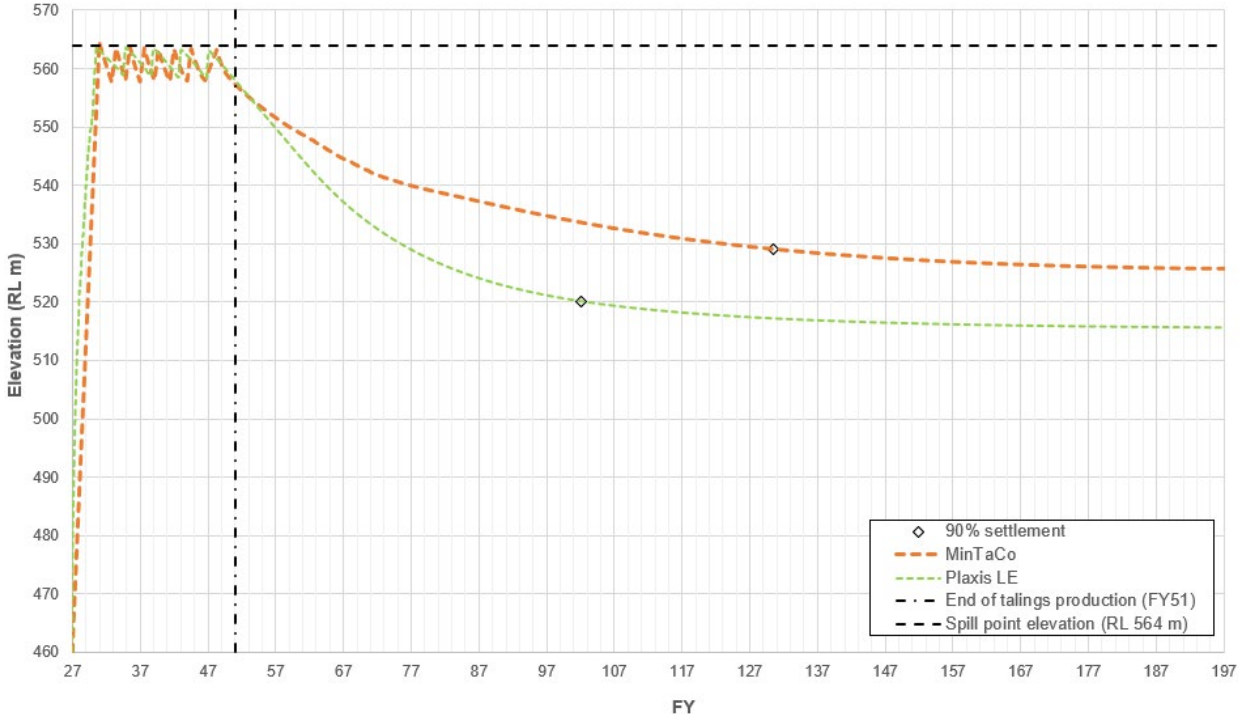


Figure 5: Settlement of software considered for the multiple filling phases

Pseudo-3D modeling

The results of 1D modeling are representative for a single location within the pit, where settlements are expected to be the greatest. It is expected that the average settlement across the pits' area will be less due to changes in the pit geometry. Pseudo-3D consolidation modeling has been undertaken to provide a better understanding of the tailings settlement profile in three-dimensional configuration. Note that pseudo-3D does not consider horizontal dissipation of pore pressure, lateral deformation, and the effects of evaporative desiccation.

The results of pseudo-3D consolidation modeling are presented in Figure 6, showing the estimated final tailings surfaces at the end of consolidation. 3D outputs showing void ratio and effective stress profiles at various timeframes in both pits are included in Appendix B. The results of the pseudo-3D modeling indicate that:

- The settlement profiles at the deepest locations within the two pits are aligned with the 1D modeling results with a total estimated post-deposition settlement of ~50 m in De Grey pit. The estimated final tailings elevation at those locations at the end of settlement are within RL 510 m and RL 520 m.
- The magnitude of settlement reduces with reducing pit depth/height of tailings column. As such there is likely to be less settlement around the edges of the pits than in the center, creating a dished tailings surface profile.

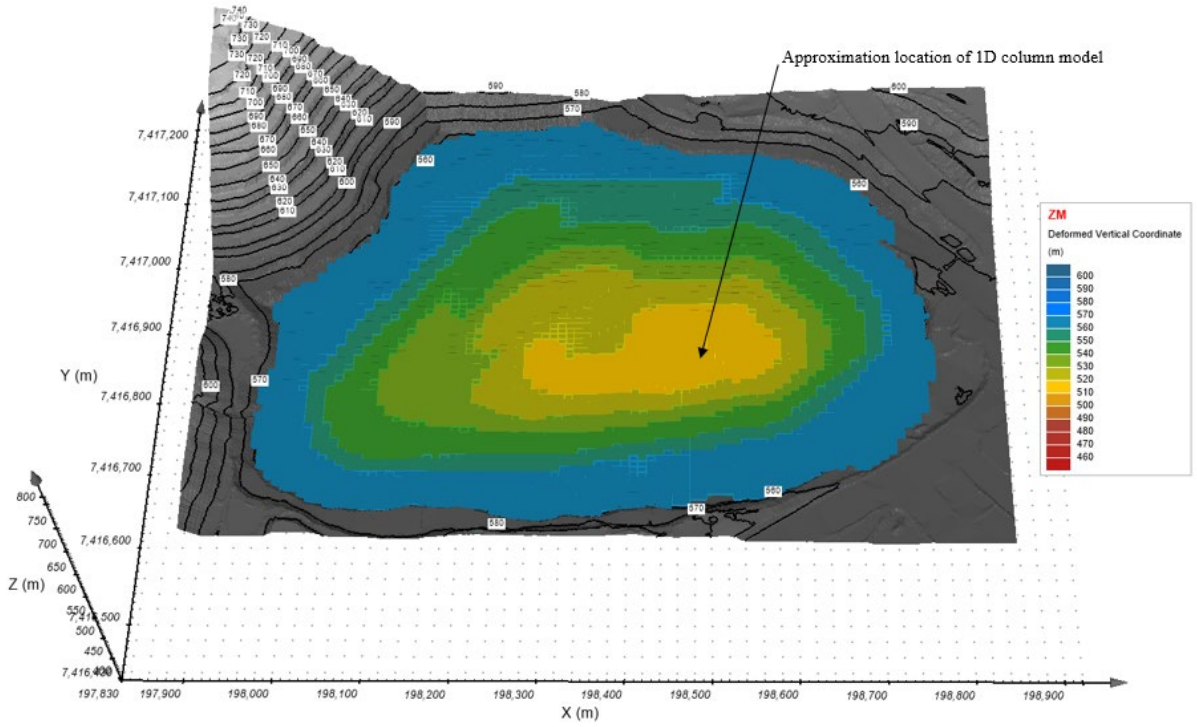


Figure 6: Pseudo-3D surface of total estimated tailings settlement in the De Grey pit

Conclusion

The numerical modeling comparison of large-strain tailings consolidation undertaken indicates the following:

- FSConsol has been primarily used by tailings practitioners in the industry for consolidation modeling due to its relatively basic GUI and the ability to model creep deformation. This is suitable for 1D consolidation models, having simple TSF geometry with limited inputs required. Plaxis LE has a more sophisticated GUI and advanced functions that allow users to model complex TSF geometry based on the actual site topography in both 1D and pseudo-3D configurations. However, this will normally require users to have relatively advanced modeling skills, with some background knowledge in 3D modeling. In comparison to Plaxis LE and FSConsol, MinTaCo has the advantage of being able to incorporate climatic conditions such as evaporation. The major drawback with MinTaCo is the lack of a user-friendly GUI and the ability to model pseudo-3D.
- The case study showed a consistent similarity between the outputs of settlement magnitude, profiles of void ratio, dry density, effective stress, and hydraulic conductivity from the three software. FSConsol showed instability in its model solver as it was not able to handle two tailings materials in comparison to Plaxis LE and MinTaCo, even though FSConsol allows the user to enter over 30 different material types. The results of pseudo-3D modeling in Plaxis LE were consistent with the 1D outcomes. When incorporating evaporation in a multiple filling scenario, MinTaCo showed a significant increase in the storage life of the TSF, which emphasizes the importance of climatic conditions to tailings consolidation process.

Acknowledgements

The author would like to thank Riccardo Fanni, Dr Peter Chapman, Brad Tiver, Tom Hills, Brendan Cummins, and Rohit Mulji for their inputs, advice and contributions to this study, as well as the Clients for the opportunity.

References

Bonet, J. 2008. *Nonlinear Continuum Mechanics for Finite Element Analysis*. Cambridge: Cambridge University Press.

Gibson, R.E. England, G.L. and Hussey, M.J.L. 1967. The theory of one-dimensional consolidation of saturated clays – Finite non-linear consolidation of thin homogeneous layers. *Géotechnique* 17(3): 261–273.

Priestley, D. 2011. *Modeling Multidimensional Large Strain Consolidation of Tailings*. The University of British Columbia.

Seneviratne, N.H., Fahey, M., Newson, T.A. and Fujiyasu, Y. 1996. Numerical modeling of consolidation and evaporation of slurried mine tailings. *International Journal for Numerical and Analytical Methods in Geomechanics* 20(9): 647–671.

Appendix A: 1D consolidation modeling outputs for the single filling phase

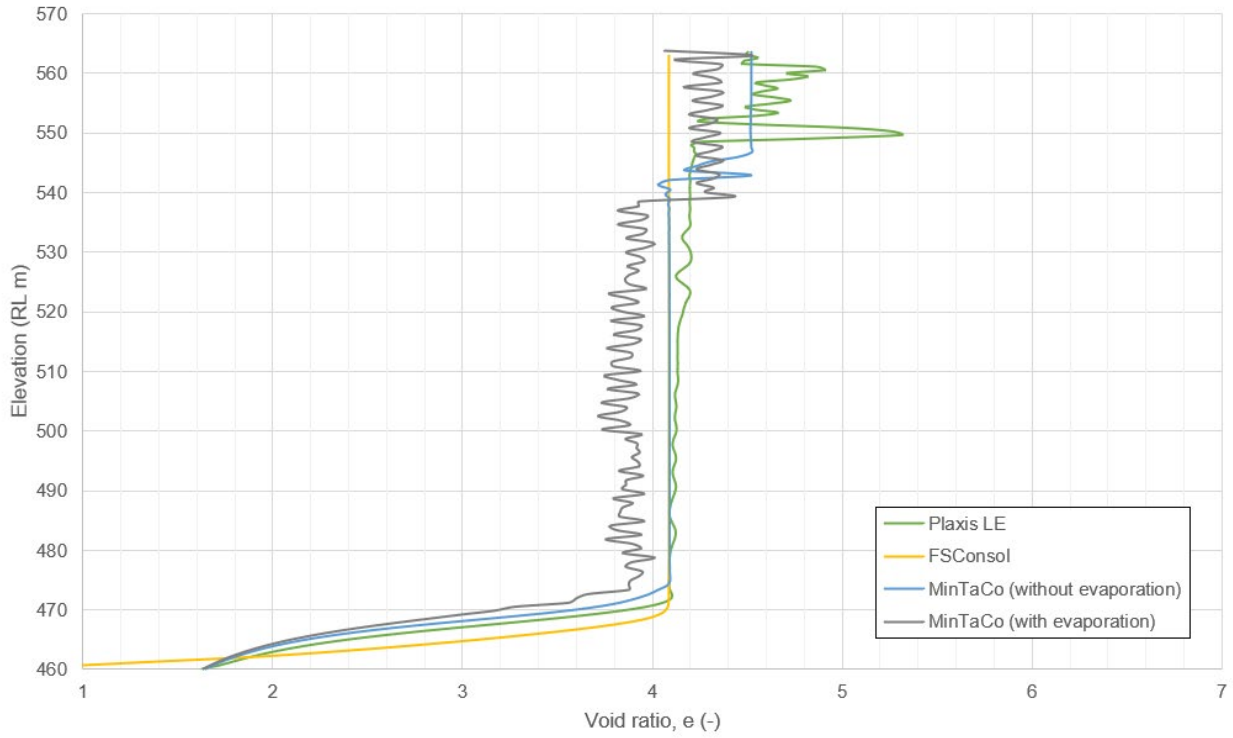


Figure A1: 1D modeling outputs for single filling phase – void ratio profiles

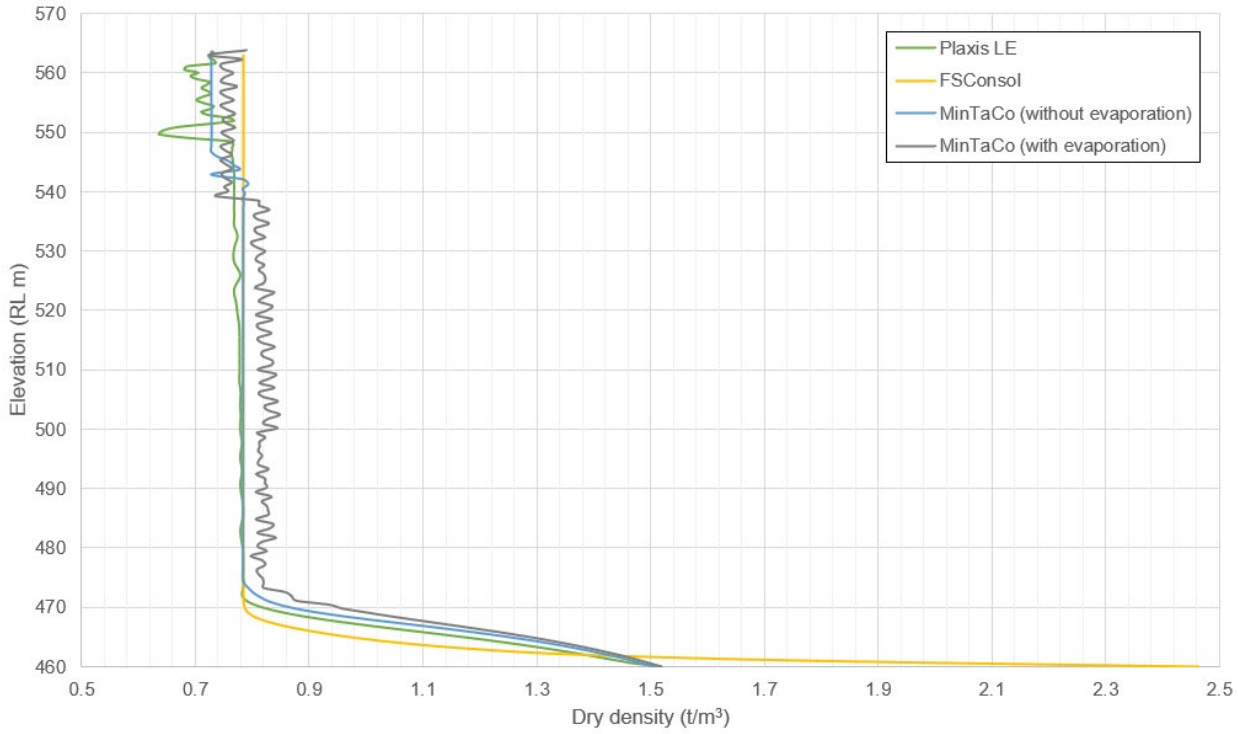


Figure A2: 1D modeling outputs for single filling phase – dry density profiles

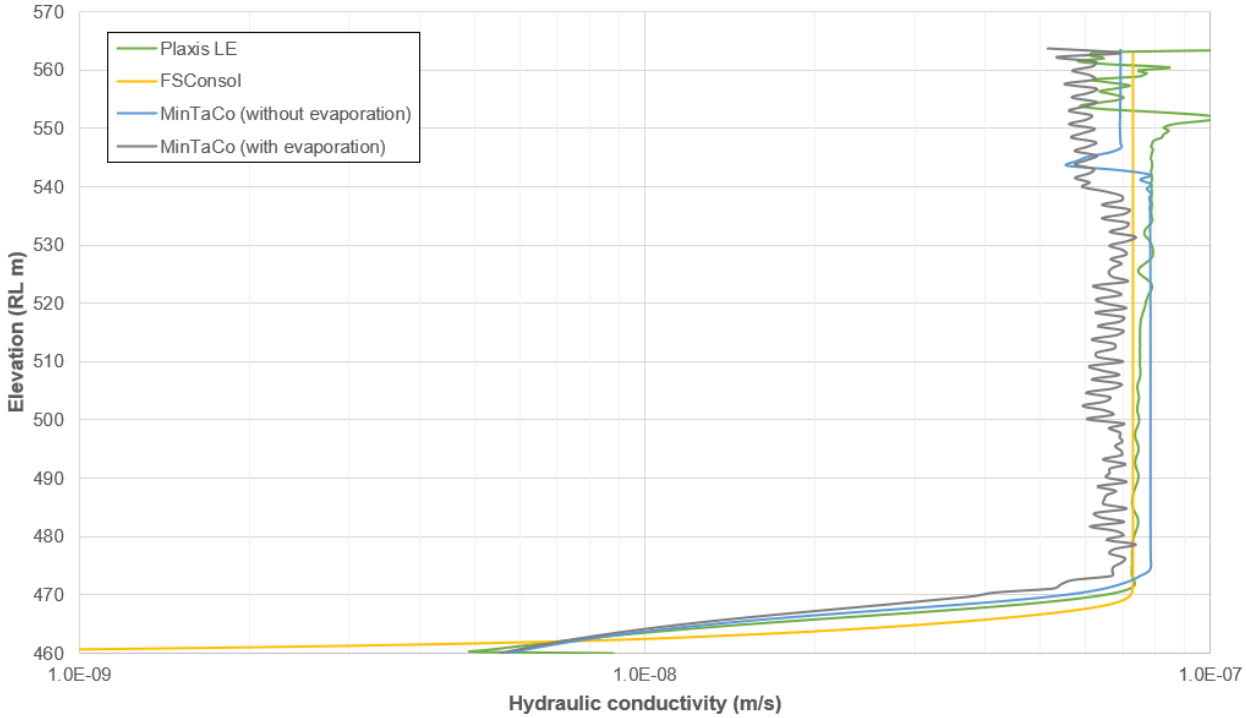


Figure A3: 1D modeling outputs for single filling phase – hydraulic conductivity profiles

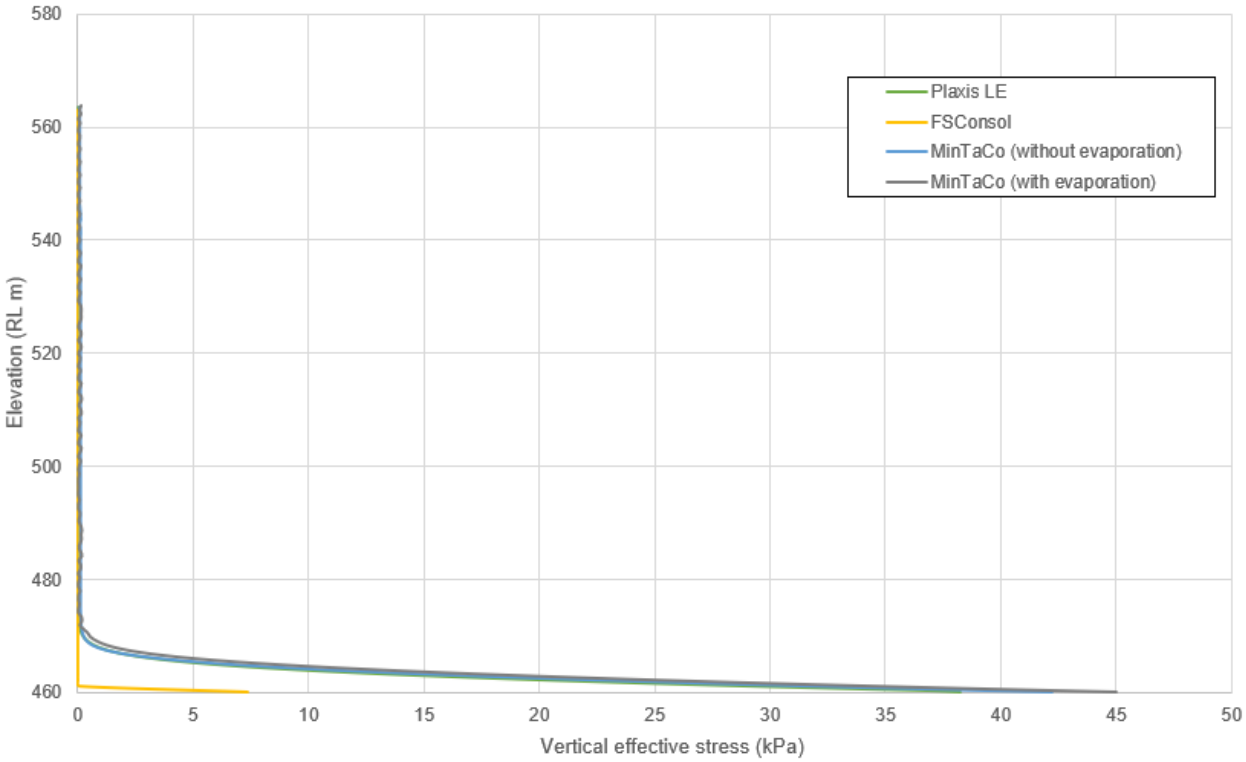


Figure A4: 1D modeling outputs for single filling phase – effective stress profiles

Appendix B: Pseudo-3D consolidation modeling outputs for multiple filling phase

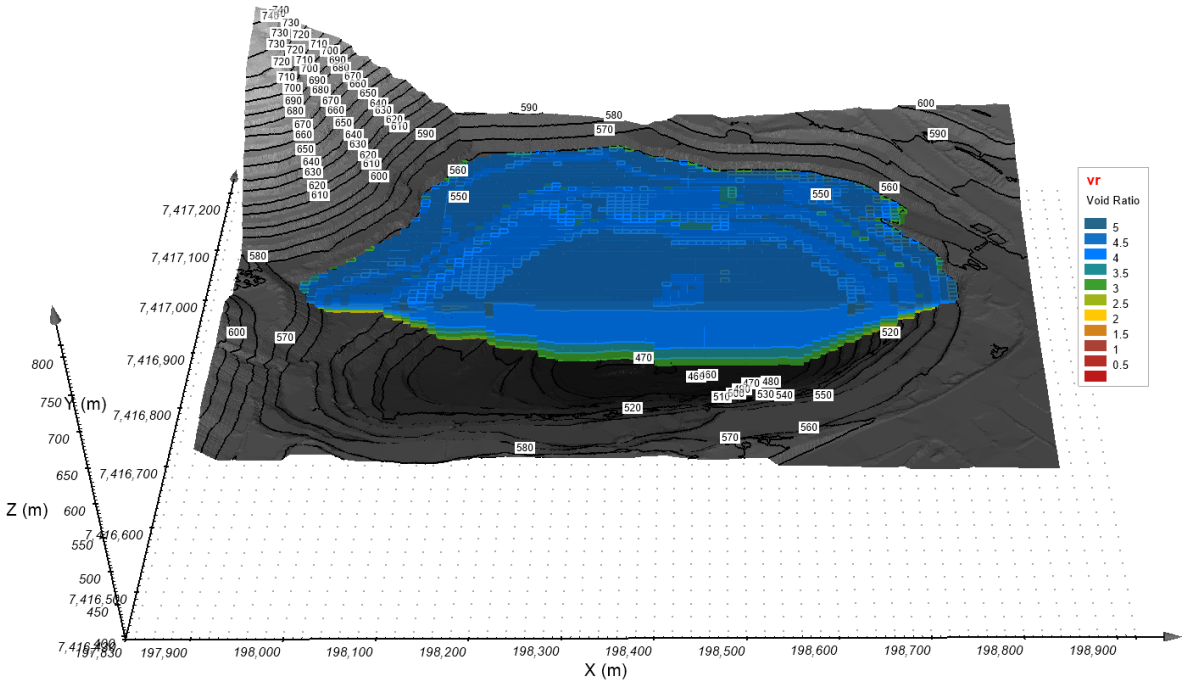


Figure B1: End of the initial deposition phase – void ratio profile

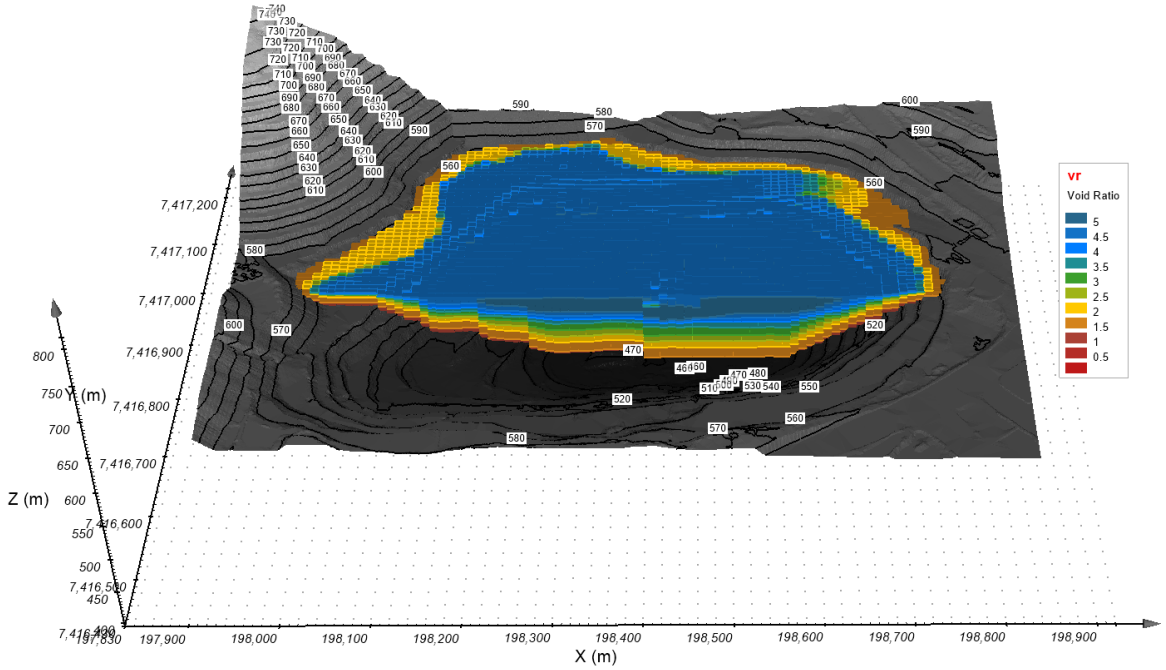


Figure B2: End of the final deposition phase – void ratio profile

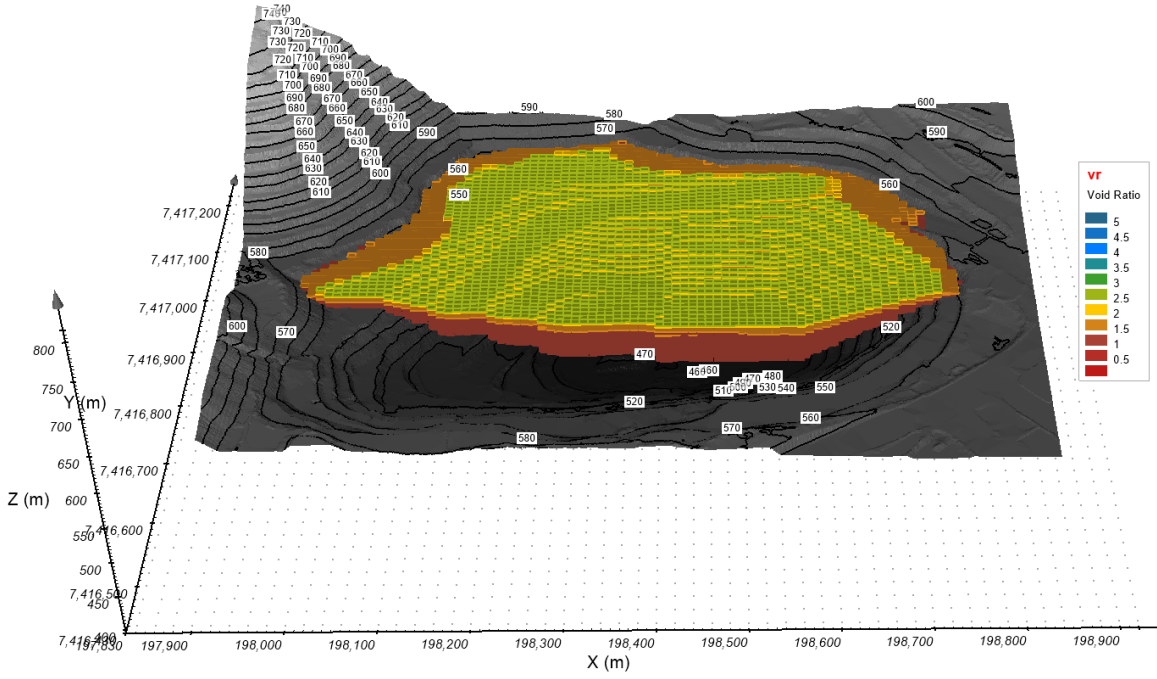


Figure B3: At total settlement – void ratio profile

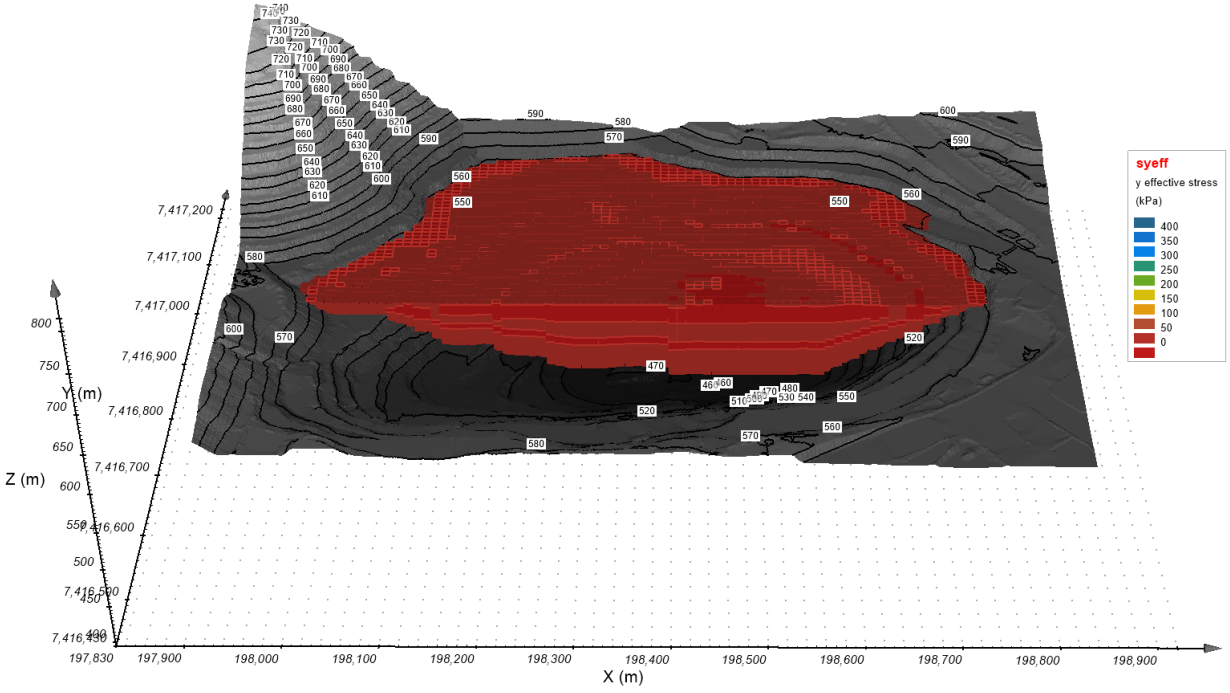


Figure B4: End of the initial deposition phase – effective stress profile

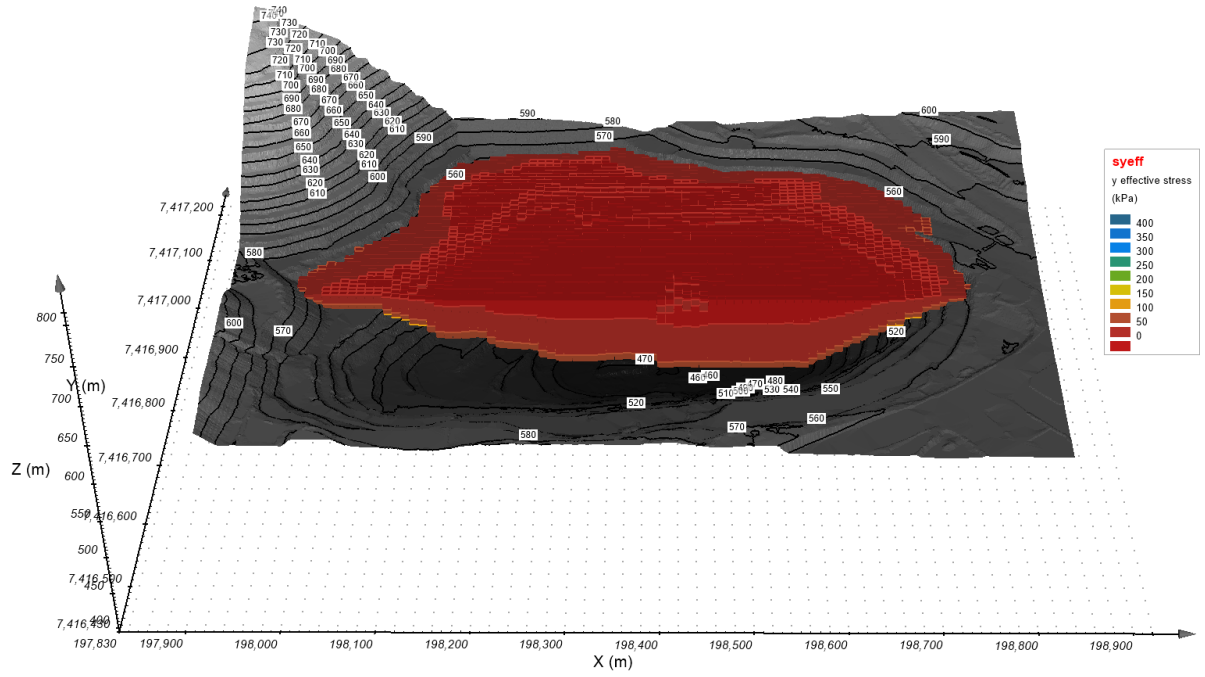


Figure B5: End of the final deposition phase – effective stress profile

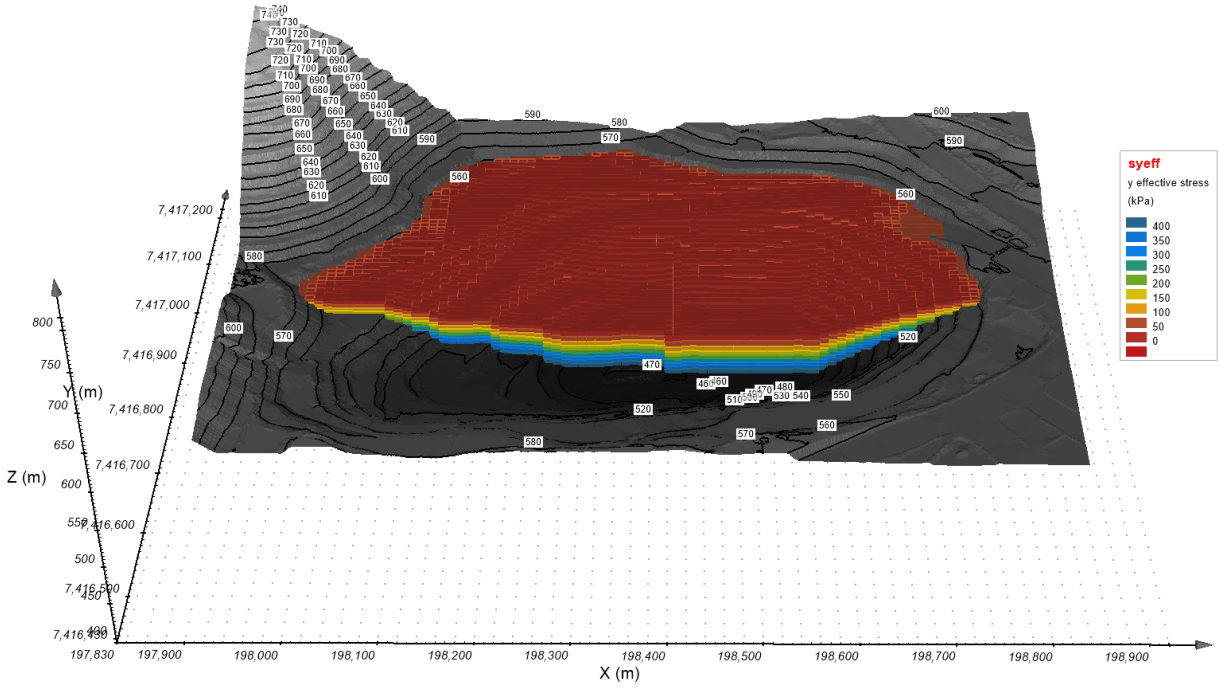


Figure B6: At total settlement – effective stress profile

Enhancing Data Management and Analysis for Mine Waste and Tailings Dam Design through Modern Data-Analytics Dashboards

Ela Talebi, Stantec, USA
Fariba Yavari, Canada
Kris Hojka, Worley Consulting Ltd, Canada

Abstract

In mine waste and tailings dam design and risk management, the mining industry has relied on traditional spreadsheet software for compiling essential data sets from field investigations, laboratory results, instrumentation, and sensor readings. While spreadsheets have been a staple due to their widespread availability and fundamental analytical capabilities, their usage has significant drawbacks and limitations. For large projects, the static nature of spreadsheets makes them inefficient for dynamic data management and highly prone to data loss and corruption. Additionally, these isolated data silos make it exceedingly difficult to perform comparative analyses against other data sources. Analyzing data within these limitations often leads to errors and challenges in correlating with historical data. This may result in a fragmented understanding of foundation conditions, leading to not well-informed decisions in tailings dam designs and their risk management.

In response to these challenges, we propose an innovative workflow that leverages the advanced capabilities of Power BI. This methodology enables a comprehensive representation of data in 2D and 3D formats, integrating information from diverse sources for multi-faceted analysis. The seamless real-time interoperability between data and visualization tools ensures continuous support throughout the project's life cycle. We provide practical examples to address visualization limitations for geotechnical engineers, and demonstrate how this technology enables a more informed and flexible response to design and risk management challenges. This improvement marks a significant enhancement in efficiency for all phases of tailings and mine waste projects, from inception to closure.

Introduction

In the field of mining waste and tailings dams design, the importance of robust data processing cannot be overstated. Traditionally, the mining industry relies on critical data sets derived from field surveys and

investigations, laboratory results, and monitoring data. However, the limitations inherent in traditional spreadsheets, such as their static nature, susceptibility to errors, and potential for data loss, impede comprehensive data management. These shortcomings pose significant challenges in addressing environmental concerns, assessing the risks of dam failure, and ensuring the long-term safety of mining operations.

Monitoring data plays a crucial role in this context, as it provides real-time insights into the behavior and performance of tailings dams. Effective monitoring can detect early signs of instability, such as changes in pore pressure, seepage, or structural deformation, allowing for timely interventions that mitigate risks. However, the vast amount of monitoring data generated can be difficult to manage and interpret using traditional methods, further complicating the ability to respond to potential issues quickly.

To overcome these obstacles, we advocate for using advanced data analysis and visualization tools, such as Power BI. Power BI's capabilities enable the integration of diverse data sources, allowing for dynamic and comprehensive analyses that surpass the static constraints of traditional spreadsheets. This innovative approach enhances decision-making processes, improves risk management strategies, and provides a deeper understanding of geotechnical and environmental conditions. By leveraging Power BI, stakeholders can gain real-time insights and a more nuanced understanding of the data, leading to more informed and proactive management of tailings dams.

Through practical examples and demonstrations, we aim to showcase the transformative potential of this method in enhancing tailings dam design and risk management practices. The integration of advanced data analytics and visualization not only streamlines data management but also fosters a culture of continuous improvement and proactive risk mitigation. By adopting these technologies, the mining industry can significantly enhance its ability to address environmental challenges, improve the safety of tailings dams, and protect both human lives and the environment.

Empowering mining projects with advanced data insights: the role of Power BI

In the field of large-scale data analysis, particularly in mining projects that deal with significant data sets, Power BI stands out as a pivotal tool for effective data exploration and decision making. Unlike Excel, which often struggles with the volume and complexity of data, Power BI excels in managing large datasets seamlessly. Modern dashboards' powerful data modeling capabilities enable the efficient storage and retrieval of various data types, ensuring that mining professionals can access and analyze critical information quickly and accurately. In addition, Power BI's dynamic visualization features enable users to create interactive dashboards and reports that provide deep insights into geological surveys, designs, and production metrics and operational efficiency.

Using Power BI's coding capabilities and advanced processing power, mining engineers can overcome the limitations of traditional spreadsheet applications and empower them to make informed decisions based on comprehensive data analysis. Additionally, Power BI's ability to create dynamic groups and hierarchies is crucial for data lifecycle analysis. In mining projects characterized by extensive data sets including investigation stages, tests, designs, and resource extraction and management, the ability to segment and visualize data dynamically is vital.

To understand operational trends and identify potential efficiencies, it facilitates this task by allowing users to define and modify dynamic groups, adapting to evolving landscapes and project requirements, from correlations and patterns that may influence decision-making processes. Using integrated data search and transformation tools, design flows can be more accurate and reduce risks associated with data management, thereby optimizing project outcomes, and ensuring sustainable resource management practices.

The role of geotechnical investigations in tailings dam design

The design of tailings dams has become critically important due to the increasing frequency of tailings dam failures, which pose severe risks to human life and cause significant environmental damage. Such incidents highlight the necessity for geotechnical engineers to meticulously attend to design details and implement rigorous safety controls. Ensuring the structural integrity and safety of tailings dams requires a comprehensive approach rooted in precise geotechnical investigations and comprehensive data processing and interpretation.

Comprehensive and detailed geotechnical investigations are essential for the design, and stability assessment of tailings dams. This process involves several key activities: drilling boreholes to obtain soil and rock samples, conducting geological profiling to understand the subsurface conditions, performing various geotechnical tests to determine material properties, and analyzing large volumes of data collected throughout different project stages. These steps are crucial for identifying vulnerable sections, potential failure modes and designing dams that can withstand both expected and extreme loading conditions.

Moreover, the data obtained from these investigations inform critical design decisions, such as selecting appropriate construction materials, determining dam geometry, and designing effective drainage and reinforcement systems. Continuous monitoring and assessment throughout the lifecycle of the dam, from construction through operation to closure, are also imperative to detect and address any emerging issues promptly. By adhering to these detailed and data-driven approaches, geotechnical engineers can significantly enhance the safety and reliability of tailings dams. Geotechnical testing is essential for ensuring the stability and safety of structures like tailings dams, encompassing a wide range of assessments on soil, rock, groundwater, and other geologic materials. In-situ soil testing methods will determine the soil strength, compactness, and consistency. Laboratory soil tests focus on parameters such as grain size

distribution, Atterberg limits, moisture content, and additional special loading tests to evaluate soil behavior under various loading conditions. These tests are crucial for predicting how soil will behave under various load conditions and environmental factors, ensuring stable foundations for tailings dams (Das, 2021).

Rock testing determines the strength and durability of rock materials, which are critical for the integrity of dam foundations and structural supports. Important parameters include compressive strength, tensile strength, and durability assessments. These parameters measured by various tests provide insights into the mechanical behavior of rock masses, ensuring they can support the construction and long-term stability of tailings dams.

Spoils permeability and pore pressure testing is used to understand seepage characteristics and potential liquefaction hazards. This information is vital for designing effective drainage systems and control of water pressures within the dam. By integrating the results of soil, rock, and groundwater tests, engineers can make informed design decisions, ensuring that tailings dams are robust, stable, and capable of withstanding both normal and extreme conditions, thereby minimizing the risk of catastrophic failures.

In addition, geotechnical research starts to use advanced methods of data analysis, including artificial intelligence algorithms and numerical simulations (Gao, 2024). These technologies enhance decision making by providing more accurate predictions of dam behavior under various loading conditions and environmental scenarios. Integrating this geotechnical research will ensure that tailings dams are designed with greater robustness, and reliability, reducing risks, and protecting human communities and natural ecosystems.

Integrating monitoring techniques with Power BI

In the field of mining waste and tailings dams design, the importance of robust data processing cannot be overstated. Traditionally, the mining industry relies on critical data sets derived from field surveys and investigations, laboratory results, and monitoring data. However, the limitations inherent in traditional spreadsheets, such as their static nature, susceptibility to errors, and potential for data loss, impede comprehensive data management. These shortcomings pose significant challenges in addressing environmental concerns, assessing the risks of dam failure, and ensuring the long-term safety of mining operations.

Monitoring is a vital component of tailings dam management, providing essential data on the dam's structural integrity and environmental impact. Common monitoring techniques include in-situ instrumentation, such as piezometers for measuring pore pressure, inclinometers for detecting slope movement, and seepage monitoring systems. Remote sensing technologies, like satellite imagery and drone surveys, are also used to monitor surface deformations and water levels. These techniques generate vast

amounts of data that are crucial for assessing the real-time condition of tailings dams and can send real time alarm, warning messages, in the event TARPs (Trigger Action Response Plan) levels are triggered.

To maximize the effectiveness of these monitoring techniques, the data they generate can be integrated into Power BI dashboards. Power BI offers a platform for real-time data visualization, enabling engineers and decision-makers to monitor the status of tailings dams continuously. By connecting monitoring instruments directly to Power BI, data such as pore pressure readings, slope stability metrics, and seepage rates can be displayed on interactive dashboards. These dashboards allow for the visualization of trends over time, alert generation when critical thresholds (TARPs) are exceeded, and the ability to perform predictive analytics. This integration empowers stakeholders to respond swiftly to emerging risks, improving safety and reducing the likelihood of catastrophic failures.

The real-time monitoring capabilities provided by integrating monitoring data with Power BI offer significant advantages. They enable proactive management by facilitating early issue detection, thus preventing them from developing into larger problems. The ability to visualize all relevant data in one platform enhances decision-making and provides a comprehensive understanding of the tailings dam's condition. This approach not only improves safety but also supports compliance with regulatory requirements and fosters a culture of continuous monitoring and improvement.

Through practical examples and demonstrations, we aim to display the transformative potential of this method in enhancing tailings dam design and risk management practices. The integration of advanced data analytics, visualization, and monitoring not only streamlines data management but also fosters a culture of continuous improvement and proactive risk mitigation. By adopting these technologies, the mining industry can significantly enhance its ability to address environmental challenges, improve the safety of tailings dams, and protect both human lives and the environment.

Ultimately, adoption of these innovations will lead to more flexible and safer tailings dam management practices, ensuring long-term sustainability and operational excellence.

Case study

A Power BI dashboard has been meticulously developed for a tailing dam geotechnical investigation project, serving as a robust tool for data analysis and visualization. This comprehensive dashboard comprises multiple pages, each dedicated to different aspects of the investigation, featuring a variety of visualizations and statistical analyses designed to present data in an intuitive and accessible manner.

The dashboard provides in-depth information on lithology, presenting intervals and classifications of different geological formations encountered during the investigation. Users can view detailed descriptions of the lithology, including rock and soil classifications, which are essential for understanding the

composition and characteristics of the subsurface materials. The location of each borehole is precisely mapped, allowing users to correlate geological data with specific geographical points.

Figure 1 exemplifies one of the pages of the report, highlighting the intricate details of lithology. This page includes rock and soil classifications along with comprehensive test results. It allows geotechnical engineers and project stakeholders to examine the properties and behaviors of various geological materials encountered.

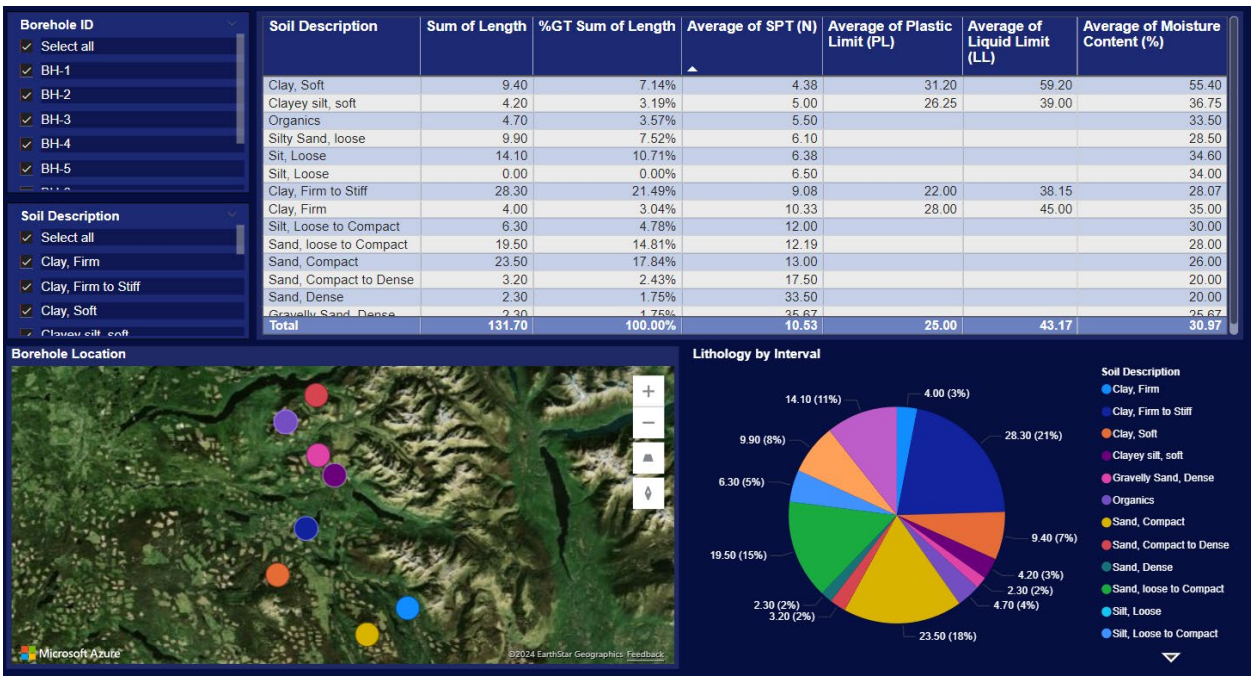


Figure 1: Detailed and dynamic lithology analysis of boreholes

The dashboard is equipped with advanced filtering capabilities, enabling users to apply various criteria and parameters to their analysis. Filters such as location, lithology, and borehole ID allow users to customize their view and focus on specific data subsets. This interactivity makes the dashboard a dynamic tool, facilitating tailored analysis and quick data retrieval based on user-defined parameters.

Figure 2 presents a borehole log, offering a thorough examination of the lithology throughout the borehole depths. This includes Standard Penetration Test (SPT) results, moisture content measurements, liquid limit, and plastic limit results. These logs are essential for understanding the mechanical properties of the soil and rock layers, which are crucial for assessing the stability and integrity of the tailing dam.

Figure 3 features an advanced 3D visualization of borehole logs, providing a spatial representation of the lithology layers across multiple boreholes. This three-dimensional perspective enables users to grasp the spatial relationships and orientations of different geological layers, enhancing their understanding of the subsurface profile. It aids in identifying weak spots, patterns, and correlations between boreholes, which can be critical for designing and implementing geotechnical solutions.

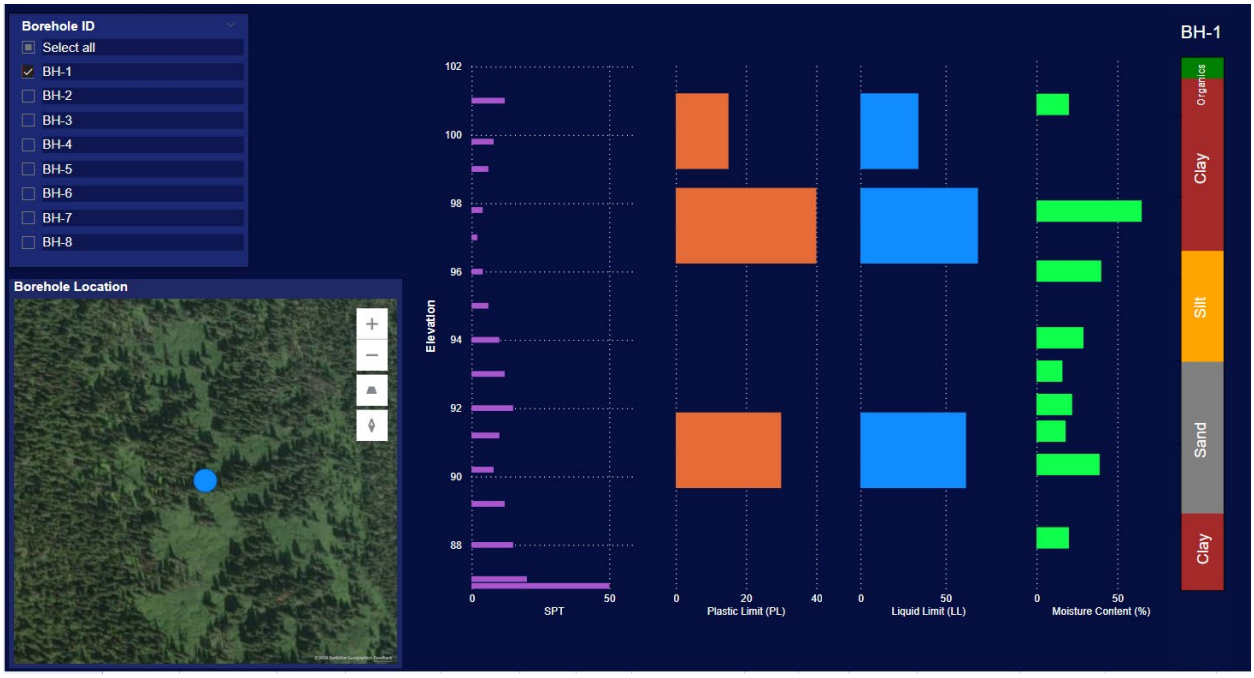


Figure 2: Detailed and dynamic analysis of borehole logs

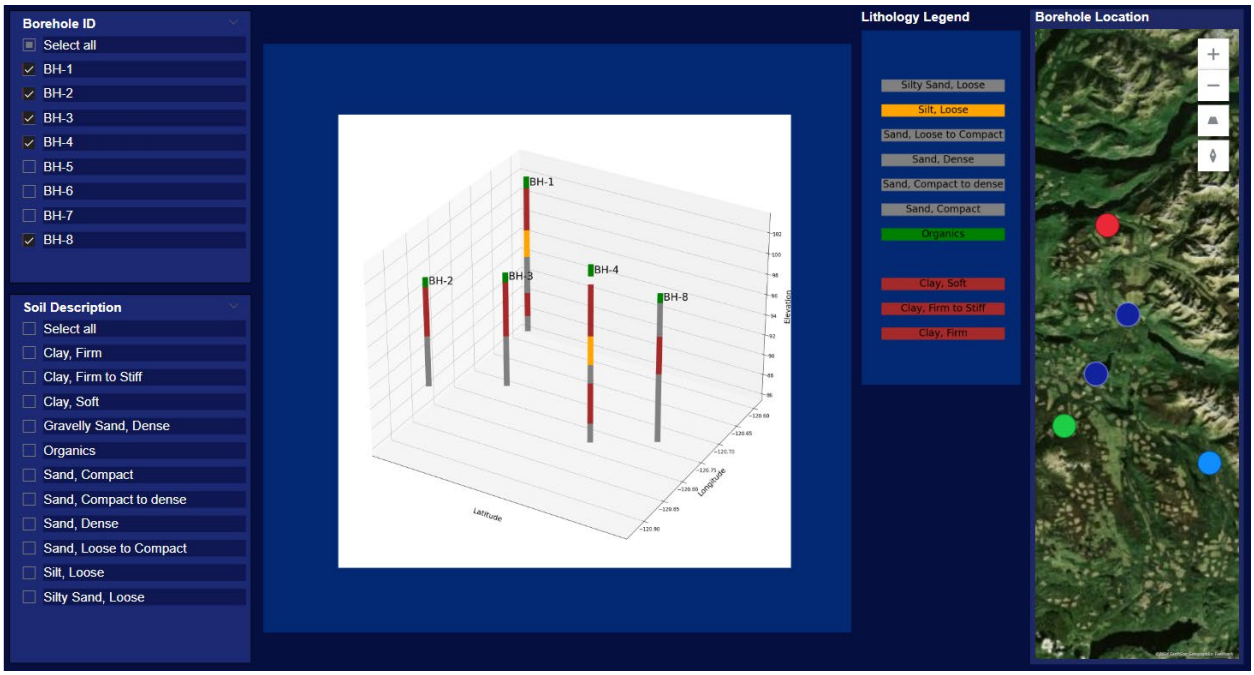


Figure 3: Detailed and dynamic 3D analysis borehole log

This Power BI dashboard features several advanced analytical tools:

- Trend analysis: Users can track changes in geological properties and test results over time or across different boreholes, enabling the identification of trends and anomalies.

- Comparative analysis: The dashboard allows for side-by-side comparisons of different boreholes or lithology layers, providing a more comprehensive understanding of the data, and
- Predictive modeling: Integrating predictive models can help forecast geological behaviors and identify potential risks associated with the tailing dam.

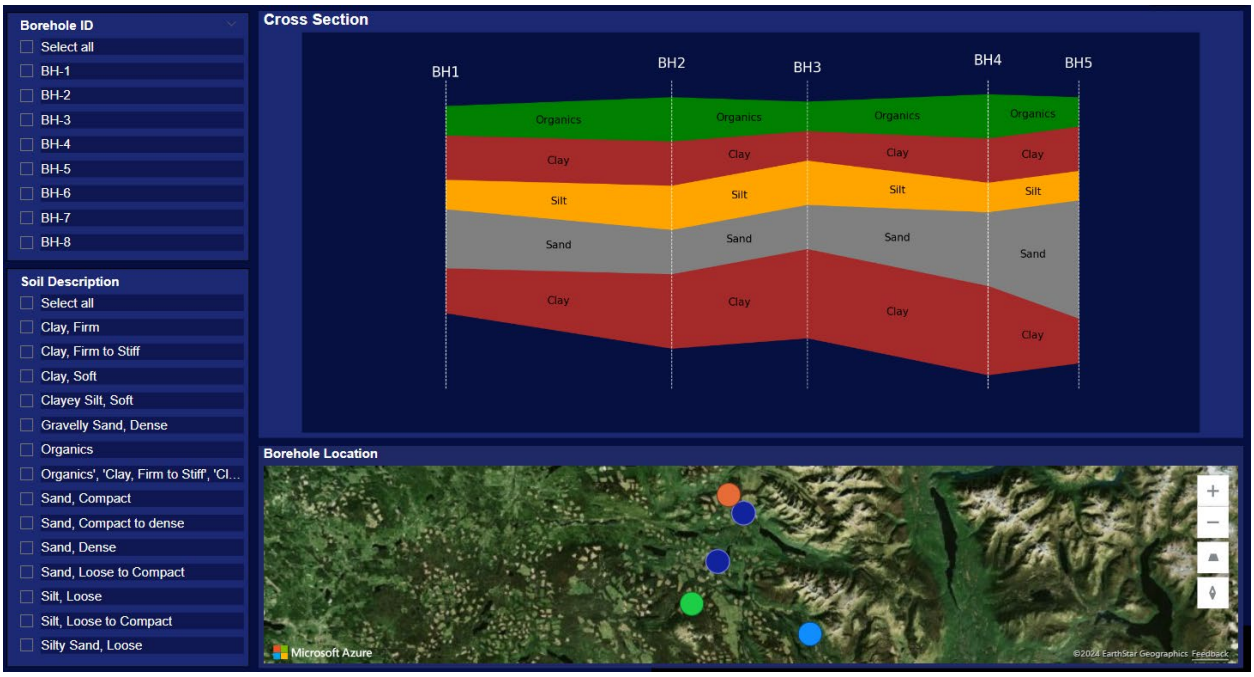


Figure 4: Cross-section of the borehole logs

In Figure 4, the geotechnical cross-sections developed in Power BI for the tailing dam design provides a comprehensive visualization of the subsurface conditions, enhancing the analysis and interpretation of geotechnical data. By plotting borehole data along a cross-section line, this tool allows for an in-depth examination of the spatial distribution and continuity of various soil layers between boreholes. The vertical lines marking each borehole location, combined with the color-coded soil layers, create a clear and intuitive representation of the subsurface profile. This detailed visualization is essential for identifying the characteristics and extent of different soil and rock formations, aiding in the design and construction of a stable tailing dam.

Furthermore, the dynamic and interactive capabilities of Power BI enhance the usability of the geotechnical cross-section. Users can filter and adjust the displayed data based on specific criteria such as borehole locations, soil types, and depth intervals, providing a tailored view of the geotechnical information relevant to their needs. This interactivity, combined with the ability to annotate and highlight key features, ensures that engineers and decision-makers can quickly and accurately assess the conditions at the tailing dam site. This tool supports more informed decision-making, contributing to the effective planning, design, and implementation of tailing dam projects.

During the presentation of this paper at the conference, we will explore how video dynamic charts improve analytical capabilities, such that these analyses lead to a broader and more accurate understanding of geotechnical information compared to traditional formats. Data storage is similar to Excel spreadsheets. This approach facilitates easy identification of missing or anomalous data and ensures comprehensive data coverage for improved design results and more reliable results.

Enhanced geotechnical data analysis for tailings dam design: mitigating liquefaction risks

Liquefaction assessment is one of the most important steps in tailings dam design and its stability assessment. Tailings dams are designed to contain safely tailings from mining processes, and their sustainability is highly dependent on accurate geotechnical analyses, including liquefaction assessment.

Liquefaction is a phenomenon in which saturated soil loses its strength and stiffness under cyclic loading such as earthquake or rapid loading during static conditions. In the field of tailings dam design, liquefaction potential evaluations are crucial to understand how dam materials behave in seismic conditions. This analysis includes a detailed evaluation of factors such as soil properties, seismic hazard levels, and dam geometry (Idriss and Boulanger, 1982).

Advanced tools like Power BI are increasingly used in these analyses due to their ability to manage large data sets and perform complex calculations efficiently. By leveraging Power BI's analytical capabilities, engineers can achieve more reliable results and more precise design adjustments. These tools enable comprehensive data analysis, including the identification of anomalies or missing data points, which are critical for sensitivity analysis and simulation of liquefaction scenarios.

The importance of data analysis in geotechnical investigations of tailings dams cannot be ignored. Accurate data analysis enables engineers to assess potential liquefaction hazards more comprehensively, thereby informing design decisions that enhance the long-term safety and sustainability of these critical structures. By integrating detailed geotechnical data analysis into the design process, it is possible to reduce the risks of missing data gaps and make more accurate interpretation of data, aiding in detection of most vulnerable zones susceptible to liquefaction.

Conclusion

A comprehensive review and comparison of traditional tailings dam design systems, including conventional geotechnical analyses and traditional databases such as Excel, reveals inherent limitations and challenges. These traditional methods often struggle with managing large volumes of data and may miss important insights due to their manual and less adaptive nature. In contrast, advances in artificial intelligence (AI) and machine learning (ML) present promising alternatives for enhancing data analysis capabilities in tailings

dam design. AI and ML algorithms can efficiently process enormous amounts of geotechnical data and identify patterns and anomalies that may not be easily visible through traditional methods. This capability enables engineers to perform more thorough sensitivity liquefaction assessments and optimize dam design to reduce risks associated with seismic events and other potential hazards.

Furthermore, the integration of AI and ML into geotechnical engineering practices promotes iterative improvements in design methods and ensures that tailings dams are not only safer, but also more resilient throughout their operational lifetimes. Using these technologies, mining companies can achieve stronger and more reliable designs for tailings dams, thereby increasing environmental sustainability and safety standards in mining operations. Continued research and implementation of AI and ML in geotechnical engineering promises more innovation and efficiency in tailings dam design, and the setting of new standards for safety and reliability in the mining industry.

The proposed methods of AI and ML play a key role in data analysis and graphs of geotechnical results, but the noteworthy point is that the experience of engineers plays a significant role in design, and a qualified, experienced engineer should be making final interpretations of geotechnical information and decisions.

References

Das, Braja M. 2021. *Principles of Geotechnical Engineering, SI Edition*. 10th edition. Cengage.

Gao, W. 2024. The application of machine learning in geotechnical engineering. *Appl. Sci.* 14(11): 4712. Accessed at https://doi.org/10.3390/app14114712

Idriss, I.M. and Boulanger, R.W. 1982. *Soil Liquefaction during Earthquakes*. Earthquake Engineering Research Institute.

PLAXIS and CASM: Formulation, Implementation, and Verification

Erick Rógenes, DF+ Engineering/University of Brasília/Bucknell University, Brazil
Ian Paes, DF+ Engineering/Pontifical Catholic University of Rio de Janeiro, Brazil
Bruno Guimarães Delgado, Vale S.A., Brazil
Alessandra Gomes, DF+ Engineering/Bucknell University, Brazil
Daniel Rocha Lanzieri, DF+ Engineering, Brazil
Felipe Cruz, DF+ Engineering/State University of Rio de Janeiro, Brazil
Alomir Fávero Neto, Bucknell University, USA
Leandro Lima Rasmussen, University of Brasília, Brazil

Abstract

The current state of practice in liquefaction studies involves analyzing this phenomenon through numerical models. In these simulations, it is often necessary to use constitutive models capable of capturing nonlinear behavior, pore pressure generation, and strength loss. The Clay and Sand Model (CASM) is one such model that can represent all these phenomena. CASM has the advantage of being applicable to both fine and granular materials, ranging from ductile to brittle behavior, and is based on a robust formulation that incorporates critical state concepts. CASM is not yet available in commercial codes, thus its application is not yet common practice. However, its potential has been confirmed through retro-analyses of recent tailings dam failure cases, such as the Brumadinho Dam collapse. In this work, we discuss CASM's formulation and present its implementation in the commercial finite element software Plaxis using its user-defined soil models functionality. The implementation is then verified through a series of numerical tests and a parametric analysis is conducted to evaluate the model's response to different input parameters. Results show that CASM is able to model important critical state mechanisms in both fine- and coarse-grained soils, such as volumetric changes, and showcase its potential for application in complex geomechanics problems, such as tailings dam failures.

Introduction

Granular and transitional soils, such as sand or silty soils, tend to contract when loosely packed and subjected to shearing. When these loose soils are saturated and rapidly loaded, their contractive tendency generates excess pore water pressures, leading the soil to behave in an undrained fashion. This process

decreases effective stress, and consequently, the soil particles lose contact with each other, reducing the soil's strength and stiffness, and causing it to behave like a fluid. This phenomenon is known as static liquefaction (Jefferies and Been, 2016).

Tailing dams constructed using the upstream method are found to be more vulnerable to failure and highly susceptible to static liquefaction (Piciullo et al., 2022). The geotechnical community has placed significant focus on the failure of upstream raised tailings dams due to static liquefaction, driven by recent incidents such as the Fundão collapse in 2015 (Morgenstern et al., 2016), the Cadia failure in 2018 (Jefferies et al., 2019), and the Brumadinho tragedy in 2019 (Arroyo and Gens, 2021), Figure 1.



Figure 1: Brumadinho tailings dam collapse snapshots

Tailings dam failures result in significant economic and environmental harm, so in order to better understand the safety and behavior of such structures, the use of numerical modeling to address the onset of flow liquefaction is increasing (Jefferies and Been, 2016). Therefore, these numerical models demand constitutive models capable of simulating the liquefaction phenomenon.

In this context, this paper addresses the constitutive model known as the Clay and Sand Model (CASM), which was first proposed by Yu (1998), and recently modified by Mánica et al. (2021). CASM was developed to represent the behavior of both sands and clays, so it is a good candidate for modeling the behavior of tailings, which encompass a wide range of grain sizes. This constitutive model has been used to retro-analyze historical tailings dam liquefaction cases, such as the Merriespruit Dam (Mánica et al., 2021) and the Brumadinho Dam (Arroyo and Gens, 2021). However, it is not currently available in commercial software, and its implementation requires a custom process.

Hence, this paper presents the CASM formulation and its implementation using an explicit integration scheme as a user-defined model in Plaxis (Brinkgreve et al. 2020). It includes a procedure to validate the implementation, along with additional parametric analyses based on a series of numerical laboratory tests. Validation results demonstrate the consistency and robustness of the formulation proposed, and the procedure described will serve as a methodology to validate future implementations.

Formulation

A description of CASM's formulation is provided in this section. For standardization purposes, the equations are written in terms of the Cambridge invariants: mean effective stress (p'), Von Mises deviatoric stress (q), and Lode angle (θ) (Wood, 2004). The parameters and main equations of the CASM model are presented in Tables 1 and 2, respectively.

Table 1: Parameters of the CASM model

Component	Parameters	
Critical State Line - CSL	Γ	CSL void ratio (e) at p' = 1 kPa, in e-ln(p') plane;
	λ	slope of CSL in e-ln(p') plane;
	M_{TC}	slope of CSL in q-p' space for triaxial compression condition;
Elasticity	ν	Poisson ratio
	κ	slope of elastic line in a e-ln(p') space
Plasticity	n	Parameter that controls the yield function shape;
	r	spacing ratio;
	m	Parameter that controls the plastic potential shape;
State	$OCR = p'_0 / p'$	over-consolidation ratio;

Table 2: Main equations of the CASM model

Component	Equation		
CSL in e x *ln* p′ plane	$e = \Gamma - \lambda \, lnp'$		Equation 1
Slope of CSL in q x p′ plane	$M_\theta = M_{TC} \left(\frac{2\,\alpha^4}{1+\alpha^4+(1-\alpha^4)\,sen3\theta}\right)^{1/4}$;	$\alpha = \frac{3}{3 + M_{TC}}$	Equation 2
Yield function	$f = \left(\frac{q}{M_\theta p'}\right)^n + \frac{1}{\ln r} \ln\left(\frac{p'}{p'_0}\right)$		Equation 3
Hardening rule	$\frac{\partial p'_0}{\partial \varepsilon_p^p} = \frac{(1+e)\,p'_0}{\lambda - \kappa}$		Equation 4
Plastic Potential	$g = \left(\frac{q}{M_\theta p'}\right)^m + \mathrm{m} - 1 - \frac{p_c\,(m-1)}{p'}$;	$p_c = \frac{p}{m-1}\left[\left(\frac{q}{M_\theta p'}\right)^m - 1\right]$	Equation 5
Elasticity	$K = \frac{(1+e)\,p'}{k}$		Equation 6

CASM is based on critical state theory and adopts an approach similar to the Cam-Clay constitutive model (Wood, 1990). It postulates a linear relationship for the critical state line in the *e* (void ratio)- *ln(p')* plane (Equation 1), with consolidation lines assumed to run parallel to the CSL.

In contrast to the Cam-Clay model, CASM replaces the normal consolidation line with the reference compression line, representing the loosest state the material might experience. According to Yu (1998), this change was made because the normal compression line of sands, unlike clays, is only reached under high stresses, uncommon in engineering problems. The position of the reference consolidation line in CASM is determined by the spatial ratio (*r*, refer to Table 1), a parameter used to measure the distance between the critical state line and the reference line.

The slightly modified version of CASM proposed by Mánica et al. (2021) is employed in this work. Mánica et al. (2021) modified the original version proposed by Yu (1998) by integrating the effect of the intermediate principal stress, captured by the change in Lode's angle on the CSL, in the *p'-q* plane. In order to account for Lode's angle changes, the authors applied the relationship presented in Equation 2, proposed by Sheng et al. (2000).

The yield function adopted in the model is presented in Equation 3, where the elastic domain is controlled by the pre-consolidation stress (p'_0). On the other hand, the hardening law (Equation 4) is based on plastic volumetric strain, similar to the Cam-Clay model.

The plastic potential function adopted by Mánica et al. (2021) was also modified from the original formulation by Yu (1998). The plastic potential employed is presented in Equation 5, where p_c must be solved for the current stress state. Notably, the plastic potential function exhibits a distinct form from the yield surface. Consequently, the CASM model incorporates non-associated flow. The parameter *m* offers flexibility in adjusting the model's response along oedometric paths, ensuring that the coefficient of at-rest lateral earth pressure (K_0) remains constant at a specified value, unaffected by plastic strains.

Finally, the elastic behavior in the CASM model is defined by constant Poisson ratio (ν), and by the bulk modulus (K). The bulk modulus is related to the slope of the unloading line (κ) and also varies with stress level and void ratio, as depicted in Equation 6.

Implementation

CASM was implemented in the finite element software Plaxis, which allows for the incorporation of new constitutive models through its "User Defined Soil Model" functionality. To integrate a user-defined constitutive model into the software, the code, written in Fortran, must be compiled into a Dynamic-link library (DLL) file and added to the program's directories.

The constitutive model will be invoked at each Gauss point, and Plaxis will provide preliminary information such as stress state, pore pressures, and state variables, along with strain increments as input

data to the user-defined script. The constitutive model will then compute stress increments according to the defined formulation, and, subsequently, Plaxis will solve the equilibrium equations using the finite element method and will pass new strains back to the constitutive model. This cycle repeats until convergence is achieved.

To make the DLL functional within the main Plaxis program, it is necessary to develop a code that communicates with specific subroutines:

1. Initialization of state variables: At this stage, initial values of user-supplied properties and state variables are defined.
2. Integration of constitutive relations: During these steps, calculations are performed to determine new stresses based on strain increments.
3. Creation of the elastoplastic stiffness matrix: This involves creating the matrix that describes the relationship between stresses and strains for elastoplastic material behavior.
4. Creation of the elastic stiffness matrix: Here, the matrix describing the relationship between stresses and strains for purely elastic material behavior is created.

The main code of the constitutive model implementation involves integrating the constitutive relations. During the integration process, an elastic prediction is first made. If it is determined that the new stress state lies outside the yield surface, a plastic correction is performed, which is necessary to ensure consistency. The generalized elastoplastic constitutive relation is presented in Equations 7 and 8.

$$\begin{Bmatrix} dp' \\ dq \end{Bmatrix} = [D] \begin{Bmatrix} d\varepsilon_p \\ d\varepsilon_q \end{Bmatrix} \quad \text{Equation 7}$$

$$[D]^{-1} = \left\{ \begin{bmatrix} {}^{1}/_{K} & 0 \\ 0 & {}^{1}/_{3G} \end{bmatrix} - \frac{1}{\frac{\partial f}{\partial s}\left(\frac{\partial s}{\partial h}\frac{\partial g}{\partial p'} + \frac{\partial s}{\partial h}\frac{\partial g}{\partial q}\right)} \begin{bmatrix} \frac{\partial f}{\partial p'}\frac{\partial g}{\partial p'} & \frac{\partial f}{\partial q}\frac{\partial g}{\partial p'} \\ \frac{\partial f}{\partial p'}\frac{\partial g}{\partial q} & \frac{\partial f}{\partial q}\frac{\partial g}{\partial q} \end{bmatrix} \right\} \quad \text{Equation 8}$$

where $d\varepsilon$ is the strain increment, with subscripts q and p representing the shear and volumetric components, respectively; *[D]* is the elastoplastic stiffness matrix; s is the hardening parameter controlling the elastic domain variation; and h is the plastic strain parameter related to s, i.e., $ds = f(dh)$.

In the CASM, the hardening parameter controlling the variation of the elastic domain is the pre-consolidation stress p_0, thus $s = p_0$. Since hardening is governed by volumetric plastic deformations, $h = \varepsilon_{vp}$. Considering that the yield function and the plastic potential function adopted in CASM are given by

Equations 3 and 5, respectively, and that the hardening law is defined by Equation 4, the following derivatives can be defined as presented in Equations 9 to 14.

$$\frac{\partial f}{\partial p'} = \left(\frac{q}{M_\theta}\right)^n \left(\frac{-n}{p'^{n+1}}\right) + \frac{1}{p' \ln r} \quad \text{Equation 9}$$

$$\frac{\partial f}{\partial q} = \left(\frac{1}{M_\theta p'}\right)^n (nq^{n-1}) \quad \text{Equation 10}$$

$$\frac{\partial g}{\partial p'} = \left(\frac{q}{M_\theta}\right)^m \left(\frac{-m}{p'^{m+1}}\right) + \frac{p' c(m-1)}{p'^2} \quad \text{Equation 11}$$

$$\frac{\partial g}{\partial q} = \left(\frac{1}{M_\theta p'}\right)^m (mq^{m-1}) \quad \text{Equation 12}$$

$$\frac{\partial f}{\partial s} = \frac{\partial f}{\partial p'_o} = \frac{-1}{ln\, r}\left(\frac{1}{p0'}\right) \quad \text{Equation 13}$$

$$\frac{\partial s}{\partial h} = \frac{\partial p'_o}{\partial \varepsilon_v^p} = \frac{(1+e0)p'_o}{\lambda - \kappa} \quad \text{Equation 14}$$

During the plastic correction process, the initial attempt is to apply the entire strain increment to integrate stresses and hardening parameters. To ensure numerical stability in this process, an explicit algorithm of automatic sub-incrementation, proposed by Sloan et al. (2001), has been adopted. If integration fails to meet the specified error level, the strain increment is reduced. This process continues until all strain is applied while respecting the specified error level.

Verification

To validate the numerical implementation of CASM, a series of numerical tests were conducted. The model developed for this stage consists of a sample under axisymmetric conditions with regular geometry, as shown in Figure 2. The parameters used in these simulations are presented in Table 3, which were defined by Arroyo and Gens (2021) to represent the fine tailings of the Brumadinho Dam.

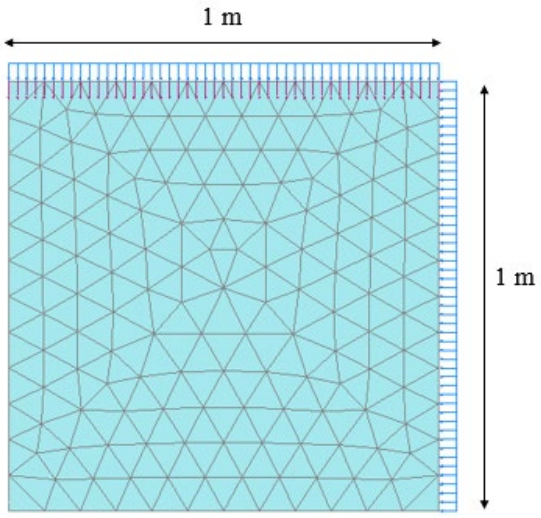


Figure 2: Boundary condition and problem setup used for CASM implementation validation

Table 3: CASM parameters applied in the validation simulations

Critical State Line - CSL		Plasticity		Plasticity and State	
Value					
Γ	1.2	n	5	ν	0.3
λ	0.053	r	35	κ	0.007
M_{tc}	1.4	m	2.3	OCR	1

For a comprehensive validation, numerical drained and undrained triaxial tests were simulated under compression and extension conditions. The results are presented in Figure 3, demonstrating the CASM ability to represent varying strength values depending on the simulated path, the hardening process under drained conditions, and the generation of pore pressures and brittle behavior under undrained conditions.

Isotropic compression and oedometer tests were also conducted. The results are presented in Figure 4a, showing an increase in stiffness with increasing confinement in both tests. It is noteworthy that in the oedometer test, the sample was initially in an isotropic condition and as it was compressed, it approached a constant K_0 value, demonstrating the model's capability to control the coefficient of lateral earth pressure, which is crucial for applications involving staged construction simulations.

An unloading followed by an undrained loading test was conducted, and the result is presented in Figure 4b alongside the results of a numerical test on a normally consolidated sample. It is observed that the model successfully captures the increase in OCR induced by unloading, leading to elastic behavior at the beginning of reloading. Such scenarios are crucial for dam de-characterization involving excavation processes and subsequent unloading.

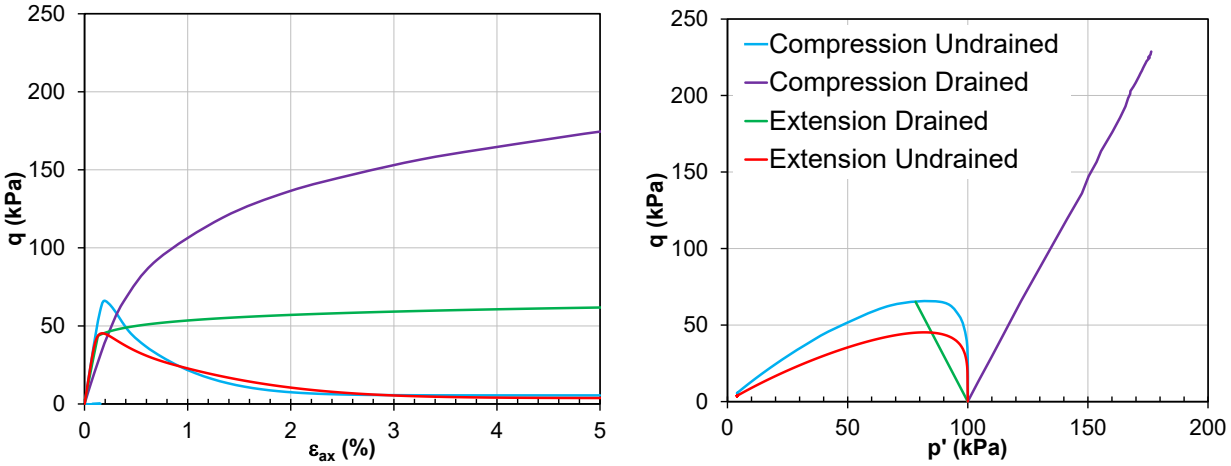


Figure 3: Validation of CASM implementation in conventional triaxial tests

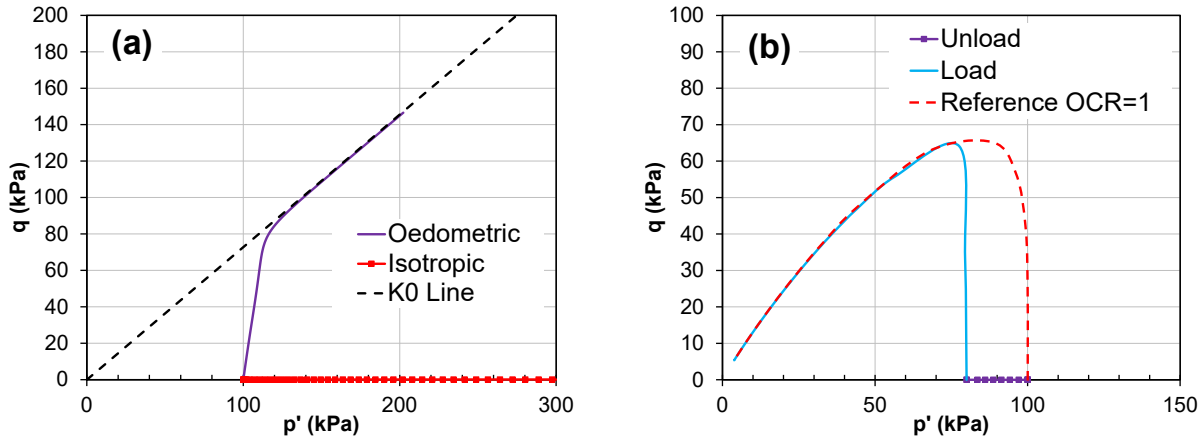


Figure 4: Validation of CASM implementation in: (a) isotropic compression and oedometer paths, and (b) unloading paths followed by undrained recompression

The numerical verification also included partially drained/undrained behavior through hydro-mechanical coupling approaches, where excess pore pressure generation is a function of strain rate, soil stiffness, and permeability. In this simulation, horizontal and vertical hydraulic conductivities of 1.00E-08 m/s and 2.00E-09 m/s, respectively, were applied, as presented by Arroyo and Gens (2021). The results obtained are shown in Figure 5, indicating that CASM can simulate partially drained behavior in triaxial compression tests by adjusting the strain rate, ranging from fully drained to undrained conditions.

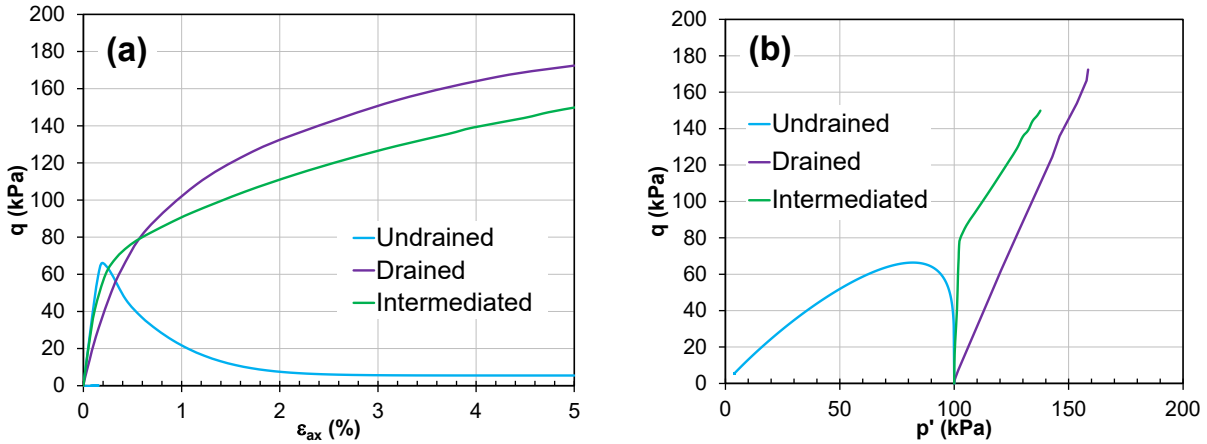


Figure 5: Validation of hydro-mechanically coupled triaxial tests using CASM

Parametric analysis

The main difference between CASM and Cam-Clay models lies in the addition of parameters n, r, and m. For instance, if $n = 2$, $r = 2$, and $m = 2$, CASM simulates behavior similar to that obtained with the Cam-Clay model, as shown in Figure 6 (Cam-Clay model parameters were extracted from Table 3). Therefore, sensitivity analyses focused on the effects of these parameters on the behavior represented in the CASM. These analyses were conducted starting from the parameters listed in Table 3.

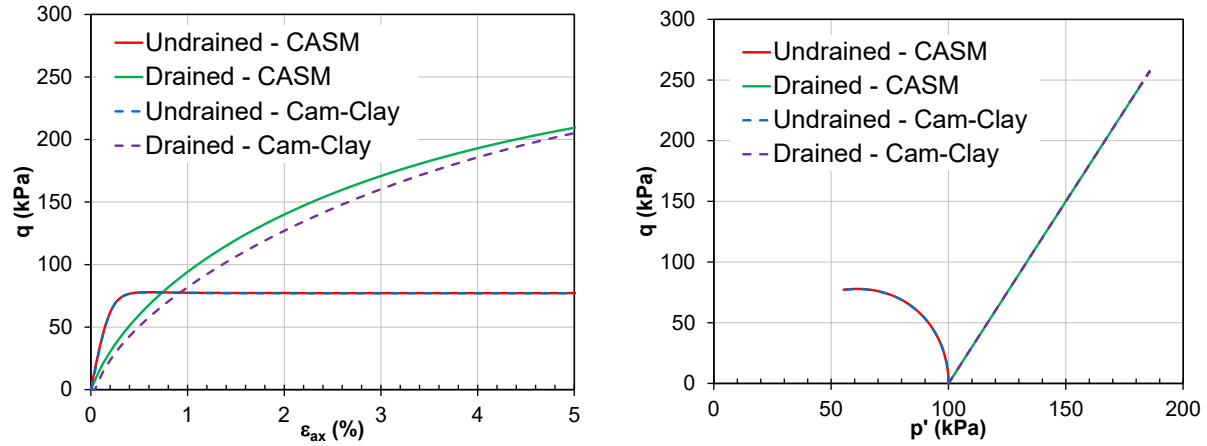


Figure 6: Comparison of triaxial compression test results using the Cam-Clay and CASM models with $r = 2$, $n = 2$, and $m = 2$

Mánica et al. (2021) presented analytically derived equations considering normally consolidated material, which establish relationships between the parameters n and r with peak undrained strengths (S_{up}) and residual strengths (S_{ur}), as shown in Equations 15 and 16. They also established a relationship between the parameters m and K_0, as given by Equation 17.

$$\exp\left[\left(\frac{1}{\sqrt[n]{n\ln r}}\right)^{n}\ln r\right]=\frac{M_{TC}}{2\frac{\sigma'_v}{S_{up}}\sqrt[n]{n\ln r}}\exp\left[\left(\frac{q_{ini}/p'_{ini}}{M_{TC}}\right)^{n}\ln r\right]\exp\left[\frac{\lambda-\kappa}{\kappa}\ln\left(\frac{M_{TC}}{2\frac{\sigma'_v}{S_{up}}\sqrt[n]{n\ln r}}\right)\right] \quad \text{Equation 15}$$

$$r=\left[\frac{M_{TC}}{6}\,(1+2K_0)\left(\frac{\sigma'_{vini}}{S_{ur}}\right)\right]^{\frac{\lambda-\kappa}{\kappa}} \quad \text{Equation 16}$$

$$\frac{3\,(\lambda-\kappa)}{2\,\lambda}=\left[\frac{M_{TC}}{m}-M_{TC}\right]\left[\left(\frac{1}{M_{TC}}\frac{3(1-K_0)}{1+2K_0}\right)-\left(\frac{1}{M_{TC}}\frac{3(1-K_0)}{1+2K_0}\right)^{1-m}\right] \quad \text{Equation 17}$$

where σ_v' is the initial vertical stress, and the subscript "ini" refers to the initial state of the material.

The parameter n modifies the shape of the yield surface, as shown in Figure 7a. It is evident that a higher n expands the elastic domain, thereby increasing the peak undrained strength, as demonstrated by Equation 17 and the parametric analyses depicted in Figure 8a and 8b.

The parameter r also influences the shape of the yield surface, as shown in Figure 8b, but its primary role is to separate the reference compression line from the critical state line. Thus, an increase in the parameter r indirectly promotes an increase in the state parameter, consequently reducing the residual undrained strength, as observed in both Equation 16 and Figure 8c and 8d.

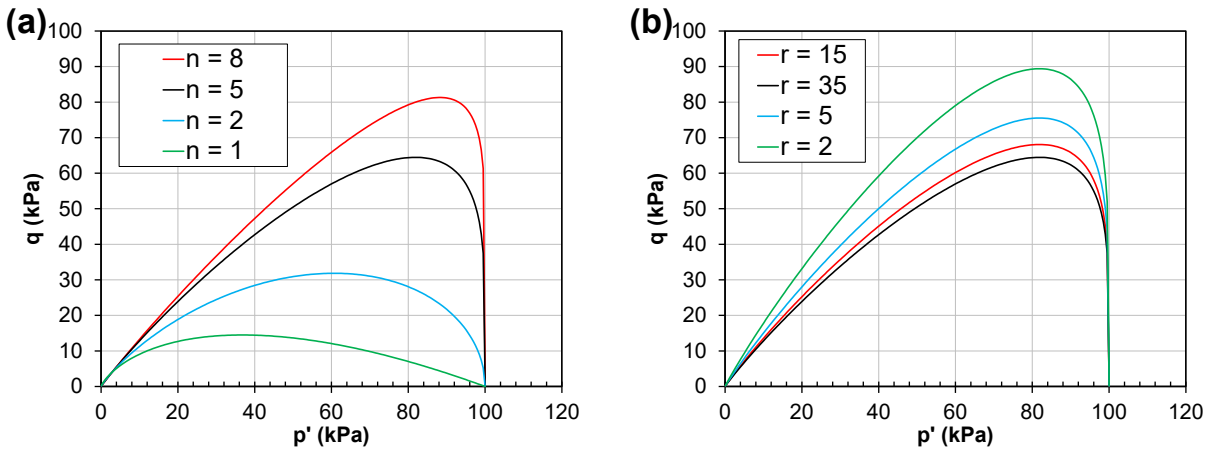


Figure 7: Changes in the yield surface shape due to variations of parameters: (a) n, and (b) r

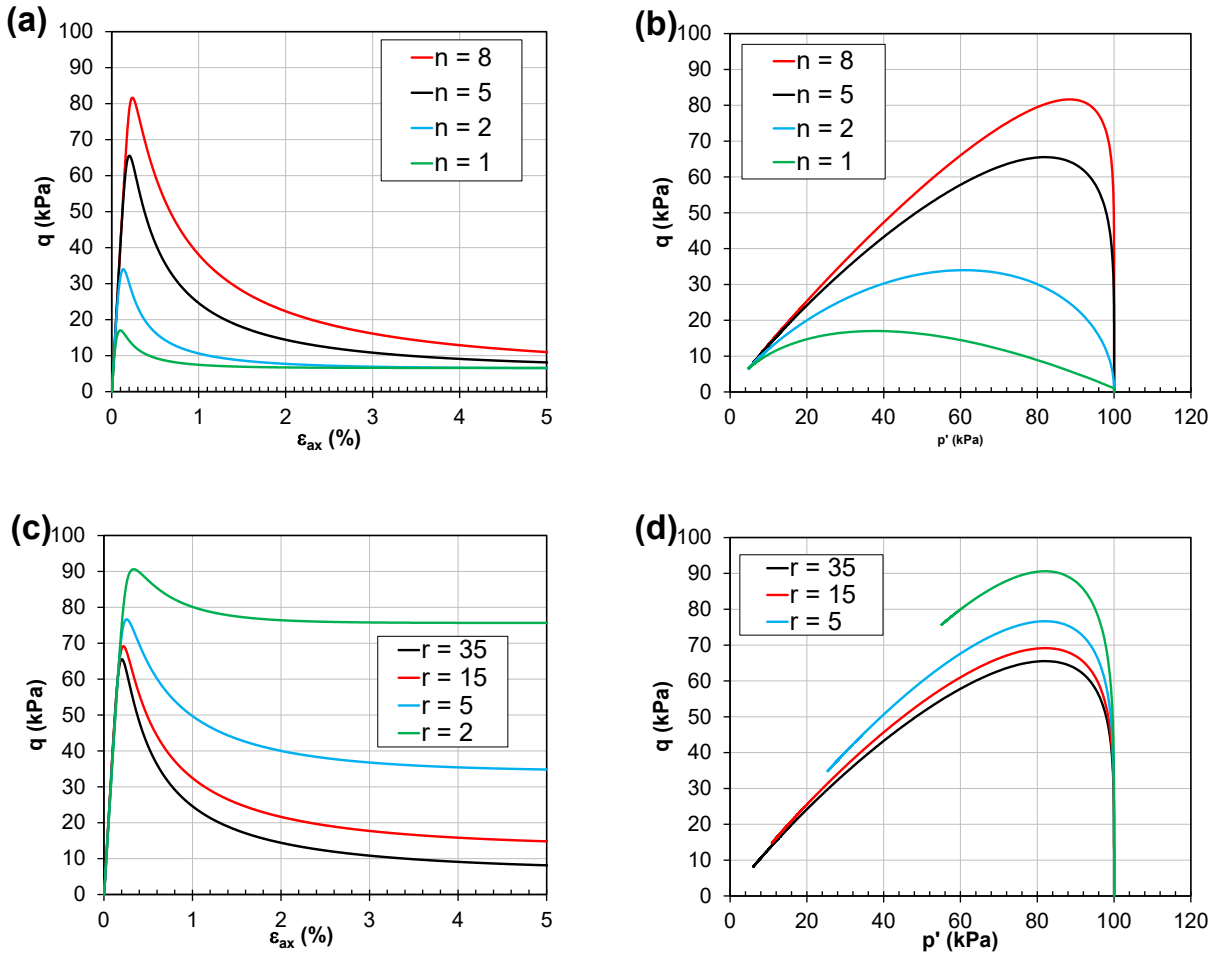


Figure 8: Sensitivity of CASM in undrained triaxial compression tests to variations of parameters: (a) and (b) n, (c) and (d) r

Given the non-associated flow rule adopted in the CASM model, the parameter m solely influences the plastic potential function. Thus, in shear loading conditions, such as in triaxial tests, this parameter affects only the deformations, while stress paths remain unchanged (Figures 9a and 9b). On the other hand, in oedometer compression conditions, m directly controls the value of the coefficient of at-rest lateral earth pressure, i.e., the slope of the K_0 line simulated in the model, as seen in Equation 17.

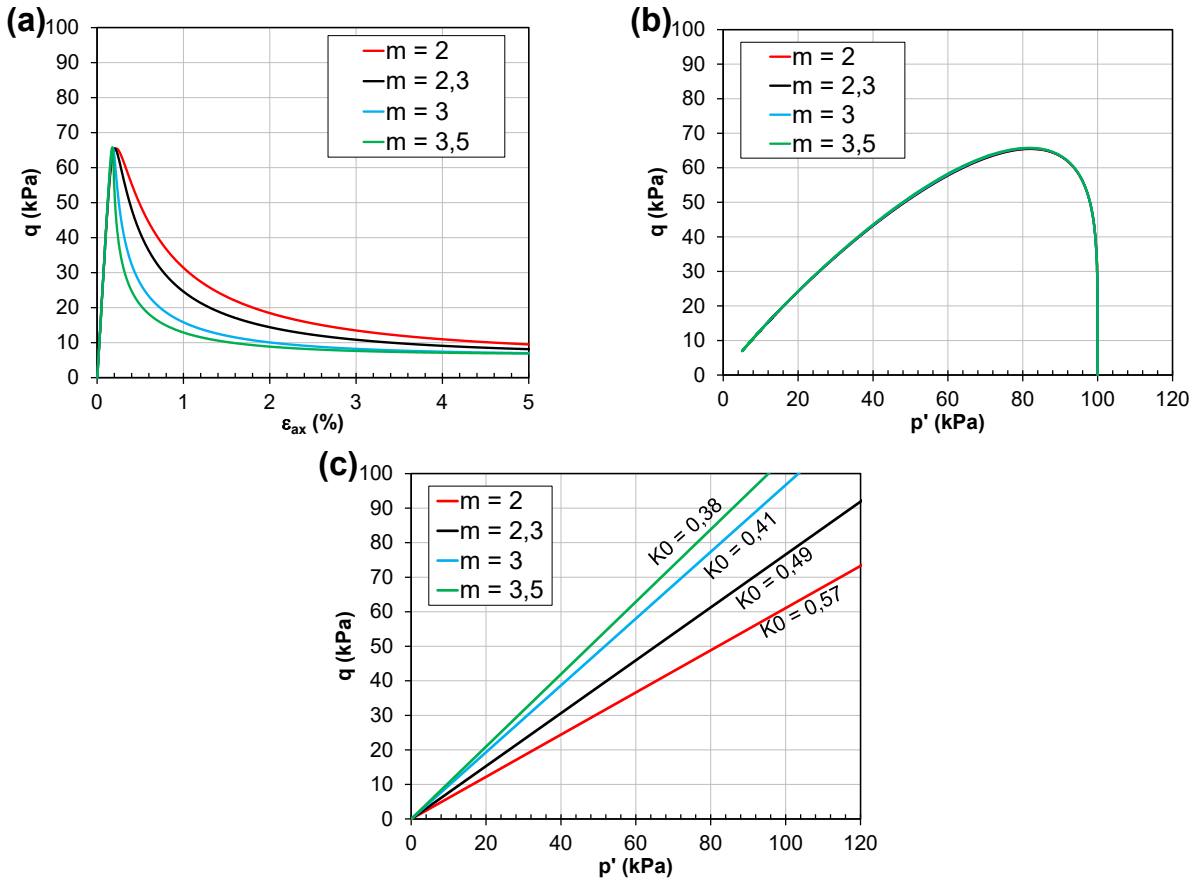


Figure 9: Sensitivity of CASM to variations of the parameter *m* in: (a) and (b) undrained triaxial compression tests, and (c) oedometer compression tests

Conclusion

Using numerical modeling to address the onset of flow liquefaction is becoming more prevalent. Consequently, there is a growing demand from the industry for constitutive models capable of simulating liquefaction phenomena. In this context, this paper focuses on the CASM model, which was developed to represent the behavior of sands and clays alike, making it a suitable candidate for characterizing tailings behavior.

The CASM formulation and its implementation using an explicit integration scheme as a user-defined model in Plaxis were presented. A validation procedure based on a series of numerical laboratory tests is also included. This procedure encompasses analyses in different stress paths and drainage conditions, demonstrating CASM's capability for transient simulations with hydro-mechanical coupling.

Additional sensitivity analyses were performed, demonstrating the relationship between CASM's parameters *n* and *r* with peak and residual undrained strength. Furthermore, CASM's ability to control the coefficient of at-rest lateral earth pressure during oedometer compression simulations was highlighted, which is crucial for applications in construction simulations.

The results of the numerical models presented in this work demonstrate the consistency and robustness of the formulation, serving as a methodology for validating future implementations. This marks the initial phase of a project aiming to utilize CASM for simulating real large-scale problems.

Acknowledgements

The authors acknowledge the support of DF+ Engineering and Vale S.A.

References

Arroyo, M. and Gens, A. 2021. Computational analyses of Dam I Failure at the Córrego de Feijao Mine in Brumadinho: Final report for VALE S.A.

Brinkgreve, R.B.J., Kumarswamy, S., Swolfs, W.M., Engin, E., Fonseca, A.F., Ragi, M.N., Zampich, L. and Zalamea, N. 2020. Plaxis 3D Connect Edition V20.03 Manuals. Bentley Systems.

Jefferies, M. and Been, K. 2016. *Soil Liquefaction: A Critical State Approach*. Second edition. Routledge Taylor and Francis Group.

Jefferies, M., Morgenstern, N.R., Van Zyl, D. and Wates, J. 2019. Report on NTSF embankment failure. Cadia Valley operations for Ashurst Australia. Independent Technical Review Board. International Centre for Numerical Methods in Engineering.

Mánica, M., Arroyo, M., Gens, A. and Monforte, L. 2021. Application of a critical state model to the Merriespruit tailings dam failure. *Geotechnical Engineering* 175(2): 151–165. DOI:10.1680/jgeen.21.00001.

Morgenstern, N.R., Vick, S.G., Viotti, C.B. and Watts, B.D. 2016. Report on the immediate causes of the failure of the Fundão dam. Fundão tailings dam review panel. Cleary Gottlieb Steen and Hamilton LLP.

Piciullo, L., Storrøsten, E.B., Liu, Z., Nadim, F. and Lacasse, S. 2022. A new look at the statistics of tailings dam failures. Engineering Geology 303: 106657.

Sheng, D., Sloan, S.W. and Yu, H.S. 2000. Aspects of finite element implementation of critical state models. *Computational Mechanics* 26(2): 185–196. DOI: 10.1007/s004660000166

Sloan, S.W., Abbo, A.J. and Sheng, D. 2001. Refined explicit integration of elastoplastic models with automatic error control. *Engineering Computations* 18(1/2): 121–154.

Wood, D. M. 2004. Geotechnical Modelling. Version 2.2. April 2004.

Yu, H.S. 1998. CASM: a unified state parameter model for clay and sand. *Int. J. Numer. Anal. Methods Geomech*. 22(8): 621–653.

A Comparison of Different Methods Used to Estimate the State Parameter to Assess the Static Liquefaction of Tailings

Fahimeh Mahdavi Naftchali, WSP Canada Inc., Canada
Mathan V. Manmatharajan, WSP Canada Inc., Canada
Hamed Behzadipour, WSP Canada Inc., Canada
Michael Etezad, WSP Canada Inc., Canada

Abstract

Static liquefaction has been one of the leading causes for the failures of tailings dam constructed using the upstream dam raise method. Cone penetration tests (CPTs) are widely used to characterize the tailings and to assess the liquefaction potential of tailings. In this study, site investigations were carried out at a mine site in Canada, which included CPTs, drilling boreholes, and index and advanced laboratory tests. CPTs were pushed to determine the in-situ characteristics of the tailings, and disturbed samples were collected to perform laboratory testing on tailings. The advanced tests included a series of triaxial compression tests to determine the tailings critical state line (CSL).

The state parameter is widely used to assess the flow liquefaction of tailings in the mining industry. In the literature, various methods have been developed to assess the flow liquefaction of natural soils and tailings based on the state parameter. The state parameter can be determined using the CSL to identify the contractive and dilative behavior of tailings. This study examines five different methods developed for the CPT to assess the flow liquefaction of tailings. The methods include those developed to determine the state parameter using the CSL and NorSand constitutive model calibration. The state parameter was calculated for each CPT using five methods. A comparison of the results obtained among different methods is provided, and the accuracy of the state parameter is determined based on these methods is discussed.

Introduction

Static liquefaction has been one of the leading causes of the failures of tailings dam constructed using the upstream dam raise method. Tailings are generally hydraulically transferred to storage facilities and deposited in a loose saturated condition within storage dams. The loosely deposited tailings are normally prone to liquefaction, posing a significant dam breach risk, where the dam is constructed on loose saturated

or near saturated tailings. Liquefaction assessment is carried out using in-situ tests (e.g., CPT) and advanced laboratory tests (e.g., triaxial tests, simple shear tests). Understanding the tailings state and behavior through in-situ tests, advanced laboratory tests, and advanced constitutive models is crucial in the current practice of tailings characterization and liquefaction assessment.

Critical state soil mechanics captures a wide range of soil behavior in a logical and quantifiable way, providing a mechanistic framework to understand soil behavior. Static liquefaction potential can be predicted under the critical state soil mechanics framework. The state parameter (ψ) introduced by Been and Jefferies (1985) was used to determine the flow (static) liquefaction susceptibility of the soils and tailings using critical state soil mechanics. The state parameter is a density index used to understand the state of the soil and is defined as the difference between void ratios at the current state and the critical state at a given stress level, and it captures the effect of both void ratio and effective stress. Soils at the same state (ψ) express similar responses and tend to have the same liquefaction potential (Manmatharajan et al., 2023). Generally, soils with a state looser than critical state ($\psi > 0$, above the critical state line) are contractive in drained shearing, and are strain softening in the deviator stress path against mean effective stress during undrained shearing; whereas soils with a state denser than critical state ($\psi < 0$, below the critical state line) are dilative in drained shearing and are strain hardening in the deviator stress path against mean effective stress during undrained shearing. Jefferies and Been (2006) suggested that soils with a state parameter higher than -0.05 ($\psi > -0.05$) will contract and will undergo strength loss during undrained shearing.

Cone penetration tests (CPTs) are widely used to characterize tailings and to assess the liquefaction potential of tailings. The CPT is one of the most reliable in-situ tests for silt-sized particles, offering accurate and repeatable data. Various methods proposed in the literature suggest correlations between the state parameter and CPT resistance (e.g., Plewes et al., 1992; Ghafghazi and Shuttle, 2008; Shuttle and Jefferies, 2016; Robertson, 2022; Ayala et al., 2023). However, these methods require some level of in-situ approximation, different levels of information on soil properties, various interpretation procedures, and some accompanying triaxial tests to determine the critical state line. This paper evaluates the estimation of state parameter from CPT resistance using five independent methods and discusses the variation in the estimated state parameter among the methods.

Laboratory testing program

Material

Two types of gold mine tailings (Tailings 1 and Tailings 2) were collected from a mine site located in Canada. The tailings were predominantly comprised of non-plastic silt-sized particles. The tailings were

deposited along the perimeter dams of the tailings storage facility with a pond maintained in the interior of the basin. Thus, the tailings were generally characterized as "saturated, non-plastic" tailings and susceptible to liquefaction under both static and dynamic loading. Figure 1 depicts the Particle Size Distributions (PSD) of the two tailings. The PSDs of the two tailings are very close and hence the two tailings are expected to yield the same CSL. Accordingly, they are considered as one material in determination of the CSL.

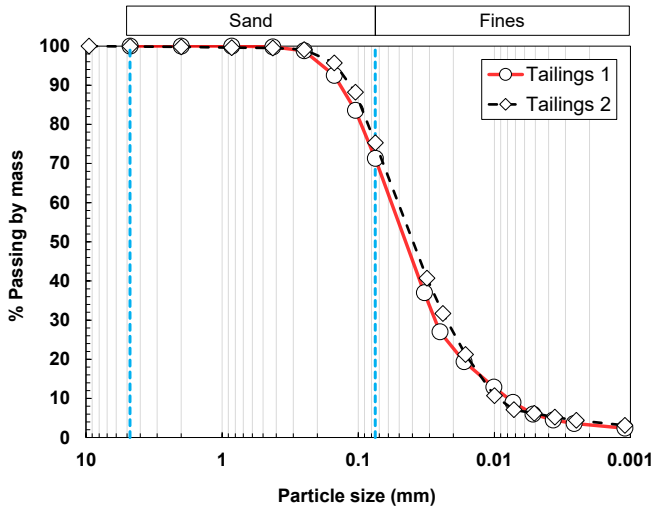


Figure 1: Particle size distribution of the Tailing 1 and Tailing 2

Triaxial test, critical state line (CSL) determination and NorSand calibration

A series of isotopically consolidated triaxial compression tests were carried out on the tailings and a CSL was determined in both e-log p' space and q-p' space. The triaxial tests were carried out following the Bishop and Henkel (1969), Jefferies and Been (2016) and ASTM D7181 and ASTM D4767 recommendations. The triaxial test specimens were reconstituted using the moist tamping method to various densities and then isotopically consolidated to a range of initial confining stresses between 75 kPa and 400 kPa. Once consolidated, the specimens were sheared at a constant rate (1% to 2% per hour) under either drained or undrained conditions until a minimum axial strain of about 20% was reached.

The tailings were initially dried in an oven at a temperature of about 60°C. Sub-samples of the oven-dried tailings were placed in plastic bags after splitting the original sample into approximately equal portions. Water was added to the sub-samples in the plastic bags to bring the moisture content to approximately 5%. The testing procedure is based on reconstituting samples, typically by placing six layers of moist soils in a reconstitution split mold. Initial densities in each layer are varied by changing the compaction effort to control how the samples are formed (trying to keep a uniform cylindrical shape) using a variation of the under-compaction method proposed by Ladd (1978) and the wet tamping technique (Ishihara, 1993). As soil properties at the critical state are assumed to be unaffected by initial fabric

(specimen reconstitution method) and density (Been et al., 1991), the choice of specimen preparation method (wet tamping) and void ratio are to obtain a set of data points to clearly define the CSL. The final moisture contents were determined by freezing the samples after concluding shearing. Figure 2 shows the CSLs in the void ratio versus *log (p')* space and in the q versus p' space. q and p'_c correspond to the deviator stress and mean effective stress at the critical state.

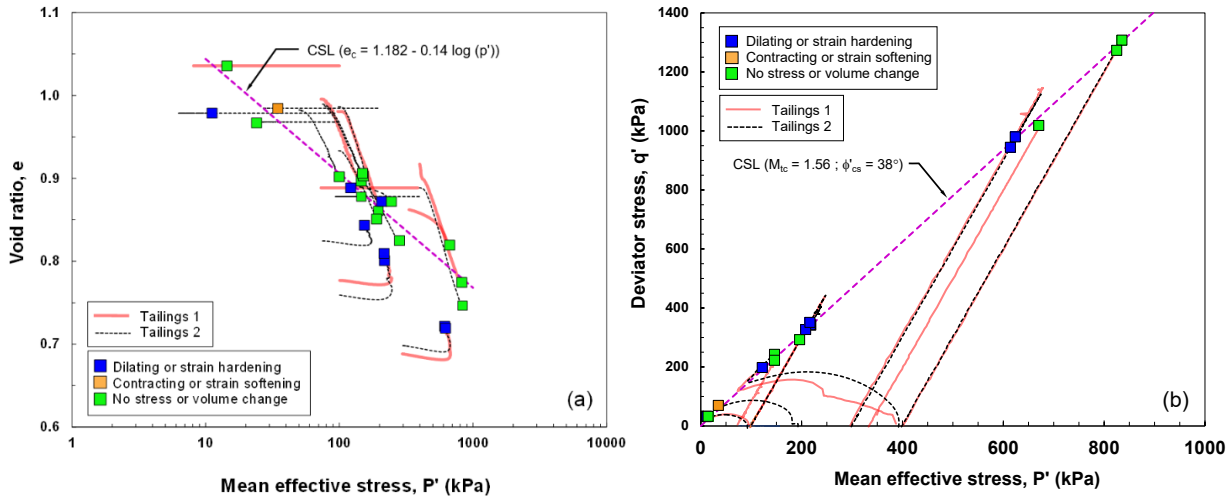


Figure 2: (a) Variation of void ratio against mean effective stress and CSL in e vs. *log (p')* (b) variation of deviator stress against mean effective stress and CSL in q vs. p'

In the void ratio *(e)* versus *log (p')* space, conventional semi-log linear CSL was considered as shown in Equation 1.

$$e_c = \Gamma - \lambda_{10} \log (p'_c) \qquad \text{(Equation 1)}$$

where e_c and p'_c correspond to the void ratio at the critical state, respectively.

Γ is the void ratio at the critical state at reference pressure of 1 kPa, and λ_{10} is the slope of the CSL in a semi-logarithm space (i.e., e vs. *log (p')*). In the q versus p' space, conventional linear CSL is defined by Equation 2.

$$q = M_{tc} p'_c \qquad \text{(Equation 2)}$$

M_{tc} is the stress ratio at critical state, where t_c refers to "triaxial compression". The stress ratio (friction angle) was estimated using dilatancy D, which is the ratio of volumetric strain to shear strain rate. The friction angle at the critical state can then be derived from the stress ratio defined by Equation 3.

$$M_{tc} = \frac{6 \sin \phi_c}{3 - \sin \phi_c} \qquad \text{(Equation 3)}$$

As shown in Figure 2, the end points denoted by green squares indicate that the tailings continue to deform under constant stresses and volumes (void ratios), which is a theoretical definition of critical state.

In practice, the tailings may not deform in such a manner due to limitations in the element tests. However, they will tend to reach the critical state. The end points denoted by orange squares indicate that the tailings are still contracting or strain softening. The end points denoted by blue squares indicate that the tailings are still dilating or strain hardening. Table 1 summarizes the CSL parameters, dilatancy, and plastic hardening parameters obtained from NorSand calibration using the triaxial test results. Figure 3 presents an example of curve fitting during NorSand calibration.

Table 1: Critical state parameters and calibrated NorSand parameters

Material	Γ	λ_{10}	M_{tc}	ϕ'_{cs} (°)	N	χ_{tc}	H	ν
Gold tailings	1.182	0.14	1.56	38	0.26	2.6	30-210ψ	0.2

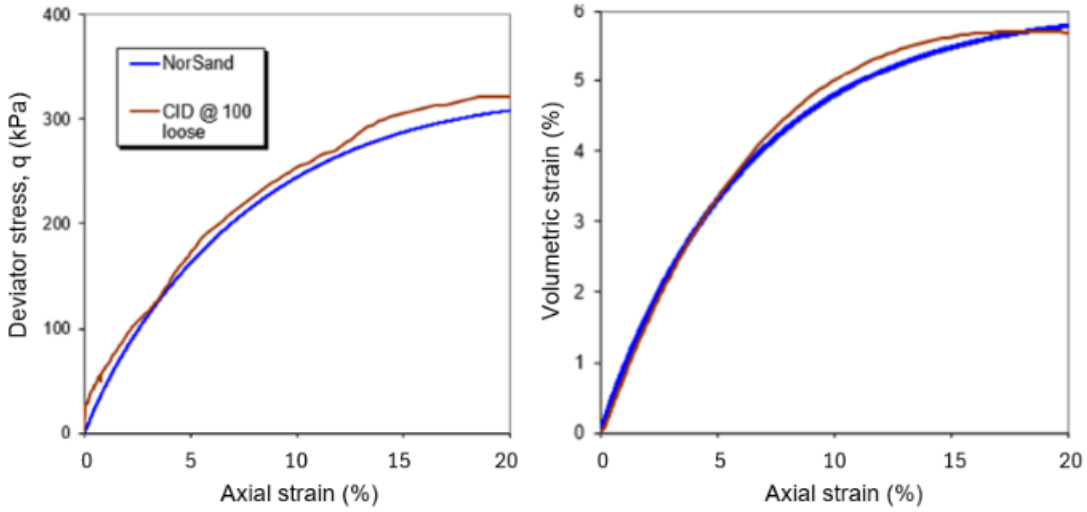


Figure 3: Example of NorSand calibration

Cone Penetration Testing (CPT) program

CPTs were advanced with a piezocone of 15 cm^2 at a standard penetration rate of 2 cm/s. The results of five CPTs are presented and discussed herein. The CPTs were performed in accordance with ASTM D5778. CPT based flow liquefaction assessment was carried out using the state parameter (Jefferies and Been, 1985). The state parameter was estimated using five independent methods proposed between the early 1990s and 2023. Some methods (empirical-based) estimate the state parameters using the CPT resistance; whereas some other methods (CSL-based) estimate the state parameter using the CPT resistance, and critical state parameters.

Methodology

Five independent methods (Plewes et al., 1992; Shuttle and Jefferies, 2016; Olaya and Bray, 2022; Robertson 2022; and Ayala et al., 2023) used in this study are discussed below. Table 2 summarizes the formulae used in the empirical-based and CSL-based methods. Details of each method can be found in the corresponding references. For the Plewes et al. (1992) method, in addition to the CSL-based method, the state parameter was determined using empirical correlation for the l_{10}. For the CSL-based methods, NorSand calibration and CPT widget were performed to get the calibrated dilatancy, elasticity, and plastic hardening parameters. Table 3 summarizes the computed coefficients. The undrained condition was considered for Shuttle and Jeffries (2016) and Ayala et al. (2023) methods.

Table 2: Methods used to estimate the state parameter (ψ)

Methods	Formula	Reference
Empirical based	$\psi = 0.56 - 0.33\ Log\ (Q_{\mathrm{tn,cs}})$	Robertson (2022)
	$\psi_0 = 0.485 - 0.314log(Q_{tn,cs})$	Olaya and Bray (2022)
CSL based	$\psi_0 = -\dfrac{ln\left[\dfrac{Q_p(1-B_q)}{(\bar{k})}\right]}{(\bar{m})}$ $\bar{k} = \left(3 + \dfrac{0.85}{l_{10}}\right)M$ $\bar{m} = 11.9 - 13.3l_{10}$ $l_{10} = \frac{F_r}{10}$ *(empirical)*	Plewes et al. (1992)
	$\psi_0 = -\dfrac{ln\left[\dfrac{Q_{sph}}{(k_{sph})}\right]}{(m_{sph})}$ $k_{sph} = a_k + b_k ln(I_r)$ $m_{sph} = a_m + b_m ln(I_r)$ $I_r = \dfrac{G_o}{p_0'}$	Shuttle and Jefferies (2016)
	$\psi_0 = -\dfrac{ln\left[\dfrac{Q_p(1-B_q)+1}{(k_{un})}\right]}{(m_{un})}$	Ayala et al. (2023)

Table 3: CPT Widget parameters

Material	Shuttle and Jefferies (2016)				Ayala et al. (2023)	
	a_k	b_k	a_m	b_m	k_{un}	m_{un}
Gold tailings	8.32	0.29	10.11	0.43	10.55	15.56

Results and discussion

Figures 4 to 8 present the CPT measured data, interpreted using CPet-IT software (v. 3.9.2.19) developed by GEOLOGISMIKI, and the estimated state parameter for five CPTs (CPTs 21-03, -04, -05, -06, and -09), respectively. Each figure presents five plots to show the variation of (a) tip resistance, (b) sleeve friction, (c) dynamic pore pressure (u_2), (d) soil behavior type index (SBTn) (I_c), and (e) state parameter (ψ) of the corresponding CPT. The contractive-dilative boundary is marked by a red dashed line representing the state parameter of -0.05 (Jefferies and Been, 2006).

In Figure 4 (CPT21-03), for the depths between the phreatic surface and 10.8 m (sand mixtures and silt mixtures), tip resistance is generally less than 5 MPa and friction is less than 50 kPa. Dynamic pore pressure shows some positive pore water development from the hydrostatic pressure and the I_c plot indicates sand and silt mixtures ($2.05 < I_c < 2.95$). In general, all the methods shown in Figure 4(e) estimate the tailings to be contractive. Estimated state parameters vary between 0.15 and -0.05 ($\Delta\psi \sim 0.2$). Plewes et al.'s (1992) empirical method estimates the state parameters to be close to 0.15 while Olaya and Bray's (2022) method estimates the state parameters closer to -0.05. Results from the rest of the methods are in between. For depths between 10.8 m and 21.2 m (sand mixtures), dynamic pore pressure closely follows the hydrostatic pressure. The estimated state parameters vary between 0 and -0.15 ($\Delta\psi \sim 0.15$).

For these depths, Plewes et al.'s (1992) method estimates the state parameters to be close to -0.15, while Shuttle and Jefferies' (2016) method provides estimates close to 0. Results from the rest of the methods are in between. Shuttle and Jefferies' (2016), Robertson's (2022), and Ayala et al.'s (2023) methods predict some layers to be contractive, while Plewes et al.'s (1992) and Olaya and Bray's (2022) methods predict a complete dilative layer. At depths between 21.2 and 24 m (clay and silt mixtures), the estimated state parameters are more scattered, and the difference among the methods is more than 0.25.

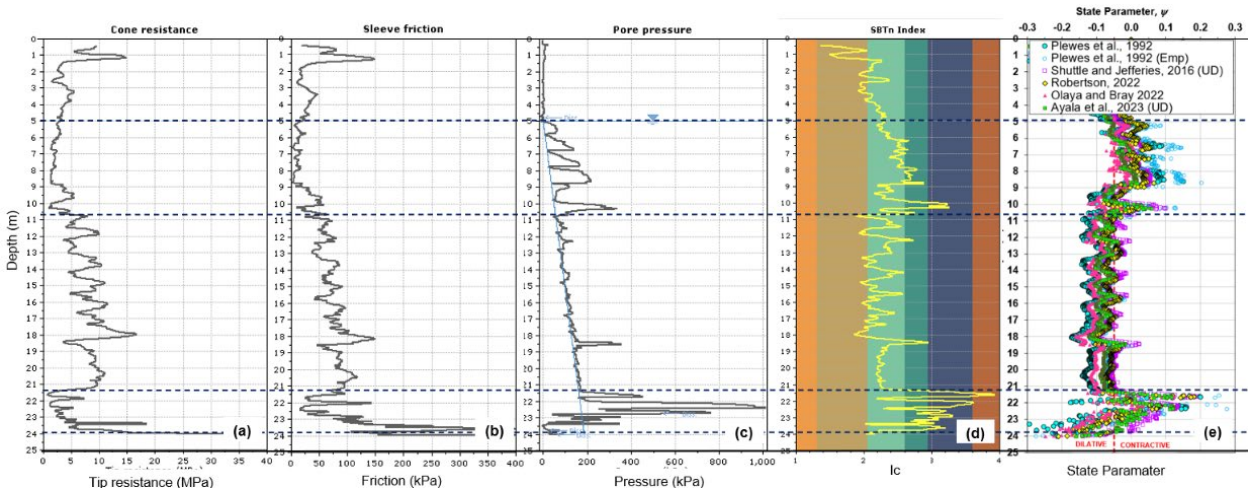


Figure 4: Results of CPT21-03 – (a) tip resistance, (b) sleeve friction, (c) dynamic pore pressure, (d) soil behavior type index, and (e) state parameter

In Figure 5 (CPT21-04), for depths between the phreatic surface and 10 m (sand mixture), all methods estimate the tailings as contractive. Estimated state parameters vary between 0.1 and 0. The estimates of Olaya and Bray's (2022) and Ayala et al.'s (2023) methods are close to 0, while the estimates of Plewes et al. (1992) empirical method are close to 0.1. Results from the rest of the methods are in between. For depths between 10 and 13.8 m (sand mixture), the estimated state parameters are very close (difference, $\Delta\psi \sim$ 0.05); However, Olaya and Bray (2022) estimate a complete dilative layer, while other methods estimate a thicker contractive layer. For depths between 13.8 and 16.3 m, the estimated state parameters are scattered.

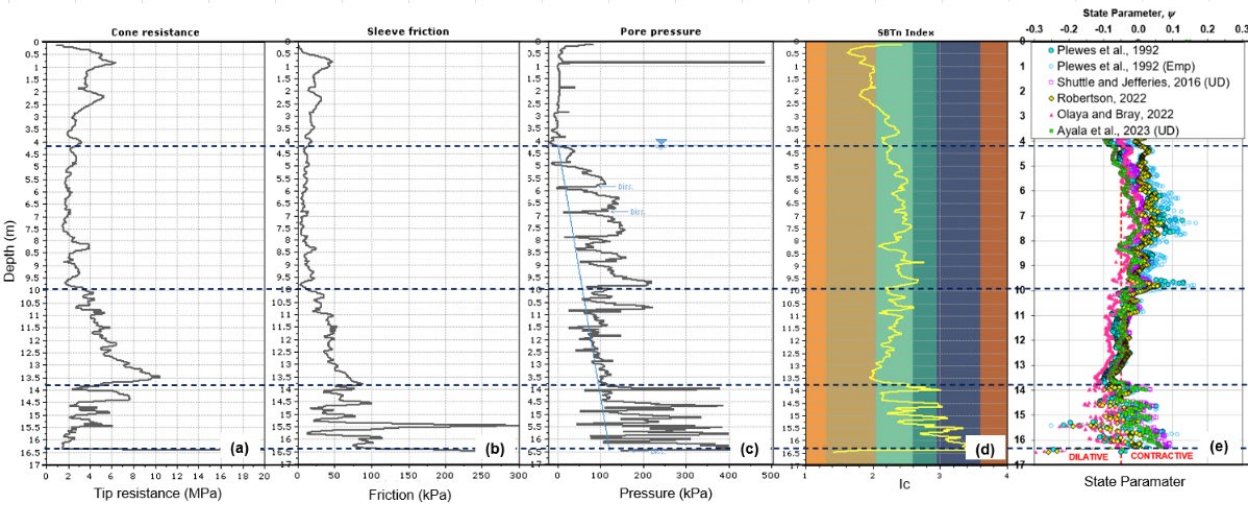


Figure 5: Results of CPT21-04 – (a) tip resistance, (b) sleeve friction, (c) dynamic pore pressure, (d) soil behavior type index, and (e) state parameter

In Figure 6 (CPT21-05), for the depths between phreatic surface and 7 m (sand mixture), three methods estimate the tailings to be contractive. The estimated state parameters vary between 0.05 and -0.06. The

methods of Olaya and Bray (2022) and Ayala et al. (2023) estimate a dilative response, while the rest of the methods estimate a contractive response. For depths between 7 and 11.5 m (sand mixture and silt mixture), the estimated state parameters vary between 0.15 and -0.05. The methods of Olaya and Bray (2022) and Ayala et al. (2023) estimate a state parameter of around 0, while the method of Plewes et al. (1992) yields estimates of around 0.15. For depths between 11.5 and 14 m (sand mixture and silt mixture), the estimated state parameters among the methods vary between 0.05 and -0.15, and they are on both sides of the contractive-dilative boundary, which is a concern for the design engineer.

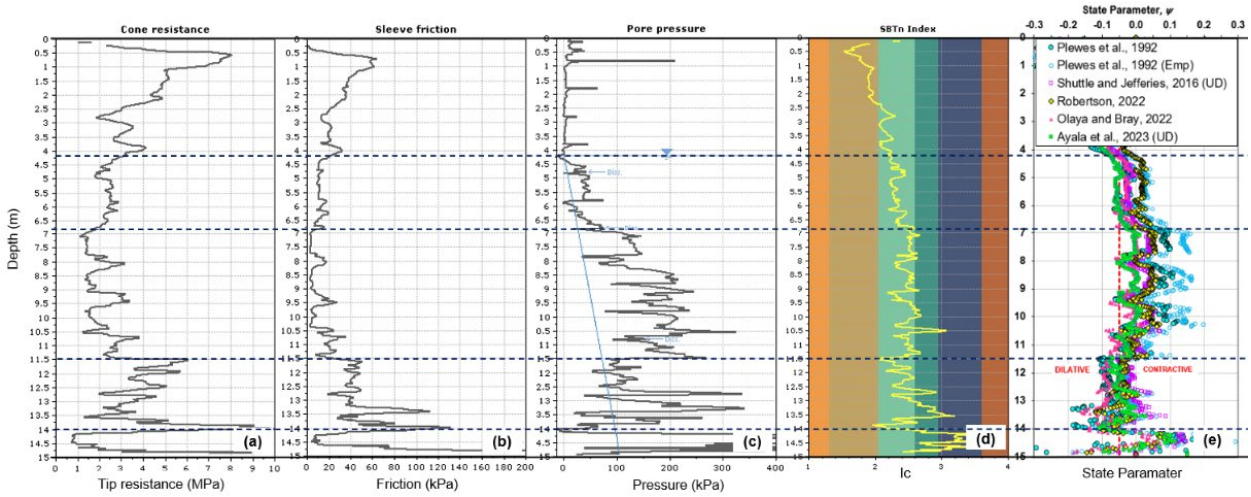


Figure 6: Results of CPT21-05 – (a) tip resistance, (b) sleeve friction, (c) dynamic pore pressure, (d) soil behavior type index, and (e) state parameter

In Figure 7 (CPT21-06), for depths between the phreatic surface and 3 m (sand mixture), a contradictive estimation of state parameter is observed. The estimated state parameters are between -0.1 and 0.05. The methods of Shuttle and Jefferies (2016) and Ayala et al. (2023) estimate a dilative response, while the other methods estimate a contractive response. For depths between 3 and 5 m (sand and silt mixtures), all methods estimate the tailings to be contractive and the estimated state parameters are between -0.03 and 0.13. For depths between 5 and 7.5 m (sand mixture), the estimated state parameters generally move from the contractive side to the dilative side with almost the same band width ($\Delta\psi \sim 0.13$). However, the Robertson (2022) method remains within the contractive side. For depths between 7.5 and 8.5 m (sand and sand mixture), all methods estimate a dilative response with about 0.1 difference in state parameter. Below 8.5 m depth (silt mixtures), the methods of Shuttle and Jefferies (2016) and Robertson (2022) estimate a contractive response, while other methods estimate a dilative response with about 0.1 difference in state parameter.

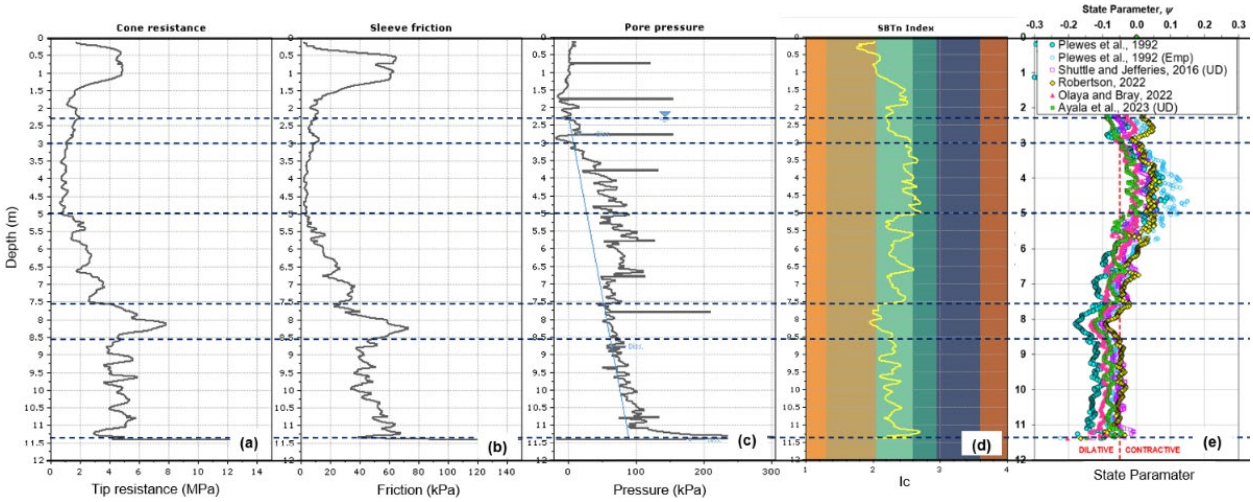


Figure 7: Results of CPT21-06 – (a) tip resistance, (b) sleeve friction, (c) dynamic pore pressure, (d) soil behavior type index, and (e) state parameter

In Figure 8 (CPT21-09), for depths between the phreatic surface (2.2 m) and 12 m (sand mixture and silt mixture), the estimated state parameters have about 0.15 difference among the methods. Plewes et al. (1992) and Olaya and Bray (2022) estimate a dilative response while Shuttle and Jefferies (2016) and Robertson (2022) estimate a contractive response. Below 12 m (silt mixtures and clay), all methods predicted a contractive response with a considerable difference in the state parameter.

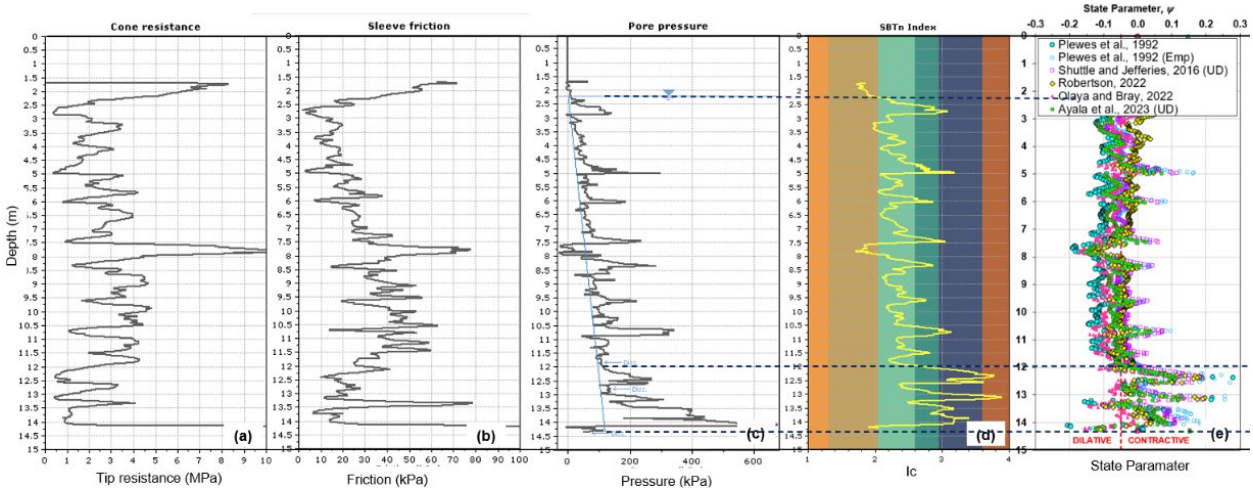


Figure 8: Results of CPT21-09 – (a) tip resistance, (b) sleeve friction, (c) dynamic pore pressure, (d) soil behavior type index, and (e) state parameter

As observed, there is a disagreement among the results obtained from the various methods in determining the state parameter of tailings. There are cases where one method indicates dilative tailings not susceptible to flow liquefaction, whereas the other method indicates contractive tailings susceptible to flow liquefaction.

Conclusion

In this study a CPT-based liquefaction susceptibility assessment of saturated, non-plastic tailings was evaluated using the state parameter approach. Five CPTs were advanced at a standard penetration rate of 2 cm/s and the CSL was determined using a series of isotopically consolidated triaxial compression tests on moist tamped tailings specimens. In total, five methods in the literature were used to determine the state parameter of tailings, and the state parameters were estimated using the CPT resistance and the combined CPT resistance, and critical state parameters. The following conclusions can be drawn from this assessment:

- Among the methods used, the difference in estimated state parameter ranges from 0.05 to 0.25.
- The greatest divergence was observed when the tailings contained finer particles (silt mixture, based on SBTn index).
- The methods exhibit less scatter for sand mixtures, based on the SBTn index.
- Based on the CPTs analyzed, no single method provides the highest (most conservative) or lowest state parameter estimates. There is not a universally accepted method available for estimating the state parameter. The state parameter, combined with the measured CPT parameters (e.g., excess pore water pressure response), should be considered in the flow liquefaction assessment.

In summary, the estimated state parameters show considerable disagreement depending on the methods used to analyze them. Without having a universally accepted and accurate method in the industry, this variation in results could lead to the adoption of a conservative approach by the design engineer to minimize the risk, which in turn may result in an overconservative design and increased cost for the project. On the other hand, if the design engineer selects a method that could result in an excessively conservative design, the risk of tailings dam instability will be increased.

Acknowledgements

Financial support from the WSP Innovation Program is gratefully acknowledged.

References

ASTM International. D4767-11, 2011. *Methods for Consolidated Undrained Triaxial Compression Test for Cohesive Soils.* West Conshohocken, PA, 2011. Doi: http://doi.org/10.1520/D4767-11

ASTM International. D5778-20, 2020. *Standard test method for electronic friction cone and piezocone penetration testing of soils*, West Conshohocken, PA. DOI: 10.1520/D5778-20

ASTM International. D7181-11, 2011. *Methods for Consolidated Drained Triaxial Compression Test for Soils.* West Conshohocken, PA, 2011. Doi: http://doi.org/10.1520/D7181-11.

Ayala, J., Fourie, A. and Reid, D. 2023. A unified approach for the analysis of CPT partial drainage effects within a critical state soil mechanics framework in mine tailings. *J. Geotech. Geoenviron. Eng.* 2023, 149(6): 04023036. DOI: 10.1061/JGGEFK.GTENG-10915.

Been, K. and Jefferies, M.G. 1985. A state parameter for sands. *Géotechnique* 35(2): 99–112.

Been, K., Jefferies, M. and Hachey, J. 1991. The critical state of sands. *Géotechnique* 41(3): 365–381.

Bishop, A. and Henkel, D. 1969. *The Measurement of Soil Properties in The Triaxial Test*. Edward Arnold Ltd. London. 228 pages.

Ghafghazi, M. and Shuttle, D. 2008. Interpretation of sand state from cone penetration resistance. *Géotechnique* 58: 623–634

Ishihara, K. 1993. Liquefaction and flow failure during earthquakes. The 33rd Rankine Lecture. *Géotechnique*, 43(2): 349–415.

Jefferies, M. and Been, K. 2006. *Soil Liquefaction: A Critical State Approach*. First Edition. Taylor and Francis. New York, USA.

Jefferies, M. and Been, K. 2016. *Soil Liquefaction: A Critical State Approach*. Second Edition. CRC Press. Taylor and Francis. Florida, USA.

Ladd, R.S. 1978. Preparing test specimens using under compaction. *Geotechnical Testing Journal*, 1(1): 16–23.

Manmatharajan, M.V., Gill, S., Liu, W., Ingabire, E.P., Sy, A. and Ghafghazi, M. 2023. Effect of particle size and particle size distribution on the critical state of loci of granular soils. *Can. Geotech. J.* 60(8): 1117–1131. https://doi.org/10.1139/cgj-2021-0643.

Olaya, F.R. and Bray, J. D. 2022. CPT case histories of post-liquefaction free-field ground settlement. Report No. UCB/GT 2022-02.

Plewes, H.D., Davies, M.P. and Jefferies, M.G. 1992. CPT based screening procedure for evaluating liquefaction susceptibility. *45th Canadian Geotechnical Conference*, Toronto, 26–28 October 1992. Canadian Geotechnical Society: 4-1–4-9.

Robertson, P.K. 2022. Evaluation of flow liquefaction and liquefied strength using the cone penetration test: an update. *Can. Geotech. J.* 59: 620–624. dx.doi.org/10.1139/cgj-2020-0657.

Shuttle, D.A. and Jefferies, M.G. 2016. Determining silt state from CPTu. *Geotechnical Research* 3(2): 90–118. http://dx.doi.org/10.1680/jgere.16.00008

Silty Sand Tailings Saturation and its Influence on Interpreted CPTu Soil Behavior Type

Andrew Burgin, Stantec Consulting Ltd, Canada
Richard Dawson, Stantec Consulting Ltd, Canada
Mauricio Pinheiro, Stantec Consulting Ltd, USA
Anelisa Vasconcelos, Belo Horizonte, Minas Gerais, Brazil

Abstract

Piezometric Cone Penetrometer (CPTu) testing is a widely used technique to investigate tailings deposits, aiding in the identification of contractive and potentially liquefiable material. Recent studies have identified a significant shift in the CPTu-interpreted behavior of silty sand tailings (from dilative to contractive / potentially liquefiable) depending on the saturation condition of the material (Russell and Reid, 2018). These findings may create uncertainty when characterizing unsaturated silty sand tailings that are expected to saturate in the future due to a rising groundwater table.

This paper investigates the effect of saturation and matric suction in the interpretation of CPTu tests conducted in an unsaturated iron ore silty sand tailings deposited at Germano Complex. The influence of suction hardening was estimated from Soil-Water Characteristic Curves determined for the tailings material. A framework was developed for characterizing the unsaturated silty sand tailings using Robertson's (2016) Modified Normalized Soil Behavior Type (Mod SBTn) that couples the saturation data with CPTu data interpretation. A protocol has been established for correcting the CPTu tip resistance to account for the influence of suction hardening as a function of overburden stress. The results show that suction hardening in the silty sand tailings at the site is significant at shallow depth (low overburden stresses) but negligible beyond ~10 m below ground surface. This provided confidence to the design team in the interpreted behavior of the tailings at depth considering closure conditions when the groundwater is expected to rise and saturate a portion of the tailings.

Introduction

Piezometric Cone Penetrometer (CPTu) testing is a common ground investigation technique that provides a continuous data profile through a deposit as a probe is advanced. CPTu testing is relatively quick and inexpensive when compared to other in-situ investigation techniques (i.e., boreholes) and has become a

preferred investigation method for tailings deposits and characterization. The continuous data profiles collected by CPTu probes include tip resistance (q_c), sleeve friction (f_s), and dynamic pore pressure (U2).

There are a range of CPTu-based semi-empirical relationships and interpretation techniques to characterize silty sand tailings. The methodology proposed by Robertson and Wride (1998) and Robertson (2010, 2016), which is based on the modified soil behavior type (Mod SBTn), has been widely used to assess the behavior and liquefaction potential of these materials. The Robertson (2016) methodology distinguishes three different soil behavior types (Sand-like, silt (Transitional) and Clay-like) but does not differentiate between saturated and unsaturated conditions.

Russell and Reid (2018) identified a significant shift in behavior (from Dilative to Contractive) of gold tailings when interpreting CPTu data when the deposit transitions from unsaturated to saturated conditions. This shift in behavior creates uncertainty associated with the characterization of unsaturated silty sand tailings using CPTu, i.e., where the data interpretation would change upon saturation (e.g., due to a rising groundwater table). Russell and Reid (2018) attributed the shift to suction hardening in the unsaturated regime, generating artificially high cone bearing resistance (q_c). The findings and the associated uncertainty led the project team to develop an in-situ and lab testing program to investigate these effects for Germano Complex's silty sand tailings.

Site characterization

The Germano Complex is a tailings storage facility located in Minas Gerais State, Brazil and comprises two primary tailings storage facilities: the Germano Pit (GP) and Germano Main Dam (GMD), both raised using the upstream construction method with hydraulically placed iron ore tailings. Constructed between 1976 and 2016, GP and GMD are approximately 55 m and 165 m high, respectively, with ~3H:1V downstream slopes. The combined tailings storage capacity of the Germano Complex is ~150 Mm^3 (Dawson et al., 2019).

Table 1: Silty sand tailings index test results

Percent Fines (<75µm)	D_{10} (mm)	Specific Gravity, G_s	Atterberg Limits	Typical Deposit (Bulk Unit Weight (kN/m^3)	Min.-Max. Void Ratio
ASTM D422	ASTM D422	ASTM D854	ASTM D4318	ASTM D7263	ASTMD4253 / ASTMD4254
45 – 55%	0.03 – 0.05	2.93	Non-Plastic	20	0.40 – 0.85

Table 1 summarizes representative index test results for the Germano silty sand tailings. According to the particle size distribution, this material classifies as a silty sand/sandy silt, denoted by the United Soil Classification System (USCS) as SM-ML, with ~50% fines (passing sieve No.200) and < 3% clay-size particles (2µm) (Dawson et al., 2019).

Methodology

The shear strength, τ, of an unsaturated soil can be described by the Bishop (1959) equation (Eq. 1) below:

$$\tau = c' + [(\sigma_n - u_a) + X(u_a - u_w)] \tan \phi' \quad \text{(Equation 1)}$$

where, c' is effective cohesion, (σ_n-u_a) is net normal stress, (u_a-u_w) is matric suction, also denoted by the symbol "s", and ϕ' is effective friction angle. X is the effective stress parameter and ranges from 0 to 1. For X = 1, reflecting fully saturated, and X = 0, effectively dry conditions, this equation reduces to the familiar Mohr-Coulomb failure criterion. X is related to the degree of saturation, S, and the saturation is related to the matric suction through the Soil-Water Characteristic Curve (SWCC). Figure 1 shows the SWCC for the Germano silty sand tailings, derived using a Tempe cell. The degree of saturation of the tailings was calculated based on an average porosity of 0.42 (e = 0.72). The residual volumetric water content, Θ_r, is estimated at 0.02.

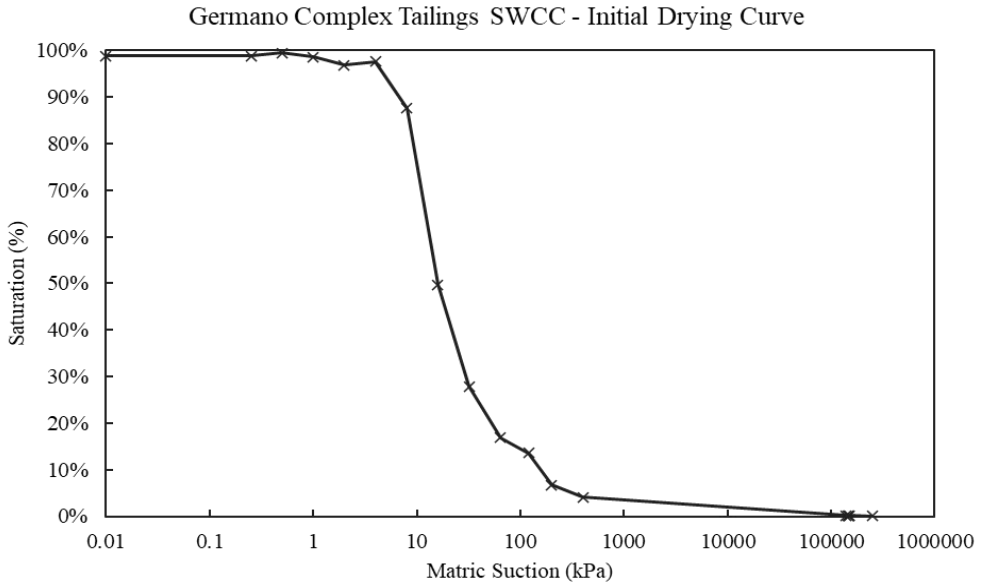


Figure 1: Germano Complex SWCC for silty sand tailings

According to Vanapalli (2009), for cohesionless materials, the additional shear strength due to matric suction is more or less parabolic when plotted against matric suction. It is null when s = 0 kPa (full saturation) and is very small beyond the residual moisture content. A peak unsaturated shear strength is reached at some intermediate matric suction. This cohesionless strength behavior model is considered representative of Germano Complex silty sand tailings behavior in the unsaturated regime.

This study is split into two phases based on the type of site investigation and data collection method, and the subsequent data analyses and interpretation, as follows:

Phase 1 – Comparison of Twinned CPTu. One (1) CPTu sounding advanced at the GMD facility, twinning a sounding advanced at the same location several years prior with a well-delineated phreatic surface. Nearby piezometers indicate a 5 to 10 m drop in the phreatic surface between the dates in which the soundings were advanced. A Fringe Zone was created where the tailings transitioned from saturated to unsaturated conditions, following cessation of tailings deposition in 2013. The data signatures of the two (2) CPTu soundings were compared for this Fringe Zone, and data profiles developed to characterize the behavior of the tailings in this zone using the Mod SBT_n framework, to identify variations between the saturated and unsaturated regime. This phase is discussed in detail in Burgin et al. (2021).

Phase 2 – Saturation Profiles. Boreholes advanced into tailings at both GP and GMD facilities, with samples collected at regular intervals for laboratory testing to characterize moisture content and specific gravity (G_s). The lab information was combined with existing oedometer test data from a previous tailings behavior characterization study of Germano silty sand tailings (Dawson et al., 2019) to estimate the degree of saturation with depth (saturation profiles), then further processed with the SWCC to develop profiles of X·s by assuming X equals the normalized volumetric water content, θ_n, calculated using the equation below (Eq. 2) (Vanapalli et al., 1996).

$$\theta_n = \frac{\theta_w - \theta_r}{\theta_{sat} - \theta_r} \quad \text{(Equation 2)}$$

where, θ_w is the volumetric water content, θ_r is the residual water content, and θ_{sat} is the saturated volumetric water content (equivalent to porosity).

Pournaghiazar et al. (2013) developed a relationship (Eq. 3) between unsaturated and saturated cone bearing, q_{cxs} and q_{c0} respectively, as a function of mean total stress, p_{no}, and X·s. A ratio approaching unity indicates similar cone bearing, while increasing values indicate the beneficial influence of suction hardening in the unsaturated regime.

$$\frac{q_{cxs}}{q_{co}} = \left(\frac{p_{n0} + X \cdot s}{p_{n0} - u_w}\right)^{0.85} \quad \text{(Equation 3)}$$

The ratio can be calculated for the full range of collected tailings samples to estimate the effect of suction hardening on CPTu data with depth.

Site data and analysis

Table 2 summarizes the site investigation activities carried out as part of the study. A total of two CPTu soundings and 14 boreholes were advanced at GP and GMD, and 229 samples were collected for moisture content and G_s testing. Samples were collected above the established groundwater table at each borehole location (i.e., sample collection was limited to the unsaturated zone). The CPTus were advanced in 2017

and 2021 at roughly the same coordinates on GMD. The unsaturated samples allowed for development of saturation profiles with depth at each borehole location.

Table 2: Summary of Site Investigation Activities

Phase	Structure	In-Situ Investigation Method	Location Count	Unsaturated Sample Count
Phase 1	GMD	CPTu	2	N/A
Phase 2	GMD	Borehole	3	46
	GP	Borehole	11	183
		Subtotal	16	229

Figure 2 compares the 2017 and 2021 CPTu datasets. The Fringe Zone, delineated by Burgin et al. (2021), is denoted as a yellow rectangle in this figure. The upper bound is about 25 m below ground surface and corresponds to the water level in 2017. The q_c profiles are generally similar although it appears the 2021 probe may be more sensitive with higher peaks and troughs. The f_s profiles appear to shift slightly right (increase) in 2021, again with higher peaks and troughs. U2 profiles bound the Fringe Zone, with (near) hydrostatic phreatic surfaces of 865 m El. and 860m El. in 2017 and 2021, respectively.

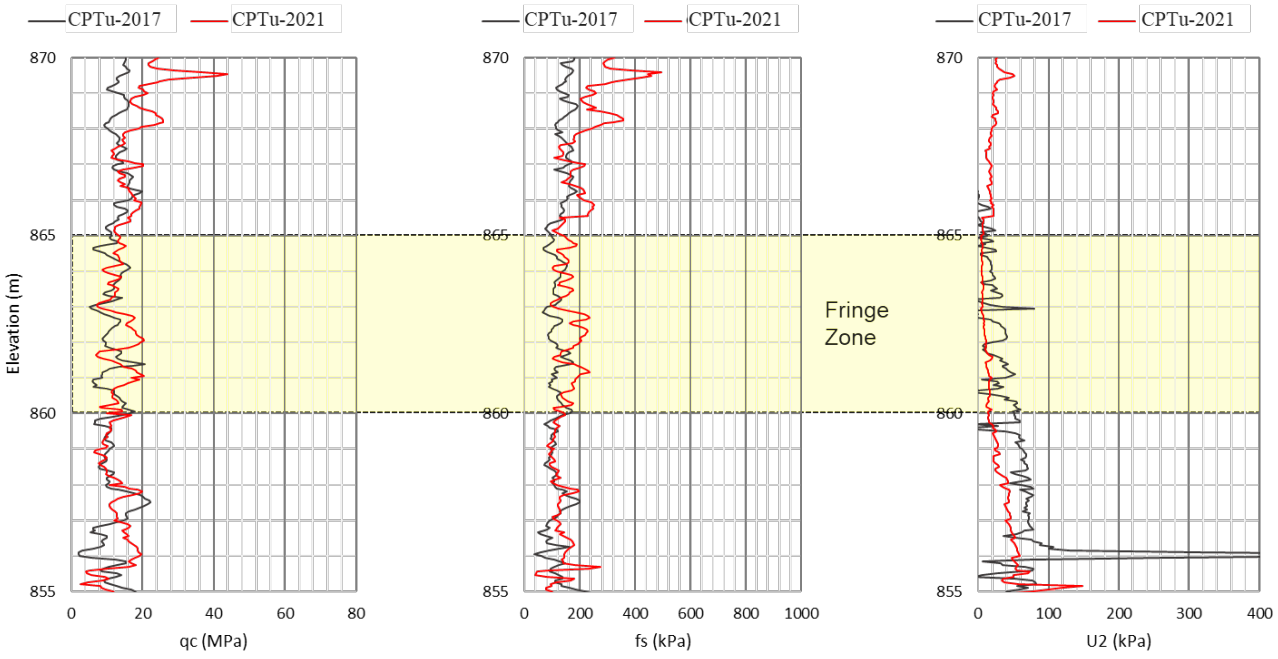


Figure 2: Phase 1 CPTu sounding data profiles, adapted from Burgin et al. (2021)

The moisture content and G_s data collected in Phase 2 can be combined with estimated void ratio to obtain the degree of saturation. The void ratio was estimated using a compression curve (p' versus e) generated by Stantec from oedometer tests carried out in a previous study (Dawson et al., 2019). Figure 3

(left) plots the resulting saturation profiles relative to depth above the estimated phreatic surface. GP and GMD samples are denoted as circles and exes, respectively. Saturation generally ranges from 10% – 50%. Almost all data points plot < 85% saturation, the minimum threshold value considered by industry upon which static liquefaction could still occur. The saturation data can be further combined with the SWCC to estimate $X^{\cdot}$s, by rearranging Equation 2 and assuming X equal to the normalized volumetric water content (Vanapalli et al., 1996). Figure 3 (right) shows that the calculated $X^{\cdot}$s data points collapse into a narrow-banded range from 7 – 9 kPa with some lower value exceptions.

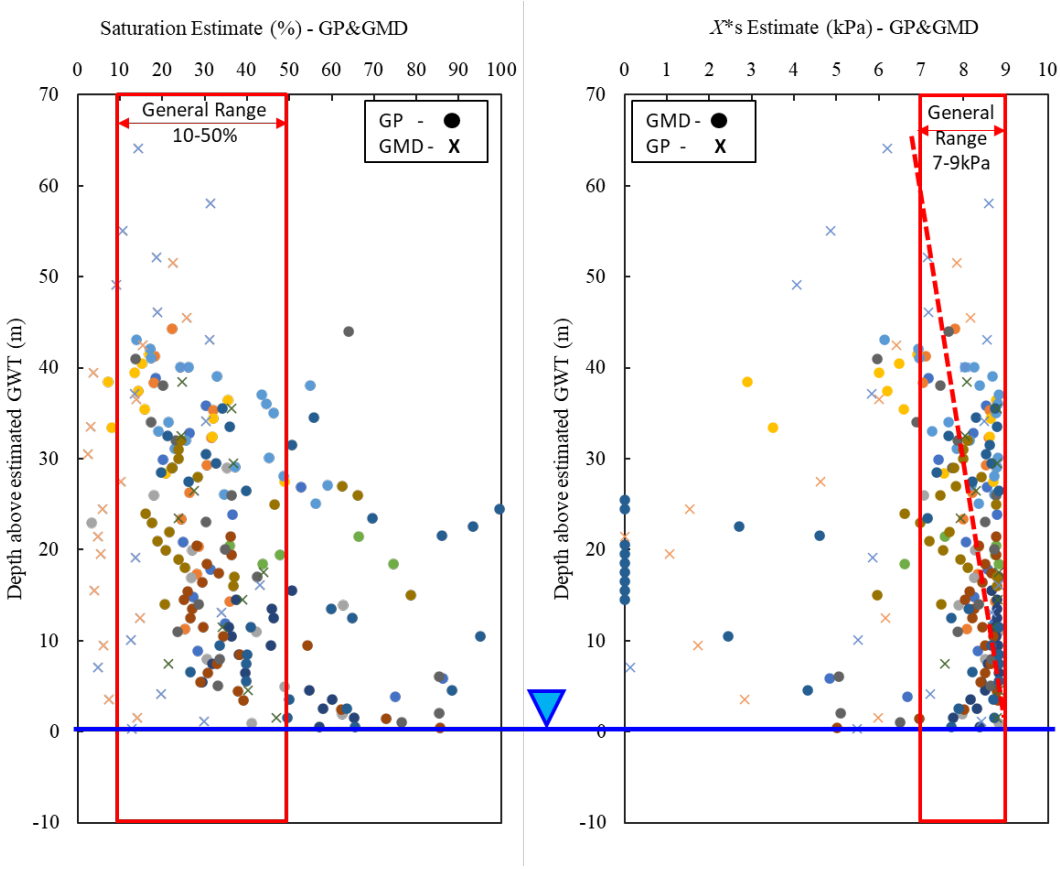


Figure 3: Phase 2 saturation data profiles (left) and $X^{\cdot}$s estimate (right)

The cone bearing ratio ($q_{c,unsat}/q_{c,sat}$), as defined by Pournaghiazar et al. (2013), can be plotted against depth below ground surface using Equation 3 by assuming a representative constant 40% saturation (for calculating normalized volumetric water content and corresponding matric suction, $X^{\cdot}$s) and K_0 of 0.5 (for calculating p_{no}). Figure 4 shows that the calculated cone bearing ratio is greater than 1.05 (dashed line) from 0 – 10 m depth and asymptotically reduces to one (1) as depth increases, demonstrating that the effect of suction hardening for the Germano silty sand tailings is negligible below this 10 m threshold.

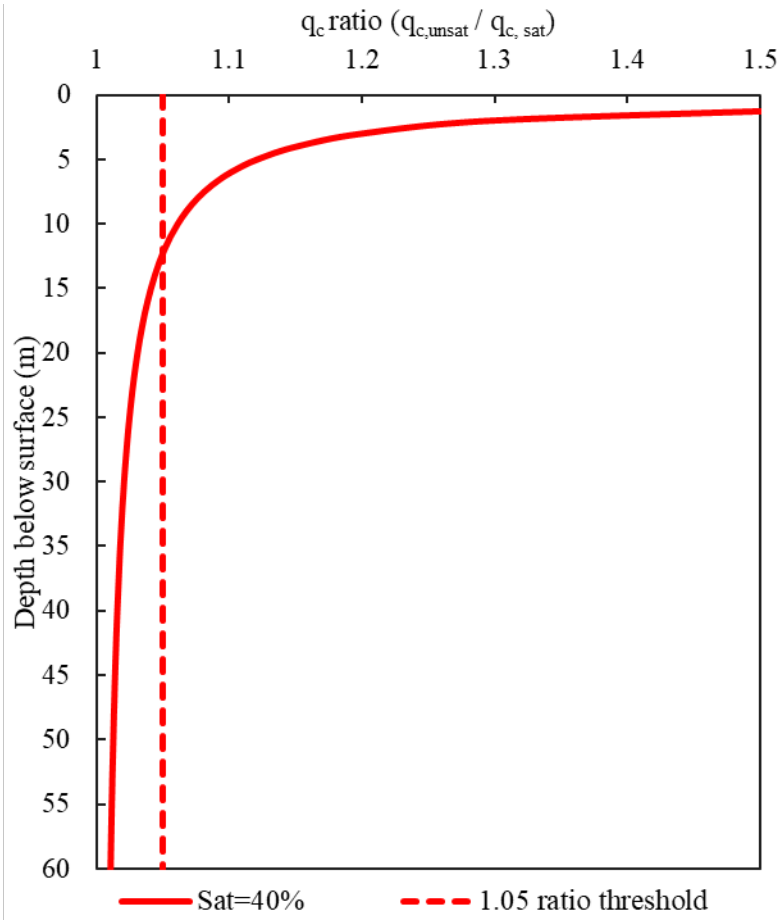


Figure 4: q_c ratio with depth, assuming constant 40% saturation and K_0 = 0.5

Saturation study discussion and findings

The data for Germano Complex indicate that the effect of matric suction on unsaturated strength of the silty sand tailings is limited to shallow overburden stresses where the relative magnitudes of overburden stress to suction hardening are comparable. This effect reduces rapidly below 5 m depth, and becomes negligible below 10 m. These findings are supported by Robertson et al. (2017), who arrived at similar observations for silty sand tailings material, that the effects of suction hardening are only significant at low overburden stresses (typically < 5 m below ground surface, where the magnitudes of effective stress and matric suction are comparable) but reduces significantly with depth as overburden stress increases.

The concept of apparent cohesion, c_{app}', is key to understanding why the twinned CPTu data profiles are similar within the Fringe Zone. Apparent cohesion describes the additional tensile stress due to surface tension of pore water in the unsaturated soil matrix and is included as a term in Bishop's equation for unsaturated shear strength. This cohesion increases the unsaturated shear strength but drops to zero as saturation approaches 100%. The apparent cohesion is calculated using the following equation:

$$c_{app}' = X \cdot (u_a - u_w) * \tan \phi' \quad \text{(Equation 4)}$$

where ϕ' is effective friction angle, which for Germano silty sand tailings is 32° (Dawson et al., 2019); $X \cdot (u_a - u_w)$ can be estimated directly from the saturation profiles with a conservative upper bound of 9 kPa from Figure 3 (right).

For an upper bound $X \cdot (u_a - u_w)$ of 9 kPa, the corresponding c_{app}' is 6 kPa, which is much less than the overburden stresses estimated within the Fringe Zone: 500 – 700 kPa (assuming a unit weight of 20 kN/m^3 for the Germano silty sand tailings). This supports the consistent q_c distributions shown in Figure 2 when comparing saturated (2017, black) vs. saturated (2021, red) data CPTu profiles. These distributions would diverge if the Fringe Zone were located at shallower depth, < 10 m, with unsaturated data inferring an artificially stronger (and possibly dilative) material due to suction hardening.

The q_c ratio profile presented in Figure 4 can be applied to correct the unsaturated CPTu data for the influence of suction hardening. The corrected q_c profile for the 2021 CPTu sounding is presented in Figure 5 in red against elevation, with the uncorrected data profile shown dashed in blue for comparison.

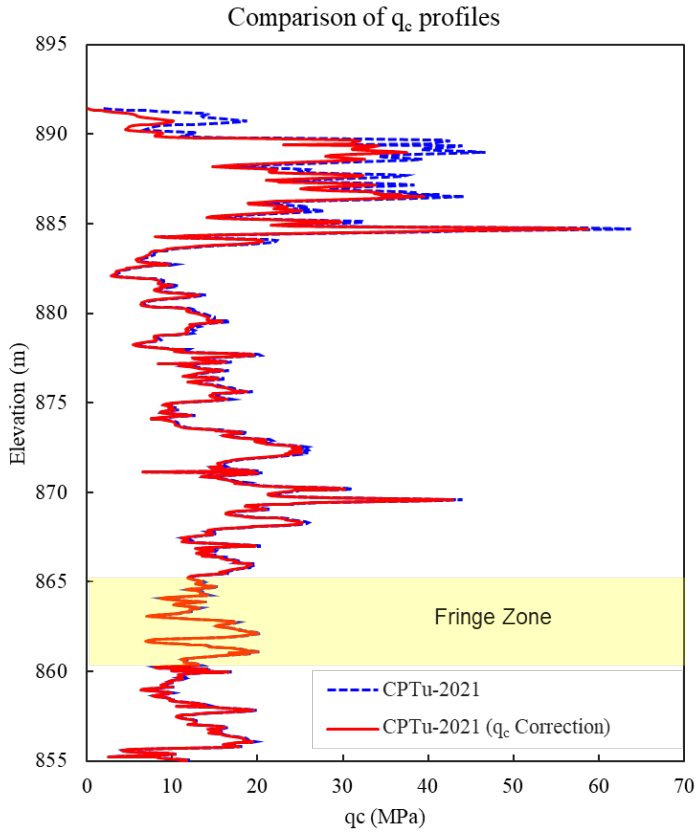


Figure 5: Comparison of raw (blue) vs. correct (red) unsaturated CPTu q_c profiles

Small differences in the two profiles appear to be present for the upper 5 m, where the corrected q_c profile is less than the uncorrected profile, and the two profiles are almost identical below elevation 886 m.

The Fringe Zone is highlighted in yellow for reference and supports the initial Phase 1 findings of similar $Q_{tn,cs}$ values when comparing 2017 to 2021 data (Burgin et al., 2021).

The relationship between decreasing q_c correction and increasing depth is further emphasized in Figure 6, that presents raw (blue) and corrected (red) 2021 CPTu data on the modified Robertson SBT_n plot for three (3) depth ranges. The leftmost plot presents data collected from 0-5 m below ground surface and highlights the pronounced effect of suction hardening at shallow depth, with a large shift in inferred soil behaviors towards increasing normalized cone resistance and reduced normalized friction when comparing the raw with corrected data. The middle plot captures data between 5–10 m depth with increasingly similar but still different soil behavior distributions, and the decreased influence of suction hardening as overburden stress increases. The rightmost plot captures data collected from 27–32 m below ground surface (Fringe Zone) with no discernable shift in raw and corrected data profiles.

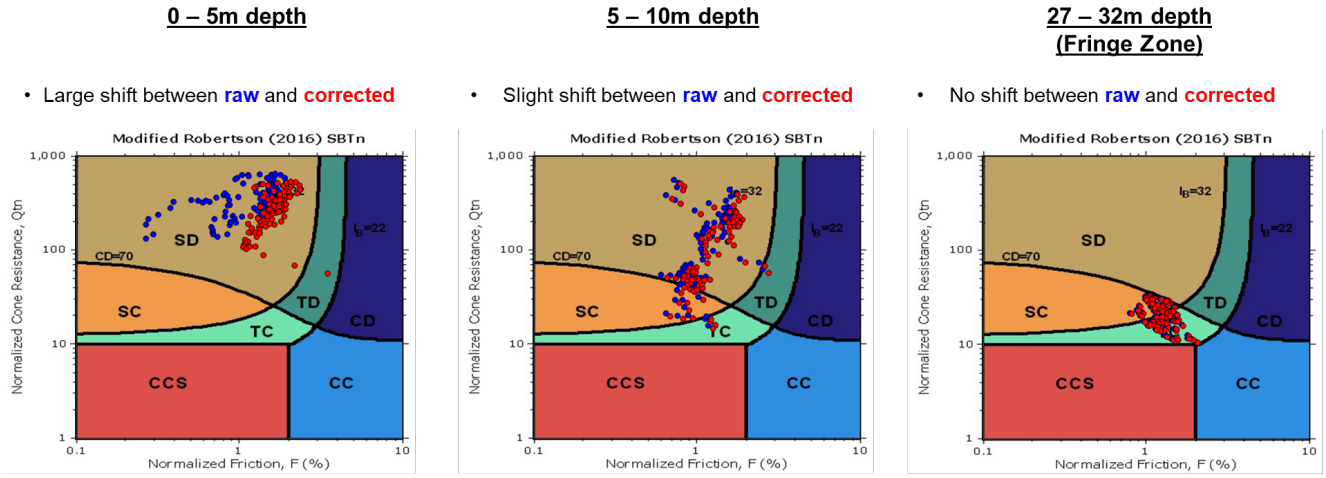


Figure 6: Comparison of raw and corrected 2021 CPTu data at different depth ranges

Conclusion

By combining the findings from both Phase 1 and Phase 2 of this unsaturated tailings study, Stantec has arrived at the following key conclusions for the unsaturated behavior of Germano silty sand tailings:

- Saturation levels at Germano Complex above the water table typically range from 10% to 50%. These values are much less than would be considered susceptible to liquefaction (i.e., S<85%).
- Impacts of suction hardening are significant up to 5 m depth and decrease to negligible beyond 10 m.
- Plots of normalized CPTu data with and without corrections for matric suction show that dilative unsaturated silty sand tailings will not shift to contractive behavior upon saturation beyond 10 m depth.

Acknowledgements

The authors wish to express our thanks to our clients, our peers in the tailings industry, and our colleagues and project team at Stantec Consulting Ltd for their support and encouragement.

References

Bishop, A.W. 1959. The principle of effective stress. *Teknisk Ukeblad.* 106: 859–863.

Burgin A., R. Dawson, M. Pinheiro, M. Wacowich and A. Vasconcelos. 2021. CPT_u assessment: investigating how a changing groundwater table may impact data collection and interpretation. *Proceedings of the 25th International Conference on Tailings and Mine Waste*. Banff, Alberta. University of Alberta Geotechnical Center: 225–233.

Dawson, R., A. Burgin, M. Wacowich, J. Bernardo and A. Vasconcelos. 2019. Laboratory and CPT_u characterization of Samarco sand tailings. *Proceedings of Tailings and Mine Waste 2019:* 1421–1433.

Pournaghiazar, M., A.R. Russell and N. Khalili. 2013. The cone penetration test in unsaturated sands. *Géotechnique* 63(14): 1209–1220.

Robertson, P.K. and Wride, C.E. 1998. Evaluating cyclic liquefaction potential using the cone penetration test. *Canadian Geotechnical Journal* 35(3): 442–459.

Robertson, P.K. 2010. Soil behaviour type from the CPT: an update. *Gregg Drilling and Testing Inc.*

Robertson, P.K. 2016. Cone penetration test (CPT)-based soil behaviour type (SBT) classification system – an update. *Canadian Geotechnical Journal* 53(12): 1910–1927.

Robertson, P.K., A. Viana de Fonseca., B. Ulrich and J. Coffin. 2017. Characterization of unsaturated mine waste: a case history. *Canadian Geotechnical Journal* 54: 1752 – 1761.

Russell, A.R. and D. Reid. 2018. Pitfalls in interpretation of cone penetration test data recovered from unsaturated geomaterials. In R.J. Jewell and A.B. Fourie (eds), *Paste 2018: Proceedings of the 21st International Seminar on Paste and Thickened Tailings*, Australian Centre for Geomechanics, Perth.

Vanapalli, S.K., D.E. Fredlund and A.W. Clifton. 1996. Model for the prediction of shear strength with respect to soil suction. *Canadian Geotechnical Journal* 33(3): 379–392.

Vanapalli S.K. 2009. Shear strength of unsaturated soils and its applications in geotechnical engineering practice. *Proceedings of 4th Asia Pacific Conference on Unsaturated Soils, Newcastle, Australia.*

A New Implicit Kinetics Method to Estimate Shear Strength Mobilized in Liquefaction Flow Failures

Jiarui Chen, University of California, Davis, USA
Scott M. Olson, University of Illinois at Urbana-Champaign, USA
Soham Banerjee, University of Vermont, USA
Mandar M. Dewoolkar, University of Vermont, USA
Yves Dubief, University of Vermont, USA

Abstract

Quantifying the shear strength mobilized during a liquefaction-induced flow failure is of great importance for mitigating related geohazards. In particular, recent high-profile failures of mine tailings and fly ash impoundments, e.g., the Kingston fossil plant (2008), the Fundão tailings dam (2015), the Cadia tailings dam (2018), the Brumadinho tailings dam (2019), etc., have illustrated an urgent need to improve estimates of liquefied shear strength. This study tentatively proposes a new implicit kinetics method to better estimate the mobilized shearing resistance of liquefied soil from liquefaction flow failures. The method was developed using a database of 20 liquefaction-induced flow failures where a sliding-block type kinetics analysis has been performed. Using the results of the kinetics analysis in conjunction with limit equilibrium stability analyses and slope angles of the pre- and post-failure geometries, the authors defined a factor to adjust shearing resistances back-calculated from limit equilibrium stability analysis to account for the kinetics effects during failure, i.e., the momentum of the failed mass, when a sliding-block type analysis cannot be performed. The proposed method is expected to benefit the quantification of liquefied shear strength mobilized during flow failures.

Introduction

Liquefaction triggered by either static or cyclic loading can result in significant deformation of the soil mass involved in the failure. If the failure involves a tailings dam, e.g., Fundão tailings dam, millions of cubic meters of mine tailings can be released (Morgenstern et al., 2016). Those tailings may pollute downstream waters and cause billions of dollars of environmental damage (Ridley and Lewis, 2019). In addition, liquefaction flow failures may lead to loss of life and destruction of infrastructure, particularly if the failure occurs without warning, e.g., Córrego do Feijão Mine Dam I failure in 2019 (Robertson et al., 2019; de

Lima et al., 2020). Evaluation of these flow failures relies heavily on quantifying the mobilized shearing resistance of the liquefied soil mass, termed herein the liquefied shear strength, s_u(liq).

Among all methods for estimating s_u(liq), the case-history based method is valuable because the back-calculated value may reflect the actual strength of the liquefied soil mobilized during the failure if the adopted analysis protocol is scientifically sound. In addition, the back-calculated shearing resistance can be linked to field test indices such as the standard penetration test (SPT) blow count and cone penetration test (CPT) tip resistance, providing relatively easy-to-use correlations for engineering practice.

The kinetics of motion have long been recognized as an essential factor to properly back-calculate s_u(liq) from case histories. Davis et al. (1988) proposed a sliding-block method to account for flow kinetics and back-calculate s_u(liq) from the Lower San Fernando Dam failure. Seed and Harder (1990) also discussed the importance of kinetics (termed momentum/dynamic effects) in estimating s_u(liq) and incorporated the effects of kinetics in an unknown number of cases in their database. However, the procedure and the cases to which it was applied were not described explicitly. Later, Olson (2001) modified the Davis et al. (1988) kinetics method and applied it to 10 out of 33 flow liquefaction cases in an expanded case history database. Shortly thereafter, Wang (2003) developed the Zero Inertial Factor (ZIF) method based on the work of Olson (2001). Most recently, Weber (2015) modified a more refined kinetics method, originally developed by Tan et al. (2000), and re-named this method the Incremental Momentum Method (IMM), which details the evolution of the failed mass movement.

In this paper, the above-mentioned methods for incorporating the effects of kinetics are briefly reviewed, including their benefits and limitations. A tentative modified method then is proposed to overcome the limitations of other methods.

Expanded flow liquefaction failure case history database

First, an expanded database has been utilized in the current study to reduce uncertainties in estimating s_u(liq) from flow liquefaction failure cases. Previously, Olson (2001) and Muhammad (2012) consistently back-analyzed s_u(liq) and s_u(liq)/σ'_{vo}, where σ'_{vo} is the initial effective vertical stress, from a total of 60 case histories. Among those cases, the Kawagishi-Cho building and Fraser River delta case histories reported by Olson (2001) possess rather limited information compared to the other cases and were excluded from the current study. To the remaining 58 case histories, Chen (2022) added 13 new flow liquefaction failure case histories that were not available previously, and which occurred more recently than 2012, or had not been analyzed consistently. These were identified and back-analyzed. Thus, the current database has a total number of 71 case histories. Table 1 summarizes the newly identified flow liquefaction failure case histories. These cases are detailed in Chen (2022).

Table 1: Liquefaction flow failure cases compiled by Chen (2022) to add to database by Olson (2001) and Muhammad (2012)

	Name	Year	Location	Type	Apparent cause of failure
1	Pinto Valley tailings impoundment	1997	Arizona, U.S.A.	Tailings dam	Undrained failure
2	Tsukidate landslide	2003	Tsukidate, Japan	Natural slope	Seismic, 2003 Miyagiken-Oki earthquake (M = 7.0)
3	Mitsuke-Ohashi bridge embankment	2004	Nagaoka City, Japan	Bridge embank-ment	Seismic, 2004 Niigata-ken Chuetsu earthquake (M_{JMA} = 6.8)
4	Kingston dredge pond	2008	Tennessee, U.S.A.	Dredge pond	Flow liquefaction
5	Bank of North River near Dechapelle	2010	Dechapelle, Haiti	Riverbank	Seismic, 2010 Haiti earthquake (M_W = 7.0)
6	Bank of Grey River near Dechapelle	2010	Dechapelle, Haiti	Riverbank	Seismic, 2010 Haiti earthquake (M_W = 7.0)
7	Las Palmas tailings dam	2010	Near Talca city, Maule region, Chile	Tailings dam	Seismic, 2010 Maule, Chile earthquake (M_W =8.8)
8	Abukuma River levee at the Edano site	2011	Near Sendai City, Japan	River levee	Seismic, 2011 Tohoku earthquake (M_{JMA} = 9.0)
9	Kayakari Dam at Ohya Mine	2011	Ohya Mine, Japan	Tailings dam	Seismic, 2011 Tohoku earthquake (M_{JMA} = 9.0)
10	Naruse River levee at the Shimo-Nakanome site	2011	Near Sendai City, Japan	River levee	Seismic, 2011 Tohoku earthquake (M_{JMA} = 9.0)
11	Fundão Tailings Dam	2015	Near Mariana, Minas Gerais, Brazil	Tailings dam	Flow liquefaction
12	Northern Tailings Storage Facility Embankment at Cadia Valley Operations	2018	Orange, New South Wales, Australia	Tailings dam	Foundation failure
13	Córrego do Feijão Mine Dam I	2019	Brumadinho, Minas Gerais, Brazil	Tailings dam	Flow liquefaction

Note: M_W – moment magnitude; M_{JMA} – magnitude reported by the Japan Meteorological Agency; M – magnitude scale not available

General procedures for the analysis

To maintain consistency, the back-analysis procedures described herein follow those used by Olson (2001) and Muhammad (2012). Specifically, the analysis in the current study focuses on flow liquefaction cases that possess sufficient details, including the geometry, phreatic surface, soil properties, etc., to perform a sliding-block type kinetics analysis, termed an explicit kinetics analysis by the authors. Those cases are classified as Class A by Chen (2022), which incorporate three components: pre-failure geometry limit equilibrium (LE) analysis, post-failure geometry LE analysis, and explicit kinetics analysis.

Limit equilibrium analysis

Limit equilibrium (LE) analysis has served as the primary method to back-analyze pre-failure and post-failure geometries of liquefaction flow failures since the work by Seed (1987). However, it is widely acknowledged that the mobilized shearing resistance back-calculated by LE analysis from the pre-failure geometry approximates the static (driving) shear stress at the time of failure, which almost always exceeds the actual liquefied shear strength. On the other hand, LE analysis of the post-failure geometry typically yields a mobilized shear strength smaller than the actual liquefied shear strength (Olson, 2001). Therefore, in nearly all field case histories, the actual s_u(liq) is bounded by the shear strengths mobilized from LE analysis of the pre- and post-failure geometries. Whether the actual liquefied shear strength is closer to the upper bound derived from the pre-failure geometry or the lower bound derived from the post-failure geometry is generally related to the travel distance of the failed mass (Weber, 2015). As such, all analyses started with the LE back-analysis of the pre- and post-failure geometries (if available).

Explicit kinetics analysis

As mentioned before, to better estimate s_u(liq), Davis et al. (1988) proposed a kinetics method based on a sliding block model (Figure 1). Assuming an initial value for s_u(liq), Newton's second law ($F = ma$) can be used to estimate the acceleration, velocity, and displacement of the sliding block along the assumed travel path of the sliding block center of gravity (CG). When the calculated CG displacement matches the observed CG displacement, the assumed liquefied shear strength becomes the "correct" value. While this method is easy to apply and enables rapid sensitivity analysis of s_u(liq) (Tan et al., 2000), the analogy of a sliding block with mass cannot provide detailed information regarding the shape of the failed mass during flow, unlike some other simplified methods (e.g., Jeyapalan, 1980).

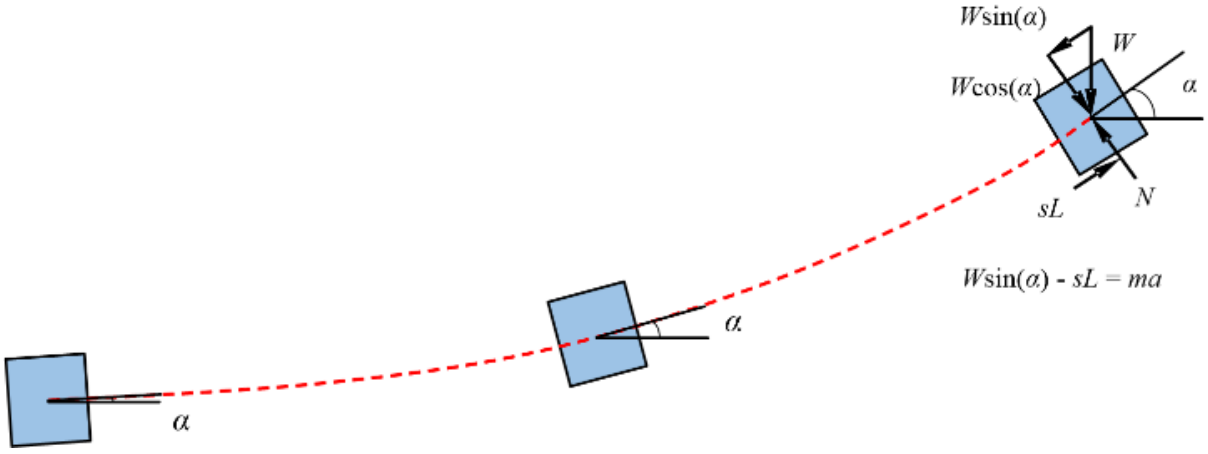


Figure 1: Sliding block analog to incorporate kinetics in the back-analysis of liquefaction flow failures

Olson (2001) proposed several modifications to the Davis et al. (1988) kinetics procedure, including (1) using a high-order polynomial rather than a hyperbola to represent the CG travel path for the failed mass; and (2) using automated functions to incorporate the evolving length of the sliding surface during flow, the shear strength of non-liquefied soil along the slip surface, and the potential effects of the failed mass sliding into a body of water (e.g., mixing and hydroplaning).

Tan et al. (2000) developed the dynamic runout analysis methodology (DRUM), applying Newton's second law to infer incremental geometries of the failed mass rather than representing the CG travel path using an equation. Building on the work of Tan et al. (2000), Weber (2015) proposed the Incremental Momentum Method (IMM). Similar to DRUM, IMM involves developing a series of estimated and feasible cross-sections that incrementally track the progression of displaced geometries from the inception of movements to the final, post-failure geometry. In essence, this details the movement of the sliding mass. As a result, both DRUM and IMM may be particularly useful in retrogressive failures. The only difference between DRUM and IMM is that IMM applies limit equilibrium analysis to each incremental movement stage. Despite the merits of DRUM and IMM, defining the incremental geometries requires significant engineering judgment, particularly if the initial and final slip surfaces are uncertain.

Expanding on the work of Davis et al. (1988) and Olson (2001), Wang (2003) developed the zero-inertial factor (ZIF) method. This method involves estimating the failed mass geometry such that the driving shear stress equals the shearing resistance (see Figure 2 [b] and [d]). At this condition, the total force, and therefore the acceleration, acting on the failed mass in the direction of movement is zero, i.e., zero inertial force. Using this concept, s_u(liq) can be back-analyzed directly from the zero-inertia geometry developed using the ZIF (i.e., the ratio between the failed mass displacement at zero acceleration and the total displacement for various points of reference in the geometry). As noted by Weber (2015), this procedure imposes another layer of uncertainty in addition to the uncertainties involved in the sliding-block analysis. Moreover, if the available case history data are not well suited for kinetics analysis, then the ZIF condition is hard to determine, and the uncertainty increases further.

Despite their differences, Chen (2022) found that s_u(liq) computed using these three methods reasonably agree, suggesting that the complexity of the kinetics analysis has a limited impact on the back-calculated values. Thus, the same kinetics method adopted by Olson (2001) and Muhammad (2012) was applied in this study. Among the four newly identified Class A cases (Table 2), only the Las Palmas tailings dam failure might be classified as a retrogressive failure, but the back-calculated s_u(liq) using the Olson (2001) method was nearly identical to that obtained by Moss et al. (2019) using IMM, suggesting that the Olson (2001) kinetics method was satisfactory for this case history.

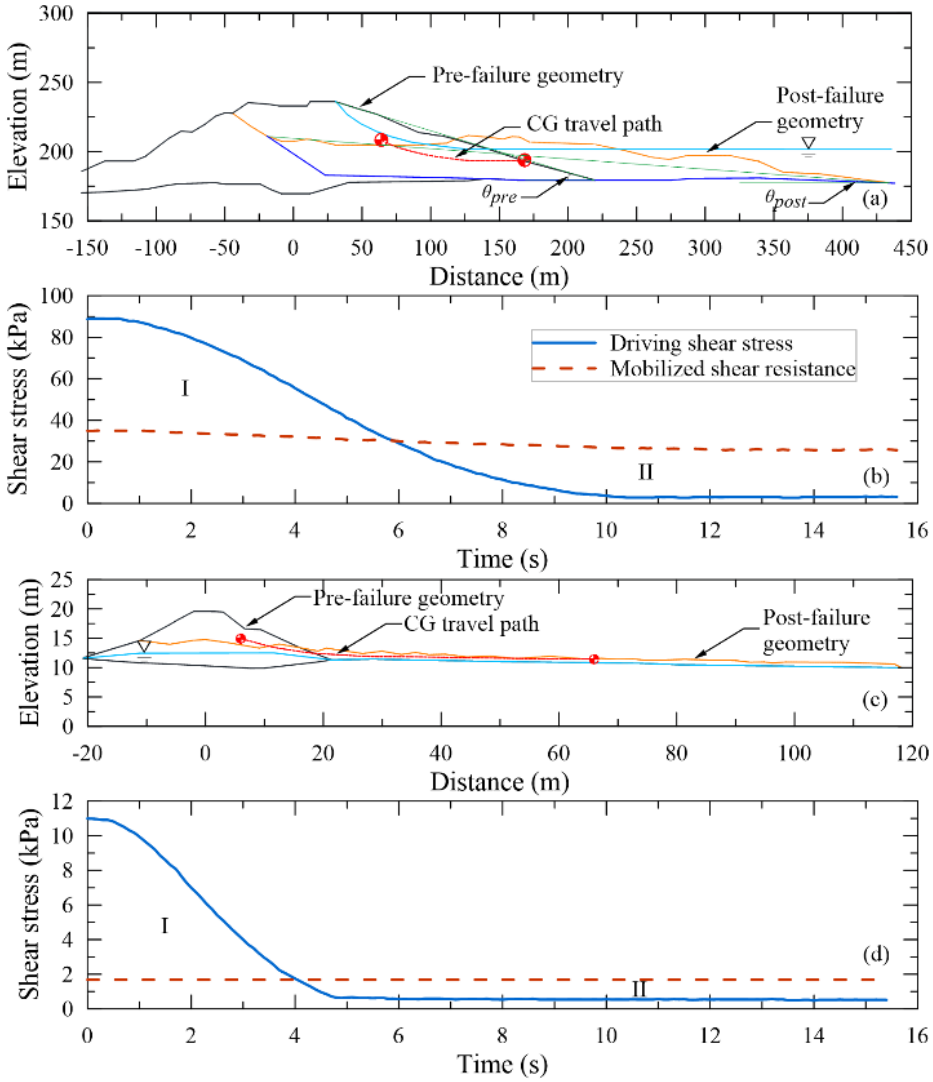


Figure 2: (a) Approximate center of gravity (CG) movement during Calaveras Dam flow failure; (b) driving shear stress and mobilized shearing resistance during Calaveras Dam failure; (c) CG movement during Uetsu railway embankment flow failure; (d) driving shear stress and mobilized shearing resistance during Uetsu railway embankment flow failure (adapted from Olson, 2001)

Proposed implicit kinetics method

Previous work and its limitations

While the explicit kinetics method, i.e., the sliding-block method, can be applied to well-documented liquefaction flow failures, an implicit method is needed to consider the effects of kinetics for cases with insufficient information to perform an explicit kinetics analysis. Weber (2015) proposed the following implicit method:

$$s_u(liq) = \xi(Weber) \times \frac{1}{2}[s_u(pre-failure\ geometry) + s_u(post-failure\ geometry)] \quad \text{(Eq. 1)}$$

where $\xi(Weber)$ is an empirical parameter that is a function of the travel path ratio (CG travel path distance divided by the initial slope height).

Weber (2015) suggested that the relationship between $\xi(Weber)$ and the travel path ratio could be well-defined. However, the applicability of the method may be poor in cases such as the subaqueous flow slide that occurred along the West Guide Bund of the Jamuna Bridge. In these cases, the initial height of the slope cannot be properly defined because the initial slide involved only a portion of a larger slope. In addition, this method also may be difficult to use for cases where the post-failure geometry is unavailable (e.g., Mochi-Koshi tailings dams or Feijão Dam I). Therefore, an alternative method was proposed in this study to overcome these limitations.

New implicit kinetics method

Wride et al. (1999) reported that the ratio between runout distance and initial slope height, which is similar to the travel path ratio defined in Weber (2015), is strongly related to the ratio between post and pre-failure slope angles ($\theta_{post}/\theta_{pre}$). Two extreme cases analyzed by Olson (2001) are shown in Figure 2. The Calaveras Dam flow failure exhibited the largest $\theta_{post}/\theta_{pre}$ among all 10 cases analyzed by Olson (2001) using an explicit kinetics analysis, while the Uetsu railway embankment exhibited the smallest $\theta_{post}/\theta_{pre}$. As illustrated in Figure 2 (b) and (d), the area of region I should be similar to the area of region II according to the impulse-momentum theorem:

$$\sum F_i \Delta t = m v_t - m v_o \quad \text{(Equation 2)}$$

$$F_i = W_i \sin \alpha_i - s_i L_i \quad \text{(Equation 3)}$$

where F_i is the net force acting on the sliding block in the direction of movement at any time t; v_o is the initial velocity of the sliding block; v_t is the final velocity of the sliding block; Δt is the time step in the numerical integration when calculating velocity and displacement for the sliding block; W_i is the weight of the failed mass at any time t; α_i is the angle between the horizontal and the tangent to the CG travel path at any time t; s_i is the mobilized resistance at the sliding block base at any time t; L_i is the slip surface length of the failed mass at any time t.

In all flow failures, the initial and final velocity, v_o and v_t, respectively, should be zero. The driving shear stresses in Figure 2 (b) and (d) reflect the evolution of the average slope angle of the failed mass, θ, where the pre-failure and post-failure average slope angles are defined in Figure 1. The initial slope angle tangent to the CG travel path (α in Figure 1 at $t = 0$) is similar to θ_{pre}. With the movement of the failed mass, α approaches θ_{post} (Figure 1). When $\theta_{post}/\theta_{pre}$ is small, the relative runout (i.e., runout distance divided by the slope height) usually is significant (Wride et al., 1999). Figure 2 (c) illustrates that, in this case, a majority of the travel time involved movement on a relatively gentle slope. Therefore, in Figure 2 (d), for Area I to match Area II, the mobilized shearing resistance must be closer to the driving shear stress near

the end of the movement, which is the back-calculated shear strength from the post-failure geometry. On the other hand, when $\theta_{post}/\theta_{pre}$ is large, the relative runout is usually small, and the shape of the driving shear stress time history (Figure 1 b) will be more-or-less centrosymmetric. In this case, for Area I to match Area II, the mobilized shearing resistance must be close to the average of the initial and final driving shear stresses, which is the average of the back-calculated shear strengths from the pre- and post-failure geometries.

Based on these observations, $\theta_{post}/\theta_{pre}$ was calculated for all well-documented cases that were analyzed by the sliding-block kinetics method in Olson (2001) and Muhammad (2012). In total, 20 cases were identified to be useful in this analysis. Key parameters are summarized in Table 2.

Table 2: Summary of geometry and kinetics analysis parameters for the Class A cases in the compiled expanded database

ID	Name	ϑ_{pre} (°)	ϑ_{post} (°)	$\vartheta_{post}/\vartheta_{pre}$	ξ
O-2	Wachusett dam - north dike	23.3	5.9	0.255	0.741
O-3	Calaveras dam	16.5	6	0.36	0.794
O-6	Fort Peck dam	14	2.9	0.204	0.586
O-10	Uetsu railway embankment	23.8	2.3	0.097	0.247
O-12	Koda Numa highway embankment	30.3	4.4	0.146	0.371
O-22	Hachiro-Gata road embankment	20.2	7.1	0.352	0.614
O-28	Lake Ackerman highway embankment	26.6	7.5	0.282	0.489
O-32	Shibecha-Cho embankment	32.2	7.2	0.224	0.541
O-33	Route 272 at Higashiarekinai	33.7	7.2	0.213	0.628
M-5	Okuli landslide	1.7	0.5	0.318	0.619
M-6	Sullivan tailings dam	21.9	3.4	0.153	0.915
M-10	Pashikuru (Route 38) road embankment	30.9	11	0.357	0.751
M-11	Itoizawa (Route 33) road embankment	27.1	6.2	0.23	0.429
M-18	Takarazuka landslide	18.3	6.9	0.377	0.903
M-20	Idenoshiri dam	26.2	7.4	0.283	0.719
M-26	Chang dam	22.4	7.8	0.349	0.741
C-2	Tsukidate landslide	11.5	5	0.433	0.716
C-7	Las Palmas tailings dam	29	5.2	0.178	0.417
C-8	Abukuma River levee, at the Edano site	25.9	10.3	0.399	1.134
C-10	Naruse River levee at the Shimo-Nakanome site	25.2	9.6	0.381	0.803

Identification (ID) nomenclature is C = Chen (2022); M = Muhammad (2012); and O = Olson (2001). Note that the numbering for M and O case histories is based on the original author's numbering to maintain consistency.

A tentative correlation between ξ and $\theta_{post}/\theta_{pre}$ follows and is illustrated in Figure 3, where:

$$\xi = 2.21\frac{\theta_{post}}{\theta_{pre}} \qquad \text{(Equation 4)}$$

and ξ was defined using shear strength ratios as follows to account for the changes in the representative initial effective vertical stress during the pre- and post-failure conditions.

$$\xi = 2\frac{s_u}{\sigma'_{vo}}\,(kinetics)/[\frac{s_u}{\sigma'_{vo}}\,(pre-failure\ geometry) + \frac{s_u}{\sigma'_{vo}}\,(post-failure\ geometry)] \qquad \text{(Eq. 5)}$$

The only outlier in Figure 3 is the Sullivan tailings dam, which was not used to regress Eq. (4). The large deviation of this case history from the trend may be attributed to its failure mechanism, which involved significant vertical displacement of a non-liquefied fill into liquefied tailings (Jefferies and Been 2006). This type of movement is not consistent with the assumed movement in the sliding-block kinetics method (Figure 1). For cases where the post-failure geometry was not available, θ_{post} was taken as the average slope angle of the ground surface where the failed mass traveled.

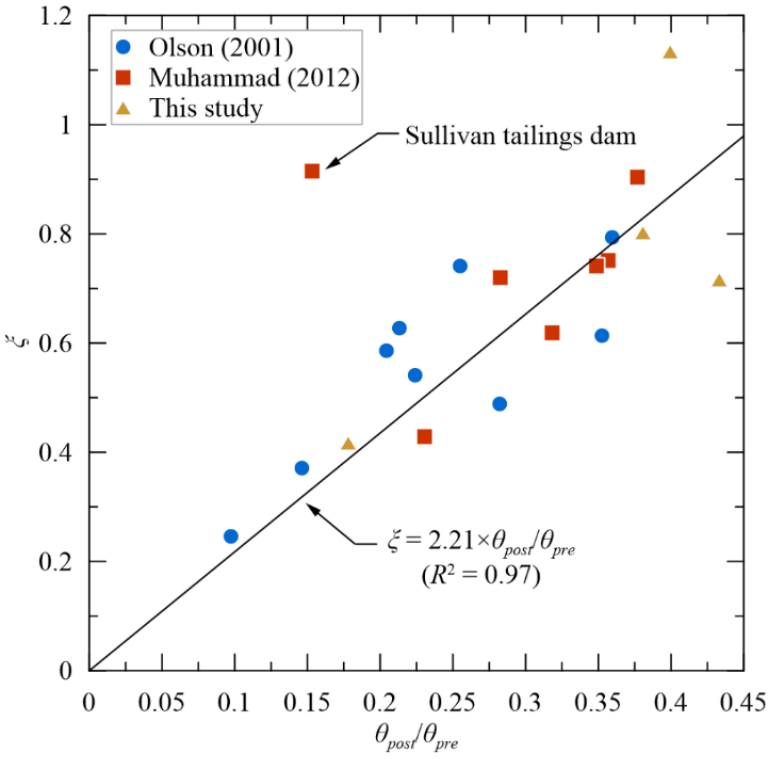


Figure 3: Tentative relationship between ξ and $\vartheta_{post}/\vartheta_{pre}$ using Class A cases in the updated field flow liquefaction failure database

Using this implicit kinetics approximation, the s_u(liq)/σ'_{vo} and s_u(liq) could be estimated tentatively for cases where an explicit kinetics analysis was not possible. It is suggested by the authors to limit ξ to a value of unity to be conservative. Thus, calculations can be done as follows.

$$\frac{s_u}{\sigma'_v}(kinetics) = \min\left(2.21\frac{\theta_{post}}{\theta_{pre}}, 1\right) \times 0.5 \times \left[\frac{s_u}{\sigma'_{vo}}(pre - failure\ geometry) + \frac{s_u}{\sigma'_{vo}}(post - failure\ geometry)\right] \quad \text{(Equation 6)}$$

$$s_u(kinetics) = \frac{s_u}{\sigma'_v}(kinetics) \times \sigma'_{vo}(post - failure\ geometry) \quad \text{(Equation 7)}$$

Additionally, the actual s_u(liq) should also be within the range of the values determined using the pre- and post-failure geometries.

Conclusion

This study focuses on an improved estimation of mobilized shearing resistance of the failed mass in a liquefaction flow failure, considering the kinetics of motion. Despite the existence of well-documented cases, over 70% of the current flow liquefaction failure case histories are not well-suited for a slide-block type kinetics analysis (termed explicit kinetics analysis by the authors), which can provide improved accuracy in estimating mobilized s_u(liq). A physics-based method is needed to enable use of case histories with less information to aid in geotechnical design of structures involving sloping ground (i.e., static shear stresses) and mitigate liquefaction-related geohazards.

As such, stemming from Newton's second law and the impulse-momentum theorem, the authors developed an implicit kinetics method, which utilizes slope geometry parameters and common LE analysis results. The tentatively proposed method should apply to a wider range of situations than other implicit kinetics methods because of the greater ease of obtaining the input parameters. Further research is ongoing to utilize the proposed implicit kinetics method to generate improved liquefied shear strength predictive models.

Acknowledgements

This work was supported by the U.S. National Science Foundation (Awards 1728199 and 1728172). Any opinions, findings, and conclusions or recommendations expressed herein are those of the authors and do not necessarily reflect the views of the National Science Foundation.

References

Chen, J. 2022. An investigation of liquefied shear strength using novel centrifuge tests, direct simple shear tests, and field case histories. Doctoral thesis, University of Illinois at Urbana-Champaign.

Davis, A.P., S.J. Poulos and G. Castro. 1988. Strengths backfigured from liquefaction case histories. In S. Prakash (ed.) *Proceedings of the 2nd International Conference on Case Histories in Geotechnical Engineering*. St. Louis: Missouri Univ. of Science and Technology: 1693–1701.

De Lima, R.E., J. de Lima Picanço, A.F. da Silva and F.A. Acordes. 2020. An anthropogenic flow type gravitational mass movement: the Córrego Do Feijão tailings dam disaster, Brumadinho, Brazil. *Landslides* 17(12): 2895–2906.

Jefferies, M.G. and K. Been. 2006. *Soil Liquefaction: A Critical State Approach*. First edition. London: Taylor and Francis.

Jeyapalan, K. 1980. Analyses of flow failures of mine tailings impoundments. Doctoral thesis, University of California, Berkeley.

Morgenstern N.R., S.G. Vick, C.B. Viotti and B.D. Watts. 2016. *Fundão Tailings Dam Review Panel: Report in the Immediate Causes of the Failure of the Fundão Da*m. New York: Cleary Gottlieb Steenand Hamilton LLP.

Muhammad, K. 2012. Case history-based analysis of liquefaction in sloping ground. Doctoral thesis, University of Illinois at Urbana-Champaign.

Olson, S.M. 2001. Liquefaction analysis of level and sloping ground using field case histories and penetration resistance. Doctoral thesis, University of Illinois at Urbana-Champaign.

Ridley, K. and B. Lewis. 2019. BHP to Defend Damages. Australia's Paydirt. 1(272): 13. https://search.informit.org/doi/10.3316/informit.488953503603013.

Robertson, P.K., L. de Melo, D.J. Williams and G.W. Wilson. 2019. *Report of the Expert Panel on the Technical Causes of the Failure of Feijão Dam I.*

Seed, H.B. 1987. Design problems in soil liquefaction. *Journal of Geotechnical Engineering* 113(8): 827–45.

Seed, R.B. and L.F. Harder. 1990. SPT-Based analysis of cyclic pore pressure generation and undrained residual strength. In J.M. Duncan (ed.) *Proceedings of the H.B. Seed Memorial Symposium,* Vancouver, BC: BiTech Publishers Ltd: 2, 351–76.

Tan, P., Y. Moriwaki, R.B. Seed and R.R. Davidson. 2000. Dynamic runout analysis methodology (DRUM). *Tailings and Mine Waste 2000*. London: CRC Press: 181–190.

Wang, C.H. 2003. Prediction of the residual strength of liquefied soils. PhD Thesis, Dept. of Civil and Environmental Engineering, University of Washington.

Weber, J.P. 2015. Engineering evaluation of post-liquefaction strength. Doctoral thesis, University of California, Berkeley.

Wride, C.E., E.C. McRoberts and P. K. Robertson. 1999. Reconsideration of case histories for estimating undrained shear strength in sandy soils. *Canadian Geotechnical Journal* 36(5): 907–33.

Seismic Deformation Analyses of Germano Main Dam Part I: Calibration of PM4Sand Model for Sand Tailings Using Field and Advanced Laboratory Test Data

Pu Yang, Stantec Consulting Services Inc., USA
Mehdi Qoreishi, Stantec Consulting Services Inc., Canada
Mauricio Pinheiro, Stantec Consulting Services Inc., USA
Evan Hsiao, Stantec Consulting Services Inc., USA

Abstract

The PM4Sand model is widely used to simulate the behavior of sand deposits subjected to seismic loading. The calibration of input parameters is essential for the model to successfully predict the pore water pressure development and resultant seismic deformations during a seismic event. This study presents a detailed calibration of the PM4Sand model for a potentially liquefiable iron ore tailings from Germano Main Dam, an upstream tailings dam located in the state of Minas Gerais in Brazil.

The calibration used site investigation data and advanced laboratory test results. Due to the thickness of the liquefiable material in the site (up to 60 m), the calibration was done in several steps to obtain stress-dependent relationships for the three primary input parameters of the constitutive model: relative density (Dr), shear modulus coefficient (G_o) and contraction rate parameter (h_{po}). First, the cone penetration testing (CPT) data together with empirical equations were used to determine the relationship between the effective vertical stress, the normalized corrected cone tip resistance (q_{c1N}), and the relative density (D_r). Second, Seismic CPT (SCPT) data were used to obtain the correlation between the confining pressure, the shear wave velocity, and the shear modulus coefficient (G_o). Third, based on the fines content of tailings, an empirical equation was introduced to correct the normalized cone tip resistance as well as the cyclic resistance ratio (CRR) curves that were computed using the CPT-based liquefaction triggering correlation by Idriss and Boulanger (2014).

A single element model was developed to simulate the stress controlled cyclic direct simple shear test to obtain hpo by matching the target cyclic stress ratio (CSR) of the simulation to the desired CRR curve. The process was repeated at multiple q_{c1N} levels to obtain a site-specific correlation between h_{po} and q_{c1N}. Finally, the laboratory cyclic direct simple shear tests were simulated to compare the simulation results against the laboratory data and to obtain the shear modulus reduction curve and the damping curve. The

simulated results were also compared with the empirical modulus reduction and damping curves from the literature for similar materials. Based on these comparisons, the last two steps were repeated until a relatively good match (based on engineering judgement) was achieved.

Introduction

The Germano Main Dam (GMD) is an upstream tailings storage facility located 25 km from Mariana, Minas Gerais, Brazil, which stores approximately 130 Mm^3 of sand tailings derived from iron ore mining and processing operations. The GMD structure spans the Córrego do Germano valley, located south of the Fundão basin and upstream of the New Santarém Dam, as shown in Figure 1.



Figure 1: Situational map of the Germano complex and battery limits for The Germano Main Dam

The facility was designed in the early 1970s, raised from a starter dam (known as Bechtel Dam), followed by multiple upstream raises, and by the decharacterization works after the Fundão failure. The impoundment received sand tailings up until the mid-1990s. Between 1997 and 2006, fine tailings and sand tailings were co-deposited throughout most of the reservoir.

Several studies, including the limit equilibrium analyses, a seismic assessment using QUAD4M, and a preliminary seismic deformation analyses using SLAMMER, have been done previously for the site in its as-is condition. However, it is necessary to introduce a detailed seismic assessment for the decharacterized

GMD in its long-term condition. The 2D finite difference method software FLAC8.0 (Itasca, 2017) was used to analyze the deformation behavior under seismic loading at the selected critical cross-section. As part of the study, this paper presents a detailed description of the calibration of advanced constitutive model PM4Sand, which is used to simulate the behavior of liquefiable material during seismic loading.

Site conditions and basic material properties

The GMD structure is composed of a variety of materials, ranging from engineered fills (Bechtel Dam, starter berm, decharacterization buttress, and rockfill drains) to contractive/dilative tailings. The structure is underlain by residual soils, which are dilative soil units that originated from weathered bedrock, and are underlain by saprolites, phyllites, and schists (simply referred to as "bedrock"). Figure 2 shows the most critical cross-section selected for the seismic deformation analysis.

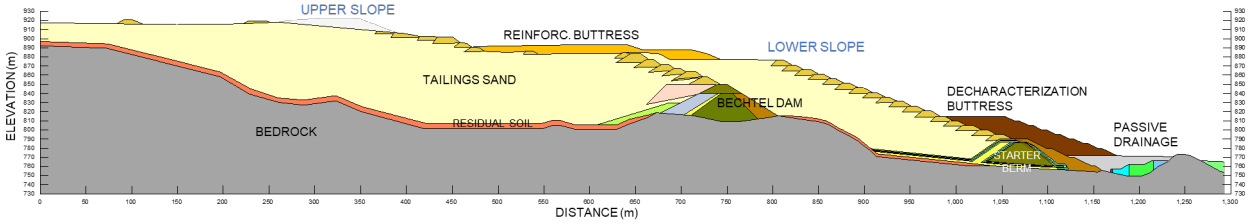


Figure 2: Selected cross-section of GMD for seismic deformation analysis

Table 1 summarizes the basic engineering properties of the materials encountered in the deformation analysis that were determined in previous analyses, together with the selected constitutive models.

Table 1: Conventional properties of materials encountered in the deformation analysis

Material	Unit weight (kN/m³)	Cohesion (kN)	Friction angle	Poisson's ratio	Density (kg/m³)	Gmax[1] (Pa)	Constitutive model
Bedrock	24	–	35°	0.30	2,250	440 MPa (Vs = 470 m/s)	Elastic
Residual Soil	18	5	25°	0.36	1,779	50% bedrock (Vs=235 m/s)	Elastic
Jet Grout	20	77	–	0.30	2,141	350 MPa	Mohr-Coulomb
Fill/Core	19	–	30°	0.35	2,040	$14000(\sigma'_m)^{0.50}$	UBCHYST
Drain/Rockfill/Buttress	20	–	35°	0.37	2,140	$43763(\sigma'_m)^{0.50}$	UBCHYST
Tailings – Compacted	20	–	33°	0.30	2,040	$23000(\sigma'_m)^{0.35}$	UBCHYST
Tailings	20	–	32°	0.30	1,781	$5400(\sigma'_m)^{0.52}$	PM4Sand/ UBCHYST

Note: [1] The equations for Gmax for different material are based on Vs data from SCPT tests performed at site

The PM4Sand is used to simulate the behavior of saturated tailings, which has the potential to liquefy during seismic events. The following section will discuss the calibration of the PM4Sand model with available field and laboratory test results. A brief description of the UBCHYST model calibration is also presented.

Calibration of the PM4Sand model

The PM4SAND model is a state-of-the-art constitutive model developed specifically for earthquake engineering purposes at the University of California at Davis (Boulanger and Ziotopoulou, 2017). Version 3.1, released on October 2017, was used in this study. The PM4SAND model follows the basic framework of the stress-ratio controlled, critical state compatible, bounding surface plasticity model for "sand-like" soil materials. The three primary parameters of PM4SAND are the apparent relative density (D_r), shear modulus coefficient (G_o), and contraction rate (h_{po}).

In this study, PM4SAND was used to represent the behavior of the saturated sand tailings material, which is potentially liquefiable during an earthquake. The field and laboratory test results were used to calibrate the model, as described in the following sections. Only the primary parameters were calibrated. The secondary parameters were set as the default values, as proposed by Boulanger and Ziotopoulou (2017).

Determination of the relative density (D_r)

As suggested by Boulanger and Ziotopoulou (2017), the relative density can be determined from the CPT results, based on the following equation:

$$D_R = 0.465\left(\frac{q_{c1N}}{C_{dq}}\right)^{0.264} - 1.063$$

where $C_{dq} = 0.9$; q_{c1N} is the normalized corrected CPT tip resistance.

The 30th percentile line from 24 CPTs from multiple site investigation campaigns was chosen to represent the penetration resistance profile (q_{c1N}) as a function of the effective vertical stress (σ_v'), as follows:

$$q_{c1N} = -\frac{1}{0.065}\ln\frac{\sigma_v'}{4283.7}$$

The selection of the 30th percentile is based on engineering judgement and on the results of the previous liquefaction analysis using QUAD4M software.

Determination of the shear modulus coefficient (G_o)

The shear modulus coefficient (G_o) can be determined from the following equations:

$$G = G_o p_A \left(\frac{p}{p_A}\right)^{1/2}$$

$$G = \rho \cdot (V_s)^2$$

where p_A is the atmosphere pressure, p is the confining stress, ρ is the density and V_s is the shear wave velocity.

The 30th percentile line from seven SCPT tests data was chosen to represent the shear wave velocity profile of the material, This was calculated as a function of the confining stress:

$$V_s = \frac{1}{0.0189} \ln \frac{\sigma'_m}{3.465}$$

Calibrating the contraction rate parameter (h_{po})

The contraction rate parameter (h_{po}) is used to obtain the target cyclic resistance ratio, which is commonly estimated based on CPT or SPT penetration resistances and liquefaction correlations. In this study, hpo was calibrated by matching the Cyclic Resistance Ratio values (CRR) from the FLAC single-element cyclic direct simple shear (CyDSS) simulations with the CRRM = 7.5 values from CPT-based liquefaction triggering correlation by Boulanger and Idriss (2014). For this purpose, a CPT-based estimate of CRR for an M = 7.5 earthquake and an effective overburden stress of 1 atm was assumed to be approximately equal to the CRR, corresponding to 15 uniform loading cycles causing a peak shear strain of 3% in CyDSS simulations.

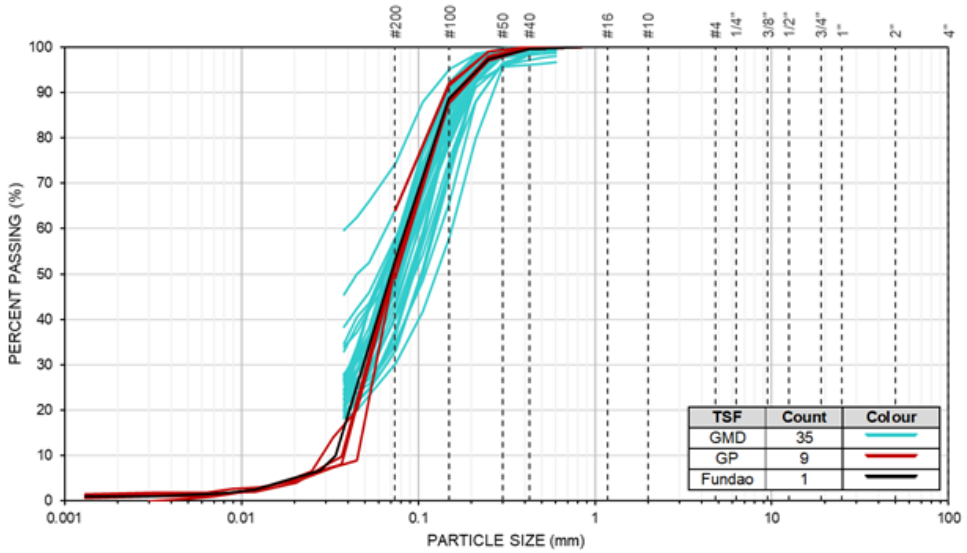


Figure 3: Particle size distribution of the tailings

Figure 3 shows the particle size distribution of the sand tailings material at Germano Mine. The tailings have a fines content of about 50%. This value was selected to correct the clean sand equivalent normalized cone tip resistance (q_{c1Ncs}) as follows:

$$\Delta q_{c1N} = \left(11.9 + \frac{q_{c1N}}{14.6}\right) \exp\left(1.63 - \frac{9.7}{FC+2} - \left(\frac{15.7}{FC+2}\right)^2\right)$$

The corrected q_{c1Ncs} was then used to calculate the CPT-based triggering correlation as follows:

$$CRR_{M=7.5,\sigma'_V=1\text{atm}} = \exp\left(\frac{q_{c1Ncs}}{113} + \left(\frac{q_{c1Ncs}}{1000}\right)^2 - \left(\frac{q_{c1Ncs}}{140}\right)^3 + \left(\frac{q_{c1Ncs}}{137}\right)^4 - 2.80\right)$$

The final selected correlation is presented in Figure 4.

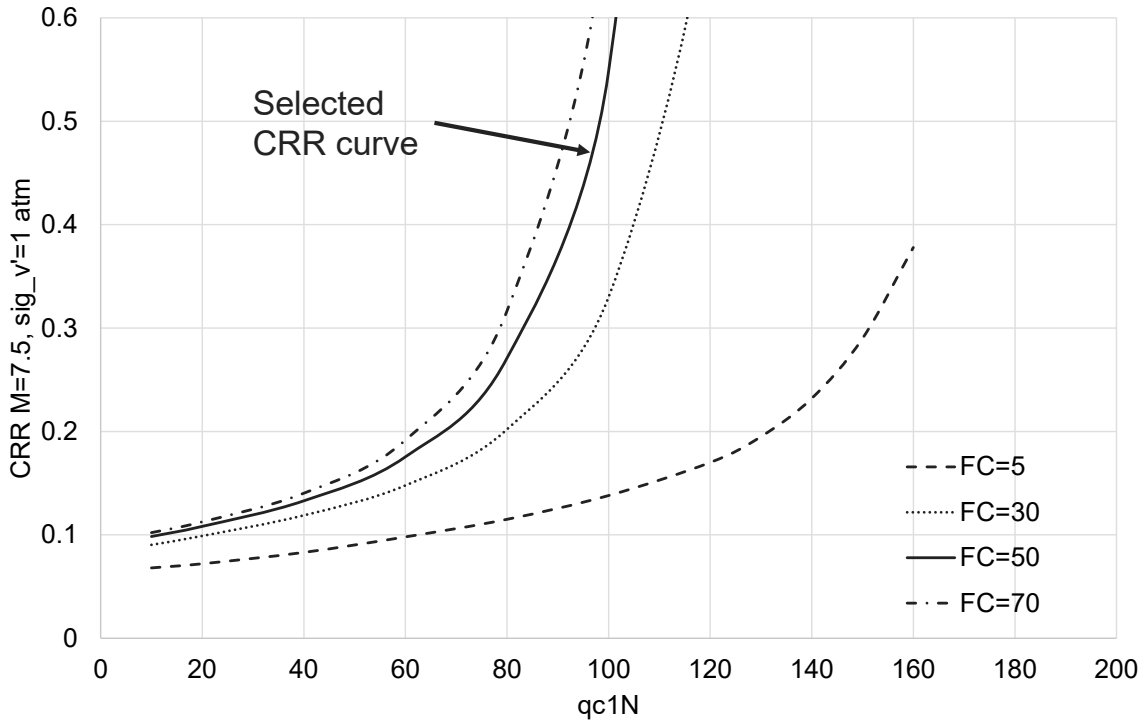


Figure 4: Deterministic CPT-based triggering correlation based on Boulanger and Idriss (2014)

Multiple single-element CyDSS simulations were then performed at various q_{c1N} levels within the modeling interest. A value of h_{po} was obtained at each q_{c1N} level by matching the CRR from simulation (reaches 3% shear strain at 15 uniform loading cycles with a confining stress of 1 atm) to the $CRR_{M=7.5}$ curve from Figure 4. Figure 5 shows the calibrated h_{po} at multiple q_{c1N} levels. A fitting function was used to correlate h_{po} with q_{c1N}, which is further related to the vertical effective stress, as previously described.

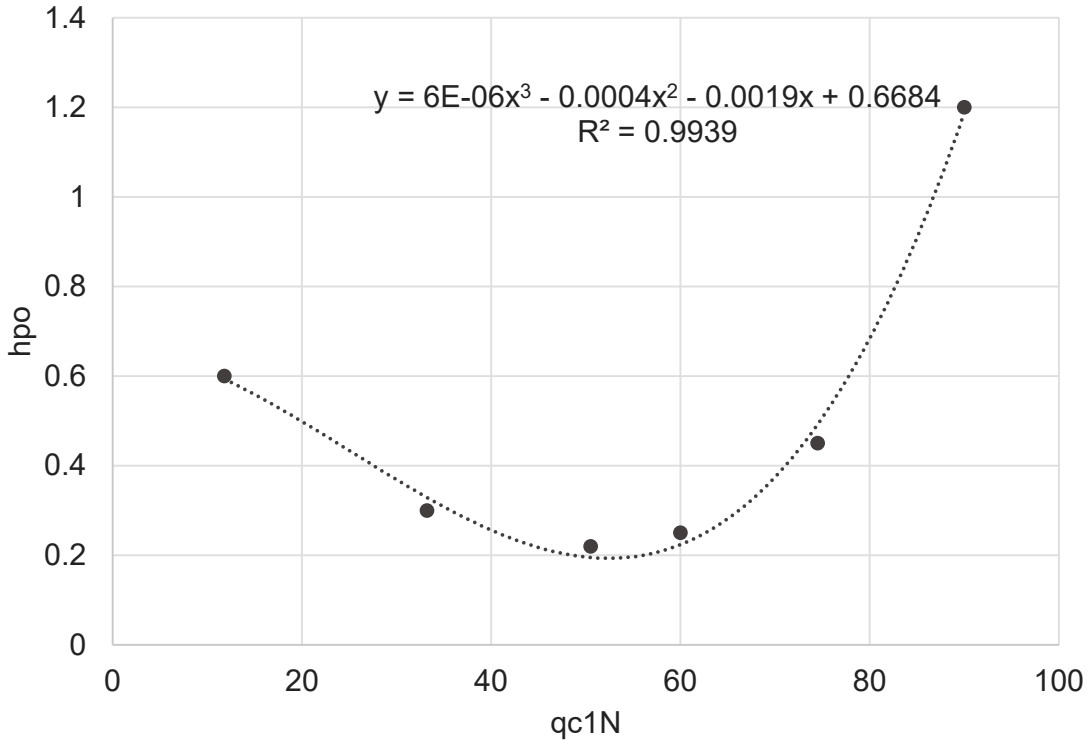


Figure 5: Calibrated h_{po} versus q_{c1N}

Verification with laboratory cyclic DSS tests

No cyclic DSS tests were carried out on the sand tailings material at GMD. However, multiple cyclic DSS tests were carried out on the sand tailings at Fundão TSF. The results are reported in Appendix D of the Fundão dam failure review panel report (Morgenstern et. al., 2016). Since the sand tailings at these two sites have similar granulometry and mineralogy, two of the cyclic DSS tests (DSS1 and DSS4) were selected to verify the calibration of the PM4Sand model in this study. A single element model was used to simulate the cyclic DSS test with the input parameters summarized in Table 2.

Table 2: Parameters used for simulating laboratory CyDSS tests

Test ID	q_{c1N}	q_{c1Ncs}	D_r	σ'_v (kPa)	σ'_m (kPa)	V_s (m/s)	G_o	h_{po}
DSS1	11.8	60.9	0.35	1,989	1,326	300	437.0	0.6
DSS4	0	46	0.2	4,284	2,856	325	349.5	0.6

The stress path, the stress strain curves, and the pore pressure ratio development were examined by comparing the simulated tests results against the laboratory data for both the DSS1 and DSS4 tests, as shown in Figure 6. A reasonable match between the simulated results and laboratory data were noticed for both the cases, which verifies the calibration of the PM4SAND model.

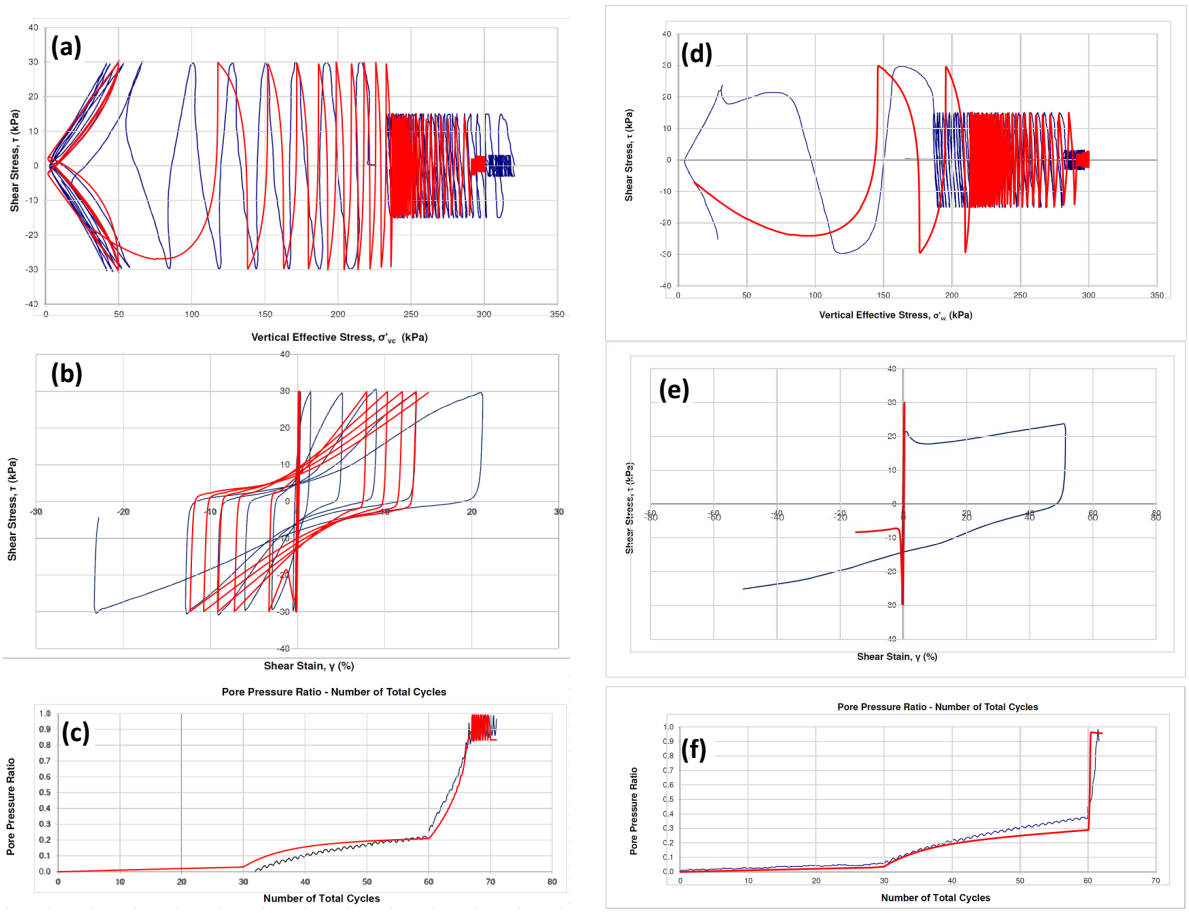


Figure 6: Simulated CyDSS test against laboratory test result of: DSS1 for (a) stress path, (b) stress-strain development, and (c) pore pressure ratio; DDS4 for (d) stress path, (e) stress-strain development, and (f) pore pressure ratio. The red line represents the simulation result and blue line represents laboratory data

Modulus reduction curves

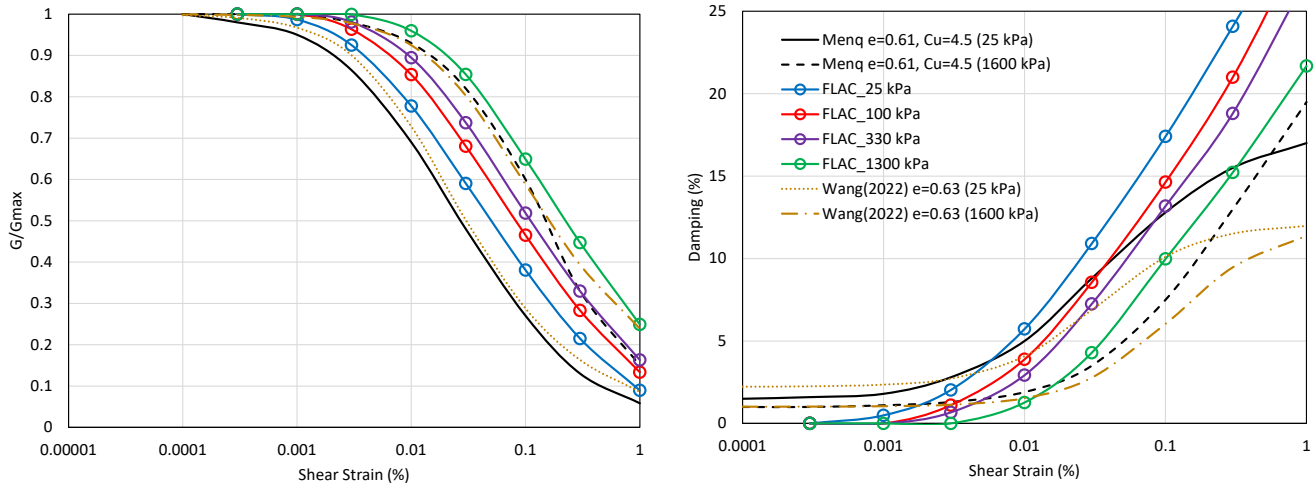


Figure 7: Modulus reduction curve for saturated tailings

Figure 7 shows the simulated shear modulus reduction curves and the damping curve for the saturated tailings, against the selected literature curves at the interested confining stress range. References used for these calibrations include (Wang and Stokoe, 2022) and (Menq, 2003). It is noted that the simulated reduction curves are generally in range with the literature reported curves, which further validates the calibration of the PM4SAND model.

Calibration of UBCHYST model

The UBCHYST model is a variation of the FLAC Mohr-Coulomb model in which the soil is considered non-linear below the failure envelope. Possible loss in stiffness and strength due to generation of excess pore pressure are not considered. The model is a user-defined model and operates within the FLAC Mohr-Coulomb model (Naesgaard, 2011).

In this study, the UBCHYST model was used to simulate the mechanical behavior of the non-liquefied materials, which include the unsaturated tailings, compacted tailings, fill/core and drain/rockfill/buttress. The selection of UBCHYST parameters is based mainly on the calibration against the previously determined modulus reduction curves, and engineering judgement. Table 3 summarizes the calibrated properties for all the materials. Figure 8 presents the calibrated modulus reduction curves against selected literature curves. References used for these calibrations include (Wang and Stokoe, 2022; Darendeli, 2001; Menq, 2003; Rollins et al., 1998).

Table 3: UBCHYST parameters calibrated for deformation analysis

Material	Density (kg/m³)	Friction Angle	Cohesion (kPa)		Rf	Hn	Modf1	Dfac	rm
Fill/Core	2,040	30°	0	$14000(\sigma'_m)^{0.50}$	0.98	0.9	1	0.1	0.8
Drain/Rock-fill/ Buttress	2,140	35°	0	$43763(\sigma'_m)^{0.50}$	0.6	1.5	1	0	0
Tailings – Compacted	2,040	33°	0	$23000(\sigma'_m)^{0.35}$	0.98	1.2	1	0.8	0.8
Tailings – Unsaturated	1,781	32°	0	$5400(\sigma'_m)^{0.52}$	0.98	2.2	1	0.8	0.8

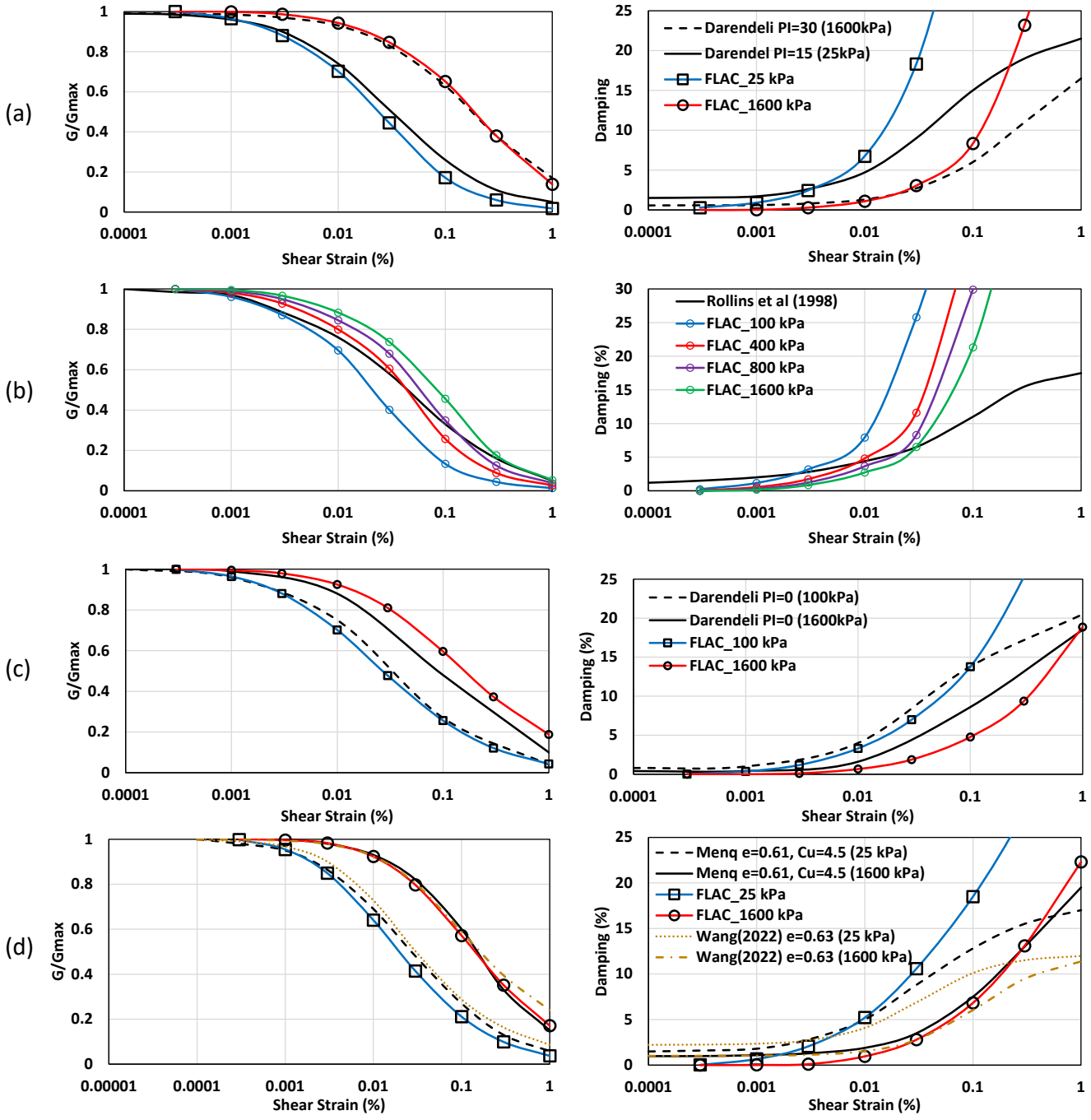


Figure 8: Calibration of UBCHYST model against modulus reduction curves from the literature for (a) fill/core, (b) drain/rockfill/buttress, (c) tailings compacted and (d) tailings unsaturated

Conclusion

This paper presents a detailed calibration of the PM4Sand model. The three primary input parameters of the constitutive model: relative density (D_r), shear modulus coefficient (G_o) and contraction rate parameter (h_{po}) were calibrated against penetration resistance based on site investigation data and verified using advanced laboratory test results. Stress-dependent relationships were obtained during the calibration process for these parameters, considering the thickness of the liquefiable material in the site (up to 60 m). The relative density (D_r) was related to the normalized corrected cone tip resistance (q_{c1N}) and effective vertical stress (σ_V') from cone penetration testing (CPT) data through empirical equations. The shear modulus coefficient (Go) was estimated based on the shear wave velocity (V_s) from seismic CPT (SCPT) data and expressed as a function of confining stress (σ_m'). An empirical equation was introduced to correct the normalized cone tip resistance (q_{c1N_CS}) and the cyclic resistance ratio (CRR) curves based on the fines content of tailings. The contraction rate parameter (h_{po}) was determined by matching the target cyclic stress ratio (CSR) of single element simulation of stress controlled cyclic direct simple shear test to the corrected CRR curve.

The process was repeated at multiple q_{c1N} levels to obtain a site-specific correlation between h_{po} and q_{c1N}. The laboratory cyclic direct simple shear tests were simulated to compare the simulation results against the laboratory data. The shear modulus reduction curve and damping curve were obtained through single element simulation of strain controlled cyclic direct simple shear test. The simulated results were also examined against the literature reported modulus reduction and damping curves for similar materials. A brief description of the UBCHYST calibration is also presented in this paper, as part of the complete calibration process that prepares all the constitutive models for the seismic deformation analysis that is to be discussed in part II of the authors' work.

Acknowledgements

The authors gratefully acknowledge support for this study from Jose Bernardo V. Rodrigues Oliveira and Jonathas Aparecido Alves Pinto from Samarco Mineração S.A. and insightful comments from Dr. Michael Beaty. Any opinions or positions expressed in this paper are those of the authors only.

References

Boulanger, R.W. and Idriss, I.M. 2014. CPT and SPT based liquefaction triggering procedures. Report No. UCD/CGM-14/1. Center for Geotechnical Modeling, University of California at Davis.

Boulanger, R.W. and Ziotopoulou, K. 2017. PM4Sand (Version 3.1): A Sand Plasticity Model for Earthquake Engineering Applications. Report No. UCD/CGM-17/01. Department of Civil and Environmental Engineering, University of California at Davis.

Darendeli, B.M. 2001. Development of a new family of normalized modulus reduction and material damping curves. Doctoral thesis, Department of Civil, Architectural, and Environmental Engineering, University of Texas at Austin.

Menq, F.Y. 2003. Dynamic properties of sandy and gravelly soils. Doctoral thesis, Department of Civil, Architectural, and Environmental Engineering, University of Texas at Austin.

Morgenstern, N.R., Vick, S.G., Viotti, C.B. and Watts, B.D. 2016. Report on the immediate causes of the failure of the Fundão Dam. Fundão Tailings Dam Review Panel.

Naesgaard, E. 2011. A hybrid effective stress – total stress procedure for analyzing soil embankments subjected to potential liquefaction and flow. Doctoral thesis, The University of British Columbia (Vancouver).

Rollins, K.M., Evans, M.D., Diehl, N.B. and Daily III, W.D. 1998. Shear modulus and damping relationships for gravels. *J. Geotech. Geoenviron. Eng*. 124(5): 396–405.

Wang, Y. and Stokoe II, K.H. 2021. Development of constitutive models for linear and nonlinear shear modulus and material damping ratio of uncemented soils. *J. Geotech. Geoenviron. Eng.* 148(3): 04021192.

Seismic Deformation Analyses of Germano Main Dam Part II Development of 2D FLAC Model and Sensitivity Studies

Pu Yang, Stantec Consulting Services Inc., USA
Mehdi Qoreishi, Stantec Consulting Services Inc., Canada
Mauricio Pinheiro, Stantec Consulting Services Inc., USA
Evan Hsiao, Stantec Consulting Services Inc., USA

Abstract

The Germano Main Dam (GMD) is an upstream tailings storage facility (TSF) situated north of Mariana, in the State of Minas Gerais, Brazil. The TSF received iron ore tailings from the late 1970s until 2013. The dam is currently going through the decharacterization process that is required by the latest local regulations. This paper presents a study of estimating the impacts of seismic events on the structure, as part of the decharacterization process.

A two-dimensional FLAC dynamic model was developed to estimate the range of excess pore water generation in the contractive tailings and the resulting seismic displacements of the structure. Existing field investigation data and laboratory tests results were used to calibrate advanced constitutive models: (a) PM4SAND for the saturated tailings, and (b) UBCHyst for unsaturated tailings and other non-liquefiable soil units. Staged construction of the structure was introduced in this study to mimic the stress conditions prior to the seismic event.

A base case analysis was first carried out to evaluate the model performance during designed earthquake time histories. Designed earthquake time histories were developed from the recorded earthquake time histories spectrally matched to the site-specific response spectra for a 10,000-year return period. Sensitivity analyses were then performed to evaluate the effect of some key factors to the model response including (a) the behavior of the model subjected to various earthquake time histories, and (b) the existence of pockets of weaker material in the tailings deposits. The development of excess pore pressures, shear strains and displacement at selected critical locations was evaluated. This study provided a systematic insight into the seismic performance of the Germano Main Dam.

Introduction

The Germano Main Dam (GMD) is an upstream tailings storage facility (TSF) located 25 km from Mariana, Minas Gerais, Brazil. GMD is the main dam of the Germano TSF, which stores approximately 130 Mm^3 of sand tailings and slimes derived from iron ore mining and processing operations. The GMD structure spans the Córrego do Germano valley, located south of the Fundão basin and upstream of the New Santarém Dam.

Several studies have been done previously to assess the seismic-induced failure potential regarding the as-is condition of the site, including simplified liquefaction assessments using QUAD4M, which concluded there was a low chance of development of liquefaction at this site. However, it is necessary to perform a detailed seismic assessment for the decharacterized GMD regarding the long-term condition to estimate the range of displacements and excess pore water pressures that would result from a seismic event. Thus, the finite difference method based 2D numerical model was developed with FLAC 8.0 to analyze the potential deformation behavior of the site under seismic loadings. As part II of the entire study, this paper describes a detailed development of a 2D FLAC model to capture the seismic deformation behavior of the selected GMD cross-section, together with two sensitivity studies that used to address the uncertainties of this study. The dam cross-section, site characterization and model calibrations are presented in Part I of this paper.

Design earthquakes and input ground motions

Table 1 summarizes the parameters of the design earthquake developed during the probabilistic site hazard analyses previously completed. The candidate seed time histories were selected from the PEER NGA-West2 database based on the following search criteria: magnitude (M) – 7.0 to 8.25; Rupture Distance (RRUP) – 35 to 195 km, 5–95%; Significant Duration – 27 seconds to 72 seconds. Figure 1 presents the final acceleration time histories used in the analyses, which are spectrally matched to design response spectra developed for this site.

Table 1: Input parameters for the design response spectra

Input parameters	Design event
M_w	7.75
R_{RUP} (km)	130
V_{S30} (m/sec)	470
Fault mechanism	Strike slip
Dip (deg)	90

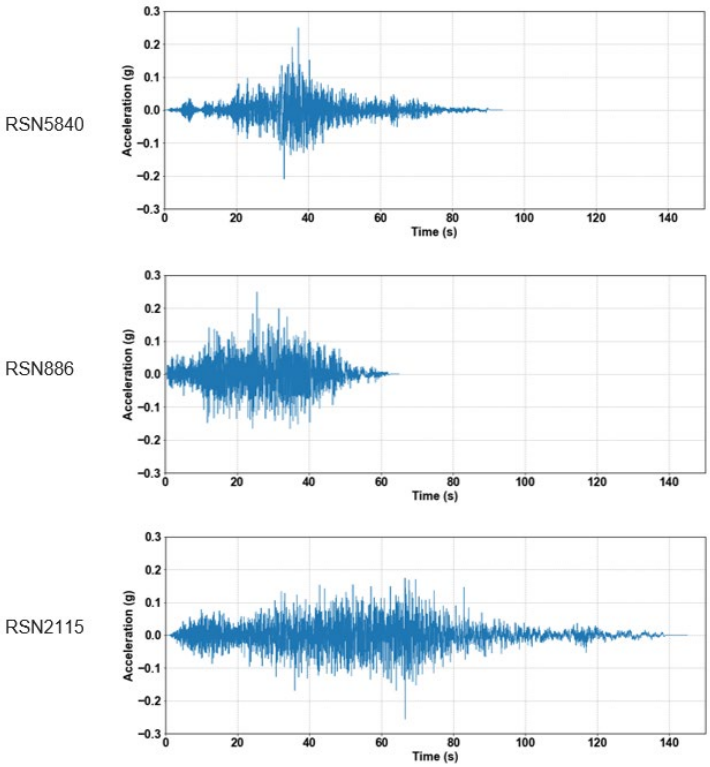


Figure 1: Acceleration time histories used in this study

Development of the base model

Material properties and constitutive models

In this study, the PM4SAND model (Boulanger and Ziotopoulou, 2017) was used for liquefiable material (saturated tailings), the UBCHYST model (Naesgaard, 2011) for all non-liquefiable materials, and the elastic model was used for bedrock. The basic engineering properties of all the materials and the detailed calibration of the PM4SAND model and the UBCHYST model were discussed in Part I of the authors' work (previous paper in this *Proceedings*).

Development of the base model in static conditions

Figure 2 shows the model geometry and the material zonation used in the FLAC analysis. A mesh size of approximately 2 m × 2 m was used in the FLAC model. A single element layer of bedrock was used at the base of the model where the ground motions will be applied during dynamic analyses. The model geometry was built in layers to approximately mimic the construction sequence of the structure, and to establish an initial stress distribution that closely represent the in-situ condition prior to the dynamic loading. For each layer of material, the density was gradually increased until the target value was reached, so as to avoid any potential stress concentration due to the sudden load from the new layer of material. The elastic model was

used for foundation material and the Mohr-Coulomb's model was used for other materials at the static stage.

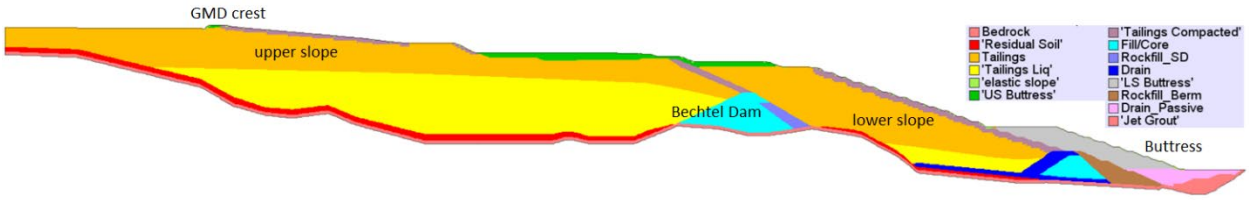


Figure 2: Geometry and material zonation of the FLAC model

The phreatic surface was introduced after all the layers had been built to initialize the pore pressure in the model domain. Figure 3 presents the initial distribution of pore water pressure, together with a solid line that represents the phreatic surface, which indicates that the pore water pressure was properly initialized.

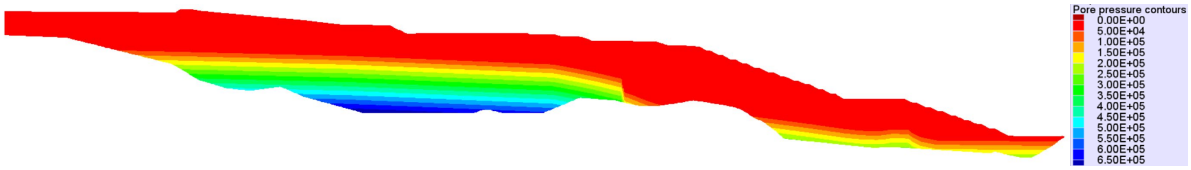


Figure 3: Initial distribution of pore pressure before dynamic analysis

Figure 4 shows the distribution of K_0 at the end of the static stage. Most of the model domain has a K_0 value close to 0.5, which is based on the results of pressure meter tests at the site. Figure 5 shows the K_α distribution at the end of the static stage (the ratio of static shear stress to vertical effective stress). The range of K_α for the majority part of the saturated tailings is less than 0.05, except for a limited area beneath the lower slope. No correction for the bias shear was considered in the modeling. Figure 6 shows the distribution of both horizontal and vertical stress at the end of static stage; no stress concentration was noticed from the figure. Such observations from these figures validate the stress initialization during the static stage.

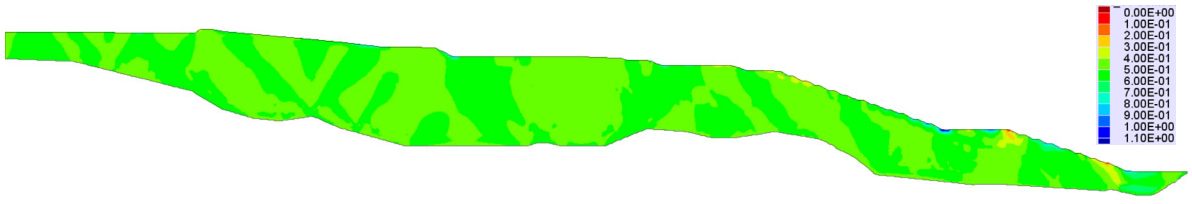


Figure 4: K_0 distribution at the end of static stage

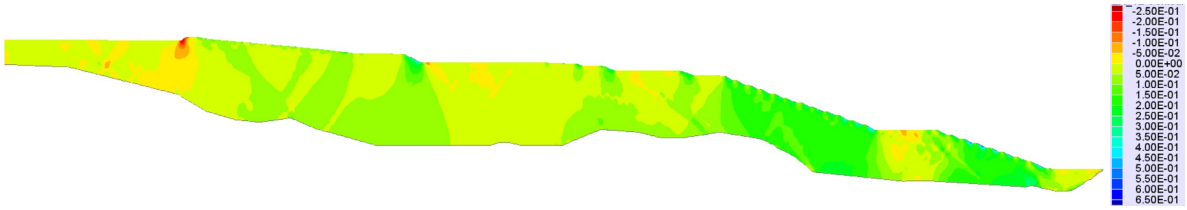


Figure 5: K_α distribution at the end of static stage

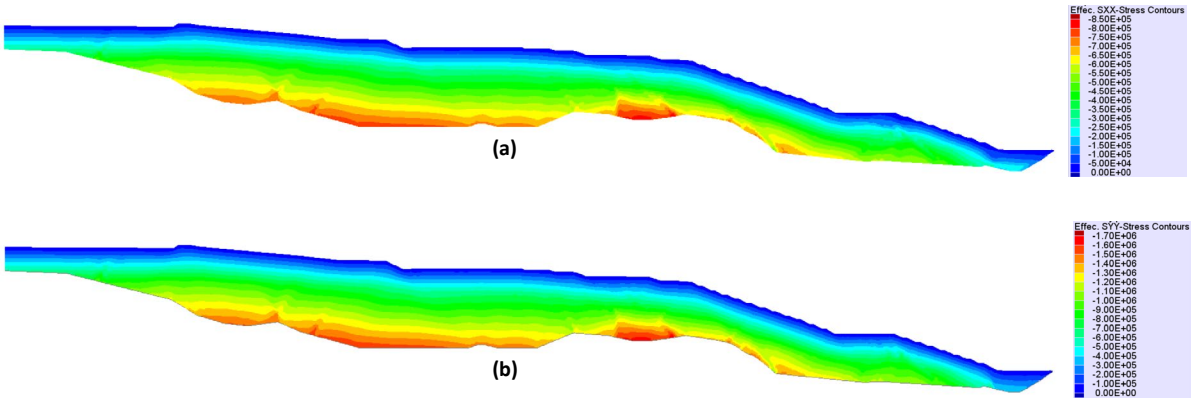


Figure 6: Distribution of (a) horizontal effective stress and (b) vertical effective stress at the end of the static stage

Model preparation for dynamic analysis

At the end of the static stage, the advanced constitutive models (UBCHYST and PM4SAND models) were initiated in the model to prepare it for the dynamic analysis. Figure 7 shows the distribution of the parameters used by PM4SAND during the initiation. The q_{c1N} ranges from 15 to 30, G_o ranges from 475 to 550 and h_{po} ranges from 0.3 to 0.6. The ranges of these parameters were in line with the PM4SAND calibration discussed in the first part of this paper, model calibrations. A Rayleigh damping of 0.5% was assigned to the base model, based on the recommendations for the PM4SAND model to prevent over damping of the saturated tailings. The dominant frequency of input motions designed for the site is 4 Hz (0.25 s). The time history RSN5840 was applied at the bottom of the bedrock layer as velocity histories.

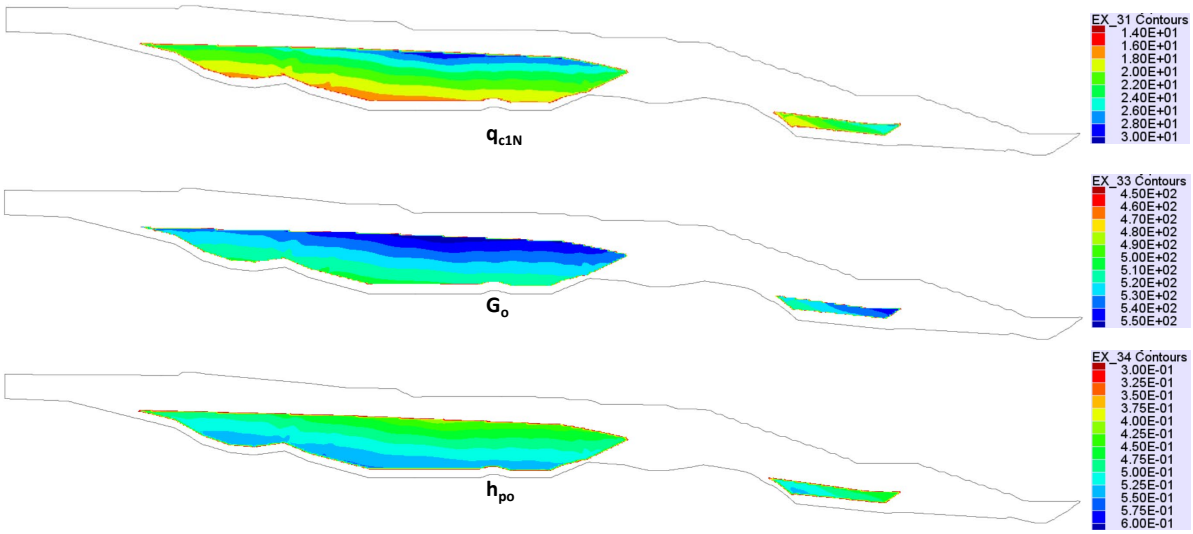


Figure 7: Distribution of PM4SAND parameters within the saturated tailings

Dynamic analysis results of the base model

The results of the seismic deformation analysis of the base model are shown in Figure 8 to Figure 13.

Figure 8 presents the deformed mesh at the end of the earthquake motion. Upwards deformation was noticed for both the upper slope toe area and the buttress toe area, which is likely due to the downwards sliding of the main body of the upper slope and the lower slope mass. On the other hand, downwards movement was observed at the crest of the lower slope, which is likely due to the sliding of the lower slope during the earthquake.

Figure 9 shows the maximum excess pore pressure ratio (Ru) distribution within the saturated tailings at the end of the dynamic analysis, with a maximum value of 40%. The presented Ru contour indicates that no liquefaction is triggered during the seismic loading for the base model.

Figure 10 presents the contour of the maximum shear strain increment at the end of the earthquake. Three potential shear planes were identified from the figure. The first shear plane starts at the upper slope crest, and passes through the bottom of the tailings deposits in the upper area and ends at the tailings – the Bechtel Dam interface, with a shear strain ranging from 0.5% to 1%. The second shear plane starts at the lower slope crest (the top of the Bechtel Dam), deeply seated into the bottom of the tailings, and reaches the base of the decharacterization buttress, with shear strain ranges from 1% to 3%. The identification of these two shear planes is consistent with the critical failure surfaces considered in the limit equilibrium analyses previously performed for the site. Additionally, a surficial shear plane was observed at the lower slope surface, with shear strain ranges from 5% to 7.5% and a depth of around 8 m.

Figures 11(a) and (b) show the horizontal and vertical displacement contours at the end of shaking. The horizontal and vertical displacements at the crest of GMD are 0.13 m and –0.21 m, respectively. The maximum horizontal and vertical displacements on the crest of Lower Slope (i.e., on the ground surface on top of Bechtel Dam) are 0.38 m and 0.17 m.

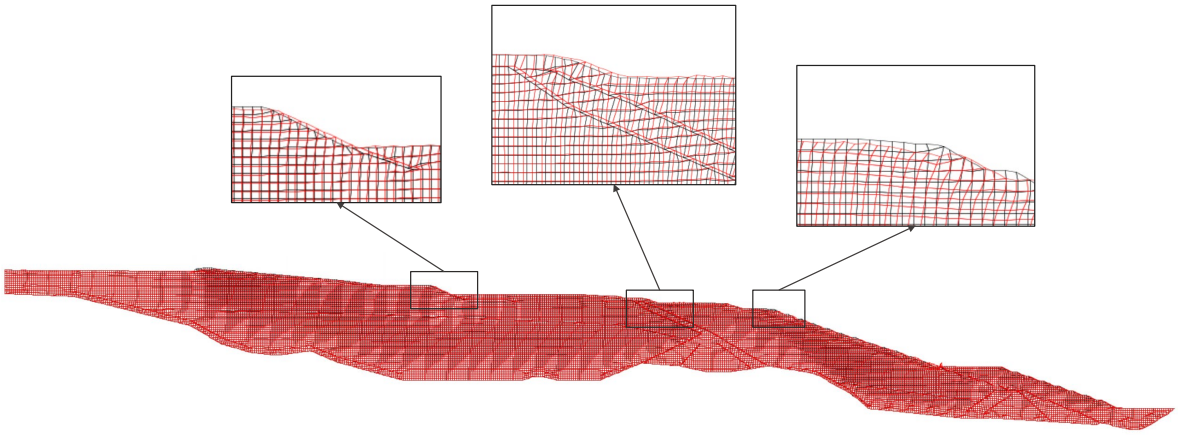


Figure 8: Deformed FLAC mesh at the end of motion, with a zoomed view at selected locations

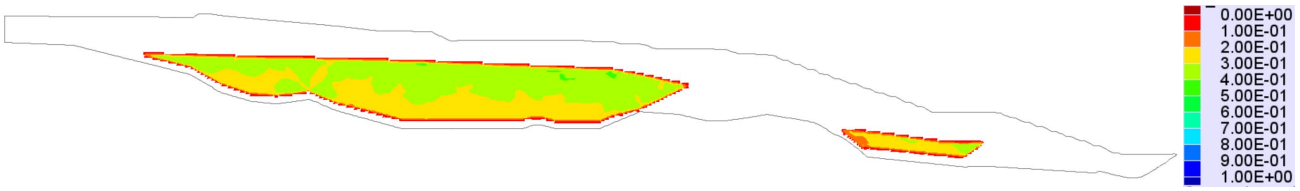


Figure 9: Maximum excess pore pressure ratio (Ru) contours at the end of motion

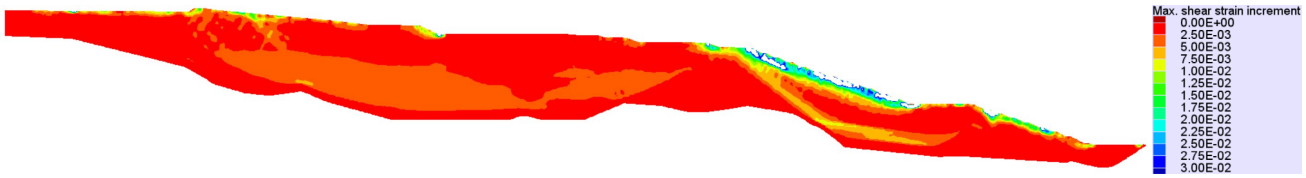


Figure 10: Maximum shear strain increment contours at the end of motion

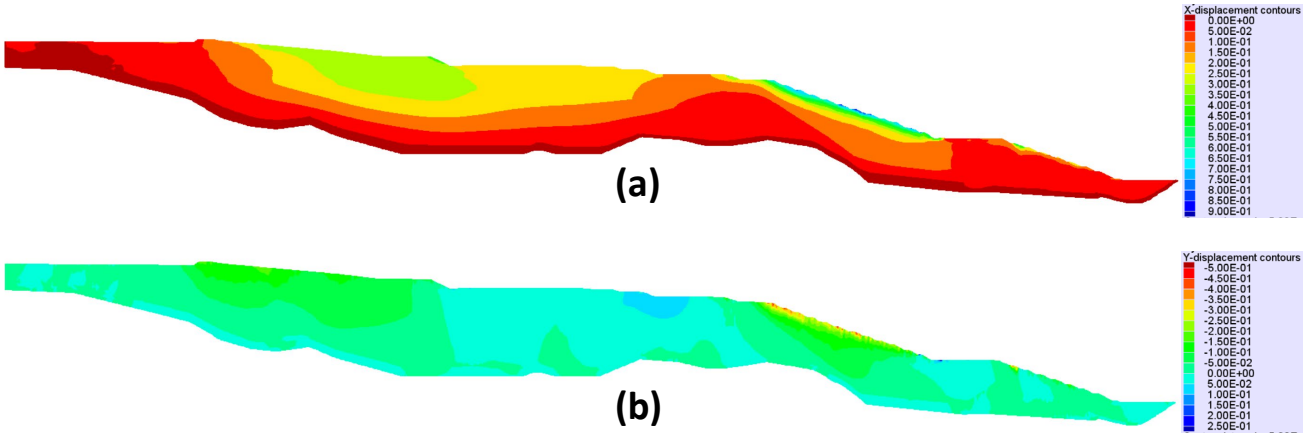


Figure 11: (a) Horizontal and (b) vertical displacement contours at the end of motion

Post-shake analyses

To perform post-earthquake analysis, the "Post-Shake" flag of the PM4SAND model was activated after 95% of the earthquake energy was transferred to the model (based on Arias Intensity). The simulation was continued for 40 more seconds past the end of shaking time in dynamic mode. Figure 12 shows the history of horizontal displacement, shear strain increment, and the Ru at selected locations. It showed negligible additional displacements during the post-earthquake phase. Minimal development of the shear strain increment was noticed initially, and it quickly reached a plateau during the post-earthquake analysis. No development of the Ru was noticed for the post-earthquake analysis. The rates of displacements are stabilized at the end of earthquake, and the movements are expected to cease at the end of shaking.

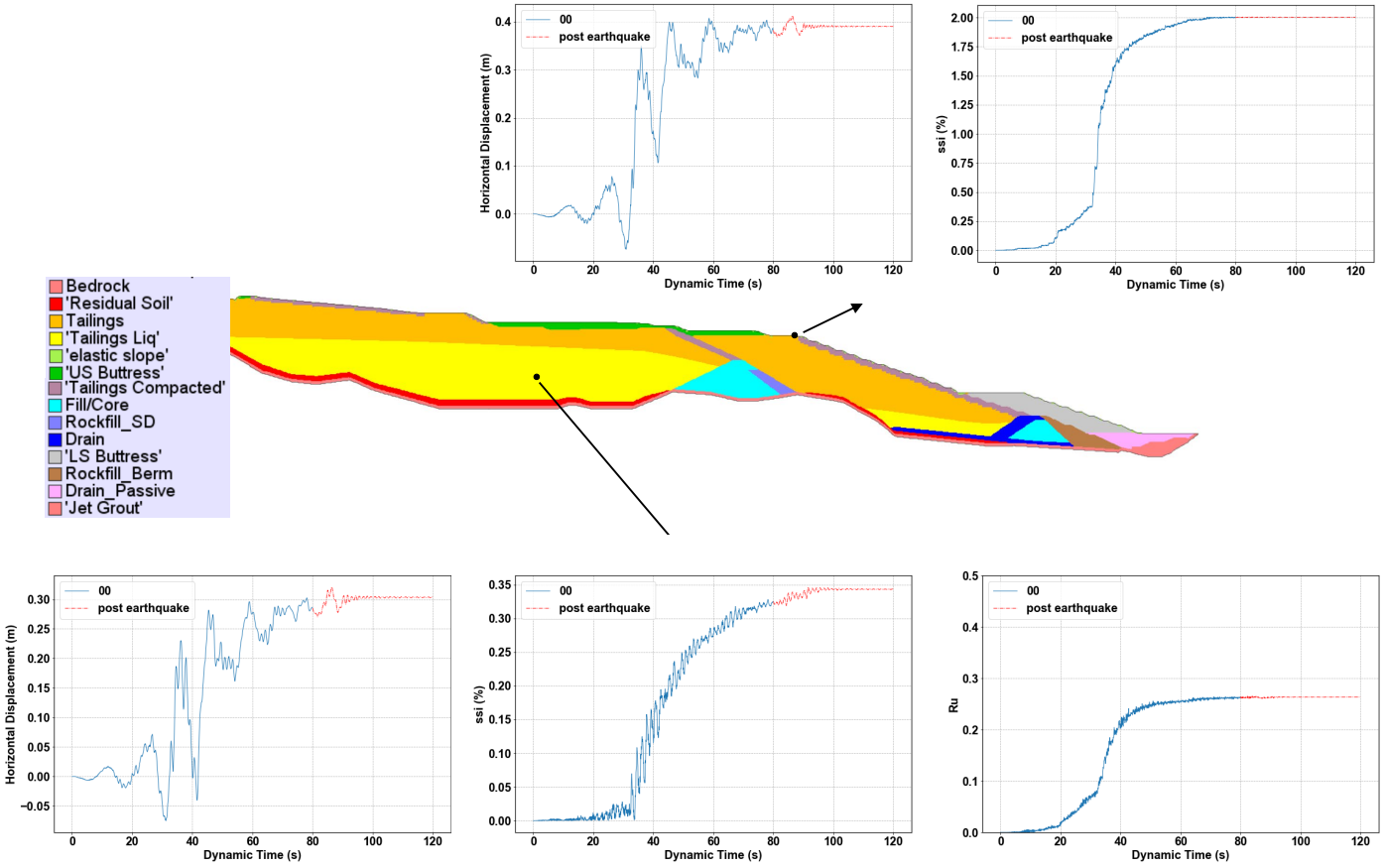


Figure 12: Element behavior at selected locations at the end of a post-earthquake analysis

Sensitivity studies

Two sensitivity studies are presented in this section to investigate the main uncertainties from the base model previously presented, which includes the uncertainty of the input ground motion, and uncertainty regarding the penetration resistance profile adopted from the CPT campaigns (30th percentile).

Earthquake motions

The two other time histories described earlier were applied to the base model to study the response of the structure; Case 41 used the ground motion RSN886 and Case 42 used the ground motion RSN2115. Figure 13 shows the contour of Ru at the end of shaking for all three ground motions and the Ru development history at selected locations. The ground motion RSN2115 leads to the largest development of Ru during shaking. A maximum Ru of 0.5 was observed at the lower slope saturated tailings, which is 67% higher than that of the base model.

Figure 14 shows the contour of shear strains at the end of shaking for all the three ground motions and the development of the shear strains at selected locations. While the results from the ground motion RSN5840 and RSN886 are in the same range, the ground motion RSN2115 leads to higher shear strains at the end of shaking. At the bottom of the lower slope saturated tailings, a maximum shear strain increment of 2.4% was observed, which was still in a reasonably low range of strains.

Table 2 summarizes the displacements at the end of shaking for all the three ground motions at selected locations. It is clearly noticed that ground motion RSN2115 (green color in Figures 13 and 14) has increased deformation compared with the other two motions. It should be noted that all three motions were spectrally matched to the same response spectra developed during the PSHA studies; however, RSN2115 has a significant duration of almost double that of the other two time histories, which contributes to the greater seismic response of the structure to this earthquake.

Table 2: Comparison of displacements at selected locations for different ground motions

Case ID	00 (RSN5840)		41 (RSN886)		42 (RSN2115)	
Location	Xdisp (m)	Ydisp (m)	Xdisp (m)	Ydisp (m)	Xdisp (m)	Ydisp (m)
GMD Crest	0.13	-0.210	0.22	-0.330	0.44	-0.580
Crest of Lower Slope	0.38	-0.170	0.53	-0.220	1.35	-0.540
Crest of Lower Buttress	0.12	-0.010	0.18	-0.015	0.35	-0.018

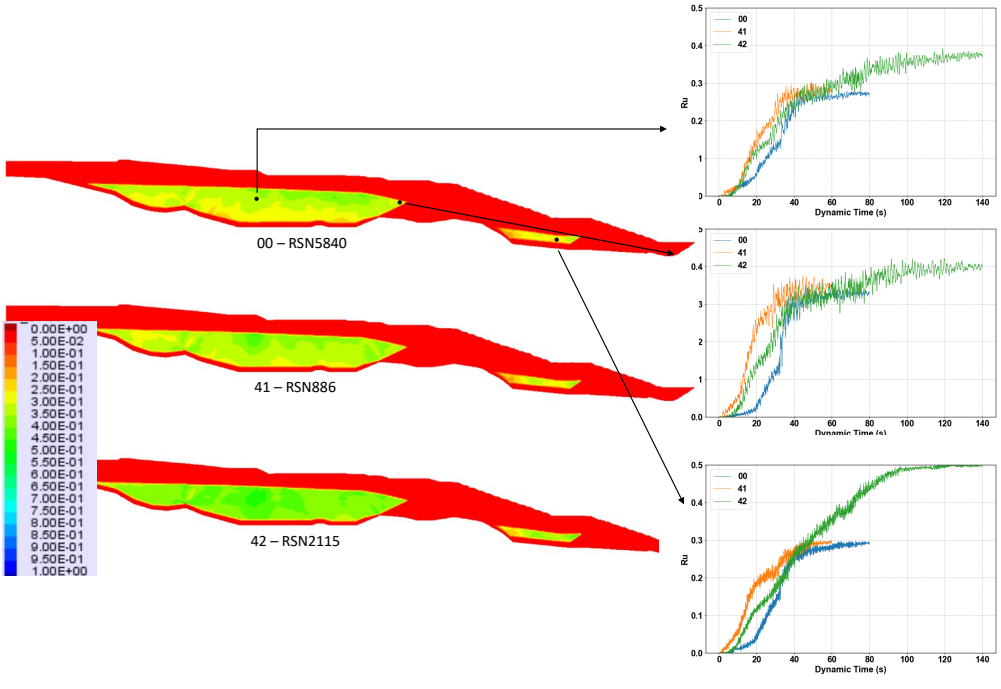


Figure 13: Ru distribution at the end of an earthquake for selected ground motions

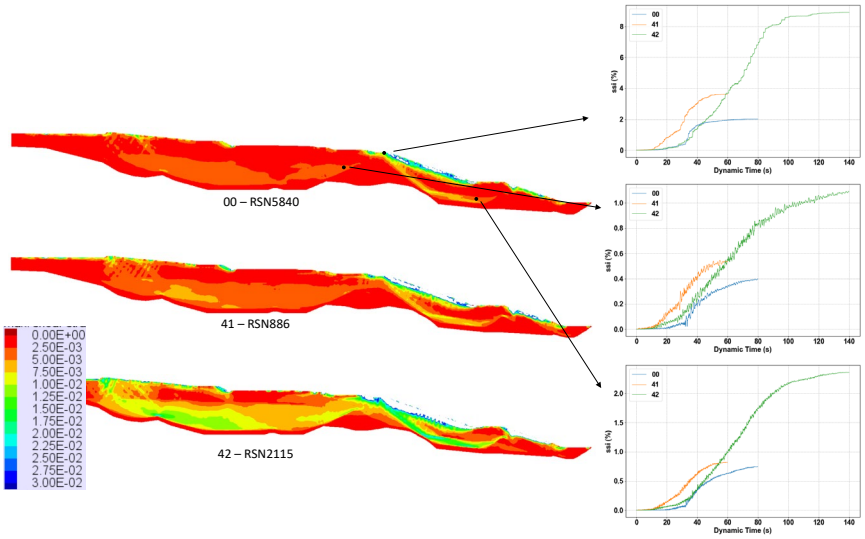


Figure 14: Maximum shear strain increment (shear strains) distribution at the end of an earthquake for selected ground motions

Tailings weak zones

Based on the existing site investigation report, weak tailings clusters may exist due to segregation of the historical depositions of tailings. These weak pockets may not use the base calibration of PM4SAND as developed for this site because their average penetration resistance may be less than the limits of the calibrated model, and they have a large deviance from the adopted 30th percentile curve. Thus, a sensitivity study was introduced to account for the effect of these weak zones on the seismic response of the structure. Figure 15 shows the three identified weak zones in saturated tailing, based on the review of available CPT data and with a conservative approach to delineate these pockets. For each of the weak zones, an iterative process has been then used to re-calibrate the parameters of PM4SAND, as listed in Table 3.

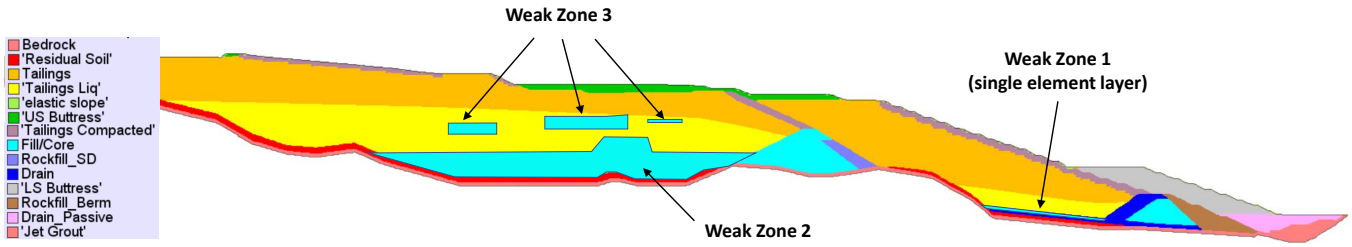


Figure 15: Location of the identified weak zones in saturated tailings

Table 3: Summary of the calibrated PM4SAND parameters for weak zones

Weak Zones	Confining Stress (kPa)	q_{c1N}	Dr	Vs (m/s)	Go	hpo
1	1,070	4.7	0.29	220	320	0.45
2	1,250	6.2	0.31	230	324	0.45
3	690	8.6	0.33	220	399	0.45

Figure 16 shows the comparison between the base model and the weak zone model for the distribution of Ru at the end of shaking. The development of Ru during shaking at selected locations is also shown in the figure. Larger excess pore pressure development was observed in all three of the weak zones, with a maximum Ru increased from 30% to 40% for weak zone 1.

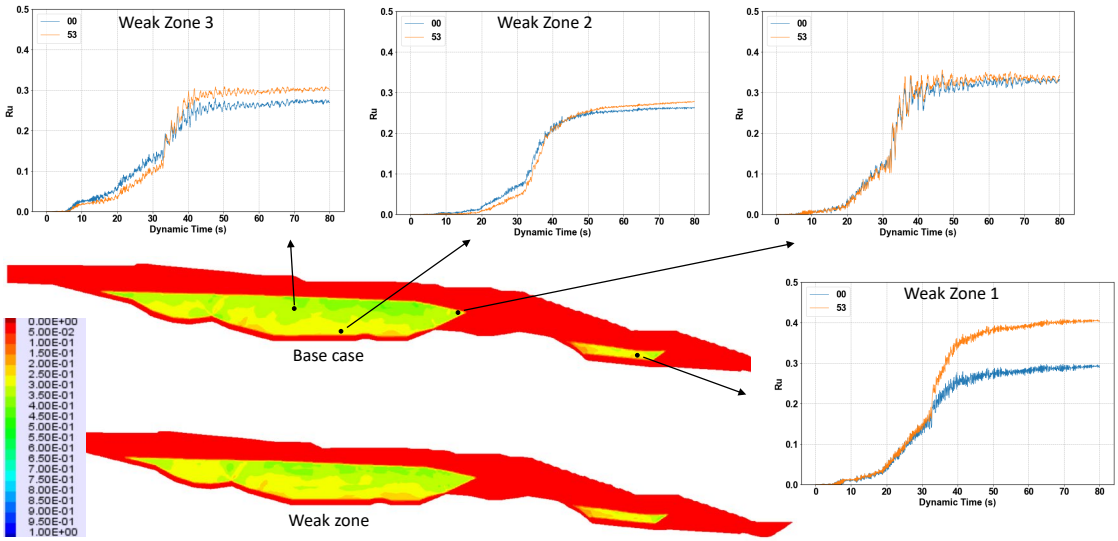


Figure 16: Comparison between the base case and the weak zone case for Ru at the end of shaking

Figure 17 shows the comparison for the maximum shear strain increment during the shaking. The range of shear strains increases considerably in the lower slope area (~100% increase) but less in other areas (~10% increase), which indicates that a potential weak layer at the bottom of the lower slope tailings deposit can significantly increase the shearing movement along the lower slope shear planes.

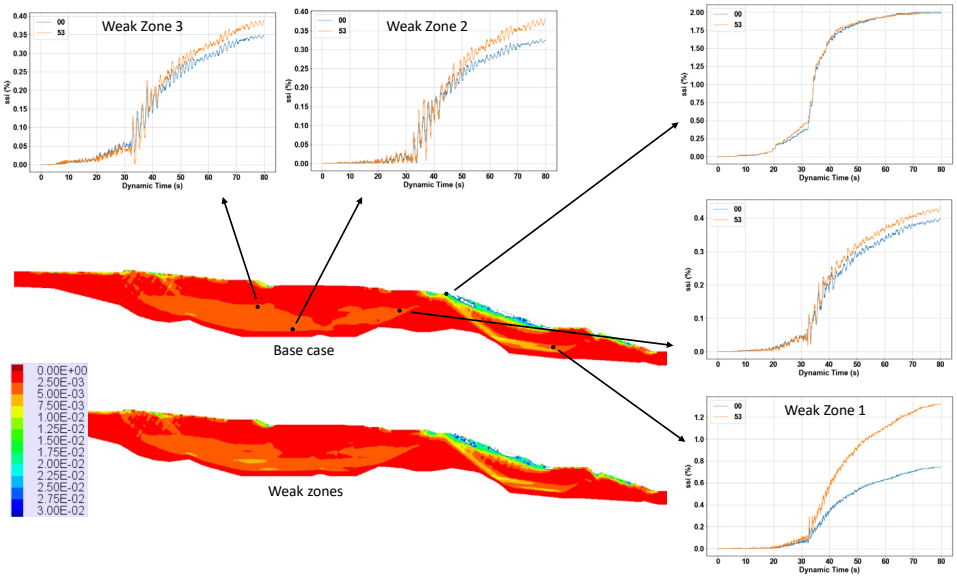


Figure 17: Comparison between the base case and the weak zone case for shear strains at the end of shaking

However, no change was observed between the two cases for the displacement at the GMD crest. At the middle of lower slope surface (where the maximum displacement of the entire model was observed), the horizontal displacement increased from 0.81 m to 0.89 m, while the vertical displacement increased from -0.19 m to -0.25 m. Overall, based on the FLAC analyses results, the existence of weak tailings can increase the deformation of the structure, especially at the toe of lower slope, while no fully developed liquefaction zones are predicted in the entire cross-section.

Conclusion

The Germano Main Dam (GMD) contains contractive tailings material. This paper presents finite difference method based 2D seismic deformation analyses to estimate the range of excess pore water pressures within tailings deposits, shear strains, and deformations resulted from seismic loading at the critical locations of GMD structure (upper slope and lower slope).

A base model was first developed to predict the seismic response of the structure with a reasonable amount of conservatism. Sensitivity analyses were then performed to address uncertainties from the base model including the input ground motion, and the existence of pockets of weak tailings. It was concluded that the most significant aspect affecting the response of the GMD structure was the input ground motions and specifically the duration of the shaking. The ground motion with the longest duration resulted in the highest seismic excess pore pressures of Ru < 50 % and maximum shear strains, $\varepsilon < 5\%$ in the entire model, which remained in the reasonably low range. It was also concluded that the existence of soft pockets of weak tailings does not significantly alter the seismic response of the dam, except at locations where the largest shear stains was observed.

Acknowledgements

The authors gratefully acknowledge support for this study from Jose Bernardo V. Rodrigues Oliveira and Jonathas Aparecido Alves Pinto from Samarco Mineração S.A., and insightful comments from Dr Michael Beaty. Any opinions or positions expressed in this paper are those of the authors only.

References

Boulanger, R.W. and Ziotopoulou, K. 2017. PM4Sand (Version 3.1): A sand plasticity model for earthquake engineering applications. Report No. UCD/CGM-17/01. Department of Civil and Environmental Engineering, University of California at Davis.

Idriss, I., Hudson, M. and Mohsen, B. 2003. Addendum to user's manual for QUAD4M for updates to QUAD4MU version. Department of Civil and Environmental Engineering, University of California at Davis.

Naesgaard, E. 2011. A hybrid effective stress – total stress procedure for analyzing soil embankments subjected to potential liquefaction and flow. Doctoral thesis, The University of British Columbia (Vancouver).

Particle Size, Hydraulic Transportation, and In-line Mixing, from a Tailings In-Line Flocculation Perspective

Raymond Guang, Paterson & Cooke Canada Inc., Canada
Trong Dang-Vu, SNF, Canada

Abstract

The method of in-line flocculation or in-line polymer addition is a niche dewatering method that is commonly used in the oil sands industry in Northern Alberta, Canada. This method promotes tailings slurry to release clear water, increase the yield stress, and create a steepened beach slope, without the need for additional capital-intensive dewatering equipment compared to a conventional tailings slurry disposal method. With coarser particles in the tailings slurry (i.e., an increased sand-to-fine ratio, SFR), the in-line flocculation process will be impacted as well as the tailings transportation. This paper will utilize typical oil sands tailings as an example of where in-line polymer injection was used as the tailings treatment method.

Adding coarse particles to treat mature fine tailings (MFT) samples has been studied in order to improve tailings dewatering characteristics (Thakurta et al., 2013; Dang-Vu et al., 2014). One of the oil sands operators – Canadian Natural Resources Limited – uses a non-segregating tailings process, in which coarse sand and fines are mixed to produce a tailings stream with improved fines capture and accelerated dewatering (CNRL, 2022). However, coarse particles will increase the deposition velocity during hydraulic transportation and also impact the rheology characteristics of the slurry. On the other hand, the higher pipeline velocity poses the challenge of potentially higher shear in the pipeline, which will impact the flocculation process that was previously designed for a specific process condition.

It is demonstrated in this paper how the variation of coarse particles in the oil sands tailings slurry (change in SFR) created an interesting yet complex issue. An improved understanding of tailings transportation, the in-line flocculation process, and of how they are interdependent, would lead to a better expectation of the tailings' Key Performance Indicators.

Introduction

In-line flocculation or in-line polymer addition typically comprises the injection of a polymer solution directly into the tailings stream (via a specially designed injector or a simple tee) at or close to the point of

discharge. The injection location may vary from several hundred meters upstream of the discharge point to the plunge pool immediately downstream. From Hogg's (2013) paper, high turbulence created by in-line mixing (i.e., injecting polymers into a pipe) has several benefits over a stirred tank. Sufficiently high turbulence could ensure high polymer-particle and particle-particle collision frequencies are achieved without the severe flocculant degradation that can be seen in a stirred tank (Hogg, 2013).

The use of static mixers for in-line flocculation has been explored by Demoz (2012, 2014) with some promising results. A different method, the application of a dynamic mixer for polymer and tailings mixing, has been commercially trialed by COSIA on fluid fine tailings (FFT) (COSIA, 2015).

Polymer and tailings mixing is always a challenging area that, when optimized, can result in maximizing the initial water release and reducing the polymer dosage. Questions are still asked about the polymer injection location in relation to the discharge point, and whether the in-pipeline mixing is sufficient for flocculation.

This paper will discuss the link between hydraulic transportation, tailings rheology, and inline mixing. Oil sands tailings are used in this study due to the authors' industry experiences.

Oil sands tailings

Oil sands tailings are the byproducts of the Clark hot water process, which separates bitumen from sand, water, and clay. The composition of oil sands tailings varies substantially, with differences in solids content, sand-to-fine ratio (SFR), clay content, and other mineral compositions.

Mining operators classify the size fractions of solid particles in the tailings as "sand," "silt," and "clay" based on several standards. In the Canadian oil sands industry, sand (coarse) particles are classified as those with a size larger than 44 microns, silt (fines) particles are classified as those with a size between 2–44 microns, and clay particles are classified as those with a size less than 2 microns (Wang et al., 2014). A finer stream PSD and a slightly coarser stream PSD can be found in Figure 1.

The three main tailings streams are coarse tailings, fine tailings, and froth treatment tailings. Coarse tailings contain approximately 55 wt% solids, mostly sand (>44 microns), with high SFR. Fine tailings consist mainly of fine mineral solids (<44 microns) with an SFR lower than 1. The last stream is froth treatment tailings, also referred to as Naphtha or Solvent Recovery Unit tailings, which contain mostly diluent.

When the resulting tailings discharge into a tailings pond, the sand particles settle quickly on the beach and at the bottom of the pond, while the fine fraction accumulates in the center of the pond and eventually settles, forming what is referred to as mature fine tailings (MFT). MFT is one of the biggest challenges for oil sands operations due to its extremely slow settling rate and poor consolidation.

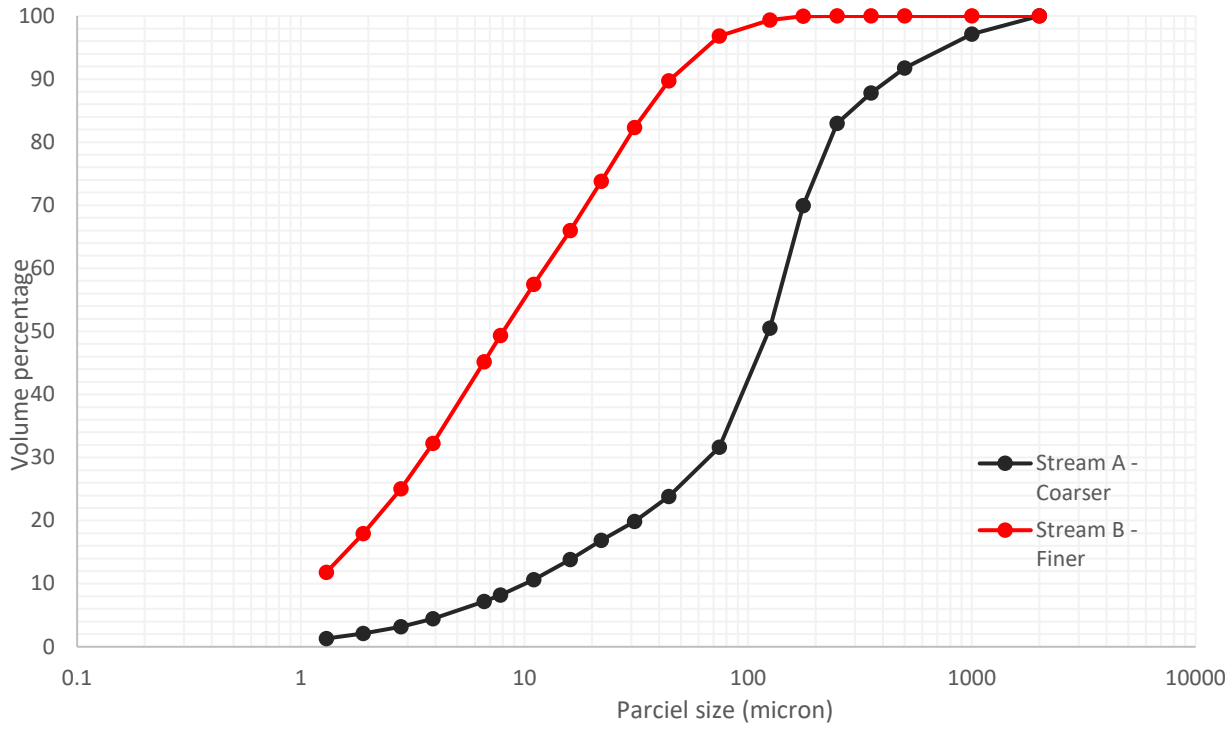


Figure 1: Typical oil sands tailings PSD

Polymer treatment and flocculation

The selection of polymer, dosages, and the flocculation process (mixing the polymer with tailings slurry) can vary greatly due to the significant variations in oil sands tailings types, their composition, and intended application. MFT is typically treated with either a single anionic flocculant or dual anionic and cationic flocculants (Najafi et al., 2014; Dang-Vu et al., 2016). Laboratory-scale procedures depend heavily on the specific applications due to the required mixing intensity and mixing duration. For example, during laboratory-scale flocculation of oil sands tailings, the sample is poured into a one-liter beaker. A given amount of polymer solution is added, followed by mixing. Mixing is conducted at 300 rpm using a portable mixer equipped with a paddle-mixing blade. After mixing, the treated tailings are allowed to settle for one minute, and the solids content of a supernatant is determined to calculate fines capture (Dang-Vu et al., 2014). Yield stress can be measured on the treated tailings using a rheometer.

To determine the dewatering rate after flocculation, gravity settling and drainage are often used. Sometimes, the capillary suction test (CST) is also applied (Wells et al., 2011).

The effect of polymers on the flocculation of tailings has been well-studied and understood since the 1950s (Henderson and Wheatley, 1987). It is reinforced in Stock (2006) that particle size, shape, and surface texture impact the effectiveness of a polymer in flocculating a tailings sample.

When coarser sandy particles are present in the tailings stream, the SFR of the tailings stream will be higher. In terms of optimum polymer dosage for flocculation, a summarized plot from Anstey and Guang (2017) is shown below:

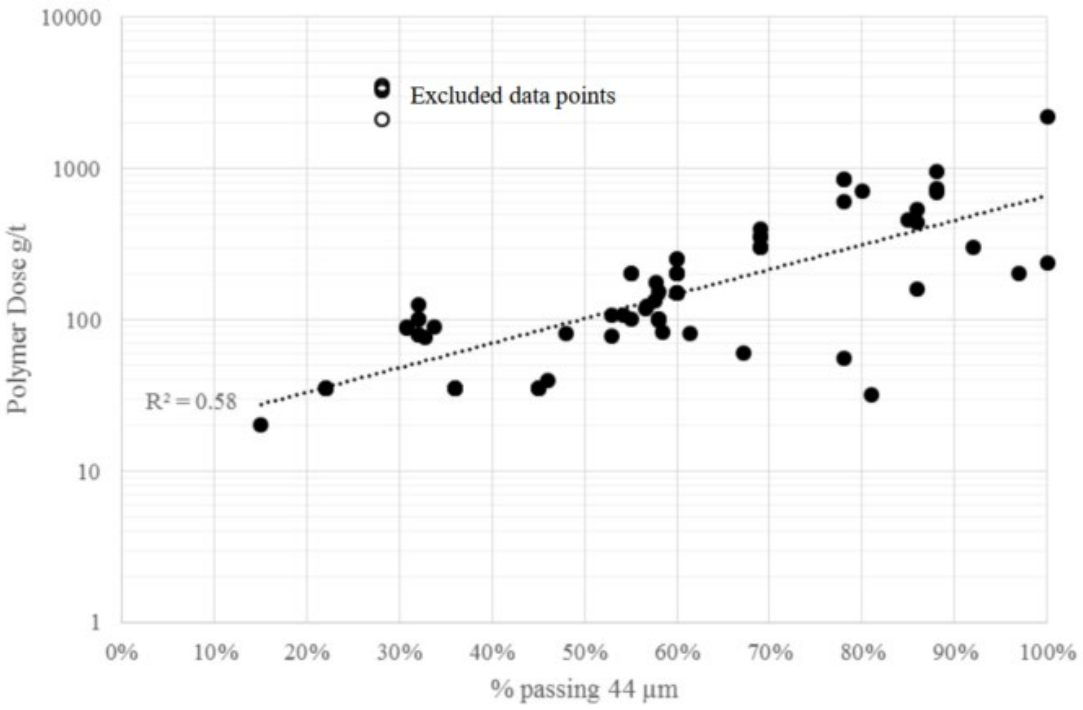


Figure 2: Optimum polymer dose versus percentage passing 44 microns (Anstey and Guang, 2017)

In the plot shown above, the optimum polymer dose was presented as a function of the proportion passing 44 microns. Despite not all the data points from the plot being oil sands tailings based, the plots nonetheless showed a strong relationship between the dosage required and the percentage passing 44 microns. A higher percentage passing 44 microns yielded a higher polymer optimum dosage. When a lower percentage passing 44 micron was recorded, a lower polymer optimum dosage was also observed. This is in line with what has previously been reported by Wells et al. (2011).

The impact of SFR on the dewatering rate was assessed by adding sand into MFT. Based on a study completed by the lead author, from Figure 3 below, it is seen that as the SFR increased from 0 (MFT) to 1 (with coarse sand addition), the net water released from the polymer-treated slurry after one hour improved from 8% to 19%. This shows that with some sand addition (i.e., elevating sample SFR), KPI in terms of net water release was trending in a favorable direction.

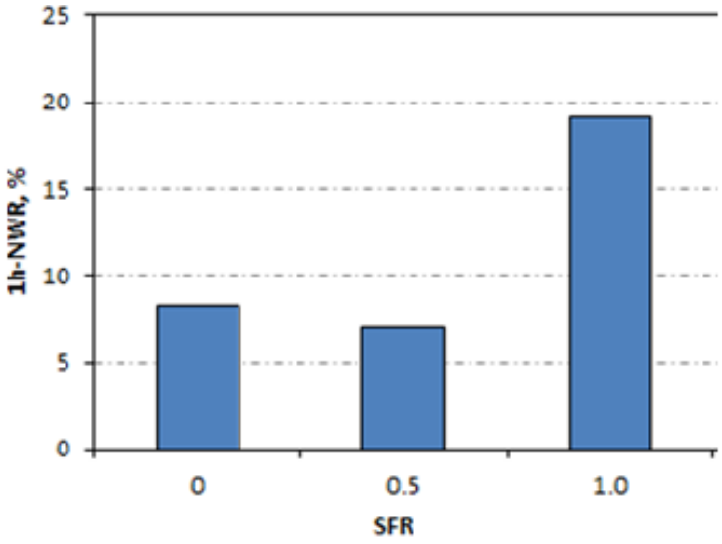


Figure 3: SFR versus one hour net water release post flocculation

Polymer and tailings mixing

As described in an earlier section, usually a mixer is used to provide mixing energy for mixing the polymer with tailings in a laboratory setting. In actual operations, the mixing mechanism differs significantly between mechanical agitation with an agitator and "in-pipeline" mixing with turbulent flow.

It is acknowledged by Costine et al. (2014) that turbulent dispersion is disadvantaged by the highly viscous nature of the underflows and large processing volumes. This statement was focused on a thickener underflow issue. However, it is also relevant to the polymer and tailings mixing in a turbulent pipeline. Nevertheless, Costine et al. (2014) proposed a chaotic topological mixer for mixing polymer and tailings in order to improve the efficacy of flocculation. Their work demonstrated that the chaotic advection improved dewatering performance and enhanced consolidation. Based on the authors' understanding, this type of device is not used in any of the current operating oil sands mines or in base metal tailings operations.

Currently, a basic in-line polymer addition method (a typical tee) is used at some oil sands tailings operations. In other words, a polymer transportation line is connected into a tailings transportation line and the polymer solution is "injected" into the tailings pipeline. The turbulence from the tailings flow is used to mix the polymer and tailings. To replicate this in a laboratory setting, a simple setup with a beaker and agitator is usually used. The agitator's mixing speed and mixing time can be controlled and monitored. In the on-site tailings operation, as pipeline sizes are fixed, velocity is controlled by the flow rate (typically varies within operational range) and the mixing efficacy is dictated by the amount of turbulence generated. It is critical that the long chain, high molecular weight anionic polymer needs to be well dispersed into the tailings stream for effective flocculation. This sounds simple enough, but is it?

Settling slurry pipeline flow

Before getting into in-pipeline mixing scenarios, the first thing to do is to understand what material is flowing in the pipeline. Generally speaking, tailings slurries can be divided into two broad categories – settling slurries and non-settling suspensions. A settling slurry consists of a diverse range of particle sizes, and is one where the turbulence present in the slurry flow is relied upon to lift and suspend the solids in order for them to be conveyed by the fluid flow. Non-settling slurries consist of finer particles that form stable homogenous mixtures exhibiting an increase in apparent viscosity, and turbulence damping (Bartosik, 2011).

A paper by Messa et al. (2021) describes three basic types of settling slurry flow. For a typical oil sands tailings stream, it is seen that the flow can be categorized as a pseudo-homogeneous regime. In this type of flow, the stream contains fine particles (typically fine sand of particle sizes between 60 and 200 microns) that flow at high velocity. The submerged weight of the solids is carried by fluid support mechanisms associated with flow turbulence (Messa et al., 2021).

The second intermediate case, where both inter-granular contact and fluid support mechanisms are significant, is called heterogeneous flow. And the other extreme case is the fully stratified flow; typically, the flow conveys large and rapidly-settling particles at a low velocity (Messa et al., 2021).

Li et al. (2016) and Fessler and Eaton (1999) wrote about the influence of solids particles on the modulation of turbulence. It is clear from a wealth of existing academic research that the behavior of solid particles in a liquid can enhance or suppress turbulence.

Turbulent behavior

When the tailings particles are mainly suspended by turbulence in the pipeline, it is prudent to understand what turbulence is and how it can be quantified.

Turbulence intensity in pipeline flow can be expressed by the Reynolds number. This dimensionless number is the ratio of inertial forces to viscous forces. The transition from laminar to turbulent flow, or the critical Reynolds number, is approximately at 2300.

With a Herschel-Bulkley fluid, which is a generalized model of a non-Newtonian fluid, the equation for a non-Newtonian Reynolds number becomes:

$$Re = \frac{8\rho V^2}{\tau_y + K\left(\frac{8V}{D}\right)^n}$$

Other than the well-known and broadly used Reynolds number, turbulent flow is also characterized by velocity fluctuations and random fluctuations of swirling regions of fluid such as eddies. Mean velocities in the X, Y, and Z directions are usually denoted by $\bar{u}$, $\bar{v}$ and $\bar{w}$, and u', v', and w' denote the velocity

fluctuations. Bulk velocity is fairly easy to calculate, whereas these velocity fluctuations require measurements obtained by specific instruments or validated simulations.

One of the methods that can be used for turbulence characteristics analysis is the quadrant analysis. This particular method is used to investigate the Reynolds stress structures and features of the large eddy.

Reynolds shear stress is caused by the x-direction velocity fluctuation u and y-direction fluctuations v having a non-zero correlation. These two quantities are the focus of the quadrant analysis. This technique is introduced by Willmarth and Lu (1972) for a turbulent boundary layer. This technique sorts contributions to the Reynolds shear stress $u'v'$ into quadrants of the u-v plane. The largest positive contributions to the turbulent energy were provided by the ejection ($u'<0$, $v'>0$) and sweep quadrants ($u'>0$, $v'<0$), while small and negative contributions were made by the interaction quadrants ($u'<0$, $v'<0$ and $u'>0$, $v'>0$). This is usually referred to as the sweep-ejection event (Kim et al., 1987).

Robinson (1991) mentioned that the near-wall turbulence production process is considered to be an intermittent, quasi-cyclic sequence. It is usually referred to as "bursting." It was described as a "violent breakup of a low-speed streak after lifting," and a "shear-layer interface sandwiched between an upstream, high-speed sweep and a downstream, low-speed ejection" (Robinson, 1991). This is a useful concept for the production of turbulent motion.

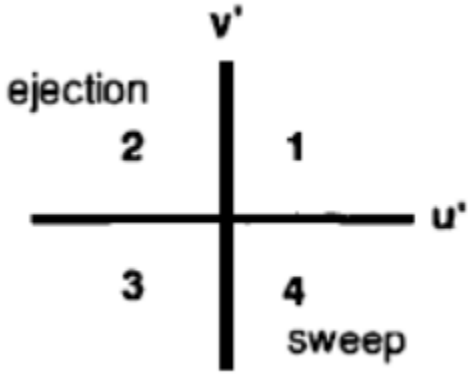


Figure 4: Quadrants of the Instantaneous u'v' plane

If the velocity fluctuation of the flow can be measured or simulated, a more quantitative quadrant analysis can be performed. An example of this can be found in both Guang (2011) and Fiorini (2017). In Guang (2011), a turbulent non-Newtonian channel flow was simulated through direct numerical simulation (DNS). Quadrant analysis was performed by obtaining the velocity fluctuation in the axial and radial direction (u' and v'). From the results, it was concluded that the largest percentage of the ejection and sweep events occurred away from the centerline and close to the side wall at approximately y/R = 0.4. It was hypothesized that the particles could be easily suspended and re-suspended in those areas.

Fiorini (2017) conducted an experimental campaign in a pipe flow facility. The Reynolds shear stress was analyzed in conjunction with the near-wall events such as ejections and sweeps. It was also concluded that with an increasing Reynolds number, the contribution of these ejection and sweep events on the total shear stress increases. Fiorini also pointed out that the ratio of contribution to the shear stress from the ejection and sweeps event is found to increase logarithmically with the distance from the wall at y/R = 0.3.

To the authors' current knowledge, the majority of the current in-line injectors used in oil sands tailings operations inject from the top of the pipe to the bottom. From the abovementioned studies, the ejection and sweep events were recorded towards the bottom of the pipe/channel. This could be an opportunity for a potential injection nozzle orientation with polymer injecting into the turbulent production regions.

In summary, ejection and sweep events can be linked to the mechanism of particle suspension. By using this quadrant analysis technique to capture the locations of Q2 and Q4 activities, better decisions could be made in terms of the best polymer injection velocity and injection location by obtaining Reynolds shear stress at specific pipeline quadrants and polymer injection pipe orientation.

Rheology impact on turbulent behavior

As described earlier, tailings particles can be categorized into fine particles and coarse particles. The particle behaviors and the turbulence in the pipeline are interdependent on each other. The finer particles (< 44 microns) became part of the carrier fluid. With higher concentrations of finer particles, especially in oil sands tailings, the rheological characteristics of the carrier fluid will change – i.e., there will be an increase in viscosity and yield stress.

If the Reynolds number was used to assess how the carrier fluid impacts turbulent behavior, as the rheology parameters of the fluid are the denominator of the Reynolds number equation, the higher the values for rheology parameters the lower the Reynolds number.

From a slightly different point of view, how does a higher yield stress or higher viscosity impact the turbulence characteristics (turbulent structures)? In a prior study by Guang et al. (2011), fluid samples with different rheological characteristics (change in yield stress) were used for DNS. It was found that in the simulation with lower yield stress values, higher turbulent production values were observed. With an increasing yield stress, the turbulent structures were weaker than in the Newtonian fluid simulation with the same viscosity.

For visualization, contours of axial velocity at a certain distance from the wall are shown in Figure 5. As the yield stress increased, the turbulent structures in simulation C were longer than the structures in the control simulation. The black structures represent low-velocity streaks. It can be seen that the streaks in simulation C were longer and wider. This further suggested that the flow was not fully developed for this

non-Newtonian fluid. The structure in the Newtonian case was smaller in scale and more random; this indicated the flow was more developed.

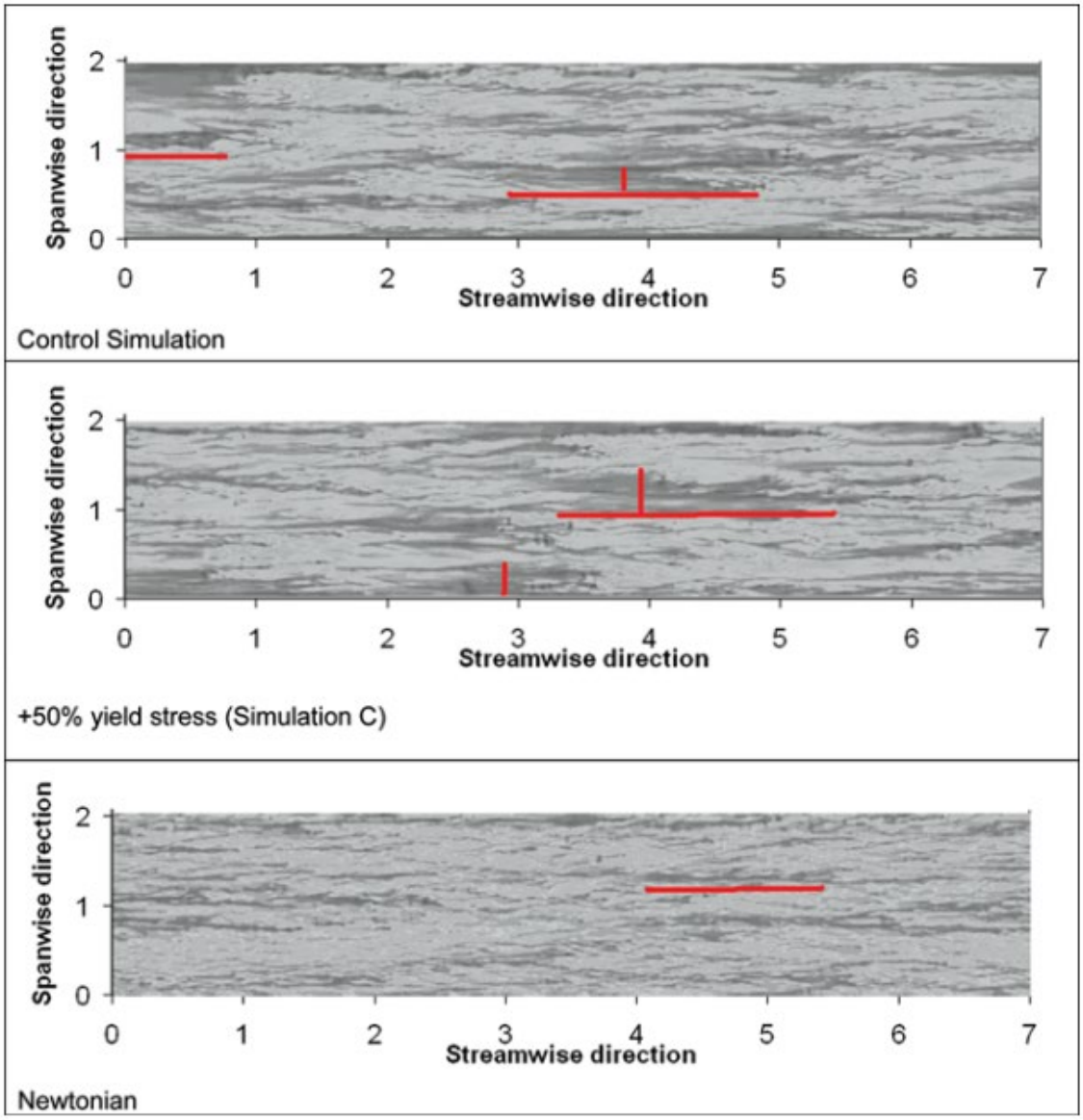


Figure 5: From top to bottom: control simulation (Re=8294), simulation C (Re=6481). White represents high velocity and black represents low velocity (Guang et al., 2011)

Discussion

To illustrate the relevance of pipeline hydraulics to flocculation, consider two different oil sands tailings streams at the same solids content, one with a higher SFR of 5.0 and one with a lower SFR of 0.1. Based on the previous section, it is expected that the stream with a higher SFR will need a lower polymer dosage, whereas the stream with a lower SFR will require a higher polymer dosage. However, assuming there is no

"injector" for the in-line injection, instead, a typical tee is used for polymer injection. The turbulence generated by the flow will be used as the mixing mechanism for polymer-tailings interaction.

Considering the above, the following is noted:

- Increased fines content (low SFR) means an increase in carrier fluid rheology.
- Fine particles become part of the carrier fluid. As the solids content of the carrier fluids increases, the apparent viscosity of the carrier fluid will increase.
- Increasing carrier fluid apparent viscosity means:
    - The deposition velocity requirement for coarse particles in this stream decreases – potentially, lower bulk velocity will be required to keep particles in suspension.
    - Turbulence is suppressed – i.e. lower turbulent energy production, weaker turbulent structure.
- Increased coarse particle content (high SFR) means a decrease in carrier fluid rheology.
- Decreased carrier fluid rheology means:
    - The required deposition velocity for coarse particles in the stream will be higher than the required deposition velocity for the low SFR stream.
    - Turbulence is enhanced.
    - Due to the higher deposition velocity requirement, the pipeline bulk velocity needs to be higher than the pipeline bulk velocity for the lower SFR scenario.

It is interesting to note that, due to the difference in rheology between the high SFR and low SFR tailings stream, even if the bulk velocity is the same, the turbulent characteristics will be different. As alluded to in previous sections, the two streams will have different carrier fluid rheology due to the SFR differences. The particle size and particle population will dictate the deposition velocity requirement. The population of the finer particles will impact the turbulent characteristics, which in turn impact the Reynolds shear stress. The Reynolds shear stress will lead to variation in the wall events, hence affecting the suspension of the coarse particles.

It may be naïve to assume that the turbulence can mix the tailings and polymer sufficiently in this complex scenario without even considering the shear sensitivity nature of the flocculated stream. At the same bulk velocity, it needs to be acknowledged that the turbulent characteristics of two different SFR materials will be different. This will ultimately impact the polymer tailings flocculation efficacy. Without fully grasping the complex nature of the physical and chemical behavior of such a large-scale of in-line mixing application, it would be easy to set an unrealistic KPI for the tailings operation.

Conclusion

This paper used the oil sands tailings treatment process as an example to illustrate the importance of tailings flow behaviors and the fluid dynamics of tailings for the design of in-line flocculation. Ideally, if all the turbulent characteristics of the flow can be measured in real-time, then it will help the engineers to understand the challenge better. Unfortunately, some of the measuring devices and/or methods are not applicable to large-scale operations.

The use of computational fluid dynamics (CFD) may offer opportunities for system optimization. The advantage of such simulations relative to physical experiments is that all the quantities of interest can be obtained for the whole flow field (McIver et al., 2000).

With the advancement of computer power, CFD is becoming an increasingly powerful tool for gaining a fundamental understanding of in-line mixing fluid mechanics. By illustrating the internal flow patterns and quantifying the turbulent characteristics, optimization could be completed by changing operating parameters without altering the configuration of the injection setup. Implementing targeted solutions will help the operation to avoid straining limited resources on numerous trial solutions.

References

Anstey, D. and Guang, R. 2017. Relationship between in-line polymer dose and tailings index properties. In Wilson, G.W., Sego, D.C. and Beier, N,A. (eds), *Tailings and mine waste 2017, Proceedings of the 21st International Conference on Tailings and Mine Waste,* Banff, Alberta, Canada.

Bartosik, A. 2011. Simulation of the friction factor in a yield-stress slurry flow which exhibits turbulence damping near the pipe wall. *Journal of Theoretical and Applied Mechanics* 49 (2): 283–300.

Canadian Natural Resources Limited. 2022. *Stewardship report to stakeholders – Canadian Natural's Sustainability Report.*

COSIA. 2015. Accelerated dewatering mixing pilot, COSIA Innovation Summit, Banff, Alberta.

Costine, A., Lester, D., Fawell, P. and Chryss, A. 2014. Shear isn't mixing: how to build larger aggregates using chaotic advection for accelerated dewatering. In D. van Zyl, R.J. Jewell and A.B. Fourie (eds), *Paste 2014, Proceedings of the 17th International Seminar on Paste and Thickened Tailings*. Vancouver, British Colombia, Canada.

Dang-Vu, T., Keele, H., Lacoste-Bouchet, P., Salehi, R., Najafi, A., Klein, C., Nelson, A. and Ramey, S. 2016. In situ deposition of treated tailings. In Sego, D.C., Wilson, G.W. and Beier, N.A. (eds), *Proceedings of the Fifth International Oil Sands Tailings Conference*. Lake Louise, Alberta, Canada.

Dang-Vu, T., Wang, N. and Ramey, S. 2014. Treatment of oil sands fresh (coarse) tailings. In D. van Zyl, R.J. Jewell and A.B. Fourie (eds), *Paste 2014, Proceedings of the 17th International Seminar on Paste and Thickened Tailings*. Vancouver, British Colombia, Canada

Demoz, A. 2012. Mixing energy density criterion for peak dewatering flocculation by static mixers. *Proceedings of the Third International Oil Sands Tailings Conference,* Edmonton, Alberta, Canada.

Demoz, A. 2014. Scaling inline static mixers for oil sand mature fine tailings flocculation. *Proceedings of the Fourth International Oil Sands Tailings Conference,* Lake Louise, Alberta, Canada.

Fessler J.R. and Eaton, J.K. 1999. Turbulence modification by particles in a backward-facing step flow. *Journal of Fluid Mechanics* 394: 97–117.

Fiorini, T. 2017. Turbulent pipe flow – high resolution measurements in CICLoPE. Thesis research, *Meccanica e scienze avanzate dell'ingegneria,* Universita' Di Bologna.

Gai, G., Hadjadj, A., Kudriakov, S. and Thomine, O, 2020. Particles-induced turbulence: a critical review of physical concepts, numerical modelings and experimental investigation. *Theoretical and Applied Mechanics Letter* 10: 241–248.

Guang, R. 2011. Particle transportation in turbulent non-Newtonian suspensions in open channels. PhD thesis, School of Civil, Environmental and Chemical Engineering, RMIT University.

Guang, R., Rudman, M., Chryss, A., Slatter, P. and Bhattacharya, S. 2011. A DNS investigation of the effect of yield stress for turbulent non-Newtonian suspension flow in open channels. *Particulate Science and Technology*
29: 209–228.

Henderson, J.M. and Wheatley, A.D. 1987. Factors affecting the efficient flocculation of tailings by polyacrylamides. *Coal Preparation* 4(1): 1–49.

Hogg, R. 2013. Bridging flocculation my polymers. *KONA Powder and Particle Journal* 30: 3–14.

Kim, J., Moin, P. and Moser, R. 1987. Turbulence statistics in fully developed channel flow at low Reynolds number, *Journal of Fluid Mechanics* 177: 133–186.

Li, D., Luo K. and Fan, J. 2016. Modulation of turbulence by dispersed solid particles in a spatially developing flat-plate boundary layer. *Journal of Fluid Mechanics* 802: 359–394.

Matas, J.P., Forris, J.F. and Guazzelli, E. 2003. Influence of particles on the transition to turbulence in pipe flow. Philosophical transactions of the Royal Society of London, Series A, Mathematical and Physical Sciences.

Messa, G.V., Yang, Q., Adedeji, O.E., Chara, Z., Duarte, C., Matousek, V., Rasteiro, M.G., Sanders, R., Silva, R.C. and de Souza, F.J. 2021. Computational fluid dynamics modelling of liquid-solid slurry flows in pipelines: state-of-the-art and future perspectives. *Processes* 9(1566).

McIver, D., Blackburn, H. and Nathan, G. 2000. Spectral element-Fourier method applied to the simulation of turbulent pipe flow. *ANZIAM Journal* 42: C954 – C977.

Najafi, A., Mian, H., Salehi, R., Lacroste-Bouchet, P., Friedrich, K., Keele, H., McWhan, C., Romero, R., Daliri, F., Jeeravipoolvarn, S., Boswell, J. and Moore, T. 2014. Flooding of in-line flocculated tailings after thin lift drying. *Proceedings of the Fourth International Oil Sands Tailings Conference,* Lake Louise, Alberta, Canada.

Peker, S.M. and Helvaci, S.S. 2008. *Solid-liquid two phase flow*. USA, Elsevier science and technology.

Robinson, S. 1991. Coherent motions in the turbulent boundary layer. *Annual Review Fluid Mechanics* 23: 601–639.

Stock, P. 2006. Chapter 6 Reagents, *Paste and Thickened Tailings – A Guide,* Third Edition, eds Jewel R.J. and Fourie, A.B., Australian Center for Geomechanics.

Thakurta, S.G., Fenderson, T., Mahmoudkhani, A., Stewart, K. and Watson, P. 2013. Effect of coarse solid addition on the dewatering of mature fine tailings. In Wilson, G.W., Sego, D.C. and Beier, N.A. (eds), *Tailings and Mine Waste 2013, Proceedings of the 17th International Conference on Tailings and Mine Waste,* Banff, Alberta, Canada.

Wang, C., Harbottle, D., Liu, Q. and Xu, Z. 2014. Current state of fine mineral tailings treatment: a critical review on theory and practice. *Minerals Engineering* 58: 113–131.

Wells, P.S., Revington, A. and Omotoso, O. 2011. Mature fine tailings drying – technology update. In R. Jewell and A.B. Fourie (eds), *Paste 2011: Proceedings of the 14th International Seminar on Paste and Thickened Tailings,* Australian Centre for Geomechanics, Perth, pp. 155-166, https://doi.org/10.36487/ACG_rep/1104_15_Wells

Willmarth, W. and Lu, S. 1972. Structure of the Reynolds stress near the wall. *Journal of Fluid Mechanics* 55: 65–92.

Wilson, K.C. and Sellgren, A. 2003. Interaction of particles and near-wall life in slurry pipelines. *Journal of Hydraulic Engineering* 129(1): 73–76.

Zahtila, T., Chan, L., Ooi, A. and Philip, J. 2023. Particle transport in a turbulent pipe flow: direct numerical simulations, phenomenological modelling and physical mechanisms. *Journal of Fluid Mechanics* 957: A1-1 to A1-40.

Preliminary Design of the Tailings Cover System Using Numerical Modeling to Perform Sensitivity Analysis

Bibhuti Panda, AECOM, USA
Rouzbeh Rasouli, AECOM, Canada
Jason Chen, AECOM, Canada
Anne-Marie Dagenais, AMD Solutions, Canada

Abstract

The purpose of a cover system for tailings is to protect the downstream receiving environment following the closure of the tailings facility. In general, a cover system provides physical stability for dust and erosion control, chemical stability to reduce containment release, and meets the land use expectation for vegetation. Five components of the cover system are normally designed: (1) a top vegetation layer, (2) a protection layer, (3) a drainage layer, (4) an impermeable layer, and (5) a capillary break layer. A pre-feasibility level study was performed to design a cover system for a tailings storage facility in Eastern Canada. A two-dimensional (2D) numerical model was developed to estimate the net percolation into tailings under the planned thickness of the cover system. The percolation from the base of the cover was estimated and this value is used as an input to the hydrogeological model for the site. The model estimated infiltration due to rainfall, snowmelt, root transpiration, surface evaporation, and runoff. The model simulated liquid and vapor phase water transport in a two-dimensional model section. The model also included a feature to simulate thin layers of geomembrane liners and considered potential defects.

Sensitivity analyses were performed to investigate the critical input parameters and a long-term (60-year) simulation was performed to find the variability of net percolation estimate in future climate change conditions. The sensitivity analyses were performed for a selected year representative of normal climate conditions to evaluate critical parameters and their effect on the net percolation and to study the effect of climatic conditions, hydraulic conductivity of the geomembrane, defects on the geomembrane, slope of the cover, vegetation parameter, protective layer thickness, et cetera. The numerical model showed that the selected cover option is suitable based on the estimated infiltration and meets closure objectives for the study site.

Introduction

The management of mine waste such as mine tailings that is either a reactive or non-reactive waste product during mining operations and closure is an important function that requires the application of numerous technologies. The design and construction of a cover system for mine tailings is the most critical aspect of mine closure. The main objective of installing a cover system over the tailings is to protect the downstream receiving environment following closure of the tailings facility. In many cases, this is achieved by reducing the net percolation of water into the tailings, thereby reducing the effluent seepage quantity. The cover system for any site is designed based on the following important design objectives (INAP, 2017):

- physical stability – dust and erosion control;
- chemical stability – reduce contaminant release; and
- meeting the land use expectation – vegetation.

In a cover system design approach, the selected methodology goals are to develop a cover system that is technically the best option, is cost-effective with the appropriate balance of capital and operating expenditure, is implementable, and meets stakeholders' expectations. Various cover systems may be employed to meet the above design criteria as discussed in the "Cold Regions Cover System Guidance Document" (MEND, 2012). The following categories of cover systems have been identified as appropriate cover systems.

1. Simple protection cover system – vegetation and erosion protection cover system that is needed in areas where vegetation can help promote evapotranspiration and reduce soil erosion.
2. Store and release cover system – these covers require climate conditions where there is greater evapotranspiration than precipitation, both seasonally and annually.
3. Enhanced store and release cover system, with a lower permeability layer, and capillary break. The objective is to further reduce net percolation during short duration seasonal events when the storage capacity of a store and release cover system might be exceeded. The capillary break layer cover system is another form of enhanced store and release cover system.
4. Barrier type cover system – a compacted clay layer. This controls the ingress of atmospheric water and in some cases atmospheric oxygen. It should include a layer with an as-built (field) saturated hydraulic conductivity of less than or equal to 1×10^{-9} m/s.
5. Cover systems with engineered layers – geosynthetic/fabric layers. These can be used either as a drainage layer or as a barrier layer that can reduce net percolation and oxygen ingress.

The selection of a cover system depends on site conditions and the design objective. Cost will depend on material sourcing and overall cover configuration, which will also depend on closure objectives and site conditions. In some cases, a combination of more than one category of cover system may be used for cover design at a specific site. The integration of landform and cover system is also an essential part of the cover system design. The important factors that control landform are geology, soil type, hydrogeology, topography, constructability, and final land use.

The selection of a cover thickness to support the chosen revegetation plan is also an important consideration in cover design. The vegetative growth medium (i.e., topsoil and fill layers) above the drainage layer is designed to adapt to future land use planning, which could include shallow rooted grasses and shrubs or deeper-rooted trees. A growth medium thickness of 76 cm (30 inches) will support the root zone depth of grasses, shrubs, and/or large trees, depending on which revegetation plan is chosen for the cover.

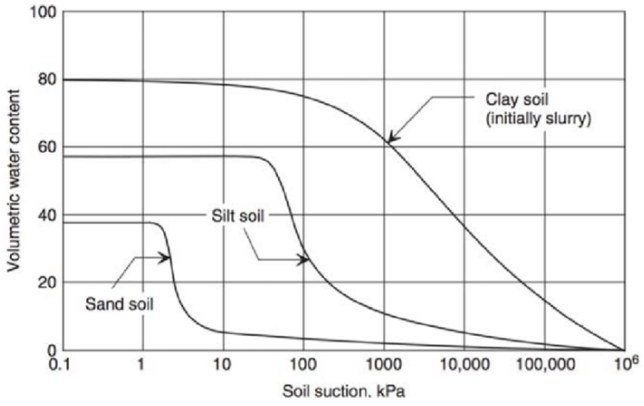
A cover system was evaluated for a tailings facility. A preliminary semi-quantitative analysis and a capital cost assessment were performed to compare different cover options. In the comparative analysis, the required thickness and characteristics of the growth medium were considered common to all cover design options. A Multi-Criteria Analysis (MCA) also called a “Multiple Accounts Analysis” (MAA) was performed to evaluate the options and facilitate a final decision. The selected cover option was evaluated using numerical modeling to perform a range of sensitivity analyses for the effect of critical parameters on a suitable cover system for the study site, located in Canada. The average climate condition at the site can be described as a humid continental climate with a significant variation in temperature between summer and winter. The 30-year average annual precipitation is about 927 mm (36.5 inches) at the study site, which typically consists of 8 months of rainfall and 4 months of snowfall.

Past studies

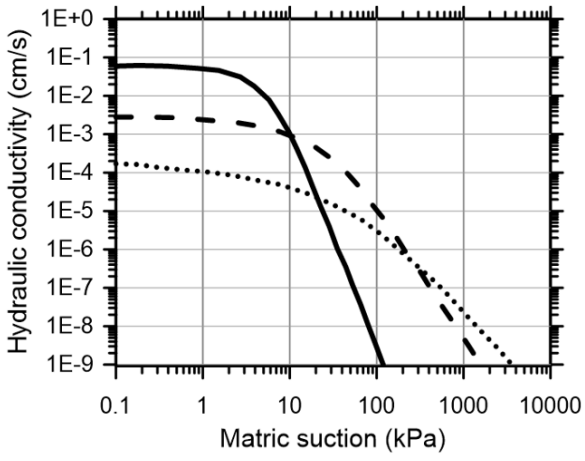
The Canadian Mine Environment Neutral Drainage (MEND) initiative developed a manual for cover systems (MEND, 2012) for waste rock and mine tailings. MEND is a co-operative research program that is directed by a partnership of the Canadian mining industry, federal and provincial governments, and non-governmental organizations (NGOs). The capillary barrier concept is commonly used in the design of mine waste cover systems and more specifically, the design of multi-layered cover systems (MEND, 2004). This system is used to maintain a tension saturated layer within the cover system and thus mitigate oxygen ingress and reduce net percolation flow. A fine-textured material placed between an underlying and overlying coarse-textured materials can result in a capillary barrier for downward as well as upward moisture migration from the sandwiched layer. The cover system may contain some, or all, of these components depending on local site conditions.

The capillary barrier layers generally consist of fine-grained soil over coarse-grained soil layers, though the fine-grained soil over a geotextile in lieu of coarse-grained soil also produces a capillary barrier effect (Zornberg et al., 2009). Water is held in the fine soil until evapotranspiration, horizontal drainage, or percolation removes the water. Differences in pore size distribution between the two layers cause infiltrated water to be retained in the upper soil layer under unsaturated flow conditions, as long as the contrast in unsaturated hydraulic conductivity of the soils in the two layers is sufficiently large (Dwyer, 2003). The upper soil layer exhibits greater moisture content than the lower soil layer at the same matric suction. Thus, a capillary barrier effect occurs when a relatively fine-grained soil overlies a relatively coarse-grained soil or a geotextile. The matric suction in the fine-grained soil layer typically must become negligible (i.e., saturated conditions) before any appreciable flow occurs into the lower coarse-grained layer (or geotextile).

The performance of a cover can be explained by the following: beginning at relatively dry conditions, that is, at high suctions, the fine-grained soil has a significantly larger hydraulic conductivity than that of the coarse-grained soil layer. With increasing water content and decreasing matric suction, the hydraulic conductivity of the fine layer will increase gradually. The hydraulic conductivity of the coarse-grained soil layer will remain comparatively low until suction corresponding to the air entry value (AEV) is overcome. Before reaching these conditions, water will not move from the fine-grained layer into the coarse layer even though the water content of the fine layer will increase during infiltration. Breakthrough into the coarse-grained soil layer occurs when the matric suction at the interface equals that of the air entry value of the coarse-grained soil layer (AEV for sand soil is low), as shown in Figure 1.



a)



b) Coarse-solid, Medium-dashed, Fine-dotted

Figure 1a: Soil-water characteristic curve for different soils (Fredlund and Rahardjo, 1993)
Figure 1b: Hydraulic conductivity vs. suction (van Genuchten and Pachepsky, 2011)

Geosynthetic layers can be used as alternatives to earthen soil material layers. Some advantages of geosynthetic layers include:

- Net percolation rate can be significantly reduced.
- A geosynthetic layer can be installed quickly and easily.
- Overall cover thickness and requisite imported materials and settlement issues can be reduced significantly. However, if a final profile surface is being driven by drainage elevations at the perimeter of the tailing's footprint, a thinner cover thickness could mean that more profile fill would be required underneath the cover to maintain the same finished drainage levels at the perimeter.
- Geosynthetic clay liner (GCL) can replace compacted clay soil when it may not be available at every site.
- GCLs are more resistant to freeze/thaw events than natural clay liners.

In any cover system, the geosynthetic layers that can be used in place of soil layers include:

- a non-woven geotextile filter layer can be used as a filter to protect a drainage layer;
- a geonet can be used as a drainage layer; and,
- geomembrane and GCL layers can be used as barrier layers.

The five components of a cover system, as discussed in MEND (2004) are:

1. A top vegetation/soil layer – an evapotranspiration layer with vegetation supported by topsoil.
2. A protection layer – protects the lower layers from physical damage and freeze/thaw impacts.
3. A drainage layer – a drainage soil or an equivalent layer of geosynthetic material.
4. A low hydraulic conductivity geomembrane/soil layer – a layer of compacted low-hydraulic conductivity soil/amended soil or an equivalent geomembrane liner.
5. A capillary break layer – a coarse-grained soil/composite geonet layer, which acts as a break in unsaturated soil conditions.

A cover system was selected from different options, similar to the one discussed above, which comprises five components system, as shown in Figure 2. A numerical model was developed to evaluate the system, as discussed in the following section.

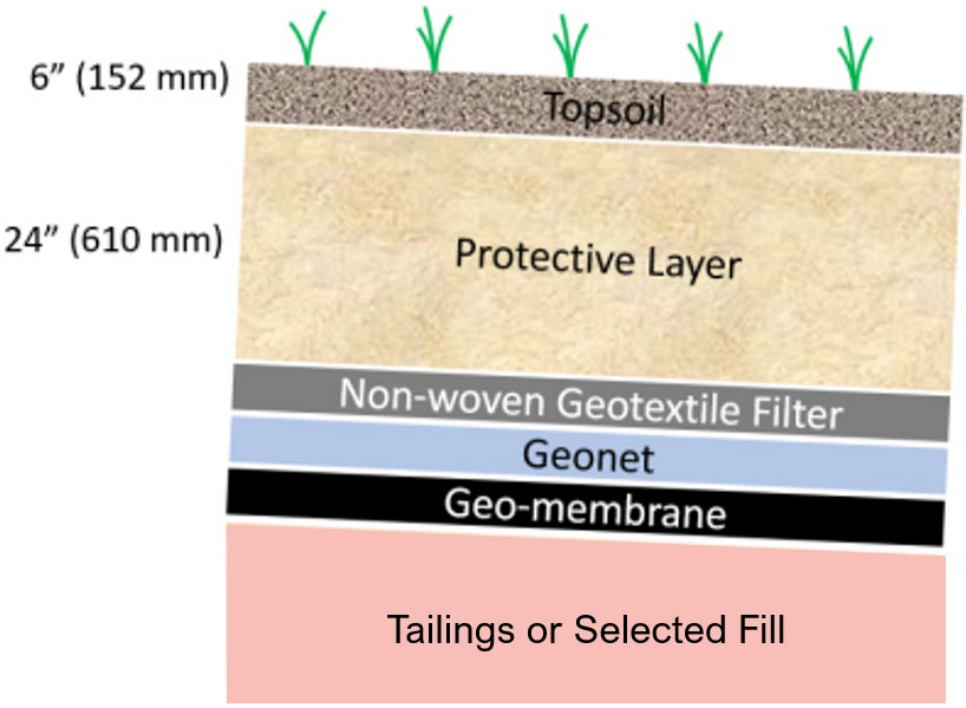


Figure 2: Different layers for cover model

Methodology

SEEP/W Version 2021 R2 finite element software was used to develop the numerical model to design the cover. SEEP/W is a commercial computer program developed by Geo-Slope International Ltd. SEEP/W can analyze the water flow from the environment across the soil surface, through the cover, and into the groundwater regime. The analysis includes infiltration due to rainfall, snowmelt, root transpiration, surface evaporation, and runoff. The model simulates liquid and vapor phase water transport in a two-dimensional cross-section. The code includes a feature to simulate geomembranes using line elements. The percolation from the base of the cover is estimated and is used as an input to the hydrogeological model for the site.

Near-surface processes of evaporation and infiltration are represented as boundary conditions applied to the surficial nodes in the finite element mesh. Infiltration during a timestep with precipitation is computed by subtracting the actual evaporation from the precipitation. The resulting value, which can be either positive (net infiltration) or negative (net evaporation), is applied as a specified flux to the surface node. However, if a positive flux value would result in the surface node becoming saturated, the boundary condition changes to a specified pressure equal to the saturated pressure head, and the net infiltration is calculated from the solution to the flow equation. In this case, runoff occurs equal to precipitation, minus actual evaporation, minus calculated infiltration. SEEP/W also has procedures for accounting for snow accumulation and snow melt.

Key features of the cover modeling in SEEP/W include:

- Material properties can be estimated relatively easily using data such as grain-size, saturated hydraulic conductivity, and saturated water content, or alternatively they can be imported from the built-in material database if this information is not known.
- Large site-specific climate datasets can be applied to the model over extended time periods using transient analyses. Climate input parameters include temperature (minimum and maximum), relative humidity (minimum and maximum), wind speed, evaporation, and rainfall. These can be specified daily or at any other time interval.

The current study was focused on the cover profile, which may include up to about 1 m (3 feet) to 2 m (6 feet) of fill material for profiling below the cover. The model consisted of a 150 mm (6 inches) layer of topsoil, 610 mm (24 inches) of protective layer, a geonet, and a geo-membrane. The fill above the water table and tailings below water level were modeled with their respective hydraulic properties. The bottom of the model and the toe end of the cover were modeled with drain boundary condition. The initial groundwater level was considered constant at 2 m (6 feet) below the cover surface at the toe of the slope. as presented in Figure 3.

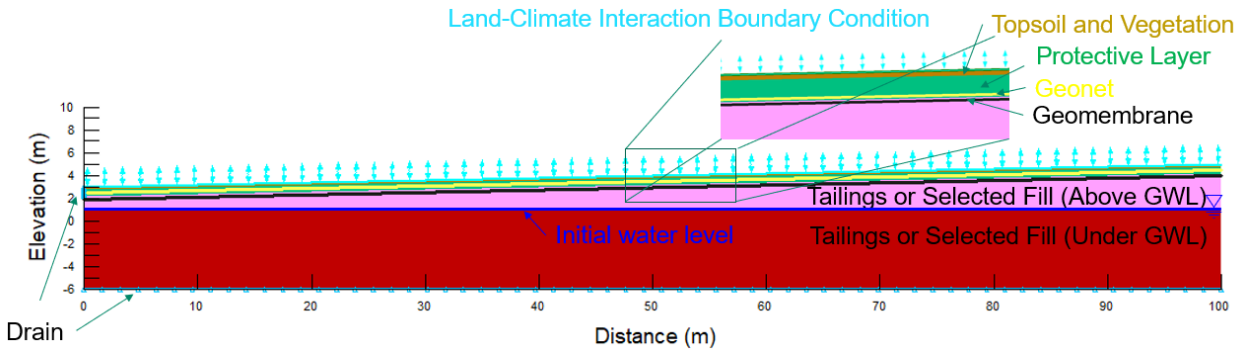


Figure 3: Two-dimensional cover model

Input parameters

The major input parameters for the model include climatic data, vegetation data, physical and hydrological properties of the cover material, fill and tailings. The climatic data for the cover design is mainly based on the available data from Environment Canada for the study site station for the past 30 years, including: air temperature (hourly); precipitation (daily); relative humidity (hourly); wind speed (hourly) and snow depth (daily).

Precipitation is the most important parameter for any cover system. The variation of total precipitation (monthly) for the last 30 years is presented in Figure 4. The average annual precipitation is presented in Figure 5.

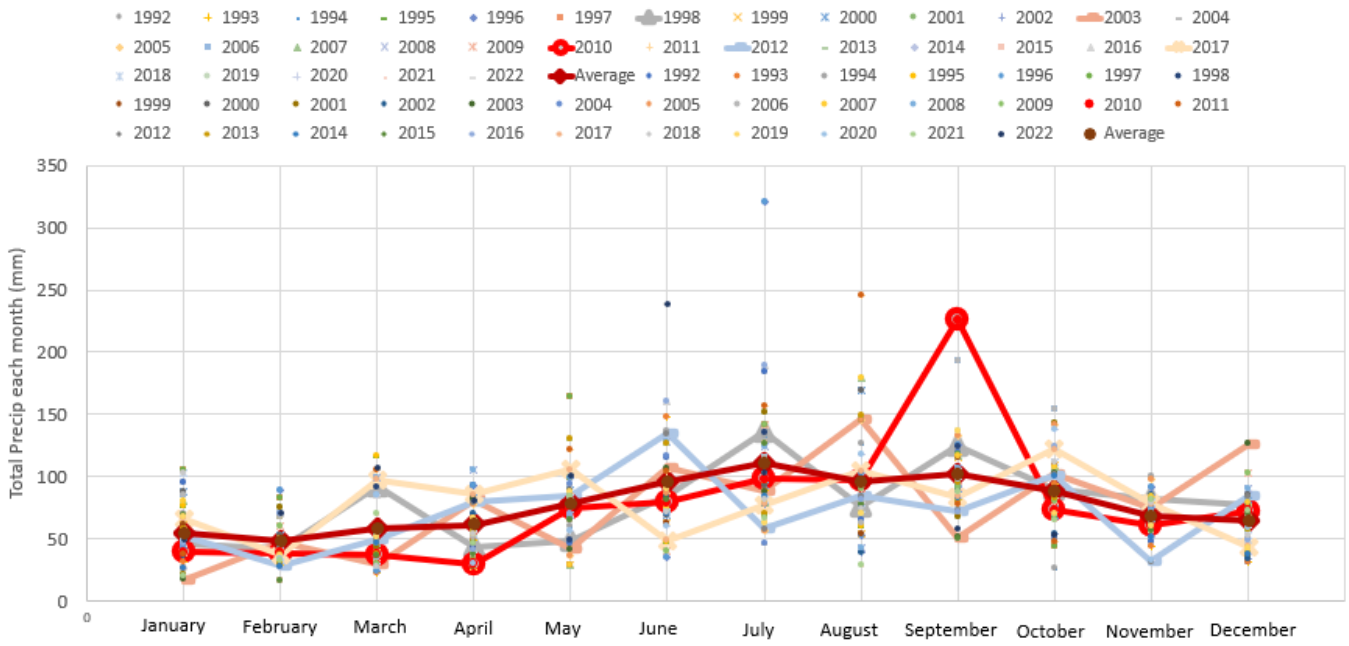


Figure 4: Monthly variation of total precipitation for the last 30 years

The vegetation data are shown in Table 1 and data are selected using a standard vegetation function stored in the SEEP/W database. The vegetation data was approximated from past studies based on expected vegetation type. The figures for leaf area index, root dimensions, and plant height are based on the assumption that the cover will evolve from grasses to shrubs. The plant moisture limit and normalized root density are derived from typical functions. The 75% soil cover fraction is a conservative assumption representing the minimum expected cover.

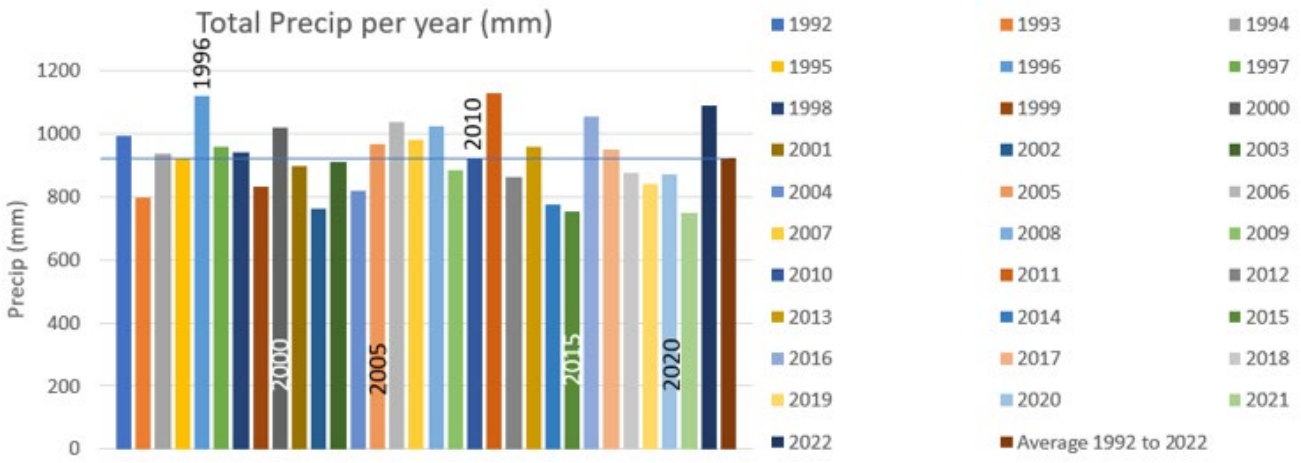


Figure 5: Variation of total annual precipitation from 1992 to 2022

Table 1: Boundary condition – vegetation data

Parameter	Input data
Leaf Area Index	Between 0 and 0.5
Root Depth	0.6 meter
Plant Moisture Limit	Limiting when water table is less than 10 m
Normalized Root Density	Linear decrease from 1 to 0
Soil Cover Fraction	0 for leaf index area less than 0.5 0.75 for leaf index area equal or more than 0.5
Vegetation Height	1.5 m

The main model parameters include hydraulic conductivity function, soil water characteristic curve, material density, hydraulic anisotropic condition, and material compressibility. The constitutive relations between water content, soil-water potential, and unsaturated hydraulic conductivity can be described using three different methods: Fredlund and Xing (1994), Green and Corey (1971), or van Genuchten (1980). Model input parameters were selected from previous modeling studies by others for the soil, fill, and tailings parameters and for geosynthetic layers from the literature.

The material parameters for the key layers are presented in Figure 6. The material parameters for the non-woven geotextile filter were not considered as this layer has no effect on the flow and is aimed at separating the protective layer from geonet only. The geonet was modeled with a saturated only material model with saturated lateral conductivity equal to 1 m/sec and a ratio of vertical to lateral conductivity (Ky/Kx) equal to 20. The geomembrane was modeled with a saturated only material model with saturated lateral conductivity equal to 1×10^{-12} m/sec and a ratio of vertical to lateral conductivity (Ky/Kx) equal to 1.

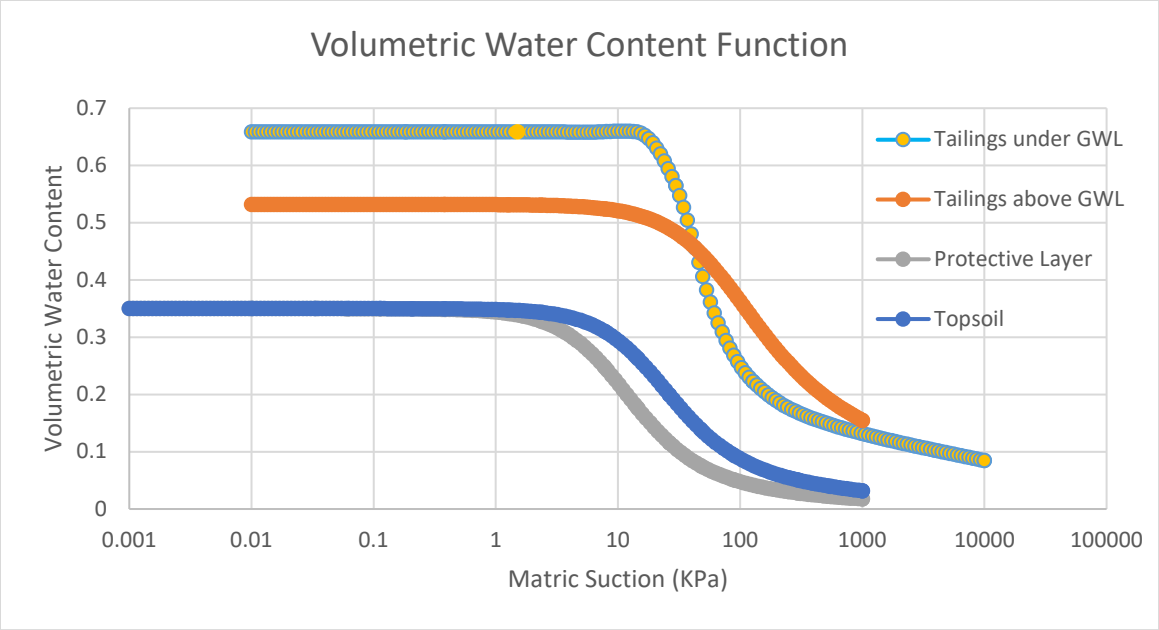


Figure 6a: Soil water characteristic curve

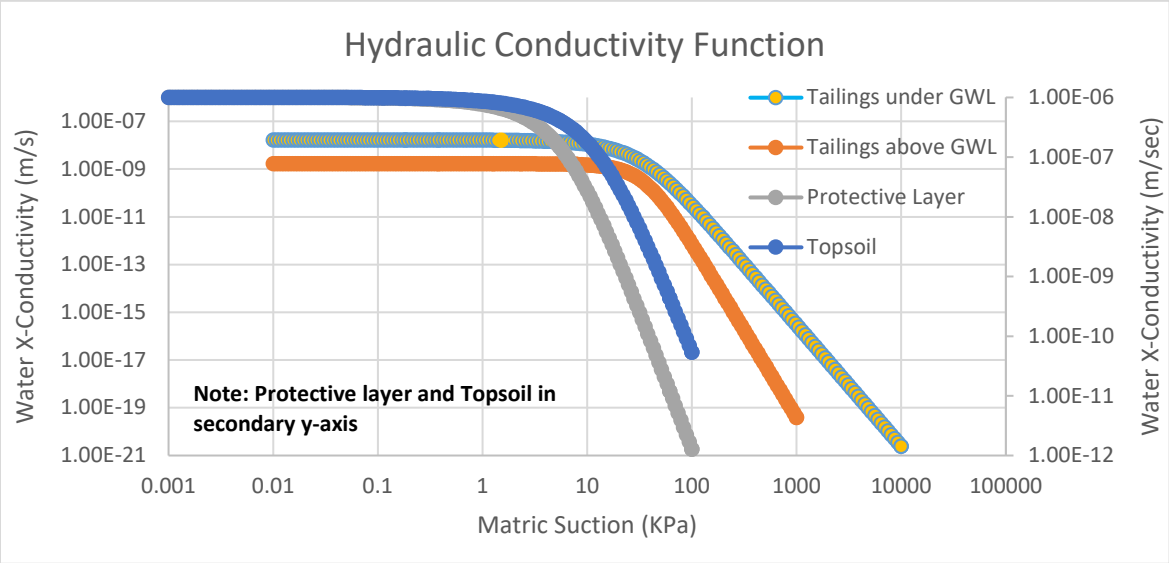


Figure 6b: Hydraulic conductivity function

The geomembrane and geonet were modeled using the interface element in SEEP/W. The thickness of each of them is 3 mm. The sensitivity analyses performed for key parameters are described in Table 2.

Table 2: Input data for sensitivity analyses

Analysis Case	Climatic Conditions	Protective Layer Thickness (inches)	Cover Slope (%)	Material Parameters (Geomembrane) Hydraulic conductivity – Thickness	Vegetation -Soil Cover Fraction (SCF)
1 (base case)	2010	24	2	1×10^{-12} m/sec-3 mm	0.75
2	2012	24	2	1×10^{-12} m/sec-3 mm	0.75
3	2017	24	2	1×10^{-12} m/sec-3 mm	0.75
4	2010	18	2	1×10^{-12} m/sec-3 mm	0.75
5	2010	30	2	1×10^{-12} m/sec-3 mm	0.75
6	2010	24	1	1×10^{-12} m/sec-3 mm	0.75
7	2010	24	3	1×10^{-12} m/sec-3 mm	0.75
8	2010	24	2	1×10^{-12} m/sec-3 mm	0.75
Y9	2010	24	2	1×10^{-12} m/sec-3 mm	0.9
10	2010	24	2	1×10^{-12} m/sec-3 mm	0.6
11	2010	24	2	1×10^{-12} m/sec-3 mm	0.4
12	2010	24	2	1×10^{-12} m/sec-one 1 cm hole/100 m	0.75
13	2010	24	2	1×10^{-11} m/sec-one 1 cm hole/100 m	0.75
14	2010	24	2	1×10^{-12} m/sec-one 10 cm hole/100 m	0.75
15	2010	24	2	1×10^{-11} m/sec-one 10 cm hole/100 m	0.75
16	2010	24	2	1×10^{-12} m/sec-one 100 cm hole/100 m	0.75
17	2010	24	2	1×10^{-11} m/sec-one 100 cm hole/100 m	0.75
18	2010	24	2	6-inch clay layer; 1×10^{-9} m/sec	0.75
19	2010	24	2	1×10^{-11} m/sec-3 mm	0.75
20	2010	24	2	1×10^{-13} m/sec-3 mm	0.75
21	2010	24	2	1×10^{-12} m/sec-3 mm-No Geonet	0.75
22	2010	24	2	24-inch clay layer; 1×10^{-9} m/sec	0.75
23	2010	24	2	1×10^{-12} m/sec-3 mm-Geonet 0.1 m/sec	0.75

Modeling results

The sensitivity analyses were performed for a one-year period to evaluate critical parameters and their effects on the net percolation. The sensitivity analyses were performed to study the effect of such parameters as climatic condition; hydraulic conductivity of geomembrane; defects on geomembrane; slope of the cover; vegetation parameter; protective layer thickness; and use of geonet. Three years of climate data from 2010, 2013 and 2017 were selected for the model to determine the baseline scenario. These three years have a total annual precipitation close to the average annual precipitation of the past 30 years. The water balance was also checked at the ground surface to verify the SEEP/W model. All three climate conditions showed similar net infiltration into the fill material below the cover. Based on this, the 2010 climate condition was selected as a baseline scenario for the sensitivity analyses as it showed slightly higher infiltration.

The infiltration results were evaluated for the different scenarios analyzed in the sensitivity analyses, and the percentage of annual infiltration with respect to annual precipitation was estimated for the different scenarios. Based on O'Kane and Ayres (2012), an infiltration percentage of lower than 5% is considered to

be very low for a cover design and between 5% to 15% is considered to be low. Results from the baseline scenario and the sensitivity analyses indicate that for most cases the infiltration is less than 5%. This cover option is considered adequate for this site.

Discussion and conclusion

The numerical model results showed that the selected cover option is suitable and effective for the study site. The sensitivity analyses showed that the infiltration is sensitive to climatic conditions, slope of the cover, hydraulic conductivity of the geomembrane, and defect in the geomembrane. Among the different parameters studied, the geomembrane permeability appeared to have the most effects.

The statistical analysis of the climatic data for the past 30 years was performed, and 3 representative years were selected for the sensitivity analyses. There was a relatively small variation in the annual precipitation of the past 30 years. As there was a relatively small variation in precipitation in each year, the sensitivity analysis with three different years' precipitation data showed minimal effects on the infiltration through the cover layer. Regarding the slope of the cover, it was found that less infiltration will occur on a steeper surface. Geomembrane degradation, modeled with an increase in permeability of an order of magnitude and/or defects with sizes ranging from 10 cm to 1 meter, which is deemed conservative, will also increase the infiltration. Vegetation parameters showed minimal to no effects on infiltration.

Based on the sensitivity analysis results, the model was developed to study the performance of the cover for a period of 60 years with an increase in average annual precipitation to consider potential climatic changes. For this scenario, it is assumed that the average annual precipitation will increase by 18% over the next 50 years.

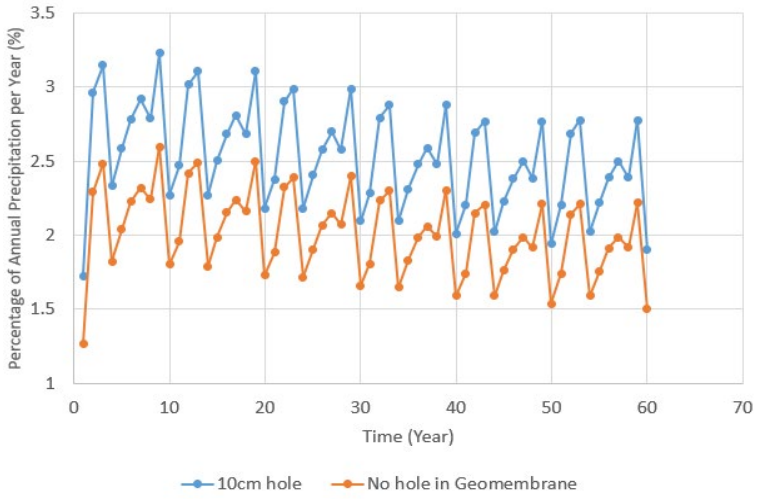


Figure 7: Percentage of infiltration with respect to precipitation

The long-term analysis results (Figure 7) showed that 1.5% to 2.5% of the annual precipitation may infiltrate through a cover with no liner defect and 2% to 3% infiltration may be expected in cover with a hypothetical liner defect (0.1% of the length), which is modeled with one 10 cm hole in every 100 m length of cover in a 2D condition. The infiltration was found to be decreasing over time over a period of 60 years, as presented in Figure 7.

References

Aubertin, M. and Chapuis, R.P. 1991. *Criteres de conception pour les ouvrages de retenue des residus miniers dans la region de l'Abitibi. Proceedings of the 1st Canadian Conference on Environmental Geotechnics:* 113–127. Montreal, Quebec, Canada. The Canadian Geotechnical Society and the St-Lawrence Centre.

Dwyer, S.F. 2003. Water balance measurements and computer simulations. PhD dissertation. University of New Mexico.

Fredlund, D.G. and Rahardjo, H. 1993. *Soil Mechanics for Unsaturated Soils*. Canada: John Wiley & Sons.

Fredlund, D.G. and Xing, A. 1994. Equations for the soil-water characteristic curve. *Canadian Geotechnical Journal* 31: 521–532.

GEOSLOPE International Ltd. 2021. Seepage modeling with SEEP/W. Brochure. Calgary, Alberta, Canada.

Green, R.E. and Corey, J.C. 1971. Calculation of hydraulic conductivity: a further evaluation of some predictive methods. *Proceedings of the Soil Science Society of America* 35: 3–8.

INAP. 2017. Global Cover Systems Design. Technical guidance document prepared by the International Network for Acid Prevention.

MEND. 2004. Mine Environment Neutral Drainage. Design, construction and performance monitoring of cover systems for waste rock and tailings, Canadian Mine Environment Neutral Drainage Program, Project 2.21.4, July.

MEND. 2012. Mine Environment Neutral Drainage. Cold regions cover system design technical guidance document, Canadian Mine Environment Neutral Drainage Program, MEND report 1.61.5c. July 2012. Edited by O'Kane Consultants, Inc. OKC Report No. 817/2-01.

O'Kane, M. and Ayres, B. 2012. Cover systems that utilize the moisture store-and-release concept – do they work and how can we improve their design and performance? *Proceedings of Mine Closure 2012,* 25−27 September, Brisbane, QLD, Australia.

van Genuchten, M. T. and Pachepsky, Y. 2011. Hydraulic properties of unsaturated soils. In J. Glinski, J. Horabik and J. Lipiec, eds. *Encyclopedia of Agrophysics*, Springer: 368–376.

van Genuchten, M.Th. 1980. A closed-form equation for predicting the hydraulic conductivity of unsaturated soils. *Soil Science Society of America Journal* 44(5): 892–898.

Zornberg, J.G., Bouazza, A. and McCartney, J.S. 2009. geosynthetic capillary barriers: principles and applications. *Proceedings of the First African Conference on Geosynthetics, GeoAfrica 2009,* Cape Town, South Africa (CD ROM).

The Evaluation of Nonlinear Dynamic Numerical Simulations of TSFs

Michael James, Agnico Eagle Mines, Canada

Abstract

The use of nonlinear dynamic (numerical) analysis (NDA) for the evaluation of the seismic stability of tailings storage facilities (TSF) is becoming more common due to rigorous standards that mandate the use of the maximum credible earthquake (MCE) or a 10,000-year recurrence interval in the presence of extreme consequences during operations or for closure. The increasing usage of NDA is also due to an increase in the capacity and expertise of consultants. However, there is considerable uncertainty in the review of NDA. There are few guidelines and no industry standards for the execution and review of NDA for TSF. As a result of this, as well as the very complex nature of NDA, the reports for such analyses may lack sufficient information to be verified and the reviewers must rely on the expertise and judgement of the consultant. Furthermore, experienced numerical modelers are relatively rare, and many modelers are specialized and lack experience and judgement in other relevant aspects of geotechnical engineering. This paper presents, in terms accessible to technical professionals who are not modelers, information and guidelines to assist in the understanding and review of NDA for TSF. This is accomplished with an explicative NDA of an example TSF. Basic guidelines for the evaluation of NDA studies for TSF are provided.

Introduction

Historically, seismic activity has not been a primary cause of the failure of tailings storage facilities (TSF). However, when it has been a cause, the consequences have been devastating. Of particular note is the El Cobre Tailings Dam failures (Chile, 1965), when three upstream raised tailings dams failed as a result of the Valparaíso earthquake (moment magnitude, M_w 7.5). The flow of 2.25 M m^3 of liquefied tailings destroyed the town of El Cobre and more than 200 lives were lost (Dobry and Alvarez, 1967). Due to the indefinite lifespans of TSF and the consequences of failure, it is imperative that all TSFs be designed or upgraded to withstand reasonably anticipated seismic loadings, even in areas of low seismicity.

This paper presents the nonlinear dynamic (numerical) analysis of an example TSF in an explicative manner to inform technical professionals not familiar with such analyses and to provide basic guidelines for the review of technical studies on this subject.

The effects of earthquakes on TSFs

Locally, earthquakes induce transient, alternating three-dimensional accelerations in the bedrock underlying a TSF. These accelerations (ground motions) are transmitted upwards from bedrock, through any overburden, and through the TSF. In practice, the ground motions are separated into three orthogonal components: 1) vertical, 2) horizontal and parallel to the alignment of a perimeter dike, and 3) horizontal and perpendicular to that alignment. The ground motion perpendicular to the alignment is of concern because it acts to reduce physical stability ($F=M \cdot A$). Generally, the most important effects are in the downstream direction. However, for dikes with upstream raises, the stability in the upstream direction may be of concern.

Within saturated, contractive materials, such as loose tailings, silts or sands, the ground motion may induce the generation of excess pore water pressures (epwp) and, ultimately, liquefaction. The loss of stiffness and strength associated with epwp generation and liquefaction can result in the deformation or failure of a perimeter dike.

Following shaking, the dissipation of epwp in an unfavorable direction can induce destabilizing seepage pressures. This is a postulated cause of failure of Dike No. 2 of the Mochikoshi TSF in Japan following the 1978 Izu-Ohshima-Kinkai earthquake (M_w of 7) (Ishihara, 1984).

Methods of evaluation

Typically, the seismic performance and stability of a TSF are evaluated using analytical methods consisting of, for each perimeter dike, a) a site response analysis, b) a simplified liquefaction analysis, c) a pseudo-static or post-liquefaction analysis, d) an estimation of permanent displacements, if applicable, and e) an evaluation of the results. However, in most instances these methods do not well represent the effects of earthquakes on TSFs. Some important phenomena are ignored, while others are treated in an overly simplistic or unrealistic manner (James et al., 2022). For example, the results of simplified liquefaction analysis in level ground conditions where there are no initial static shear stresses (e.g., within a TSF away from the influence of the perimeter dikes) agree reasonably well with numerical analysis (James and Aubertin, 2016), but tend to significantly differ near dikes, particularly below upstream raises (James 2024a, 2024b). Unrealistically, the pseudostatic method of stability analysis replaces the transient, random horizontal accelerations of an earthquake with a "static" horizontal acceleration that tends to be much more detrimental to stability; hence, there is significant conservatism that can lead to overdesign.

Generally, the results of the analytical methods are conservative. However, when a phenomenon that is critical to the seismic performance and stability of a particular dike is not represented, the results of these methods may be misleading.

The Mile High TSF

The Mile High TSF is in a board alluvial valley northeast of Denver, Colorado and was in operation from 1996 to 2014. It retains nonreactive, slurry-deposited tailings from hard rock gold mining.

Locally, the topography is relatively flat. Subsurface conditions consist of 1 to 2 m of dense alluvium (clayey sand with gravel) over bedrock of hard, relatively intact siltstone and sandstone. The groundwater table is near the surface.

The TSF is oval in plan with dimensions of 600 m north-south by 300 m east-west. The perimeter dikes are Dike 1 on the west side and Dike 2 on the east. An east-west cross-section of the TSF is shown in Figure 1.

Dike 1 is composed of a 5-m-high starter dike of compacted fill (clayey sand with gravel). The dike is founded on the native alluvium and is served by 1-m-thick granular subdrains at regular intervals. The upstream (u/s) and downstream (d/s) slopes are at 1.5:1 (H:V) and 2:1, respectively. Two 4-m-high upstream raises of compacted tailings were constructed from the starter dike. Working pads of tailings mixed with waste rock were placed on the tailings beach, prior to the construction of the raises. The inclinations of the slopes of the raises are like those of the starter dike.

Dike 2 is a rockfill structure with slopes of 1.5:1 u/s and 2:1 d/s. The u/s slope has a 1-m-thick transition filter zone. This dike is founded directly on bedrock.

The tailings in the TSF were deposited by end-of-pipe from around the perimeter to a height of 17 m, leaving a freeboard of 1 m. The surface of the tailings slopes downwards at about 1% from the perimeter towards the center.

As noted, tailings deposition ended in 2014. In 2016, a 1-m-thick multi-layer cover was placed on the tailings for closure.

The phreatic level within the TSF is relatively high, and in the long term is expected to vary seasonally from 3 to 6 m below the surface, including considerations for climate change.

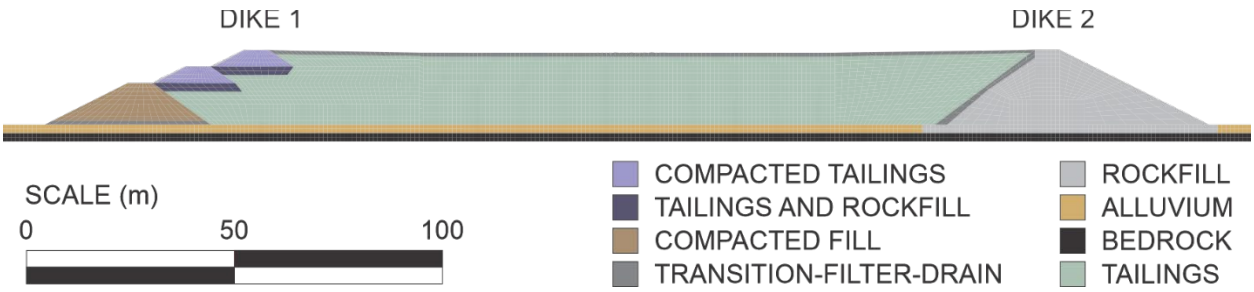


Figure 1: Cross-section of the Mile High TSF

Design Earthquake Ground Motion

For closure, the Design Earthquake Ground Motion (DEGM) corresponds to a recurrence interval of 10,000 years. The parameters for the DEGM were obtained using the ASEC Hazard Tool/ Standard ASCE/SEI 7-22 (ASCE, 2024) for Soil Class A (Hard Rock). The peak (horizontal) ground acceleration (PGA) of 0.226 g and spectral acceleration (Sa) envelope are shown in Figure 2. The PGA is not actually associated with a period, but is shown at a period of 0.001 s for convenience. The results of deaggregation analysis (Figure 3) indicate a modal magnitude-distance pairing of 5 (M_w) and 5 km (ASCE, 2024). The Arias intensity of the pairing varies from 0.01 m/s to 0.5 m/s for one horizontal direction (Bahrampouri et al., 2020).

The S_a envelope represents the probable maximum values of spectral acceleration from many different magnitude-distance pairings from different regional sources. It does not represent a single earthquake. The modal magnitude-distance pairing is the most probable pairing of those considered.

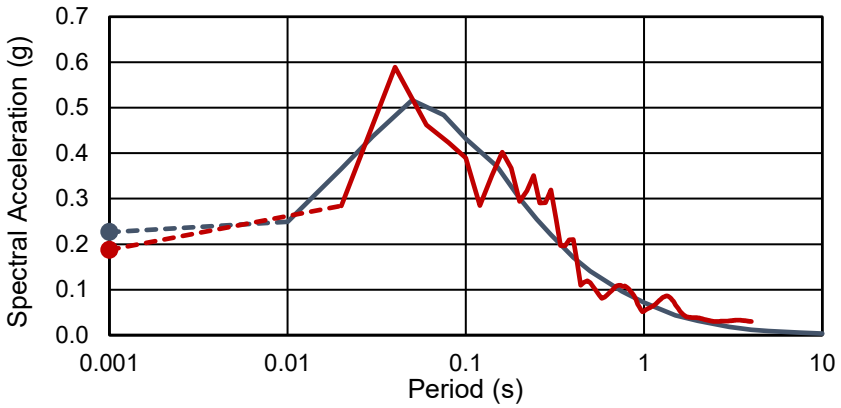


Figure 2: Spectral acceleration envelope of DEGM 5 % damping (blue) and spectral acceleration graph of ground motion H4-04 (red)

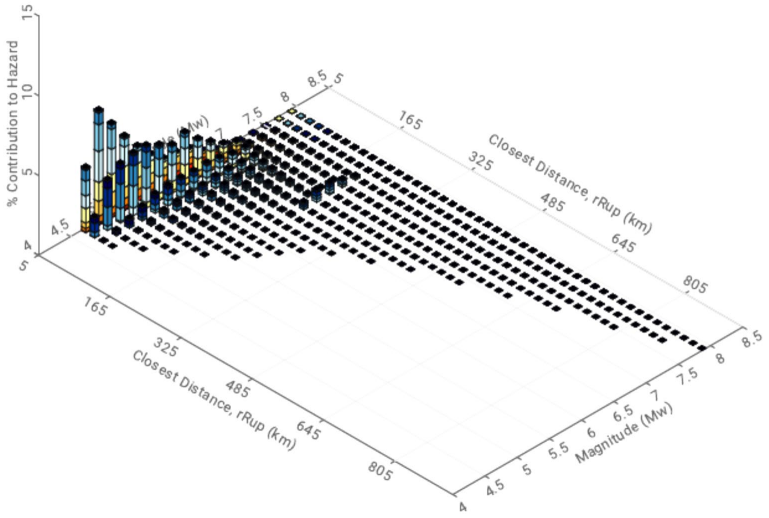


Figure 3: Graphic of deaggregation analysis (from ASCE, 2024)

Nonlinear dynamic analysis of the TSF

This section presents the NDA of the TSF. It should be noted that the methodology employed in NDA varies depending on the particularities of each case as well as the objectives of the analysis. There is no one-size-fits-all method.

Methodology

This study employed version 8 of the FLAC finite differences program (Itasca, 2016) with the dynamic and user-defined model options. The analyses were conducted in plane strain mode.

The methodology was as follows:

1. Development of grid (geometric model), establishment of mechanical boundary conditions, and assignment of constitutive models with associated material properties.
2. Analysis for mechanical equilibrium.
3. Assignment of flow boundary conditions and initial pore water pressures (to facilitate computation).
4. Analysis for flow equilibrium.
5. Analysis for coupled (mechanical and flow) equilibrium (static condition).
6. Verification of static stresses and pore water pressures within the model.
7. Dynamic analysis by the application of dynamic boundary conditions and of a ground motion record to the bottom of the model.

Geometric model, constitutive models and material properties

A geometric model of quadrilateral elements, nominally 1-m-square, was created. The 1-m-height of the elements was sufficient for the faithful transmission of the seismic waves through the model per Itasca (2016) and provided sufficient granularity for evaluation of the results. In some less critical areas, such as the shoulders of Dike 2, larger elements were used for convenience. The use of larger elements in these areas did not affect the results. The geometric model is shown in Figure 4.

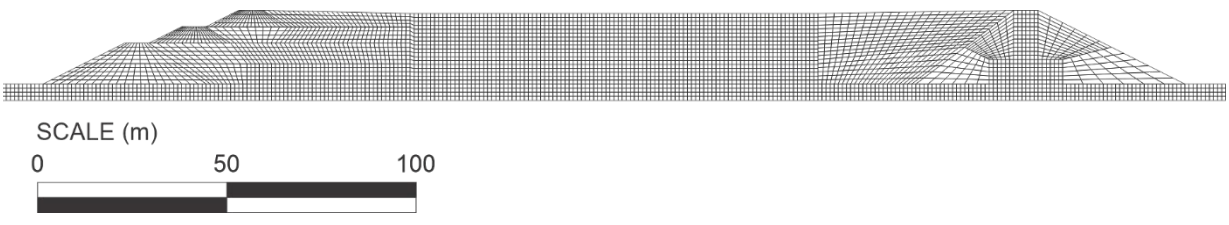


Figure 4: Geometric model of the TSF

For bedrock, a shear wave velocity, Vs, of 1,500 m/s and a total unit weight, γ, of 26.5 kg/m^3 were assumed. As the bedrock is unyielding relative to the expected loads, the elastic model was used to simulate its behavior. The bedrock was given a hydraulic conductivity of 1×10^{-8} cm/s.

As tailings deposition ended in 2014 and a granular cover was placed in 2015, it is assumed that the tailings are, or will soon be, normally consolidated. Accordingly, the properties of the tailings were derived from in-situ testing as well as laboratory testing of consolidated specimens (James, 2009). Even when normally consolidated, the tailings will be contractive and subject to excess pore water pressure (epwp) generation and liquefaction where saturated. Due to the potential for epwp generation and liquefaction, the UBCSAND constitutive model (Beaty and Byrne, 2011) was used for the tailings. The model parameters were obtained by numerically simulating the dynamic laboratory testing (James, 2009; James and Aubertin, 2016). These parameters are an average standard penetration test blow count, $(N_1)_{60\text{-}CS}$, of 10 blows/30 cm, a dry unit weight γ_{DRY} of 23.1 kN/m^3, an effective angle of internal friction, ϕ', of 35° and a porosity, n, of 0.62. The high values of γ_{DRY} and ϕ' of the tailings are a result of their mineralogy (specific gravity of 3.8). To simulate the heterogenicity typical of tailings, even after consolidation, a normal distribution factor of 2 blows/30 cm was used. As this is the primary variable with respect to epwp generation and liquefaction, it creates some randomness in the response of the individual elements of tailings. The tailings were assigned a hydraulic conductivity of 1×10^{-10} cm/s.

The raises of Dike 1 are composed of compacted tailings; this material was modeled similarly to the retained tailings but with an $(N_1)_{60\text{-}CS}$ value of 20 blows/30 cm and no randomization.

The properties of other materials are given in Table 1. The properties are from published sources and the author's experience. The Mohr-Coulomb (elastic-plastic) model was used for these materials.

Table 1: Material properties

Property	Rockfill	Alluvium	Compacted Fill	Filter-Transition	Rockfill-Tailings
γ_{DRY} (kN/m^3)	23.5	22.6	22.6	22.6	23.5
ϕ'	48°	35°	35°	34°	35°
c' (kPa)	-	50	50	-	-
n	0.15	0.15	0.15	0.15	0.1
Vs (m/s)	600	400	400	325	300
μ	0.2	0.25	0.25	0.25	0.3
K (cm/s)	100	1×10^{-5}	1×10^{-5}	1	1×10^{-4}

Where γ_{DRY} is dry unit weight, ϕ' is effective friction angle, c' is effective cohesion, n is porosity, V_s is shear wave velocity, μ is Poisson's ratio, and K is hydraulic conductivity.

A general shear modulus reduction (versus shear strain) curve (Seed and Idriss, 1970) was applied to all materials except for bedrock and the retained and compacted tailings. In FLAC, damping is estimated from the shear modulus reduction curve. This was not applied to bedrock as it is considered rigid (no appreciable shear strains) with respect to the applied loading. Nor was it applied to the tailings because shear modulus reduction and damping are implicit in the UBCSAND model. Shear modulus reduction curves are typically horizontal at very low strains, so it is necessary to include a small amount of Rayleigh damping. Through trial and error, it was found that 0.0125 of Rayleigh stiffness suited this purpose, while allowing faithful transmission of the ground motion through the model, particularly the bedrock.

Selection of ground motions

Due to the considerable variation and uncertainty in ground motions, numerical analysis should consider at least five ground motions that correspond to different magnitude-distance pairings and sources, if applicable, that satisfy the DEGM in terms of the spectral acceleration envelope and the intensity of earthquake loading as measured by the Arias intensity, I_x, and the anticipated predominant period and durations of shaking.

The Denver region has moderately low seismicity and produces earthquakes of relatively high frequency; as a result, there are very few, if any, recorded ground motions that could be reasonably scaled to simulate the DEGM. For this paper, several ground motions were created and processed using software by SeismoSoft (2022). Ground motion H4-04 (Figure 5) was then selected for use in this example. This ground motion (GM) has a PGA of 0.188 g, an Arias intensity, I_x. of 0.251 m/s, predominant and mean periods of 0.04 s and 0.22 s, respectively, a duration of 12 s, and a significant duration (between 5 and 95% of I_x) of 6.81 s. The spectral acceleration graph of the GM is shown in Figure 5.

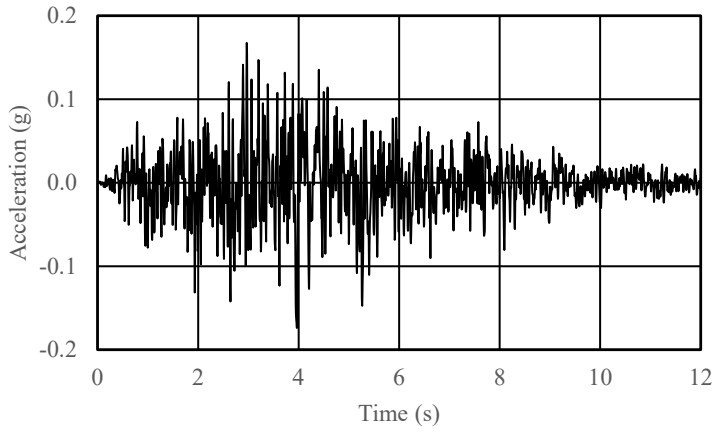


Figure 5: Ground Motion H4-04

Site response

How well a model transmits acceleration is fundamental. Given that bedrock is assumed to be rigid and unyielding, the accelerations should not be amplified or damped within the bedrock. The accelerations measured at the top of the bedrock should be nearly identical to those input at the bottom of bedrock. Figure 6a presents the input and measured accelerations. They are nearly identical, confirming faithful transmission. Had they been different, then the TSF would not have experienced the DEGM.

Figure 6b shows the accelerations in the center of the TSF near the surface. Note the appreciable amplification, which is expected in soft soil, at least until the generation of significant epwp.

The accelerations on the crests of Dikes 1 and 2 are shown respectively in Figures 6c and 6d. The ground motion within the dikes was substantially amplified. Ground motions are always amplified by embankments, typically by a factor of 1.5 to 2.5, increasing with stiffness and steepness. The accelerations on the crest of Dike 1 are a bit more chaotic due to its reliance on the tailings for support, which produces significant interaction between the dike and the tailings.

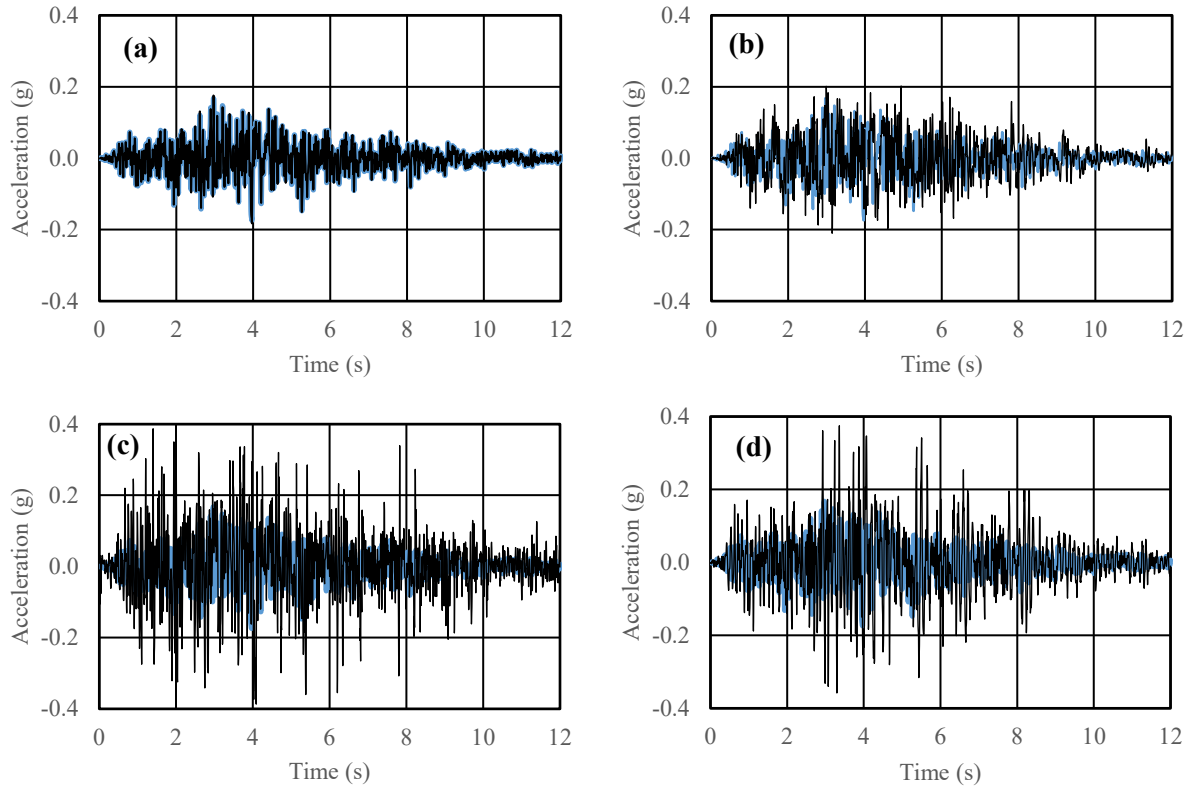


Figure 6: Accelerations – (a) GM H4-04 (blue) and measured on top of bedrock (black), (b) GM H4-04 (blue) and measured near top of tailings (black), (c) GM H4-04 (blue) and on crest of Dike 1 (black), and (d) GM H4-04 (blue) and measured on crest of Dike 2 (black)

The response of the tailings

Figures 7a, 7b, and 7c respectively present the accelerations, cyclic stress ratio, CSR, and epwp ratio, r_u, in the center of the TSF. The accelerations and CSR are at mid-height and the r_u is at 0.25, 0.5, and 0.75 of the height, H, of tailings. The CSR is the ratio of the applied shear stress on an element of soil and is mostly due to the applied accelerations (which induce shear stress) but may also be affected by stress redistribution during shaking. The parameter r_u is the ratio of the developed epwp to the initial effective vertical stress. It is zero at the start of shaking and increases as the application of CSR triggers a contractive response causing epwp generation.

The accelerations indicate appreciable amplification during shaking, as expected. The amplitudes of CSR are considerable, generally varying from about 0.05, where epwp generation typically commences, to over 0.1, where several cycles will induce liquefaction, which is defined here as an r_u of 0.7 or more. The graphics of r_u indicate that liquefaction occurred in the upper half of the tailings by the 5th second of shaking but did not occur in the lower half.

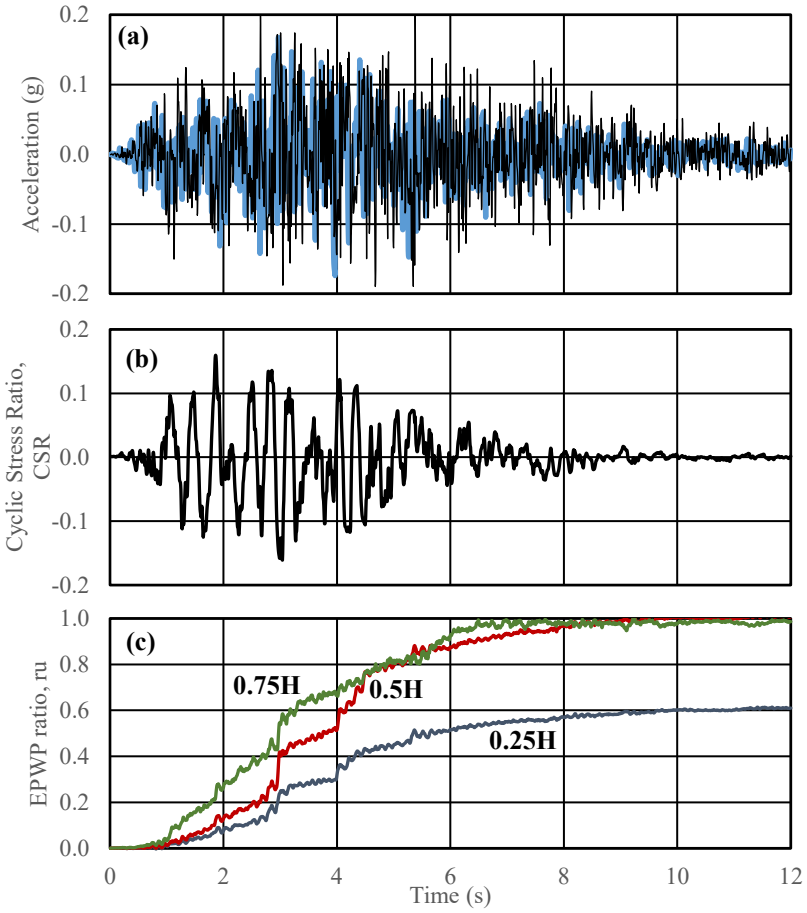


Figure 7: (a) GM H4-04 and accelerations in center of tailings at mid-height (h=0.5H), (b) CSR in center of tailings at h=0.5H, and (c) development of r_u at 0.25H, 0.5H and 0.75H

Displacements of the crests of the dikes during shaking

The horizontal (x) and vertical (y) displacements of the crests of the dikes during shaking are shown in Figure 8, where x and y are positive to the right and up, respectively. The crest of Dike 1 displaced about 10 cm d/s by the 5th second, then reversed by 5 cm before moving d/s for a displacement of about 12 cm by the end of shaking (EoS). The crest of Dike 2 followed a similar path, except that the displacement was initially u/s and then changed to d/s, with about 2 cm of d/s displacement by EoS. The vertical displacements of the crests were relatively uniform and were about 5 cm downwards for Dike 1 and 0 for Dike 2 at EoS.

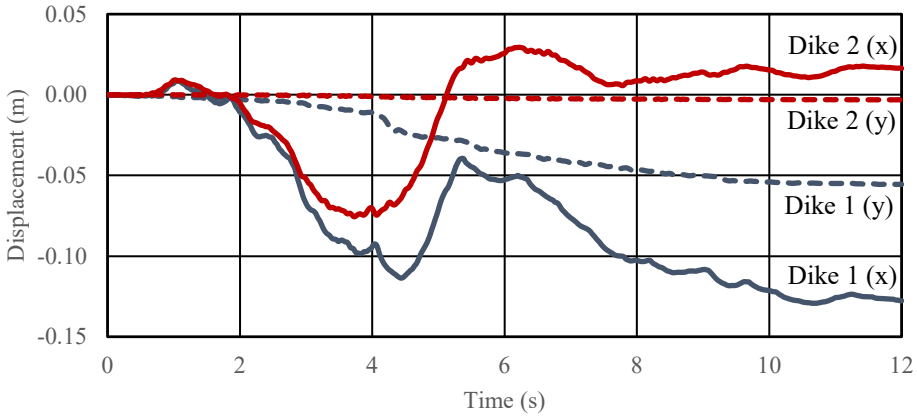


Figure 8: Displacements of the crests of Dikes 1 and 2

Conditions at the end of shaking

As shown in Figure 9 (top), there was extensive liquefaction in the upper half of the tailings. The generation of epwp and liquefaction was favorably affected by the presence of the upstream raises of Dike 1, due to the presence of initial static shear stresses. Near Dike 1, interaction between the dike and the tailings, due to their different periods, resulted in additional liquefaction at depth.

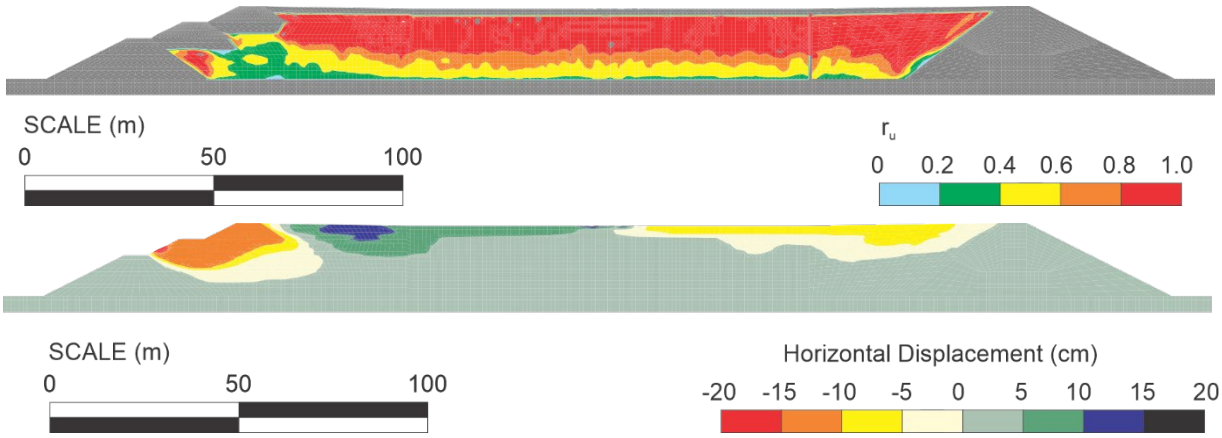


Figure 9: Conditions at the end of shaking: (top) excess porewater pressure ratio, and (bottom) horizontal displacements

Evaluation of performance and stability

Using NDA, the performance and stability of a TSF is evaluated based on the magnitudes and patterns of displacements at EoS, the magnitude and pattern of nodal velocities at EoS, or the occurrence of failure (excessive deformation) during shaking. When excessive deformation occurs during shaking, execution is stopped due to numerical instability. However, the magnitude and pattern of velocities when execution stops are usually sufficient to determine failure.

In many cases, the velocities at EoS may be indicative of continued displacement and possible failure. In such cases, a post-shaking analysis should be conducted by continuing the NDA with appropriate changes to the constitutive models or parameters in elements with liquefaction.

Depending on the configuration of the perimeter dike, epwp development at EoS may indicate a potential for epwp dissipation to cause failure. In these cases, an appropriate post-shaking analysis is needed.

Basic guidelines for review

Basic guidelines for the review of the NDA of a TSF are:

1. Life cycle considerations: The analysis should be focused on operational (current) or closure (long-term conditions).
2. The material properties should correspond to the phase in the life cycle under consideration.
3. Plots of vertical stresses and pore water pressure in the static phase, before shaking, should be provided for verification.
4. Ground motions records should be selected based on agreement with different ranges of periods of the spectral acceleration envelop of the DEGM (e.g., 0.1 to 1 s), and the anticipated Arias intensity corresponding to a given moment-distance pairing. The PGA is not a significant factor in NDA. Also, spectral matching is not recommended because the resulting ground motions are generally overly intense.
5. The constitutive models used should be capable of reasonably well simulating the behaviors of concern, for example excess pore water pressure generation and liquefaction, and this should be demonstrated by appropriate examples or the simulation of laboratory testing.
6. The ability of the model to reasonably well transmit accelerations through bedrock and through the model should be demonstrated graphically.
7. Plots of acceleration, cyclic stress ratio, and excess pore water pressure ratio at key locations should be provided for verification.

8. Plots of the condition of the model at the end of shaking, including excess pore water pressure ratio, horizontal and vertical displacement and horizontal velocity should be provided as a basis for evaluation and used to determine if post-shaking analysis is required.
9. When post-shaking analysis is conducted, it is important to establish the objective, i.e., verify that velocities will decrease with time, determine effects of post-shaking dissipation of epwp, or estimate post-shaking consolidation settlements, and modify the constitutive models and parameters as necessary.

Conclusion

Numerical modeling, particularly dynamic numerical modeling, is not an exact science. At best it is a simplified mathematical expression of very complex and interrelated phenomena, and thus cannot provide precise predictions of behaviors, strains, or displacements. What it provides is a better understanding of the various phenomena and information for comparison, to which engineering judgement must be applied.

References

American Society of Civil Engineers (ASCE). 2024. Accessed May 1, 2024 at https://ascehazardtool.org/

Bahrampouri, M., Rodriguez-Marek, A. and Green, R.A. 2020. Ground motion prediction equations for Arias Intensity using the Kik-net database. *Earthquake Spectra* 37(1): 428–448.

Beaty, M.H. and Byrne, P.M. 2011. UBCSAND constitutive model version 904aR, Documentation report.

Dobry, R. and Alvarez, L. 1967. Seismic failures of Chilean tailings dams. *Journal of the Soil Mechanics and Foundations Division* 93(SM6): 237–260.

Ishihara, K. 1984. Post-earthquake failure of a tailings dam due to liquefaction of the pond deposit. *Proceedings of the International Conference on Case Histories in Geotechnical Engineering:* 1129–1143. St-Louis, New York: ASCE.

Itasca Consulting Group (Itasca). 2016. FLAC, Fast Lagrangian Analysis of Continua, Version 7.0. Itasca Consulting Group, Minneapolis, MN.

James, M. 2009. The use of waste rock inclusions to control the effects of liquefaction in tailings impoundments. PhD thesis, Department of Civil, Geological and Mining Engineering, Polytechnique, Montréal QC.

James, M. and Aubertin, M. 2016. Comparison of numerical and analytical liquefaction analyses of tailings. *Geotechnical and Geological Engineering* 35(1): 277–291. doi.org/10.1007/s10706-016-0103-x.

James, M., Gordan, G., Znidarčić, D., Moncrieff, J., Quinn, J. and Winckler, C. 2022. Geotechnical design analysis. In *Tailings Management Handbook: A Life Cycle Approach*. Englewood CO: SM: 551–580.

James, M. 2024a. The evaluation of seismic performance of tailings storage facilities – Part 1. *Proceedings of the 77th Canadian Geotechnical Conference.* Montreal: Canadian Geotechnical Society.

James, M. 2024b. The evaluation of seismic performance of tailings storage facilities – Part 2. *Proceedings of the 77th Canadian Geotechnical Conference.* Montreal: Canadian Geotechnical Society.

Seed, H.B. and Idriss, I.M. 1970. Soil moduli and damping factors for dynamic response analyses (Report No. ERC 70-10). Berkeley CA: Earthquake Engineering Research Center.

Modeling of Embankment Scour Caused by a Tailings Pipeline Break and Potential Risk of Dam Breach

Angus Rose, WSP, Australia
Mateus Nogueira, WSP, Australia
David Accadia, WSP, Australia

Abstract

Slurry pipelines for tailings facilities can deliver tailings slurry at high pressures and flowrates. For arrangements that require discharge from an embankment, a pipe break could result in a significant scour risk to the embankment. If the break goes unnoticed and tailings delivery is not stopped, the subsequent erosion could lead to a breach of the embankment and loss of containment.

Computational Fluid Dynamics (CFD) software was used to model scour erosion of a hypothetical compacted rockfill embankment due to pipeline break at the upstream crest edge, and consequent flow of a high mass concentration tailings slurry onto the upstream face. Rheological data for the tailings slurry was used to characterize it as a non-Newtonian fluid. Geotechnical properties assigned to the embankment fill were key inputs for the erosion modeling. The modeling, undertaken for an operating facility, showed that scour erosion can progress through an embankment in a matter of hours, leading to a substantial loss of freeboard and therefore a potential embankment breach. Outcomes of the modeling prompted the installation of monitoring instruments on the embankment for early detection of a pipe break.

Introduction

This paper presents an analysis of pipe-break induced erosion of a hypothetical compacted rockfill embankment due to a failure of a tailings delivery pipeline. Many tailings storage facilities (TSFs) operate under an arrangement that requires tailings slurry deposition from an embankment, into the tailings impoundment area. For these facilities, a rupture/break of the tailings delivery pipeline could represent a large risk of erosion of the embankment, if the break were to go unnoticed, potentially resulting in loss of freeboard and loss of containment.

The scenario summarized in this paper was for a pipeline break at the crest of an embankment, with uncontrolled tailings slurry flow, causing scour of the crest and upstream face.

Assessment characterization

Embankment and pipeline layout

The tailings delivery pipeline was modeled along the upstream crest edge of the embankment, positioned about 1.2 m from the edge, with the center of the pipe assumed to be about 0.4 m above the embankment crest, allowing for pipe supports. See summary of the pipeline parameters adopted for the assessment in Table 1.

Table 1: Adopted tailings delivery pipeline parameters

Parameter	Value
Pipe internal diameter (mm)	292
Tailings slurry flow rate (m^3/hr)	600
Tailings slurry flow rate (m^3/s)	0.17

Embankment geometry and materials

The embankment was formed with compacted rockfill, with a 0.5-m-thick layer of compacted screened rockfill on the upstream face to form a bedding layer for a geosynthetic liner. The embankment geometry is summarized in Table 2 and is shown in cross-section in Figure 1. A tailings surface 6.5 m below the embankment crest was adopted for analysis and instantaneous failure of the geosynthetic liner was assumed.

Table 2: Embankment geometry

Parameter	Value
Upstream slope gradient of embankment	2.7H:1V
Embankment crest width (m)	8

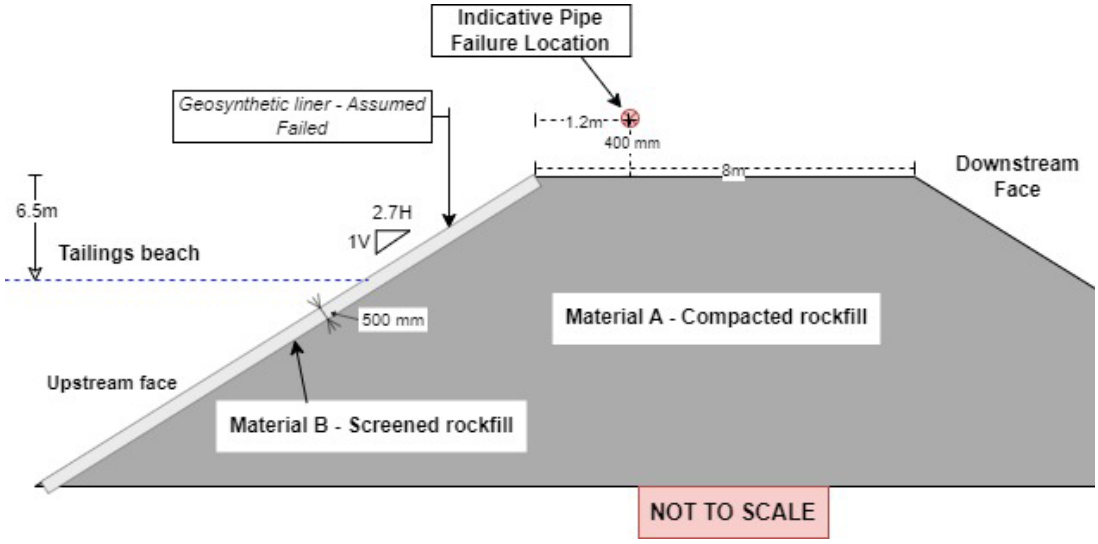


Figure 1: Cross-section of embankment arrangement for pipe break modeling

The fill materials in the embankment are as follows:

1. Material A – Compacted Rockfill: Well-graded, particles typically sand to cobble size. Soil (sand and gravel) content up to 70% by volume.
2. Material B – Screened Rockfill**:** Well-graded mine waste rock, with particles smaller than 50 mm. Characterized as sand and gravel.

Fill material parameters for analysis

The materials were assigned erodibility classifications according to the method of the U.S. Bureau of Reclamation (USBR), for comparison to modeled erosion rates (U.S. Department of the Interior – Bureau of Reclamation, 2019). These erodibility classifications, along with key material parameters that were used to characterize the embankment materials in the hydraulic modeling software, are summarized in Table 3.

Table 3: Embankment material parameters for assessment

Material	Maximum particle size (mm)	Particle density (t/m³)	Representative D_{50} (mm)	Angle of repose (°)	Layer thickness (mm)	USBR erodibility classification[1]
Material A	130	2.8	20, 40 (Note)	33	n/a	Medium to Low (IV)
Material B	50	3	10	33	500	Medium erodibility (II)

Note 1: Material A split into soil and rock component for this assessment (soil component, D_{50} = 20 mm, rock component D_{50} = 40 mm)

Tailings flow characteristics

Newtonian vs. non-Newtonian flow

Analysis of the flow of tailings slurry is generally more complex than the flow of water. Depending on the solids concentration of the slurry, the flow can possess Newtonian (e.g., water) or non-Newtonian (e.g., mud or tailings) characteristics. For Newtonian fluids, the ratio of shear stress to shear rate is constant for varying shear rates, resulting in constant viscosity. For non-Newtonian fluids, (e.g., tailings) and other fluids that do not obey Newton's Law of Viscosity, the relationship is not constant; as such, this relationship is called apparent viscosity, where viscosity changes with shear rate. This is illustrated in Figure 2 for five typical fluid types (Kilgore and Cotton, 2005).

Tailings typically exhibit yield-pseudoplastic (shear thinning) behavior, where apparent viscosity decreases with increasing shear rate. Additionally, these fluids require a minimum shear stress (yield stress) before flow is initiated. As these characteristics are dependent on the type of tailings and the concentration of solids present, the tailings can exhibit very different behavior to water at increased shear rates and should therefore be considered when modeling the flow of tailings in hydraulic analyses.

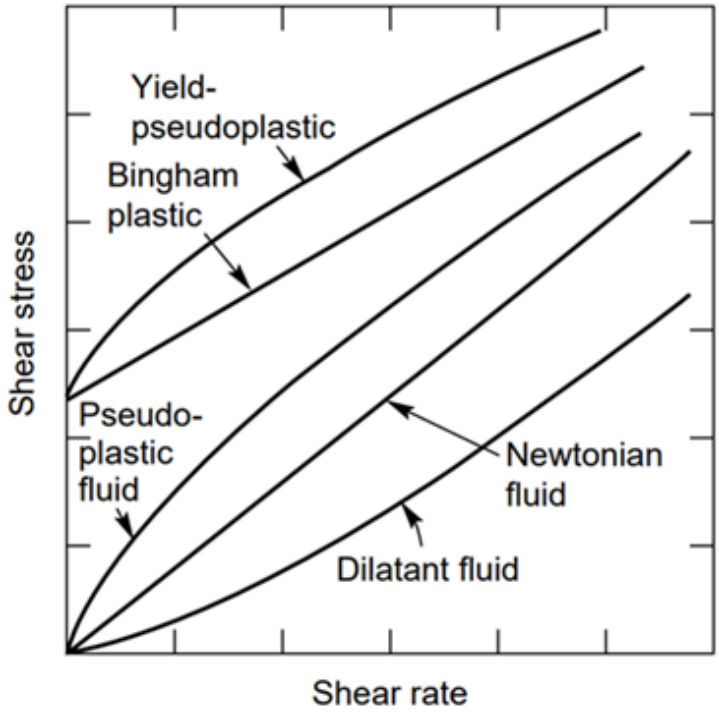


Figure 2: Illustration of shear stress as a function of shear rate (Chabbra and Richardson, 1999)

Tailings slurry rheology data

Tailings slurry rheology parameters adopted for analysis are summarized in Table 4.

Table 4: Tailings slurry rheology data

Parameter	Tailings rheology
Solids particle density, ρ_s (kg/m^3)	3,300
Process water density, ρ_{pw} (kg/m^3)	1,070
Bingham yield stress, τ_0 (Pa)	$\tau_0 = 16{,}100\ C_m^{13.5}$
Bingham plastic viscosity, μ_{BP} (Pa.s) (Note)	$\mu_{BP} = 2.08\ C_m^{8.45}$
Tested range of slurry solids concentrations, C_m (% w/w)	50.4% to 68.8%
Slurry solids concentration adopted, C_m (% w/w)	63%

Note: μ_w refers to the viscosity of water at 24° C (0.000916 Pa.s)

Yield stress (τ_y) and plastic viscosity (μ_0) data for the tailings are presented for a range of solids concentrations by mass in Figure 3. The fit lines included represent the equations noted in Table 4 for Bingham yield stress and Bingham plastic viscosity, respectively.

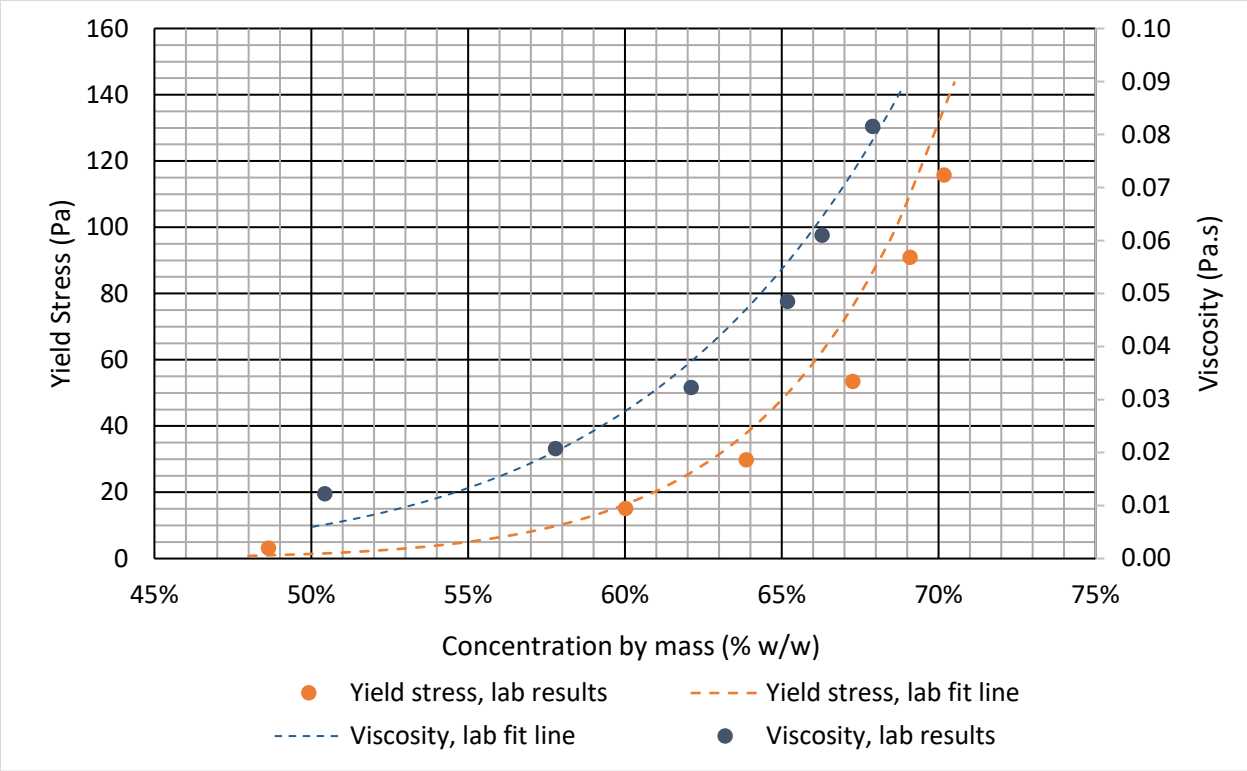


Figure 3: Yield stress vs. mass concentration, and viscosity vs. mass concentration for tailings slurry sample

Adopted tailings rheology model

The Bingham plastic model was adopted to model the tailings slurry in this assessment. In the Bingham model, the fluid is assumed to have a yield stress, which must be exceeded before the fluid will flow. Once this stress is met the fluid will flow with a constant viscosity. Mathematically, the Bingham plastic model can be expressed as the following:

$$\tau = \tau_0 + \mu_{BP}\gamma$$

Where:

- τ is shear stress (Pa)
- τ_0 is the yield stress (Pa)
- μ_{BP} is the Bingham plastic viscosity (Pa.s)
- γ is the shear rate (s^{-1})

The Bingham plastic viscosity represents the constant viscosity exhibited by the fluid once the yield stress has been exceeded.

Adopted tailings rheological parameters

Tailings rheological properties for the samples were obtained via the relationships presented in Table 4 and are presented in Table 5.

Table 5: Adopted tailings rheology parameters for the pipe break erosion analysis

Parameter	
Slurry solids concentration adopted, C_m (% w/w)	63
Slurry density, ρ_{slurry} (kg/m^3)	1,830
Yield stress, τ_0 (Pa)	31.5
Bingham plastic viscosity, μ_{BP} (Pa.s)	0.042

Hydraulic modelling

Software selection

Hydraulic modeling was completed using the FLOW-3D Hydro (Version 22.1.1.01) (Flow-3D) software package developed by Flow Science Inc (Flow Science Inc., 2022). Flow-3D is a commercially available three-dimensional (3D) computational fluid dynamics software package that includes a physics-based modeling package. It is suited to modeling the complexities of both Newtonian and non-Newtonian flows, such as tailings. An overview of the settings used for these models is presented below.

The governing equations behind the hydraulic modeling of scour erosion are empirical, and as such these models contain uncertainty and require consideration when interpreting the results.

Model geometry, mesh, and terrain extents

A digital model of a portion of the embankment surface was created for use in Flow 3D. Fine and coarse mesh sizes were adopted based on optimization of model accuracy and simulation time, as well as resolution of flow behavior. The extents of the surface analyzed for the model, as well as the mesh arrangements, are summarized in Table 6, with the respective directions indicated in Figure 4.

Table 6: Description of mesh used for analyses

Mesh direction/element	Fine mesh	Coarse mesh
Lateral extent (x direction) (m) (**Note A**)	5	9
Length (y-direction) (m) **(Note B)**	5.5	8.5
Vertical extent (z direction)	3	4.2
Cell size (cm)	10	20
Total no. cells	82,500	39,690

Notes:

(A) The lateral extent of mesh is parallel to the crest.

(B) Length of mesh parallel to embankment slope

(C) Distance measured along embankment, includes crest, face, and toe.

(D) Directions for mesh alignment are shown in Figure 4.

Model setup

General

Modeling was performed using a three-dimensional mesh, to simulate erosion of the embankment crest edge at the location of the pipe break. Due to the computationally intensive nature of the assessment, the assessment was limited to the upper portion of the embankment, rather than the entire upstream face between the crest and tailings beach, and the entire crest. Extrapolations were then made to estimate the duration for erosion through the embankment and down to the tailings surface.

In addition to the inputs and assumptions discussed in the sections above, the following model inputs and assumptions were adopted in the hydraulic modeling:

- Inflow boundary at the location of the pipe at a constant flowrate of 0.17 m^3/s.
- Outflow boundaries were adopted at the sides of the modeled region (refer to Table 6).
- Models were compared at 30 minutes (1,800 seconds) of simulated time to balance computational time and assessment of risk of scour. A longer period of simulated time was run for the coarse mesh size model (about 75 minutes of simulated time), due to shorter overall computational time.
- Turbulence was modeled using the Renormalized Group model (RNG), which is equipped to model turbulence in flows near solid surfaces.

Sediment transport

The following were adopted for the sediment transport model:

- The critical shields number for erosion, calculated via the Soulsby-Whitehouse equation (Soulsby and Whitehouse, 1997).
- The Meyer-Peter and Muller equation for bed load transfer rate, a simple excess shear relationship (Meyer-Peter and Müller, 1948).

Erosion assessment results

Erosion profiles, total eroded depths, and erosion extents into and along the embankment crest were obtained from the analysis.

General erosion behavior

The embankment profile prior to erosion is shown in Figure 4, and the surface following 30 minutes of simulated erosion is presented in Figure 5. The tailings slurry is shown as a semi-transparent surface and the extent of erosion is summarized in the section below entitled "Change in scour extent with time." For the following figures, the x-axis is along the embankment crest, the z-axis is vertical, and the y-axis is perpendicular to the embankment alignment. Note, the upstream crest edge (pre-erosion) is located at y = 0, and z = 6.5 (arbitrarily).

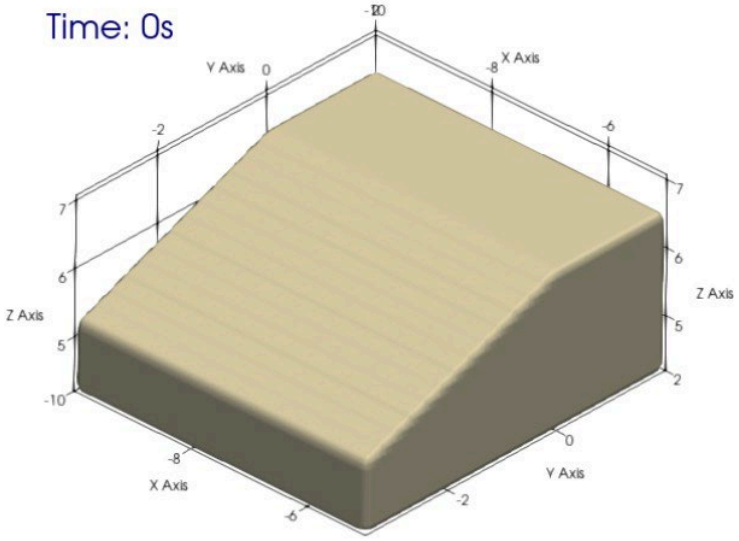


Figure 4: TSF embankment profile before pipe break simulation

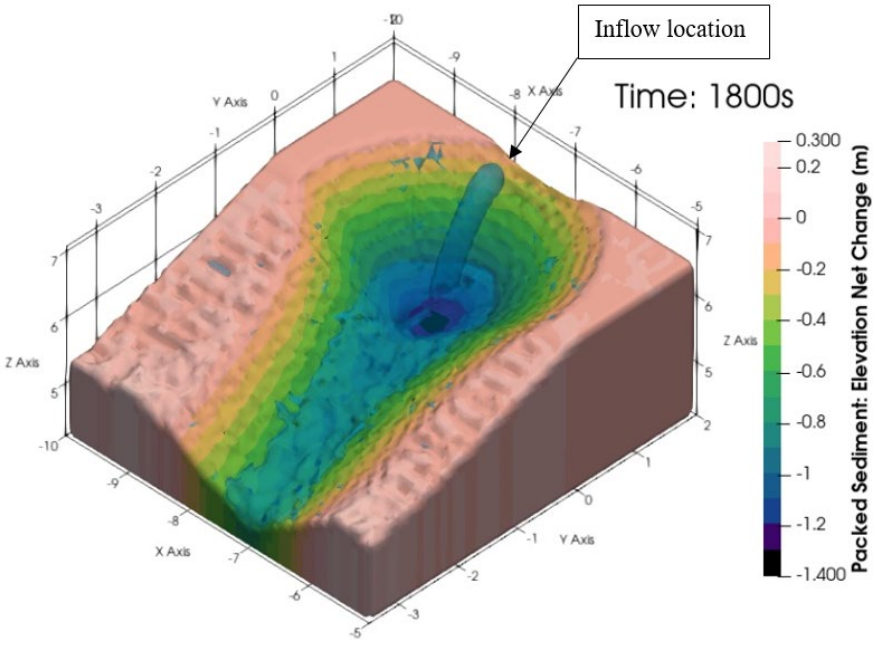


Figure 5: Flow 3D results for tailings slurry, 30 minutes of simulated erosion

Cross-sections showing the erosion profiles after 30 minutes of simulation are presented in a long section in Figure 6 along the embankment crest, and in a cross-section in Figure 7, offset from the upstream crest edge by 20 cm (approximate location of maximum eroded depth). The red dashed line indicates the original embankment crest surface prior to erosion.

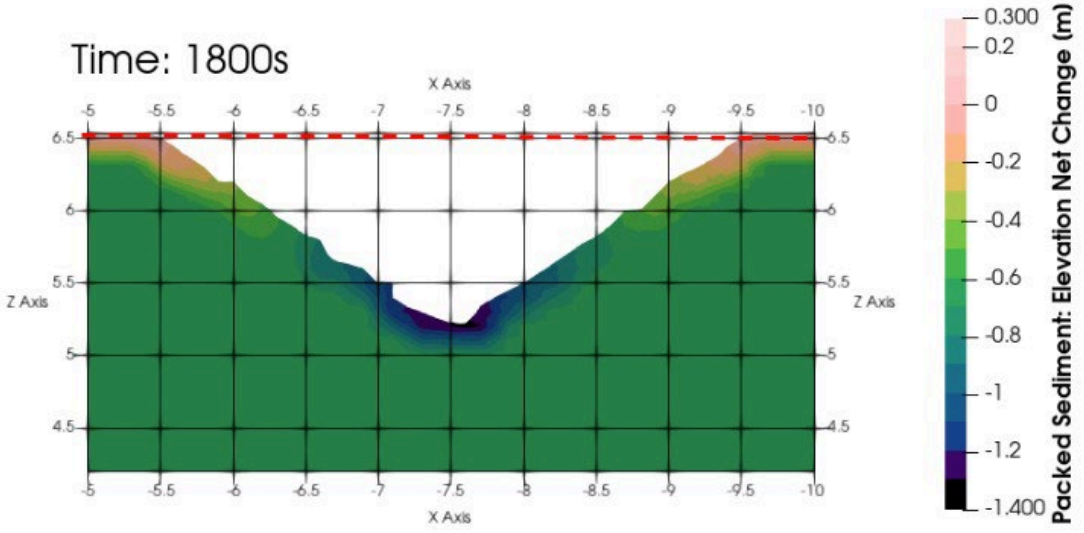


Figure 6: Flow 3D results after 30 minutes of simulated erosion, 20 cm from the upstream crest edge

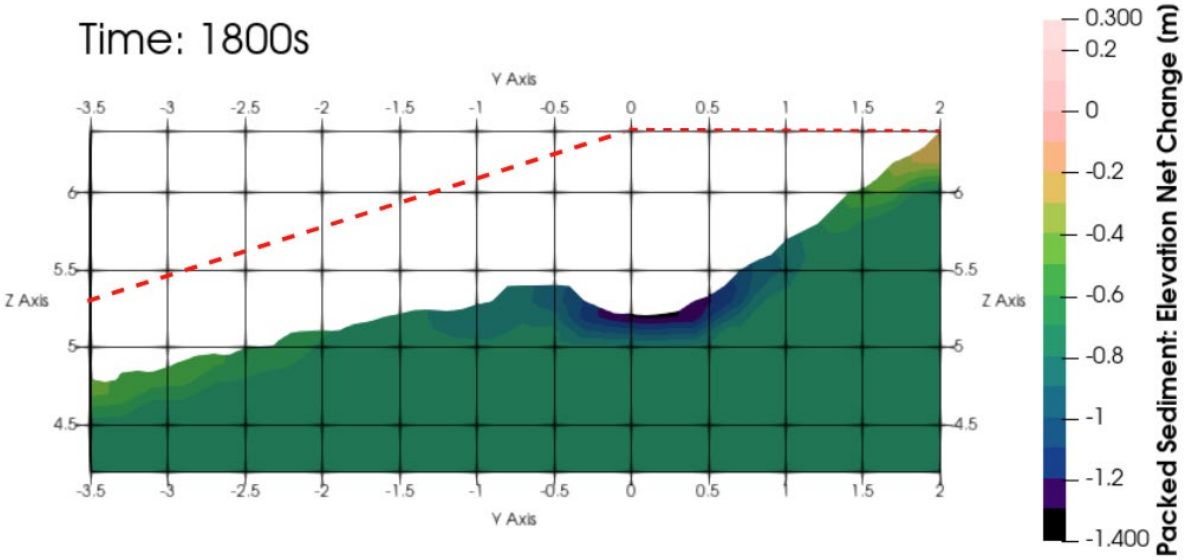


Figure 7: Flow 3D results after 30 minutes of simulated erosion, cross-section at x = -7.5 m

A top-down view of the embankment after 30 minutes of simulated erosion is presented in Figure 8, with the original upstream crest edge marked as a dashed red line.

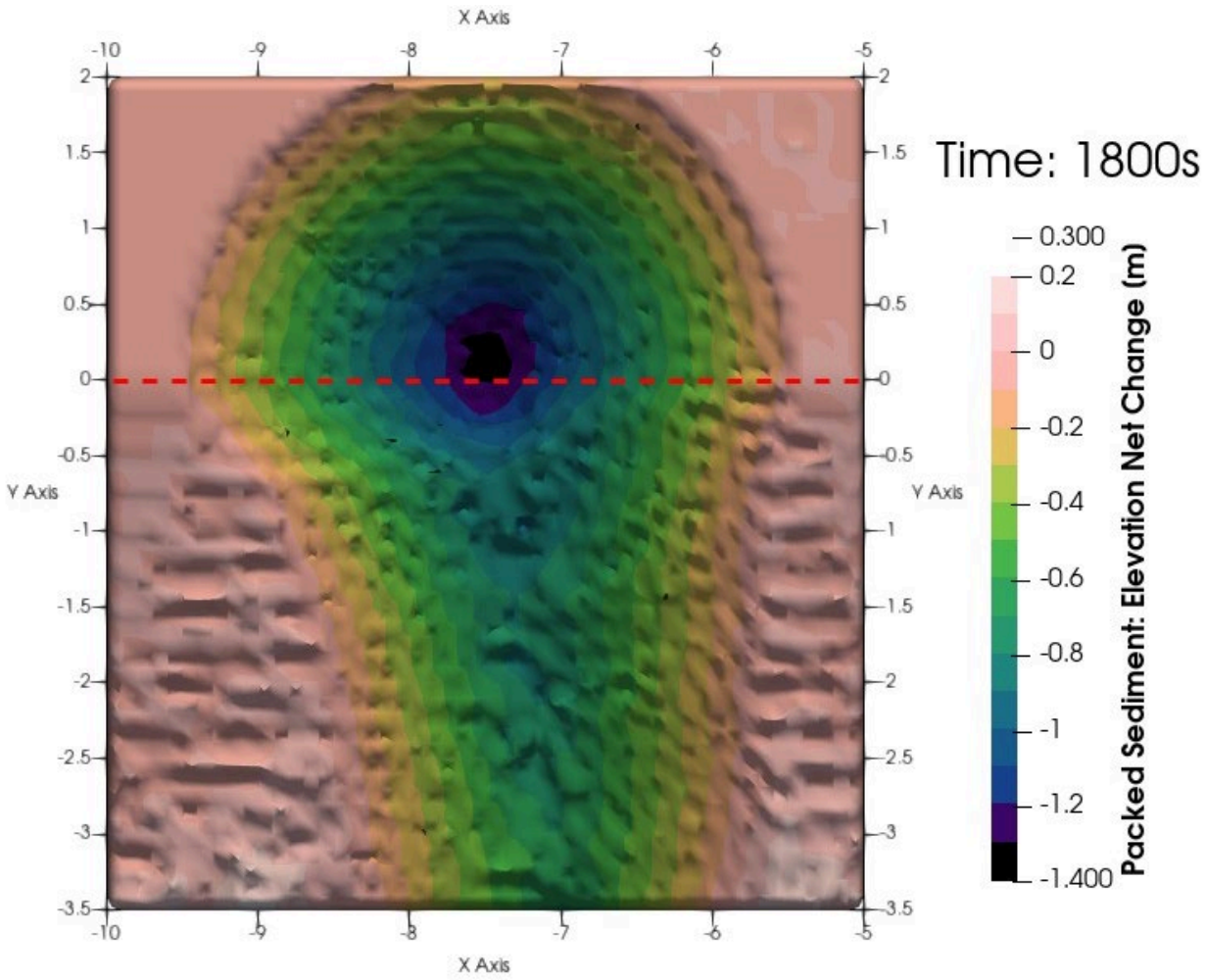


Figure 8: Flow 3D results for the embankment after 30 minutes of simulated erosion, top-down view

Change in scour extent with time

Scour estimates were linearly extrapolated to estimate the time at which the embankment crest (8 m wide) is eroded. Coarse mesh model results are also presented to give a further indication of the model behavior over time.

The rate of retreat of the erosion scarp is indicated in Figure 9, with a linear extrapolation marked as a dashed line. The extrapolation for the fine mesh model indicates erosion through the 8 m wide embankment crest over about 3.5 hours, whereas extrapolation for the coarse mesh model indicates erosion through the crest occurs over about 5.3 hours.

Note, retreat distance is in the positive y-direction indicated in Figure 7 and Figure 8. Also note that the estimated minimum scarp failure time is marked as a red dashed line.

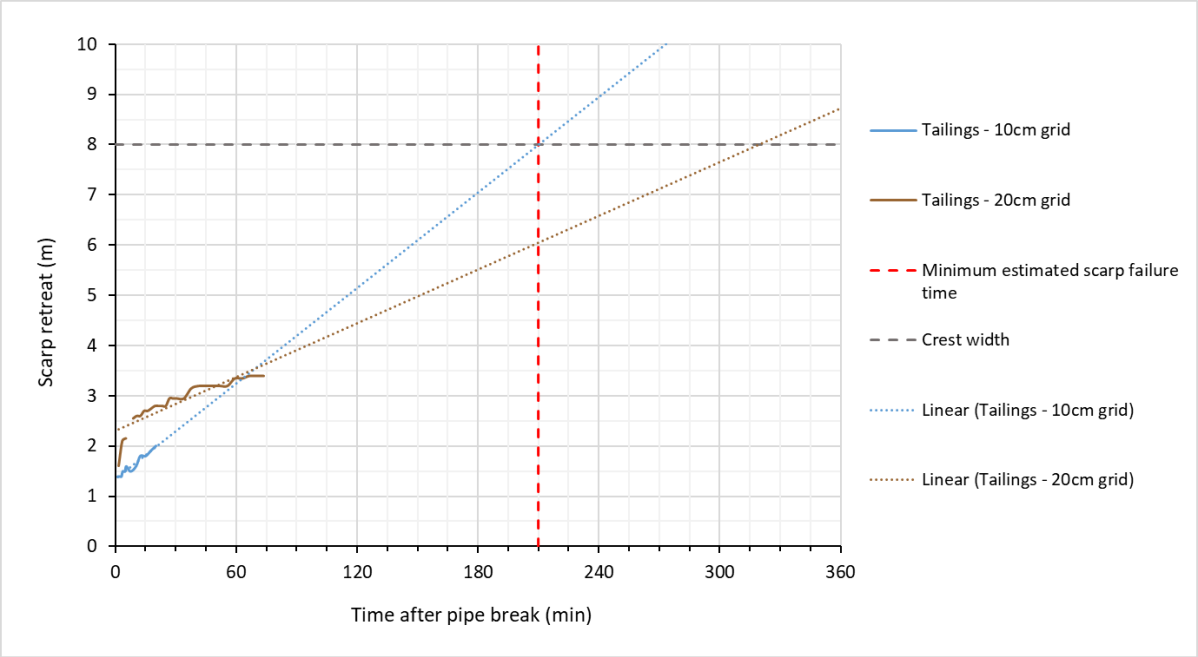


Figure 9: Flow 3D modeled scour distance through the embankment crest

Total vertical scour over time is presented in Figure 10. The estimated shortest duration for the crest to be eroded 6.5 m vertically down to the tailings beach is about 3.5 hours (see Figure 9), as shown by the red dashed line.

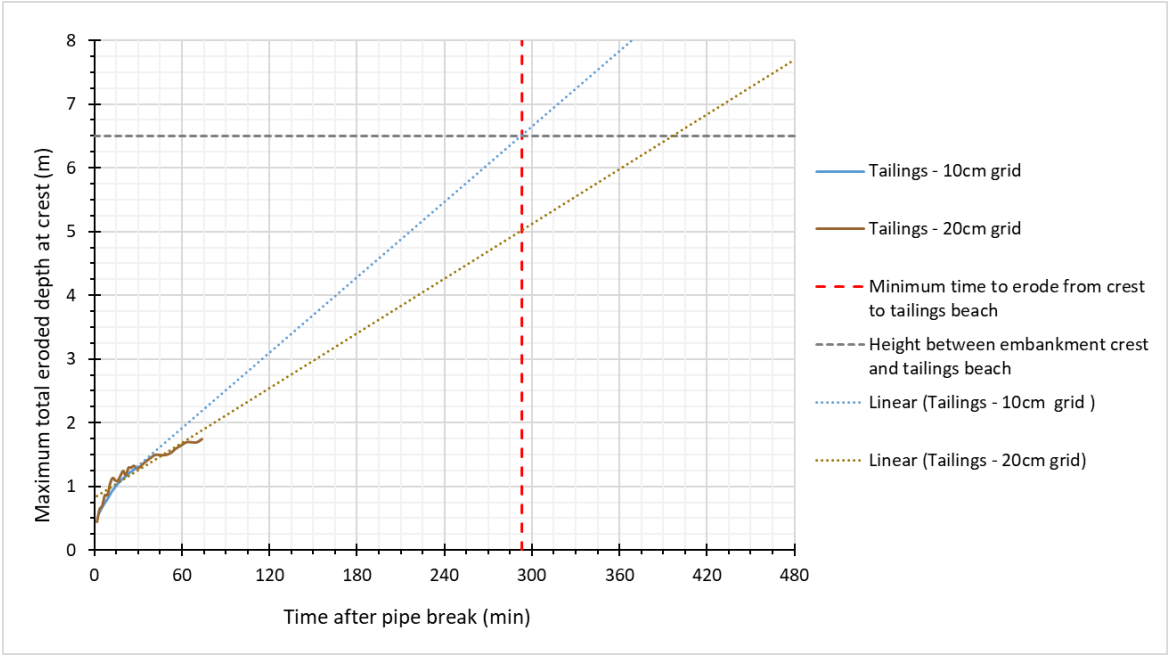


Figure 10: Maximum vertical scour comparison for Flow 3D tailings, with failure time of the scarp

Discussion

In summary, the results from the Flow 3D simulations of pipe-break induced flow of tailings slurry onto the embankment, and the linear extrapolations of these results over time, indicate the following:

- Erosion of 50% of the embankment crest width (4 m) occurs in about 90 minutes.
- Erosion of the crest width (8 m) occurs between about 3.5 and 5 hours.
- Once the erosion scarp retreats through the embankment crest (in 3.5 hours), the estimated lateral erosion extent (along the embankment alignment) is about 16 m.
- Erosion down to the intermediate tailings surface, i.e., a depth of 6.5 m from the upstream crest edge of the embankment occurs after about 4.8 hours.
- Development of a pool of tailings liquid underneath the pipe outlet location, dissipating energy from the outflowing tailings and slowing the overall rate of vertical scour.

The following considerations are provided for the interpretation of the model results:

- The analysis for the fine mesh (10 cm) was limited to a simulation time of 30 minutes for computational efficiency. A coarser mesh model (25 cm) was run for a longer simulation time (70 minutes) for comparison.
- Due to the computationally intensive nature of modeling sediment erosion, the analysis of erosion was limited to the crest and upper portion of the embankment. Linear extrapolations for duration of erosion were made based on the model results.
- Current sediment transport rate equations are empirical and were developed for water. As such there are limitations when applying these to the flow of tailings and other fluids.
- The Meyer-Peter Muller equation for bed load transport rate is empirically derived and was developed for gravel sized particles in the flow of water.

Conclusion

A pipe break event for a tailings delivery pipeline on a hypothetical embankment and slurry flow onto the upstream slope of the embankment was modeled in the Flow 3D Hydro computational fluid dynamics modeling package.

Flow from the break in the tailings delivery pipeline was assessed to estimate the rate of erosion through the embankment crest. Tailings slurry was modeled at a solids concentration of 63% w/w solids and flowing at a rate of 600 m^3/hour. Following the pipe break and slurry flow onto the upstream face of the embankment, the model showed a pool of slurry forming on the crest underneath the pipe break location. Linear extrapolations for results from a fine mesh model indicate the potential to erode through the 8 m

wide embankment crest in about 3.5 hours if flow continues without detection and without cessation of pumping. After 3.5 hours, the maximum erosion depth was estimated to be about 5 m.

References

Chabbra, R.P. and Richardson, J.F. 1999. *Non-Newtonian Flow in the Process Industries*. Oxford, UK: Butterworth-Heinemann.

Flow Science Inc. 2022. FLOW-3D HYDRO® Version 22.1.1.01 (Computer software).

Kilgore, R.T. and Cotton, G.K. 2005. Design of roadside channels with flexible linings, Hydraulic Engineering Circular No. 15, Third Edition. U.S. Department of Transportation, Federal Highway Administration.

Meyer-Peter, E. and Müller, R. 1948. Formulas for bed load transport. *Proceedings of 2nd meeting of the International Association for Hydraulic Structures Research,* Delft, 39–64.

Soulsby, R. L. and Whitehouse, R. 1997. Threshold of sediment motion in coastal environments. *Pacific Coasts and Ports '97: Proceedings of the 13th Australasian Coastal and Ocean Engineering Conference and the 6th Australasian Port and Harbour Conference*; Volume 1.

U.S. Department of the Interior – Bureau of Reclamation. 2019. Best practice in dam and levee safety risk analysis, version 4.1, Chapter D-1: Erosion of rock and soil, July 2019. In U.S. Department of the Interior Bureau of Reclamation, and U.S. Army Corps of Engineers.

A Parameter Calibration Methodology for the Clay and Sand Model (CASM) Constitutive Model

Alessandra Gomes, DF+ Engineering/Bucknell University, Brazil
Erick Rógenes, DF+ Engineering/University of Brasília/Bucknell University, Brazil
Felipe Cruz, DF+ Engineering/State University of Rio de Janeiro, Brazil
Paula Pais, DF+ Engineering, Brazil
Alomir Fávero Neto, Bucknell University, USA

Abstract

Liquefaction is a major failure mechanism in upstream tailings dams, as evidenced by the Fundão (2015) and Brumadinho (2019) disasters. This phenomenon occurs in loose and saturated materials and is triggered by destabilizing processes that induce shear in the soil, causing pore volume reduction with associated rapid excess pore pressure generation, and significant drops in effective stress and shear strength, resulting in fluid-like behavior of the material. Traditional stability analyses using the limit equilibrium method are inadequate to model liquefaction, as they fail to capture the post-peak behavior of the material and only effectively simulate failure triggers. Liquefaction analyses have been developed through the application of numerical modeling that considers stress-strain relationships within the deforming material, which requires the use of constitutive models capable of capturing liquefaction. The main constitutive models capable of representing liquefaction are based on critical state soil mechanics, such as NorSand and CASM (Clay and Sand Model), models applied in recent studies of the rupture of Dam I, Brumadinho, Minas Gerais, Brazil. CASM can simulate fine or granular materials with ductile or brittle behavior, incorporating the concept of critical state and the state parameter in its formulation. Given that CASM does not have a well-defined calibration methodology, this work presents a calibration methodology for the model and applies it to tailings materials. We show that the calibration methodology is robust and simple enough to be used by practitioners and researchers alike, contributing to the potential popularization and usage of CASM in future applications related to liquefaction of geomaterials.

Introduction

Liquefaction has been one of the main failure mechanisms in upstream tailings dams. Among recent cases of failure associated with the phenomenon are the Fundão disaster in 2015 (Morgenstern et al., 2016) and

the Brumadinho disaster in 2019 (Robertson et al., 2019; Arroyo and Gens, 2021).

The phenomenon of liquefaction involves a significant reduction in the shear strength of soil subjected to undrained loading due to the generation of excess pore pressure. This occurs because the total stress remains constant while the effective stress decreases due to the excess pore pressure (Sternik, 2014), which increases until it reaches a value equal to the normal stress component.

It is important to note that saturated, loose, granular soils are more prone to liquefaction because they exhibit contractive behavior (Been and Li., 2009). Tailings, which share similar characteristics to soils, are also susceptible to liquefaction because of their often-times loose state.

In geotechnical projects, stability analyses of dams are commonly performed using the limit equilibrium method, where the soil is assumed to exhibit a rigid failure region, and to exhibit perfectly plastic behavior along a well-defined failure surface. This assumption does not represent the mechanism of liquefaction, in which the material shows significant deformations after peak strength is reached. Additionally, limit equilibrium analyses are limited to the simulation of triggers. Given these limitations, liquefaction analyses have been developed through the application of numerical stress-strain modeling. These models are mostly developed using a continuum approach, requiring constitutive models that can capture the phenomenon of liquefaction.

The main constitutive models capable of representing liquefaction are based on critical state soil mechanics and plasticity theory concepts, such as the NorSand model (Jefferies and Been, 2016) and the Clay and Sand Model (CASM) (Yu, 2006). These models have been applied in recent studies of the rupture of Dam I in Brumadinho, Minas Gerais, Brazil (Robertson et al., 2019; Arroyo and Gens, 2021).

The NorSand model can reproduce contractive (volume reduction) or dilative (volume increase) behaviors in sands during shear loading, and originated from observations of sand behavior in large-scale hydraulic fills (Shuttle and Jefferies, 2005). Various works have introduced modifications and improvements to this model (Been and Jefferies, 1985; Jefferies, 1993; Jefferies and Shuttle, 2002; Jefferies and Shuttle, 2011). However, one can only simulate granular materials, and many parameters are required, some of which are difficult to calibrate from test specimens in the laboratory.

CASM, on the other hand, can simulate fine or granular materials with ductile or brittle behavior, incorporating the concept of critical state and the state parameter in its formulation. Given that CASM does not have a well-defined calibration methodology, this work proposes a calibration methodology for the model parameters, with applications to tailings materials.

CASM formulation

Figure 1 shows a schematic representation, on the v-ln(p') plane, of some of the parameters used in CASM, where e is the void ratio and p is the mean normal stress.

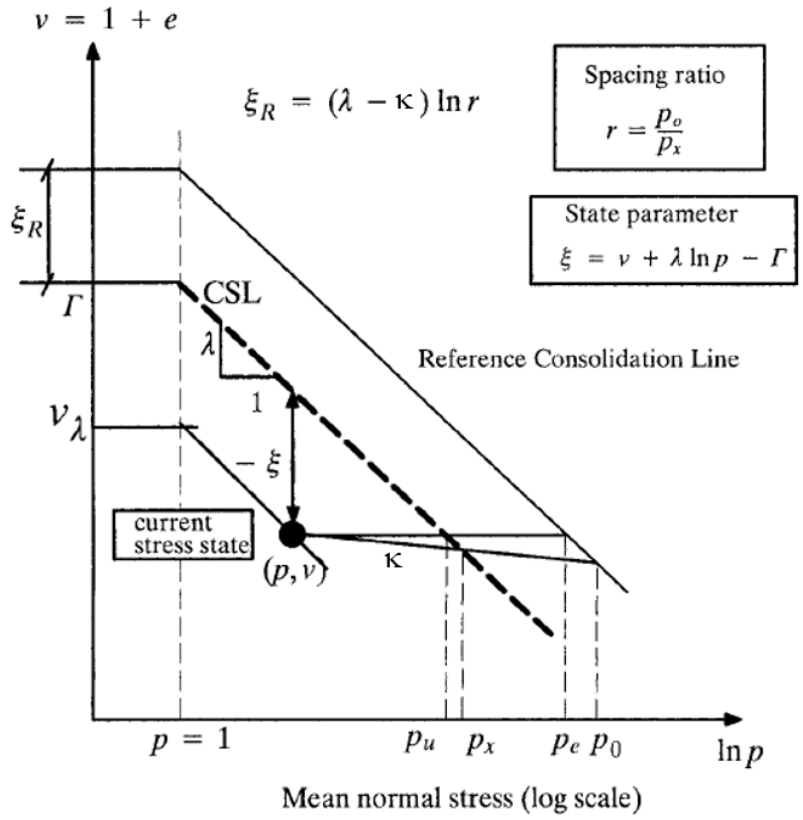


Figure 1: Schematic representation of some parameters of the CASM constitutive model (Yu, 2006)

CASM applies a similar approach to that used in the Cam-Clay constitutive model (Wood, 1990), as it assumes that the consolidation lines are parallel to the critical state line (CSL). Thus, many parameters present in Cam-Clay were retained in CASM.

Unlike the Cam-Clay model, in CASM, the isotropic virgin compression line has been replaced by a reference compression line, assumed to be the loosest probable condition to which the material may be subjected. This change was made because, according to Yu (2006), the isotropic virgin compression line of sands, unlike clays, is only reached at high stress states, higher than those commonly applied in engineering problems.

The reference consolidation line in CASM is defined based on the reference state parameter (ξ_r) or the spatial ratio (r). Both parameters represent ways to measure the distance between the critical state line and the reference line, and are, therefore, changeable parameters related by Equation 1.

$$\xi_r = (\lambda - \kappa) \ln r \qquad \text{(Equation 1)}$$

Where λ is the slope of the CSL, and κ is the elastic compressibility. Given the assumed parallelism between the critical state line and the reference consolidation line, the state parameter is directly related to the overconsolidation ratio (OCR) by Equation 2. Thus, it is observed that to represent dilative materials, it is necessary to use OCR > 1.

$$\xi = (\lambda - \kappa) \ln r \, (1 + \frac{\ln p'/p'_0}{\ln r}) \quad \text{(Equation 2)}$$

To represent elastic behavior, the CASM model uses the following input parameters: Poisson's ratio (ν) and the unloading line slope (k). The parameter k is related to the bulk modulus (K) by Equation 3.

$$K = \frac{(1 + e)\, p'}{k} \quad \text{(Equation 3)}$$

From Equation 3, the bulk modulus is not a constant value, as it tends to vary with mean stress and void ratio. Given that the model assumes a constant value for Poisson's ratio, the shear modulus consequently varies with mean stress and void ratio as well.

The yield function adopted in the model is presented in Equation 4 as a function of the state parameter, and in Equation 5 as a function of preconsolidation stress. It is noteworthy that the ratio p'_0/p' is referred to as the OCR.

$$f = (\frac{q}{M_\theta p'})^{n} + \frac{\xi}{\xi_r} - 1 \quad \text{(Equation 4)}$$

$$f = (\frac{q}{M_\theta p'})^{n} + \frac{1}{\ln r} \ln (\frac{p'}{p'_0}) \quad \text{(Equation 5)}$$

Where q is the Von Mises deviatoric stress, n is a parameter that controls the shape of the surface and M_θ is the slope of the CSL in the p'-q plane.

Arroyo and Gens (2021) modified Yu's original formulation (1998) by incorporating the effects of intermediate principal stress variation (captured by the change in Lode angle, θ into the value of M_θ. They applied the relationship presented in Equation 6, proposed by Sheng et al. (2000).

$$M_\theta = M_{TC} \, (\frac{2\,\alpha^4}{1 + \alpha^4 + (1 - \alpha^4)\, sin3\theta})^{1/4} \quad \text{(Equation 6)}$$

Where M_{TC} is the slope of the CSL under triaxial compression conditions (θ=30°), and α is a parameter that controls the shape of the function. Both are defined based on the critical state friction angle (ϕ_{cs}) by Equations 7 and 8, respectively.

$$M_{TC} = \frac{6\ sin\ \phi_{cs}}{3 -\ sin\ \phi_{cs}} \quad \text{(Equation 7)}$$

$$\alpha = \frac{3 -\ sin\ \phi_{cs}}{3 +\ sin\ \phi_{cs}} \quad \text{(Equation 8)}$$

As presented in Equation 5, the size of the elastic domain is controlled by the preconsolidation stress p'_0. In CASM, a hardening law based on plastic volumetric strains (ε_{vol}^{p}) is assumed, similar to Cam-Clay, and as shown in Equation 9.

$$\frac{\partial p'_0}{\partial \varepsilon_{vol}^{p}} = \frac{(1+e)\ p'_0}{\lambda - \kappa} \quad \text{(Equation 9)}$$

It should be noted that since the hardening law does not depend on shear deformations, the CASM model in the version applied by Arroyo and Gens (2021) cannot capture the increase in material strength after reaching the critical state line, a situation typically observed in materials with state parameter values close to zero.

Finally, the plastic potential function adopted by Arroyo and Gens (2021) also differs from Yu's original formulation (1998). The authors reported that this modification improved the numerical convergence of the model. The plastic potential applied is presented in Equation 10, proposed by Mánica et al. (2021).

$$g = \left(\frac{q}{M_\theta p'}\right)^{m} + \mathrm{m} - 1 - \frac{p_c\ (m-1)}{p'} \quad \text{(Equation 10)}$$

Where m is a parameter that controls the shape of the plastic potential, and p_c is the preconsolidation stress, given by Equation 11, which must be solved for the current stress state.

$$p_c = \frac{p}{m-1}\ \left[\left(\frac{q}{Mp'}\right)^{m} - 1\right] \quad \text{(Equation 11)}$$

It is observed that the plastic potential function is different from the yield surface (Equation 5), and therefore CASM does not have an associated flow.

Calibration methodology

For the calibration of CASM, eight input parameters are required, as presented in Table 1.

Table 1: Parameters of CASM

Component		Parameters
Critical State Line – CSL	G	CSL void ratio at p' = 1 kPa
	l	Plastic compressibility
	Mtc	Critical state slope in p'-q space
Elasticity	n	Poisson's ratio
	k	Elastic compressibility
Plasticity	m	Plastic potential shape
	r	Spacing ratio
	n	Yield shape

The methodology for determining the required input data for the constitutive model will be divided into 5 steps:

Step 1 – Determination of parameters M, Γ and λ

To determine parameters *M, Γ*, and λ, triaxial tests are conducted to establish the CSL on the *p'-q* plane (Figure 2-a), and the ln(*p'*)-*e* plane (Figure 2-b). In the *p'-q* plot, parameter *M* is obtained from the slope of the CSL, while in the ln(*p'*)-*e* plot, *Γ* corresponds to the CSL void ratio at *p'* = 1 kPa, and λ represents the slope of the CSL.

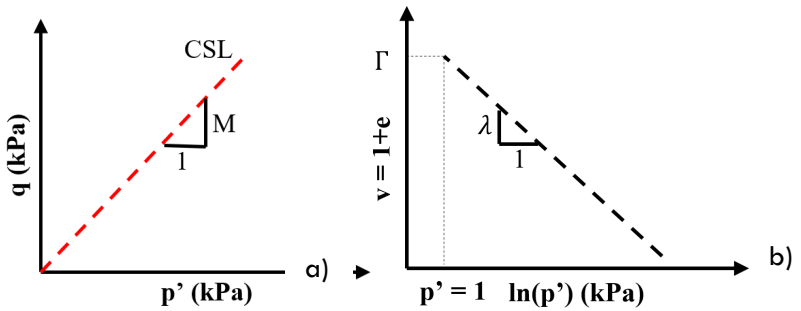


Figure 2: a) Plot to obtain parameter *M*. b) Plot to obtain parameters *Γ* and λ

Step 2 – Determination of the elastic parameters ν and κ

Parameter ν can be obtained through data from triaxial tests by plotting the axial strain (ε_a) versus radial strain (ε_r) and determining ν from the slope of the line. Alternatively, this parameter can also be obtained from literature references, as in Arroyo and Gens (2021), as it does not vary significantly.

To obtain *k*, consolidation oedometer tests are conducted and the ln(*p'*)-*v* graph is plotted (Figure 4). The value of *k* corresponds to the slope of the recompression line, as illustrated in Figure 3.

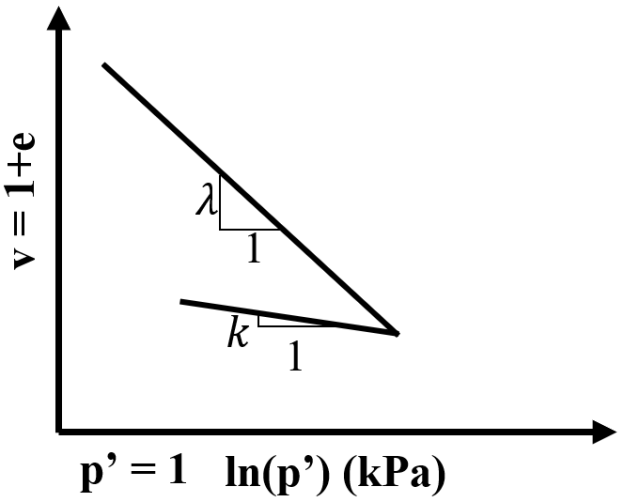


Figure 3: Graph to obtain parameter *k*

According to Mánica et al. (2021), since the parameters *v* and *κ* do not vary much, they can be estimated.

Step 3 – Determination of the plastic parameter – *m*

The parameter *m* controls the shape of the plastic potential and can be used to adjust the model's response in oedometer tests, ensuring that the coefficient of earth pressure at rest (K_0) remains at a specified value without changes due to plastic deformations. The relationship between K_0 and *m* is given by Equation 15.

$$\frac{3\,(\lambda-\kappa)}{2\,\lambda}=\left[\frac{M}{m}-M\right]\left[\left(\frac{1}{M}\frac{3(1-K_0)}{1+2K_0}\right)-\left(\frac{1}{M}\frac{3(1-K_0)}{1+2K_0}\right)^{1-m}\right] \quad \text{(Equation 15)}$$

The equation requires data related to the CSL (*M* and *λ*), determined in Step 1, and the elastic parameter (*κ*), determined in Step 2, and K_0, which can be obtained through pressuremeter tests.

Step 4 – Determination of the plastic parameter – *r*

The parameter *r* allows control of the distance between the CSL and the virgin compression line on the horizontal axis and is related to residual undrained strength (S_{ur}), determined by Equation 17.

$$r=\left[\frac{M}{6}\,(1+2K_0)\left(\frac{\sigma'_{vini}}{S_{ur}}\right)\right]^{\frac{\lambda-\kappa}{\kappa}} \quad \text{(Equation 16)}$$

The equation requires data related to the CSL (M and λ) (Step 1), the elastic parameter (κ) (Step 2), K_0 (Step 3), and the residual undrained strength of the material ($\frac{S_{ur}}{\sigma'_{vini}}$), which can be obtained through triaxial or CPTu tests.

Step 5 – Determination of the plastic parameter – *n*

The parameter n controls the shape of the yield surface and is related to peak undrained strength (S_{up}), determined by Equation 17.

$$\exp\left[\left(\frac{1}{\sqrt[n]{n\ln r}}\right)^n \ln r\right] = \frac{M}{2\frac{\sigma'_v}{S_{up}}\sqrt[n]{n\ln r}} \exp\left[\left(\frac{q_{ini}/p'_{ini}}{M}\right)^n \ln r\right] \exp\left[\frac{\lambda-\kappa}{\kappa}\ln\left(\frac{M}{2\frac{\sigma'_v}{S_{up}}\sqrt[n]{n\ln r}}\right)\right] \quad \text{(Equation 17)}$$

To determine parameter n, Equation 17 is used. The equation requires data related to CSL (M and λ) (Step 1), the elastic parameter (κ) (Step 2), the plastic parameter (r) (Step 3), and the peak undrained strength of the material ($\frac{S_{up}}{\sigma'_{vini}}$), which can be obtained through triaxial or CPTu tests.

Calibration for tailing materials

Below is presented an application of the methodology to calibrate CASM parameters for tailings materials. After obtaining the input data, p'-q and ε_{ax}-q graphs will be illustrated, comparing the calibration results with the tested material.

Step 1 – Determination of parameters *M*, *Γ* and *λ*

To determine parameters M, Γ, and λ, triaxial tests were conducted to establish the critical state line on the p'-q plane (Figure 4), and the ln(p')-e plane (Figure 5). In the p'-q graph, parameter M = 1.32, from the slope of the CSL. In the ln(p')-e graph, the values obtained were Γ = 1.79 and λ = 0.035.

It should be noted that Figure 5 presents the critical state line in the ln(p')-v plane, using only the three undrained loading confining pressures shown in Figure 4, which, in turn, presents the critical state line in the p'-q plane. However, the authors acknowledge and advise that critical state lines are more accurately represented with a minimum of eight tests, incorporating both drained and undrained loading conditions.

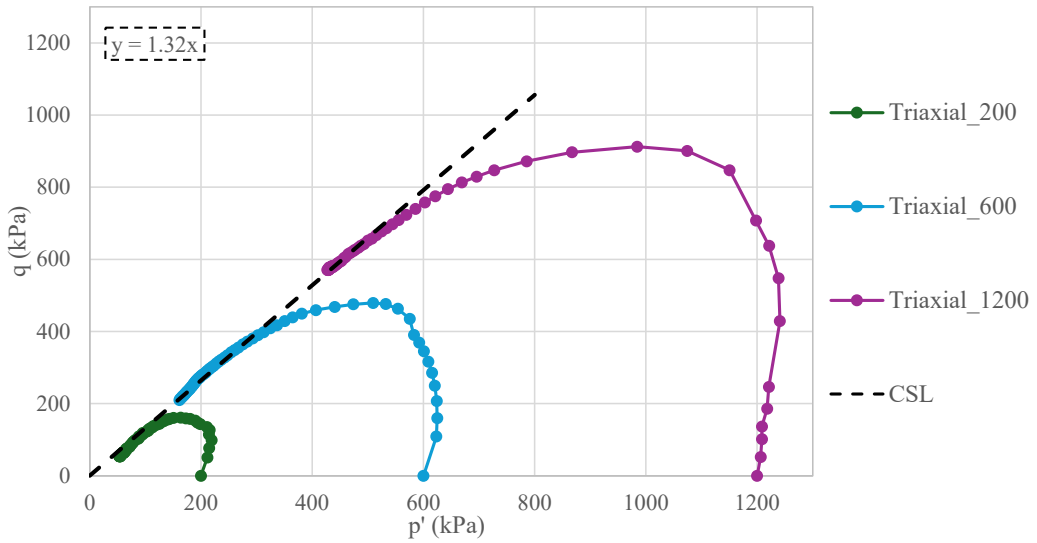


Figure 4: Critical State Line – *p'-q* plot

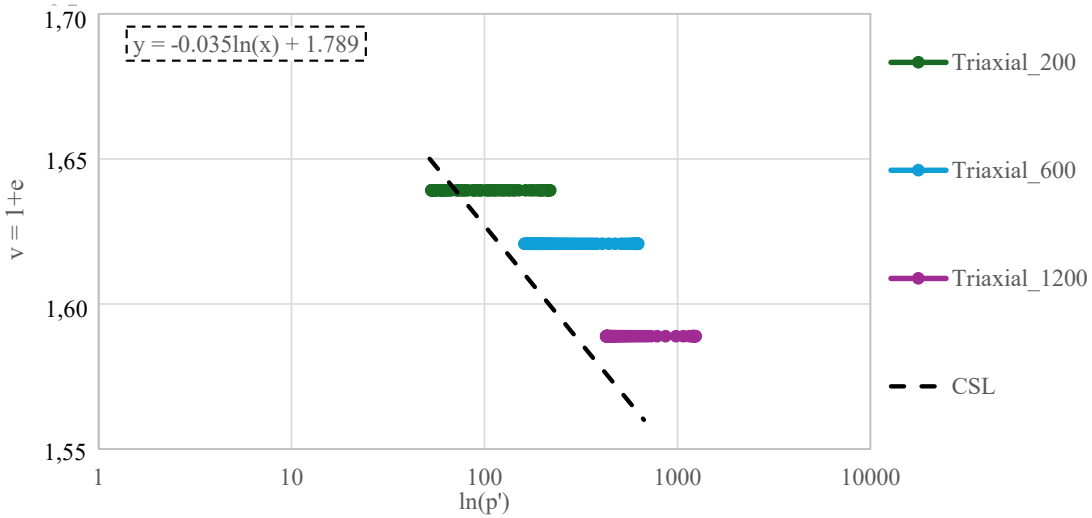


Figure 5: Critical State Line – ln(*p'*)-*v* plot

Step 2 – Determination of elastic parameters ν and κ

The parameter $\nu = 0.3$ was obtained from Arroyo and Gens (2021), as it shows little variation. Due to the lack of oedometer consolidation tests, $\kappa = 0.02$ was assumed.

Step 3 – Determination of the plastic parameter – *m*

Equation 15 requires CSL data, determined in Step 1: $M = 1.32$ and $\lambda = 0.035$, the elastic parameter determined in Step 2: $k = 0.02$, and K_0, which can be obtained through pressuremeter tests; in this case, $K_0 = 0.6$ was used. Applying these parameter values to Equation 15 yielded $m = 1.5$.

Step 4 – Determination of the plastic parameter – *r*

To determine the parameter *r*, the following values were considered: M = 1.32 and λ = 0.035 (Step 1), k = 0.02 (Step 2), and K_0 = 0.6 (Step 3). For the undrained residual strength of the material $\left(\frac{S_{ur}}{\sigma'_{vini}}\right)$, correlations were performed using the methodologies of Olson and Stark (2003) and Sandrekarime (2014) with the CPTu test data, resulting in $\frac{S_{ur}}{\sigma'_{vini}}$ = 0.13. By applying the parameter values to Equation 16, r = 20.0 was obtained.

Step 5 – Determination of the plastic parameter – *n*.

To determine the parameter n, the following values were considered: M = 1.32 e λ = 0.035 (Step 1), k = 0.02 (Step 2), and r = 20.0 (Step 4). For the undrained peak strength of the material $\left(\frac{S_{up}}{\sigma'_{vini}}\right)$, correlations were performed using the methodologies of Olson and Stark (2003) and Sandrekarime (2014) with the CPTu test data, resulting in $\frac{S_{up}}{\sigma'_{vini}}$ = 0.27. By applying the parameter values to Equation 17, n = 5.5 was obtained.

Table 2 presents a summary of CASM parameters obtained from the calibration for the tailings material.

Table 2: Parameters of CASM

Component		Parameters
Critical State Line – CSL	G	1,79
	I	0,035
	Mtc	1,32
Elasticity	n	0,30
	k	0,02
Plasticity	n	5,5
	r	20,0
	m	1,5

Once the input data resulting from the calibration were obtained, the p'-q (Figure 6) and ε_{ax}-q plots (Figure 7) were compared with the laboratory test results.

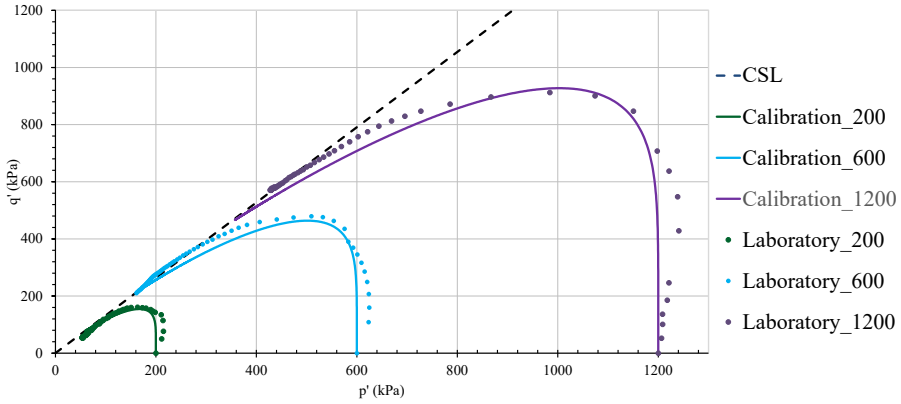


Figure 6: Calibrated versus laboratory p'-q curves

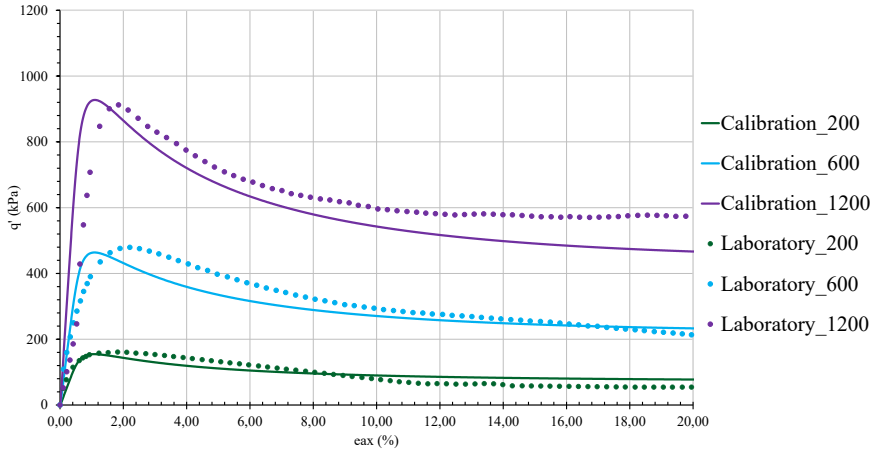


Figure 7: Calibrated versus laboratory ε_{ax}-q curves

Since the calibration should approximate the behavior of the materials simulated in the laboratory tests, it is shown that in the present example case, a consistent calibration is observed when applying the calibration methodology presented in this work.

Conclusion

This work presented the methodology for the calibration of the CASM constitutive model, illustrating the field and laboratory tests considered to obtain the input data required by the model and the necessary equations for the calibration process. Additionally, an application of the proposed calibration methodology to a tailings material was performed, and the results of the calibrated model in p'-q and ε_{ax}-q spaces agree very well with results from laboratory tests. The methodology proposed in this work results in accurate and consistent calibration of the behavior of the material. Hence, we envision that the proposed calibration methodology will serve as a reference for practitioners and researchers alike when using CASM to model

liquefaction-prone materials, such as those in tailings dams applications.

The authors assert that the calibration of the CASM constitutive model should prioritize meeting the criteria of the critical state line, ensuring its alignment both in the p'-q plane and the ln(p')-e plane. While attempts to calibrate the mechanical behavior of tailings are valid, it is challenging to replicate field conditions accurately in the laboratory. Consequently, complete convergence between the numerical simulation and the mechanical behavior observed in laboratory tests is unlikely, as stress paths may not fully align with each other.

Acknowledgements

The authors acknowledge the support of DF+ Engineering.

References

Arroyo, M. and Gens, A. 2021. *Computational analyses of Dam I Failure at the Córrego de Feijao Mine in Brumadinho: Final report for VALE S.A.*

Been, K. and Jefferies, M.G. 1985. A state parameter for sands. *Géotechnique* 35(2): 99–112.

Been, K. and Li, A.L. 2009. Soil liquefaction and paste tailings. In R. Jewell, A.B. Fourie, S. Barrera and J. Wiertz (eds), *Paste 2009: Proceedings of the Twelfth International Seminar on Paste and Thickened Tailings,* Australian Centre for Geomechanics, Perth, pp. 281–290, https://doi.org/10.36487/ACG_repo/963_32

Jefferies, M. and Been, K. 2016. *Soil Liquefaction: A Critical State Approach*. Second Edition. Florida, USA: CRC Press, Taylor & Francis.

Jefferies, M.G. 1993. Nor-sand: a simple critical state model for sand. *Géotechnique* 43(1): 91–103.

Jefferies, M.G. and Shuttle, D.A. 2002. Dilatancy in general Cambridge-type models. *Géotechnique* 52(9): 625–638.

Jefferies, M.G. and Shuttle, D.A. 2011. On the operating critical friction ratio in general stress states. *Géotechnique*, 61(8): 709–713.

Mánica, M.A., Arroyo, M., Gens, A. and Monforte, L. 2021. Application of a critical state model to the Merriespruit tailings dam failure. *Proceedings of the Institution of Civil Engineers – Geotechnical Engineering* 175 (2): 151–165.

Morgenstern, N.R., Vick, S.G., Viotti, C.B. and Watts, B.D. 2016. Fundão tailings dam review panel: Report on the immediate causes of the failure of the Fundão Dam. Tech. Rep., Cleary Gottlieb Steen and Hamilton LLP.

Olson, S.M. and Stark, T.D. 2003. Yield strength ratio and liquefaction analysis of slopes and embankments. *Journal of geotechnical and geoenvironmental engineering* 129(8): 727–737.

Robertson, P.K., Melo, L., Williams, D.J. and Wilson, G.W. 2019. *Relatório do painel de especialistas sobre as causas técnicas do rompimento da Barragem I do Córrego do Feijão.*

Sadrekarimi, A. 2014. Effect of mode of shear on static liquefaction analysis. *Journal of Geotechnical and Geoenvironmental Engineering* 140(12).

Sheng, D., Sloan, S.W. and Yu, H.S. 2000. Aspects of finite element implementation of critical state models. *Computational Mechanics* 26(2): 185–196. DOI: 10.1007/s004660000166

Shuttle, D. and Jefferies, M. 2005. *NorSand: Description, Calibration, Validation and Applications.*

Sternik, K. 2014. Prediction of static liquefaction by nor sand constitutive model. *Studia Geotechnica et Mechanica. XXXVI* (3): 75–83.

Wood D.M. 1990. *Soil Behaviour and Critical State Soil Mechanics*. Cambridge University Press. doi.org/10.1017/CBO9781139878272

Yu, H.S. 2006. *Plasticity and Geotechnics*. New York: Springer Science.

Drained Laboratory Vane Shear Testing to Characterize Nonplastic Tailings

Alvino Bezuidenhout, University of the Witwatersrand, South Africa
Luis A. Torres-Cruz, University of British Columbia, Canada and University of the Witwatersrand, South Africa

Abstract

The peak and residual undrained strength of tailings are of paramount importance when assessing their geotechnical stability. Accordingly, efforts have been made to use vane shear testing (VST) to assess the undrained strength of tailings. However, these efforts have been hindered because tailings are often nonplastic and thus exhibit relatively high permeability, making it difficult to attain undrained conditions during a VST. While much attention has focused on how to achieve, and verify, undrained VSTs in low-plasticity soils, in this paper we hypothesize that drained VSTs can provide information about the contractiveness of a soil and thus give insights into their undrained strength. We present results from a series of laboratory VSTs performed on a fine-grained angular silica sand that we use as a proxy for nonplastic tailings. Besides exploring the repeatability of the VST, the experiments also explore the effects of specimen diameter, pore medium (air vs. water), and angular velocity. We used these results to establish a test configuration that led to drained results in dry specimens and that eliminated undue interference due to an insufficiently large mold diameter. This configuration was then used to investigate the effect of the initial void ratio. The behavior of the specimens at large shearing deformations (360 vane rotations) was also investigated. Initial void ratio, and therefore potentially contractiveness, has a distinct effect on the results. This supports the possibility of using drained VSTs to assist assessments of the undrained shear strength of nonplastic tailings. We discuss additional research directions that should be addressed.

Introduction

Assessment of the peak and residual strength of tailings is a major consideration when assessing their geotechnical stability. The vane shear test (VST) has been identified as a method that can aid the characterization of the undrained strength of tailings (Hogan et al., 2022; Reid, 2016; Reid et al., 2023). During a vane shear test (VST), a vane with four blades is pushed into the ground and rotated to measure the shearing resistance of the soil (Figure 1). VSTs have several features that make them attractive as a geotechnical investigation tool:

1. A relatively simple geometry amenable to analysis.
2. The possibility of obtaining a full force vs. displacement (torque vs. rotation angle) curve to characterize the soil at any particular depth. This is unlike the cone penetration test (CPT), which provides only one reading of tip resistance, friction sleeve, and dynamic porewater pressure for any particular depth.
3. The VST can be performed both in the field at full scale (e.g. ASTM D2573) or in the laboratory at a reduced scale (e.g. ASTM D4648). This has the potential of facilitating the interpretation of the field version of the test.
4. The angular velocity of the vane can be adjusted within a wide range to promote drained or undrained conditions.

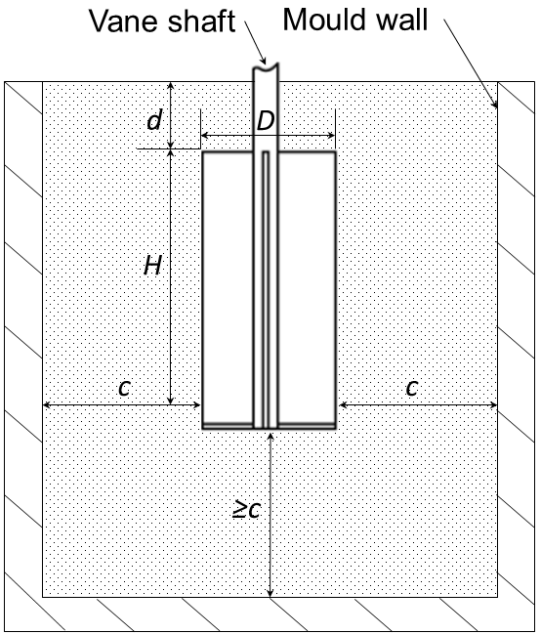


Figure 1: Setup of a laboratory vane shear test

However, a major difficulty in using VSTs to measure the undrained strength of nonplastic soils, such as many types of tailings, is that the greater permeability of these soils makes it challenging to attain undrained conditions. So far, attempts to overcome this difficulty have focused on increasing the angular velocity of the vane to promote undrained conditions (Hogan et al., 2022; Reid, 2016; Reid et al., 2023). However, regardless of how fast the vane is rotated, the situation remains challenging for at least two reasons. Firstly, drainage begins as soon as the vane reaches its target depth and before it even begins to rotate. During an in-situ testing campaign in which a deliberate effort was made to reduce the time between insertion and rotation, the average measured time was ~3 minutes (Reid et al., 2023). Clearly, significant

drainage can occur in the tailings surrounding the vane during this time. A second difficulty is the lack of a reliable criterion to determine when a VST is undrained or not (Reid et al., 2023).

Given these difficulties in performing and verifying undrained VSTs in nonplastic tailings, in this paper we focus on using drained VSTs to assess the shearing characteristics of nonplastic soils. Naturally, the undrained strength cannot be inferred directly from a drained VST. However, we show that the torque vs. rotation curve produced by a drained laboratory VST reflects the density of the specimen and thus has the potential to also reflect its contractiveness. We hypothesize that because the contractiveness of a soil is fundamentally correlated to its undrained shear strength (Jefferies and Been, 2015), it may be possible to estimate the undrained strength of low plasticity soils using the results of drained VSTs. While the data presented herein is insufficient to validate our hypothesis, it does suggest that this is a possibility worth exploring.

Materials and methods

We tested a narrowly graded silica sand with angular particles (Figure 2) as a proxy for nonplastic tailings. The sand had a maximum and minimum void ratio of e_{max} = 1.12 and e_{min} = 0.68, determined as per ASTM D4254-16 and the procedure proposed by Torres Cruz (2016), respectively. The mean particle density was ρ_s = 2.67 g/cm^3 (BS 1377).

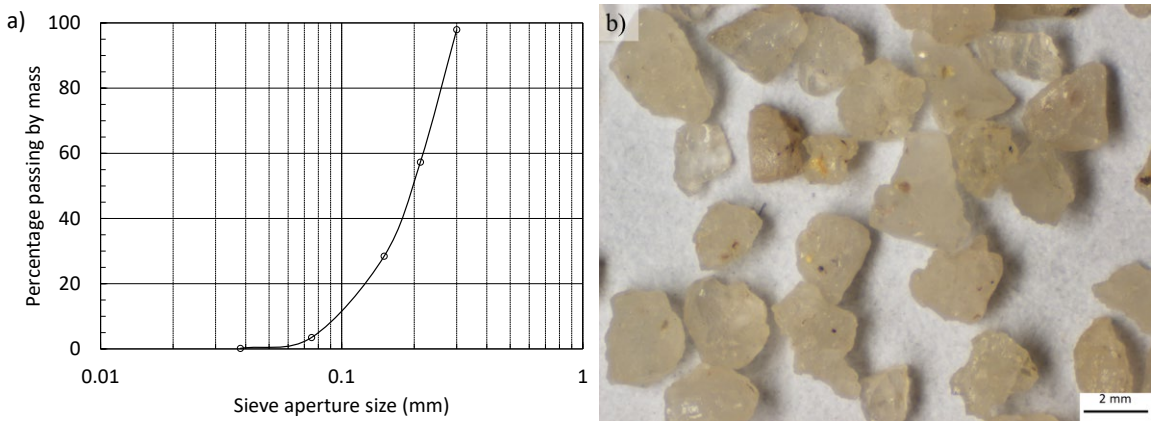


Figure 2: a) Particle size distribution and b) micrograph of the silica sand

We performed laboratory vane shear tests, generally abiding by ASTM D4648. All tests were done with a square vane with a width and height of 12.7 mm. We used a fully automatic vane shear tester capable of logging torque against angle of vane rotation. The VST device comprised a control panel and test frame that housed strain sensors (used to measure torque), a removable vane, a fully threaded spindle and handle that allowed the vertical displacement of the vane (and sensor housing unit) and a mold support bracket fixed to the base of the test frame. The control panel was connected to a desktop computer from which each

test was configured. The VST device could measure torques of up to 3 Nm, at a resolution of 0.001 Nm and operate at angular velocities from 0.06 to 1,200°/min.

Table 1 shows the features of the test that we varied during the experimental program, as well as the values or options that such features took on. We performed a total of 19 tests. Table 2 indicates their purpose and their characteristics in terms of specimen (or mold) diameter in mm (D), pore medium (M), angular velocity in °/min (V) and initial void ratio (e_0).

Table 1: Features of the VSTs that varied within the testing program

Test feature	Values or options tested
Specimen diameter *D* (mm)	37, 75.5, 101, 105
Pore medium *M*	Air (dry), water (saturated)
Angular velocity *V* (°/min)	0.15, 1.5, 4.7, 15, 47, 150
Maximum vane rotation θ_{max} (°)	150, 1,080, 3,220, 14,400, 129,600
Initial void ratio e_0	0.68 = e_{min}, 0.89, 1.11 ≈e_{max}

Table 2: Summary of the testing program

Test no.	Characteristics (D/M/V/θ_{max}/e_0)	Aspect explored
1	101/air/15/1080/0.68	Repeatability and benchmark
2	101/air/15/1080/0.68	Repeatability
3	101/air/15/1080/0.68	Repeatability
4	101/air/15/1080/0.68	Repeatability
5	37/air/15/1080/0.68	Effect of specimen diameter
6	75.5/air/15/1080/0.68	Effect of specimen diameter
7	105/air/15/1080/0.68	Effect of specimen diameter
8	101/water/15/3220/0.68	Effect of pore medium
9	101/water/0.15/150/0.68	Effect of pore medium
10	101/water/0.15/150/0.68	Effect of pore medium
11	101/air/1.5/1080/0.68	Effect of angular velocity
12	101/air/4.7/1080/0.68	Effect of angular velocity
13	101/air/47/1080/0.68	Effect of angular velocity
14	101/air/150/1080/0.68	Effect of angular velocity
15	101/air/15/1080/0.89	Effect of void ratio
16	101/air/15/1080/1.11	Effect of void ratio
17	101/air/150/129,600/0.68	Behavior at large rotation
18	101/air/150/129,600/0.89	Behavior at large rotation
19	101/air/150/129,600/1.11	Behavior at large rotation

Test 1 served as a benchmark test. As described below, for most of the remainder of the tests, different aspects of test 1 were systematically varied to isolate the effect of changes on D, M, V and e_0. However, tests 2 to 4 were set up identically to test 1 to investigate repeatability. We assessed repeatability by computing the coefficient of variation (CoV) of the torque measured by the tests 1 to 4 at any given rotation angle. The CoV was computed by calculating the standard deviation of the sample of the torque readings and dividing them by the mean torque reading.

Tests 1, 5, 6, and 7 were aimed at identifying a suitable specimen diameter D. There are good reasons both to keep D small and to make it large. On the one hand, a small D implies specimens that use less material and are quicker to form, and in which homogeneity is easier to achieve. On the other hand, if D is too small, the walls of the mold interfere with the results and can artificially increase the measured torque (Barros and Barros, 1989). An adequate D must thus be established through testing. For our benchmark configuration (test 1) and, consequently, for most of the remaining tests, we adopted $e_0 = 0.68 = e_{min}$ because we hypothesized that this dense condition was the critical one in terms of identifying a D large enough to eliminate the effect of the mold walls.

Tests 1, 8, 9, and 10 investigated the effect of pore medium, specifically, the difference between dry and saturated specimens. We considered this because, except for tests 8 to 10, all VSTs were performed on dry specimens as they are more easily prepared than saturated specimens. However, it is saturated tailings that are of practical interest as they are prone to undrained loading. We thus assumed that the results from dry specimens are relevant to saturated specimens provided that the VSTs in the saturated specimens are fully saturated. The tests on saturated specimens were designed to verify this assumption.

With tests 1, 11, 12, 13, and 14 we investigated the effect of the angular velocity V of the vane. In saturated soils, V has a significant effect because low velocities promote drained conditions while high velocities promote undrained conditions. Presumably, the effect of V on dry soils, and particularly on a sand like the one tested herein, is much smaller because the lower viscosity and greater compressibility of air may prevent the development of any air pressure (i.e., prevent the development of fully or partially undrained conditions) even when the vane is rotated relatively quickly. Notwithstanding, we ran tests to ensure that changes in V did not affect the results.

Tests 1, 15, and 16 investigated the effect of the initial void ratio e_0. Because the peak friction angle of a sand is directly correlated to its initial void ratio e_0, the peak torque during a VST is also directly correlated to e_0. We investigated this effect by running tests at e_0 close to e_{min}, close to e_{max} and close to an intermediate value.

Finally, tests 17, 18, and 19 explored the behavior of VSTs with different e_0 at large values of vane rotation. For these tests the vane was allowed to complete 360 revolutions ($\theta_{max} = 129{,}600°$). Regardless of initial density, soils attain the same critical friction ratio at large shear strains for a given mode of shearing

(Jefferies and Been, 2015). Accordingly, we hypothesized that tests with different e_0 would eventually reach the same torque values. Tests 17, 18, and 19 were run to explore this hypothesis. Given the large number of vane rotations involved in these tests, their vane rotation velocity was 150°/min.

The specimen preparation method depended on the target e_0 and pore medium. Except for tests 16 and 19, all specimens were prepared by dry tamping ten sand layers of equal mass and height. The mass of each layer was calculated as a function of the target e_0. Tests 16 and 19 were prepared at $e_0 = 1.11 \approx e_{max}$. Accordingly, these tests were prepared by gently pouring the sand into the specimen container without any tamping.

Tests 8 to 10 involved saturated specimens. Accordingly, after dry tamping, a plastic disc with 1 mm diameter holes was placed on top of the specimen. Distilled water was then poured on top of the disc, and it flowed through the 1 mm diameter holes. The disc protected the specimen from disturbance by the pouring of the water. Weighing the specimen before and after pouring the water enabled the estimation of the saturation (S), with the method typically achieving $S > 95\%$. While not perfectly saturated, herein we refer to these specimens as saturated.

For all tests, the vane was positioned in the center of the cylindrical mold (Figure 1), ensuring uniform lateral clearance that was verified using a Vernier caliper. The vane was lowered into the specimen at approximately 6 mm/min. The clearance between the bottom of the vane and the bottom of the mold was at least equal to the lateral clearance. For all dry specimens prepared at $e_0 = 0.68$, the height of soil above the upper edge of the vane (distance d in Figure 1) was equal to 25.4 mm, that is, twice the height of the vane. This resulted in a vertical effective stress of $\sigma'_v = 0.50$ kPa at the mid-height of the vane, a value that was computed using:

$$\sigma'_v = \gamma\left(d + \frac{H}{2}\right) \qquad \text{(Equation 1)}$$

$$\gamma = \left(\frac{G_s}{1 + e_0}\right)\gamma_w \qquad \text{(Equation 2)}$$

Where γ is the total unit weight, d and H are as defined in Figure 1, G_s is the specific gravity of the solids, and γ_w is the unit weight of water (9.81 kN/m^3). We increased the soil height d (Figure 1) for tests 8, 9, 10, 15, 16, 18, and 19 to achieve the same initial nominal $\sigma'_v = 0.50$ kPa at the mid-height of the vane for all tests.

Results

Figure 3 presents the results of the tests done to assess repeatability. The four curves exhibit a peak torque of ~0.045 Nm at a rotation angle of ~20° followed by a sharp drop in strength between $20° \leq \theta \leq 80°$ and a slower drop at $\theta > 80°$. The reduction in T was still ongoing at $\theta_{max} = 1080°$ when T reached ~0.014 Nm.

The CoV begins at relatively high values of ~50% but reduces quickly to <5% as T increases to its peak value. After the peak the CoV increases again to ~15% until the end of the test. The mean CoV of 13.5% is similar to the mean CoVs reported for undrained triaxial compression, direct shear, and laboratory VST performed on plastic soils and drained shear tests in sand (Phoon and Kulhawy, 1999). Overall, tests 1 to 4 suggest that the laboratory VST can perform a reliable characterization of the silica sand.

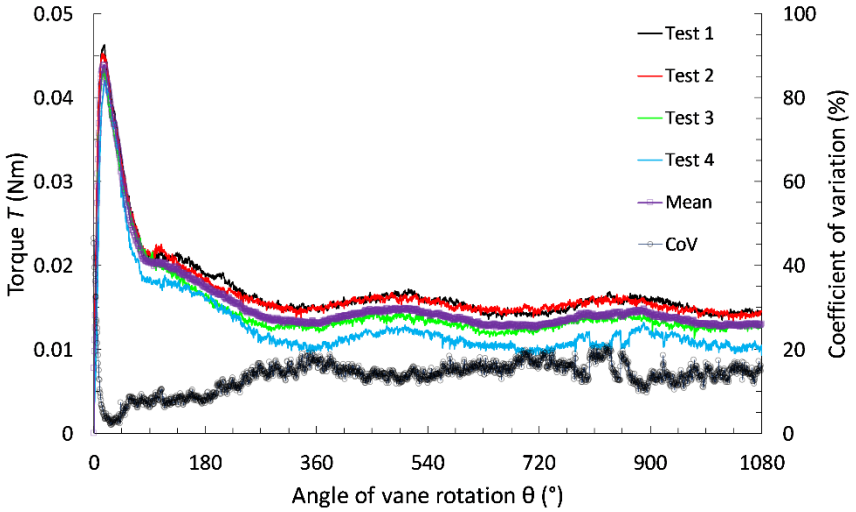


Figure 3: Repeatability assessment of the vane shear test

Figure 4 presents the results of the tests that explored the effect of specimen diameter D. For D values of 37, 75.5, and 101 mm there is an inverse correlation between D and the torque at any given value of θ. However, the curves for D = 101 mm and D = 105 mm are virtually indistinguishable suggesting that, for the sand used herein, D = 101 mm is adequate to eliminate interference from the walls of the mold.

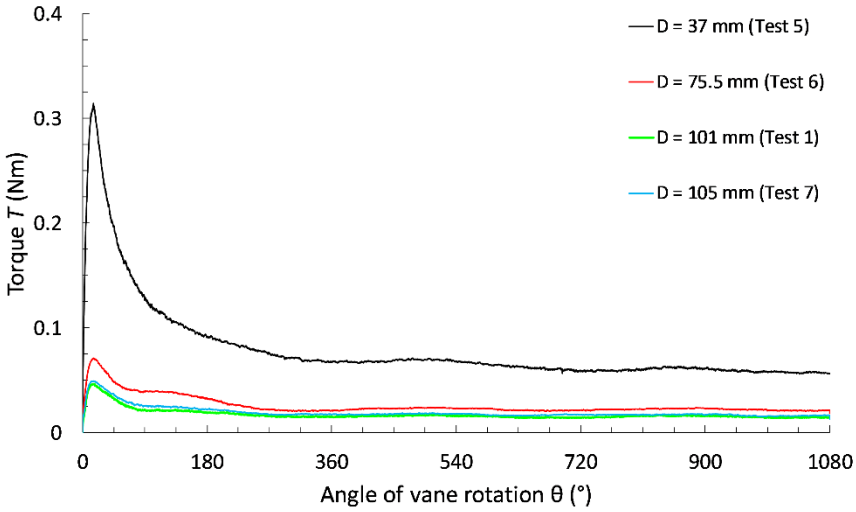


Figure 4: Effect of specimen diameter

Figure 5 presents the results of the tests done to assess the effect of pore medium. The saturated specimens (tests 8, 9, and 10) yielded torque values that are significantly larger than those measured in the dry specimen. As mentioned previously, the expectation was that the tests on dry and saturated specimens would yield the same results provided that the tests on saturated specimens were drained. Test 8 was the first test on a saturated specimen and yielded torque values that were significantly higher than the benchmark test 1. We initially attributed this difference to test 8 not being fully drained. That is, we suspected that since test 8 had $e_0 \approx e_{min}$, dilation of the dense sand was generating negative pore water pressures that were increasing the effective stress levels and therefore the shear strength. To improve drainage, for test 9 we brought down the angular velocity by two orders of magnitude from 15 to 0.15°/min. Surprisingly, test 9 yielded even higher torque values than test 8 (Figure 5). We believe the results of test 9 are spurious and that the high torque values are due to the vane shaft deviating from verticality during insertion.

Test 10 is a repetition of test 9, taking care to prevent the vane shaft from deviating from verticality. The torque values of test 10 are still significantly larger than those of test 1 that was dry (Figure 5). It is not clear to us what is causing the large difference between tests 1 and 10 since both have $e_0 = e_{min}$, D = 101 mm, initial σ'_v = 0.50 kPa at the mid-height of the vane and, presumably, both tests are fully drained. We believe that further testing is required to clarify this matter. It is also interesting to note the similarity between tests 8 and 10 despite their large differences in V (Figure 5). This apparent independence of the torque values from V is similar to a finding reported by Wilson (1963).

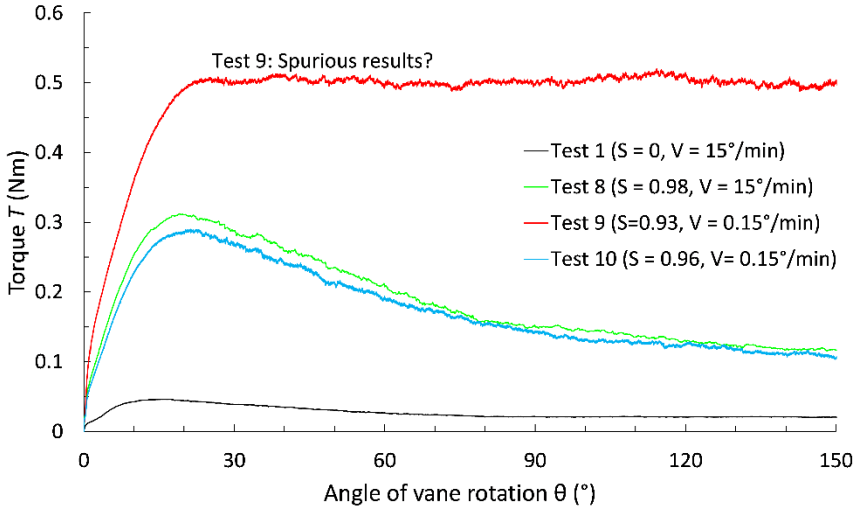


Figure 5: Comparison of specimens with air or water as a pore medium

Figure 6 shows the effect of changing the angular velocity over two orders of magnitude from 1.5 to 150°/min. While there are differences between the five curves (Figure 6a), these differences do not seem to

be systematic. That is, there appears to be no clear direct or indirect correlation between V and T at a given angle of rotation (Figure 6b). Furthermore, beyond $\theta = 360°$ the five curves are largely indistinguishable. We interpret the similarity of the results to mean that, despite differences in V, all five tests were fully drained. The similarity in results could also mean that all five tests are fully undrained. However, we believe this is unlikely considering that all specimens were dry (M = air) and that the slowest test was run at V = 1.5°/min.

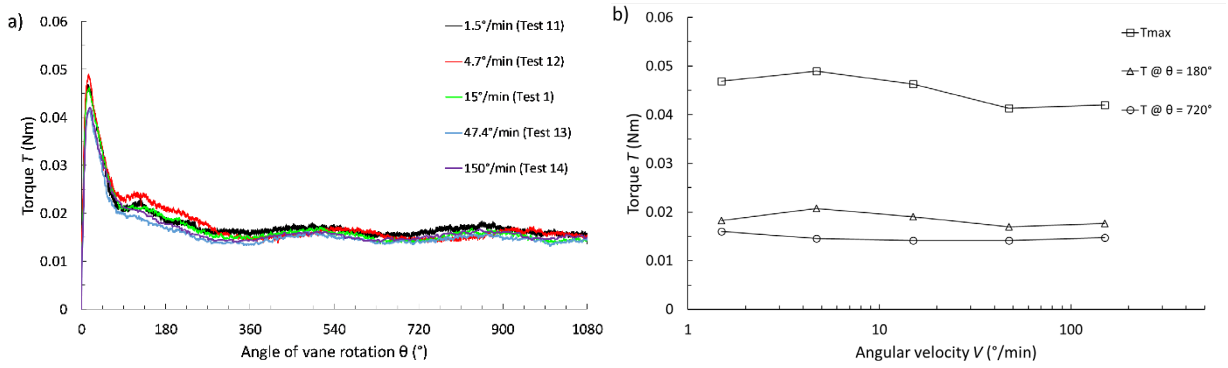


Figure 6: Effect of angular velocity

Figure 7 illustrates the effect of changes in e_0. These tests were done with D = 101 mm because this diameter proved to be adequate to eliminate the effects of the mold walls (Figure 4). The results show a clear inverse correlation between e_0 and peak torque (Figure 7a), a finding that is consistent with previous investigations (Barros and Barros, 1989; Park et al., 2016; Park et al., 2018). The ratio of the peak torque (T_{max}) to the end-of-test torque (T_{EoT}) is also significantly affected by e_0 (Figure 7b).

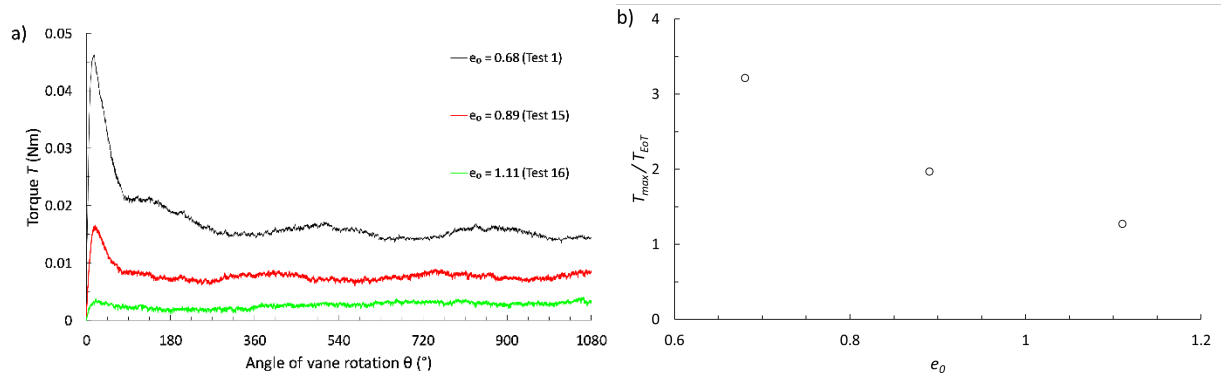


Figure 7: Effect of e_0 on a) Full torque vs. rotation curves and b) T_{max}/T_{EoT}.

Figure 8 shows the results of tests ran to 360 vane revolutions. Figure 8a suggests that tests 17 and 18 reached a steady residual torque after ~160 vane revolutions. Conversely, it appears that, despite the large number of revolutions, test 19 did not reach a truly steady residual torque, with the torque still increasing at the end of the test. Figures 8a and 8b also show that, contrary to our expectation, the three tests did not

reach the same residual torque at large strains. Instead, the residual torques are inversely correlated to e_0. We suspect this is due to a cavity that developed around the vane shaft during rotation in each test (Figure 9). This cavity reduces the shaft friction and the vertical effective stress around the vane. The geometry of the cavity appears to be influenced by e_0. Specifically, the looser the soil, the higher its susceptibility to disturbances, and the larger the diameter and depth of the cavity. In turn, this leads to a lower σ'_v around the vane and therefore lower torque values. These results highlight the experimental challenges of attaining truly constant σ'_v across tests with different e_0.

The inset in Figure 8a shows that the two denser tests (17 and 18) approached a peak torque at $\theta \approx 20°$ and then reduced to a residual torque. Conversely, test 19 shows a nearly monotonic increase in strength.

Figure 8b, which focuses on the last ten revolutions, shows that all three tests exhibit a well-defined sinusoidal shape with a periodicity of one revolution. This may be indicative of a non-uniform strength distribution along the shear surface. Although Figure 8b only shows the last ten revolutions of the tests, the periodic nature of the torque response is established much earlier, in some cases as early as in the second revolution (Figures 3, 6, 7, and inset in Figure 8a). It also appears that the amplitude of the sinusoidal response increases with specimen density.

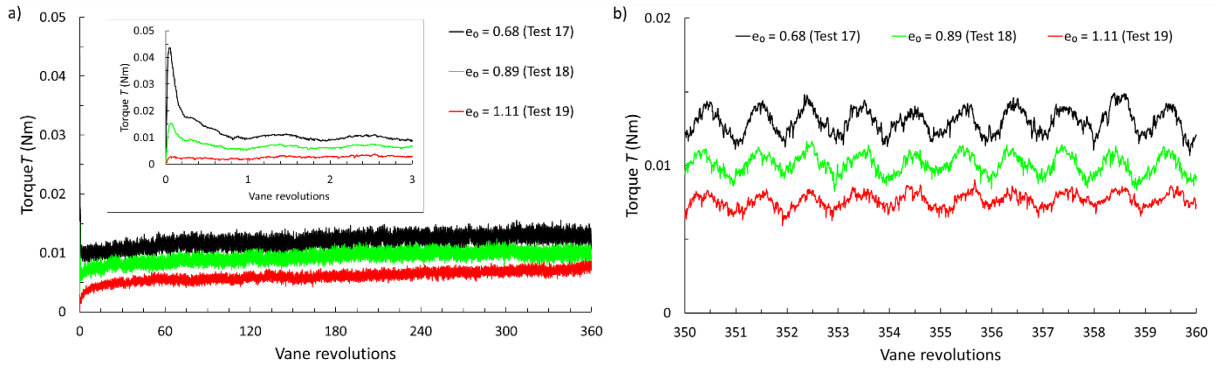


Figure 8: Tests run to 360 revolutions. a) Full results with inset showing enlargement of the first three revolutions and b) last ten revolutions

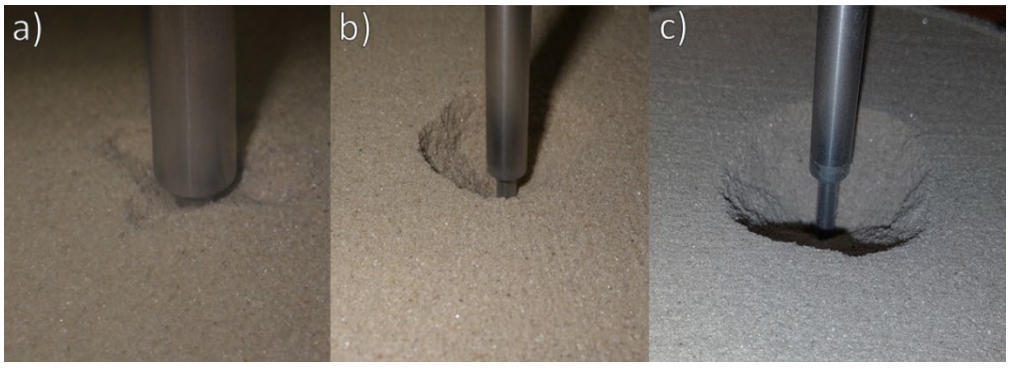


Figure 9: Cavity around the vane shaft at the end of a large deformation vane shear test. a) $e_0 = 0.68 = e_{min}$, b) $e_0 = 0.89$ and c) $e_0 = 1.11 \approx e_{max}$.

Discussion

The initial void ratio e_0 of the tests affects T_{max} and the ratio T_{max}/T_{EoT} (Figure 7). We hypothesize that these effects are related to whether the specimen is contractive or dilative. Accordingly, drained VST results appear to have the potential of aiding in the assessment of the volume change characteristics of tailings. Such characteristics are correlated to the undrained strength of tailings, suggesting that drained VSTs can ultimately assist with the assessment of undrained strength. There are several practical issues to address before these observations can be translated into a robust methodology to assess undrained strength.

Firstly, while Figure 7 shows that e_0 affects VST results, it is very likely that there is also an effect of horizontal effective stresses (not measured herein). The magnitude of these horizontal stresses also affects the contractiveness of the soil, and therefore its undrained strength, because it is the combination of void ratio and mean effective stress that controls contractiveness (Been and Jefferies, 1985).

Assuming that it is indeed possible to establish a correlation between VST results and the volume change characteristics of the soil, it is crucial to determine whether such a correlation is affected by the particle size distribution. This is relevant to hydraulically deposited tailings because they exhibit intense layering with particle size distribution varying from one layer to the next.

Another consideration is ensuring that the field VST is indeed drained. This is probably not as challenging as ensuring that the VST is fully undrained which, as mentioned in the introduction, is an approach adopted in other works. However, ensuring fully drained conditions is not necessarily straightforward because neither laboratory nor field VST probes are typically fitted with piezometers. The addition of piezometers would be a welcome enhancement. Furthermore, because of the aforementioned layering in tailings deposits, the angular velocity required to achieve drained conditions is likely to vary significantly both laterally and vertically. It is also necessary to consider the implications that these velocities will have on the duration of field VSTs.

We encountered an unexpected difference between tests in dry and saturated specimens (compare tests 1 and 10 in Figure 5) and were unable to explain them satisfactorily. Resolution of this matter is crucial to the interpretation of VST results because it is ultimately saturated or nearly saturated tailings, and not dry tailings, which mostly contribute to stability concerns of tailings deposits.

All tests presented herein were performed at a very low σ'_v of 0.50 kPa at the mid-height of the vane. Additional testing is required to investigate VST results obtained at σ'_v levels that are more representative of in-situ conditions.

Our laboratory VST results exhibited a sinusoidal pattern with a periodicity of one revolution. It appears that the amplitude of the sinusoidal response is affected by e_0. We are not aware of a similar pattern having been reported for field VSTs. We believe this is worth exploring as well as assessing the effect that the amplitude may have in result interpretation.

Finally, VST-based assessment of the in-situ undrained strength of tailings may require pairing VST results with a laboratory test, such as triaxial testing or direct simple shear, in which undrained (or constant volume) conditions can be easily imposed. Again, further research is needed to determine whether it is possible to correlate VST results with the undrained strength measured in laboratory tests.

Conclusion

We presented the results of a laboratory VST program that explored repeatability as well as the effect of specimen diameter, pore medium (dry vs. saturated), angular velocity, and initial void ratio e_0. The testing program also investigated the behavior of VSTs at very large strains (360 revolutions). Results on a clean angular silica sand show that the laboratory VST is generally repeatable, with a representative CoV of ~13%. A mold diameter of 101 mm was adequate to eliminate interference from the mold walls. For undetermined reasons, dry and saturated specimens yielded different results. We will carry out further testing to clarify this issue. On dry specimens, varying the rotation velocity from 1.5 to 150°/min did not affect the results. The results are affected by e_0, with denser specimens resisting higher torques. Cavities formed on the surface of the specimens appear to hinder efforts to run tests at different e_0 while maintaining a constant σ'_v. VSTs yield a periodic response that may begin as early as in the second revolution, but which is particularly noticeable when running tests to a large number of revolutions.

The effect of e_0 on drained VSTs suggests that it is worth exploring the possibility of using such results to estimate the in-situ undrained strength of nonplastic tailings. However, several issues discussed herein must be addressed to develop a robust methodology.

References

Barros, P.L.A., Barros, C.L.A. 1989. Vane shear test application on cohesionless soils. *Proceedings of the 12th International Conference on Soil Mechanics and Foundation Engineering*. Rio de Janeiro, Brazil: 171–174.

Been, K. and Jefferies, M.G. 1985. A state parameter for sands. *Géotechnique* 35(2): 99–112.

Hogan, A.A., Kelly, S.A., Storteboom, O. and Roberston, P.K. 2022. Modified field vane technology for improved reliability of undrained shear strength measurements in mine tailings. *Proceedings of Tailings and Mine Waste, 2022*. Denver, Colorado.

Jefferies, M.G. and Been, K. 2015. *Soil Liquefaction – a Critical State Approach*. Second edition. London: CRC Press.

Park, S.S., Zhou, A. and Kim, D.R. 2016. Vane shear test on Nakdong river sand. *Journal of the Korean Society of Civil Engineers* 36(3): 463 – 470 (in Korean).

Park, S.S., Kim, D.R. and Lee, S.B. 2018. Measurement of friction angle of sand from horizontal stress and torque acting on vane. *Journal of the Korean Society of Civil Engineers* 38(1): 63 – 71 (in Korean).

Phoon, K.K. and Kulhawy, F.H. 1999. Characterization of geotechnical variability. *Can. Geotech. J.* 36: 612 – 624.

Reid, D. 2016. Effect of rotation rate on shear vane results in a silty tailings. *Geotechnical and Geophysical Site Characterisation 5.* Australian Geomechanics Society, Sydney, Australia.

Reid, D., Rodriguez, C., Fourie, A. and Tiwari, B. 2023. Partial drainage effects during vane shear tests, with an emphasis on the measurement of remolded strengths. *Proceedings of Tailings and Mine Waste, 2023.* Vancouver, Canada.

Torres Cruz, L.A. 2016. Use of the cone penetration test to assess the liquefaction potential of tailings storage facilities. Doctoral thesis, School of Civil and Environmental Engineering, University of the Witwatersrand, South Africa.

Wilson, N.E. 1963. Laboratory vane shear tests and the influence of pore-water pressures. ASTM Special Technical Publication 351: 44–52.

Modeling Assumptions and Implications during Closure Assessments on Legacy Tailings Facilities

Benjamin Kramka, Stantec, USA
Erin Dunn, Stantec, USA
Lauren Meyer, Stantec, USA
Jason Cumbers, Stantec, USA

Abstract

Moving a legacy tailings storage facility (TSF) toward closure under the Global Industry Standard for Tailings Management (GISTM) involves comprehensive assessment and understanding of construction history, site management, and post-operation activities and procedures. Some legacy TSFs that have undergone steps toward closure prior to the GISTM may not meet the GISTM requirements for closure. Consequently, mining companies that are working toward GISTM compliance for legacy TSFs in their portfolios are having to re-evaluate previously closed or partially closed facilities with limited historical documentation on the site and dam construction, under more rigorous standards. Assumptions are often made on how a facility was built based on historical as-built information and previous consultants' investigation work, leaving data gaps in the conceptual TSF zonation and geometry used for detailed geotechnical stability analysis. Further complicating these types of modeling exercises is the presence of material property data gaps, outdated management techniques during operation, and construction field adjustments made with minimal documentation.

This paper provides recommendations for approaching stability analyses and assessing needs for further site investigation, specifically for legacy mine sites seeking closure with critical data gaps related to TSF as-built conditions. Not only are supplemental investigations to close gaps costly and time intensive, but gaining access for site investigations can be challenging and require modifications to partially closed facilities, which Owners often prefer to avoid. As stakeholders drive the industry toward more stringent requirements and better management to avoid failures, it can be more efficient to use conservative models and sensitivity analyses to evaluate data gaps and inform stakeholder decisions than to proceed with targeted investigations or closure planning. By approaching modeling with an emphasis on data gap driven sensitivities developed using case study analogies, site closure designers can effectively implement solutions more quickly.

Introduction

Achieving closure of a legacy TSF to meet current-day standards such as the GISTM can be a lengthy process. TSF liability is not only controlled by ongoing maintenance costs, but is more closely tied to risks involving embankment and dam stability under a wide range of loading conditions that could lead to a catastrophic failure event. To satisfy closure requirements and achieve critical risk-reduction measures, a common approach often involves site investigations to resolve major unknowns and attempt to fully characterize a TSF before moving forward with a closure design. While this approach seeks to minimize risk from all angles, there are drawbacks as well, specifically the amount of time and capital investment required to reach the final closure implementation.

This paper outlines the steps a closure design team can take to assist an Owner with identifying the closure status of a legacy TSF and beginning to assess the approach to design for closure. This approach seeks to identify data gaps up front and rule out factors contributing to potential instability, or identify those that can remain unknown with minimal risk. This process can be iterative and includes the following steps:

- Identifying site-specific closure criteria based on relevant standards, regulations, Owner goals and appetite for risk.
- Assessing available historical documentation, publicly available information, and data for the site and identifying data gaps and uncertainties with respect to necessary parameters for closure design.
- Developing conceptual models and sensitivity analyses for the TSF.
- Using the results of the conceptual models to update data gaps and make a decision to either revisit data needs or move forward with closure design, balancing cost and time constraints with the criticality of remaining gaps.

TSF closure criteria

TSF closure criteria typically relies on governing regulations set by states or national government agencies with jurisdiction over the TSF in addition to state-of-the-practice guidelines published by professional organizations. Since it was published in late 2020, many mining companies have aligned with the guidance from the GISTM for establishing minimum design criteria for closure of TSFs. GISTM design criteria for active TSFs are based on consequence classification. The criteria for closure are consistent for all TSF consequence classifications due to the design life or period of performance of the facility, with design for the 10,000-year recurrence interval for both seismic and hydrologic analyses (GISTM, 2020). Alternative guidance exists from various national dam associations (non-regulatory entities) such as the Canadian Dam Association (CDA) and the Australian National Committee on Large Dams (ANCOLD), among others.

These associations form the basis for guidelines or state-of-the practice standards which can also be considered and adopted by mining companies and closure design teams as deemed appropriate. Other governmental regulatory agencies may have design requirements, such as the Nuclear Regulatory Commission or Environmental Protection Agency in the United States. The GISTM has become the industry standard for TSF closure design criteria with required compliance for member organizations of the International Council on Mining and Metals (ICMM) because of its comprehensive approach that seeks to consider all stakeholders.

The key drivers for site closure generally pertain to perceived and inherent risks associated with failure of a TSF and potential impacts to the people and environment within the neighboring communities. Although all sites are different and will have their own site-specific risks (geohazards, nearby waterways, wildfires, avalanches, seasonal flooding, etc.), several apply across the board. These risks include:

- Static failure due to poor construction techniques, foundational weakness, phreatic surface changes, static liquefaction, or piping.
- Seismic failure due to liquefaction and/or material strength reduction.
- Dam breach and inundation due to hydrologic events.

Assessment of these potential failure modes is typically explored through a multi-disciplinary risk assessment and used to inform the design. For legacy TSFs, where as-built documentation is lacking, this commonly means making conservative assumptions regarding as-built conditions, construction techniques, material properties (particularly for liquefiable tailings and foundation conditions), water levels within the TSF, and identification and understanding of the known unknowns. This information is typically gathered through a thorough assessment of existing historical data.

Historical data assessment

The first step in assessing the closure status and/or planning for closure design of a legacy TSF in reference to GISTM or other regulatory criteria is to complete a desktop study and assessment of the available historical data. The engineer of record (EOR) typically completes a historical data assessment for the site. The desktop study is especially important for Owners and EORs that were not responsible for the legacy facility during operations, construction, or closure, and are not familiar with site history or its documentation. Though mining companies and EORs that were responsible for historical operations and closure should also complete a thorough review of historical data prior to developing closure designs. Documents and information that should be compiled and reviewed to support or develop a thorough historical site knowledge base include:

- Geotechnical investigation field and laboratory data.

- Design documentation.
- Operational data.
- As-built construction documentation.
- Instrumentation and monitoring data.
- Regional and site geology, geomorphology, and hydrogeology.
- Geochemistry.
- Climate data.
- Seismicity.
- Photographs (construction, aerial, site inspection).

A site visit should also be conducted by the EOR as a part of the review, to gain a better understanding of the TSF configuration and current status.

Document review

Evaluating historical site information that was collected prior to closure allows for review of key design elements with respect to critical risks and failure modes identified during a risk assessment. The document review should organize data to align with identified risks and closure criteria. Data should also be organized into the components needed to build an overall conceptual site model (CSM). For example, data should be organized by material type such as tailings, cover, embankment fill, and foundation materials. Data should also be organized to show which data may be used for planned analyses, such as liquefaction, stability, scour/erosion, or dam breach analyses. Organizing data this way allows for efficient review of data trends and identification of data gaps.

An important step of the document review is to identify data that can be used for the analyses needed to assess closure criteria conformance, the associated data gaps for the analyses, and the complete TSF knowledge base. For example, material property testing on samples collected from presumed dam raises can support general understandings for how a dam may have been initially constructed. Historical documentation, such as photographs of TSF construction and operations, should be cross-referenced and evaluated for discrepancies, and it is not uncommon to find conflicting information or data which can be challenging to navigate as a data gap.

How the data is assessed in historical documentation also matters, since the circumstances around why it was collected, or how, may by biased, or are often not fully known to the EOR or current Owner. Data should be assessed qualitatively to evaluate the level of certainty for specific parameters in the available data set. For instance, laboratory testing such as triaxial shear strength tests should be reviewed to evaluate the test methods used and overall quality of the results. If incorrect test methods were used, or if reporting of the results does not include enough information (for example, stress path plots) to evaluate

the test results in detail, this should be flagged as uncertain in the desktop review for additional evaluation during model parameter development. Additionally, historical lab data and drill log information regarding conditions of sample collection should be assessed and weighed with the tested values to see if the results are representative of broader conditions or should be discounted appropriately. Data should also be assessed quantitatively. If a dataset is too small for a specific parameter, it should be noted as uncertain in the desktop review. For example, many historical data sets lack information about the TSF foundation material properties; if there are few, to no, historical borings or laboratory tests for foundation materials, it is challenging to assess the potential for liquefaction, or identify weak foundation layers, that could pose a risk to overall stability. In this case, review of regional datasets may provide clues as to heterogeneity or continuity of native foundation layers.

Public reference information

Paired with existing site knowledge, data pulled from publicly available literature can improve the understanding of historical data and provide useful information for closing data gaps. Historical closure designs for legacy TSFs will have been developed on a set of assumptions that fit the overall TSF closure plan at that given time, requiring new EORs to conduct an independent review of the historical information to establish assumptions in line with new closure goals. Part of weighing the applicability of the site data is incorporating regional characteristics, stratigraphy, hydrogeology, and other publicly available information. This is also a good time to review relevant case histories, for example those with similar location, operational aspects, tailings composition, construction methods, or other factors where important assumptions can be drawn from the key outcomes of another closure design. Both successful closure designs and past failures should be considered in a case history review when evaluating assumptions for the TSF models.

Generally, the CSM will incorporate detailed local information and become more granular with wider uncertainty as site boundaries are reached, but there still needs to be an understanding of how the conditions of the boundary materials affect model results. An example of information to be considered while developing the CSM includes reviewing geologic studies for materials that could affect stability, hydrogeology, geochemistry, or liquefaction potential near or beneath the TSF. Data collected from the surrounding area should be organized similarly to the site-specific data, by specific model inputs as well as more general groupings. One may be easily drawn to previous assumptions and assertions regarding factors controlling TSF stability from observed historical data trends. For example, concluding that excess seepage observed through toe drain water present in a dam adjacent to a lake is from the lake, when it could be coming from the surrounding hillslope or elsewhere. A proper CSM will develop assumptions that are based

on available reference information to highlight the known and unknown information for a particular TSF equally.

Conceptual models and sensitivity analyses

Compiling a thorough site knowledge base allows for development of a more comprehensive conceptual site model (CSM), which provides a framework for assessing potential risk of failure. The key focus when transitioning from evaluating site data categorically to building the site model is revisiting the main components of the risk assessment under GISTM to prioritize details that inherently make the greatest difference in modeling and associated results. For example, a data gap for shallow bedrock strength may be less relevant than whether overlying fine-grained loess deposits were left in place over bedrock and directly below the TSF footprint. Though it is important to accurately capture all available data to build out a conceptual site model that can be relied on for a closure assessment, it is also important to incorporate quality data into the main components of the CSM that may impact closure criteria being met.

Additionally, once a framework has been created for a TSF, professional assumptions and observations that feed into the CSM should be evaluated in the field by experts in that area of practice to visualize how the closure criteria objectives are being incorporated. A basic approach is to build a database from historical information and use linear interpolation combined with statics to derive site information that is defensible and reflective of the onsite behavior; however, comparing that to the regional setting and case studies will make a CSM and modeling approach more informative on the driving factors for long-term TSF stability. This step of the closure process requires outside-of-the-box thinking to weigh the knowns with the unknowns and establish evaluation criteria that will allow identification of the data gaps needing to be addressed vs. those that can be designed around with less certainty.

Preliminary model development should be approached as a directional study intended to address the following questions:

1. Does the site meet the closure criteria for known site conditions (developed based on available data), and satisfy critical risks?
2. Does the site meet the closure criteria for worst-case conditions for model inputs with insufficient data or unknowns?

Addressing these questions may require model refinement and additional data input.

Knowns: stability model development using available historical data

The data identified for the CSM and general site history tend to be the primary focus, since most of the information on how a TSF was constructed and its general performance provides information on current TSF conditions. Model development should begin by identifying the critical areas within the TSF. For

stability analyses, this may include areas with the tallest or steepest embankment slopes, or areas with known layers of weaker materials or higher water levels. In some cases, the selected portion of the TSF used as the base case model, may externally appear to be a critical slope based on topography or dam height but may not be an area with the most critical subsurface conditions. For these conditions, one efficient approach is to develop a single model that is a hybrid of the two conditions, pairing the critical topography or geometry from one portion of the TSF with the critical subsurface conditions from another area to create a worst-case model that checks both conditions for stability. This is an example where model refinement is anticipated, but if the results meet the closure criteria, additional model refinement may not be necessary. If the results do not meet the criteria, more detailed, separate models for each condition should be prepared to evaluate and compare whether they meet criteria on their own.

Starting with generalized conservative models that qualitatively evaluate a range of conditions for legacy sites with data gaps and uncertainties, and refining the models in later iterations is an efficient way to develop preliminary models and identify key risks and closure objectives for the site. For example, if multiple data gaps for material properties important to the model are assumed to have low strength and no failure surfaces pass through these materials, it may be an indication that the known data is needing more refinement compared to the unknowns. These models should start with high level, general expected conditions, and be refined after preliminary analyses with more granular data inputs and newly collected information. Selected model inputs should be compared to expected/published values to draw comparisons against different data sets for the same parameters.

For example, strength parameters from triaxial or direct shear laboratory test results compared with calculation of strength parameters using field data tests or correlations for standard penetration tests (SPTs). These lab and calculated values should be compared to typical empirical values for similar materials. At this stage, the modeling team needs to evaluate what is an appropriate minimum or representative lower bound for model inputs to select, which will change for each parameter and sometimes for each material depending on the data reviewed. Either the most conservative value of the site data and typical comparison values can be selected for analysis, or the highest quality or quantity data could be used, even if it's not the most conservative option. This will either lead to very conservative base case models, or less conservative with additional sensitivity analyses to evaluate more conservative parameters. Regardless of the approach, it is important to evaluate each model parameter holistically by cross-checking each parameter with overall site knowledge and asking the following questions:

- Is there agreement between multiple data sources for each parameter? (e.g., field data, laboratory data, and typical values)
- Does each model input fit with the overall site understanding? (e.g., does model geometry align with known construction methods such as upstream, centerline, or downstream)

Additional data gaps may be identified in this step as data is reviewed in detail for development of the base case models. If the stability analysis results meet the closure criteria, it is important to run additional sensitivity analyses to check for potential site conditions that may not meet the criteria. Alternatively, if the results of base case analyses do not meet the criteria, back-calculation analyses can be used to identify site conditions that would meet the criteria.

Unknowns: model sensitivity analyses or back-calculation

After development of a CSM using available site data, sensitivity stability analyses should be prepared to evaluate data gaps, limited data sets, or other uncertainties identified during the historical data assessment and base case model development process. Sensitivities should evaluate key risks identified for the site. For example, if seismic liquefaction of tailings is a key risk, sensitivity analyses for post-earthquake stability should encompass potential worst-case scenarios, such as a reduced liquefied residual strength or increased saturation levels leading to more liquefiable tailings. If there is not enough data to complete a liquefaction analysis for the tailings, or if the liquefaction analysis is inconclusive, sensitivity analyses should also evaluate a maximum extent of liquefied materials or lower-bound liquefied residual strengths for tailings as well. The scale of the sensitivity analysis should be relative to the level of uncertainty for the model parameter that is being adjusted in the analysis. For parameters with high levels of uncertainty it is most efficient to model a lower bound worst-case scenario, rather than modeling a less conservative but more realistic scenario. This approach allows the modeler to quickly identify whether the parameter with a high level of uncertainty controls stability.

In some cases, sensitivity results meet the design criteria. For these scenarios the sensitivity analysis helps increase the level of confidence in meeting design criteria, even when data gaps may be present for the TSF. The results of the sensitivity analyses that do not meet closure criteria should be used to identify critical data gaps; if a change to a specific parameter results in an analysis that does not meet the closure criteria, that data gap is a critical data gap. Identification of critical data gaps can inform a targeted field investigation to fill the critical data gaps, or focused conceptual closure design alternatives, depending on whether the Owner decides to collect more data or proceed with closure design. For the data with a higher degree of confidence, the decision on addressing this sensitivity for closure will look different than for gaps where there is limited confidence for which back-analysis may better inform on feasibility of achieving satisfactory results.

If the base case does not meet the closure criteria, the components of the model should be reviewed to identify which component is most critical in causing the analysis to not meet the closure criteria. The identified component can then be back-calculated for a minimum input that would result in the analysis meeting the criteria. The back-calculated parameter should be checked against the available data or typical

values to verify it is a realistic value that could exist for the site, if more data were available. This check can help inform whether additional field investigation could be used to fill data gaps and run updated analyses that have the potential to meet the closure criteria or not. If the back-calculated parameter appears to be unrealistic for the existing conditions at the site, it may be more prudent to begin developing a conceptual closure design that would modify the TSF to meet the criteria.

Moving ahead: design or assessment of data needs

Once uncertainties and the impacts on stability are known, effective management for the end goal of closure can proceed. Comfort with the range of results derived from sensitivity analyses will inform the path forward. If conservative modeling within a reasonable range of parameters shows the TSF meets closure criteria, and the closure design team is comfortable with the results, additional steps may not be necessary. Alternatively, if modeling leaves results that are marginal or insufficient, in most cases the engineer will recommend that more data collection will be necessary to reach a place of confidence with models that represent reasonably true conditions. Data collection may include updated surface topography, geotechnical test pitting, drilling, sampling, or laboratory testing to verify assumptions or expand existing data sets.

In most cases, the key considerations for an Owner are the estimated costs and schedule for detailed data collection. GISTM compliance typically proceeds based on a set schedule based on the Owner's risk profile for sites. Depending on the cost and other risks associated with field investigations, an Owner may weigh this against simply designing stabilization measures using conservative stability model parameters to forgo the cost and delays associated with prolonged geotechnical investigation and analyses. For example, a gap showing global stability failure of foundation material could be potentially mitigated by laying back slopes at shallower angles instead of trying to characterize the foundation material in more detail. Large field programs coupled with follow-on data collection and updates to analyses can have significant impacts on schedule targets for overall compliance. Another consideration for field investigations is evaluating whether the data that could be collected in the field is likely to change the conservative model outcome which is where the back analysis plays an important role. If back-analysis results are unrealistic compared to expected or typical TSF properties, it is unlikely that field investigation will provide value in meeting closure criteria, and stabilizing measures will be necessary, regardless of the data gaps.

For the purposes of the planning an investigation, the engineering team must think strategically about the key data that will most benefit the gaps in the current stability models. The team should think long-term about questions that may arise not only during the next revision phase of the analyses but also details that may become critical during a future design phase. In many cases, questions around remaining saturation of old tailings deposits are key because this influences both static and post-earthquake stability. Estimates for

undrained strengths of saturated tailings also tend to be a key parameter for development of stability models. This process of using the field collected data can be iterative with multiple rounds of investigation and analysis updates necessary to address gaps satisfactorily prior to beginning closure design. However, as described above, the Owner should consider the option of beginning closure design with conservative models, even when some data gaps may remain. It is sometimes more efficient to develop a conservative closure design instead of completing additional field investigations until all data gaps are filled.

Risk tolerance and specific site goals dictate how this last step is addressed, and a collaborative effort between the TSF management team (Owner's) and the engineering team is critical to shaping the most efficient closure path to reach the closure objectives. Better and more information is always preferred, but professional judgement informed by a thorough analysis approach can help move a site to completion if all parties are motivated to answer the key questions within the framework of what needs to be resolved and what can remain unknown.

Conclusion

Closure of legacy TSFs can be a lengthy process with limited historical data, but to comply with GISTM, many sites have a limited timeframe to achieve compliance. These timelines can be challenging to meet when questions arise that were not anticipated or built into the analysis approach. In particular, TSF embankment stability is among critical closure risks. Closure planning for legacy sites should begin with identification of the closure criteria based on relevant guidelines, regulations, and Owner goals. After identification of the closure criteria, historical data is collected and assessed to identify data gaps prior to developing preliminary CSMs. CSMs should be developed using site data identified during the historical assessment, and sensitivity analyses should be completed to evaluate the potential range of conditions that meet closure criteria and identify critical data gaps. The CSM and sensitivity analyses may show that the site meets the closure criteria and does not require additional action.

If the CSM does not meet the closure criteria, parameters that would meet the criteria should be back-calculated to set expectations and objectives for field investigation or stabilization measures. Results of the conceptual model, sensitivity analyses and back-calculations, if completed, should then be used to decide whether to conduct targeted field investigations, or to begin closure design with conservative assumptions. If completion of additional field investigation and updates of analyses are warranted, it may be an iterative process depending on closure objectives and available schedule.

Although some stakeholders may want to know every TSF site detail, this may not always be the best and most efficient path to effective risk mitigation for site closure. TSF closure designed to mitigate the worst-case scenario in a cost-effective and timely manner to meet GISTM compliance goals is also a viable path forward. As we advance the state of practice and follow new Best Practice guidelines, filling

critical data gaps or demonstrating closure with thorough and conservative analyses should be a primary focus ahead of filling all data gaps for legacy TSFs.

References

Global Industry Standard on Tailings Management (GISTM) 2020. *Global Tailings Review.* Accessed 6/14/2024 at: https://globaltailingsreview.org

Enhancing the Safety of Tailings Dams: An Updated Approach in Fault Tree Analysis and Probabilities

Geinfranco Villalta, Stantec, Peru
Raquel Borja, Stantec, Peru

Abstract

The complexity and scale of tailings dams, along with recent catastrophic failures, highlight the need for advanced risk assessment methodologies. This study presents an updated probabilistic analysis of tailings dam failures using fault tree analysis (FTA), incorporating recent data from failure incidents and integrating contemporary failure probabilities.

A comprehensive review of tailings dam failure databases was conducted to identify prevalent failure modes and critical vulnerabilities. A sensitivity analysis was applied to the updated FTA model, identifying key events that significantly influence the overall failure probability and providing a dynamic risk assessment framework adaptable to changing conditions.

The research concludes with strategic recommendations for enhancing dam stability, including design innovations, structural modifications, and improved monitoring protocols. The methodology's effectiveness is demonstrated through a case study, advancing the field of tailings dam risk assessment and contributing to the prevention of future failures.

Introduction

Tailings dams are critical in mining operations, storing byproducts from mining processes. However, their potential for catastrophic failure poses significant environmental and economic risks. Recent failures, such as the 2015 Bento Rodrigues and 2019 Brumadinho disasters in Brazil, underscore the urgent need for enhanced risk assessment methodologies.

This paper enhances tailings dam safety through an updated FTA integrated with recent probabilistic data. By recalibrating risk factors with current incident data and applying sensitivity analysis, the study offers a dynamic risk assessment framework that identifies key vulnerabilities and informs better design and management practices.

Through a comprehensive review of failure databases, the updated FTA model systematically maps potential failure mechanisms, providing insights that guide strategic recommendations for improving dam

stability. This research advances the field by offering a robust methodology for predicting and preventing failures, contributing to the long-term safety and reliability of tailings storage facilities.

Background

Tailings dams are vital structures in mining, designed to store byproducts of operations. Their failure can result in catastrophic consequences, including loss of life, environmental damage, and significant economic costs. Historical data, such as the 2015 Bento Rodrigues and 2019 Brumadinho disasters, highlight the frequency and severity of these failures, emphasizing the need for rigorous risk assessment and management practices. Databases like the WISE-Uranium Project provide continuous updates on major failures, underscoring the ongoing risks.

Traditional risk assessment methods, like deterministic approaches, evaluate dam stability under specific conditions but often overlook uncertainties in geotechnical properties and loading. Probabilistic Risk Assessment (PRA) offers a more advanced approach by incorporating variability and uncertainty, allowing for a comprehensive understanding of risks through statistical analysis and probability distributions.

FTA is a prominent risk assessment technique for complex systems like tailings dams. It uses a top-down approach to identify and quantify the causes of failure, providing valuable insights into critical components and weak points. Studies by Hartford and Baecher (2004), along with recent advancements by Taguchi (2014) and De La Cruz (2017), demonstrate FTA's effectiveness in improving safety protocols. By focusing on primary failure modes such as earthquake-induced failures, overtopping, and slope instability, FTA supports the development of robust mitigation strategies, advancing the safety and reliability of tailings storage facilities.

Failure tailings dam events

The history of tailings dam failures is marked by numerous catastrophic events with significant environmental and human impacts. According to the International Commission on Large Dams (ICOLD), the primary causes of these failures – overtopping, slope instability, earthquakes, foundation issues, seepage, and structural failures – have evolved over decades.

Recent analyses using databases like the CSP, WISE Uranium Project, and World Mine Tailings Failures database offer detailed records on incidents, including mine locations, dam types, and failure causes. These resources, though not exhaustive, are critical for identifying trends and risk factors. By integrating data from these comprehensive sources, this research aims to develop targeted mitigation strategies and improve safety standards in the mining industry, thereby reducing the risks of future catastrophic events.

Understanding the historical context and evolving nature of tailings dam failures is essential for enhancing the safety and reliability of these structures. This research contributes to the ongoing effort to prevent future incidents and strengthen risk management practices in the mining sector.

Main failure modes identified

The classification of tailings dam failure modes has evolved significantly, incorporating a deeper understanding of their causes and interactions. Taguchi (2014) refined this classification into five key failure modes: overtopping, static liquefaction, internal erosion, static slope instability, and seismic slope instability. This classification aligns with previous studies while adding nuanced perspectives on event triggers and interrelations.

Rico et al. (2008) expanded the database on tailings dam failures, identifying additional factors such as mine subsidence, unusual rain, snowmelt, and poor management practices. They emphasized the prominence of slope instability, overtopping, and earthquakes, especially in upstream-constructed tailings facilities. This highlights the need for comprehensive risk management approaches.

Stark et al. (2022) and De La Cruz (2017) further corroborated these findings. Stark et al.'s (2022) analysis emphasized the importance of robust seismic design and ongoing monitoring to mitigate seismic instability risks. De La Cruz illustrated the complex interplay between design flaws, operational practices, and environmental factors contributing to failures. These studies underscore the necessity for advanced risk assessment methodologies like FTA to enhance the safety of tailings dams. Therefore, this paper focuses on the three main failure modes: earthquake-induced failures, overtopping, and slope instability.

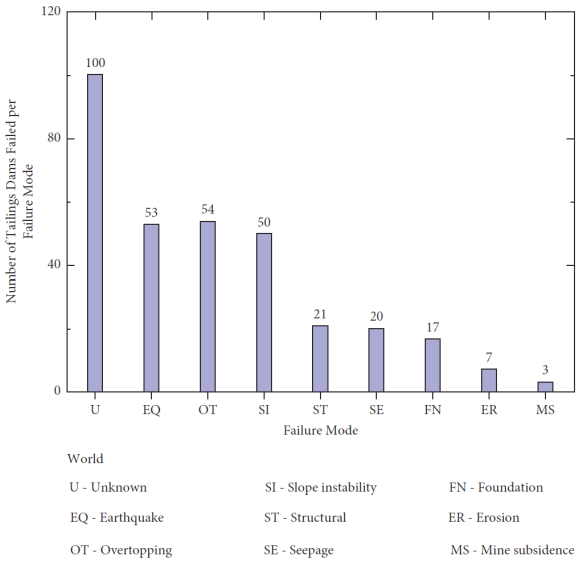


Figure 1: Updated number of tailings dam failed per failure mode in the world (Stark et al., 2022)

Figure 1, adapted from Stark et al. (2022), illustrates the number of tailings dam failures by failure mode. The most frequent causes are unknown (100 incidents), followed by earthquake-induced failures (EQ, 53 incidents), overtopping (OT, 54 incidents), and slope instability (SI, 50 incidents). Other failure modes include structural issues (21 incidents), seepage (20 incidents), foundation problems (17 incidents), erosion (7 incidents), and mine subsidence (3 incidents). This data emphasizes the need for robust design and risk assessment practices to mitigate these common failure mechanisms. For this reason, this paper will focus on discussing the three main failure modes: earthquake-induced failures, overtopping, and slope instability.

Probability of tailings dam failures

The probability of tailings dam failures has evolved significantly with advancements in engineering practices and risk assessment methodologies. Historical failure rates, as reviewed by Silva et al. (2008), have shown a trend towards lower probabilities in well-designed and managed facilities, underscoring the importance of robust engineering and comprehensive safety practices.

De La Cruz (2017) methodology integrates historical data, expert judgment, and advanced probabilistic techniques. Extensive historical failure data provides a foundation for understanding the frequency and types of basic events leading to failures. Expert opinions are elicited to estimate probabilities for events with limited data, based on their experience and understanding of failure mechanisms.

In Taguchi (2014), probabilities of basic events were estimated through historical data analysis, expert judgment, and probabilistic modeling. Historical failure data provided a basis for understanding the frequency and nature of basic events, refined through expert elicitation. Appendix A summarizes the estimated probabilities of basic events for the three main failure modes (static instability, overtopping, and seismic instability).

By integrating historical data, expert insights, and probabilistic techniques, the methodologies developed by De La Cruz and Taguchi provide a robust framework for understanding and mitigating the risks associated with tailings dam failures. This approach ensures probability estimates are reflective of real-world conditions, enhancing the reliability of risk assessments for tailings dams.

Fault tree analysis

FTA is a systematic, deductive failure analysis technique used to identify and evaluate the possible causes of a predefined undesired event, such as a failure in a tailings dam. It involves creating a fault tree, a graphical representation that uses logical gates to map out the pathways leading to the failure (Baecher and Christian, 2003). Each pathway traces back from the top event (the undesired event) to the basic events that contribute to it, allowing for a thorough examination of potential failure causes.

Procedure

The procedure begins by identifying a critical failure, known as the "top level" event, and placing it at the top of the fault tree diagram. From this top event, the possible intermediate causes leading to it are identified and analyzed. Each failure is examined step by step to identify its potential causes, moving to successively lower levels of the system until further analysis is deemed unproductive (ISO/IEC, 2009). Boolean logic is used to combine these lower-level events into the fault tree. A schematic FTA is shown in Figure 2, along with conventional logic gate symbols, is typically used to illustrate the main concepts, although some symbols specific to mechanical systems may be excluded for simplicity.

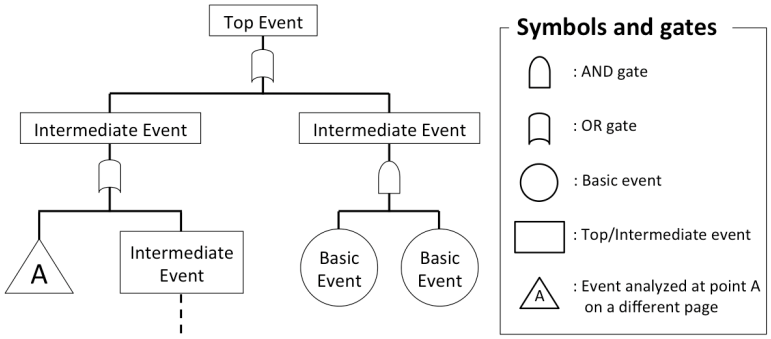


Figure 2: Example of fault tree analysis (Taguchi, 2014)

Boolean algebra for calculation of top event probability

Boolean algebra is used to combine the probabilities of basic events to calculate the total probability of the top event. The process involves using logical gates, primarily AND and OR gates, to represent how basic events contribute to intermediate events and ultimately to the top event.

AND gate

An AND gate represents a scenario where the higher-level event (output) occurs only if all the lower-level events (inputs) occur simultaneously. The probability of the event represented by an AND gate is calculated as the product of the probabilities of its input events. If E_1 and E_2 are the inputs events, the probability of P of the output event occurring is:

$$P(AND) = P(E_1)P(E_2)$$

OR gate

An OR gate represents a scenario where the higher-level event (output) occurs if at least one of the lower-level events (inputs) occurs. The probability of the event represented by an OR gate is calculated using the sum of the probabilities of the input events minus the product of their probabilities to avoid double counting. If E_1 and E_2 are the inputs events, the probability of P of the output event occurring is:

$$P(OR) = P(E_1) + P(E_2) - P(E_1)P(E_2)$$

Subjective probabilities of basic events

In FTA, assessing probabilities for basic events is crucial, especially given the limited data available. Subjective probabilities, often derived from expert judgment, play a significant role and are based on intuition, past experiences, and qualitative beliefs. However, these probabilities are prone to biases such as overconfidence, anchoring, and representativeness, which can affect the accuracy of risk assessments (Baecher and Christian, 2003; Villalta and Borja, 2023). Experiments by Fischhoff et al. (1977) and studies in geotechnical engineering by Folayan et al. (1970) and Baecher (1972) highlight the risks of overconfidence in subjective estimates. Therefore, careful elicitation and consideration of expert judgments are essential. The probabilities in Appendix A, originally defined by Taguchi (2014) and updated by Stark et al. (2022), should be applied with caution, considering site-specific variability.

Application of FTA to analyze the failure of tailings dams

The application of FTA to tailings dam failures involves constructing fault trees for different failure modes, such as seismic slope instability (SS), overtopping (OT), and static slope instability (SI). Appendix B presents the fault trees constructed for these primary failure modes. Table 1 shows the probability of failure for each mode, calculated based on the probabilities established in Appendix A and applying Boolean algebra within the FTA framework.

Table 1: Outcomes for probabilistic analysis of FTA

Failure mode	Probability of top event
Static Instability (SI)	1.7×10^{-4}
Overtopping (OT)	1.1×10^{-4}
Seismic Stability (SS)	2.3×10^{-6}

These results highlight the likelihood of failure for each mode, providing a quantitative basis for understanding the risks associated with tailings dam operations. By constructing detailed fault trees and systematically analyzing the probabilities of basic events, FTA enables a comprehensive assessment of potential failure scenarios and their impacts. This methodical approach is essential for identifying critical vulnerabilities and implementing targeted risk mitigation strategies to enhance the safety and reliability of tailings dams.

Sensitivity analysis

Sensitivity analysis is a critical component of the probabilistic risk assessment framework, providing insights into which basic events have the most significant impact on the overall probability of failure. By systematically varying the probabilities of basic events and observing the resulting changes in the top event

probability, we can identify critical factors that should be prioritized in risk management strategies.

Methodology for sensitivity analysis

The sensitivity analysis in this study involves the following steps:

1. **Identify basic events**: Determine the basic events from the fault tree models for overtopping, seismic instability, and static instability.
2. **Vary probabilities**: Systematically vary the probabilities of each basic event within a realistic range based on historical data and expert judgment.
3. **Recalculate top event probability**: For each variation, recalculate the overall probability of the top event (i.e., failure of the tailings dam).
4. **Analyze impact**: Assess the impact of changes in the basic event probabilities on the overall failure probability. This is typically visualized using Tornado plots, which show the relative influence of each basic event.

Define variation ranges

The selection of variation ranges for sensitivity analysis, as detailed in Table 1, was strategically designed to evaluate the fault tree model's sensitivity to changes in basic event probabilities. The chosen ranges (-90%, -50%, -20%, -10%, +10%, +20%, +50%, +90%) cover a broad spectrum of realistic scenarios, from minor adjustments to significant shifts, ensuring the analysis reflects potential real-world conditions (Hartford and Baecher, 2004).

These diverse variation magnitudes help identify non-linear effects and threshold points critical in complex systems like tailings dams. By including both negative and positive variations, the analysis accounts for overestimations and underestimations, providing a balanced risk assessment (Taguchi, 2014; Bowker and Chambers, 2015). The incremental steps ensure comprehensive coverage, capturing both subtle and extreme influences while maintaining probabilities within logical bounds to preserve the integrity of the analysis (Piciullo et al., 2022). These ranges, supported by historical data and expert judgment, enhance the credibility and relevance of the sensitivity analysis results (Stark et al., 2022).

Outcomes

The sensitivity analysis of tailings dam failure probabilities focused on three primary failure modes: static instability, overtopping, and seismic instability. The results provide detailed insights into how variations in basic event probabilities influence the overall failure probability, highlighting critical factors that significantly impact tailings dam stability.

Static Instability

The sensitivity analysis for static instability in tailings dams identified several key basic events that significantly influence the overall probability of failure. The findings emphasize the importance of managing these events to prevent static instability. Figure 3 shows the tornado plot for the sensitivity analysis.

Critical events

- **Over-steepened slope (SI10)**: This event demonstrates substantial sensitivity, particularly at higher positive variations (+50% and +90%). The significant increase in the total probability of static slope instability with higher probabilities of an over-steepened slope underscores the importance of maintaining safe slope parameters. Effective slope monitoring and management are essential to mitigate this critical risk (Stark et al., 2022).
- **Change in material behavior (SI3)**: Like SI10, SI3 shows a notable impact on the overall failure probability, especially at higher variation levels. This finding highlights the necessity of monitoring and managing changes in material behavior to prevent static instability. Understanding and controlling material properties are crucial (Taguchi, 2014).

Moderate impact events

- **Pore pressure increase (SI4)** and **high pool (SI5)**: These events exhibit considerable sensitivity, particularly at higher positive variations. Proper management of pore pressure and water levels within the dam is crucial to maintaining stability. Regular monitoring and proactive measures to control pore pressure and water levels can significantly reduce the risk of static instability (Hartford and Baecher, 2004).
- **Long term degradation (SI6)** and **poor pool management (SI7)**: These events display moderate sensitivity across the variation range, indicating a steady influence on the overall failure probability. Consistent maintenance practices and effective pool management strategies are necessary to mitigate these risks. Ensuring the long-term integrity of the dam structure and proper pool management can prevent gradual degradation (Piciullo et al., 2022).

Lower impact events

- **Susceptible Features in foundation (SI1)**, **unsuccessful detection (SI2)**, **runoff leading to increased water elevation (SI8)**, and **poor management of increased pool (SI9)**: These events show relatively lower sensitivity compared to others. However, they still contribute to the overall

risk, and their probabilities should be carefully monitored and controlled. Addressing these events through targeted risk management practices can further enhance dam stability.

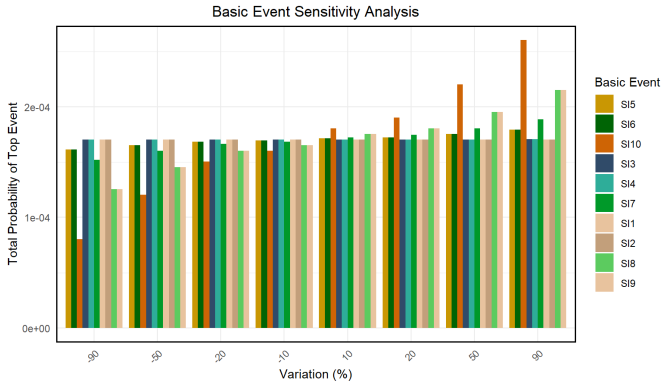


Figure 3: Tornado plot for static instability sensitivity analysis

Overtopping

The Tornado plot for the sensitivity analysis of overtopping in tailings dams provides essential insights into how variations in the probabilities of basic events influence the overall probability of overtopping failure. Figure 4 shows the tornado plot for the sensitivity analysis.

Critical events

- **Head cut advances to upstream surface (OT1)**: This event shows substantial sensitivity, particularly at higher positive variations (+50% and +90%). The significant increase in the total probability of overtopping with higher probabilities of head cut advancing to the upstream face underscores the importance of maintaining the structural integrity of the dam's upstream face. Effective monitoring and intervention are essential to mitigate this critical risk (Stark et al., 2022).
- **High pool (OT4)**: Like OT1, OT4 shows a notable impact on the overall failure probability, especially at higher variation levels. This finding highlights the necessity of maintaining adequate freeboard and effective water management practices to prevent overtopping. Proper management of water levels within the dam is crucial to maintaining stability (Taguchi, 2014).

Moderate impact events

- **Slurry inflow exceeds design capacity (OT5)** and **natural ore variability (OT6)**: These events exhibit considerable sensitivity, particularly at higher positive variations. Proper management of slurry inflow and understanding the variability of ore properties are critical to maintaining stability. Regular monitoring and proactive measures to control these factors can significantly reduce the risk of overtopping (Hartford and Baecher, 2004).

- **Design error (OT7)** and **exceedance of design criteria (OT8)**: These events display moderate sensitivity across the variation range, indicating a steady influence on the overall failure probability. Robust design standards and thorough review processes are necessary to mitigate these risks. Ensuring that the dam is designed to withstand expected loads and operational conditions can prevent design-related failures (Piciullo et al., 2022, 2022).

Lower impact events

- Runoff leading to increased string wind (OT12), earth / rockslide (OT13), high pool (OT14), unsuccessful intervention (OT11), and rapid thaw (OT10): These events show relatively lower sensitivity compared to others. However, they still contribute to the overall risk, and their probabilities should be carefully monitored and controlled. Addressing these events through targeted risk management practices can further enhance dam stability.

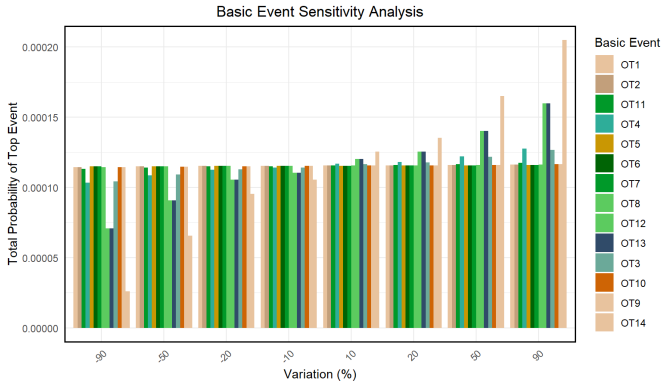


Figure 4: Tornado plot for overtopping sensitivity analysis

Seismic Instability

The sensitivity analysis for seismic instability identified the critical factors that significantly impact the failure probability during seismic events. Figure 5 shows the tornado plot for the sensitivity analysis.

Critical events

- **Ground motion exceeding design parameters (SS9)**: This event demonstrates substantial sensitivity, particularly at higher positive variations (+50% and +90%). The significant increase in the total probability of seismic instability with higher probabilities of ground motion exceeding design parameters underscores the importance of designing dams to withstand expected seismic loads and conducting regular seismic risk assessments (Stark et al., 2022). Ensuring the dam's structural integrity against seismic loads is paramount for preventing seismic instability.

- **Liquefaction (SS3)**: Similar to SS9, SS3 shows a notable impact on the overall failure probability, especially at higher variation levels. This finding highlights the necessity of implementing measures to improve soil stability and prevent liquefaction in seismically active regions (Taguchi, 2014). Effective soil stabilization and reinforcement techniques are essential to mitigate this critical risk.

Moderate impact events

- **Slope steepness (SS4)** and **pore pressure increase (SS5)**: These events exhibit considerable sensitivity, particularly at higher positive variations. Proper management of slope steepness and pore pressure is crucial to maintaining stability during seismic events. Regular monitoring and proactive measures to control these factors can significantly reduce the risk of seismic instability (Hartford and Baecher, 2004).
- **Change in material behavior (SS6)** and **tailing water release from pool (SS7)**: These events display moderate sensitivity across the variation range, indicating a steady influence on the overall failure probability. Ensuring that the dam's materials remain stable under seismic conditions and managing the release of tailing water are essential to mitigate these risks (Piciullo et al., 2022).

Lower impact events

- **Undrained situation (SS1)**, **contractive material (SS2)**, **displacement intercepts pool (SS8)**: These events show relatively lower sensitivity compared to others. However, they still contribute to the overall risk, and their probabilities should be carefully monitored and controlled. Addressing these events through targeted risk management practices can further enhance dam stability (Bowker and Chambers, 2015).

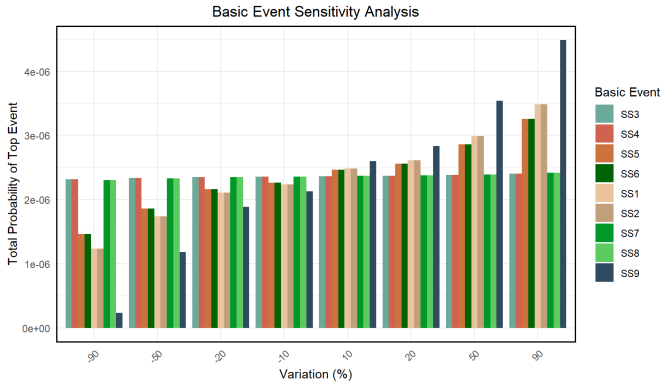


Figure 5: Tornado plot for seismic instability sensitivity analysis

Summary of findings

The sensitivity analysis across the three failure modes – static instability, overtopping, and seismic instability – provides critical insights into the factors that most significantly affect the stability of tailings dams. The key outcomes include:

- The importance of maintaining surface integrity and internal drainage to prevent static instability.
- The necessity of effective water management and drainage maintenance to mitigate overtopping risks.
- The critical need for soil stability measures and robust seismic design standards to address seismic instability.

These findings emphasize the need for targeted risk management strategies that focus on the most influential factors identified through sensitivity analysis. By addressing these critical areas, dam operators can significantly enhance the safety and reliability of tailings dams.

Conclusion

This study offers an in-depth analysis of tailings dam failure probabilities using fault tree analysis (FTA) combined with sensitivity analysis, focusing on static instability, overtopping, and seismic instability. Key findings highlight those specific basic events, such as over-steepened slopes, high pool levels, and ground motion exceeding design parameters, disproportionately impact failure probabilities, emphasizing the need for targeted risk management strategies.

The analysis underscores the importance of maintaining up-to-date probabilistic data, reflecting current conditions for accurate risk assessment. While the probabilities derived from Taguchi (2014) and updated by Stark et al. (2022) provide a foundational basis, their applicability may vary across different sites, necessitating site-specific validation. The study also recognizes that varying one probability at a time in sensitivity analysis may not fully account for interdependencies between variables, suggesting that future research should explore these relationships.

The practical applicability of this methodology is demonstrated through insights into critical risk areas, enabling the development of robust mitigation measures. By implementing these recommendations, the likelihood of catastrophic failures can be significantly reduced, safeguarding human lives, environmental health, and infrastructure integrity. This research advances tailings dam risk assessment by integrating FTA with updated probabilistic data and sensitivity analysis, offering actionable insights for improving dam safety. Future efforts should focus on refining these models and incorporating additional data to enhance the reliability and applicability of the risk assessment framework.

References

Baecher, G.B. 1972. Site exploration: a probabilistic approach. Doctoral dissertation, Massachusetts Institute of Technology.

Baecher, G.B. and Christian, J.T. 2003. *Reliability and Statistics in Geotechnical Engineering.* John Wiley & Sons.

Bowker, L.N. and Chambers, D.M. 2015. The risk, public liability, and economics of tailings storage facility failures. Available at download risk, public liability and economics of tailings storage facility failures PDF

Caldwell, J. and Charlebois, L. 2010, November. Tailings impoundment failures, black swans, incident avoidance, and checklists. *Proceedings of Tailings and Mine Waste 2010.* CRC Press.

Carvajal Arroyo, M.I. 2018. *Desarrollo de una metodología para análisis de estabilidad física de depósitos de relaves.* Universidad de Chile.

CSP. 2024. TSF failures from 1915. Center for Science in Public Participation. Accessed 10 June 2024 at http://www.csp2.org/tsf-failures-from-1915

De la Cruz, S. 2017. *Evaluación del fallo de presas de relaves con el método del árbol de fallos.* Universidad Politécnica de Madrid.

Fischhoff, B., Slovic, P. and Lichtenstein, S. 1977. Knowing with certainty: the appropriateness of extreme confidence. *Journal of Experimental Psychology: Human Perception and Performance* 3(4): 552.

Folayan, J.I., Höeg, K. and Benjamin, J.R. 1970. Decision theory applied to settlement predictions. *Journal of the Soil Mechanics and Foundations Divisio*n 96(4): 1127–1141.

Hartford, D.N. and Baecher, G.B. 2004. *Risk and Uncertainty in Dam Safety*. Thomas Telford.

ISO (International Organization for Standardization). 2009. Risk management: principles and guidelines (31000:2009). Geneva.

Piciullo, L., Storrøsten, E.B., Zhongqiang, L., Farrokh, N. and Lacasse, S. 2022. A new look at the statistics of tailings dam failures. *Engineering Geology* 303: 106657.

Rico, M., Benito, G., Salgueiro, A.R., Díez-Herrero, A. and Pereira, H.G. 2008. Reported tailings dam failures: a review of the European incidents in the worldwide context. *Journal of Hazardous Materials* 152(2): 846–852.

Silva, F., Lambe, T.W. and Marr, A. 2008. Probability and risk of slope failure. *J. Geotech. Geoenviron. Eng.* 134(12): 1691–1699.

Stark, T. D., Moya, L. and Lin, J. 2022. Rates and causes of tailings dam failures. Advances in Civil Engineering. Wiley.

Taguchi, G. 2014. Fault tree analysis of slurry and dewatered tailings management – a framework. Doctoral dissertation, University of British Columbia, Canada.

UNEP. 1998. Case Studies on Tailings Management, United Nations Environment Programme, International Council on Metals and the Environment.

Van Zyl, D., Miller, I., Milligan, V. and Tilson, W.J. 1996. Probabilistic risk assessment for tailings impoundment founded on Paleokarst. In *Uncertainty in the Geologic Environment: From Theory to Practice:* 563–585. ASCE.

Vick, S.G. 1994, October. Geotechnical risk and reliability – from theory to practice in dam safety. *Proceedings of Earth, Engineers, and Education – A Symposium in Honor of Robert V. Whitman:* 45–58. Cambridge: MIT.

Villalta, G. and Borja, R. 2023. Application of Monte Carlo simulation to the probability assessment in FMEA. *Proceeding of Tailings and Mine Waste 2023.* Vancouver, Canada.

Whitman, R.V. 1984. Evaluating calculated risk in geotechnical engineering. *Journal of Geotechnical Engineering* 110(2): 143–188.

WISE Uranium Project. 2019. Chronology of major tailings dam failures. Accessed 20 June 2024 at https://www.wise-uranium.org/mdaf.html

World Mine Tailings Failures. 2024. Accessed 15 June 2024 at https://worldminetailingsfailures.org/

Appendix A

Summary of the probabilities of each basic failure

Table A.1: Probabilities for static instability

Event ID	Description	Probability
SI1	High pool	0.0050
SI2	Long term	0.0050
SI3	Runoff from watershed leads to large increase	0.0100
SI4	Poor management of increased pool	0.0050
SI5	Change in material behavior (phi)	0.0020
SI6	Over steepened slope	0.0020
SI7	Unsuccessful intervention	0.0050
SI8	Susceptible features in foundation	0.0100
SI9	Unsuccessful detection	0.0050
SI10	Condition similar to design	0.0001

Table A.2: Probabilities for overtopping

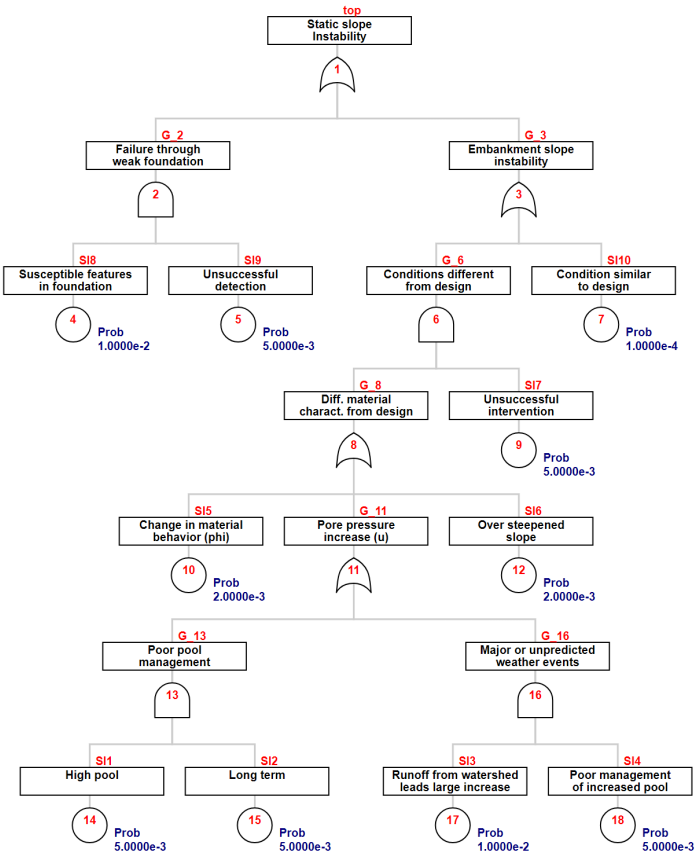
Event ID	Description	Probability
OT1	Head cut advances to upstream surface	0.0100
OT2	Head cut formation	0.0200
OT3	Crest deformation	0.0025
OT4	High pool	0.0050
OT5	Slurry inflow exceeds design capacity	0.0050
OT6	Natural ore variability	0.0050
OT7	Design error	0.0050
OT8	Exceedance of design criteria	0.0100
OT9	Heavy rain exceeds PMP	0.0100
OT10	Rapid thaw	0.0100
OT11	Unsuccessful intervention	0.0050
OT12	Strong wind	0.0100
OT13	Earth/Rockslide	0.0010
OT14	High pool	0.0050

Table A.3: Probabilities for seismic instability

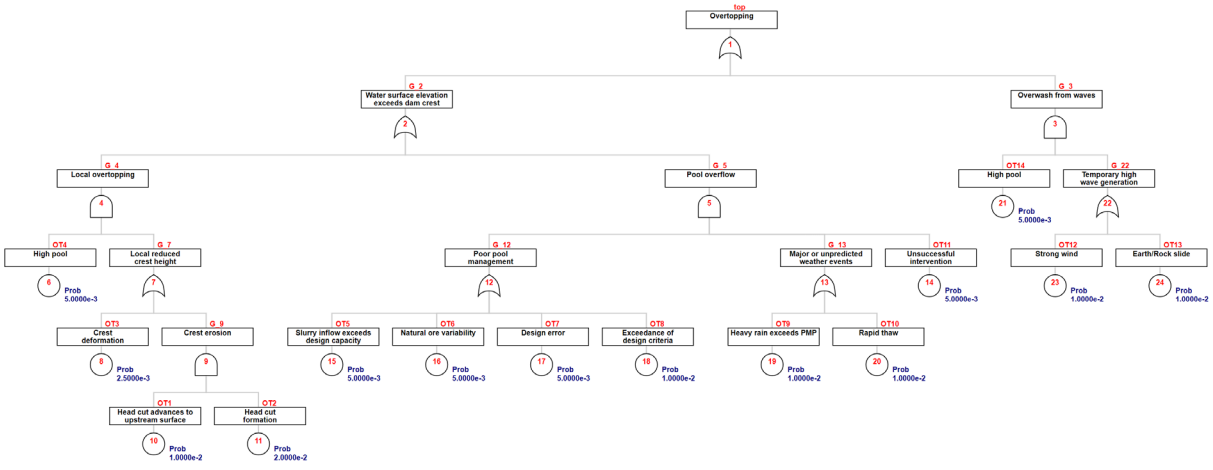
Event ID	Description	Probability
SS1	Contractive material	0.0500
SS2	Undrained situation	0.0050
SS3	Pore pressure increase due to seismic loading	0.0050
SS4	Slope too steep	0.0020
SS5	Displacement intercepts pool	0.0200
SS6	Differential horizontal displacement	0.0100
SS7	Crest deformation	0.0025
SS8	Seiche	0.0050
SS9	Ground motion exceeds design condition	0.0050

Appendix B

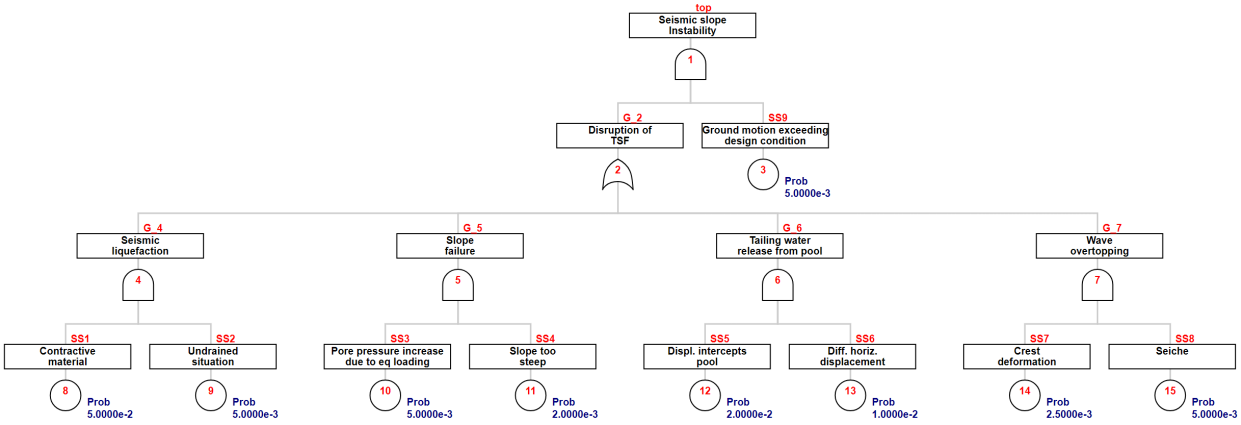
Fault tree analysis for static instability



Fault tree analysis for overtopping



Fault tree analysis for seismic instability



Analysis of the Deformation and Cracking Mechanism of the Itabiruçu Dam – Case Study

Paulo Cella, BVP Geotecnia e Hidrotecnia, Brazil
Carlos Santos, BVP Geotecnia e Hidrotecnia, Brazil
Felipe Neiva, BVP Geotecnia e Hidrotecnia, Brazil
Laura Rodríguez, Ex-BVP, Brazil

Abstract

This work aims to understand the dominant displacement mechanism that resulted in a set of longitudinal cracks, a few tens of meters long, that affected the Itabiruçu Dam, Conceição Mine, Itabira Complex, Minas Gerais, Brazil The dam is currently 71 meters high and has a crest length of around 920 meters. The appearance of cracks caused the fourth dam raise to be halted for over 2.5 years, starting in mid-2019. A significant number of field and laboratory investigations, as well as a comprehensive monitoring program implemented after construction was halted, produced a rich data set, which in this article is subjected to a careful analysis of the actual displacements caused by differential settlements of the foundation beneath the downstream shell of the dam. In addition to looking into the numerical model results (on which this paper is not specifically focused) as a basis for the monitoring evaluation, a comparison was also made with a finite element classical study (Clough and Woodward, 1967), in which the construction of an idealized dam in several stages is appraised by assigning material deformability within a range of contrasting embankment/foundation stiffness ratios. In the case study presented herein, the vertical-to-horizontal displacement ratio was found to be more likely to correspond to the pattern of components associated with the gravitational dam settlement as an isolated mechanism, rather than a potential underlying foundation shear band development.

Introduction

Loading effects in compacted soil embankments can lead to anomalies that affect the physical stability of a facility during operation and decommissioning. According to Silvera (2006), construction-related issues can develop depending on the rate at which the embankment is built on a saturated foundation or differential stiffnesses occurrence contrasts between the embankment and the foundation.

Clough and Woodward (1967) studied the pattern of displacements induced along the embankment-foundation interface of an earth dam in idealized gravity settlement models, based on different stiffness ratios between these materials, considering incremental and single-stage loading. The results showed that the distribution of horizontal and shear stresses at the embankment-foundation interface, as well as vertical and horizontal displacements, are significantly affected by the stiffness contrast between embankment and foundation.

Poulos and Davis (1972) also arrived at similar conclusions, by normalizing the displacements based on the displacement influence factor concept proposed by Poulos et. al (1972), which differs according to construction stages.

This paper presents the case of the Itabiruçu Dam (Figure 1). The dam has had a history of surface cracks. The study attempted to investigate whether the cracks were due to differential gravitational settlement, or horizontal displacement along a potential deep shear band, at the embankment-foundation interface.

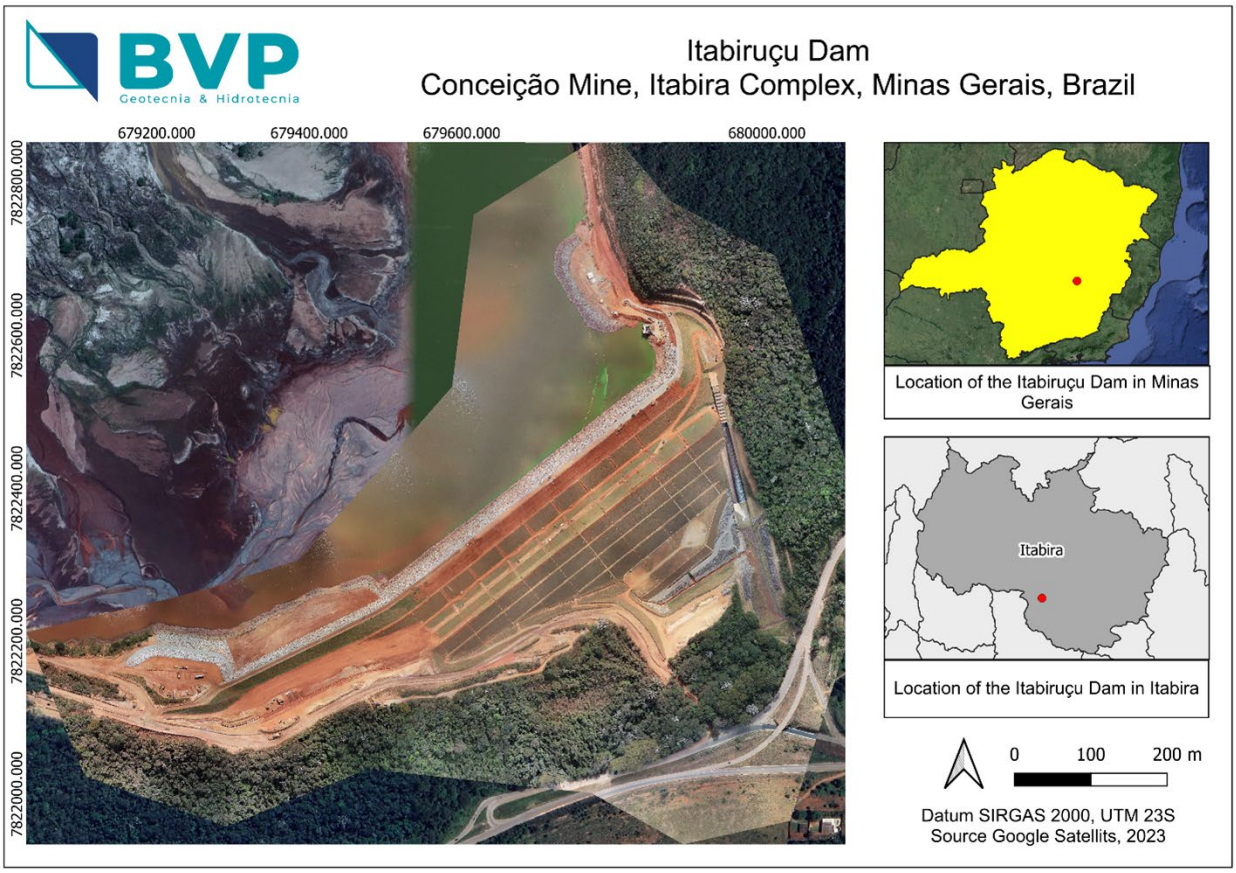


Figure 1: Location of the Itabiruçu Dam (source: Google Satellites)

Key facts about the most recent raise of the dam

Itabiruçu Dam was built at Conceição Mine, Itabira Complex, Minas Gerais, Brazil, to store iron tailings generated and provide water for ore processing. The starter dyke was built circa 1980/1981 to a crest elevation of 812.0 m. During operations, the dam has undergone four downstream raises: in 2004, to elevation 817.5 m; in 2011, to elevation 833.0 m; in 2016, to elevation 836.0 m; and in 2023, to elevation 841.0 m.

The last-mentioned raise was started in 2018, and was planned to reach an elevation of 850.0 m. However, in July 2019, after the crest reached an elevation of 819 m, construction was preventively halted following the appearance of centimetric lengthwise cracks, close to the contact between the previous raise and the new one (see Figure 2), as well as cross cracks at the left abutment. Construction resumed in May 2022 after a comprehensive field investigation program was carried out, monitoring instruments installed, and numerical simulations performed to understand the displacement mechanism. Construction was completed in July 2023, to a modified design crest elevation of 841 m, and guidelines were set out to control the rate of rise, and to establish a threshold settlement for the structure.

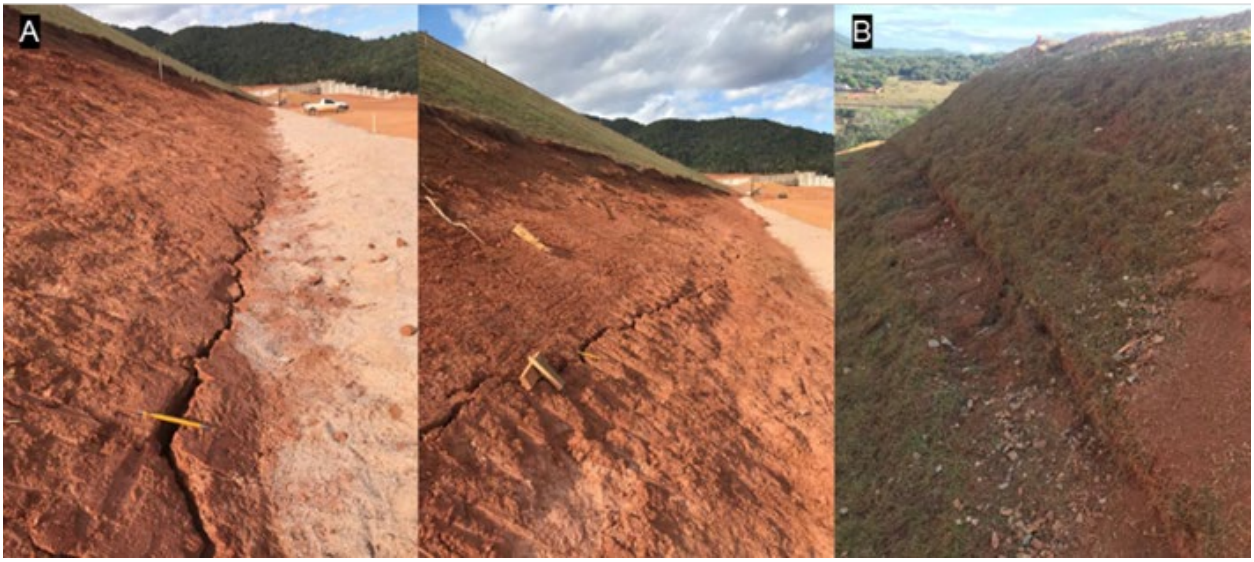


Figure 2: A) Cracks on the downstream dam shell, at the contact between the previous raise and the new one (Berm el. 818 m); B) Left abutment cracks (source: own archive)

A comprehensive field investigation program was carried out, and monitoring instruments installed. This allowed for enhanced knowledge on both foundation conditions and behavior, and evolution and gradual stabilization of facility movements. Among the studies was the numerical simulation of the dam with undrained foundation, in which constitutive model selection, mesh sizes, and medium discretization refinement, as well as important distinctions of geotechnical foundation units sectorization, were thoroughly discussed and enhanced over more than two years of work, with various professionals having

been engaged, including designers, EoR, client, Public Prosecutor's Office auditors. Stiffness, compressibility, and hydraulic conductivity parameters of the embankments were adjusted in several stages, in order to replicate the decreasing settlement rates and the piezometric levels established. The numerical model was accurately calibrated, hence data value and reliability for interpretation of dominant deformational mechanism and facility behavior trend in the medium term, as long as no significant changes occur in the patterns identified to date.

Geological-geotechnical foundation condition

Geological-geotechnical data on Itabiruçu dam is based on several site investigation programs performed during dam design and raise phases (Figure 3).

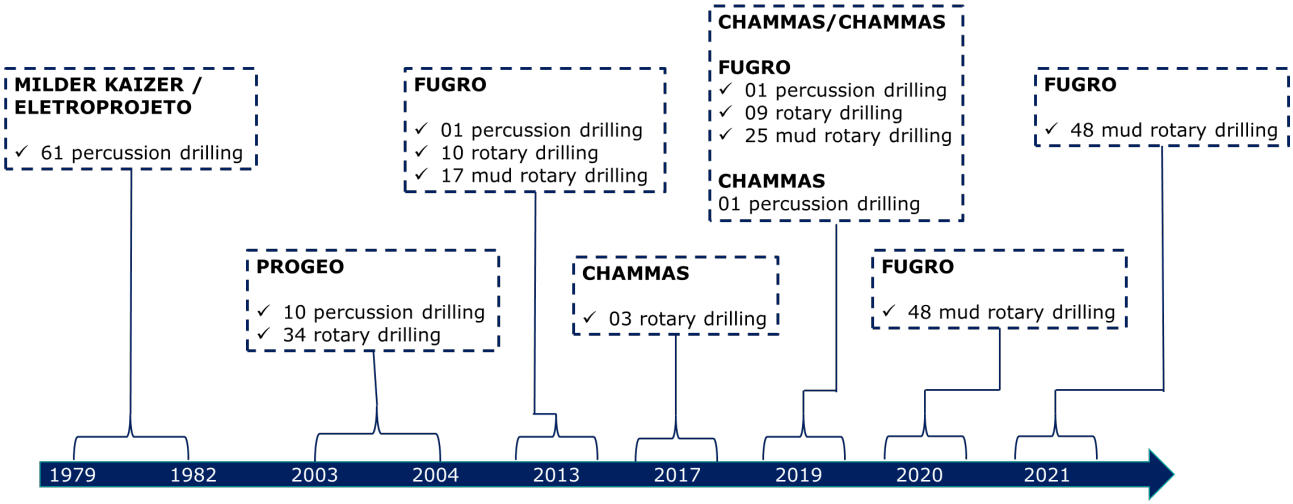


Figure 3: Itabiruçu dam investigations timeline (source: BVP, 2023c)

The dam footprint comprises weathered rocks and soils from Nova Lima Supergroup schists and Guanhães Complex migmatite gneisses. Schists occur predominantly at the dam toe and on the left abutment. They can include mafic schist, steatite, and serpentinite (talc-schist), usually as saprolite, saprolite and residual soil, generally clayey. Gneiss, on the other hand, outcrops mainly as saprolite soil along the right abutment and central portion of the dam. Within this area, large saprolite thicknesses were encountered in the boreholes, underlying clayey-sandy to sandy-clayey saprolite soil, with felsic bands. In total, there are about 7500 meters of boreholes, five CPTs, and over fifty in situ? strength tests.

Geological-geotechnical units

The geotechnical units under the Itabiruçu Dam footprint were carefully characterized following the assessment of the site investigation data. Two gneiss saprolite units were identified: a saprolite soil / young residual soil, referred to as “SAC” underlain by a well-structured saprolite soil, referred to as “SSG”. SAC

is a more compressible and less permeable unit than SSG. It has lower strength parameters and develops excess pore pressure during shear up to the maximum deviatoric stress. SSG has been shown to dissipate partly or totally the excess pore pressures in undrained triaxial tests.

These two subunits were differentiated by applying double corrections to the SPT blow count (N_{SPT}) obtained from drilling programs, especially from 2013 onwards. The corrections were required to account for the significant increase in confinement (due to placement of 40 to 45 m of embankment) compared to in situ testing carried out in 1977, 1983, and 2004, which were drilled on native ground or minor embankments, and also to account for energy losses due to much longer string lengths. Correction due to confining stress used the methodology proposed by Boulanger (2003), specific to low-plasticity silty soils (correction index lower than sand index), in order to obtain NSPT values in conditions comparable to those of the boreholes drilled in earlier investigation phases. On top of these two corrections, an additional factor of 0,7 concerning the energy efficiency. For SAC, $N_{SPT} < 10$. For SSG, $10 \leq N_{SPT} \leq 35$.

The prominent heterogeneity of saprolite horizons, with varying textures (from clayey to sandy soils) and colors, favors the adoption of a correction parameter for N_{SPT}, at the expense of reduced assertiveness in tactile-visual differentiation from the drill cores.

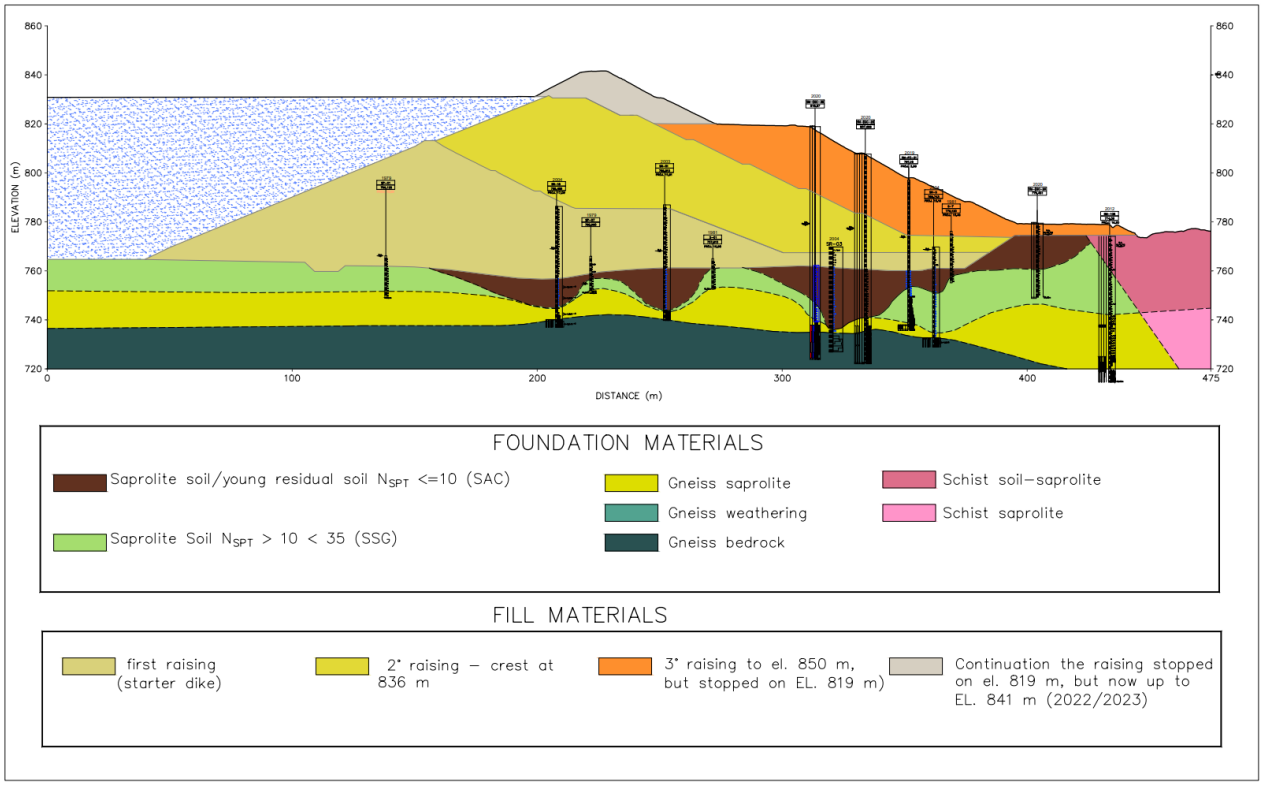


Figure 4: Sections with adjusted NSPT values, differentiating two saprolite soil horizons, one with NSPT <10 and the other with 10> NSPT <35 (source: BVP, 2023c)

The section in Figure 4 identifies the two units, SAC (in brown) overlying the less compressible soils SSG (in green). The thickness of the SAC soil ranges from 5 to 25 m, whereas the SSG ranges from 7 to 30 m. A slightly altered gneiss saprolite underlies the saprolite layer. The thickness of the saprolite ranges from 5 to 15 m. The other foundation materials are also presented.

Settlement basin

The settlements large-scale pattern in the downstream shell, as measured from the prisms/survey monuments, was shaped like a bow (or basin). The center of the basin coincided with the lengthwise crack observed at the contact between the existing embankment and the new raise. Figure 5 plots the vertical displacements over the monitoring period (from 2019 to 2023). Ranges of accumulated vertical displacement (15 to 100 mm; 100 to 300 mm, and greater than 300 mm) are shown in different colors, for reference. A maximum settlement of 420 mm was reached during the stabilization phase, before construction was resumed, and over 500 mm was reached during the final raise to the crest at elevation 841 m, starting from the downstream plateau, halted in 2019 at elevation 819 m. As a result, a 38 m wide berm was shaped along the downstream slope (Figure 4).

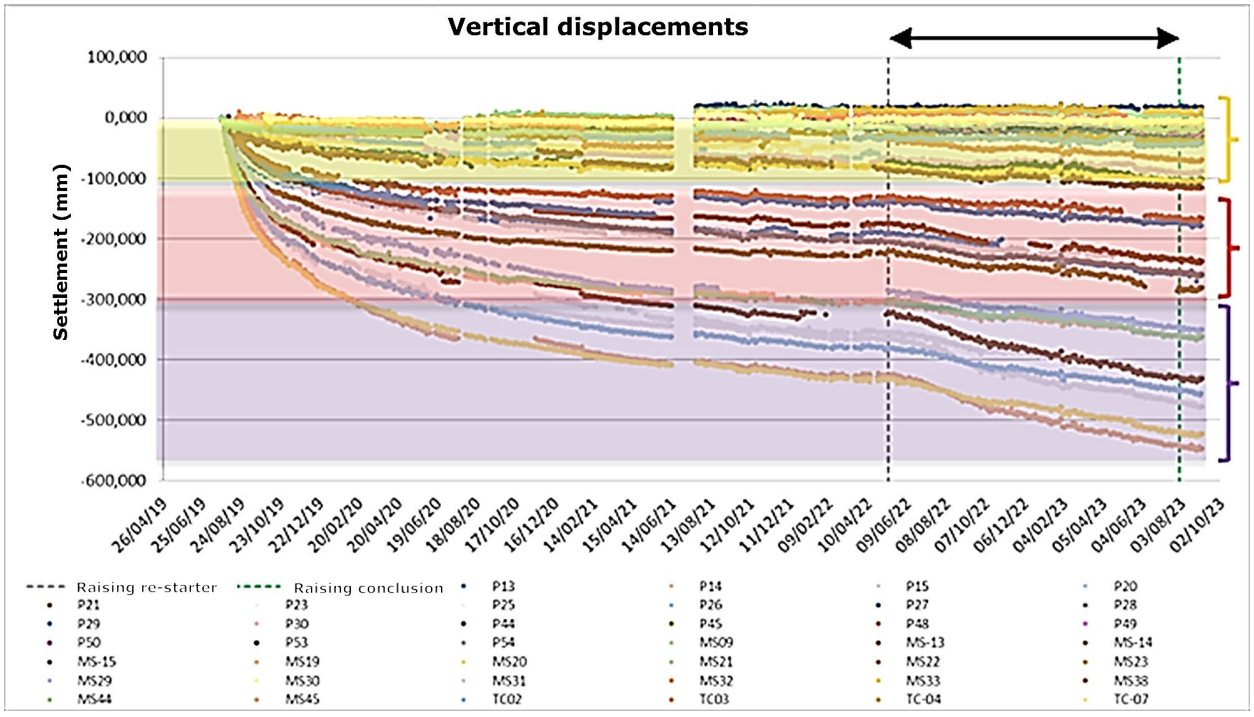


Figure 5: Prisms and survey monuments – full monitoring period – accumulated settlement. double arrow indicates works resume period (source: BVP, 2023c)

The data shows a gradual slowdown in the settlement rate during the first few years of monitoring. The decreasing settlement rate was used to calibrate the numerical model. Note that monitoring only started about two months after construction was stopped, in 2019.

Figure 6 plots contours of accumulated settlement measured from August to October 2019. The arrows plot the direction and magnitude of the horizontal displacement component at each instrument location. The contours and arrow pattern indicate the existence of a settlement basin. Figure 7 shows the settlement basin six months after construction was completed, in July 2023. The instruments MS-19 and MS-20 located at the center of the basin show vertical displacements of 548 mm and 523 mm, respectively, with full stabilization yet to be achieved.

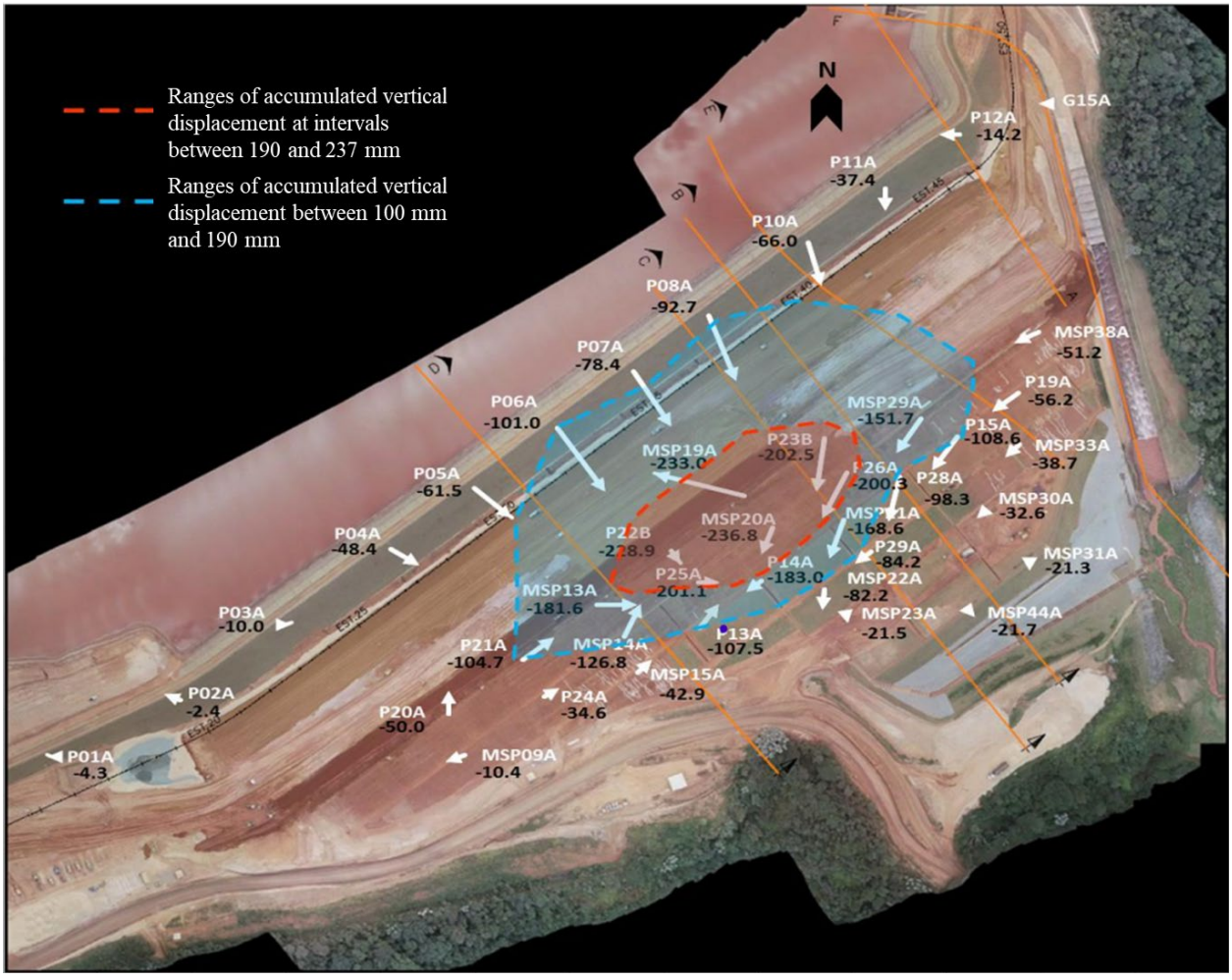


Figure 6: Settlement basin identified, considering monitoring from August to October 2019. The arrows indicate the direction and magnitude of the horizontal displacement component at each instrument location (source: BVP, 2019b)

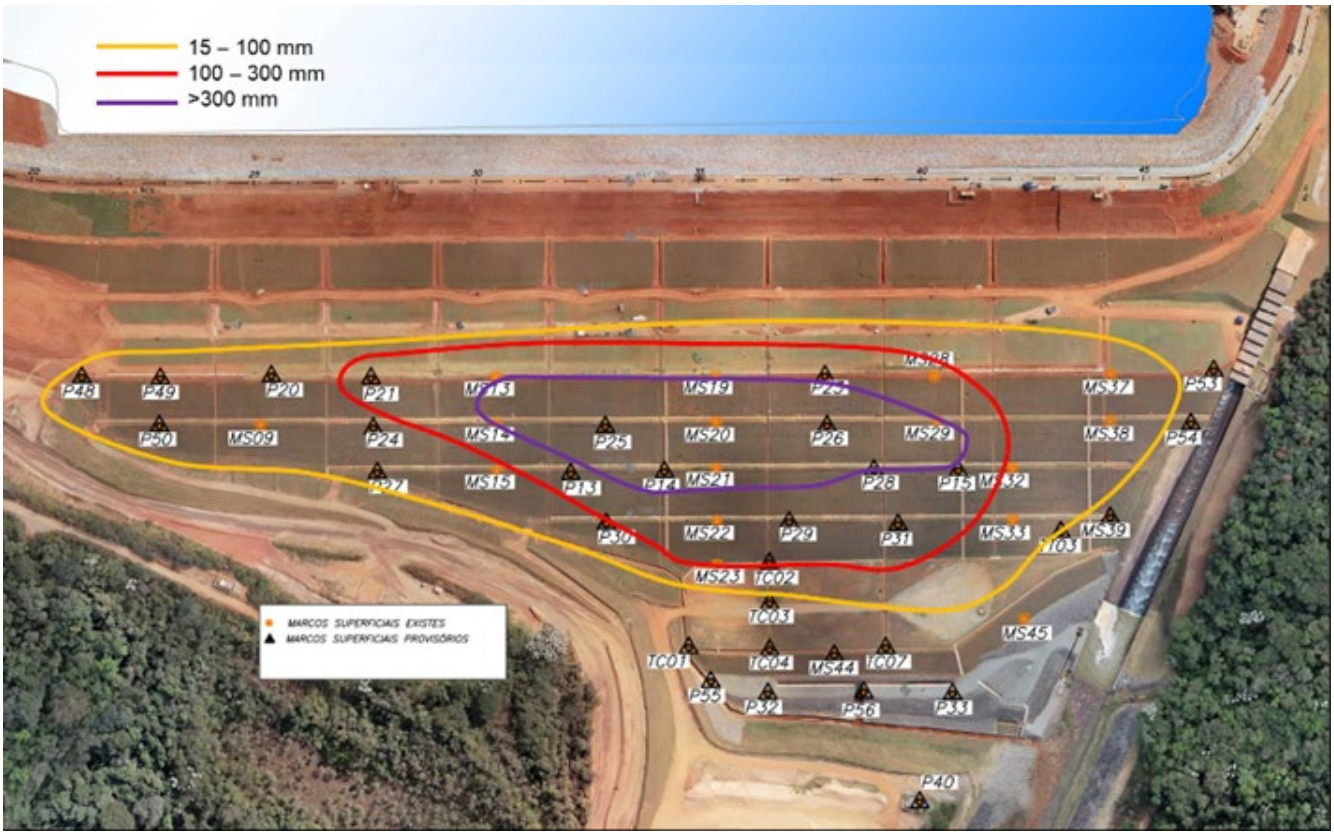


Figure 7: Settlement basin for the monitoring period between 2019 and mid-2023 (source: BVP, 2023c)

Theoretical reference model

Clough and Woodward (1967) developed a theorical model to evaluate the effects of embankment construction rate. They carried out finite element simulations of an idealized dam under construction in stages (or in a single-stage), assuming foundation to embankment stiffness ratios of 1:1, 1:2, and 1:5 (i.e., the embankment is 1×, 2× or 5× stiffer than a homogeneous foundation). For displacement pattern configuration, the theoretical study assumed a single valued embankment deformability. The dam load was applied as a gravity load in ten steps, up to the final height of the structure.

Figure 8 plots the resulting vertical and horizontal displacements at the base of the dam for the three stiffness ratio cases.

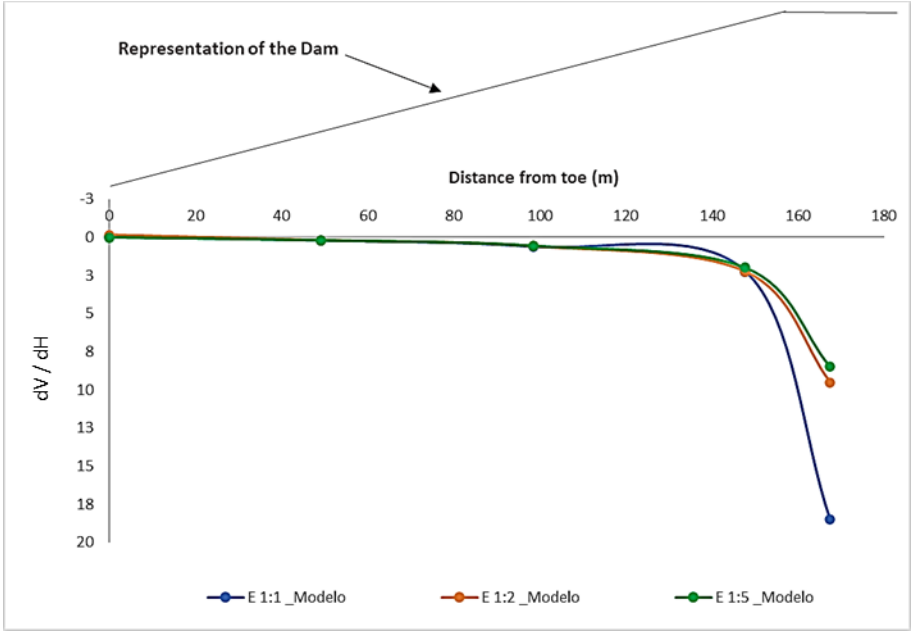


Figure 8: Vertical to horizontal displacement ratio (dv/dh) for different embankment-foundation stiffness ratios (Source: adapted from Clough and Woodward, 1967)

To apply the Clough and Woodward (1967) model to Itabiruçu Dam, the vertical displacements were divided by the horizontal displacements, as shown in Figure 9.

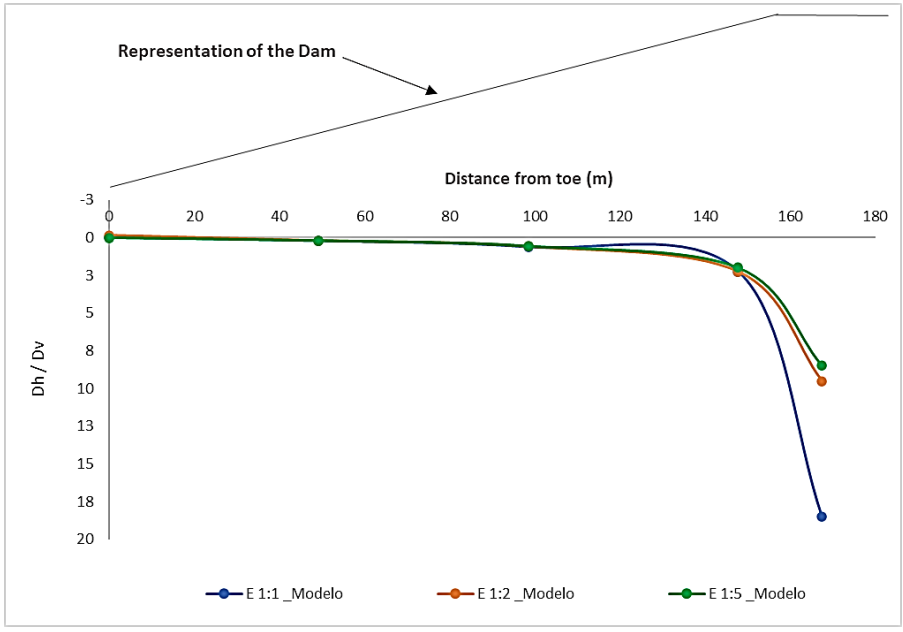


Figure 9: Vertical to horizontal displacement ratio (dv/dh) for different embankment-foundation stiffness ratios (source: adapted from Clough and Woodward, 1967)

The next section compares the model and actual vertical and horizontal displacements obtained from instruments installed near the embankment-foundation interface.

Comparison between field measurement and theoretical model

Inclinometer and settlement gauge data was used to compare field measurements with the model.

Monitoring evaluation mainly focused on checking the displacement profiles over instrument operation history, aiming at identifying any signs of raise-induced shear zone formation and mass movement. The instrumentation used to observe horizontal and vertical displacement behavior at the embankment/foundation contact is shown in Figure 10 for the typical section.

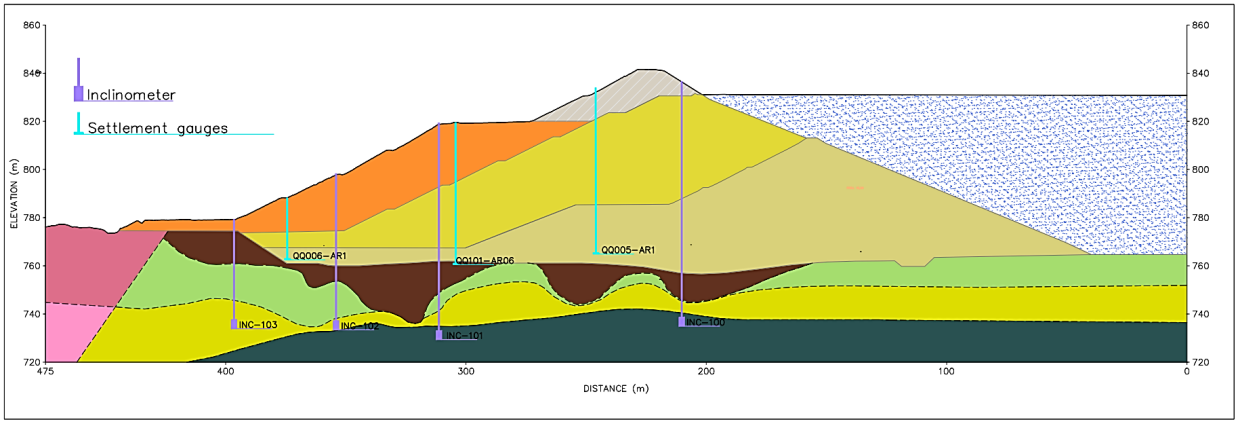


Figure 10: Typical instrumented section of a conventional earth dam. The dam embankment erected in 2022/2023 is indicated in the figure key (source: BVP, 2023c)

Also, four inclinometers anchored in competent rock are shown, from dam crest to toe, as well as three settlement gauges (RA) near the embankment/foundation interface more directly subjected to final works loading.

Figure 11 shows the horizontal displacement (Figure 11 (A)) and vertical displacement (Figure 11 (B)) profile indicated by the instrumentation, whose maximum and minimum distribution and distance from the crest is similar to Figure 9 of the theoretical reference modeling.

It is worth noting that the profiles on Figure 11 correspond to different times during the final dam raise works, making it possible to evaluate the effects of the increased load with the actual embankment and foundation stiffness contrast, conditioned in the actual case by the high SAC unit compressibility against the higher embankment stiffness. Thus, embankment/foundation stiffness relationships addressed in the idealized model are inverted.

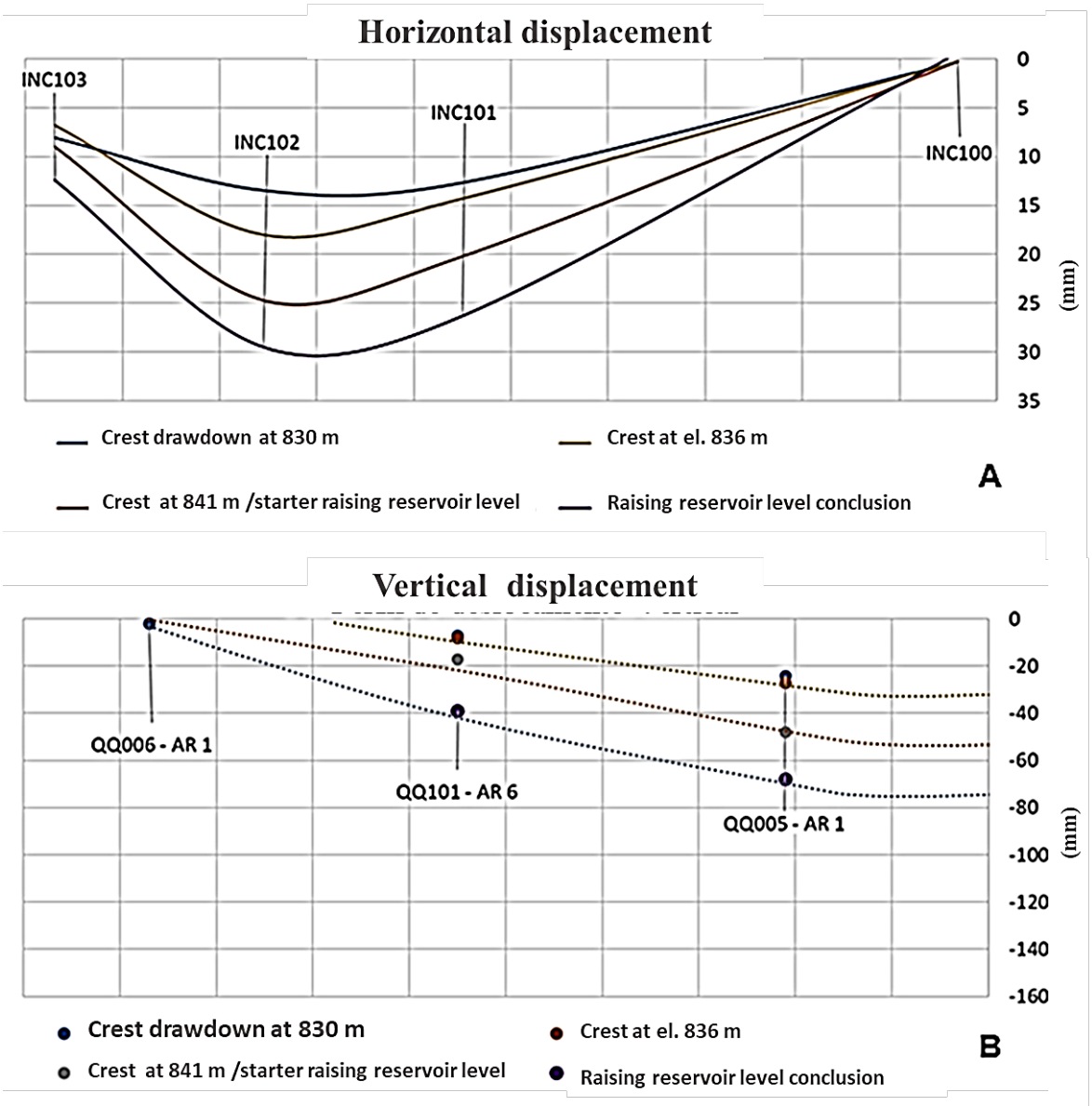


Figure 11: Monitoring data of displacements over time A) horizontal and B) vertical with behavior similar to that proposed in the theoretical model, according to Figure 8

In order to check whether the displacement pattern identified in the selected section replicates the idealized model, but with stiffness ratio inverted, the analysis included monitoring data on vertical and horizontal displacements from instruments installed in a farther section, also at depths corresponding to the embankment/foundation interface. Figure 12 shows the plot plan for additional instruments (an inclinometer and a pressure gauge) included in the comparison basis.

We believe that the considerable distance of the additional instruments from the most instrumented section is strongly significant for a typical downstream shell deformational behavior to be established, in a considerably more complex foundation condition from a geological-geotechnical standpoint.

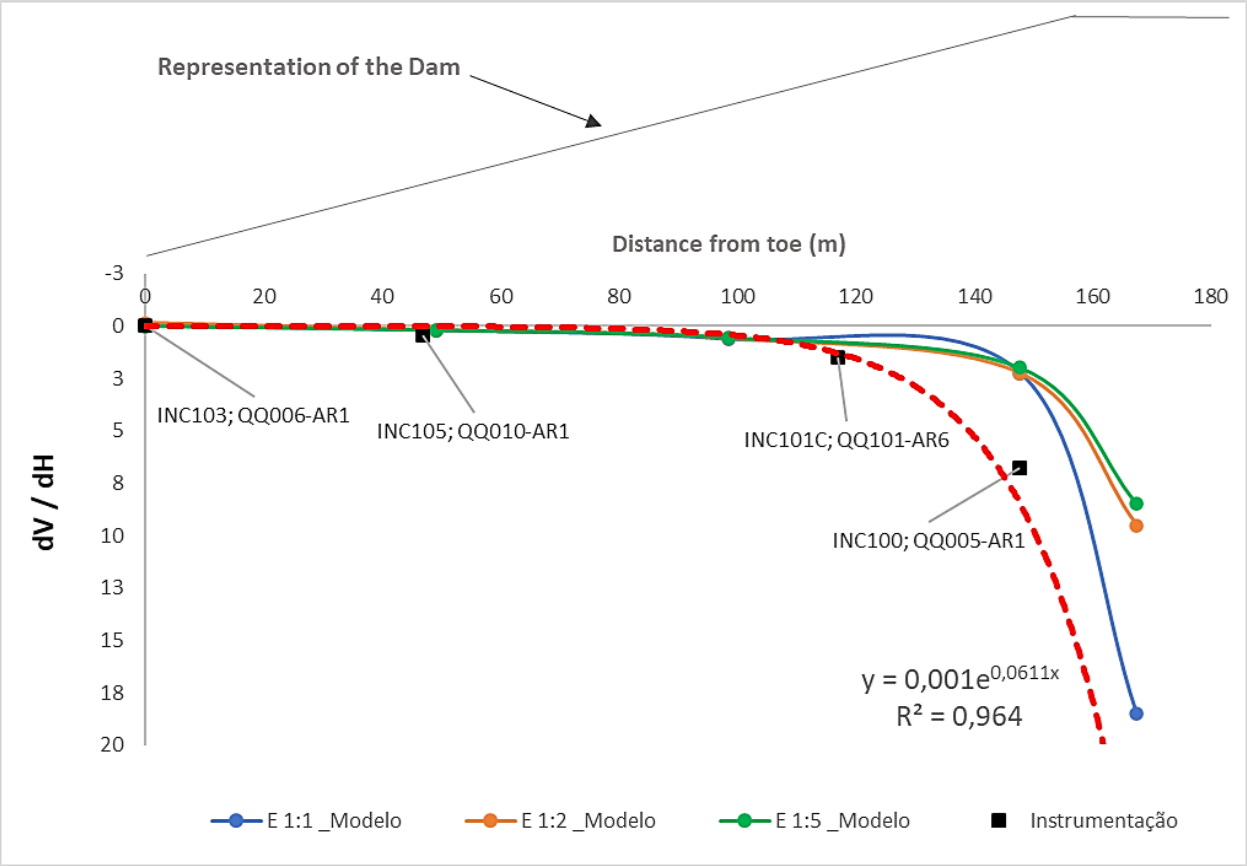


Figure 12: Comparison of site-measured vertical and horizontal displacements (dashed red line) with the theoretical model

Figure 13 shows vertical and horizontal displacement ratios recorded by the instruments considered. The relationship between vertical and horizontal displacements in the actual case (dashed red curve) quite reasonably follows idealized model ratio pattern, but it is on the opposite side to the equivalent stiffness curve (blue curve). This is clearly compatible with the actual case of the foundation being more flexible than the embankment, according to the calibrated numerical model.

The shape of the normalized curve between vertical/horizontal displacements corresponding to the actual measurements shows a similar pattern to the normalized reference model curves, which suggests the actual case behavior, in terms of settlement and horizontal displacement, is in line with deformations associated with the gravitational facility settlement, in which the actual foundation is around 2 to 2.5 times more flexible than the embankment stiffness.

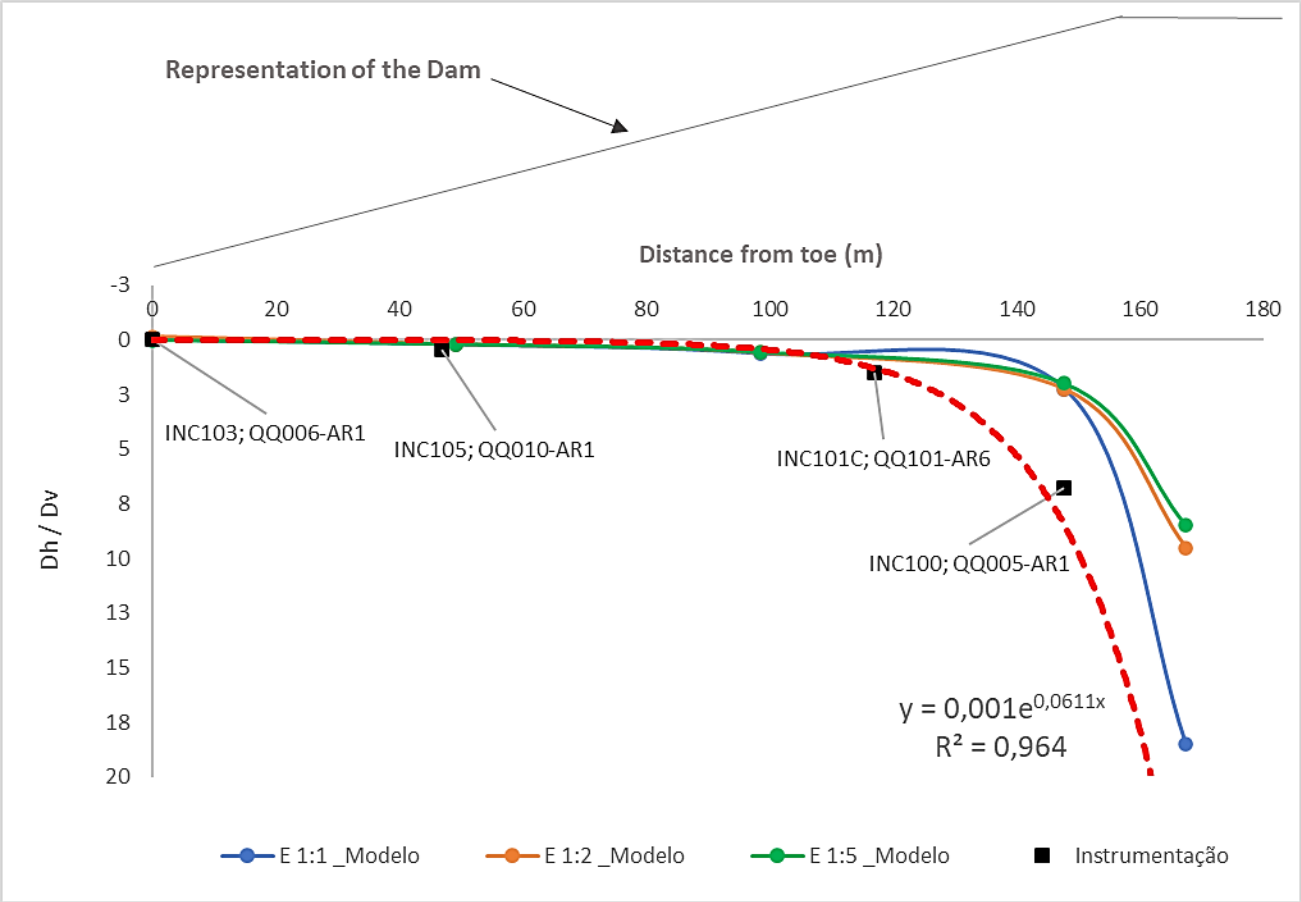


Figure 13: Comparison of site-measured vertical and horizontal displacements (dashed red line) with the theoretical model

Table 1 shows the E50 modules of the Hardening Soil model, Undrained module 'A' applied to the foundation, on the off-the-shelf program PLAXIS. These values led to the best result of comparison between the numerical Itabiruçu Dam simulation and the monitoring data, especially regarding construction pore pressure dissipation rate, as shown in Figure 14, with numerical model and settlement results over time for survey monuments 19 and 20.

Table 1: Average stiffness modulus (E50), embankment phases and foundation materials (source: BVP, 2023a)

Materials	Average stiffness modulus – E50 (kPa)
Embankment, downstream shell	6,475
Foundation	3,600

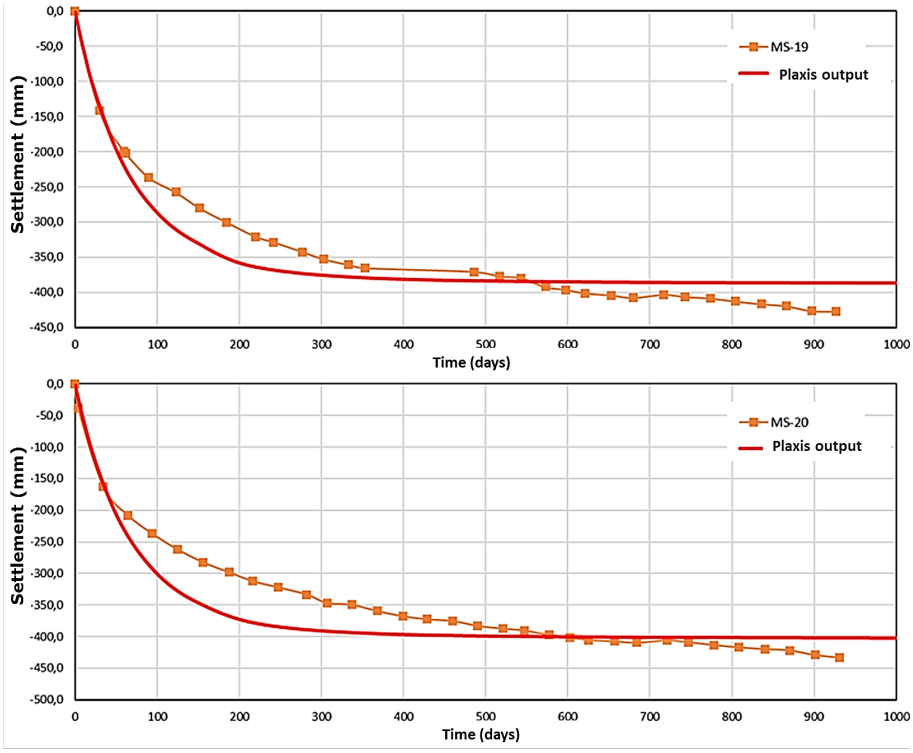


Figure 14: Comparison between the actual vertical displacement curves measured by using MS 19 and MS 20 monuments and the simulated numerical model curves (source: BVP, 2019a)

According to this analysis, the actual facility behavior, as per synthetic vertical and horizontal displacement ratios along the embankment/foundation interface downstream the dam axis (Table 1), fits the facility/foundation deformation mechanism, in which foundation is 2-2.5 times more flexible than the embankment, due to self-weight settlement.

Highlight of the discussion

Despite the presence of a highly compressible layer in the foundation as compared to the embankment stiffness, the ratio of horizontal to vertical displacements has shown full compatibility concerning the shape of the function captured in the Theoretical Reference Model in which the foundation was repeatedly stiffer than landfill in all cases modeled by the authors. This similarity suggests the dam would have experienced just gravitational settlement as the single deformational mechanism.

Conclusion

Typical horizontal and vertical displacement behavior evolution, as the downstream raise of the analyzed dam developed, has shown a similar pattern to that of the theoretical reference model of Clough and Woodward (1967), with various relative embankment/foundation stiffness ratios being considered. In the

actual case, as in the model, the horizontal displacements measured near the dam axis tend to be minimal or cancel out where vertical displacements reach their peak value, whatever the relative embankment/foundation stiffness may be. At about one-third of the distance from dam toe to crest, the horizontal displacements are more significant and decrease both upstream and downstream. Itabiruçu Dam measurements replicate with excellent adherence the idealized model pattern of deformations induced by gravitational settlement.

The curve shape of normalized displacements along the embankment/foundation interface underneath the downstream shell in the actual case is compatible with the normalized curve pattern of the theoretical self-weight settlement model, and is even coherently located on the opposite side to the theoretical curves, since the typical Itabiruçu Dam foundation stiffness turned out to be around 2 to 2.5 times lower than that of the embankment.

The main value of this finding is that the origin of the dam cracks is confirmed by differential settlement given its occurrence as pockets of most compressible soil unit (SAC), with the lowest SPT blow counts of the program, usually less than 10. To date, there have been no unequivocal findings of horizontal displacements in inclinometer logging, regardless of the depth below the facility/foundation interface, nor occurrence of cracks in drainage channel concrete downstream of the dam. Horizontal displacements recorded by the instrumentation have been proven to correspond to settlement components of SAC deformation, mainly. Over almost four years of continuous monitoring, low-angle shear bands in the facility foundation embankment have been ruled out. The most important aspect in analyses of this nature is the actual facility/foundation behavior, over the long period of instrumentation monitoring, which points to gradual and consistent settlement stabilization over time, mainly due to the dissipation of excess construction pore pressures induced in the SAC unit.

As for horizontal displacements, no behavior was recorded during the period of continuous measurements for almost four years, which could raise suspicions of a second facility movement mechanism, possibly associated with strain softening of the foundation under large deformations, as a result of potential mobilizations of foundation strength in the post-peak regime. The observations of the entire set of monitoring instruments on the dam scale show convergence with the mechanical stress-strain response in dozens of undrained and drained triaxial tests, carried out both in the SAC and in the SSG unit, which showed maximum losses of peak strength of only 10% in some tests, despite the development of positive pore pressures in the SAC up to close to the maximum deviator strength.

Finally, settlement recurrence along the reference section as raise works resumed was at lower magnitudes than those recorded immediately after work was halted, due to a maximum height loading of 17 meters in the 2022 stage, compared to a 40-meter loading between 2018 and 2019. On the other hand,

the decreasing settlement rates from the recent construction completion are similar to those of the previous long period, in our opinion caused by gravitational settlement.

References

Boulanger, R.W. 2003. High overburden stress effects in liquefaction analyses. *Journal of Geotechnical and Geoenvironmental Engineering* 129(12):1071–1082.

BVP Geotecnia e Hidrotecnia. 2019a. *Relatório Técnico RL-1850CC-G-31335 – Consolidação preliminar dos dados – Anexo.* Belo Horizonte.

BVP Geotecnia e Hidrotecnia. 2019b. *Relatório Técnico RL-1850CC-G-31337 – Consolidação Final Dos Dados – Fase 2 Modelo Adensamento – Anexo*. Belo Horizonte.

BVP Geotecnia e Hidrotecnia. 2023a. *Relatório técnico RL-1850CC-X-33700 – Parecer e análise crítica – Estudo tensão x deformação alteamento até 2022*. Belo Horizonte.

BVP Geotecnia e Hidrotecnia. 2023b. *Relatório Técnico RL-1850CC-X-33059 – Análise de tensão e deformação do alteamento utilizando Plaxis 2D.* Belo Horizonte,.

BVP Geotecnia e Hidrotecnia. 2023c. *Relatório Técnico RL-1850CC-X-33585 – Revisão Periódica de Segurança de Barragens.* Belo Horizonte.

Clough, R. and Woodward, R. 1967. Analysis of embankment stresses and deformations. *Journal of Soil Mechanics and Foundations Division* 4: 529–549.

Poulos, H.G. and Davis, E.H. 1972. *Elastic Solution for Soil and Rock Mechanics*. New York: John Wiley & Sons.

Poulos, H.G., Booker, J.R. and Ring, G.J. 1972. Simplified calculation of embankment deformations. *Soils and Foundations* 12(4): 1–17.

Silveira, J.F.A. 2006. *Instrumentation and safety of earth and rockfill dams*. São Paulo: Oficina de Textos.

Enhancing Pseudo 3D Seepage Modeling with Topographic Integration for Heap Leach Facilities

I.J. Vega, SRK Consulting, Argentina
A.G. Terlisky, SRK Consulting, Argentina
M. Noël, SRK Consulting, Canada

Abstract

The management of heap leach facilities (HLFs) is a critical aspect of sustainable mining operations. Seepage control is key in optimizing the production of mineral extraction and drainage systems, and it is also a crucial component in ensuring environmental protection and structural stability. Building upon our previously developed automated modeling tool (Noël et al., 2023), which facilitated time-dependent pseudo-3D seepage analysis using Hydrus-1D, Python, and Autodesk® Dynamo®, we introduce a significant enhancement that incorporates topographic features into the seepage modeling process. This advancement allows for a more realistic representation of the HLF environment by intersecting heap leach pads volumes with the surrounding topography.

The novel feature extends the capabilities of the existing tool by enabling the simulation of seepage through the heap leach pads as it interacts with the natural landscape. This interaction is critical for understanding how topography influences the distribution and flow of seepage, which in turn affects the design and optimization of HLF drainage systems and the assessment of potential environmental impacts. The methodology involves:

i) integrating detailed topographic data into the discretization process of the HLF shape in both space and time;

ii) analyzing the interaction between the heap leach pads and the topography to assess changes in seepage patterns; and

iii) computing the modified time-dependent total seepage over the entire base of the HLF and the variation of the water entrained by the heaps, considering the topographic constraints.

The application of this improved modeling approach is exemplified through a theoretical case study, where a simplified analysis was previously conducted. Utilizing our enhanced tool, we will intersect the topography with the HLF to validate and analyze the results. This case study not only validates the tool but also illustrates the practical implications of incorporating topographic data into seepage modeling. The tool

also supports the evaluation of seepage in various types of waste containment facilities, including waste rock dumps (WRD), tailings storage facilities (TSF), and co-disposal sites.

Introduction

Seepage modeling for various mine waste containment facilities, such as heap leach facilities (HLFs), tailings storage facilities (TSFs), "dry" stacks, waste rock dumps (WRDs), and co-disposal sites, is typically performed in 1D and 2D to predict seepage into the groundwater system. Due to the complexity and computational load, 3D simulations are rarely performed.

The modeling presented relies on Hydrus-1D, an industry-standard code for simulating water and solute transport in variably saturated porous media. The modeling tool discretizes the deposition of mine waste in time and space, enabling 1D modeling for individual blocks and stacking material as the facility is constructed. Autodesk® Dynamo® discretizes the variable 3D geometry of the TSF into independent columns at different time steps, which are then assembled into stacks representing the gradual construction of the waste facility. Python reads the inputs, runs the Hydrus simulations for each block and stack, and processes the results.

A significant enhancement to this modeling tool incorporates topographic features into the seepage modeling process. This advancement allows for a more realistic representation of the facility environment by intersecting heap leach pads volumes with the surrounding topography.

1D model considerations

The modeling was performed using Hydrus-1D software. The water transport is based on Richards' equation for the saturated/unsaturated water flow with the van Genuchten model (van Genuchten, 1980). The automatic stacking modeling was done as presented in (Noël et al., 2023). As an instance the sequence of modeling is illustrated in Figure 1 for one column.

The model was configured to extract results at the bottom surface of the heap leach and to quantify the water entrained by the heaps. Each column's seepage was modeled separately, and the total seepage and entrained water were obtained by integrating all the discretized blocks over the entire heap leach domain.

The bottom boundary was set to model a drain, representing a drainage system open to atmospheric pressure, and did not allow any water uptake in the event of negative pressures (suction). The top boundary condition was set for two conditions: irrigation of the heap and a no-flux condition when the heap was being drained. For the sake of simplicity, climatic conditions were not modeled in this study. However, future work can incorporate these factors to enhance the model's accuracy.

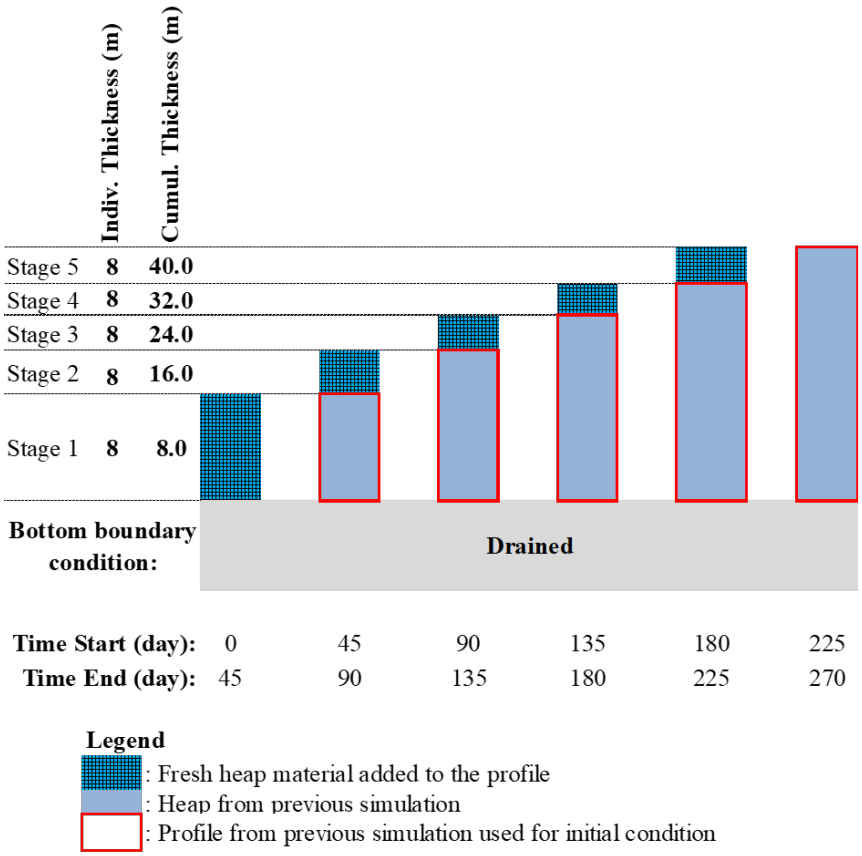


Figure 1: Discretization and the stacking sequence assembled by the Python code and modeled by Hydrus – evolution of a given column over six time stages

The initial condition for the first simulation involved specifying the volumetric water content corresponding to the degree of saturation observed in the field. Subsequent simulations used the model output as the initial condition for the already placed material. Newly placed material was assigned a volumetric water content matching the field-observed degree of saturation. This process was repeated for all simulations as the heap thickness increased.

Pseudo 3D model and sequential columns discretization

To enable Hydrus-1D to solve seepage for complex 3D geometries, a discretization into vertical columns is necessary. The volume of the heap leach pad and the topographic surface was first assembled in Autodesk® Dynamo®. The entire geometry is then automatically discretized into a grid of vertical columns covering the full heap leach footprint. Each vertical column intersects the topographic surface and the heap leach volume at different elevations.

The 3D representation of the HLF is vertically discretized into typical lift thicknesses, starting from the deepest point. Each lift's surface is further subdivided based on the surface area of the irrigation cells,

with a corresponding irrigation duration. This results in a specific number of irrigation cells for each lift. It is assumed that the first lift is completed before adding the subsequent lift. The irrigation duration is then used to establish the sequential timing for the start and end of irrigation for each cell.

Finally, the results obtained are elevation vs. time curves for each column, which are used as input for the Hydrus-1D simulations. It is important to note that each column has its own unique growth curve depending on its position in the grid and the timing. No lateral flow is considered in this model.

All these processes are automated using Python coding enabling changes such as topographic surface, grid spacing, and lift thickness to be made automatically. This makes sensitivity analysis very straightforward to perform.

Theoretical case study

A theoretical case study utilizing the tools discussed in the previous sections of this paper is presented.

Figure 2 illustrates the heap leach volume (in blue) and the topographic surface (in silver) imported into the Autodesk Dynamo® environment.

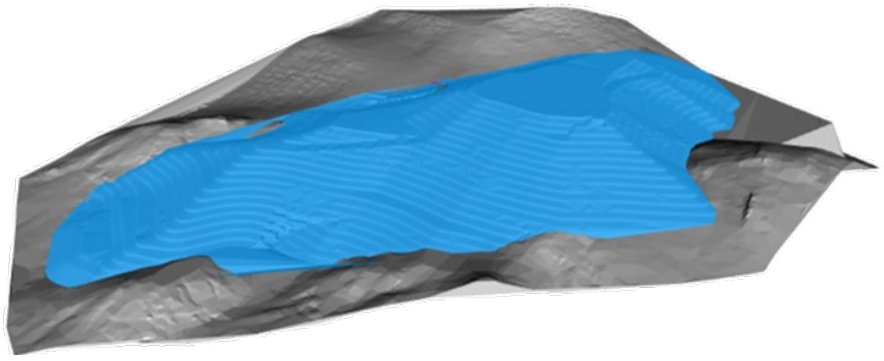


Figure 2: Heap Leach 3D volume and topographic surface

Figure 3 displays the 1D columns resulting from the discretization of the 3D heap leach volume, accounting for the intersection of the heap leach with the topographic surface.

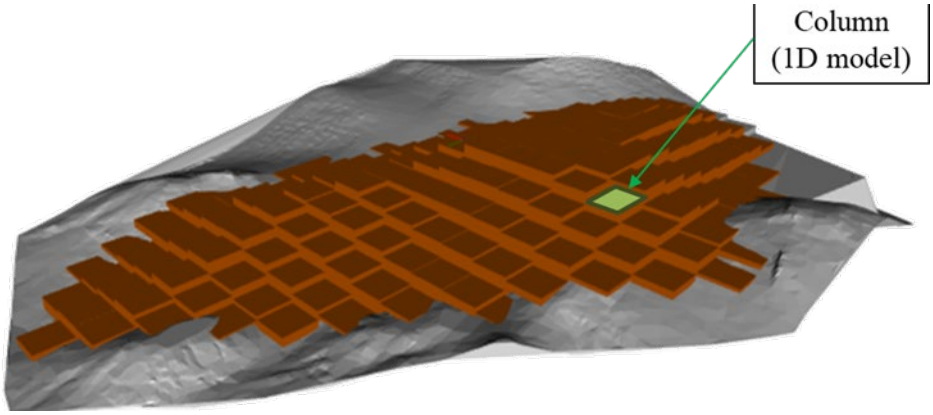


Figure 3: Grid of 1D columns discretization of the heap leach

Subsequently, the position and elevation of each column's starting and ending points are extracted as X, Y, and Z coordinates for data processing, enabling the construction of coupled space and time Hydrus 1D simulations for each 1D column.

Figure 4 illustrates the thickness of each point in the heap leach at the end of construction, depicted on the left colormap plot, which is based on the Z coordinates of each 1D column's starting and ending points. The right plot displays the 163 columns with their corresponding indexing, resulting from the grid spacing of 80 m × 80 m.

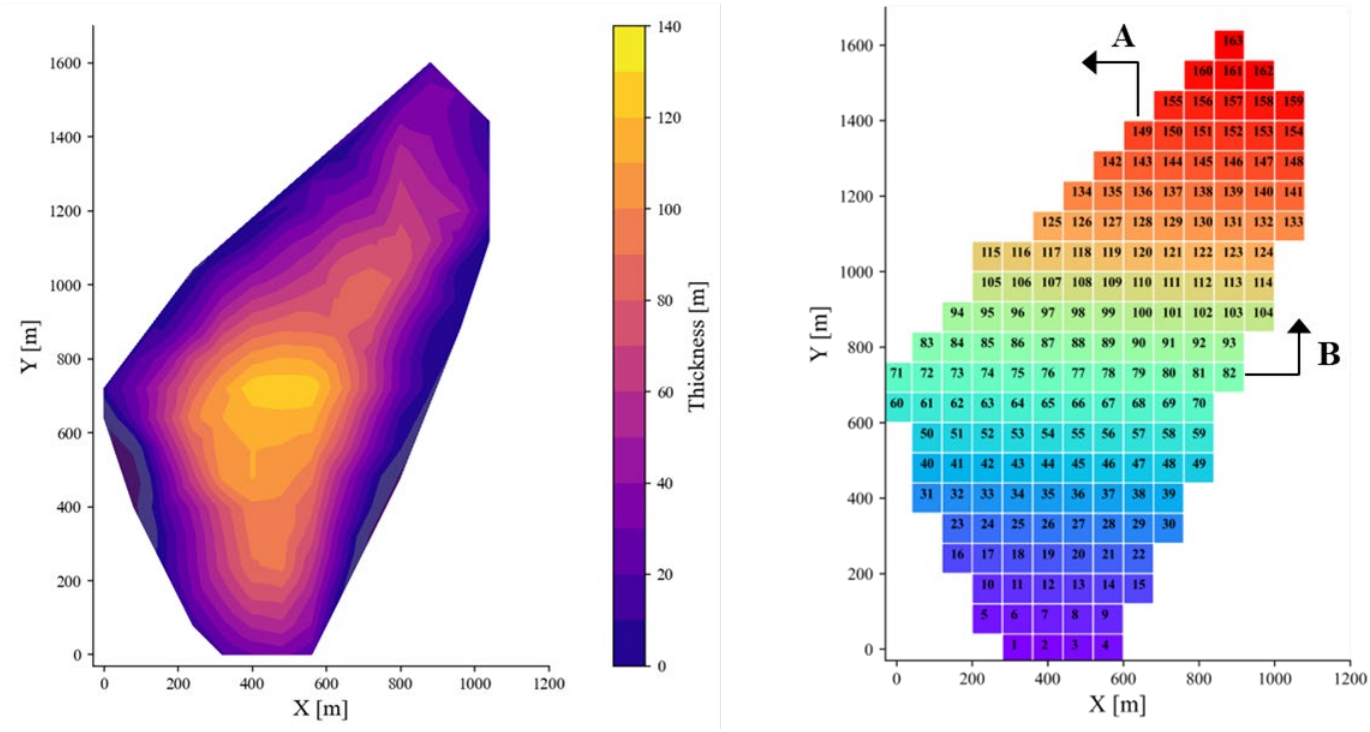


Figure 4: Heap leach 1D columns discretization: total thickness and indexing.

For a better understanding of the topography on the construction sequence, sections A and B are shown in Figure 5. The horizontal gray lines represent the typical 8-meter-thick lifts.

Examining Section A, it is observed that column 143 is the first to emerge in time, as it has the lowest intersection with the topography and will emerge at lift number 5 (i.e., 40 m). In contrast, column 15 is the last to commence, as it intersects the topography at a higher elevation.

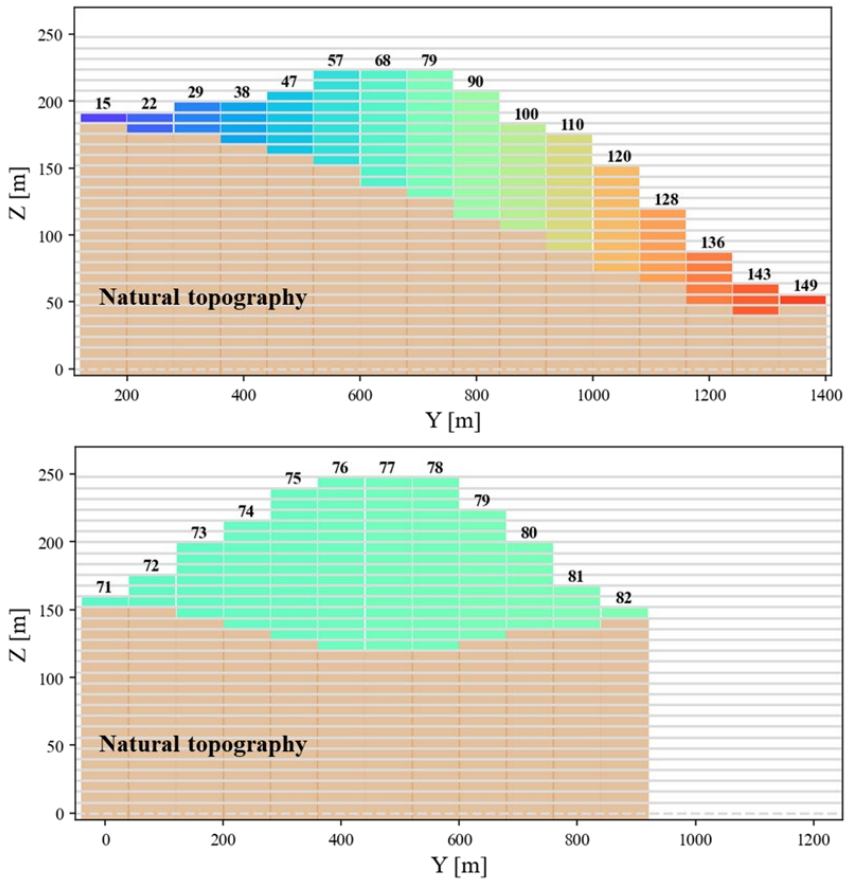


Figure 5: Section A (upper panel) and Section B (lower panel), referred to Figure 4

The surface of each lift was then discretized according to the surface of the irrigation cells, which was set to 90,000 m² with an irrigation duration of 45 days. An irrigation rate of 6 liters per hour per m² was used to model the heap when being irrigated. A quantity of irrigation cells was therefore obtained for each lift. Given that each column covers an area of 6,400 m², if a single lift encompasses more than approximately 14 columns, the lift is divided into multiple cells. It was assumed that the first lift would be completed before adding the subsequent lift. The irrigation duration was then used to establish the sequential time at which each irrigation cell would start and end irrigation.

As an initial instance, the first three lifts are illustrated in the plan view of Figure 6. Adjacent to each column footprint, a number indicates the total height of each column for a given lift. If the number is colored, it signifies that the column is increasing in height during that lift. Conversely, if the number is black, it indicates that the column has reached its final height.

In the bottom left corner of each plot, the cell surface area is displayed. As shown in Figure 6, the first three lifts do not exceed one cell, as the total area of the columns is significantly less than 90,000 m².

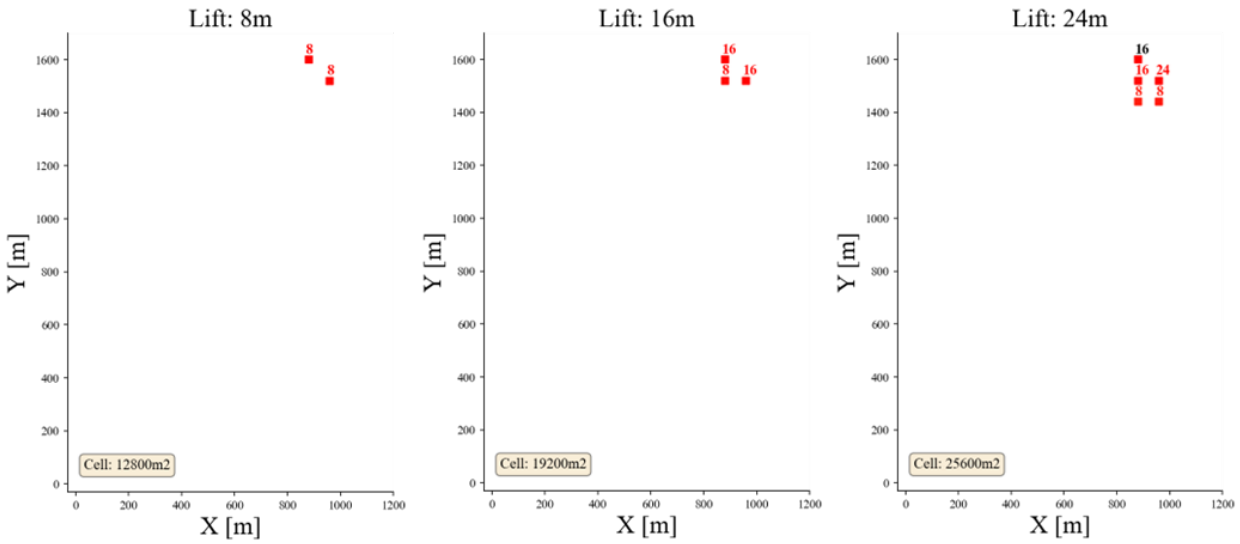


Figure 6: Construction sequence – first 3 lifts

Figure 7 depicts the lifts at 88 m and 96 m. Since the 96 m lift exceeds 90,000 m², it is divided into two irrigation cells. In addition to the previously explained color representation, if the height number is gray, it indicates that the column is part of a cell that is not being irrigated at that specific time step. Each lift corresponds to a particular time step, and if a lift has more than one cell, those cells are irrigated at different times.

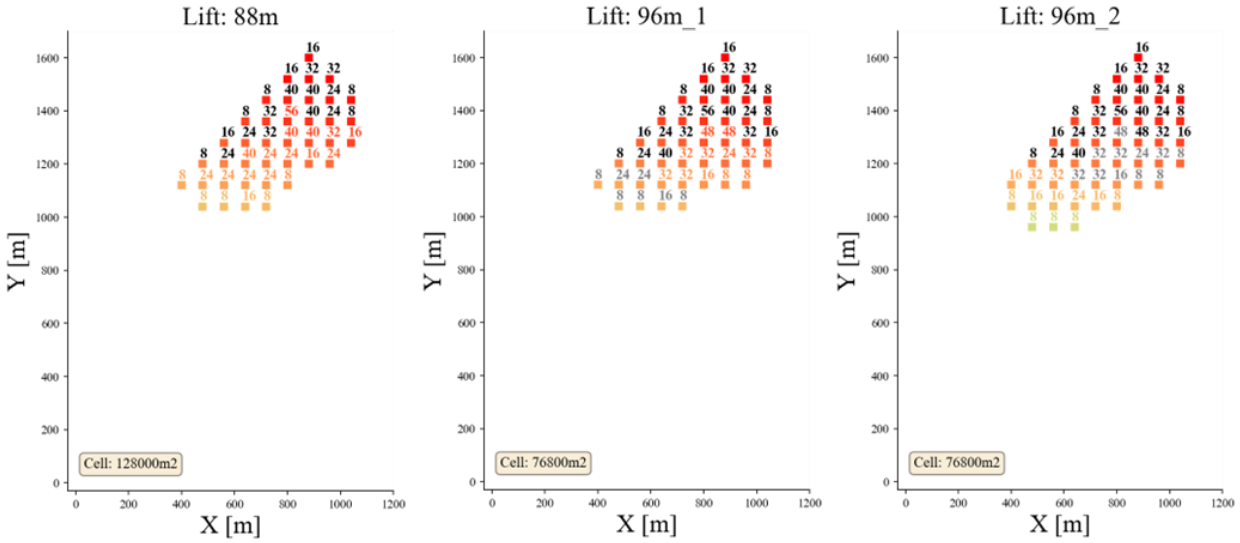


Figure 7: Construction sequence – 88 m and 96 m lifts

The final lift, corresponding to 248 m, is shown in Figure 8. The height numbers indicate the final height of each column.

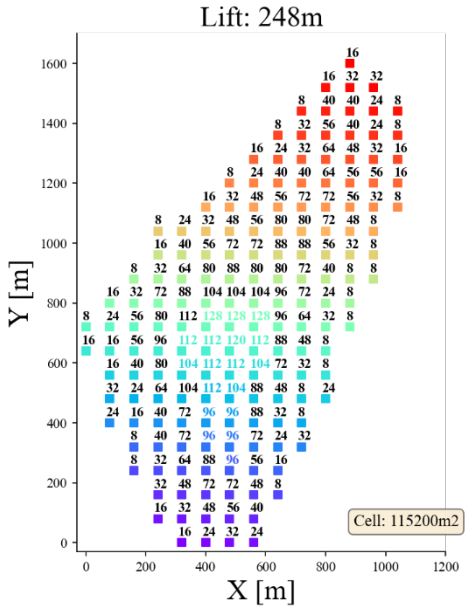


Figure 8: Construction sequence – 248 m lift

Finally, the total accumulative bottom flux volume BF_{Total} and the total entrained water EW_{Total} are calculated by adding up all the columns as shown in Equation 1 and 2, results are shown in Figure 9. Hydraulic properties of the heap leach material used to run the simulations are shown in Table 1. Additionally, the infiltration rate is shown in Figure 10.

$$(1)\ \boldsymbol{BF_{Total}(t) = \sum_{n=1}^{163} BF_{Col_n}(t)}$$

$$(2)\ \boldsymbol{EW_{Total}(t) = \sum_{n=1}^{163} EW_{Col_n}(t)}$$

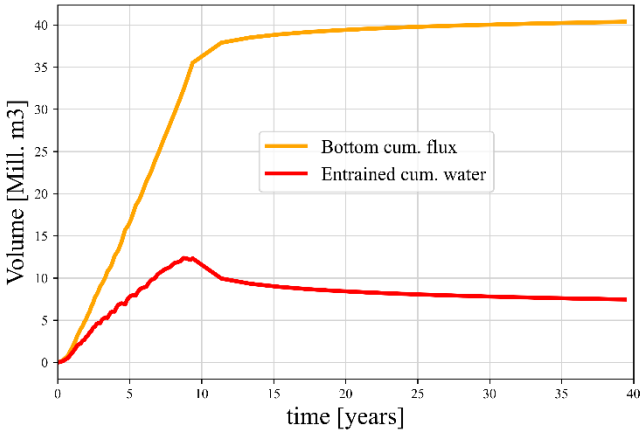


Figure 9: Total drain down – total entrained water

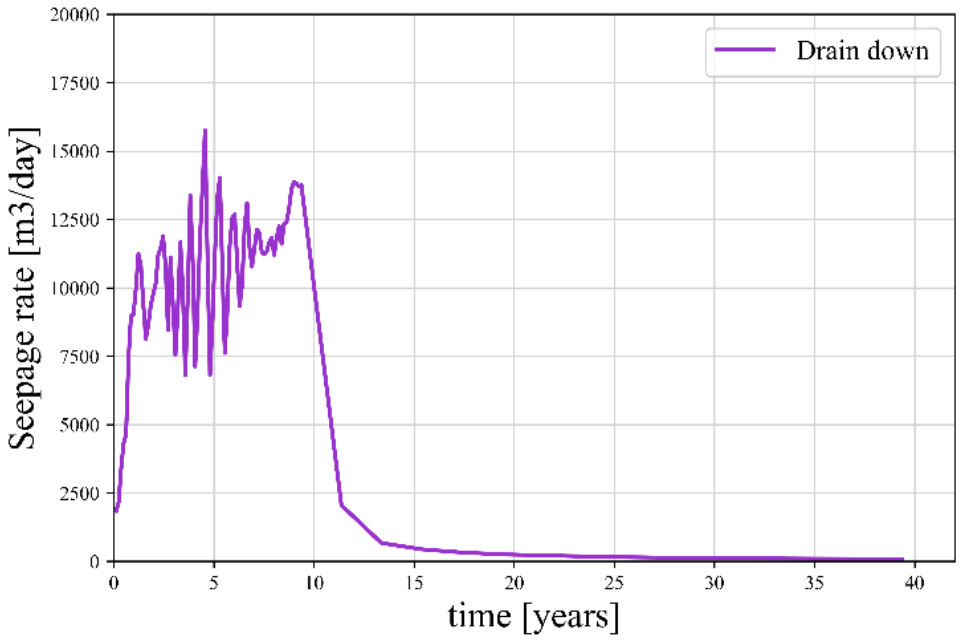


Figure 10: Total drain down rate as function of time

Table 1: Hydraulic properties of the heap leach material

Parameter	Value
θ_r	0.04 m³/m³
θ_s	0.38 m³/m³
$\theta_{initial}$	0.08 m³/m³
α	40 1/m
n	1.5
l	0.5
K_s	1.00e-5 m/sec

To analyze how topography influences the distribution and flow of seepage, colormaps of cumulative bottom flux at six different times during the construction of the heap leach are presented in Figure 10. Understanding the distribution of flow through the heap leach is crucial for the design and optimization of drainage systems.

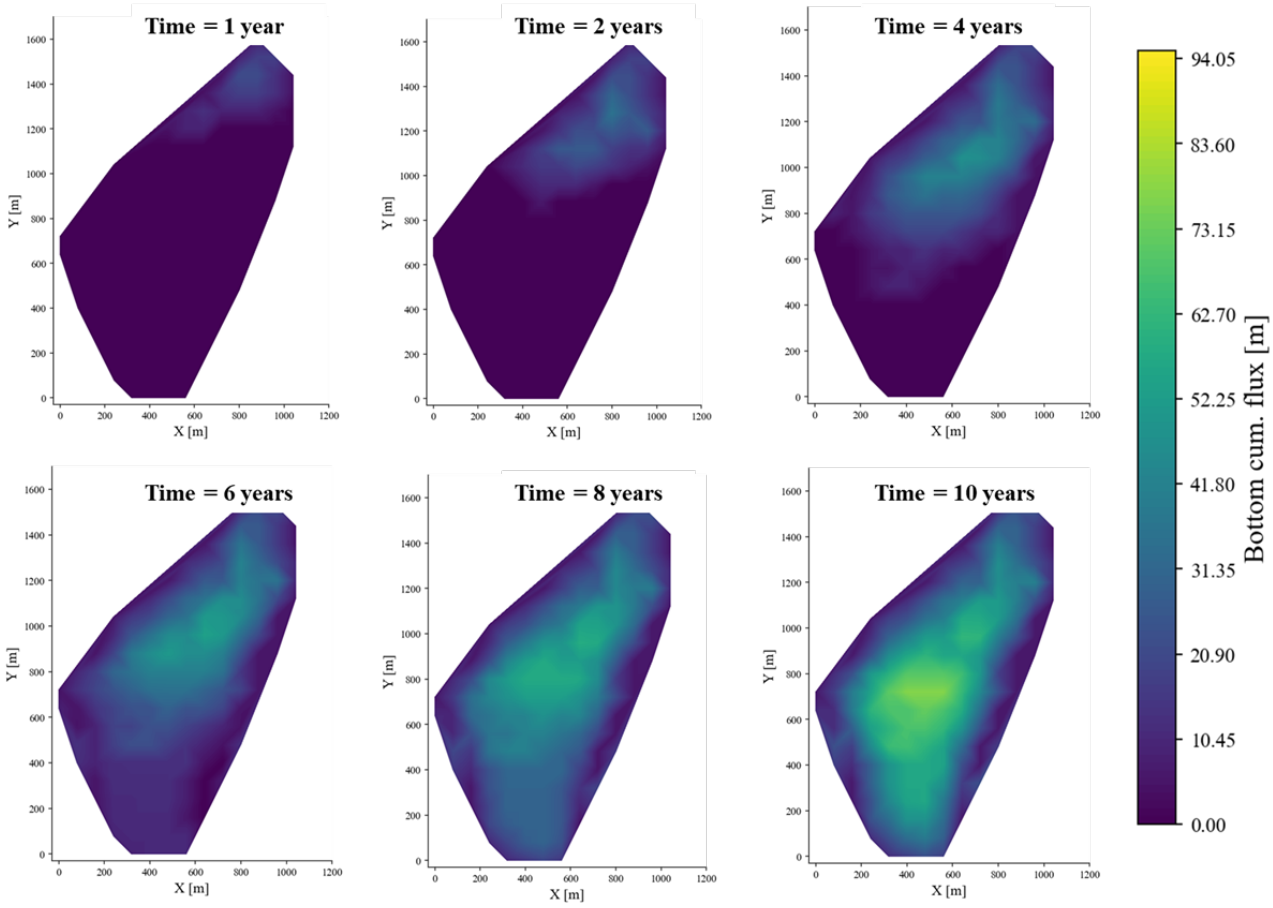


Figure 11: Bottom cumulative flux distribution as function of time during construction of the heap leach

Discussion

The pseudo-3D model presented in this study offers a valuable tool for simulating water flow in HLFs by integrating topographic features into the seepage modeling process presented in Noël et al. (2023). However, it is important to acknowledge the inherent limitations of the 1D column approach used in this model.

The main limitation is the omission of the horizontal flow component. This approach is acceptable in facilities where deposition occurs in horizontal layers and for facilities that have a geometry with a high ratio of horizontal to vertical dimensions. However, in more complex situations this simplification can become inaccurate.

Additionally, the consolidation and void ratio variation (and implicitly the saturated hydraulic conductivity) of the materials are not coupled into the analysis given the limitation of Hydrus-1D. This limitation would, however, be limited to filtered tailings, and even less for waste rock and heap leach

materials. Future research could build upon the methodologies presented by Fredlund et al. (2015) to enhance the accuracy of seepage modeling by integrating the effects of consolidation.

To address the horizontal flow limitation, it is planned to validate the model with either 3D or 2D models. This additional step will allow for the evaluation of the magnitude of horizontal flow and its impact on the distribution and flow of seepage in the HLF. It is crucial to mention these limitations in the present work to acknowledge the potential constraints of the 1D column models.

In summary, while the pseudo-3D model with topographic integration represents a significant advancement in seepage simulation in HLFs, it is essential to consider the limitations associated with the omission of horizontal flow and the uncoupled consolidation and void ratio variation.

Conclusion

The integration of topographic features marks a significant advancement in pseudo-3D seepage modeling for waste containment facilities. This study demonstrates that incorporating topographic data enhances the realism of seepage simulations, allowing for more accurate predictions of seepage distribution, which is crucial for optimizing drainage systems and assessing environmental impacts.

The enhanced tool was validated through a theoretical case study applied to an HLF, demonstrating its utility in such facilities, and incorporating irrigation sequences into the modeling. The tool can also be applied to various mine waste facilities, including waste rock dumps, tailings storage facilities, and co-disposal sites. Automation using Python facilitates easy adjustments and sensitivity analysis, enabling the evaluation of different scenarios and their impact on seepage patterns.

Additionally, the tool allows for the analysis of various deposition methods, optimizing the process to the maximum extent. It enables changes in irrigation areas, irrigation duration, irrigation quantity, and maximum heights for drain placement, considering the height of the HLF and the inclusion of impermeable layers within the heap.

Furthermore, future work will incorporate climatic conditions into the model. This will allow for the analysis of HLF performance under different climatic scenarios (humid or arid), assessing the influence of climate on water entrainment and flow. This capability will enable the evaluation of HLF functionality for any location by changing climatic conditions.

In summary, integrating topographic features into pseudo-3D seepage modeling enhances the accuracy and realism of seepage predictions and provides a robust tool for optimizing HLF drainage systems. Future improvements should focus on addressing the identified limitations and incorporating climatic conditions to further enhance the model's applicability.

References

Fredlund, M.D., Donaldson, M. and Chaudhary, K.B. 2015. Pseudo 3-D deposition and large-strain consolidation modeling of tailings deep deposits. *Proceedings of Tailings and Mine Waste, 2015.*

Noël, M., Vega, I.J., Rivarola, F., Lopez, Ezama, I., McGregor, M. and Terlisky, A.G. 2023. Coupling tailings deposition modelling with Hydrus-1D and Python for pseudo-3D seepage predictions. *Proceedings of Tailings and Mine Waste, 2023.*

Simunek, J. and van Genuchten, M. 2018. Hydrus-1D, version 4.17.0140. Code for simulating the one-dimensional movement of water, heat and multiple solutes in variably saturated porous media. Department of Environmental Sciences, University of California, Riverside. Released November 15, 2018. Available at: http://www.pc-progress.com/en/Default.aspx?H1d-downloads

van Genuchten, M.Th. 1980. A closed-form equation for predicting the hydraulic conductivity of unsaturated soils. *Soil Science Society of America Journal* 44(5): 892–898.

Comparative Analysis of Vane Shear and Fall Cone Tests for Characterizing Oil Sands Tailings in the Sandy-fine Category

Peter Kaheshi, University of Alberta, Canada
G. Ward Wilson, University of Alberta, Canada
Heather Kaminsky, Northern Alberta Institute of Technology (NAIT), Canada

Abstract

Some tailings deposits encountered in oil sands mine sites today fall into the sandy-fine category, characterized by fines content and sand-fines ratio ranging from 25% to 50% and 1 to 3, respectively. These include composite tailings and thickened tailings deposits; more can be expected to come from coarse sand and centrifuged fluid fine tailing mixtures resulting from the emerging co-deposition approach. Tailings in this category may be too fine to behave as cohesionless or too sandy to behave as cohesive, depending on the amount and properties of fines included.

Although Fall Cone tests (FCT) and Vane Shear tests (VST) are common, less complex and cheaper techniques for measuring undrained strength can certainly be used to measure strength for these materials (i.e.: Triaxial and Direct Shear tests); however, their applicability in sandy-fine oil sand tailings has not been explored. This paper compares experimental shear strength data obtained from FCT and VST to determine their applicability and repeatability in measuring strengths for sandy-fine tailings with different fines content and stress levels. Five mixtures of coarse sand and mature fines tailing (MFT) were made to obtain samples mimicking deposits within the sandy-fine category. Samples were characterized for particle size distribution and Atterberg limits before their shear strength was measured using both FCT and VST at their different stresses. Experimental data have shown a strong correlation between FCT and VST data up to 60 kPa strength. Also, a good agreement is seen between measured strength data up to 60 kPa and estimated values using the liquidity index for each sample.

Both FCT and VST are deemed suitable for sandy-fines deposits' shear strength measurements up to 60 kPa; beyond 60 kPa to 100 kPa VST gives a better estimate than FCT.

Introduction

Canada has about 167 billion barrels of oil that is viable for economic extraction with current economic conditions and technology. This ranks Canada as the fourth largest oil producer in the world, and about 97% of these reserves are in oil sands (Natural Resources Canada, 2023). Surface mining is used to extract 20% of these oil reserves as they are deposited less than 75 m below the surface. Trucks and shovels are used to load and transport the oil sand to a plant where bitumen is separated from sand by hot water extraction and froth treatment (AER, 2023; Natural Resources Canada, 2023). Byproducts known as tailings are left after the bitumen-recovering process. These contain water, silt, remnant bitumen, and clay, and traces of metals, salts, and other hydrocarbons. Since FFTs are fines-dominated, constituting mainly illite but also kaolinite and illite-smectite layers (Chalaturnyk et al., 2002), they take exceedingly long to consolidate and gain the required strength for trafficability and reclamation due to their high dispersion. This has led to the accumulation of fluid tailings (FT) in the Athabasca oil sands to about 1,392 Mm^3 in 2022 (AER, 2023).

As an initiative to manage these volumes, Directive 85 has set out the requirements for oil sands mining projects, including identifying any fluid waste coming from bitumen extraction with more than 5% solids and undrained shear strength less than 5 kPa as FT (AER, 2022). Undrained shear strength is one of the key performance indicators of oil sands tailings deposits; thus, it requires appropriate techniques to measure.

Some of the tailings deposits encountered in oil sands mine sites today have fines contents falling into the transition zone between fines and sand zones (COSIA, 2014); these include composite tailings (CT), some thickened tailings (TT) (Imperial, 2022; Oil Sands Tailings Consortium, 2012), and non-segregating tailings (NST) resulting from co-deposition of sand and FT to avoid segregation and fasten consolidation (CNRL, 2020; COSIA, 2012; Oil Sands Tailings Consortium, 2012). Shear strength measured in FT will be undrained because, with the highest composition being fines, pore pressure dissipation is not likely during measuring. It remains unknown, due to limited research on transitional oil sands tailings, whether the strength measured will be undrained or drained depending on the fine fractions and their properties, because they may be too fine to behave as cohesionless or too sandy to behave as cohesive. This research therefore intends to correlate undrained shear strength estimated from index properties to the one measured using both Vane Shear and Fall Cone tests.

Both Vane Shear and Fall Cone tests have been commonly used to measure undrained shear strength for soft cohesive soils. Das (2009) has identified Vane Shear as a tool for reliable undrained shear measurement results for medium to very soft and cohesive soils. ASTM D4648/D4648M-24 (2024) has clearly stated that vane shear test for strength does not apply to non-plastic silts and sandy soils; it has also been noted by the same standard that the use of vane shear in predominately silty soils can cause deviation from the cylindrical surface assumed, thus leading to errors in estimated strength.

The Vane Shear test involves penetrating a four-bladed vane in a sample followed by rotating it at a constant rate to determine the torque required for the vane to cause a cylindrical shear surface. This torque is then converted to a unit shearing resistance of the cylindrical surface area. Undrained shear strength by Vane Shear test is calculated using Equation 1 and Equation 2

$$\tau_v = \frac{T}{K} \quad \text{(Equation 1)}$$

$$\text{where } K = \frac{\pi D^2 H}{2} X \left(1 + \frac{D}{3H}\right) \quad \text{(Equation 2)}$$

where T is the maximum torque applied to cause failure, which is determined by the spring constant and angle of rotation, K is a constant accounting for shape and dimension of vane used, H is the height of the vane and D is the vane width. The ASTM (D4648/D4648M-24, 2024) for laboratory Vane Shear test has clearly stated that these tests are suitable for soils with undrained shear strength less than 100 kPa.

The Fall Cone test is a simple testing procedure in which a cone with known mass just touching the surface of soil specimen is released and allowed to penetrate through by its own weight; the penetration depth h is recorded. Like the Vane Shear test, the Fall Cone test is also applicable only for cohesive soils (Canelas et al., 2018; Hansbo, 1957; Koumoto and Houlsby, 2001). Equation 3 by Hansbo (1957) has been used to estimate undrained shear strength for cohesive soil; it relates cone penetration depth *h* to the shear strength of soils τ_f

$$\tau_f = \frac{KQ}{h^2} \quad \text{(Equation 3)}$$

where Q is the weight of the cone and K is a factor accounting for the cone angle. Values of K were initially estimated by Hansbo (1957) by relating cone penetration depths to field Vane Shear tests, out of which 1 and 0.3 were concluded as K values for 30º and 60º cones, respectively. Later, Wood (1985) did experimental measurements for K values and arrived at 0.85, 0.49, 0.29 and 0.19 as average cone factors for 30º, 45º, 60º and 75º cones, respectively. Recent theoretical estimation of K values by Koumoto and G. Houlsby (2001) showed a good agreement with both Hansbo (1957) and Wood (1985).

Claveau-Mallet et al. (2012) and Lu and Bryant (1997) have shown that a minimum penetration between 4 mm and 5 mm can give consistent Fall Cone test results. Working on stiff clay, Hansbo (1957) showed that the Fall Cone test can give a good strength estimation value up to 20 t/m^2, which is approximately 200 kPa while using a 400 g and 30º cone.

For decades now, undrained shear strength has been predicted by using index properties, mainly liquidity index (I_L) (Skempton, 1954, 1957). From experimental tests by Wroth and Wood (1978) on four different clays, a great correlation between liquidity index and strength was found; it was proposed that

there is a fixed approximate value of strength for liquid and plastic limit and that these values correspond to the ratio of 1:100. From this study they developed Equation 4:

$$C_u = 170e^{-4.6I_L} = 1.7 * 10^{2(1-I_L)} \text{ (kPa)} \quad \text{(Equation 4)}$$

Leroueil et al. (1983) proposed an alternative equation, Equation 5, which fits well for materials with a liquidity index ranging between 0.5 and 2.5. This is not appropriate when the I_L value is less than that range as it will result in infinite strength when 0.21 is the liquidity index.

$$C_u = \frac{1}{(I_L-0.21)^2} \text{ (kPa) for } 0.5<I_L<2.5 \quad \text{(Equation 5)}$$

For a higher liquidity index, Locat and Demers (1988) developed a correlation between undrained shear strength and liquidity index ranging from 1.5 to 6.0, as shown in Equation 6:

$$C_u = \left(\frac{1.167}{I_l}\right)^{2.44} \text{ (kPa) } 1.5<I_L<6.0 \quad \text{(Equation 6)}$$

Materials

Materials used in this study were designed to have fines contents that fall within the transitional zone of oil sand tailings (25% to 50% fines content and sand-fines ratio of 1 to 3). These samples were made by mixing coarse sand tailings (CST) and mature fluid tailings (MFT) in predetermined ratios. Because tailings from different sites could have different properties and compositions as they come from different ores with different nature and/or different froth processes were employed (Romanova et al., 2006), Sand and MFT used in this study were received from different oil sand mines' operators to cover a wider spectrum of mineral and chemical composition encountered in sites. Four resulting mixtures have been named in the format SMXX-X.X where SM stands for sand and MFT mixture, and XX and X.X stand for fines content (in percentage) and MBI value respectively for each sample. One sample was designed to include Kaolinite to assess the effect of clay mineralogy, this is named SMKXX-X.X with SMK standing for sand, MFT and Kaolinite mixture, while XX-X.X has the same meaning.

Methodology

Materials characterization

Each sample was characterized to determine PSD; sieve analysis was used to determine PSD for soil particles greater than 45 μm; whereas laser diffraction was used to analyze particles with less than 45 μm size.

Atterberg limits were measured by ASTM D4318 – 17 (ASTM International, 2017), a modified air-dried sample preparation procedure was used, and both bitumen and >425 μm particles were not removed from the sample before testing.

A Methylene Blue Index (MBI) test involved dispersing the sample for homogeneity, acidifying to remove iron oxide-hydroxide effects to titration, and finally titrating the sample with methylene blue to determine the endpoint, which is shown by a blue halo.

Fall Cone and Vane Shear strength test

Samples were allowed to drain water to reach different moisture contents by using Tempe cells. They were subjected to different suctions that were known to be below the Air Entry Value of the respective sample. At the end of water release each sample was tested for undrained shear strength using both the Vane Shear test and Fall Cone test, before getting them in the oven to measure moisture content. At least five measurements of FCT and VST were taken to determine shear strength values for each sample at a given moisture content; this made it possible to check the repeatability of measurements and omissions of outliers.

To measure undrained strength using the Fall Cone test, a metal cone was released to fall under gravity and penetrate the sample. Archived penetration depth was then measured using the gauge attached to a device. Depending on the strength of the material being tested either a 100 g or 400 g cone with 30 degrees aperture angle was used to archive a penetration depth of not less than 5 mm. The Hansbo (1957) equation (Equation 3) was then used with a constant K value of 0.85 to correlate penetration depth to undrained shear strength.

Compliance with ASTM D4648/D4648M-24 (2024) was done to measure shear strength using the Vane Shear test. In this test an electric motor-driven vane shear test equipment was used. The test involved the insertion of a 1/2" by 1/2" four-bladed vane within the sample and rotating at a constant rate of 60º/min until failure occurred. The spring deflection angle (Δ) was recorded at failure, to be used with the spring constant to determine torque (T).

Results and discussion

Materials characterization

The particle size distribution curves for the five designed mixtures are shown in Figure 1 with fines, and the clay contents are summarized in Table 1. The fines content refers to <44 μm particles. In the five samples this ranged from 27.5% to 43%, and the sand-to-fines ratio (SFR) was between 1.3 and 2.6. Sample SMK43-1.6 had the highest clay fraction (38%) because the mixture was composed of sand and kaolinite, which is almost entirely clay-sized. In contrast, other mixtures consisted of sand and mature fine tailings (MFTs) where MFT has particle sizes both below and above clay particle size (<2 μm); thus, they had lower clay

size contents in their resulting mixtures.

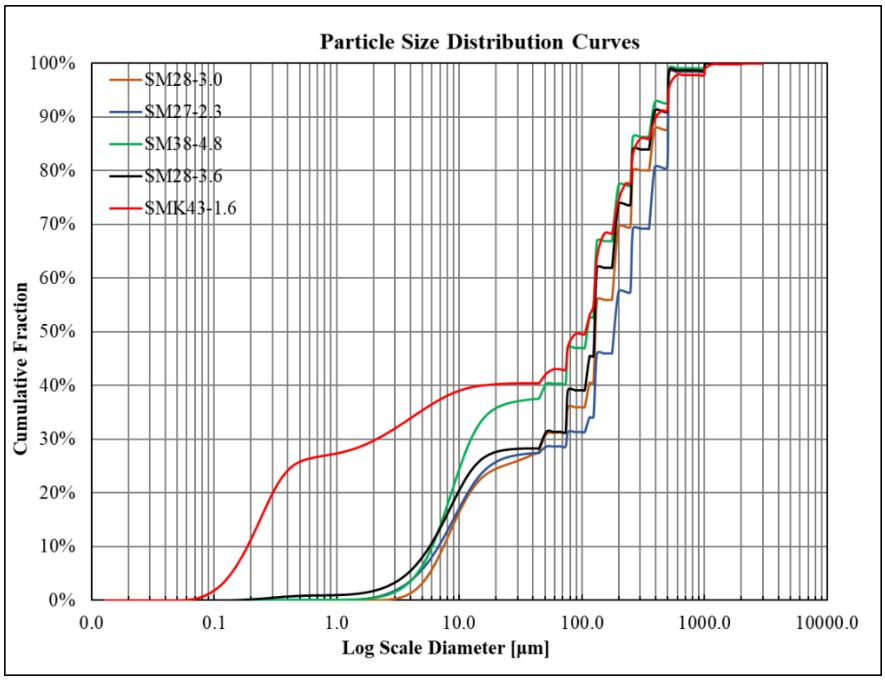


Figure 1: Particle size distribution data for the sample used in the study

Table 1 presents the Atterberg limits and clay properties for each sample. The liquid limit of the samples ranged from 21% to 29%, and the plasticity index varied between 9% and 19%. Despite sample SMK43-1.6 having the highest fines and clay contents, its methylene blue index (MBI) values were significantly lower compared to the other samples. Also, the sample did not show a significant difference in consistency limits when compared to other samples with less fines and clay contents. This discrepancy is due to SMK43-1.6 containing kaolinite, which is less active than the illite typically found in fluid tailings (FT).

Table 1: Summarized index properties for tested samples

ID	Fines (-44m)	Clay (-2µm)	MBI	Liquid Limit %	Plastic Limit %	PI (%)
SM28-3.0	28%	12%	3.0	23%	11%	13%
SM27-2.3	27%	13%	2.3	22%	9%	13%
SM38-4.8	38%	18%	4.8	29%	10%	18%
SM28-3.6	28%	16%	3.6	21%	12%	9%
SMK43-1.6	43%	38%	1.6	24%	12%	11%

FCT and VST data comparison

Figure 2 is a scatter plot for average values from both the FCT and VST data of each of the five samples. Samples SM28-3.0, SM27-2.3, SM38-4.8 and SM28-3.6 show a strong correlation between shear strength

values obtained from FCT and those obtained from VST up to 60 kPa. Beyond this point, the correlation keeps decreasing as strength increases. Also, past 60 kPa the shear strength values measured by FCT are higher than those measured by VST. This can be explained by the crust forming on the surface, thus inhibiting the penetration of the Fall Cone, which will result in an overestimation of the sample's strength, as opposed to the VST, which is inserted to measure strength at the middle portion of the sample. A very weak correlation between FCT and VST was observed for sample SMK43-1.6's data; the trend shows that the VST overestimates strength values below 80 kPa while underestimating values above that. This is the sample that constituted mainly sand and kaolinite. While the comparison is not as good as for other samples, it is still reasonable.

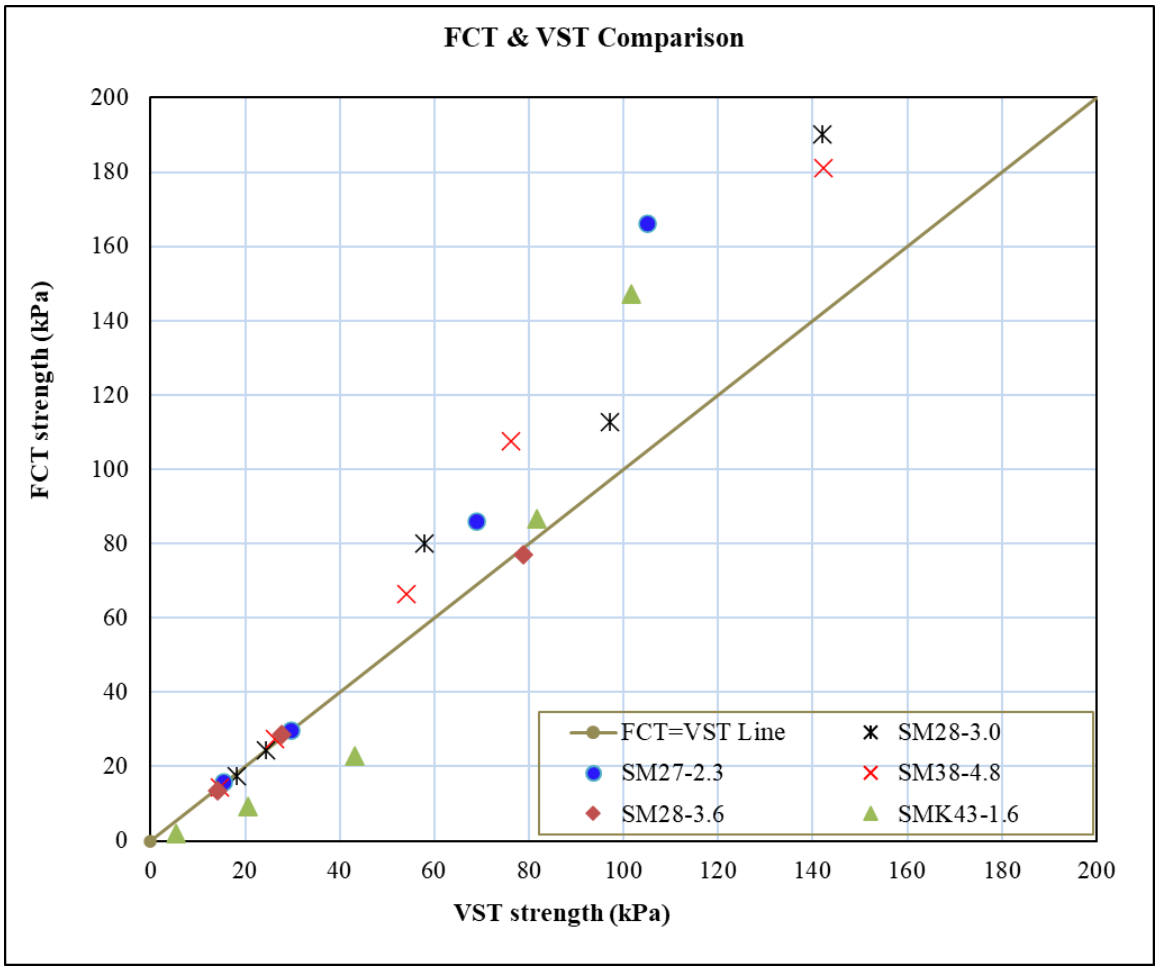


Figure 2: Data comparison between FCT and VST in transitional oil sands tailings

Figure 3 and Figure 4 show very good correlation for strength data, from both the FCT and the VST, for samples SM28-3.0, SM27-2.3, SM38-4.8, SM28-3.6 and SMK43-1.6 to undrained shear strength estimated by Leroueil et al.'s (1983) Equation 5 and Locat and Demers' (1988) Equation 6 respectively, especially in their intended range of liquidity index (greater than 0.5).

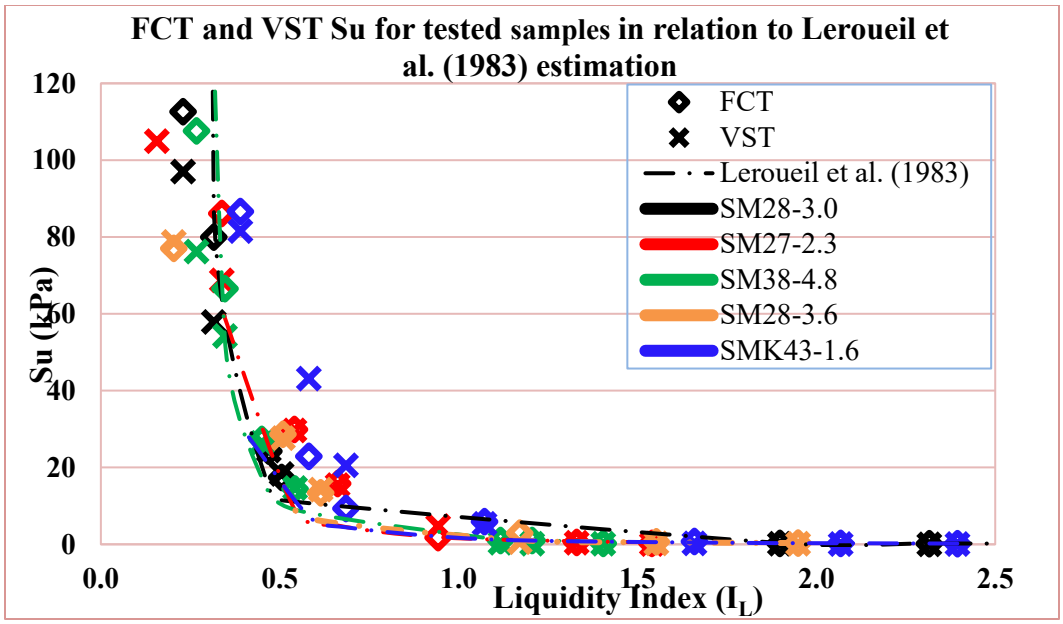


Figure 3: Shear strength correlation between the FCT experimental data, the VST experimental data and strength estimates using the Leroueil et al. (1983) approach

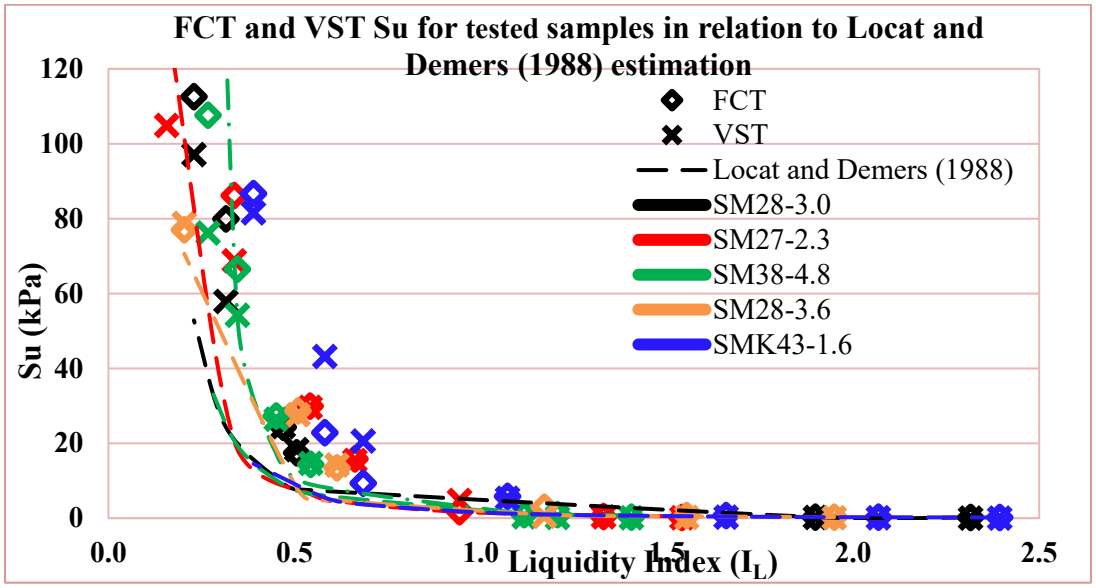


Figure 4: Shear strength correlation between the FCT experimental data, the VST experimental data and strength estimations using the Locat and Demers (1988) approach

All samples show an exponential increase in shear strength with a decrease in their water content and liquidity index, which agrees with the trend observed by Boger (2006) through experiments on various tailings samples. At first, strength increases slowly with liquidity index/water content decrease, and a quick increase is observed at the point where these materials get to a liquidity index of about 0.5. For samples

SM28-3.0, SM27-2.3, SM38-4.8, and SM28-3.6, a great correlation between measured values and estimated values by Leroueil et al. (1983) is evidenced up to 60 kPa strength. The Locat and Demers (1988) estimated values in Figure 4 show a better agreement with higher measured strengths when samples have reached less than 0.5 liquidity index values. The agreement between laboratory tests data and estimates by Leroueil et al. (1983) and Locat and Demers (1988) models that were developed based on cohesive materials provides confidence that both FCT and VST can be used in estimating undrained strength for oil sands tailings in sandy-fines category.

The correlation of FCT and VST measured strength values with both the Leroueil et al. (1983) and the Locat and Demers (1988) estimates keeps diminishing as strength values increase, especially beyond 100 kPa. A diminishing correlation can be explained by the suitability of VST and FCT to measure only up to 100 kPa and 200 kPa respectively, which means measurements are unreliable beyond and close to those limits, and also by the fact that both Leroueil et al. (1983) and Locat and Demers (1988) are designed for undrained strengths of samples with higher than 0.5 liquidity index values. Another significant factor affecting FCT measurements could be the crust forming on the top layer of the samples during their preparation in Tempe Cells, leading to a strength overestimate for the strength of the inner part of the sample. Both FCT and VST experimental data for sample SMK43-1.6 are poorly correlated to either of the two estimation approaches, even at a higher liquidity index where all other samples have shown a good correlation. From the sample characterization study, the sample SMK43-1.6 has the least activity with an MBI value of 1.6, even though it has the highest fines and clay contents. With these properties, this sample likely exhibited drained shear strength, whereas FCT and VST are meant to measure undrained shear strength, and hence the incorrect strength values.

Conclusion

Experimental data have shown a great correlation with estimated data using Atterberg properties of the samples. From this study it can be concluded that either the Vane Shear or Fall Cone test can be used to measure the shear strength of oil sands tailings in sandy-fines category for shear strength up to 60 kPa with great accuracy and repeatability. For measurements of higher strengths of these materials, it would be better to consider the use of other shear strength measurement counterparts, i.e., direct shear and triaxial tests.

If there is a need to measure strength between 60 kPa and 100 kPa while understanding the inaccuracy and reliability of the data, then VST should be used as it gives values closer to the estimated values of strength, with no effects caused by the crust forming on the surface.

Acknowledgements

The authors would like to acknowledge the research and financial support from the Natural Science and

Engineering Research Council of Canada and Canada's Oil Sands Innovation Alliance (NSERC/COSIA) Industrial Research Chair in Oil Sands Tailings Geotechnique and Industrial Research Chair for Colleges in Oil Sands Tailings Management.

References

AER. 2022. Directive 085 – Fluid tailings management for oil sands mining projects. Accessed 5/18/2024 at https://static.aer.ca/prd/documents/directives/Directive085.pdf

AER. 2023. State of fluid tailings management for mineable oil sands, 2022. Accessed 5/18/2024 at https://static.aer.ca/prd/documents/reports/State-Fluid-Tailings-Management-Mineable-OilSands.pdf

ASTM International. 2017. D4318 − 17 Standard test methods for liquid limit, plastic limit, and plasticity index of soils. ASTM International.

Boger, D. V., Scales, P.J. and Sofra, F. 2006. Rheological concepts. *Paste and Thickened Tailings – A Guide:* 25–37. Accessed 6/14/2024 at https://acg.uwa.edu.au/wp-content/uploads/2014/11/PTT_v2_sample_chapter.pdf

Canelas, D., Fernandes, I. and Da Graça Lopes, M. 2018. Use of Fall Cone Test for the determination of undrained shear strength of cohesive soils. *MATEC Web of Conferences* 251(4): 04067. DOI:10.1051/matecconf/201825104067

Chalaturnyk, R.J., Don Scott, J. and Özüm, B. 2002. Management of oil sands tailings. *Petroleum Science and Technology* 20(9–10): 1025–1046. doi:10.1081/LFT-120003695

Claveau-Mallet, D., Duhaime, F. and Chapuis, R. 2012. Practical considerations when using the Swedish Fall Cone. *Geotechnical Testing Journal* 35(4). doi:10.1520/GTJ104178

CNRL. 2020. Canadian natural Jackpine Mine fluid tailings management report. Accessed 5/22/2024 at https://static1.squarespace.com/static/52abb9b9e4b0cb06a591754d/t/5ed01229ed759012fc08d0a1/1590694462355/2019+CNRL+JPM+Fluid+Tailings+Report+%28comp%29.pdf

COSIA. 2012. Technical guide for fluid fine tailings management. Accessed 6/12/2024 at https://cosia.ca/sites/default/files/attachments/TechGuideFluidTailingsMgmt_Aug2012.pdf

COSIA. 2014. Measuring undrained shear strength of oil sands tailings deposits.

D4648/D4648M-24, A. 2024. Standard test methods for laboratory miniature vane shear test for saturated fine-grained soil. ASTM International.

Das, B.M. 2009. *Principles of Geotechnical Engineerin*g. Cengage Learning.

Hansbo, S. 1957. A new approach to the determination of the shear strength of clay by the Fall Cone Test. Stockholm, Sweden: Royal Swedish Geotechnical Institute.

Imperial. 2022. Mine plan amendment and tailings management plan integrated application. Accessed 5/19/2024 at https://dds.aer.ca/iar_query/ApplicationAttachments.aspx?AppNumber=1936482

Koumoto, T. and Houlsby, G.T. 2001. Theory and practice of the Fall Cone Test. *Géotechnique* 51(8): 701–712. doi:10.1680/geot.51.8.701.40475

Leroueil, S., Tavenas, F. and Le Bihan, J.-P. 1983. *Propriétés caractéristiques des argiles de l'est du Canada*. *Can. Geotech. J.* 20(4): 681–705. doi:10.1139/t83-076

Locat, J. and Demers, D. 1988. Viscosity, yield stress, remolded strength, and liquidity index relationships for sensitive clays. *Can. Geotech. J.* 25(4): 799–806. doi:10.1139/t88-088

Lu, T. and Bryant, W.R. 1997. Comparison of vane shear and fall cone strengths of soft marine clay. *Marine Georesources and Geotechnology* 15(1): 67–82. doi:10.1080/10641199709379935

Natural Resources Canada. 2023. *Energy Fact Book 2022–2023*. Accessed 5/18/2024 at: https://natural-resources.canada.ca/sites/nrcan/files/energy/energy_fact/2022-2023/PDF/Energy-factbook-2022-2023_EN.pdf

Oil Sands Tailings Consortium (OSTC). 2012. Technical guide for fluid fine tailings management. Calgary, AB, Canada.

Romanova, U., Valinasab, M., Stasiuk, E., Yarranton, H., Schramm, L. and Shelfantook, W. 2006. The effect of oil sands bitumen extraction conditions on froth treatment performance. *Journal of Canadian Petroleum Technology* 45(09). DOI:10.2118/2005-037

Skempton, A. 1954. Discussion: Sensitivity of clays and the c/p ratio in normally consolidated clays. *Proceedings of the American Society of Civil Engineers,* Separate 478, 19–22.

Skempton, A. 1957. Discussion: Further data on the c/p ratio in normally consolidated clays. *Proceedings of the Institution of Civil Engineers* 7: 305–307.

Wood, D. M. 1985. Some fall-cone tests. *Géotechnique* 35(1): 64–68. doi:10.1680/geot.1985.35.1.64

Wroth, C.P. and Wood, D.M. 1978. The correlation of index properties with some basic engineering properties of soils. *Can. Geotech. J.* 15(2): 137–145. doi:10.1139/t78-014

Selection of the Seismic Coefficient in Pseudostatic Slope Stability Analyses of Tailings Dams

Jonathan Bray, University of California Berkeley, USA
Jorge Macedo, Georgia Institute of Technology, USA

Abstract

The seismic coefficient used in pseudostatic slope stability analysis of tailings dams is often based on precedence without consideration of what constitutes satisfactory performance. The potential for a material to lose significant shear strength due to earthquake ground shaking should be evaluated first. A flow slide is possible if the post-liquefaction slope stability factor of safety is less than one. The seismic coefficient used in the analysis should be compatible with the allowable amount of seismic slope displacement. The seismic coefficient can be selected to achieve an assessment consistent with the amount of seismic slope displacement that would have been calculated with a seismic slope displacement procedure. The seismic slope displacement procedure employed captures the dynamic response characteristics of the slope with its fundamental period and the seismic demand with the 5% damped elastic design spectral acceleration at the degraded period of the potential sliding mass and the moment magnitude of the governing earthquake. The uncertainty in the estimates of these parameters can be captured using different percentile estimates of these values. By using a *displacement-compatible* seismic coefficient in the pseudostatic slope stability analysis, the engineer considers the amount of seismic displacement judged to be allowable and the seismic hazard at the site in the selection of the seismic coefficient.

Introduction

Pseudostatic slope stability procedures are often used in engineering practice to evaluate the seismic performance of tailings dams. These procedures have the advantage of being straightforward to use in preliminary seismic slope stability assessments. However, the parameters utilized in the analysis should reflect the potential seismic demand at the site and its impact on the seismic performance of the tailings dam to provide a reliable assessment of the potential seismic performance of the tailings dam. The seismic coefficient should be selected in a rational manner because its value determines the reasonableness of the results of a pseudostatic slope stability analysis. As seismic slope displacement provides an index of the anticipated seismic performance of the slope, the seismic coefficient used in the analysis should be

compatible with the allowable amount of seismic slope displacement of the tailings dam and the characteristics of the governing seismic hazard.

After discussing the pseudostatic slope stability procedure, a procedure is recommended that takes advantage of recent work on performance-based earthquake engineering (PBEE) seismic slope displacement procedures. This procedure calculates a seismic coefficient that is a function of the allowable seismic slope displacement, the seismic demand at the tailings dam site, and the sliding mass's properties. The way this approach can be used in engineering practice is also discussed.

Pseudostatic slope stability procedure

The pseudostatic slope stability analysis calculates a factor of safety (*FS*) using a static limit equilibrium method in which a horizontal inertial force is applied to the potential sliding mass to represent the destabilizing effects of the earthquake shaking. The horizontal inertial force is expressed as the product of a seismic coefficient (*k*) and the weight (*W*) of the potential sliding mass (see Figure 1). The pseudostatic analysis also requires the use of appropriate material dynamic strengths (*s*). The static limit equilibrium method should satisfy all three conditions of equilibrium to ensure that a reliable *FS* is calculated (Duncan et al. 2014). The seismic performance of a tailings dam is judged to be acceptable if the calculated *FS* is above a specified minimum value (which is often assumed to be 1.0, 1.1, or 1.2). The seismic coefficient, shear strength, and acceptable minimum factor of safety are often based on precedence. The basis for the selected *s, k,* and *FS* values used in a pseudostatic slope stability analysis is often unclear. The rationale for the selected values is often questionable. Justifiable values of *s*, *k*, and *FS* are required if a pseudostatic slope stability procedure is to be used reliably to assess the seismic performance of a tailings dam.

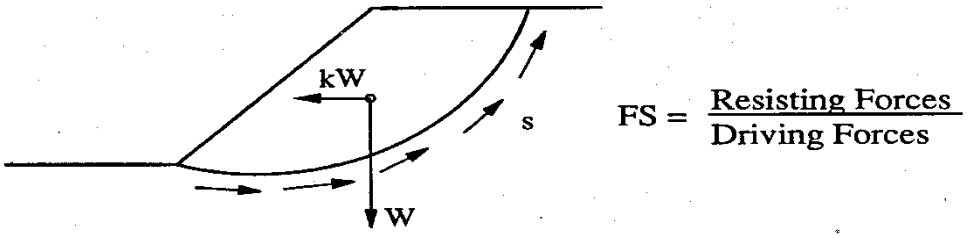


Figure 1: Pseudostatic slope stability analysis

Severe strength loss evaluation

In the evaluation of the seismic performance of a tailings dam, the engineer must first assess if there are materials in the tailings dam or in its foundation that can lose significant strength because of cyclic loading. Soil liquefaction is a primary concern, especially if flow liquefaction can occur. The pseudostatic slope stability procedure can provide misleading results if the cyclic strength of the tailings and earth materials

is not evaluated appropriately. The calculated *FS* is meaningless if pre-seismic static strength values are utilized in the analysis and these materials lose significant strength due to earthquake shaking. The potential for significant strength loss either due to liquefaction of sandy or silty materials or cyclic softening of sensitive clayey soils must be evaluated first. If it is likely that these materials will undergo severe strength loss, their post-shaking reduced shear strength values should be employed in the seismic stability evaluation. If the post-seismic slope stability *FS* approaches or falls below unity, a potentially catastrophic flow slide is possible. Therefore, the assessment of the strength loss potential of the materials in and below the tailings dam should be the initial focus of the evaluation.

Several soil liquefaction triggering procedures are available (e.g., Robertson, 2009; Boulanger and Idriss, 2016). The Chinese criteria should no longer be used to assess the liquefaction susceptibility of fine-grained soil. Updated criteria such as those developed by Bray and Sancio (2006), which are based on soil plasticity ($PI \leq 12$) and sensitivity ($w_c/LL \geq 0.85$), should be used. Additionally, soils with $PI > 12$ should be evaluated carefully, as sensitive clay flow slides have occurred, such as those in Anchorage during the 1964 Alaskan earthquake (e.g., Idriss 1985). The potential for flow slides resulting from severe strength loss due to liquefaction or post-peak strength reduction in sensitive clays should be evaluated carefully before employing a limit equilibrium stability procedure that assumes a rigid-perfectly plastic material response during shear (e.g., Bray and Macedo, 2023).

Framework for the selection of the pseudostatic coefficient

The pseudostatic slope stability method can provide reasonable results for a tailings dam if the combination of *k*, *s*, and *FS* used provides a performance assessment that is consistent with that expected from advanced analysis and field case histories. A properly calibrated pseudostatic slope stability procedure requires a compatible selection of the seismic coefficient, dynamic material strengths, and an acceptable factor of safety. All three of these critical design parameters must be specified and shown to provide reliable results in terms of the anticipated amount of seismic displacement of the tailings dam.

The horizontal force *kW* in the pseudostatic slope stability analysis represents the dynamic effects of the design earthquake. However, unlike the earthquake's actual dynamic effects, this pseudostatic force acts as a constant force in only one direction. In limit equilibrium analysis, $FS = 1.00$ occurs when the activating forces (or moments) equal the resisting forces (or moments). Hence, only the condition of incipient motion is considered. With dynamically applied earthquake-induced loads, the force may act in one direction for only a few tenths of one second before its direction is reversed. The results of these transient forces will be a series of displacement pulses (Newmark, 1965). Satisfactory performance is judged by whether the accumulated seismically induced permanent displacement is tolerable. Selecting a seismic coefficient that is a fraction of the maximum seismic demand is reasonable because exceeding the

maximum seismic resistance during a few instances will only lead to small seismic slope displacement. Thus, the results of a pseudostatic slope displacement procedure should be tied to the likely shear-induced seismic slope displacement (D_S) of the tailings dam.

A Newmark sliding block model can capture that part of the seismically induced permanent displacement attributed to shear deformation. Ground movement due to volumetric compression of the soil is not captured explicitly by a Newmark model. The top of a tailings dam can displace downward due to shear and volumetric-induced deformation. Shear-induced and volumetric-induced displacement should be estimated separately using procedures based on the sliding block model to estimate shear-induced displacement and other procedures to estimate volumetric-induced displacement (e.g., Tokimatsu and Seed, 1987 or Bray and Olaya, 2023). The sum of the shear-induced and volumetric-induced dam displacement components should be considered.

The yield coefficient (k_y) used in a Newmark-type calculation is the k value that results in a $FS = 1.00$ in the pseudostatic slope stability analysis; it represents the dam's dynamic resistance. Recognizing that k_y for a sliding mass depends exclusively on the slope characteristics is important. Although a pseudostatic slope stability analysis is performed to find k_y, one should remember the problem is inherently dynamic, so several potential slip surfaces should be considered to find the sliding mass that produces the largest D_S, which is the critical sliding surface. The most important parameter in a rigid or decoupled flexible sliding block analysis is $k_y/k_{max,}$ where k_{max} is the maximum seismic demand. The sliding mass with the lowest k_y/k_{max} value will produce the largest D_S.

The Seed (1979) pseudostatic slope stability method was developed for earth dams with materials that do not undergo severe strength loss and dam crest accelerations less than 0.75 *g*. Seismic performance is judged to be acceptable by this method using $k = 0.15$ with appropriate dynamic strength if $FS \geq 1.15$. This approach involves several simplifying assumptions and is calibrated for evaluating earth dams wherein D_S = 1 m implies satisfactory seismic performance. Another significant limitation of this method is that earthquake shaking is represented by a single seismic coefficient value ($k = 0.15$) for all cases. Instead, k should depend on the source-to-site distance (R), site conditions (V_{s30}), and the moment magnitude (M) of the design earthquake event. Additionally, the use of a minimum acceptable FS other than 1.00 leads to inconsistencies. Using $FS \geq 1.15$ ensures k_y will be greater than 0.15 by an unknown amount. The expected seismic performance is unclear because the level of conservatism resulting from $FS \geq 1.15$ is unknown.

The Hynes-Griffin and Franklin (1984) pseudostatic screening procedure is based on a conservative interpretation of the dynamic response of an earth dam to an older set of shallow crustal earthquake ground motions. They too assumed materials are not susceptible to severe strength loss, and D_S = 1 m implies satisfactory seismic performance. Their procedure applies $k = 50\%$ of the peak ground acceleration on rock (PGA_R) at the site, $s = 80\%$ of the static shear strength of the materials, and $FS \geq 1.00$. If these criteria are

met, the dam is judged to be safe as defined by D_S = 1 m being tolerable. Tying k to 50% PGA_R enables the pseudostatic slope stability analysis to consider the different seismic hazard hazards at sites worldwide, but PGA is not an optimal seismic intensity parameter for estimating D_S for tailings dams (Bray and Travasarou 2007). Seismically induced displacement of an earth structure is better captured by peak ground velocity (PGV) (Newmark 1965), or 5%-damped elastic spectral acceleration (S_a) (Bray and Travasarou, 2007).

A pseudostatic stability procedure developed by Saragoni (1993) based on observations of the performance of rigid retaining structures at ports in Valparaiso during the 1985 Chile earthquake has also been applied to evaluate the seismic performance of tailings dams. In it, $k = 0.30\ PGA/g$ for $PGA \leq 0.673\ g$ or $k = 0.22\ (PGA/g)^{0.333}$ for $PGA > 0.673\ g$. This procedure was not developed to capture the response of tailings dams, which are not rigid. Moreover, Saragoni (2014) later states "… *displacements are not related with maximum ground acceleration* …" Thus, this procedure should not be used to select the seismic coefficient in a pseudostatic slope stability analysis of a tailings dam.

Historically, engineering judgment and precedence guided the selection of k. There are now several studies that recommend the k value to be used in pseudostatic slope stability analysis. However, the basis of the recommended k value is often not linked explicitly to the properties of the potential sliding mass, the seismic hazard, and importantly, the likely amount of seismic slope displacement. With the adoption of modern PBEE approaches and an enhanced understanding of the seismic hazard, the use of a prescribed seismic coefficient value across a geographic region because it has been used previously is not justifiable. Instead, k should be selected based on the unique seismic hazard present at a site and the level of seismically induced permanent displacement that constitutes an acceptable level of seismic performance of the tailings dam. This paper presents a rational framework for selecting k in pseudostatic slope stability analysis.

PBEE seismic slope displacement model

The recommended procedure for selecting a *displacement-compatible* seismic coefficient is based on the work of Bray and Macedo (2019) for shallow crustal earthquakes and the work of Macedo et al. (2023) for interface and intraslab subduction zone earthquakes. These procedures utilize thousands of recorded ground motions from defined tectonic sources with a validated nonlinear coupled flexible stick-slip sliding model to estimate seismic slope displacement of earth structures, including tailings dams, and the uncertainty of the estimate of D_S. The methodology, model, and their limitations are described in Bray et al. (2018). This seismic slope displacement model allows the engineer to estimate D_S using two equations that calculate: (1) the probability of negligible ("zero") slope displacement (i.e., $D_S \leq 0.5$ cm), and (2) the likely amount of "nonzero" slope displacement. The probability of negligible slope displacement equation can be neglected in this application because it does not have a noticeable effect on k for a median seismic slope displacement value larger than 5 cm. Neglecting this first step yields conservative results for displacements less than 5 cm. Given the

simplifications of a sliding block model, it should not be used in cases when it estimates median D_S values greater than 5 m. It can be used when limited zones liquefy if post-liquefaction residual strengths are used.

For ordinary shallow crustal earthquake shaking, D_S (cm) is estimated as (Bray and Macedo, 2019):

$$ln(D_S) = a_1 - 2.482Ln(k_y) - 0.244\left(Ln(k_y)\right)^2 + 0.344Ln(k_y)Ln(Sa(1.3T_s)) + 2.649Ln(Sa(1.3T_s)) - 0.090\left(Ln(Sa(1.3T_s))\right)^2 + a_2T_s + a_3(T_s)^2 + 0.603M_w + \varepsilon \quad (1)$$

where k_y is the yield coefficient; T_s is the initial fundamental period of the sliding mass in seconds; a_1 = -5.981, a_2 = 3.223, and a_3 = -0.945 for systems with $T_s \geq 0.10$ s, and a_1 = -4.684, a_2 = -9.471, and a_3 = 0.0 for $T_s < 0.10$ s; S_a is the 5% damped elastic spectral acceleration of the ground motion acting on the material below the sliding mass at a period of $1.3T_s$ in the unit of g; M is the earthquake's moment magnitude; and ε is a normally-distributed random variable with zero mean and standard deviation (σ) of 0.72.

For subduction zone earthquakes, D_S (cm) is estimated as (Macedo et al., 2023):

$$ln(D_S) = a_0 + a_1ln(k_y) + a_2(ln(k_y))^2 + a_3ln(k_y)\ln\left(S_a(1.3T_s)\right) + a_4\ln\left(S_a(1.3T_s)\right) + a_5(\ln\left(S_a(1.3T_s)\right))^2 + a_6T_s + a_7(T_s)^2 + a_8M_w + \varepsilon \quad (2)$$

where the parameters are as defined previously, except the coefficients a_0 to a_8, and σ are defined in Table 1 for interface and intraslab sources.

Table 1: Coefficients for interface and intraslab earthquakes (Macedo et al., 2023)

Coefficient	Interface		Intraslab	
	$T_s < 0.1$ s	$T_s \geq 0.1$ s	$T_s < 0.1$ s	$T_s \geq 0.1$ s
a_0	-5.00	-6.19	-4.13	-5.27
a_1	-3.18	-3.18	-2.21	-2.21
a_2	-0.35	-0.35	-0.20	-0.20
a_3	0.45	0.45	0.22	0.22
a_4	2.89	2.89	2.31	2.31
a_5	-0.14	-0.14	-0.02	-0.02
a_6	-9.46	2.87	-9.45	3.63
a_7	0.0	-0.86	0.0	-1.10
a_8	0.46	0.46	0.50	0.50
σ	0.75	0.75	0.62	0.62

The Newmark (1965) rigid block sliding analysis assumes a rigid block sliding on a rigid plane that is excited by an acceleration-time history. Tailings dams are not rigid blocks, so capturing the dynamic response characteristics of their flexible sliding mass is important. This can be done approximately with the decoupled approximation or more robustly with a fully coupled model (Rathje and Bray, 2000). Kramer and Smith (1997) noted: "*If permanent displacements are assumed to be restricted to the sliding interface, the most important characteristics are the stiffness and distribution of mass within the failure mass.*" The sliding mass can be

represented by a dynamic system that captures its fundamental period and mass.

Tailings dams are part of a larger dynamic system. They may be founded on rock, or they may be founded on deep alluvium. It is a simplification to characterize the fundamental period of a tailings dam without considering the flexibility of its foundation. It is a simplification to characterize a part of the tailings dam that may slide during an earthquake without considering the flexibility of the material below the sliding plane. It is equally a simplification to characterize a structural system by its fixed-based fundamental period when it is founded on a soil deposit. Yet, these simplifications are routinely made in practice because they can provide useful insights. The fundamental period of a potential sliding mass within a larger dynamic system provides an index of its flexibility and the dynamic response characteristics of the sliding mass.

The Bray et al. (2018) sliding block model assumes a flexible sliding mass that can slide atop a rigid base, which is consistent with the approach developed by Kramer and Smith (1997). The spectral acceleration value (S_a) at $1.3T_s$ represents the seismic loading on a flexible sliding mass that is not rigid (i.e., $T_s > 0$ s). As with other rigid or flexible sliding block Newmark-type models, this approach suffers from the assumption that the earth below the sliding mass is assumed to be rigid. However, $S_a(1.3T_s)$ can be used as an index of the seismic loading on a potential sliding mass by validating its use with observations from field case histories and the results of robust advanced analyses, as was done in developing the Bray and Macedo (2019) and Macedo et al. (2023) procedures. T_s can be estimated approximately in most cases, or it can be estimated reliably using the methodology proposed by Bray and Macedo (2021).

For the base sliding case and for other deep sliding cases, use of the T_s of the dam or T_s of a large sliding mass that is a large part of the dam is reasonable for estimating the seismic demand. For shallow sliding cases, the response of the material below the potential sliding mass changes the input characteristics of the ground shaking, which can be estimated using nonlinear 1D seismic site response methods. Additionally, the estimated $S_a(1.3T_s)$ value, which approaches *PGA* as $1.3T_s$ approaches 0, should be adjusted for topographic effects (e.g., amplifying the PGA by a factor of 1.3 for moderate slopes (Rathje and Bray, 2001) or using the dam crest PGA relationship of Park and Kishida, 2019). A simplified sliding block analysis cannot capture all the aspects of the problem that can be captured by a nonlinear dynamic finite difference analysis with a robust, validated, calibrated constitutive model. However, a nonlinear, coupled flexible sliding block model that has been validated with field case history data can provide an index of the likely seismic performance of a tailings dam.

Selection of the seismic coefficient

The Bray and Macedo (2019) procedure and Macedo et al. (2023) procedure have been adapted to provide a rational basis for selecting k that is based on the expected seismic demand at the project site and the desired level of seismic performance of the tailings dam in terms of its allowable seismic displacement. Instead of calculating D_S as a function of k_y, T_s, S_a, and M, Equations (1) and (2) can be revised to solve for a

displacement-compatible k as a function of the allowable seismic displacement (D_S), T_s, S_a, and M. If this value of k is used in a pseudostatic slope stability analysis and the calculated $FS \geq 1.00$, then the selected percentile estimate of D_S will be less than or equal to D_{Sa}. Specifically, the calculated shear-induced seismic slope displacement will be less than D_{Sa} if one performs a seismic slope displacement calculation using the Bray and Macedo (2019) procedure or the Macedo et al. (2023) procedure.

The *displacement-compatible k* applied in pseudostatic stability analyses is not the yield coefficient (k_y). However, k can be linked to k_y in a pseudostatic slope stability analysis to get the same result as if one had performed a seismic slope displacement calculation. This is the approach proposed by Whitman (1990) to select k in a pseudostatic analysis of a rigid retaining wall with the value of k linked to k_y, so the analysis achieved results consistent with those of a seismic displacement analysis. If k is selected to be k_{max} and $FS \geq 1.00$ for a rigid or decoupled flexible sliding block case, $D_S = 0$ because the seismic demand never exceeds k_y (i.e., $k_y/k_{max} \geq 1.00$). If k is selected to be less than k_{max} and $FS = 1.00$ for a rigid or decoupled flexible sliding block case, D_S will be calculated to be greater than 0, because the seismic demand exceeds k_y (i.e., $k_y/k_{max} < 1.00$). As the selected k decreases for these cases when $FS = 1.00$, k_y/k_{max} also decreases, and thus D_S increases. Thus, the value of k selected in a pseudostatic slope stability analysis is tied to D_S. Although the sliding mass has a unique k_y value, an engineer can choose the value of k to use in a pseudostatic slope stability analysis, and their choice of k leads to more or less D_S being calculated in a corresponding seismic slope displacement analysis. The inversion of Equation (1) or (2) provides a value of k consistent with a Newmark-type seismic slope displacement calculation that gives the desired range of seismic slope displacement. These equations can also be used to cast the estimation of k in a fully probabilistic framework (Macedo and Candia, 2020), but in this case, the estimation of k needs the estimation of D_S hazard curves.

The Bray and Macedo (2019) site-dependent and allowable displacement-dependent value of k is:

$$k = exp\left[\frac{-a+\sqrt{b}}{0.49}\right] \geq 0.03 \quad (3a)$$

where

$$a = 2.491 - 0.344Ln(S_a(1.3T_s)) \quad (3b)$$

$$b = a^2 - 0.98(Ln(D_{Sa}) - a_1 - 2.703Ln(S_a(1.3T_s)) + 0.089Ln(S_a(1.3T_s))^2 - a_2T_s - a_3(T_s)^2 - 0.6070M - \varepsilon) \quad (3c)$$

where the model parameters and coefficients are defined previously in Equation (1). A similar manipulation of Equation (2) can be done to estimate k for interface and intraslab subduction zone earthquakes as functions of the seismic hazard and D_{Sa}, as presented in Macedo et al. (2023). The minimum design value of k is set to 0.03 regardless of what is calculated to establish a reasonable threshold. The basis of this threshold value of k are the simplifications involved in the pseudostatic slope stability analysis, the uncertainty of the seismic slope displacement procedure increases as k decreases, and the requirement to

have an adequate static factor of safety in a relatively gentle infinite slope.

The steps required to perform the pseudostatic slope stability analysis with a seismic hazard-dependent and project performance-dependent *displacement-compatible* seismic coefficient are:

1. Evaluate if there are materials that could lose severe strength during earthquake shaking (e.g., liquefaction). Use post-shaking reduced strengths for these materials and use best-estimate dynamic shear strengths for materials that do not lose significant strength (Bray and Macedo, 2023). Calculate the post-liquefaction slope stability FS. If $FS \leq 1.0$, a flow slide may develop, and the seismic displacement can be large. Evaluate and implement mitigation measures or consider using advanced analysis to assess the seismic performance of the tailings dam. If $FS > 1.1$, the pseudostatic slope stability method may be used. A pseudostatic slope stability analysis is most appropriate for evaluating a tailings dam and foundation that are composed of materials that do not lose significant strength loss due to earthquake shaking. For example, a well-compacted downstream dam built on a competent foundation (i.e., dilative materials) can be evaluated with the pseudostatic slope stability method. For this case, best-estimate strain-compatible dynamic shear strengths can be used for the dam and its foundation, but the liquefied residual shear strength should be used for the impounded saturated contractive tailings as they will likely liquefy near the start of ground shaking. Cases with limited zones of liquefied material in the dam and its foundation can also be evaluated assuming these materials reach their liquefied residual shear strength at the start of earthquake shaking. The pseudostatic slope stability method should not be used to evaluate the seismic performance of an extreme consequence upstream dam built atop liquefiable contractive tailings with a brittle response.
2. Establish the total allowable seismic displacement (D_a in cm) of the tailings dam through consultation with the owner while considering the consequences of unsatisfactory performance at displacement levels greater than this threshold. The total allowable seismic displacement is the summation of the shear-induced seismic slope displacement D_{Sa} (cm) and the allowable seismic volumetric-induced displacement D_{Va} (cm); D_a should not exceed about 300 cm, given the limitations of the pseudostatic slope stability method and volumetric-induced displacement methods. The volumetric component D_{Va} is typically relatively small in cases in which the shear component D_{Sa} is significant, so one can assume $D_{Sa} = 0.8\ D_a$. The percent exceedance of the D_{Sa} displacement threshold is typically set at the 16% exceedance level (i.e., set $\varepsilon = \sigma$ in Equation 3) considering the consequences of unsatisfactory performance of a tailings dam.
3. The seismic demand is defined in terms of the design spectral acceleration for outcropping site conditions below the sliding mass (which may include topographic amplification) at the degraded

period of the sliding mass (i.e., $S_a(1.3T_s)$) and the moment magnitude (M) of the controlling earthquake event. The ground motion hazard level should be established based on the uncertainty in the seismic hazard characterization, the criticality of the project, and the consequences of unsatisfactory performance.

4. Calculate the *displacement-compatible k* (e.g., using Eq. 3 for shallow crustal earthquakes) and apply this k in a pseudostatic slope stability analysis that satisfies all three conditions of equilibrium. If the resulting $FS \geq 1.00$, the selected percentile estimate of D_S will be less than D_{Sa} if one had performed a seismic slope displacement calculation. The preferred minimum value of the acceptable FS is 1.00 because this method has been calibrated to provide an assessment consistent with the seismic slope displacement calculated with a sliding block analysis. A spreadsheet is available on the authors' websites to simplify the calculation of the design seismic coefficient (e.g., Bray and Macedo, 2024).

Figure 2 illustrates the general relationships between k and D_S and the seismic hazard (i.e., $S_a(1.3T_s)$ and M) for a selected T_s for several seismic source mechanisms. Allowable shear-induced seismic slope displacement values of 30 cm and 1 m at the 16% exceedance level were used to illustrate the dependence of k on the selected level of allowable displacement. Results are also provided for the 1 m displacement level for two earthquake magnitude scenarios. For a selected allowable shear-induced seismic slope displacement target, the seismic coefficient increases with increasing ground motion intensity, as one would expect. It also increases as the magnitude (i.e., duration) of the earthquake event increases. Importantly, the seismic coefficient decreases significantly as the allowable displacement level increases. The seismic coefficient is shown to vary systematically as the allowable shear-induced seismic displacement threshold and design ground shaking level vary.

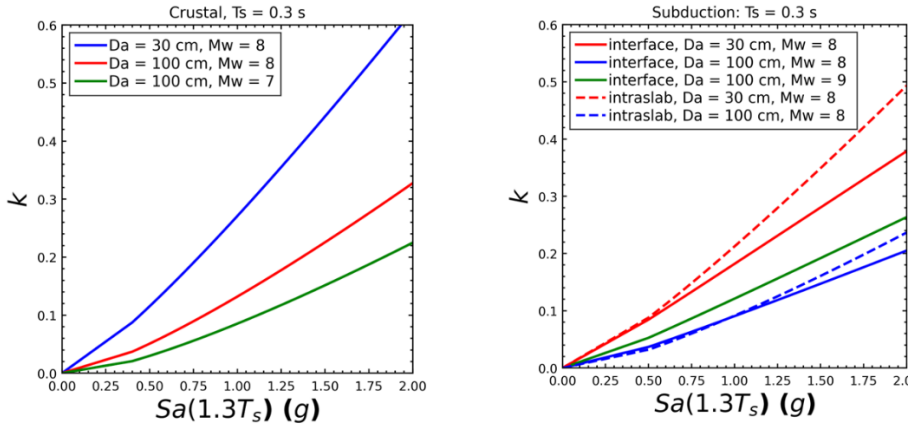


Figure 2: Variation of the seismic coefficient as a function of allowable shear-induced seismic displacement set at 30 cm and 100 cm at the 16% exceedance level and the specified seismic hazard for several cases (k < 0.03 values displayed to show trends)

The seismic coefficient also depends on the potential sliding mass's fundamental period. Relatively stiff slopes with short fundamental periods (i.e., 0.1 s < T_s < 0.3 s) tend to displace more because of resonance with the earthquake ground shaking. More flexible slopes (i.e., T_s > 0.5 s) have relatively less potential for seismic displacement. This effect can be seen by examining representative earthquake scenarios specified in Figure 3 (i.e., soft rock site at R = 20 km from a shallow crustal strike-slip M = 8 earthquake and at R = 50 km from a subduction M = 8 earthquake). After the peak k value is reached, it decreases progressively as the slope's fundamental period increases. The seismic coefficient required to limit a specified allowable seismic displacement threshold is larger for shallow stiff sliding masses than for deep flexible sliding masses (e.g., Rathje and Bray, 2000). The differing effects of interface and intraslab subduction zone earthquake sources are illustrated in Figure 3b.

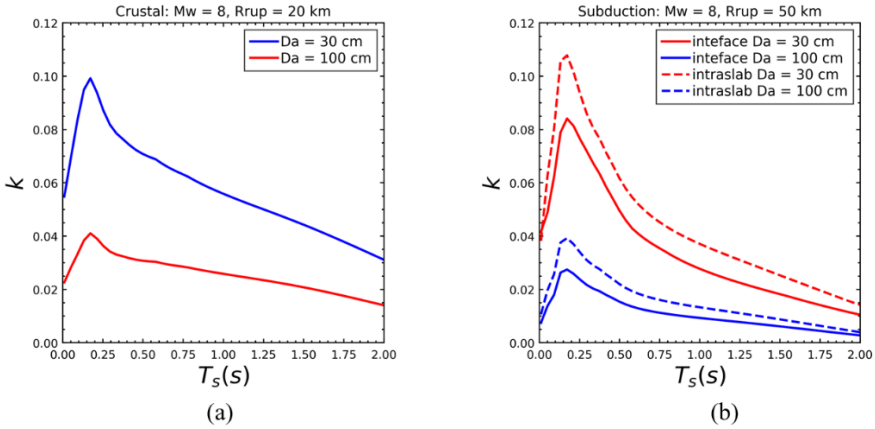


Figure 3: Dependence of the seismic coefficient on the fundamental period of the potential sliding mass for a scenario earthquake with seismic slope displacement set at 30 cm and 100 cm at the 16% exceedance level (k < 0.03 values displayed to show trends)

Example of the selection of the *displacement-compatible* seismic coefficient

The steps presented previously to perform a pseudostatic slope stability analysis with a *displacement-compatible* seismic coefficient are applied to a tailings dam shaken by the 2010 M8.8 Maule, Chile earthquake. Information on the Las Tortolas main tailings dam is provided in Valenzuela (2015) and Valenzuela et al. (2020). It is a downstream-constructed sand dam. Its cross-section, which shows the sliding mass analyzed in this example, is shown in Figure 4.

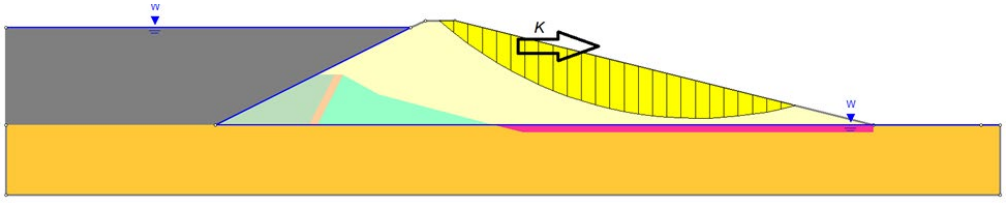


Figure 4: Idealized cross-section of the Las Tortolas main dam (from Valenzuela, 2015) with the potential sliding mass analyzed in this example shown

The selection of the *displacement-compatible* seismic coefficient for the tailings dam for the seismic demand produced by the 2010 Maule earthquake proceeds as follows:

1. No materials lose severe strength at the 2010 Maule earthquake level of shaking. Best-estimate dynamic shear strengths of the dam materials are based on the information provided by Valenzuela (2015) and Valenzuela et al. (2020). The calculated post-seismic slope stability *FS* exceeds 1.1, so the pseudostatic slope stability method can be used.
2. No significant deformation was observed at the Las Tortolas main dam after the 2010 Maule earthquake (Valenzuela, 2015). In this back-analysis of a tailings dam in which no significant deformation was observed, seismic displacement value of D_a is assumed to be negligible (i.e., less than 5 cm). The low value of D_a in this back-analysis should not be confused with the design D_a which is selected at higher level (i.e., often 1 m or more) to judge satisfactory dam performance for the design earthquake, which has a higher seismic demand. The shear-induced seismic slope displacement (D_{Sa}) is assumed to be 80% of D_a, so D_{Sa} = 4 cm. The percent exceedance of the D_{Sa} displacement threshold is set at the 16% exceedance level considering the consequences of unsatisfactory performance of a tailings dam.
3. The initial fundamental period of potential sliding mass (T_s) shown in Figure 4 is estimated as 0.52 s using $T_s = 2.6\ H/V_s$, where H = 70 m and V_s = 350 m/s based on information in Valenzuela (2015). The estimated spectral acceleration for outcropping site conditions below the sliding mass at the degraded period of the sliding mass (i.e., $S_a(1.3T_s)$) is estimated as 0.18 *g* based on $S_a(1.3T_s)$ being about equal to the outcropping *PGA* at the site reported in Valenzuela et al. (2020). The 2010 Maule earthquake is M = 8.8.
4. The *displacement-compatible k* is estimated using the Bray and Macedo (2024) spreadsheet for a subduction zone interface event, which is the tectonic setting of the Maule earthquake. With D_{Sa} = 4 cm, T_s = 0.52 s, $S_a(1.3T_s)$ = 0.18 *g*, *PGV* set to -1 to use the scalar model, M = 8.8, mechanism set to 0 for an interface event, and epsilon = 0.75 to set D_{Sa} at the 16% probability of exceedance level, k = 0.12. The value of k = 0.12 is applied in a slope stability analysis program using the Spencer (1967) method to calculate FS = 1.8 which exceeds 1.0. The result of the pseudostatic slope stability analysis indicates the earthquake-induced displacement of the Las Tortolas tailings dam during the 2010 Maule earthquake should be less than 5 cm, which is consistent with the observed performance reported by Valenzuela (2015). In a forward design analysis of the dam, the seismic demand (i.e., $S_a(1.3T_s)$ and M) would be higher and the allowable seismic displacement (D_a) would be higher, which would produce a different value of k as it is selected to be compatible with the allowable design displacement and consistent with the design seismic hazard.

Conclusion

The seismic coefficient used in a pseudostatic slope stability analysis should be selected in a rational manner. It is not rational to select an arbitrary value of k without considering the site-specific seismic hazard and determining the threshold of allowable seismic displacement that constitutes satisfactory seismic performance of the tailings dam. A rational PBEE procedure is presented that estimates k based on the consequences of different seismic displacement values and different seismic hazards. The engineer should consider the project performance criteria and the seismic hazard when selecting a *displacement-compatible* k value to apply in a pseudostatic slope stability analysis.

This approach requires the engineer to establish a project-specific allowable level of seismic displacement of the tailings dam in consultation with the owner. This is an important dialogue and is project specific. The robustness of the tailings dam and its appurtenance structures should be assessed, and the consequences of unsatisfactory performance should be considered. The site-dependent seismic demand is characterized by the 5% damped elastic design spectral acceleration at the degraded period of the potential sliding mass, either through a probabilistic or deterministic seismic hazard assessment (PSHA or DSHA). The uncertainty in the seismic demand estimate can be addressed using different fractiles in the PSHA or different percentiles of the deterministic estimate of the design spectral acceleration in the DSHA. The uncertainty of the seismic displacement estimate is handled using the 16% exceedance level of the estimated seismic displacement that is judged to be allowable.

The potential for severe strength loss of the materials within and below the tailings dam due to earthquake shaking must be evaluated before employing the pseudostatic slope stability procedure. It is critically important to assess the strength loss potential of the tailings dam and its foundation. A flow slide is possible if the post-liquefaction slope stability FS $\leq$ 1.0. Best-estimate strain-compatible dynamic shear strengths should be used for materials that do not lose significant strength, and liquefied residual shear strengths should be used for saturated contractive materials that are likely to liquefy. Additionally, it is important to remember that seismic slope performance is evaluated in terms of the potential range of seismically induced permanent displacement, even when a pseudostatic slope stability procedure is employed. The estimated seismic displacement of a tailings dam is an index of seismic performance. Thus, an appropriate level of engineering judgment should be exercised.

Acknowledgments

The Faculty Chair in Earthquake Engineering Excellence at UC Berkeley provided financial support to perform this research, which was supplemented by Georgia Tech. The PEER Center provided access to the NGA-West2 and NGA-Sub ground motion intensity measures.

References

Boulanger R.W. and Idriss I.M. 2016. CPT-based liquefaction triggering procedures. *Journal of Geotechnical and Geoenvironmental Engineering* 142(2), 04015065.

Bray, J.D. and Sancio, R.B. 2006. Assessment of the liquefaction susceptibility of fine-grained soils. *Journal of Geotechnical and Geoenvironmental Engineering* 132(9), 1165–1177.

Bray, J.D. and Travasarou, T. 2007. Simplified procedure for estimating earthquake-induced deviatoric slope displacements. *Journal of Geotechnical and Geoenvironmental Engineering* 133(4): 381–392.

Bray J.D. and Macedo, J. 2019. Procedure for estimating shear-induced seismic slope displacement for shallow crustal earthquakes. *Journal of Geotechnical and Geoenvironmental Engineering* 145(12): 04019106.

Bray J.D. and Macedo, J. 2021. Closure to Procedure for estimating shear-induced seismic slope displacement for shallow crustal earthquakes by J.D. Bray and J. Macedo. *Journal of Geotechnical and Geoenvironmental Engineering* 147(5).

Bray, J.D. and Macedo, J. 2023. Performance-based seismic assessment of slope systems. *Soil Dynamics and Earthquake Engineering J.* 168(2).

Bray, J.D. and Olaya, F.R. 2023. 2022 H. Bolton Seed Memorial Lecture: Evaluating liquefaction effects. *Journal of Geotechnical and Geoenvironmental Engineering* 149(8).

Bray, J.D. and Macedo, J. 2024. Simplified seismic slope stability excel spreadsheets. https://www.ce.berkeley.edu/people/faculty/bray/research. Accessed June 15, 2024.

Bray J.D., Macedo J. and Travasarou T. 2018. Simplified procedure for estimating seismic slope displacements for subduction zone earthquakes. *Journal of Geotechnical and Geoenvironmental Engineering* 144(3).

Duncan, J.M., Wright, S.G. and Brandon, T.L. 2014. *Soil Strength and Slope Stability*. Germany: Wiley.

Hynes-Griffin, M.E. and Franklin, A.G. 1984. Rationalizing the seismic coefficient method. Misc. Paper No. GL-84–13. U.S. Army Engineer WES, Vicksburg, MS.

Idriss, I.M. 1985. Evaluating seismic risk in engineering practice. *Proceedings of the 11th International Conference on Soil Mechanics and Foundation Engineering,* San Francisco, CA, 12–16 Aug., Vol. 1: 255–320.

Kramer, S.L. and Smith, M.W. 1997. Modified Newmark model for seismic displacements of compliant slopes. *Journal of Geotechnical and Geoenvironmental Engineering* ASCE, 123(7): 635–644.

Macedo, J., Bray, J.D. and Liu, C. 2023. Seismic slope displacement procedure for interface and intraslab subduction zone earthquakes. *Journal of Geotechnical and Geoenvironmental Engineering* 149(11): 04023104, doi: 10.1061/JGGEFK.GTENG-11445.

Macedo, J. and Candia, G. 2020. Performance-based assessment of the seismic pseudo-static coefficient used in slope stability analysis. *Soil Dynamics and Earthquake Engineering* 133:106109. doi: 10.1016/j.soildyn.2020.106109.

Newmark, N.M. 1965. Effects of earthquakes on dams and embankments. *Géotechnique* V. 15(2): 139–160.

Park D.S. and Kishida, T. 2019. Seismic response of embankment dams based on recorded strong motion data in Japan. *Earthquake Spectra* 35(2): 955–976.

Rathje, E.M. and Bray, J.D. 2000. Nonlinear coupled seismic sliding analysis of earth structures. *Journal of Geotechnical and Geoenvironmental Engineering* 126(11): 1002–1014.

Rathje, E.M. and Bray, J.D. 2001. One- and two-dimensional seismic analysis of solid-waste landfills. *Canadian Geotechnical Journal.* 384: 850–862.

Robertson P.K. 2009. Performance-based earthquake design using the CPT. *International Conference on Performance-Based Design in Earthquake Geotechnical Engineering* (Is-Tokyo 2009).

Seed, H.B. 1979. Considerations in the earthquake-resistant design of earth and rockfill dams. *Géotechnique*, V. 29(3): 215–263.

Spencer, E. 1967. A method of analysis of the stability of embankments assuming parallel inter-slice forces, *Géotechnique* V. 17(1): 11–26.

Tokimatsu, K. and Seed, H.B. 1987. Evaluation of settlements in sands due to earthquake shaking, *Journal of Geotechnical Engineering* 113(8): 861–878.

Valenzuela, L. 2015. Tailings dams and hydraulic fills. The 2015 Casagrande Lecture, at the 16th International Conference on Soil Mechanics and Geotechnical Engineering. Buenos Aires, Argentina.

Valenzuela, L., Verdugo, R., Campana, J. and Opazo, C. 2020. Safety performance of dams in Chile highly seismic environment. *Proceedings of the Fourth International Dam World Conference,* Lisbon, Portugal, Sept 21–25.

Whitman, R.V. 1990. Seismic design and behavior of gravity retaining walls. *Proceedings, Design and Performance of Earth Retaining Structures*, Geotech. SP No. 25, ASCE, NY, 817–842.

The Critical State Line Parameters of Iron Ore Tailings from Basic Laboratory Tests: Updated Insights with Additional Data

José Ccotohuanca, Klohn Crippen Berger Consultoria Ltda, Brazil
Daniel Klassen, Klohn Crippen Berger Ltd, Canada

Abstract

Characterizing iron ore tailings using the critical state soil mechanics (CSSM) framework has become standard practice in Brazil to support the static liquefaction assessments of tailings storage facilities (TSF) undergoing decommissioning processes and the design of filtered tailings stacks. This has resulted in a substantial published database of iron ore critical state (CS) parameters, as most iron ore TSF projects are situated within the Iron Quadrangle (Minas Gerais) in Brazil, an area renowned for hosting one of the world's largest reserves of iron ore.

In early 2024, the authors presented a database containing CS parameters derived from laboratory testing of 26 iron ore sources. Based on newly published data, this database has been expanded. This article compiles CS parameters from an updated database that includes 40 iron ore tailings from various sites in Brazil and worldwide. These parameters are then compared to basic laboratory data including specific gravity (G_s), fines content (FC), mean particle size (D_{50}), coefficient of uniformity (C_u), Atterberg limits represented by the plasticity index (PI) and liquid limit (LL), minimum (e_{min}) and maximum (e_{max}) void ratios as well as the iron oxide content. The aim is to establish correlations between basic iron ore tailings data and CS parameters, providing a screening approach to determine whether laboratory results fall within expected ranges, or if more detailed tests are necessary when assessing static liquefaction for iron ore TSFs.

Introduction

Static liquefaction is defined as sudden strength loss in a (near) saturated (typically granular) soil, accompanied by rapid generation of excess pore-water pressure. This could develop into a liquefaction flow failure if the soil strength drops below the applied shear stress (Lade and Yamamuro, 1997). Recent incidents, such as the failures at Fundão (Morgenstern et al., 2016) and Brumadinho (Robertson et al., 2019), have identified static liquefaction as a primary failure mechanism. These Brazilian tailings storage facility (TSF) failures have resulted in unprecedented and devastating consequences for the environment,

infrastructure damage and human losses. In response, new regulations have been enacted in Brazil, introducing the concept of "TSF decharacterization." This involves transitioning from an existing upstream-constructed tailings dam to a structure that no longer primarily serves as a tailing containment facility, thereby functionally reintegrating the facility into the environment. The failures also spurred increased interest in alternative dewatered tailings technologies (e.g., filtered tailings), due to their lower risk compared to conventional hydraulically deposited tailings.

In the Brazilian context, where decharacterization and filtered tailings projects were not commonly practiced, comprehensive geotechnical investigations were required to understand the behavior of the tailings material to support static liquefaction assessment, generally following the critical state soil mechanics (CSSM) framework. Consequently, a database of critical state (CS) parameters was developed and published. This was primarily on iron ore tailings, given the predominant location of TSFs within the Iron Quadrangle in Brazil – one of the world's largest reserves of iron ore.

While it is widely recognized that soil index properties impact critical state locus (CSL) parameters (Jefferies and Been, 2015), research linking tailings index properties to CSL parameters remains limited. Smith et. al. (2019), Torrez-Cruz and Santamarina (2020), Macedo and Vergaray (2022) and Hussien and Sgaoula (2023) are among the few related studies. Recently, an investigation targeting a unique commodity (iron ore) has been elaborated by the authors (Ccotohuanca et al., 2024).

This article aims to provide trends between CS parameters and iron ore tailings index properties (e.g., FC, D_{50}, C_u, G_s, etc.). An expanded database was compiled, including 40 iron ore tailings materials from Brazil and various global mining sites. This database, along with the correlations found, offers a valuable screening approach to discern whether laboratory results are within expected ranges, or if more detailed tests are required when assessing static liquefaction for iron ore TSFs.

Expanded iron ore tailings database

The expanded iron ore tailings database ("the IOD") consists of 40 iron ore tailings sources from several mines located throughout Brazil, Mexico, Australia, and China; 9 of them as part of this study and the rest from published literature as detailed in Table 1.

The IOD includes index properties along with CSL parameters, including: the slope on a natural logarithm base ($\lambda_e = \lambda_{10}/2.3$) and the altitude at 1 kPa (Γ), when the CSL is represented by a linear function using a semi-log idealization, $e_{cs} = \Gamma - \lambda_e \cdot \ln(p')$; and the a, b, and c coefficients, for a curved CSL represented by a power law function, $e_{cs} = a - b(p'/p_{atm})^c$. The IOD also includes the stress ratio at critical state (M_{tc}).

Table 1: Index properties and CS parameters of the expanded IOD

ID #	Index properties									Critical state parameters		Source
	D_{50} (μm)	C_u	FC (%)	LL (%)	PI (%)	G_s	Fe (%)	$e_{min}\|e_{max}$	Part. Shape	$\Gamma \mid \lambda_e$ or $a\mid b\mid$ c	M_{tc}	
1	121	2.9	25.1	–	NP	3.52	51.3	0.99|0.60	A-SA	0.905|0.032|0.63	1.37	This study
2	63	2.5	65.6	–	NP	3.64	NA	0.99|0.54	A-SA	0.870|0.061|0.360	1.35	This study
3	61	2.9	65.9	–	NP	3.70	NA	1.03|0.52	A-SA	0.896|0.08|0.334	1.35	This study
4	14	9.9	98.3	–	NP	3.71	NA	2.32|1.34	A-SA	2.110|0.983|0.117	1.38	This study
5	39	11.6	73.3	16	2	3.42	32.1	1.05|0.38	A-SA	0.759|0.126|0.350	1.35	This study
6	30	25.7	77.1	17	3	3.30	29.2	1.24|0.37	A-SA	0.865|0.235|0.185	1.32	This study
7	25	13.5	74.9	17	1	3.46	39.3	1.32|0.37	A-SA	0.755|0.090|0.355	1.33	This study
8	28	5.0	87.6	–	NP	4.65	71.9	1.30|0.68	A-SA	0.863|0.020|0.700	1.49	This study
9	41	16.7	74.8	–	NP	3.85	34.4	1.23|0.61	A-SA	0.930|0.080|0.380	1.49	This study
10	72	4.9	51.6	20	4	4.38	NA	NA	NA	1.040|0.039	1.38	Robertson et al. (2019)
11	51	4.8	70.8	21	4	3.89	50.3	NA	NA	1.120|0.039	1.38	Robertson et al. (2019)
12	120	6.1	33.7	–	NP	4.89	87.6	NA	A-SA	1.020|0.039	1.38	Robertson et al. (2019)
13	73	4.2	51.0	–	NP	2.95	11.2	1.13|0.48	A-SA	0.865|0.024	1.33	Morgenstern et al. (2016)
14	34	25.4	90.8	–	NP	3.20	23.3	1.18|0.60	NA	0.805|0.201|0.150	1.38	Carneiro (2021)
15	73	5.8	52.2	–	NP	3.05	20.9	1.28|0.51	A-SA	0.770|0.077|0.320	1.40	Oliveira (2022), Wagner et al. (2022), Consoli (2023b), Silva et al. (2024)
16	104	2.7	33.3	–	NP	2.97	17.2	0.99|0.51	A-SA	0.864|0.044|0.480	1.35	
17	96	6.3	39.1	–	NP	2.83	1.7	1.08|0.50	NA	1.000|0.150|0.245	1.30	Consoli (2023a)
18	36	9.6	86.5	–	NP	4.02	42.3	1.09|0.57	NA	0.950|0.150|0.232	1.35	Consoli (2023a)
19	92	3.3	39.1	–	NP	5.01	NA	1.33|0.63	NA	1.012|0.024|0.770	1.35	Cella and Padovani (2021)
20	34	9.2	76.7	–	NP	3.99	NA	1.37|0.71	NA	1.202|0.068	1.33	
21	72	2.5	52.1	–	NP	2.91	14.2	0.85|0.40	A-SA	0.780|0.046|0.355	1.31	Dawson et al. (2019)
22	46	3.1	79.9	–	NP	3.60	25.4	1.31|0.65	A-SA	1.130|0.230|0.270	1.35	Silva et al. (2022)
23	36	6.2	92.4	–	NP	4.55	NA	NA	NA	1.037|0.037	1.40	De Oliveira Faria et al. (2024)
24	151	3.0	11.8	–	NP	3.15	7.0	NA	NA	1.090|0.069	1.35	Carrizo et al. (2023)
25	23	6.8	93.3	25	NP	3.11	3.1	1.21|0.69	A-SA	1.157|0.085	1.40	Li and Coop (2019)
26	38	8.7	67.6	25	NP	3.14	0.0	1.10|0.59	A-SA	0.912|0.128|0.296	1.36	Li and Coop (2019)
27	232	10.4	17.9	20	NP	3.37	11.0	1.09|0.49	A-SA	0.799|0.087|0.445	1.41	Li and Coop (2019)
28	15	23.5	88.0	–	NP	2.78	NA	NA	NA	0.864|0.144|0.243	1.46	Reid et. al. (2018)
29	16	18.9	82.3	–	NP	2.96	6.0	NA	A-SA	1.539|0.813|0.059	1.39	Reid and Fanni (2020)
30	NA	NA	NA	27	5	2.99	NA	NA	NA	0.900|0.043	1.47	Smith et al. (2019)
31	NA	NA	NA	26	4	3.23	NA	NA	NA	1.035|0.053	1.33	Smith et al. (2019)
32	NA	NA	NA	-	NP	2.96	NA	NA	NA	0.925|0.045	1.42	Smith et al. (2019)
33	NA	NA	NA	37	19	3.75	NA	NA	NA	1.427|0.109	1.47	Smith et al. (2019)
34	NA	NA	NA	32	14	3.46	NA	NA	NA	1.160|0.075	1.33	Smith et al. (2019)
35	7	33.4	98.7	39	18	3.71	NA	NA	NA	1.350|0.094	1.10	Mmbando et al. (2023)
36	91	2.2	37.2	–	NP	2.72	NA	1.00|0.50	NA	1.004|0.041	1.29	Serpa (2022)
37	83	9.8	45.2	–	NP	2.95	NA	1.08|0.42	NA	0.840|0.034	1.30	Serpa (2022)
38	67	16.2	56.9	–	NP	2.98	NA	NA	NA	0.795|0.031	1.19	Serpa (2022)
39	123	3.0	23.4	–	NP	2.85	NA	NA	NA	0.829|0.049|0.401	1.42	Guimarães et al. (2023)
40	NA	NA	35.0	21	6	3.14	NA	NA	NA	1.000|0.374|0.190	1.13	Rios and Botero (2023)

Notes:
1) NA: data not available, NP: Non-plastic, FC: Fines content, C_u: Coefficient of uniformity, D_{50}: Mean particle size, LL: Liquid limit, PI: Plasticity index, G_s: Specific gravity, Fe: Iron oxide content, e_{min}, e_{max}: minimum and maximum void ratio, A: Angular, SA: Subangular, M_{tc}: Stress ratio at critical state.
2) Tailings 10 to 13 represent results from the Fundão and Brumadinho tailings failures.
3) Tailings 14 to 17 and 36 to 39 are results from filtered tailings samples.
4) $a, b,$ and c parameters are reported in cases where CSL fits a curve, while Γ and λ_e are reported for the conventional linear approach.
5) Tailings 35 exhibited two CSL values depending on the sample preparation method (slurry deposition and moist tamping). The results obtained through moist tamping were selected for inclusion in the database.

Figure 1a illustrates the particle size distribution (PSD) of the IOD database, categorized based on their FC (% passing the #200 sieve) into two groups: those with FC higher ("fine tailings") and lower ("coarse tailings") than 50%. A comparison is drawn with the PSDs of iron ore tailings from the Iron Quadrangle (in Brazil), as compiled by Carneiro et al. (2023). The PSDs of the IOD fall within the "coarse and fine" range (grey area) of the referenced study, with two samples (#4 and #35) falling within the "slimes" range (brown area). Overall, the IOD exhibits a wide range of fine content (FC = 11.8 – 98.7%) and particle diameter (D_{50} = 6.5 – 231.7 μm).

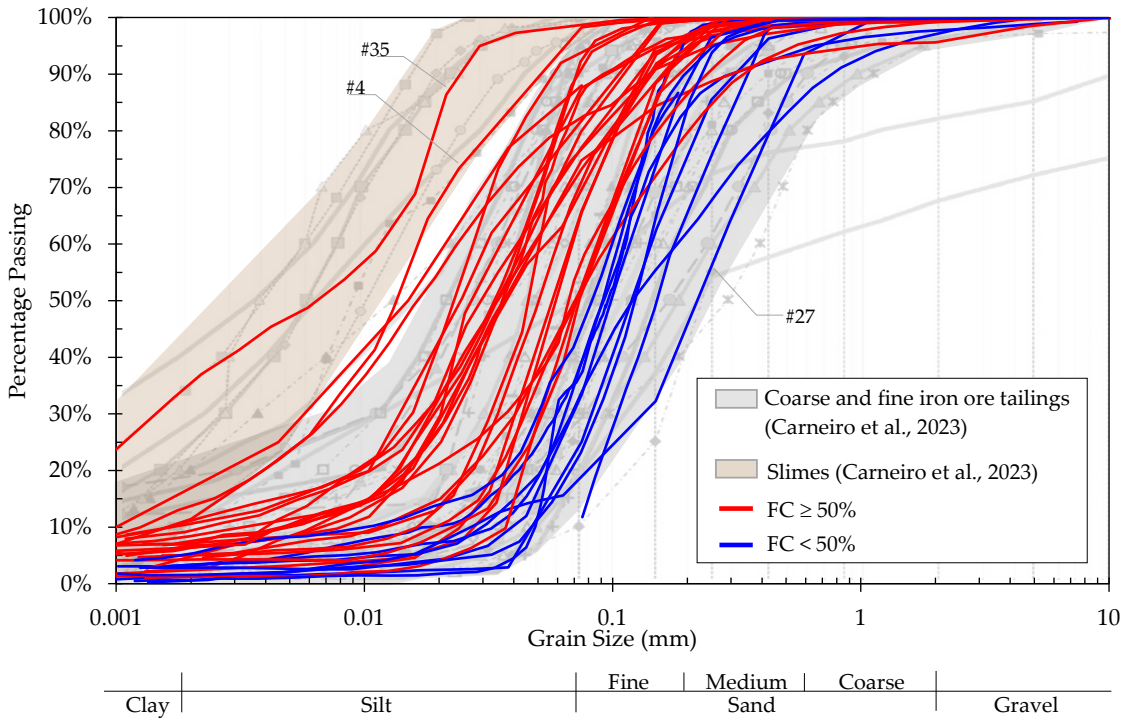
While the majority of IOD samples are typically classified as non-plastic, the iron ore tailings exhibiting plasticity were plotted in the Casagrande plasticity chart (Figure 1b). Samples #33, #34, and #35 demonstrated the highest plasticity, while the remainder exhibited a PI of less than 6%.

Given the distinctive characteristics of iron ore tailings, notably the high G_s values, a dataset comprising the percentage of iron oxide (% hematite) alongside their corresponding G_s values, which ranges from 2.78 to 5.01, was assembled. These data are visualized in Figure 1c, revealing a strong correlation, even when incorporating literature data from Espósito (2000) and Lopes (2000).

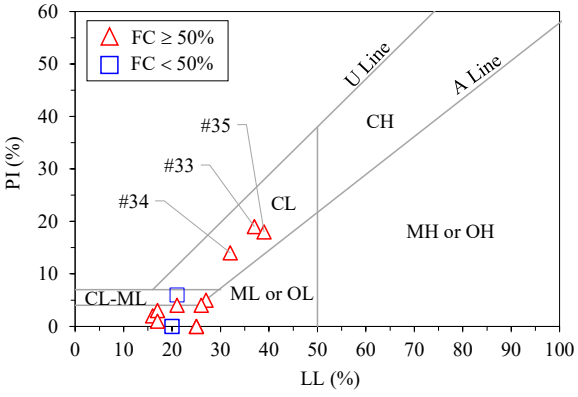
The particle shape was assessed using Scanning Electron Microscopy (SEM) images. Most of the IOD tailings exhibit an angular-subangular (A-SA) shape, regardless of the FC. Examples of typical SEM images for different FC are depicted in Figure 1d.

Figure 2a shows the distribution of the CSLs for the expanded IOD plotted over the tailings database by Macedo and Vergaray (2022) (in grey). Overall, the CSLs from the IOD align with those observed in the referenced study. The CSLs cover a broad spectrum in the e versus p' plane, the difference in e for a given p' is on the order of 0.4. Half of the CSLs follow a linear relationship (in a semi-log plot). The CSLs from samples #4 and #14 / #40 form the upper and lower boundaries for the IOD.

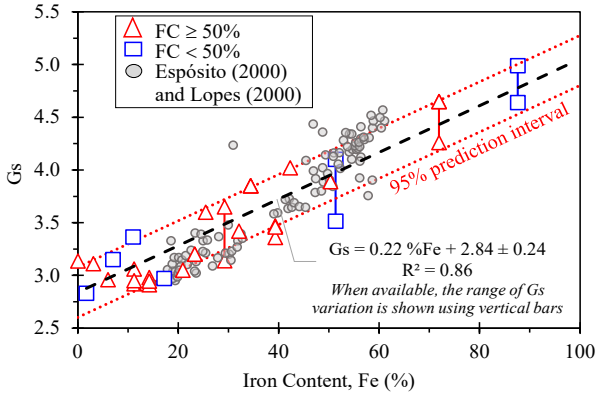
Figure 2b shows a histogram of the M_tc values for sands (from Jefferies and Been, 2015), various types of tailings (from Macedo and Vergaray, 2022), and those pertaining to the IOD. The M_tc values for mine tailings, including those of the IOD, are generally higher compared to sands. For the IOD, this parameter spans from 1.10 to 1.49, with a mean value of 1.36.



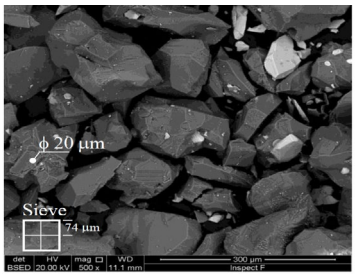
(a) PSD curves of the IOD



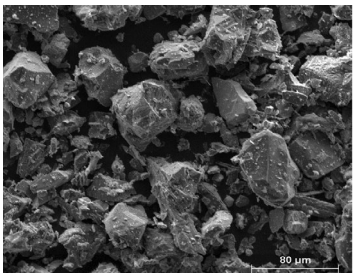
(b) Plasticity of the IOD



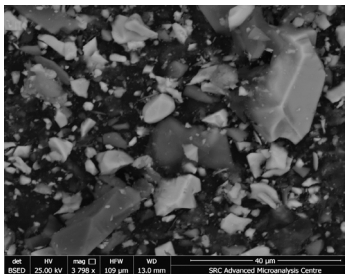
(c) % Fe content



Sample # 16: FC: 33.3%



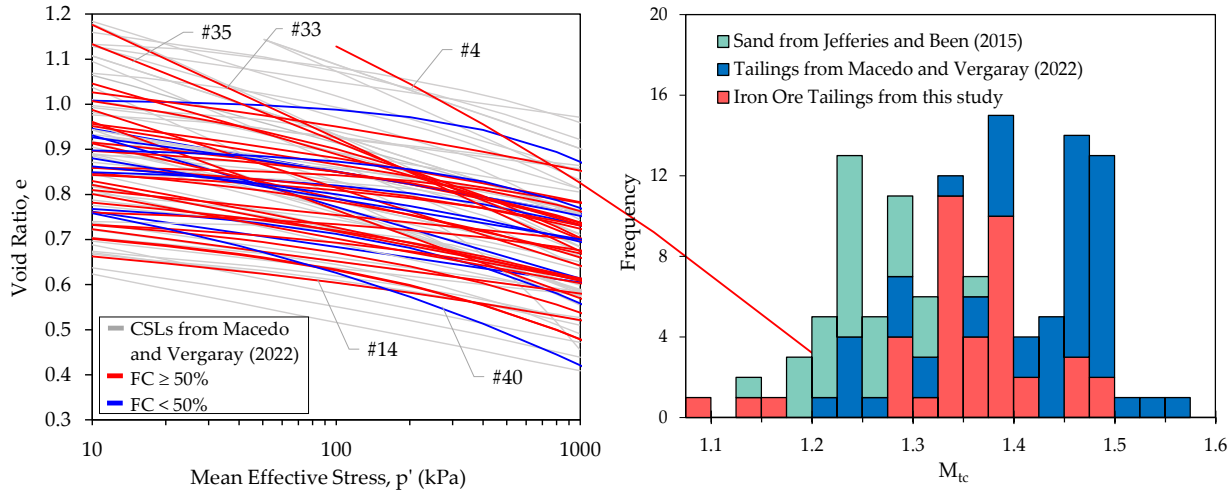
Sample #13: FC: 51.0%



Sample #4: FC: 98.3%

(d) SEM images

Figure 1: Index properties of the expanded IOD



(a) Distribution of the CSLs of the IOD

(b) Distribution of the M_{tc} values

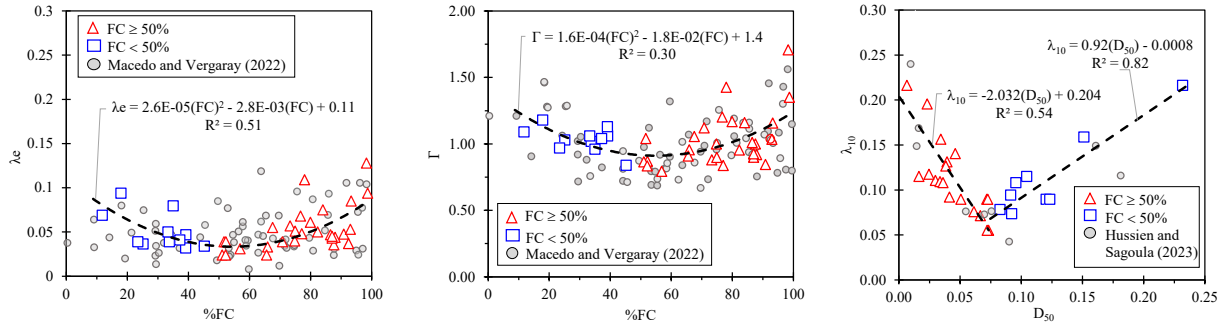
Figure 2: CSL parameters for the expanded IOD

Evaluation of trends and discussion of the results

A review of trends and correlations between CS parameters (Γ, λ_e and M_{tc}) and index properties was conducted. To investigate the influence of the PSD, three key material characteristics (D_{50}, FC and C_u) were evaluated. Plasticity was assessed via Atterberg limits (PI and LL), material state through void ratio (e_{min} and e_{max}), and mineralogy by considering the iron oxide (%Fe) content.

For the "curved" CSLs with minimal curvature, a void ratio deviation of less than 0.02 over the stress range of p' = 30 – 900kPa, which typically encompasses the range of interest for most geotechnical TSF projects, a common semi-logarithmic representation was adopted for comparison purposes.

Figure 3 displays a series of charts illustrating acceptable trends observed in the comparison between CSL and soil index parameters. When available, data from the literature on other tailings and/or natural soils have also been incorporated into these figures for comparison.



(a) (b) (c)

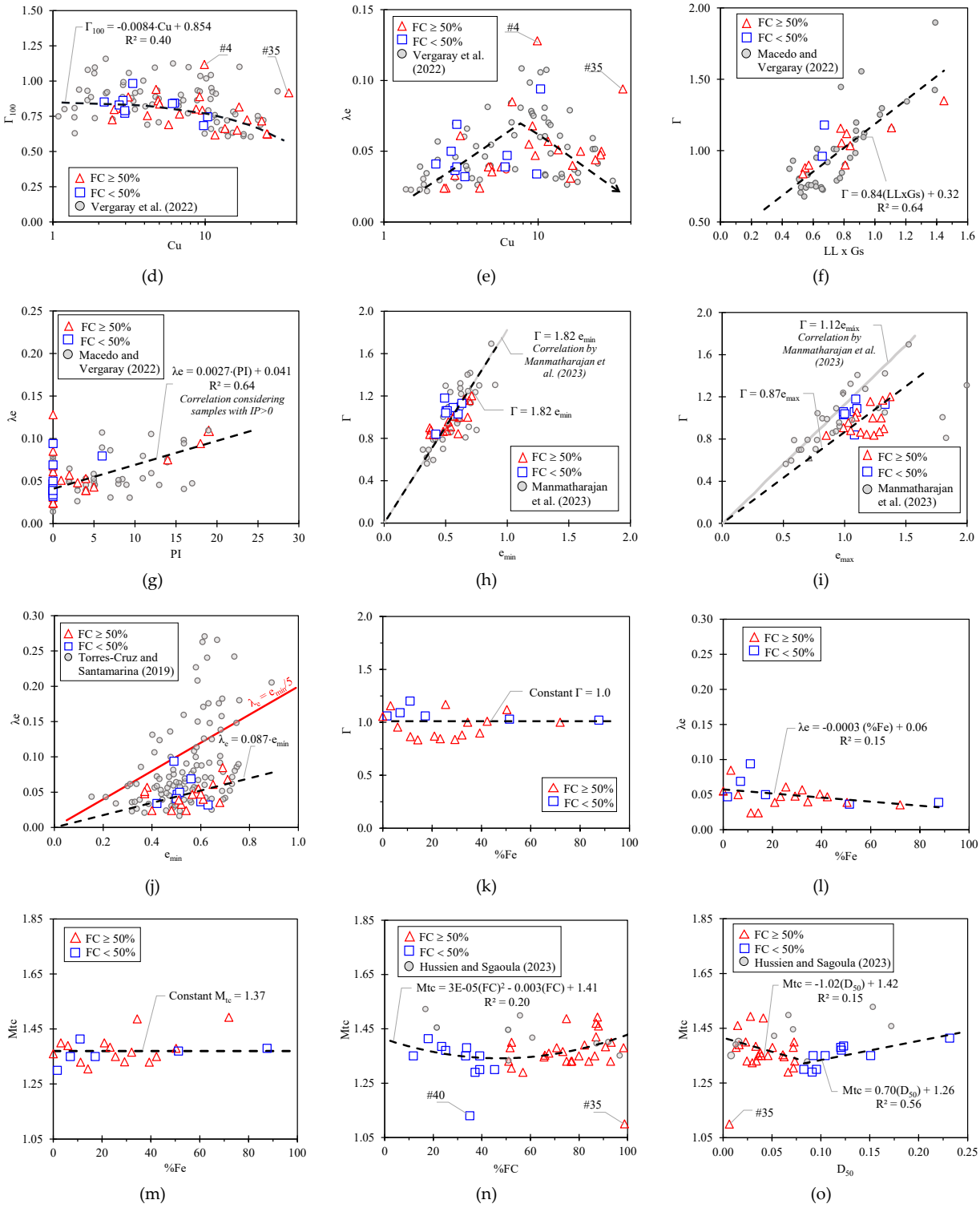


Figure 3: Evaluation of trends and correlations for the expanded IOD

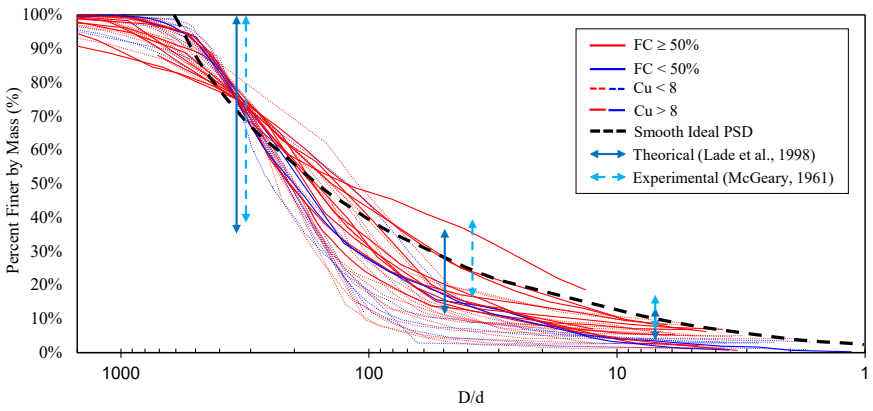


Figure 4: Normalized PSD of the IOD to evaluate particle packing according to the theories of Lade et al. (1998) and McGeary (1961)

Based on the figures, the following can be highlighted:

- Both Γ and λ_e exhibit a low to moderate correlation with FC (Figures 3a, 3b), with Γ decreasing as FC increases until it reaches approximately 50% of FC, after which this trend reverses. This pattern is consistent with findings from published studies, such as Thevanayagam et al. (2002), Carrera et al. (2011), Smith et al. (2019), Macedo and Vergaray (2022) (also represented in the figures), and Manmatharajan et al. (2023). The U-shaped trend can be attributed to the behavior of finer particles filling the voids: below 50% FC, the tailings are dominated by a sand skeleton, while above 50%, contacts are primarily influenced by silt and clay-sized particles. At around 50% FC, the finer fraction filling the voids contributes to the load-carrying skeleton, resulting in a less compressible material (i.e., lower λ_e).
- D_{50} exhibits a moderate relationship with λ_{10} (Figure 3c) and Γ (not depicted here). The trend follows a V-shaped curvature, with λ_{10} sharply decreasing as D_{50} increases until reaching approximately 0.075 mm. Beyond this point, the trend reverses, showing a smooth positive linear relationship. The results are compatible with Hussien and Sgaoula (2023), also plotted in Figure 3c.
- Figure 3d depicts the impact of material grading (using C_u as a proxy) on Γ, presented in an alternative form as Γ_{100} (i.e., the altitude of the CSL at 100kPa) as proposed by Torrez-Cruz and Santamarina (2019). The observed linear trend suggests a decrease in Γ as C_u increases. The IOD values fall within the range of results from other tests on different types of tailings and sands with lower roundness (as compiled by Macedo and Vergaray, 2022) (plotted in grey), typically characterizing the tailings of the IOD (see Figure 1d).
- Figure 3e shows λ_e in terms of C_u. It is noted that λ_e tends to increase with C_u up to values on the order of 6-8 and then decreases as C_u keeps increasing following a similar trend as showed in Macedo and Vergaray (2022). This observation suggests an enhanced particle packing with high C_u,

consistent with classical criteria for classification of "well-graded" sand by the Unified Soil Classification System (USCS), which states that a more densely packed arrangement of particles can be achieved when C_u is greater than 6 and C_c (coefficient of curvature) is between 1 and 3.

- The trends observed in Figure 3d and 3e can also be interpreted considering the ranges for PSD curves that promote optimal packing, as proposed by Lade et al. (1998) and McGeary (1961) and shown in Figure 4. When examining normalized PSD curves (normalized by D_{75}, the size at which 75% of particles are finer) for the IOD, it is evident that the PSD curves with $C_u > 8$ match the ranges of optimal particle packing indicated by the aforementioned authors. This supports the potential use of C_u as an acceptable proxy for interpreting and understanding the CSL position. Of note, a similar result was observed in a database for several tailings presented by Vergaray et al. (2022).
- While the available data on iron ore tailings with Atterberg limits are limited, the available results suggest a good linear correlation between Γ and LL when normalized by specific gravity $LL{\times}Gs$ (see Figure 3f), a trend also observed by Macedo and Vergaray (2022) and Smith et al. (2019). This correlation aligns with concepts from the CSSM framework, as outlined by Schofield and Wroth (1968). Similarly, a strong linear correlation was observed between PI and λ_e (see Figure 3g). This outcome is expected, given that both parameters serve as proxies for compressibility, in line with CSSM-based concepts. Furthermore, this is consistent with using PI (as an indicator for compressibility) in fine-grained plastic soils for analyzing liquefaction susceptibility, as proposed in the methodology of Bray and Sancio (2006).
- The spatial variability of e_{min} within a tailings deposit anticipates spatial variability of Γ, given the good correlation between these parameters (see Figure 3h). This correlation extends to other datasets of natural soils and various types of tailings (from Manmatharajan et al., 2023), as also depicted in grey in Figure 3h. Similarly, a good linear trend was observed between e_{max} and Γ (see Figure 3i). However, the slope of the linear regression for iron ore tailings is lower compared to tailings from other commodities or natural soil. It appears that iron ore tailings tend to exhibit lower Γ values than other materials for a given e_{max}.
- The range of possible λ_e values increase with e_{min} (see Figure 3j). Overall, the expected λ_e values are lower than $e_{min}/5$. The data from IOD falls within the range of most of other quartz-rich tailings (plotted in grey) based on the Torrez-Cruz and Santamarina (2020) database.
- Figures 3k, 3l and 3m suggest that the iron oxide content (% hematite) does not exert a significant influence on λ_e, Γ or M_{tc}, with only a weak linear trend observed for λ_e.
- Broader investigations by Torres-Cruz and Santamarina (2020), encompassing soils beyond tailings, suggest that the primary factor influencing M_{tc} is neither mineralogy nor particle size, but particle

shape. While this study finds no significant variation in particle shape among the examined iron ore tailings (mainly angular to subangular), a wide range of M_{tc} values was observed within the IOD. Upon examining M_{tc} values alongside index properties, it was observed that, despite weak to moderate correlations, there may be a potential influence of FC (Figure 3n) and D_{50} (Figure 3o). These trends exhibit similar U-shaped patterns as seen in Figures 3a to 3c.

- Caution is advised when analyzing very fine iron ore tailings (slimes) (refer to Figure 1a). In certain instances, such as with samples #4 and #35 in Figures 3d, 3e, the results for these samples are outliers when compared to other "Fine and Coarse" iron ore tailings.

Conclusion

In this article, we compared CSL parameters inferred from laboratory testing of iron ore mine tailings gathered from mine sites in Brazil and globally with their laboratory index properties. Our aim was to establish correlations between basic iron ore tailings data and CSL parameters. A database, expanded from an initial 26 sources to a total of 40 iron ore tailings sources, was collected.

Upon analyzing the results, we confirmed previously observed conclusions with a smaller IOD dataset. First, the trends observed using an extended iron ore tailings database did not show significantly different behavior from other types of tailings. This is evident when examining correlations with index properties such as FC, D_{50}, C_u, plasticity, and void ratio, which displayed a greater potential to influence CSL parameters compared to correlations with iron oxide ($\%Fe$) content. This suggests that inferences about tailings behavior made from other types of tailings can be reasonably adopted. Second, when particle shape remains consistent (angular to subangular particles in this study), as observed for the expanded IOD, certain index parameters such as FC and D_{50} may exert a slight influence on M_{tc} values.

References

Bray, J.D. and Sancio, R.B. 2006. Assessment of the liquefaction susceptibility of fine-grained soils. *Journal of Geotechnical and Geoenvironmental Engineering* 132(9): 1165–1177.

Carneiro, J.J.V. 2021. Characterization and behaviour of iron ore tailings: the effect of compaction and stresses. Thesis research, master's degree in civil engineering, Federal University of Viçosa – UFV, Viçosa.

Carneiro, J.J.V., Marques, E.A.G., Fonseca, A.J.P.V. and Oliveira, A.H.C. 2023. characterization of an iron ore tailing sample and the evaluation of its representativeness. *Geotechnical and Geological Engineering*, Springer: 2833–2852.

Carrera, A., Coop, M. and Lancelotta, R. 2011. Influence of grading on the mechanical behaviour of Stava tailings. *Géotechnique* 61(11): 935–946. DOI:10.1680/geot.9.P.009.

Carrizo, L., Tasso, N. and Sottile, M. 2023. *Caracterización geotécnica de un relave minero susceptible a licuar:* Geotechnical characterization of a mine tailings susceptible to liquefaction, *XXVI Congreso Argentino de Mecánica de Suelos e Ingeniería Geotécnica*, Comodoro: Rivadavia.

Ccotohuanca, J., Lanza, V. and Costa, I. 2024. The critical state line parameters of iron ore tailings from basic laboratory tests. *Proceedings of Tailings 2024*. Santiago, Chile.

Cella, P.R.C. and Padovani, F.A. 2021. Five Brazilian tailings – from laboratory and field data towards safer design criteria. *Proceedings of 7th Internacional Conference Tailings Management*, virtual event.

Consoli, N.C. 2023 (a). Critical state analysis of two compacted filtered iron ore tailings with different grading and mineralogy at different stages of treatment. *Acta Geotechnica*, Springer: 881–898, DOI: 10.1007/s11440-023-01963-9.

Consoli, N.C. 2023 (b). Determination of critical state line (CSL) for silty-sandy iron ore tailings subjected to low-high confining pressures. *Journal of Rock Mechanics and Geotechnical Engineering* 16(5): 1684–1695. DOI: 10.1016/j.jrmge.2023.06.014.

Dawson, R., Burgin, A., Macowich, M., Bernardo, J. and Vasconcelos, A. 2019. Laboratory and CPTu characterization of Samarco sand tailings. *Proceedings of Tailings and Mine Waste*. Vancouver, Canada.

De Oliveira Faria, A., Delgado, B.G., Ferreira, L.D. and Dos Santos Junior, M.P. 2024. Comparative evaluation of constitutive models for stress-strain analysis of an iron ore tailings from the Quadrilátero Ferrífero, Minas Gerais, Brazil. *Soils and Rocks: An International Journal of Geotechnical and Geoenvironmental Engineering* 47(1). DOI: 10.28927/SR.2024.011022.

Espósito, T.J. 2000. *Metodologia Probabilística e Observacional Aplicada a Barragens de Rejeito Construídas por Aterro Hidráulico*. Thesis research, Universidade de Brasília.

Guimarães, B., Viana, A., Jabur, R., Matos, B. and Coelho, D. 2023. Geomechanical behaviour of an iron ore tailings under high-stress levels for disposal by dry stacking. *Proceedings of the 1st International Conference on Geotechnics of Tailings and Mine Waste*. Ouro Preto, Minas Gerais, Brazil.

Hussien, M.N and Sgaoula, J. 2023. Tailings state from basic laboratory tests and CPT data. *Proceedings of Tailings and Mine Waste*, 2023. Vancouver, Canada.

Jefferies, M. and Been, K. 2015. *Soil Liquefaction: A Critical State Approach*. Second edition. London, UK: Taylor and Francis Group.

Lade, P., Liggio, C. and Yamamuro, J. 1998. Effects of non-plastic fines on minimum and maximum void ratios of sand. *Geotechnical Testing Journal* 21(4): 336. Doi:10.1520/gtj11373j.

Lade, P.V. and Yamamuro, J.A. 1997. Effects of non-plastic fines on static liquefaction of sands. *Can. Geotech. J.* 24(6): 918–928. DOI: 10.1139/cgj-34-6-918.

Li, W., Coop and M.R. 2019. Mechanical behaviour of Panzhihua iron tailings. *Can. Geotech. J.* 56(3). DOI: 10.1139/cgj-2018-0032.

Lopes, M.C.O. 2000. *Disposição hidráulica de rejeitos arenosos e influência nos parâmetros de resistência*. Thesis research, University of Brasília.

Macedo, J. and Vergaray, L. 2022. Properties of mine tailings for static liquefaction assessment. *Can. Geotech. J.* 59: 667–687. Canada.

Manmatharajan, M.V., Gill, S., Liu, W., Ingabire, E.P., SY, A., Ghafghazi, M. 2023. Effect of particle size and particle size distribution on critical state loci of granular soils. *Can. Geotech. J.* 60(8). DOI: 10.1139/cgj-2021-0643.

McGeary, R.K. 1961. Mechanical packing of spherical particles. *Journal of the American Ceramic Society* 44(10): 513–522. Doi:10.1111/j.1151-2916.1961.tb13716.x.

Mmbando, E., Fourie, A. and Reid, D. 2023 Mechanics of an iron ore tailings exhibiting transitional behaviour. *Geotechnical and Geological Engineering* 41: 2211–2220. DOI: 10.1007/s10706-023-02379-8.

Morgenstern, N.R., Vick, S.G., Viotti, C.B. and Watts, B.D. 2016. Report on the immediate causes of the failure of the Fundão dam. Fundão Tailings Dam Review Panel.

Oliveira, S.C. 2022. *Influência do Estado de Tensão na Obtenção dos Parâmetros de Estado Crítico de Rejeitos Filtrados de Minério de Ferro*. Thesis research, Federal University of Ouro Preto – UFOP.

Reid, D., Fanni, R. 2020. A comparison of intact and reconstituted samples of a silt tailings. *Géotechnique*, 45p, DOI: 10.1680/jgeot.20.P.020.

Reid, D., Fanni, R., Koh, K. and Orea, I. 2018. Characterisation of a subaqueously deposited silt iron ore tailings. *Géotechnique Letters* 8: 278–283. DOI: 10.1680.

Rios, E. and Botero, E. 2023. Assessment of the critical state locus in reconstituted samples and calibration of NorSand model. *Proceedings of the Rocscience International Conference*. Toronto, Canada.

Robertson, P.K., de Melo, L., Williams, D.J. and Wilson, G.W. 2019. *Report of the Expert Panel on the Technical Causes of the Failure of Feijão Dam I.*

Schofield, A. and Wroth, P. 1968. *Critical State Soil Mechanics*, First edition, McGraw-Hill.

Serpa, F. 2022. *Influência do teor de finos no comportamento geomecânico de um rejeito de minério de ferro do Quadrilátero Ferrífero*. Thesis research, Geotechnics, Federal University of Ouro Preto – UFOP.

Silva, J.P.S., Cacciari, P.P., Torres, V.F.N., Ribeiro, L.F.M. and Assis, A.P. 2022. Behavioural analysis of iron ore tailings through critical state soil mechanics. *Soils and Rocks* 45(2). DOI: 10.28927/SR.2022.071921.

Silva, J.P.S., Rissoli, A.L.C., Cacciari, P.P., Fonseca, A.J.P.V., Scheuermann, H.C., Wagner, A.C., Carvalho, J.V.A., Festugato, L. and Consoli, N.C. 2024. Triaxial testing response of compacted iron ore tailings considering a broad spectrum of confining pressures. *Soils and Foundations* 64(2).

Smith, K., Fanni, R. and Reid, D. 2019. Critical State testing of tailings – comparison between various tailings and implications for design. *Proceedings of Tailings and Mine Waste, 2019*. Vancouver, Canada.

Thevanayagam, S., Shenthan, T., Mohan, S., Liang, J. 2002. Undrained fragility of clean sands, silty sands, and sandy silts. *J. Geotech. Geoenviron. Eng.* 128(10): 849–859. DOI: 10.1061/(ASCE)1090-0241.

Torrez-Cruz, L.A. and Santamarina J.C. 2020. The critical state line of nonplastic tailings. *Canadian Geotechnical Journal* 57(10): 1508–1517. DOI: 10.1139/cgj-2019-0019.

Vergaray, L., Macedo, J., Arnold, C. and Arroyo, M. 2022. Influence of the particle size distribution on the critical state properties of mine tailings. *Proceedings of the 26th International Conference on Tailings and Mine Waste*. Vancouver, Canada.

Wagner, A.C., Silva, J.P.S., Carvalho, J.V.A., Rissoli, A.L.C., Cacciari, P.P., Chaves, H.M., Scheuermann, H.C. and Consoli, N.C. 2022. Mechanical behavior of iron ore tailings under standard compression and extension triaxial stress paths. *Journal of Rock Mechanics and Geotechnical Engineering* 15(7): 1883–1894. DOI: 10.1016/j.jrmge.2022.11.013.

Enhancing Tailings Dam Foundation Assessment: a SHANSEP Approach for a Brazilian Alluvium Soil

Carlos Besso, Worley Consulting, Australia
Sergio Capellão, Geocoba Projetos de Engenharia, Brazil
Marcus Vinicius Lima Dias, Vale, Brazil
Rodrigo Marinaro, Vale, Brazil

Abstract

This paper outlines the rational methodology applied to validate the undrained parameters for the foundation alluvium layer of an existing tailings dam, providing adequate input for slope stability analysis. A comprehensive in-situ and laboratory investigation survey revealed high coarse fraction content, partial drainage effects, slight over-consolidation, and a non-linear trend in the undrained strength ratio plot, leading to the need to define a linear intercept to properly design the undrained shear strength envelope. It is concluded that the continued use of advanced testing methodologies and SHANSEP principles is crucial for accurately assessing the slope stability of tailings dam foundations under similar geological contexts in Brazil, rather than relying on empirical correlations through standard penetration tests (SPTs).

Introduction

To comply with the new Brazilian national legislation ANM 2022, the geotechnical stability of an existing tailings dam was reassessed under undrained loading conditions for long-term scenarios. The dam's foundation comprises a clayey alluvium stratum among other layers, prompting a comprehensive site and laboratory investigations to enhance the understanding of the alluvium geomechanical behavior, especially regarding its physical properties, undrained shear strength, stress history, and drainage conditions for dissipating excess pore-water pressures.

The survey encompassed boreholes (including new SPT, rotary drilling, and undisturbed Shelby sampling), vane shear tests, piezocone tests, characterization tests, consolidation tests, and triaxial tests. The results revealed four main aspects: a high degree of coarse fraction content; a marked partial drainage effect; a slightly over-consolidated behavior; and a non-linear trend in the undrained strength ratio plot. These findings led to the usage of a linear-intercept approach to obtain more realistic undrained parameters.

This paper outlines the rational methodology applied to validate the undrained parameters for the foundation alluvium layer of an existing tailings dam, providing adequate input for slope stability analysis. It is noteworthy that, even by applying the undrained envelope with a linear intercept, the factors of safety for undrained loadings remained lower than those for drained loadings, which aligns with good engineering practice as recommended by international guidelines (e.g., ANCOLD 2019).

Characterization tests

The index properties of the material are presented in Figure 1 and Table 1. The particle size distribution results indicate that the coarse fraction content varies from 24 to 62% (including a significant gravel content), and the fine fraction content ranges from 28 to 76%. This finding suggests a high degree of heterogeneity in the alluvium material, leading to coefficients of consolidation and shear strengths that are not representative of a typical soft clay deposit, as discussed in the following sections.

Furthermore, the material exhibits medium plasticity, with a mean plasticity index (PI) of 11%, and a colloidal inactivity ($A_c < 0.75$), indicating that true cohesion is not expected, as discussed by Skempton (1953). Specific gravity values close to and above 3.0 were observed, suggesting that the mineralogy may contain oxides that could contribute to a certain degree of cementation, which could also lead to true cohesion (Leroueil and Vaughan, 1990). However, this was discounted as manual handling of the material demonstrated friable behavior.

Finally, the USCS classification (ASTM 2017) encompasses silt (ML), elastic silt (MH), clayey sand (SC), silty sand (SM), and lean clay (CL), reflecting the material's heterogeneity.

Table 1: Index properties

Sample	Gs	Atterberg Limits (%)			Granulometry (%)				A_c	USCS
		LL	LP	PI	Gravel	Sand	Silt	Clay		
S-01	2.91	39	25	14	1.0	32.0	41.0	26.0	0.54	CL
S-02	2.77	46	31	16	0.6	25.3	23.1	51.0	0.30	ML
S-03	2.52	52	41	11	0.5	23.8	40.7	35.0	0.30	MH
S-06	3.06	40	29	11	18.3	30.5	25.5	25.7	0.43	ML
S-07	2.99	25	12	13	0.0	42.9	21.1	36.0	0.36	CL
S-08	3.17	39	30	9	0.0	51.7	21.9	26.5	0.34	SC
S-09	2.81	43	33	10	0.3	32.0	34.3	33.3	0.30	ML
S-10	2.73	–	–	–	0.2	50.4	21.1	28.4	–	SC
S-12	–	24	16	8	5.6	43.4	35.9	15.1	0.53	CL
S-13	–	40	30	10	9.8	61.2	20.0	9.0	1.12	SM

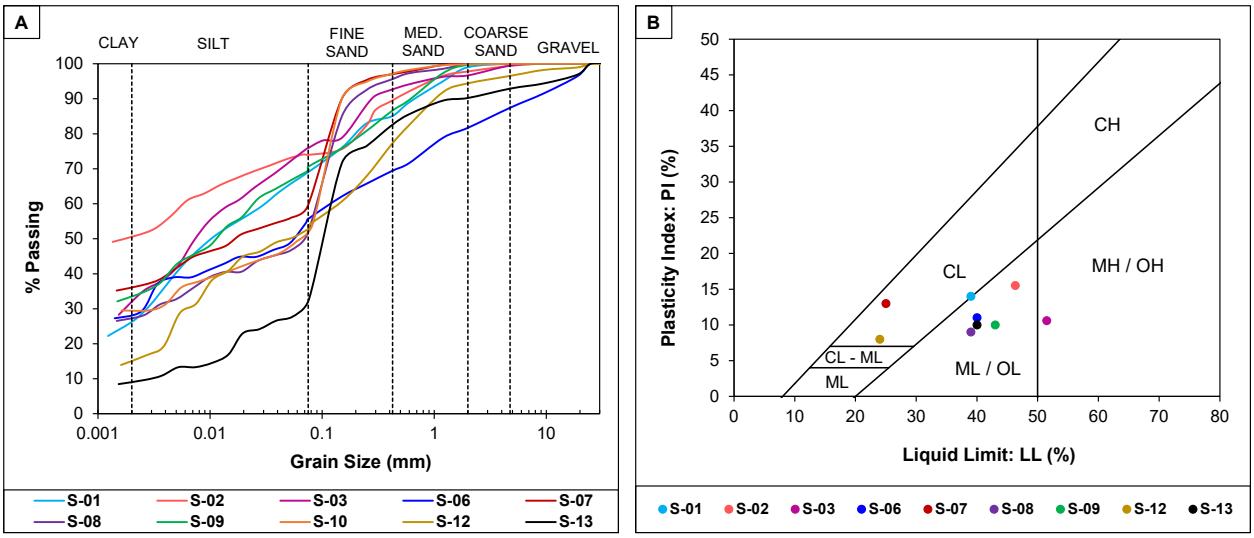


Figure 1: (A) Particle size distribution; (B) plasticity chart

Standard penetration tests (SPT)

A total of 14 SPT were conducted in the alluvium layer throughout the dam's life period. Figure 2 presents the N_{SPT} frequency histogram and profile, indicating that the values range primarily from 0 to 8 blows, with a mean value of 4, stating a low SPT resistance for the material.

This finding suggests that the alluvium may comprise a typical soft clay deposit, as the low N_{SPT} blows reflect the values obtained from Brazilian marine sedimentary deposits of soft clays (Massad, 2009). However, as discussed in the following sections, typical undrained strength parameters estimated based on SPT correlations provide overly conservative results when compared to in-situ and laboratory shearing test.

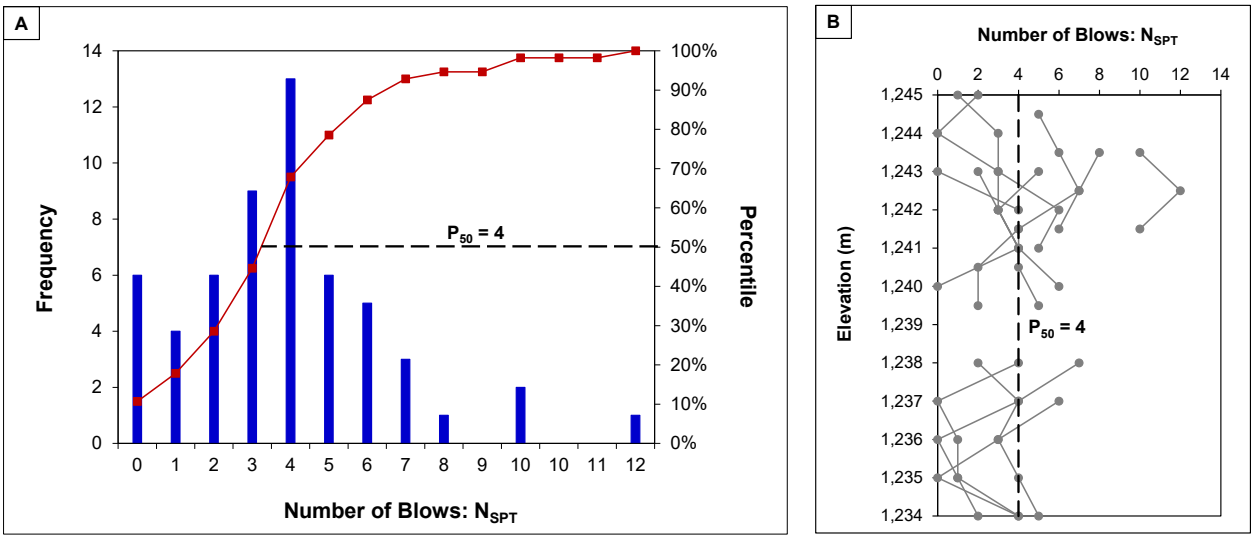


Figure 2: (A) N_{SPT} frequency histogram; (B) N_{SPT} profile

Consolidation tests

Figure 3A and Table 2 present the overall results of the oedometer consolidation tests. The coefficients of consolidation (c_v) were obtained using both Taylor (t_{50}) and Casagrande (t_{90}) methods, yielding an average value circa 10^{-2} cm²/s. Such value is found to be relatively high when compared to typical values of 10^{-4} cm²/s for traditional Brazilian marine sedimentary deposits of soft clays (Massad, 2009), likely due to the high coarse fraction content.

Similarly, the average compression index (C_c) was found to be 0.55, indicating low compressibility compared to typical values of C_c exceeding 1.0 for typical Brazilian deposits of compressible soft clays (Massad, 2009). The low compressibility is also assigned as a result of the high coarse fraction content.

Over-consolidation stresses, determined using the Pacheco Silva method, revealed over-consolidation ratios (OCR) ranging from 1.0 to 1.6, suggesting the presence of slightly over-consolidated regions within the alluvium layer. This finding supports the SHANSEP approach for the undrained shear strength envelope based on an over-consolidation stress of 400 kPa, as discussed in the following sections.

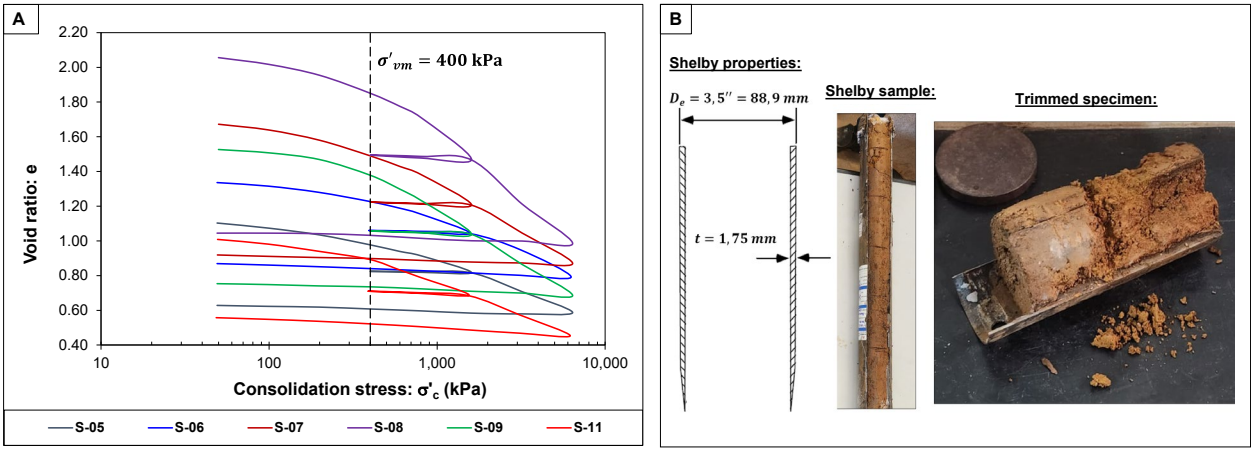


Figure 3: (A) Consolidation tests results; (B) specimen preparation

Regarding the reliability of the laboratory test results (both consolidation and triaxial), this study aimed to achieve state-of-the-art standards for obtaining undisturbed laboratory specimens. Shelby tubes with 88.9 mm (3.5 pol) diameter and 1.75 mm thickness were used for in-situ sampling, resulting in an area ratio (Ra) of 8.4%, as recommended by Clayton et al. (1998). However, the procedures outlined by Ladd and DeGroot (2004) could not be applied due to the high degree of friability during manual handling of the material, as illustrated in Figure 3B. Additionally, the gravel content obstructed cutting and trimming both the Shelby tubes and specimens with a wire saw.

Nonetheless, the obtained sample disturbance quality index ranged from good to fair, to poor according to the criteria of Lunne et al. (1997) and Coutinho et al. (1998), as presented in Table 3. Given the challenges faced during specimen preparation, the samples were ultimately considered acceptable.

Table 2: Consolidation tests results

Sample	Over-consolidation stress σ'_{vm} (kPa)	Over-consolidation ratio OCR	Coefficient of consolidation c_v (cm²/s)	Permeability k (cm/s)	Constrained modulus E_{oed} (MPa)	Compression index C_c (1/kPa)	Quality index $\Delta e/e_0$
S-05	490	1.2	1.4E-02	8.9E-07	52.3	0.33	0.13
S-06	400	1.0	8.3E-03	1.2E-07	50.2	0.36	0.09
S-07	400	1.3	1.5E-02	5.9E-07	44.4	0.53	0.09
S-08	470	1.6	3.2E-02	8.2E-07	35.7	0.79	0.08
S-09	325	1.1	1.2E-02	3.0E-07	40.0	0.59	0.07
S-11	360	1.2	1.0E-03	1.0E-08	45.6	0.36	0.11

Table 3: Quality index criteria

Criterion	OCR	Quality index, $\Delta e/e_0$			
		Very good to Excellent	Good to Fair	Poor	Very Poor
Coutinho et al. 1998	1 – 2.5	< 0.05	0.05 – 0.08	0.08 – 0.14	> 0.14
Lunne et al. 1997	1 – 2.0	< 0.04	0.04 – 0.07	0.07 – 0.14	> 0.14

Vane shear tests

A set of 4 in-situ vane shear tests (VST) were carried out in the alluvium, and the results are presented in Figure 4A. In accordance with the Brazilian national standard ABNT NBR 10905, a rotation rate of 6 degrees per minute was applied for the VST. Regarding shearing-rate corrections (Bjerrum, 1973; Morris and Williams, 1994), the medium plasticity resulted in correction factors higher than 1.0. Following a conservative approach, these corrections were not applied.

VST-01 was the sole test performed under undisturbed condition, while VST-02, VST-03 and VST-04 were conducted under remolded conditions, i.e., after 10 complete rotations of the vane. The sensitivity index (S_t) was conservatively defined by the lowest remolded strength (VST-02), resulting in a S_t value of 2.3, falling under the normal sensitivity classification according to the criteria of Skempton and Northey (1952).

Notably, partial drainage effects are suggestive when observing the drainage boundaries that indicate exceedance of 10% of porewater pressure dissipation. All the tests failed after the Blight/Chandler drainage boundary, suggesting that fully undrained strength was not mobilized. However, using the Morris and Williams drainage boundary, the undisturbed test VST-01 appears to have fully mobilized undrained

strength at failure, and thus this sole test is herein validated for peak undrained strength assessment. Further discussion on partial drainage effects will be presented in the following sections.

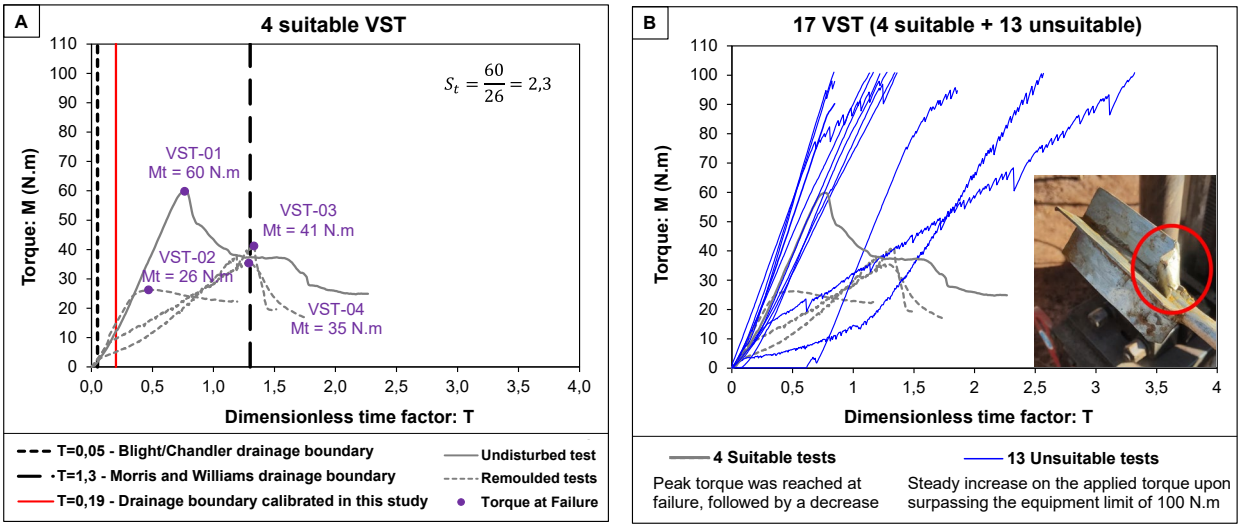


Figure 4: (A) 4 suitable vane shear tests; (B) all 17 vane shear tests

Figure 4B presents the attempts to conduct a set of 13 vane shear tests (blue contours), which were deemed unsuitable due to a steady increase in applied torque, leading to termination of the tests upon surpassing the equipment reading limit of 100 Nm. Additionally, 5 attempts to perform VST were unfeasible because torque application was impeded (possibly due to the presence of gravels, as suggested by the material's high coarse fraction content), resulting in damage to the blade, as shown in Figure 4B.

Piezocone tests

A set of 3 piezocone tests (CPTu) were carried out at 3 different locations on the dam's alluvial layer, with CPTu-01 and CPTu-02 positioned in the same section but on different embankment benches. The test results generally indicated normally consolidated (contractive) clay behavior, characterized by low tip resistances (q_t lower than 2 MPa) and high penetration pore pressures (B_q higher than 0.1). However, an exception was observed between elevations 1,242 and approximately 1,240 m, as outlined by the yellow box in Figure 5, where high tip resistances along with negative penetration pore pressures were recorded, suggesting a dilative behavior. Notably, the highest OCR values were obtained from samples S-07 and S-08, collected at elevations 1,242 and 1,241 m, respectively, near CPTu-02 borehole, corroborating the assumption of a dilative/over-consolidated region within the foundation alluvial stratum.

Results indicating contractive clay-like behavior were exclusively included in the undrained strength assessment, as shown in Figure 6B (Robertson, 2016), as high strength values within dilative zones were

disregarded. The undrained strengths were calculated using the Lunne et al. (1997) correlation, where a cone factor of N_{kt} = 14 was calibrated (Figure 6A) based on the sole vane shear test result on the undisturbed condition (VST-01), along with the net tip resistance (q_{net}) from CPTu-01 at the depth where VST-01 was conducted, as these tests were carried out at the same location with boreholes 2 m apart.

However, due to uncertainties on the drainage conditions of VST-01 and given that 13 VST surpassed the equipment reading limit, the N_{kt} was decreased to 12 to derive the S_u profile presented in Figure 5.

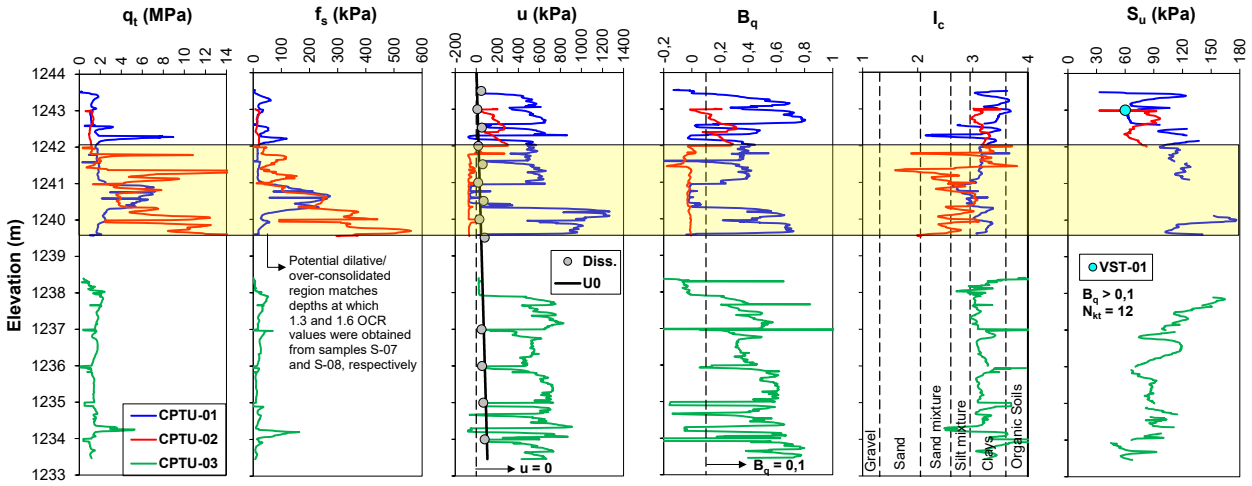


Figure 5: Piezocone tests results and interpretations

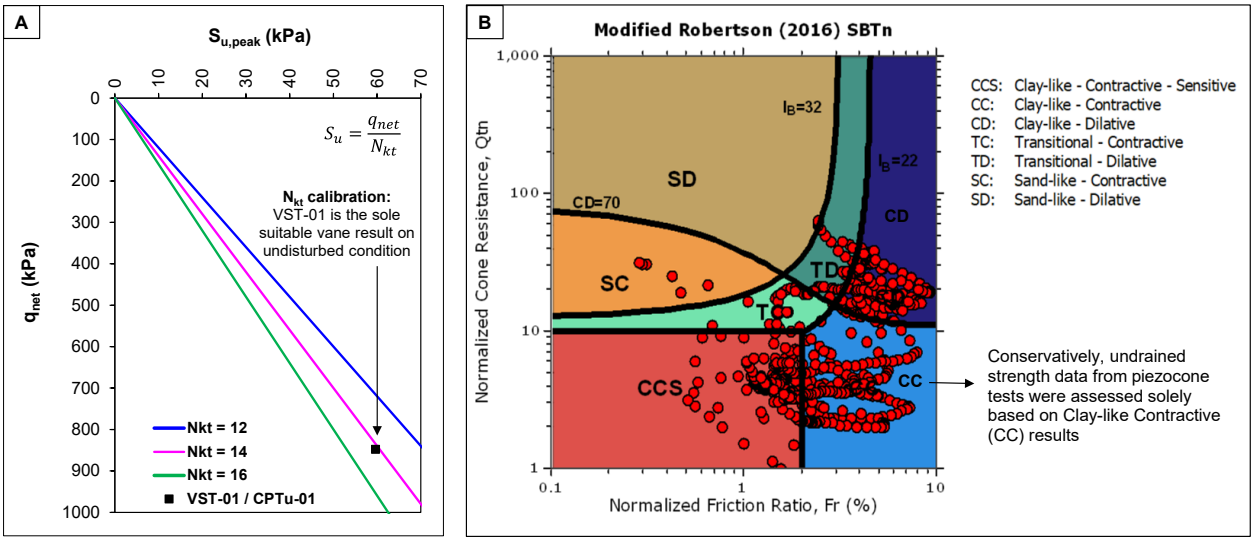


Figure 6: (A) N_{kt} calibration and sensitivity; (B) Modified soil behavior type (SBTn) chart

It is noteworthy that the hydrostatic pore-pressure profile (U0) obtained from dissipation test results was cross-verified with readings from piezometers installed near the CPTu boreholes on the same day the piezocone tests were conducted. The results showed a maximum difference of only a few dozen centimeters.

Additionally, a thorough protocol was followed to ensure the saturation of the porous stone, involving glycerin storage and subsequent rubber wrapping prior to ground penetration onset. This validation process confirmed the accuracy of the pore-pressure measurements from the piezocone tests, ensuring that the negative pore pressures observed within the dilative region were not due to cavitation effects. Finally, apparent cohesion from suction was ruled out since the material is confirmed to be saturated.

Partial drainage assessment

As shown in Figure 7A, a mean coefficient of consolidation ($c_v = 0.05$ cm^2/s) was derived from both consolidation and CPTu dissipation tests, corresponding to typical silt values (Duncan et al., 2014). Furthermore, VST results indicated partial drainage effects, as all tests fail after the Blight/Chandler drainage boundary. However, using the Morris and Williams drainage boundary, 4 VST (1 undisturbed and 3 remolded) appear to have mobilized fully undrained strength at failure, and thus these 4 tests were deemed valid for the drainage assessment. Moreover, CPTu dissipation test results indicated that 6 out of 10 tests indicate partial drainage behavior according to the DeJong and Randolph boundary, as shown in Figure 8B.

To enhance the understanding of partial drainage effects and undrained strength mobilization, further analyses were conducted. Firstly, general drainage conditions were assessed following the methodology proposed by France et al. (2015), as illustrated in Figure 7B. Considering the alluvium layer's 4-meter thickness and drainage at both the bottom and top interfaces, partial drainage is expected to occur under a rapid loading scenario applied over a hypothetical time of 1 day.

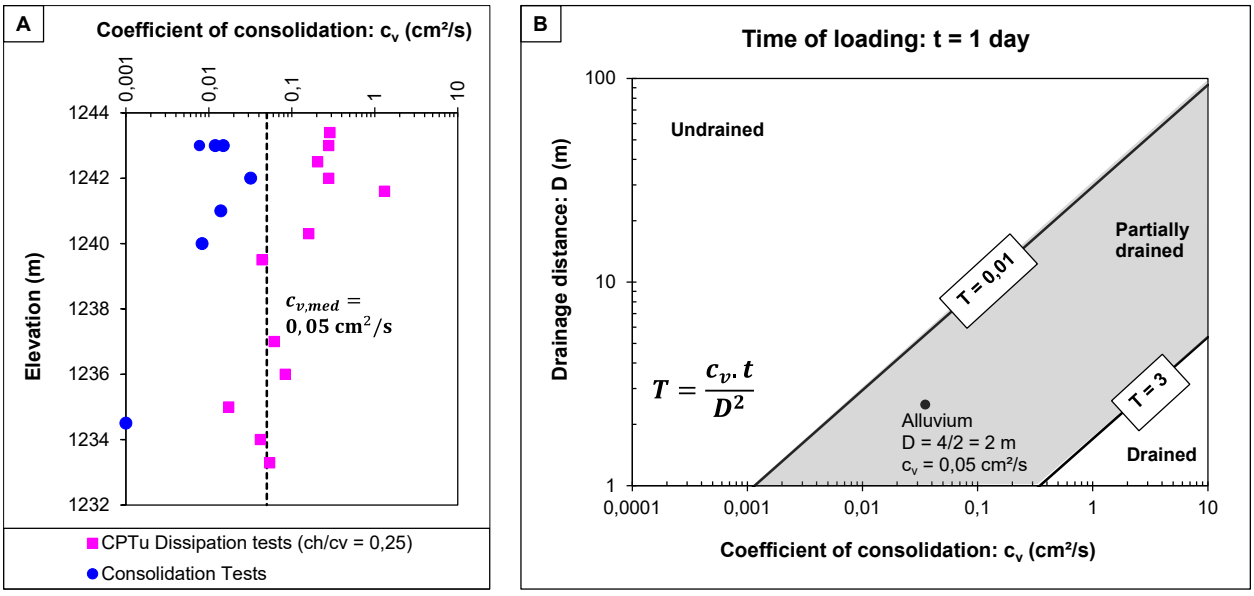


Figure 7: (A) Coefficient of consolidation mean value; (B) general drainage assessment

Further analyses encompassed calibrating the characteristic drainage curves for both vane shear and dissipation tests, as shown in Figures 8A and 8B, respectively. The theoretical curves were obtained using the methodologies of Morris and Williams (2000) for vane shear tests, and both Teh and Houlsby (1991) and DeJong and Randolph (2012) for dissipation tests. According to Morris and Williams (2000), fully undrained conditions occur until 10% of degree of drainage (U), and fully drained conditions occur after 90%. Based on this criterion, it was observed that 1 out of 14 tests (including both vane shear and dissipation tests) indicated fully undrained behavior, while the remaining 13 tests show partially drained behavior.

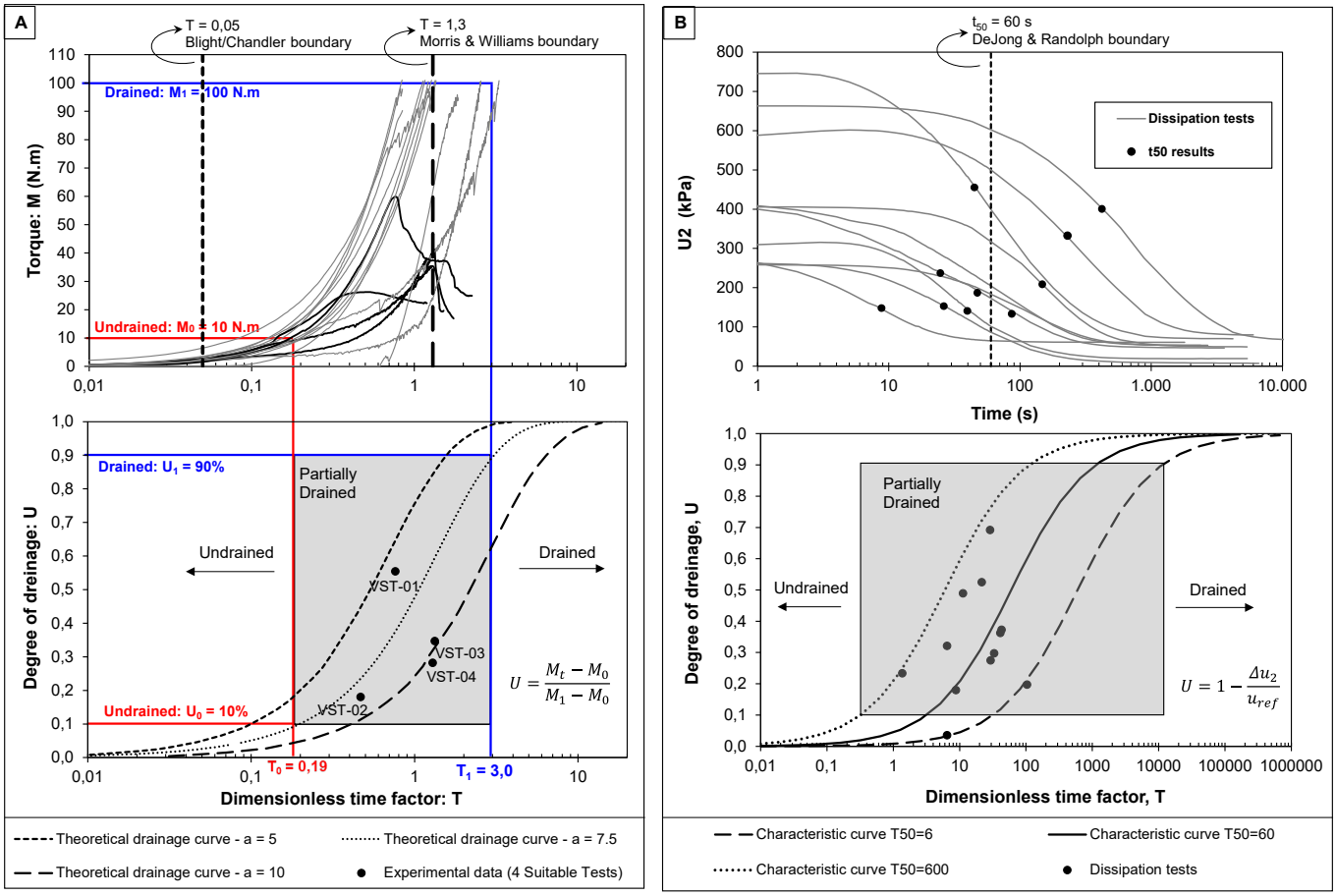


Figure 8: (A) Partial drainage in vane shear tests; (B) partial drainage in CPTu dissipation tests

Triaxial tests

A series of 11 saturated and isotopically consolidated undrained triaxial (TX-CIU) tests were carried out at confining pressures of 50, 100, 200, 400, and 600 kPa, as shown in Figure 9.

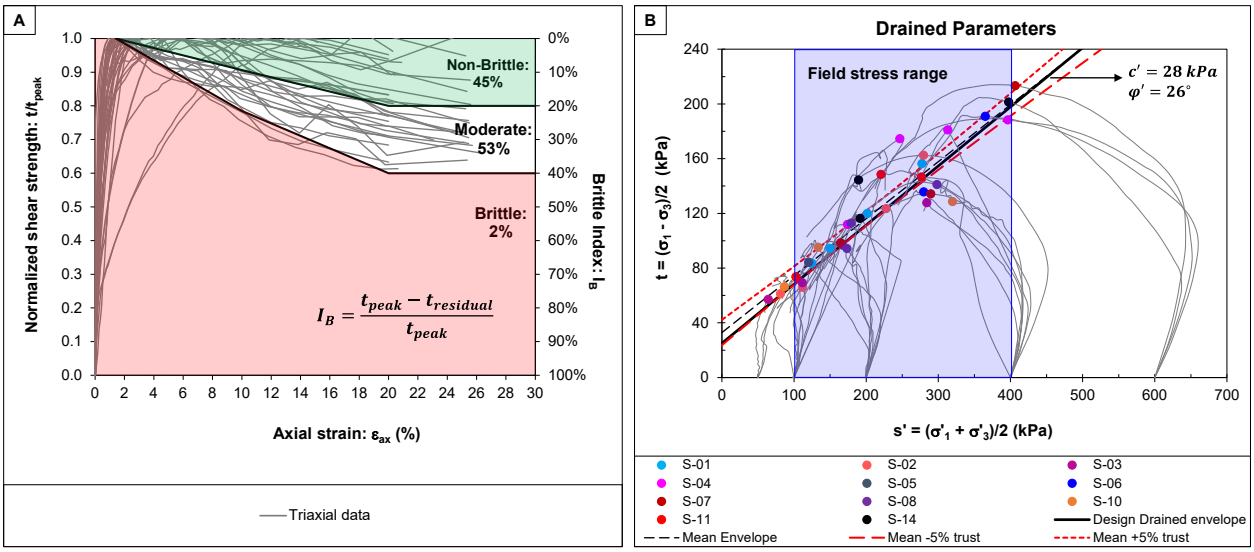


Figure 9: (A) Brittleness assessment; (B) definition of drained parameters

As illustrated in Figure 9A, the results demonstrated non to moderate brittleness, according to the criteria of Bishop (1967). Furthermore, a predominantly contractive behavior was observed, characterized by the A pore-pressure parameter ranging from 0.5 to 1.0, which classifies the material as normally consolidated clay according to the criteria of Skempton (1952). Exceptions were noted in some tests at a confining pressure of 600 kPa, where the A parameter ranged from 1.5 to 2.0, indicating a sensitive behavior per Skempton (1952). These findings highlight the need to define undrained strength parameters for the alluvium, which will be discussed in the next section.

Regarding the drained parameters, the Mohr-Coulomb criteria was assessed by the usage of maximum deviatoric stress criterion. Following the Eurocode (2007) guidelines, the drained strength envelope was designed within the field stress range, fitting the mean envelope minus 5% of the confidence interval with a t-Student value of 2.037, as illustrated in Figure 9B.

SHANSEP approach

Due to the observed dilative/over-consolidated behavior in some piezocone and consolidation tests, a SHANSEP approach was evaluated following the Ladd and Foot (1974) methodology. As shown in Figure 10A, applying an over-consolidation stress of 400 kPa revealed a non-linear trend when plotting the undrained strengths against OCR values, thereby confirming the suitability of assessing SHANSEP principles to define the alluvium undrained strength parameters, as per Gallardo (2023a, 2023b, 2022).

However, given the variation in contractive/normally consolidated and dilative/over-consolidated behaviors, it was not possible to establish an OCR profile as required for a consistent SHANSEP approach

(Duncan et al., 2014). Hence, a conservative linear envelope was defined with an intercept aimed at modelling a single relationship across all test results, as illustrated in Figure 10B.

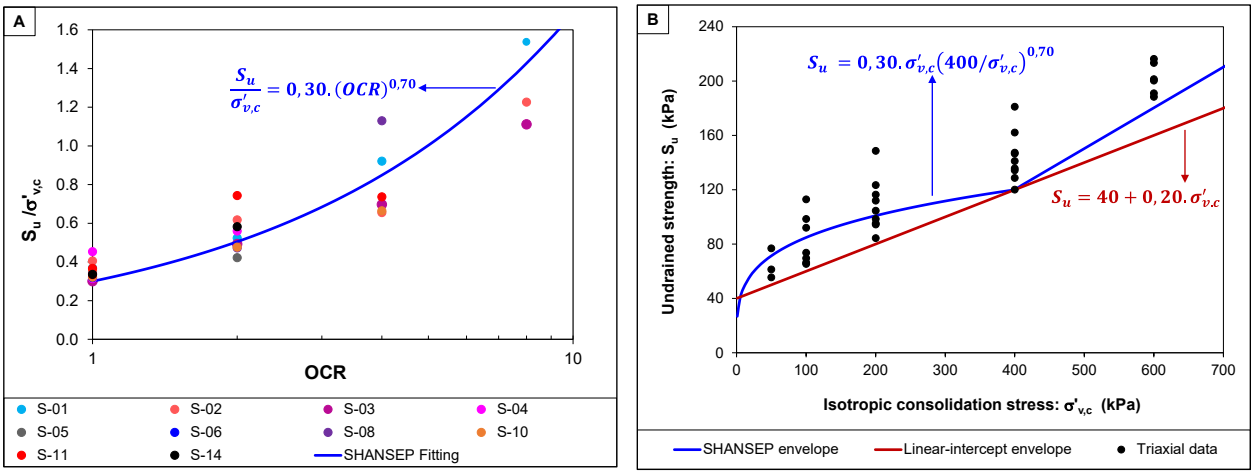


Figure 10: (A) Undrained strength ratio plot; (B) SHANSEP and linear-intercept envelopes

To define the design undrained envelope, the undrained strengths were plotted against the consolidation stresses, following Sadrekarimi and Olson (2011) and Jefferies and Been (2015). However, according to Duncan et al. (2014), undrained strengths obtained from TX-CIU tests may be unconservative due to effects of anisotropy, stress reorientation, and strain rate. The authors emphasize that such results require adjustment to be suitable for design purposes.

Therefore, a correction technique was applied to the isotropic vertical consolidation stress by introducing the anisotropic coefficient at rest (K_0), estimated using Jaky's (1944) correlation. As illustrated in Figure 11A, corrected anisotropic vertical consolidation stresses ($\sigma'_{v,0}$) 1.36 times the isotropic stresses (σ'_c) were obtained, conservatively resulting in lower slope tangent of the line. It is noteworthy that the adopted envelope was observed to fit the mean envelope minus 5% of the confidence interval with a t-Student value of 2.037 within the field stress range.

Finally, all in-situ and laboratory tests results for undrained strengths are plotted in Figure 11B, confirming that the adopted linear-intercept envelope ($S_u = 40 + 0.20\sigma'_v$) defined by triaxial tests also fairly fits the mean value of the S_u profile obtained with piezocone results based on $N_{kt} = 12$ (the CPTu-VST calibrated value of $N_{kt} = 14$ was reduced given the confirmed partial drainage observed in both tests).

Notably, Figure 11B outlines that the adopted envelope with a linear intercept of $S_u = 40$ kPa (solid contour) fits the overall results more accurately than the envelope with a cut-off of $S_{u,min} = 40$ kPa (dotted contour). In fact, the cut-off envelope, typically applied to normally consolidated material (e.g., obtained by empirical correlations through SPT results) proves to be an excessively conservative lower

boundary for the alluvium herein studied. Moreover, the upper boundary with an intercept of S_u = 80 kPa (dashed contour) states that the adopted linear intercept reflects the average trend across all tests results.

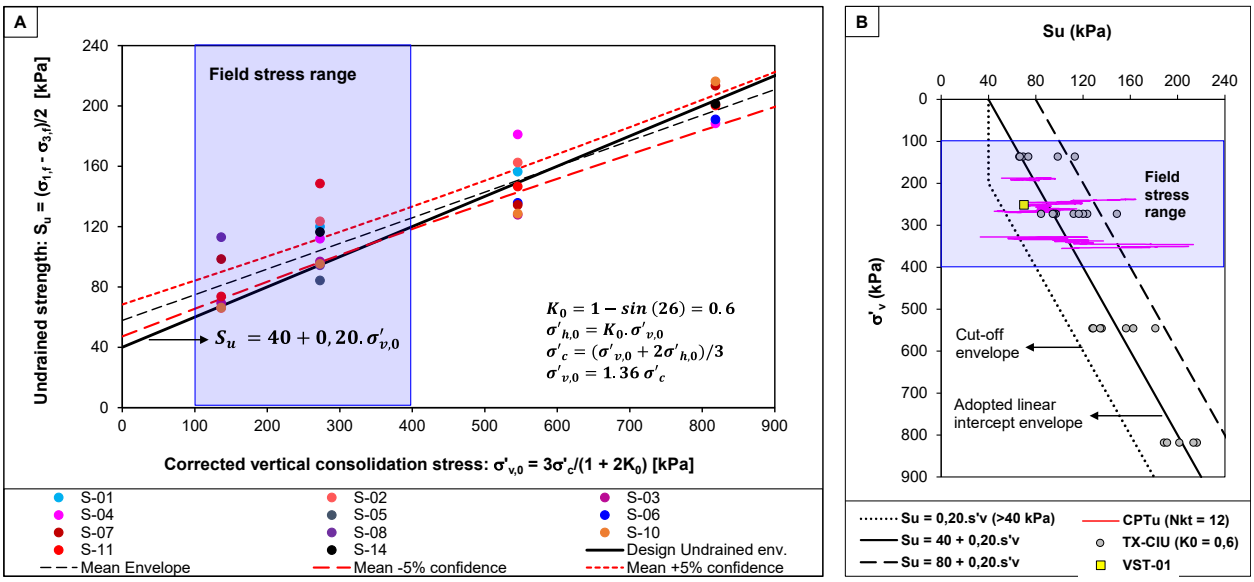


Figure 11: (A) Definition of undrained parameters; (B) in-situ and laboratory results

Conclusion

Comprehensive site and laboratory investigations on the alluvium layer of an existing tailings dam revealed significant high coarse fraction content, partial drainage effects, slightly over-consolidated behavior, and a non-linear trend in the undrained strength ratio plot. These findings led to the usage of a linear-intercept approach, resulting in more accurate undrained strength parameters and realistic factors of safety, which remained lower than those for drained conditions, aligning with established engineering guidelines.

Challenges in sampling and specimen preparation were found due to the high coarse fraction content and friability, though samples were deemed acceptable by established criteria. Vane shear and dissipation tests confirmed partial drainage behavior, suggesting that in-situ fully undrained shear strength mobilization is unlike to occur. Zones of dilative behavior in piezocone tests matched depths at which oedometer tests provided slight OCR values, indicating an over-consolidated region within the alluvial layer.

A certain degree of sensitiveness was found to the alluvium, according to sensitivity index (S_t) from vane shear test and some shear pore-pressure parameters (A) from undrained triaxial tests. Additionally, 53% of the triaxial results indicated moderate brittleness (I_B ranging from 20 to 40%), and low N_{SPT} values were observed. These findings underscore the need to define undrained strength parameters for the alluvial material, despite its in-situ partial drainage behavior and slight over-consolidated zones.

True or apparent cohesion was found to be negligible due to colloidal inactivity, friability (despite high specific gravity values suggesting potential cementation), and saturation confirmed by hydrostatic pore-pressure profile from dissipation tests and by readings from piezometers, ruling out suction effects.

A conservative linear undrained strength envelope was defined due to the inability to establish an OCR profile, given the alternation in over-consolidated/dilatant and normally consolidated/contractive behaviors. This envelope incorporates a linear intercept to model the undrained strengths obtained in all tests, ensuring consistency across the entire stratum, rather than discretizing sub-layers based on normal and over-consolidated behaviors. Additionally, a correction technique was applied to decrease the slope tangent of the obtained envelope, as TX-CIU tests typically yield unconservative undrained strength values.

The adopted linear-intercept envelope ($S_u = 40 + 0.20\sigma'_v$) exhibited greater consistency compared to the cut-off envelope ($S_u = 0.20\sigma'_v$ @ $S_u > 40$ kPa). While true cohesion is not expected for the alluvium, the high coarse fraction content, partial drainage effects, and slight over-consolidation necessitate defining a linear intercept to accurately determine the undrained strength parameters to be used in stability analysis.

Finally, it is concluded that the continued use of advanced testing methodologies and SHANSEP principles is crucial for accurately characterizing material properties to assess slope stability of tailings dam foundations under similar geological contexts in Brazil, rather than relying on empirical correlations, e.g., through SPT results.

Acknowledgements

The authors express their gratitude to VALE S.A. for facilitating this extensive investigation survey. They also extend their thanks to colleagues at deepmath solutions for providing the algorithm used to plot theoretical drainage curves for vane shear tests, utilizing the Morris and Williams (2000) solution.

References

Agência Nacional de Mineração (ANM). 2022. *Resolução Anm Nº 95, de 07 de Fevereiro de 2022*. Diário Oficial da União.

Associação Brasileira de Normas Técnicas (ABNT). 1989. NBR 10905: *Solo – Ensaio de palheta in situ*. Rio de Janeiro: ABNT.

ASTM International. 2017. Standard practice for classification of soils for engineering purposes (Unified Soil Classification System) (D2487-17). West Conshohocken, PA: ASTM International.

Australian National Committee on Large Dams (ANCOLD). 2019. Guidelines on tailings dams – planning, design, construction, operation and closure.

Bishop, A.W. 1967. Progressive failure – with special reference to the mechanism causing it. *Proceedings of Geotech. Conference,* Oslo 2, 142–150.

Bjerrum, L. 1973. Construction on soft clays. Norwegian Geotechnical Institute Publication, No. 94.

Blight, G.E. 1968. The vane test for silts and its application to South African soils. *Proceedings of the 6th International Conference on Soil Mechanics and Foundation Engineering*, Montreal, 1: 203–208. Toronto: University of Toronto Press.

Chandler, R.J. 1988. The in-situ measurement of the undrained shear strength of clays using the field vane. *In Vane Shear Strength Testing in Soils: Field and Laboratory Studies,* ASTM STP 1014: 13–44. Philadelphia: American Society for Testing and Materials.

Clayton, C.R.I., Siddique, A. and Hopper, R.J. 1998. Effects of sampler design on tube sampling disturbance—numerical and analytical investigations. *Géotechnique* 48(6): 847–867.

Coutinho, R.Q., Oliveira, J.T.R. and Oliveira, A.T.J. 1998. Estudo quantitativo da qualidade de amostras de argilas moles brasileiras – Recife e Rio de Janeiro. *XICOBRAMSEG – Cong. brasileiro de mecânica dos solos e engenharia geotécnica*, 2: 927–936, Brasília, Brasil.

DeJong, J.T. and Randolph, M. 2012. Influence of partial consolidation during cone penetration on estimated soil behavior type and pore pressure dissipation measurements. *J. Geotech. Geoenviron. Eng.* 138(7): 777–788.

Duncan, J.M., Wright, S.G. and Brandon, T.L. 2014. *Slope Stability Analysis and Design*. Engineering and Research Publication, 3rd edition.

European Committee for Standardization (CEN). 2004. Eurocode 7: Geotechnical design – Part 1: General rules. Brussels: CEN.

France, J.W., Williams, J.L., Winckler, C.J.C. and Adams, T.E. 2015. Soil shear strength selection for stability analysis – practical guidance. *Proceedings of Dam Safety 2015*, the Annual Conference of the Association of State Dam Safety Officials, New Orleans, LA, September 2015.

Gallardo, A. 2022. Peneirinha Dam; Technical Presentation N.º404; Static liquefactions and other myths. Doc. N.º 19070-AE-005-BAR-RPT-404-0. Prepared for VALE by TPF Consultores, Lisboa, Portugal.

Gallardo, A. 2023a. Peneirinha Dam; Technical Note N.º204; On the alluvial clay occurring on the left abutment – a little more of the same. Report N.º 19070-AE-005-BAR-RPT-204-0. Prepared for VALE by TPF Consultores, Lisboa, Portugal.

Gallardo, A. 2023b. Peneirinha Dam; Technical Presentation N.º407; The tale of Peneirinha and the alluvium. Doc. N.º 19070-AE-005-BAR-RPT-405-0. Prepared for VALE by TPF Consultores, Lisboa, Portugal.

Jaky, J. 1944. The coefficient of earth pressure at rest. *Journal of the Society of Hungarian Architects and Engineers* 78(22): 355–358.

Jefferies, M.G. and Been, K. 2015. *Soil Liquefaction: A Critical State Approach*. 2nd edition. New York: CRC Press.

Ladd, C.C. and DeGroot, D.J. 2004. Recommended practice for soft ground site characterization: Arthur Casagrande Lecture. In *Soil Behavior and Soft Ground Construction,* ASCE GSP 119: 1–86.

Ladd, C.C. and Foott, R. 1974. A new design procedure for stability of soft clays. *Journal of the Geotechnical Engineering Division* 100(GT7): 763–786.

Leroueil, S. and Vaughan, P.R. 1990. The general and congruent effects of structure in natural soils and weak rocks. *Géotechnique* 40(3): 467–488.

Lunne, T., Robertson, P.K. and Powell, J.J.M. 1997. *Cone Penetration Testing in Geotechnical Practice.* London: Blackie Academic and Professional.

Massad, F. 2009. *Solos Marinhos da Baixada Santista.* São Paulo: Oficina de Textos.

Morris, P.H. and Williams, D.J. 2000. A revision of Blight's model of field vane testing. *Canadian Geotechnical Journal* 37(5): 1089–1098.

Morris, P.H. and Williams, D.J. 1994. Effective stress vane shear strength correction factor correlations. *Canadian Geotechnical Journal* 31: 335–342.

Robertson, P.K. 2016. Cone penetration test (CPT)-based soil behaviour type (SBT) classification system – an update. *Canadian Geotechnical Journal* 00: 1–18 (0000)

Sadrekarimi, A. and Olson, S.M. 2011. Evaluation of the strength ratio of sands. *Geotechnical Testing Journal* 34(4): 1–9.

Skempton, A.W. 1954. The pore pressure coefficients A and B. *Géotechnique* 4(4): 143–147.

Skempton, A.W. 1953. The activity of clays. *Proceedings of the 3rd International Conference on Soil Mechanics and Foundation Engineering* 1: 57–61.

Skempton, A.W. and Northey, R.D. 1952. The sensitivity of clays. *Géotechnique* 3(1): 30–53.

Teh, C.I. and Houlsby, G.T. 1991. An analytical study of the cone penetration test in clay. *Géotechnique* 41(1): 17–34.

Interpretation of Cyclic DSS Testing under Static Bias on Underflow Copper Tailings

Alfonso Cerna Diaz, AECOM, USA
Kevin Ritter, AECOM, USA
Jason Hilgers, AECOM, USA

Abstract

This paper summarizes the results of a cyclic DSS laboratory testing program that was completed to investigate the influence of static bias load reversal on the deformation mechanisms and strength loss of copper underflow tailings, using stress-controlled cyclic direct simple shear (DSS) testing.

The influence of static bias on cyclic induced permanent deformation was evaluated for a range of initial static shear stresses. For a given number of cycles, permanent deformations under static driving shear stresses were found to be dependent on the initial state parameter, the ratio between Initial Loading Stress Ratio (LSRo) and the Image Stress Ratio (ISR), which provides an index of strain potential.

Introduction

Methods to evaluate the effect of static bias on cyclic response primarily have focused on its role in liquefaction triggering in sloping ground (i.e., ground subjected to a static driving shear stress). Due to the limited number of well-documented case histories of liquefaction in sloping ground, the majority of these methods used extensive data from single element tests (e.g., cyDSS, cyTX) to extend the widely used cyclic stress approach (Idriss and Boulanger, 2008; Seed and Idriss, 1971; Whitman, 1985) that used only level-ground liquefaction case histories.

Although significant understanding was gained into the effects of static bias on the range of triggering criteria (e.g., ~3 percent shear strain), the induced post-liquefaction shear deformation processes under sloping ground conditions are still not well understood. If liquefaction is triggered in sloping ground, a post-triggering stability analysis is performed with the liquefied shear strength assigned to the liquefied soils. In addition, derived deformations pre- and post-liquefaction are best evaluated by means of nonlinear dynamic deformation analysis using effective stress-based numerical modeling. However, cyclic laboratory data for tailings under static bias to assess the applicability of such models and evaluate the seismic performance of the tailings storage facilities (TSFs) are scarce (Reid et al., 2024).

In this study, cyclic DSS testing under level ground and initial static shear stresses were performed to evaluate liquefaction triggering and post-triggering permanent deformations and use the ratio between Initial Loading Stress Ratio (LSRo) and the Image Stress Ratio (ISR), as defined by Jefferies and Been (2016), and the state parameter (Been and Jefferies, 1985) to provide an index of strain potential.

Laboratory testing program

A laboratory testing program was completed at the Norwegian Geotechnical Institute (NGI) to investigate the influence of a static bias load on underflow tailings behavior using cyclic direct simple shear (cyDSS) testing. The laboratory testing program consisted of testing samples at similar void ratios and at vertical stress and cyclic stress ratios under a varying static bias. This allowed for an evaluation of the impact of the static bias load on the cyclic and post cyclic response.

Underflow sand tailings tested here are often characterized by contractive/ductile behavior if they are saturated, based on state-based behavior characterization. The laboratory testing program used bulk samples and Shelby tube samples which were collected during various geotechnical investigations from a TSF. The underflow sand samples were reconstituted using the slurry sedimented method.

Standard index testing was performed to characterize and classify the samples used for the cyclic DSS testing with static bias. The following tests were completed as part of the index property testing: water (moisture) content, unit weight estimation, hydrometer/sieve analyses (Figure 1), and Atterberg limits.

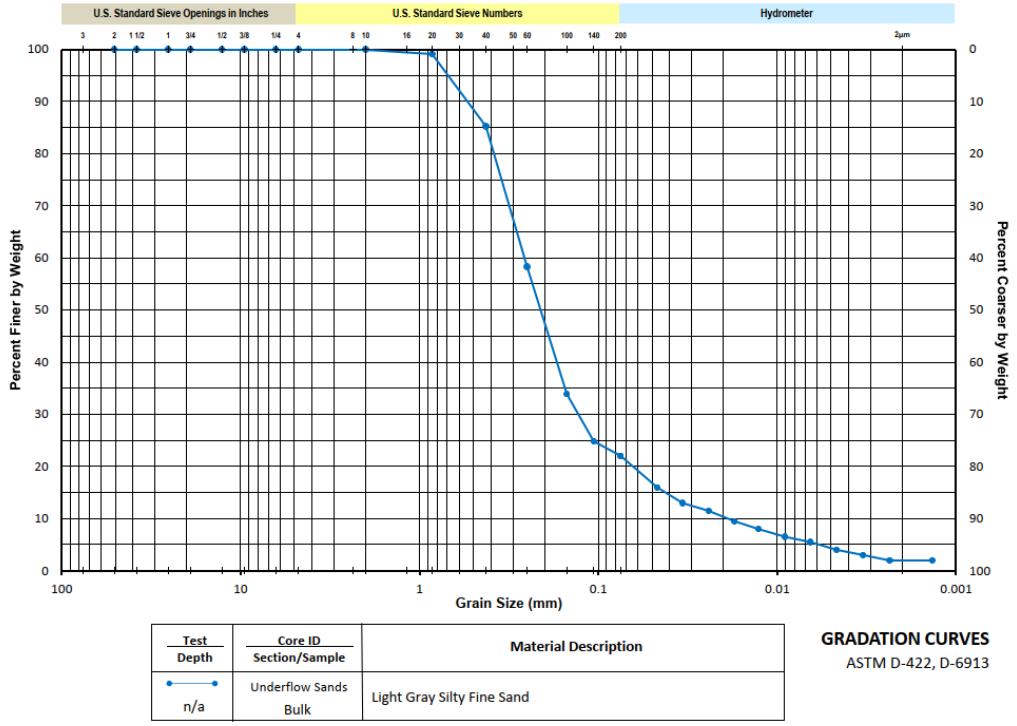


Figure 1: Typical grain size distribution of underflow sand tailings

The testing results are provided in Table 1. The results show that the underflow sand tailings are non-plastic and have a fines content of 22 percent.

Table 1: Summary of index property testing

Sample	Sample	Total unit weight (pcf)	Fines content (%)	PL	LL	PI
Underflow sands	Bulk	Various	22	NP	NP	NP

Cyclic DSS testing protocol

Cyclic DSS testing with a static shear stress bias was performed to evaluate the influence of static bias loading on the cyclic and post-cyclic behavior of the tailings material. Care was taken to vary only the static shear stress bias load. All other testing parameters, such as consolidation stress, void ratio, and cyclic stress ratio (CSR), were kept nearly constant for all samples of the same material so that the influence of the varying static bias load could be compared. From all these parameters, experimental variability in the void ratio among tests was still present. Therefore, to characterize the response of each sample, initial state parameters from all samples were estimated after consolidation.

A summary of the testing parameters is provided in Table 2.

Table 2: Summary of Cyclic DSS testing parameters

Sample	Test ID	Consolidation stress (σ'_v, psi)	Static bias ratio (bias shear stress α, psi)	Cyclic stress ratio	Initial state parameter ($\psi=e_o-e_c$)
Underflow tailings (this paper)	Base	150	0 (0)	0.17	0.07
	SB-0.2	150	0.2 (30)	0.17	0.19
	SB-0.4	150	0.4 (60)	0.17	0.04
Underflow tailings (Cerna-Diaz et al., 2022)	Various	Various	0 (0)	0.17-0.20	-0.15-0.11

The following general testing procedure was used in the completion of the cyclic DSS testing:

1. Specimen preparation: Preparation of test specimens following ASTM D6528.
2. Consolidation: One initial consolidation stress, i.e., 150 kPa, was specified for the underflow material, and all specimens were consolidated to this initial vertical effective stress.
3. Application of static bias load: for tests under static bias, the initial shear load was applied to the test specimen at a rate/increment that followed the drained stress path and did not generate excess pore pressures.

4. Cyclic loading: the cyclic stress ratio (0.17) and frequency (0.1 Hz) were specified, and all specimens were tested at this same CSR and frequency.
5. Post-cyclic loading: After cyclic loading, each specimen was sheared in a post-cyclic monotonic loading.

Cyclic DSS testing results

The results of the cyclic DSS testing at level ground (bias=0) and with static bias for the underflow tailings are summarized in the following sections.

Level ground baseline testing (no static bias)

One level ground cyclic DSS and historical test results are summarized in Figure 2. Figure 2 shows the test path (shear stress versus [vs.] vertical effective stress), shear stress vs. shear strain, excess pore pressure ratio (r_u) vs. number of cycles, and shear strain vs. number of cycles.

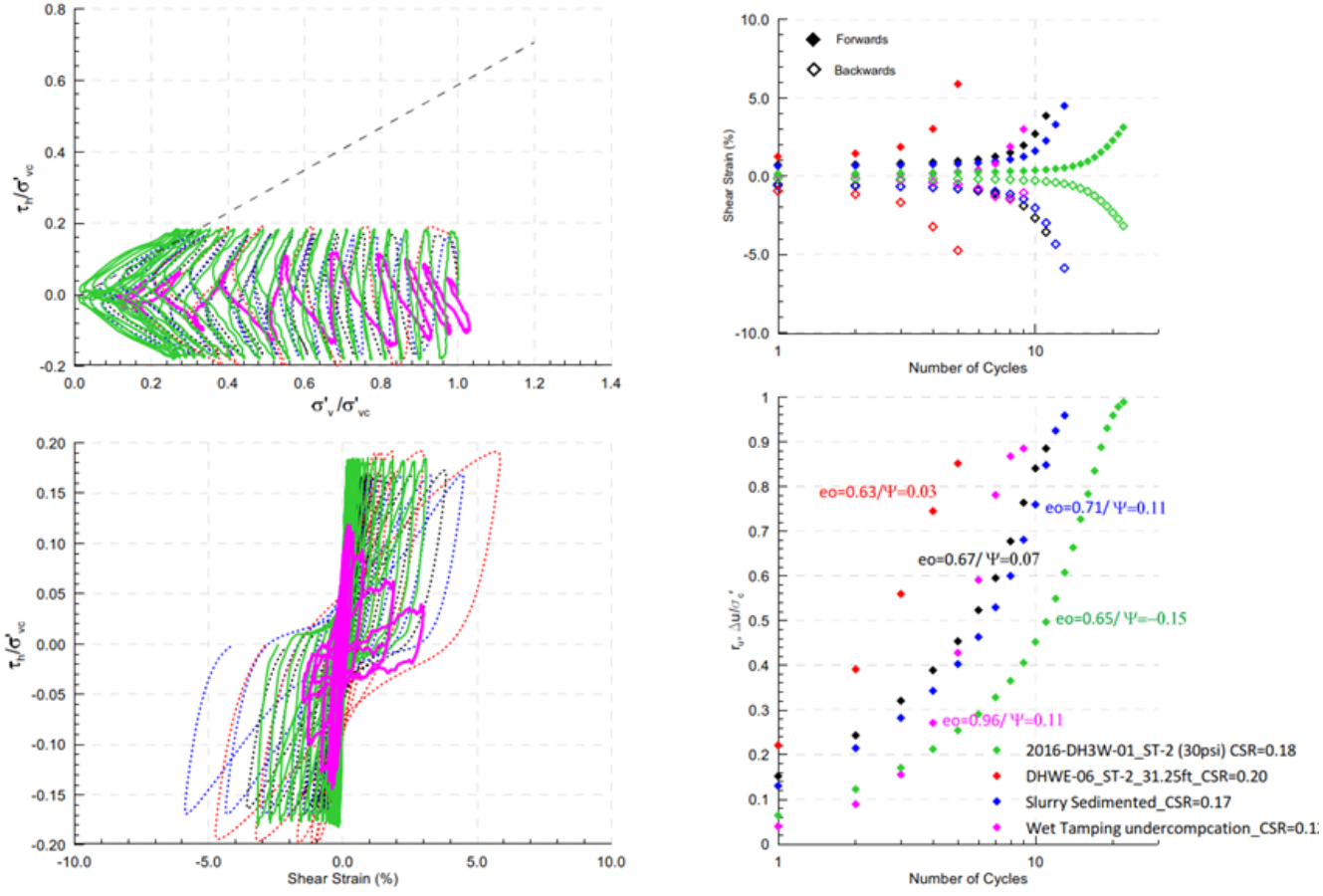


Figure 2: Cyclic level ground (no static bias) new and historical baseline DSS tests on the underflow sand tailings

Undrained cyclic loading in all level ground tests induced contractive behavior resulting in the development of positive excess pore water pressures due to the change in direction of loading, which resulted in cyclic accumulation of plastic shear strains. The accumulation of plastic shear strains and the development of excess pore pressures generally induced loss of stiffness throughout cycling; the specimens exhibited cyclic mobility type behavior with more noticeable dilatant response as the stress paths crossed the Phase Transformation Line (PTL) with subsequent cycles of softening and hardening upon proximity to the PTL at the levels of CSR imposed by the cyclic DSS tests (CSR ~ 0.17). Additionally, historical level ground cyclic DSS tests (CSR ~ 0.17-0.2). that were completed on similar underflow tailings material, as presented in Cerna-Diaz et al. (2022), are included in Figure 2.

The results of new and historical tests indicate that the level of accumulated shear strains is dependent on the initial state parameter. Samples that had a higher initial state parameter showed an increased rate of cyclically induced accumulated shear strains. The cyclic stress-strain response of the samples is governed by the void ratio and location with respect to the critical state line, as shown in Figure 3, with state parameters estimated by assuming Ko~0.6 for the DSS mean effective stresses estimates.

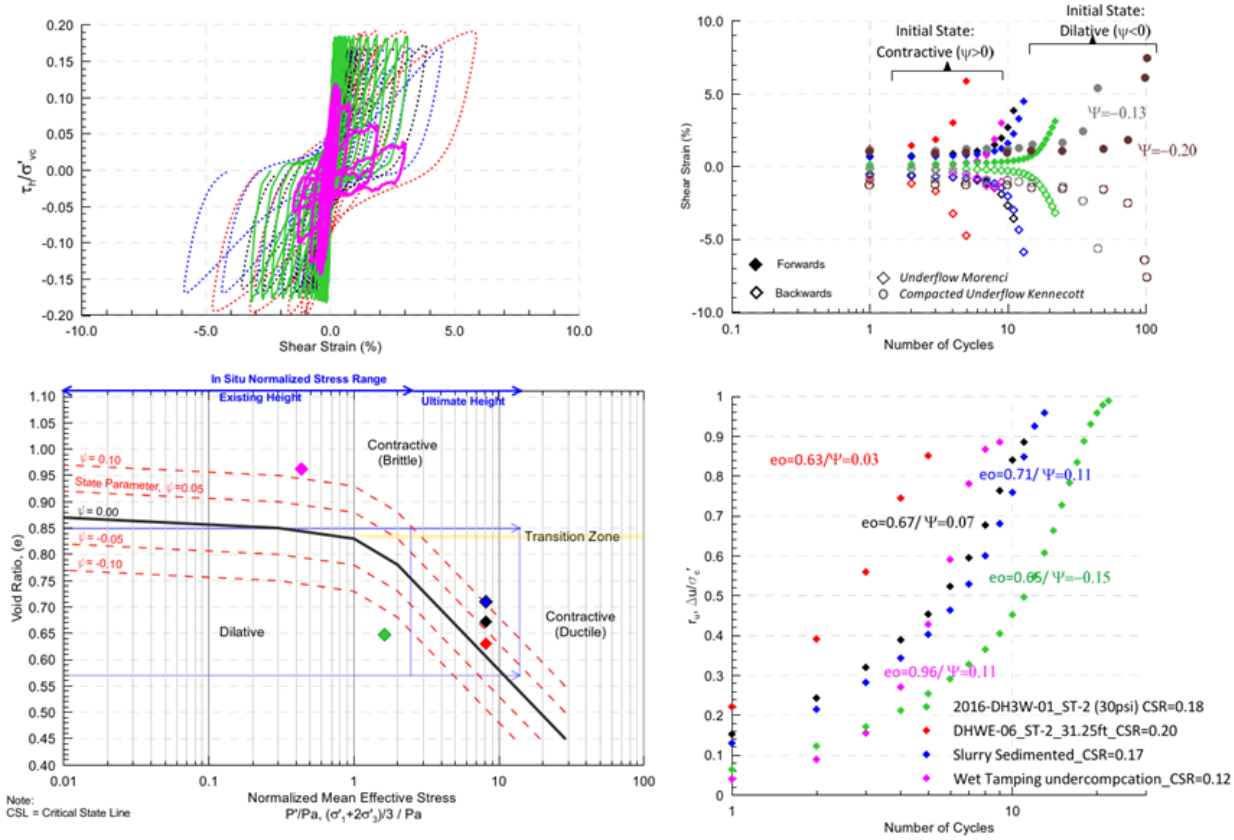


Figure 3: Cyclic level ground DSS (no static bias) baseline tests on the underflow sand tailings based on their initial state on the CSL space static bias cyclic testing results

Furthermore, a sample prepared using the wet tamping undercompaction method underwent a rapid loss of stiffness, while the pore pressures continued to increase at the fastest rate out of all of the test specimens, with the onset of triggering (e.g., the onset of strength loss) occurring at a relatively low value of r_u~0.4. This test started with an initial consolidated void ratio of 0.96 (ψ=0.11) and is in the contractive/brittle critical state line (CSL) space as defined by Robertson, 2017.

In contrast, another sample was prepared using the more realistic slurry sedimented method with an initial consolidated void ratio of 0.71. This specimen had an identical state parameter (ψ=0.11) but was tested at a higher vertical effective consolidation stress, which placed it in the contractive/ductile space. During testing, this specimen exhibited an accumulation of plastic shear strain, without a loss of strength, to levels below those induced by the cyclic CSR during cyclic loading, even upon full liquefaction of the specimen.

Static bias testing results

For the testing program completed as a part of this study, two static bias (0.2 and 0.4) cyclic DSS tests were conducted on the underflow sand tailings, and the results are plotted in Figure 4. Figure 4 shows the test path (shear stress vs. vertical effective stress), shear stress vs. shear strain, excess pore pressure ratio (r_u) vs. number of cycles, and shear strain vs. number of cycles.

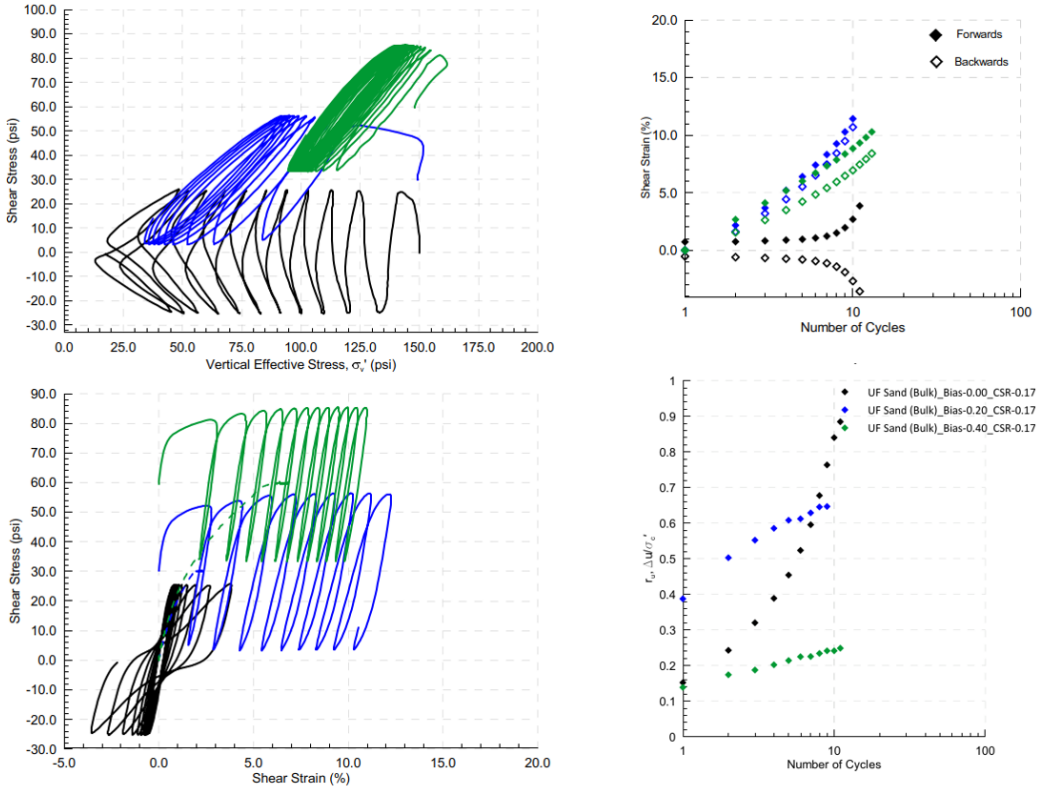


Figure 4: Cyclic DSS tests with static bias (0, 0.2. and 0.4) on the underflow sand tailings

Cyclic behavior

Similarly to level ground tests, undrained cyclic loading in all of the cyclic tests completed with static bias induced contractive behavior, resulting in the development of positive excess pore water pressures and an accumulation of shear strains, as shown in Figure 4. The testing results showed an accumulation of shear strains in the direction of the initial applied static shear stress and generation of positive excess pore pressures, which indicated a loss of stiffness with each additional cycle. The results also indicated that the samples do not exhibit loss strength to levels below those induced by the cyclic CSR as imposed by the cyclic DSS tests (CSR~0.17). This is observed as the sample continues to carry the imposed shear stress throughout the loading cycles, even after liquefaction.

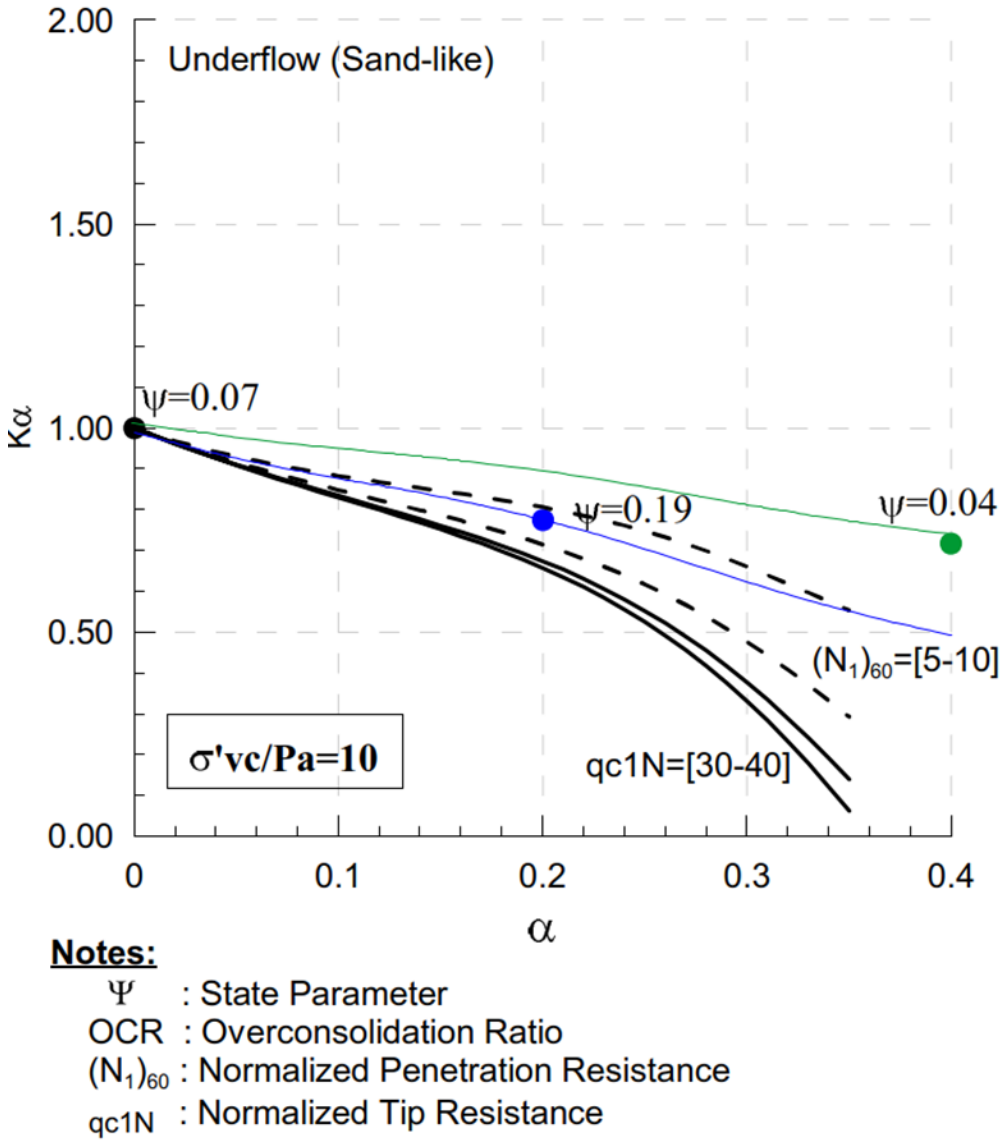


Figure 5: Sloping ground correction factor Ka from testing program vs. Boulanger (2003) relationship

In contrast to the level ground tests, the maximum induced excess pore water pressure ratio during cycling was less than 1 for each of the tests with static bias. The induced r_u ratios were the lowest for the test with the highest static bias (alpha=0.4) and the highest for the level ground level test (alpha=0.0). This is consistent with the decrease in the limiting value of the residual r_u in cyclic simple shear tests with the increase of static shear stress ratio on clean sands, as reported by Ishihara and Nagase (1980) and summarized in Idriss and Boulanger (2008). Furthermore, as shown in Figure 5, from initial screening level comparisons with Kα relationships (e.g., Boulanger, 2003) based on 3 percent single amplitude failure criteria, it appears that underflow testing suggests a lower reduction in cyclic resistance than the Boulanger (2003) correlation tailored for natural sands for similar stress and density conditions.

Initial consolidated state parameters of tested specimens, following the drained static bias phase, are plotted in the contractive ductile space of the CSL, as shown in Figure 6.

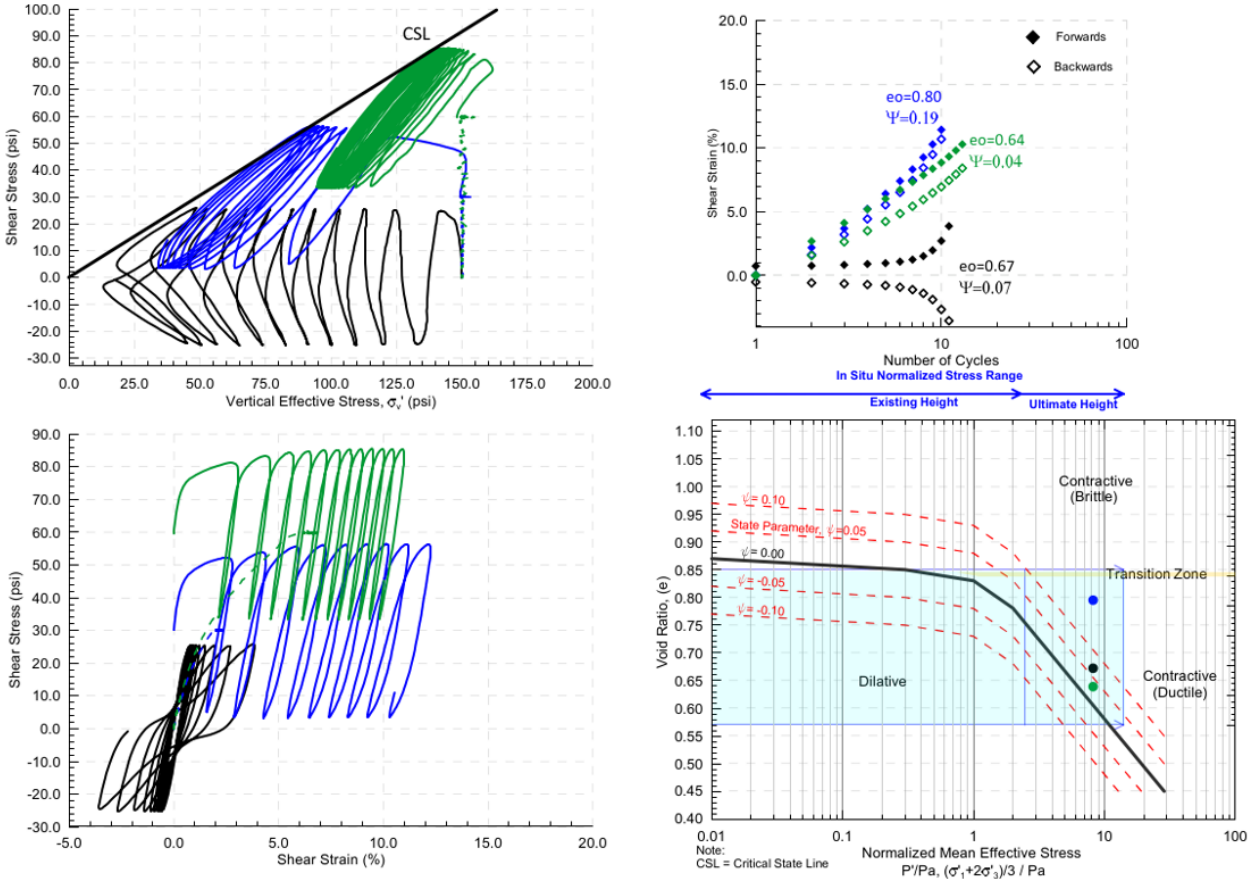


Figure 6: Cyclic DSS tests with static bias (0, 0.2. and 0.4) on the underflow sand tailings with respect to their initial state on the CSL space

The test with the largest positive state parameter (ψ=0.19) underwent the largest permanent deformation, larger than 3 percent and up to 12 percent of shear strains, for the same number of cycles, as shown in Figure 7a to Figure7e. Figure 7d also shows that although permanent strains are higher for tests

with static bias, the rate of accumulation of these deformations decreases with the number of cycles (Figure 7d) and is accompanied by a ratcheting effect showing an increase in shear stress with the number of cycles, as shown in Figure 7a and Figure 7e.

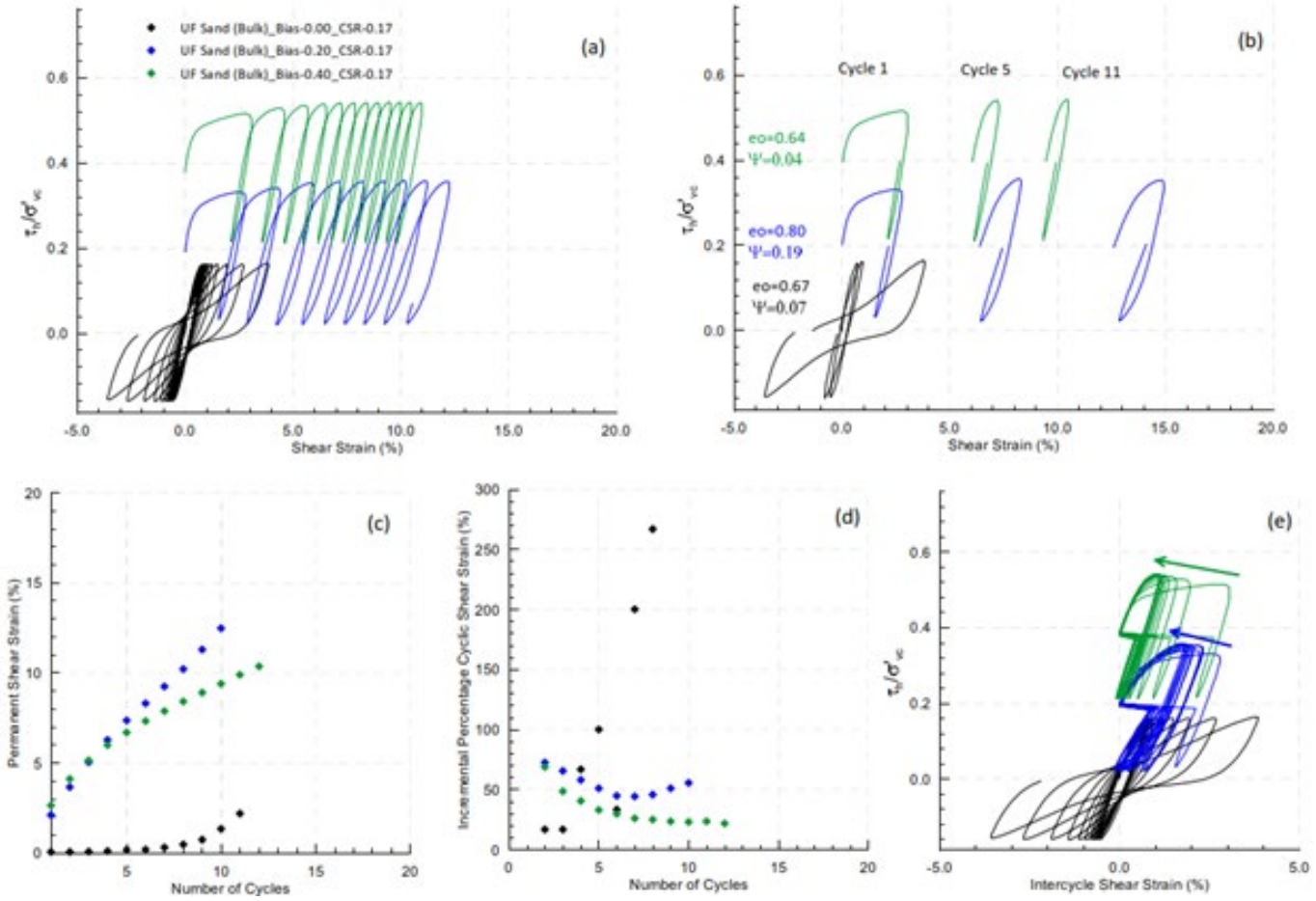


Figure 7: Cyclic DSS tests with static bias (0, 0.2, and 0.4) on the underflow sand tailings with respect to accumulation of shear strains and shear stress and initial state

The influence of static bias appears to increase the accumulation of shear strains for a given state parameter, as shown in Figure 7b, which compares the non-bias test with the test at a bias of 0.4, which is at a similar state parameter. The ISR (i.e., phase transformation line) describes the line that divides contractive and dilative behavior, and it is typically defined by monotonic tests (red lines), as observed in Figure 8. Once the stress path crosses the ISR, accumulation of strains brings the stress path close to the failure line, with a decreasing rate of permanent strain accumulation in ductile materials.

Although higher permanent deformations were recorded under static bias tests, the intercycle shear stress shear strain response indicates a slight hardening behavior for static bias tests. For instance, the sample with static bias of 0.4 (green line) starts nearly at the ISR line and begins dilating from the initial loading stage, causing a ratcheting and progressive increase in shear stress once the stress path crosses the

ISR. Analogously, the test with static bias of 0.2 (blue line) starts contracting toward the failure line, while dilation during cycles becomes more pronounced as the stress path crosses the ISR, as shown in Figure 8.

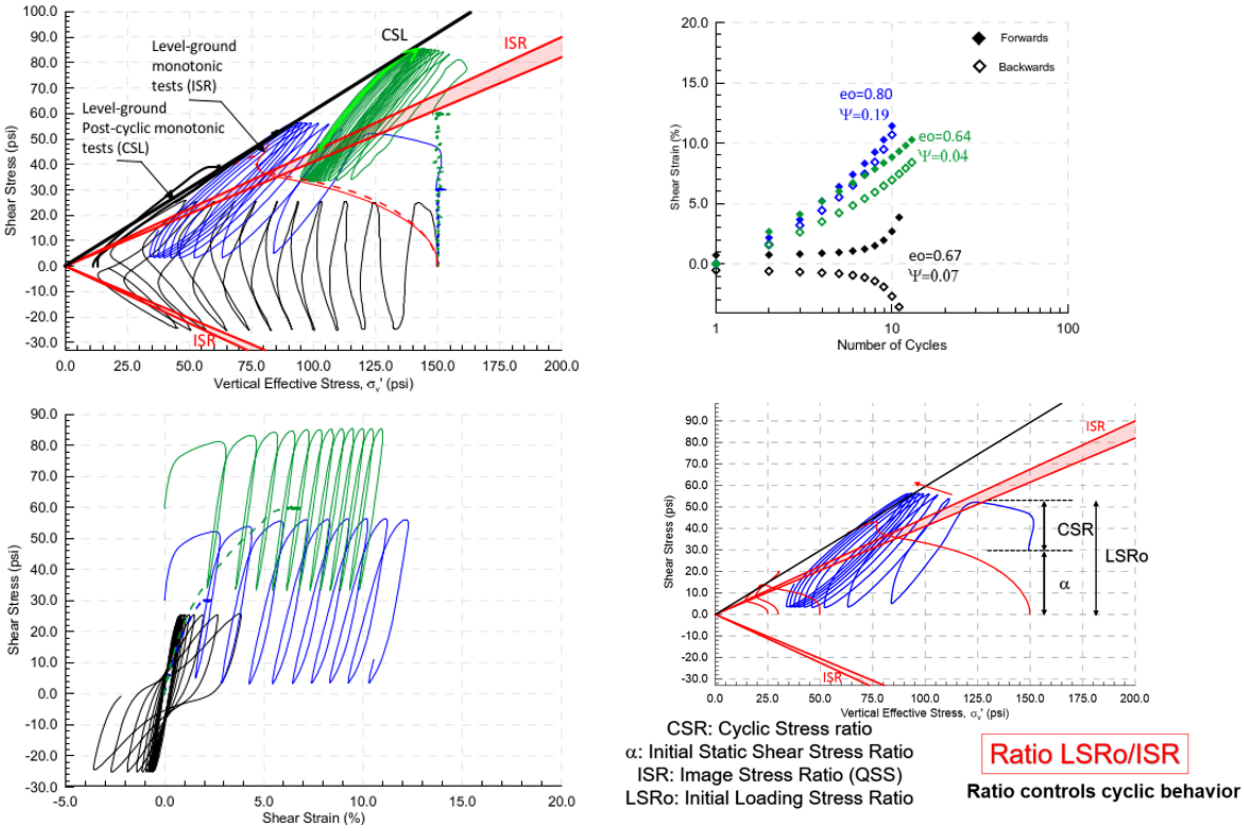


Figure 8: Cyclic DSS tests with static bias (0, 0.2. and 0.4) on the underflow sand tailings with respect to their location to ISR and illustration of Ratio of LSRo/ISR concept (Jefferies and Been, 2016)

Dilation during cycles is shown as a temporary increase in the effective vertical stress. The test with static bias of 0.2 also depicts ratcheting and progressive increase in shear stress once the stress path crosses the ISR. In summary, the tendency for tests with static bias of 0.2 and 0.4 is to enhance dilative response between cycles, accompanied by a slight increase in shear resistance during cyclic loading, depicting an additional ductile response compared to level ground tests.

As shown in Figure 9, the cyclic accumulation of strains appears to be controlled by the location of the initial static shear stress and confining pressure with respect to its ISR (Jefferies and Been, 2016), which is ratio LSRo/ISR as defined in Figure 8 for the same number of loading cycles (~10-11). This concept is introduced to gain insight into the cyclic loading behavior of underflow sands in terms of accumulation of shear strains.

Further comparisons with static bias cyclic tests on denser Monterey sands performed by Kammerer et al. (2002), as shown in Figure 9, also indicate that permanent deformations appear to be controlled by the state parameter and the LSRo/ISR ratio.

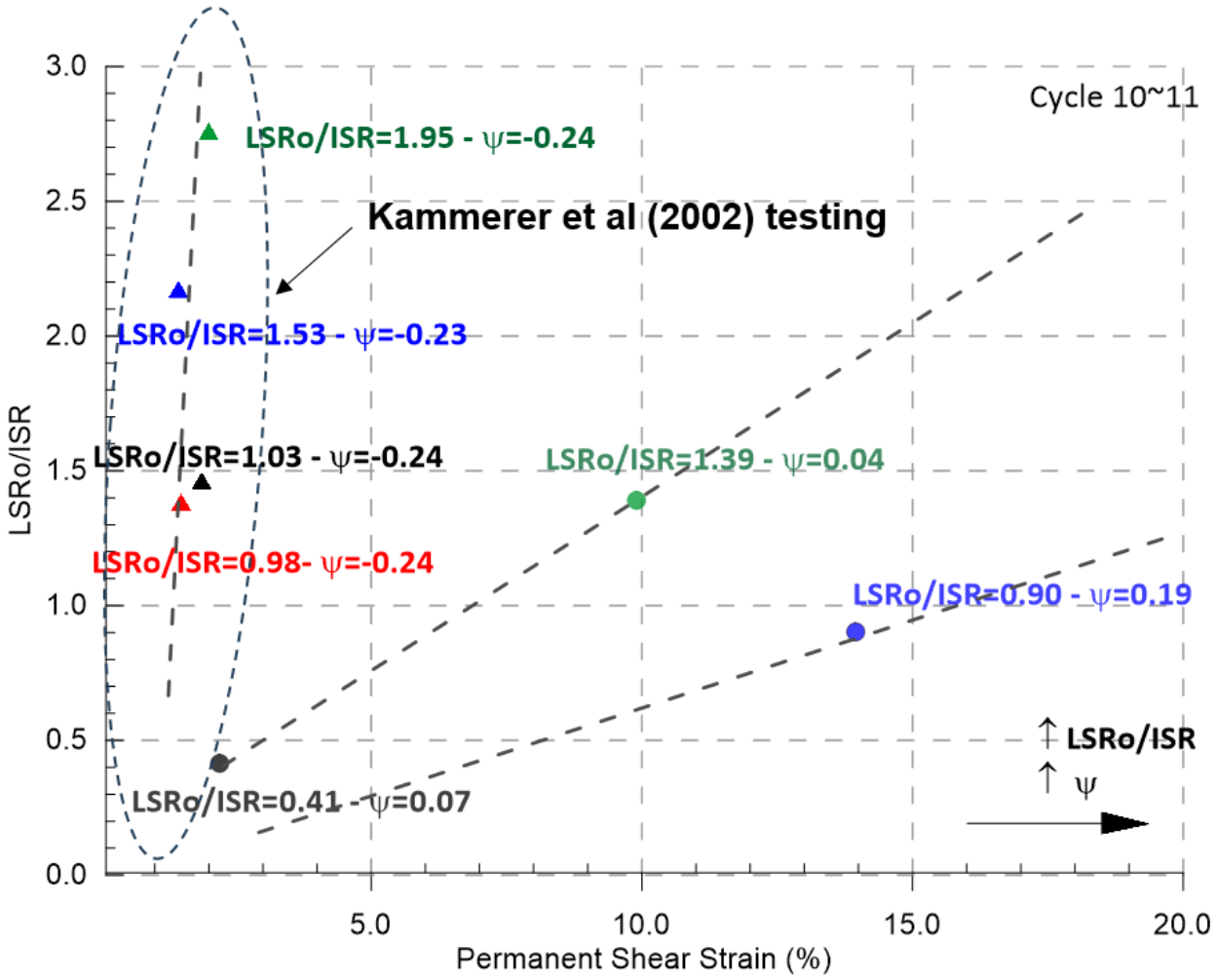


Figure 9: LSRo/ISR (Jefferies and Been, 2016) and state parameter as an index of permanent strain potential from cyclic DSS testing

Post-cyclic testing

One post-cyclic DSS test was completed on a sample of the underflow sand tailings after cyclic loading on the test with a static bias of 0.2, initial state parameter (ψ) of 0.19, and consolidated void ratio (e_c) of 0.8 to contrast with the test with non-static bias (alpha=0) with initial state parameter (ψ) of 0.07 and consolidated void ratio (e_c) of 0.67 (see Table 1). As a comparison, level ground post-cyclic testing was conducted in 2016–2017 with consolidated void ratios between 0.63 and 0.78, and initial state parameter less than 0.11 (denser).

The results of static bias and level ground tests in terms of test path (shear stress vs. vertical effective stress), shear stress vs. shear strain, and excess pore pressure ratio (r_u) vs. shear strain are shown in Figure 10. Generally, the static bias test (blue) indicates dilative excess pore water pressure response with increasing shear strain with a slight contractive behavior for shear strains larger than 12 percent. Level

ground post-cyclic testing also shows dilative excess pore water pressure response as they move to critical state conditions.

As shown in Figure 10, post-cyclic strengths were generally estimated at 15 percent strain for the level ground tests and for tests with static bias.

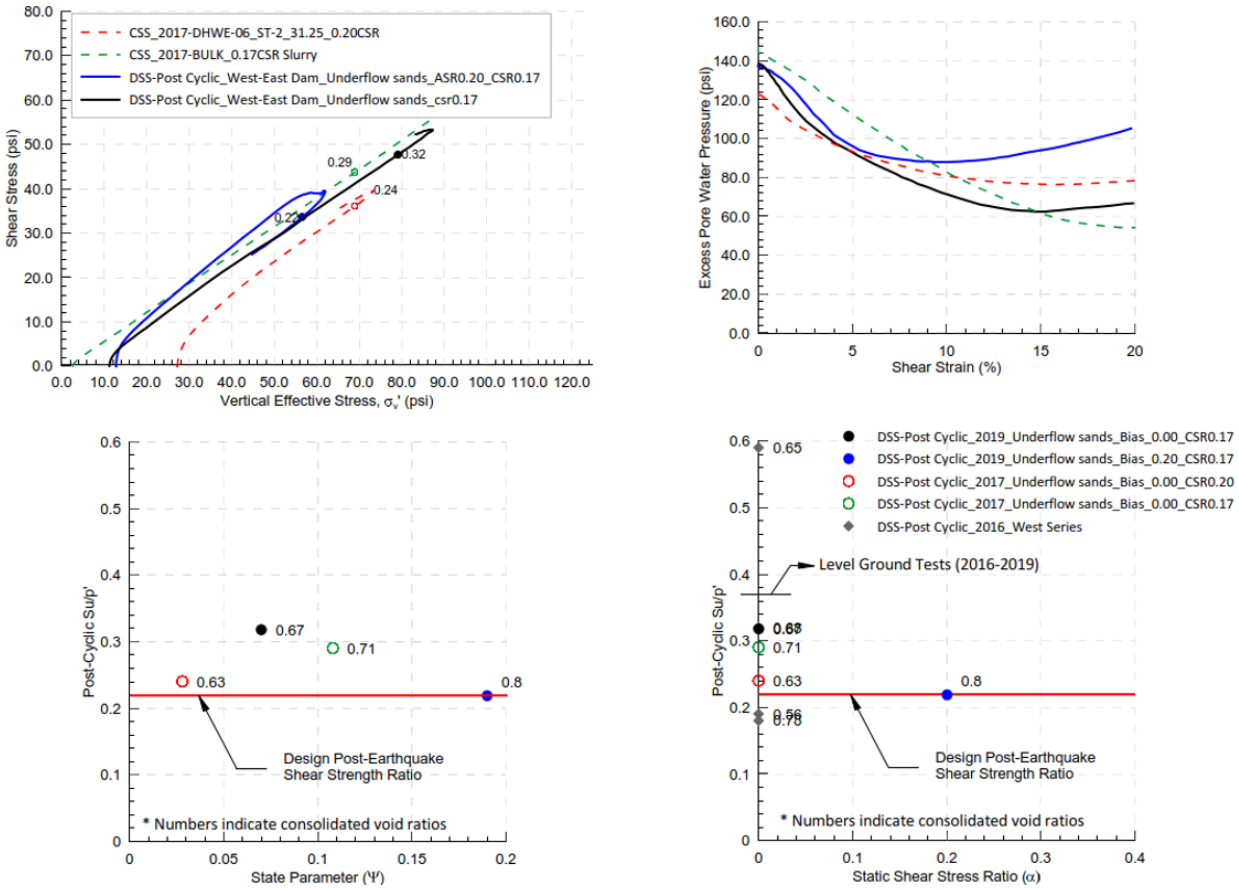


Figure 10: Underflow sands tailings post-cyclic DSS testing results

Because the volumetric response (e.g., excess PWP) levels off at around 15 percent strain, this was selected; thus, this level of strain is nearly compatible with critical state conditions. Post-cyclic monotonic loading for static bias tests indicated a post-cyclic strength ratio of about 0.22. The level ground post-cyclic tests that were conducted indicated a similar range of post-cyclic strength ratios, i.e., ratios between 0.18 and 0.32. Therefore, there is no systematic difference between level ground and static bias on post-cyclic strength results.

Conclusion and recommendations

Preliminary results of the DSS testing program on underflow sands under static bias suggest that tailings strain accumulation may be controlled by the initial state parameter and the ratio LSRo/ISR.

Static bias cyclic DSS tests on underflow sand tailings at the densities and stress states selected for this program indicated a loss of stiffness without a loss of shear strength to levels below those associated with the CSR selected for the cyclic DSS tests, which is characterized as cyclic mobility behavior. Cyclic loading caused a ratcheting and progressive increase in shear stress with accumulating cycles once the stress path crossed the ISR, which resulted in limited excess pore pressure development for a given initial static shear stress ratio.

The static bias testing has not been shown to provide a significant benefit or detrimental effect on the cyclic behavior. As compared to the level ground testing, the static bias testing results in a stress path closer to ISR or Phase Transformation Line (PTL), and thus accumulates more strain without reducing the strength during cyclic loading.

The presence of a static bias did not appear to influence the measured post-cyclic strengths, which is consistent with known critical state soil mechanics concepts.

Additional static bias testing on underflow materials at high void ratios above, slightly below/above CSL and low stresses are recommended to investigate the effect of static bias at extreme potentially brittle behavior to lightly contractive/dilatant conditions. This testing will provide insight for bounding the cyclic response under sloping ground conditions for a full range of behavior.

References

Been, K. and M.G. Jefferies. 1985. A state parameter for sands. *Géotechnique* 35(2): 99–112.

Boulanger, R.W. 2003. Relating Kα to relative state parameter index *J. Geotechnical and Geoenvironmental Eng.* 129(8): 770–73.

Cerna-Diaz, A., T. Barham, J. Hilgers, L. Yenne and R. Davidson. 2022. Role of silty sand tailings state and compressibility on cyclic induced shear deformations. *Proceedings of Tailings and Mine Waste, 2022.* Denver, Colorado.

Idriss, I.M. and R.W. Boulanger. 2008. *Soil Liquefaction During Earthquakes*. 2nd edition. Earthquake Engineering Research Institute.

Ishihara, K. and F. Yamazaki. 1980. Cyclic simple shear tests on saturated sand in multi-directional loading. *Soils and Foundations* 20(1): 45–59.

Jefferies, M.G. and K. Been. 2016. *Soil Liquefaction – A Critical State Approach*. London: Taylor and Francis.

Kammerer, A.M, J.M. Pestana and R.B. Seed. 2002. Undrained response of Monterey 0/30 sand under multidirectional cyclic simple shear loading conditions, Geotechnical Engineering Research Report No. UCB/GT/02-01, University of California, Berkeley, July 2002.

Reid, D., R. Fanni and A. Fourie. 2024. Drained static bias effects on very loose silt tailings. *Proceedings of 8th International Conference on Earthquake Geotechnical Engineering.* Osaka, Japan

Robertson, P.K. 2017. Evaluation of flow liquefaction: influence of high stresses. *Proceedings of the 3rd International Conference on Performance Based Design in Earthquake Geotechnical Engineering*. Vancouver, BC, Canada, 16–19 June 2017.

Seed, H.B. and I.M. Idriss. 1971. Simplified procedure for evaluating soil liquefaction potential. *J. Soil Mechanics and Foundations Div.* 97(SM9): 1249–273.

Whitman, R.V. 1985. On liquefaction. *Proceedings of the 11th International Conference on Soil Mechanics and Foundation Engineering.* San Francisco, CA. A.A. Balkema: 1923–926.

Cyclic Response of Mine Tailings at Field and Laboratory Scales – Example Using a Novel Database

Cody Arnold, Georgia Institute of Technology, USA
Jorge Macedo, Georgia Institute of Technology, USA

Abstract

Cyclic liquefaction induced by seismic loading from earthquakes is a major concern for countries with active mining industries and moderate seismicity such as Peru, Chile, and the USA. Cyclic liquefaction is more likely to induce flow failure as compared to other failure modes, and has been associated with a large portion of failures in seismic countries like Chile. Chile is a leading provider of copper and lithium to the global market, and the country's ability to sustain such a large mining sector could be hindered by its ability to safely store its tailings. Mine tailings have been shown to have unique mechanistic responses dissimilar to that of traditional soils (i.e., sands and clays). Much of engineering practice relies on techniques and procedures developed from data derived from sands and clays. As such, our understanding of the cyclic behavior of mine tailings needs continued research interest to extract new insights into their unique behavior. This paper utilizes a recently developed database focused on the cyclic response of mine tailings to highlight some insights into their peculiar behavior. Specifically, their unique range of material properties and resulting liquefaction curves, the applicability of existing factors in the liquefaction assessment of these materials as compared to sands, and a comparison of in-situ and laboratory-derived cyclic resistances are showcased.

Introduction

The design of sustainable tailings storage facilities (TSFs) is of major concern to both the countries they lie within and the countries that benefit from the extracted resources. The Paris Climate Agreement was adopted by 196 member countries of the United Nations in 2015. The agreement aims to keep global warming below 2 degrees Celsius through the transition from fossil fuels to more sustainable energy solutions (e.g., wind, solar, hydroelectric, electric cars, etc.). Many countries have implemented legislation to match. As an example, the U.S.A. aims to reduce its greenhouse gas emissions by 50% below 2005 levels by 2030. However, with this transition to renewables comes increased demand for the raw materials required to implement such technologies. As an example, the demand for copper, which is utilized in a wide

array of renewables, is expected to double from 25 million metric tons in 2022 to over 51 million metric tons by 2050 (S&P Global, 2022). Similarly, the demand for other metals is projected to increase as well (Eyzaguirre and Araya, 2021). This creates a major hurdle, because with the increasing demand and the degradation of ore grade (Bowker and Chambers, 2017), the amount of in-situ material that needs to be extracted for processing grows drastically. This leads to an enormous amount of waste material (tailings), which poses a direct threat to the environment and human life. Consequently, this has led to more dams being constructed in the past decade than any decades prior (Warburton et al., 2019), as well as dams being designed to hold larger volumes of waste. While the average number of yearly TSF failures has remained constant (Piciullo et al., 2022) the severity of failures (i.e., the amount of released waste) has been increasing (Piciullo et al., 2022; Bowker and Chambers, 2017).

After several high-profile TSF failures (e.g., Brumadinho, 2019; Fundao, 2015; Cadia, 2018) a consortium of agencies, one of which was the United Nations Environmental Program, released the global industry standards on tailings management (GISTM) (ICMM et al., 2020) with the goal of reducing TSF failures. Several notable tailings engineers also conducted their own studies seeking to highlight the contributing factors to these failures. One such individual was Norbert Morgenstern, who evaluated fifteen TSF incidents and classified their contributing factors into three categories: engineering, operations, and regulatory. Morgenstern (2018) determined that engineering was the primary factor in the failures. Other independent studies (Been, 2016; Jefferies, 2021) have reached similar conclusions.

In a detailed look at failure causes by Piciullo et al. (2022), the three known major causes of failure are overtopping (23%), static (16%), and dynamic liquefaction (14%). However, despite dynamic liquefaction only being the third most common cause, it sees a disproportionally higher association with flow failures as compared to overtopping and static liquefaction (Halabi et al., 2022). This makes the seismic design of TSF in countries with active mining industries and moderate to high seismicity (e.g., Peru, Chile, USA) a major concern.

For instance, Chile is the leading producer of copper ore and the second largest producer of lithium in the world at 28% and 30%, respectively (USGS, 2023a; USGS, 2023b). Chile also has the largest reserves of copper and lithium (USGS, 2023a; USGS, 2023b), and therefore its ability to safely mine and store tailings in perpetuity is crucial to the global supply. However, between 1901 and 2013 the primary cause of TSF failures in Chile was earthquake-induced (cyclic) loading (Villavicencio et al., 2013) with nearly 50% of those involving flow failure. These studies highlight the lack of knowledge surrounding the cyclic response of mine tailings and the need for further research into their unique cyclic behavior.

Mine tailings are typically classified as silts or silty sands and have characteristics that separate them from naturally occurring silts (e.g., angularity, mineralogy, etc.). This poses a challenge to tailings engineers, as most engineering approaches for seismic design have been developed from databases and case

histories of sites mainly containing sands and a few natural silts (Seed and Idriss, 1982). Additionally, several studies have highlighted that the scaling of mechanical properties in mine tailings varies from that of naturally occurring soils (Macedo and Vergaray, 2021; Jefferies and Been, 2016) even at similar gradations (Ishihara et al. 1980; Geremew and Yanful, 2012). This paper utilizes a recently developed database (Arnold and Macedo, 2024) focused on the cyclic response of mine tailings to look at unique trends in their behavior, as well as to assess existing procedures for seismic design. Specifically, the scaling factor for overburden stress (K_σ) is assessed for a selected tailing from the database in conjunction with past trends for sands. Additionally, the Boulanger and Idriss (2014) method for estimating the cyclic resistance (CRR) from cone penetration testing (CPT) is compared against laboratory-based estimates from cyclic simple shear (CSS) tests, for a selected tailing.

Database

A recently developed database (Arnold and Macedo, 2024) focused on the cyclic response of mine tailings grants a novel opportunity to study the unique response of tailings materials. As shown in Figure 1a, there is a wide range of particle size distributions (PSD) present within the database. The database contains about 130 CSS tests on 20 different mine tailings gradations. As previously mentioned, mine tailings are typically identified as non-plastic silty sands to sandy silts with fine contents (FC) typically ≥ 35%, which is indeed the case for many of the tailings in the database, as highlighted by the histograms in Figures 1b and 1c. This does however highlight an existing gap with regard to tailings that do contain plasticity, as they are not as well represented.

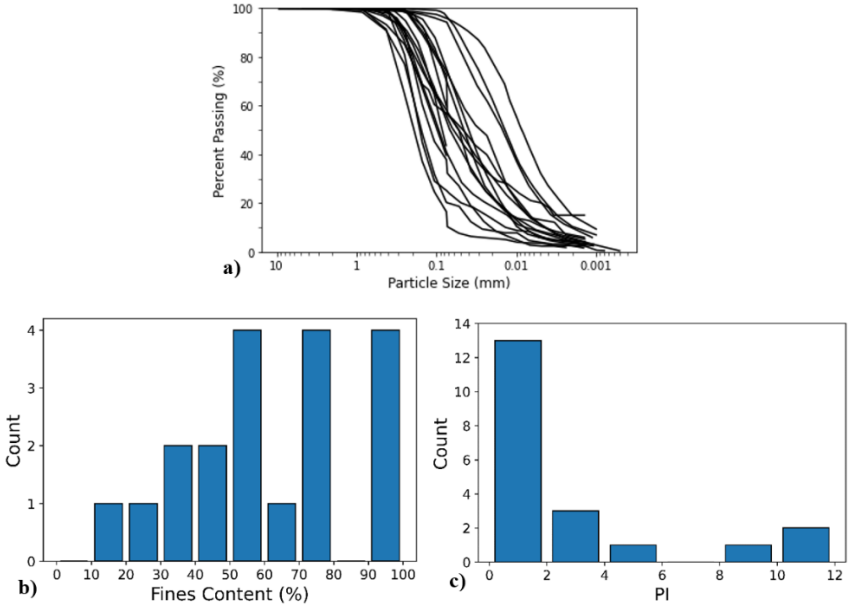


Figure 1: Range of a) PSD, b) FC, and c) PI for available mine tailings within the database (Arnold and Macedo, 2024)

The database is also unique in that it offers a robust amount of secondary information on its materials in the form of critical state line (CSL) via triaxial testing and in-situ information via CPT. To discern the materials by how much data is available on each they are placed into one of three classes: A, B, and C. Class A is the most numerous and indicates those materials containing all three data types (CSS, CSL, and CPT). Class B denotes those with CSS and one other data type (CSL or CPT), and class C denotes those with only CSS data available. Furthermore, supplemental data (e.g., FC, plasticity index (PI), ore type, etc.) regarding the materials is also made available, when possible.

Insights

The cyclic resistance of soils can be assessed in several ways but the use of CSS testing is quite commonly used. Estimating the cyclic resistance requires a minimum of 3 CSS tests to derive a liquefaction resistance curve. However, it is not uncommon for 4 or 5 tests to be used for greater accuracy. The liquefaction resistance curve relates the cyclic stress ratio (CSR) to a predefined failure criterion (N_{liq}), typically associated with a strain criterion (i.e., 3.75% single amplitude). The failure point of each test is then plotted CSR against N_{liq} in log scale and is fitted by a power law. Equation 1 represents a resistance curve with fitting parameters *a* and *b*.

$$(1)\quad \boldsymbol{CSR = aN^{-b}}$$

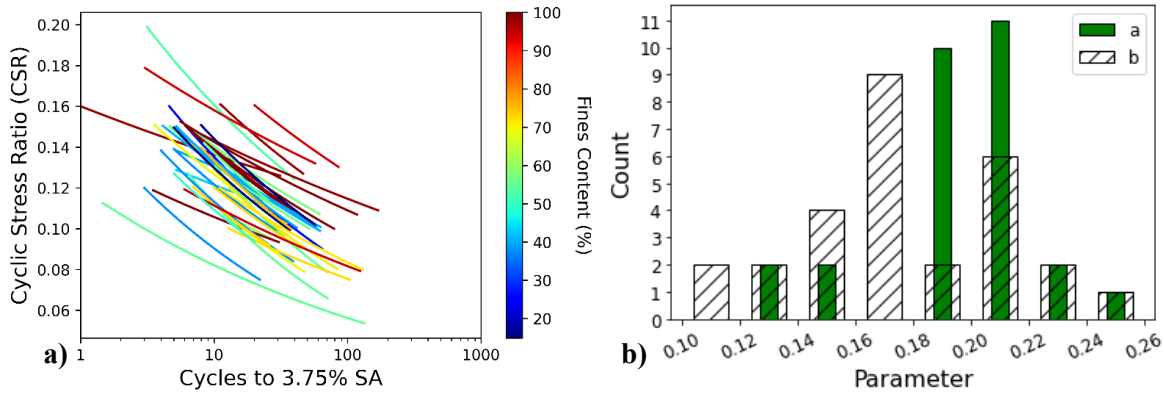


Figure 2: a) Liquefaction resistance curves for database materials labeled by FC and b) range of fitting parameters (*a* and *b*) (Arnold and Macedo, 2024)

The resistance curve is then used to further interpret a cyclic resistance of an equivalent earthquake loading. For instance, it is quite common to consider 15 cycles (CRR_{15}) in liquefaction-triggering procedures such as the Seed and Idriss (1982) procedure. Thus, deriving CRR_{15} at a given confinement and density requires the previously mentioned 3 to 5 CSS tests. Figure 2a shows the liquefaction resistance curves from the database labeled by FC, and the resulting fitting parameters are shown in Figure 2b. In general, *a* is lower than what is typically seen in sands (~ 0.27). This is further highlighted by Figure 3a

which shows that the database tailings need only relatively low CSR values to liquefy, even under high-stress states (a significant number of tests ≥ 300 kPa).

Another aspect to highlight is the slope of the resistance curves which is captured by the *b* parameter, which is on average around 0.19 (Figure 2b). This is notable as sands have typical b values on the order of 0.34 (Idriss and Boulanger, 2008). In fact, it is more similar to the *b* value seen in clays (~ 0.14 - Idriss and Boulanger, 2008) which is interesting as mine tailings would typically be expected to show a more "sand-like" response based on their material properties. For instance, considering the fact that most of these are non-plastic tailings (Figure 1c) the method from Idriss and Boulanger (2006) would classify them as sand-like (PI ≤ 7). This discrepancy highlights the challenges in designing for these materials as they exhibit "sand-like" responses but have significant compressibility more akin to clays.

The compressibility of these non-plastic tailings is further exemplified by the magnitude of their CSL slopes (λ_e). Figure 3b shows the range of λ_e for the tailings within the database, on average they are around 0.07. This is twice as large as λ_e typically reported for common testing sands (~ 0.033) and for natural sands (~ 0.037) as reported by Jefferies and Been (2016).

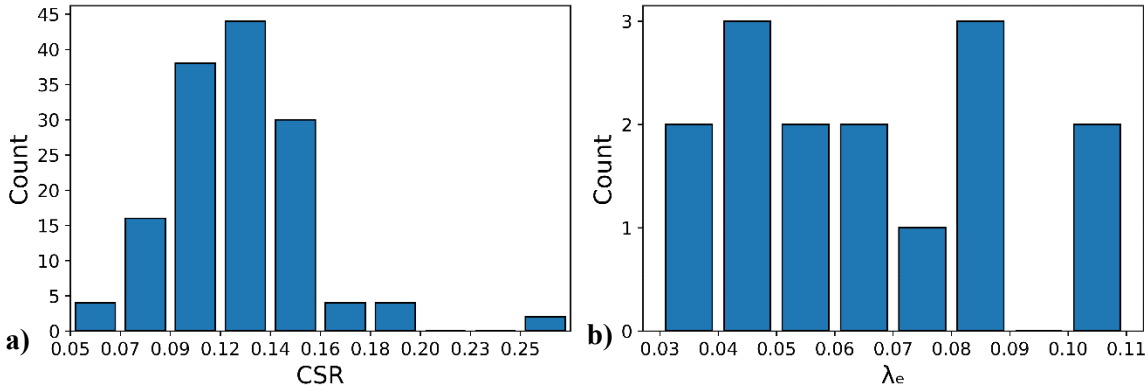


Figure 3: Range of a) CSR and b) λ_e for available mine tailings within the database (Arnold and Macedo, 2024)

Overburden stress effect

As previously discussed, the K_σ scaling factor plays an important role in the liquefaction assessment of soils. This is especially true in large TSF as the large height to which these structures are built is accompanied by large overburden stresses. The original scaling factors were derived from case histories on predominantly sandy soils. These factors denoted that increasing vertical stress would negatively affect the cyclic resistance (i.e., increasing confinement results in lower K_σ). Several authors since have proposed their own trends for K_σ in sands. For instance, shown in Figure 4 is the consensus curve proposed by Hynes et al. (1998) for sands as well as the semi-empirical trends proposed by Idriss and Boulanger (2006) based on case histories for non-cohesive soils (PI ≤ 7).

Conversely, data for mine tailings has been shown to indicate little or even a positive effect from increasing confinement. The data from Ingabire (2019) shows a base metal tailing at two varying relative densities (D_r); which are close to K_σ values of 1. A material from the database is also plotted, indicating an agreement with the Ingabire tailings. The chosen material (5_3) is non-plastic with about 40% fines. For both sands and tailings, researchers have noted that the looser the material the less impactful K_σ will be. However, for the tailings shown here even denser states have significantly less effect from K_σ than has been seen in sands. This has been noted by other authors as well (Sanin, 2005; Sanin, 2010; Verma, 2019; Al Taarhouni et al., 2011). Some authors have also noted a positive effect from K_σ (Wijewickreme et al., 2005; Sadrekarimi and Jones, 2019).

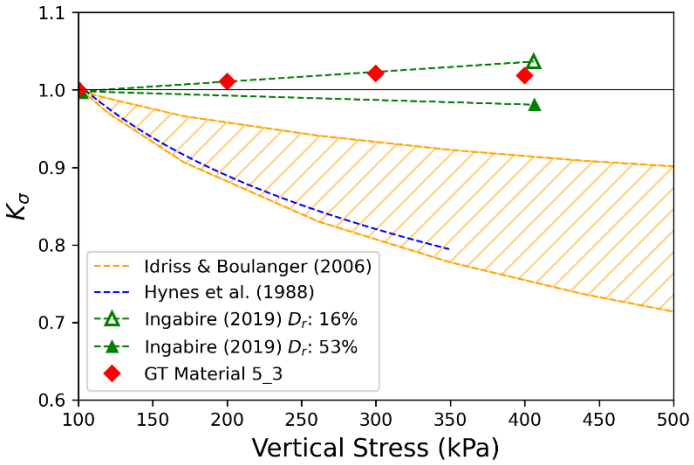


Figure 4: Kσ for GT material 5_3 compared against published trends

In summary, the effect of overburden stress and how it will ultimately affect the scaling factor (K_σ) in mine tailings is largely unknown. Despite the numerous studies that exist to date there does not yet seem to be a consensus on how to approach this for mine tailings materials. In the development of K_σ trends for sands large databases of either laboratory testing or case histories were required. This is where mine tailings suffer from a large knowledge gap as there are very few databases available to utilize. We expect that the database referred to in this study would be instrumental in allowing for further insights into the K_σ factor applicability to mine tailings by conducting more comprehensive assessments similar to those shown in Figure 4.

Comparison of field-corrected laboratory derived cyclic resistance with CPT estimates

As discussed in the previous section, the estimation of cyclic resistance for a given soil under a given demand can be estimated via laboratory testing (i.e., CSS) however, several methods (e.g., Boulanger and Idriss, 2014) exist for estimating from in-situ testing (i.e., CPT). These types of methods are very desirable, especially in the early stages of design, as it can take time to acquire samples and perform the necessary

tests. The validity of these in-situ estimations is of great interest and given the availability of CPT and CSS information within the database it is worthwhile to compare the two. Other authors have made similar comparisons, however for natural soils (Mijic et al., 2021).

Figure 5 showcases material 4_1 from the database with both the Boulanger and Idriss (2014) interpretation as well as the laboratory-derived CRR_{15}, with a correction factor of .9 (Seed, 1979). The laboratory samples were recovered from 7.5 m and 10.5 m; however, the tested specimens were reconstituted in the laboratory. Given this, it is surprising to see that the laboratory and field-derived CRR values are quite similar. Even for fully intact specimens, many factors could result in differences between the two interpretations (i.e., in-situ fabric). More comparison between in-situ and laboratory estimates, as those presented in Figure 5 are encouraged as it is quite difficult to recover undisturbed tailings samples (Wijewickreme et al., 2005), and most procedures for assessing the cyclic resistance have been developed for soils with low fines content and cannot be assumed to apply directly to tailings. The recent database developed by Arnold and Macedo (2024) could contribute to that direction, hopefully with more contributions from the tailings community.

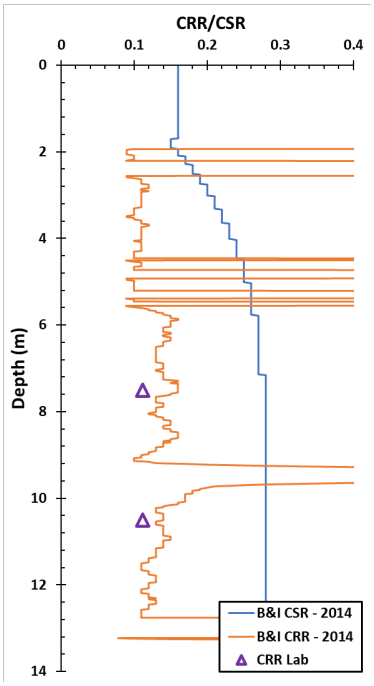


Figure 5: Comparison of field-adjusted laboratory derived CRR and field estimated CRR for material 4_1

Conclusion

This paper highlights the usefulness of a recently developed database on the cyclic response of mine tailings (Arnold and Macedo, 2024). The database provides a wide range of different mine tailings gradations with many having field (CPT), cyclic (CSS), and critical state (CSL) information available. This presents a novel

opportunity for investigating the unique behavior of these materials and assessing the applicability of procedures developed for sands and clays. Initial insights from the database are shown herein.

The database tailings are comprised of mostly non-plastic sandy silts to silty sands with FC ≥ 35%, on average. Their liquefaction resistance curves highlight a unique response that is influenced by their compressibility, which is shown to be more significant than in natural silts and sands. The overburden stress correction factor (K_σ) has been studied heavily in sands by many authors and the expected behavior is a negative effect of cyclic resistance with increasing confinement. However, a mine tailing from the database is plotted against these trends showing an inverse behavior, increasing resistance with increasing confinement. This raises questions regarding the applicability of existing K_σ relationships to mine tailings materials.

Lastly, the estimation of cyclic resistance via in-situ testing (i.e., CPT) (Boulanger and Idriss, 2014) is compared against the laboratory-derived values. The results show good agreement between the field and laboratory values, which is surprising considering that the laboratory specimens were reconstituted. This could be because mine tailings are relatively young materials geologically and there is not much difference between in-situ fabric and laboratory reconstructed specimens (e.g., lack of field bonding). Estimating the cyclic resistance from reconstituted specimens is quite common considering the challenges associated with recovering intact tailings samples. More comparisons such as this are encouraged to gain confidence in the laboratory and field-based estimates of cyclic resistance; particularly, because field-based methods have not been formulated for mine tailings specifically.

Acknowledgements

We thank Ruben Vargas and Solange Paihua from Knight Piesold for facilitating data access through materials shipped to Georgia Tech for testing and data sharing. We also thank TAILENG members who facilitated the access to some data.

References

Al Tarhouni, M., P. Simms and S. Sivathayalan. 2011. Cyclic behaviour of reconstituted and desiccated-rewet thickened gold tailings in simple shear. *Canadian Geotechnical Journal* 48(7): 1044–1060.

Arnold, C. and J. Macedo. 2024. A novel experimental database on the cyclic response of mine tailings earthquake spectra. DOI: https://doi.org/10.17603/ds2-1k0a27dt17

Been, K. 2016. Characterizing mine tailings for geotechnical design. *Geotechnical and Geophysical Site Characterisation* 5 – Lehane, Acosta-Martínez and Kelly (eds). Australian Geomechanics Society, Sydney, Australia, ISBN 978-0-9946261-1-0.

Boulanger, R.W. and I.M. Idriss. 2014. CPT and SPT based liquefaction triggering procedures. Report No. UCD/CGM-14/1. Center for Geotechnical Modeling, University of California at Davis.

Bowker, L.N. and D.M. Chambers. 2017. In the dark shadow of the supercycle tailings failure risk and public liability reach all time highs. *Environments* 4(4): 75. https://doi.org/10.3390/environments4040075

Eyzaguirre, A.G. and J.C. Araya. 2021. *El mercado de litio Desarrollo reciente y proyecciones al 2030,* Comision Chilena del Cobre, Ministerio de Mineria, N° 2021-A-12347. Accessed 6/19/2023 at https://www.cochilco.cl/Mercado%20de%20Metales/Produccio%CC%81n%20y%20consumo%20de%20litio%20hacia%20el%202030%20edicio%CC%81n%202021%20versi%C3%B3n%20def.pdf

Geremew, A.M. and E.K. Yanful. 2012. laboratory investigation of the resistance of tailings and natural sediments to cyclic loading. Geotechnical and Geological Engineering 30: 431–447. https://doi.org/10.1007/s10706-011-9478-x

Halabi, A.L.M., A.T. Siacara, V.K. Sakano, R.G. Pileggi and M.M. Futai. 2022. Tailings dam failures: a historical analysis of the risk. *Journal of Failure Analysis and Prevention* 22: 464–477. https://doi.org/10.1007/s11668-022-01355-3

Hynes, M. E., R. Olsen and D.E. Yule. 1998. The influence of confining stress in liquefaction resistance. *Proceedings of the 30th joint meeting of the US–Japan cooperative program in natural resources panel on wind and seismic effects.* Gaithersburg, MD, USA: 167–184.

ICMM (International Council on Mining and Metals), UNEP (United Nation Environment Programme), and PRI (Principles for Responsible Investment). 2020. Global Industry Standard on Tailings Management.

Idriss, I.M. and R.W. Boulanger. 2006. Semi-empirical procedures for evaluating liquefaction potential during earthquakes. *Soil Dynamics and Earthquake Engineering* 26(2–4): 115–130.

Idriss, I.M. and Boulanger, R.W. 2008. Soil liquefaction during earthquake. EERI Publication, Monograph MNO-12, Earthquake Engineering Research Institute, Oakland. https://www.eeri.org/

Ingabire, E.P. 2019. Influence of fines content on cyclic resistance and residual strength of base metal tailings. MS thesis, Department of Civil and Mineral Engineering, University of Toronto, Canada.

Ishihara, K., J. Troncoso, Y. Kawase and Y. Takahashi. 1980. *Cyclic Strength Characteristics of Tailings Materials, Soils and Foundations* 20(4): 127–142. Accessed at https://doi.org/10.3208/sandf1972.20.4127.

Jefferies, M.G. 2021. Improving governance will not be sufficient to avoid dam failures. *Proceedings of the Institution of Civil Engineers – Geotechnical Engineering* 1–15. Doi:10.1680/jgeen.21.00105

Jefferies, M.G. and K. Been. 2016. *Soil Liquefaction: A Critical State Approach.* 2nd edition. Boca Raton, FL, USA: CRC Press.

Macedo, J. and L. Vergaray. 2021. Properties of mine tailings for static liquefaction assessment, Canadian Geotechnical Journal. 59(5): 667–687. Accessed at https://doi.org/10.1139/cgj-2020-0600

Mijic, Z., J.D. Bray, M.F. Riemer, S.D. Rees and M. Cubrinovski. 2021. Cyclic and monotonic simple shear testing of native Christchurch silty soil. *Soil Dynamics and Earthquake Engineering* 148: 148106834. Accessed at https://doi.org/10.1016/j.soildyn.2021.106834.

Morgenstern, N.R. 2018. Geotechnical risk, regulation, and public policy. The Sixth Victor de Mello Lecture. *Soils and Rocks, São Paulo* 41(2): 107–129, May–August, 2018.

Piciullo, L., E. Storrøsten, L. Zhongqiang, N. Farrokh and S. Lacasse. 2022. A new look at the statistics of tailings dam failures. *Engineering Geology* 303: 106657. https://doi.org/10.1016/j.enggeo.2022.106657

S&P Global. 2022. The future of copper – will the looming supply gap short-circuit the energy transition? Accessed 6/21/2023 at https://www.spglobal.com/marketintelligence/en/mi/info/0722/futureofcopper.html

Sadrekarimi, A. and S. Jones. 2019. Effect of overburden pressure on cyclic resistance of Fraser River sand. *Proceedings of 7th International Conference on Earthquake Geotechnical Engineering*, Roma, Italy.

Sanin, M.V. 2010. Cyclic shear loading response of Fraser River Delta silt. Doctoral thesis, Department of Civil Engineering, University of British Columbia, Vancouver, Canada.

Sanin, M.V. 2005. Cyclic shear loading response of Fraser River Delta silt. M.A.Sc. thesis, Department of Civil Engineering, University of British Columbia, Vancouver, Canada.

Seed, H. B. and I.M. Idriss. 1982. Ground motions and soil liquefaction during earthquakes. Oakland, California, USA: Earthquake Engineering Research Institute.

Seed, H.B. 1979. Soil liquefaction and cyclic mobility evaluation for level ground during earthquakes. *J. Geotech. Eng. Div.* 105(GT2): 201–55. Accessed at https://doi.org/10.1016/0148-9062(79)91243-9.

Suazo, G., A. Fourie, J. Doherty and A. Hasan. 2016. Effects of confining stress, density and initial static shear stress on the cyclic shear response of fine-grained unclassified tailings *Géotechnique* 66(5): 401–412.

US Geological Survey (USGS). 2023a. Major countries in copper mine production worldwide in 2022 (in 1,000 metric tons) (Graph). In *Statista*. Accessed June 2023 at https://www.statista.com/statistics/264626/copper-production-by-country/

US Geological Survey (USGS). 2023b. Major countries in worldwide lithium mine production in 2022 (in metric tons) (Graph). In *Statista*. Accessed June 2023 at https://www.statista.com/statistics/268789/countries-with-the-largest-production-output-of-lithium/

Verma, P. 2019. Monotonic and cyclic shear loading response of natural silts from British Columbia, Canada. Doctoral thesis, Department of Civil Engineering, University of British Columbia, Vancouver, Canada.

Villavicencio, G., R. Espinace, J. Palma, A. Fourie and P. Valenzuela. 2013. Failures of sand tailings dams in a highly seismic country. *Can. Geotech. J.* 51(4): 449–464.

Warburton, M., S. Hart, J. Ledur, E. Scheyder and A.J. Levine. 2019. The looming risk of tailings dams. Reuters. Accessed June 2023 at https://www.reuters.com/graphics/MINING-TAILINGS1/0100B4S72K1/index.html

Wijewickreme, D., Sanin, M.V. and Greenaway, G.R. 2005. Cyclic shear response of fine-grained mine tailings. *Can. Geotech. J.* 42(5): 1408–1421.

Some Considerations on the Stability of Tailings Dams Subjected to Blasting Vibration

Ezra Coyle, SLR Consulting Ltd, USA
Shayan Hashemi, SLR Consulting Ltd, Canada

Abstract

Ground vibration guidelines are typically established for blasting sites to prevent damage to adjacent facilities or infrastructures. However, blast induced vibrations present significant challenges to the geotechnical engineer during design and construction of the tailings dams, in large part due to the considerable uncertainty regarding the shear strengths of the different components of the structure. In addition, blast induced vibrations are associated with short duration high frequency pulses, which are fundamentally different from ground vibrations caused by earthquakes. The objective of this study is to review the application of the pseudo-static approach in assessing the stability of tailings dams subjected to blasting vibrations.

The facility analyzed in this paper is a downstream, raised zoned rockfill embankment with a two layered filter system on the upstream slope. The facility is in operation, and drill and blast activities are planned in the tailings facility basin for rock quarrying purposes. A significant potential impact from blasting near the dam would be the impact to the integrity of the filter materials placed on the upstream slope of the dam. Dynamic loads that exceed the design peak ground acceleration can lead to potential sloughing of the filters.

This paper presents the method and results obtained by the pseudo-static approach to analyze the stability of the slopes subjected to blast vibrations. The blast vibration at the bedrock is treated as a simple harmonic motion in the horizontal direction. Maximum allowable peak particle velocity values are proposed for different critical sections of the dam. The results show that the potential slough in the filter layers upstream of the dam is identified as a credible failure mode that governs the dam safety and appropriate vibration limits. The study highlights the importance of monitoring and understanding the properties of the different components of the tailings dams that may be impacted by blasting vibrations.

Introduction

While earthquake considerations for the design of tailing storage facilities (TSFs) are commonly practiced

within the tailings industry, methods and considerations for blasting induced vibration are less common. Blast induced vibrations are associated with short duration high frequency pulses, which are fundamentally different from ground vibrations caused by earthquakes. Regardless, it is intuitive for the sake of dam safety, that some limits must be prescribed when blasting in the vicinity of TSFs. This paper explores a common method for determining appropriate blasting limits and offers some commentary on its shortcomings in the application to one specific facility, while proposing some additional methods and considerations.

Problem definition

This study was carried out to assess the impacts of blasting from a proposed quarry development on the embankments of a particular TSF. Figure 1 shows a typical cross-section of the TSF in question. The TSF is a 3.1 km long zoned rockfill embankment with an upstream slope at an inclination of 2.5H:1V and a downstream slope inclination of 2H:1V, and a crest width of approximately 10 m. The TSF was constructed with Select Mine Fill (SMF) and Mine Rock Fill (MRF), sourced from blasted rock from an adjacent open pit. SMF is a selective rock fill used at the upstream slope of the TSF as a transition layer between MRF and a coarse filter layer. This facility employs a two-layer filter system on the upstream slope of the embankment, which is composed of a fine filter material (sand) underlain by coarse filter material (gravel). The fine filter is overlain by an upstream HDPE liner. The proposed quarry was located immediately within the TSF basin.

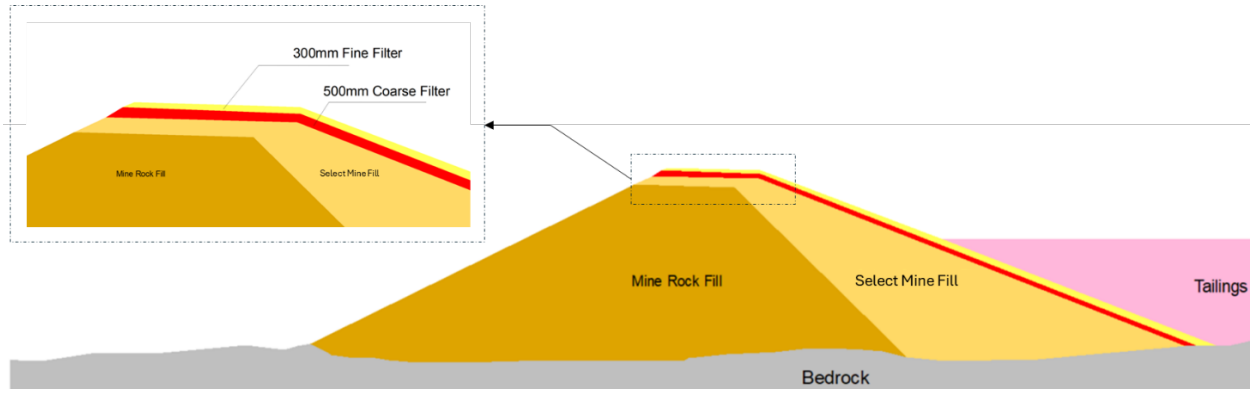


Figure 1: Typical cross-section of the TSF

Methodology

Identifying TSF critical components

Intuitively, downstream failure of the embankment is considered primarily in relation to vulnerable components and failure modes of the TSF. However, after a cursory examination of available limit equilibrium stability analyses, the fine filter on the upstream slope is identified as the most critical

component of the dam, when subjected to ground motions. If the fine filter were to slump, it would not be able to perform its primary purpose (convey seepage if there is any) and this could lead to damage or further damage of the overlying HDPE liner. Repairing the filter in the instance of a slump could be very difficult, especially if the water depth is significant, and could potentially lead to processing plant impacts.

Finding the yield acceleration

Finding the limits of the filter under pseudo-static loading was the first step in defining blast limits for our TSF. Blasting induced vibration will create an inertial force that is proportional to the mass of the slip surface:

$$F = KW$$

Where K is the response peak ground acceleration coefficient and W is the weight of the soil mass in the slip surface. A simple pseudo-static approach was utilized here, in which back analyses of the dam stability are carried out to infer a minimum operating yield acceleration, assuming the Factor of Safety (FoS) could have been as low as unity at that time.

Pseudo-static Limit Equilibrium (LE) analyses were carried out using GeoStudio SLOPW/W software to estimate the yield acceleration at critical sections. Two sections of the TSF at approximately Stations 06+00, and 11+00 have been considered in the analyses, based on proximity to the blasting area and height of the structure. Seepage analyses were carried out to estimate the steady-state phreatic surface considering the pond operating using the SEEP/W software. The Morgenstern and Price method of slices for the calculation of rigid body forces and slip surface optimization were adopted in the analyses. The geotechnical properties of the TSF were established from engineering judgement and experience with similar materials and projects. Table 1 summarizes the material parameters used in the stability analyses. No undrained materials were modeled initially.

Table 1: Material parameters used in the stability analyses

Material	Unit weight (kN/m^3)	Shear strength
Mine Rock Fill	21	ϕ' = 38, c' = 0 kPa
Select Mine Fill	20	ϕ' = 32, c' = 0 kPa
Fine Filter	19	ϕ' = 35, c' = 0 kPa
Coarse Filter	20	ϕ' = 35, c' = 0 kPa
Tailings	11	ϕ' = 0, c' = 10 kPa

The failure criterion was set based on the potential sloughing of the filter layers along the unsupported slope; therefore, the slip surface was limited to the filter layers extending from the crest to the upstream toe

of the dam. Figure 2 shows the results of the stability analyses in the studied sections. The TSF yield acceleration was assessed using the pseudo-static analysis and calculated as 0.21 g for both sections.

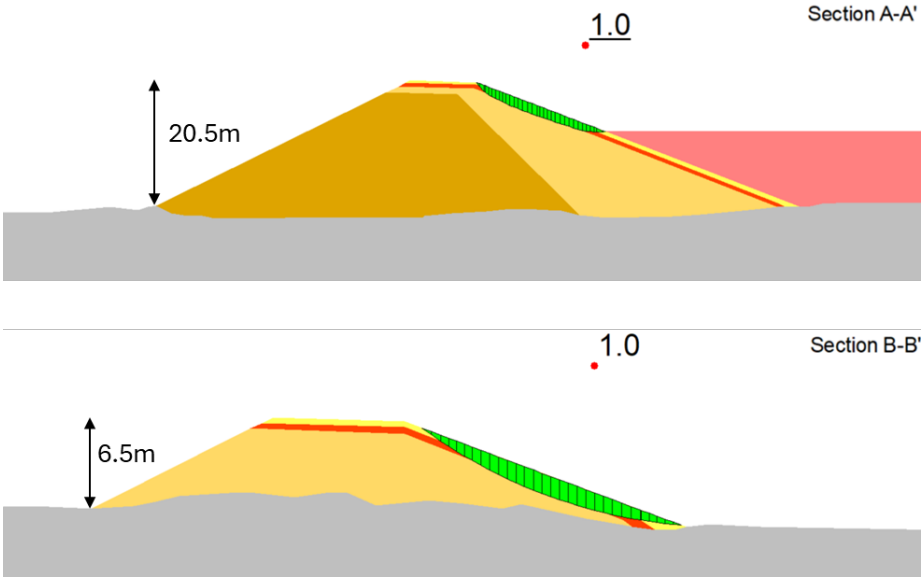


Figure 2: Stability analyses results for Sections A-A' and B-B'

Relationship to PPV

Relating blasting and TSF engineering disciplines to one another requires a relationship between yield accelerations and the associated Peak Particle Velocities (PPVs). To do so, a simple harmonic motion is firstly defined as:

$$x = PPD\sin(\omega t + \theta)$$

$$\dot{x} = PPD\cos(\omega t + \theta)$$

$$\ddot{x} = -PPA\sin(\omega t + \theta)$$

Where x is displacement, $\dot{x}$ is velocity, $\ddot{x}$ is acceleration, ω is circular frequency of the ground motion, θ is phase shift, PPD is peak particle displacement, PPV is peak particle velocity, and PPA is peak particle acceleration equal to ωPPV.

The response ground yield acceleration can be calculated from the input bedrock ground motion (Wong and Pang, 1992):

$$K = K_a(\frac{PPA}{g})$$

Where K_a is the magnification factor determined from response analysis and g is the acceleration of gravity. By combining the abovementioned equations, the limiting PPV (or PPV_c) is estimated as:

$$PPV_C = \frac{K_C g}{\omega K_a}$$

Where PPV_C is the PPV maximum limit, K_c is the yield acceleration coefficient, g is the gravitational acceleration, and ω is the circular frequency of the ground motion and K_a is the magnification factor determined from response analysis. K_a varies with the frequency of the induced vibration and the fundamental period of the slope. K_a for a damped single-degree-of-freedom system subjected to a simple harmonic forced vibration is

$$K_a = \sqrt{\frac{1 + 4\lambda^2\alpha^2}{(1-\alpha^2)^2 + 4\lambda^2\alpha^2}}$$

Where λ is the soil damping factor. A soil damping factor of 0.2 for the fundamental mode of vibration has been assumed. A can be evaluated from the division of input vibration frequency by natural frequency of slope:

$$\alpha = \frac{\omega T_1}{2\pi}$$

Where T_1 is the fundamental period of the slope. An approximate method to estimate T_1 is (Wong, 1991):

$$T_1 \approx \frac{3.3h}{S}$$

Where H and S are height and shear wave velocity of the slope, respectively. Accordingly, in blast monitoring records for similar patterns in the area, the dominant frequency of the blast ranged from 30 to 40 Hz. A design frequency of 30 Hz was conservatively assumed for the analysis. Values of ωK_a for different V_s/H and F are plotted in Figure 3 (Wong and Pang, 1992).

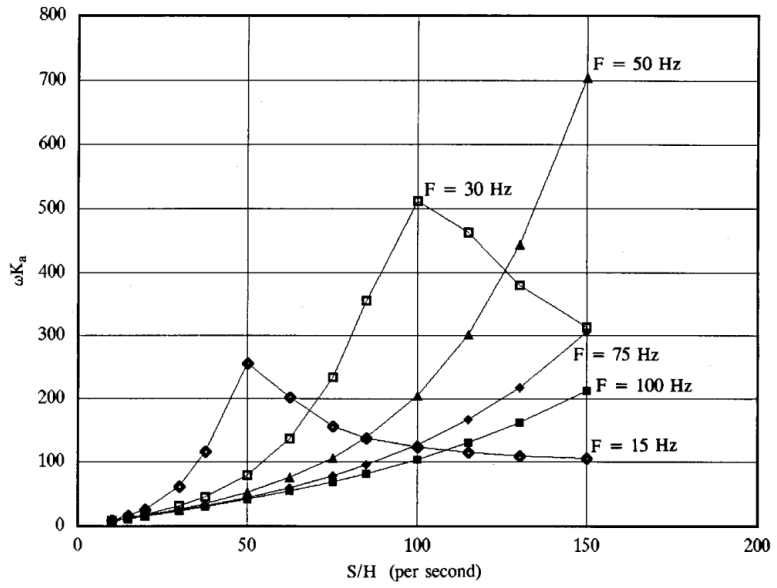


Figure 3: ωKa versus V_s/H for slopes with horizontal bedrock based on single-degree-of-freedom model (Wong and Pang, 1992)

Outcomes

Table 2 presents the calculated PPV limits for different structures within the TSF based on the single-degree-of-freedom method. Pseudo-static analyses representing the worst-case condition of the TSF filters sloughing has shown that PPV limits provided in Table 2 will produce a FoS against slope instability of greater than unity. The pseudo-static analysis approach is considered conservative (Wong and Pang, 1992). As more experience is obtained through blasting within the quarry, additional optimizations may be possible for the recommended PPVs.

Table 2: Calculated maximum PPV limits

Location	Distance from initial blasting location (m)	Yield acceleration	Limiting PPV (mm/s)
STA 06+00	300	0.21g	7
STA 11+00	480	0.21g	22

PPV attenuation model

The proposed limits were then compared with anticipated PPVs from surface blasting. A common method for predicting PPV from blasting is as per the US Bureau of Mines (1959) according to:

$$PPV = k\left(\frac{D}{\sqrt{W}}\right)^{-b}$$

Where D is distance (m), W is explosive charge per delay (kg), and k and b are site-specific factors. The blasting design was then conducted to yield anticipated PPVs at the upstream toe of the TSF below the limits shown in Table 2. Factors of safety were also added to the prescribed limits, to capture varying degrees of uncertainty associated with the analyses.

Monitoring plan and risk mitigation measures

Based on the critical parameters, the following monitoring was recommended to be conducted during the blasts at the TSF quarry:

- Monitoring PPV, PPA, and blast wave dominant frequency using seismographs as the main products of the blast.
- Porewater pressure monitoring at vibrating wire piezometer locations in the TSF to measure any excess pore pressures induced by blasting.
- Monitoring deformations to confirm that there are no excessive displacements or settlements.

The intent of the monitoring plan was to collect data to refine understanding of wave propagation so that the blast plan can be optimized for rock fill production while respecting dam safety constraints. An

important assumption of the methodology is that failure will be triggered once the blast induced parameters exceed the proposed limits.

Method shortcomings

General shortcomings

While the method outlined presents some rigor around prescription of specific blasting limits, the disastrous earthquakes in Alaska and Niigata in 1964 produced a realization that pseudo-static methods of analysis did not give reliable predictions for stability during earthquakes, with strength reduction during cyclic loading identified as one of the key issues (Jefferies and Been, 2016). Subsequently, relying on pseudo-static methods exclusively is no longer common in TSF best practice, and inconveniently, pseudo-static analyses were the basis of our blasting prescription method described above.

Undrained loading

In the instance of our facility, a saturated (or near saturated) filter could be prone to undrained failure if loaded too rapidly. As the filter is placed loosely to promote drainage, it will almost certainly be contractive and potentially be prone to undrained failure, potentially initiated by blasting. Other facilities may have materials in their cores or foundations that also may be prone to undrained failure.

While performing undrained stability analyses of the filter will give an estimation of its stability in the instance of undrained loading, it will not be linked back to the prescription of any blasting limit; i.e., any blast of any magnitude could or could not trigger undrained failure.

Liquefaction potential

Regarding potential liquefaction of the filter (if saturated), CPTu based triggering methods are not practical, given an only 300 mm layer thickness of filter. This leaves only laboratory testing to determine the filter's resistance to potential liquefaction (Cyclic Resistance Ratios [CRR]) when exposed to varying Cyclic Stress Ratios (CSRs) from blasting. Relationships for duration – number of cycles – Moment Magnitude (Mw) do exist; thus, the Magnitude Scaling Factor (MSF) for calculation of the CSR could be completed, in combination with earlier derived accelerations. Limiting anticipated blasting PPV limits to a CSR would then provide additional prescription around blasting limits.

This was not completed in our study but will be perused if further blasting of higher charge weights or higher predicted PPVs are to take place.

Conclusion

In conclusion, while earthquake considerations for the design of TSFs are commonly practiced within the

tailings industry, methods and considerations for blasting induced vibration remain less common. Despite this lack of common practice, it is essential for the sake of dam safety to prescribe limits when blasting near TSFs. This paper has explored a common method for determining appropriate blasting limits, highlighted its shortcomings in application to a specific facility and others, and proposed additional methods and considerations to enhance similar assessments.

Primary shortcomings of the method include an inability to model strength reduction during cyclic loading, including undrained behavior and potential liquefaction, if materials are susceptible. This shortcoming is not only relevant to this specific case study's fine filter, but to all dams encompassing a loose potentially saturated material, be they foundation units, embankment fills, filters and cores, or the tailings themselves in instances of upstream raises.

Some methods to safeguard against these shortcomings are identified; however, they do not do well in linking back to prescribe specific blasting limits, or to helping identify if a particular blast will impact dam stability and subsequent dam safety.

References

Duvall, W.I. and Petkof, B. 1959. Spherical propagation of explosion-generated strain pulses in rock. United States Department of the Interior, Bureau of Mines.

Jefferies, M. and Been, K. 2016. *Soil Liquefaction: A Critical State Approach*. Second Edition. Taylor and Francis Group LLC, Boca Raton, FL.

Wong, H.N. 1991. Evaluation of seismic stability of soil slopes in Hong Kong. MSc thesis, Department of Civil Engineering, Imperial College of Science, Technology & Medicine, University of London.

Wong, H.N. and Pang, P.L.R. 1992. Assessment of stability of slopes subjected to blasting vibration. *Geo Report No. 15.* Geotechnical Engineering Office, Civil Engineering Dept., The Government of the Hong Kong Special Administrative Region.

Geotechnical Controls for Piles of Filtered Iron Ore Tailings

Danilo Eloi, Vale S.A., Brazil
Rodney Silva, Vale S.A., Brazil
Miguel Paganin, Vale S.A., Brazil
Letícia Cedro, Vale S.A., Brazil
Gricor Channakian, Vale S.A., Brazil
Felipe Bonucci, Vale S.A., Brazil
Mateus Leite, BVP Geotecnia Hidrotecnia, Brazil
Adrielle Santos, Vale S.A., Brazil

The geotechnical control process for tailings stacking is crucial to ensure structural stability under both geomechanical and critical state conditions throughout operational phases and post-closure. Tailings exhibit distinctive characteristics compared to natural soils due to their production process involving physical and chemical stages, prompting extensive research into methodologies for controlling geotechnical parameters to improve compacted tailings layers.

Material compaction is regulated through various methodologies, including Hilf tests, Proctor tests, nuclear densimetry, non-nuclear densimetry, and penetrometer tests. In the stacking process of iron ore tailings, the presence of significant iron percentages (ranging approximately from 10% to 30%) poses challenges in conventional testing. Variations in density, influenced by the variability in iron content, result in compaction determinations exceeding 100%. The variation in the magnetic field influences densimetry tests. Penetrometer studies encounter difficulties due to the high resistance exhibited by tailings post-compaction.

To achieve better control over critical state parameters and susceptibility to liquefaction both during operation and post-closure, as well as indirectly monitor the degree of compaction, studies utilizing void ratio tests in the field have demonstrated linear results. In order to establish the control parameters, the critical state line of the tailings was drawn up through laboratory tests using techniques such as those described by Jefferies and Been (2016) and Viana et al. (2021). By determining the void ratio, which relates to the stresses to which the pile will be subjected at its maximum height, we determined the maximum void ratio that the layers of the pile could have, maintaining the structure on the dilatant side and thus not being susceptible to liquefaction.

Introduction

In mineral extraction activities, various quantities of materials are extracted and generated in different stages of the process. The ore extraction process, the location and depth of deposits, the available technologies at extraction sites, and the processes involved are among the several factors that determine the amount of waste generated by mining activities. The main types of waste generated are overburden and tailings. Overburden consists of materials from the extraction activity, due to the layers of soil covering the ore. Tailings result from the beneficiation process of these mineral substances within plants, which can involve purely physical or physico-chemical stages. Among the purposes of beneficiation are standardizing the size of fragments, removing minerals without economic value associated with the mined rocks or soils, and increasing the quality and physico-chemical purity of the final product. In most cases, minerals found in nature require beneficiation to improve their properties (Luz and Lins, 2018).

Figure 1 presents a schematic representation of a mineral exploration process involving physical stages.

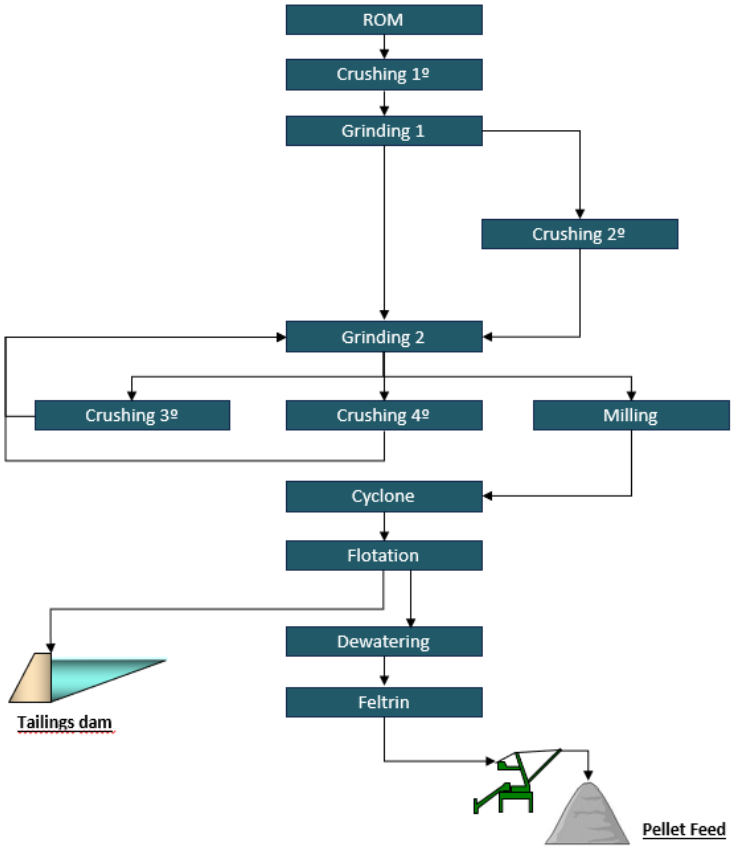


Figure 1: Macro flowchart of the mineral exploration process (Eloi et al., 2024)

Mining tailings are the materials generated in the separation process of ore from concentrate, composed of very fine particles and, in some cases, chemical residues from the ore beneficiation stage (IPEA, 2012). Since tailings result from a sequence of physical and chemical processes, they exhibit various characteristics influenced by the beneficiation process, such as particle size distribution, particle shapes, density, mineralogical composition, and moisture content. Due to these beneficiation-influenced characteristics, tailings differ from those expected of natural soils (Vick, 1983).

In the exploration of iron ore, the beneficiation process of hematite, one of the main iron oxides, is notable. During the separation process, fine-grained tailings are formed (Gomes, 2017), characterized by high saturation levels. These can be categorized based on their particle size distribution into silts and clays or sands. Silts and clays tend to exhibit characteristics of high compressibility and plasticity in their particle size distribution, making them difficult to settle. Sandy tailings, on the other hand, have high shear strength and permeability.

Due to the high saturation levels of iron ore tailings, controlled stacking processes are preferred over dam disposal methods. Filtering processes are therefore implemented to remove water from the tailings. This involves hydro cyclones with the addition of flocculants to improve material density, thickening with flocculants and coagulants to adjust saturation and separate materials, and filtration using either disc filters or filter presses, depending on the technology used. After filtration, the thickened and filtered slurry is conveyed via conveyor belts to temporary stacking areas, where the tailings are stored before being transported to the controlled stacking site.

Figure 2 illustrates an iron ore tailings filtration plant with labeled structures, operating in the context of this study.



Figure 2: Disc filter tailings filtration complex

Methodology

This work demonstrates the geotechnical control systems used in the iron ore tailings stacking process, as well as the results obtained from a case study. These processes are divided into controls for the filtration plant, controls for stacking to ensure approved layers of compacted tailings, and instrumentation controls to measure structural safety factors throughout stacking and post-closure.

The geotechnical controls at the filtration plant include iron content analyses, crucial for understanding the densities at which tailings are directed to the compaction areas, moisture content analyses of filtered tailings leaving the plant, and particle size distribution analyses of the tailings after filtration.

Geotechnical controls during the stacking process consist of field controls such as moisture control, compaction control, void ratio and particle size distribution, and laboratory control tests to assess the geomechanical parameters of strength. Additional campaigns with SCPTU tests are conducted to further verify the strength parameters of compacted tailings.

Various instruments including piezometers, inclinometers, load cells, settlement meters, water level meters, and flow meters in drains are installed in the structure to constantly monitor parameters that can affect safety factor models of the structure.

Data and discussion

The geotechnical analyses conducted in the iron ore stacking process aim at ensuring stability and operational safety of the structures. Control over material characteristics imposes limits on the process, such as the compaction energy to be applied or the rates of structure raising when assessing pore pressure dissipation. Regarding iron ore tailings, given their predominant particle size distribution of silts and sands and thus their high susceptibility to liquefaction, recent studies demonstrate the necessity of compaction control for stacking, to prevent material from exhibiting contractive behavior.

Geotechnical controls applied at the filtration plant

In the filtration process, initial controls are carried out to verify if the produced tailings are within acceptable limits for the stacking project. Should the material fall outside specified ranges, it is directed to areas where it can be disposed of without controls, such as exhausted pits or active dams.

The first test conducted is to assess the iron content in the tailings. Higher iron contents are known to be associated with increased fines, which directly influence the moisture content of the tailings. This, in turn, requires more effort in drying the material before compaction, impacting the processing times related to work areas for tailings, initial moisture content affecting drying time, and fleet capacity. Therefore, setting a limit on the iron content indirectly controls the moisture content of the material. Another geotechnical control related to iron content is the density of the material. Higher iron percentages increase

material density, leading to variations in the amount of material mass required to define stacking layers with controlled volume. In the case under study, a 25% iron content limit was implemented to indirectly control the geotechnical parameters of density, moisture, and particle size distribution.

In this studied complex, material sampling for iron content evaluation occurs every fifteen minutes, with analyses performed on a composite of every four samples mixed, thus representing hourly production of iron ore tailings.

As mentioned in the previous paragraph, moisture control directly correlates with the required work time for tailings to reach suitable compaction conditions. This ensures that the material is compacted near its optimal moisture content as determined by Proctor tests, achieving the required compaction level to maintain dilatant behavior. Moisture tests are conducted on fractions of the plant using the halogen moisture analyzer method, providing timely results. Table 1 illustrates moisture and iron content control over a 24-hour period for materials processed in this system in the year 2024.

Table 1: Moisture and iron content control

Start Date	Final Date	Iron Percentage	Moisture
28/06/2024 05:30	28/06/2024 06:29	26,19	11,19
28/06/2024 04:30	28/06/2024 05:29	25,39	11,28
28/06/2024 03:30	28/06/2024 04:29	26,75	11,14
28/06/2024 02:30	28/06/2024 03:29	25,30	11,13
28/06/2024 01:30	28/06/2024 02:29	24,87	11,18
28/06/2024 00:30	28/06/2024 01:29	24,22	11,25
27/06/2024 23:30	28/06/2024 00:29	23,85	10,96
27/06/2024 22:30	27/06/2024 23:29	23,23	11,66
27/06/2024 21:30	27/06/2024 22:29	22,73	11,83
27/06/2024 20:30	27/06/2024 21:29	22,17	11,15
27/06/2024 19:30	27/06/2024 20:29	21,78	11,40
27/06/2024 18:30	27/06/2024 19:29	22,12	11,72
27/06/2024 17:30	27/06/2024 18:29	23,29	11,11
27/06/2024 16:30	27/06/2024 17:29	24,27	11,44
27/06/2024 15:30	27/06/2024 16:29	24,79	11,07
27/06/2024 14:30	27/06/2024 15:29	25,17	12,41
27/06/2024 13:30	27/06/2024 14:29	28,17	10,80
27/06/2024 12:30	27/06/2024 13:29	26,29	11,24
27/06/2024 11:30	27/06/2024 12:29	25,05	10,83
27/06/2024 10:30	27/06/2024 11:29	24,72	10,91
27/06/2024 09:30	27/06/2024 10:29	24,05	11,62
27/06/2024 08:30	27/06/2024 09:29	23,21	11,38
27/06/2024 07:30	27/06/2024 08:29	22,85	11,92
27/06/2024 06:30	27/06/2024 07:29	23,71	11,56
27/06/2024 05:30	27/06/2024 06:29	22,52	11,80

In the samples collected at the plant, particle size distribution controls are conducted using laser granulometry tests. As mentioned, variations leading to higher fines content can affect the material's moisture content, thereby increasing drying time. Larger particle sizes can promote the formation of permeable zones within the stacking, potentially creating water pockets that may result in localized excess pore pressures and points more susceptible to liquefaction. Therefore, a particle size distribution range has been specified for this additional control of the filtered tailings.

Table 2 illustrates the particle size fractions evaluated at the plant in the same samples mentioned in Table 1.

Table 2: Particle size fractions in tailings samples

Start Date	Final Date	2mm	1mm	0,5mm	0,25mm	0,15mm	0,106mm	0,075mm	0,045mm	0,038mm	0,025mm	0,010mm	0,005mm	-0,005mm
28/06/2024 05:30	28/06/2024 06:29	0,00	0,00	0,00	6,50	16,50	13,90	12,50	13,80	3,60	7,90	13,30	6,10	5,90
28/06/2024 04:30	28/06/2024 05:29	0,00	0,00	0,00	1,00	8,70	10,20	11,30	16,00	4,80	11,10	19,30	8,90	8,70
28/06/2024 03:30	28/06/2024 04:29	0,00	0,00	0,00	1,00	9,20	10,90	12,10	16,30	4,70	10,70	18,50	8,40	8,20
28/06/2024 02:30	28/06/2024 03:29	0,00	0,00	0,00	3,00	10,40	11,30	12,30	16,10	4,50	10,10	17,20	7,70	7,40
28/06/2024 01:30	28/06/2024 02:29	0,00	0,00	0,00	2,70	12,30	12,20	12,40	15,60	4,30	9,70	16,20	7,30	7,30
28/06/2024 00:30	28/06/2024 01:29	0,00	0,00	0,00	3,10	11,90	12,40	12,80	15,90	4,30	9,50	15,90	7,20	7,00
27/06/2024 23:30	28/06/2024 00:29	0,00	0,00	0,00	3,00	13,50	13,30	13,20	15,60	4,20	9,00	14,90	6,60	6,70
27/06/2024 22:30	27/06/2024 23:29	0,00	0,00	0,00	2,20	11,80	12,50	13,10	16,20	4,40	9,60	15,90	7,10	7,20
27/06/2024 21:30	27/06/2024 22:29	0,00	0,00	0,00	2,80	13,90	14,00	13,90	16,00	4,10	8,70	13,90	6,20	6,50
27/06/2024 20:30	27/06/2024 21:29	0,00	0,00	0,00	0,40	8,20	11,00	12,40	16,50	4,70	10,50	18,40	8,70	9,20
27/06/2024 19:30	27/06/2024 20:29	0,00	0,00	0,00	5,30	16,40	14,90	13,80	14,80	3,60	7,60	12,30	5,50	5,80
27/06/2024 18:30	27/06/2024 19:29	0,00	0,00	0,00	3,90	14,30	13,90	13,60	15,60	4,00	8,30	13,70	6,20	6,50
27/06/2024 17:30	27/06/2024 18:29	0,00	0,00	0,00	2,50	11,00	11,50	12,10	15,50	4,30	9,60	17,00	8,10	8,40
27/06/2024 16:30	27/06/2024 17:29	0,00	0,00	0,00	3,90	15,50	14,40	13,00	14,20	3,80	8,30	14,10	6,30	6,50
27/06/2024 15:30	27/06/2024 16:29	0,00	0,00	0,00	6,00	17,40	14,10	12,00	12,50	3,40	7,70	13,90	6,30	6,70
27/06/2024 14:30	27/06/2024 15:29	0,00	0,00	0,00	5,40	12,80	10,20	9,50	13,00	4,20	10,10	17,90	8,40	8,50
27/06/2024 13:30	27/06/2024 14:29	0,00	0,00	0,00	3,80	8,90	8,30	9,40	14,90	4,90	11,60	20,00	9,00	9,20
27/06/2024 12:30	27/06/2024 13:29	0,00	0,00	0,00	5,10	15,40	13,30	12,20	14,20	3,90	8,50	14,10	6,40	6,90
27/06/2024 11:30	27/06/2024 12:29	0,00	0,00	0,00	7,00	17,00	14,10	12,50	13,80	3,70	8,20	13,30	5,40	5,00
27/06/2024 10:30	27/06/2024 11:29	0,00	0,00	0,50	2,30	7,70	9,50	11,20	15,60	4,60	10,50	19,20	9,20	9,70
27/06/2024 09:30	27/06/2024 10:29	0,00	0,00	0,00	5,50	14,30	12,70	12,40	14,70	4,00	8,80	14,40	6,40	6,80
27/06/2024 08:30	27/06/2024 09:29	0,00	0,00	0,00	5,10	18,00	15,90	14,00	14,10	3,40	7,30	11,60	5,10	5,50
27/06/2024 07:30	27/06/2024 08:29	0,00	0,00	0,00	4,40	15,00	13,20	12,20	14,40	4,00	8,90	14,60	6,50	6,80
27/06/2024 06:30	27/06/2024 07:29	0,00	0,00	0,00	4,50	16,50	14,40	12,90	14,10	3,70	8,10	13,30	6,00	6,50
27/06/2024 05:30	27/06/2024 06:29	0,00	0,00	0,00	3,70	16,70	15,50	14,00	14,40	3,50	7,50	12,60	5,80	6,30

Geotechnical controls applied in stacking operations

After the filtering process, the reject material meeting predetermined parameters within established limits is directed to stacking areas. These materials are transported by heavy-duty vehicles and spread out, worked to reduce moisture, and compacted in compacting squares using earthmoving equipment. In this context, the initial controls related to the rejects are those concerning the material's working moisture content in the field. To achieve this, Proctor tests with standard energy are conducted every 3,000 m³ of material to determine the working moisture content in subdivided areas in the field.

Figure 3 presents results from Proctor tests with standard energy conducted on rejects from the studied site. As indicated by the results, the optimum moisture content for compaction typically ranges between 9% and 13% in most cases. Based on conducted studies and understanding that the material can perform within these limits, it was decided to eliminate controls for deviations from the optimum moisture content

reference value and to require that the material should only be within this moisture range. Thus, according to Figure 4, it is evident that the majority of materials fall within this sample range.

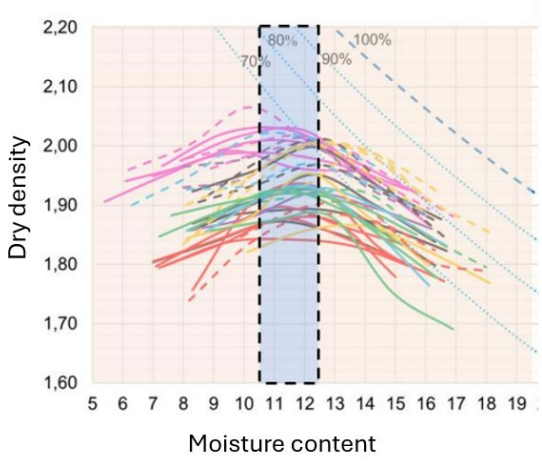


Figure 3: Proctor tests with standard energy on samples from a period

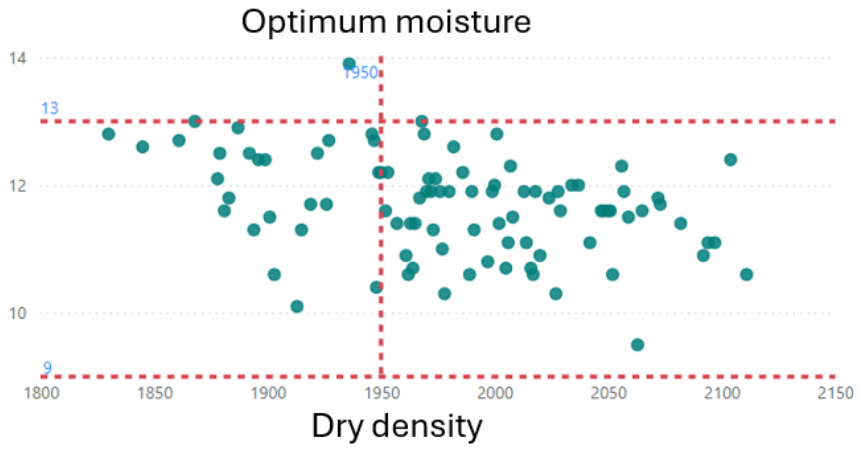


Figure 4: Relationship of moisture tests analyzed within the range over a period

With the results from Proctor tests with standard energy determining the optimum moisture content, and the material being within the established moisture range, the material is compacted in layers of 35 cm thickness with a permitted variation of 5 cm. After compaction, tests to determine the void ratio of the reject material are conducted to verify if the results maintain the material in the dilatant branch when evaluating the critical state lines of the material. Laboratory studies to determine the critical state lines have shown that these vary according to the material's gradation. For the sake of safety, the designers and the Engineer of Record for the structure have determined that the void ratio for approval of the material in this stacking case study should be 0.60. Hence, a control regarding void ratios for approval of the layers is conducted throughout the stacking process, as depicted in Figure 5.

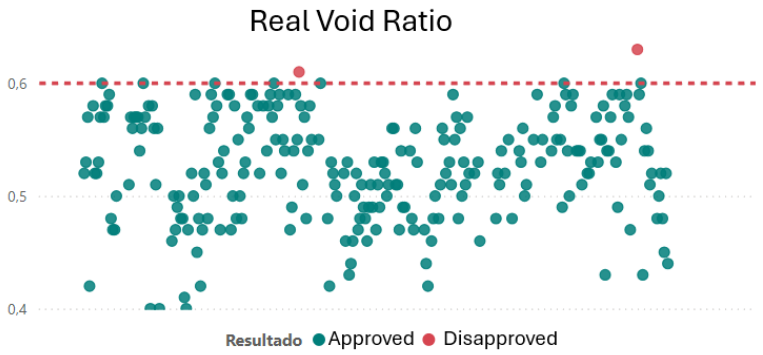


Figure 5: Relationship of tests approved by void ratio and failed tests over a period

As a reassessment parameter for plant results and to verify potential grain breakage, characterization tests such as sieving, and sedimentation tests, are conducted in accordance with ABNT NBR 7181 every 3,000 m³. These tests are not criteria for material rejection but serve solely as investigative measures to understand material characteristics after compaction.

Drained and undrained triaxial tests and oedometer tests are performed on blocks extracted every 3 meters of stack height. These tests verify the strength and compressibility parameters of the materials. The objective of these campaigns is to ensure that the parameters used in the safety factor models for the stack remain consistent. In the same blocks, tests are conducted to recharacterize the materials, ensuring that the characteristics of compacted rejects do not vary with stack height. Figures 6 and 7 illustrate the results of tests conducted on blocks from the stack under study.

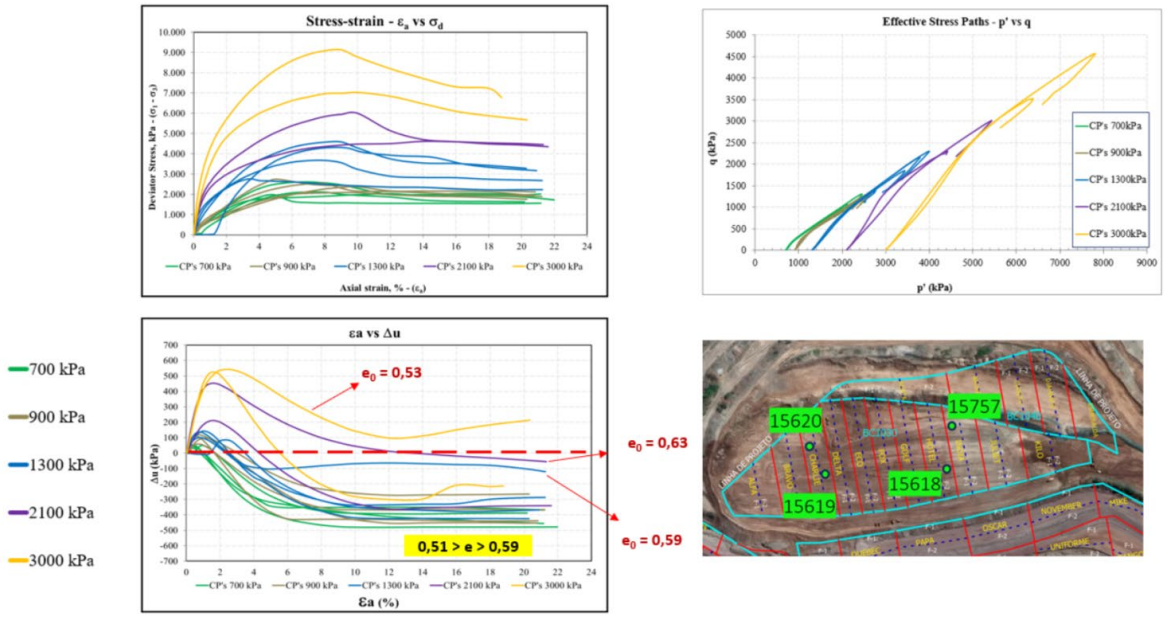


Figure 6: Results of undrained triaxial tests conducted on the reject material

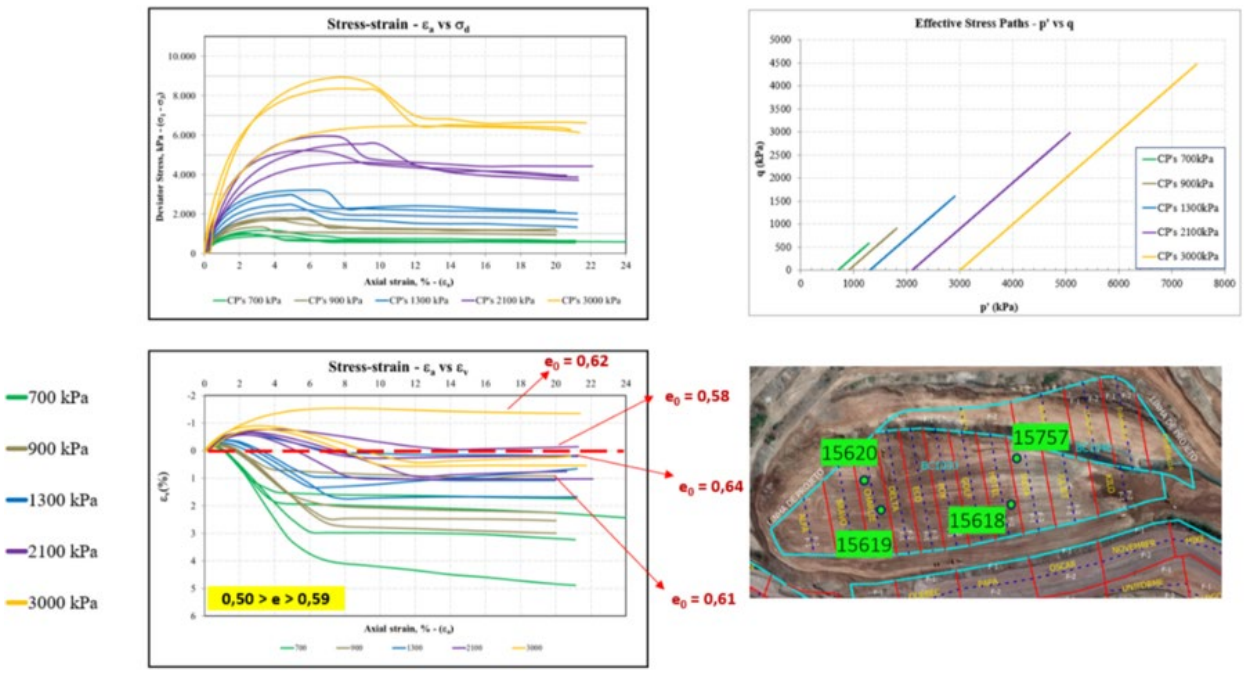


Figure 7: Results of drained triaxial tests conducted on the reject material

Geotechnical control through piezocone tests with pore pressure measurement, dissipation tests, and seismic tests are conducted with the objectives of identifying areas of excess saturation, estimating material stiffness for numerical analysis, and reevaluating material behavior. These tests are repeated annually after rainy periods, and their quantitative determination is defined by the Engineer of Record for the structure.

Geotechnical controls through instrumentation

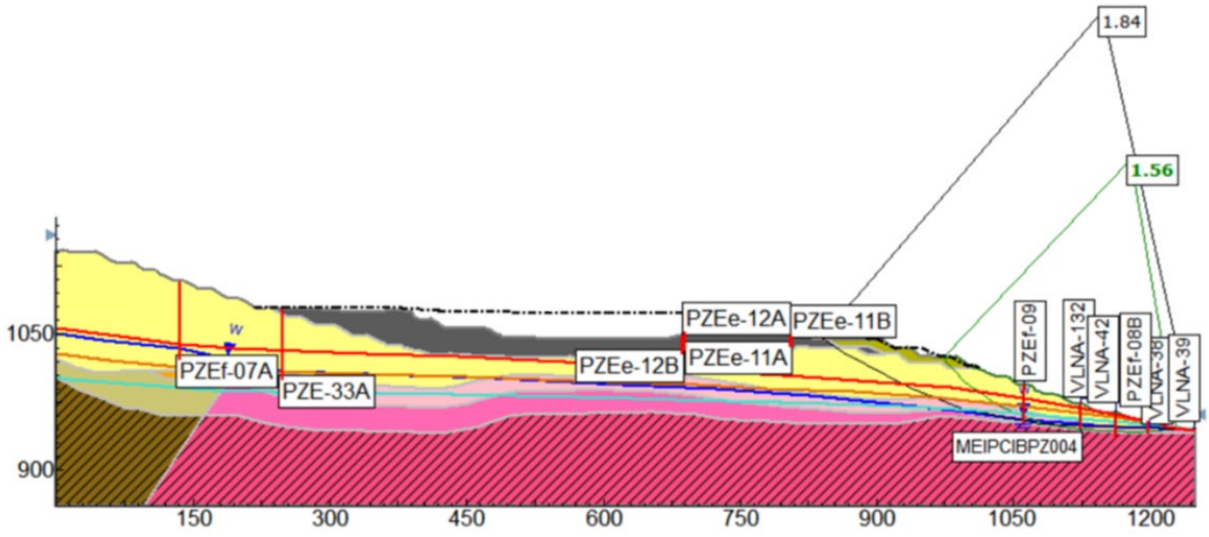


Figure 8: Safety factors of one of the structure sections evaluated based on monitoring instrument data

As described by Hawley and Cunning (2017), permanent waste and overburden stacks must have instrumentation and monitoring plans for the risks involved throughout the structure's lifespan and after closure. Among the instruments installed in iron ore tailings stacks are piezometers, load cells, settlement gauges, surface markers, geophones, inclinometers, water level meters, and flow meters in drains.

All instruments aim to assess the structure's behavior with respect to operational safety factors. To establish control levels for geotechnical structure instrumentation, as outlined by the Bureau of Reclamation (2014), potential failure modes affecting the structure must first be identified. Control levels for each instrument's purpose listed above were defined during pre-operation phases, throughout operational years, and after structure closure. Figure 8 illustrates the safety factors derived from models developed monthly by the structure's Engineer of Record, based on readings from installed instruments.

Conclusion

Geotechnical controls associated with various stages of the stacking process of filtered iron ore tailings aim to ensure the stability of structures during operational phases and post-closure. The physical and mineralogical characteristics of the tailings, such as iron content, moisture content, and particle size distribution, directly influence the workability of the material and are therefore crucial to monitor during the filtration stage.

Control during compaction stages aims to ensure that the material placed in the structure meets design strength requirements and predetermined model characteristics. Void ratio control was developed to monitor the critical state of the material, consistently maintaining its dilatant characteristics. The high susceptibility to liquefaction of tailings, due to their silty and sandy nature, necessitates careful control of these parameters, particularly highlighted after recent incidents of tailings dam failures due to liquefaction.

Studies conducted on the stacking process have shown that compacted tailings exhibit high resistance during SCPTU penetration tests, indicating a need for further development in future studies to enhance the performance of such tests.

Instrumentation of iron ore tailings stacks during operational phases serves not only to monitor anomalous behaviors but also to ensure the stability of the structure, which is evaluated in studies aimed at determining safety factors for the structure.

References

American Society of Testing and Materials – ASTM. 2011. Standard Test Method for Consolidated Undrained Triaxial Compression Test for Cohesive Soils. ASTM D4767. West Coshohocken, PA.

American Society of Testing and Materials – ASTM. 2016. Standard Test Methods for Maximum Index Density and Unit Weight of Soils Using a Vibratory Table. ASTM D4253. West Coshohocken, PA.

American Society of Testing and Materials – ASTM. 2016. Standard Test Methods for Minimum Index Density and Unit Weight of Soils and Calculation of Relative Density. ASTM D4254. West Coshohocken, PA.

American Society of Testing and Materials – ASTM. 2020. Standard Test Method for Consolidated Drained Triaxial Compression Test for Soils. ASTM D7181. West Coshohocken, PA.

Associação Brasileira de Normas Técnicas – ABNT. 2016. *Amostras de solo – Preparação para ensaios de compactação e ensaios de caracterização*. NBR 6457. Rio de Janeiro, RJ.

Associação Brasileira de Normas Técnicas – ABNT. 2016. *Grãos de pedregulho retidos na peneira de abertura 4,8 mm – Determinação da massa específica, da massa específica aparente e da absorção de água.* NBR 6458. Rio de Janeiro, RJ.

Associação Brasileira de Normas Técnicas – ABNT. 2016. *Solo – Determinação do limite de plasticidade*. NBR 7180. Rio de Janeiro, RJ.

Associação Brasileira de Normas Técnicas – ABNT. 2017. *Solo – Determinação do limite de liquidez*. NBR 6459. Rio de Janeiro, RJ.

Associação Brasileira de Normas Técnicas – ABNT. *2018. Solo – Análise granulométrica*. NBR 7181. Rio de Janeiro, RJ.

Bureau of Reclamation. 2014. Embankment Dams – Design Standards nº13. Chapter 11: Instrumentation and Monitoring.

Eloi, D.M., Silva, R. and Louzada, P. 2024. Characterization differences between iron tailings from the Iron Quadrangle and Carajás Complex, Tailings 2024, Chile.

Gomes, A.C. 2017. *Estudo de aproveitamento de rejeito de mineração. Dissertação de Mestrado em Engenharia.* Universidade Federal de Minas Gerais.

Hawley, P.M. and Cunning, J. 2017. *Guidelines for Mine Waste Dump and Stockpile Design*. CRC Press, 1st edition.

IPEA. 2012. Instituto de Pesquisa Econômica Aplicada. *Diagnostico dos Resíduos Sólidos da Atividade de Mineração de Substâncias Não Energéticas.* Brasília: 96 IPEA, 2012. Accessed at http://repositorio.ipea.gov.br/bitstream/11058/7702/1/RP_Diagn%C3%B3stic o_2012.pdf

Jefferies, M. and Been, K. 2016. *Soil Liquefaction – A Critical State Approach*. 2nd edition, 690. Boca Raton, FL.

Luz, A.B and Lins, F.A.F. 2018. Introdução ao Tratamento de Minérios. In Adão Benvindo da Luz, João Alves Sampaio and Sílvia Cristina A. França (Org.). *Tratamento de Minérios*. 6th ed. CETEM 1: 3–6.

Viana Da Fonseca, A., Cordeiro, D. and Molina Gómez, F. 2021. Recommended procedures to assess critical state locus from triaxial tests in cohesionless remoulded samples. *Geotechnics* 1(1): 95–127.

Vick, S.G. 1983. *Planning, Design, and Analysis of Tailings Dams*. Vancouver, BC, Canada: BiTech Publishers.

2D and 3D Numerical Analyses of a Trial Embankment Construction over a Tailings Storage Facility

Alfonso Cerna Diaz, AECOM, USA
Lisa Yenne, AECOM, USA
Pooya Sheykhloo, AECOM, USA
Richard Davidson, RRD LLC, USA
Theo Gerritsen, Rio Tinto, Australia

Abstract

Constructing a trial embankment over an inactive tailings storage facility (TSF) aided understanding of the consolidation and shear behavior that would take place during construction of a new embankment founded on an inactive TSF. Based on a series of 3D finite difference and 2D/3D finite element flow-deformation back analysis on a well-controlled trial embankment construction, the deformation and excess pore pressures of the tailings dam were found to be controlled by the underlying tailings state and permeability. Given the uncertainty in the use of the constitutive model, hydraulic conductivity, and dimensionality applied to tailings, this paper provides insight into the use of two-dimensional and three-dimensional plasticity-based and consolidation models to capture flow-deformation at a "system-level" to evaluate the deformation and stability of tailings dams, to be used as part of performance-based evaluations as recommended by GISTM. This back analysis study highlights the use of consolidation/coupled modeling for tailings dams involving construction limits that permit partially drained conditions.

Introduction

Key aspects to verify adequate performance of current or future tailings storage facilities (TSFs) are geotechnical evaluations to identify preferred construction methods for expansion of TSFs, assess potentially fatal flaws of design, evaluate ground improvement methods, and establish construction requirements or operational criteria. Routine geotechnical analyses are performed based on field investigations and laboratory testing, to assess the material behavior of soft and very loose tailings; these analyses are limited to the boundary conditions imposed in the laboratory and by in-situ testing. A field performance using a trial embankment offers a unique opportunity to evaluate tailings behavior on a large scale, providing a site-specific case history to a TSF project, thus helping to reduce and manage risks and

uncertainties. This leverages GISTM good practice guide recommendations on performance-based approach evaluations (ICMM, 2021).

In this paper, using the Settle3 uncoupled finite difference (FDM) approach and the 2D/3D NorSand PLAXIS fully coupled finite element method (FEM) modeling of a well-characterized trial embankment case history, the role of compressibility and permeability in capturing settlements and excess pore water pressures (PWP) is assessed. The results indicate that all modeling approaches with a "best estimate" of compressibility and permeability values, following the recorded construction sequence, can reasonably capture recorded settlements and the Excess PWP distribution with 3D coupled formulation, giving a more realistic PWP distribution during construction loading.

Field-scale construction program

A case history of the response of a 30-ft trial embankment with 4H:1V slopes on wick drain treated area, 6H:1V slopes on a non-treated area and a plan area of ~450' × 300' constructed over soft fine-grained mine tailings to capture a real-world shear and consolidation response in mine tailings. The trial embankment consists of a compacted embankment constructed over a non-wick untreated area and a wick treated area. Wicks were installed beneath one-half of the embankment on a 9 ft triangular spacing to a depth of 100 ft to reduce excess pore water pressures during construction. A detailed field monitoring program of settlements, PWP, and movements was carried out over a five-year time period from 2010 to 2015. The general subsurface conditions consist of a ~70 ft contractive decant pond clay (DPC) layer underlain by a thick dilatant whole tailings (WT) layer. The DPC in the South Impoundment was deposited in areas of the impoundment where tailings slurry was allowed to slow and pool. This included the historic decant pond areas. Flow channels formed at a sufficient distance from the single point discharges created enough quiescence for the finer-grained particles to settle out of suspension. Generally, whole tailings (WT) were deposited from the deltaic processes resulting from single point discharge and peripheral spigoting since the mid-1980s.

Details of the trial embankment, including profile instrumentation layout and construction photographs, are shown in Figure 1. Nested vibrating wire piezometers were installed at nine locations along the long axis of the embankment centerline. Three nested piezometers were installed beneath the crest, two at mid-slope, two at the toe, and two approximately 30 ft from the toe at depths ranging from 5 to 130 ft below the ground surface. Settlement plates and survey monuments were installed to evaluate settlements and horizontal movements within the trail embankment area.

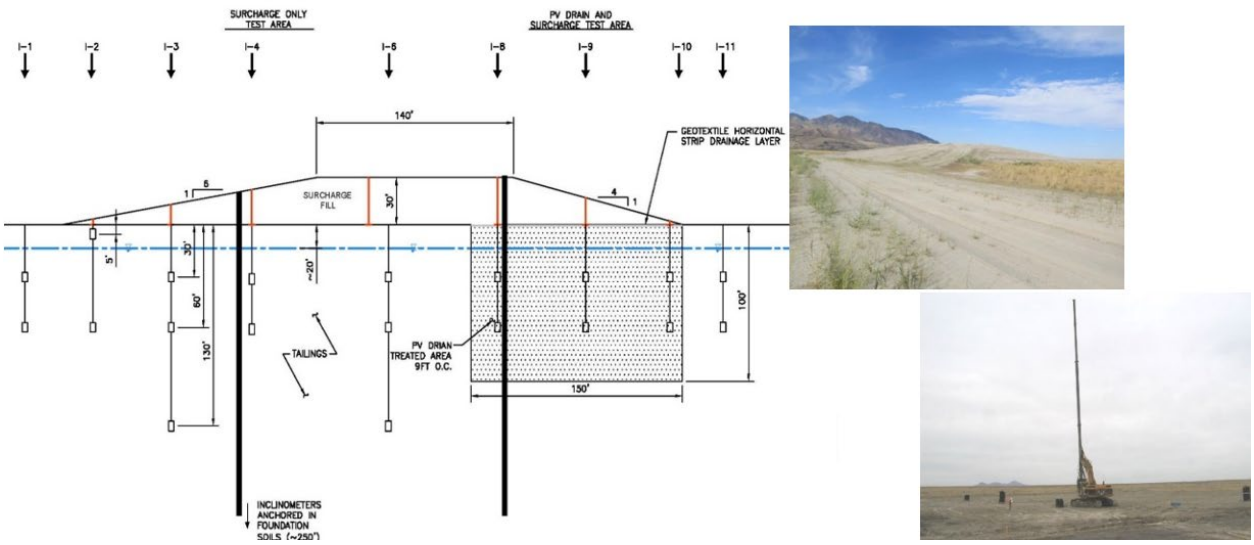


Figure 1: Trial embankment plan view, instrumentation layout and construction

The imposed trial embankment height and construction rate, along with observed field settlement and Excess PWP, are shown in Figure 2 at the non-treated locations.

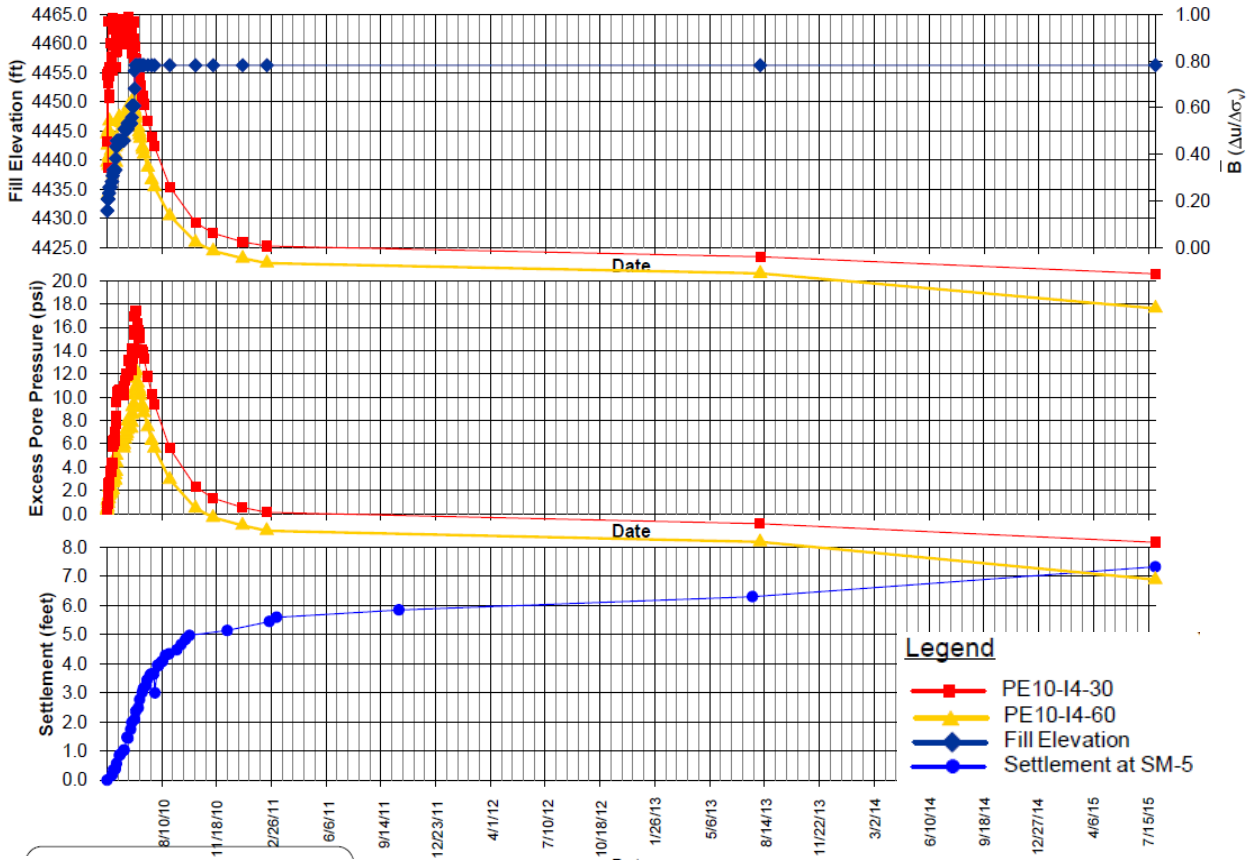


Figure 2: Trial embankment fill elevation, construction rate, B bar, Excess PWP, and settlements over 5 years

Piezometers in the untreated area indicate high loading induced Excess PWP with B-values of nearly 1.0, suggesting that the fill loads were supported in pore pressure. In contrast, deeper tailings did not generate significant Excess PWP. Wick drains reduced Excess PWP by ~50 percent. PWP returned to pre-construction eight months after the completion of the embankment in June 2010, as shown in Figure 2.

Field and laboratory testing program

The site investigation program included 2008 and 2010 CPT soundings, and 2010 and 2014 drill hole investigations. This information is summarized in Figure 3.

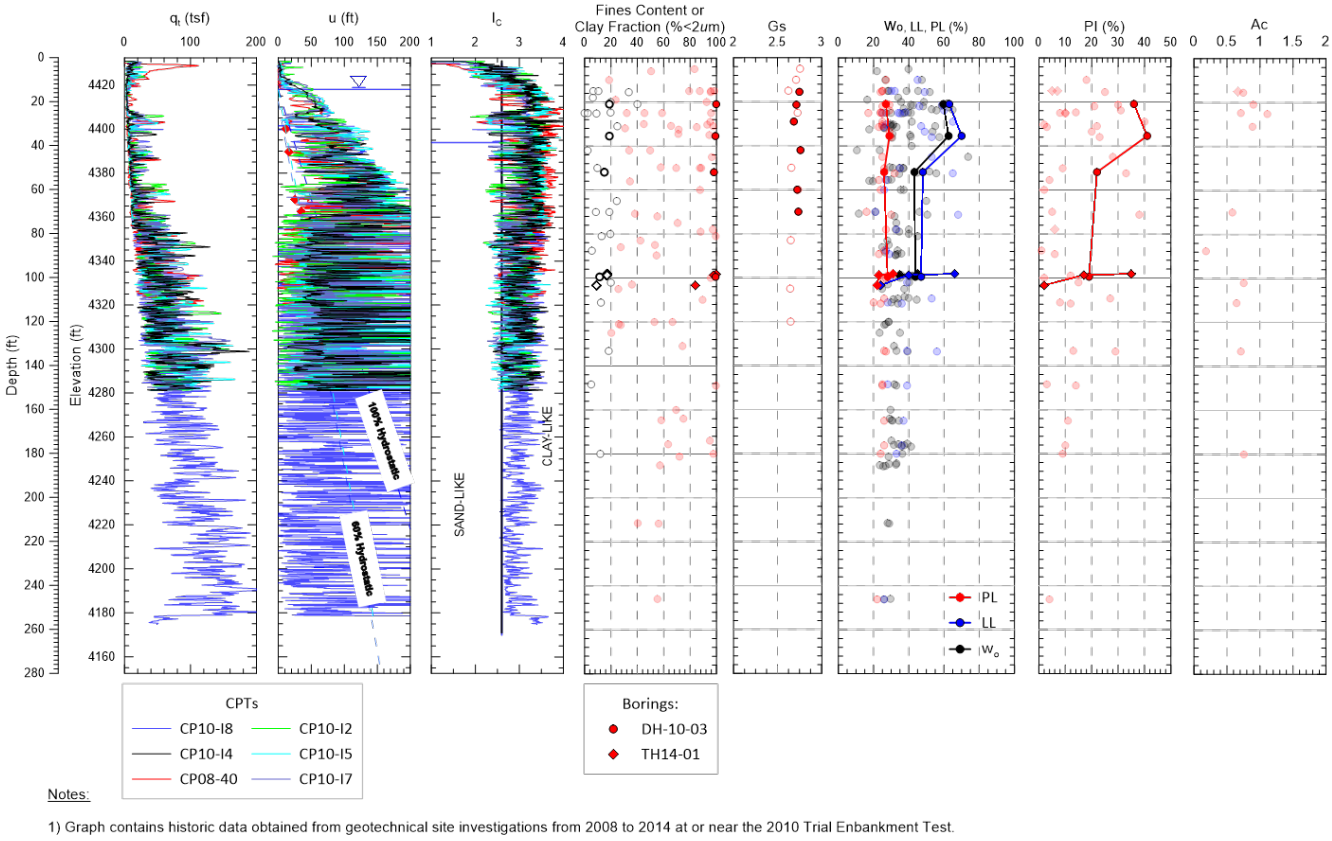


Figure 3: Trial embankment CPTs tip resistance, pore pressure response (u2), Ic, and index testing

The data from CPTs in Figure 3 shows that tip resistances are generally less than 20 tsf in the first ~60 feet, with associated contractive response (e.g., positive Excess PWP), and range from 20 tsf to less than 200 tsf from ~60 to 260 feet, with an increase of dilative response with depth (e.g., negative Excess PWP). PPD test locations and hydrostatic pore pressure measurements indicate that the percentage of hydrostatic varies between 70 to 100 percent below the trial embankment footprint. The soil behavior type index (Ic) traces show that within about the first 60 feet, the tailings material is predominantly clay-like, transitioning to slightly more sand-like behavior intercalated below 60 feet. The information gathered from

the 2010 to 2014 drill hole investigation also indicates this transition from clay-like material to sand-like material based on results from laboratory index tests results, showing a decrease in the Plasticity Index (PI) and Clay Fraction (CF) with depth.

Extensive laboratory testing programs performed during the past 30 years were used to evaluate the tailings shear and volumetric behavior. Engineering property testing included permeability, consolidation, DSS, and triaxial compression tests on undisturbed and reconstituted specimens.

Consolidation and strength tests were used to calibrate constitutive models used, while permeability testing was used to support the flow characteristics of the tailings. Triaxial testing was performed on both Shelby tube samples and reconstituted tailings to develop critical state lines for the materials (DPC and WT).

The DPC is a low to high plasticity silty clay (CL, CH) that can be found in various thicknesses along the impoundment. It has a low sensitivity based on the results of field vane shear tests and a review of the liquidity indices of the material. The material exhibits a contractive, nearly ductile, shear response under triaxial compression tests with an undrained shear strength ratio of 0.29 to 0.40. The CSL for the DPC along with shear-stress shear-strain and excess pore pressure are shown in Figure 4.

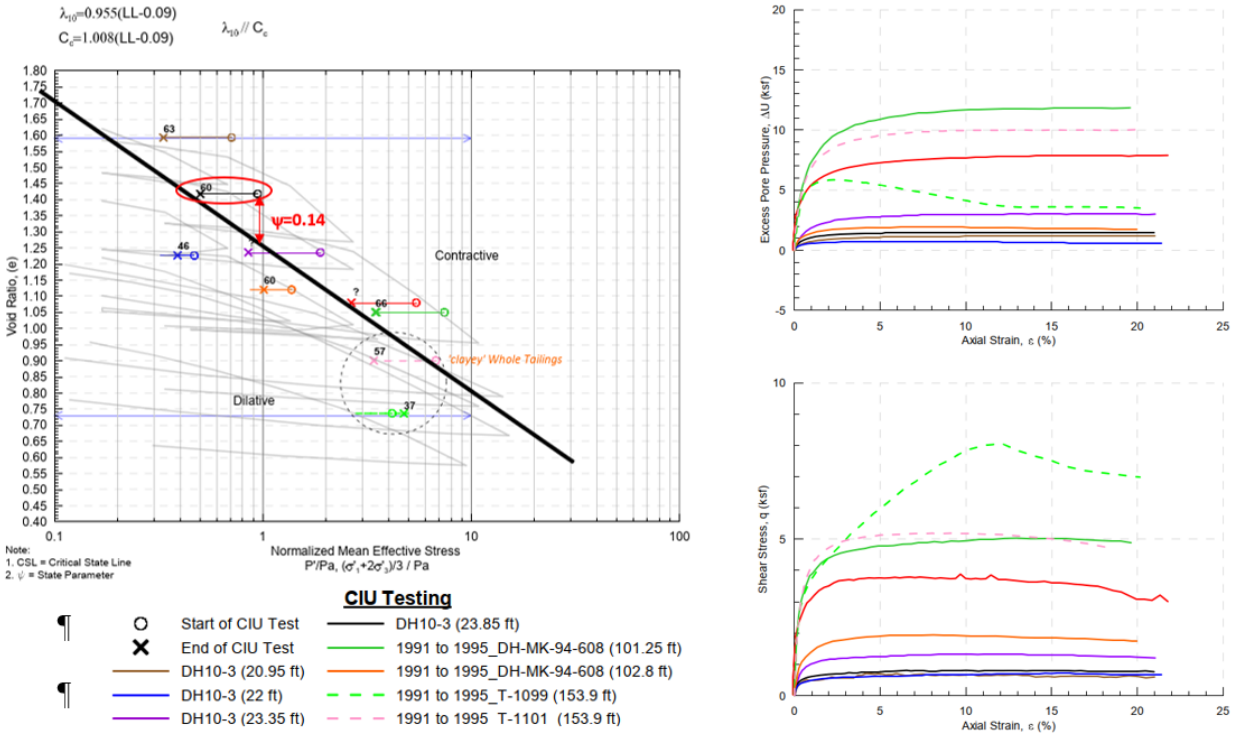


Figure 4: Decant pond clay critical state line and undrained triaxial testing results

The slope of the CSL is nearly parallel to the consolidation lines, compatible with clay-like behavior at the critical state. The DPC in the trial embankment area is slightly overconsolidated at the surface and

normally consolidated at depth. Generally, whole tailings (WT) material is characterized as contractive at surface and dilative at depth. This material was deposited from the deltaic processes resulting from single point discharge and peripheral spigoting since the mid-1980s. WT are typically composed of non-plastic to low plasticity, cohesionless tailings consisting of silty and sandy tailings. The CSLs for the whole tailings, along with shear-stress shear-strain, excess pore pressure, and stress path plots are shown in Figure 5.

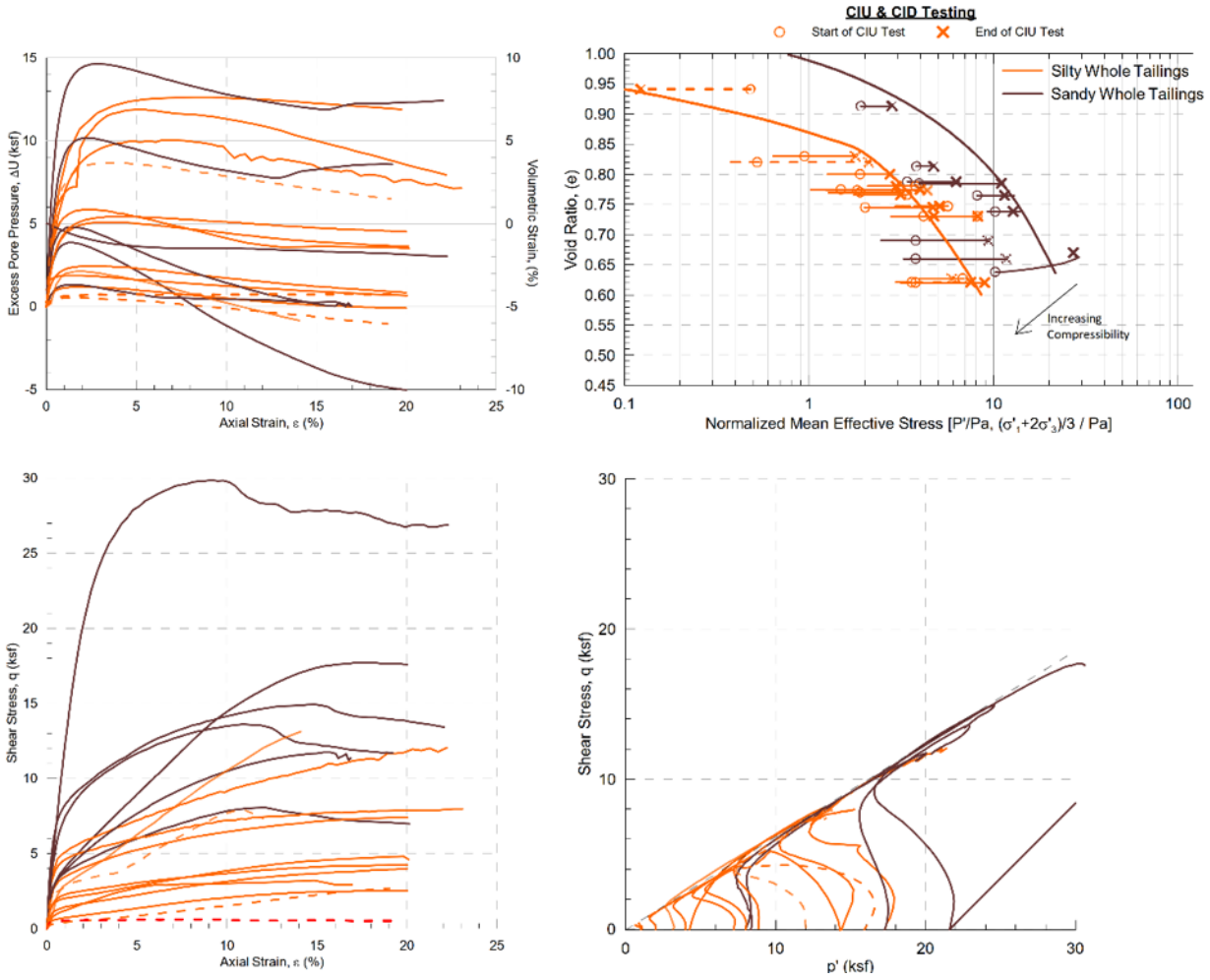


Figure 5: Whole tailings critical state lines and undrained triaxial testing results

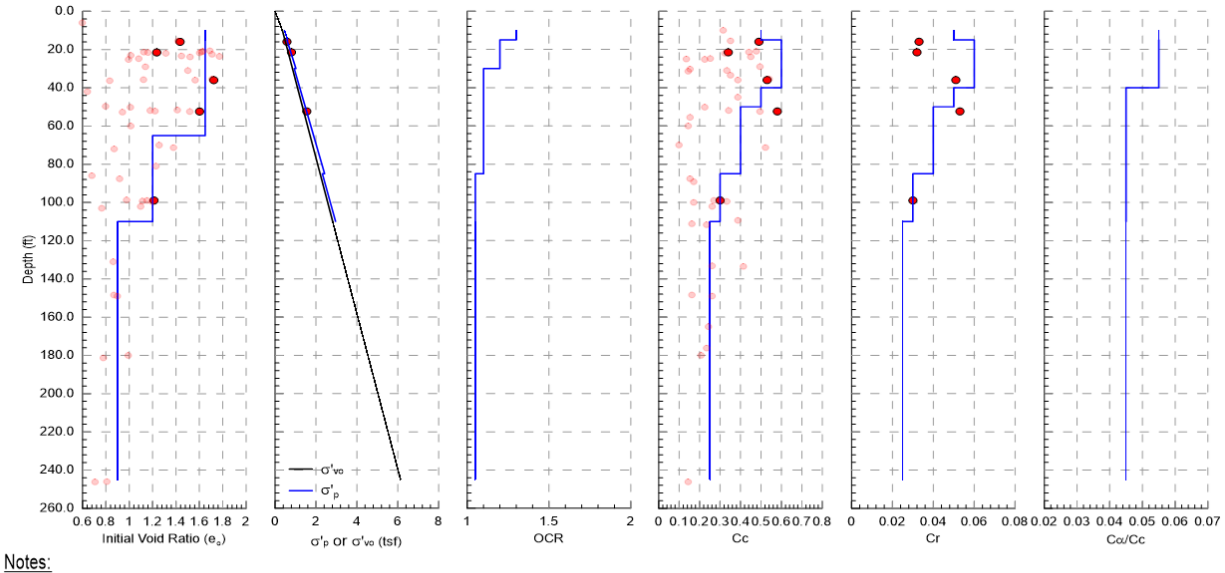
The scatter is explained by differences in gradation in the highly interbedded whole tailings materials, in which the far left CSL is representative of primarily non-plastic silty materials (ML), while the far right CSL range is associated primarily with silty sand materials (SM). Initial state parameters indicate that WT plots below/above and to the left/right of the estimated CSL, indicating dilative/contractive ductile behavior in the transition zone, consistent with CPT testing.

Numerical analyses

Pseudo 3D finite difference consolidation analysis

Settle3 is used for analyses of vertical settlement and consolidation under surface loads such as foundations, embankments, and surface excavations. Loads are calculated within the domain in three-dimensional components, while settlements and pore pressures are computed in one-dimensional form. Settle3D calculates total settlement as the sum of three components: (1) immediate settlement; (2), settlement due to primary consolidation; and (3) settlement due to secondary compression.

Immediate settlement occurs instantaneously with the application of the load and is calculated assuming linear elastic behavior using 1D constrained modulus and the change in vertical stresses. Primary consolidation settlement occurs as excess pore water pressures, generated initially by the imposed load, dissipate with time. Settle3D uses the 1D Terzaghi theory of consolidation solved via the finite different method, modified to account for changes in compressibility and permeability during primary consolidation. Settle3D uses a bi-linear material model in which the modulus is a function of the stress to describe the changes in compressibility. For the computation of secondary settlement, Settle3D uses the ratio between the secondary compression index and the compression index (Cα/Cc), denoted as the law of compressibility (Mesri and Godlewski, 1977, 1979) after the average degree of consolidation reaches 95 percent. The trial embankment was modeled using a 3D geometry based on as-built geometries, and construction staging based on actual loading (lifts) documented during construction of the embankment.



Notes:

1) Compressibility parameters (Cc, Cr) were obtained from consolidation tests at different depths marked as isolated red solid points
2) Solid lines represent values used in the consolidation model in Settle 3D

Figure 6: Compressibility parameters used for Settle3 FDM numerical model

Case history information used in the model calibration included data from an extensive consolidation laboratory testing program, whose compressibility parameters are summarized in Figure 6. Boundary conditions consisted of double drained at the base and surface, with no flow in the horizontal direction.

The results of the Settle3 analysis of the case history indicated that the model fully captured the total settlement magnitude observed at the trial embankment, as shown in Figure 7.

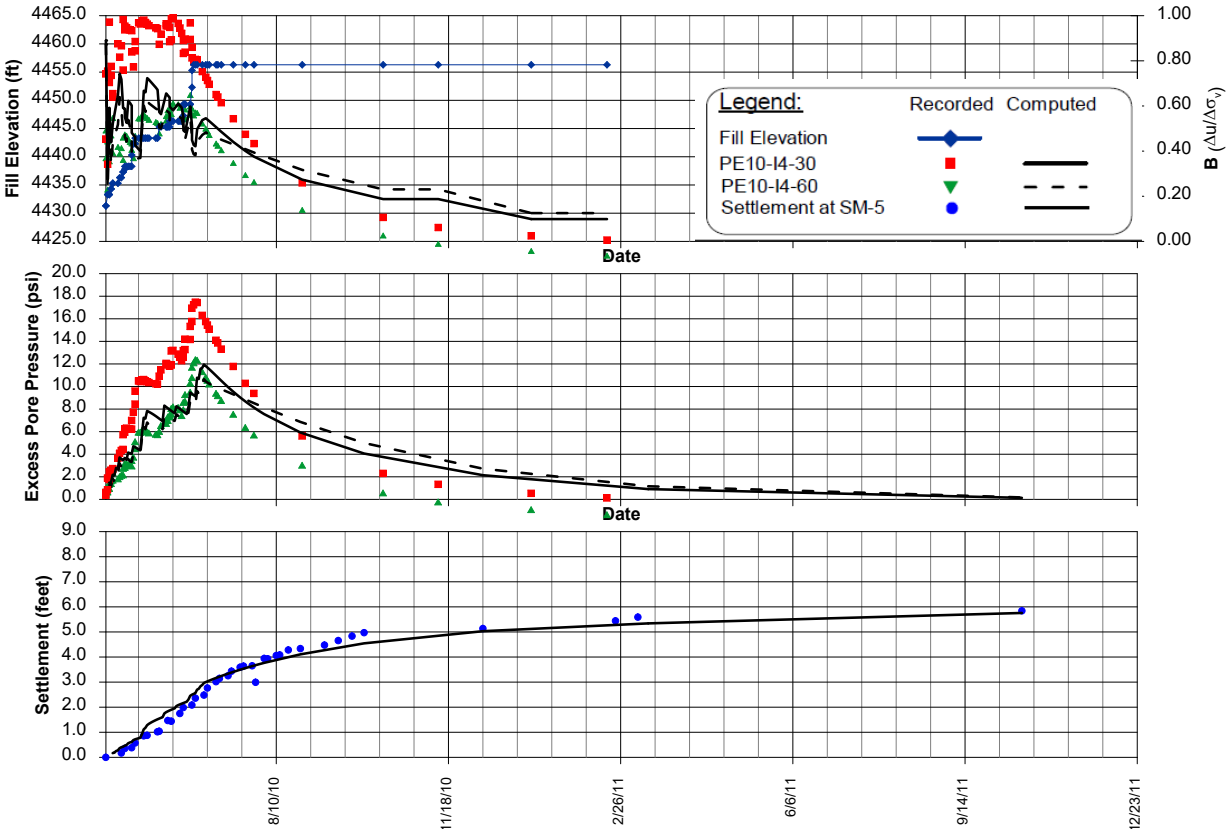


Figure 7: Computed (Settle3) and recorded settlement, excess pore water pressures and B bar for 2010 trial embankment crest (2010 to 2011) at I4 locations

The Settle3 analyses generally captured the time rate of consolidation and pore pressure generation and dissipation observed in the case history for both the non-wicked and wicked zone, as shown in Figure 8. As shown in Figures 7 and 8, the excess pore pressures generated in the non-wicked zone are slightly higher than those calculated from Settle3 and can be attributed to shear-induced pore pressures not captured due to the Settle3 formulation being derived entirely from compression loading.

Figure 9 also shows the resultant calibrated vertical permeability obtained from trial embankment case history. The calibration was carried out by systematically adjusting permeability values within an estimated range to develop a best estimate permeability distribution. As shown in Figure 9, the resultant calibrated permeability distribution with depth was found to be generally within an order of magnitude higher than the vertical permeability estimated from laboratory Incremental Load (IL) consolidation tests, flexible wall

permeability tests performed, and vertical permeability estimations from CPT Ic based correlations (Robertson and Cabal, 2015). In contrast, the calibrated permeability falls within the range of horizontal permeability (k_h) estimated from CPT correlations based on dissipation tests. This increase in the calibrated permeability accounts for the interbedded nature of the tailings that enhances horizontal flow in the field.

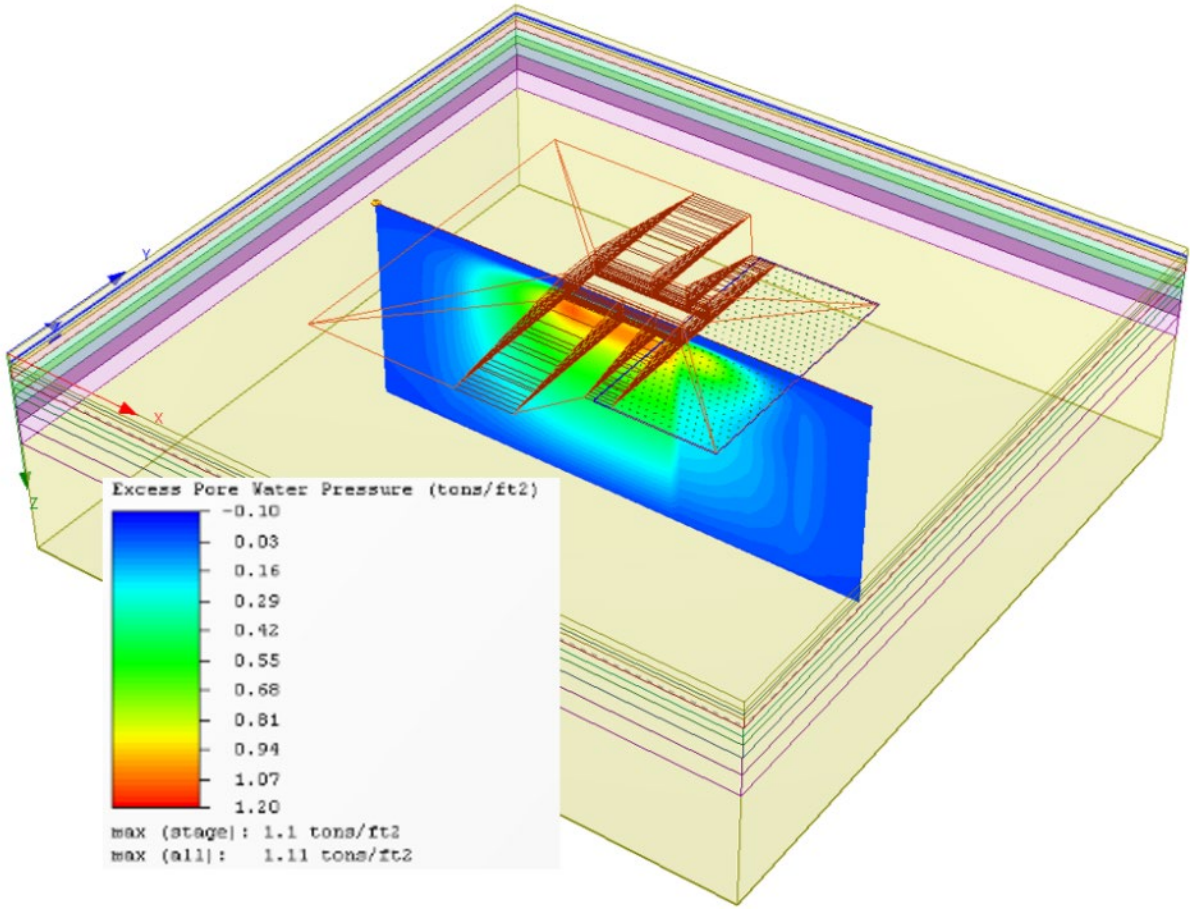


Figure 8: Trial embankment Settle3 maximum excess pore water pressures

2D Finite element NorSand analysis

The trial embankment material 2D FEM numerical model was broken down into two main materials (DPC and WT) for the PLAXIS model. The upper 60 feet are classified as soft tailings (DPC) and the lower 100 feet are classified as deep whole tailings (WT), with the phreatic surface set at 20 feet below the ground surface with 80 percent hydrostatic conditions. The NorSand constitutive model (Jefferies, 1993) was calibrated for each of these materials. NorSand was calibrated for the upper soft tailings and lower whole tailings, as shown in Table 1. Figure 10 presents the numerical calibration fits for laboratory shear strength tests on the two materials. Good fits to the laboratory data were obtained for both tests.

Table 1: Summary of trial embankment NorSand parameters

Material	Γ	λe	Mtc	N	χ	Plastic hardening (H)	Elasticity
Soft tailings (DPC)	**2.1**	**0.23**	**1.45**	**0.35**	**2.5**	**H_o=75, H_ψ=0**	**G_{ref}=176x10³ psf, n_g=1.0**
Whole tailings (WT)	**1.92**	**0.13**	**1.5**	**0.20**	**3.3**	**H_o=32, H_ψ=300**	**G_{ref}=510x10³ psf, n_g=0.65**

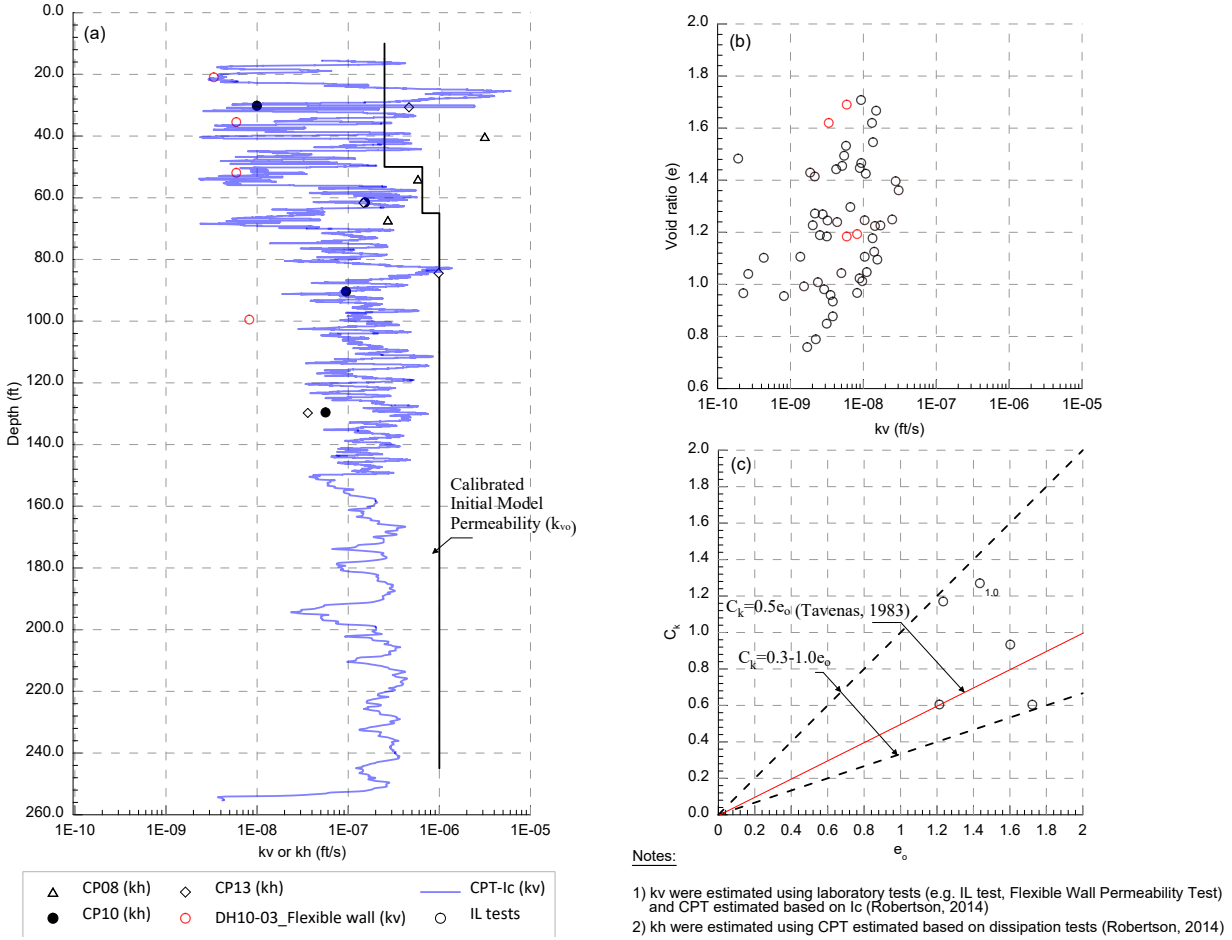


Figure 9: 2010 trial embankment laboratory, CPT, and calibrated Settle3 permeability (kv)

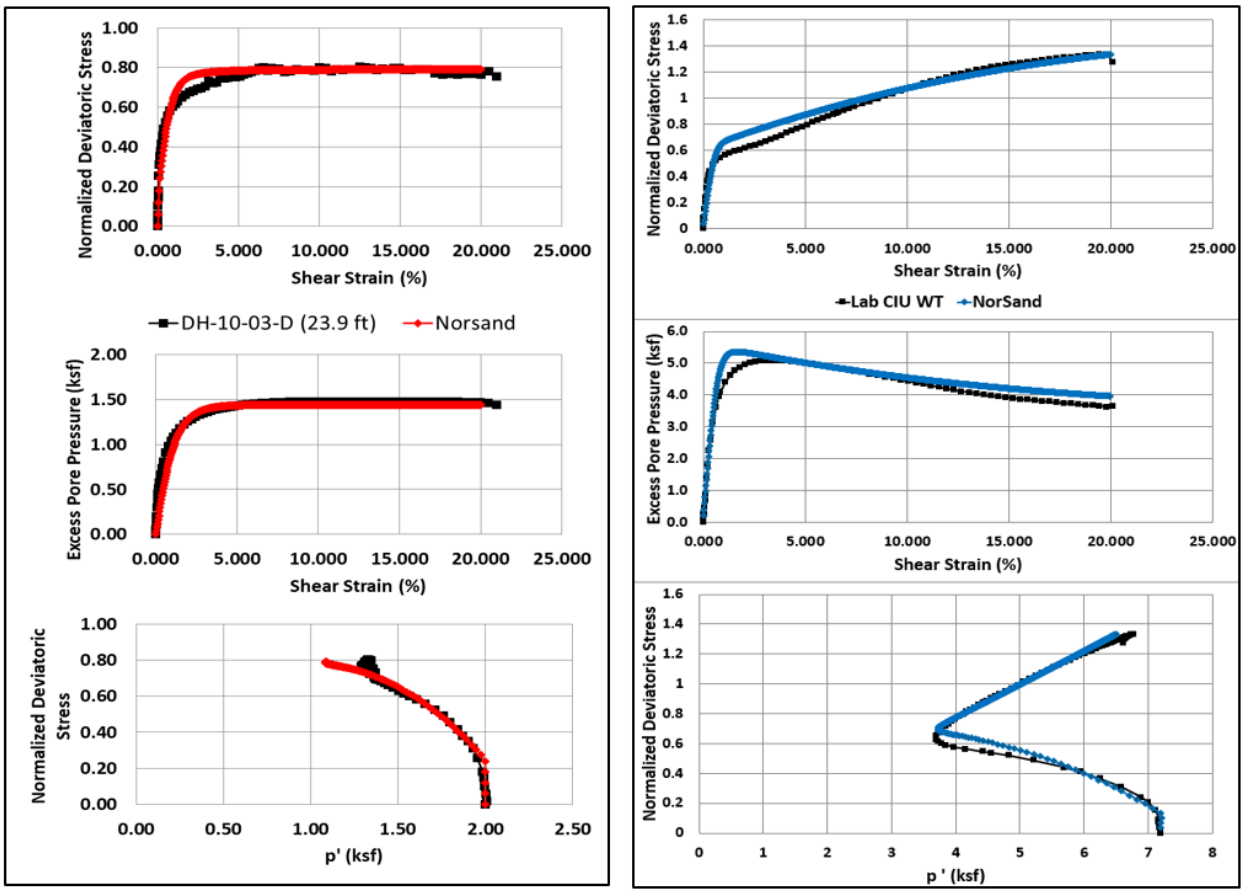


Figure 10: NorSand calibration results for soft tailings (left) and whole tailings (right)

Figure 11 presents the PLAXIS staged construction model, which includes the discretized foundation with upper soft tailings, and deep whole tailings NorSand properties. These foundation zones are further discretized into lifts of different permeability. The 30-foot-tall embankment is broken down into foot increments with loading and dissipation steps based on the actual construction sequencing with a total of 49 stages. Wicks are included on the right side of the model based on the as-built spacing. Boundary conditions consisted of allowing drainage in four directions of the model. The model was initialized with the foundation in place, using a gravity turn-on procedure and an assigned K_0.

The initial foundation state parameter and model conditions prior to embankment construction are shown in Figure 12, which presents CPT-based state parameter estimates using the Plewes method (Plewes et al., 1992) with 80th and 90th percentile lines that used G_{max} (1/5*G_{max}, 1/3*G_{max}, and G_{max}). The use of the Plewes method was considered appropriate at this stage of the study given the uncertainty in the application of the NorSand CPT widget, due to the lack of calibration chamber testing in low to high plasticity tailings to derive reasonable mapping factors (e.g., Cq, Shuttle and Jefferies, 2016).

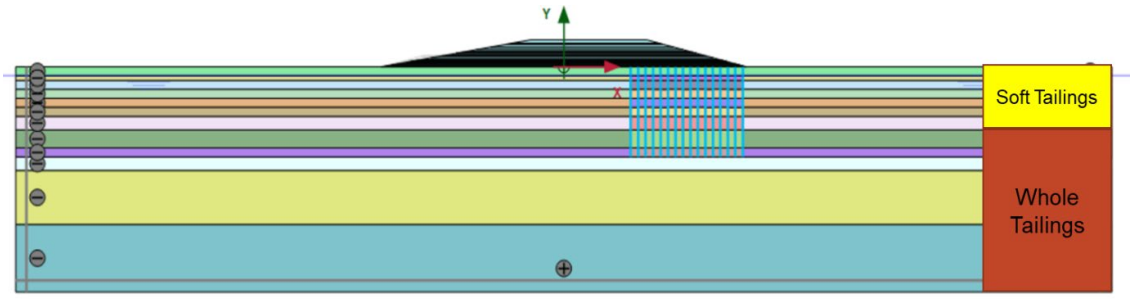


Figure 11: 2010 Trial embankment 2D FEM model (embankment, soil domain, and wick drains)

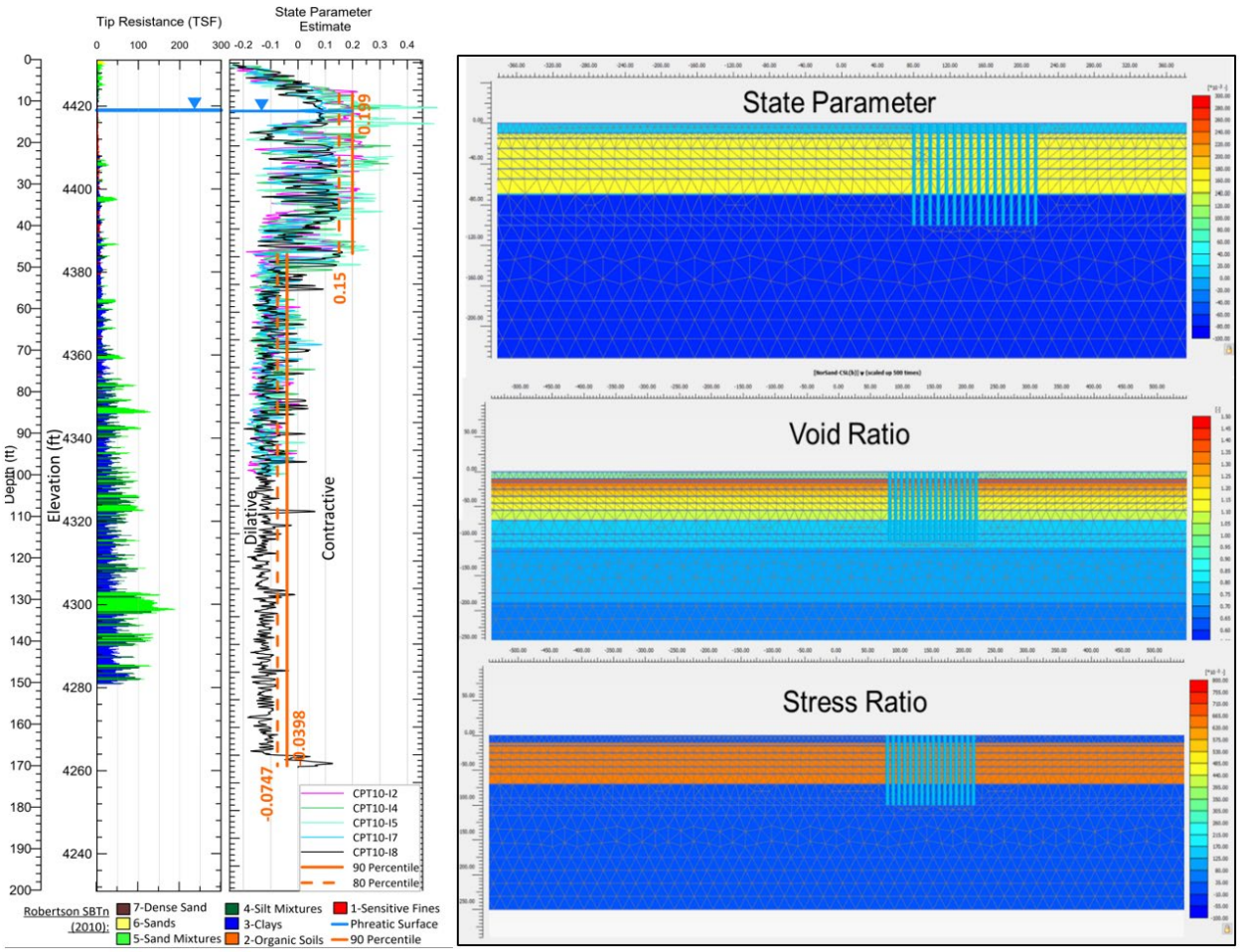


Figure 12: 2D FEM simulations using NorSand (a) initial characteristic state parameters; (b) initial model state parameter, void ratio and stress ratio profile

The goal of the model was to find the combination of a characteristic state parameter and G_{max} that results in the best time history match to settlement and pore pressures. The best match to time history data was obtained using the 80th percentile of state parameter and G_{ref} between $G_{max}/3$ and $G_{max}/5$, as shown by the settlement comparison in Figure 13, which presents the settlement time history match between settlement plates data and the NorSand model results. Consistent with this observation, as shown in Figure

14, single element calibrations of NorSand for DPC layer under oedometer compression loading paths show a better agreement with the compressibility of the IL consolidation tests for calibrations that use Gref=Gmax/5, while Gref=Gmax/3 tends to slightly underpredict the compressibility of the DPC consolidation tests. This highlights the importance of calibrating the Gref parameter for the NorSand model against key loading paths that reflect field conditions. This allows for sensitivity analyses using a range of Gref consistent with standard practice from undrained triaxial testing and drained compressibility-based testing.

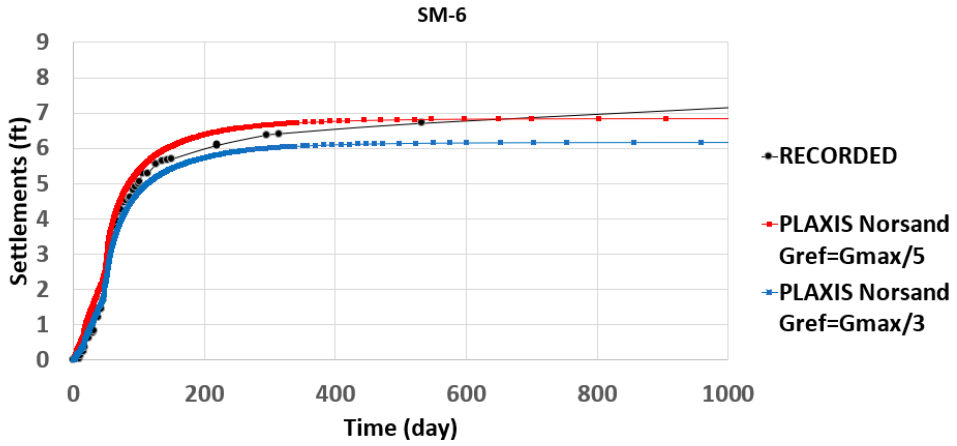


Figure 13: Trial embankment NorSand 2D FEM model settlement comparison for Gmax/5 and Gmax/3

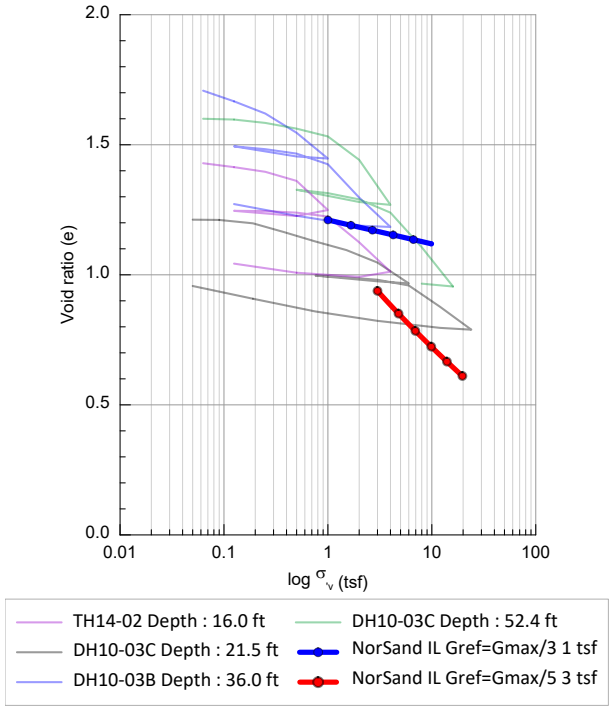


Figure 14: Trial embankment consolidation testing using oedometer in DPC and NorSand oedometer calibrations for Gmax/3 and Gmax/5

Additionally, as shown in Figures 15 and 16, consolidation beneath the trial embankment suggest that areas closer to the wick drains undergo large consolidation as Excess PWPs are dissipated much more rapidly with a state parameter above 0.18 at Ultimate Height, while areas near the left toe underwent shear-induced PWP with less dissipation throughout construction, with resulting state parameters below 0.14.

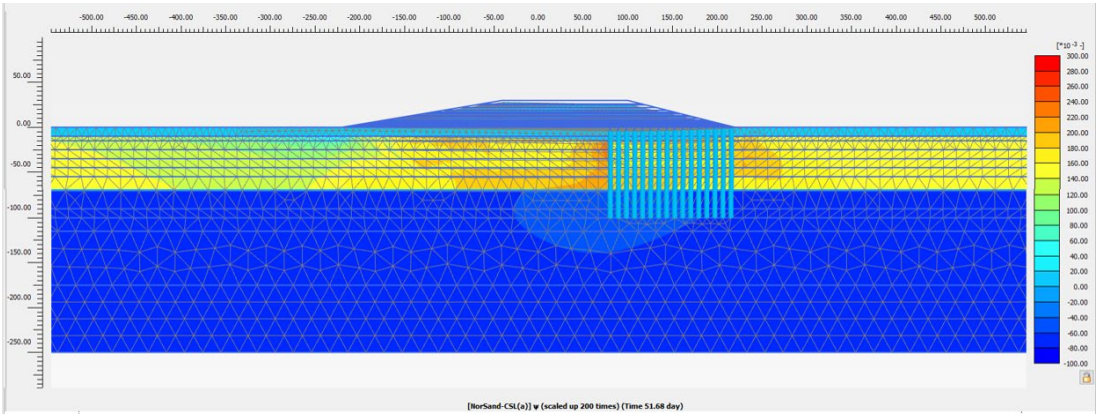


Figure 15: Trial embankment NorSand 2D FEM model state parameter at ultimate height

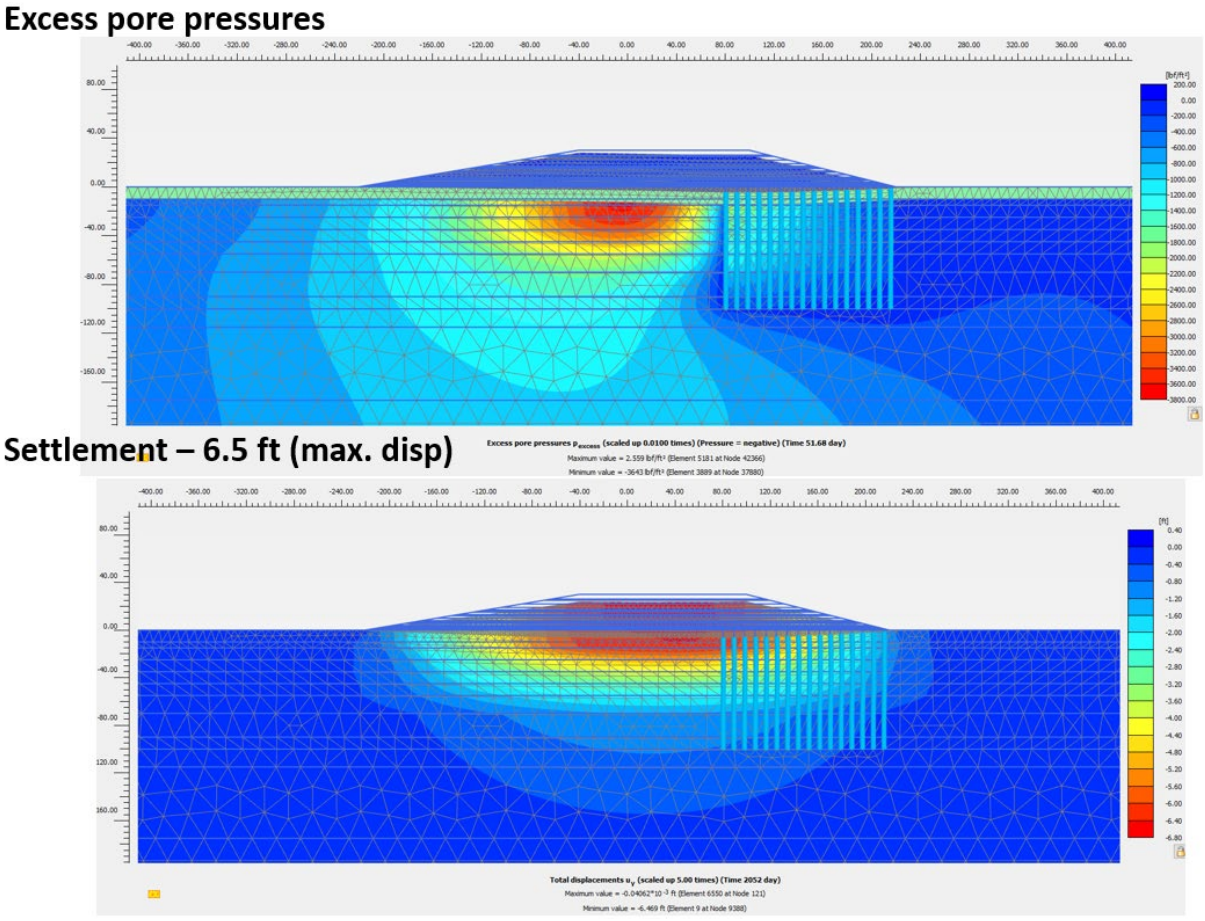


Figure 16: Trial embankment NorSand 2D FEM model Excess PWP and settlements at ultimate height

Unlike Settle3, the NorSand model was able to match the consolidation and shear-induced PWP time history and settlement behavior of the soft foundation tailings well, although it overpredicted the initial induced PWP for the piezometer located at 60 ft (PE10-I4-60), as shown in Figure 17. Internal results using the soft soil model (Vermeer and Neher, 1999) are also shown for comparison, showing good results with less shear-induced PWP for the piezometer located at 30 ft (PE10-I4-30).

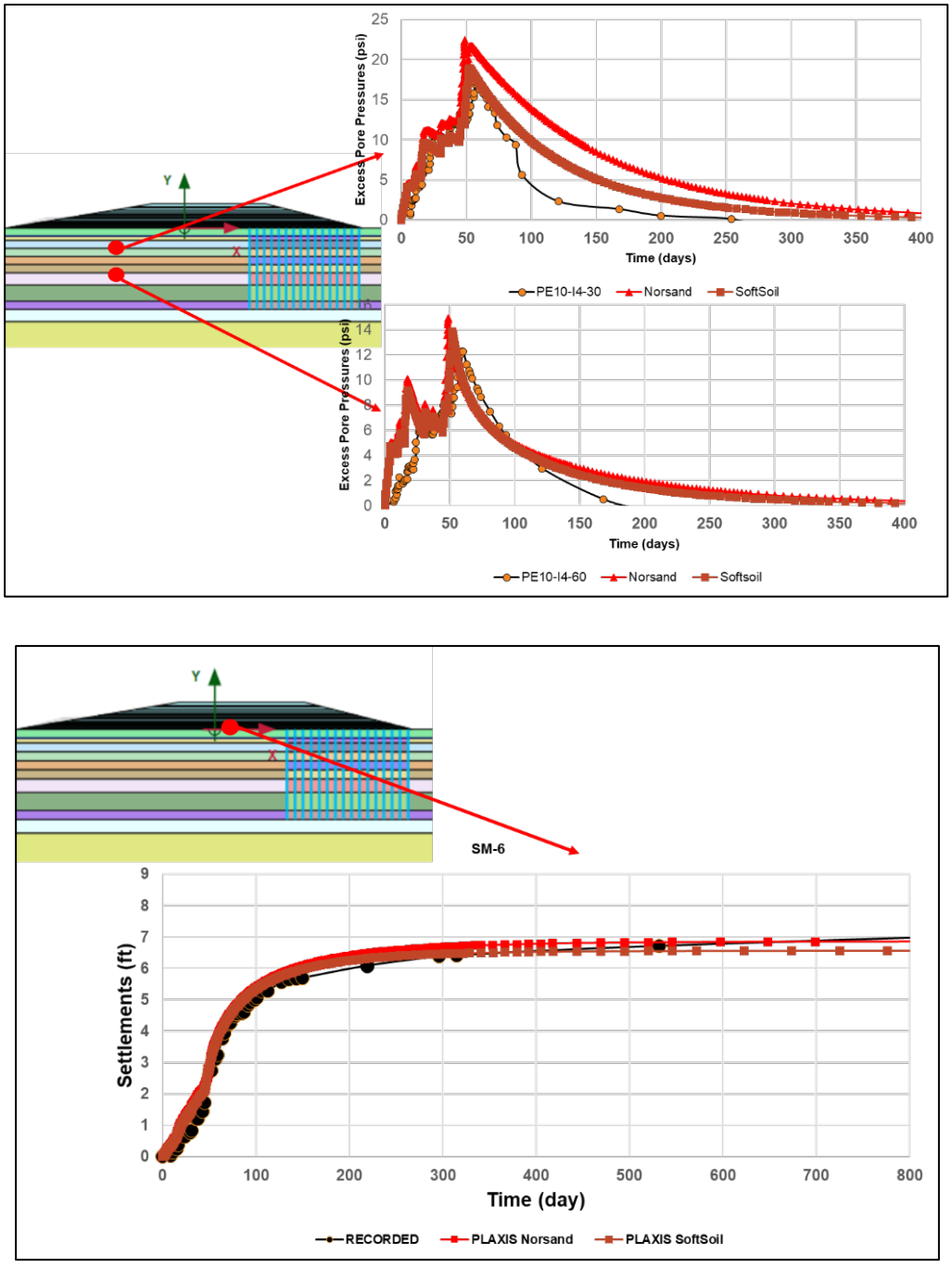


Figure 17: Comparison between recorded response and the 2D FEM model using NorSand and soft soil constitutive models (a) Excess PWP; (b) settlement

3D Finite Element NorSand analysis

As shown in Figure 18, a simplified preliminary 3D FEM model using NorSand was generated using the 3D formulation in PLAXIS 3D. It consisted of a 3D staged construction sequence, using a fully coupled consolidation scheme, and was established to mimic the approximate construction sequence. This 3D is compatible with the 2D simulations in terms of construction sequence, initial state parameter and PWP conditions, constitutive model parameters, and flow parameters (with the addition of a third-dimension component), although simplifications were made regarding distinguishing stages from loading/dissipation, along with the simplification of not including wick drains for the preliminary 3D analyses shown in this paper.

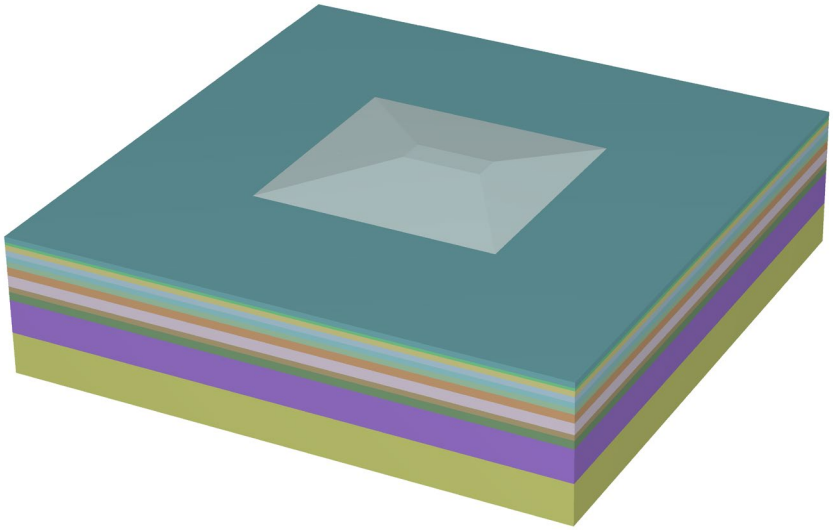


Figure 18: 2010 Trial embankment 3D FEM model (embankment, soil domain)

Additionally, as shown in Figure 19, similarly to PLAXIS 2D, the PLAXIS 3D model is able to capture reasonably well the recorded settlements beneath the trial embankment while capturing better the Excess PWP at 60 ft (PE10-I4-60), as shown in Figure 20. PLAXIS 3D dissipates much slower after loading, likely due to the inclusion of the wick drains. The better agreement of PLAXIS 3D with the NorSand model for the Excess PWP time history at depth is related to the stress distribution being different than plane strain conditions, as assumed in the PLAXIS2D model, although PLAXIS 3D shows slower dissipation of Excess PWP, likely due to simplifications made regarding wick drains exclusions. The trial embankment plan dimensions of ~ 450’ × 300’ were then better approximated by the 3D model due to its truly 3D loading nature. As observed in Figure 20, the PLAXIS 3D model shows a much shallower stress distribution with settlements above 1 ft concentrating within the first 120 ft, while PLAXIS 2D suggest a much deeper settlement distribution up to 160 ft for values above 1 ft, likely due to the overprediction of effective stresses at depth.

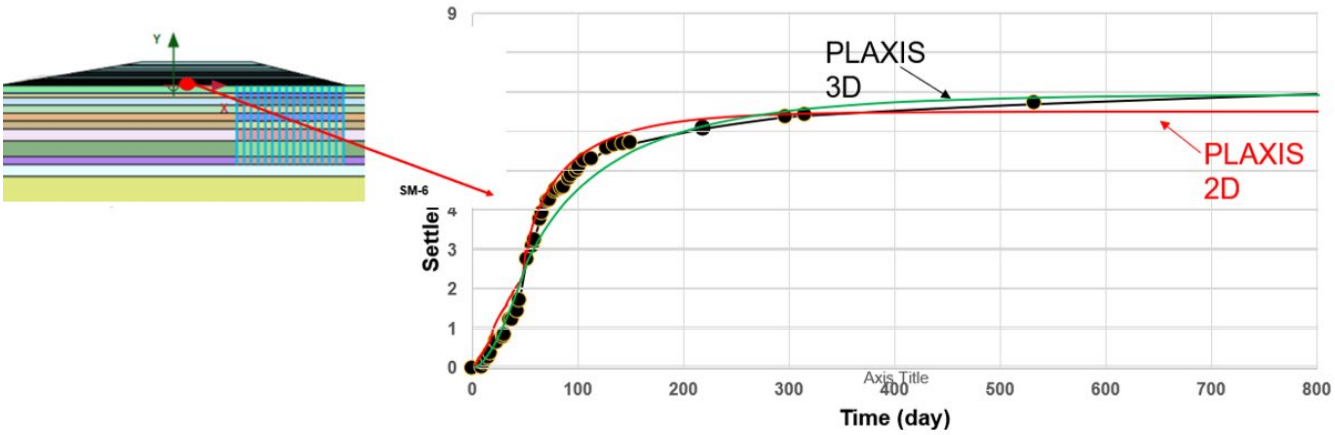


Figure 19: Recorded and computed settlement response from PLAXIS 2D and 3D NorSand models

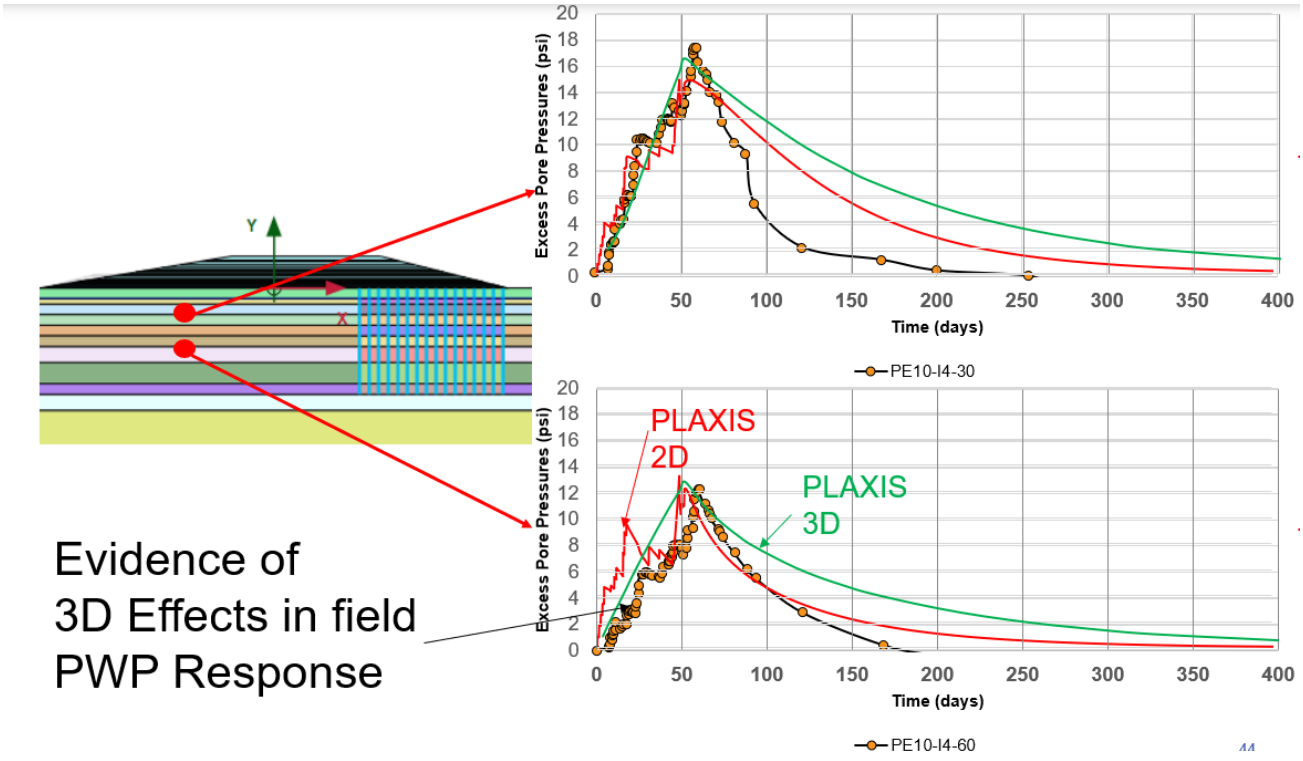


Figure 20: Recorded and computed PWP response from PLAXIS 2D and 3D NorSand models

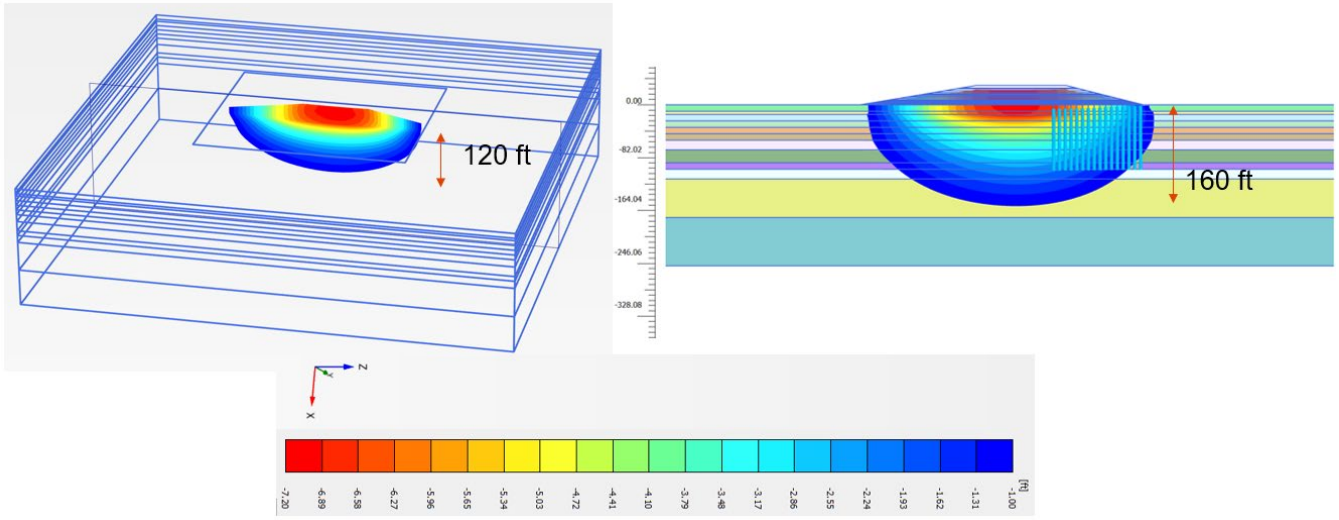


Figure 21: Comparison between computed settlement response from PLAXIS 2D and 3D NorSand models

Summary of 2D and 3D calibrated permeabilities

Figure 22 shows the resultant calibrated vertical permeability (Settle3), and the horizontal and vertical permeabilities from PLAXIS2D and PLAXIS3D that simulated the trial embankment case history. The resultant calibrated permeability distribution between PLAXIS 2D and 3D with depth were found to be compatible in the first 70 ft, while generally the PLAXIS3D model suggesting a half an order of magnitude lower than the vertical permeability derived from PLAXIS2D. The resultant permeability anisotropy values from PLAXIS2D and 3D are consistent with compositional changes that affect the system permeability in interbedded tailings, as suggested by Cerna-Diaz et al. (2024).

The calibrated bounds from PLAXIS3D exhibit better agreement with laboratory Incremental Load (IL) consolidation tests, flexible wall permeability tests performed, and permeability distribution estimates from CPT Ic based correlations (Robertson and Cabal, 2015). This decrease in the calibrated permeability in the vertical direction for PLAXIS3D occurs due to 3D modeling capturing flow in the three directions consistent with realistic flow patterns in the field, while PLAXIS 2D assumes no flow into the page direction and Settle3 assumes only dissipation in the vertical direction.

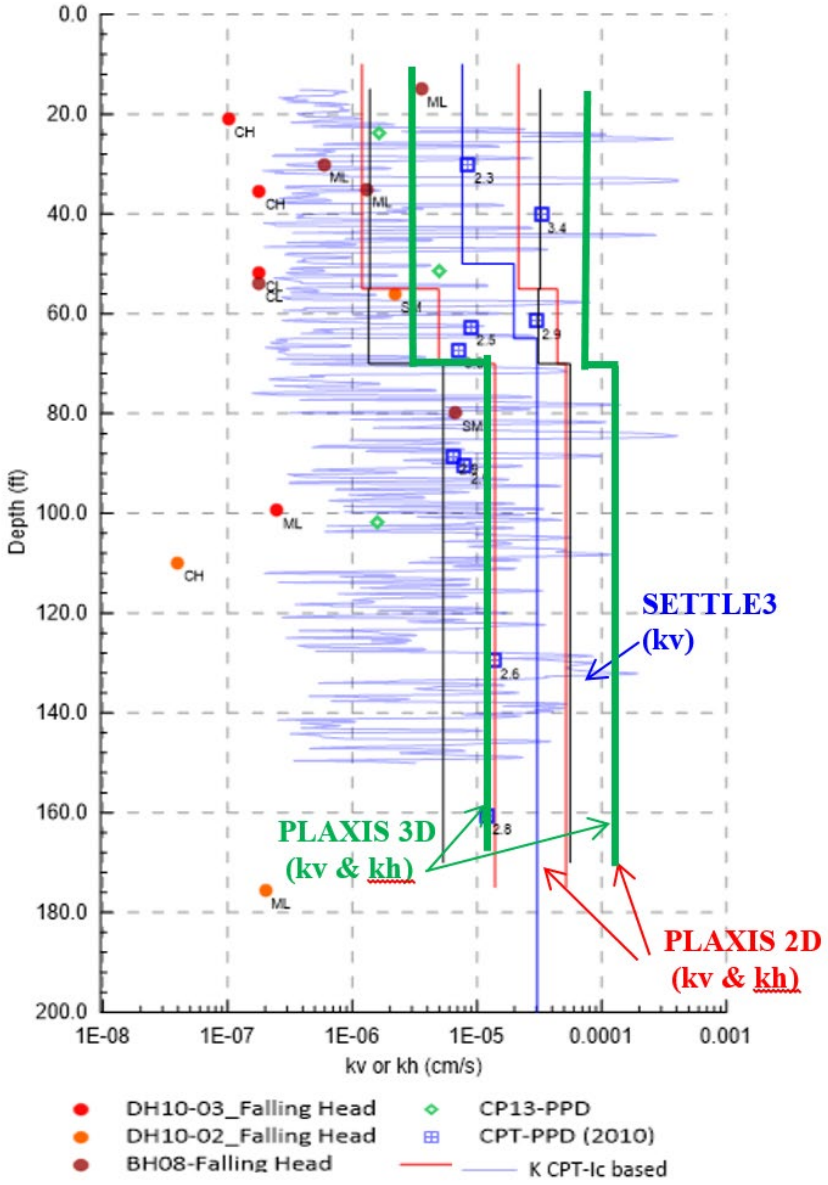


Figure 22: 2010 Trial embankment laboratory, CPT, and calibrated Settle3 (black), PLAXIS 2D (red), and PLAXIS 3D (green) permeabilities (kv and kh)

Conclusion and recommendations

Using a well-documented consolidation of a trial embankment construction over an existing TSF, this paper evaluated the role of 2D and 3D numerical analyses on the back-analyses of settlements and Excess PWP using a simple bilinear FDM consolidation model (Settle3) and a NorSand critical state-based constitutive plasticity model in PLAXIS2D and PLAXIS3D. For all modeling approaches, the results show generally good agreement in the computed settlements among the three modeling techniques used here, while a closer computed PWP response was obtained with NorSand as it captures shear-induced PWP. The NorSand 3D

model was able to best capture the PWP distribution at depth as it captured the dimensionality of trial embankment more realistically. The computed responses also show distinct state parameters, illustrating how drainage conditions can affect consolidation (e.g., consolidation stresses) and shear behavior during the partially drained loading exerted by the trial embankment. In addition, the extracted "system-level" state and permeability that produced computed results in reasonable agreement with the recorded response used an initial-state parameter profile compatible with the 80th percentile, a NorSand G_{ref} between $G_{max}/3$ and $G_{max}/5$, and a combination of permeabilities (kv and kh) consistent with CPT dissipation tests and laboratory testing, and a somewhat improved extracted permeability distribution with 3D FEM analysis using NorSand. Lasty, these analyses highlight the importance of integrating TSF performance monitoring program with large-scale testing to aid recommendations stemming from GISTM performance-based evaluations.

References

Cerna-Diaz, A. Olson, S. Chen, J. and Barham, T. 2024. Role of permeability on undrained instability triggering during copper tailings dam static liquefaction. USSD 2024 Annual Conference – Seattle.

ICMM. 2021. Tailings Management, Good Practice Guidelines. International Council on Mining and Metals, London.

Jefferies, M.G. 1993. NorSand: a simple critical state model for sand. *Géotechnique* 43: 91–103.

Mesri, G. and Godlewski, P.M. 1977. Time and stress compressibility interrelationship. *Journal of Geotechnical and Geoenvironmental Engineering* 103(5): 417–430.

Mesri, G. and Godlewski, P.M. 1979. Closure: Time and stress compressibility interrelationship. *Journal of Geotechnical and Geoenvironmental Engineering* 105(1): 106–113.

Plewes, H.D., Davies, M.P. and Jefferies, M.G. 1992. CPT based screening procedure for evaluating liquefaction susceptibility. *Proceedings of the 45th Canadian Geotechnical Conference* 4: 1–9.

Robertson, P.K. and Cabal, K.L. 2015. *Guide to Cone Penetration Testing for Geotechnical Engineering*. Sixth edition, Signal Hill, CA: Gregg Drilling and Testing.

Shuttle, D.A. and Jefferies, M.G. 2016. Determining silt state from CPTu. *Geotechnical Research* 3(2): 90–118.

Vermeer P.A. and Neher, H.P. 1999. A soft soil model that accounts for creep. In R.B.J. Brinkgreve (ed.), *Beyond 2000 in Computational Geotechnics*. Rotterdam: Balkema, 249–261.

Fabric Effects on the Onset of Static Liquefaction under Drained Conditions – Implications for Mine Tailings

Srinivas Vivek Bokkisa, Georgia Institute of Technology, USA
Jorge Macedo, Georgia Institute of Technology, USA

Abstract

This study investigates the onset of static liquefaction under constant shear drained (CSD) stress paths, considering fabric anisotropy and loading characteristics. The SANISAND-F constitutive model based on the Anisotropic Critical State Theory (ACST) is utilized for the analysis. An analytical criterion is derived to assess the onset of static liquefaction in the CSD stress path, accounting for constitutive parameters, loading-induced anisotropy, and fabric. Numerical results reveal the significant influence of fabric anisotropy on the stress ratio at the point of instability. It is observed that the stress ratio decreases with an increase in Lode angle and major principal stress deviation from the vertical, while increasing with higher initial fabric intensity. These findings are consistent with existing experimental evidence obtained under typical experimental setups. However, we also found that the interaction between Lode angle and loading/fabric directions could potentially alter these trends. The implications of these findings for assessing static liquefaction in mine tailings under generalized loading conditions are discussed.

Introduction

Static liquefaction has led to catastrophic failures in slope systems such as tailings storage facilities (TSFs) and water dams in the past decade (Embankments and Committee, 2021; Jefferies et al., 2019; Morgenstern et al., 2016; Robertson et al., 2019). It is well established that loose particulate materials can experience static liquefaction under undrained shear loading conditions (Ishihara, 1996; Kramer, 1996), but case history failures have shown that it can also be triggered under completely drained loading conditions. Examples include the Wachusett Dam failure in 1907 (Olson, 2000), Fundão in 2015 (Morgenstern et al., 2016), Cadia in 2018 (Jefferies et al., 2019), and the Edenville-Sanford dam failure in 2020 (Embankments, Dams and Slopes Committee, 2021).

Figure 1a illustrates the schematic failure mechanism of the 1907 Wachusett dam failure. Under drained conditions, a rise in the water table caused a significant decrease in effective vertical stresses, while shear stress remained relatively unchanged (Olson, 2000). This stress change can be simulated through a

constant shear drained (CSD) test, as shown in Figure 1b, which involves two stages: initial triaxial loading to reach the desired deviatoric loading (q), followed by releasing the vertical and confining stresses while maintaining a constant q. The response of a loose material in a CSD test, depicted in Figure 1(b, c), exhibits instability characterized by the stress ratio ($\eta = q/p'$) on the instability line. Instability is triggered when the mobilized stress ratio η exceeds the critical stress ratio $\eta_f = \left(\frac{q}{p'}\right)_f$ (Lade, 1992). Later in the paper, we provide more detailed discussions on the conditions for instability triggering and the definition of the instability stress ratio (η_f).

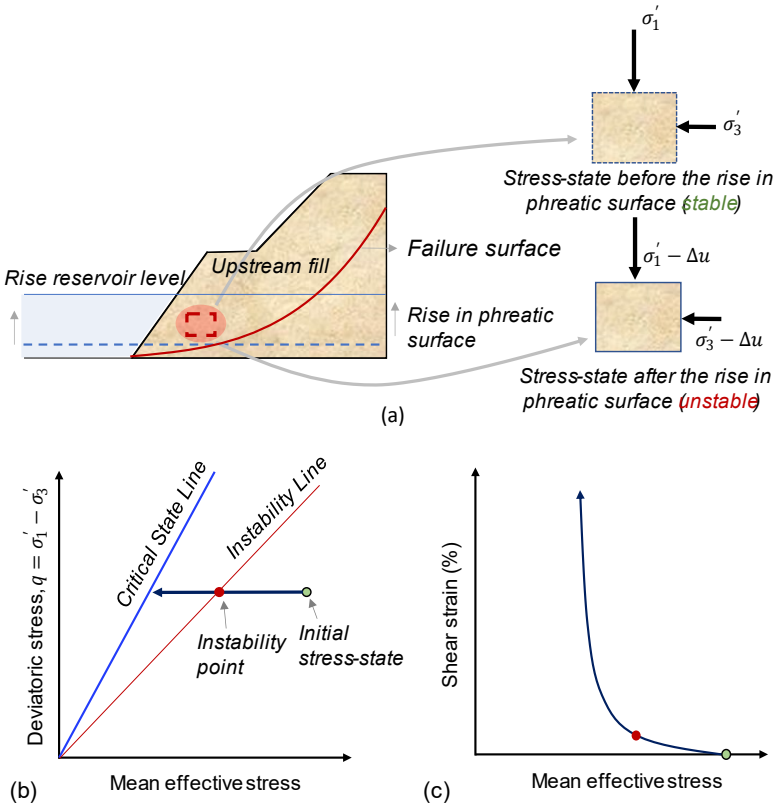


Figure 1: (a) Illustration of the cross-section through the failed portion of the North Dike of Wachusett Dam (b, c) Schematic of the behavior of loose granular material subjected to CSD loading

Prior experimental studies have extensively investigated instability onset under CSD loading, primarily focusing on triaxial conditions and varying densities and stresses (Chu et al., 2003; Dong et al., 2016; Fotovvat et al., 2022; Sasitharan et al., 1993). However, research examining non-triaxial conditions is limited. For instance, Wanatowski et al. (2010) and Wanatowski and Chu (2012) explored sand instability in plane-strain conditions under CSD stress paths, discovering a lower η_f compared to triaxial conditions. Recently, Fanni et al. (2022) conducted experiments using a hollow cylinder setup to investigate the influence of induced and inherent fabric on instability onset under CSD stress path. Their findings indicated

that fabric anisotropy significantly influence η_f, with lower values observed for higher Lode angles and stress orientations further from the vertical. However, the number of loading conditions was limited due to experimental limitations.

Previous numerical studies have examined instability onset under CSD stress paths, primarily focusing on triaxial conditions with different constitutive models (Alipour and Lashkari, 2018; Ramos et al., 2012; Sibille et al., 2007). However, fabric anisotropy effects on CSD stress paths have been rarely explored in these studies. In this context, one of the main contributions of this study is to assess the effect of induced and inherent fabric anisotropic on the instability onset under CSD stress paths comprehensively. Importantly, our simulations also provide insights for scenarios that are difficult to represent experimentally and have not been assessed in previous efforts due to the inherent. Towards this end, we derive an analytical instability criterion for granular materials under CSD loading using ACST and use it to numerically investigate fabric anisotropy's effects on triggering instability. Specifically, we explore the effect of rotation of principal stress direction, intermediate stress ratio, and initial fabric intensity on η_f.

ACST model, instability criteria and performance

The SANISAND-F model

The SANISAND-F model, proposed by Petalas et al. (2020), is an extension of the Dafalias and Manzari (2004) model and is formulated within the ACST framework (Li and Dafalias, 2012). It introduces a fabric tensor $\boldsymbol{F}$ as a state variable to measure the relative orientation between the loading and fabric directions. The model enhances critical state conditions and incorporates a scalar Fabric Anisotropy Variable ($A = \boldsymbol{F}:\boldsymbol{n}'$). The isotropic state parameter ψ (Been and Jefferies, 1985) is further influenced by fabric through the dilatancy state parameter ζ. This new state parameter determines the estimated dilatancy, which varies with fabric anisotropy. For more details, readers are referred to Li and Dafalias (2012) and Petalas et al. (2020).

Instability criteria for CSD stress path

Hill (1958) defined the stability of particulate materials based on positive second-order work, $d^2W = d\,\boldsymbol{\sigma}' d\boldsymbol{\varepsilon} > 0$. Instability occurs when $d^2W = d\,\boldsymbol{\sigma}' d\boldsymbol{\varepsilon} = 0$, where $\boldsymbol{\sigma}'$ and $\boldsymbol{\varepsilon}$ are stress and strain tensors. The instability condition can be expressed as $d\boldsymbol{s}:d\boldsymbol{e} + \frac{1}{3}dp'd\varepsilon_v = 0$, where $\boldsymbol{s}$ is the deviatoric stress, $\boldsymbol{e}$ is the deviatoric strain, p' is the mean effective stress, and ε_v is the volumetric strain. For a constant deviatoric stress ($d\boldsymbol{s} = \boldsymbol{0}$) under a CSD stress path, the instability condition simplifies to $dp'd\varepsilon_v = 0$, yielding two potential instability types: Type 1 ($d\varepsilon_v = 0, dp' \neq 0$) and Type 2 ($dp' = 0, d\varepsilon_v \neq 0$).

Applying constraints for Type-1 instability ($d\varepsilon_v = 0$, $d\boldsymbol{s} = \mathbf{0}$ and $dp' \neq 0$) to the SANISAND-F constitutive equations, the instability criterion $H^1 = K_p - K_{p,f} = 0$ is derived, where K_p is the current plastic modulus and $K_{p,f} = KD\boldsymbol{n}:\boldsymbol{r}$ is the estimated plastic modulus at the instability. K is the bulk modulus, D is the dilatancy, $\boldsymbol{n}$ is loading direction and $\boldsymbol{r}$ is deviatoric stress ratio tensor. Similarly, for Type-2 instability ($dp' = 0$, $d\boldsymbol{s} = \mathbf{0}$ and $d\varepsilon_v \neq 0$), the instability criterion is $H^2 = K_p - K_{p,f} = 0$, where $K_{p,f} = 0$. The instability criteria H^1 and H^2 depend on fabric anisotropy through the dilatancy state parameter ζ and the fabric anisotropic variable A. These dependencies allow for the consideration of fabric anisotropy effects on instability in the CSD loading path. Detailed step-by-step procedures for deriving the instability criteria for each instability type can be found in Bokkisa et al. (2023).

Table 1: Material parameters of the SANISAND-F model

Description	Symbol	Firoozkuh sand	Silica fine sand
Elasticity	G_0	120	120
	v	0.1	0.05
Critical state	e_{ref}	0.923	0.755
	ξ	0.527	0.27
	λ	0.0569	0.032
	M_c	1.24	1.21
	c	0.8	0.66
Plastic modulus	h_1	12	6
	c_h	0.93	0.9
	n^b	2.5	2.2
Yield surface	m	0.01	0.01
Dilatancy	A_0	0.35	1.2
	n^d	7.5	8
Fabric	e_A	0.01	0.06
	F_{in}	0.5	0.7
	c_0	1.0	10
	h_2	1.2	1.1
	$\boldsymbol{n}_F$	$\begin{bmatrix} 2/\sqrt{6} & 0 & 0 \\ 0 & -1/\sqrt{6} & 0 \\ 0 & 0 & -1/\sqrt{6} \end{bmatrix}$	

Performance of SANISAND-F in simulating CSD stress paths

Bokkisa et al. (2023) assessed SANISAND-F's ability to simulate CSD stress paths for Firoozkuh sand and Silica Fine Sand. Table 1 provides the calibrated material parameters for these sands. The satisfactory

performance of SANISAND-F is demonstrated in Figure 2, even when considering complex stress paths with varying levels of anisotropy in loading (α_σ and b) for Silica Fine Sand. For a comprehensive understanding of the calibration procedure and performance of the model under CSD stress paths, readers are advised to refer to Bokkisa et al. (2023).

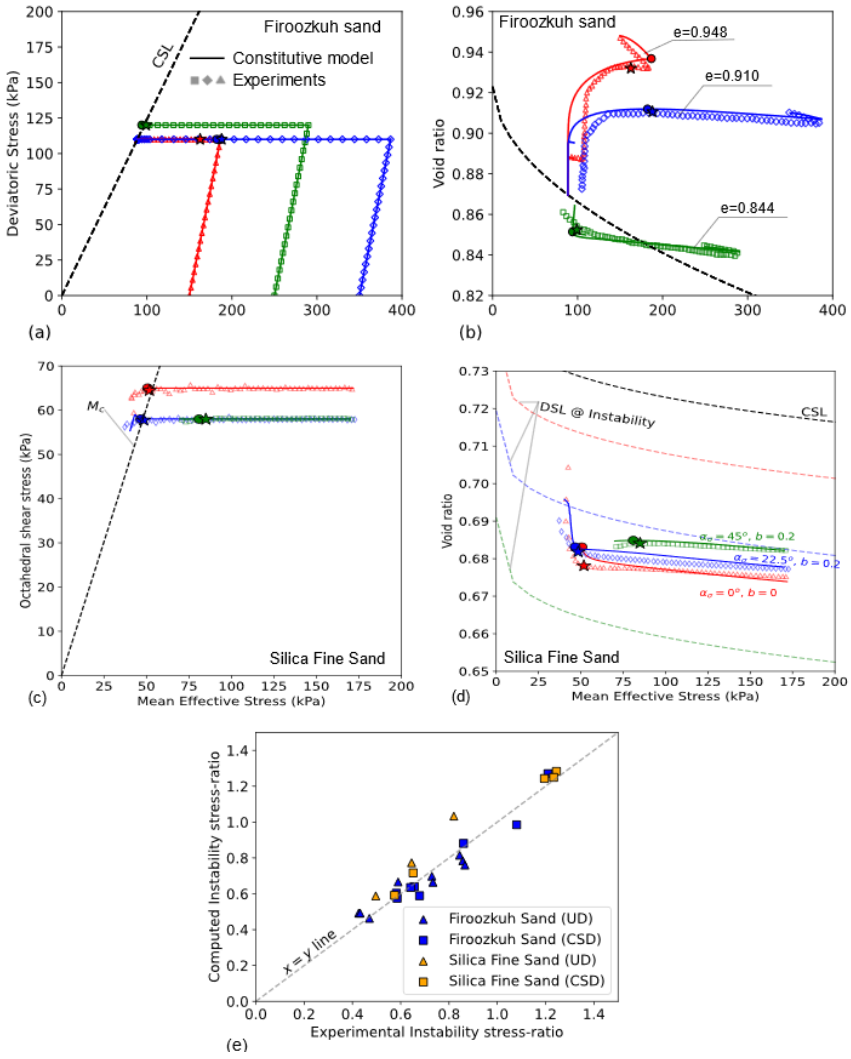


Figure 2: Performance of SANDISAND-F model for CSD stress paths (from Bokkisa et al., 2023)

Fabric effects on the instability onset under CSD stress paths

In this section, numerical simulations are conducted to examine the impact of stress principal axis rotations (α_σ), Lode angle (θ), and initial fabric intensity (F_{in}) on the initiation of instability under a CSD stress path. The stress principal axis rotation (α_σ) represents the constant rotation between the principal stresses and the deposition axis during drained shearing. The simulations are compared against experimental observations where available, with a focus on exploring general trends. The analysis utilizes calibrated

parameters for Firoozkuh sand. The shear stresses and shear strains are expressed in the octahedral form as q_{oct} and γ_{oct}, respectively.

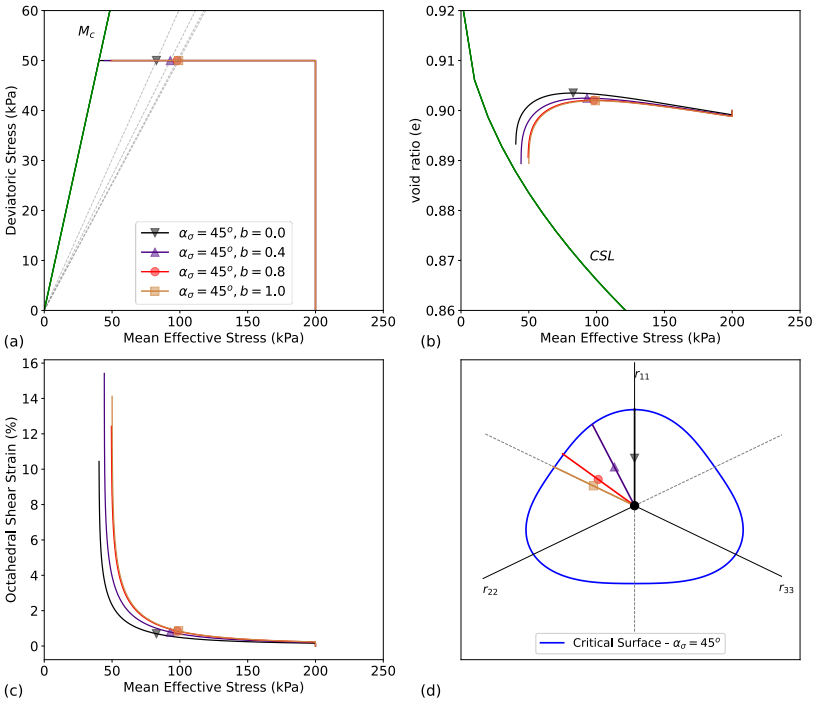


Figure 3: SANISAND-F model responses exploring Lode angle effect on instability

Effect of Lode angle (θ)

Figure 3 shows the simulations of CSD paths considering $\alpha_\sigma = 45^o$, $e_{in} = 0.9$, $p'_{in} = 200$ kPa, a targeted q_{oct} of 50 kPa, and different Lode angles, θ =[$0^o, 23.4^o, 49.1^o, 60^o$] (corresponding to b=[0,0.4,0.8,1.0]). η_f is estimated using the H^1 criterion and highlighted with different markers on each loading path. Figure 3 also shows the M_c line representing the critical state stress ratio for $b = 0$ for reference. Note that, in general, the critical state stress ratio is Lode angle dependent. It can be observed in Figure 3a that as b increases, η_f decreases. Figure 3b shows that instability occurs at the transition between volume increase and decrease responses, consistently with the loose initial state. After the instability onset, the octahedral shear strains also start to increase significantly, as illustrated by Figure 3c. Last, Figure 3d shows the stress paths in the π −plane, where differences in the loading path that cannot be appreciated in the $p' - q$ space are now evident. As b is constant, the stress paths in the π -plane are straight lines. In terms of previous efforts assessing the role of b on η_f under CSD stress paths, we are only aware of the experimental study of Wanatowski et al. (2010), who compared η_f for triaxial paths (i.e., α_σ=0^o, $b = 0$) and plane strain conditions, observing larger η_f in triaxial conditions. Even though b was not estimated by Wanatowski et

al. (2010), previous studies have suggested b varying in the range between 0.25 and 0.5 (Yoshimine et al., 1999) for plane strain conditions. Thus, the experimental observations by Wanatowski et al. (2010) are, in general, consistent with the trends in Figure 3.

To illustrate the assessment of a broader range of b values, we conducted additional simulations considering $\alpha_\sigma = 45^o$ and varying θ from 0^o to 360^o. The η_f estimated at instability for these simulations can be plotted in the π −plane of the principal deviatoric stress-ratio space to construct an instability surface. Figure 4 shows such a surface, where the axes in the π-plane are adjusted to have the distance from the origin to the instability surface also representing η_f in the $p' - q$ space. Figure 4 also highlights the instability points corresponding to $b = [0,0.4,0.8,1.0]$. The interpretation of the instability surface in Figure 4 is that it separates stable from unstable states for any Lode angle; hence, it provides a full assessment of η_f in multiaxial space.

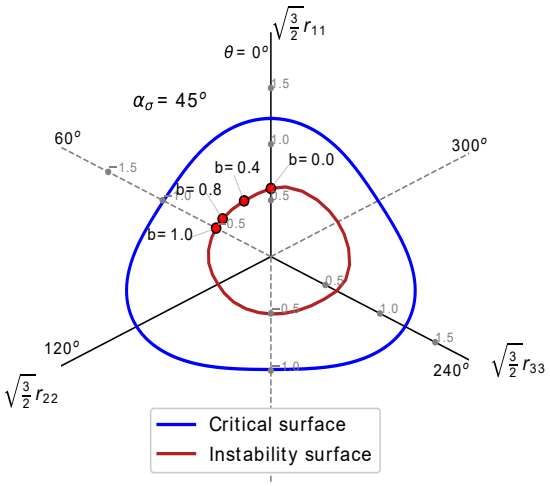


Figure 4: Instability surface obtained for whole range of Lode angels, $0^o - 360^o$

Effect of principal stress axis rotation (α_σ)

Figure 5 shows the simulations of CSD paths considering $\theta = 0^o$ ($b = 0.0$), $e_{in} = 0.9$, $p'_{in} = 200$ kPa, a targeted q_{oct} of 50 kPa, and α_σ =$[0^o, 30^o, 60^o, 90^o]$. The η_f estimated using the H^1 criterion are also highlighted. It can be observed that α_σ significantly affects the instability triggering and η_f. Indeed, η_f decreases as α_σ increases (see Figure 5a). Figure 5b shows that the increase in volume before the instability is less as α_σ increases, and Figure 5c shows that strains increase significantly as the CSD loading progresses after the instability, consistent with previous observations. The difference in the stress paths with respect to α_σ can be better distinguished in Figure 5d where the stress paths are plotted in the global deviatoric stress-ratio space, i.e., $r_z - r_r - r_\theta$ and viewed along the r_r axis. It can be observed that as the α_σ increases, the stress paths rotate more with respect to the vertical (i.e., r_z axis). In terms of previous

studies exploring the effects of α_σ under CSD loading, we are only aware of the experimental study by Fanni et al. (2022), who considered α_σ values of 22.5^o and 45^o. The aforementioned trends are consistent with the observations by Fanni et al. (2022) (i.e., η_f decreases as α_σ increases).

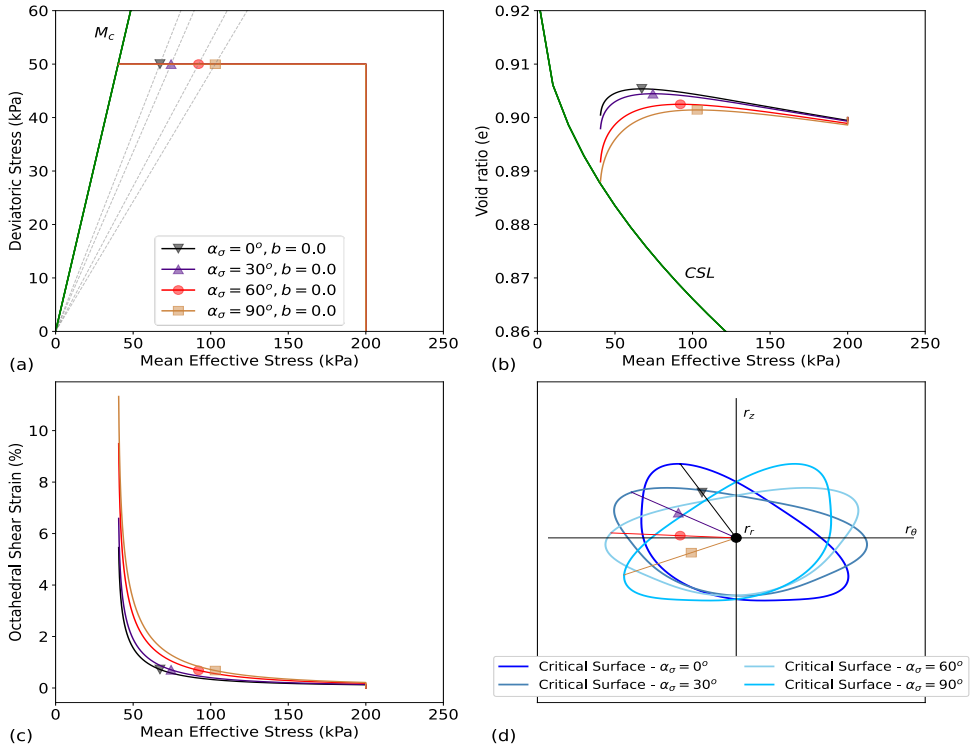


Figure 5: SANISAND-F model responses exploring effect of α_σ on instability

Figure 6 shows the instability surfaces for different α_σ values, considering the full range of θ values. It is interesting to see how the shapes of instability surfaces change as $\alpha_\sigma$varies, affecting interactions with different Lode angles. For example, for low Lode angles, i.e., $\theta = 0^o$ to 60^o, η_f decreases as α_σ increases; however, this trend is reversed for large Lode angles, i.e., $\theta = 120^o$ to 240^o. These trends are associated with the coupling between the Lode angle, α_σ, and the initial fabric direction (represented by the fabric tensor in Table 1). The trend of η_f decreasing as α_σ increases has been observed experimentally for Lode angles and initial fabric directions that are expected to be consistent with those in our simulations (i.e., the Fanni et al. [2022] study previously discussed). However, experimental studies considering interactions of α_σ, initial fabric, and a wide range of Lode angles, as considered in this study, are unavailable. Future experimental studies should inspect this further.

Effect of initial fabric intensity (F_{in})

In this section, numerical simulations are conducted to examine the influence of initial fabric intensity on instability triggering and η_f under CSD loading. The simulations vary the fabric intensity (F_{in}), while

keeping other parameters constant. Figure 7 illustrates the results for simulations with $\alpha_\sigma = 0°$, $\theta = 0°$, $e_{in} = 0.9$, $p'_{in} = 200$ kPa, a targeted q_{oct} of 50 kPa, and different fabric intensities (F_{in}=[0.01,0.5,1.0]) representing nearly isotropic to highly anisotropic fabrics. As F_{in} increases, the initial volume increase during stress relief under CSD loading becomes more pronounced, resulting in higher η_f values (see Figure 7a and 7b). This behavior is linked to the evolution of the fabric anisotropic variable ($A = FN$), which controls dilatancy. For the considered cross-anisotropic fabric with $b = 0$, where the loading direction aligns with the fabric direction ($N = 1$), A equals F. Larger F_{in} values correspond to greater A, leading to a smaller dilatancy state parameter (ζ) and an intensified dilative response. The evolution of shear strains follows the patterns observed in previous simulations, and the stress paths in the π-plane exhibit vertical upward movements ($\theta = 0°$), with instability points occurring at different distances from the critical surface due to varying initial fabric intensities (see Figure 7d).

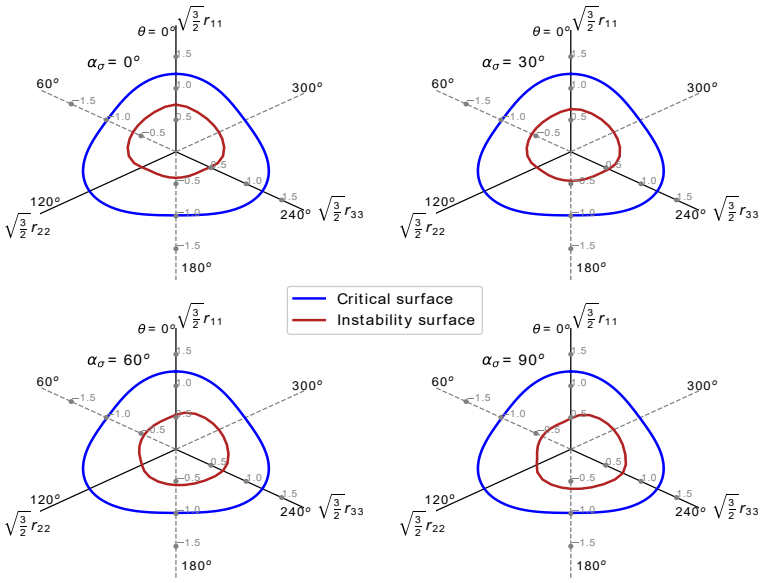


Figure 6: Instability surfaces obtained for various α_σ values

Figure 8 shows instability surfaces estimated for different F_{in}, α_σ of 0^o and 45^o, for the full range of Lode angles. Considering $\alpha_\sigma = 0^o$, it can be observed that for the isotropic fabric ($F_{in} = 0.01$), the instability surface is almost symmetric with respect to the origin. In contrast, the instability surface estimated for the anisotropic fabric ($F_{in} = 1.0$) is not symmetric and particularly distorted for $\theta = 0^o$ and $\theta = 180^o$, where η_f has its maximum and minimum values and also changes more significantly relative to the $F_{in} = 0.01$ instability surface. In the case of $\alpha_\sigma = 45^o$, a significant change in the instability surfaces and η_f relative to the $\alpha_\sigma = 0^o$ cases can be observed. For instance, there is a significant decrease in η_f for cases with a high fabric intensity ($F_{in} = 1.0$) and Lode angles between 0^o and 60^o. Again, these changes

are influenced by the coupling between the Lode angle, α_σ, and the initial fabric direction. As previously discussed, the only study we know of exploring α_σ effects under CSD loading is the Fanni et al. (2022) study, where the authors also considered different reconstitution procedures to represent different fabrics. They observed that dry-pluviated specimens showed a greater reduction in η_f when α_σ is increased for b values in the order of 0.2. Moreover, Yang et al. (2008) highlighted that both dry pluviation and moist tamping produce cross-anisotropic fabrics; however, the fabric anisotropy is higher for dry pluviation. Thus, our results (i.e., Figures 8 and 9) are in qualitative agreement with the experimental observations by Fanni et al. (2022) and Yang et al. (2008).

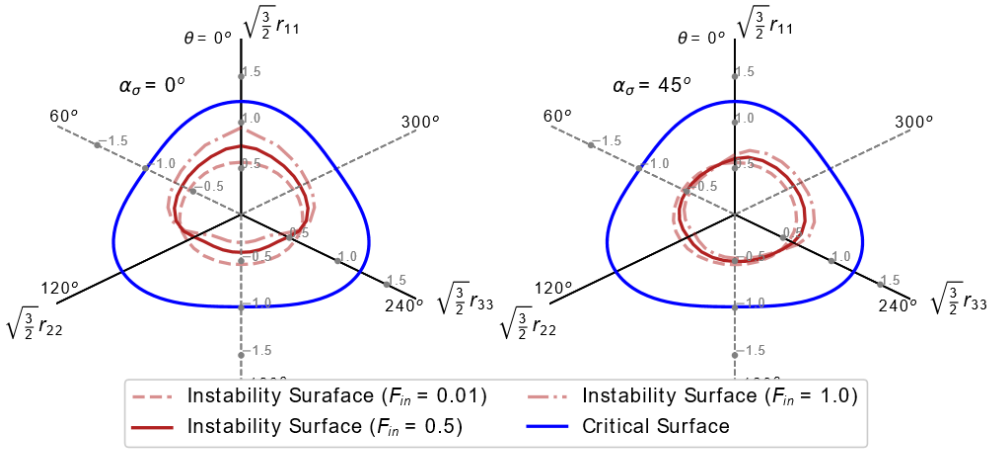


Figure 8: Effect of F_{in} on the instability surfaces obtained for $\alpha_\sigma = 0^o$ and $\alpha_\sigma = 45^o$

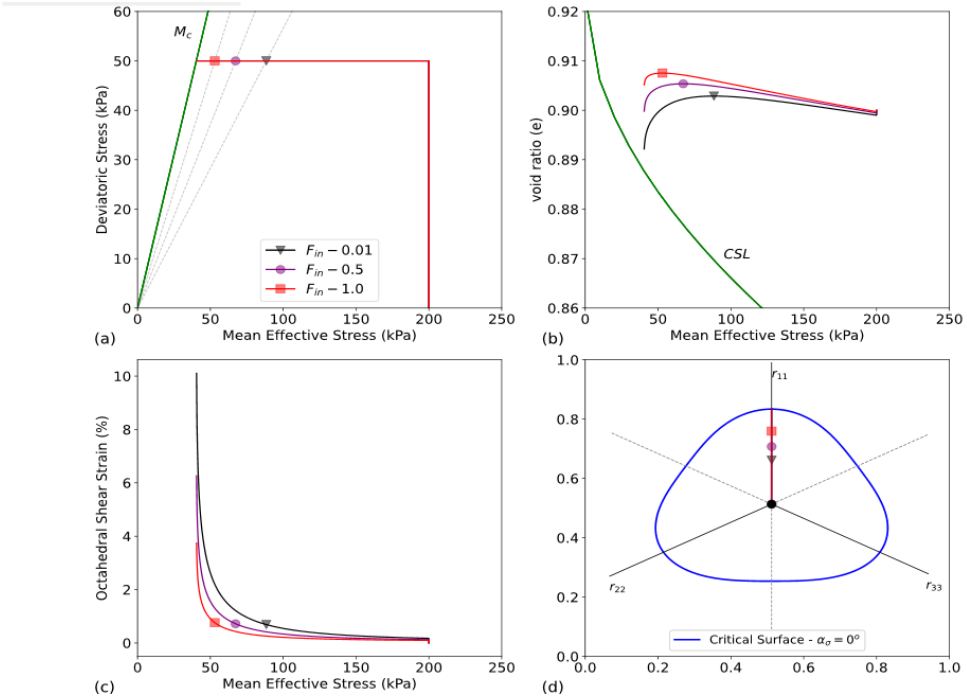


Figure 9: SANISAND-F model responses exploring effect of F_{in} on instability

Implications for mine tailing deposits

Previous sections assessed the effects of inherent and induced fabric on mechanical properties using Firoozkuh sand as an example. However, it is important to note that the constitutive models developed within the ACST framework can be applied to any particulate material, including mine tailings, by accounting for the appropriate mechanical properties (Macedo and Vergaray, 2022). Therefore, the qualitative observations discussed earlier are expected to apply to mine tailings as well. To quantify the responses of mine tailings with fabric anisotropy, it is necessary to have well-calibrated SANISAND-F material parameters for different gradations of mine tailings. In the design or assessment of TSFs, geotechnical engineers typically evaluate the TSF's response to static liquefaction, an important engineering consideration. However, fabric effects, which are expected to be significant, are often overlooked in engineering practice due to their challenging incorporation. Nevertheless, the ACST framework, coupled with well-calibrated models, provides an opportunity to incorporate fabric effects in engineering assessments. Along the slope, various stress states such as triaxial compression, rotated principal stresses, simple shear, and triaxial extension are evident. Considering the findings discussed earlier in this paper, it is anticipated that the inherent fabric of the tailings, combined with different loading paths and initial consolidation states, play a crucial role in triggering the static liquefaction instability. The proposed criteria in this study represent a step forward in incorporating inherent and induced fabric effects once the mechanical properties are quantified.

Conclusion

In this study, we have used the ACST framework to investigate the instability conditions under CSD stress paths, considering the role of fabric anisotropy, multiaxial loading, and state in a comprehensive manner, something that has not been addressed in previous efforts. The performance of the ACST-based SANISAND-F constitutive model under CSD stress paths was found to be satisfactory. Fabric effects were incorporated into defining different instability criteria, resulting in fabric-dependent and loading condition-dependent instability surfaces. The ACST framework with the SANISAND-F model provided valuable insights into assessing the relative effects of fabric (inherent and induced), α_σ, and Lode angle on instability under CSD stress paths. Our numerical findings were consistent with experimental results for conditions representative of the limited experimental information available regarding anisotropic effects. η_f decreased with increasing Lode angle and α_σ within typical experimental ranges.

Additionally, η_f increased with higher initial fabric intensity (F_{in}), and the decrease in η_f with increasing α_σ was more significant for higher F_{in} values, consistent with the experimental study by Fanni et al. (2022). Our findings emphasize the interplay among the Lode angle, α_σ, and F_{in}. In scenarios not

previously examined, the onset of instability can either be promoted or hindered for a given Lode angle and increasing α_σ, depending on the interactions between loading and fabric directions. Further experimental investigations encompassing wider ranges of Lode angle, α_σ, and F_{in} would yield additional insights in this regard.

Acknowledgements

This material is based upon work supported by the National Science Foundation under Grant No. 2013947. Any opinions, findings, and conclusions or recommendations expressed in this material are those of the authors and do not necessarily reflect the views of the National Science Foundation.

References

Alipour, M.J. and Lashkari, A. 2018. Sand instability under constant shear drained stress path. *International Journal of Solids and Structures* 150: 66–82. https://doi.org/10.1016/j.ijsolstr.2018.06.003

Been, K. and Jefferies, M.G. 1985. A state parameter for sands. *Géotechnique* 35(2): 99–112.

Bokkisa, S.V., Macedo, J. and Petalas, A.L. 2023. Fabric anisotropy effects on static liquefaction under constant shear drained loading. *Computers and Geotechnics* 163: 105724.

Chu, J., Leroueil, S. and Leong, W.K. 2003. Unstable behaviour of sand and its implication for slope instability. *Canadian Geotechnical Journal* 40(5): 873–885.

Dafalias, Y.F. and Manzari, M.T. 2004. Simple plasticity sand model accounting for fabric change effects. *Journal of Engineering Mechanics* 130(6): 622–634.

Dong, Q., Xu, C., Cai, Y., Juang, H., Wang, J., Yang, Z. and Gu, C. 2016. Drained instability in loose granular material. *International Journal of Geomechanics* 16(2). Accessed at https://doi.org/10.1061/(asce)gm.1943-5622.0000524

Embankments, Dams and Slopes Committee of the Geo-Institute of ASCE. 2021. *Edenville and Sanford Dam Failures: Field Reconnaissance Report*.

Fanni, R., Reid, D. and Fourie, A. 2022. Effect of principal stress direction on the instability of sand under the constant shear drained stress path. *Géotechnique* 74(9): 875–891.

Fotovvat, A., Sadrekarimi, A. and Etezad, M. 2022. Instability of gold mine tailings subjected to undrained and drained unloading stress paths. *Géotechnique* 74(2):174–192.

Ishihara, K. 1996. *Soil Behaviour in Earthquake Geotechnics*. Clarendon Press.

Jefferies, M., Morgenstern, N.R., van Zyl, D. and Wates, J. 2019. *Report on NTSF embankment failure, Cadia valley operations for Ashurst Australia*. Newcrest Mining Ltd.

Kramer, S.L. 1996. *Geotechnical Earthquake Engineering*. Pearson Education India.

Lade, P.V. 1992. Static instability and liquefaction of loose fine sandy slopes. *Journal of Geotechnical Engineering* 118(1): 51–71.

Li, X.S. and Dafalias, Y.F. 2012. Anisotropic critical state theory: role of fabric. *Journal of Engineering Mechanics*, 138(3): 263–275. https://doi.org/10.1061/(asce)em.1943–7889.0000324

Macedo, J. and Vergaray, L. 2022. Properties of mine tailings for static liquefaction assessment. *Canadian Geotechnical Journal* 59(5): 667–687.

Morgenstern, N.R., Vick, S.G., Viotti, C.B. and Watts, B.D. 2016. Report on the immediate causes of the failure of the Fundão Dam. Fundão Tailings Dam Review Panel.

Olson, S.M., Stark, T.D., Walton, W.H. and Castro, G. 2000. 1907 Static liquefaction flow failure on the North Dike of Wachusett dam. *Journal of Geotechnical and Geoenvironmental Engineering* 126(12): 1184–1193.

Petalas, A.L., Dafalias, Y.F. and Papadimitriou, A.G. 2020. SANISAND-F: Sand constitutive model with evolving fabric anisotropy. *International Journal of Solids and Structures* 188–189: 12–31. https://doi.org/10.1016/j.ijsolstr.2019.09.005

Ramos, A.M., Andrade, J.E. and Lizcano, A. 2012. Modelling diffuse instabilities in sands under drained conditions. *Géotechnique* 62(6): 471–478. https://doi.org/10.1680/geot.10.P.109

Robertson, P.K., de Melo, L., Williams, D.J. and Wilson, G.W. 2019. *Report of the Expert Panel on the Technical Causes of the Failure of Feijão Dam I.*

Sasitharan, S., Robertson, P.K., Sego, D.C. and Morgenstern, N.R. 1993. Collapse behavior of sand. *Canadian Geotechnical Journal* 30(4): 569–577. https://doi.org/10.1139/t93-049

Sibille, L., Nicot, F., Donze, F.V and Darve, F. 2007. Material instability in granular assemblies from fundamentally different models. *International Journal for Numerical and Analytical Methods in Geomechanics* 31(3): 457–481.

Wanatowski, D. and Chu, J. 2012. Factors affecting pre-failure instability of sand under plane-strain conditions. *Géotechnique* 62(2): 121–135.

Wanatowski, D., Chu, J. and Loke, W.L. 2010. Drained instability of sand in plane strain. *Canadian Geotechnical Journal* 47(4): 400–412.

Yang, Z.X., Li, X.S. and Yang, J. 2008. Quantifying and modelling fabric anisotropy of granular soils. *Géotechnique* 58(4): 237–248.

Yoshimine, M., Özay, R., Sezen, A. and Ansal, A. 1999. Undrained plane strain shear tests on saturated sand using a hollow cylinder torsional shear apparatus. *Soils and Foundations* 39(2): 131–136.

Numerical Modeling Evaluation of Consolidation Behavior of Saturated/Unsaturated Fluid Fine Tailings Consolidated Using the Applied Suction Method

Bereket Fisseha, Tetra Tech Canada, Canada
G. Ward Wilson, University of Alberta, Canada
Delwyn G. Fredlund, University of Alberta, Canada

Abstract

This paper explores the consolidation behavior of treated fluid fine tailings (FFT) using an applied suction method, incorporating both experimental studies and numerical modeling to enhance dewaterability and management of mine tailings. The study utilized a meso-scale column apparatus to apply negative pore-water pressure, simulating field conditions that impact FFT consolidation, including environmental effects like evaporation and desiccation in arid and semi-arid climates.

Key experimental findings demonstrated that varying atmospheric fluxes significantly influence the drying and consolidation rates of FFT, affecting the soil's transition from fully saturated to partially saturated states. Numerical models, specifically the SVFLUX-SVSOLID and UNSATCON modules, were employed to validate these experimental results and further refine our understanding of FFT behavior under applied suction conditions. The models adjusted for soil properties based on empirical data from laboratory tests, providing insights into the dynamics of self-weight and suction-induced consolidation.

Overall, the integrated approach of experimental validation and numerical modeling presented in this study offers potential strategies for improving the handling and reclamation of tailings, particularly in challenging environmental conditions. Future work will focus on refining these models to enhance their predictive capabilities and practical application in tailings management.

Introduction

The global mining industry faces significant challenges in managing the waste generated by mining activities, particularly tailings, a by-product of mining and mineral processing. Tailings consist of sand, fines (silt and clay-sized materials), and, in the case of oil sand operations, bitumen. These tailings are characterized by slow settling rates and low hydraulic conductivity due to their fines-dominated composition. The high fines content is further amplified during extraction processes by additives such as

dispersing agents (Beier et al., 2009). Upon deposition, tailings segregate, with coarser particles forming beaches and dykes, while the finer particles are stored in ponds. In oil sand operations, these fine particles in ponds are referred to as fluid fine tailings (FFT). The sedimentation process in these ponds, which is influenced by the composition of fine particles, typically results in the solids content reaching 30–35% within two to three years. However, these deposits are slow to consolidate, and once sedimentation ends, the process of self-weight compression determines the final solids content. Mine operators generally use containment structures to store FFTs, which create a large surface footprint and pose ongoing engineering challenges for reclamation.

Several operators are conducting research to improve the dewaterability of tailings and enhance their post-deposition trafficability. Techniques being explored include composite tailings, conventional thickening, centrifugation, inline flocculation and thickening, as well as various combinations of these methods. Additionally, thin-lift deposition and rim-ditching are under consideration. These initiatives focus on increasing tailings dewatering through desiccation via evaporation, drainage, or freeze-thaw and consolidation (Morgenstern and Scott, 1995).

It is well established that geotechnical engineering challenges, such as high-volume change deposits (consolidation), stability of earth-fill structures, and reclamation of tailings impoundments, are best analyzed using the fundamental principles of saturated and unsaturated soil mechanics. For instance, unsaturated flow behavior has been employed to predict the dewaterability of thin or multilayer tailings deposits, including high-density hard rock tailings, as well as to model evaporation and drainage processes (Fisseha et al., 2010; Simms et al., 2007; Simms et al., 2010; Sulfate et al., 2010).

An experimental study on the consolidation behavior of fluid fine tailings (FFT) was conducted using a meso-scale column apparatus, applying negative pore-water pressure (suction) techniques (Fisseha et al., 2017b). This study highlighted the critical role of negative pore-water pressure, an unsaturated soil principle, in the consolidation, drying, and desiccation of deposited tailings, particularly in arid and semi-arid environments with high atmospheric fluxes (Fisseha, 2020).

This paper presents a consolidation model exercise aimed at calibrating experimental results on self-weight consolidation and the applied suction method for treated FFT. The numerical analysis will enhance the understanding of tailings consolidation properties, including self-weight consolidation and suction effects due to evaporation.

Background

This section briefly reviews the objectives of the experimental study, focusing particularly on the need for the consolidation process using applied negative pore-water pressure (suction technique) and its interactions with the saturated, transition, and unsaturated zones.

The study aimed to consolidate soft tailings using the suction technique to better understand and characterize these tailings in relation to saturated and unsaturated zones. This was performed under controlled stress conditions in a laboratory setting using a column apparatus. The fundamentals and advantages of this method are detailed in Fisseha et al. (2017b) and Fisseha (2020).

In the field, desaturation, drying, and desiccation processes occur at the surface of fully saturated tailings due to atmospheric conditions, including evaporation and evapotranspiration. These processes lead to the formation of a transition or interlayer zone, influenced by changes in the water table within the soil profile from rainfall and evaporation cycles.

Figure 1 illustrates a generic transition or interlayer zone between unsaturated and saturated conditions. In the experiment, fully saturated tailings were placed in the column, and water was periodically withdrawn using an incremental applied suction method from the bottom boundary. This apparatus allowed for the investigation and characterization of the transition zone under controlled conditions, simulating field conditions of drying and desiccation. The experiments demonstrated similar development of the transition zone to what was observed in conceptual field trials, although the direction of flux differed. Consolidation and desiccation processes progressed in the column and field, regardless of the direction of flux – whether from applied suction at the bottom or from evaporation and rainfall at the surface.

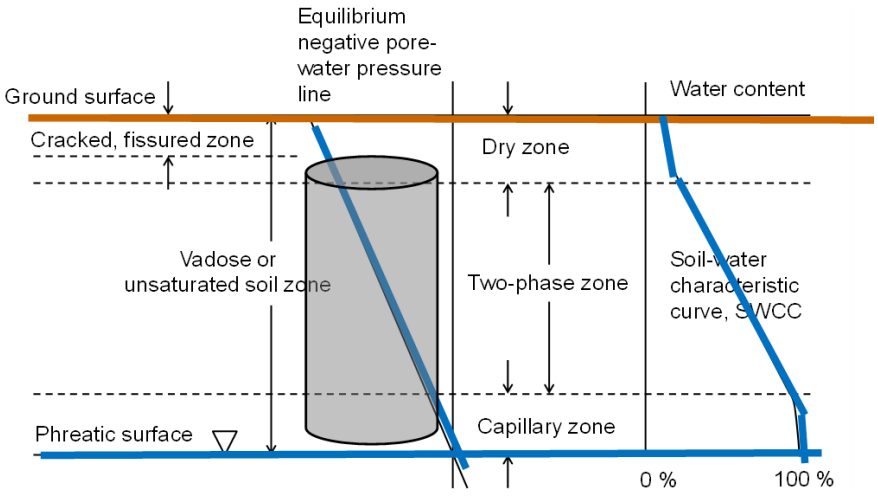


Figure 1: Column used to characterize the consolidation of tailings using applied suction in relation to conceptual unsaturated zones

Materials and methods

Materials

The study utilized flocculated FFT and flocculated centrifuged tailings cake (FCTC), with FFT prepared at 38% solids content and FCTC at 55%. Geotechnical index properties were tested to establish baseline

characteristics, using an anionic polymer A3338 as the flocculant. The preparation methods align with those reported in previous studies (Mizani et al., 2013; Fisseha, 2020). The FCTC materials were prepared off-site and are not discussed in this paper.

Table 1: Summary of geotechnical index properties of FFT and FCTC

Properties	Flocculated FFT	FCTC
MBI (meq/100 g)	3.75	–
Bitumen Content (%)**	2.57	0.37
D50, D60 (μm)	3.2, 6.3	1.4, 2.4
Specific Gravity, Gs	2.2	2.48
Liquid Limit (%)	42	57
Plastic Limit (%)	30	26
Fines content (< 44 μm) (%)	81	87
Clay size particle (%)	40.5	53
SFR	0.24	0.15

Note: MBI – Methyl blue index; SFR – sand to fine ratio; ** Bitumen content – calculated using total bitumen divided by dry tailings. Major ions in pore fluid were not measured

Testing methods

A number of standard laboratory tests was carried out to characterize and obtain the engineering properties of flocculated FFT and FCTC materials. Detail descriptions of testing procedures for settling test, soil-water characteristic curve (SWCC), shrinkage curve (SC), and large-strain consolidation tests (LSC) to obtain compressibility and hydraulic conductivity curves are presented in Fisseha et al. (2017a) and Fisseha (2020). A brief description of the methodology for consolidation using the applied suction technique (Fisseha et al. 2017b) during the experimental study is presented herein.

Consolidation using applied suction test

LSC testing of flocculated FFT was conducted using a meso-scale column apparatus, constructed from Plexiglas with a PVC base and a high air-entry value ceramic disc. The column had dimensions of 300 mm in diameter and 500 mm in height. This apparatus employed an applied negative water pressure technique to consolidate the materials placed within it.

Initially, flocculated FFT in Column 1 and FCTC in Column 2 underwent self-weight consolidation. This phase was complete when changes in height became infinitesimal. Following this, the accumulated bleed water resulting from settlement was decanted. It is crucial to remove this bleed water before applying negative pore-water pressure at the base of the column, to preserve the natural sedimentation process.

During the settlement/self-weight consolidation phase, the water flow was upward. This direction reversed to downward when negative water pressure was applied at the column's base. After decanting the

bleed water, sufficient time was allowed for the materials to reach equilibrium from the loading and unloading processes. The consolidation using applied negative water pressure was then continued by applying incremental vacuum pressure.

Further details on the new column apparatus can be found in Fisseha et al. (2017b).

Modeling approach

Numerical analyses were conducted to validate the experimental results from this study on the consolidation of FFTs. These analyses primarily focused on the behavior of tailing consolidation coupled with unsaturated flow properties. The literature underscores the significant role of evaporation in dewatering slurry tailings and facilitating tailings management and mine reclamation. It highlights how soil-atmosphere interactions can influence consolidation rates due to notable changes in soil suction. The study builds on these findings by providing detailed insights into how these processes interact under varied conditions, thereby offering potential improvements in tailings management and reclamation strategies.

Literature review

Models such as PLEXIS 2D (formerly known as 1D consolidation from SOILVISION), FSCONSOL, and CONSOL employ large-strain consolidation formulations. Additional models like CONDES, MinTaCo, and UNSATCON specifically integrate unsaturated flow or desiccation processes to account for dynamic soil conditions near tailings surfaces. These models are crucial for understanding the varying degrees of saturation and their impact on tailings behavior, particularly when the soil transitions from fully to partially saturated.

Numerical analysis in the experimental study utilized two stages of modeling to replicate the experimental tests as detailed in Fisseha (2020) and Fisseha et al. (2022). These stages are self-weight consolidation and consolidation using applied suction.

Stage 1: Self-weight consolidation

PLEXIS 2D (formerly known as 1D consolidation from SOILVISION SYSTEMS) was used to model the self-weight consolidation phase of flocculated FFT. This stage involved adjusting material properties based on laboratory results to align model predictions with empirical data, focusing specifically on the self-weight consolidation of FFT, not FCTC.

Model setting

The initial stage of self-weight consolidation analysis was performed using the SVFLUX-SVSOLID (consolidation) GT module from SoilVision®, chosen for its availability and compatibility with our data.

The material properties, alongside initial and boundary conditions for Stage 1, were derived from engineering properties obtained through laboratory testing, and are summarized in Table 2.

Table 2: Summary of geometry, material properties, initial and boundary conditions used during the self-weight consolidation modeling exercise for the flocculated FFT

Geometry				
Description	unit	Base reference (y-axis)	Thickness of material	
Deposited tailings	m	0	0.505	
Material property				
Model type and description	Used functions	Fitting method	Parameters	
SVSOLID	Compressibility function	Weibull function under Elasto-plastic category	*A*	0.585
			B	-0.821
			E	-0.688
			F	-0.269
		Elastic parameters	Poisson's ratio	0.3
			Minimum stress limit (*kPa*)	0.15
SVFLUX	Saturated hydraulic conductivity	Single power function	*C* (*m*/*day*)	1.750E-07
			D	8.71
Initial condition				
Model type and description	Assigned parameters	unit	Type	Value
SVFLUX	Initial head	m	calculated	–
SVSOLID	initial void ratio	–	constant	4.07
Boundary condition				
Model type and description	Boundary regions	Assigned parameters	Y– direction	Value (kPa)
SVSOLID	Top	Displacement	Free	–
	Bottom		Fixed	–
SVFLUX	Top	No boundary condition (No BC)	Excess pore pressure constant	0
	Bottom	No boundary condition (No BC)	Zero flux	–
Stage setting				
Stage name	Description	Duration (days)	Total duration (days)	Increments
1st Stage	initiation	0.1	0.1	1
2nd Stage	construction	99.9	100	1

Key parameters used include:

- Poisson's ratio: assumed within an acceptable range based on standard engineering practices.
- Hydraulic conductivity: adjusted from a measured value of 8.64E-07 m/day to 1.75E-07 m/day. This modification was necessary to align simulation results with the observed total settlement.
- Compressibility curves: modeled using the Weibull function to accurately represent the significant volumetric changes observed in flocculated FFT.

These adjustments ensured the convergence of the model and improved the agreement between the simulated results and the empirical data.

Stage 2: Consolidation using increments of applied suction

Current commercial software generally lacks the capability to model consolidation processes that involve applying increments of suction. UNSATCON, a developmental model, was employed to simulate these conditions and to validate the experimental results from incrementally applied suction. Model parameters were carefully adjusted to reflect observed behaviors, such as changes in hydraulic conductivity and volume compression, ensuring accuracy in the simulations. This streamlined summary focuses on the critical elements and results of the modeling efforts, omitting redundant details and emphasizing the outcomes and adjustments made during the modeling stages.

Model setting

The UNSATCON model was used to validate the measured results during stage 2. As an example, only results for the flocculated FFT were modeled and compared with the measured results. The results displayed the change in suction distribution over time with profile.

Table 3: Summary of fitting parameters for the tailings used during the testing program

Modified State Surface Model (SSM)								
Volume change behavior								
Fitting parameters	a – controls initial e	b – related to average slope of compression line and SWCC	c – curva-ture of compres sion curve	d – curva-ture of SWCC	f – curva-ture of compres sion curve	g – curvature of SWCC	κ	K_s
Flocculated FFT	5.3	0.85	0.06	0.006	1620	1000	0.015	0.0015
Water retention behavior								
Parameters	$C_{drying\ –\ postion\ SWCC}$		$C_{wetting}$	$\lambda_{se\ -dependence\ SWCC\ on\ e}$		$\lambda_{sr\ -\ slope\ SWCC}$	λ_{ss}	
Flocculated FFT	2.5		1.5	0.15		0.4145	0.115	

The required parameters were determined by fitting with the empirical formula described in the UNSATCON model (Qi et al., 2017, 2018). The parameters used from the state surface model (SSM) and the hydraulic conductivity functions are summarized in Table 3 and Table 4, respectively.

Table 4: Summary of parameters obtained using the power and exponential functions for the flocculated FFT

Permeability function parameter	Flocculated FFT	
	Power function	Exponential function
k1	1.0E-11	8E-12
k2	8.7089	3.1541
k3	0.75	0.5

The initial and boundary conditions assigned during the modeling exercise are presented in Table 3 and Table 4, respectively. The initial conditions were the thickness of the deposited tailings, number of depositions, initial void ratio, specific gravity, and duration of time for the model to run.

Table 5 and Table 6 summarize the initial condition and boundary conditions used during the modeling exercise for the flocculated FFT, respectively. The boundary condition given for the first 100 days described self-weight consolidation at the top that includes decantation. The bottom boundary condition describing incrementally applied negative water pressure (suction) was given the following day 100 until the end of the experimental test (i.e., 450 days).

Table 5: Initial conditions used during the modeling exercise

Description	Symbol	Units	Flocculated FFT
Total tailings height	*h*	*m*	0.5
Number of depositions	1	*unitless*	1
Initial void ratio	e	*unitless*	4.01
Specific gravity	G_s	*unitless*	2.22
Total run time	*t*	*days*	450

Table 6: Boundary conditions used during the modeling exercise

Description	Stage 2	Flocculated FFT
Top boundary	No boundary condition	Decantation
Bottom boundary	Consolidation using applied suction	Incremental suction with time

Results

The modeling exercise output with the laboratory measured results for the flocculated FFT. These results are presented in this section. The results are organized under stage 1 (self-weight consolidation) and stage 2 (consolidation using applied suction).

Stage 1: Self-weight consolidation

The output results obtained from the model are presented in this section. Figure 2 presents the final output results showing the final change in height and void ratio distribution for the self-weight consolidation process of the flocculated FFT. A comparison of measured results with modeled outputs is presented in the discussion below.

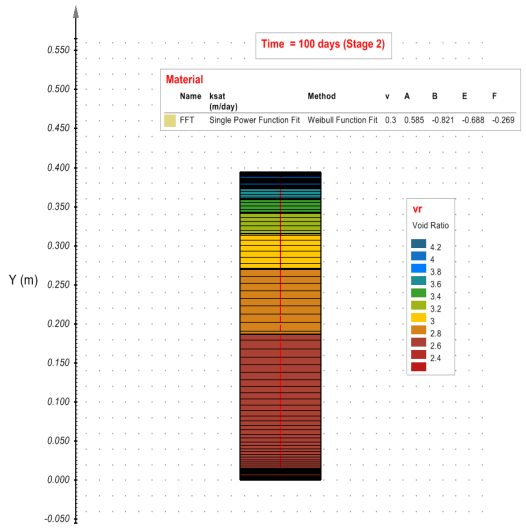


Figure 2: Model output results from SVSOLID coupled SVFLUX

Void ratio

The void ratio distribution within the flocculated FFT profile varies with depth, as expected. The initial void ratio assigned was 4.07 and was uniform for the entire profile. Figure 2 shows an output results

comparison between the model output and average void ratio measured. The modeled output results are presented as "Day 1" and the measured values are presented as "e-avg_Day 1." The output from the self-weight model results shows a smaller void ratio near the bottom of the column with variations along the entire material thickness, as shown in Figure 3.

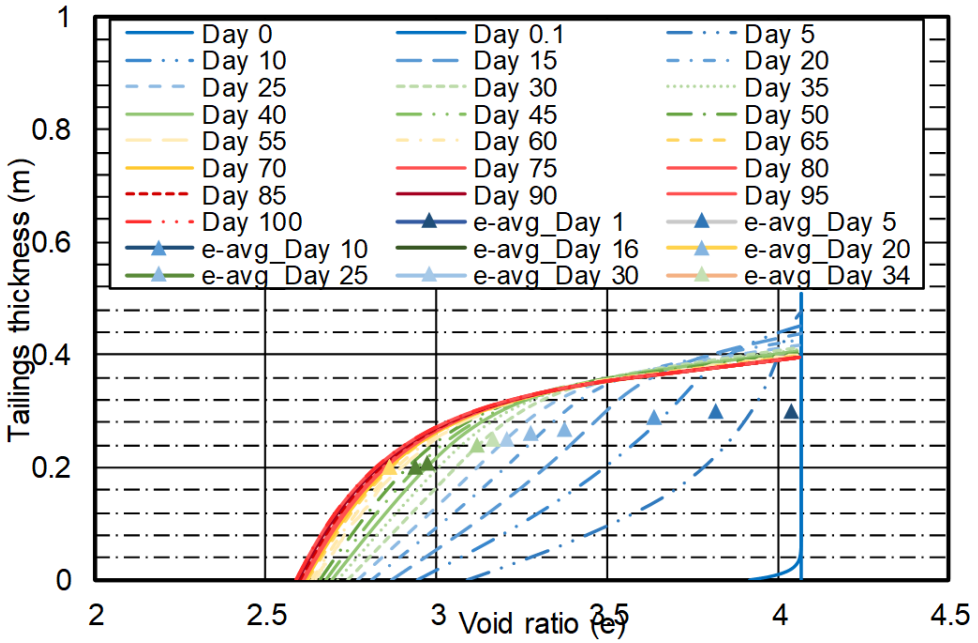


Figure 3: Modeled and measured average void ratio for the FFT during stage 1

For instance, a final void ratio of 2.2 was observed at the column's bottom and 4.07 near the surface at the end of the self-weight consolidation process, as illustrated in Figure 3, which depicts changes in void ratio with depth and time. The model output was assessed against the average void ratio across the entire tailings column, calculated daily and plotted as single data points. The measured and predicted results generally aligned, with discrepancies likely due to averaging the void ratios for the entire column thickness instead of using a more detailed model approach.

Settlement

The modeled settlement results for the flocculated FFT are presented in Figure 4. These results were in reasonable agreement with measured results. The model slightly over-predicted the settlement for the first 30 days and under-predicted the settlement from day 60 until the end of the self-weight consolidation process.

In general, the model output was in agreement with the average measured settlement. It should be noted that the settlement measurements were conducted using three-point measurement and that the averaged methods from the surface since the tailings surface were not flat and smooth.

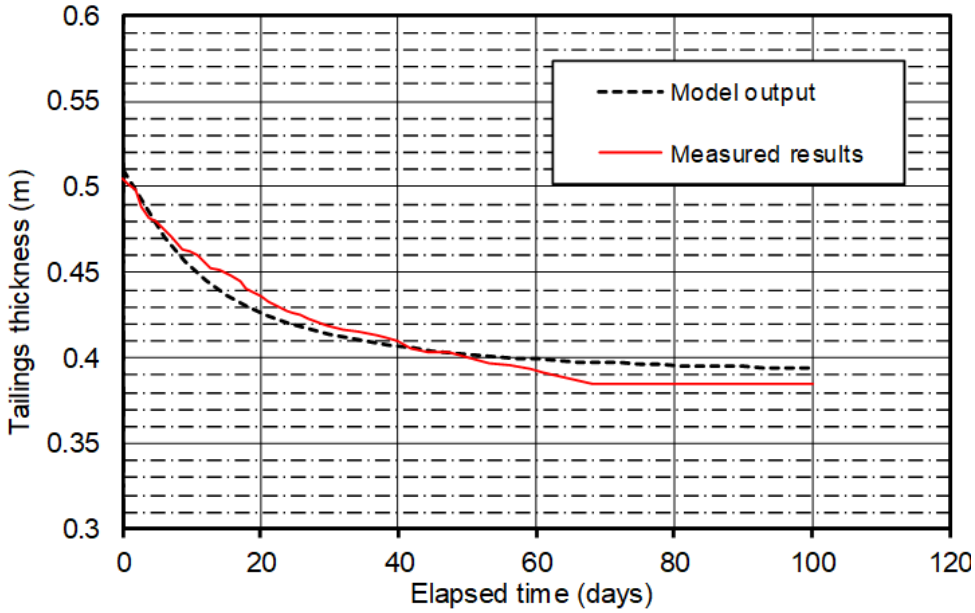


Figure 4: Total vertical settlement for the FFT during Stage 1

Excess pore pressure

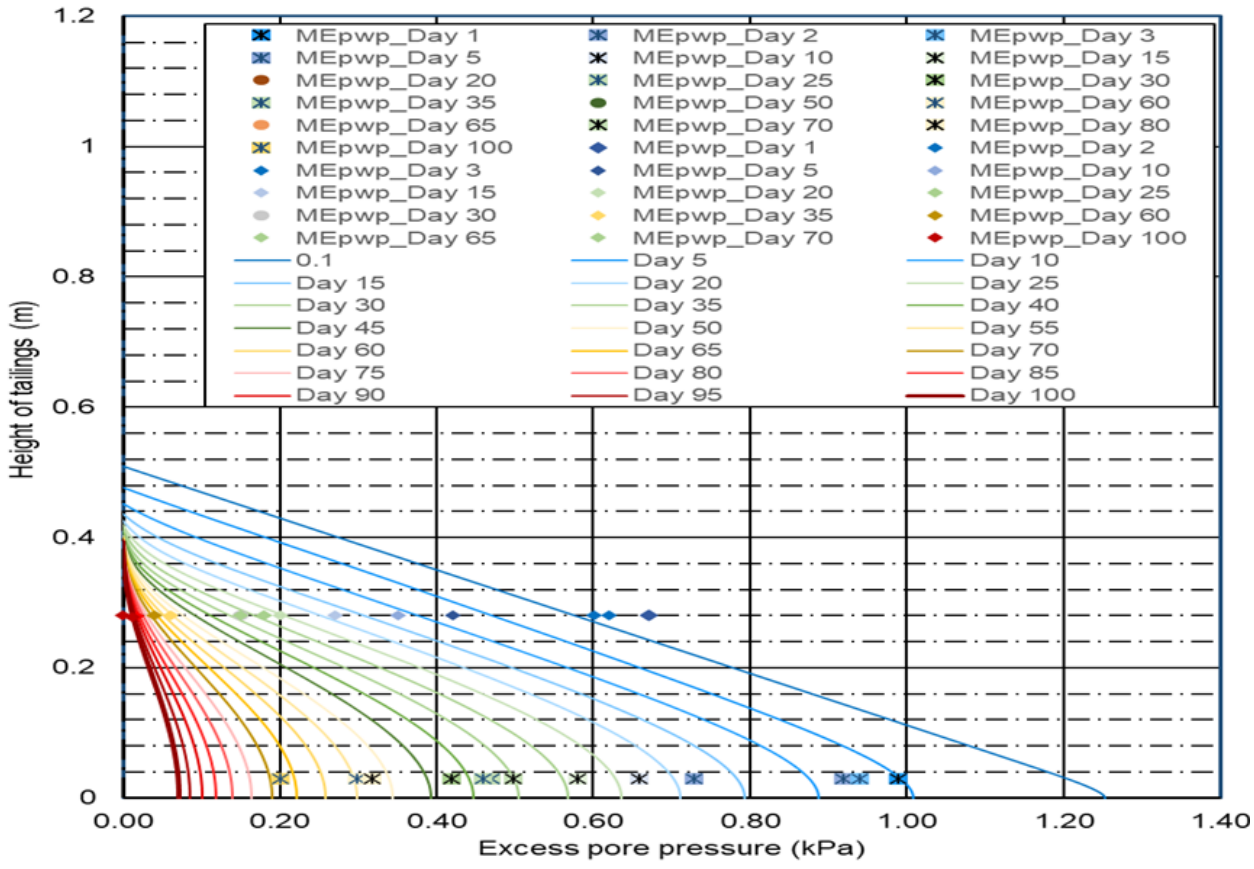


Figure 5: Excess pore pressure dissipation for the flocculated FFT during Stage 1

The results of excess pore pressure dissipation from the model output and measurement are presented in Figure 5. A comparison of the modeled and measured results shows good and reasonable agreement. Pore pressure results are described as "MEpwp_Day 1" for the measured excess pore pressure and "Day 1" for the model output. Possible excitation values were incorporated that can increase the sensitivity values of the sensor. Roughly up to +/- 5% of error can be included due to excitation and other factors.

The measured data points are presented with the same color for the corresponding dissipation time presented by the model. The model and measured results are presented as line and data points in Figure 5 for the corresponding elevation, i.e., sensor located 3 cm and 28 cm above the column base. The same colors are used between measured and modeled excess pore pressure for the same corresponding times. Overall, a good agreement was predicted between the modeled and measured dissipation of excess pore pressure results.

Effective stress

The effective stress results calculated using the model are presented in Figure 6. The model output was compared with the calculated effective stress results using the change in total density calculated.

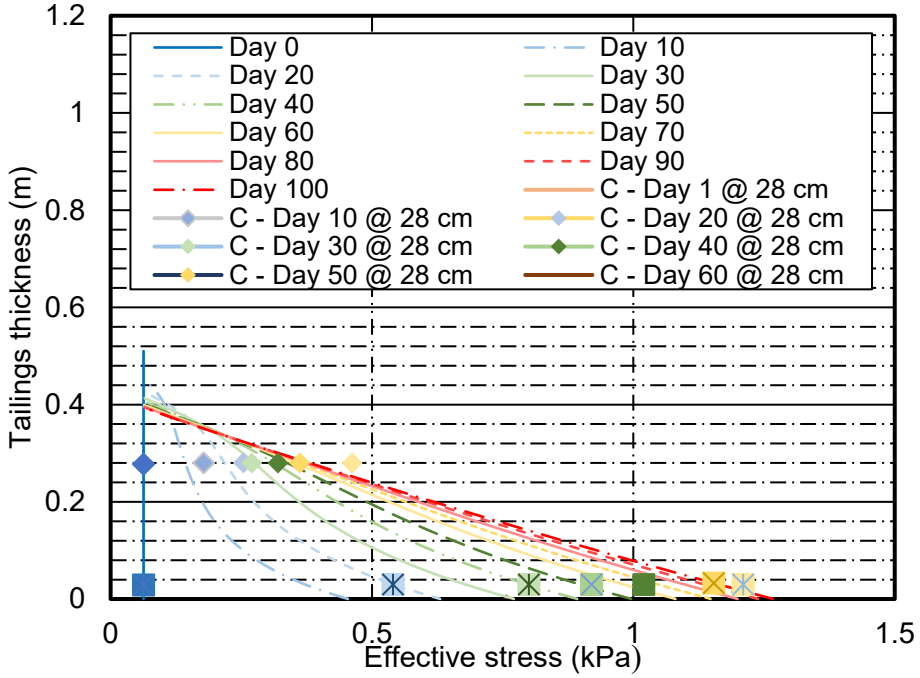


Figure 6: Effective stress computed from model output for the FFT during Stage 1

The calculated effective stress values are presented as individual data points for a given time and described in the legend as "C – Day 10 @ 28 cm" to indicate the calculated, day 10 located at 28 cm from the base of the column. The model results are given as a line in the plot. The calculated effective stress results were higher than the effective stress predicted using the model. For example, the calculated effective

stress was 2.6 kPa near the base of the column by the end of the self-weight consolidation period, in comparison to 1.2 kPa predicted by the model. The calculated effective stress values were reasonable in agreement assuming error values of 0.4 – 1.3 kPa over time.

Stage 2: Consolidation using applied suction modeling

The results from the UNSATCON model were changed in total height, gravimetric water content, solids content, void ratio, and distribution of suction with deposited tailings thickness, and are discussed in the following section.

The model requires additional calibration and refinement to achieve reasonable agreement with the measured results. The scope of this thesis does not include development of the software, refinement, and calibration.

Change in total height

The measured and modeled change in total height (vertical strain) for the applied suction test are presented in Figure 7. The final height was 0.23 m and 0.25 m for the measured and model, respectively. Overall, reasonable and acceptable agreement was obtained between the measured and modeled results.

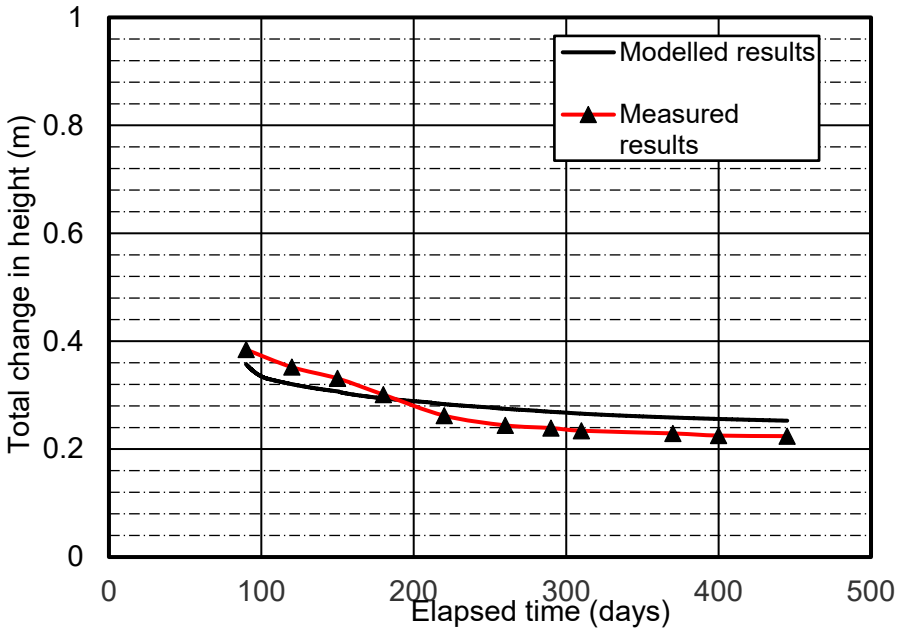


Figure 7: Comparison of measured and modeled vertical strain results

Solids content

The solids content, calculated from the gravimetric water content, averaged 72%. Figure 8 shows an overall acceptable agreement, with unsaturated soil properties slightly underpredicting the results at 68%. Three

months after the mesoscale test, the solids content increased, likely due to evaporation, as no additional suction was applied following completion of the test.

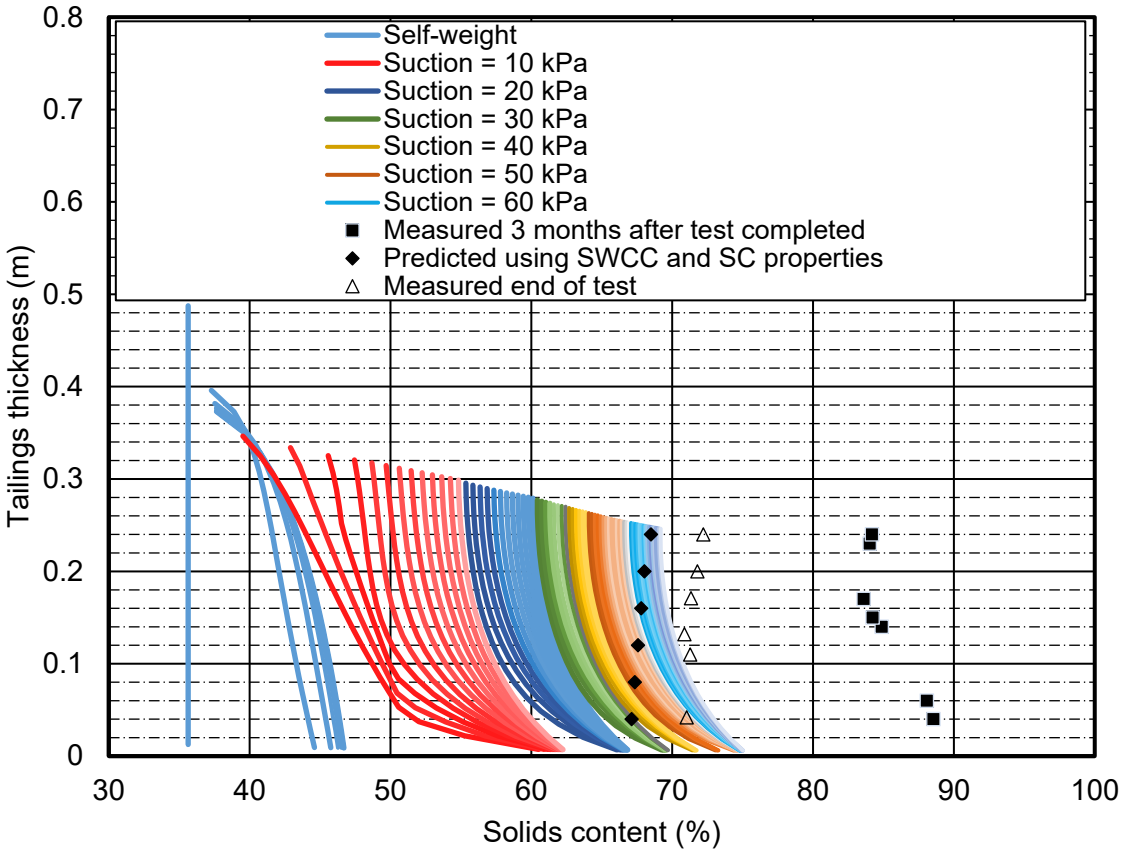


Figure 8: Comparison of measured and modeled solids content results

Void ratio

Figure 9 shows the measured and modeled void ratios, with the measured values accounting for lateral deformation. The average measured void ratio across the tailings thickness is represented by a colored diamond, corresponding to the suction line colors in the figure. Averaging the void ratios affected the values, especially when there was a significant difference between the surface and bottom of the tailings. The final average measured void ratio was 1.07, while the modeled ratio was 1.35. Reasonable agreement was observed at lower suction values, but as suction increased, significant differences emerged between the measured and modeled void ratios. Further model refinement is recommended for further accurate results.

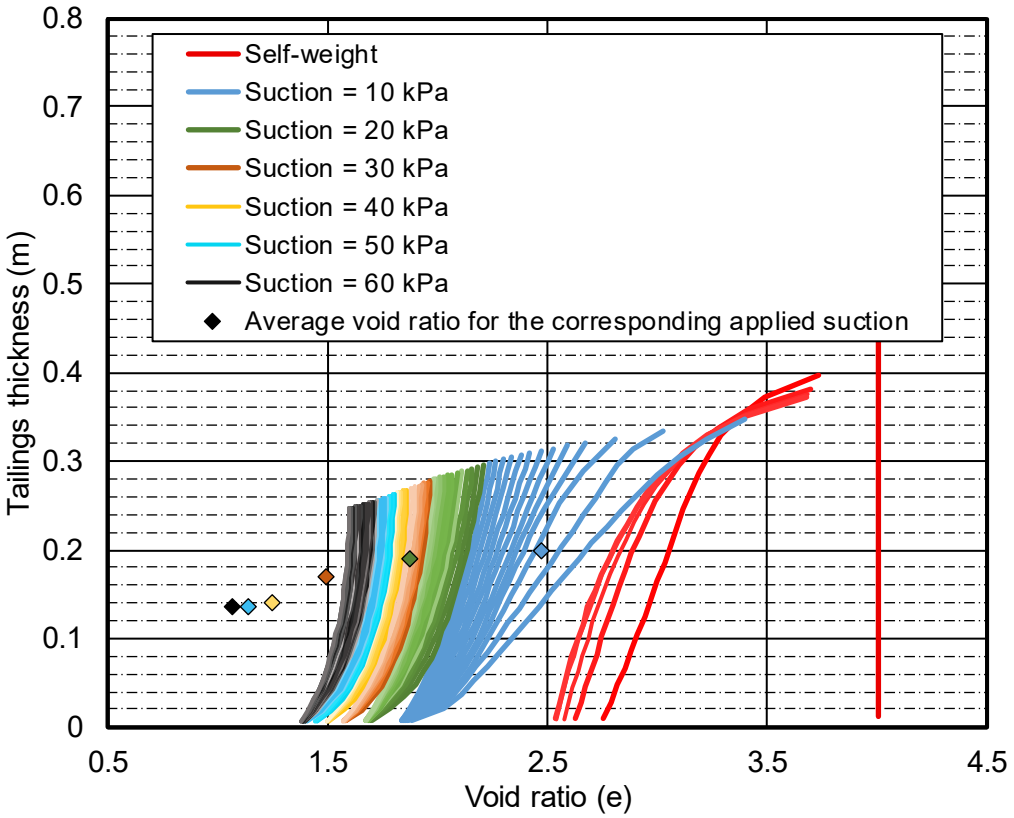


Figure 9: Comparison of measured average void ratio and modeled void ratio results

Conclusion

In conclusion, the SVFLUX_SVSOLID model closely aligns with experimental results for self-weight consolidation, as seen in Figures 2 to 5, covering void ratio, total settlement, excess pore pressure dissipation, and effective stress distribution. The UNSATCON model provided a good match for surface settlement compared to mesoscale testing. While solids content showed reasonable overall agreement, the trends varied with depth between measured and modeled results. However, the suction results showed no agreement between the model and measurements.

The UNSATCON model offers significant capabilities in simulating the consolidation behavior of unsaturated soils, making it a valuable tool in engineering design and analysis. By accurately modeling the complex interactions between soil structure, moisture content, and suction, UNSATCON allows for a more reasonable prediction of settlement and consolidation in unsaturated soils, which are often challenging to assess with traditional methods. This enhanced understanding facilitates more reliable designs, particularly in geotechnical applications where soil behavior under varying moisture conditions is critical, such as subject to various drying and wetting cycle. The model's ability to incorporate unsaturated soil mechanics

into consolidation analysis provides engineers with a more comprehensive framework, ultimately leading to safer and more efficient design solutions in civil engineering projects.

References

Beier, N., Alostaz, M. and Sego, D. 2009. Natural dewatering strategies for oil sands fine tailings. *Proceedings of Tailings and Mine Waste 2009 Conference*, Banff, Alberta, and November 1–4: 845–858.

Fisseha, B., Bryan, R. and Simms, P. 2010. Evaporation, unsaturated flow, and salt accumulation in multilayer deposits of "paste" gold tailings. *Journal of Geotechnical and Geoenvironmental Engineering* 136(12): 1703–1712.

Fisseha, B., Wilson, G.W. and Fredlund, D.G. 2017a. Assessment of large-strain consolidation and shear strength of saturated/unsaturated fluid fine tailings. *Proceedings of 70th Canadian Geotechnical Conference and the 12th Joint CGS/IAH-CNC Groundwater Conference,* Ottawa, Ontario, October 1–4.

Fisseha, B., Wilson, G.W and Fredlund, D.G. 2017b. Large-strain consolidation column with applied negative water pressure. *Pan-Am-UNSAT2017, Proceedings of Second Pan American Conference on Unsaturated Soils*, Dallas, Texas, USA, Nov 12–15.

Fisseha, B. 2020. Experimental study on consolidation behaviour and shear strength gain for saturated/unsaturated treated fluid fine tailings. Ph.D. thesis, Department of Civil and Environmental Engineering, University of Alberta, Edmonton, AB, Canada.

Fisseha, B., Wilson, G.W and Fredlund, D.G. 2022. Assessment of large-strain consolidation and shear strength of saturated/unsaturated fluid fine tailings*. Proceedings of the 26th International Conference on Tailings and Mine Waste*, Denver, Colorado. USA. Nov 6th – 9th, 2022.

Fredlund, D.G., Rahardjo, H. and Fredlund, M.D. 2012. *Unsaturated Soil Mechanics in Engineering Practice*. John Wiley & Sons.

Mizani, S., He, X. and Simms, P. 2013. Application of lubrication theory to modelling stack geometry of high density mine tailings. *Journal of Non-Newtonian Fluid Mechanics* 198: 59–70.

Mizani, S., Simms, P., Dunmola, A., Cote, C. and Freeman, G. 2014. Rheology for surface deposition of polymer amended fine tailings*. Rheologica Acta* 56(2).

Morgenstern, N.R. and Scott, J.D. 1995. Geotechnics of fine tailings management. In *Geoenvironment 2000: Characterization, Containment, Remediation, and Performance in Environmental Geotechnics.* Y.B. Acar and D.E. Daniel (eds). ASCE, New York, NY, USA, Geotechnical Special Publication no. 46: 1663–1683.

Qi, S., Simms, P. and Vanapalli, S. 2017. Piecewise-linear formulation of coupled large-strain consolidation and unsaturated flow. I: model development and implementation*. Journal of Geotechnical and Geoenvironmental Engineering* 143(7). DOI: 10.1061/(ASCE)GT.1943-5606.0001657.

Qi, S., Simms, P. 2018. Analysis of dewatering and desaturation of generic field deposition scenarios for thickened tailings. *Proceedings of the 21st International Seminar on Paste and Thickened Tailings*, Perth, Western Australia. DOI: 10.36487/ACG_rep/1805_33_Simms.

Simms P., Grabinsky M.W. and Zhan, G. 2007. Modelling evaporation of paste tailings at the Bulyanhulu mine. *Canadian Geotechnical Journal* 44(12): 1417–1432.

Simms, P., Dunmola, A., Fisseha, B. and Bryan, R. 2010. Generic modelling of desiccation for cyclic deposition of thickened tailings to maximize density and to minimize oxidation. *Proceedings of the 13th International Conference on Paste and Thickened Tailings,* Toronto, Ontario: 293–301.

Sulfate, E.B., Wilson, W., Wijiewickreme, D. and Simms, P. 2010. Predicting void ratio in surface deposited paste tailings. *Proceedings of Mine Waste 2010,* Perth, Australia: 473–48.

SVFLUX, Software package form SoilVision Systems Ltd. SVFLUX Tutorial Manual.

The Use of Waste Rock in Geotechnical Projects: The Challenge to Achieve the Geotechnical Parameters

Danilo Eloi, Vale S.A., Brazil
Miguel Paganin, Vale S.A., Brazil
Letícia Cedro, Vale S.A., Brazil
Rayssa Silva, Vale S.A., Brazil
Marina Ferreira, Vale S.A., Brazil
Gricor Channakian, Vale S.A., Brazil
Rodney Silva, Vale S.A., Brazil

Abstract

In recent decades, there has been a significant increase in the demand for mineral resources, driving advancements in mining technologies and processes. This has led to the rapid expansion of mining complexes and associated geotechnical structures such as slopes, waste piles, and dams. Consequently, there is a growing need for geotechnical studies, analysis, and projects. In some mining complexes such as the Itabira Mining Complex in Brazil, geotechnical parameters for fragmented waste rock used in projects are often qualitatively inferred or based on relationships proposed in literature, due to limitations in quantitatively defining these parameters from large-scale samplings. This qualitative approach introduces uncertainties in safety factors and geotechnical design criteria confidence.

To address this, the Itabira Mining Complex has developed a method to quantitatively characterize waste rock for more precise use in geotechnical projects. Studies on friable samples have shown more conservative parameters compared to those for rocky samples, serving as an initial step in understanding these materials and evaluating whether parameters derived from literature are suitable references for design studies on waste rock piles. Laboratory testing campaigns, particularly triaxial tests, have been conducted on various lithologies within the Itabira complex to primarily determine strength parameters such as friction angle and cohesion. These tests, supplemented by characterization tests, enhance our understanding of the lithologies and their behavior. The test results presented in this study outline the approach used in the Itabira Mining Complex to quantitatively characterize waste rock for more accurate and informed utilization in geotechnical projects, particularly in waste rock piles and shared tailings and waste rock piles.

Introduction

The Itabira mining complex is situated in the extreme northeast of the Iron Quadrilateral, within the central region of Minas Gerais state, Brazil. It comprises the Conceição, Minas do Meio, Periquito, Dois Córregos, Onça, Camarinha, Chacrinha, and Cauê mines, encircled by their respective geotechnical structures. Open-pit iron ore extraction is a primary economic pursuit in Itabira, a municipality in Minas Gerais state. Established in 1942 in Itabira city, Vale S.A. presently holds the distinction of being one of the world's largest iron ore producers. The Itabira mining complex presently yields approximately 25 million tons of iron ore annually. The cessation of mine operations is projected to happen around 2042.

Nearly 80 years of operational history have engendered vast, deep, open-pit excavations and significantly elevated heaps of waste rock, some of which exceed 300 meters in height. Given its adjacency and constraints relative to urban locales, the ensuing two decades will witness an augmentation in extant geotechnical structures, encompassing waste rock heaps, alongside the initiation of novel structures. Moreover, alterations in long-term mine planning over the years and shifts in the acceptance of geotechnical design criteria necessitate the reinforcement of certain extant waste structures.

In all instances, fragmented rock waste is integrated as an elemental constituent within projects. The term "fragmented" denotes materials subjected to detonation. Principal applications encompass its utilization within drainage systems, safeguarding the slope facets of waste piles constituted of altered material, and, notably, serving as a geotechnical reinforcement material (buttress). Diverse designers and consultants undertake project execution. The variability in quality and geotechnical proficiency of waste rock stems from constraints in quantitatively delineating geotechnical parameters from fragmented waste rock. These parameters are qualitatively inferred or established via relationships posited in literature, leveraging fundamental parameters of friable materials, which have undergone extensive scrutiny.

Regional and local geology

The Iron Quadrilateral is located at the southern extremity of the São Francisco Craton (Almeida, 1977). It is the result of various tectonic and deformational activities involving two major orogeneses: the Trans-Amazonian, which occurred over approximately 2,000 to 2,200 million years and the Brasiliano, which occurred over 650 to 500 million years (Alkmim and Marshak, 1998; Dorr, 1969). These two orogenic events at different times led to the formation of high-grade ores (Rosière et al., 2001; Rosière and Chemale, 2000). The rocks of this formation are divided into three lithologies: the Metamorphic Complex, consisting of gneisses, migmatites, and granitoids; the Rio das Velhas Supergroup, a metavolcanic sedimentary sequence of the greenstone belt type; and the Minas Supergroup, composed of clastic and chemical metasedimentary rocks (Castro et al., 2020; Dorr, 1969). The combination of hypogene and supergene

processes explains the formation of high-grade iron ores in the iron quadrilateral (Rosière et al., 2008). In the geological formation process, high-grade iron ores replaced itabirites in locations where faults occurred in the rocks due to tectonic activities (Rosière et al., 2008).

In the Itabira mining complex, the formation of marine metasedimentary rocks is observed (Dorr, 1969). These consist of itabirites, dolomitic itabirites, amphibolitic itabirites, and, subordinately, phyllites, quartzites, schists, and marbles of the Cauê Formation. Rossi et al. (2019) demonstrate that within this mining complex, depicted in Figure 1, four geological units are identified, constituting the Itabira synclinorium: basement gneisses, volcano-sedimentary sequence of the Rio das Velhas Supergroup, metasedimentary units corresponding to the Minas Supergroup, and granitoid bodies. All of these sequences are intruded by intrusive rocks. Additionally, there are recent sedimentary coverings throughout the region.

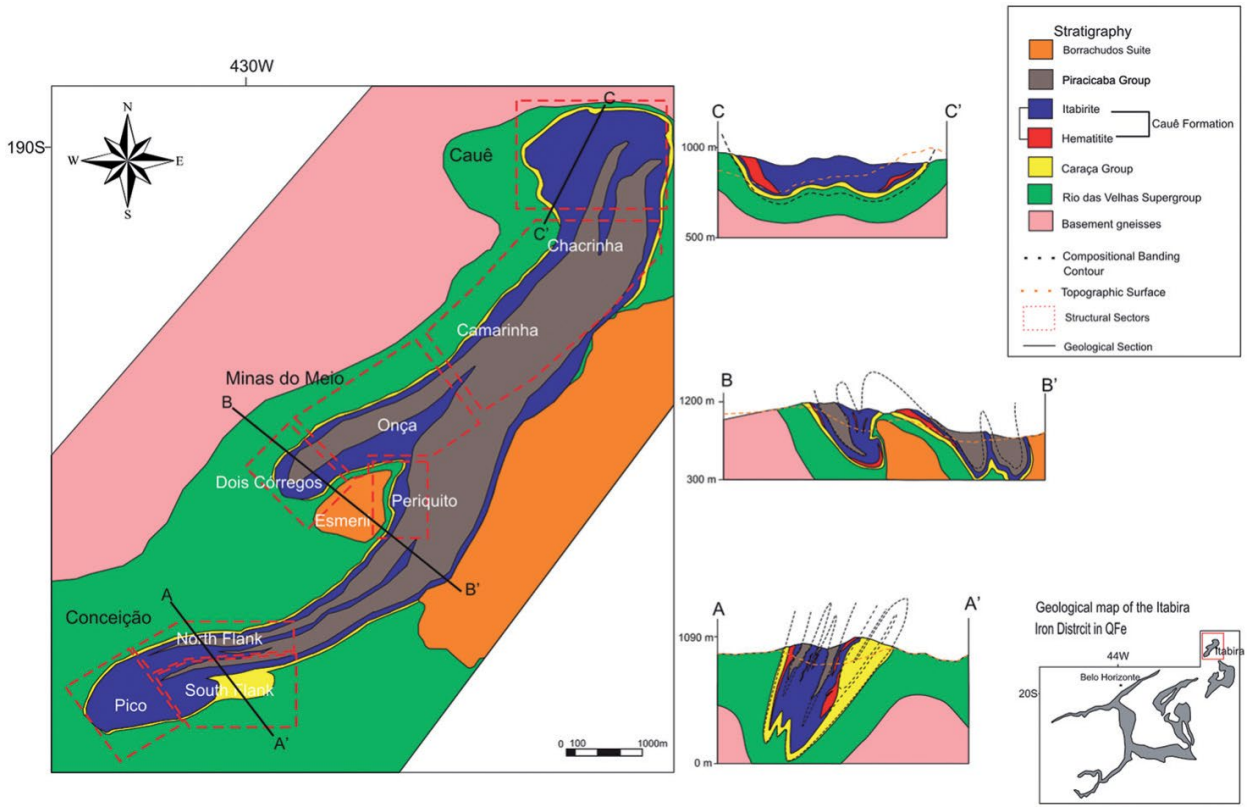


Figure 1: Geological map of the Itabira Mining Complex, location of the mines, structural sectors, and vertical geological section of the mines (extracted from Endo et al., 2019)

Geotechnical characterization of the Itabira complex waste materials

The imperatives of sustainability and economic efficiency are fundamental realities in the mining sector, driving the imperative to innovate and modernize operational processes while optimizing the utilization of available materials in mineral extraction endeavors. Alongside the persistent aim of maximizing metal retrieval from ores, ensuring continued access to mining sites and safeguarding the stability of waste rocks

and tailings management infrastructure such as piles and dams create a critical necessity for comprehensive studies and analyses of the geotechnical properties of these materials. However, the assessment of such properties for waste materials within areas of ancient rock formations, subject to diverse weathering processes as observed in Itabira, poses challenges due to the inherent complexity and variability of these materials. Consequently, geotechnical parameters are often qualitatively inferred or derived from established relationships found in the literature. The comprehensive characterization of fragmented waste materials on a large scale to accurately quantify geotechnical parameters remains a significant challenge in the mining industry, prompting reliance on characterizations primarily based on easily disaggregated rocks in locations such as Itabira. The presence of cavities in the Itabira massifs signals a prevalent occurrence of waste materials derived from easily weathered and fragmented rocks, predominantly composed of quartzites and schists. Therefore, a testing campaign on these materials was conducted to determine their strength and characterization parameters for waste pile projects.

Friable quartzites

Two primary types of quartzite material exist in the Itabira Complex, categorized as Micaceous Quartzite and Ferruginous Quartzite. These materials were classified using the Bieniawski method as completely weathered rock (W5) and highly weathered rock (W4) (ISRM, 1981). Subsequently, the strength varied from very weak rock (R1) to weak rock (R2) (ISRM, 1981). Characterization tests were conducted on various samples to determine the particle size distribution, demonstrated in Figure 2; the Atterberg limits to determine the plasticity of these materials, presented in Figure 3; and specific mass. All tests are executed by the Brazilian Association of Technical Standards (ABNT).

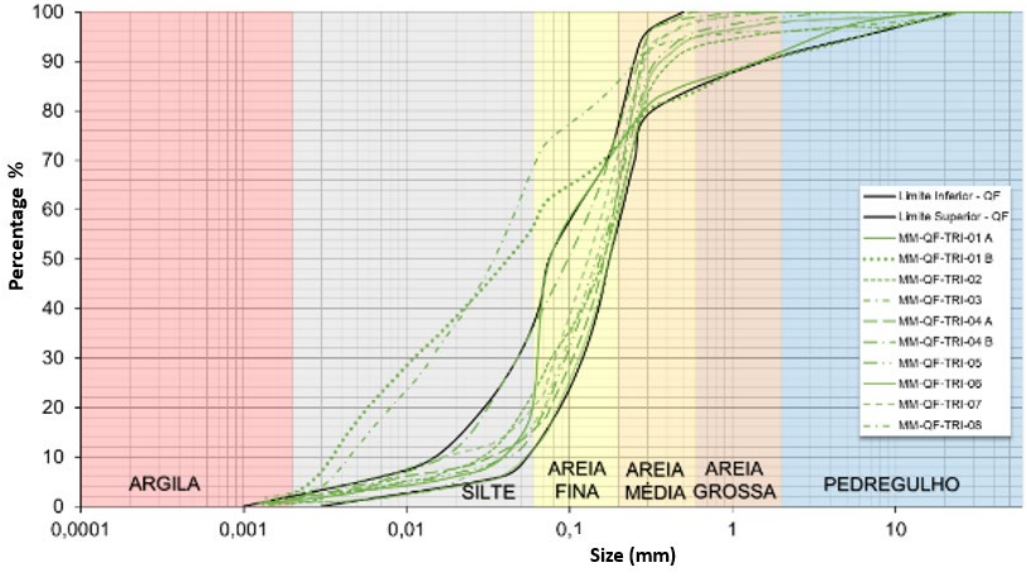


Figure 2: Particle size curves of friable quartzite

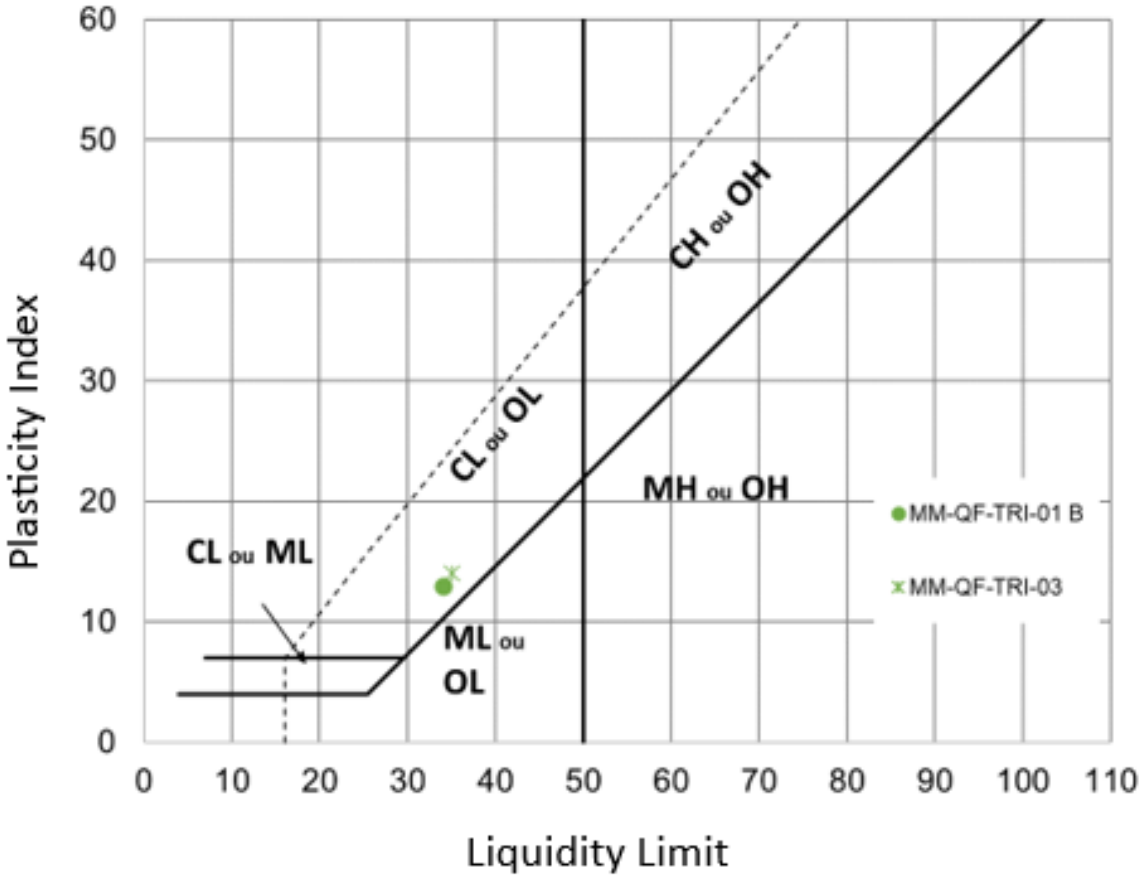


Figure 3: Plasticity chart of friable quartzite

Based on the particle size curves, the friable quartzite was categorized by ABTN as poorly graded silty sand with fines, comprising approximately 20% of materials passing through the sieve with an aperture of 0.075 mm. The fine fraction of the materials predominantly exhibits low plasticity or non-plastic characteristics. The specific mass ranged from 2.70 g/cm³ to 3.51 g/cm³, with higher values attributed to elevated concentrations of ferrous oxides.

Drained and undrained triaxial compression tests were conducted on samples reconstituted to a dry density of approximately 85% of the maximum dry unit weight, determined through standard compaction tests, under confining stresses of 200, 400, 800, 1,600, and 3,200 kPa.

The drained test results are illustrated in Figure 4, revealing dilative behavior under the three lowest confining pressures (200, 400, and 800 kPa) and contractive behavior under the two highest confining pressures (1,600 and 3,200 kPa).

The results of the undrained tests are depicted in Figure 5, indicating an increase in pore pressure due to shear for all 5 confining pressures. This behavior suggests a contractive material and aligns with the drained test outcomes discussed earlier.

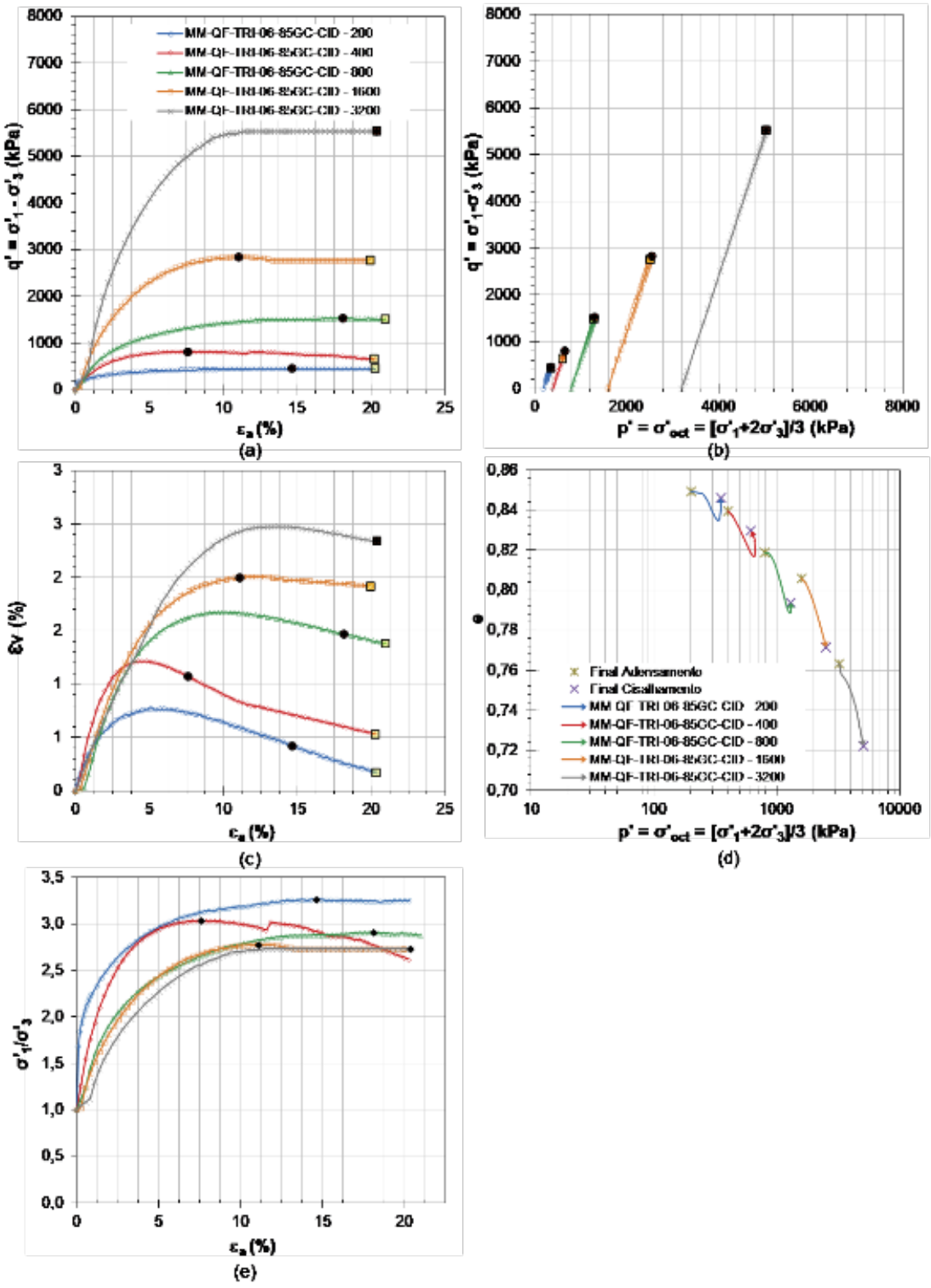


Figure 4: Drainage tests on friable quartzite

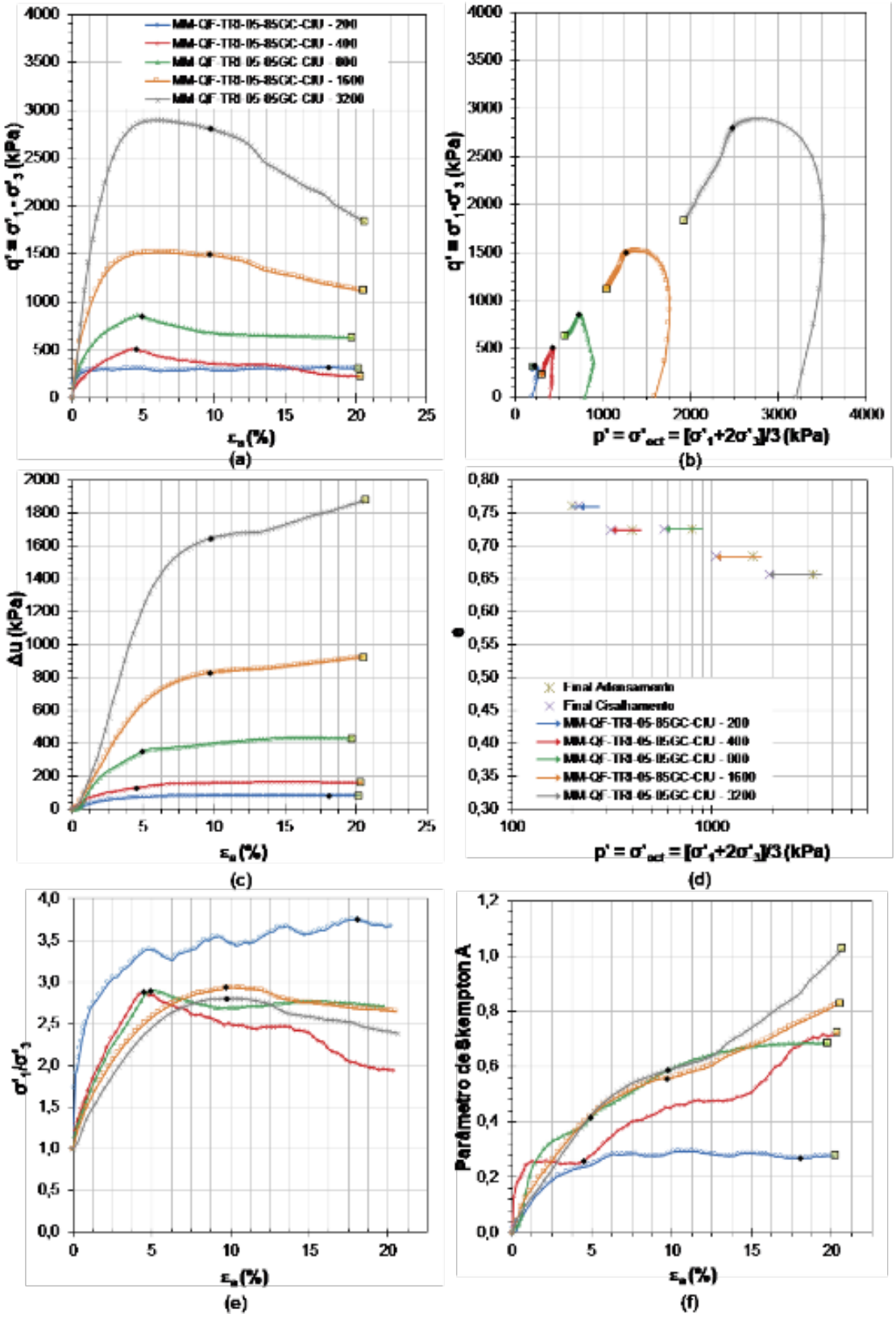


Figure 5: Undrained friable quartzite tests

Friable schist

The friable schist material is characterized as saprolitic schist with intercalations of phyllite. The material's weathering degree was determined as completely weathered (W5), and its resistance level was classified as very weak (R1), in accordance with ISRM (1981) standards. Various samples underwent characterization tests to acquire the particle size curve, depicted in Figure 6, the Atterberg limits, shown in Figure 7, and specific mass measurements of the friable quartzites. All tests were executed by the Brazilian Association of Technical Standards (ABNT).

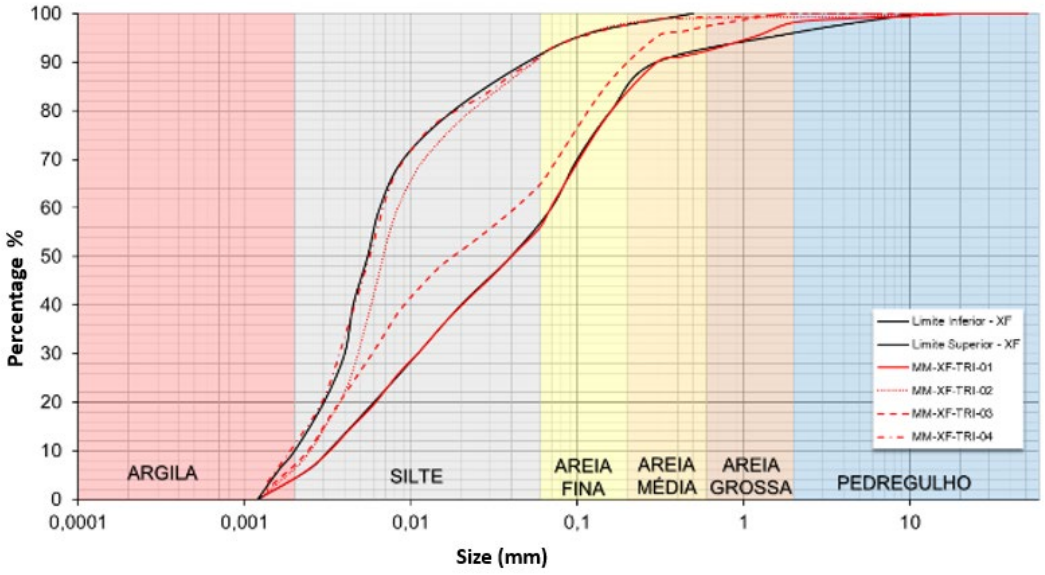


Figure 6: Particle size curves of friable schist

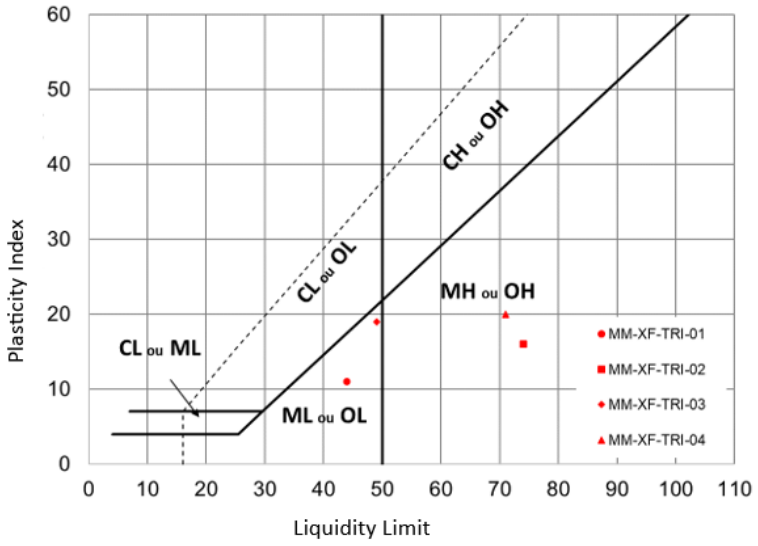


Figure 7: Plasticity chart of friable schist

The results of the particle size characterization tests classified the friable schist as a fine-grained material, with 52% to 85% of the total mass passing through the sieve with openings of 0.075 mm. The fines were categorized as low to high plasticity silt based on the results of the Atterberg limits. The specific mass of the materials averaged 2.86 g/cm³. Triaxial tests show that friable schist tends to generate positive pore pressures in undrained conditions and undergoes contraction, reducing the void ratio, in drained conditions. Figures 8 and 9 illustrate the results obtained in the drained and undrained tests for stresses ranging from 200 to 3,200 kPa. The materials showed contractive behavior in both cases.

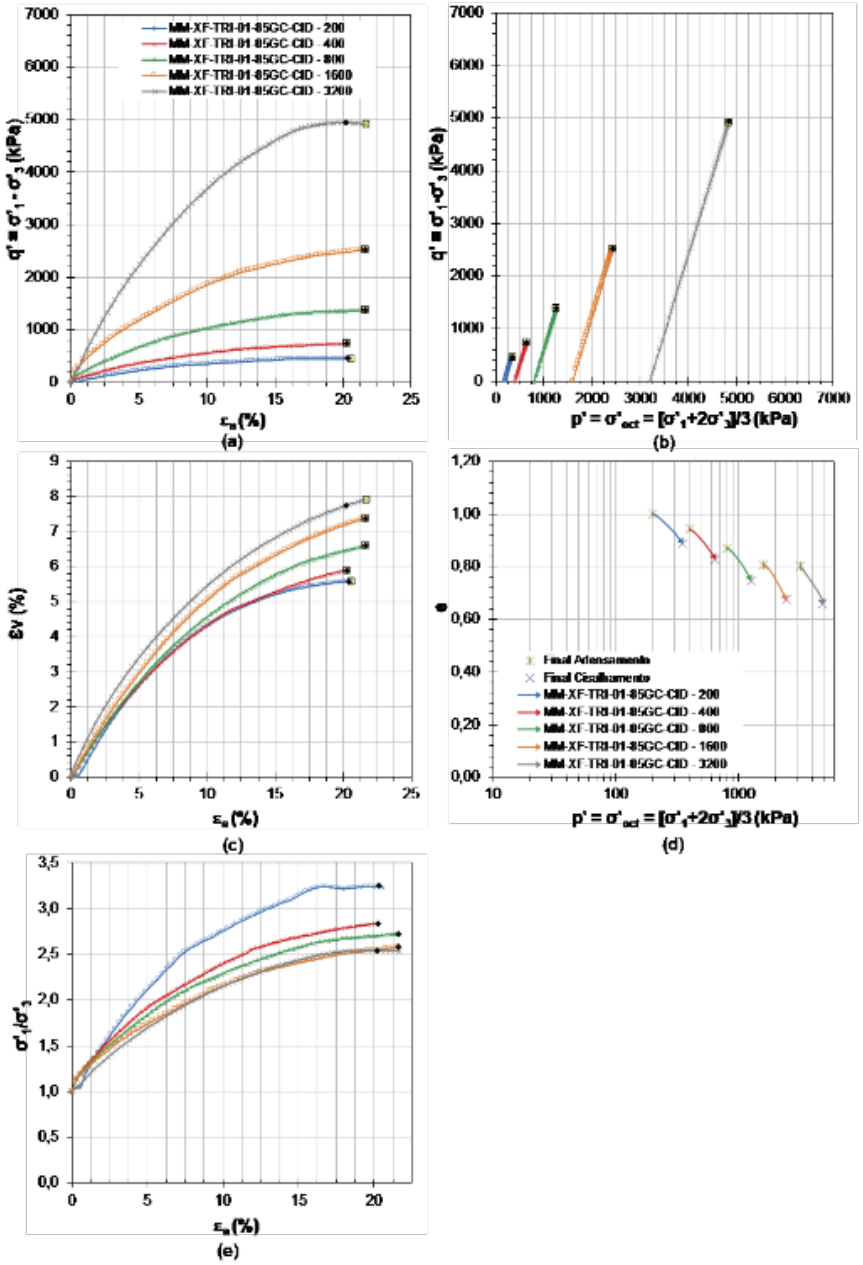


Figure 8: Drained tests friable schist

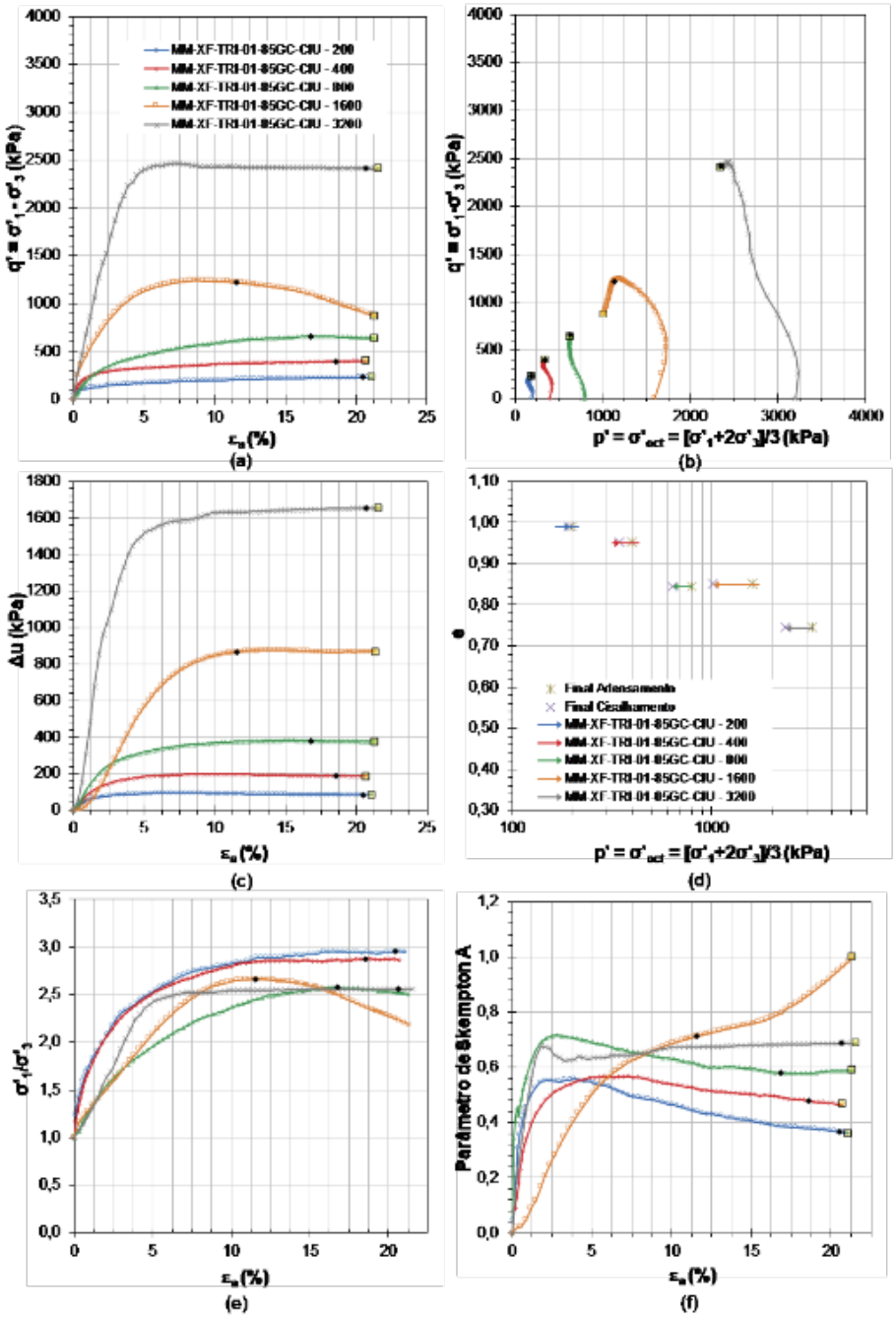


Figure 9: Undrained friable schist tests

Conclusion

Due to the depth of the mines in the Itabira complex, the waste materials consist of friable and rocky materials from blasting. The results of this study classified the behavior of friable materials, demonstrating that at low (200 kPa) and high (3,200 kPa) stresses, these materials tend to behave preferentially in a contractive manner. However, as observed in the test on sample MM-QF-TRI-06, the friable quartzite

exhibited dilative behavior at low stresses when compacted to 85% of standard Proctor density. These findings prompted a revision of the designs to enhance the geotechnical parameters of the waste rock piles, given that friable materials contribute to increased structural fragility. Despite this behavior, none of the samples underwent static liquefaction in any of the tests, indicating that pore pressures did not exceed effective stresses. Although there were discrepancies in the behavior of quartzites and schists, it is assumed as a design premise in the Itabira Complex that the most critical condition of these materials, in each evaluated parameter, should be adopted to ensure greater accuracy in the safety factors of the structures.

Studies focused on the parameters of rocky materials should be conducted to potentially enable the segregation of materials in pile structures, aiming to identify areas where friable materials can be disposed of in a confined manner, in case the geotechnical parameters of rocky materials exhibit characteristics that increase safety factors.

References

Alkmim, F.F. and Marshak, S. 1998. Transamazonian Orogeny in the Southern São Francisco Craton Region, Minas Gerais, Brazil: evidence for Paleoproterozoic collision and collapse in the Quadrilátero Ferrífero. *Precambrian Research* 90(1–2): 29–58.

Almeida, F.F.M. 1977. O Cráton de São Francisco. *Revista Brasileira de Geociências* 7(4): 349–364.

American Society of Testing and Materials – ASTM. 2011. Standard Test Method for Consolidated Undrained Triaxial Compression Test for Cohesive Soils. ASTM D4767. West Coshohocken, PA.

American Society of Testing and Materials – ASTM. 2020. Standard Test Method for Consolidated Drained Triaxial Compression Test for Soils. ASTM D7181. West Coshohocken, PA.

Associação Brasileira de Normas Técnicas – ABNT. 2016. *Grãos de pedregulho retidos na peneira de abertura 4,8 mm – Determinação da massa específica, da massa específica aparente e da absorção de água*. NBR 6458. Rio de Janeiro, RJ.

Associação Brasileira de Normas Técnicas – ABNT. 2016. *Solo — Determinação do limite de plasticidade*. NBR 7180. Rio de Janeiro, RJ.

Associação Brasileira de Normas Técnicas – ABNT. 2017. *Solo – Determinação do limite de liquidez*. NBR 6459. Rio de Janeiro, RJ.

Associação Brasileira de Normas Técnicas – ABNT. 2018. *Solo – Análise granulométrica.* NBR 7181. Rio de Janeiro, RJ.

Castro, P.T.A., Endo, I., Gandini, A. L. 2020. *Quadrilátero Ferrífero: avanços do conhecimento nos últimos 50 anos.* 3rd edition. Belo Horizonte. ISBN 978-65-990542-8-0. www.qfe2050.ufop.br

Dorr, J. V. N. II. 1969. Physiographic, stratigraphic and structural development of the Quadrilátero Ferrífero, Minas Gerais, Brazil. USGS/DNPM. Professional Paper 641-A. 110p.

Endo, I., Delgado, C. E. R. Oliveira, M. M. F. de, Zapparoli A. de C., Carlos D. U., Galbiatti H. F., Castro P. de T. A., Suita M. T. de F., Barbosa M. S. C., Lana C. E., Moura L. G. B. de. 2019b. *Estratigrafia e Arcabouço Estrutural do Quadrilátero Ferrífero: Nota Explicativa do Mapa Geológico do Quadrilátero Ferrífero, Minas Gerais, Brasil. Escala 1:150.000*. Ouro Preto, Departamento de Geologia da Escola de Minas – UFOP – Centro de Estudos Avançados do Quadrilátero Ferrífero: www.qfe2050.ufop.br.

Rosière, C.A. and Chemale, F. 2000. Brazilian iron formations and their geological setting. *Revista Brasileira de Geociências* 30: 274–278.

Rosière, C.A., Siemes, H. Quade, H., Brokmeier, H.-G. and Jansen, E.M. 2001a. Microstructures, textures and deformation mechanisms in hematite. *Journal of Structural Geology* 23(8).

Rosiere, C.A., Spier, C.A., Rios, F.J. and Suckau, V.E. 2008. The itabirite from the Quadrilátero Ferrífero and related high-grade ores: an overview. *Reviews in Economic Geology* 15: 223–254.

Rossi, D. Q., Endo, I., Gabriel, E. G. 2019. Structural framework of the iron district of Itabira, Iron Quadrangle, Minas Gerais. *International Engineering Journal* 72(1): 39–45.

Feijão Dam I 3D Numerical Simulation: A Comprehensive Approach, from Triggering to Dam Breach

Alfredo Arenas, ATC Williams, Australia
Nicolas Pereira, Red Earth Engineering a Geosyntec Company, Australia

Abstract

The failure of Dam I at Vale's Córrego do Feijão iron ore mine on 25 January 2019 resulted in significant human, environmental, and economic losses. Efforts have focused on understanding the triggering mechanisms behind the failure, traditionally modeled using commercial software based on continuum mechanics and small strain theory. However, these approaches are limited to capturing only the initiation of events.

This study employs the Material Point Method (MPM), a robust numerical technique capable of modeling large deformations, to bridge the gap between small and large strain theories. Unlike conventional methods like FLAC3D, MPM offers a more comprehensive analysis of the complex triggering mechanisms and initial stages of dam breach events.

The paper summarizes liquefaction triggering analyses of the tailings storage facility (TSF) and details the integration of post-triggering states from FLAC3D into the MPM framework. This approach avoids the arbitrary assignment of residual strengths typical in traditional dam breach analyses. The study outlines the iterative propagation process of failure using MPM-PUCRio and presents detailed results from the dam breach analysis conducted with this method.

Introduction

The failure of Dam I at Vale's Córrego do Feijão Iron Ore Mine on 25 January 2019 resulted in tragic consequences, including over 270 fatalities and significant economic and environmental damage. This event, along with other recent catastrophic failures of tailings storage facilities (TSFs), have prompted extensive efforts to enhance TSF safety (ICOLD, 2022; Morrison 2022).

Despite the clear visual evidence of flow liquefaction captured in video footage of the failure, there remains substantial debate regarding its triggering event. Two primary investigations have been conducted. First, the Expert Panel (EP) released a report in December 2019 (Robertson et al., 2019). This group

attributed the failure to a combination of reduced surficial suction due to increased rainfall and drained creep. They explicitly dismissed drilling activities conducted at the time as a plausible cause. Second, CIMNE published a report in August 2021 (Arroyo and Gens, 2021). They identified drilling-induced liquefaction as the primary trigger, while discounting creep and suction reduction as potential causes.

The work herein summarizes the methodology and findings of the triggering mechanism that led Dam I to failure. The FLAC3D triggering mechanism assessment is part of an undergoing work, with an already finished set of analyses, which is an extension of the work presented at NUMGE 2023 (Arenas et al., 2023) from plain strain analysis (2D) to a full 3D model.

Specifically for the work presented herein, a series of FISH codes were implemented in FLAC3D to export mesh state into MPM-PUCRio. The mesh analyzed in FLAC3D is exactly the same mesh used in MPM-PUCRio. Among the exported data from FLAC3D are the grid points, the material groups, stress tensor, strains, liquefaction state, and the pore water pressure.

MPM-PUCRio was run iteratively to simulate the propagation of the failure under large strain deformation. The triggering mechanism framework is imported as defined in FLAC3D. Through a C# code the progression of the solution is iteratively carried out in MPM-PUCRio, where a solution is saved as time in the model advances.

FLAC3D numerical modeling

Geometry

The numerical model geometry was derived from publicly available information, notably the EP report on Feijão dam. This information consists mainly of plain images and tables, lacking digital data such as UTM coordinates or elevations.

To address this challenge, Geo Meshing v4.3.2 software was employed to convert this information into a detailed 3D numerical model. Geo Meshing utilizes parametric inputs, such as crest width, to generate 2D/3D meshes without requiring 3D surfaces or volumes. It was also utilized for interpolating Ψ values within tailings elements, inferred from Cone Penetration Testing (CPTu) data.

A discretization size of 3.5 × 3.5 × 3.5 meters was used, resulting in a model with approximately 1 million elements. Figure 1 provides insights into the 3D model details. Note the model's cutting plane is located at section "SM13," named after the borehole position, being drilled at the failure moment (BH SM13). The model was created using tetrahedra elements, to make it 1:1 compatible with the MPM solver.

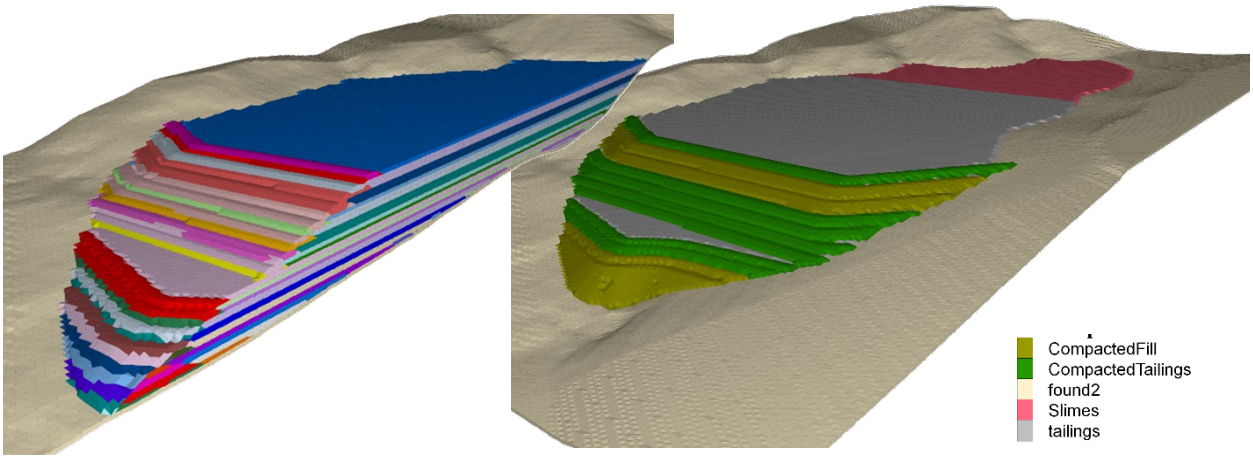


Figure 1: FLAC3D model. Left: FLAC3D model cut at section SM13, showing construction stage layers. Right: full 3D model describing main geotechnical units

Constitutive models

Each material during the Dam I construction sequence was simulated using the Mohr-Coulomb (MC) constitutive model (Itasca, 2022), with parameters detailed in Table 1. In addition, and during the triggering process, the NorSand model was used to capture the excess pore pressure generation that loose and brittle tailings generate before crossing the instability line in Table 2.

While the use of MC for stiff foundations or compacted embankments is common, even in advanced modeling, its application to saturated, contractive, and brittle tailings necessitates further discussion.

The decision to employ a modified form of the MC model, for those tailings element crossing the instability line, is supported by several factors:

(i) no constitutive model, to the best of the authors' knowledge, reliably captures behavior along the critical state line (constant shear drained stress path) in boundary value problems for loose, contractive, brittle soils; and

(ii) the use of any constitutive model, regardless of its sophistication, inherently assumes or explicitly defines in-situ values of parameters like the lateral earth coefficient at rest (K_0), the principal stress ratio (Kc), and the Lode Angle, which are crucial for identifying instability initiation when verifying if the stress ratio η (the ratio of deviatoric stress, q, to mean effective stress, p') is higher than the stress ratio at the instability line (ηIL).

To address these challenges, the MC model was adapted during the construction sequence with a Poisson's ratio selected to target a specific K_0 below ground level, set at 0.7 in this instance. This approach enables a reasonable estimation of in-situ K_0, which is not always feasible with more complex models. In addition, this value avoids setting off the proposed triggering scheme at the end of construction.

Table 1: Mohr Coulomb material properties. Drained properties. Construction only

Material	Shear Modulus Reference[1] (kPa)	Friction (°)	Cohesion (kPa)
Foundation	1,472,000[2]	N/A[3]	N/A[2]
Slimes	1,285	0	$0.22(\sigma'_v)$
Compacted Tailings	3,496	40	0
Compacted Fill	2,525	35	10
Ultra fine Ore	2,525	35	10
Fine Tailings	1,028	33.2	5
Coarse Tailings	1,028	34.6	5

Note[1] $G = G_0 P_a \left(\frac{p\prime}{P_a}\right)^n$, where G_0 is the Shear reference modulus

Note[2] Constant Value

Note[3] Elastic constitutive model adopted

Table 2: NorSand material properties

Material	CSL			N	Xtc	H_0	Gref	n	Mtc	H_Y	Pois-on
	a	b	c								
Fine Tailings	1.04	0.037	0.0	0.15	6.0	60	24,800	0.62	1.4	300	0.2
Coarse Tailings	1,31	0.145	0.235	0.136	3.0	35	25,000	0.55	1.34	218	0.2

Pa = 101.3 kPa

Instability initiation is identified by monitoring η across all saturated tailings elements using routines developed by the authors. Elements where η exceeds ηIL are then assigned liquefied strengths as cohesion inputs, effectively transitioning the failure criterion from MC to Tresca.

It is important to note that during static construction phases, the MC strength criterion is utilized as a review of material plastic states within the model, consequently indicating that elastic input parameters control the in-situ stress state. During triggering analyses, modifications implemented by the authors, along with the NorSand constitutive model, govern instability and liquefied strength, a process detailed subsequently in this study.

Construction sequence, in-situ state and tailing types

The construction sequence simulation of the Feijão TSF was organized into 13 stages, with each stage further divided into approximately 3.5-meter layers. This division resulted in 33 lifts for the embankment and 27 lifts for the tailings, activated sequentially and alternately to simulate TSF construction. A K_0 value of 0.7 was applied during the construction of the 3D model, chosen initially to ensure numerical stability before triggering testing. Figure 2 guided the selection of K_0 to closely approach the instability line while keeping in-situ stresses for the most contractive materials below it.

At the end of each construction stage, the phreatic level was updated based on seepage analysis conducted by the EP.

Regarding tailings in-situ state at the end of the construction sequence simulation, both ηIL and su(LIQ)/σ'vc values utilized in the modeling are functions of Ψ, highlighting the critical importance of Ψ interpretation and its assumed in-situ distribution for analysis outcomes.

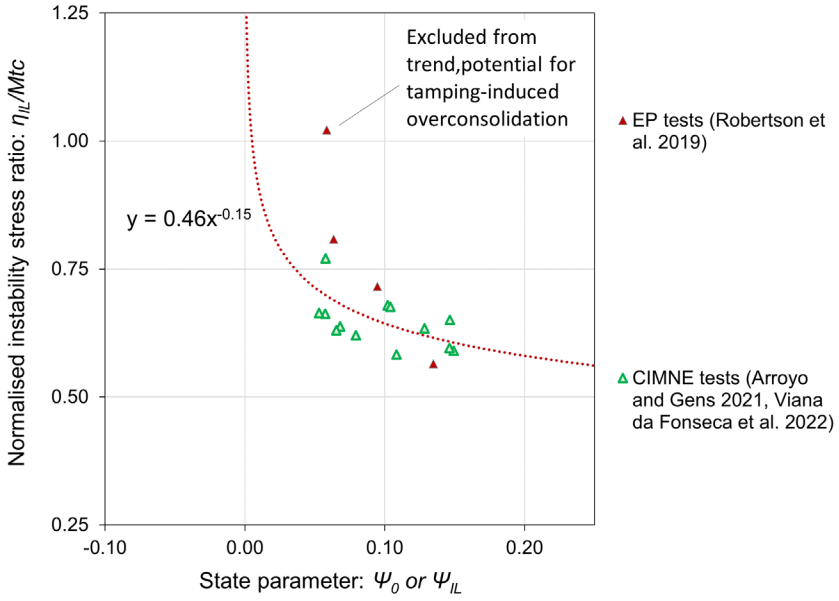


Figure 2: Normalized instability stress ratio versus state parameter (Arenas et al., 2023)

Using Geo Meshing v4.3.2, Ψ values were interpolated from CPTu using the built-in data feature. The interpolation scheme utilized a bin height of 1.75 meters (half of the numerical element height) and 50th percentile Ψ values, chosen after testing various bin sizes to minimize mesh bias. The 50th percentile was found to offer a balanced representation of field conditions for Ψ, avoiding excessive conservatism. While Jefferies and Been (2015) recommend using 80% Ψ for domain-wide representation, such an approach would be overly conservative for this detailed numerical analysis at the element level. Ψ values were estimated from CPTu data using the inversion method (Plewes et al., 1992), with Figure 3 illustrating the interpreted Ψ distribution.

Residual strength

The liquefied strength ratios for the tailings were determined following the "best practice trends" outlined by Jefferies and Been (2015). In this approach, su(liq)/σ'vc is treated as a function of Ψ, informed by both the back analysis of flow liquefaction case histories and Continuous Surface Subsidence Monitoring (CSSM). This method is preferred over the "steady state approach" due to compelling evidence of flow liquefaction occurrences in deposits with Ψ ranging from -0.05 to +0.05.

Triggering

A critical component of the triggering analysis conducted in this study is the adoption of the ηIL value specific to in-situ tailings, particularly the relationship between ηIL and Ψ (e.g., Yang 2002). To establish this relationship for Feijão tailings, the triaxial compression test data from both investigative groups were synthesized, as depicted in Figure 2. While electronic data from CIMNE tests were accessible (Viana da Fonseca et al., 2022), data from the EP tests was unavailable to the authors, necessitating the use of previously digitized data (Reid et al., 2022).

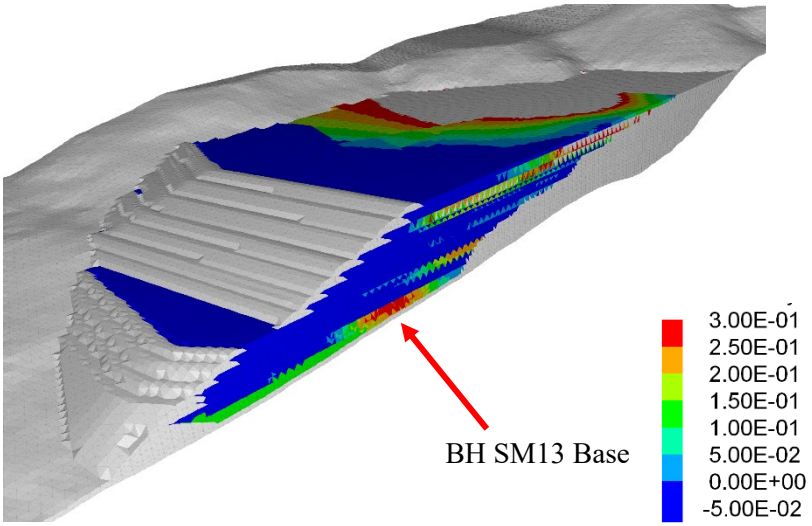


Figure 3: Tailings interpolated state parameter over the FLAC3D model

The data presented in Figure 2 and the selected trend are normalized by Mtc, with Mtc being the normalization factor for the triaxial compression tests shown. This normalization allows the triaxial compression data to be reasonably extrapolated to the in-situ conditions of the 3D numerical model. It should be noted that one of the EP tests was excluded from the synthesis in Figure 3 (as indicated) due to concerns that tamping-induced overconsolidation may have influenced the resulting peak strength/ηIL (Reid et al., 2022).

It is important to highlight the absence of suitable strength tests for the Feijão slimes within the framework of Figure 3, which is a significant limitation given the potential presence of slimes at the base of BH SM13. Consequently, the same trend observed for fine/coarse tailings was applied to the slimes, with adjustments based on the inferred lower Mtc/M for the slimes, as was indicated in Table 2.

Once the model reached equilibrium under the aforementioned conditions, an assessment of potential instability triggering around borehole SM13 during drilling was conducted. This process involved two primary stages: (i) establishing a pore pressure regime around the borehole; and (ii) checking for triggering. This approach represents a modified version of that adopted by Reid et al. (2021). Specifically, this

simplified procedure systematically evaluates all elements of saturated tailings within a numerical model. The procedure involves assessing whether the in-situ η exceeds a critical instability value ηIL at any location. If ηIL is exceeded, liquefied strengths are assigned to triggered elements, stability is reassessed, and the process is iteratively repeated to determine whether the model converges. This approach was chosen for its suitability in analyzing a constant shear drained (CSD) stress path, typical around boreholes where increased pore pressures can occur, particularly in brittle, loose tailings.

Results

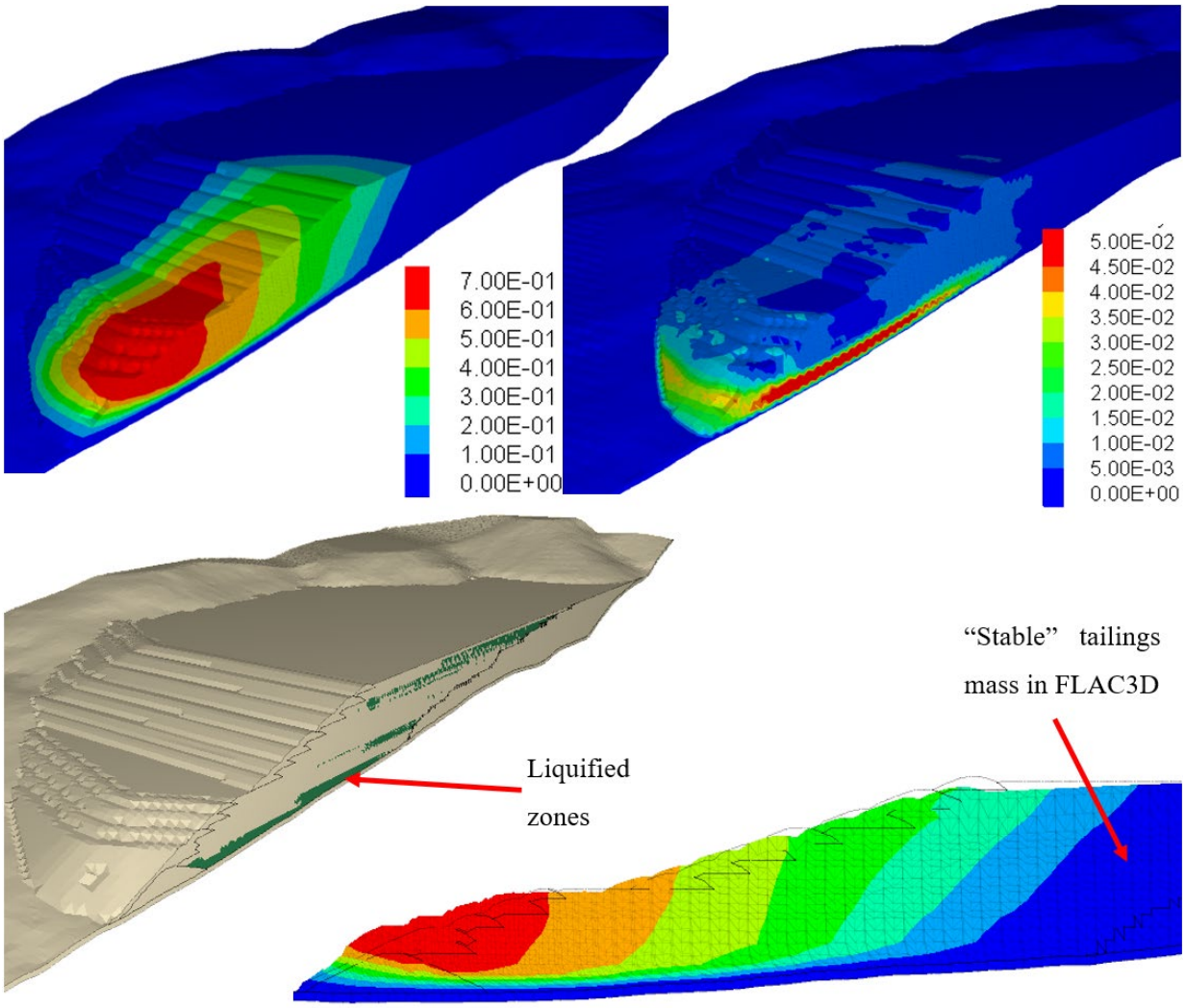


Figure 4: FLAC3D triggering results. All figures have a cutting plane at SM13. Upper left: displacement magnitude. Upper right: maximum shear strain. Lower left: liquified zones in Green. Lower right: displacement magnitude at SM13. Contours deformed and delineated original configuration

It is important to clarify that the FLAC3D model developed to run MPM analysis was run only long enough to establish the triggering mechanism. Therefore, displacement and shear strain magnitudes are small when

compared to the detailed FLAC3D model (not presented herein). The detailed model presents displacements that reach over 10 m and shear strain above 30%. This was also noted in the 2D model presented by Arenas et al. (2023).

Figure 4 shows partial results of the FLAC3D comprehensive stability assessment. The upper left figure illustrates the magnitude of displacements in meters. The upper right figure depicts shear strain, capped at a maximum value of 5%. The lower left figure identifies liquefied zones (areas where $\eta > \eta IL$, in green). Finally, the lower right figure replicates the same information as the first figure, but with the mesh deformation exaggerated and the original position of the slope delineated with a black line. Notice the bulged area below the setback resembling the first movement observed in the Feijão failure footage.

Limitations

Even though FLAC3D is a very robust platform, its continuous mesh nature prevents assessing analysis with extremely large deformations, even when the "large strain" option is active. This characteristic precludes the shear stress shifting that happens when a mass of soil moves and unconfines the soil right behind the moving front. In essence, shear stresses and pore water pressure will not increase in the "stable" soil mass, and the cascading failure effect will not be reproduced.

Figure 4 shows the "stable" mass. At these zones shear stresses are not transferred from the liquefied zones, as was happening during the expansion of the failure surface during the triggering assessment. Therefore, those zones beyond the failure surface will not generate excess pore pressure and/or increment in shear stresses, precluding activating the triggering mechanism in a software such as FLAC3D. In order to mobilize those zones, large strains are needed to produce the necessary reduction of lateral stress, with the consequent increment in shear stress and triggering.

MPM analysis

MPM is a computational technique employed to simulate large deformation processes in various scenarios. Rather than representing individual soil grains, MPM discretizes the continuum into material points, each embodying a volume of the solid.

The methodology involves two computational meshes, one serving as a background grid, and a second one representing the material points. This hybrid approach, described by Soga et al. (2016) and Yerro et al. (2022), mitigates distortion issues commonly encountered in traditional methods like finite element or finite difference approaches. By transferring data between grid and material points at each step, MPM can capture large deformation processes such as those seen in dam failures.

Similar approaches have been considered in the past for Tailings Dam Breach Analyses (TDBA): Zabala and Alonso (2011) presented the first application of MPM to model tailings dam failure; Robertson

et al. (2019) presented a 2D MPM dam breach model of Dam 1; and Pierce (2021) used MPM to identify the key factors controlling the runout of the Cadia tailings dam failure of 2018 in Australia.

The runoff modeling was conducted using MPM-PUCRio software. It includes various constitutive models and incorporates memory parallelization techniques, allowing for simulations with a large number of material points (Pierce, 2021).

Geometry

The MPM mesh was exported from FLAC3D, allowing for the integration of materials and their distribution. Figure 5 presents an isometric view of the resulting MPM mesh geometry and material distribution.

Given the size of the elements in the FLAC3D mesh, a regular structured cubic background grid of 3.5 meters was used for the material point simulation.

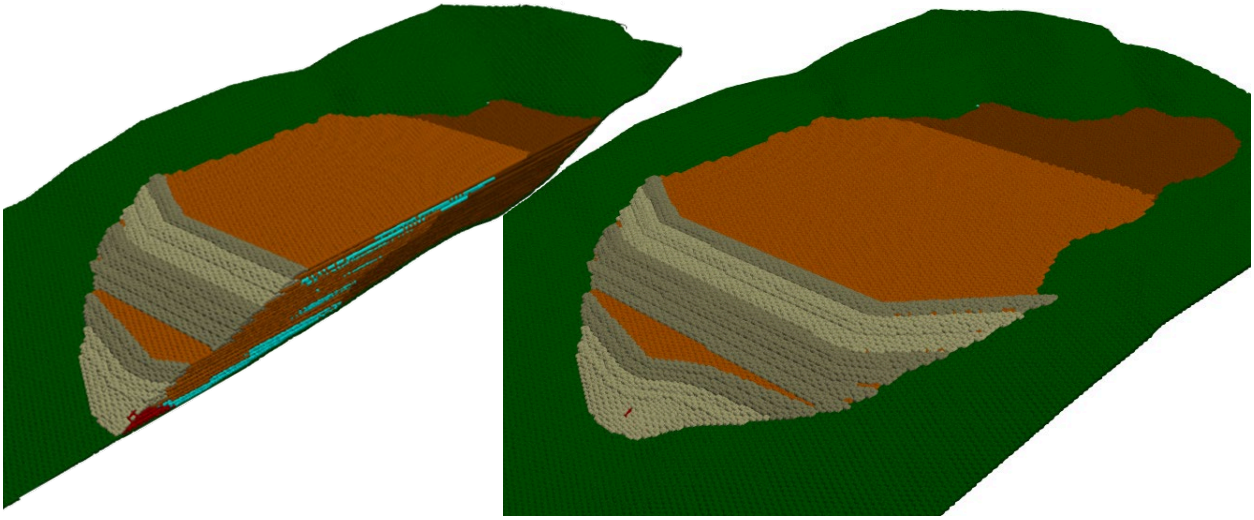


Figure 5: MPM model. Left: MPM model cut at SM13. Liquefied zones shown in light blue as imported from FLAC3D. Right: full 3D MPM model

State from FLAC3D

After analyzing the triggering in FLAC3D, the mesh and material configuration was imported into MPM-PUCRio. Along with this information, the strain and stress tensor as well as the pore water pressure was preserved for each zone/material point. Finally, the liquefied condition reached in the FLAC3D analysis was also transferred into MPM-PUCRio; thus, it constitutes the initial condition for triggering the failure.

The major advantages of using this approach are: first, the stresses generated with the detailed construction sequence replicated in FLAC3D are preserved, which in turn preserves K_0 conditions. This last feature is key when analyzing CSD triggering mechanisms. This is a mayor advancement since MPM software packages usually define a single stage for initial conditions, gravity loading, which provides an inconsistent K_0 distribution across the model. Second, it eliminates the guess work related to the initial

triggering. Most of the time, standard practice using MPM methodology assigns residual properties to an arbitrary area of the facility to initiate the simulation.

Constitutive models

Differing from FLAC3D analysis, the response of the embankment and tailings materials were modeled with MC. This model does not explicitly consider the effects and evolution of pore water pressure as NorSand does, and therefore it is expected that fewer zones would potentially liquefy during the analysis. It is important to note that once the material point reaches liquefied conditions, it was modeled with the MC using residual strength properties, as was done in FLAC3D.

The foundation materials were considered linearly elastic, and the inherent MPM contact algorithm controlled the interaction of all materials.

Triggering in MPM

As previously mentioned, the triggering mechanism used in the MPM analysis is the same as is used in the FLAC3D analysis. Given the large strain capabilities of the MPM solution, it allows for a significant change in the deviatoric stresses in the mass immediately behind the moving front (which after a few seconds in the simulation becomes the new front). Therefore, the effectiveness of the triggering mechanism to expand across the impoundment is much greater.

Results

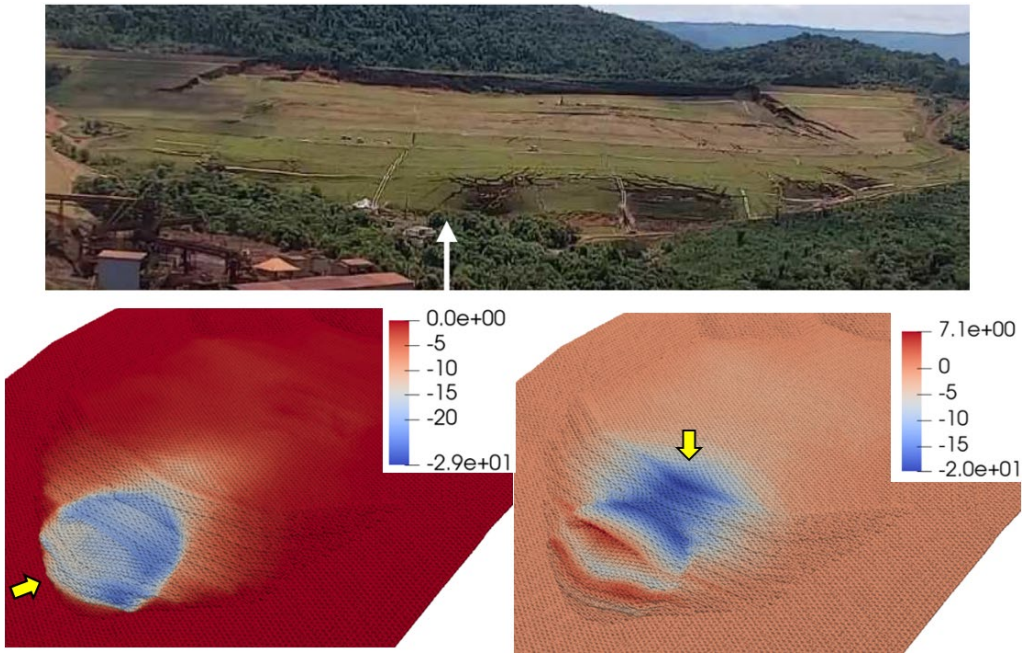


Figure 6: Above: video footage captured at 5.5 s after the initiation of the failure. Below: MPM runout simulation at 5.5 s. Left: horizontal displacements. Right: vertical displacements

The upper portion of Figure 6 shows the Feijão Dam I capture at 5.5 s since the initiation of the failure (Robertson et al., 2019). Similarly, the lower part of Figure 6 shows the runout analysis at 5.5 seconds after initiating the analysis. The bulging below the TSF step back and the crest settlement can be clearly observed.

Figure 7 shows the displacement magnitude of the MPM runout simulation. The left- and right-hand figures show the displacement magnitude after 20 seconds and 54 seconds (respectively) after triggering the failure. Note how the mobilized mass has extended into the impoundment.

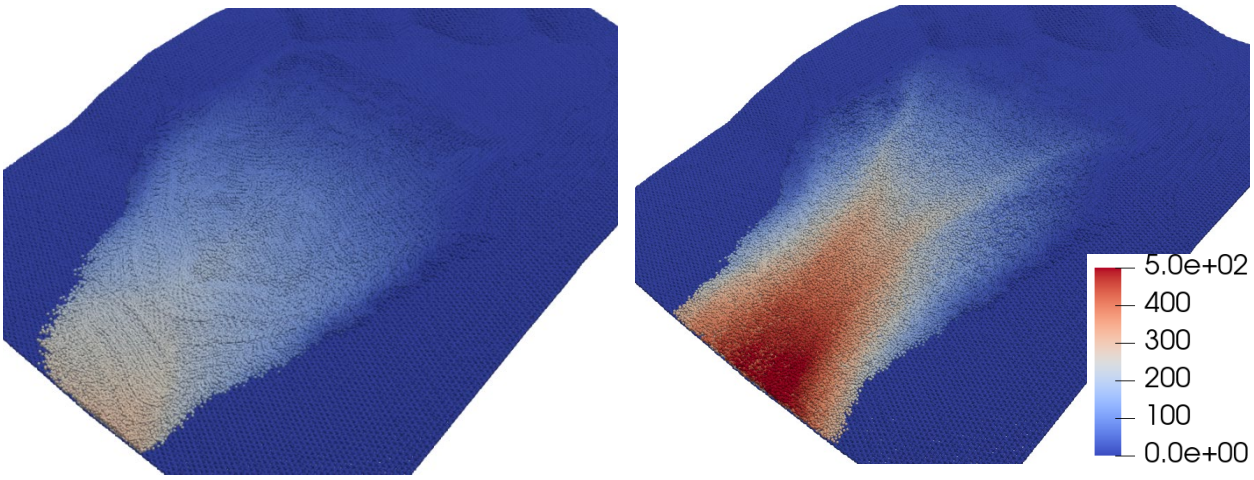


Figure 7: MPM runout simulation. Left: displacement magnitude at 20 seconds. Right: displacement magnitude at 54 seconds

Conclusion

The following conclusions can be drawn from the present work:

- The current analysis and methodology, as per Reid et al. (2021), enhances our understanding of why the TSF could have failed during the drilling of borehole SM13.The authors trust the mechanism of triggering presented herein is plausible and credible, as it has a strong foundation in a robust theoretical framework, and it uses advanced, proven 3D modeling techniques and the reliable NorSand constitutive model. Subsequently, the results observed from either FLAC3D or MPM- PUCRio encompass those observed during the failure.
- The adopted methodology offers a practical framework for analyzing and predicting liquefaction triggering mechanisms. This methodology eliminates the more traditional guess work of where to apply residual conditions to tailings within the impoundment. And therefore, it is applicable to existing facilities with no distress conditions.
- MPM-PUCRio offers large strains solutions that allow the implemented triggering to efficiently propagate throughout the tailings impoundment where liquefaction potential exists.

- The presented runout simulation closely replicates essential features of the failure captured on the video footage, such as the bulging below the TSF setback and the initial crest settlement.

References

Arenas, A., Reid, D., Fanni, R., Smith, K. and Fourie, A. 2023. *Numerical assessment of drilling-induced static liquefaction triggering of Feijão Dam I. Proceedings of 10th European Conference on Numerical Methods in Geotechnical Engineering (Numge 2023).* doi.org/10.53243/NUMGE2023-161

Arroyo, M. and Gens, A. 2021. *Computational analyses of Dam I Failure at the Córrego de Feijao Mine in Brumadinho: Final report for VALE S.A.*

Fernández, F. 2020. *Modelagem numérica de problemas geotécnicos de grandes deformações mediante o método do ponto material*. Doctoral dissertation, Pontifícia Universidade Católica de Rio de Janeiro.

Finke Morrison, K. 2022. *Tailings Management Handbook: A LifeCycle Approach*. Society for Mining, Metallurgy and Exploration (SME).

Geo Meshing. 2023. v4.3.2. Retrieved from https://www.geomeshing.com

ICOLD. 2022. Tailings Dam Safety Bulletin – Draft.

Itasca. 2022. FLAC3D Manual.

Jefferies, M. and Been, K. 2015. *Soil Liquefaction: A Critical State Approach*. Second Edition. Taylor and Francis Group LLC, Boca Raton, FL.

Pierce, I. 2021. *Applying the material point method to identify key factors controlling runout of the Cadia tailings dam failure of 2018*. Doctoral dissertation, Virginia Tech.

Plewes, H.D., Davies, M.P. and Jefferies, M.G. 1992. CPT based screening procedure for evaluating liquefaction susceptibility. *Proceedings of the 45th Canadian Geotechnical Conference* 4: 1–9.

Reid, D., Dickinson, S., Mital, U., Fanni, R. and Fourie, A. 2021. On some uncertainties related to static liquefaction triggering assessments. *Proceedings of the Institution of Civil Engineers: Geotechnical Engineering* 175: 181–199.

Reid, D., Fanni, R. and Fourie, A. 2022. *Effect of tamping conditions on the shear strength of tailings*. *International Journal of Geomechanics* 22(6): 04021288.

Robertson, P.K., de Melo, L., Williams, D.J. and Wilson, G.W. 2019. *Report of the Expert Panel on the Technical Causes of the Failure of Feijão Dam I.*

Soga, K., Alonso, E., Yerro, A., Kumar, K. and Bandara, S. 2016. Trends in large-deformation analysis of landslide mass movements with particular emphasis on the material point method. *Géotechnique* 66(3): 248–263.

Viana da Fonseca, A., Cordeiro, D., Molina-Gómez, F., Besenzon, D., Fonseca, A. and Ferreira, C. 2022. The mechanics of iron tailings from laboratory tests on reconstituted samples collected in post-mortem Dam I in Brumadinho. *Soils and Rocks* 45(1): 1–20.

Yang, J. 2002. *Non-uniqueness of flow liquefaction line for loose sand*. *Géotechnique* 52(10): 757–760.

Yerro, A., Girardi, V., Martinelli, M. and Ceccato, F. 2022. Modelling unsaturated soils with the material point method: A discussion of the state-of-the-art. *Geomechanics for Energy and the Environment* 32: 100415.

Zabala, F. and Alonso, E. 2011. Progressive failure of Aznalcóllar dam using the material point method. *Géotechnique* 61(9): 795–808.

The Use of Programming Language in GISTM Compliance for the Holden Mine

Summer Y. Sun, Stantec, USA
Phillip E. Crouse, Stantec, USA

Abstract

Since the release of the Global Industry Standard on Tailings Management (GISTM) in 2020, Rio Tinto and other ICMM member mining companies have been reassessing the stability of their legacy tailings storage facilities (TSFs). Reassessing the stability of these tailings storage facilities necessitates effective handling and analysis of vast amounts of geotechnical data. The advent of information technology has enabled the collection of this data in digital formats, prompting the utilization of software platforms such as ArcGIS, DAARWIN, EarthSoft, gINT, and Access for data organization and visualization. However, integrating data into these platforms often requires substantial initial efforts.

This paper presents a case study of reassessing the stability of the Holden Mine Tailings Piles using the R programming language. The study showcases the capabilities of programming languages in handling decades-worth of data, organizing it into suitable formats, and integrating it into a comprehensive three-dimensional model. This paper highlighted key advantages of programming, including efficiency in automating repetitive tasks, and its flexibility in designing customized plots tailored to specific geotechnical parameters. The extensive open-source graphics packages foster collaboration and innovation within the geotechnical engineering community, contributing to continuous improvement in data management and analysis practices.

Furthermore, the paper demonstrates the utilization of R's statistical packages to develop site-specific correlations between field and laboratory test results, including the Standard Penetration Testing, Cone Penetration Testing, and Index Testing. These correlations are an important part of assessing legacy tailings piles for GISTM compliance. The paper presents the site-specific correlation between unit weight and cone tip resistance, as well as the observed trend between the degree of saturation and dynamic pore water pressure. This paper presents the process to develop these correlations, which are tailored to the unique conditions of Holden Mine Tailing, and which provide more accurate and precise estimations of geotechnical parameters. The efficiency of programming enabled us to leverage data management, analysis,

and visualization, which enabled stakeholders to make more informed decisions regarding the design, monitoring, and maintenance of TSFs, ultimately advancing safety and sustainability in the mining industry.

Introduction

Rio Tinto reclaimed the Holden Mine between 2010 and 2016 which included reconfiguring the tailings piles that had been operated between 1937 and 1957. The Holden Mine is a former underground copper mine that was developed and operated by the Howe Sound Mining Company (Howe Sound). The mine is in the northwestern U.S. in north central Washington State near Lake Chelan. Rio Tinto never owned or operated the mine; they are managing and funded the reclamation and currently performing operating and maintenance of the closed facility. Since the release of the Global Industry Standard on Tailings Management (GISTM) in 2020, Rio Tinto and other ICMM member mining companies have been reassessing the stability of their legacy tailings storage facilities. Reassessing the stability of these tailings storage facilities (TSFs) necessitates effective handling and analysis of vast amounts of geotechnical data. It is especially difficult to integrate such wide range of data types when they come from various sources and formats. This study proposes an alternative tool for geotechnical data management using R programming language and demonstrated a workflow to use the tool for a tailings storage facility (TSF).

Geographic Information System (GIS) technology is widely used in the industry as an efficient tool to store, organize, analyze, and display this type of data in the form of digital layers and maps (Player, 2006). GIS provides promising outcomes for integrating multiple data types, such as photos, scanned maps, Shapefiles or computer-aided drafting (CAD) files (Singh, 2018). However, GIS is not designed for geotechnical data analysis and is mostly used to visualize the final results of the geotechnical analysis. It lacks the specialized functionalities tailored to the unique characteristics of geotechnical data, such as geospatial analysis and geotechnical calculations, which hinders the real-time visualization of the analysis results.

As a popular programming environment for statistical computing and graphics, R can be the one-stop solution for both powerful data calculations and high-quality plots. It is especially valuable for geotechnical data where visualization data through plots, maps, and charts helps understand patterns, trends, and relationships in the data. R's flexible plotting functionalities allow customization and interactive exploration of the data. R is an open-source software, which means it is freely available to use. Companies can encourage geotechnical engineers to explore the capabilities of R without incurring substantial software licensing expenses. Table 1 shows the comparison between the GIS-based software and the open-source programming code in the application of geotechnical data processing.

Table 1: Comparison between GIS-based software and open-source programming code

	GIS-based software	Open-source programming code
Data integration	Usually requires significant initial efforts to build the model	Relatively less efforts to build the model
Data visualization	Strong at integrating multiple data types and displaying the data in layers, including maps and photos	Not a tool designed to display maps and photos, but the graphics packages can present spatially relationships of data
Data processing	Not a tool tailed for calculations and spatial analysis of geotechnical data	Allows the customization and interactive exploration of data
Learning curve	Steep	Steep with no prior programming experiences
Cost	Usually not free	Usually free of charge

Figure 1 illustrates a simplified process of data management discussed in this work that includes three steps: data acquisition, data integration and data processing. Instead of providing a synthesized manual to data management, this study aims to demonstrate a workflow using R and therefore only the key steps within the workflow are listed in Figure 1. The workflow is flexible to adapt to additional data needs. Section 2 of this paper discusses in more detail each step in the workflow.

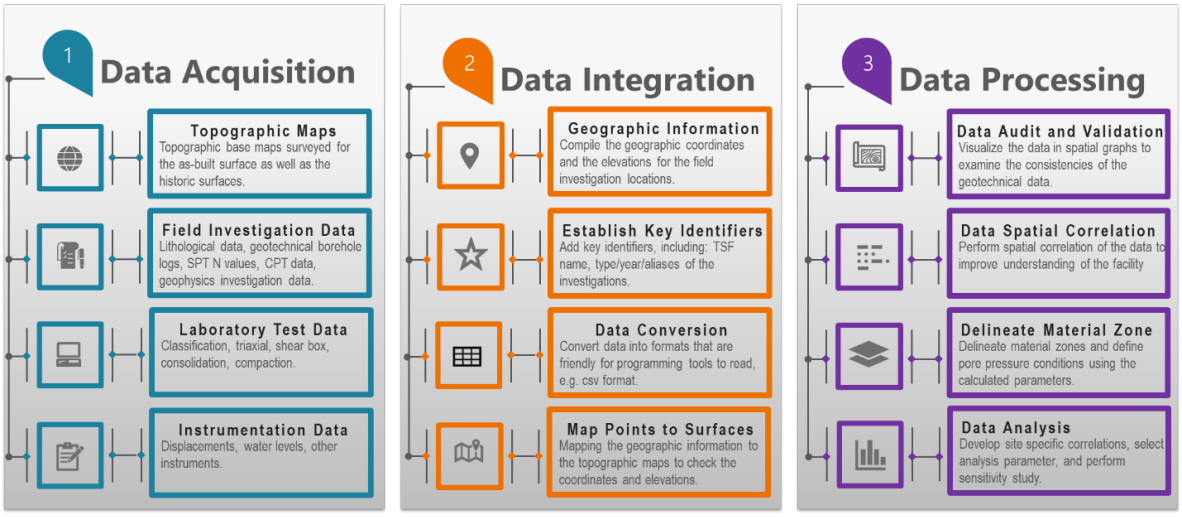


Figure 1: Diagram of the streamlined workflow for data acquisition, integration and processing

Geotechnical data acquisition and integration

Data acquisition

Data acquisition can involve several sources of information including topographic maps, field investigation data, laboratory test results and instrumentation monitoring data. Topographic maps are the basis to develop a three-dimensional (3D) model to incorporate geotechnical information into a spatial database. Topographic maps of the area, not only for the as-built surface but also for the surfaces over the life of the

facility, should be gathered to improve the accuracy and resolution of the 3D model.

Field investigation data, laboratory test results and instrumentation monitoring data can vary in complexity depending on the specific investigation or monitoring instrument. Prior to performing a geotechnical investigation, a desktop study should be conducted to collect existing information about the site. This helps to select the investigation locations and define the objectives of the subsequent investigation. Electronic formats of the collected data should be gathered to minimize manual data entry in the next steps of the analysis.

Data integration

Data integration is a process to map the geotechnical data into a 3D model. The first step is to compile the geographic data of the investigation and to align them spatially with the coordinate system used in the 3D model. This step ensures that the geotechnical data can be accurately referenced within the 3D model. The second step is to identify the key identifiers that can be used to sort, filter, and differentiate the data. Examples of the commonly used identifiers include names of the facilities, types of the investigations, and dates of the investigations. The third step is to convert the data to formats that are computer-friendly. It is crucial to minimize manual data entry, as this will reduce time and cost, and also the potential for human error. R supports integration with various data formats commonly used in geotechnical engineering, such as CSV, Excel, and databases. This enables seamless importing and exporting of data from various sources and tools. Figure 2 shows the steps used to sort the available geotechnical data according to their sources and to utilize geographic coordinates to associate the data to a spatially represented point in the 3D model.

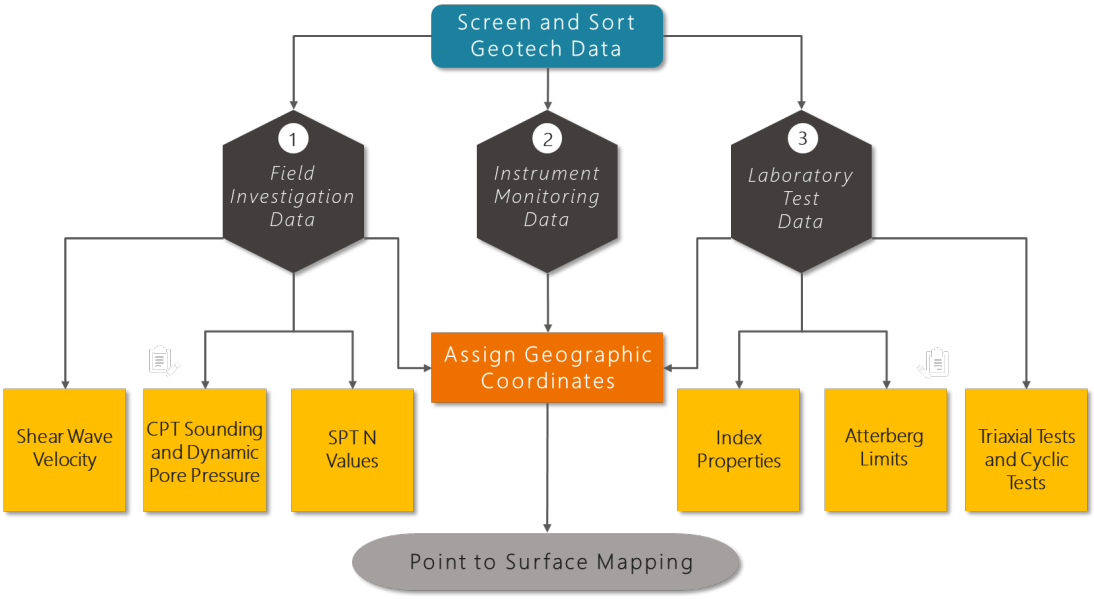


Figure 2: Steps to screen and sort geotechnical data

The most preferred method for data entry is to import data directly from the testing equipment, such as the laboratory apparatus, the monitoring devices, and the CPT rigs. If legacy data are stored in PDF files, internet tools are available to analyze the scanned documents or images and convert the texts into machine-readable data using technologies such as artificial intelligence (Jaksa and Liu, 2021). If the above two mentioned strategies cannot be applied, one can use template-based data entry. This is the least preferred method for data entry and should be used only if handwritten texts are the sole source of information. It is recommended that standardized data entry templates are designed to match specific data requirements and to be readable by computer (Deaton, 2018). Template-based data entry is also useful when migrating data from the legacy reports to the new database.

Geotechnical data processing

Data audit and validation

R can support data validation by assisting with visualizing data in one-dimensional, two-dimensional, and three-dimensional plots. The data validation aims to check the following aspects.

- If major features (e.g., depth of the tailings, thickness of the cover material) indicated by the CPTs or boreholes agree with or contradict the topographic surfaces established.
- If data collected by different methods, including field investigation data, laboratory test results and instrumentation monitoring data, show similar stratigraphic layers.

Figure 3 provides an example of a comparison between the information gathered from a mud rotary drilled borehole (TSF-BH-C10) and a companion CPT (TSF-CPT-B14) that is 45 ft away. The example in Figure 3 includes the field description of the soils, the field blow counts, and the composition of soil types by weight from the borehole investigation, as well as the tip resistance, the dynamic pore water pressure, and the clean sand equivalent normalized tip resistance (Qtncs). The vertical axis is labeled with both the elevations and the depths for the various geotechnical properties, which enables comparison of the data at similar depths. Figure 3 also includes additional annotations to enhance the desired emphasis on important thresholds or reference values.

For example, the Qtncs plot includes Qtncs = 70 as a reference line between the contractive and dilative behaviors, which is defined by Robertson and Wride (1998) and is associated with the state parameter of Jefferies and Been (2006). CPT results show a contractive behavior in the depth between 45 ft and 85 ft as well the bottom 10 ft, where low field blow counts are observed in the collated SPT profile. The comparison between boreholes and CPT data enables geotechnical engineers to find contact surfaces between the stratigraphic layers.

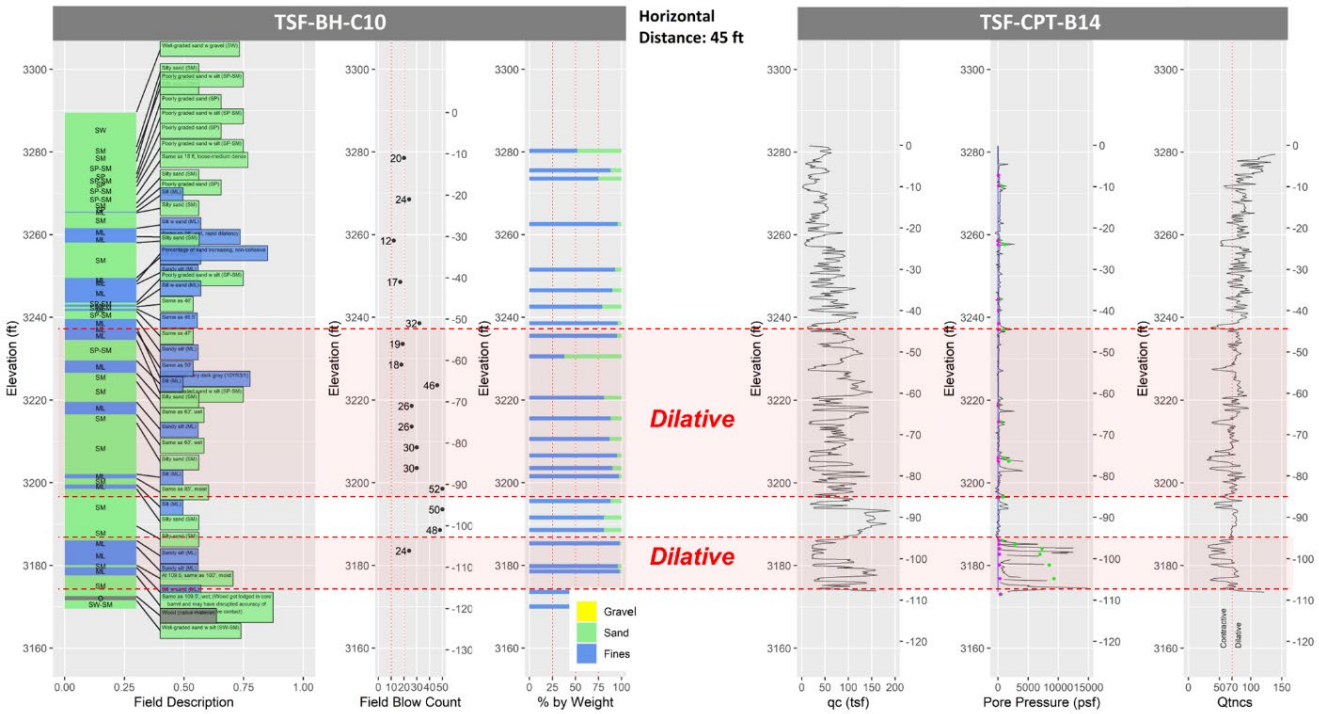


Figure 3: Comparison between CPT and borehole data

Data spatial correlation

Evaluation of mine facilities often requires manipulations and correlations of a large amount of spatial information. The 3D plots produced by R can be customized to show desired parameters of the field and the laboratory data. Figures 4 and 5 provided two examples of the 3D visualization of the information gathered from CPT within the TSF. In Figures 4 and 5, normalized cone tip resistance Qtncs and dynamic pore water pressure u2 are shown as color columns that are associated with their northings, eastings, and elevations. The magnitudes of the geotechnical parameters are coded by colors. It is important that spatial reference points are included in the 3D model so that the positions of the data are readable. In Figures 4 and 5, the locations of the CPT data are vertically projected to the terrain contours to represent their relative positions within the TSF. As shown in Figures 4 and 5, the Qtncs and u2 plots can be compared to examine the subsurface conditions and locate areas with contractive and saturated tailings. The views can be rotated, and zoomed in and out, to provide a comprehensive view of the geotechnical data within the site context.

The 3D model can assist in the process of selecting slope cross-sections for the stability analyses to determine the factors of safety against slope failures. In the next section, a 2D cross-section was generated by R to delineate the tailings profiles within the TSF.

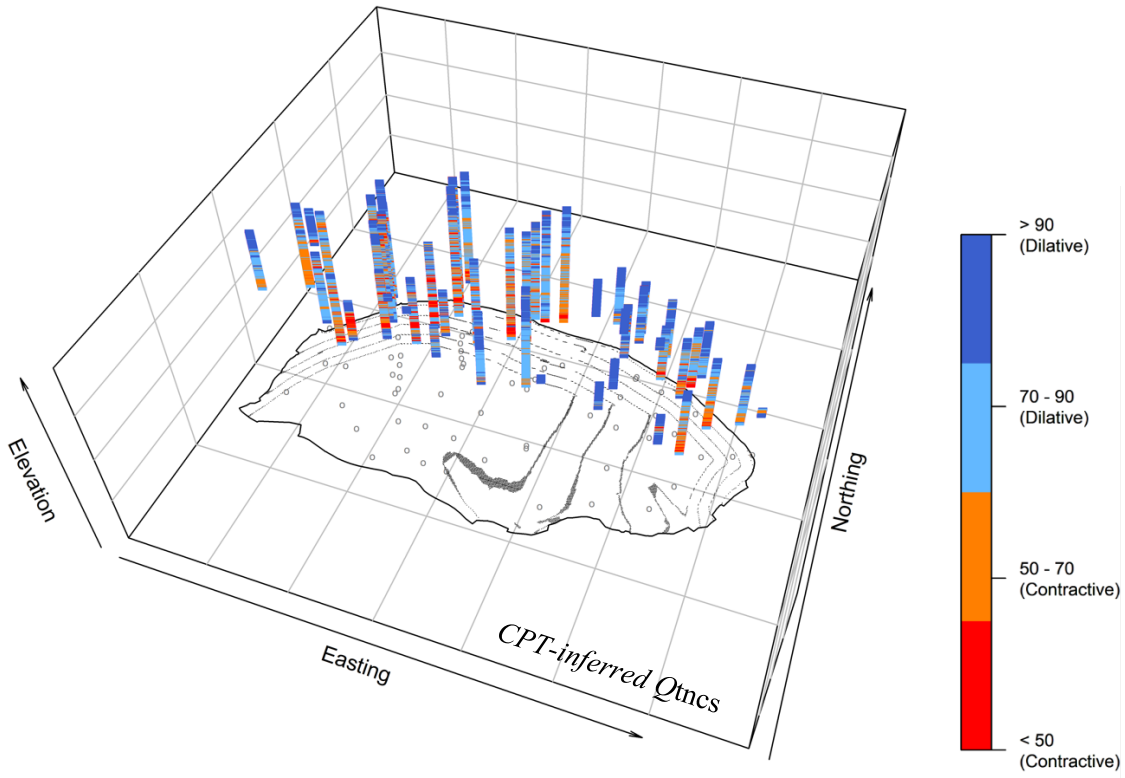


Figure 4: Spatial visualization of CPT-inferred clean sand corrected tip resistance

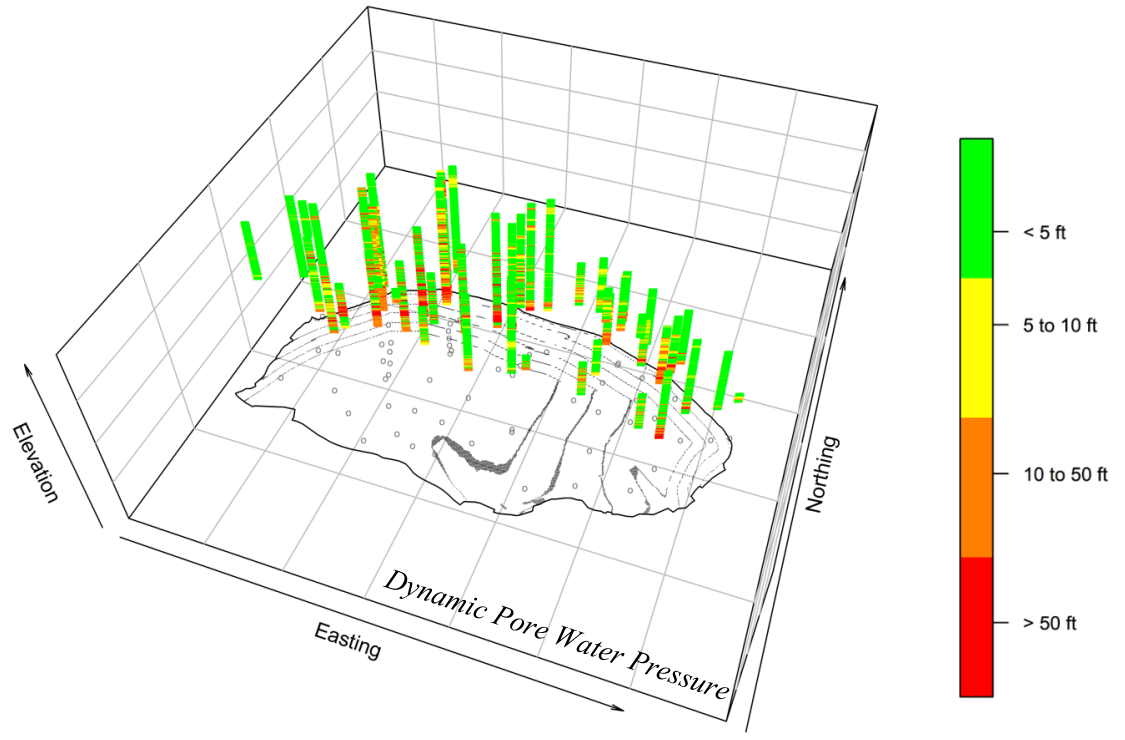


Figure 5: Spatial visualization of dynamic pore water pressure

Delineate material zones

R can produce 2D cross-sections that enable layer delineation by evaluating multiple sources of data. Figures 6 and 7 provided two examples of the 2D cross-sections of a TSF with the information gathered from CPT. Instead of the actual configuration of Holden Tailings Piles, a simplified cross-section is used to demonstrate the process of the data analysis. In Figures 6 and 7, two variables were projected to the cross-sections: dynamic pore water pressure u_2 and normalized tip resistance Qtncs. The foreground black lines combined with the background color bars indicate both the trend and the magnitudes of the parameters.

An essential step to ensure the correct location of the projected data is to interpolate the spatial coordinates along the selected cross-section to calculate the lateral distance, which is shown as the horizontal axis in Figures 6 and 7. Instead of showing multiple geotechnical parameters across the board, we noted that the 2D geotechnical model needs to be focused on one or two parameters in the same plots to maintain readability.

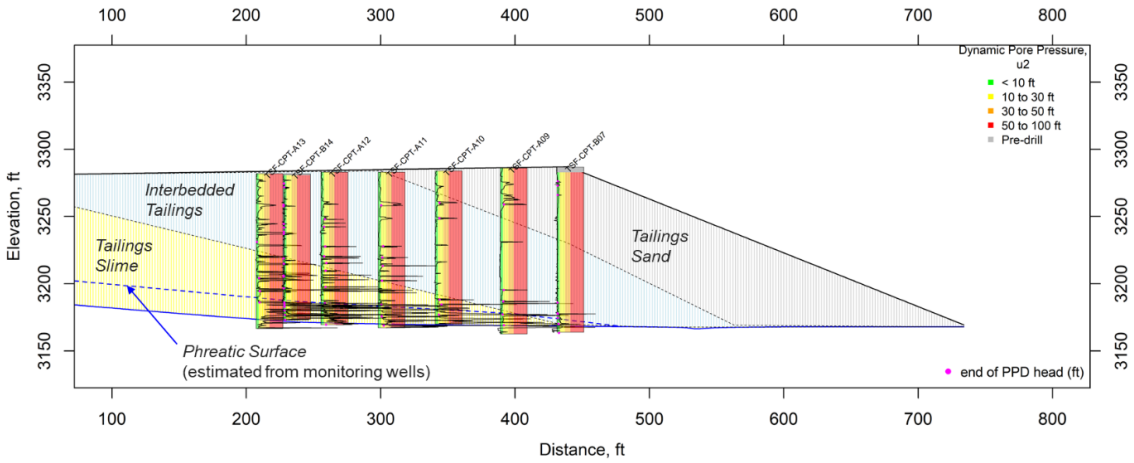


Figure 6: Dynamic pore water pressure and delineated tailings profile

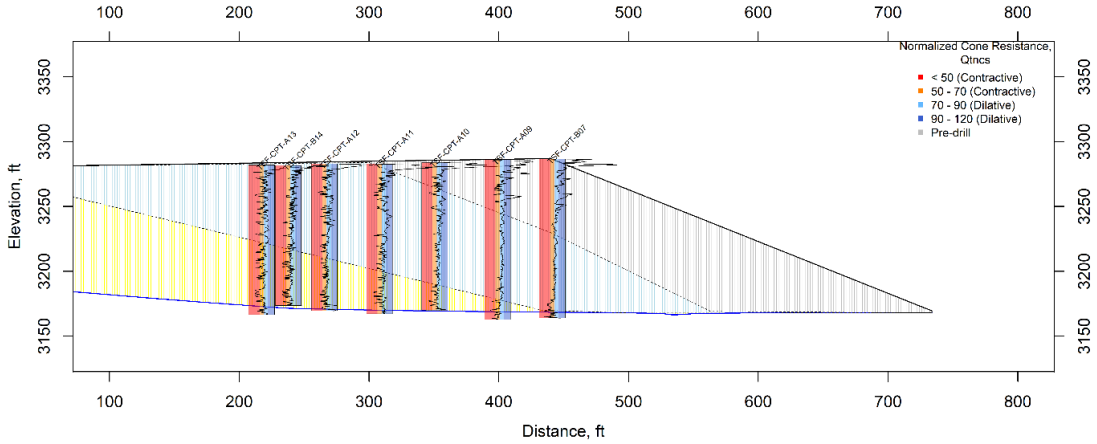


Figure 7: Clean sand tip resistance and delineated tailings profile

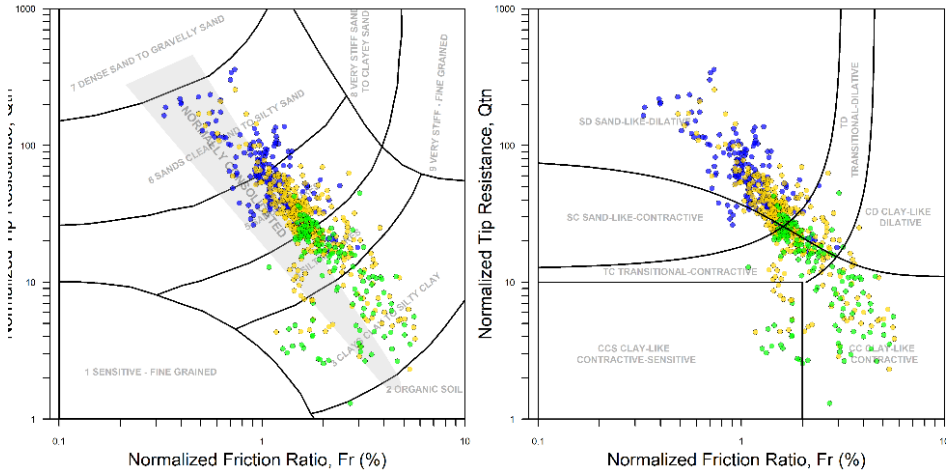


Figure 8: Evaluation of tailings response in the CPT soil behavior charts

The 2D cross-sections can be used for the following purposes:

- Delineate tailings profile. In Figure 6, a total of three tailings groups were identified between the as-built topographic surface and the bottom of the tailings: the contractive tailings slimes, the dilative tailings sand, and the interbedded tailings with intercalated behaviors between the contractive. Also shown in Figure 8, the tailings slime zone is located within the contractive zone in the potential liquefaction chart, which indicates a possible strength loss (flow-liquefaction) and cyclic softening (Robertson, 2010).
- Understand pore water pressure condition. The dynamic pore water pressure within the cross-section and the phreatic surface depicted from the monitoring wells are shown in Figure 7. In Figure 7, the pressure head at the end of pore pressure dissipation tests is shown to assist in evaluating the saturated zones. For this exercise, it is considered that the tailings slime is saturated and is potentially liquefiable, the tailings sand is not saturated, and the interbedded tailings are partially saturated.

The next section will demonstrate sensitivity predictions using R that show how the pore pressure condition changes the liquefaction trigger analysis result.

Data analysis

Once the material zones are delineated, the geotechnical data within each material zone can be extracted for further data analysis. Figure 9 shows the residual strength ratio profiles, and Figure 10 shows the cumulative distribution curves for the residual shear strength ratio calculated for the tailings sand, the interbedded tailings and tailings slimes delineated in the cross-section. The values in Figure 10 can be used to develop the geotechnical parameters that can be used in subsequent stability analyses of this section.

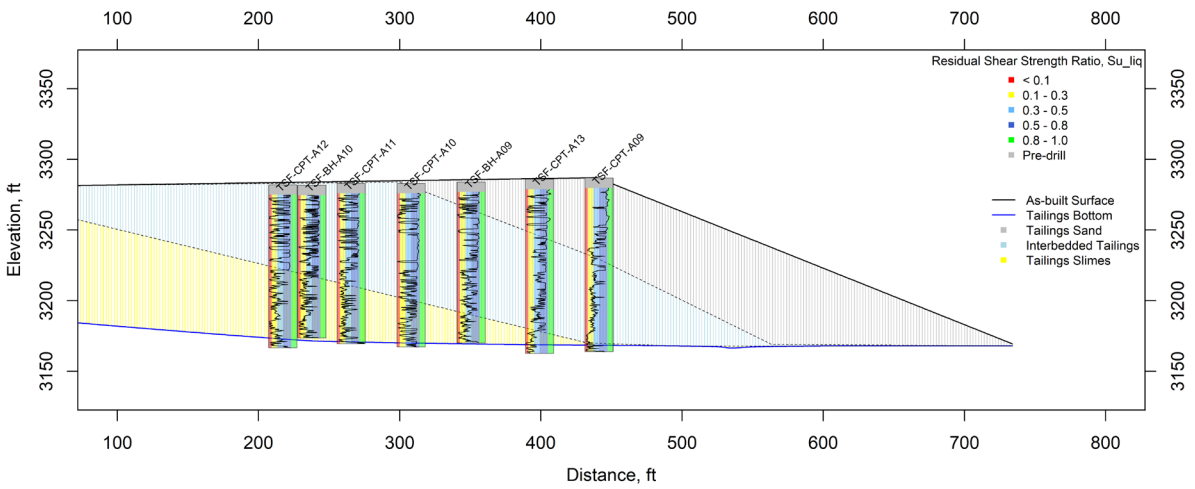


Figure 9: Tailings residual shear strength ratio

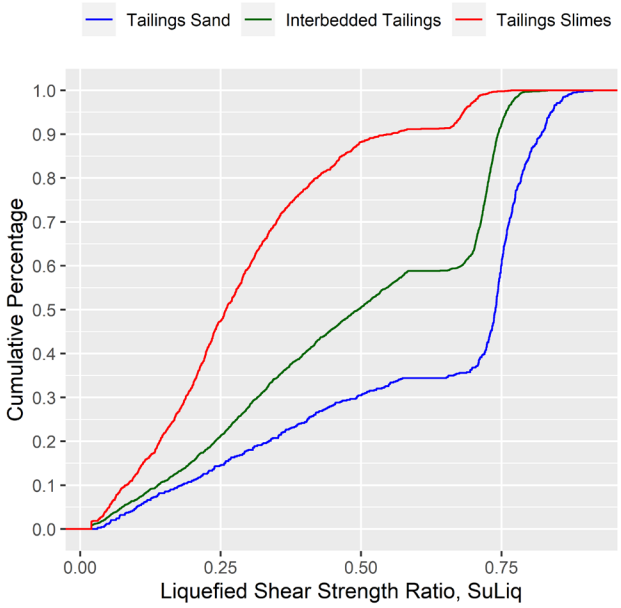


Figure 10: Cumulative distribution curves of liquefied shear strength ratio

After identifying the potentially liquefiable zones, CPT-based empirical correlations were used to calculate the factor of safety against liquefaction (FoS_{Liq}) for the identified saturated zones. In this example, FoS_{Liq} was calculated using the correlation in Boulanger and Idriss (2014). In Figure11, the FoS_{Liq} under various design earthquake return periods are calculated by assuming two scenarios for the saturated zones. In Figure 11 (a) and (b), both the slime and interbedded tailings are considered saturated, while in Figure 11 (c) and (d) only the slime tailings are saturated. Through this exercise, the conclusions were drawn that the assumption of fully saturated slime is reasonable, and that most of the interbedded tailings at the bottom half of the TSF, although partially saturated, are not susceptible to liquefaction.

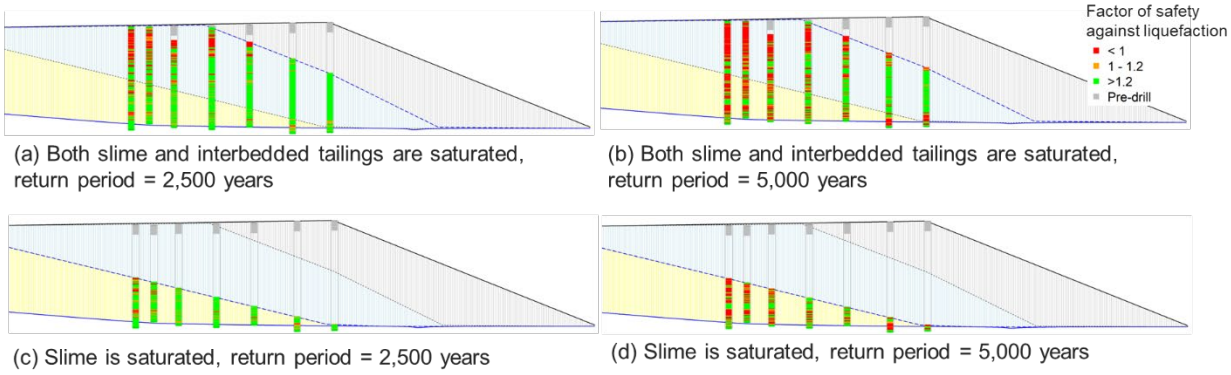


Figure 11: Calculated factors of safety against liquefaction for different saturation assumptions and design earthquake return periods

Discussion and conclusion

This paper presented a workflow to integrate geotechnical data into a database and utilized R to process the geotechnical data. The examples demonstrated the efficiency of R, which enables the automation of repetitive tasks involved in the data processing, as well as the flexibility of R, which designs plots specifically tailored to incorporate desired geotechnical parameters for visualization.

The techniques discussed in this study are demonstrated to be easy to adapt and can be utilized for not only the TSFs but also other mine domains, such as the waste stockpile. It is noted that the complexity of the models will require basic knowledge in programming and, most importantly, the developer's technical expertise in geotechnical engineering, mining, and the related engineering disciplines. The site and engineering knowledge are more important than the programming skills. To adapt to the new needs in the industry and to improve the quality of the solutions, continuous learning for geotechnical engineers in programming and data science should be encouraged by consulting companies.

Acknowledgements

We are grateful to Rio Tinto for their invaluable support and approval to publish the information presented in this study. Their collaboration and willingness to share information have significantly contributed to advancing knowledge in the mining industry. We believe that sharing this approach has the potential to greatly improve our available tools for data management in the mining industry.

References

Boulanger, R.W. and I.M. Idriss. 2014. CPT and SPT based liquefaction triggering procedures. Report No. UCD/CGM-14/1. Center for Geotechnical Modeling, University of California at Davis.

Deaton, S.L. 2018. What are the benefits of geotechnical data interchange? Prepared for the 69th Highway Geology Symposium, September, 2018.

ICMM. 2019. *Integrated Mine Closure Good Practice Guide*. 2nd edition.

Jaksa, M. and Z. Liu. 2021. Editorial for special issue "Applications of artificial intelligence and machine learning in geotechnical engineering." *Geosciences* 11(10): 399. https://doi.org/10.3390/geosciences11100399

Jefferies, M. and K. Been, 2006. *Soil Liquefaction: A Critical State Approach.* First edition. London: CRC Press.

Jefferies, M.G. and K. Been. 2015. *Soil Liquefaction – A Critical State Approach*. Second edition. CRC press.

Player, R.S.V. 2006. Geographic Information System (GIS) use in geotechnical engineering. *Proceedings of GeoCongress 2006: Geotechnical Engineering in the Information Technology Age.* Reston, VA, USA: 1–6.

Robertson, P.K. 2010. Evaluation of flow liquefaction and liquefied strength using the cone penetration test. *Journal of Geotechnical and Environmental Engineering* 136(6): 842–853.

Robertson, P.K. and C.E. Wride. 1998. Evaluating cyclic liquefaction potential using the cone penetration test. *Canadian Geotechnical Journal* 35(3): 442–459.

Singh, A., S. Noor, R. Chitra and M. Gupta. 2018. Applications of GIS in geotechnical engineering: some case studies. *International Journal of Scientific Engineering and Science* 2(3): 34–38.

Chapter Three

Application of GISTM

TAILINGS AND
MINE WASTE 2024



ALARP: Where are We Going and How Do We Get There?

Malcolm Barker, GHD, Australia
Chris Topham, GHD, Australia
Nick Glover, GHD, Australia
Manuel de Membrillera Ortuño, GHD, Australia

Abstract

The water dam industry has been using the ALARP (As Low as Reasonably Practicable) principle for many years in order to assess the tolerability of public safety risks. Consideration of the ALARP principle is inherently subjective, and it is necessary to develop a repeatable and defendable process. This paper presents the current guidance from experience in Australia and other countries on how to address the primary and secondary considerations in determining an ALARP risk position for tailings facilities, using both the International Council on Mining and Metals (ICMM) publication and the Global Industry Standard on Tailings Management (GISTM), together with the Australian National Committee on Large Dams (ANCOLD) 2022 Risk Assessment Guidelines, as well as other sources where the ALARP principle is considered, in order to propose a process for tailings dams.

The paper then provides a case study using quantitative and qualitative risk analysis in the application of the ALARP principle and reflects on the resulting justification to both pursue and avoid dam safety upgrades to small and large tailings dams.

What is ALARP?

Recent research shows that approximately 20,230 Tailings Storage Facilities (TSFs) have been constructed in the period 1965 to 2020, and that the annual number of constructed TSFs increased three-fold over this period (Rana et al., 2022). The average annual probability of failure of a TSF over that period is approximately 2.7×10^{-2} (1 in 37 years), that is, two orders of magnitude greater than water dams.

Among other issues, that is the reason why the mining and tailings dams industry has been addressing the question of "How do we reduce the risks to As Low as Reasonably Practicable (ALARP)?" in recent years.

In this regard, it is important to note that there is no clear guidance in GISTM or ICMM as to which method of risk assessment should be used for evaluating ALARP. This paper aims to provide a process that can be used for any of the risk assessment approaches, including quantitative, semiquantitative and qualitative methods for facilities that may range from Low to Extreme consequence classification, or using the applicable regulation or guidance in each country.

According to GISTM Requirement 4.7:

*"… the Accountable Executive shall approve and document the implementation of measures to reduce **both** the probability and the consequences of a tailings facility failure in order to reduce the risk to a level as low as reasonably practicable (ALARP). The **basis and timing** for addressing the upgrade of existing tailings facilities shall be **risk-informed** and carried out as soon as reasonably practicable."(Emphases added by author)*

According to the Glossary in GISTM:

ALARP requires that all reasonable measures be taken with respect to 'tolerable' or acceptable risks to reduce them even further until the cost and other impacts of additional risk reduction are grossly disproportionate to the benefit.

According to the *ICMM Tailings Management Good Practice Guide*, factors involved in applying ALARP after a remedial action and/or enhanced operational practices or surveillance have been implemented include:

- Application of relevant good practice. This can be applied to all aspects of the facility including operation, maintenance, surveillance, construction, and emergency planning.
- The level of incremental risk in relation to the established risk guidelines.
- The cost-effectiveness of the risk reduction measures in relation to likelihood and/or consequence.
- Remaining life of the facility and potential alignment with closure planning that may reduce likelihood and/or consequence.
- Societal concerns as revealed by consultation with the community and other stakeholders.
- Other factors such as:
    - consideration of standards-based approaches,
    - benchmarking,
    - direct business impacts,
    - constructability,
    - implementation schedule, and

- environmental consequences.

Each of these factors is considered in the ALARP approach proposed for facilities varying from Low to Extreme risk, as shown in Figure 1.

It should be noted (ANCOLD, 2022) that the additional understanding that comes from the risk assessment process for reducing risks to ALARP may reveal that a less costly solution to a dam safety problem could be justified, but it could just as easily be that a risk assessment shows that a more stringent safety level, and thus a more costly solution, should be implemented.

Risk assessment approaches

Figure 1 presents a risk matrix based on a previous paper (Barker, 2023) and the ANCOLD Guidelines on the Consequence Categories for Dams (ANCOLD, 2012). This shows an indicative way forward for the use of the various risk assessment methods when evaluating ALARP, including ratings for population at risk (PAR), potential life loss (PLL), environment, social effects, infrastructure and economics, and company reputation.

		Potential Life Loss				
		None <0.1	Unlikely 0.1 - 1	Possible 1 - 5	Likely 5 - 50	Many >50
		Population at Risk				
		None	1 - 10	10 - 100	100 - 1000	>1000
		Consequences				
Likelihood Description	**Likelihood AEP Range**	**Low**	**Significant**	**High**	**Very High**	**Extreme**
Very High	1E-2 to 1E-3	Medium SQRA	High Hybrid/ QRA	High Hybrid/ QRA	Extreme QRA	Extreme QRA
High	1E-3 to 1E-4	Medium SQRA	Medium SQRA	High Hybrid/ QRA	Extreme QRA	Extreme QRA
Moderate	1E-4 to 1E-5	Low Qualitative Matrix	Medium SQRA	Matrix to Full QRA	High Hybrid/ QRA	Extreme QRA
Low	1E-5 to 1E-6	Low Qualitative Matrix	Low Qualitative Matrix	Medium SQRA	High Hybrid/ QRA	High Hybrid/ QRA
Remote	1E-6 to 1E-7	Low Qualitative Matrix	Low Qualitative Matrix	Low Qualitative Matrix	Medium SQRA	High Hybrid/ QRA
Environment		Minimal Loss	Not Significant	Significant	Major	Catastrophic
Health Social and Culture (People affected)		Minimal Effects	Significant Disruption	100-1000 People	1000 People affected	5000 people affected
Infrastructure & Economics		<US$1M	<US$10M	<US$100M	<US$1B	>US$1B
Company Reputation		Minor Temporary	Measurable - Limited	Substantial - State	Serious - National	Severe – Global
Severity Factor		10	30	100	300	1000

Figure 1: Risk assessment approaches selected using a risk matrix example (Barker, 2023)

The selection of the risk approaches does not negate the use of more detailed risk analyses for low-risk facilities where data is available and there is a requirement to comply with the tailings storage facility

owner's risk management framework or a Regulator's requirements. The more detailed risk analyses are preferred where there is a population at risk; however, where a tailings facility has little or no PAR or PLL, then the simplified analyses are appropriate, particularly since the cost benefit ratios are limited in value for the ALARP evaluation.

Process for achieving an ALARP solution

The process for achieving an ALARP solution has been further developed, as presented in Figure 2, which shows the bigger picture spiraling into the focal point of the ALARP solution, as discussed below.

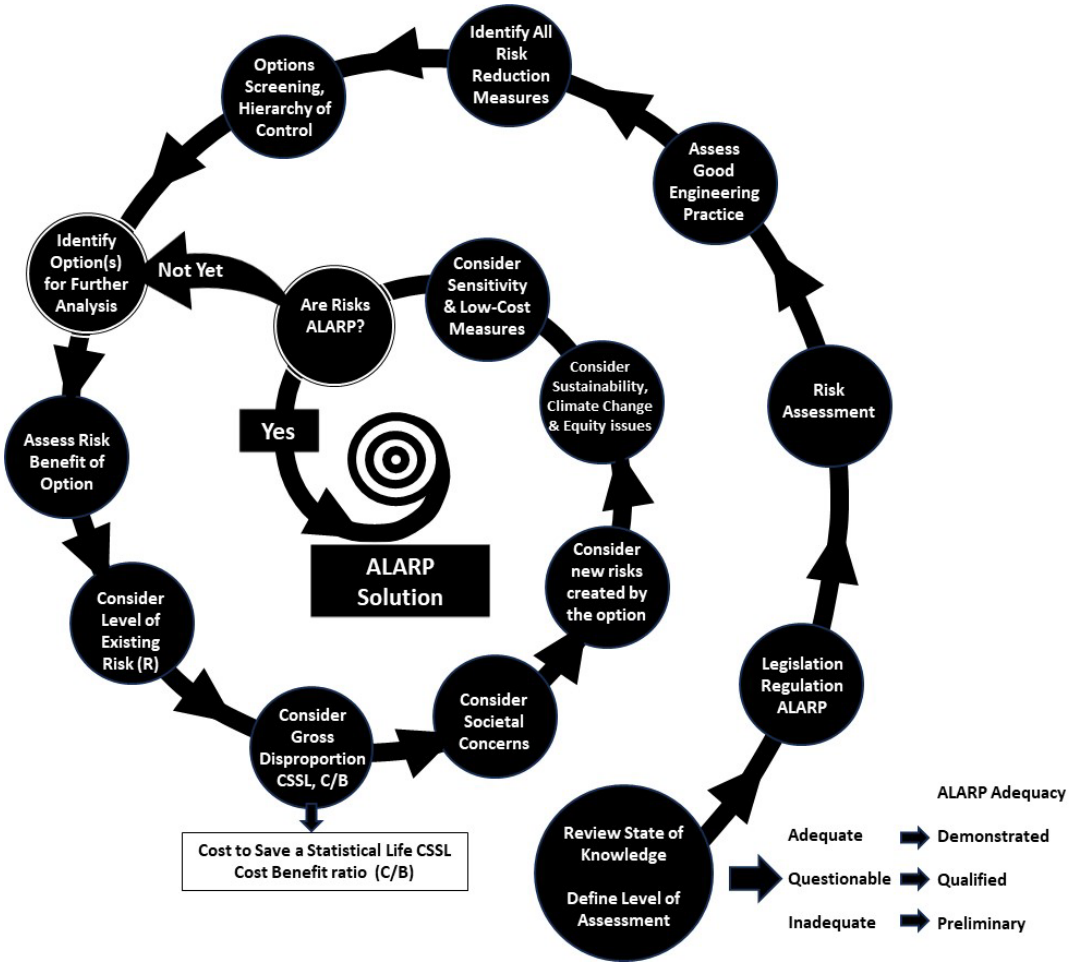


Figure 2: Conceptual representation of the iterative process to circle in on a risk position that is ALARP for a single dam (modified after Topham et al., 2024)

State of knowledge and level of ALARP assessment

A useful approach to a state of knowledge assessment is provided below, based on Pearse et al. (2022). This approach is a screening tool to qualify the outcomes of the assessment. The assessment is subdivided into four categories to assess the adequacy of the information in terms of these points:

- Level of detail and currency of risk assessment.
- Engineering inputs, which are used for the potential failure modes and likelihood assessment.
- Consequence assessment inputs.
- Understanding of risk control measures (existing and additional).

For each of these categories, the assessment team makes a judgement on the degree of adequacy (inadequate, questionable, or adequate) for the dam system. The lowest "adequacy level" will generally dictate whether the ALARP assessment is Preliminary, Qualified, or Demonstrated.

Legislative and regulatory context

The facility owner may have obligations for the ALARP assessment to be compliant with the following:

- GISTM, which "provides a framework for safe tailings facility management while affording Operators flexibility as to how best to achieve this goal."
- Legal duty to reduce risks to ALARP under both statute and common law (in the UK and Australia).
- Any requirements their regulator may have in regard to ALARP.

Risk assessment

The level of knowledge, regulatory requirements and internal company policies, together with the initial evaluation of risk using a failure modes and effects analysis (FMEA) approach are used to determine whether the quantitative or qualitative approach is to be used for the risk assessment, as shown in Figure 3.

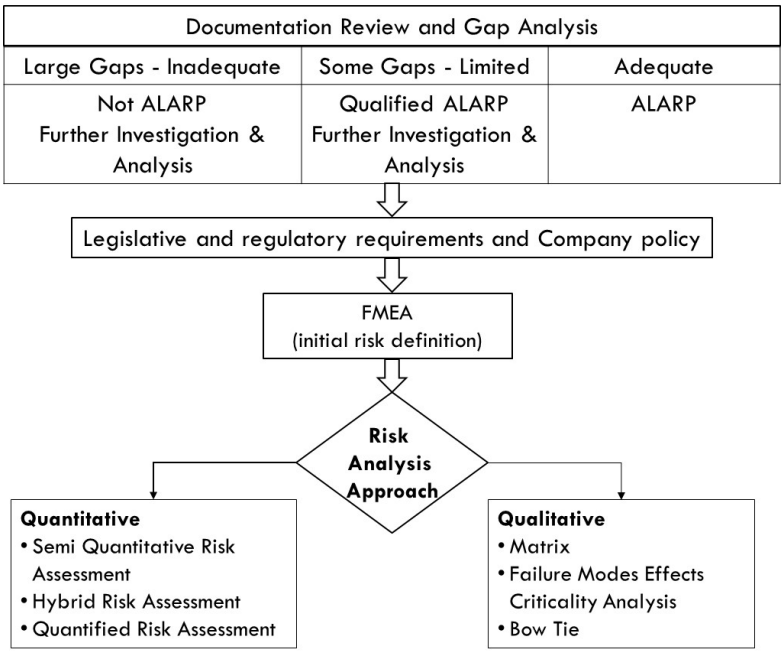


Figure 3: Selection process for risk assessment approach (Barker et al., 2022)

Where a qualitative risk assessment is used, a criticality rating system like the example shown in Table 1 can be used for evaluating the likelihood of failure or a descriptive system based only on the Initiation (I) shown in Table A1 in the Appendix.

Criticality as an alternative for probability in qualitative analysis

In order to evaluate the likelihood or criticality of a failure mode, three numerical ratings are multiplied together to calculate the overall "criticality," as the following example shows:

Table 1: Example criticality rating system (adapted from GHD, 2023)

Symbol	Rating name	Description	Score range
I	Initiation	Likelihood of the initiating mechanism being present or occurring. Includes all events up to and including the point at which the failure mode initiates	Score of 1 (rare) to 5 (almost certain)
P	Progression	Likelihood the failure mode, once initiated, will progress to a catastrophic consequence	Score of 1 (rare) to 5 (almost certain)
E	Control effectiveness	Effectiveness of existing controls that PREVENT and DETECT the failure mode event, and/or INTERVENE to lessen the consequences. This is a measure of the effectiveness of the controls listed in a TSF Bow Tie analysis, FMEA, (and any others) relevant to each failure mode	Score of 1 (highly effective) to 5 (absent)

Note that the "initiation" portion of event ends once the failure mode has been initiated. The progression rating can then be applied to the subsequent events leading to an extreme or catastrophic failure. Importantly, such rating systems can be further tailored to suit the TSF owner.

Hence, to calculate the Criticality (C) of a failure mode:

Criticality (C) = I × P × E, a numerical value ranging from 1 – 125.

In the case that there is a desire to convert criticality to annual exceedance probability (AEP), this could be done on a log basis, as shown in Figure 4.

Tables A1 to A3 in the Appendix provide guidance when selecting these criticality parameters. As with a quantified approach for risk analysis, it is important for the failure mode to be well understood and described to ensure that it is credible and can be understood for the application of the ALARP process.

Tables A4 to A6 in the Appendix provide a means of rating the consequences resulting from a failure for potential life loss, economic loss and company reputation, and social and environmental losses. This

rating system can then be used to evaluate the effectiveness of risk reduction measures (RRMs), using plots of either the calculated probability of failure or the Criticality values against the various consequences.

It should be noted that when plotting data and using it for reducing risks ALARP, as shown in Figure 4, there should not a limit of tolerability for acceptance, as there may still be remedial measures that are needed even when a tolerability limit is reached. Notwithstanding this, it is known that some corporations do include a limit of tolerability, and this should be used with caution.

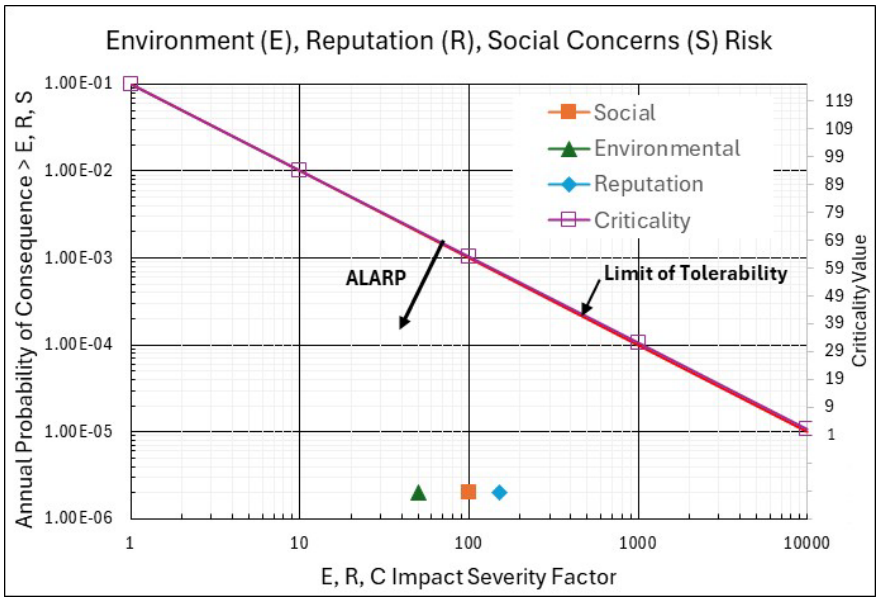


Figure 4: Risk plot of annual probability or criticality versus impact severity factor for environmental, reputational and social concern

Assess good practice and precedent

The UK Health and Safety Executive (HSE) guidance material states that good practice is defined as "*those standards for controlling risk that HSE has judged and recognised as satisfying the law, when applied to a particular relevant case, in an appropriate manner.*" Some sources of good practice include:

- industry standards;
- guidelines;
- precedence – be careful as some aspects of precedence may not be appropriate for your TSF; and
- benchmarking.

Identify risk reduction measures

In practical terms, mitigations against each failure mode identified in the risk analysis can be described in terms of recognized good practice.

Screen options using hierarchy of controls

Having identified the RRMs, a ranking and screening tool is used to assist in the selection of the RRMs for further analysis. A typical multi-criteria analysis (MCA) tool can be used to rate each measure against categories relevant to the ALARP assessment, as shown in the example in Table 2 below for the qualitative and quantitative assessments. An example of the multi-criteria screening tool is shown in Table 3, noting that elements and metrics of such rating systems can be tailored to suit the TSF owner, and weightings can be applied to metrics depending on their relative importance within the context being considered. The MCA total rating in this example is the addition of each of the weighted scores.

Table 2: Risk reduction measures screening factors

Qualitative Assessment	Quantitative Assessment
Understand Failure Modes	Understand Failure Modes
Hierarchy of Controls (How well does the RRM address the Controls?)	Hierarchy of Controls (How well does the RRM address the Controls?)
Implementation cost	Implementation cost
Level of risk reduction achieved (Matrix)	Level of risk reduction achieved (R-value per ANCOLD, 2022). See below
Interdependency with other RRMs	Percentage of total risk contribution addressed by RRM
Additional risk introduced by the RRM	Interdependency with other RRMs
	Additional risk introduced by the RRM

Table 3: Example of multi criteria analysis screening tool score categories

Implementation Cost	Weighted score
>$30M	0
$15M to $30M	1
$10M to $15M	2
$5 to $10M	3
$2M to $5M	4
$1M to $2M	5
$750k to $1M	6
$500k to $750k	7
$250k to $500k	8
$100k to $250k	9
<$100k	10

Order of magnitude of Risk Reduction (Total Cummulative F - Total Cummulative F with RRM)	Weighted score
<0.01	0
0.01-0.1	1
0.1-0.2	2
0.2-0.3	3
0.3-0.4	4
0.4-0.5	5
0.5-0.6	6
0.6-0.7	7
0.7-0.8	8
0.8-0.9	9
>0.9	10

Percentage of total risk contribution addressed by RRM (%)	Weighted score
<1	0
1.0-10.0	1
10.0-20	2
20-30	3
30-40	4
40-50	5
50-60	6
60-70	7
70-80	8
80-90	9
>90	10

Interdependency on success of other RRM	Weighted score
Nil	0
1 RRM	-2
2 RRM	-4
3 RRM	-6
4 RRM	-8
5 RRM or more	-10

Additional risk to implement/construct RRM	Weighted score
Nil	0
Insignificant - mangaged with inspection and monitoring	-2
Minor - managed with simple control	-4
Moderate - comprehensive operation required	-6
Significant - comprehensive controls and detailed analyses required	-8
Catastrophic - unlikely to be controlled	-10

Heirarchy of Controls	Weighted score
Eliminate the Hazard	0
Substitute the Hazard	1
Isolate the Hazard	2
Engineering Controls	3
Administrative Controls	4
PPE	5

Existing risk level and risk reduction benefit of options

An example of the existing risk level and risk benefit for a RRM is shown in Figure 5 for a quantitative and qualitative risk quantification.

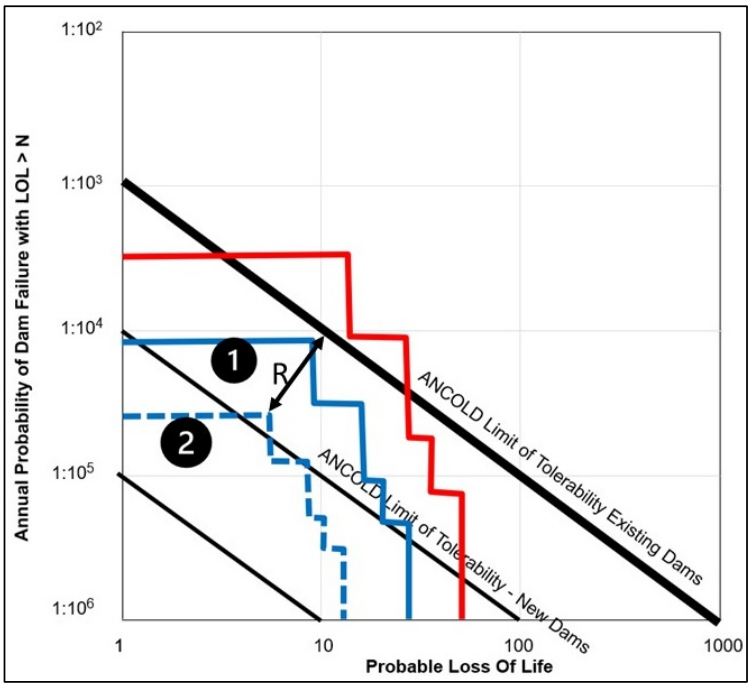


Figure 5: Risk level and risk reduction benefit for quantitative (FN) risk analyses

Where the ALARP assessment is based on a quantitative risk analysis, the level of risk (R) shown for the quantitative assessment can be calculated as defined in the equation below (ANCOLD, 2022).

$$R = -\log\frac{Worst\ risk\ point\ on\ F-N\ Curve}{Limit\ of\ Tolerability} = -\log\frac{(F\times N)_{MAX}}{10^{-3}}$$

Where:

- R is the level of risk expressed in orders of magnitude below the Limit of Tolerability
- $(F\times N)_{MAX}$ is the product for the worst risk pair of F and N
- F is the cumulative annual probability of failure with expected loss of life ≥N

For individual risk:

$$R = -\log\frac{Individual\ Risk}{Limit\ of\ Tolerability}$$

The value R is also used in assigning the disproportion factor for estimation of the Cost to Save a Statistical Life (CSSL) defined by ANCOLD (2022). Recommendations for the interpretation based on the considerations above are shown in Figure 5 for the quantitative risk analysis.

Figure 6 includes an example of how to portray the level of risk reduction for a qualitative matrix approach, where that reduction can be established by a simple ratio of the change of numerical value in the matrix. In the example shown in Figure 6, this ratio would be 9/4=2.25.

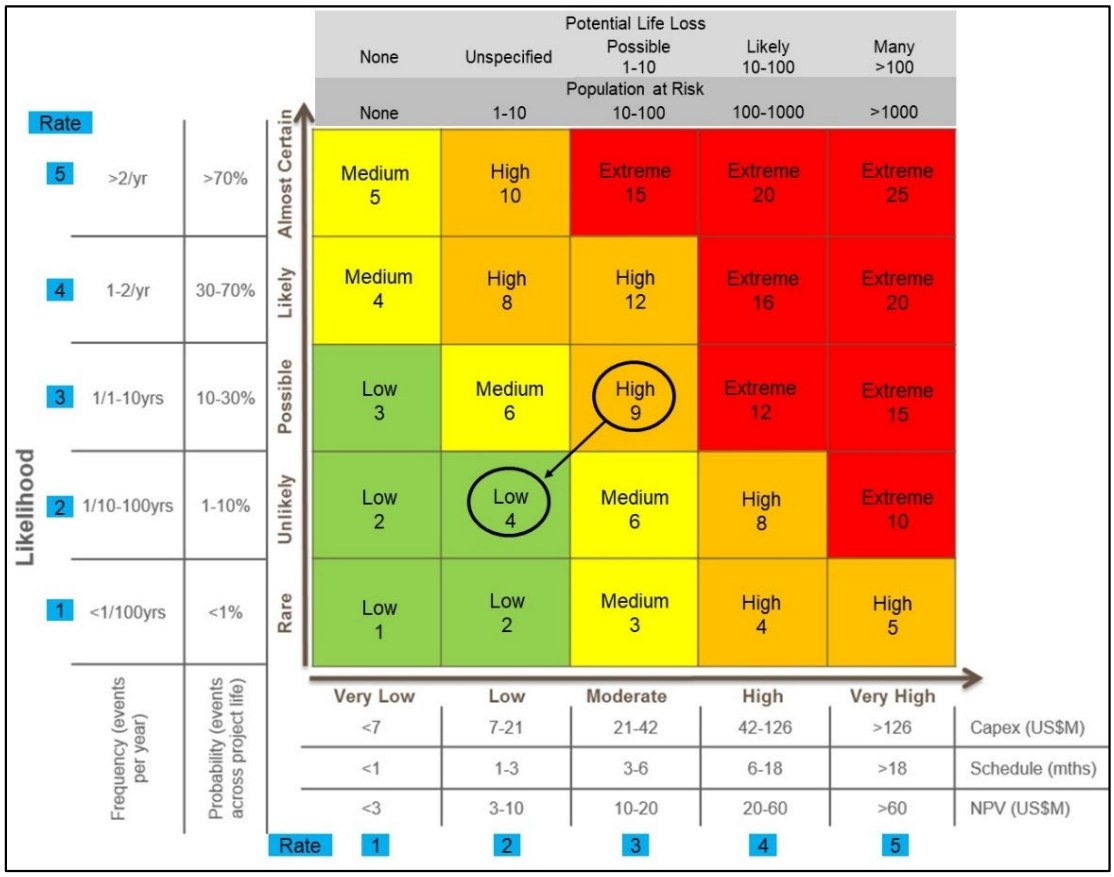


Figure 6: Risk level and risk reduction benefit for qualitative (matrix) risk analyses

Cost effectiveness

Quantitative assessment of cost effectiveness

The R-values achieved by each combination of RRMs, when plotted against the cumulative cost of implementation, can provide a useful visual assessment of when the cost of the next most viable RRM is grossly disproportionate to the risk benefit achieved, and also be used as a RRM prioritization sequence.

Figure 7 presents an example plot for a dam, which clearly shows the benefit gained from the considerable expenditure to deliver RRM 5 and RRM 6 is grossly disproportionate to the risk benefit (when compared to RRMs 1 – 4).

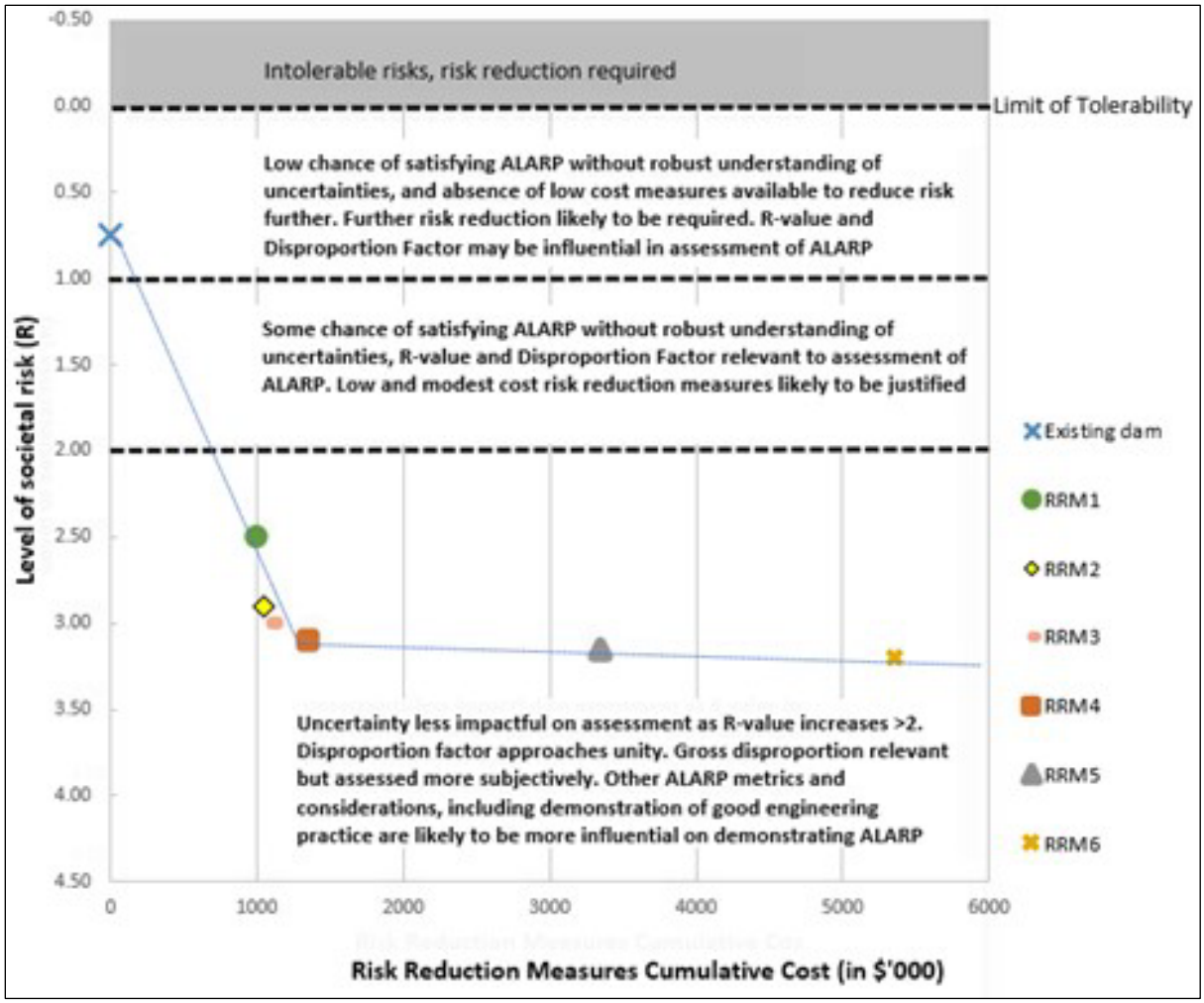


Figure 7: Level of reducing existing risk (R) as additional measures are added versus cumulative cost (Topham et al., 2024)

ANCOLD (2022) provides an approach to evaluate the gross disproportionality of costs relative to the Limit of Tolerability using the R value and CSSL, as well as a cost benefit ratio (CBR). In the authors' experience, once the risk is lowered below the Limit of Tolerability, the CSSL and CBR are not generally strong drivers for ALARP, but rather the remaining factors.

Qualitative assessment of cost effectiveness

In the case of the matrix approach, it would be mandatory for the risk to be lowered to at least the Medium to High range. As discussed above, the level of risk reduction can be established by a simple ratio of the change of numerical value in the matrix, which is 2.25 in Figure 6. The axis in Figure 6 would be adjusted to suit the range of risk reduction, and a similar plot would be produced for each RRM.

Societal concerns

If the TSF in question has characteristics that would suggest an elevated level of societal concern regarding a failure, then a lower risk target may be warranted, compared to a more remote, less critical TSF. Relevant considerations are as follows:

- The hazards and uncertainty regarding the risks.
- High Consequences. Dread owing to the scale of consequences. Will society have greater leverage for reducing risks to ALARP?
- Vulnerable People. Who are they and where are they with respect to any potential failure scenario, and can they be moved to another location in order to eliminate the risk?
- Critical Infrastructure/loss of services. Is there any critical infrastructure affected for the future operation of the site or affected areas in the event of a failure?
- Equity of distribution of risk and benefits. Where would it be best to implement changes in operation of infrastructure to achieve equitable risk reduction across the system?
- Climate Change. Has climate change been considered in the ALARP decision?

Table A5 in the Appendix provides a descriptive means for quantifying societal concerns that can be used as a direct measure for seeing the impact in changes of likelihood for each RRM.

Creation of new risks

Creation of new risks where the remedial works change the configuration of a site or result in placement of material over areas that may be affected in future operations. This is particularly important where a "temporary fix" becomes a "permanent fix" and the resulting effects on the structure can lead to failure if the failure modes are not well understood.

Environmental and sustainability

The potential differentiation between risk reduction measures on the basis of environment or sustainability should be considered, in line with the owner's corporate strategy and risk appetite as well as any legislative or regulatory requirements.

Table A6 in the Appendix provides a descriptive means for quantifying environmental impacts that can be used as a direct measure for seeing the impact in changes of likelihood for each RRM.

Low-cost measures

In accordance with ANCOLD (2022), measures that are sufficiently low-cost should be adopted regardless of whether they provide a material or measurable risk reduction benefit, especially if they represent recognized good practice.

Case study (Dam A)

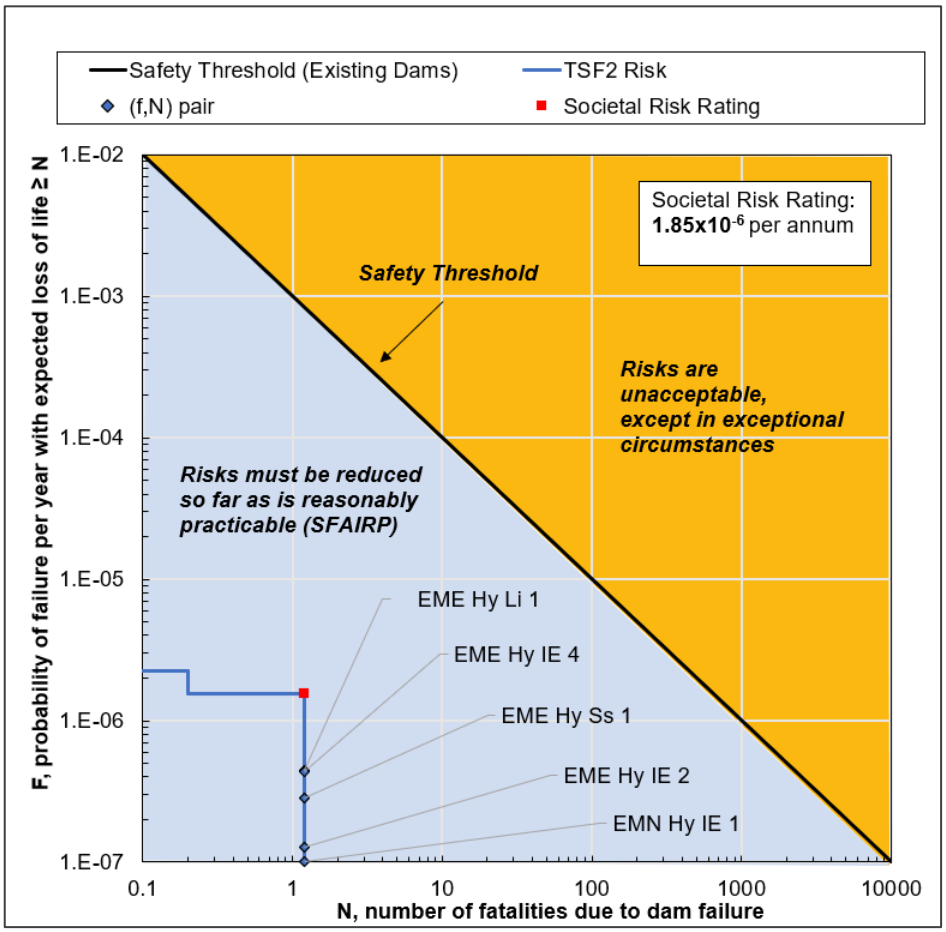
The following case study is provided to demonstrate the application of ALARP using the quantitative and qualitative approaches. The qualitative approach assumes that we do not have the probabilistic AEP for failure and an overall probability of failure is taken based on the failure modes.

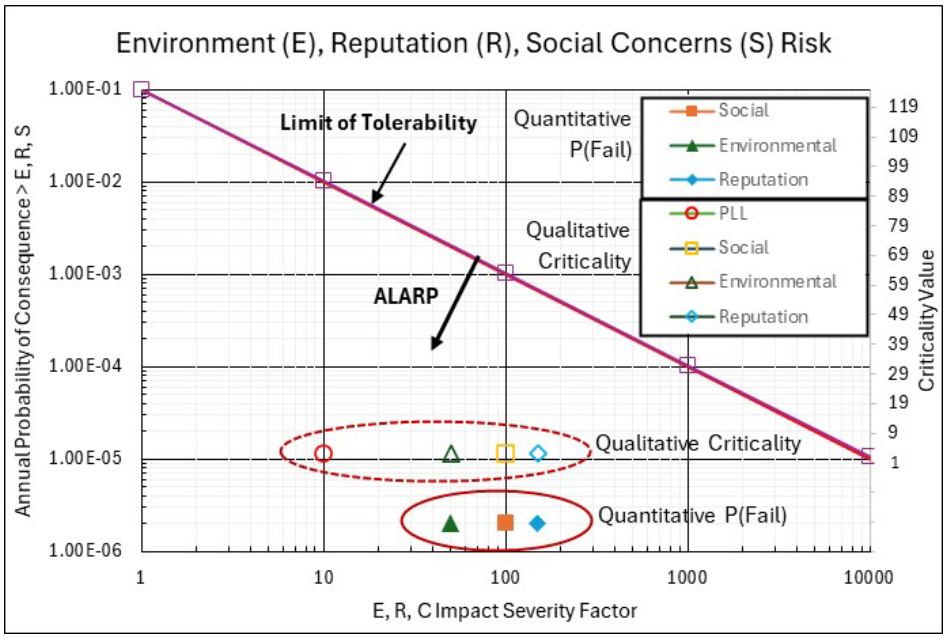
The structure is a 29 m high TSF with four embankments constructed via either centerline or upstream raises, creating a turkey's nest structure (an off-river storage that does not capture any external surface water). The decant system includes a tower located at the center of the tailings impoundment and a conduit that goes under one of the TSF walls to return water to a process water pond. The assessment is taken for the closure condition with the TSF at maximum height and a free overflow spillway, following a final downstream raise expected to be finished in three years. The key metrics relevant to the ALARP assessment are presented in Table 4.

Table 4: Characteristics relevant to ALARP assessment for Dam A at closure

Description of Dam	29 m high center line and upstream raised TSF embankment using clay and tailings for construction, with 3,500 m long perimeter embankments. The starter embankment was constructed in 2012 and there have been 2 upstream raises and 2 center line raises to date. Closure condition assumes a final downstream raise and capping.
Consequence Category	Downstream consequences include flooding of the mine site, underground mine works, and public land. Population at Risk estimated to be up to 17 persons, with potential loss of life around 1 person. Quantitative PLL: 1 Qualitative PLL Severity: 5 (uncertainty as to 1 PLL) Social Concerns Severity: 100 Environmental Severity: 50 Reputation Severity: 150
Summary of Risk Position	This dam is well below the Limit of Tolerability (LoT) or Safety Threshold for the quantitative assessment (R = 2.7), with key contributors to total risk position as follows: • Flow liquefaction of the eastern wall embankment and tailings under loading conditions including blasting, machinery vibrations, drillings, phreatic level changes, etc. leading to a brittle failure mechanism and breach of the embankment (27%) • Internal erosion and piping at the foundation due to presence of the decant conduit (26%) • Slope instability through embankment leading to settlement and loss of freeboard under normal loading (17%) Qualitative Criticality • Initiation 1 (Good knowledge and practice in design and construction) • Progression 2 (Possibility cannot be ruled out) • Control 1 (Effective and reliable) • Criticality = 1x2x1 = 2
	RRM 1: additional downstream berm to reduce the likelihood of failure by slope stability, internal erosion and flow liquefaction. RRM 2: stockpile of materials in the dam break flow path to direct dam break inundation away from the underground works tunnel entrance (and hence avoid PLL)

Risk Overview





ALARP Element	Conclusions
State of Knowledge	The dam is a relatively new tailings structure, with the starter embankment constructed in 2012. The most recent raises, stage 3 and stage 4, were designed with reference to many current design codes, such as relevant Australian Standards and ANCOLD design guidelines for tailings, which represent recognized good practice. There is good design and construction documentation including photographs and QA documentation. The operation and maintenance manual and emergency response plan are in place and well prepared. The ALARP assessment can be considered to be adequate given the state of knowledge.
Legislation and Regulation	The ALARP assessment is to be completed using the ANCOLD guidelines and the Water Act.
Recognized Good Practice	At closure, existing known risks will be resolved in line with recognized good practice. The critical failure mode for this dam relates to the risk of liquefaction of the tailings retained by the eastern embankment. This risk is mitigated by the centerline/downstream raise of the structure, which provides additional stability against both slope stability and liquefaction of tailings and represents recognized good practice. Following recognized good practice, the dam owner is already upgrading the surveillance/monitoring system and decommissioning the decant conduit.
Gross Disproportion – Cost Analyses	**Quantitative Assessment** At closure, the dam plots almost 3 orders of magnitude under the limit of tolerability for an existing structure using quantitative analysis. It is therefore expected that the cost of all conceivable RRMs would be grossly disproportionate to the risk reduction achieved. To prove that this is the case, a modified CSSL assessment was completed which indicated a "Poor" justification rating for any RRM which costs above $3,100. **Qualitative assessment** Based on good design and construction for closure, the Progression can be reduced to a value of 1 resulting in a Criticality of 1
Gross Disproportion – Level of Risk vs. Cost	RRM 1 (Large downstream filter and rockfill berm intersecting the foundation) is estimated to cost several million dollars and hence meets the gross disproportionality threshold, demonstrating it is not justified. The cost of RRM 2 (stockpile of materials to direct dam break flow path away from works and towards the water process ponds) is a lost opportunity cost (to use this area for another purpose), but with stockpile of materials to proceed regardless of location, this can be considered negligible. Its impact on the Societal (F–N) curve would be to limit the Potential Loss of Life to itinerants, and hence achieve material risk reduction for low cost, meeting a key ALARP test. Hence RRM 2 was recommended.
Creation of New Risks	For the low-cost option, consideration must be given to the location of the redirected dam break flow path to ensure no new risks are created by the RRM. The redirected flow pathway does not result in additional environmental or life safety risks because it would be directed towards the water process ponds.
Societal concerns	Given the potential for loss of jobs and dislocation of people, the severity factor was set at 100 for the existing facility and for RRM 2, this was reduced to 20, as shown in Figure 8.
Equity/Efficiency	Considered neutral to ALARP determination.
Environmental	Environmental risks during construction are considered manageable given the Stage 4 raise currently taking place; however, it was considered likely that fauna and stock would be affected, and the existing dam was given a severity factor of 50 and following RRM 2, this was reduced to 10.
Low-cost measures	RRM 2 is considered to be a practicable, low-cost measure with a meaningful reduction in life safety risk and is therefore included in measures recommended to reach an ALARP risk position. Along with these two risk reduction measures, the dam owner is currently implementing several measures following recognized good practice by default, including an upgrade of the monitoring system, a TSF safety review and risk assessment, update of the consequence assessment and emergency action plan (non-structural measures).

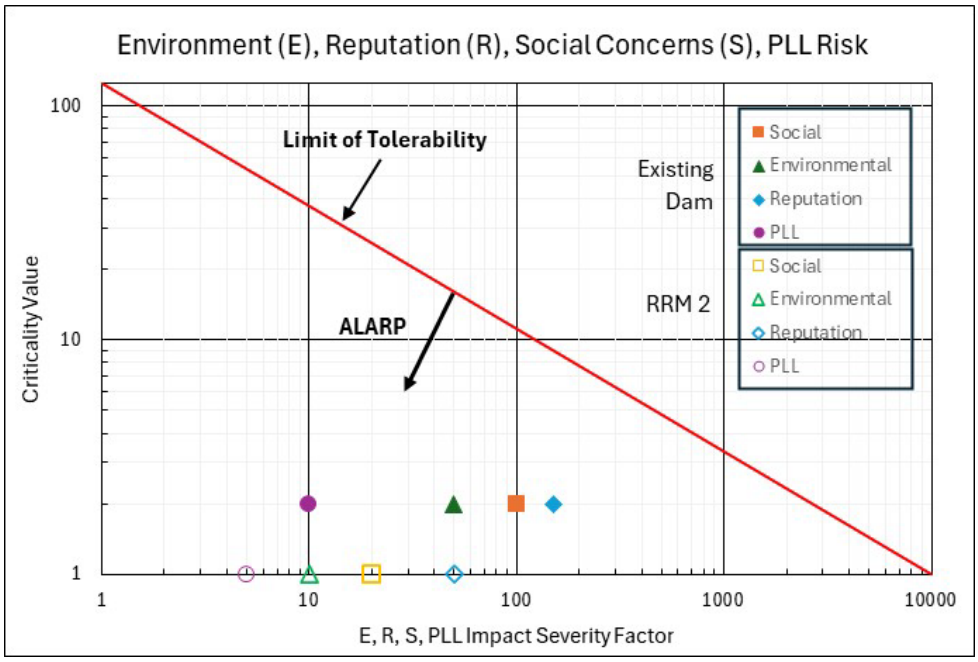


Figure 8: Qualitative presentation of existing risk and RRM 2 risk reduction

This dam represents an example of where the ALARP approach can justify avoidance of an expensive structural risk mitigation measure on the basis that the costs are grossly disproportionate to the risk benefit gained, particularly considering the existing low-risk position. However, the identification of RRM 2 to use stockpiled materials to train dam break flows away from the mine is a very low-cost measure, which would have a material risk benefit, as shown in Figure 8. RRM 2 represents a simple measure that lowers the risk position so far as is reasonably practicable, as long as no new risks are created by the redirection of the potential dam break flood. Along with these two risk reduction measures, the dam owner is currently implementing several measures following recognized good practice.

Conclusion

The question we normally ask is: "Do you think the risk profile of the dam is ALARP?" However, a better question is: "Have we documented our ALARP considerations effectively?" Always remembering that if the dam failed and there were fatal consequences or environmental damage, you would want to be able to confidently answer in the affirmative to the question: "Has ALARP been achieved, or were all reasonably practicable actions completed with respect to the known event?"

The proposed approach to ALARP solutions provides a means of documenting the process of reaching an ALARP solution for risk reduction for both quantitative and qualitative risk assessment approaches.

Documentation of ALARP determinations as shown above can be compared to the intent of a Safety Case of a high hazard facility, to document and justify the managed risk profile.

References

ANCOLD. 2012. Guidelines on the Consequence Categories for Dams, October 2012.

ANCOLD. 2022. Guidelines on Risk Assessment.

Barker, M., Laxman, M. and Methiwala, J. 2023. Did someone say ALARP? If so, how do we get there? *Proceedings of Tailings and Mine Waste, 2023.*

GHD. 2023. TSF FMECA, Cell 1 and Cell 2 Facility X.

GISTM. 2020. ICCM, UN and PRI. 2020. Global Industry Standard on Tailings Management (GISTM). Accessed at https://globaltailingsreview.org/global-industry-standard/

HSE. 2001. Reducing risks, protecting people (R2P2). Discussion Paper, Risk Assessment Policy Unit, Health and Safety Executive, United Kingdom: Health and Safety Executive, London.

ICMM. 2021. International Council on Mining and Metals. *Mining with Principles, Tailings Management Good Practice Guide,* May 2021.

Pearse, M., Foster, M., Hill, P., Banzi, S., Hameed, M. and Liu, B. 2022 Application of the SFAIRP principle to a diverse portfolio of dams. *Proceedings of ANCOLD conference*. Sydney, 26–28 October, 2022.

Rana, N.M., Ghahramanai, N., Evans, S.G., Small, A., Skermer, N. McDougall, S. and Take, W.A. 2022. Global magnitude-frequency statistics of the failures and impacts of large water-retention dams and mine tailings impoundments. *Earth-Science Reviews* 232: 104144.

Topham et al. 2024. ICOLD. *To do or not to do, that is the question: how ALARP justifies dam upgrade decisions.* In press.

Appendix

Criticality rating tables

Table A1: Example of Initiation Rating (I) Progression Rating (P) (Adapted from GHD, 2023. Dam X containing GHD technical memo dated 15 June 2022, proposed new Criticality Ranking System for FMEA)

Numerical Value (I, P)	Qualitative Rating	Indicative Quantitative Probability Range (AEP)	Likelihood Descriptor
1	Rare	< 1E-4	A failure pathway can be described; however, several events must occur concurrently or in series to cause failure. All the events individually have a low likelihood of occurrence.
2	Unlikely	1E-3 to 1E-4	The event has been known to occur elsewhere, however, at present the conditions do not exist for this event to occur and the failure pathway cannot be specified with confidence. The possibility of this failure mode occurring cannot be ruled out but there is no evidence that suggests it has occurred or that the fundamental condition has been met that could lead to it occurring.
3	Possible	1E-2 to 1E-3	Postulated physical processes or conditions exist that can be described and specified. AND/OR The fundamental defect or condition required for the failure mode to take place exists. OR Existing evidence suggests the failure mode is weighted towards "less likely" than "more likely."
4	Likely	1E-1 to 1E-2	Known physical processes and conditions exist that can be described and specified with confidence. Similar conditions have caused a known failure for a comparable structure OR The fundamental defect or condition required for the failure mode to take place exists. OR Existing evidence suggests the failure mode is weighted towards "more likely" than "less likely."
5	Almost Certain	1 to E-1	Known physical processes and conditions exist that can be described and specified with confidence. Similar conditions have caused known failures elsewhere OR Existing evidence suggests this failure mode has initiated or is expected to occur in near future, or has a frequent initiator

Table A2: Example of control effectiveness (E)

Numerical Value of E	Qualitative Rating	Likelihood descriptor
1	Effective and Reliable	In combination, the Control(s) are considered to be adequately designed, reliable, and operating effectively. In line with good practice
2	Satisfactory, could be improved. OR Effective but limited influence on FM	In combination, the Control(s) are considered to be adequately designed, but may not be reliable in all situations, or there are some operating difficulties. Mostly effective. Largely in line with contemporary industry practice for this failure mode. Control(s) effective but have limited influence on Failure Mode
3	Marginal	In combination, the Control(s) are not considered to be adequately designed, or may be unreliable to impact this failure mode, or at a frequency that is not suited to the failure mode. Partially effective. Below contemporary industry practice for this Failure Mode
4	Weak ineffective	Few controls relevant to this Failure Mode. Control(s) are considered weak, or ineffective for this Failure Mode
5	Absent	No Controls

Table A3: Criticality rating (C)

Numerical Value of C	Qualitative rating
1 to 12	Low: Failure mode not expected and/or well managed. Continue to monitor and maintain effectiveness of controls to prevent, detect and intervene.
13 to 60	Moderate: Failure mode is of material concern. Look for opportunities to better understand mechanism, lower the likelihood of failure mode initiating and progressing to failure. Improve controls reliability. Review consequence management controls for improvements.
61 to 125	High: Urgent focus required to lower the likelihood of failure mode initiating and progressing to failure. Improve controls reliability. Review consequence management controls for improvements

Consequences tables

Table A4: Life, economic and company consequences

Factor	Minimal Loss	Not Significant	Significant	Major	Catastrophic
Population at Risk	None	1 – 10	10 – 100	100 – 1000	> 1000
Potential Life Loss	<0.1	0.1 – 1	1 – 5	5 – 50	> 50
Infrastructure and Economics ($US)	< 1M	1M – 10M	10M – 100M	100M – 10B	>10B
Company Reputation	Minor	Limited Region	Substantial State	Serious National	Severe Global
Severity Factor	1	10	100	1000	10,000

Table A5: Health and societal impacts

Severity Level	Description (time months)	Human Health and Loss of Services (People affected)	Loss of Heritage	Dislocation of People (person months)	Employment (jobs lost)	Severity Factor
5	Severe (Catastrophic) (12)	1000	International facility	1000	100	10,000
4	Serious (Major) (6 to12)	100	National facility	100	50	1,000
3	Substantial (Medium) (2 to 6)	10	Regional facility	10	10	100
2	Measurable but Limited (Low) (1 to 2)	1	Local facility	1	5	10
1	Minor (<1)	<1	Local buildings	<1	1	1

Table A6: Environmental impacts severity level

Severity Level	Description	Area of Impact (km^2)	Stock and Fauna	Ecosystem recovery	Rare and Endangered Species	Severity Factor
5	Severe	>20	Significant health impacts from contaminates water supply	> 10 yrs	Permanent loss of species	10,000
4	Serious	10 to 20	Measurable health impacts from contaminates water supply	3 to 10 yrs	Severe impact recovery over number of years	1,000
3	Substantial	5 to 10	Contaminates water supply used by stock and fauna	1 to 3 yrs	Recover over a number of years	100
2	Measurable but Limited	1 to 5	Contaminates water supply used by stock and fauna health impacts not expected	<1 yr	Minimal Species damage	10
1	Minor	<1	No contamination of water supply	Recovers with little intervention	No species affected	1

Conformance vs. Compliance: Contrasting the Voluntary GISTM to 9 years of Federal CCR Regulations

Lucas P. Carr, Ramboll Americas Engineering Solutions, USA
Steven F. Fecht, Ramboll Americas Engineering Solutions, USA
Nguyet Nguyen (Wit Win), Ramboll Americas Engineering Solutions, USA

Abstract

The failures of tailings facilities at metals mines in the mid to late 2010s were preceded by similar failures of coal combustion residual (CCR, which is sometimes considered a type of tailings) surface impoundments that occurred at Kingston in 2008 (Tennessee, USA) and Dan River in 2014 (North Carolina, USA, 2014). The Kingston failure involved the static liquefaction of an industrial waste impoundment and a corresponding catastrophic flow-failure and offsite release of industrial waste. Similarly to the later tailings facility failures, the CCR failures also led to offsite environmental impacts, significant public scrutiny, a loss of public trust and social license to operate for the impoundment owners, damage claims and litigation, and corresponding efforts by stakeholders to develop systems to prevent similar failures from occurring again.

The prevention systems to reduce the occurrence of future failures differ significantly for CCR and tailings. For CCR, the system is one of mandatory compliance through federal regulation by the United States Environmental Protection Agency (USEPA) under 40 C.F.R. Part 257 (CCR Rule). This approach has been successful, as no failures have since occurred. However, the CCR Rule utilizes prescriptive technical criteria, provides limited allowance for risk quantification or site-specific variations, is the subject of ongoing litigation, and was significantly expanded in scope by USEPA in 2024. This approach is significantly different than the 2020 Global Industry Standard for Tailings Management (GISTM), which is a system of voluntary conformance[1] through a stakeholder-developed program that allows for site-specific variations, while requiring robust levels of governance and overlapping review. This paper will

[1] All members of the International Council of Mining and Metals (ICMM) have committed to conforming with the ICMM. Conformance with the GISTM is voluntary for non-ICMM members, although many non-ICMM member companies have committed to GISTM conformance.

contrast the two methods of prevention – compliance[2] vs. conformance[3] – and elaborate on the relative advantages of the GISTM over the CCR rule, as well as lessons learned from CCR compliance that may prove helpful for GISTM practitioners.

Introduction

Coal combustion residuals (CCRs) are a class of residual materials left over from the burning of thermal coal (i.e., ash), primarily for electric utility generation. They are sometimes considered to be a type of tailings. Most CCRs consist of fly ash, typically silt-sized, and bottom ash, typically sand-sized, though some power plants equipped with scrubber systems produce silt-sized gypsum. CCRs have historically been managed like mine tailings. This has included storing CCRs in wet-sluiced industrial waste impoundments, which often share design features, construction methods, operations, environmental concerns, and failure mechanisms with mine tailings storage facilities. CCR impoundments are common in countries relying on thermal coal for electricity, including, but not limited to, the United States (US), China and India. This paper will focus on CCR disposal facilities in the US, where nearly 700 impoundments (USEPA, 2016) are estimated to be present.

CCR surface impoundments gained significant publicity after the catastrophic 2008 Kingston failure in Tennessee, which released around 5.4 million cubic yards of CCR and wastewater into the Clinch River (AECOM, 2009). Public outcry over the Kingston failure and concerns related to groundwater and surface water contamination at other impoundments prompted USEPA to begin the process of regulating CCR at the Federal level in 2010 (USEPA, 2024a), leading to the promulgation of 40 Code of Federal Regulations (C.F.R), Part §257, known as the "CCR Rule." This rule provides comprehensive environmental, structural, and closure regulation of CCR surface impoundments and landfills.

There are many parallels between the events that ultimately led to the promulgation of the CCR Rule and the development of the Global Industry Standard for Tailings Management (GISTM) (Global Tailings Review, 2020) in 2020. However, the overarching systems developed to improve management and prevent failures for each waste stream – regulatory compliance for CCR and stakeholder standard conformance for tailings – are fundamentally different. This paper will evaluate the differences between each system and provide lessons learned from the experience of the authors supporting impoundment owner/operators in supporting both CCR Rule regulatory compliance and GISTM standard conformance activities. The authors

[2] "Compliance" is defined, for the purposes of this paper, as an activity that an entity (*i.e.*, waste impoundment owner/operator) is mandated to perform by an external governmental agency under legal authority, and where a lack of compliance may directly subject the entity to litigation and/or other legal penalties.

[3] "Conformance" is defined, for the purposes of this paper, as an activity that an entity voluntary performs and is in accordance with standards and/or guidance documents developed by 3rd-party non-governmental organizations (i.e., stakeholder groups), and where a lack of conformance may subject the entity to stakeholder scrutiny, but is unlikely to directly subject the entity to litigation and/or legal penalties.

aim to provide a case study that will benefit tailings impoundment owners and practitioners, based on these lessons learned. Additionally, this paper will address the challenges posed to the industrial waste management industry by a mandatory Federal regulatory program, as well as some of the potential challenges and shortcomings associated with a voluntary and stakeholder-based program like the GISTM relative to a mandatory program.

CCR impoundment management practices and waste characteristics

Most CCR impoundments in the US were initially constructed in the 1950s through the 1970s to support the widespread construction and operation of coal-fired power plants associated with postwar industrialization and economic growth. Impoundments were often constructed adjacent to the power plants, which were nearly always adjacent to a large water body (i.e., river, lake, or reservoir) that provided cooling water. Most impoundments were initially constructed with an earthen starter dike with later capacity increases using dike raises. CCR was typically wet-sluiced into the facility, and dike raises for some, but not all impoundments, were constructed using the upstream method, where the raises were constructed wholly or partially over a foundation of wet-sluiced industrial waste. However, not many CCR surface impoundments used single-stage or downstream earthen construction methods, due to site characteristics and other factors.

The geotechnical behavior of wet-sluiced CCRs is in many ways similar to wet-sluiced tailings. This generally includes susceptibility to brittle behavior (i.e., static and seismic liquefaction), flow failure when co-stored with water, and a relatively high shear strength at relative low strains during drained loading.

CCR impoundment failures

The most significant CCR impoundment failure occurred at the Tennessee Valley Authority (TVA) Kingston Fossil Plant (KIF) in Roane County, Tennessee, on December 22, 2008. The event was a catastrophic flow-failure of an 84-acre (34-hectare) CCR dredge cell, resulting in the release of approximately 5.4 million cubic yards (4.1 million cubic meters) of CCR over an approximately 300-acre (121 hectare) area (Figure 1). The release occurred without warning at approximately 1:00 AM local time and impacted the adjacent Emory River, along with onsite and offsite areas. It caused serious damage to several residences but did not result in any injuries or fatalities (AECOM, 2009; WBIR, 2018).



Figure 1: Post-failure photographs of Kingston CCR impoundment failure (USEPA, 2017)

A root cause analysis commissioned by the TVA (AECOM, 2009) identified that the failure was clearly a static liquefaction event induced by excessive deformation in upstream-constructed containment dikes. The report noted that the deformation was induced by the construction of the starter dike and subsequent dike raises over a previously unknown thin foundation layer of weak slimes. The effects of the deformations were exacerbated by strain incompatibility between the relatively plastic foundation slimes and the saturated, contractive CCR within the impoundment that behaved in a semi-brittle manner. After the dike deformed enough to trigger a breach, the flow-failure event was initiated and rapidly occurred.

The Kingston failure was followed by the Dan River failure in Eden, North Carolina, USA, in 2014. The Dan River failure occurred when a stormwater conduit buried beneath an inactive CCR surface impoundment failed, causing approximately 82,000 tons of CCR and 27 million gallons of CCR wastewater to flow into the Dan River (USEPA, n.d.). While the Dan River failure was significantly smaller than the Kingston failure, it was also driven by the tendency of CCR to exhibit flow-failure behavior, and it caused striking visual impacts to approximately 70 miles of the Dan River downstream from the site (NC DEQ, 2014) (Figure 2).

Both failures were similar to several of the tailings facility failures that occurred in the 2010s, including the sudden and unexpected nature of the events, the flow-failure of the material, and significant impacts to offsite areas. Both failures also received widespread press coverage in the US and significant attention by non-governmental organizations (NGOs), environmental groups, state environmental regulatory agencies, and Federal regulatory agencies.



Figure 2: Post-failure CCR impacts in the Dan River (NC DEQ, 2014)

The USEPA CCR Rule

In 2010, USEPA proposed to regulate CCR under the Resource Conservation and Recovery Waste (RCRA) of 1976, to reduce the risks posted by CCR surface impoundments and landfills. After a multi-year rule development and multiple public comment periods, USEPA issued the final CCR Rule on December 14, 2014, thereby regulating CCR under Subtitle D of RCRA (USEPA, 2024a), with an effective date of April 15, 2015.

Features of the Rule

The CCR Rule was initially "self-implementing," as USEPA did not have direct enforcement authority under RCRA Subtitle D in 2015. Instead, the enforcement of the rule was left to citizen lawsuits. Direct enforcement of the CCR Rule was later granted to USEPA under the Water Infrastructure Improvements for the Nation Act (WIIN Act) in 2016; this act also allowed states to implement their own CCR permit programs after USEPA review and approval. As of the date of this paper, only three state permit programs

(Oklahoma, Georgia, and Texas) have been approved while one program (Alabama) has been denied by USEPA (USEPA, 2024b).

Compliance with the CCR Rule is required to be demonstrated via a public internet website, hosted by the CCR unit owner/operator, and required to contain multiple Professional Engineer-certified documents, including, but not limited to, location restrictions (§257.60-64), design criteria (§257.71), structural integrity (§257.73), air criteria (§257.80), hydrologic and hydraulic capacity (§257.82), routine inspections (§257.83), groundwater monitoring and corrective action (§257.90-98), and closure and post-closure care (§257.103-104).

Comparison to the Global Tailings Standard

This section will compare several, but not all, of the key portions of the CCR Rule to the GISTM. Both the CCR Rule and GISTM are extensive and far-reaching documents; a comparison of all requirements of both documents is beyond the scope of this paper.

Implementation and adoption

Compliance with the CCR Rule is mandatory for all electric utilities and independent power producers in the US. While there were some exemptions in the CCR Rule based on the operational status of the power plant in 2015, many of these exemptions were later removed under an expansion of the CCR Rule in 2024, termed the "CCR Legacy Rule." Non-compliance or non-adoption with the CCR Rule can result in direct enforcement action by USEPA or citizen lawsuits under RCRA Subtitle D (i.e., self-implementation).

All members of the International Council on Mining and Metals (ICMM) have committed to implementing the GISTM, along with multiple non-ICMM members. However, there is no requirement for non-ICMM members to adopt the GISTM. The non-ICMM members who have committed to the GISTM have done so voluntarily, although sometimes at the request of investors and/or other stakeholders. The GISTM is also self-implementing, with implementation overseen by the tailings facility owner/operator directly as opposed to a dedicated and independent external agency[4]. This is similar to the initial implementation of the CCR Rule, prior to the WIIN act.

Community and project-affected people engagement

Community and project-affected people engagement within the CCR Rule is limited to public postings of various hydrogeologic and engineering certification documents, annual inspection reports, and routine groundwater and fugitive dust monitoring reports. The CCR Rule also requires CCR unit owner/operators

[4] As of the date of this paper, an external 3rd party auditing program for GISTM conformance is in the early stages of development, but is likely several years away from being implemented.

to list contact information for submitting questions. No other requirements for the engagement of the local community or project-affected people are included in the CCR Rule; this includes a lack of engagement requirements for design or planning-related activities, such as the siting of a new CCR unit or the closure of an existing CCR unit, and a lack of a mechanism for grievances to be reported and addressed. However, it should be noted that many state regulatory programs (i.e., water quality, dam safety, landfill permitting programs) do have public meeting requirements that are outside of the CCR Rule.

The GISTM, in Principle 1 and Principle 2, requires the meaningful engagement of project-affected people and the community. This includes documenting the engagement of project-affected people and developing a grievance mechanism to address the complaints of project-affected people. Additionally, the GISTM requires that the design of the tailings facility consider the local environmental, social, and economic context, and that the potential impacts of a tailings facility failure be considered during the complete lifecycle of the tailings facility (Principle 3).

Design criteria

The CCR Rule includes prescriptive criteria for the hazard potential classification, minimum slope stability factors of safety for multiple dike stability loading conditions (§257.73), rainfall frequencies for the inflow design flood control plan (§257.82), and seismic event return intervals. The slope stability factors of safety and seismic design events are the same regardless of the hazard potential classification, while the frequency of the inflow design flood control plan varies based on the hazard potential classification. Design criteria are the same for an operational and a closed unit. The maximum flood frequency is the probable maximum flood (PMF) for a "High" hazard potential classification CCR unit. There are no mechanisms that explicitly allow for temporary non-compliance with the design criteria; non-compliance may trigger mandatory closure of the impoundment, enforcement action by USEPA, or citizen lawsuits.

For operating facilities, the GISTM includes prescriptive criteria for flood and seismic events ranging from a 1/200-year to a 1/10,000-year event, based on the consequence classification of the facility. For facilities in a state of passive-care closure (i.e., "safe closure"), 1/10,000-year seismic and flood events are required. Other seismic events such as the Maximum Credible Earthquake (MCE) or Maximum Design Earthquake (MDE) may also be used for closure design, although these concepts are not explicitly mentioned in the GISTM. Specific safety factors or analysis methodology are not included for geotechnical and hydraulic analysis. Instead, the GISTM requires that the design criteria of the tailing facility be selected in a site-specific manner considering multiple factors, including the risk posed by the facility (Principle 4). Additionally, instances of non-compliance with the GISTM can be addressed through the development and implementation of risk mitigation plans, when approved by tailings facility owner/operator governance systems and external reviewers (Principle 4).

Risk assessments

The CCR Rule does not include any requirements for CCR unit owner/operators to perform risk assessments, potential failure mode assessments, or failure mode and effects analyses. Instead, the CCR Rule relies on the certification by a Professional Engineer that the facility meets §257.73 and §257.82 structural stability design criteria requirements for all facilities. In the experience of the authors, some CCR unit owner/operators voluntarily and proactively performed risk assessments as part of internal risk management and governance program. However, these assessments were not mandated, and the CCR Rule does not include the over-arching concept of continual risk reduction to "as low as reasonably practicable" (ALARP) that is a central focus of the GISTM. In fact, outside of the inflow design flood event, the CCR Rule inherently treats the design criteria for CCR units in a "one-size-fits-all manner" (i.e., factors of safety, monitoring an OMS requirement, dam safety reviews), regardless of the level of risk posed by the facility (i.e., potential environmental and human impacts of a failure, size and location of the CCR unit).

The GISTM requires risk assessments to be performed for all tailings facilities and utilized to inform the design of the facility. Additionally, the GISTM, in Principles 4 and 5, requires that designs be robust, consider all identified failure modes, and reduce risk to ALARP. The GISTM also inherently allows for the use of RIDM to provide for flexible and site-specific design criteria. This approach inherently allows for each tailings facility to be viewed independently, with an implied goal of allocating additional resources and applying more conservative design criteria to high-risk facilities.

Management of change

The CCR Rule requires the update of certifications for the structural integrity (§257.73) and hydraulic and hydrologic capacity (§257.82) every five years, regardless of the hazard potential classification of the impoundment. This process is similar to a Dam Safety Review (DSR), as opposed to a formalized Management of Change process. Documentation of changes to the local social, environmental, and economic context outside of the facility are not required as part of the periodic certification process or any other CCR Rule requirements.

The GISTM requires the ongoing review and evaluation of material changes not only to tailings facilities but also to the surrounding social, environmental, and economic context. Tailings facility owners and operators are required to define material changes and update multiple documents, including but not limited to, impact assessments, breach assessments, and design basis reports, based on material changes (Principles 2, 3, and 4).

Management and governance

There are substantial differences in the role of corporate management and governance between the CCR Rule and the GISTM, as discussed in this section.

Role of the Engineer of Record

CCR Rule

The CCR Rule requires certifications for various rule requirements to be prepared and posted to a public website. These certifications must include the seal and signature of a qualified Professional Engineer in the state with where the CCR Unit is located (e.g., the Certifying Engineer). No specific requirements are listed for the minimum qualifications for the Certifying Engineer. CCR Rule certifications are prepared for multiple portions of the CCR rule, including but not limited to, the design and operating criteria (§257.71-73, 82) and certifications for both closure plans and closure completion (§257.102-103). The scope of the certification only includes the explicit regulatory requirements.

It is commonplace for multiple Certifying Engineers, often from multiple consulting firms, to certify different sections of the CCR Rule for the same CCR unit within a given year (e.g., a different Certifying Engineer for annual inspections vs. the initial design and operating criteria). It is also not uncommon for Certifying Engineers to be changed between initial and periodic certifications. The CCR Rule does not require or imply that the various Certifying Engineers need to communicate with one another. Additionally, the CCR Rule does not contain any requirements for continued engagement or communication between the Certifying Engineer(s) and CCR Unit owner/operators between required certifications. When Certifying Engineers are changed, there are no requirements for the new Certifying Engineers to communicate with the previous Certifying Engineers.

GISTM

The GISTM requires the formal engagement of an Engineer of Record (EoR) for all active tailings facilities and closed facilities with a "High" or higher consequence classification (Principle 9). The GISTM requires that the EoR have relevant experience, skills, and time to fulfill the role. The EoR must be empowered through a written agreement explaining the obligations of the EoR and owner/operator to each other, and the EoR's activities must be governed by a quality management program. Additionally, the GISTM stipulates that EoR selection decisions be made by the Accountable Executive rather than by procurement personnel. Furthermore, the GISTM requires the development of a knowledge transfer plan in case of a change in the EoR.

The EoR is also expected to be continually involved in the tailings facility's design and operation. This includes preparing an Annual Inspection Report; reviewing operational, monitoring, and surveillance (OMS) data; and communicating with the Responsible Tailings Facility Engineer.

Corporate governance

The CCR Rule requires CCR Unit owner/operators to certify compliance with certain portions of the CCR Rule (i.e., Part A demonstrations via §257.103). Most other requirements of the CCR Rule are expected to

be implemented via certifications prepared by Certifying Engineers. The CCR Rule does not include any specific provisions or requirements for owner/operators to implement corporate governance programs for managing their CCR units. However, some CCR unit owner/operators have self-implemented corporate governance programs.

The GISTM includes multiple requirements for corporate governance (Topic IV). These requirements include, but are not limited to, appointing an Accountable Executive to oversee tailings management; reporting to the Board of Directors; appointing a Responsible Tailings Facility Engineer for each tailings facility; providing training for workers involved in tailings management; implementing lessons learned from internal and external failures; developing a whistleblower protection system; and implementing both Tailings Management Systems and Environmental and Social Management Systems.

Independent reviews

The CCR Rule does not include any provisions for the independent review of certifications and assessments performed by Certifying Engineers. The CCR Rule does not prohibit a sole Certifying Engineer from preparing a certification with no independent or external review, although in practice, most certifications are prepared by engineering firms and reviewed by internal subject matter experts independent of the Certifying Engineer prior to completion. Once a certification has been prepared, it may be reviewed by a state permit agency (if present), USEPA, or an individual or non-governmental agency (NGO) and potentially challenged via a citizen lawsuit. Challenges to the certification statements would then be addressed via a prolonged regulatory review and/or litigation processes, instead of via an independent review process performed prior to finalizing design activities.

The GISTM requires multiple levels of independent review. This includes assigning a Senior Independent Technical Reviewer or an Independent Tailings Review Board (ITRB) to provide high-level review of most documents and studies prepared by the EoR. Additionally, the GISTM requires auditing of compliance with the Tailings Management System (TMS) and Environmental and Social Management System (ESMS), along with periodic risk assessments using a multi-disciplinary team. Furthermore, the GISTM requires the Accountable Executive (AE) to be involved in technical decision making for certain high-risk tailings facilities.

Dam safety reviews

The CCR Rule requires periodic certification of structural integrity (§257.73) and hydrologic and hydraulic capacity (§257.82) to be prepared on a five-year basis for all surface impoundments. Initial certifications were required in 2016, the first periodic certifications were prepared in 2021, and the next periodic certifications will be required in 2026. While the scope of the periodic certifications is somewhat similar to a Dam Safety Review (DSR), the CCR Rule does not include specific guidance other than certifying that

the CCR Unit still meets all of the structural integrity and hydraulic capacity requirements. The CCR Rule also does not have any independence requirements for periodic certifications; they can be prepared by the initial Certifying Engineer or any other qualified Certifying Engineer, including allowing the same Certifying Engineer to prepare multiple concurrent periodic certifications. In practice, periodic certifications often involve a review of monitoring data for the impoundment over the past 5 years, a site visit, and updated engineering analyses to verify that the impoundment still meets the CCR Rule criteria.

The GISTM requires that a DSR be performed at least every five years for high-consequence facilities and every ten years for all other facilities. The DSR engineer must be different from the EoR, and the same DSR engineer cannot conduct consecutive DSRs at the same facility. Additionally, the DSR engineer must certify their avoidance of conflicts of interest.

Closure planning and design

The CCR Rule contains a detailed closure performance standard in §257.102 including the preparation of a closure plan; requirements to remove liquids from the CCR unit; prescriptive final cover requirements, such as an 18-inch-thick compacted clay low-permeability layer or a geomembrane with an 18-inch-thick protective cover and six inches of topsoil; and requirements for a closure to be completed within five years of initiation unless an extension is prepared. Additionally, as part of the 2024 Legacy Rule updates, §257.102 was revised by USEPA to include a more restrictive performance standard regarding the removal of both impounded free liquids and free liquids contained within the CCR mass, and to clarify that CCR units could no longer be closed where the waste is in contact with groundwater under long-term, post-closure conditions.

The GISTM requires that the closure design be performed under the same requirements as the design of an active facility. Specific information related to the final cover system design or the management of liquids within the tailings facility is not included in the GISTM. However, the GISTM does not preclude closure of a facility in accordance with local regulations that may be more restrictive than the GISTM itself.

Post-closure care

The CCR Rule requires a minimum 30-year post-closure care period for all CCR units (§257.104) that are closed in place. The post-closure care period may extend beyond 30 years if groundwater impacts attributable to the CCR unit remain present. There is no upper limit to how long a CCR unit with groundwater impacts must remain in post-closure care. During post-closure care, the CCR Rule requires that the owner/operator maintain the final cover system and embankments, conduct groundwater monitoring, and maintain any leachate collection systems.

The GISTM divides the closure lifecycle of a tailings facility into “active care closure” and “passive care closure,” also known as “safe closure.” The GISTM does not include any minimum or maximum

durations for post-closure care, presumably due to varying requirements in local regulations. However, the GISTM's "safe closure" concept requires an extensive assessment by the EoR, with review by a Senior Independent Technical Reviewer or ITRB, to demonstrate that the tailings facility no longer poses a risk to the environment or people.

Groundwater monitoring and corrective action

The CCR Rule requires active groundwater monitoring of all CCR surface impoundments that are not in a post-closure care state, per §257.90-94. This includes the design and certification of a groundwater monitoring program by a Certifying Engineer, and the routine collection of groundwater samples for specific constituents with the results posted to a public website. If a statistically significant increase above background levels is noted in one constituent, the CCR Unit must enter an assessment monitoring program (§257.95). Depending on the results of the assessment monitoring, groundwater corrective measures may be performed (§257.96-98).

The GISTM does not include detailed requirements for groundwater monitoring or groundwater corrective action. However, the GISTM does require documentation of the social, economic, and environmental context of the tailings facility (Topic II), as well as environmental monitoring (Principle 7) and implementation of an ESMS to observe the effects of the tailings facility on the environment (Principle 6). It should be noted that many tailings facilities may still have groundwater monitoring and corrective action requirements as part of state regulatory programs.

Legacy sites

CCR Rule

The CCR Rule initially was restricted to apply only to power stations where the coal-fired boiler was active on or after October 15, 2015. For these stations, the CCR Rule only applied to units that contained CCR and liquids on or after this date and were not in a state of being "capped or otherwise maintained (i.e., in a state of post-closure care with no liquids remaining). If the power station was inactive prior to October 15, 2015, all CCR surface impoundments at the station were exempted from regulation. These exemptions resulted in a significant number of impoundments that were not initially regulated by the CCR Rule.

In 2024, USEPA significantly expanded the scope of the CCR Rule by issuing the "Legacy Rule," which rescinded many of these exemptions and expanded the rule to include CCR disposed of outside of CCR units on the power plant site for uses such as structural fill. These legacy CCR surface impoundments and management units will now have to comply with many of the requirements of the 2015 rule, including, but not limited to, design criteria, structural stability, groundwater monitoring, and closure. The first litigation regarding the legacy rule was filed on June 13, 2024 (City Utilities of Springfield, Missouri vs. EPA, No. 24-1200, D.C. Circ.) and additional litigation is expected.

GISTM

The GISTM does not include an exemption for legacy tailings facilities at active mine sites or legacy mine sites. Per the definition of a "tailings facility" in the GISTM, these legacy tailings disposal areas are generally interpreted to still be a tailings facility, are in a state of active-care closure, and are still subject to all the requirements of the GISTM until they are demonstrated to be in a state of "safe closure." The GISTM does not include explicit provisions for an accelerated or more limited safe-closure demonstration for legacy tailings facilities, even though some of these tailings facilities have been closed and/or reclaimed for decades and may have little resemblance to an active tailings facility. However, the GISTM does not explicitly prohibit an accelerated path for safe-closure for these facilities, which can leave these facilities in a grey are.

Conclusion

The GISTM and CCR Rule offer fundamentally different approaches to supporting the safe and environmentally responsible management of otherwise similar types of industrial waste. Some of this difference stems from the CCR Rule being developed via a multi-year agency rulemaking process with thousands of public comments, as required under US law (e.g., compliance), while the GISTM was developed in an accelerated manner outside of a regulatory setting using the input from various industry and external stakeholder groups (e.g., conformance). This section will discuss conclusions regarding the effectiveness of both approaches for failure prevention, key advantages of the GISTM over the CCR Rule, and potential challenges that GISTM implementation may pose relative to the CCR Rule.

Success of the CCR Rule in failure prevention relative to the GISTM

Anecdotally, the mandatory CCR Rule has been highly effective in preventing failures of CCR impoundments in the US. The authors are not aware of any significant releases of CCR from surface impoundments in the US that have occurred since Dan River in 2014, nor of any catastrophic flow-failures that have occurred in the US since Kingston in 2008.

However, it is the authors' opinion that multiple other factors beyond the CCR Rule have contributed to the effective elimination of CCR surface impoundment failures. For example, many CCR unit owners and operators self-implemented strategic CCR management and governance programs after the Kingston and Dan River events. These programs often included performing detailed engineering studies and risk assessments that, in many cases, exceeded the minimum requirements of the CCR Rule. These programs also resulted in the implementation of risk mitigation projects (i.e., buttressing of embankments, spillway improvements, enhanced monitoring and surveillance programs). Many of these programs and mitigation projects were implemented or in the process of implementation prior to the effective date of the

CCR Rule in 2015. Additionally, many unit owners/operators proactively transitioned some of their plants from wet disposal to CCR dewatering with waste storage in regulated landfills, to reduce impoundment-related risks.

Another potential factor in the successful elimination of CCR impoundment failures is the decline in CCR storage volume in the US. Production decreased by nearly 50% between 2008 and 2021, while the percentage of CCR utilized for beneficial use increased from approximately 47% to 67% over the same period (American Coal Ash Association, 2022). This is due to the closure of multiple coal-fired power plants, which also led to an increased demand of CCR for beneficial use applications such as concrete. Many CCR surface impoundments were also dewatered and closed due to either plant closure and/or CCR Rule-related closure triggers. Therefore, the lack of CCR impoundment failures may also be influenced by significant declines in both the volume of new CCR making it into impoundments, as well as the total number of remaining active impoundments.

Conversely, the GISTM is still a relatively new standard, with initial implementation for high-risk facilities completed in August 2023 for ICMM members. Lower-risk facilities are not required to be conformant with the GISTM until August 2025, while non-ICMM members who choose to implement the GISTM are not bound by a formal conformance schedule. While multiple failures of tailings facilities and heap leach pads have occurred since the GISTM was promulgated, such as the Jagersfontein collapse in South Africa and the Williamson failure in Tanzania, the authors are not aware of any failures involving a tailings facility that has successfully implemented the GISTM.

Unlike CCR, both the number and size of active tailings facilities is expected to increase significantly in the future, due to increased demand for metals. Additional time will be required to assess the success of the GISTM in failure prevention and "zero harm," particularly for new and larger tailings facilities that will be constructed in the future. This also may provide a future opportunity to study the incident and/or failure rate of GISTM-conformant tailings facilities compared to those that have are not conformant or have not adopted the GISTM.

Advantages of the GISTM over the CCR Rule

In many ways, the GISTM is a more robust and holistic standard than the CCR Rule, due to the incorporation of concepts that are not part of the CCR Rule. These concepts include, but are not limited to:

- Active community and project-affected people engagement throughout all aspects of the tailings facility lifecycle, including a community grievance mechanism, as opposed to one-way engagement via certification document postings.
- Significant requirements for corporate governance, including the assignment of specific governance roles for all tailings facilities.

- Robust requirements to document minimum qualifications for key tailings related roles, based on site-specific circumstances.
- Requiring the long-term engagement of a single Engineer of Record or Designer of Record to providing ongoing, sustained support for the facility, rather than multiple Certifying Engineers who are not required to be involved in facility operation outside of certification preparation.
- Requirements for multiple layers of overlapping, independent review of work performed by the Engineer of Record, including independent reviewers or review boards and dam safety reviews performed by independent engineers, rather than allowing certifications to be based on the judgment of a single Certifying Engineer.
- Requirements to utilize site-specific risk assessments to drive decision-making, using a multi-disciplinary team, and requirements that the design of the facilities consider the risk assessments.
- Including the concept of minimizing risk to "as low as reasonably practicable" for all known failure modes.
- Allowance for significant differences in the design of tailings facilities (i.e., minimum safety factors, design freeboard, analysis methods) based on local and regional practices and the overall risks posed by the tailings facility.
- Providing an intensive process for terminating post-closure care, including a demonstration with independent review that the tailings facility no longer a risk to people or the environment, as opposed to maintenance over a defined period and reliance on groundwater monitoring results.
- Wording requirements in a manner that is sufficiently flexible to accommodate site-specific considerations based on local regulatory practices, as opposed to requiring detailed interpretation of a Federal regulation, which may be subjected to ongoing litigation and changes in interpretation (i.e., Utility Solid Waste Activities Group vs. EPA. No. 15-1219, D.C. Circ. June 14, 2016).

Potential challenges of the GISTM relative to the CCR Rule

There are several aspects of the GISTM that may prove challenging during continued adoption and conformance activities, based on observations by the authors in supporting CCR Rule compliance activities. These aspects include, but are not limited to:

- For non-ICMM members, the GISTM is a voluntary standard. While many non-ICMM members have chosen to implement the GISTM, others may forego implementation. Therefore, the ability of the GISTM to achieve "zero harm" caused by tailings facilities may always be limited by the number of tailings facility owners and operators who choose to implement the standard.

- The GISTM is primarily focused on preventing catastrophic failures of tailings facilities through corporate governance and multiple layers of review. The GISTM includes more limited requirements to address other environmental impacts caused by tailings facilities, such as fugitive dust emissions, groundwater impacts, and surface water discharge impacts. While these impacts are mentioned within the GISTM (via the requirements for Impact Assessments, maintaining a knowledge base, and TMS and ESMS programs), they are generally non-specific and overshadowed by the focus failure prevention requirements. Based on the experience of the authors with the CCR Rule, public and regulatory attention may shift away from catastrophic failure prevention and towards long-term environmental impacts near the end-of-life for tailings facilities, particularly during the transition to closure. This may lead to the potential for future public, regulatory, and corresponding cost uncertainties related to long-term environmental remediation, particularly if closure-related regulations become more stringent.
    - This has occurred for CCR surface impoundments, as 2024 updates to the CCR Rule by USEPA have effectively prohibited surface impoundments to be closed in a manner where the CCR will remain in contact with groundwater under post-closure conditions, regardless of known or predicted future impacts to groundwater, human health, and ecological health.
    - Additionally, many environmental groups and/or NGOs publicly advocate for the closure of essentially all CCR surface impoundments by excavating all CCR from the impoundments and placing it regulated landfills (e.g., closure-by-removal), for the perceived benefit of reducing groundwater impacts. This type of closure method can have a very high cost and can be disruptive to local areas due to the required construction disturbance and/or hauling of material on adjacent roadways.
- With the GISTM being a flexible and self-implementing standard, much like the pre-WIIN CCR Rule was, there is the potential for significantly different interpretation of its requirements among tailings facility owners. While the GISTM will undoubtedly result in more consistent and robust tailings management practices, interpretation differences may cause challenges for EoR/DoR firms working for multiple tailings facility owners, as well as third-party stakeholders reviewing tailings disclosures. This may also cause challenges for future 3rd party audits of GISTM conformance, as auditors may have different opinions than facility owner/operators and their EoRs, with both opinions being valid interpretations of the GISTM.
- The current lack in a formalized 3rd-party audit program may also prove challenging, as future auditors may encounter significantly different tailings management and GISTM conformance

practices for different facilities and owner/operators, several years after those owner/operators have started GISTM conformance activities.

- Addressing legacy sites will continue to be a challenge for the GISTM. With the CCR Rule, legacy facilities were initially unregulated for nearly 9 years, which allowed the industry significant time to focus resources on active CCR surface impoundments, which typically have a higher risk profile. However, legacy tailings facilities, which like legacy CCR facilities typically, but not always, have a lower risk profile, are not exempted by GISTM, nor is conformance on a different schedule than active facilities. The GISTM also lacks an explicit, accelerated "safe closure" pathway for these facilities. Bringing these legacy facilities into GISTM conformance, prior to completing a safe closure demonstration, may be a substantial effort and may divert key engineering and financial resources away from often higher-risk, active tailings facilities.
    - The CCR industry is currently undergoing a similar challenge due to the 2024 Legacy Rule, which is inducing a chronic shortage in CCR engineering and environmental resources.
    - One potential way to address this for tailings impoundments would be to revise the GISTM to include an explicit accelerated safe closure demonstration mechanism for low-risk legacy impoundments that have been inactive or reclaimed for years, pose little risk to people or the environment, and in many cases may no longer visually resemble a tailings facility.
- Currently the authors are not aware of significant efforts at the Federal level in the US to regulate tailings facilities in a manner like the CCR Rule. However, in the event of new country-wide regulations, whether in the US or another country where tailings are not regulated at the federal level, challenges may occur for tailings facility owners to conform with the GISTM requirements, country-wide regulatory requirements, and local regulatory requirements. This may cause different types of assessments, certifications, and documents to be prepared and posted to disclosure websites or provided to regulatory agencies. This is currently occurring in some states in the US who have developed state-specific CCR regulatory programs that are not yet approved by USEPA, such as Illinois, which can result in burdens for the regulated entities.

Conclusion

It is the intent of the authors to highlight the relative advantages and corresponding challenges of a voluntary, stakeholder-developed standard like the GISTM over a mandatory regulatory approach such as the CCR Rule for achieving the safe and environmentally responsible management of industrial waste storage facilities. The authors are not advocating for the voluntary adoption of the GISTM for CCR unit

owner/operators. The authors would consider such an approach to be duplicative and potentially unnecessary, due to the nearly 10 years of successful failure prevention and risk management achieved by the CCR Rule. The authors hope that this paper is helpful for tailings practitioners and facility owners/operations in realizing the importance of GISTM implementation to achieve successful failure prevention, social responsibility, and environmental responsibility in a voluntary manner, as well as some of the challenges they may encounter while implementing a conformance-based program.

References

AECOM. 2009. Root cause analysis of TVA Kingston dredge pond failure on December 22, 2008.

American Coal Ash Association. 2022. Coal Ash recycling rate increases slightly in 2021; use of harvested ash grows significantly. Accessed 6/20/2024 at: https://acaa-usa.org/wp-content/uploads/2022/12/News-Release-Coal-Ash-Production-and-Use-2021.pdf

Global Tailings Review. 2020. Global Industry Standard on Tailings Management (GISTM). GlobalTailingsReview.org

North Carolina Department of Environmental Quality (NC DEQ) (2014). Dan River Coal Ash Skill. Accessed 6/20/2024 at: https://www.deq.nc.gov/news/key-issues/coal-ash-excavation/coal-ash-archive/dan-river-coal-ash-spill

United States Environmental Protection Agency (USEPA) (no date). Eden NC Coal Ash Spill. Accessed 6/20/2024 at: https://response.epa.gov/site/site_profile.aspx?site_id=9065

USEPA 2016. Effort to assess coal combustion residuals disposal units. Accessed 6/20/2024 at: https://www.epa.gov/coalash/effort-assess-coal-combustion-residuals-disposal-units

USEPA 2017. TVA Kingston site case study.

USEPA 2024a. Disposal of coal combustion residuals from electric utilities rulemakings. Accessed 6/20/2024 at: https://www.epa.gov/coalash/coal-ash-rule#history

USEPA 2024b. Permit programs for coal combustion residual disposal units. Accessed 6/20/2024 at: https://www.epa.gov/coalash/permit-programs-coal-combustion-residual-disposal-units

WBIR 2018. Historic Disaster: 10 years after the ash spill. Accessed 6/20/2024 at: https://www.wbir.com/article/news/historic-disaster-10-years-after-the-ash-spill/51-3125fb4d-93bc-4dd8-9ce1-63a449fa6ff9

A Screening Approach for Preliminary ALARP Assessments of Societal Risks of Existing Tailings Dams

Chao Han, Red Earth Engineering – A Geosyntec Company, Australia
Wade Ludlow, Red Earth Engineering – A Geosyntec Company, Australia

Abstract

The ALARP (As Low as Reasonably Practicable) principle has recently been applied to tailings dams via the Global Industry Standard for Tailings Management (GISTM, 2020) and is used to inform risk reduction to a level that is tolerable and justified by the benefits. ALARP assessment involves risk identification, assessment, and evaluating the risk reduction measures. ALARP assessment considers the existing risks and the risk reduction measures, and determines whether the risks are tolerable, provided that they are reduced to the lowest level that is reasonably practicable and can be justified by the benefits. ALARP assessment is a complex and subjective process that requires the involvement and acceptance of various stakeholders, such as regulators, operators, communities, and investors. Currently, the authors consider that there is a lack of consensus on how to conduct ALARP assessment for tailings dams, especially for the societal risks that affect the public safety and welfare.

This paper discusses the approaches for ALARP assessment of tailing dams outlined in various standards and guidelines and proposes a screening-level approach for the ALARP assessment of the societal risks of existing dams, based on the cost benefit analysis method in ANCOLD (Australian National Committee on Large Dams) guidelines. The key parameters, assumptions, methodology, and results for the proposed approach are presented, along with a flow chart that illustrates the main steps and decision points. The paper also highlights the key threshold features beyond which a more comprehensive ALARP assessment among wider stakeholders is warranted and demonstrates the application of the proposed approach via an example. The authors also discuss some of the shortcomings of the current ALARP assessments used for tailings dams and some proposed improvements.

The proposed approach can provide a useful tool for a high-level screening of the necessity and feasibility of risk reduction measures and can support the decision-making process for achieving ALARP outcomes.

Introduction

ALARP stands for As Low as Reasonably Practicable, which is a principle that guides the management of risks in various industries, such as mining, oil and gas, nuclear, and civil engineering. According to this principle, risks should be reduced to a level that is acceptable to society and the regulator, taking into account the costs and benefits of risk reduction measures. ALARP assessment is a process of evaluating the existing and residual risks of a system or an activity and demonstrating that they are tolerable, and that further risk reduction is either impractical or disproportionate to the improvement gained.

The ALARP principles have historically been used for water dam safety related decision making and have recently been adopted for tailings dams via requirements set out in the Global Industry Standard on Tailings Management (GISTM, 2020). However, there is no universally accepted framework or methodology for conducting and documenting ALARP assessments. Different countries and organizations have adopted different approaches, criteria, and terminology for defining and demonstrating ALARP, which may lead to inconsistencies and ambiguities in the evaluation and communication of risks.

The International Commission on Large Dams Bulletin 189 (ICOLD, 2020) has documented the responses submitted by national committee members to a survey conducted in 2019. The survey contained a range of questions regarding legal, regulatory, and enforcement arrangements, as well as general considerations and risk analysis, evaluation, management and communication. The questions most relevant to risk evaluation and ALARP principles are extracted below, with the responses summarized in Table 1.

Q 4.5: What are the criteria or guidelines for risk tolerability/acceptability used to address societal concerns?

Q 4.11: Is the principle of As Low as Reasonably Practicable (ALARP) applied and if it is, what is the legal context within which it is applied and how it is used in demonstrating the tolerability of risk?

Table 1: Survey results summary based on ICOLD (2020)

Country	References	Q 4.5 Societal Risk Tolerability		Q 4.11 ALARP Demonstration
		Individual	Cumulative	
Argentina	Program underdevelopment	Not specified	Not specified	Not applied
Australia	ANCOLD (2003)	1×10^{-4} (existing); 1×10^{-5} (new)	Limit of tolerability	Good practice + cost-effectiveness
Canada	No criteria	Not specified	Not specified	Not applied
Czech Republic	No criteria	Not specified	Not specified	Not applied
France	No criteria	Not specified	Not specified	Limited use
Italy	No criteria	Not specified	Not specified	Not applied

Country	References	Q 4.5 Societal Risk Tolerability		Q 4.11 ALARP Demonstration
		Individual	Cumulative	
The Netherlands	Not specified	Not specified	Not specified	Not applied
USA	FERC (2016)	1 x 10^{-4}	Tolerable risk reference line	Good practice + cost-effectiveness
	USACE (2014)	1 x 10^{-4}	Societal risk limit line	Good practice + cost-effectiveness
	USBR (2019)	1 x 10^{-4}	Expected annualized life loss of 1E-3 per facility	Not specified

It is clearly demonstrated that concepts of ALARP principles are not equally familiar to the survey participants around the world. That is, respondents answered that ALARP Demonstration is not applied in Argentina, Canada, Czech Republic, France, Italy and the Netherlands, while the survey indicated it is applied as good practice in Australia and the USA. The ICOLD survey was largely based on water dams, so the ALARP concept is even less apparent in the tailings dam industry.

The GISTM (2020) and Tailings Management *Good Practice Guide* (2021) created by the International Council on Mining and Metals (ICMM) require that the operators of tailing dams follow a risk-based approach to manage the risks of their facilities to ALARP, and that they apply the best available technology and the best available practices to prevent and minimize the potential impacts of the failure. However, they do not provide specific guidance on how to conduct ALARP assessment for tailing dams; instead, they recommend that the operators follow the existing regulations or guidelines that are applicable to their jurisdictions to conduct ALARP assessment and demonstrate the acceptability of their risks.

The ANCOLD Tailings Guidelines (2020) reference ANCOLD (2003) for risk assessment of higher and extreme consequence dams to quantify the risk tolerability of specific elements or features of a tailings dam, such as spillway capacity. However, no guidance has been provided for the overall risks of tailings facilities. ANCOLD (2003) was recently revised in ANCOLD (2022).

This paper presents a simplified screening approach based on ANCOLD (2022) methodology to facilitate the ALARP demonstration process for the societal risks of existing tailings facilities.

Methodology

ANCOLD method

ANCOLD (2022) acknowledges that risk evaluation is a matter for dam owners, who need to ensure that the risks meet, or are lower than, any legal requirements and relevant guiding criteria, and that dam owners need to be aware that they may have a legal duty to reduce risks to ALARP under both statute and common

law. The criteria relevant to community, public safety, and workers' risks are highlighted below:

- For existing dams, an individual risk to the person who is most at risk that is higher than 10^{-4} per annum is unacceptable, except in exceptional circumstances. This limit has considered the background risk to the population, which varies with age, as shown in Figure 1, based on data from the Australian Government Actuary, 2017. The limit value of 10^{-4} is slightly higher than two times the minimum average background risk for females aged 12.
- For existing and new dams, a societal risk that is higher than the limit line, shown in Figure 2, is unacceptable, except in exceptional circumstances. The anchor point (i.e., F value of 10^{-3} at N=l) and the slope of the line (i.e., a slope of -1.0 for equal log scales on both axes representative of a risk neutral position) that define the F-N criterion line have been chosen by review of societal risk criteria by Ball and Floyd (1998). The concept of a vertical truncation adopted by other authorities is not considered practical or appropriate and hence is not included in Figure 2.
- The concept of "broadly acceptable" level of risk that was used historically has been abandoned by ANCOLD, which instead provides that ALARP should be applied indefinitely below the limit of tolerability as the primary basis for determining the tolerable risk in a particular case.
- The above guidelines on the tolerability of public safety risk were also put forward for the risks to workers at the dam and at integral workplaces below the dam.

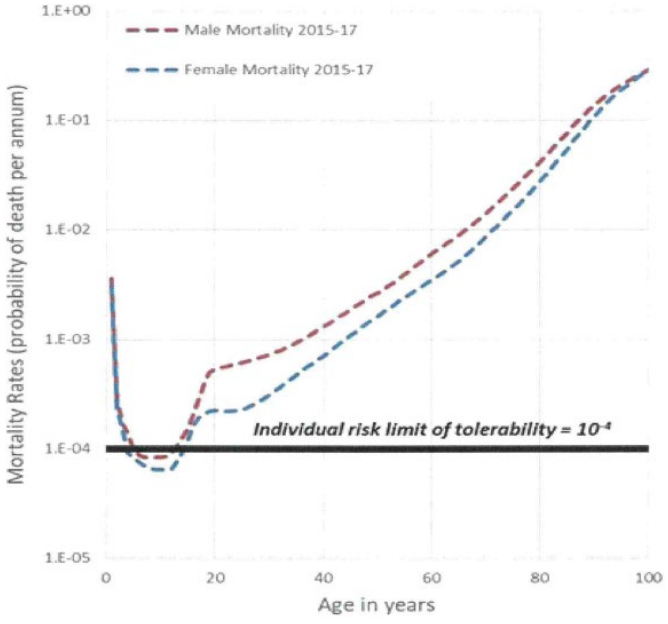


Figure 1: Average background risk (Australian Government Actuary, 2017) and ANCOLD (2022) Individual Risk Guidelines

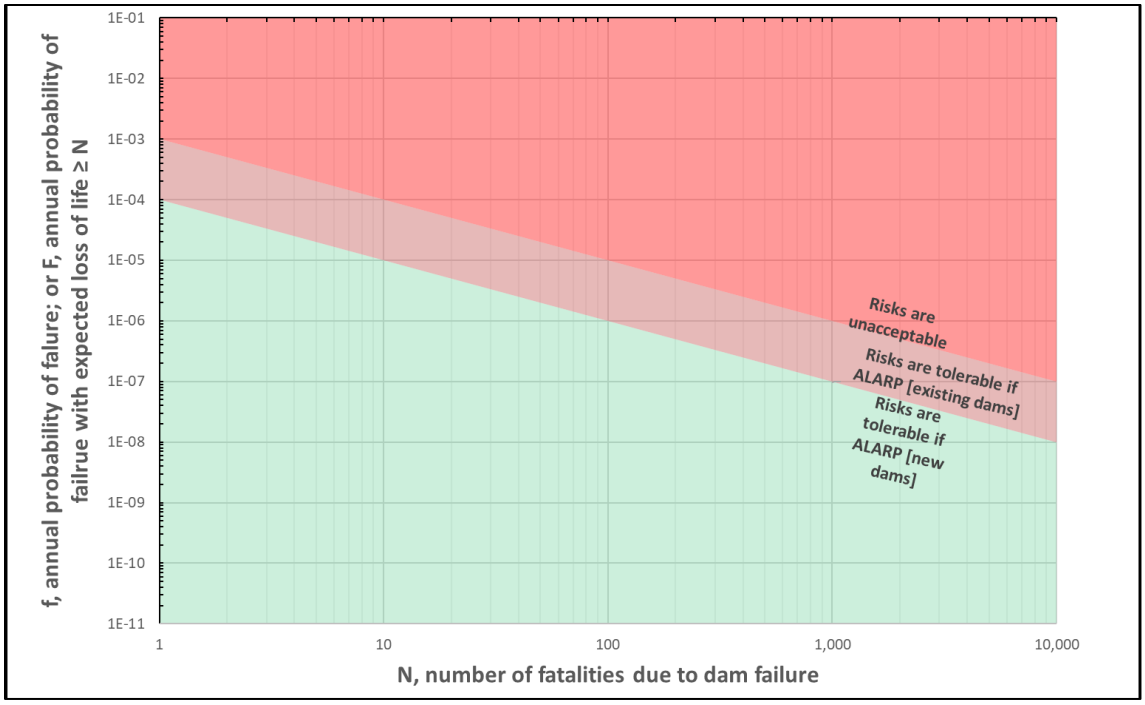


Figure 2: ANCOLD (2022) societal risk guideline

ANCOLD (2022) stipulates that if risks are above the tolerable limits for individual and societal risks, then necessary risk reduction methods are required, regardless of any cost considerations. If the risks are below the tolerable limits, then a demonstration for ALARP can be undertaken. C11-7-4 summarizes the steps required to demonstrate ALARP, which includes the assessment of the dam and its components for compliance with current standards-based good practice, and subsequent determination of a justification rating of cost-to-save-a-statistical-life (CSSL) for those measures that can practicably be implemented. Compliance with current standards-based good practice can be assessed through conventional engineering approaches, which is excluded from the current paper topics. The calculation of adjusted CSSL can be undertaken using Equation 1:

$$CSSL(A) = \frac{(C_A\text{-}(E[R{:}e]\text{-}E[R{:}pr])\text{-}([O{:}e]\text{-}[O{:}pr])\text{-}F_D(E[S{:}e]\text{-}E[S{:}pr])}{(E[L{:}e]\text{-}E[L{:}pr])} \quad \text{(Equation 1)}$$

Where:

- *CSSL(A)*: Adjusted cost-to-save-a-statistical-life, with the provision that a negative value is taken as zero.
- C_A: Annualized cost of implementing risk reduction measure, dollars per annum.
- *E[R:e]*: Expected value of economic and financial consequences of dam failure (failure probability times monetary losses) for the existing dam, dollars per annum.

- *E[R:pr]*: Expected value of economic and financial consequences of dam failure (failure probability times monetary losses) post-risk reduction, dollars per annum.
- *E[L:e]*: Expected value of life loss for existing dam, lives per annum.
- *E[L:pr]*: Expected value of life loss post-risk reduction, lives per annum.
- *O:e*: Existing operating costs, dollars per annum.
- *O:pr*: Operating costs post-risk reduction, dollars per annum.
- F_D: Disproportion factor, dimensionless. Table 8.6 of ANCOLD (2022) provides guidance on F_D values for maximum potential loss of N ranging from 0 to 10, and suggests that for N greater than 10, the N = 10 values apply.
- *E[S:e]*: Expected value of the costs of safety benefits for the existing dam, dollars per annum. Benefits can include avoidance of deployment of emergency services and avoidance of countermeasures such as evacuation and post-accident decontamination.
- *E[S:pr]*: Expected value of safety benefits post-risk reduction, dollars per annum.

The justification rating of CSSL can be determined using Table 2, where:

- VPF: Value in preventing a facility, $AU7.7 million by end of September 2021 quarter, based on a 50% increase on the Office of Best Practice Regulation (OBPR, 2021) value of $AU5.1 million, which is considered a defensible adjustment by Abelson (2007). According to the Reserve Bank of Australia (RBA) Inflation Calculator (2024), the equivalent VFP by end of March 2024 quarter is $AU8.8 million.
- A "Poor" Justification Rating indicates the corresponding risk reduction cost can be shown to be grossly disproportionate.

Table 2: Demonstration of gross disproportion (modified from ANCOLD, 2022)

Justification Rating	Range of CSSL ($AU/Life)	
	Greater than or equal to	Less than
Very Strong	0	0.05 x F_D x VPF
Strong	0.05 x F_D x VPF	0.2 x F_D x VPF
Moderate	0.2 x F_D x VPF	F_D x VPF
Poor	F_D x VPF	–

Analysis details

A series of cost-effectiveness analyses have been carried out using the ANCOLD methodology outlined above to inform the practicality of demonstrating ALARP for societal risks of hypothetical existing dams

based on the Justification Rating in Table 2. These analyses are subsequently used to develop a proposed screening approach to assess the necessity and feasibility of risk reduction measures. To facilitate the simplified approach, the following assumptions have been incorporated into the analyses:

- E[S:e] - E[S:pr] ≈ 0, indicating the net safety benefits between the existing and post-risk reduction scenarios are negligible, compared to the cost of implementing risk reduction measures.
- [O:e] - [O:pr] ≈ 0, indicating the same operating costs between the existing and post-risk reduction scenarios.
- A range of assumed existing risks are tabulated in Table 3, which represent zero to three orders of magnitude (OoM) lower than the limit of tolerability of 10^{-3} lives per annum. For each scenario the post-risk reduction societal risks are assumed to have a failure probability of one to three orders of magnitude lower than the existing risks, without any changes to the failure consequence. An illustration of Risk ID 3 with a two order-of-magnitude reduction is shown in Figure 3.
- A range of assigned monetary losses due to dam failure are summarized in Table 4, which represent the possible combination of the ANCOLD (2020) failure impact severity level and the potential life loss (PLL, equivalent maximum N in Table 3) in the consequence category assessment. The monetary loss values have been assigned to be ten times higher than the lower bound of infrastructure damage cost for the corresponding severity level. The impact durations have been assigned to be the lower bound of the corresponding severity level, so that a reasonably high annual monetary loss can be calculated using the Capital Recovery Method in Equation 2, where the discount rate is assumed to be 7%.

$$Annualised\ Monetary\ Loss = Monetary\ Loss \times \frac{Discount\ Rate}{1-(1+Discount\ Rate)^{-Impact\ Duration}} \quad \text{(Equation 2)}$$

Table 3: Assumed existing risk scenarios

Risk ID	Order of Magnitude below Limit of Tolerability	Maximum number of fatalities, N	Existing Risk	
			Probability of Failure	Expected Life Loss, E[L:e]
			–	(Lives per annum)
1	1	1	5.0E-04	5.0E-04
2	1	10	5.0E-04	9.5E-04
3	1	100	5.0E-04	1.4E-03
4	2	1	5.0E-05	5.0E-05
5	2	10	5.0E-05	9.5E-05
6	2	100	5.0E-05	1.4E-04

Risk ID	Order of Magnitude below Limit of Tolerability	Maximum number of fatalities, N	Existing Risk	
			Probability of Failure	Expected Life Loss, E[L:e]
			–	(Lives per annum)
7	3	1	5.0E-06	5.0E-06
8	3	10	5.0E-06	9.5E-06
9	3	100	5.0E-06	1.4E-05

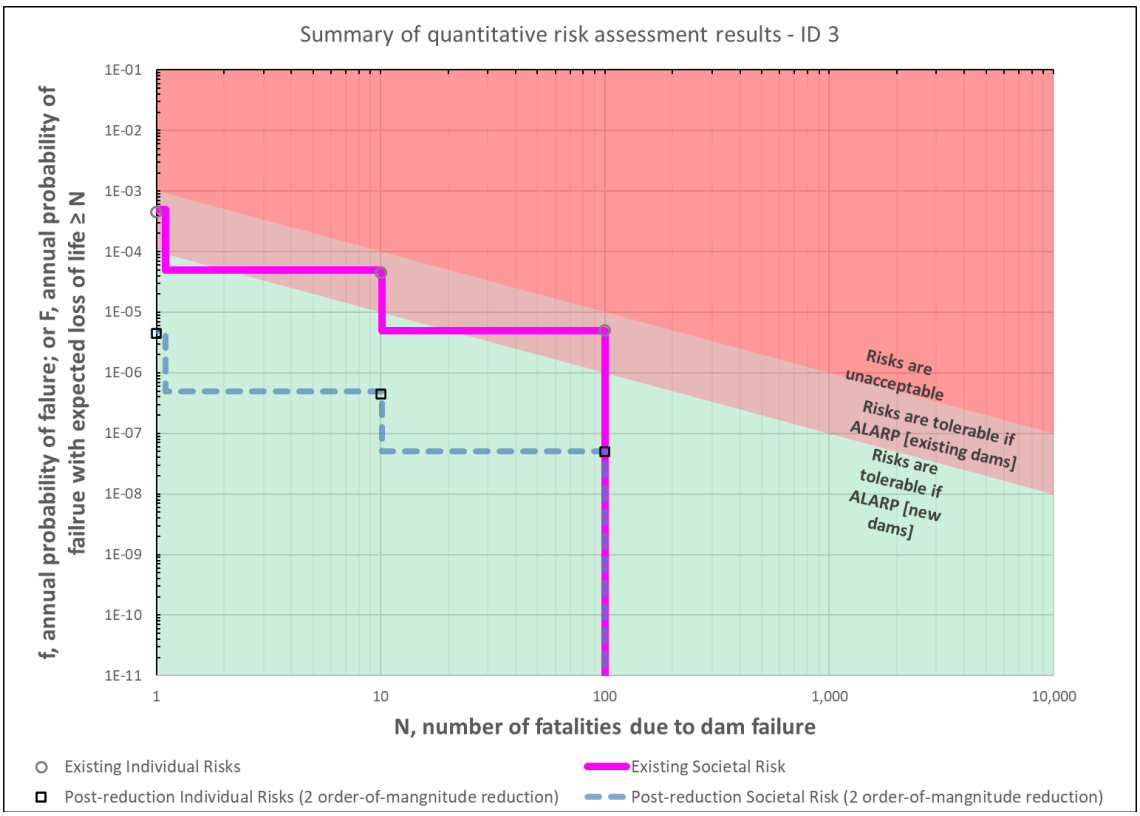


Figure 3: Illustration of existing risk ID 3 and two order-of-magnitude reduction

Table 2: Assigned severity levels

Failure Impact Severity Level	Monetary Loss ($AU)	Impact Duration (year)	Capital Recovery Factor at 7% Discount Rate	Monetary Loss per Annum ($AU)
Medium	$100,000,000	1	1.07000	$107,000,000
Major	$1,000,000,000	5	0.24389	$243,890,694
Catastrophic	$10,000,000,000	20	0.09439	$943,929,257

Based on the above assumptions, the threshold value of C_A to define gross disproportion in Table 2 can be calculated by rearranging Equation 1 and adopting CSSL = F_D × VPF, where VPF = is $AU8.8

million by the end of the March 2024 quarter. The calculations were undertaken in spreadsheets with all possible combinations of the input parameters tabulated in a table. It is worth reiterating that for this assessment it is assumed that the N value (loss of life) is not reduced as part of the risk reduction measure.

Results and discussions

A total of 81 scenarios were calculated, and the threshold value of C_A are shown in Figure 4. Based on the authors' experience with tailings facilities, it is generally difficult to identify any effective risk reduction measures with a cost less than $AU100,000 per annum, reflected by the red dashed line in Figure 4. The results have led to the following observations:

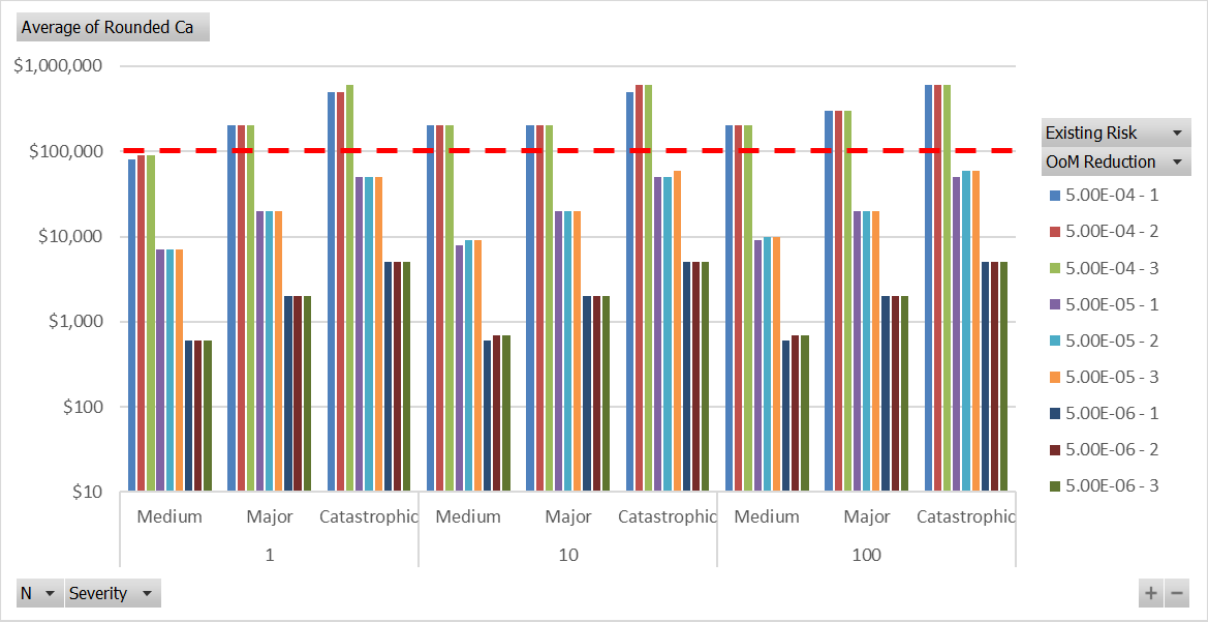


Figure 4: Analysis result summary

- The effectiveness of risk reduction methods represented by the OoM risk reduction has limited impact on the threshold value of C_A, compared to other input parameters such as existing risks and failure consequences.
- The calculated threshold value of C_A increases with severity level and decreases with reduced existing risk. The sensitivity to maximum N is less pronounced given a certain combination of existing risks and severity level. Therefore, the dominant factor in determining the threshold value of C_A is the product of severity level and existing risk.
- The results indicate that for tailings facilities with an existing societal risk in the range of 10^{-4} to 10^{-3} lives per annum, it is likely that there exist risk reduction measures with very strong to

moderate justification ratings, unless the potential dam failure would result in medium severity consequence and no more than a single fatality.

- It is also suggested that for tailings facilities with an existing societal risk lower than 10^{-4} lives per annum, it is most likely that any risk reduction measures would have a poor justification rating (i.e., would be defined as grossly disproportionate).

For tailings facilities at which the impact severity level is governed by the combined effect of infrastructure cost and impact duration, their consequence categories can be determined from Table 5. Therefore, the equivalent consequence category assessed in this study ranges from High C to Extreme. The above discussed results indicate:

- For High C or lower consequence category dams, they could be considered to meet ALARP if their existing risks are lower than the limit of tolerability.
- For High B or higher consequence category dams, they could be considered to meet ALARP if their existing risks are more than two orders of magnitude lower than the limit of tolerability.
- ALARP demonstration with cost-effectiveness considerations is expected for High B or higher consequence category dams with existing risks less than two orders of magnitude lower than the limit of tolerability.
- The above points are interesting outcomes of the assessment; however, each facility may have other risks, issues, or constraints that may require additional consideration or review.

Table 5: ANCOLD (2012) Consequence Category Table based on PLL

Potential Loss of Life (PLL)	Severity of Damage and Loss			
	Minor	Medium	Major	Catastrophic
<0.1	Very Low	Low	Significant	High C
≥0.1 to <1	Significant	Significant	High C	High B
≥1 to <5	*(Note 1)*	High C	High B	High A
≥5 to <50		High A *(Note 2)*	High A	Extreme
≥50		*(Note 1)*	Extreme	Extreme

Note 1: *With a PLL equal to or greater than one (1), it is unlikely Damage will be minor. Similarly with a PLL in excess of 50 it is unlikely Damage will be classified as Medium.*
Note 2: *Where PLL is in the range ≥5 to<10, the Category level can be reduced to* ***High B.***

Proposed screening approach

Based on the above results, a simplified screening approach is developed, as shown in Figure 5. Due to the assumptions incorporated into the analyses, the proposed approach should only be used for the following scenarios:

- The differences in safety benefits between existing and post-risk reduction scenarios should be negligible.
- The differences in operational costs between existing and post-risk reduction scenarios should be negligible.
- The risk reduction measures should focus on reducing failure probability with a minimal change to failure consequences.

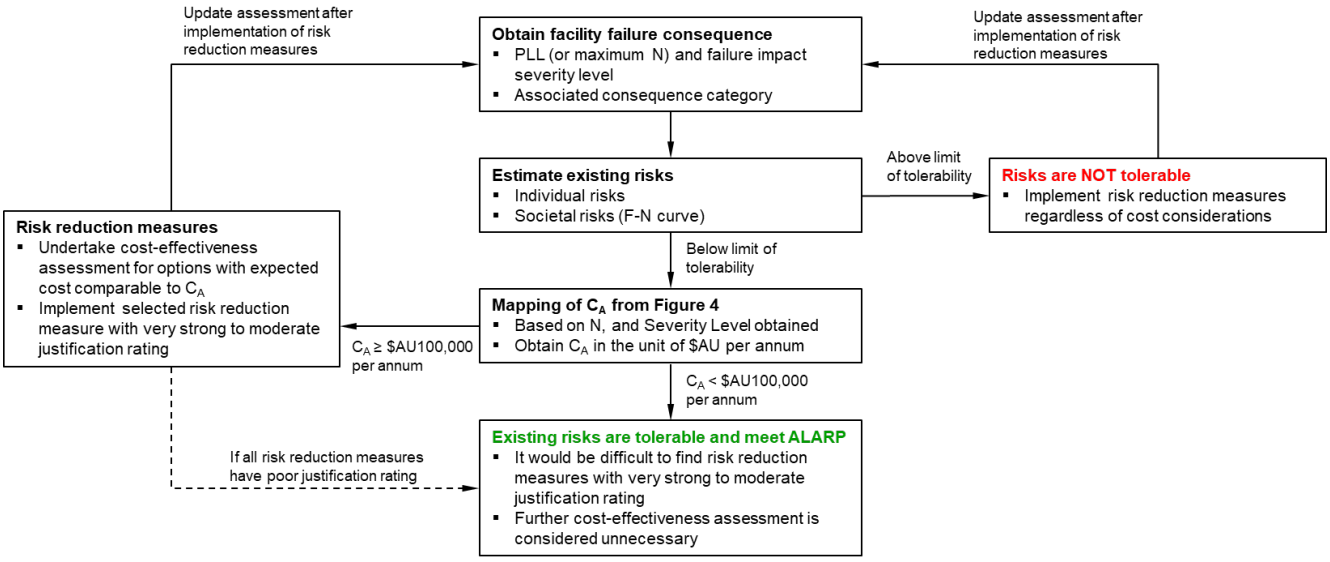


Figure 1: Proposed ALARP screening approach

Application example

A hypothetical mining company has a number of tailings facilities, with the risk profiles summarized in Table 6. Forming part of the GISTM compliance requirements, the company's appointed Accountable Executive is required to endorse the documentation stating the ALARP status of their tailings facilities. As a starting point, the company needs to decide which facilities have intolerable risks that require further risk reduction measures regardless of cost; which facilities can be considered to meet ALARP with a high confidence level; and which facilities require additional resource allocations to demonstrate ALARP with more detailed cost-effective assessments.

The company decided to use the proposed screening approach, and the results shown in Table 7 demonstrate that the existing risks for Facilities 2 and 3 are likely to meet ALARP. For Facility 1, ALARP

is unlikely to be achieved with the existing risks and the risk reduction Option B is preferred, with a detailed cost benefit analysis recommended to support this option.

Table 6: Summary of application example

Facility ID	Consequence Category	Existing Societal Risks		Risk Reduction Options	ALARP Demonstration Required based on Screening?
		Risk Rating	Max. N		
1	Extreme	10^{-4}	10	A. Buttress C_A of at least \$1 million per annum B. Improve Monitoring System C_A below \$100,000 per annum	A. Screening suggests option is unlikely to be cost-effective B. Screening suggests ALARP needs to be demonstrated
2	High B	10^{-5}	1	Buttress C_A of at least \$1 million per annum	Screening suggests already ALARP
3	Significant	10^{-4}	<1	Larger pumps to control water (C_A of at least \$1 million per annum)	Screening suggests already ALARP

ALARP limitations

While the authors have found ALARP to be a fairly rigorous review of risk ratings and a good tool to communicate the benefit of risk reduction options, it is limited to Potential Loss of Life. It does not account for environmental, cultural heritage risks, reputational, and other similar risks. A number of approaches are available to attempt an ALARP assessment as follows.

One option is to review the current and residual risks and look at the reduction on the risk matrix. This goes some way towards showing the reduction of risk and gives an indication of an ALARP condition, and can be used for environmental, cultural heritage, and business reputation risks that cannot be quantified on an F-N plot. An example is shown in Figure 6 using the AS/NZS 4360: 2004 Risk Management Guidelines, in which the ALARP boundary should be defined by the dam owners based on the individual company's risk appetite. This is an area that requires further development so that ALARP conditions can be demonstrated for risks other than loss of life.

Level	Criteria	Description
1	Rare	Almost never happened
2	Unlikely	Rarely happening
3	Possible	Can happen every once in a while
4	Likely	Often occur
5	Almost Certain	Can happen any time

Source: Likelihood criteria adopted from standard AS/NZS 4360: 2004.

Level	Criteria	Description
1	Insignificant	No injury and/or no disease caused and/or no effect on the environment, small financial loss
2	Minor	Minor injury and/or illness with mild symptoms and/or small effect on the environment, small financial loss
3	Moderate	Moderate injury and/or chronic illness requires medical treatment and/or moderate effect on the environment, sizeable financial loss
4	Major	Serious injury and/or chronic illness require medical treatment and/or serious and long-term environmental damage, big loss, production disruption
5	Catastrophic	Fatal and/or chronic diseases require serious medical treatment and/or very serious and long-term environmental damage, huge losses and very broad impacts, cessation of all activities

Source: Severity criteria adopted from standard AS/NZS 4360: 2004.

Likelihood	Severity				
	Insignificant (1)	Minor (2)	Moderate (3)	Major (4)	Catastrophic (5)
Almost Certain (5)	M	H	VH	VH	VH
Likely (4)	L	M	H	VH	VH
Possible (3)	L	M	H	VH	VH
Unlikely (2)	L	L	M	H	VH
Rare (1)	L	L	M	H	H

ALARP

R1 R2 R3

Source: Risk assessment matrix adopted from AS/NZS 4360: 2004 standard.

Figure 6: Example of ALARP approach to environmental risks

Another option would be to assume a monetary loss commensurate with the environmental risk assessed. Based on the severity level for a dam failure in ANCOLD (2020) in Figure 7, a medium risk environmental consequence could be assumed to have a similar dollar value consequence in the table ($10M to $100M) and the practitioner would select a suitable value within this range for the cost benefit assessment.

Both of the above methods need further development, but as GISTM requirements become more widespread and further experience is gained, it will be necessary to demonstrate ALARP for all major risks including potential loss of life, environmental, cultural heritage, etc.

DAMAGE TYPE	MINOR	MEDIUM	MAJOR	CATASTROPHIC
Infrastructure (dam, houses, commerce, farms, community)	<$10M	$10M-$100M	$100M-$1B	>$1B
Business importance	Some restrictions	Significant impacts	Severe to crippling	Business dissolution, bankruptcy
Public health	<100 people affected	100-1000 people affected	<1000 people affected for more than one month	>10,000 people affected for over one year
Social dislocation	<100 person or <20 business months	100-1000 person months or 20-2000 business months	>1000 person months or >200 business months	>10,000 person months or numerous business failures
Impact Area	<1km²	<5km²	<20km²	>20km²
Impact Duration	<1 year	<5 years	<20 years	>20 years
Impact on natural environment	Damage limited to items of low conservation value (e.g. degraded or cleared land, ephemeral streams, non-endangered flora and fauna). Remediation possible.	Significant effects on rural land and local flora & fauna. Limited effects on: A. Item(s) of local & state natural heritage. B. Native flora and fauna within forestry, aquatic and conservation reserves, or recognised habitat corridors, wetlands or fish breeding areas.	Extensive rural effects. Significant effects on river system and areas A & B. Limited effects on: C. Item(s) of National or World natural heritage. D. Native flora and fauna within national parks, recognised wilderness areas, RAMSAR wetlands and nationally protected aquatic reserves. Remediation difficult	Extensively affects areas A & B. Significantly affects areas C & D. Remediation involves significantly altered ecosystems.

Figure 7: Example of assigning dollar values based on environmental impacts (ANCOLD, 2020)

Conclusion

This paper reviews relevant standards and guidelines that recommend ALARP assessment of tailings dams and suggests a screening-level approach for ALARP assessment of the societal risks for existing tailings dams, based on the cost benefit analysis method in ANCOLD guidelines. The paper presents the main

parameters, methodology, assumptions, and supporting results for the suggested approach, supported with a flow chart that shows the main steps and decision points. The paper also shows the key threshold features that require a more detailed ALARP assessment among wider stakeholders and applies the proposed approach to the risk evaluation of hypothetical tailing dams via an example. The shortcomings of the current ALARP assessments used for tailings dams such as environmental, cultural heritage, and business reputation risks are also discussed, and the proposed improvement options are suggested.

The suggested approach can help identify the existing tailings facilities that meet ALARP with the existing risks, since it would be difficult to find risk reduction measures with strong to moderate justification ratings. For the facilities that do not meet ALARP with the existing risk, this approach can help screen for the need for and feasibility of risk reduction measures for subsequent detailed ALARP demonstration.

References

Abelson, P. 2007. *Establishing a Monetary Value for Lives Saved: Issues and Controversies*, Working Papers in Cost Benefit Analysis WP 2008-2.

Australian Government Actuary. 2017. *Australian Life Tables 2015–17*. Accessed 06/01/2024 at https://aga.gov.au/publications/life-tables/australian-life-tables-2015-17

Australian National Committee on Large Dams (ANCOLD). 2003. *Guidelines on Risk Assessment*. ANCOLD, Australia.

Australian National Committee on Large Dams (ANCOLD). 2012. *Guidelines on Assessment of the Consequences of Dam Failure*. ANCOLD, Australia.

Australian National Committee on Large Dams (ANCOLD). 2020. *Guidelines on Tailings Dams*. ANCOLD, Australia.

Australian National Committee on Large Dams (ANCOLD). 2022. *Guidelines on Risk Assessment*. ANCOLD, Australia.

Ball, D.J. and Floyd, P.J. 1998 *Societal Risks.* Report prepared for UK Health and Safety Executive.

Federal Energy Regulatory Commission (FERC). 2016. *FERC Risk-Informed Decision Making Chapter 3, Risk Assessment.* Accessed 06/01/2024 at https://www.ferc.gov/sites/default/files/2020-04/chapter-3.pdf

International Commission on Large Dams (ICOLD). 2020. *Bulletin 189*: *Current state-of-practice in risk-informed decision-making for the safety of dams and levees.*

International Council on Mining and Metals (ICMM). 2020. *Global Industry Standard on Tailings Management.*

International Council on Mining and Metals (ICMM). 2020. *Tailings Management Good Practice Guide.*

Reserve Bank Australia (RBA). 2024. *Inflation Calculator.* Accessed 06/01/2024 at https://www.rba.gov.au/calculator/

The Office of Best Practice Regulation. 2021. *Best Practice Regulation Guidance Note: Value of statistical life, Office of Best Practice Regulation,* Department of Prime Minister and Cabinet, Australia, August

US Army Corps of Engineers (USACE). 2014. *ER 1110-2-1156*: *Engineering and Design Safety of Dams – Policy and Procedure.*

US Bureau of Reclamation (USBR). 2019. *Best Practices in Dam and Levee Risk Analysis, Chapter A-9 Governance and Guidelines.*

Integrating Geometric Deposition and Hydrological Water Balance in Tailings Management: a Semi-Probabilistic Approach

Paulo Victor S.A. De Castro, GeoMerry, Brazil
Miguel Palape, Minebridge, Chile
Roberto Cezar Rego Silva, WSP, Brazil
João Marcus S.A. De Castro, GeoMerry, Brazil

Abstract

This paper introduces an innovative approach to tailings disposal, merging geometric deposition techniques with hydrological water balance within a semi-probabilistic framework. The primary tools employed in this methodology are Muk3D for geometric deposition and GoldSim for hydrological water balance. The process is dynamic and iterative, effectively tracking tailings from their source to the pond, identifying deposition points, and establishing the tailings surface. This methodology significantly enhances accuracy in estimating volumes of tailings and lakes, ensuring that errors stay within predetermined permissible error margins for both tailings and pond volumes.

The dynamic nature of the model facilitates automated dam raising, treated as discrete events, thereby ensuring immediate updates to reservoir geometry. This is accomplished through a Python-based programming environment, which boosts efficiency and facilitates independent processing. By incorporating semi-probabilistic techniques and selecting a cumulative probability volume, this method not only improves long-term decision-making, but also addresses uncertainties inherent in tailings management effectively.

The implementation of this integrated strategy offers valuable insights into efficient tailings management and robust risk assessment. It represents a potential paradigm shift in industry standards, providing a comprehensive and advanced approach to overcoming the challenges faced in the mining industry. The findings from this study are expected to make a significant contribution to the field of tailings management, setting a new benchmark for future practices.

Introduction

The management of tailings in the mining industry is a complex and evolving challenge, demanding

innovative approaches to ensure environmental safety and operational efficiency. This paper introduces a novel methodology for tailings disposal, combining geometric deposition techniques with hydrological water balance within a semi-probabilistic framework. The primary tools employed in this methodology are Muk3D for geometric deposition and GoldSim for hydrological water balance, integrated within a dynamic and iterative process that tracks tailings from their source to the pond, identifies deposition points, and establishes the tailings surface. This approach significantly enhances the accuracy of volume estimations for both tailings and lakes, maintaining errors within predefined permissible margins.

The dynamic model facilitates automated dam raising, treated as discrete events, ensuring immediate updates to reservoir geometry. This process is executed within a Python-based programming environment, enhancing efficiency and allowing for independent processing. By incorporating semi-probabilistic techniques and selecting a cumulative probability volume, the methodology not only improves long-term decision-making but also effectively addresses the uncertainties inherent in tailings management. Oboni and Oboni (2020) highlight the significance of innovative approaches in tailings management, emphasizing the need for accurate and reliable methods to mitigate environmental impacts and enhance operational efficiency.

In the numerical simulation of reservoir filling, this paper proposes the use of Muk3D software. The model applied in Muk3D for simulating tailings disposal follows an iterative process of geometric approximation between the lake volumes and the tailings to be disposed of in the reservoir. To ensure the final configuration is physically consistent, the geometric approximation adheres to the following constraints:

- beach angles of the tailings;
- positioning of spigots as the highest point of the tailings surface;
- location of the lake; and
- maximum elevation of the lake.

Consequently, the tailings surfaces are defined by the beach angles and the spigot positions, with the beach angle varying when in contact with the horizontal lake surface. The iterative process ensures the dynamic interaction between tailings and lake surfaces is accurately modeled.

The implementation of this integrated strategy offers valuable insights into efficient tailings management and robust risk assessment. It represents a potential paradigm shift in industry standards, providing a comprehensive and advanced approach to overcoming the challenges faced in the mining industry. The findings from this study are expected to make a significant contribution to the field of tailings management, setting a new benchmark for future practices.

Methodology

For the numerical simulation of reservoir filling, Muk3D software was utilized. The model employed in Muk3D for tailings disposal simulation involves an iterative process of geometric approximation between the lake volumes and the tailings to be disposed of in the reservoir. To ensure the final configuration is physically consistent, the geometric approximation adheres to the following constraints:

- beach angles of the tailings: the lake's interaction area affects the subaqueous and subaerial angles. Because of the particle deposition pace along the tailings beach, a bigger lake area in a reservoir results in a different angle shift (from subaerial to subaqueous) than a smaller lake;
- positioning of spigots as the highest point of the tailings surface;
- location of the lake; and
- maximum elevation of the lake.

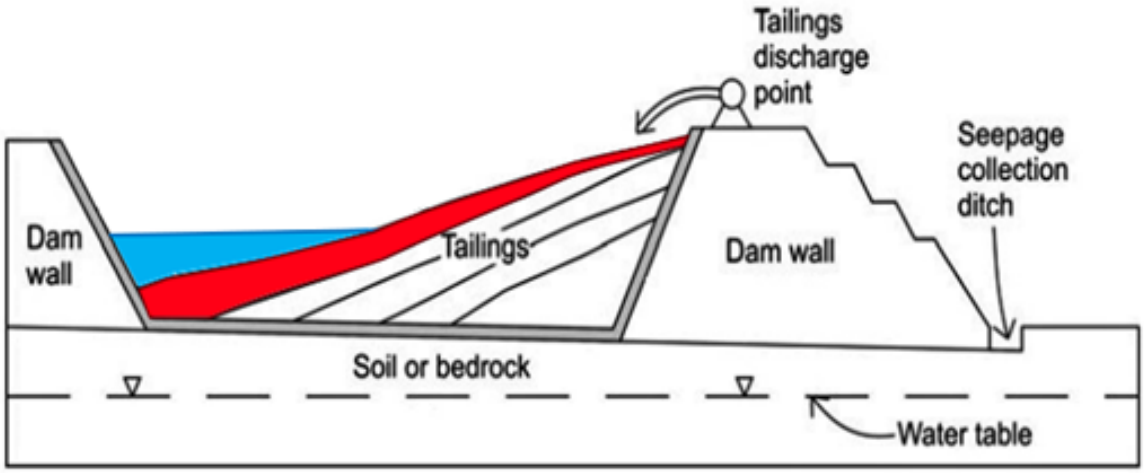


Figure 1: General view of a tailings deposition plan

The diagram in Figure 2 illustrates the automated model workflow, integrating GoldSim, Python, and Muk3D. GoldSim handles the water balance and hydrological assessments, managing tailings volumes and raising areas. Muk3D simulates tailings geometric deposition and dam raising. Python coordinates the processes, linking elevation, area, and volume data between GoldSim and Muk3D. This iterative loop ensures continuous updates and adjustments, enhancing accuracy and efficiency.

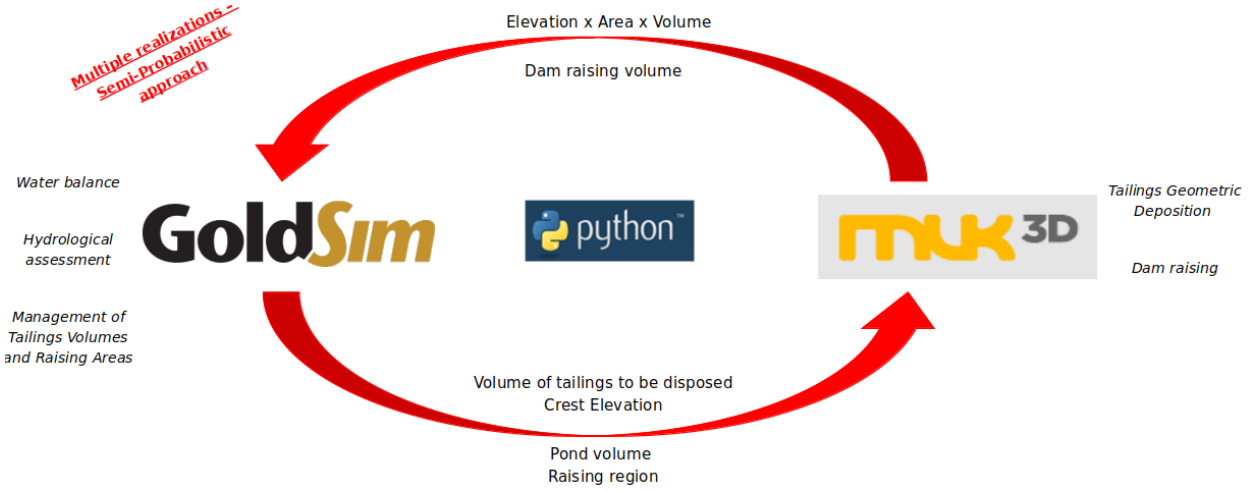


Figure 2: Simulation process interaction

Thus, the tailings surfaces are defined by the beach angles and the position of the spigots. The beach angle varies when in contact with the horizontal lake surface, and the iterative process is defined to achieve the configuration as presented.

The spigot positions over time determine the deposition points considered in the model for surface formation. This iterative process approximates the lake and tailings volumes until the error between the target volume and the calculated volume is within acceptable limits:

- tailings volume = 1%
- lake volume = 10%

The disposal plan considers continuous dam raising, using tailings as the material for construction. The model manages the regions to be raised based on reservoir filling, constructing in 1-meter layers and following a counterclockwise cycle.

In the geometric deposition of tailings, curves representing elevation versus area are generated. For model optimization, only vectorized curves of elevation versus area are imported into GoldSim. For hydrological verifications, GoldSim's numerical integration tool determines the corresponding volume for a given elevation and area pair by integrating the entire interval up to that pair. Thus, interactions with lake elevation, area, or volume elements update the lookup table with data generated from Muk3D.

The semi-probabilistic approach described in the study integrates a probability distribution for lake volumes. Given the computational limitations, specific lake volumes with cumulative probabilities are used for geometric deposition modeling. This approach accounts for the intrinsic variability of input variables such as rainfall, evaporation, tailings production rates, moisture content, beach angles, and uncertainties in tailings properties.

This model has the advantage of accommodating all these variabilities, allowing the simulation of disposal scenarios that better represent risk conditions, including both extreme and more probable scenarios. The adjustments to this coupled model can significantly assist in risk management for structures that, for example, require maintaining a lake near the catchment area, have discharge restrictions, need verification of the contingency storage volume, among other aspects. By considering scenarios with cumulative probabilities, the model can provide a comprehensive assessment of risks and help in strategic decision-making for tailings management throughout the mine's life.

Results

The results of the hypothetical case study demonstrate the application of the integrated, automated model for tailings and water management. The probabilistic volume of the lake over time, the volume of tailings disposed of over time, and the crest elevation of the dam were analyzed under non-linear probabilistic conditions.

Probabilistic lake volume over time

The model's output for the lake volume over time incorporates the variability of rainfall, evaporation, and other hydrological factors. The lake volume was tracked at cumulative probabilities. This analysis helps in understanding the range of potential scenarios for water management, as shown in Figure 3.

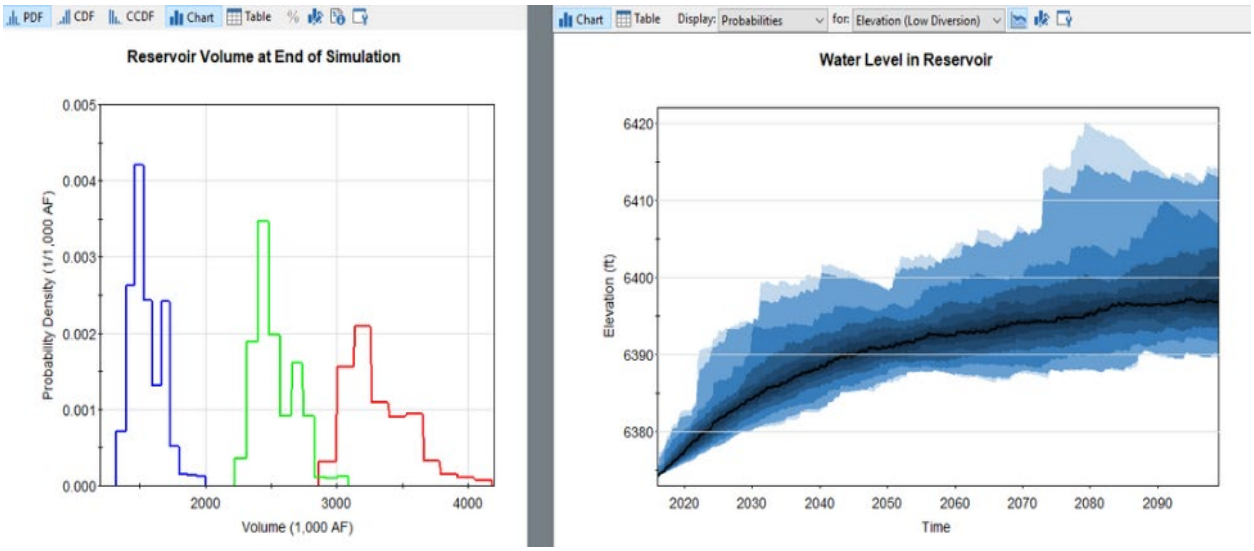


Figure 3: Probabilistic lake volume over time

Volume of tailings disposed over time

The volume of tailings disposed of was monitored, showing the impact of varying production rates and tailings properties. This probabilistic approach provides insights into the expected range of tailings volumes, aiding in strategic planning for tailings management as shown in Figure 4.

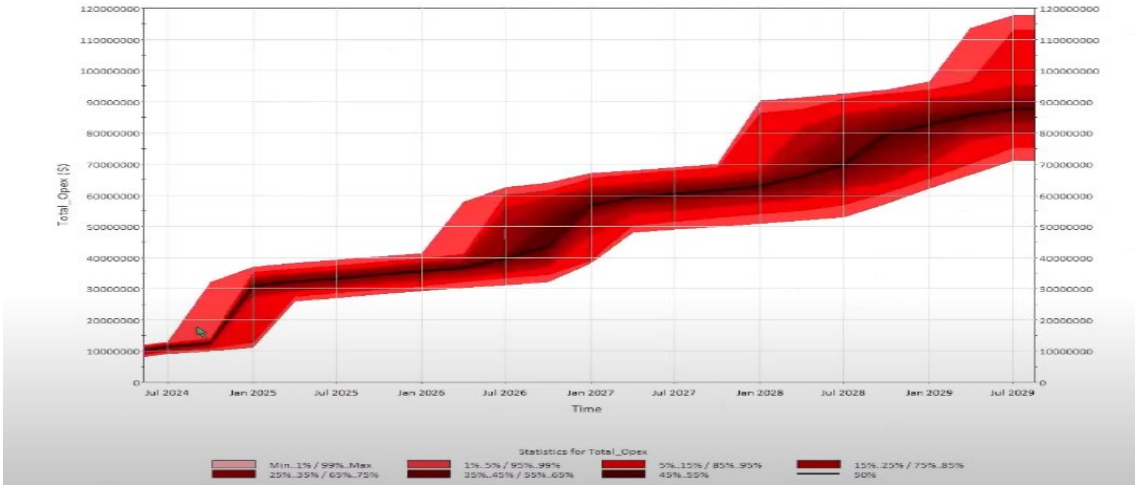


Figure 4: OpEx for tailings disposed over time

Crest elevation of the dam

The crest elevation of the dam was adjusted iteratively, based on the deposition model. The results, presented in Figure 5, show how the dam height changes with the cumulative probability scenarios, highlighting the importance of accurate modeling for effective dam raising. The more information provided about the criteria that the operation evaluates for the most current date and future perspectives, the more accurate the model is. The accuracy of the modeling directly influences the operationality of the structure, providing the necessary volumes and timelines for the raising, while also correlating the modification of auxiliary structures with the crest elevation increase, such as the alteration of the spillway channel, modification of tailings pipelines, and other auxiliary structures.

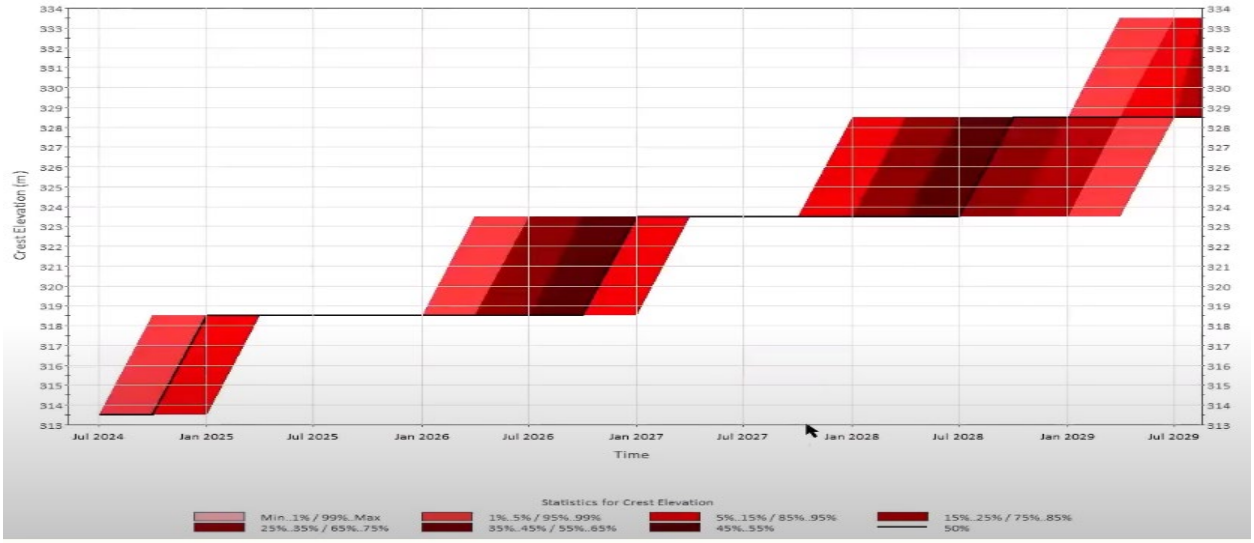


Figure 5: Crest elevation of the dam

Discussion

The probabilistic approach highlights the non-linear responses of the system under varying conditions. The ability to simulate different scenarios provides a robust framework for assessing risks and planning for tailings management. This hypothetical case study lays the groundwork for detailed modeling of real-world cases, incorporating the specific nuances and complexities of each site. The results underscore the potential of this integrated model to improve decision-making and operational efficiency in tailings and water management.

Conclusion

The integrated and automated use of geometric deposition models and hydrological balance presented in this article demonstrates significant potential for enhancing tailings management. The ability to automate control of various variables, such as flood transit verification, overflow volumes, and occurrence probabilities, offers a comprehensive approach to managing tailings. This method ensures effective dam raising, addresses water demand risks for industrial plants, and manages operational contingencies. Additionally, the automated identification and positioning of tailings discharge points streamline operations, providing a robust framework for improved safety and efficiency in tailings management.

Understanding these risks and their dimensional knowledge clarifies strategic decision-making for tailings management directions throughout the life of the mine. This comprehensive understanding is crucial for optimizing long-term planning and ensuring the sustainability and safety of mining operations.

Acknowledgements

We extend our gratitude to MineBridge Software for their support and access to Muk3D software, which was pivotal for our geometric deposition simulations. We also thank GeoMerry for their expert guidance and collaboration in waste disposal and management planning, which significantly contributed to the success of this study.

References

Finke Morrison, K. 2022. *Tailings Management Handbook: A Life-Cycle Approach*. Society for Mining, Metallurgy & Exploration.

GoldSim Technology Group. 2024. GoldSim user guide. Retrieved from GoldSim Technology Group.

MineBridge Software Inc. 2024. Muk3D user manual. Accessed at https://support.muk3d.com/

Oboni, F. and Oboni, C. 2019. *Tailings Dam Management for the Twenty-First Century: What Mining Companies Need to Know and Do to Thrive in Our Complex World*. Springer.

Praskievicz, S. and Chung, H. 2009. A review of hydrological modelling of basin-scale climate change and urban development impacts. *Progress in Physical Geography Earth and Environment* 33(5): 650–671.

SimplXit. 2023. GoldSim webinar tutorial: model and application cases.

Incorporating Lifespan Considerations into ALARP Decision-Making for TSFs: a Practical Methodology

Ignacio A. Cueto, SRK Consulting, Argentina
Osvaldo N. Ledesma, SRK Consulting, Canada
Franco Oboni, SRK Consulting, Canada

Abstract

ALARP (As Low as Reasonably Practicable) is featured in several state-of-the-art guidelines, such as those of the Canadian Dam Association (CDA), the Mining Association of Canada (MAC), and the Australian National Committee on Large Dams (ANCOLD), as well as in GISTM/ICMM, which all address risk evaluation and recommend the use of ALARP. In some literature ALARP is essentially represented as the trade-off equilibrium between mitigation costs and risk reduction benefits. However, its most modern definition is that a residual risk, i.e. the risk after mitigation, shall be as low as reasonably practicable, and to be considered ALARP it must be possible to demonstrate that the cost involved in reducing it further would be grossly disproportionate to the benefit gained.

Being able to demonstrate ALARP status, that is locating the minimum ALARP point (LMALARP) is therefore paramount to owners, the Engineer of Record (EoR), the public, insurers, lenders and regulators.

Rationally, LMALARP yields better decisions, enhances the value of projects and avoids mitigative Capital Expenditure (CAPEX) squandering. LMALARP should not be seen as a static process, as it has to encompass various time horizons in the life of a project/facility. Indeed, the short-term ALARP may be very different from the long-term one due to different uncertainties, changing system conditions and external evolution, such as for example land use around the considered facility, which will require adaptation.

This paper showcases how to quantitatively incorporate lifespan in the ALARP assessment when looking at a specific mitigation program and/or to compare different mitigation options. To do so, annualized quantitative risks must be evaluated for each mitigative alternative, and the cost of the various mitigative actions estimated. For each time horizon the result is the trade-off equilibrium between mitigation costs and risk reduction benefits, which represents the minimum theoretical ALARP point. Various considerations can then guide decision-makers to select the point where the cost involved in reducing it further would be grossly disproportionate to the benefit gained.

This process has been applied to existing facilities, showing how the optimum solution varies, not only when the weighting of the different consequences is shifted (environmental vs. financial vs. reputation, etc.), but also when the lifespan of the structured is considered.

Introduction

ALARP (As Low as Reasonably Practicable) is featured in several state-of-the-art guidelines, such as those from the Canadian Dam Association (CDA), the Mining Association of Canada (MAC), and the Australian National Committee on Large Dams (ANCOLD), as well as in GISTM (Global Tailings Review, 2020) and ICMM, which all address risk evaluation and recommend the use of ALARP.

In some literature, ALARP is essentially represented as the trade-off equilibrium between mitigation costs and risk reduction benefits. However, its most modern definition is that a residual risk, i.e. the risk after mitigation, shall be as low as reasonably practicable, and that to be considered ALARP it must be possible to demonstrate that the cost involved in reducing it further would be grossly disproportionate to the benefit gained.

This paper shows quantitative solutions to Locate Minimum ALARP (LMALARP) threshold level, the trade-off equilibrium point cited above, and how to integrate various time horizons to this evaluation. The disproportionate mitigation investment lies to the right of the LMALARP in Figure 1b.

ALARP concept evolution

The principle of ALARP was originated in British case law, with examples dating back to 1949. One of these cases dealt with whether it was reasonably practicable to prevent any possibility of a rock fall in coal mines, and established the concept of "reasonably practicable," distinguishing it from being "physically possible," as these terms are applied to risk mitigation measures. Thus, it can be said that ALARP was born from mining applications. The court at that time established that: *"Reasonably practicable is a narrower term than 'physically possible' and implies that a computation must be made ... in which the quantum of risk is placed in one scale and the sacrifice involved in the measures necessary for averting the risk (whether in time, trouble or money) is placed in the other and that, if it be shown that there is a great disproportion between them – the risk being insignificant in relation to the sacrifice – the person upon whom the obligation is imposed discharges the onus which is upon him."* (Edwards vs. National Coal Board, 1949) to do so. Interestingly, the judge used the word "computation" and did not even consider a qualitative approach.

Historic definitions

The UK Health and Safety at Work Act of 1974 (HSWA) formally adopted the ALARP principle (HSE,

2024). Several countries around the world have employed elements of the ALARP concept including Australia, Abu Dhabi, Belgium, Brazil, Denmark, Hong Kong, Ireland, Netherlands, Saudi Arabia, and the U.S.A. In the U.S.A., the ALARP principle has been employed by the U.S. Army Corps of Engineers (USCE) since 2009 (USCE, 2009, 2019)

Historically, ALARP was defined as a probability level, paired with a number of potential fatalities (see Figure 1a, from Hain, 2015), i.e., a risk measured with a fatality metric. Some studies even defined ALARP as a fixed probability threshold.

Unfortunately, such a graph does not allow the determination of ALARP, not even as a trade-off, but states that if a failure is below the intolerable region, then it is ALARP or, for lower values, even broadly acceptable. Beyond the arbitrary nature of the risk levels, we find that mixing the definition of ALARP with tolerance creates unnecessary confusion. Furthermore, the fatality metric does not allow the evaluation of ALARP for multidimensional consequences (compounded fatalities, environmental, direct losses, indirect losses), which are the ones generating risk in notorious mining events.

In some literature, however, ALARP is essentially represented as the trade-off equilibrium between mitigation costs and risk reduction benefits. The ALARP framework implicitly assumes that full elimination of risks cannot be achieved and that there is always some trade-off between residual risk after mitigation and the associated mitigative cost. Figure 1b shows the ICMM guidance (ICMM, 2021) which depicts ALARP as the trade-off point.

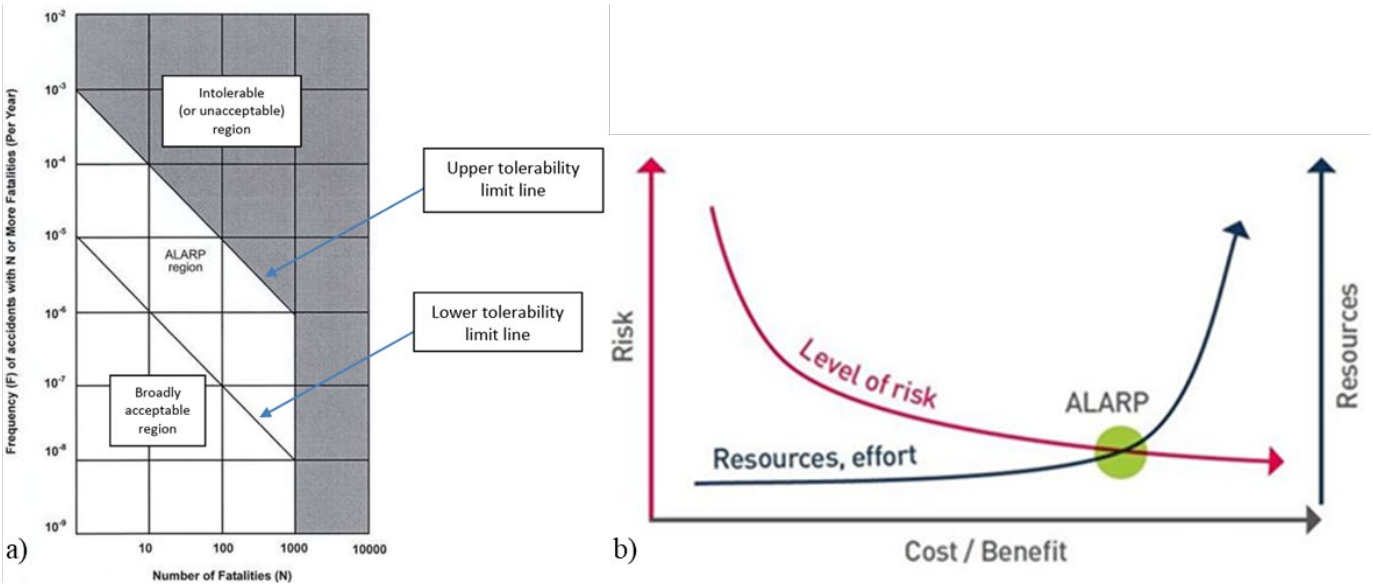


Figure 1: a) A generic ALARP graph (Hain, 2015). b) ICMM 2021's concept of assessing benefit of mitigation effort to residual risks with ALARP at trade-off point, called herein LMALARP (ICMM, 2021)

These definitions appear in many studies and papers and create some confusion because the definition nowadays has shifted, as shown in the next section.

Modern definitions

It appears that the definition of ALARP is now back to its origins (Edwards vs. Coal Board, 1949), i.e. a residual risk, the risk after mitigation, for which it must be possible to demonstrate that the cost involved in reducing it further would be grossly disproportionate to the benefit gained (Hain, 2015). The minimum trade-off point (the intersection between the two curves shown in Figure 1b, which we call the LMALARP, the location of the minimum ALARP) can be evaluated using quantitative risk evaluations (Oboni and Oboni, 2022a; 2022b; 2022c), while the final decision on what constitutes disproportion , i.e. the shifting of ALARP to the right of the horizontal axis of Figure 1b, relies on human judgement.

This definition thus encompasses demonstrating disproportionate investment for limited risk reduction (to the right of the trade-off point of Figure 1b). It is our opinion that the shift to the right is strongly influenced by public opinion, which has become a fundamental driver recognized by a UNEP partner (Roche et al., 2017), Oboni and Oboni (2019), and then GISTM.

Determining the trade-off to elicit a rational decision on ALARP

Who is interested in rational estimates of ALARP?

As a result of the prior discussion, being able to find the LMALARP is paramount to owners, the Engineer of Record (EoR), the public, insurers, lenders, and regulators.

The ability to rationally discern the LMALARP fosters better decision making, enhances the value of projects, and avoids mitigative CAPEX squandering.

Why should ALARP consider various planning time horizons?

The LMALARP should not be seen as a static process, as it has to encompass various planning time horizons over the life of a project/facility. Indeed, the short-term ALARP may be very different from the long-term one due to various uncertainties, changing system conditions, and external evolution, such as for example land use around the considered facility. Because of this it is paramount to be able to deliver a view of ALARP evolution for increasing time horizons, while keeping in mind that inevitably conditions will change, making it necessary to adapt and review in the future.

Finding a solution

Analysis concepts

This paper showcases a development allowing users to quantitatively incorporate lifespans in the ALARP assessment when looking at a specific mitigation program and/or to compare different mitigation options. The methodology proposes the quantitative inclusion of the time/lifespan concept into the ALARP principle. To do so, annualized quantitative risks have to be evaluated for each mitigative alternative and the cost of the various mitigative actions estimated. For each time horizon the result is the trade-off equilibrium between mitigation costs and risk reduction benefits, which represents the minimum theoretical ALARP point. Various considerations can then guide the decision-makers to select the point where the cost involved in reducing it further would be grossly disproportionate to the benefit gained.

For this methodology to be useful the total quantitative annualized risk must be evaluated using multidimensional quantified consequences, i.e., the sum of harm to people, environmental damages, direct and indirect costs, and estimated reputational consequences converted into a single metric such as monetary quantity. The evaluation system is generally discussed with corporate key stakeholders and reflects the company's criteria. To use the scheme shown in Figure 1b, both curves must have the same units, since having two different axes means the intersection point depends on the axis scale. As a result, the annualized residual risks (after each mitigation scenario) are expressed as the multiplication of the annualized probability of failure by the potential consequences in monetary value per annum, for instance USD/yr. With that, a classic optimization problem can be defined as the sum of the mitigation cost and the annualized risk over a planning time horizon, a schematic of the objective function plotted against the different scenarios can be seen in Figure 2. It should be noted that this plot corresponds to a specific maximum time horizon selected for each study. The planning time horizon should not exceed a few decades, and it should be clearly stated that beyond this, re-evaluation should be expected.

For each assessed planning time horizon, a different mitigation alternative might come as the optimum solution, resulting in multiple plots, such as those shown in Figure 2. A different way to look at this is to plot the mitigation alternatives total cost as a function of the planning time horizon, as shown in Figure 3, where the y-axis at time equal zero represents the mitigation cost, and the slope of the line is the annualized risk after mitigation. Figure 3 shows when a mitigation alternative becomes more attractive than others: in the example shown, after year 7, alternative 2 (the green line) becomes more attractive.

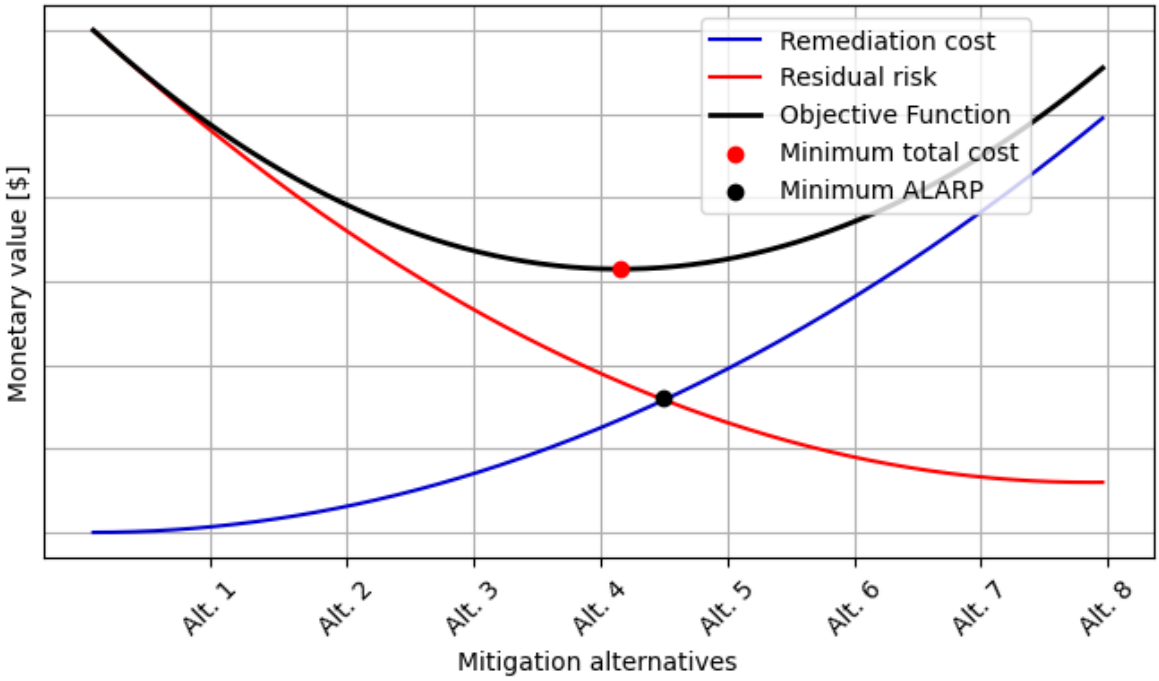


Figure 2: Objective function definition based on the mitigation and residual risk cost for a given time horizon

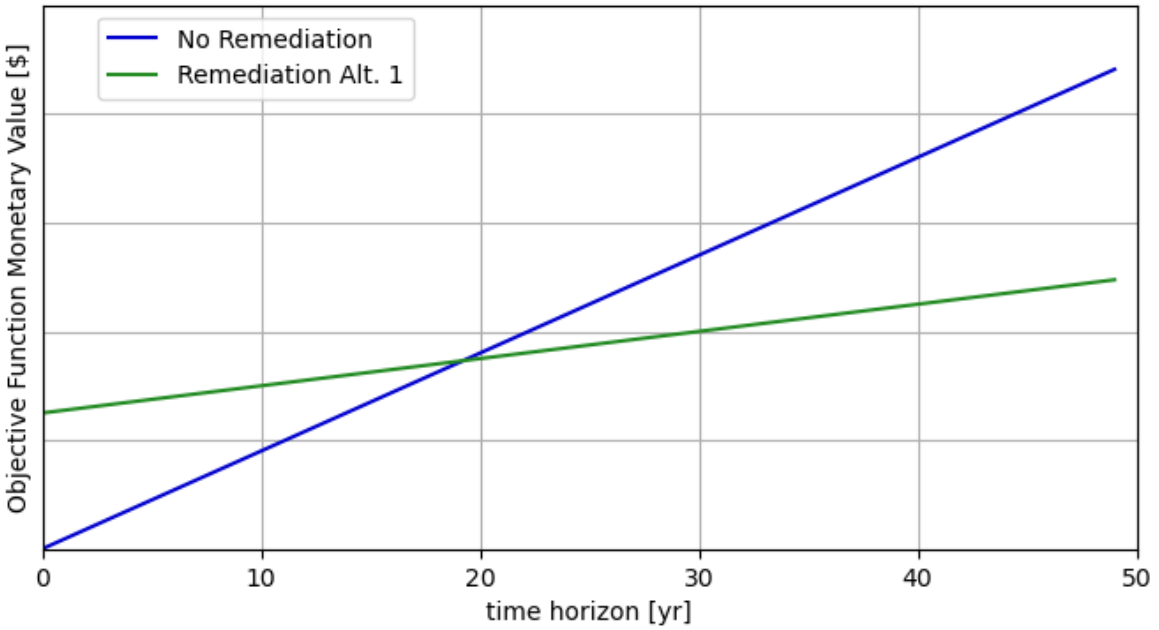


Figure 3: Objective function vs. time horizon for two different risk mitigation alternatives

Application example

This process has been applied to existing facilities, and has shown how the optimum solution varies, not only when the relative value of the various consequence dimensions changes (environmental vs. financial

vs. reputation, etc.), but also as a function of the structure's lifespan.

The tailings management area of this example (similar to a real-life case the authors studied in the recent past) is composed of 2 tailings storage facilities (TSFs) referred to as TSFS A and TSF B. A river that is the habitat of several species runs at 100 to 150 meters from the toe of both facilities, and a small population is located downstream across the river.

The TSF's current condition and several mitigation alternatives were evaluated with a quantitative risk assessment (QRA), using a bow tie structure linking hazards to consequences. The bow tie includes fault trees for the various failure modes/causalities on the left side (event probability side), and an event tree enabling the evaluation of consequences, on the consequence side. The potential mitigations considered for this example are buttressing the facilities, population relocation, and a combination of both. The obtained annualized risk per mitigation alternative is summarized in Table 1.

Table 1: Risk and mitigation cost

Mitigation alternative	TSF A annualized risk (M USD/yr)	TSF B annualized risk (M USD/yr)	Total annual risk (M USD/yr)	Mitigation cost (M USD)
Current	3.0	11.0	14.0	0.0
Buttress on A	1.0	11.0	12.0	12.0
Buttress on B	3.0	4.0	7.0	93.0
Buttress on A & B	1.0	4.0	5.0	105.0
Population Relocation	2.8	7.0	9.8	20.0
Buttress on A & B + Population relocation	0.9	3.0	3.9	125.0

Figure 4 shows an analysis of total monetary value (mitigation cost and annualized risk) for different time horizons: 3, 12, and 30 years. It can be seen how the optimum solution changes for the different time horizons considered. Of course, these evaluations will require adaptation and re-evaluation, especially for longer time periods.

Figure 5 shows how, depending on the planning time horizon being considered, the mitigation alternative that yields a minimum objective function changes.

If the time horizon for mitigation was shorter than 5 years, and the closure design considered stabilization of the facilities and an improvement of the surface water management system, the optimum alternative is to do nothing. But on the other hand, if this time was longer and there were more than 18 years of operation ahead, the optimum mitigation alternative is to buttress TSF A and B and relocate the downstream population. If the projected time to mitigation was in between those values a relocation of the population would be shown to be the optimum solution.

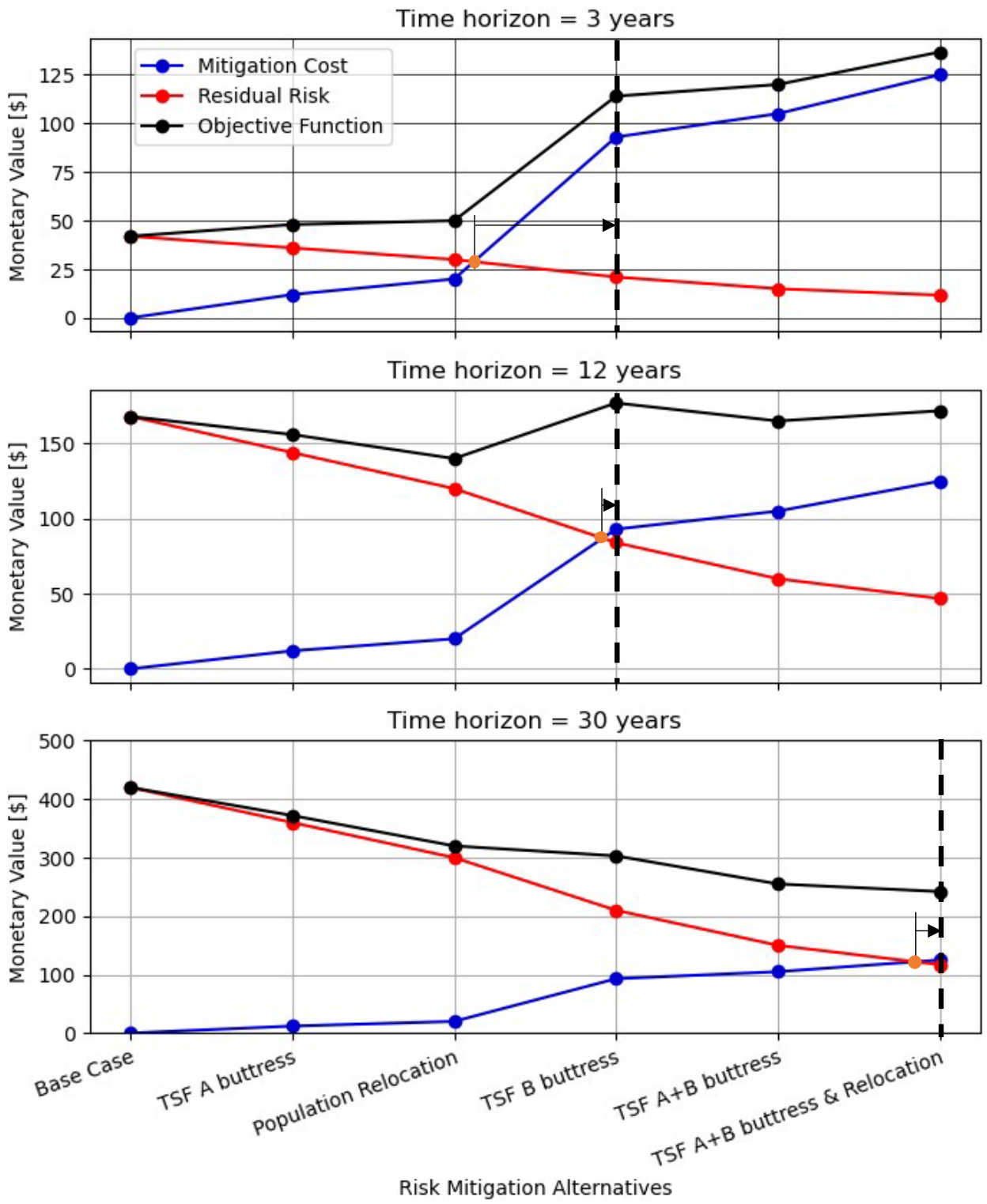


Figure 4: Objective function, mitigation, and risk cost for a 3-, 12- and 30-year time horizon

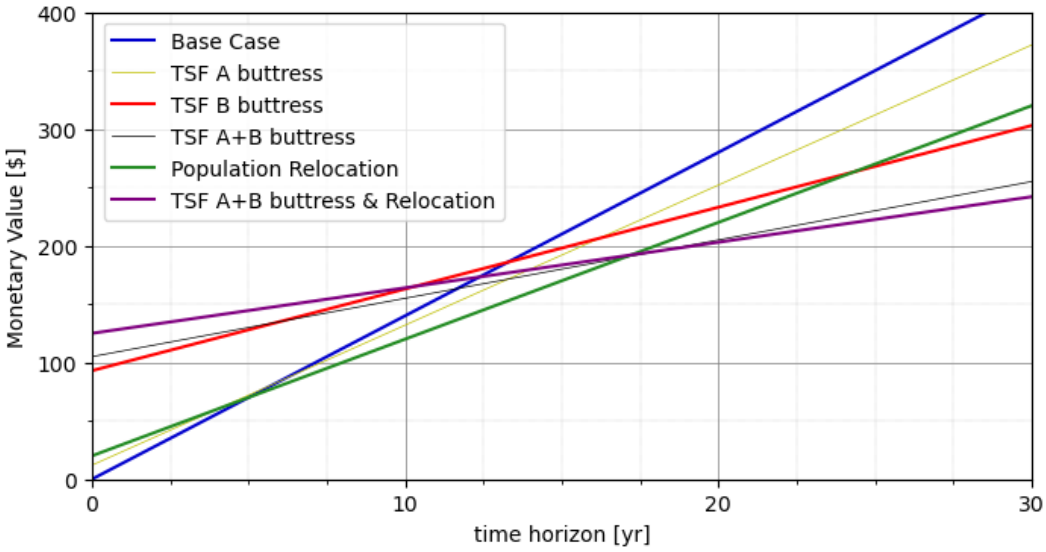


Figure 5: Objective function value vs. time horizon for each risk mitigation alternative

Conclusion

This paper presents a methodology for incorporating lifespan considerations into ALARP decision-making. The approach emphasizes the necessity of evaluating all mitigation costs, risk estimations, and risk reductions in consistent units, specifically, annualized values. This consistency is crucial for accurately determining the minimum ALARP point, which represents the trade-off equilibrium between mitigation costs and risk reduction benefits.

The optimization of system mitigation must account for the time horizon as a variable. The findings indicate that the minimum ALARP point is not static, but varies with the selected time horizon. Shorter time horizons may justify lower mitigation levels as minimum ALARP points, whereas longer horizons may necessitate more comprehensive mitigations to achieve a minimum ALARP point. This temporal variability underscores the importance of a dynamic approach to ALARP assessments, one that adapts to changing conditions and evolving system states.

The methodology presented in this paper allows for the quantitative inclusion of lifespan in ALARP assessments. By evaluating annualized quantitative risks for each mitigative alternative and estimating the associated costs, decision-makers can identify the theoretical minimum ALARP point for various time horizons. This process facilitates a rational decision-making framework that enhances the value of projects and prevents unnecessary capital expenditure on mitigative measures.

The application of this methodology to existing facilities demonstrates its practical utility. The example reveals how the optimum mitigation solution varies not only with the weighting of different consequence dimensions (environmental, financial, reputational) but also with the lifespan of the structure.

The results highlight the importance of considering multiple time horizons in ALARP assessments to ensure that mitigation strategies remain effective and economically viable over the long term.

Furthermore, this process must recognize that conditions will inevitably change, necessitating periodic reviews and adaptations of the assessments. The method aims to support the evaluation of the minimum ALARP, which is then subject to discussions that incorporate public perception and the interests of other stakeholders. This inclusive approach ensures that ALARP assessments remain relevant and responsive to the evolving landscape of TSF management.

In conclusion, the integration of lifespan considerations into ALARP decision-making provides a robust framework for optimizing risk mitigation strategies. By adopting this methodology, stakeholders can achieve a balanced approach that aligns with regulatory requirements, enhances project value, and addresses public and environmental concerns.

References

Edwards vs. National Coal Board. 1949. Accessed 06/25/2024 at https://www.safetyphoto.co.uk/subsite/case%20e%20f%20g%20h/edwards_v_national_coal_board.htm

Global Tailings Review. 2020. Global Industry Standard on Tailings Management (GISTM).

Haine, S. 2015. Safety and enforcement division staff White Paper on As Low as Reasonably Practicable (ALARP) risk-informed decision framework applied to public utility safety. California Public Utilities Commission.

HSE. 2024. ALARP at a glance risk management expert guidance on risk management. Accessed 06/23/2024 at https://www.hse.gov.uk/enforce/expert/alarpglance.htm

ICMM. 2021. Tailings management good practice guide.

Oboni, F. and Oboni, C. 2022a. Optimizing mitigation of tailings dams portfolios. Proceedings of Tailings and Mine Waste, 2022. Denver, Colorado, November.

Oboni C. and Oboni, F. 2022b. Tailings dam risk mitigation through risk informed decision making. *Planning for Closure, 2022.* Santiago, Chile.

Oboni C. and Oboni, F. 2022c. A case study on ALARP optimization. *Proceedings of Tailings, 2022*. Santiago, Chile.

Oboni, F. and Oboni, C. 2019. *Tailings Dam Management for the Twenty-First Century: What Mining Companies Need to Know and Do to Thrive in Our Complex World*. Springer.

Roche, C., Thygesen, K. and Baker, E. 2017. Mine tailings storage: safety is no accident. UN Environment, GRID-Arendal.

USCE. 2009. Interim tolerable risk guidelines for US Army Corps of Engineers Dams. Available at http://www.nfrmp.us/TRG2010/docs/USSD_2009_Corps_Tolerable_RisK_Dam_Safety_10_Feb_09.pdf

USCE. 2019. Best practices in dam and levee safety risk analysis – public risk tolerance and risk guidelines. Available at https://usbr.gov/ssle/damsafety/risk/BestPractices/Chapters/1-BestPracticesCover.pdf

A Risk-Based Approach for Management of Change of Tailings Storage Facilities

Bryan Bale, Teck Resources Ltd., Canada
Shawn Gravel, Teck Metals Ltd., Canada
Adam Chiorando, Teck Alaska Inc., USA

Abstract

The Global Industry Standard on Tailings Management requires a formal change management system that triggers the evaluation, review, approval, and documentation of changes to design, construction, operation or monitoring of a tailings storage facility (Principle 6.5). Teck has guidance for change management processes at the corporate and site levels and has recently trialed a proposed approach for management of technical changes at tailings facilities. This paper presents a risk-based approach for management of change that is appropriate as part of a change management system for complex and significant technical or operational changes. Guidance for use of the approach, including stakeholder preparation, risk assessment, change management actions, and decision approval are presented. The approach was developed through two management of change examples at Teck's operating mine sites. The management of change approach was used to identify the risks that these changes would introduce as well as the actions required to lessen these risks.

Introduction

The Global Industry Standard on Tailings Management (GISTM) requires that tailings storage facility owners implement a formal change management system (Principle 6.5). The change management system has the objective of disciplining and coordinating the change process, and should include an evaluation of the change, a review and formal approval of the change, followed by detailed documentation including action plans (Global Tailings Review, 2020). These requirements for management of change are included in the site and company management systems at Teck. To facilitate fully implementing the GISTM requirements, Teck developed and trialed a suggested procedure for management of change for tailings facilities.

This paper presents a risk-based approach for a management of change process that is appropriate for complex and significant technical and operational changes that impact a tailings storage facility. The

approach was developed through two real scenarios where a significant change was considered at Teck's tailings storage facilities. The suggested process evolved during these scenarios as lessons were learned along the way, to the point where the authors concluded that the approach was ready for implementation as a standard method. It was also recognized that sharing this approach with the broader industry would be worthwhile. This paper presents the two case studies where this management of change approach was developed, the lessons learned through these examples, and recommendations for use. The key steps in the risk-based approach include stakeholder preparation, risk assessment, change management actions, and decision approval. The approach also meets the GISTM requirements and definitions. We also learned that management of change should be considered in parallel with a structured decision-making approach.

Management of change for tailings storage facilities

"Management of change" can be defined as "a systematic approach to managing changes to ensure that they are implemented safely, efficiently, and effectively" (Center for Chemical Process Safety, 2008a). "Management of change" refers to the technical aspect of the change, while "change management" often refers to the behavioral aspect of the change. Management of change is the more appropriate term for the expectations described by the GISTM.

The management of change approach as presented in this paper can be considered as an element of a change management system. The management of change process defined by Teck includes the steps shown in Figure 1.



Figure 1: Management of change steps

Teck's Management of Change Standard aligns with these steps, and a key aspect of the standard is the requirement for risk assessment.

Identify the change

The first step in management of change is to recognize that a change is proposed or occurring (Identify the Change step in Figure 1). As per GISTM, the changes can be to the design, construction, operation or monitoring of the tailings facility. This requires diligent review of these aspects and is primarily the responsibility of the Responsible Tailings Facility Engineer supported by the Engineer of Record (ICMM, 2021).

The Change Management System should provide guidance on the management of change procedure to use. Not all changes require a formal risk assessment. For example, a minor deviation in construction may be handled with a non-conformance report with acceptance and corrective actions included. More complex changes may warrant a risk-based approach as described in this paper.

Teck's Red Dog Mine has a useful management of change screening tool checklist as part of their Change Management System. The checklist is intended to be completed with a group of stakeholder representatives, and it lists questions that could trigger more rigorous management of change requirements. Questions cover topics related to various stakeholder's perspectives including environmental, regulatory, design, safety, cost, standard operating procedures, training, human resources, maintenance, external communities and more. The screening tool also serves to document if a risk-based management of change approach is warranted, who should be involved, and approval to proceed with further study of the proposed change (Pre-Approval step in Figure 1).

Risk assessment

A risk assessment is central to the management of change process for more complex or significant changes (refer to Figure 1). There are numerous risk-assessment approaches that can be considered. A "What-If Analysis" (Center for Chemical Process Safety, 2008b) was selected as an appropriate risk-assessment method for the proposed change examples described in this paper.

As defined in a procedure for Teck Metals' Trail Refinery, a What-If Analysis technique follows a brainstorming approach in which a group of experienced people familiar with the subject process ask questions or voice concerns about possible undesired events that could occur because of the proposed change. The purpose of a What-If Analysis is to identify hazards, hazardous situations, or specific event sequences that could produce undesirable consequences. The approach requires the group to identify possible abnormal situations, their consequences, existing safeguards, and then suggest alternatives for risk reduction where obvious improvement opportunities are identified or where safeguards are judged to be inadequate. The method can involve examination of possible deviations from the design, construction, modification, or operating intent. It requires a basic understanding of the process intention, along with the ability to mentally combine possible deviations from the design intent that could result in an incident.

Figure 2 illustrates the What-If Analysis approach with suggested questions for the facilitator, and Figure 3 shows the analysis worksheet.

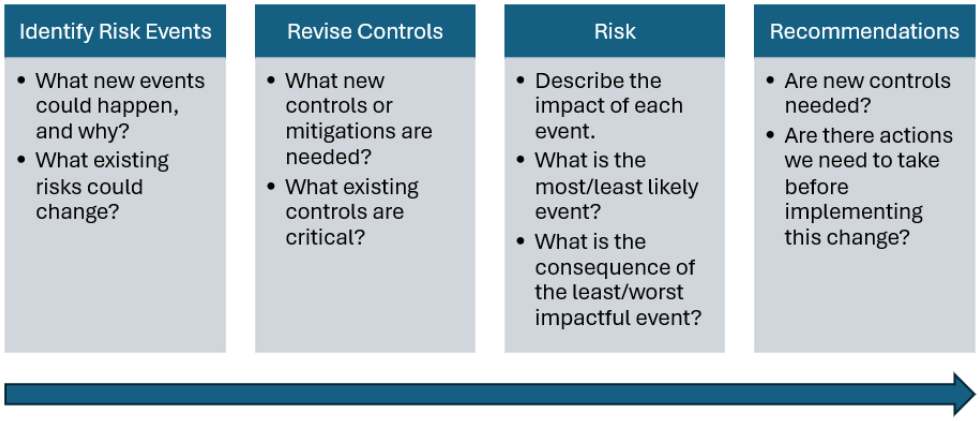


Figure 2: Thought process and facilitator questions for a "What-If" analysis

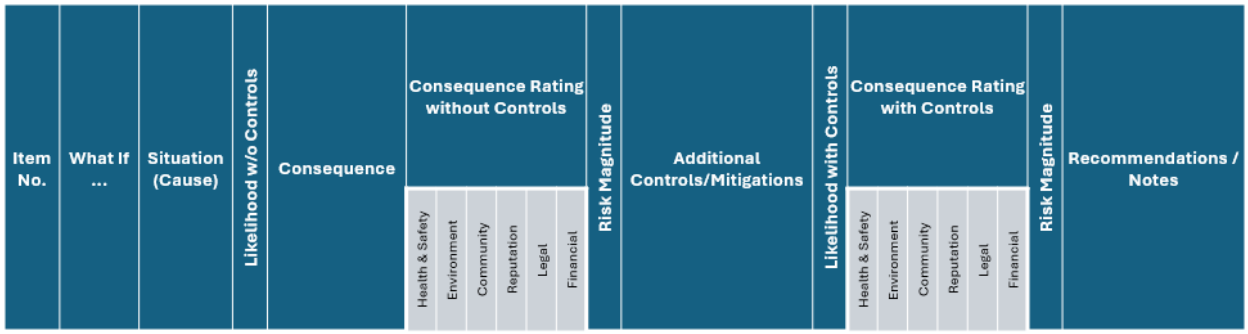


Figure 3: Teck's "What-If" analysis worksheet

The brainstorming provided by this method is valuable to gather a list of risk events without constraining the thinking to findings of previous risk assessments. The use of third-party and cross-functional participants minimizes bias and encourages broader thinking. Additional controls, mitigations, and recommendations should be suggested freely throughout the brainstorming portion. The details of the risk-evaluation portion can be completed after, with a smaller group using the standard risk-classification system for the company and considering the risk with and without additional controls. The method is appropriate for a tailing storage facility change where there is access to subject matter experts. Examples of this risk assessment are provided next as they were important to evaluate the utility of this risk assessment method.

Example #1 – Red Dog Mine – tailings pipeline on dam

Problem and proposed change

Teck's Red Dog Mine is a zinc and lead mine located in Alaska, USA. Tailings are deposited as a slurry

within a tailings storage facility. Two dams form the containment on opposite ends of a valley, with a water pond covering most of the tailings surface. Tailings are deposited near the dams to form a beach above water to maintain separation between the dams and the water pond, and this requires tailings pipelines running along the upstream side of the dams.

The tailings deposition pipelines along the dam have traditionally been placed on a compacted tailings pipe grade located on the tailings beach adjacent to the dam. This presented challenges as the construction of the pipe bench would occasionally damage the liner, requiring repairs. The pipe bench also had to be raised incrementally after each dam raise, which resulted in the deposition pipelines often being too low and missing the opportunity to maximize the beach width. Employees also had to access valves on the pipe bench, requiring difficult access down the lined dam face. The proposed operational change was to move the tailings deposition pipeline onto the dam crest, and to use slotted downspouts to ensure that the deposition pipes would not plug as the tailings beach elevation increased and buried the deposition pipes. Figure 4 illustrates the proposed change.

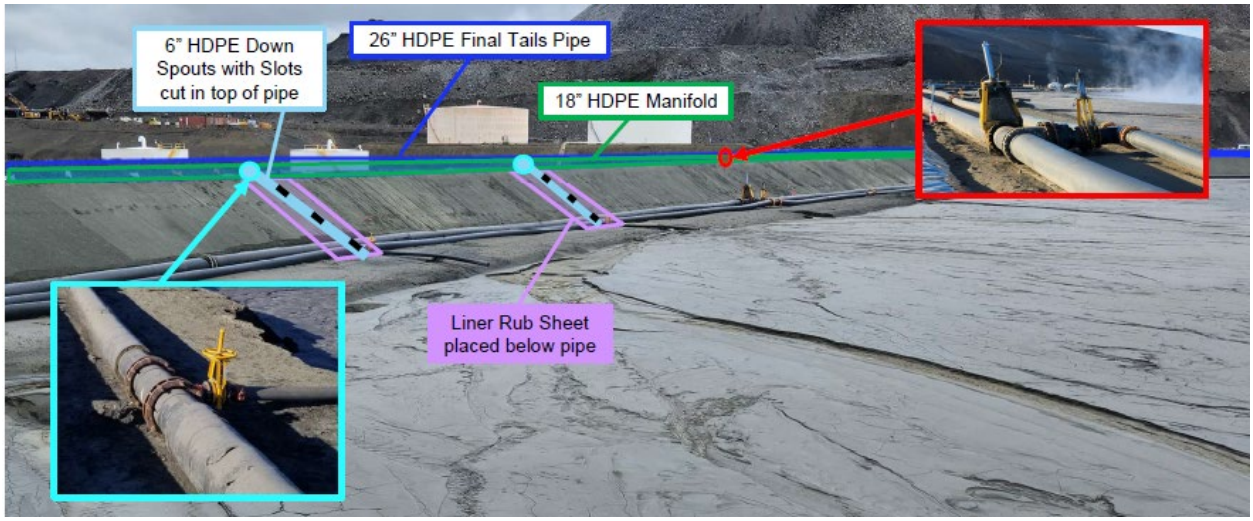


Figure 4: Proposed change to move the tailings deposition pipeline onto the dam crest

Management of change approach

The management of change screening questionnaire developed by Red Dog Mine was used as a first step once the change was identified. A group of stakeholders from the mine met to review the problem statement and proposed change. The questionnaire was used to document the potential implications of the proposed change discussed at this meeting. It was recognized that the proposed change of moving the deposition pipeline onto the dam crest could introduce a risk of tailings spills onto the dam, as well as other implications. The proposed change could affect numerous groups, including maintenance crews, operators, tailings planners, the Engineer of Record, and local community groups. The recommendation from the group, guided by the questionnaire, was to pursue a formal risk-based management of change process. This

screening questionnaire served to identify the change, justify using a risk-based management of change approach, and document the pre-approval to consider the change from site management.

At this stage, the Tailings Department staff at Red Dog Mine recognized that they would need to develop a risk-based approach that was appropriate for this scenario. They reached out for support within Teck, and a What-If Analysis was suggested. The What-If Analysis approach was suggested as it is a standard method in use at Teck Metals' Trail Refinery and is common in the Process Safety field.

The risk assessment was conducted in two sessions. The first 2-hour session began with setting a common understanding amongst the varied stakeholder groups and introduced the risk-assessment approach. The problem statement and proposed change were discussed. The Engineer of Record provided their perspective on the proposed change as a technical deliverable, including assessment of the flow rate that would occur during a pipe break, and the low potential for erosion on the dam. Events that could occur because of the proposed change were suggested using a brainstorming approach. Additional controls, mitigations, and recommendations were suggested throughout the discussion. Upon completion of the event list, the likelihood and consequences of some of the risk events were completed as a group, and the rest were completed after the meetings by the facilitator. A second 1-hour session was required to review and finalize the risk-assessment results.

Results and lessons learned

The risk events introduced by the change are summarized in Table 1. All risk events can be managed without an increase in risk level with the addition of new controls and mitigation measures.

Table 1: Summary of risk events introduced by pipeline relocation

What-If Event	New Controls/Mitigations
Pipe leaks tailings onto dam crest	Place geomembrane under valves and flanges, Install containment berm, Reduce number of flanges, Implement installation QC program, Modify daily inspection form, Develop Safe Work Plan for pipe moves, Develop pipe condition assessment, Install traffic control and vehicle barriers.
Downspout damages liner	Install a rub sheet.
Pipe maintenance is needed	Install spill containment under valve.
Snow drifts form behind pipe	Use snowblowers rather than loader, Delineate pipeline location.

Based on the conclusion that the new risks can be managed without an increase in the risk level, the recommendation to proceed with the proposed change was made. The Engineer of Record provided a report documenting the design for the change and the new controls and mitigations, with the risk assessment appended as a basis for their recommendations. A standard Decision Memorandum was used to document the change, gather approval signatures from management, and document the new controls and mitigations that need to be implemented (Final Approval and Planning steps in Figure 1). These new controls and mitigations were tracked using an existing site system prior to relocating the tailings pipeline (Implementation step in Figure 1). The proposed change was also presented to the Independent Tailings Review Board prior to commissioning. New controls including inspection forms were developed to verify the new controls and were added to the Operation, Maintenance and Surveillance Manual (Verification step in Figure 1).

The management of change approach tested for this case followed all steps as described in Figure 1. The approach was robust and effective. It was helpful that Red Dog Mine had a pre-existing change screening questionnaire that served to identify the change, identify stakeholders, and document the approval from management to proceed with a formal risk-based approach. It was also noted that the initial meetings were hampered by discussion of other alternatives that had been previously eliminated, and that the risk assessment was time-consuming. These lessons were carried forward to the next example for optimization.

Example #2 – Highland Valley Copper operations – modification of a spillway intake gate

Problem and proposed change



Figure 5: Highmont tailings storage facility spillway intake channel and control gate

Teck's Highland Valley Copper Mine is in British Columbia, Canada. There are several closed tailings facilities on the property, including the Highmont Tailings Storage Facility. There is a control gate located in the spillway intake channel that is used to temporarily store water during the spring snowmelt and allow most of the water to be diverted for use in the site process. It was identified that more water could be temporarily stored if the control gate was modified to be 75 cm taller, which would reduce the frequency that the flow would discharge to the receiving environment. The implications of this change on the dam safety profile required further consideration. Figure 5 shows the spillway inlet channel with the control gate structure.

Management of change approach

The proposed change presented potential trade-offs between dam safety and environmental management perspectives. The Highland Valley Copper tailings staff requested support to manage this change. Considering the recent trial with the Red Dog Mine site, the same team offered to facilitate this change using the template developed at Red Dog Mine, with the goal of creating a standard approach for the company.

Several lessons were learned from the Red Dog Mine example that were incorporated for this second case. It was recognized that a lot of time was invested by a large group for the Red Dog Mine case, and reducing the total time for this task was a goal. To accomplish this, a site Change Owner and facilitator were assigned to lead the work, with less reliance on the full team.

Like the Red Dog Mine example, the first meeting was a brief (30-minute) session to set a common understanding with all stakeholders and introduce the risk-assessment method. Although the goal was just to understand the problem statement and proposed change, inevitably there were suggestions of the risks to consider, alternate solutions, and suggested actions. These were captured in the risk-assessment worksheet for the next session. It was interesting to note that the discussion was again complicated when other alternative solutions were suggested during this session, indicating that we had not properly informed all stakeholders of the alternative evaluations completed previously.

Following the introductory session, the Change Owner and facilitator pre-populated the What-If Analysis with events they identified. The second session (2-hours) was then held with a cross-functional group of stakeholders, including the Engineer of Record, to review the event list and suggest other events. It was noted that several new events were suggested, likely because the obvious technical events were pre-populated leaving more time for brainstorming. New controls/mitigations and recommendations were captured for each. Lastly, a few events were assigned risk scores, focusing on the most and least impactful events leveraging the cross-functional team. The facilitator and Change Owner completed the risk assessment after the meeting, using the events scored with the group as benchmarks to evaluate the rest.

Results and lessons learned

The risk events introduced by the change are summarized in Table 2. Identified new events that could occur because of the change have a lower risk score than the "do-nothing" case. The Engineer of Record demonstrated that the water pond volume would be temporarily increased by a relatively small amount, while maintaining freeboard or stability requirements.

Table 2: Summary of risk events introduced by gate raise

What-If Event	New Controls/Mitigations
The risk profile for the dam increases (perceived)	Review change with Independent Tailings Review Board and Community Groups, Perform commissioning testing of the gate, Update Operations Manual.
Vegetation around the pond is drowned	Develop plan to revegetate with flood tolerant species.
Water quality is worsened	Develop monitoring plan to identify if this occurs and be prepared to reverse the change.
Wildlife is displaced	Establish new vegetation that supports existing wildlife use.

The results of the risk-assessment workshop were provided in a report from the facilitator and submitted to the stakeholder group for review. Highland Valley Copper is progressing through this change, with the next steps to follow a similar approach as was used in the Red Dog Mine example. This will include formal documentation of the proposed change from the Engineer of Record, review by the Independent Tailings Review Board, management approval using a Decision Memorandum, and tracking of completion of the new controls and mitigations.

After using this management of change approach twice, the time required for the broader team was reduced. This was mostly due to pre-populating the event list and using the team meetings to focus on identifying events that were missed and assigning risk ratings to only a few events with the rest completed by the Change Owner and facilitator. Including the "do-nothing" case was also a useful addition.

Part of a structured decision-making approach

It was noted that both examples were complicated when new ideas were suggested during the workshop. It was realized that management of change and structured decision-making are related, and both should be considered in parallel. In hindsight, the same cross-functional team should be involved as alternatives are considered or be informed prior to proceeding the management of change of the preferred option. Figure 6 illustrates the steps in a structured decision-making approach.

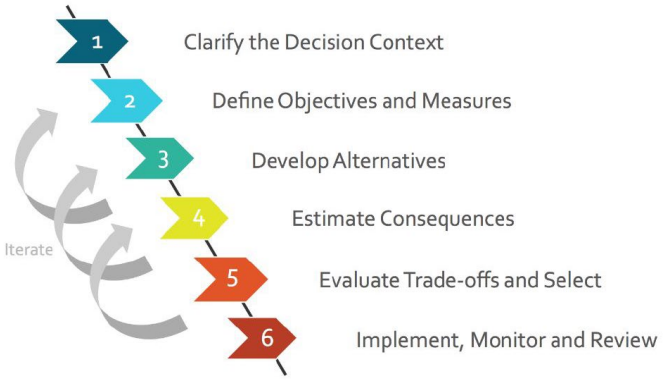


Figure 6: Steps in a structured decision-making approach (Compass Resource Management, 2024)

Recommended approach for management of change

Based on these examples, the following approach is recommended for management of change of technical and operational changes for a tailings storage facility.

1. Evaluate alternate options for the problem as part of a structured decision process. Ensure that all feasible options are considered and documented before starting on the management of change for the preferred option. Note that rushing into management of change will be derailed as other ideas are suggested if this is not done. A document listing the alternate ideas and the reason for pursuing the proposed change can be used in preparing the group for the risk assessment.
2. Identify the change – the questionnaire form used by the Red Dog Mine was useful. Implications of the proposed change from various stakeholders' perspectives and the decision that a formal risk assessment was required were captured using this form. Considering the time investment to conduct a good risk assessment, this screening tool is very useful.
3. Pre-approval of the proposed change – ensure that management agrees with the concept for the change and endorses the subsequent risk assessment. Multiple stakeholders will need to participate, and they may need direction to do so. Again, the form used by Red Dog Mine documented this approval and was effective.
4. Risk assessment – the What-If Analysis described here is recommended as a suitable format that identifies new risk events that arise from the event, or changes to the existing risks. Cross-functional representation is valuable to both identify the new risks that could be introduced, and to evaluate the consequences. Ensure that any new participants are oriented to the problem, alternatives, and proposed change prior to beginning this step. Leverage the group for the key brainstorming of risk events and risk calibrations and complete the rest with a smaller team to minimize the time commitment. The risk assessment method should be scaled appropriately depending on the significance of the change. The "do-nothing" case should be considered.

5. Final approval – the approval for the change should be documented. A Decision Memorandum with signatures from the appropriate management level is a suitable tool. The risk assessment documentation and endorsement from the Engineer of Record can be appended. The Deviance Accountability Report should also be updated to document the change.
6. Planning – including identification of the additional actions and controls addressed during the risk assessment. These can be documented in the Decision Memorandum as for Step 5.
7. Implementation of the change – the new actions and controls should be tracked to completion using formal systems before the change is made.
8. Verification of the change should be embedded into the Operations, Maintenance and Surveillance Manual, and other similar documents.

Conclusion

The GISTM requires that tailings storage facility owners implement a formal change management system. It was identified that developing an appropriate, standardized system for the technical and operational changes that arise for tailings storage facilities would be useful. This paper presented a suggested approach for management of change using a risk assessment. The management of change approach was developed through two real scenarios at Teck operating mine sites where a significant change was considered.

A "What-If Analysis" was selected as an appropriate risk-assessment method. The brainstorming provided by this method was valuable to gather a list of risk events without constraining the thinking to findings of previous risk assessments. The use of third-party and cross-functional participants minimized bias and encouraged broader thinking. The approach was trialed at two sites and was found to be effective in identifying the new controls and mitigations that were required to safely implement the change.

Lessons were learned through the example cases that were incorporated into the recommended approach. A key finding was the realization that management of change is related to structured decision-making, and that omitting this idea-generating step can side-track the risk assessment. It was also apparent that the change identification questionnaire used by Red Dog Mine was very useful and aligns with this approach. Including the "do-nothing" case was also a valuable consideration. Lastly, it was important to have a facilitator and site Change Owner to minimize the amount of time required from the broader cross-functional group.

An 8-step management of change approach was suggested that includes stakeholder preparation, risk assessment, change management actions, and decision approval. Recommendations for use of a screening tool, the risk-assessment method, and decision approval documentation were provided. The management of change approach described could be adopted as a procedure or guideline under a company's broader Change Management system.

References

Center for Chemical Process Safety. 2008a. *Guidelines for the Management of Change for Process Safety*. New York: John Wiley & Sons.

Center for Chemical Process Safety. 2008b. *Guidelines for Hazard Evaluation Procedures*. Third edition. New York: John Wiley & Sons.

Compass Resource Management. 2024. *Structured Decision Making.* Accessed 6/20/2024 at https://compassrm.com/what-we-do/services/decision-analysis/.

Global Tailings Review. 2020. Global Industry Standard on Tailings Management*. Global Tailings Review.* Accessed 6/17/2024 at https://globaltailingsreview.org/wp-content/uploads/2020/08/global-industry-standard_EN.pdf

ICMM, 2021. Tailings Management Good Practice Guide. *ICMM.* Accessed 8/13/2024 at https://www.icmm.com/website/publications/pdfs/environmental-stewardship/2021/guidance_tailings-management.pdf?cb=60002.

Global Climate Change due to Earth Cycles and Implications for GISTM Standards

Kris Hojka, Worley Consulting Ltd, Canada
Fariba Yavari, AtkinsRéalis, Canada

Abstract

Tailings storage facilities (TSFs) face critical challenges during passive closure, adhering to GISTM standards that mandate a flood design criteria equivalent to a 1/10,000-year return period. While 10,000 years is a brief period geologically, it spans over a significant period of human history, when civilizations have been lost due to natural climate changes. This study explores our civilization's vulnerability to natural climate change over 10,000 years, driven by the Earth's cycles, particularly the Milankovitch cycles – Earth's Eccentricity, Obliquity, and Axial Precession. Historical climate transformations, from Biblical floods shaping the Black Sea and Persian Gulf to changes in the Sahara and Great Lakes, highlight these cycles' profound impacts.

Statistical models typically use a 100-year precipitation record to estimate severe rainfall events, often overlooking natural global climate changes. Predicting extreme events like a 1-in-10,000-year flood is challenging due to climate change's unpredictability over such a long timeframe. Therefore, the focus should shift from a 1-in-10,000-year flood parameter to eliminating risks through innovative tailings disposal technologies. Methods like dry stacking, in-pit disposal, and paste disposal offer viable alternatives for risk reduction and environmental rehabilitation. For operational or actively closing TSFs, a 1-in-10,000 flood criterion minimizes current risk but escalates during passive closure due to global climate change. This necessitates continuous evaluation and proactive measures to address evolving climate challenges. In summary, this study advocates for a comprehensive approach to TSF management, recognizing the intertwined nature of geological, climatic, and technological factors. It emphasizes shifting from predicting extreme events to actively eliminating risks, promoting sustainability and resilience in TSFs.

Introduction

Climate change has long been a powerful influence on Earth, shaping coastlines, landscapes, and ecosystems over millions of years. Its primary drivers have been geological processes such as volcanic activity and the movement of continents, as well as Orbital Earth Cycles. These cycles have led to at least

five major ice ages in the last 2 billion years. The most recent ice age began 3 million years ago and persists to this day. We are currently in a warm interglacial period that started 11,000 years ago.

Milankovitch cycles and global climate change

Milankovitch (Orbital) cycles have a profound influence on Earth's climate and the mechanisms through which changes in Earth's orbit and axial tilt shape long-term climate trends. Milotin-Milankovic's groundbreaking hypothesis proposed that changes in the Earth's position relative to the Sun, known as Milankovitch cycles, played a key role in climate change and the onset of the ice ages. Three key orbital motions, including eccentricity, tilt, and precession, are examined in detail for their influence on the distribution of solar radiation and weather patterns.

Eccentricity refers to the shape of the Earth's orbit around the Sun, with variations affecting the distance between the Earth and the Sun and the amount of solar radiation received. The tilt of the Earth's axis affects the intensity of seasons and the extent of glacial periods, and larger tilt angles favor deglaciation. Precession, the direction of the Earth's axis of rotation, contributes to changes in the timing and distribution of solar radiation, especially in high latitude regions.

The Milankovitch cycles contribute to the periodic onset of ice ages, which occur every 41,000 years, and the transition to longer interglacial periods, which occur every 100,000 years. While the exact mechanisms behind this transition remain a matter of science, Milankovitch's theory has been widely accepted and supported by subsequent research. Evidence from deep-sea sediment cores and ice cores in Greenland and Antarctica supports the role of Milankovitch cycles in driving major climate changes on geological time scales (NASA Science Editorial Team, 2020). Despite ongoing research to further understand the complex interactions between Earth's rotation and climate dynamics, the Milankovitch cycle theory of glacial-interglacial cycles is well established in the scientific community.

According to the Milankovitch cycle, the Earth is currently in a position where its long-term cooling trend, which began 6,000 years ago, is projected to persist for the next 23,000 years. Over the next 100,000 years, Earth's orbit will become less eccentric, resulting in changes dominated by variations in obliquity rather than eccentricity. Consequently, it is unlikely that there will be a significant decline in insolation to trigger a new glacial period within the next 50,000 years (NASA Science Editorial Team, 2020). However, it is essential to note that while orbital variations provide insights into future climate, other factors such as human-induced greenhouse gas emissions can significantly influence climate dynamics.

In the context of contemporary climate debates, the potential for another ice age remains a topic of debate among scientists and researchers. While some argue that future ice ages are less likely as the Earth warms, disrupting traditional weather patterns and intensifying greenhouse gas concentrations, others focus on the role of long-term atmospheric forces due to the Milankovitch cycle.

Proponents of the orbital forcing theory believe that despite current human influences on climate, natural astronomical cycles will eventually push Earth into another ice age, albeit on a time scale of tens of thousands of years. Studies on celestial mechanics and climate change show the complex interplay of orbital parameters in modulating Earth's climate over geological timescales and emphasize the complex relationship between celestial mechanics and terrestrial climate dynamics (Abouelmagd et al., 2024).

Finally, the outlook for future ice ages is uncertain, as competing hypotheses and models offer different predictions. Continued research on past climate events, along with advances in climate modeling and observational techniques, will be necessary to elucidate the complex mechanisms governing Earth's climate change and to predict the long-term trajectory of global climate change.

Changes to the climate during the last 10,000 years

Ice ages are integral seasons of Earth's climate history, characterized by extensive glaciation and much colder temperatures compared to interglacial periods. These ice ages, defined by the expansion of the polar ice sheets and the lowering of global sea levels, have occurred repeatedly throughout Earth's existence. Scientific evidence suggests that there have been at least five or six major ice ages in the planet's geological past, interspersed with numerous smaller ice ages. Figure 1 illustrates the present-day interglacial state (a), and the Quaternary glacial state (b).

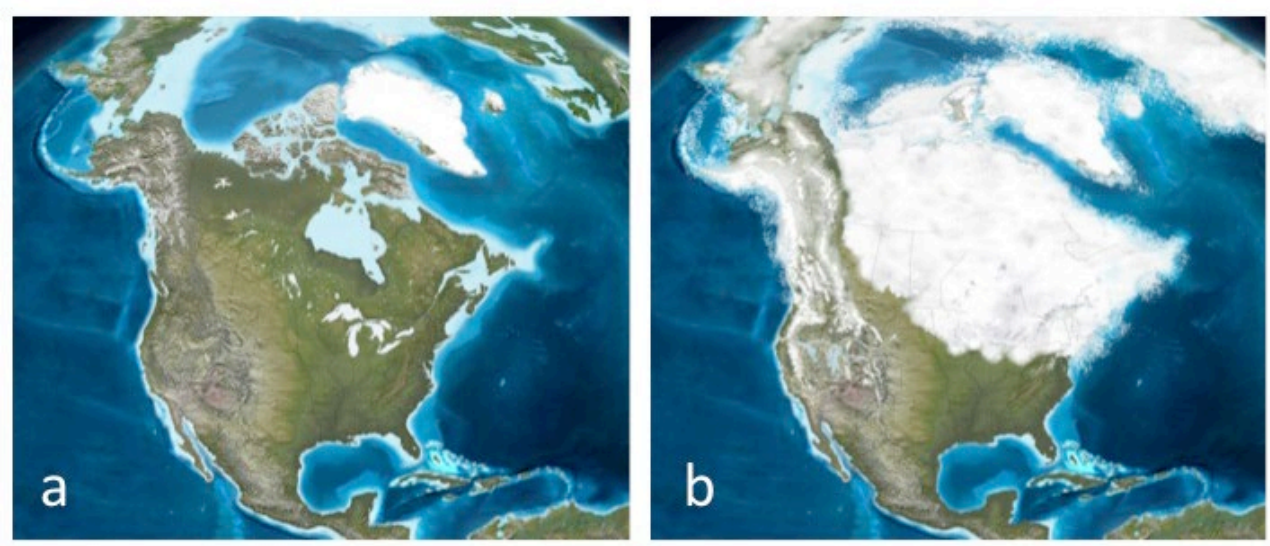


Figure 1: (a) Present-day interglacial state, (b) Quaternary glacial state (Glaciation, 2017)

Each ice age is usually followed by a warming period known as an interglacial period. Currently, Earth is experiencing one of these interglacial phases, which began approximately 10,000 years ago after the last Great Ice Age peaked about 21,000 years ago. During this interglacial period, the global temperature

gradually increased, leading to the retreat of glaciers, and creating more hospitable conditions for life. The effects of climate change since the last ice age have been manifested in many ways and are profoundly affecting natural systems and human societies.

About 13,000 to 15,000 years ago in North America, melting and receding ice formed the Great Lakes and flooded many areas in today's Washington state, Oregon, and Utah. The sea-level rose, attributed to the thermal expansion of seawater and the melting of land glaciers.

The Black Sea Flood hypothesis, proposed by William Ryan, Walter Pitman, Petko Dimitrov and colleagues in 1997, provides a convincing explanation for a major geological event about 8,400 years ago. According to this hypothesis, rising sea levels in the Mediterranean breached the natural barriers and flooded the former freshwater lake of the Black Sea about 7,600 years ago, marking a transformative moment in the region's ecological history (Figure 2). Evidence supporting this hypothesis includes sedimentary deposits and submerged archaeological sites discovered in the Black Sea Basin, which provide tangible clues to past geological and climatic dynamics. At the same time, the Persian Gulf was formed due to rising sea levels.

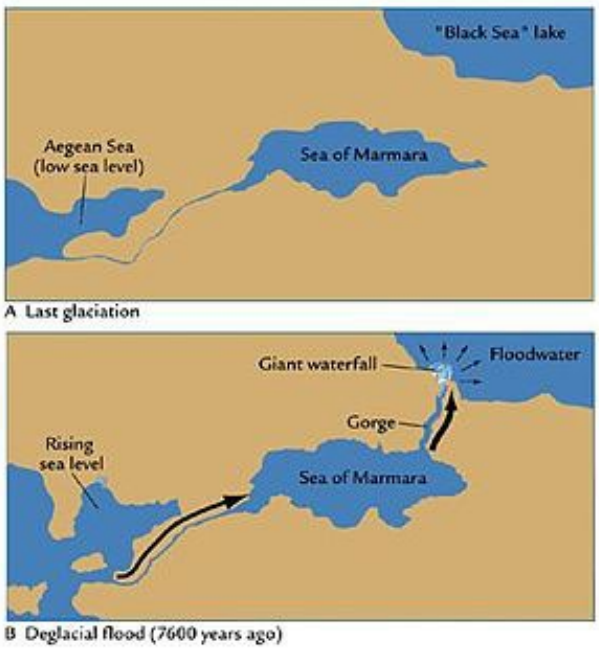


Figure 2: A vast area of the Black Sea flooded, causing sea levels to rise and coastlines to change (Fields, 2014)

Most floods generated by melting ice were catastrophic, destroying anything in their pathway. In 1996, William Pitman, a geologist, provided an illustrative catastrophic description and evidence of the Black Sea flood in his controversial theory of the Great Deluge (Glaciation, 2017):

1. By the end of the last ice age (around 12500 BC), glacial meltwater formed huge freshwater lakes, including the present-day Black Sea. Meltwater also cascaded into the world's oceans, raising sea levels by 400 feet.
2. According to the flood hypothesis, the rising Aegean Sea overran a natural barrier at the present-day Bosporus strait. Carbon dating of the shells of the first marine mollusks to arrive in the Black Sea dates the flood to 5600 BC.
3. Evidence indicates seawater rushed into the Black Sea region at a rate 200 times greater than Niagara Falls, turning the lake brackish.
4. The resulting flood would eventually have covered 60,000 square miles of land in about one year, expanding the Black Sea to its present boundaries.
5. Stone tablets inscribed with the Epic of Gilgamesh were discovered at Nineveh, 560 miles from the Black Sea. The flood story in Gilgamesh may be inspired by the Black Sea event.
6. The Genesis story of Noah, which dates to the ninth century BC, is derived from the epic of Gilgamesh, which incorporates sources as old as 2100 BC. Similar flood stories are also found in the epic literatures of Greece, India, Burma, and Borneo.

Human-induced climate changes

While natural factors such as changes in solar radiation and volcanic activity have historically played a key role in the initiation of ice ages, human-induced changes in the atmosphere, particularly increased greenhouse gas emissions, are now contributing to unprecedented changes in the dynamics of global weather.

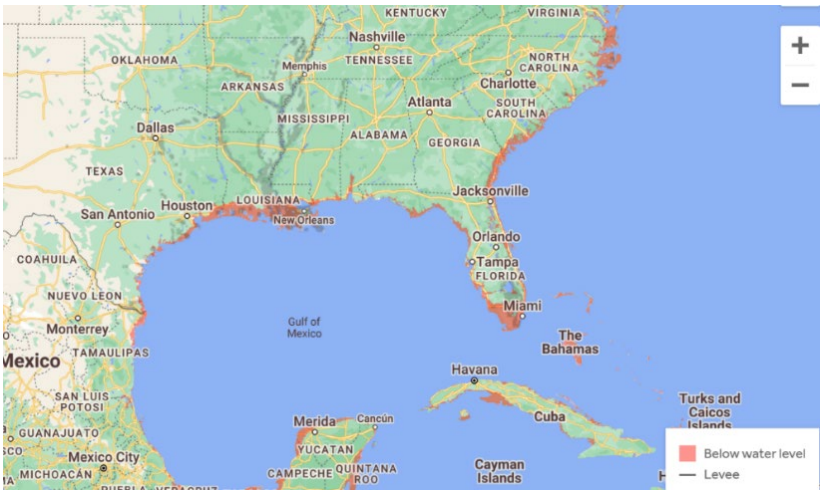


Figure 3: Gulf of Mexico coastal area simulated 5 m rise in sea level (source: Climate Central, 2024)

The effects of climate change since the last ice age have been manifested in many ways and are profoundly affecting natural systems and human societies. Sea-level rise, attributed to the thermal expansion of seawater and the melting of land ice, poses significant threats to coastal communities around the world. Global sea levels rose by an average of 8 inches (20 cm) from 1880 to 2009, according to a 2019 study published in the journal *Nature*. Forecasts indicate a rapid increase in sea level in the next few decades due to continuous melting of ice and thermal-induced water expansion. Based on NASA predictions, by the year 2500 global ocean levels may rise by 5 m, or even by 14 m in the worst-case scenario.

Climate change increases the frequency and severity of droughts, floods, and fires, and exacerbates risks to ecosystems, agriculture, water resources, and human settlements. Research published in the *Proceedings of the National Academy of Sciences (PNAS)* in 2020 identified a significant increase in the frequency of extreme precipitation events worldwide, leading to increased flood risks in many regions. Similarly, the increased incidence of extreme droughts, such as the prolonged drought documented in this study from 915 to 1025, as well as the intensification of wildfires, underscores the wide-ranging impacts of climate change on social stability and ecological resilience.

Closure criteria for tailings storage facilities

According to the Global Industry Standards on Tailings Management (GISTM) outlined by the International Council on Mining and Metals (ICMM, 2020), passive closure for all tailings facilities mandates resilience against the impact of earthquakes or floods equivalent to a 1-in-10,000-year event. But what does this entail specifically for flood design criteria? Let us delve into that in this paper.

Requirement 5.3 of the GISTM states: *"Develop, implement and maintain a water balance model and associated water management plans for the tailings facility, taking into account the knowledge base including climate change, upstream and downstream hydrological and hydrogeological basins, the mine site, mine planning and overall operations and the integrity of the tailings facility throughout its lifecycle. The water management program must be designed to protect against unintentional releases."*

From the above, the design must be resilient enough to address the following key points:

- floodwater at the site;
- floodwater originating from upstream sources;
- floodwater flowing from downstream sources;
- changes to groundwater; and
- anticipating the impacts of climate change.

Hence, for passive closure to be effective, the design must fulfill all these criteria, ensuring resilience against the extreme scenario of 1-in-10,000-year flood event.

How extreme rainfalls are estimated

How do we go about estimating a storm event that occurs only once in 10,000 years if our climate data spans less than a century, or even less than 50 years? In such situations statistical techniques are employed to extrapolate to a 1,000- or 10,000-year event. Numerous statical methods exist, with each tailored to the distribution of existing rainfall events. These methods typically aim to identify the most suitable fitting curve for the available data.

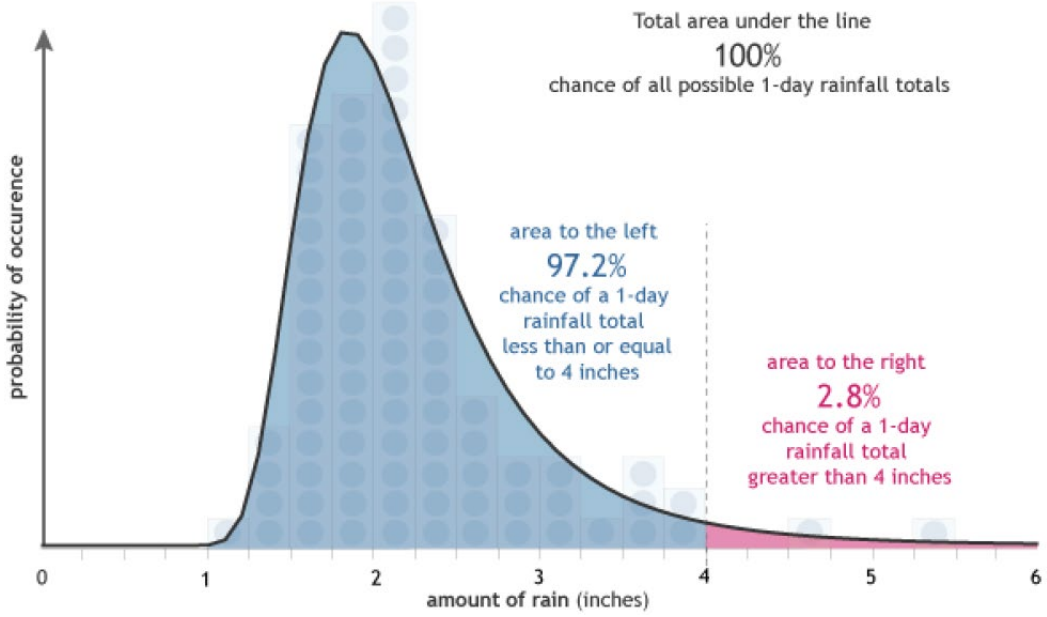


Figure 4: Statistical distribution of 1-day rainfall events. 82-year histogram of annual daily maximum precipitation totals for Beckley, West Virginia (source: Climate Central, 2024)

Figure 5 illustrates the distribution of individual recorded rainfall depicted as dots. The best fit distribution trendline (the curved line) delineates a theoretical spectrum of all potential extreme rainfall events, ensuring that the total area beneath it equals 1.0 or 100%. To determine the likelihood of a rain event exceeding a certain amount, the percentage of the total area to the right of that rainfall threshold is calculated. Conversely, the probability of a rain event falling below or equal to a specific threshold is derived by subtracting the area to the right of that threshold from 100%. Figure 4 indicates, for instance, a 2.8% chance of experiencing rainfall equal to or greater than 4 inches on any given day.

With the ability to determine the probability of a given rainfall amount, we can also ascertain which rainfall amounts correspond to specific probabilities, such as 0.1%. In other words, we can identify a rainfall threshold for events like a one-in-1,000-year event, as shown in Figure 5.

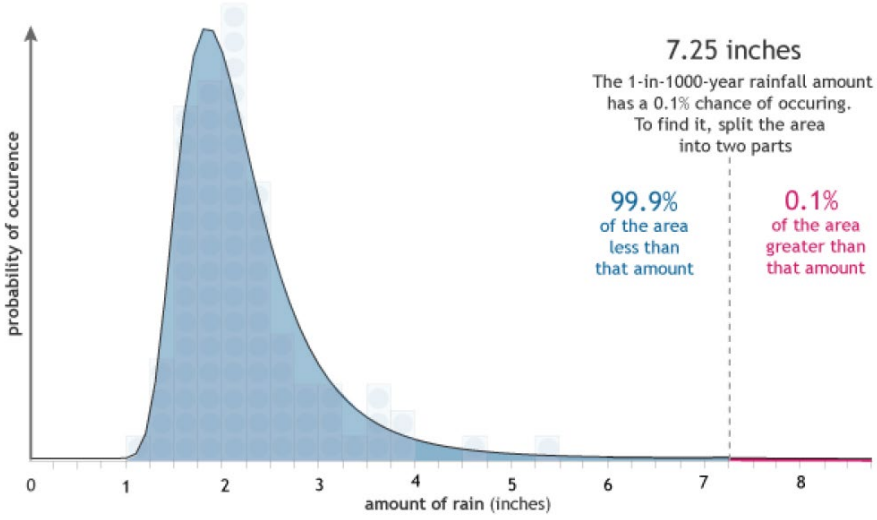


Figure 5: Determining 1-in-1,000-year rainfall, based on Figure 4 histogram

It is possible to extend the frequency analysis to estimate even more extreme events such as a 10,000-year event by extrapolating from the statistical distribution of rainfall data. However, beyond 1-in-1,000 or -2,000 events the reliability of the method is not certain, and the larger the Annual Exceedance Probability (AEP), the larger the uncertainty. It is thought that the estimated AEP for the probable maximum precipitation (PMP) events may have an estimated error in the range of two orders of magnitude (Nathan et al., 2013), as shown in Figure 6. Conversely, the estimated rainfall value for the given AEP is also uncertain and may have a wide error.

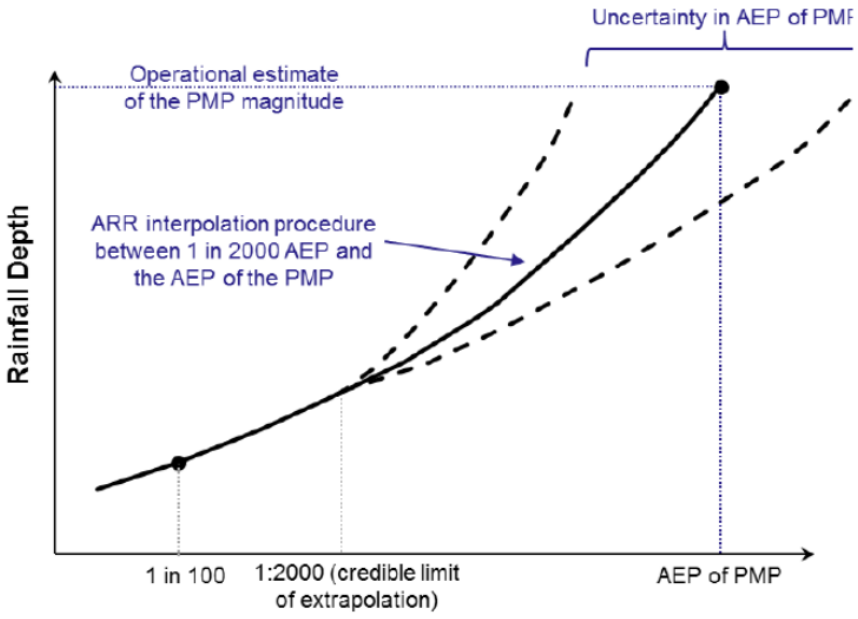


Figure 6: AEP and PMP uncertainty (source Nathan et al., 2013)

Climate change impact on rainfall frequency analyses

Can climate change impact the statistics of rainfall frequency analyses? Absolutely! Climate change significantly complicates this process. When scientists rely on past observations to understand climate patterns, they ideally seek a stable climate. A changing climate makes this task more challenging because historical data may no longer accurately represent current or future conditions. Global warming has the potential to completely shift the natural distribution of climate variables. More and more often, we observe 1-in-100 or 1-in-1,000-year rainfall events reported around the globe, and climate change is likely to increase the frequency of extreme precipitation events. What was once considered a rare occurrence, like a 1-in-20 year extreme 24-hour precipitation event, may become more common in the future, occurring with a frequency closer to 1 in 5 years. This presents a dilemma for scientists: they must assess the rarity of extreme events based on historical data, while also acknowledging that climate change is altering the likelihood of these events occurring. This will alter the statistics of flood frequency analyses and increase uncertainty regarding the estimation of extreme flood events.

In essence, climate change introduces a level of uncertainty into the analysis of past climate data and the prediction of future climate scenarios. Scientists must navigate this uncertainty to provide accurate assessments of climate-related risks and impacts. This underscores the importance of continually updating methodologies and models to account for the dynamic nature of the climate system under the influence of climate change.

Climate change modeling relies heavily on understanding the fundamental physical processes that underpin how precipitation patterns may change in a warming world. With rising temperatures, increased evaporation and surface drying can contribute to the intensification and prolongation of droughts in certain regions. However, it is essential to consider the impact of warmer air on the air's capacity to hold moisture, as described by the Clausius-Clapeyron equation. For every 1°C rise in temperature, the air can typically hold around 7% more moisture. Consequently, a world approximately 4°C warmer than the pre-industrial era would potentially have about 28% more water vapor in the atmosphere. However, this additional moisture will not be distributed uniformly across the globe. Some regions may experience heightened precipitation, while others may witness reduced rainfall due to shifting weather patterns and various influencing factors. This complex interplay of physical processes underscores the dynamic nature of climate change's impact on precipitation patterns, highlighting the importance of comprehensive and nuanced analysis in understanding regional climate variations and potential future scenarios.

Uncertain predictability of climate change

Utilizing current climate change models, scientists can project the trajectory of global climate patterns for

the next century, primarily driven by human activity-induced changes in atmospheric moisture, temperature, and rainfall distribution. These models enable the estimation of the likelihood of extreme weather events, such as rainfall with a 1-in-100-year return period. However, the precision of these projections diminishes when examining rainfall frequencies beyond the 1-in-100-year threshold, particularly for events ranging from 1-in-1,000 to 1-in-10,000 years. The uncertainty surrounding these rare events underscores the complexity of predicting long-term climate trends with absolute certainty.

In addition to anthropogenic influences, climate change stemming from natural factors like the Milankovitch cycle also plays a significant role in shaping global climate over millennia. This astronomical phenomenon, occurring on a scale of approximately 20,000 years, introduces potential cooling effects that could counteract the warming attributed to human activity. However, the compounded impact of both human-induced and Milankovitch-driven climate changes remains poorly understood. Consequently, certain regions may experience heightened precipitation, while others may face increasing aridity, leading to shifts in landscape and climate zones.

Furthermore, the melting of ice from polar regions, such as Antarctica and glaciers, poses a substantial threat by raising sea levels and inundating low-lying coastal areas. This influx of water not only alters coastal landscapes but also contributes to changes in the patterns of ocean currents, potentially intensifying storm systems and exacerbating flooding events. The resultant increase in violent storms and widespread inundation poses significant challenges for coastal communities and infrastructure resilience. There are many different climate change models, and researchers cannot agree about how climate change may go, and which areas will become wetter or drier. However, all of them agree that significant changes are coming, one way or another, by the end of this century. Figure 5 shows the results of two climate change models. The one on the left predicts hotter, drier climate and the one on the left predicts hotter, wetter climate. The truth could be somewhere in between: some areas may become drier and some areas wetter, and some areas may experience violent extremes in weather changes over a short period of time.

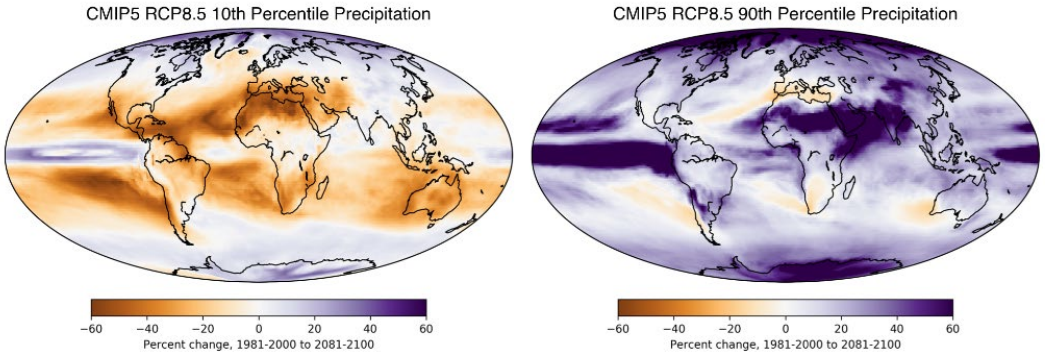


Figure 7: Two models for global climate change: 10th percentile of mean precipitation changes (left map) and 90th percentile (right map) for total precipitation (rain and snow) for each 1×1 latitude/longitude grid cell between 1981–2000 and 2081–2100 (source: Carbon Brief, 2018)

As climate zones and geographical boundaries undergo transformation, formerly arid regions may witness the emergence of lakes and rivers, while deserts may experience shifts towards more humid conditions. These changes to the natural landscape will have profound implications for ecosystems, water resource management, human settlements, and infrastructure.

Design of resilient tailings storage facilities

Consequently, the long-term implications of climate change on tailing storage facility (TSF) design criteria remain uncertain. Even TSFs designed to withstand current climate conditions may become vulnerable to the evolving climate landscape, necessitating adaptive measures to mitigate risks associated with increasingly unpredictable weather patterns. In other words, if the TSF is designed for 1-in-10,000 years based on current statistical models, it does not necessarily mean that the structure will survive 10,000 years, it simply means that the current risk of annual exceedance is 0.0001, and this risk will increase with climate change. The potential for much greater rainfall events, alterations to regional landscapes, and heightened vulnerability of existing TSFs highlight the urgent need for proactive planning and resilient design strategies in the face of ongoing climate change.

Examples of more resilient strategies for TSF disposal would include:

- Utilizing underground and in-pit disposal methods.
- For closure, preferring dry covers over wet covers.
- Implementing filtered tailings technology, which is less prone to failures and more suitable with dry covers.
- Stabilizing tailings with chemical additives such as fly ash and polymers.
- Focusing on process and metallurgy techniques that eliminate toxic compounds at the process level, ensuring the waste is non-hazardous.

Selection of each strategy should be performed based on the evaluation of multiple accounts including geological settings, topography, climate and expected changes to the environment. Paste technologies with underground disposal as well as in-pit disposal methods seem to have the least environmental footprint and are the most resilient to erosion and future climate changes. However, these methods are not always possible and economically justified. Dry stacking of filtered tailings would be the second choice for the most resilient tailings strategy. After closure, these facilities are assumed to be fully drained, and therefore the potential for failure is minimal. The slopes can be covered with erosion protection material and the slopes can be further stabilized by berms or armor for long-term stability and erosion protection. The last choice should be conventional slurry tailings disposal facilities. These structures are difficult to manage and may

entrap pore water within tailings. This is difficult to drain and may create a risk of liquefaction and failure for many years after closure.

Conclusion

The last 10,000 years of global climate history have demonstrated that radical climate shifts can occur, leading to significant changes in coastlines and landscapes. Current climate prediction models may be unreliable, as they are based on limited data and fail to consider all factors, such as the Milankovitch cycles, changing ocean levels, and currents. Compounding the effect of human-made climate change and Milankovitch cycles is not well understood. We must prepare for significant climate changes over the next 10,000 years, though the severity and geography of these changes are unpredictable. Many arid regions may become more arid or wet, while humid areas may become wetter. Numerous areas may be inundated by new rivers, lakes, or oceans. Many TSF sites, even those designed to the highest GISTM standards, could become inundated or eroded.

The potential for increased rainfall, flooding, alterations to regional landscapes, and the heightened vulnerability of existing TSFs, underscores the urgent need for proactive planning and resilient design strategies in response to ongoing climate change.

References

Abouelmagd, E., Ibrahim, M. and Garcia, J. 2024. Advances in celestial mechanics and space dynamics. Accessed 6/08/2024 at Advances in Celestial Mechanics and Space Dynamics | SpringerLink

Carbon Brief. 2018. *Climate modelling, explainer: what climate models tell us about future rainfall.* Accessed 6/05/2024 at: https://www.carbonbrief.org/explainer-what-climate-models-tell-us-about-future-rainfall/

Climate Central. 2024. *Interactive Maps.* Accessed 6/05/2024 at: https://coastal.climatecentral.org/map/6/-80.6073/25.8722/?theme=sea_level_rise&map_type=ice_sheet&basemap=roadmap&contiguous=true&elevation_model=best_available&ice_loss_level=14.8&ice_sheet=antarctic&refresh=true&water_unit=m

Fields, C. 2014. The whole world remembers Noah's flood. Accessed 6/08/2024 at The Whole World Remembers Noah's Flood – The Creation Club | A Place for Biblical Creationists to Share and Learn

Glaciation. 2017. Accessed 6/08/2024 at: Glaciation | Canadian Cryospheric Information Network (ccin.ca)

ICMM. 2020. *Global Industry Standards on Tailings Management, Accessed 6/05/2024* at: https://www.icmm.com/en-gb/our-principles/tailings/global-industry-standard-on-tailings-management

NASA Science Editorial Team. 2020. Accessed 6/08/2024 at: https://science.nasa.gov/science-research/earth-science/milankovitch-orbital-cycles-and-their-role-in-earths-climate/

Nathan, R., Scorah, M., Jordan, P., Lang, S., Kuczera, G., Schaefer, M.G. and Weinmann, E. 2013. A tail of two models: estimating the annual exceedance probability of probable maximum precipitation. *36th Hydrology and Water Resources Symposium: The art and science of water.* Barton, ACT: Engineers Australia, 2015: 133-143. ISBN: 9781922107497.

NOAA Climate.gov. 2016. How can we call something a thousand-year storm if we don't have a thousand years of climate observations? Accessed 6/05/2024 at https://www.climate.gov/news-features/event-tracker/how-can-we-call-something-thousand-year-storm-if-we-don%E2%80%99t-have-thousand

Credible Failure Modes: Considerations for Assessment and Application

Scott Martens, Teck Resources, Canada
Angela Kupper, BGC Engineering, Canada

Abstract

A core requirement of the Global Industry Standard on Tailings Management (GISTM) is to minimize risk for all credible failure modes for all phases of a tailings facility lifecycle. The intention of this requirement is to confirm that all potential failure modes are considered in the risk evaluation and that the related hazards and consequences are appropriately controlled to minimize the associated risk with all credible failure modes.

Identifying and addressing all credible failure modes is essential to support the development of robust risk management systems to prevent the hazards from causing failures. The credibility of potential failure modes is generally evaluated against a standard of negligibility, and the bar to demonstrate negligibility must be set very high. Removing potential failure modes from consideration without sufficient rigor may lead to inadequate: design oversight, construction quality control, adherence to operating requirements, or surveillance and monitoring, all of which could be seen to be unnecessary if credible failure modes are incorrectly removed from consideration. A robust failure modes assessment must consider not just the reserve capacity of the system under "extreme" loading, but also the potential for uncertainties due to insufficient site investigations, mischaracterization of materials, numerical models that do not fully capture soil or rock behavior, construction defects, computational errors, non-adherence to the operating procedures, other human errors, and the inherent uncertainties associated with geotechnical engineering.

With robust designs using multiple layers of defense based on comprehensive site investigations that adopt redundant and complementary tools and methods, rigorous construction quality control, and comprehensive performance monitoring, tailings and mine waste facilities can achieve the very high levels of safety and reliability that are required of all critical infrastructure. For this, proper identification and management of credible failure modes are essential.

Introduction

The GISTM was released in 2020 to support safe management of tailings facilities, following catastrophic tailings dam failures. A core requirement of the GISTM is to minimize risk for all credible failure modes for all phases of a tailings facility lifecycle. The GISTM and the International Council on Metals and Mining (ICMM) Tailings Management Good Practice Guide (GPG), (and other systems for responsible tailings management practice) require that all credible failure modes be identified and that robust controls be implemented to manage the hazards that could lead to a failure with unacceptable consequences. However, there has been debate on the interpretation and approach to consider credible failure modes. Although the GISTM sparked the debate for tailings facilities, the discussion in this paper is also applicable to other mine waste facilities. This paper discusses credible failure modes and the concepts and approaches to assess them, such that all potential failure modes are considered in the risk evaluation, the list of credible failure modes is comprehensive and complete, and all hazards and consequences are appropriately controlled to minimize the associated risk to a "negligible" level. The bar to demonstrate negligibility must be set very high.

There are unfortunate examples where engineering systems that were believed or assumed to have no credible failure modes have failed, or where risks have been significantly underestimated. Most of these have resulted from the lack of robustness around the identification and evaluation of potential failure modes. Not recognizing the existence and credibility of potential failure modes can lead to inadequate: design oversight, construction quality control, adherence to operating requirements, and/or surveillance, all of which could be seen to be unnecessary if there are believed to be no credible failure modes.

A structure can be very safe and still have credible failure modes, provided they are all appropriately managed to a very low risk level. There is minimal correlation between the number of credible failure modes and actual safety. This is evident from commercial aviation, where learning from past failures and adoption of a safety culture has resulted in very high levels of safety, despite there being hundreds or thousands of credible failure modes for each aircraft. Aviation safety incorporates design reviews and testing, redundant systems, personnel training (pilots and maintenance personnel among others), operational procedures including air traffic control, inspections and maintenance, and emergency planning, that together result in an exceptionally low probability of serious incidents. In 2023 there was a single fatal accident of a scheduled commercial aircraft out of 38 million flights (about 100,000 flights per day), which resulted in a fatal accident rate per flight of 3×10^{-8}, and a 5-year average from 2019 to 2023 of 1×10^{-7} (IATA, 2024). The flight fatal accident rate has consistently reduced over time through a combination of improvements in engineering, manufacturing quality, procedures and technology. Despite the differences between the tailings and aviation industries, this analogy demonstrates that it is possible for complex systems to be operated very safely when the risks of potential failure modes are controlled.

A failure modes assessment starts by developing a comprehensive catalogue of all physically possible failure modes, from which the credible failure modes are assessed, and risk treatment plans are developed. The aim of a failure modes assessment should be to identify all credible failure modes, so that the hazards and consequences can be managed appropriately. Acknowledging the reality and credibility of potential failure modes is essential to develop robust risk management systems to prevent the hazards from causing failures. Starting from a corporate safety culture that is declared and supported at the level of the Board of Directors, implemented with robust designs using redundant tools and multiple layers of defense, rigorous construction quality control, and comprehensive performance monitoring, tailings and mine waste facilities can also achieve the very high levels of safety and reliability that is required of all critical infrastructure. For this, proper identification and management of all potential failure modes is essential.

Definitions of credible failure modes

FEMA (2015) defined credible potential failure modes as: "*A potential failure mode that is considered to affect the total risk at a given dam and for which action could potentially be taken to reduce risk. A non-credible potential failure mode is a potential failure mode which is judged to have very low risks and for which a strong case can be made to that affect. Non-credible potential failure modes are often judged to represent a risk that is well below tolerable risk guidelines and orders of magnitude less than that of the more dominant potential failure modes at a given dam.*"

The GISTM (2020) definition is as follows: "*Credible Failure Mode / Scenario – Refers to technically feasible failure mechanisms given the materials present in the structure and its foundation, the properties of these materials, the configuration of the structure, drainage conditions and surface water control at the facility, throughout of its lifecycle. Credible failure modes can and do typically vary during the lifecycle of the facility as the conditions above vary. A facility that is appropriately designed and operated considers all of these credible failure modes and includes sufficient resilience against each. Different failure modes will result in different failure scenarios. Credible catastrophic failure modes do not exist for all tailings facilities. The term 'credible failure mode' is not associated with a probability of this event occurring and having credible failure modes is not a reflection of facility safety*."

The intent of the last sentence in the GISTM (2020) definition was to highlight that the existence of credible failure modes is not related to the safety of a facility since acknowledging a credible failure mode is not a statement of whether its probability is high or low. The probability of occurrence of any credible failure mode (and the safety of the facility) is associated with how that failure mode is managed. However, determining a failure mode to be a non-credible failure mode must be associated with an extremely low ("negligible") probability of occurrence as discussed further below.

FERC (2021) gave the following definition and discussion: "*Credible – A term used to indicate that a potential failure mode is considered to be physically possible and the likelihood of the potential failure mode is not considered so remote as to be negligible*." FERC notes that "*So remote as to be considered clearly negligible"* means that *"the likelihood of the potential failure mode (PFM) leading to failure is so minute so as not to be considered credible, and in quantitative terms, an annual frequency less than 1/1,000,000.*"

Threshold of negligibility

As implied by the three definitions above, there is not a single, widely accepted understanding of what conditions need to be satisfied for a failure mode to be considered non-credible (Small et al., 2023). It is common to consider that failure modes that are considered to have a "negligible" probability of occurrence are non-credible failure modes. "Negligible" is commonly defined as "*so small or unimportant as to be not worth considering*."

Some organizations have established a threshold of negligibility to be in the range of an annual probability of exceedance of 1/1,000,000 to 1/10,000,000 (10^{-6} to 10^{-7}) (FERC, 2021 and Morrison and Byler, 2022, respectively). However, we note that the threshold of what is "so small or unimportant as to be not worth considering" is dependent on the consequences. The FEMA (2015) definition referred to "risks" thus acknowledging both probability and consequence. Negligible events are commonly considered to be not only the ones that occur exceedingly infrequently (such as meteor strikes on dams) but also the ones with minor consequences. For example, a relatively high probability of getting a scratch from a tree branch while hiking in Banff could be considered a negligible event; a much lower probability of encountering a grizzly bear on the same hike would not be considered negligible, or "so small or unimportant as to be not worth considering." If the consequence is minor, an event "not worth considering" may be relatively common, whereas for a very severe consequence, even an annual probability of 10^{-6} may require further consideration. If large numbers of lives are at risk, this annual probability of occurrence would need to be even lower. This notion is honored in the As Low as Reasonably Practicable (ALARP) criteria that were originally developed by HSE (2001) and modified by others for application to dams. It is noteworthy that a fatal commercial aviation accident rate of 1/38 million would be considered negligible based only on the probability ranges above, but the aviation industry and regulators consider the failure modes to be credible and strive to further reduce the risk of these failure modes, consistent with the principles of ALARP.

It is conceptually important that the range of probabilities associated with negligibility is much lower than an "Extreme" event with an annual probability of exceedance of 10^{-4}. The annual probability of exceedance for design loading associated with Extreme consequence of failure facilities recommended by

the GISTM and other guidelines (CDA 2007; ICOLD 2022) of 10^{-4} is not meant to be an acceptable risk level or the threshold of negligibility; the system must still have a low probability of failure given the occurrence of the extreme event. For example, to meet a 10^{-6} annual probability of failure criterion, a seismic stability assessment would need to demonstrate not just that the slopes are designed to withstand seismic ground motions with an annual probability of exceedance of 10^{-4}, but also that the conditional probability of loss of containment, given the occurrence of that level of ground motion, would be no more than 1% (since 1/10,000*1/100 = 10^{-6}). This understanding assists in setting the performance expectation for seismic loading, if the failure mode is to be considered non-credible and assuming the potential consequences of a failure support 10^{-6} as an acceptable level. While it is not necessary to invoke a specific numerical threshold for negligibility, the ranges noted above provide an idea of the robustness necessary for designs such that potential failure modes meet a condition of negligibility.

These probabilities provide a conceptual indication of the threshold of negligibility; however, it is cautioned that humans are very poor at estimating low probabilities, and very frequently estimate values that are much lower than reality (Vick, 2014). NASA is widely regarded as one of the most technologically sophisticated organizations in the world, yet NASA senior management believed that the probability of a catastrophic loss of a Space Shuttle was 1/100,000 (Vick, 2002); the actual value was 1/68 (two catastrophic vehicle losses in 135 flights). It is particularly difficult to quantify the probability of failure in cases where there is only a small number of case histories for the loading event or failure occurrence (unlike for floods and seismic events where the return period can be estimated statistically).

Assessment of credible failure modes

A multi-disciplinary team should be engaged to assess potential failure modes. The team's composition would be determined for each specific case, but it could include geologists, dam designers (all relevant disciplines: soil and rock mechanics, seismic specialists, hydrology and hydraulics, modelling, etc.), construction personnel, operations personnel, the monitoring team and others. The variety of viewpoints and experiences in a multi-disciplinary team is critical to the robustness of the assessment.

The team should start by focusing on producing a comprehensive and complete list of potential failure modes. The potential failure modes assessment process can be viewed as a series of gates. First, only failure modes that are clearly not physically possible can be eliminated without additional consideration. Second, some potential failure modes may also be determined to be non-credible if sufficient evidence already exists to conclude that the probability and/or the consequences of failure are clearly negligible. Third, all other potential failure modes would be assessed in detail using investigation data and analyses to determine whether they meet criteria for negligibility, have already been managed to an acceptably low level of risk or need to be managed to an acceptable level of risk. The final result of the assessment should be a list of

all potential failure modes and the basis for determining them to be either non-credible, already at an acceptable risk level, or required to be managed to an acceptable and ALARP risk level.

A robust credible failure modes assessment must consider not just the system reserve capacity under "extreme" loading, but also the potential uncertainties due to insufficient site investigation, mischaracterization of materials, numerical models that don't fully capture soil or rock behavior, construction defects, computational errors, limitations to the current level of human knowledge in all technical disciplines, non-adherence to the operating procedures, other human errors, and as noted by Morgenstern (2024) the inherent uncertainties in geotechnical engineering. A degree of humility is required in assessing the above, in particular the ranges of uncertainty. As stated by Donald Rumsfeld in a US Department of Defense briefing in 2002 "… as we know, there are known knowns; there are things we know we know. We also know there are known unknowns; that is to say we know there are some things we do not know. But there are also unknown unknowns – the ones we don't know we don't know" (United States Department of Defense, 2002). A robust credible failure modes assessment should therefore also contemplate the potential for "unknown unknowns."

Detailed documentation of all the above should be prepared to allow independent review of the assessment and to demonstrate the thoroughness of the process. Moreover, potential and credible failure modes change with time and the assessment needs to be reviewed and revised as required. Credible failure modes may change if there are changes to the downstream condition or changes to the facility and its operations, such as additional raises, change in pond management, re-start after a long pause, etc. FERC (2021) recommends "Just because a potential failure mode is clearly negligible does not mean that it should not be re-evaluated under each subsequent PFMA (potential failure modes assessment)" and therefore should be retained in the documentation in case conditions change since the previous assessment. Detailed documentation provides a good basis for starting a reassessment of potential failure modes and the impact of changes or for reviewing the assessment after changes in staff or ownership. There are several case histories of failures caused by a poor understanding of the failure modes after a long pause in operations and/or change in ownership (Stava in Italy in 1985 killing 268 people, Jagersfontein in South Africa in 2022).

An assessment of credible failure modes must consider both primary and secondary, or dependent, failure mechanisms. For example, direct overtopping of a tailings facility may have a negligible probability if the facility is designed to store significantly more than the Probable Maximum Flood (PMF) or pass this through a spillway. However, that should not immediately lead to the conclusion that failure due to overtopping is not credible since secondary mechanisms, such as a rapid landslide into the pond that is triggered by the elevated pond water level in conjunction with heavy precipitation, could create a wave that overtops the dam. An example of this was the Vajont dam in Italy in 1963, where a large, rapid landslide

created a 250 m high wave that overtopped the dam, leading to the deaths of about 2000 people. In that case, the possibility of a landslide creating a wave that could overtop the dam had been considered, and based on model studies concluded that the effects of a wave would cause negligible damage, and that this conclusion "can be considered absolutely certain with regard to even the most foreseeable catastrophic landslide event" (Datei, 2005). In that case, the confidence on the model predictions was tragically overstated; a reminder of the need to consider uncertainties in the assessment of potential failure modes.

Table 1 is a non-exhaustive list of factors that should be considered in assessing the credibility of failure modes. The quality of the data, its representativeness and the uncertainties associated with each of the factors must be considered in evaluating credible failure modes. It is important to be aware that the level of knowledge is constantly evolving, and any current assessment will have limitations.

Table 1: Examples of factors to be considered in assessing credible failure modes

Is the spacing of boreholes sufficiently close that a geologically plausible weak material large enough to compromise the integrity of the structure could not exist between boreholes?
Are the boreholes deep enough that any weak material below the base of the boreholes could not compromise the integrity of the structure?
Are the soil properties understood well enough that there is no plausible condition where the soil strength would be less than considered in the analysis (including considerations of undrained vs. drained strength, and residual vs. peak strength)
Are the constitutive models for soil and rock behavior correct, or are there some aspects of the material behavior that may not be accurately modelled?
Do the materials vary at a scale that is not practical to replicate in analytical models (such as thin sand and silt layers in a tailings beach)?
Is material behavior well understood over the full range of stresses? Is the design outside of precedence for stress range, for the materials in the embankment and foundation?
Could there be a change in saturation in the long term due to continuous operation, infiltration and/or rise in groundwater levels, or a change in material properties due to chemical effects?
Could a gap in the construction quality control (QC) have resulted in a defect large enough to cause a failure?
Do multiple models using different approaches (analytical vs empirical, different but appropriate models of material behavior, etc.) all result in the same conclusion ("converging lines of evidence").
Could there be a landslide into the reservoir or the top of the facility?
Does the safety of the facility rely on any human action, such as operating a return water/fluid system?
Is monitoring required to identify the need for corrective action?
Could a spillway or water diversion system become blocked by debris?
Could the spillway itself fail (similar to the Oroville dam) and could this lead to retrogression into the facility or a different failure mode?
Do predictions of extreme events account for factors such as climate change?
Could internal erosion occur due to: Changes in the water table? Failure of a seepage control element, such as a drain or an internal collector pipe drain? Biological or chemical clogging of a filter or drain? Seepage through the abutment of the facility? Insufficiently compacted layers? Inconsistency of fill gradation? Defects in a geosynthetic liner? Chemical alteration or Dissolution of soluble elements in the foundation or abutments?

Validity check

A check on the validity of a conclusion that a particular failure mode is non-credible is that it should logically lead to the absence of a requirement for critical controls for that failure mode. Changes to the facility that increase the robustness through passive measures such as toe berms could render failure modes non-credible. However, any system that requires active human input or intervention to prevent a failure has credible failure modes, though a well-designed system with redundant checks and balances could render the probability of failure sufficiently low to be considered safe. For a non-credible failure mode, it should be confirmed that the full possible range of potential human error or inaction would not result in the loss of integrity of the facility. If there are no credible modes, the facility would not rely on monitoring systems to manage risk, however having monitoring systems as a redundancy is helpful to confirm system performance.

There may be situations where there are no credible failure modes during early stages of construction, when the dam section is very wide relative to its height, but where instrumentation monitoring is necessary to establish the performance for evaluation of the design assumptions and the safety at later stages of construction.

The following conditions are, on their own, insufficient to demonstrate that a failure mode is non-credible, though a combination of these could be part of the safety case, or well-reasoned argument to demonstrate that the facility meets acceptable safety standards:

- Designing to meet regulatory requirements and good industry practice. The technical quality of regulatory requirements is quite variable globally. Adherence to updated, high quality regulatory requirements and industry guidelines may provide a solid basis for managing the risk of potential failure modes, but it may not be sufficient in all cases.
- Attaining a specific factor of safety. As noted by Lupo (2018), prescriptive factor of safety criteria “do not convey any information regarding risk to the design, construction nor operation of the TSF (tailings storage facility).” This is because there are several factors that must be considered to select appropriate design factors of safety to manage risks on each project (Küpper, 2023). There are multiple instances where tailings storage facilities have failed with large calculated factors of safety, where the factor of safety was calculated on the basis of an incorrect understanding of a potential failure mechanism or the adopted design parameters were not adequate to represent the actual material behavior, such as using drained strengths for contractive, brittle materials or due to lack of data, uncertainties or errors. Examples where pre-failure factors of safety were calculated to meet or exceed the regulatory requirements but the facility failed, include: Mt. Polley at 1.5+ (B.C. Chief Inspector of Mines, 2015),

Brumadinho at 1.6 to 2.1 using drained parameters (CIAEA,2020), Wachusett Dam with a drained factor of safety of 2.4 (Reid and Fourie, 2019), and examples by Carrier (1991) and Morgenstern (2024) of dams that failed with factors of safety of 1.7 and 1.8, respectively. If incorrect or inappropriate parameters are used for the analysis, then a high calculated factor of safety is not an assurance of actual safety.

- Having the calculated capacity to withstand extreme loading (earthquake or flood). Loading estimations can have a large degree of uncertainty, calculations can be in error, failure mechanisms can be missed, and secondary failure mechanisms can occur.
- Model predictions of good performance during normal and extreme loading conditions. No models can perfectly capture all aspects of soil and rock behavior, nor the inherent material variability within a test hole, or the unknown ground variability between test holes. Models can provide valuable insights into the system behavior, and the uncertainty in the predictions can be reduced through performance-based updating, as described by Morgenstern (2018). Achieving model equivalence and calibrating the model to measured performance supports performance-based risk management. However, uncertainty is always present, and the advice of the statistician George Box remains prescient: "All models are wrong, but some models are useful."
- Good performance as demonstrated by monitoring, surveillance, or maintenance. Any potential failure mode that requires monitoring is a credible failure mode. An operator may choose, out of an abundance of caution, to continue monitoring despite the conclusion that there are no credible failure modes, however, that conclusion must not depend on the monitoring if the failure modes are to be truly non-credible.
- Previously assigned low probability of failure for a given failure mode. The results of previous risk assessments should be reviewed to check if the previous conclusions were rigorous and remain valid.

Caution on failure mode assessments

The most important caution that must be taken when conducting potential failure mode assessments is to not discount possible potential failure modes. In assessing the credibility of failure modes, the team must be aware of the potential for goal-seeking and confirmation bias. Confirmation bias (Kahneman, 2011; Vick, 2002) is the natural human tendency to seek out information that validates our pre-existing beliefs or hopes, and discounting information that would contradict these. There is an inherent desire to not have credible failure modes for tailings and mine waste facilities. However, the desire to have no credible failure modes can lead to confirmation bias. Other biases and heuristics described by Kahneman (2011) and Vick

(2002) such as the availability bias, representativeness bias, and overconfidence, can cause even experts to underestimate the level or risk and/or overestimate their ability to control the risk.

Potential failure modes and their probability change throughout the lifetime of each facility and thus the assessment must be re-done periodically, and each assessment should be considered an interim determination. The failure mode assessment should be reviewed and repeated whenever a condition occurs that would invalidate any of the premises for the previous assessment; an example could be climate change impacts on the Probable Maximum Flood that could render an older design condition no longer representative of a credible extreme. A potential failure mode and risk assessment at the design stage is helpful to check that all potential failure modes have been adequately addressed. However, there could be features that are only discovered during construction. Moreover, many engineering failures have been caused by changes in plans during construction, or inadequate construction quality assurance and quality control (QA/QC). For these reasons, a potential failure mode and risk assessment should always be re-done during and post-construction to assess if pre-construction or interim determinations remain valid and if modifications to the design are worthwhile or required to attain an appropriate level of risk management.

For new facilities, one aspect of risk management is to eliminate or mitigate as many potential failure modes as is practical in the design. An example of eliminating a failure mode would be excavating out a weak layer within the footprint of the dam as part of the foundation treatment. However, most if not all tailings and mine waste facilities will have credible failure modes that require mitigation.

There may be situations where, at the current stage of construction of a facility, a rigorous assessment of potential failure modes meets the standard to declare that there are no credible failure modes. However, future raises or expansion of the facility, or changes downstream that increase the potential consequences, may introduce credible failure modes. Construction quality control and instrumentation monitoring may be necessary to confirm the safety of the facility at later stages of construction. In that case, it may be prudent to avoid an early declaration that there are no credible failure modes, since that could cause organizational resources to be redirected to other priorities and detract from the vigilance that is needed to maintain the safety of the structure. “Regardless of non-credibility of failure modes, monitoring is most often still required to demonstrate performance and ensure that the failure mode remains non-credible with time” (LePoudre and Morrison, 2022). For “safe closure” it is generally necessary to confirm that there are not and will not be any credible catastrophic failure modes (ICMM, 2021).

Credible failure modes and risk management

The bow-tie risk management model is an example of a tool that illustrates how hazards can lead to an unwanted event, and consequences that can result from that event. In the bow-tie model (Figure 1), the hazards are on the left side of the figure, the unwanted event or incident in the middle, and the consequences

on the right. Potential failure modes can be represented by the unwanted event in the middle of the Bow-Tie. The risk management system uses controls (barriers) between the hazards and the unwanted event – these prevent or reduce the probability of the event from occurring, given the existence of the hazards. If the event should occur despite the presence of the barriers, recovery measures on the right side of the bow-tie prevent or mitigate the consequences.

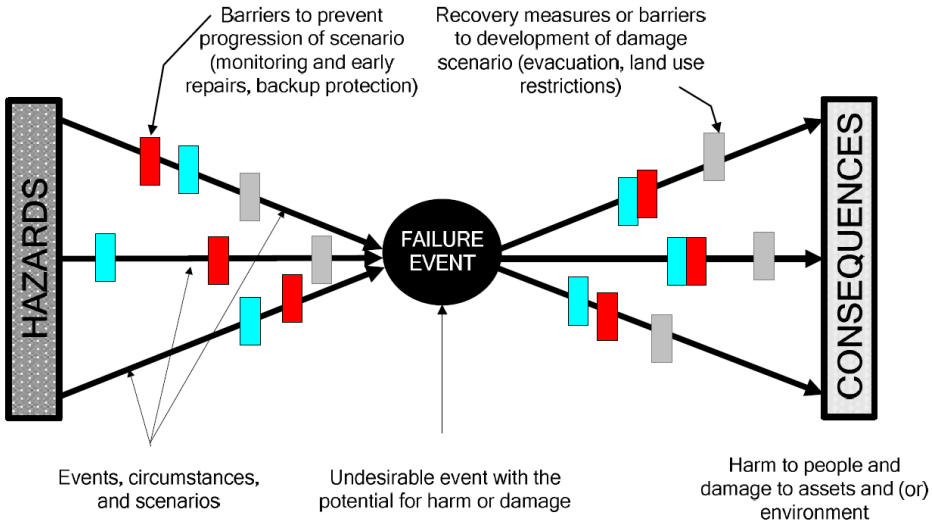


Figure 1: Bow-tie risk management model (CDA, 2007)

Acknowledgement of credible failure modes is a necessary aspect of mitigating hazards so that risks are controlled to acceptably low and ALARP levels. If potential failure modes are discounted as being non-credible without a sufficiently rigorous assessment, hazards that should be subject to controls may be left uncontrolled, increasing the risk of failures. An illustration of this is the sinking of the Titanic, with the loss of 1500 lives.

The Titanic was believed to be "unsinkable," which was effectively saying that it had no credible catastrophic failure modes. This belief drove risk taking on both sides of the bow-tie. the captain didn't slow down, and entered the iceberg field at 22 knots, which was full speed for the ship – there was no reason to slow down as a precaution, since the ship was unsinkable. The ship only held lifeboats for 50% of the people on board, and the crew were not trained and did not practice emergency deployment of the lifeboats that were carried. There was no need to since there were no credible failure modes! Had the owner, the designer, and the captain instead been realistic about the failure modes and focused on managing risk and operating safely considering the existence of credible failure modes, there could have been zero fatalities – they would have slowed down in the iceberg field to manage the risk of a collision that could catastrophically damage the ship (left-hand side of the bow-tie). furthermore, even if they didn't slow down, the 2.5 hours between hitting the iceberg and sinking was enough time to evacuate if they had enough

lifeboats and were trained to use them (right-hand side of the bow-tie). The belief that there were no credible failure modes was the direct cause of the enormous loss of life.

While the operations of the Titanic appeared to have been consistent with the international standards at the time, a robust assessment of potential failure modes would have indicated that additional risk controls were needed to reduce the risk. Inappropriately discounting the credibility of potential failure modes can take away the level of awareness and focus on the part of the dam owner and the engineer, that would otherwise contribute to a heightened diligence in risk management. The sinking of the Titanic is also a reminder that while it is important to meet international standards for each type of project, it may not be sufficient in all cases.

Acknowledgement and communication of risk

There is a perception among some groups and individuals that tailings and mine waste facilities should have zero risk. This is antithetical to existence of pervasive risk throughout society – virtually all infrastructure, from tall buildings to bridges and airplanes, have credible failure modes and hence some, typically small, risk of failure. This is also a mischaracterization of the statement "zero tolerance for human fatality" (GISTM, 2020) which does not mean zero risk – there is always risk of fatality with operating vehicles, with working underground, with working in tall office buildings. Accepting a small risk of a negative outcome doesn't mean that the outcome is tolerated. Despite the very low probability of fatal commercial aviation accidents of 1/38 million, the industry and regulators continue to work to improve safety further. The mining industry must also continually work to reduce the risk from all potential failure modes towards the goal of "zero fatalities and catastrophic events" (ICMM, 2021).

When communicating risk, it is important to understand the cultural and social context of the audience and adjust the communication accordingly. It is increasingly more common for mine owners to have developed relationships with the host communities and an understanding of the social context such that communications can be specifically tailored to work best in each situation. Sandman (2012) notes that the common perception in risk communication is that "the way to reassure people is to tell them only reassuring things." From this perspective, it would be attractive to be able to declare to stakeholders that a facility has no credible failure modes. However, Sandman (2012) further notes "Instead of convincing us that there is nothing to worry about, the conventional strategy often convinces us that you are not taking the risk seriously enough." Rather than telling people that there is nothing to be concerned about, it is generally more reassuring to confirm that we do recognize that there is a small degree of risk, which we are taking very seriously and will continue to manage. "If you tell me not to worry about anything, I will end up worrying about everything. I will worry less once I know you are worrying for me." (Sandman, 2012).

The aviation analogy is apt again. It is much more comforting to know that there is a large team of well-prepared professionals worried about the safety of the aircraft, than if those professionals said that there was no possible way for an aircraft to crash and therefore nothing to worry about.

Future considerations

This paper is not the last word on the topic. There has been significant discussion on the topic of credible failure modes and risk management, even during the preparation of this paper. It is clearly an issue that is evolving in the tailings dam safety community.

A future refinement may be to de-emphasize the assessment of the credibility of failure modes and focus on an assessment of all potential failure modes using the ALARP framework where both probabilities and consequences are considered. A failure mode that is non-credible would by definition satisfy the requirements of acceptable risks within the ALARP framework. In the future, the tailings dam safety community might reconsider the terms credible and credibility. The qualitative (and possibly subjective) nature of these terms is not helpful when facing the complexity and difficulty of assessing and quantifying the very small probabilities of occurrence of certain potential failure modes. Assessing and managing risks within the framework of ALARP may be easier to explain and support. Moreover, both the GISTM (2020) and the GPG (ICMM, 2021) require that risks be managed to ALARP so using a single framework streamlines the process. The same rigor described in this paper is required for an ALARP assessment.

Regardless of the system used to assess and manage risks, it must be done with rigor so that all risks that could result in unacceptable outcomes are identified and managed.

Conclusion

Robust risk management should aim to identify all potential failure modes and manage the associated risk. Failures of tailings and mine waste facilities are unacceptable and can have profoundly tragic consequences. Mining leaders and professionals must work to design, construct, operate and close tailings and mine waste facilities that are safe, robust, and resilient throughout all stages of their life cycle. Risk assessments are a key part of this: striving to identify all potential failure modes, appropriately controlling the hazards (the left side of the bow-tie), minimizing the consequences where possible, and enacting effective emergency response plans if a loss of control does occur (the right side of the bow-tie).

Tailings and mine waste facility risks must be managed to acceptably low levels and further reduced using the ALARP principle, so that these facilities do not meaningfully increase physical or environmental risks to the nearby populations or the environment itself. The assessment of risk using the ALARP principle or an assessment against a standard of negligibility should consider both the probability and the consequences of a potential failure.

Most safe tailings and mine waste facilities will have credible failure modes, just as bridges, tall buildings, commercial aircraft, and medical surgeries do. The presence of credible failure modes does not imply that a system is unsafe. These systems all have credible failure modes, but if the hazards are properly identified and controlled, the probability of failure can be acceptably low and consistent with the goal of zero fatalities and no catastrophic events.

Leading mining companies have adopted rigorous procedures for potential failure modes assessments and management of risks that include using the ALARP principle. Broad adoption of these principles and procedures would result in a significant improvement in tailings facility safety. The point of this paper is not to undermine the confidence in well-designed and well-constructed tailings facilities that are responsibly operated and maintained. The objective is to challenge all mining companies and professionals to a high standard of rigor in identifying and assessing potential and credible failure modes so that the risks are effectively managed to such a low level that we can demonstrate consistently safe, reliable performance of tailings and mine waste facilities. As with other critical infrastructure, where the risks are appropriately managed, the public can have confidence in the safety of these facilities.

Acknowledgements

The authors' perspectives have evolved and benefitted from many valuable discussions with colleagues, including Dr Norbert Morgenstern, Dr Roy Mayfield, Tamara Johndrow, Greg Puro, Andy Small, Chad LePoudre, Jennifer Brash, Alex Strouth and the anonymous reviewers. We hope that this paper will stimulate further discussion that will lead towards strengthened systems for safe and reliable tailings and mine waste structures.

References

British Columbia Ministry of Energy and Mines. 2015. *Investigation Report of the Chief Inspector of Mines Mount Polley Mine Tailings Storage Facility Breach*. Accessed at https://www2.gov.bc.ca/assets/gov/farming-natural-resources-and-industry/mineral-exploration-mining/documents/directives-alerts-incidents/chief-inspector-s-report-page/m-200_mount_polley_2015-11-30_ci_investigation_report.pdf

Carrier, D. 1991. Stability of Tailings Dams. *XV Ciclo di Conferenze di Geotecnica di Torino 1991.*

Canadian Dam Association. 2007. *Dam Safety Guidelines*.

Datei, C. 2005. *Vajont la storia idraulica.* 2nd ed. Padua: International bookshop Cortina: 119–130.

Extraordinary Independent Consulting Committee for Investigation (CIAEA). 2020. *Executive Summary of the Independent Investigation Report. Failure of Dam 1 of the Córrego do Feijão Mine – Brumadinho, MG.* Accessed 15/06/2024 at https://vale.com/documents/d/guest/20-02-20_ciaea_report_i-1

Federal Emergency Management Agency (FEMA). 2015. *Federal Guidelines for Dam Safety Risk Management*.

Federal Energy Regulatory Commission (FERC). 2021. Chapter 17 – Potential Failure Mode Analysis. *Engineering Guidelines for the Evaluation of Hydropower Projects*. Washington.

Global Tailings Review. 2020. *Global Industry Standard on Tailings Managemen*t.

Health and Safety Executive (HSE). 2001. *Reducing Risks, Protecting People: HSE's Decision-Making Process*. London, UK: Risk Assessment Policy Unit, her Majesty's Stationery Office.

International Air Transport Association (IATA). 2024. *IATA Annual Safety Report Executive Summary and Safety Overview.* 60th Edition. Accessed 04/07/2024 at https://www.iata.org/contentassets/a8e49941e8824a058fee3f5ae0c005d9/safety-report-executive-and-safety-overview-2023.pdf

International Commission on Large Dams (ICOLD). 2022. *Tailings Dam Safety*. Bulletin 194.

International Council on Mining and Metals (ICMM). 2021. *Tailings Management Good Practice Guide.*

Kahneman, D. 2011. *Thinking, Fast and Slow*. Farrar, Straus and Giroux.

Küpper, A. 2023. Tailings Management: Where are we today and where do we go from here? Keynote address *Tailings and Mine Waste, 2023.* Vancouver, BC. Accessed 02/07/2024 at https://tailingsandminewaste.com/wp-content/uploads/TMW-2023-A-Kupper-Nov-6-2023.pdf

LePoudre, D.C. and Morrison, K. 2022 Tailings management systems. Chapter 37. *Tailings Management Handbook*. Society for Mining, Metallurgy and Exploration (SME).

Lupo, J. 2018. TSFs, risk, and the human element. *Tailings and Mine Waste 2018*, Keystone: pp 3–8.

Morgenstern, N.R. 2018. Geotechnical risk, regulation, and public policy. The Sixth Victor de Mello Lecture. *Soils and Rocks, São Paulo* 41(2): 107–129, May–August, 2018.

Morgenstern, N. 2024. *From Certainty to Uncertainty in 64 Years*. University of Alberta Geotechnical Centre. Accessed 08/06/2024 at https://www.youtube.com/watch?v=MNDMSySTagw

Morrison, K. and Byler, B. 2022. Risk assessment and risk management. Chapter 38. *Tailings Management Handbook*. Society for Mining, Metallurgy and Exploration (SME).

Reid, D. and Fourie, A. 2019. Static liquefaction workshop. Calgary, Canada.

Sandman, P. 2012. *Responding to community outrage: strategies for effective risk communication.* Self-published. https://www.psandman.com/media/RespondingtoCommunityOutrage.pdf

Small, A., Kupper, A., Johndrow, T. and Al-Mamun, M. 2023. Credible failure modes – summary of 2021 and 2023 workshops. Tailings and Mine Waste 2023, Vancouver: pp. 1245–1255

United States Department of Defense. 2002. Defense.gov News Transcript: DoD News Briefing – Secretary Rumsfeld and Gen. Myers. February 12, 2002. Archived from the original on April 6, 2016.

Vick, S. 2002. *Degrees of Belief: Subjective Probability and Engineering Judgment*. American Society of Civil Engineers (ASCE) Press.

Vick, S. 2014. The use and abuse of risk analysis. *Proceedings of Tailings and Mine Waste 2014*. Colorado, USA: 49–56.

Practical Remedies to Improve the Defenses of Tailings Structures

Jeremy Boswell, Thurber Engineering Ltd, Canada
Anan Morshed, Thurber Engineering Ltd, Canada
Thomas Kujawa, Thurber Engineering Ltd, Canada
Meghan Barton, Thurber Engineering Ltd, Canada

Abstract

The high-profile failures of tailings storage facilities (TSFs) and the associated loss of life over the last decade have generated substantial volumes of new legislation and guidance and an enormous workload of validation and compliance effort in industry response. Improvements in standards and new design are noticeable, especially for facilities owned by multinational mining companies and members of the ICMM and those who have voluntarily subscribed to the principles of GISTM. However, even after all this effort, the industry has continued to witness several more failures worldwide over the past two years, some of which have involved loss of life. The primary causes of the recent Jagersfontein tailings disaster in South Africa, which failed in 2022 after publication of the above-mentioned industry responses to Brumadinho, are summarized in this paper.

The most relevant risks that have led to recent tailings dam failures have been identified and many have been well publicized: storage of water and fluid tailings behind tailings dams; tailings or foundation liquefaction; combination mechanisms of failure, such as pond overtopping followed by erosion of embankments and liquefaction flow failure; weak engineering; facility dormancy; the failure of dam management systems, and human error.

While all the effort in confirming compliance is laudable, have we become somewhat distracted? It is suggested in this paper that renewed and continued attention should be focused on the practical improvement of the defenses of tailings structures. This paper outlines several practical and operational defenses: understanding deposition history in limiting rate of rise; avoiding the banana skin of very weak layers deposited in critical areas; prioritization of subaerial beaching and maximizing beach length and beach compaction to reduce the risks of liquefaction, internal erosion or embankment failure; and vigilance in tracking leading indicators and exercising duty of care. Key defenses relating to pond size reduction and

elimination of water storage have been addressed in papers by the lead author at previous Tailings and Mine Waste conferences in Colorado.

It has been estimated that there are around 30,000 TSFs worldwide, many of which have not been fully closed over the past century but are simply dormant. The paper concludes with a call to action to recognize the risk of dormancy, to address the risks posed by facilities that are no longer operational, and to take action to ensure that our industry leaves a positive legacy for future generations.

Introduction

In November 2023 in Vancouver, delegates to the Tailings and Mine Waste 2023 conference heard an excellent keynote address by Dr Ed McRoberts (McRoberts, 2023). In his address, McRoberts pointed out afresh the grave dangers of a weak layer of fines deposited operationally near the base of a tailings storage facility (TSF). Over the years this problem layer has become known colloquially in the industry as the "banana skin." Further detail is provided later in this paper. In response to a question "How does one avoid the banana skin?" McRoberts affirmed that one does one's utmost to not build such a layer and to prevent its creation. The conference discussion provoked interest from the authors of this paper and generated momentum to list some practical remedies for the banana skin problem. Some of these remedies also address some of the other more common mechanisms and risks of failure of TSFs.

Defining the "banana skin"

Weak layers are frequently responsible for the failure of TSFs. Many authors have described in great detail the dangers of unaddressed weak foundations. The Mount Polley failure in 2014 (Morgenstern et al., 2015) and the Los Frailes failure in 1998 (Alonso and Gens, 2006) are good examples. However, the banana skin under consideration here is not a weak foundation layer: it is a weak layer on the floor of the TSF basin that is typically created by the storage of water and fines during commissioning. If not immediately removed, the fines settle and form the banana skin, which becomes most problematic for global slope stability once the structure has risen in height.

In the typical design of starter earthworks for a TSF, as shown in Figure 1, a toe drain near the starter embankment and sometimes also a blanket drain some distance from the toe are provided for drainage of the tailings and depression of the phreatic surface, to enhance stability. However, if fines are allowed to accumulate above the drain, the drain becomes blinded and is rendered impermeable and ineffective. Even more seriously, the fines if left in place serve to create a soft clay/fines layer at the base of the TSF. This is the banana skin – created by maloperation. The banana skin formed no part of the design, planning, or construction phases. For the later stage raises of the TSF, the supernatant pond is removed. However, the

banana skin is left behind. This banana skin leaves a substantially weak pathway of preferred weakness in the TSF.

Also shown in Figure 1 is the impact of the banana skin (weak layer) on global stability, and the improvement in stability if a banana skin is avoided, since the failure plane is then unlikely to pass through the same zone.

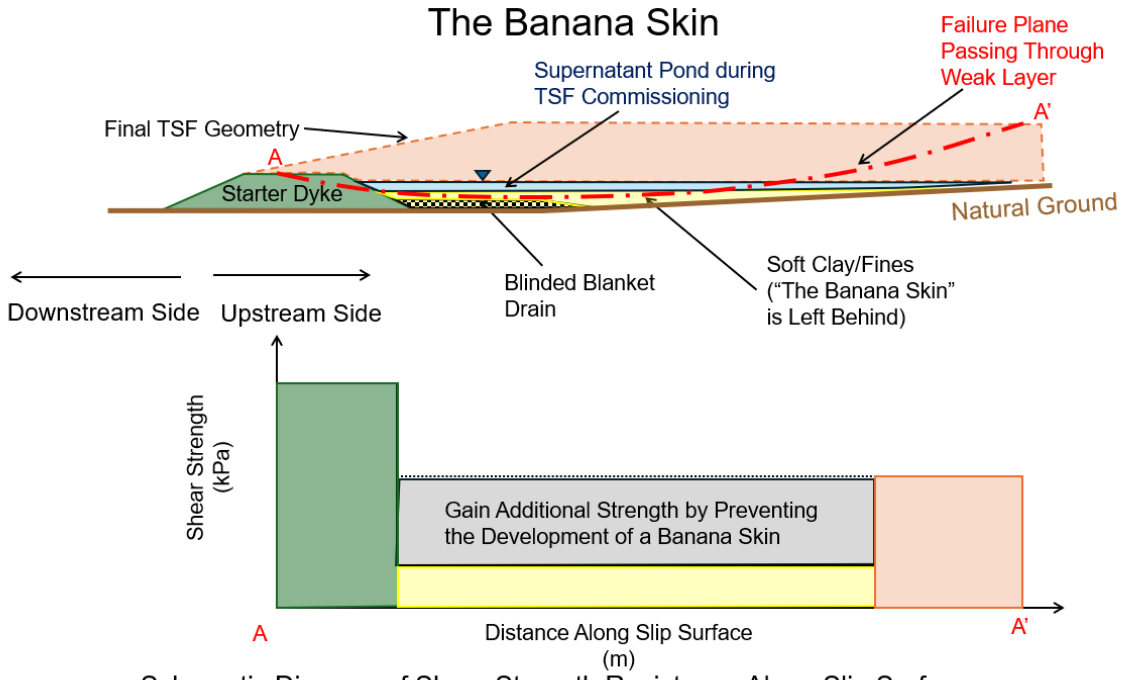


Figure 1: Defining the "banana skin"

In order to defend the TSF against the risks of the banana skin, the commissioning phase is critical. However, commissioning is not even considered by many engineers as being of any great significance, as illustrated in Figure 2. Recognition of the vital elements of the commissioning phase goes a long way towards safe TSF operation. This paper addresses several different defenses that may be employed to guard against the banana skin, especially during the commissioning phase of the TSF life cycle.

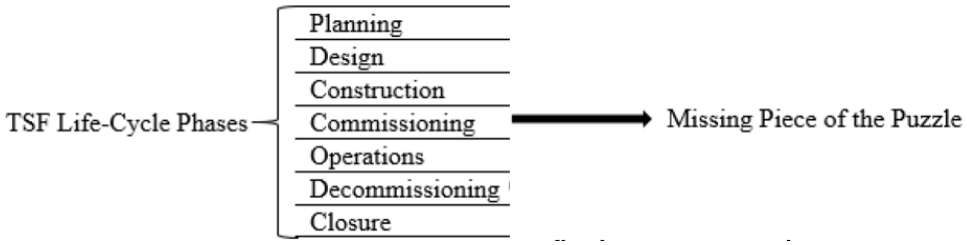


Figure 2: Life cycle of a tailings storage facility

Lefkochrysos platinum TSF case study

The erstwhile Lefkochrysos Platinum Mine (Lefkochrysos meaning "white gold") is a platinum mine which was developed in the mid-1980s near the town of Brits, South Africa, some 100 km northwest of Johannesburg. After the initial design and commissioning, the mine underwent several changes of name and ownership. As an interesting metallurgical aside, the mine was the first platinum mine to successfully mine and commercially process UG2 ore without the usual need to blend it with Merensky reef to beneficiate the ore. This opened up opportunities for other mines to successfully extract platinum group metals more directly from UG2 reef.

One of the challenges of the Lefkochrysos TSF design was that the mineralogy of the (somewhat chrome rich) processed ore and tailings was unknown prior to production, owing to the innovative nature of the mining project. Thus, the usual tailings characteristics of particle size distribution, particle specific gravity, slurry relative density, tailings mineralogy, permeability and governing rates of rise were substantially unknown and had to be assumed. In essence, the tailings design was required to be conservative and defensive, and as subsequent events were to prove, was successful. This case study of the design of the TSF shows various defenses which were employed against several operational risks, including the banana skin. The 14 defenses that the Lefkochrysos design embraced to prevent development of a banana skin are listed below and shown in Figure 3:

1. Spigoted discharge from multiple deposition points to direct and develop beaching away from the starter embankment.
2. Sufficiently large deposition areas to allow for Beach Above Water (BAW) (subaerial) deposition, managed rates of rise and associated desiccation and consolidation. Beach compaction (e.g., track packing) may also be added to accelerate consolidation and improve embankment stability.
3. Cross walls to immediately direct deposition away from the drains and prevent blinding of drains.
4. Bypass lines and cells for deposition of wastewater, flushing water and off spec or dilute tailings.
5. A constructed sacrificial beach (not shown) under the tailings to prevent accumulation of fines near the toe by introducing immediate gradient to initial beach deposition profiles.
6. Wing walls around the decants, which increase beach length, reduce beaching velocity and momentum, improve settling of fines, and prevent beach erosion and channel short-cutting.

7. Temporary decant towers (penstock inlets) to progressively remove supernatant at the point of accumulation in a timely manner, while at the same time allowing progressive and planned migration of the decant points away from outer embankments.
8. Permanent decants, with wing walls to improve beaching and settling of fines, and to prevent pond migration.



Figure 3: Lefkochrysos platinum TSF case study

9. Toe drains (not shown) below the tailings, providing immediate and early drainage of the deposit.
10. Blanket drains at natural ground level (not shown) and offset from the toe to improve drainage of the deposit and to assist with longer term phreatic surface management.
11. Finger drains that collect supernatant during deposition from areas more remote from the decants. The design intent was that in time the finger drains could be allowed to plug or be decommissioned, which was successfully accomplished.
12. Elevated drains (installed later on the beach when the TSF has undergone several raises), which improve drainage of the mature beach and prevent phreatic surface encroachment towards outer embankments. Chimney drains or vertical drains are also a critical element of

TSF design, especially for downstream and centerline construction, in controlling seepage and internal erosion. Vertical drains are seldom employed in upstream construction designs, and they were not considered for this design.

13. A silt trap, which enables rapid removal of turbid supernatant and emergency response to upset events, and allows for settling and capture of fines under controlled conditions. The silt trap was designed to be removable from the recycle water circuit, using a simple gated gravity bifurcation, thus allowing for desilting of the dam without interrupting operation of the TSF or the process plant and mine.
14. A recycle dam to prevent the storage of water on top of tailings, and to contain flood events.

These 14 defenses may be divided into four categories, as explained below.

Geotechnical and hydrotechnical design

Geotechnical and hydrotechnical remedies require foresight and anticipation of commissioning and operational issues of a TSF. These proactive measures need to be designed and specifically applied to the TSF. Cross walls direct the tailings away from drainage structures, reducing the chance of the drainage being blinded or blocked. Wing walls increase the length of the beach and improve the settling of fines to prevent beach erosion and channel short-cutting. The recycle dam is used to prevent water storage on top of tailings. The silt trap removes turbid material from the supernatant pond and allows the fines to settle under controlled conditions.

Drainage

Drainage can be implemented prior to, during and after TSF operation to manage and maintain the flow of water through and around the TSF. The construction and use of toe drains, or ground surface blanket drains, would require pre-emptive design and planning to ensure the drain is located, sized, and designed to be able to convey the design flow volumes. Finger drains collect the supernatant during deposition and may be decommissioned later. On the other hand, elevated drains are installed later when the tailings surface has been raised. Elevated drains improve the drainage of mature beaches and eliminate phreatic surface encroachment towards the outer embankment.

Buttressing with the inclusion of reverse filters can improve stability and remedy seepage and internal erosion risks. Many of these drainage elements would provide immediate drainage during the commissioning phase of the TSF, minimizing the size of the supernatant pond and removing the likelihood of fine material being deposited on top of drains or in vulnerable areas.

Slurry discharge, decant and supernatant control

Depositional cells promote the settlement of tailings material and allow water to drain into the recycle dam or a secluded area of the beach. A bypass line would redirect off-spec product, flushing of tailings lines, and additional wastewater runoff. Additional decant towers (both permanent and temporary) allow the operator and owner to better manage and maintain water levels within the TSF. Active supernatant control and removal reduces potential impacts of poor depositional management or off-spec deposition of tailings material and improves the quality of recycled water.

Beaching and deposition

Spigots, cyclones, or open-ended discharges from multiple deposition points are used to direct the beach away from the starter dam. The sacrificial beach prevents the accumulation of fine tailings material too near to the outer embankments. Off-spec cells create an area of the facility that is used for emergency deposition so that an upset condition does not impact the global stability or efficiency of the TSF. Sound beaching and deposition practice relies on a sufficiently large depositional area, controlled rates of rise, and allowing the material to be deposited above water in a sub-aerial environment rather than in a subaqueous environment. This prevents the long-term suspension of fine tailings material, promotes faster settling, and enhances tailings consolidation.

Premium on duty of care and attention to detail

The Lefkochrysos case study described above holds significant implications for tailings management:

- Owners, designers, and operators have significant responsibility to ensure that their responsibilities are discharged with the commensurate duty of care (Boswell and Sobkowicz, 2011). This applies especially to the commissioning phase.
- The defenses described above are not extremely complicated or demanding and in several cases are not even expensive. Timely and assiduous implementation of defensive measures (of which the 14 listed above are examples) will go a long way to assuring the safety of TSFs.
- Attention to detail is demanded during the implementation of defensive measures. Slipshod or partial compliance will provide no defense, since a chain is only as strong as its weakest link.

Jagersfontein tailings disaster case study

Pre-2010 history

The Jagersfontein mine in South Africa was operated by the New Jagersfontein Company from 1882 until 1932, when De Beers Consolidated Mines Ltd (De Beers) acquired the mine. Large-scale commercial mining by De Beers commenced in 1949 (Lochner et al., 2024), operating as an underground mine until

1972. Following the South African transition to democracy in 1994, the new Mineral and Petroleum Resources Development Act (MPRDA) came into force and the Minerals Act of 1991 was repealed. Under the new act, the Jagersfontein tailings facility was reclassified as an ordinary dam in 2002 and had no need to comply with mining legislation (Lochner et al., 2024). This enabled large-scale re-mining activities to proceed where conventional mining regulations did not apply.

Superkolong Consortium, a broad-based black economic empowerment (BEE) holding company, acquired the mine from De Beers in 2010 (Writer, 2022) to reprocess the legacy coarse reject kimberlite dumps and reopen the TSF after almost 40 years of dormancy. Jagersfontein Development Ltd, a partnership between Reinet Investments S.C.A. (Reinet) and Sonop Diamond Mining Ltd, acquired shares in Superkolong in 2011 (Brown and van Wyk, 2022). In April 2022, Reinet sold its consortium share to Stargems Group, a Dubai-based diamond trading company, just months before the tailings disaster.

Jagersfontein TSF operational history after 2010

In 2010, after the onset of coarse reject mine waste dump reprocessing, the original TSF was expanded to the west and almost doubled in size by 2013 (Torres-Cruz and O'Donovan, 2023). Construction of the east TSF extension was underway in 2015 and completed by 2017. Tailings deposition from the west expansion eventually allowed tailings to flow from the west extension to the original TSF and east extension via two furrows in an internal wall. Continued eastward migration of tailings eventually completely buried the furrows and internal wall. In 2019, erosion gullies and slope instability were observed in the downstream southeastern wall, and buttressing efforts commenced to increase the wall thickness in this area.

The tailings facility was shut down in 2020 by the provincial government as the facility exceeded authorized water levels (Banya, 2022). Operations were allowed to continue under a new license in June 2021. An inspection of the TSF by engineers in July 2022 found that the water volumes were within limits and that the dam was safe (Banya, 2022). On September 11, 2022, the TSF failed, causing at least one loss of life, destroying several homes and causing significant environmental damage. About 5 million cubic meters of tailings material (Rivet, 2023) were released, creating a downstream tailings plume about 8.5 km long and 1.5 km wide (Petley, 2022). Tailings continued to flow along approximately 56 km of streams and rivers.

Contributing factors

Investigations of the failure concluded that several operational practices contributed to the breach of the Jagersfontein TSF, including:

- Too much slurry was pumped into the TSF, resulting in a full supernatant pond with water right up to the perimeter wall.

- There was tailings deposition from only one discharge location on the west dam wall of the TSF. The lack of perimeter tailings deposition prevented the development of beach freeboard.
- The absence of beach freeboard and lack of capacity did not leave available storage to manage extreme precipitation events.



Figure 4: Aerial photographs of the Jagersfontein tailings facility in 2010, 2021, and September 2022 (photographs courtesy of Google Earth)

- Ponding of surface water at the downstream toe of the southwest dam wall, likely from seepage through the TSF foundation or the dam wall, contributed to slope instability.
- There was a lack of toe drainage or seepage control measures around the perimeter of the TSF.
- There was a lack of compartmentalization.
- There had been many changes in ownership, and therefore there was a lack of continuity of the TSF operating staff.
- There was a lack of regulatory oversight during the years of the TSF dormancy.

- There was a change in regulatory jurisdiction and a re-classification of the Jagersfontein tailings dam as an ordinary dam, which enabled re-mining activities to proceed outside of regular mining regulations.
- There was human error, including:
    - Failure to recognize warning signs, such as the development of seepage and erosion gullies in the area of the breach in 2019 (Torres-Cruz and O'Donovan, 2023).
    - Failure of the operator to listen to workers' concerns about overfilling of the TSF.
    - Dismissal of calls from residents about "rumbling sounds" hours prior to the failure (Brown and Van Wyk, 2022).

Some lesser known but valuable facility management defenses

Whistleblower policy

As discussed in the Jagersfontein case study, employees are often the first to realize if there is something seriously wrong with the TSF. However, it is not easy to speak up about this concern in front of their hierarchies, as it may lead to subsequent discrimination or disadvantage later on. Some people are also afraid of harassment and victimization. This will lead them not to report their concerns.

The Mining Association of Canada (MAC) and other statutory and vocational bodies and guidance (such as GISTM, 2020 – also embracing the principle of Free Prior and Informed Consent), encourage whistleblower policy and practice to enable employees and communities to raise serious concerns without fear. Moreover, this promotes openness, honesty, and accountability.

Change management procedures

Change management procedures are a key component of the operation and surveillance of a TSF. Any significant changes to ownership, regulatory oversight, operations, personnel, monitoring, or design require a change management procedure. Change management systems, processes, and procedures are specified in several sections of GISTM 2020 and ICMM 2021.

Significant risks are associated with the TSF when changing key personnel (e.g., Engineer of Record, Responsible Tailings and Facility Engineer, etc.). Apart from this, a procedure should be developed for mine ownership and production changes. The Jagersfontein disaster showed the tragic consequences of not having these change management procedures in place.

Compartmentalization as an operational defense

The TSF that consists of a single compartment does not present options for continued tailings operation in the event of a substantial malfunction with the TSF containment (i.e., overtopping failure, internal erosion,

etc., of an individual embankment). Multiple compartments would assist in an emergency. One hates to repeat the cliché "Don't put all your eggs in one basket" – however, it was never truer than in this case.

Documented and detailed contingency planning

No tailings management plan should be without early and comprehensive contingency planning. Contingency measures for tailings deposition are considered an essential feature of tailings planning, without which the operator is left with little defense in the case of an operational upset, site incident, flood event, or other extreme situation. The greater the risk of upset events or conditions, the more effort should be applied to contingency planning.

Some example components of contingency planning include:

- Hard and soft copies of maps, the Emergency Preparedness and Response Plan (EPRP), Operation Maintenance and Surveillance (OMS) documents, the Design Basis Report (DBR), Risk assessment documents, and other emergency documents should be available and easily accessible at the TSF. With these emergency documents, a "war room" must be prepared for an emergency situation when digital records may be inaccessible.
- A secondary power source, availability of mobile plant, heavy equipment, and emergency materials should be on standby for the TSF to tackle emergency situations.
- A backup of human resources for emergency situations is required, especially for key operational personnel.
- Communication procedures with the downstream population and emergency services should be developed. An early warning system and a formal flood notification procedure should be in place to warn anyone located downstream. This should also include table-top and on-site practical drills and rehearsals.

Specialist training for key operations personnel

Successful commissioning of a tailings facility is a key foundational aspect of a stable and well-maintained TSF. By establishing and communicating clear design, construction, and commission-staged goals, the personnel involved in the TSF can understand and operate in the best interests of facility performance.

Additional precautions

When commissioning a TSF, there is a heightened requirement for foresight so that design engineers, owners, and operators can understand and implement the best methods to mitigate the creation and impact of a banana skin or fine silt layer. Accordingly, a few further precautions are emphasized below:

- Ensure that the tailings material has been comprehensively characterized and accounted for in the facility design. In the absence of such characterization, the design must be developed with an abundance of caution and precaution in mind.
- Ensure that the initial depositional volumes during commissioning are monitored and surveyed for quality assurance/control studies to confirm the design engineers' assumptions, especially in regard to production tonnages, water volumes, tailings PSD, slurry density, and beach slope.
- Manage deposition so as to reduce the likelihood of poor-quality material eroding and damaging facility defenses. Examples include the use of wing walls, buttresses, sacrificial beaches, swales, and bypass lines.
- Ensure the area of beach is large enough, and available soon enough, to accommodate rate of rise limitations and maintain minimum beach lengths. The beach is also used to control pond location, limit migration of the supernatant pond, prevent overtopping and, under normal operating conditions, to create and maintain above-water tailings deposition.
- Ensure drainage measures and design features are well established and protected through commissioning and operational phases.
- Practice careful vigilance in regard to the development and application of change management procedures.

Conclusion

The Jagersfontein tailings failure in 2022, and more recent heap leach failures at Çöpler Mine in Turkey in February 2024 in which nine lives were lost, and at Eagle Gold Mine in Yukon in June 2024, are unfortunately showing that our defenses continue to need substantial improvement. It may be argued that TSF owners who are members of or subscribe to the ICMM Tailings Practice Standard (ICMM 2021) and GISTM (2020) and other newly revised jurisdictional regulations have upped their game considerably, and that standards in this sector have improved significantly. However, this represents less than 5% of all the TSFs worldwide. As an industry we clearly still have a long way to go, to get to zero harm.

This paper has listed several practical remedies to improve the defenses of tailings structures. At the same time, there has to be a concomitant shift in dam safety culture towards duty of care and attention to detail in many areas, including change management procedures, contingency planning, operator training, and community and employee awareness.

While several mine owners have embarked on the arduous journey to true closure of tailings structures, far too many dormant structures have simply been abandoned. Stronger action is needed to ensure that our industry leaves a positive legacy for future generations.

Acknowledgments

The authors wish to express our thanks to our clients, our associates in the industry, and our colleagues at Thurber Engineering for their support, collaboration and insight, which contributed to this paper.

References

Alonso, E. and Gens, A. 2006. Los Frailes Anzacóllar dam failure part 1 field observations and material properties. *Géotechnique* 56(3): 165–183.

Banya, N. 2022. Troubled South African tailings dam had history of high water levels. Accessed 22/05/2024 at https://www.reuters.com/world/africa/troubled-south-african-tailings-dam-had-history-high-water-levels-2022-09-12/

Boswell, J.E.S. and Sobkowicz, J.C. 2011. Duty of care applied to tailings operations. Plenary Paper in *Proceedings of Tailings and Mine Waste, 2011.* Vancouver, November 2011.

Boswell, J.E.S. and Sobkowicz, J.C. 2018. Leading versus lagging indicators of tailings dam integrity. *Proceedings of Tailings and Mine Waste, 2018.* Keystone, CO, September 2018.

Brown, M. and Van Wyk, D. 2022. Report on the Jagersfontein Tailings Disaster. Bench Marks Foundation.

GISTM. 2020. International Council on Mining and Metals (ICMM), United Nations Environment Program (UNEP), the Principles for Responsible Investment (PRI). 2020. Global Industry Standard on Tailings Management (GISTM), August 05, 2020.ju

ICMM. 2021. International Council on Mining and Metals (ICMM). Tailings Management Good Practice Guide, May 2021.

Lochner, M, Kemp, D., van der Walt, P., Matebesi, S., Cloete, J. Harris, J., Ang Li Ern, M. and Own, J.R. 2024. The catastrophic failure of the Jagersfontein tailings dam: an industrial disaster 150 years in the making. *International Journal of Disaster Risk Reduction* 109: 104585. Elsevier Ltd.

McRoberts, E. 2023. Questions and thoughts on liquified strength of sand: an overview. Keynote in *Proceedings of Tailings and Mine Waste, 2023.*

Morgenstern, N.R., Vick, S. and van Zyl, D. 2015. Report on Mount Polley Tailings Storage Facility Breach, Independent Expert Investigation and Review Panel. Victoria, Province of British Columbia, Canada. https://www.mountpolleyreviewpanel.ca/final-report

Njini, F. 2022. Dubai-based owner of South Africa mine waste dam probing beach. Accessed 22/05/2024 at https://www.bloomberg.com/news/articles/2022-09-11/dam-collapse-at-abandoned-south-african-diamond-mine-kills-three

Petley, D. 2022. The 11 September 2022 Jagersfontein tailings dam failure. The landslide blog. Accessed 22/05/2024 at https://blogs.agu.org/landslideblog/2022/09/12/jagersfontein/

Rivet, S. 2023. Preliminary survey report for Jagersfontein. Orthophotos, topographic surveys (DEM) and reconstructed surfaces produced from archive satellite imagery. PhotoSat Information Ltd.

Torres-Cruz, L.A. and C. O'Donovan. 2023. Public remotely sensed data raise concerns about history of failed Jagersfontein dam. *Scientific Reports. Springer Nature* 13: 4953. Accessed 24/05/2024 at https://doi.org/10.1038/s41598-023-31633-5

Writer, S. 2022. Jagersfontein mine owner Stargems says tailings was safe and secure. Accessed 16/09/2022 at https://www.miningmx.com/news/diamonds/50736-jagersfontein-mine-owner-stargems-says-tailings-facility-wassafe-and-secure/

Update on GISTM Implementation at BHP – Lessons Learned on the Journey

Chad LePoudre, BHP Group Ltd, Canada
Tenaya Brown, BHP Group Ltd, USA
Justin Willis, BHP Group Ltd, Australia
Chris Sonntag, BHP Group Ltd, USA

Abstract

BHP Group Limited (BHP) is a multinational mining and metals company headquartered in Melbourne, Australia, and a founding member of the International Council on Mining and Metals (ICMM). This paper summarizes BHP's journey and lessons learned through implementation of the Global Industry Standard on Tailings Management (GISTM) across a global portfolio of multiple operating and legacy assets. BHP self-declared conformance with GISTM for its 22 very high and extreme consequence tailings storage facilities (priority TSFs) in August 2023, and is working towards conformance for the remaining TSFs by August 2025. BHP is also currently progressing the independent validation component of GISTM conformance for the priority TSFs.

Three broad topics are included in this paper: (1) BHP's GISTM journey, including internal and external work; (2) challenges and lessons learned from technical and non-technical perspectives; and (3) summary of findings and next steps.

This paper highlights the complex and iterative nature of GISTM implementation across the organization and highlights the importance of ongoing support and continuous improvement initiatives. An emphasis on lessons learned and practical solutions to technical and non-technical challenges faced by BHP is intended to contribute to the industry knowledge base around good tailings management practices.

Introduction

The Global Industry Standard (the standard) on Tailings Management (GTR, 2020) was publicly released in August of 2020 by the Global Tailings Review (GTR) panel, co-convened by the International Council of Mining and Metals (ICMM), the United Nations Environment Programme (UNEP), and Principals for Responsible Investment (PRI) (GTR, 2020). As a founding member of ICMM, BHP is committed to demonstrating alignment with GISTM across our global portfolio of tailings facilities.

BHP operates a portfolio of 74 tailings storage facilities (TSFs) including 22 very high and extreme consequence TSFs (referred to as priority TSFs). BHP self-declared conformance with GISTM for its very high and extreme consequence TSFs in August 2023, and is working towards conformance for the remaining TSFs by August 2025. This paper highlights the GISTM implementation approached adopted by BHP and describes the alignment framework, internal and external workstreams, challenges and lessons learned from technical and non-technical perspectives, summary of findings, and opportunities for next steps. BHP is on a journey of continuous improvement in tailings management, including GISTM implementation and conformance. The intent of this paper is to contribute to the industry knowledge base around good tailings management practices and share the learnings and potential opportunities for continuous improvement identified though BHP's experience with GISTM implementation.

Overview of BHP's GISTM journey

Background

Preparation for implementation of GISTM within BHP began before GISTM was published. First, as an ICMM member, BHP had the privilege to participate in the review of various versions of the GISTM drafts. For each version of the drafts, internal Subject Matter Experts (SMEs) reviewed and provided comment on components of the standard respective to their expertise. These comments were collated and provided to an ICMM coordinator who, in turn, collated all comments received from ICMM members and then submitted these comments to the GTR panel. It was important to BHP to participate in this process so that we had an early opportunity to understand the content, could participate in advancing good tailings practice, and to help ensure that the standard was also practically achievable. The achievable portion was important to BHP for our own facilities, but we also recognized early the importance of achievability in not discouraging non-ICMM members from GISTM uptake. BHP was also among ICMM members that began working on documents to support GISTM implementation, namely the Tailings Management Good Practice Guide (ICMM, 2021a) and Global Industry Standard on Tailings Management Conformance Protocols (ICMM, 2021b) (more discussion below).

BHP's approach

BHP operates in accordance with the three-lines assurance process (IIA, 2020). BHP's operating model places a large degree of autonomy on the individual asset (first line), supported by group level functional teams such as the centralized tailings excellence (TEx) team (second line), with occasional reviews by an internal audit team with accountability to the board (third line). Figure 1 describes the types of roles and responsibilities typically associated with each line (BHP, 2022).

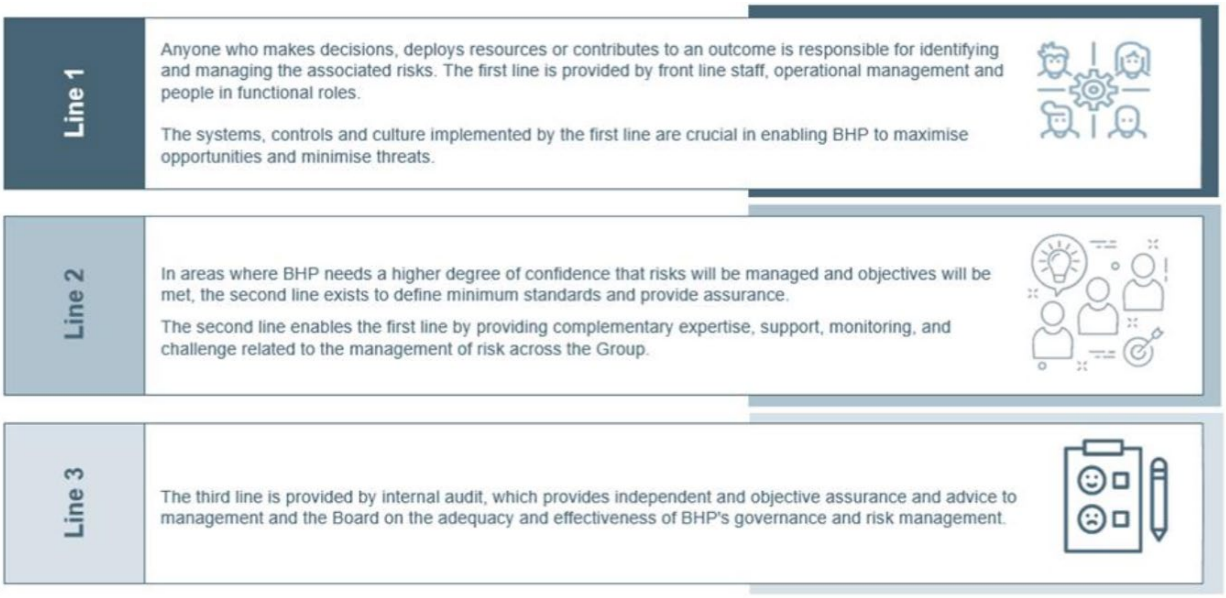


Figure 1: BHP three lines model (BHP, 2022)

For GISTM each asset was responsible for conformance themselves, as they own the work within the first line. The central TEx team provided support, coordination, and guidance, and collected and summarized implementation progress for reporting to BHP management. BHP's approach to GISTM alignment began with the creation of a board-endorsed tailings management policy and revision to our internal Global Standard for tailings, specifying the need to conform with GISTM. The TEx team prepared and updated guidance documents, prepared a GISTM "Mapping Tool," and consulted with internal stakeholders on the rollout and conformance as part of defined second line activities. The mapping tool was a table that included each of the requirements, conformance protocols, examples of evidence for conformance, and multi-disciplinary resources (internal and external) to assist the asset with implementation of each of the GISTM.

BHP assessed conformance to GISTM based on a number of principles, described in full in our Public disclosure document (BHP, 2023), and summarized below:

- Conformance is based on evidence that demonstrates that the understood intent of the GISTM requirement criteria have been met with underlying systems, processes, and practices in place to meet the requirements.
- Requirements may be assessed as not applicable in specific situations.
- Major engineering works required to meet a GISTM requirement scheduled for completion beyond the ICMM timeframe are considered acceptable with a suitably detailed and prioritized work plan.
- For requirements that reflect on-going processes (for example requirements 1.2, 1.3, 3.1, 5.8, 6.1, 6.2, 9.3, 13.4, 14.2 – 14.5, 15.2 and 15.3), a "Meets with a plan" level of conformance is acceptable

when can be demonstrated that the work has been substantially progressed and is supported by systems and processes. Additionally, in the event of a tailings facility failure, there should be no realistic prospect that claiming conformance for these requirements could be considered as a potential cause of failure. Where processes are in a cycle of review and updated in accordance with BHP's regular business practices, evidence that reflects that current practices and demonstrates systems and processes are in place that meet the intent of the requirement, will be taken as conformance.

For sites with very high or extreme consequence classifications (Prioritized Sites), BHP set internal conformance deadlines leading up to the August 2023 deadline. These internal deadlines provided time for internal review and verification of the self-assessment outcomes and provided evidence. Sites with high or lower consequence classifications are now in the process of being brought into alignment with GISTM requirements, with an internal target date of December 2024. To facilitate learnings across assets, a GISTM champions group was established with regular routines for the sharing of experiences and approaches between the asset teams.

Internal work

The conformance push leveraged internally developed mapping and self-assessment tools that were informed by the Tailings Management Good Practice Guide (ICMM, 2021a) and Global Industry Standard on Tailings Management Conformance Protocols (ICMM, 2021b). The tools were utilized to conduct gap assessments and identify work streams for each tailings facility to achieve conformance. Identified work streams were either completed by site teams or contracted to external parties. The internal work focused on updating and developing documentation and driving further integration between the tailings team and other functional groups within the organization, including Health, Safety and Environment, Corporate Affairs, Tailings Excellence, and the Accountable Executive. Externally contracted work focused on production of documents such as the DAR, DBR, etc.

The TEx team coordinated regular meetings (approximately every two weeks) with asset representatives that had accountability for GISTM conformance. These representatives were referred to as the "GISTM Champions." The meetings covered a wide range of topics, but were nearly always focused on various technical issues and challenges associated with GISTM implementation. This forum also allowed for the sharing of lessons learned between assets, where some assets had advanced various portions of GISTM already. Needs of the assets were discussed, such as resourcing support or additional guidance needed, and the TEx team would work to help facilitate solutions.

During the conformance push, a quarterly self-assessment and audit readiness review was conducted by each asset. The review enabled the asset teams to track progress towards conformance and capture any

lessons learned or guidance from the organization. It also facilitated benchmarking from a quality perspective and effective resource allocation to ensure sufficient progress was being accomplished across the portfolio.

External work

BHP was also among ICMM members that began working on documents to support industry GISTM implementation, namely the Tailings Management Good Practice Guide (ICMM, 2021a) and the Global Industry Standard on Tailings Management Conformance Protocols (ICMM, 2021b). The Tailings Working Group of ICMM facilitated a series of meetings between member companies to conduct knowledge shares on technical subjects related to GISTM. Further, ICMM prepared training materials, including videos of voiceover presentations to support the Good Practice Guide. It may be noted that the Good Practice Guide, the Conformance Materials, and the training materials were made available, free of charge to anyone, on the ICMM website.

A key component of the GISTM conformance push for many assets was further defining the scope of support required from the Engineer of Record (EOR) and Independent Tailings Review Board (ITRB). While much of this understanding and capacity was already developed, some asset teams had to appoint and empower new resources to achieve conformance. In several instances, GISTM requirements required substantial increases in external resource utilization to generate and/or consolidate the necessary technical information in an auditable format.

While the preparation for GISTM was focused on preparing for external independent conformance validation, BHP's August 2023 conformance declaration was based on self-assessment results. To provide confidence in the self-assessment results, BHP ran a verification program using an external auditing team that reviewed a sample of evidence across the GISTM requirements and high priority TSFs. This verification was completed toward the end of 2022, with several technical and non-technical lessons learned from this verification program. These items will be discussed in the following sections.

Challenges and lessons learned

Throughout BHP's GISTM journey, there have been many challenges and lessons learned ranging from detailed technical aspects to non-technical items such as approvals processes. This section presents the technical and non-technical challenges and lessons learned, compiled from the authors' personal experiences and the results of a detailed questionnaire sent out from TEx to the priority TSF teams after GISTM declaration.

GISTM survey results

Following completion of the GISTM self-assessed conformance declaration, TEx solicited feedback from

the assets through a survey, with responses received from three assets. The survey questions and feedback are summarized in Table 1.

Table 1: Survey results

Questions	Survey response summary
What was the one, most challenging part of GISTM implementation from your perspective?	Three consistent challenges were noted across assets. (1) ALARP, (2) definition of conformance, (3) internal reporting requirements.
Were the ICMM conformance protocols useful, did you refer to them at all or often?	Yes. The conformance protocols became a key element of demonstrating conformance rather than achieving compliance. Particularly during external verification.
Was the ICMM Good Practice Guide helpful?	Yes. However, not to the extent of the conformance protocols. Served as more of a reference guide than a driver for work.
Was the BHP mapping tool helpful? What changes would have helped?	Yes. However, several improvement opportunities were noted. These opportunities led to some updates to the mapping tool and other available resources.
Did you find that BHP OR, standards and/or guidance notes were helpful with implementation of GISTM? Please provide comments.	The guidance documents were found to be useful, but often not released sufficiently early. In some cases, changes to guidance documentation caused re-work.
Did you get adequate support from asset leadership with conformance?	Yes. However, several assets noted that coordination and communication was challenging due to changes in leadership positions over the period.
Would additional communication from TEx to asset leadership be helpful? Suggestions?	Assets requested continual support around GISTM effort rather than a one-off, as well as additional guidance on how to communicate the ALARP journey to senior management and the Accountable Executive.
Was support from TEX helpful, and/or what additional support from TEx or other functions would have been helpful?	Several assets suggested that sharing examples of "what good looks like" for various requirements could be helpful and improve practices across the organization.
The Public Disclosure details will need to be verified every year. How did you find the process this time? What would you suggest could be done to improve it?	Development of a routine with long lead times and a consistent approach were identified as key improvements. Some challenges were noted around the requirements changing through implementation.
Were you given sufficient opportunity to review and comment on the public disclosure?	The assets had mixed results but indicated that more time may have been needed if major changes to the public disclosure had been required.
An audit readiness review is now needed to internally verify conformance, prior to external and public auditing (such as GTMI). Do you have suggestions for this review?	Clarity around scope and timing was requested and emphasis was placed on communicating BHP's understanding of current conformance.
What would you do differently for GISTM conformance next time?	Two primary items were noted: (1) Improve efficiency to gain approvals and sign-offs with asset leadership teams and Accountable Executive, (2) ensuring timely guidance and resourcing based on asset needs.

Questions	Survey response summary
What went well with the GISTM conformance process?	Substantial organizational support for GISTM conformance push, starting early on key scopes, approvals, and processes.
Please rank difficulty (low, medium, high) and provide comments regarding the 15 principles of the GISTM	A relatively wide variety of responses were recorded. Principles found to present a **high** level of difficulty were: **Principle 3: Design, Construction, Operation and Monitoring of the Tailings Facility.** This presented a challenge at some sites due to the level of engagement required with the Accountable Executive. **Principle 15: Publicly disclose and provide access to information about the tailings facility to support public accountability.** This was difficult because of the number of reviews, changing templates, and multiple iterations for each disclosure. Principles found to present a **medium** level of difficulty were: **Principle 1: Respect the rights of project-affected people and meaningfully engage them at all phases of the tailings facility lifecycle, including closure.** This was identified as an early struggle before appropriate SMEs and functional groups were brought in to support the efforts. All other Principles were either found to require **low** effort or were not commented on by the assets.

Technical challenges and lessons learned

Technical challenges to achieving GISTM conformance were primarily related to interpretation of the requirements and understanding what level is considered sufficient to meet the intent. While the Conformance Protocols and Good Practices guides were useful references, in practice they provided sufficient flexibility for organizations to incorporate their own risk frameworks and operating standards, which meant that different interpretations and views of conformance could exist. At BHP this flexibility was leveraged to update existing processes, systems, and documents to make them suitable for GISTM, rather than wholesale creation of new systems and documents. This reduced the workload on the asset teams, while ensuring sustainability of the GISTM implementation. Using existing systems, process and documents did present a number of challenges though, specifically with the Deviance Accountability Reports (DAR) and ALARP. Design Basis Reports (DBR) also presented challenges at some legacy TSFs, where construction design basis and documentation are often limited. These challenges and lessons learned are discussed in more detail below.

Definition of conformance

There was challenge within BHP, and the mining industry, regarding the definition of conformance. For

example, there are different interpretations and intent behind the words "compliance" and "conformance," or "verification" and "validation." For many of the requirements of GISTM, it is difficult to meet the higher standard associated with "compliance" and "verification" as compared to "conformance" and "validation." For example, Requirement 2.2 pertains to site characterization, but all persons associated with tailings management will understand that site characterization is almost never complete (perhaps only in some instances of passive closure). Similar challenges exist with many other requirements. Therefore, BHP's position regarding conformance was based on the principle of "where work is substantially progressed and supported by systems and processes."

Using Requirement 2.2 again, if it was demonstrated that a site characterization was substantially progressed in accordance with the requirement, and there was an effective governance and assurance system in place (EoR responsible for the site characterization, ITRB periodically reviewing the site characterization and assessing gaps, Dam Safety Reviews conducted on schedule, etc.), then the Requirement would most likely satisfy the "meets" threshold. Therefore, an asset could conform with the requirement where they could demonstrate good practice, even if there was work in progress to address potential gaps in knowledge identified through the aforementioned processes and systems. Further, independent validation could be conducted using the same criteria.

There were some who disagreed with this approach, both within and external to BHP, creating one of the significant challenges experienced and even becoming the topic of some discussion at ICMM Tailings Working Group meetings. Persons who dealt with other sustainability commitments were more accustomed to the compliance model. However, other sustainability initiatives tend to apply to a more policy-oriented approach, with questions such as "does a human rights policy exist?" where GISTM requires companies to "conduct human rights due diligence to inform management decisions throughout the tailings facility lifecycle and address the human rights risks of tailings facility credible failure scenarios." Since management decisions are ongoing and credible failure scenarios are constantly being reviewed and revised, BHPs position was that evaluation of conformance with the requirement is more appropriate than compliance.

The independent validation process is the quality control on this approach to conformance. BHP is now going through the process of independent validation of conformance using independent consultants, in accordance with the ICMM Conformance Protocols. The evidence for each requirement is reviewed and those independent reviewers provide feedback to BHP on whether the criteria for conformance has been met.

Interpretation of GISTM requirements

The BHP guidance documents to support GISTM interpretation sought to provide sufficient guidance so

that GISTM was interpreted and implemented consistently across the assets, and was aligned with BHP's overarching risk and governance frameworks without introducing rework, while also providing enough flexibility to be implemented leveraging asset specific systems, processes, and documents. In practice this was a tight balancing act that was difficult to get correct, with some guidance ending up being too broad, while the more specific guidance did not cover every situation present in BHP. As noted in the survey feedback, the guidance was sometimes not issued in a timely manner, and a number of opportunities for improvement have been identified that are currently being addressed. While developing guidance documents is not necessary to achieve GISTM compliance, guidance and support from the second line enables adoption of a consistent approach to GISTM across an organization, more efficient use of existing systems and process, and alignment with overarching BHP frameworks.

Legacy TSFs

Demonstrating conformance for legacy TSFs presented a significant technical challenge as many of the facilities are between 50 to100 years old and/or were never operated by BHP. Many supporting technical documents met the intent of GISTM but were not in a state that enabled easy verification or auditing. Characterization studies and reports, design documents, and construction records and details were often limited in scope, partially complete, or unavailable. While legacy TSFs did have sufficient detail within the knowledge base to make a determination on the TSFs integrity, the data was not in the formats specified in GISTM such as the DBR, DAR, CDIV, etc. When considering the evidence needed to demonstrate conformance, it became necessary to make judgement calls on if/when to conduct additional characterization data, complete additional engineering studies and when necessary, remediation projects, all the while considering resource availability.

Additionally, many communities and first responders located near legacy assets had a limited history of engagement with the sites. "Principle 1: Respect the rights of project-affected people and meaningfully engage them at all phases of the tailings facility lifecycle, including closure" (GTR, 2020) required tailings SMEs for legacy TSFs to generate alignment with Corporate Affairs on the best approach to GISTM as external discussions around tailings and their potential impacts should proceed on the shoulder of established relationships with communities and first responders.

Design basis reports (DBR)

DBRs for operating facilities were generally already developed and met the intent of GISTM. However, at many legacy sites, the basis of design was not documented, and documentation to support a design basis was found across a variety of different documents. Further, in many cases, documenting the design basis required additional geotechnical and environmental characterization and analysis to fill gaps in the existing knowledge base. One of the approaches adopted by BHP was to implement a Knowledge Base Report

(KBR) in lieu of the DBR at some sites. The KBR compiles references to relevant historical documentation, including available as-built and characterization documentation, operational history and design or assessment criteria. It is structured similarly to a DBR but focuses on leveraging existing documentation and ensuring that is categorized and available in a manner that meets the intent of the DBR, rather than summarizing the information found in each report across a long operational history. This practice was found to be effective and supported demonstration of conformance with several other GISTM requirements.

As Low as Reasonably Practicable (ALARP)

From a technical perspective, the demonstration of ALARP was, and continues to be a key challenge across assets along the GISTM journey. The ALARP concept involves highly subjective terms, and there are a number of ways to demonstrate that risks have been reduced to ALARP. For BHP, the desire was to use existing site and BHP wide systems and process as much as possible, while also aligning with BHP's risk management framework, reflected in the guidance developed by the TEx team. After an approach had been developed each TSF needed to be considered to assess if the risks could be demonstrated as being at ALARP or not. Key to demonstrating ALARP is an assessment of risk reduction options and a decision on whether to proceed or not with these options. This required extensive internal communication and engagement, including with asset leadership and the Accountable Executive. Prompt and proactive planning and communication regarding risk and risk status are considered key to successfully meeting Requirement 5.7 of GISTM.

Non-technical challenges and lessons learned

Throughout the GISTM journey, multiple non-technical challenges and lessons learned were identified. These consisted of managing the large volume of evidence, obtaining management support and buy-in on our GISTM journey, generating required approvals from the Accountable Executive and delegates, developing consistent approach across BHP, managing workloads for EoRs and internal teams and reporting status of implementation. These are discussed in detail below.

Evidence management system

To demonstrate conformance to GISTM, many pieces of evidence need to be prepared, compiled, reviewed, approved, and ultimately issued for external validation. BHP elected to use an internal web-based tool for managing evidence for the assortment of external standards that BHP has committed to comply with. This tool, called the Sustainability Standards Portal (SSP), while not exclusively for GISTM, was under development concurrently with assets working towards priority TSF conformance, with the GISTM evidence a trial use of the tool.

Three key challenges arose during implementation. (1) Addressing issues and bugs with the new tool as the evidence was being uploaded; (2) rolling the tool out to assets; and (3) providing user training on the tool. After rollout, assets provided feedback on the system and were able to identify several improvements that have positively influenced efficiency and usability of the tool. Key improvements included updates to the Quick Reference Guide, development of SSP training videos for new and existing personnel, allowing for bulk processing and downloading of documents and data, and changes to some of the validation and comments functions to improve user experience. While the tool provides improved long-term documentation and auditability, additional resources and time were needed for uploading, verifying, and approving conformance documentation that put a strain on several assets.

Management support and buy-in

Obtaining asset leadership support and buy-in around GISTM presented a challenge, particularly at operating assets. For example, in one instance an asset asked, "Who do you think you are and why do you think you can make us do this?" In these cases, asset leadership was primarily concerned with costs, potential impact to production, and complexity from changes or improvements to operating systems and procedures. Tailings SMEs consistently found that communicating the "why" behind many of the new requirements was necessary. Early and proactive communication was determined to be the most effective approach to generating buy-in. Buy-in was also achieved through being able to clearly and accurately demonstrate how GISTM conformance activities impacted cost, production, and risk outlook at the site. However, it was also necessary to have established commitment to GISTM from BHP executives in writing to demonstrate to assets that this was not an optional exercise. It was also noted that some "healthy tension" between management and technical SMEs was a good thing as it pushed asset leadership to improve understanding and support for good tailings management practices, while also motivating technical SMEs to be efficient and well thought-through in their approach.

Approvals – accountable executive and asset management

Developing a clear, consistent mechanism for asset management and Accountable Executive approvals required substantial coordination and communication from TEx and tailings SMEs. Three primary challenges were encountered when obtaining AE and management approvals. (1) Upward communication and acceptance of the role and responsibilities of the accountable executive; (2) defining the delegations and approvals framework and process; and (3) obtaining signoff on required documents in a timely manner.

Once the delegations and approvals framework has been developed, the most influential and effective approach to obtaining approval/signoff was the generation of a single signoff package rather than obtaining approval on each required deliverable separately. As the Accountable Executives spanned multiple assets, the signoff packages needed to be relatively consistent across each asset and need to have a structure that

enabled key site-specific information to be communicated succinctly. In addition, practitioners needed to be prepared when engaging directly with the AE and senior leadership to answer questions or concerns in a format specified by management.

Developing consistent approach across BHP

BHP's asset lead GISTM approach was accompanied by the risk that each asset would interpret the requirements differently, resulting in different standards across BHP. As noted above, this risk was managed by the development of guidelines, and a verification program run by a third party. As this was the first time implementing the standard, the internal guidance was not able to address all scenarios and required updating, which resulted in re-work for some assets. The verification program identified areas of inconsistency that required re-work also, and the timing of these updates resulted in short timeframes for updating ahead of the GISTM implementation deadline. The journey to achieve a consistent standard across BHP continues, and additional planning for the non-priority TSFs is underway in an attempt to avoid repeating the same level of re-work.

Managing workloads

Throughout the GISTM journey, challenges with tailings team workload were encountered, due in part to the limited availability of experienced tailings practitioners within both operations and consulting functions. A balance needed to be found between managing the projects and technical studies that would improve tailings facility safety and mitigate risks, and preparing evidence to support implementation and report GISTM progress. Simplifying and improving internal tracking and reporting systems to enable the site teams to focus on TSF integrity was a key lesson, while making sure that the validation team has suitable experience to assess implementation as opposed to simply box ticking. As noted by the ICMM conformance protocols, this reduces the need for "bullet proof" evidence.

To achieve conformance two of BHP's assets created specific GISTM positions or teams, while the remainder managed the workload within existing teams. Where the workload was managed within existing teams, this was often accompanied by greater use of the EOR and external consultants.

For the GISTM requirements requiring support from the EoR or other external consultants, deliverable timeliness and quality became a challenge in many instances due to the sheer quantity of work and the need to prioritize work, resulting in short turnaround times on certain work scopes. It was found that in an era of high workloads for experienced consulting support, early planning, communication, and prioritization of work leads to better outcomes.

Summary of findings and next steps

This section summarizes the TEx survey results, technical and non-technical challenges and lessons learned

as discussed in the sections above and the next steps identified within BHP. The survey was conducted across varying assets and teams and showed that technical guidance and resources related to the GISTM conformance push were generally appropriate and available. However, the survey also indicated that ALARP, demonstration of conformance, and internal reporting requirements were often challenging to implement. Principles 3, 14, and 15 were found to be the most difficult with a rating of "high" and Principle 1 was rated the next most difficult with a rating of "Medium." All other Principles were rated as "low" difficulty or not commented on by the assets.

Several technical and non-technical challenges and lessons learned were identified along the GISTM journey. Technical challenges primarily consisted of interpretation of GISTM requirements, developing DBRs, demonstration of conformance at legacy TSFs, and ALARP. In many instances, these challenges were interconnected and interdisciplinary in nature, which required extensive coordination and collaboration between the business, SMEs, and internal and external stakeholders. Technical lessons learned were to focus on obtaining early and thorough technical guidance, using benchmarking across sites to determine what "good" looks like, and setting up clear routines/cadence for updates and review of documentation.

From a non-technical perspective, challenges primarily consisted of developing and implementing an evidence management system, obtaining management support and buy-in, clarity on the approvals process with senior management and the accountable executive, developing a consistent GISTM conformance approach across the organization, and managing workloads. Lessons learned focused on early and proactive communication around GISTM, and the importance and necessity of defining routines, expectations, and lead times that are reasonable and achievable. Further, it is important to continue to integrate GISTM alignment as it is a continuous process rather than a destination and one-time conformance push. A key portion of the lessons learned was also the ability and advantage of leveraging experience from the 2023 conformance push for high priority sites to the 2025 conformance push for lower priority sites.

As BHP moves towards conformance for all TSFs by August 2025, we are updating all relevant guidance, maintaining routines for sharing lessons, tracking progress of conformance, and scheduling out key engagements and internal deadlines considering the lessons gained from the priority TSFs.

Conclusion

Throughout the GISTM journey, BHP personnel committed to an immense amount of internal effort and external coordination to achieve conformance for the high priority sites by 2023. As part of the continuous improvement process, the lessons learned along the way have been incorporated into the conformance push for low priority sites that is currently underway. Three topics were included in the paper: (1) BHP's GISTM journey, including internal and external work; (2) challenges and lessons learned from technical and non-

technical perspectives; and (3) summary of findings and next steps.

This paper details the complex and iterative nature of GISTM implementation across the organization and emphasizes the importance of ongoing support and continuous improvement initiatives. The findings further herein illustrated the importance and benefits of maintaining a robust and integrated three lines of defense model that is supported at the highest levels of the organization. The emphasis on lessons learned and practical solutions to technical and non-technical challenges faced by BHP is intended to contribute to the industry knowledge base around good tailings management practices.

Acknowledgements

First and foremost, the authors would like to acknowledge everyone within BHP who has contributed their valuable time and effort to the GISTM journey. Without their tremendous effort and commitment, achieving GISTM conformance at all would not have been possible. The authors also acknowledge the thoughtful survey responses from various SMEs across the organization that are discussed in this paper. Their responses demonstrate an unbroken commitment to continuous improvement of tailings management practices. Lastly, the authors would like to acknowledge the support of BHP leadership along the GISTM journey. Their commitment to GISTM aligns with our core values of "doing what's right," "seeking better ways," and "making a difference" and has resulted in a strong and robust safety culture across the organization.

References

BHP. 2020. Water and Tailings Storage Facilities. Our Requirements. BHP Group Ltd.

BHP. 2022. Risk Management Guidance Note.

BHP. 2023. Tailings Management System – Legacy Assets. BHP Group Ltd.

GTR. 2020. Global Industry Standard on Tailings Management. Global Tailings Review.

ICMM. 2021a. Tailings Management Good Practice Guide. London: Internation Council of Mining and Metals.

ICMM. 2021b. Conformance Protocols Global Industry Standard on Tailings Management. London: International Council on Mining and Metals.

IIA. 2020. The IIA's Three Lines Model. The Institute of Internal Auditors.

Meteorological Inputs to Tailings Storage Facility Assessments and Risk Assessments – Experience and Lessons Learned

Bill Kappel, Applied Weather Associates, USA
Doug Hultstrand, Applied Weather Associates, USA
Andy Small, Klohn Crippen Berger, Canada

Abstract

As a result of the issuance of the Global Industry Standard on Tailings Management (GISTM) in 2020, the International Council on Mining and Metals Tailings Management Good Practice Guide (ICMM GPG), and ICOLD's Bulletin 194, Tailings Dam Safety, there is a drive to designing tailings storage facilities (TSFs) to handle the Probable Maximum Flood (PMF) during closure and, in many cases, during operations. Quantifying the effects of extreme precipitation and changing meteorological conditions on the safety of tailings storage facilities during operations and closure is critically important. This paper provides guidance with respect to the PMP and how climate change should be accounted for in the PMP estimate. Additionally, guidance is provided on how to couple wind speeds during extreme precipitation events to determine suitable freeboard.

Applied Weather Associates (AWA) has completed hundreds of site-specific PMP, precipitation frequency, and climate change assessments around the world; many for large dams and complex mining operations. These studies have included both deterministic and probabilistic evaluations. For TSFs with ponds, the results have been used to determine spillway adequacy and freeboard requirements, to understand water balance, to evaluate extreme precipitation depths and seasonality, and to provide input for evaluation of hydrologic runoff responses. These studies are also applicable for cover designs and designing erosion protection systems.

AWA develops the PMP following the storm-based approach, which provides deterministic values that are commonly used for evaluation of spillway adequacy and design. Until recently, these deterministically derived values did not have a probability associated with them, and therefore quantifying where those values fell within the risk spectrum was not possible. For nearly ten years now, AWA has applied a regional Lmoments process along with a stochastic storm transposition process to quantify the probability of the PMP depths. This also provides unique outputs that include several recurrence intervals,

including the 10,000-year event. This combination of deterministic and probabilistic outcomes is very valuable for assessing risks associated with a TSF.

Over the last few years, AWA has also included climate change projections specifically related to extreme rainfall and PMP. This presentation will provide details on PMP development, the application of probability assessments, and how climate change assessments are applied to those outcomes. These will be discussed with specific examples related to tailings storage facility safety. Several locations around the world will be considered. This analysis is very important for informing likelihoods in risk assessments.

AWA also has provided input to estimating the required freeboard that is required to protect from overtopping of tailings dams during extreme precipitation events. Proper consideration of extreme meteorological events (precipitation and wind) are key data inputs to assist designers and owners on how to best allocate funding for ongoing safe operations and closure.

The GISTM and ICMM GPG introduced the concept of credible failure modes, a key component of which is understanding if a potential failure mode is physically possible. This paper will provide input to physically impossible thresholds related to extreme precipitation events.

Introduction

Understanding and quantifying the hazards from meteorological and climatological events that can affect tailings storage facilities (TSFs) is critical to ensuring safety and reducing risk. Many of the meteorological and climatological inputs include a large amount of uncertainty and subjective judgement. It is very important that these analyses are completed by experienced and qualified experts in this field. Another critical aspect is communication of development process, areas of uncertainty, and how those affect results to the practitioners and regulators. Discussions in this paper will describe several of the key meteorological processes that are used for design inputs for TSFs. These include Probable Maximum Precipitation (PMP), precipitation frequency, climate change assessments, and wind speed assessments.

Probable Maximum Precipitation development

Probable Maximum Precipitation (PMP) is a critical input for estimating the Probable Maximum Flood (PMF) with a rainfall-runoff relationship, which is an input to hydrologic design. However, a deterministically derived PMP represents the theoretical upper limit of rainfall (WMO, 2009) which is based on subjective storm adjustments, uncertain storm analyses, and other meteorological judgements. Further, deterministically derived PMP depths have not included any probability or frequency of occurrence. Therefore, although PMP is often provided as a specific depth representing the best estimate for various durations for a given area size or location, it must be recognized that there is uncertainty around that value. Therefore, it is important to quantify areas of uncertainty in the PMP development process, determine the

effect of those uncertainties, communicate those uncertainties, and work with the engineering team to ensure reasonable application is completed. To further complicate the issue, climate change projections should also be evaluated to determine if they predict changes that are outside of the bounds of uncertainty and natural variability already accounted for in the PMP development process.

Since the early 2000s, Applied Weather Associates (AWA) has continued to refine the deterministically derived PMP depths to quantify uncertainty and reduce risk. Part of this process includes quantifying the amount of uncertainty associated with each major input parameter. These include selection of storms, storm transposition limits, storm adjustment factors, quantification of rainfall accumulation in time, space, and magnitude, and other key parameters. The range of variance of each of these can be evaluated and combined to provide a total amount of uncertainty around the best estimated PMP depths (Mikovic et al., 2015; Kappel et al., 2020; Kappel et al., 2023).

Another recent advancement AWA has refined to provide a probabilistic estimation of PMP is the process to calculate annual exceedance probabilities (AEP) for various durations out to 10^{-10}. This is completed by applying the regional Lmoments process and stochastic storm transpositioning process to develop statistically robust data sets from which to derive the required recurrence intervals with confidence bounds (Kappel et al., 2024). Deterministically derived PMP depths can then be plotted or compared to the AEP output to understand the rarity of the PMP depths. This provides a valuable sensitivity of the PMP depths, which can support risk assessments.

These processes are, of course, dependent on the amount, spatial coverage, and quality of data available. The more data available both spatially and temporally, the more accurate the results will be. This relates to the storm analyses, storm adjustments, precipitation frequency development, temporal characteristics, and spatial patterns.

The final piece of the puzzle is to test climate change projections related to extreme rainfall against the range of uncertainty that has been calculated using deterministic and probabilistic methods. AWA has completed nearly a hundred such studies globally using regionally downscaled models (RCM) derived from the suite of global climate models (GCM) available from the various Intergovernmental Panel on Climate Change (IPCC, 2017) outputs. Initial work used the 5th generation of models, CMIP5 (2017) and now uses CMIP6 (2021). This suite of climate change projections provides daily temperature, precipitation, atmospheric moisture, and other meteorological parameters needed to understand the amount and rate of change through 2100 that are important for PMP development. These projections can then be compared against the information derived from observational data and the baseline climatology of a given location. Recommendations related to the most likely outcome can then be developed and provided for evaluation and sensitivity analyses.

Example of deterministic PMP development

PMP depths are used in the computation of the Probable Maximum Flood (PMF) for relatively small catchments, generally for the design of high-consequence structures, such as TSFs. PMP depths developed in the example below were focused on the area size of the contributing basin to a TSF at a mine site in Utah (1.23-mi^2) as shown in Figure 1.1. AWA used our database of storm analysis and PMP information from adjacent studies that are specifically relevant to this location (Figure 1.1). PMP depth estimates calculated for this location were evaluated against the previous studies and regional work.

Methods used to derive PMP values included consideration of numerous extreme rainfall events that have been appropriately adjusted to the basin and representing each PMP storm type important for this location, local and general storms. Storm lists that have been previously applied and reviewed in detail by several independent review boards in adjacent studies were considered to develop the initial list of storms. These were evaluated in detail to determine which could potentially be important for PMP development for this particular basin (Figure 2). The large number of storm events covering a large spatial region and long period of record provided enough data from which to derive the PMP depths within an acceptable amount of uncertainty.

The process of combining maximized storm events by storm type into a hypothetical PMP design storm resulted in a reliable PMP estimation by combining the worst-case combination of meteorological factors which represent a PMP design storm that is physically possible over of the basin considered. The method assumed that a sufficient period of record was available to identify extreme storm events within the region and that at least a few of those storms attained or came close to attaining the maximum storm efficiency possible for converting atmospheric moisture to rainfall. In essence, the process is trading time for space to capture PMP processes.

The PMP development process assumes that if additional atmospheric moisture had been available, an individual extreme storm would have maintained the same efficiency for converting atmospheric moisture to rainfall. The amount of moisture is represented by available precipitable water in the atmosphere and is calculated by assuming a saturated atmospheric column based on observed dew points. Therefore, the ratio of the maximized rainfall amounts to the actual rainfall amounts would be the same as the ratio of the precipitable water observed versus the climatological maximum in the atmosphere associated with each storm.

It is important to remember that the methods used to derive PMP and the hydrological procedures which transform PMP depths into runoff need to adhere to the requirement of being “physically possible.” In other words, various levels of conservatism and/or extreme aspects of storms that could not physically occur in a PMP storm environment should not be used to produce combinations of storm characteristics that are not physically consistent in determining PMP depths or for the associated hydrologic applications.

Although the term "probable" is included in the PMP term, this does not relate to probability. Instead, it refers to the physical possible element associated with the design storm. Any PMP event is considered to be extremely rare and represent a physical upper limit of rainfall potential.

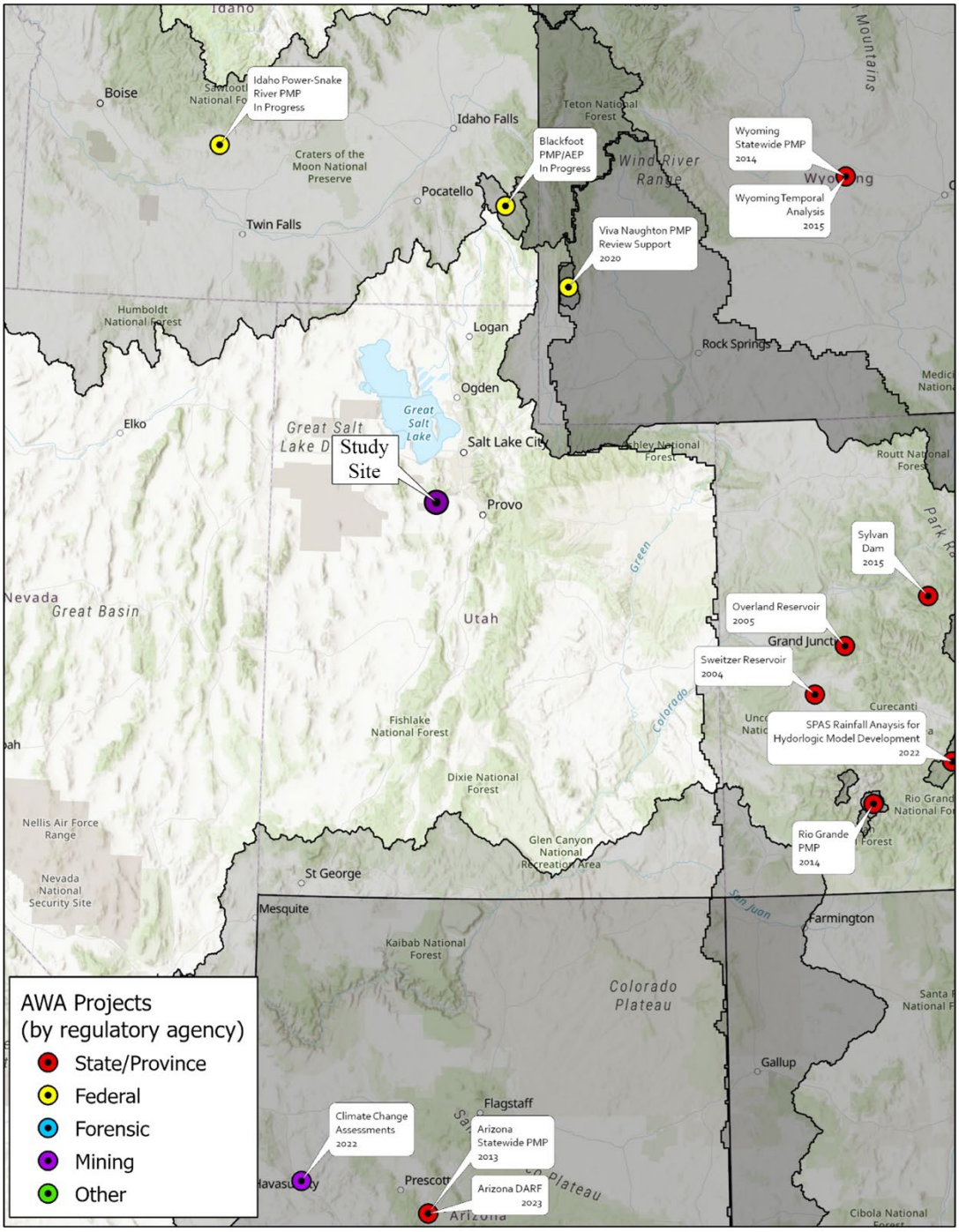


Figure 1: Probable Maximum Precipitation study location and surrounding studies that were evaluated for data

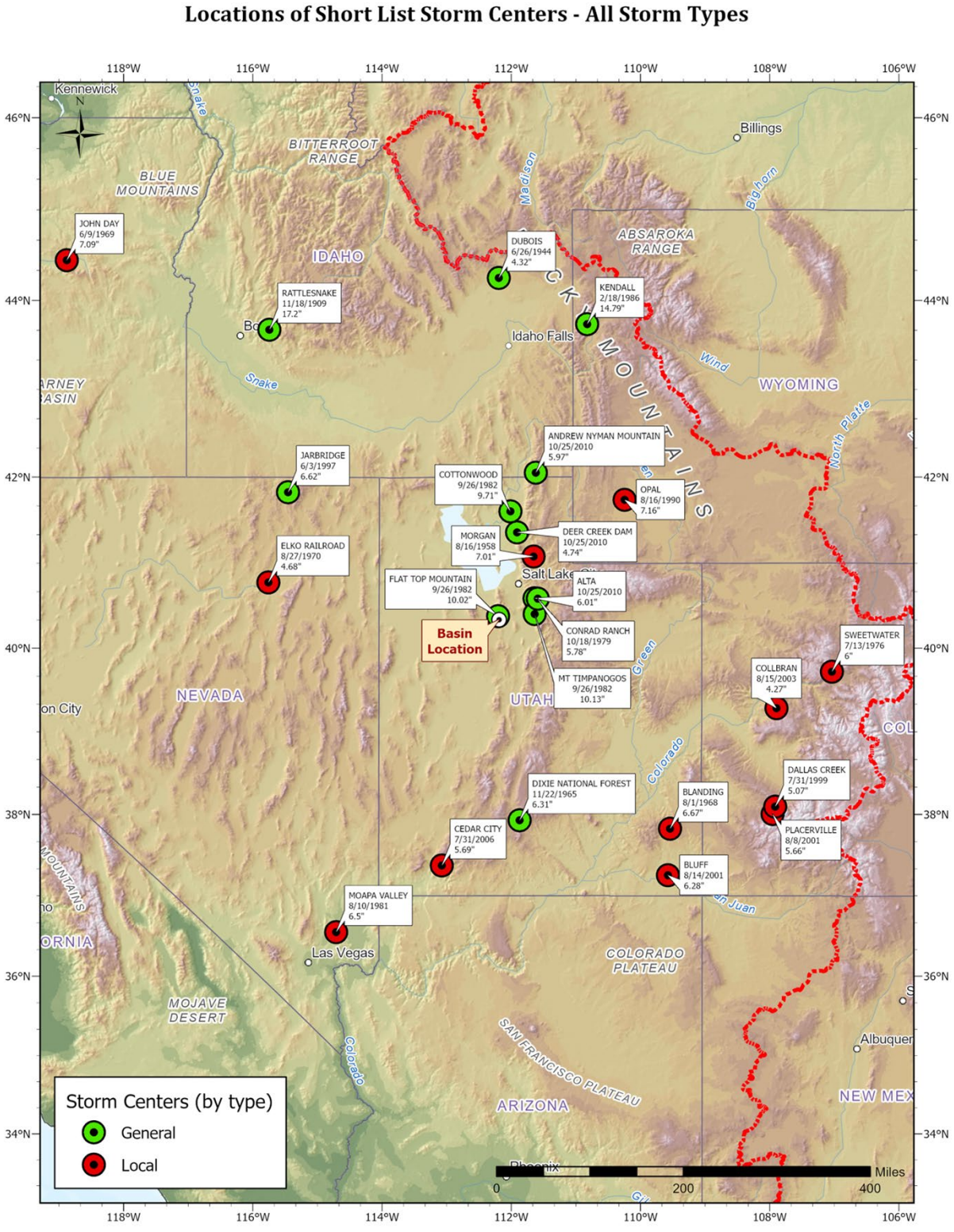


Figure 2: Locations of storm centers used for PMP development in relation to the basin location

To calculate the PMP, the Total Adjustment Factor (TAF) for each storm must be applied to the rainfall depths calculated using the Storm Precipitation Analysis System (SPAS) analyzed depth-area-duration (DAD) value for the area size and duration of interest to yield a total adjusted rainfall value. The storm's total adjusted rainfall value is then compared with the other total adjusted rainfall depths of every storm considered transposable to the basin location. The largest adjusted rainfall depth becomes the PMP for that point at a given duration. This process must be repeated for each applicable duration and storm type.

This study provides basin-specific PMP depths based on the area-size of the basin and the durations most relevant for PMF evaluations. Depth-duration charts plotting the adjusted rainfall depths for both storm types are provided in Figure 3 and Figure 4. The controlling storm for each duration can be determined from the depth-duration charts and it is important to note that several storms control PMP as the duration changes and there are generally a good number of storms supporting the controlling storm PMP depths.

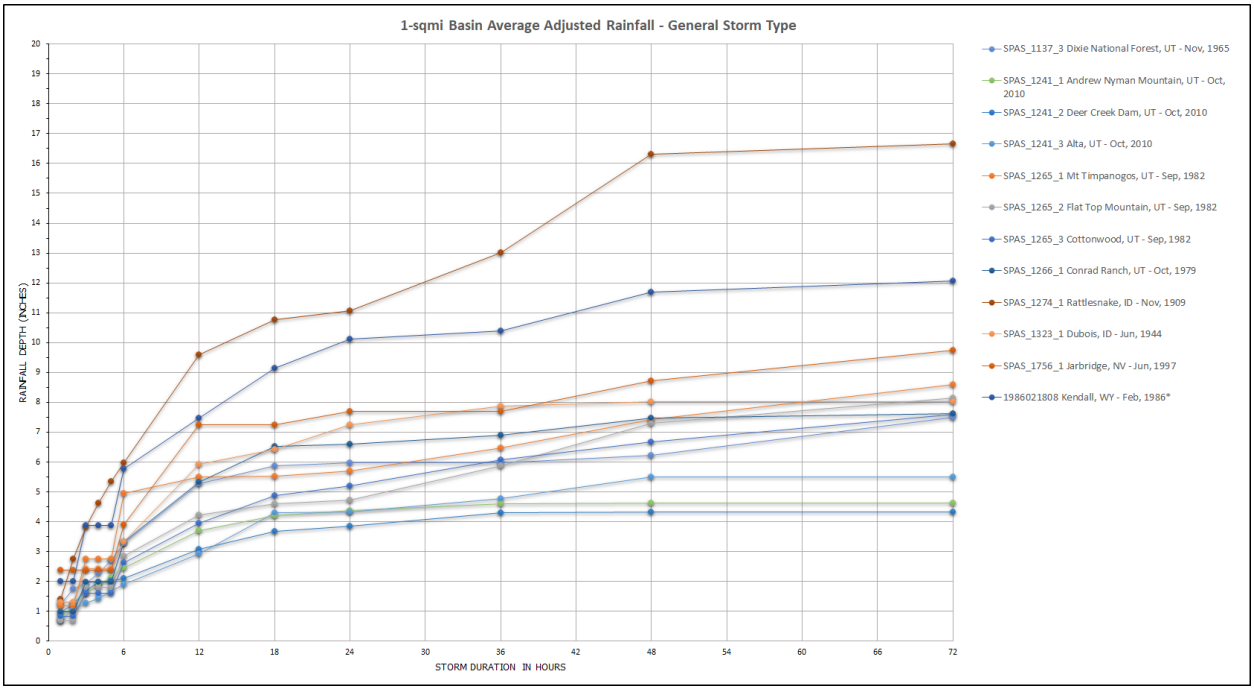


Figure 3: General storm PMP depth-area chart

It is important to note that a very specific combination of atmospheric parameters is required to produce a PMP event or similar rare precipitation frequency. After an extreme event occurs (e.g. 100-year, 1,000-year, or PMP type storm) the atmosphere needs time to recharge and reset. The time for that reset increases depending on the rarity of the event. Therefore, it is not reasonable to expect back-to-back PMP events. There is limited guidance on this for several reasons. One is that we have not observed many PMP

level events from which to determine this timeframe. Next, this would vary by storm type and location. For example, it is much more likely that tropical systems could affect a similar region within a few days of each other. This is partially because those storms are moving in from a location outside of a particular location and therefore the atmospheric parameters that develop those storms are not directly affected by the previous storm until reaching the location. Conversely, a severe local storm required high levels of local instability and moisture inflow. If severe storms were to occur in a given location, it would affect the atmospheric conditions around that region. This would lower the instability and sap the moisture from the atmosphere. Therefore, it would likely take several days to weeks before another storm would happen in the same location.

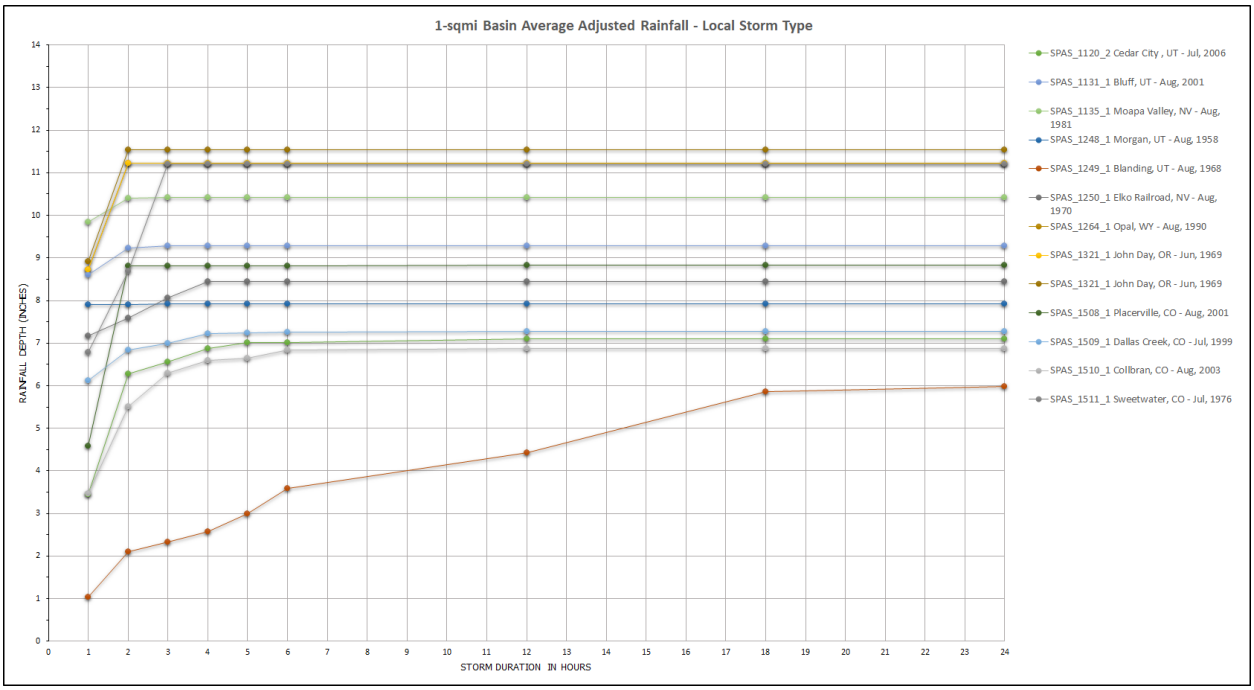


Figure 4: Local storm PMP depth-area chart

There is general guidance from some agencies related to the timeframe between major events. For example, the Federal Energy Regulatory Commission (FERC) recommends a 100-year rainfall three days prior to the PMP with dry conditions in between. The nuclear Regulatory Commission also provides guidance. However, in both cases, the guidance is somewhat arbitrary, and more work needs to be completed to better define these antecedent conditions. As the timeframe after a given event extends, the possibility of another event increases, but this should be considered weeks at a minimum depending on the storm type and seasonality as a given location.

These discussions are only related to the precipitation aspects. Consideration also needs to be given to the hydrologic assumptions and the rarity of each of those assumptions and how they could occur prior to and between PMP events.

This is very important for analyzing the reasonableness of the PMP depths and ensuring appropriate envelopment and consistency through time. The PMP depths should be utilized for subsequent PMF development. These represent depths that incorporate the current state-of-the-science methods for PMP development along with an updated storm database.

Example of Annual Exceedance Probability development

In this example study, AWA analyzed precipitation-frequency relationships to derive the Annual Exceedance Probabilities (AEP) for 24-hour and 72-hour precipitation for the location. A regional L-moment analysis based on methods described in Hosking and Wallis (1997) and utilizing the R-statistical software packages lmom and lmomRFA developed by Hosking (2015a; 2015b) was followed.

A regional frequency analysis approach utilizes L-moment statistics instead of product moment statistics, which decreases the uncertainty of rainfall frequency estimates for more rare events and dampens the influence of outlier precipitation amounts from extreme storms (Hosking and Wallis, 1997). The basis of a regional frequency analysis is that data from sites within a homogeneous region can be pooled to improve the reliability of the magnitude-frequency estimates for all sites. A homogeneous region may be a geographic area delineated by meteorological climatologies or may be a collection of sites having similar characteristics pertinent to the phenomenon being investigated. The data methods used are listed in the following sub-sections.

Precipitation data and annual maximum series data

For this study locations, a search to identify individual stations in the region was conducted using precipitation data sources from official National Weather Service (NWS) stations, Remote Automated Weather Stations (RAWS), US Geological Survey (USGS), and other meteorological networks. Each station's period of record (POR) was evaluated to determine which stations were appropriate for use in the final regional analysis.

The term "annual maximum" refers to a single 24-hour and 72-hour precipitation maximum being selected for each precipitation gauge for each year of record. Several procedures were required for assembly of the precipitation annual maximum series (AMS) dataset. Figure 5 shows the extent of the study area and the stations used in the analysis after the completion of these procedures and all subsequent quality checks. Regional L-moment statistics (Hosking and Wallis, 1997) were computed for the annual maximum data for

stations shown in Figure 5. Detailed methods and examples of the Lmoments precipitation development are provided in several references (e.g., Kappel et al., 2024).

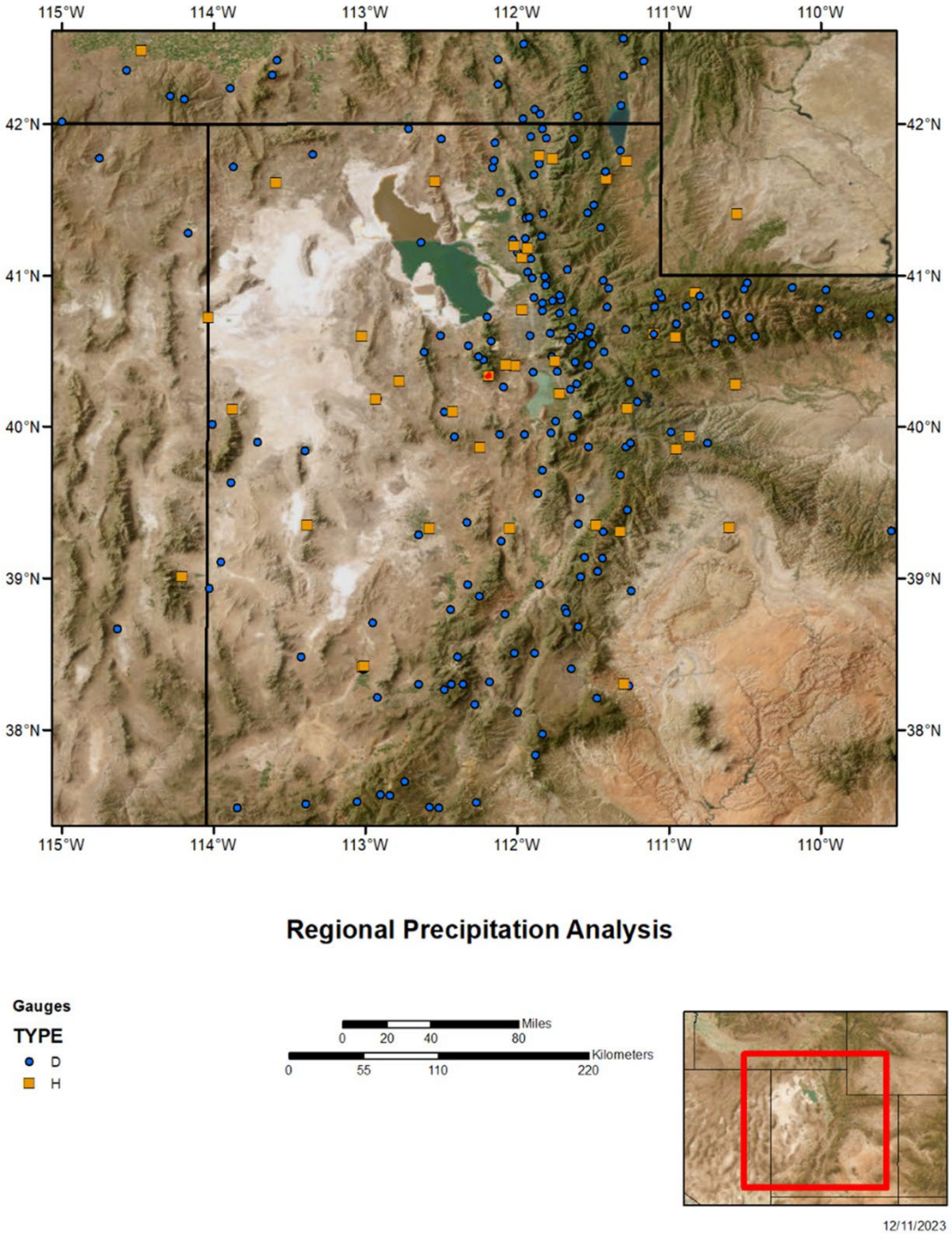


Figure 5: Locations of stations used for regional frequency analysis. The red outline is the basin, orange squares are hourly stations and blue circles are daily stations used for the 24- and 72-hour analysis

The output from this process is a series of gridded datasets that produce the at-site mean annual maximum (MAM) statistics described in the above sections and were used to scale the GEV distribution regional curve for each duration on a grid-cell by grid-cell basis. This allowed spatial mapping of precipitation-frequency estimates for selected recurrence intervals for the durations of 24-hours and 72-hours. Eighteen average recurrence interval (ARI) grids per duration were prepared from this information for point precipitation maxima for 1, 2, 5, 10, 25, 50, 100, 200, 500, 1,000, 5,000, 10,000, 100,000, 1,000,000, 10,000,000, 100,000,000, 1,000,000,000, and 10,000,000,000 years. The final 24-hour 100-year ARI and 72-hour 100-year ARI are shown in Figure 6 and Figure 7.

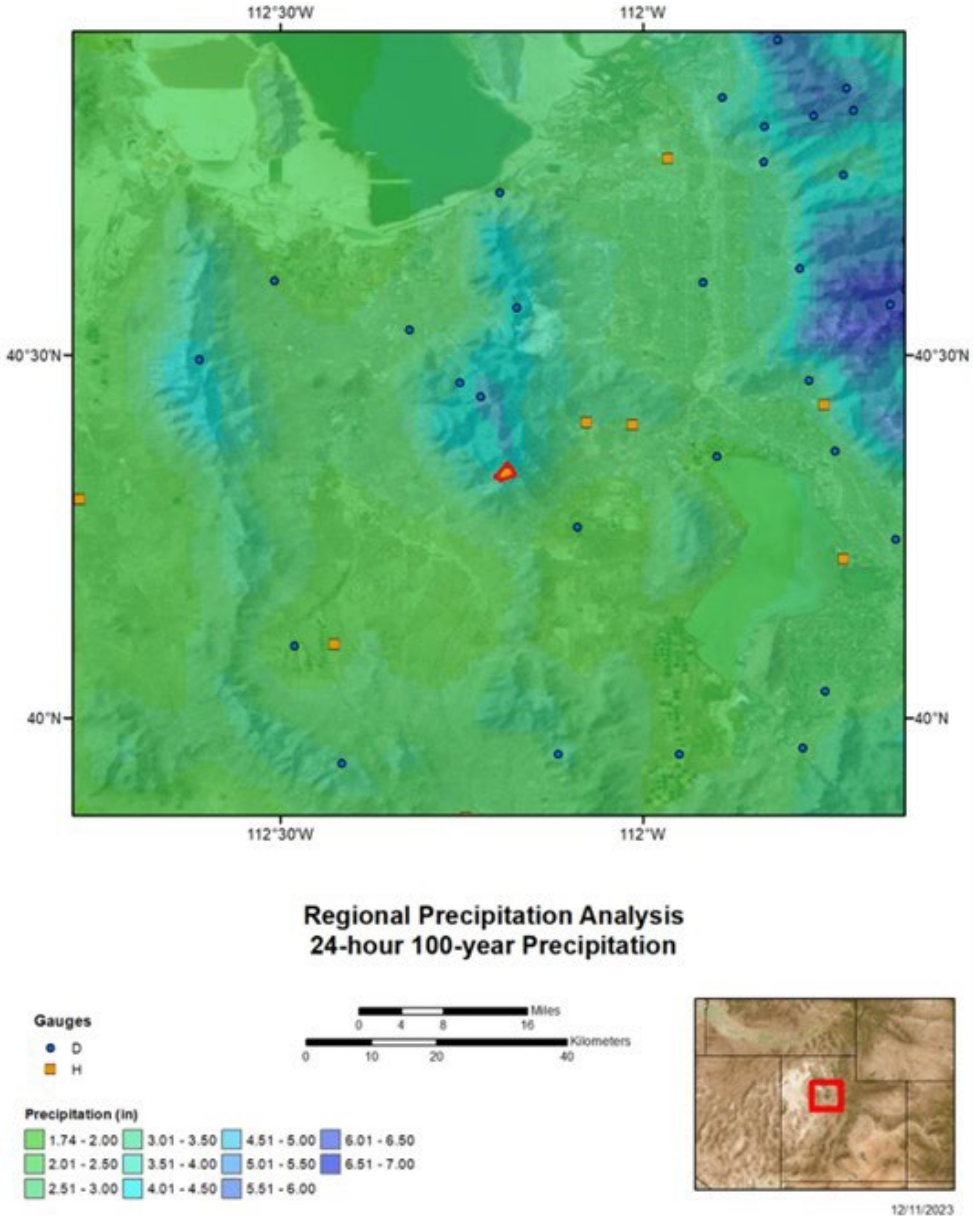


Figure 6: Spatially mapped 24-hour 100-year precipitation

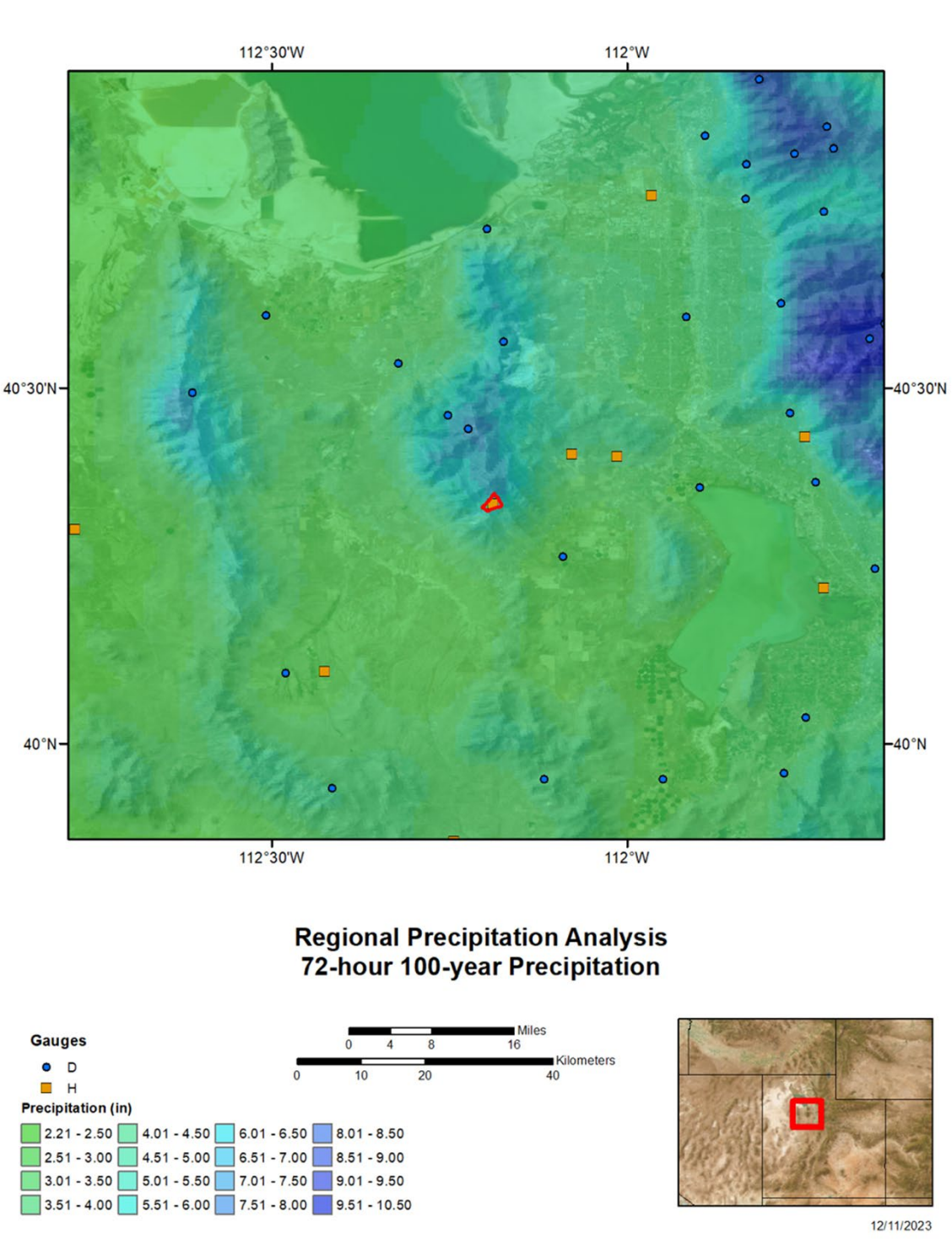


Figure 7: Spatially mapped 72-hour 100-year precipitation

Annual Exceedance Probability (AEP) grids for the 24-hour and 72-hour were used to extract the basin average AEPs. The 24-hour and 72-hour basin average AEP values are provided in Table 1 and illustrated in Figure 8 and Figure 9.

Table 1: 24- and 72-hour AEP values in inches. The 50% data represent the best estimate of precipitation magnitudes, while the 5% and 95% data represent the upper and lower bounds

Study Site		24-hour			72-hour		
ARI	AEP	50%	5%	95%	50%	5%	95%
1	9.9^{-1}	0.9	0.8	1.0	1.3	1.1	1.4
2	5.0^{-1}	1.8	1.6	1.8	2.6	2.4	2.6
5	2.0^{-1}	2.3	2.1	2.4	3.4	3.1	3.5
10	1.0^{-1}	2.7	2.5	2.8	4.0	3.7	4.1
25	4.0^{-2}	3.2	2.9	3.3	4.8	4.3	5.0
50	2.0^{-2}	3.6	3.2	3.8	5.4	4.8	5.7
100	1.0^{-2}	4.0	3.5	4.3	6.1	5.3	6.4
200	5.0^{-3}	4.5	3.9	4.8	6.7	5.8	7.2
500	2.0^{-3}	5.0	4.3	5.5	7.6	6.5	8.4
1,000	1.0^{-3}	5.5	4.6	6.2	8.4	7.0	9.3
5,000	2.0^{-4}	6.7	5.4	7.7	10.2	8.3	11.8
10,000	1.0^{-4}	7.2	5.8	8.5	11.0	8.8	13.0
100,000	1.0^{-5}	9.1	6.9	11.5	14.0	10.7	17.6
1,000,000	1.0^{-6}	11.3	8.1	15.2	17.5	12.6	23.5
10,000,000	1.0^{-7}	13.8	9.4	19.7	21.5	14.6	30.8
100,000,000	1.0^{-8}	16.6	10.6	25.6	26.0	16.7	40.1
1,000,000,000	1.0^{-9}	19.9	11.9	32.9	31.3	18.8	51.9
10,000,000,000	1.0^{-10}	23.5	13.2	42.1	37.4	21.0	66.7

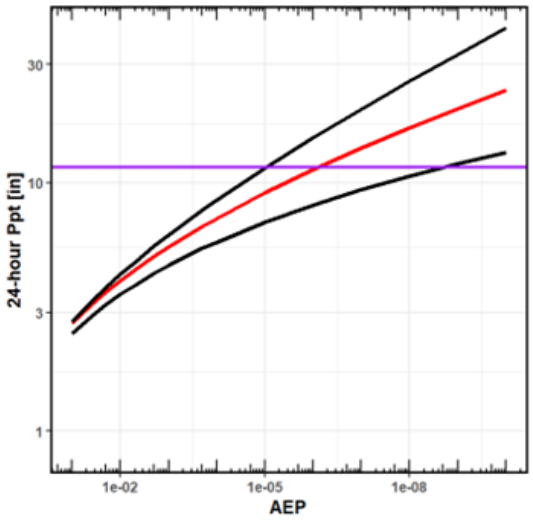


Figure 8: 24-hour regional L-moment frequency curve and uncertainty bounds representing the 5% and 95% confidence intervals. The purple line represents the estimated basin 24-hour PMP

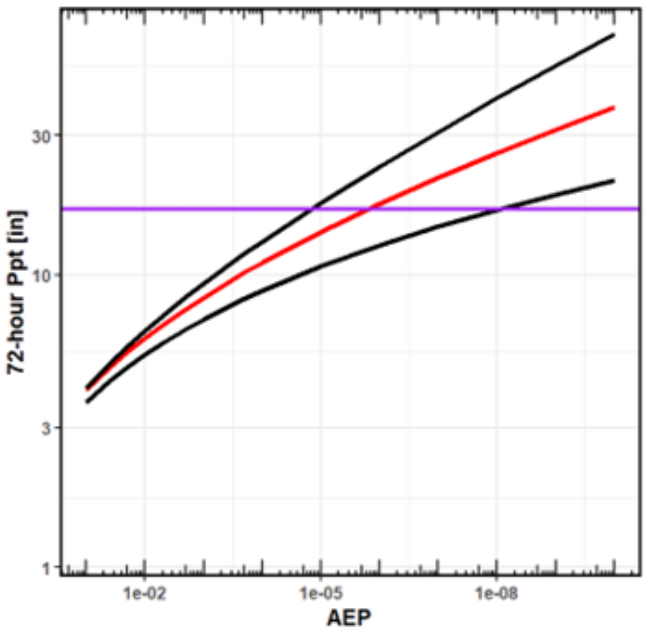


Figure 9: 72-hour regional L-moment frequency curve and uncertainty bounds representing the 5% and 95% confidence intervals. Purple line represents the estimated basin 72-hour PMP

Annual Exceedance Probability (AEP) for the 24-hour (11.5-inches) and 72-hour (16.74-inches) PMP were estimated. The 24-hour PMP has an AEP of 10^{-7} (Table 2) and the 72-hour PMP has an AEP of 10^{-6} (Table 2). It is important to note that there is significant uncertainty at these very low AEP ranges. Uncertainty bounds are provided for reference. However, even with the extreme uncertainty at very rare AEPs, this still provides valuable information and sensitivity inputs for risk analyses and probability assessments.

Table 2: AEP for 24-hour and 72-hour PMP

Basin	PMP (24 hr, 72 hr)		AEP (24 hr, 72 hr)		AEP Upper (24 hr, 72 hr)		AEP Lower (24 hr, 72 hr)	
Study site	11.5	16.7	10^{-7}	10^{-6}	10^{-6}	10^{-5}	10^{-9}	10^{-9}

Climate change assessments

Climate is changing, always has been changing, and always will change as long as the energy received from the sun across the Earth's surface and atmosphere is not distributed evenly. Accounting for future changes in climate is important to reduce risk and develop resiliency to potential future changes. The magnitude and rate of change at any given location for important meteorological parameters often must be modeled. However, we currently have an incomplete understanding of the Earth's climate system and future estimates of atmospheric composition. Therefore, model projections of the Earth's climate system and how that

climate system responds to greenhouse gases are applied using global climate models (GCMs), which are computationally intensive and are therefore run at low resolution both in time and space. The GCMs are developed by various governmental, academic, and research agencies around the world in coordination with the Intergovernmental Panel on Climate Change (IPCC). For detailed analysis at a given site, the resolution of the GCMs is inadequate to capture the spatial variations. To overcome this, projections from GCMs are downscaled using a statistical process into regional downscaled model projections (Regional Climate Models, or RCMs) through the CORDEX interface. The RCM process can provide projections of future climate conditions on a much smaller scale (e.g., 25-km by 25-km) supporting more detailed site-specific information allowing for adaptation assessment and planning (Figure 10).

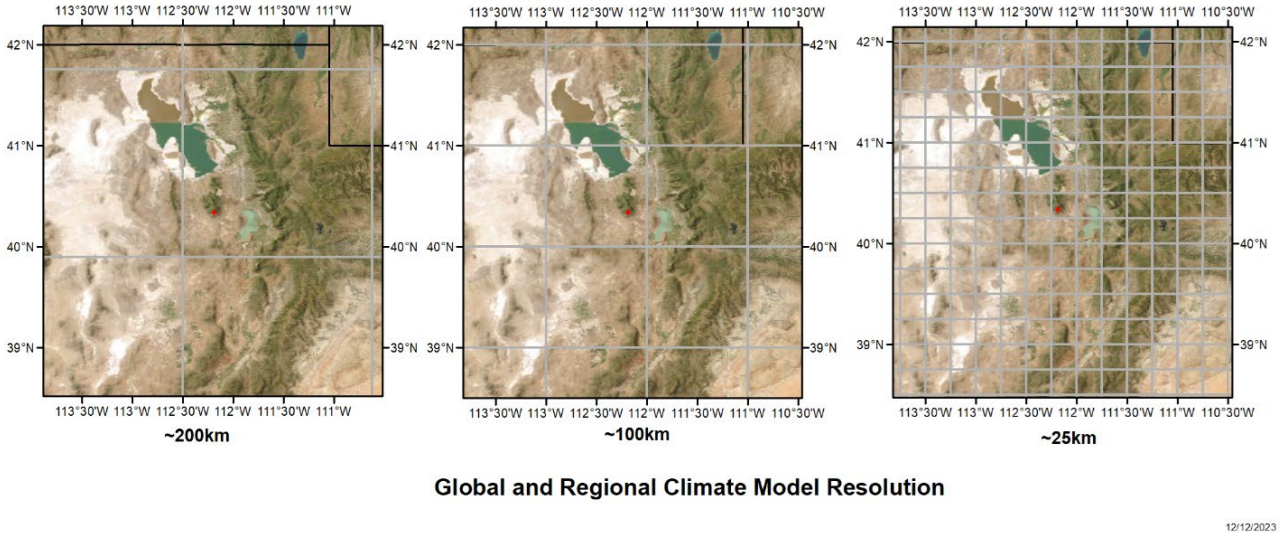


Figure 10: Climate change analysis region showing grids from GCM and RCMs

From these RCM projections, the potential effects of climate change on meteorological characterization within the study region were assessed. Various emissions scenarios that are used to force the GCMs are described by Shared Socioeconomic Pathways (SSPs). SSPs are scenarios of projected socioeconomic global changes and greenhouse gas concentration trajectory that are considered possible in the future (Figure 11).

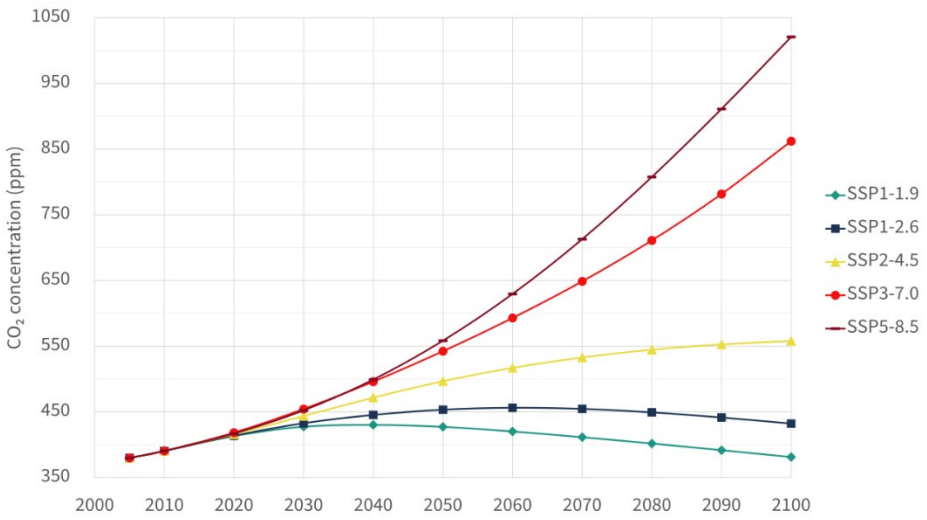


Figure 11: Shared Socioeconomic Pathways (SSP) trajectories. Reproduced from IPCC (2021)

The key climate model parameters used in this analysis were precipitation (Ppt), air temperature (Ta), dew point temperature (Td), wind speed (Ws), solar radiation (Srad), and evaporation (Evap). The parameters of relative humidity (RH) and Ta were used to derive the estimates of dew point (Td). Twenty-six RCM projections had the parameters needed for the climate change analysis. The climate projections historical period is based on daily data from 1950 through 2014, and the future periods are based on daily data from 2015 through 2100. The projections are evaluated using several methodologies. This helps inform the range of outcomes and uncertainty in the projections and produce a more reliable estimation.

Climate change projection analysis methods

Trend analysis

Mann-Kendall trend analysis (Mann, 1945; Hipel and McLeod, 2005) was performed on three climate stations located near the mine site for 1-day, 3-day, and annual durations. Results of these station-based trend analysis are shown in Table 3. The climate station trend results were used to assess the historic model projections.

Table 3: Climate stations used for trend analysis, evaluated at the 0.05 significant level

	Precipitation			Temperature
	1-day	**3-day**	**Annual**	**1-day**
Station 1	no trend	no trend	no trend	no trend
Station 2	no trend	decrease	no trend	decrease
Station 3	no trend	no trend	N/A	no trend

In addition, Mann-Kendall trend analysis (Mann, 1945; Hipel and McLeod, 2005) was performed on twenty-six climate model projections using the three scenarios (historic, SSP4.5, SSP8.5) for durations of 1-day, 3-day, 30-day, 90-day, and annual. Results for all climate model projection trend analyses are summarized in Table 4.

Table 4: Climate stations used for trend analysis, evaluated at the 0.05 significant level

	Precipitation					Temperature
	1-day	**3-day**	**30-day**	**90-day**	**Annual**	**1-day**
Historic	24 – no trend 2 – increase 0 – decrease	23 – no trend 3 – increase 0 – decrease	25 – no trend 1 – increase 0 – decrease	24 – no trend 2 – increase 0 –decrease	26 – no trend 0 – increase 0 – decrease	6 – no trend 20 – increase 0 – decrease
SSP45	20 – no trend 6 – increase 0 – decrease	22 – no trend 4 – increase 0 – decrease	20 – no trend 6 – increase 0 – decrease	17 – no trend 9 – increase 0 – decrease	20 – no trend 5 – increase 1 – decrease	0 – no trend 26 – increase 0 – decrease
SSP85	8 – no trend 18 – increase 0 – decrease	9 – no trend 17 – increase 0 – decrease	11 – no trend 15 – increase 0 – decrease	11 – no trend 15 – increase 0 – decrease	12 – no trend 13 – increase 1– decrease	0 – no trend 26 – increase 0 – decrease

Precipitation frequency analysis

Methods to account for non-stationarity in projections were not addressed, the projections were applied assuming stationarity. For the precipitation frequency analysis, AWA utilized the daily climate model projections to perform frequency analysis on the 1-day, 3-day, 30-day, 90-day, and annual durations.

AWA evaluates the climate change projections for the entire period available from 2015 through 2100. However, because the projections are provided on a daily time step, other evaluation periods can be considered applying a rate of change through time. For example, one may evaluate the projections through the year 2050 and then do a separate analysis for the years 2050–2100. This may result in slightly different outcomes depending on the climate change projections amount of change through time.

AWA identified, extracted, and quality controlled maximum daily precipitation projections for the twenty-six models and three projection scenarios. Annual Maximum Series (AMS) were then subjected to the frequency analysis methods described earlier in the AEP section. Example results from this analysis are shown in Figure 12 and separated by season for the 1-hour duration. Figure 13 provides example results of the summaries of climate change assessments that can be applied for evaluation. For most high hazard structures, the median of the SSP4.5 is recommended for application.

*** 1-Day Precipitation

	10yr	50yr	100yr	500yr	1000yr	Pct Change					Average
Historical	29.6	35.9	38.3	43.6	45.8	-	-	-	-	-	
SSP45	31.6	36.7	38.4	41.5	42.6	7%	2%	0%	-5%	-7%	**0%**
SSP85	32.2	38.3	40.7	45.8	47.8	9%	7%	6%	5%	4%	**6%**

*** 1-Day Summer

	10yr	50yr	100yr	500yr	1000yr	Pct Change					Average
Historical	25.6	31.3	33.4	37.5	39.0	-	-	-	-	-	
SSP45	27.0	34.6	37.5	43.4	45.6	6%	11%	12%	16%	17%	**12%**
SSP85	26.8	32.3	34.3	38.0	39.3	5%	3%	3%	1%	1%	**3%**

*** 1-Day Winter

	10yr	50yr	100yr	500yr	1000yr	Pct Change					Average
Historical	27.9	34.7	37.5	43.7	46.3	-	-	-	-	-	
SSP45	29.8	35.3	37.3	41.3	42.8	7%	2%	-1%	-6%	-8%	**-1%**
SSP85	31.1	37.9	40.6	46.6	49.0	11%	9%	8%	6%	6%	**8%**

Figure 12: Example results for 1-day precipitation frequency analysis for climate projection from Model 1

	SSP45				SSP85			
	Mean	Median	10th	90th	Mean	Median	10th	90th
Temperature 1-Day; C	**2.8**	**2.8**	1.7	3.8	**6.3**	**6.5**	4.2	8.0
Temperature 1-Day Summer; C	**2.8**	**2.8**	1.7	3.8	**6.3**	**6.5**	4.1	8.0
Temperature 1-Day Winter PF; C	**3.0**	**3.2**	1.9	3.9	**6.6**	**6.4**	5.0	8.8
*Precipitation 1-Day PF; %	**12**	**9**	-1	27	**14**	**13**	0	25
Precipitation 1-Day Summer PF; %	**8**	**12**	-6	19	**12**	**12**	-4	28
Precipitation 1-Day Winter PF; %	**13**	**12**	-1	26	**18**	**20**	3	34
*Precipitation 3-Day PF; %	**23**	**18**	1	37	**29**	**24**	3	63
Precipitation 3-Day Summer PF; %	**15**	**9**	-7	49	**20**	**19**	-7	47
Precipitation 3-Day Winter PF; %	**20**	**21**	-6	45	**29**	**28**	2	60
Precipitation 30-Day PF; %	**14**	**13**	-4	27	**21**	**20**	-1	48
Precipitation 90-Day PF; %	**15**	**13**	-2	32	**19**	**17**	-1	41
Precipitation Annual PF; %	**10**	**10**	-5	27	**15**	**11**	0	34
Moisture Maximization 1-Day, %	**No Change**				**No Change**			
Moisture Maximization 3-Day; %	**No Change**				**No Change**			

Figure 13: Climate change projection results through 2100

Wind-wave run up

Another aspect that is critical for TSF and dam design is the need to properly quantify the potential of wave

action on top of a PMP/PMF event. In many studies reviewed by AWA, the wind wave run up analysis have been inadequate and not representative of the wind patterns that could occur during and immediately following a PMP/PMF event. As part of the wind wave run up analysis, wind speed and direction analysis are completed for various durations and directions. The critical timeframe for wind wave set up and the critical fetch(s) given the design of the TSF pond or reservoir must be evaluated. The analysis can be completed using a frequency analysis based on observed data at the site and within similar regions.

However, the main issue that is often found and corrected by AWA site-specific studies is related to understanding of the unique synoptic meteorological conditions that would be associated with the PMP event and the wind fields that would be generated during these events over the location of interest. During the PMP design storm, significant wind would only occur within a specific range of directions as a PMP event develops, matures, and moves through based on the synoptic patterns associated with the storm environment as well as the local topographic and exposure conditions.

The specific characteristics that occur with the PMP design storm and the site location must be considered. And the specific wind direction(s) that could occur should during the storms must be accurately considered when developing the wind speed and direction inputs for wind wave run up. In other words, if the wind with the PMP design storm could only come from the northwest yet the critical direction for the fetch of the location is from the southwest, then the maximum wind speeds only from the northwest should be used. Winds from other directions (e.g. southwest) should not be used as they are not critical for the wave development over the TSF. For locations that are affected by tropical systems, the wind direction will change through time as the storm progresses through the region. During the course of the storm, wind directions may shift from each direction of the wind rose. In these situations, the frequency analysis and development of wind speed climatologies should only be done for the direction(s) that are along the fetch and would result in the maximum wind wave set up. Conversely the wind speeds from the other directions should not influence the wind speed climatologies. Therefore, applying the worst-case wind speed and wind direction outputs without proper consideration for how these parameters would develop during a PMP design storm is not correct and should not be applied.

It is important to note that the storm characteristics vary by location and storm type. For example, along the west coast of the North America, wind is associated with low pressure systems moving off the Pacific Ocean generally from northwest through southwest and PMP events would not occur with winds from the northeast through southeast. In this region, many reservoirs drain from the east to the west following the river systems and topography. Therefore, the critical fetch for many of these locations does not align with the most critical wind direction and the wind wave run up analysis should only consider the critical directions. This would likely result in smaller wave set up and less freeboard requirements.

In central regions of North America, low pressure systems often form on the lee side of the Rocky Mountains. In these areas winds from the north through the east through the south are most common during heavy rainfall events as low pressure move through the region. However, most reservoirs drain orthogonal to these directions as they drain from west to east from the higher to lower elevations. However, in these regions, the strongest winds often occur associated with strong upper-level winds crossing the mountains and down sloping off the mountains towards the adjacent plains. These are sometimes termed “Chinook” winds. In these situations, the weather pattern is dry, but the winds can be sustained well over 100mph for several hours. In addition, these are often occurring in a direction that represents the worst-case fetch of a given reservoir. In cases where the PMP/PMF has recently occurred and the reservoir is still relatively full, this event could occur at a timeframe when the strongest winds and high-water surface elevations co-occur.

Another example would be the eastern Atlantic coast of North America where tropical system s affect the region. In these areas this type of storm moves in from the south through the east. However, these storms are associated with a closed circulation until they transition to an extra tropical storm. Therefore, wind from these vents can come from any direction depending on the path of the storm in relation to the given TSF or reservoir. However, the wind speed from the different directions varies significantly during the lifetime of the storm. In this example, the strongest winds are associated with the right front quadrant of the storm and if this quadrant of the storm could not affect a given location, only the wind speed form the appropriate quadrants should be used. Again, many of the reservoir systems in this region flow from west to east or south to north and the reservoirs also follow these directions. Therefore, the wind speed associated with the right front quadrant would in the opposite direction of the critical fetch of these reservoir examples. Instead, the wind direction associated with the direction of the critical fetch would be evaluated, for example the left front quadrant or northwest to west wind speed associated with the tropical system.

The goal of this discussion is to be sure the analysis is specifically reflective of the local characteristics of the TSF or reservoir site, the direction and distance related to the fetch, and how those relate to the meteorological patterns that would produce strong winds during a PMP design storm event.

Conclusion

The development and application of important meteorological input parameters for TSF design and evaluation was discussed, with examples provided of deterministic PMP and probability assessments. Comments were provided on the proper pairing of extreme mereological events and wind and how those should be applied based on the site-specific location. In addition, the application of climate change assessments and how those affect these outputs was shown. It is important to note that unrealistic combinations of outcomes and overly conservative applications should not be applied. For dam safety assessments and design the key messages are as follows:

- Do not combine PMP back-to-back. The timing between events should reflect the physical conditions of the location, atmosphere, and storm type.
- Quantifying the probability of extreme events, including PMP, is very useful for risk assessments and risk informed decision making process, and to ensure your design is appropriately rare.
- Consideration of climate change should be assessed to determine how changes may affect extreme events for a given location and how to ensure resiliency of design.
- Site specific evaluation of extreme wind conditions that could occur in relation to the PMP storm event and the topography/exposure of your site should be completed to ensure inappropriate combinations of extreme parameters are not combined.

References

Hipel, K.W. and McLeod, A.I. 2005. *Time Series Modelling of Water Resources and Environmental Systems*. Electronic reprint of book originally published in 1994. http://www.stats. uwo.ca/faculty/aim/1994Book/.

Hosking, J.R.M. 2015a. L-moments. R package, version 2.5. http://CRAN.R-project.org/package=lmom.

Hosking, J.R.M. 2015b. Regional frequency analysis using L-moments. R package, version 3.0-1. http://CRAN.R-project.org/package=lmomRFA.

Hosking, J.R.M. and Wallis, J.R. 1997. *Regional Frequency Analysis, An Approach Based on L-Moments*. Cambridge University Press.

IPCC. 2017. Intergovernmental Panel on Climate Change (IPCC) Fifth Assessment Report (AR5) Observed Climate Change Impacts Database, Version 2.01. Palisades, NY: NASA Socioeconomic Data and Applications Center (SEDAC). https://doi.org/10.7927/H4FT8J0X.

IPCC. 2021. *Climate Change 2021. The Physical Science Basis*. Contribution of Working Group I to the Sixth Assessment Report of the Intergovernmental Panel on Climate Change (Masson-Delmotte, V., P. Zhai, A. Pirani, S.L. Connors, C. Péan, S. Berger, N. Caud, Y. Chen, L. Goldfarb, M.I. Gomis, M. Huang, K. Leitzell, E. Lonnoy, J.B.R. Matthews, T.K. Maycock, T. Waterfield, O. Yelekçi, R. Yu and B. Zhou [eds.]). Cambridge University Press.

Kappel, W.D. 2020. PMP estimation for mine tailings dams in data limited regions. *Journal of Dam Safety* 17(2): 30–45.

Kappel, W.D., Hultstrand, D.M., Muhlestein, G.A., Rodel, J.T., Steinhilber, K. and Venticinque, M. 2023. Site-specific probable maximum precipitation and regional precipitation frequency analysis for the Cerro Verde mine and surrounding regions, Chile. Prepared for Freeport-McMoRan.

Kappel, W.D., Hultstrand, D.M., Rodel, J.T., Muhlestein, G.A., Venticinque, M and Steinhilber, K., May 2024. Site-specific probable maximum precipitation and climate change assessment for Faro mine, Yukon Territory. Prepared for SRK.

Kappel, W.D., Hultstrand, D.M., Rodel, J.T., Muhlestein, G.A., Venticinque, M, Cheke, D. and Steinhilber, K., June 2024. Statewide probable maximum precipitation for New Jersey. Prepared for the New Jersey Dept. of Environmental Protection Dam Safety.

Kappel, W.D., Hultstrand, D.M., Steinhilber, K. and Rodel, J.T. 2020. Climate change and PMP: are these storms changing? *Journal of Dam Safety* 17(3).

Mann, H.B., 1945. Nonparametric tests against trend. *Econometric* 13: 245–259.

Micovic, Z., Schaefer, M.G. and G.H. Taylor, 2015. Uncertainty analysis for probable maximum precipitation estimates. J. Hydrology. 521: 360–373.

World Meteorological Organization, 2009. Manual for estimation of probable maximum precipitation, Operational Hydrology Report No 1045, WMO, Geneva, 259 pp.

GISTM – Effective Implementation

Lis Boczek, South32, Australia
Richard Zayler, South32, Australia
Gideon Steyl, South32, Australia

Abstract

The Global Industry Standard on Tailings Management (GISTM) is an important standard for mining companies to implement for both investors and insurers. GISTM focuses on the importance of social, environmental and engineering aspects to ensure the safety of tailings storage facilities (TSFs) and the communities that may be affected by mining operations and their associated structures. A key aspect in obtaining value from GISTM alignment is breaking down the silos that exist within the operations and corporate functions of a mining company. GISTM cannot be successfully implemented if it is solely focused on being compliance driven. It requires structural changes in the organization to achieve the intent on a continual basis during the life of the TSF. Prior to the standard, interaction of the groups required to implement and sustain GISTM would only occur to achieve regulatory outcomes, and the relationship would not continue into the operational space once the TSF was built.

The implementation journey of GISTM within South32 has highlighted two components that influence successful implementation: collaboration and improved operational practices.

This paper attempts to provide a response to the question: "Can GISTM drive the change needed to achieve improved operational performance to increase the safety of the TSF?" We will outline the journey taken by South32 to implement GISTM across our operations and the benefits obtained from the process. In addition, the paper aims to highlight the lessons learnt and improvements undertaken to implement GISTM for not just compliance, but to improve the overall safety, social performance, and environmental outcomes associated with our TSFs.

Introduction

The Global Industry Standard on Tailings Management (GISTM) was developed following the 2019 catastrophic failure of a tailings storage facility (TSF) at Córrego do Feijão mine in Brumadinho, where 272 people lost their lives and there were significant impacts to local flora and fauna. An integrated approach to tailings management with transparency, accountability, and safeguards for the rights of project-

affected people were key pillars of the GISTM implementation. ICMM member companies committed to implement the standard for Very High and Extreme facilities by August 2023 and all remaining TSFs by August 2025. The ICMM drafted conformance protocols to support implementation of the 77 GISTM requirements and these protocols are used as a basis by many mining companies, including South32, to assess conformance to GISTM.

Several GISTM papers have been published since it was introduced in 2020 and it continues to be a source of discussion. There are many ideas on how to implement GISTM within companies. Consultants have made numerous interpretations of each of the Principles and the best way to implement these in a mining environment. It is well understood that to implement GISTM effectively, collaboration across the different disciplines within a mining company is required. Due to the expanding literature support on GISTM, the industry is evolving in its understanding through collaboration and shared learnings within the ICMM member companies.

This paper discusses the journey undertaken by South32 on the path to GISTM conformance, and how this conformance can influence the safety of our TSFs.

South32's journey

Roles and accountabilities

The GISTM implementation at South32 began as a centrally managed project with each operation being responsible for the implementation. Each operation was initially given the freedom to implement GISTM for TSFs with guidance on the minimum requirements to meet conformance by South32's Tailings Dams Governance group, prior to the publishing of the ICMM protocols.

An initial gap assessment was completed at each operation to inform the budget and timeline to achieve GISTM implementation. Accountable Executives (AE) were appointed based on geographical region and a Responsible Tailings Facility Engineers (RTFE) for each operation was employed. The RTFE mandate was to achieve GISTM conformance at their respective operation. Subsequently, Engineers of Record (EOR), Independent Tailings Review Board (ITRB) Members and Independent Technical Reviewers (IRs) were shortlisted for each operation and appointed to their roles by the AE.

The hardest role to fill in all operations was the RTFE. The minimum qualification requirements were defined by the Tailings Dams Governance group and our operations endeavored to recruit appropriately qualified RTFEs. This proved a significant challenge as the experience and qualifications defined were in high demand across the whole industry. The parallel implementation of GISTM among all ICMM members resulted in a chronic shortage of candidates.

Most operations employed a project manager to facilitate the implementation, which led to a compliance mindset around commissioning and completing documentation. At some operations, the GISTM implementation commenced prior to appointment of the RTFE role.

The ITRB/IRs conducted site visits to all operations and channels were set up between our RTFEs, EORs, and ITRB/IRs to allow for regular communication and feedback.

Development of documentation

To achieve ICMM GISTM conformance, modification of existing documentation and in some cases new reports to fill in the gaps identified were required. The development of engineering documentation, retrospective construction documentation, and potentially long lead items were identified as priorities for our RTFEs and EORs to address. The finished documents generally met the GISTM requirements; however, when internal technical reviews were undertaken, gaps were identified where the whole requirement, or the intent of the requirement, was not being met.

Three key questions arose regarding the documentation being produced. Firstly, was it fit for purpose? Secondly, was it sufficient to fit the risk classification of the facility? Finally, was it suitable for the available resources and experience of personnel at the operation? This was especially relevant in the case of our Tailings Management Plans (TMP), Water Management Plans (WMP) and Operation Maintenance and Surveillance Manuals (OMS), where the documentation must be appropriate for the end user to implement.

To ensure all information was available in a centralized location for all our operations and functions, an internal Microsoft SharePoint site for GISTM documentation was created.

Engagement with stakeholders (internal and external)

One of the key pillars of GISTM is meaningful engagement with project-affected and Indigenous peoples. Our operations already had systems in place to engage with our local communities and Indigenous populations on a variety of issues, and we leveraged those existing systems to start engagement specifically on our TSFs. A key learning from the TSF specific stakeholder engagement is the significance to communities of environmental impacts on waterways and land areas. When these are not heritage sites, they would not have been identified during desktop reviews. Historically, consequence classification assessments were undertaken by consultants without engagement across all groups to inform them of all impacts. Whild engagement cannot be retrospectively implemented for existing facilities, modifications can be made to the future design and closure of the facility that may provide a better outcome for those impacted.

Internal stakeholder engagement included cross-functional and operational teams. In South32 we identified very early on that our Environmental and External Affairs teams are key players to achieve meaningful conformance to GISTM. We also recognized that GISTM conformance would not be achieved in an effective manner without improving the profile of our TSFs and our facility performance within the

greater South32 business. Site visits, workshops, and virtual meetings were conducted across all South32 functions to promote awareness of our TSFs. Furthermore, educational and tailings related materials were updated for our operations to help raise the perceived importance of our TSFs. The increase in profile significantly helped our cross-functional teams to achieve conformance for our environment and community-focused requirements.

Cross-functional meetings at various levels, implemented initially to promote GISTM conformance, have continued and evolved into more informal information sharing between functions within the business. This has helped maintain collaboration and relationships with stakeholders, and ensures that the importance of our TSFs is not lost among the wider business.

How did we measure conformance?

What does GISTM conformance look like?

To enable measuring of GISTM conformance, companies score themselves as "meets," "partially meets," and "does not meet" against each of the GISTMs 77 requirements. Meeting with a plan has also been accepted by the industry for some requirements where conformance will take longer due to additional works, etc. This is particularly evident in relation to as low as reasonably practical (ALARP) risk reduction measures.

Understanding what is required to meet conformance may sound simple but interpretation can vary, and the requirements of conformance can also vary depending on the type of TSF, size, consequence classification, and construction methodology. To define the minimum requirements, the first step taken by South32 was to review the consequence classification of each TSF, confirm whether all TSFs met the definition of a TSF under GISTM, and identify existing facilities that should be excluded. This step was important, as the definition of a TSF for the purpose of an internal standard and/or stewardship activity often includes other waste types/facilities that do not strictly meet the industry definition for tailings.

Conformance criteria

ICMM GISTM conformance protocols set out guidance for measuring conformance, and an initial gap assessment of implementation works to date was conducted in early 2021 by South32 Tailings Dams Governance group.

The criteria used for self-assessment were those presented in the ICMM Conformance Protocols; however, for better quantification/precision for the "partially meets" criteria, South32 adopted three different levels of conformance achievement (25%, 50% and 75%), considering sufficiency status as evidence for meeting the requirement as per Table 1. Conformance to GISTM was measured across each operation as a percentage compliance.

Table 1: GISTM requirement assessment criteria

Criteria	Adherence
Does Not Meet – No information as evidence	0%
Partially Meets – Information exists but is insufficient and actions/purchase order are not in place	25%
Partially Meets – Information exists but is insufficient and actions/purchase order do not cover whole requirement	50%
Partially Meets – Information exists but is insufficient and actions/purchase order covers whole requirement	75%
Meets – Information exists as evidence	100%
Not Applicable – This specific requirement is not applicable in the context of the asset and does not participate in the calculation of the average	N/A

All the operations' self-assessments were collated into a Monthly Report that was issued to key internal stakeholders. Internal validation of the operations' self-assessments was undertaken by South32 Tailings Dams Governance group and third-party KPMG for our FY23 disclosure.

Addressing the safety of our facilities

Conformance to GISTM alone, while it provides a deeper understanding of the condition of our TSFs, does not fully address the safety of the TSF. Without good operational systems and practices, the safety of our TSFs can be compromised. Thus, a significant focus has been placed on ensuring that our documentation is fit for purpose; our people are well trained; and the risks to the TSFs are well understood and communicated from an operational perspective.

One of the keys to the safety of our TSFs is ensuring that risks around water management are well understood. The role that water plays in increasing the risk of failure and the impact of failure has been made clear to our operations. Our South32 Dam Management Standard mandates that all decant pond sizes should be less than 10% of the operational area in a TSF, unless designed to be greater and approved in writing by the EOR. Secondly, the design storm must be removed within 30 days by available infrastructure to ensure the safe operation of the TSF and promote maximum in-situ tailings density.

Monthly reporting by our RTFEs within the business includes GISTM conformance and TSF performance metrics such as:

- decant pond size;
- trigger action response plan (TARP) condition;
- instrumentation condition;
- inspection reports;

- maintenance status;
- survey reports (LiDAR, InSAR, monuments); and
- status of critical controls.

South32 also implemented a centralized monitoring platform to allow for real-time oversight of the physical performance of each of our TSFs, which includes the above performance metrics.

Moving from conformance to effective implementation

At the beginning of South32's journey, the mindset of the business was around compliance to GISTM, with targets set to achieve 100% conformance by the implementation timelines. This focus led to a mindset of ticking boxes rather than using the GISTM to change our operations to embed it. Through internal review processes, it became evident that the dialogue needed to shift from pure GISTM compliance and focus more on changing the way we operate while achieving conformance to the GISTM.

South32 achieved compliance to GISTM for their very high consequence classified facilities by August 2023 and are well on the way to achieving full compliance for all other facilities by August 2025. As a business we are committed to maintaining conformance with GISTM. If we unpack what a sustained conformance to GISTM looks like at an operational level, it requires a change from work undertaken to achieve and maintain conformance, to work required to embed GISTM into the way we operate. Although a subtle difference, the embedment of GISTM requires all areas of the organization at both an operational level and a corporate level to work together and think with a proactive and engaged mindset that is driven by improvements in how we operate. It requires sustained ownership and commitment to facilitate the embedment of GISTM.

As we mature in our journey and we move closer to achieving GISTM conformance across our business, we have shifted from making GISTM conformance the goal, to making sure GISTM becomes part of the way we operate. This involves ensuring those cross-functional relationships are maintained and strengthened with systems to support and ensure that we have ongoing communication and that we meet our commitments within South32. It also includes ensuring that any documentation related to the operation of the TSF aligns with actions undertaken especially around the OMS, water management plan, trigger, action and response plan, and emergency response plans. The outcome of this supports South32's guarantee that we all go home safe and well and is an integrated part of how we operate.

Learnings and outcomes

Learnings

The implementation of the GISTM within South32 had, and still has, some challenges and learnings. These include:

- GISTM being viewed as a Project to be implemented and once completed we are compliant in the long term. There is and has been significant effort made to promote and educate stakeholders to understand that ongoing commitment to GISTM requires a sustained effort to maintain conformance going forward.
- Maintaining momentum throughout the GISTM implementation at each operation as it approached full conformance. It is challenging, as the last 5% to reach 100% conformance required 50% of the effort, and ongoing education was needed as stakeholders changed over the journey.
- External engagement was left to the latter half of the implementation, but this engagement would have benefited from early education on our TSFs, or from being gradually introduced to our TSFs from the start, using our existing external engagement systems.
- The deliverables for the GISTM varied greatly across the operations. This was in part due to the initial momentum of the implementation with different RTFEs, EORs, and consultants involved. Effort was made to standardize key documentation and reporting requirements, but in hindsight, this would have benefited from a slower initial implementation that was phased in to align with set goals for South32.
- Starting implementation before the ICMM conformance protocols were published and fully understood. South32 started implementation in December 2020 with gap assessments and actions to fill the identified gaps completed in February 2021. RTFEs and EORs had commenced actions, and it was not until mid- to late-2021 that the conformance protocols were reviewed against the actions, resulting in additional gaps identified, which caused delays and required rework.
- TSF Projects in late Feasibility Study and Execution phases were impacted by South32s commitment to implement GISTM, as these projects could not be delayed due to their business sustaining nature and have been treated as “existing facilities” under GISTM. This led to stakeholder engagement and requirements being retroactively applied.
- Management plans and documentation produced to conform with GISTM requirements was not always used effectively by the operation to enhance our TSF knowledge base or support improvements in operational safety.
- Effective change management and early intervention in the change management process to enable continued implementation of GISTM. Due to the continued changing structure in the operational environment, effective handovers between staff required management to allow for sufficient knowledge transfer between individuals and familiarization with systems.

Positive outcomes

There have been many positive outcomes for our business with the implementation of GISTM. These include:

- Centralizing our Tailings Knowledge Base to allow for easy access to all documentation related to our TSFs. This allows for information to be viewed by all areas of the organization (not just at the operation).
- Promotion of our TSFs and people has allowed for a higher level of TSF awareness across the business and at the operation.
- Greater understanding of the risk of our TSFs and improvements in how we manage those risks.
- More detailed and live monitoring of our TSFs, with regular reporting to a larger group of stakeholders on TSF status.
- Collaboration between stakeholders with inclusion of tailings team members at an early stage in projects and working groups.
- Operational integration of the tailings team in the wider team to help maintain relationships and improve decision-making processes.
- Improved water management at our operations through enhanced understanding of the role water plays in managing the risks associated with a TSF and the potential impact of failure.
- Identification of areas that require additional attention moving forward, and where we can continue to improve our operations to reduce TSF-related risks.

Conclusion

South32 is still progressing on the learning journey to bring all areas of the operations and functions together to achieve embedment of, and maintain conformance to, GISTM. Conformance at face value can be achieved without collaboration, but ongoing maintenance and effectiveness cannot. South32 still has a road to travel to achieve the level of collaboration and density of communication to provide for a business-as-usual mindset, but with progressive integration into the South32 operating system it is achievable. In addition, a focus on moving forward to maintain effective implementation is ensuring that documentation produced is fit for purpose and, where gaps still exist, working to improve these areas to ensure alignment. While a standardized approach is preferred for ease of governance and alignment across the business, implementation of the GISTM needs to be specific to each operation, and conditions of the TSF and cannot be a one-size-fits-all approach.

References

International Council on Mining and Metals (ICMM). 2020a. Global Industry Standard on Tailings Management. International Council on Mining and Metals.

International Council on Mining and Metals (ICMM). 2020b. Global Industry Standard on Tailings Management Conformance Protocols. International Council on Mining and Metals.

A Case Study on ALARP for Safety Management of Tailings Storage Facilities

Theo Gerritsen, Rio Tinto, Australia
Yi Zhu, Rio Tinto, USA

Abstract

ALARP – *As Low as Reasonably Practicable* – refers to the principle of testing risk reduction against the cost of the corresponding risk reduction effort. The principle of societal risk acknowledges that there is no absolute safety (zero risk) from engineered systems, and neither society nor a company have infinite resources to spend on managing risks. However, it requires risk management to reduce risks to *"As Low as Reasonably Practicable."* ALARP is built into requirements under the Global Industry Standard on Tailings Management (GISTM, 2020). Rio Tinto presented its ALARP roadmap for demonstrating dam safety to an ALARP requirement in relation to tailings storage facilities during the 2023 Tailings and Mine Waste Conference in Vancouver (Zhu and Pascoe, 2023). This paper presents the details of when one of its active tailings storage facilities followed that roadmap for ALARP demonstration.

Introduction

ALARP – *As Low as Reasonably Practicable* – refers to the principle of testing risk reduction against the cost or sacrifice of the corresponding risk reduction effort. The ALARP principle is referenced across multiple Rio Tinto Standards and Group Procedures. Rio Tinto's risk management standard and HSE management system standard both require that health and safety risks are managed to ALARP. To facilitate Rio Tinto's commitment to the implementation of GISTM for its tailings storage facilities (TSFs), Rio Tinto has developed a process (roadmap) to demonstrate ALARP related requirements in the GISTM (Zhu and Pascoe, 2023). This paper presents a short summary on that roadmap and the details when the roadmap was followed for ALARP demonstration by its Oyu Tolgoi mine tailings storage facility (OT TSF).

The Oyu Tolgoi copper-gold mine (OT) is located in the southern Gobi Desert region of Mongolia, approximately 550 km south of the Mongolia capital, Ulaanbaatar, and 80 km north from the border with China. OT operates a multi-cell paddock type TSF, as shown in Figure 1. TC1 of the TSF was active and TC2 was undergoing its stage 1 (initial) construction (during the ALARP demonstration exercise presented in this paper). The OT TSF supports a nominal ore processing rate of approximately 110,000 tonnes per

day (for an annual tailings production of approximately 40 million tonnes). It receives thickened tailings slurry with an average solids content (by weight) of about 60%.

TC1 is a roughly-2km square ring-dike facility constructed with containment embankments raised in the downstream direction. Construction of TC1 started in February 2011 and tailings deposition commenced in March 2012. The embankments are raised each year and are scheduled to reach the final height of approximately 70 m to provide about 240 million m^3 of storage volume for storing about 360 million tonnes (Mt) of tailings solids.



Figure 1: OT TSF

TC2 was constructed to the north of TC1, with the northern embankment of TC1 forming the southern embankment of TC2. TC2 has a total footprint area of approximately 480 hectares in a sub-pentagonal shape. The adopted design footprint of TC2 is moderately larger than the 400 hectares of TC1 and this has led to a larger design storage volume of 282 Mm^3 for TC2 than TC1 of 240 Mm^3. TC2 design has largely followed the same for TC1 but has incorporated the operational experience and lessons learned from TC1.

Rio Tinto ALARP roadmap for dam safety

As presented in Figure 2, the Rio Tinto ALARP roadmap for dam safety requires both good practice demonstration and ALARP demonstration.

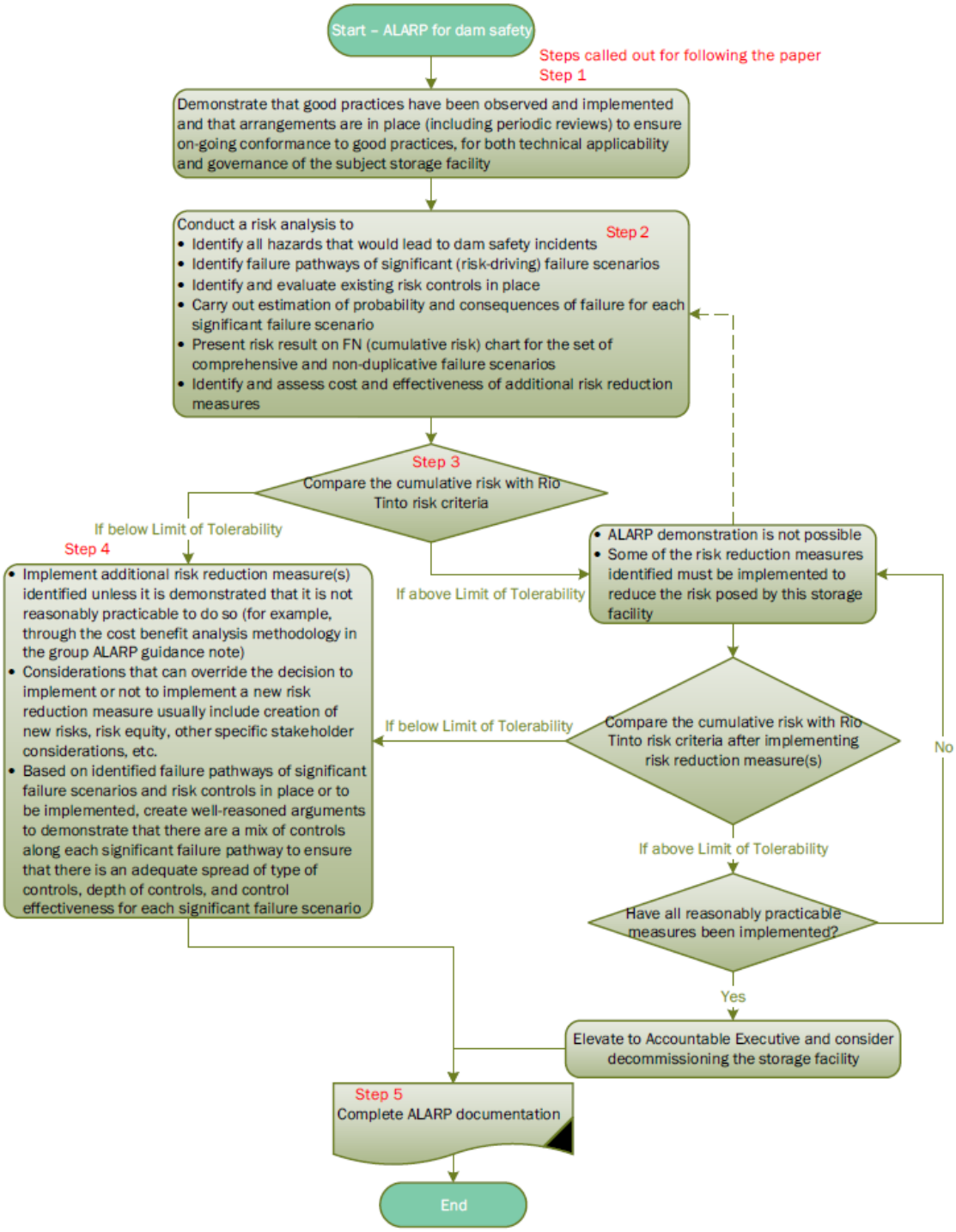


Figure 2: Rio Tinto ALARP roadmap for dam safety

Good practice demonstration (Step 1 in Figure 2)

To the extent possible, Rio Tinto requires an examination of the implementation of specific applicable good practice to each of its TSFs, from both engineering and governance points of view. This is done before the quantitative risk analysis based ALARP demonstration.

For OT TSF, the good practice demonstration includes a detailed examination on the implementation of the Tailings Management System (TMS) at OT and the state-of-practices followed by the engineering and operations for the TSF.

Implementation of TMS for the OT TSF

The specific implementation of the TMS for the OT TSF is embodied by the following:

1. A clear understanding of the responsibilities and accountabilities for roles related to the tailings management. OT has established both internal roles and external roles for its tailings management, including the Accountable Executive, Nominated Manager, Qualified Site Representative, and Responsible Dam Engineer. OT has a qualified Engineer of Record (EoR) and deputy EoR, an ITRB, and independent operational and design reviewers.
2. Regular reviews of both short- and long-range tailings management plans to ensure adequate funding/planning for tailings management.
3. Following the processes (in Rio Tinto D5 safety standard on tailings storage and GISTM) to deliver quality designs or design changes.
4. Following the processes (in D5 and GISTM) to deliver constructions that meet the design intent.
5. Maintaining an effective Operations Maintenance and Surveillance (OMS) manual and conducting proper TSF operations, TSF maintenance, and TSF surveillance activities, accordingly, including:
    - maintaining a defined operational freeboard;
    - maintaining a defined size of reclaim pond;
    - maintaining an effective TSF monitoring system with the trigger action response plan (TARP) defined and regularly reviewed; and
    - conducting regular planning and maintaining a mature level of preparedness for upset and emergency scenarios.
6. Maintaining an effective tailings response plan (for loss of containment dam failure scenarios) and conducting regular response drills.
7. Following the Rio Tinto 3-lines-of-defense assurance delivery model:
    - First line of activities by OT site-based team and the Rio Tinto Copper technical team for a proper implementation of D5 and GISTM.
    - Second line of activities by the Rio Tinto Group Technical Major Hazards team.

Good practices for engineering and operations

OT TSF is a modern tailings storage facility with a thoroughly documented development history. Engineering study started in the 2000's and over almost 20 years Knight Piésold, KCB, Golder, and ATC Williams have amassed engineering data and reports for the OT TSF. The cumulative understanding of the site condition is thorough and up to date through several programs of site investigation and laboratory testing. The current engineering assessment methodology is at the state-of-practice, for material characterization, pore pressure response behavior characterization, and geotechnical analyses including liquefaction evaluation, slope stability, and seismic deformation. The adopted dam raising methodology for the TSF is to raise the containment embankments in the downstream direction. A review board was established earlier in the TSF development process. For the current TC2 initial construction, the EoR has full time supervision onsite led by an experienced construction engineer.

The TSF is founded on Cretaceous clay and the potential geotechnical (in)stability associated with it remains to be the most visible risk-driving failure mode (leading to a potential loss of containment of tailings and water). This was confirmed through a recent (October 2022) hybrid risk analysis (HBRA) presented later in this paper.

While clayey foundation is of general concern for its undrained behavior during shearing and its potential to reach a residual strength condition, the current adopted shear strength characterization of the clay for OT TSF design is appropriate, and this conclusion is based on significant number of efforts including carrying out multiple comprehensive field and laboratory investigation programs, employing state-of-the-art geotechnical analyzing techniques, and conducting multiple reviews. OT continues its working with the EoR on recommendations from the ITRB to further improve the confidence on and verify/confirm the appropriateness of the shear strength characterization of the clay for design.

A weakness of engineering during TC1 initial construction in 2011 was the decision not to install a purposely designed seepage collection (drainage) system; this decision, compounded with a few other chains of events, has led to the high salinity incident officially registered in November 2021. However, TC2 has clearly rectified this engineering weakness.

An internal review in 2019 raised its concerns on limited appreciation of the regional hydrogeological setting and the potential interaction between TSF seepage and the surface/groundwater system. Since then, significant works have been completed by Piteau Associates on the subject, including hydrogeologic well testing, site hydrogeological characterization, and numerical modeling on seepage and water chemistry. This work has informed the TC2 design on seepage management.

A comprehensive TSF OMS manual was last updated in August 2022. The OMS includes the full scope from tailings delivery, tailings deposition, water returns, and embankment performance monitoring with proper TARPs defined. The tailings depositional practice has refined over the years and has since early

2019 been performing well in terms of encouraging proper tailings beach development and tailings consolidation, minimizing water loss through evaporation, and maintaining the operating freeboard and size of the reclaim water pond.

OT maintains a system of comprehensive geotechnical instrumentations on telemetry (on Tableau system) to monitor pore pressures and displacements, with well-defined/reviewed TARPs. Multiple daily inspections are conducted by several TSF related teams. Deformation remote monitoring by InSAR is included in the system as well. Continuous evaluation on the currency and adequacy of dam instrumentations is evident. EoR team is well connected with activities onsite and independent operational reviews are carried out per a defined schedule.

The monitoring of the growth of the TSF basin at OT with bathymetric surveys can be improved. Although the state of tailings does not control stability of the TSF, an improved understanding on the overall in-placed dry density of the stored tailings mass and its spatial distribution enhances tailings response planning, refines the TSF life (duration) estimates, and leads to a more efficient closure design.

Tailings response plan, included in the OMS manual, was last updated in August 2022. The OMS includes TARPs to trigger the tailings response plan. The response plan is based on failure impact scenarios simulated in the dam break studies. OT carried out a drill for tailings response in 2019 during which OT was able to contact potential population to be impacted within one hour. Another drill was carried out in 2023.

ALARP demonstration

Rio Tinto has designed a risk analysis (HBRA) to be conducted to support the ALARP demonstration. The HBRA largely follows what is practiced by the Bureau of Reclamation of US Department of the Interior and US Army Corps of Engineers (BOR and USACE, 2019) and US Federal Energy Regulatory Commission (FERC, 2021) as quantitative risk analysis (QRA) for dam safety. The state-of-practice of risk characterization for dam safety relies in part on subjective probability estimates (quantification of expert judgment). Such a risk analysis was carried out for OT TSF in October 2022 (Step 2 in Figure 2) and formed the basis for its ALARP demonstration exercise presented in this paper.

Societal risk tolerability (Steps 2 and 3 in Figure 2)

The risk analysis identified eight risk-driving failure scenarios for the OT TSF:

1. Failure of TC1 embankment in the area of the northwestern corner due to rising pore pressures at toe resulting from sealing of foundation pore pressure relief wells.
2. Failure of TC1 embankment in the area of the northwestern corner due to design with nonconservative parameters adopted for the foundation.

3. Failure of TC1 embankment in the area of the northwestern corner under normal static condition.
4. Failure of TC1 embankment in the area of the northwestern corner under seismic loading condition.
5. Failure of TC1 embankment in the area of the northeastern corner under normal static condition.
6. Failure of TC1 embankment in the area of the northeastern corner under seismic loading condition.
7. Failure of TC1 embankment in the area of the northeastern corner due to foundation liquefaction or strain softening caused by rapid loading (fast rise of water level in the reclaim pond).
8. Failure of TC1 west embankment under seismic loading condition.

It is noted that all the above failure scenarios are the so-called geotechnical instability failure mode which is about the static and seismic instability of the embankment-foundation system (the structural containment system). During the risk analysis, there was consensus that any overtopping or internal erosion-based failure mode is not significant (or risk-driving) for the OT TSF due to the rigorous design and construction of the TSF. The risk characterization from the risk analysis led to Figure 3 presenting the risk level posed by the TSF.

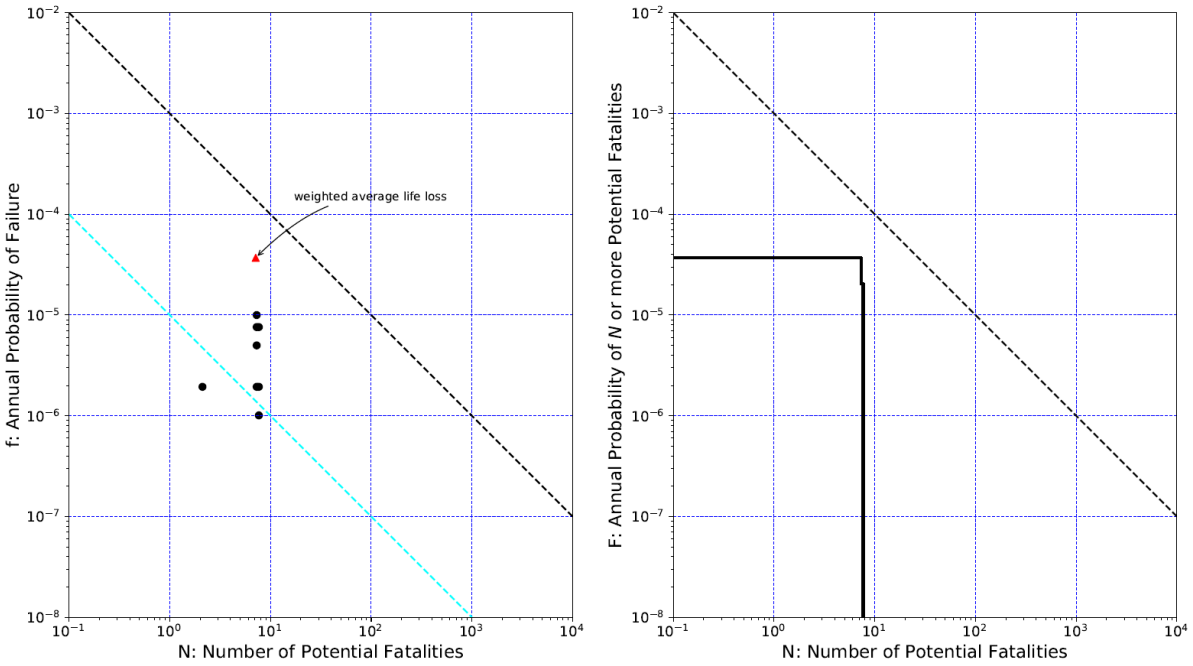


Figure 3: Existing risk posed by OT TSF (based on risk analysis in October 2022)

The *F*-*N* chart (Figure 3) presents cumulative (combined) risk effect required for societal risk (public safety) evaluations. *F*-*N* is the relation between the estimated number of fatalities (*N*) and the estimated annual probability of failure of the dam (*F*) causing loss of life ≥ *N*. As detailed in Zhu and Pascoe (2023), risks falling within the ALARP region (such as shown in Figure 3) are not considered to be tolerable until after assessing continuous risk reduction measures. These are risks that we do not regard as negligible but rather something we need to keep under review and reduce further if we can. The Rio Tinto ALARP

roadmap for dam safety does not involve the concept of "broadly acceptable risk" that is at normally two orders of magnitude lower than the Limit of Tolerability (LoT). Good dam safety management practice requires continuous risk monitoring and reviews even for risks at two orders of magnitude lower than the LoT. The Rio Tinto ALARP roadmap requires assessing continuous risk reduction measures for all risk levels; by doing so, it maintains a downward thrust on an already low risk level.

Continuing risk reduction measures (Steps 2 and 4 in Figure 2)

For the OT TSF, during the risk analysis in October 2022 (Step 2 in Figure 2) the following further risk reduction/mitigation measures were identified and assessed:

- Risk reduction measure (RRM) #1: Undertake study to assess pore pressure impacts on stability performance related to sealing off foundation pressure relief wells along the north embankment of TC1.
- Risk reduction measure (RRM) #2: Assess the extent and orientation of clay fissuring within the clay foundation and update material properties used with the stability models to reflect the outcomes of the study.

Both RRM #1 and RRM #2 are about characterization of the foundation for the TSF. The Rio Tinto ALARP process considers such efforts as part of good engineering practice, as such, these efforts should be carried out *regardless of cost or time*. The consensus during the risk analysis is that, once these studies are completed, the perceived risk would be lower, as presented in Figure 4.

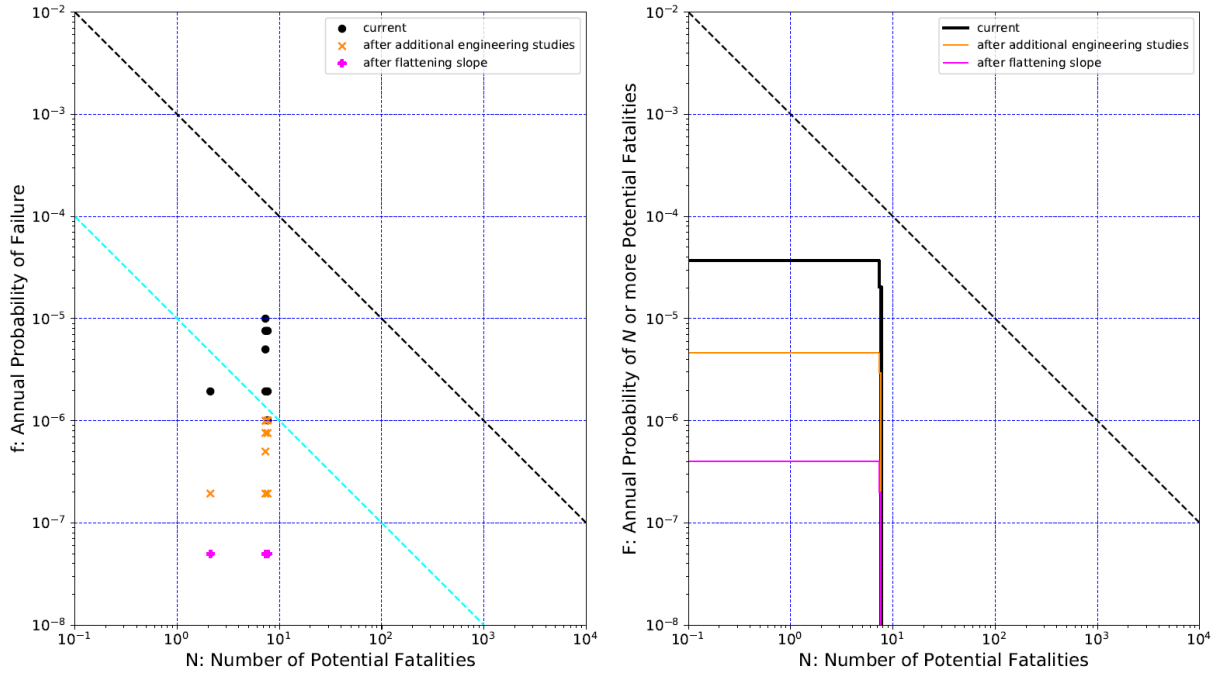


Figure 4: Summary of risks posed by OT TSF

The risk analysis (Step 2 in Figure 2) did not identify other risk reduction measures due to the robustness of the OT TSF (as briefly summarized above in the Section on *good practices for engineering and operations* as part of Step 1 on *good practice demonstration*). However, for the purpose of demonstrating ALARP regarding the benefit of further risk reduction versus the additional effort (sacrifice) required, Figure 4 also includes a hypothetical risk level after further flattening the downstream slopes. Following the Rio Tinto group ALARP guidance, Table 1 presents the cost benefit evaluation for this risk reduction measure of flattening the downstream slopes, based on the following inputs:

- Current existing risk (the expected value of annual life loss) = 2.78×10^{-4} (this is the area under black lines on the FN chart in Figure 3 or Figure 4).
- Flattening the existing downstream slopes would achieve a risk reduction of 2.75×10^{-4} that would lead to a residual risk of 2.99×10^{-6} (indicated by the magenta lines on the FN chart in Figure 4).
- The cost of such measure is US$5M capital spending. In reality, any type of flattening the current 4H:1V downstream slopes would incur a cost much higher (hence leading to an even higher disproportion factor in Table 1).

Table 1 indicates that it is *not reasonably practicable* to implement such a risk reduction measure.

Table 1: Cost benefit evaluation for flattening the downstream slopes

Description of the proposed Risk Reduction Option:		*flattening downstream slope*	
Base Data			
Value for preventing a single fatality (VPF)	12,000,000	*USD*	**See ALARP Guidance note*
Disproportion factor (PF)	10		**See ALARP Guidance note*
Scenario Data			
Existing risk (base case)	2.78E-04	*pa*	**Taken from relevant quantitative risk annalysis. This is the cumulative individual risk calculated or the expected value of annual life loss (calculated with FN curves, based on 'stationary stochastic process' assumption)*
Risk with implemented risk reduction option	2.99E-06	*pa*	
Risk reduction offered	2.75E-04		
Cost to implement solution			*The 'cost' and 'value' should be in common Net Present Value (NPV) terms.*
Capital cost	5,000,000	*USD*	**Cost estimate to implement solution*
Life of facility until closure	15	*years*	**expected life of facility until closure*
Operational expenditure per year	0	*USD*	**Ongoing yearly operational cost*
Yearly cost	333,333		
Cost for preventing a fatality (CPF)	1,214,053,986	*USD*	
Disproportion Factor (PF)	101.2		
Conclusion on Risk Reduction option	Don't implement risk reduction option		

Effectiveness and sufficiency of risk controls (Steps 2 and 4 in Figure 2 continued)

The Rio Tinto ALARP roadmap for dam safety lastly requires a review of the effectiveness and sufficiency of risk controls. This review leads to well-reasoned arguments demonstrating that there are a mix of controls

along each significant potential failure development pathway to ensure that there is an adequate spread of type of controls, depth of controls, and control effectiveness for each significant failure scenario.

For OT TSF the risk analysis in October 2022 (Step 2 in Figure 2) identified the following risk controls including both preventive and mitigative controls:

- Proper engineering designs, including:
  - A qualified design consultant for providing the design.
  - Adequate site and laboratory investigation programs to properly characterize the subsurface conditions, the dam construction materials, and the tailings material.
  - Proper seismic hazard study.
- Proper hydrogeological study on the regional groundwater system overall and pore pressure regime in the TSF foundation in particular.
- Proper hydrological study and adequate surface water management (upstream diversion) to minimize recharge into the groundwater system directly underneath the TSF.
- Proper independent reviews.
- Proper TSF constructions, and construction QCQA.
- Proper water balance study and modeling to guide the operation of the supernatant pond and monitoring of the water level of the supernatant pond.
- Sufficient monitoring of the growth of the TSF basin with bathymetric surveys, and proper planning and execution of tailings deposition.
- Adequate and sufficient TSF monitoring with TARPs defined and reviewed regularly and implemented with the monitoring and mitigation plans defined with the TARP levels.
- Preparedness and response planning for upset and emergency scenarios.
- Specifically for the risk of environmental impact (by seepage from TSF), controls include a properly designed and constructed seepage management system (drainage, cutoff, seepage collection and a pump back system when required to capture seepage leaving the compliance boundary), proper seepage monitoring, and water compliance monitoring.
- Failure impact assessment based on proper dam break studies and a proper tailings response plan with periodic mock exercises.

These risk controls are mapped out against the potential development of a failure pathway leading to downstream consequences. This detailed mapping of risk controls shows that there is an adequate spread of type of controls, depth of controls, and control effectiveness for each significant failure scenario analyzed during the October 2022 risk analysis (Step 2 in Figure 2). These detailed mappings are also well-reasoned arguments that there are effective risk controls in place to keep the risk posed by the OT TSF low. Due to

page limitations this paper is unable to include these detailed mappings of risk controls for OT TSF. Interested readers are encouraged to contact the paper authors.

ALARP documentation (Step 5 in Figure 2)

Deciding whether a risk is reduced to ALARP is a deliberate and separate exercise from seeking continuous improvement of dam safety management. The result of an ALARP assessment could be one of the following (Zhu and Pascoe, 2023):

- Existing risk is confirmed to be ALARP.
- Risk would be ALARP after implementing action(s).
- The confidence level for the risk characterization is low so that additional studies are required before an ALARP conclusion.
- ALARP is not possible, and other actions are required, e.g. the removal of the storage facility should be considered.

This deliberate ALARP assessment exercise should be properly documented (Step 5 in Figure 2). For the case presented in this paper, a document was prepared to support the assessment result that the risk posed by the OT TSF was reduced to ALARP based on the four pillars of evidence (Zhu and Pascoe, 2023). This document was approved by AE and became one of the integrated knowledge base files of the project.

Conclusion

A well-designed, constructed, and operated TSF is expected to pose a low risk. The application of the ALARP principle is consistent with the requirements of Rio Tinto's risk management standards, maintains a downward thrust on this already low risk, ensures that the risk situation does not deteriorate, and drives continuous improvement of dam safety management.

Determining whether a risk has been reduced to ALARP requires judgment. Risk characterization is an iterative, analytical-deliberative process. There is no simple formula for computing what is ALARP. Rio Tinto has adopted an ALARP roadmap for dam safety (Zhu and Pascoe, 2023) to help practitioners to meet the need for ALARP demonstration. This paper presents the details of a real case on ALARP demonstration by following the Rio Tinto ALARP roadmap for dam safety. The same process is being applied to the rest of TSFs in its portfolio. While deciding whether a risk posed by a tailings storage facility is reduced to ALARP is a deliberate and separate exercise, seeking improvement of dam safety management and conformance with good practice is continuous throughout the lifecycle of the TSF.

Acknowledgements

The authors appreciate the permission of Rio Tinto and the Oyu Tolgoi mine to publish this paper to advance the risk related engineering designs and approaches for tailings storage facilities.

References

BOR and USACE. 2019. *Best practices in dam and levee safety risk analysis, version 4.1*. July 2019. Bureau of Reclamation of US Department of the Interior and US Army Corps of Engineers.

FERC. 2021. *Engineering guidelines for the evaluation of hydropower projects, chapter 17 – potential failure mode analysis*. December 2021.

GISTM. 2020. *Global Industry Standard on Tailings Management by the Global Tailings Review*, 2020.

Zhu, Y. and M. Pascoe. 2023. ALARP for safety management of tailings storage facilities. *Proceedings of Tailings and Mine Waste, 20b23*. November 5–8, 2023, Vancouver, Canada: 1041–1053.

Importance of Environmental Components in Assessing Risks under GISTM

Karen Bechard, Geosyntec Consultants Inc., Canada
Heather Townsend, Geosyntec Consultants Inc., Canada
Rachel James, Geosyntec Consultants Inc., Canada

Abstract

Risk management is a key component under the Global Industry Standard for Tailings Management (GISTM), which strives towards zero harm to people and the environment. Under this standard, a large part of assessing potential risk to people and the environment is understanding the geotechnical stability and tolerance of a Tailings Storage Facility (TSF) to withstand certain events (e.g., weather, seismic). However, understanding how environmental factors affect the risk potential of a TSF can be important, and the evaluation of environmental risks under the GISTM is not clearly defined. When evaluating the potential risk of harm to people and the environment, it is imperative to understand the conceptual site model, for example, how various environmental components interact spatially and temporally, to understand the full spectrum of risks and how to most effectively manage them. Environmental considerations cover many topics, two examples of which are geoenvironmental and ecological factors.

Geoenvironmental factors consider impacts from surface water, groundwater and pore water transport, interactions with the local hydrology (water balance), chemistry/geochemistry of mine wastes (i.e., acid generation potential and longevity of acid generation, and metal leaching potential) and impacts to geotechnical stability. Ecological factors consider ecological community structure, whether that may include the presence of endangered species, or valued ecosystem components (e.g., fish spawning area). Under GISTM, the information listed above comprises a large part of the environmental Integrated Knowledge Base (IKB). This paper describes how environmental components are threaded throughout the GISTM, along with geotechnical stability components, how they are included in the decision processes within the GISTM risk evaluation framework, and ultimately how they feed into risk management design considerations and closure planning. Examples of potential impacts and design input based on the authors' experience with closed mine site projects will be provided.

Introduction

A Tailings Storage Facility (TSF) at Vale's Córrego de Feijão mine in Brumadinho, Brazil collapsed in January 2019, causing the deaths of 270 people. In response to this event, the Global Industry Standard for Tailings Management (GISTM) (PRI et al., 2020), a program voluntarily entered by mining companies, was developed with the intent of increasing the level of safety to people and the environment by improving tailings governance and management. The GISTM contains 77 auditable Requirements, distributed among 15 Principles, which in turn are grouped into the following six topic areas:

1. affected communities;
2. integrated knowledge base;
3. design, construction, operation and monitoring of the tailings' facility;
4. management and governance;
5. emergency response and long-term recovery; and
6. public disclosure and access to information (PRI et al., 2020)

Environmental components are woven throughout these six topic areas of GISTM, either directly, or indirectly and hold increased weight with respect to interpretation of material impacts as described below. This paper will discuss:

- the environmental components of GISTM;
- the environmental "what's new" under GISTM;
- interpreting connections between environmental disciplines and other technical areas of GISTM; and
- integration of environmental components into the assessment of risk and risk management.

Environmental components within GISTM

The majority of the direct environmental aspects of GISTM are addressed through Topic Areas II (Integrated Knowledge Base [IKB]) and III (design, construction, operation and monitoring of the tailings facility), as summarized in Figure 1. While requirements underlined in Figure 1 indicate direct environmental deliverables and/or input to TSF management, the subsequent discussion in this paper emphasizes that environmental characterization and evaluations should be completed to inform all components of TSF design and design implementation (e.g., construction, operational, and progressive closure and reclamation).

Under topic areas II and III, environmental components like Comprehensive Site Characterization Report (Requirement 2.2), Water Balance Model (Requirement 5.3), Environmental Surveys, and

Environmental Impact Assessments (Requirement 3.3) are clearly defined (PRI et al., 2020) and are associated with clear deliverables to be incorporated into the sites IKB.

Topic 2: Integrated Knowledge Base		Topic 3: Design, Construction, Operation and Monitoring of the Tailings Facility			
Principle 2	**Principle 3**	**Principle 4**	**Principle 5**	**Principle 6**	**Principle 7**
2.1 Document and update knowledge about social, environmental, and local economic context of TSF **2.2** Prepare, document, and update comprehensive site characterization **2.3** Develop and document dam breach analysis **2.4** Assess and document potential human exposure and vulnerability to TSF failure scenarios	**3.1** Adaptively manage TSF using climate change knowledge **3.2** Analyze multi-criteria alternatives for tailings management (new TSF) OR periodic review of technology and design (existing TSF) **3.3** For new TSFs, assess lifestyle impacts including climate change factors **3.4** Define 'material change' for social, environmental, and local economic impacts; Adaptively manage impacts	**4.1** Determine consequence of failure classification **4.2** Determine external loading criteria (new TSF) AND perform 5yr DSR; ITRB/SITR review **4.3** Adopt classification and flexibility for future upgrades (AE) **4.4** Identify and document the design criteria (DBR) **4.5** Apply design criteria, considering material properties, slope stability, seepage and deformation **4.6** Identify and address brittle failure modes **4.7** Implement ALARP in upgrades, signed by EOR/AE if not feasible **4.8** Prepare DBR (by EoR); ITRB/SITR review	**5.1** Incorporate multi-criteria alternatives (new TSF) **5.2** Develop a robust design demonstrating feasibility of safe closure **5.3** Develop a water balance model **5.4** Address all potential failure modes to ALARP **5.5** Develop design for each stage of construction **5.6** Design closure to demonstrate feasibility, incl. progressive closure and reclamation **5.7** Approval by AE of design to ALARP **5.8** Conform with standards for resettlement	**6.1** Build, operate, close TSF according to design intent **6.2** Implement QA/QC and Construction Design Intent Verification **6.3** Prepare "As-Built" reports, signed by RTFE/EOR **6.4** Develop, implement, review, and update OMS **6.5** Implement change management system and Deviation Accountability Report signed by AE **6.6** Include new and emerging technologies and approaches in TSF design	**7.1** Design, implement, and operate a performance monitoring program **7.2** Design, implement, and operate engineering monitoring for potential failure modes **7.3** Establish specific and measurable performance criteria for monitoring **7.4** Analyze monitoring data; Identify and address deviations through Trigger Action Response Plan **7.5** Report monitoring results with approval of EoR/RTFE

Numbered requirements are listed under each Principle; Requirements with direct environmental deliverables/input are underlined.
TSF = Tailings Storage Facility, AE = Accountable Executive, ITRB = Independent Tailings Review Board, SITR = Senior Independent Technical Reviewer, DSR = Dam Safety Review, ALARP = As Low As Reasonably Practicable, DBR = Design Basis Report, EoR = Engineer of Record, RTFE = Responsible Tailings Facility Engineer, QA/QC = Quality Assurance/Quality Control

Figure 1: Requirements under GISTM with direct environmental deliverables/input

A brief description of key environmental disciplines (excluding those related to stability evaluations, which are well understood under geotechnical engineering, seismicity, and physics) that support GISTM, and how they provide technical inputs integral to interpretations of environmental conditions under GISTM are listed as follows:

- **Geology** – The geologic setting, including both regional and local geology, plays a critical role in understanding the natural environment and forms the foundational understanding for several other GISTM components, including hydrology, geochemistry, hydrogeology, and geotechnical studies. Geological investigations identify potential risks such as active faults and unstable slopes as well as initial characterization of soil and rock formations.
- **Hydrology** – Hydrologic components, defined to include site and regional surface water volume, flow rate, and conveyance, are considered within a tailing's facilities' design, operation, monitoring and closure. GISTM requires a solid understanding of the mine site hydrology through IKB components such as: site characterization, hydrological modelling, and the Water Balance Model (WBM). It is also linked to flood (RA), as well as through monitoring and reporting.

- **Geochemistry** – Geochemistry utilizes knowledge of the regional geology alongside targeted environmental testing to assess the acid generating and metal leaching (ML) potential of stored mine waste to understand the risk of producing acid rock drainage (ARD). Geochemical characterization is a core component to environmental RA for each type of mine waste such as waste rock, overburden, tailings, and process water. Geochemical characterization forms the basis of the geochemical conceptual model (GCM) which integrates with mine waste and mine water management plans to predict site wide water quality and downstream environmental impacts. Hence, geochemical assessment supports environmental assessments and plays an important role in the selection of potential contaminants of concern.
- **Hydrogeology** – Groundwater at mine sites is most frequently impacted by seepage into the subsurface from waste disposal sites. The fate and transport of those contaminants is controlled by the hydraulic parameters of the water-holding subsurface rock and soil layers, which transmit groundwater along the hydraulic gradient. Thus, hydrogeological investigations characterize the subsurface to understand the flow of groundwater and to identify areas where surface contaminants may more easily impact groundwater quality or where groundwater may discharge to the surface and impact downstream ecosystems. Within GISTM, hydrogeological investigations support site characterization, the WBM and Site Water Quality Model (WQM), and closure planning.
- **Ecology** – Ecology supports the IKB and environmental consequence classification by allowing an understanding of the rare or endangered species within the area, and the quality of habitat in the surrounding environment that could be potentially impacted. Ecology is integrated into the GISTM to ensure environmentally responsible practices that minimize impacts on ecosystems. This includes conducting baseline ecological studies/surveys and Environmental Impact Assessments (EIAs), avoiding sensitive habitat, and designing facilities to minimize ecological impacts. Biodiversity conservation plans, long-term ecological monitoring, and adaptive management strategies are implemented to protect local habitats and species. Effective water management practices safeguard aquatic ecosystems, while RAs and emergency response plans address potential ecological threats. Closure and post-closure plans include ecological restoration and sustainable land use to promote ecosystem recovery.
- **Ecotoxicology** – The evaluation of ecotoxicity is dependent on understanding the presence of contaminants or constituents with the potential to become toxic over time or under specific conditions. In other words, it is dependent on an understanding of water quality, geochemistry and the receiving environment ecosystem. It evaluates the potential for toxic effects to ecosystems and is a component of the environmental consequence classification, Ecological RAs and EIAs under

GISTM. Ecotoxicology is one of the main reasons that chronic loss of contaminants may require mitigation plans.

- **Water chemistry** – This includes the chemical characterization of existing surface water and groundwater, and projected chemistry of TSF impacted water. Tracking water quality and field water chemical parameters over time allows for the identification of potential transport of TSF-impacted water that can aid in site water management planning. Site water chemistry projections are conducted by utilizing the outputs and interpretation from geochemical laboratory testing (and hence GCM) and WBM to develop the Conceptual Site Model (CSM) and WQM; which then further inform the overall environmental and social impact assessments.
- **Meteorology/climatology** – Meteorological and climatological data inform accurate water balance calculations, essential for planning water management systems. These data help predict extreme weather events whose probable maximum precipitation (PMP) values support climate evaluations of tailings dam structures and inundation mapping in the event of a catastrophic failure. Meteorological data are used in hydrological models to simulate water movement and to inform design flood levels, while climatological data aids in long-term planning and RA.

The authors interpretation of the connections of the listed environmental disciplines to key components of the Environmental IKB, as well as how the IKB feeds into the RA framework under GISTM are shown in Figure 2.

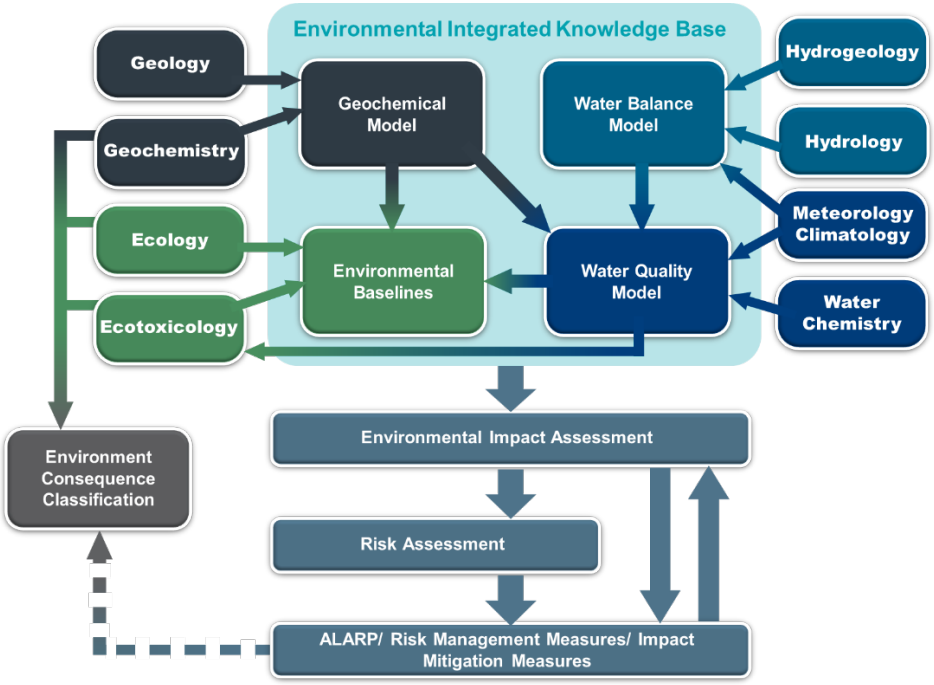


Figure 2: Environmental disciplines supporting GISTM framework

Another clear environmental component within GISTM can be found within Principle 3 "Use all elements of the knowledge base – social, environmental, local, economic and technical – to inform decisions throughout the tailings facility lifecycle, including closure" within the definition of material impacts (PRI et al., 2020), which leads to a new interpretation of 'loss of contaminant', as discussed below.

The environmental "what's new" under GISTM

Prior to the formation of the GISTM standard, loss of containment at a tailings dam at operational sites was mainly considered to be a dam failure. The GISTM, however, acknowledges that there are other avenues through which loss of containment can occur via its inclusion of 'chronic impacts' and 'long-term impacts' in its explanation of potential material impacts to a tailings facility which would require impact mitigation and management plans (for new tailings facilities; Requirement 3.3), or an update to the tailings facility management following adaptive management best practices (for all tailings facilities; Requirement 3.4). In other words, GISTM allows that material impacts can occur through loss of containment over time (e.g., chronic loss), instead of solely by an acute catastrophic event. There are two main environmental contributors that fulfill the chronic impact meaning, and both fall under the environmental umbrella: contaminant loss due to dust transport, and contaminant loss due to seepage. The authors acknowledge that, particularly for closed sites, contaminant loss due to these types of plumes were an identified risk prior to GISTM, however the inclusion of these within GISTM pushes these considerations forward into earlier planning stages within a mine's life.

Given the inclusion of chronic contaminant loss events as material impacts, long-term chronic downstream effects are put into question. The implications of this are discussed further under the topics of RA and Risk Management below.

Interpreting connections between environmental components and others technical areas under GISTM

While the preceding section identified the obvious, or 'direct', environmental components under GISTM, this section discusses the role that environmental components may have as an 'indirect' factor. For example, where environmental input is not specifically identified, but where that component may be influenced by environmental factors or outcomes. Figure 3 shows a high-level framework for GISTM, highlighting those areas where environmental components are linked in some capacity either directly, or indirectly, for example, as a predecessor where input from the environmental team is essential to achieve the intent of GISTM. It highlights the integral nature of environmental components/input throughout the duration of GISTM integration.

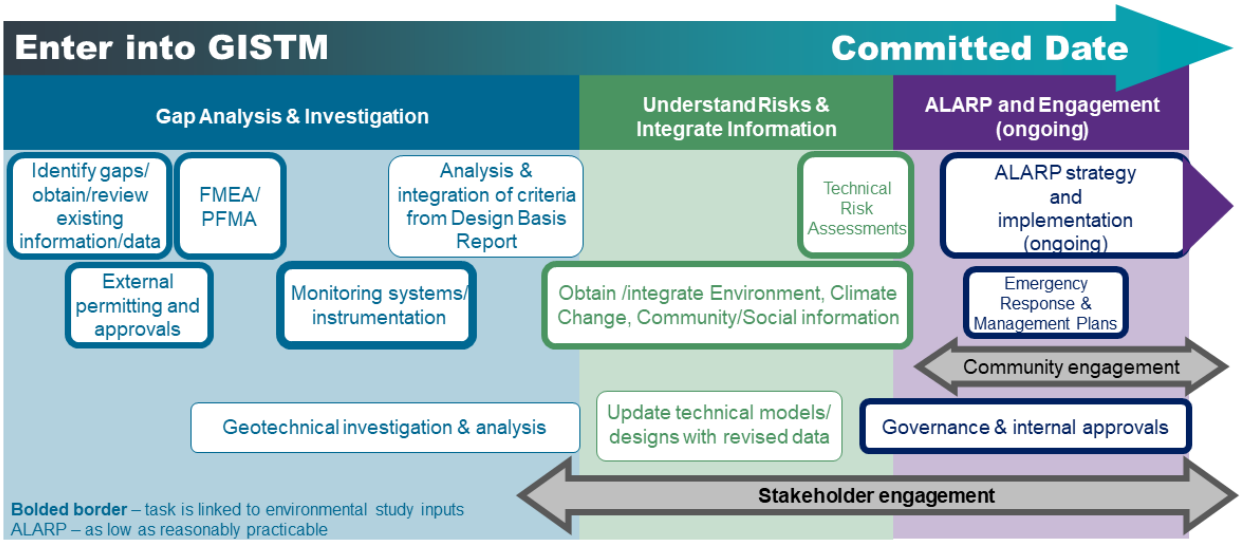


Figure 3: High-level schedule GISTM roadmap showing environmental study touchpoints

An example of an indirect relationship would be the dependency that dam breach analyses (non-environmental component) have on the climate change RA (environmental component), which provides necessary inputs such as PMP values and frequency of extreme storm events required for the assessment to use climate change knowledge according to the practice of adaptive management.

Another example of an indirect relationship would entail utilization of environmental site characterization information (e.g., tailings geochemical characterization and projected water quality under the GCM and WQM components) to inform operational, closure and reclamation, and overall site waste management and water conveyance design. An example of this indirect component and its importance under GISTM is further detailed below.

Weaving environmental components into the assessment of risk and risk management

Environmental component in RA

The evaluation of risk occurs within the 'Risk Assessment' box in Figure 2 and can be evaluated because it encompasses the knowledge of the environmental IKB and relevant EIAs. Formal RAs are required under GISTM in two key places. Foremost is the assessment of risk to potential failure modes of the TSF structure, foundation, etc. (Requirement 5.4). Typically, this is achieved through a Potential Failure Modes Analysis (PFMA) and is sometimes combined with a Failure Mode and Effects Analysis (FMEA). RAs must consider all potential failure modes until they are deemed non-credible (ICMM, 2021). Thus, environmental components must be considered in this process if they are a credible risk. The relevant environmental components evaluated are Site-specific. For instance, a site with existing or potential ARD

will include significant geochemical considerations compared to one with no ARD potential. In general, data (including environmental data) is reviewed in the context of the design and closure plan to identify potential failures that could occur, as well as the potential impact those failure modes could have from an environmental perspective. This requires a solid understanding of the site characterization data, including the water balance model, GCM, surrounding habitat quality, and other relevant environmental information.

Requirement 10.1 of the standard requires that a multi-disciplinary RA (MDRA) be conducted every three years, or in response to a material change to any of the RA components – this includes tailings facility, social, environment, or local economic changes. Environmental data is one of the main components for an MDRA, especially the environmental studies interpretation "…*which emphasizes the human relationship with the environment and the social and political dimensions thereof."* (Britannica online, 2024). The outcomes of the RA feed into the as low as reasonably practicable (ALARP) process under GISTM along with the implementation of impact mitigation measures and risk management measures. Two examples of how environmental data could lead to significant risks are included below. The examples highlight why the Canadian Dam Association (CDA) Environmental Consequence Classification (ECC) framework (Nikl et al., 2022) includes 'intrinsic hazard of contents' in the classification system, along with ecological impact and duration of impact.

Example of environmental component with potential for significant risks (geochemical)

TSF contact water can contain elevated concentrations of metals, sulphate and other parameters of concern; the source of these parameters can be in situ reactions of residual minerals in the tailings solids, or process water discharged with the tailings slurry. The geochemical evolution of a TSF may also influence the physical characteristics of TSF solids, impacting flow and stability through the tailings. An example of this occurred in 2019 at Córrego do Feijão mine near Brumadinho, Brazil where the failure of Dam-I was partly attributed to geochemical evolution. Iron oxidation products, observed by scanning electron microscopy (Robertson et al., 2019), resulted in bonding between coarse tailings particles. Interpretation of pre-failure cone penetration test results in the context of in situ shear wave velocity (Vs) profiles suggest the "development of microstructure due to a small amount of bonding" (Robertson et al., 2019).

Thus, it is possible that the bonding created by iron oxidation products could have contributed to the development of a microstructure in coarse tailings, impacting geotechnical parameters of the solid tailings (Robertson et al., 2019). Robertson et al. (2019) concluded that the bonding between particles created stiff tailings, that were potentially very brittle if triggered to become undrained. It was also noted that the "unusual mineralogy" of the tailings also impacted the interpretation of standard methods used to evaluate

material parameters that are considered in deformation and stability analyses (Section 6.6, Robertson et al., 2019).

Geochemical alteration is evaluated in the GCM, which accounts for the interaction of the solid tailings and process water with the tailing's particle properties, as well as water transportation (i.e., hydrogeological regime) across the site. Processes that are considered in the integrative GCM for TSF stability include:

- Dissolution of acid generating (e.g., sulfides) and neutralization minerals (e.g., calcite, dolomite) may alter tailings mass, which can in turn affect geotechnical stability through reduction in grain size and changes to hydrogeological regime.
- Secondary mineral formation from porewater saturated with products from previously dissolved minerals. Precipitation of secondary minerals may lead to changes in the hydrogeological regime through decreased porosity/permeability, which may also change the hydrogeological regime and affect geotechnical stability.
- Changes in pH from mineral dissolution and precipitation reactions may impact tailings porewater pH, and thus the physical strength of clay minerals which may be present in TSF foundation or embankment materials thereby affecting their structural integrity (Durocher et al., 2022).

Example of environmental component with potential for significant risks (ecological)

Habitat destruction or contamination due to either inundation from a dam failure, or long-term deposition through dust dispersion or seeps can also lead to significant risks. The former, impact to habitat due to a dam failure, can be identified via an assessment of the ecological impact e.g. as recommended under the ECC framework recommended by Nikl et al. (2022). This assessment includes components such as identifying species of special interest (threatened/endangered/species at risk/species of special concern), defining the region of study, as well as identifying similar habitat in the region.

In an ECC conducted by the authors evaluating the potential ecological impacts related to a modeled inundation area in the event of a dam failure, potential impacts to a trout spawning area, supporting a nearby healthy sport-fishing industry, was a main consideration of the ecological impact assessment included in the ECC (Confidential Site, Montana). The Montana Natural Heritage Program have classified the specific trout species as an "S2-species of greatest conservation need," meaning they are "at risk because of very limited and/or potentially declining population numbers, range and/or habitat, making it vulnerable to global extinction or extirpation in the state" (MFWP, 2022). Habitat impacts and restoration implications, including both costs and duration, are considered in the ECC within the GISTM (ICMM, 2020; Annex 2, Table 1).

The conundrum of environmental protection in risk management

Including long-term effects as material impacts that require management is a game changer for the tailings industry and introduces many more questions on how these impacts should be assessed and managed. For sites that are active, chronic environmental impacts can often be managed at an operational level through maintenance actions like dust suppression and pump-and-treat of TSF-impacted water that may seep off-site from the facility. For sites on their way to closure, management of risks posed by chronic environmental impacts can be more of a challenge.

Key considerations along with pertinent questions requiring thought as an industry, especially for sites entering closure, are listed in Figure 4.

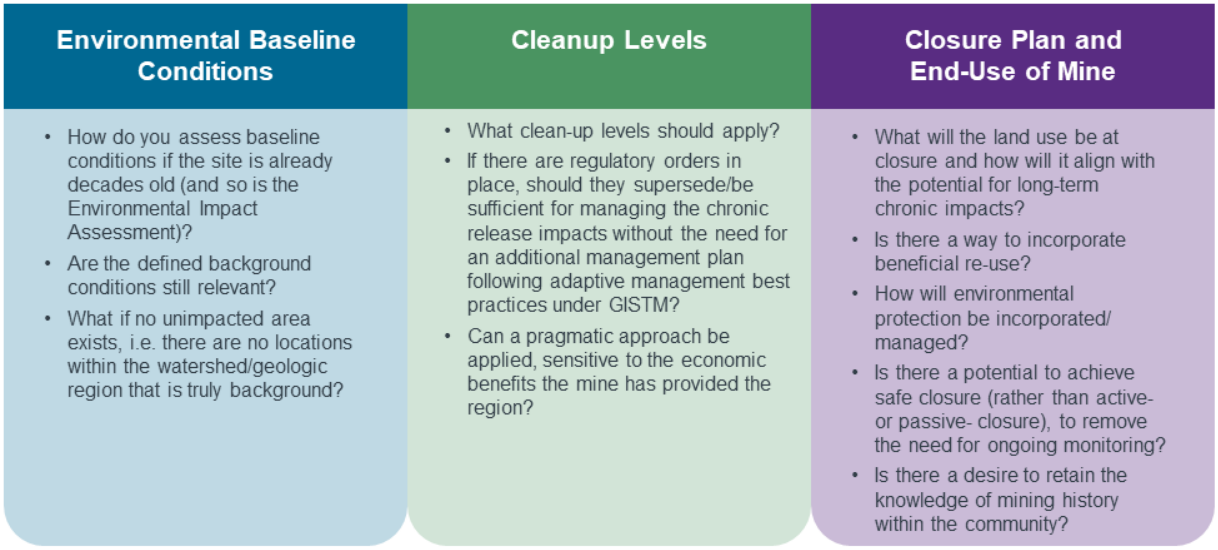


Figure 4: Key considerations for management of chronic environmental impacts

In brief, the questions to be asked as an industry relate to defining environmental baseline conditions, what we are willing to accept as a society with respect to cleanup levels, and how chronic environmental impacts effect the closure plan and end-use of a mine. Ideally, considerations on the benefits that mining has bestowed upon the community and region will be considered in management planning. By permitting a mine, there is an inherent understanding that there will be some associated level of environmental impacts.

Conclusion

This paper discusses how the environmental components under GISTM play an important role in understanding site conditions and how they link with other technical areas within the GISTM framework. Environmental components are integral to assessing the risk for a TSF. Metal leaching and acid rock drainage (ML/ARD) may affect downstream environments directly through degradation of water quality

and habitat and indirectly by increasing the risk of geotechnical instability, while understanding the water balance is integral to closure planning. Further, due to chronic releases being included within GISTM as material impacts, environmental components are an important factor to consider in both the long-term management and on-going assessments of tailings facilities.

References

Britannica online. 2024. Available online at: https://www.britannica.com/science/environmental-science

Durocher, J., D. Sprague and B. Usher. 2022. Geochemical interactions and long-term TSF stability: an update. *Proceedings of Tailings and Mine Waste*. Denver, Colorado, USA. November 6–9, 2022.

ICMM. 2021. Conformance Protocols – Global Industry Standard on Tailings Management. May 2021. Available online at: ICMM – Conformance Protocols: Global Industry Standard on Tailings Management

International Council on Mining and Metals (ICMM). 2020. Global Industry Standard on Tailings Management. August. Available online at Global Industry Standard on Tailings Management – Global Tailings Review

Montana Fish, Wildlife and Parks (MFWP). 2022. Westslope Cutthroat trout conservation strategy for the Missouri river headwaters of Southwest Montana. January 7, 2022. Available online at: https://myfwp.mt.gov/getRepositoryFile?objectID=105196

Nikl, L., Steele, J., Robertson, L., Davidson, S. and R. Schryburt. 2022. An update to the Canadian environmental consequence classification methods for mine dam failures. Canadian Dam Association Conference, October 19, 2022.

PRI (Principles for Responsible Investment), ICMM and UNEP (United Nations Environment Programme). 2020. Global Industry Standard on Tailings Management available online at: global-industry-standard_EN.pdf (globaltailingsreview.org)

Robertson, P.K., de Melo, L., Williams, D.J. and Wilson, G.W. 2019. *Report of the Expert Panel on the Technical Causes of the Failure of Feijão Dam I.* Retrieved from https://bdrb1investigationstacc.z15.web.core.windows.net/assets/Feijao-Dam-I-Expert-Panel-Report-ENG.pdf

Maintaining Continuity Lessons – Learned from a TSF Incident Linked to Engineer Transitions

George Afriyie, Newmont Corporation, USA
Jeremiah Williams, Newmont Corporation, Ghana
Rashida Umar, Newmont Corporation, Ghana
Ankomah Bosomtwi, Newmont Corporation, Ghana

Abstract

Effective management of a tailings storage facility (TSF) requires key roles to be in place for the design, construction, and operations of the facility. These key roles collaborate and need to work closely for the successful management of the facility. One of these key roles is that of the Engineer of Record (EoR).

The EoR role is defined by the Global Industry Standard on Tailings Management (GISTM) as the "qualified engineering firm that supports a mining firm in confirming that a TSF is designed, constructed and decommissioned with the appropriate level of integrity that aligns and meets applicable regulations, statutes, guidelines, codes and standards." To effectively achieve this, the named EoR for a TSF must be a long-term role that is involved in the life cycle of the facility. Prior to the GISTM, the role of the EoR and other key roles were not mandated within many mining companies (and still are not) unless it was an explicit requirement of the jurisdiction in which the facility was located. To this end, many operational TSFs did not have EoRs in place and may have used different consultants for the design of the various construction stages, often driven largely by competitive bidding processes (i.e., supply chain). This approach is discouraged as institutional knowledge of the facility is lost through the changeover and introduces the risk of loss or miscommunication of certain key information from consultant to consultant. In addition to this, the lowest cost consultant may not necessarily be the most qualified to be the EoR. These can lead to undesirable outcomes in the operation and monitoring of these facilities, such as the development of an incomplete knowledge base, leading to untimely response to upset conditions or deviations from normal condition. This paper discusses how changes in EoR led to an incident on a TSF.

Introduction

The safe and proactive management of tailings storage facilities (TSFs) require key roles to be in place for the operations, maintenance and surveillance of these facilities. These key roles collaborate and work

closely to successfully manage these facilities (ICMM, 2021). One of these key roles is the Engineer of Record (EoR).

Prior to the Global Industry Standard on Tailings Management (GISTM, GTR 2020), the role of the EoR and other key roles such as the Responsible Tailings Facility Engineer (RTFE) were not a requirement in some jurisdictions where mining companies operated. The GISTM defines the EoR role as the "qualified engineering firm that supports a mining firm in confirming that a TSF is designed, constructed and decommissioned with the appropriate level of integrity that aligns and meets applicable regulations, statutes, guidelines, codes and standards." To effectively achieve the intent of this role, the named EoR (external or internal) for a TSF must be a long-term position that is involved in the life cycle of the facility (Sova et al., 2023; Morrison et al., 2017). Considering the jurisdictions where this role was not a requirement, some operational TSFs did not have long-term EoRs (external or internal) and may have used different consultants for the design of the various TSF expansions. The EoR may have often been selected via competitive bidding. This approach is discouraged as it can lead to undesirable outcomes such as loss of institutional knowledge of the facility through the changeover; it introduces the risk of miscommunicating certain key information from one consultant to another; it impacts on longer-term planning for the facility considering the TSF lifecycle; it may not necessarily result in the selection of the most qualified candidate; and it may potentially impact the timely response to upset conditions or deviations from normal operations, in the management of these facilities.

This approach was practiced at one of the mines within the portfolio of the organization prior to the appointment of the current EoR. The loss of knowledge from change in consultants led to an internal erosion incident, but without release of tailings, as a result of a construction defect.

Overview of the facility

The TSF embankments are constructed by the downstream method, comprising the use of local borrow on the upstream portion with the downstream shell constructed with run of mine waste rock from an open pit. Geotextile was previously placed in between the two material types to act as a transition from the local borrow to the waste rock. The embankment upstream slopes on the southern portion have a composite liner system, which consists of a compacted low permeability clay and a High-Density Polyethylene (HDPE) geomembrane liner, whereas embankments in the northern portion have a low permeability clay with riprap on the upstream face. The rate of rise for the TSF is about 2 m per year. The south and southeast embankments are buttressed by a waste rock facility (WRF). Further downstream of the south embankment is an open pit where mining activities have ceased. The spillway of the facility is located at the right abutment of the south embankment and, if activated, flows into the open pit downstream of the embankment.

The supernatant pond is maintained at the southeast corner of the impoundment. The TSF has an overliner drainage system to promote dewatering and consolidation of the tailings on the southern half of the TSF where the pond is located. In addition to the overliner drainage system, a leak collection and recovery system (LCRS) is installed beneath the composite liner to mitigate seepage from the TSF into the surrounding environment. The northern half is lined with a compacted clay liner. In the design and construction of the facility over the last decade, the services of three different consultants have been used.

Governance structure for TSFs

The organization uses the Line-of-Defense (LoD) model, as shown in Figure 1, for the responsible management of the facilities in the portfolio. The model has key roles at the site and corporate levels with defined roles to manage the facilities.

1st Line of Defense	**Site-based implementation** The site teams that actively manage the facilities include the site's General Manager (GM); a Responsible Tailings Facility Engineer (RTFE), who is responsible for the integrity of the site's tailings facility (or facilities) and oversees their design, construction and monitoring; and a dedicated Engineer of Record (EoR) and EoR team, who provide technical expertise and assurance that the tailings facility is safely designed, constructed and operated. The Regional Leadership Team (RLT) is responsible for the respective site team.
2nd Line of Defense	**Systematic third-party review** This process includes Independent Tailings Review Boards (ITRBs) for all active operations and legacy sites with an "extreme" or "very high" consequence classification, senior independent technical reviews for other tailings facilities and periodic dam safety reviews (DSRs) by an independent consulting team.
3rd Line of Defense	**Functional accountability** An Accountable Executive (AE), who reports directly to the CEO, communicates regularly with the Board and is accountable for the safety of Newmont's tailings facilities. The Corporate Tailings and Dams Team (CTDT), serves as a delegate to many of the AE's responsibilities, providing centralized leadership, oversight and support for all tailings facilities (including inactive and legacy operations).
4th Line of Defense	**Leadership commitment** Newmont's Executive Leadership Team (ELT) and the Board of Directors commit to the safe management of Newmont's tailings facilities. The Board's Safety and Sustainability Committee provides oversight, and the AE communicates with the Board through the Committee.

Figure 1: Line-of-defense model

In terms of the site, the governance structure (first LoD) was not fully in place for the TSF under consideration prior to 2020; an RTFE was not appointed. An EoR was appointed for the facility. However, there were changes of the EoR firm based on the outcome of competitive bidding that was organized periodically. Although there were corporate stakeholders involved in management of the facility, they were not required to be involved in decisions to change EoRs or the adjudication of the competitive bids. An RTFE was not appointed for the facility until 2020. In terms of the second LoD, an Independent Tailings Review Board (ITRB) has been in place since 2018. The third and fourth LoDs were implemented as part of tailings management activities in 2020.

Following the full implementation of the governance framework in 2020, changes in EoRs or key roles through competitive bidding that was the previous practice is no longer the case. A guideline is in

place within the organization, which lays out the requirements and interactions required for the different levels around the management and decision-making for the facility.

Changes in EoR

The facility has been in operation over the last two decades and during this period, three different consultants have had some involvement in the design, construction supervision, monitoring, and regulatory reporting for the facility. Figure 2 shows the various stages for the design and construction that these companies were involved in the project. Company 1 was involved in the project from the feasibility stages initiating the design for the starter through to stage 10 of the facility. With regards to the construction supervision, quality assurance (QA) and the construction completion report, Company 1 was responsible for the initial stages until stages 9 and 10, early works. The involvement of Company 1 with the project came to an end in 2014 following adjudication of competitive bids undertaken by the organization.

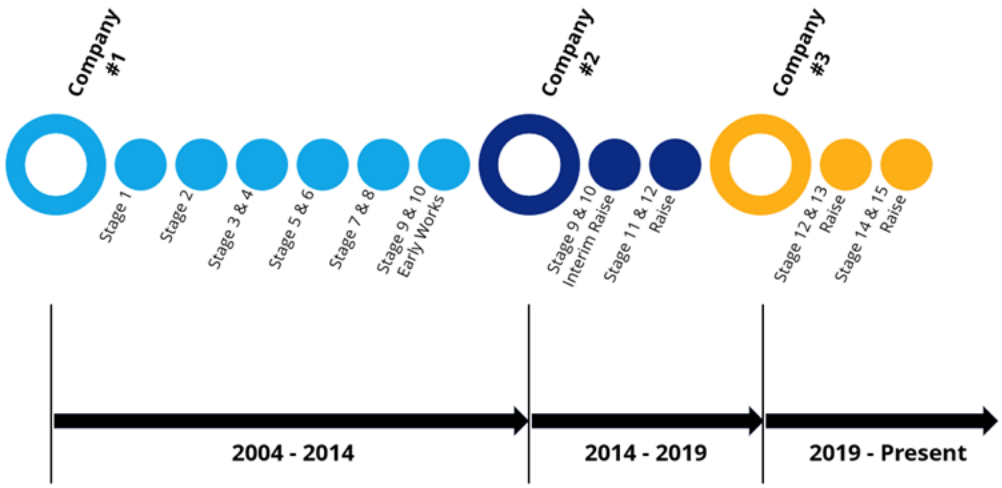


Figure 2: Chronology of EoR involvement with project

Company 2 was contracted in 2014 to replace Company 1 mainly in reviewing the construction supervision documents, quality control (QC) and QA documentation for interim raise of stage 9 and stage 10 undertaken by the organization. This company also compiled the construction completion report. Following the completion of the initial scope, the stages 12 and 13 expansion contract which had design, construction supervision and QA as part of the scope was awarded to Company 2. Following completion of the scope in 2019, Company 2 was replaced by Company 3 through competitive bids.

Company 3 has been involved with the project since 2019. The contract covers the design, construction supervision, QA, and regulatory reporting for the TSF. A terms of reference is in place between

the organization and company 3. The document details the scope of services, authority, roles, and responsibilities of the EoR, as well as the organization's obligations, and forms the basis of the long-term contract that is in place.

For the different changeovers there was no handover period or review, prior to contract execution. During these changes there were no communications around non-conformances or deviations from design with regards to the TSF management or construction. For periods of transition between EoRs, the site undertook the construction supervision and QA activities.

Effects of EoR transitions

This section discusses the observations made through the different changeovers at the site.

Long-term TSF panning

The changes of the EoR as well as the site not having an RTFE has affected the longer-term plans that could have been put in place for the TSF. These changes had the effect that each company that was involved was reviewing previous activities, rather than continuously improving the existing design, monitoring, or management practices. The lack of long-term planning has led to the delay of certain activities such as instrumentation planning and data collection to fill design gaps in a timely manner. Following the appointment of a longer-term EoR, many important activities that could have been completed in previous years are required to be completed within a shorter period of time.

Operational changes and inconsistency

The changes in EoR led to inconsistency with certain construction activities like instrument raises for the facility. In addition to this, certain operational requirements that may have been aligned to a design intent were changed without implementation of appropriate management of change processes. With a longer-term EoR in place, changes are considered over the facility life cycle to understand the impacts prior to completing such changes, and this provides an opportunity for a more systematic approach to improving practices on the facility.

Dam safety concerns

In situations where key information is not adequately passed on to a new EoR, it can lead to undesirable outcomes. For this TSF, such changes led to a change in the manner in which vertical raises of TSF instrumentation through the geomembrane liner, as shown in Figure 3, were completed. This event presented a condition with increased risk of internal erosion of one of the facility embankments. Due to the lack of the appropriate QC and QA activities during the vertical raise through the geomembrane liner, a

pipe developed via the liner boot. In addition to this, operational volume on the pond was not strictly followed in between transitions.



Figure 3: Extrusion weld around the piezometer extension

Internal erosion mechanism

A cross-functional internal forensic team together with the current EoR investigated the conditions that led to the internal erosion incident. The investigation concluded that the incident occurred vertically along the extended standpipe of the instrument, as shown in Figure 4, after the geomembrane liner tore along the extrusion weld of the HDPE geomembrane boot, which can be observed in Figure 3. The instrument was a standpipe that had been converted to a vibrating wire piezometer (VWP); hence, the vertical raise through the liner was to extend the cable for readings to be taken.

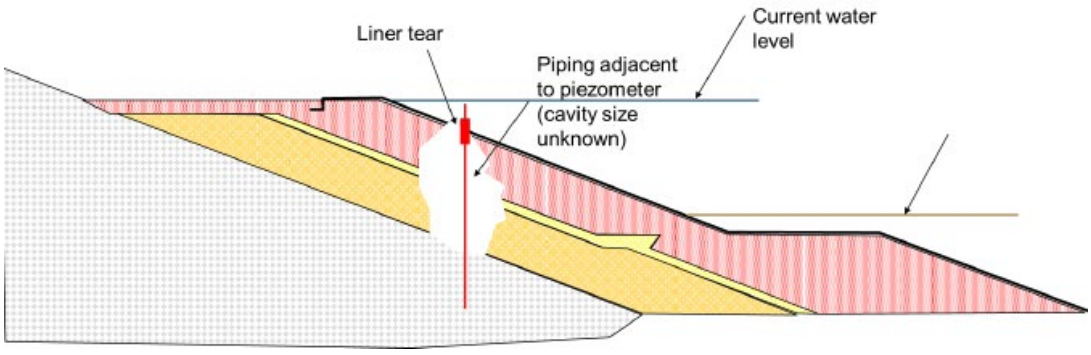


Figure 4: Illustration of piping incident along piezometer penetrating the geomembrane

Considering the robustness of the downstream rock shell, minor damage was observed on the upstream slope of the embankment beneath the liner. The established procedures within the organization were followed by the site in responding to the incident as well as the completion of the repair process.

Lessons learned from the EoR transitions

The lessons learned through the EoR transitions, and the internal erosion event included the following:

- The change of consultants at various stages of facility expansion led to knowledge of the facility not being retained or passed on. This has been evident in the planning for the facility considering the complete lifecycle. Having an appointed EoR in place has ensured that longer-term planning for the design and/or operational practices are aligned to the closure and post-closure goals.
- Appropriate documentation should be developed for key tasks that form part of TSF raises. The instrument raise through the liner that is required with each raise for this TSF was not clearly captured in previous construction completion records and no procedure was developed. To this end, the change in supervisory personnel without a reference led to poor QC and QA of the instrument raise.
- Although competitive bidding can be effective in meeting the commercial objectives of an organization, in the instance of a facility built over multiple years like a TSF such an approach does not necessarily yield the desired value. For this TSF, the amount of money spent to repair the internal erosion incident quickly eroded the difference in cost during the competitive evaluation of the consultants.
- A robust governance structure in place for a TSF is essential in ensuring that management and decision making involves a cross-functional team. The governance structure in place prior to the transitions did not require stakeholder engagement for such changes regarding the EoRs. The robust governance currently in place requires such decisions to be approved by the Accountable Executive or their delegate.
- There was cross-functional collaboration from different departments on site, regional, and corporate level as well as the EoR in the monitoring and repair of the internal erosion incident. This ensured that all components of TSF management were taken into consideration. Collaboration and transparency with the regulators built a stronger relationship and trust with the organization. The forensic report from the investigation was shared with the regulator.
- A well-documented and effective Operation, Maintenance and Surveillance (OMS) manual with well-defined Trigger Action Response Plans (TARPs) are effective in guiding the site to determine deviations from normal operations.

Conclusion

Change of EoRs at various stages of design and construction with inadequate handover had adverse effects on the management and operations of a TSF facility. Over the last two decades of operations, three different

companies were involved in the design and construction supervision of the different stages of the tailings facility. Following lessons learned on an internal erosion incident and effects on long-term planning for the facility, effective changes have been implemented to ensure that a long-term EoR contract is in place. A more robust governance structure is in place within the organization to ensure that such decisions concerning EoR changes, if required, involve other stakeholders at the site, regional, and corporate levels.

The internal erosion incident was due to failure of an extrusion weld around an instrument that penetrated the HDPE geomembrane liner. The continuous use of a single consultant would have most likely prevented the occurrence as the instrument raise deviated from practices used for previous construction raises. The practice of changing consultants as a result of competitive bidding is strongly discouraged (or should be highly scrutinized if required), as the design and construction of these facilities benefit greatly from a long-term consultant (EoR) to ensure learnings are effectively incorporated into the management of these critical infrastructures.

Repairs related to the incident on the TSF have been completed. Lessons from these incidents have been shared across the organization to prevent reoccurrence.

References

Global Tailings Review (GTR). 2020. Global Industry Standard on Tailings Management. Accessed 06/01/2024 at https://globaltailingsreview.org/global-industry-standard/

International Council on Mining and Metals (ICMM). 2021. Tailings management good practice guide. Accessed 06/15/2024 at https://www.icmm.com/website/publications/pdfs/environmental-stewardship/2021/guidance_tailings-management.pdf?cb=60002

Morrison, K.F., Snow, R.E., Ridlen, P. and Hatton, C.N. 2017. What does it mean to be the Engineer of Record (EoR) for a tailings storage facility (TSF)? *Proceedings of Tailings and Mine Waste, 2017*. Accessed 06/15/2024 at https://www.researchgate.net/publication/336130546

Sova, M.R., Erturk, H.S. and Hatton, C.N. 2023. Effective EoR succession planning recommendations for implementation of GISTM. *Proceedings of Tailings and Mine Waste, 2023.* Vancouver.

Preventing Potential Consequences of a TSF Failure: Addressing the Other Side of the Risk Equation

Susan Joyce, On Common Ground Consultants, Canada
Keiran Doyle, Satarla, UK

Abstract

Implementing the new GISTM is introducing a series of challenges to operating companies as they seek to upgrade their geotechnical stability, adjust tailings management systems and organizational structures, and to adapt existing technical decision-making modalities to the new demands of GISTM requirements. Companies have frequently focused on Topic III: Design, Construction, Operation and Monitoring of the Tailings Facility, and Topic IV: Management and Governance. Many companies have sought to integrate into existing operational systems the new components of integrated decision-making laid out in Topic II. Some requirements of Topic II are poorly understood and lagging in implementation, even though they contribute to the overall objective of building and managing TSFs for safer outcomes, and inform decision-making processes required by Topics III – VI.

With a strong focus on reducing probability of failure, less has been reported to date on steps to eliminate or reduce potential consequences of a TSF failure. This paper considers requirements within GISTM that support understanding and decision-making directed at reducing potential consequences of credible tailings failures, and argues that this process should take place in parallel with efforts to reduce the probability of failure. It presents two shifts in approach to address this gap; first, we propose a strategic shift in risk assessment approaches to put "safety of people" at the center of the risk analysis rather than "TSF failure." Building on that shift, we propose a pathway – a sequence of short-term actions for assessing and reducing potential consequences to prevent harm to people. We argue that this allows sites to apply all levels of the risk-control hierarchy, employing proactive controls aimed at eliminating or reducing consequences, in contrast to the current practice of proactive engineering controls combined with primarily reactive mitigation measures as a response to actual impacts on people's lives.

Introduction

Increasing production and forecasts of resource extraction, particularly for copper, suggest a continued trend towards larger tailings storage facility (TSF) structures containing more tailings that are potentially

deposited more quickly, all of which increase the probability of TSF failures (Robertson, 2018). They already represent some of the largest engineered structures on earth, and by deduction, the largest hazards created by humans.

The Global Industry Standard for Tailings Management (GISTM or the Standard) came into play in 2020 due to the steep rise in TSF failures, and fatalities arising from them. ICMM companies committed to the implementation of the GISTM standard, and to ensure that very high and extreme Consequence Classification dams are "compliant" by August 2023, with two additional years to bring other TSFs online. Considerable work has been done to align management systems and put in place "levels of defense" – Dam Safety Reviews, Change Management, Independent Tailings Review Boards, Responsible Tailings Facility Engineers, and so on. Considerable effort has been expended by companies to improve the design and construction of geotechnical containment structures to optimize the stability of existing TSFs and their ongoing management.

While not possible to quantify from the available data, it is reasonable to assume that the effort and investment to date in complying with GISTM has been predominantly focused on reducing the probability of failure. This work, given the underlying uncertainty in geotechnical parameters and the pre-existing instability or information gaps identified in recent failures, is critically important. However, geotechnical studies and subsequent strategies to improve stability take time and resources, so providing for safer facilities is not usually a quick solution. Further, industry recognizes that engineering and monitoring improvements are not going to eliminate the risks of failure; they may even increase the risk in the short term, such as in the Cadia embankment failure of 2018 (Jeffries et al., 2019). Meanwhile, the assessment of the very real consequences for at-risk populations situated downstream of these facilities, and actions to eliminate or manage those consequences, are far less mature.

Understanding and quantifying the consequences for people is important – critical in fact – because it is the threat to people that is at the core of the standard – and it is what drives many specialists doing this work. Kemp introduced disaster literature to the discussion of TSF failures in 2020 by contextualizing TSF failure events in terms of their human cost. The example used was of a hurricane offshore that is just a hurricane unless it wreaks havoc with peoples' lives and property, in which case it becomes a disaster. Equally a tailings dam failure is not a disaster unless there are people – and property, infrastructure, etc. killed or damaged – although it may still constitute an environmental disaster. For a TSF failure to be considered a disaster requires people, their livelihoods, infrastructure, or critical ecosystems to be in the path of a TSF failure, and for it to cause serious disruption to the functioning of affected people through losses and impacts (Kemp, 2020).

A similar focus was put forward by Robertson in 2018 when he conceptualized TSF management in terms of a system that includes what is at risk downstream. He put forward a systems approach to tailings

governance that identified three components of the system that must be assessed – 1) the stability of the TSF; 2) the failure path or route; and 3) the receiving environment. In Robertson's terms, each of these components of the system needs to be identified, assessed, and strengthened in order to manage risk and improve resilience at the level of the TSF system (Robertson, 2018). The agreement between the two approaches is that the TSF containment failure is a disaster depending on what happens downstream.

Discussion

Different understandings of risk assessment

The definition of risk from the perspective of threats to objectives is simple enough; the *Oxford English Dictionary (OED)* defines risk as simply a "hazard or danger, or exposure to a mischance or peril" (RAIS, 2024). A TSF presents a hazard to people, property and the environment – there is no probability associated with the existence or reality of the concept. Through the development of risk assessment as a decision tool, which the *OED* dates to 1957 as a term, one of the tools for assessing and prioritizing response to risk is the assessment of risk as a relationship between consequences and probability. Risk assessment is a core practice and tool used by tailings professionals to identify and understand the hazards that pose a threat, and to allow prioritization of the actions to be taken to reduce the risk(s) associated with that threat. Prioritization is helpful and even necessary in a world of limited time and resources in which to respond to a hazard.

Risk conceptually considers both probability and consequences when it is used to evaluate options in a complex situation and to direct proportionate effort and money towards the most important contributors to the risk. But how you ask the initial questions, or how you posit what the risk is, will determine how you assess the root causes, pathways, consequences, and subsequently the controls that are developed. The people usually at the table – frequently all trained in the same ways of thinking and analyzing TSF risk (Ospina and Chovan, 2022) agree on the risk question: how to stop TSF failures. They then agree on control measures that are put in place to prevent or respond to the unwanted event, identified as the TSF failure. In doing so, operators are only addressing the risk probability and are missing a range of potential tools and actions available for consideration that place greater emphasis on eliminating or reducing potential consequences.

This is not consistent with GISTM intent, which includes several requirements aimed at identifying and assessing potential consequences and, when these are high, requires operators to take actions to reduce the consequences in case of a failure. The most explicit, Requirement 5.7, states that for new facilities classified as High, Very High and Extreme, "… the Accountable Executive … shall approve additional reasonable steps …to further reduce potential consequences to people and the environment." And that for existing TSFs, the Accountable Executive "... shall seek to identify and implement additional reasonable

steps that may be taken to further reduce potential consequences to people and the environment." (GISTM, 2020).

Risk assessment is also applied to the field of Business and Human Rights, but the approach differs in several important ways from environmental or safety risk management. When considering risks to human rights there are the requirements that: 1) all risks to human rights caused by companies should be eliminated; 2) there are no "offsets" to compensate for negative impacts to human rights; and 3) mitigation is defined as reducing the probability of an impact occurring and is employed when elimination of the risk is not possible (UNHCHR, 2012). Prioritization of actions is based principally on the assessed severity of the risk based on context and scope (extent), scale (gravity of the harm), and the ability to remediate the harm done.

The most significant difference when assessing risks to human rights is that the probability of the risk occurring is considered, but it is a secondary level consideration to ensure adequate attention is paid to high-severity, low-probability impacts (UNGP Reporting Framework, 2024). Severity is the predominant factor considered; the probability of the harm occurring "may be relevant in helping prioritize the order in which potential impacts are addressed" (UNHCHR, 2012).

In contrast with risk assessments formulated as "probability x consequences," severe risks to humans should not be qualified by the probability of it occurring; actions should be taken to eliminate the risk. Hence, companies need to take action to reduce the severity of human rights risks (i.e., consequences) in parallel with reducing probabilities.

Using risk assessment for proactively reducing consequences

One of the most versatile and widely used tools for risk assessment and communication is the bowtie analysis. Disaster analysis and process safety management provided the impetus for developing the bowtie tool, the use of which is driven by the need to understand high consequence hazards that endanger multiple lives and have far-reaching impacts. Bowtie analysis facilitates the mapping of pathways to and from unwanted events across defined occurrence time-zones to inform and strategize the development of proactive and reactive controls.

As illustrated in Figure 1, proactive controls are typically applied to causes, with reactive controls implemented to directly or indirectly mitigate consequences or impacts after they have occurred. If the risk assessment identifies embankment failure as the critical Unwanted Event, that is the focal point of the bowtie and control measures are built based on that. Controls aimed at prevention – the left side of the bowtie – are subsequently focused on TSF stability from an engineering perspective. Harm to people is a consequence and by design, subject to only reactive controls.

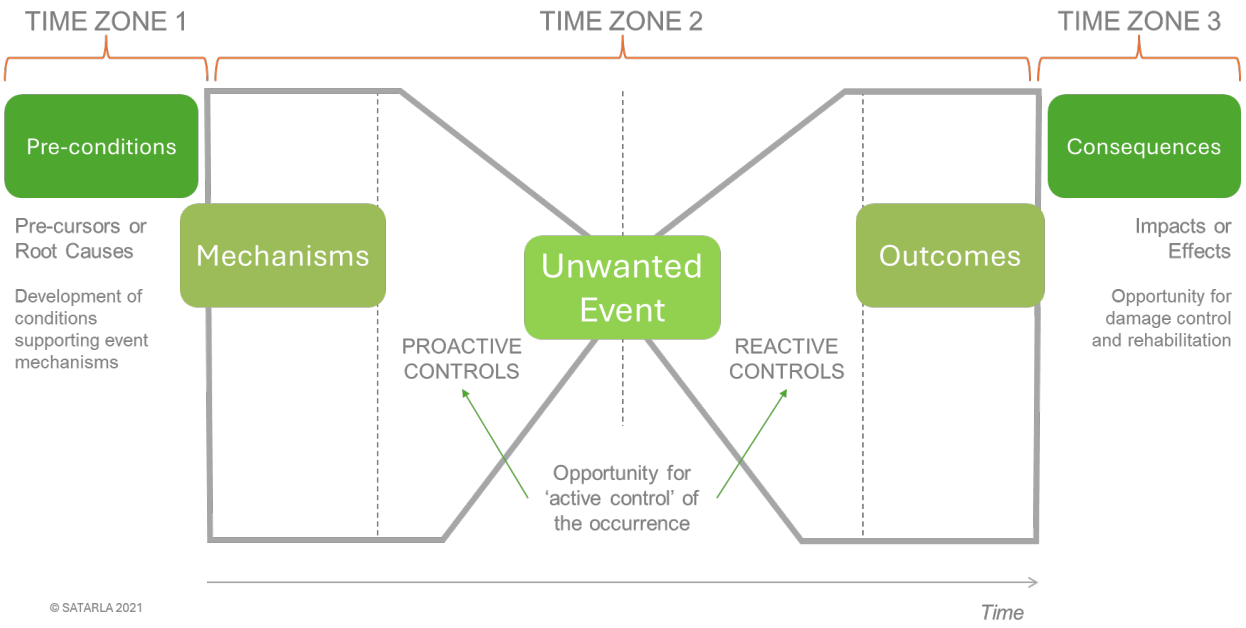


Figure 1: Generalized time sequence of events in bowtie analysis. Doyle (2024) with influence from Viner (1991)

If the chosen material unwanted event is "harm to people," an effective bowtie analysis should enable the identification of a range of pre-conditions, contributing causes/mechanisms requiring the implementation of preventive controls. This likely would include TSF instability, and it also would generate additional causes relative to what puts people in the pathway of a failure; what exposes them to the hazard; and what makes them vulnerable to harm if it occurs. This "risk statement" should lead to identification of both direct and indirect reasons for why people are exposed to harm by the hazard, e.g., location of people and facilities, poor construction of downstream homes, unavailability of surface water in other potential locations, etc. (see Kemp, 2020, for a detailed discussion of exposure and vulnerability).

If the intent is to identify effective controls for preventing "harm to people," then positioning that as the problem or unwanted event results in a bowtie analysis that is more focused on the causal pathways that put people at risk and consequently supports development of preventive and proactive controls to remove or reduce that exposure to harm, not just preventive and proactive controls considered relevant to geotechnical stability.

Review of the GISTM approach to reducing risk as a consequence-based standard

GISTM requirements provide a pathway to deliver on improved safety of tailings management in the short term, through the identification of people who are exposed to the TSF hazard, how they are exposed to the specific outcomes (e.g., liquified tailings inundation or base slump, etc.) and steps to be taken to prevent consequences and to be prepared to respond – engaging controls on both sides of the bowtie analysis. These are actions the operator can implement during the time required for upgrading geotechnical stability of

existing facilities. This proposed sequence is even more critical for operators of those facilities where geotechnical instability has been identified, or with limitations to being upgraded as required by the standard (see Requirement 4.7).

As has been discussed at earlier conferences (Small et al., 2023), the mandate for the Expert Panel that developed GISTM was to use a consequence-based approach to inform requirements for design and other aspects of TSF management such that consequence and probability of failure are evaluated independently. The consequence-based approach aligns with a human rights principle, which is to eliminate the risks associated with an event if the consequences are high or extreme, even if the relative probability is low (UN Guiding Principles Reporting Framework, 2024).

A sequence of key requirements for preventing harm and reducing consequences

Implementing the 77 requirements of the GISTM requirements requires delivering on over 200 deliverables across the 15 Principles (McNab et al., 2023), and determining which deliverables and requirements are highest priority is a challenge and is influenced by decision-makers' areas of expertise. Built into the GISTM are a series of requirements or actions designed to provide operators with the information needed to act on worker and community safety relative to a potential TSF failure, and social performance expertise in the tailings management team can fine-tune this sequence to the specific situation.

Using that expertise, a sequence of actions for existing TSFs can be construed from the requirements that has the potential to provide a basis for decisions on reducing potential consequences in the short term, while additional studies are underway and/or geotechnical engineering upgrades are being put in place. This same sequence serves as the basis for a more comprehensive set of controls when the studies and assessments making up the Integrated Knowledge Base have been completed. This allows development of a deeper and more robust analysis of how people are exposed to various forms of harm from potential TSF failures (Kemp, 2020; Owen et al., 2020), as per the assessment of causal pathways in a bowtie analysis and the disruption of those pathways through proactive controls to prevent harm.

The assessment of potential human exposure and vulnerability (Requirement 2.4) is the linchpin in this process and cannot be carried out without meaningful engagement of those at risk (Requirement 1.3). This assessment starts with the outputs of the Dam Breach Analyses for credible failure modes (Requirement 2.3) and the resultant inundation maps. Based on these inputs, social specialists should be mobilized to carry out a targeted engagement and assessment of potential impacts to people's lives and livelihoods to understand who and how people are exposed in the case of a TSF failure, including the workforce, contractors, and itinerant users of downstream areas.

In urgent situations such as at-risk populations downstream from an unstable TSF, the approach may be drawn from well-established social research methodologies such as Rapid Rural Appraisal (Townsley,

1996), or others appropriate to the context. The information obtained is fundamental to inform short-term decision-making around safety, to support safety-focused risk assessments (as per the bowtie analysis approach discussed above), and to inform decisions on the allocation of key resources to address both stability (probability) and safety (consequences). Finally, this information is necessary to inform reactive controls to mitigate consequences, in particular emergency response preparedness – just in case.

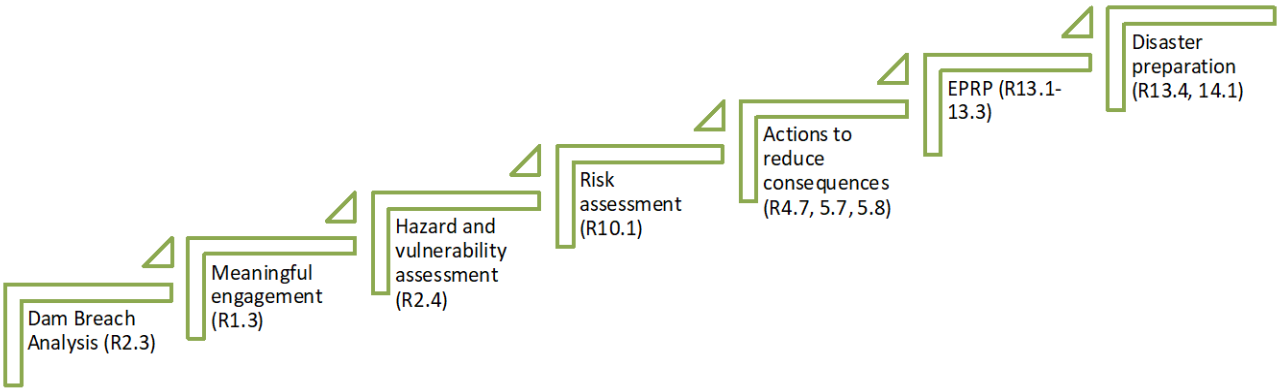


Figure 2: GISTM Harm Prevention Sequence for an existing TSF

This Harm Prevention Sequence also requires meaningful engagement and disclosure of the risks people are under to complete the remaining steps effectively and deliver safer outcomes. Involvement and ongoing engagement with at-risk stakeholders are built into the remaining requirements of the Sequence as they are into the Standard:

- At risk groups should be represented at and participate in risk assessment workshops as part of the multi-disciplinary and multi-stakeholder input to ensure that a diversity of perspectives and perceptions are included and to avoid bias, overly like-minded thinking, and over-confidence in reduction of probability as being sufficient for the reduction of risk (Ospina and Chovan, 2022).
- Identification of proactive controls aimed at reducing consequences for at-risk people will require disclosure and their participation in decision-making.
- Emergency Preparedness and Response Planning (EPRP) cannot be effective, nor it is aligned with GISTM Requirements 13.1–13.3, unless it is carried out collaboratively with first responders and local authorities as well as directly with at-risk workers, contractors, and community members.
- Disaster preparation and planning is fundamentally about engaging with public sector actors, first responder and authorities, as well as at-risk people.

This sequence, and GISTM in general, requires an effective internal and external engagement process; the importance of building internal cross-functional literacy and capacity between social and engineering teams while negotiating these stages, should not be underestimated (Ospina and Chovin, 2022).

In time, an initial rapid assessment focused on short-term actions to reduce consequences and inform emergency planning should be built into in-depth social and environmental impact assessments of the inundation zone(s) and more robust exposure and vulnerability assessments, in line with the requirements of Topics I and II of GISTM but also as the required knowledge base for the integrated decision-making embedded across the standard. The intention behind identifying a key sequence of actions to prevent harm is that these studies take time to carry out effectively and comprehensively, as do geotechnical investigations, and those responsible for high-risk TSFs should be informed on how to reduce potential consequences as soon as possible.

The Requirements presented here provide a proposed set of actions to be implemented in sequence, and to ensure that each step informs the next and that consecutive steps are aligned with the intent of keeping people safe. The information inputs, analyses, and engagement processes allow for informed decision-making on the appropriate and acceptable (to the people at risk) steps for proactively reducing consequences. This also provides a credible process whereby the Accountable Executive can attest to and demonstrate that further actions have been taken to reduce consequences (Requirements 4.7 and 5.7). While geotechnical improvements are fundamental to long-term safety, this approach recognizes that TSF failures remain possible – if less probable – and that people need to be kept safe.

Key for safety – EPRP

The Emergency Preparedness and Response Plan is an output of the risk assessment process, and it is typically identified as a reactive control for consequences articulated on the reactive right-hand side of bowtie analyses. An operation-wide EPRP is a standard part of a mining operation's physical security and OHS safety programs, with scenarios described, planned, and in principle trained on for all identified potential emergencies through pre-arranged drills and simulations. The emergency response kicks in when the event is imminent or has occurred, so it is by definition a set of reactive controls and intended to mitigate or minimize negative impacts, not to prevent them. The intent of the EPRP is to limit the damage done by the TSF failure to the greatest extent possible through response preparedness, training, availability of specific equipment and resources, etc.

The pre-GISTM practice of developing EPRPs only for hazards or emergencies identified within the footprint of the operation presents a problematic gap in both management and governance if not addressed explicitly through the engagement and coordination required by the Standard. On-site safety teams may have no mandate off-site, and TSF teams have no mandate or expertise in emergency planning or response. Probably neither of these functional areas have any knowledge of or expertise to understand types of exposure of downstream populations. Hence, the planning, coordination, training, and testing associated with emergency preparedness for hazards/emergencies that leave the operational footprint may require an

entirely new approach, organizational structure, and team to ensure clear assignment of responsibility and accountability for this critical task.

Drawing on the strategic shift in risk assessment proposed above, emergency planning associated with potential TSF hazards can be implemented in ways that make it more of a proactive control, contributing to reducing community exposure to hazards and improving resilience. This can be accomplished by conducting EPRP development with communities at risk from TSF failures in line with the UN APELL (Awareness and Preparedness for Emergencies at Local Level) approach (UNEP, 2015). In the process of engaging and training for emergency response to a TSF failure, a broader capacity to identify and eliminate direct consequences, or mitigate and prepare for a wider range of hazards present for the community can be constructed.

Conclusion

The arguments for acting in the short term to reduce potential consequences in parallel with the measures adopted to reduce the probability of a failure are two-fold. First, it is aligned with GISTM intent and will support the responsibility that the Accountable Executive has relative to this issue. Secondly, carrying out consequence prevention measures to address the exposure of at-risk people to harm provides additional tools with a higher visibility with the local community and potentially a faster delivery than many engineering fixes. Thirdly, prevention is more cost-effective than remediation, as evidenced by the costs associated with the three largest and most deadly TSF disasters of the last decade; Mt. Polley, San Marco, and Brumadinho. The investments made by BHP and Vale in recovery programs through the Renova Foundation after the San Marco failure are likely to be higher than the cost of averting the failure from the start (Kemp, 2022). Quantifying the probable cost of a disaster can focus decision-making onto taking measures that will reduce consequences in case of a failure; the win-win associated with these actions is the probable positive contribution to quality of housing or security of tenure, etc., for at risk people as actions are taken to address their vulnerability.

The argument is not to stop making TSFs more stable – as is widely recognized, dams that have failed and killed people were found after the fact to have been unstable prior to failure. However, in facing hazards with the potential to lead to major disasters, represented by multiple fatalities and significant damage to livelihoods, ecosystems, and social infrastructure, reducing probability is not sufficient. And neither are the requirements of GISTM solely focused on reducing probability. Tackling the problem from multiple fronts, due to multiple causal pathways, makes greater sense and reflects an urgency that is not always perceived. If we can broaden the scope of activities being undertaken to more than engineering, we have a wider range of tools available, which subsequently broadens the scope of action and focus of efforts.

Accountability for decisions to reduce consequences is clearly defined in GISTM as sitting with the Accountable Executive; there remains work to determine who has responsibility and the capability to ensure that this work is being done on site. As discussed above, reducing consequences requires carrying out assessments of exposure, vulnerability of people to the failure modes, and engaging with them to address the risks they face, the solutions for these may be varied and need to be determined with them. In other words, the work is bringing the core practices of social performance specialists to the table in managing TSF risk.

There needs to be a clear focus in the GISTM implementation on keeping people safe in the face of the real and ongoing hazard presented by TSFs, and there are tools at hand to do so. If people are permanently situated in the pathway of a credible failure, the potential for harm to them is almost never eliminated through geotechnical stability and TSF management alone. The point is to ensure that there is a risk management strategy in place that puts "avoiding harm to people" at the core – as the unwanted event, so that consequences are being reduced when lives are at risk. The two dimensions of reducing risk – probability and consequences – can and should take place in parallel, mobilizing different internal teams so that different resources are channeled to the relevant controls aimed at prevention of the unwanted event, rather than solely reacting to it.

Acknowledgements

We would like to acknowledge the contribution of Dr Deanna Kemp for bringing disaster literature and perspective to the work of the Global Tailings Review Expert Panel that developed the GISTM, and for her ongoing critical thinking relative to root causes of human exposure and vulnerability to TSF failures in conjunction with her colleague Dr John Owen. Dr Keiran Doyle and Chris Neal's previous work on the use of bowtie analysis has shaped our understanding of its potential effectiveness in this context. Any and all errors are ours.

References

Doyle, K. 2024. Generalised Time Sequence Model for Bowtie Analysis, Satarla. *With Influence from Neal, C. 2023*. Unpublished.

Hopkins, A. and D. Kemp 2021. *Credibility Crisis: Brumadinho and the Politics of Mining Industry Reform.* Sydney: Wolters Kluwer.

Jeffries, M., N.R. Morgenstern, D. Van Zyl and J. Wates. 2019. Report of ITRB on NTSF Embankment Failure, Cadia Valley Operations for Ashurst Australia. Accessed April 28, 2024, at https://www.newcrest.com/sites/default/files/2019-10/190417_Report%20on%20NTSF%20Embankment%20Failure%20at%20Cadia%20for%20Ashurst.pdf

Kemp, D. 2020. Lessons for mining from international disaster research. In *Towards Zero Harm: A Compendium of Papers Prepared for the Global Tailings Review.* Accessed 20/10/2020 at https://globaltailingsreview.org/: 37–46.

McNab, Louise, J. Boshoff, J. Gutierrez, E. Zegarra, D. Honores, N.A. Mensa, F. Rodriguez and J. Rogers. 2023. GISTM – defining substantial conformance: Gold Fields' substantial implementation of the GISTM at the Cerro Corona mine in Peru and Tarkwa mine in Ghana. In Joe Goodwill (editor), *Proceedings of Tailings and Mine Waste 2023,* Vancouver, BC, Canada: 1245–1255.

Ospina, M. and Chovan, K. 2022. The social side of tailings management: reflections on environment, social and governance compliance. *Proceedings of the 8th International Conference on Tailings Management*. Gecamin Publications. Accessed 06/19/2024 at https://www.gecaminpublications.com/tailings-2022/

Owen, J.R., D. Kemp, É. Lèbre, K. Svobodova and G. Pérez Murillo.2020. Catastrophic tailings dam failures and disaster risk disclosure. *International Journal of Disaster Risk Reduction* 42: 101361. Accessed 02/20/2023 at: https://www.sciencedirect.com/science/article/pii/S2212420919306648

RAIS. 2024. The risk assessment information system. Accessed June 10, 2024, at https://rais.ornl.gov/tutorials/whatisra.html#:~:text=The%20Oxford%20English%20Dictionary%20(Oxford,injury%2C%20damage%2C%20or%20loss.

Robertson, Andrew M. 2018. Corporate governance for management of tailings dams; 3RT approach to assessment and management. Presented at the Mines Waste and Tailings 2018 Conference Tailings Course.

Small, Andy, Angela Küpper, Tamara Johndrow and Mohammad Al-Mamun. 2023. Credible failure modes – summary of 2021 and 2023 workshops. In Joe Goodwill (editor), *Proceedings of Tailings and Mine Waste 2023,* Vancouver, BC, Canada: 1245–1255.

Townsley, Philip. 1996. Rapid rural appraisal, participatory rural appraisal and aquaculture. Rome, Italy: Food and Agriculture Organization of the United Nations. Accessed 08/12/2z024 at: https://www.fao.org/4/w2352e/W2352E03.htm

UNGP Reporting Framework. 2024. UN Guiding Principles Reporting Framework. Salient human rights issues. Accessed 05/12/2024 at https://www.ungpreporting.org/resources/salient-human-rights-issues/.

UNEP. 2015. Awareness and preparedness for emergencies at local level (APELL). Accessed 08/10/2024 at https://www.preventionweb.net/publication/apell-handbook-process-improving-community-awareness-and-preparedness-technological

UNHCHR. 2012. *Corporate Responsibility to Respect HR: An Interpretive Guide*. Accessed 06/24.2016 at https://www.ohchr.org/sites/default/files/Documents/publications/hr.puB.12.2_en.pdf

Viner, D.B.L. 1991. *Accident Analysis and Risk Control*. Melbourne, Australia: Derek Viner Pty Ltd.

Surveying the Landscape: Understanding Engineer of Record Challenges and Perceptions in the Brazilian Tailings Industry

Luciano Souza, Federal University of Rio de Janeiro, Brazil
Luciana Praça, DF+ Engenharia, Brazil
Matteus Hamade, Associação Brasileira de Mecânica dos Solos ABMS, Brazil
Mauro dos Santos, Pimenta de Ávila Consultoria, Brazil
Raika Silva, RP Soluções Engenharia, Brazil

Abstract

This study investigates the perceptions and experiences of professionals in the Brazilian tailings engineering sector regarding the Engineer of Record (EoR) role. The research utilized a comprehensive survey inspired by similar studies in North America, adjusted for the Brazilian context, to gather data on participants' involvement, aspirations, risk perceptions, and understanding of the legal implications associated with the EoR role. The surveys also captured important information regarding experience level, demographics, and education of the tailings community in Brazil. The findings reveal a significant hesitation among professionals to assume EoR responsibilities, largely due to the recent high-profile dam failures in Brazil and the associated legal consequences. The survey also highlighted a demographic disparity within the industry, with notable gender and race gaps, and an alarming trend of Junior professionals overestimating their competency. These insights suggest a need for improved education and clearer communication of legal responsibilities to the involved professional, alongside initiatives to address demographic imbalances in the field.

Introduction

The demand for qualified professionals in the tailings engineering job market in Brazil surged significantly, starting in 2015 with the Fundão failure and accentuated by the Brumadinho failure in 2019. The high demand was experienced by consultant companies that were suddenly inundated with an enormous demand for new projects to improve the safety of existing tailings facilities in the country. This demand was not all driven by the proactive motivation of dam owners to improve current operations, but rather was mainly motivated by the myriad of state and national legislation updated since 2016, which became stricter in just

a couple of months following 2019, as explained by Braga (2021), due to new international standards, such as the GISTM (Global Industry Standard on Tailings Management, 2020).

Suddenly, the Brazilian tailings job market, which has a stablished consultancy hub located in the city of Belo Horizonte (Minas Gerais), experienced an influx of professionals from different parts of the country. New consultancy companies were established and experienced a rapid growth, and senior international firms expanded work in Brazil. As expected, the demand was higher than the supply of qualified professionals, especially Senior engineers, who suddenly saw tailings engineering as an opportunity for professional growth after a decade of slow economic growth for engineering firms in Brazil. This new marketplace was now composed of a few experienced tailings engineers and an immense number of professionals who either had previous experience with engineering (outside of the tailings environment) or were completely new to the profession.

In 2024, five years after this sudden shock to the market, the demand for new projects seems to be slowing, but the challenges remain. The most recent one was the inclusion of the Engineer of Record (EoR) as a mandatory role for tailings facilities in Brazilian national legislation in 2022, following the guidelines of the GISTM.

Looking to the future of the profession to explore our capacity for meeting the current and future demand for qualified professionals, this paper presents the results of a survey conducted online with tailings professionals with different backgrounds who are currently working in the tailings engineering job market. Initially, the efforts were motivated by the work of Prince and Boswell (2023) who surveyed 164 young engineers and investigated via multiple means their willingness to become EoRs in the future. The authors decided to broaden this investigation by asking professionals working in the tailings industry with different sets of experiences about their perceptions of the EoR role and the tailings industry.

The following sections will present the methodology, outline the limitations, and detail the findings of the survey. The diverse pool of respondents has yielded a rich dataset that potentially presents a substantial number of combinations to be explored in future research. For this paper, the authors decided to present a broader overview of the data, with the aim of presenting a comprehensive understanding of the current state of the tailings community in Brazil. As this work progresses with the engagement of national and international peers, this research will be expanded to include more participants, fostering a more comprehensive understanding of the Brazilian tailings management landscape.

Survey methodology

The survey was anonymously conducted using the Google Forms platform. Anonymity was guaranteed and no personal information was collected. This step was important because the authors are active members of the tailings community, working for different companies, and the participants might feel intimidated to

sincerely share their views.

The survey was divided into the following sections: demographics, which included questions regarding gender, age, experience, and area of expertise; academic experiences, which included a brief survey of the educational background of the respondents; professional experience, which surveyed the current level of professional classification and if the participant is currently affiliated with any professional association; professional perception, which included questions aiming at understanding the participants` self-perception on topics such as professional experience, field work, regulatory knowledge, risk profile and soft skills; Engineer of Records, which included questions that are generally based on the work of Prince and Boswell (2023), with some specific adjustments to include Brazilian characteristics.

The survey was mainly advertised using the authors' own social media and message groups, with some contribution from participants in their network. The survey was also shared by the Minas Gerais branch of the Brazilian Association of Soil Mechanics (ABMS) in an email message.

With a total of 165 participants, the authors believe that the number of responses is an adequate number to represent the tailings industry in Brazil. However, considering the pool of respondents, the following limitations were noted:

- More than 80% of the respondents are currently working in areas related to consultancy and only 14% are employed by mining companies. Hence, most of the results presented in this research are representative of the views of professionals working in the consultancy industry.
- Approximately 80% of the respondents work in geotechnical engineering, while the others are divided into water management, geology, and project management roles. Thus, the results drawn in this research are limited to a general overview of the current state of geotechnical consultants working in tailings engineering.

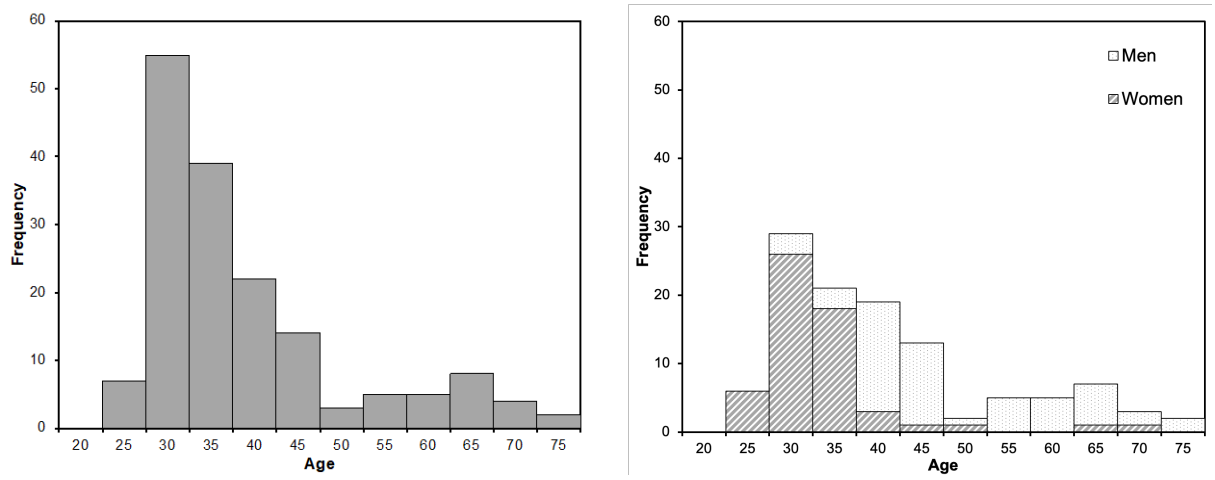
Results

Demographics

The demographics results showed that 64.8% and 35.2% were men and women, respectively. These results, while they reflect gender inequality in the tailings technical community, are aligned with other surveys conducted around the world. The results also showed racial inequality, as 70.3% of the respondents identified themselves as white, while 22.4% identified as mixed race *("Pardo")* and only 5.5% as black *("preto")* and 1.2% as Asian *("Amarelo")*. Comparing these rates with the last national census results (IBGE, 2022), one can deduce a high level of racial inequality, since the division for the census was 45.3% mixed race, 43.5% white, 10.2 % black and 0,4% Asian.

With respect to age, Figure 1 presents a histogram with the age groups. As one can see, the great majority of the respondents (>70%) were less than 40 years of age (38% less than 30 years; 37% between 30 and 40 years). From the histogram presented in Figure 1, it is possible to observe an age gap around the ages of 40 to 50 years (10% of respondents), with an increasing number of respondents older than 60 years. Although this inference is limited to the representativeness of the number of respondents considering the whole tailings community, this result corroborates the general impression of the market that professionals with around 25 years of experience (around 50 years of age) are the scarcest in the market.

Dividing the histogram to account for gender distribution (see Figure 1 [b]), it is possible to confirm something that is easily observed in the tailings community: the low number of female Senior professionals. For professionals older than 40 years, the number of female engineers is almost zero, highlighting that the gender gap identified in the general pool of respondents is linked to age groups. Based on the results presented in Figure 1 (b), one can infer that gender inequality tends to lower with passing time, as this gap reduces in professionals under 35 years of age.



(a) (b)

Figure 1: Age distribution histogram – (a) general (b) by gender

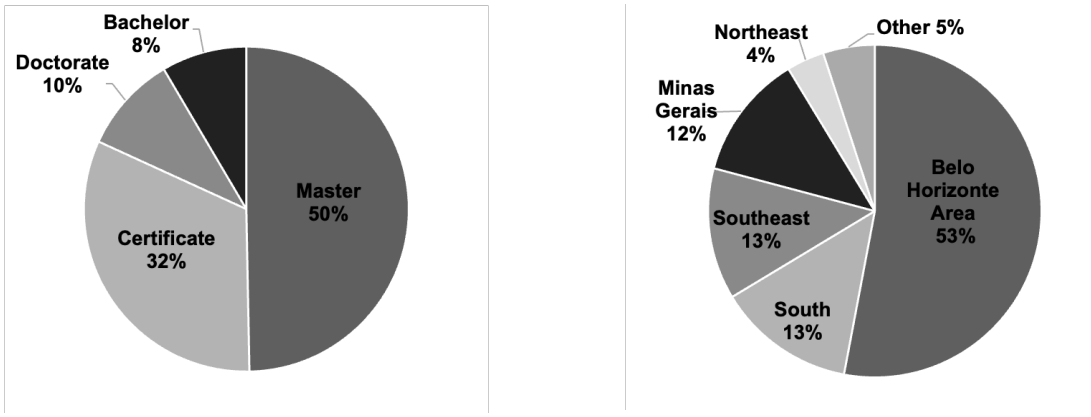
Education

Another important aspect of the initial assessment of the survey was the investigation of the educational level of the respondents. In total, half of the respondents had a master's degree, 32% had an equivalent to a certificate degree (Lato Sensu Graduate), 10% had a doctorate degree, and only 8% had a bachelor level (Figure 2 [a]). These results highlight the high level of specialization required to work in this field, and that only a small percentage do not go further than the bachelor level degree.

An additional aspect investigated in this study was the evaluation of the academic institutions where these professionals graduated. There is a general perception that the tailings job market in Brazil, which is

mainly concentrated in Belo Horizonte (Minas Gerais state), lack diversity in terms of the presence of professionals coming from different universities, and that the majority of the professionals graduated in institutions located in Minas Gerais (the location of the headquarters of most mines and consultancy companies).

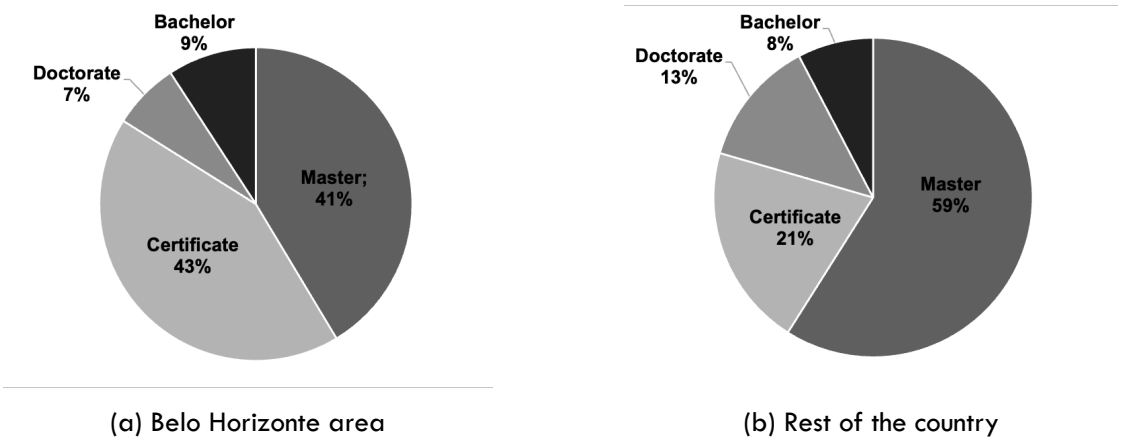
The results presented in Figure 2 (b) corroborate this general impression, since 53% of the participants did their undergraduate degree in universities close to Belo Horizonte (< 100 km), while the rest of the country had fairly uniform numbers, ~12% for each region, including the rest of Minas Gerais state, and the southeast and south regions. The states in the north, northeast and central parts of the country produced only 8% of the respondents, while 1% did their undergraduate studies abroad. This reflects a lack of diversity, despite recent efforts to include professionals from different parts of Brazil in the last years due to the need of qualified professionals. In terms of the type of institution, 76% of the respondents studied in public universities, while 23% studied in private universities and 1% in foreign universities.



(a) Educational level (b) Location of undergraduate studies

Figure 2: Educational background – (a) level of education; (b) region of undergraduate studies

Another finding is related to the level of education based on where the respondents did their undergraduate studies. The participants who did their undergraduate studies in universities in the Belo Horizonte area preferred to continue their education with a master's and doctorate degree, while just a small fraction (21%) preferred the professional certificate degree (Figure 3 [b]). Participants who did their undergraduate studies in universities in the Belo Horizonte area almost equally chose master's degrees or a certificates degree to advance in their higher education study (Figure 3[a]).



(a) Belo Horizonte area (b) Rest of the country

Figure 3: Educational level by location of undergraduate studies: (a) Belo Horizonte area (b) rest of the country

These results indicate another general trend observed in the market. Professionals who studied in the Belo Horizonte area had the opportunity to complete internships in tailings consultant companies that facilitated their passage to an appropriate job. After they secured their job living in the Belo Horizonte area, a high number of people preferred to do a certificate degree, since it is easier to combine this with a full-time job (Figure 3 [a]), as reflected by the low supply of master's degrees in this region. On the other hand, the majority of the participants (~75%) who did their university degree in the rest of the country chose either a master's degree or a doctorate degree to increase their educational level (Figure 3[b]). With less opportunity for internships in their hometowns, professionals had to further improve their educational level in order to secure jobs.

Experience

The research investigated how long the respondents had been working in general engineering versus in tailings. The results show that 75% of responses were from professionals who had been working in tailings for less than 10 years. Within this group, 22% were professionals with more than 10 years of general engineering experience who started working in the tailings job market after the tailings dam disasters in 2015 and 2019 in Brazil.

Regarding the job category of the respondents, the survey showed parity in the representativeness of each level (Junior, Intermediate, Senior, and Expert) with around the same number of respondents for each category. Nonetheless, an important aspect of the current job market was observed: the inconsistency in experience across job categories, as shown in Figure 4. For Experts, for example, the answers varied from 11 to 50 years of experience; for Senior level, from 3 to 32 years; for Intermediate level, from 4 to 17 years and, finally, for Junior level from 1 to 11 years of experience as an engineer. It is important to highlight,

however, that since the question was formulated as an open question, multiple types of answers were given. Hence, filtering and categorizing were necessary to ensure that the data could be analyzed effectively.

The average values for each category showed some coherent trends, as seen in Figure 4. Nonetheless, as seen in the number of years of work experience mentioned above, there is no clear separation between the Junior and Intermediate categories, which had very similar years of experience. It was noted that Senior engineers were usually professionals with more than 10 years of engineering experience. However, it was also noted that this position is held by professionals with less experience with tailings than is usually adequate (<10 years of tailings experience). As expected, for Experts, Consultants or Master (a type of classification created in Brazil), the distribution is even more diverse, and it is clear that there is no clear criteria to which to attribute this classification.

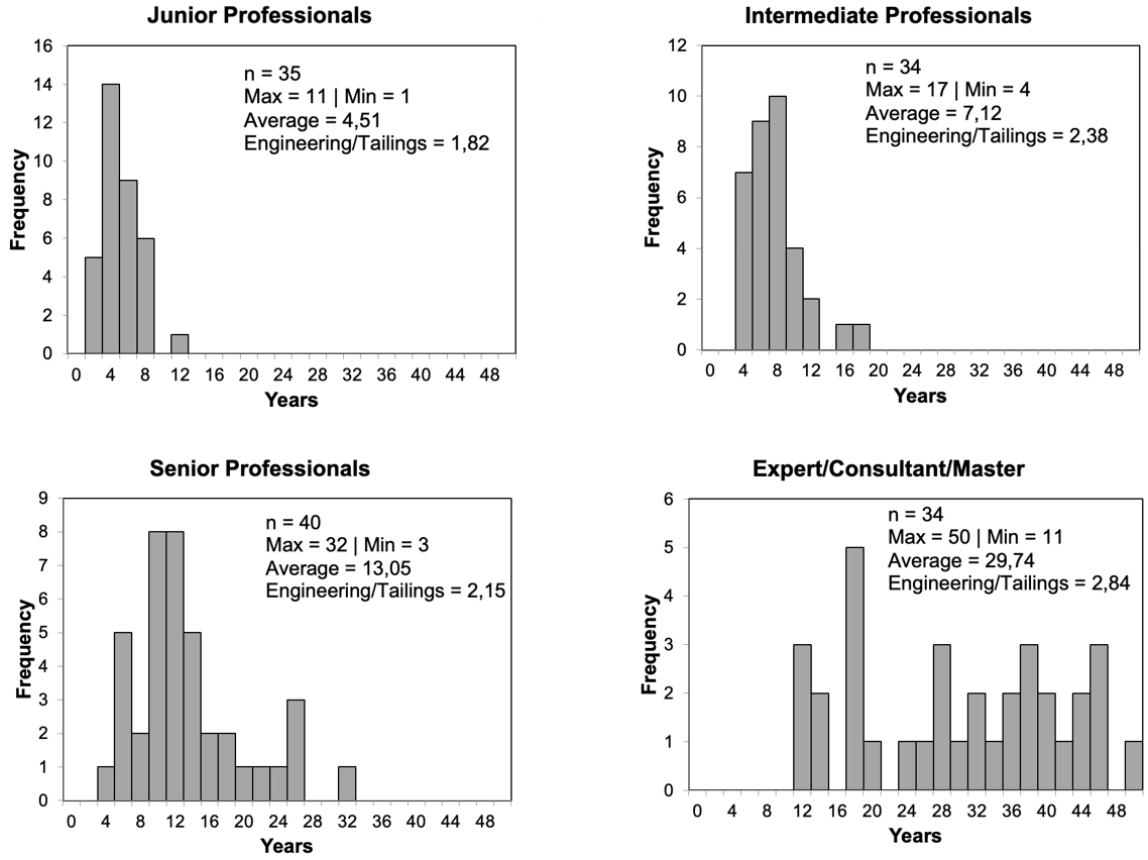


Figure 4: Years of engineering experience: distribution histogram per job category

The authors believe these results accurately depict the current state of tailings engineering in Brazil, where the demand for qualified professionals surpasses the available supply. This imbalance leads to a distortion of the relationship between job category (Junior/Intermediate/Senior/Consultant) and time of experience. Caution should be exercised by the industry so as to allow adequate time for professional

development before people are able to take on large commitments and significant responsibilities within such complex structures.

Professional perception

The Professional Perception section of the questionnaire aimed to research the participants' opinions on Professional Experience, Field Work, and Regulatory Knowledge. The responses reflect a self-evaluation of various career markers considered by the authors to be important in tailings practice. Most of the questions on this section could be responded to with Strongly Agree (SA), Agree (A), Indifferent (I), Disagree (D), Strongly Disagree (SD). The participants also responded to a question on whether academic experience or professional experience is more important for professional development, and self-evaluated their level of understanding of the tailings practice.

The data shows that 37% of the participants find that available working hours are insufficient for their assigned workload. A possible interpretation of this response is that there is still a need for more qualified professionals – an interpretation that is in agreement with the current market understanding (Hatton et al., 2020). Most of the participants (>75%) believe that their assigned responsibilities, job category, and professional progression are coherent with their experience level. More than 80% of the participants responded that academic experience and professional experience are equally important for professional development.

The vast majority (>95%) of the participants understand the importance of field work. The authors consider this to be an interesting finding given that this research population is strongly represented by geotechnical engineers working in consultancy, which has a primarily office workload. Although 80% of the participants claim to have done fieldwork for professional development, 56% would like still more fieldwork experience. This result could also be understood from the perspective of the study population.

Responses show that 83% of the participants claim to have an understanding of national regulations that is coherent with their job category, which is consistent with the current heavily regulated tailings engineering environment in Brazil. Also, 72% claim to understand international regulations such as CDA, GISTM, ICLOLD and MAC. The authors found it noteworthy that 56% of the participants claim to be indifferent or to not understand the civil and criminal liability associated with their work. Additionally, more than 55% are indifferent or do not understand the CREA (Brazilian NSPE corresponded) regulations, which defines technical attributes and liability. This complementary information shows that, even in a job market that boomed after the failure of two major structures, which resulted in civil and criminal lawsuits, most of the engineers are not aware of the potential judicial consequences associated with their work and have not tried to learn more about it.

The participants also responded to a self-evaluation of their level of understanding of the tailings engineering practice by choosing one of three pre-set responses developed by the authors to simulate a Junior, Intermediate and Senior level knowledge, as follows:

- Junior: "I execute assigned tasks with basic understanding of the information and existing tools, but not necessarily understanding the results and implications."
- Intermediate: "I have advanced understanding of the physics and engineering of a project, as well as the nuances of the structure's operation, and have the ability to contribute to problems based on previous experience."
- Senior: "I possess deep understanding of all the technical areas related to the structure and the current state of practice, am able to fluently communicate them to all stakeholders, and possess the feeling of ownership of the structure."

The self-evaluation responses by the participants resulted in 12.1% with Junior knowledge, 67.3% with Intermediate knowledge and 20.6% with Senior knowledge. These numbers should be compared to the demographics of this study: 21% are Juniors, 45% are Intermediate/Seniors, and 21% are Expert/Consultants/Masters. The authors' interpretation is that Junior participants judge themselves to have a better understanding of the tailings engineering practice than is expected for their category. Unfortunately, this might reflect a typical Dunning–Kruger effect.

EoR

The EoR section of the survey included questions generally based on the Prince and Boswell (2023) work, with adjustments to include Brazilian characteristics. The questions were developed to understand:

1. the participants' involvement with EoR practice;
2. their aspirations to become an EoR in the future;
3. their risk perception regarding assuming this role;
4. their understanding of the lawsuits against engineers involved in the Brazilian failures; and
5. their main concerns as an EoR in the event of a failure.

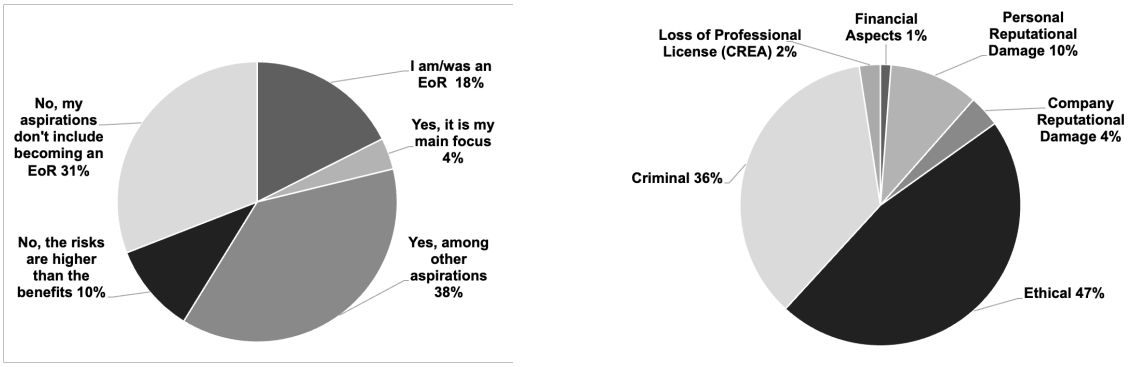
All responses in this section should be understood in the context of the participants' demographics, education, and experience, as previously presented.

Within the response pool, only 14% claim to be assigned an EoR or Deputy EoR role; nonetheless, 64% claim to be working in an EoR team. This data is coherent with the authors' understanding of the Brazilian consulting industry: as the EoR has become a mandatory role for high DPA (Associated Potential Damage, as per ANM, 2022), teams were created in the consulting industry to provide this service to the mines, but only a minority of existing Seniors can assume this role. Signing off on a structure's stability, either as an EoR or with a DCE (Declaration of Stability, as per ANM, 2022) – which is commonly done

by a small niche of Senior professionals – has become a major industry demand, as confirmed by this data. But will the industry be able to fill these positions with the upcoming generation?

In the responses to the questions "Do you aspire to assume an EoR role at any point in your career?" and "How do you see the personal risks of assuming an EoR role?", nearly half of the participants (41%) responded negatively to the first question – although with varying justifications – and 42% responded "risky" or "unacceptable" to the latter. The authors compared these findings to those of Prince and Boswell (2023), who found that only 16% of respondents (who were in Canada, the USA, South America, Australia, and South Africa) were not interested in this role, and that 33% responded with "risky" or "unacceptable." The authors offer as a possible interpretation that the two Brazilian failures are not only more recent, but also had a higher fatality rate than the Mount Polley failure in Canada. Furthermore, Brazil currently has 64 mine dams at an emergency level (ANM, 2024), which could also impact participants' personal wiliness to assume the associated liability.

A related question was: "How did the civil and criminal repercussions of the professionals involved with the recent failures influence your decision to assume an EoR role?" More than half (55%) of the participants responded "negatively" to this question, compared to the 33% found by Prince and Boswell (2023). Also, only 5.4% of the Brazilian professionals claimed to have no understanding of the repercussions, comparing to 35% found in the primarily North American population (Prince and Boswell, 2023). The latter comparison could indicate that participants found the consequences to the involved engineers in Brazil following the failures unacceptable.



(a) Do you aspire to assume an EoR role at any point of your career?

(b) What would be your biggest concern as an EoR in a failure event?

Figure 5: Survey results for questions (a) and (b) regarding EoR

When asked what their biggest concern as an EoR in a failure event would be, 47% responded "Moral/Ethical," 36% "Criminal," 10% "Personal Reputation," and 7% chose either "Financial Aspects," "Loss of License," or "Firm Reputation" (Figure 5 (b)). This result is comparable to data presented for the primarily North American industry (Prince and Boswell, 2023). The responses to this question could be

motivated by what is socially acceptable. The authors were surprised as they expected a larger percentage to have criminal concern. This might be explained by a lack of awareness of the potential judicial consequences associated with the professional work, as shown in the previous sections.

Discussion

Based on the strong survey turnout, the authors believe that the results presented in the last section represent well the entire technical tailings consulting community in Brazil. The survey gathered responses from professionals with diverse backgrounds and experiences, and the age distribution shown in the histogram reflects market conditions. There is a high number of Junior and Intermediate professionals, with relatively few Senior or Expert professionals.

The demographic results reveal a considerable gender and race gap in the consultancy industry, which any attentive professional might have anticipated. The gender gap is particularly pronounced among seasoned professionals, while it is almost non-existent in rookie roles. Optimistically, one could argue that within 10 to 15 years, the gender gap in the consultancy industry may close, given that equal numbers of men and women are entering the job market at Junior positions. However, understanding the historical and current reality of the job market for women, it is crucial to continue implementing gender equality initiatives to further reduce the gap.

The numbers presented reflect the significant racial inequality in Brazil, making it difficult to draw specific conclusions. It is essential to implement additional measures to reduce this disparity, as university-level affirmative action alone has not sufficiently increased the representation of black and mixed-race individuals in the highly specialized engineering job market.

The experience section of the survey indicates that there is a clearly dysfunctional relationship between experience and professional category. The authors believe that sector-wide research – possibly funded by market stakeholders and developed by an experienced human resource company – could be a strong tool to expedite the rebalancing of the job market after the recent rapid growth.

Regarding the professional perception section, the authors believe that there is space for further segmentation of the results, which should focus on finding relationships between gender, educational level, and experience to the answers provided in this section. Nonetheless, the current analysis showed interesting data on the professional perceptions of topics such as workload and field work. However, concerning results are presented next.

The first is related to the level of understanding regarding civil/criminal liability related to their jobs. Considering the repercussions for the professionals who were involved in the past disasters, the authors believe that schools, professional associations and other institutions should target educational programs to

provide better information regarding the judicial aspect of the job as a method of empowerment of technical professionals.

The second concerning finding is that Junior professionals reported a self-evaluation of tailings understanding that does not coincide with their age or experience. As mentioned above, this could be a clear sign of the Dunning-Kruger effect, but it would be troubling if a Junior professional is responsible for a project of high consequence. Unfortunately, in Brazil, there is no restriction preventing Junior professionals from signing off on a project.

Finally, with respect to the EoR section of the survey, the majority of the participants claimed that they either work or have worked with EoR projects. Nonetheless, when it comes to assuming the role of EoR, there was a negative tendency in the results, which was more pronounced than in the work of Prince and Boswell (2023) for the primarily North American industry. The vast majority seemed to be aware of the negative repercussions for professionals in Brumadinho and Fundão, and this might have had an impact regarding the personal risks of assuming the role of EoR. Also, living in Belo Horizonte, a common negative aspect of working with tailings dams is that they are frequently in the news and, as expected, are often portrayed negatively.

As the mines in Brazil continue to grow, the industry will need to create ways to adapt to the lack of capable professionals for tailings structures. Following the international trend, educational initiatives combining multiple stakeholders should be explored as a possible solution. Nonetheless, there needs to be a change in the public reputation of the companies and professionals in order to attract new talent.

Conclusion

The survey results provide a valuable snapshot of the current state of the Brazilian tailings engineering sector, particularly regarding the EoR role. There is a clear reluctance among professionals to take on this responsibility, driven by the high risks and severe legal consequences highlighted by recent disasters. This reluctance is compounded by a lack of understanding of civil and criminal liabilities among young engineers, suggesting an urgent need for targeted educational programs. The findings also indicate significant gender and racial disparities within the industry, which require ongoing efforts to ensure diversity and equality. Overall, the study underscores the importance of addressing these issues to foster a more knowledgeable, cautious, and inclusive professional community capable of safely managing Brazil's tailings dams. Further research is needed to research a more diverse pool of respondents that includes professionals working for mining companies and professionals specialized in other areas than geotechnics. Also, further data segmentation is required to identify trends in answer related to age, gender, and experience.

Acknowledgements and disclaimer

The authors acknowledge the contribution of the 165 participants who kindly provided information to this paper. We also extend acknowledgement to those who assisted in the distribution of the survey to a larger public than was possible within only the authors' own network – notably the Minas Gerais branch of ABMS (Brazilian Association of Soil Mechanics and Geotechnical Engineering). The opinions expressed herein are solely those of the authors and do not express the views or opinions of their employers.

References

Agência Nacional de Mineração (ANM) 2022. *Resolução ANM Nº 95, de 07 de fevereiro de 2022*. Consolidates the regulatory acts concerning the safety of mining dams. Amended by Resolução ANM Nº 130/2023 and by Resolução ANM Nº 175/2024. Available at ANM website. Accessed on: August 21, 2024.

Agência Nacional de Mineração (ANM) 2024. *Relatório Sintético Campanha de Entrega DCE Março 2024*, Agência Nacional de Mineração ANM, Governo Federal, Brasil, 2024.

Braga, M. 2021 *Mudanças de política ambiental motivadas por catástrofes: lições dos rompimentos de duas barragens de rejeitos no Brasil*. 2021. 156 f. Dissertação (Mestrado em Engenharia Ambiental) – Núcleo de Pesquisas e Pós-Graduação em Recursos Hídricos, Universidade Federal de Ouro Preto, Ouro Preto, 2021.

GISTM. 2020. Global Industry Standard on Tailings Management. Accessed at global-industry-standard_EN.pdf (globaltailingsreview.org)

Hatton, C.N., Spencer, D., Bareither, C. and Ward, K. 2020. All hands on deck! – a semi-quantitative attempt to characterize the impending qualified tailings professional resource shortage. In *Proceedings of Tailings and Mine Waste, 2020.* Denver, CO: 551–565.

Prince, M. and Boswell, J. 2023. *The willingness of young engineers to assume the role of EOR for TSFs.* In *Proceedings of Tailings and Mine Waste, 2023.* Vancouver, Canada. https://doi.org/10.14288/1.0438104

The Role of Engineer of Record – a Reflection of the Current State of Practice from an Australian Perspective

Theo Gerritsen, Rio Tinto, Australia
Laura Fidel, WSP, Canada
Lis Boczek, South 32, Australia
Chris Hatton, WSP, USA

Abstract

The role of Engineer of Record (EoR) was predominantly implemented in the United States and Canada, with origins in the civil engineering sector dating back to 1927, prior to the inception of the Global Industry Standard for Tailings Management (GISTM) in 2020. Since the adoption of GISTM across the mining sector, the EoR role has been adopted internationally, with countries like Australia becoming more familiar with the role. This has led to ongoing discussions in professional committee forums, comprised of both Owner and engineering consultancy groups, on the appropriate implementation of the role. The Queensland Tailings Group (QTG) held a series of workshops and discussions beginning in November 2023 and attended by over 40 Australian-based EoR practitioners from 12 Mining Engineering Consultants. The workshops were attended by Laura Fidel, who was nominated as the EoR at the time of the 2014 Mount Polley Failure. This paper discusses the role of the EoR (from an Australian perspective) against the backdrop of Laura's experience, and with input from the workshop attendees. Discussion points included:

- Australian EoR guidelines and references;
- personal and legal risk;
- EoR as a career path – risk and reward;
- EoR – quality and career development and succession;
- setting up for success;
- are mining companies employing the EoR correctly; and
- why become an EoR.

The key objective of the workshop was to listen to the people who are EoRs and ask them their views, instead of relying completely on the various standards and guidelines describing what an EoR should be. In other words, "What about me, does my opinion count?"

Introduction

A key component of the mining industry, albeit not the most glamorous, is the management of waste from the mining process. The facilities designed to store and manage this waste can range from simple to extremely complex. The absence of properly designed and managed facilities has led to a considerable number of tailings storage facility (TSF) failures across the industry on a global level, and these continue to occur with some level of regularity. It must also be recognized that these structures are ever-expanding in size – both vertically and laterally – continually raising the tailings engineering and operational bars to a whole new level (Morrison and Hatton, 2016). As such, the industry has pushed to increase the level of accountability and responsibility for those tasked with maintaining the safety and integrity of these facilities. Does it make sense to expect professionals to willingly put this onus in part on themselves by undertaking such roles when the repercussions of any degree of error seem to profoundly outweigh the advantages? An example of this is the emergence of the role of the Engineer of Record (EoR), in which this paper will summarize the opinions of several practitioners from an Australian perspective.

History of the EoR role

The term EoR is believed to have been first used in the civil works industry, related to the design of structures (buildings). It is known to date back to at least 1927 in North America. It was later codified in 1976 by AISC in their code of standard practice. The use of EoR terminology in other areas of engineering, including the design of dams and tailings storage facilities, is less certain. The government of British Columbia (BC) introduced the Dam Safety Regulation in 2000 (Government of British Columbia, 2000), which included a requirement for mining companies to employ professional engineers to certify the design and construction of tailings dams. This requirement was reinforced and further evolved following the Mount Polley tailings dam failure in 2014. This led to the creation of a formal Tailings Review Task Force and a new regulation that established the EoR role as a mandatory requirement for all new tailings facilities.

The Mount Polley tailing dam failure brought to the forefront the challenges and pitfalls of having multiple engineering firms involved with tailing dam design and was a catalyst for the development of EoR guidance that established a single responsible individual backed by an experienced firm.

The catastrophic tailings dam failure in Brumadinho in 2019 pushed further accentuated the need for appropriate action to enhance the safety of TSFs across the globe. The tragic event motivated the United Nations Environment Programme (UNEP), the International Council on Mining and Metals (ICMM), and Principles for Responsible Investment (PRI) to convene the Global Tailings Review to develop an international standard for safer management of TSFs. It was called the Global Industry Standard on Tailings

Management (GISTM) (ICMM, 2021). The GISTM effectively globalized the EoR role in 2020. Figure 1 shows a partial history of the development of the EoR role as we know it today.

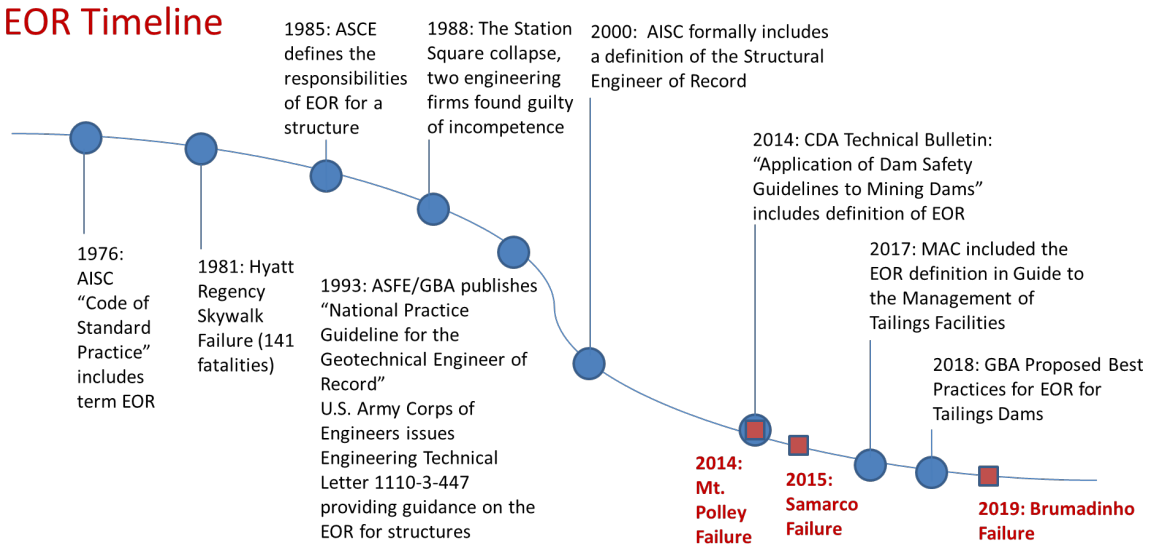


Figure 1: Abbreviated history of the EoR (courtesy of Paul Ridlen and Amanda Adams)

EoR guidelines and references

There are many guidelines and papers outlining the requirements of an EoR for the TSF governance process, with some references providing additional detail on what qualities and experience an EoR must possess. These requirements have progressed and evolved, particularly in the years following the Mount Polley failure. Specific to Australia, the Australian National Committee on Large Dams (ANCOLD) provides some guidance. The following is a list of currently published general requirements expected of an EoR for tailings dams:

- ANCOLD (ANCOLD, 2019)
    - In addition to the responsible Site Person, there should be a Responsible Technical Person assigned to each tailings dam, this person, named the "Engineer of Record" in some jurisdictions, must be appropriately qualified and experienced in the scale and type of dam involved.
- Canadian Dam Association (CDA) (CDA, 2019)
    - Experience and knowledge commensurate with the complexity and potential consequences of a failure. Typically, have at least 10 years of related experience.
    - Current knowledge of applicable regulation and good practice
    - Registration and good standing with the engineering association in the local jurisdiction.

- Engineers and Geoscientists of British Columbia (EGBC)
    - A minimum Bachelor of Science level degree but a Master of Science with specialization in geotechnical is more typical (EGBC, 2021).
    - 15 years of geotechnical engineering practice with at least 10 years in progressively increasing responsibility for tailings dam design, operation, monitoring, risk assessment, and emergency response action planning … for dams that are not complex or not very high-risk dams (EGBC, 2021).
    - 20 years or more for complex and high-risk tailings dams (EGBC, 2021).
    - Supported by a firm that has Dam Safety professionals and specialists who can provide the necessary support and oversight. The EoR cannot be a firm (EGBC, 2023),
- GISTM (GISTM, 2020)
    - Engage an engineering firm with expertise and experience in the design and construction of Tailings Facilities and for close facilities with "High," "Very High" and "Extreme" Consequence Classification that are in the active closure phase,
    - The firm nominates a senior engineer, approved by the Operator, to represent the firm as the EoR.
    - Necessary expertise, skills, and time to fulfill this role.
    - Must be competent and have experience appropriate to the Consequence Classification and complexity of the tailings facility.
- Ministry of Energy, Mines and Low Carbon Innovation (EMLI)
    - Technical expertise and experience commensurate with the complexity of the TSF or dam.

The EoR in Australia

The role of the EoR and its implementation within the respective local governance framework has varying levels of maturity, depending on the geographical location of the practitioners. The EoR, in some jurisdictions such as Canada, is a position with legal ramifications. In Australia, the EoR role is heavily associated with the GISTM governance, with little if any recognition of the role outside of mining organizations committed to GISTM implementation.

From the references summarized above, it is apparent that there is good international guidance on EoR responsibilities, and on why the role of EoR should be adopted. There is also some guidance on EoR requirements. However, when focusing on Australian and Australian-based practitioners, ANCOLD seems to be the only Australian-based/focused reference and it does not refer to EoR but to "Responsible Technical Person." The later adoption of the EoR concept by Australian practitioners and mining companies, together

with still limited guidance, may be the catalyst for the ongoing discussion in Australia on the various aspects of the role of EoR. The numerous discussions the authors have had and observed prompted the organizing of the QTG EoR Workshop in November 2023.

The Queensland Tailings Group EoR workshop

The Queensland Tailings Group (QTG) EoR workshop brought together some 40 Australian-based tailings practitioners who currently had one or more EoR commissions, or had previously worked as an EoR. Representatives from the Consulting and Owner side attended the workshop, with Laura Fidel drawing on her experience as the assumed EoR for Mount Polly to prompt the group discussions.

Laura Fidel's presentation captivated the audience and received positive praise. More importantly, her work and discussions brought to the forefront key issues that are relevant to the EoR position. The current guidance focuses on the technical aspects and qualification of the individual EoR. However, there are so many more questions that need to be answered and addressed as we move forward. Laura Fidel's presentation addressed some of these non-technical subjects including:

- Personal and legal risks.
- The EoR as a career path and the associated risks and rewards.
- The quality of the EoR, continuing development and succession.
- Setting our new EoRs up for success.
- Are Owners presently applying the EoR correctly?
- Why become an EoR?

Personal and legal risk

What is the personal risk for an engineer who takes on the role of EoR? Based on discussions at the QTG events, individual discussions among many of the Australians practicing EoR, and views shared during the November 23 workshop, the risk is too high. The experience shared by Laura Fidel during the workshop confirmed this sentiment for a majority of the participants.

Having been in the industry's spotlight for years, due to the exhaustive punitive process initiated by Engineers and Geoscientists of British Columbia (EGBC) following the Mount Polley failure, Ms. Fidel's experience sheds valuable light on the level of personal risk EoRs face. She had naïvely assumed the EoR for the Mount Polley TSF at the time of the 2014 failure. The decision was innocently made out of a sense of duty to the company in an attempt to do the right thing for the company and the Owner. She was intended to be a stopgap until more senior resources could be identified. This altruistic decision was subsequently viciously targeted by EGBC and underwent a lengthy inquiry. She shared that the investigation stage involved frequently providing supporting evidence of her professional experience as well as all

documentation related to the project, legal representation at the company's level, a day-long fact-finding interview, and being the subject of a subcommittee's findings report.

The progression to the disciplinary stage involved different legal representation, now at a personal level, retaining an industry expert to opine on her behalf, submitting multiple documents and retorts to evolving allegations, and among other things, being the subject of an intense hearing that lasted two full weeks. The formal disciplinary decisions involved the temporary suspension of her license to practice engineering in BC and mandated completion of three technical courses. However, there was a high level of risk that the disciplinary outcome could have been much more severe, involving permanent loss of her license to practice engineering and destroying her career, and costing hundreds of thousands of dollars in fines and legal costs. This process highlights the extreme measures that can be taken by governing bodies regarding the EoR role, however unnecessary or heinous they may be.

It is easy to focus on the risk to the monetary outcomes; however, it does not end there. The risk extends to having personal and/or professional reputation tainted, negative effects on mental health, and even strained personal relationships. Ms. Fidel's ability to weather the storm created by EGBC overstepping its authority is a testament to her fortitude and legacy.

Only one or two workshop attendees indicated they had some sort of personal indemnity as part of the contract they had with their employer. This brings to attention that the following issues should be called out for further discussion between the Consulting Industry, the Owner's side, and regulatory bodies and working groups:

- If and where feasible, implement a process where the Consultant protects the EoR employee from personal risk.
- Should the Owner invest in the EoR by way of secondment while in training as part of their development?
- Can limitations be set within regulatory bodies regarding the degree of prosecution applied to individual EoRs, as opposed to their consultant?

EoR as a career path – risk and reward

A topic of considerable discussion was focused on the EoR as a career path, within the Consultant organizations. The following development areas resulted from the discussion:

- The reward for undertaking an EoR role needs to start better aligning with the risk involved should there be a failure of the facility. This is especially true for the case where the EoR is taking responsibility for a facility that they have not designed. There was a widely shared sentiment at the workshop that the risk and responsibility/accountability carried by the EoR are not in proportion to the general compensation currently received by those undertaking the role. Should an EoR be paid

more than an engineer with the same experience who does not take on an EoR role? Other professions such as surgeons, aircraft pilots, rocket scientists, or lawyers are generally compensated based on the level of risk that is involved, so why is the same logic not being applied to EoRs?

- Should the Consultant provide a career path for people who want to dedicate themselves to the role of EoR, including appropriate compensation? Currently, EoR roles are fulfilled by Principal Engineers with significant experience in the design, construction, and operation of tailings storage facilities and are in short supply. This would mean that there may be a discrepancy between general Principal Tailings Engineering design work and the role of EoR.
- As an EoR, are you an Owner-facing representative of a larger team or are you the responsible person regardless of the team? The benefits for individuals are not clear.
- Is becoming an EoR career limiting? Once a person is responsible for two to three sites, there is limited opportunity for involvement in emerging projects within the business. The EoR role becomes the only focus.

EoR – quality and career development and succession

The shortage of appropriately experienced engineers to fulfill EoR roles is forcing the recruitment of engineers from other discipline areas. Will having EoRs from other disciplines be considered acceptable, considering the precedence set by EGBC regarding geotechnical experience (EGBC, 2021) and the high number of years of "related experience" that various existing guidelines include as minimum qualifications (CDA, 2019)?

These guidelines certainly suggest that internationally this would not be acceptable. In other jurisdictions, how are these engineers developed to ensure they have the appropriate understanding to perform in the EoR role? Should there be a tailings discipline associated with the National Professional Engineers Register? There need to be minimum requirements outlined and accepted internationally for the EoR as an individual and representing a company in a guidance document.

Setting up for success

For the EoR role to be successful, a trusting relationship between the Owner and Consultant needs to be established. The following comments were made during discussions around the development of trust and improving the role of EoR:

- How are (technical) disagreements approached and resolved: is there a formal process, does the Owner's side have a review and performance process in place which is factual and non-emotive, is there sufficient opportunity for recourse and feedback, and does the EoR have a method for escalation to the Accountable Executive (AE) or leadership beyond the day-to-day

reporting (i.e. Tailings Superintendent or equal)? These issues are a critical part of working on and keeping the trusted relationship growing and developing.

- How is the scope of work defined: is the scope and remittance of the EoR fully described and understood by both parties? The procurement team often has too much input into the scope, or the scope is written generically or by Owner personnel with limited understanding of the specific requirements of the operations.
- Is the EoR working with the Owner's operational and corporate technical teams as one team: there should be little or no barriers in terms of the decision-making process and where possible, the EoR should be integrated and attend the various asset technical meetings. The EoR should also have regular contact with the Owner's representatives in the Community and Social Performance and Environmental, Social, and Governance departments to ensure the impact of the TSF on said disciplines is understood, so that risk can be anticipated and mitigated. This is key to the effective implementation of the GISTM.
- Does the EoR have access to an external support network? Contact and regular communication with the Responsible Tailings Facility Engineer/Responsible Dam Engineer, Independent Tailings Review Board, AE, and Owner's subject matter expert (SME) are essential.

Are mining companies employing the EoR correctly?

The implementation of the EoR in the governance structure and adoption of the EoR role, in the Australian context, suggests experience with the following issues:

- The procurement processes must be improved on the Owner side to provide clear requirements and expectations for the role commensurate with the consequence classification of the facility. The intent of the EoR is to form a long-term partnership between the consulting firm and the mining company, not for a set period where, at the end, the role is to be re-tendered. The procurement process is often too long, complicated, and too onerous; sometimes the procurement department has undue influence on both the selection of tenderer's and terms and conditions – even though the GISTM suggests this must not be the case.
- The EoR is too often used as a design house without consideration of the role outside of facility design. The EoR has a design function, but the main purpose is to act as a safeguard on risk. To do this, the EoR needs to be involved in all areas of the operation, not just design. In some cases, the EoR company struggles to perform in the EoR role and deliver on design packages due to a lack of resources or projects not specifically related to the TSF being included in their remit. The Owner could help with the EoR workload by allowing pro-active

prioritization of design and analysis works, particularly when a facility has significant safety performance requirements to meet.

- The term EoR tends to be broadly used, but is applied universally and often interpreted in varying ways by owners, regulatory bodies, and professionals working in the industry. For this reason, both Owners and consultants can very easily misunderstand the role.
- On the Owner side – a high degree of commitment and sacrifice is expected of the EoR, and the limits of obligations are blurred.
- On the consultant's side – there is a misunderstanding of the role in terms of the required support team, and an improperly documented scope framework.
- It is important to detail the requirements, responsibilities, and obligations of an EoR and also of the owner that they are to be contracted to. EoRs should never be hired by procurement personnel or based on commercial reasoning. EoR appointments should not be subject to competitive bidding-type processes but rather selected based on the best-fit candidate to satisfy the unique requirements of the facility.
- The EoR should form a partner relationship with the Owner and be empowered to affect change in designs around the tailings storage facilities they are responsible for.
- Competitively tendering design work and introducing a Designer of Record (DoR) and EoR complicates the role of the EoR and their ability to take responsibility for a design from a different company. The EoR should be given the first right of refusal and if a DoR is required, the EoR must be involved from inception, including the choice of DoR. However, if possible, combining a DoR and EoR from different companies on the same project should be avoided.
- Terms of Reference are key to providing clear expectations of both the EoR and the Owner. The United States Society on Dams (USSD) EoR working group is currently working on developing a guidance document that looks at frameworks for terms of reference. They note: *"A term of reference (TOR) for Engineer of Record (EoR) engagement is an important document that details the requirements, responsibilities, and obligations of the engineer of record and the mine owner that engages the EoR. It is an essential component of the EoR/Owner relationship to set up the team for success."*

Why become an EoR?

It is a demanding, risky, stressful, moderately rewarded, all-encompassing, time-consuming, ever-evolving role that requires an incredibly high level of knowledge and experience. Hands up in the air for all those interested.

For some, it may be an extraordinary opportunity to grow as a professional. A successful EoR should be communicative, have a solid foundation of technical knowledge, demonstrate emotional intelligence and leadership, have operational understanding and management, regulatory comprehension, and awareness, among other attributes. However, personal and professional growth tends to prompt a limited level of drive to be in an EoR role for many. It currently seems to be a role that is performed out of necessity more than anything else. Is this the anticipated future for the role, or will transformation occur?

Conclusions from the workshop

At the conclusion of the workshop, the attendees felt that a Charter should be developed for the EoR role in Australia.

Is it possible to make an EoR a desirable role? It must be. The EoR role is increasingly becoming a mandatory requirement for mine owners to employ and adopt. The standard for the responsibilities of the EoR is also significantly increasing. An example of this is the recently updated publication of the HSRC in British Columbia, which, among other changes, puts the onus on the EoR over any other professional engineer for many sections of the code (EMLI, 2024).

So, what are the key selling points, and how will the role be positively promoted? Questions like these must be posed to every individual and company who is involved in the business of managing mine waste, from the mine owner to the governing regulatory body to the engineering consultant.

The responses make it clear that major changes are essential to cultivate a culture where developing professionals are eager and interested in becoming an EoR, and where those already established in the role have a sense of satisfaction and security. Local and global governance initiatives are gaining traction towards providing consistency in clarity regarding the expected responsibilities of an EoR; however, improvements are needed in many areas.

Areas needing further development include:

- granting individual professional legal indemnity;
- increasing compensation;
- strengthening employer and Owner support;
- providing easy access to continued training and development; and
- promoting EoR role awareness and exposure within tertiary or post-secondary education.

The EoR role for mine waste facilities should not be the role that no one knows about outside of the mining industry. They should be well-known experts that the public admires for the intense amount of effort, expertise, and responsibility they hold for keeping the public and environment safe from disaster.

Perhaps most importantly, the role of EoR and its requirements should be developed with and by EoR's and prospective EoR's and their (often) personal sacrifice should be understood and supported by the Owner.

Suggestions for further discussions, in Australia and perhaps elsewhere

Perhaps a round table or working group modeled on or led by the USSD/CDA EoR working group could help to further dissect the issues raised. This paper does not claim to represent all EoRs, nor does it claim to represent the voice or opinion of EoRs based outside Australia. The views collected in this paper are based only on the voices of the participants in the November 23 QTG workshop. The following topics are suggested for further discussion, with the Owner as well as the consultants.

- clear career path;
- legal protection/indemnity/positive;
- risk vs. reward (appropriate compensation); and
- promotion/professional registration including: increased CPD, working with universities for (advanced) courses to supplement EoR experience, supplement experience with placements in different fields/regions.

References

Canadian Dam Association (CDA). 2019. Technical Bulletin: Application of Dam Safety Guidelines to Mining Dams (2019 Edition).

EMLI (Ministry of Energy, Mines and Low Carbon Innovation). 2024. Health, Safety and Reclamation Code for Mines in British Columbia. April 2024.

EGBC (Engineers and Geoscientists of British Columbia). 2021. In the Matter of Laura Fidel, P.Eng. EGBC File No. T15-048 – Determination of the Discipline Committee. July 12, 2021.

EGBC. (Engineers and Geoscientists of British Columbia). 2023. Legislated Dam Safety Reviews in BC. Version 4. September 2023.

Government of British Columbia, 2000. British Columbia Dam Safety Regulation B.C. Reg. 44/2000. Accessed 08/20/2024 at Dam Safety Regulation – Province of British Columbia (gov.bc.ca)

International Council on Mining and Metals (ICMM). 2021. Conformance Protocols – Global Industry Standard on Tailings Management. May 2021.

Morrison, K.F. and C.N. Hatton, 2016. Addressing the issue of Engineer of Record for tailings storage facilities. *GBA Business Brief.*

Beyond HR: Embedding GISTM Principle 11 in Leadership for Transformative Tailings Management

Johan du Toit, Data Riders Consulting & Education, Portugal
Fernando Damasio, Data Riders Consulting & Education, Brazil

Abstract

Leadership in mining must embrace Principle 11 of the GISTM (Global Industry Standard for Tailings Management) as a solemn duty, thereby avoiding the tempting and all-too-easy option of delegation to Human Resources. Principle 11 seeks to replace cultures of fear with ones of learning and open communication, in which surprises and deviations are not treated as issues to be hidden but as catalysts for early learning and knowledge sharing. This allows productive problem-solving, where issues are openly discussed and become shared experiences to help prevent unwanted events.

This shift is not just procedural, but strategic. Mining leaders are encouraged to do what only they can do. Use their positions-of-power deliberately and diligently to permit previously "undiscussable" discussions to be aired (versus "don't bring me problems … bring me solutions"). By treating unexpected events as invitations for learning, leaders can build the basis of effective tailings management. The responsibility for this transformation lies not just with support departments, but with the operational leadership at every level, showing their pivotal role in the creation of safe tailings facilities *and* a robust safety culture.

Introduction

The Global Industry Standard on Tailings Management (GISTM, 2020) was launched in August 2020 by the ICMM, the United Nations Environment Programme, and Principles for Responsible Investment. The GISTM was created in response to the catastrophic dam collapse at Vale's Córrego do Feijão mine in Brumadinho, Brazil, in 2019, which drove home the need for enhanced safety and effective governance of tailings facilities globally.

Origin of the Global Industry Standard for Tailings Management

The GISTM aims to achieve the goal of zero harm to people and the environment and applies to current and future tailings facilities. The Standard comprises six topic areas, 15 principles, and 77 auditable

requirements, and is supported by implementation protocols that provide more detailed guidance for certification or assurance and equivalence with other standards.

ICMM members have committed to implementing the GISTM by August 2023 (for extreme and very high-consequence facilities) and August 2025 (for all other facilities).

Importance of the GISTM Principle 11

Principle 11. Develop an Organizational Culture that Promotes Learning, Communication and Early Problem Recognition (GISTM, 2020).

Consider a hypothetical organization that has a culture characterized by a *lack* of learning, communication, and early problem recognition *in a complex, high-intensity industry*. That alarming state of affairs would surely be a huge red flag for all the stakeholders. Hence the pressing need to foster the positive culture required by Principle 11 (du Toit, 2022).

The problem with the GISTM, in this one case, is that while the original Standards document does a very fine job of laying out the five Requirements for Principle 11, the subsequent Conformance Protocols document (GISTM, 2021) adduces examples and clarification notes that reduce Principle 11 to an impoverished version of its original form.

Methodology used in this paper to demonstrate the "complication" with Principle 11

Content analysis is a research method used to systematically analyze texts, images, videos, and other communication materials (Wikipedia). Researchers code or label the content into categories, which allows them to quantitatively analyze patterns using statistics or qualitatively examine meanings. Content analysis practices vary across disciplines, but typically involve defining the data being analyzed, its context, boundaries, and what is being measured. The approach used for this paper is qualitative: exploring intentionality and implications behind the content.

This paper uses seminal documents (GISTM, 2020 and GISTM, 2021) to investigate whether their underlying intentions are consistent. To do this consistency check, use is made of prominent frameworks in the Human Resources domain: Ulrich's (2008) book titled *HR Competencies: Mastery at the Intersection of People and Business* and the *People-Capability Maturity Model* (Curtis et al., 2009). The relatedness, if not equivalence, of the maturity levels between the Ulrich and P-CMM frameworks has been demonstrated (du Toit, 2010), as shown in Figure 1. The evidence that the principle 11 Requirements are misaligned with the Conformance protocols is based primarily on analyzing the content between the two key GISTM documents and the precise levels-based language in the encyclopedic P-CMM (2009).

The People-Capability Maturity Model (P-CMM) Version 2.0 is a framework designed to help organizations improve their workforce practices and enhance overall organizational performance. It provides a structured approach for characterizing the maturity of workforce practices, establishing

continuous workforce development programs, and setting priorities for improvement actions. The P-CMM consists of progressive maturity levels, each focusing on different aspects of workforce management and development. By implementing the P-CMM, organizations can systematically address critical people issues and align workforce activities with business objectives, creating a culture of excellence and continuous improvement.

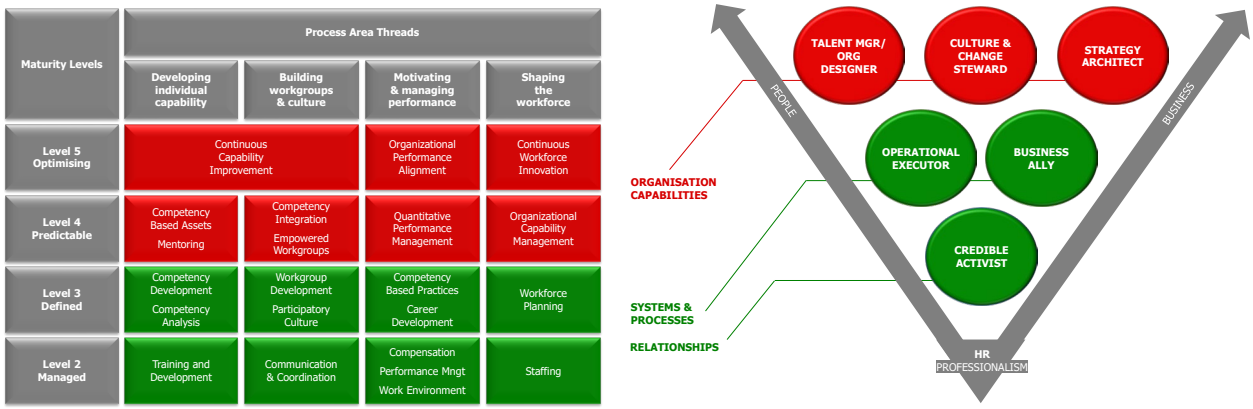


Figure 1: P-CMM 2.0 process areas (left) compared to Ulrich's HR competencies (right)

Evidence of impoverishing Principle 11 at the Conformance protocols stage

Table 1: Textual comparison between GISTM Standards and protocols statements

Req. #	Requirements of Principles 11	Examples of Conformance protocols
11.1	"Educate personnel … how their job … relate[s] to the prevention of failure"	"Training needs analysis" "Training logs"/"attendance sheets"
11.2	"Establish mechanisms that incorporate workers' experience-based knowledge into … all phases of the tailings facility lifecycle"	"Involved in development of … [systems]" "Providing training to new workers" "Incorporating the … experience they have … into action plans"
11.3	"Establish mechanisms that promote cross-functional collaboration to ensure effective data and knowledge sharing, communication … "	"Information sharing … "
11.4	" … implement lessons from … investigations and incident reports [with] attention to human and organizational factors"	"Limitations of humans" "Resilient to human error"
11.5	"Establish mechanisms that recognize, reward and protect from retaliation, [those] who report problems or identify opportunities"	"Grievance mechanisms" = partially equivalent to conformance

The impoverishment of Principle 11 at the Conformance protocols stage is likely to go unnoticed, because it has the effect of silently shifting critical work from operational executives and managers to support

functions (like HR). Consider the simple phrase "Establish mechanisms …". The danger lies in underestimating the significance contained in requirements 11.2, 11.3 and 11.5. To avoid that, it is useful to examine definitions of "establish" and "mechanism" (taken from the top entries for both words in the online *Merriam-Webster Dictionary*):

es·tab·lish

1: to institute (as a law) permanently by enactment or agreement

2: to make firm or stable

3: to bring into existence: FOUND

mech·a·nism

1a: a piece of machinery

b: a process, technique, or system for achieving a result

By applying these definitions one can fairly construct this meaning for "establish mechanisms that [x]" = "bring into existence, to make firm or stable, a process, technique or system for achieving result [x]."

Using content analysis, we show more fully in Appendix 1 that the Principle 11 requirements and the corresponding Conformance protocols are "at different levels." We use the P-CMM (People-Capability Maturity Model) 2.0 to demonstrate that the requirements from the principle employ language that is more progressed than from the examples-of-conformance (e.g., "educate" versus "training").

The People-Capability Maturity Model supports our findings that the Requirements' language is more generally located at the higher two maturity levels (Level 4: Predictable and Level 5: Optimizing), whereas the Conformance language is generally located at the lower two maturity levels (Level 2: Managed and Level 3: Defined).

What then does managerial leadership involvement in Principle 11 look like?

Since Principle 11 is about how to "develop an organizational culture … " it is instructive to consider what "levers" are available for leaders to affect cultural change (a more sophisticated perspective of organizations as *complex adaptive systems* is in Appendix 2 to expand the insights provided below).

Psychological Safety: The positive result of all-in leadership involvement

The modern work of Amy Edmondson and Timothy Clark, standing on the shoulders of giants like Rogers, Schein, Bennis and Deming (Psychological Safety – Wikipedia), has mainstreamed the urgently needed and useful concept of Psychological Safety.

Edmondson (2018), the latter-day pioneer in this field, cuts to the chase with her latest book titled, *The Fearless Organization: Creating Psychological Safety in the Workplace for Learning, Innovation, and Growth*. Clark (2020) has also made a pivotal contribution with *The Four Stages of Psychological Safety.*

This highly accessible work lays out a conceptual model of the four "stages" of psychological safety that teams and team members need to progressively move through:

1. *Inclusion Safety,* where members feel safe to belong to the team.
2. *Learner Safety,* where members learn through asking questions.
3. *Contributor Safety* ,where members feel safe to offer their own ideas, without fear of embarrassment or ridicule.
4. *Challenger Safety,* where members can question others' ideas (particularly those in authority) or suggest significant changes to ideas, plans, or ways of working.

Inclusion Safety is viable where normative practices are progressive, which is typical of many Western businesses (see the ubiquity of DEI [diversity, equity and inclusion] policies). *Learner Safety* is feasible where semantic practices are customized to link organizational performance to individual and team contributions, which is standard in most Western businesses (see the omnipresence of "cascaded" performance measurement constructs like Balanced Scorecards and OKRs).

Contributor and *Challenger Safety* are much more fragile. It is useful here to recall the definition of "political dynamics" (in Organization Learning Practices listed in Appendix 2): affect *which knowledge is valued* and how information flows. They also influence who has the *authority to make decisions and how conflicts are resolved* (italics are the authors).

Admit that power is the enabler or blocker

"Power is America's last dirty word. Rosabeth Moss Kanter (1997) from Harvard Business School was the first to brazenly state that "It is easier to talk about money – and much easier to talk about sex – than it is to talk about power ". This sentiment was reiterated over a decade later by Jeffrey Pfeffer, a professor of organizational behavior at Stanford Graduate School of Business. It seems that after a generation has passed these truisms have to be restated to not be forgotten.

In his book *Power: Why Some People Have It and Others Don't* (2010), Pfeffer argues that power is a crucial aspect of organizational life, and that understanding and navigating power dynamics is essential for personal and organizational success. He also notes that power is often overlooked or downplayed in American culture, leading to a lack of awareness and understanding of its role in shaping individual and organizational outcomes.

Seek Operating System "balance"

Marquet's book *Leadership is Language* (2020) presents compelling concepts like the Red and Blue Operating Systems, to help achieve positive outcomes in high-stakes environments.

Red Operating System:

- Referred to as "red work," this system focuses on execution and reducing variability.
- It involves strict goals, steep hierarchies, and a "prove and perform" mindset.
- It is effective in the short term for achieving results, but less adaptive in the long run.

Blue Operating System:

- Referred to as "blue work," this system focuses on thinking, decision-making, and embracing variability.
- It involves collaboration, learning, and a "learn and grow" mindset.
- It is more adaptive in the long run but may not yield immediate results.

Enable Share of Voice

Marquet (2020) also introduces the powerful concept of Share of Voice, which emphasizes distributing decision-making authority and influence within an organization. It pushes leaders to give everyone a voice in decision-making processes, rather than relying solely on their perspective.

Key aspects of Marquet's Share of Voice include:

- Distributing decision-making authority to team members, allowing them to take ownership and contribute to the organization's success.
- Amplifying diverse perspectives to inform more innovative decision-making.
- Fostering a culture of inclusivity where everyone feels empowered to contribute regardless of their position or background.
- Developing leadership skills at all levels of the organization.
- Fostering engagement by truly involving team members in decision-making.

Effective leadership should balance, and shift as needed, between both *systems* (mentioned in the previous section), by using and acknowledging that language plays a pivotal role in keeping this balance.

Conclusion

The GISTM was launched in response to the need for enhanced safety and governance of tailings facilities globally and aims to achieve zero harm to people and the environment. The GISTM has received an industry-wide commitment, with ICMM members pledging to implement the Standard for all their tailings facilities by August 2025.

There is potentially a serious misalignment between what the original GISTM (2020) standard espouses and what the later GISTM Conformance (2021) protocols seek to measure. Once this "measurement impoverishment" is recognized, it requires operational executives acting on evidence-based practices that will keep operational leaders in-the-loop, striving to:

- Create deep Psychological Safety that enables learning, innovation, and growth (Edmondson, 2018) that requires leaders to diligently address covert "power" dynamics that can make sensitive subjects "undiscussable" (Smith, 2024).
- Recognize respected academic research that shows that Organizational Learning is a consequence of collective behaviors, that depend on asymmetric power relationships.
- Embrace Marquet's practical emphasis on balancing the Red and Blue Operating Systems, where language plays a key role.
- Allow Share-of-Voice to be more equal as it is a powerful enabler in creating a more collaborative, inclusive, and effective work environment.

References

Beauregard, N., Lemyre, L. and Barrette, J. 2015. The domains of organizational learning practices: an agency-structure perspective. *Societies* 5: 713–733. doi:10.3390/soc5040713

Clark, T.R. 2020. *The Four Stages of Psychological Safety*. Berrett-Koehler Publishers.

Curtis, B., B. Hefler and S. Miller. 2009. *The People-Capability Maturity Model (P-CMM) Version 2.0,* Second Edition. Software Engineering Institute. Accessed 6/07/2024 at https://insights.sei.cmu.edu/documents/808/2009_005_001_15095.pdf

du Toit, J. 2010. OD's role in shaping tomorrow's leaders … or, OD in the Anomic Age. Talk presented at the Re-Inventing Organizational Development 2010 conference, Johannesburg, South Africa, June 2010.

du Toit, J. 2022. How operational integrity stewarded by geotechnical professionals enables catastrophic risk management. In R. Cameron and B. Simonian (eds), *CIMBC22. Proceedings of the 2022 CIM Convention*. Vancouver, British Columbia, Canada from May 1–4, 2022: https://store.cim.org/en/how-operational-integrity-stewarded-by-geotechnical-professionals-enables-catastrophic-risk-management

Edmondson, A. 2018. *The Fearless Organization: Creating Psychological Safety in the Workplace for Learning, Innovation, and Growth*. Wiley.

ESG Reporting Intelligence, 2024. Understanding DEI policies and tracking DEI data amid changing regulations. Accessed 14/06/2024 at: https://esgri.com/understanding-dei-policies-and-tracking-dei-data-amid-changing-regulations/

GISTM. 2020. Global Industry Standard on Tailings Management. Accessed 6/06/2024 at: global-industry-standard_EN.pdf (globaltailingsreview.org)

GISTM. 2021. Conformance Protocols: Global Industry Standard on Tailings Management. Accessed 6/06/2024 at https://www.icmm.com/en-gb/our-principles/tailings/tailings-conformance-protocols

Kanter, R.M. 1979. Power failure in management circuits. *Harvard Business Review* 57(4): 65–75.

Marquet, L. David. 2020. *Leadership is Language: The Hidden Power of What You Say – And What You Don't*. Penguin Publishing Group.

Martin, R.L. 2022. *A New Way to Think: Your Guide to Superior Management Effectiveness*. Harvard Business Review Press.

Merriam-Webster.com Dictionary. 2024. *Merriam-Webster*. Accessed 6/11/2024 at https://www.merriam-webster.com/dictionary/establish

Nonaka, I. 1994. A dynamic theory of organizational knowledge creation. *Organization Science* 5(1):14–37.

Patterson, K., J. Grenny, R. McMillan and A. Switzler. 2005. *Crucial Confrontations: Tools for Resolving Broken Promises, Violated Expectations, and Bad Behavior*. McGraw-Hill.

Pfeffer, J. 2010. *Power: Why Some People Have It and Others Don't*. Harper Collins.

Smith, D.D. 2024. How to discuss the undiscussables on your team. *Harvard Business Review*. Accessed 14/06/2024 at https://hbr.org/2024/04/how-to-discuss-the-undiscussables-on-your-team

Ulrich, D. 2008. *HR Competencies: Mastery at the Intersection of People and Business.* Society for Human Resource Management.

Wikipedia. 2024. Content Analysis. Retrieved 6/20/2024 from https://en.wikipedia.org/wiki/Content_analysis

Wikipedia. 2024. Psychological Safety. Accessed 6/20/2024 at: https://en.wikipedia.org/wiki/Psychological_safety

Appendix 1: Detailed content analysis

The analysis below is extracted from the "Evidence of impoverishing Principle 11 at the Conformance protocols stage" section of the paper and placed in an Appendix. This helps smooth the flow in the paper.

Table A1: Textual implications between GISTM Requirements and Conformance statements

Req. #	Requirements for Principles	Examples of Conformance
11.1	"Educate" => *critical thinking, problem solving and communications skills*	"training" => *specific job skills or competencies*
11.2	The relevant advanced practices for Principle 11 from P-CMM are mostly from the two upper levels of maturity ("upper half"; the red blocks in Fig. 2)	One example from "lower half" – Workgroup Development at Level 3
11.3	Relevant "knowledge sharing" for Principle 11 from P-CMM are found at Level 4 (Commitment 1 of Competency Based Assets process area)	"Information sharing" appears once in PCMM ("strategic HR management")
11.4	Relevant "lessons learned" for Principle 11 from P-CMM are more from upper levels of maturity ("upper half"; the red blocks in Fig. 2)	Wrong model of accident causation used (people-safety versus process-safety paradigms)
11.5	Highest two levels of P-CMM give the correct view of recognition and rewards (not the "outstanding (individual) contribution" mentioned in lower levels)	The lower levels (the green blocks in Fig. 2) of P-CMM are where the recognition and rewards effort is driven by "formulas" owned by HR

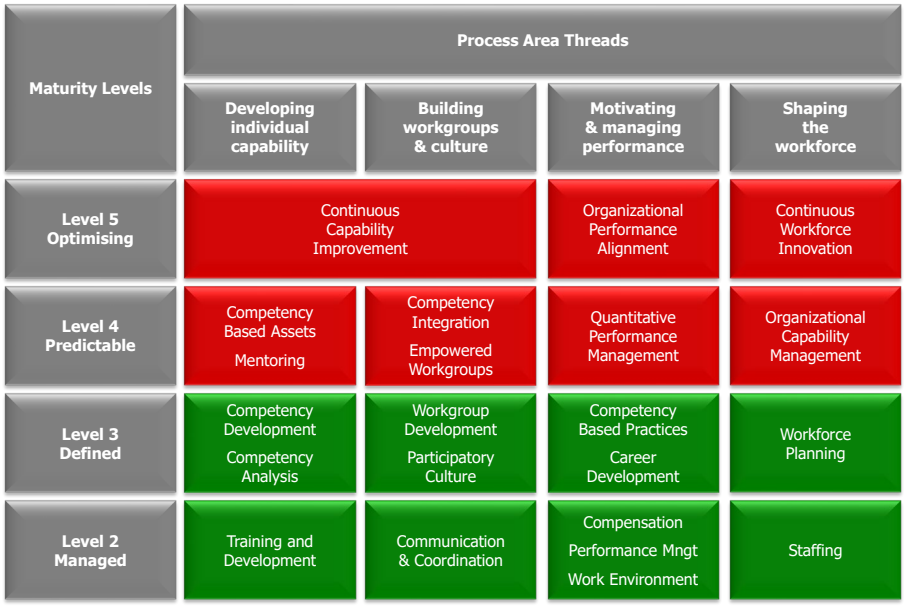


Figure A1: P-CMM 2.0 framework distinguishing lower and upper levels

Example of misalignment for requirement 11.5

"Awareness of, and orientation to, the organization's recognition and reward system" (Curtis et al., 2009). If the recognition and reward system is an example of an OLP (organizational learning practice), then its political, normative, and semantic dynamics need to be made explicit.

Table A2: Comparison of lower- and higher-maturity practices

Dynamic	Lower maturity competencies	Higher maturity capabilities
Political	"Rules of the game" = formal HR policy	"Rules of the game" = Organizational culture
Normative	"Outstanding performance" desired	"Improving workgroup performance" desired
Semantic	"High potentials," "rank-and-yank"	"Continuous improvement," "transparency"

"Recognition and rewards are made to reinforce the skills and behaviors that the organization values." The intent of the Managed and Defined maturity levels is Compliance and Conformance (Control). At the higher levels of Predictable and Optimizing it is Performance (Control plus Continuous Improvement). What a less mature "Control" organization values is different from what a more mature "Performance" organization values. With requirement 11.5 this is painfully clear. The "establish mechanisms" language seeks positive impact, by firstly, "recogniz[ing] and reward[ing] [those] who report problems or identify opportunities *for improving tailings facility management*" (italics are the authors). Secondly, the qualifier is added that these workers should also be protected from retaliation if their contributions are not welcomed, for instance by insecure management. The lofty ambition of 11.5 is to unlock the vast potential of "early problem recognition."

An indication that the Conformance protocols misunderstand this vital point, is evident from listing "grievance mechanisms" as partially meeting 11.5 and is also repeated under requirements 12.1 and 12.2. Perhaps this is due to the unfortunate sequencing of having Principle 12, that deals with whistleblowing related to potentially unlawful activities, being straight after Principle 11 that speaks of a positive, healthy organizational culture of learning, communication, and early problem recognition.

The P-CMM uses language at its lowest level of maturity (Level 2: Managed) that resonates with the language of "grievance:"

- Handling problem employees,
- Documenting and managing unsatisfactory performance.

At the highest-level of P-CMM (Level 5: Optimizing) is the process area of Continuous Capability Improvement. It has an instructive entry under Practice 15: *"The organization's workforce practices are adjusted, as needed, to accommodate continuous improvement activities by individuals and workgroups."* An example of where such adjustment may be needed is "Recognition and Rewards."

The lesson from P-CMM for 11.5 is that there is an urgent need to adjust the workforce practice of "Recognition and Rewards." The Conformance protocol examples do not have a single reference to recognition and rewards; just this lower-maturity reference to "*acknowledgement and feedback when problems and opportunities are raised."* The latter example could quite readily be provided by a system-generated email when the person raising the problem uses one of the "channels" to report the matters (since

confidentiality and anonymity are a design-feature and an option on these channels, it is hard to see how that will help with recognizing and rewarding the people doing the reporting).

Example of requirement 11.3 misalignment

"Establish mechanisms that promote cross-functional collaboration to ensure effective data and knowledge sharing, communication and implementation of management measures *to support public safety and the integrity of the tailings facility*" (GISTM, 2020) (italics are the authors). The language used in the Conformance protocols is mainly pre-occupied with "information sharing." This is the same language found in the lower-maturity P-CMM related to the process area of Communication and Coordination (Level 2, Managed). Collaboration is a more mature practice than coordination (just as knowledge management is a more advanced endeavor than information management).

The ambitions of 11.3 are not modest. This goal of cross-functional collaboration is intended to promote the safety of the public and the integrity of the critical assets.

"The organization's stated values encourage knowledge sharing between individuals and workgroups." Competency-Based assets (CBA) process area, Level 4, Predictable)

The purpose of CBA is *" to capture the knowledge, experience, and artifacts developed in performing competency-based processes for use in enhancing capability and performance."* (Curtis et al., 2009)

Example of requirement 11.2 misalignment

"To achieve … Maturity Level 4, the organization quantifies and manages the capability of its workforce and competency-based processes […]. The organization creates a culture of measurement and *exploits shared experience*." (P-CMM 2009, p.37) (italics are the authors). The intention of requirement 11.2 is relatable to the maturation to Level 4. Refer to the 11.3 example above where CBA is already covered.

The intention here is about *deliberate* processes (c.f. SECI model of knowledge management [Nonaka, 1994]) of turning workers' *tacit* knowledge (privately held) into *explicit* knowledge (a corporate asset). It is hard to see how the examples adduced in the Conformance protocols meet this standard (see Table 1). The emphasis in requirement 11.2 is "externalization" (tacit to explicit); the conformance protocol for 11.2 is closer to Nonaka's "socialization" (tacit to tacit). The latter is easier to try and verify, but like all the other examples covered before it is verifying a much-impoverished version of what the Standard intends.

Appendix 2: Culture as an emergent property of complex adaptive systems

Organizational culture change: steering mechanisms and organizational learning practices

Roger Martin's latest book, *A New Way to Think* (2022), declares that cultural change cannot be affected directly, or mandated by leaders. Instead, they should influence the way organizational members interact

and work together, through the formal mechanisms under their control ("steering," not "driving").

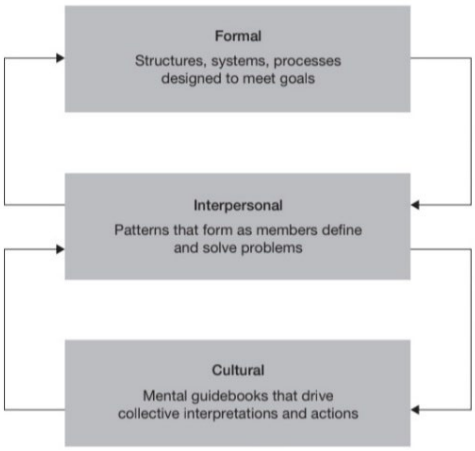


Figure A2: Martin's steering mechanisms for cultural change

Martin's pragmatic advice (from a business consultant and business school dean with over 40 years of experience) is well aligned with rigorous academic research from the Organizational Learning school. Organizational Learning Practices (OLP) – as a critical precursor for the desired organizational culture – are defined (Beauregard et al., 2015) as a set of *collectively shared practices* held by members of a given organization embedded in normative, political, and semantic dynamics.

- Normative Dynamics: the shared norms, values, and expectations that guide members' behavior within an organization. They shape the organizational culture and provide a framework for acceptable practices and routines (compare with the Helps and Hindrances of Patterson et al., 2005).
- Political Dynamics: the power structures and political interactions that occur within an organization. Political dynamics can affect which knowledge is valued and how information flows. They also influence who has the authority to make decisions and how conflicts are resolved (compare with the Bridges and Barriers of Patterson et al., 2005).
- Semantic Dynamics: the meaning and understanding of language and symbols within an organization. Semantic dynamics are about how knowledge is interpreted and communicated among members.

These dynamics interact with each other to shape the *learning environment* of an organization, influencing how knowledge is created, shared, and utilized to achieve organizational goals. This research also reveals some of the more vexing dimensions needed for change, like the issue of power and politics.

Global Industry Standard on Tailings Management (GISTM) – Some Aspects of Implementation

Marcelo Roberto Barbosa, MB CONSULTORIA MINERAL, Brazil
Lucas Samuel Santos Brasil, GWS Engenharia, Brazil
Flavia Cruz Pereira, Lm4tech, Brazil
Denise Capanema, Vale S.A., Brazil
Marina Borges, Vale S.A., Brazil

Abstract

The release of the Global Industry Standard on Tailings Management (GISTM) in August 2020 marked a turning point in the management of tailings storage facilities (TSFs). This comprehensive guide brought together a robust range of technical and non-technical themes, which was unprecedented considering the parties involved in its development. Highlighting its significance, all global mining companies that are members of the International Council on Mining and Metals (ICMM) have committed to its adoption.

At first glance, the Standard may seem complex and difficult to implement, but it is not, as long as it is viewed as a cultural transformation in the company's tailings management. This work presents some aspects of GISTM implementation in companies, highlighting the case of Vale S.A., which achieved compliance in 48 TSFs between 2020 and 2023. Through a governance framework diagram, the macro-processes of the pre-implementation phase will be discussed, suggesting ways to prepare for, achieve, and maintain compliance with the Standard. This aims to encourage other mining companies to voluntarily engage with GISTM, continuously improving processes and enhancing the safety of TSFs.

Introduction

The document "Global Industry Standard on Tailings Management" (GISTM), (ICMM, 2020), referred to in this article as the "Tailings Standard" or simply "Standard," marked a watershed moment for the mining industry in managing tailings storage facilities (TSFs) more responsibly and sustainably. It consolidated a comprehensive range of technical and non-technical themes, unprecedented in scope, given the diverse and robust documentation of guidelines and best practices on tailings already available globally.

The development of the GISTM, published in August 2020, was triggered by previous tailings dam failures, culminating in the Brumadinho incident in Brazil in 2019. Williams (2021) reinforces this initiative

by noting that the progressive raising of tailings dams has led to an unacceptable rate of catastrophic failures, resulting in deaths and environmental and infrastructural damage. The author also points out that the failure rate of tailings dams is about two orders of magnitude higher than that of water dams.

The GISTM was the result of collaboration between the International Council on Mining and Metals (ICMM), the United Nations Environment Programme (UNEP), and the Principles for Responsible Investment (PRI). This unprecedented consortium brought together a productive mix of objectives and values, creating a comprehensive set of guidelines and requirements aimed at safer management, not only in engineering and geotechnics but also in social, environmental, and governance aspects for tailings dams throughout their lifecycle, from design and construction to operation, closure, and post-closure. The Standard also stipulates that it applies to both current and future dams.

Regarding implementation timelines, the GISTM recommended that ICMM member companies implement and disclose their compliance by August 2023 for dams classified as having extreme and very high consequences. For other tailings dams, the final compliance deadline is August 2025.

For clarification, "compliance" means that the company can demonstrate the existence of systems and processes to implement all applicable requirements of the Standard without conflicting with relevant existing legislation.

Several authors have highlighted the importance of the GISTM for the industry. Romero (2023) notes that the Standard strongly emphasizes preventing catastrophic failures by promoting risk-based approaches to ensure the safety of workers, communities, and the environment. He adds that it also encourages the adoption of best practices to minimize environmental impact, and includes measures to reduce water consumption, prevent pollution, and promote rehabilitation and recovery to restore affected ecosystems. The author concludes by saying that the Standard emphasizes the importance of transparency, accountability, and stakeholder engagement, encouraging mining companies to disclose relevant information about their dams and interact with affected communities.

Sova et al. (2023) state that mine owners, regulators, and engineering consultants had already been reporting on dams, but with the new Standard, they now report at a previously unrequired or undefined level. The typical lifecycle of a dam can last from 10 to 100 years, and facilities often undergo progressive construction, keeping them active. The author also notes that complying with the Standard has been a significant challenge for the industry, requiring greater accountability from engineers and dam owners.

This work aims to present some aspects of GISTM implementation in companies, sharing the case of Vale S.A., which implemented the Standard between 2020 and 2023 for 48 tailings dams in Brazil and Canada.

About the GISTM and the conformance protocols

The GISTM (ICMM, 2020) is a document comprising six Topics, subdivided into fifteen Principles, which in turn are divided into seventy-seven auditable Requirements. Table 1 provides a summarized overview of the interrelated themes throughout the Tailings Standard, emphasizing that a significant number of them are, in some way, covered by the National Dam Safety Policy (NDSP).

Table 1: Interrelated themes of the GISTM's Topics, Principles, and Requirements

6 Topics	15 Principles	77 Requirements
1. 1. Affected Communities	1. Human Rights	4
2. Integrated Knowledge Base	2. Knowledge	4
	3. Information for Decision-Making	4
3. Design, Construction, Operation, and Monitoring of Tailings Disposal Structures	4. Planning	8
	5. Design	8
	6. Risks	6
	7. Monitoring	5
4. Management and Governance	8. Policies	7
	9. EoR (Engineer of Record)	5
	10. Review	7
	11. Culture	5
	12. Whistleblower	2
5. Emergency Response and Long-Term Recovery	13. Emergency	4
	14. Recovery	5
6. Public Disclosure and Access to Information	15. Disclosure	3

The current Standard is designed to establish a normative framework that encompasses the critical elements of cultural transformation within geotechnical teams operating tailings storage facilities (TSFs), thus proposing an integrative perspective. This approach supports the premise that organizational structures must be responsible for all interacting areas that create and sustain the teams responsible for TSFs. Uniquely, this Standard can be applied throughout the entire lifecycle of the dam, maintaining relevance and effectiveness over time through continuous maintenance processes. Additionally, one of the Standard's innovations is the customization of internal compliance and specific evaluations for each TSF, alongside external audits aimed at certification. This creates a more personalized approach and a clearer understanding of risks and compliance. Finally, the Standard requires organizations to establish new roles and responsibilities, ensuring an ongoing process that spans the entire chain of command, thereby guaranteeing

the effectiveness of corporate governance and an unwavering commitment to the safety and sustainability of TSFs as assets within the mining sector's production process.

The Conformance Protocols

The document "The Conformance Protocols" (ICMM, 2021) was developed by the ICMM and published in May 2021. This document was created in collaboration with two international consulting firms and the ICMM Tailings Working Group, which comprises professionals from 21 ICMM member companies, including the author of this article (Figure 1).

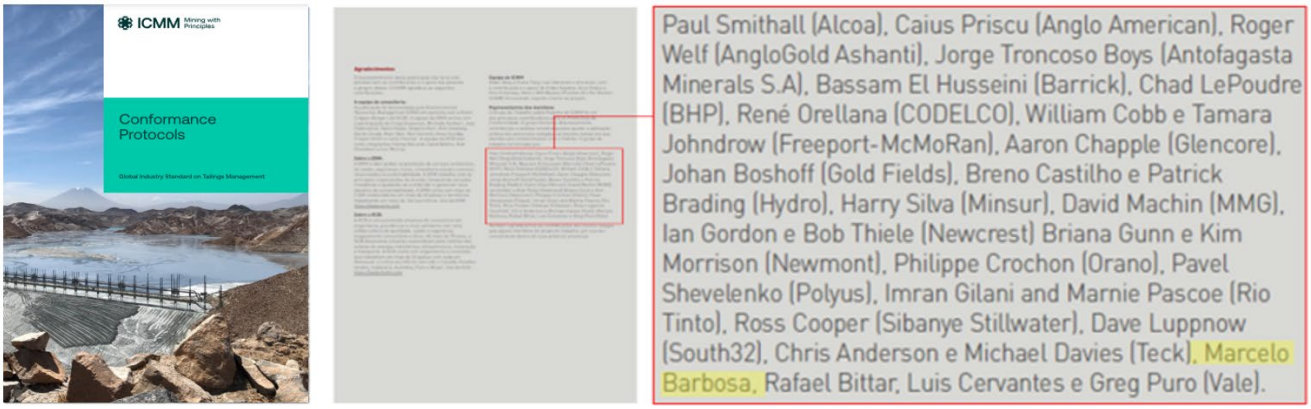


Figure 1: Acknowledgments page of the document "The GISTM Compliance Protocols." The highlighted name is that of the lead author of this paper

The primary objective of these protocols is to serve as a guide for companies and independent third parties to evaluate the implementation of requirements and confirm compliance with the GISTM. The document is in the form of checklists, with criteria on how the requirements should be assessed, and includes examples of documentation, activities, and initiatives that can be presented as evidence for the 77 auditable requirements of the Standard. It is important to emphasize that despite these guidelines, the content of the requirements should be thoroughly studied, interpreted, and understood by the teams involved in the implementation, as they encompass a wide range of disciplines and should be fully utilized to significantly aid in the engagement and integration of the teams.

Therefore, through the ICMM's compliance protocols, the Standard will help demonstrate to all stakeholders that responsible practices are being applied throughout the entire lifecycle of the company's TSFs. Finally, it is important to highlight a recommendation from this document: that ICMM member companies commit to demonstrating their compliance based on, at a minimum, self-assessments within the agreed timelines. However, these companies should engage independent third parties to conduct validation or verification as soon as reasonably possible to confirm the claims made in their self-assessments.

GISTM governance macroprocesses and aspects of implementation

The GISTM governance framework required for a successful implementation within companies, due to the unique characteristics of each organization and the diverse range of factors governing their tailings structures, suggests that there is no "silver bullet" of ready-made or ideal methodologies and frameworks. Gore and Moghaddam (2023) indicate that each portfolio of structures within a company will need its own methodology and transformation journey when adopting the GISTM. This process unfolds over time, benefiting from implementation experiences shared across the global industry, which is precisely the intention of this article.

The macroprocess diagram displayed synthesizes the strategy developed during the implementation period. This timeframe allowed for a detailed analysis and an in-depth understanding of the GISTM requirements. Figure 2 illustrates the sequence of macroprocesses and their interrelationships with the three suggested implementation phases.

It is important to note that the Maintenance Phase should operate as a circular process, where the activities for assessing compliance with the requirements are defined with some periodicity/recurrence, focusing primarily on adherence to the GISTM principles.

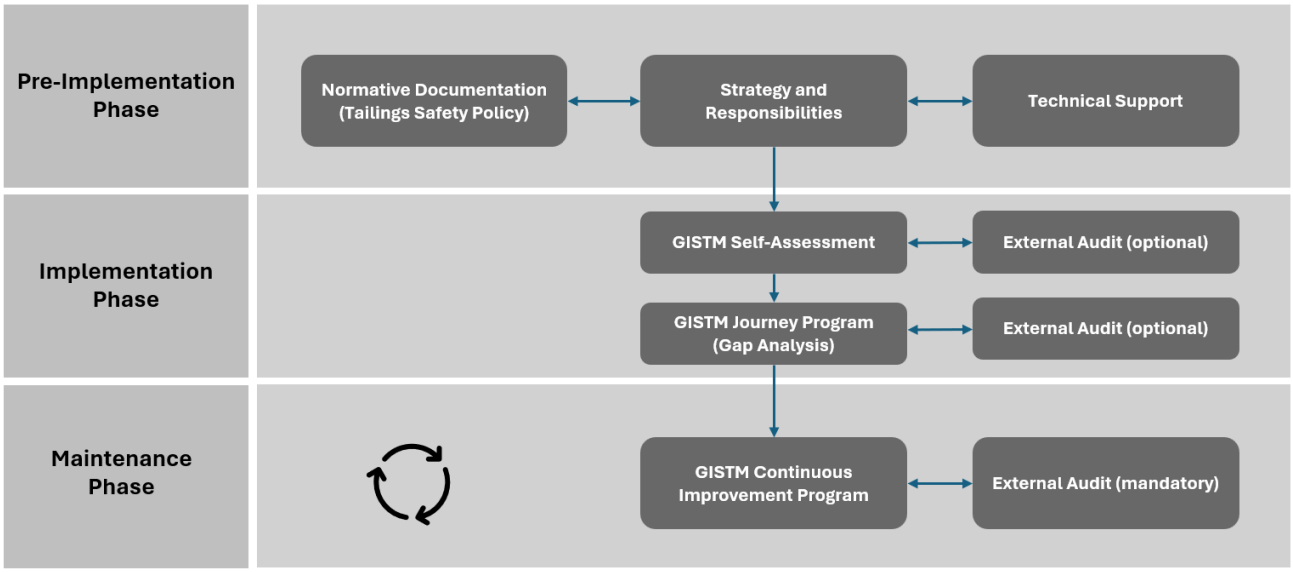


Figure 2: The three phases of GISTM governance macroprocesses: pre-implementation, implementation, and maintenance

All macroprocesses are divided into numerous processes and products. However, this article will focus solely on the macroprocesses of the Pre-implementation Phase, discussing their critical points and key aspects.

Pre-implementation phase macroprocesses of the GISTM

Experience has shown that by focusing on the three macroprocesses of this phase, if well-discussed and planned internally, companies can achieve good visibility on how the Standard will be integrated into the company's processes in the future. The macroprocesses discussed below are interdependent and do not necessarily have a defined timeframe for completion.

Pre-implementation Phase – macroprocess – normative documentation (tailings safety policy)

This macroprocess can be considered the "starting point" for implementing the Standard within the company. It is an extremely important document that may already exist internally alongside other company regulations and/or have other names, but in general, it should be developed and titled as the "Tailings Safety Policy." This document affirms the top management's commitment to responsible tailings management and the implementation of the GISTM, or it can reference another compliance standard, whether external, internal, national, or international.

This document must be signed by the highest level of the company's hierarchy and widely disseminated both internally and publicly, ensuring the necessary seriousness and credibility for employees and the market.

Pre-implementation Phase – macroprocess – strategy and responsibilities

This macroprocess highlights three points of attention to be considered:

Implementation timeline: for non-ICMM member companies, engagement with the Standard is voluntary, and therefore, this timeline is flexible and should be adjusted based on the company's needs and feasibility.

- **Case of Vale S.A.:** It took three years to achieve GISTM compliance for 48 dams.
- **Lesson:** The premise should be a realistic and feasible schedule with progressive goals. The important thing is to plan to achieve the goals gradually, creating a continuous loop of motivation for the involved teams and top management.

Human resources: the "GISTM team" should ideally be dedicated and independent of the operational teams of the dams. The benefit of dedication lies in the fact that, due to the multidisciplinary nature of the Standard's requirements, a central technical liaison is more productive and integrative. This team becomes a reference and focal point in the implementation developments and does not overburden the operational teams with new demands. This dedicated team should include at least one senior professional with expertise in mining geotechnics.

- **Case of Vale S.A.:** the GISTM team consisted of ten professionals (two full-time Vale S.A. employees, one senior and one trainee, and eight contracted from third-party geotechnics and

technology firms, including three full-time mid-level professionals, three part-time junior and mid-level professionals, and two on-demand senior professionals).

- **Lesson:** a small and dedicated GISTM team is sufficient to drive and engage the company in the implementation processes.

Financial resources: The budget to be allocated is another subject of open discussion within the company, directly related to the number of tailings structures and, obviously, the availability of funds. This will have a visible impact on three important points: the implementation timeline, the dedicated team, and the technical support, whether from consulting or technology.

- **Case of Vale S.A.:** The company opted for a long-term implementation (following the ICMM's recommended three-year period), a lean GISTM team, and a preference for developing its own technology platform for management and control.
- **Lesson:** As the timeline, team, and infrastructure can be adapted, so can the implementation budget. The key message is that it is better to start the implementation at a "low profile" pace than to postpone or not start at all.

Pre-implementation Phase – macroprocess – technical support

This macroprocess highlights two points of attention to be considered:

External technical expertise: this point addresses the need to seek external technical knowledge to support the implementation of the Standard, which can be done in three main ways:

1. **Technical consulting:** this form of support is not required by the Standard and is therefore optional and at the company's discretion, based on its need to acquire knowledge for implementation. This could involve hiring companies or independent consultants to guide the initial steps in the GISTM and/or to follow up on the implementation developments.
    - **Case of Vale S.A.:** two companies were contracted to oversee the entire implementation until compliance was achieved. One was an engineering and geotechnics company (providing support in technical and non-technical areas of the Standard), and the other was a technology and project/process management company (providing support in the digital environment for storage, management, performance indicator [KPI] control, and visibility of results).
    - **Lesson:** due to the multidisciplinary nature of the Standard and its broad themes, it is not essential to hire or assemble a large team, as discussed

above. However, acquiring prior knowledge of the Standard, at least for planning a good roadmap, is highly advisable.

2. **Independent professional:** this form of support is recommended by the Standard for result validation, which can also be referred to as verification or audit. This activity is important when the company has already begun the implementation work and decides it needs to calibrate its methodology and ongoing results, or confirm the level of compliance achieved at that point. The Compliance Protocols refer to this activity as "third-party validation" or "third-party audit," which should be conducted by a senior professional or auditor with the necessary experience, skills, and knowledge to expertly confirm the reasonableness and authenticity of the company's self-assessment claims, or to perform an autonomous audit.

It is important to note the timelines, as the Standard recommends that companies hire auditors to conduct third-party validation as soon as possible to confirm the claims of self-assessments. Subsequently, the intervals between independent audits should not exceed three years for dams classified as "Extreme" or "Very High" consequence, and five years for all others.

- **Case of Vale S.A.:** two companies were contracted for auditing at two different periods. The first round was a "calibration audit" after the first self-assessment of the dams (to analyze the methodology and the level of compliance achieved up to that point), and the second round was a "verification and validation audit" before disclosing compliance to the market (to ensure the reliability of the results).
- **Lesson:** although these calibrations, validations, verifications, or audits are not mandatory but are recommendations of the Standard, the important thing is to ensure the quality and trust in the implementation results. The best way to achieve this assurance is through an external and independent perspective.

1. **Independent Tailings Review Board (ITRB) and Independent Senior Technical Reviewer:** this form of support is mandatory according to the Standard. Several requirements, particularly those focused on risks and emergencies, stipulate that some activities, documents, and/or products presented as evidence of meeting these requirements must be reviewed by an ITRB (a group of two or more Independent Reviewers with over 25 years of experience) or an Independent Reviewer (a single professional with over 25 years of experience). The choice between an ITRB or an Independent Reviewer is at the discretion of the hiring company, which may depend on the number of dams (the larger the number, the better it is to have the opinion of a group of experts), or on the level of criticality or risk of the asset at that time, which might also require the opinion of more than one expert.

- **Case of Vale S.A.:** both forms of support were contracted.
- **Lesson:** it is important to meet this requirement of the Standard, as it is a fundamental procedure, especially for the physical safety of the dams.

2. **Digital transformation:** this point of attention addresses the promotion of a digital environment within the company, which is also at the company's discretion and can be adjusted based on the availability of human, technological, and financial resources. It is important to emphasize that these digital environments are generally scalable, starting with basic, low-cost tools and progressively building improvements and robustness. This point is sensitive and should be seen as the optimal way to organize, record, and maintain the entire governance process. Additionally, it has the potential to serve as the "calling card" for the GISTM implementation, both internally and externally, especially in anticipation of future audits.

This suggested digital transformation has at least three objectives:

- **Data registration on a corporate network:** avoid registering and handling data and information on isolated machines. Consider front-end interfaces that are more user-friendly, standardized, and include metadata. This promotes auditability, ensuring data reliability and preventing the production and dissemination of conflicting information within the company.
- **Centralized storage of data and evidence (uploads and downloads):** avoid directories on isolated and uncontrolled machines. Consider more robust repositories for digital evidence files, with cybersecurity, access control, and a backlog of changes and modifications. This aims to demonstrate the integrity of the environment end-to-end, which is important during audits.
- **Data processing, management, and disclosure:** avoid tools without error alert rules for typos and redundancies. Consider developing performance indicators (KPIs) with outputs on customizable dashboard panels, and parameterizable reports and maps.
    - **Case of Vale S.A.:** An appropriate and scalable digital environment was developed.
    - **Lesson:** A digital environment is extremely important and serves as a foundation and stimulus for cultural transformation, providing visibility of the implementation and progressive results.

Conclusion

A proposed GISTM governance framework was suggested, and the Macroprocesses of the Pre-Implementation Phase were discussed, based on the learnings from Vale S.A., which implemented the Standard and achieved compliance for 48 TSFs over a three-year period.

The main message of the discussed Phase highlights the flexibility of the GISTM implementation process for non-ICMM member companies in terms of timeline, team, and financial resources. These can be adjusted to fit any company profile, which helps to alleviate some of the apparent restrictions or complexities due to the Standard's magnitude. This serves as an invitation for other mining companies to voluntarily engage and begin their transformation journeys brought by the Standard.

Acknowledgements

The authors thank Vale S.A. for authorizing the use of the facts described from its implementation.

References

ICMM. 2020. Global Industry Standard on Tailings Management (GISTM).

ICMM. 2021. The Conformance Protocols.

Gore, M.S. and Moghaddam, A.N. 2023. Utilized approaches in the application of GISTM to legacy tailing facilities. *Proceedings of Tailings and Mine Waste 2023.* Vancouver, Canada: 169–180.

Romero, J.E. 2023. Engineers of record, professional registration, and the mining industry in Mexico. *Proceedings of Tailings and Mine Waste 2023.* Vancouver, Canada: 201–212.

Sova, M.R., Erturk, H.S. and Hatton, C.N. 2023. Effective EoR succession planning. Recommendations for implementation of GISTM. *Proceedings of Tailings and Mine Waste 2023.* Vancouver, Canada: 213–224.

Williams, D.J. 2021. Lessons from tailings dam failures – where to go from here? *Minerals* 11(853). 34P. Accessed 10/03/2024 at https://doi.org/10.3390/min11080853

Risk-Based Planning of Monitoring Programs for TARPs

Richard Sisson, Geosyntec Consultants International Inc., USA
Dirk van Zyl, Independent Geotechnical Consultant, USA

Abstract

This paper describes a rational, risk-based method for developing monitoring programs and trigger action response plans (TARPs) for tailings facilities. It emphasizes the importance of the link between planning instrumentation programs and the risk assessment for the facility. The objective of the instrumentation program should be to either provide specific information regarding potential failure modes, confirm assumptions used to establish that a failure mode is not credible, or provide information that will provide significant value in the future design of similar structures. This paper describes a process that begins with identification of hazards and an assessment of the expected performance and risks for a facility. It continues with a description of the design of the monitoring program so that it is effective and avoids the pitfalls the authors have observed.

Introduction

In 2000, Martin and Davies wrote:

> *"Many tailings dam failure modes are preceded by warning signs that can be readily detected well in advance with a proper dam surveillance program. If the warning signs are promptly detected, and appropriately appreciated, time is available for the implementation of remedial measures. For many of these detectable failure modes, a good dam surveillance program, in concert with emergency preparedness and response plans, represents a highly cost effective, proactive risk management tool relative to the options of a failure or an unnecessarily excessive and expensive degree of design conservatism. It does not however provide a means of safely stewarding a facility whose design and or construction is flawed. A number of failure modes that do not provide readily apparent advanced warning signs and it is important to recognize that these failure modes cannot be properly addressed using the observational method and cannot be appropriately addressed by a dam surveillance program. The only way to deal with*

these latter failure modes is to devise appropriate design and construction measurements."

Almost 25 years later, this philosophy remains prevalent. Trigger action response plans (TARPs) are considered good practice for detecting warning signs of failure modes for tailings storage facilities (TSFs) and are required by some regulators. The purpose of a TARP is to define a range of trigger levels and the associated responses to be initiated if a trigger level is reached. The concept is a useful one, and TARPs have been applied with considerable success for managing hazards in related endeavors, such as pit slope engineering.

Good TARPs have prerequisites. They must:

1. be based on a thorough identification of failure modes;
2. not be so conservative that numerous false alarms occur;
3. not be unconservative resulting in undetected adverse behavior; and
4. identify an appropriate path for escalation of response.

Despite widespread acceptance of the value of TARPS, published case histories describing successful detection of adverse behavior are rare, largely because of the potential impacts of negative publicity. The authors have reviewed multiple projects where TARPS were flawed because triggers were exceeded without implementation of the documented action plan, or where response plans were unnecessarily triggered because the link to an identified failure mode was illogical.

Even well-respected references such as the *Tailings Management Handbook* (Finke Morrison, 2022) provide dubious advice. In the chapter on monitoring, an example of a red slope stability trigger is vibrating wire piezometer data indicating a factor of safety less than 1.3. The chapter indicates "a red trigger indicates conditions close to failure and evacuation should occur." Yet using relationships between factor of safety and annual probability of failure based on actual engineering projects and developed through quantified engineering judgement, Silva et al. (2008) estimate an annual probability of failure of 10^{-4} for a structure with a factor of safety of 1.3 if it is designed and built using best practices for engineering and construction. In the absence of other indicators, the calculated safety factor of 1.3 is not a clear indication that the structure is "close to failure."

This paper describes principles for designing instrumentation programs and establishing effective TARPs while avoiding the pitfalls previously described. While none of these principles are new, it is hoped that this review reinforces principles for improved process for developing TARPs for TSFs. In this paper, the process is organized as follows:

1. Identify hazards and potential failure modes.
2. Identify warning signs that can monitored to provide warning of adverse behavior.

3. Establish actions that could be undertaken to mitigate a potential failure if it began to develop.
4. Determine values of the behavior that would trigger escalating risk management.
5. Select instrumentation to obtain the necessary measurements. Establish how the instrumentation data should be analyzed and reported.
6. Identify responsibilities when a trigger value is exceeded.
7. Document the entire process in the OMS.

The following sections of the paper describe this process.

Failure mode identification

The design of instrumentation should be based on an evaluation of hazards, identification of failure modes, and an assessment of the likelihood that the failure mode will develop. Each failure mode is examined to determine warning signs, and surveillance measures are identified considering the probability that the mode will develop. Much attention has been given to methods assessing risks for tailings dam. Discussion and evaluation of methodology are beyond the scope of this paper, but Figure 1 illustrates the concept described by Martin and Davies (2000). In practice, detailed event trees are needed to link warning signs to failure modes.

Once failure modes and their warning signs are identified, it is essential to separate brittle and ductile failure mechanisms. Brittle failures should be treated using the precautionary method, not the observational method, and are outside the scope of this paper. Although instrumentation may provide advance warning of adverse behavior preceding brittle failures and would typically be considered prudent, monitoring should not be relied upon to significantly reduce the risk of such failures. However, ductile failures may be addressed using the observational method, providing that monitoring is planned and implemented with sufficient diligence that adverse behavior is detected and remediated before it has unacceptable consequences.

In addition to identifiable failure modes, the monitoring program must consider "unknown-unknowns:" the inherent risk (generally very low), that is associated with every dam no matter how apparently well-designed and safe it may be (Dunnicliff, 2017; Stateler et al., 1995; Martin and Davies, 2000.) Two common sources of this inherent risk are construction defects and unidentified weak foundation units. Unless foundation conditions are very competent and consistent and the structure is very robust, and depending on the consequences of failure, instrumentation should be considered as one prudent defense. The size of a likely failure provides an initial guide to instrument density. However, a monitoring program does not eliminate the need for an adequate characterization of the geological environments of deposition in the dam foundation and carefully controlled construction.

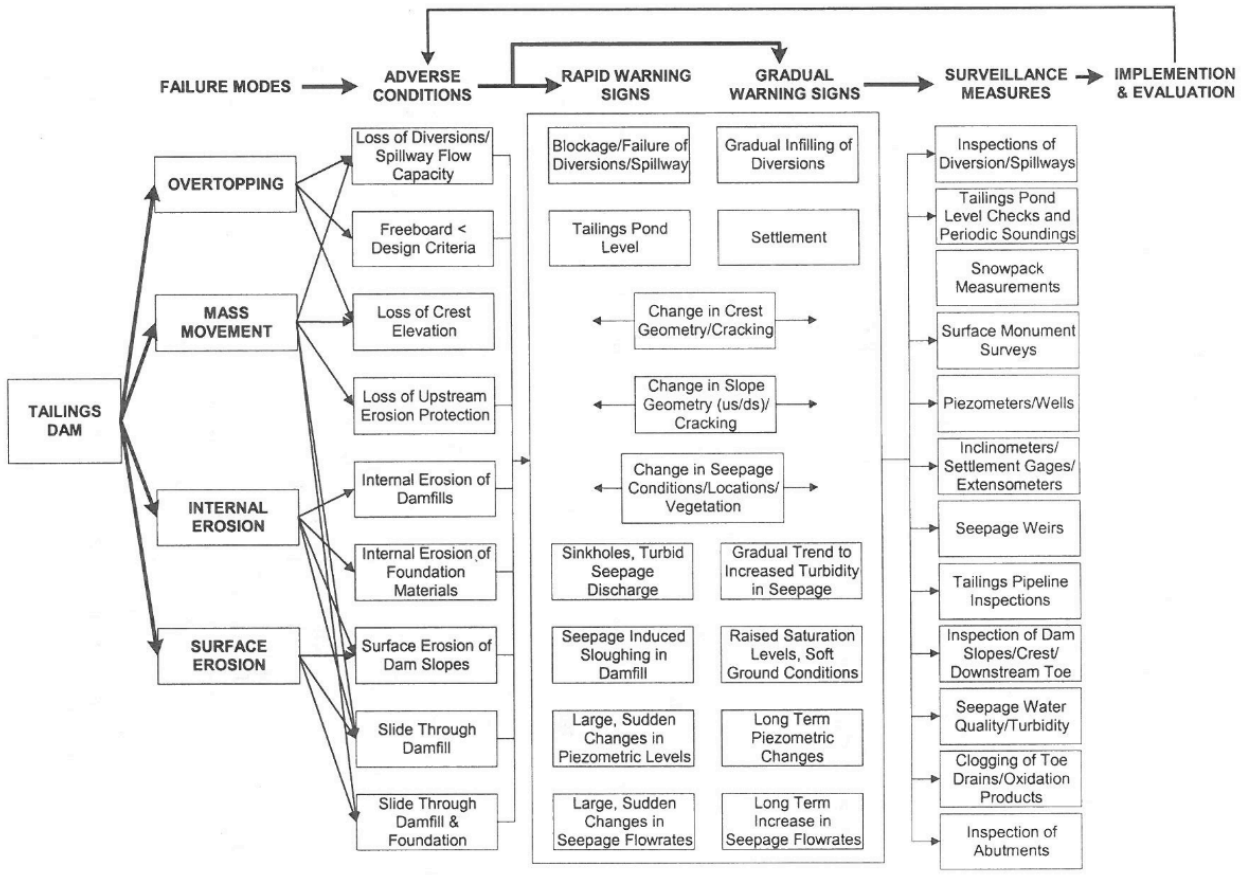


Figure 1: Tailings facility failure modes and observations (Martin and Davies, 2000)

Warning signs

Warning signs should be developed based both on analyses performed during design to predict behavior and on experience gained from thorough understanding of applicable case histories. Expected performance should be defined during the design, as well as key engineering parameters impacting that performance. The uncertainty surrounding those parameters and implications for behavior at the upper and lower limits of those parameters should be evaluated and described. Concepts for contingencies and opportunities that could be implemented if performance deviates from expected should be cataloged. The value of visual observation as warning signs should not be overlooked, as USBR practices have resulted in relating visual observations to the majority of key monitoring parameters (Stateler et al., 1995).

Response plans

Establishing TARPS requires identifying escalating actions if performance deviates from expectations. Actions that might be undertaken in response to instrumentation include:

- Rereading or checking instruments promptly, depending on whether they are read manually or remotely.
- Notifying the Responsible Tailings Facility Engineer (RTFE) and the Engineer of Record (EOR) and increasing monitoring frequency or density, and adding additional types of instrumentation.
- Notifying the Operating Manager and the Accountable Executive.
- Developing construction plans for conceptual mitigative actions.
- Implementing a mitigation action.
- Preparing to evacuate.
- Evacuating.

However, it is generally undesirable to have separate triggers for each response, because in many cases it is difficult to predict performance with sufficient resolution to assign meaningful trigger levels to each action. The authors have seen response plans with up to six trigger levels. While appreciating the value in establishing a structured, systematic response plan to mitigate human error in stressful situations, the authors believe that this objective must be balanced against the flexibility needed to address unique conditions that exist at each site. To provide this flexible crisis response, it is important to have an emergency call-out procedure with sufficient levels of notification to rapidly mobilize leadership. In addition, the range of foreseeable responses should be clearly and succinctly documented so that they are available in a crisis.

Recognizing that regulatory requirements may mandate including specific actions (e.g., evacuation), a three-tier system (green, yellow, and red) would cover the following three conditions:

Green

The structure is performing as planned.

Yellow

The structure is or may not be performing as planned, but an immediate release of fluids is unlikely. The EOR should be involved, monitoring intensity should be increased, and TARPS should be reviewed and, if appropriate, revised. If the condition persists, detailed mitigation plans should be developed. The condition should be reported to the Operating Manager and Accountable Executive (AE) as part of regular reporting.

Red

Intervention is necessary because, without it, a release of fluids is not unlikely. Mitigation must be implemented, and the Operating Manager and AE should be notified immediately. It may be necessary to activate emergency response procedures.

Trigger values

Trigger values typically must be established for the common failure modes of overtopping, piping, and instability due to deformation, but it is often difficult to do so for deformation and piping. Both theory and experience, if available, should be considered. Other failure modes such as surface erosion and subsurface subsidence may also need to be addressed on a site-specific basis.

Triggers for notifying external stakeholders should be carefully developed so that communication protects the public but is not unnecessarily alarmist. The system needs to be carefully designed so that it has a very high probability of detecting imminent failures but a very low probability of false triggering; however, it is not clear that such a system yet exists. Transparency with stakeholders is a key principle of the Global Industry Standard for Tailings Management (GISTM), and appropriate measures should be developed for communicating the performance of tailings facilities. However, false alarms for evacuation will unnecessarily erode public trust and may result in some stakeholders ignoring true emergency situations if they occur in the future. Ideally, response plans for triggers prior to implementing the emergency action plan should consider installing additional instrumentation to better inform the decision as to whether to implement the ERP, especially when the trigger requires a response of evacuation.

Overtopping

Overtopping is a failure mode where trigger values usually can be logically established using analyses. The risk of overtopping can be evaluated using hydrologic and hydrotechnical analyses, with due consideration of the uncertainty in estimates of low frequency high intensity events.

Piping

Piping failures are relatively uncommon for tailings dams, in part because a beach above water often exists at the upstream face of the embankment. The results of the risk assessment should include identification of defense mechanisms against piping and evaluation of how they might not function effectively. If these systems do not function as intended, the TARP should be triggered. Examples would be a beach that does not meet design assumptions or a drain that does not function as intended. While seepage patterns and volumes can be predicted analytically, stratigraphic details may result in significant but localized differences between model predictions and field observations that may not be detected with a reasonable number of instruments. Thus, visual monitoring is a key defense against piping.

Peck (2010) describes practical aspects of piping, and several piping incidents for water dams, and recommends practices for monitoring seepage that provide extremely useful guidance in identifying warning signs and developing monitoring plans for risks related to piping. Gradients or measured flows that change suddenly or are higher than assumed in design would trigger an increased intensity in

monitoring and perhaps mitigation. Seepage that is turbid or exits the structure where it is unfiltered would typically trigger mitigative actions or even implementing the emergency response plan.

Instability

It is often not possible to establish meaningful trigger levels for instability using empirical data for tailings dams, because it is unusual to have sufficient data of adverse performance applicable to a specific site. Initial triggers may be based on a change relative to historical levels, but interpreting monitoring data to predict the likelihood of failure due to instability remains challenging. Methods such as inverse velocity (Fukuzono, 1990) have been developed but experience indicates they need to be calibrated for specific materials being considered. Only a few failures have been publicly documented in detail and most have been brittle undrained failures. As a result, few if any sites exist where case histories provide an appropriate analogy for drained deformation, except for clay shales at residual strength. This situation is different from pit slopes, where the design philosophy is to accept failures that do not threaten human life or create unacceptable impacts on mine costs and production. As a result, instability is not uncommon, and often sufficient site-specific performance data exists to establish appropriate trigger action levels. Documented performance from other sites may also be useful.

Like the use of empirical data, theoretically based analyses have limited value for establishing trigger levels. For most well-designed dams, the design avoids plastic behavior. Thus, stress-deformation models typically predict only elastic deformation (either linear or non-linear), which does not directly create a credible failure mechanism. State-of-the-practice static stress-deformation models do not provide information on time-dependent movements, which are more likely to indicate a failure risk than initial response to loading. Apparent time-dependent deformation is frequently observed in deformation monitoring records for tailings facilities, but it cannot usually be determined what percentages of the deformation can be attributed to elastic response during ongoing construction, changes in details of loading (e.g. upstream tailings properties and geometry), pore pressure dissipation in fine grain soils, time-dependent plastic or viscoelastic deformation, and instrument noise. Triggers also should not be overly reliant on safety factors calculated using limit equilibrium analyses, as there is not a unique correlation between safety factor and probability of failure (Silva et al., 2008).

While neither empirical nor analytical approaches are sufficient to establish meaningful action levels for instruments used to monitor piping and instability, they are useful to develop triggers for major action (mitigation, public notifications) to address ductile instability when combined with expert judgement. In the absence of other indications of adverse behavior such as visual observations, triggers involving major actions such as constructing mitigations or public notification should not be activated solely based on:

- a single instrument;
- instruments that do not directly measure deformation such as piezometers; or
- calculated safety factors.

Instead, sufficient measurement and visual observation of deformation should be initiated when the response plan is first triggered to provide multiple warnings of progressing instability, possibly in conjunction with refinement of the next level TARP. Even with the addition of expert judgement, the level of uncertainty associated with this methodology should be recognized. The industry would benefit from research and pilot testing of instrumentation designed specifically to quickly warn that a loss of fluids is occurring in tailings facilities.

Selection of monitoring instruments

In his classic book on geotechnical instrumentation, Dunnicliff (1988) wrote: "Every instrument on a project should be selected and placed to assist with answering a specific question: if there is no question, there should be no instrumentation." Instruments should be established either to provide specific information regarding potential failure modes, or to confirm assumptions used to establish that a failure mode is not credible.

In planning the scope of a monitoring program, the probability should be evaluated that adverse behavior will develop, instrumentation will detect it, and failure will be avoided. The evaluation should recognize that deformation monitoring of tailings dams often does not achieve the accuracy of which the instruments are capable. (This could probably be improved by using careful design and installation, plus experienced staff who are well trained to follow thoughtful procedures.) Modifying the TSF design should be considered if the probability of adverse behavior is significant, and it is costly or impractical to implement and staff monitoring programs that have a high probability of detecting the behavior and providing warning with sufficient time for successful mitigation.

If the structure will perform adequately for the full range of input parameters and opportunities for design optimization are not significant, instrumentation is only justified by the potential for "unknown-unknowns or by the value of monitoring data for improving future designs." Not enough attention has been paid to monitoring "unknown-unknowns." If construction defects and foundation defects do not create a credible failure mode (likely a rare situation), it could be argued that the probability of unknown unknowns is so low that only visual monitoring is needed for instability.

USACE (2020) provides reasonably up to date summary of available instruments and procedures for use. Specific issues that should be considered in selecting instrumentation are:

- Selection should consider the sensitivity needed to detect performance deviations.
- Routine manual surveying will result in variability (noise) that prevents interpreting anything except long-term trends, unless very high-quality survey methods are used.
- Manually read inclinometers are capable of accuracy within several millimeters and of providing a displacement profile with depth. However, they require diligent, well-trained staff using consistent and appropriate procedures for installation, raising the casing, and regular monitoring. If the instrumentation designer is not confident that these conditions exist, alternate instrumentation may be preferable.
- GPS receivers can provide measurements with sub-millimeter accuracy when appropriate interpretation methods are applied to deal with issues such as changes in atmospheric conditions. However, experience shows that the level of diligence and expertise necessary to do so is often not achieved for tailings facilities. Details of GPS methods and capabilities for monitoring tailings dams must be thoroughly researched during the design process.
- The challenges associated with monitoring downstream construction also appear to be under appreciated. Either the instruments must be incrementally raised as fill is placed around them, or they must be removed and replaced during fill placement. In either case, the instruments often do not capture deformation during fill placement, when it is most likely to be important.
- For high tailings dams, buckling due to casing downdrag must also be considered for inclinometers and piezometers.

These issues can be minimized but not eliminated by planning, procuring, installing, and monitoring instruments with meticulous attention to guidance provided by Dunnicliff (1993, 2017), but mine operators are often reluctant to expend the money and effort, and Engineers of Record are not always insistent.

Implementation of monitoring program

Not infrequently, data from tailings management facility is less precise than the fundamental capability of the instrument, likely due to sub-optimal installation and monitoring procedures. Challenges for the mining industry in conducting surveillance programs are summarized in Table 1, adapted from Martin and Davies (2000). More recent assessments of challenges in monitoring tailings facilities indicate they have not been entirely overcome (Clarkson et al., 2020).

Table 1: Monitoring challenges in the mining environment
(adopted from Martin and Davies, 2000)

Challenge	Requirement
Constructed and operated by organizations whose focus and expertise are in mining, not building dams.	Operations personnel require training, support, and commitment from corporate to mine management and operations levels
Mining must be economic to continue operation. Tailings seen as cost center.	Tailings dam owners must resist the inevitable temptation to cut back on surveillance programs in favor of devoting more resources to profit centers. Resources for surveillance must be independent of cyclical business environments.
Tailings management in general and dam surveillance in particular are not career paths for miners.	Need continuity and clarity in communication between site and Engineer of Record. Procedures need to be documented to facilitate staff turnover

Instrument installation

A "golden rule" described by Dunnicliff (2017) for monitoring tailings facilities is that *"Tasks should be assigned to the people who have the greatest motivation to achieve high quality data."* In many cases, this is the EOR or Responsible Tailings Facility Engineer (RTFE). Current practice, however, is that instrument installation is either performed by the construction contractor or by a specialty subcontractor. The priority in the procurement process should be selecting a well-qualified contractor, not price. If a bidding process is selected, specifications and drawings must be prepared that may include details on the required type of instrument, the installation locations, the qualifications of the installation personnel and their supervision, the method and frequency of reading, environmental concerns, and the payment method (USSD, 2013).

Written procedures should be developed for the installation of monitoring instruments. Documentation of installation procedures is important and should include the procedures for installation as well as the steps necessary for operation (i.e., troubleshooting concerns, connection to data loggers, etc.). Documentation should include the technical requirements of the instruments, calibration requirements, installation details, and servicing requirements and methods (USSD, 2013).

For downstream construction, careful thought should be given to procedures for raising the instruments as construction progresses. One issue is that compaction around the instrument is difficult, and the consequences of a local loose zone around the instrument should be considered. Just as importantly, if the instrument cannot be read during loading, important data may be missed.

Data acquisition

Consistently acquiring accurate data is essential to successfully implementing a TARP. Data can be gathered manually, through automated data acquisition systems, and by documented visual observations. While automated data acquisition systems reduce the potential for human error, errors due to factors such as damaged or mis-identified leads and incorrect calibration factors can and do occur. It is essential to have

trained staff regularly and diligently observing site conditions. Not all instruments are readily automated.

Considerations for manually read instruments are:

- readings should ideally be performed by the same individual using the same equipment;
- the details of procedures are important and need to be clearly documented;
- staff turnover is almost inevitable, so succession planning and training programs are important; and
- sufficient resources must be available to deal with non-routine issues, such as anomalous readings and damaged instruments, so that instruments are re-read promptly when unusual readings are recorded and essential instruments are repaired or replaced promptly if damaged.

Data reduction and interpretation

Once data is collected, deviations from previous readings should be identified within 24 hours so that the instrument can be re-read promptly if anomalies exist. Machine learning may provide opportunities to enhance and streamline this anomaly detection. Once the data is considered reliable, data analyses and presentation can be delegated to junior staff, but it is important for data to be interpreted by experienced staff who understand potential failure modes and design of monitoring program.

Responsibilities

A RACI chart and a notification matrix should be developed for each trigger point to define roles and notification processes. The roles and responsibilities for "red" triggers should be developed working with the teams for mine emergency response and external stakeholder communication and should be endorsed by the accountable executive.

Documentation

Requirements for documentation during the design and implementation of the monitoring program have been described. This documentation should be incorporated into the Operations, Maintenance, and Surveillance Manual. An auditing program should be considered to confirm that implementation of the monitoring program is consistent with the Manual and follows best practices, and to identify whether areas for improvement exist.

Conclusion

While the principles for developing monitoring plans for tailings facilities have been well described going back at least as far as Dunnicliff (1993), implementation must be improved. Literature and the authors' experience indicate that the keys to establishing effective TARPS are:

- The starting point should be a thorough risk assessment that identifies failure modes in detail and associated warning signs for the potential failure mode.
- Establishing TARPS for brittle failure modes may not significantly reduce risk and should be carefully evaluated.
- Logical TARPS are often difficult to establish for many TSFs because documented instances of adverse behavior are rare for analogous situations and analytical models frequently do not capture the complexity of soil behavior.
- The response plan should be appropriate for the severity of the triggering behavior. Once a plan is developed, it should be followed meticulously. Excessive caution should be avoided, but false positives can damage credibility.
- The "achievable" accuracy of instruments is sometimes not achieved. Careful attention should be paid to the procedures for installation and monitoring of instruments. These procedures should be well documented. Staff need to be trained to understand the potential failure modes, the use of the instruments for detecting failures, the use of the procedures, interpretation of the data, and response to the results. Succession planning and training programs are essential to managing staff turnover.

References cited in this paper provide details. Although not referenced here, the U.S. Federal Energy Regulatory Commission also provides detailed information on risk assessment and dam instrumentation. The concepts described by Stateler et al. (1995) are described in further detail in publications available from the U.S. Bureau of Reclamation. Designers of surveillance modes would benefit from studying literature describing failures unrelated to tailings management facilities and the psychology of decision making and risk management (e.g., Kahneman, 2012; Taleb, 2021).

References

Clarkson, L., Williams, D.J. and Seppälä, J. 2020. Real-time monitoring of tailings dams. *Georisk Assessment and Management of Risk for Engineered Systems and Geohazards* 15(2): 113–127.

Dunnicliff, J. 1993. *Geotechnical Instrumentation for Monitoring Field Performance*. New York: Wiley.

Dunnicliff, J. 2017. A 13-Step procedure for systematic planning of monitoring programs using geotechnical instrumentation. *Geotechnical Instrumentation News,* January.

Finke Morrison, K. 2022. *Tailings Management Handbook: A LifeCycle Approach*. Society for Mining, Metallurgy & Exploration (SME).

Fukuzono, T. 1990. Recent studies on time prediction of slope failure. *Landslide News* 9–12.

Kahneman, D. 2012. *Thinking, Fast and Slow*. Penguin.

Martin, T.E. and Davies, M.P. 2000. Development and review of surveillance programs for tailings dams. Association of State Dam Safety Officials. Las Vegas, Nevada.

Peck, R.B. 2008. National dam safety: seepage and piping (Parts 1 and 2). Federal Emergency Management Agency – FEMA P-717DVD – Case Histories and causes of failure. Expert Video Series, the National Dam Safety Program, https://www.youtube.com/watch?v=ZMHUoEdbgkA,

Silva, F., Lambe, T.W. and Marr, W.A. 2008. Probability and risk of slope failure. *Journal of Geotechnical and Geoenvironmental Engineering* 134(12): 1691–99.

Stateler, J., Von Thun, L., Scott, G. and Boernge, J. 1995. Development of performance parameters for dam safety monitoring. *Geotechnical Instrumentation News,* December.

Taleb, N. 2021. *Incerto: Fooled by Randomness, The Black Swan, The Bed of Procrustes, Antifragile, Skin in the Game*. Random House Trade Paperbacks

U.S. Army Corps of Engineers 2022. Instrumentation of embankment dams and levees. Manual, November 30. https://www.publications.usace.army.mil/Portals/76/Users/182/86/2486/EM%201110-2-1908.pdf.

USSD Committee on Monitoring of Dams and their Foundations. 2013. Development of a dam safety instrumentation program. U.S. Society on Dams.

Chapter Four

Breach and Inundation Estimates

TAILINGS AND MINE WASTE 2024



Application of USACE LifeSim to the Feijão Dam B-1 Tailings Storage Facility Failure of January 25, 2019

William Johnstone, Spatial Vision Consulting Ltd, Canada
Jesse Morrill-Winter, US Army Corps of Engineers, USA

Abstract

Interest in methods and models that estimate potential life loss consequences for tailings storage facility (TSF) incidents and failures has become more prevalent in the last few years. Consequences estimation models such as the US Army Corps of Engineers' (USACE) LifeSim simulator are regularly used to analyze risks posed by water dam and levee systems; however, only a few studies have explored how LifeSim can be applied to the TSF life loss consequences estimation problem. On January 25, 2019, the Feijão Dam B-1 Tailings Storage Facility (TSF) at Minas Córrego do Feijão mine in the State of Minas Gerais, Brazil, failed catastrophically, releasing a devastating downstream mudflow that inflicted extensive damage to buildings and infrastructure, and caused a historic 270 fatalities. In the summer of 2022, the Risk Management Center (RMC) of USACE initiated the Córrego do Feijão Dam B-1 Tailings Dam Failure Case Study to explore how consequences simulators could be used to analyze historic TSF failures and to provide insights into how life loss might be estimated for these types of events. The study goals were to: 1) investigate how LifeSim V2 can applied to TSF failure events and incidents; 2) identify important similarities and differences between water dam and tailings dam failure events; 3) identify strengths and weaknesses in current loss estimation methods; 4) show how LifeSim outputs can be used to classify proposed, active, inactive, and decommissioned TSFs; and 5) identify potential near-term modifications to the LifeSim methodology and simulator, and also longer-term research needs. The results of this study confirm that LifeSim can indeed inform TSF life loss consequences studies. Possible modifications to current methods are proposed, including adjusting building strength characteristics to account for the physical properties of the tailings and introducing evacuation behaviors calibrated to industrial populations.

Introduction

Interest in the capability to estimate potential life loss consequences for Tailings Storage Facilities (TSF) has become more prevalent within the international dam safety community. LifeSim is an agent-based model developed by the US Army Corps of Engineers' (USACE) to estimate potential life loss and direct

economic damages due to water dam and levee failure events (USACE RMC, 2024). However, there is currently only a very small number of application studies that have applied LifeSim to the TSF life loss consequences estimation problem.

On January 25, 2019, the Feijão Dam B-1 Tailings Storage Facility (TSF) at Minas Córrego do Feijão mine in the State of Minas Gerais, Brazil, failed catastrophically, releasing a devastating downstream mudflow that caused a historic 270 fatalities. The Feijão Dam B-1 event provided an important opportunity to demonstrate how LifeSim can be used to analyze a historic TSF failure event, to show how agent-based simulation methods can be used to estimate life loss for these types of events, and to demonstrate how this approach could be used to inform consequences estimation and risk assessments for proposed, active, inactive, and decommissioned TSFs.

In the summer of 2022, the Risk Management Center (RMC) of USACE initiated the Córrego do Feijão Dam B-1 Tailings Dam Failure Case Study. The primary goals for this study were to: investigate how LifeSim V2 can be applied to TSF failure events; identify important similarities and differences between water dam and tailings dam failure extreme flooding and failure events; identify strengths and weaknesses in the current LifeSim methodology and simulator; show how LifeSim outputs can be used to classify TSFs using the Global Industry Standard on Tailings Management (GISTM) (ICMM and UNEP, 2020) and Anglo American's Consequences Classification of Structures (CCS) standard (Anglo American, 2019); and identify potential near-term and longer-term research needs to enhance the applicability of these types of models.

USACE Feijão Dam B-1 LifeSim validation case study

Methodology and timeline

The Feijão Dam B-1 LifeSim Case Study followed an iterative development process in which successively more detailed, representative, and calibrated models of the event were designed, developed, and assessed. Project work began in August 2022 and was substantially complete by January 2024. Two types of model were developed: an event validation model, which attempts to re-create the historic event using LifeSim, and a process validation model, which uses the USACE Modeling, Mapping and Consequence (MMC) Production Center's Standard Operating Procedure (SOP) to estimate potential consequences, assuming that a failure has yet to occur (USACE MMC, 2022).

The first type of analysis asks, "Will our consequences tools give us results similar to what actually took place?" and the second type asks, "If we did not know what happened, would our current approach get us there?" Four tasks were typically performed within each iteration of the validation work: 1. Planning and experimental design; 2. Data discovery and compilation; 3. LifeSim model development; and 4. Reporting and feedback.

History and failure of Córrego do Feijão Dam B-1

The Córrego do Feijão Iron Mine started its operations in 1956 through Companhia de Mineração Ferro e Carvão, and the first production at the facility began in 1963. In 1973 the mine came under the control of Ferteco Mineração, followed by Vale since April 27, 2001. The mine operated 24 hours a day, 7 days a week. It employed 613 direct employees and a number of third-party contractors who worked in three shifts, one of which was six hours and two of which were nine hours (Assembleia Ligislativa do Minas Gerais, 2019; Government of Brazil, 2019b; Robertson et al., 2019; Secretaria de Estado de Meio Ambiente e Desenvolvimento Sustentável and Governo do Estado de Minas Gerais, 2018).

Figure 1 presents a simplified layout of the southern portion of the Vale mine and the primary downstream impact zones where the Population at Risk (PAR) were located. The Feijão Dam B-1 TSF is shown at the upper right.

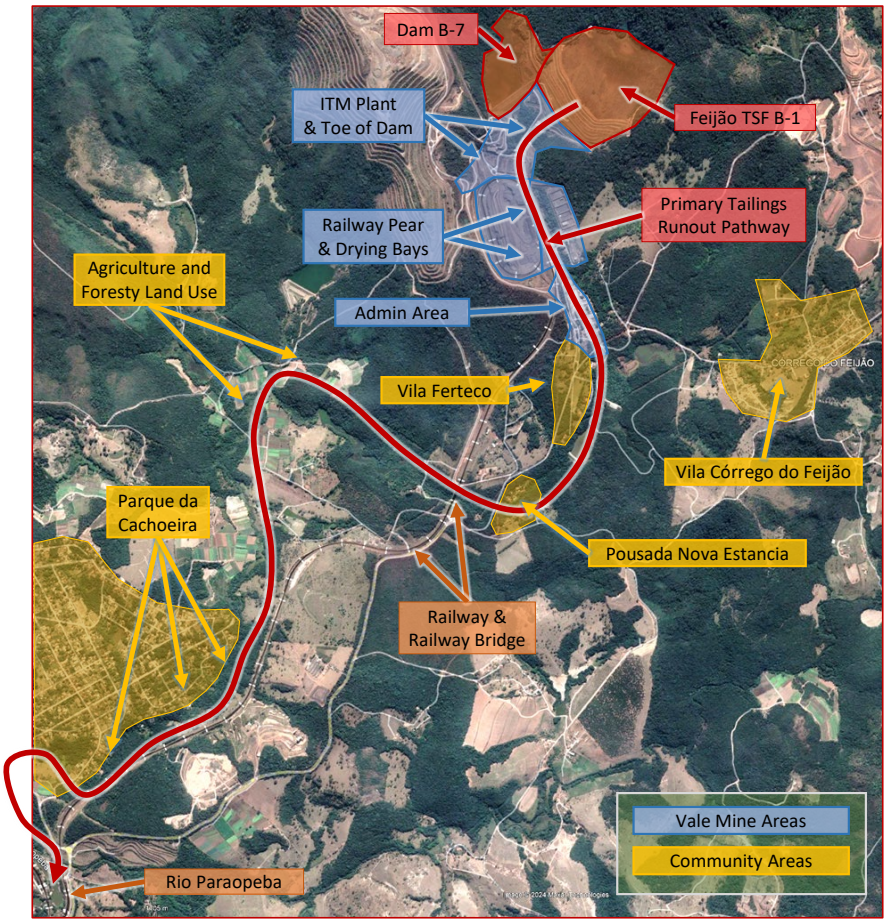


Figure 1: Extent of the primary downstream impact zone from Feijão TSF B-1 to the Rio Paraopeba, and the primary locations of the PAR

The primary purpose of the structure was to dewater and store the tailings from a processing plant called the ITM, where crushing and ore concentration was performed. The starter dam for TSF B-1 was

constructed in 1976, the final raise was constructed in 2013, and tailings disposal ceased in July 2016 (Robertson et al., 2019). At the time of its failure, Dam B-1 did not have a supernatant pond.

Key occupied locations immediately downstream of the TSF included the area below the toe of the dam, the ITM processing plant, the drying bays, the materials storage/transfer/railway area, and the administration area (all shown as blue fill). Downstream communities and locations of interest include Vila Ferteco, Vila Córrego do Feijão, the Pousada Nova Estancia resort, agriculture and forestry land use, and the community of Parque da Cachoeira (shown as yellow fill). Other key locations are the railway right-of-way and bridge crossing, and the confluence of the tailings flow pathway with the Rio Paraopeba.

On January 25, 2019, at approximately 12:28 p.m. local time, Dam B-1 failed, releasing a catastrophic mudflow that travelled rapidly downstream. The initial failure surface extended across much of the breadth of the dam, and the collapse of the slope was complete within ten seconds. While the dam was extensively monitored using survey monuments along the crest of the dam, inclinometers, ground-based radar, piezometers, and other instruments, Robertson et al. (2019) observe that none of these methods detected any significant deformations or changes prior to failure. An estimated 9.7 million cubic meters (Mm^3) of material, representing approximately 75 percent of the stored tailings, flowed out of the dam in less than five minutes (Robertson et al., 2019). The primary impact zone extended 10 km from the dam down to a confluence with the main channel of the Rio Paraopeba.

The primary outflow pathway of the tailings is indicated on Figure 1 with a simplified red line. While the full extent of the impact zone continues beyond the river confluence much further down the Rio Paraopeba river channel, the extent shown here is the primary zone of interest for understanding the exposed PAR and the life losses for the historic event. Rana et al. (2021) observe that the initial tailings outflows moved as a debris avalanche that achieved a peak velocity of 28 m/s (~101 km/hr) with a flow depth of 30 m. Approximately 700 m downstream, the tailings runout transitioned to a high-energy debris flow moving at approximately 18 m/s (~65 km/hr). Simulated maximum flow depths for structures located below the toe of the dam and then downstream to the railway bridge ranged from 25 m down to 10 m.

Most sources report the observed life loss (*N_LL)* as 270 individuals; however, since two of those victims were pregnant, some sources list the total life loss as N_LL = 272 (Assembleia Ligislativa do Minas Gerais, 2019; Passos and Quierati, 2023). While detailed estimates of the PAR were not reported, or statements about the size of the PAR were either incomplete or considered to be not credible, key sources such as Passos and de Freitas (2021) indicate that detailed lists of the full set of PAR (survivors and victims) were developed, possibly down to the occupancy of individual industrial and community structures, outdoor areas, and vehicles. This study recommends that future researchers should locate and use these datasets so that even more detailed consequences validation work can be performed.

Data discovery, assessment, compilation and indexing

The research approach used in this study was based on an earlier Life Safety Model validation study performed by Johnstone et al. (2003) for the Malpasset Dam failure. These methods were updated for the Feijão Dam B-1 case study. The types of data these studies require include a Digital Elevation Model (DEM) surface, TSF runout model, road network, buildings, Emergency Action Plan (EAP), and outcome data such as the observed losses of structures and people. Fortunately, extensive forensic investigations had been conducted by government agencies and research organizations, which means that there were many credible sources. A paper by Lumbroso et al. (2021) and an available non-Newtonian HEC-RAS hazard model of the event developed by Gibson et al. (2022) also helped the study team to develop a more complete understanding of the severity of the hazard within the different downstream zones. Key data discovery and management activities included:

- Google was the primary research tool. Documents and websites were translated from Brazilian Portuguese into English using Google Translate, and news videos were translated using YouTube.
- Key GIS sources were also consulted including: OpenStreetMap, Esri's Living Atlas, Google Maps, NASA, European Space Agency, Government of Brazil GIS websites, and satellite imagery.
- Important sources included the Brazilian Federal and State government agencies, news outlets, university researchers, and international agencies. The materials were compiled at three geographic scales: macro (the whole extent, simple maps, high-level), meso (regional and local land use and ground cover down to collections of buildings and outdoor areas, GIS "polygons"), and micro (detailed GIS points/lines/areas, individual roads, buildings, vehicles, people, destinations).
- The full body of PDFs, MS Office files, GIS files, photos, videos, etc. encompassed 90+ primary folders, 1,300+ files and 15.3 gigabytes of disk storage.

Experimental design of the LifeSim model simulations and alternatives

After completing the data discovery phase, the study team iteratively developed an experimental design for the event and process validation models. Guidance was provided by the US National Institute of Standards and Technology (NIST, 2024). As shown in Table 1, three validation groupings were developed: Event Validation, Process Validation, and Model Verification. A total of fifty-nine alternatives were created, grouped into twelve simulations that focused on key goals of the study. Key aspects of the design included:

- LifeSim's default stabilities for building objects were modified to explore differences between the physical properties of water dam and tailings runouts. Four building strength calibrations were used: 100% (the default settings for water dams); reduced building strength to 75% and 50% of default values to reflect the potential for more severe impacts of higher density tailings outflows

(i.e., extreme damage to a structure and the potential for high hazard life loss is more likely at lower depth-velocity products for tailings flows); and 150% strength (i.e., much stronger than for "water" to assess model sensitivity to stronger structures. The set of four strength calibrations (150%, 100%, 75%, 50%) were used in most of the Event and Process analyses.

- For Event Validation:
    - Model sensitivity variations included: 1) assess whether losses increase if the PAR takes more time to mobilize after initial awareness; 2) model structures as two-story buildings to assess whether sheltering-in-place with additional vertical height can reduce losses; 3) shift LifeSim's high hazard life loss fatality rates higher by 5% and 10% to reflect the observation that tailings appeared to pose more extreme hazards to buildings, vehicles, and people than water; 4) assess sensitivity to the most extreme possible (100%) loss rate; and 5) vary the starting locations and quantity of the employees and contractors within the Vale operations and administration areas.
    - A set of loss mitigation sensitivity variations were also developed: 1) calibrate the protective action initiation times for employees and contractors to reflect their emergency preparedness training so that they respond much faster than community PAR to the approaching tailings flows (i.e., within five minutes, now called a "Fire Drill" calibration); 2) calibrate all PAR (industrial and community) so that everyone in the impact zone responds immediately using the Fire Drill calibration; 3) adjust building locations to assess sensitivity to starting positions; and 4) explore the potential reduction in losses if an early warning could have been issued two to six hours before the moment of breach initiation and TSF failure.
- For Process Validation:
    - USACE's MMC SOP was applied using two types of warning: **Minimal Warning**, in which the community warning and mobilization process starts zero to two hours before failure, and **Ample Warning**, in which warning and mobilization is started two to six hours before failure.
    - A set of "tailings volume" alternatives were also created to model a set of three TSF outflow scenarios that show how consequences can be estimated as a function of a structure's height and storage volume at various stages of an asset's lifecycle. Two additional breach outflow and runout scenarios of 66% and 33% of the historic outflow volume were developed using HEC-RAS. This provided three breach simulations: 100% (the historic event), 66% and 33%.
- Model Verification is a special case with one alternative that was used to confirm that the team had created an Evacuation Route System (ERS) model in LifeSim that correctly reflected Vale's Emergency Action Plan (EAP) for TSF B-1 (Vale and Walm Engenharia, 2018a, 2018b).

Table 1: LifeSim/Feijão Dam B-1 experimental design: simulations, alternatives, key properties

Validation Group		Simulations		Alternatives	Key Properties
Group	Name	Group	LifeSim Name	#	
1. Event	Event Validation	1 Event Validation	*B1_Evac*	4	Friday, January 25, 2019, 12:28:24 PM Local Time. The majority of simulations consider four stability criteria settings: 150%, 100%, 75% and 50%
	Validation Sensitivity	2 Slower PAR Response	*B1_Evac_Slow*	4	Investigate if losses could be higher if the PAR took much longer to mobilize before trying to evacuate
		3 Two Story Structures	*B1_NumStories*	4	Investigate potential value of shelter-in-place / vertical evacuation
		4 Vary Fatality Rates	*B1_5% shift*	4	Shift High Hazard fatality rate curve higher by 5%
			B1_10% shift	4	Shift High Hazard fatality rate curve higher by 10%
			B1_100% Loss Rate	4	Set High Hazard fatallty rate curve to always 100% loss
		5 Vary PAR Size and Location	*B1_PAR_Sensitivity*	3	Uniform PAR: Rather than concentrating the PAR, allocate them uniformly at other structures within the mine area to explore whether losses are sensitive to starting locations. Large PAR: Model a much larger number of industrial PAR as reported by one news agency.
	Assess Mitigations	6. Fire Drill Vale	*B1_Evac_FireDrill*	4	Calibrate protective action response by Industrial PAR (employees and contractors only) using "Fire Drill". These industrial PAR mobilize to 100% within 5 minutes.
		7. Fire Drill All	*B1_Evac_FireDrill_All*	4	Calibrate protective action response by Industrial (employees and contractors) and Community PAR using "Fire Drill". All PAR mobilize to 100% within 5 minutes.
		8. Move	*B1_AdjBldgLoc'ns*	1	Adjust building locations to explore sensitivity
		9. Early Warning	*B1_EarlyWarn*	4	Warn PAR 2 to 6 hours before failure.
2. Process	Process Validation	10. MMC SOP	*B1_MMC_SOP*	6	PAR are allocated for 2:00 am (02:00) and 2:00 pm (14:00). The Vale mine is staffed 24x7, and residential areas have more PAR at nighttime than for daytime.
		11. Vary Tailings Volumes	*B1_100%_Volume*	4	Calibrations are similar to "Event Validation". The only difference is the released volume of tailings.
			B1_66%_Volume	4	
			B1_33%_Volume	4	
3. Verify	Model Verification	12. Verify Road and Trail Network	*Verify_RoadNetwork*	1	Verify correct evacuations along the Road and Trail network pathways to the destinations defined in Vale's PAEBM (EAP)
Total # Sims & Alts-->		12		59	

Preparation of key LifeSim model inputs

This section provides a brief description of the development of the primary data inputs used to create the LifeSim alternatives:

- **Key Sources:** Examples of key sources include the Robertson et al. (2019) expert panel report, a book by the journalist Arbex (2022), post-disaster investigations and support by Brazil's Federal and State of Minas Gerais legislatures, ministries and agencies (Assembleia Ligislativa do Minas Gerais, 2019; Government of Brazil, 2019a, 2019b), reports from media outlets (e.g., Globo, 2019), journal papers by Lumbroso et al. (2021) who developed a post-failure model of the event using the HRW Life Safety Model and by Passos and de Freitas (2021) who describe the immediate post-failure response and longer-term work by the firemen of Minas Gerais to locate and recover the remains of the victims, and work by the Instituto Medico Legal in Belo Horizonte to organize, identify, and return these remains (da Rocha et al., 2022; Quierati, 2019) and to determine causes of death (Araujo et al., 2022).

- **Basemaps and Satellite Imagery/Ground Cover and Land Use:** Web-based sources such as Google, Esri, and OpenStreetMap (OSM Foundation, 2024) were used to provide before and after base mapping and imagery of the full extent of the impact zone and surrounding region.
- **Tailings Dam Breach Analysis (TDBA) Hazard Runout Models:** Four breach outflow and runout models of the event were identified by this study: a pre-failure model developed by Walm Engineering to inform EAP development (Vale and Walm Engenharia, 2018a, 2018b), post-failure models developed by Lumbroso et al. (2021) and by Gibson et al. (2022), and more recent work by Adria et al. (2023) to investigate the properties and arrival times of the runout downstream to the Rio Paraopeba. This study used the HEC-RAS model developed by Gibson et al. (2022) as the 100% (i.e., "historic") event. As noted above, two additional 66% and 33% volume hazards were also developed.
- **Structures and Outdoor Areas:** Structures and outdoor areas located in and around the tailings runout zone were compiled starting with a baseline dataset from Lumbroso et al. (2021). More structures, outdoor areas, and details were then added using pre-failure Google and Esri satellite imagery, and OSM basemap sources. Multiple structure datasets were created to model variations in population sizes and distribution, number of stories, stability criteria and structure location. Four population allocations were used to account for variations in the PAR: population model 1 estimates the final Event PAR size and distribution; model 2 estimates a much larger PAR based on information provided on the day of the failure; model 3 distributes the event PAR more uniformly across the mine administration area; and model 4 uses the USACE's production-level method which varies PAR by time of day.
- **Population:** Two types of population were developed for the area in and surrounding the Vale mine: an "industrial PAR" comprising Vale employees and contractors who were working onsite, and a "community PAR" to represent people located in the impact zone outside of the assumed mine property boundary. Estimates of the number and location of industrial PAR were developed iteratively using many sources. Estimates of the community PAR assumed a nominal number of individuals who occupied their homes at the time of failure. Estimation of the PAR at Pousada Nova Estancia was determined using the list of victims combined with news items and narratives in Arbex (2022).
- **Evacuation Route System (ERS):** Development of the road and trail network started with a downloaded copy of the OpenStreetMap dataset. This dataset was extensive, detailed, and provided a very useful basemap. Additional GIS editing effort was required to ensure that the network model had correct nodal connections at street intersections. This created the need to add a model verification alternative (#59) so that a zero-hazard model could be run to confirm that evacuating

PAR moves correctly along the roadways towards their target destinations. This single ERS dataset was used in all the event and process simulations.

- **Emergency Planning Zones (EPZs) and Destinations:** A GIS polygon layer was created to define the EPZs that are used to vary the community warning and evacuation times. This allowed the LifeSim modelers to set up different ranges of warning times. A new calibration called "Fire Drill" was created to simulate the rapid protective actions of well-trained industrial PAR at the Vale mine site. A related GIS points layer was created to define the set of target evacuation destinations outside of the impact zone. This was based on Vale's emergency action plan design (PAEBM) (Vale and Walm Engenharia, 2018a, 2018b).

Results: historic event simulations

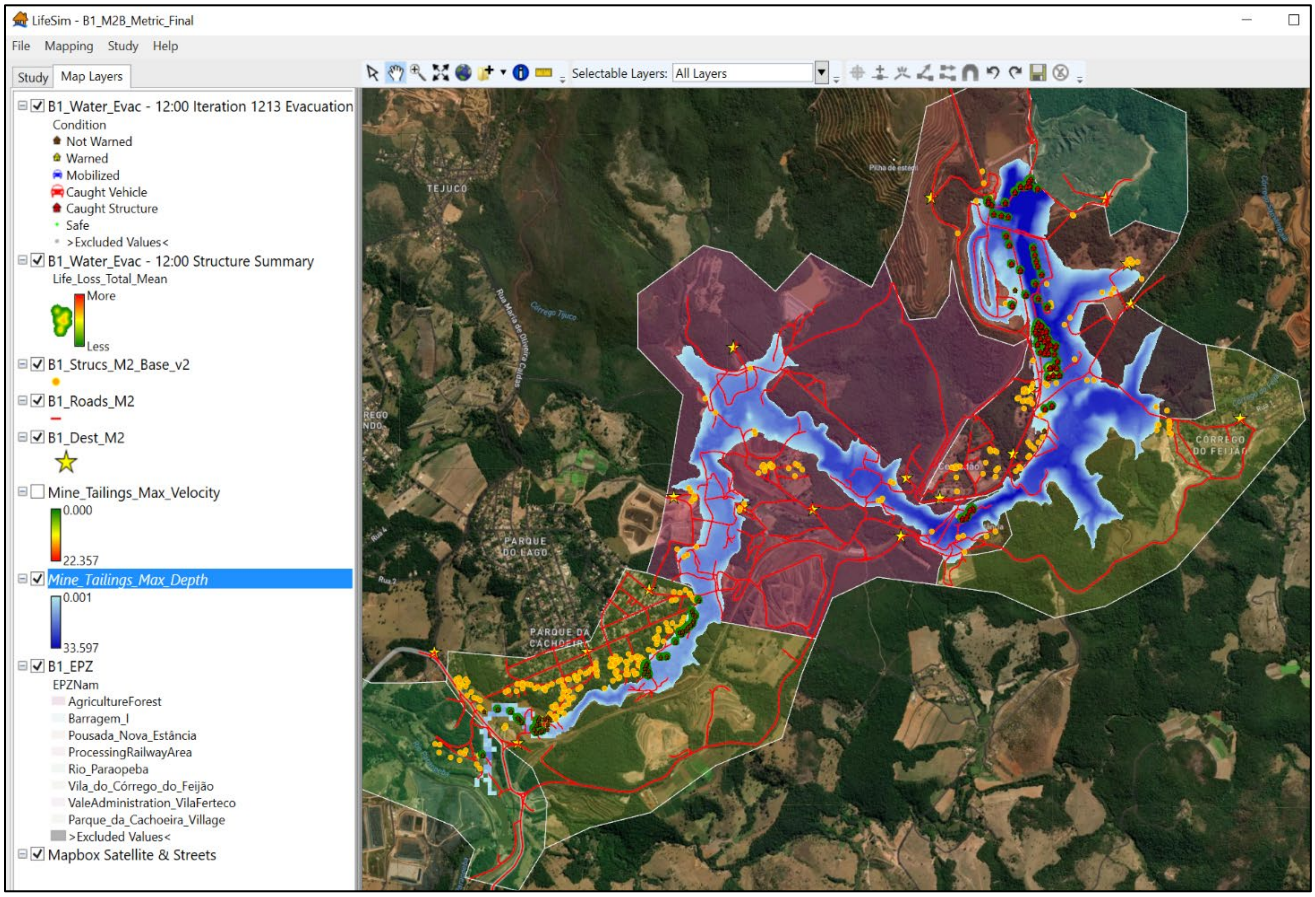


Figure 2: Event validation map for Alternative #2: B1_Water_Evac

Figure 2 presents an example consequences map for one alternative that includes a basemap satellite image, the road network, the tailings outflow maximum depth, building loss or survival, and life loss outcomes. Figure 3 presents a LifeSim whisker diagram, which provides summary statistics for the total estimated life loss for the 100%, 75% and 50% stability calibrations. The observed historic life loss of

N_LL = 270 is indicated in all the whisker diagrams using a vertical red line. Each of the alternatives have uncertainty bands that encompass the historic life loss, and each whisker plot presents the minimum, quartiles, mean, median and maximum. The blue bars indicate the 25% to 75% quartile boundaries. In general, the central tendency of most of these estimates fall below the observed historic value of 270 lives lost.

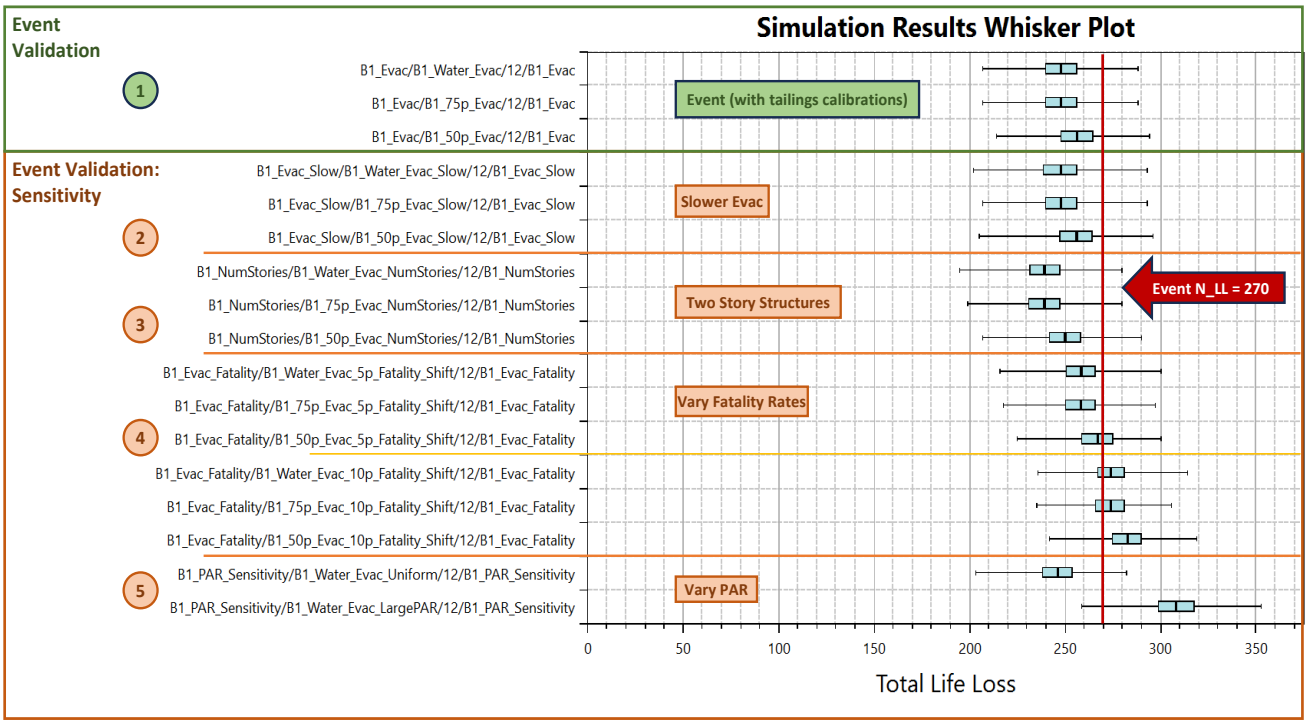


Figure 3: Historic event validation simulations: LifeSim consequences whisker diagram

The assessment of slower evacuations by the PAR did not greatly increase the losses, which suggests that even with self-mobilization, the PAR would be unable to react quickly enough to reduce losses. Modeling the availability of a second story to allow for vertical evacuation also did not reduce losses significantly, which suggests that a shelter-in-place protective action strategy would not have been effective for this event. The shifting of fatality rates by 5% and 10% did indeed increase the life loss distributions marginally so that the central tendency more closely matches this historic event. This might provide some support for the question as to whether outflows from tailings dams are more dangerous to the PAR than outflows from water dams.

The sensitivity of losses to a more uniform allocation of the PAR across the Vale mine site and administration were also not very high, which suggests that the starting locations of the PAR would have had minimal influence on loss and survival outcomes. This is another possible indicator of the extreme severity of the tailings outflows. The Large PAR sensitivity runs were used to explore a news report which

suggested a much larger population at risk within the impact zone. The simulation results suggest that if this higher estimate of the exposed industrial population at risk was correct, then LifeSim would also estimate much higher life losses than the observed value.

Finally, the assessment of variations of building stability parameters indicates that life losses are relatively insensitive to these calibrations. This suggests that the extremity of the flow depths and velocities within the mining operations and administration areas were so high that the LifeSim life loss algorithm was already "maxing out" to yield very high life loss estimates. Reducing the calibrated strength capacities of buildings, vehicles, and people did little to further increase the estimated losses.

Results: MMC SOP process simulations

USACE relies on a consistent production level approach to support its Dam Safety Program by building dam breach consequence models. The MMC is responsible for establishing the standard production level approach that all dam breach modeling efforts follow. The MMC SOP uses two warning scenarios: a minimal warning scenario which samples a uniform uncertainty distribution about the hazard identification time from -2 hours prior to breach through +0 hours at the time of breach, and an ample warning scenario, which samples from -6 hours prior to breach to -2 hours prior to breach.

Both warning scenarios allow for an increased opportunity time for PAR to take protective actions and evacuate to safety (USACE MMC, 2022). Figure 4 presents the LifeSim life loss whisker diagram for these cases. The scenarios model 2:00 a.m. and 2:00 p.m. scenarios. The industrial PAR is located in the mining operation 24-7, and a larger community PAR was assumed to be located at home at nighttime. The plotted results all have central tendencies and uncertainty bands that are well below the historic observed loss, the minimal warning losses are higher than for ample warning, and the upper limit of the 2:00 a.m. event approaches the historic observed loss.

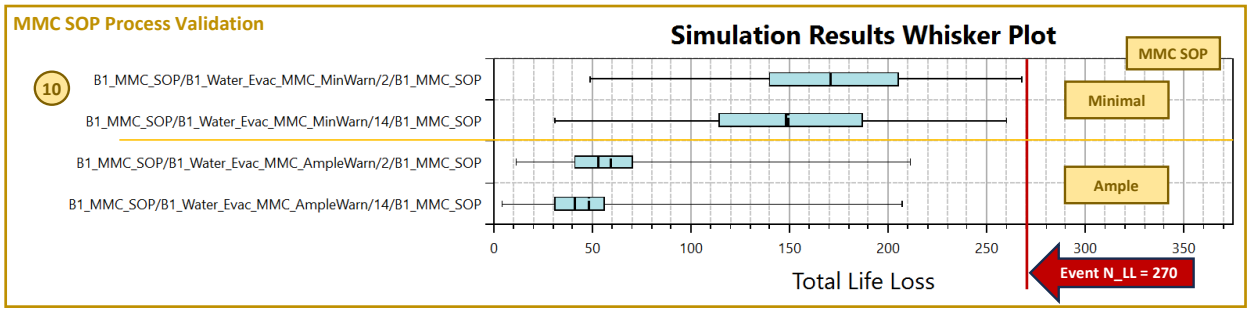


Figure 4: MMC SOP simulations: whisker diagram for minimal and ample warning

An important aspect of the historic event is that a very large number of the industrial PAR were in the cafeteria and the arrival time under minimal warning was so fast that more than 90% of the PAR in that zone could be exposed to the tailings runout. The additional warning time provided under the MMC SOP

ample warning scenario can substantially reduce the number of PAR exposed to the tailings and exhibits a wider variation in outcomes with the central tendency greatly reduced towards N_LL = 50.

The sensitivity of life loss to the volume of breach outflows was also investigated. The results demonstrated the expected reductions in the sizes of the exposed PAR and of life loss as the outflow volumes declined. Building stability calibrations also had a clear influence on the life loss outcomes at the lowest flow scenario (33%). This supports a recommendation that the physical effects of tailings flows on structures, vehicles, and people should be studied further.

Summary

The Feijão Dam B-1 Tailings Dam Failure can be viewed as an industrial disaster with very high mortality rates for the employees and contractors. It was also a societal disaster with many community members and tourists killed. At the macro scale, the observed life loss was N_LL = 270, the total exposed population is estimated to be N_PAR = 418, and the estimated gross mortality rate is F_LL = 65%. This is a very high loss rate. The loss of the industrial PAR below the TSF and in the administration area dominated the life loss consequences. The losses at the Pousada Nova Estancia resort were also severe. Further downstream, the town of Parque da Cachoeira had the highest community exposures but the lowest life losses and mortality rates.

Only self-awareness, immediate evacuation, and a few post-failure rescues saved lives. Important gaps remain with the data used to characterize the location and quantities of PAR and life loss at the micro-scale level (e.g., at individual structures and key outdoor areas such as the "railway pear," drying bays and administration area below TSF B-1, and further downstream in Parque da Cachoeira). It should be possible to eventually gain access to more detailed records so that these uncertainties can be further reduced.

Conclusions and recommendations

The Feijão Dam B-1 Tailings Dam Failure case study successfully demonstrated how LifeSim can be used to develop a useful model of this historic event. Most of the event validity life loss estimates encompass the observed consequences. The study also showed how USACE's MMC SOP can be applied. It was possible to characterize the PAR for a range of location types (e.g. residential, industrial, agricultural), for variations by time of day, to estimate life loss for a range of TSF breach outflow scenarios, and to explore how variations in EAPs and community preparedness can influence outcomes. The MMC SOP simulations appear to correctly characterize the range of possible consequences, with the central tendency of the Ample Warning scenarios falling well below the actual losses, as would be expected, and with the Minimal Warning scenarios presenting more extreme consequences that in some cases approach the observed extreme event. While the study confirmed the strengths of the LifeSim simulator and methodology, and no fundamental

gaps were found, modifications and adjustments to existing methods could increase the value of the simulator for modeling TSF failure and runout events. This includes:

- Develop a better understanding of how tailings flows affect buildings, vehicles, and people via mechanisms such as adhesion, fouling, and deposition. Examples include more building damage, loss of transport (vehicles cannot move, vehicles stall), impacts on pedestrians, and compromised first-responder rescues (deposited tailings become barriers to emergency vehicles).
- Investigate how object stability calibrations can be adjusted to account for the physical properties tailings flows, and whether there is also a need to adjust the mortality rate curves.
- Add the "Fire Drill" Protective Action Initiation (PAI) response pattern to represent well-trained industrial PAR.
- Since the Feijão Dam B-1 failure is only one of four types of Tailings Dam Breach Analysis event identified by the CDA's 2021 Bulletin, the LifeSim methodology (and possibly the simulator) may need to be extended to also support modeling TSF failure events that have both a supernatant pond and liquefiable tailings.
- Finally, given the extremity of the Feijão Dam B-1 Tailings Dam Failure event, it will be important to study other TSF incidents and failures with different characteristics such as: larger communities, larger PAR, the potential for earlier detection and warning, medium- to lower-intensity tailings flows, longer downstream runout distances, lower life loss rates, and successful evacuations.

Acknowledgements

The study team extends sincere thanks to Jason Needham, Woody Fields, and Paul Risher of USACE RMC for their leadership and support, to Stanford Gibson of USACE HEC for developing the HEC-RAS Feijão Dam B-1 TSF failure runout model, and to the USACE LifeSim consequences estimation working group.

References

Adria, D. A. M., Ghahramani, N., Rana, N. M., Martin, V., McDougall, S., Evans, S. G. and Take, W.A. 2023. Insights from the compilation and critical assessment of breach and runout characteristics from historical tailings dam failures: implications for numerical modelling. *Mine Water and the Environment* 42: 650–669. doi:https://doi.org/10.1007/s10230-023-00964-0

Anglo American. 2019. Anglo American Technical Standard AA TS 602 001 Mineral Residue Facilities and Water Management Structures Standard and Technical Specifications, version 5.2, September 2019 (Original version released February 2014).

Araujo, R.M., Lemos, Y.A., do Nascimento, E.D., Paraizo, A.H., Wainstein, A.J.A. and Drummond-Lage, A.P. 2022. Identification of victims of the collapse of a mine tailings dam in Brumadinho. *Journal of Forensic Sciences Research* 7(4): 580–589.

Arbex, D. 2022. *Arrastados: Os bastidores do rompimento da barragem de Brumadinho, o maior desasatre humanitario do Brasil: Intrinseca.*

Assembleia Ligislativa do Minas Gerais. 2019. *Comissao Parlamentar de Inquerito: da Barragem de Brumadinho, Relatorio Final; Causas do rompimento de barragem de rejeitos da mineradora Vale em 25 de janeiro de 2019.* Belo Horizonte

da Rocha, C.S., Silva, L.S. and da Silva, J.M. 2022. *Vivências dos trabalhadores do instituto médico legal de belo horizonte, minas gerais, frente ao desatre de massa: Rompimento de barragem. New Trends Qualitative Research (NTQR)* 13. doi:https://doi.org/10.36367/ntqr.13.2022.e730

Gibson, S., Moura, L.Z., Ackerman, C., Ortman, N., Amorim, R., Floyd, I., . . . Sánchez, A. 2022. prototype scale evaluation of non-Newtonian algorithms in HEC-RAS: mud and debris flow case studies of Santa Barbara and Brumadinho. *In Geosciences* 12: 134–157.

Globo. 2019. Tragédia em Brumadinho; FOTOS. Globo. Retrieved from https://g1.globo.com/mg/minas-gerais/noticia/2019/01/25/barragem-da-vale-se-rompe-em-brumadinho-mg-fotos.ghtml

Government of Brazil. 2019a. *Commissao Parlamentar de Inquerito Rompimento da Barragem de Brumadinho, Relatorio.* (Outobro de 2019). Camara dos Deputados.

Government of Brazil. 2019b. *Relatório de Análise de Acidente de Trabalho, Rompimento da barragem B I da Vale S.A. em Brumadinho/MG em 25/01/2019.*

ICMM and UNEP. 2020. Global Industry Standard on Tailings Management (GISTM). International Council on Mining and Metals (ICMM) and United Nations Environment Programme (UNEP).

Johnstone, W.M., Assaf, H., Sakamoto, D. and Hartford, D. 2003. Analysis of the Malpasset dam failure using GIS and engineering models. Paper presented at the GeoTec 2003, Vancouver, BC.

Lumbroso, D., Davison, M., Body, R. and Petkovšek, G. 2021. Modelling the Brumadinho tailings dam failure, the subsequent loss of life and how it could have been reduced. *Natural Hazards and Earth System Sciences* 21: 21–37. doi:10.5194/nhess-21-21-2021

NIST. 2024. 5.1 – Process Improvement, 5.1.1 – What is Experimental Design? Washington, DC: National Institute of Standards and Technology, US Department of Commerce. Accessed at https://www.itl.nist.gov/div898/handbook/pri/pri.htm

OSM Foundation. 2024. Open Street Map. Accessed at www.openstreetmap.org

Passos, A. and de Freitas, J.S. 2021. *A Inteligencia Operacional Aplicada aos Resgates em Desasastres: A Atuacao dos Bombeiros no Rompimento da Barragem de Mineracao em Brumadinho/MG – Brasil. Territorium: Revista Internacional de Riscos, Territorium* 28(1): 35–51. doi:10.14195/1647-7723_28-1_3

Passos, A. and Quierati, L. 2023. *Brumadinho 272 – relato de um comandante do Corpo de Bombeiros sobre as buscas e as vidas impactadas pelo desastre da barragem*. Jau, Brazil: 11 Letras da 11 Editora.

Quierati, L. 2019. *Por identificações, Brumadinho cria software para montar corpos e pede aval raro do MP (2019/07/24).* Accessed at https://noticias.uol.com.br/cotidiano/ultimas-noticias/2019/07/24/brumadinho-seis-meses-trabalho-de-identificacao.htm

Rana, N.M., Ghahramani, N., Evans, S.G., McDougall, S., Small, A. and Take, W.A. 2021. Catastrophic mass flows resulting from tailings impoundment failures. *Engineering Geology* 292. doi:https://doi.org/10.1016/j.enggeo.2021.106262

Robertson, P.K., de Melo, L., Williams, D.J. and Wilson, G.W. 2019. *Report of the Expert Panel on the Technical Causes of the Failure of Feijão Dam I.*

Secretaria de Estado de Meio Ambiente e Desenvolvimento Sustentável, and Governo do Estado de Minas Gerais. 2018. Licenciamento Ambiental Parecer Unico No 0786757/2018 (SIAM) issued by: Governo do Estado de Minas Gerais, Secretaria de Estado de Meio Ambiente e Desenvolvimento Sustentável, Subsecretaria de Regularização Ambiental – SURAM, Superintendência de Projetos Prioritários – SUPPRI (0786757/2018).

USACE MMC. 2022. Technical Manual for Dams: Modeling, Mapping, and Consequences. In FY2023 (MMC Information Hub URL: https://mmc.sec.usace.army.mil/usace-dams-sop.html): US Army Corps of Engineers, Modeling, Mapping, and Consequences Production Center.

USACE RMC. 2024. LifeSim – RMC Software and Tools. Retrieved from https://www.rmc.usace.army.mil/Software/LifeSim/

Vale and Walm Engenharia. 2018a. Document 3.3.3.8.6.6.1.1.2 – ENCARTES_PAEBM_I_2018_07 – Rota de Fuga em Caso de Emergência – Anexo A, B, C. Zona Rural – Brumadinho/MG, Vide Mapa: WBH34-17-VALE-DES-0169.

Vale and Walm Engenharia. 2018b. Document 3.3.3.8.6.6.1.1.3 – MAPAS_PAEBM_I_2018_07 – Complexo Paraopeba – Mina Córrego do Feijão – Barragem I Estudo de Cenários (Dam Break) Mapa de Envoltória Máxima de Inundação Cenário de Ruptura Dia Chuvoso (Rainy Day) – Folha 1/2 and 2/2.

The Importance of Considering Dilute to Dry Tailings Rheology Formulations in Practical Tailings Dam Break Modeling

Reinaldo Garcia, Hydronia LLC, Pembroke Pines, USA
Jacinto Artigas, Hydronia LLC, Pembroke Pines, USA
Sergio Martinez, LIFTEC/CSIC-Universidad Zaragoza, Spain
Pilar Garcia-Navarro, LIFTEC/CSIC-Universidad Zaragoza, Spain
Javier Murillo, LIFTEC/CSIC-Universidad Zaragoza, Spain
Nick Calero, Hydronia LLC, Pembroke Pines, USA
Adolfo Correa, BrazilHydro, Brazil

Abstract

After mine tailings dam failures, the flowing material often consists of a mix of water and multiple solid phases with different sediment size classes, organic components, chemical solutes, metals, and numerous sediment types in the dam itself. In turn, the high-speed flow can entrain soil from the existing terrain and, under low energy conditions, can deposit or stop altogether.

To determine the areas that could be impacted by tailings, it is critical to utilize models that consider rheology formulations that correctly represent the dam materials and tailings, whether dilute or dry. Also, if conditions require, the model should be able to incorporate the interaction of the tailings flow with existing water bodies such as water reservoirs or rivers.

In this paper, we present a practical application of the RiverFlow2D MT two-phase model for tailings dam risk assessments to the Córrego do Feijão tailings dam near Brumadinho, Brazil, that include rheological formulations applicable to non-Newtonian fluids representing initially dilute tailings but also those originating from dry stacks. The model considers the variability of the soil characteristics in the initial terrain and tailings as well as how fluid properties such as density, viscosity, and yield stress change in time and space as the materials flow and interact with the terrain soils and other water bodies.

The application shows that using a rheological formulation that does not adequately represent the tailings flow would lead to erroneous runout distances. The results highlight the importance of considering an appropriate rheological formulation for tailings deposits and the dynamic interaction of tailings with their surrounding environment. This paper may be of interest to professionals involved in assessing risk and mitigation measures related to tailings dam breaks.

Introduction

Flows of high-density mine tailings are one of the most challenging and difficult to assess gravity-driven flows in environmental processes. In this kind of flow, the fluid in motion consists of a mixture of water and multiple solid phases of different natures, such as different sediment size classes, organic materials, and heavy metals, moving rapidly downstream over steep terrain. Typically, the slurries and debris are considered highly solid-laden fluids, in which the density of the mixture can be more than two or three times the water density, and the bulk solid phase represents 40 to 80% of the flow volume (Iverson, 1997). Tailings flows lie can include hyperconcentrated flows and dry materials avalanches (Hungr et al., 2001). Most of the numerical models reported for highly solid-laden flows use a single-phase approach, neglecting the mixture density in the shallow-flow mass and momentum conservation equations (Murillo and García-Navarro, 2012). Two-phase approaches consider the depth-averaged mass and momentum conservation for the liquid and solid phases separately (George and Iverson, 2011). Note that some tailings flow models depict two layers of different flow behavior, such as upper alluvial sediment flow and an underlaying layer of uniform material mud flow. These models, inaccurately called two-phase models, establish a non-physically based interaction between the layers and therefore cannot be considered realistic two-phase models, and are not tested against experimental results and do not show real event data.

Erosion and sedimentation

The mass exchange between flow layer and the erodible bed involves complicated physical processes, and the understanding of the theoretical basis remains unclear. Experiments in large-scale channels (Iverson et al., 2011) and field observations of real events (McCoy et al., 2012) indicate that the entrainment volume in steep beds can be of the same order of magnitude as the initial volume mobilized. Tailings flows can gain significant mass and momentum as they move over steep slopes as a consequence of the material entrainment from the erodible bed, before deposition begins on flatter terrain downstream. One of the biggest challenges for the application of depth-averaged models to realistic large-scale, long-term mud/debris flows is the computational effort required. These kinds of unsteady flows usually occur over very steep and irregular terrain, which requires the use of a refined non-structured spatial discretization in order to capture the terrain complexity, increasing the computational times exponentially.

Furthermore, the complexity of the numerical resolution and the computational cost of the solvers also increase considerably with the number of equations involved, and the coupling between flow variables adds special features to the mathematical model. Most of the numerical models specially designed for mud/debris flow are one-dimensional, or their resolution procedures are based on square-structured meshes in the case of 2D models. There is a lack of efficient and robust two-dimensional numerical models specifically designed for mud/debris flows and able to work with non-structured triangular meshes. In the

last five years, the use of Graphic Processing Units (GPU) hardware accelerators for sequential computation has proved to be an efficient and low-cost alternative to the traditional multi-CPU strategies (Lacasta et al., 2015).

This paper presents a two-phase two-dimensional model for multi-grain tailings flows over nonuniform erodible beds. We first present the fundamental equations, and then we summarize the results of simulations of a real tailings dam break event using the quadratic rheological formulation suitable for relatively dilute tailings and the granular formulation appropriate for dry stacks.

Two-phase tailings flow model

The model for mud/tailings flow is based on that described in detail in Martínez-Aranda et al. (2022), and involves the following assumptions:

- A shallow-two-phase solid-water flow approach.
- A multicomponent flow: the mixture of water and sediment particles is described by using the continuum approach and assuming the same velocity for the liquid and the solid phase.
- The different sediment size-classes present in the flow are distributed uniformly in the flow column.
- The reference coordinate system is horizontal-vertical, but the pressure and stress forces act along the direction tangential to the bed surface.
- Dynamic pore-fluid pressures can be developed in the liquid phase, affecting the frictional shear stress between solid grains.
- The model formulation is physically based and has been thoroughly validated with experimental data and real events (Martínez-Aranda et al., 2022).
- The two-dimensional mud/tailings flow model over erodible bed consists of 3 + N + 1 partial differential equations, including the depth-averaged equations for the water-sediment mixture mass and momentum conservation:

$$\frac{\partial}{\partial t}(\rho h) + \frac{\partial}{\partial x}(\rho h u) + \frac{\partial}{\partial y}(\rho h v) = -\sum_{p=1}^{N} \rho_{b,p} \frac{D_p - E_p}{1 - \xi_p} \quad (1)$$

$$\frac{\partial}{\partial t}(\rho h u) + \frac{\partial}{\partial x}(\rho h u^2 + \frac{1}{2} g_\psi \rho h^2) + \frac{\partial}{\partial y}(\rho h u v) = -g_\psi \rho h \frac{\partial z_b}{\partial x} - \tau_{bx} \quad (2)$$

$$\frac{\partial}{\partial t}(\rho h v) + \frac{\partial}{\partial x}(\rho h u v) + \frac{\partial}{\partial y}(\rho h v^2 + \frac{1}{2} g_\psi \rho h^2) = -g_\psi \rho h \frac{\partial z_b}{\partial y} - \tau_{by} \quad (3)$$

the continuity equation for each sediment size-class p = 1, ...,N, expressed as:

$$\frac{\partial}{\partial t}(h\,\phi_p) + \frac{\partial}{\partial x}(hu\,\phi_p) + \frac{\partial}{\partial y}(hv\,\phi_p) = -(D_p - E_p) \qquad 4$$

as well as the mass conservation equation for the bed layer considering N sediment size-classes:

$$\frac{\partial z_b}{\partial t} = \sum_{p=1}^{N} \frac{D_p - E_p}{1 - \xi_p} \qquad 5$$

where ρ is the bulk mixture density, h is the flow depth, (u, v) are the components of the depth averaged flow velocity vector **u** along the x and y coordinates respectively, ϕ_p represents the depth-averaged volumetric concentration of the p^{th} sediment size-class, N is the number of sediment size-classes transported, and (τ_{bx}, τ_{by}) are the components of the basal resistance vector τ_b along the x and y coordinates respectively. Moreover, z_b is the bed elevation, ξ_p is the deposition porosity for the p^{th} sediment class and $\rho_{b,p}$ the associated bulk density in the bed layer, D_p and E_p are the size specific deposition and entrainment exchange rates respectively, and $g_\psi = g\cos^2\psi$ is the bed-normal projection of the gravity, g is the gravitational acceleration and cos ψ is the direction cosine of the bed normal with respect to the vertical axis (Juez et al., 2013). Accordingly, the normalized bulk density r is given by:

$$r = \frac{\rho}{\rho_w} = 1 + \phi^\chi \qquad \text{with:} \quad \phi^\chi = \sum_{p=1}^{N} \frac{\rho_{s,p} - \rho_w}{\rho_w}\,\phi_p \qquad 6$$

where ϕ_χ is the buoyant solid concentration, ρ_w is pore-water density and $\rho_{s,p}$ is the density of the sediment particles for each sediment size-class.

Rheological formulations

A detailed explanation of the depth-averaged non-Newtonian basal resistance models used for the RiverFlow2D MT model can be found in Martinez-Aranda et al. (2022). Here, only the most important points are summarized.

The rheological formulations available in RiverFlow2D MT are summarized in Table 1.

Table 1: Rheological basal resistance formulations used in RiverFlow2D MT

ID	MODEL	BASAL RESISTANCE	FLOW TYPE
1	Turbulent Manning	$\tau_b = \tau_f + \rho g_\psi \frac{n^2 \lvert\mathbf{u}\rvert^2}{h^{1/3}}$	Turbulent Newtonian
2	Full Bingham	$2\tau_b^3 - 3\left(\tau_y + 2\mu_B \frac{\lvert\mathbf{u}\rvert}{h}\right)\tau_b^2 + \tau_y^3 = 0$	Cohesive viscoplastic
3	Simplified Bingham	$\tau_b = \frac{3}{2}\tau_y + 3\mu_B \frac{\lvert\mathbf{u}\rvert}{h}$	Cohesive viscoplastic
4	Turbulent Coulomb	$\tau_b = \tau_f + \rho g_\psi \frac{n^2 \lvert\mathbf{u}\rvert^2}{h^{1/3}}$	Frictional turbulent with $\tau_f = \left(\rho g_\psi h - \mathcal{P}_b\right)\tan\delta_f$
5	Turbulent Yield	$\tau_b = \tau_y + \rho g_\psi \frac{n^2 \lvert\mathbf{u}\rvert^2}{h^{1/3}}$	Cohesive turbulent
6	Turbulent Coulomb/Yield	$\tau_b = \min(\tau_y, \tau_f) + \rho g_\psi \frac{n^2 \lvert\mathbf{u}\rvert^2}{h^{1/3}}$	Frictional/cohesive turbulent with $\tau_f = \left(\rho g_\psi h - \mathcal{P}_b\right)\tan\delta_f$
7	Quadratic	$\tau_b = \tau_y + \frac{k_0}{8}\mu_B \frac{\lvert\mathbf{u}\rvert}{h} + \rho g_\psi \frac{n^2 \lvert\mathbf{u}\rvert^2}{h^{1/3}}$	Cohesive viscous/turbulent with $k_0 = 24$
8	Granular	$\tau_b = \rho g_\psi\, h \tan\delta_f$	Dry pure-frictional
9	Viscoplastic Coulomb	$\tau_b = \tau_f + \left(\frac{2m+1}{m}\right)^m \mu_P \left(\frac{\lvert\mathbf{u}\rvert}{h}\right)^m$	Frictional shear-thinning $m < 1$ or shear-thickening $m > 1$, with $\tau_f = \left(\rho g_\psi h - \mathcal{P}_b\right)\tan\delta_f$

Numerical solution

The equations described in the above section are solved by a fully conservative finite-volume method, detailed in Martinez-Aranda et al. (2022). The spatial domain is divided into triangular computational cells using an unstructured mesh. The time step is limited by the Courant-Friedrichs-Lewy (CFL) condition. The numerical computation can take advantage of multiple-core Graphical Processing Units (GPU) that allow reducing model runs up to 1,000 times with respect to non-parallelized models.

Results

This application aims to illustrate the importance of selecting the rheological formulation that better captures the non-Newtonian behavior of the tailings we would need to deal with. Using a formula that is not appropriate for the type of tailings would require using values of the key parameters (e.g., viscosity, yield stress) that could be unrealistic. In this test we compared the results for two different rheological formulas, while keeping the same parameters for both cases. On 25 January 2019 (at 12:28 p.m.), Dam I at the Córrego do Feijão Iron Ore Mine, located 9 km north-east of Brumadinho in the state of Minas Gerais, Brazil, suffered a sudden and catastrophic failure, resulting in an extremely violent mud flow that traveled downstream for more than 10 km and reached the Paraopeba River. The initial failure extended across the face of the dam and the slope collapse was complete in less than ten seconds. Most of the dam material flowed out of the dam in less than five minutes. The tailings in the dam showed a sudden and significant loss of strength and rapidly became a heavy liquid that flowed downstream at a high speed (about 120 km/h

in some zones). The data used to characterize the tailings, and the main parameters used in the test, are summarized in Table 2.

Table 2: Parameters used in the simulations

Parameters used in the simulations						
Liquid density ρ_w (kg/m^3)	1,000					
Initial mixture density ρ (kg/m^3)	2,247.5					
Internal stability angle ϕ_b(°)	5					
Manning roughness coeff. n (s m -1/3)	0.003					
Pore press. excess coeff. γ_{pp} (–)	2.05					
Global critical Shields stress θ_c (–)	0.03					
Transport capacity parameter β_T (–)	0.5					
Number of solid phases	6					
Solid phase material	**Sand**	**Silt**	**Fe**	**Al**	**Mn**	**Ti**
Medium diameter d_p (mm)	0.4	0.075	0.075	0.075	0.075	0.075
Initial volume concentration ϕ_p (–)	0.19	0.224	0.075	0.009	0.0015	0.0003
Solid density ρ_p (kg/m^3)	2,700	2,700	7,874	2,700	7210	4,506
Bed fraction $F_{b,p}$ (–)	0.38	0.62	0.0	0.0	0.0	0.0
Deposition porosity p_p (–	0.35	0.45	0.45	0.45	0.45	0.45
Critical Shields stress $\theta_{c,p}$ (–)	0.020	0.067	0.067	0.067	0.067	0.067

Tailings were composed of a mixture of water, sediments and heavy metals, mainly iron (Fe) 264.9 mg/g, aluminum 10.8 mg/g, manganese 4.8 mg/g, and titanium 0.5 mg/g (Vergilio et al., 2020). The size distribution consisted basically of a mineral sand fraction (38%) and a fines fraction (62%), accounting for mineral silt-clay and metals particles. The water content before the failure was estimated to be around 50% by volume with a specific weight of 22 to 26 kN/m^3 (Robertson et al., 2019).

Figure 1 shows an aerial image of the mine site after the dam collapse, including the dam location and the original tailings elevation in meters above sea level.

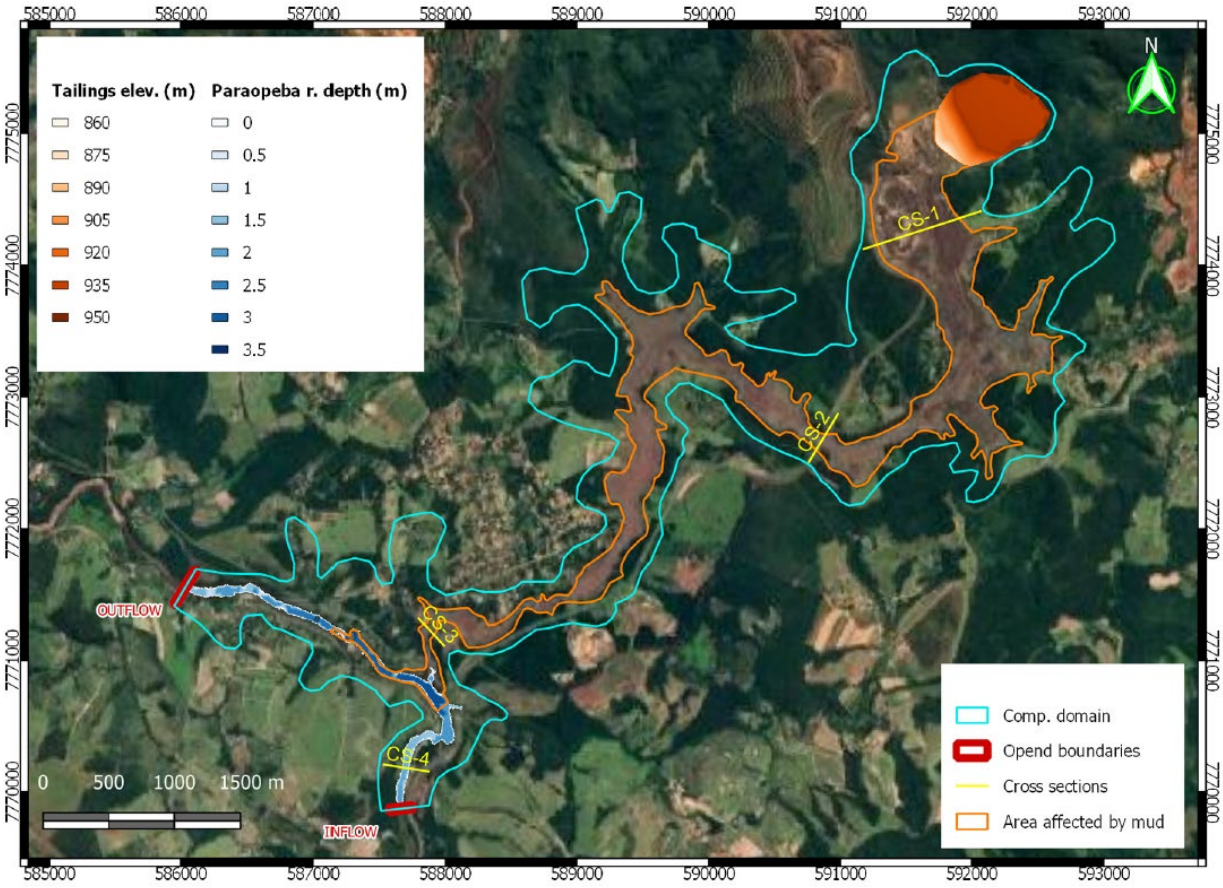


Figure 1: Aerial image of the area affected by the mud and the computational domain used in the simulation

The area affected by the mud was 3.3 × 106 m^2, not including the original dam area. In order to perform the simulations, a spatial domain of 10.396 × 10^6 m^2 is discretized using an unstructured triangular mesh, with the RiverFlow2D MT model containing approximately 20,000 cells ranging from 15 m to 50 m in size.

For the simulations the tailings mixture is considered fully saturated with an initial global volumetric concentration of solids φ_0 = 0.5, leading to a mixture density ρ = 2247.5 kg/m^3. The specific initial volumetric concentration for each solid phase φ_p is estimated from the available literature (Robertson et al., 2019).

Figure 2 shows the mud flow depth at 5 minutes, 10 minutes, and 35 minutes after the dam collapse, assuming the Quadratic and the Granular rheological formulation. Figure 3 depicts the volumetric concentration of the mixture.

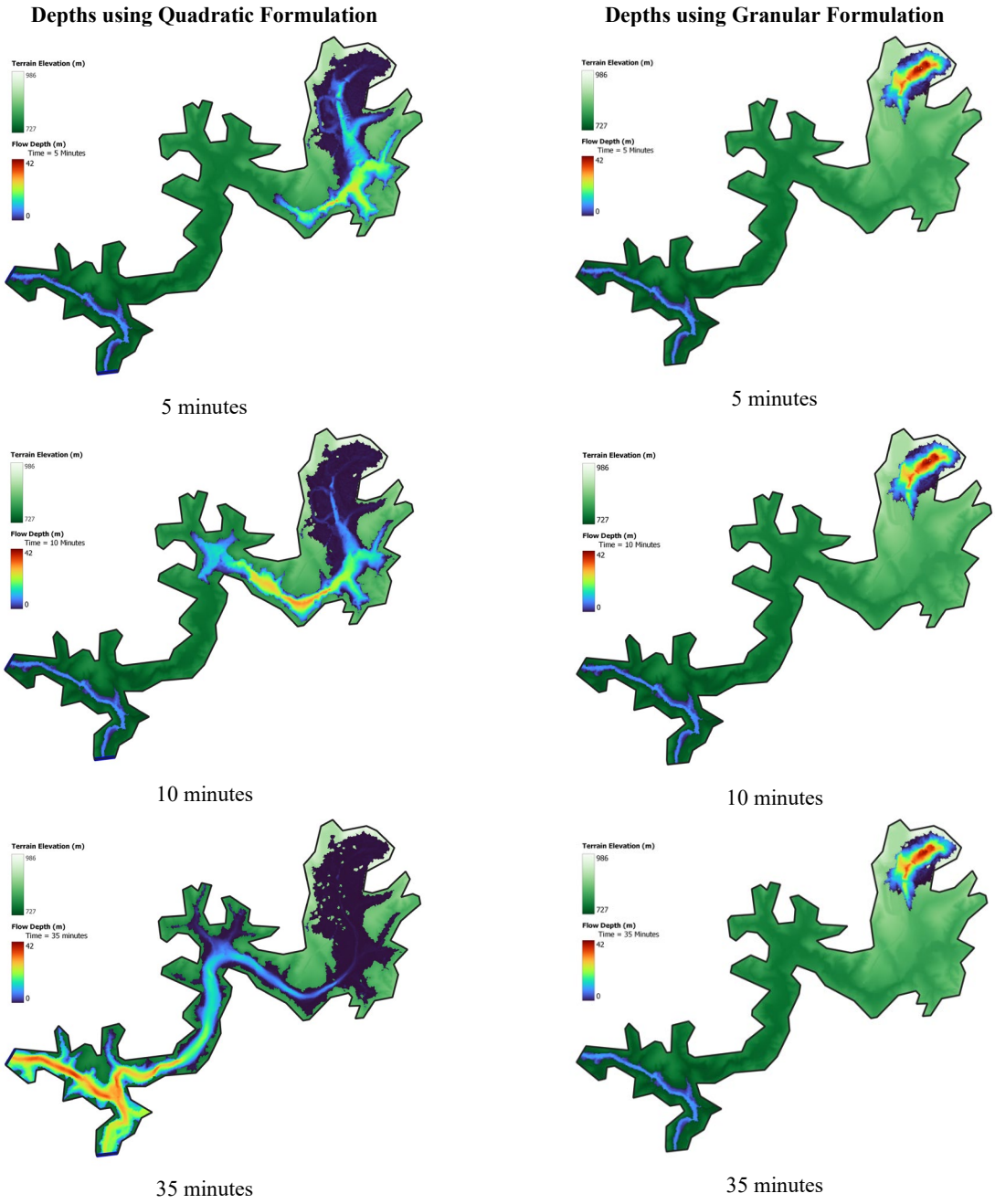


Figure 2: Flow depth maps at different times obtained using the Quadratic (left) and Granular (right) formulations

The numerical results using the quadratic formulation show that almost the entire initial tailings volume flowed out of the dam in the first five minutes after the dam collapse. The mud wave moved downstream with a computed height of more than 25 m and with velocities greater than 15 m/s (54 km/h) in some zones during the first minutes. On the other hand, assuming the granular formulation, the flow stops quickly at a short distance from the original deposits.

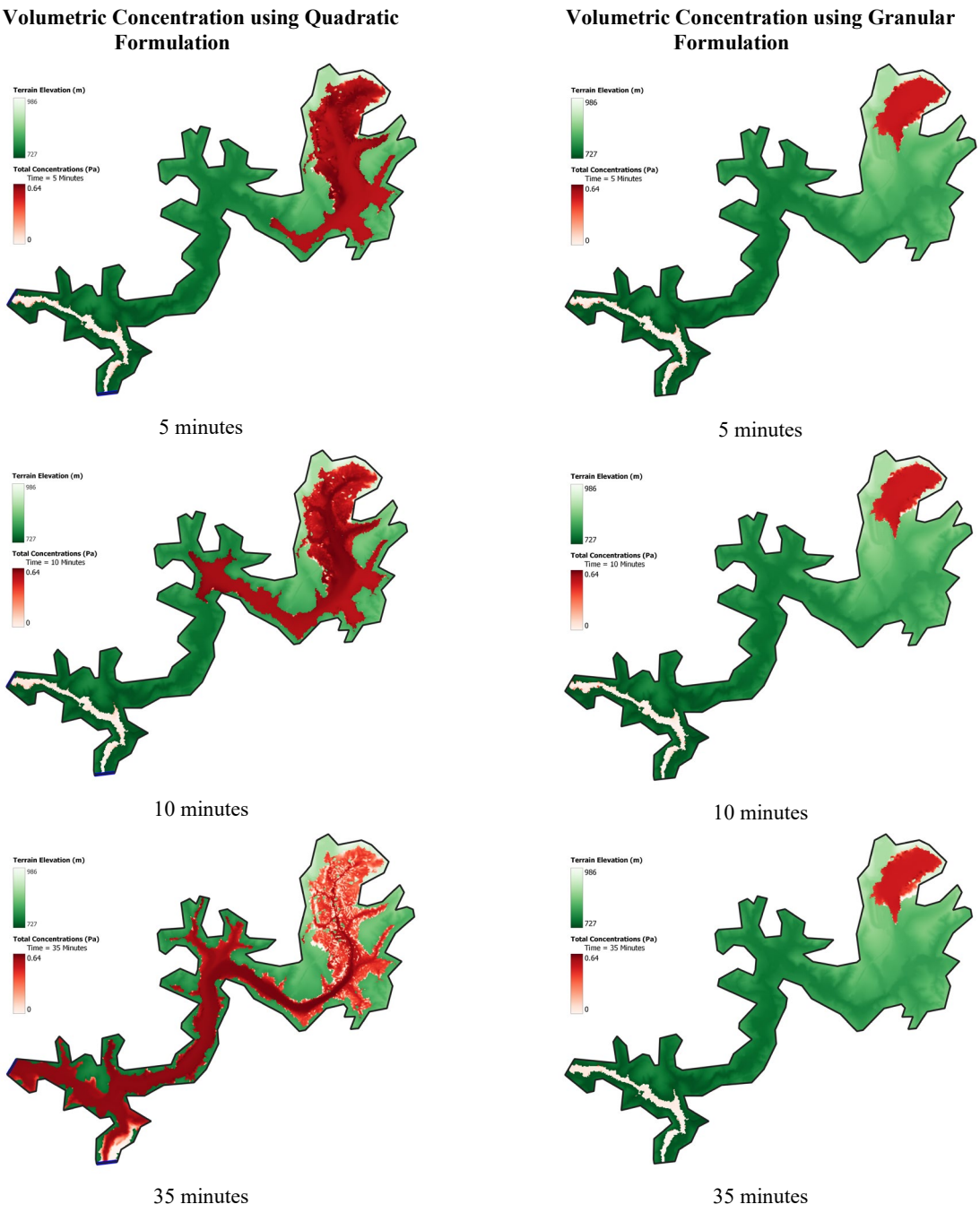


Figure 3: Material volumetric concentration maps at different times obtained using the Quadratic (left) and Granular (right) formulations

Conclusion

After mine tailings dam failures, the flowing fluid often consists of a mix of water and multiple solid phases with different sediment size classes, organic materials, chemical solutes, metals, and numerous sediment types from the dam itself. In turn, the high-speed flow can entrain soil from the existing terrain and, under

low energy conditions, can deposit or stop altogether.

To determine the areas that could be affected by tailings, it is critical to utilize models that consider rheology formulations that correctly represent the dam materials and tailings, whether dilute or dry. Also, if conditions require, the model should be able to incorporate the interaction of the tailings flow with existing water bodies such as water reservoirs or rivers.

This paper presents a practical application of the RiverFlow2D MT two-phase model for tailings dam risk assessments using as base data the case of the Córrego do Feijão dam break that occurred in Brazil in 2019. The simulations were performed with Quadratic and a Granular rheological formulation applicable to non-Newtonian fluids. The first one can be used to represent initially dilute tailings, while the latter can be used for those originating from dry stacks. The model considers the variability of the soil characteristics in the initial terrain and tailings as well as how fluid properties such as density, viscosity, and yield stress change in time and space as the materials flow and interact with terrain soils and other water bodies.

The application presented shows the importance of considering an appropriate rheological formulation for the tailings deposit and the dynamic interaction of tailings with their surrounding environment. Assuming the quadratic formula, the tailings flow several kilometers downstream from the dam location, while considering the Granular formulation the tailings flow only a few hundred meters from the initial deposit until they come to a full stop.

Acknowledgements

We would like to acknowledge the support of the Interamerican Development Bank through the HydroBID Flood initiative, Hydronia LLC (USA), Hydronia Europe (Spain), and the Computational Hydraulics Group of the Universidad de Zaragoza (Spain).

References

George, L. and Iverson, M., 2011. *A two-phase debris-flow model that includes coupled evolution of volume fractions, granular dilatancy and pore-fluid pressure*. *Proceedings of 5th International Conference on Debris-Flow Hazards: Mitigation, Mechanics, Prediction and Assessment,* 10.

Hungr, O., Evans, S.G., Bovis, M.J. and Hutchinson, J.N. 2001. A review of the classification of landslides of the flow type. *Environ. Eng. Geosci*. 7 (3): 221–238.

Iverson, R.M. 1997. The physics of debris flows. *Rev. Geophys*. 35 (3): 245–296.

Iverson, R.M., Reid, M.E., Logan, M., LaHusen, R.G., Godt, J.W. and Griswold, J.P. 2011. Positive feedback and momentum growth during debris-flow entrainment of wet bed sediment. *Nature Geosci.* 4: 116–121.

Juez, C., Murillo, J. and García-Navarro, P. 2013. 2D simulation of granular flow over irregular steep slopes using global and local coordinates. *J. Comput. Phys*. 255: 166–204.

Lacasta, A., Juez, C., Murillo, J. and García-Navarro, P. 2015. An efficient solution for hazardous geophysical flows simulation using GPUs. *Computers and Geosciences* 78: 63–72.

Martínez-Aranda, S., Murillo, J. and García-Navarro, P. 2022. A GPU-accelerated Efficient Simulation Tool (EST) for 2D variable-density mud/debris flows over non-uniform erodible beds. *Engineering Geology* 296: 106462.

McCoy, S.W., Kean, J.W., Coe, J.A., Tucker, G.E., Staley, D.M. and Wasklewicz, T.A. 2012. Sediment entrainment by debris flows: in situ measurements from the headwaters of a steep catchment. *J. Geophys. Res. Atmos.* 117: F03016.

Murillo, J., García-Navarro, P., 2012. Wave Riemann description of friction terms in unsteady shallow flows: application to water and mud/debris floods. *J. Comput. Phys* 231: 1963–2001.

Robertson, P.K., de Melo, L., Williams, D.J. and Wilson, G.W. 2019. *Report of the Expert Panel on the Technical Causes of the Failure of Feijão Dam I.*

Vergilio, C.d.S., Lacerda, D., Oliveira, B.C.V.d., Sartori, E., Campos, G.M., Pereira, A.L.d.S., Aguiar, D.B.d., Souza, T.d.S., Almeida, M.G.d., Thompson, F. and Rezende, C.E. d. 2020. *Metal concentrations and biological effects from one of the largest mining disasters in the world (Brumadinho, Minas Gerais, Brazil).* Sci. Rep. 10(1): 5936.

Wu, W. 2007. *Computational River Dynamics*. NetLibrary, Inc. CRC Press.

Dam Breach Analysis: A Methodology for Non-Newtonian Hazard Mapping and Fatality Rate Estimates

Mark Walden, NewFields Mining Design and Technical Services LLC, USA
Martin Rust, NewFields Mining Design and Technical Services LLC, USA
Nick Rocco, NewFields Mining Design and Technical Services LLC, USA
Sarah Melberg, NewFields Mining Design and Technical Services LLC, USA
Reinaldo Garcia, Hydronia LLC, USA

Abstract

One of the results of the tailings dam breach modeling process is the creation of a hazard map that classifies areas of the inundation into different hazard categories based on the depth and velocity of the flood. The hazard map is commonly used to estimate the Potential Loss of Life (PLL). Current industry practice is to employ hazard map categories and corresponding fatality rates developed based on water (Newtonian) flood properties. This paper presents a robust analytical framework for addressing the non-Newtonian characteristics of tailings floods, specifically focusing on its application in hazard mapping and fatality rate estimation. The case studies presented in this paper indicate that accounting for fluid density can significantly increase the estimated PLL; however, PLL is also dependent on the sediment concentration, location of the downstream residences, and depth and velocity of the flow. When the modeled flow is deep and fast, adjusting for density does not have a significant effect; however, where flows are wider, shallower, and/or slower, the differences can be substantial. The presented methodology offers a straightforward and practical tool for engineers and practitioners to estimate the true potential impacts of tailings dam breaches, leading to more informed decision-making and potentially saving lives.

Introduction

General

The non-Newtonian properties of tailings flows are typically considered during tailings dam breach modeling; however, current industry practice when estimating potential loss is to employ Newtonian methodologies and corresponding fatality rates that are available from the literature. Tailings flows typically have much higher sediment concentrations, densities, yield stress, and viscosity, than those associated with water floods. A higher-density fluid will result in a higher force exerted on objects in the flow path. In

general, a high density, yield stress, and viscosity flow causes more damage and is much harder for people caught within the flood to escape. This indicates that tailings flows should have higher associated fatality rates than those determined for water floods when all other variables are constant.

The United States Bureau of Reclamation (USBR, 2015) provides fatality rates that are based on case studies of water dam (Newtonian) failures that aggregate many factors. A similar case study for tailings dam failures that relates fatality rates to depth times velocity, warning time, and sediment concentration does not exist.

A sound mathematical approach to account for the non-Newtonian properties of tailings floods for hazard mapping and fatality rate estimates is summarized herein. This paper provides guidance on how the mathematical approach can be efficiently applied in practice and presents case studies supporting validation of the methodology and highlighting the potential severity of predicted impacts. The USBR fatality rate charts and other Newtonian-based analytical approaches to determining the impacts resulting from a hypothetical dam breach scenario can continue to be used, provided that the methodology described in this paper is followed and the depth times velocity values are adjusted to account for the fluid density of a specific tailings flow.

Derivation

The following methodology builds upon the concept discussed by Correa et al. (2021) and the previously developed procedure by Walden et al. (2022). The methodology utilizes the moment instability equation developed by Jonkman and Penning-Roswell (2008), as follows:

$$\boldsymbol{D \times V = \left(m \times \frac{2g \cdot cos(\alpha) \cdot L}{C_D \cdot B \cdot \rho} \right)^{0.5}} \quad (1)$$

Where, D × V is the critical depth times velocity of the flow, m is the mass of the person, B is the average body width exposed normal to the flow (m), L is the height of the person, C_D is the drag coefficient (unitless), g is the acceleration due to gravity (9.81 m/s^2), ρ is the density of the flowing fluid (kg/m^3), and α is the angle from the pivot point to the center of mass. A typical dam breach analysis assumes typical parameters for the theoretical population caught within the flood and m, B, L, g, α, and C_D can be combined into a single constant (K), and the resulting simplified equation is:

$$\boldsymbol{D \times V = \left(K \times \frac{1}{\rho} \right)^{0.5}} \quad (2)$$

Equation 2 clearly shows that the critical D × V is directly proportional to $\sqrt[2]{\boldsymbol{1/\rho}}$. The D × V of a non-Newtonian tailings (slurry) flood can be set equal to that of a clear water flood provided a conversion factor (X) is applied, as is depicted in Equations 3, 4, and 5.

$$\boldsymbol{D_{water} \times V_{water} = X \times D_{Slurry} \times V_{Slurry}} \quad (3)$$

(4) $$\left(K \times \frac{1}{\rho_{water}}\right)^{0.5} = X\left(K \times \frac{1}{\rho_{slurry}}\right)^{0.5}$$

(5) $$X = \left(\frac{\rho_{slurry}}{\rho_{water}}\right)^{0.5}$$

Where, X is the density ratio, V_{slurry} is the velocity of the non-Newtonian flood, V_{water} is the velocity of the Newtonian clear water flood, D_{slurry} is the depth of the non-Newtonian flood, D_{water} is the depth of the Newtonian clear water flood, ρ_{slurry}, is the density of the non-Newtonian flood, and ρ_{water} is the density of water.

The density ratio (X) can be applied to determine the equivalent clear water depth times velocity, which can be directly applied to hazard mapping as it is typically based on the depth times velocity values of the flood. The equivalent clear water depth times velocity equation (Equivalent Clear Water Hazard Map (ECWHM) equation) is as follows:

(6) $$ECWHM = D_{Slurry} \times V_{Slurry} \times X$$

Where the ECWHM equation can be applied to a dam breach model in order to convert a non-Newtonian hazard map into an equivalent Newtonian hazard map, as is described in the following section.

Application

The ECWHM equation can be applied through the use of a raster calculator once a tailings dam breach analysis model has been simulated. A raster is a matrix of cells (or pixels) where each cell contains a value representing information, such as the sediment concentration of the flood. Determining the slurry density raster is imperative for the accurate computation of the ECWHM, as defined by Equation 6. Conventional outputs from prevalent 2D dam breach modeling software, such as Riverflow2D, Flow2D, and HEC-RAS, do not include density rasters. Instead, these software packages typically produce a raster representing sediment concentration (C_v), and a conversion is necessary to transform the C_v raster into a density raster. This conversion is achieved through the application of the subsequent formula, which utilizes the specific gravity of solids (G_s):

(7) $$\rho_{slurry} = C_V \times (G_s \times \rho_{water}) + (1 - C_V) \times \rho_{water}$$

Case study

Background

The Brumadinho (Córrego do Feijão- Dam 1) tailings dam failure was selected for a case study to validate the previously presented ECWHM approach to fatality rate estimates. The Brumadinho failure released approximately 10 million (M) cubic meters (m^3) of mining waste and flowed at depths greater than 10 meters. The dam collapsed quickly and the peak flow (90,000 m^3/s) at the breach opening was estimated to

occur 5 seconds after the initiation of the failure. Images of Córrego do Feijão- Dam 1 pre- and during failure are presented on Figure 1. Loss of life resulting from the dam collapse has been estimated to be between 270 and 320 people (Lumbroso, 2021).

Results from previous dam breach modeling of the failure indicated that the computed results align with the observed data (Martinez-Aranda et al., 2022). The maximum depth times velocity raster from the previous study was used as a basis to validate the ECWHM methodology.



Figure 1: Córrego do Feijão Dam 1 pre-failure (left) and during failure (right)

Identification of structures and populations

The exact number of people residing within each inundated structure at the time of the failure are either not well documented or are not publicly available at this time. Therefore, inhabitable structures were identified using satellite imagery from the area prior to the failure. To estimate the number of persons within each flood hazard zone, it was assumed that three people resided within each structure, per the recommendations of the Department of Homeland Security (DHS, 2011). An estimated 200 individuals were present in the canteen immediately downstream of the facility (Lumbroso et al., 2021) at the time of the breach and were also accounted for in this study.

Methodology for estimating fatality rates

The generalized Reclamation Consequence Estimating Methodology (RCEM) approach (USBR, 2015) was utilized to estimate the fatality rate at each inundated location. The RCEM approach primarily considers flood severity (DxV) and warning time as the driving factors for determining the fatality rate associated with populations within the inundation area of a Newtonian flood. Although practitioners frequently apply the RCEM approach to individual structures, its primary design characterizes regional population fatality rates, offering a broad-scale assessment rather than structure-specific risks (Feinberg et al., 2016). Consequently, when using RCEM for individual structures, it is essential to adopt a conservative fatality rate limit from the relevant RCEM chart to avoid potential underestimation of fatality risks. The RCEM

methodology provides two charts that were developed for selecting fatality rates. One chart corresponds to failures that have little to no warning and the other corresponds to failures with adequate warning. The chart corresponding to little to no warning time was selected for use in this study as it best represents the actual event. The chart, presented on Figure 2, provides a suggested limit for estimating fatality rates corresponding to specific DxV values.

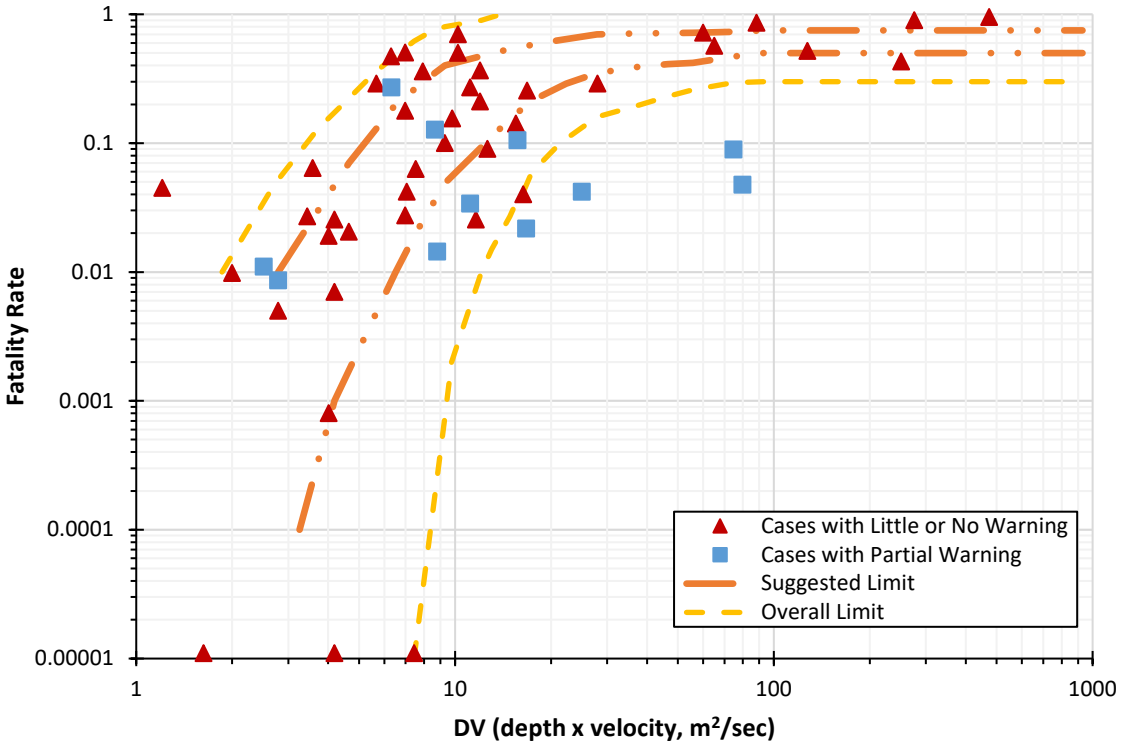


Figure 2: RCEM depth times velocity chart (adapted from USBR, 2015)

The suggested upper limit was used as a basis for estimating the fatality rates associated with the failure. For simplicity, ease of use, and efficiency, the DxV values were binned according to the flood hazard categories from Federal Emergency Management Agency (FEMA) Guidance for Flood Risk Analysis and Mapping (FEMA, 2020), which categorizes the DxV values based on flood severity. The categories are based on studies in Australia (Hawkesbury-Nepean Floodplain Management Steering Committee, 2006).

The bin listed by FEMA for extreme was considered to provide too large of a range in fatality rates and was further subdivided into four additional sub-categories. The categories and their corresponding DxV and fatality rates are presented in Figure 3 and are tabulated in Table 1. Although the fatality rates in Table 1 corresponding to the low and medium categories are listed as 0 because the associated fatality rates are so low (~0.00005) that they are unlikely to affect Potential Loss of Life (PLL) estimates.

Table 1: Depth times velocity zones and corresponding fatality rates

Category	Depth Times Velocity Range (m^2/s)	Fatality Rate
Low	<0.2	0
Medium	0.2-0.5	0
High	0.5-1.5	0.0001
Very High	1.5-2.5	0.005
Extreme I	2.5-5.2	0.05
Extreme II	5.2-9.3	0.25
Extreme III	9.3-27.9	0.55
Extreme IV	>27.9	0.75

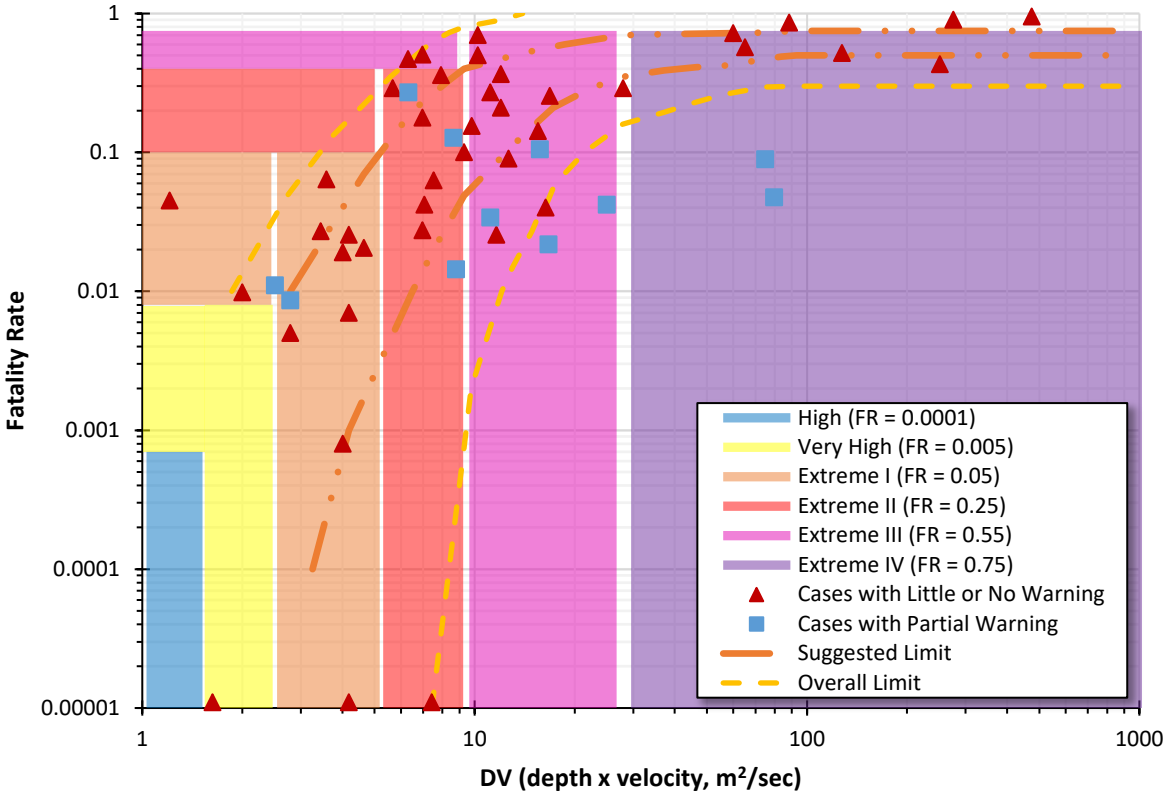


Figure 3: Zoned depth times velocity chart

Determining the tailings flood density

A raster of the maximum flood density during the breach was produced using Equation 7. The density raster for the tailings flow is presented in Figure 4. The densities of the tailings flood were found to range from

as high as 2,248 kg/m^3, representative of a thick mudflow, to as low as 1,001 kg/m^3, representative of clear water flow. The average density was 2,157 kg/m^3. Most areas impacted by the flood experienced flow densities between 2,100 kg/m^3 and 2,250 kg/m^3.

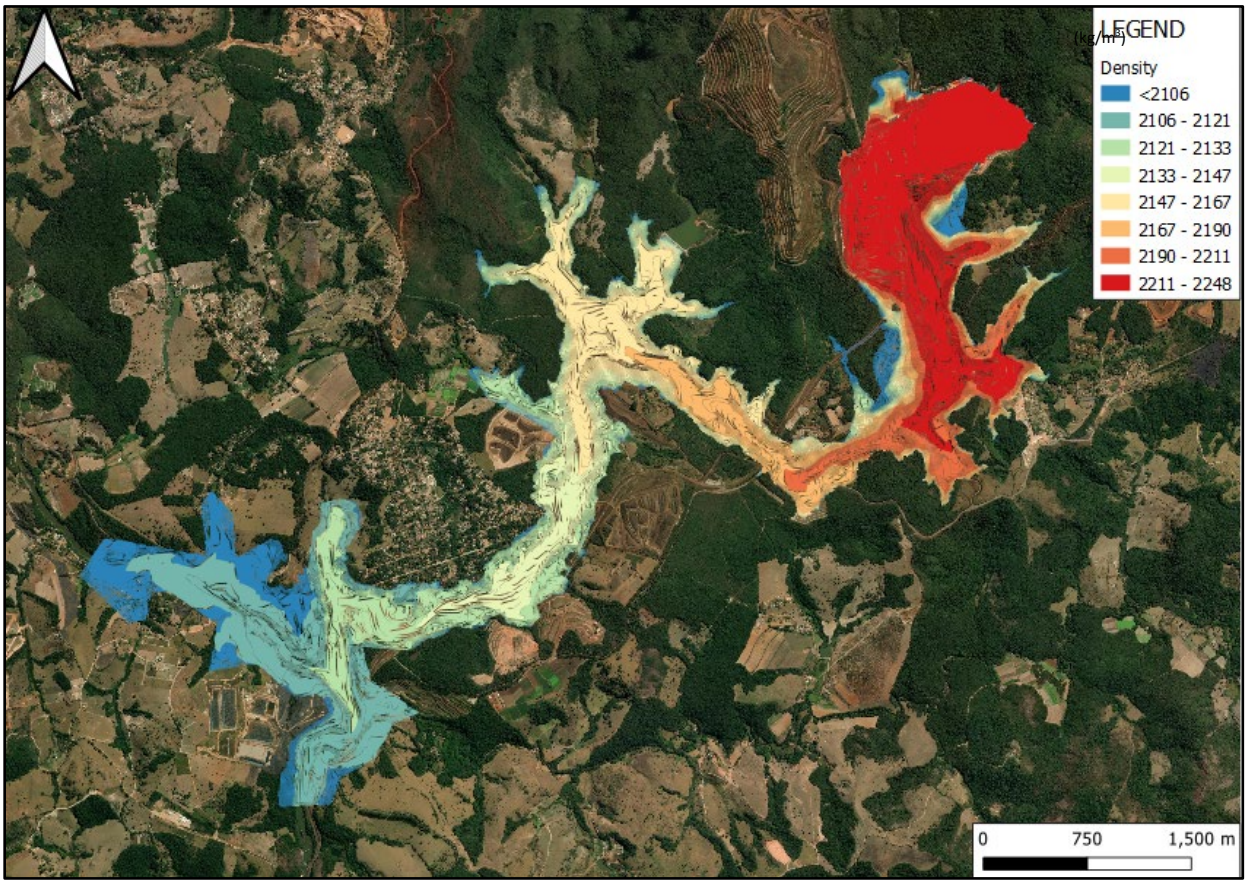


Figure 4: Brumadinho failure fluid density

Generating the equivalent clear water hazard map

The ECWHM was generated using the simplified approach previously described. In general, a raster calculator was used to produce the ECWHM using a raster of the density ratio and the original hazard map (depth times velocity raster) generated by the breach flow model. The density ratio, employed for the conversion of the original hazard map raster into an ECWHM, was determined utilizing Equation 5.

The density ratio values ranged from ~1.0 (indicating no change from the original raster) to as high as 1.5 (indicating a 1.5 times increase in the ECWHM depth times velocity value). The average value was 1.47, and approximately 99 percent of the values were above 1.40. In general, the density ratio indicates that the depth times velocity values in the original hazard map should be approximately 1.5 times greater to produce an equivalent clear water hazard map.

Results

Densities

The results indicate that Brumadinho tailings dam failure produced very high-density flows, generating instability at lower depths and velocities than equivalent Newtonian flows.

In the case of the Brumadinho tailings dam failure, the fluid densities were typically between 2,100 kg/m^3 and 2,250 kg/m^3 due to the large release of solid mine waste from the facility, lack of a significant supernatant pond, and lack of substantial dilution as the flood transitioned downstream.

Hazard mapping

The original hazard map is presented in Figure 5 and the ECWHM is presented on Figure 6. Each hazard map presents the breach location, hazard map, and location of inundated structures (presented as circles that are color-coordinated with their hazard rating). A high-level overview indicates that there is little difference between the two hazard maps, which is due to the very high flood depths and velocities associated with the failure. However, closer review indicates that notable differences are apparent on the fringes (outer 100 to 300 meters) of the floodplain, as presented in Figure 7.

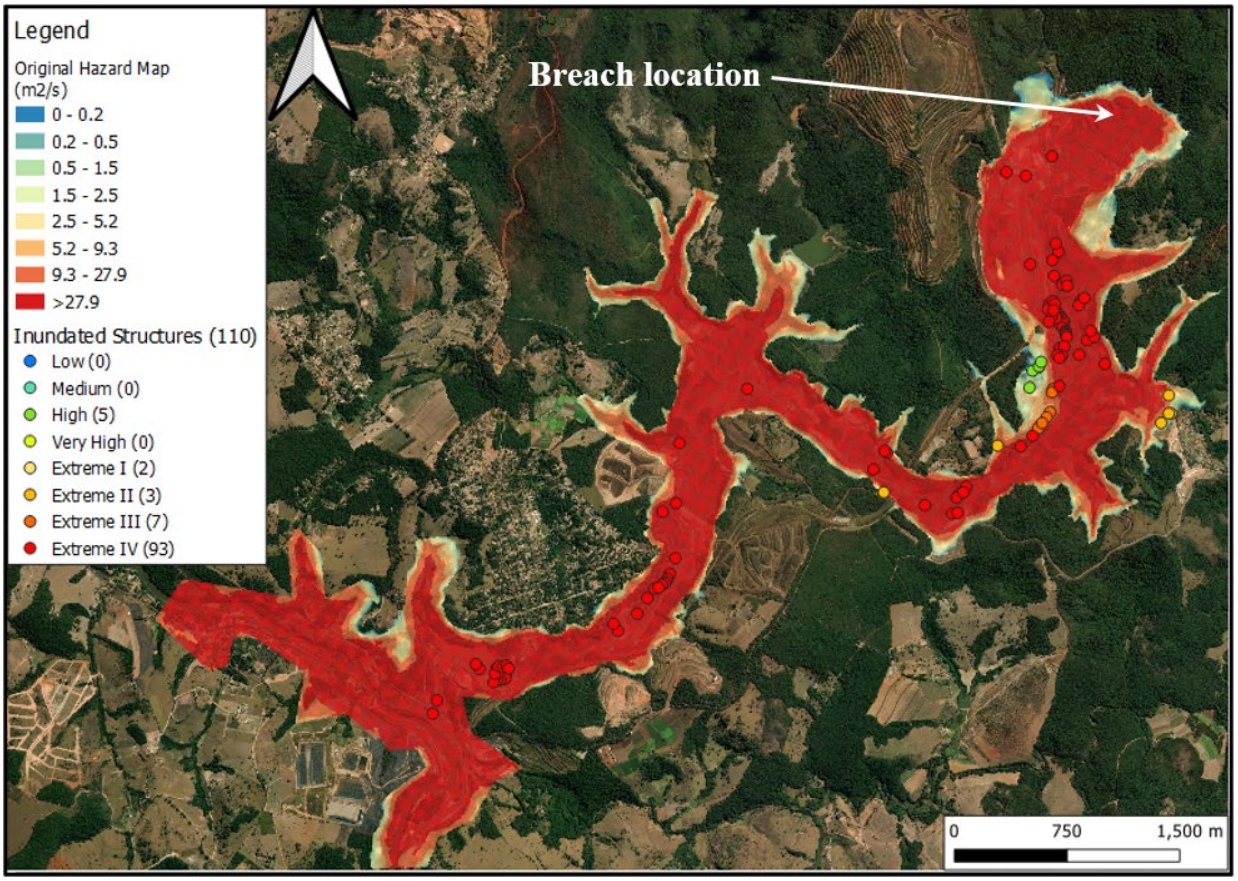


Figure 5: Original hazard map

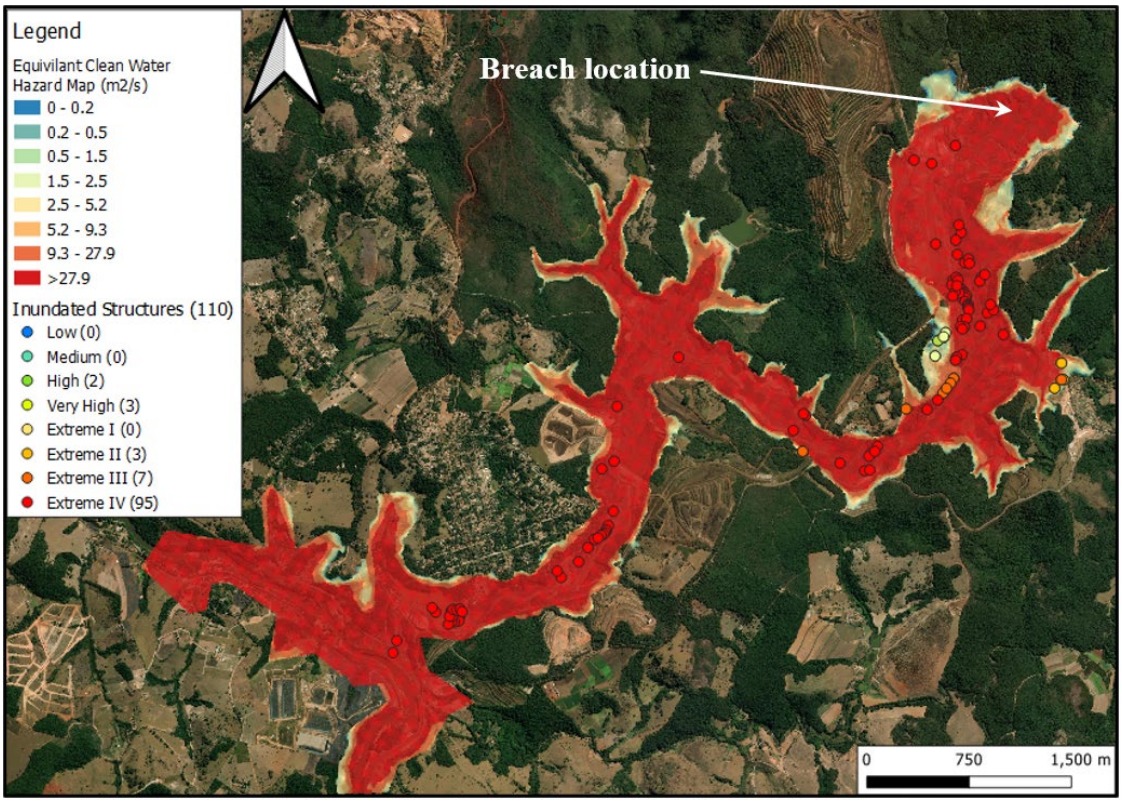


Figure 6: ECWHM hazard map

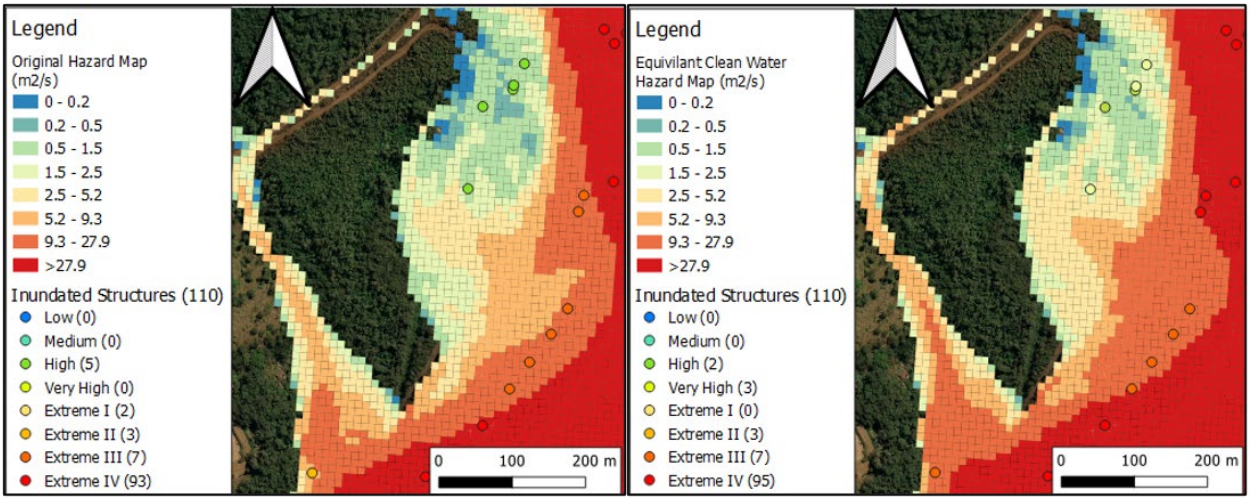


Figure 7: Original hazard map (left) vs. ECWHM hazard map (right)

The data from each hazard map was evaluated statistically to further investigate the differences between the results. Table 2 presents the average, maximum, minimum, and standard deviation depth times velocity values for each hazard map, along with the percent of raster values within each hazard class. As expected, the ECWHM has higher depth times velocity values, which represents higher associated hazard levels.

Table 2: Depth times velocity zones and corresponding fatality rates for the Brumadinho failure

Category	Newtonian	ECWHM
Average (m^2/s)	117	173
Minimum (m^2/s)	<0.01	<0.01
Maximum (m^2/s)	693	1,039
Standard Deviation (m^2/s)	123	182
Low Hazard (% of raster values)	<1%	<1%
Medium Hazard (% of raster values)	<1%	<1%
High Hazard (% of raster values)	3%	2%
Very High Hazard (% of raster values)	2%	2%
Extreme I Hazard (% of raster values)	5%	4%
Extreme II Hazard (% of raster values)	5%	4%
Extreme III Hazard (% of raster values)	14%	12%
Extreme IV Hazard (% of raster values)	70%	75%

Loss of life

The procedure for estimating the population at risk (PAR) and assigning fatality rates was previously discussed. Lumbroso et al. (2021) states that the total number of deaths from the dam failure ranged between 270 and 320 people. A comparison of the resulting difference in number of inundated structures, PAR, and PLL between the original hazard map and the ECWHM is presented in Table 3. The resulting hazard maps were previously presented in Figure 5 and Figure 6.

Table 3: Inundated structures, PAR, and PLL for non-Newtonian flood for the Brumadinho failure

Hazard	Structures		PAR		PLL	
	Original	ECWHM	Original	ECWHM	Original	ECWHM
Low	0	0	0	0	0.0	0.0
Medium	0	0	0	0	0.0	0.0
High	5	2	15	6	0.0	0.0
Very High	0	3	0	9	0.0	0.0
Extreme I	2	0	6	0	0.3	0.0
Extreme II	3	3	9	9	2.3	2.3
Extreme III	7	7	21	21	11.6	11.6
Extreme IV	93	95	476	482	357.0	361.5
TOTAL	**110**	**110**	**527**	**527**	**371.1**	**375.3**

Discussion

Case study summary

The case study resulted in an overall increase in PLL of approximately 4.2 people when the ECWHM methodology is compared to the standard Newtonian methodology. The total PLL for the ECWHM was 375.3, which is close to the high end of the range of estimated fatalities (270-320) and in general, indicates that the methodology used provides a reasonable and conservative approximation. The minor difference in PLL (~4.5 people) between the Newtonian and ECWHM methodologies indicates that, in the case of the Brumadinho failure, application of the ECWHM method does not have a significant impact on the resulting PLL. However, it should be noted that the minor difference in PLL can be attributed to the following:

1. **The unique and violent release of tailings during the dam failure.** The dam collapsed quickly and the peak flow of mine waste (estimated to be 90,000 m^3/s) from the breach opening was estimated to occur 5 seconds after the initiation of the failure (Lumbroso et al., 2021). The extremely high depth and velocity flood wave caused the majority of the depth times velocity values to be above 27.9 (the highest risk category (Extreme IV) associated with a 75% fatality rate) prior to adjustment with the ECWHM methodology. Therefore, although the ECWHM methodology increased the depth times velocity values, most remained in the Extreme IV hazard category.
2. **The location of the inundated structures**. The majority of the structures were located in the center of the flood path which falls in the Extreme IV risk category regardless of whether slurry density is taken into account or not. In countries with more stringent regulations for land development near rivers and floodplains the structures are more likely to be located on the fringes of the inundation due to regulatory requirements.

In scenarios beyond the scope of the present case study, the utilization of ECWHM may yield substantial differences compared to predictions derived from Newtonian methodologies, as is discussed in in the following section.

Impact of Implementation in other cases

The impact of applying the ECWHM methodology was evaluated for four hypothetical dam breach scenarios. These hypothetical Dam Breach Analyses were completed for mine sites at various locations around the world using appropriate standards, as described by the Canadian Dam Association (2021). The ECWHM methodology was not originally applied but was implemented to compare the original results to the ECWHM methodology. The results are presented in Table 4.

Table 4: ECWHM impacts on other tailings dam breaches

Case	Methodology	Average Slurry Density (kg/m³)	Structures	PAR	PLL	ECWHM Increase in PLL (%)
Case 1	Original	1,883	139	417	77.6	41
	ECWHM				109.6	
Case 2	Original	1,843	54	162	10.9	59
	ECWHM				17.3	
Case 3	Original	1,765	270	810	19.1	83
	ECWHM				35.0	
Case 4	Original	1,881	37	111	9.5	26
	ECWHM				12.0	
Brumadinho Case Study	Original	2,157	66	198	133.1	3
	ECWHM				137.6	

Note: All cases consider fair weather (sunny day) failure modes.

The impacts (regarding PLL) of applying the ECWHM to each of these cases are significantly larger than those established from the Brumadinho case study.

It should also be noted that use of the ECWHM method results in an increase in the PLL consequence classification (in terms of the Global Industry Standard for Tailings Management guidelines [Global Tailings Review, 2020]) for both Case 1 and Case 4. The PLL consequence classification for Case 1 would increase from Very High (10-100 PLL) to Extreme (>100 PLL), and the PLL consequence classification for Case 4 would increase from High (1-10 PLL) to Very High. Cases 2 and 3 had higher percent increases than Cases 1 and 4; however, the PLL consequence classification does not increase as the original PLL values were on the low end of the Very High consequence classification category and both scenarios require increases greater than 500% to transition to the Extreme hazard category.

The large difference in the PLL increase between the hypothetical cases and the Brumadinho case study can be best explained by the variance in the distribution of structures within each hazard zone. As indicated in Table 3, approximately 85% of the inundated structures were within the Extreme IV hazard zone without application of the ECWHM and have already been assigned the maximum fatality rate. In comparison, Table 5 presents the resulting difference in number of inundated structures, PAR, and PLL between the original hazard map and the ECWHM for Case 1. As indicated in Table 5, none of the inundated structures were within the Extreme IV hazard zone. This implies that the larger impact to PLL realized when the ECWHM is applied is due to either the populations being located further from the area of maximum depth and velocity (safer locations) and/or the flood generated from the DBA was of lower depth

and velocity than the Brumadinho failure. This result aligns with the fact that the violent Brumadinho failure was somewhat unique and the indication that many of the dwellings were constructed without much consideration for potential flood hazards, meaning that they were closer to the area of maximum depth and velocity. The results indicate that when the modeled flow is deep and fast, adjusting for density does not have a significant effect; however, where flows are wider, shallower, and/or slower, the differences can be substantial.

Table 5: Inundated structures, PAR, and PLL for non-Newtonian flood for Case 1

Hazard	Structures		PAR		PLL	
	Original	ECWHM	Original	ECWHM	Original	ECWHM
Low	14	12	42	36	0	0
Medium	8	6	24	18	0	0
High	20	14	60	42	0.1	0
Very High	14	16	42	48	0.4	0.5
Extreme I	33	27	99	81	5	4.1
Extreme II	27	26	81	78	20.3	19.5
Extreme III	23	38	69	114	51.8	85.5
Extreme IV	0	0	0	0	0	0
Total	**139**	**139**	**417**	**417**	**77.6**	**109.6**

Other methods of application

The ECWHM methodology can be applied to the USBR RCEM guidance as outlined in this paper, or any variation thereof. It should also be noted that the methodology could also be applied to LifeSim (2021) models, which utilizes depth and velocity measurements to evaluate flood impacts. Specifically, the ECWHM methodology can be used to understand the economic impacts of the inundation and evaluate the potential damage to inundation structures.

Engineering judgement

The methodology outlined in this paper is intended to be a tool to help account for the impacts caused by high-density non-Newtonian flows and should not be utilized without the application of sound engineering judgment. There are many ways that the assumptions utilized in the methodology can be adjusted for specific cases. For example, the case study presented here-in estimated that three people resided within each of the inundated structures. However, there may be some cases where it is appropriate to assume more, or less, than three people reside within each structure. Accurate structure type classification is also a crucial

consideration, as engineered structures are generally more resilient to collapse. Transient populations can be another area of uncertainty, requiring additional consideration.

Consideration of the time step that the maximum depth, velocity, and sediment concentration (density) occur is also important. The flow model results provide the spatial variability of each of these metrics over the entire simulation, and maximum values inherently occur at different times of the simulation. Using the maximum of all three variables would produce conservative results; however, it would be more accurate to use the depth, velocity, and sediment concentration values from the timestep that produces the most critical results.

Conclusion

Non-Newtonian tailings properties are typically considered during tailings dam breach modeling, but are not commonly accounted for when estimating PLL since there is limited guidance on how these properties influence fatality rates. When determining the consequences of the impacts of a tailings dam breach the current standard of practice is to employ Newtonian-based methodologies, which can lead to underestimating the true potential impacts of the breach. Tailings flows typically have much higher sediment concentrations and fluid densities than those associated with water floods, which in turn leads to greater impacts at equivalent Newtonian depths and velocities.

This presented procedure provides a reasonably simple methodology for adjusting the depth times velocity values such that the existing Newtonian methods for estimating PLL can be utilized.

It should be noted that, although the approach outlined in this document is technically feasible, it has only been validated based on a single real-world case study. Further work should be completed in this area to further refine and build upon the methodologies outlined in this paper. The authors recommend completion of the following to support further development and refinement:

1. Additional back-analysis case studies should be completed to further validate the work and assumptions outlined in this paper.
2. Additional studies should be completed to assess the impacts of using this methodology in consequence-estimating software such as LifeSim.
3. Additional studies should be completed to further validate this methodology in terms of application to damage to structures and economic impact.

In general, more tools directly related to non-Newtonian tailings floods, rather than Newtonian water floods, are essential for continual development and improvement in predictive dam breach modeling. The procedure presented herein is a positive step in that direction.

References

Canadian Dam Association. 2021. Technical Bulletin: Tailings Dam Breach Analysis.

Correa, G., de Paula, G.L., Nascimento, M., Brandao, M. and Sa, J. 2021. Flood hazard classification for a hyperconcentrated flow. *Proceedings of the Tailings and Mine Waste Conference, 2021*. Banff, Canada.

Federal Emergency Management Agency. 2020. Guidance for Flood Risk Analysis and Mapping. Guidance Document 14. December.

Feinberg, B., Engemmoen, W., Fiedler, W. and Osmun, D. 2016. Reclamation's empirical method for estimating life loss due to dam failure. *Proceedings of FLOODrisk 2016 – 3rd European Conference on Flood Risk Management.* DOI:10.1051/e3sconf/20160706002.

Global Tailings Review. 2020. Global Industry Standard on Tailings Management.

Hawkesbury-Nepean Floodplain Management Steering Committee. 2006. Designing Safer Subdivisions. Guidance on Subdivision Design in Flood Prone Areas.

Jonkman, S.N. and Penning-Rowsell, E. 2008. Human instability in flood flows. *Journal of the American Water Resources Association*. August.

Lumbroso, D., Davison, M., Boyd, R. and Petkovsek, G. 2021. Modelling the Brumadinho tailings dam failure, the subsequent loss of life and how it could have been reduced. *Nat. Hazards Earth Syst. Sci*. 21: 21–37.

Martinez-Aranda, S., Murillo, J. and Garcia-Navarro, P. 2022. A GPU-accelerated Efficient Simulation Tool (EST) for 2D variable-density mud/debris flows over non-uniform erodible beds. *Fluid Dynamic Technologies-I3A,* University of Zaragoza, Spain.

United States Department of Homeland Security. 2011. Dams Sectors – Estimating Loss of Life for Dam Failure Scenarios.

United States Department of the Interior Bureau of Reclamation (USBR). 2015. RCEM – Reclamation Consequence Estimating Methodology – Interim Guidelines for Estimating Life Loss for Dam Safety Risk Analysis.

US Army Corps of Engineers Risk Management Center. 2021. LifeSim 2.0. Retrieved from US Army Corps of Engineers Risk Management Center's LifeSim page.

Walden, M., Rust, M. and Rocco, N. 2022. Considerations for defining fatality rates associated with non-Newtonian flows from tailings dam failures. *Proceedings of the Tailings and Mine Waste Conference, 2022*. Denver, Colorado.

Multi-model Analyses of Tailings Impoundment Failure and Runout: Part III

Armin Saeedi, Carleton University, Canada
Mario Martinelli, Carleton University/Deltares, Canada/Netherlands
Paul Simms, Carleton University, Canada

Abstract

Continuing the line of research presented previously at Tailings and Mine Waste 2022 and 2023, in order to better understand and eliminate uncertainties associated with tailings impoundment failures and the prediction of subsequent runout characteristics, the Merriespruit case study is re-analyzed using a geomechanics-based MPM software employing Norsand in undrained conditions. Work reported in the earlier papers did not employ Norsand in MPM, nor did it consider pore-water pressure. Parameters were constrained by element test data. The MPM model employing Norsand is able to accurately describe the progressive nature of the failure, and is also able to capture other features, for example the shallower failure zone upstream of the main failure. The state parameter that best matched the retrogression pattern produced a runout considerably shorter than reported (500 m compared to > 1.2 km). It is argued that this is at least partially an artefact of 2D conditions, hypothesized for two reasons i) the less sheared tailings trap a substantial amount of mobilized tailings, which would not necessarily occur in 3D, ii) the shallow part of the failure extends much wider than the breach in reality; therefore, there is a lower volume of low strength tailings available to flow in the 2D simulation compared to the real 3D case. It is also clear that the shape of the CSL at low stresses will have a strong influence on the volume of flowable tailings, whereas the CSL is usually defined using laboratory and/or field data obtained at much higher stress than runout conditions.

Introduction

Approaches to numerical modeling of both the initial failure of a tailings impoundment and the subsequent runout are being developed by many researchers. The initial failure is often simulated using geomechanics-based software, taking into account complex constitutive behavior, pore-water pressure coupling, 3D geometry and appropriate mechanical and hydraulic boundary conditions (e.g. Zabolotnii et al., 2022), whereas runout is simulated in practice using flow models with various rheological constitutive models, most of which use a depth-average solution of the momentum equation (as summarized by Rana et al.,

2021). This simplification allows for inundation mapping over a real topography. These two types of models probably define the ends of the spectrum of available tools, whereas a number of other models try to consider both rheology and geomechanics, usually providing additional complexity at the cost of increased computer resources, or simulating only 2D profiles of the runout.

This paper is the continuation of research presented at the Tailings and Mine Waste 2022 and 2023 conferences (Saeedi et al., 2022, 2023), where three different models (FLAC3D, Anura 3D, and UINTAH-VBR) were applied to analyze the failure and the subsequent tailings runout i) at the Merriespruit mine, as well as ii) in centrifuge and small flume experiments for clayey tailings. The models were a 3D geomechanics model (FLAC3D) using the Norsand constitutive model and considering 3D geometry; a 2D geomechanics model (Anura 3D), using the material point method numerical approach (MPM), and simulating the tailings failure using a Mohr-Coulomb constitutive model but ignoring pore-water pressure; whereas the third was a 3D viscosity bifurcation rheology model (also implemented in a MPM framework. The finding of the first paper (Saeedi et al., 2022) was that the more geomechanics-based models could apparently reproduce the failure surface and mobilized volume for a reasonable set of parameters, but substantially underpredicted both the runout distance and overpredicted the speed of the runout. By contrast, for a reasonable set of parameters, the rheology model could give a good approximation of the observed runout speed and extent, but overpredicted the volume of tailings mobilized during the failure and could not correctly simulate failure initiation, and would therefore require an independent estimate of the "hydrograph" of mobilized tailings.

The second paper in the series (Saeedi et al., 2023) focused on analyzing a centrifuge test on a 3 m tall clayey tailings embankment using a rheology and a geomechanics-based constitutive models: both constitutive models simulated degradation of strength from a peak to a residual value. In the rheological model this occurred as a function of strain rate; in the geomechanics model strength decreased through accumulated plastic strain. Both constitutive models, calibrated to the same laboratory data, gave very similar predictions of runout. It was concluded from the relatively small height (3 m) that momentum of the mobilized tailings was dissipated in each model by the de-structuration process; and that the flow during the runout phase was slow enough that either method could reasonably describe the deceleration of the flow.

The present paper returns to the analysis of Merriespruit, but now employs a more sophisticated constitutive model in the MPM software, namely the Norsand constitutive model implemented to allow undrained simulations that consider existing pore-water pressure. Some effort is made to explain what the Norsand model actually does, from a practical perspective.

Numerical formulation and constitutive model (Norsand)

MPM formulation

In the current study, the Anura-Deltares MPM software is employed. The MPM implementation is described by Martinelli and Galavi (2022) and verified for several constitutive models. It uses an explicit dynamic formulation, and an automatic adaptation of time step size based on the Courant–Friedrichs–Lewy (CFL) criterion, to promote computational stability and numerical efficiency. The CFL criterion is very common and was originally used in computational fluid dynamics to maintain numerical stability. This and other features that promote numerical stability allow for the efficient use of more complex constitutive models, such as Norsand. While 3D simulations are possible, at present they take considerable time and are less stable. This paper only reports 2D analyses.

Norsand implementation

Here we include a brief qualitative description of Norsand, in an attempt to convey some understanding of how it actually works. The Norsand model is based on critical strength concepts, where during undrained shear the geomaterial will approach an ultimate shear stress that is a function of the friction angle and the critical state line in void ratio (e) and mean effective stress (p') space. Conventionally, where the critical state line is expressed in a semi-logarithmic relationship, $e_c = \Gamma - \lambda \ln(p')$, e_c being a void ratio on the CSL, the ultimate undrained strength will then be $M/2 \exp((\Gamma - e_c)/\lambda)$, M being the slope of the critical state line in q (deviatoric stress) – p' space. This ultimate strength therefore depends on the friction angle and the slope of the CSL, increasing with density; and importantly, is therefore independent of stress path. But more important is the initial state of the soil before undrained loading. If the soil, at a given e, is at a higher mean effective stress than the CSL, the peak strength will be higher than the residual, leading to the possibility that a particular tailings impoundment is susceptible to brittle failure, which may contribute to substantial acceleration of the tailings as the resisting forces decrease during failure.

Figure 1 gives an idea of how the model functions. This group of figures shows the stress path under undrained loading for three samples, one starting on the CSL, and two others starting at void ratios above and below the CSL, but starting at the same mean effective stress. If we consider the points on the right as three initial possible states in a tailings impoundment – each has been arrived at by presumably some combination of depositional stress history, including consolidation, potentially desiccation, or perhaps some alteration due to compaction; all three have the same identical initial condition in terms of stress. For undrained loading, the loading path is horizontal in e -p' space (no volume change), and the final shear strength depends only on the initial value of e. But how the stress the path progresses in terms of shear depends strongly on the initial state, and to a lesser degree on the elastic and plastic parameters of Norsand.

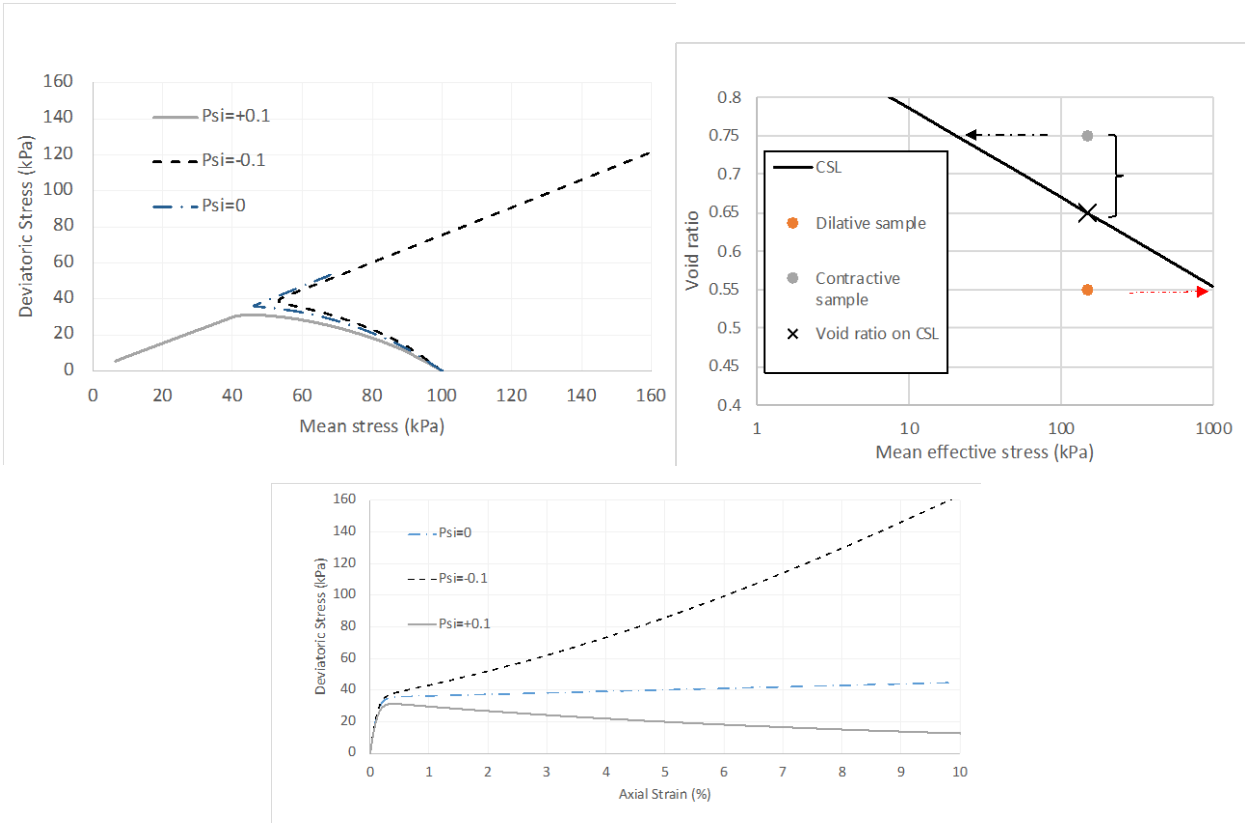


Figure 1: Basic function of Norsand model

The initial state of the geomaterial is described by the state parameter (ψ), which is the vertical change of void ratio between its initial value, and the void ratio on the CSL at the same mean effective stress, as shown in Figure 1. For example, consider the stress path of the sample with ψ = 0.1. This contractive sample moves towards the CSL to the left in e-p' space, arriving at its unique (and low value of) p'. This is reflected in Figure 1 b, where the critical state is reached at a value of q = M p'. The peak strength is also the lowest among these example samples, though the variance between peak strengths is much smaller than the variance in the critical state strengths. Thus, Norsand and similar models transit the geomaterial between a peak strength largely dependent on the initial stress state; to the critical state, largely dependent on void ratio.

The field case

The Merriespruit dam failure is a relatively well documented case (Fourie et al., 2001; Fourie and Papageorgiou, 2001; Wagener, 1997). The failure is generally attributed to an overtopping trigger, while the length of the runout is thought to be due to static liquefaction as the failure progressed, possibly exacerbated by the presence of a significant pond of water that accumulated near the dam, co-incident with the

overtopping event. The height of the tailings near the breach was 30 m, and the width of the breach was approximately 150 m. Cross-sections of the impoundment geometry before and after the breach are shown in Figure 2.

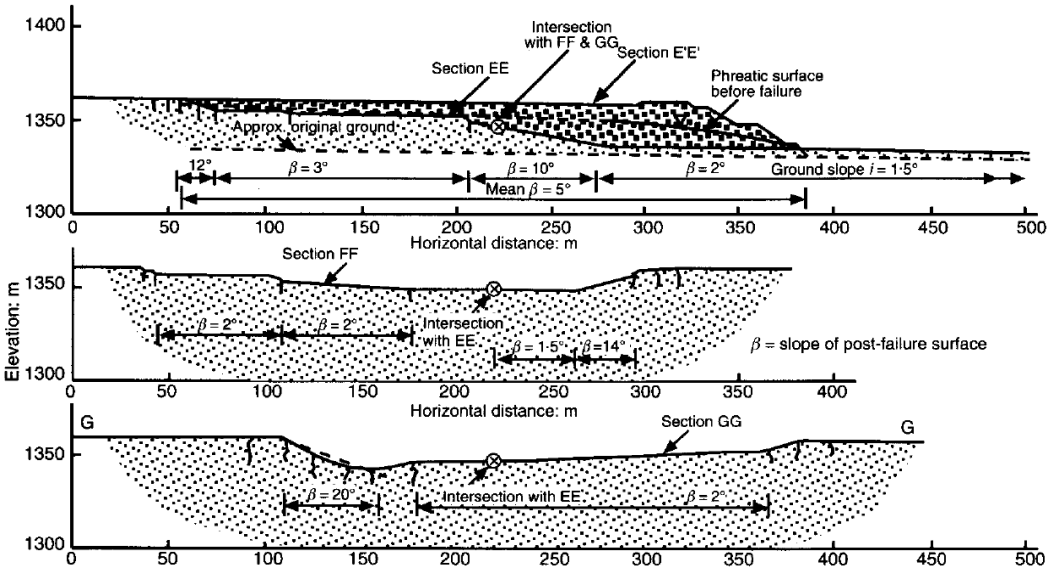


Figure 2: Failure surface, redrawn from Fourie et al. (2001)

The runout of the tailings is variously reported as between 1.2 km, 1.96 km, 2 km in 5 minutes, and 3 km (Wagener, 1997; Niekerk and Viljoen, 2005; Rana et al., 2021; Fourie et al., 2001). Some spreading parallel to the dam is evidenced in several pictures after the failure, appearing to be no more than twice the breach width. Evidence from damaged buildings points to a maximum thickness of the flow of 2.5 m at 300 m from the breach. Eyewitness accounts suggest the travel time to reach the maximum distance was approximately five minutes (Fourie et al., 2001).

From in-situ measurements (such as reported in Strydom and Williams, 1999), an in-situ void ratio of 0.8 appears to be representative of about the bottom two-thirds of the tailings. The critical state line and critical state friction angles are obtained taken from the triaxial tests conducted by Fourie and Papageorgiou (2001) on reconstituted samples from their M4 samples. The CSL fit is shown in Figure 4 (from Fourie and Papageorgiou, 2001). Comparing with the in-situ measurement of void ratio of 0.8, we can show the implied distribution of void ratio with mean effective stress by the choice of state parameter. The chosen state parameter values of 0.035 and 0.1 seem to bracket the reported void ratio of 0.8 for the range of effective stresses likely for the bottom 20 m of the impoundment. The remainder of the Norsand parameters are obtained by calibrating to the M4 triaxial experiments, using average values reported by Been and Jeffries (2015) as the initial parameter set. We find a good fit to these triaxial tests by only varying the H parameter, with all others kept at their initially assumed mid-range value.

Table 1: Calibrated and typical Norsand parameters

Parameters	Description	Calibrated Merriespruit	Typical range for sands/tailings
G_{ref}	Shear modulus factor	200	100-500
ν	Poisson's ratio	0.2	0.1-0.3
A	Exponent of the stiffness relation	0.5	Fixed
e_{cs0}	Critical state void ratio at p=0	0.8	Measured independently
λ	Slope of the critical state line	0.05	As above
M	Exponent of the critical state line	0.6	As above
M_{tc}	Critical state q/p' line at failure	1.58	As above
N	Dilatancy parameter	0.3	0.2–0.5
H	Hardening modulus	75	25-500; Estimated by 103-9810 ψ_0
X_{tc}	Hardening/softening coefficient	3	2-5

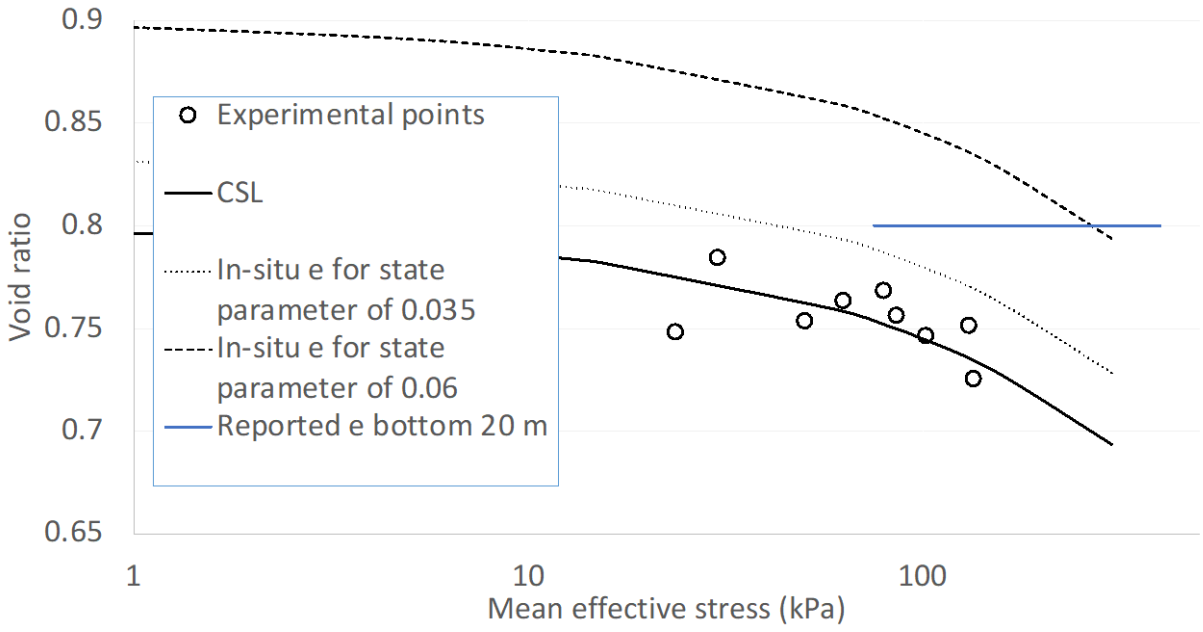


Figure 3: The CSL in e-p' space, the distribution of void ratio with effective stress implied by two different state parameters, and estimated void ratio in bottom 2/3 ratio of the impoundment

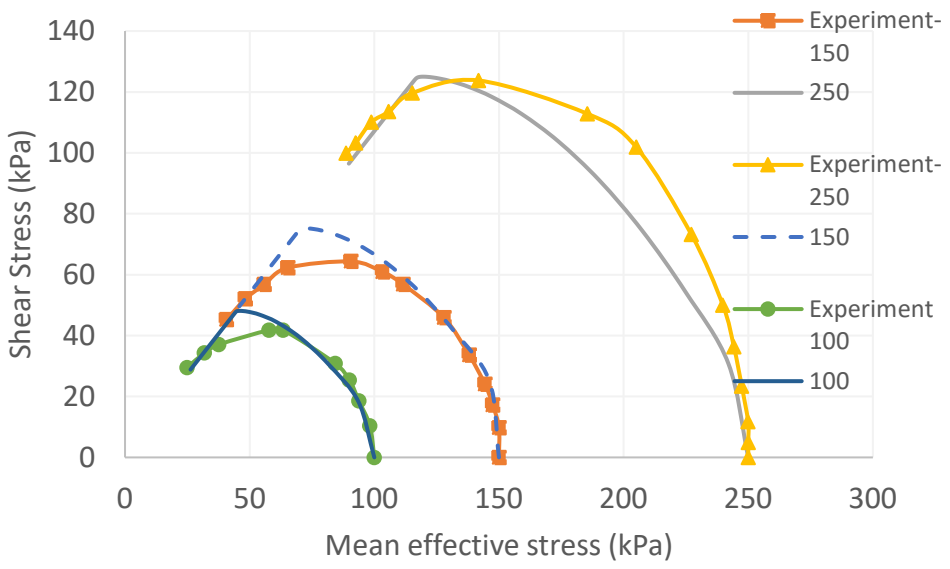


Figure 4: Calibration of Norsand using triaxial data on M4 samples from Fourie and Papageorgiou (2001)

Model geometry and boundary conditions

The model uses a simplified version of the geometry. Except for the starter dyke, the whole of the section is modeled as the tailings, using the Norsand parameters. The starter dyke is modeled as a Mohr-Coulomb material with an initial friction angle of 30°. This is progressively reduced to initiate the failure, to simulate the erosion of the front dyke due the supposed overtopping trigger. The phreatic surface is a simplified version of initial surfaces estimated in other studies (e.g., Figure 2). The bottom boundary condition is fixed. The mesh size is in the order of 1 m, and it was not possible to substantially reduce the mesh size while keeping a stable model. The back boundary is fixed. The assumed geometry downslope from the toe is a plane that dips downwards at 1.5 °, for the whole distance of the flow. The presence of buildings or any other geometric features are ignored.

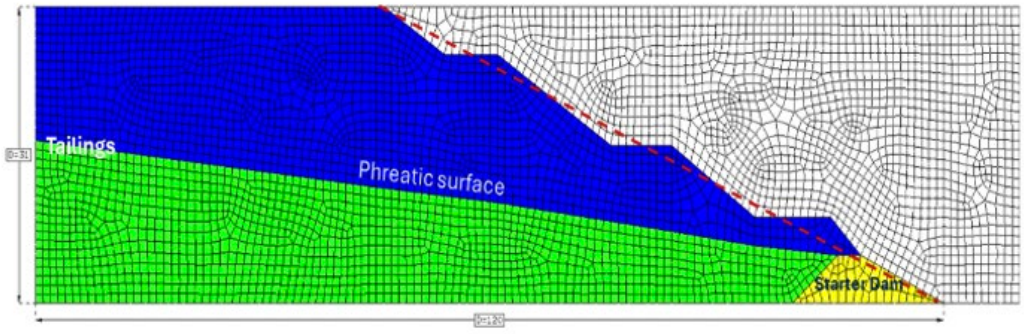
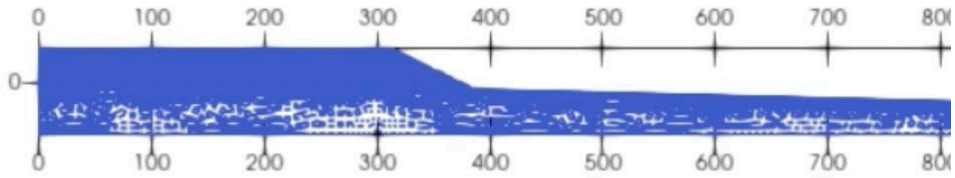


Figure 5: Idealized 2D geometry and mesh

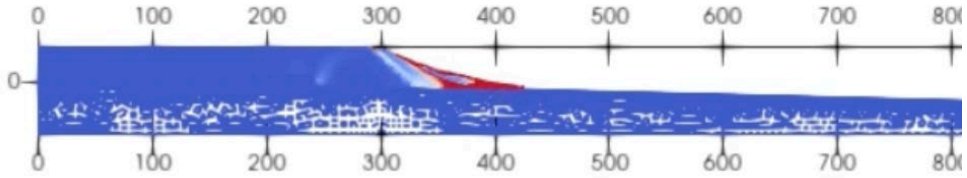
Results

We performed simulations using state parameters ranging from 0.02 to 0.1. We found a good reproduction of the postulated progressive failure geometry and the tailings mobilized during retrogression using a state parameter of 0.035. For lower values, the tailings do not retrogress to the same extent; for higher values the retrogression exceeds that reported; and for state parameters greater than 0.06 the whole deposit in the modeling domain is mobilized, with the runout not stopping before the domain boundary is reached.

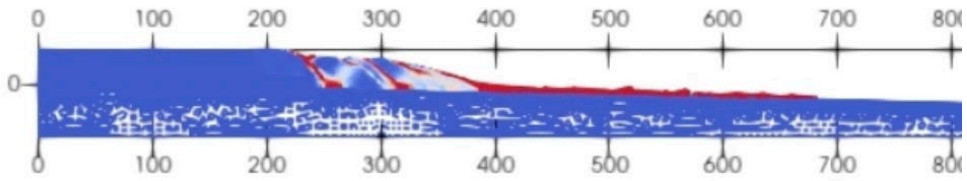
The simulation for $\psi = 0.035$ is shown in Figure 6. The failure is progressive, showing an initial failure closer to the toe in Figure 6 (b), but then developing two additional slip planes father back from the original toe in Figure 6 (c). These slip planes result in two zones of unsheared tailings. Tailings mobilized by further retrogression seem to flow on top of these unsheared zones. Unlike the true event, the unsheared zones "trap" material between themselves and the eventually stable face of the post-failure impoundment. This is an artifact of the 2D model, and it is likely that fracturing in 3D would in reality allow the mobilized tailings to drain. The runout predicted for this state parameter is 550 m, much less the observed value (>1.2 km), but this trapping of the material obviously reduces the predicted extent.



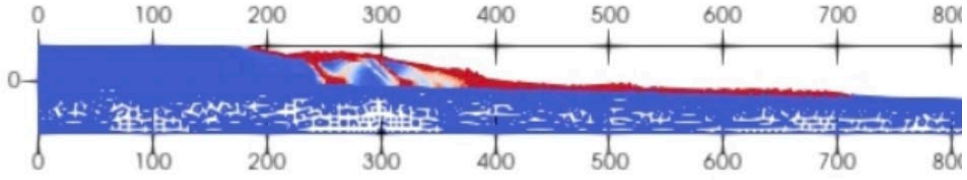
(a)



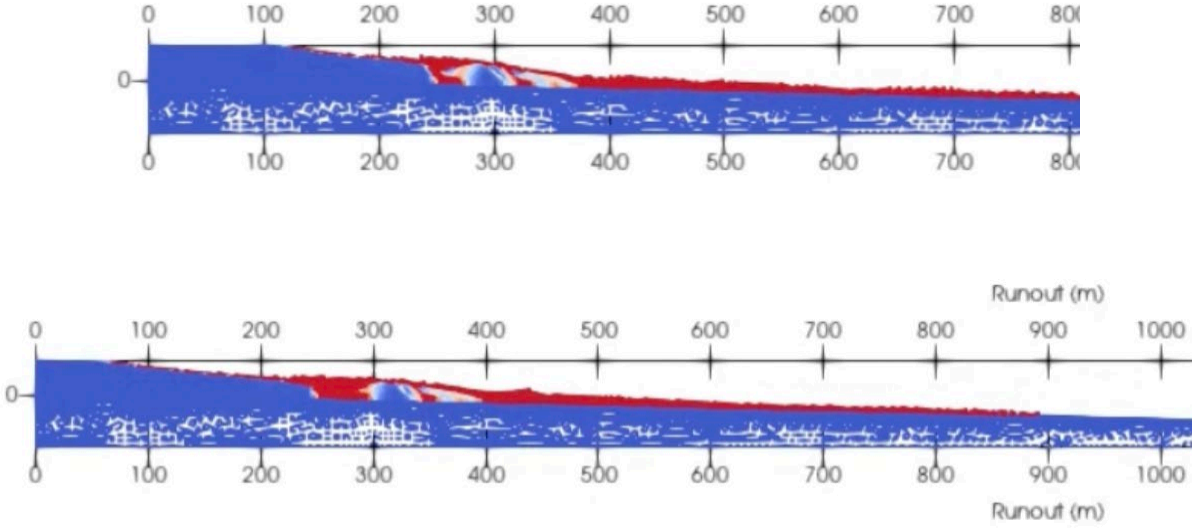
(b)



(c)



(d)



(e)

Figure 6: Simulation for state parameter of 0.035, which has the best agreement with a) initial geometry; b) initiation of first flow slide; c) initiation of 2 more slip surfaces, material already mobilized flows in front of toe; d) shallow regression behind initial failures, tailings continue to flow on top of unsheared slope remnants; (e) final geometry, runout from the toe about 500 m; the remnants have been pushed about 25 m



Figure 7: Photograph showing the accumulation of material near the breach (photograph supplied by Andy Fourie, personal communication)

The accumulation of unsheared material seems to play a role in shaping the actual failure surface. The portion of the failure surface furthest back from the toe is very shallow, and it possibly remains shallow due to some stability imparted by the less sheared material in front. Again, the presence of unsheared material, or at least stronger material in the immediate area of the failure, seems to be clear in Figure 7.

The chosen initial state assuming $\psi = 0.035$ indicates a range of initial void ratio, most less than 0.8, but with a range in 10 kPa effective stress or less with $e > 0.8$. Given the formulation of the CSL, this material greater than 0.8 will never touch the CSL in undrained loading in e-p' space; though it will follow the M line in q-p' space, q decreasing as the tailings thin out during their flow. For reference, the critical state strength at $e = 0.798$ is 300 Pa, at $e = 0.775$ it is 20 kPa, at $e = 0.75$ it is 60 kPa.

Considering that this case has been modeled by rheometry models with yield stress of 300 Pa (e.g., Saeedi et al., 2022) or even less, this points to the tailings contributing to flow as those being in the relatively shallow zones of the impoundment. This would seem to also provide some indication of where to focus remediation /better control of deposition, given that the "dangerous tailings" are easily classified.

Interestingly, this also points to another explanation of the low runout. As can be seen from Figure 7, the zone of shallow failure behind the dam extends to a greater width than the breach, especially to the left from the perspective of the reader looking at Figure 7. Converted into a 2D situation, there would be a greater volume of shallow mobilized tailings, which could flow over the remnants and contribute to longer runout. As mentioned previously, in 3D the tailings trapped behind the remnants would likely be able to flow out and also contribute to longer runout. This requires further investigation: as pointed out by an

anonymous reviewer, 3D effects associated with the sides of the breach might have an inhibiting effect on the runout.

Summary and conclusion

To summarize the analyses and the discussion:

1. The Merriespruit failure was analyzed using MPM, employing the Norsand constitutive model in an undrained condition
2. The CSL in e-p' and p-q' space was determined using the M4 sample of triaxial tests undertaken by Fourie and Papageorgiou (2001).
3. Other plasticity parameters were obtained by starting with mid-range values and calibrating to measured triaxial stress paths. Agreement could be obtained with the mid-range values suggested by Been and Jeffries (1985).
4. A range of state parameters (0.035 to 0.1) were considered, based on the fitted CSL in e-p' space and the reported void ratio of 0.8 at depth by Strydom and Williams (1999).
5. Using 0.035, the nature and location of retrogressing failure surface could be well captured. Using higher state parameters pushed the retrogression back beyond what was reported. State parameters > 0.06 resulted in full mobilization of all tailings in the domain.
6. For the ψ=0.035 simulation, the runout is well short of the reported range (~ 500 m compared > 1.2 km). This is hypothesized to be an artefact of 2D conditions, such as the remnants of unsheared trapping in some of the mobilized tailings, which would be less likely to occur in 3D. Also, in the real failure, the shallow zone extended to greater width than the breach.
7. It is demonstrated that critical state theory implies that the shallow tailings would be the ones mobilized to larger distances, which is reproduced in the model.
8. It is clear that the shape of the CSL at low effective stresses will bear strongly on the generation of flowable tailings.

References

Been, K. and Jefferies, M.G. 1985. A state parameter for sands. *Géotechnique* 35(2): 99–112.

Fourie, A.B., Blight, G.E. and Papageorgiou, G. 2001. Static liquefaction as a possible explanation for the Merriespruit tailings dam failure. *Canadian Geotechnical Journal* 38(4): 707–719. NRC Research Press Ottawa, Canada.

Fourie, A.B. and Papageorgiou, G. 2001. Defining an appropriate steady state line for Merriespruit gold tailings. *Canadian Geotechnical Journal* 38(4).

Henriquez, J. and Simms, P. 2009. Dynamic imaging and modelling of multilayer deposition of gold paste tailings. *Minerals Engineering* 22(2): 128–139. Elsevier.

Jefferies, M. and Been, K. 2015. *Soil Liquefaction: A Critical State Approach*. Second edition. CRC press.

Martinelli, M. and Pisano, F. 2022. Relating cone penetration resistance to sand state using the material point method. *Géotechnique* 12(2):131–138. https://doi.org/10.1680/jgele.21.00145

Martinelli, M. and Galavi, V. 2022. An explicit coupled MPM formulation to simulate penetration problems in soils using quadrilateral elements. *Computers and Geotechnics* 145: 104697.

Saeedi, A., Xia, X., Esfandiari, Z., Zabolotnii, E. and Simms, P. 2022. Multi-model assessment of dam failure and runout. *Proceedings of Tailings and Mine Waste, 2022:* 513–522.

Saeedi, A., Esfandiari, Z., Xia, X., Zabolotnii, E., Martinelli, M., Beier, N.A. and Zambrano, G. Multi-model analyses of physical simulations of tailings impoundment failure and runout: Part II. *Proceedings of Tailings and Mine Waste, 2023:* 297–308.

Rana, N.W., Ghahramani, N., Evans, S.G., McDougall, S., Small, A., and Take, A.W. 2021. Catastrophic mass flows resulting from tailings impoundment failures, *Engineering Geology* 292: 106262. https://doi.org/10.1016/j.enggeo.2021.106262.

Strydom, J.H. and Williams, A.A.B. 1999. A review of important and interesting technical findings regarding the tailings dam failure at Merriespruit. *Journal of the South African Institution of Civil Engineering* 41(4): 1–10.

Wagener, F. 1997. The Merriespruit slimes dam failure: overview and lessons learnt: technical paper. *Journal of the South African Institution of Civil Engineering (Joernaal van die Suid-Afrikaanse Instituut van Siviele Ingenieurswese)* 39(3): 11–15. South African Institution of Civil Engineering (SAICE).

Van Niekerk, H.J. and Viljoen, M.J. 2005. Causes and consequences of the Merriespruit and other tailings-dam failures. *Land Degradation and Development* 16(2): 201–212. Wiley Online Library.

Zabolotnii, Morgenstern, N.R. and Wilson, G. Ward. 2022. Mechanism of failure of the Mount Polley Tailings Storage Facility. *Canadian Geotechnical Journal* 59(8): 1503–1518.

"Failing Forward" to Secure Oil Sands Tailings Impoundments against Catastrophic Failures: Preliminary Results

Armin Saeedi, Carleton University, Canada
Louai Alshafti, Carleton University, Canada
Xuexin Xia, Carleton University Canada
Gonzalo Zambrano Narvaez, University of Alberta, Canada
Nicholas Beier, University of Alberta, Canada
Mario Martinelli, Deltares, Netherlands
Paul Simms, Carleton University, Canada

Abstract

The "failing forward" project is conducted at Carleton University and the University of Alberta to assess the risk of flowability and egress of clayey tailings off-site at different stages of the tailings facility (pre- and post-closure). The research is conducted using physical experiments at different scales (flume tests, multi-meter high prototype embankments, and centrifuge tests) to verify understanding of possible failure mechanisms and post-failure runout behavior. The physical experiments are interpreted using geotechnical and rheological characterization tests, in concert with a suite of numerical analysis tools. The latter includes both geotechnical and rheological based large deformation software. Preliminary results and analysis of experiments on both oil sands tailings and a soft clay analogue are reported.

Introduction

The "failing forward" project is conducted at Carleton University and the University of Alberta, funded by Canada's Oil Sands Innovation Alliance (COSIA), a research consortium of the oil sands surface miners. The goal of the project is to develop criteria for tailings flowability. Flowability can be defined as the capacity of tailings to flow substantial distances off-property in the event of breach, but also speaks to other safety hazards, such as those that might be encountered during reclamation, where a loss of strength may result in a serious accident, even though no breach occurs. The scope of the project is aimed at clayey tailings, similar to various treatments of oils sands fines dominated tailings, but also other clay tailings such as bauxite red muds.

The "failing forward" clause refers to experiments at various scales that physically model the failure of tailings. These experiments are required as the number of failures are relatively few, and/or not characterized sufficiently to establish criteria related to flowability on themselves. The physical experiments replace, in essence, large databases on well documented failures, that provide clear geotechnical information on what type of failure can result in landslides of substantial volume and runout. As an example, correlations have been developed for failures of Eastern Canadian Clays, as shown in Figure 1, in terms of sensitivity and remolded shear strength. The failures are divided into "retrogressive" and "landslides," the first pertaining to failures generating substantial runouts.

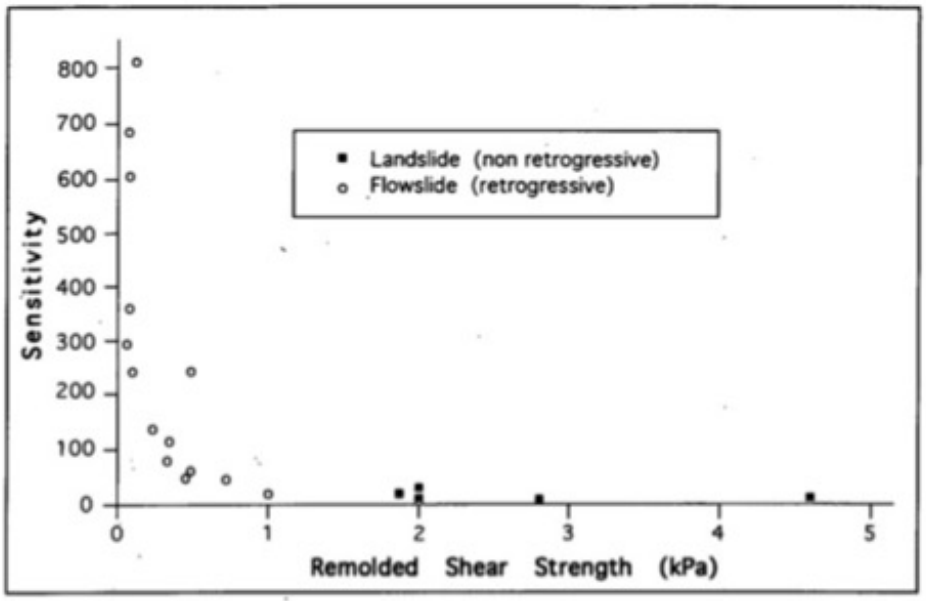


Figure 1: Example of a flowability criteria build on database of real slope stability failures (Lefebvre, 1981)

The different types of physical experiments are shown in Figure 2. Due to tailings availability, most tests on oil sands tailings are restricted to the flume and centrifuge experiments, with a clay analogue being used for the largest experiments.

The physical tests are then used as targets for different types of numerical simulations, including FLAC and material point methods (MPM) codes, incorporating both geotechnical and rheological constitutive models of varying complexity, supported by shear strength and rheology testing. Combining these physical tests and numerical analyses, we hope to better understand clayey tailings flowability. The characterization of tailings flowability is crucial for oil sands operators to design closure progression, to ensure minimal risks and/or consequences for long-term reclamation plans (Miller et al., 2022).

In this paper, we report select analysis on centrifuge and flume tests, using also a subset of numerical analyses.

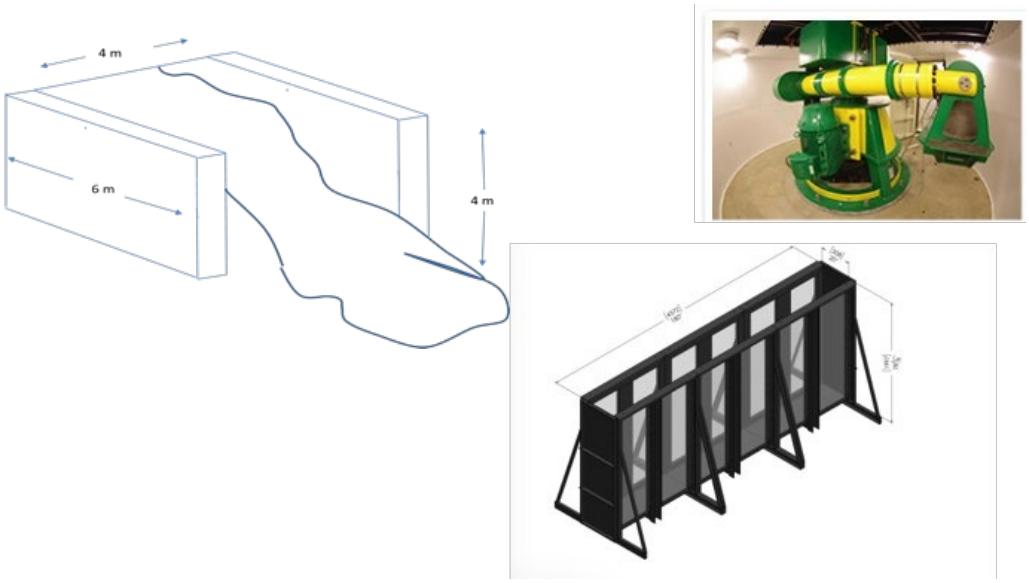


Figure 2: Physical models used in the project, including 4 m high test pit, 8 m long flume (bottom), and centrifuge tests in various configurations

Methods

Numerical models

In this paper, we show simulations using MPM codes, using two relatively simple constitutive models. Both models are explained in more detail in other publications (Saeedi et al., 2022; Simms et al., 2023). Both models essentially transition the material between a peak strength and a residual strength. In the geotechnical constitutive model (Mohr-Colomb Strain Softening or MCSS), strain softening occurs through accumulated plastic shear strain:

$$S = S_{residual} + (S_{\max} - S_{residual})e^{-\eta\varepsilon_{pd}} \quad \text{(Equation 1)}$$

Where S, the shear strength, is reduced from the peak value of S_{max} as a function of plastic shear strain (ε_{pd}), the limiting value being the residual shear stress $S_{residual.}$ The parameter η, the shape factor, regulates the decrease in strength with plastic shear strain. The shape factor can be obtained by fitting Equation 1 to element test data; however, the application of Equation 1 is affected by strain localization (Zabolotni et al., 2022), and therefore the shape factor that will predict a given runout distance may change with mesh size (Martinelli and Remmerswaal, 2023). One strategy to calibrate the shape factor is to simulate an element with the same mesh size as would be used in the failure and runout simulation.

In the rheology model (viscosity bifurcation or VBR), the change in shear strength is a result of incremental changes in the state of the model as a function of strain rate as opposed to accumulated shear strain. For low strain rates, the material will build structure and increase in viscosity and strength, the high strain rates, the material will disintegrate and viscosity and strength will degrade. Aside from the peak and

the residual shear strength, the model also requires rheology test data ,which provides i) the viscosity at the fully sheared state, and ii) rate of viscosity increase or decrease at a given strain rate. The VBR model is described more fully in Saeedi et al. (2022). Its practical advantage is its strain rate dependency limits issues of localization, and it is more stable in 3D. The geotechnical strain weakening model, however, is more intuitive to those with a geotechnical perspective.

Experiments

All of the tests reported employ Leda Clay as an analogue to clayey tailings. The LL and PL are 52% and 27% respectively, the clay mineralogy predominantly Illite (80%) with some Kaolinite (10%). Leda Clay, also called Champlain Sea Clay, is extensively studied in the geotechnical literature.

Here we report tests from a i) small flume tests, and ii) centrifuge experiments, as pictured in Figure 3. The flumes are 0.3 m high by 0.15 m wide, where a reservoir 0.3 m long is failed by gate lifting. The centrifuge experiment was tested at the 2-m radius beam centrifuge at the GeoCERF facility at the University of Alberta. The model was 0.3 m high, 0.3m wide, and 0.5 m long, with a bench 0.1 m long at the top. The embankment was failed when it was spun up to a prototype height of 2.8 m (18 g).



Figure 3: Picture of Flume Test 4

The flume tests are performed at water contents approximately 1.85 × LL, but are performed at different rest times. Each test has the same residual shear strength (0.265 kPs), but the peak shear strength varies with rest time. The shear strength development during the rest time is monitored by fall cone using. a special frame to allow testing of the surface of the material in the reservoir. This frame also allows for shear strength measurements in the tailings or clay after failure. Pore-water pressure is monitored at two depths as well during the rest time.

The centrifuge tests were performed at 1.1 × LL, and a rest time sufficient to generate a peak strength of 7 kPa, while the measured residual strength was 2 kPa. Peak strength, as well the strength in the flowed material after failure, was tested using a fall cone supported by a similar apparatus as in the flume tests.

To date, there are about twenty flume tests, and two centrifuge tests. Three of the flume tests have been performed on oil sands tailings, but all the remaining tests have been performed using Leda Clay. The tests reported in this paper are summarized in Table 1.

Table 1: Tests reported in this paper

Type of test	Rest time	Water content	Residual, peak strength (kPa)
Flume test 4	< 5 minutes	1.89 x LL	0.265, 0.27
Flume test 9	24 hours	1.86 x LL	0.28, 1.3
Centrifuge test 1	3 weeks	1.1 x LL	2, 7

Results

Flume test 4

The post-failure geometry of this test is shown in Figure 3. It is typical of such tests done on high water content / unconsolidated soft soils or tailings, the runout being higher than would be predicted by simple analytical methods based on yield stress alone (for example, see the lubrication theory equations in Henriquez and Simms, 2009), due to the momentum generated by the mode of failure. However, this test can be well-simulated by the MCSS model using the measured shear strength (peak strength = residual strength), as shown in Figure 4.

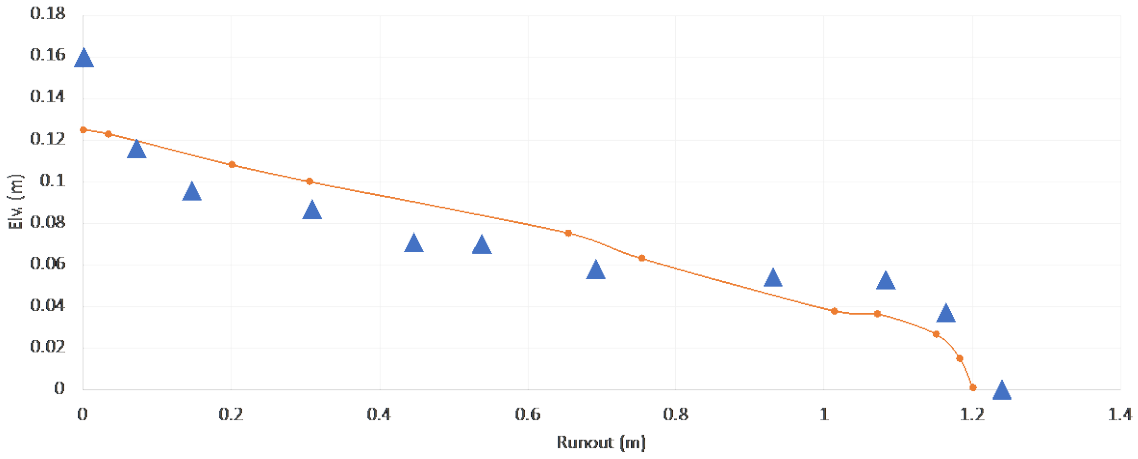


Figure 4: MCSS model simulation of Flume Test 4 using $S_{peak} = S_{residual} = 0.27$ kPa

Flume test 9

This test presents more complex behavior. Pictures of the flume test are shown in Figure 5 along with simulations snapshots at similar times using the MCSS model. The consolidation time of 24 hours has

generated sufficient peak strength that there are regions at the bottom and at the top that do not yield, and after initial yielding and deformation, a slip surface forms, and part of the top of the samples slides on this failure surface, some of it remaining effectively a rigid body, while the bottom part subsequently de-structures and joins the leading yielding material at the front of the toe.

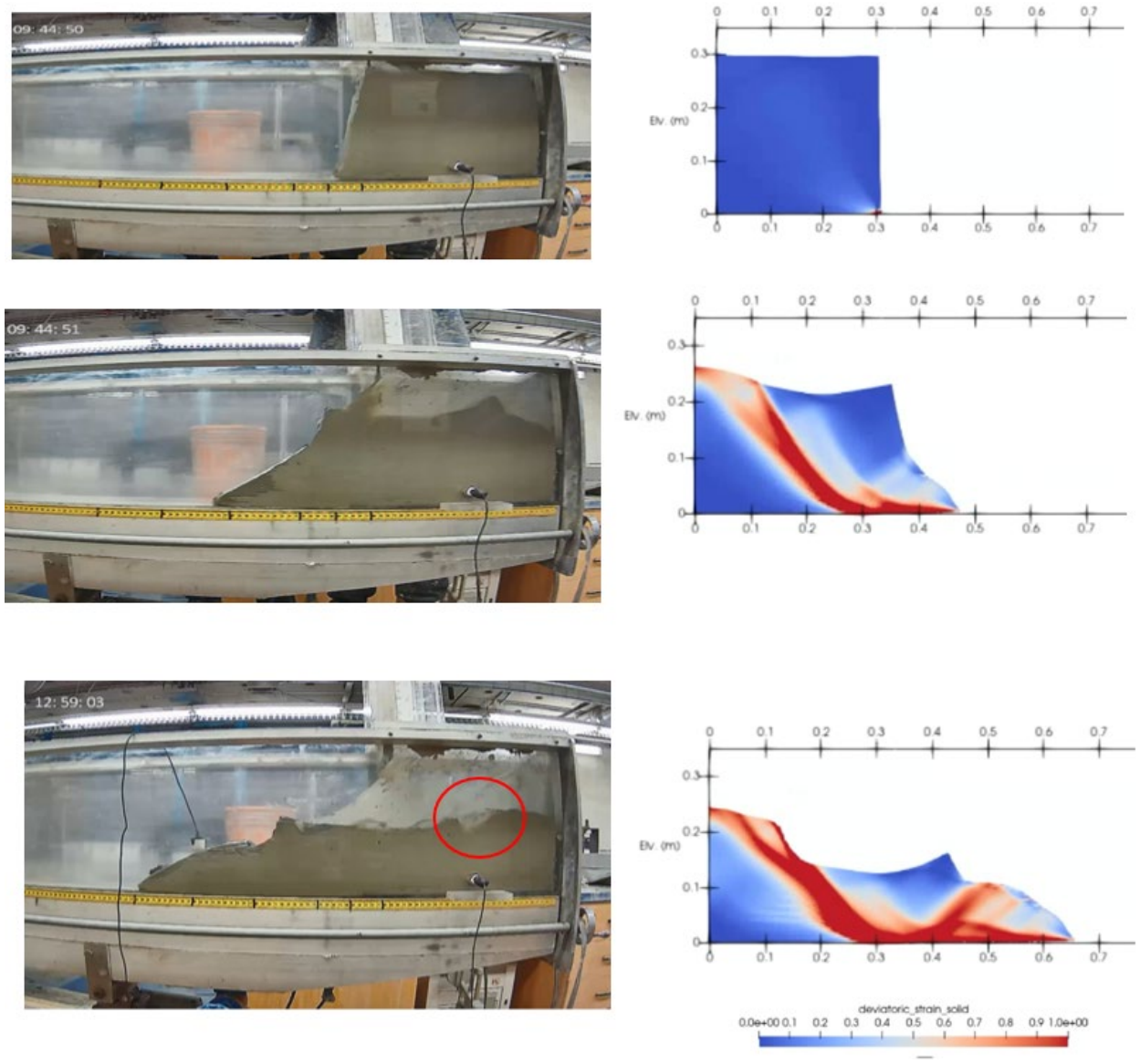


Figure 5: Pictures of Flume Test 9 paired with simulation results at similar times. MCSS model using a shape factor of 5

Most of this behavior is captured by the MCSS model, a notable exception is that the real material separates readily from the back wall, but this does not occur in the model, where the backwall is a boundary condition fixed in the x-direction. Still, the shape during failure, the final profile, and the runout are well-

captured by the model, as shown in Figure 6. The best agreement with runout is provided by a shape factor between 5 and 10 (Figure 7).

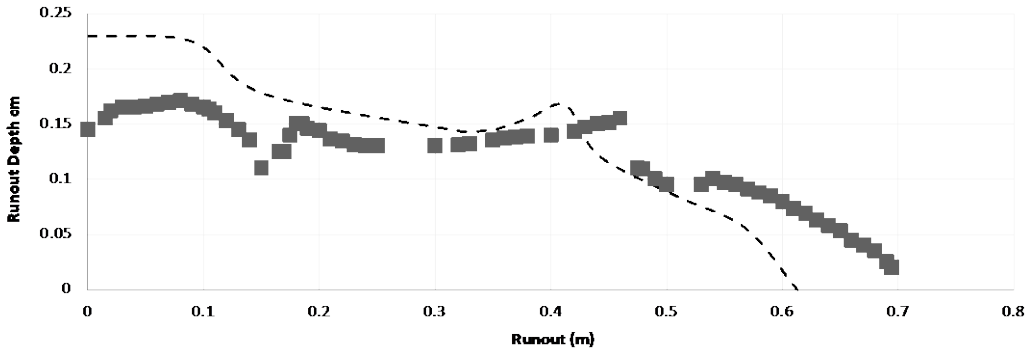


Figure 6: MCSS simulation of Flume test 9, final profile, shape factor of 5

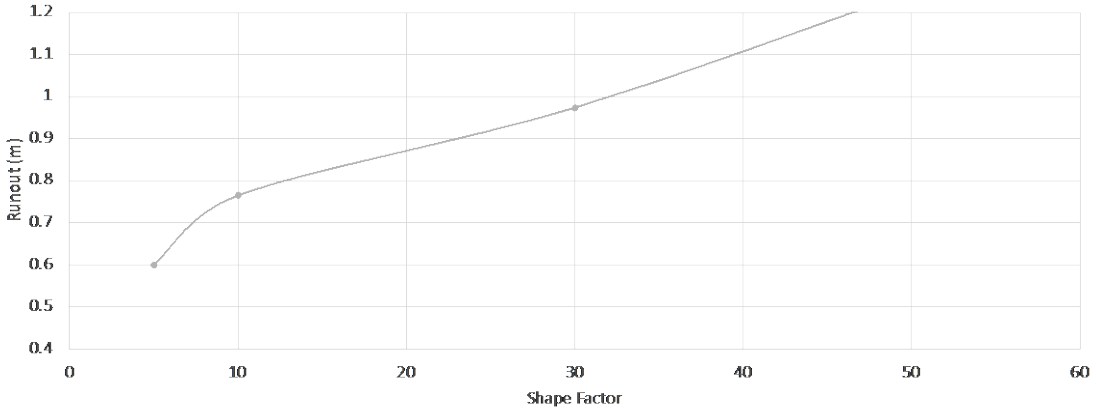


Figure 7: Sensitivity of runout to shape factor in simulations of Flume Test 9

VBR model

Figure 8 shows snapshots from the 3D VBR model. Its relative better stability and speed in 3D allow us to study effects such as the finite time of raising of the gate, and the influence of sidewalls. The raising of the gate time (< 0.5 s) makes very little difference compared to instantaneous removal (~ 1 cm of runout). The sidewalls, however, can have a significant influence, depending on what boundary condition is used. Using a no flow / full stick boundary condition could result in a decrease in runout by as much as 5 cm. However, as discussed later, this does not seem to be the case in the flume tests, where the effect of sidewalls was investigated experimentally.

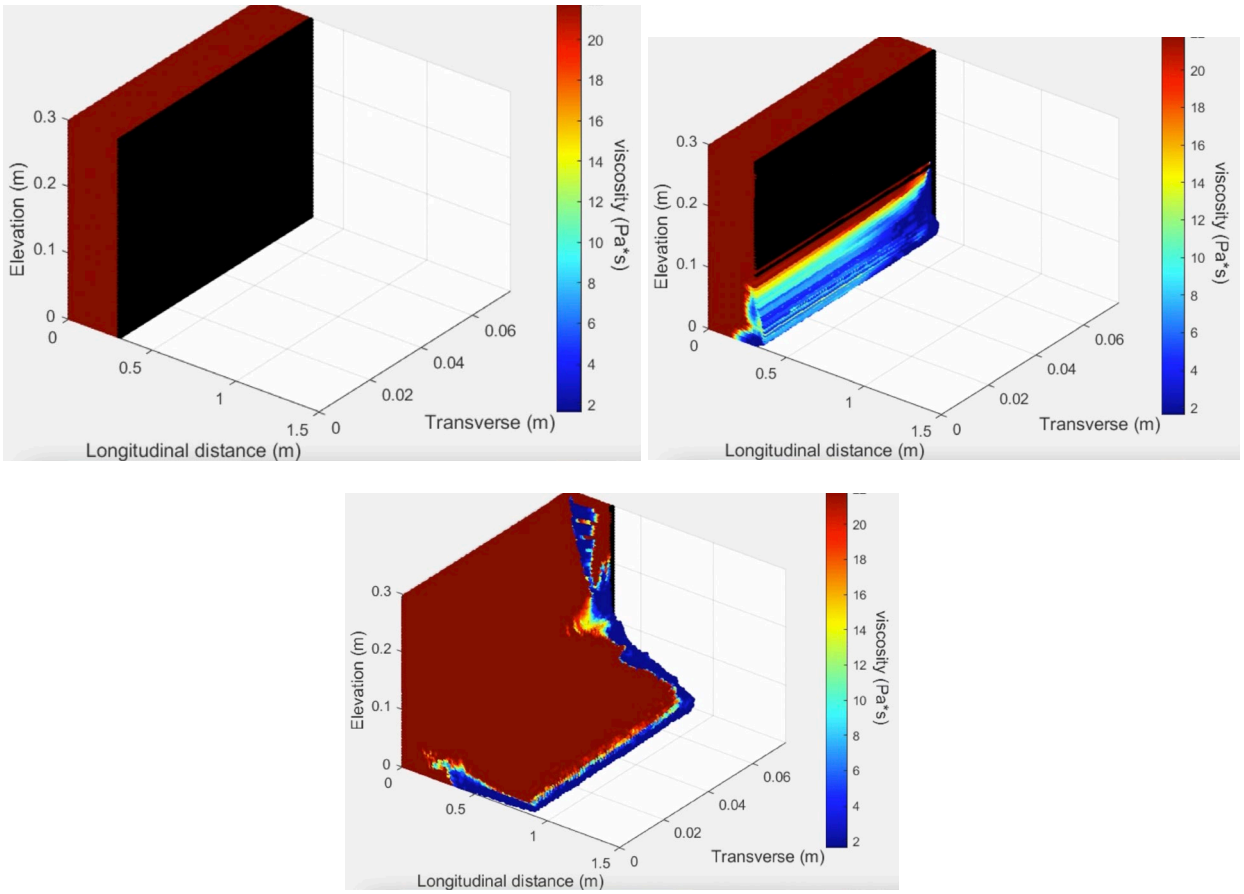


Figure 8: 3D rheology model simulation of flume test 4, showing its capacities to simulate raising of the gate, and simulation of the sidewall boundary conditions

Centrifuge Test 1

The centrifuge test, previously discussed in Saeedi et al. (2023), is shown in Figure 9 in its pre-flight and post-failure state. The reader should remember that the height is actually less than 0. 3 m, spun up to its prototype height of 2.8 m at the time of failure.

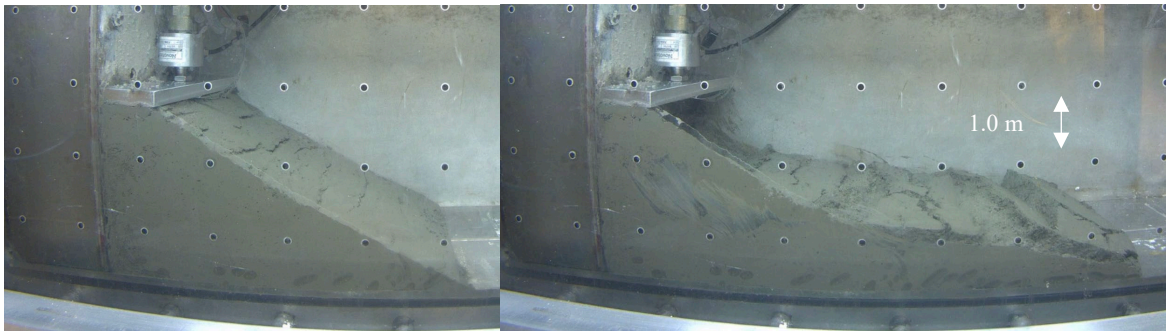


Figure 9: Centrifuge model test of aged clay at 1.2 LL, (2.8 m high, 5 m long with 1 m bench in prototype), intact strength 7 kPa, remolded strength 2 kPa

This centrifuge test experiences failure in a successive pattern, an original failure surface forming before much deformation occurs. and then after the tailings start to move, two successive shear bands or zones of shear bands form, coincident with the material farther from the toe stopping, while material towards the toe continues to move. This behavior is evident in the real tests by the large cracks that form at the surface. The behavior is replicated in the model, as evidenced by the pattern shown in Figure 10.

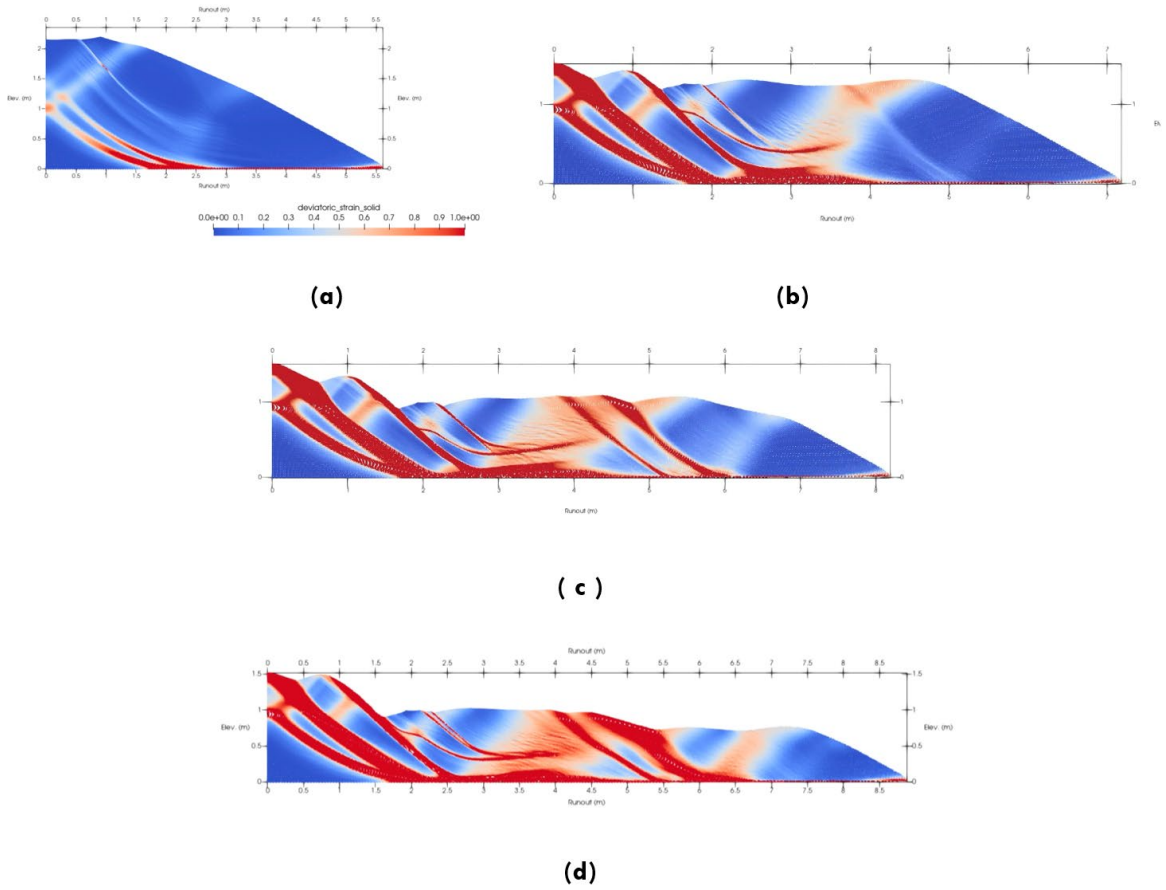


Figure 10: Best centrifuge simulation with MCSS , shape factor of 0.5 (a) initial shear band formation, (b) translation of material in front of initial shear band (c) formation of secondary shear bands (d) material in front of new shear bands translates, material behind has stopped

With the formation of the initial shear band, the whole material in front of the shear band moves, but then a secondary series of bands develops. Thereafter the material in front of the new shear bands continues to move, but the material between the old and new zones of shear bands stops.

This behavior is again quite different from the previous two flume tests. Here, the initially relatively stronger material experiences most of its deformation as successive translations of rigid body elements, sliding over relatively discrete shear zones. While Flume Test 4 experiences almost uniform degrees of shear strain, Flume Test 9 exhibits a combination of behaviors in Flume Test 4 and this centrifuge test.

Discussion on the shape factor

The flume test was best fitted with a shape factor between 5 and 10, while the runout in the centrifuge test was best fitted using a shape factor of 0.5 or 1. The higher range of shape factors in the flume test are more realistic: a value of 10 implies 2/3rd s reduction in strength by 10% shear strain, a value of 1 implies only a 10% reduction in shear strength by 10% shear strain. As discussed in Saeedi et al. (2023), it was thought that this low shape factor might be parameterizing the effects of the sidewalls. Evidence collected in the flume tests by varying width suggest minimal action by the sidewalls. However, the interaction between the clay and walls could be quite different for the initially stronger clay material in the centrifuge: investigations are ongoing.

Conclusions and ongoing work

Physical modeling studies are ongoing to study failure and runout at different scales, to properly characterize flowability in clayey tailings. Preliminary tests have used a well-studied clay as an analogue. The physical experiments have been interpreted using multiple models. In this paper, we report on the analysis of two flume tests and a centrifuge test using an MPM code using the MCSS model. The following conclusions are made:

1. The two flume tests and centrifuge test use material of different initial water contents, and different "rest times" to change the sensitivity as a function of consolidation. All three tests exhibited distinct behaviors as a result of these differences. The weakest material yielded throughout homogeneously, whereas the strongest material was dominated by translation of zones of unyielding material over discrete shear bands.
2. The relatively simple MCSS model could replicate the qualitative evolution of shape in all these tests, despite these strong differences in initial state and consequent behavior.
3. The flume tests runout is best replicated by a shape factor of 5 to 10, while for the centrifuge this value was 0.5 or 1. This large discrepancy is thought be due to substantial interaction with the sidewalls in the centrifuge test where the material is stronger, but this requires further investigation.

Ongoing and future work includes expanding the physical tests to larger tests in 1 g (up to 3 m height) as well as much larger prototype heights in the centrifuge. Modeling work includes simulation of the expanding database of physical tests with the suite of models already described, but also beginning to use critical state models for clays (such as the SCLAY family) to compare with the straightforward but relatively simple MCSS model.

Acknowledgements

The authors gratefully acknowledge funding provided by Canada's Oil Sands Innovation Alliance and the Natural Science and Engineering Research Council of Canada (NSERC).

References

Henriquez, J. and Simms, P. 2009. Dynamic imaging and modelling of multilayer deposition of gold paste tailings. *Minerals Engineering* 22: 128–139.

Lefebvre, G. 1981. Fourth Canadian Geotechnical Colloquium: Strength and slope stability in Canadian soft clay deposits. *Can. Geotech. J.* 18: 420–442.

Martinelli, M. and Remmerswaal, G. 2023. Evaluation of a Gauss integration scheme in MPM for strain-dependent soils. *Proceedings of 10th European Conference on Numerical Methods in Geotechnical Engineering.*

Miller, G. and 10 others. 2022. Assessment tool for landforms containing potentially flowable tailings. *Proceedings of the 2022 International Oil Sands Tailings Conference*. December 3–5, Edmonton, Alberta.

Saeedi, A., Xia, X., Esfandiari, Z., Zabolotnii, E. and Simms, P. 2022. Multi-model assessment of dam failure and runout. *Proceedings of Tailings and Mine Waste 2022*. Denver, Colorado, Nov. 22–25th.

Simms, P., Xia, X., Patel, A., Parent, E., Beier, N.A. and Zambrano-Narvaez, G. 2023. Rheology for deposition control and deposit failure risk analysis. *Paste 2023: 25th International Conference on Paste, Thickened and Filtered Tailings.* April 28th –30th, Banff, Alberta.

Zabolotnii, N., Morgenstern, R. and Wilson, G. Ward. 2022. Mechanism of failure of the Mount Polley Tailings Storage Facility. *Canadian Geotechnical Journal* 59(8): 1503–1518.

Probability Distributions of Tailings Dam Breach Volumes by Failure Mode as Part of a Risk Screening-Level Tool

Stephanie Bale, BGC Engineering Inc., Canada
Vincenzo Coia, BGC Engineering Inc., Canada
Brad Russell, BGC Engineering Inc., Canada
Daley Clohan, BGC Engineering Inc., Canada

Abstract

The mining industry is constrained by available qualified professionals to perform detailed risk assessments for tailings storage facilities. As such, a suite of simple spreadsheet models and guidance to support assessment of tailings dam risk using a combination of failure statistics and engineering judgment is being developed by the authors. The objective of this work is to complement expert-based quantitative or semi-quantitative risk assessment methods and accelerate the adoption of risk-informed decision making in all phases of tailings dam management. Designers and dam owners can apply this framework to improve consideration of risk in site selection and preliminary design; support rapid screening and prioritization of large portfolios of dams; inform expert-based assignments of failure mode probabilities; help assess the reasonableness of risk assessment results generated using more rigorous methods; and inform the range of dam breach analysis scenarios that should be conducted in consideration of the risk drivers.

The current work, and the focus of this paper, is estimating tailings release volume using a statistical approach to assign preliminary probability distributions of the release volume by failure mode. Guidance is provided for adjusting the baseline release volume distributions according to site conditions, such as impounded tailings volume, pond volume, liquefaction susceptibility, dam height, fill materials, and dam configuration.

Introduction

Best practice guidance for the tailings dam industry includes requirements to perform and regularly update risk assessments, including identification and characterization of potential failure modes (Global Tailings Review [2020] and International Commission of Large Dams [ICOLD, 2022]). Best practices have been adopted from the water dam industry and include expert-based quantitative or semi-quantitative risk

assessment; however, these efforts are constrained by limited availability of personnel with the required expertise to support assessment for the global inventory of tailings storage facilities (TSFs), which exceeds 20,000 (Rana et al., 2022). In addition to the number of TSFs that require an assessment, substantial effort is needed to prepare each risk assessment, including conducting tailings dam breach assessments (TDBAs) that allow for the evaluation of consequences associated with the potential failure modes.

While there is industry guidance to base a TDBA on so called "credible flow failure scenarios," they are often based on conservative assumptions leading to results representing "worst-case" scenarios that manifest the most extreme consequence. This approach does not lend itself well to the risk assessment process as it focuses only on a single scenario. To support a risk assessment, TDBAs would need to be performed for each failure mode, or at least the risk driving scenarios, recognizing that the probability associated with each failure mode is unique and dam breach characteristics related to each failure mode vary.

Considering these constraints, there is a need to develop tools to assist with the risk assessment process associated with TDBAs. Previous work by Porter et al. (2023) involved the development of a screening-level tool to support expert-based assignment of probability of failure estimates for common failure modes. This work included developing simple spreadsheet models based on review of recent publications on tailings dam inventories and failure databases (including Rana et al., 2022; Stark et al., 2022). Baseline failure probabilities by dam raise method and failure statistics were then used to identify the average relative contribution of common failure modes to the total probability of failure. Guidance is provided to adjust the industry-average probability of failure estimates based on site conditions, design criteria, and level of governance practice.

Expanding on the work by Porter et al. (2023), the authors have developed a framework for an extension of this screening-level tool to support the selection of tailings dam breach volumes to assist with screening-level assessments and TDBAs. The statistical approach outlined by Porter et al. (2023) has been adopted to assign a preliminary baseline probability distribution to release volumes for common failure modes. Preliminary guidance has also been developed to adjust the baseline release volumes according to site conditions, which is described in this paper.

This work is part of an overall screening-level risk tool envisioned by the authors to complement expert-based quantitative or semi-quantitative risk assessment methods and accelerate the adoption of risk-informed decision making in all phases of tailings dam management. The probability of failure and probabilistic release volume tools can feed into other simplified models to estimate runout extents and flow velocity, providing a spatial probability estimate. Combined with other exposure models, life loss and economic loss could be estimated, leading to an estimate of total annualized risk that can be plotted on a

plot of frequency of event vs. number of fatalities (i.e., F-N) and compared against established risk tolerance criteria.

Development of preliminary baseline probability distributions for dam breach release volume by failure mode

While statistical relationships for TDBA release volumes have been explored by others (including Rico et al., 2008; Larrauri and Lall, 2018), few have explored the relationship between release volume and failure mode. This has, however, been recently explored by Lin et al. (2022) who present proportion of sand burst (proportion of released volume to impounded volume, referred to as release volume proportion hereafter) by common failure modes, as shown in Figure 1.

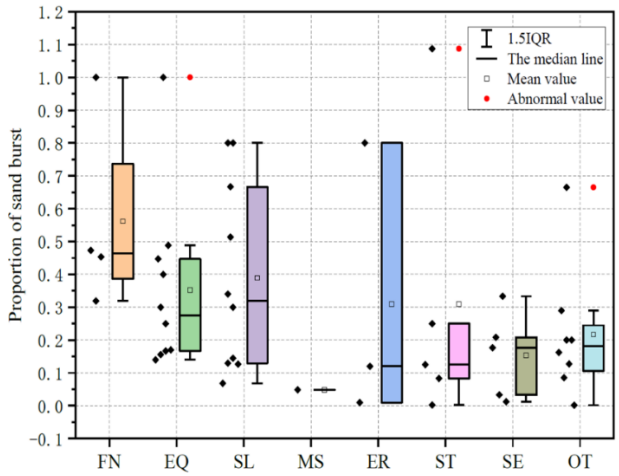


Figure 1: Dam breach release volume proportion by failure mode, as reported by Lin et al. (2022). Failure modes include Foundation (FN), Earthquake (EQ), Slope Instability (SL), Mine Subsidence (MS), Erosion (ER), Structural (ST), Seepage (SE), and Overtopping (OT)

The data by Lin et al. (2022) has been used in conjunction with expert judgement to develop baseline probability distributions for dam breach release volume proportions for each failure mode. For this work, the authors have adopted a Beta probability distribution using the dam failure data summarized by Lin et al. (2022), which was chosen because it is bounded between 0 and 1, and due to its flexibility in shape. These baseline distributions are summarized in Table 1 and are considered preliminary for the purposes of developing the framework for the screening-level tool. Future work is planned to use an expanded dataset, and to use a more objective implementation of expert judgement such as through Bayesian statistics.

The Beta family of distributions is defined by two parameters, $\alpha > 0$ and $\beta > 0$, and has density

$$f(x) = \frac{x^{\alpha-1}(1-x)^{\beta-1}}{B(\alpha,\beta)}$$

for $0 < x < 1$, where $B(\alpha, \beta) = \Gamma(\alpha)\Gamma(\beta)/\Gamma(\alpha + \beta)$ is the beta function, and $\Gamma(z) = \int_0^\infty t^{z-1}\, exp(-t)\, \mathrm{d}t$ is the gamma function for $z > 0$. When compressed to have a minimum of x^* and a maximum of 1, the density function becomes

$$\frac{1}{1 - x^*} f\left(\frac{x - x^*}{1 - x^*}\right).$$

Table 1: Parameters (α, β, minimum) defining the Beta distributions for release volume proportion for two failure modes under consideration for this paper. The median and interquartile ranges of the distributions are also included

Failure mode	α	β	Minimum	Median	Interquartile range
Foundation (FN)	2.40	3.88	0.25	0.53	0.43 – 0.63
Overtopping (OT)	1.86	4.31	0.01	0.29	0.18 – 0.42

Development of preliminary guidance to adjust baseline volume distributions for site-specific conditions

Guidance was developed to adjust the baseline dam breach release volume proportion distributions for site-specific conditions. A preliminary list of site conditions was developed based on judgement and includes impounded tailings volume, pond volume, liquefaction susceptibility, dam height, fill materials, and dam configuration. These conditions were incorporated into 4 site factors as summarized in Table 2. Preliminary guidance has been developed for each site factor relating to foundation and overtopping failure modes. These failure modes were selected for initial development of the tool as they are commonly investigated failure modes and some of the site factors, specifically dam fill configuration, affect each quite differently.

Table 2: Site factors

Site Factor	Inputs	Description
Release Potential	Impoundment Volume (V), Dam Height (H)	Adopted from Piciullo et al. (2022) and provides an indication of the release potential during a breach. A high dam doesn't necessarily mean a large release potential if there is a small impoundment volume behind it, and vice versa: the potential is dependent on both variables.
Liquefaction Susceptibility	High, Low	Based on tailings susceptibility to liquefaction and provides an indication of tailings mobility. Preliminary estimates are based on judgement of how much of the tailings deposit is contractive, and how high the phreatic level is within the deposit.
Pond Ratio	Surface Area (Pond, Impoundment)	Defined as pond surface area ÷ impoundment surface area. This factor relates to the erosional potential to transport tailings sediments from the deposit through the failure process. If tailings liquefaction susceptibility is low, then pond ratio becomes a factor.
Dam Type / Fill Configuration	Construction Method (Upstream, Centerline, Downstream, Water Retention); Fill Material (Tailings, Rockfill, Earthfill)	Considers construction methods and dam fill materials and configurations that are typically used with each method. Different configurations have different susceptibility to failure, and corresponding magnitude, especially for failure modes involving erosion.

Scaling factors are proposed as a method of adjusting a baseline distribution of release volume proportion, V_U. However, as V_U cannot be scaled without potentially exceeding the 100% release proportion limit, the *release volume excess ratio,* V_E is scaled, which is the release volume (V_U) divided by the volume not released ($1 - V_U$), as shown below. After scaling, the release volume proportion can be back-calculated.

$$V_E = \frac{V_U}{1-V_U} \quad \text{(Equation 1)}$$

The baseline volume (V_U) distributions for the foundation and overtopping failure modes, as developed from the data provided by Lin et al. (2022), are shown in black in Figure 2. Distributions of V_U after scaling V_E by 0.5 and by 2 are also shown. Scaling by 0.5 moves the baseline distribution towards smaller values, while scaling by 2 moves the baseline distribution towards larger values. Note that the scaled distributions are no longer Beta distributions.

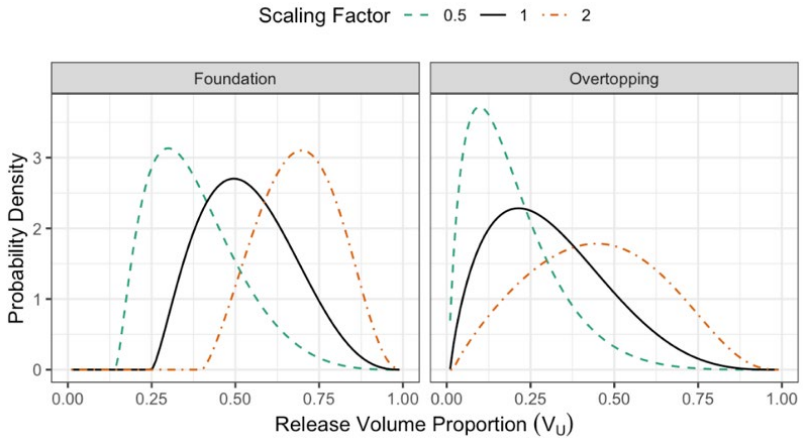


Figure 2: Preliminary probability distributions for dam breach release volume proportion by failure mode based on data provided by Lin et al. (2022). Baseline distributions are presented in black. Adjustment to baseline distributions by applying a scaling factor of 0.5 and 2 are also presented

At this stage of the development of the tool, the objective was to develop a framework for which scaling factors could be developed for each site factor. Scaling factors presented in this paper have been developed using a combination of empirical evidence (Piciullo et al., 2022) and engineering judgement, and require refinement as part of future work. Specifically, the selection of site conditions, inputs, and scaling factors should be refined through discussion with subject matter experts. Additionally, scaling factors should be refined following a process that involves testing the tool on tailings dam failure case histories. The baseline distribution should also be refined (narrowed) to more accurately represent sites with a scaling factor of 1, rather than representing the full spread of release volume proportions. This can be achieved through investigation of the residuals of a regression analysis for the failure database used to develop the baseline probability distributions.

Scaling factors developed for the proposed site factors (Table 2) are presented in the following sub-sections. The geometric mean of the four scaling factors is proposed to be considered for adjusting the baseline release volume proportion distributions for site-specific conditions, akin to an ensemble mean of four separate models. The resulting distribution of V_U is then issued as the predictive distribution, and the median is taken as a deterministic prediction.

Release potential

An empirical relationship of release volume (R in m^3) was established by Piciullo et al. (2022) using the impoundment volume (V in m^3) and dam height (H in m), which has been used to inform a preliminary empirically-driven scaling factor for the release potential. The relationship is

$$log_{10} R = 0.330 + 0.611\, log_{10} V + 0.944\, log_{10} H + \varepsilon. \quad \text{(Equation 2)}$$

The non-ε terms make up the mean log release volume, whereas the ε term is a random variable capturing the volume distribution with mean zero. To inform the scaling factor, the release volume excess ratio V_E, has been defined as

$$V_E = \frac{\mathrm{R}}{\mathrm{V-R}}. \quad \text{(Equation 3)}$$

Scaling factors can be calculated for sites with different dam heights and release volumes as the site-specific predicted V_E divided by the average predicted V_E across all sites considered in the failure database used to generate the baseline probability distribution, as

$$\text{Scaling Factor} = V_{E,\text{Site-Specific}}/V_{E,\text{Average}}. \quad \text{(Equation 4)}$$

Further work is required to improve the empirically driven scaling factor for the release volume, such as limiting release volumes to less than or equal to the total impoundment volume, which has not been accounted for in the relationship developed by Piciullo et al. (2022).

Liquefaction susceptibility

Preliminary scaling for liquefaction susceptibility is determined using engineering judgement. If the tailings are highly susceptible to liquefaction, then scaling factors of 2 and 1.5 are applied as preliminary scaling factors for foundation and overtopping failures, respectively. The authors judged that the release volume proportion for tailings susceptible to liquefaction would be higher for a foundation failure, compared to an overtopping failure. The rationale is that a foundation failure results in a sudden loss of confinement, and with that, liquefiable tailings would become very mobile. Overtopping failures generally tend to be more gradual with a progressive loss of confinement, and so may result in tailings being less mobile. These values could be refined by adding more granularity to the scaling range based on estimated percentages of contractive tailings within an impoundment and the degree of saturation.

If the liquefaction susceptibility of tailings is low, then no scaling factor is proposed. In this case, the pond ratio site factor should be considered, as described in the next section.

Pond ratio

The volume of tailings that may be released during a potential dam breach is influenced by the size and location of ponded water stored withing the TSF. Generally speaking, the volume of tailings released increases as the volume of stored water and/or the ratio of pond area to tailings area increases as the stored water provides increased erosive effects, increasing tailings mobility, during the breach. Furthermore, the closer the pond is to the TSF dam the larger the release potential becomes. Integrating the scaling relationship associated with pond location is outside the purview of this work. Instead, the authors focused on developing a relationship between pond area versus tailings surface area. Proposed scaling factors are presented in Table 3.

Table 3: Site-specific input assignment

Pond Ration (PR)	Scaling factor	Comment
PR<0.1	0.5	A low PR suggest lower release volume proportions
0.1<PR<0.4	1	Considered to represent average conditions
0.4<PR<0.8	1.5	A higher PR suggest higher release volume proportions
0.8<PR<1.0	2	

It was assumed that the same pond scaling factors can be used for foundation and overtopping failure modes. Future work will explore the efficacy of the proposed scaling factors over the range of possible pond ratios.

Dam type/fill configuration

Dam fill configurations were considered for upstream, centerline, and downstream construction methods, as well as water retention dams, which typically do not have a tailings beach present (Table 4). Judgement was used to assign relative rankings based on how susceptible the configuration is to external erosion. A downstream-constructed dam zoned with a rockfill shell is deemed to be the least susceptible, whereas an upstream-constructed dam with a tailings shell is deemed the most susceptible. Preliminary scaling factors for overtopping are proposed to range from 0.5 to 2 as presented in Table 3. No scaling factor is proposed for the foundation failure mode, as in this case the full dam is involved in the failure process and therefore assumed not susceptible to subsequent erosional processes.

Table 4: Dam type/fill configurations and preliminary scaling factors

Dam type	Dam fill configuration	Preliminary scaling factor
Upstream	Tailings Shell	2
	Rockfill Shell	1.7
	Wide Compacted Tailings Zone	1.3
Centerline	Tailings	1.5
	Earthfill	1.0
	Zoned with Rockfill Shell	0.7
Downstream	Tailings	1.3
	Earthfill	0.8
	Zoned with Rockfill Shell	0.5
Water Retention Dam (No Beach)	Earthfill	1.2
	Zoned with Rockfill Shell	0.8

Example use of probabilistic release volume tool

The following section presents results using the preliminary probabilistic release volume tool for three tailings dam failure case histories: Mount Polley, Brumadinho, and Merriespruit. These failure case histories were selected considering they are well-documented and represent a range of release volume proportions from failure modes of focus within this framework development.

Compared to the failure case histories in Lin et al. (2022), Mount Polley represents a typical foundation failure (FN), that had a pond present at the time of failure; the resulting outcome of the failure was a large volume; however, it is generally a lower value within the range of release volume proportion for this failure mode.

Brumadinho is considered a relatively extreme failure case study in that a high release volume proportion occurred, even with no pond present in the impoundment. Although this failure is categorized as a slope instability (SI) failure mode, the authors have included it for this assessment and consider it reasonable to compare as a foundation failure (FN).

Merriespruit represents a typical overtopping failure (OT) and although it had catastrophic consequences, it had a relatively low release volume proportion for the failure mode.

Table 5 summarizes the site-specific input assignments for each dam and Table 6 presents the calculated scaling factors following the framework presented in this paper, along with the resulting median estimated release volume proportion compared to the actual release volume proportion reported in case history literature.

Table 5: Site-specific input assignment

	Mount Polley	Brumadinho	Merriespruit
Impoundment Volume, V (Mm^3)[1]	74	12	7
Dam Height, H (m)	40	87	31
Liquefaction Susceptibility	Low	High	High
Pond Ratio	0.4 – 0.8	0 – 0.1	0.4 – 0.8
Dam Type	Centerline	Upstream	Upstream
Dam Fill Configuration	Zoned with Rockfill Shell	Tailings Shell	Tailings Shell

Table 6: Preliminary results for three tailings dam failure case histories

		Mount Polley		Brumadinho		Merriespruit	
		FN	OT	FN	OT	FN	OT
Release Potential	Release Volume, R (Mm^3) (Eq. 2)	5.4		4.4		1.1	
	Release Volume Excess Ratio, V_E (Eq. 3)	0.08		0.58		0.15	
	Release Volume Proportion, V_U (Eq. 1)	0.07		0.37		0.13	
Scaling Factors	Release Potential (Eq. 4)	1.0	0.9	7.7	6.6	2.1	1.8
	Liquefaction Susceptibility	1	1	2	1.5	2	1.5
	Pond Ratio (Table 3)	1.5	1.5	1	1	1	1
	Dam Type / Fill Configuration (Table 4)	1	0.7	1	2	1	2
	Combined Scaling Factor (Geometric Mean)	1.12	0.99	1.98	2.11	1.43	1.52
Predictions after Scaling	Release Volume Proportion, V_U (median, Interquartile Range)	0.55 (0.46–0.66)	0.28 (0.17–0.42)	0.69 (0.60–0.77)	0.46 (0.31–0.60)	0.61 (0.52–0.71)	0.38 (0.24–0.52)
	Release Volume, (Mm^3)	41	21	8.3	5.5	4.3	2.7
Reported from Case Histories	Actual Release Volume Proportion	0.32		0.80		0.09	
	Predicted Exceedance Probability	0.99	0.43	0.18	0.04	1	0.96
	Actual Release Volume (Mm^3)	23.6		9.57		0.6	
	Failure Mode	FN		SI		OT	

[1] The convention 1 $Mm^3 = 10^6$ m^3 is used here, as opposed to the metric system convention, following common use in the industry.

Model performance can be evaluated through investigation of exceedance probabilities. These are calculated as the predicted probability of exceeding the observed V_U; if f is the predictive (scaled) density function, then the exceedance probability is $\int_{V_U}^{1} f(x)\mathrm{d}x$. If predictive distributions are calibrated, then exceedance probabilities should be uniformly distributed. Table 6 shows that exceedance probabilities tend to be closer to 0 or 1, indicating the need for further calibration of expert judgement and integration of data. Despite this, predictions are more certain than random guessing (i.e., the Uniform distribution), as seen from the interquartile ranges spanning roughly 0.2 to 0.3 units compared to the Uniform distribution's 0.5. A metric to consider during the refinement stage is the Continuous Ranked Probability Score, which combines calibration with prediction certainty.

The probability distribution from the tool produces an exceedance probability of nearly 100% compared to the actual value for Mount Polley, which is expected considering the failure was at the lower bound of release volume proportions in the failure case dataset.

The predicted value for Brumadinho (using a foundation failure for simplicity in this framework) is lower than the actual value, but it is recognized that Brumadinho was considered a relatively extreme failure scenario. The probability distribution from the tool produces an exceedance probability of 18% compared to the actual value, which aligns with the expected result.

The predicted value for Merriespruit is higher than the actual value, with a corresponding 96% exceedance probability compared to the actual value.

These values, in general, are considered reasonable though they do suggest additional refinement of the scaling factors should be completed through comparison to additional failure case studies. Additional refinement can be achieved by considering additional site factors in case the selected ones are not sufficient at capturing the characteristics of failure case. Additionally, other interaction effects may need to be considered; for instance, in the current model, the pond ratio effect is only applied when liquefaction is low.

Discussion

Applications

This paper outlines the authors vision to develop a screening-level risk tool which could be used to support improved consideration of risk in site selection and preliminary design, rapid screening and prioritization of large portfolios of dams, and assessment of the reasonableness of risk assessment results generated using more rigorous methods.

Independent of full risk screening, the probabilistic release volume tool has some interesting applications, including informing the range of TDBA scenarios that should be conducted in consideration of the risk drivers. The probabilistic release volume tool when used in combination with the previously

developed probability of failure calculator (Porter et al., 2023) can help identify the risk driving breach scenarios and prioritize the number of TDBA scenarios. For example, depending on the unique site conditions, the probability of failure due to a foundation and seepage failure may be identified as contributing the most to the dam's overall total annual probability of failure. Based on the estimated dam-specific release volume distributions for these two failure modes, one may observe that the release potential for a foundation failure is significantly greater than for a seepage failure. This could allow for an informed decision to prioritize assessment of the foundation failure mode, Additionally, generating probability distributions for release volumes allows practitioners to make informed decisions on what release volume to use in a TDBA, such as the 50^{th} or 90^{th} percentile, based on a consideration of uncertainty in characterizing the failure. This method also highlights the full range of release potential rather than relying on average values as is often seen in current practice.

Further work is also planned by the authors to extend the tool to include a probabilistic framework for breach hydrograph development as discussed in the following sub-section.

Extending to a probabilistic breach hydrograph framework

While there is uncertainty associated with characterizing credible failure modes and mechanisms (especially in absolute terms), the physical processes that lead to a failure are generally understood. However, the way in which the failure evolves and releases stored material is complex and still a maturing science (Clohan and Kidner, 2020). As such, there are currently no physically based models that are capable of accurately estimating the rate of tailings released over time (i.e., tailings breach hydrograph). Instead, empirically/semi-empirically based models that are based on clear-water breach events are used to develop tailings dam breach hydrographs using estimates of breach bottom width (BBW) and time of failure (ToF).

The Canadian Dam Association (CDA, 2021) provides high-level guidelines on the development of tailings dam breach hydrographs using estimates of BBW and ToF. However, there are no industry specific technical standards for determining these parameters, and the typically referenced equations used to estimate embankment breach parameters are, in most cases, empirical (DSO, 1998) and largely based on past failures of water-retaining dams less than 30 m high, which is not particularly applicable to large tailings dams or tailings dams in general (Clohan and Kidner, 2020).

The current state-of-practice for determining BBW's and ToF's is to use one of the following techniques:

1. Use a single correlation between estimates of release volumes and dam characteristics. For example, use DSO (1998) to estimate the BBW and ToF.
2. Assume that discrete estimates of BBW and ToF represent a range of potential estimates and develop a probability distribution function over the range of estimates.

The validity of the first technique is generally undisputed as there is an implicit correlation between the BBW and ToF that suggests the parameters should not be mixed and matched. However, as one equation can predict a relatively larger BBW with a relatively longer ToF and another equation can predict a relatively smaller BBW with a relatively shorter ToF for the same inputs, it is often unclear which equation is the most conservative or which generally represents an "average" condition.

The authors acknowledge some may contest the mixing and matching of breach parameters and that technique 2 may not be valid. However, Ahmadisharaf et al. (2016) has shown that the correlation between BBW and ToF is relatively weak, and that mixing and matching breach parameters is a useful approach for developing a probabilistic framework to selecting a breach hydrograph.

By understanding the probability of a given hydrograph, a connection with the probably of failure and the probability of release volume can be made to develop a true probabilistic breach hydrograph.

Limitations of screening-level risk tools

The use of a screening-level tool must be used for the appropriate application and in consideration of the limitations of the tool at its current stage of development. The risk screening-level tool described is meant to complement more rigorous risk assessment methods such as quantitative or semi-quantitative assessments that are supported by subject matter experts.

The development of baseline distributions and adjustment factors presented in this paper are considered preliminary and will be refined as part of future work planned by the authors, as described in the above sections. For example, an investigation as to what scaling factors are empirically achievable would facilitate the selection by expert judgement. The expectation is that the tool will improve over time as more data becomes available to support a statistical basis and by the incorporation of more expert involvement and testing.

Acknowledgements

The authors would like to acknowledge Michael Porter and Rob Millar from BGC Engineering Inc. for their contributions.

References

Ahmadisharaf, E., A.J. Kalyanapu, B.A. Thames and J. Lillywhite. 2016. A probabilistic framework for comparison of dam breach parameters and outflow hydrograph generated by different empirical prediction methods. *Journal of Environmental Modelling and Software* 86: 248–263.

Canadian Dam Association (CDA). 2021. Technical Bulletin: Guidelines for Tailings Dam Breach Analysis.

Clohan, D. and E. Kidner. 2020. Tailings Breach Studies and Inundation Mapping. In K.F. Morrison (ed.), *Tailings Management Handbook: A Life-Cycle Approach.*

Dam Safety Office (DSO). 1998. Prediction of embankment dam breach parameters – a literature review and needs assessment. DSO-98-004, Water Resources Research Laboratory, Bureau of Reclamation, US Department of the Interior.

Global Tailings Review. 2020. Global Industry Standard on Tailings Management. Co-convened by International Council on Mining and Metals, UN Environment Programme, and Principles for Responsible Investment.

International Commission on Large Dams (ICOLD). 2022. Bulletin No. 194, Version 1.0, Tailings Dam Safety (Final Version Submitted for Publishing), November 16, 2022.

Larrauri. P.C. and U. Lall. 2018. Tailings dam failures: Updated statistical model for discharge volume and runout. *Environment* 5(2).

Lin, S., G. Wang, W. Liu, B. Zhao, Y. Shen, M. Wang and X. Li. 2022. Regional distribution and causes of global mine tailings dam failures. *Metals* 12(6): 905.

Piciullo, L., E.B. Storrøsten, L. Zhongqiang, N. Farrokh and S. Lacasse. 2022. A new look at the statistics of tailings dam failures. *Engineering Geology* 303: 106657.

Porter, M., B. Russell and B. Watts. 2023. Using statistics and judgement to generate screening-level estimates of tailings dam risk. *Proceedings of Tailings and Mine Waste 2023.* Vancouver, Canada, November 2023.

Rana, N.M., N. Ghahramani, S.G. Evans, A. Small, N. Skermer, S. McDougall and W.A. Take. 2022. Global magnitude-frequency statistics of the failures and impacts of large water-retention dams and mine tailings impoundments. *Earth-Science Reviews* 232: 104144.

Rico, M., G. Benito and A. Diez-Herrero. 2008. Floods from tailings dam failures. *Journal of Hazardous Materials* 154: 79–97.

Stark, T.D., L. Moya and J. Lin. 2022. Rates and causes of tailings dam failures. *Advances in Civil Engineering*. https://doi.org/10.1155/2022/7895880

Volumes of Dam Material Mobilized by Erosion During Tailings Dam Failure Events

Daniel Adria, Knight Piésold, Canada
Violeta Martin, Knight Piésold, Canada
Heleman Wong, Knight Piésold, Canada

Abstract

The breach size and shape, and the rate at which it is formed, are key characteristics that must be estimated for conducting a dam breach analysis. A frequently used simplification in such analysis is that the breach channel through a dam is trapezoidal in cross section. This convention allows for consistent comparison between historical dam breaches (water and tailings dams alike) and is useful for numerical modelling of the breach hydrograph and downstream flood wave or runout propagation. However, a breach channel is three-dimensional, and an assessment of the volume of the dam material mobilized for a given two-dimensional trapezoidal breach geometry represents an additional useful parameter to consider when conducting the breach analysis.

The breach geometry and the mobilized dam volumes in a tailings dam breach event could vary substantially depending on the construction type, the dam geometry, and the construction materials used. The breach characteristics can also be impacted by the breach mechanism, which appears to be different for erosional type mechanisms (i.e., overtopping and internal erosion) compared to non-erosional type mechanisms (e.g., slope instability, foundation failure, liquefaction). It is important to include such considerations when conducting tailings dam breach analyses, as they may present physical constraints for the breach development.

Two empirical equations for calculating the eroded dam volume and the dam erosion rate are presented in this paper. Multiple linear regression equations were developed for a combination of historical erosional breach events of water and tailings dams, which use the breach height and the breach outflow volume as inputs. Also presented is a method to estimate whether the supernatant pond volume is sufficiently large for an erosional breach to progress to the foundation based on these equations.

Introduction

The breach size and shape, and the rate at which it is formed, are the key characteristics that must be

estimated when conducting a tailings dam breach analysis (TDBA). A frequently used simplification is that the breach channel through a dam is trapezoidal in cross section. This convention allows for consistent comparison between historical dam breaches (water and tailings dams alike) and is useful for numerical modelling of the breach hydrograph and downstream flood wave or runout propagation using the parametric breach approach (Froehlich, 2008; Wahl, 1998). The parametric breach approach is available in commonly used software for TDBAs (e.g., HEC-RAS, FLO-2D, RiverFlow2D). Many empirical equations developed for water retaining dam breaches use this convention as well.

A breach channel is three-dimensional, however, and an assessment of the volume of the dam material mobilized for a given two-dimensional trapezoidal breach geometry represents an additional useful parameter to consider when conducting the breach analysis. The breath or thickness of tailings dams can range substantially between facilities and dam construction methods (e.g., upstream, centerline, or downstream). All else being equal, it is intuitive that a larger breach channel would develop in a narrower upstream or centerline constructed dam compared to a wider downstream constructed dam (Figure 1), as the same amount of energy would be available for eroding through a much larger dam volume.

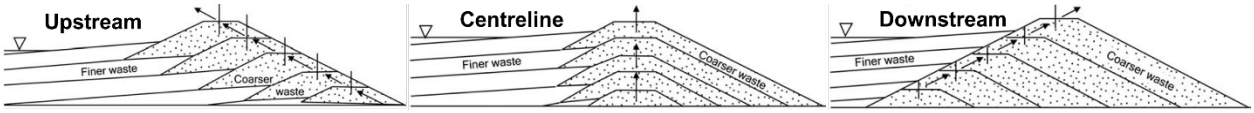


Figure 1: Comparison of tailings dam geometries (adapted from Blight, 2010)

Despite this, most common empirical equations would suggest the same formation time and breach width for both tailings dams, which limits the inclusion of either adverse or favorable site-specific conditions such as the dam size and geometry. Furthermore, these empirical equations are not appropriate to use when the failure is caused by non-erosional mechanisms (e.g., slope instability, foundation failure, liquefaction, etc.), because they were developed for overtopping and internal erosion type failures. The outflow volume, breach geometry and formation time, as well as the peak flow and hydrograph shape are strongly impacted by whether a dam is breached through erosional or non-erosional mechanisms, as discussed in this paper.

Adria et al. (2023a) presented a paper at the 2023 Canadian Dam Association (CDA) conference, in which they introduced two empirical equations for calculating the eroded dam volume and the dam erosion rate for erosional breach scenarios. While these equations are applicable to both water and tailings dams, their applicability to tailings dams and some of the examples presented in that paper are further discussed herein. These examples include specific considerations such as a method to estimate whether the supernatant pond volume is sufficiently large for an erosional breach to progress to the foundation. Additional work is ongoing to expand on the understanding and the dataset related to erosional breaches of tailings dams.

Dam breach processes

Deep understanding of the physical processes during the breach and subsequent flood wave propagation are key requirements for conducting successful breach studies (Rana et al., 2021a). For context within this paper, these processes and existing conventions are summarized below.

Breach geometry conventions

The breach geometry is typically represented with a trapezoid (Figure 2), using the breach height, the average breach width (B_{Avg}), and the breach side slopes (Z_L and Z_R). The bottom breach width (B_B), or alternatively the top breach width (B_T) could be used. The ultimate breach geometry for erosional breaches can be formed by a V-shape cut that progresses downwards until it encounters materials that are substantially less erodible than the dam material, after which it starts widening until the outflow no longer has the capacity to further enlarge the breach opening. The period from when the V-shape begins cutting down into the dam to when the ultimate breach geometry is reached is considered the breach formation time. The formation time excludes the comparatively minor head-cutting phase that occurs during the initial overtopping or internal erosion development (Wahl, 1998), prior to the main breach progression. The breach geometry for non-erosional breaches appear to have more rounded shapes (e.g., U-shapes), but could be reasonably approximated with the same trapezoidal convention (Adria et al., 2023b).

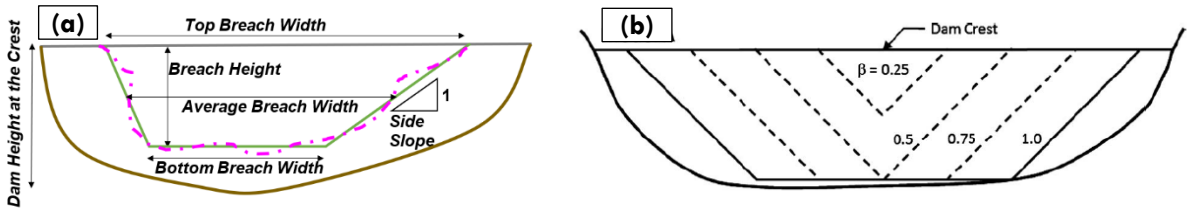


Figure 2: Trapezoidal breach: a) geometry and b) breach formation (Froehlich, 2008)

Breach and outflow processes

Breach processes and characteristics developed through internal erosion and overtopping of water retaining dams are well understood and documented (e.g., USBR, 1988; Wahl, 1998; Froehlich, 2008; Wahl, 2014; Walsh et al., 2021). These processes primarily involve erosion of the dam materials by water flowing over the crest or through the dam over a period of minutes to hours. Failures can also be caused by slope instability, foundation failure, structural failure, liquefaction, or other mechanisms that could remove the containment structure within seconds to minutes. In such "non-erosional" type failures, erosion does not play a key role, as these failures are dominated by geotechnical characteristics (e.g., slip surfaces, residual undrained shear strength ratios, etc.) rather than pond volumes.

The breach outflow volume for tailings dam breaches depends on whether there is a pond present in the TSF, and whether the tailings are susceptible to liquefaction (Small et al., 2017; CDA, 2021). The CDA

TDBA guidelines (2021) further identify two processes to qualitatively describe the discharge mechanisms associated with the outflow of the supernatant pond and/or flowable tailings. Process I is the discharge of the supernatant pond that carries tailings and dam materials mobilized through erosion, which can often be analyzed using Newtonian fluid approximations. Process II is the outflow of flowable tailings that are mobilized due to liquefaction or progressive slumping of unsupported tailings until a stable tailings slope is achieved (backscarp). The outflow from Process II would be primarily comprised of tailings solids and interstitial water, and therefore would have a much lower water content (i.e., higher solids content) compared to Process I. Process II outflows must be analyzed using non-Newtonian fluid approximations and associated rheological properties for the tailings material. A breach can, but does not have to, include both Process I and Process II outflows, which can occur in either order, or simultaneously.

As the breach opening develops and the outflows propagate downstream, the physical impacts of the two discharge mechanisms typically are notably different. Process I breach outflows have a relatively low solids content and are highly erosive, as was observed in the Mount Polley failure in 2014 with the erosion of Hazeltine Creek (Morgenstern et al., 2015; Cuervo et al., 2017). In contrast, Process II runouts have a high solids content and typically result in limited erosion. For example, the liquefied tailings outflow from the Prestavèl TSF in Italy (i.e., Stava) had a high fluidity and an intensive destructive power, but the downstream creek channel itself did not undergo much erosion or deposition (Berti et al., 1988). Takahashi (2014) stated that no erosion occurred because the solids fraction inside the water-sediment mixture of the Prestavèl tailings was so high (approximately 48% by volume) that the flow could not become denser through additional erosion. Hungr et al. (2005) similarly stated that flows with lower sediment concentrations can be expected to be more erosive than flows with higher sediment concentrations.

In this paper, the focus is on erosional breach processes through the embankment, which is considered separate from the downstream erosion of stream-channels and their floodplains.

Development of eroded dam volume equations

Adria et al. (2023a) developed two empirical equations to estimate the eroded dam volume (V_{ED}) and the mean eroded dam volume rate (M), which make use of the combined and verified databases for water retaining dam breaches from Wahl (1998, 2014) and erosional tailings dam breaches from Adria et al. (2023b). The proposed relationships are based on multiple linear regressions (MLRs) of dam height and outflow volume. MLRs have better predictive capabilities than the methods in which each input is used individually or combined (as in the height-volume product in MacDonald and Langridge-Monopolis, 1984). The two MLR equations are defined as follows:

$$V_{ED} = 1.26 {H_W}^{1.803} {V_{Out}}^{0.338} \quad (1)$$

$$M = \frac{V_{ED}}{T_f} = 415\ {H_W}^{2.296} {V_{Out}}^{-0.098} \quad (2)$$

In these equations V_{ED} is the volume of the eroded dam material [m³], H_w is the height of water above the breach [m], V_{Out} is the volume of breach outflow that typically includes the supernatant pond and the eroded tailings material [m³], M is the mean eroded dam volume rate [m³/hr], and T_f is the breach formation time [hr]. The variable V_{ED} is the same as V_M or V_{Er} used by MacDonald and Langridge-Monopolis (1984) or Wahl (1998), however, the labelling is changed to prevent confusion with eroded tailings volumes, or dam materials that mobilize through non-erosional breach processes. The events used to develop the empirical equations are compiled in Tables A1 and A2 of the Appendix to this paper.

Figure 3, reproduced from Adria et al. (2023), compares the predicted values for: (a) the eroded dam volume using Equation 1, and (b) the mean eroded dam volume rate using Equation 2 with observed values, while the insets show a box and whisker plot of the predicted to observed ratios. The dashed lines represent half an order of magnitude above and below the 1:1 line, indicating the approximate range of the error. Ideally, the boxplots have a mean and median close to unity (indicating little error on average) and a narrow interquartile range (indicating lower variability in estimated value accuracy). The interquartile ranges for the two equations are comparable to or are smaller than observed in earlier equations, indicating good predictive ability (Wahl, 2004).

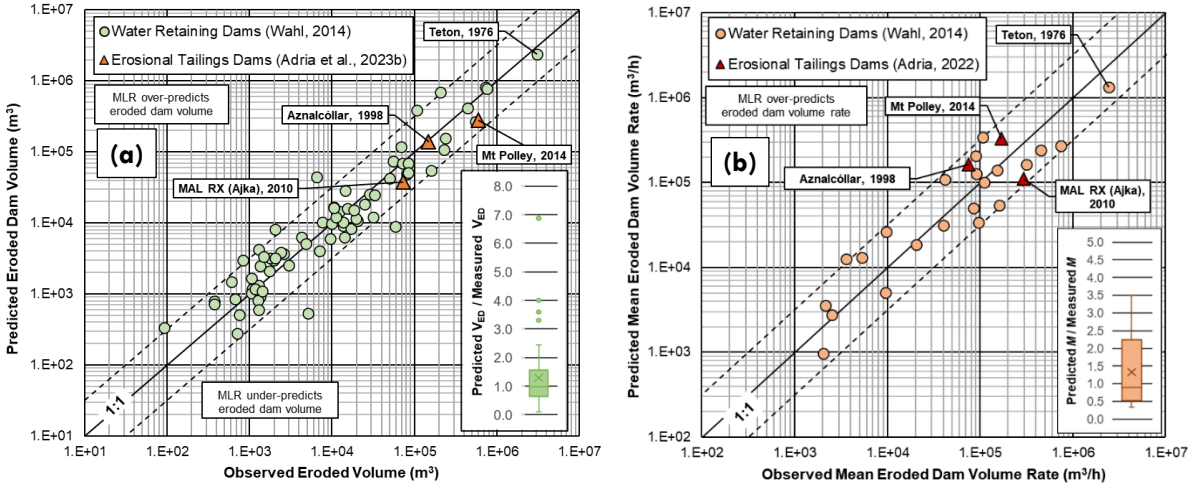


Figure 3: Comparison of observed and predicted values for: (a) eroded dam volume, and (b) mean eroded dam volume rate (from Adria et al., 2023)

For Equations 1 and 2, the volume of tailings that are eroded with the supernatant pond during Process I outflows is included in V_{Out}, while the liquefied tailings volume discharged in Process II outflows is not included in V_{Out} in consideration of the limited erosive potential of Process II flows (this can be changed depending on project-specific conditions). Equations 1 and 2 are not meant to be applied to non-

erosional breach events, for which the breach develops due to drivers other than erosion. For the tailings dam breach events that were included in the development of regression equations shown in Figure 3, the estimated volumes of tailings eroded during the supernatant pond discharge (i.e. Process I) were included in the analysis. A Process II outflow volume may be estimated separately after the breach geometry is selected, and the runout from Process II either evaluated separately or included in the final outflow hydrograph, as appropriate for the project-specific conditions.

The eroded dam volume rate varies during the breach development, with higher rates occurring during the peak outflow and lower rates during the rising and receding limbs of the breach hydrograph. The value predicted by Equation 2 represents the average or the mean rate. The mean eroded dam volume rate itself cannot be used as an input for most dam breach hydrograph modelling approaches, but needs to be combined with an estimate of the eroded dam volume to inform the breach formation time. The eroded dam volume can be estimated either by using Equation 1, or by using other regression equations to determine the breach width and side slopes (e.g., Froehlich, 2008; Xu and Zhang, 2009), and then converted to the eroded dam volume using relatively simple geometric equations. The Washington Guidelines (2007) include discussion on these geometric equations, or 3D CAD modelling can also be used to calculate the eroded dam volume based on the estimated breach geometry for more complex dam geometries if required (e.g., buttresses, or varying slopes). The primary advantage of estimating the mean eroded dam volume rate is to support the selection of both the breach geometry and the breach formation time.

Applications of eroded dam volume equations to tailings dams

Adria et al. (2023a) presented several examples that illustrate the impact of outflow volume or dam geometry on the breach size or the rate of breach development. They also included examples to demonstrate how topographic constraints may impact the breach development, and a discussion on how to use sensitivity analysis to support the final selection of breach parameters. Some of those examples relevant to tailings dams are included herein.

Determining breach widths and breach heights

Breach analysis ideally considers the dam geometry in a rational, non-subjective way. The characteristics of three TSFs that are 50 m tall are summarized in Table 1. These TSFs are hypothetical, but the geometries and pond volumes are comparable with the range the authors have observed for real TDBAs. TSF 1 and TSF 2 have the same pond volume, but TSF 1 has a thinner geometry (i.e., smaller crest width, steeper downstream slope, and a centerline dam construction with nearly vertical upstream slope). TSF 2 and TSF 3 are both downstream constructed dams with the same dam geometry, but the supernatant pond volumes are different. The tailings are considered non-liquefiable (i.e., they would represent Case 1B according to CDA,

2021); however, a portion of the tailings would be eroded and mobilized during the breach development. The eroded tailings volume in Process I was calculated using a 30% volumetric solids concentration in the outflow and a void ratio of 1 for the tailings material (Fontaine and Martin, 2015; CDA, 2021).

In Table 1, Equation 1 was used to calculate the Eroded Dam Volume for all three dams, which was then used to estimate the breach height and the bottom width given the outflow volume. The assumed breach side slopes for all three dams are 1H:1V. TSF 1 and TSF 2 are used to demonstrate how Equation 1 can be used to quantitatively consider the dam geometry (i.e., the dam thickness), rather than relying on subjective adjustments to empirical equation results. For both TSFs the same volume of dam material is predicted to erode (as the pond volumes, and thus, the breach outflow volumes, V_{Out}, are identical); however, the breach width for the downstream constructed dam must be narrower to erode the same dam volume given the same breach height.

Table 1: Comparison of estimated breach heights for different TSF characteristics

Parameter	TSF 1: Large pond centerline dam	TSF 2: Large pond downstream dam	TSF 3: Small pond downstream dam
Supernatant Pond Volume (m^3)	1,800,000	1,800,000	400,000
Eroded Tailings Volume (m^3)	2,700,000	2,700,000	600,000
Total Outflow Volume (m^3)	4,500,000	4,500,000	1,000,000
Crest Width (m)	5	20	20
Upstream and Downstream Slopes (xH:1V)	0 and 2	1 and 4	1 and 4
Calculated Eroded Dam Volume (m^3)	258,000	258,000	62,000
Calculated Breach Height (m)	50	50	30
Calculated Breach Bottom Width (m)	60	0	0

The second pair of TSFs (TSF 2 and TSF 3) that have different supernatant pond volumes is used to demonstrate the relationship between the breach outflow volume and the possible breach height to reach the predicted eroded dam volume from Equation 1. In this process, the breach height can be determined as follows:

1. The required volume of the dam that must be eroded for a breach to reach a given elevation is calculated using the geometric relation between breach geometry and eroded dam volume as per the Washington Guidelines (2007). The breach geometry uses a breach side slope of 1H:1V (or alternate as selected), a bottom breach width of 0, and a given dam geometry (i.e., crest width, upstream dam slope, and downstream dam slope). The calculation is performed at regular breach depth intervals, moving downwards from the crest elevation, to represent a V-shape erosion progression from Froehlich (2008).

2. The potential eroded dam volume that could be eroded for each breach height is calculated using Equation 1 for the same intervals using the predetermined outflow volume and varying the breach height.
3. The two eroded dam volume curves are plotted, and the breach elevation where the required eroded dam volume (Step 1) exceeds the potential eroded dam volume (Step 2) (i.e., the intersection of the two curves) represents the ultimate breach height. If the two curves do not intercept, the breach could progress down to natural ground.

This process is shown in Figure 4 (reproduced from Adria et al., 2023), using the hypothetical example of TSF 2 and TSF 3 from Table 1. The eroded dam volumes are placed on the x-axis to align the breach elevation (y-axis) vertically with the breach geometry schematic; the eroded dam volume remains as the independent variable in this procedure. The small pond is unable to erode the dam to its foundation, while the large pond is sufficient to erode it to the foundation. A pond larger than 1,800,000 m³ would be able to erode the downstream constructed dam to foundation and proceed to lateral erosion and breach widening, as described by Froehlich (2008). Dam features that also could arrest breach should be identified to support an estimated breach elevation that is above the foundation elevation. For example, a large buttress or bench is a plausible cause for the vertical breach progression to be slowed or stopped.

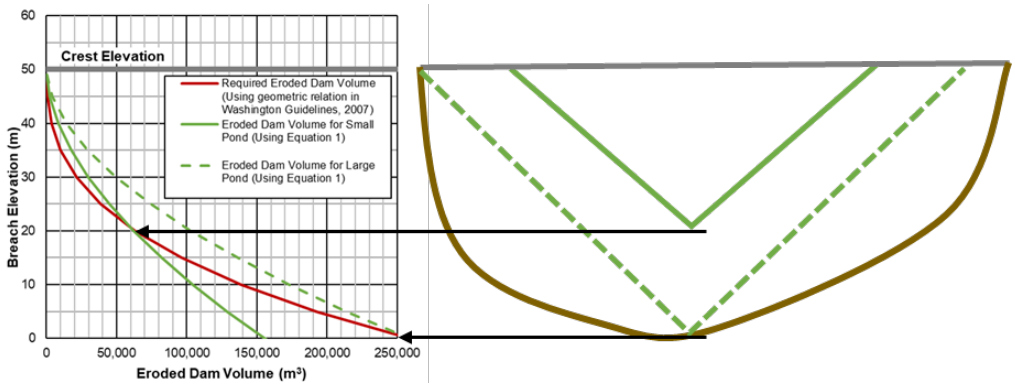


Figure 4: Comparison of the calculated eroded dam volume against the dam volume that would need to be eroded to reach a specific breach height with the V-shape breach

Refining formation times for sensitivity scenarios

A practitioner may ultimately choose more conservative inputs than what is estimated from any one regression equation; however, the combination of these conservative choices should remain within reason, which can be supported using the mean dam erosion rate equation. A larger breach, faster breach, or a combination of a larger and a faster breach could be assessed; however, these scenarios could result in physically impossible and extreme breach outflows. By using Equation 2 and the scatter in Figure 3b, an upper and lower bound on the mean eroded dam volume rate can be estimated for the sensitivity scenarios.

Using TSF 1 from Table 1 as an example, a breach bottom width and a breach formation time were estimated for the base case using Froehlich (2008). The values selected for the sensitivity scenarios (wide or fast breach) were based on the results from Froehlich (2008), and adjusted using the error guidance for these parameters from Wahl (2004). The selected breach side slope for this example was 1H:1V. The example results are shown in Table 2 (from Adria et al., 2023), where the breach width and formation time were calculated using Froelich (2008), V_{ED} was calculated using the geometric relations in Washington Guidelines (2007), and M was calculated using the dam breach formation time from Froehlich (2008) and the eroded dam volume from Washington Guidelines (2007).

Table 2: Mean eroded dam volume rates for sensitivity scenarios for a centerline dam

Parameter	Base Case	Wide Breach	Fast Breach	Wide and Fast Breach
Average Breach Width (m)	55	110	55	110
Bottom Breach Width (m)	5	60	5	60
Breach Formation Time (hr)	0.24	0.24	0.12	0.12
Eroded Dam Volume (m^3)	110,000	260,000	110,000	260,000
Eroded Dam Volume Rate (m^3/hr)	458,000	1,080,000	917,000	2,170,000

In comparison, Equation 2 predicts a mean eroded dam volume rate of 736,000 m^3/h. The maximum error for Equation 2 is approximately 0.5 orders of magnitude, therefore the maximum and minimum M values could be as high as 2,327,000 m^3/h and as low as 233,000 m^3/h, respectively. The base case values, as predicted using Froehlich (2008), result in an M value that is less than the predicted value from Equation 2. This is due to the implicit assumption in Froehlich (2008) that the dam would be downstream constructed and would have more dam material that could be eroded during a breach. A simple change from a centerline dam to a downstream dam that has an upstream dam slope of 2H:1V would result in a similar M value when using Froehlich (2008) to that calculated using Equation 2.

The wide breach and fast breach scenarios have an M value (i.e., 1,080,000 m^3/hr and 917,000 m^3/hr) that is between the best estimate and the maximum M value from Equation 2 (i.e., 736,000 m^3/hr and 2,327,000 m^3/hr, respectively) for the example dam. The wide and fast breach scenario has an M (2,170,000 m^3/hr) that is about the same as the maximum M value from Equation 2. The adjustments in the breach width and formation time used for these hypothetical sensitivity cases are not extreme and are less than the typical uncertainties when using multiple empirical equations (Adria et al., 2023a) but result in an extreme outcome when combined. Depending on the project-specific conditions, the wide and fast breach sensitivity scenario may not be physically possible, or it could be representative of a worst-case scenario for an erosional breach.

It is noted that credible non-erosional breach scenarios could still result in a wider and faster breach than a worst-case erosional breach; however, it is also possible that a non-erosional breach is smaller than the erosional breach and may not represent the worst-case scenario (e.g., a decapitation or a shallow surface slip type failure).

Comparisons to case histories

There are numerous uncertainties in TDBAs every step along the way. It is therefore prudent and beneficial to compare the final selection of breach parameters against case histories to assess whether the selections are reasonable and sufficiently conservative. To assess the predicted mobilized tailings volume in a TDBA, the outflow volume can be compared to the impounded volume. This comparison is shown in Figure 5 (reproduced from Adria et al., 2023), which is adapted from Rana et al. (2021a and 2021b).

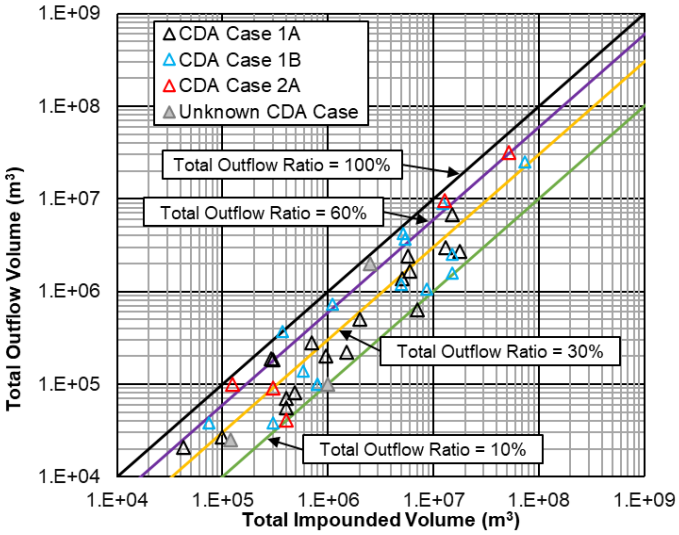


Figure 5: Total outflow ratios for past tailings dam failures (adapted from Rana et al., 2021a)

Other types of comparisons are shown in the Appendix and include scatter plots of: (A) breach heights to average breach widths, (B) eroded dam volumes, (C) mean erosion rates/breach formation times, and (D) mean dam erosion rates. The plots were developed using data compiled by Wahl (1998, 2014), Walder and O'Connor (1997), Rana et al. (2021b), and Adria et al. (2023b). Colored lines that represent relevant ratios are included on these plots for reference. As an example, if the dam evaluated in the TDBA has a broad geometry and is constructed of erosion-resistant materials, it should plot closer to the lower ratios shown with blue lines on the Appendix figures.

Conclusion

This paper discusses the processes that occur during breach formation that need to be understood to prevent

the application of non-analogous case studies or empirical equations to forward-analysis. Two empirical equations from Adria et al. (2023a) are presented that estimate the eroded dam volume and the eroded dam volume rate. These equations can provide additional tools for breach parameter selection, particularly for dam geometries that are outside of the typical conditions in existing dam failure databases. The authors find these equations to be useful tools in their day-to-day practice, as they provide a different measure for checking the reasonableness of the selected breach parameters, given the inherent uncertainties associated with the breach analysis.

Acknowledgements

The authors gratefully acknowledge their clients and colleagues for valuable inputs and support during actual dam breach assessments and preparation of this manuscript. The contributions of Dr Scott McDougall, who collaborated on the CDA 2023 paper, are also greatly appreciated. Various members of the CanBreach Research Program were also instrumental in the development of several key databases used in this paper and contributed thoughtful discussions on several of the themes in this paper over the years. The authors also thank the two reviewers of this manuscript for their constructive comments.-k

References

Adria, D.A.M., Martin, V., McDougall, S., 2023a. The role of sensitivity analysis in selecting dam breach parameters. *Proceedings of the CDA 2023 Annual Conference*, October 22–25, Winnipeg, Canada.

Adria, D.A.M., N. Ghahramani, N.M. Rana, V. Martin, S. McDougall, S.G. Evans and W.A. Take, 2023b. Insights from the compilation and critical assessment of breach and runout characteristics from historical tailings dam failures: Implications for numerical modelling. *Mine Water and the Environment* 42: 650–669. https://doi.org/10.1007/s10230-023-00964-0

Berti, G., F. Villa, D. Dovera, R. Genevois and J. Brauns. 1988. Disaster of Stava, Northern Italy. *Proceedings of the Specialty Conference on Hydraulic Fill Structures:* 492–509.

Blight, G.E. 2010. *Geotechnical Engineering for Mine Waste Storage Facilities*. London, UK: CRC Press/Balkema.

CDA (Canadian Dam Association). 2021. *Technical Bulletin: Tailings Dam Breach Analysis*.

Cuervo, V., L. Burge, H. Beaugrand, M. Hendershot and S.G. Evans. 2017. Downstream geomorphic response of the 2014 Mount Polley tailings dam failure, British Columbia. *Proceedings of the Fourth World Landslide Forum.* Ljubljana, Slovenia. May 29–June 2.

Fontaine, D. and V. Martin. 2015. Tailings mobilization estimates for dam breach studies. *Proceedings of Tailings and Mine Waste 2015,* Vancouver, BC, October 26 to 28: 342–356.

Froehlich, D.C. 2008. Embankment dam breach parameters and their uncertainties. *J Hydraul Eng* 134(12): 1708–1721.

Hungr, O., S. McDougall and M. Bovis. 2005. Entrainment of material by debris flows. *Debris-flow Hazards and Related Phenomena,* M. Jakob and O. Hungr (eds): 135–158. Springer, Berlin.

MacDonald, T.C. and J. Langridge-Monopolis. 1984. Beaching characteristics of dam failures. *J Hydraul Eng* 110(5): 567–586. https://doi.org/10.1061/(ASCE)0733-9429(1984)110:5(567)

Martin, V. and Akkerman, A. Challenges with conducting tailings dam breach assessments. *Proceedings of the International Commission on Large Dams 2017 Annual Meeting, ICOLD,* July 3–7, Prague, Czech Republic (2017).

Morgenstern, N.R., S.G. Vick and D. Van Zyl. 2015. *Independent Expert Engineering Investigation and Review Panel Report on Mount Polley Tailings Storage Facility Breach*

Rana, N.M., N. Ghahramani, S.G. Evans, S. McDougall, A. Small and W.A. Take. 2021a. Catastrophic mass flows resulting from tailings impoundment failures. *Engineering Geology* 292: 106262. https://doi.org/10.1016/j.enggeo.2021.106262

Rana, N.M., N. Ghahramani, S.G. Evans, S. McDougall, A. Small and W.A. Take. 2021b. *A Comprehensive Global Database of Tailings Flows.* Borealis, the Canadian Dataverse Repository. https://doi.org/10.5683/SP2/NXMXTI

Small, A., M. James and M. Al-Mamun. 2017. Advancing the state of practice for tailings dam breach assessment using empirical correlations. *Proceedings of Canadian Dam Association Annual Conference.* Kelowna, BC, Canada. October 16–18.

Takahashi, T. 2014. Chapter 7: Debris flow disasters and their reproduction by computer simulations. In *Debris Flow: Mechanics, Prediction and Countermeasures* (2nd edition, p. 572). CRC Press. Boca Raton.

USBR (US Bureau of Reclamation). 1998. Downstream Hazard Classification Guidelines. Department of the Interior.

Wahl, T.L. 1998. Prediction of Embankment Dam Breach Parameters: Literature Review and Needs Assessment., Water Resources Research Laboratory Report DSO-98-004.

Wahl, T.L. 2004. Uncertainty of Predictions of Embankment Dam Breach Parameters. *J Hydraul Eng* 130(5): 389–397.

Wahl, T.L. 2014. Evaluation of Erodibility-Based Embankment Dam Breach Equations. Water Resources Research Laboratory Report HL-2014-02.

Walder J.S. and J.E. O'Connor. 1997. Methods for predicting peak discharge of floods caused by failure of natural and constructed earthen dams. *Water Resour. Res.* 33(10): 2337–2348.

Walsh, A., S. McDougall, S.G Evans and W. A. Take. 2021. Effect of upstream dam geometry on peak discharge during overtopping breach in noncohesive homogeneous embankment dams; implications for tailings dams. *Water Resour. Res*. 57. Accessed at https://doi.org/10.1029/2020WR029358

Washington State Department of Ecology (Washington Guidelines). 2007. *Dam Safety Guidelines: Technical Note 1 Dam Break Inundation Analysis and Downstream Hazard Classification.*

Xu. Y. and L.M. Zhang. 2009. Breaching Parameters for Earth and Rockfill Dams. *J. Geotech. Geoenviron. Eng.* 135(12): 1957–1970.

Appendix

Table A1: Events used to develop equations – water retaining dams (Wahl, 2014)

Event	Height of Water above Breach invert (m)	Outflow Volume (m^3)	Formation Time (h)	Eroded Dam Volume (m^3)
Apishapa, USA, 1923	27.8	22,202,640	0.75	238,000
Baldwin Hills, USA, 1963	18.3	910,308	0.33	31,700
Bearwallow Lake, USA, 1976	5.8	49,300	–	1,090
Buckhaven No. 2, USA, Unknown	6.1	24,700	–	1,070
Bullock Draw Dike, USA, 1971	3.1	740,088	–	1,350
Butler, USA, 1982	7.2	2,380,000	–	4,310
Castlewood, USA, 1993	21.7	9,251,100	0.50	55,700
Caulk Lake, USA, Unknown	11.4	698,000	–	13,700
Clearwater Lake, USA, 1994	4.1	466,000	–	1,290
East Fork Pond River, USA, 1978	9.8	1,870,000	–	7,630
Elk City, USA, 1936	9.4	1,180,000	–	16,900
Emery, USA, Unknown	6.6	425,000	0.83	1,970
Euclides da Cunha, Brazil, 1977	58.3	57,973,560	–	726,000
Fogelman, USA, Unknown	11.1	493,000	–	2,050
Frankfurt, Germany, 1977	8.2	351,542	–	1,290
French Landing, USA, 1925	8.5	3,873,127	2.58	13,800
Frenchman Creek, USA, 1952	10.8	16,035,240	–	28,400
Goose Creek, USA, 1916	4.5	579,736	0.50	1,070
Grand Rapids, USA, 1900	7.5	255,000	–	1,800
Haas Pond, USA, Unknown	4	23,400	–	708
Hart, USA, 1986	10.7	6,350,000	–	24,800
Hatchtown, USA, 1914	16.8	14,800,000	1.00	161,000
Hell Hole, USA, 1964	35.1	30,590,304	0.75	555,000
Horse Creek, USA, 1914	7	12,800,000	–	20,500
Hutchinson, USA, 1994	4.4	1,170,000	–	1,750
Ireland #5, USA, 1984	3.8	160,000	0.50	1,260
Johnstown (South Fork Dam), USA, 1889	24.6	18,921,583	0.75	68,800
Johnston City, USA, 1981	3.1	574,802	–	673
Kelly Barnes, USA, 1977	11.3	777,092	–	9,940
Kraftsmen's Lake, USA, 1994	3.7	177,000	–	376
La Fruta, USA, 1930	7.9	78,900,000	–	32,900
Lake Avalon, USA, 1904	13.7	31,500,000	2.00	81,000
Lake Frances, USA, 1899	14	789,427	–	12,400
Lake Genevieve, USA, Unknown	6.7	680,000	–	2,630
Lake Latonka, USA, 1966	6.3	4,090,000	–	9,540
Lake Philema, USA, 1994	9	4,780,000	–	11,300

Lambert Lake, USA, Unknown	12.8	296,000	–	5,870
Laurel Run, USA, 1982	12.8	382,379	–	19,500
Lawn Lake, USA, 1982	6.7	798,000	–	2,400
Little Deer Creek, USA, 1963	22.9	1,360,000	0.33	50,600
Long Branch Canyon, USA, Unknown	3.2	284,000	–	378
Lower Latham, USA, 1973	5.8	7,080,000	1.50	14,300
Lower Otay, USA, 1916	39.6	49,300,000	1.00	107,000
Lyman, USA, 1915	16.2	35,770,920	–	71,900
Lynde Brook, USA, 1876	12.2	2,874,008	–	15,300
Melville, USA, 1909	7.9	24,700,000	–	10,600
Merimac Upper Lake, USA, 1994	3.4	69,600	–	758
Mossy Lake, USA, 1994	4.4	4,130,000	–	2,040
Oros, Brazil, 1960	35.4	650,043,960	8.50	765,000
Otter Lake, USA, Unknown	5	109,000	–	1,170
Potato Hill Lake, USA, 1977	7.8	105,000	–	3,010
Quail Creek, USA, 1989	16.7	30,800,000	1.00	84,400
Rainbow Lake, USA, 1986	10	6,780,000	–	10,500
Renegade Resort Lake, USA, Unknown	3.7	13,900	–	92
Rito Manzanares, USA, 1975	4.6	24,670	–	1,290
Salles Oliveira, Brazil, 1977	38.4	71,541,840	–	440,000
Schaeffer Reservoir, USA, 1921	30.5	4,440,528	0.50	227,000
Scott Farm Dam no. 2, Canada, Unknown	10.4	86,000	–	7,020
Sheep Creek, USA, 1970	14	910,000	–	18,300
Sinker Creek, USA, 1943	21.4	3,330,396	2.00	84,100
Spring Lake, USA, 1889	5.5	135,683	–	612
Statham Lake, USA, 1994	5.6	564,000	–	1,350
Teton, USA, 1976	77.4	309,603,480	1.25	3,060,000
Trial Lake, USA, Unknown	5.2	1,480,000	–	829
Trout Lake, USA, Unknown	8.5	493,000	–	4,830
Wheatland no. 1, USA, 1969	12.2	11,594,712	1.50	14,600
Wilkinson Lake, USA, 1994	3.6	533,000	–	1,420
Winston, USA, 1912	6.4	662,379	–	1,480

Table A2: Events used to develop equations – tailings storage facilities (Adria et al., 2023b)

Event	Height of Water above Breach Invert (m)	Outflow Volume (m^3)	Formation Time (h)	Eroded Dam Volume (m^3)
Aznalcóllar, Spain, 1998	26	15,000,000	2.0	150,000
MAL Reservoir X (Ajka), Hungary, 2010	21.8	1,200,000	0.25	74,000
Mount Polley, Canada, 2014	37.7	24,400,00	3.5	600,000

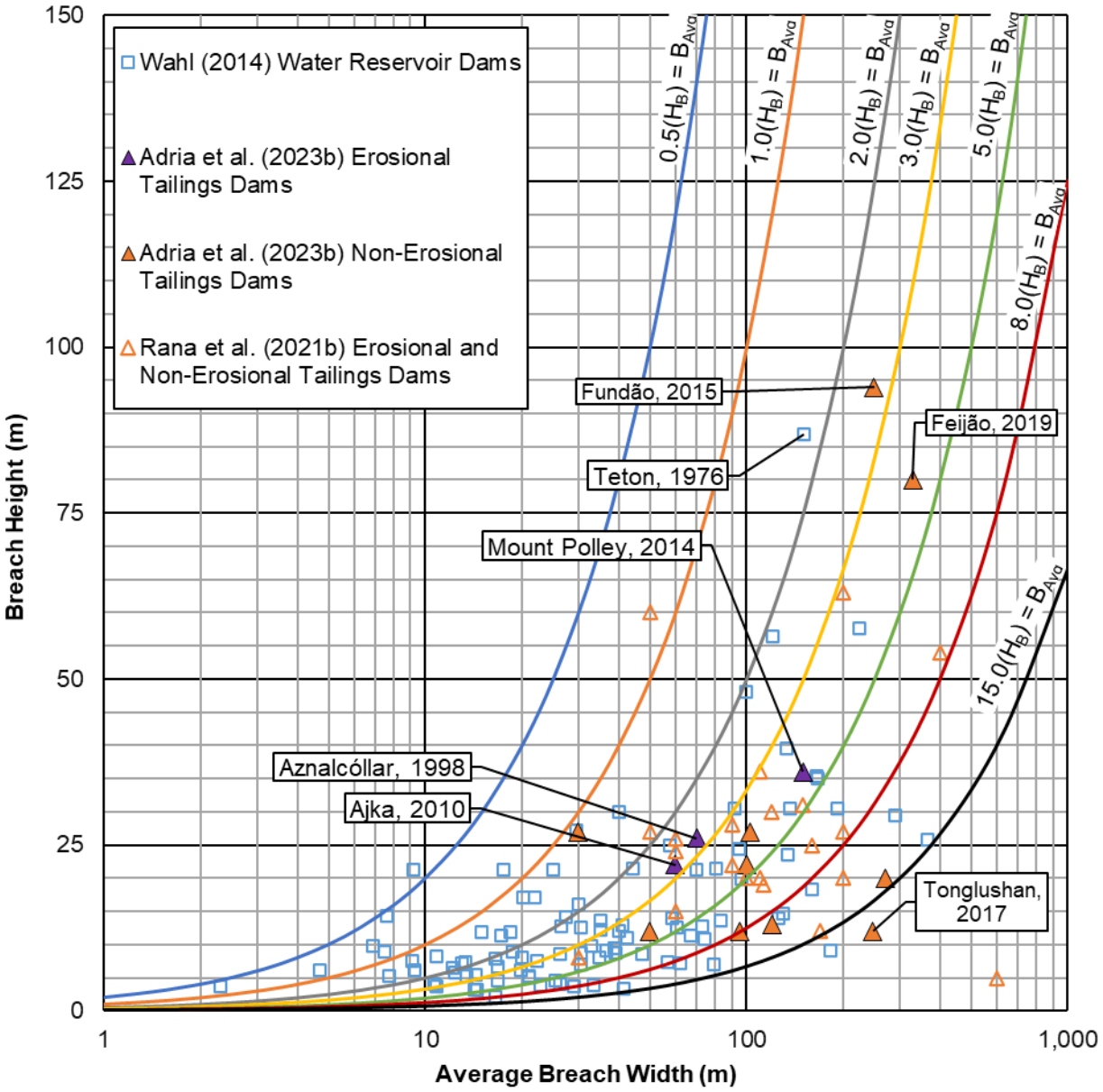


Figure A1: Breach height to breach width ratios (adapted from Wahl, 1998)

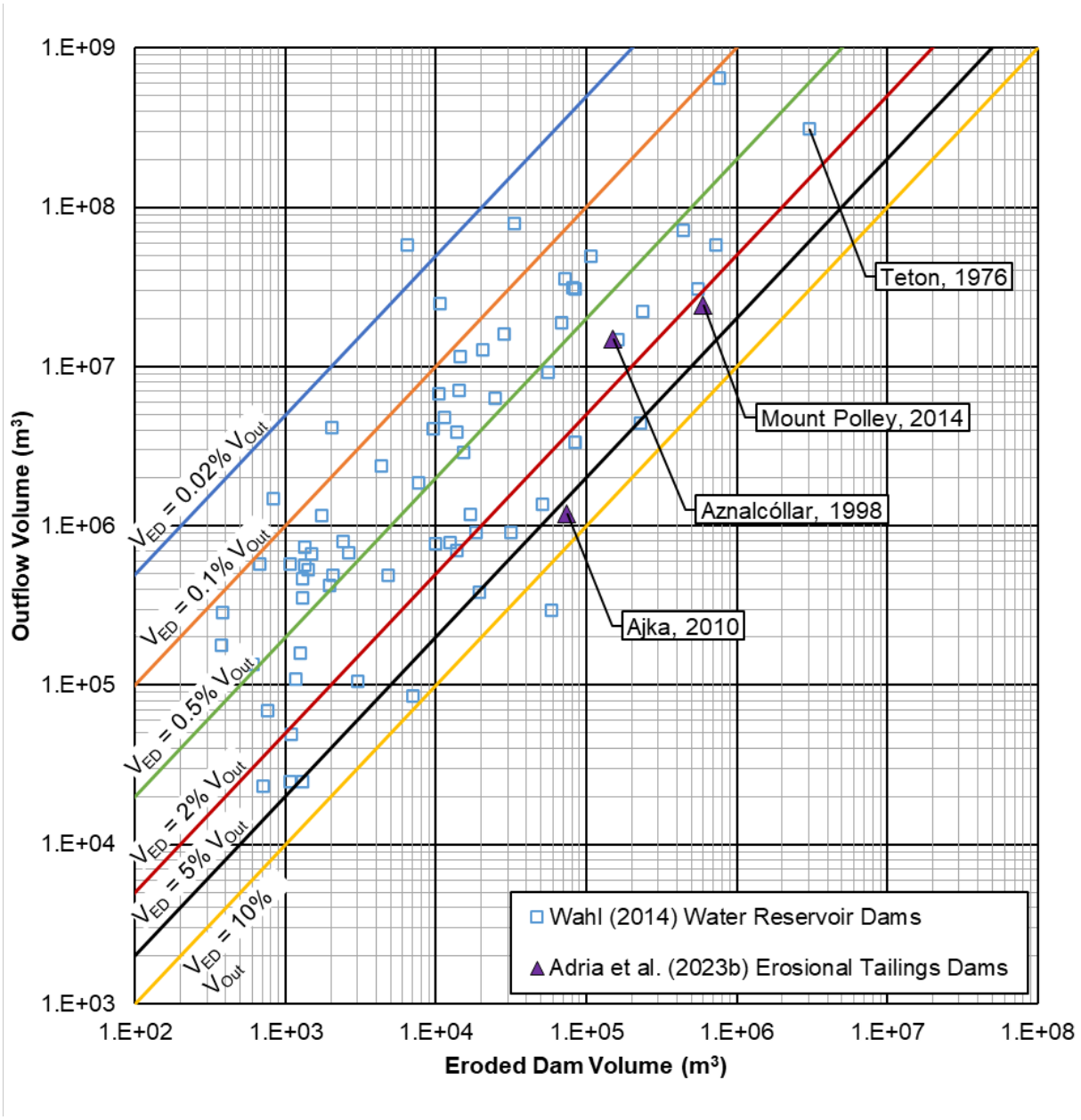


Figure A2: Outflow volume to eroded dam volume ratio

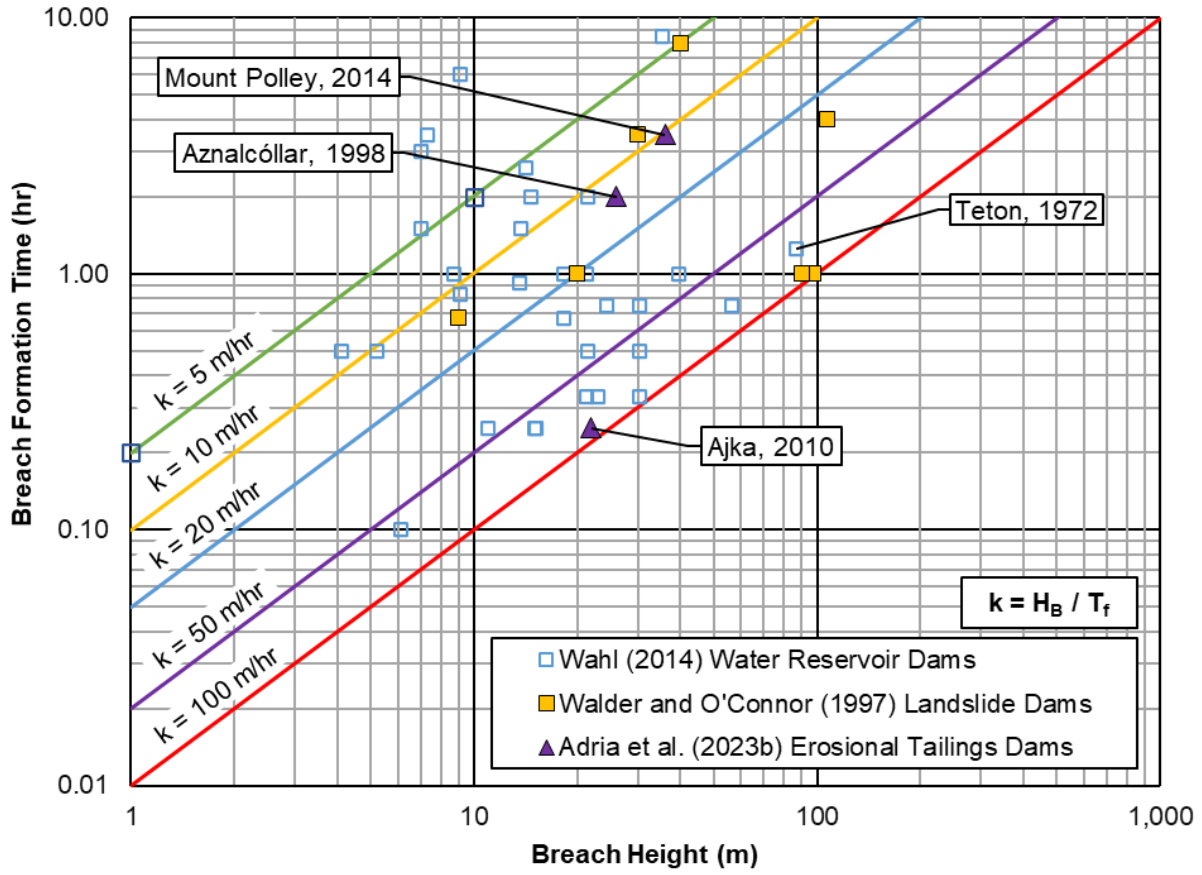


Figure A3: Mean erosion rates for various types of dam failures

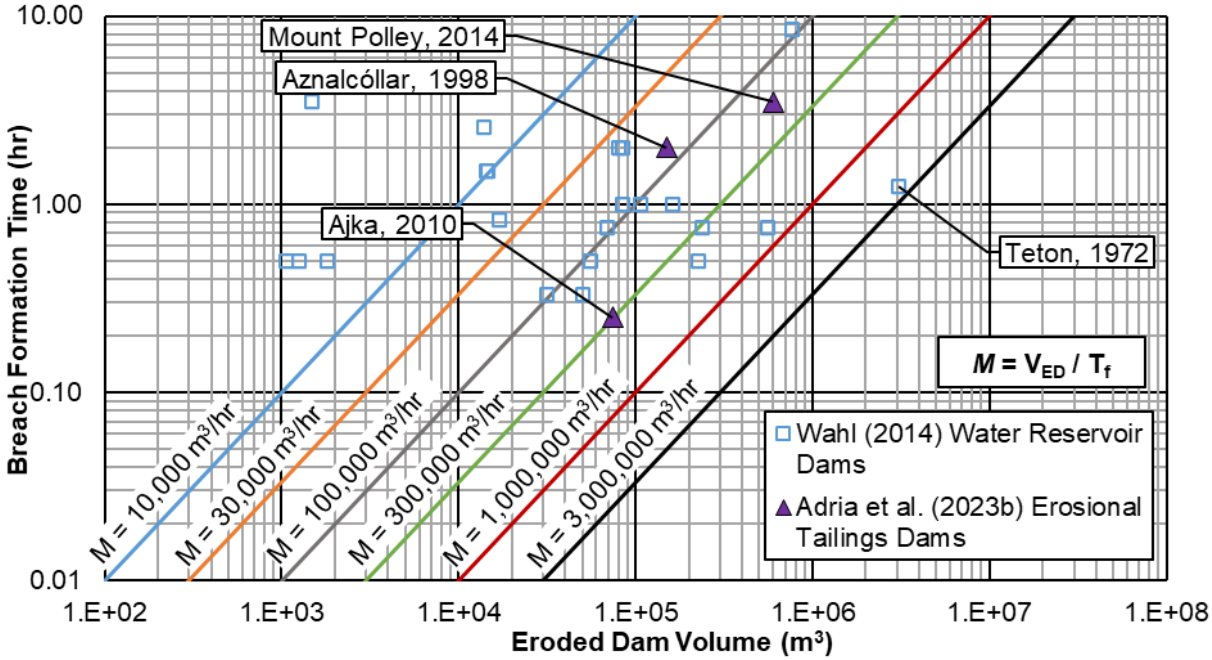


Figure A4: Mean eroded dam volume rates for various types of dam failures

Estimation of Outflow Runout Distance in Tailings Dam Using an Artificial Intelligence Technique

Mohammad Rashidi, Stantec, USA
Sam Abbaszadeh, Stantec, USA
Jenisha Chhetri, Stantec, USA

Abstract

There are about 3,500 tailings dams worldwide storing billions of tons of mill and waste tailings from mineral processing activity at mine sites. A number of particular characteristics make these tailings dams more vulnerable to failure than traditional water storage dams, such as multi-stage raising, constructing embankments using mine waste materials, and the lack of regulations in certain regions. More than a third of the existing tailings dams are at high risk of causing catastrophic damage to the downstream communities, socio-economic activities, and ecological systems. The extent of tailings dam failure is often estimated as part of the risk assessment process, utilizing available empirical and semi-empirical approaches. While these methods are helpful, they are not developed specifically for estimating the runout distance for tailings dams. Some critical parameters that affect outflow runout distance, such as break mechanisms, breach size, and the geometry of the downstream valley, are not incorporated in these methods.

This study introduces a new method to predict potential mine waste runout distance using information from historical tailings dam failures. The new method is based on artificial intelligence and uses the Genetic Programming (GP) method. Parameters such as tailings height at the time of failure, volume of tailings released, and slope of the downstream area are considered as the input parameters in the proposed GP models. The results obtained from comparing the proposed artificial intelligence method and existing empirical relationships showed that the proposed method is capable of estimating the runout distance for tailings dams.

Although the accuracy of any runout estimations should be approached with great caution, the proposed method can be utilized as a simple tool to provide an estimation of the runout distance. This information can be used by the project team to better understand the failure consequences and potential risks and impacts to the downstream population.

Introduction

Tailings dams play a crucial role in storing vast amounts of mill and waste tailings generated from mineral processing activities at mine sites worldwide. With approximately 3,500 tailings dams worldwide, storing billions of tons of tailings, these structures present unique challenges and risks to the communities and environment, in terms of their vulnerability to failure compared to traditional water storage dams (Davies et al., 2000). Factors such as multi-stage raising, the use of mine waste materials in embankment construction, and the absence of adequate regulations in certain regions contribute to the heightened risk associated with tailings dams (Adamo et al., 2020).

Alarming statistics indicate that over one-third of existing tailings dams have a high risk of catastrophic failure, which could lead to severe damage to downstream communities, socio-economic activities, and ecological systems (Rourke and Luppnow, 2015). Accurate estimation of the runout distance resulting from such failures is a crucial aspect of risk assessment, as it helps in understanding the potential consequences and impacts on the downstream population, which is required by most guidelines and standards such as GISTM (Global Tailings Review, 2020).

Current empirical and semi-empirical approaches used for estimating the extent of tailings dam failure, although valuable, do not specifically account for the unique characteristics and parameters influencing runout distance of tailings dams. Critical factors such as break mechanisms, breach size, and the geometry of the downstream valley may have been overlooked in these methods.

To address the limitations of existing approaches, previous studies have sought alternative methods to predict the runout distance of tailings dam failures. Rico et al. (2008) proposed an empirical relationship by analyzing historical data on tailings storage facility (TSF) failures. Their approach incorporated parameters such as tailings height, total tailings volume, and released tailings volume, as represented in Equation 1. The study demonstrated the effectiveness of this approach in estimating runout distance. However, an important factor that was not considered in their estimation was the influence of downstream topography. The omission of downstream topography as a parameter in their analysis represents a gap in their methodology.

$$D_{max} = 1.61 \times (H \times V_R)^{0.66} \quad (1)$$

Where D_{max} is maximum runout distance (km), H is the dam height (m), and V_R is released outflow volume ($\times 10^6 m^3$).

In this study, a novel method is presented for predicting the runout distance of tailings dam failures by leveraging historical data from past incidents and utilizing artificial intelligence, specifically the Genetic Programming (GP) method. By incorporating key input parameters such as tailings height at the time of failure, volume of released tailings, and the slope of the downstream area, our proposed GP model aims to provide accurate estimations of the runout distance. By integrating these critical factors, the proposed

method seeks to overcome the limitations of previous approaches and improve the reliability of runout distance predictions for tailings dam failures.

While the proposed method may serve as a simple tool, it can provide valuable insights for project teams in comprehending the potential risks, impacts, and failure consequences to downstream populations. By integrating the estimation of runout distance into risk assessments, decision-makers can make more informed choices regarding tailings dam management, emergency preparedness, and disaster response.

In the subsequent sections of this paper, we will delve into the methodology employed, present the results of the comparative analysis, and discuss the implications of the proposed method for tailings dam failure mitigation.

Study of database

The height at the time of failure (H), TSF capacity (V_T), released volume (V_R), and the distance traveled by the tailings (D_{max}) are inputs in Rico et al.'s (2008) method (Equation 1). Of the 29 tailings dam failure cases analyzed by Rico et al., nine of them did not have complete information, particularly the downstream slopes of TSF (S). Therefore, the remaining 20 tailings dam failures were used to develop and validate the correlation presented in this study, as illustrated in Table 1. Figure 1 indicates the location of the tailings dam failures reported in Table 1.

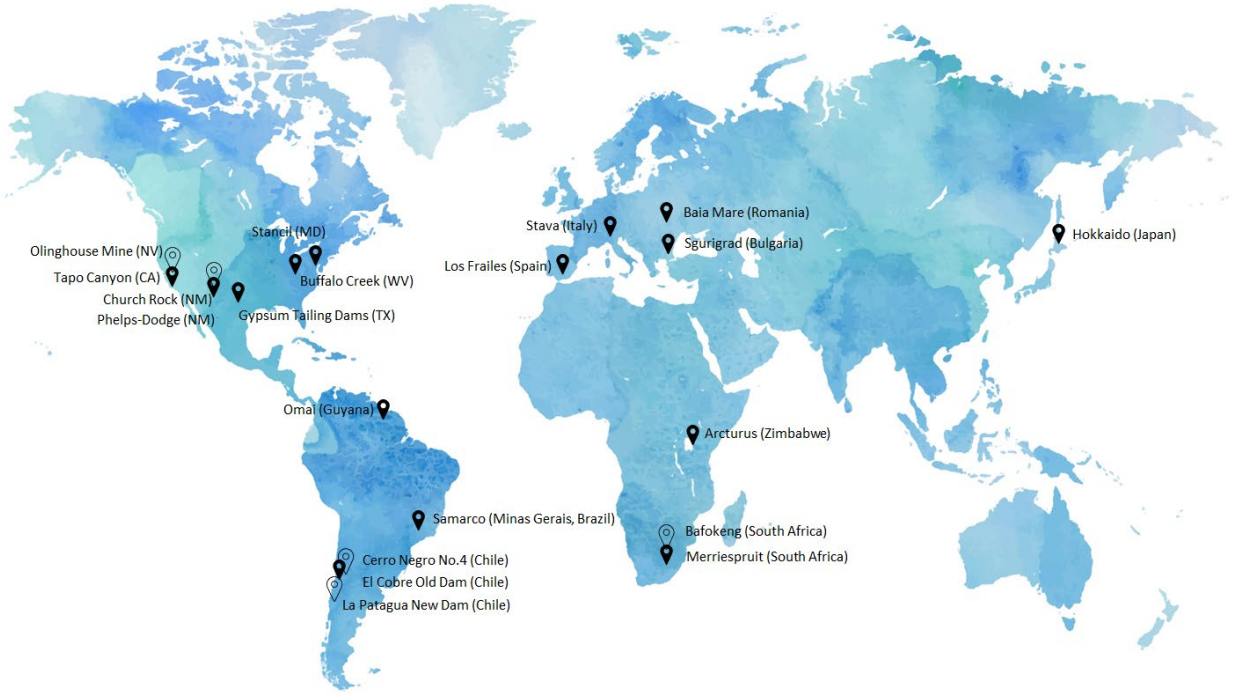


Figure 1: Relative location of the tailings dam failures used in the study

Table 1: Database of tailings dam failures used in the study

No	Dam name	Year of failure	Height of dam (m)	Released 43 ($\times 10^6 m^3$)	Total volume ($\times 10^6 m^3$)	Downstream slope (%)	Runout distance (km)
1	Arcturus (Zimbabwe)	1978	25	0.0211	0.911	6.7	0.3
2	Bafokeng (South Africa)	1974	20	3	13	1.6	45
3	Baia Mare (Romania)	2000	7	0.1	0.8	5.6	0.18
4	Buffalo Creek (USA)	1972	16	0.5	0.5	1.1	64.4
5	Cerro Negro No.4 (Chile)	1985	40	0.5	2	1.9	8
6	La Patagua NewDam (Chile)	1965	15	0.035	0.3	2.1	5
7	El Cobre Old Dam (Chile)	1965	35	1.9	4.25	1.1	12
8	Gypsum Tailings Dam (USA)	1966	11	0.98	3.44	6.7	0.3
9	Hokkaido (Japan)	1968	12	0.09	0.3	12.7	0.15
10	Los Frailes (Spain)	1998	27	4.6	17.5	0.3	41
11	Sgurigrad (Bulgaria)	1966	45	0.22	1.52	6.1	6
12	Merriespruit (South Africa)	1994	31	1.23	7.04	5.9	2
13	Phelps-Dodge (USA)	1980	66	2	2.5	2.1	8
14	Stancil (USA)	1989	9	0.038	0.074	4.0	0.1
15	Stava (Italy)	1985	29.5	0.19	0.3	10.2	4.2
16	Tapo Canyon (USA)	1994	24	0.08	0.16	7.8	0.18
17	Churchrock (USA)	1979	11	0.37	0.37	0.6	104
18	Ollinghouse (USA)	1985	5	0.025	0.12	10.5	1.5
19	Omai (Guyana)	1995	44	4.2	5.25	2.2	80
20	Cerro Negro No.3 (Chile)	1965	20	0.085	0.5	2.2	5

Genetic programming

Genetic programming is a subfield of artificial intelligence that extends the principles of genetic algorithms (GAs) (Goldberg, 1989). GP begins with an initial population consisting of randomly generated computer programs, represented as syntax trees, composed of functions and terminals suitable for the given problem domain. Functions encompass standard arithmetic operations, programming operations, mathematical functions, logical functions, and domain-specific functions. Terminals, on the other hand, represent constants or variables. Through a supervised trial and error process, the initial functions and terminals undergo adjustments to obtain refined functions and terminals that accurately estimate the desired output.

GP, much like nature, is inherently a random process and cannot guarantee specific results. However, the stochastic nature of GP enables it to escape traps that deterministic methods may encounter. This randomness has proven to be a key factor in the success of GP, as it allows for the evolution of innovative and unexpected solutions to complex problems.

In GP, programs are commonly represented as syntax trees, as opposed to traditional lines of code. For instance, Figure 2 depicts a tree representation of the program "max(x + y, x – 6)," where x and y are independent variables, and 6 is a constant. In GP, the leaves of the tree, such as variables and constants, are referred to as terminals, while the internal nodes, such as arithmetic operations and functions like "max," are called functions. The collective set of allowed functions and terminals forms the primitive set of a GP system.

Similarly to other evolutionary algorithms, GP involves the generation of an initial population of individuals, typically generated randomly. Various approaches exist for generating this initial population, including the full and grow methods, which are simpler and earlier techniques, as well as a widely used combination of the two known as ramped half and half (Koza, 1992). Genetic operators in GP, such as crossover and mutation, are applied to individuals who are probabilistically selected based on their fitness, as determined by the objective function.

By leveraging the principles of GP, researchers and practitioners can explore the potential of evolving novel solutions and addressing complex problems through adaptive and self-improving computational processes.

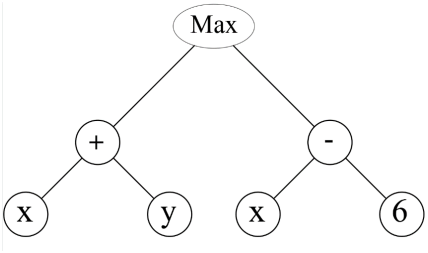


Figure 2: Representation of an expression tree in GP ("Max" represents the maximum function)

The advantage of GP over other soft computing techniques (such as artificial neural networks and adaptive neuro fuzzy inference systems) is that GP is not a black box and outputs are in the form of semi-complex mathematical solutions, which could be applicable to the actual problems. The GP approach is relatively new in the field of dam engineering, although some studies have been dedicated to their application recently (Rashidi et al., 2021; Noorzad et al., 2014).

In this study the data set was divided into training (80%), and validation (20%) subsets to prevent overfitting. The performance of the testing set is critical because it determines the accuracy and generalization capability of the model.

Two statistical evaluation criteria were used to assess the performance of the intelligent methods. These criteria are Root Mean Square Error (RMSE) and determination coefficient (R^2), respectively, given by Equations 2 and 3.

$$RMSE = \sqrt{(\frac{1}{n})\sum_{i=1}^{n}(a_i - p_i)^2} \quad (2)$$

$$R^2 = (\frac{\sum_{i=1}^{n}(p_i - p^-)(a_i - a^-)}{\sqrt{\sum_{i=1}^{n}(p_i - p^-)^2(a_i - a^-)^2}})^2 \quad (3)$$

where a is the actual value and p is the predicted value, a^- and p^- are the mean of actual and predicted values respectively, a is the absolute error, $a_i - p_i$; a- is the mean of absolute error, 1n and n is the number of data sets. Evidently, a model with good performance (i.e., RMSE close to 0 or R^2 close to 1) will be the best model among several candidates.

Results and discussions

Sensitivity analysis

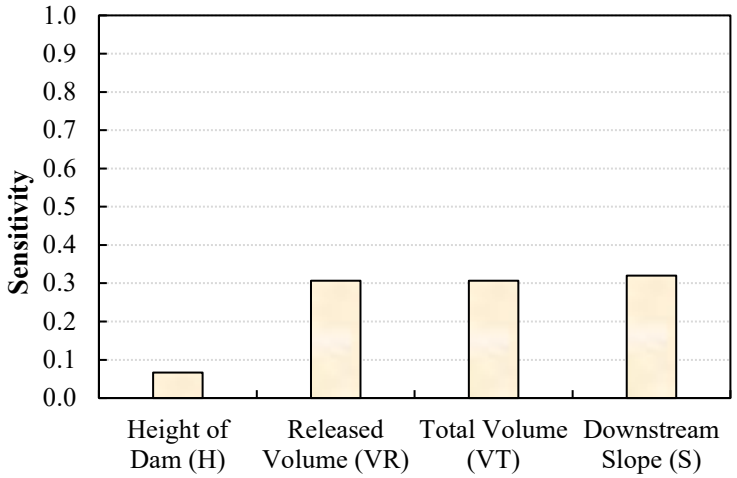


Figure 3: Sensitivity of the runout distance to the tailings dam features

Figure 3 illustrates the results of the sensitivity analysis conducted on the GP model developed in this study. The sensitivity function provides insights into the relative impact of input parameters on the estimation of runout distance. A negligible magnitude of the sensitivity function indicates that the corresponding input parameter has minimal influence on the model's output, whereas a higher value signifies a greater impact of the tailings dam features on the estimated runout distance.

Based on the sensitivity analysis results presented in Figure 3, it is evident that the downstream slope of the tailings storage facility (TSF) exhibits the highest influence on the maximum runout distance of a tailings dam. Following the downstream slope, the total and released volume of tailings were identified as the next most influential parameters affecting the outflow runout distance. Conversely, the height of the tailings dam was found to have the lowest influence compared to the other parameters. These findings highlight the critical impact of the downstream slope in determining the runout distance of tailings dams. Understanding the significant influence of these parameters allows for more informed decision-making and improved risk assessment in the management of tailings facilities.

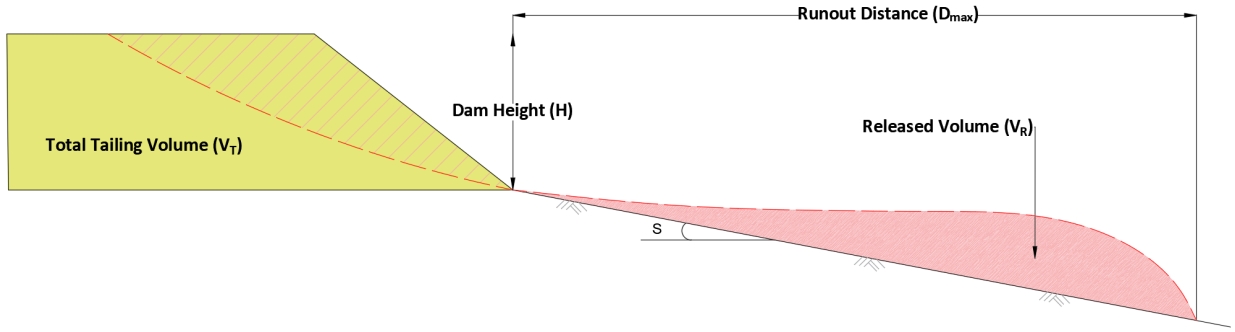


Figure 4: Cross-sectional illustration of the tailings dam failure for a tailing dam

Genetic programming model

Genetic programming was utilized to construct a prediction model for estimating the outflow runout distance of tailings dams. The GP method was employed to develop Equation 4, which incorporated data from 20 case studies and considered three key input parameters: the height of the dam, the released volume of tailings, and the downstream slopes of the TSF:

$$D_{max} = V_T + {V_R}^3 - (\frac{7.21}{S^S} - \frac{113}{V_T + S^{2^S}}) \quad (4)$$

Where D_{max} is maximum outflow runout distance in km, V_R is the released volume of tailings in million m^3, V_T is the total volume of tailings in million m^3, and the S is downstream slopes of the TSF in percentage.

For prediction of runout distance, out of the 20 sets of data, 16 sets (80%) were considered for training and the remaining 4 sets (20%) were considered for validation. The training and validation data sets were selected randomly from the database. Figure 5 shows the relationship between actual runout distance and predictions of GP for Equation 4.

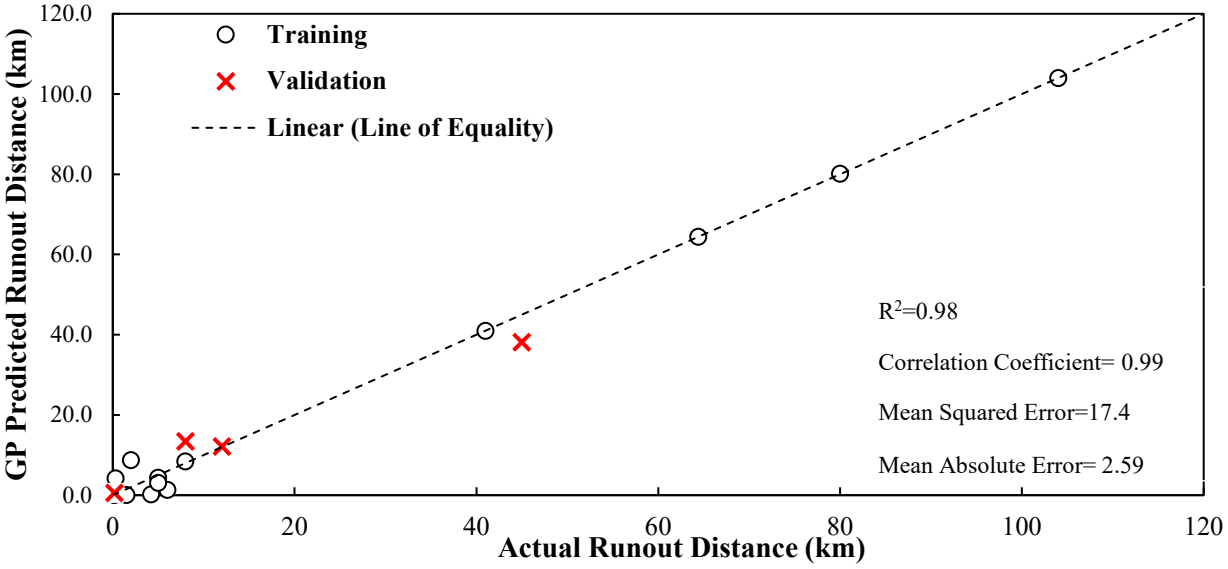


Figure 5: Predicted runout distance using GP versus actual runout distance

Comparison between GP Model and experimental relationships

Figure 6 shows the comparison between the actual runout distance, estimated runout distance using GP model, and experimental relationship developed by Rico et al. (2008). As observed in the plot, the coefficient of determination for empirical relationship was 0.364, which is the indication of low accuracy of this equation in predicting of outflow runout distance of TSF.

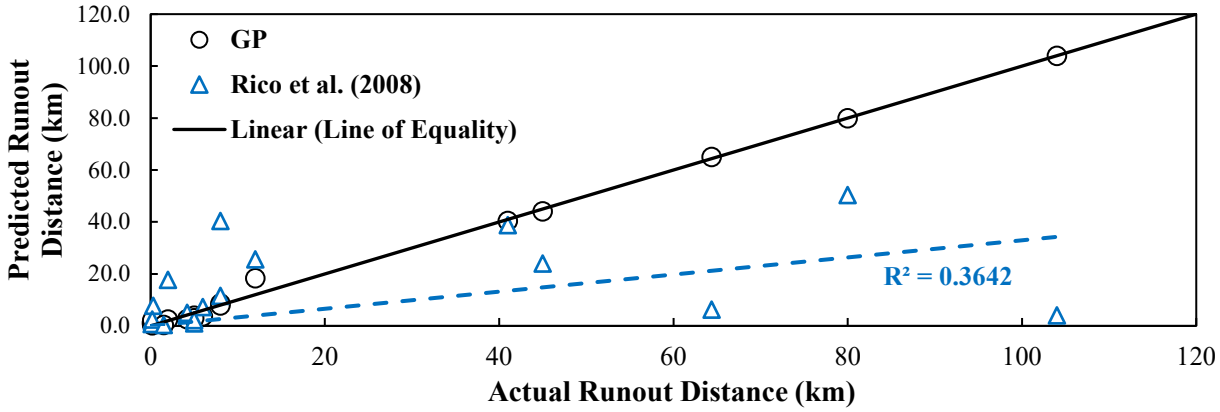


Figure 6: Coefficient of determination between the actual runout distance and predicted intelligent models (GP [Eq. 4]) and experimental relationships [Rico et al., 2008] [Eq. 1])

The limitations of existing empirical relationships can be attributed to their reliance on only two factors: tailings height and size. To achieve more robust and practical equations, it is essential to incorporate additional parameters, particularly downstream topography, which enhances the intelligence and predictive capability of the resulting relationships.

Figure 7 illustrates a comparison of the prediction performance between the GP models developed in this study and the empirical relationship proposed by Rico et al. It appears that the Rico et al. equation mostly underestimates the actual runout distance. These equations exhibit limited ability in predicting higher values of D_{max}. In contrast, the proposed GP model demonstrates significantly improved accuracy when compared to the Rico et al. relationship. By incorporating a wider range of input parameters, the proposed GP equation proves to be more applicable and reliable for estimating runout distance.

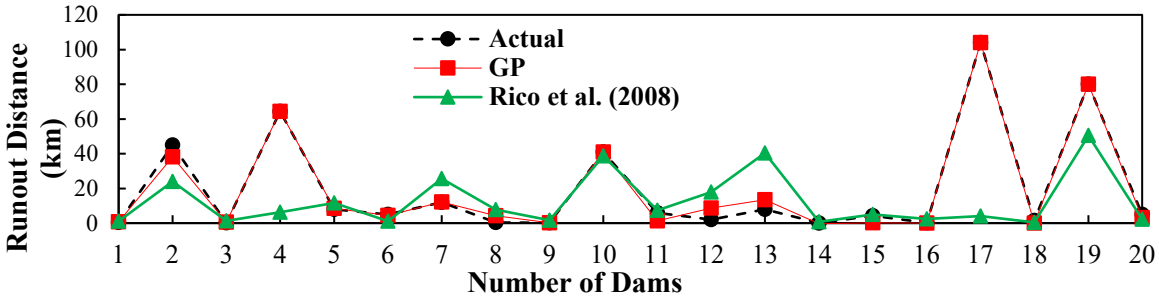


Figure 7: Comparing the actual runout distance and predicted intelligent models (GP [Eq. 4]) and experimental relationships (Rico et al. [Eq. 1])

Validation

The proposed equation using GP was validated using the Dynamic Run-out Methodology (DRUM) on a hypothetical upstream-constructed tailings dam model. This method satisfies Newton's second law of motion and uses an idealized kinematic boundary. In this method, the slide mass is assumed to slide along the slip surface, controlled by shear strength along the interface, as schematically shown in Figure 8.

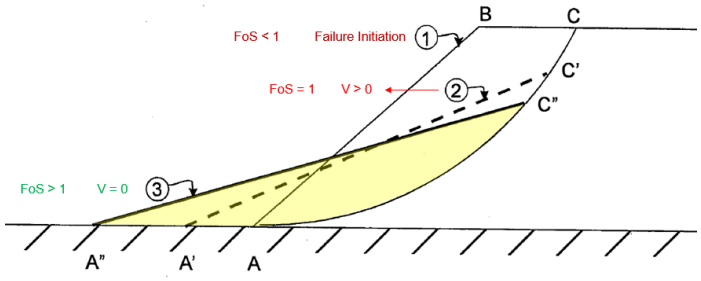


Figure 8: Configurations and conditions during flow slide in DRUM method (Moriwaki et al., 2000)

A hypothetical upstream-constructed tailings dam model was used to perform DRUM analyses and verify the newly developed equation using GP. The model contained three different tailings materials: coarse tailings, fine tailings, and slimes, as shown in Figure 9. Available field and laboratory data from a tailings project in North America were used for characterization, as summarized in Table 1. The Cone Penetration Tests (CPTs) and their dynamic pore pressure profiles were used to establish saturation.

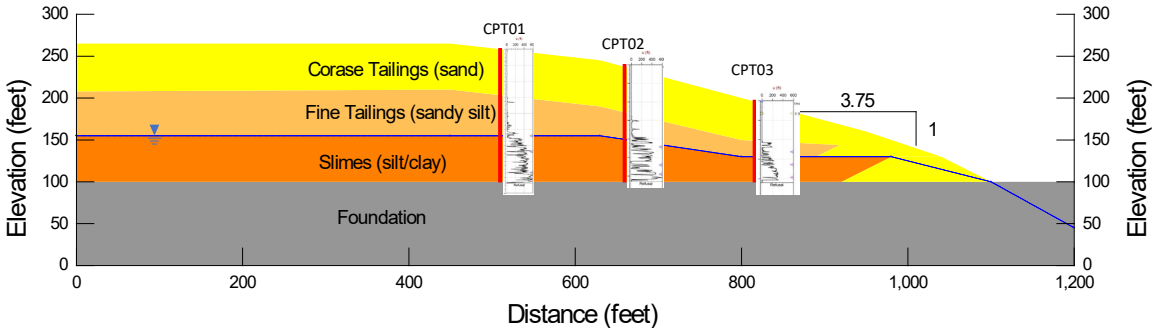


Figure 9: Analyzed cross-section geometry and tailings zone delineation

Table 2: Material properties summary

Materials	Cohesion, c' (pcf)	Friction Angle, ϕ' (degrees)	Residual Undrained Shear Strength	Peak Undrained Shear Strength	Total Unit Weight (pcf)
Coarse Tailings	0	37	–	–	110
Fine Tailings	100	30	–	–	120
Slimes	–	26	0.10	0.25	120
Foundation	1,000	38	–	–	135

Critical slip surfaces for the DRUM analysis were selected based on the results of seismic deformation analyses on the hypothetical model. A large seismic load with PGA=1.0 and M=7.9 was used to trigger liquefaction in the hypothetical model and develop a flow runout. The slip surface and released tailings area were derived from displacement results from the FLAC analysis, as shown in Figure 10.

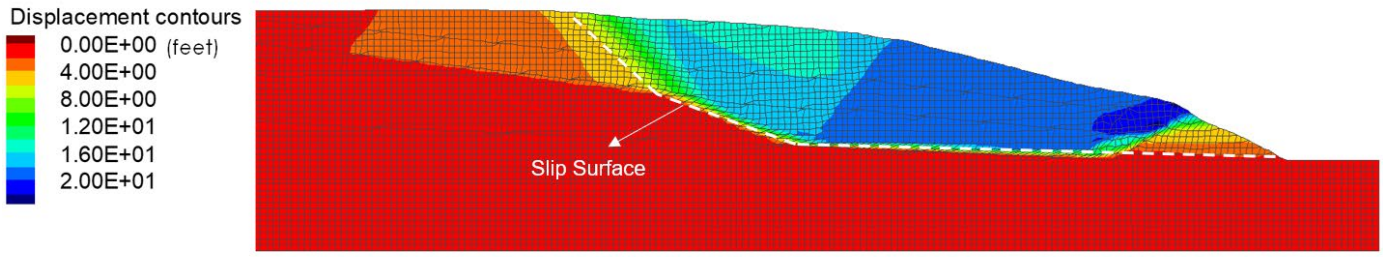


Figure 10: Calculated slip surfaces from seismic deformation

Since FLAC is not effective at estimating large magnitudes of deformation following a flow failure instability, the full flow runout calculation for the hypothetical model was performed using DRUM analyses. Calculations continued until the slide mass velocity approached zero, indicating a dynamically stable slide configuration. The total run-out distance for the hypothetical model was 2,200 ft, with a maximum velocity of 14 feet per second (ft/s). Figure 11 shows the time histories of computed runout distance and velocity.

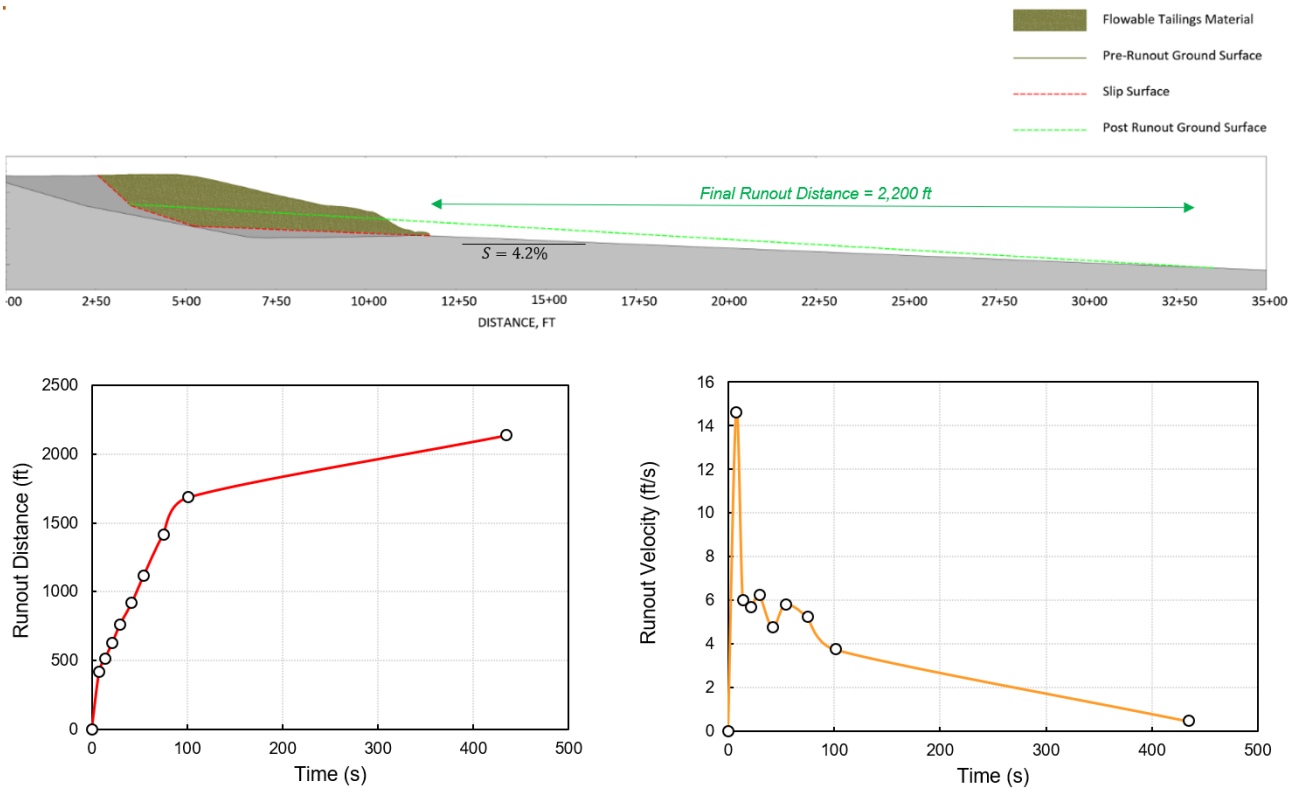


Figure 11: DRUM analysis results

The estimated total and released tailings volume, downstream slope, and dam height for the hypothetical model were 1,000,000 m³, 225,000 m³, 4.2%, and 55 m, respectively. Based on the newly developed GP equation, the runout distance for the hypothetical model should be approximately 2,066 ft, which closely matched the 2,200 feet result from DRUM analyses:

$$D_{max} = 1 + 0.225^3 - \left(\frac{7.21}{4.2^{4.2}} - \frac{113}{1 + 4.2^{2^{4.2}}}\right) = 0.63\ km = 2{,}066\ ft$$

Therefore, this validation shows the newly developed model can roughly estimate the runout distance of tailings storage facilities. The improved accuracy of the GP model, coupled with its consideration of additional input parameters, enhances its runout distance prediction capabilities. The utilization of the GP model in predicting runout distance offers a valuable tool for better understanding the potential consequences and risks associated with tailings dam failures. Although accuracy of any runout estimations should be approached with great caution, the proposed method can be utilized as a simple screening tool to provide an estimation of the runout distance. This information can be used by the project team to better understand the failure consequences and potential risks and impacts to the downstream population.

Conclusion

This study utilized Genetic Programming to predict the outflow runout distance of tailings storage facilities (TSFs) by analyzing data from 20 documented tailings dam failures globally. The models incorporated parameters such as total and released tailings volume, downstream slope, and height of the dam, revealing that downstream topography considerably affects the runout distance. The newly developed GP equation was validated using the DRUM analysis on a hypothetical upstream constructed tailings dam model, estimating a runout distance of approximately 2,066 feet, which is in close agreement with the 2,200 feet calculated based on the DRUM method. This validation shows that the GP models can be effectively used in estimating runout distances.

The findings of this study indicate that intelligent methods like Genetic Programming are well-suited for addressing complex problems involving multiple influential factors, such as predicting runout distances in tailings dams. Despite inherent uncertainties and complexities in tailings dam failures, this method seems to provide reasonable estimations that can aid project teams in understanding potential consequences and risks, and their impacts on downstream populations. This paper demonstrates the potential effectiveness of using advanced AI techniques to improve predictions and risk assessments in the context of tailings dam management.

References

Adamo, N., Al-Ansari, N., Sissakian, V., Laue, J. and Knutsson, S. 2020. Dam safety: the question of tailings dams. *Journal of Earth Sciences and Geotechnical Engineering* 11(1): 1-26.

Davies, M.P., Martin, T. and Lighthall, P. 2000. Mine tailings dams: when things go wrong. *Proceedings of Tailings Dams 2000*: 261–273. Association of State Dam Safety Officials.

Global Tailings Review. 2020. Global Industry Standard on Tailings Management. August 2020.

Goldberg, D.E. 1989. *Genetic Algorithms in Search, Optimization and Machine Learning*. Boston, MA: Addison-Wesley Longman Publishing.

Koza, J.R. 1992. *Genetic Expression Programming: on the Programming of Computers by Means of Natural Selection*. Cambridge, MA: MIT Press.

Noorzad, A., Behnia, D., Moeinossadat, S. R., and Ahangari, K. 2014. Prediction of crest settlement of concrete-faced rockfill dams using a new approach. *Proceedings of the International Symposium on Dams in a Global Environmental Challenge,* ICOLD, Bali.

Rashidi, M., Saghafi, M. and Takhtfiroozeh, H. 2021. Genetic programming model for estimation of settlement in earth dams. *International Journal of Geotechnical Engineering* 15(3): 1–10.

Rico, M., Benito, G. and Diez-Herrero, A. 2008. Floods from tailings dam failures. *Journal of Hazardous Materials* 154(1–3): 79–87.

Rourke, H. and Luppnow, D. 2015. The risks of excess water on tailings facilities and its application to dam-break studies. *Proceedings of Tailings and Mine Waste Management for the 21st Century:* 225–230.

Good Practices for the Elaboration of Hypothetical Dam Break Studies in Brazil

Caique Simões Renna Costa, AECOM, Brazil
Fernando Pereira Aguilar, AECOM, Brazil
Mônica Torres dos Santos de Almeida, AECOM, Brazil
Vicente Mello, AECOM, Brazil

Abstract

Recently, two catastrophes involving tailings dam ruptures in Brazil occurred: in 2015, the Fundão Dam failure in Mariana City, and in 2019, the B-I Dam failure in Brumadinho City, both in the state of Minas Gerais. These two events resulted in the loss of human lives and severe socio-environmental impacts on nearby communities, thereby necessitating an increase in risk management and dam safety in Brazil, as well as in local legislation and regulations.

The quality of a hypothetical rupture study is directly proportional to the knowledge of the dam structure and the materials deposited in its reservoir. For hydraulic propagation modeling, a precise understanding of the downstream region significantly impacts the flood boundary results, affecting its cross-sectional coverage, the arrival time of the rupture wave, and the distance reached by the flood boundary. The use of robust software and appropriate modeling allows available information to be used for more reliable and representative results.

This paper suggests good practices for studying and modeling hypothetical failures based on the knowledge acquired by AECOM in evaluating more than 220 tailings containment structures in Brazil.

Introduction

Reflecting Brazil's advances in dam safety in recent years, AECOM has been established as an independent technical advisor to the National Mining Agency of Brazil (ANM) in auditing more than 220 mining dams. This has enabled AECOM to understand the sensitivity of information and parameters in the development of dam break studies and, consequently, in estimating the resulting floodplain.

Additionally, as a result of the dam failure events in the state of Minas Gerais, the company Vale, owner of the B-I Dam, signed a Term of Covenant with the Public Prosecutors Office of the State of Minas Gerais (MPMG) to update all its hypothetical rupture studies. To ensure the quality of the studies, Vale

prepared the document “Guidelines for Studies of Hypothetical Rupture of Mining Dams” in 2020, which AECOM audited. Brazilian regulatory institutions have also created more restrictive resolutions to ensure the quality of studies, such as ANM resolution 95 of 2022, later modified by resolution 175 of 2024. These resolutions establish a classification for mining dams based on their associated potential damage, which is categorized as low, medium, and high. This damage is defined as that which may occur due to the rupture, leakage, infiltration into the soil, or malfunction of a dam, regardless of its probability of occurrence, to be graded according to the loss of human lives, social, economic, and environmental impacts.

It has been determined that all mining dams must have an updated hypothetical rupture study with high technical rigor, primary data obtained through direct investigations, and two-dimensional hydrodynamic modeling. It is also worth mentioning that other Brazilian institutions have prepared or are preparing documents to guide hypothetical rupture studies and establish minimum quality standards. As an example, a term of reference has already been prepared by the Minas Gerais State Foundation for the Environment (FEAM) in 2021, and a specific technical standard is being discussed by the Brazilian Association of Technical Standards (ABNT).

At the same time, there have also been advances in the guidelines for preparing these studies outside Brazil, such as the guidelines proposed by the Canadian Dam Association in 2021 in its technical bulletin, which details in depth the aspects related to hypothetical rupture studies. Additionally, there is the role of the engineer of record, who has knowledge of the structure and can validate the failure mode proposed by the designer.

Although Brazilian and international normative/regulatory institutions are evolving in their guidelines and requirements for preparing hypothetical dam break studies, there are still gaps, such as the lack of specification in certain points of the legislation, like the definition of freeboard, where it is not clear if the wind wave height needs to be considered to ensure a 1-meter freeboard. Additionally, designers face challenges in preparing detailed studies due to a lack of basic data, such as adequately precise topographic surveys. Furthermore, small entrepreneurs often lack a robust technical team and do not have specialized professionals capable of developing high-quality studies as required by the legislation. The guideline documents only sometimes reflect the difficulties encountered by designers, as in the case of mining dams in Brazil.

Thus, this article aims to present the main criteria and essential data to be used to prepare the hypothetical dam break studies in accordance with the best Brazilian and international practices. In addition, it considers the experience acquired by AECOM during the audit process in more than 220 mining dams in Brazil.

Discussion

A hypothetical dam break studies (HDBS)'s quality is important for understanding the dam and the materials deposited in its reservoir. Historical information about the structure contributes to understanding its weaknesses and defining failure modes and volumes to be mobilized for the scenarios with the most significant impacts. Thus, the HDBS should be prepared with the best technical knowledge of the structures. For this purpose, the essential data are listed below:

- Documents related to the design and safety of the structure, such as Executive Design, As Built or As Is, Regular and Periodic Safety Inspection Reports.
- Detailed topographic and cadastral survey of the dam and reservoir area, updated topobathymetry of the reservoir, and primitive topography. The developer will be able to use additional information, such as geological-geotechnical investigations of the reservoir and dam, which allows for improving the precision of the primitive topography. Topographic inconsistencies can significantly interfere with the mobilized volumes of the study and, consequently, with the results of the floodplain.
- Complete geological-geotechnical investigations of the embankment and foundation dam to obtain the resistance factors that will support the studies for evaluating the failure modes.
- Geotechnical characterization of the reservoir through geological-geotechnical tests and investigations. The following information must be considered, at a minimum, regarding tailings, residues, or sediments deposited in the reservoir: information on the water table; contact between the deposited material and the natural terrain; angle of repose; Atterberg limits; specific weight of the grains; granulometry; void index and moisture content in situ; and saturation and classification of the material according to the risk to health and the environment. This minimum characterization of the materials is mentioned in the guidelines document elaborated by Vale in 2020, and in the FEAM term of reference and ANM resolution 95 of 2022.
- Rheological characterization of the material disposed of in the reservoir (where applicable).

For tailings accumulation dams, it is essential to know the characteristics of the material disposed in the reservoir in order to know with greater precision about the deformations and flow of the fluid in rupture studies. Fluids composed of a mixture of water and solids may be classified as hyperconcentrated, depending on the calculated volumetric concentration (VC) and the rheological characteristic of the mixture contained in the reservoir. The most common equations for representations of hyperconcentrated flows use the parameters of dynamic viscosity, yield stress, and specific weight. For the proper rheological characterization of a fluid, it is necessary to define the number of samples/assays and their VCs for the

study. It is recommended that the tests be performed for different VC values, allowing correlations among the different conditions of the samples (VC curves versus shear stress and viscosity).

Sensitivity analyses of rheological parameters, input parameters for hydrological studies, downstream topographic surveys, and primitive topography are desirable to understand how a given material will propagate in the downstream valley. In this sense, it is recommended that the designer carry out preliminary modeling to understand the impact of variations in VCs and rheological parameters on the propagation of the rupture wave through the downstream valley. This will contribute to selecting the most critical scenario, as long as it is credible.

Downstream valley investigations are also essential. They should comprise at least the following:

- Precision mapping/topography of the downstream valley.
- Land use and occupation.
- Inventory of the main structures, urban equipment, and population downstream (industrial structures, public equipment, areas of environmental and cultural interest, among others).
- Inventory of structures that can exert hydraulic or synergistic controls with the breaking wave (e.g., dams, tailings piles, bridges, embankments, among others).
- Bathymetry of the downstream valley when there is a watercourse in the region.

Such information should guide the refinement of the simulation model to adequately represent flooding in the regions of interest.

The topographic survey in the valley downstream of the dam must be updated and carried out with adequate precision, preferably with contour lines at a minimum of every meter. For regions with human occupation, very flat topography or other singularities require greater accuracy. It is recommended that bathymetric sections along the downstream river valley be surveyed, ensuring more significant detail in the river channel and a better representation of the geometry in the modeling. It is worth mentioning that the treatment of the topographic survey for the elaboration of the digital terrain model (DTM) is of paramount importance for the study, because hydrodynamic modeling is sensitive to inconsistent or low-resolution topographic data, and the use of inadequate DTMs may generate incoherent and unrealistic results. All topographic surveys must be accompanied by technical reports with information about the applied methodology, topographic landmarks, auxiliary control points, cartographic projection systems, software, and models used to process the geographic product.

Figure 1 presents an example of the importance of data quality. The first image shows a low-resolution digital surface model, while the second image represents the same location with a high-resolution digital terrain survey, adequately processed and with integrated bathymetry.

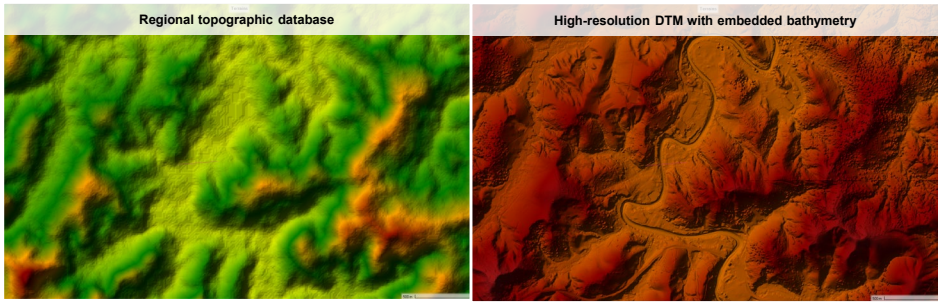


Figure 1: Difference in the quality between DSM and DTM

Evaluated scenarios

The HDBS should evaluate different simulation scenarios, adopting different hypotheses of rupture or extreme conditions. The scenarios evaluated should include at least the following items:

Scenarios without dam break: these must be developed to evaluate the impacts of natural floods in the downstream valley without the influence of the rupture wave, considering different return times:

- Ordinary natural flood: natural floods in the downstream valley can completely fill smaller beds (e.g., floods associated with a 2-year return period).
- Severe natural flood: natural floods in the downstream valley with an extreme return period (e.g., a flood with a 100-year return period, which is the flood assessed for flood insurance in the U.S. and tracked by the Federal Emergency Management Agency – FEMA). For large drainage areas, the flood attenuation of the downstream valley reference can be assessed along the propagation of the rupture wave.

Scenarios with dam break: Two rupture scenarios must be minimally modeled, each of them being associated with one hydrological condition of the downstream valley:

- Dam break – fair weather: rupture scenario associated with ordinary natural flooding in the downstream valley and the reservoir's water level at the spillway threshold.
- Dam break – rainy day: rupture scenario associated with severe natural flooding in the downstream valley and the water level in the reservoir being at least at the maximum maximorum or at the dam crest. These levels should be determined in the reservoir flood study. The reservoir flooding analyses utilized to develop the scenario must be fully documented and presented.

Additional scenarios: for some structures, additional scenarios can be evaluated, such as:

- For reservoirs with multiple embankments, rupture scenarios must be developed for all dams that could be mobilized in a rupture event.

- For structures with upstream tailings piles, synergistic failure scenarios between the dam and pile should be evaluated.
- For structures with long dam crests, different locations for breaches should be evaluated, defining a maximum potential envelope of the impact area around the structure.

Failure modes and rupture hydrograph

The failure mode adopted as a reference should be credible and represent the worst-case scenario, regardless of its probability, as mentioned in ANM Resolution 95/2022. In this context, a sensitivity analysis must be conducted when there are two or more credible failure modes. The sensitivity analysis results must be presented in the study (e.g., compare the rupture hydrographs of the credible modes). Various failure modes can be assessed, including but not limited to overtopping, internal erosion, and collapse (liquefaction, instability, tipping, sliding), among others.

The breach parameters of a rupture are intrinsic to the failure mode adopted. In traditional rupture scenarios such as overtopping and internal erosion in earth dams, the breach parameters determine the peak flow and duration time. This type of hydrograph has classic characteristics of rise, peak, and bust. Conversely, instantaneous ruptures such as liquefaction and destabilization result in hydrographs characterized by an extremely high peak, immediate onset, short duration, and rapid recession. Hydrographs with high peaks often lead to more severe flooding, even when the same volume is mobilized across all rupture scenarios.

The elaboration of the rupture hydrograph for cases of overtopping and internal erosion is usually done with parametric models, which are based on real dam failures and are elaborated by means of mathematical regressions adjusted to the geometric and hydraulic parameters measured during and after the opening of the breach. The most established parametric models for dams are Froehlich (1995), MacDonald and Langridge-Monopolis (1984), Von Thun and Gillette (1990), and Xu and Zhang (2009). The hydrograph developed in these models is based on data such as reservoir volume and dam height.

Conversely, instantaneous breach formations, such as liquefaction, are more accurately defined using hydraulic modeling software. This is because they depend on the immediate topographic features of the valley downstream of the structure.

As an example of the behavior of different hydrographs, Figure 2 illustrates three distinct types: overtopping, internal erosion, and liquefaction/instability hydrographs. It is observed that overtopping and internal erosion hydrographs have similar shapes, while the liquefaction/instability hydrograph exhibits markedly different characteristics from the others. It is important to highlight that although overtopping and internal erosion (piping) hydrographs have similar shapes and peaks, the different failure modes

significantly influence the wave arrival time. This occurs because the development of the hydrograph can accelerate the occurrence of the peak, resulting in a shorter arrival time.

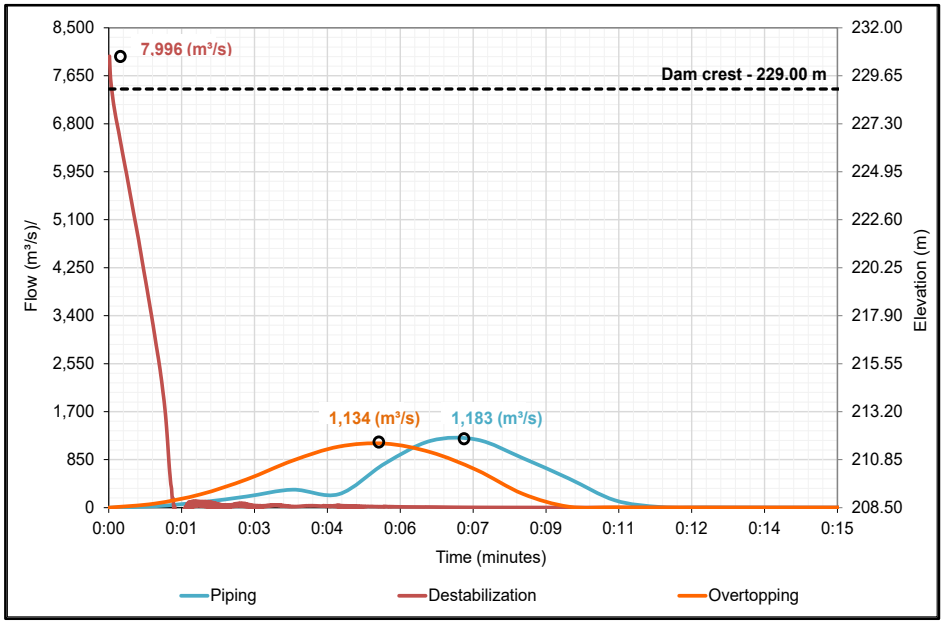


Figure 2: Comparison of rupture hydrographs from different failure modes

Potential mobilized volume

The justification for the mobilized volume should be based on physical and credible processes, aiming to adopt the largest possible mobilized volume. The volume can be defined through geotechnical and rheological parameters of the deposited material (when there are reserved solids). The mobilized volume must be divided into at least three components: volume of water, volume of mobilized solids in the reservoir, and volume of the rupture breach. It is common practice to define the mobilized portions as 100% of the volume of water in the reservoir and the breach. However, the solids portion of the reservoir can vary depending on the rigor of the designer, with the residual angle of repose of the material disposed in the reservoir often being used as a reference. Some of these good practices are further explored in the guidelines prepared by Vale in 2020. The figure presents a summary of the proportions of the potential volume mobilized.

Flood wave propagation

The propagation of the rupture wave must be carried out using at least two-dimensional hydraulic modeling software. Structures in which mobilized volume composition generates hyperconcentrated flows must be modeled in software with non-Newtonian flow modules. Cases in which the rupture wave initially presents a hyperconcentrated flow may present a dilution of the solid contents and a consequent change in the flow parameters. This possibility considers the transport of water transport by natural floods and/or other

downstream flow interferences.

Synergy between structures/dams/piles

Resolutions 32/2020 and 95/2022 of the National Mining Agency (ANM) stipulate that the entrepreneur must evaluate synergistic rupture scenarios if dams are identified in the downstream stretch. However, these regulations do not consider the synergistic effects with other structures, such as stacking and other structures located upstream of the reservoir. It is important to highlight that the synergy between structures can be triggered by factors such as the direct impact of the rupture wave, and earthquakes resulting from an initial rupture, among others. Figure 3 illustrates some possible scenarios where different structures may present synergistic rupture effects with the evaluated structure.

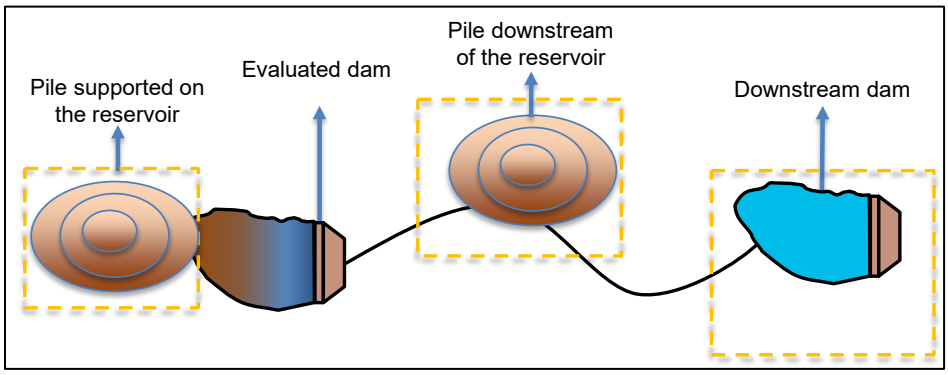


Figure 3: Examples of configurations that may result in synergistic effects

Examples of configurations that may result in synergistic effects include:

- A pile supported by the dam reservoir;
- A pile downstream of the reservoir; and
- a downstream dam.

Synergistic scenarios should be evaluated when structures (upstream or downstream) can be mobilized due to dam failure.

When a reservoir is identified in the wave propagation section, the passage of the rupture wave through the structure (dam) must be detailed to show whether the rupture wave causes elevation above safety levels, such as the crest of the downstream structure, and thus consequent synergistic effect (cascade disruption). For more representative results, it is recommended to evaluate the stability of the downstream structure even in the case of non-overtopping, as well as to perform calibration/sensitivity of the flow under natural conditions in the downstream valley.

Minimal results

The results to be extracted from the model must be represented in maps and tables containing the hydraulic

parameters by cross-sections, as also mentioned in Brazilian regulations, such as ANM Resolution 95/2022. The maps to be prepared must include, but are not limited to:

- Maps resulting from the hydrodynamic model: inundation boundary, maximum depth, and velocity; arrival time of the rupture wave; hydrodynamic risk/ flood hazard.
- The segmentation of the Self-Rescue Zone and the Secondary Rescue Zone: It should be noted that this map is extremely important, as the Self-Rescue Zone is characterized as the region of the valley downstream of the dam in which it is considered that warning notices to the population are the responsibility of the entrepreneur, as there is not enough time for an intervention of competent authorities in emergencies. In Brazil, the Self-Rescue Zone is defined as the greatest distance, 10 km or 30 minutes of propagation of the rupture wave.
- Registration of interferences along the floodplain.

The flow cross-sections complement the maps and must be drawn at an appropriate interval. Locations and elements at risk must have more sections, to guarantee more detailed information in sensitive areas. The cross-section results must be presented in hydrodynamic results tables for each scenario modeled in the rupture study. The minimum information to be presented for each section in the table is: riverbed elevation, maximum depths, and velocities reached for the natural situation and for the situation after rupture, maximum flow achieved, rupture wave arrival time, and rupture wave arrival time (peak). It is worth mentioning that FEAM (2021) and ANM (2023 and 2024b) published a term of reference and resolution and manual, respectively, for the presentation of the results and maps of flood studies.

Termination point of incremental hazard evaluation

The hypothetical rupture study must explain how the termination point of incremental hazard evaluation was defined. That point defines where the increase in downstream water surface elevation, caused by the breach, is not sufficient to cause incremental damage. As a reference, we can evaluate the point where the elevation caused by the rupture wave does not exceed the limit of the gutter and/or natural flood plain and presents velocities and flows close to those of the natural flood, where there is a concentration of buildings or infrastructures or larger rivers, among others.

It is relevant to mention that the Federal Emergency Management Agency (FEMA, 2013) establishes the stopping criterion for the assessment of incremental floods at the point where a 2-foot (0.61 m) rise above the natural flood level is no longer identified. However, a thorough evaluation by the designer is crucial, as a 2-foot (0.61 m) rise can be significant in very flat regions, where even small depths can result in a considerable increase in impact. Conversely, in incised channels, a 2-foot rise can substantially hinder the propagation of the rupture, as it may not result in significant incremental damage.

Conclusion

The objective of this paper was to comment on minimum standards of technical rigor for hypothetical dam break studies according to Brazilian standards and legislation, in addition to the experience in the analysis of more than 220 hypothetical dam break studies conducted by AECOM. It is worth mentioning that the study in question is highly dependent on the available data, the technical knowledge of all the professionals involved, and interdisciplinary interaction. This knowledge makes it possible to establish the most representative and credible failure modes and volumes to be mobilized. It was also important to know the downstream valley through detailed topobathymetric surveys, mapping structures that can exert hydraulic and/or synergistic controls, and determining hydrological conditions in the downstream valley. In addition, appropriate software and calculation methods will allow the entire information framework to be used for solid results, which will be more representative of an eventual rupture, and therefore adequate for the creation of emergency action plans.

However, studies on hypothetical rupture still have a long way to go for improvement. Items to be further refined in the future include:

- More accurate characterization of Self-Rescue Zone and Secondary Rescue Zone.
- Use of robust (3D) computational models.
- Geotechnical aspects of Fault Modes.
- Accurate characterization of tailings rheology.
- Better characterization of hydrological scenarios.
- Relationship between Failure Modes and Deployable Volumes.
- Full characterization of the downstream section.

References

Associação Brasileira de Normas Técnicas (ABNT). 2017. Norma Brasileira, *NBR 13.028*. Brasília, DF, Brazil.

Agência Nacional de Mineração (ANM). 2022. *Resolução n° 95, de 7 de fevereiro de 2022*. Brasília, DF, Brazil.

Agência Nacional de Mineração (ANM). 2023. *Resolução n° 130, de 24 de fevereiro de 2023*. Brasília, DF, Brazil.

Agência Nacional de Mineração (ANM). 2023. *Resolução n° 142, de 16 de outubro de 2023*. Brasília, DF, Brazil.

Agência Nacional de Mineração (ANM). 2024a. *Resolução n° 175, de 01 de agosto de 2024*. Brasília, DF, Brazil.

Agência Nacional de Mineração (ANM). 2024b. *Manual de Entrega da Mancha de Inundação*. Brasília, DF, Brazil.

Canadian Dam Association (CDA). 2021. Technical Bulletin – *Tailings Dam Breach Analysis*.

Fundação Estadual do Meio Ambiente (FEAM). 2021. *Termo de Referência para a Entrega de Estudos de Ruptura Hipotética de Barragens*. Belo Horizonte, MG, Brazil.

Federal Emergency Management Agency (FEMA). 2013. *Federal Guidelines for Inundation Mapping of Flood Risks Associated with Dam Incidents and Failures*.

MacDonald, T.C. and J. Langridge-Monopolis. 1984. Breaching characteristics of dam failures. *Journal of Hydraulic Engineering* 110(5): 567–586.

Von Thun, J.L. and D.R. Gillette. 1990. *Guidance on Breach Parameters*. Unpublished internal document, U.S. Bureau of Reclamation, Denver, Colorado. March 1990.

Vale. 2020. *Diretrizes de Rompimento Hipotético de Barragens de Mineração*.

Vale. 2023. *Diretrizes de Estudos de Ruptura Hipotética de Barragens na Mineração*. Fase 2.

Xu, Y. and L.M. Zhang. 2009. Breaching parameters for earth and rockfill dams. *Journal of Geotechnical and Geoenvironmental Engineering* 135(12): 1957–1970.

Good Practices for Hydraulic Safety for Mining Dams in Brazil

Fernando Pereira Aguilar, AECOM, Brazil
Manuelle Prado Cardoso Pereira, AECOM, Brazil
Vicente Mello, AECOM, Brazil

Abstract

This paper presents information and recommendations regarding hydrology and hydraulic issues related to mining dams, based on observations made during audits, as well as on technical safety consultancy work carried out for more than 220 dams throughout Brazil.

It is essential to consider the hydrological routine and hydraulic checks for mining structures, especially tailings dams, in an environment of climate change, in which extreme events of greater magnitude and frequency of occurrence are expected. Insufficient overflow capacity of spillways and decants, inappropriate freeboard, or inefficient surface drainage systems are deficiencies frequently observed in mining structures.

Introduction

Recently, two catastrophes have occurred involving tailings dam ruptures in Brazil: in 2015, the Fundão Dam failures in Mariana City, and in 2019, the B-I Dam failures in Brumadinho City, both in Minas Gerais. These two events caused loss of human life and severe socio-environmental impacts on nearby communities, thus demanding an increase in risk management and dam safety in Brazil and in local legislation and regulations. Despite these occurrences not being caused by failures in hydraulic structures, this aspect is also crucial to ensure the safety of dams against extreme flood events and thus prevent further catastrophic failures.

Brazilian normative and regulatory institutions are evolving in their guidelines and requirements to enhance the hydraulic safety of dams. Despite this progress, there are still gaps in the available standards and regulations. Moreover, the standards merely guide the development of studies and projects, necessitating that the designer uses established methodologies and adopts best technical practices for secure evaluation of the structures. For instance, the available standards indicate return periods associated with risks to be met in the design of hydraulic structures of a dam. However, they do not specify the

methodologies to be adopted in developing studies and the precautions necessary to mitigate risks to people, infrastructure, and the environment.

Furthermore, it is essential to emphasize that nowadays, climate change is increasingly an issue, as extreme events with greater magnitude and frequency are observed, requiring additional care in the assessments of the performances of hydraulic structures, as it is understood that legislations and standards do not always allow for these changes. Thus, there is a growing need for routines to update hydrological studies and hydraulic verifications in mining structures, especially in tailings dams that exhibit dynamic behavior concerning their geometry and uses in their contributing watershed. Insufficient performance of spillways and inadequate freeboards for the dam and other hydraulic structures, including surface drainage systems, are deficiencies frequently observed in mining structures. This paper presents information and recommendations regarding hydrology and hydraulics issues related to mining dams based on observations during audits and technical safety consultancy work carried out by AECOM at more than 220 dams throughout the Brazilian territory.

Discussion

Study of intense rainfall

The study of intense rainfall is one of the inputs in analyzing reservoir flooding, in addition to helping to verify surface drainage structures. As a good practice for studies of intense rainfall, it is important to evaluate rainfall stations located close to the studied structure. The selected stations must represent the hydrological behavior of the study region, being able to assess variables such as distance from the structure, altitude, relief, and extension of the historical series, among others.

Intense rainfall studies include the definition of the hydrological season, a complete annual maximum rainfall historical series, a graph with the various adjustments of probability distributions, statistics from probabilistic adherence tests, trend analysis, and a table with rainfall quantiles for different duration times and recurrence intervals. Essential information and evaluations are expected for each aspect presented, as indicated below.

Historical series: a daily historical series is recommended, with a minimum of 20 years corresponding to the most recent period possible. Data consistency analyses and assessment of possible outliers must be presented.

Adjustments to probability distributions: this consists of plotting the historical data observed in the Weibull distribution using more common methods, such as Gumbel, Gamma, GEV, Log-Normal, Exponential, Pearson III, and Log-Pearson III, enabling visualization of the adherence of each statistical curve to the sample used. It is usual to present adherence tests demonstrating deviations from the studied probabilistic distributions, but not limited to these, since the visual analysis of trends translates into an

important criterion for choosing the statistical distribution depending on the sample data, especially for the curve extrapolation region. Figure 1 presents an example of how to display the probabilistic distribution fitting of the rainfall study.

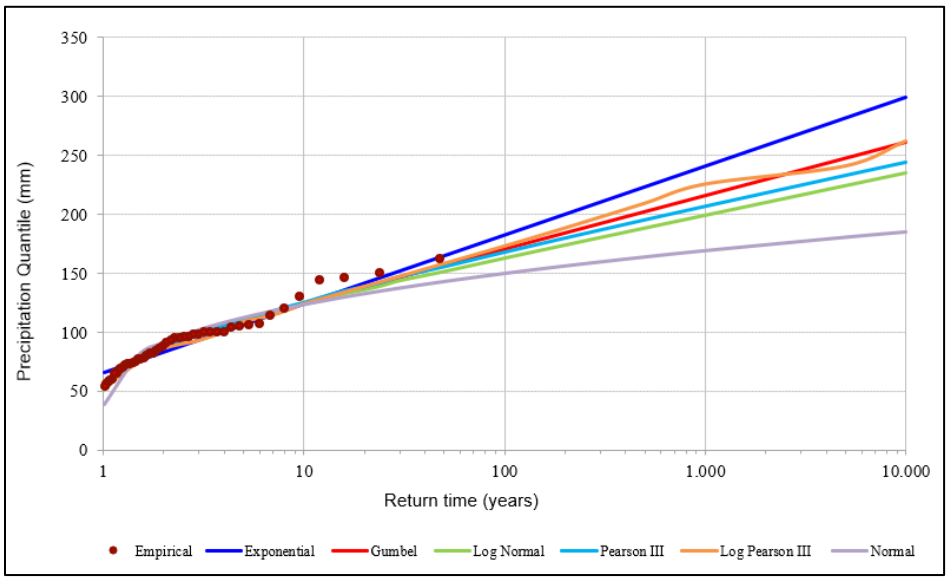


Figure 1: An example of adjustments to probability distributions

Disaggregation of rainfall quantiles: generally, rainfall data comes from daily information obtained from rain gauges, requiring the conversion of daily quantiles into 24-hour quantiles and disaggregation for shorter durations. Among the available disaggregation methodologies we can highlight, for Brazilian conditions, the isozone method presented by Taborga Torrico (1974), the technical note by Silveira (2000), the CETESB Project Manual (1980), or intensity-duration-frequency curves developed for a specific station or nearby and representative stations.

Probable Maximum Precipitation (PMP): hydraulic verification of a dam for the occurrence of a PMP, which represents the maximum rain event physically possible to occur in a given region, can be requested for structures that present high Associated Potential Damage or for decharacterization and closure projects. There are two classic methods for calculating the PMP of a region: the deterministic or meteorological method, and the statistical method. Consistent hydrometeorological data must be used to apply the deterministic method. The statistical method is based on rainfall data series, which must also be properly constituted. The most recognized statistical methodology is recommended by the World Meteorological Organization (WMO, 2009), for which parameters were developed for North American regions. However, several studies in Brazil suggest that calculating the maximization factor using data from rainfall stations in the area of interest would be more representative. The PMP study, however, reflects a

regional characteristic; therefore, it is recommended that a careful analysis be carried out to select stations that reflect the regional meteorological condition.

Reservoirs flooding

The reservoir flooding analysis is one of the main products of the safety analysis of a dam in the face of extreme floods, which consists of defining the greatest surface elevation that will be reached inside the reservoir, associated with the most significant outflow. This study is based on the classic modified Puls method (Butler, 1957), which consists of a balance of inflow and outflow. The main inputs of this study are inflow, storage volume, and the downstream hydraulic control, which define the outflow.

The inflow can be obtained using two approaches, direct or indirect, that should be applied depending on data availability. The direct method allows the calculation of flows through direct measurements of the variable of interest. The indirect method consists of obtaining flow through formulations with correlated variables, such as converting rainfall into flow.

Mining dams are generally found at the headwaters of watersheds, where, in general, there are gaps in flow monitoring. So, indirect methods are used to define the influent flow. The main methods currently used are the NRCS (Natural Resource Soil Conservation Service) method and the Rational method, which is recommended for basins smaller than one km².

To apply the NRCS method, it is necessary to characterize and define the drainage area, time of concentration, land use and occupation, and curve number, among others. The main aspects that must be observed when defining these parameters are described below.

Drainage area: to delimit the drainage area, it is essential to use an updated cartographic base with adequate precision, which also allows extraction of information about its physical characteristics, such as axial length, maximum difference in level, and equivalent average slope, among others. It is recommended that the limits of the drainage area be presented, preferably with contour lines. Based on the physical characteristics of the contribution area, the need for subdivision of the drainage areas must be assessed. In the case of anthropic areas, the direction of the flow and surface drainage infrastructure that can alter the contributions to the reservoir must be carefully evaluated. In these cases, it is important to carry out a detailed local topographic survey in addition to providing a registry of hydraulic infrastructure.

Time of concentration: The methods most used to calculate the time of concentration, which represents the watershed's response time, are the Kirpich method, the G.B. Williams method, and the kinematic method (Pinheiro, 2011). Silveira (2005) also presents numerous methods for calculating the time of concentration in urban and rural basins. It is recommended to evaluate the empirical conditions considered for the development of each methodology and look for appropriate similarities with the case under study.

Curve Number (CN): This is the index of the NRCS method for generating an effective hyetograph from total precipitation, depending on land use and occupation, soil hydrological group (related to soil typology), and antecedent humidity. This index provides great sensitivity to calculations regarding its variation. In the literature, there are tables that present these relationships, as presented by Tucci (2015) and Chow et al. (1988). Figure 2 is an example of a map of land use and occupation.

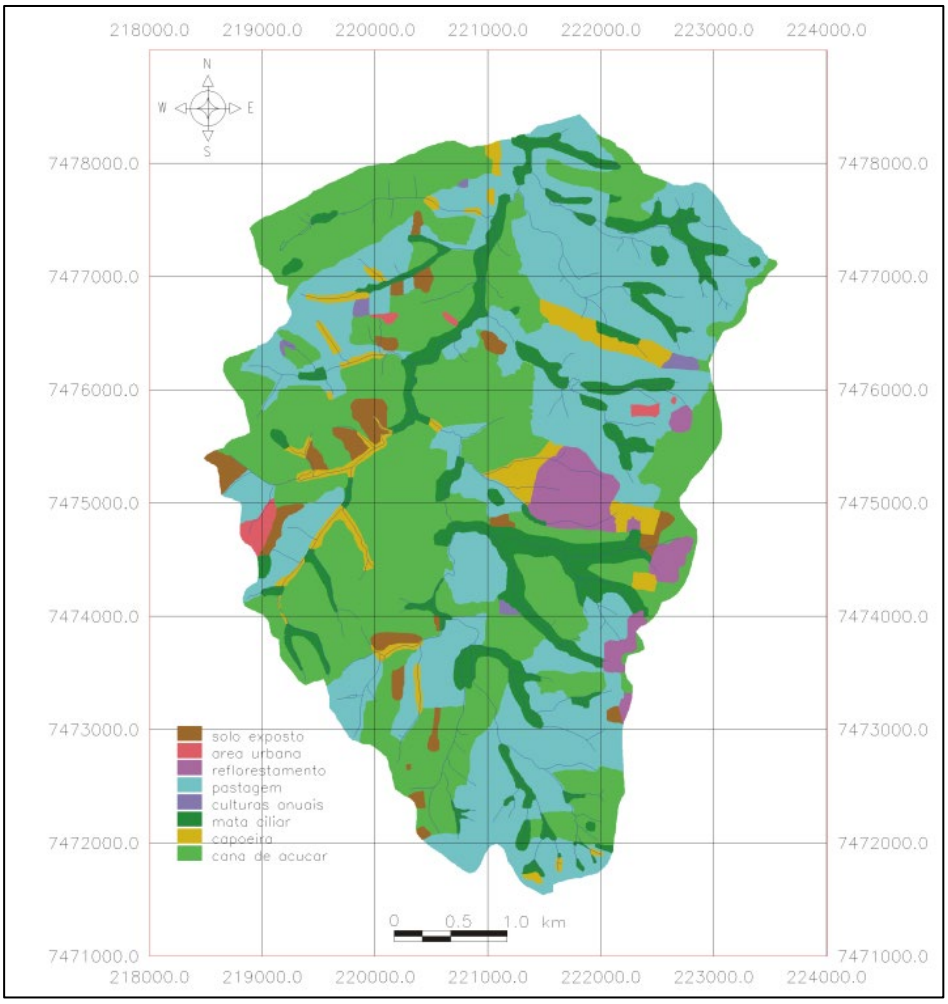


Figure 2: Map of land use and occupation of micro basin hydrographic Ribeirão dos Marins (source: Sartori, 2004)

Hydrologic soil group: Once the types of soil present in the drainage area have been identified, the respective hydrological groups must be associated. To justify the choice of groups, it is recommended to base it on established bibliographical references such as the studies by Sartori (2004 and 2010). For areas affected by anthropogenic activity, where the soil revealed on the surface does not present its natural condition (e.g., tailings pile and pit), it is important to note that the reference mapping may not reflect the current condition for the potential for infiltration and runoff generation. Therefore, the classification of the

soil hydrological group must take the altered condition into account. Figure 3 is an example of a map with different soil classifications.

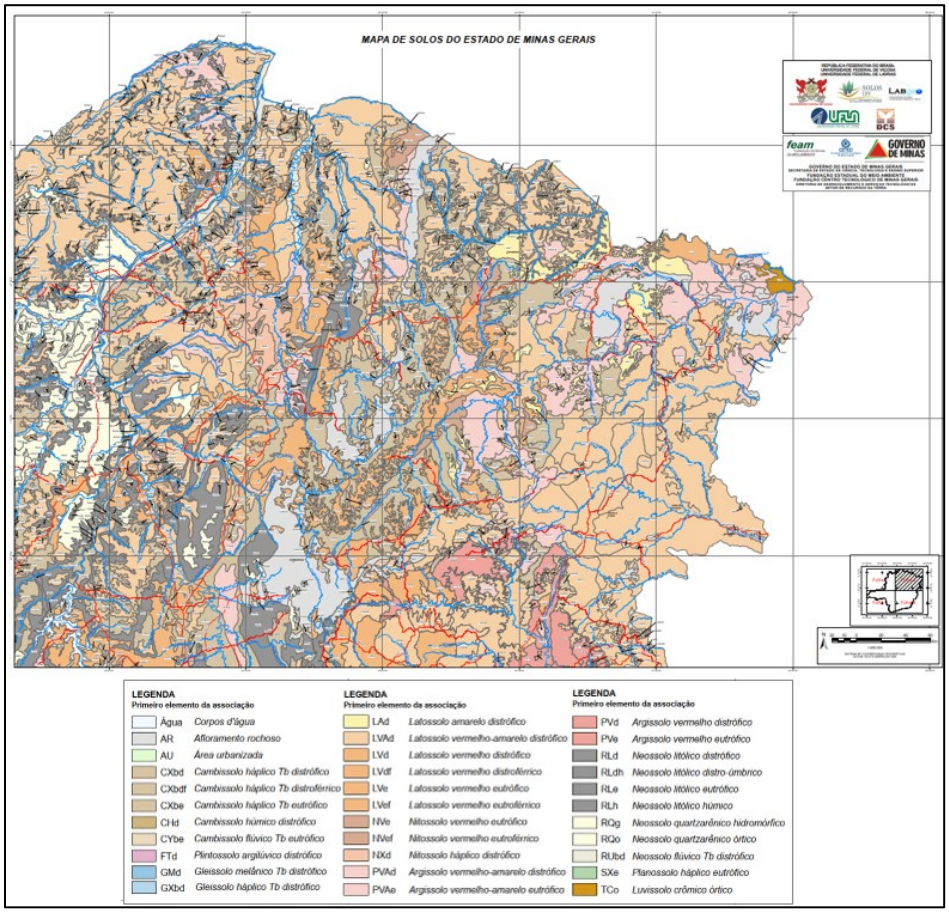


Figure 3: Soil classification of part of the state of Minas Gerais, Brazil
(Source: Universidade Federal de Viçosa; Fundação Centro Tecnológico de Minas Gerais; Universidade Federal de Lavras; Fundação Estadual do Meio Ambiente, 2010)

Calibration and hydrological modeling

As recommended by the National Mining Agency (ANM) Resolution 95 of February 7, 2022, Art. 24 § 5, *"the mining company must calibrate the data from the basins and sub-basins of his dam with data obtained from instruments with sufficient time for calibration aiming at adequate dimensioning of the spillways with real data, comprising 2 (two) hydrological cycles with significant maximum events."*

The mining company must prepare a monitoring plan to monitor and calibrate flow data to meet this requirement. There are several ways to carry out this monitoring, and it is recommended to use precision measuring instruments to measure and store data on rainfall, flow, and water levels in reservoirs for short durations (intervals of 5 minutes or less).

From the data acquired, precipitation events can be related to the study of intense rainfall for the region and, consequently, to assess the measured flows so that the adopted hydrological parameters can be calibrated. Such as:

- time of concentration;
- curve number;
- initial abstraction;
- etc.

Field information must be acquired and must be carried out together office work, such as geological mapping.

Minimum freeboard in reservoirs

The concept of freeboard is the space allocated between the maximum flood level and the crest elevation of the embankment, with the purpose of absorbing the effects of waves formed by winds or adding additional security for possible settlement of the crest.

The most used methodology for determining the required freeboard to accommodate wind-generated waves was formulated by Saville et al. (1962) by determining the fetch (extent of the surface over which the wind is present).

The U.S. Bureau of Reclamation, Design of Small Dams – USBR (1987) recommends adopting the value of 1 meter as the minimum freeboard above the maximum flood level. Resolution 95/2022, issued by the National Mining Agency – AN M, stipulates a minimum freeboard of 1 meter for dams with downstream populations. Figure 4 presents a layout of the spillway with the recommended minimum freeboard.

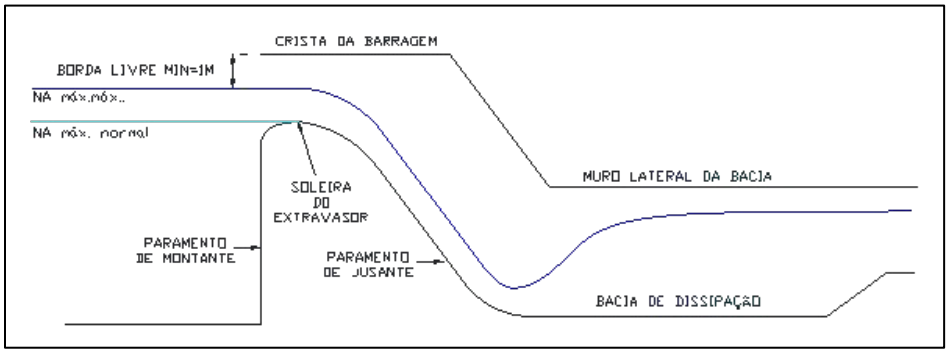


Figure 4: Layout of a spillway with minimum freeboard

Hydraulic check of the spillway system

The hydraulic verification of the overflow system must be based on a topographic survey of the structure with the presentation of plans, profiles, and sections that demonstrate the As Built geometry. Information

on all the relevant sections, such as the inlet, gallery, steps, smooth channel, stilling basin, and restitution channel must be presented.

From the characterization of the spillway, it is possible to evaluate the most appropriate methods for defining the relations between quota and discharge. Currently, it has been usual to obtain discharge curves by hydraulic modeling using established software such as HEC-RAS (Hydrologic Engineering Center – River Analysis System). For this analysis, it is important to identify all hydraulic control points along the spillway.

It is essential to develop hydraulic simulations to show the flow restriction conditions of the structures. In open-pit structures, software for one-dimensional modeling can be used to simulate the worst performance of the overflow system, such as the silting conditions of the approach channel. For structures with culverts or galleries, it is usual to present their elevation discharge curves to identify hydraulic controls and generate the most restrictive curve. Finally, for more complex structures, two-dimensional, three-dimensional, and physical model studies can be used to obtain more representative curves and understand the limits of the structure.

It is necessary to carry out the hydraulic verification of the entire spillway system for the design flow defined in the flood transit studies, with results presented through tables and graphs, as well as the waterline profile and velocities along the structure. Tables should include different sections of the structure, such as transitions, curved sections, steps, culverts, transition boxes, smooth channels, dissipation basin, and restitution channel, with variables such as maximum speed, flow depth, free edge, and Froude number, among other information.

Stilling basins and restitution channels should be checked using appropriate methodologies according to their geometry, coating, etc. As a good practice for stilling basins and restitution channels in riprap, it is recommended to present the average diameter of the blocks (D50) to withstand the design floods. Finally, stilling basins must dissipate energy efficiently without causing degradation or disturbance in the restitution channel.

Hydraulic check of the surface drainage system

The hydraulic verification of the surface drainage systems of the structures is important for managing the dam's conservation state. This verification should follow the recommendations in the Brazilian Technical Standard – NBR 13.028/2017 (ABNT, 2017) – adopting a recurrence time of 100 years for small flow devices, such as berm channels, and 500 years for large flow devices, such as peripheral channels.

To characterize the surface drainage system, it is crucial to use the cadastral topographic survey of drainage devices to identify its layout, geometries, and coatings.

Surface drainage devices usually have small drainage areas, less than one km², so it is recommended to use the rational method for calculating flows, with the premise of adopting the intensity of the design rainfall with a duration equal to the time of concentration of the catchment.

The results should include all drainage devices, and may be in tabular format, with information such as geometry, dimensions, coating, time of concentration, maximum requested flow, maximum allowable flow, maximum velocities and depth, and freeboards at its various points.

It is noteworthy that there are dams with special drainage structures, such as belt channels, whose function is to reduce the contribution of tributary flows to the reservoir. Therefore, they are usually dimensioned for the return time equivalent to that adopted in the reservoir flooding analysis. It is important to carry out reservoir flooding studies, disregarding the presence of these channels, since they may present operational failures/obstructions throughout the useful life of the dam.

Conclusion

Considering the current scenario of climate change to which tailings dams are subjected, in which increasing and frequent extreme weather events are possible, the evaluation of the hydrological and hydraulic safety of tailings containment structures requires frequent checks to evaluate aspects such as freeboards of dams/reservoirs, capacity of hydraulic structures (overflow and surface drainage systems), as well as adequate restitution of flows before discharge to the receiving water body.

The frequent assessment of the structure's hydrological and hydraulic safety will allow for the timely introduction of corrective measures, ensuring the safety of the facilities and affected communities and increasing the resilience of the structures in the face of extreme weather events.

References

Associação Brasileira De Normas Técnicas (ABNT). 2017. Norma Brasileira, NBR 13.028 – *Mineração – Elaboração e apresentação de projeto de barragens para disposição de rejeitos, contenção de sedimentos e reservação de água*.

Butler, S. 1957. *Engineering Hydrology*. 2nd edition, edited by N.M. Newmark. Englewood Cliffs, NJ: Prentice-Hall.

Chow, V.T., M.R. Maidment and L.W. Mays. 1988. *Applied Hydrology*. McGraw-Hill International Editions.

Companhia de Tecnologia e Saneamento do Estado de São Paulo (CETESB). 1980. *Drenagem Urbana – Manual de Projeto*. São Paulo, SP.

Pinheiro, M.C. 2011. *Diretrizes para elaboração de estudos hidrológicos e dimensionamentos hidráulicos em obras de mineração*. 1st edition, organized by ABRH. Porto Alegre, RS.

Sartori, A. 2004. *Avaliação da Classificação Hidrológica do Solo para a Determinação do Excesso de Chuva do Método do Serviço de Conservação do Solo dos Estados Unidos.* Master Dissertation, Faculdade de Engenharia Civil, Arquitetura e Urbanismo, Universidade Estadual de Campinas, Campinas, SP.

Sartori, A. 2010. *Desenvolvimento de critérios para Classificação Hidrológica de Solos e Determinação de Valores de Referência para o parâmetro CN.* Doctoral thesis, Universidade Estadual de Campinas, Campinas, SP.

Sartori, A., F.L. Neto and A.M. Genovez. 2005a. *Classificação Hidrológica de Solos Brasileiros para a Estimativa de Chuvas Excedentes com o Método Serviço de Conservação do Solo dos Estados Unidos. Parte I: Aplicação*. Revista Brasileira de Recursos Hídricos 10(4).

Sartori, A., F.L. Neto and A.M. Genovez. 2005b. *Classificação Hidrológica de Solos Brasileiros para a Estimativa de Chuvas Excedentes com o Método Serviço de Conservação do Solo dos Estados Unidos. Parte II: Aplicação*. Revista Brasileira de Recursos Hídricos 10(4).

Saville, T., E.W. McClendon and A.L. Cochran. 1962. *Freeboard Allowances for Waters in Inland Reservoir*. ASCE Journal of Waterways and Harbors Division.

Silveira, A.L. 2000. *Equação para os Coeficientes de Desagregação de Chuva*. Revista Brasileira de Recursos Hídricos 5(4): 143–147. Porto Alegre, RS.

Silveira, A.L. 2005. *Desempenho de Fórmulas de Tempo de Concentração em Bacias Urbanas e Rurais*. Revista Brasileira de Recursos Hídricos 10(1).

Taborga Torrico, J.J. 1974. *Práticas Hidrológicas*. 120p, Transcon, Rio de Janeiro, RJ.

Tucci, C.E.M. 2015. *Hidrologia: Ciência e Aplicação*. 4th edition. Editora da Universidade, Porto Alegre, RS.

U.S. Bureau of Reclamation (USBR). 1987. *Design of Small Dams*. Washington, DC.

Universidade Federal de Viçosa; Fundação Centro Tecnológico de Minas Gerais; Universidade Federal de Lavras; Fundação Estadual do Meio Ambiente. 2010. *Mapa de solos do Estado de Minas Gerais.* Fundação Estadual do Meio Ambiente, *Belo Horizonte*, MG.

World Meteorological Organization (WMO). 2009. *Manual on Estimation of Probable Maximum Precipitation (PMP)*. No. 1045. ISBN: 978-926-3101045-9. Geneva.

Chapter Five

Case Histories

TAILINGS AND
MINE WASTE 2024



Agnico Eagle LaRonde Filtered Tailings Project, Concept to Commissioning

Ajit Baruah, Metso Canada Inc., Canada
Paul de la Duarantaye, Metso Canada Inc., Canada

Abstract

Agnico Eagle Mine (AEM) Limited is a senior Canadian gold mining company, producing precious metals from operations in Canada, Australia, Finland, and Mexico. In 2018, to make their operations more sustainable at LaRonde concentrator in Quebec, Canada, AEM decided to review its tailings management system with alternate tailing storage methods including thickened, paste and filtered tailings. As the existing tailings storage facility was reaching its capacity limit, it was imperative for AEM to move ahead with an alternate tailings storage system in order to keep the operation going. After review and a detailed study of various options of dry stacked filtered tailings, a system was evaluated as the best feasible option to enhance the tailing storage facility's (TSF's) life and to transition towards a more sustainable solution for tailings management.

This paper presents the storyline of the AEM filtered tailings project, from concept to successful commissioning stage. The tailings filter plant was designed for a rated capacity of 10,000 tpd of tailings generated from both the LaRonde and the LZ5 operations, with different mineralogical characteristics. The project began with laboratory testing through an independent testing agency, followed by confirmatory filtration testwork by Metso, the original equipment manufacturer (OEM) eventually selected as the preferred supplier for the filtration technology. The filtration plant was commissioned in October 2022 with AEM's special attention to integrating state of the art control systems to ensure maximum operational efficiency. The filter plant has been running satisfactorily for the last nine months, meeting the required performance parameters.

Introduction

In 2019 a bidding process was started and RFQs were issued to reputable equipment suppliers for dewatering equipment including thickener, pressure filters, and other auxiliaries for the proposed filter plant to handle 10,000 tonnes per day of tailings with a cake moisture target of 16%. Patterson and Cooke, the third-party consulting company involved in the early phase of the project, was responsible for the collection of various samples and for completing the review process with multiple dewatering equipment suppliers.

Individual original equipment manufacturers (OEMs) conducted confirmatory testwork in support of offering dewatering solutions, including thickeners and filters. After carefully reviewing the test results and being offered solutions by individual OEMs for filtration systems including thickening and filtration, Metso was selected as the successful bidder. The selection was made primarily based on the following criteria.

- Ability to meet the targeted cake moisture and capacity.
- Flexibility of equipment operation for feed with multiple characteristics.
- Optimized quantity of filters considering the significant impact on the overall filtration building size and cost.
- Maintenance requirements and operating costs.
- Expandability features for future increases in capacity.
- Ability to integrate AEM's preferred control system (Mine 4.0) with the OEM supplied equipment control.
- Proven references with AEM and other operators for similar operations.

Filtration testwork

In October 2019, Metso conducted dewatering testwork for thickening and filtration to review and optimize the equipment selection and to provide necessary the process guarantee. As the tailings to be fed to the filtration plant would be reporting from two different concentrators, namely LaRonde and LZ5, with significantly different characteristics, testwork was conducted with various blend ratios, as listed below.

Table 1: Material properties for the filtration testwork

Blend ratio	SG	P80	% Solid
LaRonde/LZ5		(µm)	(%w/w)
75/25	1.688	74	60.0%
50/50	1.697	56	60.0%
0/100	1.648	30	58.5%



Figure 1: Labox 100 test unit

A Metso proprietary pressure filtration test equipment, Labox100, with a 0.02m^2 filtration area, was used to conduct pressure filtration tests for various blends of samples. Some findings from the pressure filtration testwork are listed below.

Table 2: Summary of filtration testwork results

Blend	Unit	Sample 1		Sample 2		Sample 3	
(Laronde/LZ5)		75/25		50/50		0/100	
Feed % Solid	%w/w	60.2	60.2	61.1	61.1	58.3	58.3
Feed Pressure	Bar	7	7	7	7	7	7
Pres. Pressure	Bar	12	12	12	12	12	12
Chamber depth	mm	45	45	45	45	45	45
Cycle time	min	8.25	8.25	8.75	8.25	10.5	8.5
Cake moisture	%w/w	12.99	12.84	13.87	14.52	17.2	16.8
Filtration rate	KgDS/m^2/hr	278.4	254.0	245.1	261.1	191.7	232

The following conclusions were reached after the completion of the filtration test work.

- Cake thickness of ~+40 mm cake thickness was achieved using a 45 mm chamber.
- 12 bar membrane squeezing pressure was required for effective membrane pressing.
- The impact of air drying was significant on the final cake moisture content, and could easily reduce the cake moisture by 6–7%.
- The LZ5 material was the most difficult material for filtration, and the final cake moisture achieved was ~17%.



Figure 2: Cake with and without air drying (Sample 1: 75/25 blend)

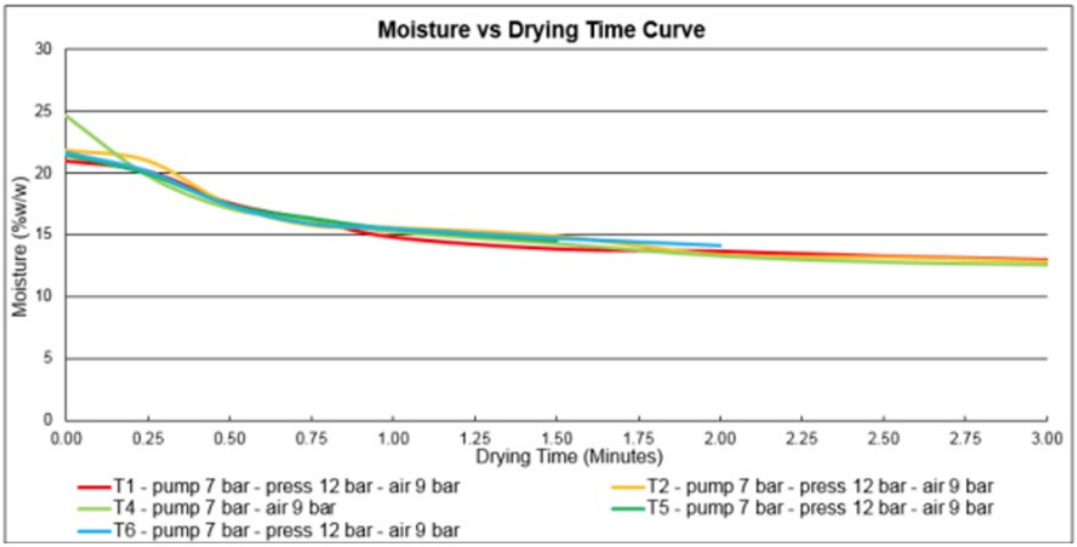


Figure 3: Sample 1: 75/25 Blend – effect of drying time on moisture

Filter sizing

After a detailed review of the filtration testwork runs and a careful review of the individual parameters, the production plant filter units were sized for the below mentioned process conditions.

Table 3: Process data

Design capacity	444 tph
Solid SG	3.06
Feed % solid	58.3% (%w/w)
Slurry density	1,645 g/l
pH	10.7
P80	56 µm
Cake moisture target 16.0%	

Table 4: Filter sizing parameters

Filling and filtration	3.0 min @ 7 bar
Pressing	0.5 min @12 bar
Cake air drying	1.5 min. @ 9 bar
Technical Time	4.5 min
Total cycle time	**8.5 min**
Estimated cake thickness for sizing	39 mm
Estimated solid fraction in cake	51% % vol/vol
Filtration rate for sizing	214 kg/m^2/hr
Calculated filtration area requirement	831 m^2

Selected filter

Metso Larox FFP3512 62/74 M45 3 units

Table 5: Technical specifications of each filter unit

Filtration area per filter with 62 chambers	831 m^2
Filtration area per filter with expansion 74 chambers	992 m^2
Chamber thickness	45 mm
Total chamber volume with 62 chambers	16.7 m^3
Total chamber volume with 74 chambers	20.0 m^3
Total installed power per filter(only)	96 kW
Filter Plate size	3.5 m x 2.5 m

Project execution

Three units for Mesto FFP3512 62/74 M45 filters were selected for the final plant configuration based on various considerations for operating methodology, as well as different feed scenarios. A 36 m diameter High-Rate tailings thickener was installed alongside the filtration building to feed the filters at a desired solid concentration, as established by the testwork for optimum performance. The building layout was decided upon in light of the various maintenance requirements that would be critical with multiple units of large pressure filter units.

After careful consideration of the layout based on the selected filters and other associated equipment, engineering work started in January 2019. Cold commissioning began in June 2022 and full-scale production started in December 2022.



Figure 4: Metso 36 m high-rate tailings thickener and 3xFFP3512 62/74 M45 filter

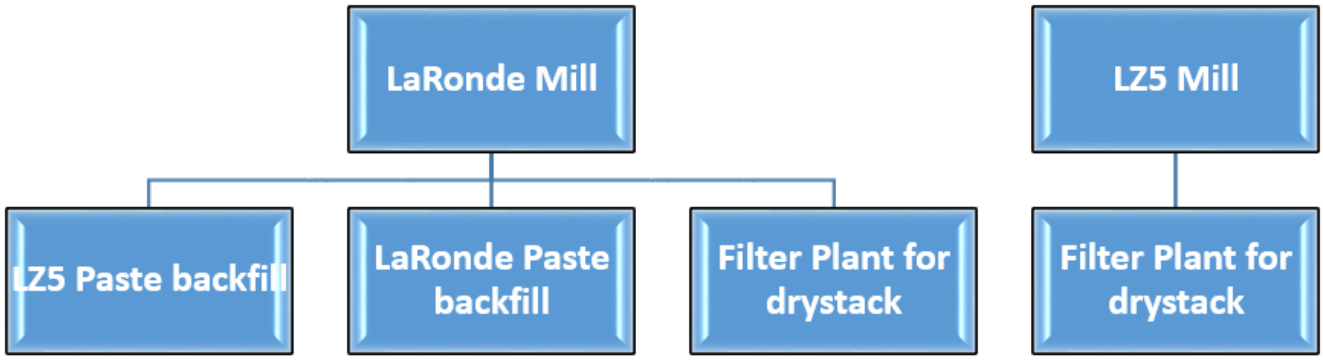
High level project milestones

High level project milestones are shown below.

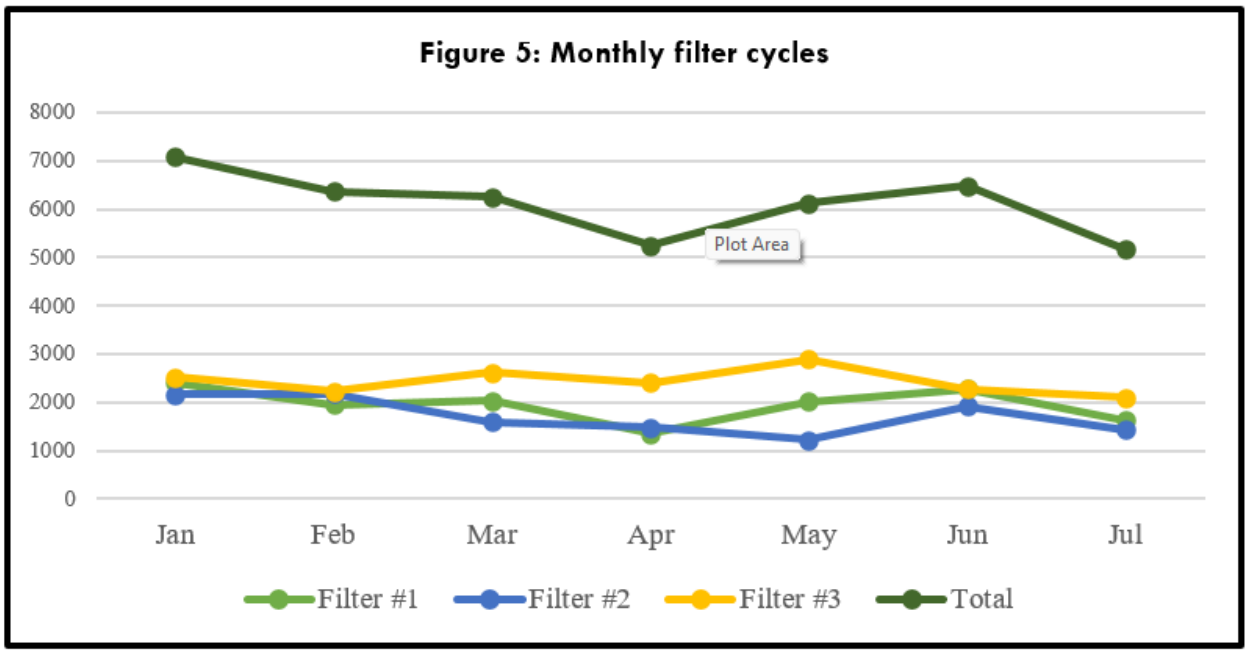


Filter plant operation

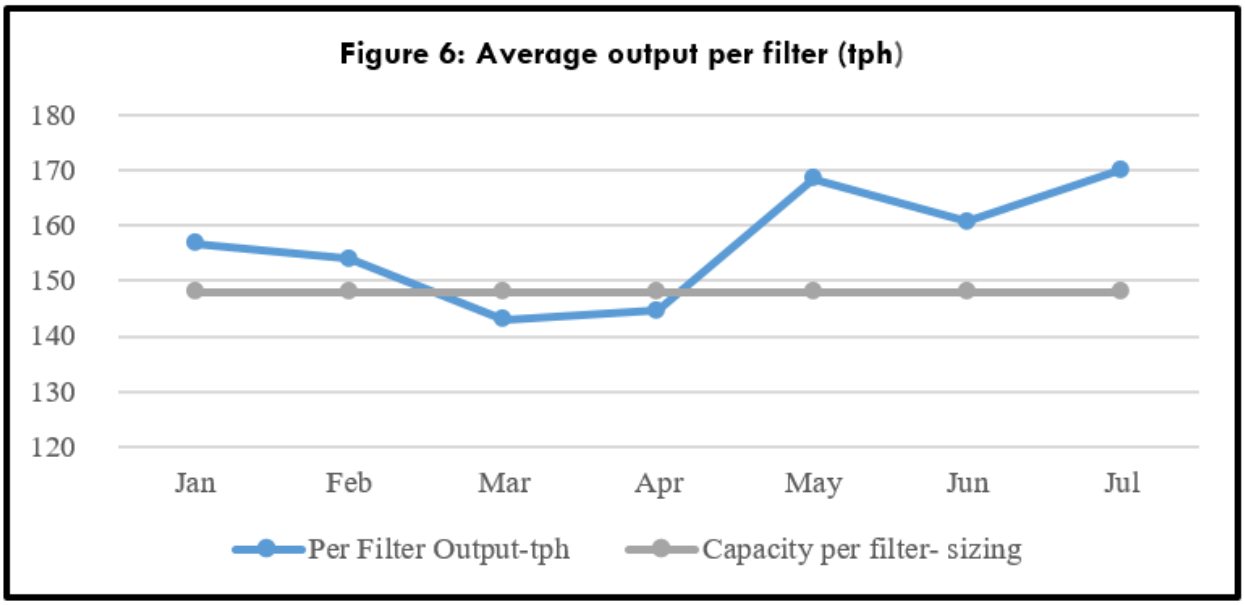
The filter plant was commissioned in August 2022, and full-scale production started on December 2022. It was designed for 444 tph nominal throughput rate; however, depending on the demand of the paste backfill for underground operation, feed to the filter plant averaged at 202 tph for the period of January to July 2023.



To ensure maximum availability of the three filters, a unique operational methodology was implemented to operate only two filters at a time and evenly distribute the operating hours for the individual filters. Figure 5 indicates the total cycles operated with the individual filters on a monthly basis.



The throughput rates from each individual filter were consistent over the seven months of the reported period, consistently meeting or exceeding the design numbers, with some level of variability based on feed characteristics. Some of the operating data have been presented in the following figures.



The cycle times of the individual filters were consistent, ranging between 8.5 to 10 minutes versus the sizing basis of 8.5 minutes. However, cake moisture content was consistent. The change in cycle time was attributed to target moisture content and manual intervention to change the cycle time, depending on

whether LZ5 mill was operating or not. Since August 2023, the filter plant has been fed with a lower ratio of tailings from the LZ5 mill (as the LZ5 mill is not operating) and cycles time were in the range of 7 to 8 minutes during this period.

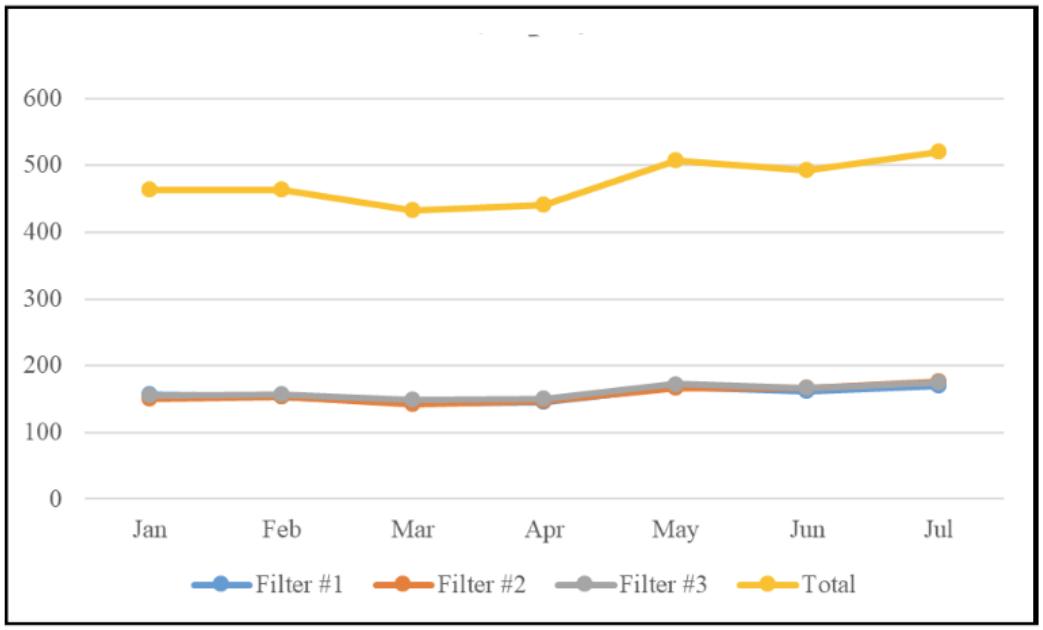


Figure 7: Individual filter production rate (tph)

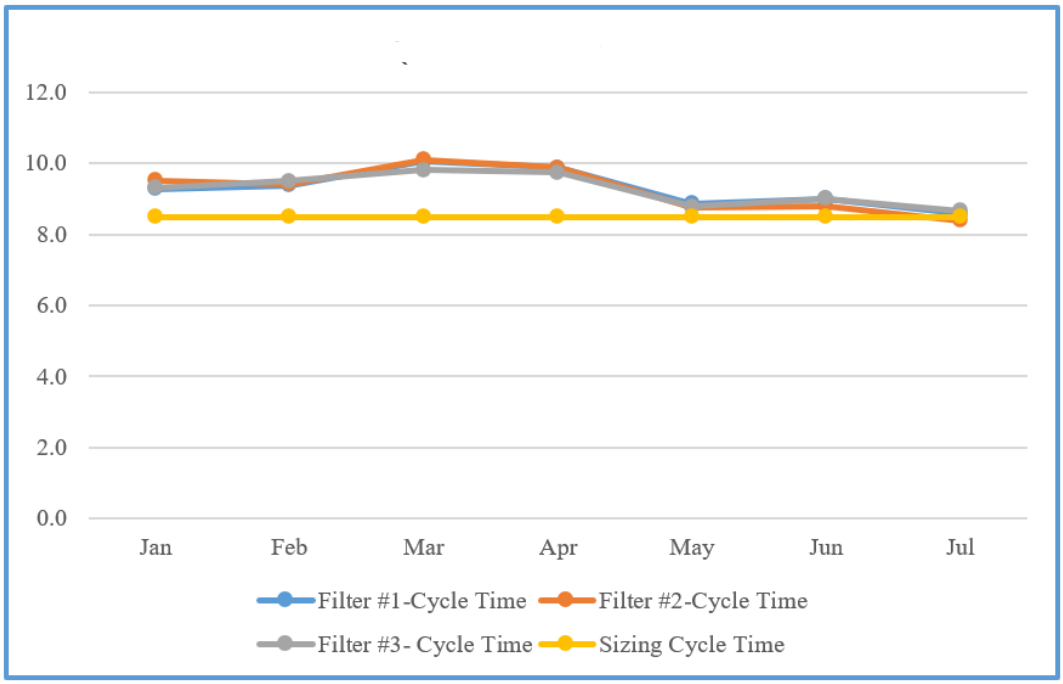


Figure 8: Cycle time

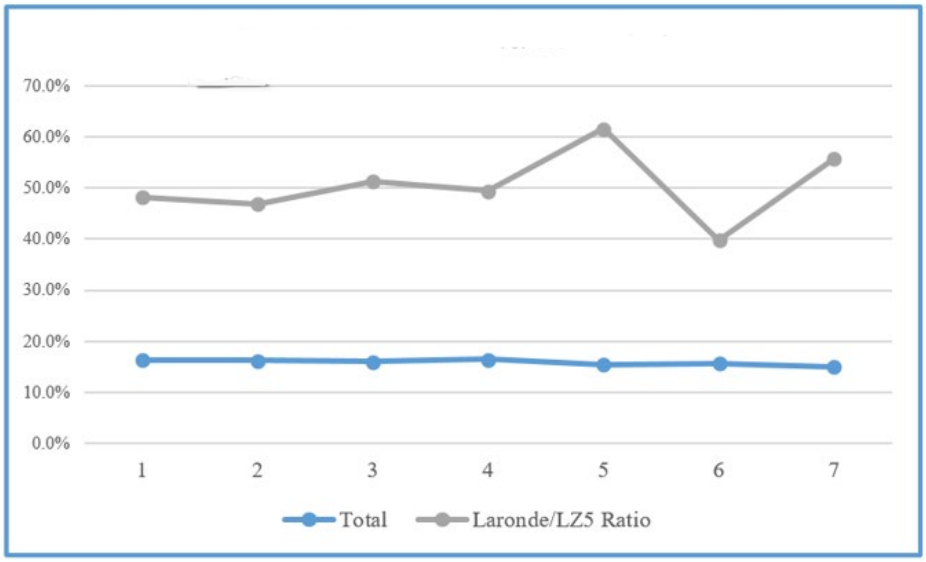


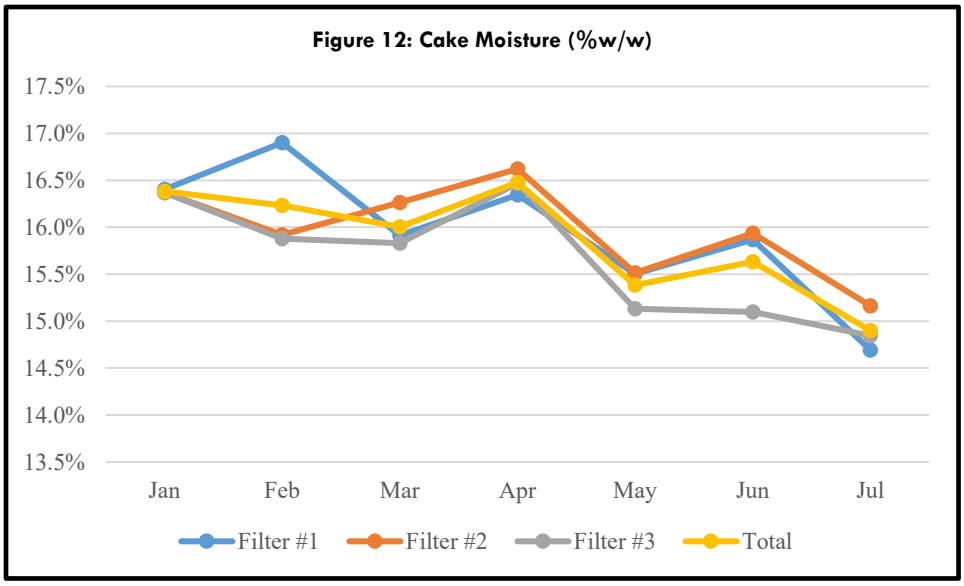
Figure 9: Cake moisture vs. ore blend ratio



Figure 10: Filtered tailings cake from discharge conveyor



Figure 11: Filtered tailings stockpile



Consumables

Cloth life is currently 4,300 cycles and no diaphragms or feed shoes have been replaced. The filter cloth being used currently is made with Polyamide material, a monofilament fabric with an air permeability specification of 140 l/dm^2/min @200Pa.

Conclusion

The LaRonde filtered tailings project has been operating since December 2022. The filter plant is consistently meeting the targeted process performance parameters. The success of this project has been attributed to the following:

- Significant work was done in the early phase of the project with an extensive amount of laboratory-scale test work to mitigate any process risks due to possible changes in ore characteristics.
- Emphasis was given to the proper selection of dewatering technologies and to developing a building design that would ensure seamless maintenance practices and the highest level of safety standards for its operators and maintenance crews.
- Existing Laronde concentrator personnel were transferred during the commissioning stage, in order to develop a clear understanding and knowledge of filter plant equipment and operations prior to start-up.

This project has been considered as a step forward to meet Agnico Eagle Mine's long-term sustainability targets.

The Closure of the Germano Pit Tailings Storage Facility

Mauricio Pinheiro, Stantec, USA
Richard Dawson, Stantec, Canada
Andrew Burgin, Stantec, Canada
Mathieu Wacowich, Stantec, USA
Rogerio Torres, formerl Stantec, Brazil
Jose Bernardo, Samarco, Brazil
Anelisa Vasconcelos, Samarco, Brazil

Abstract

Germano Pit (GP) is a decharacterized tailings storage facility located in an iron ore mined-out pit, about 25 km north of Mariana, Minas Gerais, Brazil. Operations started in 2000 and stopped in 2015 following the Fundão dam failure. Long-term plans to reestablish operations at GP were discontinued once the facility was reclassified as an upstream tailings structure by the regulator, and therefore became subject to decharacterization as per the regulatory requirements that came into effect in 2019. "Decharacterization" is a term coined by the Brazilian mining dam regulator to describe the process in which a facility is safely removed from operation and remediated to eliminate catastrophic failure and improve environmental performance. Decharacterization is thus the first step towards closure of upstream tailings facilities under the new regulations. Construction activities associated with the decharacterization of GP started in 2019 and were completed in June 2023. These activities involved construction of a reinforcement wasterock buttress and underdrains; regrading of the reservoir to eliminate ponding; and construction of a surface water management system to convey runoff flow away from the structure. As of January 2024, the State regulatory body endorsed the decharacterization of GP, the first upstream tailings facility to be decharacterized in Brazil. This paper shares some of the key aspects of the project, including Stantec's involvement as designer of record, engagement with technical auditors and other review bodies, and impacts of an evolving regulatory environment.

Introduction

The failures of Fundão and B1 tailings storage facilities (TSFs) changed the regulatory scene in Brazil as it

pertains to the management of TSFs. On February 15, 2019, immediately after the Brumadinho failure, the National Mining Association (ANM) instated Resolution No. 4/2019, prohibiting the use of the upstream construction method of tailings dams, and enforcing the decharacterization of upstream constructed tailings dams (and dams of unknown construction method) in Brazil (ANM, 2019a). Concurrently, in the state of Minas Gerais, the environmental regulatory entities Secretaria de Estado de Meio Ambiente e Desenvolvimento Sustentável (SEMAD) and Fundação Estadual do Meio Ambiente (FEAM) passed Joint Resolution No. 2784 on March 21, 2019 (SEMAD/FEAM, 2019), requiring mining dam owners in the state to prepare plans for the decharacterization of their upstream tailings dams.

The term "decharacterized mining dam," first defined by Ordinance No. 70.389/2017 issued on May 17, 2017 (DNPM, 2017), was further elaborated with Resolution No. 4 as being a structure that does not receive tailings and/or sediments from mining activities; a structure that does not have the characteristics or does not function as a dam according to its intended design. To provide more clarity to the definition, the following activities were described in Resolution No. 4 as part of the decharacterization process:

- Cessation of active tailings deposition operations and decommissioning of associated infrastructure (e.g., slurry pipelines, conveyors).
- Implementation of measures to minimize or eliminate runoff and groundwater flows towards the reservoir.
- Implementation of measures to ensure the long-term physical and chemical stability of the structure.
- Monitoring as required to substantiate the effectiveness of the design measures.

Resolution ANM No. 13/2019, issued on August 13, 2019, replaced Resolution No. 4 and instituted new target dates for the decharacterization of upstream tailings dams, but did not effect changes to the definition or interpretation of a decharacterized structure (ANM, 2019b). A few years later, ANM issued Resolution No. 95/2022 on February 7, 2022 (and Resolution No. 130/2023 on February 27, 2023), to consolidate several national regulations pertaining to the safety of mining dams into a single updated document (ANM, 2022, 2023). The definition of a decharacterized structure was maintained, except for establishing a minimum monitoring period of two years post-construction of the decharacterization design.

These regulatory changes affected 74 TSFs in the country (IBRAM, 2024). Germano Pit (GP), a TSF operated by Samarco Mineração S.A. (Samarco), a joint venture between Vale S.A. and BHP Billiton, is one of them. Formerly regarded as a drained stack, the facility was reclassified by the regulator in 2019 as an upstream tailings dam – and as such, subject to the new regulations and to the decharacterization process. GP is located at the Germano Mine, 140 km south of Belo Horizonte, Minas Gerais, Brazil. The facility is contained within the mined-out Germano Pit. Figure 1 shows a situational map of the facility, which is

situated just upstream of the former Fundão and Germano TSFs. The structure is about 50 m high and stores about 14 Mm^3 of sand tailings derived from iron ore mining and processing operations.

This case study paper describes key aspects of the decharacterization project of GP, Stantec's involvement as designers, the impacts of an evolving regulatory environment, and our engagement with technical auditors and review bodies.

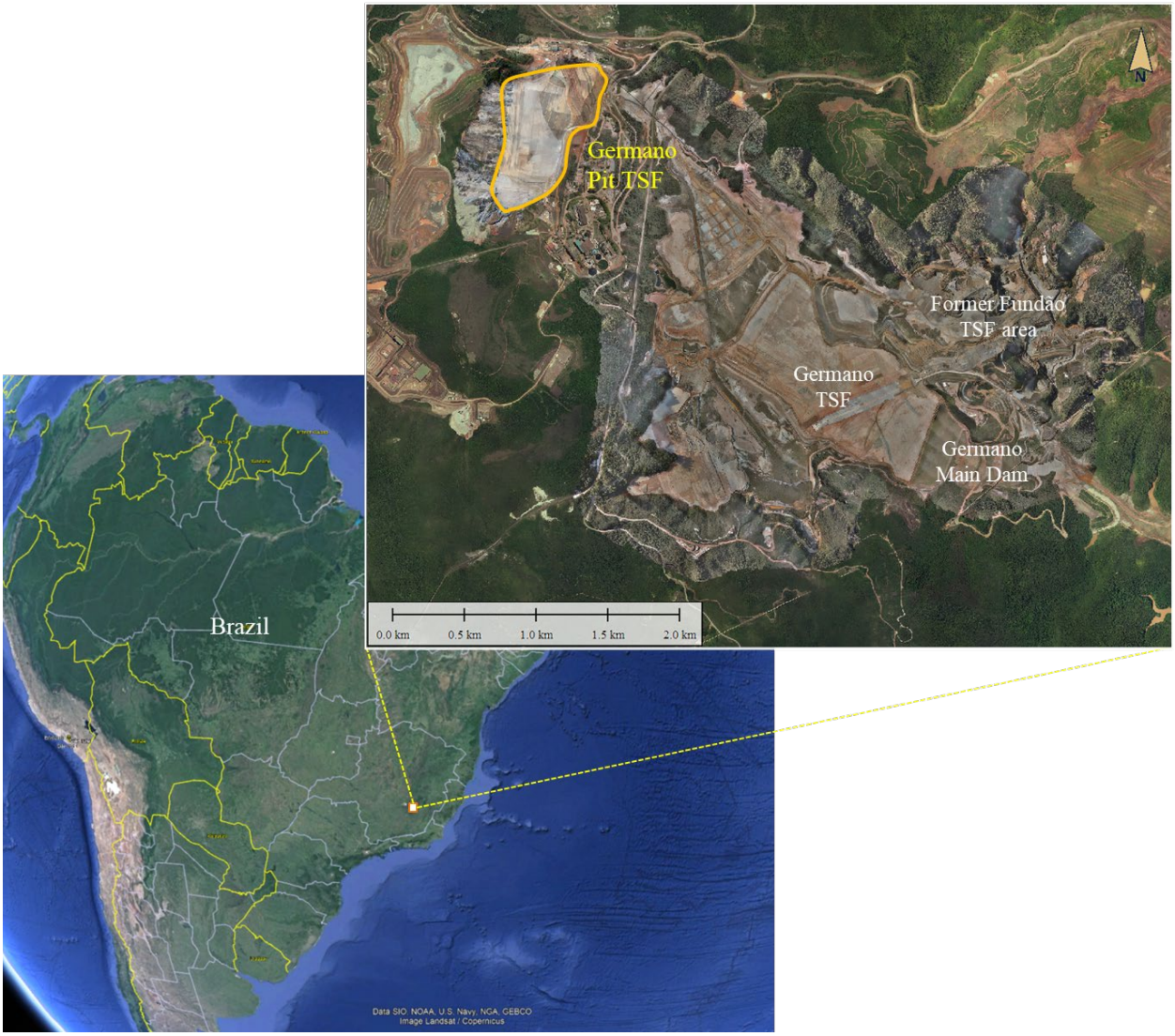


Figure 1: Situational map of the Germano Pit TSF

Germano Pit: history and site conditions

Iron ore was mined at Germano pit from late 1970s to the 1990s. After that, the pit was repurposed as a tailings storage facility, receiving underflow feed. Tailings operations started in 2000 and were suddenly halted in November 2015 in the aftermath of the Fundão dam failure.

The Germano Pit tailings is a silty-sand / sandy-silt material, with average fines (particle diameter less than 75 μm) content of about 52%, and clay percent less than 1%. The tailings mineralogy comprises mostly silica (70–75% SiO2) and iron (17–22% Fe) (Pereira, 2005). Crystalline minerals of quartzites, silicates, iron and aluminum oxides are also present. Very low (trace) levels of other metals (i.e., Sb, As, Ba, Co, Cu, Pb, Ni, Ag, V, and Zn) are present in the tailings. The silica has angular to sub-rounded grains. The tailings were deposited hydraulically from spigots. Beach development during operations resulted in a sand-like tailings structure throughout most of the facility and a slightly segregated clay-like tailings at the back of the facility, where the supernatant pond was maintained.

The site is located in a tropical climate, with well-defined rainy and dry seasons. The rainy season typically occurs from October to March, and the dry season occurs from April to September. The average annual rainfall at the site is 1,554 mm (Stantec, 2022). The area also experiences significant levels of evapotranspiration, with an annual average value of 840 mm (Stantec, 2022). The catchment area of the facility is about 140 ha.

Groundwater flows towards the south and east of the facility, mostly through aquifer Itabirite Formation.

The mine is located on a relatively low seismic zone with no significant ($M_w > 3$) regional earthquakes recorded. A peak ground acceleration (PGA) of 0.168g and peak ground velocity (PGV) of 6.3 m/s were estimated from a site-specific probabilistic seismic hazard assessment (PSHA) for an annual exceedance probability of 10,000 years (Stantec, 2022).

Decharacterization design

With the failure of B1/Brumadinho dam in 2019, and the inception of new mining dam regulations, ANM reinterpreted GP as an upstream tailings dam. A Term of Commitment was then signed in 2019 between the mine owner and various government federal and state bodies to decharacterize Germano Pit within three years, i.e., by late 2022.

A conceptual plan for the decharacterization of GP was immediately developed. The plan was advanced based on the new federal and state regulations and existing international guidelines, like those published by the Canadian Dam Association (CDA, 2014, 2019). The CDA guidelines recognize closure as a progressive multi-phased process extending over several years. Three stages are distinguished in the guidelines: (a) Transition – during this stage the tailings structure is no longer in operation, and activities are undertaken to prepare for closure care stages; (b) Closure / Active Care – when the closure elements are monitored for performance and a substantial maintenance component is set in place; (c) Closure / Passive Care – following cessation of active mining activities on site, when the structure has attained steady-state conditions and the monitoring history demonstrates no further intervention is required by the owner or other

parties. Although the term “decharacterization” is new to the international mining industry, it essentially defines a stage in the closure process similar to Active Care as defined by CDA.

Decharacterization objectives were then defined for the project, in alignment with Resolution No. 13/2019 and existing CDA guidelines. However, with the advent of the Global Industry Standard on Tailings Management (GISTM) (GTR, 2020) and ANM Resolution No. 95/2022, the objectives were updated but maintained their initial core elements, as follows:

- Objective #1: Eliminate “credible” high consequence failure mechanisms or render them non-credible. The Brazilian practice is to classify mining dams according to the associated failure consequence. Failure of a “high” consequence structure would result in significant loss of life, large environmental damages, and/or large reparation costs (similar to Extreme consequence as defined by CDA). An important decharacterization objective for GP is to eliminate or mitigate credible high consequence failure modes, especially those associated with liquefaction or other mechanisms that would lead to a breach and flow of tailings.
- Objective #2: Manage surface water to minimize ponding and erosion. Excessive ponding from heavy rainfall events is a hazard that could lead to overtopping and uncontrolled erosion. This objective attempt to eliminate permanent ponding and minimize temporary stormwater storage on the tailings deposit by designing a water management system that collects surface flows and diverts them downstream, away from the TSF, via positive flow gradients. The surface water management system at GP must also minimize erosion for flows over the structure.
- Objective #3: Manage long-term seepage and drainage performance. GP reservoir is a recharge area. The decharacterization design must consider how to collect these seepage flows and convey them downstream and away from the structure. Understanding the long-term steady state condition in the structure is key to evaluating and mitigating high consequence failure modes related to Objective #1.
- Objective #4: Identify Active Care and Passive Care stage monitoring and maintenance requirements. The types of monitoring (e.g., visual inspections, measurements, parameters, etc.) and maintenance (e.g., erosion control, revegetation, channel repairs) will be selected according to the resource requirements at each stage.
- Objective #5: Accommodate design compatible with future land use objectives, which involved repurposing the facility to store filtered tailings.

Key design elements

With the decharacterization objectives outlined, the following key design elements were proposed and implemented for GP:

- A reinforcing engineered buttress at the toe of the facility, sized for a minimum post-liquefaction factor of safety of 1.2; considering the existing underdrainage system would clog / degrade over time and reduce its effective hydraulic conductivity, and assuming residual strength (post-liquefaction undrained strength ratio) for the saturated tailings below the long-term water table. Figure 2 presents plan and cross-section views of the buttress, comprising a plateau area and benches. The extended plateau area was required to provide support for the future conveyor belt lines (shown in green in the figure).
- Extension of the existing underdrainage system. The new system comprises: (a) a 1 m thick sand blanket under the footprint of the buttress and (b) a rockfill drain network. This underdrainage system collects seepage flows from the existing drainage system and conveys them to a culvert outlet that crosses an internal access road and the state highway MG-129, as shown in Figure 3. The system will require long-term monitoring and periodic maintenance to ensure that seepage and drainage are not interrupted.
- A surface water management system, consisting of bench channels, left and right abutment secondary channels, and a Main Drainage Channel, located in the right abutment (see Figure 2). Sized for the probable maximum precipitation (PMP) event, with updated considerations on climate change, the Main Drainage Channel is the primary conveyance structure for the GP watershed. It combines open channels, stepped channels, culverts, and dissipation basin, as shown in Figure 2. With an approximate length of 462 m and a total elevation difference of 42 m, this structure begins at the GP crest, where it receives runoff from the tailings deposit and pitwall, and discharges downstream through a pair of culverts passing underneath the highway MG-129. Secondary channels tie-in to the Main Drainage Channel at various locations along the structure.
- Re-grading of the reservoir towards the in-pit perimeter channel, to eliminate permanent ponding of stormwater runoff on the deposit.
- An instrumentation, monitoring, and maintenance plan, to assess performance and conformity with basis of design, particularly over the next two years of Closure / Active Care as specified by Resolution No. 95, and to provide early warning of defects or impending threat to stability.

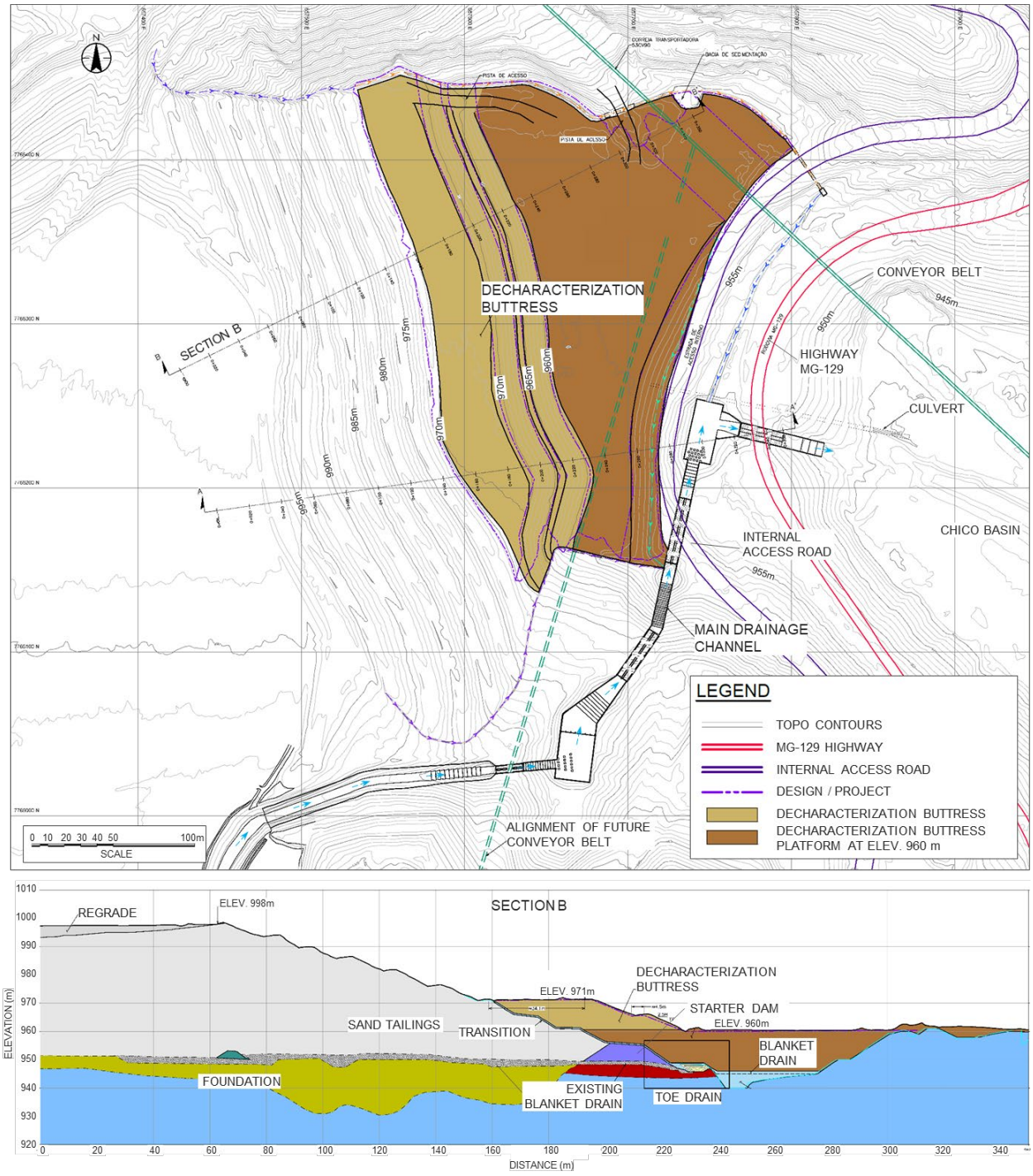


Figure 2: Decharacterization buttress and main drainage channel

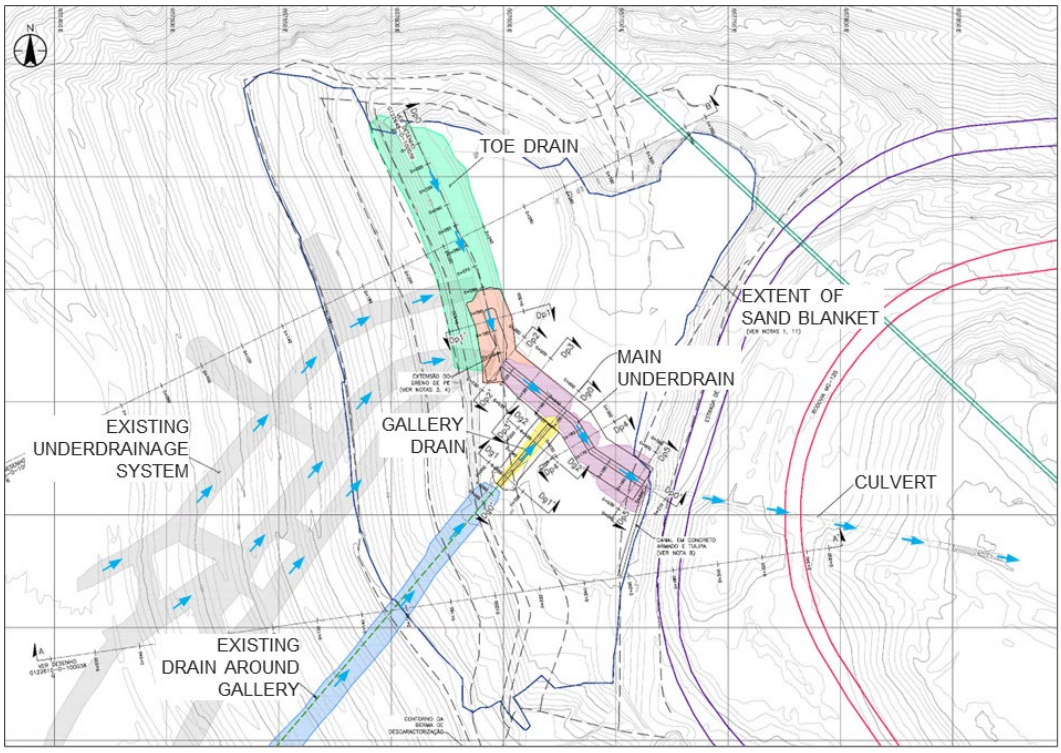


Figure 3: Connection between existing and new underdrainage system

Construction

Construction activities associated with the decharacterization of the facility started in 2020 and were safely completed by mid-2023. These activities included:

- Removal of vegetation and interferences, such as a non-operational segment of a conveyor belt, buildings, and electricity poles.
- Plugging of a 460 m long bullet-shape reinforced concrete gallery, located at the right abutment, and extending from the reservoir up to the downstream toe of the facility. The gallery was used during operations to decant the supernatant pond.
- Regrading of the reservoir surface, which involved the placement and compaction of 516,000 m^3 of filtered sand tailings.
- Construction of the decharacterization buttress, which consisted of removal of unsuitable foundation material, and placement of nearly 412,000 m^3 compacted waste rock. This activity also included construction of the sand blanket drain and the new rock underdrain system.
- Construction of the Main Drainage Channel, and secondary channels. Due to schedule constraints, the secondary channels and stretches of the Main Drainage Channel were constructed with precast concrete elements.

- Construction of a twin culvert/tunnel under the state highway MG-129, as part of the main drainage channel.
- Decommissioning or raising of existing instruments and installation of new instruments.
- Revegetation of slopes and a portion of the reservoir.
- Implementation of the instrumentation and monitoring plan. This included the decommissioning of selected instruments (e.g. prisms, a malfunctioning Shape Accel Array (SAA) inclinometer, one slope inclinometer, two flowmeters, four piezometers), the raising of instruments under the footprint of the buttress, and the installation of new slope inclinometers, tiltmeters, piezometers, prisms, geophones/ accelerometers, and a flowmeter (to measure seepage flows). Most of the instruments are automated. Readings are measured remotely, continuously and in real time, and communicated to a central data management system.

In addition to these activities, the Operations, Maintenance and Surveillance (OMS) manual, Trigger Action Response Plan (TARP) and Emergency Preparedness and Response Plan (EPRP) were updated to reflect the as-built conditions of the structure. Figure 4 shows a drone photo of GP post-decharacterization works.



Figure 4: Germano Pit post-decharacterization construction (Source: Samarco)

As per Article 8 of Resolution No. 13, the decharacterization of Germano Pit had to be completed by December 15, 2022. However, the COVID-19 outbreak, contractor performance, weather constraints (long raining season), heterogeneous wasterock sources, and rise in phreatic levels during reservoir regrade work impacted project timeline. A revised Term of Commitment between Ministério Público de Minas Gerais (MPMG), Ministério Público Federal (MPF), SEMAD, and FEAM, with the intervention of ANM, was then prepared and signed in 2022, extending the target date for the decharacterization of the structure to October 2023.

Auditing, review engagement and regulatory context

In 2019, with the enactment of ANM Resolution No. 4 (and then No. 13) and local state regulations, MPMG retained an external expert consultant to provide independent technical auditing of several decharacterization projects in the State, including Germano Pit. As a government institution responsible for defending the rights of citizens and interests of society, MPMG's role includes minimizing the risks associated with catastrophic failure of upstream construction TSFs. The auditing scope for GP included areas of geotechnical engineering, dam safety, surface water management, hydrogeology, environmental engineering, instrumentation/monitoring, and construction quality.

During construction, the auditors conducted monthly site visits to inspect the construction, document site conditions, and identify nonconformities/anomalies that needed to be remediated. Reported nonconformities were logged by Samarco, and a responsible person and target completion date were assigned to each nonconformity.

The site visit was followed by a one or two-day technical session, in which Stantec, other consultants and the client's engineering and operations groups presented various aspects of their work, provided updates about field activities and response/trends of the monitoring instruments. These were often fruitful and collaborative sessions in which the state auditors not only challenged the design basis and methodology of assessment but also provided recommendations to minimize risks and improve the resilience and robustness of the design. On one occasion, following the presentation of a Computational Fluid Dynamics (CFD) assessment to support the detailed design of the Main Drainage Channel, the auditors raised concerns about the selection of user-defined hydraulic parameters and their potential impact on flow depths and assessment of freeboard allowance along the channel under PMF condition. They recommended building a physical model of the channel to calibrate the input parameters and benchmark the CFD model for various stormwater return periods. Samarco honored the recommendation and partnered with Fundação Centro Tecnológico de Hidráulica (FCTH) of the University of Sao Paulo (USP) to construct a 1:10 scale model of the channel and run the hydraulic tests (Figure 5). The work spurred the development of a doctorate and

two Master of Science research projects. The results of the reduced scale model led to optimizations to the original design that were implemented during construction.

In addition to the technical auditor team, an Independent Tailings/Technical Review Board (ITRB) provided a similar review scope, although with a less “boots on ground” involvement and a more “big picture” / senior perspective than the auditing team. Initially, the ITRB sessions were held quarterly; however, by the end of the construction phase, meetings were held twice a year. The sessions comprised a site visit and technical meetings with consultants and client’s engineering and operations groups, followed by a wrap-up session with the Accountable Executive.

The GP project also had other levels of external reviews provided by an independent consultant team representing Samarco, and the other two independent consulting firms, each representing the two main shareholders: Vale and BHP.

The multi-tiered review process at GP was an important part of the process to restore stakeholder confidence following the Fundão and Brumadinho disasters. These reviews needed to be carefully integrated into the project design and construction planning process to minimize delays and optimize the value-added benefit they provided. This was a unique and necessary aspect of the project which can be expected on other tailings projects in Brazil to improve public perception and prevent future catastrophic failures.



Figure 5: Constructed physical model at the FCTH Hydraulics Laboratory Facility

Conclusion

The decharacterization of Germano Pit TSF spanned several years – a period that included the implementation of strict national regulations for upstream-constructed TSFs and the development of global standards for the safe management of tailings facilities, towards the goal of zero harm. The design and construction of the decharacterization works for GP were closely examined and evaluated by teams of technical expert auditors, the ITRB, and other independent reviewers representing Samarco and its shareholders. Concerns raised and recommendations proposed during the multi-tiered review process were carefully integrated into the design and construction to minimize risks, to improve the robustness and resilience of the design and its as-built elements, and to restore stakeholder confidence. In June 2023, Samarco concluded the construction of the decharacterization works of the facility. After assessments by ANM, the local regulators and the external state auditor, the decharacterization of Germano Pit was endorsed in January 2024, making it the first upstream tailings facility to complete the "decharacterization" process in Brazil. Other decharacterization projects completed prior to GP involved either partial or complete removal of the tailings deposit (e.g., Gonçalves et al., 2023). In June 2024, the Brazilian Mining Institute (IBRAM) announced that 22 out of 74 TSFs that fell under the regulations had been decharacterized in the country (IBRAM, 2024). The national objective is to complete 90% of the decharacterization projects over the next three years.

Acknowledgements

The authors acknowledge the successful planning and execution of the Germano Pit decharacterization project by its various contributors – Samarco's engineering and operations groups (especially Jonathas Pinto, former Samarco), contractors, QC/QA teams, technical auditors, reviewers, and Stantec's design team and field personnel.

References

ANM, 2019a. *Resolução No. 4, de 15 de fevereiro de 2019*. Agência Nacional de Mineração.

ANM, 2019b. *Resolução No. 13, de 8 de agosto de 2019*. Agência Nacional de Mineração.

ANM, 2022. *Resolução No. 95, de 07 de fevereiro de 2022*. Agência Nacional de Mineração.

ANM, 2023. *Resolução No. 130 de 24 de fevereiro de 2023.* Agência Nacional de Mineração.

CDA, 2014. *Technical Bulletin: Application of Dam Safety Guidelines to Mining Dams*. Canadian Dam Association.

CDA, 2019. *Technical Bulletin: Application of Dam Safety Guidelines to Mining Dams*. Canadian Dam Association (2019 Edition).

DNPM, 2017. *Portaria Nº 70.389, de 17 de maio de 2017*. Departamento Nacional de Produção Mineral.

Gonçalves, T.M., Ramos, R.C., Pereira, F.M.S., Vizcarra, G.C. and Castro, A.L. (2023) *Case study: decharacterization of tailings dike in the iron quadrangle, Minas Gerais, Brazil.* In *Proceedings of Tailings and Mine Waste, 2023,* Vancouver, Canada: 375–386.

GTR, 2020. *Global Industry Standard on Tailings Management (GISTM)*. August 2020. Global Tailings Review.

IBRAM, 2024. *Mineração: IBRAM passa a divulgar periodicamente avanços na segurança de barragens*. Accessed June 22, 2024, at https://ibram.org.br/noticia/mineracao-ibram-passa-a-divulgar-periodicamente-avancos-na-seguranca-de-barragens/

SEMAD/FEAM, 2019. *Resolução Conjunta SEMAD/ FEAM nº 2.784, de 21 de março 2019*. Secretaria de Estado de Meio Ambiente e Desenvolvimento Sustentável (SEMAD), Fundação Estadual do Meio Ambiente (FEAM).

Stantec, 2022. Germano – Geral / Cava do Germano / Descaracterização da Cava do Germano / Memorial Descritivo do Projeto / Projeto Executivo. 166818010-WP411-RPT-03.

A Safe Approach to Assess the Trafficability of Tailings Beaches for Operation and Closure Construction Activities

Delakshan Inparajah, WSP Canada Inc., Canada
Gordon W. Pollock, WSP Canada Inc., Canada
Ahreum Lee, WSP Canada Inc., Canada
Anthony Faulder, WSP Canada Inc., Canada
Jason Chen, Suncor Energy Inc., Canada

Abstract

Infrastructure construction on tailings beaches is necessary for multiple reasons, including tailings deposition and pond closure activities. The main challenges for infrastructure construction on a tailings beach are the proximity to the pond's edge and the presence of a potentially liquefiable tailings beach within the construction area. Construction activities on a tailings beach could trigger liquefaction, and assessing this potential is a key factor in managing risk. Liquefaction failures could occur rapidly and do not manifest any early signs or warnings, limiting the ability to react promptly to safeguard personnel, infrastructure, and equipment. Therefore, assessing the trafficability of construction equipment and developing a safe operating procedure prior to infrastructure construction is critical to tailings operation and managing risk during construction.

This paper will discuss case studies involving the construction of tailings infrastructure to facilitate the safe deposition of tailings and the construction of infrastructure to conduct a field trial for the closure of a tailings pond. The approach adopted in these case studies has been successfully implemented in several other tailings ponds in Northern Alberta, Canada. The proposed approach can also be used as a general guideline for tailings facilities other than oilsands to manage the risk of infrastructure construction on the tailings beaches.

Introduction

Infrastructure construction on tailings beaches is essential for berm/corridor construction for tailings deposition, closure work, and operational support activities such as barge launch and maintenance. Energy Safety Canada (2021) recommends conducting a trafficability assessment, a process that necessitates the

approval and expertise of a geotechnical engineer who plays a key role in assessing the risk and developing a safe work plan when ground conditions are unknown in tailings facilities. Therefore, assessing the trafficability of a tailings deposit, such as a tailings beach, is critical for the safe operation of the equipment, managing the risk, and reducing delays during construction.

The approach discussed in this paper for trafficability assessment can be used for infrastructure construction on tailings beaches and to manage the risk during the track packing or beach conditioning activities with different dozers. The impact of operating the equipment on the tailings beach can be assessed by performing cone penetration testing (CPT) before and after the trafficability trial (i.e., the before and after CPTs will show whether operating the equipment, such as dozers, has changed the tailings deposit state from contractive to dilative to a certain depth below the ground).

The trafficability trial must be conducted on unfrozen ground and in a ground condition comparable to, or better than, that expected during the infrastructure construction. The following steps are carried out as part of the desktop study to plan the trafficability trial:

- Understand the project needs (proposed infrastructure, access, timing of the construction, etc.) and selection of the trafficability study area.
- Conduct an aerial photographic review and assess the available geotechnical information for the specific site.
- Assess the available CPT and other relevant data for liquefaction susceptibility.
- Review available laboratory test results to understand the particle size distribution (PSD) of the tailings beach.
- Establish the trafficability lanes that cover the project area and meet the project needs.
- Finalize the equipment list for the trial based on the project needs.
- Develop the site-specific trafficability study procedures and safety measures.

Trafficability study planning and desktop study

Good trafficability is defined as the ability of construction equipment to travel on a tailings surface relatively unhindered, i.e., without excessive rutting or getting stuck in the tailings beach. The density and the undrained shear strength of the tailings deposit, liquefaction susceptibility, and the equipment's ground-bearing pressure govern the equipment's trafficability on a tailings deposit. The soft tailings deposit typically varies between a slurry and a solid, with a shear strength from 1 kPa to 100 kPa (McKenna, 2009). If the tailings deposit predominantly consists of fine sand that is susceptible to liquefaction, the shear strength range noted above corresponds to the liquefied strength of the tailings sand beach.

A desktop study must be carried out to characterize the tailings deposit and the depositional history of the project site. Additionally, understanding the purpose of the trafficability study and the relevant background information such as details of the proposed infrastructure, construction methodology being considered, access to the site, the timing of the construction, available geotechnical testing (CPT and laboratory testing), etc. are essential to developing a site-specific trafficability study that caters to the project requirements. As part of the desktop study, satellite imagery of the pond (preferably since the beginning of the active deposition of tailings) and pond level data from different years are reviewed to identify the areas of potential soft and wet zones. As part of the desktop study, the available CPT data is also assessed for liquefaction susceptibility based on the latest criteria, such as the Robertson's (2022) method. In the absence of CPT information, a CPT investigation using an amphibious CPT rig is recommended prior to the trafficability study. The following information is also gathered as part of the desktop study:

- The client-specific guidelines for working close to a water body and the province or territory's occupational health and safety regulations.
- Beaching locations within the trafficability study area and the duration of beaching.
- Type of tailings beach, i.e., coarse sand, fluid fine tailings, or treated tailings.
- Existing field and laboratory testing data for the tailings beach.
- Normal operating pond level, the highest pond level in recent years, and the expected pond level during the field trial and actual construction stage.

Based on the above information and the project requirements, trafficability lanes for the trial area are selected to assess the performance of the tailings beach under the equipment loading. As part of the trafficability study at the oil sands tailings facility, no personnel or equipment are allowed within 30 m from the edge of the pond (measured from the point closest to the pond). If personnel or equipment need to enter within the 30 m zone close to the pond, more rigorous site-specific guidelines/safety measures must be developed. Figure 1 shows the typical trafficability trial lanes developed for a berm/corridor construction for the tailings deposition at an oil sands tailings pond. As part of the trafficability trial, test pits are also excavated with a hand shovel or with a smaller excavator (based on the trafficability study findings to access the test pit location) to observe the subsurface conditions, describe the soil/tailings deposition, and collect samples for laboratory testing such as sieve analysis and hydrometer testing. Figure 1 shows the four test pit locations within the proposed corridor for tailings deposition.

Equipment for the trafficability study and the infrastructure construction

The construction equipment used for the trafficability study should be comparable to the equipment required for the infrastructure construction at the site. Additional equipment might have to be added to the

trafficability study to provide flexibility for the execution team during the infrastructure construction stage. All trafficability studies must start with an amphibious vehicle, such as an Argo.

Different bulldozers, such as low ground-bearing pressure (LGP) bulldozers, regular bulldozers, and articulated trucks (wiggle wagons) with and without the payload, are typically used in all field trials. Depending on the project requirements, special construction equipment such as pipe loaders and side booms may also be considered for the field trial.

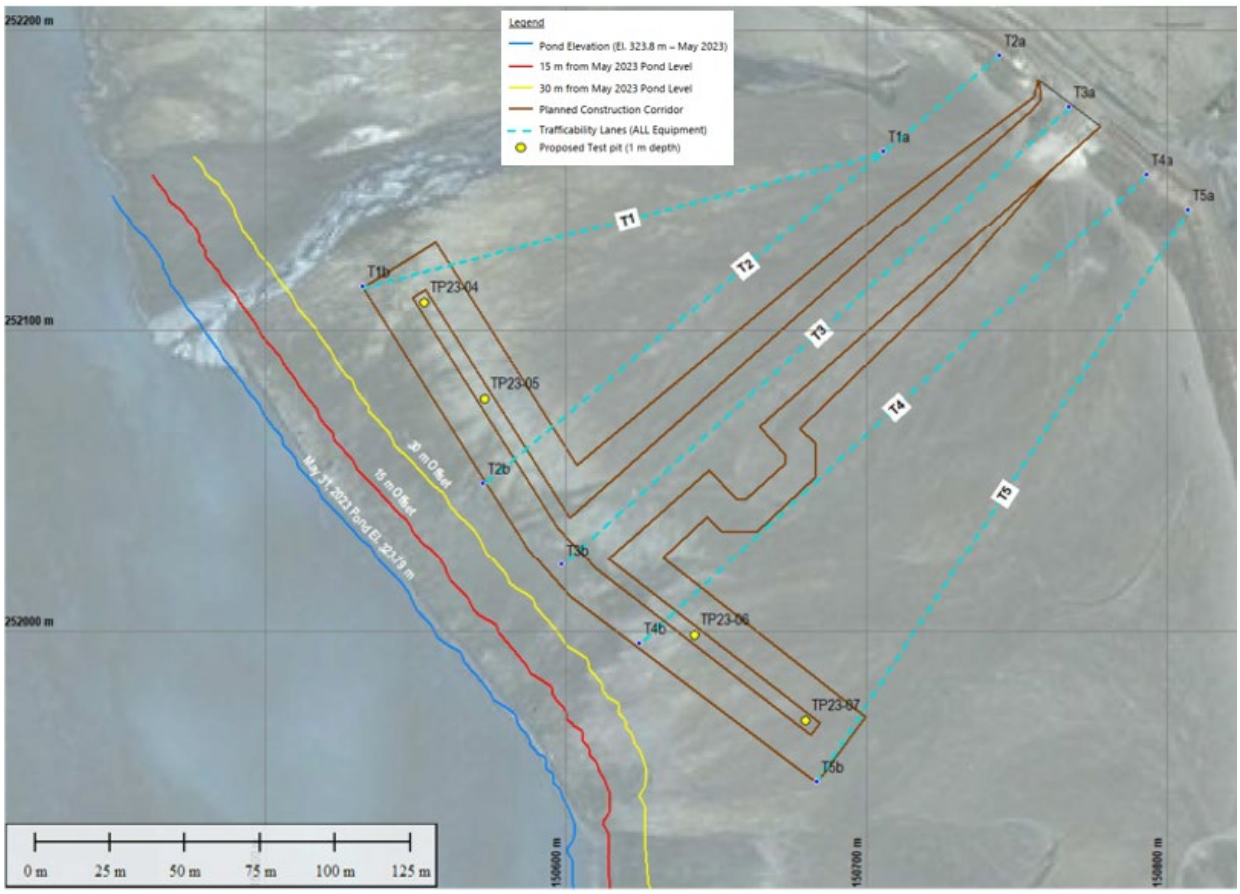


Figure 1: Project site with pond offsets and trafficability lanes based on the desktop study

Additionally, a large bulldozer, such as a CAT D10 or equivalent with a long cable sling, is required for the trafficability trial to retrieve (with winching/towing) any equipment that gets mired during the trial. This large bulldozer must be perched on a competent ground close to the trafficability study area, and it is not expected to travel along the trafficability lanes.

The weight of the equipment and the ground-bearing pressures are assessed as part of the desktop study to develop the details of the field trial. The typical equipment used in the oil sands tailings beaches for various infrastructure construction is summarized in Figure 2 with the relevant information.

The required construction equipment for the trafficability study should be readily available at the site at the time of the trial, as the sequence of the equipment is a key factor in the field trial. The sequencing requirements for the equipment are further discussed in the general guidelines section below.



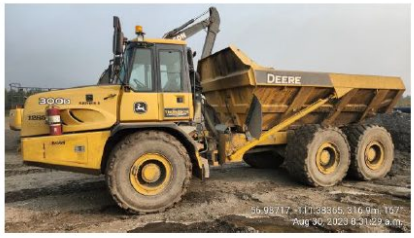
ARGO on tracks



John Deere 650J WLT Dozer



John Deere 850 WLT Dozer



John Deere 300D Truck



Volvo A40G Truck

Equipment	Weight (kg)	Approximate Bearing Pressure (kPa)
ARGO	635	4.6
John Deere 650J LGP Dozer	8,977	26.2
John Deere 850L WLT Dozer	22,800	40.4
John Deere 300D Truck (Unloaded)	19,500	85
John Deere 300D Truck (Loaded)	46,800	208
Volvo A40G Truck (Unloaded)	29,900	115
Volvo A40G Truck (Loaded)	66,901	270

Figure 2: Equipment typically used for trafficability study on an oil sands tailings beach

General guidelines for the trafficability study

The general guidelines discussed in this section have been successfully followed in several trafficability studies in the oil sands industry. However, additional guidelines and safety measures might have to be considered for other tailings storage facilities based on the findings of the desktop study for the specific site. The general guidelines and safety measures adopted for the trafficability studies at various tailings sand ponds at an oil sands facility are summarized below:

- As part of the trafficability study, personnel and equipment should not be allowed to travel within 30 m (100 ft) from the edge of the pond (measured from the point closest to the pond).
- The surveyors must use an amphibious vehicle, such as an Argo, to install the survey stakes for the 30 m offset limit from the pond edge and the trafficability lanes prior to the field trial.
- The trafficability study should not be carried out if fog, smoke, wind, ice, or snow obscure the pond edge, 30 m offset limit stakes, and the trafficability lanes.

- All equipment must travel along the competent ground (such as on the dyke crest) up to the trafficability lane locations.
- A larger bulldozer should be on standby with a long cable sling on the competent ground to retrieve any equipment in the event it gets mired during the trial (an amphibious vehicle such as an Argo can be used to transport the operator of the mired equipment, and the operator of the equipment must be trained in self-rescue).
- During the trial, all equipment should travel at a low speed (at the oil sands tailings beaches, trafficability studies are conducted with equipment traveling at approximately 5 km/hr) along the trafficability lanes.
- All equipment should travel within 5 m of the specified trafficability lanes during the field trial.
- The traverse of the sequentially heavier equipment along a trafficability lane should be within 2 m of the nearest path of the previously trafficked lighter equipment.
- All equipment operators must avoid sharp turns, including the operator of the Argo.
- The amphibious vehicle (such as an Argo) must be used as the first equipment for all the trafficability lanes, and the trial along a particular lane is continued by sequentially sending equipment with increasingly higher ground-bearing pressure.
- The empty articulated truck must travel along the lanes before sending the loaded articulated truck (with payload) along the same trafficability lane.
- All equipment should travel straight down the trafficability lanes toward the 30 m limit from the pond edge and then travel straight back until reaching competent ground within the beach. All equipment should avoid turning or reversing near the end of the trafficability lane that is close to the pond edge or near a location of poor trafficability previously identified along a trafficability lane. The loaded articulated trucks must be reversed down the beach along the trafficability lanes (with a competent person traveling on the Argo in radio communication with the operator of the truck all the time) to allow the operator to dump the load and drive forward to the competent ground if the loaded truck becomes mired during the trial.
- Equipment traveling parallel to the pond is exposed to a higher risk, which must be avoided at the site.
- Heavier equipment should not travel/approach the location where lighter equipment had poor trafficability or became mired, and should not go past the zone where lighter equipment had issues. The location where the lighter equipment had poor trafficability or got mired should be staked in the field to indicate the limit for the heavier equipment.

- The equipment operator must be prepared to reverse out (loaded trucks will travel in a reverse direction towards the pond, so they will have to drive forward) of any soft areas. The competent person traveling on the Argo parallel to the equipment will act as the spotter and must communicate with the operator if they identify any potential soft or problematic areas along the trafficability lanes.
- In saturated tailings sand, it is common to have water coming to the surface in the form of sand boils (see Figure 3) during the trafficability trial. This indicates the densification of the beach due to the equipment loading. To benefit from the densification, the area should be left undisturbed to allow pore pressure dissipation. In such events, the trafficability trial can be moved to the next trafficability lane until the sand boils are settled in the previous lane. Once the sand boils are settled/reduced, the remainder of the equipment can be allowed to travel along the areas that manifested sand boils.

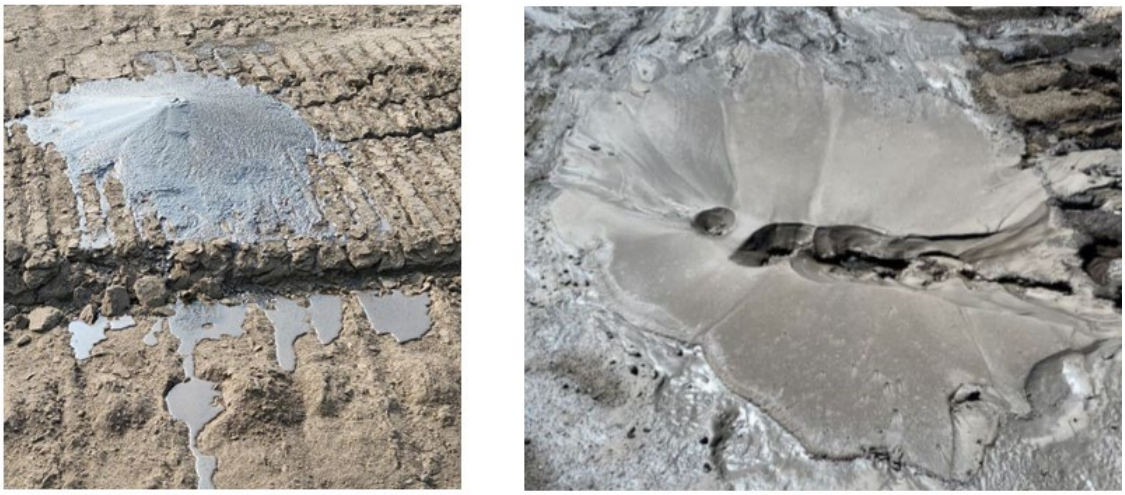


Figure 3: Sand boils observed during the trafficability study

In addition to the above guidelines, it is critical to have competent geotechnical staff at the site and a qualified geotechnical engineer (with experience conducting trafficability studies) who understands the project objectives and operational risks plan and oversees the trafficability study.

CPT testing and test pits

If the desktop study indicates a lack of geotechnical data at the site, CPT testing with field vane shear testing, along with dissipation testing, is typically carried out before, or as part of the field trial. The selected CPT test holes can be done before and after the trafficability trials to understand the densification and pore pressure conditions of the tailings beach due to the equipment loading as part of the trafficability trial. The CPT investigation on the tailings beach must be carried out using an amphibious rig.

The field staff overseeing the trafficability trial can perform the test pitting at the site, make observations of the test pit (the soil profile, depth to the water table, and the performance of the test pit slopes), and collect samples from the site for laboratory testing. The test pits can be left open until the completion of the trafficability trial to perform a follow-up observation of the test pit side slopes performance and the amount of water accumulated within the test pits. At the end of the field trial, the test pits must be backfilled with the material excavated at the site.

Field trafficability study and execution phase

The client representative, competent geotechnical staff, and experienced equipment operators must meet at the site to review the safety procedures for working close to a water body, verify the survey stake locations, and confirm that the site conditions meet the general guidelines provided above for the trafficability study. Additionally, the competent geotechnical staff overseeing the trafficability study is responsible for the following tasks:

- Recording the field activities and the weather conditions during the days of the field trial.
- Recording information for each piece of equipment used in the field trial, including photographs capturing the equipment brand, model, unit number, tire size, and any other relevant information.
- Measuring the ground contact area for each piece of equipment.
    - For the equipment with tracks, measure the width of the track and the portion of the length that is in contact with the ground.
    - For the equipment with tires, measure the width of the tires and the tire length that is in contact with the ground. If the equipment has dual tires, measure the effective contact area outside the two tires.
- Travel in an amphibious vehicle parallel to the equipment performing the trafficability trial, document the observations, and communicate with the equipment operator when signs of poor trafficability are recognized, or when it is necessary to stop the trial.
- Record the location (with a handheld GPS) where each type of equipment started the trial and had poor trafficability conditions or got mired during the trials. Place a survey stake where poor trafficability conditions were observed, and where the trafficability trial for a particular piece of equipment along a trafficability lane was terminated.
- Ensure that heavier equipment along the same trafficability lanes does not pass beyond the termination location for the lighter equipment.
- Capture photographic documentation of sand boils, ground rolling, cracking, and seepage locations.

- Measure the rut depth for each piece of equipment at various locations along the trafficability lanes.
- Communicate with the experienced geotechnical engineer frequently (when practical) regarding the observations, findings, and the progress of the field trial, in order to assess the risk continuously.

Poor trafficability conditions are indicated by deep ruts, excessive roll (ground surface manifesting a wave motion) representing high pore pressures in the soil below the surficial crest, excessive cracks, and excessive seepage water expressed at the surface along the trafficability lanes. If poor trafficability conditions are observed at the site, the trial must be paused, and the site condition must be reassessed by the field staff, client representative, and the geotechnical engineer, based on the safety requirements. Prematurely finishing a trial will limit the construction equipment's access and may result in the construction of the infrastructure being impractical.

Delaying the termination of the trial might result in safety issues, such as equipment getting stuck and potentially sinking by triggering liquefaction within a larger area. Therefore, it is critical to have an experienced field geotechnical staff overseeing and coordinating the field trial in consultation with a geotechnical engineer, as trafficability trials involve significant engineering judgment. Performing a thorough desktop study, following the trafficability study approach discussed in this paper in conjunction with the site-specific conditions, and having an experienced geotechnical staff to conduct the field trial is paramount, not only for the safety of the field trial but also to assess the feasibility of the project/infrastructure construction.

After the completion of the trafficability trial, field observations, information from the test pits, and the start and end points of different equipment are reviewed along with the information from the desktop study and the project requirements. Based on the findings, the project area may need to be relocated or reduced to manage the risk during the infrastructure construction. The findings and recommendations for the permissible limits of construction equipment access on the tailings beach for construction activities are developed, and the recommendations are typically summarized in a drawing. The drawings summarizing the recommendations for the two recent trafficability studies at an oil sands tailings facility are provided as part of the case studies below.

Trafficability study case studies

Case study 1: construction of a corridor to support the tailings operations

The tailings sand beach at this site consists of treated tailings, and the trafficability trial was conducted to develop a strategy for a berm/corridor construction to support the tailings deposition. Four test pits were also excavated with a hand shovel at selected locations to perform visual characterization/observations of

the tailings beach. Figure 1 shows the proposed infrastructure, trafficability lanes, and the test pit locations for this trafficability study.

A desktop study was carried out for this site, which included reviewing aerial photos, existing CPT data, and laboratory test results. The approach for the trafficability study provided in this paper was adopted in the field trial for this site. Sand boils (see Figure 3) and ground rolling (see Figure 4) were observed in some areas of the beach during the trial. The trafficability trial was completed successfully, and the recommendations provided to the client for equipment access for the corridor construction are shown in Figure 5.



Figure 4: Ground rolling observed close to the end of a trafficability lane

Figure 5 shows a color-coded map for the construction equipment safe access limits; the green hatched area represents the area where all equipment up to a 40-ton loaded truck can be permitted during the construction; the yellow hatched area is limited to a 30-ton loaded truck and smaller equipment tested during the field trial; and the red hatched area was limited to Argos and bulldozers comparable to a John Deere 850WLT model or smaller bulldozers.

The termination points for each type of equipment along the trafficability lanes are also shown in Figure 5 (for example, the T3-300D(E) location marked on the figure indicates the furthest point the 30-ton empty truck travelled along Trafficability Lane 3). The recommendations were reviewed with the client's construction and execution teams, and these recommendations were successfully implemented at the site during the construction.

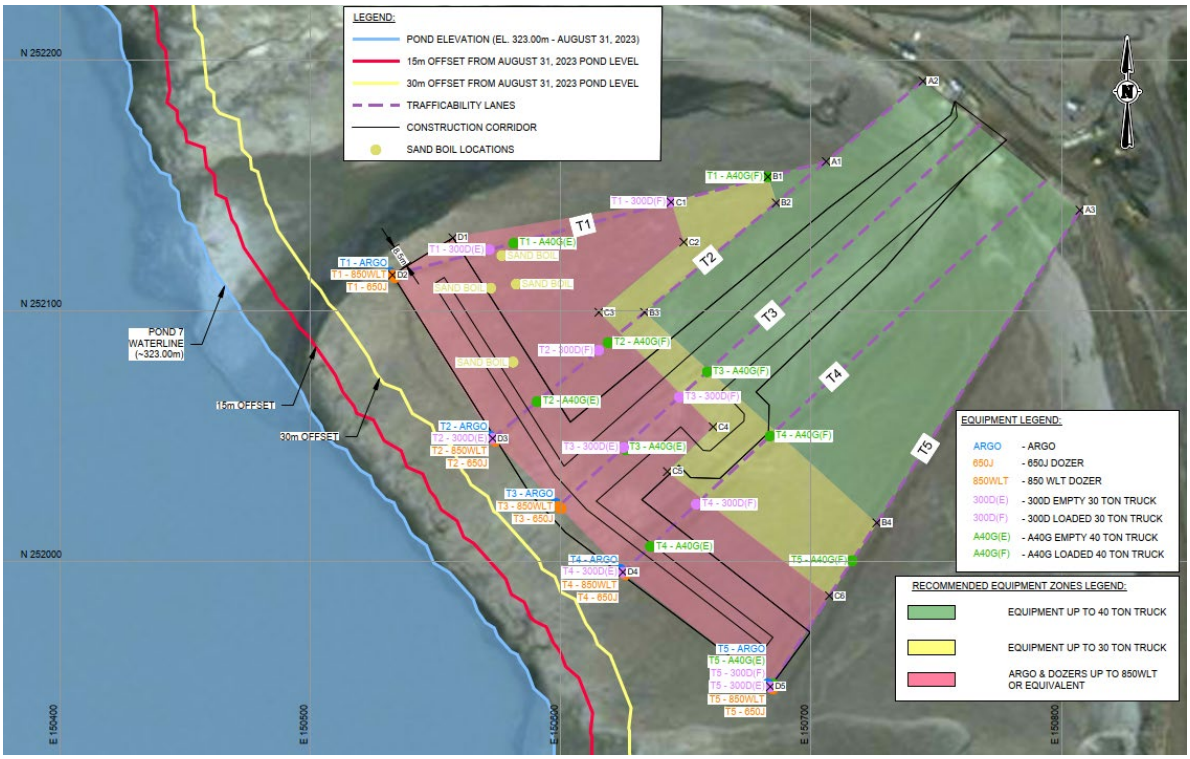


Figure 5: Trafficability study recommendations for the spur construction

Case study 2: infrastructure construction for closure trial at an oil sands tailings pond

The tailings sand beach at this site consists of composite tailings, and the trafficability study was conducted to develop an infrastructure construction plan on the tailings sand beach to perform a closure trial for the tailings pond. Ten test pits were excavated as part of the field trial at selected locations, to perform visual descriptions and observations of the tailings beach and to collect samples for laboratory testing to characterize the composite tailings beach.



Figure 6: Sand boils and seepage along the trafficability lanes in Case Study 2

A desktop study was carried out for this site, which included reviewing aerial photographs, existing CPT data, and laboratory test results. The construction on the tailings sand beach consisted of a stockpile, a solid handling area, a mixing hopper, pipelines, and other associated infrastructure. Sand boils, excessive seepage, and soft ground conditions were observed close to the competent ground along Trafficability Lanes 1 and 2 (see Figure 6).

During the trafficability trial, the loaded truck got mired close to the starting point of Trafficability Lane 1 due to the presence of soft ground conditions underneath the surficial crust (see Figure 7). Encountering sand boils, excessive seepage, and soft ground conditions was not uncommon on tailings sand beaches, and similar observations were also observed at different oil sands tailings sand beaches, as summarized in Martens et al. (2008).



Figure 7: Loaded truck mired close to the starting point of Trafficability Lane 1

Figure 8 (on the next page) shows the trafficability lanes, initially planned access ramp location, infrastructure locations, revised ramp location based on the trafficability study findings, and recommendations for equipment access limits. Due to the soft ground conditions and the poor performance observed in the northern part of the trial area (Trafficability Lanes 1 and 2), the initially planned access ramp location was deemed unsuitable for the construction equipment and the operation of the proposed infrastructure for the closure trial.

During the trial, the client and the geotechnical engineering consultant team assessed alternative locations for the access ramp, and the proposed infrastructure was shifted to the south, based on the revised access ramp location. The collaborative effort and the initial understanding of the site based on the desktop study were critical to implementing the design change without creating major downtime for the fieldwork during the trial. In addition to the typical construction equipment (see Figure 2), a side boom was also required for the construction of the infrastructure at the site. A trafficability trial was conducted with a side boom, and a spin test with the counterweight was also conducted as part of the field trial to simulate the construction.

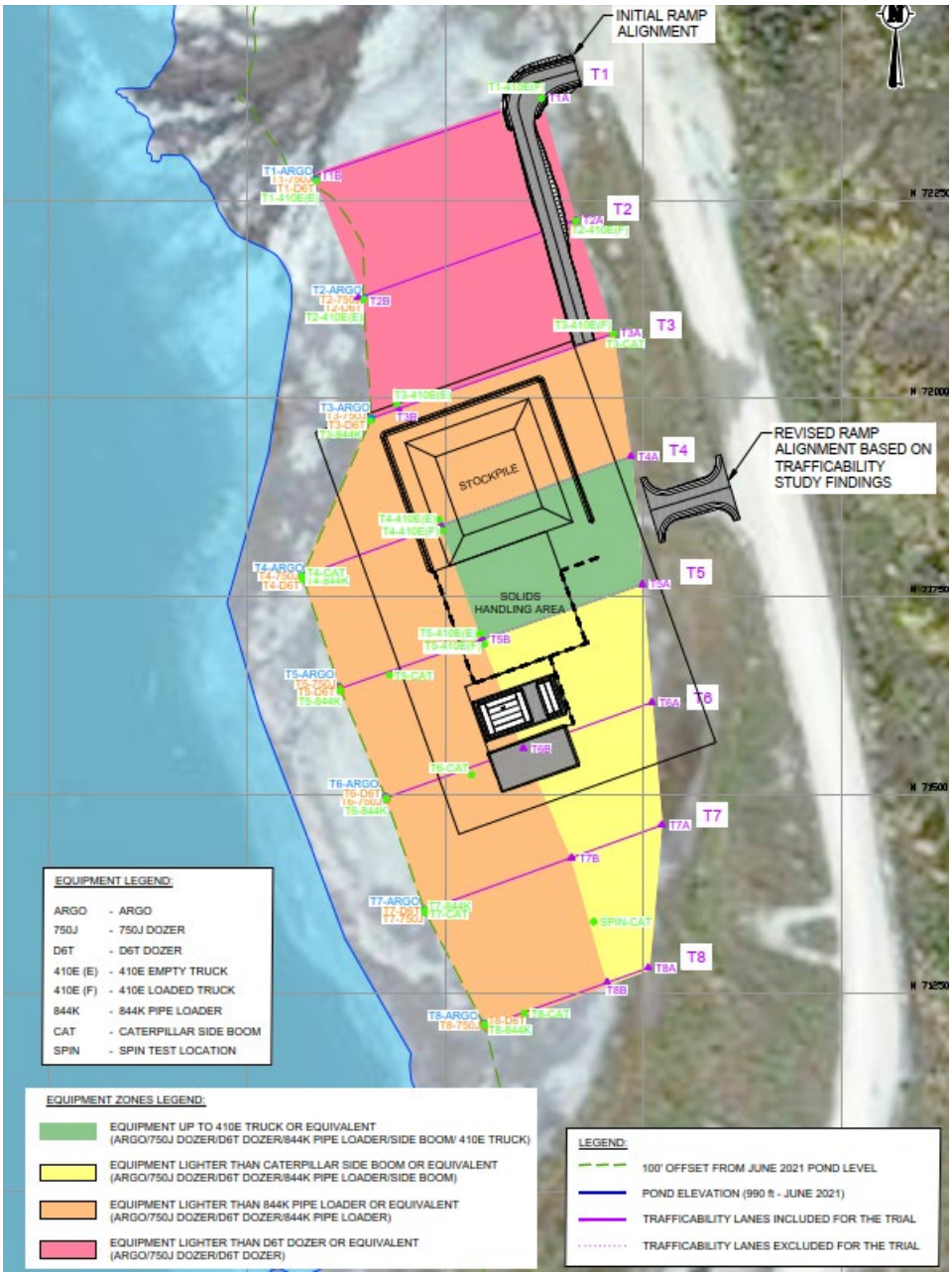


Figure 8: Trafficability study recommendation for the closure trial infrastructure construction

Figure 8 shows a color-coded map for the construction equipment safe access limits based on the desktop study and the findings from the field trafficability assessment. As shown in Figure 8, the general area close to Trafficability Lanes 1 and 2 is limited to only small bulldozers or Argo access; hence, the proposed infrastructure was shifted southward to align with the revised access ramp location. The recommendations were reviewed with the client's construction and execution teams, and the infrastructure construction was successfully completed at the site without any safety issues or delays.

Conclusion

This paper provides a safe approach for conducting a trafficability study and developing safe access limits for construction equipment on tailings beaches. The proposed approach has been successfully used in various oil sands tailings beaches to reduce the risk and uncertainty during field trials and infrastructure construction.

Acknowledgments

The authors would like to thank Jason Rhee and Suncor Field staff for supporting and coordinating the field trials and Martin Gautier and Kyle Holm of WSP for their support during the field trafficability trials. The authors also wish to recognize W.K. (Dan) Chan of WSP for his technical guidance during the development of these trafficability study guidelines.

Disclaimer

Suncor Energy Inc. and its affiliates (collectively "Suncor") do not make any express or implied representations or warranties as to the accuracy, timeliness, or completeness of the statements, information, data, and content contained in this paper and any materials or information (written or otherwise) provided in conjunction with this paper (collectively, the "Information"). The Information has been prepared solely for informational purposes and should not be relied upon. Suncor is not responsible for and is hereby released from any liabilities whatsoever for any errors or omissions in the Information and/or arising from a person's use of, or reliance on, the Information.

References

Energy Safety Canada. 2021. Working on and around oil sands tailings ponds. A program development guideline. Accessed at https://www.energysafetycanada.com/Attachments/DownloadResource?attachmentGuid=7cebfbf4-b763-43ea-8940-1b9e843cbf87&open=True

Martens, S., Lappin, T. and Godwaldt, R. 2008. Compaction of upstream construction tailings dam beaches using dozers. *Proceedings of the Canadian Geotechnical Conference 2008, Edmonton, Alberta, Canada.*

McKenna, G. 2009. Techniques for creating mining landforms with natural appearance. *Proceedings of Tailings and Mine Waste 2009.* Banff, Alberta, Canada.

Robertson, P.K. 2021. Evaluation of flow liquefaction and liquefied strength using the cone penetration test: an update. *Can. Geotech. J.* 59(4):620–624.

Long-term Performance of a Coarse-Grained Monolayer Cover on a Pre-oxidized Mine Site

Karine Sylvain, Research Institute on Mines and Environment (RIME), Université du Québec en Abitibi-Témiscamingue, Canada

Isabelle Demers, Research Institute on Mines and Environment (RIME), Université du Québec en Abitibi-Témiscamingue, Canada

Thomas Pabst, Norwegian Geotechnical Institute (NGI), Norway

Sophie Turcotte, Ministère des Ressources naturelles et des Forêts, Canada

Andréane Samson, Ministère des Ressources naturelles et des Forêts, Canada

Abstract

Reclamation of old and sometimes abandoned mine sites can pose significant environmental challenges, due to the pre-oxidized (weathered) nature of tailings and the long-term occurrence of acid mine drainage. The abandoned mine site Aldermac, a legacy of metal mining during the 1930s in the Abitibi-Témiscamingue region, Quebec, Canada, was one of the most contaminated mine sites in Quebec prior to its reclamation. The multimillion-dollar reclamation project built in 2011 has subsequently improved site conditions and reduced the environmental impacts. The southern sector was reclaimed using a landfill cell with a high-density polyethylene (HDPE) geomembrane. The selected reclamation method of the northern part of the site consisted of a monolayer cover combined with the elevated water table technique. The elevated water table, positioned above the tailings, was designed to maintain the reactive tailings saturated, thus reducing direct oxidation of sulfides. A monolayer cover composed of coarse-grained (sand and gravel, also known as an evaporation barrier cover) was placed on the reactive tailings to minimize the evaporation while promoting infiltration. In this study, four monitoring stations were installed near observation wells to assess the performance of the cover. Each station was equipped with suction and volumetric water content probes, while pressure sensors were installed in observation wells to continuously monitor water table variations. Field observations indicated that the water table was maintained above the tailings during the monitoring period. This case study demonstrates the capacity of a monolayer cover of coarse-grained materials to effectively reduce evaporation fluxes by enhancing the site water balance. Presented results provide valuable insights for the development of new strategies to enhance climate resilience in reclamation methods using coarse cover.

Introduction

Abandoned mines represent a legacy of safety and environmental concerns across Canada, with around 10,000 abandoned sites across the country (Mackasey, 2000). Abandoned mine sites typically present a complex set of environmental challenges, which are largely caused by prior inadequate mine wastes management. Common issues encountered at abandoned mine sites include a variety of conditions, including spills of tailings in the environment (Maqsoud et al., 2016), dam failures (Ranđelović et al., 2020), the presence of unknown and heterogeneous mine wastes (Cornelissen et al., 2019), wind erosion and transportation of contaminants (Rodríguez et al., 2009; Corriveau et al., 2011), modification of landscape (Mhlongo and Amponsah-Dacosta, 2016), accumulation of contaminants (Navarro et al., 2008), and extensive generation of acid mine drainage (AMD) (Seal II et al., 2008).

Tailings that are produced at the concentrator to extract the metals of interest can contain sulfide minerals, which can generate AMD in contact with oxygen and water (Blowes et al., 2014). AMD is characterized by high concentrations of sulfates, metals, and metalloids, and low pH (Jambor et al., 2005). In abandoned mine sites, tailings have typically been exposed for decades without any method of mitigation, and in some cases the low pH (2 to 4 standard units) and the presence of ferric iron (Fe^{3+}) can further contribute to the persistence of AMD (RoyChowdhury et al., 2015). The low pH can increase significantly the mobility of metals such as Fe, Cd, Ni, Zn, and Pb in the interstitial water and the final influent (Blowes et al., 2014). Typically, secondary minerals are accumulated (Jönsson et al., 2006; Favas et al., 2016) and in some cases can generate cemented layers or hardpan (Hakkou et al., 2008; Quispe et al., 2013), which cause high heterogeneity of the hydrogeological properties (McGregor and Blowes, 2002; Elghali et al., 2019). Therefore, reclamation of abandoned mine sites requires complex fieldwork to select the appropriate methods of reclamation, such as building dams, reprofiling slopes, excavating tailings that have been spilled into the environment, and characterizing the mine waste and the underlying geology (Kubit et al., 2015).

Under humid climate conditions, the exclusion of oxygen is considered the most efficient method of AMD mitigation (Bussière and Guittony, 2021). The low oxygen diffusion rate in water (10,000 times lower than in air) inhibits the direct oxidation reactions leading to AMD (Aubertin et al., 2016). Among the available techniques, the elevated water table technique (EWT), combined with the monolayer cover, consist of raising the water table to half of the air entry value (AEV) of the reactive tailings (Pabst, 2021) and adding a coarse layer on the top to control the water balance (Dagenais et al., 2006; Ouangrawa et al, 2010). The cover reduces evaporation, tailings erosion and favors infiltration. In cases of highly pre-oxidized tailings, the water table can be raised up to the surface of the tailings (Pabst et al., 2018) or in the cover (Maqsoud, 2017).

In this paper, the reclamation work performed on the abandoned Aldermac site is presented. The study specifically concentrates on the northern part of the site, where the selected method of reclamation was the

EWT combined with a monolayer cover of sand and gravel. The water table was raised into the cover because of prior extensive oxidation (Maqsoud, 2017; Maqsoud et al., 2022). The sector of this site has been monitored since 2011 by the Ministry of Natural Resources and Forest of Quebec (MNRF) and the Mineral Technology Research and Service Unit (URSTM). Instrumentation stations were installed for continuous monitoring from 2020 to 2022 for this research project. This case study demonstrates the efficiency of a monolayer cover made of coarse-grained materials as an evaporation barrier to enhance the site water balance. The effectiveness of the method was also evaluated in response to extremely dry climate conditions recorded in summer 2021.

Methodology

Site description

Aldermac mine site is located 15 km west of Rouyn-Noranda, in Abitibi-Temiscamingue, Quebec. The mine site was operated for copper and zinc mining from 1931 to 1943. During this period, approximately 1.3 million tonnes of tailings were generated and deposited on approximately 50 hectares and exposed to atmospheric conditions (SNC Lavalin, 2007). The tailings spilled over a surrounding area of 26 hectares along 10 km of Creek 1 and the Arnoux River, following the failure of a dam in 1942 due to the limited means of confining. These tailings contained a significant concentration of sulfide minerals, ranging from 20% to 30% of pyrite and pyrrhotite, and were generating AMD (e.g., pH ranging from 2.3 to 5). On-site observations revealed the presence of a 5 cm to 30 cm thick hardpan, characterized as goethite, jarosite, natrojarosite and gypsum (Bédard, 2000). Heavy metal concentrations (such as iron, copper, and zinc) exceeded provincial legislative criteria, affecting water quality in adjacent receiving environments including the Arnoux River and Lake Arnoux (Mocq and Hare, 2018).

The planning for the reclamation began in 2005 and the reclamation construction was completed between 2008 and 2010. The site was divided into three sectors: the Southern sector with higher elevation, the Intermediate sector, and the Northern sector in a valley. The Southern sector was reclaimed using a landfill cell with the tailings deposited on the surface of a high-density polyethylene (HDPE) geomembrane. The tailings of the Intermediate sector and the spill area were excavated and transported to the North sector.

The selected method for the North sector was the elevated water table (EWT) combined with a monolayer cover. The constitutive material of the monolayer cover was sand and gravel, extracted from a borrow pit directly on the site. The target thickness of the cover was 1 m. The fieldwork included the construction of three dams (F, G, and H in Figure 1) and the enhancement of dam E to maintain the water table positions close to the surface of the tailings. The Northern sector was divided into two sections to optimize the placement of tailings excavated from the spill by a central dam (dam G). Terrace 1 was 3 m higher than the final elevation of Terrace 2. Four spillways were built on dam G to control overflow from

the accumulation areas and the water table position of Terrace 2. After the placement of the cover during winter 2011, differential displacements were observed, and the site was reprofiled by adding additional cover material (except for 5 hectares in Terrace 2 where a swamp formed).



Figure 1: Northern part of the Aldermac site reclaimed using the elevated water table technique combined with a monolayer cover of sand and gravel (aerial photo from Google Earth).
Observation wells T1 to T6 and Station 1 to 4 are shown with blue circles and green squares, respectively

A total of twelve piezometers and observation wells were installed in the Northern area of Aldermac following the reclamation to monitor the groundwater and surface water quality. Six observation wells, labeled T1 to T6, were installed in the cover close to the interface of the tailings to monitor the water table position. The performance of the reclamation method has been evaluated through multiple water level monitoring and water sampling campaigns since 2011 (Maqsoud et al., 2013; Maqsoud, 2017; Maqsoud et al., 2022), and the site continues to be monitored by the Ministry of Natural Resources and Forest of Quebec (MNRF).

Climate conditions at the Aldermac site

The Aldermac site is in a humid climate, and the yearly water balance is positive. The annual climate was estimated using the Daymet method on a 1 km grid (Thornton et al., 2020). The total precipitation, which included snow and liquid precipitation, was on average 910 mm from 1994 to 2023 (Table 1). The minimum annual total precipitation estimated during the monitoring period (2020 to 2022) was 770 mm (2021), which was also the minimum annual total precipitation for the period 1994 to 2023. The maximum total precipitation was 1,030 mm (2022), which was the second-highest total annual precipitation since 1994.

The climate is temperate and cold during the winter. The average temperature for the period 1994 to 2023 was 2.4°C.

Table 1: Annual climate data over the last 30 years (1994 to 2023)

	Total precipitation annually (mm)	Temperature (°C)
Minimum	770 (2021)	-43.1(1994)
Maximum	1,050 (2008)	35.9 (2005)
Average (1994 to 2023)	910	2.4

Monitoring program in the Northern area

The aims of the monitoring program were the evaluation of the cover performance to maintain the water table above the tailings. During the fall of 2020, four instrumented stations (S1 to S4) were installed, close to the observation wells T3 to T6 to characterize the hydrological behavior of the covers. Trenches were excavated to install pore-water pressure probes (Watermark ±1 kPa) and volumetric water content probes (GS3 ±0.03 m^3/m^3) at depths of 30 cm, 60 cm, and 90 cm under the surface of the cover. At Station S1, the probes were installed at 20 cm, 45 cm, and 75 cm due to high water table position. A total of four pressure sensors were placed in the observation well T3 to T6 to continuously monitor the water table level (Figure1). Cover material and tailings were also collected for characterization. The atmospheric conditions data were collected at the meteorological station Rouyn Noranda 15 km from the mine site and compared to the dataset from Daymet (Table 1). The potential evapotranspiration was calculated with Penman-Monteith model using PyDaymet from HyRiver (Chegini et al., 2021).

Material in-situ properties

Tailings were sampled under the cover and their particle size distributions (PSD) were obtained using laser diffraction analysis (Malvern Mastersizer). The PSD of the cover samples was determined according to ASTM D6913 (2021) (Figure 2a). The water retention curves were obtained with the MK model (Aubertin et al., 2003) for both materials (Figure 2b). The in-situ porosity of the cover was determined using a nuclear densimeter, and varied from 0.22 to 0.30 on the site. A significant contrast between the water retention curve (WRC) of the cover and the WRC of the tailings suggested an effective capillary break. The low air entry value (AEV) of the cover can prevent capillary rise, thereby limiting evaporation (Ouangrawa et al., 2010).

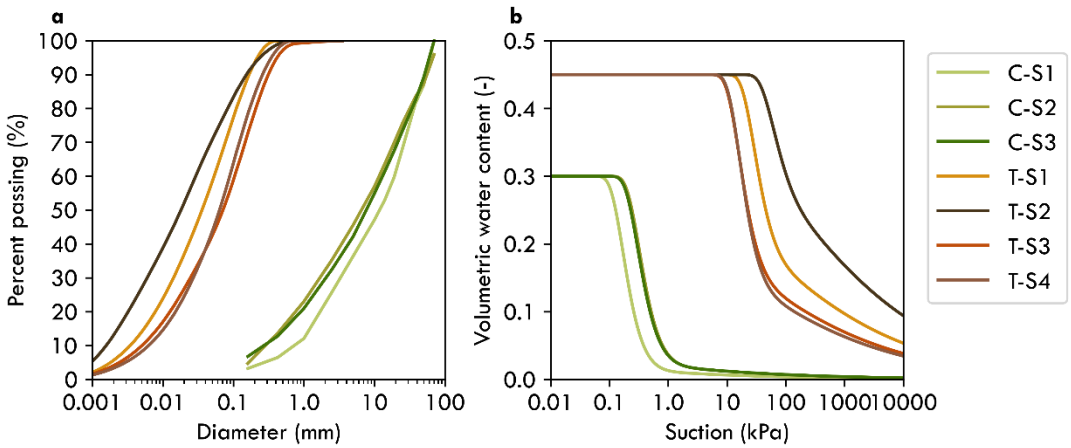


Figure 2: (a) Particle size distribution and (b) water retention curves of the tailings (T) at the stations S1 to S4 and cover material (C) at the stations S1 to S3

Results and discussion

Water table position by manual measurements (2011 to 2023)

The water table position was measured manually over the period 2011 to 2023, initially by URSTM from 2011 to 2015 (Maqsoud et al., 2022), subsequently by the MNRF from 2015 to the present and during this research project from 2020 to 2022. The water table elevation in Terrace 1 was approximately 3 m greater than the water table elevation in Terrace 2. T1 is located downstream of the energy dissipation basin, and T2 is located downstream of the Intermediate Sector basin, separated by dam H. The water table remained close to the surface of the cover as those basins controlled the water table position. In Terrace 2, near T4, a swamp formed because of vertical displacement of the cover and tailings during the early years of the reclamation works (see section Site description above) (Figures 3e and f).

The position of the water table in Terrace 1 was monitored using manual measurements in observation wells T1 to T3 (Figure 3a, b, and c). For T1 and T2, the water table level remained close to the surface and occasionally exceeded the surface level of the cover. Water table elevation in the observation well T3 (Figure 3c) was lower than T1 and T2 (e.g., 0.25 m to 0.45 m; Figures b and c) because of the proximity to dam G, which is built with four spillways to control the water table position in Terrace 2. Fluctuations of +/-0.7 m were observed in observation well T3.

Terrace 2 water level was monitored using observation wells T4, T5, and T6 (Figures 3d, e, and f). The water table elevation in T4 was close to the surface or above the surface during the entire observation period (Figure 3d). Significant fluctuations of the water table position in T5 and T6 (up to 0.9 m) were also observed.

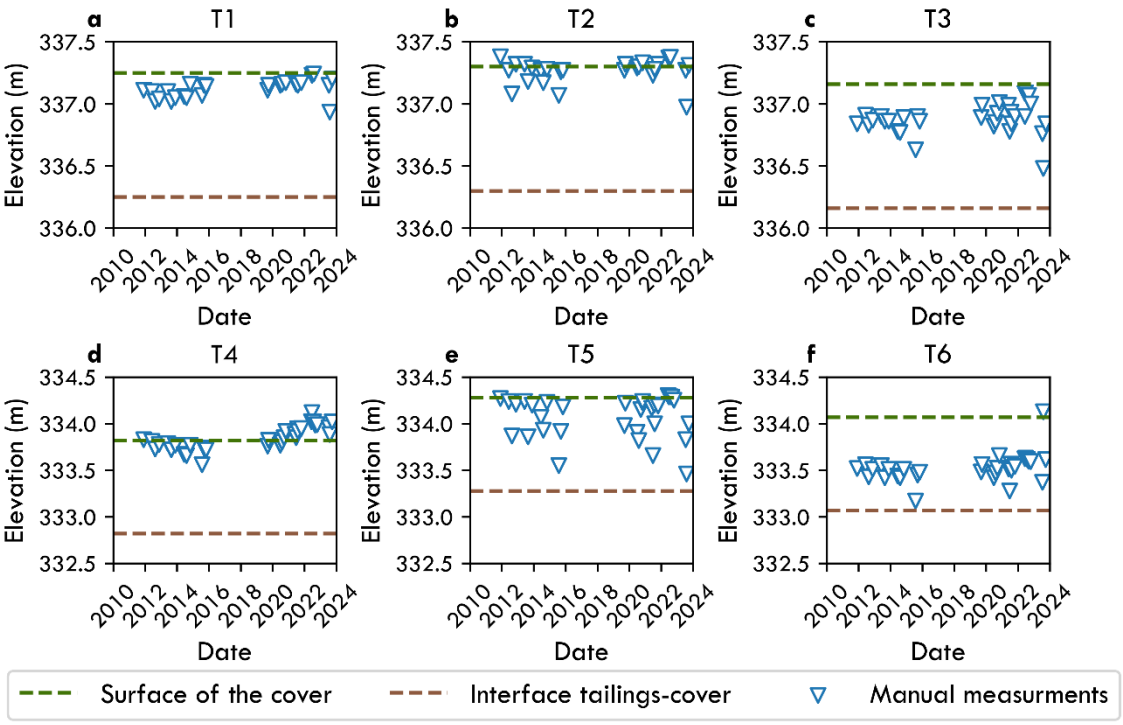


Figure 3: Water table elevation (m) obtained by manual measurements of the observation wells for the monitoring period (2011 to 2023). The dashed brown line presents the tailings interface approximated by Maqsoud et al. (2022) during the installation of the observation wells, and the green dashed line presents the estimated cover surface elevation

The performance of the reclamation method was previously analyzed by Maqsoud et al. (2022) for the 2011 to 2015 monitored period. The manual measurements of the water table level in all observation wells (T1 to T6) suggested that, during this period, the water table was maintained above the tailings, within the cover, which could suggest that direct oxidation of the tailings was efficiently controlled (Maqsoud, 2017; Maqsoud et al., 2022). These findings were correlated with a decrease in electrical conductivity and dissolved elements in the groundwater (Maqsoud et al., 2022), as well as improvement of water quality downstream in the Lake Arnoux just one year after the reclamation of Aldermac mine site (Mocq and Hare, 2018). The manual measurements campaigns conducted between 2016 and 2023 by the MNRF and the authors suggested that the water table has remained above the tailings, and within the cover since its reclamation. This indicated that the tailings remained saturated (Figure 2b) and the reclamation was deemed efficient.

Continuous monitoring of the water table (2020 – 2022)

The water table elevations were measured continuously in the observation wells T3, T4, T5, and T6 from 2020 to 2022. The year 2021 was the driest recorded in the past 30 years (total annual precipitation

770 mm), while 2022 had above-average yearly precipitations (1,030 mm). A significant difference in the water table elevation was observed between 2021 and 2022. For example, near station 1 during the summer of 2021, the water table in T3 ranged from 336.6 m to 337.1 m with significant variations of 0.5 m. In contrast, during the summer of 2022, the water table remained close to the surface of the cover at 337.2 m, with significantly smaller amplitudes of maximum 0.2 m (Figure 4a). The same trend was observed in observation well T5 near Station 2, although greater amplitudes were recorded in 2021 (e.g., 0.9 m; Fig 4b).

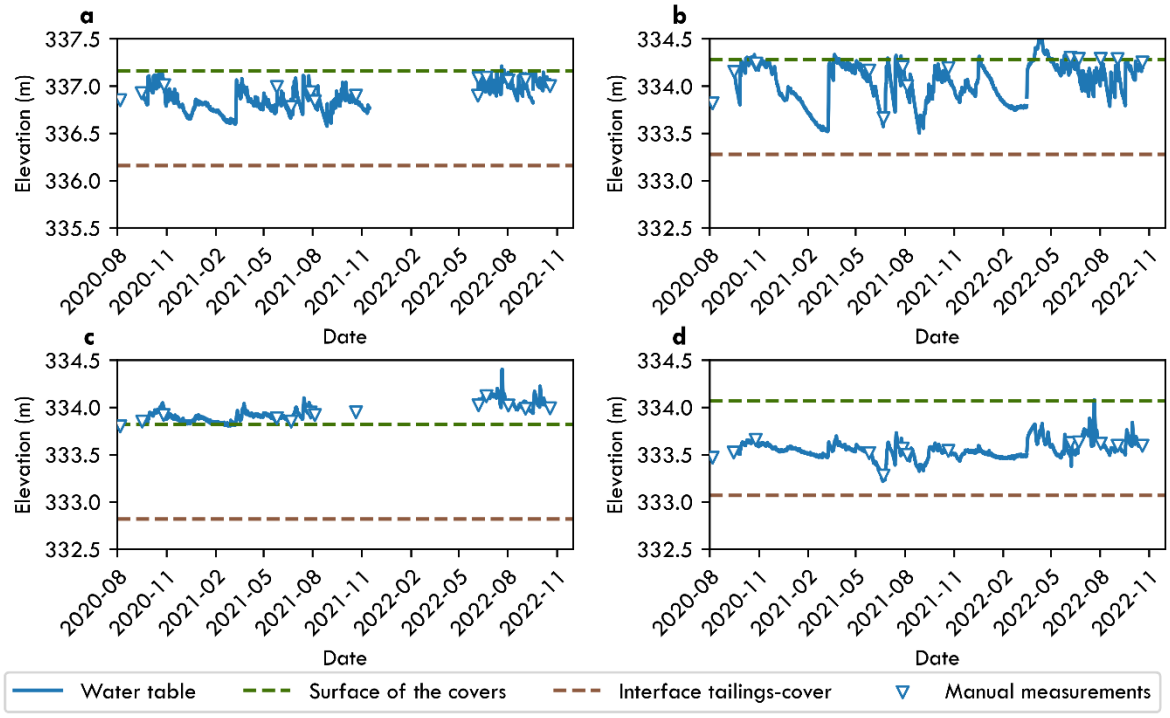


Figure 4: Continuous water table elevation in observation well at Terrace 1 a) T3 (Station 1), and at Terrace 2 b) T5 (Station 2) c) T4 (Station 3) and d) T6 (Station 4).
The gaps of measurement of the water table in a) and c) are due to equipment failures

The water table was continuously above the cover in the observation wells T4 (Figure 4c). The water table elevation in the observation well T6, which is located near the final effluent, remained above the interface of the tailings for the monitoring period, although the water table significantly decreased during the summer of 2021 (Figure 4d). The monitored period revealed that the water table elevation was intrinsically sensitive to the climatic conditions, as a great increase of the water table elevation was observed on-site.

Dry years (2021)

From spring to the fall of 2021, two months, May and August, were characterized by a potential water deficit period where precipitation fell below the potential evapotranspiration (PET) (Table 2). August was particularly dry, with total precipitation of 47 mm, an estimation of 93 mm of PET, and a maximum of 15

consecutive days without precipitation. During this period, the water table in the observation wells decreased by 0.6 m in T5 in Station 2, 0.4 m in T3 in Station 1 and 0.3 m in T6 (Figure 5). The water level remained above the cover in T4, near station 3, so the results are not presented here.

Table 2: Precipitations and PET comparison from May to September

	Rainfall (mm)	Estimated potential evapotranspiration (mm)	Maximum number of consecutive days without precipitation	Date
May	61	75	5	26 to 30
June	116	85	4	14 to 17
July	136	90	6	7 to 12
August	47	93	15	13 to 27
September	119	53	3	1 to 3, 18 to 20, 28-30

Generally, the water table at Stations 1, 2, and 4 were sensitive to periods of precipitation and evaporation (Figure 5). For example, the water table level at Station 2 (T5) and at Station 1 (T3) rose by approximately 0.7 m and 0.6 m, respectively, after an intense rainfall of 50 mm on July 15th. The water table at Station 4 (T6) was at the lowest elevation of the North sector, with a depth of 0.4 m to 0.5 m from the surface of the cover, and exhibited smoother increases in response to periods of rainfall and evaporation.

The volumetric water content in the probes at the bottom of the cover remained at saturation in all Stations 1, 2, and 4 (red line; Figure 5), as the water table level remained above the probes throughout the period. In Station 1 and Station 2, the water table was generally above the middle probes, positioned at depths of 0.45 m and 0.6 m respectively, with occasional measurements at greater depth corresponding to a decrease in the volumetric water content (orange line; Figure 5). In Station 4, the water table fluctuated between depths of 0.4 m to 0.8 m, resulting in periods of saturation and periods where volumetric water content decreased as observed in the middle probes. Finally, the volumetric water content of surface probes (purple) was near saturation when the water table was increasing after rainfall, and remained at residual volumetric water content when the water table was deeper than the probes.

Therefore, during a particularly dry year, the water table remained above the interface between the tailings and the cover, which indicates that the cover effectively maintained saturation in the tailings by preventing evaporation, thereby minimizing the direct oxidation of the tailings. However, the results showed that the water table is sensitive to an extensive period of evaporation and drainage as the water table decreased between 0.3 m to 0.9 m during a period without any rainfall, or with low rainfall. The low AEV of the cover maintained a capillary break, and therefore no capillary rise to the surface, which did reduce the evaporation.

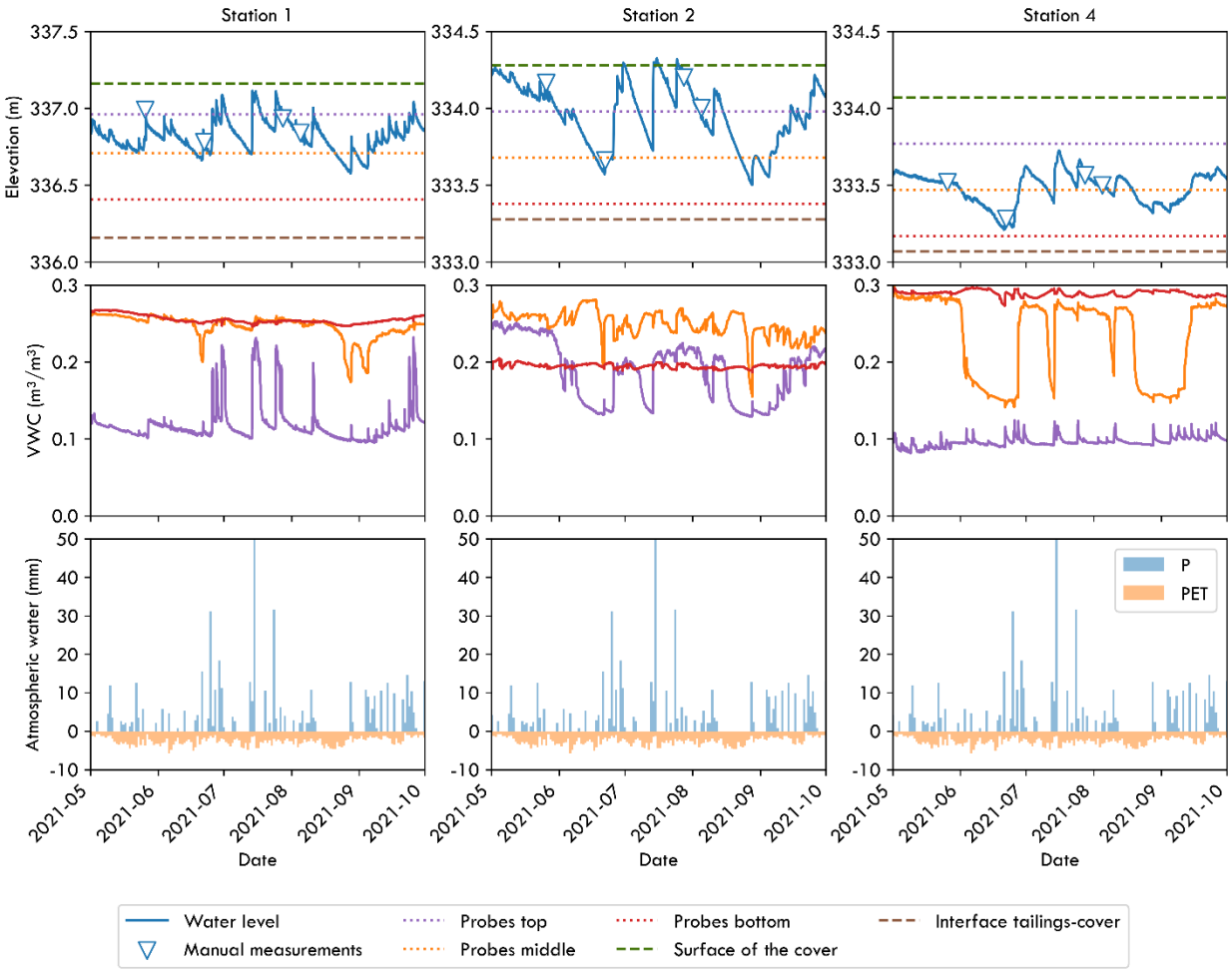


Figure 5 : Evolution of the water table elevation (m), volumetric water content regarding the atmospheric water balance of precipitation (p) and potential evapotranspiration (PET) of Station 1, 2 and 4

Conclusion

The water table at the Aldermac site was raised in the cover to control AMD generation of the pre-oxidized tailings. The water table level was maintained above the tailings from 2011 to 2023, as shown by the manual measurements campaign. Continuous measurements of the water table level and the volumetric water content were performed at four stations for 2020 to 2022, providing insights into the amplitude of the water table fluctuations. Specifically, an analysis of the water table and the volumetric water content during the driest recorded year (770 mm of total precipitations) since 1994 indicated that the water table remained above the tailings, which suggests the importance of the coarse-grained layer to prevent excessive evaporation. However, during the intense period of drought in August 2021, the water table decreased by 0.4 m to 0.7 m in the Stations 1, 2 and 4, which indicated the sensitivity of the water table regarding the period of water deficits. Future work involves modeling climatic scenarios to assess the performance of the cover during periods of intense droughts.

Acknowledgements

We extend our gratitude to MNRF for their contributions to the project, as well as the technicians at URSTM and Polytechnique Montreal. Financial support was provided by the Natural Sciences and Engineering Research Council of Canada (NSERC) through an Alliance grant, with the participation of MRNF, Iamgold Corporation and Agnico Eagle Mines Ltd.

References

Aubertin, M., Bussière, B., Pabst, T., James, M. and Mbonimpa, M. 2016. Review of the reclamation techniques for acid-generating mine wastes upon closure of disposal sites. *Proceedings of Geo-Chicago 2016*: 343–358.

Aubertin, M., Mbonimpa, M., Bussière, B. and Chapuis, R. 2003. A model to predict the water retention curve from basic geotechnical properties. *Canadian Geotechnical Journal* 40(6): 1104–1122.

Bédard, I. 2000. Techniques de réhabilitation des zones d'épanchement du parc à résidus miniers Aldermac, École Polytechnique de Montréal.

Blowes, D., Ptacek, C., Jambor, J., Weisener, C., Paktunc, D., Gould, W. and Johnson, D. 2014. *The Geochemistry of Acid Mine Drainage*. DOI:10.1016/B978-0-08-095975-7.00905-0

Bussière, B. and Guittonny, M. 2021. *Hard Rock Mine Reclamation: From Prediction to Management of Acid Mine Drainage*. Routledge Taylor & Francis Group.

Chegini, T., Li, H.-Y., and Leung, L.R. 2021. HyRiver: Hydroclimate data retriever. *The Journal of Open Source Software* 6(66): 3175. https://doi.org/10.21105/joss.0317

Cornelissen, H., Watson, I., Adam, E. and Malefetse, T. 2019. Challenges and strategies of abandoned mine rehabilitation in South Africa: The case of asbestos mine rehabilitation. *Journal of Geochemical Exploration* 205: 106354.

Corriveau, M., Jamieson, H., Parsons, M., Campbell, J. and Lanzirotti, A. 2011. Direct characterization of airborne particles associated with arsenic-rich mine tailings: Particle size, mineralogy and texture. *Applied Geochemistry* 26(9–10): 1639–1648.

Dagenais, A.-M., Aubertin, M. and Bussière, B. 2006. Parametric study on the water content profiles and oxidation rates in nearly saturated tailings above the water table. *Proceedings of the 7th International Conference on Acid Rock Drainage (ICARD):* 2630: 405420.

Elghali, A., Benzaazoua, M., Bussière, B., Kennedy, C., Parwani, R. and Graham, S. 2019. The role of hardpan formation on the reactivity of sulfidic mine tailings: A case study at Joutel mine (Québec). *Science of the Total Environment* 654: 118–128.

Favas, P., Sarkar, S., Rakshit, D., Venkatachalam, P. and Prasad, M. 2016. Acid mine drainages from abandoned mines: hydrochemistry, environmental impact, resource recovery, and prevention of pollution. In

Environmental Materials and Waste: Resource Recovery and Pollution Prevention: 413–462 (Prasad, M.N.V. and Shih, K., eds). Elsevier.

Hakkou, R., Benzaazoua, M. and Bussière, B. 2008. Acid mine drainage at the abandoned Kettara Mine (Morocco): 1. Environmental characterization. *Proceedings of Mine Water and the Environment* 27: 145–159.

Jambor, J., Ptacek, C., Blowes, D. and Moncur, M. 2005. Acid drainage from the oxidation of iron sulfides and sphalerite. *Proceedings of Lead & Zinc '05*.

Jönsson, J., Jönsson, J. and Lövgren, L. 2006. Precipitation of secondary Fe (III) minerals from acid mine drainage. *Applied Geochemistry* 21(3): 437–445.

Kubit, O.E., Pluhar, C.J. and De Graff, J. V. 2015. A model for prioritizing sites and reclamation methods at abandoned mines. *Environmental Earth Sciences* 73: 7915–7931.

Mackasey, W.O. 2000. *Abandoned Mines in Canada*. WOM Geological Associates Inc.

Maqsoud, A. 2017. Mine site reclamation Challenge through some examples in Québec (Canada). *International Journal of Environmental Science* 2: 12.

Maqsoud, A., Mbonimpa, M. and Bussière, B. 2013. *Réhabilitation du site minier abandonné Aldermac: résultats préliminaires du suivi de la nappe surélevée*. Presented at GeoMontréal, Montréal, 2013.

Maqsoud, A., Mbonimpa, M., Benzaazoua, M. and Turcotte, S. 2022. Evaluation of the performances of a monolayer cover with an elevated water table used for the reclamation of the abandoned Aldermac mine site (Québec, Canada). *Mining* 2(1): 65–85.

Maqsoud, A., Neculita, C.M., Bussière, B., Benzaazoua, M. and Dionne, J. 2016. Impact of fresh tailing deposition on the evolution of groundwater hydrogeochemistry at the abandoned Manitou mine site, Quebec, Canada. *Environmental Science and Pollution Research* 23: 9054–9072.

McGregor, R. and Blowes, D. 2002. The physical, chemical and mineralogical properties of three cemented layers within sulfide-bearing mine tailings. *Journal of Geochemical Exploration* 76(3): 195–207.

Mhlongo, S.E. and Amponsah-Dacosta, F. 2016. A review of problems and solutions of abandoned mines in South Africa. *International Journal of Mining, Reclamation and Environment* 30(4): 279–294.

Mocq, J. and Hare, L. 2018. Influence of acid mine drainage, and its remediation, on lakewater quality and benthic invertebrate communities. *Water, Air, and Soil Pollution* 229: 1–15.

Navarro, M., Pérez-Sirvent, C., Martínez-Sánchez, M., Vidal, J., Tovar, P. and Bech, J. 2008. Abandoned mine sites as a source of contamination by heavy metals: a case study in a semi-arid zone. *Journal of Geochemical Exploration* 96(2–3): 183–193.

Ouangrawa, M., Aubertin, M., Molson, J. W., Bussière, B. and Zagury, G. J. 2010. Preventing acid mine drainage with an elevated water table: Long-term column experiments and parameter analysis. *Water, Air, and Soil Pollution* 213(1–4): 437–458.

Pabst, T. 2021. Elevated water table with monolayer covers. In *Hard Rock Mine Reclamation. From Prediction to Management of Acid Mine Drainage* (eds: Bussière, B. and Guittonny, M.)

Pabst, T., Bussière, B., Aubertin, M. and Molson, J. 2018. Comparative performance of cover systems to prevent acid mine drainage from pre-oxidized tailings: A numerical hydro-geochemical assessment. *Journal of Contaminant Hydrology* 214: 39–53.

Quispe, D., Pérez-López, R., Acero, P., Ayora, C., Nieto, J. M. and Tucoulou, R. 2013. Formation of a hardpan in the co-disposal of fly ash and sulfide mine tailings and its influence on the generation of acid mine drainage. *Chemical Geology* 355: 45–55.

Ranđelović, D., Mutić, J., Marjanović, P., Đorđević, T. and Kašanin-Grubin, M. 2020. Geochemical distribution of selected elements in flotation tailings and soils/sediments from the dam spill at the abandoned antimony mine Stolice, Serbia. *Environmental Science and Pollution Research* 27: 6253–6268.

Rodríguez, L., Ruiz, E., Alonso-Azcárate, J. and Rincón, J. 2009. Heavy metal distribution and chemical speciation in tailings and soils around a Pb–Zn mine in Spain. *Journal of Environmental Management* 90(2): 1106–1116.

RoyChowdhury, A., Sarkar, D. and Datta, R. 2015. Remediation of acid mine drainage-impacted water. *Current Pollution Reports* 1: 131–141.

Seal II, R.R., Hammarstrom, J.M., Johnson, A. N., Piatak, N.M. and Wandless, G. A. 2008. Environmental geochemistry of a Kuroko-type massive sulfide deposit at the abandoned Valzinco mine, Virginia, USA. *Applied Geochemistry* 23(2): 320–342.

SNC Lavalin. 2007. *Plan de restauration du site minier Aldermac.* Ministère des ressources naturelles et de la faune.

Thornton, M., Wei, Y., Thornton, P., Shrestha, R. and Kao, S.-C. 2020. Daymet: station-level inputs and cross-validation result for North America, version 4. ORNL DAAC.

Geotechnical Failure of a Waste Rock and Heap Leach Facility at the Bellavista Gold Project

Terry Braun, SRK Consulting, USA

Abstract

On October 24, 2007, a slow-moving landslide damaged an active waste rock stockpile and a "downstream" gold heap leach facility. The deep-seated landslide under the waste rock stockpile and heap leach facility involved approximately 35,000 cubic meters of material. The combined failure resulted in permanent shutdown of the open mine after two years of operations. The contributing factors to the failure included insufficient investment in geotechnical characterization of the foundation below the waste rock stockpile, disputed interpretations of the complex geomorphology and geologic conditions underlying the site, limited emphasis on the engineering design of the waste rock stockpile, surface water and groundwater management challenges associated within a high rainfall environment, and ineffective technical communications within the owner and external project teams.

This paper evaluates the applicability of the observational method relied upon during the design-build process for the waste rock and heap leach facilities at the Bellavista Gold Mine. The paper also explores various governance aspects and engineering design and oversight failures that contributed to the geotechnical failure.

Introduction

The Bellavista Gold Mine, located near Miramar, Costa Rica, started operations in 2005 as a 4,500 ore tonnes per day open pit gold operation, heap leach facility (HLF), and waste rock stockpile. Table 1 presents the project milestones leading to and following the geotechnical failure. Figure 1 presents the general layout of the facilities. The October 2007 deep-seated landslide damaged the HLF and process plant after two years of commercial operations. Figure 1 also shows the approximate extent of the deep-seated failure area. Rapid movement of the landslide stopped by the end of November 2007. No lives were lost and Glencairn Gold (Glencairn) reported no release of cyanide into the environment. Glencairn and successor entities continued geotechnical monitoring of the post-failure landscape for several years. Monitoring included water quality sampling upgradient, on-site and downgradient in the watershed, in coordination with the responsible governmental authorities.

Table 1: Bellavista project milestones

Date	Milestone
June 29, 2005	Glencairn announces first gold pour and plans to ramp-up the open pit and heap leach operation to a design rate of 60,000 ounces of gold per year.
Mid-2006	Glencairn commissioned design of "uphill" expansion of the HLF.
2006 Annual Financial Report	Cumulative total of 1.67 million tonnes (3 million cubic meters) of heap leach ore under active leach. Approximately 2.9 million tonnes (5.2 million cubic meters) of waste rock in the stockpile
Q1 2007 Report	Quarterly gold sales of 10,475 ounces, contributing to the life of mine gold sales of 53,055 ounces and revenue of US31.8 million.
July 27, 2007	Glencairn announces suspension of mine operations due to concerns over recent ground movements. 33% decrease in market capitalization of Glencairn (TSX:GGG).
August 14, 2007	Glencairn confirms rinsing the HLF as a precautionary measure to reduce cyanide in the HLF and announces the start of an extensive ground monitoring program.
September 13, 2007	Glencairn announces that a deep-seated ground creep had occurred between the processing plant and the HLF.
October 24, 2007	Glencairn reports an overnight landslide, resulting from ground movement and continuing heavy rains, which caused significant damage to the structure of the gold recovery plant.
December 2010	Central Sun Mining (successor to Glencairn) filed a conceptual study to re-start mining operations with new off-site infrastructure and flotation-type metallurgical process technology.

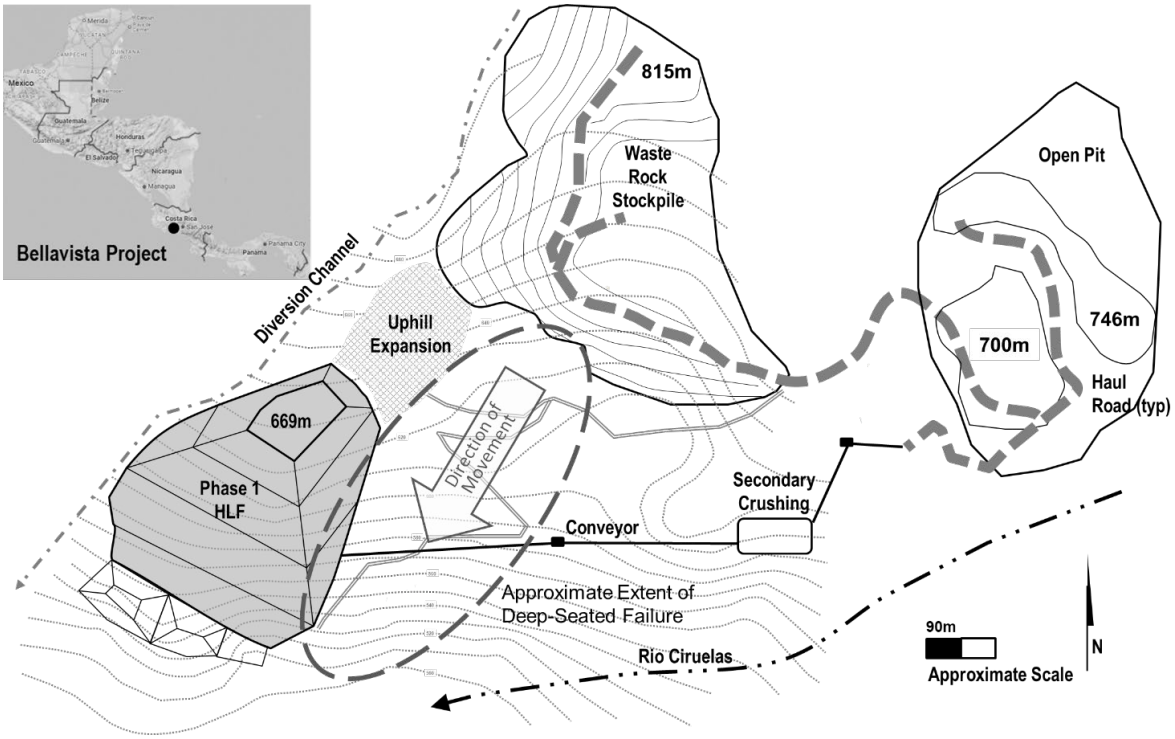


Figure 1: Site location and general layout

Within a few years after the failure, successor entities to Glencairn brought a lawsuit that named multiple design firms involved in the Prefeasibility and Feasibility Studies for the Project and the detailed design of the HLF. All claims were settled by November 2017.

Financial perspective

Glencairn acquired the Bellavista project on October 31, 2002, through issuance of 750,000 common shares (valued at CAD 240,000) and CAD 140,000 in cash. On October 17, 2003, Glencairn acquired the El Limon mine, an existing 1,000 tonnes per day underground gold mine in Nicaragua. Glencairn funded both acquisitions and subsequent capital investments through a series of equity financings in late 2003 and 2004.

Equity finance is common in the junior mining sector. It allows mining companies with limited cash resources and limited ability to service debt to finance project acquisition or development through the issuance of new equity shares. This method of finance dilutes the equity ownership of existing shareholders with the strategy that the associated acquisition or development activities increase total equity value at a higher rate than the dilution incurred, generating net shareholder value. Successful junior mining companies typically focus on the advance and/or delivery of development projects, which often includes the requirement to raise significant funds. During the project development and delivery phase, junior mining companies manage primary technical, financial, and schedule risks through the efficient use of capital. Projects that require unforeseen capital investment or experience production delays are part of the risk profile of investors in the junior mining sector. Delays or cost overruns commonly trigger additional equity raises, which dilute shareholders at a faster rate than the associated value-add activities, and can result in net value destruction for shareholders.

In 2003, Glencairn planned to build the Bellavista mine while operating the newly acquired El Limon mine. This business strategy offered equity investors a degree of confidence with potential financial returns from an operating gold mine and the near-term delivery of the Bellavista project that would match, and then exceed, the annual gold production from El Limon.

Project development

The Bellavista gold deposit is in the Tilarán-Montes del Aguacate gold belt, a 100 km long by 30 km wide region in the western part of the San José Quadrangle. The mine site is approximately 70 kilometers northwest of San Jose and 3 kilometers northeast of the town of Miramar, a district of the Montes de Oro canton in Costa Rica. Mining activity started pre-World War I with a 100 tonnes per day stamp mill and cyanide vat leaching process. Artisanal mining took place through the 1950s. Junior Canadian companies started work on the property in the 1970s (PAH, 2002).

Ownership history

Wheaton River Minerals (Wheaton) advanced the project to the feasibility level in April 1999, held, and then sold the project to Glencairn in 2002. Glencairn commissioned a National Instrument 43-101 Technical Report for the project in December 2002 (PAH, 2002). Glencairn obtained the financing to fund the project in 2003 and started construction in early 2004. In November 2007, Glencairn became Central Sun Mining, which was purchased by B2Gold in April 2009.

Physical setting

The topography surrounding the mine site varies from less than 100 meters above sea level to over 1,000 meters in the northern part of the mine property. The average elevation of the mine site is 750 meters. The Ciruelas River lies near the southern boundary of the property and is the primary drainage for the sub-basin that contains the mine site. The region is seismically active. The University of Costa Rica estimated the maximum credible earthquake as Richter magnitude 7.0 on the Barranca fault, which is at a distance of 11 km from the site.

Geology

The Costa Rican Gold Belt includes the Montes de Oro District, which hosts the Bellavista epithermal gold-silver deposit. PAH (2002) described three lithologic units in the project area. The underlying Tilarán Group forms the bedrock over approximately 80% of the project area. The Liz Fault is the most dominant structural feature at Bellavista and is pre-Monteverde Formation (Alan et al., 1992).

The Monteverde Formation unconformably overlies the rocks of the Tilarán Group and consists of interbedded andesitic lava flows, pyroclastic rocks, ignimbrites, and lahars. The volcanic sediments were deposited in paleo-topographic lows on an undulating bedrock surface composed of the weathered rocks of the Tilarán Group. The Monteverde Formation outcrops mainly in the north and north-western part of the project area.

Figure 2 shows the exposed lahar contact at the site. PAH (2002) described the base of the Monteverde Formation as a lahar unit consisting of large round and subangular blocks of varying igneous composition deposited on an irregular surface of Aguacate rocks (Alan et al., 1992). This basal sequence is up to 80 meters thick in the Bellavista project area.

Geomorphology

The dominant topography in the project area exhibits flat-undulated and flat-concave slopes followed by rough or very rough and steep hills. PAH (2002) reported a thick weathered horizon of bedrock due to tropical weathering and high annual rainfall. Site data indicate that the bedrock surface is weathered to

depths of between 10 and 40 meters depending on location. As a result, non-weathered outcrops of bedrock are mainly confined to locations within steeply incised drainages.

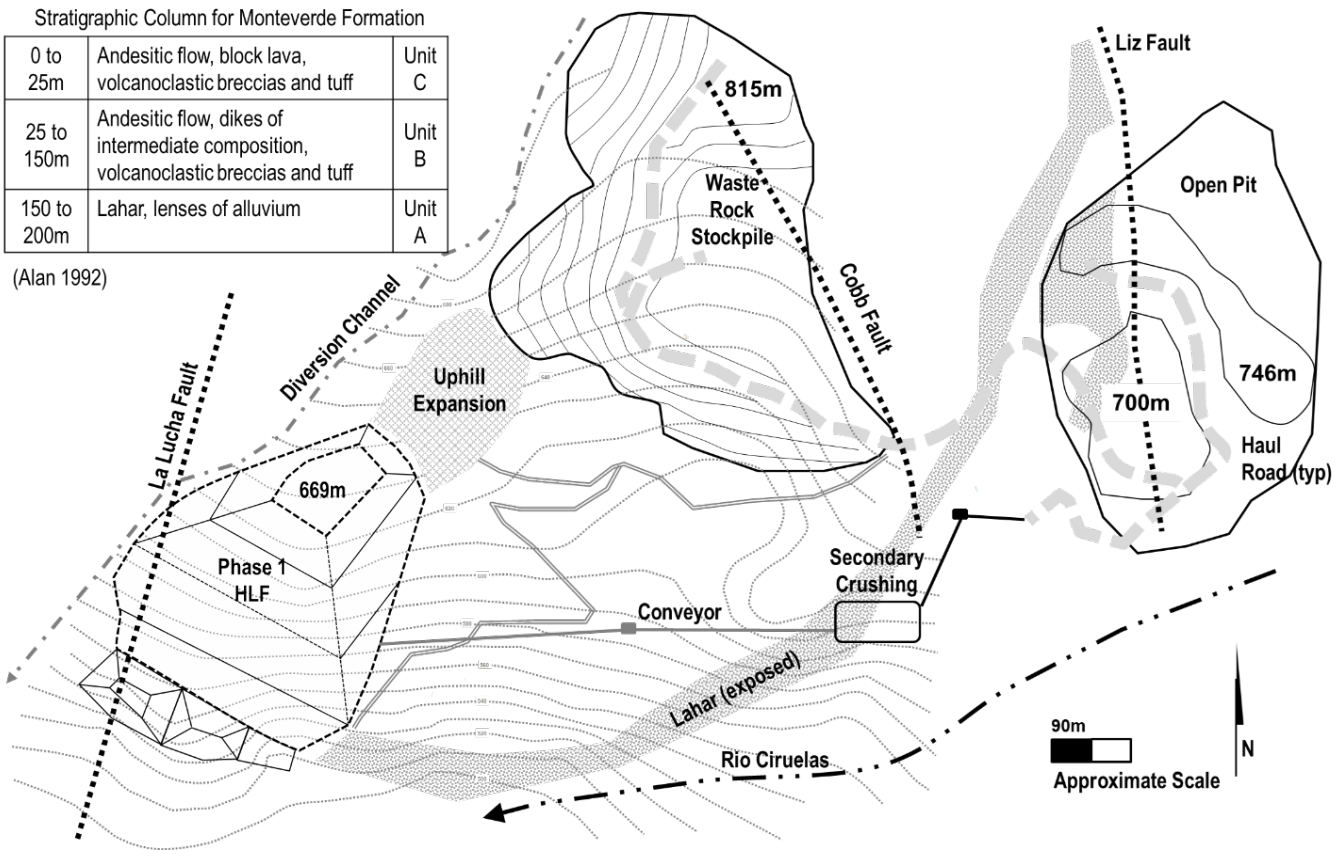


Figure 2: Site geology and structure

Pre-design site work included the review of aerial photography of the waste rock stockpile site. This geomorphological interpretation of the terraced topography suggested a large landslide. Geologic mapping, combined with drilling and geophysical data, indicate the Monteverde Formation consists of inter-layered pyroclastic tuffs, lahars, and breccias. Under this geomorphological interpretation, the terraced topography was due to rapid and deep weathering of the bedrock surface coincident with recent faulting. These contrasting interpretations led to uncertainty in the conceptual geotechnical model.

Hydrogeology

Within the project area, the Monteverde Formation contains groundwater within fractured lava flows and brecciated areas. This formation includes an intermittent clay matrix that contributes to the isolation of saturated zones. The twelve springs in the vicinity of the waste rock stockpile and HLF occur near the Monteverde-Tilaran contact. Outflow from the Monteverde Formation feeds two perennial springs (Montezuma 1 and 2) east of the HLF and south of the Waste Rock Stockpile.

Heap leach facility and waste rock stockpile

The Feasibility Study (1999) presented the Phase 1 HLF detailed engineering design and a future, conceptual phase as a lateral, eastward expansion of the Phase 1 HLF. The presence of the Montezuma Springs within the proposed second phase footprint removed this concept from further consideration. The Phase 1 Detailed Engineering design included approximately 3.2 million tonnes of ore (5.76 million cubic meters), stacked in 21 lifts to a top heap elevation of 680 meters.

The Feasibility Study for the waste rock stockpile contemplated an ultimate storage capacity of approximately 14.9 million tonnes. The average strip ratio for the first 2.5 years of operations was 1.75 (Wheaton, 1999); therefore, the required waste rock stockpile capacity associated with the Phase 1 HLF was approximately 5.6 million tonnes (10.08 million cubic meters). The Feasibility Study included a conceptual layout of the waste rock stockpile. There was no detailed engineering design of the waste rock stockpile.

The project went on hiatus between 2000 and 2002 until Wheaton sold the project to Glencairn, who re-started project development in mid-2003. Waste rock stripping activities and Phase 1 HLF construction commenced in late 2003. The mine operations team scheduled and placed waste rock in accordance with the mine plan developed by the owner's team.

Glencairn announced completion of the Phase 1 HLF in late 2005 and, in 2006, commissioned detailed engineering for an uphill expansion of the HLF (avoiding the footprint of the proposed Phase 2 HLF). Construction of the uphill expansion started in early 2007. Braun (2022) provided a more detailed timeline which highlighted the challenges of maintaining an integrated knowledge base with transitions in project ownership and multiple external engineering firms.

HLF design

For the Bellavista project, an external Engineer of Record (EOR) oversaw construction of the Phase 1 HLF and design of the uphill expansion. The design firm of the EOR provided field construction quality assurance (CQA) during Phase 1 HLF construction. The design firm de-mobilized their field CQA staff following construction of the complete Phase 1 HLF lined footprint and surrounding engineering controls. Field staff for the design firm returned to the site for the uphill expansion project.

The design firm for the Phase 1 HLF and uphill expansion provided a HLF Operations Manual. This document provided guidance related to loading of the pad, construction sequence for pad development and stacking through the life of mine. The manual included survey monitoring requirements, piezometer monitoring and normal operating ranges for monitoring results. Glencairn's contract miner, under the supervision of the operations team, placed ore on the Phase 1 HLF. Glencairn's operations team collected and reported operational monitoring data.

Waste rock stockpile design

The design of waste rock stockpile started with the volumetric requirements, the geochemical characterization of the material and the site layout defined in the 1999 Feasibility Study. The owner's team assumed responsibility for site preparation, scheduling and placement of waste rock. The owner requested technical support from the HLF engineers of record and the pit slope design consultant during operations and construction of the waste rock stockpile. Unlike the Phase 1 HLF or uphill HLF expansion, the waste rock stockpile did not have a designated engineer of record.

Pit slope design

While the pit slope design consultant and owner's team anticipated, encountered and ultimately mitigated the geotechnical challenges posed by the lahar contact in the northwest open pit, this experience did not translate into a better understanding of the conceptual geotechnical model for the waste rock stockpile and HLF. When viewed as a lesson learned, this missed opportunity was a failure to integrate the site knowledge base.

Conceptual geotechnical model

Hawley and Cunning (2017) describe the conceptual geotechnical model during the initial site selection as a combination of site geology, geochemistry, hydrogeology and hydrology. As the project moves from conceptual to prefeasibility to feasibility level, the geotechnical model progresses from conceptual to preliminary to advanced. At the preliminary feasibility study level for site selection, site characterization work supports preliminary stability analyses and site selection while the feasibility study level defines stability criteria for the advanced stability analysis and supports the final site selection. The detailed design is an optimization process, including year by year stability assessments as the facility is built. Hawley and Cunning (2017) note that much of the necessary data are collected at stages throughout the process and site selection inevitably becomes an iterative process.

The Feasibility Study and Environmental Impact Study for the Bellavista project incorporated site characterization work through 2000. The study team developed a conceptual geotechnical model and conducted 2-D stability analyses of sections through the waste rock dump and through the heap leach facility. Over the course of the PFS and FS, the 2-D stability analyses included variable water tables in the underlying Monteverde Formation.

During the Phase 1 HLF design, the design team used site sampling and test work to assign strength parameters to the upper Monteverde Formation. The owner and design team debated the presence of potential deep-seated failure surfaces (within the Monteverde Formation and/or within the weathered interface zone of the upper portion of the Tilarán Formation) shown in Figure 3. The limited vertical and

horizontal extent of geotechnical investigation led to uncertainties in geologic interpretation of the interface between the Monteverde and Tilarán Formations as well as uncertainties regarding the strength parameters for the two units and the weathered interface zone.

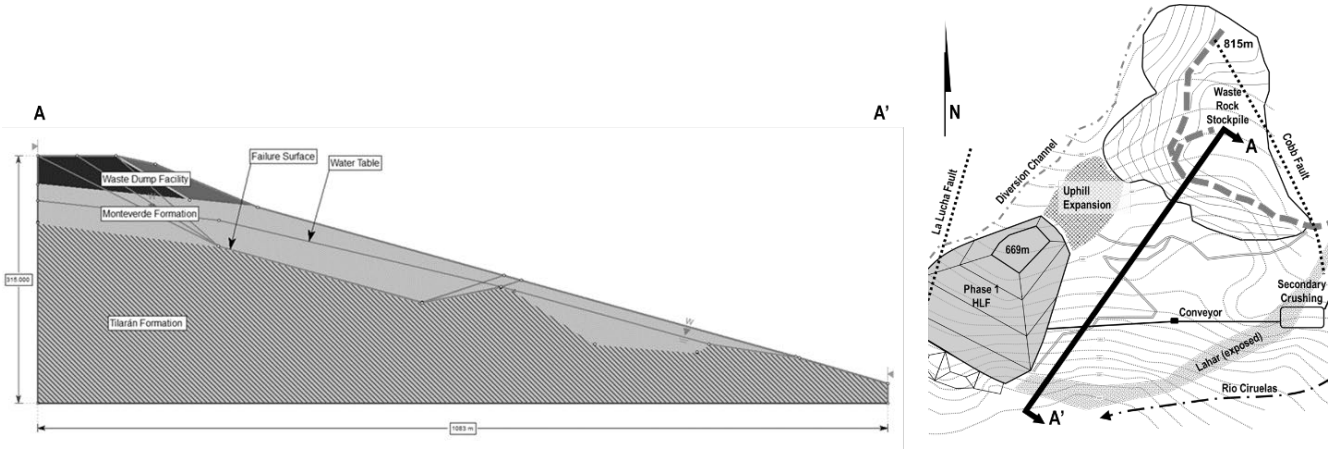


Figure 3: Conceptual geotechnical model

At the time, the design firm, owner and third-party engineer postulated that the Observational Method approach, when combined with potential modification of the HLF design and specification of monitoring systems, would allow the waste rock dump and HLF to be built, operated and closed safely despite the uncertainties in the foundation characterization at the time of project development. This sequence of decisions also assumed a slow-moving deep-seated failure could be mitigated with adequate monitoring and sufficient notice to implement a contingency plan.

Observational method and mine waste facility design

Chapter 41 of the Tailings Management Handbook (TMH) (Morrison, 2022) states the "application of the observational method is a carefully orchestrated **proactive** process" that requires "continued engagement and consistent attention." These authors reiterate this method "allows the mining community to move closer to monitoring the "critical issues" and allows proactive responses to monitoring results". When applied to tailings facilities, the proactive process requires the geotechnical engineer to transform a potentially complex foundation stratigraphy into a simplified site model and consider site-specific design criteria, including the change in load of the facility over time and the potential interaction with adjacent facilities.

Peck's (1969) framework for the observational method includes the assessment of the most probable conditions and the **most unfavorable conceivable deviations** from these conditions. This assessment leads to selection, in advance, of a course of action or modification of design for "every foreseeable significant deviation" of the observational findings from those predicted. Morrison (2022) also references four key

requirements by Powderham (1996) for successful application of the observational method, including the requirements that design alterations are possible during construction and that monitoring can identify trends in "separate key construction-induced events from background to secondary effects."

Original implementation

The three-year delay between completion of the detailed engineering design for the Phase 1 HLF and the re-start of detailed planning and mobilization in late 2003 was long enough for meaningful turnover within the technical and operational teams, including the handover from Wheaton to Glencairn in late 2002. Where there was continuity in the technical team, the ability to build and maintain the integrated knowledge base was limited. Braun (2022) notes the geotechnical model of the open pit was sensitive to the geologic contact of the Tilarán and Monteverde Formations. The incumbent geotechnical consultant factored this observation into the design of the north walls of the open pit from the start of pit operations.

HLF and waste rock stockpile construction commenced around the same time as the open pit. The owner construction team retained a contract miner for open pit and waste rock operations and site surface water infrastructure. The new HLF design firm provided field construction quality assurance.

The as-built field monitoring program included conventional survey prisms on and adjacent to the HLF, water level measurements in piezometers installed at the base of the HLF, water level measurements in shallow groundwater monitor wells upgradient and downgradient of the facilities and daily inspections of construction activities. Field crews surveyed the prisms on a manual basis. Field technicians monitoring groundwater levels in monitoring wells upgradient and downgradient of the HLF and waste rock stockpile. Construction started in the dry season and carried into the wet season. Field quality control measures at the HLF included subgrade inspection and conventional destructive and non-destructive testing of the liner material. Contractors cleared organic matter and installed drains at the bottom of the waste rock stockpile prior to placement of waste rock.

Surface water management relied on temporary and permanent diversion channels and ponds to facilitate construction activities. Figure 4 presents the conceptual surface water management system. Daily field reports during the wet season emphasized the day-to-day challenge of surface water management to maintain effective working platform for liner installation and equipment access. Given the heterogeneity of the Monteverde Formation, surface water precipitation at a given location would either recharge or runoff rapidly. Construction related surface water management likely increased recharge into the Monteverde Formation relative to pre-mining conditions. This excess recharge would have increased the saturation of the lahar contact with the Tilarán Formation.

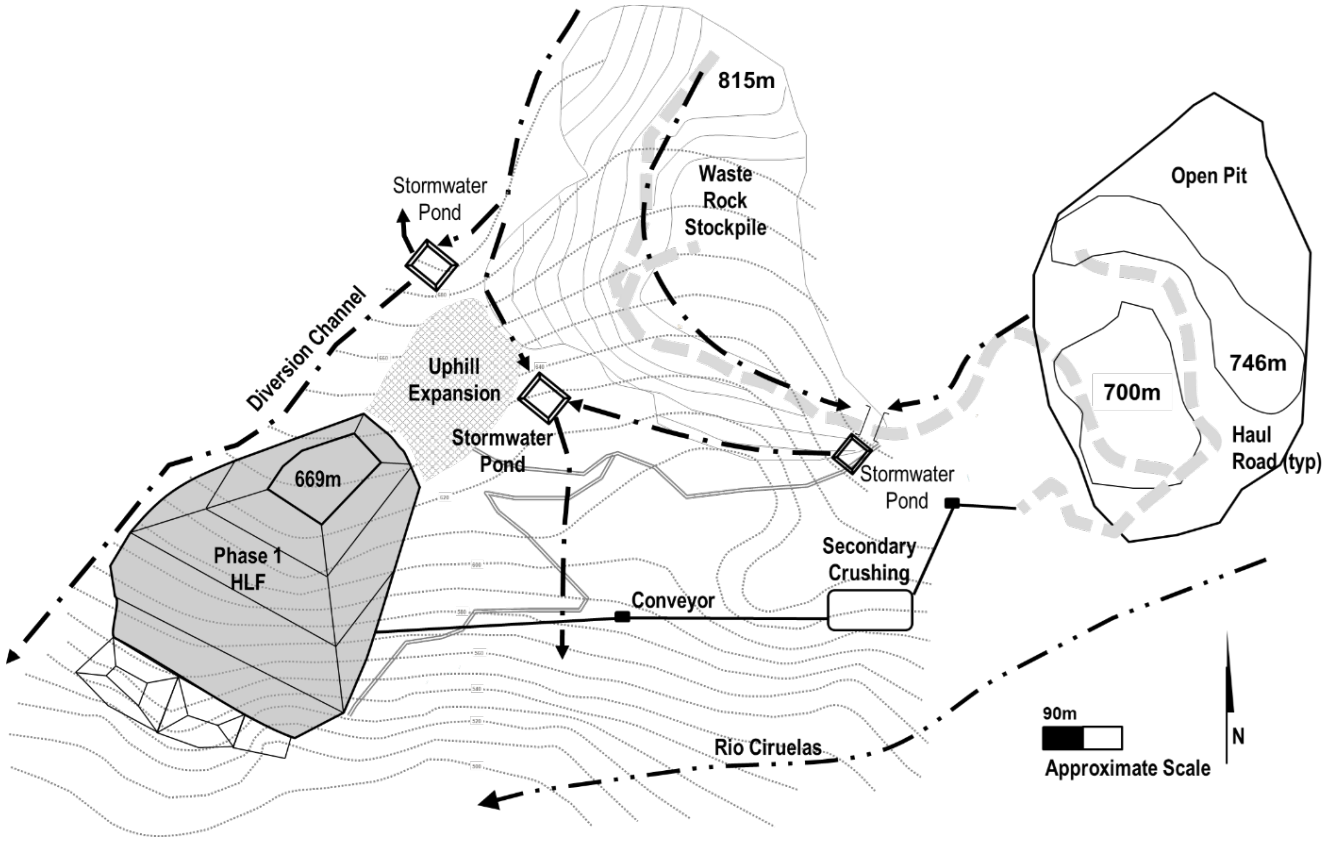


Figure 4: Conceptual surface water management system

Remedial measures

Given the deep-seated nature of the landslide, the report of initial ground movement between the processing plant and HLF, and the size of the waste rock stockpile above the landslide zone, the author assessed three types of remedial measures to mitigate the risk of the deep-seated failure:

- **Water Control:** improve hydraulic control of the saturated zone within the Monteverde Formation, including upgraded surface water controls to reduce enhance recharge in disturbed areas and use of shallow dewatering wells
- **Waste Rock Stockpile Unload:** reduce the waste rock mass in the credible failure zone
- **Engineered Buttress:** design and build a structural buttress near the toe of the credible failure zone

Table 2 summarizes each scenario for this screening level assessment. The precursor monitoring period starts once the monitoring plan detects the potential failure condition. The design-construct period is the estimated duration to design and implement the contingency measure.

Table 2: Remedial measures for potential mitigation of deep-seated failure

Scenario – goal	Description	Pre-cursor monitoring period	Design-construct period
Water Control: improve hydraulic control of the saturated zone within the Monteverde Formation	Upgrade surface water controls to reduce enhance recharge in disturbed areas	Timing subject to integration with construction planning and production scheduling	3 to 6 months with construction in December and March (dry season) Operations and post-closure
	Install shallow dewatering wells	3 to 6 months of site characterization and public consultation related to protection of Montezuma I and II springs	6 months to complete installation and surface works Operations and potentially post-closure
Waste Rock Stockpile Unload: reduce the weight of waste rock stored in the credible failure zone	Consider in-pit disposal with potential reduction of mine life	6 months to assess viable alternatives; additional 12 to 24 months to amend operating license	3 months for mine plan revisions
Engineered Buttress: increase the resistance to ground movement near the approximate toe of the credible failure zone	Subsurface structure anchored in bedrock or engineered embankment to restrict ground movement	6 to 12 months for site characterization and analysis 12 to 24 months to amend operating license	9 to 12 months

Improved hydraulic control of the saturated zone within the Monteverde Formation would offer the fastest implementation and short-term benefit in terms of managing the upper water table at or below pre-mining levels. Shallow dewatering wells below the waste rock stockpile could pose a potential risk to the perennial flows at the Montezuma I and II springs and, potentially, an indefinite obligation to operate and maintain.

Waste rock stockpile unloading would require an alternative storage location for relocated material and for future waste rock materials. Haul distances could increase. A new location would likely require a siting study, site characterization, application to amend existing permits, and mine plan revisions. If in-pit disposal is considered, the mine life could be curtailed if mine scheduling could not accommodate the required storage volume.

The engineered buttress would carry the most significant upfront capital. The precursor period would involve geotechnical characterization of the foundation conditions in the vicinity of the exposed lahar surface. This effort would include re-use of inert waste rock materials, where possible, and development of borrow materials for the buttress fill. Following development of the engineering design, construction of the buttress would require an application to amend existing permits.

This simplified assessment of remedial measures includes a wider possible range of design alterations to potentially mitigate the risk of a deep-seated failure. These design alterations carry additional initial cost

for site characterization and design work. In addition, the time required for permitting and construction would likely curtail or stop mine operations. Once mine operations re-started, the mineral reserve statement for the project would be impaired. The additional cost, the potential for curtailment or suspension of mine operations and likely reduction of mineral reserves are material business risks for a junior mining company working toward profitability.

Governance

The *Guide to the Management of Tailings Facilities* (MAC, 2021) and the Global International Standard for Tailings Management (GISTM, 2020) re-opened and updated the governance associated with design, operations and closure of tailings facilities. In terms of governance, these guidelines identify the importance of accountability in the owner's management team, of a designated design professional, and of a facility-specific Operation, Maintenance and Surveillance Manual. GISTM emphasizes the role of an integrated life-of-asset knowledge base to inform and guide the owner and design professionals during personnel transitions or asset transition from operations to closure. These tailings-related governance items are relevant to HLF and waste rock stockpile design.

Conclusion

The external design firms and the successive ownership's technical team offered substantive project experience relevant to the Bellavista project. The coordination and continuity challenges during project development and construction contributed to underlying technical uncertainties in the conceptual geotechnical model and in the interpretation of the monitoring program, including the relevant operational learnings from pit slope instability. Early recognition of this uncertainty and conceptual development of a wider range of critical controls was a missed opportunity. Further, the engineering design process for the waste rock stockpile lacked continuity of responsible oversight.

The author suggests the original monitoring plan for the HLF could have provided sufficient warning for the owner to conduct emergency HLF rinsing and to assess more substantial remedial measures. These remedial measures would require additional initial cost for site characterization and design work and permitting/construction timelines that would likely curtail or stop mine operations. Once mine operations re-started, the mineral reserve statement for the project would be restated and likely be impaired.

Equity markets react negatively to material disclosures such as suspended operations and/or reduction of mineable reserves. These are material business risks for a junior mining company and many companies in this situation successfully disclose, adopt, and implement a recovery plan. In July 2007, the only viable remedial plan for the Bellavista property was an accelerated permanent shutdown. If the project team had identified timely and viable alternative remedial measures for the worst-case deep-seated failure scenario,

the owner could have stopped production, implemented the remedial measures and followed a staged return to production. In retrospect, Glencairn, as a junior mining company, needed to prioritize mitigation of some operational risks over others during development and operations at the Bellavista property. As a result, the risk of the deep-seated geotechnical failure scenario near the HLF and Waste Rock stockpile was understated in the project risk register.

References

Alan, M.A., Quesada, J.D., Seaward, M. and Hutton, D. 1992. Economic geology of the Bellavista gold deposit, Costa Rica. Paper presented at the Annual Meeting of the Society for Mining, Metallurgy, and Exploration, Phoenix, Arizona, February 24–27.

Braun, T. 2022. Rumble in the jungle: Lessons learned from a waste rock dump failure. SME Annual Meeting, Feb. 27 – March 2, 2022, Salt Lake City, UT.

Financial Times. 2019. Company Announcements Mineral and Financial Investments Ltd Investment in Golden Sun Resources Ltd. Via secured convertible note, June 13.

GISTM. 2020. Global Industry Standard on Tailings Management. Accessed 6/06/2024 at: global-industry-standard_EN.pdf (globaltailingsreview.org)

Hawley, M. and Cunning, J. 2017. *Guidelines for Mine Waste Dump and Stockpile Design*. CSIRO Publishing.

Mining Association of Canada (MAC). 2021. *A Guide to the Management of Tailings Facilities, Version 3.2*.

Morrison, K.F. 2022. *Tailings Management Handbook, A Life-Cycle Approach*. Society for Mining, Metallurgy and Exploration.

Peck, R.B. 1969. Advantages and limitations of the observational method in applied soil mechanics. *Géotechnique* 19(2): 171–187.

PAH (Pincock Allen and Holt). 2002. Bellavista Gold Project, Costa Rica. Technical report, prepared for Glencairn Gold Corporation, December 10.

Powderham, A.J. and Nicholson, D.P. 1996. *The Observational Method in Geotechnical Engineering*.

B2Gold Corp, December 1.

Wheaton River Minerals. 1999. Feasibility study for the Bellavista Mine, April.

Tailings Disposal Management in Large Reservoirs – Case Study for Mirim Dam, Salobo Mine, Brazil

Gustavo Belotto, Vale S.A., Brazil
Carlos Alex Alves Lima, Vale S.A., Brazil
Henrique Tropia Granja Guerzoni, Vale S.A., Brazil
João Paulo Rodrigues Costa, Vale S.A., Brazil
Felipe Campolina, Vale S.A., Brazil
Jefferson Oliveira, Vale S.A., Brazil
José Henrique Coelho Wanderley Costa, Vale S.A., Brazil

Abstract

Tailings hydraulically disposed are prone to gravity separation processes throughout reservoir occupation, which brings high complexity to the disposal model in terms of predictability of occupancy and operational quality control. Initial design conditions based on laboratory tests may present limitations in response reliability over years of operation, given the large number of variables impacting the behavior of tailings in disposal, such as: ore characteristics; comminution process stability; discharge flow rate; solids content in slurry; and specific weight of minerals. The vast array of variables can impact the robustness and quality of the Tailings Disposal Plan, aimed at maximizing volumetric occupancy.

Salobo Mine implemented the PDCA (Plan, Do, Check, Act) methodology, to systematize data acquisition methods, modeling, and operational management (Control + Key Performance Indicators – KPIs) of copper tailings disposal at the Mirim Tailings Dam. The Mirim Dam currently has 110 Mm^3 of accumulated tailings and will, at the end of its useful life, store 758 Mm^3 after the extraction of approximately 1 billion tons of copper. It is expected to become the largest tailings dam in Brazil.

Topobathymetric data acquisition is routinely conducted to assess the evolution of tailings disposal. Aerial surveys are conducted using a DJI Phantom 4 RTK drone and bathymetry with a Syqwest Bathy-500HD equipment. The resulting data is processed using Deswik.CAD software, specialized in compliance evaluation to volume disposal plans.

The employed methodology applied spatial zoning in the reservoir, enabling the evaluation of operational adherence to the tailings disposal plan and feeding back parameters of the geotechnical-hydraulic disposal model. The KPIs used resemble those used in the mine planning process, such as planned and disposed volumes; planned and not disposed; unplanned and disposed; as well as indexes that assess

the adherence and geometric/volumetric compliance to the tailings disposal plan. Such tools enable short- and medium-term plan adjustments to reduce the impact on optimal (planned) reservoir occupancy and minimize future needs for mechanized tailings management or robust pumping systems.

Real data on tailings behavior in disposal, such as angles of repose and dry consolidated density, were recalibrated with data from the reservoir itself, enhancing the geometric predictability of tailings occupancy.

Introduction

Worldwide production of tailings increases with every decade. Mining operations in the late 1800s and early 1900s produced only about 1–100 t/d (metric tons per day), while modern mining operations can produce 1 million t/d (Morrison and Lammers, 2020). It is estimated that every 30 years, the maximum height of hydraulically filled tailing reservoirs doubles and that in the same period, the volume of tailings and water processed by the mineral industry multiplies by the order of 10 times (Robertson, 2011). The challenges of tailings management in large reservoirs increase constantly in order to meet global industry standards (GISTM) and guarantee the governance and management of tailings in a safer manner (International Council on Mining and Metals, 2020).

Most conventional tailings store facilities (TSFs) are designed, constructed, and operated considering staged development based on the mine plan, particularly the schedule for ore production and waste rock removal and processing for facility construction. Staged development is intended to match TSF capacity with tailings generation to satisfy operational requirements and incremental tailings dam raises or lateral expansion (Snow, 2020).

The Mirim TSF began operations in 2012 and since then, raising have been and will be carried out to achieve the project geometry, in order to meet a storage volume of 758Mm³ of tailings (current mineral reserve at the Salobo mine). In 2024 the volume occupied by tailings is approximately 124Mm³.

The development of tailings facilities depends, necessarily, of the production volume and behavior of tailings during disposal. Aiming to maximize reservoir occupancy, tailings disposal plans are developed to support operational and financial decisions (water management, geotechnical, hydraulic and environmental risks) of short, medium and long-term scenarios, while being adherent to national and internation standards as well as local legislation. This process results in cycling the discharge points, causing each sector to have periods of active and inactive discharge. (Mussé, 2020). Subaerial and subaqueous beach slopes are usually determined by laboratory tests where they are performed to determine those (and other) parameters (physical, chemical, rheology, etc.). Sometimes, flume tests are used to get an indication of deposition slopes; however, they are used more to show, for example, the degree of segregation of the tailings from the spigot discharge based on a range of solids contents. Most typical examples of uncertainties include tailings beach slopes (and their changes along the surface and the time), size and location of supernatant

pond (for slurry tailings), and tailings geotechnical/rheological properties. The deposited tailings will acquire some slope and density, depending on the characteristics and discharge flow energy. The range of variability (as well as the complexity of the topography configuration) can demand comprehensive sensitivity analyses.(Mussé, 2020). In order to comply with the sensitivity analysis necessary to identify any gaps between the modeling of the Mirim Dam's tailings disposal plan and the beach geometry achieved during the TSF's operation, it is proposed to use indicators of adherence and compliance with planned geometry, such as those used in the open pit mining performance indicators proposed by Câmara et al. (2014).

Nader et. al (2012) suggested that mining performance indicators are used within the mining context, with the aim of implementing control measures and consequently defining them as key result indicators (KRI), result indicators (RI), performance indicators (PI) and finally, key performance indicators (KPI), where KRI determines how activities should be carried out, RI indicates what was done, PI determines what needs to be done and, finally, the KPI that informs which parameters generate a significant increase in performance.

Mining indicators are also used to manage waste disposal in waste piles, with the same geometric indices being used to measure adherence and compliance of waste management. The evaluation of the geometry of the waste piles according to what was planned in relation to what was executed, has a desirable methodology for replication in relation to the management of tailings disposal within the perimeter of an TSF. It is understood that losses in adherence to tailings management lead to higher costs, regulatory difficulties, and reputational issues during the operation and closure process, as is becoming increasingly well understood is that closure of a TSF is "a process" rather than "an event," and that this process is no less challenging or costly than the design, construction, and operation components themselves (Andrews et al., 2020).

Study area: Mirim Tailings Dam

The Mirim Tailings Dam is part of the Salobo Project, which is located in the Tapirapé-Aquiri National Forest, in the municipality of Marabá, Pará, Brazil, as illustrated in Figure 1.

The TSF was designed to store tailings from the Salobo mine's copper ore processing, in addition to providing raw water to the three processing plants. Its main embankment is located in the narrow-enclosed valley of the Mirim creek. The morphology of the area allowed the construction of a relatively short embankment, with approximately 320 meters long and 40 meters wide at the crest. Currently the reservoir occupies an area of 9.0 km^2 and is located within a 33.0 km^2 watershed.

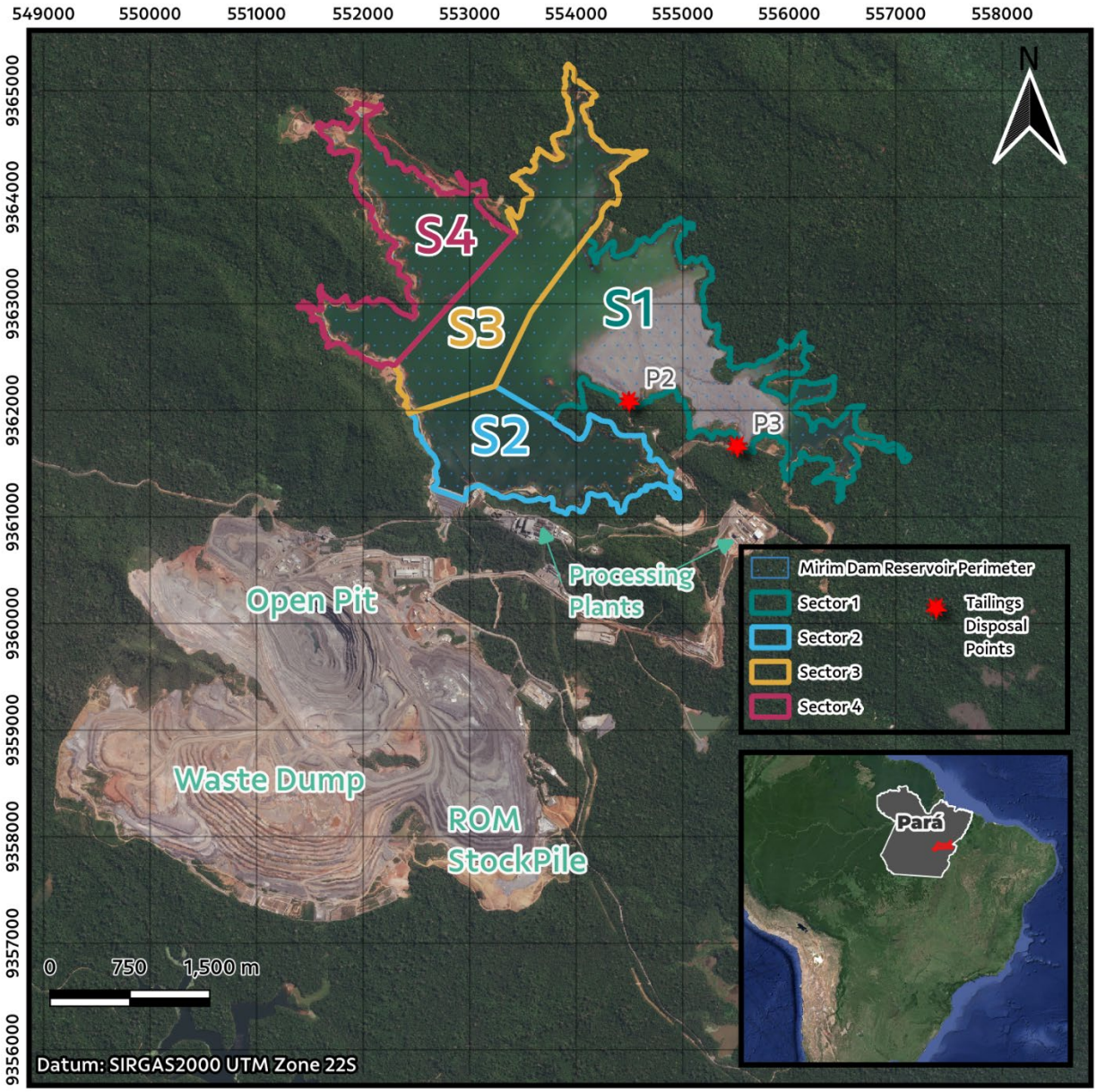


Figure 1: Site location of the Mirim Tailings Dam

The internal structure of the embankment is composed on its upstream zone of a schist rockfill, transitioning to a sieved quartzite and an impermeable clay core. The embankment downstream zone is composed of a transition filter located after the clay core. The filter comprises medium sand, fine gravel (4.8 – 9.5 mm) and coarse gravel (25 – 50 mm) in contact with the schist rockfill. The embankment is situated on a quartzite bedrock with some intrusions of mafic rocks and pegmatite veins. The mafic intrusions and pegmatite veins generated a reddish and whitish clayey soil respectively.

Tailings disposal timeline

Salobo mine has an estimated production of 36 Mt of ore per year. The tailings disposal plan plays an important role in declaring the mine's reserves and resources, as the mine has an estimated life until 2057. The disposal plan foresees the tailings discharge in the upstream part of the reservoir at an elevation close to the main embankment crest. This causes the subaerial beach slope to be around 0.5%, while the submerged tailings slope is around 2.5%. Raw water is collected for the processing plants close to the embankment, in a location with greater water depth.

The operation of Mirim TSF began in April 2012. The first discharge point was called P2 (see Figure 1). In 2017, the discharge point changed from P2 to P3, located further upstream of the TSF watershed, in order to improve the operation of the raw water pumping system. The elevation of P3 is very close to the current elevation of the spillway threshold.

According to the analysis of the topobathymetry surveyed in April 2023, the reservoir can be separated into four distinct sectors (see Figure 1). Sector 1, the main beach, contains the largest quantity of tailings. On the beach, it is possible to find slopes between 0.2 and 0.5%, and a pattern of increasing angles as it goes further downstream on the beach. Sector 2, located in the region of the main embankment, has the highest slopes, with values up to 2.7%, and the highest water column. Sectors 3 and 4 have little tailings stored and are furthest from the beach and the main embankment. In these sectors, water occupies the largest space.

Tailings management methodology

Tailings management systems

The management of tailings according to the methodology proposed by the authors aligns with the process described by the PDCA (Plan-Do-Check-Act) framework, as defined by the Mining Association of Canada (2021) for managing mining projects from conception to closure. This approach is further detailed by LePoudre and Morrison (2020):

- **Tailings disposal plan (Plan):** establish objectives, processes, and plans necessary to meet objectives (policy and commitment, planning).
- **Tailings disposal (Do):** implement processes and plans within a structured management framework (implementing the tailings management framework).
- **Geometrical analysis of tailings disposal adherence to plan (Check):** Measure and monitor all aspects of performance and analyze and report results (performance evaluation).

- **Route adjusting (Act):** Review performance, identify areas of nonconformance and opportunities for improvement. Take action to maintain and continually improve (management review for continual improvement).

The objective of this article is to establish easily reproducible metrics that provide key performance indicators, as outlined by Nader et al. (2012). These metrics enable the proper implementation of the PDCA methodology, following industry best practices.

Topobathymetric surveys

Topobathymetric surveys are carried out routinely at Mirim TSF to evaluate the evolution of tailings disposal. For the current study, surveys from June 2021 and April 2023 were used. The survey carried out in June 2021 was also used as the basis for the most recent tailings disposal plan at Mirim TSF.

The aerial survey is carried out with DJI's Phantom 4 RTK drone and bathymetric survey with SyQwest Bathy 500 equipment, GPS Trimble R12i (on the base) and GPS Trimble R10 (as rover). Data processing is carried out using Pix4Dmapper version 4.3.31 and Hypack 2020 software for noise cleaning and surface generation.

Bathymetry and aerial survey data are compiled in Deswik.CAD 2023.2 and visual maps are generated in QGIS 3.32. Solids are also generated in Deswik.CAD to calculate volumes and define performance indicators, through the geometric evaluation of solids inside or outside the originally planned surface.

Performance indicators for tailings disposal

In this study, performance indicators commonly applied to mine planning were used. Reis and Nader (2023) argue that, given the obligation to ensure the planned Run of Mine (ROM) mass values for the site, two key performance indicators are established to measure the effectiveness of the mining plan:

- The Adherence Index (AI), which determines how assertive the pre-established assumptions were, the operational maturity to follow the predetermined geometry, and hence the effectiveness of the planning in performing the geometry of the plan.
- The Compliance Index (CI), which measures the assertiveness in defining the parameters for the execution of the plan, how disciplined the operation is for the execution of the proposed geometry, the assertiveness of the block model, and the original topography for the elaboration of the plan.

In turn, the AI and CI indicators are determined by the difference between geometries. These differences between geometries generate three indicators:

- Planned Executed (PE), which determines the volume that was mined/deposited and was within the mining plan.

- Executed Not Planned (ENP), which measures the mined/deposited volume that was outside the proposed geometry.
- Planned Not Executed (PNE), which measures the volume that was within the mining/disposal plan and was not mined/deposited.

Figure 2 schematically illustrates the adoption of these criteria (PE, ENP, PNE) for tailings disposal. The identification of these parameters occurs through the comparison between planned and actual topographies over a certain time interval.

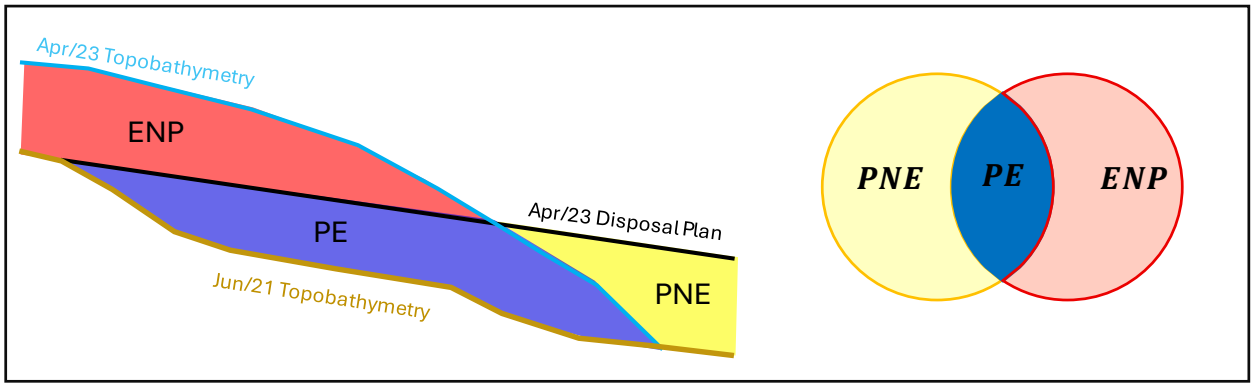


Figure 2: Schematic drawing of tailings disposal indicators used in the study

The following formulas are suggested for the calculation of the Adherence and Compliance Indexes (Costa, 2015):

$$AI = \frac{PE}{PE + ENP} \quad \text{(Equation 1)}$$

$$CI = \frac{PE}{PE + PNE} \quad \text{(Equation 2)}$$

Results and discussion

In the following sections, the results obtained in the assessment of tailings disposal between June 2021 and April 2023 will be presented, as well as indicators and indexes of disposal performance. For a better spatial understanding, the analysis was performed for the four sectors of the reservoir, defined based on the deposition patterns observed in the period (see Figure 1).

Tailings deposition assessment

Figure 3 presents the results of the topobathymetric surveys carried out in June 2021 (Figure 3-A) and April 2023 (Figure 3-B). It is also possible to compare with the surface predicted on the disposal plan for April 2023 (Figure 3-C). It is observed that most of the changes occurred within sector 1 (S1), in which elevations

increased from approximately 242 m to 250 m. The comparison between the disposal plan and topobathymetry shows that higher beach elevations were expected in the disposal plan, mainly in the most upstream portion of the basin, but they were not achieved, according to the survey. There was also an expectation of a greater tailings deposition in Sector 2, which has not happened.

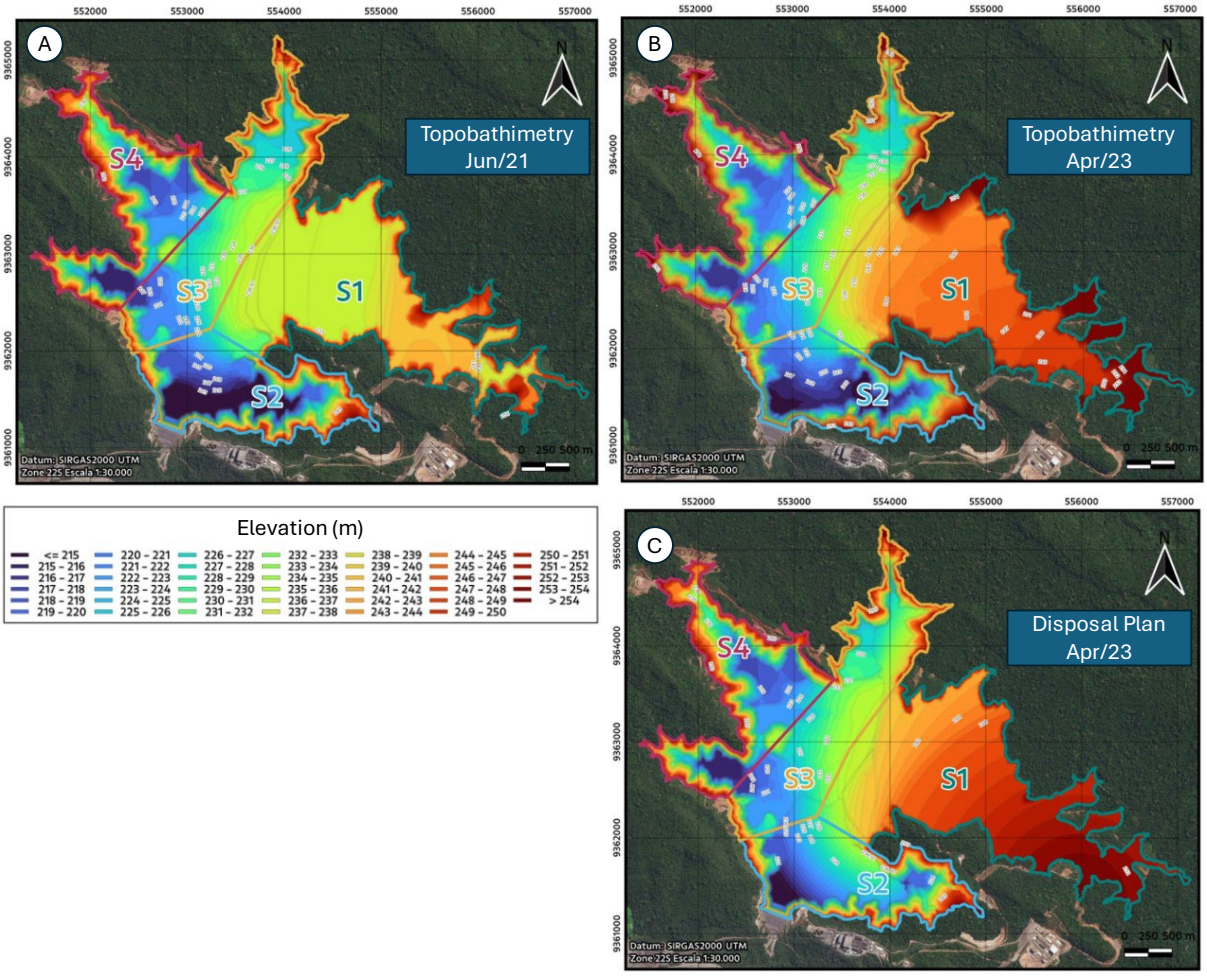


Figure 3: Topobathymetric surveys carried out in June 2021 and April 2023 and disposal plan for April 2023

Figure 4 shows a heat map with the deposition thicknesses expected by the tailings disposal plan (Figure 4-A) and measured from topobathymetric surveys (Figure 4-B). In this figure, the discrepancies between the disposal plan and the executed can be observed, as previously indicated.

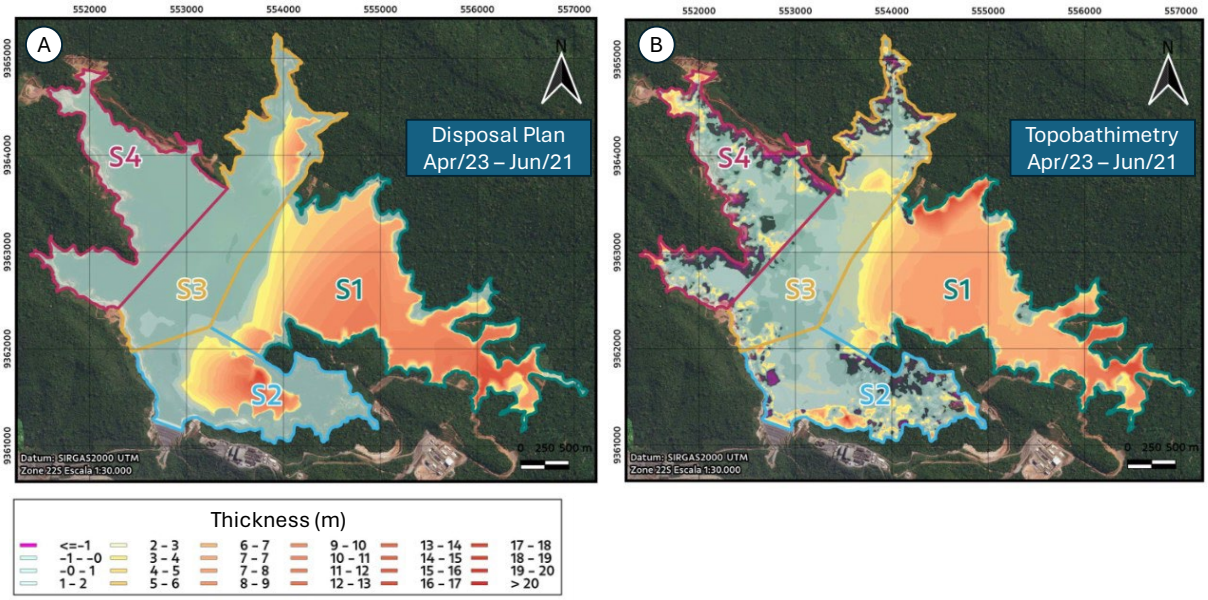


Figure 4: Thicknesses expected by the tailings disposal plan and measured from topobathymetric surveys

Performance indicators of tailings disposal

Using the geospatial assessment of the executed and planned tailings disposal, heat maps were generated for the disposal indicators of "Planned Executed" – PE (Figure 5-A), "Planned Not Executed" – PNE (Figure 5-B) and "Executed Not Planned" – ENP (Figure 5-C).

In relation to PE, it is noted that most of the disposal occurred according to the plan in Sector 1, with the deposition of 18.0 Mm^3 of tailings, followed by Sector 2 with 0.8 Mm^3 and Sector 3 with 0.4 Mm^3.

The PNE deposition was mainly concentrated in the upstream portion of Sector 1, in which a greater thickness of tailings was expected, and in the central-northern portion of Sector 2. The disposal of 4.6 and 4.7 Mm^3 of tailings in these regions were expected respectively. In Sector 3, 1.4 Mm^3 of tailings were not deposited as planned.

ENP tailings disposal occurred mainly in sectors 1 and 3. Sector 1 had tailings mainly located in the north and central-west areas, both in the downstream portion of the sector. 3.7 Mm^3 of non-planned tailings were disposed in this sector. In sector 3 there was an unplanned volume of 2.1 Mm^3 in its central portion.

The plot in Figure 5-D shows the total deposition of each sector divided into PE, ENP, and PNE indicators. Since there was no plan to received tailings in Sector 4 and it is understood that the tailings were not able to reach the area, the indicators in this sector were disregarded in subsequent calculations.

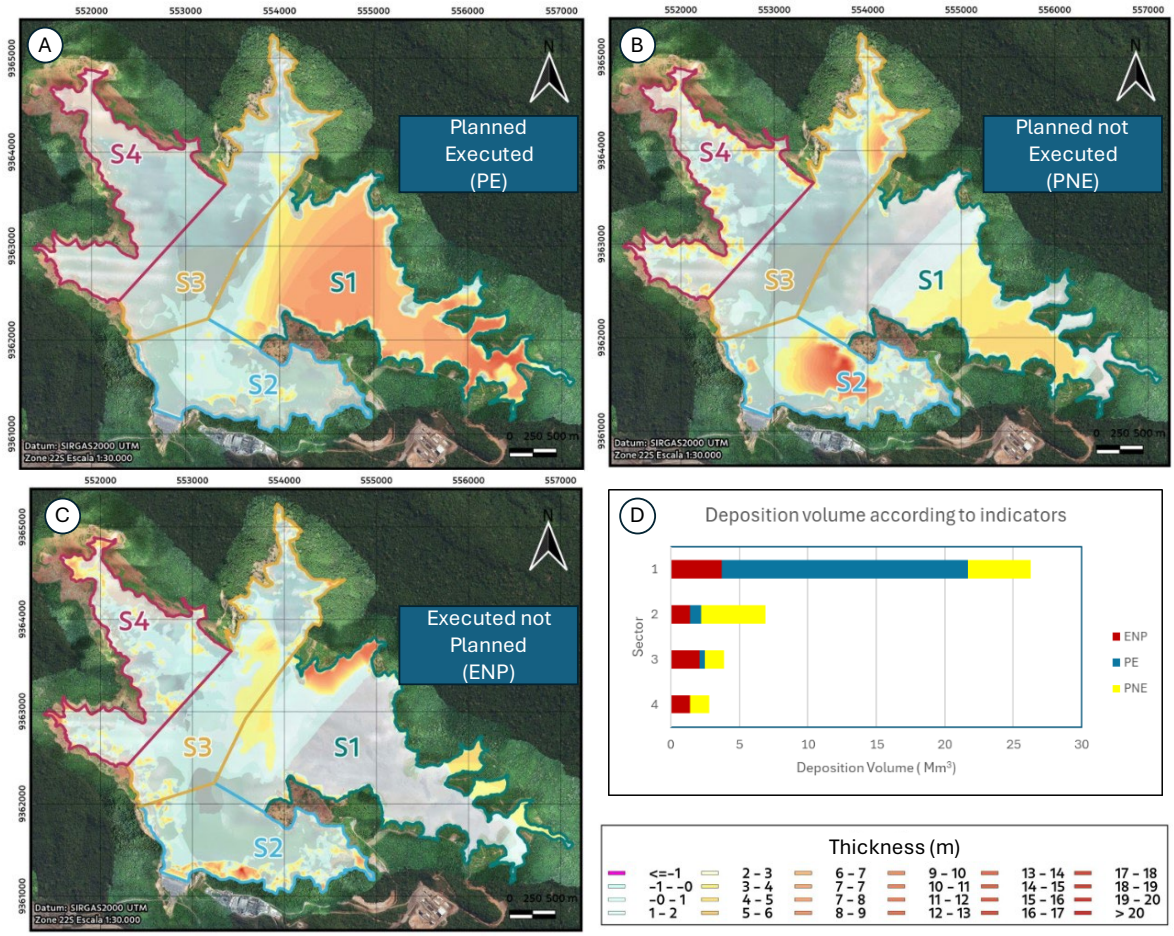


Figure 5: Performance indicators of tailings disposal

The IA and IC indices were calculated for each sector according to equations 1 and 2. The results are presented in Table 1 below.

Table 1: Key Performance Indicators for tailings management from July/2021 to April/2024

Sector	ENP (Mm³)	PE (Mm³)	PNE (Mm³)	CI	AI
1	3.7	18.0	4.6	80%	83%
2	1.4	0.8	4.7	14%	36%
3	2.1	0.4	1.4	22%	16%
4	1.4	0.001	1.4	0%	0%
Total	7.1	19.2	10.7	64%	73%

The evaluation indicated adequate adherence and compliance to the planned disposal in Sector 1, responsible for the largest deposited volume of tailings. However, Sectors 2 and 3 showed low adherence and compliance, where tailings did not reach the projected elevations specified in the disposal plan.

Conclusion

The implementation of commonly applied KPIs in mine planning has brought new perspectives to tailings management at the Mirim Tailings Dam. It allowed for evaluating the physical occupancy of the reservoir, identifying areas not occupied by tailings (individualized sectors), assessing the alignment between tailings production from the plant and measurements from topobathymetry, ensuring predictability in the tailings management plan for maximum, safe, and optimized reservoir occupancy, and developing a closure plan with minimal environmental impact.

Continued assessments based on new bathymetric data, collected semi-annually, offer an opportunity to support revisions of the tailings disposal plans, as well as the implementation of operational measures to ensure the correct geometrical conformance of end-of-life tailings surface on the reservoir.

References

Andrews, J., Crouse, P., Handerson, M., McKenna, G., Slingerland, N., Williams, D. J. and Morrison, K. F. 2020. Closure Planning and Landform Design. In *K F. Morrison, Tailings Management Handbook – A Lifecycle Approach* (pp. 235–276). Denver: Society for Mining, Metallurgy and Exploration (SME).

Câmara, T. R., Kuckartz, B., Peroni, R. L., Fontoura, D. M. and Capponi, L. N. 2014. Reconciliação: Ferramentas de Avaliação do Fator Mina/Usina. *Proceedings of 8º Congresso Brasileiro de Mina a Céu Aberto / 8º Congresso Brasileiro de Mina Subterrânea*. Belo Horizonte.

Costa, F. V. 2015. Análise dos principais indicadores de desempenho usados no planejamento de lavra. Post graduation in Mineral Engineering – PPGEM.

International Council on Mining and Metals. 2020. Global Industry Standard on Tailings Management. Global Tailings Review Org.

LePoudre, D. C., Morrison, K. F. 2020. Tailings Management Systems. In K. *F. Morrison, Tailings Management Handbook – A Lifecycle Approach* (pp. 731–748). Denver: Society for Mining, Metallurgy and Exploration (SME).

Mining Association of Canada (MAC). 2021. A Guide to the Management of Tailings Facilities, Version 3.2.

Morrison, K. F., Lammers, H. 2020. What are Tailings? In *K. F. Morrison, Tailings Management Handbook – A Lifecycle Approach* (p. 6). Denver: Society for Mining, Metallurgy and Exploration (SME).

Mussé, M. 2020. Tailings Deposition Planning. In *K. F. Morrison, Tailings Management Handbook – A Lifecycle Approach* (pp. 659–684). Denver: Society for Mining, Metallurgy and Exploration (SME).

Nader, B., Tomi, G., Passos, A. O. 2012. Indicadores-chave de desempenho e a gestão integrada da mineração. Rem: Revista Escola de Minas: 537–542.

Reis, V. C., Nader, B. 2023. Performance indicators and their importance for effective short-term and operational mine planning. REM: Revista Escola de Minas: 101–107.

Robertson A. 2011. Mine waste management in the 21st century—challenges and solutions beyond incremental changes. *Proceedings in International Conference on Tailings and Mine Waste*. Vancouver, Canada: University of British Columbia.

Snow, R. E. 2020. Conventional Tailings Management. In *K. F. Morrison, Tailings Management Handbook – A Lifecycle Approach* (pp. 65–83). Denver: Society for Mining, Metallurgy and Exploration (SME).

Dam Safety Remediation Measures at the Aitik Tailings Management Facility, Northern Sweden

Romain Girard, Boliden Mineral AB, Sweden
Joseph Quinn, Klohn Crippen Berger, Canada

Abstract

At the Aitik tailings management facility (TMF), recent (2019–2023) extensive site investigations in the dams' foundations and the deposited tailings mass have highlighted the need to undertake a large program of dam safety remediation measures to improve the stability of the roughly 70 m high embankments, and to help achieve the requirements set out in the Global Industry Standard on Tailings Management (GISTM).

The techniques and management strategies used were uniquely selected to satisfy critical performance requirements, as needed to manage continuous operation and tailings deposition, and to safely execute the remediation works. They include buttressing of the existing clarification pond, construction of an extensive shear key at the toe of one of the embankments, and establishment of an exclusion zone for tailings deposition through the construction of rockfill piers across the tailings beach surface. In addition, the works involve the construction, decommissioning, or relocation of key mine infrastructure (haul roads, services, and water management features such as spillways, pump houses, and pipes).

Over the course of the 32 months duration of the project, over 45 Mt of rockfill will have been hauled to the dams and the scope, scale, timeline, and logistical complexity of the works will have impacted the entire mine site.

Summary of the Aitik tailings management facility

The Aitik TMF

The Aitik tailings management facility (TMF), located near the town of Gällivare in the arctic region of northern Sweden, receives between 40 and 45 million tonnes (Mt) of tailings annually from the enrichment plant of the largest open pit copper mine in Europe (from the main Aitik open pit and the now depleted Salmijärvi satellite pit). The mine and the TMF have been in operation since the 1960s. Tailings generated from mineral ore processing at the mine are deposited hydraulically within the Aitik TMF for storage, with approximately 1,000 Mt of tailings deposited to date. The current TMF footprint covers an area of ≈15 km^2, impounded by 10 km of continuous perimeter embankments. The main TMF impoundment is used to store

low sulfur tailings and includes Dams A-B and C-D on the east side of the facility and Dams E-F and G-H on the west side of the facility. The HS tailings impoundment, used to store the high sulfur tailings stream, is separated from the main TMF impoundment by Dam HS. The clarification pond downstream of Dam E-F is an auxiliary structure of the TMF. The embankment heights vary from ca 40 m (Dams A-B and C-D) to ca 70 m (Dams E-F and G-H) and all are currently being raised using the upstream construction method. The supernatant water is currently managed through two functioning spillways: the U2 spillway, which will soon reach its service life and be replaced by the U3 spillway, with supernatant water reporting from both spillways to the clarification pond. Figure 1 shows an overview of the Aitik Mine and its TMF.



Figure 1: Overview of the Aitik TMF prior to remediation project (June 2021)

Overview of site characterization for Dams E-F and G-H

From 2019 to 2023, site investigations were undertaken at the Aitik TMF to improve the site characterization, and over the course of the four years both the tailings and foundation were investigated using a wide array of investigation methods. While investigations occurred all around the TMF, the emphasis of the programs was on Dams E-F and G-H, as they are the highest dams and are also the dams with the highest consequence classification (Very High according to the GISTM). It is also at these dams that the investigations showed the most challenging conditions, and these dams were the focus of the subsequent stabilization remediation measures instituted, and presented in this paper.

Foundation soils

The foundation soils at Dam G-H typically comprise a series of peat and glacial deposits overlying bedrock, whereas at Dam E-F, those glacial soils are typically overlain by a layer of tailings deposited over recent years in the clarification pond. Below Dam G-H, the thickness of the glacial soils generally ranges between 4 m and 17 m, with a localized 100 m wide section where the deposit attains a thickness of 26 m. This soil unit includes the presence of loose layers located at varying depths, but generally to a maximum of around 10 m depth.

Beneath Dam E-F, the glacial soil thickness typically varies between 5 m and 18 m and includes loose layers located at varying depths. Loose layers in the glacial soils have been identified using in-situ test data from Swedish weight soundings (HfA), as well as Standard Penetration Tests (SPT) and Cone Penetration Tests (CPT).

Tailings in the clarification pond

In the clarification pond, recent deposited tailings are present, originating mostly through discharge of tailings through the U2 spillway. The thickness of these tailings varies between 1 m and 7 m and these deposits extend some 600 m to 800 m from the U2 spillway outlet into the clarification pond.

TMF tailings

The properties and condition of the deposited tailings within the TMF, whether fine grained silts to coarse grained sands, as well as whether dense or loose can generally be related to the deposition method. During early operation (1960s to late 1990s), tailings were discharged subaerially from Dam A-B and flowed towards Dams E-F and G-H where a large supernatant pond was maintained, meaning that the finer fraction and slimes settled subaqueously. During more recent operation (from the early 2000s), spigot deposition was implemented around the perimeter embankments, but with limited subaerial beach length at Dams E-F and G-H due to supernatant pond management requirements through the U2 spillway.

Typically, the subaqueously deposited tailings are fine-grained and loose, exhibiting contractive properties and potential for brittle behavior.

Stabilization measures design description

After the site characterization, the stability analyses for Dams E-F and G-H with the strengths and extents of the liquefiable foundation soils combined with the post-liquefaction strength of the tailings showed that the factor of safety criteria were not met for the post-liquefaction condition, and that immediate stabilization measures were needed to meet stability requirements. Due to the size of the facility, the height of the dams, and the presence of key infrastructure immediately downstream of the dam toes, it quickly became evident

that these remediation measures were going to be significant and would impact the entire site. The dam remediation measures were subsequently designed to fulfill key criteria. Firstly, they should be sufficient to fulfil all stability criteria. Secondly, they should not jeopardize the dams' stability while they were being implemented. Lastly, they should not compromise production. To meet the above criteria, specific remediation measures were designed for Dams E-F, which differed from those for Dams G-H, and specific tailings and water management measures were designed and implemented. Lastly, the impacts of the remediation measures on site infrastructure were assessed and significant changes designed and implemented as part of the remediation project.

The TMF remediation project was approved by the company management and board in April 2022 and construction activities started immediately. They are expected to be completed in December 2024.

Dams E-F

An assessment of potential stabilization methods was made to review alternatives. Stabilization methods reviewed included grouting (jet grouting and soil mixing), densification (e.g., dynamic compaction and vibro-compaction), desaturation and consolidation, excavation and replacement of loose soils, and buttressing. The pros and cons of each method were evaluated at a high level; ultimately, buttressing was selected as the preferred alternative for being the lowest risk approach and the one most likely to meet the tight schedule. Other methods would require either partial or complete dewatering of the clarification pond (e.g., for excavation and replacement methods) and/or excavating or applying significant energy to the toe of the dam (e.g., densification methods), which were considered to have a risk of potentially destabilizing the dam. The buttressing sequencing was estimated to require around two years and would improve stability of the dam continuously once the initial lifts of the buttress were complete, whereas other methods would take more time to implement and could have a temporary negative effect on the dam stability. Additionally, buttressing addressed the remediation needs for both the foundation and the tailings, whereas the other remediation methods studied were focused on the foundation improvements and would have still required subsequent buttressing to address the issue posed by the loose tailings.

The main drawback to buttressing was that it extends some 300 m into the clarification pond, hence losing about 20% of capacity in the clarification pond – from 18 Mm^3 of water down to approximately 14 Mm^3 post-remediation. It also interfered with existing infrastructure (e.g., the reclaim water pump, current spillway outlet, and train terminal) and required a large quantity of rockfill to implement.

Based on the assessed strengths for the loose glacial soils and the clarification pond tailings, the overall gradient of the buttress was required to be in the order of 10H:1V. This shallow-sloped buttress was taken forward through various design phases up to start of construction over the course of six months, and the

conceptual buttress design and the final buttress construction are shown in Figures 2 and 6. The buttress design estimated that around 18 Mt of waste rock was required to meet stability requirements.

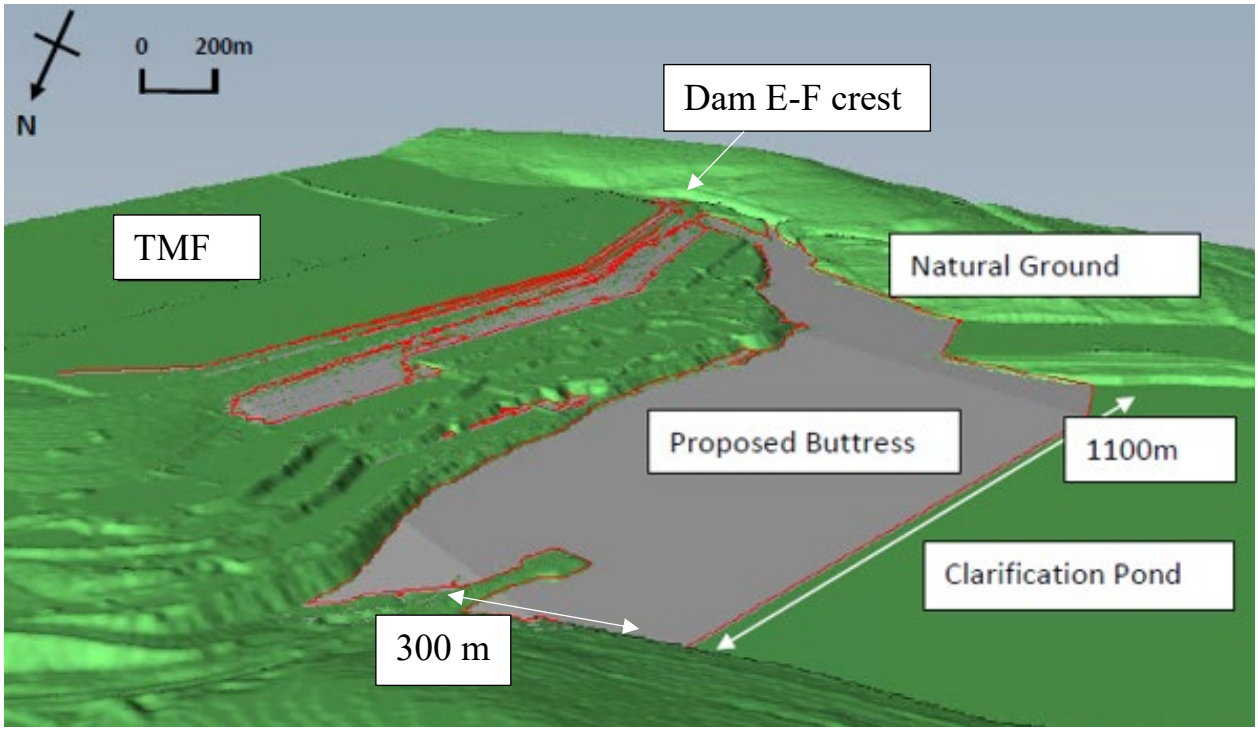


Figure 2: Oblique view of the E-F Dam buttress

Dam G-H

Like Dam E-F, stability analyses indicated that the factor of safety criteria for the post-liquefaction stability cases were not met with the strengths and extents of loose foundation soils identified from the site characterization. To increase stability at Dam G-H, different options were considered, similar to the assessment for Dam E-F, and many of the alternatives were rejected for similar reasons. However, the absence of water at the toe of Dam G-H made the option of improving the foundation conditions a more achievable and attractive option than it was for Dam E-F. Therefore, the solution that was selected was a combined shear key (excavation of unsuitable soils and replacement by suitably competent fill material) and subsequent buttressing, addressing the stability issues from the weak foundation soils and the weak tailings, respectively. This was selected as the preferred option because it reduces the land and fill requirements compared with constructing a shallow sloped buttress, and it was deemed that construction could be achieved safely within the timeframe available.

Figure 3 shows a typical section of the proposed remediation solution, while Figure 4 shows the extents of the shear key and buttress at conceptual level. The shear key dimensions are approximately 40 m base width, with 1V:3H side slopes, 8 to 10 m deep and approximately 1,500 m long alongside the Dam G-H toe. The subsequent buttressing work required placement of buttress fill some 40 m high, totaling around

16 Mt of material. The buttressing does not extend to the full width of the constructed shear key to allow for potential extension of the shear key in the future without destabilizing the existing buttress.

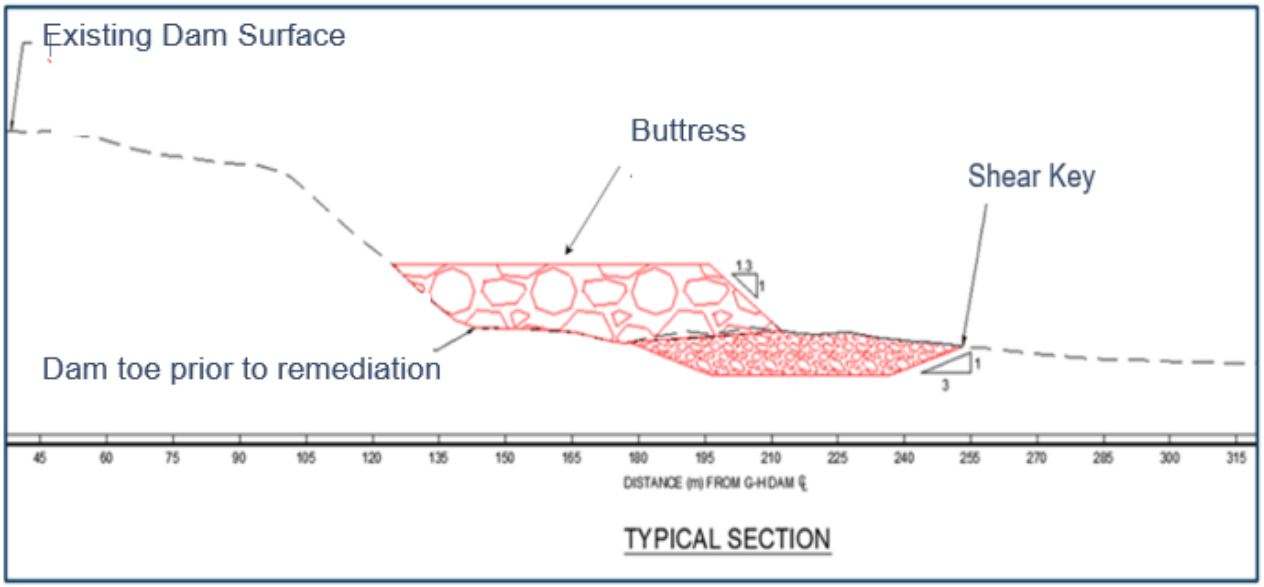


Figure 3: Proposed concept of Dam G-H shear key and buttress section

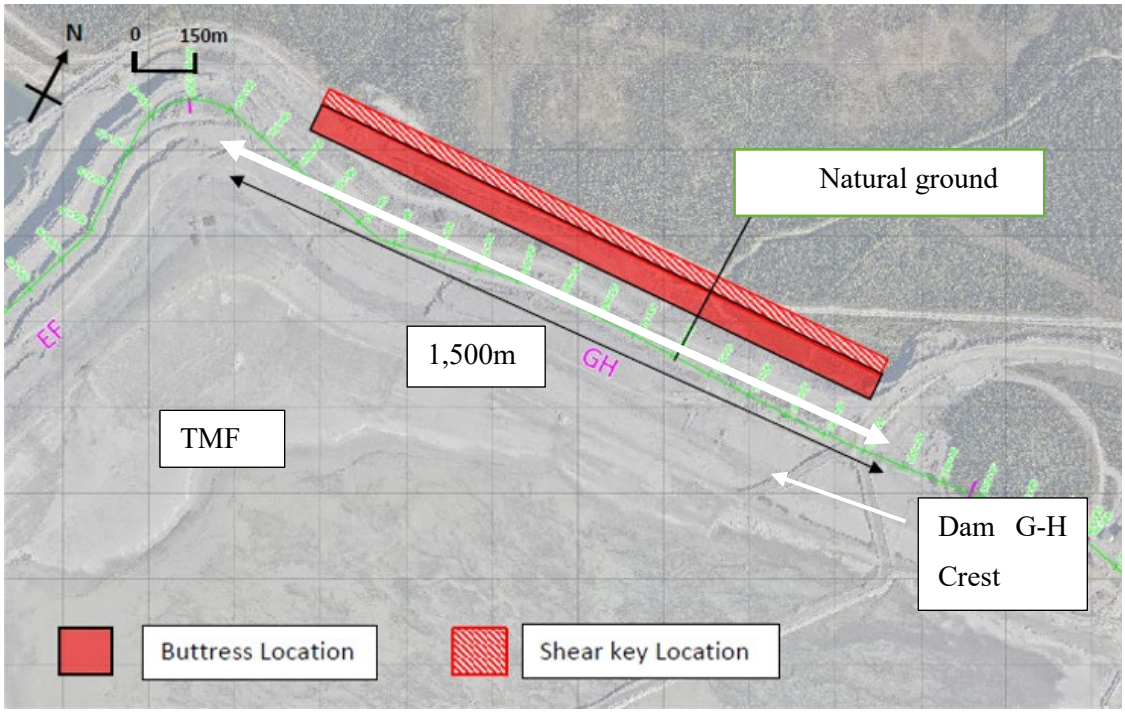


Figure 4: Proposed Dam G-H shear key and buttress location

Dam stabilization measures: construction, sequencing and risk mitigation

Dam E-F

The construction of the buttress was sequenced to allow Boliden to relocate key infrastructure while the buttressing work was ongoing. In particular, the outlet of the U2 spillway as well as the existing pump station in the clarification pond, had to be kept in operation for 4 months and 14 months, respectively, until alternative infrastructure could be built, allowing for this existing infrastructure to be decommissioned. Also, prior to the buttress construction, it was necessary to construct a new haul road to the dam area to achieve the shortest possible haulage distance to the dams, while also keeping the road out of the Life of Mine dam footprint. This haul road was also intended to avoid traffic on the dams' existing buttresses to improve dam and worker safety from the large number of trucks that were going to be used to haul the material. The construction of the haul road took place from May 2022 to October 2022 and required 4 Mt of waste rock to be placed.

The buttress was constructed from run-of-mine or stockpiled waste rock, typically a minus 500 mm material, hauled by contractors using 100 t and 160 t trucks with bulldozers receiving and spreading out the material. This material was placed loose in large lifts when deposited into water in the clarification pond, and subsequently placed in 3 m lifts and compacted with haul traffic once the buttress surface was out of the water. Ice build-ups in the clarification pond were removed ahead of the buttress placement working front, and snow was cleared on the buttress material during placement.

To avoid potential initialization of instability in the underlying loose sediments, the buttress construction started from a ramp located adjacent to the reclaim water pump station and advanced into the clarification pond from there, thus avoiding the need to traffic on the existing buttress. The aim was for the newly placed buttressing to provide support to the existing buttress. Subsequently, the buttress construction sequence was designed to be constructed at the farthest distance from the existing buttress before incrementally constructing inwards towards the existing buttress. This is illustrated in Figure 5. All buttressing work was then progressed from lower levels to higher levels to ensure that factors of safety were always improving with buttress placement, and not inducing potential local instability.

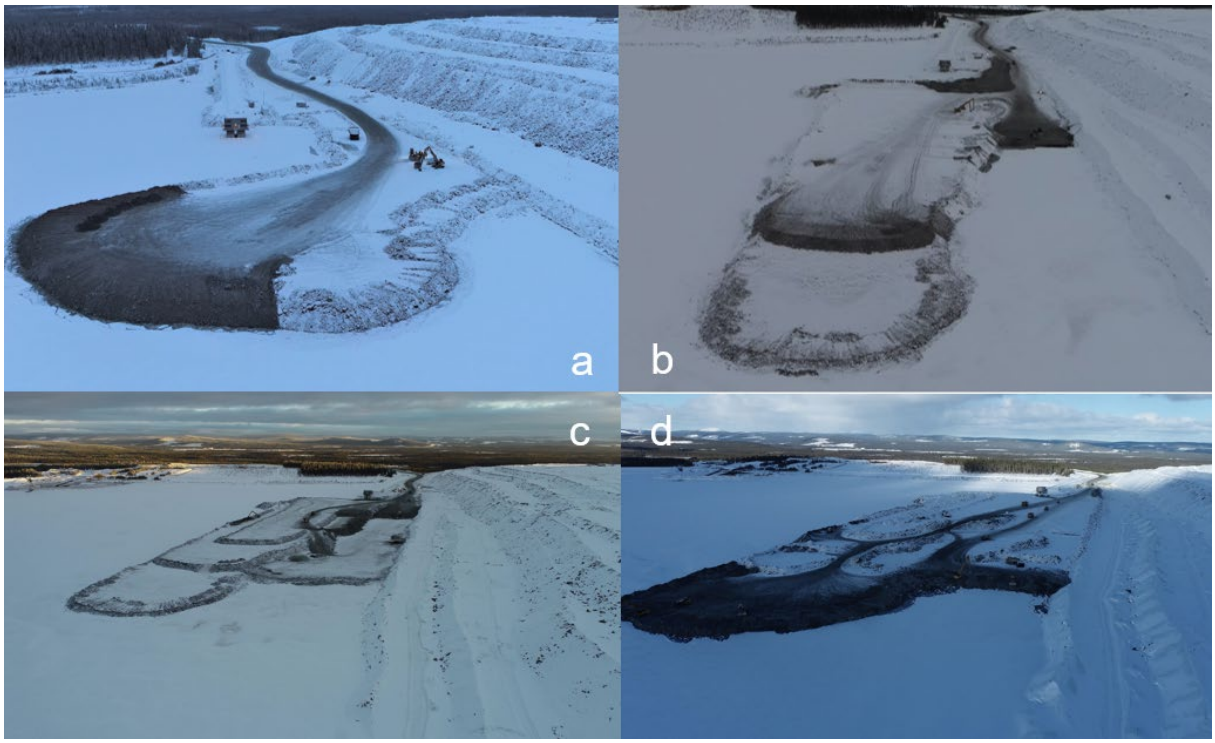


Figure 5: Early staged construction of the Dam E-F buttress in the clarification pond (a – November 2022; b – January 2023; c – March 2023; d – April 2023)

Buttressing started at Dam E-F in November 2022 and was successfully completed in May 2024. Over the 18-month period, more than 18 Mt of mine waste rock was placed and the final buttress construction is shown in Figure 6. During the most intensive construction months, up to 70,000 t were placed daily at the Dam E-F buttress area.



Figure 6: Final remediation buttress construction at Dam E-F

Dam G-H

The shear key excavation, backfilling and subsequent buttress placement was to be implemented through a construction sequence comprising three main stages.

Stage 1 was the construction enabling works, comprising the removal and relocation of existing infrastructure and dewatering activities. The infrastructure in the area comprised a pump station and associated settling basin with a lined channel, which were decommissioned in two parts to allow for a staged excavation of the shear key. The dewatering activities were done in advance of the main excavation works through the excavation of drains at regular intervals within the future shear key area to help with the lowering of the water table prior to the main excavation work, and assist with the dewatering of the excavated area (e.g., from precipitation and additional seepage) during the excavation work. This work started in May 2023 and was completed around November 2023.

Stage 2 was the excavation and backfilling of the shear key, with concurrent construction of the filter layers. Over the 10-month shear key construction period (August 2023 to June 2024), approximately 1.2 Mm^3 of material was excavated from the shear key and replaced by the equivalent volume of suitable fill (Figure 7).

The shear key backfill was designed to be free draining and dense. As such, it was specified to be constructed of coarse rockfill and compacted in 2 m thick lifts. A material of gradation between 50 mm and 400 mm was specifically produced through crushing and screening from the waste rock stockpile material. This gradation was chosen to eliminate fines in the backfill material and to maximize the effect of the compaction efforts. This rockfill is not filter-compatible with the adjacent glacial soils and requires a filter layer to prevent migration of fine particles and mitigate the potential for a piping failure mechanism. This filter layer was designed as a two-layer system comprising a “coarse filter” layer adjacent to rockfill and a “fine filter” layer adjacent to finer soil units located alongside the upstream excavation face of the shear key.

To prevent the shear key excavation causing instability of the dam or buttress slope, and to maintain stability during shear key construction, the shear key excavation area was offset approximately 40 m (calculated from numerical modeling) from the dam toe and the shear key was excavated in “panels” of approximately 50 m sections (parallel to the dam long axis), and backfilling progressively to limit the “open excavation” area to the width of the panel. The excavation slopes were constructed at the designed gradient of 3H:1V to prevent excessive erosion during construction.

To assist with winter construction and avoid the potential for ice forming at the base of the excavation that could create layers of weakness within the fill or loosen the basal foundation soils layers, the groundwater table was maintained below the base of the excavation through localized pumping and the use of previously excavated drains. Additionally, the backfilling of any excavated foundation area was

undertaken within 24 hours of the excavation and the snow and ice were removed from excavated zones or fill areas prior to fill placement using the free draining backfill material.

Stage 3 is the construction of the buttress over the shear key. This work started in June 2024 and is expected to be completed in December 2024. Over the 7-month period, over 15 Mt of waste rock will be placed to stabilize the dam, and the construction will be undertaken using a mix of the mine fleet (300 t trucks) and contractor equipment (similar to that used for the Dam E-F buttressing). In early June 2024, the rate of buttress placement exceeded 90,000 t per day.

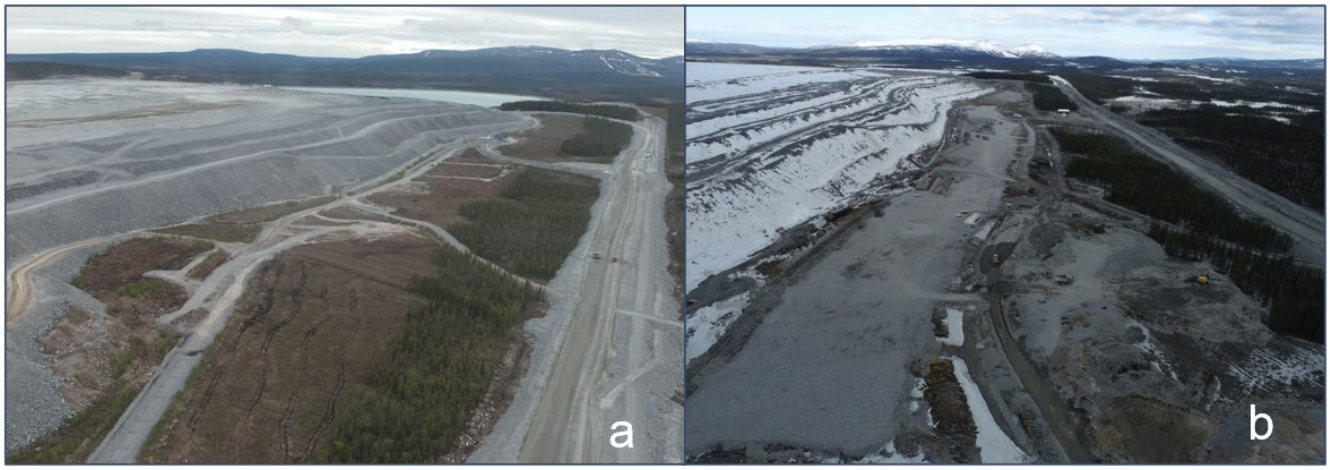


Figure 7: Toe of Dam G-H; a – during drainage work; b – at near-completion of shear key

Surveillance and monitoring during construction

Surveillance and monitoring activities were critical during the implementation of the dam safety remediation measures. A wide range and number of instruments (inclinometers, vibrating wire piezometers, survey monuments), either previously installed as part of the dam monitoring network, or specifically installed ahead of the remediation work construction, was monitored on an ongoing basis throughout the construction period, and post construction. From there, a Trigger Action Response Plan (TARP) was defined for use during construction. The TARP was based upon visual observations and instrumentation monitoring during construction. If the observations or the instrumentation were to indicate that construction activities were initiating displacements or pore pressure increases outside the pre-defined TARP threshold values, construction would have been suspended and a revised construction plan would have been developed. Additionally, regular surveillance and surveying activities (through visual inspection, regular surveying activities, drone surveys, and acquisition of satellite photos) were undertaken to assess the performance of the construction and the existing dams, and to monitor the progress of the construction work. Lastly, extensive quality control and quality assurance activities were undertaken, where required, to fulfil the technical specification requirements, which included visual inspections, surveys, and compaction records, sampling and testing of construction material, and approval of work.

Continued operation (tailings deposition and water management) during remediation

To fulfil one of the key criteria defined from the outset of the remediation project and allow continued operations while the remediation project was undertaken, an updated deposition and water management strategy was specifically designed, as shown conceptually in Figure 8.

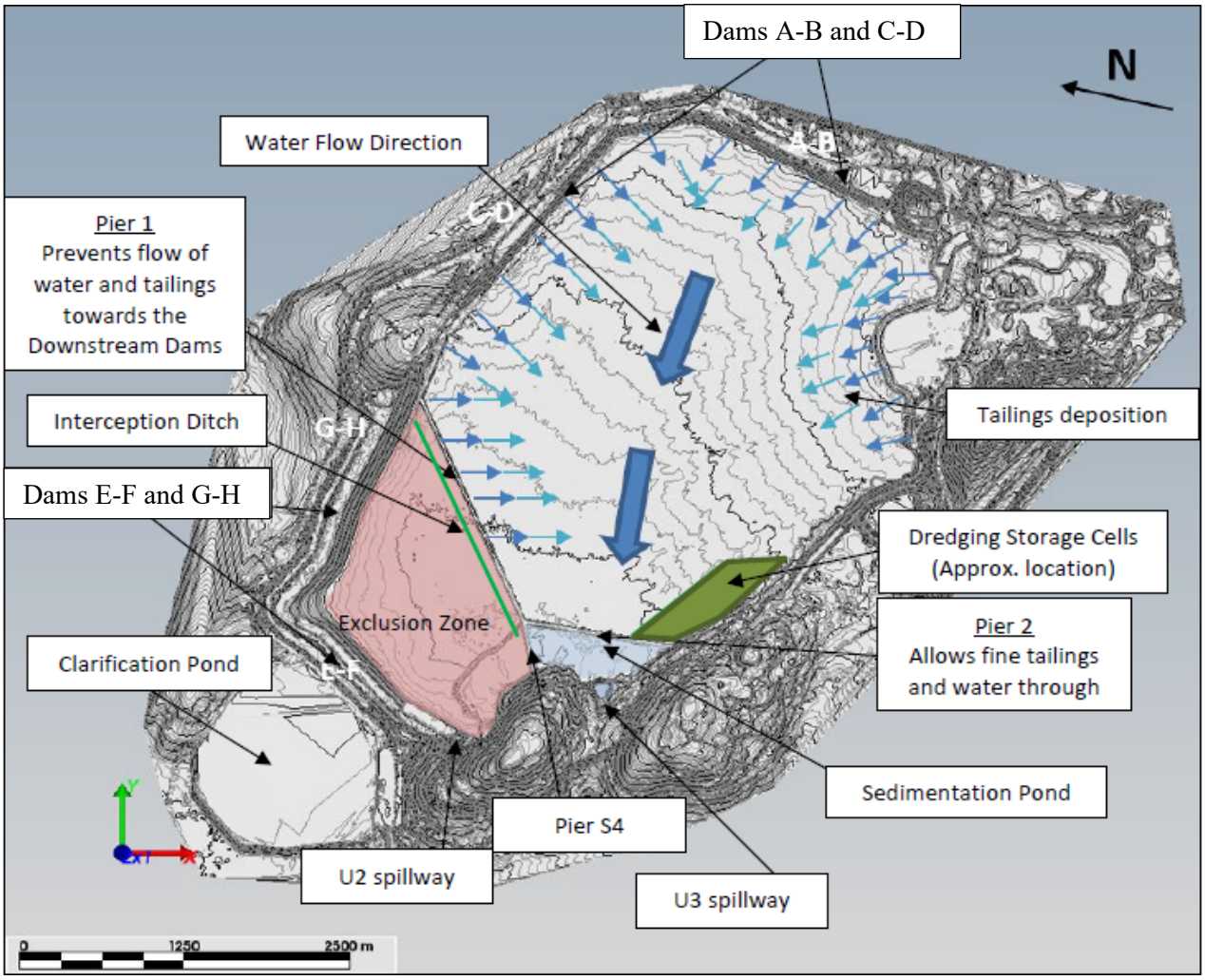


Figure 8: Deposition and water management strategy during the remediation work

An exclusion zone was demarcated on the surface of the tailings impoundment via the construction of rockfill piers to redirect deposition of tailings and water away from Dams E-F and G-H and thus prevent further loading or increases of pore pressure. These piers comprise a 20 m wide crest with a typical height of 5 m from the existing tailings surface at the time of construction.

The focus of the deposition strategy from Dams A-B and C-D was to adjust the practice of tailings deposition (which previously included extensive use of end-of-pipe deposition, leading to high velocity flows and widespread erosion) to maximize the use of the available storage volume in the facility, and

formation of a tailings beach that would gradually slope towards the U3 spillway. These strategies included alternate methods of deposition, such as more extensive, controlled, and consistent use of spigots, extending spigot lines into the facility following initial deposition, and the use of splitter boxes to minimize the impact of end of pipes flows (Thuysbaert et al., 2024). Deposition of tailings and water was directed towards the U3 spillway where Pier P2 was constructed. Water could pass through Pier P2, and the operational supernatant pond was established in the region upstream of the existing U3 Spillway pier (referred to as "the sedimentation pond").

Due to the lowest crest dam (Dam E-F) not being raised, the maximum allowable water level within the facility could not be changed and remained constant during the remediation period to keep sufficient freeboard. However, as the tailings were deposited upstream of the piers and the overall tailings level in the facility increased, it was necessary to undertake dredging operations during the summer of 2023 and 2024 in the sedimentation pond to ensure continuous pre-clarification of the supernatant water before discharge to the clarification pond. A total of approximately 1 Mt of tailings will have been dredged by the time Dams E-F and G-H are raised again in 2025. The tailings dredged from the sedimentation pond were discharged into a series of "dredging cells" located within the TMF (see Figure 8).

While remediation works were ongoing, it was necessary to add two sets of additional piers upstream of Pier P1 and P2 to enable tailings deposition to continue outside the exclusion zone. Additional piers are offset a minimum distance of 300 m upstream of Pier 1 and Pier 2 to maintain an overall slope of the piers and tailings upstream of the exclusion zone to less than 2% to limit the potential for tailings to flow into the exclusion zone should instability develop in the piers (less than typical post-liquefaction runout slopes). Also, both the U2 and U3 spillways remained open to safely convey flood water to the clarification pond.



Figure 9: View of Piers P1 to P4 used for tailings and water management

Each set of piers was constructed over an initial two-month period, and then required regular addition of fill to counter the effect of settlement (approximately 1 to 2 m of settlement were measured over the first 12 months of the piers being constructed). The total amount of material required to build piers P1 to P6 is estimated at ca 6 Mt, and the piers were constructed using contractor equipment (bulldozers and 60 t and 100 t dumpers and trucks) (see Figure 9). No major issues were encountered during the construction of the piers, with typically very little heave or cracking being observed.

Infrastructure work as part of the remediation project

The extent of required remediation work at Dams E-F and G-H and in particular the overall loss of operational water volume in the clarification pond due to the buttress construction had a significant impact on much of the site infrastructure. In particular, the overall site-wide water management had to be redesigned and several key water management components (including a spillway, pump stations, and associated pipelines) at the site required either decommissioning, rerouting, or new construction, as described earlier. In addition, the satellite pit (Salmijärvi) was intended to be used as the main clarification pond to offset the loss of volume in the current clarification pond, and significant infrastructure had to be constructed to ensure water could be pumped into and from the existing clarification pond to the Salmijärvi pit and then to the process plant. The work with the infrastructure had to be staged to meet continuous process operational demands, while ensuring the remediation work could be undertaken within the planned timeframe.

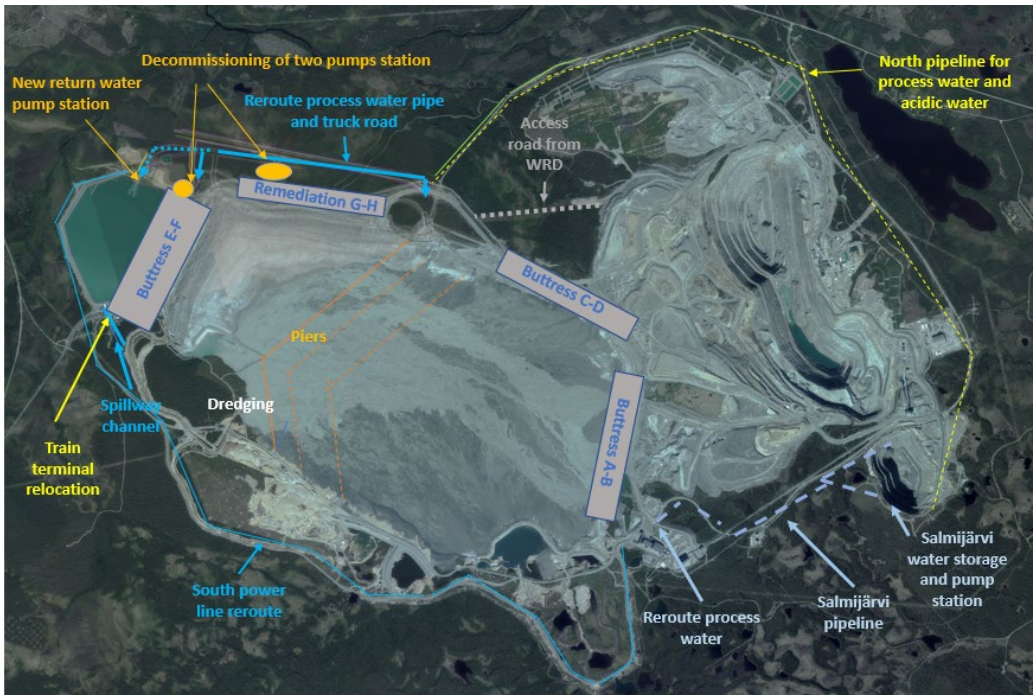


Figure 10: Overview of the remediation project scope of work

In addition, buttress construction was undertaken at Dams A-B and C-D during the remediation work, as a continuation of the buttress construction that had previously been required as part of the design requirement for the continuous safe operation of these embankments. During the period 2022 to 2024, over 5 Mt of rock was placed to buttress Dams A-B and C-D.

Figure 10 shows the overall extent of impact of the dams' remediation measures on key infrastructure. Figure 11 shows an overview of the facility in May 2024, with the following areas of interest: buttressing at Dam E-F completed, shear key excavation and backfill at Dam G-H near completion and buttressing started, successful establishment of the exclusion zone (revegetated with grass to assist with dust prevention), successful construction of Piers P1 to P6, ongoing dredging in the sedimentation pond, and the different areas of buttressing.

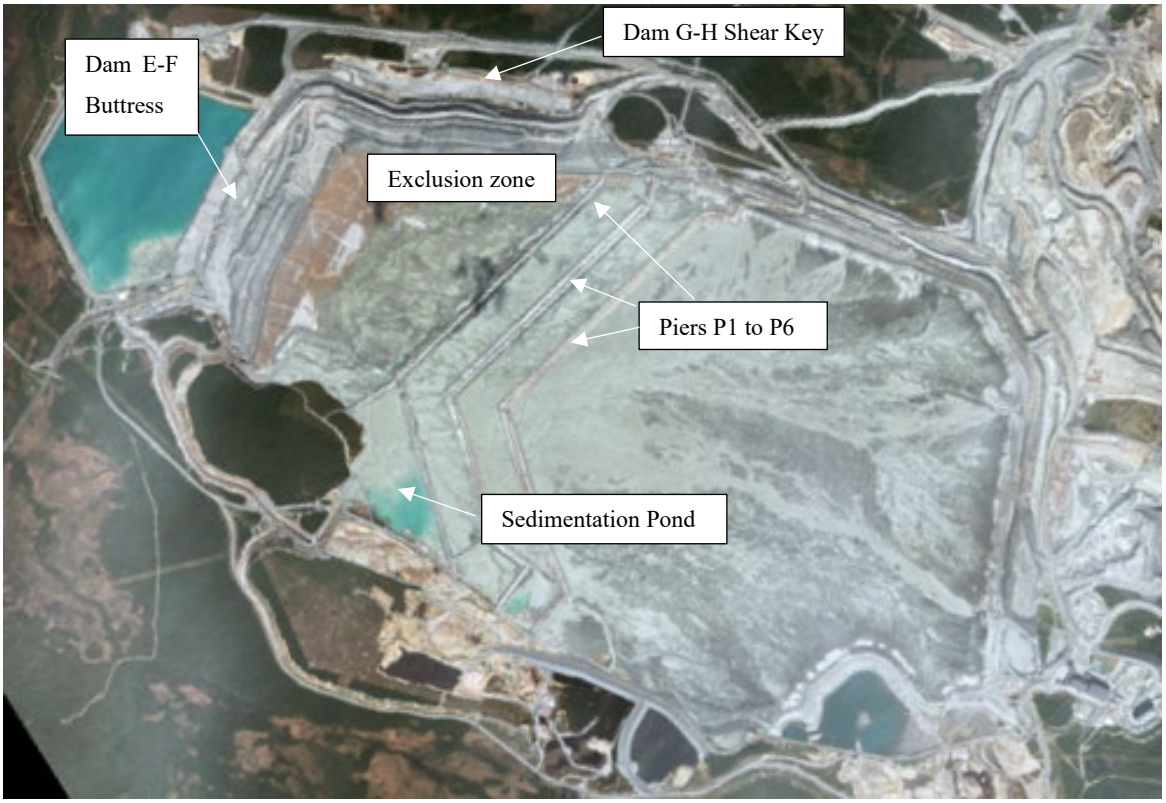


Figure 11: Overview of the Aitik TMF during the remediation work (May 2024)

Conclusion

The Aitik TMF remediation project was approved by the Boliden management and board in April 2022, and construction started immediately. The Dam E-F buttressing work was completed in May 2024, and the remediation work at Dam G-H is expected to be completed in December 2024. Deposition from these dams is planned to restart in the spring of 2025. During the 32-month project, over 45 Mt of rockfill will have

been hauled to the TMF area to allow for the remediation measures to be constructed, and the mine site will have undergone significant changes. These changes are necessary to allow for safe and sustainable storage of tailings and to prevent a loss of production while implementing the remediation works.

References

ICMM. 2020. Global Industry Standard on Tailings Management. International Council on Mining and Metals.

Thuysbaert, J., J. Piccolo-Lawrence, J. Quinn and R. Girard. 2024. Improving tailings deposition: a drone and satellite survey validation framework for enhanced facility management. *Proceedings of Tailings and Mine Waste 2024*. Colorado. USA.

Tailings Pond Sedimentation Capacity: A Practical Approach

Michael Louws, Klohn Crippen Berger Ltd, Canada
Karina Stapleton, Klohn Crippen Berger Ltd, Canada
Andrew Witte, Klohn Crippen Berger Ltd, Canada
Sam Nunoo, Gibraltar Mines Ltd, Canada
Faegheh Niyazi, Gibraltar Mines Ltd, Canada

Abstract

An important aspect of the operation of many conventional mine tailings storage facilities (TSFs) is providing sufficient tailings pond sedimentation capacity to meet total suspended solids (TSS) water quality requirements for direct discharge to the environment or reclaim for re-use in milling. While maintaining a larger pond volume/area will typically correspond to greater sedimentation capacity (i.e., residence time), minimizing the tailings pond size can be important for reducing the risk of the facility. For sites with negative water balances/water deficits (i.e., outflows and losses exceeding inflows), managing the TSF with a small pond and maintaining sufficient water for re-use in milling can be important for operational resilience and water conservation. Previous guidance has highlighted the challenges of purely theoretical approaches for the sizing of TSF pond areas for adequate sedimentation and have suggested "rules of thumb" for minimum pond sizing that tend to be conservatively large when compared to observed pond sizes for operational facilities.

This paper presents a summary of observed tailings pond sizes and reported mill throughput for several conventional TSFs across North America and South America, and a case study for a conventional TSF at an open pit copper mine. Based on the results of the case study and observations for other sites, a practical approach is presented for setting operational targets for pond sizing in terms of tailings production rates and estimated material settling velocities, and for assessing when additional TSS controls may be required (e.g., berms to increase flow path lengths, silt curtains, or filtered intake structures).

Introduction

For many conventional mine tailings storage facilities (TSFs), providing sufficient tailings pond sedimentation capacity to meet total suspended solids (TSS) water quality requirements for direct discharge

to the environment or reclaim for re-use in milling is an important aspect of operations. While sedimentation in tailings ponds is similar to sediment ponds designed to settle out sediment loads from hydrologic events, there are several unique characteristics and uncertainties that can be challenging for the operation of conventional TSFs with TSS requirements for direct discharge to the environment or reclaim for re-use in milling. Of particular concern is the pond area available for sedimentation, which can vary significantly depending on facility geometry and natural ground topography, as well as the spatial and temporal variability in tailings deposition. Previous guidance such as that suggested by Coates and Yu (1977) has highlighted the challenges of purely theoretical approaches for the sizing of TSF pond areas for adequate sedimentation and suggested "rules of thumb" for minimum pond sizing that tend to be conservatively large when compared to observed pond sizes for operational facilities.

This paper presents a summary of observed reclaim pond sizes and reported tailings production for operational conventional TSFs in North and South America, which can be used as a screening tool for pond sizing or assessment of TSS controls for sites that have TSS requirements for water reclaimed or discharged from the facility. A case study is presented to illustrate the use of the benchmarking dataset and theoretical settling pond design calculations to assess the pond sizing requirements and TSS control requirements for a large conventional TSF.

Background

Sedimentation, or particle settling, is the process of removing solids from suspension in a liquid under the force of gravity. Sedimentation is common practice for conventional TSFs and as part of tailings thickening processes for thickened tailings applications (Li, 2024). For conventional TSFs a tailings slurry is typically deposited on a tailings beach where sedimentation of the coarser fraction of the tailings occurs; water "bleeds" down the beach slope into a tailings pond, where remaining finer particles settle out of suspension, and an overflow/decant or pumping system (e.g., a barge and pump system) is operated to reclaim water from the facility. The tailings particle settling behavior, tailings pond geometry, and the hydraulic characteristics of the system govern the design constraints of the system when there is a requirement to minimize TSS in reclaimed or discharged water.

Settling behavior can be categorized by four types depending on concentration and particle interactions: discrete particle settling (the focus of this paper), flocculant settling, hindered settling, and compression settling (Kynch, 1952). The discrete settling of a single particle in a fluid under ideal conditions can be described by Stokes' law, which can be applied to estimate settling velocities of tailings particles with adjustments for non-ideal particle shapes and fluid temperature. Laboratory testing is the preferred approach to estimate settling velocities of tailings solids (i.e., a settling column test). In practice, the sedimentation properties of any suspended material may be influenced by many factors that include

local solids content, states of aggregation or flocculation, particle size, shape, and distribution, particle specific gravity and mineralogy, and the properties of the fluid (Li, 2024; Coates and Yu, 1977).

Beyond the settling behavior of tailings particles, the sedimentation capacity of a particular pond can be heavily influenced by the pond geometry and hydraulic characteristics, which include the pond depth and surface area, pond water temperature and pH, inflow and outflow rates, and hydrodynamic conditions in the pond such as turbulence or wave-induced resuspension.

In contrast to the design of sediment ponds that are generally designed with a permanent pond geometry and sediment load driven by hydrologic events, tailings ponds can have several unique characteristics:

- The variability in when and where tailings are deposited can affect both the sediment load reaching the pond and the effective pond sedimentation area (i.e., the deposition location relative to the outflow location can vary substantially resulting in large portions of the pond being unavailable for settling, or higher sediment loads in the pond).
- The requirement for sedimentation capacity in operational TSFs can be driven by sedimentation of tailings from slurry deposition rather than mobilized sediment from extreme hydrologic events.
- The dynamic process of tailings deposition and progressive dam raises can also result in significant variation in pond geometry over the life of mine.
- Reclaim pond geometry and corresponding effective pond sedimentation area can be heavily influenced by natural topography and often cannot be practically altered in the same manner as typical sediment ponds.
- The surface area of tailings ponds tends to be quite large, and therefore more susceptible to wind impacts.

Methodology

The methodology adopted in this paper assumes TSS criteria for reclaim or discharge water (which may not be the case for all conventional TSFs) and includes the following key steps discussed in the sections that follow:

1. Conduct an initial screening of critical TSF pond configurations to assess whether a detailed analysis is warranted for the planned pond configuration, based on benchmarking for other similar sites.

2. Conduct theoretical calculation of a settling capacity factor, defined as the ratio of effective sedimentation area over the required sedimentation area, considering site-specific constraints in future TSF operations, considering the following:
    - deposition geometry (i.e., effective sedimentation area and distance from inflow to outflow);
    - tailings throughput and material sedimentation properties (inflow sediment load);
    - tailings material particle size or outflow concentration of interest (outflow sediment load).

Benchmarking

Current and historical conventional tailings operations in North and South America were assessed using Google Earth aerial imagery. Facilities are categorized as either: those with observable additional controls for TSS (e.g., rockfill filtered intake structures, or berms around the intake area), or those with no readily observable physical TSS controls and uncertain TSS constraints for reclaim or discharge.

This benchmarking exercise is based on publicly available tailings tonnage data and conditions interpreted from publicly available aerial imagery. The area of discharge into the pond was approximated for each TSF to determine the effective pond area available for settling (the "effective sedimentation area") to account for the effects of "dead storage" areas in the ponds (i.e., areas of the pond that are effectively short-circuited and provide minimal settling capacity).

For the benchmarking exercise the pond area was plotted against mill throughput. This is a simplification and does not account for situations where pond depth may also influence sedimentation capacity (e.g., in very shallow ponds) or where mill throughput is a poor proxy for the tailings loading in the pond (e.g., the potential for cycloning operations to deposit a finer fraction of the whole tailings on the beach). As discussed in the theoretical approach section, estimation of sediment loading also depends on when and where tailings are deposited on the tailings beach. In general, 100% of the tailings throughput is assumed to contribute to sediment loading in the estimated effective pond sedimentation areas. This assumption is likely to overestimate the sediment loading in some cases, since tailings deposition may sometimes be concentrated in specific areas of the beach. The information for this benchmarking exercise could be refined with additional site data (e.g., tailings deposition details, pond depths, TSS requirements for reclaim, and TSS controls).

Figure 1 presents schematics of three TSF configurations illustrating the relationship between tailings deposition locations and inflows to the pond, and approximated areas of effective sedimentation and areas of dead storage. Case (a) shows a ring-dyke facility on relatively flat terrain with a reclaim pond located at

the center of the facility and with deposition occurring from the portion of the ring dyke at a point in time such that a large fraction of the pond is not available for sedimentation. Case (b) presents a facility in mountainous terrain where the natural topography isolates a large fraction of the pond making it unavailable to provide sedimentation capacity. Case (c) presents a case in mountainous terrain where most of the pond area is effective for sedimentation.

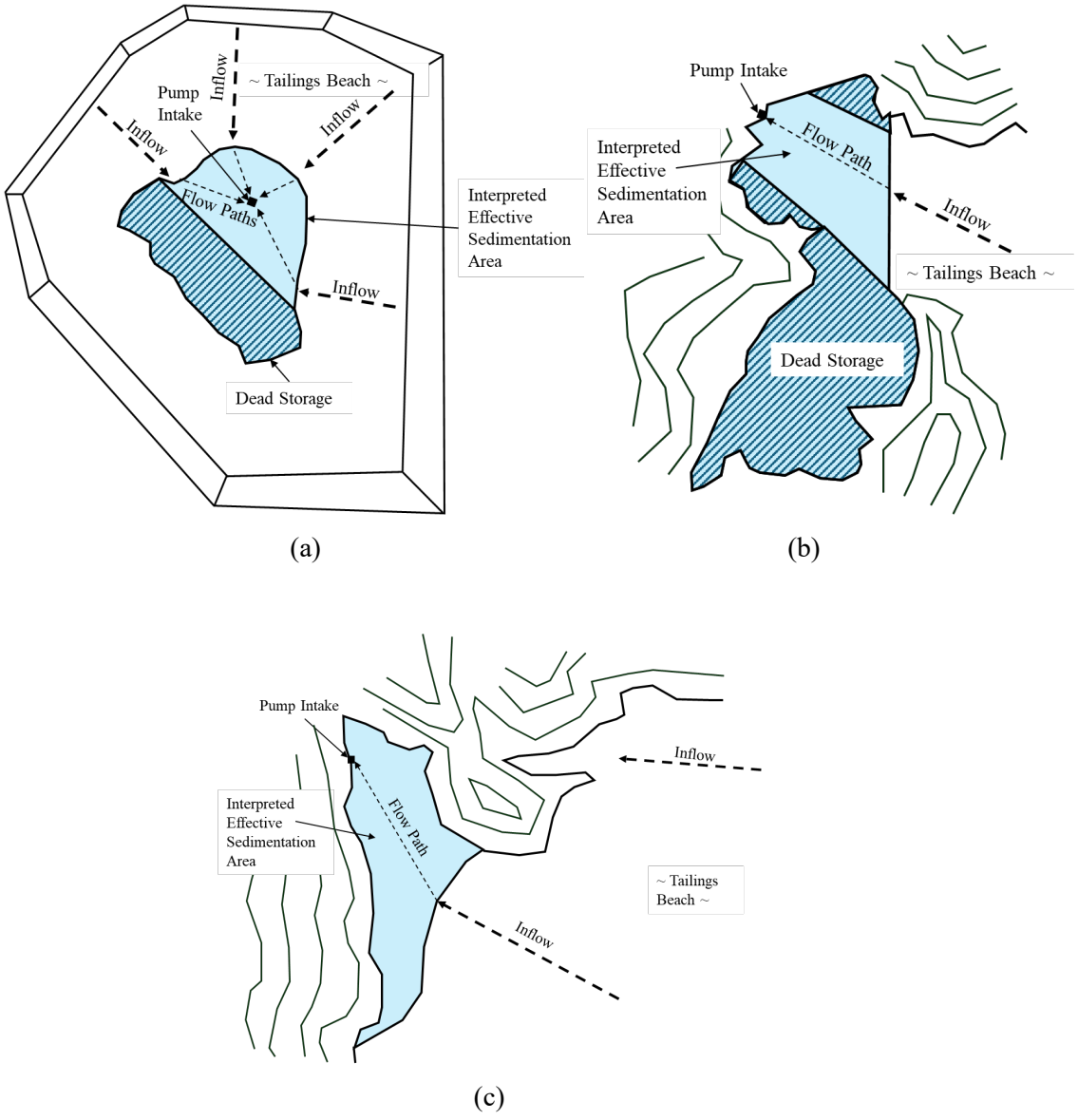


Figure 1: Interpreted effective pond sedimentation area vs. dead storage for example sites

Figure 2 presents a comparison of the trends in tailings throughput (in metric tonnes per day, TPD) vs. the estimated effective sedimentation area, divided into sites with observed physical controls for TSS and those with uncertain physical controls. The shaded blue zone represents the approximate range of most data points for sites without / uncertain physical controls for TSS. Coates and Yu's (1977) "rule of thumb"

for tailings pond sizing (15 acre/1,000 TPD or about 0.60 km^2/10,000 TPD) is also shown. Tailings throughput is compared against pond area in the plot to compare against the Coates and Yu "rule of thumb', noting that pond area is a proxy for the distance of the flow path between the inflow and outflow (i.e., pond length), assuming dead storage has been accounted for in the estimation of the pond area. An approximate length to width ratio is commonly assumed when relating pond length and width to pond area.

The site data suggests that irrespective of site-specific constraints for TSS and uncertainties, recent TSF operations tend to operate with effective pond sedimentation areas lower than that suggested by Coates and Yu. Scatter in the points reflects uncertainties in inputs (due to limitations of publicly available data) and/or differences between the sites. Uncertainties in inputs include the tailings throughput contributing to the tailings pond, and estimated effective sedimentation areas. Differences between sites could include tailings properties (e.g., particle size distribution (PSD), shape, and specific gravity), pond depth, and reclaim rates.

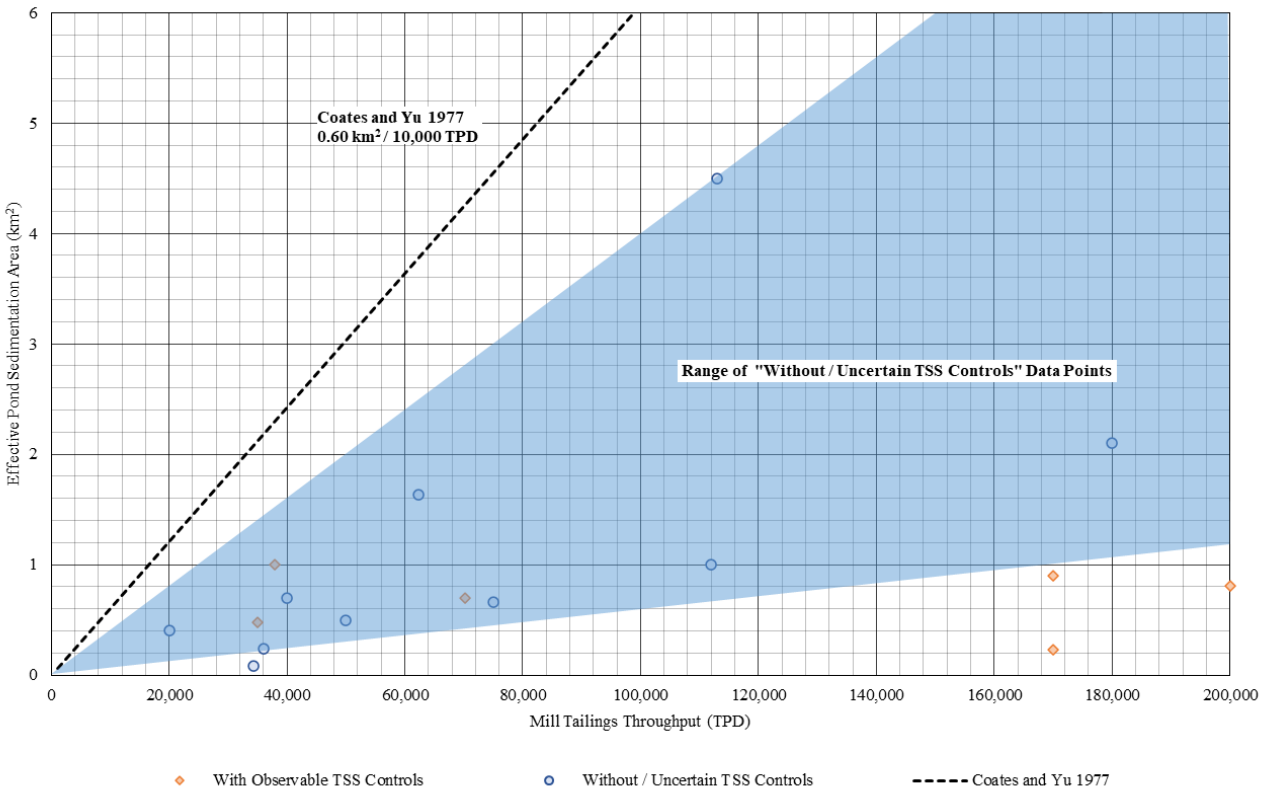


Figure 2: Effective pond sedimentation area vs. mill tailings throughput

Figure 2 could be applied as a screening-criteria for sites that have TSS criteria for mill reclaim or effluent discharge. Site estimates of the effective pond sedimentation area for future configurations of the mine life along with the estimated tailings throughput expected to contribute to the effective pond

sedimentation area should be plotted on Figure 2 and compared to the benchmarking and historical datasets. If the site data:

a. plots near the Coates and Yu (1977) line and above the blue zone, then pond sedimentation capacity is likely adequate;
b. plots within the blue zone, then theoretical analysis should be considered particularly if towards the lower end of the zone; or
c. plots near or below the bottom of the blue zone, then theoretical analysis is warranted and additional TSS controls will likely be required.

Theoretical approach

This assessment had the following steps:

1. Develop a conceptual model of the TSF and tailings pond geometry (usually based on an output of tailings deposition planning and modelling, and considering a range of possible future combinations of tailings deposition locations and pond geometry to identify critical configurations throughout the life of mine):
    a. Estimate the locations where tailings deposition is concentrated; and
    b. Estimate the effective pond sedimentation area (i.e., non-dead storage area) based on the facility and pond geometry, and considering a range of length to width ratios (values between 3:1 and 5:1 are typically recommended in literature (ENV, 2015; EPA, 1976)); and
    c. Estimate the corresponding total tonnage deposition contributing to the area of interest.
2. Estimate settling velocities of the tailings material of interest using settling column testing including testing of TSS for the settling column supernatant water (or, if no settling tests are available, using Stokes' law).
3. Calculate a "pond settling capacity" factor based on the ratio of effective pond sedimentation area vs. required pond area to settle out a particle size of interest.
    a. The required pond surface area based on the following equation (EPA, 1976):

$$A = F_s \frac{Q}{v_s}$$

Where Q is the outflow rate from the pond, m^3/s
A is the effective sedimentation area of the pond, m^2

F_s is a settling factor to account for short-circuiting or other non-ideal settling conditions (typically assumed to be between 1.2 and 2.0; ENV, 2015), unitless

v_s is the settling velocity of sediment particle size of interest, m/s

b. The effective pond sedimentation area as estimated in (1) above.

In general, particles sizes smaller than about 4 μm diameter cannot practically be removed by discrete settling (Haan et al., 1994), and it is common to assume that removal of 5 μm to 10 μm particles will result in sufficient water quality (ENV, 2015). However, it is important to understand the PSD of the tailings in question – if the tailings contain a high proportion of silt and clay-sized particles the water quality requirements may not be met if relying on only discrete particle settling. Laboratory testing to estimate the material PSD and settling velocity is recommended to inform the settling velocity of the particle size, which is critical to meeting the target water quality criteria.

Case study

The case study is for an open pit copper mine that produces and deposits tailings in a conventional TSF at a rate of about 77,000 TPD. Since around the mid-2000s, the TSF supernatant pond volume has been progressively reduced from a volume of about 70 Mm^3 to a volume of about 16 Mm^3 to support overall risk reduction for the facility, with the objective of operating the facility with a small supernatant pond of about 5 Mm^3. The water quality in water pumped from the TSF supernatant pond is required to meet a TSS criterion of 25 mg/L.

The objectives of the case study were to assess the feasibility of operating the TSF with a reduced pond volume considering the planned tailings production and deposition plan, and to set operational targets for if and/or when additional physical TSS controls (e.g., rockfill berms or protection of the pump intake structure) would be required.

For future configurations, the estimated critical (i.e., smallest) effective sedimentation area is estimated to be 0.14 km^2, which plots close to the benchmarking data where additional TSS controls were observed, and substantially lower than the Coates and Yu suggested pond sizing. Therefore, a theoretical approach was adopted to assess the feasibility of the planned pond sizing to meet TSS constraints. Major assumptions made for this assessment included:

a. Guidelines for sediment pond design recommend that 5 μm to 10 μm particles be settled out of suspension to meet water quality standards (ENV, 2015). Results of settling column test results were assumed to represent sufficient water quality for reclaim water, i.e., the settling velocity of the supernatant and solids interface is assumed to represent approximately the tailings d_{10} (approx. 5 μm), and the supernatant water quality is sufficient to meet water quality

requirements. The pond depth is assumed to be sufficient for settling to be primarily discrete particle settling.

b. The tailings loading assumed for this assessment assumes that the effects of varying solids contents on settling velocities could be neglected since tailings inflows to the pond will generally be at or lower than solids contents of whole or cyclone overflow tailings.
    - A key uncertainty in this process is the estimation of the effective pond sedimentation area and corresponding length to width ratios. Ratios of approximately 4:1 were assessed for historical pond areas. For future configurations, a ratio of 5:1 was conservatively assumed (i.e., pond area was calculated based on the estimated distance from inflow to outflow and the assumed 5:1 length: width ratio). Future configurations of the TSF were based on tailings deposition modelling that are subject to uncertainties in tailings beach slopes and potential changes to tailings deposition strategies.

c. A pond settling capacity factor of 2.0 was adopted for this assessment, considering the possibility of non-ideal settling conditions such as wind and wave action on the pond surface or scouring and sediment resuspension. Resuspension of solids due to influence of the pump intake is considered by including a buffer below the pump intake.

Figure 3 (on the next page) presents a schematic of the case study tailings beach and pond configuration, illustrating the pond area available for sedimentation considering a critical configuration of tailings deposition near the pump intake. In this case, due to both natural topography and tailings deposition strategies, a large portion of the pond is unavailable for sedimentation.

Table 1 summarizes the results of the case study calculations. The base case considers an estimated future critical configuration of the facility considering a relocated barge and pump; sensitivity cases were considered for a higher outflow rate and a reduced effective pond sedimentation area. The results were benchmarked against historical TSF pond configurations using the same methodology.

Table 1: Base case and sensitivity cases for future operations and historical benchmarking

Parameter	Base case	Sensitivity cases		Historical benchmarks	
		Increased outflow	Reduced pond sedimentation area	June 2023	October 2023
Effective sedimentation area (km^2)	0.14	0.14	**0.12**	0.11	0.07
Pond length:width ratio	5:1	5:1	5:1	4:1	4:1
Equivalent distance to outflow (m)	850	850	**800**	670	510
Outflow rate (m^3/s)	2.0	**2.5**	2.0	1.8	1.9
Settling capacity factor	1.3	1.0	1.1	1.1	0.7

Note: **Bold** text indicates differences for the sensitivity cases compared to the base case.

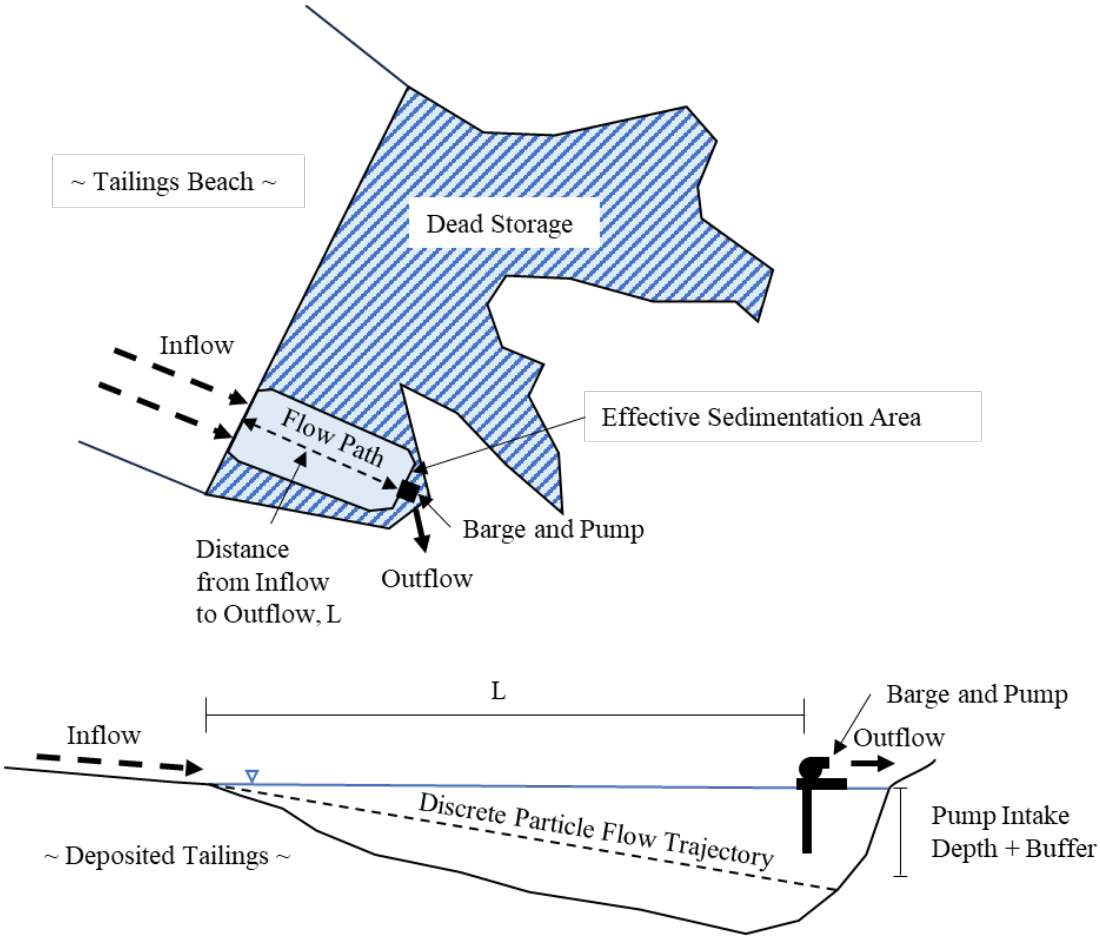


Figure 3: Schematic TSF plan and section illustrating sediment flow trajectory

The results suggest that an increased outflow rate and reduced effective pond sedimentation area both significantly affect the settling capacity, as reflected by the reduced settling capacity factor. The historical benchmarking cases demonstrate that the reduction in distance from tailings inflow to outflow between June 2023 and October 2023 resulted in a settling capacity factor below one, which is supported by TSS data: June 2023, pond TSS was about 12 mg/L, and October 2023, pond TSS was about 32 mg/L, which validates the adopted approach for estimation of pond settling capacity for the future TSF configurations.

The results of this assessment suggest that the planned future operations are likely to be close to a settling capacity factor of one, and therefore it is probable that additional physical or chemical controls to reduce TSS in the pond will likely be required assuming even minor deviations compared to the assumed tailings deposition properties and plan. Considering these results, the barge and pump has been moved to a more favorable and protected location farther from the tailings beach edge, and the distance from inflow (i.e., beach edge) to outflow (i.e., the barge and pump location) has been adopted as a target metric for ongoing tailings deposition and water balance planning.

Conclusion

The capacity of tailings ponds to settle out solids in dynamic TSF beach and pond systems is a complex process subject to many uncertainties. Assessment of pond settling capacity should consider the settling properties of tailings materials (ideally estimated via laboratory testing), and critical configurations of the facility over time, considering tailings throughput and deposition locations, effective pond sedimentation area, and outflow rates. While it may be preferred to operate with a small supernatant pond considering the facility risk and/or site hydrologic conditions, in many cases, pond geometry and tailings deposition strategies will dictate that large fractions of the pond area will not contribute to pond settling capacity (i.e., be dead storage areas).

The benchmarking data presented in this paper for North and South American copper mine TSFs could be used as a screening tool to assess whether significant further study is warranted for proposed facility configurations. The theoretical approach adopted for this study is a practical (and simplified) approach based on methods commonly used for sediment pond design. It could be used to inform key performance indicators for tailings deposition planning, and to inform decision-making for long-term pond sizing and potential requirements for additional chemical controls such as flocculants, or physical controls such as protected or pump intakes or berms to increase the flow path of tailings on the beach.

A more detailed analysis may be warranted where an estimated outflow sediment concentration or actual pond sedimentation efficiency is needed (e.g., to inform water treatment design), or for shallow ponds where discrete particle settling may not govern and where resuspension is more likely. The approach in this paper requires several assumptions for aspects of sedimentation that cannot be readily measured or observed, notably the application of idealized settling behaviors in a non-ideal setting environment, the potential for non-quiescent pond conditions and resuspension of solids (particularly around intake structures), and variability in sediment loads reaching the pond. Careful consideration should be paid to these uncertainties given the site context, and sensitivity or uncertainty analysis should be conducted to inform the sensitivity of any conclusion to variability in key input assumptions. These uncertainties could be used to inform key performance indicators for tailings deposition planning and for pond shape and location management, e.g., the distance from pond edge to pump location.

References

British Columbia Ministry of Environment. (ENV). 2015. Assessing the design, size, and operation of sediment ponds used in mining – Version 1.0. December.

Coates, D., and Yu, Y. 1977. Waste embankments. *Pit Slope Manual.* Canada Centre for Mineral and Energy Technology, Ottawa, Report 77-1.

Environmental Protection Agency. (EPA). 1976. Effectiveness of surface mine sedimentation ponds. EPA-600/2-76-117.

Haan, C.T., Barfield, B.J. and Hayes, J.C. 1994. *Design Hydrology and Sedimentology for Small Catchments.* San Diego: Elsevier Academic Press.

Kynch, G.J. 1952. A theory of sedimentation. *Transactions of the Faraday Soc*iety 48: 166–176.

Li, Y. and D. van Zyl. 2024. Experimental study on the overall settling behavior of copper tailings suspension. *Minerals Engineering* 208: 108580.

Key Parameters that Influence the Operation of Tailings Dry Stack Disposal, Considering Various International Practices

Gino Vizcarra, Vale S.A., Brazil
Kathy Tehrani, ATC Williams, Australia
Fernando Sgavioli, Vale S.A., Brazil
Thatyane Martins Gonçalves, Vale S.A., Brazil
Frank Pereira, Vale S.A., Brazil

Abstract

The mining industry has increasingly prioritized the use of tailings dry stacking as an alternative to traditional tailings disposal methods. This shift aims to minimize the potential for dam failures and tailings runout, offering both environmental and safety advantages. However, it is important to note that the behavior of tailings dry stacks can vary significantly due to differences in site conditions such as temperature, humidity, precipitation, and seismic activity across various regions. Brazil, Peru, and Australia are among the countries that have implemented tailings dry stacking disposal, each facing unique challenges and adopting specific approaches to address them. This study seeks to examine how the operation of a tailings dry stack is affected by different environmental conditions and evaluate its effectiveness as a method for disposing of tailings.

In Peru, the dry stacks are at a high altitude and in mountainous regions, which can present challenges such as low temperatures and increased risk of landslides. In contrast, in Brazil, where tropical conditions prevail, the main concerns are heavy rainfall and the potential for erosion. Additionally, in Australia, where drought conditions are common, high temperatures and lack of precipitation have an impact on the stability and drying behavior of the dry stacks.

By analyzing international practices and case studies, several key parameters have been identified that significantly influence the operation of tailings dry stack disposal, such as the type and density of the tailings material, the moisture content and compaction of the stack, and the design for closure considering local conditions and climate change scenarios. Understanding and properly considering these parameters is crucial for ensuring the successful and sustainable operation of tailings dry stack disposal facilities. In summary, the operation of tailings dry stack disposal is influenced by various key parameters such as

environmental conditions, site-specific challenges, and proper design and implementation that need to be carefully considered and addressed to achieve optimal environmental and safety outcomes.

Introduction

Dry stacking is an innovative method of tailings disposal that involves the dewatering of tailings to create a stable, low-moisture material that can be stacked and compacted. This approach reduces the risks associated with traditional tailings impoundments, such as embankment failures and tailings runout, and offers significant environmental and safety advantages by minimizing water usage and potential contamination. This study compares the operation of tailings dry stacks at three different sites located in distinct climates: high altitude and mountainous regions of Peru, tropical conditions in Brazil, and arid, drought-prone areas of Australia. Each site presents unique environmental challenges, necessitating tailored strategies and design adjustments to accommodate changes to mine plans and ensure the stability and effectiveness of the dry stacks.

Site I: Minas Gerais, Brazil

Overview

The site is an operating 68,000 tonne-per-day open pit iron ore mine located in the state of Minas Gerais, Brazil, approximately 200 km east of Belo Horizonte. During the dry season, about 8,000 tonnes per day of filtered tailings are stored in a filtered tailings storage facility (TSF). This decreases to 3,000 tonnes per day during the wet season. Figure 1 depicts the tailings dry stacking facility.



Figure 1: Tailings storage facility in Minas Gerais (source: Google Earth)

Site conditions

The site is located in a high rainfall, temperate climate environment. The mean annual precipitation is approximately 1,200 mm, which is roughly equivalent to the local evaporation rate. Periods of heavy rainfall lasting several days are common. The mean annual temperature is approximately 22° C. The site does not have high seismicity.

TSF operations

The tailings have a specific gravity of approximately 3 g/cm^3 and a P80 ranging from 0.1 to 0.2 mm. The tailings contain around 15 % hematite. The TSF operation and monitoring are conducted by the operator, with periodic inspection carried out by external consultants. During the engineering design phase, a trial field was created to evaluate the thickness layer, velocity of roller compactor, water application and compaction, in order to ensure that the final tailings deposit will achieve the desired slope and moisture content for a stable dry stack (Rodari Gutierrez and Agustin Oldecop, 2021). The stacking of filtered tailings involves dumping by trucks, while the fill construction consists of building embankments and placing compacted approved material in areas where unsuitable material has been removed. The tailings are placed in controlled, compacted layers not exceeding 30 cm (compacted) using approved compaction equipment, ensuring uniform raising and achieving a minimum compaction level of 95 percent maximum dry density. During fill placement, there is continuous full-time observation, and field tests are performed under the supervision of an QA/QC team. If the required compaction is not recorded during testing, additional effort has to be exerted, along with adjustments to moisture content, until at least 95 percent compaction is achieved. The TSF is constructed above a drainage system designed to collect seepage and rising water tables. The global slope for the TSF is 15º and the local slope is 2.5H:1V (22º).

Site II: Cerro Lindo, Peru

Overview

The Cerro Lindo Mine is situated in the province of Chincha, department of Ica, approximately 200 km south of Lima, Peru. The mine currently processes 7,000 metric tonnes per day to extract polymetallic minerals including zinc, lead, and copper, utilizing the sub-level stoping mining method. The mineral processing results in the generation of concentrates that account for roughly 10% of the processed material. Of the generated tailings, 55% is used for underground paste backfill, while the remaining 45% is deposited on the surface as filtered tailings.



Figure 2: Cerro Lindo TSF (source: Google Earth)

Site conditions

The mine is located in the occidental Andes at an average elevation of 2,000 masl. The yearly average precipitation and evaporation are 200 and 1,500 mm, respectively. The zone has an arid climate, with average yearly temperatures of 19°C, and with some rain concentrated in the months of December to March. For the rest of the year precipitation is rare and sporadic (Lara and León, 2011).

The mine is located in a high seismicity area, less than 100 km from the Peru-Chile trench. Earthquakes in the area are expected up to a magnitude of Mw = 9.0 (for the maximum credible earthquake) with maximum accelerations at a basal rock level of 0.45 g (Lara and León, 2011). In 2007 a significant seismic event of magnitude Mw = 8.0 occurred, considered as a maximum operation earthquake for the project area, with a return period of 500 years. The Cerro Lindo tailings TSF sustained no damage during and after this earthquake.

The TSF is located in the Quebrada Pahuaypite, which has an approximate watershed area of 0.45 km^2. The average gradient of the bottom of the Quebrada Pahuaypite is 20–25%, and the valley side slopes are also variable between 25 and 45%. From a hydrogeological point of view, the quebrada does not have water flow at all times of the year and there is no evidence of water seepage. The groundwater level is more than 40 m deep in the area of the tailings deposit (Lara and León, 2011).

TSF operations

The filtered tailings deposit is composed of two desiccation platforms of approximately 2,250 m^2 and 14,050 m^2 each, located at elevations 2,028 and 2,082 masl, respectively. In these platforms, filtered tailings are discharged, spread by sectors to obtain desiccation and to allow further compacting. The tailings deposit has been designed to store 14 Mt of tailings and is built as a large fill that will have an overall slope of 2.8H:1V (19°). The tailings storage construction has benches that have a minimum width of 10 m each, and are 20 m high. As a part of the tailings deposit, a basal drainage system has been provided for seepage collection from the tailings deposit. The filtered tailings require compaction in layers due to the elevated site topography and the high seismic activity of the location.

Site III: Karara, Australia

Overview

The Karara mine is a magnetite mining and processing facility situated in the Mid-West region of Western Australia, approximately 225 km east-southeast of Geraldton and 320 km north-northeast of Perth. The mine operation comprises an open-pit mining excavation, a beneficiation processing plant, a waste rock disposal area and TSFs.



Figure 3: Karara TSF (source: Google Earth)

Site conditions

The local climate is characterized by an extended dry season lasting seven to eight months, accompanied by cold, wet winters and hot, dry summers. Average temperatures during the warmer months in Morawa range from a daily minimum of 13°C to a maximum of 38°C, while in the cooler months, the average temperature span is 6°C to 28°C. The average annual precipitation is 300 to 400 mm, fluctuating from a monthly low of 8 mm in December to a high of 60 mm in June. Extreme rainfall events exceeding 160 mm can be anticipated, and a 1-in-20-year, 72-hour rainfall event could produce over 100 mm of precipitation. The number of days with measurable rainfall varies significantly, with less than 2 days per month on average during the November through February period, compared to approximately 8 days per month during the winter season.

TSF operations

The mineral processing at the Karara mine generates tailings characterized by a high silica content and fine to ultrafine particle size. Due to limitations within the processing plant, the mine operator has implemented a tailings management approach utilizing both conventional wet tailings facilities and a dry stack tailings facility. The dry tailings are deposited at a moisture content of approximately 15%, while the wet tailings are pumped to the tailings dam at around 45% solids. The dry tailings are stacked using a radial stacking technique involving a series of conveyor extensions that sweep across the deposition area. The conveyor system operates in an arcing motion, depositing the dry tailings in layers. As each arc is completed, the conveyor is shifted to the next arc, and the tailings deposition continues. The tailings storage facility is surrounded by toe drains to collect any runoff and seepage, which are then directed to drainage collection sumps. The slopes of the tailings facility are maintained between 43° and 45° during construction and tailings placement. Upon closure, the tailings facility landform will be shaped to achieve a stable slope configuration.

Key parameters influencing tailings dry stack operation

By analyzing international practices and case studies, several key parameters have been identified that significantly influence the operation of tailings dry stack disposal. These are discussed below.

Environmental and site-specific challenges

Brazil: tropical conditions

Brazil's tropical conditions pose challenges. Heavy rainfall can lead to erosion and increased moisture content in the tailings, which affects their stability and compaction. Additionally, the high humidity levels

can slow down the drying process, making it difficult to maintain the desired moisture content in the tailings.

Peru: high altitude and mountainous regions

In Peru, tailings dry stacks are often located in high-altitude and mountainous regions. These areas present unique challenges, such as low temperatures and an increased risk of landslides. The cold climate can affect the dewatering process and the compaction of the tailings, potentially leading to stability issues. Furthermore, the steep terrain increases the risk of landslides, which can compromise the integrity of the dry stack.

Australia: drought conditions

In Australia, drought conditions are a primary concern. High temperatures and lack of precipitation can accelerate the drying process, potentially leading to overly dry and brittle tailings. This can cause dust generation and pose a health hazard. Moreover, the arid conditions can affect the stability of the stack, as excessively dry materials may not compact well.

Table 1: Average annual rainfall and evaporation in studied sites

Site	Average annual precipitation	Average annual evaporation
Minas Gerais	1,200 mm	1,200 mm
Cerro Lindo	200 mm	1,500 mm
Karara	400 mm	2,000 mm

Type and density of the tailings material

The type of tailings material and its density are critical factors in the design and operation of dry stacks. Different minerals and processing methods result in tailings with varying particle sizes, shapes, and densities. These properties influence the stack's stability, permeability, and compaction behavior. Accurately characterizing the tailings material is essential to design a containment structure that can accommodate its specific properties. Table 2 summarizes the type, specific gravity, and fines content of the tailings material in the three sites.

Table 2: Type and density of tailings material

Site	Tailings type	Specific gravity, Gs	Fines content, %
Minas Gerais	Iron ore	2.95 – 3.10	40 – 65
Cerro Lindo	Zinc, Copper, Lead	4 – 4.2	56 – 58
Karara	Iron ore	2.94 - 3	75 – 90

Moisture content and compaction

The moisture content of the tailings is a vital parameter affecting the stack's stability and behavior. Proper dewatering is necessary to achieve the right moisture content for compaction. Overly wet tailings can lead to instability and erosion, while overly dry tailings can become dusty and difficult to compact. Regular monitoring and adjustment of the moisture content are crucial for maintaining the stack's integrity. Table 3 summarizes the average moisture content (MC) and average in-situ dry density of tailings in the sites.

Table 3: Moisture content and in-situ dry density of tailings

Site	Average MC after compaction	Average in-situ dry density	Layer thickness
Minas Gerais	10.5 – 13 %	1.9 – 2 tonne/m^3	0.3 m
Cerro Lindo	5 – 7 %	2.7 – 2.8 tonne/m^3	0.3 m
Karara (Amoah et al, 2018)	13 – 15 %	1.7 tonne/m^3	24 – 26 m

Design and construction of the containment structure

The containment structure's design and construction are fundamental to tailings dry stacking's success. The structure must be engineered to support the tailings' load and withstand environmental stresses such as rainfall, temperature fluctuations, and seismic activity. Proper drainage systems, erosion control measures, and reinforcement techniques must be incorporated to ensure long-term stability. Table 4 presents the key design parameters of the dry stack in the studied sites.

Table 4: Key design parameters

Site	Stacking rate Tpd	Volume Mm^3	Area Ha	Max height m	Global slope H:V
Minas Gerais	3,000 – 8,000	8	42	60	3.75:1
Cerro Lindo	5,000	4.93	60	160	2.8:1
Karara	33,000	449	486	60	2.6:1

Conclusion

The operation of tailings dry stack disposal is influenced by various key parameters such as environmental conditions, site-specific challenges, and proper design and implementation. Understanding and properly considering these parameters is crucial for ensuring the successful and sustainable operation of tailings dry stack disposal facilities. Each region presents unique challenges that require tailored approaches to achieve optimal environmental and safety outcomes.

Ongoing monitoring and maintenance are essential for the sustainable operation of tailings dry stacks. Regular inspections and monitoring of the stack's moisture content, compaction, and structural integrity can help identify potential issues before they become critical. Implementing a robust maintenance plan that includes erosion control, dust suppression, and stability monitoring can enhance the stack's performance and safety.

By learning from international practices and adapting strategies to local conditions, the mining industry can enhance the effectiveness of tailings dry stacking as a safer and more environmentally friendly disposal method.

References

Amoah, N., Dressel, W. and Fourie, A.B. 2018, Characterisation of unsaturated geotechnical properties of filtered magnetite tailings in a dry stack facility, in R.J. Jewell and A.B. Fourie (eds), *Paste 2018: Proceedings of the 21st International Seminar on Paste and Thickened Tailings*, Australian Centre for Geomechanics, Perth, pp. 375–388, https://doi.org/10.36487/ACG_rep/1805_31_Amoah

Karara Mining Limited. 2022. Karara Iron Ore Project – Mine Life Extension Revised Proposal Environmental Protection Act Section 38 Referral Supporting Document.

Lara, J.L. and León, E. 2011. Design and operational experience of the Cerro Lindo filtered tailings deposit. In R.J. Jewell and A.B. Fourie (eds), *Paste 2011: Proceedings of the 14th International Seminar on Paste and Thickened Tailings,* Australian Centre for Geomechanics, Perth, https://doi.org/10.36487/ACG_rep/1104_03_Lara

Rodari Gutierrez, G.J. and Agustin Oldecop, L. 2021. Test plot study of a tailings stack final cover prototype. MATEC Web Conf. 2021, PanAm-Unsat 2021: 3rd Pan-American Conference on Unsaturated Soils: 04006. https://doi.org/10.1051/matecconf/202133704006

Characterization of Flocculated Fluid Fine Tailings Using On-line Microscopy

Paul Mikula, Kalium Research, Alberta, Canada
Nan Wang, Syncrude Research, Alberta, Canada
Adeola Bello-Hamilton, Syncrude Research, Alberta, Canada
Randy Mikula, Kalium Research, Alberta, Canada

Abstract

Oilsands fine fluid tailings (FFT) can be processed using flocculation to separate water from the tailings by adding polymer to a coagulant treated FFT. Variations of this process are in use at the Suncor and Imperial surface mined oilsands operations. At the Syncrude oilsands facility this process is called Floc-T. The degree of flocculation in the FFT, and the effectiveness of the dewatering process, are determined by the polymer dosage and how well it is mixed. Presently the performance of the Floc-T process is measured using capillary suction time (CST) tests roughly every three hours, so adjustments to the process can be made. Using online microscopy imaging technology to determine the performance of the flocculation process allows for adjustments to be made more frequently in response to changes in the FFT feed. Computer analysis of the optical images is used to determine key statistical quantities such as the median brightness and the inter-quartile range, which can be correlated with FFT feed and mixing parameters and ultimately used to control the polymer dosage and mixing conditions. Unlike the CST test, the image analysis gives a direct assessment of the degree of flocculation independent of the feed density. The microscopic image analysis therefore provides a real-time assessment of the mixing and flocculation in the FFT, without the need for sample testing, allowing for a rapid response to changes in the FFT feed. Results from full-scale commercial application of the technology are presented along with a strategy for automation.

Introduction

The Syncrude Floc-T process involves mixing polymer into the fine fluid tailings (FFT) to flocculate or clump the solid mineral particles together, allowing easier separation of the solids and the water. For this process to work effectively, the polymer dosage needs to be correct, and it needs to be sufficiently mixed into the FFT. Figure 1 shows a schematic of the Floc-T process as operated at Syncrude. The residence time tank shown was used in the pilot testing, but not in the commercial operation since there is enough pipeline

residence time to ensure proper coagulant treatment of the fluid fine tailings. Since the polymer used is a significant cost, optimizing this process involves keeping polymer dosages as low as possible as well as ensuring the FFT is properly flocculated. The current procedure for measuring the effectiveness of the process involves taking samples at regular intervals and measuring the capillary suction time to determine how easily water drains from the sample. This does not allow for rapid changes in the process to be made to account for changes in FFT feed that could vary significantly between sampling intervals. Using an on-line imaging device to take pictures of the FFT in the pipe can inform operators of real-time changes to the FFT mixing and flocculation without relying on sampling.

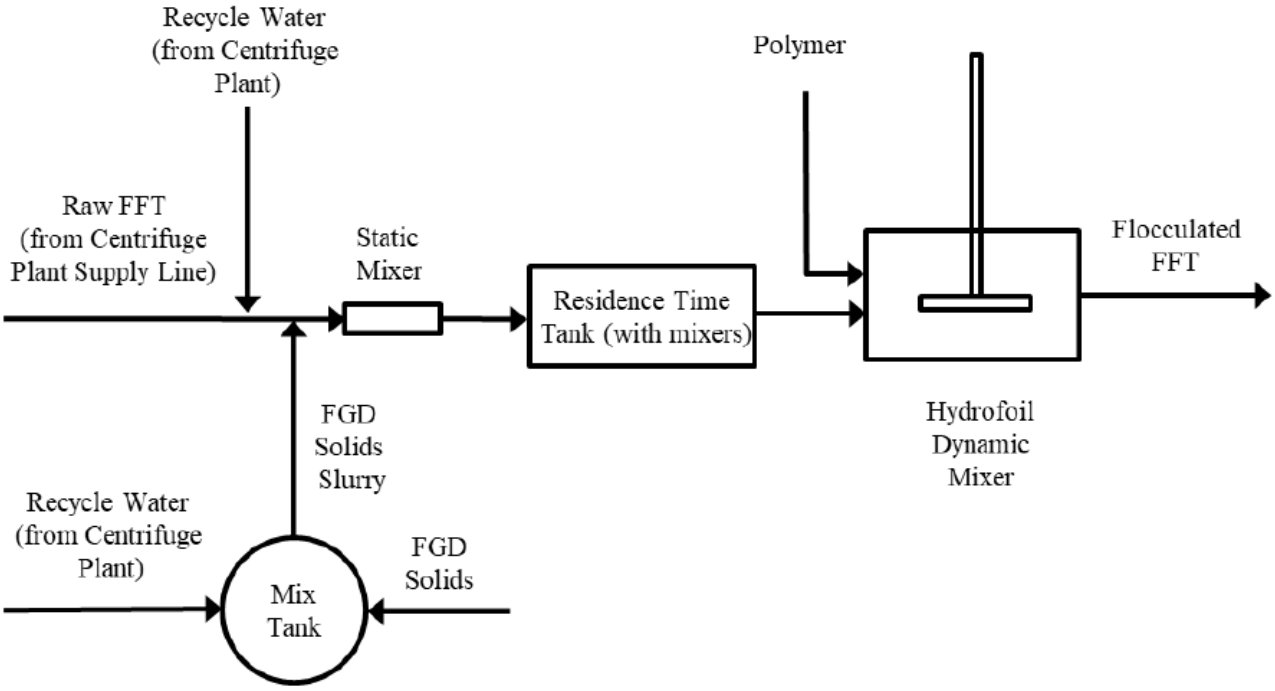


Figure 1: Schematic of the Floc-T tailings treatment process at Syncrude

The image capture system used for the Syncrude Floc-T process testing was a Mettler Toledo PVM system. This has the capability of automated illumination to maintain consistent image brightness, or the option of fixed illumination. Images can be captured and stored in files that can be accessed to perform the necessary image analysis to quantify the degree of flocculation. The image time interval can be modified to match the process dynamics or process response time. The probe was mounted approximately 15 m downstream of the in-line dynamic mixers and perpendicular to the flocculated FFT flow. The probe in the PVM is a 19 mm steel tube approximately 40 cm in length with a sapphire window in contact with the FFT flow. The optical system is controlled by a head unit at the end of the steel tube. The head unit is connected to a power supply and image acquisition unit by a fiber optic cable about 3 m in length. The power supply and image acquisition unit is in turn connected to a laptop computer for image output and general system

control (illumination level, image capture interval etc.). The power supply, optic control unit and associated laptop computer were housed in a weatherproof enclosure, while the probe was mounted on the pipe and exposed to the elements. It is important to note that the probe was left in place throughout the three-month program and there was never any evidence of blinding or contamination of the optical window.

In the images, brighter regions represent higher solids concentrations and dark regions represent water. A well flocculated sample will show clumps of solids separated by water, while poorly flocculated samples will appear more homogeneous. Previous work with imaging of FFT has shown that there is a clear difference in the distribution of pixels in images of FFT depending on the level of flocculation in the sample. Figure 2 shows an image with poor flocculation, along with the distribution of pixel brightness. Figure 3 shows a sample with good flocculation along with the distribution. The average and inter-quartile range (IQR) of each distribution are indicated.

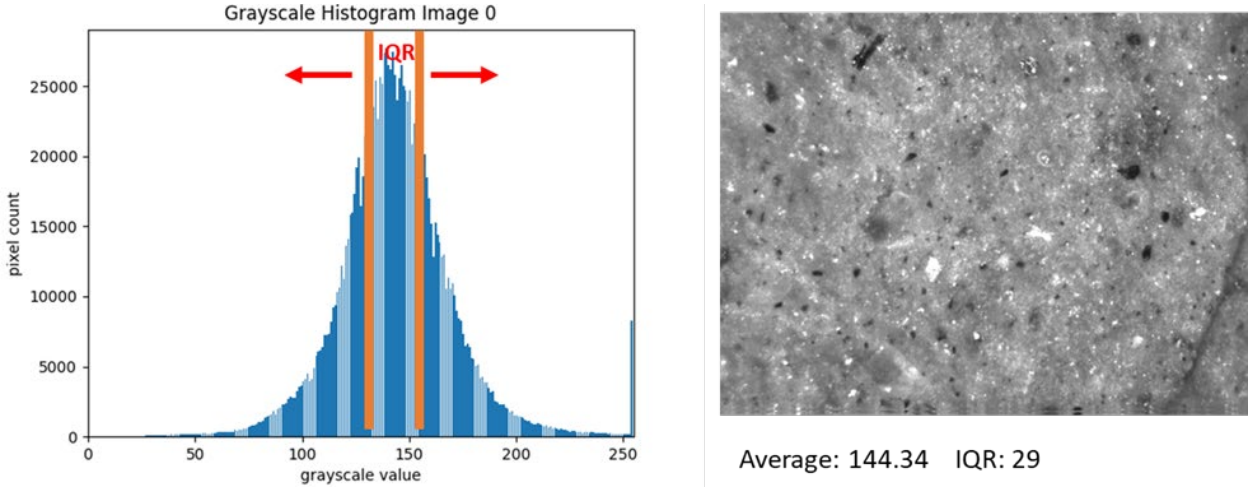


Figure 2: Image and pixel distribution for well flocculated MFT

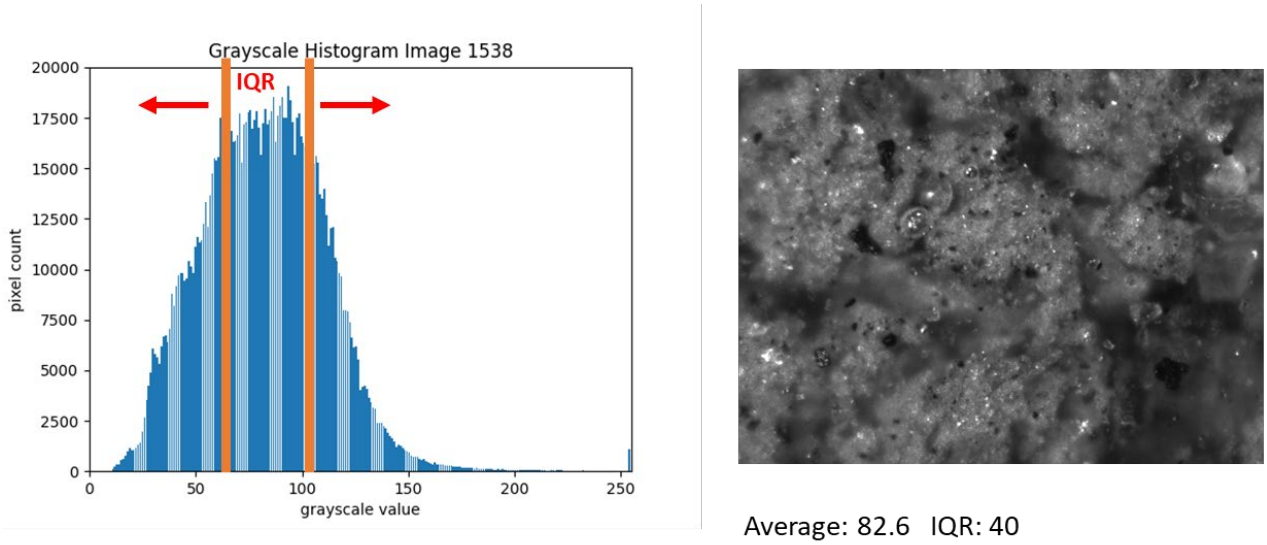


Figure 3: Image and pixel distribution for ideally mixed polymer and MFT

The analysis of images collected during the Floc-T process allows for real time adjustments to mixing and polymer dosage that can optimize the process without relying on infrequent CST testing. Furthermore, it represents a significant improvement over other proposed methods for on-line process monitoring. Previous suggestions for controlling the flocculation process involve near infrared spectrometers and density gauges to determine clay content and therefore polymer dosage, as well as instruments to measure flocc size (Junaid, 2020). All this complication is avoided with this direct assessment of the degree of flocculation using image data.

Results and discussion

PVM images were collected on train 1 in Syncrude's Floc-T process plant for 11 different intervals between September 14th and 25th. Most of the data was collected while changes were being made to the mixing speed, to see the effect of mixing on the PVM images. The 11 intervals (or runs) are labelled A through K in chronological order. This study will only discuss intervals B, C, and D in detail; the results of the other intervals agree with what is found in those three. During each of these intervals changes were made to the mixer speed, resulting in changes to the degree of flocculation observed.

The two quantities used to describe the image pixel distributions are the median brightness and the IQR. The median is an indicator of the overall brightness of the image, and the IQR is an indicator of the width of the distribution. Data from the Floc-T process (mixer speed, flow rate, etc.) is collected roughly every 10 seconds while images are taken as fast as twice a second in some cases. In order to match images with process data, a linear interpolation is used between pairs of data points. In this report, the FFT density and the mixer speed are compared with median brightness and the IQR from the images.

This section will highlight the important features of the imaging data. To reduce some of the variability in the imaging data, the charts in this report plot the data as a 20-point running average. For the runs considered here this is an average over 10 seconds, which is the same interval over which most of the flocculation process data is collected. The first run considered is run B, where images are collected with a variable brightness gain determined by the PVM software.

Figure 4 shows how the median brightness compares with the mixer speed over the run, and Figure 5 shows how the median brightness compares with the density over the run. Figure 6 shows the IQR and the mixer speed during the run. The important part of this run is the changes to the mixer speed, which starts at 30% of the maximum (roughly 525 RPM), then is dropped to 0, and increased by 10% of the maximum in 1-minute intervals up to 70%, then decreased in the same intervals back to 30%.

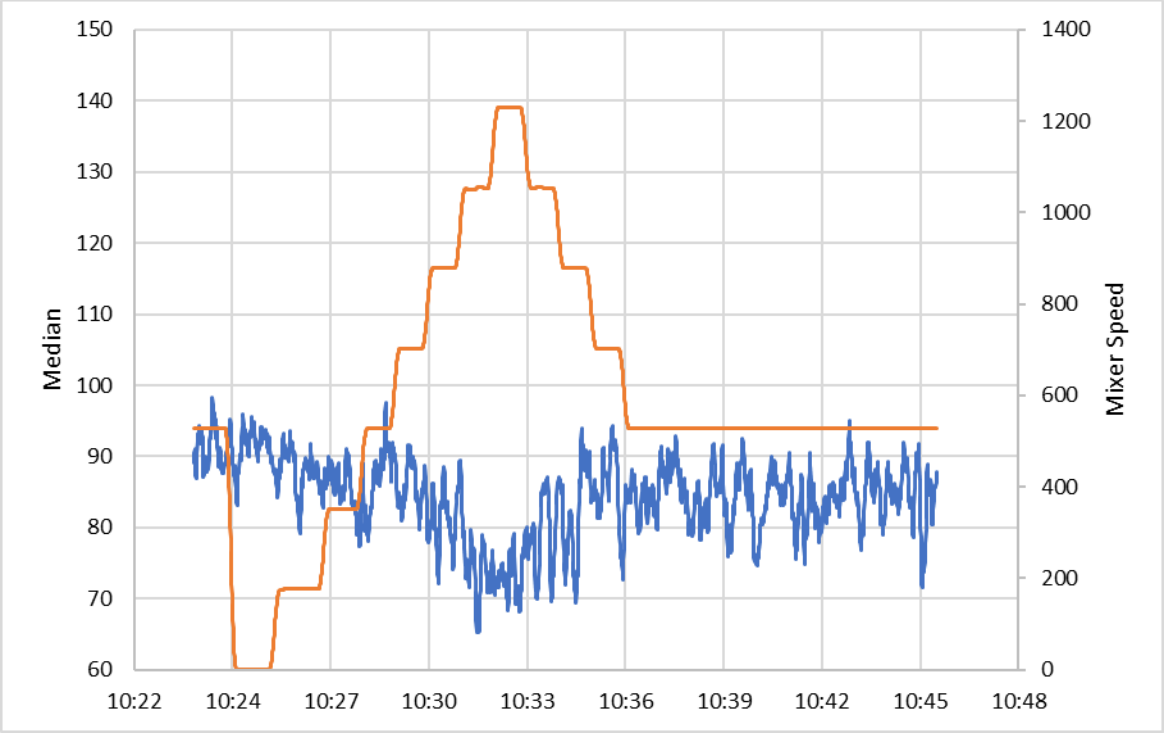


Figure 4: Median brightness (blue) and mixer speed (orange) for run B

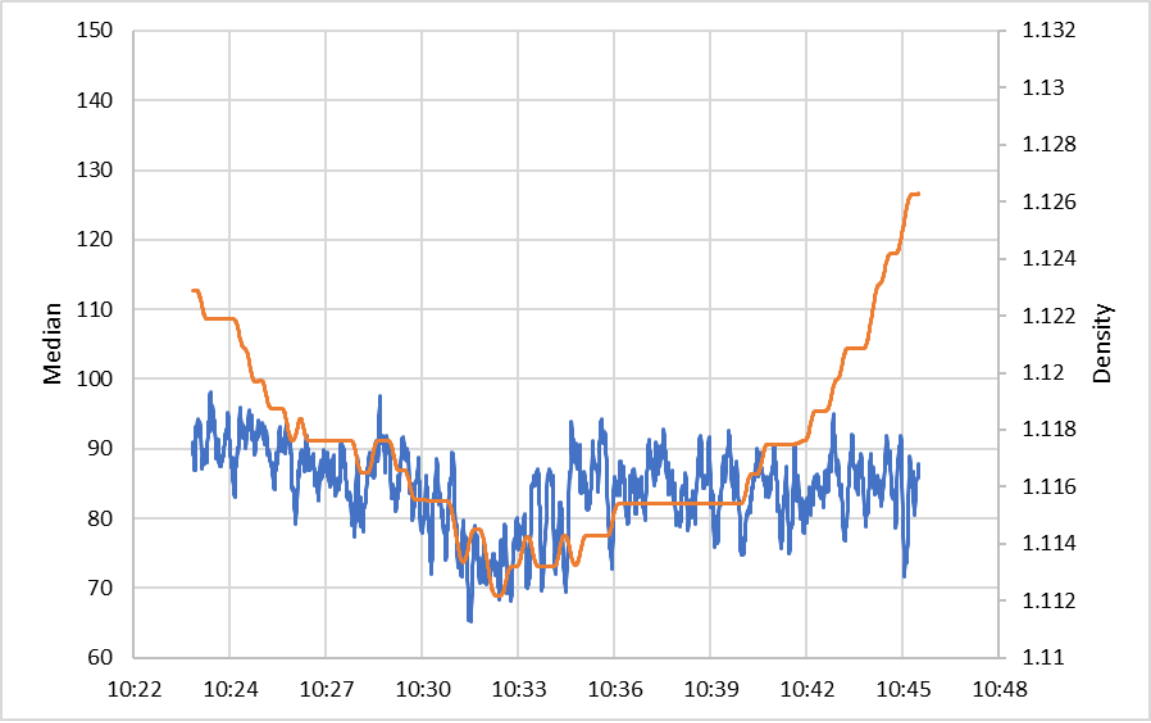


Figure 5: Median brightness (blue) and density (orange) for run B

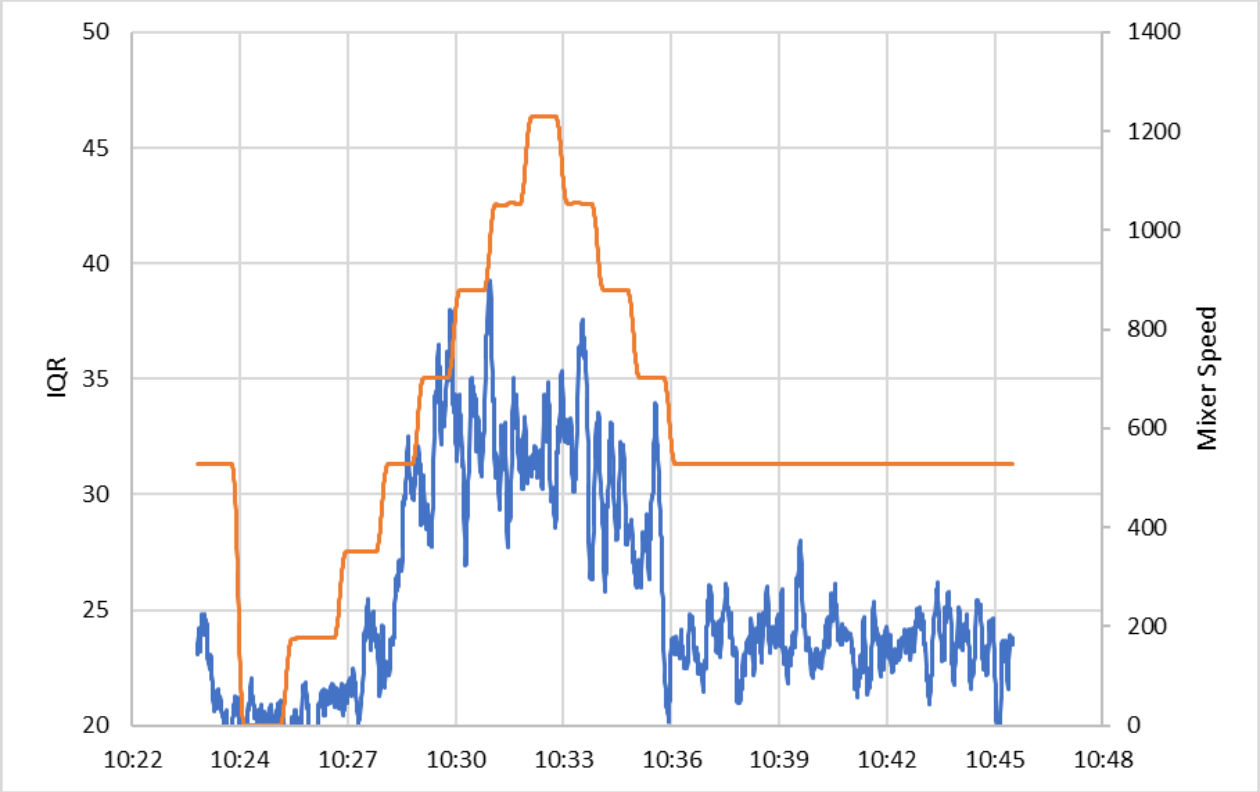


Figure 6: IQR (blue) and mixer speed (orange) for run B

Figure 4 shows only a slight dip in the median brightness during run B despite the changes to the mixer speed and density. The lack of change in the median brightness for run B is due to the PVM imaging software applying a variable gain to the images. For all the runs after A and B, a fixed imaging gain was used so that changes in average brightness could be observed in the images, which might better reflect changes in flocculation. Despite the variable gain, the width of the distribution as measured by the IQR still correlates with the mixing speed. Increased mixing leads to a wider distribution of brightness in the image, indicating better flocculation. It is also worth noting that the IQR representation of flocculation was also sensitive to the flocculation differences at low mixer speeds.

During run C, a similar test with the mixer speed is performed, with the speed increased by 10% increments from 0% up to 70% of the maximum speed, then back to 0. For this run the mixer speed begins and ends at 20% (roughly 350 RPM), and the PVM images are collected with a fixed gain. Figure 7 and Figure 8 show how the median brightness and IQR vary with the mixer speed. In addition to showing changes to the median brightness, fixing the gain has also reduced the variability in both the median and IQR from image to image.

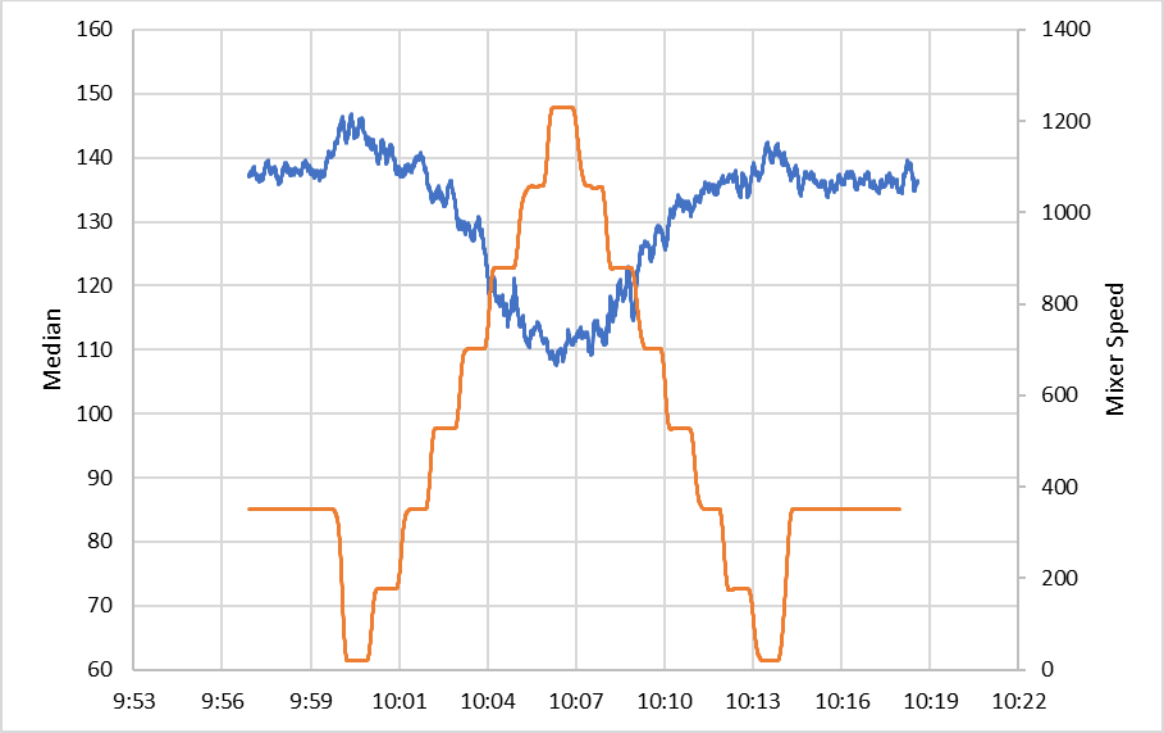


Figure 7: Median brightness (blue) and mixer speed (orange) for run C

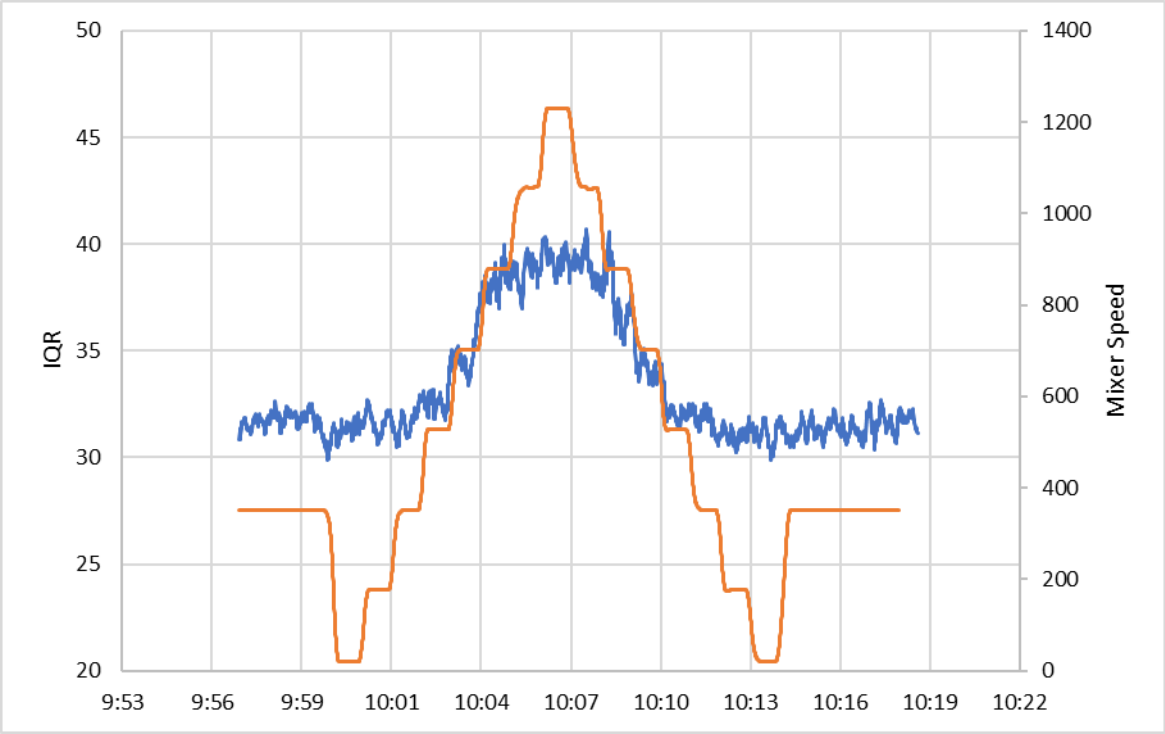


Figure 8: IQR (blue) and mixer speed (orange) for run C

From Figures 7 and 8, the effect of the mixing speed on the median and IQR image data suggests that the flocculant mixing performance can be improved by increasing the mixing speed. Figure 7 shows an obvious effect of the mixing speed on the median brightness compared to Figure 4 with variable gain. Lower median brightness (darker image with more water) and higher IQR (a wider distribution is a less homogeneous image) are both indicators of improved flocculation performance. In Figure 8, there is no significant effect on the IQR from reducing the mixer speed to 0; this is due to the short time period for the changes to mixer speed. For this run the IQR levels off once the mixer speed reaches 50%. This suggests that in this case optimal mixing has been achieved, and even higher mixing speeds may lead to overmixing and decreased flocculation performance.

Like the previous runs, run D also features significant changes to the mixer speed throughout; however, during run D the changes in the feed density are also significant. Figures 9 and 10 show the median brightness and IQR respectively along with the density throughout the run. Figures 11 and 12 show the median brightness and IQR respectively along with the mixer speed during the run. Although most CST data is collected every three hours, during run D CST tests were conducted at three different times, corresponding to different mixing speeds. The results of the CST tests for this run are indicated on Figure 12 and summarized in Table 1, which shows clear variation in the CST as the mixing speed changes.

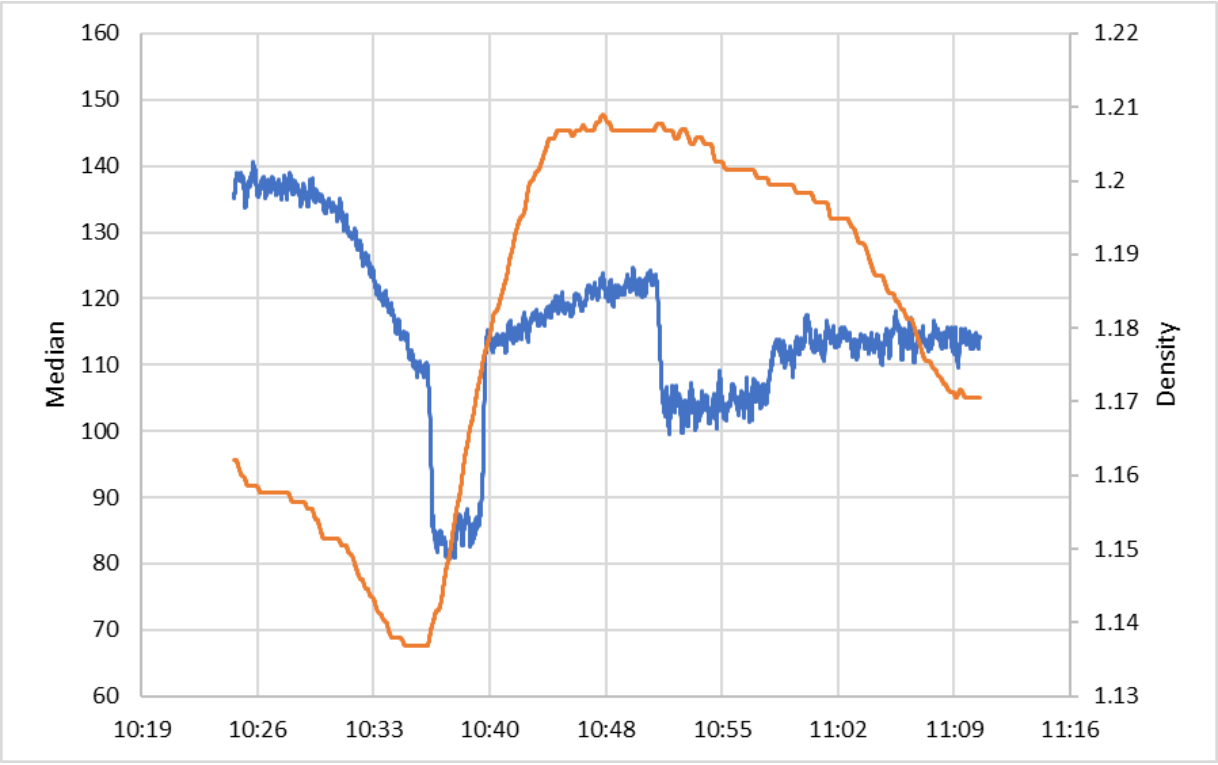


Figure 9: Median brightness (blue) and density (orange) for run D

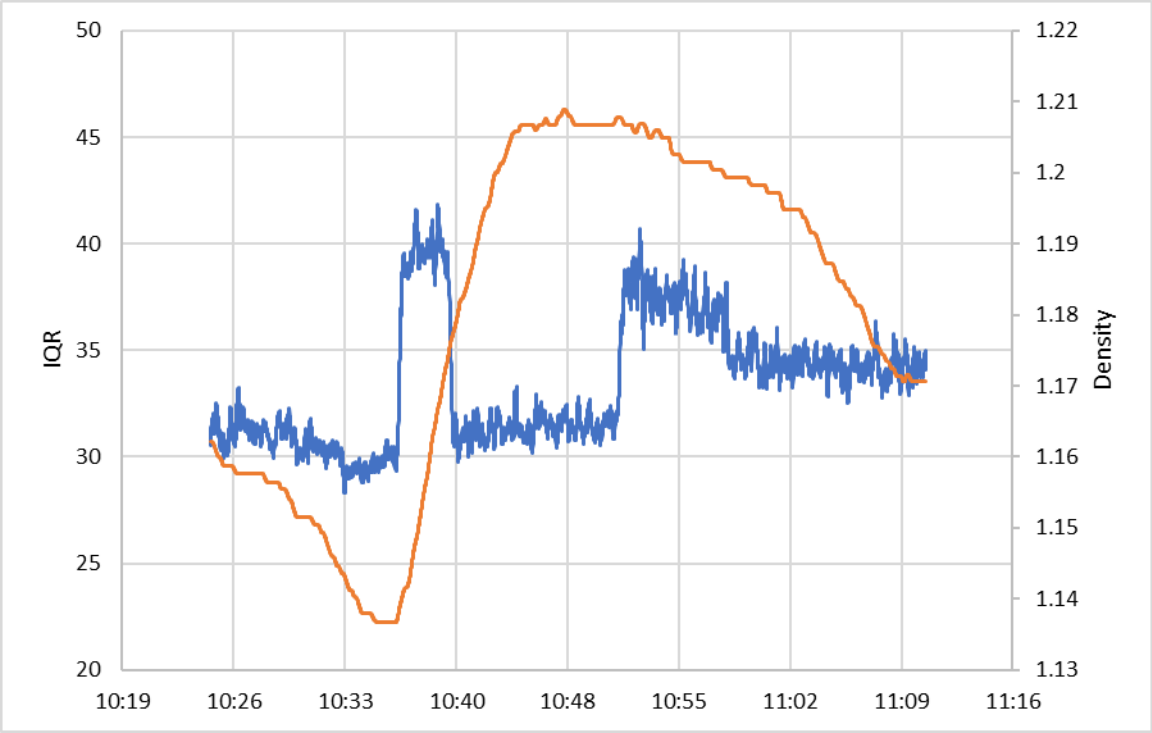


Figure 10: IQR (blue) and density (orange) for run D

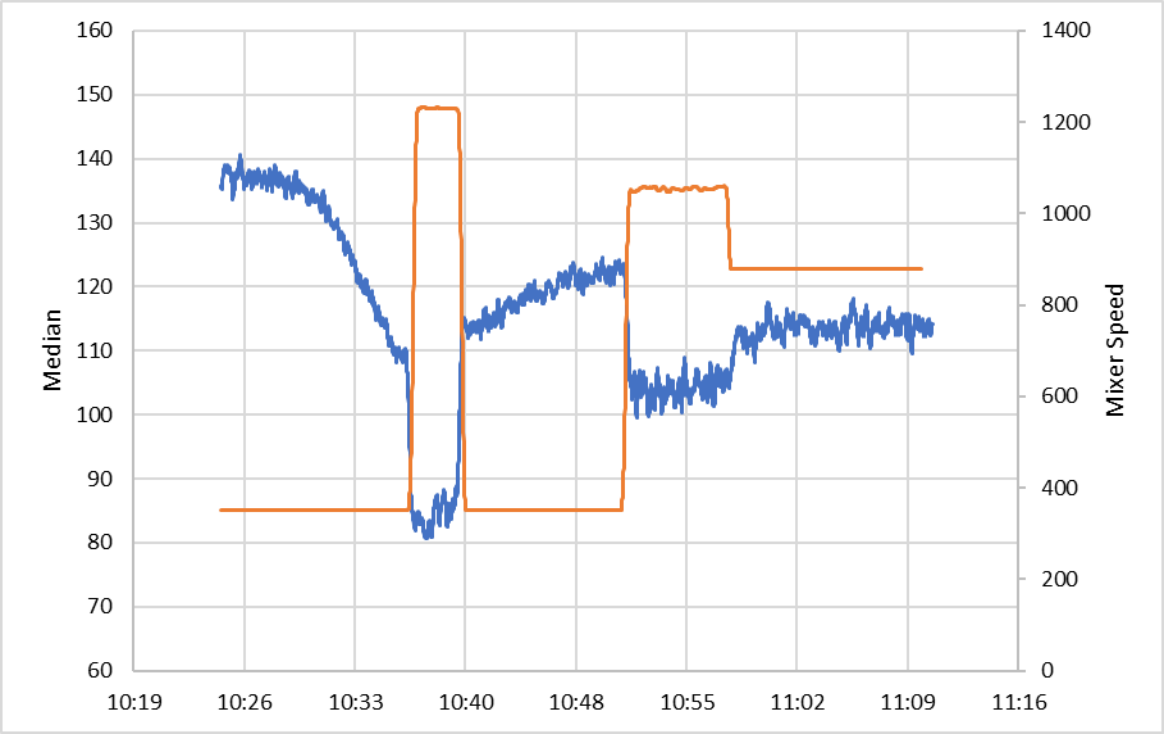


Figure 11: Median brightness (blue) and mixer speed (orange) for run D

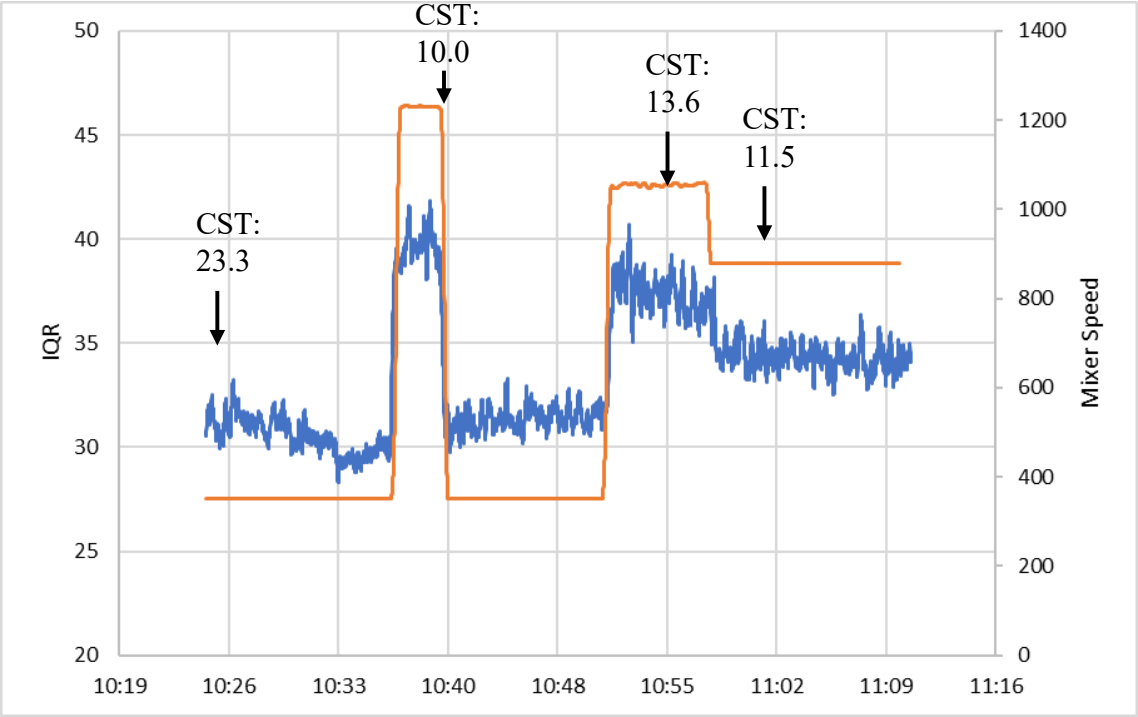


Figure 12: IQR (blue) and mixer speed (orange) for run D, with CST values

Table 1: CST data for run D

Time	Mixer speed	Average CST
10:25	20%	23.3 s
10:40	70%	10.0 s
10:55	60%	13.6 s
11:00	50%	11.5 s

In Figure 9 the effect of the density variations on the median brightness can be clearly seen at the start of the run before the mixer speed begins to change; however, the IQR does not change significantly with the density, as shown in Figure 11. Although lower density will typically result in a lower CST, the feed density is outside of the operator's control and this lower CST does not necessarily represent improved plant operation. Since the IQR does not significantly change with density, changes to the IQR are a better representation of changes to the flocculation in the FFT, which can be optimized through control of polymer dosage and mixer speed by the operator.

This result is extremely important since it shows that the IQR representation of the sample image is independent of FFT density. Figure 13 shows sample images corresponding to each of the recorded CST values over the run.

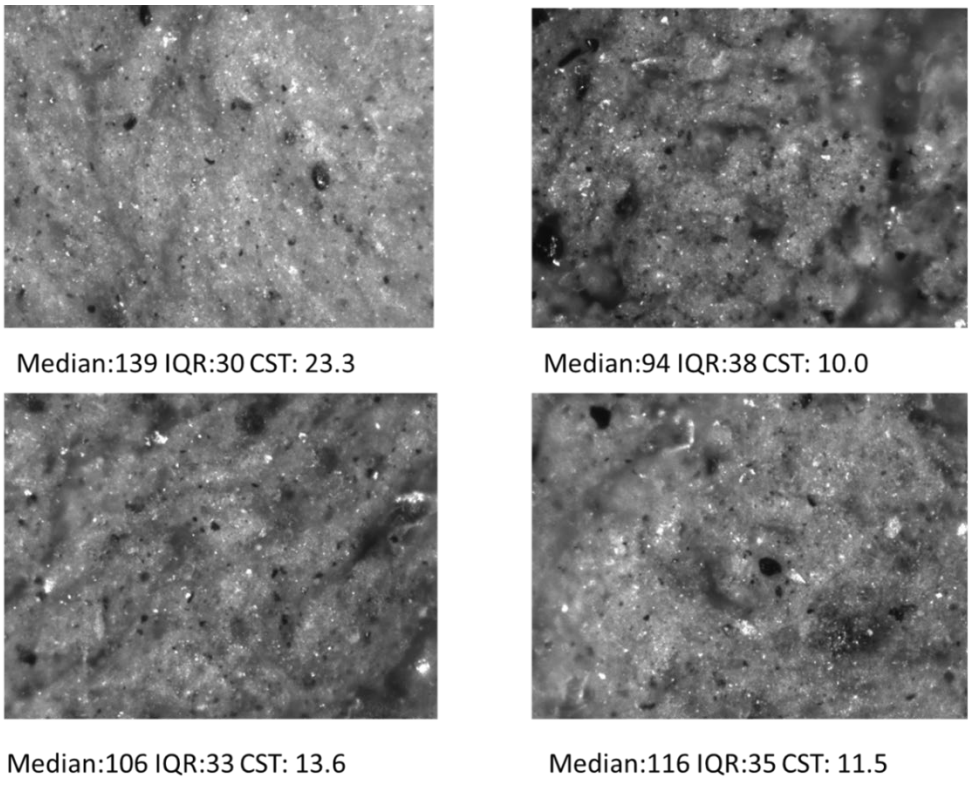


Figure 13: Sample images corresponding to each recorded CST value

Process or flocculation optimization is determined by establishing the lowest possible CST value, and this is challenging when the density is changing because lower FFT density will result in a lower CST. The link between CST and density can then cloud the optimum mixing and polymer dosage. Using the IQR data from the image allows for optimization of the flocculation independent of FFT feed density.

Conclusion

The PVM image analysis provides an on-line method for measuring Floc-T performance that could allow for changes to the process to be made in real time to optimize performance. The main feature of the PVM images that correlates with the flocculation in the FFT is the width of the distribution of pixel brightness, which can be quantified using the IQR. Reducing the images to a single number (the IQR) allows for the development of simple algorithms to guide (or eventually automate) control of the mixing and polymer dose. These types of algorithmic process controls could also be used to reduce overall polymer usage without negatively impacting the flocculation mixing performance.

References

Junaid, A. et al. 2020. Method of Dewatering a Tailings Stream. Canadian Patent 2 937 452, filed July 28, 2016, awarded Dec 15, 2020.

Reducing Mine Closure Cost Risks by Employing Effective Construction Management Strategies

Michael Nahir, Parsons Inc., Canada
Marie Rousseau, Parsons Inc. Canada,
Geoff Karcher, Crown Indigenous Relations Northern Affairs Canada, Canada

Abstract

Mine closure projects have several complex and multidisciplinary construction activities. Typically, these include construction of water treatment plants, tailings and waste rock covers, diversions, development of landforms, demolition and disposal, excavation, and remediation of contaminated soils. Managing these construction works, often in remote areas, is complex with very significant costs and schedule risks. Most large civil projects employ staff with construction management expertise, which is recognized as an important skill set to drive project goals and reduce costs and schedule risks.

Driven by the goal of averting such consequences and risks, our paper aims to present strategic and proven approaches for effective project execution. Using recent experiences and a case study, the authors wish to offer comprehensive insights into the intricacies of managing mine remediation and closure projects. Examples of tailored strategies that will be discussed are the critical role of logistics and supply chain management, adaptive scheduling methodologies, constructability assessments, workforce safety and equipment resilience in extreme climates, the functional delineation of roles within the construction management team and the importance of aligning contractor expertise with the unique challenges presented by remote projects. We examine the seasonality of work in remote regions, delving into the types of tasks feasible under varying climatic conditions and the optimal sequencing of these activities. The construction manager is primarily responsible for delivering on the objectives of the owner.

Construction management

After completion of site assessments, options analysis and preliminary design, it is time to start planning for the implementation of the mine site remediation and closure works. A construction project is defined by having a scope, schedule and a budget. Of primary significance is to ensure that the objectives of the client are met in all aspects of the project delivery. The scope of the project is determined by the design team using science and engineering principles to solve problems. However, the project must be constructable.

The importance of constructability requires that the designers work collaboratively with the construction managers to ensure that the work is feasible to implement. Feasibility is not only determined by schedule and budget but also by adherence to building codes, safety requirements, and labor compliance.

Construction management is a specialized field within the construction industry that involves overseeing and coordinating all aspects of a construction project from inception to completion. It encompasses a wide range of activities and responsibilities aimed at ensuring that projects are completed on time, within budget, to the required quality standards, and meeting other expectations required by the owner. The following sections highlight key aspects and considerations for construction management in mining remediation and closure projects including a Case Study on the Faro Mine Remediation Project, Yukon Canada, North Fork Rose Creek Diversion Project.

The following are key aspects of construction management:

- **Project Planning and Development**: Construction managers are involved in the early stages of a project, working with clients, engineers, and other stakeholders to develop project plans, establish goals and objectives, and define project scopes. They help create realistic timelines and budgets, taking into account factors such as site conditions, regulatory requirements, and client preferences. In all cases a Project Execution Plan is prepared to layout the project and the processes.
- **Budgeting and cost control**: Construction managers are responsible for managing project budgets and controlling costs. They develop cost estimates, track project expenses, and monitor financial performance throughout the project lifecycle. They identify potential cost overruns, implement cost-saving measures, and ensure that the project stays within budget.
- **Scheduling and sequencing management**: Construction managers create project schedules, set milestones, and sequence activities to ensure that the project progresses according to plan. They monitor progress, identify potential delays, and implement strategies to keep the project on schedule. They also manage critical paths and prioritize tasks to optimize project timelines.
- **Design integration and constructability**: Construction managers are brought in to review the project design at key milestones. This is to reduce the likelihood of constructability or omission surprises and subsequent change orders at the construction stage.
- **Resource management**: Construction managers oversee the allocation of resources such as labor, materials, equipment, and subcontractors. They ensure that resources are used efficiently and effectively, coordinating deliveries, managing subcontractor relationships, and resolving resource conflicts as they arise.
- **Quality assurance and control**: Construction managers are responsible for ensuring that work is performed to the required quality standards and specifications. They conduct quality inspections,

enforce quality control measures, and address any issues or deficiencies that arise during construction. They also monitor compliance with building codes, regulations, and industry standards.

- **Safety management**: Construction managers prioritize safety on the job site and implement safety protocols to protect workers, subcontractors, and the public. They develop safety plans, conduct safety training, enforce safety regulations, and investigate accidents or incidents to prevent recurrence.
- **Communication and stakeholder management**: Construction managers serve as the primary point of contact for the main stakeholders involved in the project. They communicate project updates, address concerns, resolve conflicts and effectively manage interactions to ensure that all parties are aligned and informed throughout the construction process.
- **Risk management**: Construction managers identify, assess, and mitigate risks associated with the project. They anticipate potential challenges, such as weather delays, supply chain disruptions, or labor shortages, and develop contingency plans to minimize their impact on the project.

Overall, construction management requires a combination of technical expertise, leadership skills, communication skills, and project management capabilities. Construction managers must possess strong communication, problem-solving, and decision-making skills to effectively manage all aspects of the construction process and deliver successful projects.

The complexity of mine remediation and closure construction

Mine remediation and closure projects are typically multi-year and multimillion dollar projects with high cost and schedule risk. Designs are often based on imperfect assessments where a hundred percent characterization is nearly impossible. As a result, there is significant uncertainty in the extent of the mine waste issues such as volumes and depth as well as subsurface and hydrogeological conditions. Surface water management is also based on projections that are changing with changing climate estimates.

Coupled with design uncertainty is construction uncertainty and risk. As risks increase so does the potential for large cost increases and schedule slippage. Table 1 describes the multidisciplinary aspects of the various remediation and closure components, typical solutions and construction methods involved in mine remediation and closure. The sequencing of various trades and specialties requires a high degree of coordination and management. In the construction industry the construction manager is responsible for this aspect of the work.

The standard of mine remediation and closure has increased in the recent past and as a result the construction standard is higher. Early days of mine closure entailed simple solutions like waste

consolidation and basic soil covers. Whereas today's designs are science based with detailed engineering of complex solutions such as hydraulic designs of diversions, multilayered cover systems and water treatment plants. The role of the construction manager is now seen as an important way to reduce costs and schedule risks.

Table 1: Mine closure components, closure options and construction skill sets

Closure component	Example closure options	Construction skill sets
Underground workings	Seal the openings Flood Fill with tailings/waste rock	Concrete Piping Mechanical Conveyance Electrical Pumping
Open pits	Berms Fill with water Fill with tailings/waste rock	Heavy civil Piping Mechanical Conveyance Pumping
Rock and overburden piles	Shape Shape and simple cover Shape and complex cover Relocate to pit	Heavy civil Surveying Liners Conveyance Hydraulic monitoring
Tailings impoundments	Upgrade dams Simple cover Complex cover Revegetate	Expert civil Heavy civil Surveying Liner placement Conveyance Hydraulic monitoring Revegetation
Water management and treatment facilities	Diversions WTP Passive treatment Groundwater collection Surface water collection	Heavy civil Instrumentation Operations Electrical Mechanical Structural Drilling Well installation Pumping Piping
Buildings and equipment	Resell Demolition	Heavy civil Hazardous material removal

Closure component	Example closure options	Construction skill sets
	Nonhazardous landfills	Liner placement Surveying
Wastes, hazardous materials, and contaminated soil	Onsite treatment of contaminated soils Offsite disposal of contaminated soils Onsite disposal of hazardous materials Offsite disposal of hazardous materials	Bioremediation Hazardous soils Heavy civil Liner Placement Surveying
Infrastructure	Resell Onsite disposal	Heavy civil Liner placement Surveying
Environmental Monitoring	Applies to all components	Environmental science

Remote construction risks

Construction management risks in mine closure projects like the Faro Mine are significant due to their complexity and environmental impact, particularly in remote settings.

Remote work locations are characterized by their physical or geopolitical isolation, resulting in labor, materials, plant, and communication risks. The availability and accessibility of human resources are major factors that pose challenges to organizations attempting to manage projects in remote settings effectively. Figure 1 shows an example of a logistical challenge associated with remote work in northern regions.



Figure 1: Subcontractor welding ice cleats on excavator in the winter

Remote construction sites, such as the Faro in the Yukon Territory, are subject to higher risks than those located in well-developed areas. These risks include extreme working conditions that can negatively impact productivity and make it difficult for off-site management staff to track workforce productivity.

Additionally, remote teams may take advantage of the situation, leading to inefficiencies and cost overruns. Faro is known for its harsh weather conditions, which can include long and cold winters with temperatures dropping as low as -40°C (-40°F) and very short summers with temperatures ranging from 10°C to 20°C (50°F to 68°F). See Figure 2. The area also experiences heavy snowfall and strong winds during the winter months. Snow can be expected from around end of September / beginning of October until mid-April. Winter daylight hours are short, as they range from 4.5 hours in December to 15 hours in April. These extreme conditions can pose significant challenges for workers and construction projects in the area and the picture below provides an example.



Figure 2: Subcontractor working in the dark and the cold

Remote projects are also vulnerable to unexpected weather conditions, geological factors, and natural disasters. The 2023 wildfires in Yellowknife are an example of a natural disaster affecting a remove site and delaying construction at Giant Mine.

Communication can be challenging at remote sites due to limited cell service and Wi-Fi coverage. Time-sensitive decisions may also be delayed due to physical distance and communication challenges.

Remote sites are often far from law enforcement and emergency services, which can increase response times in emergencies. Workers may also have difficulty communicating for help due to poor mobile signal or data coverage.

Logistics can represent a significant challenge due to underdeveloped road infrastructure, limited local suppliers, harsh weather conditions, and poor communication and coordination. This leads to longer lead times for deliveries at site that must be planned accordingly.

Security risks include theft and vandalism due to a lack of constant supervision or surveillance options. Harsh weather conditions and wildlife can also pose unique security challenges.

In addition to these risks specific to remote sites, typical construction management risks include occupational health and safety hazards such as exposure to hazardous materials like zinc and lead in Faro; ensuring adherence with environmental laws; managing contaminated soils; implementing appropriate remediation and closure techniques; addressing community concerns; obtaining necessary approvals including from affected First Nations and dealing with bureaucracy.

Effective risk management requires meticulous planning, robust monitoring, adaptive strategies that mitigate multifaceted challenges ensuring successful sustainable mine closure projects. Strategies to mitigate project risks. Figure 3 shows the CM managing risks associated with specialized skill sets.

Aside from technical challenges, the owner's objectives often include the socio-economic needs of a project which provide benefits to the local communities including the indigenous peoples. Having an adequate supply of trained labor and construction resources is often limited and add a degree of uncertainty.



Figure 3: Installation of transformer supported by CM experts

Mitigating construction risks

While planning and managing construction risks, the CM considers a number of factors that will affect the success of the closure project. These factors are described below.

Skilled workforce management at site

In remote construction projects, having a 3rd party entity on site 24/7/365 to provide care and maintenance, procurement, and construction management services on behalf of the client is essential. To maintain high productivity and quality, it is necessary to recruit and retain skilled workers, on rotation, while providing ongoing training. Project progress and overall performance by subcontractors are closely monitored, no matter what the expertise required.

Construction maintenance in a remote location requires a team at site that includes a director, project managers, project coordinators, a quality manager, superintendents, inspectors. Adequate accommodation, transportation and welfare facilities for workers on remote sites are also provided. For example, an older hotel facility was purchased along with some housing at the Town of Faro and there is also a work camp at the mine site.

Service level agreement

Detailed and comprehensive Service Level Agreements are a useful tool that are often developed by a CM in collaboration with the client. The purpose of these agreements is to define the overarching principles of the relationship between CM and client, the vision, roles and responsibilities, and the exercise of decision-making authorities with respect to the delivery of specific work packages.

They include agreements on subjects like: Submittals, RFIs, Shop Drawings, Change Management, Quality Management, Commissioning, Reporting, As-built drawings.

Comprehensive planning and risk assessment

The CM conducts thorough constructability and risk assessments before executing every single work package, to identify potential issues early. The CM goes through the process of identifying every possible threat that creates potential loss exposure for our client, categorizes them and assesses the impacts. Detailed cost estimates are prepared for budget and procurement management. The CM develops project plans, including mitigation measures and contingency plans for those risks we identify.

Technological integration and innovation

Advanced technologies such as drones, GPS, aerial mapping, a construction management software (Kahua) and AI technology are in use at the Faro Mine Complex for better oversight in this remote location. The project team is also getting ready to implement remote monitoring systems to track progress and detect

issues promptly. Examples of innovation recently used include:

1. The CM, the owner and their Engineer of Record, and subcontractors use project management software for efficiently managing construction. The CM often has their own project management software and offers a sophisticated construction management tool for the delivery of all work packages.
2. Drones are used for dam and pit inspections and photogrammetry.
3. The software Propeller Aero is used, which offers cutting-edge drone technology and data solutions for construction. This tool is used for aerial mapping, data capture and analysis and surveying. Propeller brings real-time precision and efficiency to work packages at the Faro Mine Site.
4. The OpenSpaceAI Enterprise system and software are used for construction supervision, as-built drawings verification, quality reviews and project audits.

Procurement

One of the critical CM functions is the procurement of subcontractors to execute work packages. The CM works to identify and put in place the right tendering process and contractual arrangements. This work starts well in advance of the contract start date to make sure the design and procurement are well prepared and tested.

For most work packages, the CM conducts online bidders meetings to reduce cost and time commitment. Meetings include drone footage and photography. For complex and high risk work it is necessary to bring contractors to site.

The CM conducts frequent quality assurance inspections and audits to ensure compliance with the requirements set out in the plans and specifications.

Regulatory compliance management and environmental protection

The CM must ensure regulatory compliance on site at all times. Commonly the CM will have an environment team which overseas that all the environmental requirements are met. This could include all the monitoring of water and air as dictated in environmental permits. If there are water treatment plants, then discharge criteria must be met. Reporting requirements are tracked and adjustments made to meet compliance.

The CM is required to inspect, monitor, and document any environmental impacts should they occur. They also assist in adjusting practices to minimize harm. For subcontracts, the environmental team ensures to provide a detailed orientation to all new staff scheduled to work at site and their work is inspected daily to ensure compliance.

Budget and financial management

Budget and financial management is critical for the success of any construction project, particularly in remote locations such as the Faro Mine. To ensure that budgets are managed effectively, detailed work breakdown structures (WBS) are developed and agreed upon with subcontractors for each work package. This allows for a clear understanding of the scope of work and associated costs, enabling accurate budgeting and cost control.

Monitoring expenses closely is also essential to avoid overruns. This involves tracking actual costs against budgeted costs on a regular basis to identify any discrepancies and take corrective action as needed. Upon written approval, adjustments may be made to budgets based on changes in scope or unforeseen circumstances that impact project costs.

Change happens. Particularly in mine remediation and closure there are many site components which are uncertain due to the limitation of assessments. Costs are very sensitive to volume estimates such as in cover material and borrow sources. Due to these assessment limitations appropriate contingencies must be rationalized and budgeted. The change control process must be transparent and timely in order to avoid further costs due to work stoppage and extended review of unacceptable invoices. As a best practice the CM meets with the owners representatives and the subcontractors on a regular basis to ensure smooth and efficient account management.

In addition to WBS development and expense monitoring, effective budget and financial management at the Faro Mine Site also involves establishing clear communication channels with all stakeholders involved in the project. This includes regular reporting on project progress, financial performance, and any issues or risks that may impact budgets.

Community and stakeholder engagement

The project team engages with local communities and stakeholders to better understand their interests and expectations for the project. To meet owner's socio-economic objectives the CM may do a market study to evaluate the labor supply and required skill sets for the project are locally available. Based on the study specific objectives can be determined and built into the procurement plan. To give local community's contractors time to plan for major works, the CM presents their master schedule at community sessions. Feedback from the community is important to validate resource assumptions.

Supply chain and logistics optimization

Reliable supply chain strategies are essential for managing the timely delivery of materials and equipment in remote construction projects. To this end, agreements are required for deliveries of various supplies such as water treatment lime, diesel, gasoline, drinking water, spare parts, and other critical items. Local supply chains are also utilized where possible to reduce dependency on distant suppliers.

To ensure appropriate testing and quality assurance prior to shipping to the sites, the CM will visit suppliers and plants where infrastructure is fabricated for construction purposes. This approach eases logistics planning and helps to ensure that materials meet required standards. For instance, the CM's quality manager may visit an office complex trailer manufacturer before trailers are shipped to the site to better evaluate construction approach and adherence to specifications.

Health and safety protocols

Stringent health and safety protocols have been implemented to protect workers. There is also a detailed process for site access by visitors, and for consultants and subcontractors planning to work at sites. The CM provides regular safety training and ensure access to medical facilities and emergency services.

Case Study: Faro Mine Remediation Project, North Fork Rose Creek Diversion Project

The Faro Mine Site, referred to as Tse Zul by the local Indigenous community is located approximately 15 km from the town of Faro Yukon, and is within the traditional territory of the Kaska Nation. The Ross River Dena Council is located approximately 90 km from the site and is the closest Kaska community. The Faro Mine site is in a remote area approximately 4 hours from the City of Whitehorse. The mine ceased operation in 1998 having once been one of the largest lead zinc mines in the world. It is considered one of the most complex mine remediation projects in Canada. While the project navigates the regulatory process to allow for implementation of the final remediation, the completion of urgent works is required to ensure protection of the environment. In this context, urgent works can be considered as the implementation of all, or components of, select final remediation measures before the full remediation project. The North Fork Rose Creek (NFRC) Realignment Project was identified as an urgent work and has two parts, the non-contact water diversion channel (NCWD) and the contact water collection system (CWS). See Figure 4 for the NFRC and mine layout.

The need for the NFRC realignment was based on seepage from the adjacent waste rock creating an exceedance of zinc concentrations in the receiving environment beyond the requirements established in the Fisheries Act.

Based on the inability of investigative drilling and interim measures to identify and mitigate the source of the contaminants and considering a Letter of Direction from Environment and Climate Change Canada; a decision was made to advance the design and implementation of a 1.9 km section of the clean water diversion channel accompanied by an associated contact water collection system.

Crown Indigenous Relations Northern Affairs Canada (CIRNAC) engaged a design engineer to provide options, design, and specifications for the diversion. The designer acted as the owner's engineer

throughout the life of the project. CIRNAC also contracted a construction manager (CM). In this capacity the CM was responsible to support constructability review, cost estimates, sequencing, and work package structure to meet project procurement technical objectives, support project socio-economic objectives, provide project oversight and to take on responsibilities related to quality and environmental management.

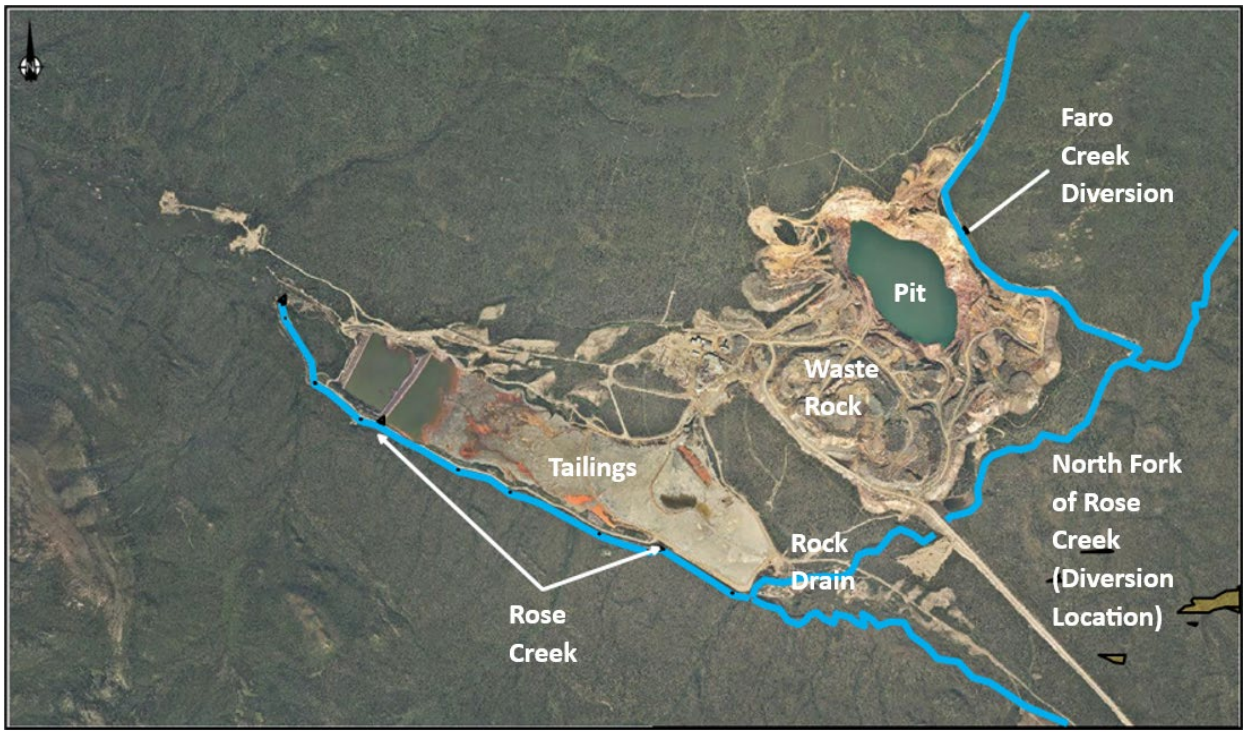


Figure 4: New diversion construction area

The issue for tender (IFT) package for the NCWD was developed as a single contract during the design phase. To meet socio-economic requirements within Parsons' CM contract that had been established by CIRNAC, Parsons as CM broke out the work into thirteen smaller packages to provide greater opportunity for Indigenous and local contractors to be successful in bidding on the work. The CM played an instrumental role in reviewing the work and determining how best to deconstruct the work to meet the CIRNAC objective. This approach helped the project to achieve one of its over-arching objectives to maximize local and Yukon socio-economic benefits. While it resulted in significant additional work for the designer and Parsons at the outset, some associated delay and increased implementation complexity, the result provided for positive owner outcomes.

The primary planned source of non-acid generating clean fill (NAG) for the new channel was from the existing haul road which needed to be excavated to facilitate the construction of the diversion. However, the haul road was found to have insufficient NAG rock requiring development of new sources of borrow at greater expense and increased project risk since many of the potential source locations had not yet been

evaluated for their geochemical and structural properties based on the early state of overall remediation plan development. To facilitate this work the CM supported the evaluation of options and recommendations for the development of an alternative borrow source. Because of borrow delays some of the planned winter work had to be rescheduled to the spring where the increased risk of perma-frost thaw created other challenges such as loss of thermal blanket (an insulating rock layer that protects existing permafrost) . When permafrost thaws, it settles and become unstable: so, winter work are preferable in this case. Also, construction restrictions due to conflicts with the bird nesting window (May 3rd – Aug 23rd) and the fish spawning window (April 1st – July 1st) became a factor. However, the CM was ultimately able to work with the design team to design and fast track the construction of a new borrow source to support the continued advancement of the urgent work.

In addition to the above, and obviously unplanned, was the onset of the COVID 19 Pandemic during construction. Recognizing the urgency of completing this work for the client, the unknowns and risks associated with a pandemic and the need to effectively manage safety at site, Parsons worked closely with their subcontractors and CIRNAC, as owner, to consider and develop options that would allow for the safe continuation of work. Through the implementation of reduced shift rotations, two-week isolation in Whitehorse for all out-of-territory staff, prior to coming to site to meet health requirements of the Yukon Territory, and diligent management on site Parsons was able to continue the construction of the project through the pandemic keeping workers safe while minimizing additional delays to the urgent work.

Completion of the realignment of the North Fork Rose Creek represented a critical step in ensuring that clean water and valuable fish habitat are protected from the contaminated water originating in the nearby waste rock. The delivery of this project using the CM model provided the client, CIRNAC, with delivery sequencing and structures that helped them to achieve their socio-economic objectives for the local First Nations and Yukoners in general. The construction manager was able to effectively identify challenges such as acid generating rock in the haul road, insufficient borrow, and even the COVID 19 Pandemic and The CM identified and recommended solutions and mitigations to the client that recognized the urgency of the project and supported its continued advancement limiting delays and cost impacts.

Figure 5 shows the construction channel to the right alongside the permanent channel running through the old haul road and rock drain to the left.



Figure 5: Completed new channel along-side temporary construction channel on right

Conclusion

With more mine site remediation and closures taking place and the complexity of the construction increasing, the deployment of a construction manager is a necessary value add to control project schedule and costs. The following is a summary of the benefits of having a construction manager.

Prioritize owner's interests: The CM acts as the Owner's Representative to ensure all decisions are to the benefit of the project.

Provide benefit to the project: by prioritizing the owner's interests, the CM can prevent scope creep, manage expectations, and ensure that the project delivers the desired outcomes without incurring additional costs.

Front-end loading: Good planning up front by the CM reduces risk of cost, change orders, and schedule overruns. The cost devil is in the details.

Reduce risks: By addressing potential issues early, the CM can mitigate risks related to cost overruns, change orders, and schedule delays. Detailed planning helps identify and resolve problems before they escalate, leading to more accurate budgeting and fewer surprises.

Develop construction costs alongside design: The CM oversees competitive bidding and develops realistic budgets to ensure the project is completed cost-effectively through the efficient use of resources.

Ensure cost-effective completion: By integrating cost considerations into the design phase, the CM ensures that the project is designed within budget constraints. This approach helps avoid costly redesigns and ensures efficient use of resources.

Commence construction as design is completed: The CM works closely with the Owner's design team through the design phase and in transition to construction stage to ensure the project is buildable and cost-effective.

Ensure a smooth transition to construction: By ensuring that the design is complete and feasible, the CM can avoid delays and additional costs associated with design changes during construction.

Maximize communication and minimize conflict: The CM uses a collaborative and inclusive approach to build mutual trust during the project's early stages. As the design develops, the CM provides expertise on the main requirements of constructability, cost, schedule, value engineering, and material selection.

Provide expertise on key requirements: The CM provides expertise on constructability, cost, schedule, value engineering, and material selection. This guidance helps avoid conflicts and ensures that the project is executed efficiently and within budget.

Provide a central point and single line of communication, control and responsibility: The CM is the one who has a thorough understanding of the project's big picture. They receive input from multiple sources, manage the flow of information, integrate project participants, and ensure the work is completed on schedule and on budget.

Effective management: by having a single point of control, the CM can ensure that the project stays on schedule and within budget. This centralized approach reduces the risk of miscommunication and ensures that all project participants are working towards the same goals.

Provide a highly qualified project team: The CM applies extensive industry knowledge to advise on which contractors are best suited to deliver the needs of the project. This greatly reduces the risk of change orders as there are fewer surprises.

Reduce risk of change orders: By selecting the right contractors and ensuring that they understand the project requirements, the CM can minimize surprises and reduce the likelihood of change orders, which can significantly impact the project budget.

Proposal for Guidelines on Filtered Tailings Disposal: Detailing the Hypothetical Rupture Studies

Elaine Soares, AECOM, Brazil
Waldemar Felitti, AECOM, Brazil
Fernando Pereira Aguilar, AECOM, Brazil
Alex Castro, AECOM, Brazil
Luiz Vilas Bôas, AECOM, Brazil

Abstract

AECOM has amassed considerable expertise in mining tailings management through intensive analyses and inspections in collaboration with Brazilian authorities. The catastrophic dam failures in 2015 and 2019 spurred the strengthening of countries' legislation and underscored the need to adhere to global standards to prevent future disasters. The pursuit of new technologies, such as filtered tailings storage facilities (FTSFs), is growing, although in-depth studies and standardization are still needed. Tailings disposal demands technical rigor and governance, considering long-term risks and environmental adaptability.

The multidisciplinary team at AECOM developed technical guidelines for the disposal of filtered tailings. The guidelines cover the entire life cycle of the projects, including conception, operation, and post-closure phases. The process involved multiple stages of drafting, validation, and review, enhanced by input from an external committee. The guidelines span preliminary studies, site and material characterization, hydrological and hydrogeological studies, numerical analyses, and Hypothetical Rupture Studies (HRS).

This paper provides detailed information on HRS to highlight the developed methodology, as the existing literature is very limited for this type of analysis. HRS evaluate the potential impact and necessary emergency actions in case an FTSF fails, with a focus on defining the Impact Zone. They are based on premises such as the uncertainty of the rupture location, the long lifespan of such structures, and the immediate impact in case of rupture while considering the worst-case damage scenario. The studies require understanding the mobilizable volume, defined by the failure mode, critical scenarios, and sectorization of the FTSF. A mass flow similar to landslides is expected for the propagation analysis, but methodologies and references on the subject are still sparse. The Impact Zone must graphically represent the maximum extent of impact. The proposed methodology seeks to standardize practices and should be refined as knowledge as this field grows.

Introduction

Over the past eight years, AECOM has collaborated with a multidisciplinary team of experts working alongside Brazilian authorities in emergency response, impact assessment, and post-breach reparations. This collaboration has generated an extensive and independent database resulting from more than 1.5 million hours of analysis, field inspections, and technical presentations, culminating in approximately 60,000 conclusions and recommendations in Technical Reports and Notes submitted to government authorities. This experience has revealed various possibilities for contributions to tailings management based on lessons learned.

The catastrophic dam failures in Brazil in 2015 and 2019 highlighted a discrepancy between documented information and these structures' actual stability and risks. AECOM has identified a lack of technical understanding of the real risks during construction, inadequate documentation, and insufficient financial resources for secure closure and repair as key lessons from these incidents. Consequently, these events have cause significant strengthening of local legislation, positioning it among the most stringent worldwide. They have also underscored the importance of adopting global standards and compliance initiatives, particularly in environmental, social, and corporate governance (ESG), to ensure responsible industry management and prevent future disasters. Equally important to establishing standards is the verification process, which must be robust, transparent, and supported by documentation, inspections, interviews, and independent analyses in line with advancements in legislation (Neri et al., 2024).

Furthermore, these developments have driven the development and adoption of innovative tailings management technologies, catalyzing demand for solutions that ensure operational continuity and mitigate associated impacts and costs. In this context, FTSF have become an alternative of interest, primarily due to their ability to reduce liquefaction risks and environmental impacts by minimizing water content in tailings, leading to an increased need for research, licensing, and implementation of such structures.

While pursuing new technologies represents progress, the practice of filtered tailings disposal has not yet been extensively studied or standardized. Overlooking the lessons learned from previous tailings dam failures could lead to repeating past mistakes, potentially creating new risks for communities.

Historically, the stacking of materials in mining has been a practice mainly limited to waste rock and has also been related to global catastrophes, such as the Aberfan tragedy in 1966. However, filtered tailings disposal demands more stringent technical rigor than waste rock disposal alone. Concerns such as the risk of tailings liquefaction, chemical safety, and the potential synergistic effects with downstream structures in the event of a breach are paramount. Furthermore, adopting FTSFs as an alternative for tailings disposal introduces additional governance challenges, requiring careful adjustment of production rates to ensure the safety of construction and operation (Neri et al., 2024).

The long-term nature of tailings disposal structures is also noteworthy. These structures provide a final destination for waste materials, with implications that extend well beyond the immediate future, potentially lasting decades or centuries, alongside associated risks. Consequently, it is vital to plan mining complexes with a complete life-cycle perspective of these structures, designed, constructed, and operated with the foresight of secure closure, considering their long-term presence and adaptability to current and future environmental changes. This planning must include allocating and accumulating the necessary resources for closure throughout the operational life cycle.

Considering these risks, AECOM developed technical guidelines for the disposal of tailings in FTSFs to initiate technical discussions, regulation, and standardization. This initiative, part of a broader project addressing tailings management, aims to provide a proactive framework for mining waste structures. The summary presented here reflects the outcomes of work completed in June 2023.

Methodology

A multidisciplinary team of experts developed the guidelines, identifying technical criteria and drafting initial guidelines. These drafts underwent rigorous review by an expert panel, ensuring robust validation. The multi-phased process included successive drafting, validation, and content review stages. The final version was enriched by the evaluation and contributions of an external committee of consultants, culminating in the definitive set of guidelines.

Technical guidelines for filtered tailings disposal

The development of the guidelines aimed to encompass the entire life cycle of tailings disposal in FTSF, from project conception to the post-closure phase, including existing structures.

The guidelines also sought to address not only the disposal of tailings alone but also the disposal of mixtures of tailings and waste rock, as this is a common practice in the industry that presents significant challenges due to its complexity. The two major methodologies for tailings disposal in the industry are: (i) shared or segregated disposal when there is no mixing of the two materials, which remain separated in distinct compartments of the structure, such as sectors, layers, or cells, with the disposal of these materials not necessarily being contemporaneous; and (ii) co-disposal or blending where there is a mixture of materials during the disposal activity (Aragão, 2008; Silva, 2014).

Both methodologies present complexities related to the proportion of the mixture of these two materials; the definition of representative parameters of the resulting material in the case of co-disposal; and the dimensions and definition of a representative geological-geotechnical model that allows for a realistic analysis of the structure.

The technical guidelines are composed of 17 chapters covering the following topics:

Preliminary Studies: Key preliminary studies include evaluating tailings dewatering alternatives, which should encompass economic and environmental cost-benefit analyses. Initial tests should be conducted on a smaller scale in the laboratory, followed by real-scale tests considering the local conditions. This stage should also involve studying locational alternatives to identify conditions to be avoided or those that would favor implementing the structure at the site (Neri et al., 2024).

Investigation and Basic Data: Basic information necessary for the development of studies should be collected from the initial phases, with a gradual increase in detail as the studies progress. Key data includes information related to detailed and up-to-date topography and cartography. Site characterization involves stages of existing data research, geological mapping, direct and indirect investigations, sample collection, and field tests. These activities aim to develop a local geological-geotechnical and hydrogeological model. Material characterization involves characterizing and parameterizing the materials of the geological-geotechnical model. This includes field and laboratory tests and evaluation of the susceptibility of these materials to liquefaction. Chemical characterization aims to determine the chemical composition, physical properties, and mineralogical composition of the materials placed. It helps define disposal practices, operational management of the structure, and environmental control involving geochemical characterization and the potential for acid drainage. Trial embankments should be conducted before the start of operations and whenever there are variations in operations. This aims to characterize the procedures and criteria to be adopted during disposal and compaction activities to support operational quality control. Seismic studies aim to determine the seismicity of the structure's location. When necessary, they should include a Probabilistic Seismic Hazard Analysis (PSHA) and Deterministic Seismic Hazard Analysis (DSHA) to define the design of earthquakes to be considered (Neri et al., 2024).

Hydrological Studies: Developed to support the design and verification of the hydraulic structures of a FTSF, including internal and surface drainage. They involve studies and surveys of hydrometeorology, design flows, intense rainfall, and probable maximum precipitation (PMP) (Neri et al., 2024).

Hydrosedimentological Studies: These studies are necessary to design sediment containment structures originating from the FTSF (Neri et al., 2024).

Hydrogeological Studies: These studies aim to characterize the water dynamics within the FTSF, the effects of groundwater presence on the structure, and the potential impacts on surface and groundwater resources due to the structure’s installation. They are based on understanding the hydrogeological behavior of materials, surface runoff, subsurface flow systems, and the interaction of these factors with the structure. This involves developing a conceptual hydrogeological model during the conceptual design phase and numerical models to simulate specific scenarios (Neri et al., 2024).

Water Balance: The water balance aims to account for the inflows and outflows of water within the system, providing a foundation for determining the design flows used in sizing the FTSF internal drainage.

Drainage: The FTSF's drainage may be divided into two main groups. Surface drainage aims to manage surface water, reducing infiltration into the FTSF and minimizing damage caused by concentrated water flow. Internal drainage is constructed along with the FTSF and is designed based on water balance studies. This includes basal drainage at the interface between the foundation and the FTSF and, if necessary, intermediate drainage constructed along the structure's elevation, as well as deep drainage.

Numerical analyses: Numerical analyses are conducted to verify the safety conditions of the FTSF regarding physical stability, demonstrating compliance with minimum acceptance criteria stipulated by engineering standards and best practices while optimizing geometry and construction sequence. This requires defining the geological-geotechnical model, specifying material parameters involved in the analyses, and understanding potential failure modes. Typically, these analyses involve limited equilibrium methods, necessitating the establishment of methodologies, criteria for defining analysis sections, scenarios, and acceptance criteria. Percolation analyses should also be developed to estimate percolation rates, neutral pressures, suction gradients, and hydraulic gradients that may develop within the mass and foundation, supporting the verification of structure safety conditions, with attention to material saturation risks. In cases of complex geometry, high stresses, and stratified foundations, stress-strain analyses should be elaborated to determine displacements, deformations, and stress accumulation regions (Neri et al., 2024).

Instrumentation and Monitoring: Monitoring is an essential activity to ensure safe operating conditions. It involves developing a geotechnical monitoring plan that includes the necessary actions and instrumentation for monitoring. This plan must be included in the structure's Operation Manual and should define routine in situ visual inspections and the instrumentation systems installed for monitoring. The monitoring systems should include instrumentation for measuring deformations, pore pressures, groundwater levels, internal drainage flow rates, surface water, hydrometeorological data, and hydrogeochemical monitoring (Neri et al., 2024).

Safety Evaluation: The safety evaluation aims to verify if the structure's performance aligns with the design assumptions. It is based on the collection of inspection information and historical monitoring data, providing support for new stability analyses, which should be conducted periodically (Neri et al., 2024).

Hypothetical Rupture Studies: These studies evaluate the potential damage associated with the structure in case of failure. It aims to define the area that could be impacted in the event of a failure, known as the Impact Zone. This involves understanding the Mobilized Volume, Propagation Analysis, and characterizing the area downstream of the FTSF (Neri et al., 2024).

Risk Analysis: This activity focuses on identifying, analyzing, and evaluating risks, aiming to reduce or mitigate the effects of uncertainties on the safety of structures (Neri et al., 2024).

Climate Change Resilience: This phase aims to develop more robust projects to address changes caused by extreme climatic events. This includes sensitivity analyses and adaptation actions.

Project Phases: This chapter aims to establish the minimum recommended contents for each project phase. To this end, a phased approach has been proposed, divided into Conceptual Design, Basic Design, and Detailed Design. Accompanying these stages, some primary documents should be included, such as Technical Specifications, As Built, As Is, Operation Manual, and Monitoring Levels (Neri et al., 2024).

Implementation and Construction: This phase includes activities related to preparing the foundation and necessary structures for the start of operation, including the initial stacking stage until a level working platform is reached. The activities involved in implementation include Preliminary Services for Vegetation Removal and Site Clearing, Topographic Surveying and Earthworks, Construction Access, Foundation Preparation, and the Construction of Internal Drainage (Neri et al., 2024).

Operation: The operation phase begins after completing all activities related to the implementation of the FTSF. It includes only the activities associated with the placement of materials and related services until the structure reaches its final design geometry. Key activities during this phase include constructing operational accesses, technological monitoring and ensuring construction quality, operational procedures, sediment management, temporary coverings, planning for the rainy season, and preparing periodic As Built reports. Technological monitoring aims to ensure that the quality and assumptions specified in the design are met and to assist in quality management (Neri et al., 2024).

Closure: Deactivating and closing the structure should result in the area being functionally reintegrated into the environment, considering that it will remain at the site for an indefinite but extremely long period. Closure criteria should account for the physical permanence of the structure and the inherent risks of its existence. The closure project should define the closure concept and the necessary monitoring to ensure the physical and chemical stability of the FTSF. Activities involved in closure include the Closure Project, Final Covering, Final as Built, Post-Closure Inspection, and Performance-Based Post-Closure Monitoring (Neri et al., 2024).

Detailing the Hypothetical Rupture Studies (HRS)

The topic of filtered tailings disposal is relatively recent, with limited published references, especially regarding Hypothetical Rupture Studies (HRS). AECOM proposed a specific methodology for conducting these studies to develop the guidelines. HRS for FTSFs are essential for assessing potential damages in the event of a structural failure and establishing necessary emergency actions. These studies are driven by these structures' inherent risks and impacts, and their findings should form the basis for project risk assessments. Therefore, HRS results must meet these expectations. The proposed methodology identifies key questions that HRS should address to provide relevant data for risk analysis:

- Where: What area might be impacted?
- When: Is it possible to define a time frame within which the event might occur?

- Duration: Once the event has started, will there be time for action?

The study's primary goal is to identify the Impact Zone, the area potentially affected by a rupture.

A primary concern regarding the stacking of tailings is their liquefaction potential. The guideline is based on the principle of making tailings stacking feasible, ensuring that the materials placed will not undergo liquefaction. This requires that they (i) display dilatant behavior, achieved through rigorous compaction methods, and (ii) remain unsaturated. Current experience indicates that filtered silty-sandy tailings have achieved the best outcomes. However, the required characteristics of the tailings for their disposal and compaction to meet these conditions may vary depending on the specific properties of each material. They should be evaluated on a case-by-case basis. There is consensus that proper compaction involves layering these materials in thin strata with moisture content close to the optimal level.

Assuming that FTSF will not be susceptible to liquefaction, the expected failure modes are related to mass instability, typically assessed through limit equilibrium analyses. Nevertheless, the potential for operational errors or deficiencies in adhering to design criteria during the construction process cannot be overlooked. Therefore, the potential for liquefaction of the disposed material or other credible failure modes should be evaluated whenever plausible.

Based on these considerations, eight premises were defined to guide the development of the proposed methodology and studies (Neri et al., 2024):

- uncertainty in defining the location of the rupture;
- defining the zone with the greatest possible damage, regardless of the probability of occurrence;
- considering the time of arrival of the impact wave as instantaneous when the adopted methodology does not allow the definition of the arrival time of the impact wave;
- predicting interaction with or impact on other structures;
- considering the long lifespan of this type of structure, including the post-closure period;
- adherence to project phases and construction stages, with continuous data updates;
- defining geological-geotechnical sections and material parameterization based on projects, investigations, and technological controls; and
- overcoming uncertainties inherent in the applied methodologies by adopting conservative criteria.

Additionally, discussing the distinctions between FTSF and traditional tailings dams concerning HRS is essential. While there is a tendency to compare them and draw parallels from tailings dams to FTSF, such comparisons are not always applicable. Dams typically feature linear structures with a predominant slope direction, designed to contain materials that lack self-support in the upstream reservoir. In contrast, FTSF exhibit complex geometries with multiple slope directions and are constructed using the same materials they are intended to hold, necessitating self-support.

When considering the rupture of these structures and the sequence of events involved, dams go through a complex sequence of events, from the dam breach to the propagation of the reservoir material downstream. In contrast, when transferring this analysis to FTSF, these elements do not directly apply. The rupture process is simpler, focusing on the mass rupturing and propagating downstream from the breach area. However, pinpointing the rupture location in FTSF is more intricate than in tailings dams due to their complex geometry. In tailings dams, the critical location is typically the highest section. Minor variations in the location do not significantly affect the outcome or the affected area, as it primarily relates to reservoir dynamics rather than breach location. In contrast, for FTSF, the rupture involves only the structure mass, making the outcome highly dependent on the rupture location. Additionally, as there are multiple slope directions, there are numerous critical sections to consider.

To conduct the HRS, primary data need to be acquired. This includes topography/cartography of the entire FTSF and adjacent areas, FTSF projects, material characterization (including the disposed materials and those of the foundation and internal drainage structures), and data on structures that could be affected by the rupture, such as sediment containment dams or other FTSF (Neri et al., 2024).

The HRS development involves understanding three main components: Mobilized Volume, Propagation Analysis, and the Downstream Area.

Mobilized volume

The mobilized volume refers to defining the volume that will be mobilized during a rupture. This involves the FTSF geometry and material characterization (obtained from basic data). It also includes determining the failure mode, critical scenarios, location of the critical section, and rupture wedge (Neri et al., 2024).

Failure modes

The definition of the Failure Mode, which is usually expected to be mass destabilization, must be individually assessed based on the specific characteristics of each structure. HRS should evaluate all possible failure mechanisms, even if they are unlikely, to identify the most critical scenarios regarding the generation of the Impact Zone. For existing FTSFs, if materials with contractive behavior are present due to design or construction quality control errors, rupture by liquefaction should be assessed, even if these materials are not saturated (Neri et al., 2024).

Critical scenarios

To consider the most critical scenarios for potential rupture, various factors that could lead to FTSF failure should be evaluated, including operational non-compliance with the project plan and malfunctions such as improper material disposal, inadequate compaction, and internal and surface drainage systems failures. Stability analyses should account for the most critical conditions the structure may face throughout its lifespan, such as earthquakes, water table fluctuations, pore pressure generation, changes in materials, and

uncertainties in resistance parameters.

After conducting stability analyses across different failure modes and scenarios, various failure surfaces will likely be identified. However, the surface with the lowest safety factor might have smaller dimensions compared to others. In such cases, the designer should determine which scenarios to use for the propagation study, even if they do not represent the lowest safety factor. Similarly, the scenario with the highest mobilized volume may not be the most critical regarding the Impact Zone. For instance, the rupture propagation from a larger unsaturated deep wedge might be less severe than the liquefaction of a smaller volume. Another crucial aspect is the formation of successive rupture surfaces following initial instability. After the first failure, it is necessary to assess whether the remaining surface remains stable (safety factor > 1). If not, the formation of a second rupture wedge should be evaluated, and so on, i.e., a cascading failure scenario (Neri et al., 2024).

FTSF sectorization

Due to the spatial configuration and the topographical and construction characteristics of a FTSF, there can be several critical sections that, in the event of a rupture, may generate different affected areas. It should be considered that the rupture can occur at any location within the structure, not just in the most critical section (Neri et al., 2024). Therefore, sectorization of the FTSF must be performed to define sectors with homogeneous characteristics based on specific criteria, such as:

- geometry (height and slope inclination);
- disposed material;
- foundation conditions;
- downstream topographic condition;
- original topographical configuration;
- stability conditions and failure modes.

For each sector, the location of the critical section should be evaluated, considering possible failure modes and the Impact Zone to be generated.

Propagation analysis

Gravitational forces primarily drive the movement of the mass. However, propagation analysis is a physically complex phenomenon influenced by other variables such as topography, climate, geological and geotechnical properties, rheological properties, groundwater level, etc.

Analysis methods

The choice of the model to be used and the data parameterization for the analysis should consider the failure mode, volumetric concentration, and saturation of the mobilized mass. In this context, the types of flow, as

proposed by O'Brien and Julien (1985), can be classified into: (i) aqueous, (ii) mud flood, (iii) mudflow, and (iv) landslide. Aqueous and mud flood flows exhibit more fluid characteristics, whereas mud flow demonstrates plastic and cohesive deformation. Conversely, landslide flow is characterized by block sliding or granular flow. For FTSF, it is anticipated that the flows resulting from a potential rupture will be based on the landslide type, where the ruptured mass primarily consists of earth or rock materials with low water content. According to the classification by Cruden and Varnes (1996) for mass movements in natural slopes, the expected landslide types in FTSF would predominantly be translational or rotational landslides or debris flows, depending on the material involved and the modes of movement.

The methods for analyzing rupture propagation in slopes, which can also be applied to FTSF, are divided into two main categories: (i) empirical-statistical and (ii) analytical/numerical. For the design or evaluation of a FTSF, both methods can be employed depending on the project's stage of development. Empirical-statistical methods are based on correlations from historical events. Due to their simplicity, they can be used for initial estimates. However, because of their low accuracy, the propagation of the mobilized volume should be estimated using analytical/numerical methods as the project advances. Analytical/numerical methods involve solving equations that describe the movement of masses. These methods consider the geometry and mechanism of potential slippage and can provide information such as flow velocity, depths, and the distribution of the rupture area (Neri et al., 2024). Table 1 presents some models that can be used for rupture propagation studies in FTSFs.

Table 1: Examples of models that can be used for propagation studies

Model	Description
FLO-2 D	Two-dimensional hydrodynamic model
Flow-R	Empirically based model for regional susceptibility assessments of debris flows
D-Claw	Open-source software for modeling granular fluid flows (landslides, debris flows, etc.)
HEC-RAS	One-dimensional and two-dimensional hydrodynamic model
MADFLOW	A two-dimensional numerical simulation tool for analyzing the mobility of tailings, soil, rock, and/or gravity-driven water mixtures
RAMMS	Two-dimensional hydrodynamic model
RiverFlow2D	Two-dimensional hydrodynamic model
Flow-3D	Three-dimensional hydrodynamic model
Anura3D	Software for modeling large deformations and soil-water-structure interaction using the material point method (MPM)

Hydrological scenarios

Assessing the hydrological scenarios in HRS is fundamental for both recharge studies and defining the intensity of rainfall that should be incorporated into the rupture hypothesis. This directly impacts the analysis of the propagation of mobilized and drained material.

There may be sediment retention dams or other structures downstream of the FTSF. If credible or possible, the cascading rupture scenario of the FTSF and downstream dams should be evaluated. In such cases, to assess the scenario with the greatest possible damage, it is recommended to consider at least one rupture scenario under severe hydrological conditions. This includes considering intense rainfall with a return period (TR) of 10,000 years or the Probable Maximum Precipitation (PMP) event in the upstream contributing basin and a natural flood in the downstream valley, with a TR of 100 years for the rainy-day rupture and a TR of 2 years for the sunny-day rupture. The premise of overlaying the rupture hydrograph onto the peak of the reference natural flood should be used, as it is impossible to predict whether there will be an overlay of these two hydrographs or where it will occur (Neri et al., 2024).

Interaction with other structures

Assessing the interaction with other structures is necessary when evaluating areas that may be affected by a rupture, in addition to the topographic characterization and the survey of land use and occupancy. The mass movement generated by the rupture of the FTSF can impact downstream structures. When these affected structures have mobilizable volumes, there is an interaction between the mass movement originating from the FTSF and the movement of the newly mobilized mass. In cases where the cascading mobilization of a dam is plausible, the HRS should incorporate the dam rupture into the model. During the design phases, preliminary HRS can define expected impact areas and facilitate the planning and implementation of structures with potential interaction in the event of a rupture, such as sediment retention dams, in areas outside the anticipated impact zone (Neri et al., 2024).

Impact zone

The Impact Zone should be represented cartographically as the result of an HRS corresponding to the maximum boundaries around the FTSF. The final Impact Zone of the FTSF will be the cumulative boundary of the various impact zones defined for each analyzed sector and those resulting from secondary impacts.

The final impact zone should be considered during various project stages, assuming the complete construction of the FTSF. However, during operation, it is recommended that the impact zone for each stage of raising is continually updated. This allows for predicting the expected impact zones for each stage based on updated information on geometry, material characterization, and downstream area conditions, optimizing the use of impact areas and the resources required for preventive actions when necessary. For the closure stage, the final impact zone should also be updated, considering the most current information and data obtained during the structure's operation.

The definition of the impact zone will facilitate the identification of potential impacts, risk management, the planning of alert systems, the formulation of emergency plans, and the determination of downstream land uses and activities (Neri et al., 2024).

Conclusion

The development of these guidelines was driven by a need to proactively address the technical standards applicable to mining waste structures. Through broad stakeholder discussions, this work aims to contribute to a comprehensive standardization and regulation of filtered tailings storage facilities (FTSF). It emphasizes the importance of a complete life-cycle approach to ensure quality and safety in the construction and operation of disposal systems. While some topics are emerging and evolving, such as HRS, the proposed methodology serves as a starting point for best practices that will be refined as the body of knowledge expands. Crucially, the stability of a tailings disposal structure relies on appropriate engineering, governance, operation, monitoring, maintenance, and closure practices. The multisectoral approach has left a lasting impact on society, contributing to improving safety and preserving life, reinforcing the Culture of Safety and Prevention.

Acknowledgments

We would like to express our sincere gratitude to the Public Prosecutors Office of the State of Minas Gerais (MPMG) for their initiative in promoting the development of guidelines for filtered tailings disposal. Their commitment to integrating technical knowledge into the Brazilian mining sector and supporting discussions on the subject is invaluable and essential for enhancing practices and standards in our industry, as well as improving socio-environmental safety.

References

Aragão, G.A.S. 2008. *Classificação de pilhas de estéril na mineração de ferro*. Thesis research for Master's degree, Universidade Federal de Ouro Preto, UFOP.

Cruden, D.M. and Varnes, D.J. 1996. Landslide types and processes. Transportation Research Board, US National Academy of Sciences, Special Report 247: 36–75.

Neri, A.C., Soares, E.N., Sánchez, L.E., Castro, A.L., Aguilar, F.P., Carmo, F.F. Dupin, P.C., Felitti, W. F., Kamino, L.H.Y., Massignan, R.S., Mello, V., Silva-Sánchez, S., Vilas Bôas, L.E. 2024. *Diretrizes Técnicas e Socioambientais para Projetos de Pilhas de Disposição de Rejeitos de Mineração.* São Paulo: Fundação para o Desenvolvimento Tecnológico da Engenharia.

O'Brien, J.S. and Julien, P.Y. 1985. Physical properties and mechanics of hyperconcentrated sediment flows. *Proceedings of Specialty Conference on Delineation of Landslide, Flashflood, and Debris Flow Hazards in Utah* (ed. D.S. Bowles), Logan, Utah: 260–279.

Silva, R.K.A. 2014. *Co-disposição e disposição compartilhada de rejeitos e estéreis em cava exaurida*. Thesis research for Master's degree, Universidade Federal de Ouro Preto, UFOP.

The Use of an O-pile System for Foundation Seepage Control during Tailings Dam Construction: A Case Study

Rui Couto, WSP Canada Inc., Canada
Siavash Farhangi, WSP Canada Inc., Canada

Abstract

Seepage control is a critical aspect in the design, construction, and operation of a tailings dam to ensure the stability of the dam and to limit the amount of pond water that can pass through the foundation. This becomes apparent when unexpected field conditions are encountered during construction, which occurred during the raising of a tailings facility at a mine site in Northern Ontario, Canada.

Due to uncertainties about the long-term performance and durability of the PVC and GCL membranes in one of the main dikes, raising of the facility necessitated the construction of a new till-core earthfill dike downstream of the existing dike, founded on dense glacial till and/or bedrock. During the foundation excavation, a boulder field was encountered within the glacial till layer, preventing safe excavation to the required foundation depth and construction of the "keyed-in" core that would provide seepage control. Test pit and borehole investigations were initiated to confirm both the elevation of the bedrock along the dike centerline and the hydraulic conductivity of the boulder field to best inform alternative design options. Based on the results of the site investigations and numerical seepage and stability assessments, an O-pile (modified sheet pile wall) system was selected for the seepage cut-off, as it provided the lowest risk to the project schedule, while maintaining the original dike alignment and design intent.

The O-piles consisted of a steel tube installed via percussive rotary drilling. Upon completion of the O-pile installation, grout was injected through the bottom 0.6 m of the pile, encasing it within the bedrock, while the remainder of the O-pile was backfilled with a bentonite-amended sand. Once construction of the dike was completed, data collected from instrumentation installed within the foundation upstream of the dike indicated progressively rising water levels, providing confidence that the O-piles were functioning as intended.

Introduction

Seepage control is a critical aspect in the design, construction, and operation of a tailings dam to ensure the stability of the dam and to limit the amount of pond water that can pass through the foundation. This

becomes apparent when unexpected field conditions are encountered during construction, which occurred during the raising of a tailings management facility (TMF) at a gold mine in Northern Ontario, Canada.

An aerial view of the TMF is shown in Figure 1. The TMF consists of two ponds: a Primary Pond and a Secondary Pond. Tailings are deposited in the Primary Pond, while the Secondary Pond acts as a polishing pond, providing time for additional clarification prior to discharging excess water into the environment. The Primary Pond consists of five Dikes, numbered Dikes 1 through 5, that contain tailings within a historical lake. An offline dike barrier (ODB) was constructed downstream of Dikes 1 and 4 in order to reclassify the TMF as an "offline" structure (i.e., not overprinting/impacting any existing waterbodies) within the provincial regulatory framework, and to minimize Dike 1 seepage to the environment.



Figure 1: Tailings management facility plan view

The original dike (Dike 1) was an earth fill dam, constructed in 1988 to an elevation of 416 m, employing a 30 mil PVC membrane beneath the upstream slope as the main water retaining element. Additional dikes were built during mine operations, as shown on Table 1, raised by the downstream method of construction, as dictated by the tailings deposition requirements. Figure 2 shows a typical cross-section of the Dike 1 raises. In 2011, Dike 1 was raised by the downstream method to a crest elevation of 418.3 m (AMEC, 2012). At that time, a geosynthetic clay liner (GCL) was used as the water-retaining barrier, which was overlapped (minimum 1.0 m) with the existing PVC membrane, with bentonite placed between the seams. A second raise to a crest elevation of 424 m also continued the use of the GCL. Due to uncertainties in the long-term performance and durability of the PVC and GCL membranes, raising of the facility necessitated the construction of a new till-core earthfill dike, downstream of the existing dike.

Table 1: Construction history for primary pond

Year	Construction history
1988	• Construction of Dike 1 starter dam
2011	• Raising of Dike 1 to elevation 418.3 m and construction of Dike 2 to an elevation of 420 m and Dikes 3 and 4 to an elevation of 418.3 m • Emergency spillway constructed along Dike 3 to invert elevation of 417 m • Construction of seepage collection ponds
2015	• Raising of all dikes to a crest elevation of 424 m • Emergency spillway raised to invert elevation of 422.8 m
2019	• Construction of an Offline Dike Barrier to a crest elevation varying from 410.5 m to 409.5 m
2020 – 2021	• Completion of dike raise to a crest elevation of 427 m, including construction of new Dike 1 downstream of the existing Dike 1

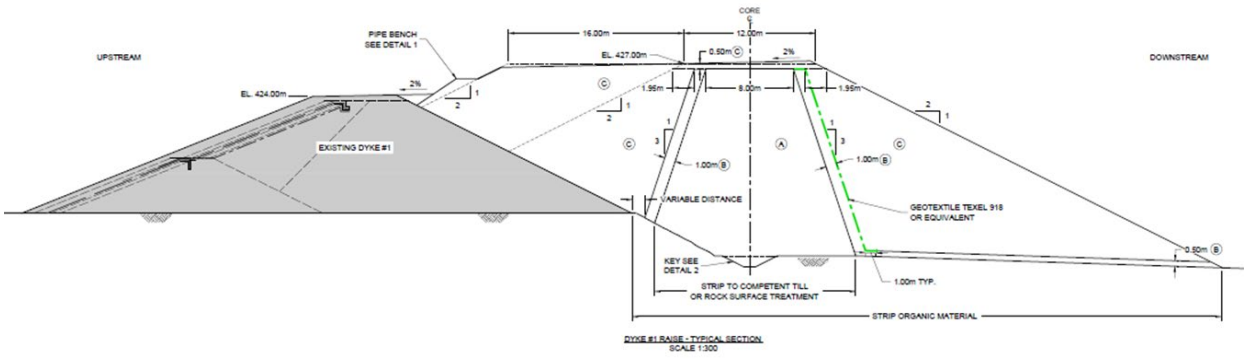


Figure 2: Typical section for Dike 1 raise (Wood, 2018)

Excavation for the new Dike 1 foundation commenced during the summer of 2020. During the removal of organics and unsuitable soils along the central portion of the proposed Dike 1 footprint, a zone consisting of sand and gravel till with cobbles and boulders (up to 2 m in diameter) was encountered at an elevation of about 407 m, spanning a length of about 40 m from Sta. 0+232.5 m to Sta. 0+272.5 m. Steeply dipping bedrock was encountered both to the south and north of the excavation. The groundwater table was also at about elevation 407 m. Attempts to excavate into the boulder zone were hampered both by the density of boulders and the rapid inflow of water into the excavation. At the time, the ultimate depth to bedrock was unknown, though it was estimated to be anywhere from 6 m to 10 m based on a historical borehole log (BH-04-15) advanced in 2015. Figure 3 provides a borehole stratigraphy profile for Dike 1 that indicates the borehole in question.

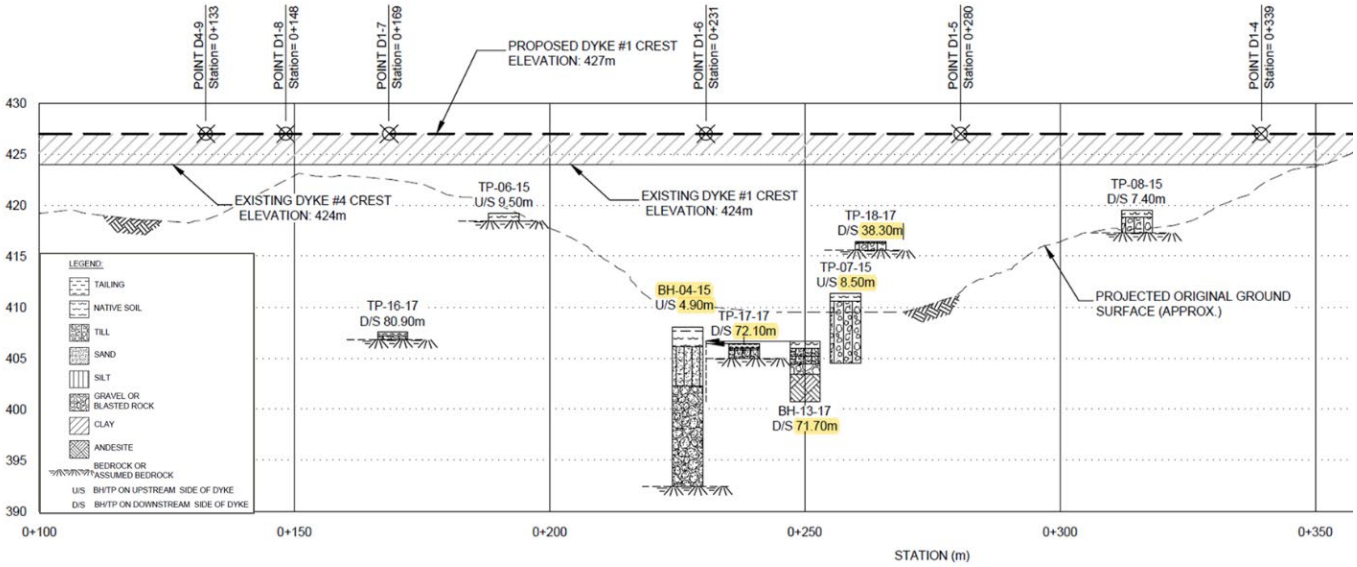


Figure 3: Dike 1 stratigraphy profile

Geotechnical investigations

To better ascertain the depth of the bedrock in the area of the boulder zone, a bedrock probing investigation and well installation program was undertaken in early September 2020. A total of eight boreholes were advanced to competent bedrock; five were located along the centerline of the proposed Dike 1 and three were located approximately 10 m downstream of the centerline. Figure 4 provides an inferred bedrock profile based on the data collected during the investigation.

The investigation indicated that the depth of bedrock varied from about 2 m below the subgrade level at the north and south ends of the boulder zone, dipping down to a maximum of 8 m below subgrade at an elevation of 399 m.

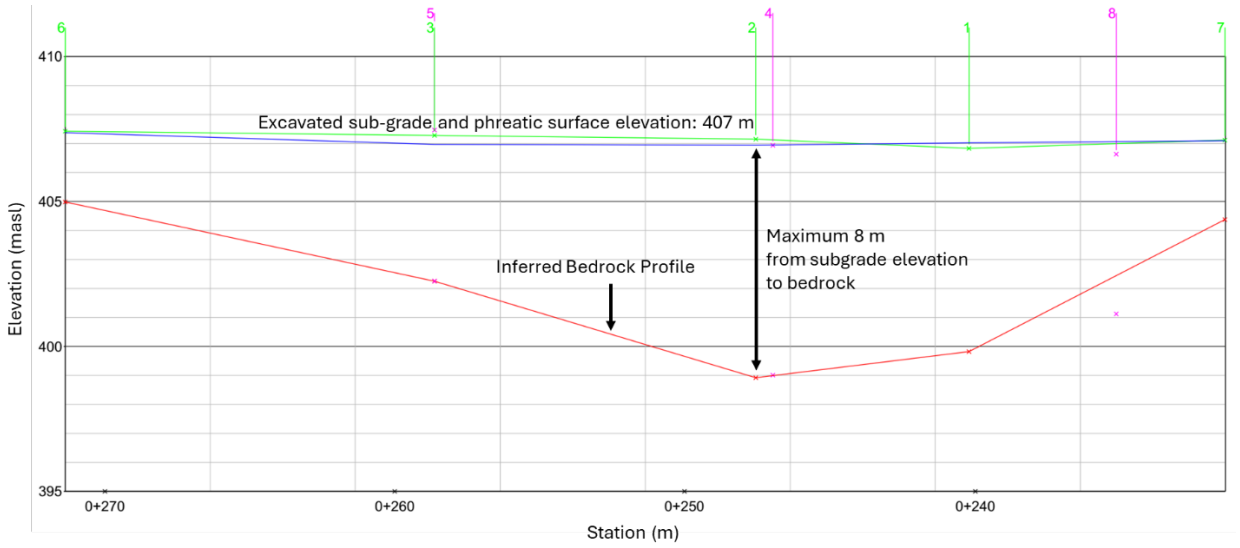


Figure 4: Dike 1 centerline bedrock profile

Stability and seepage analyses

Using the available historical data and the results of the bedrock probing investigation, a series of stability analyses were undertaken to confirm the stability of the existing Dike 1 under the temporary excavated condition at the toe. In addition, seepage analyses were completed to analyze what the effect would be on seepage rates through the foundation between construction of the new Dike 1 on top of a treated versus untreated boulder zone.

Stability analyses were carried out using the limit equilibrium modelling software slope/W, which was coupled with the finite element seepage modelling software seep/W, both of which form part of the GeoStudio modelling package developed by Geoslope International Ltd.

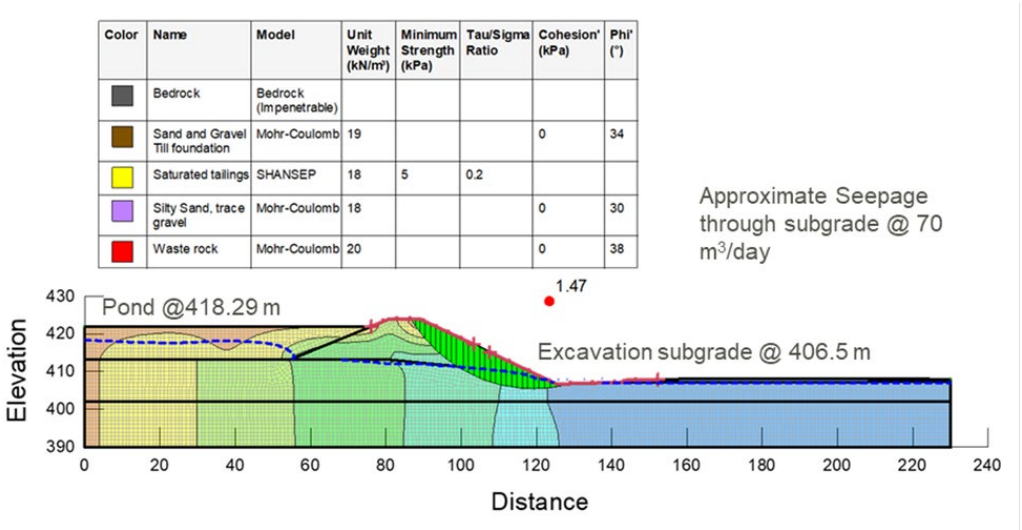


Figure 5: Dike 1 stability and seepage – temporary excavated condition

Figure 5 shows the seepage and stability analysis results for the static loading conditions at Dike 1 based on the pond level and toe elevation during construction. The analysis indicated a factor of safety against slope failure of 1.47 and a seepage rate at the toe of the dike of around 70 m3/day across the exposed length of the excavation. This seepage rate is consistent with the amount of seepage that was reporting to the downstream seepage collection station.

Figure 6 and Figure 7 provide the seepage and stability analysis results for a fully constructed new Dike 1 at a crest elevation of 427 m with upstream pond elevation of 423.5 m (approximate normal operating pond elevation) for an untreated and treated boulder zone, respectively.

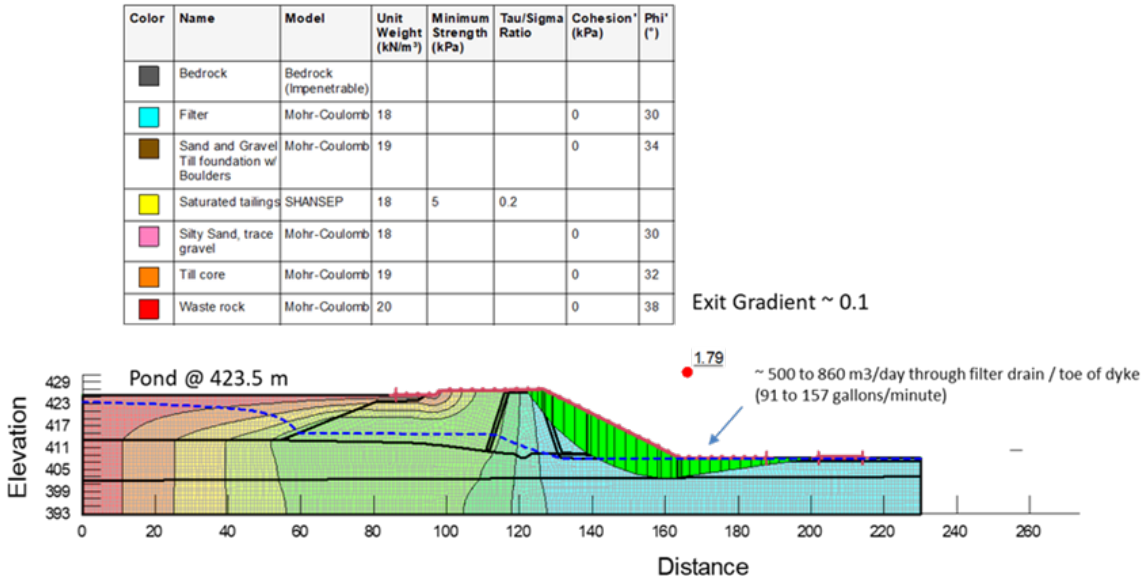


Figure 6: Dike 1 Seepage and stability – crest elevation 427 m with untreated boulder zone

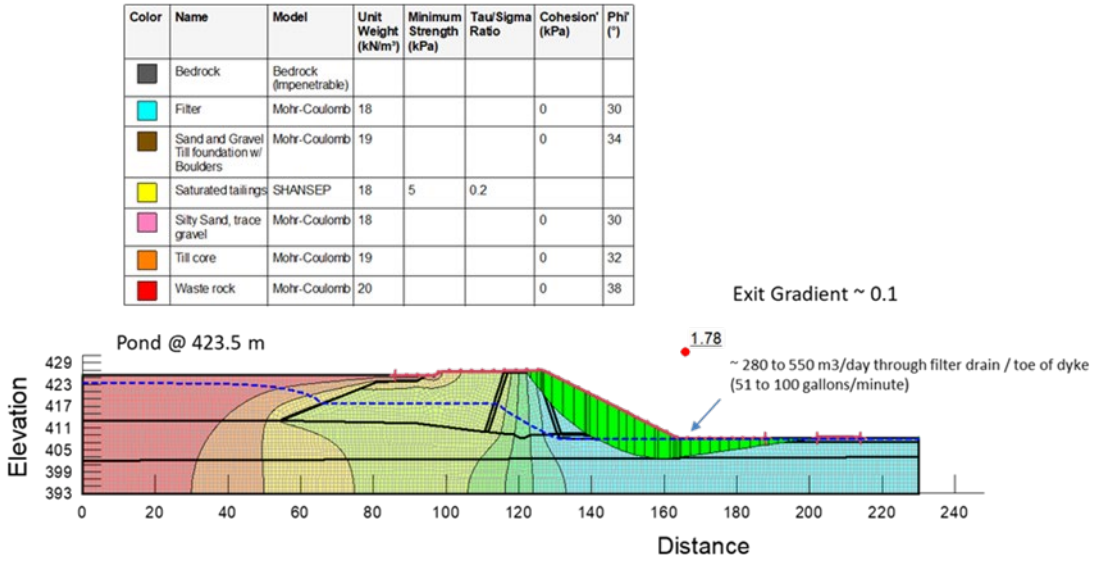


Figure 7: Dike 1 seepage and stability – crest elevation 427 m with treated boulder zone

In this case, the treated boulder zone was modelled with a hydraulic conductivity (k) of one order of magnitude less than the untreated boulder zone (10-6 m/s compared with 10-5 m/s). The results indicated that stability of Dike 1 is not a concern and that by treating the boulder zone to reduce its permeability, the long-term seepage rates through the dike foundation can be approximately halved.

Seepage cut-off wall options assessment

Various options to treat the Dike 1 foundation were reviewed in discussions with earthwork and specialist contractors, which included the following:

- A stepped excavation down to bedrock with upstream dewatering well points. The excavation would be backfilled with compacted till borrow. For stability of the excavation, this option would require a downstream step-out of the Dike 1 centerline of anywhere from 6 m to 12 m.
- Jet-grouting of the boulder zone down to bedrock.
- An engineering cut-off embedded in Bedrock consisting of either a Secant Pile Wall, or O-piles.

Table 2 provides a summary of the comparison that was undertaken for the boulder zone treatment options based on various design, engineering and stability considerations, relative cost, and risk to project schedule.

Based on the comparison conducted, the chosen method of foundation treatment was the installation of an O-pile cut-off wall as it presented the lowest risk to the project schedule and would allow the centerline of the new Dike 1 to remain the same as the original design and best achieve the design objectives as per the original design (Wood 2018).

Table 2: Seepage cut-off treatment options

Option	Treatment goal achievable?	Design, engineering, and stability considerations	Relative cost	Risk to project schedule
Excavation and Replacement	Yes	• Relies on dewatering being successful. • Does not maintain original design alignment - would require about a 12 m step out of Dike 1 centerline for excavation slope stability. • Existing Dike 1 stability and groundwater control a concern at deepest part of excavation	Lowest	High
Jet Grouting	Uncertain	• Difficult to achieve and verify continuous cut-off (shadowing effects around boulders and lack of quality control (QC))	Moderate to High	High

O-pile	Yes	• Need to ensure adequate tie-ins to competent bedrock, Dike 1 core, and competent till / bedrock. • Some form of permeability testing required pre- and post-installation to confirm design criteria achieved	High	Moderate
Secant Pile Wall	Yes	• Similar considerations to O-pile wall, though 2 to 3 overlapping rows required as opposed to one row of O-piles. • Risks of damage due to pile interlocking • Slower construction compared O-pile installation	High	High

O-pile design and installation

Figure 8 provides typical shop drawing plan view and cross-section details for the O-piles as provided by the subcontractor.

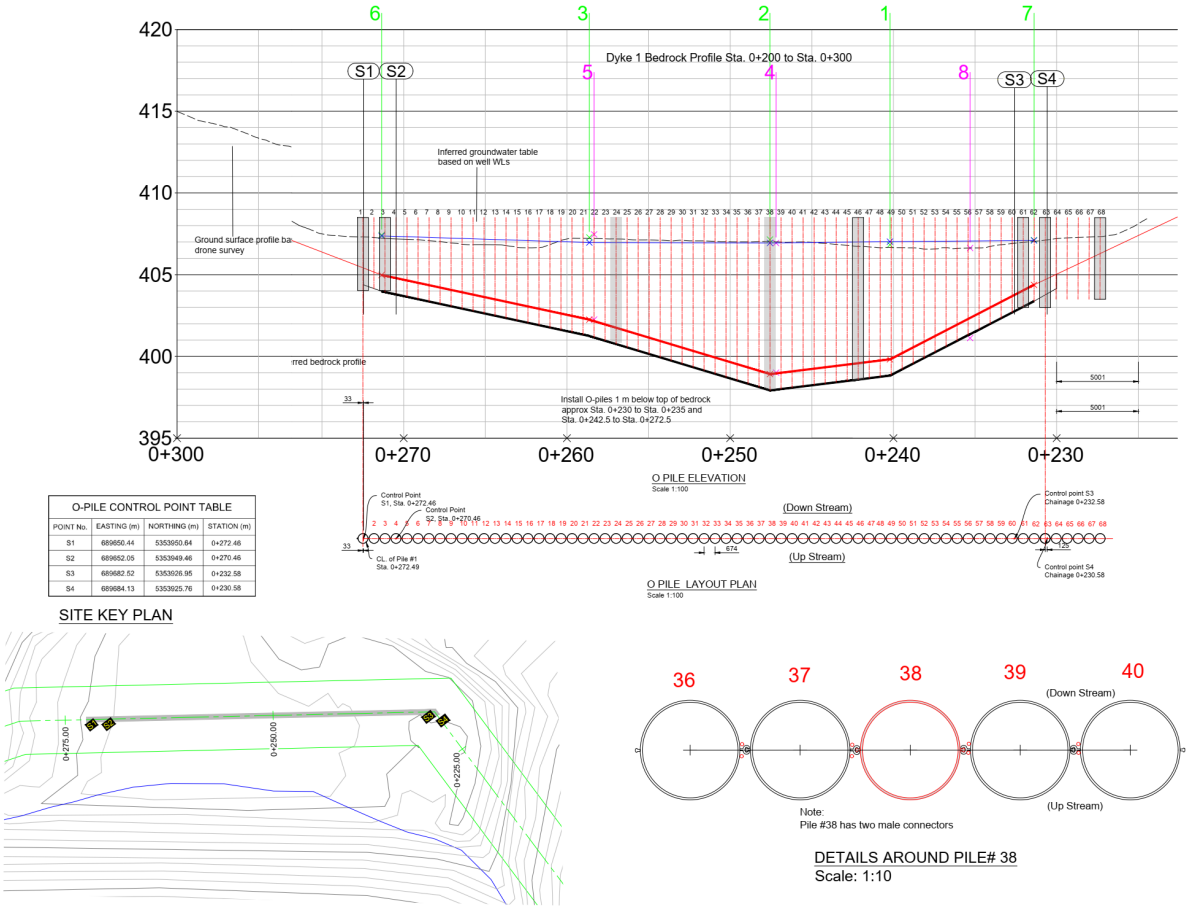


Figure 8: O-pile plan, profile, and cross-section views

The O-piles consist of an inner diameter of 600 mm that is installed via a percussive rotary drill rig. The O-piles connect to each other via an interlocking C-section as shown in detail 4 in Figure 9, with a sealant installed inside the female end of the connector. Upon completion of the installation, grout is injected through the bottom 0.6 m of the pile to encase it within the bedrock. The remainder of the O-pile length is then backfilled with earthfill material to serve as ballast.

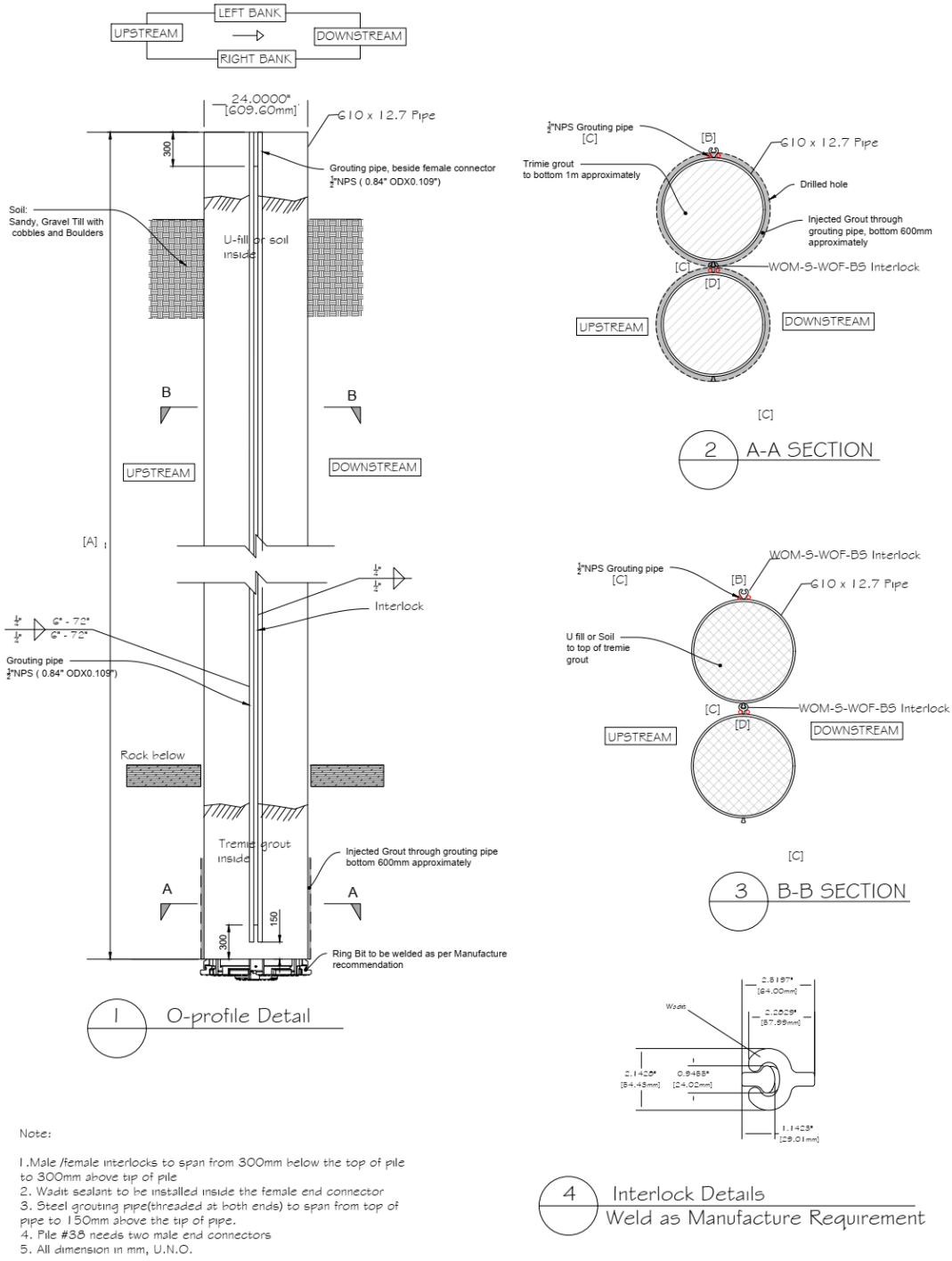


Figure 9: O-pile installation details

Figure 10 provides the as-built profile for the O-pile wall. The O-pile wall was constructed from about Sta. 0+227.5 m to Sta. 0+272.5 m to allow for adequate tie-in to the till core and bedrock abutments at the north and south ends of the excavation, with a minimum 2.0 m overlap between the O-pile wall and the till core, a minimum 1.0 m embedment of the top of the O-pile into the till core above the subgrade elevation, and a minimum 1.0 m embedment into competent bedrock. A provision was made for additional jet grouting between the O-pile connections if damage or verticality issues were noted in the connections during installation, however this was not required based on QC data collected during the installation.

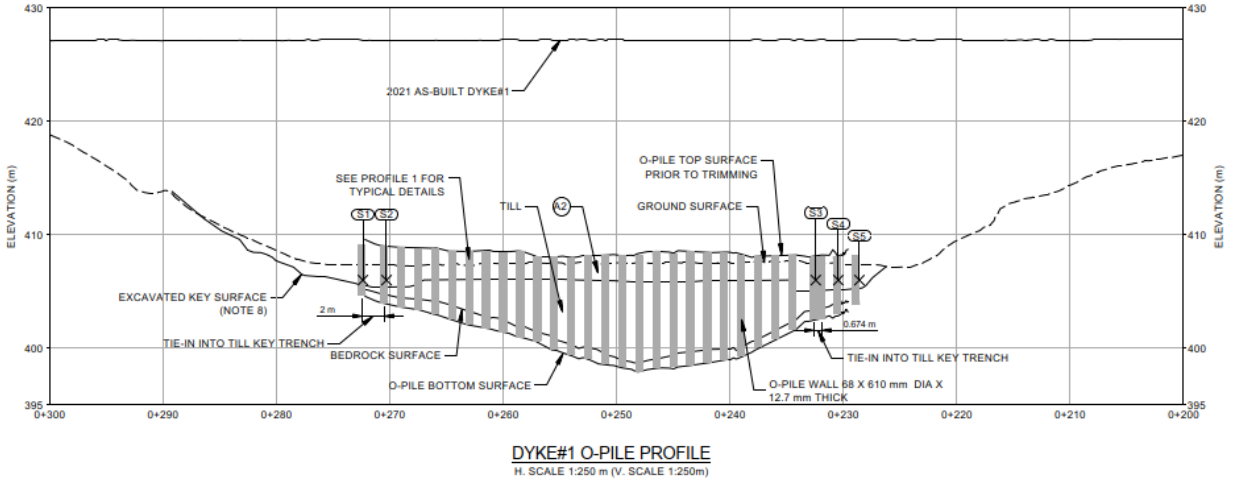


Figure 10: As-built profile of O-pile wall

Pre-/post-installation monitoring and dike performance

Pump tests

Pumping tests to monitor the drawdown cone of a suction pump (Pentair STA-RITE SNE-L 1 hp) were conducted prior to and following the installation of the O-Piles in order to ascertain the hydraulic conductivity of the Dike 1 foundation.

Drawdown data from the pump well both during the pre-O-pile installation test and the post O-pile installation test showed that the bulk hydraulic conductivity of the till in the immediate vicinity around the O-pile was about 2 x 10^{-5} m/s. This is consistent with original assumptions for the hydraulic conductivity of the till formation in the seepage analyses conducted, though did not necessarily reflect potential local hydraulic conductivity values in areas of higher boulder presence, which was believed to be higher.

Total drawdown of the upstream wells over time between the pre-test and the post-test were similar, however the response time (i.e., lag in time between when the pump well flow rate reached steady state and when the upstream wells began to first show a decrease in water table elevation) was slower for the post-test by a factor of 4 across all wells that were instrumented with level loggers. These results show that the

O-pile wall had an effect in the transmissivity rate between upstream and downstream ends. However, trying to quantify how that translated to a change in hydraulic conductivity is complex due to the increased seepage rate / pathway around and below the O-pile wall (Golder, 2020).

Dike instrumentation and seepage pump-back rates

Additional evidence on the effectiveness of the O-pile wall was gathered in the form of vibrating wire piezometer (VWP) data from instruments installed upstream and downstream of the dike as well as seepage pump back rates from the seepage collection pump back station located downstream of the dike. Figure 11 provides a summary of the VWP data collected from the time of the installation of the VWPs until the end of 2023.

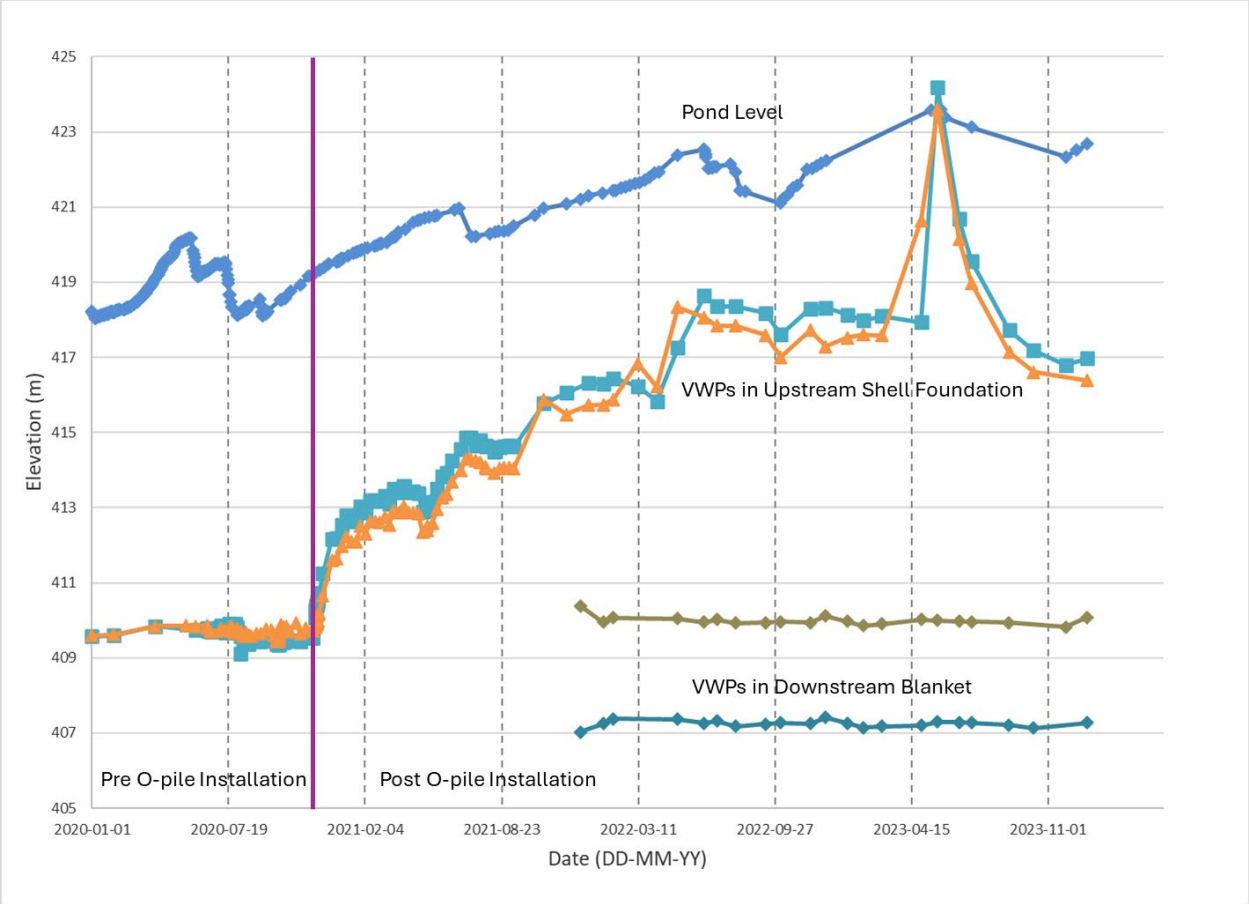


Figure 11: Dike 1 vibrating wire piezometer data compared with primary pond water level

The data indicated an increase in the phreatic surface upstream of the dike immediately after installation of the O-piles, with the trend continuing in subsequent years until the piezometric levels in the instrument begin to mimic that of the pond level fluctuation of the tailings pond. Data from the downstream VWPs show little to no change over time and is consistent with background groundwater levels, indicating that the phreatic surface through the Dike 1 core is decreasing as intended (WSP, 2024). Seepage pump-

back rates have typically ranged on average between 300 m^3/day to 500 m^3/day since the installation of the O-pile wall, which is consistent with the seepage analysis estimate prepared for the design and provided in Figure 7 for a "treated boulder zone".

Conclusion

During the construction of a tailings dam, unexpected foundation conditions may arise that necessitate the collection of additional geotechnical information within a relatively short period of time to modify the design and/or update construction methodology approaches so as to safely execute the work, while maintaining the design intent of the facility. In this instance, the discovery of a boulder field within the foundation glacial till deposit required additional test pitting, monitoring of well installations, and testing of the pump to characterize the subsurface conditions and inform the best foundation preparation approach for seepage control beneath Dike 1. Based on stability and seepage assessments, combined with a comparison of constructability considerations, the O-pile wall approach was decided to likely be the most feasible and effective solution that could be completed within the proposed construction time window. Post construction monitoring of the phreatic surface within Dike 1 as well as downstream seepage pump-back data indicated that the installed O-pile wall appeared to be functioning as intended, ultimately demonstrating that an O-pile cut off wall can be an effective solution for seepage control on par with traditional sheet-pile or grout curtain cut-off wall methods through boulder filled glacial till deposits.

References

AMEC Environment and Infrastructure. 2012. Construction Report 2012 Island Gold Tailings Impoundment. Document TX 11 1179 03. April 2012.

Golder Associates Ltd. 2020. Temporary Vibrating Wire Piezometer TARP for Primary Pond Dyke Construction, Dubreuilville, Ontario. Document No. 19134811, August 2020.

Wood Plc. 2018. Alamos Gold Mine, Design Report – Tailings Storage Facility, Primary Pond – Dykes Raising Project, El. 427 m, Dubreuilville, Ontario. TX17015403-00000-RGE-0001-0, December 21, 2018.

WSP Canada Inc. 2024. Dam Safety Inspection Report, Island Gold Mine TMF. Document No. CA-GLD-22578682, March 2024.

Seismic Imaging Techniques in Mine Closure Planning: Case Studies Across Multiple Abandoned Mines

Majid Mirzanejad, Tetra Tech, USA
Zach Spence, Tetra Tech, USA
Lincoln Steele, Tetra Tech, USA
Will Levandowski, Tetra Tech, USA
Dan O'Connell, Tetra Tech, USA

Abstract

The mining industry has significantly impacted our economies and infrastructures, leaving behind environmental concerns such as abandoned mines that require careful monitoring and remediation. Seismic imaging techniques offer non-intrusive solutions for mapping underground mine workings and estimating subsurface material properties. This includes non-invasive solutions to challenges in monitoring for potential environmental catastrophes and remediation efforts. This study overviews existing seismic techniques and proposes unique geophysical solutions to mine closure and remediation efforts.

Introduction

Mine closure, as the final phase of the mining cycle, has gained attention due to environmental impacts. Unplanned closures lead to issues such as toxic material release and soil degradation. Due to the importance of this matter, the US Congress has established CERCLA to address contaminated sites since 1980. Often, project management teams use data from invasive and non-invasive techniques to plan closures and rely on various geophysical methods for subsurface characterization. Non-invasive techniques are based on geophysical methods and should be chosen based on specific project requirements.

Gravity-based techniques use gravitational fields to associate variations in the Earth's gravity measurements with differences in rock densities. They are ideal for covering large areas and can delineate volumes of material with anomalously low and high gravity values (Tuckwell et al., 2008; Ibrahim and Lat, 2004). Magnetic methods measure the magnetic field to locate concentrations of magnetic materials or determine depths to the basement. They are suitable for mapping large geological structures and characterizing bedrock in land-based and aerial applications (Thompson et al., 1980; Naghibian et al., 2005).

Electrical methods use electric fields generated by currents in the ground to study earth resistivity. These methods involve various measurements to analyze current flow, electric potential, and electromagnetic fields within the subsurface material to gather information about the underlying soil and rock. Essential methods include DC resistivity (Binley and Kemna, 2005), induced polarization (Sumner, 2012), self-potential (Panthulu et al., 2001), electromagnetic (Xue et al., 2019), and magnetotelluric (Chave and Jones, 2012).

Seismic methods are used to determine subsurface properties. Active methods include multichannel analysis of surface waves (Park et al., 1999), seismic refraction tomography (White, 1989; Guedes et al., 2022), and full-waveform inversion (Mirzanejad and Tran, 2019; Tran et al., 2019). Passive methods include MAPS (Baglari et al., 2018), ReMi (Louie, 2001), and HVSR curve analysis (Bignardi et al., 2018). Active methods offer higher resolution but are not always feasible. This paper presents two case studies using active source FWI and passive microtremor HVSR to detect legacy mine adits and assist with slope stability analysis of an abandoned coal mine.

Methodology and implementation

Seismic methods for near-surface characterization utilize various information embedded in the recorded seismic waves. For instance, multichannel analysis of surface waves (MASW) uses information in the recorded data dispersion characteristic to estimate shear-wave (Vs) variation; seismic refraction tomography (SRT) uses first arrival travel times to estimate P-wave velocity (Vp) variation; and full waveform inversion (FWI) uses information embedded in the entire seismic waveform to estimate Vp and Vs in the subsurface soil and rock volume. The following provides a brief methodology of each of these techniques. The interested reader is referred to the sources mentioned in the previous section for a more thorough discussion.

Full waveform inversion (FWI)

Full-waveform inversion (FWI) is a non-linear data-fitting procedure aiming at obtaining detailed estimates of subsurface properties from seismic data, which can result from either passive or active seismic experiments. Given an initial guess of the subsurface parameters (a model), the data are predicted by solving a wave equation. The model is then updated to reduce the misfit between the observed and predicted data. This is repeated iteratively until the data misfit is sufficiently small. The FWI can be performed using surface-based and downhole source configurations with nodes on the surface or inside boreholes for deeper characterization. The maximum characterization depth is a function of the wavelength of the propagating wave and is usually approximately one-half the length of maximum coverage area on the surface. The FWI method does not have the limitations of the more traditional seismic techniques such as MASW and ReMi

and is suited to detecting inverse profiles as well as voids and tunnels. See Tran et al., 2019 for a complete discussion of the methodology.

Multichannel analysis of surface waves (MASW)

The MASW imaging method employed in these case studies is based on the dispersion curve inversion using a constrained ensemble Kalman-filtering method introduced by Albers et al. (2019) and demonstrated in an inversion problem by Seylabi et al. (2022). The generation of the dispersion curve was based on the phase shift method by Park et al. (1999). The MASW technique is useful for providing a quick understanding of subsurface layering and shear-wave velocity structure and is often used to generate initial models for a more thorough analysis using FWI.

Horizontal-to-vertical spectral ratio (HVSR)

The HVSR method calculates the HVSR curve used in earthquake hazard assessment. It predicts depth to bedrock and site amplification response. The produced curve can generate a shear wave velocity profile and is based on single three-component node data. The analysis herein is performed using the OpenHVSR software (Bignardi et al., 2018), known for its capabilities in obtaining and inverting the HVSR curve. The HVSR technique is more suitable for determining the depth of bedrock and is not as useful in finding accurate velocity values due to the non-uniqueness of the amplitude of the fundamental and higher modes. For more details, refer to the paper by Bignardi et al. (2018).

Case studies

The following two case studies of mine closure and remediation projects are discussed to highlight the utility of these surface-based seismic methods:

Case study I: Seismic evaluation of an abandoned mine adit

The case study presents the findings of a 3D seismic evaluation and near-surface characterization at the Silver Dyke Mine in Montana. The goal was to locate an abandoned adit, identify drilling targets, and aid in site remediation. Seismic data were collected from 63 receivers and 105 source locations (Figure 1), and a 3D full-waveform tomography analysis was performed over the abandoned adit. The Carpenter Snow Creek Mining District site spanned 9,000 acres in the Little Belt Mountains of southern Cascade County, Montana. It included mine tailings, waste rock, and mine-influenced waters from numerous inactive and abandoned mines. The EPA identified about 96 abandoned mines at the site, with at least 21 being probable contamination sources. Historic mining operations caused soil, groundwater, surface water, and sediment contamination with metals and hazardous chemicals. The Silver Dyke Mining Complex was the largest

mine in the district, featuring the Silver Dyke Glory Hole, associated underground workings, mill facilities, and eroded tailings in Carpenter Creek's floodplain areas.

The field crew collected data over a 36,382 square feet 3D survey area using 63 wireless seismic nodes and 105 source locations. The nodes were positioned with a receiver spacing of 10×20 feet using GPS coordinates and survey tapes. After installation, the nodes conducted self-diagnostic routines and recorded GPS positions for efficient data processing. A manual slide hammer with a timestamp trigger recording device was used to generate seismic signals. The ground under the hammer was struck at least five times at each source location to improve the signal-to-noise ratio. The data were collected, combined, and filtered to remove noise. Faulty channels were identified and removed. The filtered data were used for FWI analysis along with an initial MASW model. Model parameters were updated iteratively to match the seismic response to field data. The resulting Vs and Vp parameters were used to detect subsurface anomalies.

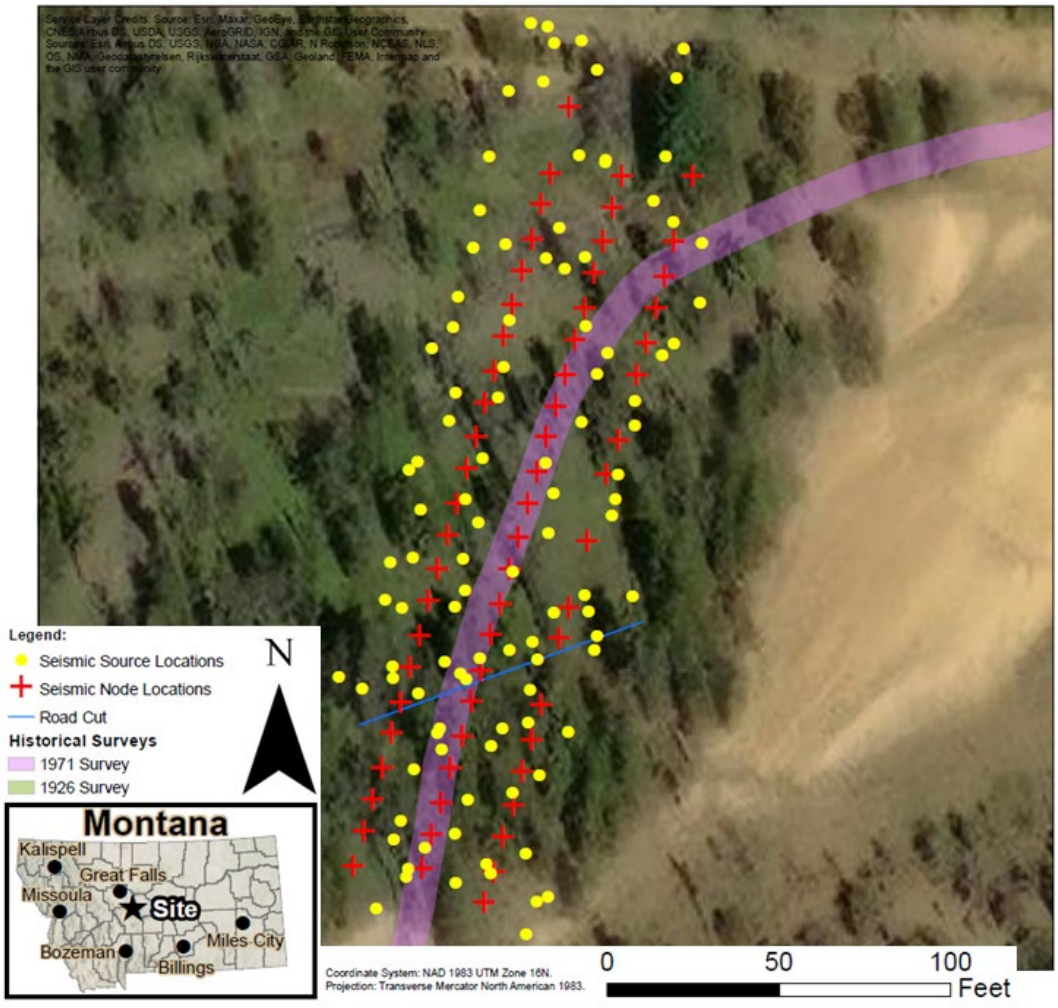


Figure 1: Silver Dyke Mine seismic survey overview

Figure 2 shows a vertical slice view of the final inverted shear-wave velocity 3D volume. There is a clear indication of various anomalies through individual slices. In particular, the anomaly shown by T1 in Figure 2a corresponded to the location of the mining adit that was expected to exist at the site from the project records. We note that the actual as-built location was not known, and the geophysics investigation was used to facilitate its finding. This adit was oriented in the southwest to northeast direction with a depth of around 45 ft from the ground surface southwest to about 60 ft towards the northeast of the survey volume. The second feature of interest is anomaly T2, shown in Figure 2b, which shows contrasting shear-wave velocity values compared to the adjacent material located at a deeper depth of about 90 ft to 100 ft from the surface and oriented west to east of the survey volume. The shear-wave velocities at the location of the T2 anomaly have not been reduced as much as the T1 anomaly during the inversion process due to it being deeper, or possibly due to being filled with a material other than air or water. There was no record of a second adit, and this anomaly was only detected through seismic testing.

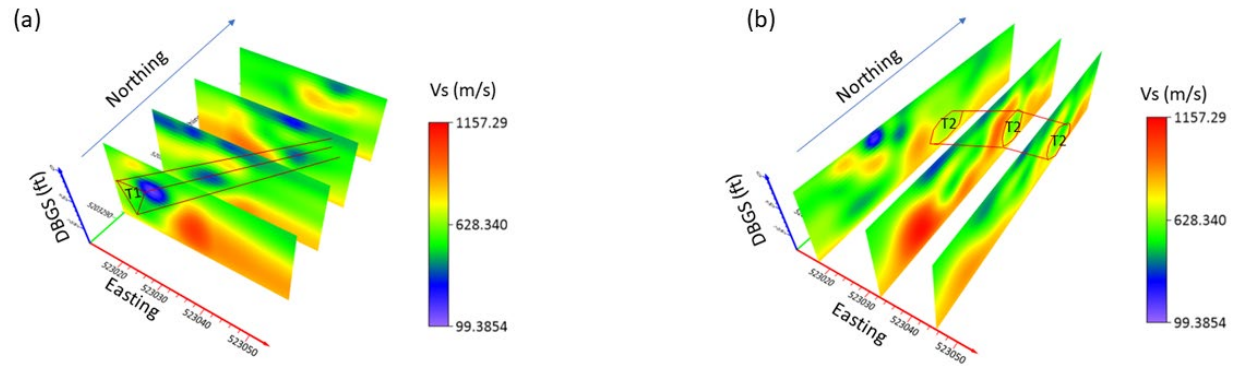


Figure 2: Vertical slices through the inverted shear-wave velocity 3D volume showing features of the mining adits and other subsurface anomalies. The vertical axis shows depth below the ground surface (DBGS) in feet, and the horizontal axis shows easting and northing UTM coordinates in meters

Figure 3 shows sample horizontal slices through the shear-wave velocity 3D volume overlay on the Google Earth satellite imagery base map of the site. The expected path of the mining adit from ground surveys and historical data is also shown, spanning from the southwest towards the glory hole (not shown) located to the northeast of the survey area. There is a concentration of low-velocity anomalies in the 10-ft slice shown in Figure 3a along the expected path of the adit because of less stiff or loose soil and overburden material at those locations.

The T1 and T2 anomalies are shown in panels (b) and (c) of Figure 3, corresponding to vertical slices at 60 ft and 90 ft depths, respectively. The directions of both anomalies are in good agreement with the expected direction of the adit, with the shallower T1 anomaly oriented slightly to the south of the expected orientation.

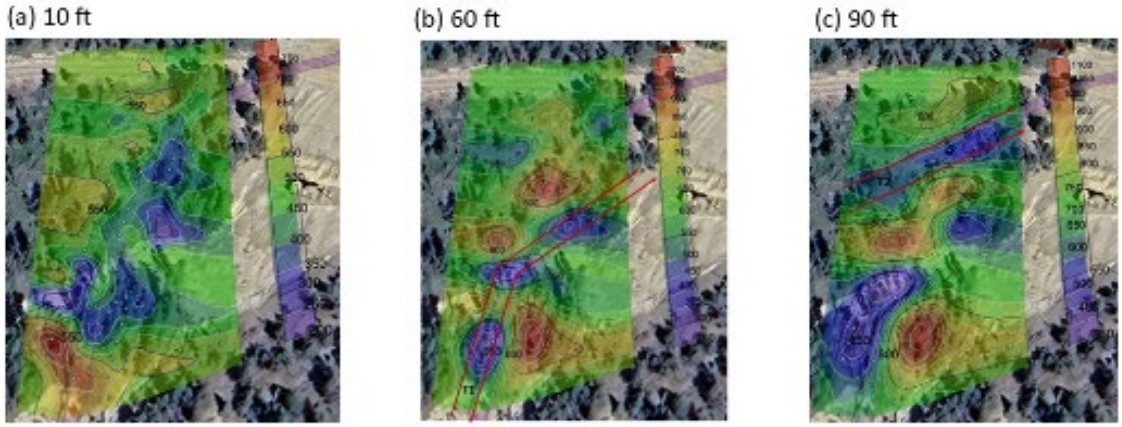


Figure 3: Horizontal slices through the inverted shear-wave velocity volume at depths of 10, 60, and 90 ft below ground surface. The extent of anomalies T1 and T2 are shown in panels (b) and (c) for the 60 ft and 90 ft depths, respectively

Case study II: Estimating shear wave velocities and slope stability analysis at an abandoned coal mine

This study was conducted to assess subsurface conditions and slope stability at the Wise Hill Reclamation Site in Craig, Colorado. The main objective was to measure shear-wave velocities across the slope to support the slope stability assessment. The borehole data was only obtained at the top of the slope with no data at the toe to support a well-informed slope stability analysis due to permitting issues at the time of drilling operations, and the HVSR technique was used to fill this data gap. The site was located on an abandoned coal mine with multiple unknown access tunnels over 200 feet deep. Borehole thermocouple measurements revealed temperatures exceeding 300°F, indicating the presence of coal mine fires across the site. Visual inspections of the slope showed open chimneys and surface cracks, with visible smoke and water vapor emanating from subsurface coal fires.

A microtremor HVSR survey was conducted using sixteen nodes along four lines, as shown in Figure 4. Seismic data were recorded using three-component seismic nodes connected to a digitizer and powered by an external battery. After recording ambient noise data, approximately 5 GB of three-component seismic data were extracted and converted to SEG-Y format for processing. The data were divided into 1-hour segments for HVSR analysis. HVSR curves were compared across the recorded time to ensure they represented subsurface properties and were not influenced by industrial noise.

Figure 5 displays the final horizontal-to-vertical spectral ratio (HVSR) curves for specific sample node locations. The fundamental frequency on these curves represents the depth to the bedrock across the site. Various regression techniques are available to determine the depth of bedrock based on the fundamental frequency shown in Figure 6 (Ibs-von Seht and Wohlenberg, 1999; Parolai et al., 2002). Comparing the fundamental frequency values with the regression lines shows upper and lower limits of

depth to bedrock, as shown in Table 1. Based on these regressions, the average depth to bedrock is 23 feet across all the channels, with variations along different inlines and crosslines, ranging from 5 to 36 feet.

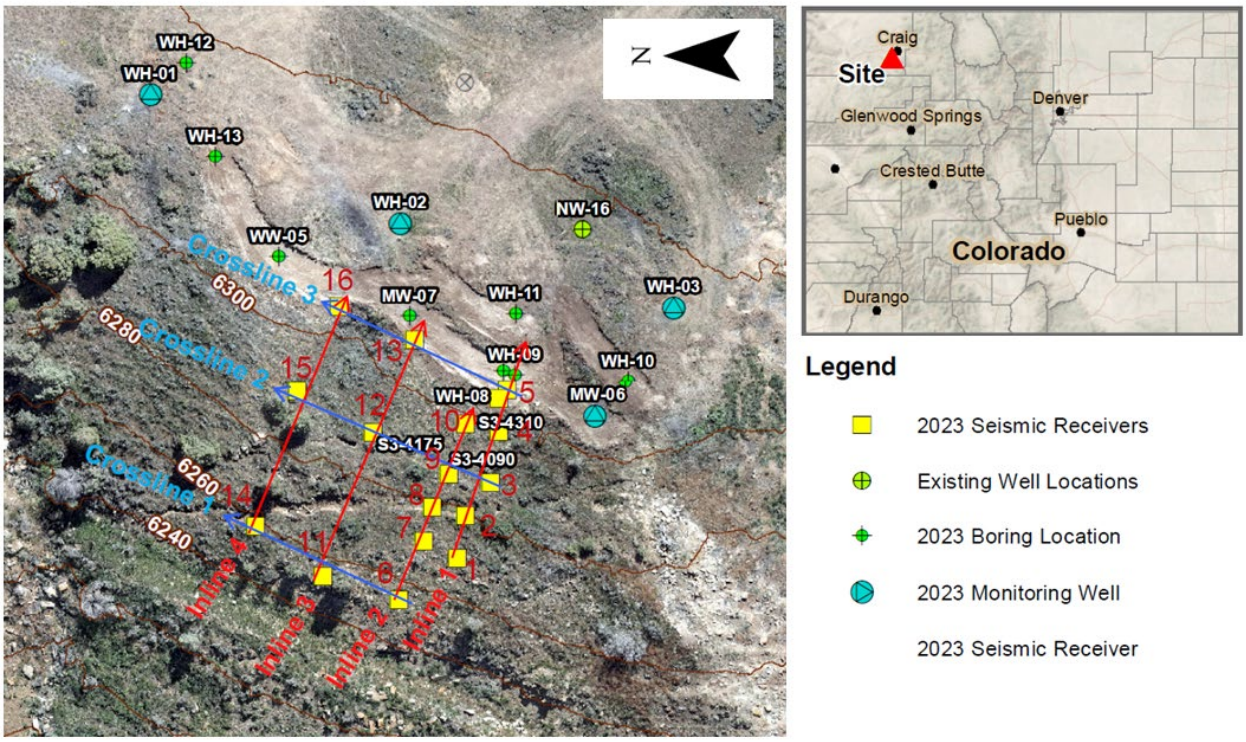


Figure 4: Wise Hill seismic survey overview

To further quantify and visualize velocity variations across the site, the produced HVSR curves were used in a Monte Carlo-based inversion method to match the amplitude and slope of the HVSR curve to that of a theoretical curve. The process perturbed various parameters, including P-wave velocity (Vp), layer thickness (H), viscoelastic medium parameters (QS, QP), density (ρ), and shear-wave velocity (Vs) to generate the best match of the theoretical and experimental HVSR curve that was obtained from the field. Generating many trial models using the Monte Carlo approach allows for exploring the parameter space while looking for new and better-fitting models.

Figure 7 shows velocity variations across sample seismic in-lines and crosslines using a Kriging interpolation method with the 1D velocity profiles from HVSR analysis as input. Based on information from MASW analysis and available drilling logs close to the survey lines, contour lines of 1,500 ft/s to 2,500 ft/s best delineate the range of elevations corresponding to the sandstone bedrock. Based on these results and Table 1, a shallower depth to the bedrock existed downslope of the survey area (nodes 1, 2, 6, 7, 11, and 14), which intercepted deeper slip surfaces and may prevent catastrophic slope failure. We note

that the velocities obtained from HVSR inversion are not unique and require a secondary geophysics method such as MASW, or drilling data to tie with the subsurface geology.

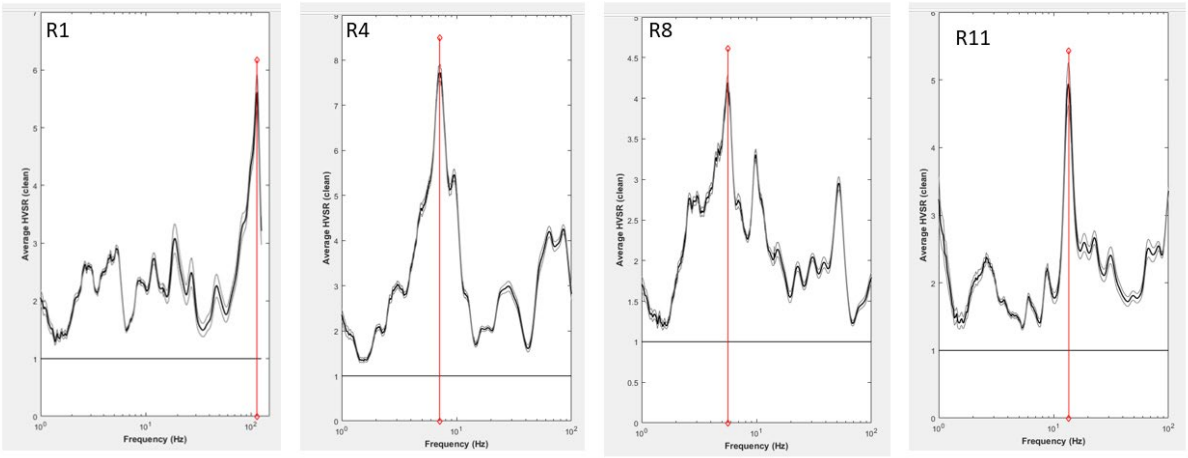


Figure 5: Sample HVSR curves

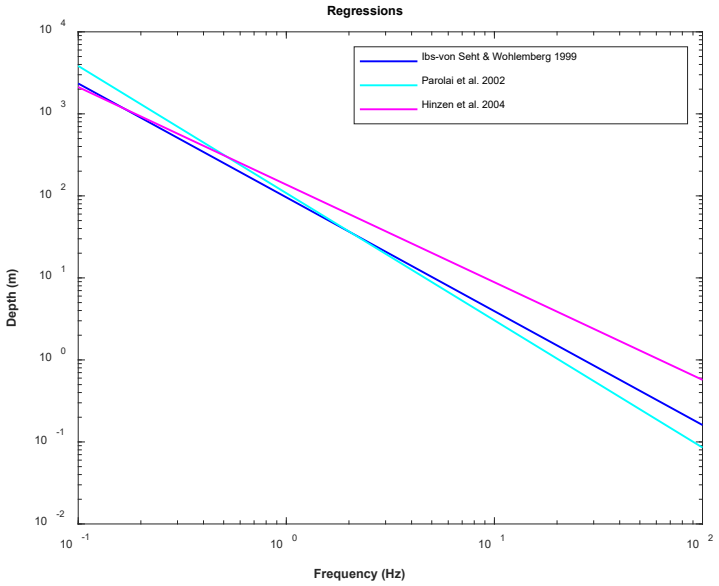


Figure 6: Depth-to-bedrock regression curves

Figures 8 and 9 show the results of a slope stability analysis based on the shear-wave velocity profiles (Figure 7) and Table 1 from the seismic survey for the minimum and maximum estimates of depth to bedrock along crosslines 1, 2, and 3. The slope stability analysis is based on the limit equilibrium formulation and the method of slices for force and moment equilibrium (Zhu et al., 2003). The outputs shown are factors of safety for several potential failure surfaces with the smaller factor of safety outlined. In this context, the factor of safety is defined as the factor by which the soil strength must be reduced so

that the potential sliding mass is at the point of limiting equilibrium. Typically, a critical factor of safety larger than 1.3 is good to ensure that the slope will be stable, with 1.5 preferred for long-term stability. The most comprehensive method implemented in the limit equilibrium formulation is the Morgenstern-Price or the Spencer method (Duncan and Wright, 1980), which provides the most accurate force closure diagram on the slices and is used in this analysis. A Mohr-Coulomb material model is employed with the shear strength parameters defined as tau=C+sigma*tan(ϕ), where C is inherent shear strength, also known as cohesion (can be assumed zero for most critical conditions), ϕ is the angle of internal friction, and sigma is the normal stress. Sigma is obtained from geometry and layering thickness and estimated based on the material unit weight.

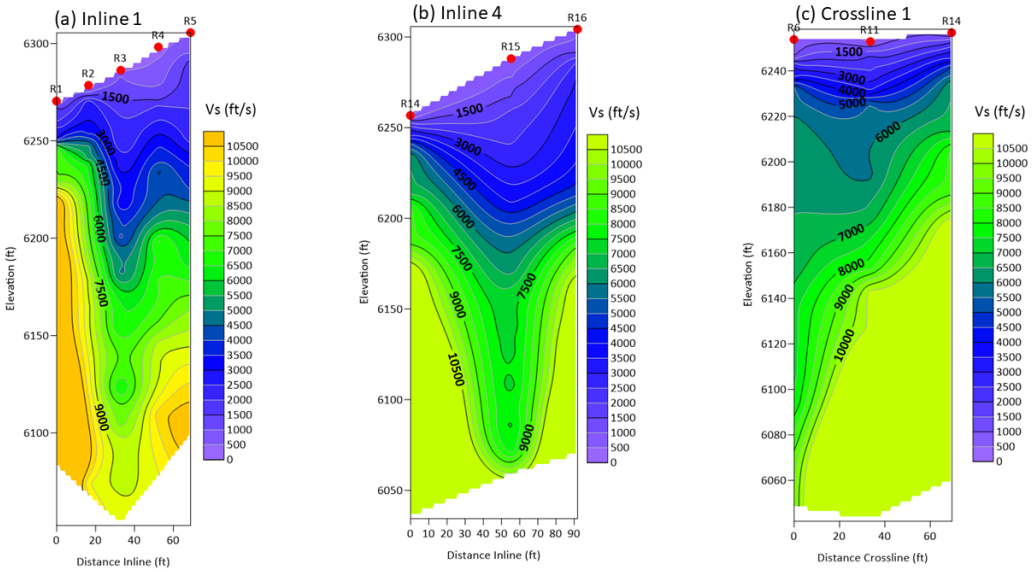


Figure 7: Sample inline and crossline interpolated shear-wave velocity profiles

Based on the performed analysis, the most critical factor of safety for the profile with the lowest estimate of depth to bedrock (Figure 8) is 1.356 for the limiting case of zero cohesion or inherent shear strength, which is an idealized case and may occur as a result of lack of moisture, lack of vegetation or lack of fine grain material or a combination of all these factors. This safety factor for the most optimistic estimate of depth to bedrock is higher than the 1.3 required for short-term stable slope conditions.

Similarly, the most critical safety factor for the profile with the highest estimate of depth to bedrock across crosslines (Figure 9) is 1.175 for the limiting case of zero cohesion, which is lower than the 1.3 value required for the short-term stable slope conditions. The shallow bedrock, as suggested by the HVSR analyses, minimizes the size of the slipping material volume. However, it does not prevent slope failure or possible movement of material onto the road downslope of the analyzed domain. We note that zero cohesion is very unlikely to occur in a real-world case scenario and was used here due to a lack of more accurate

geotechnical data and to show-case variations in the effect of depth to bedrock suggested from the HVSR analysis on the slope stability.

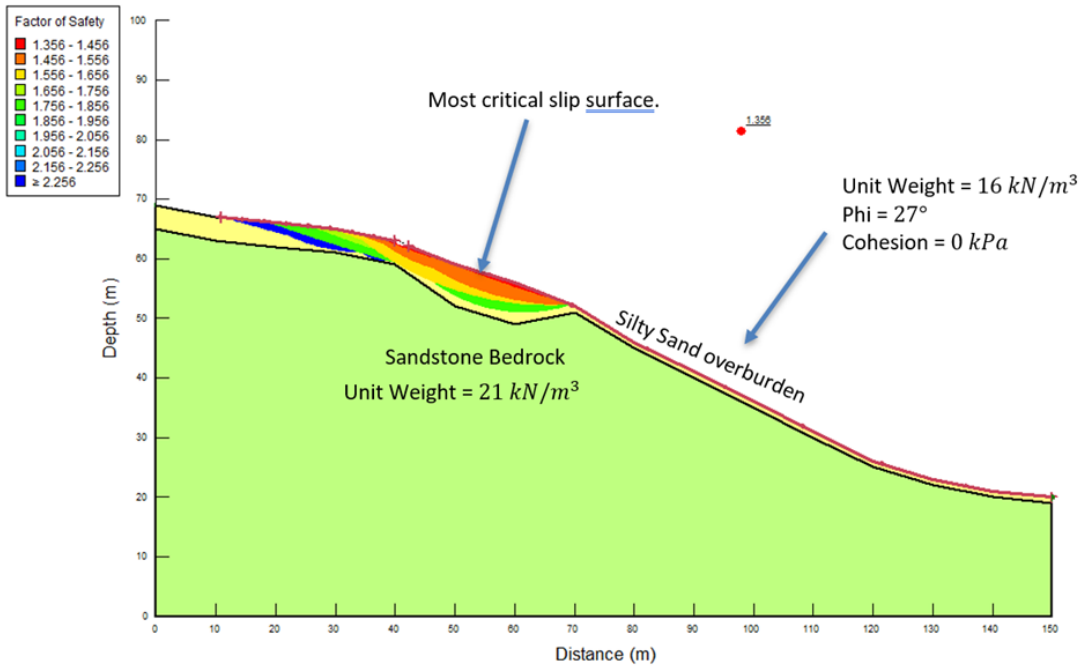


Figure 8: Slope stability analysis showing a probable range of failure surfaces based on the most optimistic estimate of depth to bedrock variation from Table 1

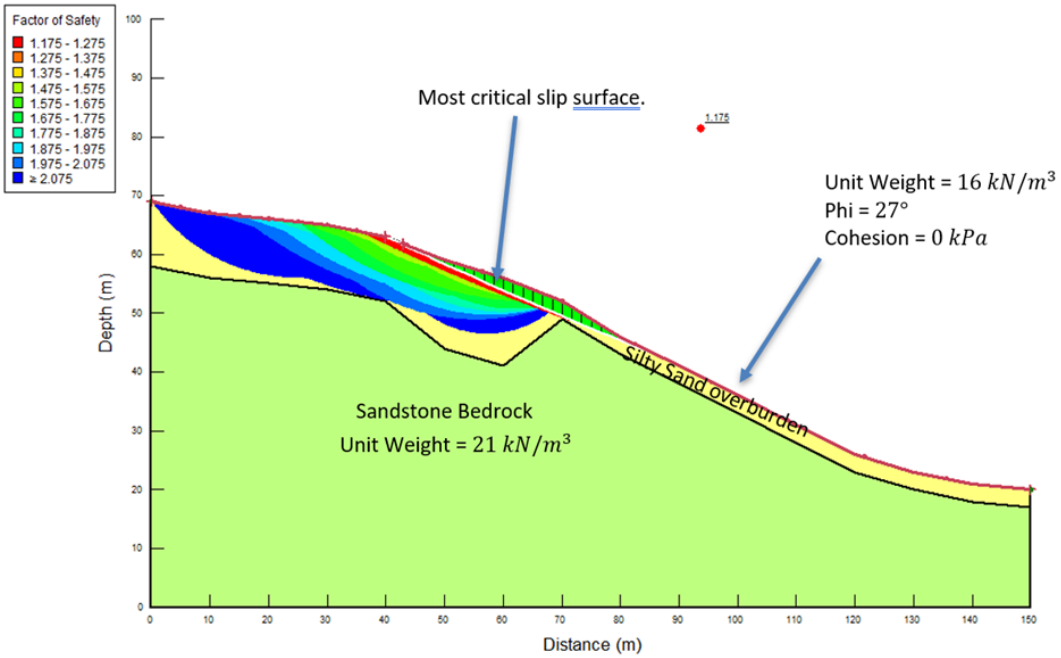


Figure 9: Slope stability analysis showing a probable range of failure surfaces based on the most conservative estimate of depth to bedrock variation from Table 1

Table 1: Estimated depth to bedrock range using HVSR curves

Node ID	Estimated Depth to bedrock					
	Minimum Estimate		Maximum Estimate		Average Estimate	
	m	ft	m	ft	m	ft
R1	0.08	0.262467	0.6	1.968504	0.34	1.1154856
R2	7	22.96588	18	59.05512	12.5	41.0105
R3	9	29.52756	20	65.6168	14.5	47.57218
R4	5	16.4042	12	39.37008	8.5	27.88714
R5	5	16.4042	12	39.37008	8.5	27.88714
R6	0.6	0.262467	0.08	1.968504	0.34	1.1154856
R7	0.1	0.328084	0.8	2.624672	0.45	1.476378
R8	7	22.96588	18	59.05512	12.5	41.0105
R9	5	16.4042	12	39.37008	8.5	27.88714
R10	5	16.4042	12	39.37008	8.5	27.88714
R11	2	6.56168	6	19.68504	4	13.12336
R12	9	29.52756	20	65.6168	14.5	47.57218
R13	5	16.4042	12	39.37008	8.5	27.88714
R14	0.3	0.984252	1	3.28084	0.65	2.132546
R15	4	13.12336	10	32.8084	7	22.96588
R16	3	9.84252	9	29.52756	6	19.68504
Average Inline 1	5.21	17.11	12.52	41.07	8.86	29.09
Average Inline 2	3.43	11.27	8.68	28.47	6.05	19.87
Average Inline 3	5.33	17.49	12.66	41.55	9	29.52
Average Inline 4	2.43	7.98	6.66	21.87	4.55	14.92
Average Crossline 1	0.79	2.60	2.53	8.31	1.66	5.45
Average Crossline 2	6.75	22.14	15.5	50.8	11.125	36.49
Average Crossline 3	4.3	14.21	11	36.08	7.66	25.15
Average of all Nodes	4.16	13.648	10.25	33.628	7.205	23.63

Conclusion

Two case studies demonstrated the effectiveness of active and passive seismic techniques in mine closure and remediation planning. The first study used the active source FWI technique to locate an abandoned mine adit and identify drill targets. The second study used microtremor HVSR analysis to estimate shear wave velocities for slope stability analysis at an abandoned coal mine. The findings indicated the utility of seismic techniques in reducing uncertainty in the mine closure and remediation planning process and reducing the gaps in the data from invasive testing methods.

References

Albers, D.J., Blancquart, P.A., Levine, M.E., Seylabi, E.E. and Stuart, A. 2019. Ensemble Kalman methods with constraints. *Inverse Problems* 35(9). DOI:10.1088/1361-6420/ab1c09

Binley, A. and Kemna, A. 2005. DC resistivity and induced polarization methods. In *Hydrogeophysics:* 129–156. Dordrecht: Springer Netherlands.

Bignardi, S., Yezzi, A.J., Fiussello, S. and Comelli, A. 2018. OpenHVSR-Processing toolkit: Enhanced HVSR processing of distributed microtremor measurements and spatial variation of their informative content. *Computers & Geosciences* 120(2): 10–20.

Baglari, D., Dey, A. and Taipodia, J. 2018. A state-of-the-art review of passive MASW survey for subsurface profiling. *Innovative Infrastructure Solutions* 3: 1–13.

Chave, A.D. and Jones, A.G. 2012. *The Magnetotelluric Method: Theory and Practice*. Cambridge University Press.

Duncan, J.M. and Wright, S.G. 1980. The accuracy of equilibrium methods of slope stability analysis. *Engineering Geology* 16(1–2): 5–17.

Guedes, V.J.C.B., Maciel, S.T.R. and Rocha, M.P. 2022. Refrapy: A Python program for seismic refraction data analysis. *Computers and Geosciences* 159: 105020.

Ibrahim, A.T.H. and Lat, C.N. 2004. Detecting subsurface voids using the microgravity method – A case study from Kuala Lipis, Pahang.

Ibs-von Seht, M. and Wohlenberg, J. 1999. Microtremor measurements used to map thickness of soft sediments. *Bulletin of the Seismological Society of America* 89(1): 250–259.

Louie, J.N. 2001. Faster, better: shear-wave velocity to 100 meters depth from refraction microtremor arrays. *Bulletin of the Seismological Society of America* 91(2): 347–364.

Mirzanejad, M. and Tran, K.T. 2019. 3D viscoelastic full waveform inversion of seismic waves for geotechnical site investigation. *Soil Dynamics and Earthquake Engineering* 122: 67–78.

Nabighian, M.N., Grauch, V.J.S., Hansen, R.O., LaFehr, T.R., Li, Y., Peirce, J.W., Phillips, J.D. and Ruder, M.E. 2005. The historical development of the magnetic method in exploration. *Geophysics* 70(6).

Park, C.B., Miller, R.D. and Xia, J. 1999. Multichannel analysis of surface waves. *Geophysics* 64(3): 800–808.

Parolai, S., Bormann, P. and Milkereit, C. 2002. New relationships between Vs, thickness of sediments, and resonance frequency calculated by the H/V ratio of seismic noise for the Cologne area (Germany). *Bulletin of the Seismological Society of America* 92(6): 2521–2527.

Panthulu, T.V., Krishnaiah, C. and Shirke, J.M. 2001. Detection of seepage paths in earth dams using self-potential and electrical resistivity methods. *Engineering Geology* 59(3–4): 281–295.

Qiang, W.U. and Songying, L.I. 2018. Positive and negative environmental effects of closed mines and its countermeasures. Journal of China Coal Society (1).

Sasaki, Y. 1989. Two-dimensional joint inversion of magnetotelluric and dipole-dipole resistivity data. *Geophysics* 54(2): 254–262.

Seylabi, E., Hallal, M.M. and Cox, B.R. 2022. Site characterization at Treasure Island and Delaney Park downhole arrays by heterogeneous data assimilation. *Earthquake Spectra* 38(4): 2398–2421.

Sumner, J.S. 2012. *Principles of Induced Polarization for Geophysical Exploration*. Elsevier.

Tuckwell, G., Grossey, T., Owen, S. and Stearns, P. 2008. The use of microgravity to detect small distributed voids and low-density ground. *Quarterly Journal of Engineering Geology and Hydrogeology* 41(3): 371–380.

Thompson, R., Stober, J.C., Turner, G.M., Oldfield, F., Bloemendal, J., Dearing, J.A. and Rummery, T.A. 1980. Environmental applications of magnetic measurements. *Science* 207(4430): 481–486.

Tran, K.T., Mirzanejad, M., McVay, M. and Horhota, D. 2019. 3-D time-domain Gauss-Newton full waveform inversion for near-surface site characterization. *Geophysical Journal International* 217(1): 206–218.

White, D.J. 1989. Two-dimensional seismic refraction tomography. *Geophysical Journal International* 97(2): 223–245.

Xue, G., Chen, W., Cheng, J., Liu, S., Yu, J., Lei, K., Guo, W. and Feng, X. 2019. A review of electrical and electromagnetic methods for coal mine exploration in China. *IEEE Access* 7: 177332–177341.

Zhu, D.Y., Lee, C.F. and Jiang, H.D. 2003. Generalised framework of limit equilibrium methods for slope stability analysis. *Géotechnique* 53(4): 377–395.

Tailings Risk Mitigations at Hudbay Flin Flon: Prioritization Approach and Implementation of Multiple Mitigation Measures

Brad Russell, BGC Engineering Inc., Canada
Trevor Ross, Hudbay Minerals Inc., Canada
Matt Dugie, BGC Engineering Inc., Canada
Matthew Schafer, BGC Engineering Inc., Canada
Ed Carey, BGC Engineering Inc., Canada

Abstract

Review of foundation conditions of legacy dams and liquefaction susceptibility assessment at the Flin Flon Tailings Impoundment System identified that several perimeter embankments at the facility were not meeting target safety factors for undrained peak and post-liquefaction loading conditions. It was recognized that remediation of these dams would require extensive investigation and engineering and a thoughtful construction approach on sensitive foundations; a process that would require multiple years to complete.

Several risk reduction measures were identified that could be implemented at the facility. In a phased approach, the project was advanced in a prioritized manner based on the assessed level of risk associated with the various structures, consideration for impacts to operations, as well as practical limitations. The prioritization and sequencing of mitigation measures were based on a qualitative assessment with risk reduction measures ranging from simple measures that could be adopted within a matter of days to complex engineered solutions that required several years to implement, all while monitoring performance.

These measures included: changes in tailings deposition strategy and location; construction of open channel spillways to improve water management and reduce ponding water levels in the TSF; upgrades to the monitoring program and emergency response plans to enable improved identification and response to adverse dam performance including installation of a novel fiber optic cable monitoring system intended to identify large displacement events; control berms to isolate the community from the tailings facility; and dam upgrades that primarily consisted of toe berms to provide buttressing weight on the downstream side of the structures.

This paper describes the means of prioritizing risks, where several hazards were identified with conflicting considerations. The prioritization method enabled practical sequencing and successful

implementation of risk mitigation measures. The designs of key features are described, along with identification of some of the main design constraints and how these were addressed.

Introduction

The Flin Flon Tailings Impoundment System (FFTIS), shown in Figure 1, is a part of the Flin Flon Metallurgical Complex (FFMC). The FFTIS was commissioned in the early 1930s when Hudson Bay Mining & Smelting Co., Limited (HBM&S), which later became Hudbay Minerals Inc. (Hudbay), began depositing tailings in the natural water body that was Flin Flon Lake. As storage capacity requirements increased, containment structures were constructed on an as-needed basis. As a result of the depositional history of tailings and construction practices at the FFTIS, many of the containment structures are founded on hydraulically placed tailings and constructed in an upstream orientation.

Following the catastrophic tailings flow liquefaction failures of the Fundão Dam at the Samarco Mine and the Feijão Dam at Brumadinho in Brazil in 2015 and 2019, respectively, a review of tailings dam safety was initiated by the mining industry. The focus of the review was mainly on tailings dams constructed in the upstream manner, and more specifically, tailings dams that have brittle contractive materials providing a portion of the support or foundation. Further, the incidents prompted updates to design standards and guidelines, including the design approach that if potentially liquefiable materials exist in an embankment or foundation, then the design should progress based on the assumption that liquefaction will occur and use post-liquefaction strengths in stability analysis (Morgenstern, 2018) with an appropriate target factor of safety (FOS).

In 2016, based on screening-level assessment of historical cone penetration test (CPT) data, it was identified that potentially liquefiable tailings existed within the foundations of several dams at the FFTIS. Detailed investigations began in 2017 to assess the liquefaction susceptibility of foundation materials within a critical state soil mechanics framework, characterize undrained peak and post-liquefaction (residual) shear strengths for liquefiable materials, and evaluate the FOS for the FFTIS dam structures based on two-dimensional limit equilibrium analyses. Field work included seismic refraction (SR) and multichannel analysis of surface waves (MASW), geophysical, seismic CPT with pore pressure measurement (SCPTu), and geotechnical drilling with in-situ standard rate and variable rate shear vane testing (VST) and fixed-piston Shelby tube sampling. Laboratory work included index and advanced testing, including triaxial testing following the methods detailed by Jefferies and Been (2016) to support defining critical state soil properties.

Several structures, with a combined length of over 9 km, were identified that did not meet the target FOS criteria developed for the site based on industry guidelines (1.5 for peak undrained strength and 1.1

for post-liquefaction strength loading conditions). In response to the findings, Hudbay initiated a phased approach for upgrades to the facility, referred to as the Legacy Dam Upgrades (LDU) project.



Figure 1: Overview of FFTIS (2018 image). Structures included within LDU project colored orange

Site description

The FFMC is located west of the City of Flin Flon, Manitoba and immediately north of the Town of Creighton, Saskatchewan. The FFTIS generally consists of separate impoundments for each of the mill tailings, zinc pressure leach (ZPL) tailings, and zinc oxide residue. Impoundments for each of the ZPL tailings and zinc oxide residue were constructed immediately adjacent to structures that were constructed at earlier stages in site development to contain mill tailings. Tailings production and deposition at the facility ceased in July 2022 and the facility is currently in a care and maintenance phase. The site is separated into several discrete ponds which served to manage the different tailings streams during operations, as well as surface water management and treatment which continues in the care and maintenance phase.

The site is an undulating landscape typical of the Canadian Shield with elevated bedrock outcrops and a typical lithological sequence in depressions consisting of peat, fine grained glaciolacustrine soils and/or glaciofluvial sand, and glacial till overlying bedrock. The glaciolacustrine clay is typically normally consolidated; however, in many areas an overconsolidated upper layer (crust) is present. The site is located within a relatively low seismicity part of central Canada.

Approach to prioritization sequencing

Several risk mitigation measures were identified that could be implemented at the facility. In a phased approach, the LDU project was advanced in a prioritized manner based on the assessed level of risk associated with the various structures, consideration for impacts to operations, as well as practical limitations. It was recognized that efforts should be made to minimize potential adverse changes in loading conditions at any of the structures not meeting target FOS, and to the extent possible, reduce loading. It was also recognized that stability upgrade construction itself was capable of triggering liquefaction and the assessment of foundation conditions, design, and construction approach would require consideration of this potential.

The prioritization and sequencing of mitigation measures were based on a qualitative assessment that generally considered the following:

1. Existence of a population at risk (PAR) in the downstream area.
2. Effectiveness of the mitigation measure(s) to reduce impact to PAR (consequence reduction).
3. Effectiveness of the mitigation measure(s) to reduce probability of failure (PoF).
4. Requirements for mitigation measure implementation to support continued operations (deposition location or crest raise requirement).
5. Effectiveness of the mitigation measure(s) to reduce risks from multiple hazard sources.
6. The relative timeline required for assessment, engineering, and construction to implement the mitigation measure.
7. The relative cost and resource requirement to complete the mitigation measure.

Based on these considerations, project phasing was developed as described below, along with the related rationale:

- Phase 1: included mitigation measures that could be implemented with relatively minimal investigation and analysis and would have relatively immediate benefit to either reduce potential consequence or PoF (selected initial mitigation measures are described below), including stability upgrades required to support continued tailings deposition of ZPL tailings (i.e. East ZPL Dam toe berm and South ZPL Dam toe berm). A focus of this phase was also to reduce potential impacts (consequence) to the adjacent community of Creighton (i.e. Environmental Control Berms, described below). Through this phase, the necessary investigation, analyses, and engineering for the stability upgrades planned for the subsequent phases was undertaken.
- Phase 2: focused on stability upgrades to reduce potential impact to the highway located adjacent to the facility.

- Phase 3: the early portion of this phase focused on stability upgrades that would reduce potential impacts to the downstream community of Flin Flon (located further downstream compared to Creighton). The balance of this phase was for stability upgrades to structures that had potential impacts that were expected to remain within the limits of the site.

Initial mitigation measures

The initial mitigation measures, shown in Figure 2, were implemented at the site including:

1. Relocation of tailings deposition away from dams with FOS below target
2. Construction of the Oxide Pond Dam (OPD) Spillway; to reduce likelihood of high pond levels (and large pond volumes stored) against the OPD
3. Construction of the South Causeway Spillway; to reduce likelihood of high pond levels (and large pond volumes stored) against several dams
4. Construction of the SZPL Spillway; to reduce likelihood of high pond levels (and large pond volumes stored) against the EZPL Dam and SZPL Dam.

Further, measures were taken to improve monitoring and emergency response capabilities at the facility, including a revision of the emergency preparedness and response plans. Monitoring upgrades included installation of additional conventional geotechnical instruments including piezometers, slope inclinometers, shape arrays, survey prisms, and settlement pins; the instruments were enabled with near real-time data acquisition and upload via cellular network to a data storage and viewing platform.

A significant initial upgrade included installation of a continuous fiber optic cable across the crest of approximately 6 km of tailings dam structures at the facility (Forbes et al., 2021). The purpose of the fiber optic cable was to provide near real-time monitoring (i.e., detection) of a dam failure event and be capable of configuration to an external alarm system. The fiber optic cable, and associated system, was not intended to provide an early warning of a developing dam failure, given the rapid nature and minimal precursor indicators of a potential flow liquefaction-type failure. An interrogation unit, and related processing equipment, monitored the fiber alignment at a sampling rate of at least 1 kHz (i.e., 1,000 cycles per second) with a 10 m channel spacing (i.e., a measurement every 10 m along the alignment). Two types of alarm thresholds were configured to detect potential dam breach scenarios: 1) a Fiber Break Alarm and 2) a Near Fiber Break Alarm. A near real-time notification system was configured to send alerts in the event of a triggered alarm; test alarm scenarios indicated that the system could detect an alarm exceedance and provide the location of the alarm along the fiber optic cable (georeferenced location along the tailings dam) within seconds of the test.



Figure 2: Overview of FFTIS (2019 image). Initial mitigation measures highlighted green

Environmental control berms

As an early consequence reduction measure, Hudbay took an innovative approach to build Environmental Control Berms (ECBs) to isolate the neighboring community from the tailings facility and reduce the potential risk of a dam breach to the nearby population.

A tailings dam breach assessment was performed to inform selection of the alignments and crest elevations. A broad spatial distribution of potential breach locations within the south end of the FFTIS were assessed and extreme breach scenarios were also evaluated in consideration of the potential for an extensive flow liquefaction slope failure, with a wider than typical breach width, such as that which occurred at the Feijão Dam at Brumadinho.

The ECBs (Berm 1, Berm 2, and Berm 3) were designed to span three topographic lows as rockfill embankments, with 6 m wide crests, 1.5H:1V north slopes, and 3H:1V south slopes facing the neighboring community to allow for revegetation. The approximate berm dimensions are as follows: Berm 1 – 5 m high and 130 m long, Berm 2 – 14 m high and 370 m long, and Berm 3 – 6 m high and 60 m long. The berm designs included provisions to maintain drainage through the structures. A simplified design cross-section is shown in Figure 3 while Figure 4 provides an overview photo of the completed structures.

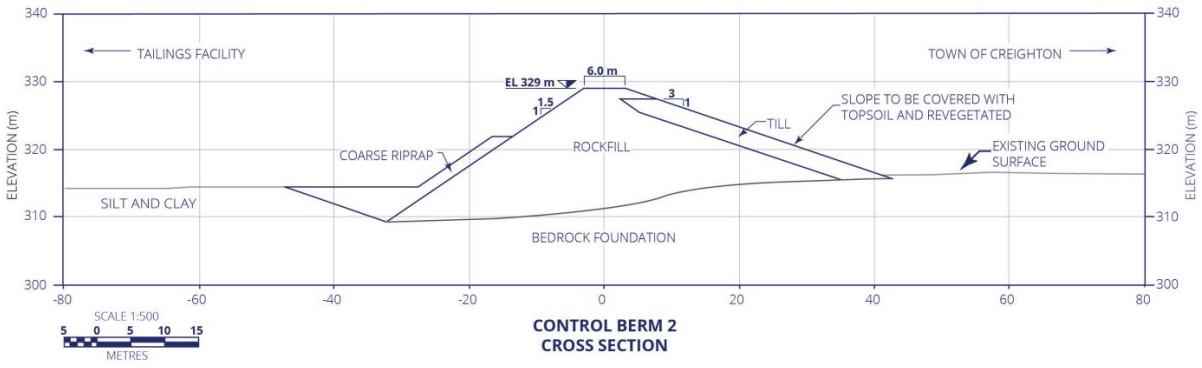


Figure 3: ECB 2 design cross-section



Figure 4: Overview photograph of ECBs

Toe berm design and engineering assessments

Engineering assessments

Between 2017 and 2022, 104 CPTs and 105 drill holes were completed on the site, along with two instrumented test fills, a test excavation, and two dewatering/pumping tests as means to better characterize the materials and the foundation conditions, and plan construction implementation.

Engineering analyses included CPT-based liquefaction susceptibility assessment using methods including Plewes et al. (1992), Robertson (2016), and the CPT-inversion approach of Jefferies and Been (2016). Undrained peak and post-liquefaction (residual) shear strengths were developed based on in-situ variable rate vane shear tests as well as laboratory and case-history based methods available in literature including Olson and Stark (2003), Sadrekarimi (2014), Robertson (2022), and Jefferies and Been (2016).

Stability analyses included primarily two-dimensional limit equilibrium analyses along with selected finite element analyses with the Norsand critical state constitutive model.

The design process considered a number of stability upgrade alternatives including toe berms, de-watering, and ground improvement; details of the options considered are summarized in Table 1.

Table 1: Summary of stability upgrade alternatives considered.

Stability Upgrade Category	Description	Option
Increasing the resistance force	Can be done by adding weight at the toe of the dam or reducing the pore water pressures. Both options result in an increase in effective stress of the soil, and consequently increase in undrained strength leading to increase in FOS	Building a toe berm Dewatering wells
Decreasing the driving force	The general way to decrease the driving force is to remove weight from the upstream of the failure surface	Crest and slope cut
In situ ground improvement	This option is used to increase the shear strength of the soil usually by adding cementitious material into the soil or densifying the soil	Cutter soil mixing Large diameter soil mixing Trench cutting and soil mixing Jet grouting Compaction grouting Vibro compaction Dynamic compaction
Soil replacement	Replacing the weak stratum with well compacted granular soil, crushed stones, or concrete columns in order to increase the shear strength and consequently, FOS values.	Rigid inclusions Stone columns Granular shear keys
Structural reinforcement	Adding structural elements to the slope or foundation soil to stop or increase the resistance along the path of failure planes.	Sheet piles Bored piles Retaining structure

Shear resistance alternatives were evaluated as the most feasible solution to provide the required stability upgrades at the structures considering: 1) toe berms and shear keys are conventional dam stability upgrade approaches with past precedence at the site; 2) toe berm construction would progressively increase the FOS; and 3) toe berms and shear keys would require relatively less engineering effort and time compared to ground improvement options. Further, additional project benefits could be realized by utilizing local contractors with extensive site experience. The stability upgrade design also incorporated removal (borrow) of historical tailings deposits and dams as both a source of toe berm fill but also as a means of reducing driving forces where possible and assist in the overall upgrade strategy. Shear keys, excavated to bedrock, were incorporated into the toe berm designs where practical and/or where site constraints required

a composite design solution. Surface water features and site drainage channels were realigned and upgraded to account for the toe berm footprints and to better align with long-term closure objectives for the site.

Details of the dam stability upgrade designs for select structures, the South Weir Dam (SWD) and Southeast Dam (SED), are provided in the subsequent sections.

South Weir Dam stability upgrade

The original starter dam construction at the SWD began in the 1940s to span across a topographic low between bedrock ridges where the historical Flin Flon Lake narrowed to approximately 50 m wide. The dam fills comprise compacted tailings and waste rock fill with smaller amounts of slag fill and natural sand and gravel for drains and filter layers; it was generally raised in an upstream direction. The Clarification Pond is situated immediately downstream of the structure with a typical water level of El. 318 m; the pond is used primarily for polishing of effluent quality. During early periods of operation, tailings migrated hydraulically from the southern discharge and had dispersed throughout the footprint of the proposed SWD toe berm.

The SWD toe berm, shown in Figure 5, was designed to provide buttressing weight (resistance to driving forces) at the SWD toe and downstream area. The toe berm foundation stratigraphy was dominated by a relatively narrow bedrock topographic low that extends upstream to downstream underlying the Clarification Pond. The topographic low gradually widens in the downstream direction and was infilled with natural sediments including peat several meters thick and glaciolacustrine clay up to approximately 15 m in thickness. The bedrock elevation within the low ranges from El. 285 m to 295 m (approximately 23 m to 33 m below Clarification Pond level).

The toe berm was designed to span between the shorelines of the Clarification Pond to form a "working platform" at El. 319.5 m. This fill was to be placed subaqueously and compacted in a manner to displace the Clarification Pond sludge material in a downstream direction and penetrate the underlying tailings material. A "mud wave" of displaced sludge was expected to form downstream of the placed fills; the material was excavated and hauled away to avoid restricting the penetration of the rockfill. The design included two benches over the working platform, to El. 322.5 m over a 170 m width and El. 324 m over a 60 m width, which was constructed of rockfill in compacted lifts. A simplified design cross-section is shown in Figure 6.

As construction progressed, a total of 14 SCPTu's and seven drill holes were completed within the toe berm footprint as part of design confirmation with the intent: 1) to confirm toe berm fill and foundation stratigraphy including the bottom of rockfill elevation target at El. 314 m was being achieved, 2) to investigate the foundation soils using CPT and VST to confirm selected design inputs, 3) to install instrumentation to support both short-term construction monitoring and long-term performance monitoring

of the toe berm. The drilling was completed in three phases during construction to allow stratigraphy (including bottom of rockfill) to be confirmed as working pad construction progressed. It also allowed instrumentation including piezometers, settlement plates, and slope inclinometers to be installed and thus, monitored relatively close to the leading slope of the working pad over the duration of the work to help promote worker and dam safety. The encountered toe berm fill and foundation stratigraphy were generally in agreement with the SWD toe berm design inputs and generally confirmed the design basis. Localized areas of thicker peat and glaciolacustrine clay were encountered at some locations within the topographic low underlying the toe berm. At one location, measured PWP conditions following working pad construction were higher than design expectations. In this area, a test fill was completed to confirm the understanding of the PWP conditions prior to completing Stage 2 toe berm construction above El. 319.5 m.

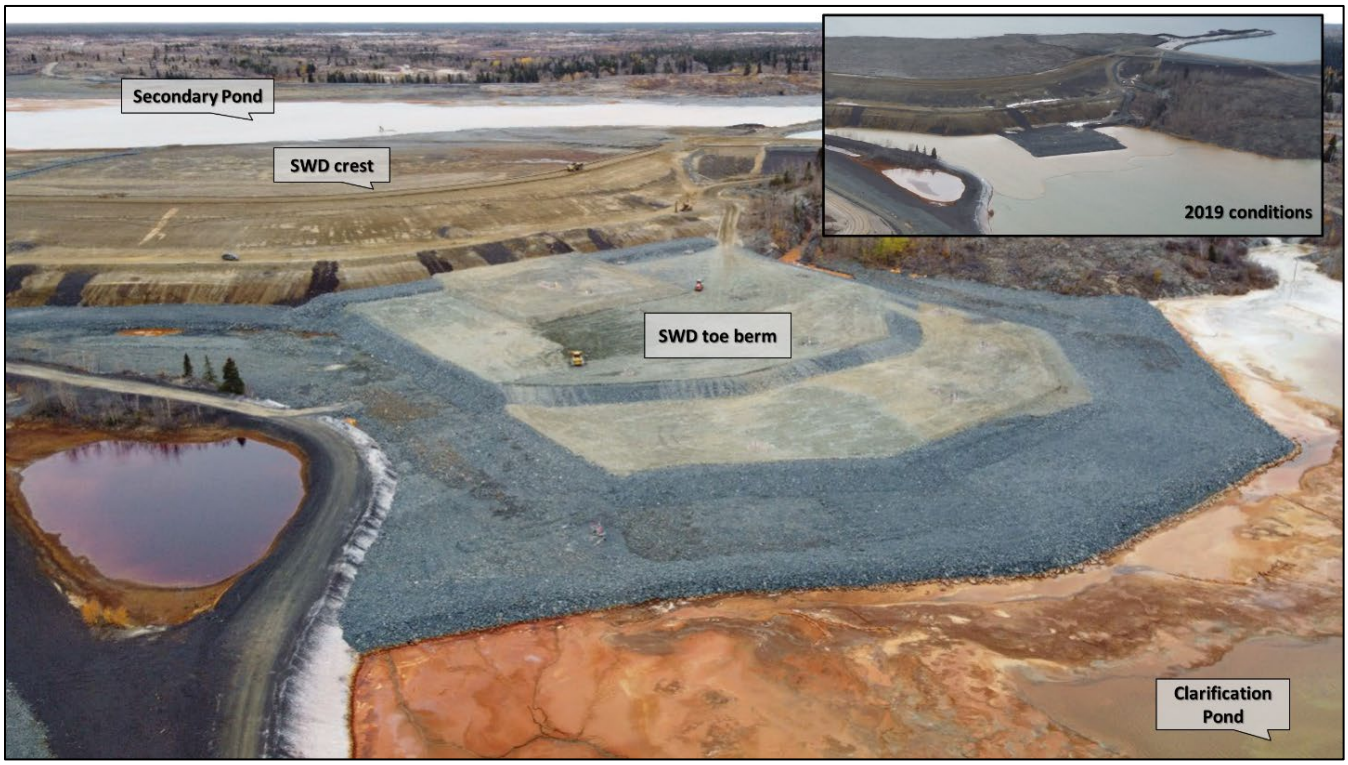


Figure 5: SWD toe berm construction; nearing completion and initial conditions (inset)

Southeast Dam stability upgrade

The Southeast Dam is one of the oldest structures within the Flin Flon Tailings Impoundment System. Construction activities began in 1927. The original starter dam was constructed across historical Flin Flon Lake between bedrock highs where the lake narrowed to approximately 125 m. The starter dam was generally founded on soft to firm normally consolidated glaciolacustrine clay up to approximately 6 m in thickness. The dam was raised in an upstream direction as required, using waste rock, slag, and compacted tailings. The dam comprises several terraces where previous construction included set-backs to reduce the

seepage gradient through the structure. The terraces were constructed over existing tailings beaches up to approximately 40 m in thickness beneath the structure.

The SED stability upgrade design involved the combination of a toe berm and shear key. Inclusion of the shear key was necessary due to constraints imposed by surface water management infrastructure (the Lake Bottom Sump) located at the downstream toe of the structure. Prior to the start of construction, a shear key field excavation trial was constructed over a plan area of approximately 25 m by 5 m. The trial work confirmed that shear key construction in a series of overlapping panels was feasible. The shear key design and construction involved the excavation of glaciolacustrine soil to bedrock over the design footprint and backfilling with compacted rockfill. A sand and gravel filter was placed along the upstream perimeter of the shear key to limit the potential of internal erosion of the foundation soil into the rockfill.

The toe berm at the lower terrace consisted of a single 85 m wide bench graded between El. 321 m to El. 319 m with perimeter slopes of 1.5H:1V. The toe berm is comprised of three primary material zones (from downstream to upstream): 1) a 3.8 m wide zone of coarse rockfill for erosion protection; 2) a 15 m wide zone of compacted rockfill; and 3) a 0 m to 30 m wide zone of compacted tailings. The toe berm included an internal drainage system that comprised three finger drains that tied into the existing slag downstream slope and a toe drain connecting the finger drains. The toe berm included benches in the upper portion of the structure; each of these were primarily constructed of compacted tailings with a 0.5 m thick layer of rockfill erosion protection. A simplified design cross-section is shown in Figure 7.

Monitoring and performance

The LDU project relied on an extensive network of instrumentation monitoring soil behavior. Over 200 automated piezometers, two automated shape arrays, 13 slope inclinometers (read daily), and 60 survey prisms (read daily) supported the evaluation of measured soil behavior versus expected performance. Further, the fiber optic detection system was monitored throughout the work and offered insight during quarry blasting activities and the subsequent assessment and field inspections to permit resumption of activities.

A construction monitoring and emergency preparedness plan was developed and updated throughout the project. The plan included the responsibilities of various parties involved in the construction works, site specific emergency response procedures, and dam safety monitoring requirements, including instrumentation reading frequencies and trigger levels for action.

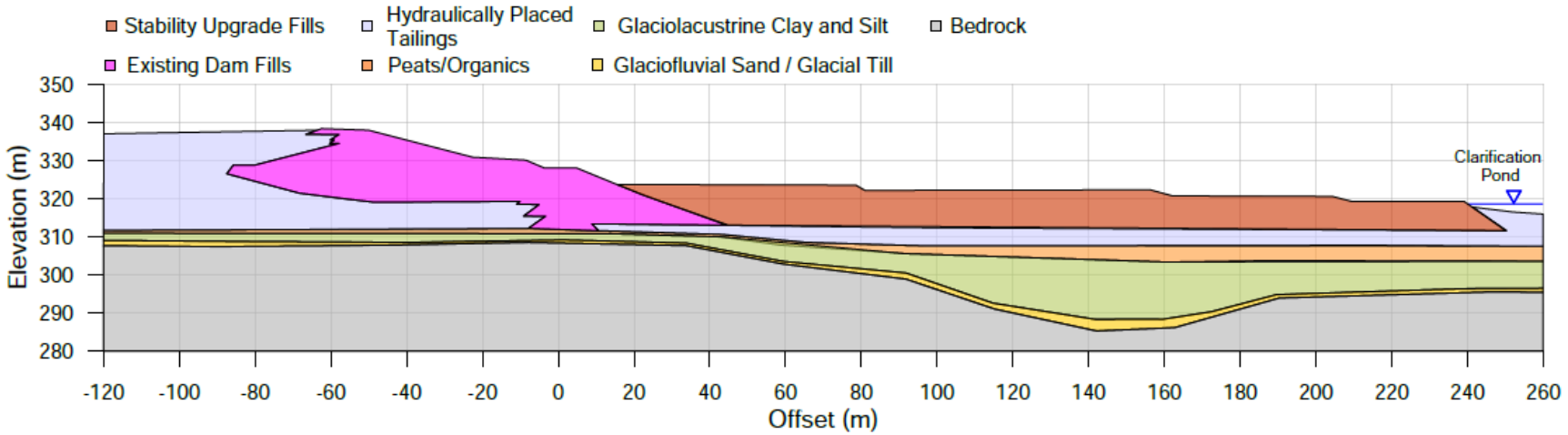


Figure 6: SWD stability upgrade design cross-section

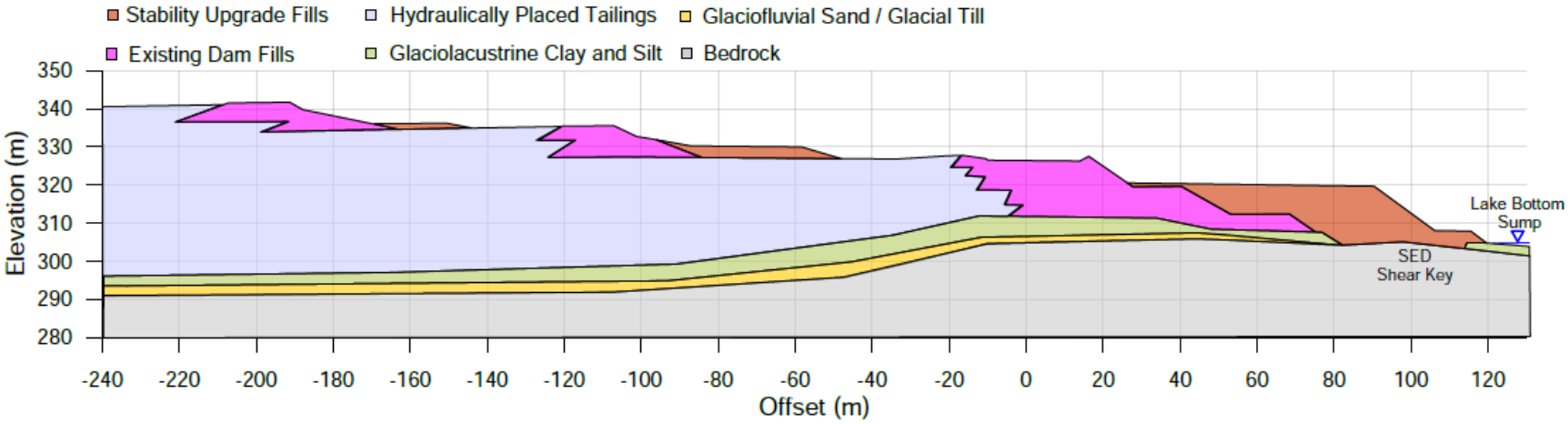


Figure 7: SED stability upgrade design cross-section

Conclusion

The LDU project at the FFTIS included approximately 1.5 million m^3 of fill placed, which significantly transformed the overall landscape of the facility and improved conditions towards being a long-term stable landform. The project represented a significant reduction in risk of a legacy tailings facility in close proximity to a population area.

This paper describes the means of prioritizing risk reduction measures where several hazards were identified with conflicting considerations. The prioritization method enabled practical sequencing and successful implementation of risk mitigation measures. The project encountered design constraints and varied conditions that required a balance of novel techniques and assessments, along with conventional methods, to achieve the project objectives.

References

Forbes, B., Ouellet, S., Suszek, N., Lato, M. and Russell, B. 2021. Application of distributed acoustic sensing within a tailings dam warning system. *Proceedings of Tailings and Mine Waste 2021.* Edmonton: 469–477.

Jefferies, M. and Been, K. 2016. *Soil Liquefaction: A Critical State Approach.* Boca Raton: CRC press.

Morgenstern, N.R. 2018. Geotechnical risk, regulation, and public policy. *Soils and Rocks, São Paulo* 41(2): 107–129. May – August, 2018.

Olson, S.M. and Stark, T.D. 2003. Yield strength ratio and liquefaction analysis of slopes and embankments. *Journal of Geotechnical and Geoenvironmental Engineering* 129(8): 727–737.

Plewes, H.D., Davies, M.P. and Jefferies, M.G. 1992. CPT based screening procedure for evaluating liquefaction susceptibility. *Proceedings of the 45th Canadian Geotechnical Conference.* Toronto.

Robertson, P.K. 2016. Cone penetration test (CPT)-based soil behaviour type (SBT) classification system – an update. *Canadian Geotechnical Journal* 53(12): 1910–1927.

Robertson, P.K. 2022. Evaluation of flow liquefaction and liquefied strength using the cone penetration test: An update. *Canadian Geotechnical Journal* 59(4): 620–624.

Sadrekarimi, A. 2014. Effect of the mode of shear on static liquefaction analysis. *Journal of Geotechnical and Geoenvironmental Engineering* 26(4): 563–567.

Case Study of Optimizing Design by Performing Field Trials of a Filter Selection for a Rockfill Embankment

Jason Hilgers, AECOM, USA
Thomas Barham, AECOM, USA
Julia Jarriel, AECOM, USA
Tiffiany Cromey, PAECOM, USA
Robert Snow, PAECOM, USA
Devinne Ramirez, Freeport McMoRan Bagdad Inc., USA
Ranjiv Gupta, Freeport McMoRan Bagdad Inc., USA

Abstract

This paper presents a case study of efforts by Freeport-McMoRan Bagdad Inc. (FMBI) to optimize the design of a filter zone for a rockfill embankment that provides containment of a tailings storage facility (TSF). The efforts included large-scale trials to optimize placement requirements and demonstrate acceptable self-healing performance of a proposed filter material with relatively high fines content.

Large-scale testing procedures to evaluate the placement and performance of the proposed filter are described, including lessons learned. The case study highlights the performance of a filter material with higher fines content than typical filters, describes the methods used to optimize filter placement, and demonstrates acceptable self-healing behavior of the proposed filter material to mitigate construction defects and cracks in the filter.

Site and TSF overview

Freeport-McMoRan Bagdad Inc. (FMBI) is an open-pit copper and molybdenum mining, milling, and leaching operation in Arizona. The mine operates at a variable production rate, depending on the rock type being milled, with an annual average of approximately 77,000 tons per day. Tailings from the mill are thickened and pumped to the mine's Upper Mammoth TSF through two tailings delivery pipelines for deposition via on-dam cyclones, single-point discharge, and perimeter spigots.

The centerline underflow sand embankment is constructed using on-dam cyclones placed at 50-foot intervals along a structural steel jacking header system. Approximately 100 cyclones are currently installed, and operators typically run 60 cyclones at a time during active deposition.

The Upper Mammoth Secondary Dam (UMSD) is a continuation of the Upper Mammoth TSF embankment. The UMSD is the right abutment for the underflow sand embankment and provides impoundment containment on the northern and eastern extents of the TSF up to the design elevation. The design for the UMSD includes six 50-foot-high centerline rockfill raises. Each raise is constructed using run-of-mine rockfill from the open pit. The upstream slope of each raise includes a two-stage filter zone to prevent migration of tailings into the rockfill. Whole tailings are deposited upstream of the UMSD, using spigots. A typical section is shown in Figure 1.

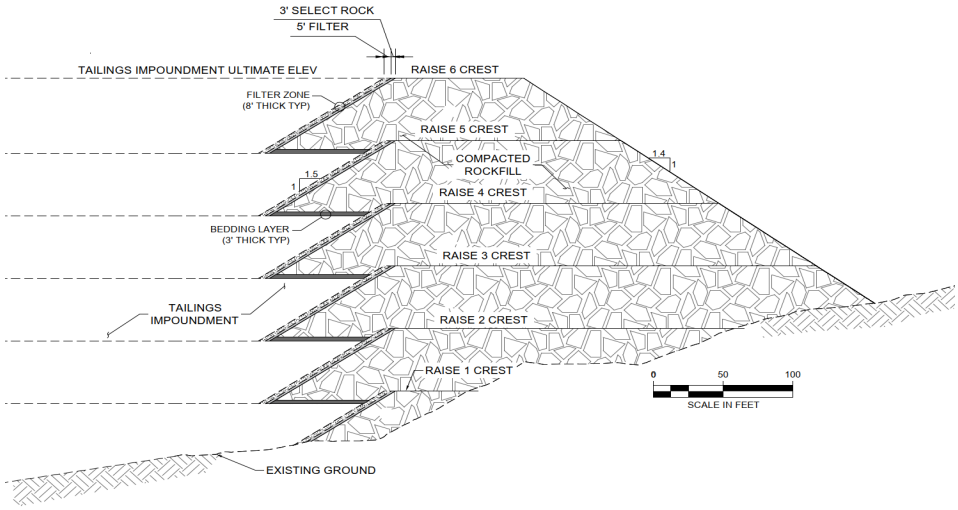


Figure 1: Typical Upper Mammoth Secondary Dam section

Introduction

During early design phases of the Upper Mammoth TSF project, a run-of-mine rockfill test fill program and filter compatibility evaluations indicated the need for a filter zone between the rockfill and the spigotted whole tailings. Filter zone gradations were developed using the Natural Resources Conservation Service (NRCS) filter design criteria outlined in Part 633 of the National Engineering Handbook (NRCS, 1994). The NRCS filter design criteria include requirements for filter compatibility and permeability that are reflected in the design procedure. Filter erosion boundary criteria developed by Foster and Fell (2001) were also considered to evaluate material susceptibility to erosion and optimize the design. These filter criteria were developed for earthen water-retaining structures, which are typically subject to the relatively high seepage gradients that are inherent in such structures. The primary function of the filter zone at the Upper Mammoth TSF was to provide separation and filter compatibility between the rockfill and the whole tailings to prevent erosion, piping, and sinkholes. Permeability of the materials was not a driving factor because of the arid climate of the site and because the reclaim pond was to be managed thousands of feet from the crest of the UMSD, resulting in seepage gradients lower than those at most water-retaining structures.

The filter zone was designed with an overall thickness of 8 feet, to balance constructability, technical requirements, and economy. The filter zone, which overlies the rockfill upstream slope, was designed with 3 feet of Select Rock and 5 feet of Filter measured horizontally. Figure 2 shows the materials used in the construction of the UMSD, from left to right; Rockfill, Select Rock, and Filter respectively.



Figure 2: Rockfill, select rock, and filter (shown left to right)

At the time of the study, FMBI operated a small crusher on-site to produce stemming material for blast holes in the open pit. The small crusher was operated near the location of the UMSD and was identified as the preferred source for the generation of the filter zone materials. The stemming material gradation is finer than the Rockfill and coarser than the initial filter design gradation and was adopted as Select Rock without modification. The byproduct of stemming material production is similar to the initial filter design gradation bands, except that the byproduct has higher fines (5 percent to 15 percent) and more fine sand. Modifications to the crusher to produce a byproduct with lower fines content and less fine sand were evaluated; however, the fines content could not be reduced to the target of 5 percent or less without the additional effort and cost of washing the material.

Given that the primary purpose of the filter zone is to provide separation and prevent migration of material between the Rockfill and whole tailings, the potential for reduced construction cost, and the opportunity for reduced environmental impacts, the stemming byproduct was proposed as filter for the project without modification. However, compaction of a filter with relatively high fines content had the potential to result in a stiff material with more potential to hold a crack or defect.

AECOM performed seepage and slope stability analyses to evaluate the geotechnical impacts of potential cracks, erosion, and piping of material into the pore spaces of the Rockfill, which could potentially result in an elevated phreatic surface or reduced shear strength in the rockfill. Based on the geotechnical analyses performed, cracks and erosion of the proposed filter material would have minimal impacts on the UMSD's performance. FMBI and AECOM, with input from the Independent Technical Review Board, decided that the proposed filter should be evaluated for erodibility, self-healing, and dispersivity.

Laboratory testing demonstrated non-dispersive behavior of all samples tested, and a procedure was developed to evaluate the self-healing behavior of the proposed filter material.

Filter erodibility test procedures

A literature review did not identify a standardized method for filter erodibility testing, so a testing procedure was developed as described herein. The purpose of the filter erodibility testing was to evaluate the ability of the proposed filter to self-heal under different placement and compaction techniques in the event of the formation of a crack or presence of a construction defect.

A total of 15 filter erodibility tests were performed by AECOM and FMBI. The first nine tests were used to refine the setup and testing procedure and are excluded from discussion in this paper for brevity. The procedure used for the last six filter erodibility tests is summarized below:

1. Test pads were constructed with a 1- to 2-foot-thick graded and compacted Select Rock layer overlain by 1 to 2 feet of filter material, as shown in Figure 3. The test pads were graded to a flat working surface.

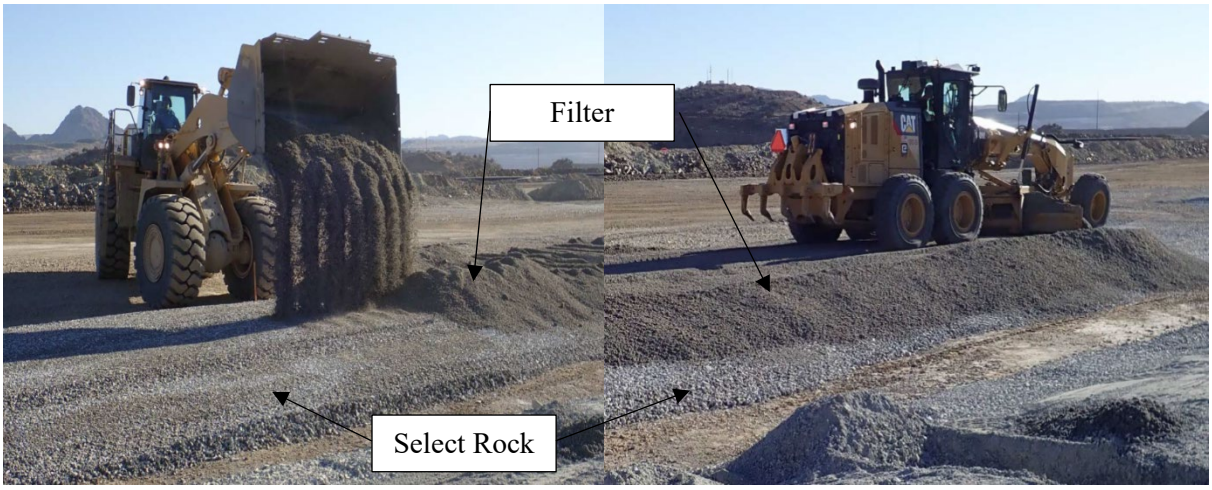


Figure 3: Test pad filter placement (left) and grading (right)

2. A trench was then excavated within the filter material down to the contact at the top of the Select Rock. Two steel plates were used for the various tests: one of the plates was 1 foot high by 2 feet long and the other was 2 feet high by 3 feet long. Both plates were ¼ inch in thickness. The plate was inserted vertically into the trench until it made contact with the Select Rock. Filter material was backfilled and compacted around the plate, using variable compactive methods (backhoe tamping or two to eight passes of a vibratory smooth drum roller). Steel plate placement is shown in Figure 4.

3. For three of the tests (up to 6 inches of underflow sand were placed on top of the filter material to simulate interaction of the underflow sand with the proposed filter and Select Rock. The underflow sand provided some surficial support and reduced the applied water stress on the crack, with the result that its self-healing ability could be better assessed.
4. Approximately 10 gallons of water were slowly added to the surface, near the plate, to moisten the materials and to minimize absorption of water during the test. Once all the water had infiltrated into the filter material, a minimum of four nuclear density gauge tests were performed to measure the density and moisture content of the compacted filter material.
5. A rubber-tire backhoe used a rope strap to remove the plate and simulate a crack in the filter material. The boom of the backhoe was used to pull the steel plate up vertically to minimize lateral disturbance of the filter material and underflow sand (if used). The steel plate just prior to removal is shown in Figure 4 (right photograph).



Figure 4: Backfilling of steel plate (left) and compacted surface prior to removal (right)

6. Orange surveyors paint was used to mark the crack location and help identify the migration of filter and underflow sand (if used). A photograph of the setup just prior to adding water to the simulated crack is shown in Figure 5.
7. Water was then poured from a 5-gallon bucket at a controlled rate across the filter material or underflow sand surface (if used) toward the crack. When the crack was visibly closed at the surface and water was observed to pond, water application was stopped, and the amount of water used was noted. Once the ponded water had infiltrated into the filter, additional water was poured, and that process was repeated until the planned quantity of water had been added to the test area.

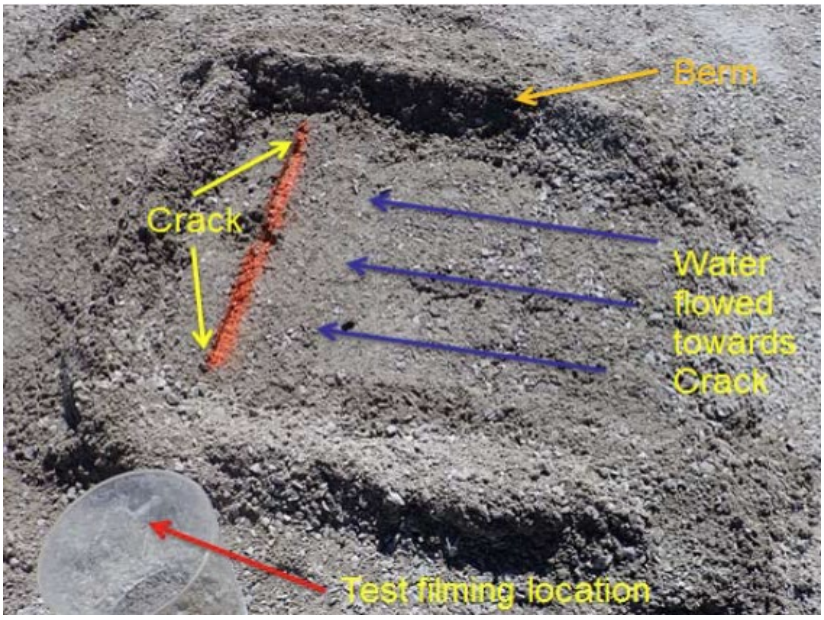


Figure 5: Simulated crack prior to adding water

8. After all the water had infiltrated, a vertical excavation within the filter material was performed at the location of the simulated crack. Visual observations were made by AECOM staff to document whether the crack had self-healed and whether the filter material had migrated into the Select Rock among other notable observations. A typical photograph of the vertical excavation is shown in Figure 6.

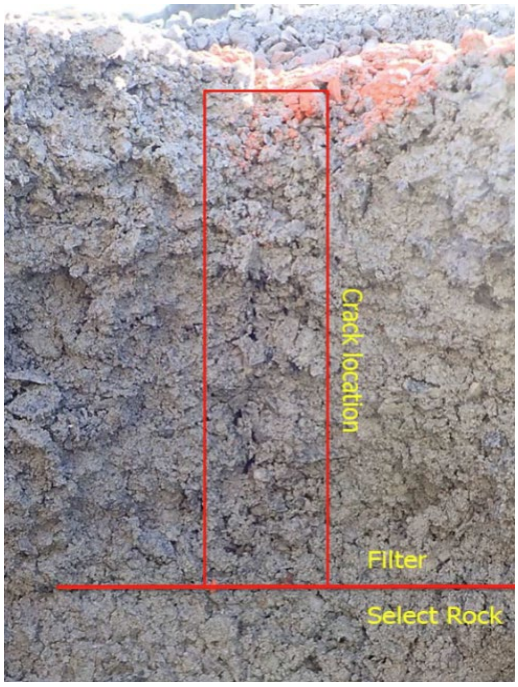


Figure 6: Vertical excavation of simulated crack

9. Samples of the filter material and Select Rock from each test were collected for particle size analysis, Atterberg limits, and dispersion testing.

Detailed observation logs noting the compaction method, crack size (steel plate), water application rate, and presence of underflow sand were kept. The observation logs also recorded how many gallons of water flowed into the crack before it started to heal, and they included numerous photographs and videos.

Filter erodibility test results

Laboratory testing performed on samples collected during the filter erodibility test identified the material as a clean to clayey fine gravel (GP-GC, GC) or clean to clayey fine gravel/sand (SP-SC) with fines ranging from 9.1 to 14 percent. The plasticity index ranged from 7 percent to 15 percent, depending on the source rock.

Two photographs identified as representative of good self-healing tests have been included in Figures 7 and 8. Figure 7 includes a photograph from Test 11 showing the simulated crack prior to plate removal and after the test and excavation to show the degree of self-healing in cross-section. This test did not include underflow sand on top of the filter material.



Figure 7: Simulated crack for Test 11 with no underflow tailings on top

Figure 8 includes a photograph from Test 13, which had 6 inches of tailings placed on top of the filter material, showing the simulated crack and the degree of self-healing in cross-section. The underflow sand entered the crack; however, the underflow sand did not reach the Select Rock. Underflow sand entering the crack is not surprising, as water flowed over the underflow sand (which easily erodes) before entering the crack. In both photographs, the orange paint applied to the surface of the crack was visible at the top of the Select Rock, indicating a crack through the material was successfully created. The distribution of orange paint within the crack illustrates the self-healing of the crack.



Figure 8: Simulated crack for Test 13 with underflow tailings on top

Test 10 through Test 15 are described in detail in Table 1, and the results of these tests, which are presented as dry density versus volume of water applied until surface ponding occurred, are shown in Figure 9. The following comments and conclusions were made based on the final six tests.

- The tests performed with less compactive effort (looser with lower dry density and void ratio) demonstrated faster self-healing performance, with just a few gallons of water flowing over the surface before the water started to pond. Minimal compactive effort (light tamping) was included in the revised project specifications based on this observation.
- From Figure 9, we can observe that while the general conclusion of lower density results in better self-healing, it is apparent that the addition of underflow to the filter surface slowed the self-healing process. The authors believe the self-healing process slowed because less sheet flow erosion was occurring at the filter surface (due to support provided by the underflow), requiring more inflow to self-heal, and

this likely better represents in-situ conditions. Thus, the authors feel large-scale tests should include representative base materials on top of the filter.

- From Figure 9 and Table 1, it can be concluded that Test 12 is an outlier, requiring about 15 gallons to self-heal and begin ponding versus 5 gallons for a similar test setup and density. Based on index property testing, the filter material requiring more water to self-heal had a slightly higher plasticity, enabling it to sustain a crack longer before eventually self-healing. Limits on plasticity were included in the project specifications based on this observation.

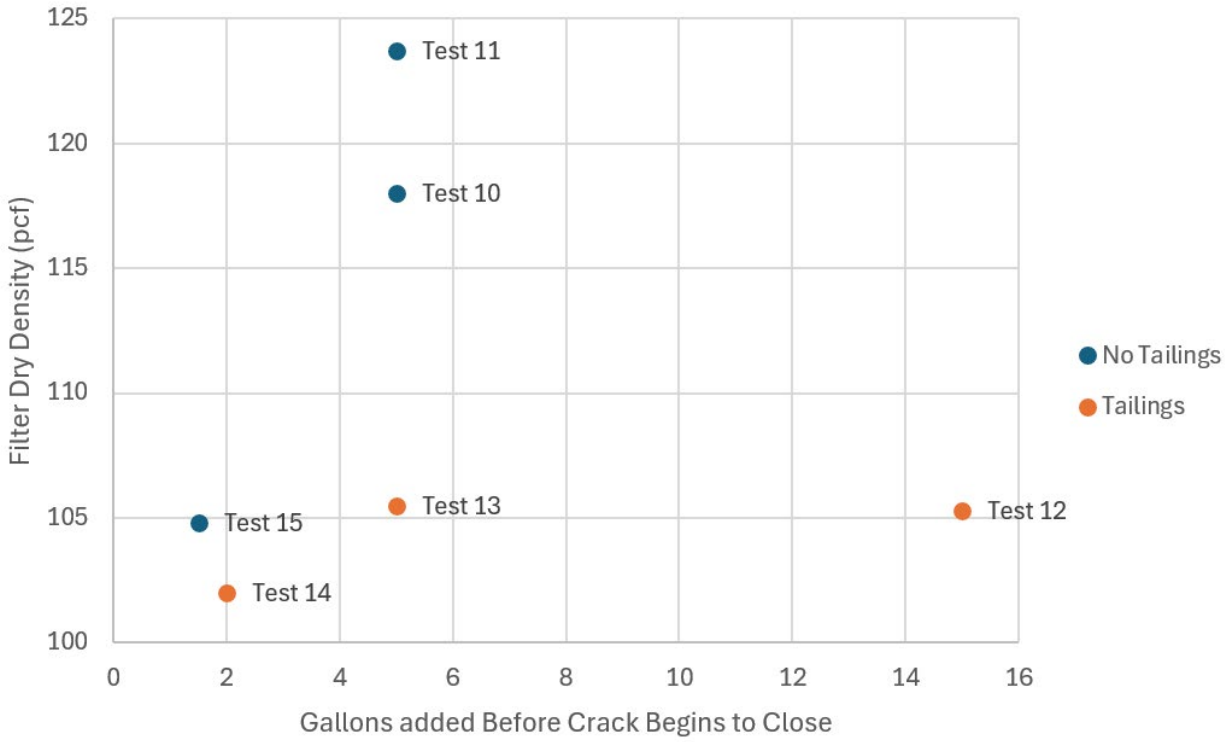


Figure 9: Summary of results from Tests 10 through 15

Table 1: Large-scale filter erodibility testing summary

Test No	Compaction Method	Depth of Tailings Placed (in)	Steel Plate Size	Water Application Rate	Water Applied Before Crack Starts to Close (gal)	Filter Dry Density (pcf)	Notes
10	2 passes vibratory compaction	0	1'x2'x¼'	15 gal/2 min	5	118.0	Crack visible at surface when plate removed. First 5 gallons flowed into crack and then began to pond at the surface. Ponding slowly dissipated into the crack area. Crack location visible in excavation down to Select Rock, but not open; had "healed" filter material.
11	8 passes vibratory compaction	0	1'x2'x¼'	15 gal/2 min	5	123.7	Crack visible at surface when plate removed, with some surface disturbance as filter material stuck to plate. First 5 gallons flowed into crack and then began to pond at the surface. Ponding slowly dissipated into the crack area. Visible surface settlement at crack location. Crack visible but mostly self-healed with filter material.
15	Surface tamped with backhoe	0	1'x2'x¼'	15 gal/2.5 min	1.5	104.8	Water flowed into crack freely for several seconds until edge of filter broke/caved off and started to plug filter. Additional 2.5 gallons of water added; minor seepage preference to crack, but flow backed up quickly. Line of crack clearly visible, minor voids present between bridging locations, small amount of paint down to surface of Select Rock.
12	Surface tamped with backhoe	6	2'x3'x¼'	35 gal/10 min	15	105.3	Underflow sand removed around plate prior to removal to prevent collapse. Crack visible when plate was removed. 15 gallons flowed into crack before it began to close. After 30 gallons, layer of fine-grained underflow sand formed covering the crack. Orange paint observed at Select Rock contact and crack self-healed and partially filled with tailings.
13	Surface tamped with backhoe	6	1'x2'x¼'	15 gal/5.5 min	5	105.5	Underflow sand removed around plate prior to removal to prevent collapse. Crack visible when plate was removed. 1-2 gallons flowed into crack before it began to pond. Orange paint observed at Select Rock contact and crack self-healed and partially filled with underflow where inflow was observed.
14	Surface tamped with backhoe	6	2'x3'x¼'	15 gal/8 min	2	102.0	Underflow sand removed around plate prior to removal to prevent collapse. Crack visible when plate was removed. 1 to 2 gallons flowed into crack before it began to pond. Crack self-healed minor infilling of underflow where inflow was observed.

Conclusion

This paper presented a large-scale field-testing procedure to evaluate the self-healing potential of filter material potentially susceptible to cracking due to relatively high fines content under various compactive efforts. AECOM and FMBI developed the testing program because a standardized method for filter erodibility testing was not identified in the literature. The procedure was useful in evaluating the self-healing potential of the proposed filter and optimizing placement requirements. By documenting and sharing our program, it is hoped that this procedure can be further refined and used as a starting point for other projects. The large-scale testing procedure evolved during the field trial and the key takeaways we wish to highlight are listed below.

- Filter material should be moistened to minimize absorption of water during the test prior to removing the steel plate.
- Surficial painting of the crack provides an insightful method to track water progression and self-healing.
- Detailed documentation of compacted filter density, applied water, and post-test excavation photographs were critical to assessing and interpreting test results.
- Water application during the test should be performed in a controlled and repeatable manner.
- Filter density versus volume of water required to self-heal (as inferred from ponding at the surface) was a useful metric for comparing tests.

The results of the case study highlight the following conclusions.

- The primary function of the filter zone at the Upper Mammoth TSF was to provide separation and filter compatibility between the rockfill and the whole tailings to prevent erosion, piping, and sinkholes. The permeability of the materials was not a driving factor because of the arid climate of the site and because the reclaim pond was to be managed thousands of feet from the upstream crest of the UMSD, creating seepage gradients lower than those at most water-retaining structures. Therefore, materials with higher fines content than typical filters can be considered for use as filter, provided the proposed materials meet the compatibility requirements for no erosion, demonstrate self-healing behavior, and provided that geotechnical seepage and stability impacts are minimized.
- Large-scale tests demonstrate that filter placement with minimal compactive effort resulted in the fastest self-healing. This finding was incorporated into the updated project specifications.
- Filter material with higher plasticity was observed to self-heal more slowly than filter material with lower plasticity. This finding was incorporated into the updated project specifications.

- The results of this case study were used by FMBI to optimize the design and operational life-cycle stages of a UMSD filter zone at the Upper Mammoth TSF. The proposed filter material was used for construction of the UMSD filter zone after appropriate modifications to the design, project specifications, and monitoring requirements. These changes resulted in reductions in construction costs and the environmental impacts associated with producing typical filter materials.

References

Foster, M., and Fell, R. 2001. Assessing embankment dam filters that do not satisfy design criteria. *Journal of Geotechnical and Geoenvironmental Engineering* 127(5).

NRCS (Natural Resources Conservation Service). 1994. *National Engineering Handbook, Part 633, Chapter 26, Gradation Design of Sand and Gravel Filters (NEH-633-26)*. Washington D.C: United States Department of Agriculture, Natural Resources Conservation Service.

Game-changing Technology for Large-scale Filtered Tailings

Oliver Whatnall, Jord International Inc., USA
Sam Caldwell, Jord International Pty Ltd, Australia
Stuart Wilson, Jord International Pty Ltd, Australia
Ricardo Santander, Jord International Inc., USA
Juan Ccarita, Jord Chile SpA., Peru

Abstract

Introducing vibration energy to tailings often induces liquefaction (release of water) and/or a thixotropic response (shear thinning). Performing filtration simultaneously delivers game-changing filtration performance.

This is the basis of Viper, the vibration-enhanced vacuum belt filtration technology that continuously produces filtered tailings with desirable moisture content at high production rates. This paper introduces the technology and shares case study data from various projects around the world, including pilot plant and industrial equipment – answering the question "how much difference can vibration make?"

The conclusion contemplates the resultant filtration plant, explaining how Viper unlocks a step change reduction in cost and complexity as well as delivering operational and maintenance advantages relative to competing technologies. It is for these reasons that Viper is enjoying interest, investigation, and implementation from a number of the world's leading mining and minerals organizations.

Introduction

Awareness, investigation and implementation of Viper filtration technology continues to grow, fueled by the enduring demand for technology for large-scale tailings filtration and encouraged by significant investments by modern miners.

Viper is a differentiated technology, leveraging vibration and vacuum for superior dewatering performance, while also facilitating a step-change simplification of the operational and maintenance requirements (relative to currently available technology). The game-changing technology is being operated and maintained at throughputs up to and exceeding 50,000 tpd, with future applications above 100,000 tpd currently under investigation.

This paper explains the fundamentals of the technology and provides relevant examples of successful application at various stages of project lifecycle, before closing with the value proposition of overcoming the cost and scalability deterrents inherent to filtered tailings.

Seven years since the 2017 report commissioned by the Mine Environment Neutral Drainage (MEND) Project Secretariat Study of Tailings Management Technologies identified that "cost and scalability of filtered tailings is one of the deterrents for mining companies," most other major filtration equipment companies continue to develop incremental improvements to existing technology. This approach may not deliver the step-change required.

Viper technology

Introducing vibration energy to tailings often induces liquefaction (release of water) and/or a thixotropic response (shear thinning). Performing filtration simultaneously delivers game-changing filtration performance.

This is the basis of Viper, the vibration-enhanced vacuum belt filtration technology which continuously produces filtered tailings with desirable moisture content at high production rates. A process description summary is included as an appendix.

The 3D model screenshot in Figure 1 illustrates a Viper vacuum belt filter. Note the green Viper modules; these are the additions to the Jord OEM conventional vacuum belt filter.

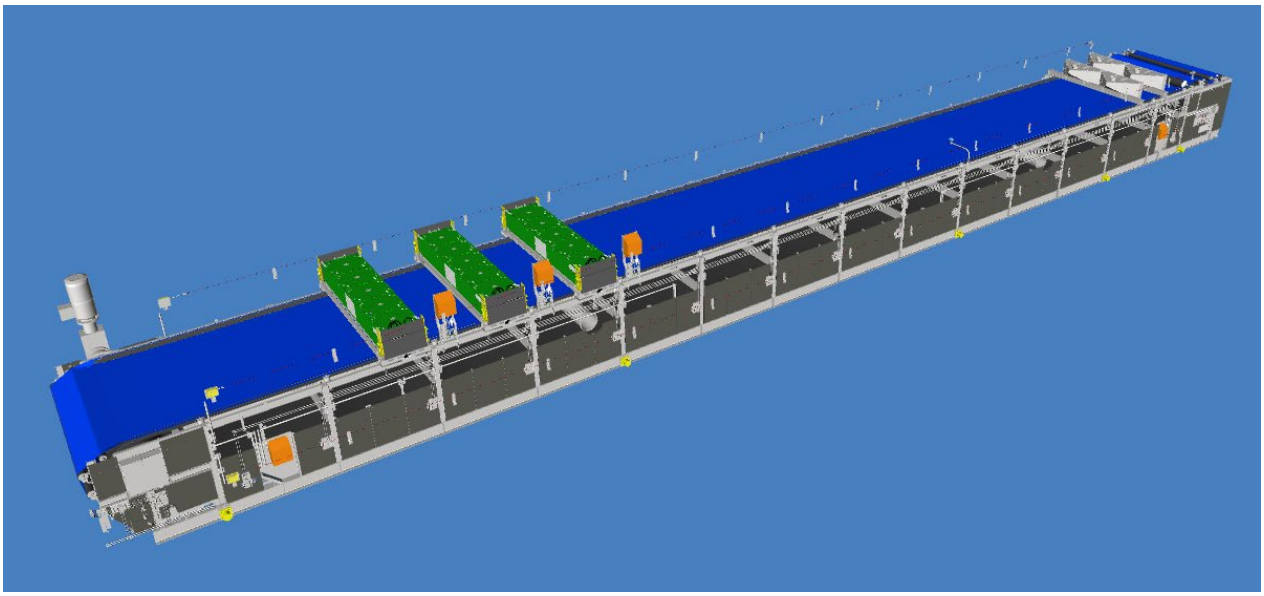


Figure 1: Viper vacuum belt filter

Critically, despite the addition of Viper modules, all fundamentals of vacuum belt filter plant design, operational and maintenance practices, which are generally well understood by the mining industry, remain valid. These include:

- Continuous process.
- Robust and reliable with high equipment availability.
- Simple, scalable technology with more than 30 years of operational history in the industry.
- Operates with a single filter cloth with typical lifetime 6 months.
- No operator intervention for cake discharge.
- Cake (from one or multiple filters) can be discharged directly to overland conveyor.
- Minimized civil and structural costs, often installed low to the ground and outside without cover (climate permitting).
- Low supporting infrastructure costs and complexity.

In many cases, including case one and case two below, the overall Viper solution is providing such an exceptional value proposition that it was selected over alternative, conventional filtration solutions despite the early stage of technology maturity at the time.

Full-scale operational plants



Figure 2: Viper technology in operation

Although Viper is a relatively young technology, numerous references exist in both the Americas and in Australia. Three of these applications are discussed below.

In combination, an industry significant, large-scale operation, at 60,000 tpd capacity (see case one), numerous gold tailings applications, including one with fine grind (see case two) and one at 4,000 masl elevation (see case three), provide compelling evidence to demonstrate industry confidence and the proven ability to unlock filtered tailings by applying the Viper technology to their process.

Future customers are in the enviable position of being "first to be second."

Case one

Through 2024, operational ramp up continues on the 60,000 tpd Viper vacuum belt filter plant in Western Australia for fine magnetite concentrate. This plant, complete with eight (8) 158m^2 filters is shown in Figure 3. The process plant produces 20 million tonnes per annum of concentrate via a proprietary process flow sheet. The process plant produces 100% of its production as slurry concentrate which is filtered below the transportable moisture limit (TML) of approximately 10%w/w.



Figure 3: 60,000 tpd Viper vacuum belt filter plant during ramp-up

Case two

In 2017, a conventional vacuum belt filter was installed to wash (i.e., remove cyanide) and filter deslimed tailings from a conventional carbon-in-pulp (CIP) processing plant. Subsequently, the tailings specification was changed which eliminated the desliming process and sent full-stream tailings (with a finer particle size distribution (PSD) of solids) to the filter, which could not be effectively dewatered at the required rate from the existing vacuum belt filter.

A paper was published in *Proceedings of Tailings and Mine Waste 2020,* "Enhancing vacuum belt filter dewatering to adapt to finer tailings grind – a case study" (Whatnall et al., 2020). This paper indicated the suitability of Viper in this application. The following year, the first full-scale commercial Viper system was commissioned filtering the full stream tailings.

Figure 4 compares the performance (production rate and cake moisture) of the conventional vacuum belt filter with the performance of the Viper vacuum belt filter over a 48-hour period during commissioning in August 2021. When operating with the Viper vacuum belt filter, the cake moisture is approximately 4 points lower and the throughput rate is increased by 35%.

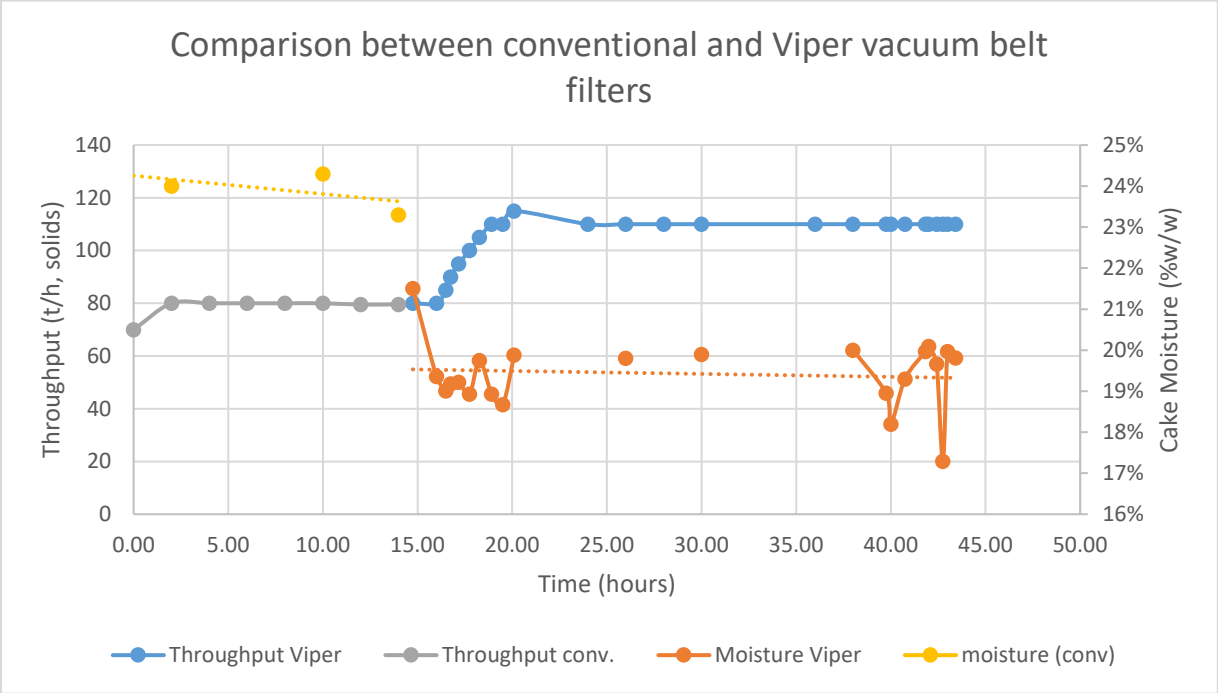


Figure 4: Comparison between conventional and Viper vacuum belt filters

Over the subsequent twelve months through 2022, a summary of weekly metallurgist notes confirm production priorities changed to preference throughput over final moisture resulting in:

- Throughput rates of 110–130 tph.
- Cake moisture content of 20–21% w/w.

Case three

One of the early adopters of filtered tailings in the 1990's, at an altitude of 4,000 masl, a Chilean precious metal miner operates a Meryl Crowe process plant with a fleet of vacuum belt filters for tailings.

This site has maintained interest in Viper technology for many years, and in 2022 engaged in a test work program to investigate the opportunity is to reduce cake moisture and increase production rate from their existing tailings belts filters by retrofitting them with Viper and reduce (or eliminate) the bottleneck for production when processing future tailings.

Work published by (2023) provided a summary of results. Fast-forward to Q1 2024, and Viper equipment has been retrofitted on one of their vacuum belt filters. See Figure 5 below, which is a snapshot taken during initial operation.

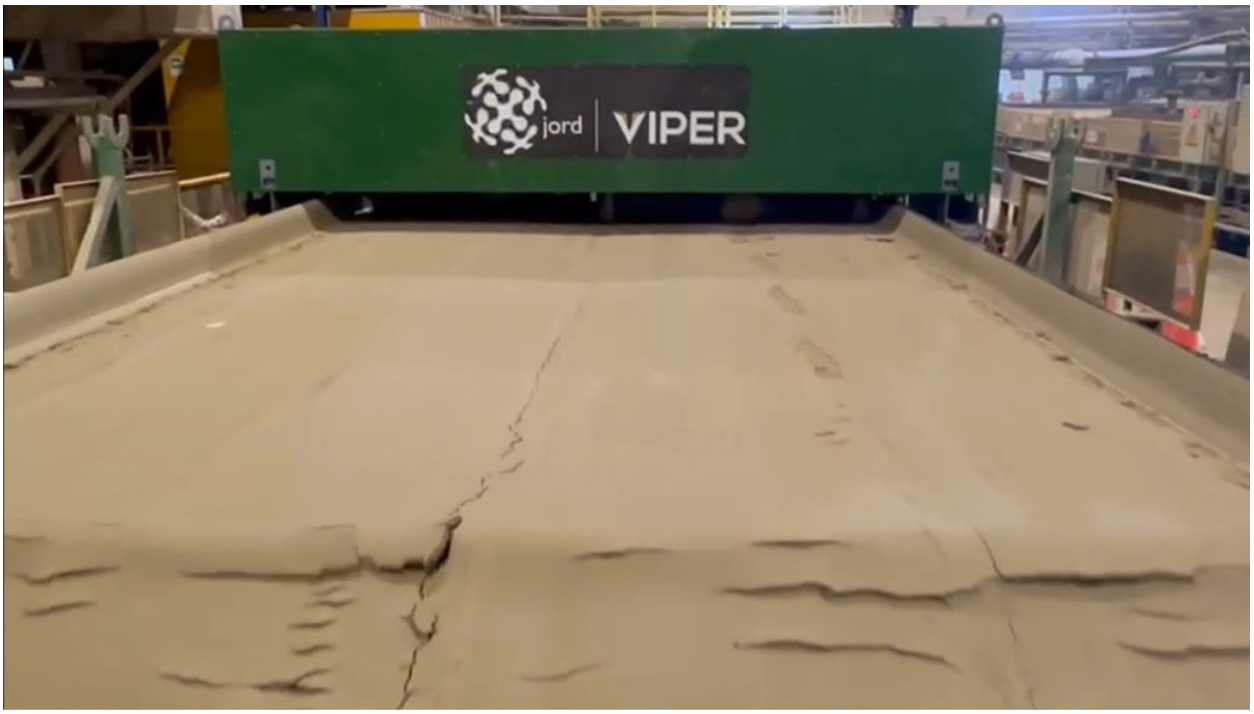


Figure 5: Initial operation of Viper retrofit

Initial results have been encouraging, with a typical moisture reduction, compared to no Viper, of ~1 point when operating one Viper module and 3-5 points when operating two Viper modules in series. Refer Figure 6 below. Work is continuing to optimize the equipment and the process to best meet the needs of the process plant going forward, including to deliver throughput increase in addition to lower cake moisture.

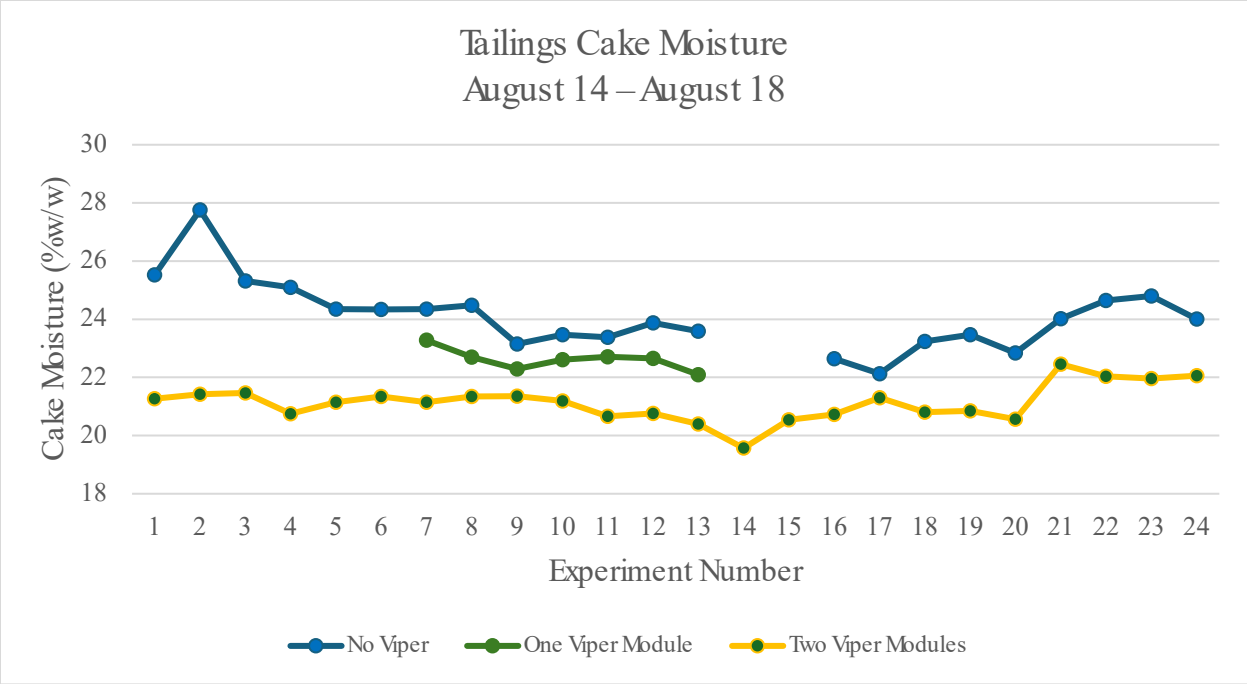


Figure 6: Comparison of cake moisture between Viper and no-Viper operation

Viper investigation examples

The past 12 months have seen significant interest and investigation of Viper technology from operations and projects.

Two further cases are summarized below to provide some examples of the opportunities and potential applications. The cases presented have contracted the supply of pilot Viper equipment to support project design and performance guarantees.

Case four

A large multinational company with operating iron ore mines in Brazil, commissioned test work to determine whether the addition of vibration would make vacuum filtration feasible for their fine iron ore tailings materials. The opportunity is to unlock a cost-effective, manageable filtration plant that would allow their strategic goal for filtered tailings to be realized.

The results from the work were encouraging, indicating that the addition of vibration to the filtration process resulted in acceptable cake moisture (~14%w/w), triggering preparation of a concept plant design (to verify the value proposition) then an agreement to mobilize our pilot plant to the site location for a campaign expected in late 2024.

This project is a useful example of a typical project cycle, investigation with bench test work, concept study then pilot plant campaign. If warranted by results and the project, typical next steps include feasibility study, commencement engineering then project execution with detailed design and equipment/plant supply.

Case five

This case study focusses on the pilot campaign conducted at site, an opportunity in the USA for filtering phosphogypsum slurry, a tailing from fertilizer production.

The pilot plant includes the vacuum belt filter with vibration rollers, filtrate receivers, filtrate pumps, vacuum pump and ancillary equipment, such as the belt conveyors. See Figure 10 for an overview of the equipment arrangement.

The vacuum belt filter has a filtration area of up to 17ft^2 (15" wide × 157" long), the effective length can be reduced if required to reduce the capacity of the system. Installed on to the vacuum belt filter are up to four vibration roller assemblies. The overall system was designed and operated at a throughput rate approximately 1 tph solids.

The objective of the pilot campaign was twofold. Firstly, to generate a large stockpile of filtered cake to verify the materials handling characteristics of the produced and secondly to verify the process performance of the Viper filter to allow detailed design and for the purposes of performance guarantees.

Initially work focused on the production of a large stockpile of filter cake, the target was a 10′ high stack. Figure 7 shows the initial production to allow the increase in the angle of the discharge conveyor, Figure 8 shows the resultant 10′ high stockpile.



Figure 7: Stockpile generation



Figure 8: 10' high filter cake stockpile

Once the stockpile was complete, the filter cake was removed for materials handling testing and analysis (by others). The focus was shifted to process performance of the filtration. The key outcomes from the testing were:

- Vibration helps produce lower cake moisture, the more vibration iterations, the lower the cake moisture.
    - No vibration = moisture 35+% w/w.
    - 4 vibration rollers = moisture typically 26-27%w/w as low as 25%w/w.
    - 3 vibration rollers = moisture 27-29%w/w.
    - 2 vibration rollers = moisture ~30% w/w.
    - 1 vibration roller = moisture >30% w/w.
- Thinner cake helps produce lower cake moisture.
    - ½" cakes = moisture ~26% w/w.
    - 5/8" cakes = moisture ~27% w/w.
    - 5/8" – ¾" cakes = moisture ~28% w/w.
    - ¾" – 1" cakes, no data.
    - 1" or thicker cakes = moisture ≥ 30% w/w.
- Consistency of sampling is critical for reliable data. As per Figure 9, the stockpile was visibly "steaming," it was necessary to attempt to quantify the impact for a given time period of

atmospheric exposure. Zero minutes (i.e., immediate sealing) and 10 minutes atmospheric exposure were chosen, and the summarized data is presented below.

- Cool evening (30°F), no wind = average 1.7 points moisture reduction.
- Midafternoon (50°F), no wind = average 1.9 points moisture reduction.
- Midafternoon (50°F), wind ~10 mph = average 2.6 points moisture reduction.



Figure 9: "Steaming" stockpile

At the time of publishing, work is continuing to document and analyze the generated data to meet the objectives of the pilot plant campaign.

State of practice

Supported by the growth and projected demand for the Viper technology, additional resources have been established in strategic locations to provide support from project identification, project development and delivery through to aftermarket.

Critical to the uptake of the Viper technology is the opportunity to test and demonstrate the performance and operability of the technology. To this end, various options are available for consideration:

- Laboratory-scale testing, providing qualitative process performance results. This requires a relatively small sample size and facilitates a rapid assessment of the suitability for a given application.
- Pilot-scale testing (see container mounted equipment in Figure 10), providing quantitative process performance results and exposure to technology operability and maintenance. Pilot-scale testing requires larger sample size, in the order of 5-20 tpd (instantaneous rate).

- Demonstration-scale testing, a single-train full-scale Viper vacuum belt filter system (see Figure 11) providing industrial-scale performance results and operation and maintenance experience. Production rate in the order of 5,000 to 10,000 tpd for one individual filter.



Figure 10: Viper pilot plant

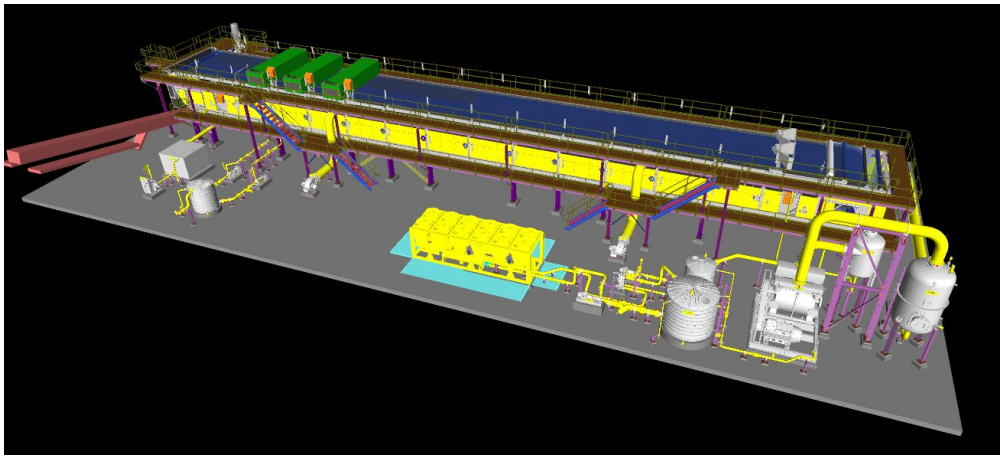


Figure 11: Viper demonstration plant

For Viper retrofit scenarios (i.e. existing conventional vacuum belt filter plants), a fourth option is leasing full-scale Viper modules to be installed onto the existing equipment providing a fast, cost-effective path to determine performance prior to roll out across the entire plant. A range of hire equipment is readily available to suit standard conventional belt filter sizes or site-specific equipment can be provided on this basis.

Conclusion

This paper explores Viper as a desirable technology solution to overcome the well-known cost and scalability challenges of tailings filtration.

The Viper technology enhances filtration performance through the addition of vibration to the process of conventional vacuum belt filtration. Critically, the addition of Viper modules changes none of the fundamentals of vacuum belt filter plant design, operational and maintenance practices, which are generally well understood by the mining industry remain valid.

In 2021, the first full-scale commercial Viper system was commissioned on tailings and shortly afterwards a 60,000 tpd Viper filtration plant was commissioned. Uptake and investigation are growing, supported by a range of testing capabilities. This includes both bench, pilot and demonstration plant options. The project cycle from investigation through study, design, delivery, installation, commissioning and on-going aftermarket services is supported by relevant technical experts.

References

Mine Environment Neutral Drainage (MEND) Program. 2017. Study of Tailings Management Technologies. *MEND Report 2.50.1.* Accessed 10/2017 at: http://mend-nedem.org/wp-content/uploads/2.50.1Tailings_Management_TechnologiesL.pdf

Whatnall, O., Barber, K. and Robinson, P. 2020. Enhancing vacuum belt filter dewatering to adapt to finer tailings grind – a case study. *Proceedings of Tailings and Mine Waste 2020.*

Whatnall, O., Santander, R., Wilson, S. and Caldwell, S. 2023. Extending the habitat of Viper filtration. Implementing the technology in the Americas. *Proceedings of Tailings and Mine Waste 2023*.

Appendix

Viper vacuum belt filter process description

Viper vacuum belt filters are continuous production machines, often numerous machines are operated in parallel, however, single filter operations are common.

Slurry is fed into the feed pipe manifold at low pressure suitable for an open pipe discharge. The feed pipe manifold distributes the slurry evenly to each of the feed slurry inlets of the feed box located at the tail end of the belt filter. The feed box distributes the feed slurry evenly across the width of the moving filter cloth.

The filter cloth is the filter media, it is supported on the rubber carrier belt. The carrier belt has recessed grooves cut into it, across its width, and holes along its centerline. Under the holes, the carrier belt passes across the vacuum box. The water/liquor in the feed slurry is drawn by vacuum through the solids and the filter cloth as filtrate. The filtrate is channeled along the carrier belt drainage grooves and through the filtrate holes into the vacuum box. Air from atmosphere is also drawn via the vacuum through the filter cake and follows the same path as the filtrate into the vacuum box. Filtrate and air are drawn from the vacuum box via filtrate hoses to the filtrate manifold to the terminal point. Piping connects the filtrate manifold to the filtrate receiver which is ultimately connected to a vacuum pump creating vacuum in the system. Once the filtrate enters the filtrate receiver, the liquid is separated from the air flow and falls to the bottom of the receiver where it is pumped away via a filtrate pump.

The carrier belt is supported on cushions of air above perforated air tables each side of the vacuum box. A high volume blower fan supplies air which is ducted to the underside of the air tables.

Sealing the stationary vacuum box against the moving carrier belt are two wear belts traveling in recessed channels of guide plates which straddle the open top of the vacuum box. Clean water is supplied to the wear belt, guide plate, carrier belt interface to cool, lubricate and provide a vacuum seal.

The drive motor and gearbox turn the filter's head pulley which drives the carrier belt. The speed of the carrier belt can be adjusted via a VSD to suit the filter feed rate and optimize the filter cake thickness. Cake thickness can be automatically controlled by varying the belt speed with reference to radar cake thickness monitors installed on the filter.

The carrier belt, filter cloth and filter cake move together from the tail end towards the head end of the filter.

Viper modules are installed at one or more locations along the top of the belt filter. Each Viper module consists of two vibrating roller assemblies (cartridges) housed within an enclosure. When engaged, both cartridges lower a roller down into the filter cake passing below. Vibration passes from the roller into the cake enhancing the dewatering performance. The roller is driven by the cake with adhesion reduced through use of low surface energy materials and high vibration frequencies.

Vibration speed is VSD controlled to optimize process and mechanical performance. Vibration amplitude can be changed by manual adjustment of the internal exciter mechanism, typically done during commissioning.

The weight of Viper cartridges on the filter cake is controlled by a "Preload System." The preload system uses a pressure control valve to inflate rubber air bellows which lift the roller. Preload is controlled by a radar level sensor directly in front of each roller. If the roller sinks into the filter cake pressure is increased. If the roller floats over the cake pressure is reduced.

Each Viper is also equipped with a set of lift bellows which raise and lower the entire module. When turned on the bellows lower the Viper on to the belt filter. When turned off the bellows lift the Viper away from the filter.

Following the last Viper, the carrier belt, filter cloth and filter cake continue down the belt filter. At the discharge end the carrier belt turns down around the head pulley while the filter cloth and filter cake travel forward over a final cake cracking roller. Finaly the cloth turns down dropping the broken cake into the discharge chute.

The carrier belt and filter cloth, now on the return side of the filter, pass through a series of spray bars which clean the cloth from both sides and remove any solids from the grooves of the carrier belt. The returning wash water, including solids, is collected in the wash return hopper and discharged.

The clean filter cloth and carrier belt are supported by separate rubber lined return rollers as they return to the tail end of the filter. A tension roller rests on top of the cloth using gravity to maintain the correct tension. If the tension roller drops too low, indicating a loose cloth, a proximity sensor will alert the operator. Cloth tracking is maintained by a pair of pneumatic valves actuated by the edge of the filter cloth. These valves control the angle of the pneumatically driven cloth tracking roller which steers the cloth back to center. Should the carrier belt or the filter cloth track outside allowable limits drift switches at the head and tail of the filter trigger and the filter is stopped to prevent damage.

Once at the tail the cloth is directed up to the top of the filter, under a bowed roller to reduce creasing, and over an idler roller, before rejoining the carrier belt under the dam roller in preparation for feed slurry.

Characterizing Creep Behavior of a Fine-grained Zinc Pressure Leach Tailings

Jade Chung, BGC Engineering Inc., Canada
Adrian Wightman, BGC Engineering Inc., Canada
Stephanie Alexander, Hudbay Minerals Inc., Canada

Abstract

The settlement of mineral tailings is commonly represented with only primary consolidation, as this mechanism is typically considered responsible for most of the decrease in thickness of the tailings deposit. However, materials containing certain hydrated minerals additionally undergo large vertical strains due to secondary compression (creep). The total decrease in thickness caused by creep over the lifespan of some material deposits can be greater than the decrease in thickness resulting from primary consolidation, as evidenced in case history reviews by various authors (Singh and Mitchell, 1968; Mesri, 2003).

In this study, the creep behavior of Zinc Pressure Leach (ZPL) tailings was assessed, using site survey data and results from laboratory testing. Survey data of the tailings beach surface and the upstream-constructed dam surface showed greater rates of settlement continuing over longer time periods than typical for silt-sized mineral tailings particles. Results of laboratory creep testing of the tailings material were consistent with the site survey data and showed elevated rates of vertical deformation beyond the interpreted end of primary consolidation.

Various theoretical, semi-empirical, and empirical models were considered and compared to assess their suitability to represent the consolidation and compression of the ZPL tailings. The outcome of this study was the selection of a combination of semi-empirical (Bjerrum, 1967; Garlanger, 1972) and empirical (Singh and Mitchell, 1969) methods as the basis for analysis of the ZPL tailings compression observed to date and the estimation of settlements projected to occur in the future. The concepts of sets of parallel compression curves (Bjerrum, 1967) and estimation of quasi-preconsolidation stress (Garlanger, 1972) formed the theoretical framework for differentiating the effect of consolidation from the effect of creep. The power law representation of creep strain rates (Singh and Mitchell, 1969) was used to support the analysis of available test data and for comparison to observed in-situ settlements.

Introduction

Zinc Pressure Leach (ZPL) tailings are the residue from a method of processing a finely ground zinc concentrate with sulfuric acid and oxygen in a pressurized multi-compartment autoclave. In this process, iron sulfate, gypsum, jarosite, elemental sulfur, and other precipitates are generated as the residue and the zinc sulfate solution is processed further to recover the economic and precious metals. A result of the ZPL process is that the residue, mixed with water, transported, and placed in the tailings facility.

During zinc processing and active deposition at the ZPL Tailings Facility mine personnel were typically present to observe and monitor the effects of compression of the ZPL tailings over time, such as: development of cracks at the surface of upstream constructed dams, decreased freeboard, or formation of depressions in the ZPL tailings surface. However, active deposition in the facility ended in 2022, and the facility is transitioning to care and maintenance and closure phases. Hudbay Minerals Inc (Hudbay) is intending to develop plans with reduced monitoring effort and progress toward post-closure landforms. Closure options being considered include the placement of cover materials and the effects of this additional load and the long-term compression of ZPL tailings is the premise for this study.

Background

Tailings deposit and facility description

Deposition of ZPL tailings into the ZPLTF commenced in 1992. The ZPL tailings were transported as a slurry of tailings solids and water via a 300 mm (12") diameter pipeline, exiting through a single point outlet at the ZPLTF, the position of which has varied throughout active deposition (1992 to 2022). The ZPL tailings are contained by a series of four perimeter dams (Figure 1): West, North, and East ZPL Dams, which have been incrementally raised in a combination of centerline and upstream configurations over the years; and the South ZPL Dam, which has been raised incrementally in centerline and downstream configurations.



Figure 1: Aerial photograph of ZPL tailings facility in 2022

ZPL tailings description

The ZPL tailings have generally been described as laminated, orangish red, nonplastic silt with trace sand, soft, moist to wet and with a metallic odor. Particles of ZPL tailings have been observed to form very thin, elongated, needle-shaped agglomerations, visible to the naked eye.

The approximate in-pipe gravimetric water content of the ZPL tailings slurry was estimated as 360%, based on volumetric water to solids ratio of 10:1 (as reported by the operator), with an average specific gravity of solids of 2.77. The water content of ZPL tailings samples recovered from ZPL tailings deposits underlying the dam fills ranged from 20% to 70%. The general trend of the water content data was decreasing water content with decreasing elevation (see Figure 2a).

The particle size distribution of ZPL tailings samples typically comprised 100% fines (<0.075 mm), 92% to 95% being silt-sized particles and 5% to 8% being clay-sized particles (Figure 2b). In accordance with the ASTM 4318-17 standard for Atterberg limits testing, the ZPL tailings samples were reported to be "nonplastic." The ZPL tailings samples were classified using the USCS as "Silt," with USCS symbol "ML."

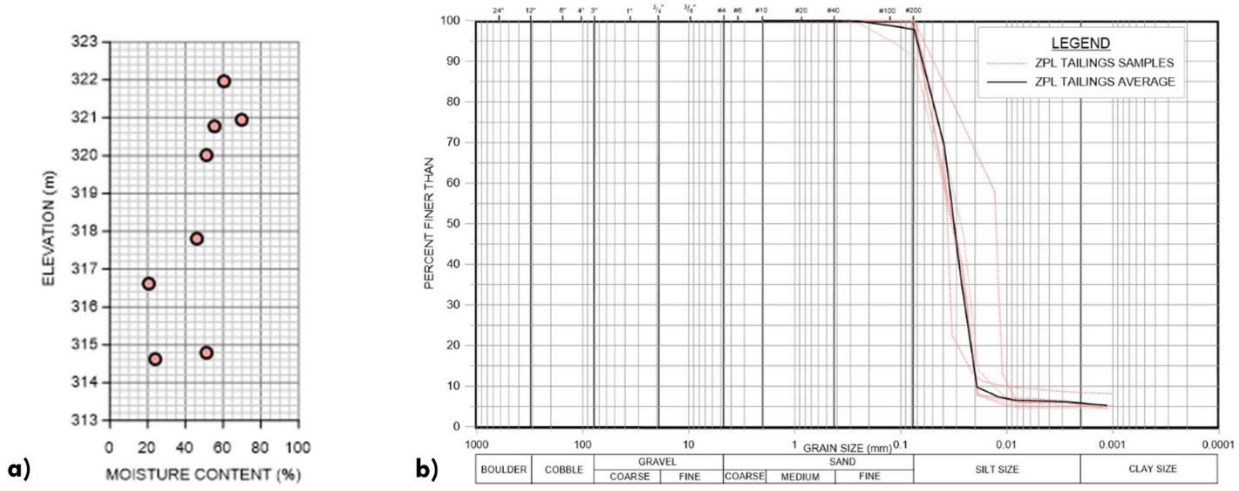


Figure 2: Results of laboratory tests on ZPL tailings samples (a) water content, (b) particle size distribution

The specific gravity of three samples of ZPL tailings solids were tested using the water pycnometer method (ASTM D854-14). The specific gravity of the ZPL tailings samples ranged from 2.6 to 2.9, with an average value of 2.8. The unit weights were assigned based on the measured mass of a known volume of ZPL tailings, which were recovered in thin-walled (Shelby) tubes using fixed piston samplers in conjunction with mud rotary drilling using side-discharge tricone bits. The assigned unit weights of ZPL tailings were as follows:

a. The saturated unit weight was 17.6 kN/m^3.
b. The dry unit weight was 11.4 kN/m^3.

c. The moist unit weight was calculated as 14.5 kN/m^3.

Trace minerals, trace metals, X-ray diffraction, and scanning electron microscopy tests were completed by SGS Canada (Lakefield) on two representative samples of ZPL tailings. The results of the tests indicated that the samples comprised primarily iron sulfates (50% to 55%), gypsum (20% to 30%) and iron oxides (10% to 25%). Gypsum is a hydrated calcium sulfate (CaSO4•2H2O) mineral, that is soluble in water and subject to rheological (flow) behavior that is time, stress, and humidity dependent.

Compression mechanisms in fine grained soil

The decrease in thickness (compression) of a fine-grained mineral soil is conventionally described as resulting from two mechanisms occurring sequentially: primary consolidation, followed by creep. Primary consolidation is the decrease in volume of the fine-grained soil as the excess pore pressures are dissipating, and the effective stress (load exerted on the particle to particle contact area) is increasing. Creep[1] describes the decrease in volume at a constant (macro-scale) effective stress (constant applied load), after excess pore pressures have dissipated.

Primary consolidation

The magnitude of volume decrease occurring in primary consolidation is a function of the magnitude of the stress increase relative to the initial effective stress and the greatest effective stress to which the soil had previously been subjected (preconsolidation stress). The relationship between effective stress and volume decrease of a given material is represented with two parameters:

1. The compression index (C_c) relating the volume (represented as void ratio) decrease to effective stresses exceeding the preconsolidation stress (p_c).
2. The recompression index (C_r) relating the volume decrease (void ratio) to effective stresses exceeding the initial effective stress, yet less than the preconsolidation stress.

The C_c and C_r can be interpreted from laboratory consolidation testing of either remolded/reconstituted samples or intact samples (Schmertmann, 1953). The typical laboratory consolidation test used to define these parameters is one-dimensional loading of the sample in an oedometer, either by:

1. Maintaining a constant rate of strain, by increasing the vertical load at whatever rate is necessary and continuously monitoring/recording the applied load and vertical displacement.
2. Incremental loading, with the duration of each load increment continued until the end of primary consolidation.

[1] Note that the terminology to describe the decrease in volume of a material deposit at a constant applied load or constant macro-scale effective stress is inconsistent in the available references. This behavior has also been referred to as “delayed consolidation,” “secondary consolidation,” “secondary compression,” and “solidification.”

The amount of time required for completion of primary consolidation (dissipation of excess pore pressures) is dependent on the permeability of the fine-grained material, the thickness of the material, and the drainage conditions. The completion of primary consolidation for each load increment in a laboratory consolidation test is interpreted using the logarithm of time method (Casagrande and Fadum, 1940), or the square root of time method (Taylor, 1942). From the assessment of time required for completion of primary consolidation for a given increase in effective stress, the coefficient of consolidation (c_v) can be assessed.

Secondary compression (creep)

The time-dependent decrease in volume of a material that occurs under constant applied load (creep) remains inconsistently defined and variably characterized in industry applications and in peer-reviewed published works. Creep has been described as occurring under either drained or undrained conditions (Mitchell and Soga, 2005); it has also been described as occurring under constant effective stress (Bjerrum, 1967). In recent publications, common terminology describes creep as occurring under a constant applied load, with drainage and pore pressure conditions described on a case-by-case basis (increasing, decreasing, remaining constant, or negligible; Mitchell and Soga, 2005; Terzaghi et al., 1996), rather than integral to the definition of creep.

The mechanisms thought to be responsible for creep are numerous, and include both microscopic and macroscopic behaviors, such as the following:

1. Deformation due to structural viscosity (Terzaghi, 1941; Taylor, 1942; Bjerrum 1967; Fredlund and Rahardjo, 1993) and the water flow from micro-pores to macro-pores (Zeevart, 1986; Navarro and Alonso, 2001; Mitchell and Soga, 2005).
2. Sliding between soil particles (Grim, 1962; Gupta, 1964; Kuhn and Mitchell, 1993).
3. The breakdown of interparticle bonds (Taylor and Merchant, 1940; Terzaghi, 1941; Crooks et al., 1984; Mesri, 2003).
4. Deformation due to "jumping" of bonds/exceedance of activation energy (Mitchell et al., 1968; Kwok and Bolton, 2010).

A commonality between the above listed mechanisms is the co-involvement of water particles and mineral particles. It is the ongoing interaction between the water particles and mineral particles that permits continued volume change. Thus, minerals that contain "bound water" (hydrous materials), such as most clay minerals, gypsum, and some other micaceous minerals, are subject to much greater magnitudes of volume decrease than anhydrous minerals such as quartz.

Mathematical modeling of creep

Many mathematical models have been developed with the goal of quantifying the volume decrease associated with creep. Some of the more common mathematical models used to estimate the volumetric

change due to creep include:

1. Empirical
    a. Semilogarithmic relationship between void ratio (or strain) and logarithm of time (Mesri and Godlewski, 1977; Walker and Raymond, 1968; Yin, 1999).
    b. Power law relationship between strain rate, stress, and time (Singh and Mitchell, 1969; Ting, 1983).
2. Semi-empirical
    a. Semilogarithmic time-dependent compression (Bjerrum, 1967) and quasi-preconsolidation stress (Garlanger, 1972).
    b. Elastic-viscous-plastic logarithmic and power functions (Yin and Graham, 1994).
3. General Stress-Strain-Time/Elastic-viscoplastic Models
    a. Overstress Theory (Adachi et al., 1996; Desai and Zhang, 1987).
    b. Nonstationary flow models (Sekiguchi and Ohta, 1977; Nova, 1982; Matsui and Abe, 1985).

The selected basis for analysis of the ZPL tailings creep behavior is a combination of semi-empirical (Bjerrum, 1967; Garlanger, 1972) and empirical (Singh and Mitchell, 1969) methods. The concepts of sets of parallel compression curves (Bjerrum, 1967) and estimation of quasi-preconsolidation stress (Garlanger, 1972) formed the theoretical framework for differentiating consolidation and creep. The power law representation of creep strain rates (Singh and Mitchell, 1969) provided a mathematical model to interpret creep test data and estimate settlements.

Bjerrum (1967) describes the compression behaviors of clays (fine grained soils) that are subject to delayed or secondary consolidation (creep), as being represented by a system of approximately parallel lines on the void ratio vs. vertical stress (log scale) diagram (see Figure 3a), rather than by a single curve. Each of the lines represents the void ratio – vertical stress relationship for a given duration of sustained loading (Bjerrum, 1967). The load-deformation "path" of soil undergoing compression follows along one of these parallel curves as the effective load increases. When the effective stress stabilizes (constant) the load-deformation path progresses vertically between one compression curve to a parallel compression curve that is characteristic of the duration of the sustained load (Figure 3a). Garlanger (1972) expanded on this parallel compression curve concept, providing a conceptual framework and computational solution for the "quasi" preconsolidation stress, the analogous maximum effective stress with an equivalent effect on void ratio and future loading, resulting from the creep occurring under a sustained lower magnitude vertical effective stress (Figure 3b).

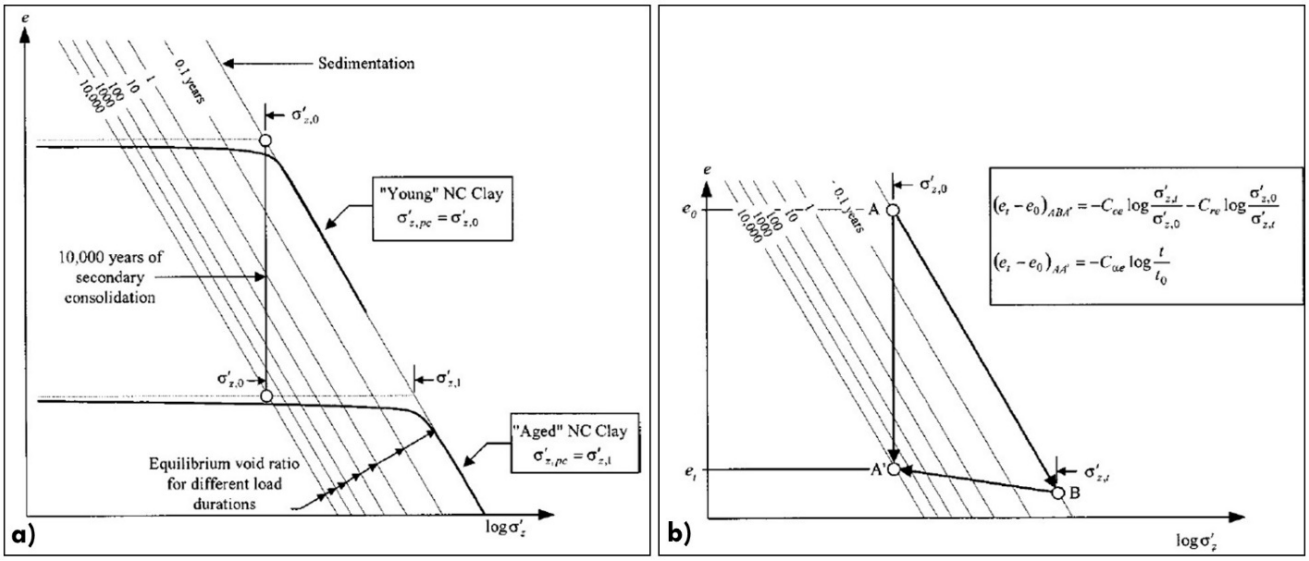


Figure 3: (a) Consolidation curves for loads of varying duration; (b) Quasi-preconsolidation stress resulting from creep (Liingaard et al., 2004, after Bjerrum, 1967)

Singh and Mitchell (1968) proposed a three-parameter power law relationship to represent the strain rate ($\dot{\varepsilon}$) as a function of the applied load (D) and elapsed time after application of load (t), for a selected unit of time (t1). The three parameters, unique to a given soil, being:

1. A = y-intercept of the linear trend of ln $\dot{\varepsilon}$ versus D plot (for unit time t1) (Figure 4a).
2. α = constant slope of the ln $\dot{\varepsilon}$ versus D plot, where all $\dot{\varepsilon}$ interpreted at same elapsed time (Figure 4a).
3. m = constant (negative) slope of the log ε̇ versus log time plot (Figure 4b).

The Singh and Mitchell (1968) strain rate function is shown in Equation 1. By integrating the Singh and Mitchell (1968) strain rate equation with respect to time, the strain accumulated from an initial time (t_0) to a subsequent elapsed time (t_f) is represented using Equation 2.

$$\dot{\varepsilon} = Ae^{\alpha D}\left(\frac{t_1}{t}\right)^m \quad \text{(Equation 1)}$$

$$\varepsilon = \int_{t_0}^{tf} Ae^{\alpha D}\left(\frac{t_1}{t}\right)^m = \frac{Ae^{\alpha D}}{(1-m)}\left[{t_f}^{(1-m)} - {t_0}^{(1-m)}\right] \quad \text{(Equation 2)}$$

Where $t_1 = 1$ (unit time)

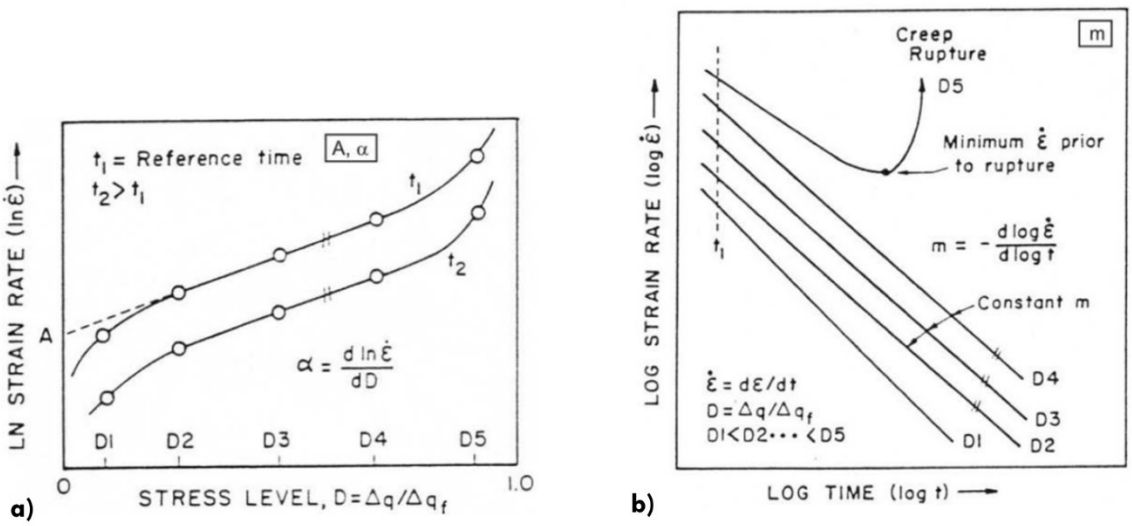


Figure 4: Singh and Mitchell (a) "A" and "α" parameters; (b) "m" parameter (Lacasse and Berre, 2005, after Mitchell, 1976)

Methodology

The compression of the ZPL tailings in-situ, and the resulting effects on tailings surface elevation and dam fill settlement, are controlled by the mechanical behaviors of the ZPL tailings varying with load and duration under a given load. The primary consolidation and secondary compression parameters of ZPL tailings were interpreted from the results of 1D (oedometer) consolidation tests completed at the BGC Advanced Laboratory in Fredericton, NB, Canada, as described in the following sections.

Laboratory test for interpretation of primary consolidation parameters

The compression index (C_c) and coefficient of vertical consolidation (c_v) of the ZPL tailings were interpreted from the results of 1D (oedometer) consolidation testing on specimens prepared using a slurry reconstitution of a ZPL tailings sample recovered in a thin-walled (Shelby) tube using the stationary piston sampling method within a drillhole advanced using mud rotary drilling methods and a baffled tricone bit. The intent of completing a consolidation test on a slurry reconstituted sample was to obtain data that could represent the ZPL tailings slurry consolidation shortly post-deposition, and prior to development of any "quasi" preconsolidation-stress due to creep effects (Figure 3b).

The slurry reconstituted sample was produced from the thin-walled Shelby tube using the following steps:

1. Mixing ZPL tailings from Shelby tube SH-04 (DH-BGC20-39) with ZPL tailings pond water (Figure 5a) to a slurry with water content of approximately 370% (by mass). The water content was selected to be consistent with the estimated in-pipe water to tailings ratio of 10:1 as reported by Hudbay (January 12, 2022).

2. Placing the liquid form slurry into a sedimentation column (Figure 5b) consisting of double porous stones at the base, the oedometer ring, and a membrane-lined extension column (with equal inner diameter as the consolidation ring).
3. Allowing the ZPL tailings to settle out of suspension (sedimentation) into the oedometer ring at the base of the settling column setup. Removing the membrane-lined extension column following the completion of sedimentation of the ZPL tailings solids.
4. Trimming the ZPL tailings sample to the top of the oedometer ring (Figure 5c).
5. Placing only the porous stone and top cap onto the sample as a low "seating load" to maintain a relatively low quasi-preconsolidation stress while promoting the necessary contact between the top cap and sample to promote accurate displacement readings for the test load increments (Figure 5d).
6. Maintaining "moist" conditions using saturated paper towels and plastic coverings for the ZPL tailings specimen during testing (Figure 6a), rather than submerged conditions (due to the high solubility of some compounds in the tailings, particularly when subject to increased pressure).
7. Completing the incremental load consolidation test in general accordance with ASTM International standard D2435M-11 (ASTM, 2020). Each load increment was ended after completion of primary consolidation (as interpreted using the square root of time method [Taylor, 1942]). One offload-reload cycle was completed prior to the final offloading of the sample.

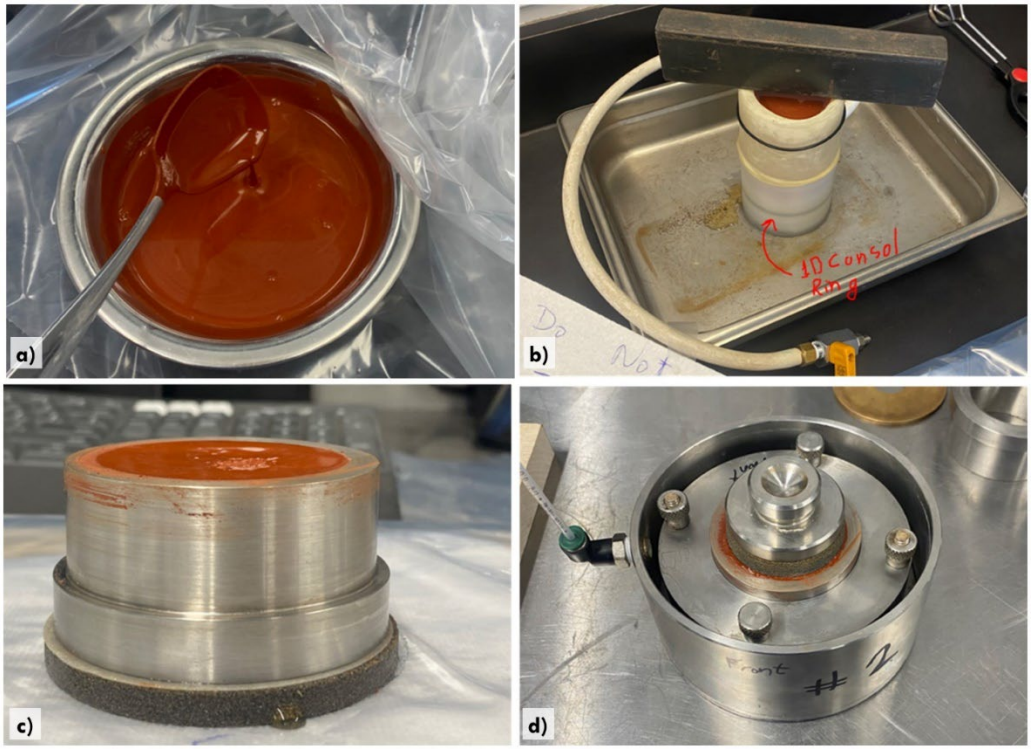


Figure 5: Preparation of slurry reconstituted specimen: (a) ZPL tailings and water slurry; (b) sedimentation column; (c) Trimmed specimen in oedometer ring; (d) Top cap as "seating load"

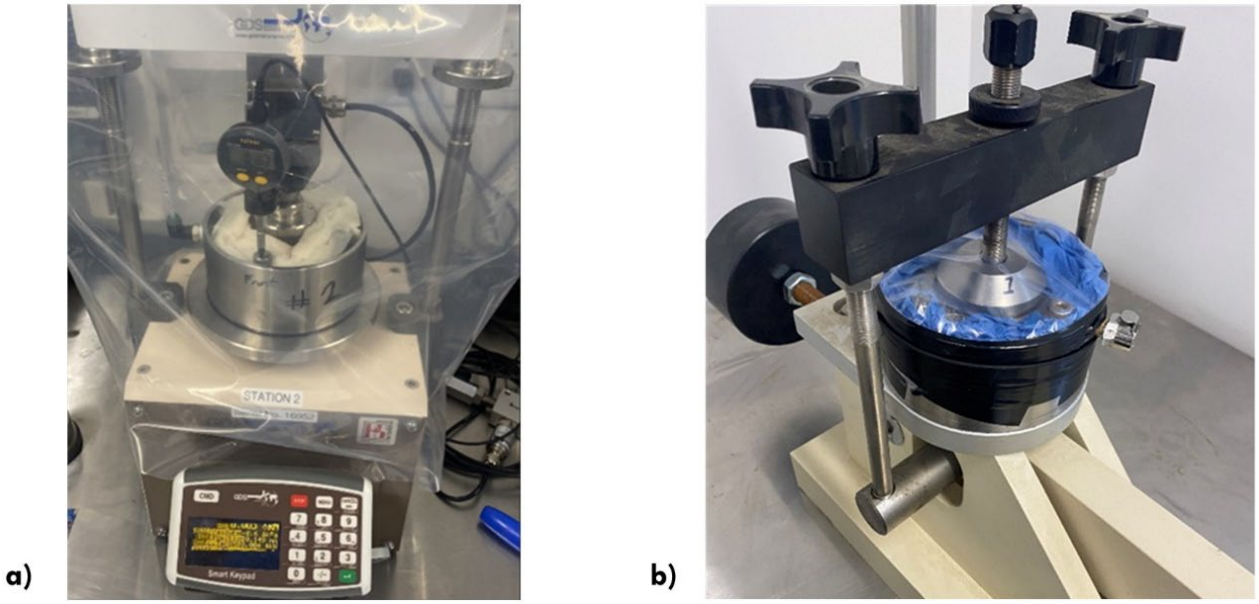


Figure 6: Oedometer equipment and materials set up for moist conditions for: (a) consolidation of slurry reconstituted test specimen; (b) intact

Laboratory test for interpretation of creep parameters

The creep behavior of ZPL tailings was assessed based on results of two long-term creep tests on specimens prepared from intact Shelby tube samples of ZPL tailings recovered using stationary piston methods, from drillholes advanced with mud rotary techniques and a side discharge tricone bit. The creep tests were completed at the BGC advanced soil testing laboratory in Fredericton, NB, Canada, using dead-weight consolidation load frame equipment and mechanical displacement gauges. Manual loading and displacement readings were intentionally selected to exclude issues of data loss that were considered likely with the use of digital systems for test durations exceeding one year.

The creep tests were completed under the one-dimensional (1D) loading conditions of consolidometer (oedometer) equipment. Test specimens were prepared in general accordance with ASTM D2435M-11 (ASTM, 2020). Test specimens were maintained in "moist" conditions during the creep test, using saturated rags and plastic coverings sealed to the cell with electrical tape (Figure 6b).

Loading of the test specimen was applied incrementally (load ratio of 2), up to the target creep loads of 201 kPa (Test C4) and 416 kPa (Test C3). Each load increment below the target creep load was applied for a duration of 24 hours. The creep test loads were applied for durations of 429 days (Test C4) and 416 days (Test C3). Following the creep test load application, incremental load increases were continued to the maximum loads of 2992 kPa (Test C4) and 3273 kPa (Test C3), as limited by the equipment setup. The tests were then completed with incremental offloading, to establish the rebound load-deformation curve.

Data and discussion

Primary consolidation

The consolidation curve (void ratio [e] versus log vertical effective stress plot) for the test on slurry constituted ZPL tailings specimen (C0) is shown in Figure 7. The interpreted C_c value was 0.42 (modified compression index, $C_c' = C_c/(1+e_0) = 0.16$). The interpreted c_v within the stress range of 10 kPa to 400 kPa (representative of typical in-situ conditions) was 1×10^{-5} m^2/s. The consolidation curves for two 1D consolidation tests completed on intact ZPL tailings samples are also shown in Figure 7 for comparison.

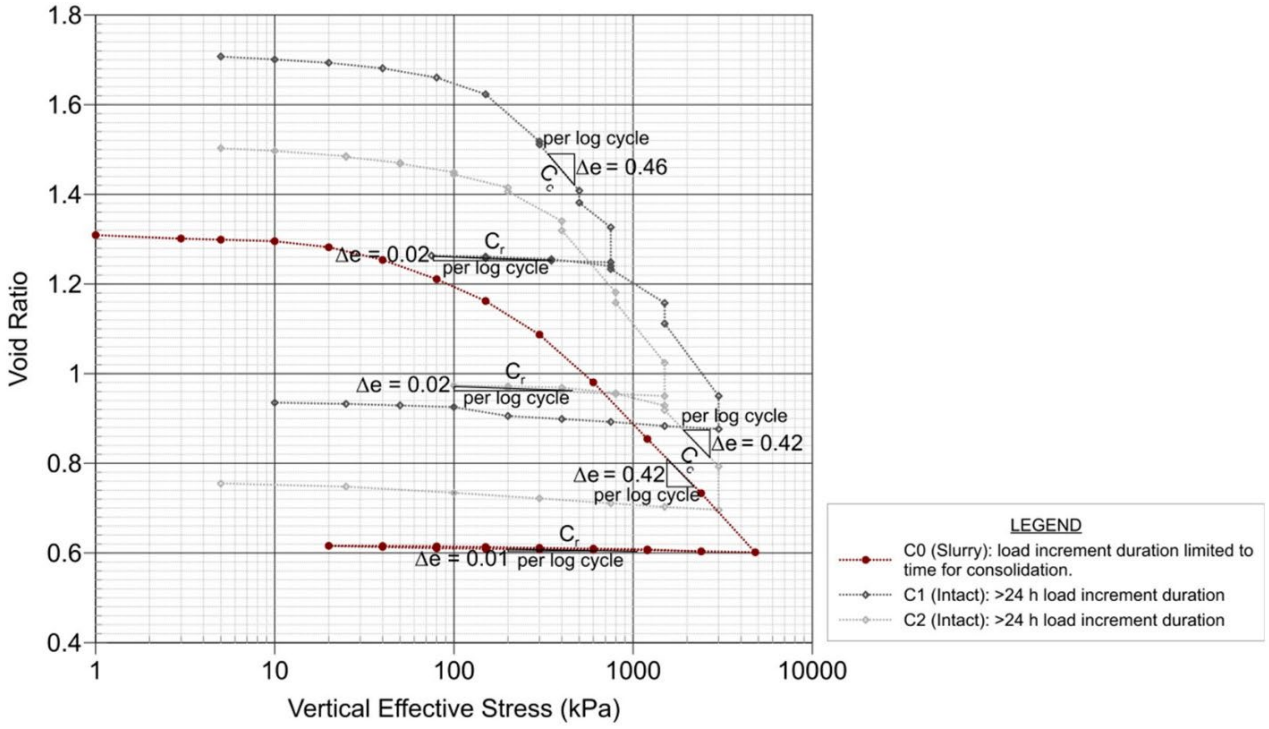


Figure 7: Consolidation of curve of slurry reconstituted and intact ZPL tailings sample

The interpreted recompression index (C_r) value was interpreted from reloading stages of the 1D consolidation test on the slurry reconsolidated specimen, in addition to the reloading stages on four 1D oedometer consolidation tests on intact ZPL tailings specimens (C1, C2, C3, and C4; Table 1). The reconsolidation curves for the test on the slurry reconsolidated specimen (C0) and two of the intact specimens (C1 and C2) are shown in Figure 7. The interpreted C_r values ranged from 0.006 to 0.020, and the assigned representative C_r value was 0.01 (modified recompression index, $C_r' = C_r/(1+e_0) = 0.006$).

Table 1: Results of reloading stages of 1D consolidation test

Depth (m)	Test ID	Test specimen type	Test conditions	Initial void ratio	Initial water content (%)	C_r	C_r' $[C_r/(1+e_0)]$
9.40 to 10.00	C0	Slurry reconstituted	Moist[1]	1.64	75.1	0.006	0.002
13.90 to 14.50	C1	Intact	Submerged[2]	1.71	55.5	0.015	0.006
20.06 to 20.70	C2	Intact	Submerged[2]	1.50	51.3	0.020	0.008
17.00 to 17.60	C3[3]	Intact	Moist[4]	1.25	49.9	0.006	0.003
9.40 to 10.00	C4[3]	Intact	Moist[4]	1.74	74.7	0.011	0.004

Notes:
1. Moist test conditions refer to use of humidification and covered cell conditions, as shown in Figure 6a.
2. Submerged test conditions refer to use of tap water to maintain the submerged condition of the test specimen within the oedometer cell. Crystals were observed to form along the surface of the water bath at the oedometer cell wall during the test. It was inferred that the source of the material forming the crystals was some soluble portion of the sample specimen that dissolved in the (tap) water bath.
3. Creep test completed on this test specimen (C3 creep test at 200 kPa load increment, C4 creep test at 400 kPa load increment).
4. Moist test conditions refer to use of humidification and enclosed cell condition shown in Figure 6b.

There was limited available published data on the consolidation parameters of similar tailings materials. A study on gypsum tailings (from phosphoric acid production [Blight, 1979]) indicated a tailings c_v of 3×10^{-5} m/s. The compression index of a fine iron tailings (Hu et al., 2019), with slightly lower fines content (78%) and void ratio of 1.4, was found to be 0.26. The compression index of a copper-zinc tailings with 90% fines content and void ratio between 1.2 and 1.4 was found to range from 0.24 to 0.30 (Fan and Rowe, 2022). The C_c of ZPL tailings was more similar to $C_c = 0.40$ of coal wash tailings (low plasticity, 66% fines, $e_0 \sim 1.6$) as reported by Qiu and Sego (2001).

Creep parameters

The creep behavior of ZPL tailings was assessed based on the results of two long-term creep tests loads applied for durations of 429 days (Test C4) and 416 days (Test C3). The strain vs. √time and strain vs. log time plots for the creep test load increments of Test C3 and C4 are shown in Figures 8a and 8b, respectively. Data from an ASTM "reference clay" is also plotted for comparison of the non-creep susceptible behavior of the "reference clay" and the ZPL tailings behavior.

The Singh and Mitchell (1969) creep parameters were interpreted from the displacement-time data of the creep load increments, using linear and exponential trendline fitting to plots of the following:

1. Ln strain rate vs. vertical stress (Figure 9a).
2. Log strain rate vs. log time (Figure 9b).

The Singh and Mitchell creep parameters interpreted for the ZPL tailings were as follows:

1. $m = 0.9$.
2. $\alpha = 0.0017$.
3. $A = 0.5$ % per day.

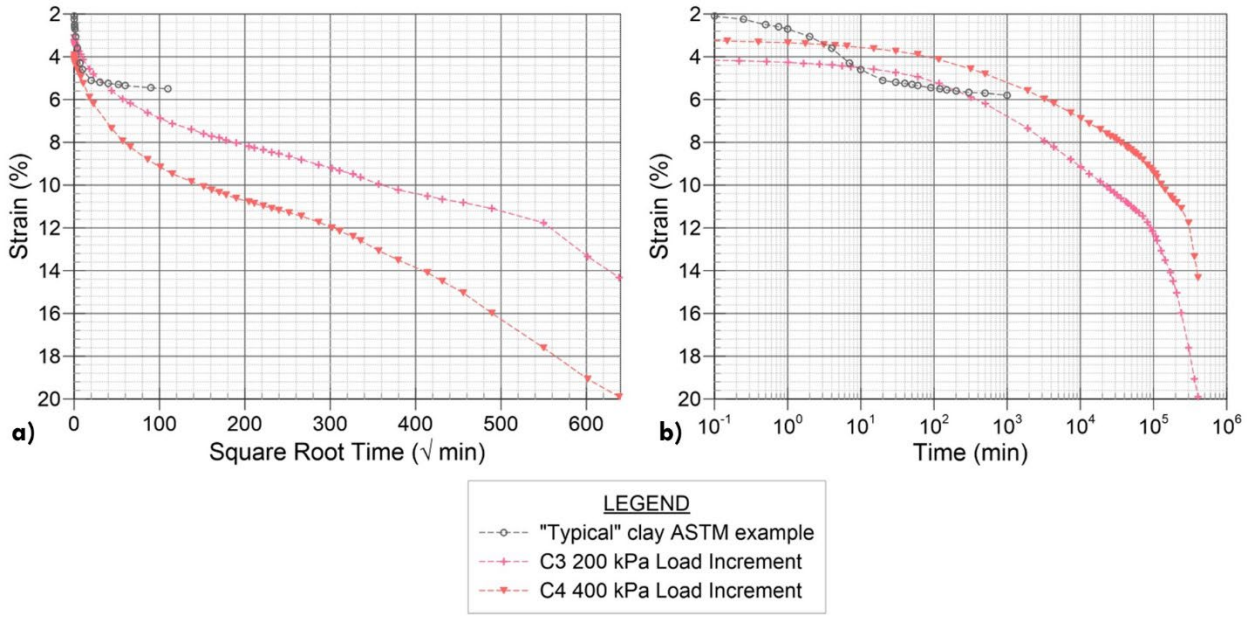


Figure 8: Strain accumulated during creep tests on intact specimens plotted against: (a) square root time; (b) log time

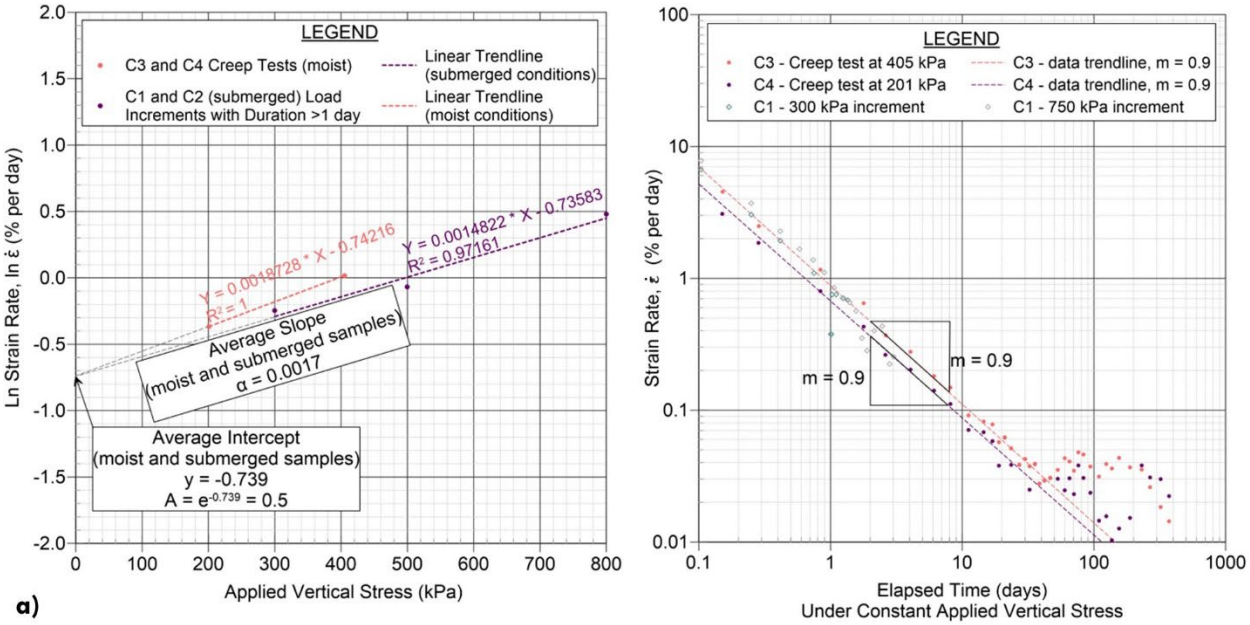


Figure 9: Interpretation of Singh and Mitchell (1969) creep parameters "A," "α," and "m" from (a) Ln strain rate vs. applied vertical stress, and (b) strain rate vs. log time plots

A comparison of the creep deformation modeled using the interpreted parameters and the creep test data is shown in Figure 10.

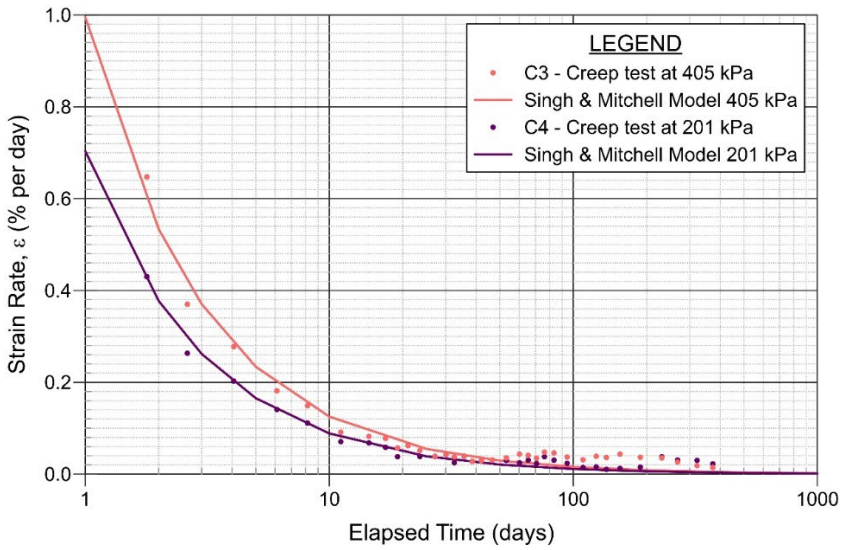


Figure 10: Comparison of laboratory creep test data and modeled creep strain rate using Singh and Mitchell (1969) parameters

Most published case histories of creep behavior describe the compression of organic materials, high plastic clays, or frozen sand units. No case histories of Singh and Mitchell power law modeling of creep in fine grained (mineral) tailings were found during the literature search. Comparison of creep behavior of the ZPL tailings to subaqueous deposits of clay/silty clay may be relevant because of the common (hydrated) mineral-water interaction in both clay minerals and gypsum, and the high water and void content resulting from subaqueous depositional environments. The Singh and Mitchell parameters of two potentially relevant case histories are provided in Table 2. Note the similarity of the "m" parameter relating the change in strain rate over time for the Bohai Bay sediment, San Francisco Bay mud and ZPL tailings.

Table 2: Comparison of Singh and Mitchell creep parameters of mineral soils in published case histories and ZPL tailings

Material	m	A (% per day)	Authors	Notes
Silty Clay Sediment (Bohai Bay Tianjin, China)	[1]0.83	[2]0.22	Li et al. (2019)	1. from 1-m = 0.17 2. from $A^*t_1/[1-m]$ = 0.37%/min 3. $\bar{\alpha}$, not α, was presented in study. $\bar{\alpha}$ correlates a normalized stress value to strain rate.
San Francisco Bay Mud	0.84	0.72	Lacasse and Berre (2005)	Samples tested in anisotropic triaxial compression. $\bar{\alpha}$, not α, was presented in study. $\bar{\alpha}$ correlates a normalized stress value to strain rate.
ZPL Tailings	0.9	0.5	(this study)	Samples tested with 1D loading in oedometer.

Conclusions and limitations

Based on the comparison of the estimated settlements and surveyed data, the selected mathematical model

and input parameters appear to be suitable to represent the compression behavior of the ZPL tailings. The mathematical modeling of the ZPL tailings compression includes assumptions and simplifications that result in inherent limitations of the model. Some of the key assumptions and simplifications applied in the mathematical modeling include:

1. Constant parameter values were interpreted to be generally applicable to ZPL tailings material; there is no accounting for spatial variability of the material parameters.
2. Interpretation of material parameters from one-dimensional loading in the laboratory test (laterally confined conditions in the standard oedometer equipment).

Because these assumptions and simplifications do not fully capture the complexity of the actual load conditions and potential spatial variability of material at the ZPL tailings facility, there is uncertainty to be considered when using the interpreted parameters and power law model for estimating settlements at the facility.

References

Adachi, T., Oka, F. and Mimura, M. 1996. Modeling aspects associated with time dependent behavior of soils. Measuring and modeling time dependent soil behavior. *Geotechnical Special Publication* 61: 61–95. American Society of Civil Engineers.

ASTM International. 2020. Standard Test Methods for One-Dimensional Consolidation Properties of Soil Using Incremental Loading (ASTM D2435M-11). https://doi.org/10.1520/D2435_D2435M-11R20.

Bjerrum, L. 1967. Seventh Rankine Lecture: Engineering geology of Norwegian normally-consolidated marine clays as related to settlements of buildings. *Géotechnique* 17: 81–118.

Casagrande, A. and Fadum, R.E. 1940. Notes on soil tests for engineering purposes. *Soil Mechanics Series* 8. Boston, USA: Harvard Graduate School of Engineering.

Crooks, J.H.A, Becker, D.E., Jefferies, M.G. and McKenzie, K. 1984. Yield behavior and consolidation – pore water response. In *Proceedings of Symposium on Sedimentation Consolidation Models: Prediction and Validation*. San Francisco, USA: American Society of Civil Engineers.

Desai, C.S. and Zhang, D. 1987. Viscoplastic model for geological materials with generalized flow rule. *International Journal for Numerical and Analytical Methods in Geomechanics* 11(6): 603–620.

Fan, J. and Rowe, R.K. 2022. Seepage through a circular geomembrane hole when covered by fine grained tailings under filter incompatible conditions. *Canadian Geotechnical Journal* 59: 410–423.

Fredlund, D.G. and Rahardjo, H. 1993. *Soil Mechanics for Unsaturated Soils*. Hoboken, USA: John Wiley & Sons, Inc.

Garlanger, J.E. 1972. The consolidation of soils exhibiting creep under constant effective stress. *Géotechnique* 22(1): 71–78.

Grim, R.E. 1962. *Applied Clay Mineralogy*. New York, USA: McGraw Hill.

Gupta, B. 1964. Creep of saturated soil at different temperatures. (MSc thesis). University of British Columbia, Vancouver, Canada. Accessed at https://open.library.ubc.ca/soa/cIRcle/collections/ubctheses/831/items/1.0050621

Hu, L., Wu, H., Zhang, L., Zhang, P. and Wen, Q. 2019. Geotechnical properties of mine tailings. *Journal of Materials in Civil Engineering* 29(2). https://doi.org/10.1061/(ASCE)MT.1943-5533.0001736

Kuhn, M.R. and Mitchell, J.K. 1993. New perspectives on soil creep. *Journal of Geotechnical Engineering* 119 (3): 507.

Kwok, C.-Y. and Bolton, M.D. 2010. DEM simulations of thermally activated creep in soils. *Géotechnique* 60 (6). https://doi.org/10.1680/geot.2010.60.6.425

Lacasse, S. and Berre, T. 2005. Undrained creep susceptibility of clays. *Proceedings of the 16th International Conference on Soil Mechanics and Geotechnical Engineering.*

Li, G., Yan, Z., Zhang, J., Liu, J. and Xi, Y. 2019. Test study on the creep behavior of Tianjin clays. IOP Conference Series: Earth and Environmental Science, 304. https://doi.org/10.1088/1755-1315/304/5/052037

Liingaard, M., Augustesen, A. and Lade, P.V. 2004. Characterization of models for time-dependent behavior of soils. *International Journal of Geomechanics* 4(3): 157–177. https://doi.org/10.1061/(ASCE)1532-3641(2004)4:3(157)

Matsui, T. and Abe, N. 1985. Undrained creep characteristics of normally consolidated clay based on the flow surface model. *Proceedings of the 11th International Conference on Soil Mechanics and Foundation Engineering:*140–143.

Mesri, G. 2003. Primary compression and secondary compression. *Geotechnical Special Publication* 119: 122–166.

Mesri, G. and Godlewski, P.M. 1977. Time and stress compressibility interrelationship. *Journal of Geotechnical Engineering* 103(5): 417–430.

Mitchell, J.K. 1976. *Fundamentals of Soil Behavior*. New York: Wiley & Sons.

Mitchell, J.K. and Soga, K. 2005. Time effects on strength and deformation. In *Fundamentals of Soil Behavior.* Hoboken, USA: John Wiley & Sons.

Mitchell, J.K., Campanella, R.G. and Singh, A. 1968. Soil creep as a rate process. *Journal of the Soil Mechanics and Foundation Division* 94(1).

Navarro, V. and Alonso, E.E. 2001. Secondary compression of clay as a local dehydration process. *Géotechnique* 51: 859–869.

Nova, R. 1982. A viscoplastic constitutive model for normally consolidated clay. International Union of Theoretical and Applied Mechanics Conference on Deformation and Failure of Granular Materials (pp. 287–295). Delft, Netherlands.

Qiu, Y. and Sego, D.C. 2001. Laboratory properties of mine tailings. *Canadian Geotechnical Journal* 38: 183–190.

Schmertmann, J.H. 1953. Estimating the true consolidation behavior of clay from laboratory test results. In *Proceedings of the American Society of Civil Engineers* 79: 1–26.

Sekiguchi, H. and Ohta, H. 1977. Induced anisotropy and time dependency in clays. In *Proceedings of the 9th International Conference on Soil Mechanics and Foundation Engineering* (pp. 229–238). Tokyo, Japan.

Singh, A. and Mitchell, J.K. 1968. General stress-strain-time function for soils. *Journal of Soil Mechanics and Foundations Division*, January 1968. American Society of Civil Engineers.

Singh, A. and Mitchell, J.K. 1969. Creep potential and creep rupture of soils. In *Soil Mechanics and Foundation Engineering Conference Proceedings* (pp. 379–384). Mexico City, Mexico.

Taylor, D.W. 1942. Research on Consolidation of Clays, Serial No. 82. Cambridge, USA: Massachusetts Institute of Technology, Department of Civil and Sanitary Engineering.

Taylor, D.W. and Merchant, W.A. 1940. A theory of clay consolidation accounting for secondary compression. *Studies in Applied Mathematics* 19(1–4): 167–185.

Terzaghi, K. 1941. Undisturbed clay samples and undisturbed clays. *Journal of the Boston Society of Civil Engineers* 28(3): 45–65.

Terzaghi, K., Peck, R.B, and Mesri, G. 1996. Compressibility of confined layers of soil. In *Soil Mechanics in Engineering Practice.* Third edition. New York, USA: John Wiley & Sons, Inc.

Ting, J.M. 1983. Tertiary creep model for frozen sands. *Journal of Geotechnical Engineering*, 109(7): 932–945.

Walker, L.K. and Raymond, G.P. 1968. The prediction of consolidation rates in a cemented clay. *Canadian Geotechnical Journal*, 5(4): 192–216.

Yin, J.H. 1999. Nonlinear creep of soils in oedometer tests. *Géotechnique* 49(2): 192–216.

Yin, J.H. and Graham, J. 1994. Equivalent times and one-dimensional elastic viscoplastic modelling of time-dependent stress-strain behavior of clays. *Canadian Geotechnical Journal* 31: 42–52.

Zeevart, L. 1986. Consolidation in the intergranular viscosity of highly compressible soils. In *Consolidation of Soils: Testing and Evaluation* 892: 257–281. Philadelphia, USA: ASTM Special Technical Publications.

InSAR Study into Pre- and Post-Failure Deformations of the Jagersfontein Tailings Dam

Divya Sekhar Vaka, GEOFEM, Cyprus
Skevi Perdikou, GEOFEM, Cyprus

Abstract

Tailings storage facilities (TSFs) are critical for storing large volumes of flowable material; however, there are potential catastrophic consequences if failures occur. Interferometric Synthetic Aperture Radar (InSAR) has proven cost-effective and efficient for monitoring TSFs. This study focuses on the application of InSAR, particularly the Small Baseline Subset (SBAS) technique, for monitoring the Jagersfontein TSF in South Africa before and after its collapse in September 2022. Historical satellite remote sensing analyses using fifty-one pre-collapse, and fifty post-collapse Sentinel-1 single look complex (SLC) images reveal significant displacement trends. Pre-collapse analysis shows pronounced displacement along TSF edges, with notable subsidence identified over the legacy and reclaimed mine waste stockpiles, and adjacent to the water reservoir. Two uplift zones are observed near the reclaimed mine waste stockpile and at the breach location, possibly indicating horizontal movement of the south wall prior to collapse, as suggested by widened wall observations from optical satellite imagery. Maximum displacements include -57 mm at the eastern point from January 2021 to August 2022, and -114 mm at the northern point from September 2022 to May 2024. Post-collapse analysis confirms intensified displacements along TSF edges, highlighting ongoing instability. The study underscores InSAR's effectiveness in detecting pre-collapse deformation patterns and monitoring post-collapse dynamics, emphasizing the importance of continuous monitoring to mitigate risks associated with TSF failures and to enhance safety protocols globally.

Introduction

Tailing storage facilities (TSFs) store considerable volumes of flowable material, which can result in loss of life and irreparable damage to infrastructure and the environment if accidentally released. Historical TSF failure events underscore the critical importance of implementing proactive monitoring systems at TSF sites to ensure safe performance (Perdikou and Lees, 2023). A key objective in TSF monitoring is to detect potential signs of instability by analyzing spatiotemporal rates of displacement (Rana et al., 2024). Conventional TSF monitoring methods include field observations and in-situ measurements using

inclinometers, extensometers, LiDAR, GPS, and manual settlement plates. However, Interferometric Synthetic Aperture Radar (InSAR) has emerged as a complementary and efficient tool for TSF monitoring due to its cost-effectiveness (Mohamadi, 2024; Sciortino et al., 2021; Thomas et al., 2019).

The availability of extensive both free and commercial synthetic aperture radar (SAR) data with global coverage enables regular, accurate, and simultaneous monitoring of TSFs using various InSAR techniques. One of these, Differential InSAR (DInSAR) measures the phase difference between two SAR images and converts this phase difference into line-of-sight (LOS) displacement. DInSAR is widely used in the mining industry to monitor short-term and rapidly moving displacements. Nevertheless, DInSAR has limitations due to decorrelation and atmospheric variations between two image acquisitions.

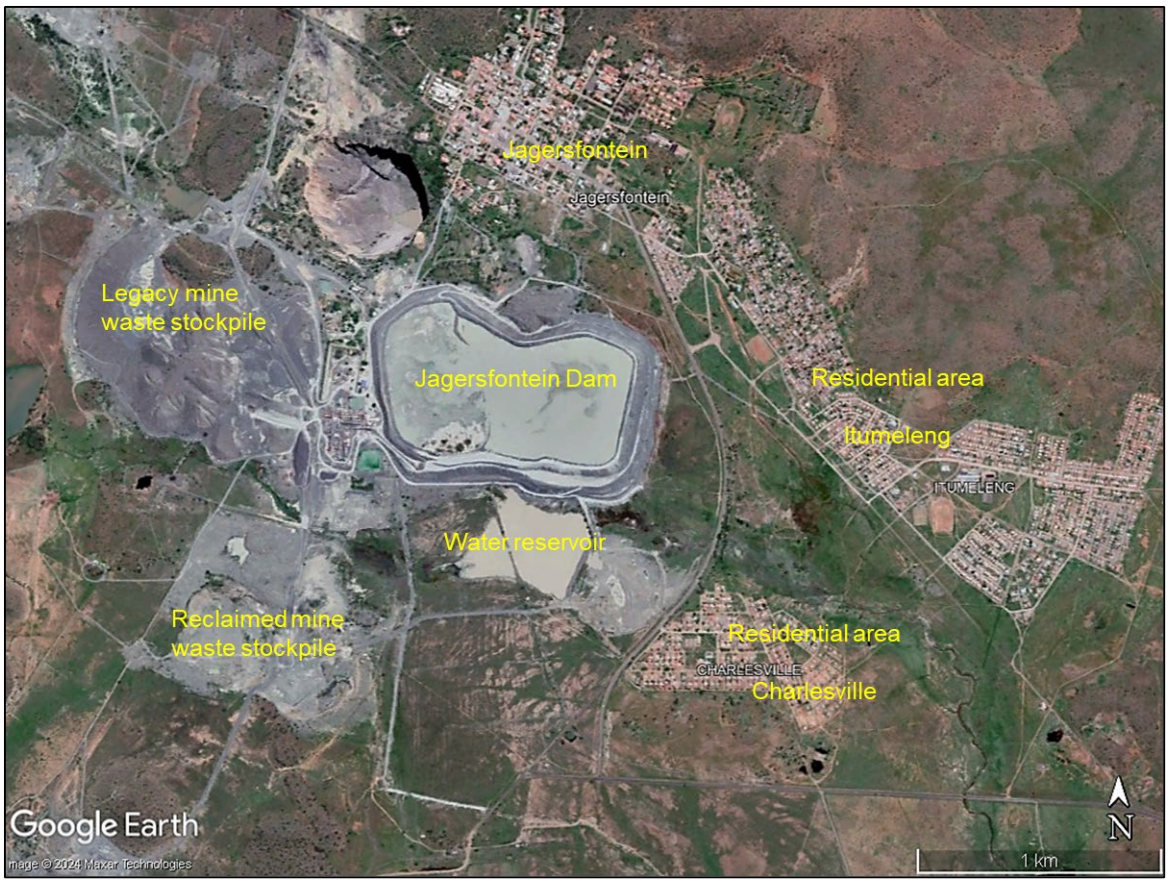


Figure 1: Google Earth imagery of the Jagersfontein Dam in February 2021 (19 months before its collapse). Labels are modified from Torres-Cruz and O'Donovan (2023)

In contrast, time series InSAR can measure millimetric-scale displacements by employing multiple SAR images for displacement monitoring (Hooper et al., 2012). Time series InSAR techniques, such as Persistent Scatterer Interferometry (PSI) and Small Baseline Subset (SBAS), are effective in monitoring TSFs exhibiting slow, long-term deformations. Additionally, time series InSAR techniques overcome the limitations of DInSAR by analyzing a network of interferograms and utilizing filtering operations (Vaka et

al., 2023). Additionally, In SAR monitoring provides a means to detect precursor accelerations that could inform time-to-failure predictions (Rana et al., 2024; Vaka et al., 2023).

On September 11, 2022, a diamond tailings dam in Jagersfontein (see Figure 1) breached, releasing sludge that killed at least one person and damaged numerous houses. The objective of this study was to monitor the Jagersfontein TSF in South Africa using InSAR. Specifically, we utilized SBAS to detect pre-collapse and post-collapse surface displacements of the Jagersfontein TSF. This article focuses on the results of historical satellite remote sensing analyses and the utility of InSAR for pre-collapse and post-collapse monitoring of the Jagersfontein TSF in South Africa.

Study area

The city of Jagersfontein has a long history of mining activities, dating back to the 1870s. In 1931, the De Beers Group acquired the mine and operated it until 1971, when underground ore extraction ceased. The mine changed ownership multiple times: it was sold in 2010 and subsequently sold two more times, with the last sale occurring some months before the dam collapse. The final owner was Jagersfontein Developments, a subsidiary company (Torres-Cruz and O'Donovan, 2023).

On September 11, 2022, the dam collapsed at its southeastern corner in two locations, as visible from Google Earth imagery captured in September 2022 (Figure 2b). A recent study by Torres-Cruz and O'Donovan (2023), using optical satellite image analysis, revealed that in May 2019, erosion gullies had developed on the internal face of the northern wall as well as on the external face of the southeastern wall where the failure occurred. Additionally, Google Earth imagery from May 2019 shows evidence of erosion or instability at the same location where the dam later collapsed (Figure 2a).

Method

For the analysis presented in this paper, fifty-one and fifty images were analyzed using the Small Baseline Subset (SBAS) technique in the pre-collapse and post-collapse periods, respectively. The SBAS technique reconstructs the phase history of a pixel with respect to the first acquisition from a network of interferograms with small temporal and perpendicular baselines, ensuring maximum interferometric coherence (Berardino et al., 2002). Interferograms were generated by setting a temporal baseline threshold of 40 days. The topographic phase was removed using a Shuttle Radar Topography Mission (SRTM) Digital Elevation Model (DEM). The differential interferograms were filtered using a Goldstein filter and multi-looked to form approximately 15 m pixels. An unwrapped coherence threshold of 0.1 was used to mask low coherence areas during phase unwrapping, which was performed using the Minimum Cost Flow (MCF) approach. The unwrapped interferograms are subsequently inverted to generate displacement time series for each pixel. These time series are displayed as points, with their colors indicating velocity: warmer colors

represent subsidence, while cooler colors denote uplift. The entire InSAR processing was carried out using ENVI SARscape.



Figure 2: Google Earth imagery of the Jagersfontein Dam a) showing erosion gullies in May 2019 b) after the breach in September 2022.
The inferred location of the erosion is marked with a red circle

Table 1: Details of the data used for the pre-collapse and post-collapse analysis

Period	Data	No. of images	No. of interferograms
Pre-collapse	02-01-2021 to 25-08-2022	51	111
Post-collapse	18-09-2022 to 22-05-2024	50	133

Results

Pre-collapse InSAR time series displacement

Figure 3 illustrates the surface displacement results from the SBAS analysis in the Jagersfontein area in the pre-collapse period. The analysis reveals significant displacement along the edges of the TSF prior to its collapse. The results are interpreted as follows: subsidence, indicated by warm colors, represents movement away from the radar, while uplift, shown in cool colors, represents movement towards the radar. Besides the TSF edges, the results identify three subsidence locations: over the legacy mine waste stockpile, the reclaimed mine waste stockpile, and to the right of the water reservoir, as shown in Figure 4.

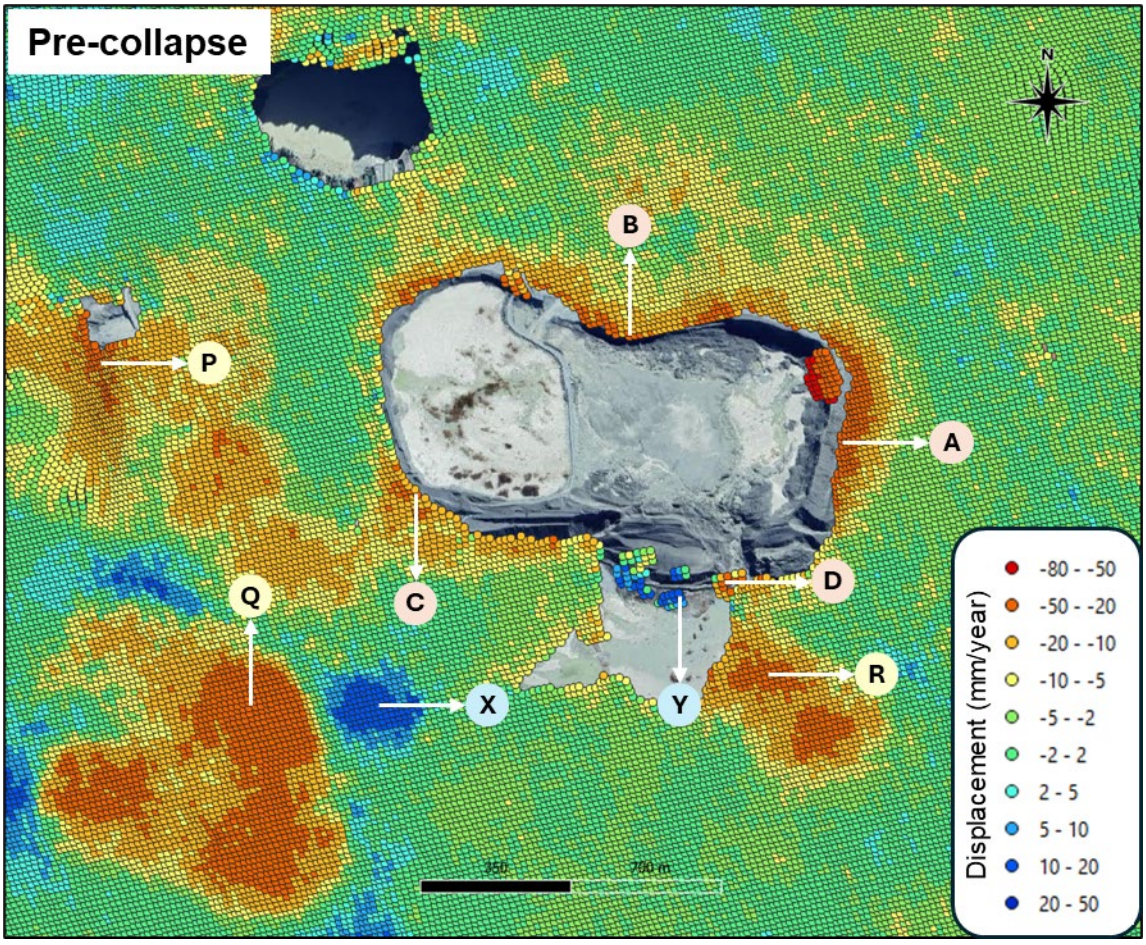


Figure 3: InSAR LOS displacement rate (mm/year) during the pre-collapse period from January 2021 to August 2022.
The subsidence time series is displayed in Figure 4 along the edges of the TSF (points A, B, C, D), at the mine waste piles (points P, Q), and to the right of the water reservoir (point R). The uplift time series is displayed at points X and Y

Additionally, the analysis indicates two uplift locations near the reclaimed mine waste stockpile and at the breach location. The uplift at the breach location may represent horizontal movement towards the

satellite before the collapse, as inferred from optical satellite images that report a widened wall at this location (Torres-Cruz and O'Donovan, 2023). The uplift at the other locations could suggest a new dumping site, warranting further detailed study.

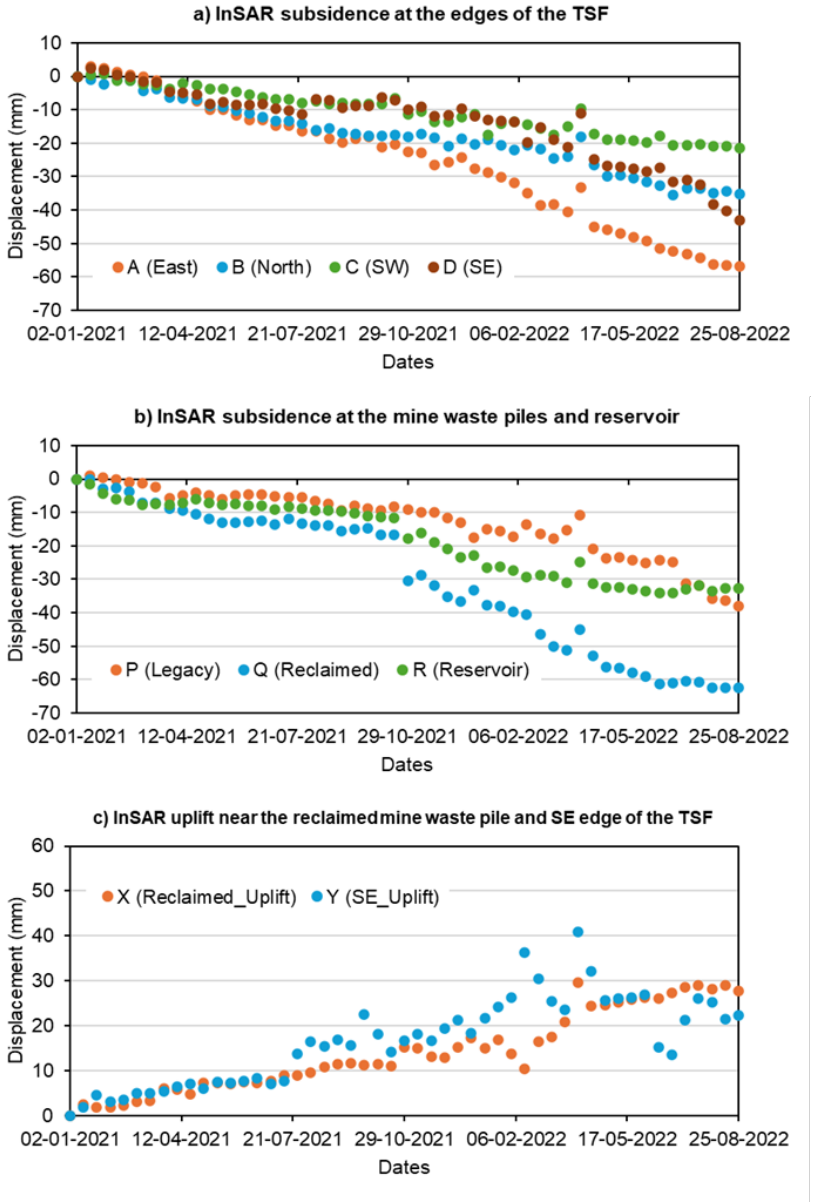


Figure 4: InSAR displacement time series before the collapse a) InSAR subsidence time series at the perimeters of the TSF (points A, B, C, D). b) InSAR subsidence time series at the mine waste stockpiles (points P, Q) and adjacent to the water reservoir (point R). c) InSAR uplift time series at the reclaimed mine waste stockpile and the breach location (points X and Y)

Figure 4 depicts the displacement time series (subsidence and uplift) at various points shown in Figure 3. The eastern point exhibited a maximum displacement of -57 mm from January 2021 to August 2022. Similarly, the northern, southwestern, and southeastern points showed maximum displacements of -35 mm,

-21 mm, and -43 mm, respectively. Notably, the southeastern corner indicated subsidence fluctuations of greater than -4 mm in February, April, June, and August 2022. Overall, significant displacement was observed along the eastern and southeastern walls during the pre-collapse period.

Post-collapse InSAR time series displacement

Figure 5 depicts the surface displacement results obtained from the SBAS analysis conducted in the Jagersfontein area during the post-collapse period. The analysis highlights increased displacement along the edges of the TSF leading in the post-collapse period. Clear subsidence signatures are evident along the TSF boundaries compared to the pre-collapse period. Additionally, three distinct subsidence areas are identified: over the legacy mine waste stockpile, the reclaimed mine waste stockpile, and to the right of the water reservoir, as depicted in Figure 5. Although fewer deformation points are observed at the legacy mine waste stockpile, a discernible subsidence trend is evident.

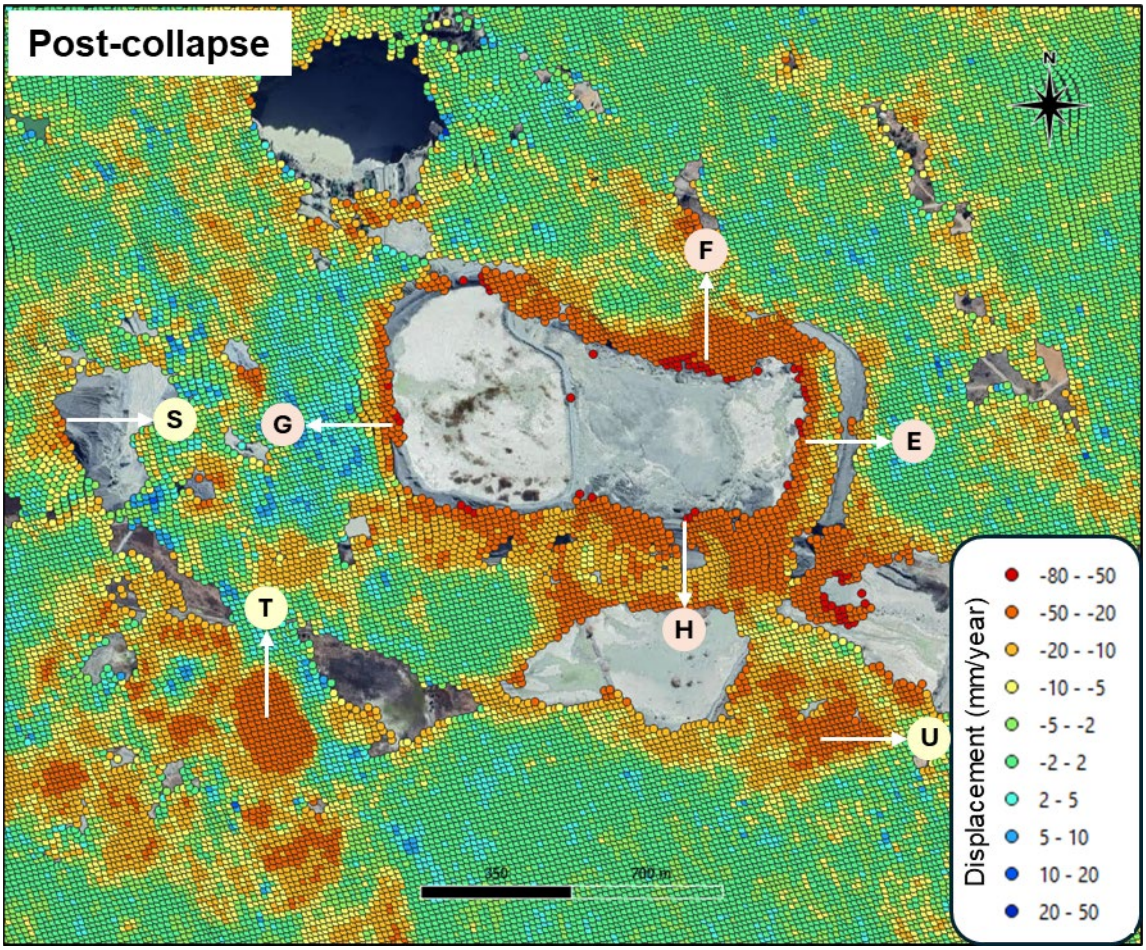


Figure 5: InSAR LOS displacement rate (mm/year) during the post-collapse period from September 2022 to May 2024.
The subsidence time series is displayed in Figure 6 along the edges of the TSF (points E, F, G, H), at the mine waste piles (points S, T), and to the right of the water reservoir (point U)

Notably, the uplift zones observed in the pre-collapse analysis are absent in the post-collapse results. While the absence of the uplift zone near the breach location was anticipated, further investigation is required to understand why the other uplift zone disappeared in the post-collapse analysis.

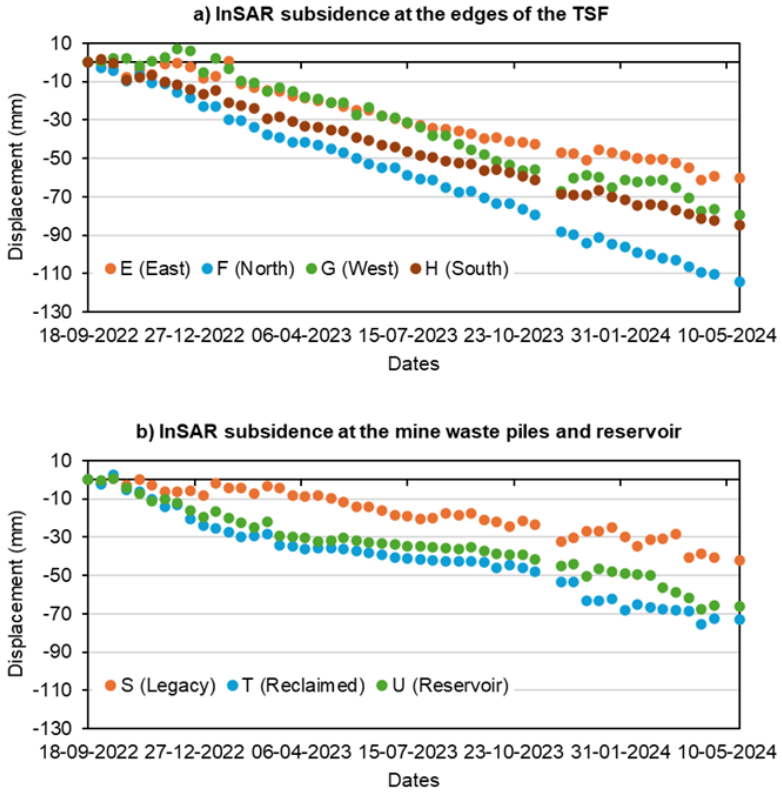


Figure 6: InSAR displacement time series after the collapse a) InSAR subsidence time series at the perimeters of the TSF (points E, F, G, H). b) InSAR subsidence time series at the mine waste stockpiles (points S, T) and adjacent to the water reservoir (point U).

Figure 6 illustrates the time series of displacement (subsidence and uplift) at several locations indicated in Figure 5. The northern point experienced the highest displacement, reaching -114 mm from September 2022 to May 2024. Likewise, the east, west, and south points exhibited maximum displacements of -61 mm, -80 mm, and -85 mm, respectively. The northern and southern edges, which collapsed during the event, show the most significant displacements.

Conclusion

The study underscores the efficacy of InSAR, particularly SBAS, in monitoring the Jagersfontein TSF both before and after its collapse in September 2022. Pre-collapse analyses revealed significant displacements along TSF boundaries and identified specific subsidence areas over legacy and reclaimed mine waste stockpiles. This highlights InSAR's capability in providing detailed insights for TSF monitoring and its

potential in early detection of instability indicators. Additionally, the pre-collapse analysis identified an uplift zone at one of the breach locations, potentially indicating horizontal movement of the south wall of the TSF. Future studies could employ amplitude tracking exercises to measure this horizontal movement accurately. Sudden accelerations observed in the displacement time series (in the pre-collapse period) can help identify potential time windows for failure. This data, in combination with deformation monitoring at specific locations and engineering experience, would provide indications as to how dam failure can be predicted as well as the necessary steps towards mitigating disaster risks and ensuring stability. Post-collapse observations further emphasized intensified displacements along TSF edges, indicative of ongoing instability. These findings underscore the critical need for continuous and effective monitoring of collapsed TSFs, which could serve as sources of future slope instability.

References

Berardino, P., Fornaro, G., Lanari, R. and Sansosti, E. 2002. A new algorithm for surface deformation monitoring based on small baseline differential SAR interferograms. *IEEE Transactions on Geoscience and Remote Sensing.* 40(11): 2375–2383.

Hooper, A., Bekaert, D., Spaans, K. and Arıkan, M. 2012. Recent advances in SAR interferometry time series analysis for measuring crustal deformation. *Tectonophysics* 514–517: 1–13.

Mohamadi, B. 2024. Utilizing InSAR for surface stability monitoring in mining sites: A case study of Sukari gold mine in Egypt. *Int. Arch. Photogramm. Remote Sens. Spat. Inf. Sci.* XLVIII-1-2024, 523–528.

Perdikou, S. and Lees, A. 2013. Could regular satellite InSAR monitoring have helped prevent the Jagersfontein tailings dam failure? *Geosaskatoon 2023. Proceedings of the 76th Annual Canadian Geotechnical Society (CGS) Conference.* Saskatoon, Canada.

Rana, N.M., Delaney, K.B., Evans, S.G., Deane, E., Small, A., Adria, D.A.M., McDougall, S., Ghahramani, N. and Take, W.A. 2024. Application of Sentinel-1 InSAR to monitor tailings dams and predict geotechnical instability: practical considerations based on case study insights. *Bull. Eng. Geol. Environ.* 83, 204.

Sciortino, A., Antonielli, B., Scancella, S., Bozzano, F., Mazzanti, P. and Moretto, S. 2021. Satellite InSAR for assessing deformation processes at the Zelazny Most Tailings Dam (Poland). *Proceedings of the 7th International Conference on Tailings Management.*

Thomas, A., Edwards, S.J., Engels, J., McCormack, H., Hopkins, V., Holley, R. 2019. Earth observation data and satellite InSAR for the remote monitoring of tailings storage facilities: a case study of Cadia Mine, Australia. In A.J.C. Paterson, A.B. Fourie & D. Reid (eds), *Paste 2019: Proceedings of the 22nd International Conference on Paste, Thickened and Filtered Tailings*, Australian Centre for Geomechanics, Perth, pp. 183-195, https://doi.org/10.36487/ACG_rep/1910_11_Thomas

Torres-Cruz, L.A and O'Donovan, C. 2023. Public remotely sensed data raise concerns about the history of failed Jagersfontein dam. *Sci. Rep.* 13: 4953.

Vaka, D.S., Rao, Y.S. and Bhattacharya, A. 2023. Time series analysis of the pre-seismic and post-seismic surface deformation of the 2017 Iran–Iraq earthquake derived from Sentinel-1 InSAR data. *J. Earth Syst. Sci.* 13: 64.

The Barriers to Widespread Adoption of Tailings Dewatering Technologies

Ljiljana Josic, AtkinsRéalis, Canada
Ashley Verge, AtkinsRéalis, Canada
Kasra Majdanishabestari, AtkinsRéalis, Canada

Abstract

Mining is an important contributor to the world economy, but tailings management is, and will continue to be in the coming decades, an increasingly difficult issue for governments, communities, regulators, and mining companies. It has been estimated that nickel, lithium, and cobalt production need to increase by 150% to supply the electric vehicle and clean energy sector in the coming years. This significant increase in metals production will result in a correspondingly significant increase in tailings production and a need for proper management. Currently, most tailings are managed conventionally. Conventionally deposited tailings contain a large amount of water, making tailings management facilities more complex and less stable. Recent catastrophic failures have resulted in enhanced oversight and calls for change. Identifying, developing, and adopting new technologies could help to eliminate the risks posed by the nature of conventional tailings facilities, which have been responsible for the failures that have occurred, and possibly remove them altogether. Dewatering of tailings is imperative for safer tailings management. By decreasing water content in the tailings, significant safety improvements can be achieved, and the risk of catastrophic dam failure and tailings runout could be eliminated.

This paper discusses tailings dewatering technologies currently available and in use. The adoption of different tailings dewatering techniques over time across the mining industry is analyzed, with particular attention to the proportion of mines using or planning to use dewatering techniques. The impact of industry-wide factors such as the catastrophic tailings dam failures that have occurred in the past decade, and the introduction of the Global Industry Standard on Tailings Management on the use of dewatering techniques, are examined. What are the key factors in making decisions on the deposition methodology selection, and what are the barriers to widespread adoption of dewatered tailings technologies? Comparison of tailings management technologies with respect to different aspects such as social, technical, environmental, and economics are presented in the paper.

Introduction

The consistency of tailings can be described on a continuum from conventional slurry (which is thickened only to the point that it can be pumped using centrifugal pumps) to a filtered tailings "dry cake," with increasing levels of dewatering. Storage of slurry tailings usually requires containment dams, with dam size typically decreasing with increasing dewatering of tailings. A major appeal of filtered tailings is the potential for stacking of the dewatered tailings without the need for any containment dams. Of particular concern are upstream dams, where portions of the dam are constructed on previously deposited tailings.

Tailings dam failures have led to catastrophic environmental and human tragedies. The Center for Science in Public Participation (CSP2, 2022) maintains a database of tailings storage facility failures worldwide that occurred between 1915 and 2022. The database documents 368 failures that resulted in 3,241 deaths and the release of over 250 million cubic meters of contaminated residues into the environment (CSP2, 2022). These failures almost exclusively occurred at conventional slurry tailings impoundments. If they reach a river, materials released from these failures can travel hundreds of kilometers. The threat of tailings dam failures can be expected to worsen in the coming years and decades due to the increasing severity and frequency of extreme weather events related to climate change. With a decrease in water content of the tailings via dewatering, the extent of runout from a failure and the resulting consequences are correspondingly minimized.

On August 4, 2014, a breach occurred in a section of the Perimeter Dam at the Mount Polley Mine Tailings Storage Facility in British Columbia, Canada. Although thankfully there was no loss of life, there were significant environmental impacts to the downstream area. The subsequent Report on Mount Polley Tailings Storage Facility Breach (Morgenstern et al., 2015) concluded that a move to application of best available technology (BAT) was required. Examples of BAT were given as filtered, unsaturated, compacted tailings, and reduction in the use of water covers commonly used to limit oxygen ingress to prevent acid mine drainage.

Two catastrophic failures in Brazil (the November 5, 2015, collapse of the Fundão Dam in Minas Gerais and the January 25, 2019, failure at the Córrego de Feijão Mine in Brumadinho), which together claimed the lives of approximately 289 people, prompted further actions by concerned parties. As part of the response, the International Council on Mining and Metals (ICMM), the United Nations Environment Programme (UNEP) and the Principles for Responsible Investment (PRI) co-convened a Global Tailings Review to establish an international standard for best practices on tailings storage facilities. The Global Industry Standard on Tailings Management (GISTM, GlobalTailingsReview.org, 2020) was launched in 2020, with ICMM member companies pledging to adopt the standard as a condition of membership. The GISTM requires the consideration of dewatering technologies for new facilities as well as expansions to existing facilities. At the same time, institutional investors are increasing their focus on environmental,

social, and governance (ESG) issues. Common ESG metrics used as investment criteria by some institutions, such as water use and total waste, can be directly improved by the adoption of dewatered tailings technologies (Karajeh, 2023).

Industry dewatering trends

Dewatering of tailings may be achieved using cyclones, centrifuges and various types of filters (vacuum filters including drum, disc, and belt types, or pressure filters including plate and frame and belt presses), or most simply, by spreading the tailings out and drying them in the sun. Farming of tailings using very low ground pressure equipment is used on red mud in Australia, and has been tested on other types of tailings including coal tailings, fly ash, and Canadian oil sands (Williams, 2021). Different methods of filtering tailings are summarized by Ulrich and Coffin (2013). Due to the removal of a significant amount (but not all) of the water in the tailings, filtered tailings are often referred to as "dry," with the disposal facilities often termed "dry stacks." Issues with this terminology have been discussed by others (e.g., Davies, 2011; Ulrich and Coffin, 2013). As such, the potentially misleading term "dry stack" will be avoided in this paper. Tailings may also be mixed with waste rock, which is referred to as co-disposal.

The use of cyclone separation can be considered the first stage in tailings dewatering, which was introduced in the 1960s to produce an economic coarse tailings product for embankment construction and increased water recovery. Thickened tailings were developed in the mid-1970s, filtered tailings in the mid-1980s, and paste operations around 1990 (Davies et al., 2011). As per Davies et al. (2011), while none of the dewatering methods besides cycloning had significant initial acceptance, all of these methods have been increasing in popularity since about 2000.

Vick (1990) reported on the contemporary state of practice that tailings collected from the thickener were "almost universally transported in slurry form to the tailings impoundment," which is described as a matter of convenience since the tailings are already mixed with water in the mill, with further dewatering to allow dry handling usually deemed economically prohibitive. Vick (1990) also reports "considerable controversy" regarding the economics, feasibility and advantages of belt filtration for tailings disposal, noting that the method is justified only when it is required for ore processing (e.g., in uranium milling that had been used extensively in France and South Africa by that time), rather than as a supplementary dewatering method.

As per Oxenford and Lord (2006), Canadian mines have been at the forefront of applications of paste and thickened tailings for surface disposal, beginning with the 1973 implementation of the first thickened tailings operation for surface disposal using the Robinsky method at Kidd Operations in Ontario. Filter stacking was also implemented in Canada at the Line Creek Coal Mine in British Columbia in 1981. Oxenford and Lord (2006) provide seven examples of mines in Canada that used paste, thickened or filtered

tailings technology as of 2006. While in each highlighted example there were various site-specific economic/engineering and environmental/social reasons to implement dewatering technologies, Oxenford and Lord (2006) also recognize the reduced risk of a tailings incident as a primary benefit of such technologies.

Ulrich (2008) reported on a poll of gold producers regarding their tailings dewatering practices in Nevada, which produces approximately 85% of the gold mined in the USA. This poll found that all responding facilities were operating conventional tailings facilities, with the region lagging behind the industry in dewatering techniques at that time. This was attributed to Nevada's regulatory framework, where the full basin area requires a liner system to achieve zero discharge. Ulrich (2008) suggested that a full lining system in addition to tailings dewatering was not economical.

Davies et al. (2011) summarized industry trends towards tailings dewatering, noting that the main objective for use of dewatering technologies was to reduce water consumption and water losses, rather than to reduce the risk of failure. The use of tailings filtration at a number of projects in Chile was noted, as were paste tailings – including Chile's first large-scale paste tailings project that was expected to soon be in operation. Davies et al. (2011) note that Chilean regulations encourage different types of tailings dewatering methods. Canada's use of tailings dewatering is noted as a slow but steady increasing trend, with greater adoption and greater success found in northern regions such as the Raglan Mine in northern Québec, and similarly at the Pogo Project in Alaska, both of which are filter stack facilities. While Australia was noted as the leader in thickened tailings application, it lagged behind other regions in the adoption of filtered tailings.

Research by dewatering equipment manufacturer Metso indicated that only 5% of the worldwide tailings produced in 2018 were dewatered to create thickened tailings or paste, and less than 1% were filtered for stacking. Metso is confident that this proportion will increase, estimating that, by 2025, 13% of all generated tailings will be subjected to some form of dewatering (Leonida, 2020).

Vargas and Campomanes (2022) discuss the current practice in Chile and Peru, where most tailings disposal is noted to be in conventional tailings impoundments; however, 11 filter stack facilities in Chile and six in Peru are profiled, demonstrating a significant contribution to the industry's experience in this technology. Copeland et al. (2023) present a summary of the South African adoption of dewatering technologies, stating that, although tailings filtration is commonly considered during trade-off studies, it is rarely implemented in South Africa, except in arid regions.

Very little information on China's tailings management practices was found in the publicly available literature. Wang et al. (2022) report that of China's 7,800 tailings storage facilities (the most of any country), 70% were built as conventional slurry impoundments. The remaining 30% of alternative tailings technologies represent the highest adoption rate of dewatering technologies found during the research for

this paper. The GRID-Arendal (2020) database contains data on only nine tailings storage facilities in China, eight of which use conventional tailings storage, with one example of in-pit disposal. Clearly, much of the true picture is missing from available public databases.

The Global Tailings Portal (GRID-Arendal, 2020) provides information disclosed by publicly listed companies. At the time of writing, a total of 2,056 facilities are listed. The database is noted to be incomplete due to the absence of information from non-publicly listed companies, including state-owned and privately owned companies, as well as many mid-size and junior companies. Tailings facilities in China and Chile are under-represented, with larger facilities being over-represented. Figure 1 presents the total number of tailings facilities constructed per year as well as the percentage of those that use filtered technology based on the GRID-Arendal (2020) dataset. Although the data is incomplete, it actually suggests a deceasing trend of filtered tailings facilities being constructed since the mid-2010s, with a peak in 2000 with 17% of constructed facilities using filtered tailings.

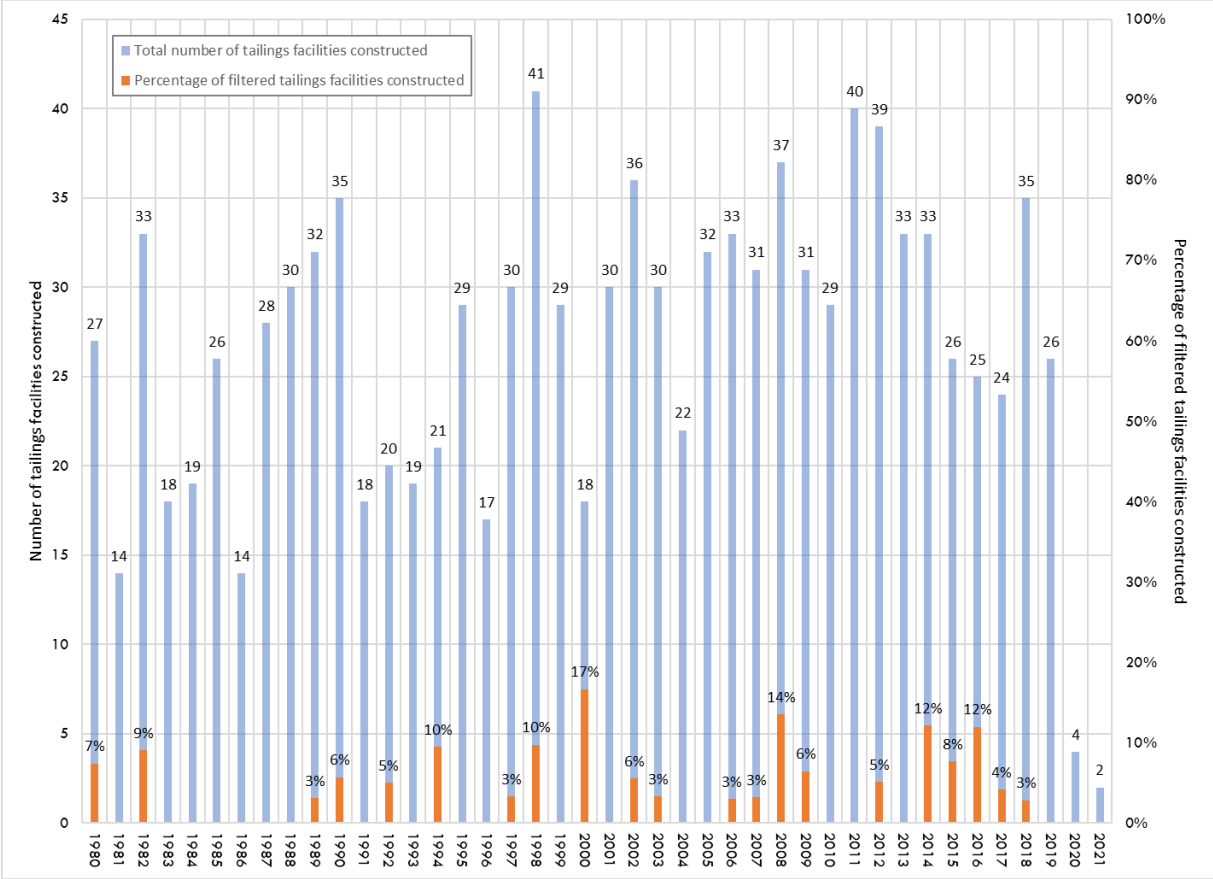


Figure 1: Total tailings facilities constructed and percentage of filtered tailings facilities (1980 to 2021)

Key decision criteria for tailings dewatering technologies

Trade-off studies are typically completed at the pre-feasibility stage of a project to determine optimal site selection, and increasingly, the selected tailings dewatering technology. GISTM Requirement 3.2 requires an analysis of alternatives for all new tailings facilities to rigorously consider all available options throughout the project life cycle, considering environmental, technical and socioeconomic aspects. Figure 2 illustrates schematically the authors' assessment of how some of the key decision criteria typically vary based on the chosen tailings dewatering technology (further comparisons provided by Boger and Hart, 2008; Carneiro and Fourie, 2019; Ulrich, 2019; Williams, 2021; Vargas and Campomanes, 2022). This is further compared in Table 1, providing the authors' more comparison of additional criteria such as footprint, potential environmental impact, and costs.

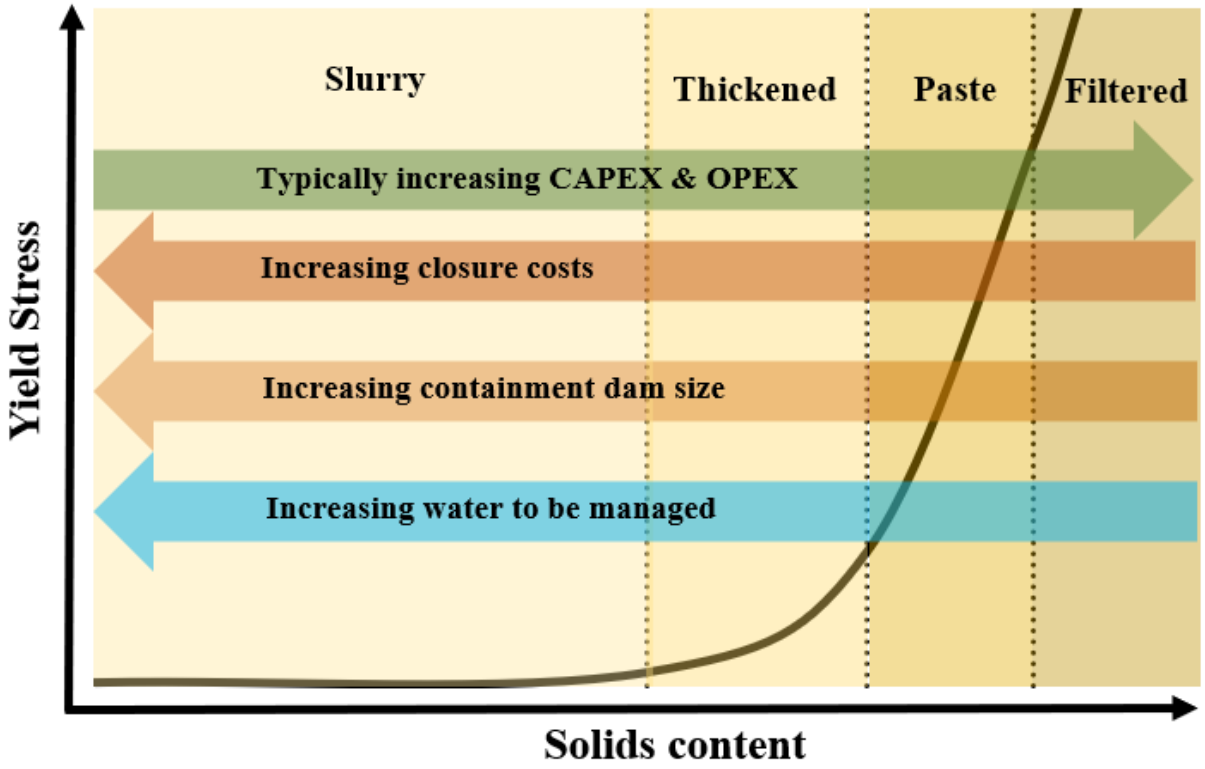


Figure 2: The tailings continuum (from slurry to filtered tailings) and key decision criteria

Table 1: Comparison of tailings disposal technologies

Criteria	Tailings disposal technology				
	Conventional slurry	Thickened	Filtered	Paste	Co-disposal
Storage technique	Surface, in-pit, offshore	Surface, in-pit	Surface, in-pit	Surface, underground backfill	Surface, in-pit
Water at disposal facility	More	Less	Less	Less	More
Footprint	Large	Smaller than conventional	Smaller and more flexible	Smaller	Reduced for tailings/waste rock combined
Risk of dam failure/environmental impact	High	Lower (small dams)	Low (no dam)	Less to none	High to moderate
CAPEX	Low	Moderate	High	High	Moderate
OPEX	Low	Moderate	High	High	Low
Sustaining capital	High	Low to moderate	Low	Low	Moderate to high
Closure cost	High	Moderate	Moderate but progressive	Low to none	High
Post-closure cost	High	Moderate	Low	Low to none	Moderate to high

Barriers to adoption of tailings dewatering technologies

While it is generally accepted that there is no one best method for tailings disposal that can be applied to any site, it seems apparent from the review of industry trends that tailings dewatering is not reaching its full potential. Typical arguments against the use of tailings dewatering technologies may be grouped into 3 categories: technical, cost and other.

Technical arguments

Historically, filtered tailings stacks were most often considered for sites located in arid regions (such as Chile and parts of Australia) or in cold regions (such as northern Canada and Alaska). In wetter climates, water management measures are essential, as described by Davies (2011). Trafficability during tailings placement can also be an issue in wetter climates. In regions with distinct rainy and dry seasons, filter stacks are often designed with an outer slope region that requires more stringent compaction criteria and need to be placed in favorable weather conditions. This outer slope region provides stability to the structure and allows for tailings placement in the interior portion of the stack during the rainy season at a lower compactive effort, which can greatly reduce trafficability concerns (Ulrich and Coffin, 2013). Torex Gold's El Limón Guajes Mine in Guerrero, Mexico is an example of a site with a filter stack designed for a climate

with a rainy season characterized by short-term, high-precipitation events (Torex Gold, 2020). Davies (2011) concludes that filter stacks can be effective in very wet climates with appropriate water management measures in place. With the relative dryness of the tailings in a filter stack, the generation of dust inevitably becomes more of an issue. Dust can be partially managed by progressive reclamation of the filter stack with placement of the closure cover to prevent erosion and usually to support vegetation growth (Davies, 2011). Binder material or chemical agglomeration can also be used to manage dust at filter stacks. Sites in windy areas could use tubular "pipe" conveyor belts to transport tailings to prevent dust generation prior to placement (Vargas and Campomanes, 2022).

Previously there were some concerns that fine tailings (particularly those with clay mineralogy) cannot be feasibly filtered; however, as reported by Ulrich and Coffin (2013), advances in filter technology are now allowing production of clayier filtered tailings. While the design and construction of filter stacks for finer tailings must adequately consider the behavior of these tailings, finer particle size does not necessarily preclude the use of a filter stack.

Acid mine drainage is caused when sulfide minerals that are often present in tailings oxidize in the presence of air and water. Traditionally, acid-generating tailings were kept saturated to prevent oxidation by subaqueous deposition in a conventional tailings impoundment with a water cover that must be maintained in perpetuity. The need to limit oxidation of acid-generating tailings may be seen as an argument to operate a conventional slurry tailings facility. As per Davies et al. (2011), attempts to prevent oxidation of acid-generating tailings using thickened and paste technology have been unsuccessful. The geochemical stability of acid-generating tailings in filter stacks depends on mineralogy, water content and mineral availability, and is the subject of ongoing research (e.g., Surrette et al., 2023). The construction of a filter stack for acid-generating tailings generally requires an encapsulation system consisting of a base liner under the stack and a cover that may be progressively placed. These additional costs may deter use of filtered tailings for acid-generating tailings, except in jurisdictions where a base liner is required for all tailings facilities, such as Québec and Nevada.

Production rates at thickened and paste facilities as of 2011 were mostly under 30,000 tonnes per day (tpd), with filtered facilities generally under 10,000 tpd. As per Ulrich (2019), filtered tailings technology has so far seen implementation at a limited number of relatively low-production tailings facilities, although higher production rate facilities are being tested. As noted by Crystal et al. (2018), further advancements in the industry can be expected, and the elimination of filter stacking as an option should not be solely based on high production rate. Vargas and Campomanes (2022) report on operating and planned filter stack facilities with maximum throughput of 50,000 tpd at Karara in Australia and Chingola in Zambia. Two significantly higher production facilities – Rosemont Copper in Arizona (75,000 tpd) and Metales in Mexico (120,000 tpd) – are noted to be in the regulatory approval or construction permitting process.

Many active conventional tailings impoundments have been in operation for decades. Due to increasing regulatory difficulty in opening new mines, the trend will likely be for fewer new facilities in favor of expanding existing facilities. If the existing facility is a conventional tailings impoundment (as most are), it is most likely that that process will be continued. Morgenstern et al. (2015) recommends against retrofitting existing conventional tailings impoundments with filtered tailings technology due to the continued risk of undrained shear failure or liquefaction of the underlying saturated tailings. On the other hand, GISTM Requirement 5.1 calls for investigation into the potential to refine the tailings technology for expansions to existing tailings facilities. Several examples of filtered tailings placement over existing conventional tailings were found in the literature. At the LaRonde Gold Mine in Québec, slurry tailings deposition was transitioned to filtered tailings placement in 2022 to reduce the risks related to slurry tailings management. In this case, a waste rock platform was constructed on the slurry tailings surface for trafficability to allow placement of the filtered tailings (Masengo et al., 2023). Examples like this can provide valuable insight for other conventional tailings facilities considering the implementation of dewatering technologies. Dewatering technologies could be used at existing mines where the conventional tailings impoundment is nearing capacity. Reducing the water content and thereby increasing the tailings density will result in a longer storage life for the tailings impoundment. However, as noted by Williams (2021), change will most easily be achieved for new mining projects, so the impact of these changes will necessarily be slow.

In summary, as stated by Morgenstern et al. (2015), “There are no overriding technical impediments to more widespread adoption of filtered tailings technology.”

Cost

Morgenstern et al. (2015) state that the primary reason for the limited industry adoption of filtered tailings to date is economic, noting that risk costs for the potential failure of conventional tailings dams are generally not considered in cost comparisons used for tailings methodology selection. The average losses resulting from a single large catastrophic tailings dam failure has been reported at $543 million based on seven dam failures that occurred between 1994 and 2008 (refer to Bowker and Chambers, 2015 for further details).

With the increasing adoption of tailings dewatering technologies, both capital and operating costs can be expected to improve due to economies of scale and advances in technology and design, as noted by Davies et al. (2011). Additionally, water use costs are increasing in many areas of the world, resulting in projects where tailings dewatering is the most economical choice.

Describing the South African state of practice, Copeland et al. (2023) report that costs remain a key factor in selecting a tailings management system, with the filter stacking option having higher capital and operating costs in most cases. However, an increasing number of projects are assessing risks and other

benefits in terms of reputation, sustainability and responsible mining, increasing the likelihood of adoption of dewatering technologies.

Carneiro and Fourie (2019) present a realistic hypothetical cost comparison for various tailings management solutions for a gold mine in Australia, using a total life cycle cost approach. They showed that using the commonly used net present value (NPV) approach, the slurry disposal method demonstrated lower costs compared to the filtered option, as may be expected. However, when compared using a total life cycle cost approach (considering potential increased rehabilitation costs as well as water costs, land use costs and carbon taxes), the filtered tailings option was found to be the most cost-effective option. Although these results may not hold true in cases with no or low water and land use costs, the filtered tailings option was also found to be the most resilient of the studied options, since there is less uncertainty regarding mine closure and future regulatory changes.

Williams (2021) suggests taking this a step further, and that a change in thinking is required in how the industry views the economics of tailings management – specifically, relying on a NPV approach with a high discount factor, rather than consideration of the full life-cycle costs. The NPV approach favors lower cost options in the short term and therefore tends to favor slurry deposition and the deferral of rehabilitation costs. As quoted by Boger and Hart (2008), this accounting approach reflects the attitude that the future matters less than the present. Espinoza and Castro (2022) describe a decoupled NPV method of financial analysis for a mining project, where risks (such as tailings dam failures) are evaluated as costs. This method allows for reductions in risk (for example, by adopting dewatering methods) to be translated to decreased cost to the project, compared to the traditional NPV approach where future rehabilitation or remediation costs are discounted and therefore additional upfront costs for dewatering technologies cannot be economically justified.

Cox et al. (2022) state that one of the current obstacles to greater adoption of tailings dewatering technologies is a poor understanding of the actual costs of conventional tailings storage. The study presents a unified costing metric to understand the actual cost of tailings facilities from the pre-feasibility stage to final closure. The study reported that data presented in the Canadian National Instrument 43-101 technical reporting standard typically underreports tailings facility costs due to data consolidation across varying cost categories and expense types. This is an issue that the authors have faced in the preparation of this paper as well as in trade-off studies for the selection of tailings disposal methods. The metric proposed by Cox et al. (2022) avoids the use of NPV and cost discounting for the reasons discussed earlier. It should be noted that the metric excludes risk costs of tailings dam failure due to the unavailability of a framework for establishing those costs; however, the metric could be expanded to include those risk costs. Although the proposed metric does not address filtered tailings storage, a clearer picture of the actual costs of conventional tailings disposal is likely to encourage greater adoption of tailings dewatering technologies.

Other factors

In their keynote address at Paste 2008, Boger and Hart (2008) explored the reasons why a larger proportion of the industry had not adopted more sustainable practices such as filtered tailings stacks. Their conclusion was that additional regulations mandating the use of a certain tailings disposal method was unlikely to be feasible. Following the two recent and significant failures of tailings facilities in Brazil, unprecedented changes were made to Brazilian regulations, including a total ban on upstream tailings dams. All existing upstream tailings dams in the country must also be decommissioned to remove the risk of failure. While not mandating the use of dewatering technologies, the regulations require consideration of alternative construction methods with the prioritization of safer methods.

On the conservative nature of the mining industry, Leonida (2020) invokes the old adage that miners prefer to be "first to be second" when it comes to adopting new technologies. It is understandable that mine owners wish to avoid the risk of technical issues related to being the early adopters of a given technology. One potential solution to this could be for more mines to implement partial dewatering of their tailings, allowing them to gain experience and confidence in the process while maintaining systems for managing conventional tailings. Leonida (2020) reports that the operational savings in terms of water and power savings could quickly offset the initial high capital cost of the filtration system, in addition to increasing the service life of existing tailings impoundments.

Additionally, in many regions of the world, there is no local experience with tailings dewatering technologies. In such an environment and in the absence of drivers such as regulations, the status quo may continue to prevail. As noted by Williams (2021), forms of tailings containment used in a given location appear to be primarily a result of past experience and established regional practices, which are noted to be difficult to change.

Conclusion

In 2011, Davies (2011) stated that "conventional tailings impoundments remain the best alternative for the majority of operating and proposed mines around the world." Notwithstanding the site-specific nature of dewatering technology selection, the authors question whether this statement stands in the post-GISTM landscape. Supporting this sentiment, Leonida (2020) noted near unanimous agreement among dewatering equipment suppliers, engineering firms, and mining companies that filter stacking is the most promising and broadly applicable method for tailings storage in the future.

A review of industry trends suggests that tailings dewatering technologies are not reaching their full potential. While there are technical arguments and other relevant factors such as resistance to change, the primary reason for this state of affairs, in the authors' view, comes down to cost. As stated by Morgenstern

et al. (2015) in the wake of the Mount Polley failure, "While economic factors cannot be neglected, neither can they continue to pre-empt best technology."

As per Williams (2021), "There is a commonly held perception that transporting tailings as a slurry is the most economical option." While this seems to be the prevailing belief in the industry, the authors question whether it reflects reality when the true costs of closure (sometimes requiring active management in perpetuity), risk of failure, and uncertainty are appropriately accounted for. The traditional NPV approach commonly used in selecting the tailings disposal option implicitly prioritizes minimizing up-front costs.

The following recommendations are suggested to support greater adoption of dewatering technologies:

- Research into technical aspects of tailings dewatering technologies should be continued to resolve remaining areas of uncertainty, such as consideration of tailings runout potential for dewatered tailings.
- Tailings management costs should be considered using a total life cycle cost approach, avoiding the use of NPV and cost discounting.
- Greater transparency in the costs of tailings management should be included in disclosures.
- The sharing of industry experience in conferences and the participation of practitioners worldwide is important in expanding the implementation of dewatering technologies in new regions.

Although it is too early to truly measure the impact of recent events such as the release of the GISTM on the adoption of tailings dewatering technologies, it does appear that there is growing knowledge of the benefits of dewatering in the industry and greater emphasis being placed on socioeconomic factors where filtered tailings demonstrate benefits over conventional tailings facilities. Transformative change is often triggered by catastrophic disasters, of which there have been many recent examples in the mining industry. It is our hope that the industry will continue to adopt dewatering methods at a greater rate for more sustainable and safer tailings management, without waiting for further loss of life.

Acknowledgements

The authors gratefully acknowledge the AtkinsRéalis management team for support in the preparation of this paper.

References

Boger, D.V. and B.C. Hart. 2008. Making an unsustainable industry more sustainable. In A.B. Fourie, R.J. Jewell, A. Paterson and P. Slatter (eds*), Paste 2008*. Kasane, Botswana. Australian Centre for Geomechanics: 3–13.

Bowker, L.N. and D.M. Chambers. 2015. The risk, public liability and economics of tailings storage facility failures. Accessed 5/29/2024 at: https://www.resolutionmineeis.us/documents/bowker-chambers-2015

Carneiro, A. and A.B. Fourie. 2019. An integrated approach to cost comparisons of different tailings management options. In A.J.C. Paterson, A.B. Fourie and D. Reid (editors), *Paste 2019: Proceedings of the 22nd International Seminar on Paste, Thickened and Filtered Tailings*. Cape Town, South Africa. Australian Centre for Geomechanics: 115–126. DOI:10.36487/ACG_rep/1910_05_Carneiro

Copeland, A., V. Daigle and A. Strauss. 2023. Is the implementation of dry stacking for tailings storage increasing? A Southern African perspective. In G.W. Wilson, N.A. Beier, D.C. Sego, A.B. Fourie and D. Reid (editors), *Paste 2023: Proceedings of the 25th International Conference on Paste, Thickened and Filtered Tailings,* University of Alberta, Edmonton, and Australian Centre for Geomechanics, Perth, pp. 611-619,

Cox, B., S. Innis, A. Mortaza, N.C. Kunz and J. Steen. 2022. A unified metric for costing tailings dams and the consequences for tailings management. *Resources Policy* 102862(78).

Crystal, C., C. Hore and I. Ezama. 2018. Filter-pressed dry stacking: design considerations based on practical experience. *Proceedings of Tailings and Mine Waste 2018*. Keystone, CO.

CSP2. Center for Science in Public Participation. 2022. TSF failures from 1915. Accessed 5/24/2024 at http://www.csp2.org/tsf-failures-from-1915

Davies, M. 2011. Filtered dry stacked tailings – the fundamentals. *Proceedings of Tailings and Mine Waste 2011*. Vancouver, BC.

Davies, M., J. Lupo, T. Martin, E. McRoberts, M. Musse, D. Ritchie. 2011. Dewatered tailings practice – trends and observations. *Proceedings of the 14th International Conference on Tailings and Mine Waste*. Vail, CO.

Espinoza, D. and G. Castro. 2022. Incorporating TSF management in mine valuations: the integration of physical and market risks using DNPV. *Proceedings of Tailings and Mine Waste 2022*. Denver, CO.

GlobalTailingsReview.org. 2020. Global Industry Standard on Tailings Management. Accessed 5/16/2024 at https://globaltailingsreview.org/global-industry-standard/

GRID-Arendal. 2020. Global Tailings Portal. Accessed 5/14/2024 at https://tailing.grida.no/

Karajeh, I. 2023. The new norm for gold miners and how change in mine waste management could help. In G.W. Wilson, N.A. Beier, D.C. Sego, A.B. Fourie and D. Reid (editors), *Paste 2023*. *Proceedings of the 25th International Conference on Paste, Thickened and Filtered Tailings*, University of Alberta, Edmonton, and Australian Centre for Geomechanics, Perth, pp. 799–811, https://doi.org/10.36487/ACG_repo/2355_63

Leonida, C. 2020. How to make filtered tailings feasible. *Engineering and Mining Journal*. Accessed 5/24/2024 at https://www.e-mj.com/features/how-to-make-filtered-tailings-feasible/

Masengo, E., E.-P. Ingabire, S. Boily, Y. Letourneau, P. Laporte, F. Guay, M. Limoges Shaigetz, J. Huza and M.R. Julien. 2023. Transition to filtered tailings at LaRonde Gold Mine. *Proceedings of Tailings and Mine Waste 2023*. Vancouver, BC.

Morgenstern, N.R., S.G. Vick and D. van Zyl. 2015. *Independent Expert Engineering Investigation and Review Panel Report on Mount Polley Tailings Storage Facility Breach*. Province of British Columbia.

Oxenford, J. and E.R. Lord. 2006. Canadian experience in the application of paste and thickened tailings for surface disposal. In R.J. Jewell, S. Lawson and P. Newman (eds), *Paste 2006: Proceedings of the Ninth International Seminar on Paste and Thickened Tailings,* Australian Centre for Geomechanics, Perth, pp. 93–105, https://doi.org/10.36487/ACG_repo/663_9

Surrette, A., G.L. Dzemua, H. Falck, K. Beatty, C. Gibson and H. Jamieson. 2023. Characterization of potentially acid-generating tailings for filtered tailings storage design. *Proceedings of Tailings and Mine Waste 2023*. Vancouver, BC.

Torex Gold. 2020. Tailings Management Report. Accessed 5/29/2024 at tailings_20management_20report_20-_20february_202020-20200207080431.pdf (torexgold.com)

Ulrich, B.F. 2008. State of practice for tailings thickening in the state of Nevada, USA. In A.B. Fourie, R.J. Jewell, A. Paterson and P. Slatter (editors), *Paste 2008*. *Proceedings of the Eleventh International Seminar on Paste and Thickened Tailings,* Australian Centre for Geomechanics, Perth, pp. 165–169, https://doi.org/10.36487/ACG_repo/863_15

Ulrich, B. 2019. Practical thoughts regarding filtered tailings. In A.J.C. Paterson, A.B. Fourie and D. Reid (editors), *Paste 2019*. Cape Town, South Africa. Australian Centre for Geomechanics: 71–80.

Ulrich, B. and J. Coffin. 2013. Considerations for tailings facility design and operation using filtered tailings. In R.J. Jewell, A.B. Fourie, J. Caldwell and J. Pimenta (editors), *Paste 2013: Proceedings of the 16th International Seminar on Paste and Thickened Tailings,* Australian Centre for Geomechanics, Perth, pp. 201-210, https://doi.org/10.36487/ACG_rep/1363_15_Ulrich

Vargas, C.C. and G.P. Campomanes. 2022. Practical experience of filtered tailings technology in Chile and Peru: an environmentally friendly solution. *Minerals* 889(12).

Vick, S.G. 1990. *Planning, Design, and Analysis of Tailings Dams*. Vancouver: BiTech Publishers Ltd.

Wang, K., Z. Zhang, L. Zhu, X. Yang, M. Chen and C. Yang. 2022. Comparative life cycle assessment of conventional and dry stack tailings disposal schemes: a case study in northern China. *Minerals* 1603(12).

Williams, D.J. 2021. The role of technology and innovation in improving tailings management. In *Towards Zero Harm – A Compendium of Papers Prepared for the Global Tailings Review*. Accessed at https://globaltailingsreview.org, pp. 64–83.

Monitoring Tailings Saturation at a TSF Using Tensiometers and Laboratory SWCC

Mahmoud N. Hussien, WSP, Canada
Soumia El Mansouri, WSP, Canada
Vu Tran, Eldorado Gold, Canada
Eric Cloutier, Eldorado Gold, Canada

Abstract

This study investigates the significance of understanding and accounting for the unsaturated nature of tailings in the mining industry. It presents a case study of an upstream-raised dam in Quebec, Canada, covering the geotechnical campaign and material characterization carried out to determine the saturation condition of the tailings above phreatic surface. This article discusses the installation of tensiometer sensors to measure the matric suction and indirectly estimate the tailings' degree of saturation, as well as a brief overview of the calibration procedure used to improve the precision of water content measurements in these sensors. Data was collected using an automated system and the results, when combined with laboratory results in terms of soil water characteristic curves (SWCC) of tailings, show that the sensor properly represented the expected saturation profile, with saturations near 100% below the water table and progressively declining toward the tailings surface. The outcomes of this study stress the need for characterizing the unsaturated zone of tailings above the phreatic surface to gain a better understanding of the TSF's overall performance and to ensure robust design.

Introduction

Significant research has recently been undertaken on the degree of saturation in tailings above the water table (e.g., Rust and Rust, 2023; Souza et al., 2023). This type of assessment is critical when determining the extent of the liquefiable zone in a tailings profile, particularly when using the traditional subaerial deposition method with slurry tailings. The concept of full saturation below the phreatic surface and at the capillary fringe is well understood. Above this level, the profile usually comprises moist layers of finer (silty) and coarser (sandy) tailings, indicating desiccation, with pore water retained under suction (negative pressure). These strata have no hydraulic connection to the groundwater profile beneath them and will remain saturated until the suction surpasses the tailings' air entry value (AEV).

This study investigates the importance of recognizing and accounting for the unsaturated nature of tailings above the phreatic surface in the mining industry. It presents a case study of an upstream-raised dam in Quebec, Canada, including the geotechnical campaign and material characterization used to evaluate the saturation condition of tailings above the phreatic surface. This article discusses the installation of tensiometers sensors to measure the matric suction and indirectly estimate the tailings' degree of saturation, as well as a brief overview of the calibration procedure used to improve the precision of water content measurements in these sensors. The findings of this study highlight the importance of defining the unsaturated zone of tailings above the phreatic surface to get a better understanding of the TSF's overall performance and ensure robust design.

Case study: tailings storage facility

The tailings storage facility (TSF) is in Quebec, Canada, and tailings are deposited via traditional slurry deposition. The TSF was constructed utilizing the upstream method, in which each stage of the dyke was progressively raised on top of previously deposited tailings, causing the dyke's crest to shift inward (upstream) with each raise. Figure 1 shows one cross-section of the TSF's dykes, the geotechnical units that comprise the section, and the phreatic condition.

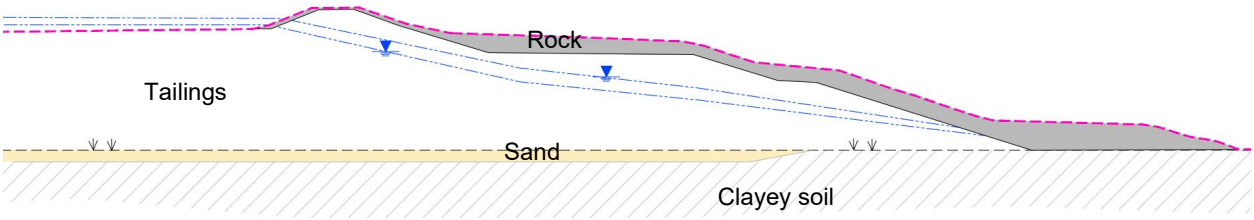


Figure 1: One cross-section of the TSF's dykes

Field investigation for tensiometers installation

As part of the continual improvement of the TSF operation, twenty tensiometers (TEROS-21, GEN 2 from Meter Group) were strategically installed at various depths in four geotechnical boreholes (5 tensiometers in each borehole) at three critical sections around the TSF to characterize the unsaturated areas of deposited tailings. The tensiometers were installed in the same locations as the existing piezometers to gain a complete understanding of both positive and negative water pressures at these sections. A geotechnical field investigation as well as laboratory tests were also completed, to measure the matric suction of deposited tailings and quantify their mechanical responses to feed the geotechnical model and to aid the detailed engineering design. The basic information regarding boreholes and tensiometers is summarized in Table 1.

The TEROS-21 system consists of a ceramic-tipped sensor, a datalogger, and a power supply. Figure 2 illustrates the components of a TEROS-21 sensor that can be used to measure the water potential and temperature of soil with porous ceramic discs. More specifically, the water potential is obtained from measuring the changes of moisture content of two engineered ceramic discs sandwiched between stainless steel screens and the circuit board.

Table 1: Basic information of tensiometers installed in each borehole

Borehole No.	No. of tensiometer	Elevation of the tensiometer (m)
TN-21-01	T-01	312.20
	T-02	313.20
	T-03	314.20
	T-04	315.20
	T-05	316.20
TN-21-02	T-06	313.00
	T-07	314.00
	T-08	315.00
	T-09	316.00
	T-10	317.00
TN-21-03	T-11	312.00
	T-12	313.00
	T-13	314.00
	T-14	315.00
	T-15	316.00
TN-21-04	T-16	313.00
	T-17	314.00
	T-18	316.00
	T-19	317.00
	T-20	319.00

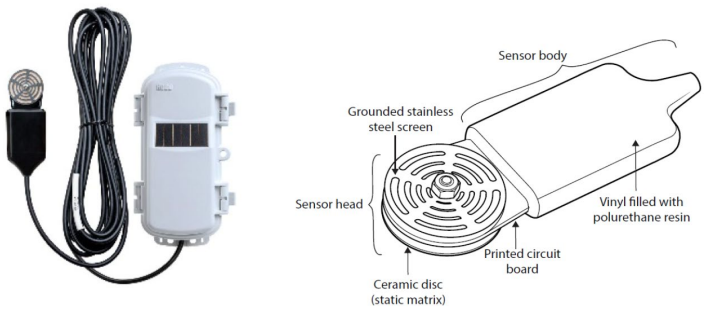


Figure 2: TEROS-21 sensor (source: TEROS-21 sensor manuals)

Five tensiometers were installed in each borehole (20 tensiometers were installed in total). The waste rock layer on top of the tailings layer was locally removed before starting the drilling. Figure 3 schematically illustrates the five tensiometers installed in a typical borehole.

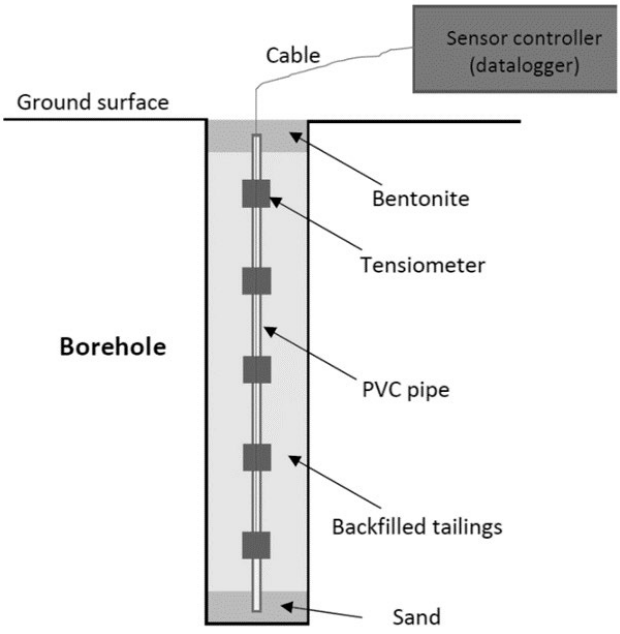


Figure 3: The schematical cross-section for tensiometers installed in a borehole

A split spoon was used to collect tailings samples from predefined elevations, and a tensiometer assembly (five tensiometers tied to a PVC pipe at a predetermined spacing) was carefully placed at each of the four drilled holes. As shown in Figure 3, a sand layer and backfilled tailings were placed on the borehole, whose top was sealed with Bentonite pellets. The datalogger (HOBO RX3000) is programmed and is being used for data collection.

Tensiometers calibration

TEROS-21 was designed to be a maintenance-free matric potential sensor designed for long-term, continuous field measurements. The TEROS-21 measures the dielectric permittivity of a solid matrix to determine the water content of the solid matrix. The relationship between water content and matric potential, known as the soil moisture characteristic curve, is used to calculate the soil matric potential. TEROS-21 is calibrated at a saturated state (0 kPa), at a dry state equivalent to −100,000 kPa, and at four calibration points between 0 and −100 kPa, resulting in accuracy of ± (10% of reading + 2 kPa) over the range of −9 to −100 kPa.

TEROS-21 calibration is not affected by soil type because the sensors only measure the water potential of the ceramic discs in equilibrium with the soil.

Laboratory tests

Basic laboratory tests (water content, specific gravity, and grain size analyses) on tailings samples extracted from tensiometers boreholes were completed in December 2022. The water content of the tailings was measured for 22 samples taken from the site. It varies between 9.40 % (TN-21-01) and 26.50 % (TN-21-04). For borehole TN-21-04, it is seen that the water content of tailings generally increases from the top to bottom, indicating an increased degree of saturation from surface to phreatic surface. This tendency is also observed for borehole TN-21-03.

Specific gravity of the tailings measured for 6 tailings samples vary between 2.751 (TN-21-03) and 2.856 (TN-21-04).

A total of four grain size analyses, by both sieve and hydrometer, were conducted on the tailings' samples at different depths. The results of sieve and sedimentation analyses for coarse and fine particles are illustrated in Figure 4.

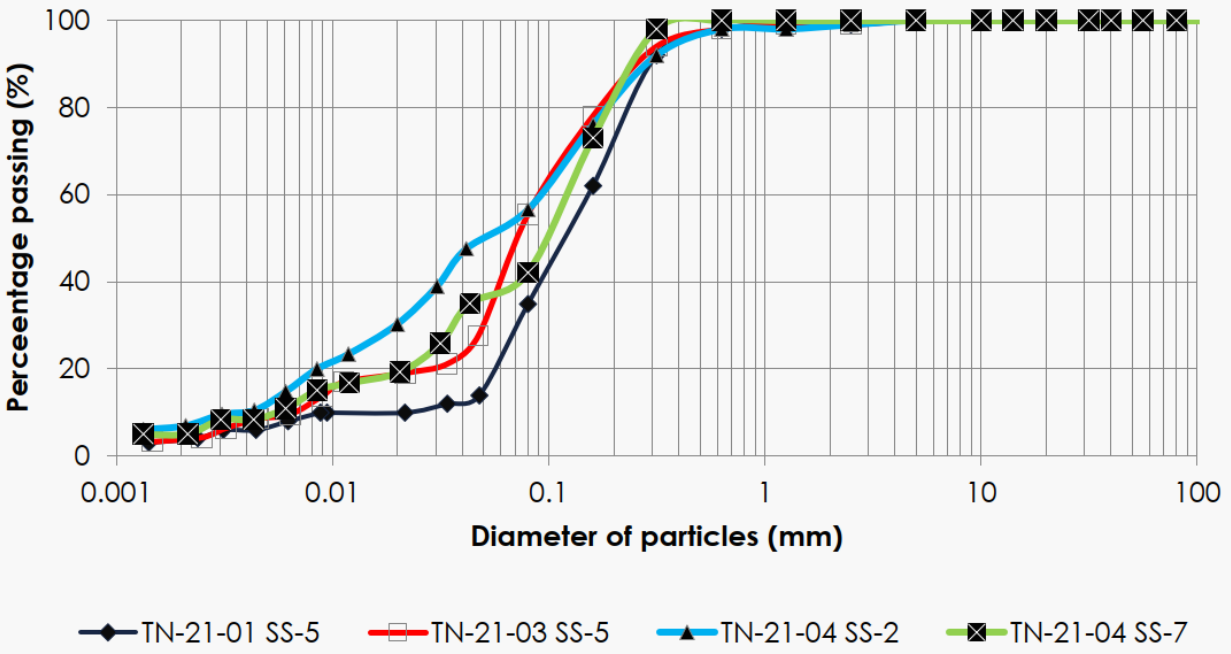


Figure 4: Particle size distribution of tailings samples

In December 2023, additional tailings samples were taken from the TSF from two additional boreholes drilled at 3 to 5 m away from the existing tensiometers boreholes (TN-21-01 and TN-21-04) to avoid disturbance. The driller went destructively to the target elevations and then the tailings were sampled using a split-spoon. These tailings samples were sent to a laboratory for Fredlund GCTS Soil Water Characteristic Curve (SWCC) testing to aid in the ongoing interpretation of the recorded tensiometer data. The SWCC defines the soil's ability to hold or release water. The curve depicts the mathematical relationship between

suction within a soil and water content or level of saturation. The curve generally exhibits two significant slope changes. The first change is the air entry value (AEV), which reflects the suction at which the soil transitions from saturated to partially saturated and is related with negative pore pressure. The second slope change indicates a state of equilibrium, which is known as residual moisture content. Figure 5 shows a typical SWCC.

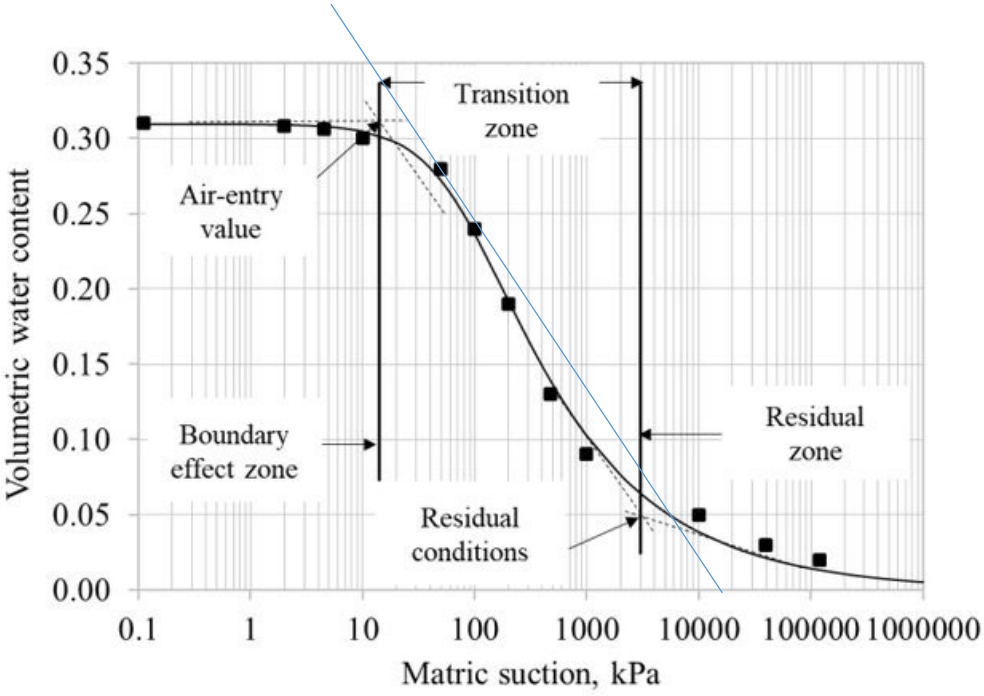


Figure 5: Typical soil water characteristic curve (SWCC)

One SWCC test was done, and the results are given in Figure 6. Figure 6 demonstrates that the AEV is 2 kPa, while the suction corresponds to %85 saturation of 17 kPa.

Tensiometers data interpretation

Figure 7 depicts a cross-section of the TSF dyke, along with the geotechnical units that make up the section and the phreatic condition. The tensiometer assembly TN-21-01 (T-01 to T-05) was installed in the same area as the piezometer (PW-21-30) to get a thorough understanding of both positive and negative water pressures in this section. Figure 8 shows the corresponding real-time data (piezometric data of PW-21-30 and suction of T-01). Suctions corresponding to the air entry value (AEV) and (%85 saturation) determined from a laboratory SWCC (Figure 6) are also shown in Figure 8 for comparison.

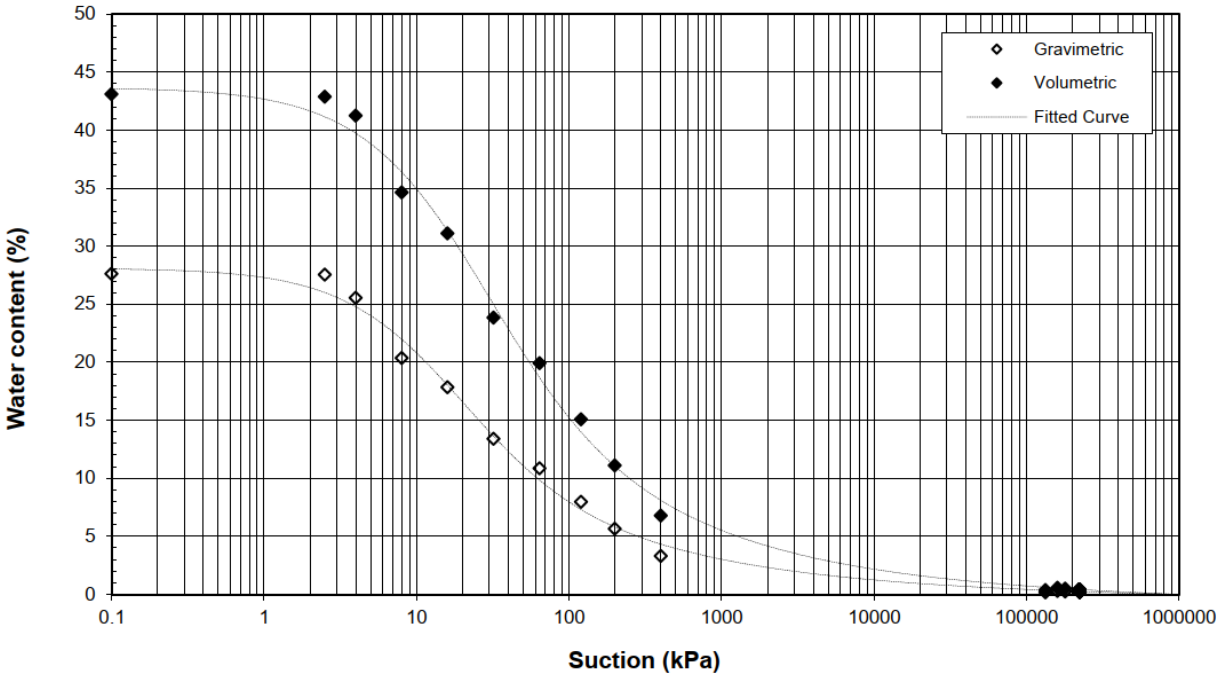


Figure 6: Laboratory soil water characteristic curve (SWCC) of tailings

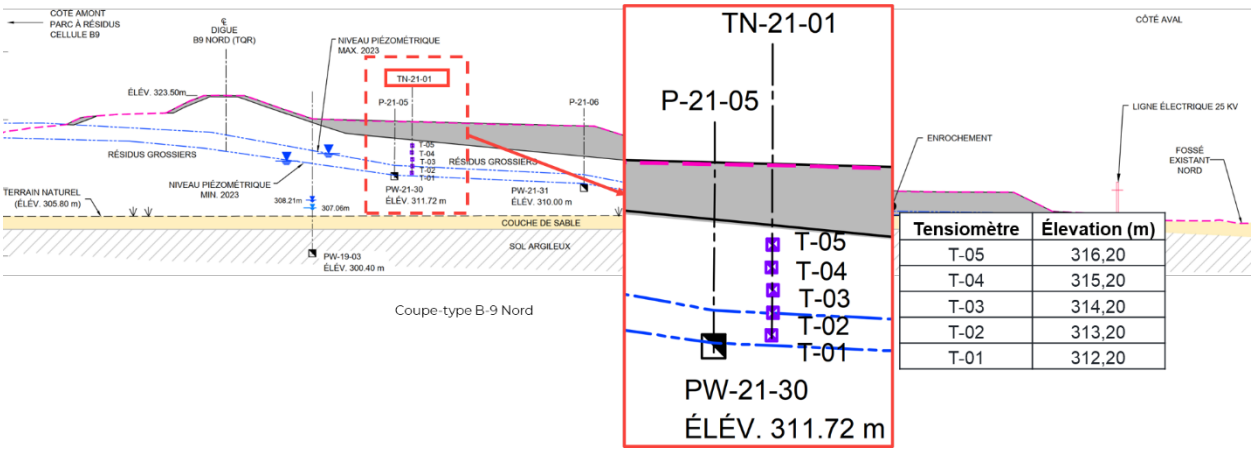


Figure 7: Tensiometers installed in the north dyke of B9 Cell

T-01 is the tensiometer that is closest to the phreatic surface. It was installed slightly above the phreatic surface and is subject to the fluctuation of water level. Figure 8 demonstrates that the tailings at the tensiometer T-01 have been typically saturated for the past year, with a trend toward unsaturation as suction gradually increases over winter (from March to May). However, the tailings at this level did not attain a true unsaturated condition since the suction value never exceeded the suction corresponding to %85 saturation (the dashed red line on the plot).

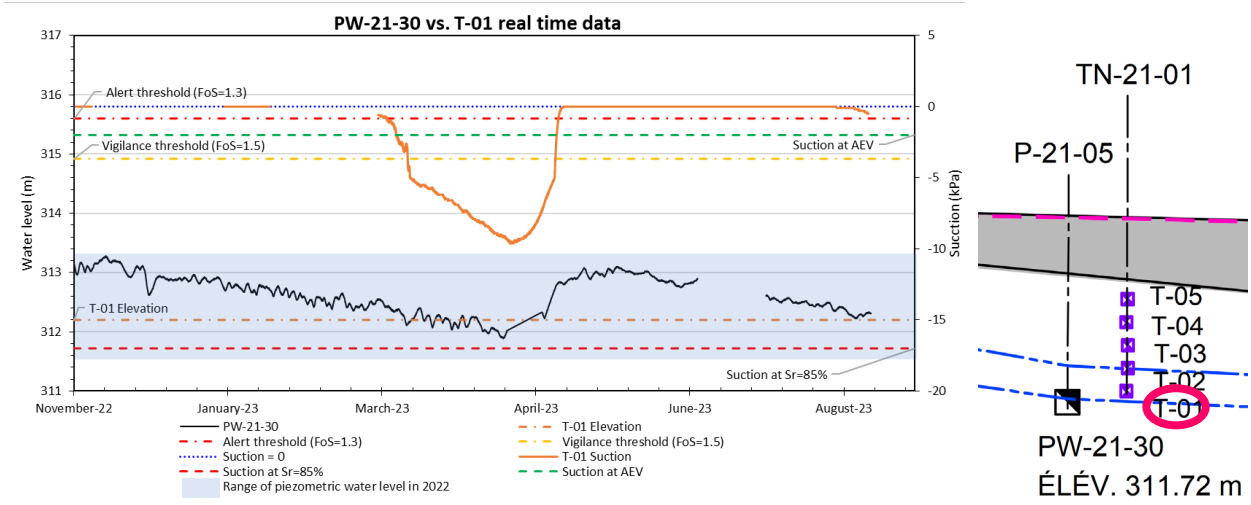


Figure 8: Real time data of piezometers (PW-21-30) and tensiometers (T-01)

Figure 9 shows the real-time data (piezometric data of PW-21-30 and suction of T-05). Suctions corresponding to AEV and (%85 saturation) are also shown on Figure 9 for comparison. T-05 is the tensiometer that is closest to the tailings surface. Figure 9 demonstrates that the tailings at the tensiometer T-05 have been typically unsaturated for the past year, and the recorded suctions exceeded the suction corresponding to %85 saturation at several occasions during the past year.

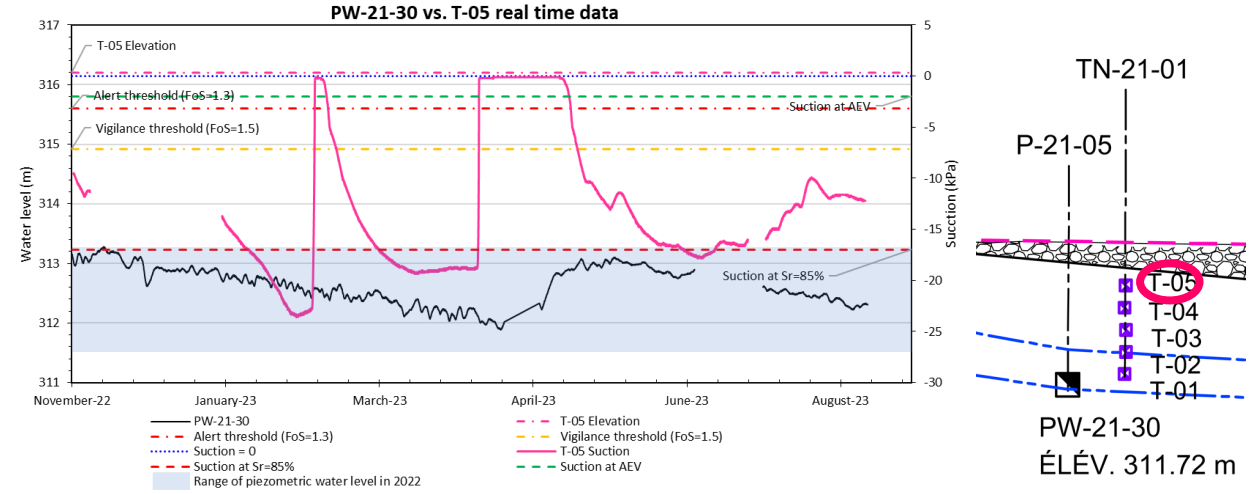


Figure 9: Real time data of piezometers (PW-21-30) and tensiometers (T-05)

Conclusion

This article discusses the installation of tensiometers sensors to measure the matric suction and indirectly estimate the tailings' degree of saturation. Data was collected using an automated system and the results, when combined with laboratory results in terms of soil water characteristic curves (SWCC) of tailings,

show that the sensor properly represented the expected saturation profile, with saturations near 100% below the water table and progressively declining toward the tailings surface. The outcomes of this study stress the need for characterizing the unsaturated zone of tailings above the phreatic surface to gain a better understanding of the TSF's overall performance and to ensure robust design.

References

Rust, E. and Rust, M. 2023. Determination of the degree of saturation above the water table from CPTu probing in tailings. *Proceedings of Tailings and Mine Waste 2023*, November 5–8, 2023, Vancouver, Canada

Souza, L., Gonçalves, T., Santos, E., Ccotohuanca, J., Silva, J. P., Small, A. and Pereira, P. 2023. Monitoring of iron tailings saturation using water moisture sensors. *Proceedings of Tailings and Mine Waste 2023*, November 5–8, 2023, Vancouver, Canada.

A Framework to Determine Tailings Liquefaction – GISTM Conformance for the Holden Mine

Mohammad Rashidi, Stantec, USA
Phillip E. Crouse, Stantec, USA
Summer Y. Sun, Stantec, USA

Abstract

There are about 3,500 tailings dams worldwide storing billions of tons of mill and waste tailings from mineral processing activity at mine sites. Unlike traditional water storage dams, these structures possess distinct vulnerabilities due to factors such as multi-stage raising, utilization of mine waste materials in embankment construction, and regulatory deficiencies in certain regions. Alarmingly, over a third of these dams pose significant risks of catastrophic failure, endangering downstream communities, socio-economic activities, and ecological systems. One of the major risks associated with tailings dams is their potential vulnerability to liquefaction. This paper addresses this critical concern by presenting a practical, step-by-step liquefaction assessment process tailored for tailings dam engineers and practitioners.

The assessment methodology encompasses initial screening and straightforward liquefaction triggering analyses leveraging available field data, such as the cone penetration test (CPT) or the standard penetration test (SPT), followed by more in-depth numerical analyses. Furthermore, this study delineates the essential procedures for seismic deformation analyses of liquefiable tailings materials, encompassing aspects like constitutive model selection and calibration, site-specific modulus reduction and damping curve, and critical state line development.

Illustrating the application of this process, a case study of Holden mine (a legacy tailings storage facility) in the state of Washington is presented. The findings offer valuable insights into evaluating the liquefaction risk associated with tailings dams, serving as a preliminary guide for safer and more efficient tailings management practices and for achieving GISTM compliance.

Introduction

During the past decade, the mining industry has experienced a number of catastrophic tailings dam failures such as Mount Polley in the Cariboo region of central British Columbia in Canada (August 2014), and Samarco (November 2015), and Brumadinho (January 2019) in Brazil. Due to the severity of these major failures, the mining industry has significantly increased efforts to improve the design, construction,

operation, and management of TSFs. This increasing awareness has led to the development of the Global Industry Standard on Tailings Management (GISTM) (GTR, 2020). A fundamental part of these evolving guidelines is the emphasis on proper identification and evaluation of critical risks. For example, Principle 10 of the GISTM requires mine owners to establish and implement levels of review as part of a strong quality and risk management system for all phases of the tailings facility lifecycle, including closure.

Liquefaction has been one of the causes of the recent TSF failures. Therefore, a critical part of the risk assessment for any TSF is the liquefaction risk assessment. This assessment often involves two important parts: assessment of extent and location of where liquefaction is likely, and evaluation of the likely consequences of liquefaction.

Liquefaction occurs when saturated soil loses a substantial amount of its original shear strength due to pore pressure generation resulting from an earthquake. Static liquefaction is also possible due to redistribution of pore pressure. The pore pressure is generated during an earthquake because the soil particles tend to compact rather quickly without allowing for the generated excess pore pressures to dissipate. This increase in pore pressure, in turn, reduces the effective stress and shear strength. The risk of liquefaction is higher in contractive tailings materials, including relatively loose natural soils and poorly compacted or uncompacted fill materials.

Approach

A step-by-step approach to evaluate the liquefaction risk for Holden's tailings piles is illustrated in Figure 1 and discussed below. It should be noted that the approach proposed here is focused on the liquefaction of tailings material, with the assumption that the foundation materials are competent and non-liquefiable. However, the same approach may be applied to perform liquefaction assessment of the foundation or any other zone in a tailings dam.

Step 1: Seismic Hazard Assessment (SHA)

Deterministic seismic hazard analysis (DSHA) and probabilistic seismic hazard analysis (PSHA) are two distinct methods for assessing seismic hazards. DSHA involves selecting a specific earthquake scenario, typically the largest credible earthquake, to determine its effects on a site, providing a single estimate of ground motion parameters for this worst-case event. It is often used for critical active tailings storage facilities projects. In contrast, PSHA considers the probabilities of all potential earthquakes and their combined impact, producing probabilistic estimates of ground motion over time, typically presented as hazard curves and used in inactive tailings storage facilities and risk assessments. DSHA focuses on understanding the maximum potential impact from a single event, while PSHA provides a comprehensive view of seismic risk by integrating the likelihood of various earthquakes.

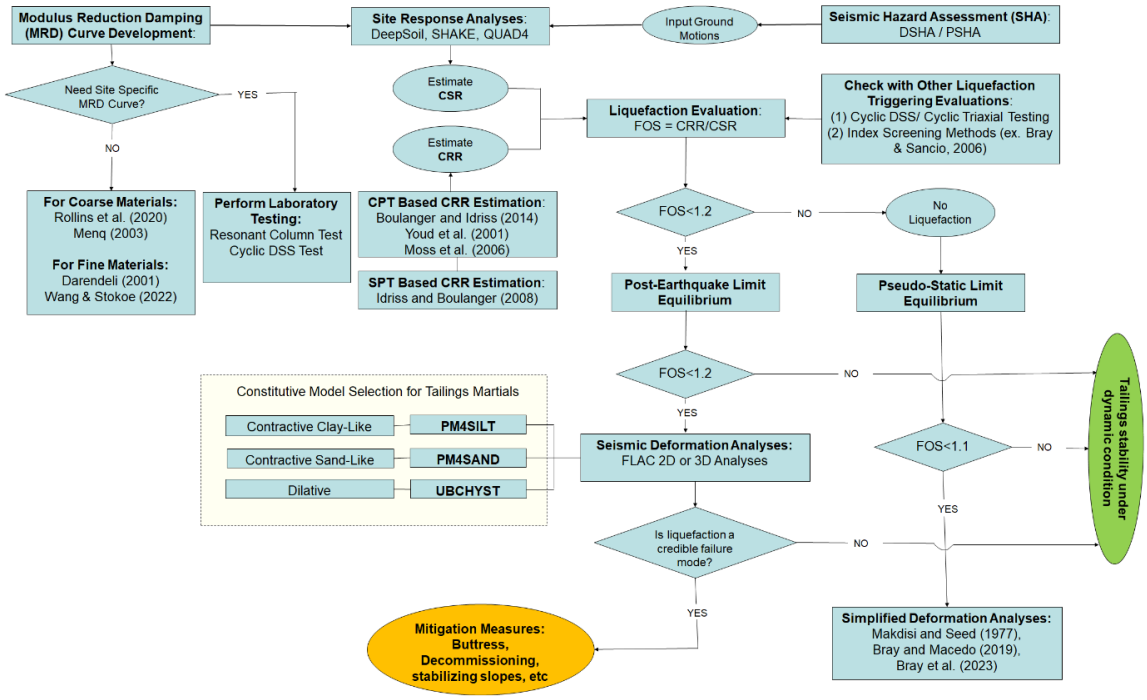


Figure 1: Assessment framework for tailings liquefaction in GISTM compliance

PSHA was used for seismic hazard assessment of Holden's tailings piles. An earthquake moment magnitude (Mw) of 6.3 and peak ground acceleration (PGA) of 0.33g for an earthquake, corresponding to an event with an annual exceedance probability of 1:10,000, was developed.

Seven time-histories corresponding to the three controlling earthquakes (including 1 Interface, 3 Intraslab, and 3 Crustal) were developed for seismic deformation analysis of Holden's mine tailings piles.

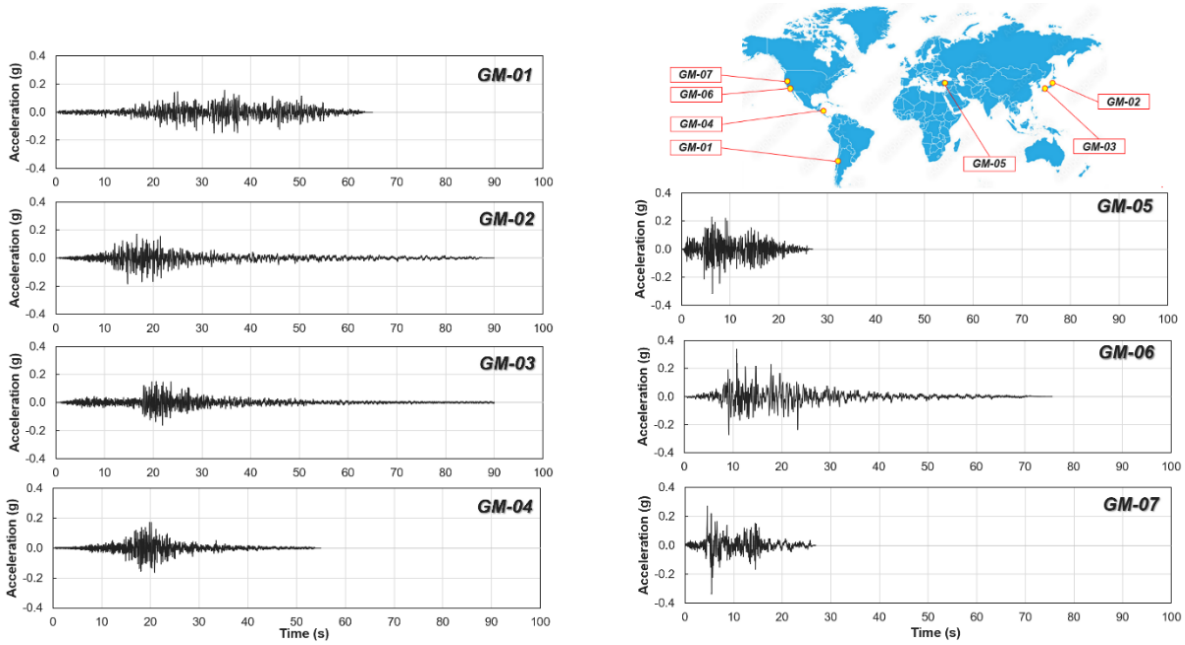


Figure 2: Developed time histories

Step 2: Shear modulus and damping curves

Shear modulus reduction and damping curves provide the change in stiffness and damping properties of tailings with increasing shear strain. These curves are non-linear and illustrate the behavior of tailings material during seismic events. They are used in the site response and dynamic deformation analyses.

The shear modulus reduction curve and equivalent damping ratio curve can be developed from laboratory test results, including resonant column tests for lower shear strains (<0.03%) and cyclic direct simple shear (DSS) tests for higher shear strains (>0.1%). Figure 3 illustrates the modulus reduction and damping curves developed for Holden's tailings materials from laboratory data obtained through cyclic DSS and resonant column tests.

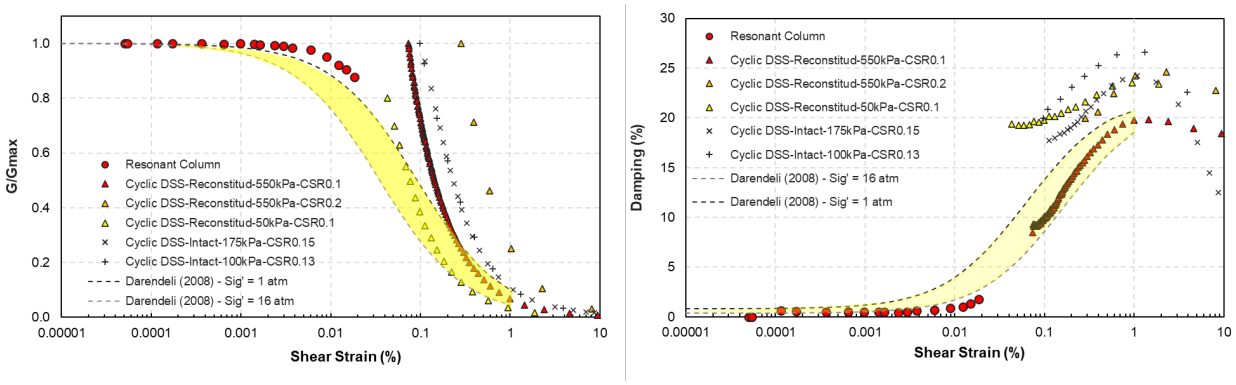


Figure 3: Shear modulus reduction and equivalent damping ratios (Holden Mine)

In the absence of laboratory data, empirical curves can be used to estimate the modulus reduction and damping curves. For coarse materials, references include Rollins et al. (1998) and Menq (2003), while for fine materials, references include Darendeli (2001) and Wang and Stokoe (2021). The developed curves for Holden tailings piles were compared with Darendeli (2001) for verification, as shown in Figure 3.

Step 3: Liquefaction triggering assessment

Liquefaction triggering analysis is used to assess the liquefaction potential of saturated tailings. In this project, a degree of saturation of over 80% was used as the basis for defining liquefaction in the tailings piles. However, this threshold may vary between 80% and 90% for other sites. The analysis consists of comparing calculated cyclic resistance ratio (CRR), as calculated from field exploration data, to the cyclic stress ratio (CSR) values calculated from the 2D site response analysis.

Cyclic stress ratio (CSR)

The site response analysis is to assess the ground motions and induced cyclic stress ratio (CSR) in response to the design earthquake event. The CSR can be developed using software such as QUAD4M, SHAKE, DEEPSOIL, QUAKE/W, FLAC, or PLAXIS. The results from the site response analysis are used to develop

a general understanding of the tailings impoundment seismic response, identify potentially liquefiable zones (e.g., using CPT- or SPT-based liquefaction triggering analysis) and subsequent consequences, and to assess the induced CSRs to guide the laboratory testing program (e.g., cyclic simple shear and cyclic triaxial tests).

Cyclic resistance ratio (CRR)

Both the cone penetration test (CPT) and the standard penetration test (SPT) can be used to estimate CRR. Multiple approaches are available to calculate CRR from CPT data by utilizing different empirical equations, including Boulanger and Idriss (2014), Youd and Idriss (2001), and Moss et al. (2006). The method developed by Idriss and Boulanger (2008) is used in industry for estimation of CRR from SPT data. The factor of safety (FoS) for liquefaction triggering analyses is estimated with the following equation:

$$FOS = \frac{CRR}{CSR}$$

A target FoS of 1.2, as recommended by Idriss and Boulanger (2008), was adopted to determine if seismic liquefaction would be triggered. Figure 4 presents the liquefaction triggering analyses for one of the TP-2 cross sections. As shown in the plot, liquefaction triggering analysis indicated that most of the saturated materials are prone to the liquefaction.

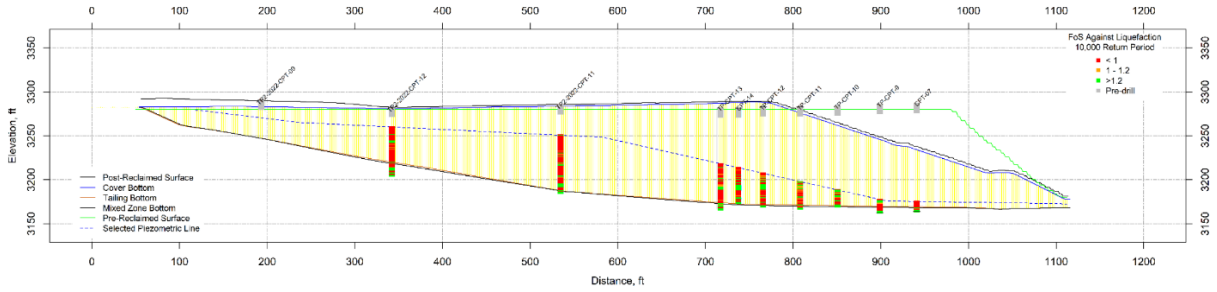


Figure 4: Liquefaction triggering analyses for TP-2

There are a few other checks for liquefaction triggering analyses of tailings materials that can be performed based on the available laboratory test results. These are:

1. cyclic testing methods (cyclic triaxial or DSS test), and
2. index screening methods.

The index screening method (Bray and Sancio, 2006) was performed for available samples. The results indicate that most of the samples fall in susceptible liquefaction zones, as shown in Figure 5, which was in line with performed liquefaction triggering analyses results.

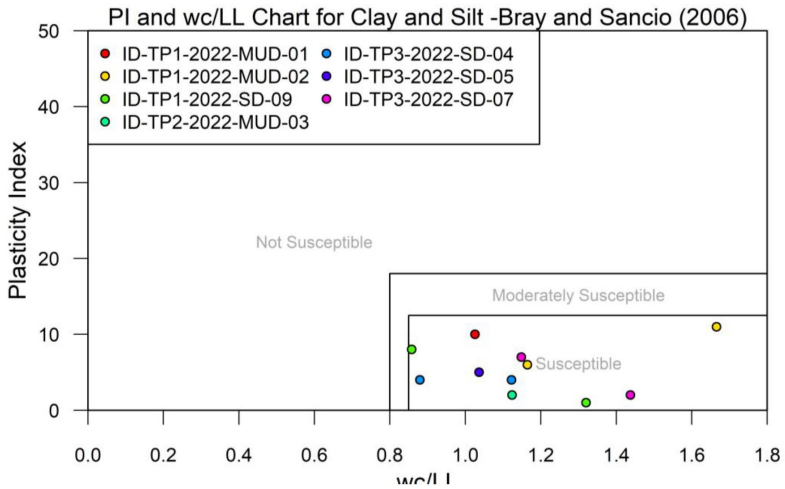


Figure 5: Index screening methods (Bray and Sancio, 2006)

Step 4: Post-earthquake limit equilibrium analyses

Upon completion of the previous step, the project team will have a good understanding of the potentially liquefiable zones within their TSF. If the analyses showed zones with a liquefaction FoS of less than 1.2, it indicates that these zones are potentially liquefiable. The next step would be to perform a post-earthquake stability analysis to evaluate the post-liquefaction stability of the tailings dam. This analysis can be done using a limit-equilibrium or other methods. In this analysis, the zones with a liquefaction FoS lower than 1.2 are assumed to liquefy, and therefore are given a post-liquefaction residual shear strength. Zones that are judged to be non-liquefiable but are not expected to be free draining (i.e., granular) will be modelled using a reduced strength to allow for potential strain softening during shaking.

Post-earthquake conditions reflect the state of the tailings immediately following the design earthquake. During such events, earthquakes can induce excess pore pressures in the saturated tailings materials. These increased pore pressures may result in liquefaction, cyclic mobility, or a reduction in strength, depending on whether the materials are in a contractive or dilatant state. The liquefied strength properties of the tailings materials were determined based on the results of liquefaction triggering analyses.

The calculated post-earthquake FoS can be used to evaluate the seismic stability of the tailings dam and judge whether large seismic displacements are expected. If the calculated FoS is larger than 1.2, it is typically indicative of the overall seismic stability with minimal anticipated seismic-induced deformations. If the FoS is between 1.0 and 1.2, performing a seismic deformation analysis may be warranted to estimate likely seismic deformations. A FoS of less than 1.0 is a likely indicator of large displacements, which also needs to be evaluated by performing a seismic deformation analysis.

Post-earthquake limit equilibrium analyses for the Holden tailings impoundment revealed that the FOS ranged from 0.9 to 1.6, with one of the eleven selected cross-sections falling below 1.0. Consequently,

we conducted seismic deformation analyses using FLAC (Fast Lagrangian Analysis of Continua). Detailed results of these analyses are presented in the next section.

Step 5: Seismic deformation analyses

Material properties for tailings materials

Tailings groups were assigned from group A through E based on the estimated fines content as demonstrated in Table 1. The material properties for each tailings materials group includes unit weight (γ), effective friction angle (ϕ'), peak and liquified undrained shear strength ratios, Poisson's ratio (v), and shear wave velocity (Vs).

Table 1: Tailings grouping criteria

Tailings group	Group A	Group B	Group C	Group D	Group E
Fines content limits	< 36%	> 36% and < 60%	> 60% and < 76%	> 76% and < 88%	> 88%

Selection of constitutive models and calibration process

This section provides the selection process for the constitutive models in each tailings gradation bandwidth group and calibration approach for the seismic deformation analyses. Constitutive models provide the numerical framework that relates increments of strain to increments of stress. The response of the constitutive model will determine the amount of plastic strain that occurs in the tailings material and therefore how much permanent deformation of the tailings pile is predicted. The response of the constitutive model depends on the initial conditions (i.e., state of stress from static initialization), the input parameters of the model, and the imposed loading. The behavior of nonlinear constitutive models may evolve during the analysis based on the loading and the response of the global analysis model.

The choice of constitutive models for advanced analysis should be based on how well each model represents the soil behavior that is considered important to the problem under consideration. Bedrock was assigned elastic behavior based on the consideration that these materials are not expected to experience significant nonlinearity. The Mohr-Coulomb constitutive model (linear elastic-plastic) was assigned to alluvium/glacial till, recompacted tailings, sludge filter, compacted waste rock, cover materials, and jet grout columns.

We tried to utilize more sophisticated constitutive models to simulate hardening/softening behavior and capture stiffness degradation and pore water pressure development for tailings materials. The constitutive models assigned to the tailings materials in the Holden mine project are shown in Figure 6.

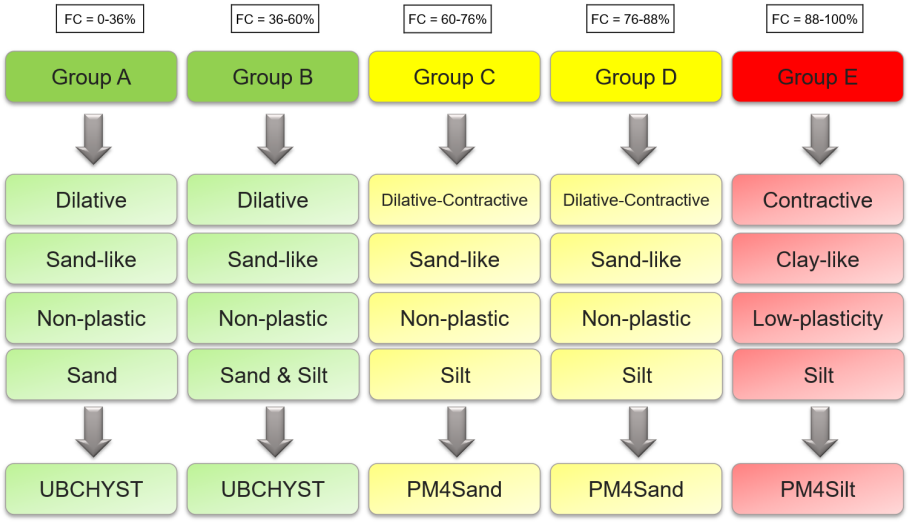


Figure 6: Selection of constitutive model for different tailings materials

As demonstrated in Figure 6, coarse tailings (groups A and B with fine content ranging from 0 to 60%) were assigned to the UBCHYST model (Naesgaard et al., 2011) as one of the robust constitutive models to simulate non-liquefiable soils subjected to earthquake loading. These layers are non-plastic dilative sand and silt, which are mainly located in the unsaturated tailings zones and are not susceptible to liquefaction.

Fine tailings materials (groups C, D, and E with fine content ranging from 60% to 100%) were assigned the PM4Silt and PM4Sand constitutive model to capture potential cyclic softening of the liquifiable tailings layers. PM4Sand and PM4Silt are nonlinear effective stress models that are coupled with pore water pressure response that can simulate flow liquefaction during a seismic event. As shown in Figure 6, PM4Sand was assigned to groups C and D since these tailings materials are sand-like non-plastic silt, while PM4Silt was assigned to the group E (finest group), which was categorized as a clay-like low-plasticity silt.

The PM4Silt (Boulanger and Ziotopoulou, 2018) model includes modifications, relative to PM4Sand (Boulanger and Ziotopoulou, 2015) that improve its ability to approximate the monotonic undrained strength, cyclic undrained strength, and secant shear modulus and equivalent damping ratio behaviors of low plasticity clays and silts, as opposed to those for purely non-plastic silts or sands. The calibration process for the UBCHYST, PM4Sand, and PM4Silt constitutive models were performed. The following section summarizes the calibration process for PM4Silt as an example.

PM4Silt calibration

The materials assigned the PM4Silt model were calibrated, using a single-element model to simulate monotonic direct simple shear (DSS) loading, cyclic DSS loading with uniform cyclic stress ratios, and

cyclic DSS loading at different cyclic strain amplitudes to obtain secant shear moduli and equivalent damping ratios. Figure 7 shows the calibration process for the PM4Silt constitutive model, which requires eight steps.

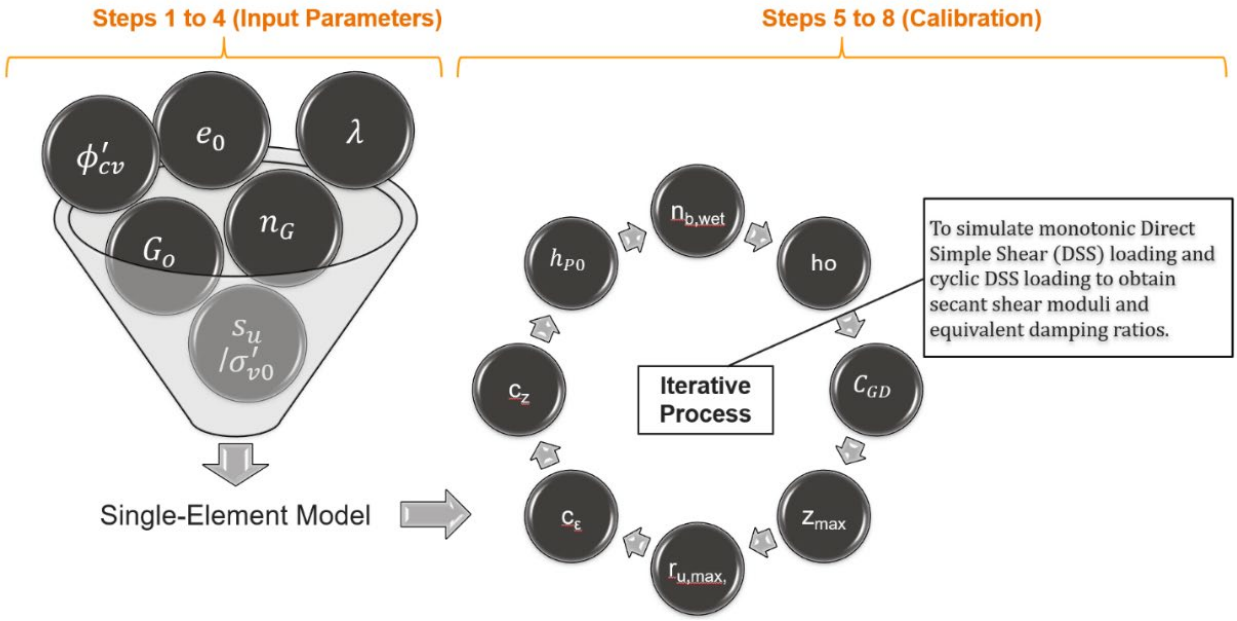


Figure 7: PM4Silt calibration process

Figure 8 demonstrates how the slope of slope of the critical state line (λ), shear modulus coefficients (G_o and n_G), monotonic loading asjuster ($n_{b,wet}$), and contraction rate parameter (h_0) were estimated or calibrated based on the available laboratory and field-testing results. Figure 9 shows that the fabric growth parameter (c_z), strain accumulation rate factor (c_ε), fabric term (Z_{max}), **and** modulus degradation factor (C_{GD}) have been calibrated to match stress path responses in undrained cyclic DSS loading.

Seismic deformation analysis results

The computer program FLAC was utilized to perform nonlinear seismic deformation analysis. The discretized analysis sections for TP-1 are shown in Figure 10. The seismic deformation analysis results indicated maximum horizontal deformations of 4, 6.5, and 5.5 for TP-1, TP-2, and TP-3, respectively. Figure 11 and Figure 12 present the total horizontal displacement and excess pore water pressure ratio for TP-1. As shown in the plot, there are limited zones where the pore water pressure ratios exceeded 0.85 (blue zones), indicating liquefaction. These deformations are considered acceptable since they occur near the upper section of the tailings piles and not at the toe.

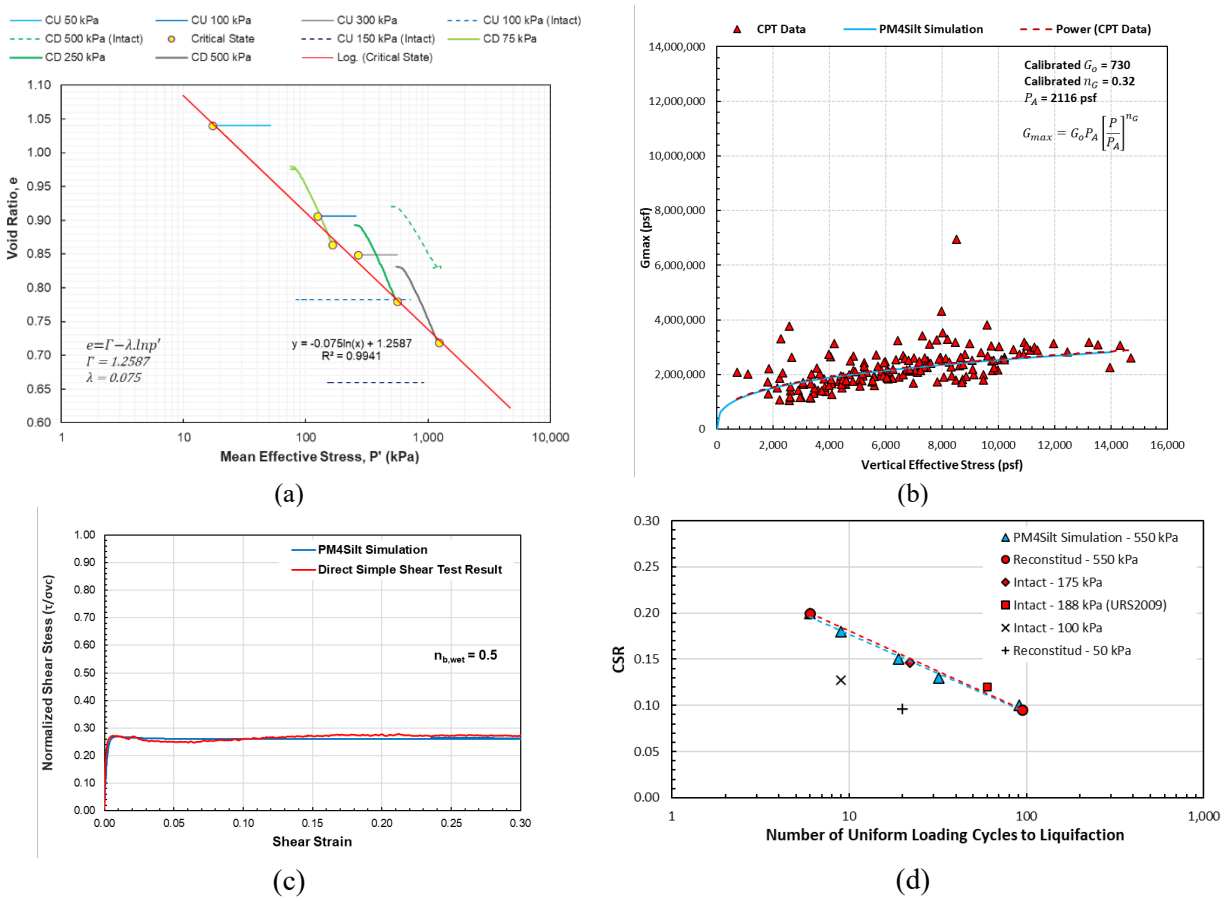


Figure 8: PM4Silt calibration: (a) slope of critical state line, (b) shear modulus coefficient, (c) monotonic loading asjuster ($n_{b,wet}$), and (d) contraction rate parameter

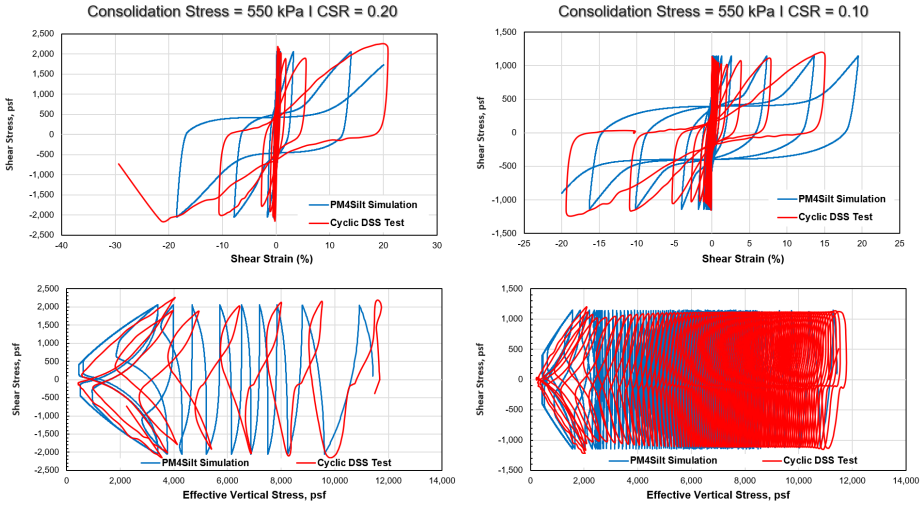


Figure 9: Stress path responses in undrained cyclic DSS loading

Three factors, including high confining pressure, high fine content, and a deeper groundwater table in Holden's tailings piles, inhibit the liquefaction process in the saturated slime layer. Observations from

various case histories reveal that the potential liquefaction zone typically spans from the ground surface down to a maximum depth of 30 feet (10 meters). It is noteworthy that deeper soil layers, influenced by augmented confining pressures, as indicated by Day (2010), tend not to undergo liquefaction due to these increased pressures. Examination of all tailings piles (TPs) shows that the layer prone to liquefaction resides at depths greater than 50 feet. This depth places these layers under excessive overburden pressure from the upper tailings materials.

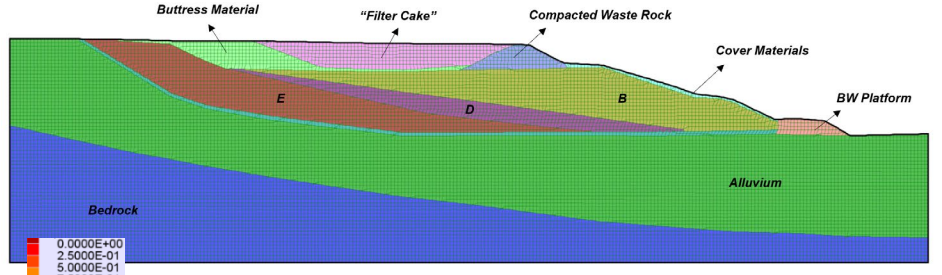


Figure 10: Discretized analysis section for TP-1

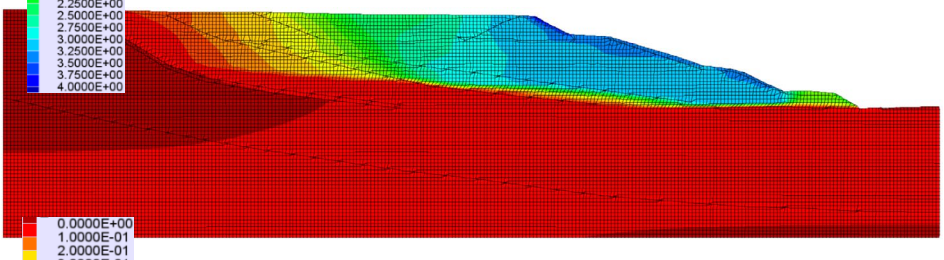


Figure 11: Horizontal displacement for TP-1

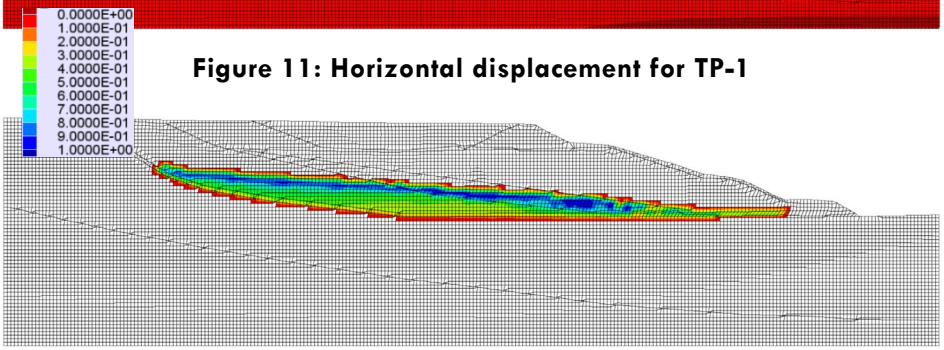


Figure 12: Excess pore water pressure ratio for TP-1

Conclusion

This paper outlined a methodology for assessing liquefaction risk in tailings dams, which possess unique vulnerabilities due to their construction methods and materials. The Holden mine case study applied the outlined assessment framework for tailings liquefaction in GISTM compliance. The study identified zones susceptible to liquefaction, conducted post-earthquake stability analyses, and used advanced numerical methods for seismic deformation analysis. These analyses indicated that while certain sections of the tailings piles were prone to liquefaction, the overall deformation levels were within acceptable limits. This comprehensive evaluation not only highlighted the specific risks associated with the Holden mine but also

validated the effectiveness of the proposed assessment process in real-world scenarios. By adopting this structured assessment process, engineers and practitioners can enhance the safety and efficiency of tailings management practices. The methodology aligns with the GISTM, providing a practical guide for compliance and risk mitigation. Ultimately, this approach helps to protect downstream communities, preserve ecological systems, and provide long-term sustainability of mining operations.

References

Boulanger, R.W. and I.M. Idriss. 2014. CPT and SPT based liquefaction triggering procedures. Report No. UCD/CGM-14/1. Center for Geotechnical Modeling, University of California at Davis.

Boulanger, R.W. and Ziotopoulou, K. 2015. PM4Sand: A sand plasticity model for earthquake engineering applications. University of California at Davis: Center for Geotechnical Modeling Report No. UCD/CGM-15/01, Department of Civil and Environmental Engineering.

Boulanger, R.W. and Ziotopoulou, K. 2018. PM4Silt: A silt plasticity model for earthquake engineering applications. Department of Civil and Environmental Engineering, University of California, Davis, CA: Report No. UCD/CGM-18/01, Center for Geotechnical Modeling.

Bray, J.D. and Sancio, R. B. 2006. Assessment of the liquefaction susceptibility of fine-grained soils. *Journal of geotechnical and geoenvironmental engineering* 132(9): 1165–1177.

Darendeli, M.B. 2001. Development of a new family of normalized modulus reduction and material damping curves. PhD dissertation, University of Texas at Austin.

Day, R.W. 2010. *Foundation Engineering Handbook: Design and Construction with the 2009 International Building Code*. McGraw-Hill Education.

GTR (Global Tailings Review). 2020. Global Industry Standard on Tailings Management. https://globaltailingsreview.org/wp-content/uploads/2020/08/global-industry-standard_EN.pdf . Accessed August 2020.

Idriss, I.M. and Boulanger, R.W. 2008. Soil liquefaction during earthquakes. Monograph MNO-12, Earthquake Engineering Research Institute, Oakland, CA, 261 pp.

Itasca. 2016. FLAC Version 8.1, Itasca Consulting Group, Minneapolis, MN.

Menq, F. 2003. *Dynamic Properties of Sandy and Gravelly Soils*. Austin: University of Texas.

Moss, R.E., Seed, R.B., Kayen, R.E., Stewart, J.P., Der Kiureghian, A. and Cetin, K. O. 2006. CPT-based probabilistic and deterministic assessment of in situ seismic soil liquefaction potential. *Journal of Geotechnical and Geoenvironmental Engineering* 132(8): 1032–1051.

Naesgaard, E., Byrne, P. and Amini, A. 2011. Hysteretic model for non-liquefiable soils (UBCHYST5d). *UBCHYST5d Memo*.

Rollins, K., Evans, M., Diehl, N. and Daily, W. 1998. Shear modulus and damping relationships for gravels. *Journal of Geotechnical and Geoenvironmental Engineering* 124(5): 396–405.

Wang, Y. and Stokoe II, K.H. 2021. Development of constitutive models for linear and nonlinear shear modulus and material damping ratio of uncemented soils. *J. Geotech. Geoenviron. Eng.* 148(3): 04021192.

Youd, T.L. and Idriss, I. M. 2001. Liquefaction resistance of soils: summary report from the 1996 NCEER and 1998 NCEER/NSF workshops on evaluation of liquefaction resistance of soils. *Journal of Geotechnical and Geoenvironmental Engineering* 127(4): 297–313.

Challenges and Mitigations to Bring a Historical Tailings Facility into Compliance with Modern Standards

Anthony Zhang, Tetra Tech, Canada
Chris Johns, Tetra Tech, Canada

Abstract

This paper presents a summary of the work undertaken by Klondike Silver and Tetra Tech to assess and manage risk associated with tailings management facility (TMF) infrastructure at a lead-zinc mine in interior BC. The underground lead-zinc mine was developed in a historic mining district and the TMF was constructed in a steep-sided river valley in mountainous terrain. The TMF was originally constructed in the 1970s and built as three adjacent cells that were raised in stages using a variety of methods and materials. Klondike and Tetra Tech worked together towards compliance with modern standards for an inactive facility. Preliminary work included review of historic documentation and site visits to identify key hazards and develop plans to manage risk. Tetra Tech undertook consultations with the regulator and the owner, and undertook geohazard, hydrological, and geotechnical assessments to identify key risks and establish priority work. Design work progressed, and construction was initiated on erosion protection works to manage the primary risk, which was determined to be from perimeter erosion from potential debris floods and debris flows in adjacent creek channels. Geotechnical investigation, piezometer instrumentation, and stability assessment were undertaken to better understand and manage geotechnical risk. An instrumentation monitoring plan was developed and incorporated into the TMF Operation, Maintenance, and Surveillance Manual to support TMF risk management.

Introduction

Historical tailings facilities often grapple with a variety of common issues, primarily stemming from their outdated designs and inadequate documentation. Many of these facilities have limited design and construction records, or were constructed based on old codes that no longer meet current regulatory standards. This can present significant challenges, as these facilities must now comply with more stringent design and assessment criteria than those that were in place at the time of construction. The absence of detailed construction records and historical information further complicates the assessment of risk and compliance. Additionally, regulatory compliance requires these facilities to adhere to current standards,

which include comprehensive dam safety management systems, and include Operations, Maintenance, and Surveillance (OMS) manuals, Emergency Preparedness and Response Plans, risk registers, etc. Multiple ownership changes can exacerbate these problems, and lead to inconsistent monitoring and maintenance practices, and a lack of continuity in record-keeping. Moreover, financial constraints on junior mining companies, particularly in non-producing mines, add another layer of difficulty in ensuring the proper upkeep and compliance of historical tailings facilities.

Project background

The Silvana Mine is located near the town of Sandon, approximately 15 kilometers east of New Denver, BC, Canada. The lead-zinc and silver underground mine is located on a historical mining property with a mill and supporting infrastructure. The operation of the mine has been in care and maintenance with ongoing exploration activity since 2013.

The Silvana TMF comprises three adjacent tailing cells constructed in the Carpenter Creek Valley (Figure 1). The three cells, identified as Pond 1, Pond 2, and Pond 3, are side-hill impoundments. The TMF has been classified as "High Consequence" under the criteria of the Canadian Dam Association (CDA) guidelines (CDA, 2013). The combined capacity was estimated at 400,000 tonnes, with the facility covering approximately 6.4 ha. Ponds 1 and 2 are currently at their storage capacity, and Pond 3 is near its capacity.

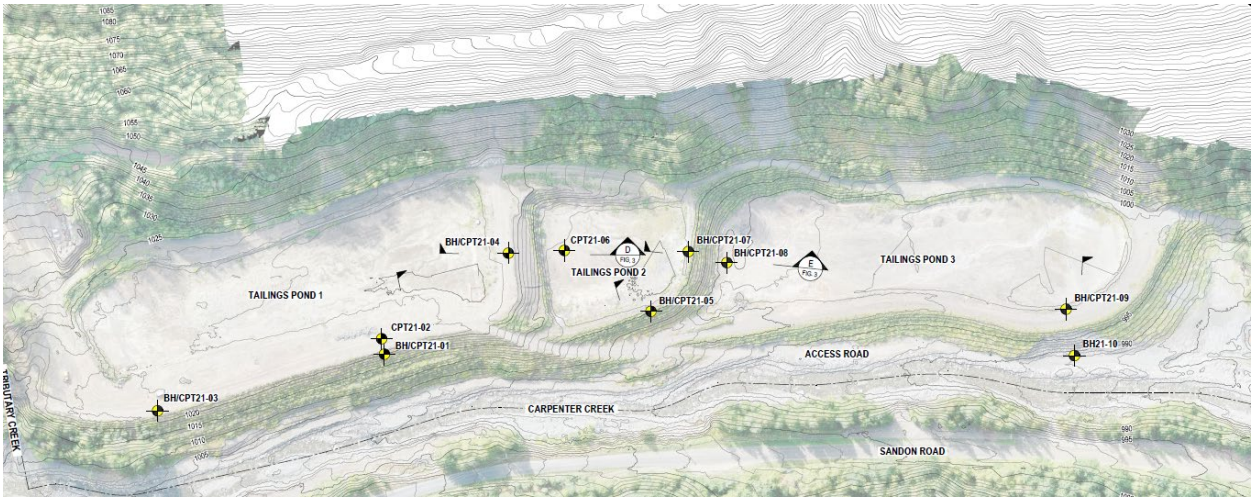


Figure 1: Layout of the Silvana TMF

The construction of the TMF commenced in 1970 with Pond 1 and 2 starter dams, and the ponds were both raised in stages between 1970 and 1980. Historical construction records indicate that Pond 1 was raised

by upstream methods and Pond 2 by centerline methods. Pond 1 was subsequently raised between 1982 and 1984 to its current configuration of approximately 22 m height and approximately 10 m crest width.

Construction of the pond starter dam was completed in 1988. A geotextile and sand filter zone on the upstream slope were part of the starter dyke. Pond 3 was raised by the downstream construction method in 1990 and 1992 to its current configuration.

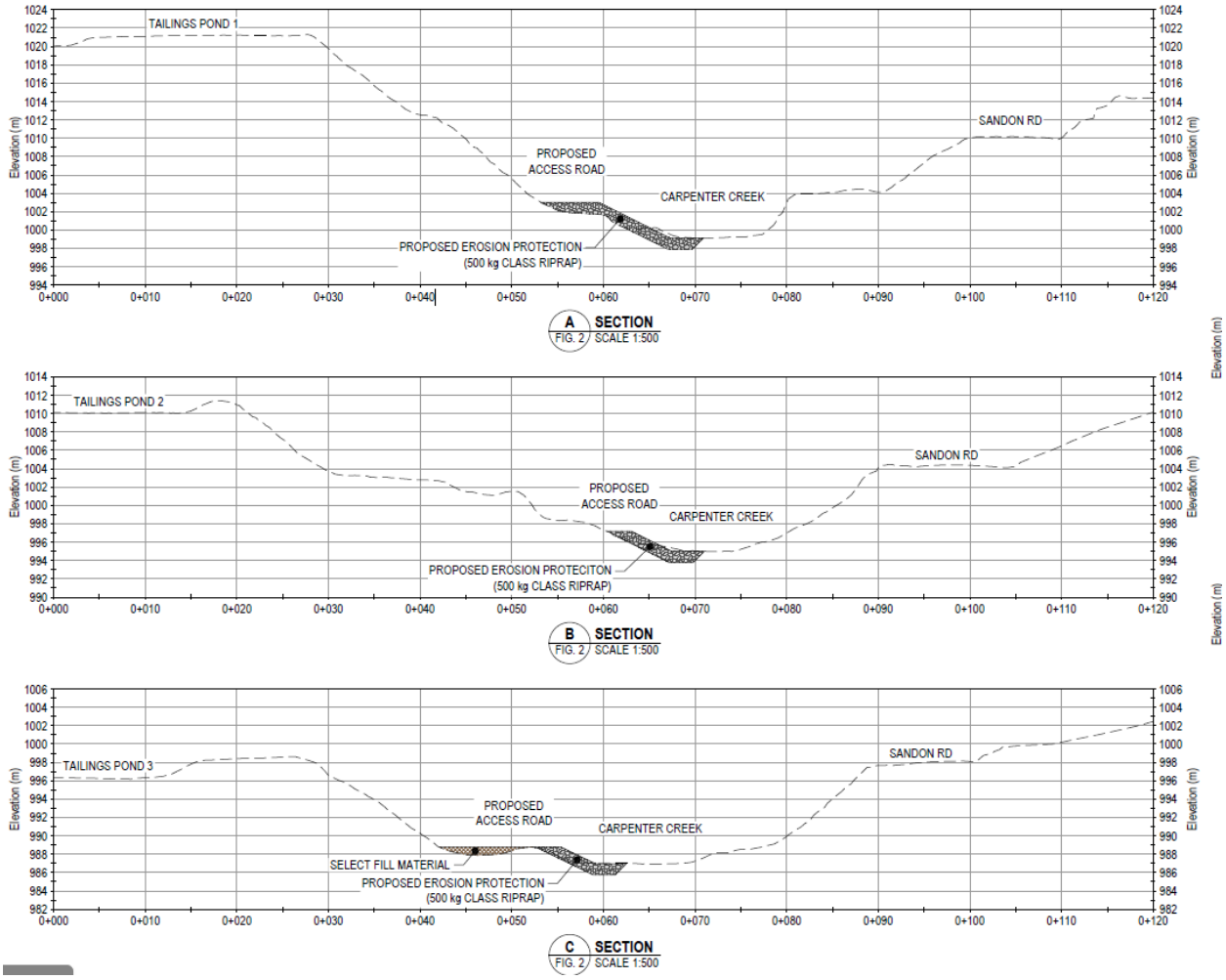


Figure 2: Selected cross-sections of Ponds 1, 2, and 3

No further raises of the TMF were reported after 1992. Construction activities reported other than regular maintenance include:

- In 2016, upgrades were completed to the TMF slopes to protect against a 1 in 200-year flow.
- In 2020, repair was completed along a washout area on the downstream slope of Pond 3.

The stratigraphy of the soils underlying the ponds consists of fluvial sands and gravels with historic tailings material. The perimeter embankments were generally constructed of granular fill excavated from

the adjoining hillside. Some Pond 1 and Pond 2 raises were constructed using coarse tailings sands with an external zone of native granular fill. The toe of the TMF embankments along Carpenter Creek were locally armored with rip-rap. The tailings material was considered non-acid generating.

Previous assessments by others had determined that Pond 1 did not meet minimum design requirements for stability and that TMF water management upgrades were required. In June 2020, regionally high spring runoff impacted the site and resulted in some erosion of the Pond 3 toe.



Photo 1: Wash-out event in June 2020

Geohazard assessment

Objective

A geohazard assessment of the Silvana TMF was undertaken to assess the facility's vulnerability to geohazard events. The assessment complemented a concurrent hydrotechnical evaluation to determine design flood events in the valley. The primary objectives of the geohazard assessment were to determine the likelihood of future geohazard processes impacting the TMF and to identify and recommend practical mitigation measures to protect the facility.

Approach

The assessment followed a systematic approach incorporating desktop reviews, historical air photograph interpretation, and field investigation. A comprehensive review of topographic mapping, bedrock geology, terrain stability, and other related technical reports was conducted. Historical air photographs and images from 1939 to 2018 were analyzed to identify previous slope and channel instabilities, documenting key geomorphological processes and historical landslide activities. The field investigation, conducted between September 28 and October 1, 2020, included traverses of Tributary Creek, Carpenter Creek, and the slopes above the TMF, noting subsurface soil conditions at road and creek exposures.

Findings

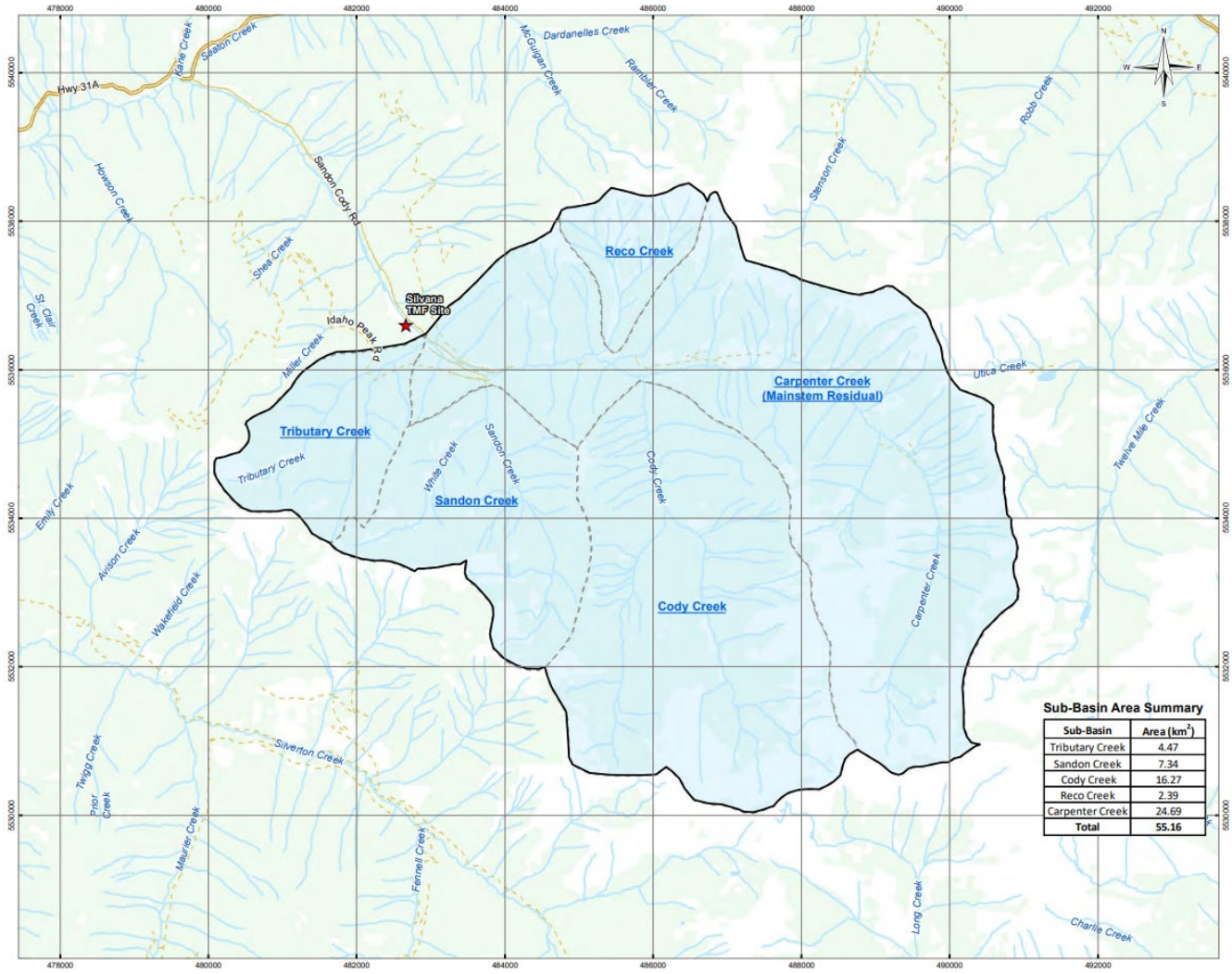


Figure 3: Terrain and Location of the TMF

The TMF site lies in a physiographic region where Carpenter Creek is a fourth-order stream with a watershed area of about 206 km². The creek flows 7.0 km from Mount Carlyle (el. 2,520 m) to Slocan Lake

(el. 820 m) at the community of New Denver, BC. The TMF is located upstream of Three Forks at ~1,000 m elevation, with a catchment area upstream of the TMF site being ~55 km². The bedrock geology consists of Triassic-aged sedimentary rocks, including argillite, slate, quartzite, limestone, and granitic dyke intrusions. Terrain stability mapping indicates that the area is generally stable. Historical flood and landslide events, such as those in 1894, 1933, 1934, 1955, 1999, and the significant event in May-June 2020, highlight the region's vulnerability to natural hazards.

Carpenter Creek, upstream of the TMF, is susceptible to debris floods, particularly downstream of Reco Creek, which is a significant sediment source. The stream channel gradient from the headwaters down to the TMF site shows that headwater reaches have steep channel gradients (25% to 45%) and are predominantly bedrock-controlled. Mid-watershed reaches extend from Cody Creek through the Sandon townsite to the TMF, with an average gradient of 5–10% and high connectivity to adjacent valley side slopes, making them significant sediment sources. The channel is incised within the banks near the TMF, with gradients becoming gentler (4–6%) but remaining highly confined.

Tributary Creek is capable of producing a full range of geomorphic events, from clear water floods to debris floods and debris flows. The middle reaches of Tributary Creek have numerous sediment sources, including large landslides observed during field investigations. The stream channel gradient in these reaches ranges from 18% to 30%, with the channel being tightly constrained by adjacent steep valley side slopes.

Mitigation recommendations

To enhance the resilience of the TMF against future geohazard events, several mitigation measures are recommended. Constructing a berm along the south boundary of Pond 1, increasing sediment storage capacity in the lower reach of Tributary Creek, and installing greater protection against slope material raveling are recommended. Continuous monitoring and maintenance of the lower reach of Tributary Creek are essential. Additionally, the geohazard assessment should be revisited after significant flood, debris flow, or slide events to document changes that may affect potential hazard and risk levels.

Conclusion

The geohazard assessment for the Silvana TMF provided a thorough evaluation of potential geohazard risks and offered practical mitigation measures to enhance the facility's resilience. This assessment underscored the importance of continuous monitoring and adaptive management to safeguard the TMF against future geohazard events.

Hydrotechnical assessment and erosion protection design

Objective

The primary objective of the hydrotechnical assessment was to propose a series of channel upgrades to protect the integrity of the Silvana TMF. The scope of work encompassed four main components: background review, hydrologic analysis, hydraulic analysis, and preliminary design. The background review included a site visit and review of historical data and contextual information. The hydrologic analysis assessed the intensity and frequency of recent freshet events and the design flows for Carpenter and Tributary Creek. The hydraulic analysis evaluated existing channel capacities and erosion mechanisms. The preliminary design work included erosion and geohazard protection measures.

Field investigation

The field investigation had several objectives:

- Inspection of Creeks: Inspect Carpenter Creek and Tributary Creek to identify signs of historical flood events, erosion, and debris flow. This inspection included visual assessments and photographic documentation of the creek banks, bed conditions, and any existing erosion protection measures.
- Assessment of 2020 Freshet Event: Evaluate the impact of the 2020 freshet event, which caused significant erosion and debris deposition. This assessment aimed to quantify the extent of the damage and identify areas most vulnerable to future events.
- Documentation of Emergency Measures: Document emergency erosion protection measures that were implemented in response to the 2020 freshet. These measures included temporary structures and modifications aimed at preventing further erosion and protecting critical infrastructure.
- Data Collection: Collect data using orthographic images and LiDAR surveys. This data was used for creating accurate hydraulic models and developing initial design plans for erosion and geohazard protection. Additionally, anecdotal historical flood information provided by the Klondike Silver was used to validate and supplement the field data.

Hydrologic and hydraulic analysis

The hydrologic and hydraulic analyses provided a detailed assessment of the water flow and erosion patterns affecting Carpenter Creek and Tributary Creek. Key components of these analyses included:

- Hydrologic Analysis: Estimating the intensity and frequency of freshet events. This analysis helped in understanding the severity and potential impact of extreme hydrological events on the mine site.

- Hydraulic Analysis: Assessing the current channel capacities of Carpenter Creek and Tributary Creek. This involved evaluating the validity of bulking factors and identifying erosion mechanisms. The hydraulic analysis aimed to determine the ability of the creek channels to convey floodwaters without causing significant erosion or damage to the embankments.
- Channel Erosion Mechanisms: Understanding the mechanisms driving channel erosion and identifying the areas most susceptible to erosion. This information was used for designing effective erosion protection measures for the long-term stability of the creek channels.

Design and recommendations

Based on the findings from the stability, hydrologic, and hydraulic analyses, preliminary designs were developed for erosion and geohazard protection measures. These designs included specific recommendations to enhance the structural integrity of the tailing pond embankments and protect against future hydrotechnical events.

Conclusion

The hydrotechnical study provided a comprehensive assessment of the hydrotechnical challenges faced at the Silvana TMF. The study findings highlighted the need for targeted erosion protection and stability enhancement measures to safeguard the tailing ponds and surrounding infrastructure. By addressing these challenges, the study aimed to support a safe and secure TMF and compliance with regulatory standards. The detailed recommendations and preliminary design plans provided a roadmap for implementing effective hydrotechnical management strategies and mitigating the impact of future hydrological events.

Geotechnical investigation, assessment, and conceptual design

Objective

The Silvana TMF geotechnical assessment evaluated the stability and compliance of the TMF structures with regulatory standards, including the Health, Safety, and Reclamation Code (HSRC) for Mines in British Columbia. The primary goal was to assess the stability of the TMF structures, identify potential risks, and recommend potential remedial actions to maintain safety and regulatory compliance.

Field investigation

A field investigation was conducted in April 2021 that included geotechnical drilling, vibrating wire piezometer (VWP) installation, Standard Penetration Tests (SPT), Cone Penetration Tests (CPT), and Seismic Cone Penetration Testing (SCPT). These activities aimed to gather comprehensive information on soil stratigraphy, strength parameters, and groundwater conditions to support stability analyses. VWPs were installed at six locations to facilitate groundwater level monitoring. The data collected from these

investigations was used to advance the understanding of the subsurface conditions and support stability assessment of the TMF structures.

Stability analyses

The stability analyses focused on assessing the stability of the tailing pond embankments under various conditions. Key components of the stability analyses included:

- TMF Stability Acceptance Criteria: Establishing criteria for acceptable stability levels based on regulatory guidelines and industry standards.
- Slope Stability Model Geometry: Defining the geometry of the slope stability models based on the physical characteristics of the embankments and surrounding terrain. Accurate modeling of the slope geometry supports reliable stability assessments.
- Material Properties: Analyzing the material properties of the embankment soils, including strength parameters such as cohesion and internal friction angle. These properties were determined from field and laboratory testing of samples collected during field investigations.
- Seismic Parameter Selection: Selecting appropriate seismic parameters for the stability analyses. This involved calculating a horizontal seismic coefficient (Kh) based on the site-specific Peak Ground Acceleration (PGA) value.
- Analyses Methodology: Implementing the generalized limit equilibrium method of Morgenstern-Price using Slope/W software (GeoStudio 2019). This method involved iterative calculations to identify potential slip surfaces and determine factors of safety (FoS) under both static and seismic conditions. The analyses also considered potential liquefaction of soil layers under seismic loading, which could impact the TMF stability. The liquefaction assessment involved evaluating the potential for cyclic loading during an earthquake to cause a loss of strength in the tailings and foundation materials.

Stability analyses summary

Summarizing the results of the stability analyses. The analyses indicated that most cross-sections of the tailing pond embankments met the target FoS, except for the static analysis of Section A-A' (Pond 1). It was determined that the liquefaction potential of the tailings and embankment foundation materials was low under design seismic events, but further work was needed to advance this assessment. Remedial design concepts were developed for sections requiring reinforcement to improve stability.

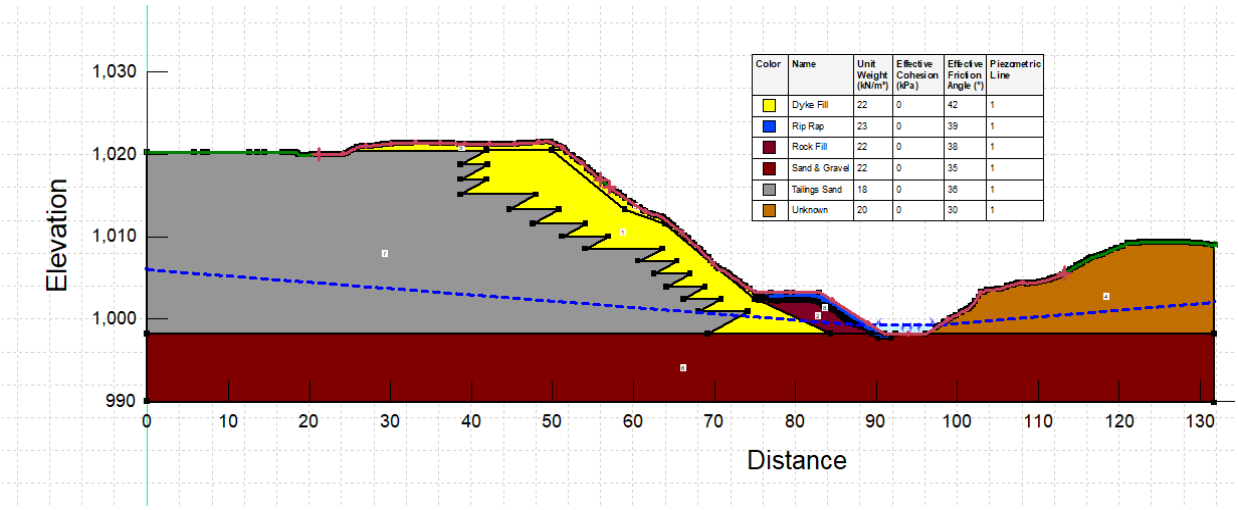


Figure 4: Existing condition of Pond 1

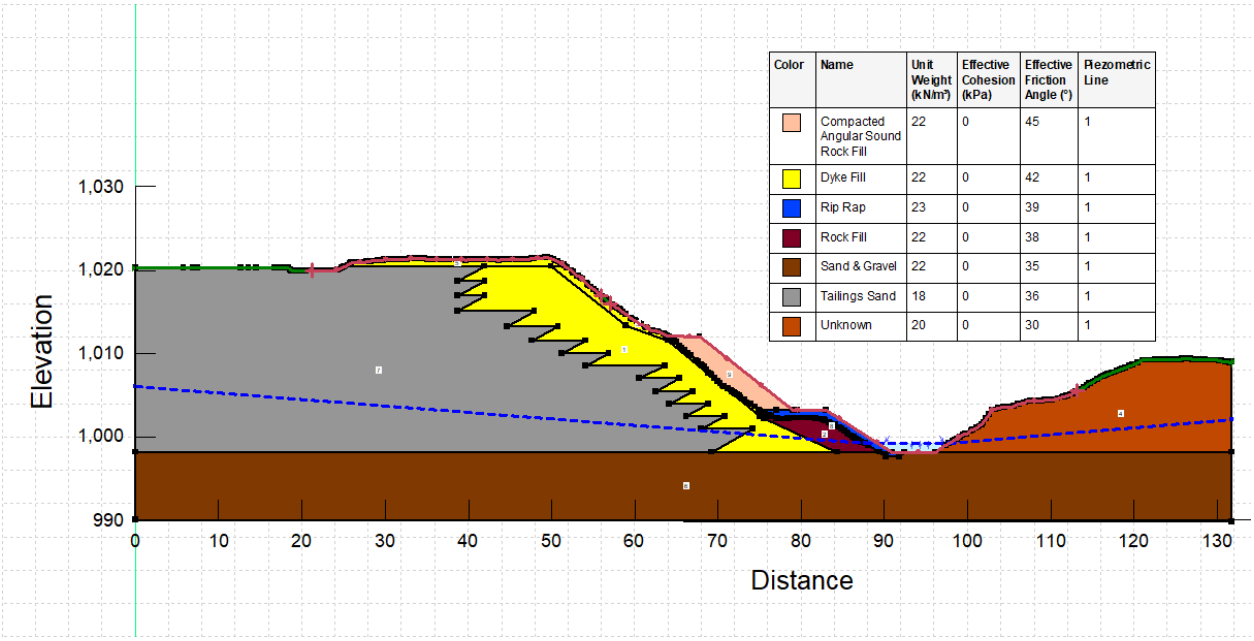


Figure 5: Conceptual remediation design

Conclusion

The stability results indicated that while most areas of the TMF met design criteria, a section of Pond 1 required remedial work to improve stability and comply with regulatory standards.

To enhance the stability of Pond 1, a conceptual remedial design involving a buttress has been proposed. The remedial measures include several recommendations for improving the slope stability of Pond 1 and mitigating potential geotechnical risks. A comprehensive program of visual inspection and instrumentation monitoring was recommended to develop further understanding of the TMF performance and to manage risk.

Regulatory and operation support

Addressing the complexities associated with historical tailings facilities necessitates a collaborative approach with owners, consultants, regulators, and stakeholders to establish a robust dam safety management system. The approach adopted at for the Silvana TMF included regular dam safety inspections, the development and implementation of an updated OMS manual, a TMF specific Emergency Preparedness and Response Plan, and the engagement of an Independent Tailings Review Board. The system includes continuous improvement protocols to incorporate new insights from ongoing evaluations and updating annually.

A collaborative approach was adopted to prioritize tasks and formulate a practical work plan that prioritized work on significant dam safety risks. The effort included regular liaison between consultants, owners and regulators. Support included periodic updates to a regulatory compliance tracking system.

Conclusion

Several challenges were encountered in identifying and addressing design and regulatory compliance issues at the Silvana TMF. Many of these issues are commonly encountered at other historical and inactive tailings storage facilities at properties where exploration and project development are the main focus. Recognizing these challenges, Tetra Tech employed a systematic approach to work closely with the owner and the regulator to develop a tailored plan that addressed the unique issues and circumstances of the TMF. This approach began with the compilation and review of historical information, providing a foundational understanding of the facility's past performance and existing conditions.

Effective communication with the client is an important component of the process to ensure that constraints, whether regulatory or financial, are fully understood and considered in the planning stages. This dialogue helps in aligning the project goals with the client's needs. A preliminary risk evaluation was carried out to identify potential issues and prioritize the tasks based on their risk and benefit. This risk-based prioritization lays the groundwork for a structured and phased approach to the plan.

The execution of the plan at Silvana TMF was carried out in distinct phases, and significant work has been completed to date. Initially, a geohazard assessment and a hydrotechnical assessment were conducted to identify and propose potential mitigation options for risks associated with natural hazards and surface water management. Preliminary design work of erosion protection and flood mitigation measures was then undertaken to address priority risks. A comprehensive geotechnical investigation and assessment was performed that provided advanced insight into the subsurface conditions and supported the design of remedial measures.

An important component of the plan was the development and implementation of a Dam Safety Management System. This system provided a structured framework for the ongoing monitoring and maintenance of the dam. The consultative and phased risk-based approach was focused on effective identification and management of dam safety risk.

References

Canadian Dam Association (CDA). 2013. *Dam Safety Guidelines 2007* (2013 edition).

Canadian Dam Association (CDA). 2019. *Application of Dam Safety Guidelines to Mining Dams*.

CFME. 2006. *Canadian Foundation Engineering Manual,* 4th edition. Canadian Geotechnical Society.

EMPR (Ministry of Energy, Mines and Petroleum Resources). 2016. Health, Safety and Reclamation Code for Mines in British Columbia Guidance Document. British Columbia: Ministry of Energy, Mines and Petroleum Resources.

EMPR (Ministry of Energy, Mines and Petroleum Resources). 2017. Health, Safety and Reclamation Code for Mines in British Columbia. British Columbia: Ministry of Energy, Mines and Petroleum Resources.

Idriss, I.M. and Boulanger, R.W. 2008. Soil liquefaction during earthquake. EERI publication, Monograph MNO-12, Earthquake Engineering Research Institute, Oakland.

Tetra Tech. 2020. Silvana Mine Hydrotechnical Assessment and Erosion Protection Preliminary Design. Tetra Tech Canada Inc. report prepared for Klondike Silver Corp, Nov. 2020.

Tetra Tech. 2021. Klondike Silver Silvana Mine Tailings Management Facility Geotechnical Assessment Report. Tetra Tech Canada Ltd. Report prepared for Klondike Silver Corp, Sept. 2021.

Tetra Tech. 2021. Silvana Mine Dam Safety Inspection, Klondike Silver Silvana Mine Tailings Management Facility. Tetra Tech Canada Ltd. Report prepared for Klondike Silver Corp, March 2021.

Chapter Six

Closure Issues

TAILINGS AND
MINE WASTE 2024



Effect of Temperature on the Generation of Arsenic from Waste Rock from an Arctic Mine: A Laboratory Investigation

Elaura Seutin, Université du Québec en Abitibi-Témiscamingue, Canada
Bruno Bussière, Université du Québec en Abitibi-Témiscamingue, Canada
Benoît Plante, Université du Québec en Abitibi-Témiscamingue, Canada
Vincent Boulanger-Martel, Université du Québec en Abitibi-Témiscamingue, Canada

Abstract

Mine waste rock is often produced in large volumes during mining, particularly when ore is extracted from an open pit. When exposed to atmospheric conditions, waste rock can react and generate contaminated mine drainage, characterized by concentrations in various metals and metalloids that exceed regulatory limits. The reactivity of waste rock is a function of different parameters such as grain size distribution, mineral type and content, water content, and temperature. In the context of mine reclamation in Arctic environments, it is often proposed to favor the aggradation of permafrost within potentially problematic waste rock storage facilities to reduce chemical reactivity and to control contaminant transport by freezing the pore water. Previous studies have demonstrated the impact of temperature on the oxidation rate of sulfide minerals.

However, much less is known about the influence of temperature on the reactivity of arsenic-bearing minerals. In waste rock, these minerals are frequently found in the form of sulfides or sulfosalts such as gersdorffite (NiAsS), and it is often assumed that the latter will react in the same way as sulfides when the temperature is lowered. To gain a better understanding of the influence of temperature on As-generating waste rock, three column tests were set up using materials from an active mine located in the Canadian low Arctic. Arsenic in the tested waste rock was mainly contained in gersdorffite. Column tests were performed at temperatures of 21, 5, and –2°C to assess the effects of temperature on arsenic leaching. Columns were submitted to twenty wetting and drying cycles. Volumetric water contents and temperatures were monitored throughout the tests and water quality was analyzed at each flush. The results showed that arsenic release decreased with temperature, from 15 mg/L at 21°C to 7 mg/L at –2°C, indicating that none of the tested temperatures completely prevented arsenic leaching.

Introduction

The mining industry has a significant positive impact on the Canadian economy, but is also known to generate significant volumes of solid and liquid waste during operations. Of these, waste rock is one of the most important, quantitatively speaking. Waste rock is a non-economic material that needs to be excavated to reach ore-bearing rock. It is usually stored in piles at the surface, where it is exposed to atmospheric conditions. As a result, many waste rock facilities end up generating acid mine drainage (AMD) due to the oxidation of the sulfide minerals. Contaminated neutral drainage (CND) is another type of mine drainage that is also a source of concern. In CND, the pH remains neutral but concentrations of various problematic elements such as arsenic, copper, nickel, lead, and zinc can exceed legislative limits. The focus of this article is on arsenic-contaminated neutral drainage (As-CND), through the study of an arsenic-generating waste rock from a mine located in Arctic conditions.

The studied waste rock material came from a mine in a subarctic environment. The actual mine closure plan consists of reducing the reactivity of the material and, consequently, the As generation, by using an insulation cover. To ensure that the remediation system will work properly, it is important to assess the relationship between temperature and arsenic generation.

In this study, the effect of temperature on arsenic generation was characterized by monitoring leaching columns at different temperatures (21°C, 5°C, and –2°C). These columns were run for 40 weeks. Results were then used to assess the arsenic generation reaction rate as a function of temperature for the tested material using the Arrhenius equation.

Materials and methods

Material selection and properties

The material selected to test the effect of temperature on arsenic leaching (identified hereinafter as NK) was chosen because, according to previous preliminary studies, it was the most at risk to generate arsenic. The material was collected onsite directly after blasting in order to obtain fresh, non-weathered samples. The sample was sieved onsite to produce five different particle sizes: 50–15 mm, 15–5 mm, 5–2.4 mm, 2.4–0.85 mm, and <0.85 mm (Figure 1). The different NK materials were then sent to the *Unité de recherche et de Service en Technologie Minérale – Université du Québec en Abitibi-Témiscamingue (URSTM-UQAT)* laboratory where they were homogenized and characterized.

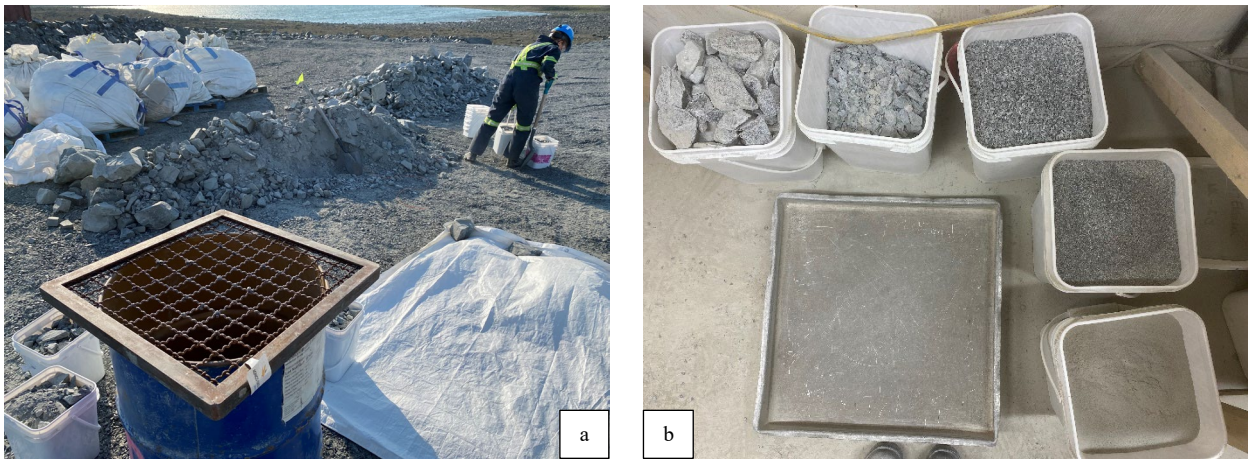


Figure 1: 50 mm hand sieving using a grid placed on a barrel (a) and the result of finer sieving using a mechanical sieve shaker, from left to right: 50–15 mm, 15–5 mm, 5–2.4 mm, 2.4–0.85 mm, and <0.85 mm (b)

The particle size chosen to assess the influence of temperature on arsenic generation was the second finest, between 2.4 and 0.85 mm. This particle size fraction was chosen after several flushes of leaching tests on all the size fractions at laboratory temperature. This choice was made because it offered the best compromise between arsenic leaching and ease of flushing (a pump had to be installed on one of the columns, complicating the collection of leachates).

The relative density and particle size distribution were assessed at the URSTM laboratory. The particle size distribution was obtained by dry mechanical sieving (ASTM D422-63, 2007e2) and laser analysis (Merkus, 2009) with an accuracy better than 1% on particle size estimation, depending on the sample and its preparation (Malvern Instruments Limited, MRK 1954-01-FR-01). Specific gravity (Gs) was measured using a helium pycnometer (ASTM D5550-14, 2014) with an accuracy of 0.003%.

The sulfur and carbon contents, major and trace element contents, acid-generating potential, and sulfur speciation were assessed to characterize the environmental properties of the material. The sulfur and carbon contents were measured using an induction furnace ELTRA CS-2000 Carbon/sulfur determinator (ELTRA GmbH Germany, 2005). Trace and major element contents were measured using inductively coupled plasma atomic emission spectroscopy and mass spectrometry (ICP-AES and ICP-MS) solid analyses and whole rock analyses. Acid generation potential was assessed using the modified Sobek test procedure (Lawrence and Wang, 1997). The sulfate sulfur was determined with a 40% HCl extraction based on Sobek et al. (1978). All chemical analyses were carried out with a relative error of approximately 5%.

The quantitative and semi-quantitative mineralogical analyses consisted of X-ray diffraction (XRD) analyses with the Diffrac.EVA v5.2.03 and Rietveld-TOPAS v4.2 software. The quantification method and automated mineralogy were conducted with a detection limit of 0.5 to 2%, which strongly depended on the crystallinity of the mineral.

The particle size distribution of the material showed a grain diameter at 50% (D_{50}, 50% of the particles have a diameter smaller than this value) of 1.45 mm, a coefficient of uniformity ($C_U = D_{60}/D_{10}$) of 1.67, a coefficient of curvature ($Cc = (D_{30}^2)/(D_{10}/D_{60})$) of 0.97, and a specific gravity (G_S) of 2.86. The material was classified by the USCS classification system as a well graded sand (SW; McCarthy, 2007; ASTM 2021). The hydrogeological characterization showed a saturated hydraulic conductivity of 2.5×10^{-5}m.s^{-1}, an air entry value (AEV is the suction at which the air starts to enter in the saturated material) of 1kPa, and van Genuchten parameters α_{vG} (cm^{-1}), m_{vG}, and n_{vG} of 0.076, 0.866, and 7.478, respectively (van Genuchten, 1980).

The porosity was calculated based on mass-volume relationships at 0.49. The mineralogical composition showed a majority of silicates (56%) with anthophyllite as the main silicate (22%) followed by carbonates (43%) with a group of carbonates undifferentiated by the analytical laboratory as "mixed carbonate" followed by dolomite (5%) and a gersdorffite content of 0.09%.

Other sulfides such as pyrrhotite (0.15%) or pyrite (0.02%) were found in such low concentrations that we considered them negligible for this study. The material showed a Net Neutralization Potential (NNP) greater than +20 kg$CaCO_3$/t, which categorized it as non-acid generating (MEND, 2009); this was validated by a low sulfur concentration (0.1%) and a higher carbon concentration (1.82%). Table 1 summarizes the results of these characterizations.

Table 1: Physical, hydrogeological, chemical, and mineralogical parameters of the material

Parameters	NK 2.4–0.85	Parameters	NK 2.4–0.85
D_{10} (mm)	0.97	S_{tot} (%)	0.10
D_{30} (mm)	1.23	C_{tot} (%)	1.82
D_{50} (mm)	1.45	AP (kg $CaCO_3$/t)	3.1
Cu	1.67	NP (kg $CaCO_3$/t)	151
Cc	0.97	NNP	148
Gs	2.89	NP/AP	49
k_{sat} (m.s^{-1})	2.5x10^{-5}	Gersdorffite (wt%)	0.09
AEV (kPa)	1	Other minerals in order of importance: dolomite, calcite, antophyllite, chlinochlore, biotite, quartz (wt%)	95.9
n	0.49		
α_{vG} (cm^{-1})	0.076		
m_{vG}	0.866		
n_{vG}	7.478		

Water quality measurements from the column tests included pH, oxidation reduction potential (ORP), electrical conductivity, acidity, alkalinity, and elemental concentrations. The pH measurement was performed with a SympHony B30PCI with an accuracy of 0.002 pH units. The same device was used to measure the ORP with a relative precision of 0.2 mV. The electrical conductivity was measured with a VWR Traceable expand range conductivity meter with an accuracy of ±1%. The acidity and alkalinity of each solution were measured with a Metrohm 848 Titrino plus automatic titrator with a relative error of 5%. Inductively coupled plasma optical emission spectroscopy (ICP-OES) analyses were then performed with the Agilent ICP-OES 5800.

Arsenic speciation was defined using the following method. First, the SAX (strong anions) and SCX (strong cations) cartridges were preconditioned with deionized water, methanol, and phosphoric acid; then, 30mL of water sample was passed through the cartridges. Positively charged organic arsenic (V) was retained on the SCX cartridge, while negatively charged inorganic arsenic (V) was retained on the SAX cartridge. Uncharged arsenic (III) was not retained and ended up in the residual water. The various cartridges were then rinsed with acetic and nitric acid to recover the different species (Watts et al., 2010; Bondu et al., 2017; Rakotonimaro et al., 2019). Each sample was then analyzed by ICP-AES to quantify the different arsenic species present in solution.

Column configuration and instrumentation

The columns used for the tests were made of transparent acrylic and were 14 cm wide and 100 cm long. A geotextile was placed at the base of each column to avoid loss of fine particles in the leachates. The columns were filled in 15 to 20 cm lifts. The lifts were put in place by pouring 5 kg of materials and compacting with the energy required to reach the targeted height. The final height of the columns was 90 cm (approximately 20 kg of dry NK materials), yielding a porosity of 0.49. The volumetric water content and temperature were monitored continuously by METER Group Teros 11 (T11) probes with an accuracy of $0.03 m^3/m^3$ and 0.5°C.

A calibration curve was developed to obtain more precise volumetric water content measurements (Cobos and Chambers, HOBO Data Loggers). Temperature was also monitored by a nickel temperature sensor (RT1 sensor from METER Group) with an accuracy better than 1°C. Those sensors were located in the middle of each column, at 45 cm below the surface (Figure 2). The frequency of measurement depended on the stage of the rinse cycle: measurements were taken every 5 minutes during the wetting stage, every hour during the draining stage, and every 4 hours during the drying stage.

Each column was then stored in its environment: the column at 21°C (C4) was stored directly in the laboratory and subjected to the laboratory's ambient temperature; the column at 5°C (C4') was stored in a refrigerator normally used to store liquid samples, where the temperature was maintained at 5°C at all times;

and the column at –2°C (C4") was stored in a large cold room with other columns and other tests in progress, where the temperature was maintained at –2°C.

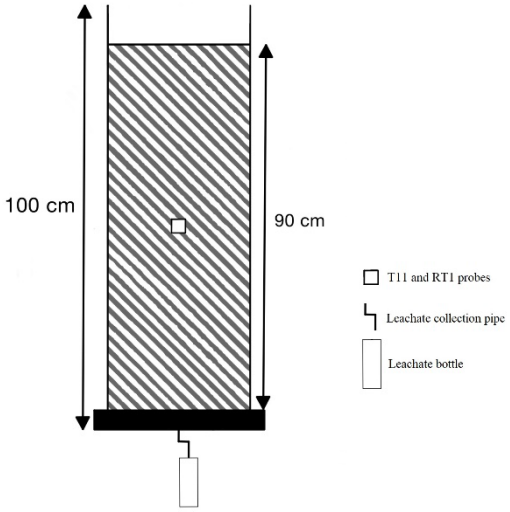


Figure 2: Schematic diagram of a mounted and instrumented column

Flushes were carried out once every fortnight using 1.54L of water; every column underwent 20 rinses. The quantity of water used was selected based on previous studies (e.g., Kandji et al., 2017; Roy et al., 2020, 2023; Poaty et al., 2021) that showed a good correlation between real and laboratory water quality at this flushing volume. Additionally, the selection was based on typical monthly rainfall for rainy months in humid climate conditions (i.e., approximately 100 mm). This wetting period was followed by a drainage period of 24 hours and a drying period of 13 days before the beginning of the next cycle. The column stored at –2°C was thawed for 3 days prior to each rinse and then reinstalled in the cold room for its drying period (Figure 3).

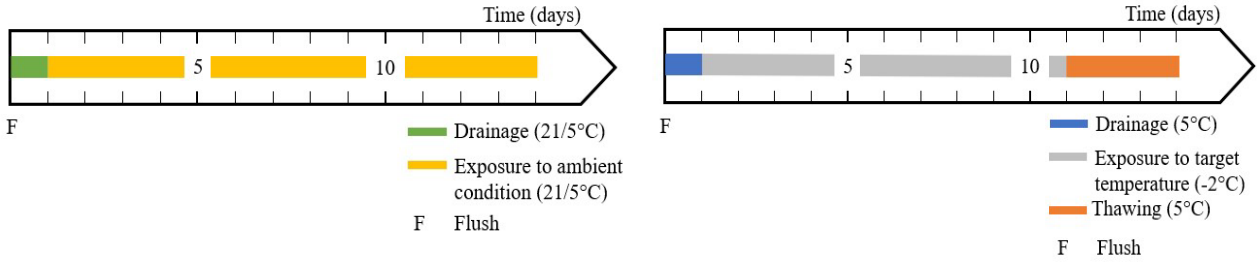


Figure 3: Typical testing cycles at ambient (21 and 5°C) on the left and target temperature (–2°C) on the right

The leachate was collected at the end of the drainage period and analyzed for geochemical parameters including pH, ORP, electrical conductivity, acidity, alkalinity, and dissolved species.

Results

Evolution of temperature

The temperatures monitored throughout the leaching tests are provided in Figure 4. Relatively stable temperatures were observed for the columns stored at 21 and 5°C. Some minor anomalies were observed due to a refrigerator breakdown (i.e., day 42) and power outages for the column at 5°C. For the column stored at 21°C, we observed a maximum of 23.5°C, a minimum of 18.2°C, and an average of 20.6°C. For the column stored at 5°C we observed a maximum of 8.0°C, a minimum of 2.9°C, and an average of 4.4°C.

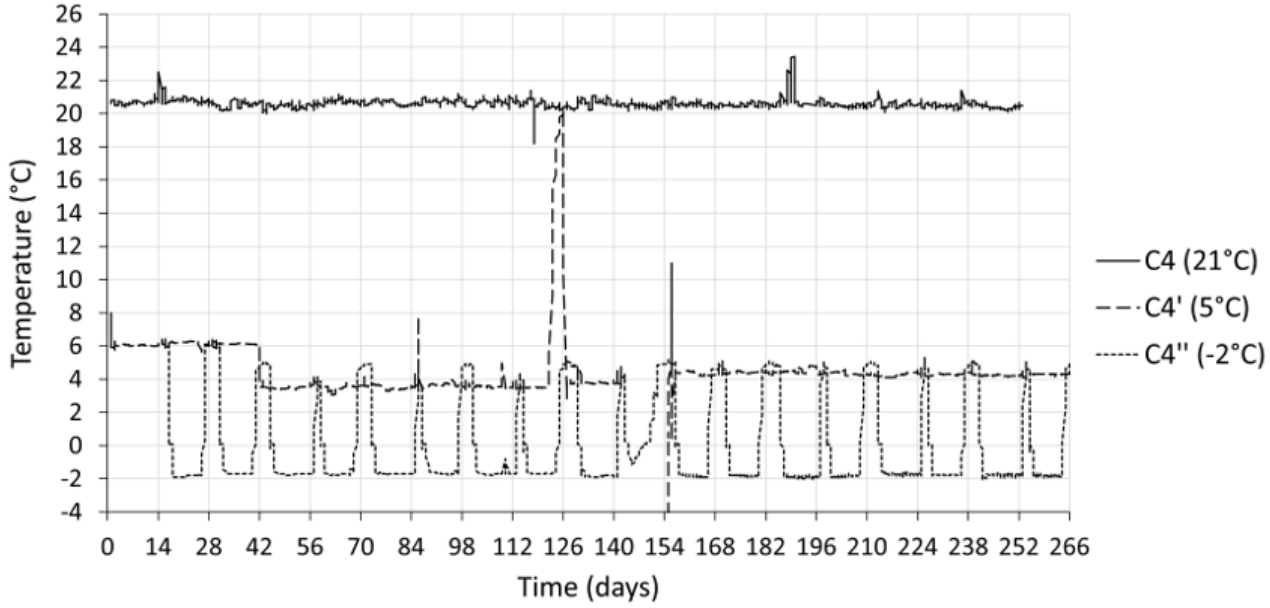


Figure 4: Evolution of the temperature during the experimentation

Figure 4 also shows the freeze-thaw cycles that were applied to the column at –2°C. Thawing events were performed at a temperature of 5°C for 3 days before the column was returned to the cold room at –2°C after the drainage phase. For this column, we observed a maximum of 6.1°C, a minimum of –2.0°C, and an average of –1.7°C when stored in the cold room and 4.8°C when stored in the 5°C environment.

Evolution of water quality

Changes in physicochemical parameters and water quality over the course of twenty rinses (266 days) are presented in Figure 5.

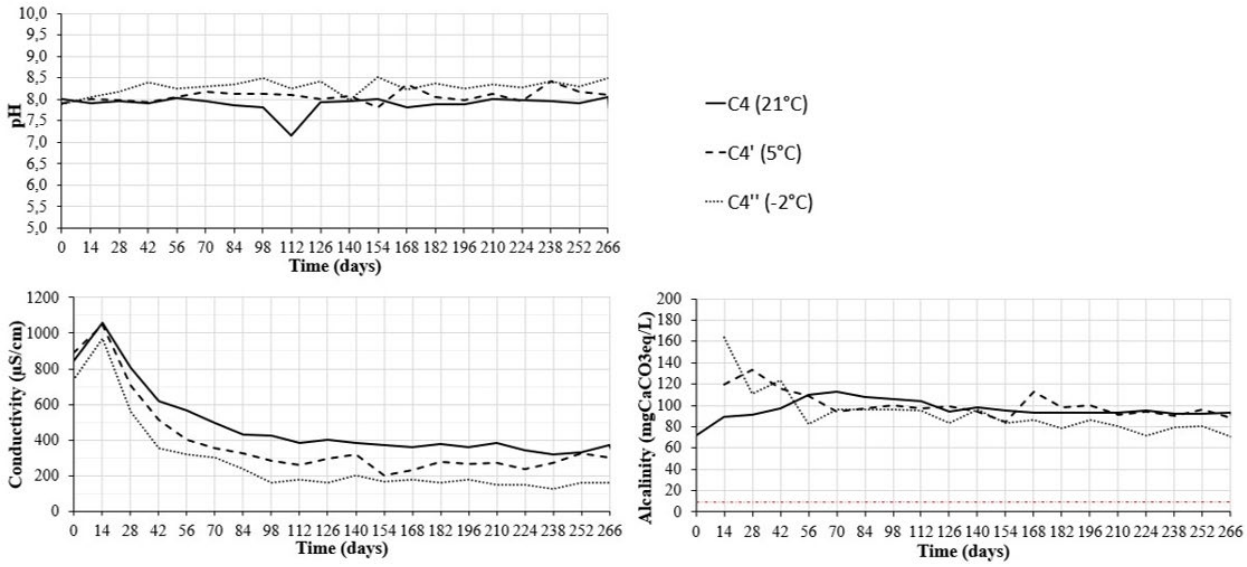


Figure 5: Evolution of pH, electrical conductivity, and alkalinity during the column tests

The pH showed a stable and similar trend for all three temperatures: it ranged from 7.2 to 8.5, with an average of 7.9, 8.1, and 8.3, respectively, for 21, 5, and –2°C. The redox potential (not shown here) showed no particular trend and ranged from 731 to 396 mV, with an average of 619, 570, and 564 mV, respectively, for 21, 5, and –2°C. The electrical conductivity of the three columns followed a similar pattern, starting at relatively high values of approximately 1,000 µS/cm before stabilizing around 400, 300, and 200 µS/cm for temperatures of 21, 5, and –2°C, respectively.

Acidity (not shown here) was systematically measured at less than 10 $mgCaCO_{3eq}/L$ for the three temperatures. Alkalinity showed a relatively stable trend at around 100 $mgCaCO3_{eq}/L$ for the three temperatures (96 for 21 and 5°C, and 84 for –2°C; see Figure 5).

Evolution of arsenic quantities and arsenic speciation

Arsenic was the main element of concern in this study. The quantity of arsenic in the leachates was monitored every fortnight until stabilization and then every month thereafter. The results shown in Figure 6 exhibit similar trends for columns C4 and C4', where a rapid increase in arsenic concentration during the first rinses was observed, followed by a stabilization. Column C4'' had a different behavior, with a progressive increase in arsenic concentrations followed by a stabilization. Stabilized arsenic concentrations were 16, 14, and 7 mg/L for the columns at temperatures of 21, 5, and –2°C, respectively. Based on the observed results over the entire test period, the arsenic generation rate was 32, 25, and 24 mg/kg/week for the 21, 5, and –2°C columns, respectively.

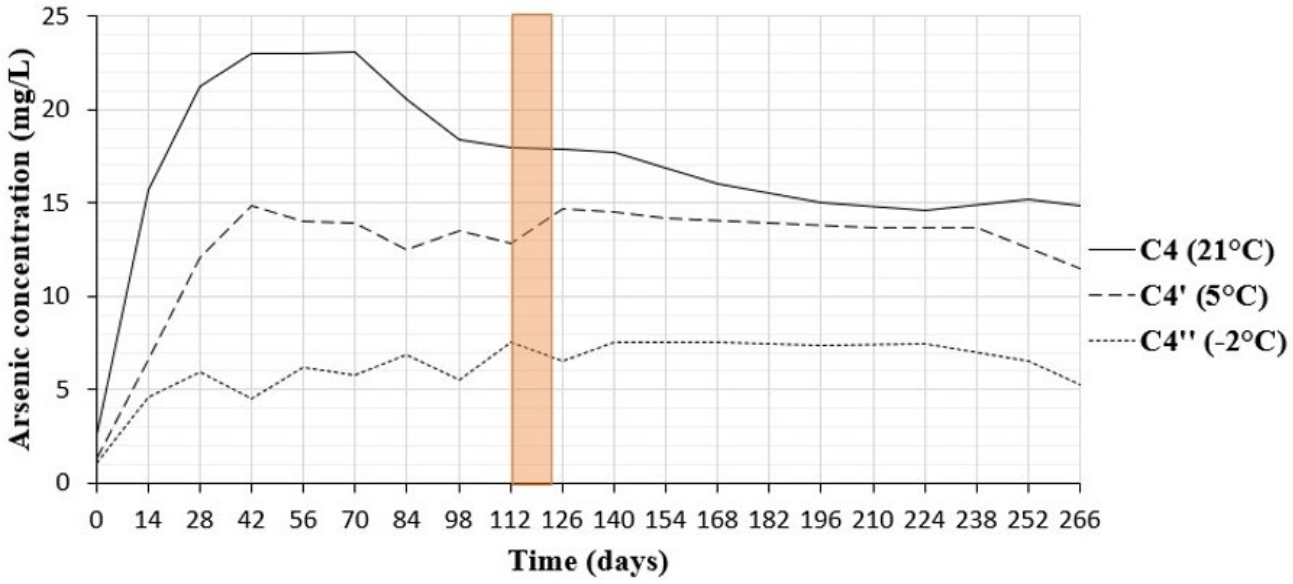


Figure 6: Arsenic concentrations during the experiment. The colored band shows when the arsenic speciation analyses were carried out

Using Eh and pH data and Pourbaix diagrams (Figure 7a), it was hypothesized that arsenic was found mainly in the form of $HAsO_4^{2-}$ or in the form of As(V) arsenates. Water concentrations of other metals were also measured, but showed low values, as for iron, where the concentration varied between 0 and 0.015 mg/L for the three columns. Although concentrations are low, we are in the hematite precipitation range (Figure7b), which could affect not only the amount of iron present in the water, but also the amount of arsenic, as iron oxyhydroxides can sorb and/or coprecipitate arsenic.

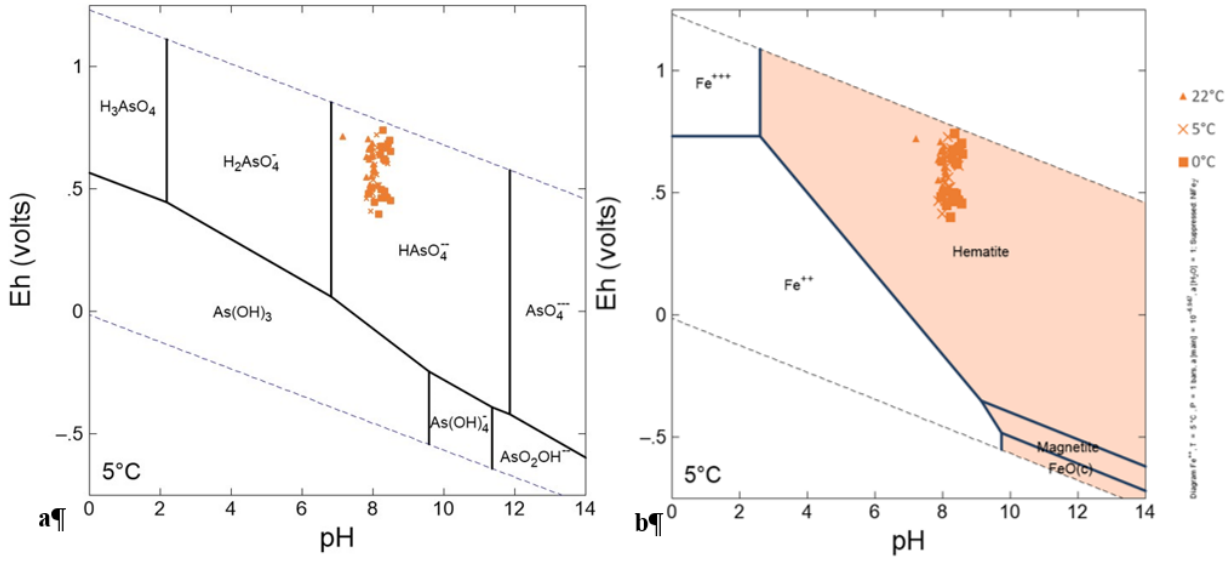


Figure 7: Plotting of Eh and pH values measured during the tests in a Pourbaix diagram for an average arsenic concentration (a) of 8.51x10^{-5}mol/L and iron concentration (b) of 1.13x10^{-7}mol/L at 5°C and 1 bar

The Pourbaix diagram presented in Figure 7 was constructed using the Geochemist's Workbench software for typical arsenic concentrations (8.51×10^{-5}mol/L) and iron concentrations (1.13×10^{-7}mol/L) found in the samples at 5°C and 1 bar.

These data for arsenic speciation were obtained by using Bond Elut SAX and SCX ion exchange cartridges to separate As(III) and As(V) in the leachates. ICP-OES analyses showed less than 0.15% of the total As was in the As(III) form, confirming the results predicted with the Pourbaix diagrams.

Conclusion

The three column tests showed that the pH remained stable during the testing period at values close to 8, regardless of temperature. These results were expected considering the low acid generating potential of the NK material. Water quality measurements also showed that Eh, acidity, and alkalinity were not significantly affected by temperature. However, electrical conductivity tended to fall as temperature decreased. The total mass of As decreased with decreasing temperature. The stabilized concentrations were similar (≈15 mg/L) at 21 and 5°C, and lower (≈6 mg/L) at –2°C.

Reducing the storage temperature of As-CND-generating waste rock that contains gersdorffite from a mine located in a cold region does not appear to be sufficient to totally prevent arsenic production in leachates when water percolates through the waste rock, unfrozen for a short period of time. This implies that to eliminate the risk of arsenic generation, the pore water within the waste rock facilities would have to stay continuously frozen. This requires that an insulation cover placed on top of this waste rock unit must have a configuration and thickness that is optimized to contain the active layer within the cover materials. This condition should be met for the actual climate context, but also for future climatic conditions that will be affected by climate change.

Results presented in this article are integrated into a larger study on the As leaching potential of waste rock located in cold climatic conditions. Presently, other column tests are being analyzed to assess the influence of grain size distribution. The column test results will also be used to calibrate a reactive transport model with the MIN3P software (Mayer et al., 2018). The calibrated model will then be used to make long-term projections for more realistic geometries and climate conditions.

Acknowledgements

This work was made possible thanks to the financial support of the NSERC-UQAT Industrial Chair on Mine Sites Reclamation funded by the Natural Sciences and Engineering Research Council of Canada (NSERC) and five industrial partners: Agnico Eagle Mines, Iamgold, Rio Tinto Iron and Titanium, Raglan Mine a Glencore company, and Newmont. The authors would also like to thank the URSTM-UQAT staff for their

assistance with laboratory work and the mine staff for their support and provision of equipment and materials.

References

ASTM. 2007e2. Standard Test Method for Particle-Size Analysis of Soils (D422-63) (Withdrawn 2016). ASTM International.

ASTM. 2014. *Standard Test Method for Specific Gravity of Solids by Gas Pycnometer* (D5550-14). ASTM International.

ASTM. 2021. *Standard Test Method for Particle-Size Distribution (Gradation) of Soils Using Sieve Analysis* (D6913-17). ASTM International.

Bondu, R., Cloutier, V., Rosa, E. and Benzaazoua, M. 2017. *Mobility and speciation of geogenic arsenic in bedrock groundwater from the Canadian Shield in western Quebec, Canada*. *Science of the Total Environment* 574: 509–519.

Cobos, D. and Chambers, C. *Calibrating ECH$_2$O Soil Moisture Sensors Application Note.* HOBO Data Loggers.

ELTRA GmbH Germany. 2005. *Operation Manual,* Germany.

Lawrence, R.W. and Wang, Y. 1997. *Determination of neutralization potential in the prediction of acid rock drainage*. *Proceedings of International Conference on Acid Rock Drainage (ICARD),* Vancouver, BC, Canada: 451–464.

McCarthy, D.F. 2007. *Essentials of Soil Mechanics and Foundations: Basic Geotechnics.* Upper Saddle River: Pearson Prentice Hall.

Mayer, K.U., Xie, M. and Su, D. 2018. MIN3P-THCm a three-dimensional numerical model for multicomponent reactive transport in variably saturated porous media. Theory Manual.

MEND. 2009. Prediction manual for drainage chemistry from sulphidic geologic materials. 1.20.1: 579.

Merkus, H.G. 2009. *Particle Size Measurements.* Springer.

Rakotonimaro, T.V., Guittony, M., Neculita, C.M., Trépanier, F. and Pépin, G. 2019. Evaluation of arsenic leaching potential in gold mine tailings amended with peat and mine drainage treatment sludge. *Journal of Environmental Quality* 48: 735–745.

Sobek, A.A., Schuller, W.A., Freeman, J.R. and Smith, R.M. 1978. Field and laboratory methods applicable to overburdens and mine soils. Environmental Protection Technology Series. U.S. Environmental Protection Agency, Washington, DC.

van Genuchten, M.T. 1980. A closed-form equation for predicting the hydraulic conductivity of unsaturated soils. *Soil Science Society of America Journal* 44(5): 892–898.

Watts, M. J., O'Reilly, J., Marcilla, A.L., Shaw, R.A. and Ward, N. I. 2010. Field based speciation of arsenic in UK and Argentinean water samples. *Environmental Geochemistry and Health* 32: 479–490.

Lessons Learned from Designing a Soil Cover System for a Tailings Storage Facility Exposed to an Arid Climate

Vincent Castonguay, AtkinsRéalis, Canada
Elissar Ozeir, AtkinsRéalis, Canada
Miguel Medina, AtkinsRéalis, Canada
Fannie Lessard, AtkinsRéalis, Canada

Abstract

Designing an efficient soil cover system for a tailings storage facility (TSF) is crucial for long-term reclamation. The efficiency of a soil cover system depends on factors like the nature of the mine waste, local climate, and regulatory objectives. Modern design relies on numerical modeling using 1D, 2D, or 3D domains, as well as incorporating climate conditions as flux boundary conditions. Sensitivity analyses help us to understand the dynamics of cover system elements by altering soil water retention and hydraulic conductivity curves, layer thicknesses, and geometrical arrangements. These simulations are challenging due to extended run-times, complex results, and large data volumes.

The authors recently conducted a conceptual study for the design of a soil cover system for a TSF in an arid climate to reduce tailings infiltration and manage surface runoff. Two distinct cover systems were proposed and applied at strategic locations on the TSF: a store-and-release (SR) concept, and a flow control layer (FCL) with drainage ditches. Groundwater flow simulations were conducted using GeoStudio's SEEP/W module. The arid climate's sudden precipitation patterns required careful consideration of time step size, convergence criteria, and geometry adjustments. Boundary condition setups were trialed to reflect the effect of the drainage ditches accurately. The hydrogeotechnical properties' uncertainty was addressed through sensitivity analyses. This paper reviews the challenges faced while performing the numerical modeling required for the conceptual study and provides recommendations for similar analyses.

Introduction

Description of the mine site

This study is conducted for designing a soil cover system for a tailings storage facility (TSF) located in a region subjected to an arid climate. The TSF has a rectangular shape with peripheral dikes and an area of

around 400 ha. Over the years, several dams were built to manage the tailings deposition. The tailings and process water are deposited on alternating sides of the TSF using the central deposition method. The tailings have little to no potential for acid mine drainage (AMD) generation and show arsenic leaching potential. Cyanide contamination could occur in the short to medium term and it is carefully monitored for.

Climate conditions

The TSF is exposed to a semi-arid climate characterized by an intense rainy season, where high rainfall events are measured over short periods of time. The potential evaporation greatly exceeds rainfall on a yearly basis. The average annual rainfall and evaporation at the site are approximately 430 mm and 3,000 mm, respectively. Strong seasonality is observed; most of the annual rainfall occurs from June to September, during the summer months. However, the potential evaporation being substantially higher than rainfall results in an overall negative water balance for the entire year. Figure 1 shows typical daily temperature, rainfall, humidity, and wind speed readings recorded at the mine site over a typical year.

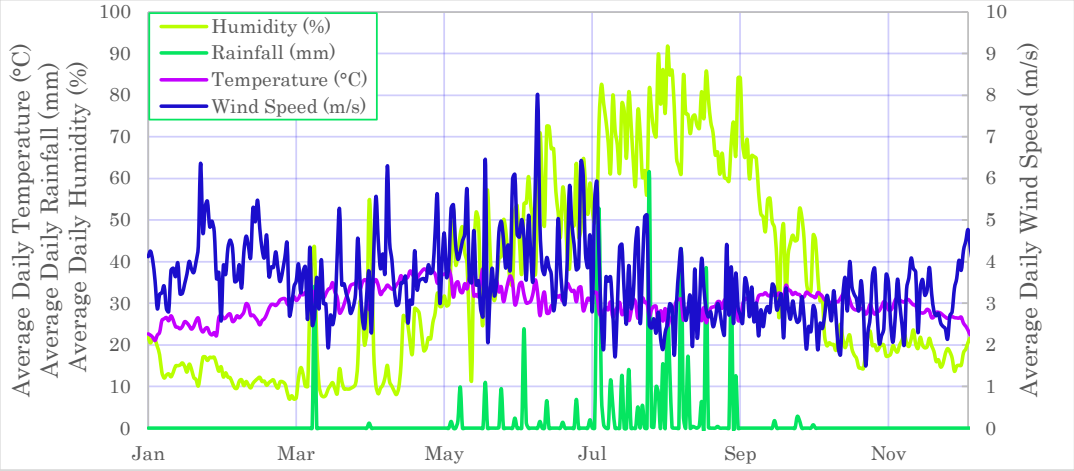


Figure 1: Typical climatic conditions recorded at the mine site

Soil cover systems

The main design objectives of soil cover systems are to limit water percolation into the tailings, ensure efficient surface water drainage, limit wind erosion, promote beneficial land use for local communities, and ensure long-term stability and sustainability with minimal maintenance requirements, all while being adapted to the specific environmental conditions of the site. In arid or semi-arid climates, cover systems experience extended dry periods, which significantly impacts evapotranspiration. However, subjecting the cover system to evaporative demands can be beneficial in such climates, leading to reduced infiltration into the underlying waste material (Bussière and Guittonny, 2021). The store-and-release (SR) cover system relies on the cover material's ability to retain sufficient moisture. Water infiltrating the cover system is "stored" within the cover material during wet periods and subsequently "released" into the atmosphere

through evapotranspiration during dry periods. As a result, net percolation into the underlying waste is minimized, making the SR cover system an appropriate option for arid climates. A typical SR cover consists of a SR layer (usually a fine-grained soil) placed over a capillary break (CB) layer (usually a coarse-grained material). The CB is created by the difference in hydraulic properties between the layers, particularly the pore size, which disrupts capillary action and effectively limits water infiltration. The flow control layer (FCL) with CB is another suitable cover system for a mine site subjected to an arid climate. The principle of the FCL relies on the capillary break effect to ensure a lateral deviation of rainfall water toward drainage ditches and prevent deep water percolation into the underlying waste material, as well as minimize soil erosion. This cover system is generally composed of a coarse-grained material (lower layer) to allow a rapid lateral transport of the water and a fine-grained material (upper layer) to create the CB and limit water infiltration. These two soil cover systems were studied for the TSF discussed in this paper.

Numerical model setup

Distinct numerical models were set up to evaluate the performance of the two soil cover systems designed for the site. While the materials used for both models were identical, the geometry definition and the boundary conditions used differed. The following sections detail the methodology followed for the study.

Methodology

The numerical simulations of water flow through the soil cover and the tailings are carried out using the SEEP/W module from GeoStudio (Seequent. 2024). The transient water flow dynamics in unsaturated soils was analyzed through finite element calculations, over a simulated period of 7 years to consider a wide range of possible climatic conditions. The steps carried out for these analyses are as follows: geometry and mesh definition; boundary and initial conditions definition; materials definition; time step adjustment; model convergence check; water percolation calculation.

Geometry definition

Geometry simplification is essential in numerical analysis, especially in preliminary engineering phases where laboratory data for hydrogeotechnical properties are not yet available, such as is the case for this project. Using a detailed 3D model for a complex mine site can sometimes create more problems than it solves. Simplifying the site into 2D or even 1D domains is often essential. While oversimplification is a risk, a 1D analysis can be useful for infiltration-percolation studies, helping identify potential convergence issues with complex boundary conditions. This study uses a 1D domain of the proposed SR cover system (Figure 2), consisting of 0.7 m of sand and 0.3 m of gravel. The lower portion of the domain consists of 9 m of tailings representing the mine waste deposit to be covered.

Vertical percolation is assumed to be the dominant seepage mechanism for the portions of the TSF where the SR cover system is used. The lateral slope in these areas is negligeable compared to the site extent. Since lateral flow should be minimal, the 1D idealization is deemed acceptable.

The second geometry defined for this study is a 2D representation of the proposed FCL cover system, consisting of the same material layers configuration used for the SR cover. The combination of an inclined surface and an effective capillary barrier promotes lateral flow through the upper sand layer toward a drainage ditch. These drainage ditches are to be located at regular intervals throughout the proposed FCL cover. Hence, only a cross section of the TSF is modeled, as shown in Figure 3.

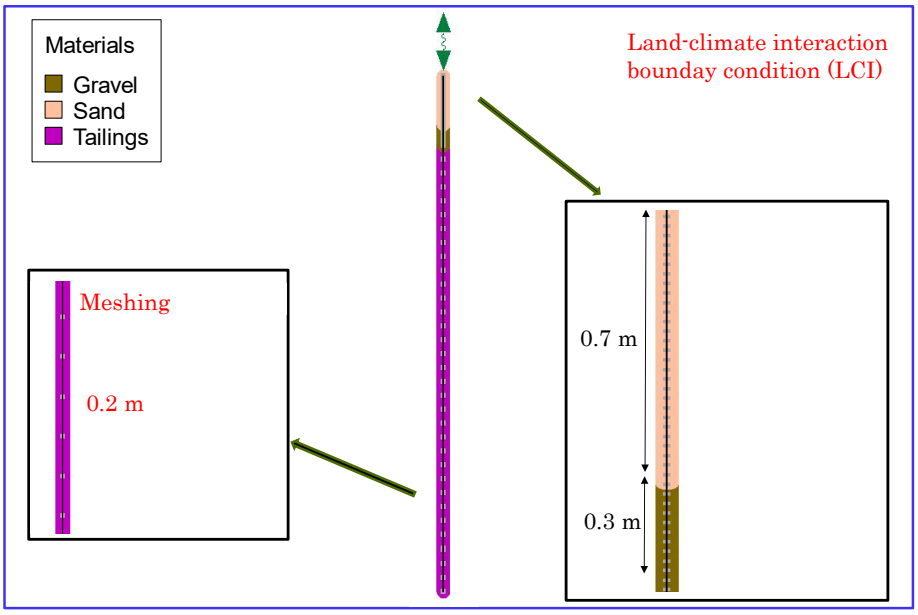


Figure 2: 1D geometry of the store and release cover system, meshing and boundary conditions

Finite elements mesh and time steps

Defining a high-quality mesh and associated time step size is paramount for the performance of any finite element analysis, whether in terms of solution accuracy or run-time. Mesh refinement is especially important at the top of domains where transient boundary conditions are applied, as is the case for this study. Where water transfers are not as important, a coarser mesh should be defined to promote faster solving. Time step size should be defined proportionally to the mesh density. Finer meshes will require smaller time steps, and conversely, so that convergence issues are avoided.

Meshing for both geometries defined for this study is shown in Figures 2 and 3. For the 1D geometry (Figure 2), the mesh size is set at 0.006 m for the sand and gravel layers. While a 0.01 m mesh size is generally a good starting point when land-climate interaction boundary conditions are used, it was decided to use a finer mesh to solve convergence issues (discussed further down). The mesh size is set at 0.2 m for the tailings layer, where water transfers are less important than in the upper layers.

For the 2D geometry (Figure 3), the mesh size is set at 0.1 m by 1 m. This mesh is considered relatively coarse, especially when compared to the 1D geometry. Since water flow can occur both vertically and laterally in 2D, convergence is not a concern as it can become in 1D. The coarser mesh size defined in 2D also promotes faster run-time, which can become substantial for such large domains.

Finally, time steps are set at 1 h for both geometries. Calculation results, however, are only saved every 24 steps, which amounts to a single save point per day. Given that the simulations cover a 7-year period, saving results every time step would result in over 60,000 save points, at every node in the domain. Saving every 24 steps reduces the number of saved points to around 2,500, which is more manageable. Note that the climate data used to define the land-climate interaction boundary condition varies daily.

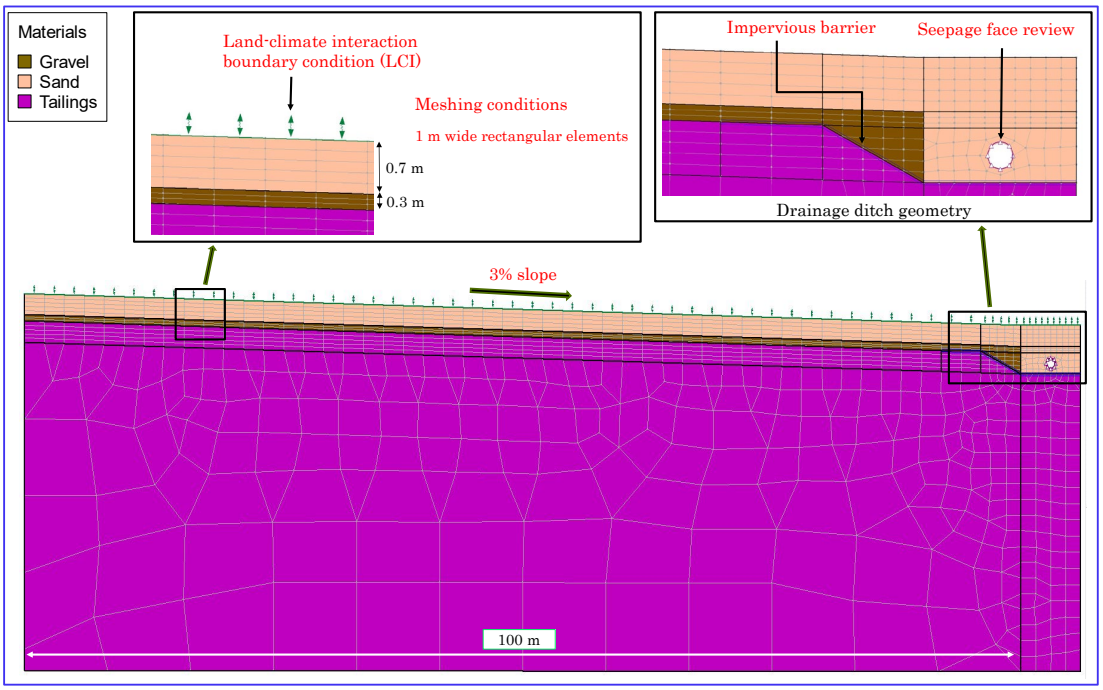


Figure 3: 2D geometry of the flow control layer cover system, meshing and boundary conditions

Boundary conditions

Similarly to defining meshing conditions, accurately defining boundary conditions is an essential step in any numerical model. Poorly defined boundary conditions significantly impact the simulation results and lead to misinterpretation of the physical situation that is modeled. These input parameters must be carefully thought through to simulate realistic study conditions.

For the two soil cover system designs, a land-climate interaction (LCI) boundary condition was applied to the very top of the domain. This boundary condition simulates actual climatic conditions measured at the site over a 7-year period, requiring the compilation of temperature, humidity, rainfall, solar

radiation and wind speed data for the period considered. Transpiration through root uptake was neglected at this stage of the engineering design process.

For both geometries, the bottom of the domain is considered impervious to represent the presence of a geomembrane installed at the bottom of the TSF on top of the natural foundation. Although it is expected that some water flow will occur through the geomembrane, it is numerically convenient to assume it to be completely impervious at this stage of the engineering design process.

Finally, the 2D model for the FCL cover system includes a drainage ditch to be lined locally with a geomembrane which will be installed on top of the tailings deposit. A drainage boundary condition is applied to the drain itself, which allows water flow when the pore water pressure at the interface reaches 0 kPa.

Initial conditions

Transient analyses require initial conditions. These generally come from a parent steady state analysis, or another transient analysis. For this study, transient "spin-up" analyses were set up for both geometries used. These analyses include the LCI boundary condition to be used for the 7-year analyses, but only applied for a limited 1-year period. The spin-up analyses are initiated using a parent steady state analysis where a 1 m total head boundary condition is applied at the bottom of the domain. The goal of the spin up analyses is to mitigate the impact of the steady state initial conditions used by letting the porewater pressure and water content within the domain respond to a full year of climate data. The results of the spin-up analyses are passed down to the child 7-year transient analyses and serve as initial conditions. Whenever LCI boundary conditions are used, spin-up analyses should be used, unless the initial conditions can be properly defined otherwise. This type of analysis is also very common for numerical simulations of thermal flow problems.

The version of GeoStudio used (2024.1) does not support spin-up analyses natively. If a parent spin-up analysis feeds its results to a child transient analysis, this analysis' start time will obligatorily be tied to the spin-up analysis. So, a 1-year spin-up analysis will force the subsequent 7-year analysis to start at the 1-year mark. Fortunately, a workaround is possible: if the spin-up analysis lives in another file, then GeoStudio allows for the transient analysis' start time to be reset to whatever value is desired by the user.

Materials definition

One of the major challenges in this study arises from the limited hydrogeotechnical data available for on-site materials. To generate the water retention curves and hydraulic conductivity functions for the simulated materials, estimation tools available in SEEP/W were used at this preliminary engineering stage. Grain-size distributions available for on-site materials were used to define the soil water retention curves and hydraulic conductivity functions shown in Figure 4 via SEEP/W's estimation functions. As shown in Figure 4, a sand material is defined, and two gravels are considered.

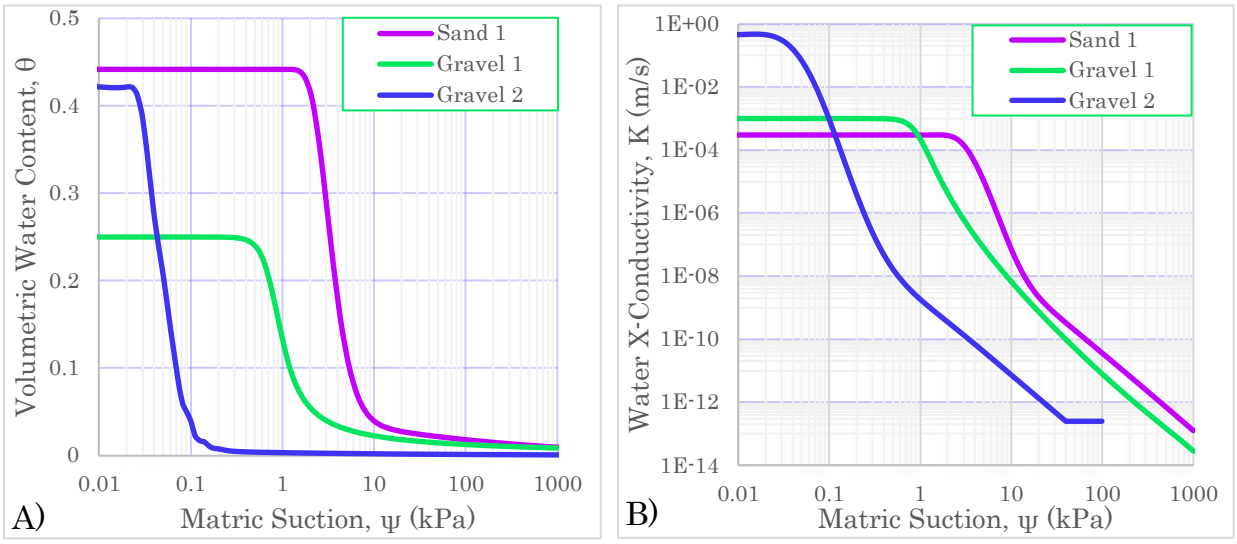


Figure 4: Soil water retention curves (A) and hydraulic conductivity functions (B)

Challenging numerical results in 1D

Extensive numerical simulations using the simpler 1D geometry ensured a proper understanding of the flow dynamics affecting the cover system before transitioning to the more challenging 2D geometry. Initiating modeling with a 1D domain facilitates detection of numerical challenges arising from complex boundary conditions. For infiltration-percolation analyses, applying the land-climate interaction (LCI) boundary conditions is crucial to simulate realistic study scenarios. However, such conditions can bring significant numerical issues due to the intrinsic temporal fluctuations of the climate data.

While 1D modeling significantly simplifies the numerical exercise, it does not prevent convergence issues. Monitoring convergence is essential to achieve accurate results. The use of LCI boundary conditions renders convergence monitoring even more resource intensive than for other types of analyses: unconverged pressure head nodes must be monitored, together with water balance checks.

Water balance interpretation

To assess the performance of the studied soil cover system, water percolation was calculated based on the water balance results obtained from the numerical model. In Figure 5, results for cumulative rainfall, runoff, infiltration, evaporation and percolation are shown for a full year. Infiltration refers to any water entering the domain via the soil-climate interaction boundary condition. Whenever the top node of the domain is unsaturated, infiltration is possible if rainfall occurs. If the top node is saturated, runoff occurs. Percolation represents water that infiltrates through the sand and gravel cover layers and penetrates the underlying tailings. A performant design minimizes percolation. Percolation being a subset of infiltration, it is always less than or equal to infiltration, and does not contribute to the overall water balance.

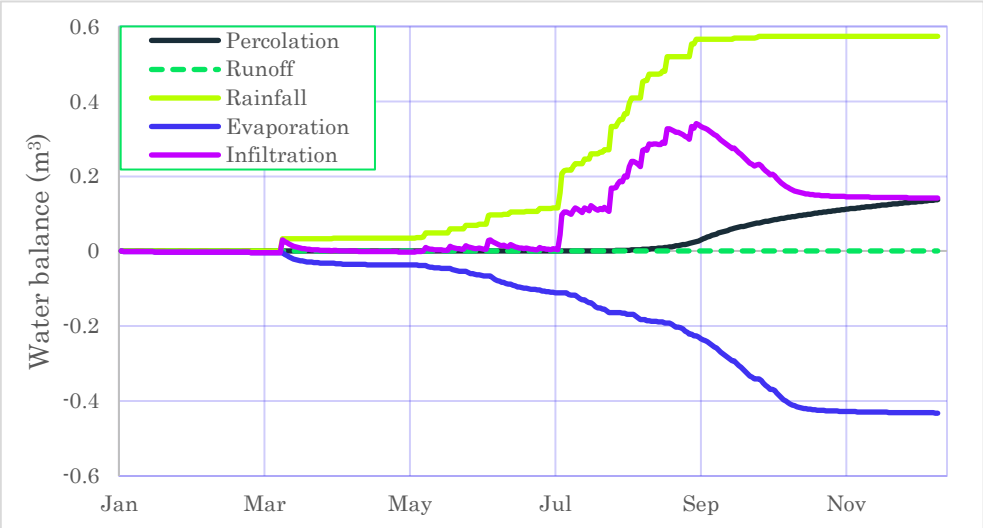


Figure 5: Water balance at the tope node of the 1D domain

As part of the convergence check requirements, the sum of infiltration, evaporation and runoff must be equal to rainfall. Water change in the domain via the boundary conditions must also be checked: the cumulative water mass transiting through boundary conditions (the LCI boundary condition in this case) must be equal to the cumulative change in water mass inside the domain. The error between these two measures must be minimized by appropriately adjusting the time steps, mesh size and convergence criteria.

Challenging convergence

Together with water balance convergence, pressure head convergence must also be monitored to ensure accurate results. By plotting the number of unconverged pressure head nodes for each solve step, remediation actions can be taken if non convergence is observed. As described by Castonguay (2023), unsaturated flow calculations are inherently prone to convergence issues because of the iterating procedure required to solve the finite element equations when nonlinear hydraulic conductivity functions are used.

To remediate pressure head convergence issues, the under-relaxation criteria used in SEEP/W can be altered. By setting the initial rate and minimum rate of under-relaxation to 0.65 and 0.01, respectively, the solver will inject a larger proportion of the previous calculated results into the current results to cautiously proceed toward the appropriate solution. This adjustment should be made to the solver's parameters whenever repeated substitution is observed when inspecting the unconverged pressure head plot.

Very low unsaturated hydraulic conductivity values should also be removed from the materials' definition if they cause convergence issue. This can be readily viewed when inspecting the hydraulic conductivity plot displaying the target functions versus the used functions. As a rule of thumb, hydraulic conductivities lower than $1x10^{-13}$ m/s can generally be removed without much effect on the general results.

Even when no pressure head convergence issues are apparent, water balance error can still occur. Rounding errors resulting from the application of the convergence criteria used in SEEP/W can sometimes cause these errors. From one iteration to the next, pressure head values at a given node will be deemed "converged" if equal once rounded down to two significant digits (default value). For most larger-scale flow problems, this is acceptable. However, it might be quite different for smaller-scale flow problems, such as those where LCI boundary conditions are applied to regions meshed at 0.01 m (or lower) intervals. Significant rounding errors can arise when accumulated over the numerous time steps used for LCI-type simulations. Increasing the convergence criterion relating to significant digits to a larger value is a way to minimize these possible rounding errors, which become apparent when monitoring the water balance.

Failure to meet the objectives of the soil cover system

The water balance results (Figure 5) showed percolation rates into the tailings reaching above 20 % of the total rainfall, irrespective of the available gravel material options used. Using the sand and gravel materials readily available at the mine site without any modification to their original grain size, although practical and economical, does not lead to adequate performances for the cover system. In this context, synthetic hydrogeotechnical properties for the granular materials were devised to perform sensitivity analyses and identify material combinations that would lead to adequate performance in terms of percolation through the tailings. Two new water retention curves and hydraulic conductivity functions were generated for both the Sand 1 and the Gravel 1 materials. The original curves were translated horizontally by 40% and 250%, as shown in Figure 6.

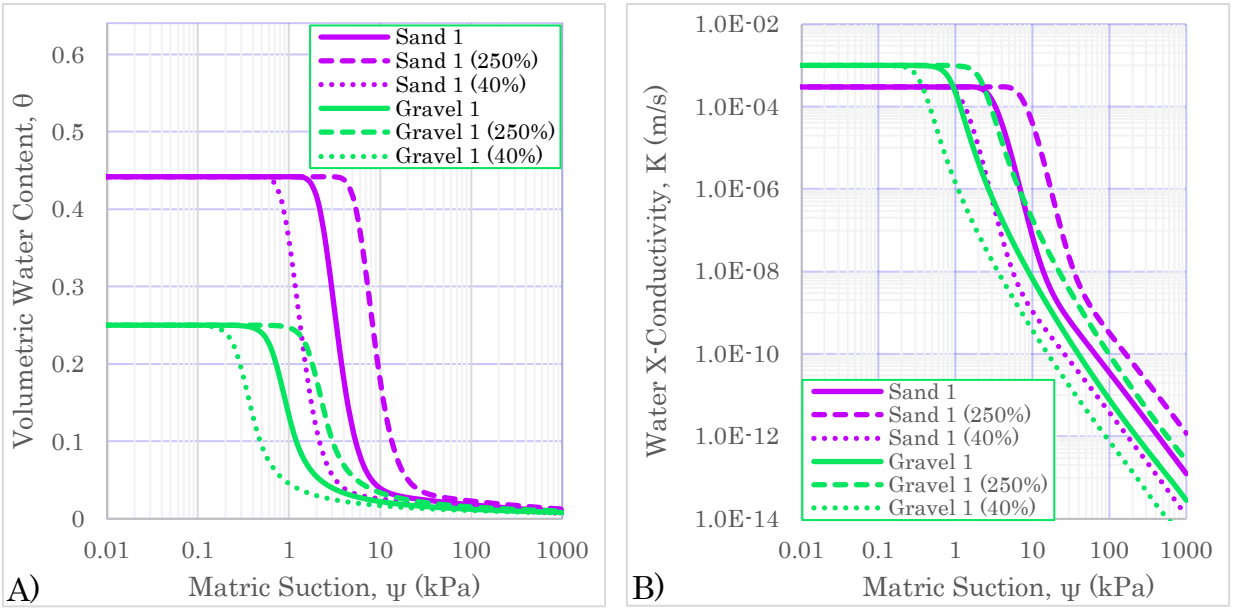


Figure 6: Soil water retention curves and hydraulic conductivity functions for site/existing and synthetic materials

The proposed water retention curves and hydraulic conductivity functions were intentionally designed to create and control the relative size of the capillary break zone between the two cover materials. Capillary break occurs when an underlying material becomes less permeable than its overlying counterpart as matric suction increases. For example, the capillary break zone that exists between the original Sand 1 and Gravel 1 materials extends from matric suction values of 1 kPa and larger. The thickness of this capillary break zone is however quite modest, which results in very comparable hydraulic conductivities, even when the capillary break exists.

On the other hand, the capillary break zone for Sand 1 (250%) and Gravel 1 (40%) extends from matric suction values of 0.4 kPa and larger, and is of very large size, creating a significant hydraulic conductivity contrast between the two materials at any given matric suction larger than 0.4 kPa. The new water balance results obtained from these sensitivity analyses yield significant improvements in the cover system performance. Very low percolation rates were observed, particularly for material pairs which showed larger capillary break zones.

Challenging numerical results in 2D

The experience gained through the 1D numerical analyses was used to tackle the increased complexity of the flow control layer cover system's 2D geometry. Irrespective of convergence issues that still might arise both in 1D and in 2D geometries, the latter brings additional challenges in terms of managing extended run-time and file size. A full 7-year numerical simulation would now extend beyond a 24-hour run time and create file size reaching over 10 GB. While extended run times can be managed through careful planning, heavy file sizes can pose significant performance issues when viewing and plotting simulation results.

Convergence issues remain one of the main challenges for 2D geometries. Close examination of the results often reveals that non-convergence arises on days where rainfall becomes suddenly intense. The sudden and stark changes in rainfall quantities inherent to the site's climatic conditions heavily contribute to numerical instability. To tackle these convergence issues, time step sizes were reduced for periods where intense rainfall occurs, which further exacerbates the already extensive run times.

An additional challenge for 2D simulations relates to meshing conditions. While generating good quality meshes is straightforward for simple geometries, integrating complex geometry features like a drainage ditch makes meshing intricate and requires careful consideration. Rectangular finite elements generated by SEEP/W's "surface layers" tool are generally easier to work with for LCI type problems, as they allow for easy mesh discretization in the vertical direction and larger dimensions in the horizontal direction. This will however only work well if the 2D geometry does not include more complex geometry features. In such cases, clever meshing strategies must be devised to obtain an efficient mesh, such as specifying the number of divisions on lateral sides of regions and forcing the use of rectangular elements.

Requirement for a drainage ditch

To simplify 2D domains, the model geometry is defined as a slice of the real field geometry. But where should the geometry extend to? A reflex might be to model a section where no feature intersects the geometry, making it representative of field conditions between distinct structures (like dykes or drainage ditches). This would be ideal if there was a way to allow lateral water flow in and out of the sides of the 2D geometry to represent an infinite domain. However, no such boundary conditions exist. The "drainage" boundary condition, which allows water to flow out of the domain, is not suitable as it only permits water to exit if the pore-water pressure reaches 0. Figure 7 shows the right-side edge of the 2D geometry where a drainage boundary condition is applied to the lateral edge of the sand and gravel layers. During a high rainfall event around the 195-day mark, saturation increases in front of the drainage boundary condition, but since complete saturation is never reached, the drainage boundary condition does not allow water to seep out. Instead, water travels downward and backward, breaching the capillary break and promoting percolation toward the tailings, as shown in Figure 8A.

For this project, the only efficient way to account for lateral flow at the edge of the 2D domain was to properly model a drainage ditch, as shown in Figure 3. Lateral water flow exits the domain via the drainage boundary condition inside the ditch. The impervious bottom (geomembrane) of the ditch allows water to accumulate and eventually exit the domain via the drainage boundary condition. Figure 8B shows how water flows to the drain instead of through the tailings once the drainage ditch is modeled.

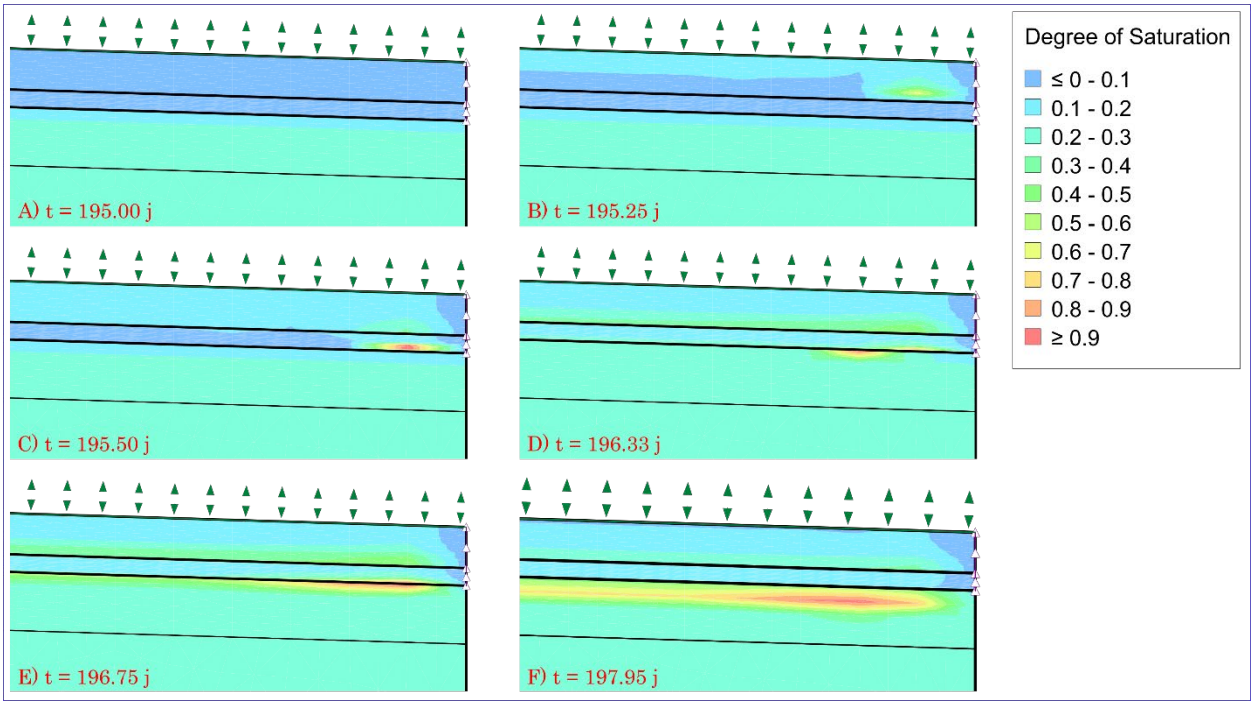


Figure 7: Retro-saturation of the flow control layer caused by the drainage boundary condition

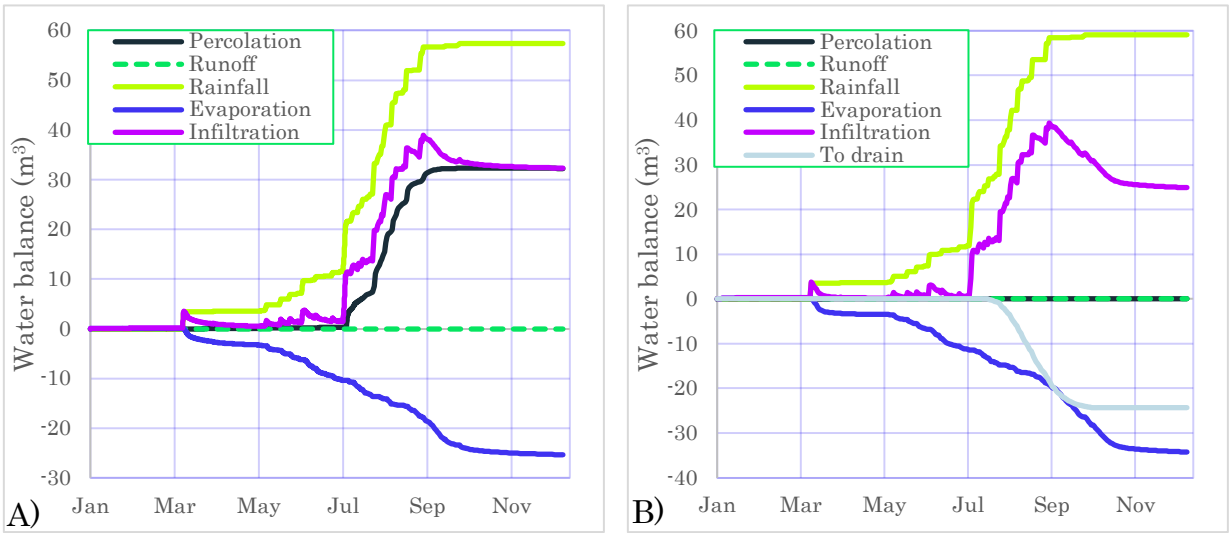


Figure 8: Water balance without (A) and with (B) the drainage ditch

Conclusion and recommendations

Modern soil cover system design for tailings storage facility relies on challenging numerical modeling, especially in arid climates with sudden and intense precipitation patterns. This study elaborates several practical steps that can be followed to simplify these simulations and ensure reliable solutions. Starting the exercise with a simple 1D geometry is a critical step to identify the numerical challenges before tackling more complex 2D geometries. Finer meshes with smaller time steps are required for domains subjected to transient boundary conditions. Coarser meshes can generally be used in 2D analyses because of the possibility of lateral flow. To tackle convergences issues in a structured manner, various elements must be checked including the porewater pressure convergence, water balance components, and consistent water changes in the domain. Finally, 2D geometries require careful consideration to elaborate consistent boundary conditions at the lateral edges of the domain to properly allow or restrict water flow, as required. The next step for the project discussed herein is to measure hydrogeotechnical properties of the soils used for the various soil covers design, account for the presence of vegetation, and refine the overall designs.

References

Bussière, B. and Guittonny, M. (eds). 2021. *Hard Rock Mine Reclamation: From Prediction to Management of Acid Mine Drainage* (first edition). CRC Press.

Castonguay, V. 2023. Toward greater confidence in numerical analysis results in geotechnical engineering. *76th Canadian Geotechnical Conference*, Saskatoon, Canada.

Seequent. 2024. GeoStudio 2024.1.0. Accessed 2024-05-21 at https://www.seequent.com.

Modeling Cover Systems for Tailings Facilities: Integrating Hydrus-1D and Python for Enhanced Seepage Prediction

Ariel Terlisky, SRK Consulting, Argentina
Imanol Vega, SRK Consulting, Argentina
Gastón Quaglia, SRK Consulting, Argentina
Jonathon Doherty, SRK Consulting, Canada
Michel Noël, SRK Consulting, Canada

Abstract

Effective management of tailings storage facilities (TSFs) is a critical aspect of sustainable mining operations, particularly post-closure. Cover systems are key elements for sustainability to help maintain the long-term stability of the TSF, particularly when designed to reduce infiltration and oxygen ingress so as to limit the rates of sulfide oxidation, thereby reducing the potential for acid rock drainage (ARD) and metal leaching (ML). We propose a novel modeling process applied to cover systems that harnesses the analytical strengths of Hydrus-1D coupled with the versatility of Python scripting and the data management and analysis capabilities of Power BI. Our methodology provides an understanding of the cover's infiltration and degree of saturation, which is crucial for determining the efficacy of cover systems and their enhanced variants with additional low hydraulic conductivity layers. Our research is expected to contribute to the body of knowledge in TSF management and closure and to provide a foundation for future innovations in cover system design.

The practical application of our modeling approach is demonstrated through a theoretical example where the automated modeling approach is used to examine key variables of the cover system performance over a wide range of input values. These variables include hydraulic conductivity, soil water characteristic curves, cover thickness, and the influence of climatic conditions as boundary constraints. The analysis results provide an understanding of the cover's degree of saturation, which is crucial for determining the efficacy of limiting oxygen transport as well as relative rates of infiltration, which in turn is crucial for predicting the performance of systems designed to reduce the potentially impacted seepage (ARD/ML) downstream of the TSF. The simulation outputs are graphically depicted using a 2D color gradient plot that dynamically represents the fluctuation of saturation levels across different temporal and spatial dimensions.

Introduction

This paper presents the integrated use of Hydrus-1D, Python, and Power BI as tools for cover design and evaluation. Hydrus-1D is an industry-standard one-dimensional time-dependent code that simulates water and solute transport in variably saturated porous media. Python is employed to automate the input process, communicating with Hydrus-1D to run the models and retrieve the outputs (Noël et al., 2023). Power BI is used to perform post-processing of the outputs and aid the engineer to interpret and easily compare the results of multiple models. This integration significantly enhances the efficiency and value of the modeling process for the engineering design.

The proposed tool is aligned with existing cover design studies in the literature, as outlined by the Mine Environment Neutral Drainage program (MEND, 2004) and the International Network for Acid Prevention (INAP, 2017).

To demonstrate the application of this integrated process, a cover example was conducted to assess the expected performance of a tailings storage facility (TSF) cover system as part of a mine project. The TSF contains potentially acid-generating (PAG) and metal leaching (ML) mine waste that could affect the water quality of the seepage leaving the TSF. The cover system function is to limit water infiltration and oxygen ingress. If the cover remains at a high degree of saturation, it will limit oxygen ingress, and the impact of the PAG/ML mine waste into the TSF seepage.

The primary focus of the modeling exercise is to determine the degree of saturation of the cover material after the TSF has drained drown, as the degree of saturation is one of the controlling variables on rates of oxygen ingress through the cover. A threshold of a minimum 0.8 degrees of saturation was established for the cover to perform effectively as an oxygen barrier.

Four types of cover configurations were evaluated. Additionally, a range of saturated hydraulic conductivity values for one of the configurations was analyzed. Average climate conditions (precipitation and evapotranspiration) were also studied in detail for both cold humid and cold arid zones, as the exercise can be repeated regardless of the TSF location. The key objective is to ensure that the cover is effective under quasi-steady state conditions for a range of climatic and material property scenarios.

Cover system

The primary functions of the cover system considered in this paper are: 1) to function as an oxygen ingress barrier for the underlying waste material by maintaining a high degree of saturation within a layer of the cover system, thereby minimizing the effective oxygen diffusion coefficient and increasing the loss of oxygen concentration; and 2) to function as a barrier to reduce water infiltration to the underlying waste material, thereby reducing the quantity of poor water quality seepage leaving the TSF.

The appropriate type of cover system primarily depends on the climate, which is defined by factors such as annual precipitation, potential evapotranspiration, and temperature. Figure 1 illustrates the optimal cover system options based on these variables (GARD Guide, 2011).

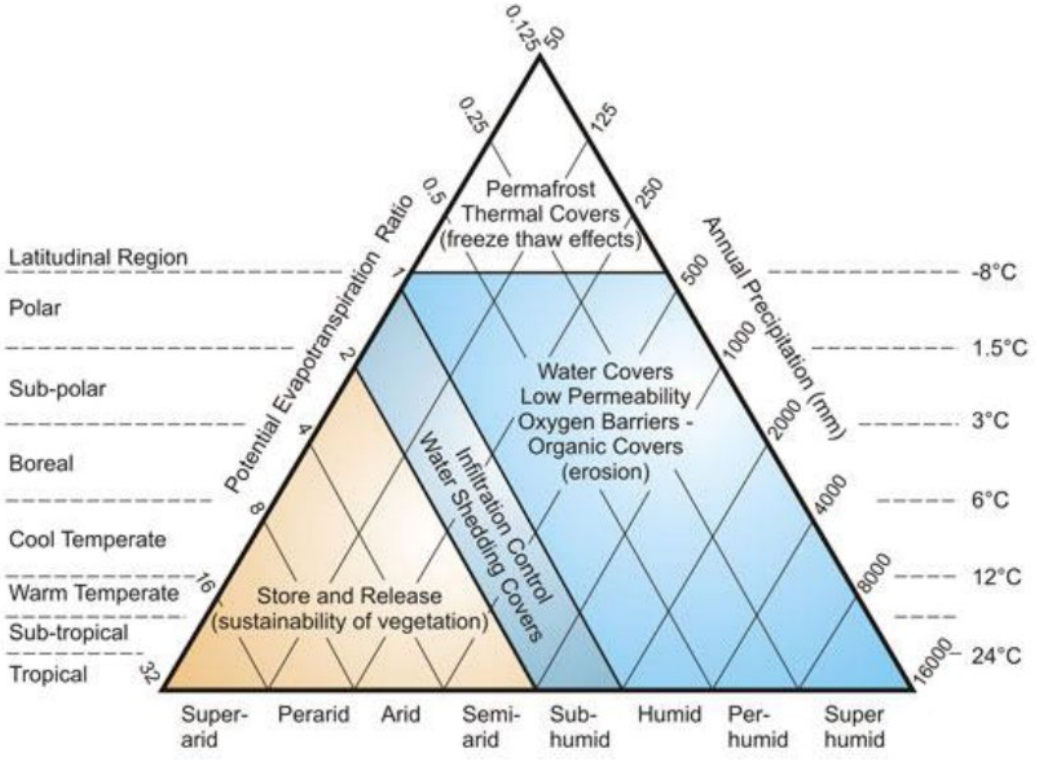


Figure 1: Cover systems and climate types (GARD Guide, 2011)

The design of a cover system for mine closure must balance cost-effectiveness with achieving an acceptable level of risk. The design should minimize additional rework and have minimal sustaining capital expenditure associated with ongoing monitoring and maintenance after closure.

Effect on degree of saturation

The degree of saturation in fine-grained materials has a strong impact on the oxygen diffusion coefficient. Figure 2 illustrates an example of the change in the diffusion coefficient of oxygen, decreasing rapidly as the degree of saturation increases. This occurs because higher saturation limits the movement of oxygen due to its lower solubility in water.

During slurry tailings deposition, the degree of saturation is high. However, after tailings deposition ceases, drain down occurs, and the phreatic surface lowers, allowing greater penetration of oxygen. As the tailings drain, the degree of saturation decreases. Oxygen diffusion is expected to be the dominant oxygen transport mechanism in tailings, whereas oxygen transport via advection and convection are also expected to be significant transport mechanisms in the waste rock environment.

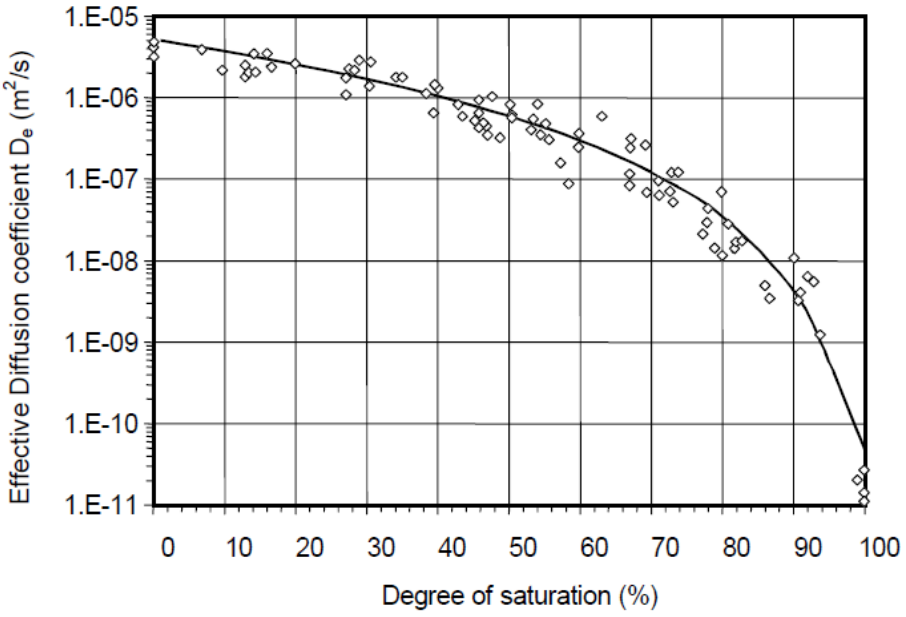


Figure 2: Effect of the degree of saturation on the oxygen diffusion coefficient (Mbonimpa et al., 2003)

Methodology

Description of Hydrus-1D and its capabilities

Unsaturated flow modeling is performed using Hydrus-1D software. The water transport is based on Richards' equation for the saturated/unsaturated water flow with various types of boundary conditions, and material properties such as the soil water characteristic curves (SWCC) and hydraulic conductivity functions are represented by theoretical models like van Genuchten (1980).

Boundary and initial conditions are crucial in simulations as they significantly influence the accuracy and reliability of the results. Hydrus-1D can accommodate detailed boundary conditions, which are also available in the modeling tool presented here. The initial conditions are set by specifying the water content or pressure head along the model's profile.

Integration with Python and Power BI for automation

The integration of Python and Power BI with Hydrus-1D represents a significant advancement in automating the flow models. A Python script was developed to streamline the modeling process. The script reads the input data (e.g., cover properties, boundary conditions, initial conditions) provided via text or spreadsheet files by the user, prepares the Hydrus-1D input files, runs the simulations, and processes the outputs. This automation has the benefit of significantly reducing the user time to conduct sensitivity analyses, which include variations of one or multiple parameters at a time such as hydraulic conductivity, cover thicknesses, saturation levels, and climatic conditions.

The Power BI is primarily used to visualize and compare the pre-processing variables and post-processing results outside the Graphic User Interface (GUI) of Hydrus-1D, enabling the creation of user-defined plots, and comparing the results of multiple models on the same plot.

Cover example

Geometry

The base case modeled geometry consists of a 6-meter cover material placed atop 10 meters of tailings, as illustrated in Figure 3. This exercise uses a cover composed of non-acid generating tailings, built during deposition above the PAG tailings. This can be a cost-effective solution, and provides the designer with flexibility to modify the cover thickness, thanks to the availability of the material. The water table (WT) was assumed to be below the model domain, and the top boundary was defined by climatic conditions. Three cover configurations include a single 6-meter cover layer, and one of the configurations involved placing a thin layer of the best-performing cover material on top of another cover material.

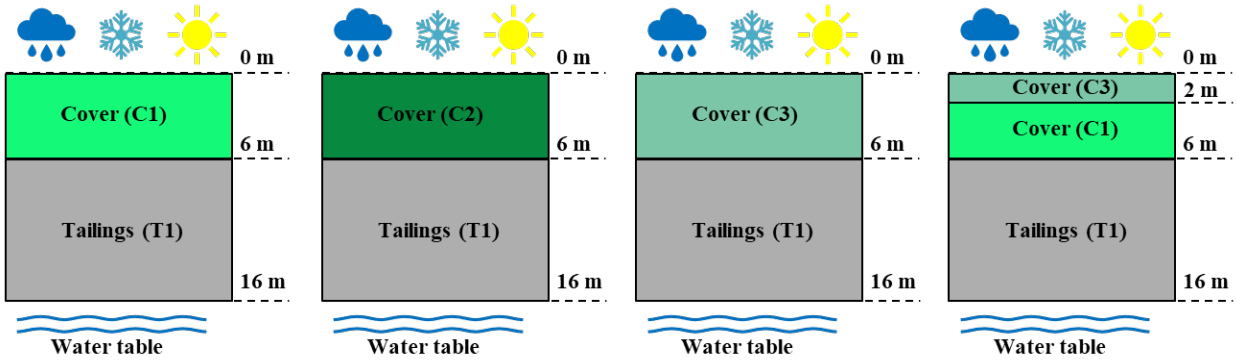


Figure 3: Cover profiles

Material properties

Four material types were used as inputs for the seepage modeling: cover (C1, C2, C3) above the tailings (T1). The properties for these materials are usually derived from geotechnical laboratory testing. As part of a testing program, a series of SWCC, saturated hydraulic conductivity, and particle size distribution (PSD) tests are conducted to characterize the hydraulic properties of the cover. It is essential that the tested samples represent densities expected in situ to ensure accurate results. If information on the PSD is available but SWCC data is lacking, the Rosetta Lite v1.1 tool (Schaap et al., 2001) inside Hydrus-1D can be employed to obtain the necessary van Genuchten parameters.

The selected hydraulic properties are fitted using the van Genuchten model (van Genuchten, 1980). The selected soil water characteristic curves for the cover and tailings are illustrated in Figure 4. The

corresponding parameters are listed in Table 1. Hydraulic properties employed in this exercise were made up by increasing the porosity and Air Entry Value (AEV).

When examining the van Genuchten parameters, it should be noted that the α parameter is inversely proportional to AEV, while the n parameter is directly related to the steepness of the SWCC slope. The AEV represents the suction state at which air begins to enter and desaturate the soil.

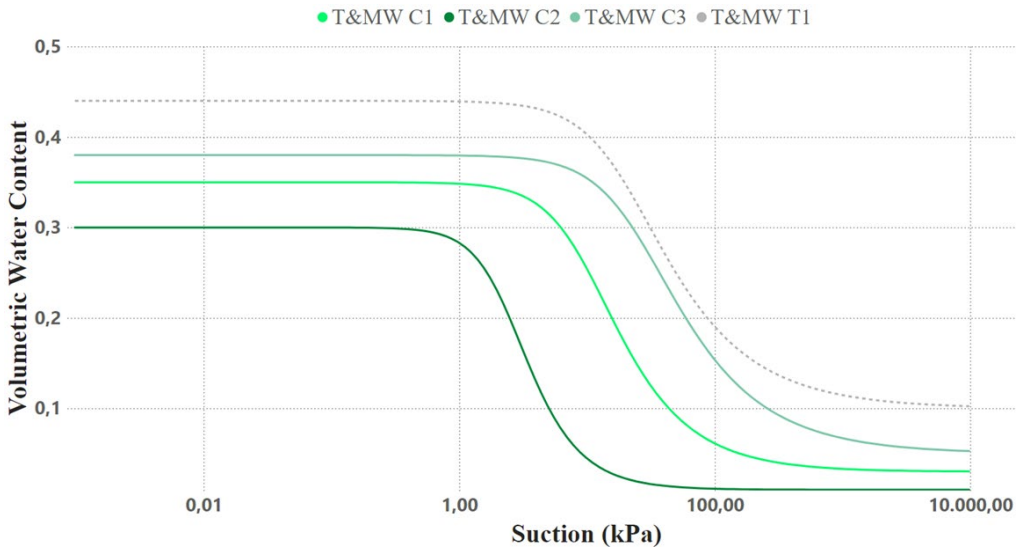


Figure 4: SWCC covers and tailings

Table 1: Hydraulic properties of the cover and tailings

Parameter	C1	C2	C3	T1
θ_r [m^3/m^3]	0.03	0.01	0.05	0.10
θ_s [m^3/m^3]	0.35	0.30	0.38	0.44
α [1/m]	1	4	0.4	0.5
n [-]	2.0	2.5	1.8	1.8
l [-]	0.5	0.5	0.5	0.5
K_s [m/sec]	1.00e-8	1.00e-8	1.00e-8	1.00e-7

Initial conditions and model time

The initial conditions were set by specifying a water content at or near saturation for both the cover and tailings, reflecting the state of the slurry tailings at the end of deposition in the TSF. These near-saturation conditions were chosen to facilitate the numerical convergence of the model.

All simulations were conducted over a five-year period to minimize the influence of the initial conditions and ensure quasi-steady state conditions (e.g., degree of saturation and infiltration) along the model's profile. The results were interpreted based on output print times at monthly intervals throughout the duration of the simulation.

Top boundary conditions

The top boundary was assigned as atmospheric, incorporating climatic data. The climate inputs for both the cold humid and cold arid scenarios were derived from Daymet, which provides long-term, continuous, gridded estimates of daily weather and climatology variables. The mean annual precipitation (MAP) from 1979 to 2019 is 252 mm for the arid scenario, while it is 360 mm for the humid scenario, representing a 40% increase. The difference in mean annual evapotranspiration is even more pronounced, with the arid scenario at 1,246 mm and the humid scenario at 247 mm, indicating that the arid scenario experiences approximately five times higher evapotranspiration.

Figure 5 shows the variation of the ambient air temperature presented as the daily average over the 40-year dataset. The daily average variation of the potential evapotranspiration is also shown in Figure 5, along with the daily average ambient air temperature, illustrating the dependency of potential evapotranspiration on ambient air temperature.

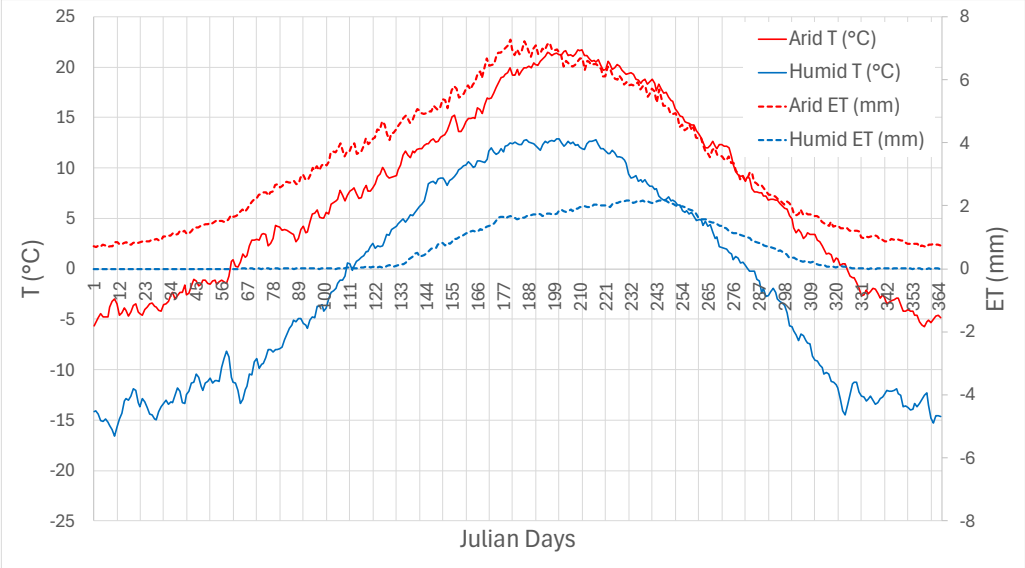


Figure 5: Average of daily ambient air temperature and evapotranspiration

An average year of precipitation and evapotranspiration from the 40-year dataset was selected for the humid climate and for the arid climate.

Daily precipitation and evapotranspiration values of each average year were specified as the top boundary conditions. The values of the average year were cycled over the entire five-year simulation period.

Bottom boundary conditions

The cover models assume that the WT position is within or near the bottom of the TSF, which is situated beneath the model domain. The bottom boundary was then assigned a free-draining condition, assuming that the base of the profile will be drained with no water uptake and that water will flow due to gravity.

Results

The main output presented in this section, as previously described, is the effective degree of saturation in the cover. Profiles are shown as lines at specific time intervals, with a color gradient (light to bold color) indicating the advance of time.

An improvement for interpretation over the line plots is the use of saturation profile plots that combine in a single figure the changes in the degree of saturation over time and depth (e.g., Figure 8). The x-axis represents time, while the y-axis represents depth. Regions with saturation levels exceeding 0.8 are denoted by dotted hatching, indicating high saturation levels. Areas with saturation levels ranging between 0.6 and 0.8 are represented by slanted hatching, distinguishing them from other regions. This comprehensive presentation of results allows for a visual understanding of how saturation levels evolve over time and depth, alongside the influence of precipitation and evapotranspiration dynamics. By using the Power BI tool to incorporate simulation results, the volume of water in the system is plotted over time.

A set of 33 simulations was run, and only the most relevant ones are shown in this paper. The title above the plot indicates the simulation number (n), cover material (C), tailings material (T), climate used as the top boundary condition (H or A), and the number of years considered in the simulation (yrs). The title may include additional parameters corresponding to further variations.

Base case

For the base case scenarios, cover material C1 was evaluated under both humid and arid climate conditions. The results are shown in Figures 6 to 9. Figure 6 illustrates the drain down. It can be observed that within the first two years the evolution from saturation to a quasi-steady state is achieved for the humid climate, but not for the arid climate. Figure 7 shows the final two years of the simulation, highlighting the upper portion of the cover as the “active zone” affected by the boundary conditions in the humid scenario. In the arid scenario, the saturation of the cover profiles continues to decrease over time, achieving the quasi-steady state by the end of the fifth year. These two figures show the limitation of the modeler to have both the detailed transition (e.g., 3 months or less) and long-term data (e.g. 5 years or more), requiring creating multiple figures and separate evaluations.

Figure 8 presents an improved view of the line profiles, as described in the results introduction, consolidating all results into a single figure, which allows depicting a fine resolution (as low as desired, in this case one month was selected), for any time period, along the entire vertical profile. While steady state can be defined in terms of the degree of saturation, when no change (or repeated variation) is reached, Figure 9 aids in interpreting the profile results, showing the moisture storage in the entire profile, and steady state is achieved when no change (or repeated variation) of the moisture storage volume is achieved.

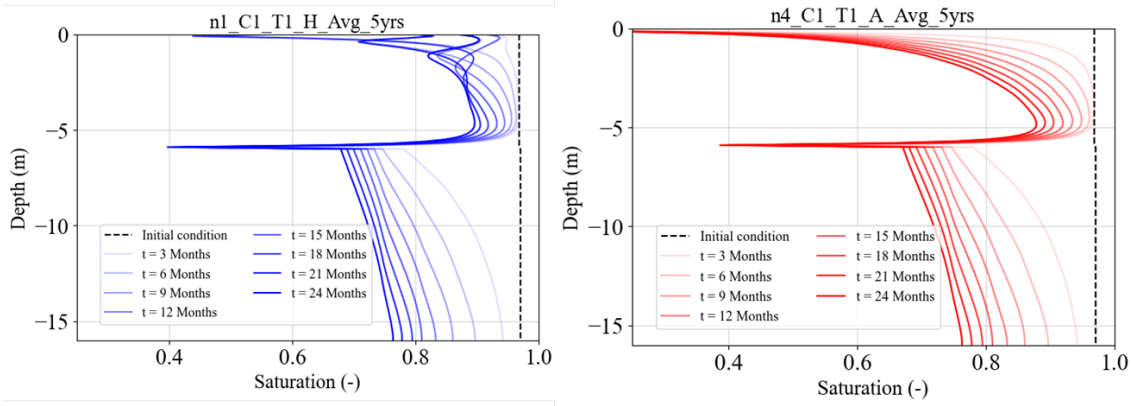


Figure 6: Saturation profile in the first two years (humid left, arid right)

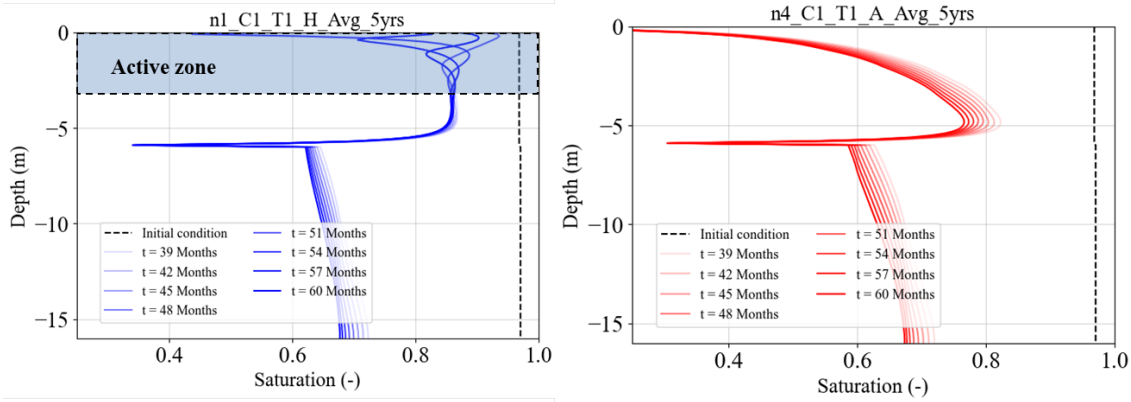


Figure 7: Saturation profile in the final two years (humid left, arid right)

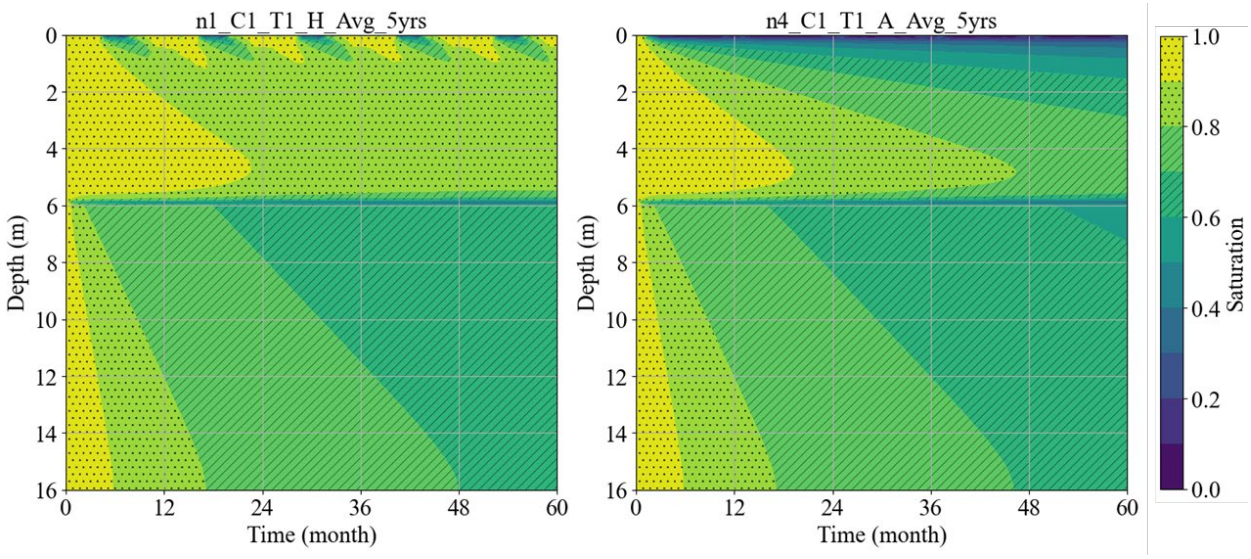


Figure 8: Base case saturation profile (humid left, arid right)

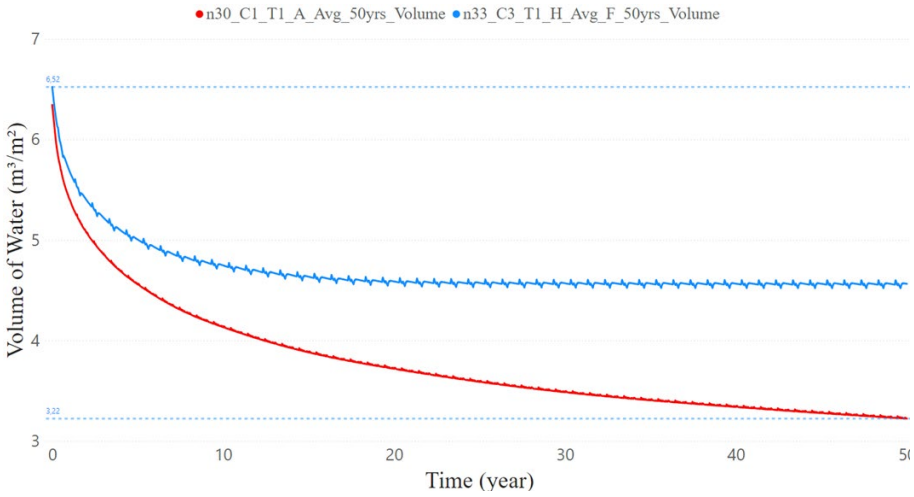


Figure 9: Volume of water of the entire system for base case – 50 years simulation

Cover material C2 and C3

The cover material was modified to C2 and C3, to evaluate the impact of different soil-water characteristic curves (SWCCs). The system shows that C3 provides superior performance, maintaining a higher degree of saturation as a result of a higher AEV (Figure 10). Consequently, C3 was used in the subsequent subsections.

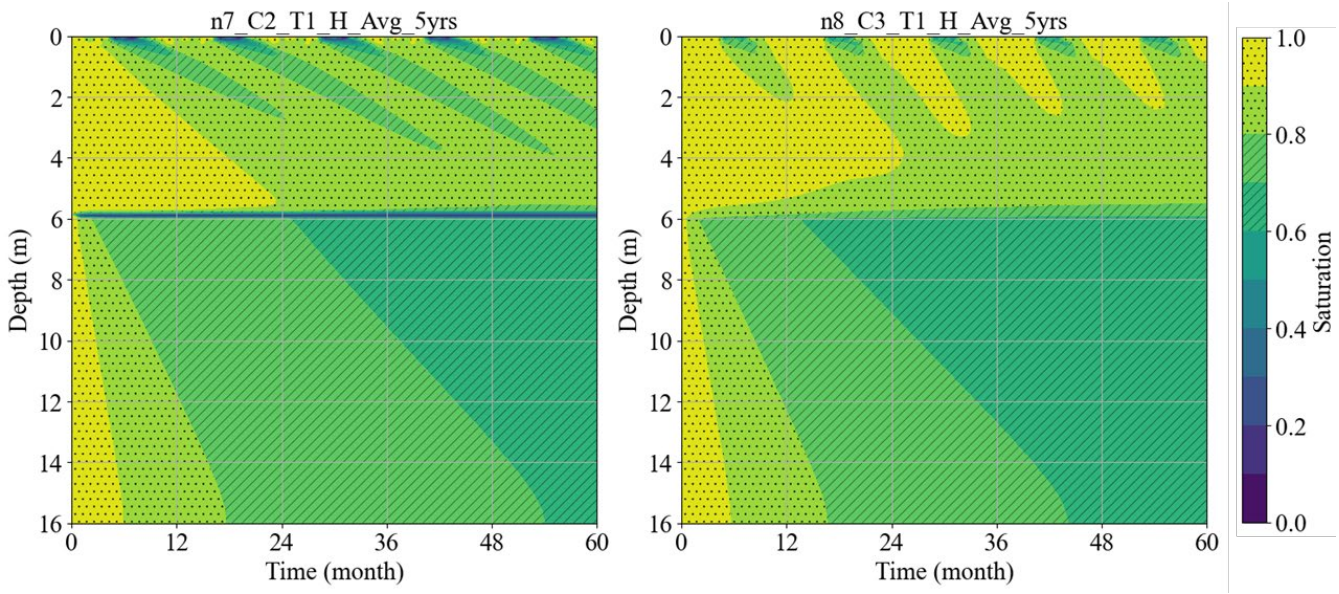


Figure 10: Saturation profile for cover materials C2 (left) and C3 (right)

Climate sensitivity analyses

Daily precipitation values were applied for the base case over 6-hour daily periods. In this section, 2 and 24-hour periods of precipitation were considered. Figure 11 shows that when precipitation is considered throughout an entire day, the degree of saturation increases considerably.

Given that the cold humid climate selection experiences a frozen period of more than 150 days (daily temperature below 0°C), a dry frozen scenario was included as a sensitivity case (Figure 12). The frozen period was assumed to occur between November and March, while the unfrozen period was assumed to occur between April and October. No precipitation was applied during the frozen period; instead, the precipitation quantity was totaled as the volume of water available during the freshet. This volume was then uniformly applied over the April period to emulate the freshet at the beginning of the unfrozen period. Snow losses due to wind and sublimation were estimated at 20%. The precipitation event in April was simply added to the freshet flux over a 14-day period. Freeze-thaw cycles impacted cover performance, potentially failing objectives due to the lack of infiltration during winter.

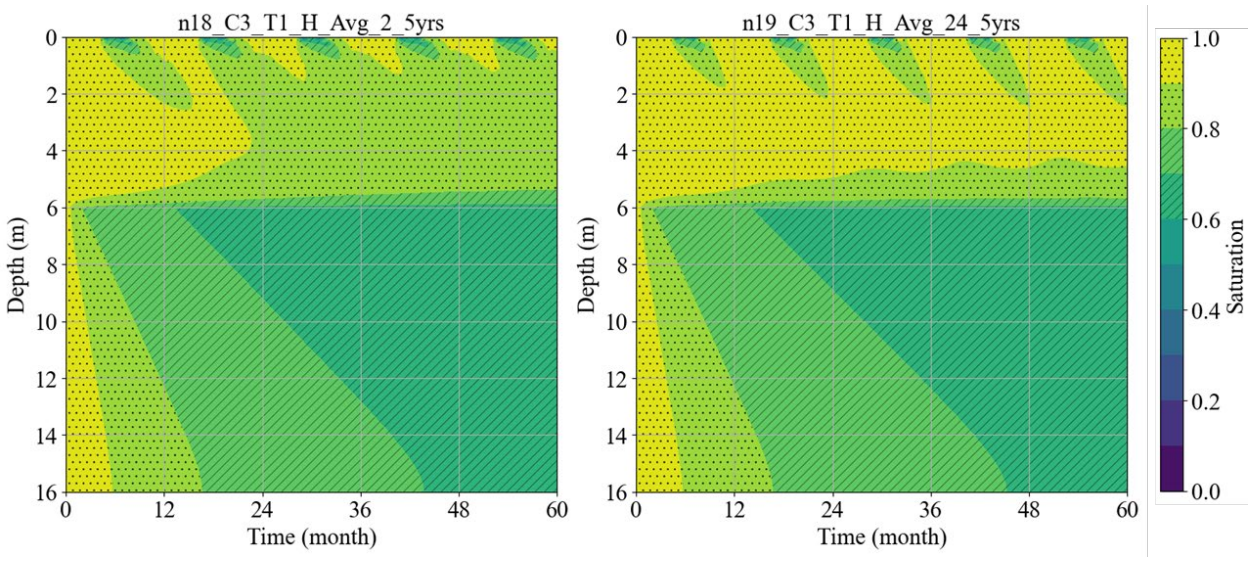


Figure 11: Saturation profile for daily precipitation with 2 hours (left) and 24 hours (right)

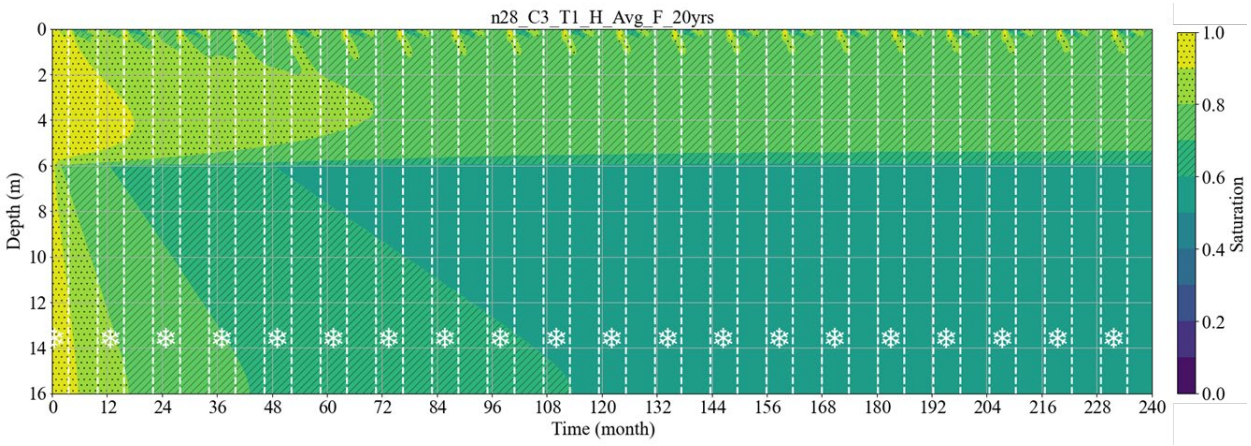


Figure 12: Saturation profile considering freeze periods of 150 days

Permeability sensitivity analyses

While maintaining the SWCC as considered, the saturated hydraulic conductivity of the cover layer was adjusted to vary between 1.00e-10 and 1.00e-6 m/s (Figure 13). The lower hydraulic conductivity maintains a higher saturation in the cover.

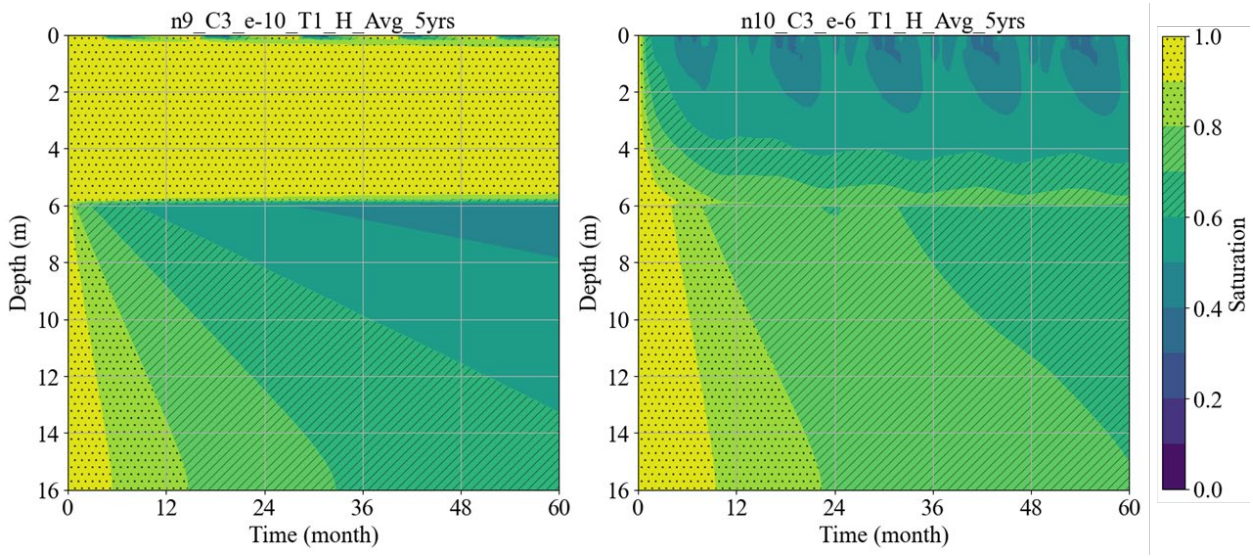


Figure 13: Saturation profile lower (left) and higher (right) Ks

Cover: thin layer of the best-performing material sensitivity analyses

A scenario featuring the best-performing cover material, C3, 2-meters, over the C1 material, which is about 4 meters, is presented (Figure 14).

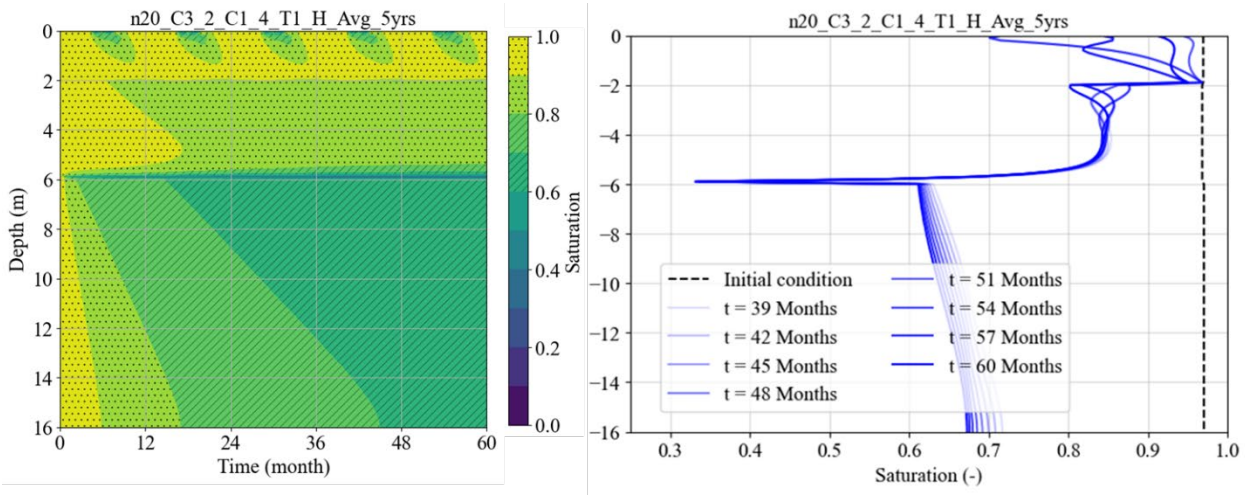


Figure 14: Saturation profile 2-meters C3 over 4-meters C1

Discussion

In this exercise the properties of the cover material were modified to assess the cover performance and find the optimal solutions (e.g., decrease hydraulic conductivity and increase moisture retention). For the engineering design there are several methods that can be considered to meet these requirements with the available non-acid generating tailing's materials, such as compaction, cycloning, material mixing, etcetera. Proper construction practices and rigorous quality control are crucial for the long-term performance of cover systems. Issues like the thickness of growth media, compaction, material placement, and construction schedules must be managed meticulously to prevent negative impacts on the cover's effectiveness and durability, as highlighted in MEND (2004).

The hydraulic properties of soils used in water balance covers can change over time (Benson, 2009), and the magnitude of these changes is closely related to the as-built condition of the cover system. Understanding these temporal changes is crucial for accurately predicting the long-term performance of cover systems in controlling water infiltration and oxygen ingress. In the analysis presented in this paper, properties were considered constant.

Finally, the modeling presented herein was restricted to vertical flow due to the use of Hydrus-1D. It did not include horizontal flow. This limitation could become important in terrain with sloping topography, as this could promote lateral flow under certain conditions.

Conclusion

An automated modeling tool that integrates Hydrus-1D, Python and Power BI was developed to model the degree of saturation for a TSF cover example. The automated process facilitates the execution of multiple scenarios, sensitivity analyses, comparisons, and modifications to cover configurations.

The cover example demonstrated a workflow for designing and modeling a proposed cover system aimed at limiting rates of oxygen ingress into the underlying mine waste materials. Key findings identified within the cover example included:

- Daily climate values have a significant impact on the cover's performance. From the base cover example, the humid scenario achieves good performance in less than 5 years, while the arid scenario did not meet the design criteria and failed to reach a quasi-steady state even after 50 years of simulation.
- An active zone, where a quasi-steady state was reached, can be observed in the base case humid scenario. This suggests that instrumentation and control may be needed only in that zone.

- Among all the cover materials, material number three demonstrated the best performance due to its higher AEV. If this material is not available on-site, a two-layer cover profile can be achieved with a highly saturated cover at the top to minimize the volume of material needed.
- The daily precipitation period had a significant impact on the profile, and well-defined and precise climate data is important for understanding the impact of climate variations on cover performance.
- If the climate includes long periods of temperatures below 0°C, it is important to consider freeze and thaw cycles, as these can affect the cover's behavior and performance, potentially falling below the required objectives due to the lack of infiltration during winter.
- A cover layer with a saturated hydraulic conductivity value not close to or lower than 1.00e-08 m/s may significantly decrease saturation levels, leading to increased infiltration and rates of oxygen transport through the cover.

References

GARD Guide. 2011. Global Acid Rock Drainage Guide. Prepared by the International Network for Acid Prevention. Accessed at http://www.gardguide.com/

INAP. 2017. Global Cover Systems Design. Technical guidance document prepared by the International Network for Acid Prevention.

Mbonimpa, M., Aubertin, M., Aachib, M. and Bussière, B. 2003. Diffusion and consumption of oxygen in unsaturated cover materials. *Canadian Geotechnical Journal* 40(5): 916–932.

MEND, 2004. Design, Construction and performance monitoring of cover systems for waste rock and tailings volume 1. MEND Report 2.21.4a. Prepared by O'Kane Consultants.

Noël, M., Vega, I.J., Rivarola, F., Lopez, Ezama, I., McGregor, M. and Terlisky, A.G. 2023. Coupling tailings deposition modelling with Hydrus-1D and Python for pseudo-3D seepage predictions. *Proceedings of Tailings and Mine Waste 2023.*

Schaap, M.G., Leij, F.J. and van Genuchten, M.Th. 2001. Rosetta: A computer program for estimating soil hydraulic parameters with hierarchical pedotransfer functions. *Journal of Hydrology* 251:163–176.

Simunek, J. and van Genuchten, M. 2018. Hydrus-1D, version 4.17.0140. Code for simulating the one-dimensional movement of water, heat and multiple solutes in variably saturated porous media. Department of Environmental Sciences, University of California, Riverside. Released: November 15, 2018. Available at: http://www.pc-progress.com/en/Default.aspx?H1d-downloads

van Genuchten, M.T. 1980. A closed-form equation for predicting the hydraulic conductivity of unsaturated soils. *Soil Science Society of America Journal* 44(5): 892–898.

The Vibro-consolidation Technique for Tailings Management and Dam Decommissioning Works

Gustavo Marçal de Sousa, Vale S.A., Brazil
Ana Torres, Vale S.A./UFOP, Brazil
Felipe Moraes Russo, Vale S.A., Brazil
Lucio Schiavon Yamamoto, Vale S.A./USP, Brazil

Abstract

Reservoir management and the search for tailings dam decharacterization solutions have become challenges that the Brazilian mining industry has to face nowadays. Based on a saturated sandy soil consolidation proposition, a promising alternative to such issues has arisen: in-situ mechanical consolidation. In particular, a technique referred to as vibro-consolidation, which consists of applying load and vibration to the tailings layer, thus forcing particles to be rearranged through tailings consolidation and expelling water up to the surface in a localized fashion, by using potentially efficient equipment for the disposed tailings particle size range, whose undersize percentage through 200 mesh sieve (0.075 mm) is not over 70%.

Thus, this work aims to introduce an experiment to contribute to new technologies aimed at assisting tailings management and/or dam decharacterization processes by applying the vibro-consolidation process, through the simulation of tailings reclamation operations from the reservoir of an iron ore tailings dam within the area referred to as Iron Quadrangle in the state of Minas Gerais, Brazil. The research uses an experimental methodology, with tests based on the proposition of a dam mining method, on an industrial scale, focusing on the vibro-consolidation technique. By applying the proposed mining methodology, enhanced mining and disposal operations workability and, consequently, geotechnical stability of the mine faces is attained. In addition to applying this technique to dam reservoirs, a promising potential might be to manage tailings in bays, existing reservoirs, and most hydraulic embankments made of iron ore tailings.

Introduction

Mining activities positively impact society by providing raw materials, job generation, state and local tax revenue, and manufacturing products required for the modern human lifestyle. Nevertheless, negative impacts also stem from such activities, and continue to impact the environment even after mining activities are discontinued (Flores and Lima, 2012). Within this context, tailings dams have always been the subject

of discussions on dam break impacts and risks. In general, tailings disposal facilities have a large footprint and demand special attention from project owners.

Currently in Brazil, hydraulic fill embankment dam stability and potential environmental impact have come in for questioning, especially following the dam breaks of Fundão, in 2015 (Carmo et al., 2017; Queiroz et al., 2018), and Brumadinho, in 2019 (Petley, 2020), for which reparation costs may be very high, even more than the costs associated with the original project and its operations.

In this context, dam decommissioning solutions have increasingly become attractive, since they do away with stability risks, as well as required on-site monitoring and periodic follow-up activities by the project owner. As recommended by Muir et al. (2005), these projects should preferably be designed by considering solutions that generate fewer geotechnical risks associated with factors such as seepage, erosion, and stability, as well as the safety of downstream communities and the minimization of environmental liabilities.

Safe dam decommissioning is a crucial variable for the decision-making process associated with a dam decharacterization or tailings reuse project. The tailings deposited in dams, in most reservoirs, are saturated, with their excavation being rather difficult (Alves, 2015). Even in legacy facilities that have been shut down for several years, there may be saturated horizons that pose risks to mining activities.

Therefore, studies must be developed to develop new technologies to allow for lower-saturation disposal and safe tailings dam mining. Associated with geotechnical designs, pilot tests and investigations, both in-situ and laboratory, are important for defining material properties, which enables safer designs to be developed (Sousa, 2020).

Hence, based on scale tests, this paper aims at assessing the feasibility of the vibro-consolidation technique in a reservoir for simulation of iron ore tailings dam mining, within the Iron Quadrangle region in the state of Minas Gerais, Brazil. Major benefits in geotechnical parameters of tailings are evaluated. The study was based on the vibro-consolidation technique for tailings, underpinned by the proposition of sandy, saturated, and soft soil consolidation, introduced by Esfahanizadeh and Atashband (2012), along with the strip-mining technique proposed in the mine and production plan developed for the pilot dam.

The major outcomes of this work include the development of the methodology and conception of a new piece of equipment whose activity cycle can potentially condition tailings disposed as slurry, which starts performing with the characteristics of materials disposed with moisture content between 20% and 30%, and may later be drained and stacked in definitive or provisional deposits.

Methodology

Production scale test description

The production scale mining test developed to enhance the in-situ vibro-consolidation technique for tailings

was performed in a conventional compacted soil dam, located in the state of Minas Gerais, Brazil, whose reservoir is used for iron ore tailings disposal. Figure 1 shows the area in which the production scale test was performed, characterized by low-consistency saturated and soft tailings.

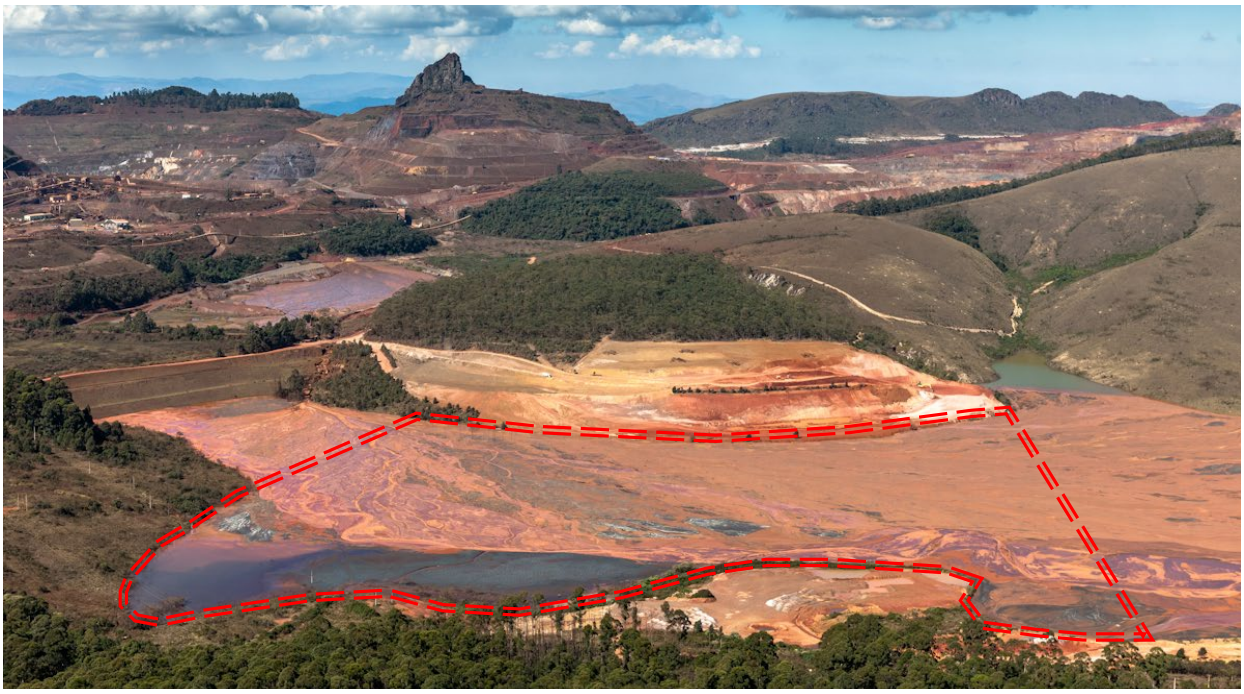


Figure 1: Production scale test area

The tests were performed over a 12-month period, with average monthly output targeted at 360,000m^3. Furthermore, test scheduling considered mine productivity variations due to rainy season months.

Data and discussion

Prior to the test period, the tailings were characterized within the mine development area, with average values obtained for major rates being shown in Tables 1 and 2.

Table 1: Average particle size of tailings disposed at the dam

Sieve	Diameter (mm)	(%) Undersize
10	2,000	95
30	0.590	85
50	0.297	82
100	0.149	80
200	0.075	69
400	0.037	42
500	0.025	38

Table 2: Average values obtained in the characterization tests

Characterization					Permeability
LL (%)	PL (%)	Gs	ρs (g/cm³)	w (%)	K (cm/s)
17	15	3.35	1.85	25.7	$9{,}7 \times 10^{-4}$

In-situ tailings were saturated and similar to soft soil, which resulted in unstable excavation slopes, thus requiring engineering solutions to ensure stability for mining activities to commence, as well as the use of special equipment for previous consolidation. Thus, activities were performed by applying standardized methodology comprising tailings consolidation, excavation, and disposal cycles. Excavations were performed in ranges, with 3-meter-high benches, in order to simulate strip mining of the reservoir with maximum 6-meter-deep excavation. This was obtained with bearing layer reclamation or direct advancement to a maximum 3-meter depth underneath the bearing layer threshold, provided that a 5-meter support meter was maintained, with a 45° slope, as shown in Figure 2.

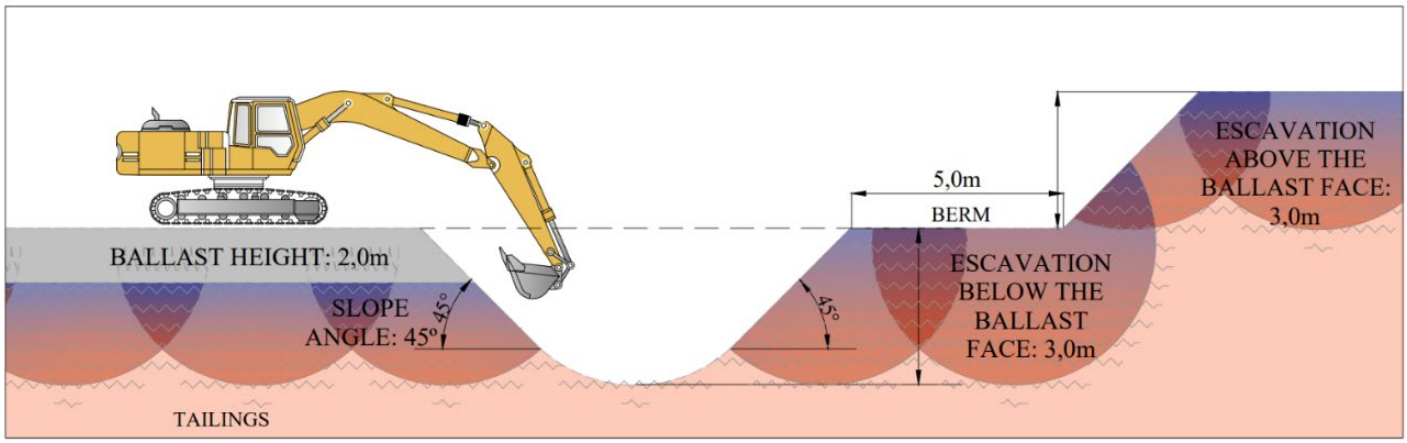


Figure 2: Operational detail of mining involving bearing layer/advancement down to a 6-meter depth

This allowed partial or total mining of a tailings reservoir, even under saturated conditions. Subsequently, the high moisture content of tailings was the challenge to be faced for material spreading, compaction, and haulage operations to be carried out, as a high moisture content might hinder haul trucks (35 tonnes) from being fully loaded.

Therefore, the tailings vibro-consolidation stage was implemented (the focus of this paper), by applying common earthworks equipment and adapting existing equipment, as shown in Figure 3, so as to enhance mining and disposal operations workability and, consequently, the geotechnical stability of mining faces.



(a) (b) (c) (d)

Figure 3: Main equipment used: (a) high-output long reach excavator (45 tonnes, 1.90 m³ bucket); (b) pump excavator suitable for pumping water and solids (20 tonnes); (c) amphibious excavator used for tailings consolidation (20 tonnes; (d) vibrating plate compactor adapted for vibro-consolidation (35 tonnes)

Mechanical consolidation proposition, vibro-consolidation, consists of applying load and/or vibration to the tailings layer, thus forcing particles to rearrange themselves by softening tailings and expelling water up to the surface in a localized fashion, followed by soil mass volume reduction. A consolidation settlement is then attained, similarly to what is proposed by Esfahanizadeh and Atashband (2012). The activity was supported by equipment potentially effective for the particle size range of the tailings disposed in the reservoir.

The test was performed over a 364-day monitoring period, with 3 daily eight-hour shifts, 7 days a week. The 12-month period has allowed for operations performance to be assessed under both dry and wet weather conditions, with hardships imposed by climate conditions to this type of operation being duly mapped out. Figures 4 and 5 (on the next page) depict the operational sequencing performed during the test in the consolidation and excavation stages.

Removed material from trial excavation were disposed of in a provisional deposit, in 2-meter-thick layers (maximum), ascending fashion, with 10-meter-high benches, 5-meter operational berms, and an angle between berms of 22° (2.5:1). An area of approximately 300,000 m^2, divided into 7 sub-areas, was prepared. In each sub-area, a 30-day cycle (minimum) was planned, comprising placement, drying, spreading, and compaction stages. A minimum 95% Normal Proctor compaction, with layer top, middle, and base checks, was set as a release criterion for the placement of each subsequent layer.

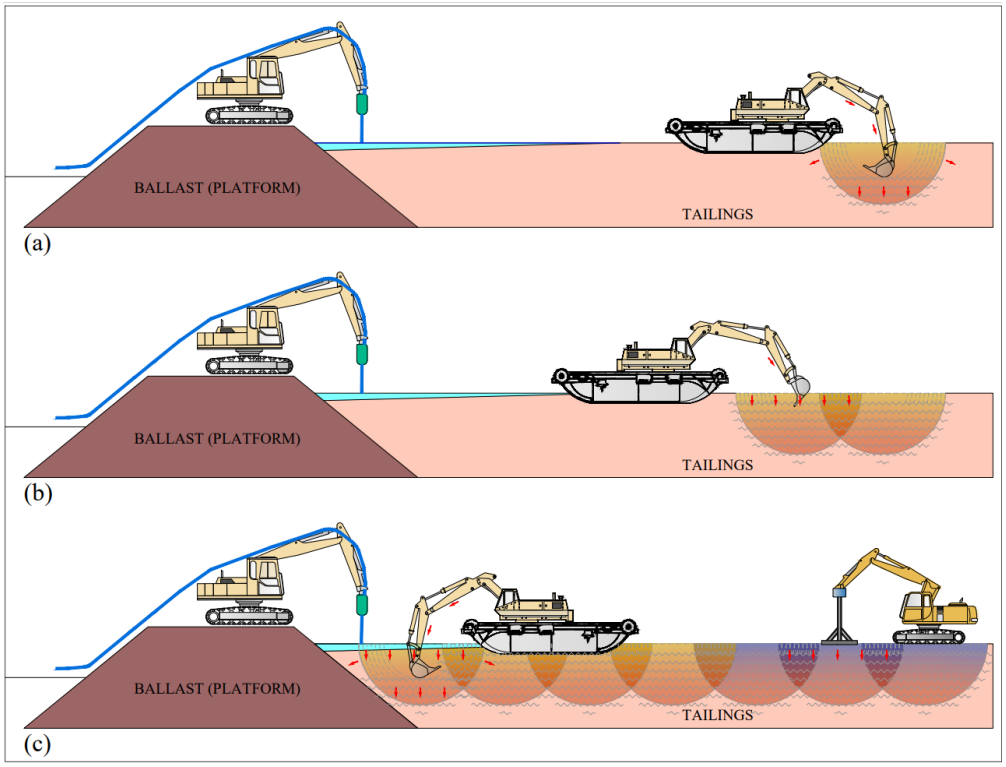


Figure 4: Vibro-consolidation execution sequence: (a) initial upward agitation at a 3-m depth by an amphibious excavator; (b) process completion up to the surface with 5 m x 5 m grid advancement; (c) employment of vibrating plate compactor for better efficiency in a 3 m x 3 m grid

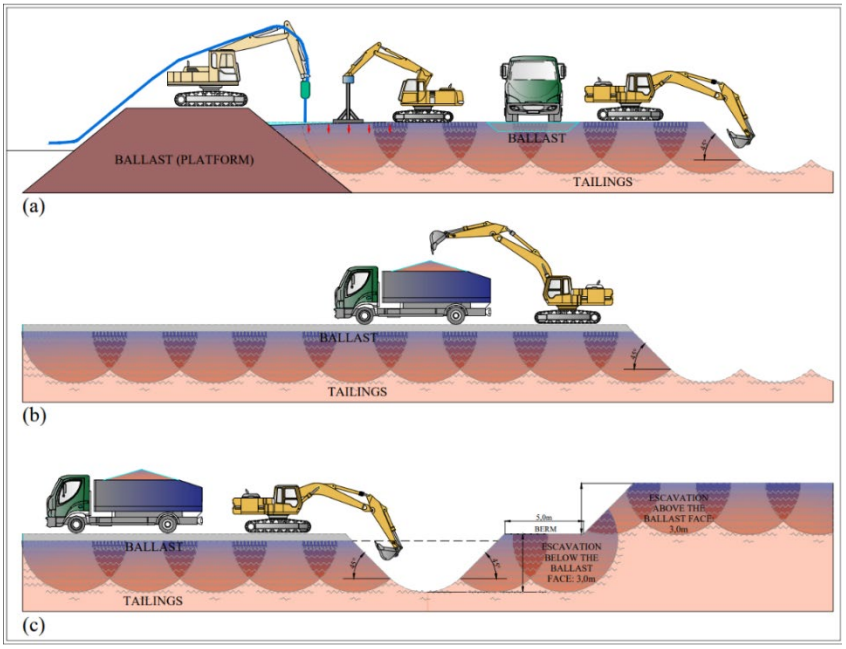


Figure 5: Planned excavation sequence upon vibro-consolidation completion: (a) start of excavation simultaneously to the vibro-consolidation process; (b) initial advancement upon consolidated material; (c) advancement with bearing layer reclamation

Results

Production scale results: production scale mining – application of vibro-consolidation technique

Due to the provisional character of excavations and to the adoption of highly restrictive geometries regarding height, and in order to cut down on potential dam break damages, a minimum Factor of Safety (FoS) of 1.15 was set for excavation slope sizing, calculated with scenarios simulating undrained conditions, where shear-induced pore pressures originating from stress relief actions during test mine stages would act. With the adoption of in-situ consolidation, tailings were considered to assume a thoroughly drained behavior, thus significantly improving safety conditions when compared to areas where the technique had not been applied.

Provided that it is appropriately executed, the geometry proposed for the test could ensure Factors of Safety (FoS) previously associated with the geotechnical stability of excavation slopes, as shown in Table 3, based on in-situ parameters.

Table 3: Geotechnical parameters and factors of safety for production scale testing

Scenario	Parameter				FoS	
	ϕ' (°)	ϕ' (°)	ru	Su (kPa)		
σ'Effective	29	–	0.40	–	1.21	(1)
σTotal	–	20	–	–	1.16	(1)
Su	–	–	–	0.23σ'v	1.15	(1)
σ'Effective	29	–	–	–	1.37	(2)

(1) Normal in-situ condition; (2) Inclusion of the vibro-consolidation stage

Figure 6 shows the tailings vibro-consolidation stage, which allowed for enhanced mining and disposal operations workability.



(a) (b)

Figure 6: Mechanical consolidation: (a) vibrating plate compactor; (b) amphibious excavator

In fact, the amphibious excavator and the vibrating plate compactor employed in the test produced good results, cutting down on the average moisture content of the tailings disposed in the embankment from 25.7% to 20.6%, thus significantly changing its consistency and improving productivity rates in all mining stages.

The best efficiency of the equipment employed for mechanical consolidation and dewatering of tailings, which allowed for a reduction of the previously shown moisture content, fell within the particle size range shown in Figure 7 (Zone B). Out of this range, in its lower bound (Zone A), dewatering is slow, and the outcome is not always satisfactory. When tailings are off their upper bound (Zone C), their consistency and moisture allow for direct load to be applied, without the consolidation process being required. Particle size variations observed occur due to hydraulic segregation of tailings particles at various mine points.

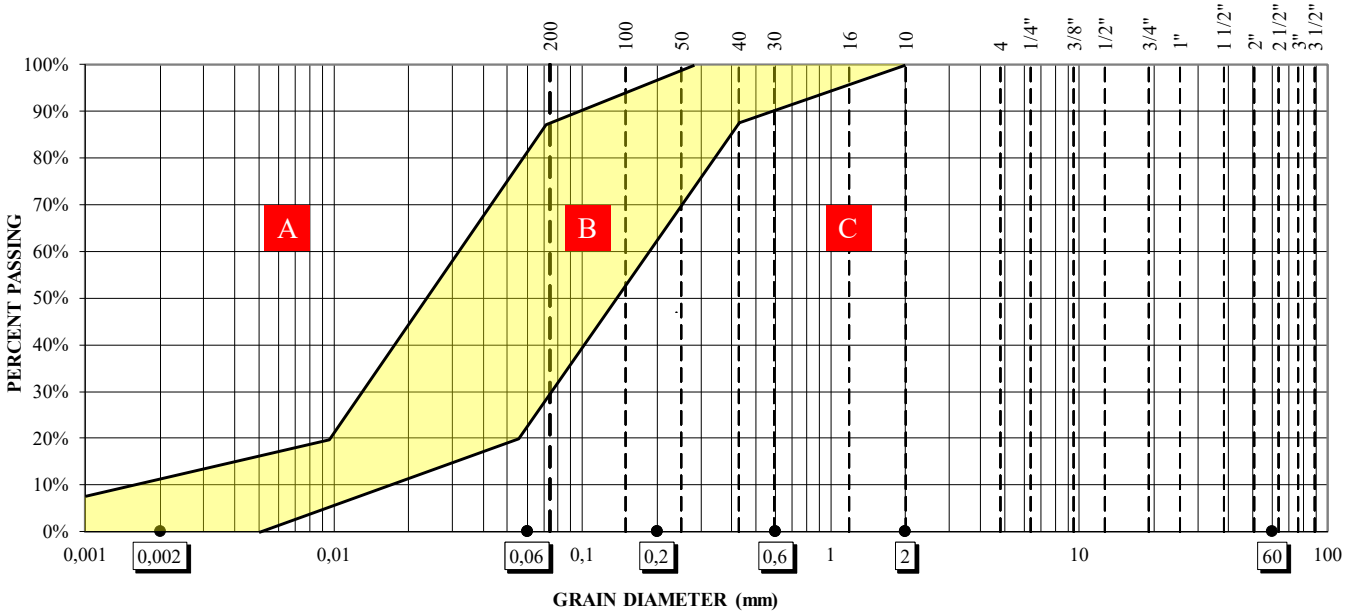


Figure 7: Efficiency of vibro-consolidation with application of the equipment described for production-scale mining test

The mining operation was standardized in average 30-day cycles from filling, rest, vibro-consolidation, and mining, as shown in Figure 8. Figure 9 shows some of these stages.



Figure 8: Management cycle through mining

Figure 9a shows the stratified structure resulting from hydraulic segregation in the particles of the tailings deposited in the reservoir. Figure 9b shows depositional layer break following vibro-consolidation, with formation of a dense and uniform horizon, where stratified layers are no longer observed.



(a) (b)

Figure 9: Various aspects of mining in the same area:
(a) before consolidation process; (b) after consolidation process

Including the vibro-consolidation stage before tailings mining has significantly improved the operational conditions, both at excavation faces and at offloading points in the deposit, thus allowing the area to be released for a new disposal cycle within the 30-day drying cycle and ensuring an exceptional stacking condition. Table 4 shows the average of random sampling for moisture content and dry apparent specific mass, carried out at mining faces and in the permitted deposit close to the dam.

Table 4: Average moisture and dry apparent specific mass values for production scale test

Collection point	avg-w (%)	avg-ρs (g/cm³)	Number of tests
Mine	20.60	1.920	43
Offloading pad	18.90	1.954	57
After 30 days	12.64	1.976	16

For moisture contents around 20%, removal to the deposit was easier, thus allowing the haul truck to be directly loaded and a dump box (haul bed) to be fully filled up. Following operations standardization, a moisture content threshold of 23% was set for mining to avoid collapses and maintain the operational condition of the deposit. Above this value, mine face operations were halted, and the material was reworked with the application of vibro-densification until it fell within the reference moisture content. Table 5 summarizes test scheduling and execution and highlights the productivity rate attained, as well as the average values measured for physical availability of tested equipment.

Table 5: Summary of production scale test performed

Period	Worked hours		Volume (m³)		Accumulated precipitation (mm)
	Estimated	Actual	Estimated	Actual	
March 2017 to May 2017	1,330	1,254	526	547.32	143.80
June 2017 to August 2017	1,710	1,672	944	1007.35	30.3
September 2017 to November 2017	1,140	1,425	870	920.60	410.7
December 2017 to February 2018	1,045	1,140	700	343.905	704.1

Even though worked days were more than estimated, the productivity rate obtained in the test was 7.8% below, which reflects the fact that the physical availability of equipment was below expectations in some months, once fleet sizing had forecasted an average productivity rate of 8,300 m^3/day. Such productivity expectation was only attained or surpassed under ideal operational conditions, i.e., without any interferences or excessive equipment breakdown.

Tested earthworks equipment has proven to be appropriate for fine tailings excavation, with approximately 70% 200 mesh sieve undersize (0.075 mm), and high specific grain mass (Gs = 3.31 g/cm^3), with productivity peaks above expectations attained. The operation is extremely sensitive to rainfall, with varying downtime due to precipitation volume.

Strength gain in the vibro-densification process

Strength gain with the application of the vibro-consolidation process was assessed by CPTu tests in a specific portion of the test area, both before and after the process, by using only the amphibious excavator to handle the material. Figure 10 shows the results before and after the use of the amphibious excavator, respectively, for a reference depth of 3 m. Tests have evidenced tip resistance gains close to or higher than

100% increment from baseline data down to a depth of 2 m. From this point downward, no significant strength gain has been evidenced.

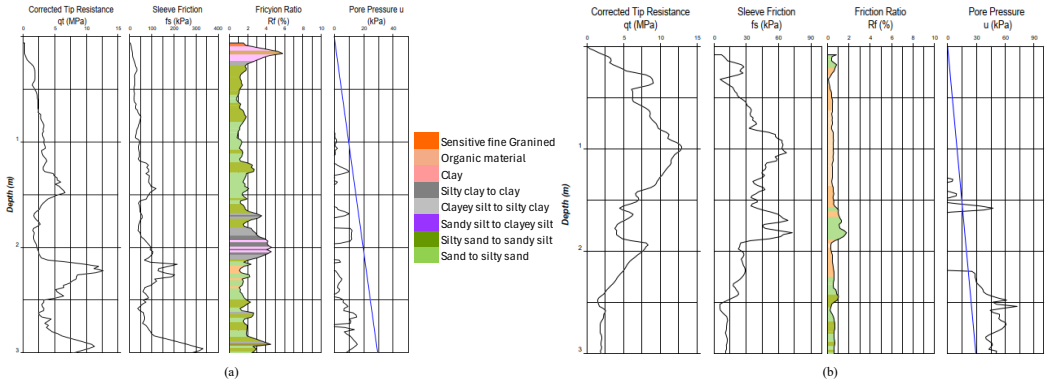


Figure 10: Test carried out: (a) before and (b) after vibro-consolidation

Also, upon observing SBTn classification abacus for soils, based on CPT tests (modified from Robertson, 1990), dispersion of results is reduced and migration of ranges 3, 4, and 5 of clays, silty clays, and clayey silts to ranges 6, 7, and 8 of clayey silts, sandy silts, and silty sands can be observed. As for pore pressure generation, in spite of the low values recorded in both tests, the generation over the first 2 m following vibro-consolidation might be considered null, which stands for gains in the stability condition, in addition to enhanced material workability.

Initially, process efficiency was expected to reach a depth of at least 3 m, which did not occur as per the test performed. One of the major reasons for this is that the amphibious excavator boom and size limited the conditioning to a maximum depth of 2 m and, even if a complementary stage with the vibrating plate excavator had been performed, initial strength gain would hinder applied energy from being transmitted beyond the previously consolidated depth.

Therefore, a proposition to overcome such constraint and reach the expected 3 m would be the fabrication of a hybrid piece of equipment, representing a mix of an amphibious excavator and a vibrating plate excavator, as shown in Figure 11. This would allow for an increase in vibro-consolidation process efficiency, as well as reaching the expected 3 m depth and working anywhere within the reservoir, in a thoroughly autonomous way.

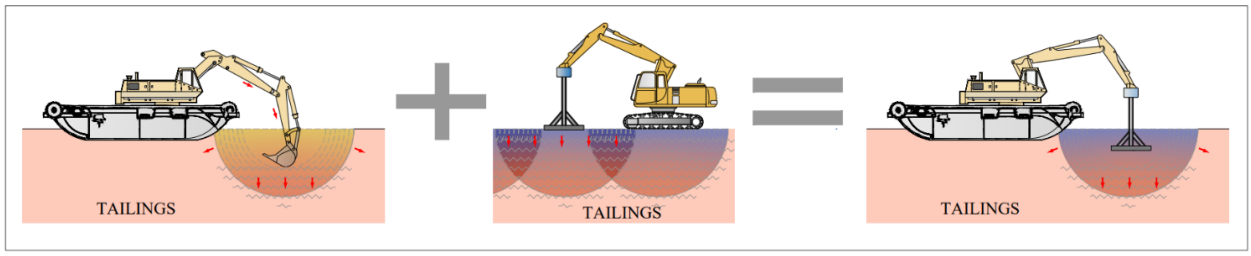


Figure 11: Proposal for the development of a new piece of equipment called amphibious plate

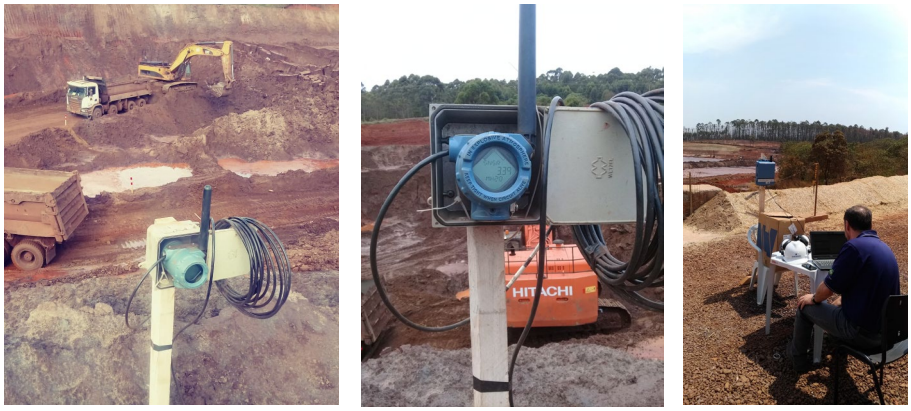
Vibration and pore pressure monitoring

During test performance, vibro-consolidation and excavation operations were monitored with vibration and pore pressure measurements at a fixed location 20 m away from the operations. Vibrations were measured from the surface by Micromate engineering seismographs, manufactured by Instatel (Figure 12), while pore pressure was measured at a 5.5 m depth by an electric piezometer manufactured by Emerson Measurement Instrumentation (Figure 14).



(a) (b) (c)

Figure 12: Vibration monitoring during operations cycle:
(a) geophone installation; (b) equipment display; (c) data acquisition



(a) (b) (c)

Figure 13: Pore pressure monitoring during operations cycles:
(a) position in relation to site; (b) equipment display; (c) remote data acquisition

Average results obtained are shown in Tables 6 and 7 below.

Table 6: Summary of production scale test performed

Reference	Parameter			
	Resulting Particle Velocity – VpR (mm/s)	Particle Displacement (mm)		Acceleration (g)
Average Value	0.2296	0.2296	0.0041	0.0057

Table 7: Summary of production scale test performed

Reference	Pore pressure (kPa)		
	Initial Phase	Vibro-consolidation Phase	Excavation Phase
Average Value	48.05	44.23	34.71

Vibration measurement records were not very significant, being close to the natural ground condition. As for pore pressures, a decrease in vibro-consolidation and excavation phases was observed against the initial condition. Records assessment allows for classification of the operational cycle applied in the test with localized interferences and without any relevance towards overall stability. A potential vibration-induced liquefaction due to the application of the technique would not be of any relevance either.

Disposal in a transitional storage facility

The excavation material was hauled and disposed of at a storage facility 3 km away from the dam, in an area duly permitted for tailings and waste disposal, as shown in Figure 14. Following excavated tailings spreading at the storage facility, with no rainfall, quick moisture loss was clear to see, even with no internal drainage element underneath tailings. Nonetheless, the best operational results were observed 30 days after material placement.



(a) (b) (c)

Figure 14: Transitional storage facility: (a) placement; (b) spreading; (c) compaction

Table 8 shows the average values obtained in the compaction control performed by random sampling after test completion, in 1 m deep trenches.

Table 8: Compaction control after test completion (average values)

Woptimum (%)	ρsmax (g/cm³)	Compaction degree (%)	Number of samples
11.6	2.180	100.2	9

The average Compaction Degree (CD) for the sampling points reached values above 100% of the Proctor test energy. This was a characteristic of the material when dry compacted, below the optimum moisture. Adopting the geometry previously described, along with the construction cycle, has ensured geotechnical stability to stacking, providing flexibility to potential mining aiming at management or decommissioning, and allowing for intermediate storage facilities to be established between the mine face and the processing plant.

Conclusion

Tailings harvesting is quite a recent approach in Brazil, with few cases having been described in literature, almost always focusing on the treatment process to be applied to disposed tailings, with mining methodology and geotechnical safety matters not being approached for this type of operation. Hence the required previous tests with equipment to provide elements to allow for a coherent technical assessment, with appropriate mining method selection to inform the development of a production plan aiming at technical and economic feasibility analyses, as recommended by Muir et al. (2005).

The results obtained from the trial using tailings vibro-consolidation technique enhancement showed that mechanized tailings excavation is a technically feasible alternative, with potential for handling large volumes of tailings. Vibration generation during excavations was moderate, with low magnitudes, in a localized fashion, only close to mine faces. Along these lines, when mining is a decommissioning solution, eliminating a tailings dam can be very worthwhile for the project owner.

Design criteria presented were specifically determined to be applied during the test phase. Upon progressing to a final design, new specific technical and economic assessments are crucial for project owner's decision-making on associated risks, so as to ensure total geotechnical safety, thus preventing accidents during excavation phases. Less daring geometries should be designed, so as to ensure higher factors of safety than the ones considered for the test.

It is noteworthy that a possible liquefaction induced by vibration to be potentially triggered by the use of the technique is punctual and has proven to be of little relevance to global stability, however, studies monitoring vibrations and additional pore pressures are ongoing, associated with representative numerical models for a complete validation of the technique applied to hydraulic landfills.

Reclamation of tailings disposed in dams stands for a clear alternative to closure, decommissioning, and/or management, which may be feasible, provided that it is well studied and developed. For this purpose,

six stages are required: Reservoir characterization; qualitative and quantitative tailings modeling; mine plan development; definition of process route/disposal location; operationalized layout; and performance of production scale tests.

All the development described in this paper is for academic purposes, aiming at contributing to the development of dam mining project engineering at a conceptual level, for each project has its own specific features, in addition to legal and environmental requirements, with direct application of results not being recommended.

Acknowledgments

The authors would especially like to thank Vale for its financial support to the project and for allowing the use and dissemination of test results, as well as the Federal University of Ouro Preto – UFOP, represented by NUGEO, for its partnership in technological development focused on sustainable mining.

References

Alves, H.O. 2015. *Estudo comparativo de duas técnicas de lavra em barragem de rejeito sob o ponto de vista geotécnico.* Thesis research, Federal University of Minas Gerais.

Carmo, F.F., Kamino, L., Junior, R.T., Campos, I.C., Carmo, F.F. Silvino, G. and Pinto, C.E.F. 2017. Fundão tailings dam failures: the environmental tragedy of the largest technological disaster of Brazilian mining in global context. *Perspectives in ecology and conservation* 15(3): 145–151.

Esfahanizadeh, M. and Atashband, S. 2012. Vibro-probe technique evaluation in soil improvement against liquefaction. *Proceedings of 15WCEE-15th World Conference on Earthquake Engineering.* Lisbon. Portugal.

Flores, J.C.C. and Lima, H.M. 2012. *Fechamento de mina: aspectos técnicos, jurídicos e socioambientais*. Ouro Preto: Federal University of Ouro Preto.

Muir, A., Mitchell, J., Flatman, S.R. and Sabbagha, C.A. 2005. Practical guide to re-treatment of gold processing residues. *Minerals Engineering* 18(8): 811–824.

Petley, D. 2020. Brumadinho: the expert panel report on the failure of the Feijão tailings dam. *American Geophysical Union Blogosphere.* Accessed 22/05/2024 at: https://blogs.agu.org/landslideblog/2020/01/20/brumadinho-tailings-disaster/

Queiroz, H.M., Nóbrega, G.N., Ferreira, T.O., Almeida, L.S., Romero, T.B., Santaella, S.T. and Otero, X.L. 2018. The Samarco mine tailing disaster: a possible time-bomb for heavy metals contamination? *Science of the Total Environment*. 637: 498–506.

Robertson, P. K. 1990. Soil classification using the cone penetration test. *Canadian Geotechnical Journal* 27(1): 151.

Sousa, G.M. 2020. *Proposta de metodologia para lavra de barragens de rejeitos de ferro construídas pela técnica de aterro hidráulico*. Doctoral thesis, Federal University of Ouro Preto.

Design, Construction, Monitoring and Numerical Modeling of Large-scale Field Trials: Assessing Cover Performance for Reclamation Method Selection

Karine Sylvain, WSP Canada Inc., Canada
Marie-Lin Breard Lanoix, WSP Canada Inc., Canada

Abstract

The selection of the reclamation method for tailings storage facilities (TSF) can pose significant challenges, necessitating innovative approaches to its comprehensive evaluation. Four large-scale field cells were constructed at Canadian Malartic Mine (Quebec, Canada) to address specific considerations for selection of the reclamation method, particularly in terms of the constructability and performance of the covers. Each cell was instrumented with a dense system of hydrogeological and oxygen probes. Two meteorological stations were installed to record local climate conditions. The index properties of the cover materials were used to estimate the hydrogeological properties. Field data, comprising thorough monitoring of climate conditions and hydrogeological evolution, were integrated into a 2D transient numerical model in SEEP/w.

This paper presents the methodology and the calibration results of the numerical model of one low permeability cover cell. The numerical model calibration involved the estimation of the spatial distribution of the material properties such as porosity, hydraulic conductivity, and the water retention curve. The calibrated results were consistent with observed field data, highlighting the reliability of the numerical model when combined with extensive monitoring and characterization to accurately represent the complex hydrogeological dynamics in the multi-layer covers. This case study demonstrates the capacity of a numerical model to effectively represent the hydrological evolution of the covers, and how large-scale field trials combined with comprehensive data can enhance confidence in the selection of the reclamation method.

Introduction

One of the main challenges of the mining industry is the long-term management of the tailings storage facilities (TSF) in terms of geochemical stability. Tailings can contain sulfide minerals which, when exposed to atmospheric oxygen and water, can react to generate acid mine drainage (AMD) which is characterized by acidic pH, high concentrations of sulfates and metal(oid)s (Blowes et al., 2014). One of

the primary objectives of mine site reclamation is to prevent AMD in the long-term (Aubertin et al., 2016). Typically, reclamation methods to prevent AMD are based on inhibiting oxidation reactions by limiting the concentration of one of the reactants of the oxidation reaction: water, oxygen or sulfides (Aubertin et al., 2016). The selection of the method depends primarily on the water balance and climate of the mine site but also the topography and natural material availability near the site (Bussière and Guittonny, 2021). For example, under humid and temperate climates, such as encountered in Quebec, Canada, oxygen exclusion is one of the most effective reclamation methods (SKR, 1989). The diffusion of oxygen in water is significantly lower than in air, which can inhibit the oxidation reaction (Yanful, 1993; Nicholson et al., 1989). Consequently, in a saturated porous medium, oxygen diffusion is limited, which can inhibit the oxidation reaction (Mbonimpa et al., 2003). This can be achieved by maintaining the tailings in a high degree of saturation by maintaining an elevated water table position combined with a monolayer cover or using multi-layered cover such as cover with capillary barrier effects (CCBE).

Selecting the most appropriate method for a mine site involves extensive studies which imply thorough analysis of site-specific conditions. For example, Aubertin et al. (2002) outlined eight major key steps for designing the reclamation method, as demonstrated in a case involving a CCBE : 1) Comprehensive characterization of mine waste and cover constitutive material, 2) Gathering climatic and environment data, 3) Preliminary evaluation study, 4) Numerical modeling, 5) Laboratory physical modeling, 6) In-situ test plots, 7) Final design selection and the 8) construction and long-term monitoring.

This conference paper describes both the methodology and the integration of the results of large-scale field trials and 2D numerical simulations, which are key steps leading to the final selection of the reclamation method. Particularly, this case study demonstrates the numerical model ability to represent field conditions, while highlighting the importance of large-scale field trials and extensive data that can lead to a greater confidence in the selection of the reclamation method, guiding towards the selection of the final design.

Site and large-scale field trials description

Site overview

The Canadian Malartic (CM) mine site owned by Agnico Eagle Mines (AEM) is one of Canada's largest open-pit gold mines. It is located in the northwest of Quebec Province, in the Abitibi region. The operation began in 2011 in the CM pit, which was mined until 2023. The operation is still ongoing with the Barnat pit and the Odyssey underground sector. Since 2011, the mine has produced thickened tailings, mainly potential acid-generating (PAG) tailings, which have been stored in a TSF constructed over an abandoned tailings facility (East Malartic). The actual TSF is now composed of seven deposition cells confined by starter embankments raised by the upstream method and the waste rock pile to the North. Over the years,

the perimeter TSF berms were raised at an overall slope between 10H:1V to 20H:1V, except for the recent confining structures. which are made of a single embankment with 2H:1V to 3H:1V slopes. Each upstream raise is 2 m high and composed of waste rocks and a separation of geotextile fabric. In 2024, the TSF has almost reached its full capacity with the tailings deposition moving along in the CM pit.

Large-scale field trials configuration

The CM mine has conducted several studies over the years in preparation for the TSF closure. Among them was the design of four large-scale field trials constructed directly on the TSF to address the constructability and performance of the reclamation methods (see Figure 1). The location was selected to evaluate the hydrogeological cover performance on both waste rocks upstream raises and tailings plateau. Each cell was built on an area that was approximately 250 m long by 15 m wide, and was isolated on each side by low permeability material. Two cells were constructed with covers with capillary barrier effects (CCBE), to reduce oxygen fluxes through the tailings, while the other two cells consisted of low permeability covers designed to limit water percolation into the tailings and promote runoff. Each cell was instrumented with a dense system of hydrogeological (e.g., volumetric water content and suction) and oxygen probes at different locations and depths. A total of approximately 1,200 probes were installed as water-collecting systems to measure runoff and water flow through specific layers of the covers (e.g., Parshall flume and water flow meter). Volumetric water content probes were initially calibrated in a laboratory.

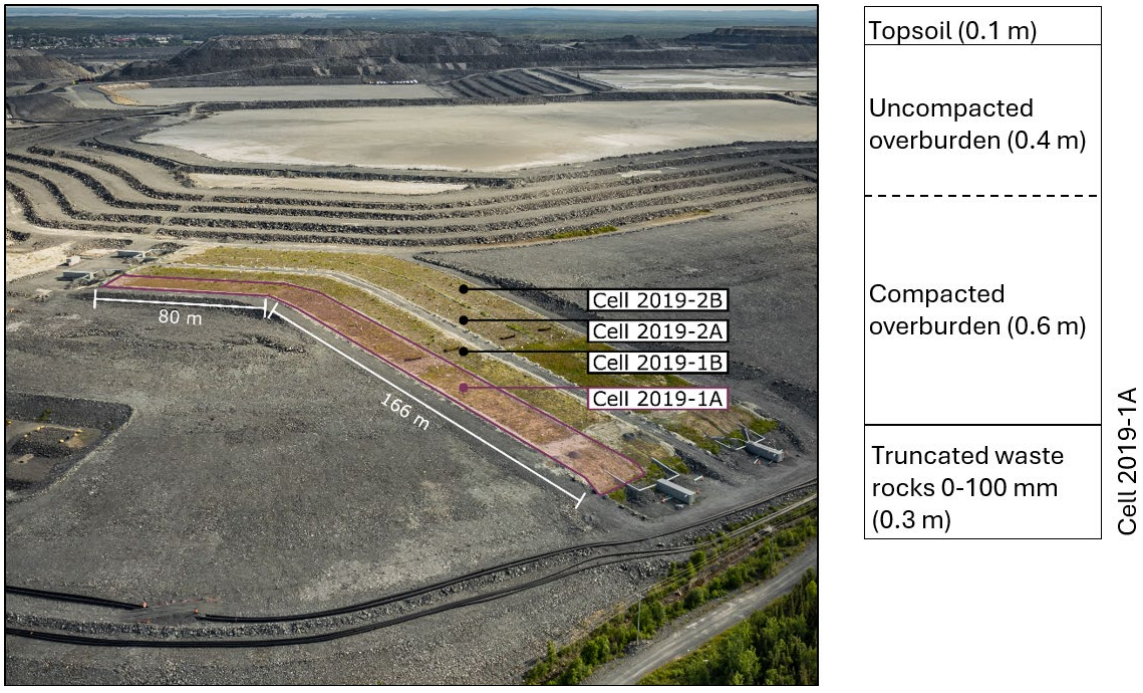


Figure 1: Large-scale field reclamation cover trials at the Canadian Malartic Mine. The field cell 2019-1A (purple) was selected for this study

Specifically, the field cell 2019-1A was selected for this study due to the similarity of the actual cover geometry considered by the mine. The cover configuration from top to bottom of the 2019-1A cell consists of 0.1 m of uncompacted topsoil, 0.4 m of uncompacted overburden, 0.6 m of compacted overburden, and 0.3 m of truncated waste rocks (e.g., particle grain size between 0 mm and 100 mm). On the plateau, an additional waste rock layer (pit run) is present between the transition waste rocks layer (0-100 mm) and the existing tailings for trafficability during the construction. On the downstream slope, the upstream raises have been first reprofiled with a continuous slope of 10H:1V and an intermediate horizontal section.

Methodology

Cover materials properties

In-situ and index laboratory testing has been performed to characterize the different cover materials during the construction of the large-scale field trials. The range of porosity was estimated, with the in-situ density measured with the nuclear densimeter and the sand cone method, based on the specific gravity (G_s) obtained in the laboratory.

A total of 20 samples of the overburden soil were collected to perform particle size distribution tests according to BNQ 2501-025, and 5 samples were collected to perform Atterberg limits tests. The overburden was classified as a clayey silt to silty clay (CL-ML) to a clayey silt (CL). The hydraulic conductivity was obtained on the field using a Guelph permeameter and compared to predictive methods such as the Kozeny-Carman model (KC; Chapuis and Aubertin, 2003), the modified KC (KCM; Mbonimpa et al., 2002) and Chapuis (Chapuis, 2012). The estimated hydraulic conductivities of the overburden varied between 8E-11 m/s and 9E- 07 m/s. The water retention curve (WRC) was predicted using the Modified Kovacs model (MK; Aubertin et al., 2002) and compared to the in-situ WRC expressed using the van Genuchten (1980) equation and the field suction and volumetric water content (VWC) measured with instruments (Figure 2a), which included hysteresis phenomena (not presented here). The permeability functions were calculated from the WRC using the van Genuchten model (Figure 2b). The heterogeneity of the overburden properties was simplified for numerical purpose in four sets of parameters associated with their locations (plateau [PL] vs. slope [SL]), and the compaction (uncompacted layer vs. compacted layer).

The particle size distribution (PSD) of the waste rocks (0-100 mm) was obtained in laboratory for 6 samples and the result showed little variability between them. The index properties were used to estimate the hydraulic conductivity using the Shepherd model (1989), KCM, KC, and Chapuis. The WRC and the permeability function were obtained using the Fredlund et al. (1994) model, which is more accurate for coarser material such as waste rocks. The hydrogeological properties of the uncompacted topsoil were estimated using field porosity and the laboratory G_s.

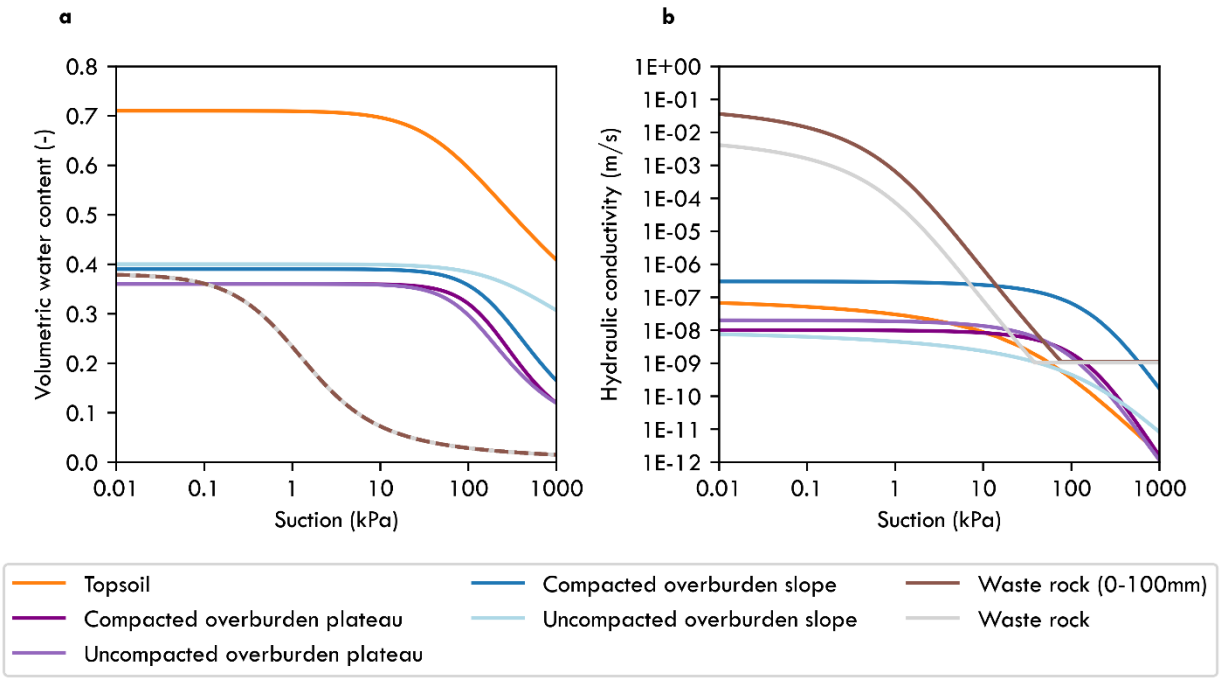


Figure 2: WRC and permeability functions of the cover materials applied in the numerical model

Climate data

The CM mine is located approximately 20 km from the town of Val-d'Or, where meteorological stations have been acquiring data since 1951. Between 1951 and 2023, the mean annual temperature is 1.6°C. The hottest month is July, with a mean temperature of 17.4°C, and the coolest month is January with a mean temperature of -16.6°C. Generally, the temperature is above 0°C around mid-April to early November. The mean annual total precipitation for the same period (i.e., 1951 to 2023) was 908 mm, with a minimum of 704 mm in 2021 and a maximum of 1,183 mm in 1979.

Specifically, the CM mine had installed two meteorological stations on the large-scale field trial area, one on the plateau and another on the slope. These two meteorological stations were in operation since July 2018, monitoring the local climate conditions (e.g., precipitations, temperature, relative humidity, solar radiation, and wind speed), including measurements of snow heights during winter to capture snowmelt infiltration and its contribution to the water balance. The measurement period used for the calibration of the numerical model corresponds to the first year of monitoring, from October 1, 2020, to September 30, 2021. The model integrated the relative humidity, the air temperature, the precipitation, the wind speed, the snow cover thickness, and the solar radiation (Figure 3). The solar radiation was estimated in the numerical model based on the latitude of the site (48.1°) and the albedo was assumed as a constant value of 0.3, due to a lack of solar radiation data over the monitored period.

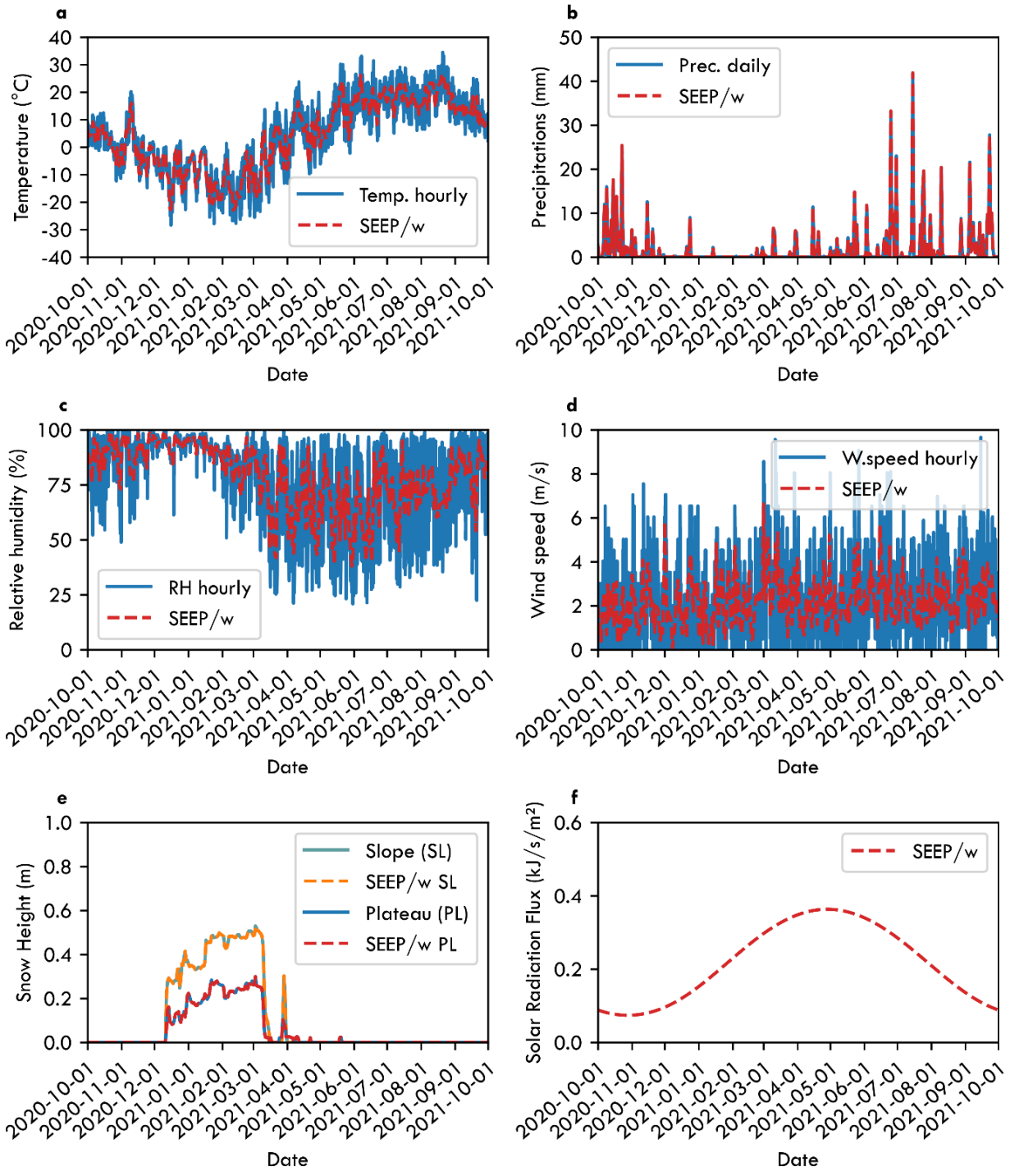


Figure 3: Climate from the weather stations (solid line) and the input parameters in the numerical model SEEP/w (dashed line) for a) Temperature (°C), b) Precipitation (mm), c) Relative humidity (%), d) Wind speed (m/s) e) Snow height (m) of the slope (SL) and the plateau (PL) f) Solar radiation approximated in the numerical model from the latitude (kJ/s/m²)

Numerical model methodology

The numerical analyses of the large field trials were performed using the finite element software SEEP/w (GeoStudio, 2023). The geometry of the model was represented by a 2D configuration and showed a 740 m-long cross-section in the large-scale field trial sector intercepting the initial toe berm, the different upstream raises, and the tailings surface. The cover configuration of the 2019-1A cell was built with the functionality of a Surface Layer to generate a fine discretization near the surface, with a resolution varying between 0.05 m and 0.07 m. The regions below the cover were built using quadrilateral and triangular elements, with an element edge length between 1 m and 5 m. Adjustments of the under-relaxation criteria due to the non-linearity of the input functions (e.g., particularly waste rocks and Land-Climate Interaction [LCI] conditions) were applied in the model by changing the initial rate of the under-relaxation criteria at 0.65 and reducing the minimum rate at 0.01. The numerical modeling approach for this study was selected to optimize the convergence and the time calculation.

The validation of the numerical model was performed by simulating the first year of data acquisition (i.e., before vegetation establishment, except for the lower portion of the slope) and comparing the temporal numerical VWC results with the VWC measured by the instruments at a similar elevation (e.g., daily time step). More specifically, three criteria were selected to choose the probes for the calibration of the numerical model: 1) similarity of the particle grain size distribution; and 2) the porosity (maximum variation of ± 0.02) between the in-situ and the modeled material; and 3) the raw data range used for the probe calibration in laboratory compared with the range measured by the instruments on the field. The modeled material properties were adjusted iteratively, based on the range of values obtained in the laboratory. The validation was based on the fit between the numerical results and the measured VWC using the Root Mean Square Error (RMSE) and the Mean Absolute Error (MAE), in addition to qualitative observations of the general behavior of the VWC (e.g., the increase of the VWC after a rainfall event followed by the rate of desaturation).

The verification of the numerical stability was performed in a four-year cycle to confirm that the initial steady state parameters did not influence the response of the transient model using the LCI boundary condition. The water balance result was similar in the second, third, and fourth year of simulation. The long-term behavior of the cover was modeled using the cumulative net infiltration of the second year and applied to a steady state model coupled with the transient model. The 2019-1A cover was also modeled on two other cross-sections of the CM TSF to verify the influence of the upstream raises geometry and the impact of the waste rock pile directly in contact with the tailings (not presented in this paper).

Results

Numerical validation of the VWC on the plateau and the slope

The numerical validations were performed for the unfrozen period from June to October, because minimal variations in VWC were observed. Such an approach is used in comparative studies (Pabst et al., 2017; Éthier et al., 2018). Simulated VWC fluctuations correlated with the seasonal variations and followed the same general trends of the field for the plateau (see Figure 4). For example, the simulated VWC of the topsoil (orange dashed lines) at a depth of 7 cm on the plateau at station PL-S1 increased after a rainfall and subsequently decreased due to drainage and evaporation, which is consistent with field VWC fluctuations. However, the VWC of the field was more varied due to the greater field porosity measurements. The RMSE and MAE were respectively 0.06 and 0.05 for the topsoil. Furthermore, the overburden layers (purple dashed lines) also had a good correlation with the field measurements. For example, the RMSE and MAE were both equal to 0.01 for the probes at a depth of 91 cm, with SEEP/w result and the field VWC at 90 cm. The maximum RMSE and MAE calculated for the compacted and uncompacted overburden were 0.05 for station PL-S1 on the plateau.

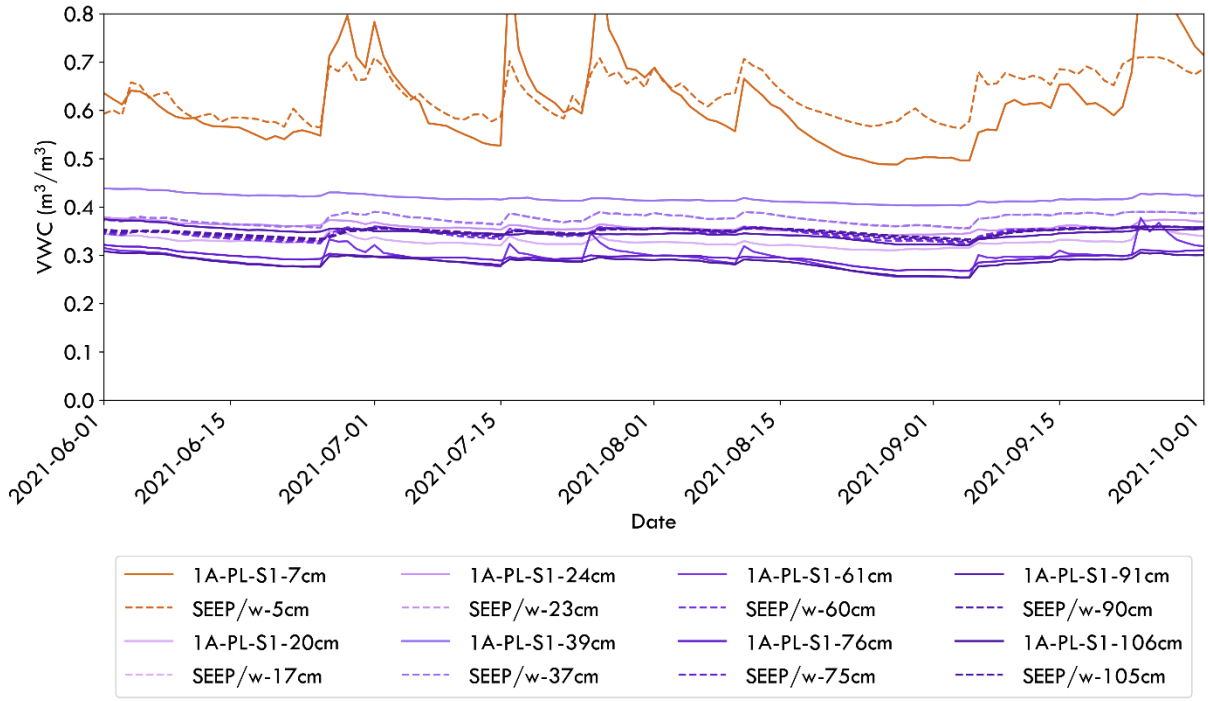


Figure 4: Evolution of the volumetric water content of the cover materials after winter. The dashed lines present the SEEP/w results, and the continuous lines present the results of the probes on the plateau (PL) at the station PL-S1

The results at the upper part of the slope at the station SL-S1 were also well represented by the numerical model (Figure 5). For example, after a rainfall, the VWC of the topsoil (orange lines) increased

substantially, followed by a decrease due to drainage and evaporation. The VWC of the overburden (blue lines) had the lowest amplitude, and the RMSE and MAE were lower than 0.05.

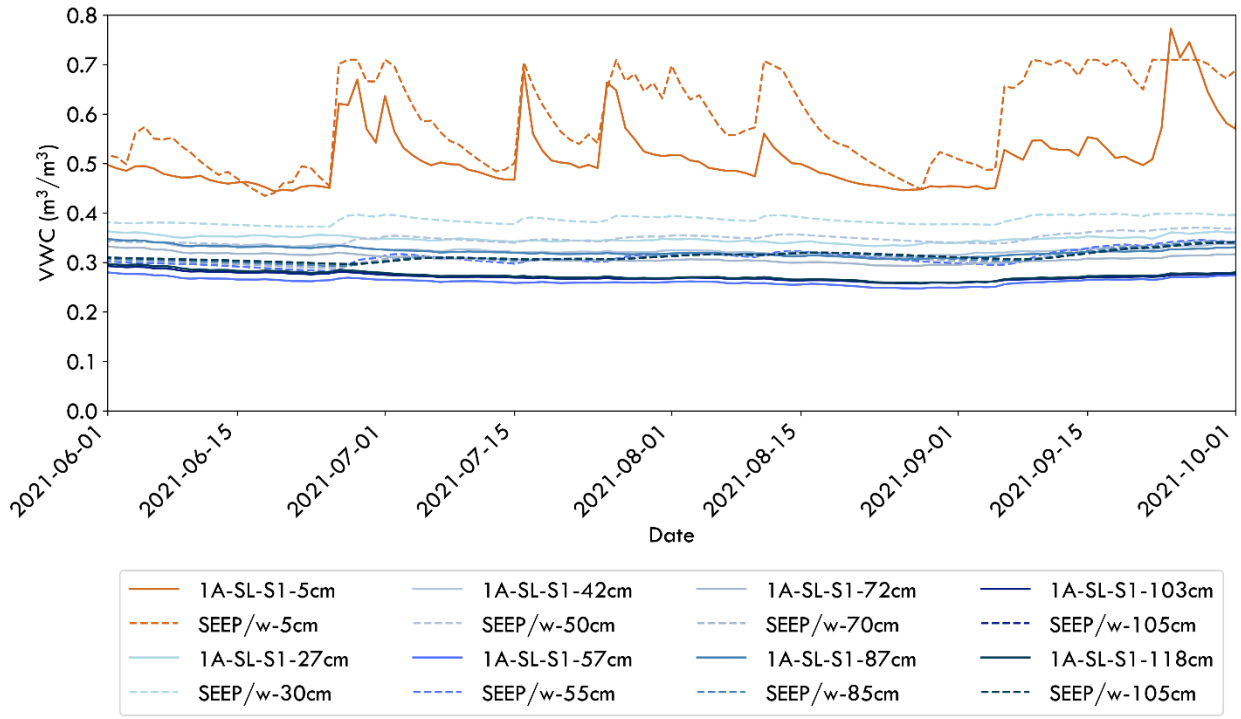


Figure 5: Evolution of the volumetric water content of the cover materials after winter. The dashed lines present the SEEP/w results, and the solid lines present the results of the probes on the upper part of the slope (SL) at the station SL-S1

The transient simulation was able to represent the general behavior of the VWC for the instrument stations and the probes on the plateau, along the upper and middle portion of the slope. The model was therefore considered representative of the field conditions and was validated for further analysis of the hydrogeological behavior of the cover system.

Water balance estimation

The water balance of a one-year cycle was analyzed to understand the influence of the cover configuration 2019-1A compared to a scenario without cover, which was considered as the reference case representing the actual state for the same cross-section (Table 1). For both scenarios, the vegetation aspect was not simulated. It was assumed that the vegetation would have the same influence on both water balance results and thus are only reliable for comparison. The addition of the 2019-1A cover on this TSF sector reduced the net infiltration, decreasing from 215 mm/y to 140 mm/y on the plateau and 255 mm/y to 55 mm/y on the slope. The runoff portion increased with the cover placement and the reprofiled slope. For both scenarios, the actual evaporation was similar, varying between 50% and 60%. The numerical results showed the effectiveness of the cover in reducing infiltration into the TSF.

Table 1: Water balance estimation (SEEP/w)

Model	Location	Net infiltration (mm/y)	Net Infiltration (%)	Runoff (%)	Actual evaporation (%)
Reference case (without cover)	Plateau	215	32	10	58
	Slope before reprofiling	255	39	1	60
2019-1A cover configuration	Plateau	140	23	22	55
	Slope reprofiled 10H:1V	55	10	40	50

Cover performance over the long term

The long-term behavior of the cover was modeled using the cumulative net infiltration of the second year (e.g., 140 mm/y on the plateau and the intermediate plateau and 55 mm/y on the slopes) and applied to a steady state model coupled with the transient model. The degree of saturation (S_r) in the center of the compacted overburden layer (continuous lines) and the uncompacted overburden layer (dashed lines) were represented for two time steps: end of July (orange lines) and for the steady state (blue lines; Figure 6). The compacted and uncompacted overburden layers maintain the same S_r on the plateau (e.g., 99% at the steady state and approximately 92% at the end of July). The compacted layer desaturated on the slope portions to reach a minimum S_r of 94% at the steady state and 80% at the end of July. The results are compared to S_r of 85%, representing the threshold value where the oxygen diffusion is significantly reduced (Collin and Rasmuson 1987; Aubertin et al., 2002). In the case of the 2019-1A cover, oxygen reduction was not part of the cover design criteria, but its evaluation was used to understand the hydrogeological behavior along the cross-section and the impact of the slope sections.

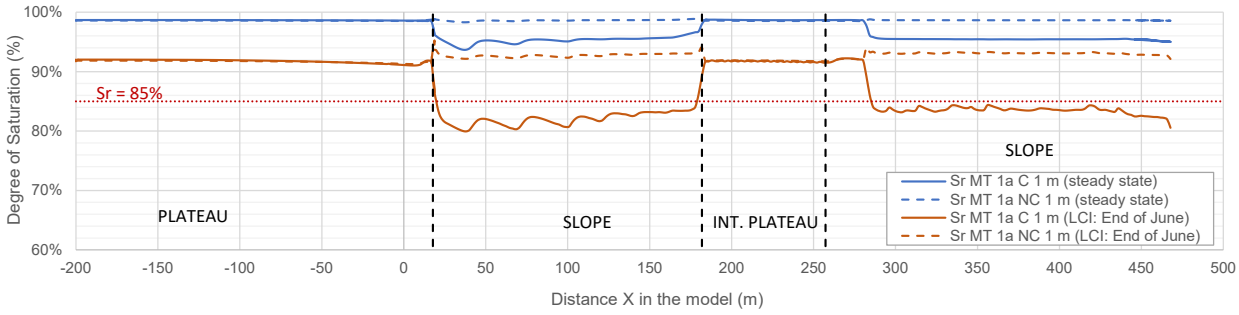


Figure 6: Degree of saturation of the uncompacted and compacted overburden layer at the end of June and in steady state condition

Discussion

Model calibration involved estimating the spatial distribution of the material properties, and the simplifications were required to manage feasibility while maintaining model accuracy. Field data included

numerous probes to capture variations in VWC, of which some disparity in porosity and behavior was observed within a given layer. The mean porosities of each layer were used in the simulation, which could explain the main difference in the field VWC data and the simulations. The manufacturer's calibration of the probes was also a specific validation criterion, and the measurement range was specifically addressed when selecting the probes for numerical validation. The WRC and permeability functions of the waste rocks were typically steep. Therefore, the permeability function was cut at 1E-09 m/s to ensure convergence of the numerical model, which implied that no capillary break between the overburden and the waste rocks was simulated.

The instrumentation stations located on the lower portion of the slope were not considered for the numerical calibration as vegetation had grown and only barren soil was simulated. VWC measurements in this sector were influenced by the vegetation during the unfrozen period. Vegetation establishment can significantly modify the water balance in cover systems (Yves-Dady et al., 2018). For example, vegetation can intercept rainwater and limit erosion (Zhang et al., 2022). Vegetation can also increase infiltration and significantly increase evapotranspiration rates, which can reduce deep percolation (Nicholls et al., 2019). Finally, vegetation can modify the soil albedo, which has a direct influence on radiation and therefore on evaporation. The impact of the vegetation establishment will be evaluated in further studies.

Conclusion

Selecting the most appropriate method for TSF closure involves extensive studies, and might consider site-specific conditions such as climate, material availability, geometry, and social aspect. This case study presented the methodology used to integrate the CM large-scale field trial data (probe results and meteorological in-situ data) to calibrate a 2D transient numerical model using SEEP/w. The material properties of the numerical model were adjusted using the index laboratory results and the in-situ WRC. The modeled material properties were adjusted iteratively based on the fit between the numerical results and the measured VWC using the RMSE and the MAE, in addition to qualitative observations such as the general behavior of the VWC and the hydrogeological properties ranges. The correlation between the general behavior of the VWC measured and simulated demonstrates the numerical model's ability to represent field conditions. At this stage, the numerical results were used to compare different cover configurations, layer thicknesses, and TSF geometry. In further studies, it is planned to better understand the influence of the vegetation, as well as the impact of climate change on the cover performance.

Acknowledgements

The authors would like to acknowledge the contribution of Canadian Malartic's Agnico Eagle Mines personnel for the large-scale trials and their support. The authors also acknowledge the contribution of their

WSP colleagues, particularly Vincent Martin and Myriam Roy, who directly contributed to the numerical simulation work.

References

Aubertin, M., Bussière, B. and Bernier, L. 2002. *Environnement et gestion des rejets miniers*. Presses Internationales de Polytechnique, Corporation de l'École Polytechnique de Montréal, Montréal. http://www.presses-polytechnique.ca/fr/environnement-et-gestion-des-rejets-miniers

Aubertin, M., Bussière, B., Pabst, T., James, M. and Mbonimpa, M. 2016. Review of the reclamation techniques for acid-generating mine wastes upon closure of disposal sites. *Proceedings of Geo-Chicago 2016:* 343–358.

Blowes, D., Ptacek, C., Jambor, J., Weisener, C., Paktunc, D., Gould, W. and Johnson, D. 2014. The geochemistry of acid mine drainage. DOI:10.1016/B978-0-08-095975-7.00905-0

Bussière, B. and Guittonny, M.. 2021. *Hard Rock Mine Reclamation: From Prediction to Management of Acid Mine Drainage* (first edition). CRC Press.

Chapuis, R.P. 2012. Predicting the saturated hydraulic conductivity of soils: a review. *Bulletin of Engineering Geology and the Environment* 71(3): 401–434. doi:10.1007/s10064-012-0418-7

Chapuis, R.P. and Aubertin, M. 2003. On the use of the Kozeny Carman equation to predict the hydraulic conductivity of soils. *Canadian Geotechnical Journal* 40(3): 616–628.

Collin, M. and Rasmuson, A. 1987. Mathematical modeling of water and oxygen transport in layered soil covers for deposits of pyritic mine tailings. Licenciate treatise. Royal Institute of Technology. Department of Chemical Engineering. S-10044 Stockholm, Sweden.

Ethier, M.-P., Bussière, B., Broda, S. and Aubertin, M. 2018. Three-dimensional hydrogeological modeling to assess the elevated-water-table technique for controlling acid generation from an abandoned tailings site in Quebec, Canada. *Hydrogeology Journal* 26(4): 1201–1219.

Fredlund, D., Xing, A. and Huang, S. 1994. Predicting the permeability function for unsaturated soils using the soil-water characteristic curve. *Canadian Geotechnical Journal* 31(4): 533–546.

Mbonimpa, M., Aubertin, M., Aachib, M. and Bussière, B. 2003. Diffusion and consumption of oxygen in unsaturated cover materials. *Canadian Geotechnical Journal* 40(5): 916–932.

Mbonimpa, M., Aubertin, M., Chapuis, R. and Bussière, B. 2002. Practical pedotransfer functions for estimating the saturated hydraulic conductivity. *Geotechnical and Geological Engineering* 20(3): 235–259.

Nicholls, E.M., Drewitt, G.B., Fraser, S. and Carey, S. K. 2019. The influence of vegetation cover on evapotranspiration atop waste rock piles, Elk Valley, British Columbia. *Hydrological Processes* 33(20): 2594–2606.

Nicholson, R.V., Gillham, R.W., Cherry, J.A. and Reardon, E.J. 1989. Reduction of acid generation in mine tailings through the use of moisture-retaining cover layers as oxygen barriers. *Canadian Geotechnical Journal* 26(1): 1–8.

Nordstrom, D.K., Blowes, D.W. and Ptacek, C.J. 2015. Hydrogeochemistry and microbiology of mine drainage: an update. *Applied Geochemistry* 57: 3–16.

Pabst, T., Aubertin, M., Bussière, B. and Molson, J. 2017. Experimental and numerical evaluation of single-layer covers placed on acid-generating tailings. *Geotechnical and Geological Engineering* 35(4): 1421–1438.

Shepherd, R.G. 1989. Correlations of permeability and grain size. *Groundwater* 27(5): 633–638.

SRK. 1989. Draft acid rock drainage. Technical Guide Vol. 1, British Columbia Acid Mine Drainage Task Force Report. Prepared by Steffen, Robertson, Kirsten in Association with Norecol Environmental Consultants and Gormely Process Engineering.

van Genuchten, M.T. 1980. A closed-form equation for predicting the hydraulic conductivity of unsaturated soils. *Soil Science Society of America Journal* 44(5): 892–898.

Yanful, E.K. 1993. Oxygen diffusion through soil covers on sulphidic mine tailings. *Journal of Geotechnical Engineering* 119(8): 1207–1228.

Yves-Dady, B., Marie, G., Bruno, B. and AbdelNabir, M. 2018. Influence of vegetation on water balance of engineered cover systems for reclaimed mine sites: literature review and outlooks. Communication presented at the 6th International Symposium on Sediment Management San Cristóbal de Las Casas, Chiapas, Mexico June 19–23, 2018 (p. 45).

Zhang, Q., Lv, X., Yu, X., Ni, Y., Ma, L. and Liu, Z. 2022. Species and spatial differences in vegetation rainfall interception capacity: A synthesis and meta-analysis in China. CATENA 213 106223. https://doi.org/10.1016/j.catena.2022.106223.

Kidston Hydro Electric Power: Re-purposing an Abandoned Mine

Malcolm Barker, GHD, Australia
Tony Ford, Genex, Australia
Peter Gaylard, Construction Joint Venture (John Holland & McConnell Dowell), Australia

Abstract

Hydroelectric power using pump storage is one of the significant renewable energy sources for Australia. The Kidston Hydro Electric Power (HEP) project provides a first for Australia in the use of a disused mine to provide both the storage capacity and the head to develop a scheme with 250 MW capacity.

.The scheme comprises an upper storage, Wises Dam, with two vertical shafts leading to the underground powerhouse discharging into the lower Eldridge pit, creating a head of over 200 m for the power generation. Pumping back to the upper storage is achieved using the turbines with solar and grid power.

The Wises Dam was constructed using waste rockfill from the mine excavation with a high-density polyethylene (HDPE) liner for the water barrier. Considerable review of the foundation conditions, including the use of a 3D leapfrog model, was required for the evaluation of the foundation depths for the HDPE plinth and the underground tunnels and powerhouse. Construction techniques for the Wises Dam liner preparation were challenging and the contractor made significant contributions to the design changes, which improved the constructability and sustainability of the works.

The Wises storage dam is now complete and the underground power station is progressing with expected power production commencing in 2025. This paper presents information on the scheme and some of the design and construction challenges from the perspectives of the Owner, Construction Joint Venture and Designer.

Introduction

The Kidston project is a 250 MW pumped storage hydro scheme located in far north Queensland on the site of the old Kidston gold mine. Gold has been mined at or near the site intermittently from 1907 up to 2001, when the mine was closed. The project incorporates the use of the two existing mining pits, Wises and Eldridge, which are shown in Figure 1 and Figure 2.

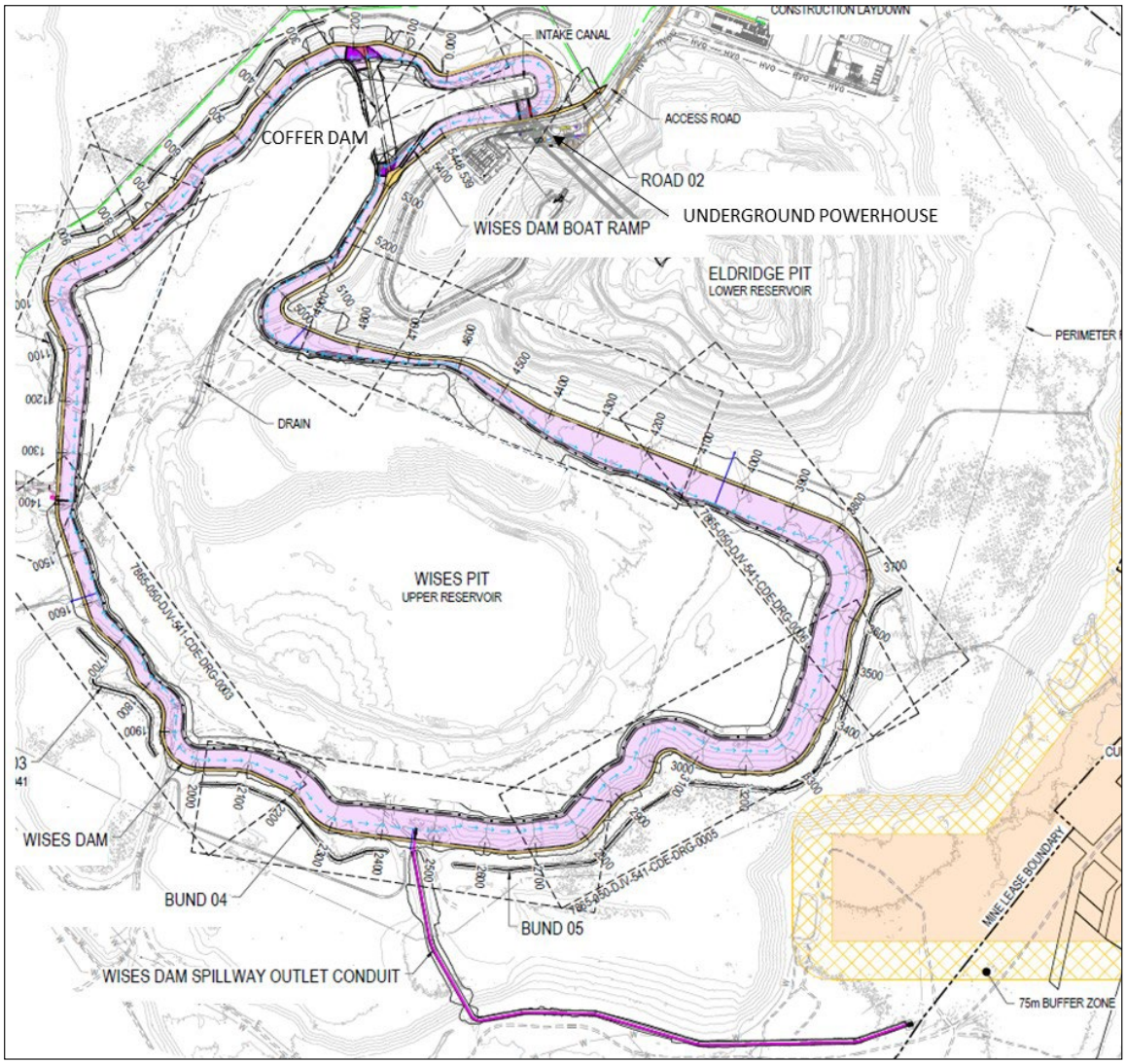


Figure 1: Project layout

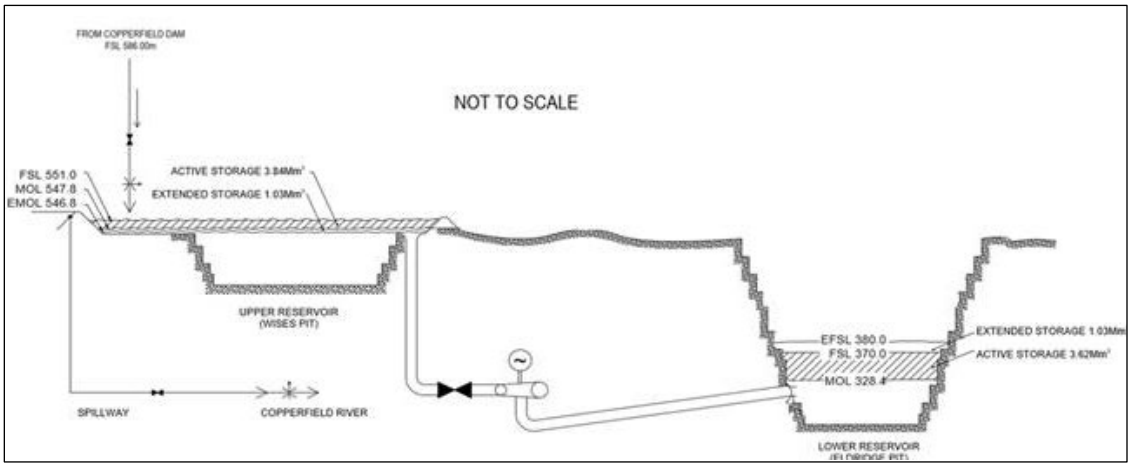


Figure 2: Project section (CJV water management plan)

Due to the historic nature of the site and the contamination from the old mining activity, seepage water from the waste rockfill area is collected from the surrounding area and pumped back into Wises Dam to prevent contamination of the environment. The Copperfield Dam, located about 20 km south of the mine, was constructed for water supply to the mine, and the existing pipeline will be used to provide makeup water where necessary. The nearby Copperfield River can accept spillway flows from the Wises storage in conditions where release is allowed by the regulating authority.

Figure 2 shows the schematic of the pumped hydro scheme, which has the underground powerhouse and tailrace into Eldridge pit connected to Wises Dam via two vertical lined morning glory shafts. The available head for power generation varies and is in the order of 200 m.

Wises Dam design

The Wises Dam has been designed as a waste rockfill embankment from the mine excavation with a 2 mm thick high-density Polyethylene (HDPE) liner for the water barrier. The design concept for the dam was based on the principles for a concrete-faced rockfill design in accordance with the International Commission on Large Dams (ICOLD) Bulletin 174.

The design was a joint venture between GHD and Mott Macdonald with the construction being completed by the McConnell Dowell John Holland Joint Venture for the client Genex. The dam, as shown in Figures 1 to 4, includes the following major components:

- Upper reservoir Wises Dam
- Inlet channel to the two vertical shafts for the pump/generator turbine units
- Rockfill embankment with cement stabilized crusher dust surface for the HDPE membrane
- HDPE upstream membrane with geotextile underlay
- Excavated cut-off trench with concrete plinth for liner locking down
- Pipe spillway including inlet with inclined slide gate, pipeline to valve control pit and Copperfield River discharge structure
- Inlet pipeline from Copperfield Dam
- Coffer Dam for early works pumping of Eldridge water into Wises Dam

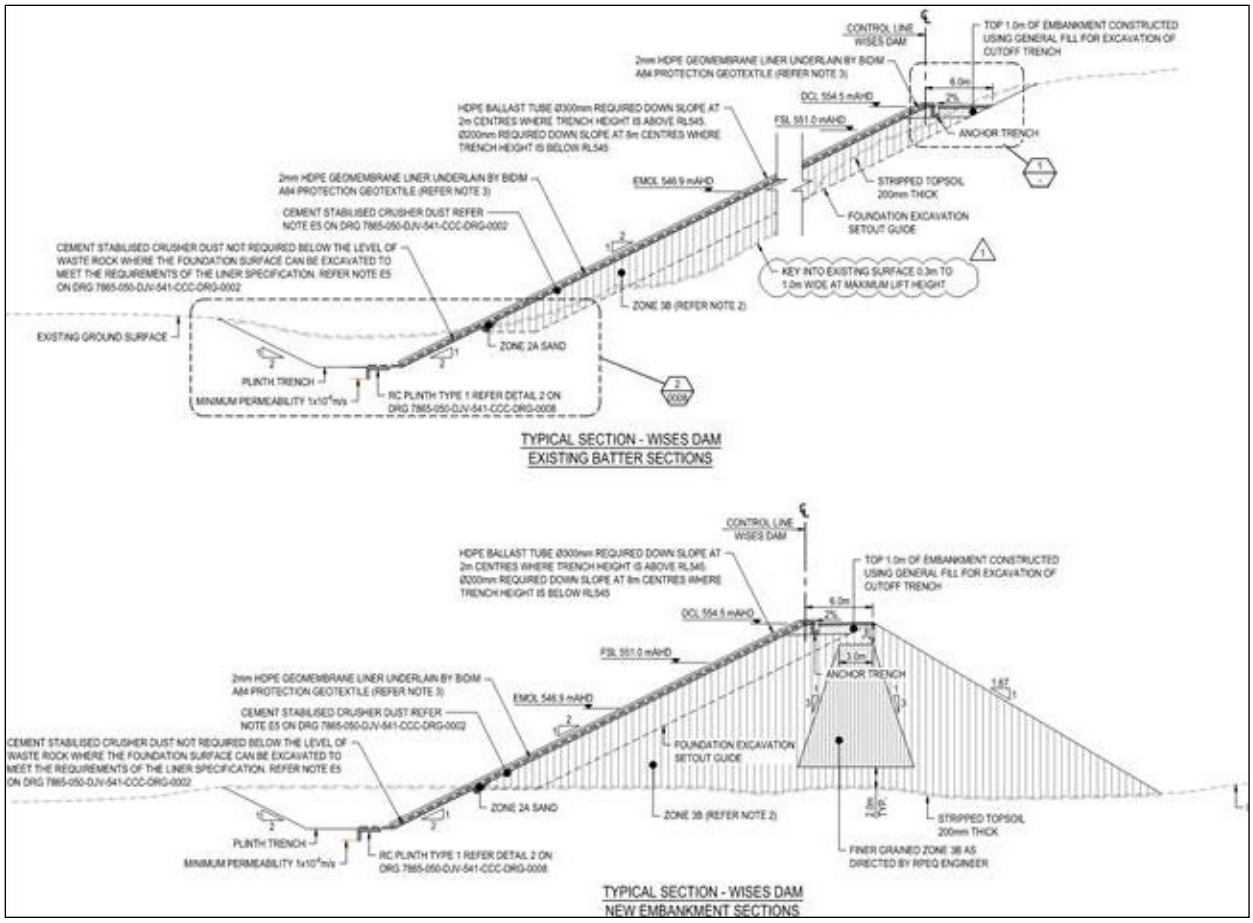


Figure 3: Embankment cross-sections

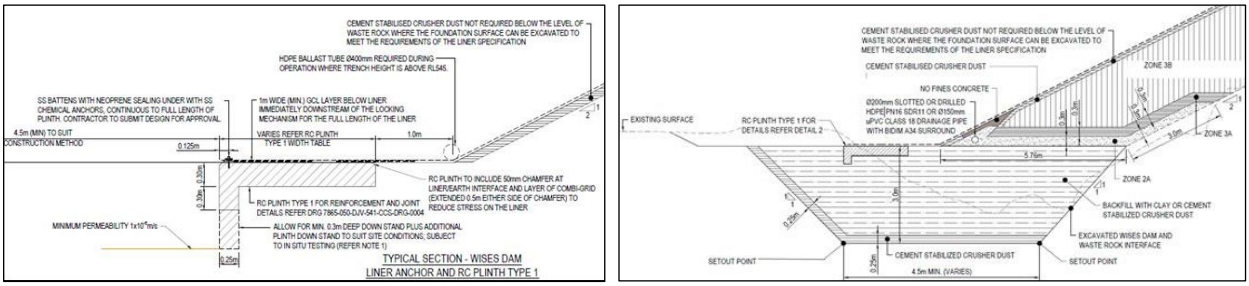


Figure 4: Plinth details. Left: rock foundation. Right: embankment plug excavate and replace

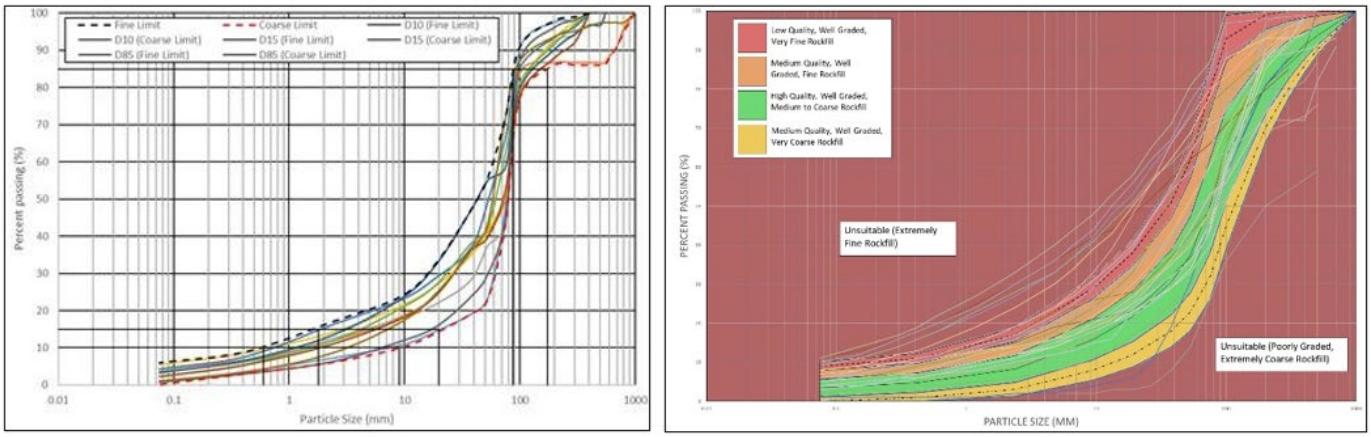


Figure 5: Zone 3B particle size distribution (Entura, 2017) left and as built right

Foundation

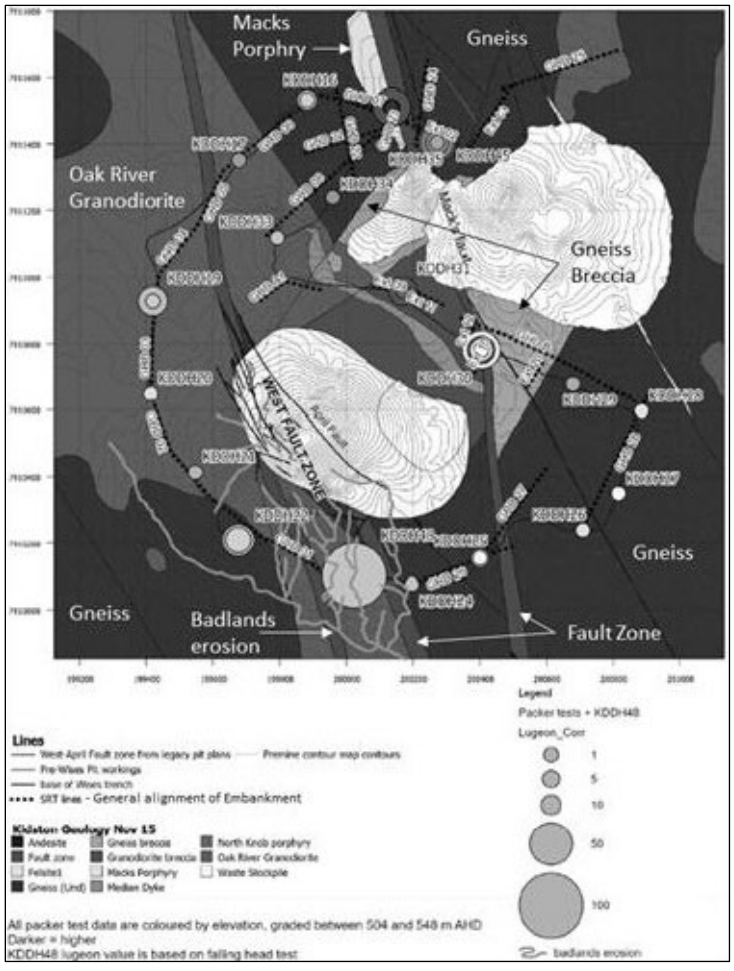


Figure 6: Geological plan at 490 m AHD level – with BH packer test permeability data

As shown in Figure 6, the bedrock beneath Wises Dam and the intake channel have been significantly affected by large-scale NNW striking faults. These are:

- Macks Fault – passing through the pillar of rock between Wises and Eldridge pits and through the intake channel.
- West Fault (zone) – passing through the western side of Wises pit and under the proposed embankment dam at two locations.
- April Fault – a "splay" off the West Fault that defines the eastern edge of the West Fault Zone and passes beneath the southern section of the embankment dam footprint.

Pre-mining topographic contour mapping showed that the now-buried topography exhibited "badlands" style erosion of the residual soil in the area where the West Fault Zone is projected to pass beneath the dam, as annotated in Figure 6.

At the time of writing this document, the filling of Wises Dam was complete. Excessive losses from the system through the "badlands" had not occurred; however, seepage loss is occurring through the foundation and liner seepage control system, which is either being pumped back into the Wises Dam from the southern areas or is flowing directly back into Eldrige pit from the northern embankment area.

Key challenges

Contractor's perspective

From a Contractor's perspective, some key challenges included the following.

Availability of geotechnical data to inform the contract price

- Geophysics are excellent for FEED studies and reference designs; however, in entering into a contract it would be better for both Contractor and Principal to have a greater level of certainty in the geotechnical data used as the basis for pricing. This would include:
    - Boreholes to at least 10 m below proposed foundation level, on the proposed alignment at about 250 m – 500 m centers. At Kidston this would have been 16 holes and only ~600 – 750 m of drilling. A very small investment to manage a risk that had implications 10 to 20 times the cost of the investigation.
    - Cut-volume increased ~40% due to the limit of accuracy on the geophysical data that was relied upon.

Materials testing

- Availability (source) of Zone 2a, 3a, 3b materials must be proven by test data at a rate of about 1 test per 250,000m^3 of proposed borrow.
- As depicted in Figures 7 and 8, the single biggest challenge was the suitability of mine waste as rock-fill.

One of the earliest reports that informed the Wises Dam design and its construction methodology was the 2017 document "Kidston Pumped Storage Project Bankable Feasibility Study – Geotechnical Report – Part B – Interpretive, Entura-B398A" provided by the Principal. It described the waste rock found onsite as "relatively consistent" and usable as for a rockfill dam embankment

On this basis the Contractor prepared the detailed design, methodology, and sequence as illustrated below, noting and observing that this method was efficient and at this stage works would be done in a timely manner without any impact to the project schedule.

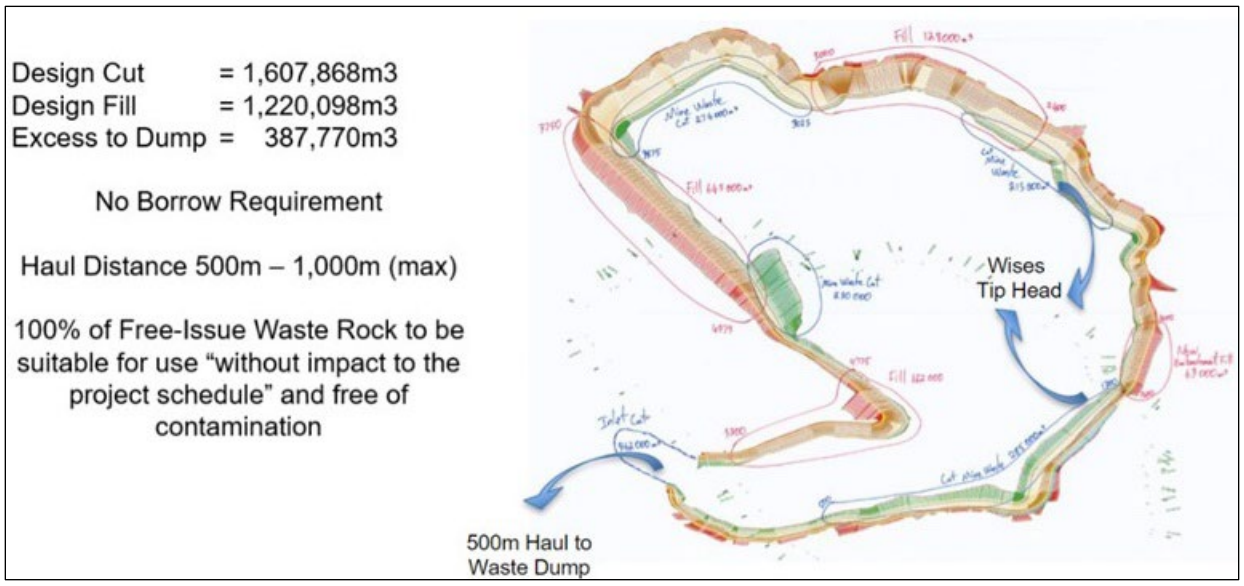


Figure 7: Planned cut-fill plan

Once significant quantities of the materials were identified as unsuitable and contaminated, the Contractor needed to revise their methodology, resulting in significant time and cost impacts due to:

- Increased haulage distances
- 387,770 m^3 of material planned to be dumped to waste stockpile increased over 400% to 1,566,576 m^3
- 1,153,134 m^3 needed to be sourced from borrow pits outside of the Wises Dam footprint – not contemplated at time of contract signing.

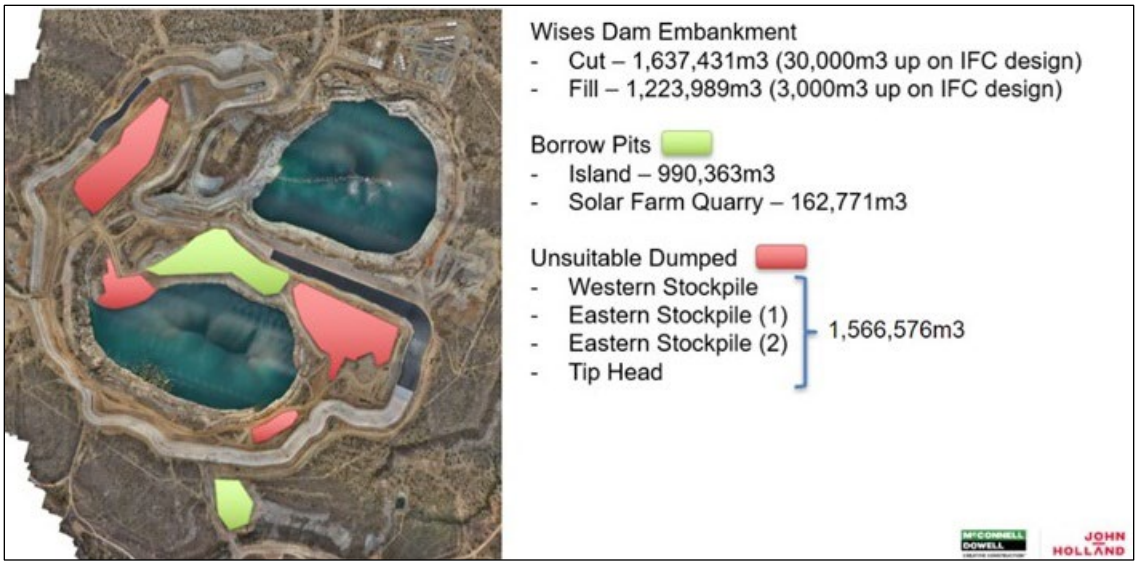


Figure 8: Revised cut-fill plan

- Rockfill grading curves. The concept design grading curves for mine waste were unrepresentative of what was actually encountered, as shown in Figure 9. Notwithstanding this, the densities and permeabilities achieved were in compliance with the design requirements.



Figure 9: Poorly graded rockfill (left) and well graded rockfill (right)

- Safety in design vs. cost
    - Batter slope of 2:1 was used for the HDPE slope to reduce costs. This steep slope presented significant construction safety risks that were very difficult and very complex to manage.
    - Dam crests must address safety in construction
        - Edge protection bunds/barriers
        - Width for heavy plant to pass if the embankment is any longer than ~500 m

Owner's perspective (Genex, 2023)

Embankment placement

To ensure settlement of the embankment, material was controlled and a minimum density of 1,950 kg/m^3 was initially specified, but was increased to 2,100 kg/m^3. This density was achieved. The grading of the rockfill needed to comply with a grading limit specification to ensure a reasonably well graded material was utilized to ensure compaction requirements were achieved, but did not contain too many fines as to reduce the permeability of the material, noting that it was required to be free draining. A trial embankment section (on permanent works) was undertaken to ensure a method specification for compaction was understood based on layer placement height and number of passes of specific machinery and quantity of water added. Increased testing frequency was adopted during the trial embankment section.

A key challenge was ensuring material and placement compliance was achieved consistently, which is very much a function of the construction team and machinery operators. In practice, this really meant that the operator loading dump trucks with rockfill material had significant control over what types of materials were being loaded at any one time to blend rock types for achieving material compliance. Initially this was very much a learning curve with testing to confirm compliance.

To expedite the process and reduce risk, a materials ready reckoner was prepared by the engineering team for the operators to refer to in terms of material compliance expectations. This involved a simple sheet, together with photographs of types of suitable rockfill blends. The importance of achieving rock fill material compliance was communicated and workshopped with the construction team and operators so that the whole dam construction team understood its importance. Once implemented, the level of rework for ensuring compliance is drastically reduced.

The rockfill compaction was achieved using only a bulldozer pushing the material into place and tracking over the material in lifts up to 1 m depth. The challenge of achieving the required density and rockfill grading confirmed the importance of undertaking a trial embankment for the purpose of developing a method specification for material placement and the implementation of a materials compliance ready reckoner to allow the operators to better determine in the field the material to be selected for utilization.

Seepage collection pipe

A seepage collection pipe is located within the rockfill material below the dam liner, to collect any leakage that may find its way through the HDPE liner and underneath the concrete cut-off plinth.

The installation of the seepage pipe and backfill details were developed in joint consultation between the design and construction team. Upon initial installation, it was observed that a better, faster and safer way for installation could be achieved. This involved modification to the pipe backfill configuration without

any lessening of design intent. The ability of the design and construction teams to work together post-design enabled this solution to be worked through and ultimately adopted.

The lesson learned relates to the ongoing design and construction interface during both the design and construction phases to ensure constructability improvements, ensuring a better, faster and safer outcome is continuously promoted, and if economically viable, then adopted.

Material preparation under the liner

The original design specified a select fill layer that was to be placed and compacted in layers to the upstream face of the rockfill material, against which the HDPE with underlying geofabric was to be placed. The challenge was that the specification of such a layer is common for HDPE-lined structures, but has had constructability issues (if the main embankment is unable to be constructed using similar materials), and there is a risk of rework due to erosion, should rain occur and the face is not protected with the liner.

A crushing and screening plant was established for the production of road base materials and concrete aggregates using the material found in the existing waste stockpiles. As part of the crushing process, a fines byproduct was produced providing a relatively consistent fines gravel (i.e. <5 mm in size). The percentage of manufactured product to byproduct waste fines was approximately a 70 to 30 split respectively. As such, a considerable quantity of waste fine material was available.

An alternate cement screed product was developed by the CJV in consultation with the designer using the waste fines to produce a low slump cementitious material that could be applied to the upstream dam face. This was an environmentally friendly solution as it used waste material, which would otherwise have a limited use, for the balance of the works, and provided a rain-resistant surface.

The installation of the cement screed utilized a combination of two long reach excavators working in tandem, as shown in Figure 10, with one excavator taking the product from the concrete truck and placing the cement screed on the dam face and roughly spreading it to level using a normal mud bucket attachment, while the other excavator smoothed out the screed to a final finish utilizing a project-developed customized screed attachment. With the excavators having a finite reach for placement, the screed was installed in sections as the dam embankment was placed to final level.

The challenge of providing a founding layer for the HDPE appropriate to the field conditions was solved by investigating opportunities for reuse of materials onsite to provide a product that satisfied design requirements/intent and also provided a protective surface to completed works in the event of wet weather. The design/construction interface and out of the box thinking enabled this solution to progress.



Figure 10: Placement of cement screed

HDPE liner placement

The upstream face of the entire dam is lined with a 2 mm high density polyethylene (HDPE) liner membrane with underlying geofabric to provide cushioning. The liner is secured under a trench backfilled with stabilized backfill on the dam crest, secured at the bottom with a stainless-steel fixing and battening system, and affixed to the reinforced concrete plinth. While this is a proven anchoring system, care was needed to ensure that the liner was secured at a relatively neutral temperature (prior to being filled with water) to ensure that the expansion and contraction of the liner remained within certain limits and did not pull away from the fixings. Some areas of the liner were up to 70 m long, resulting in considerable movement up and down the slope during the day and night.

Individual rolls of HDPE are seam welded together to ensure a continuous liner membrane. Each seam was tested onsite, together with off-site testing undertaken on HDPE liner samples that were cut from the HDPE rolls.

The lesson learned for the HDPE liner is that it is important to have the early engagement of subject matter experts to ensure that the liner specification is fit for purpose and that it achieves the specified 30-year design life.

Transfer of water from Eldridge pit to Wises Dam

Wises Dam was filled using water existing within Eldridge pit. This was achieved with a one-off transfer of water, using a bespoke pumping system comprising six 3.3 KV x 850 kW electric pumps, mounted on a pontoon structure. In total, approximately 28 GL of water needed to be pumped. The dewatering pumping station was designed to provide a flow rate ranging from 1,700 L/s to 1,250 L/s at the lowest level in Eldridge pit (where the pumping head is greatest), where the dewatering will allow access to the tail race tunnel portal. This is approximately 200 m of water level that was to be pumped into Wises Dam over a planned period of approximately 200 days under continuous operation.

The pumping system was designed, manufactured, installed, and commissioned by a panel of international suppliers and experts. Overall, the system has functioned well to date. Initial concerns about high bearing temperatures were overcome with the replacement of a larger bearing arrangement. This downtime did not impact the overall program.

The pontoon that houses the pumps and motors is put into position by three winches that can locate the pontoon within Eldridge pit. This was fundamental to being able to control the position of the pontoon, as the water level dropped in order for the pontoon to be navigated away from known features in the pit, which are remnant haul roads and platforms from mining operations.



Figure 11: Dewatering system from Eldridge pit to Wises Dam

Overcoming the challenge of the Eldridge pit dewatering was achieved by the integral commitment by all involved. All were committed to input their respective expertise into the design, manufacture, installation and commissioning phases for a successful outcome.

The challenge now evident is that there is excess water in Eldridge pit and Genex is using four misters to evaporate the water in order to lower the level by a further 40 m, after pumping into Wise Dam to a level of 1.3 m below the dam crest level. This level is above the peak expected water level allowing for the Probable Maximum Flood and is, in effect, providing a full “first fill test.”

Consultant’s perspective

What was originally planned and what was built provided significant challenges for the design team, including the following.

Foundation – depth; permeability; seepage

The concept level design assumed a relatively shallow founding depth for the concrete plinth. However, on investigation using test pitting, additional seismic traversing and Leapfrog 3D foundation modeling, it was

evident that the founding depths were quite variable and significantly lower than the concept design.

The challenge was identifying the foundation level that would provide adequate foundation strength for the concrete plinth, while having sufficiently low permeability to reduce seepage losses through the highly weathered granodiorite foundation rock to an acceptable level.

The geotechnical investigation scope incorporated a series of permeability tests targeting the overlying residual soils and extremely weathered rock mass. These tests included:

- Laboratory constant head permeability and oedometer permeability tests.
- In-situ soak-away falling head permeability tests in excavated test pits.
- In-situ Bill Cromer permeameter constant head permeability tests completed every 100 m along the plinth foundation level, with additional holes as needed in areas suspected of having a higher permeability. Figure 12 shows a Cromer (Cromer, 2015) permeameter test on material, similar to the founding level for the plinth.



Figure 12: Cromer permeameter test (Cromer, 2015)

The suitable cut-off trench level for the Wises Dam embankment methodology following the observation of low permeability testing results (<1 x 10-6 m/s) was the natural surface. To determine the natural variability of the cut-off trench (natural surface) depth between investigation locations the pre-mining survey was used as the benchmark. Observation of the variance between the pre-mine surface contours and the available borehole waste rock/natural interface was used to develop a statistical analysis of the natural surface level. The variance was plotted on a normal distribution plot at various additional depths to the pre-mine contour and a depth of the pre-mine contour plus 1.5 m additional excavation was

found to be suitable for founding the plinth. This depth was found to be very close to the final levels achieved during the construction.

Embankment – materials and quantity

The challenges described above in the owners' section were faced by the designers when ensuring that the material was of sufficient quality to ensure minimal deformation, while at the same time achieving the required permeability to ensure that there was no buildup of pore pressure within the rockfill.

Lining – material type; placement

The lining material was selected on the basis of the lowest cost suitable for the purpose. A challenge for the placement was the slope of the face at 2H:1V, which required the use of ropes for all personnel working on the face to smooth the cement stabilized crusher dust. The placement of the facing material using the long reach excavators, while achieving an overall satisfactory slope, resulted in a lot of hand labor being required to smooth out irregularities in order to achieve a maximum step of 10 mm in the facing, so as to prevent overstressing of the HDPE, potentially leading to failure.

Plinth length – jointing

The reinforcement for the liner plinth was sized based on the requirement to eliminate transverse joints, thereby minimizing seepage risks and simplifying construction with the removal of waterstops within the cutoff. The reinforcement design was performed in accordance with CIRIA C766, adopting full end restraint. N24 longitudinal bars were required at 150 mm centers to control crack widths to less than 0.3 mm. Nominal N16 bars at 200 mm centers were provided in the transverse direction. This reinforcement arrangement proved to be effective.

Drainage system

The drainage system initially considered was to have a collection pipe at the base of the slope downstream of the plinth with sumps at the low points along the plinth, in order to pump any seepage water back into the Wises Dam. This was subsequently replaced by a gravity system to avoid pumping costs, resulting in a system that would not relieve seepage flowing through the foundation below the plinth, where the water is now flowing into the seepage collection ponds surrounding the waste stockpiles.

Wises pit and waste rock interface

The sloping cut-off trench and RC plinth methodology proposed across Wises Dam was unsuitable for a portion of the embankment where the existing Wises pit (backfilled with mine waste rock) encroached on the Eldridge/Wises pit walls. The cut-off trench would be founded within the mine waste rock. Given the 1:2 (V:H) slope, it would continually extend outwards from the near vertical Wises pit walls.

Several solutions were considered but were ultimately rejected, in part due to the significant costs associated with each option. A summary of the options and the factors impacting feasibility are included in Table 1.

Table 1: A summary of the options and the factors impacting feasibility

Options	Key infeasibility factors
Modified dam/embankment designs	
Roller Compacted Concrete (RCC) dam body	Extreme cost of construction and challenges associated with connecting from and to the existing embankment design within the reduced footprint.
Conventional Vibrated Concrete (CVC) retaining wall	Must be an impermeable concrete structure including complex water stops that are required to tie into the impermeable foundation and HDPE liner.
Existing embankment designs with foundation improvement	
Zone 1A clay blanket	Granite belt geomorphology resulting in less than 1 m of residual soils across the site.
CVC blanket	Thermal and differential cracking due to the thickness of >3 m.
RCC blanket	High ambient air temperatures (>40 degrees) and insufficient volume (5,000 m^3) to introduce an additional material type with associated testing.

The foundation improvement using removal and replacement of the waste rock interface with a clay bentonite plug was determined to be the preferred solution. This uses an impermeable material (<1 x 10-7 m/s) tying into the low permeability XW rock target foundation material and forming a horizontal blanket overlying the mine waste rock. Details of this solution are shown in Figure 4.

Conclusion

The Kidston Hydro Electric Power (HEP) project provides a first for Australia in the use of a disused mine to provide both the storage capacity and the head to develop a scheme with 250 MW capacity.

The design and construction of the Wises Dam encountered a number of challenges, which were addressed with practical solutions. These included the following:

- Variable foundation conditions that were unavoidable due to the position of previous mining pits.
- Buried natural surfaces beneath meters of permeable mine waste rock.
- Variable mine waste rock deposits requiring careful adaption of the plinth design using the bentonite treated fill “plug.”
- Compaction of rockfill using bulldozer without vibration.
- Use of a continuous reinforced concrete plinth of 6,180 m, which has achieved the required maximum crack size of 0.3 mm.
- Rockfill face screeding using cement stabilized crusher dust for placement of the HDPE.

- Water transfer from Eldridge pit into Wises Dam.

Some of the challenges were expensive, but this has not prevented the CJV from continuing to provide a high-quality product for the hydropower generation.

Acknowledgements

The authors would like to acknowledge GENEX for their contribution and permission to prepare this paper as well as the contribution from the construction Joint Venture.

References

Cromer, B. 2015. Cromer constant head field permeameter. Accessed at http://www.williamccromer.com/products/permeameter/

Entura. 2017. Kidston Pumped Storage Project Bankable Feasibility Study – Geotechnical Report – Part B – Interpretive, Entura-B398A.

Genex. 2023. Lessons-Learnt-Report-9-20231205_public-version

Enhancement of Tailings Properties by Cement Amendment for their Valorization in Cover Systems to Reclaim Active or Closed Tailings Storage Facilities

Audrey Jalce, Université du Québec en Abitibi-Témiscamingue (UQAT), Canada
Isabelle Demers, Université du Québec en Abitibi-Témiscamingue (UQAT), Canada
Benoît Plante, Université du Québec en Abitibi-Témiscamingue (UQAT), Canada
Thomas Genty, Agnico Eagle Mines Ltd, Canada
Eric Brouard, Holcim Innovation Center, France
Marie-Pier Éthier, Raglan Mine, A Glencore Company, Canada
Sophie Turcotte, Ministry of Natural Resources and Forests, Canada
Marie-Andrée Guindon, Lafarge Canada Incorporated, Canada

Abstract

Mine waste facilities reclamation and acid mine drainage (AMD) prevention usually involve the construction of cover systems on tailings impoundments, requiring significant amounts of materials with specific hydro-geotechnical properties. However, if materials are unavailable locally, their extraction and transportation cause environmental and financial impacts. For legacy or closed mine sites, oxidation processes of sulfidic minerals may have already generated AMD and can make the reclamation more sensitive to geochemical conditions. Tailings valorization in cover systems can reduce environmental impacts and costs. However, using reactive tailings may require a treatment to prevent metal leaching. Among treatments, cement-based solidification/stabilization may effectively improve hydrogeotechnical properties and reduce contamination potential. Stabilized tailings could be used to create a surface layer with low water permeability on tailings storage facilities.

This research evaluated the effectiveness of adding Portland-Limestone (GUL) cement and slag-based cement at 5% or 7% binder dosages on the unconfined compressive strength (UCS), hydraulic conductivity, and oxygen consumption (OC) of cemented tailings pastes. Fresh filtered tailings provided from two active mines (samples R1 and L1) currently in operation in Québec and weathered tailings provided from an inactive closed mine (sample M1) located in Abitibi-Temiscamingue were tested. The experiment results showed that for tailings R1 and L1, slag-based cement was more effective than GUL in reducing hydraulic conductivity and increasing UCS. However, for tailings L1, a significant loss of strength was observed after 28 days of curing. One reason could be the oxidation of sulfidic minerals as observed during OC tests,

leading to a decrease in the pH of the cement matrix and dissolution of the cement hydrates. For tailings M1, with a paste pH value of 2.58, GUL was the most effective binder. However, adding 5% of lime kiln dust, as an alkaline additive, in the slag-based cement resulted in higher short-term mechanical strength.

Introduction

The mining industry produces large quantities of solid wastes, particularly waste rock and tailings, which must be stored in a manner that assures their long-term physical and chemical stability. Indeed, many geotechnical and environmental challenges are associated with mining waste storage areas. One of the main environmental challenges is the generation of acid mine drainage (AMD). AMD occurs when sulfidic minerals oxidize in atmospheric conditions (Aubertin et al., 2002). Tailings storage facilities (TSF) closure and reclamation methods have been developed to control water infiltration and/or oxygen diffusion in waste storage facilities, via cover systems built on TSF. More details are presented in the literature (Aubertin et al., 2002, 2016; Bussière et al., 2005; Bussière and Guittonny, 2021). Generally, covers require significant amounts of natural materials with specific hydro-geotechnical properties. However, access to sufficient quantities of adequate materials can be problematic, especially for large TSF or remote sites. For legacy or closed mine sites, oxidation processes of sulfidic minerals may have already generated AMD and can make the reclamation more sensitive to geochemical conditions. Indeed, on these sites, water quality can be highly contaminated with metal/metalloids, and a high concentration of Fe^{3+} in pore water can oxidize sulfidic minerals. Despite the application of reclamation methods, oxidation reactions can be difficult to stop. In this case, TSF reclamation must both prevent new contamination, by limiting water or oxygen infiltration, and treat previous contamination (Bussière et al., 2005).

To reduce the quantities of borrowed natural material and/or transportation over long distances for the construction of cover systems, valorization of in-situ mine tailings can be done. However, tailings do not always have adequate hydrogeotechnical properties. Moreover, for reactive tailings, a treatment is required to prevent AMD and metal leaching. Among treatments, cement-based solidification/stabilization (S/S) may effectively improve hydrogeotechnical properties, reduce the reactivity potential of sulfides and limit contamination by stabilizing metals and metalloids in non-soluble compounds. Cement-based S/S processes are widely used in the mine backfill industry (hydraulic fill, rockfill and cemented paste backfill). In previous studies, low-carbon cements have shown great potential for stabilizing oxidized and reactive tailings. Binder hydration creates a low-permeability cementitious matrix, in which contaminants are encapsulated, preventing leaching and pollutants from moving. The reactive surface of tailings is also reduced (Deschamps et al., 2006). The efficiency of cement-based S/S treatment depends on the binder hydration processes, controlled by intrinsic and extrinsic parameters, and on the geochemical stability of cement hydrates. Among intrinsic parameters, a significant sulfidic minerals content can harm the integrity

of the matrix, if oxidation of sulfidic minerals happens, resulting in a sulfate attack. Sulfate attack is a process due to the formation and expansion of secondary minerals, leading to cracking, strength loss, and disintegration of the matrix (Benzaazoua et al., 2002).

Cement-based S/S treatment could improve hydro-geotechnical properties and reduce the contamination potential of hazardous tailings, prior to their valorization. However, there is a lack of experience in using cemented tailings pastes as cover materials. In addition, a surface layer made of such materials will be exposed to atmospheric conditions. Limiting sulfidic oxidation could therefore be a real challenge.

So, the objective of the current research is to assess the feasibility of the valorization of cemented tailings pastes in cover systems. In this study, Portland-Limestone (GUL) cement and slag-based cement were used to solidify and stabilize tailings from three different mine sites (two active and one inactive). The unconfined compressive strength, (UCS), the saturated hydraulic conductivity (k_{sat}), and the oxygen consumption (OC) of the cemented tailings prepared with 5% or 7% binder content were evaluated to obtain the most appropriate binder and binder dosage. UCS and k_{sat} were used in this study as the first indicators of cement hydrate formation that favor contaminant stabilization. OC was used as an indicator of sulfide mineral passivation.

Methodology

Materials

In this study, three different tailings were used to prepare cemented tailings pastes. Fresh filtered tailings were taken from Raglan Mine (R1) and LaRonde Mine (L1), two operating mine sites located in the north of Quebec and in Abitibi-Temiscamingue (A.-T.), respectively. Weathered tailings were sampled from Manitou (M1), an inactive closed mine site in A.-T. After transferring the tailings to the laboratory, samples of all materials were homogenized using a spade to avoid, as much as possible, heterogeneities in the chemical and mineralogical properties. Reactive tailings R1 and L1 were submerged in water before being sealed in plastic containers to prevent oxidation. Weathered tailings M1 were oven-dried at 60°C and sieved to remove coarse fractions over 450 µm before carrying out the homogenization, characterization, and preparation processes. Porland-Limestone (GUL) cement and a blend of 20 wt.% of GU cement and 80 wt.% of ground granulated blast furnace slag (Slag) (20GU/80Slag) were used as the main binding agents. A mixture of 20GU/80Slag and lime kiln dust as an alkaline additive (5 wt.%) was also used as a binding agent. Deionized water was used for the preparation of cemented tailings paste samples to eliminate the effects of water chemistry on cemented tailings behavior.

Methods

Physical, mineralogical, chemical, and hydrogeological characterizations

The specific gravity (Gs) of tailings was measured using a Micrometrics helium pycnometer (Ultrapyc 1200e, Quantachrome Instruments). Tailings particle size distribution (PSD) was analyzed using a laser diffraction particle size analyzer (Malvern Mastersizer S3000, Malvern Panalytical, Canada).

The mineralogical composition of tailings was semi-quantified with X-ray diffractometry (XRD) using a Bruker AXS D8 Advance X-ray diffractometer. Identification of mineral species was carried out using DIFFRAC.EVA software (version 5.2.0.3) and their quantification was done by Rietveld-TOPAS software (version 4.2).

The paste pH of tailings was analyzed using a pH meter, after adding 5 ml of deionized water to 10 g of tailings. The interstitial water in the tailings was diluted with deionized water and collected by vacuum pumping. The chemical composition of interstitial water was then analyzed by ICP-AES on the liquid samples acidified with 2% HNO_3.

The k_{sat} of tailings was estimated using the model developed by Mbonimpa et al. (2002a). k_{sat} was evaluated using a rigid-wall compaction-mold permeameter (ASTM-D5856-95, 2002).

Preparation, curing and testing of the cemented tailings paste mixtures

Uniaxial compressive strength (UCS) tests

To use stabilized tailings as cover materials to create a surface layer on a TSF, a minimum UCS of 1 MPa of cemented tailings pastes after 28 days of curing was targeted in this study (Belem et al., 2009). Tailings paste mixtures were prepared with 5 wt.% and 7 wt.% GUL and 20GU/80Slag.

All the tailings paste mixtures were prepared in the laboratory, using these steps:

Half of the deionized water was mixed with the binder in a Hobart mixer bowl (capacity of 4.8 L) using a hand spatula. The tailings and the remaining water were added progressively to the mixture and mixing continued for up to 5 minutes to achieve a homogeneous paste. Immediately after preparation, the consistency of the cemented tailings pastes was measured by the mini-slump test. The slump test was also used to determine the optimum water requirement for each paste mix by aiming for a slump between 7-8 inches. Water was added to reach the desired consistency.

The cemented tailings paste mixtures were poured into 2 × 4 inches cylindrical plastic molds (50.8 diameter × 101.6 mm height) in a single layer. Molds were drilled to allow drainage. After molding, the cylinders were tapped 25 times using a steel rod with a diameter of 9.53 mm (3/8 in) to expel the air bubbles from the pastes. The prepared drained cylindrical samples were labeled and stored in the laboratory (approximately 60% relative humidity and 22°C) to cure for 3, 7, 14, 28, and 56 days before testing. The

conditions remained unchanged over the curing period to ensure the comparability of tests and to limit the number of influencing factors.

The strength evolution in the pastes was assessed by performing UCS tests on three separate specimens for each recipe. UCS tests were carried out based on the ASTM C39 standard by a computer-controlled mechanical press with a normal loading capacity of 50 kN and a 1 mm/min displacement rate, and the stress-strain data were recorded for each sample. The samples were taken out of molds after 3, 7, 14, 28, and 56 days of curing for UCS testing. The base and top of the cylinders were flattened parallel to the plates of the mechanical press before the UCS tests. The maximum stress value before failure during the compression test was measured. All the measurements were carried out in triplicate and the average values were taken as the final compressive strengths. The UCS test results were used to select the most appropriate binding agent and dosage. After UCS tests, the cemented samples were oven-dried at 90°C to determine the water content. The paste pH was then analyzed using a pH meter after adding 5 mL of deionized water to 10 g of cemented samples.

For the cemented tailings paste samples tested that reached the targeted UCS of 1 MPa after 28 days of curing, new mixtures with the same recipes were prepared for the k_{sat} and OC tests.

Saturated hydraulic conductivity (k_{sat}) tests

Cemented tailings paste mixtures were cast into 4 × 8 inches cylindrical plastic drained molds in three layers. Each layer was tapped 25 times using a steel rod with a diameter of 9.53 mm (3/8 in) to expel the air bubbles from the pastes. Samples were stored in the laboratory under controlled temperature and moisture conditions (22°C and 50% respectively) to cure for 28 and 56 days before testing. The k_{sat} of cemented tailings was evaluated using a flexible-wall mold permeameter (ASTM-D5856-95, 2002).

Oxygen consumption (OC) tests

Oxygen consumption tests were used to determine the sulfide oxidation rates in the tailings and cemented tailings pastes. In OC tests, paste mixtures were poured into drained cylinder molds with dimensions of 5.90 × 1 inches. Samples were stored in the laboratory and cured under controlled temperature and moisture conditions (22°C and 50% respectively) for 3, 7, 14, and 28 days before testing. The cylinder was then closed and sealed for oxygen concentration measurements with an oxygen sensor for a period of two to five hours (Oxygen dipping probe type PSt7, PreSens Precision Sensing GmbH, resolution at 0.01 % O_2 at 1 % O_2 and 0.05 % O_2 at 20.9 % O_2). High oxygen decrease means a high sulfide oxidation rate. To evaluate the effect of binder, OC tests were also performed on control samples (i.e. tailings without binder). For control samples, tailings were poured into cylinder molds with dimensions of 5.90 × 1 inches at a porosity n= 0,45 and a degree of saturation around 50% to favor oxidation conditions.

Results and discussion

The results of the initial characterization of the materials and mechanical strength, hydraulic conductivity and oxygen consumption of cemented tailings pastes samples are presented in this section.

Physical, mineralogical and chemical characterization

The physical properties are presented in Table 1. The G_s values of fresh tailings R1 and L1 were higher than the oxidized tailings M1: 3.05 for both R1 and L1, and 2.72 for M1. Figure 1 depicts the cumulative PSD of the tailings, and some commonly used indicators associated with PSD are presented in Table 1. The PSD values showed that 45% of tailings R1 and L1 are less than 20 µm in diameter. 90% of tailings R1 and tailings L1 are less than 120 µm and 100 µm in diameter, respectively. Tailings M1 showed a coarser PSD than the other tailings. The D_{50} and D_{90}, which correspond to 50% and 90% passing on the cumulative particle-size distribution curve, were 51 µm and 382 µm, respectively.

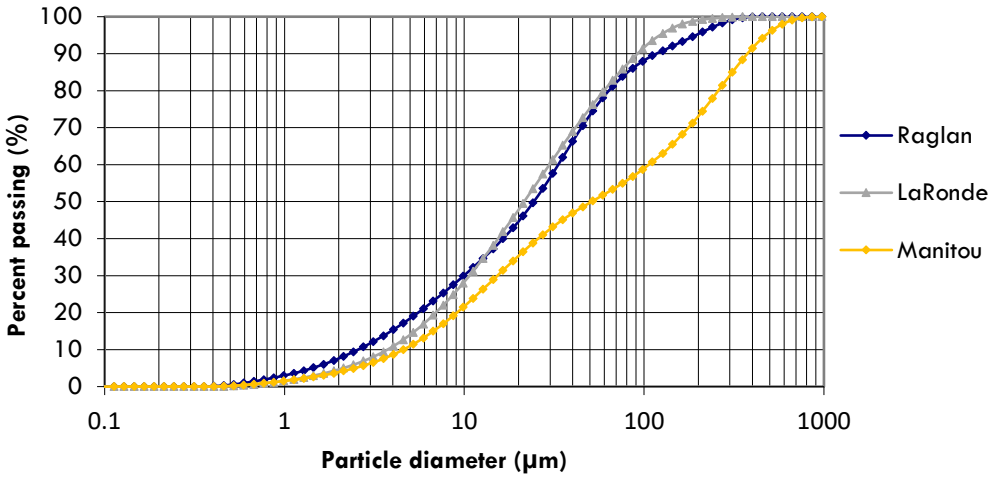


Figure 1: Particle size distribution of the studied tailings samples

Table 1: Physical characteristics of the tailings samples

Parameter	D_{50}	D_{90}	$Cu=D_{60}/D_{10}$	$Cc = D_{30}^2/(D_{60}*D_{10})$	$U = (D_{90}-D_{10})/D_{50}$	G_s
Unit	(µm)	(µm)	(-)	(-)	(-)	(kg/m³)
Raglan R1	24.3	117	13.01	1.16	4.71	3,055
LaRonde L1	21.5	92	7.99	1.03	4.11	3,052
Manitou M1	50.8	382	23.14	0.48	7.43	2,721

The mineralogical composition of tailings samples is presented in Table 2. For fresh reactive tailings R1 and L1, sulfide contents (mainly pyrrhotite for R1 and pyrite for L1) were 20.3 wt.% and 14.9 wt.% for

R1 and L1, whereas carbonate contents were 0.9 wt.% and 2.8 wt.% for R1 and L1, respectively. Mineralogical compositions of tailings M1 were completely different. Sulfides, carbonates and secondary minerals content were 0.3 wt.%, 0.2 wt.% and 1.5 wt.% respectively.

Table 2: Mineralogical properties of the tailing samples

	Raglan R1	La Ronde L1	Manitou M1
Sulfides	20.3	14.9	0.3
Carbonates	0.9	2.8	0.2
Sulfates	0.0	2.7	1.5
Fe- oxyhydroxides	2.8	0.0	0.1
Others	76.0	79.6	97.9

Table 3 presents the paste pH of the tailings. As fresh tailings, R1 and L1 present a near-neutral paste pH, contrary to M1 oxidized tailings with an acidic paste pH of 2.58, characteristic of AMD production.

Table 3: Paste pH of the tailing samples

	Raglan R1	La Ronde L1	Manitou M1
Paste pH	7.28	6.91	2.58

Hydrogeological properties

The predicted and measured k_{sat} values are shown in Table 4. The measured k_{sat} values for R1 and L1 were 7.49E-8 m/s and 4.52E-8 m/s, respectively. The k_{sat} value for oxidized tailings M1 was 2.53E-7 m/s. The predicted k_{sat} values were within an order of magnitude of the measured values.

Table 4: Measured and predicted saturated hydraulic conductivities k_{sat}

Tailings	Porosity	Predicted k_{sat} (m/s)	Measured k_{sat} (m/s)
Raglan R1	0.42	1.80E-07	7.49E-08
LaRonde L1	0.42	3.10E-07	4.52E-08
Manitou M1	0.42	5.60E-07	2.53E-07

Pore water chemical composition

The pore-water chemical composition of the tailings samples is presented in Table 5.

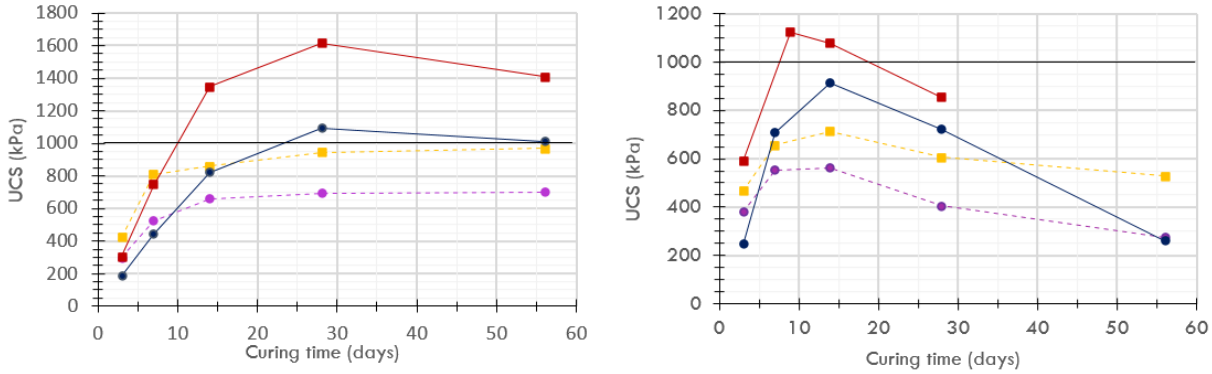
Table 5: Results of the pore-water chemical composition of the tailings samples

Tailings		Raglan mg/L	LaRonde mg/L	Manitou mg/L
Main pore-water chemical components	Cu	0.158	OQ*	67
	Fe	OQ*	OQ*	125
	Ni	15	OQ*	0
	Pb	OQ*	OQ*	0,23
	Zn	OQ*	0,218	84
Ions sulfates	SO_4^{2-}	11,708	23,528	23,946

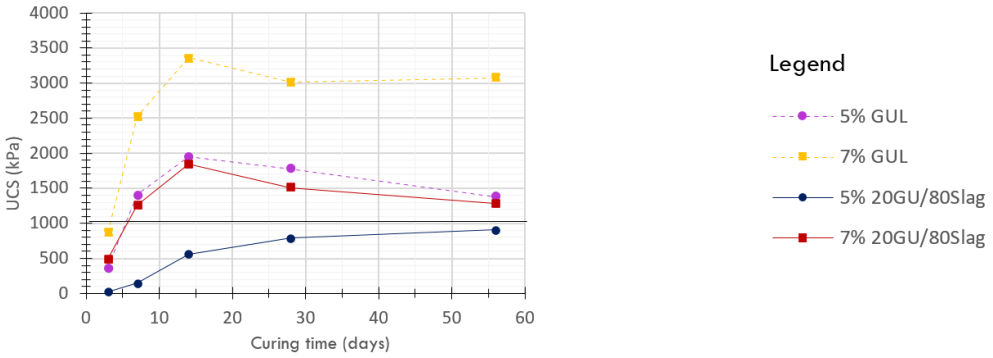
*LOQ: limit of quantification

The results show high concentrations of sulfates in the porewater of all tailings samples, especially for L1 and M1. M1 tailings have the highest concentration of Fe, which can be explained by the acidic conditions of the tailings. M1 have also higher concentrations of Cu and Zn.

Cemented tailings mechanical strength results



2a) Raglan R1 2b) LaRonde L1



2c) Manitou M1

Figure 2: Results of UCS tests on the cemented tailings samples prepared with GUL cement and slag-based cement (20GU/80Slag)

Figure 2 shows the relationship between uniaxial compressive strength and curing time of the cemented tailings paste samples prepared at 5 wt.% and 7 wt.% binder content using GUL and 20GU/80Slag for each tailings type.

For R1 tailings (Figure 2a), after 28 days, UCS increased significantly with curing age for both binder types and both binder dosages tested. However, samples prepared with GU failed to reach the targeted 28-day UCS of 1 MPa. Only the samples prepared with 20GU/80Slag binder for both binder dosages achieved it. Although a slight decrease in strength was observed after 56 days of curing, the targeted UCS was always achieved. For L1 tailings, Figure 2b shows that after 14 days of curing, UCS increased appreciably with curing age for both binder types and percentages. Slag-based cement gave the best results, probably due to its high sulfate resistance.

However, after 28 days of curing, a significant loss of strength was observed. As the samples were stored unsealed in the laboratory under atmospheric conditions, oxidation of the sulfide minerals must have occurred, leading to a decrease in the pH of the cement matrix and dissolution of the cement hydrates (ettringite, hydrated calcium silicate [C-S-H]) responsible for the strength gain. Paste pH was measured for each sample of L1 tailings prepared with 7% of GUL and 20GU/80Slag at 3, 7, 14, 28, and 56 days of curing. For both recipes, an increase in the paste pH at the beginning of the cement hydration was observed. Indeed, after 3 days of curing, the paste pH was around 11.0 and 10.1 for samples prepared with GUL and 20GU/80Slag binders respectively. Then, it decreased and dropped below 9.5 and 8.5 after 56 days of curing. For tailings M1 (Figure 2c), with an acidic paste pH of 2.44, GUL was the most effective binder. Samples prepared with 5 wt.% and 7 wt.% GUL gave UCS values above the target at 14 days. A slight loss of resistance was observed, but strengths were still superior to 1 MPa. For samples prepared with 20GU/80Slag cement, only 7 wt.% dosage was efficient in reaching the target UCS of 1 MPa. GUL cement was more efficient in rapidly increasing the pH of the cement matrix, which could contribute to the formation and stability of cement hydrates responsible for the strength. Moreover, the coarser particle size of tailings M1 could explain these high UCS values.

To evaluate the effect of the type of binder on strength development, new samples were prepared with M1 tailings and 5 wt.% of 20GU/80Slag cement where 5% of lime kiln dust was added as an alkaline additive. Figure 3 shows the relationship between uniaxial compressive strength and curing time for this alternative recipe. It resulted in higher short-term mechanical strengths, and a UCS of 1 MPa was achieved at 28 days. However, at 56 days of curing, the strength decreased to 950 kPa. The addition of an alkaline material could raise the pH value to a sufficient alkaline level, making cement hydrates more stable.

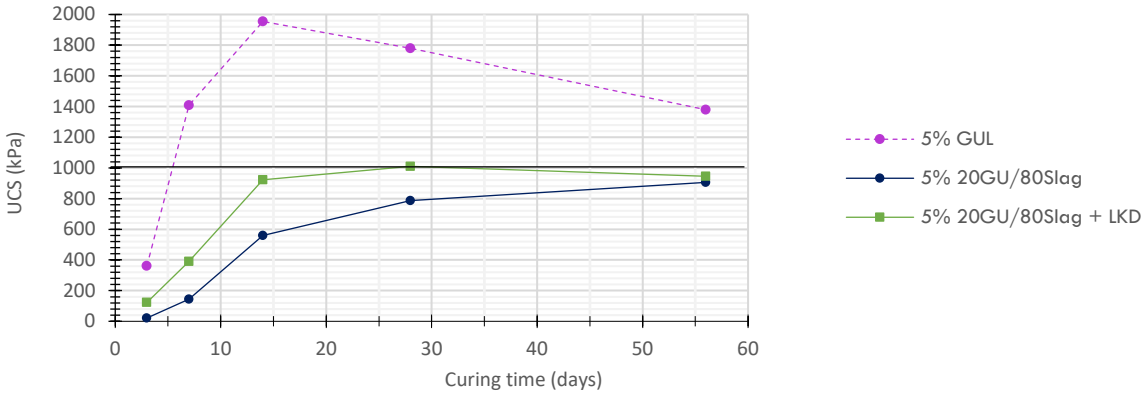
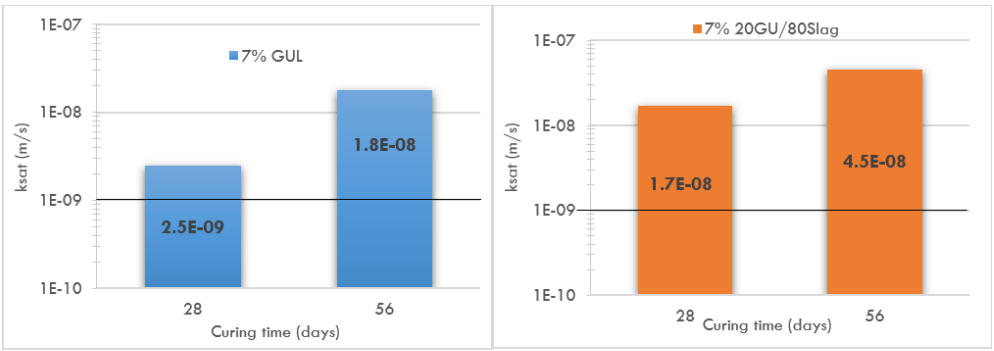
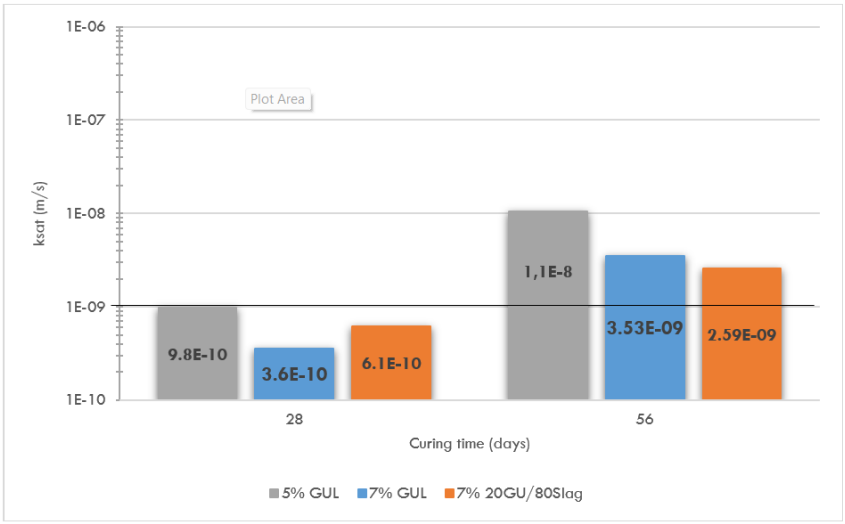


Figure 3: The effects of the PSD and the type of binder on the UCS of cemented Manitou tailings prepared with 5% of GUL and GU/Slag/LKD binders

Cemented tailings saturated hydraulic conductivity results



4a)·Raglan·R1·4b)·LaRonde·L1¶



4c) Manitou M1

Figure 4: Results of saturated hydraulic conductivity tests on the cemented tailings samples prepared with GUL cement and slag-based cement (20GU/80Slag)

Figure 4 presents the results of saturated hydraulic conductivity tests of cemented tailings pastes samples that reached the targeted 28 days UCS of 1 MPa.

In all cases the results showed a significant reduction of k_{sat} when binder was added to tailings (initial tailings with k_{sat} around 10^{-7} – 10^{-8} m/s). For R1 tailings (Figure 4a), with a binder proportion of 7% GUL, k_{sat} decreased by a factor of approximately 1½ order of magnitude after 28 days of curing. However, it remained superior to 1×10^{-9} m/s. For L1 tailings (Figure 4b), when 7% of 20GU/80Slag cement was added, k_{sat} value of the tailings decreased only by a factor of approximately ½ order of magnitude after 28 days of curing and remained superior to 1×10^{-8} m/s, which does not take into account the hydraulic barrier condition. This slight decrease in k_{sat}, despite the addition of binder, can be explained by the significant loss of strength after 28 days of curing, which suggests a dissolution of the cement hydrates of the matrix and an increase in porosity. For M1 tailings (Figure 4c), a reduction of k_{sat} of between 2½ and 3 orders of magnitude can be observed according to the mixture recipes.

Figure 4c also shows that the binder type and the proportion influence k_{sat} evolution. The GUL cement significantly impacts k_{sat} more than the 20GU/80Slag binder after 28 and 56 days of curing for the same proportion of binder. After 28 days of curing, for 7% binder content, k_{sat} is about ½ an order of magnitude lower than the one with the 20GU/80Slag binder. These results show that the k_{sat} of the samples can be negatively correlated to the UCS values (Figure 2c). The higher the UCS value is, the lower the saturated hydraulic conductivity is. At 28 days of curing, with 5% of GUL, k_{sat} was reduced at a lower amplitude than with 7% GUL, and at 56 days of curing, k_{sat} increased nearly 1 order of magnitude (from 9.8×10^{-10} m/s to 1.1×10^{-8} m/s). A crack was observed along the sample, which represents a preferential flow path for water movement and could explain the higher k_{sat} value.

Cemented tailings oxygen consumption results

The oxygen consumption (OC) tests were performed using an empty space (chamber headspace) of height h of 7.5 cm at the top, and measurements were conducted every minute for 200 minutes and 300 minutes. The percentage of oxygen consumed in the headspace ($[O_2]_{consumed}$) during OC tests is calculated as follows:

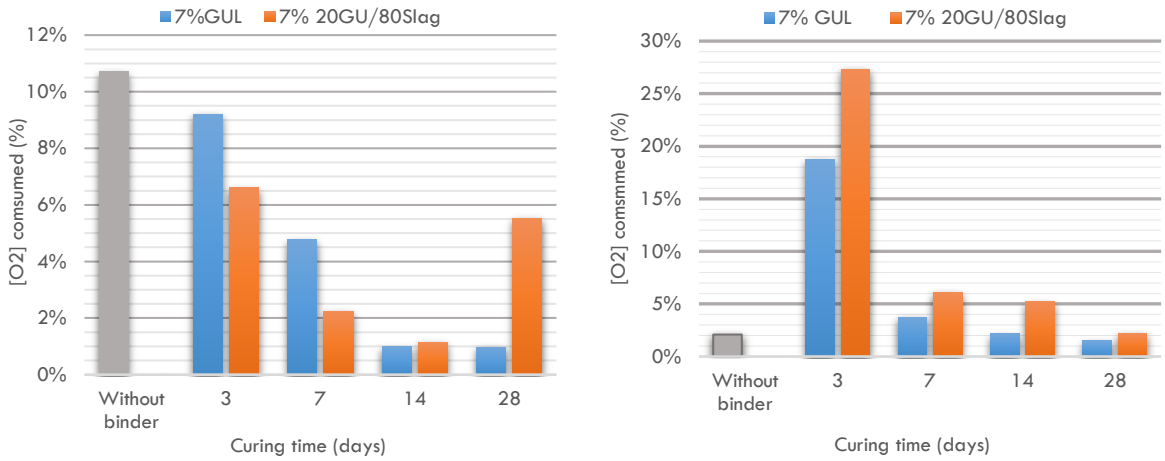
$$[O_2]_{consumed} = \frac{C_0 - C_f}{C_0} \times 100 \qquad \text{(Equation 1)}$$

where C_0 and C_f are the oxygen concentrations [ML^{-3} or $molL^{-3}$] at the beginning and the end of the OC tests, respectively.

Figures 5 presents the results of the OC tests for cemented R1 and L1 tailings paste mixtures with a binder proportion of 7% GUL and 7% 20GU/80Slag cement at 3, 7, 14, and 28 days of curing. For tailings R1 (Figure 5a), the addition of binder reduces the oxygen concentration consumed by the tailings in a short

time. Indeed, for the control sample, $[O_2]_{consumed}$ was more than 11% in the 7.5 cm headspace (over a period of 200 minutes); whereas, for both paste mixtures, the oxygen consumed in the top chamber during tests decreased with time and dropped below 1.5% after 14 days of curing. Slag-based cement seems to be more efficient in reducing the oxygen consumed by the oxidation of sulfide minerals than GUL cement. Even if an increase of $[O_2]_{consumed}$ was observed at 28 days of curing with 7% 20GU/80Slag, it remained inferior to the control sample. For tailings L1 (Figure 5b), it was observed that $[O_2]_{consumed}$ by cemented paste mixtures is 9 and 13 times higher than the control sample at 3 days of curing with 7% GUL and 7% 20GU/80Slag cement respectively.

This could be explained by the curing conditions in the laboratory. Indeed, drained unsealed molds were used in the experiment, which favored water drainage and evaporation of the samples. Consequently, the saturated conditions of the paste mixtures were not guaranteed to limit oxygen diffusion through cemented tailings paste during the curing time. After 7 days of curing, the percentage of oxygen consumed in the top chamber during the tests decreased, and a $[O_2]_{consumed}$ in the headspace less than 2% was reached for both mixtures cured at 28 days.



5a) Raglan tailings 5b) LaRonde tailings

Figure 5: O_2 concentration consumed in the chamber headspace during OC tests at 3, 7, 14, and 28 days of curing compared to control sample at 1 day

OC tests were also performed with Manitou tailings (with and without binder). However, for these tests, a total consumption of O_2 less than 1% in the 7.5 cm headspace (over a period up to 5h) was obtained. Manitou tailings can be considered as low-sulfide tailings (0.3% of sulfides) and seemed to not consume the O_2 flux into cemented paste tailings. AMD generation in these tailings is mainly driven by oxidation with ferric ions or dissolution of secondary iron oxyhydroxides (Bussière and Guittonny, 2021).

Conclusion

Based on the results of this study, it can be concluded that:

- The addition of 5% and 7% of binder increased the strength of the tailings paste mixtures and reduced the saturated hydraulic conductivity; however, both targeted UCS > 1 MPa, and k_{sat} < 1E-9 m/s after 28 days of curing were usually achieved with 7% of binder.
- Cemented paste mixtures prepared using 20GU/80Slag cement showed higher strength for tailings having neutral paste pH than the samples prepared with tailings with acidic paste pH; in that case, samples prepared with GUL cement showed higher UCS. However, adding 5% of alkaline additives can increase strength by raising the pH value to a sufficient alkaline level and making cement hydrates more stable.
- One reason for strength reduction in the cemented tailings paste at LaRonde is the dissolution of the cemented hydrates responsible for the strength, due to the oxidation of sulfide minerals during a short curing time, and thus a reduction of the paste pH of the cemented matrix.

Acknowledgements

The authors would like to acknowledge the CRSNG Alliance program for their financial support, along with partners Lafarge-Holcim, Ministry of Natural Resources and Forestry, Agnico Eagle, Raglan Mine, Iamgold corp. The authors would also like to thank the URSTM team for their technical support during the laboratory tests.

References

Aubertin, M., Bussière, B. and Bernier, L. 2002. *Environnement et gestion des résidus miniers*. Presses Internationales de Polytechnique, Corporation de l'École Polytechnique de Montréal, Montréal.

Aubertin, M., Pabst, T., Bussière, B., James, M., Mbonimpa, M., Benzaazoua, M. and Maqsoud, A. 2015. *Revue des meilleures pratiques de restauration des sites d'entreposage de rejets miniers générateurs de DMA*. In Symposium 2015 sur l'environnement et les mines.

Belem, T., Fall, M., Aubertin, M. and Li, L. 2009. *Développement d'une méthode intégrée d'analyse de stabilité des chantiers miniers remblayés.* IRSST Report No R-622, 1–97.

Benzaazoua, M., Belem, T. et Bussière, B. 2002. Chemical factors that influence the performance of mine sulphidic paste backfill. *Cement and Concrete Research* 32(7): 1133–1144.

Bussière, B. and Guittonny, M. 2021. *Hard Rock Mine Reclamation: From Prediction to Management of Acid Mine Drainage* (1st edition). CRC Press.

Bussière, B., Aubertin, M., Zagury, G. J., Potvin, R., and Benzaazoua, M. 2005. *Principaux défis et pistes de solution pour la restauration des aires d'entreposage de rejets miniers abandonnées*. Paper presented at *Symposium 2005 sur l'environnement et les mines*.

Deschamps, T., Benzaazoua, M., Bussière, B., Belem, T., and Mbonimpa, M. 2006. Mécanismes de rétention des métaux lourds en phase solide: cas de la stabilisation des sols contaminés et des déchets industriels. *VertigO-la revue électronique en sciences de l'environnement* 7(2).

Mbonimpa, M., Aubertin, M., Bussière, B. and Aachib, M. 2002a. Oxygen diffusion and consumption in unsaturated cover materials. Technical Report no. EPM-RT2002-04. https://publications.polymtl.ca/2597/

Mbonimpa, M., Aubertin, M., Chapuis, R. and Bussière, B. 2002b. Practical pedotransfer functions for estimating the saturated hydraulic conductivity. *Geotechnical and Geological Engineering* 20(3): 235–259.

TRIM4Post-Mining: Geotechnical Input for Transition Information Modeling for Post-mining Landscapes

Gerald Verbeek, Eijkelkamp North America, USA
Gustavo Hamu, Royal Eijkelkamp, The Netherlands

Abstract

As part of the recent TRIM4 research project, Royal Eijkelkamp performed various soil investigation techniques. The results of these techniques can be used as input for information modeling to support decision making and planning during the transition from mine exploitation to a re-vitalized post-mining landscape. In this paper the use of soil sampling using a sonic drill rig, the Monitoring While Drilling technique (including the use of the obtained results for subsurface characterization), as well as Sonic Cone Penetration Testing (whereby a vibration is superimposed on the standardized downward movement of a cone into the soil) are described as they were applied at the test site for the research project. The emphasis of the descriptions in this paper are the main findings that were reported in the final report of the TRIM4 research project. The paper also summarizes future development work recommended for these techniques.

Introduction

The development of effective solutions to transform mining locations into sites with new perspectives that are socially and economically viable is a fundamental part of responsible post-mining management. To promote an integrated approach for such developments, the European Union initiated the TRIM4Post Mining research project, which focused on Transition Information Modeling for post-mining landscapes. At an active lignite mine in Germany just south of Leipzig, Germany (the United Schleeenhain Coal Mine), a group of companies applied various techniques to generate the required input data for such modeling. Royal Eijkelkamp participated in this effort and contributed by performing various geotechnical techniques, such as soil sampling using sonic drilling, Monitoring While Drilling (MWD) and using the results for geotechnical sub-surface characterization, Sonic Cone Penetration Testing (CPT) to expand the use Standard CPT in challenging soil conditions, and the use of a CPT module to obtain images of the soil profile as the cone was pushed into the soil. The results of the last-mentioned are described in an accompanying paper, while those of the first three are described in this paper.

TRIM4 Research Project

The TRIM4Post-Mining Research Project was a project funded by the European Union that brought together a consortium of European experts from industry and academia to develop an integrated information modeling system, designed to support decision making and planning during the transition from coal exploitation to a revitalized post-mining landscape, enabling infrastructure development for agricultural and industrial utilization, and contributing to the recovery of energy and materials from coal mining dumps.

The basis of this system is a high-resolution spatiotemporal database, utilizing state-of-the-art multi-scale and multi-sensor monitoring technologies, which allow characterization of dynamic processes in mining waste dumps related to timely, dependent deformation and geochemical processes. It integrates efficient methods for operational and post-mining monitoring, comprehensive spatiotemporal data analytics, feature extraction, and predictive modeling; this then allows for the identification of potential contamination areas and the forecasting of geotechnical risks and ground conditions. For the interactive exploration of alternative land-use planning scenarios – in terms of residual risks, technical feasibility, environmental and social impact, and affordability – up-to-date data and models are embedded in an interactive planning system, forming a TRIM – a Transition Information Modeling System. This system is designed to support decision making and planning during the transition from mine exploitation to a re-vitalized post-mining landscape, enabling infrastructure development for agricultural and industrial utilization, and also to contribute to recovering energy and materials from coal mining dumps.

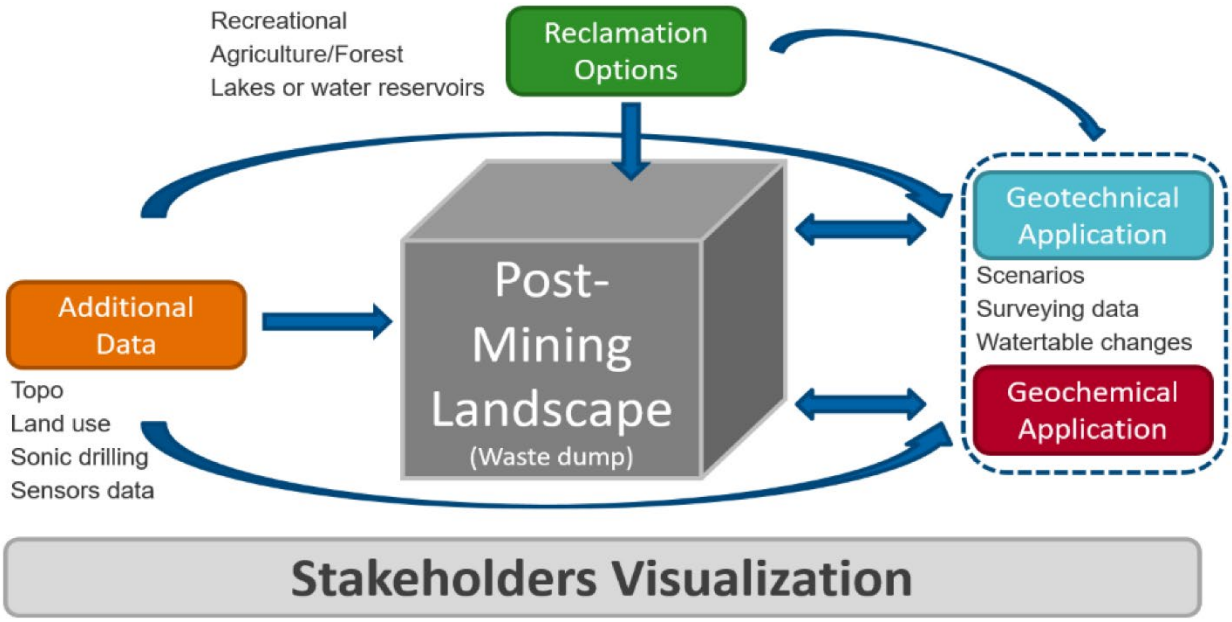


Figure 1: Considerations for the transition from mine exploitation to a revitalized post-mining landscape

Sonic sampling

For the analyses done within the Trim4PostMining project, it was of high importance that high-quality and highly representative drill cores were acquired. Any disturbances in the drill cores have a direct impact on the final test results and thus induce an error in the models that are created. To minimize these disturbances the sonic drilling method was chosen. Sonic drilling is known for its high drilling speeds, high core quality and high representation between drill core and drilled lithology.

The high performance of a sonic rig is due to the motion that a sonic rig applies on the drill string. Besides the more conventional, rotational motion, a vibrational motion is applied to the drill string. This negates the friction forces on the drill string by liquefying the soil at the drill bit and around the drill string. In rock lithology this sonic vibration results in efficient breaking of the rock, also resulting in high penetration rates and clean "cuts" of the rock lithology.

The goals for the sonic sampling campaign within the Trim4PostMining project were the extraction of drill cores to a depth of 50 m (165 ft) at two test locations, with high representativeness and core recovery rates of the drill cores. The drilling crew was able to successfully achieve both goals, and achieve core recovery rates that are seemingly unrealistic compared to conventional drilling recovery rates.



Figure 2: Drill cores acquired during the Schleenhain campaign in May 2022

Table 1: Results of sonic sampling

	Borehole 1	Borehole 2
Reached Depth (m)	50	50
Total Recoverable (m)	40.5	40.6
Total Slurries/Cavities (m)	9.5	9.4
Total Recovered (m)	39.45	40.2
Average Recovery (%)	97.4	99.0

As shown in Table 1, not all layers of the drilled lithology were acquired with sonic drilling as shown in the recovery percentage. During the drilling operation the operator noticed that in some instances the drill string did not encounter any resistance, indicating the presence of groundwater or very loose soils. In these conditions it is impossible to sample effectively as the material is flushed away or will just fall out of the drill string, which makes layers where these conditions exist unrecoverable.

Nonetheless, when viewed overall the recovery percentage of the sonic rig was very high. Also, comparing the drilled cores with the known dump model of the test locations, it was concluded that the drill core were representable for the present lithologies at the post-mining site.

Monitoring while drilling and geotechnics while drilling

The Monitoring While Drilling (MWD) system is a state-of-the-art data acquisition system that plays an increasingly crucial role in the drilling industry. This system logs various physical drilling parameters so as to optimize the performance of a drilling machine and improve the efficiency of the drilling operation by providing the drilling operator with relevant information about rig performance and soil profile.

Table 2: MWD parameters

Measured parameter	Parameter of interest	Presentation unit
Depth	Borehole depth, Relative depth	m, m
Sonic hydraulic pressure	Sonic pressure	Bar
Sonic hydraulic debit	Sonic frequency	Hz
Rotation hydraulic pressure	Torque	Nm
Rotational hydraulic debit	Rotary speed	RPM
Pull up pressure	Pull up pressure	Bar
Pull down pressure	Pull down pressure, Total downward force	Bar, kN
Flushing fluid pressure	Flushing pressure	Bar
Flushing fluid debit	Flushing flow	l/min
Location	Location	Lat, Lon
Inclination X, Y	Drilling angle	deg.
Acceleration	G-force, THD+N[1], True sonic frequency	g, %, Hz
Temperature	Borehole temperature	°C

[1] THD+N stands for total harmonic distortion including noise, which is defined as the power of the harmonics and noise divided by the total signal power. The harmonic power and noise can be calculated by subtracting the fundamental frequency power form the total output power.

Geotechnics While Drilling (GWD) is a feature that extends the MWD system, focusing on the study of subsurface ground conditions and the prediction of soil properties in real time while drilling is in progress. While the MWD system measures input parameters related to the sonic drilling process, the GWD system uses these values to derive interesting mechanical soil properties such as density, porosity, cohesion, frictional angle, etc. In this way, the GWD feature provides valuable information about soil properties in real time and presents it in such a way that it allows for quick assessment of latent conditions.

The analysis of the data obtained at the two test locations showed that various parameters, such as the pulldown pressure, sonic pressure, torque, and rate of penetration, provide valuable insights into the properties of the materials being drilled. The pulldown pressure reflects the total downward force and can indicate the type of rock or soil: softer materials may require a lower pulldown pressure, while harder materials require more. A significant decrease in the rate of penetration may indicate that the drill has encountered a harder layer, while an increase may indicate a softer layer. Additionally, torque is a good indicator of soil cohesion and varies in response to changes in soil friction to maintain a constant rotational speed. Finally, sonic pressure fluctuates in response to changes in soil friction to maintain a constant sonic frequency. The graphs below show an example of how these parameters change with depth.

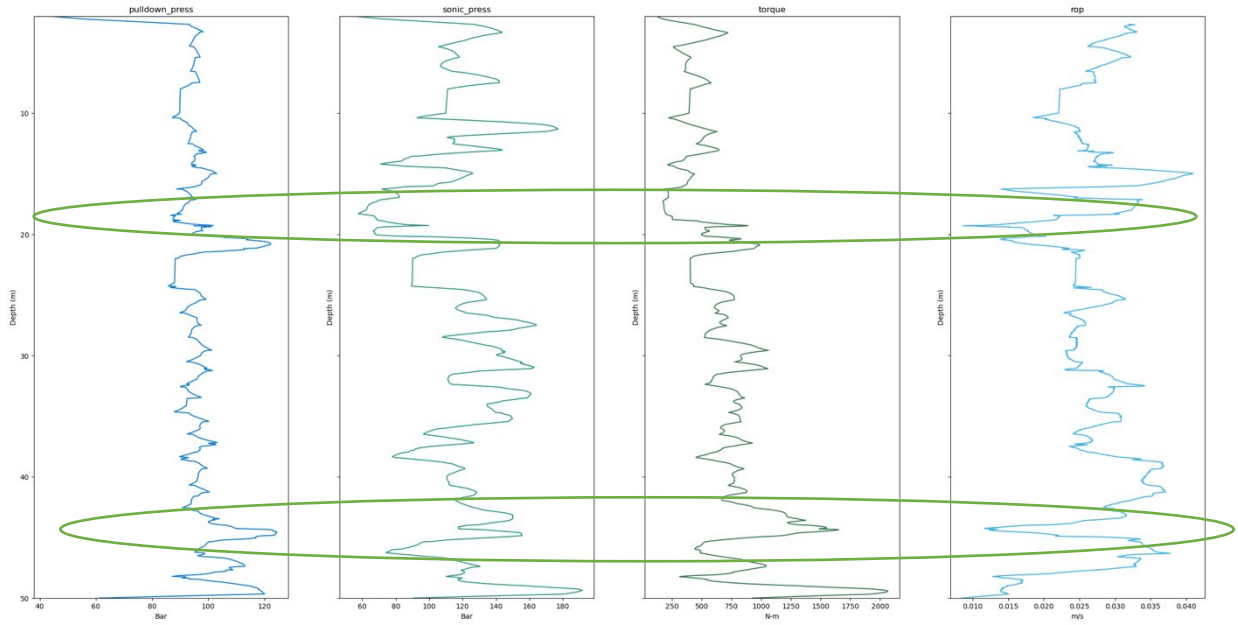


Figure 3: Pulldown pressure, sonic pressure, torque, and rate of penetration vs. depth, with the values at 20 m and 45 m highlighted as they are further discussed in the body of the paper

An intriguing pattern was observed at a depth of approximately 20 meters, where a sharp increase in pulldown pressure, sonic pressure, and torque corresponded with a noticeable drop in the rate of penetration. This demonstrates a clear relationship between the parameters and can be used to infer the characteristics of the subsurface materials being drilled. In this case it can be concluded that at that depth a resistant soil

layer is present, requiring greater pulldown pressure to advance the drill bit, higher sonic pressure to oscillate the drill bit, and increased torque to rotate and steer the drill bit.

A similar trend was observed again at a depth of approximately 45 meters, where pulldown pressure, sonic pressure, and torque displayed an upward trend, corresponding to a decline in the rate of penetration. Conversely, at a depth of approximately 40 meters, an opposite pattern was observed, with the rate of penetration increasing as torque, sonic pressure, and pulldown pressure decreased. This suggests that the soil at this interval offered less resistance to penetration.

At the same locations where the drilling was performed, soil samples were obtained at various depths. These soil samples were analyzed in the laboratory and various soil parameters were correlated with GWD features from the same sampling. This showed a moderate to strong negative correlation between bulk density, dry density, volume loss, constrain modulus low and effective angle, and torque, rate of penetration, and rotational speed. This negative correlation indicates that as these soil properties increased, the torque, rate of penetration, and rotational speed decreased. On the other hand, the constrained modulus and the effective cohesion have a moderate to strong positive correlation with torque, rate of penetration and rotational speed. This suggests that as these soil properties increased, the torque, rate of penetration, and rotational speed also increased.

These correlations were established with minimal geotechnical data and therefore these correlations are indicative only, but they can be used to guide further research and experimentation. Another area of future research should be ranking the MWD parameters listed in Table 2 on their relevance for GWD.

Sonic cone penetration testing

Sonic CPT is an exciting and rapidly developing technique that is reducing early refusals in CPT soundings by carefully applying a vibration, when needed, to the CPT string. The technique actually has a history dating back almost 40 years to 1982, when 1982 Sasaki and Koga reported their work to develop and deploy their vibratory cone, which they used for liquefaction analysis. They compared tip resistance with and without vibration and found that in loose soils the tip resistance was substantially lower in vibratory mode due to the additional excess pore pressure generated, whereas in stiff soils the vibration did not create additional excess pore pressure and the tip resistance was similar.

Royal Eijkelkamp's expertise in sonic drilling technology has allowed us to take this pioneering work much further and develop it into three key areas of application. The first application is to deal with layers of very hard soil above or between layers of softer material. With conventional CPT it is impossible to push through these layers and the test must be terminated. Sometimes destructive drilling will be performed, which is costly and provides no data. However, with Sonic CPT it is often possible to use the vibratory

action to penetrate the hard layer before Standard CPT pushing can be continued in the softer material below.

The second application is that by applying vibration to the CPT rod string, friction between the rods and soil is largely eliminated, allowing a higher percentage of the pushing force to be transferred to the cone, which enables the cone to be pushed deeper into the soil. This is particularly useful in stiff cohesive material, such as London Clay, where almost one ton of pushing force per meter can be required to overcome rod friction. This can also improve the applicability of lower weight CPT rigs, which provide a smaller reaction force.

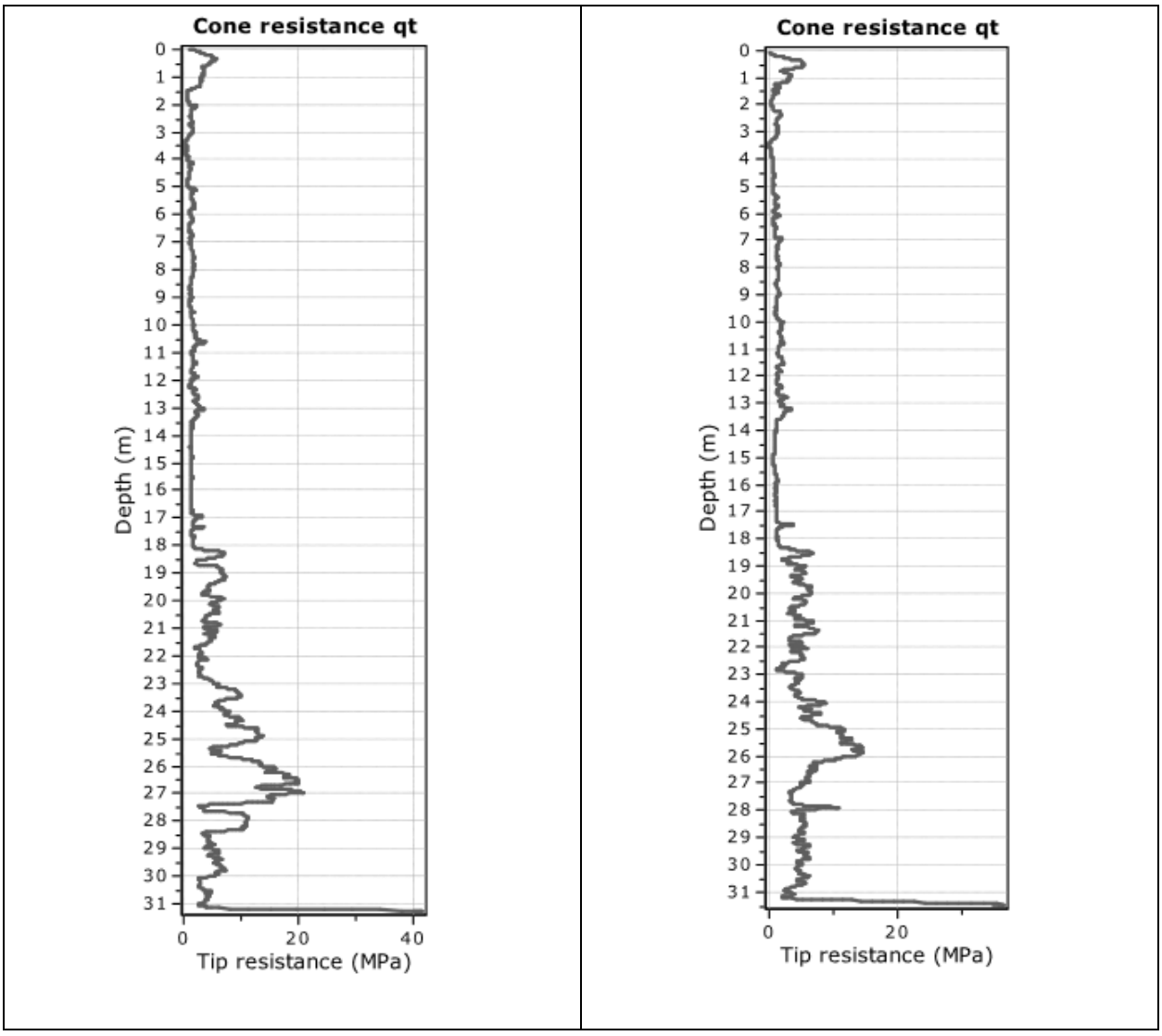


Figure 4: Comparison of tip resistance during Standard CPT (left) and Sonic CPT (right) – location 1

The third application is for producing pile driving simulations for vibratory hammer piling. Standard CPT data has long provided excellent input for impact hammer pile driving simulations, but is less suitable

for piling using a vibratory hammer. With Sonic CPT we can approach or even match the frequency of a vibratory hammer to test the influence of the vibrations on the soil.

For this project, Standard CPT and Sonic CPT were applied side-by-side. Sonic CPT was performed at approximately 100 Hz to assess the impact on the tip resistance. However, as shown in Figure 4, the reduction in the tip resistance was minimal, simply because the soil was largely cohesive. Only in the granular soil layers at depths exceeding 25 m were the tip resistances as expected (especially noticeable at a depth of 26 m), with the maximum value dropping from 21.08 MPa to 14.74 MPa. Unfortunately, it was deemed impossible to penetrate through the stiff sand layer at a depth of 31 m, as at that depth the difference in tip resistance would have been more distinct.

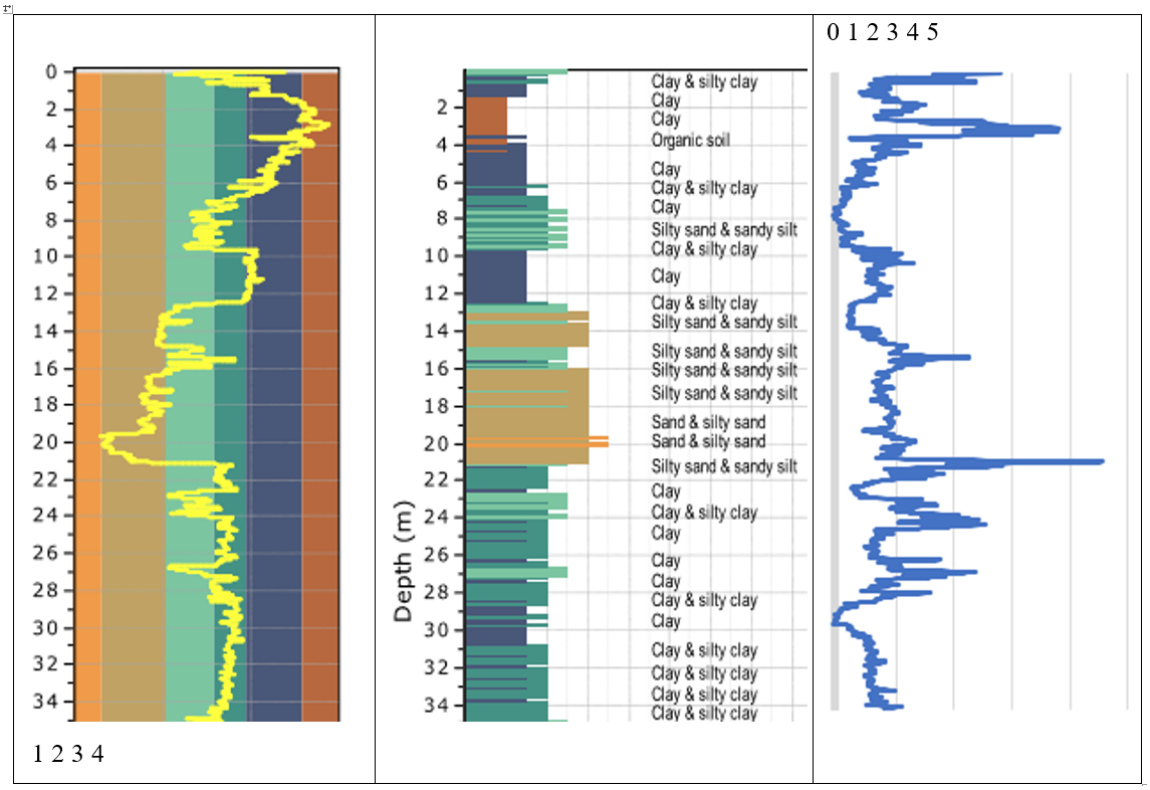
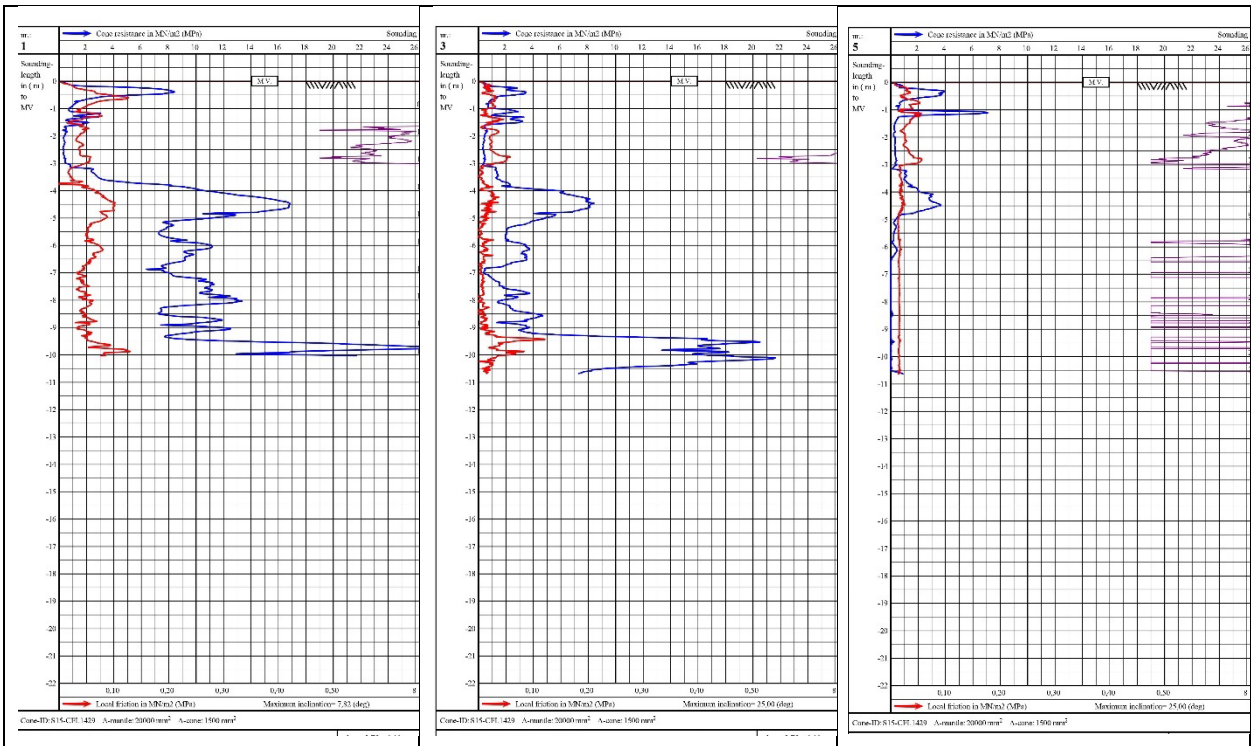


Figure 5: Tip resistance ratio Sonic CPT vs. Standard CPT, location 2, with the soil behavior type index derived from the CPT data on the left

Sonic CPT was also performed at location 2, albeit only to a depth of approximately 35 m. Figure 5 shows the tip resistance ratio between the Sonic CPT and the Standard CPT, with the soil behavior type shown on the left side of the figure. While in most cases the ratio is less than 1, there are many instances where the ratio is (much) higher than 1. At present there is no explanation for these high values, especially since there seems to be no consistency. In Figure 5 the soil behavior type index is shown as well. Initially (to a depth of approximately 16 m) there seems to be some correlation between the tip resistance ratio and the index value, but at greater depths this correlation is completely missing. Obviously more research needs

to be done to allow for a better interpretation of the Sonic CPT data. This is further complicated by the fact that the execution of Sonic CPT introduces a new variable: the frequency of the applied vibration.

Previous testing performed by Royal Eijkelkamp shows that the frequency used has a large impact on the resultant data. As shown in Figure 6, vibrating the cone at 100 Hz greatly reduces the resultant tip resistance (shown in blue), meaning the cone can penetrate harder layers more easily, but the profile does not reflect the profile of the Standard CPT. However, when the frequency is reduced to 50 Hz the shape of the profile resembles the profile of the Standard CPT and is therefore more instructive of the soil conditions. This means that if the objective is simply to make the cone go through stiffer layers (in line with the first two objectives mentioned above) the use of a higher frequency makes perfect sense. If on the other hand the objective is to derive soil parameters from the acquired data, performing Sonic CPT at a lower frequency is essential.



Standard CPT	Sonic CPT – 50 Hz	Sonic CPT – 100 Hz

Figure 6: Comparison of Standard CPT and Sonic CPT (50 Hz and 100 Hz)

Conclusion

As demonstrated during the TRIM4 project, the geotechnical soil investigation techniques described in this paper all belong in the tool box of engineers involved in characterizing mining landscapes. Soil sampling using a sonic drill rig allows for sampling in a wide range of materials, including those found in a mining

landscape, with a very high recovery percentage. The Monitoring While Drilling technique is well established to enhance the drilling efficiency and the drill rig maintenance, but more work is required to use the obtained results for subsurface characterization. The correlations generated during the TRIM4 project provide solid guidance, but before it becomes a routine operation, similar to soil behavior characterization based on the CPT data, more data is required. Finally Sonic Cone Penetration Testing is a well-established technique to minimize refusal, but once again more research is required to correlate the data obtained during Sonic CPT with the soil(behavior) type when it is performed on a stand-alone basis.

References

Benoit, J. and Souza, B. 2024. Measurement while drilling. *GeoStrata* 27(6). https://doi.org/10.1061/geosek.0000514

Sasaki, Y. and Koga, Y. 1982. Vibratory cone penetrometer to assess the liquefaction potential of the ground. *Proceedings, 1982.* 541–555.

TRIM4Post Mining website. 2024. Accessed at https://trim4postming.com

Utilization of Novel Electrokinetic Geosynthetics for Stabilization of Ultra-fine Tailings

Nilan Jayasiri, The University of Western Australia, Australia
Andy Fourie, The University of Western Australia, Australia
Cristina Vulpe, The University of Western Australia, Australia

Abstract

Dewatering by means of electroosmosis involves placing a series of electrodes into the ground and applying a potential difference between the electrodes to induce water molecules to move towards the negative electrode from the positive electrode. Despite well documented applications of this technique for improving fine and ultra-fine sediments, the mining industry has yet to embrace this technology at field scale. One of the main impediments is the rapid electrode corrosion of conventional metal electrodes. Severe corrosion of electrodes can hinder the efficiency of this technique over time, which leads to increased energy consumption. The advancement of electrically conductive geosynthetics, also known as electrokinetic geosynthetics (EKGs), presents a significant opportunity to improve the industrial uptake of this technique by replacing conventional metallic electrodes, owing to EKGs vastly superior anti-corrosive properties. The current study investigated the performance of novel EKG electrodes in dewatering ultra-fine tailings using a laboratory-scale experimental approach. The dewatering efficiencies using EKG electrodes were compared with that of conventional metal electrodes (mild steel) by assessing the volume of water expelled, strength gain, end-of-test water content, and energy consumption. The results showed that for dewatering fine, slurried tailings, the novel EKG electrodes proved to be just as effective as their traditional metal counterparts, and usually better, since corrosion effects did not hinder the electroosmosis process. Although the variation in water content between the tests conducted with the two types of electrodes under the same voltage gradients was marginal, the use of EKGs has led to a significant enhancement in undrained shear strength. This constitutes one of the main advantages of utilizing EKGs for treating ultra-fine tailings.

Introduction

Stabilizing slurried, ultra-fine tailings is one of the significant challenges faced by the owners and operators of tailings storage facilities, particularly when it comes to closure and rehabilitation. While there are several conventional practices in the industry to enhance consolidation, these techniques are sometimes only

moderately effective or impractical. Consolidation by means of electroosmosis offers a promising approach for treating slurried tailings. This technique involves placing a series of electrodes into the ground and applying an electrical potential difference between the electrodes to induce water molecules to move toward the negatively charged electrode from the vicinity of the positively charged electrode. When drainage is facilitated at the cathode, consolidation of material takes place in an amount equal to the quantity of water extracted.

One of the abiding factors that has impeded the widespread use of electroosmosis dewatering technique at the field scale is the severe corrosion of metal electrodes. Previous studies have demonstrated that metallic electrodes such as steel, copper, and aluminum are highly prone to corrosion, which negatively impacts efficiency and power consumption, which in turn impacts achieving the required degree of consolidation (Xue et al., 2015). Studies conducted with titanium and gold electrodes have shown little or no corrosion due to the corrosion-resistive properties, but the extremely high cost of these materials makes their usage in large-scale field applications not viable (Loch et al., 2010). In addition, non-metallic electrode types such as graphite have solved the corrosion issue to a considerable extent, although the disadvantages of these include: (1) lesser efficiency and (2) high brittleness (Malekzadeh et al., 2016).

The advancement of electrically conductive geosynthetics, also known as electrokinetic geosynthetics (EKGs), presents a significant opportunity to improve the industrial uptake of this technique by replacing conventional metallic electrodes, owing to EKGs' vastly superior anti-corrosive properties. The current study investigated the performance of novel EKG electrodes in dewatering ultra-fine tailings using a laboratory-scale experimental approach. The dewatering efficiencies using EKG electrodes were compared with those of conventional metal electrodes (mild steel) by assessing the volume of water expelled, strength gain, end-of-test water content, electrochemical changes and energy consumption.

Experimental methodology

Test materials

Commercially available kaolin clay was used to prepare the slurry specimens required for the testing. The basic physicochemical properties of kaolin are summarized in Table 1.

Table 1: Basic physicochemical properties of kaolin

Specific gravity	Liquid limit (%)	Plastic limit (%)	Clay content (%)	Silt content (%)	pH	Conductivity (mS/cm)
2.6	73.7	44.4	74.6	25.4	4.98	0.65

Experimental setup

The experiments were carried out using 20 L capacity (380 x 280 x 200 mm) tubs, as shown schematically

in Figure 1. The electrodes utilized in the experiments were composed of either mild steel or EKGs. Both types of electrodes had the same nominal dimensions of 180 × 83 × 3 mm, whereas the weights of mild steel and EKG electrodes were approximately 226 g and 46 g, respectively. While there are various types of EKGs, the specific EKG electrodes used in the study are identical in size to a conventional prefabricated vertical drain but manufactured from electrically conductive polymer. A perforated polyvinyl chloride (PVC) tube encased in nonwoven geotextile facilitated drainage through a small hole at the bottom of the PVC tube, and the drained water was subsequently collected into a measuring cylinder.

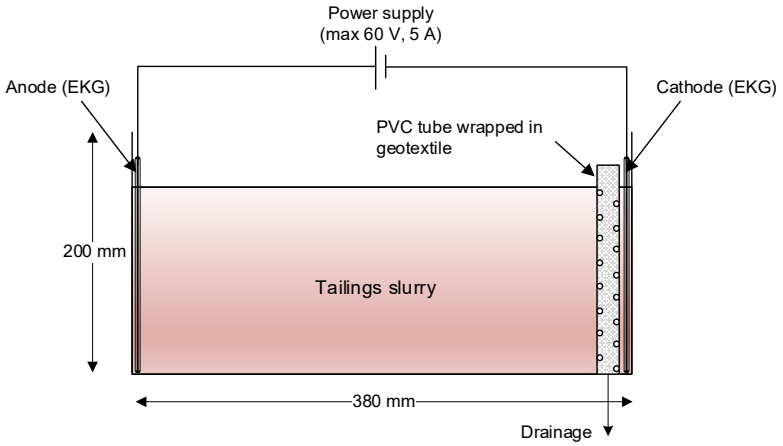


Figure 1: Schematic of the test setup

Test program

The kaolin slurry was prepared by mixing kaolin with deionized water to a water content of 150%. After 24 hours, the slurry was carefully poured into the tub to an initial height of approximately 160 mm. To prevent any moisture loss due to evaporation, the top surface of the tub was covered with clear plastic wrap. The volume of drained water and current were monitored at one-hour intervals, and the tests were terminated once the discharge rate fell below a threshold of 10 ml/hour. Once a test was completed, post-treatment moisture content and undrained shear strength were measured between the electrodes. Details of the test program are provided in Table 2.

Table 2: Details of the testing program

Test designation	Electrode material	Voltage gradient (V/m)	Voltage (V)
SE1	Mild steel	50	19
SE2	Mild steel	100	38
SE3	Mild steel	150	57
EK1	EKG	50	19
EK2	EKG	100	38
EK3	EKG	150	57

Results and discussion

Variation of drainage volume

The temporal variation of cumulative drainage volume for both types of electrode material is depicted in Figure 2a. As can be seen, the final cumulative discharges for tests conducted with EKGs under 150 and 100 V/m voltage gradients were 5.9% and 8.1% higher than those carried out with metal electrodes, respectively. In contrast, when the experiment was carried out at a relatively low voltage gradient (50 V/m), the test with the EKGs (EK1) resulted in an 11.5% lower discharge volume compared to the test with mild steel electrodes. Given that the electrode degradation rate is a function of the amount of electric charge according to Faraday's law, the reason for this behavior could be mainly attributed to the low corrosion rate occurring in the metal electrodes at lower voltage gradients. However, the corrosion effects may start to govern in metal electrodes even at low voltage gradients under field conditions since the dewatering usually extends for prolonged periods (Lockhart and Stickland, 1984).

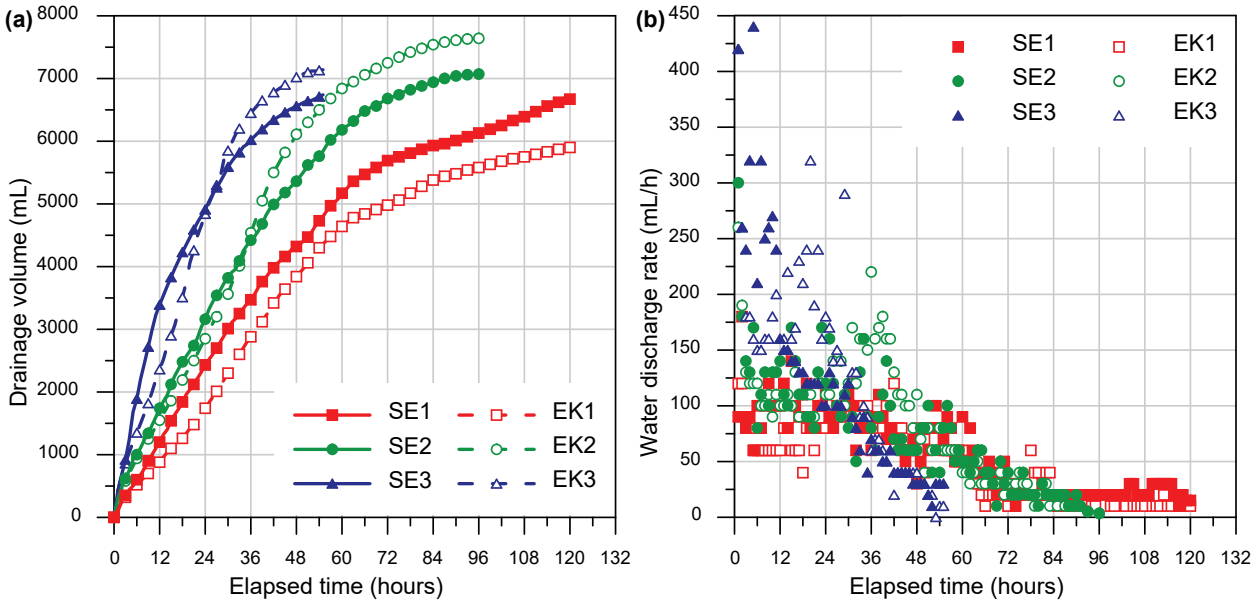


Figure 2: (a) Variation of drainage volume with time; (b) variation of drainage rate with time

It is apparent that the highest voltage gradient resulted in a lower discharge volume than that of the intermediate voltage gradient, regardless of the electrode type. This is predominantly due to the rapid desaturation of material in the vicinity of the anode, with other reasons being (1) loss of contact area between the electrode and soil, (2) electrochemical changes and (3) loss of applied voltage at the electrode interface.

According to Figure 2b, the water discharge rate was relatively constant for a longer time period in tests conducted with EKGs. Although the drainage rate was higher within the first few hours of the experiments with metal electrodes, a progressive declining rate over time can be seen since the early stages

of the tests, particularly for SE2 and SE3. This ever-declining rate is an indication of corrosion occurring at the metal electrodes, which is also reflected by the electric current drawn during the tests, depicted in Figure 3a.

Power consumption

Figure 3a shows that the amount of current drawn was relatively constant for a longer period in tests with EKG at higher voltage gradients, whereas the current tends to drop earlier for the experiments with metal electrodes. Particularly in the case of SE3, the amount of electric current drawn dramatically reduced within the first 12 hours after the commencement of the test, hindering the water discharge rate. This behavior is closely related to the corrosion effects and subsequent voltage loss at the electrode-material interface, which is discussed in the forthcoming sections. Another noteworthy observation pertaining to test EK2 is that after fluctuating around 0.08 A for more than 24 hours, there is a sudden increase in the current drawn, peaking at around 0.16 A. While the prime factor that triggered this spike is not clear, previous studies have shown that changes in ionic concentrations, formation of additional conductive pathways for ion movement within the treated material, and pore structure changes of the material could alter the amount of current drawn during electroosmosis treatment (Liu et al., 2024; Pandey et al., 2024).

The electric current was then used to determine power consumption during the electrically assisted dewatering, and to facilitate comparisons between the tests, the power consumption was interpreted in terms of kWh/dry tonnes of treated material:

$$P = \int_0^t VIdt/W_s$$

where, P is the power consumption, V is the average voltage, I is the average current, t is the treatment time and W_s is the dry weight of the material calculated from the initial solids content.

As depicted in Figure 3b, dewatering with EKG electrodes under 50, 100, and 150 V/m consumed approximately 7.6%, 31.6% and 18.9% more power, respectively, compared to mild steel electrodes under the same voltage gradients. This is mainly because the amount of current drawn during the dewatering process is generally high (resulting from lesser corrosion effects) when EKGs are utilized. Although the power consumption is only marginally higher at the lowest voltage gradient (50 V/m), a noticeable increase in the power consumption can be seen at higher voltage gradients (100 and 150 V/m). However, this can be justified by the higher volume of water extracted using EKGs under 100 and 150 V/m voltage gradients. The currently available power consumption evaluation methods do not account for the degree of treatment achieved. This highlights the necessity for a better measure of power consumption, i.e., an approach that includes changes in material characteristics.

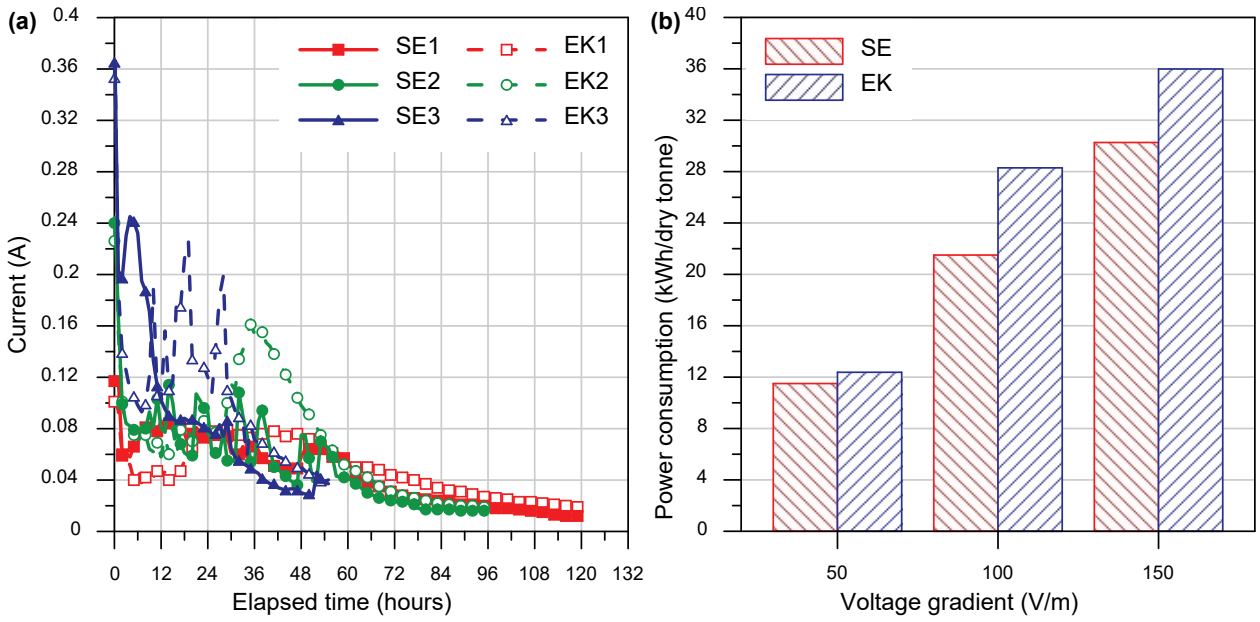


Figure 3: (a) Variation of current drawn with time; (b) power consumption in terms of kWh/dry tonnes of treated material

Electrochemical and corrosion effects

As dewatering progressed using the metal electrodes, the color of the surficial material adjacent to the anode was changed from its initial white to a yellow-brown color. Further investigation at the completion of the tests revealed that similar discoloration was present throughout the material stratum, irrespective of the applied voltage. This is a consequence of anode corrosion and subsequent accumulation of degraded substances in kaolin adjacent to the anode. Application of DC current between the electrodes not only induces the electroosmosis process, but also causes electrochemical reactions to occur adjacent to the electrodes (Mitchell and Soga, 2005). Oxidation will take place at the anode, generating oxygen gas and creating an acid front (due to the reduction in pH) in the vicinity of the anode. If the anode material is reactive (e.g., metal such as mild steel), it could oxidize and release ions into the adjacent soil matrix, causing anode corrosion, as observed in Figure 4a. Similarly, hydrolysis will occur at the cathode, generating hydrogen gas and creating a basic front (due to the increase in pH) in the vicinity of the cathode.

At the end of each test, the weight of the electrodes was recorded to determine the degree of electrode degradation based on the loss of weight during the electroosmosis dewatering. The degrees of anode degradation for the tests with steel electrodes under 50, 100, and 150 V/m voltage gradients were 3.27%, 2.91%, and 2.64%, respectively, whereas for the tests with EKGs, the anode degradation under the same voltage gradients were 0.51%, 0.13%, and 0%, respectively. It is clear that steel anodes undergo corrosion and subsequent degradation due to electrochemical reactions, whereas the EKG-type anodes demonstrated better corrosion resistance. Although the EKG electrodes exhibited minimal signs of corrosion in terms of

the degree of degradation, upon close examination of the electrodes at the conclusion of the tests, some had formed bubbles (smaller than 1 mm in size) on the surfaces of the EKG. Unlike steel electrodes, where corrosion only occurred in areas where the electrode was in contact with the material, the bubbling effect in EKGs was observed beyond those areas, for instance, the section above the material surface horizon. Hence, it is unclear whether the "bubbling" effect is solely due to electrochemical reactions or rather a ramification of applying DC current. Although the polymers do not technically "corrode" as a metallic material (Schweitzer, 2009), it is nevertheless important to further investigate the root cause for this effect as it could compromise the durability of EKGs in long-term field applications.

Regardless of the electrode material, the degree of cathode degradation under all voltage gradients was less than 0.1%, indicating no signs of corrosion as explained by electrochemical theories (Micic et al., 2001). Another noteworthy observation regarding the steel electrodes is the formation of a thin, dark layer in the sections where the electrode is in contact with the material. This is believed to be oxide precipitates resulting from electrochemical reactions. According to Xue et al. (2015), X-ray diffraction tests have revealed that these types of substances present extremely low conductive characteristics. The formation of precipitate films adjacent to electrodes could result in significant potential loss at the soil-electrode interfaces and subsequently lead to a sharp increase in resistivity. No such behavior was observed in EKG electrodes, which may be the reason for the relatively steady water extraction rate during the dewatering process (Figure 2b).

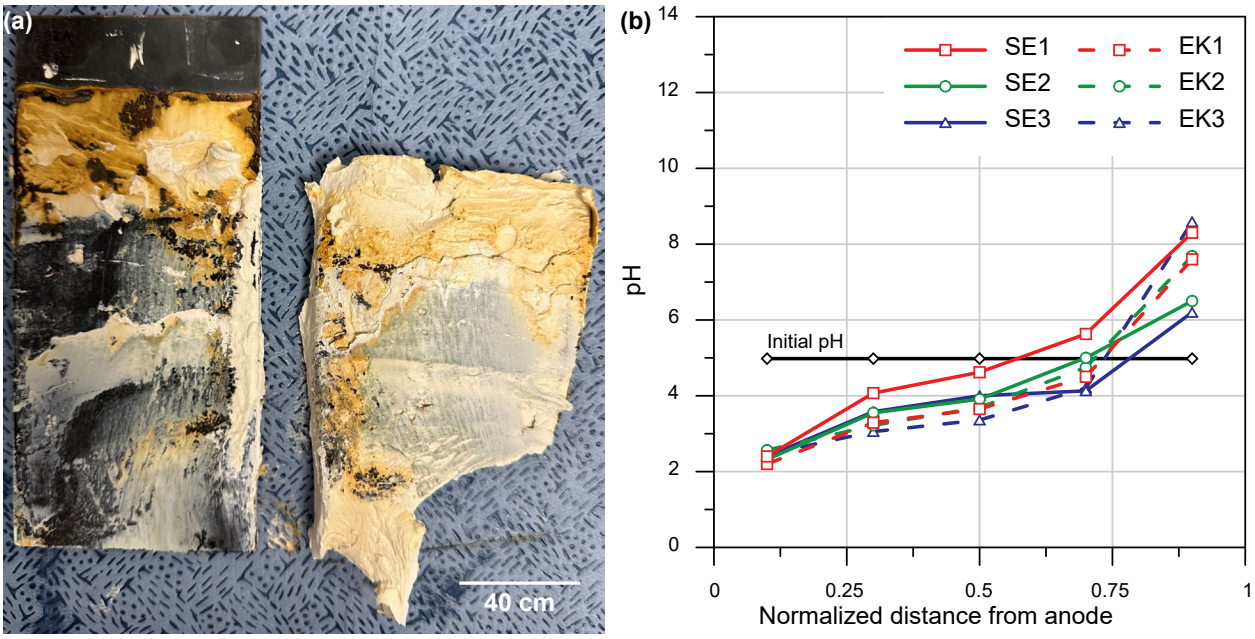


Figure 4: (a) Corrosion observed in anode and adjacent soil at test SE2; (b) variation of pH between the electrodes

Figure 4b shows the pH variation between the electrodes with respect to the normalized distance from the anode (distance to the sampling point from the anode normalized by the distance between electrodes). As expected, the material near the anode exhibited acidic conditions due to hydrogen ion (H^+) release. The pH value of the anodic zone was generally about 2.4, irrespective of the electrode type and the voltage gradient, indicating a twofold decrease from the initial state. In contrast, the pH in the vicinity of the cathode increased due to the release of hydroxide ions (OH^-); nonetheless, the pH values demonstrated considerable variability. The post-treatment pH value of the material near the cathode ranged from 6.2 to 8.6, which is approximately a 50% average increase from the pre-treatment pH. As depicted in Figure 4b, the material away from the electrodes (0.3 – 0.5 normalized distance from the anode) experienced a lesser change in pH. Interestingly, the posttreatment pH of the tailings treated with EKGs was comparable to that of metal electrodes, despite the EKGs being manufactured from non-metallic polymer material.

Variation of water content

The distribution of water content between the anode and cathode is presented in Figure 5. On average, the water content of the slurry reduced approximately 70% from the initial value of 150% due to the electroosmosis treatment. As expected, EK1 has the lowest average reduction in water content (88%) and is 7% higher than the water content obtained from the test with metal electrodes under the same voltage gradient. In contrast, the post-treatment average water contents for tests conducted with EKGs under 150 and 100 V/m voltage gradients are 4.2% and 8.8% lower than those carried out with metal electrodes, respectively. The obtained water content values are generally in line with the extracted water volumes presented in Figure 2. Overall, the results of water content measurements further showed that the EKGs performed slightly better in dewatering compared to metal electrodes at high voltage gradients.

The electroosmosis process causes the water molecules to move toward the cathode from the vicinity of the anode and as a result, the water content at the anode is generally lower than that at the cathode. However, no such variation was found in the present study. According to Figure 5, the water content is generally low at the closest sampling point to the anode, but as the sampling location moves towards the cathode, it starts to increase before starting to decrease again, indicating the highest water content at the section before the halfway point between the electrodes (0.3 – 0.5 normalized distance from the anode). The reason for this behavior could be mainly attributed to the formation of shrinkage cracks perpendicular to the flow path (Figure 6), which subsequently resulted in disrupting the conductivity and electroosmotic flow (Jayasiri et al., 2024). It appears that the shrinkage cracks may have acted as a barrier up to a certain degree, preventing water molecules from passing from the anode section to the cathode. Besides the above, loss of contact area between the electrode and soil cluster due to electrode detachment could also contribute to this peculiar behavior.

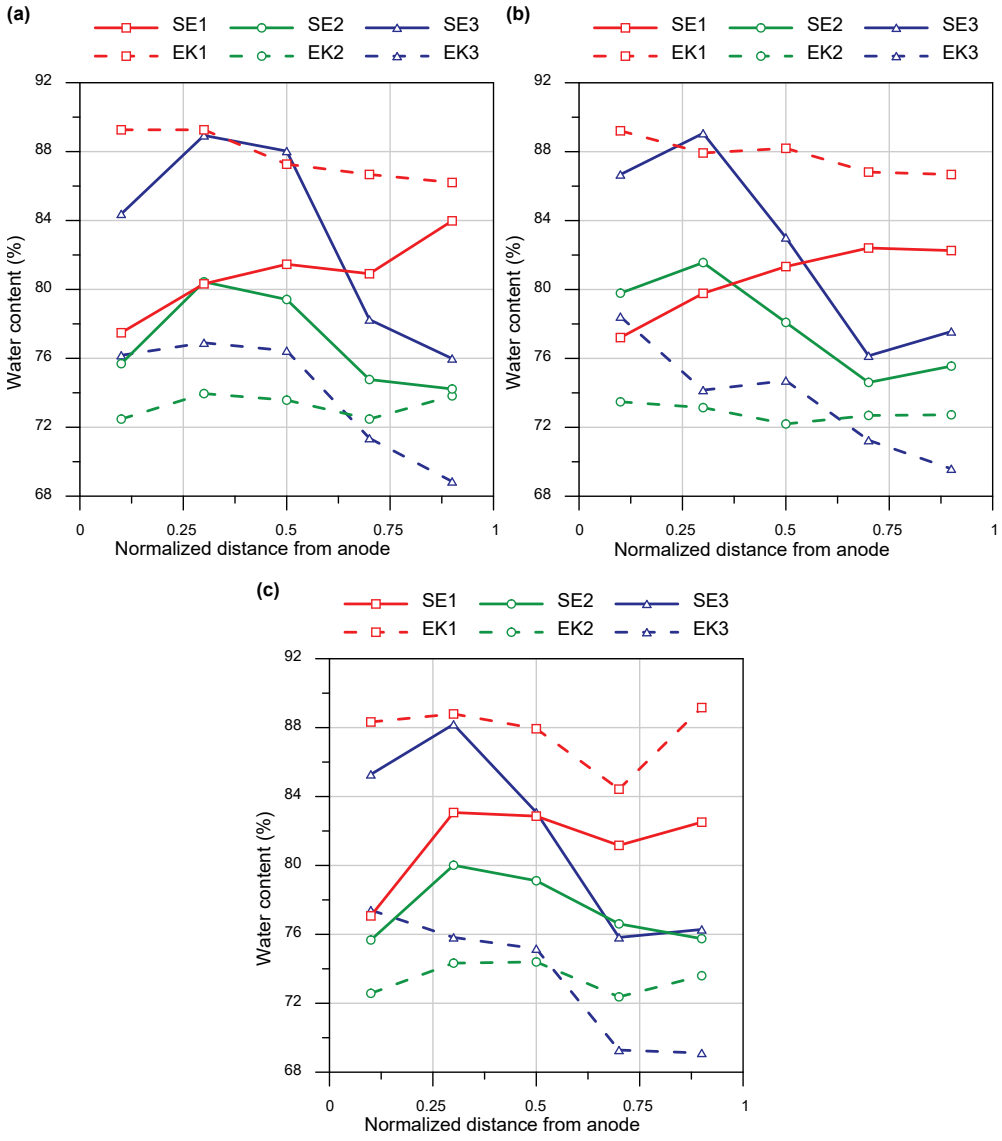


Figure 5: Variation of water content in (a) top layer; (b) mid-depth layer; (c) bottom layer

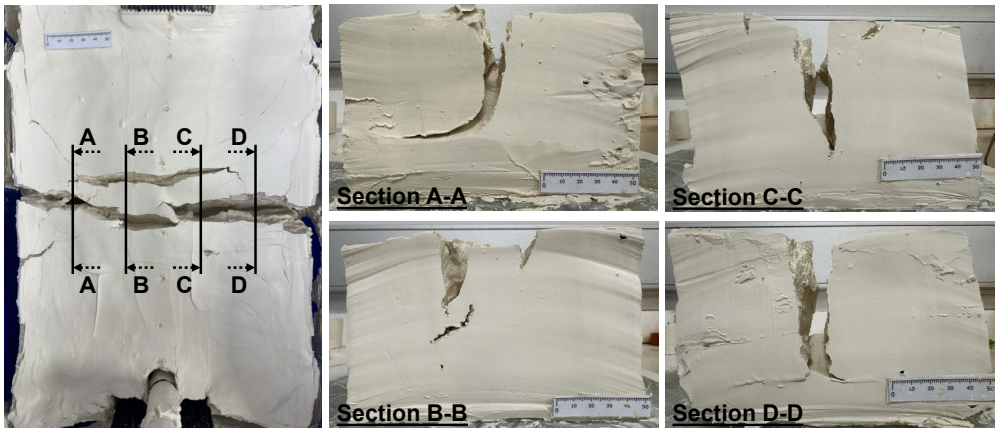


Figure 6: Cross-sections showing the formation of shrinkage cracks in test EK2

Variation of undrained shear strength

Figure 7 depicts the distribution of approximate undrained shear strength between the electrodes. The measured undrained shear strength variation generally agrees with the observed water content trend presented in Figure 5. On average, the electroosmosis treatment enhanced the undrained shear strength of the material by 24 times compared to the pretreatment shear strength of 0.3 kPa. Under the low voltage gradient (50 V/m), the test conducted with mild steel electrodes indicated a marginal 16.3% increase in shear strength compared with the test conducted with EKG.

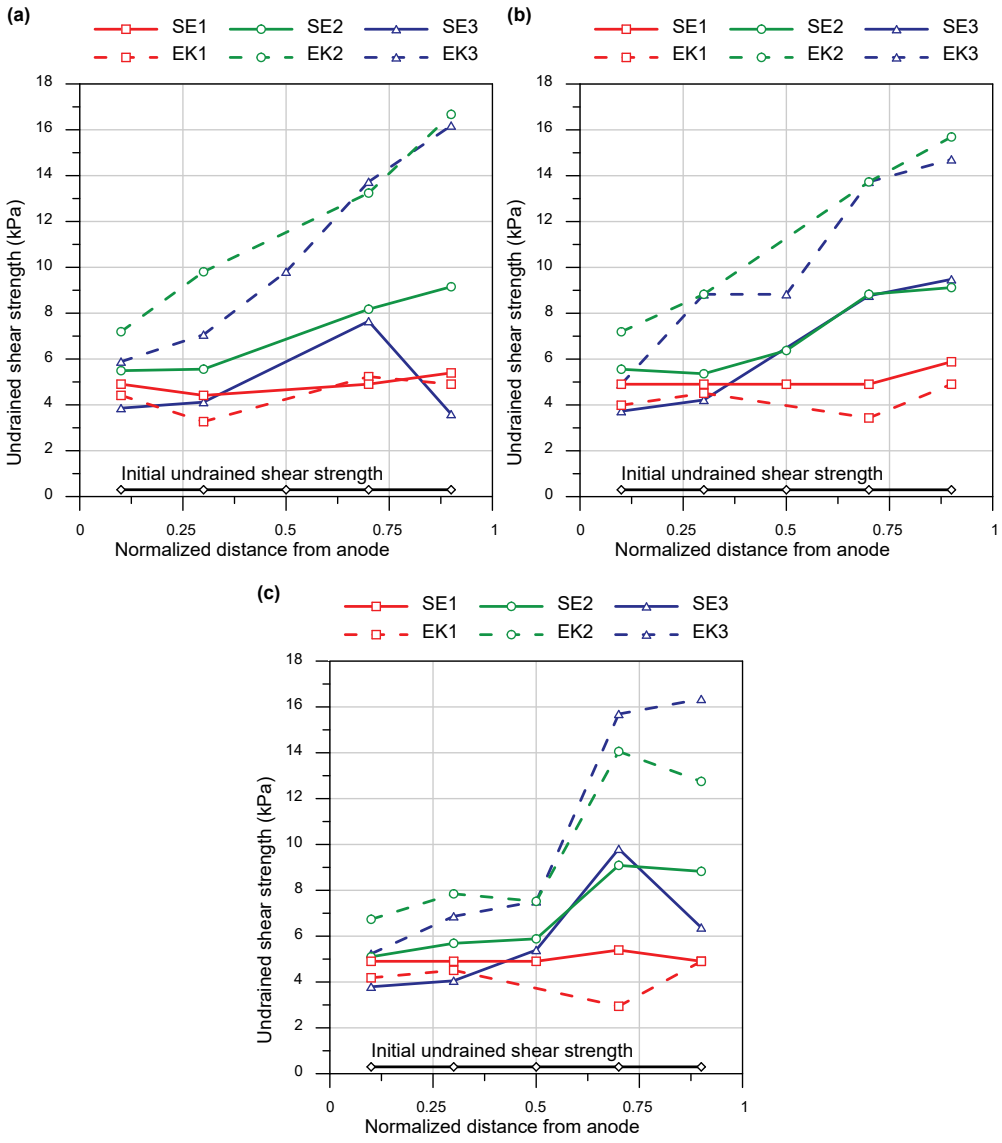


Figure 7: Variation of undrained shear strength in (a) top layer; (b) mid-depth layer; (c) bottom layer

At 150 and 100 V/m voltage gradients, the average post-treatment strengths of the tests that utilized EKGs were 79.3% and 55% higher than those conducted with mild steel electrodes, respectively. In

contrast, the post-treatment average water contents for tests performed with EKGs under the same voltage gradients were only 4.2% and 8.8% lower than those carried out with metal electrodes. Although the change in water content between the tests conducted with the two types of electrodes is marginal, the use of EKGs has led to a significant enhancement in undrained shear strength. This constitutes one of the main advantages of utilizing EKGs for treating ultra-fine tailings. However, further research is required to investigate the factors contributing to this effect and to quantify the enhancement not reflected by the change in water content.

Conclusion

Severe corrosion of metal electrodes is one of the major barriers that impede the widespread use of the electroosmotic dewatering technique in stabilizing ultra-fine tailings. The current study investigated the performance of novel electrokinetic geosynthetic (EKG) electrodes, which are manufactured from electrically conductive polymer in dewatering ultra-fine tailings, compared to conventional metallic electrodes. Based on the outcomes of this study, the following key conclusions can be drawn:

- EKGs performed well at higher voltage gradients (150 and 100 V/m) compared to conventional metal electrodes, whereas under a lower voltage gradient (50 V/m) metal electrodes resulted in a relatively better discharge volume.
- The better performance at lower gradient and the poor performance under higher voltage gradients could be mainly attributed to the lower corrosion rate in the metal electrodes at lower voltage gradients. However, the corrosion effects may start to govern in metal electrodes even at low voltage gradients under field conditions since the dewatering usually extends for prolonged periods.
- Dewatering with EKG electrodes under 100 and 150 V/m consumed approximately 31.6% and 18.9% more power, respectively, compared to mild steel electrodes under the same voltage gradients. This is mainly because the amount of current drawn during the dewatering process (resulting from lesser corrosion effects) is generally higher when EKGs are utilized.
- Dewatering with EKG electrodes under 100 and 150 V/m consumed approximately 31.6% and 18.9% more power, respectively, compared to mild steel electrodes under the same voltage gradients. This is mainly because the amount of current drawn during the dewatering process (resulting from lesser corrosion effects) is generally higher when EKGs are utilized.
- Post-treatment water content and undrained shear strength assessments showed that although the change in water content between the tests conducted with the two types of electrodes under the same voltage gradients is marginal, the use of EKGs has led to a significant enhancement in undrained shear strength. This constitutes one of the main advantages of utilizing EKGs for treating ultra-fine tailings.

In summary, the results showed that for dewatering fine, slurried tailings, the novel EKG electrodes proved to be just as effective as their traditional metal counterparts, and usually better, as corrosion effects did not hinder the electroosmosis process. While the present work only focused on the corrosion issue of conventional metal electrodes and investigating the viability of replacing them with EKGs at laboratory scale, other aspects such as long-term performance under field conditions, scale effects, capital and operational costs and logistics, etc., should be broadly investigated to promote the application of electroosmosis dewatering technique in large scale field applications.

Acknowledgments

This research was financially supported by the Australian Government through the Australian Research Council Linkage Project (LP200200216). The first author would like to acknowledge the Scholarship for International Research Fees, Ad Hoc Postgraduate Scholarship and MRIWA Postgraduate Research Scholarship supported by the University of Western Australia and Minerals Research Institute of Western Australia, respectively. The support from the Geotechnical Engineering technical staff at the University of Western Australia is gratefully acknowledged.

References

Jayasiri, N., A. Fourie and C. Vulpe. 2024. A comparative study on the performance of electroosmotic consolidation of fluid fine tailings under constant voltage and constant current configurations. In *Mine Closure 2024: Proceedings of the 17th International Conference on Mine Closure.*

Liu, J., W. Cui, B. He, X. Qin, Z. Zhou, B. Xu, S. Yu, G. Qin, K. Liu, X. Peng, X. Nie, F. Ma, P. Han and X. Bai. 2024. Experimental study on electroosmosis-solidification of engineering slurry pretreated by composite flocculant. *Constr Build Mater* 411: 134356.

Loch, J.P.G., A.T. Lima and P.J. Kleingeld. 2010. Geochemical effects of electro-osmosis in clays. *J. Appl. Electrochem*. 40(6): 1249–1254.

Lockhart, N.C. and R.E. Stickland. 1984. Dewatering coal washery tailings ponds by electroosmosis. *J. Powder Technol.* 40(1–3): 215–221.

Malekzadeh, M., J. Lovisa and N. Sivakugan. 2016. An overview of electrokinetic consolidation of soils. *Geotechnical and Geological Engineering* 34(3): 759–776.

Micic, S., J.Q. Shang, K.Y. Lo, Y.N. Lee and S.W. Lee. 2001. Electrokinetic strengthening of a marine sediment using intermittent current. *Canadian Geotechnical Journal* 38(2): 287–302.

Mitchell, J.K. and K. Soga. 2005. *Fundamentals of Soil Behavior,* 3rd edition. John Wiley & Sons.

Pandey, B.K., S. Rajesh and S. Chandra. 2024. Engineering and physicochemical response of soft clay with electrokinetic consolidation process. *Acta Geotechnica* 19(8): 1–17. doi: 10.1007/s11440-024-02227-w.

Rozas, F. and M. Castellote. 2012. Electrokinetic remediation of dredged sediments polluted with heavy metals with different enhancing electrolytes. *Electrochimica Acta* 86: 102–109.

Schweitzer, P.A. 2009. *Fundamentals of Corrosion. Mechanisms, Causes, and Preventative Methods.* CRC Press. Taylor & Francis Group.

Xue, Z., X. Tang, Q. Yang, Y. Wan and G. Yang. 2015. Comparison of electro-osmosis experiments on marine sludge with different electrode materials. *Drying Technology* 33(8): 986–995.

Enhanced Conceptualization of Reactive Filtered Tailings Oxidation Using a Reactive Transport Model

Katherine Raymond, Okane Consultants, Canada
Jared Robertson, Okane Consultants, Canada
Julie Zettl, Okane Consultants, Canada
Mike O'Kane, Okane Consultants, Canada

Abstract

An increasing concern within the mining industry is the need for balance between geotechnical and geochemical stability for long-term tailings storage. Often, filtered tailings (otherwise known as dry stack tailings) can enhance geotechnical stability, reducing risk associated with tailings dam failures. Typically, in the conceptualization of sulfidic (reactive) filtered tailings, there is an increased risk of metal leaching and acid rock drainage (ML/ARD) because the material is unsaturated, allowing for additional sulfide mineral oxidation. This conceptualization can lead to inherent conservatism in long-term predictions in seepage water quality where numerical models assume the entire tailings profile becomes oxic. Here, we explore incorporating a "reasonable expectation" conceptual model for tailings oxidation that includes mechanistic processes (e.g., including diffusion limitations and oxygen consumption by sulfide oxidation), which can be used to run sensitivity analyses and enhance understanding of site-specific ML/ARD risk for reactive filtered tailings storage facilities (TSFs). To support this conceptual model, reactive transport models of Potentially Acid Generating (PAG) sulfidic tailings were simulated to demonstrate mechanistic processes controlling oxygen ingress and pyrite weathering over time under different climate, TSF design, and pyrite reactivity rate scenarios. Under more reactive pyrite conditions (i.e., pyrite with faster rate kinetics), oxygen ingress may be limited to the top several meters over the first few decades, similar to conventionally deposited tailings simulations. While filtered tailings have the potential to generate greater quantities of metal loads long-term, model results show poor quality seepage produced may take many more decades, or over a century, to be observed in basal seepage. This demonstrates the importance of managing surface runoff during operations through closure in both filtered and conventional TSFs and highlights opportunities to design cover systems that manage runoff, and decrease infiltration and/or oxygen ingress, to meet regional closure objectives.

Introduction

Production of tailings is projected to rise in the coming decades to satisfy increasing societal demands for metals, as well as declining ore grades (Mudd, 2010; Northey et al., 2014). In light of recent global tailings dam failures, mining companies are investigating alternative tailings storage facility (TSF) designs from conventional tailings (where tailings are typically piped as a slurry to a storage facility at a relatively low solids content and retained behind containment dams). One such alternative is the use of filtered tailings, which involves dewatering tailings prior to mechanical deposition by truck or conveyor (MEND, 2017). Typical conceptualization of sulfidic (reactive) filtered tailings assumes an increased risk of metal leaching and acid rock drainage (ML/ARD) because the material is unsaturated, allowing for greater sulfide oxidation due to oxygen availability. The conceptualization of additional oxygen availability may lead to long-term predictions in seepage water quality where numerical models assume the entire tailings profile becomes oxic to maintain conservatism. This study proposes a "reasonable expectation" conceptual model for tailings oxidation, investigating the depth of oxygen ingress over time as a function of pyrite reactivity and water content. To evaluate this conceptual model, a series of reactive transport models are presented to compare release of ML/ARD products under a range of conventional and reactive filtered tailings scenarios, including variations in climate and material reactivity. Simulated water quality and oxygen concentrations are presented as a function of depth and time. Although conceptual in nature, model simulations highlight the mechanistic processes applicable to various TSFs under different site-specific conditions and are used to demonstrate the diffusion-limited depth of oxygen ingress and timing of release of ML/ARD constituents.

Conceptual model

Oxygen ingress into finer-textured materials such as tailings is dominated by diffusion across exposed surfaces (Aubertin et al., 2000). Diffusive flux can be described by Fick's first law:

$$F = -D_e \frac{\partial C}{\partial z}$$

where F is the gas flux (mol m^{-2} s^{-1}), D_e is the effective diffusion coefficient (m s^{-2}), C is gas concentration (mol m^{-3}) and z is depth (m). D_e is a function of porosity, saturation, and the free phase diffusion coefficient; lower porosity and higher water saturation corresponds to lower D_e for the gas phase (Millington, 1959).

Oxygen ingress can therefore be limited to shallower depths within a tailings profile if there is a higher degree of water saturation, or through a low porosity cover system that limits oxygen ingress at the surface (INAP, 2017; Bussière and Guittonny, 2021; Barritt et al., 2022; Barber et al., 2015). Increased saturation

or decreased porosity acts to limit sulfide mineral oxidation by oxygen, as shown in the example of pyrite oxidation by oxygen:

$$FeS_2 + \frac{7}{2}O_2 + H_2O \rightarrow Fe^{2+} + 2SO_4^{2-} + 2H^+$$

When oxygen is available in the pore spaces, depending on sulfide mineral reactivity, shallower sulfide mineral oxidation may rapidly consume oxygen entering the tailings through diffusion, limiting availability of oxygen to react with sulfide grains at depth. Conceptually, this process is self-limiting, as diffusion rates decrease with increasing depth of the oxidation front (i.e., the concentration gradient decreases), which travels slowly downwards as sulfide minerals are consumed near the surface (Figure 1) (Mayer et al., 2015; Zhang et al., 2023). Adversely impacted tailings porewater is first focused above the oxidation front, where the acidity generated is a function of exposure time, tailings reactivity, water content, and surface area.

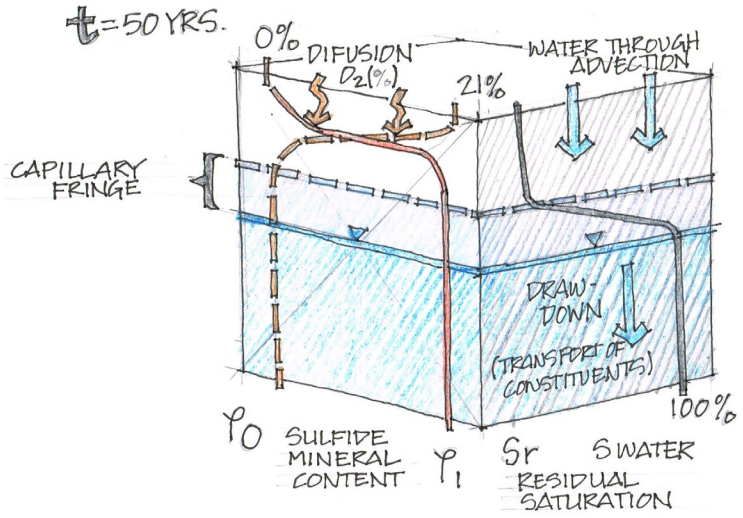


Figure 1: Sulfide mineral oxidation limited by oxygen diffusion in a tailings column, where oxidation products are transported downwards by water through advection

As filtered tailings are put in place in a drier state than conventional tailings, a "wetting up" process occurs prior to seepage emanating from the base of the landform. Over time, net infiltration across the tailings surface, or net percolation through the cover system, may result in a largely vertical porewater pressure response leading to basal seepage from the landform. Acidity generated from upper lift surface exposure during construction will then be transported downward through the landform, where the water quality of basal seepage is influenced by solids and porewater chemistry along the flow path. The time for this seepage to reach the landform's base will be a function of the flow path length (i.e., facility height) and porewater velocity. Drain-down/seepage from consolidation may also contribute to seepage rates, depending on site-specific conditions. It may take several decades for ML/ARD impacted porewater to

reach the landform's base; hence, in most cases, surface runoff is the primary pathway for manifestation of ML/ARD risk in filtered TSFs during operations and in post-closure. This timing aspect of the conceptual model highlights the importance of runoff management from TSFs to water stewardship at mine sites.

These processes of oxygen ingress, consumption, and transport of constituents from the surface downwards can be visualized through a conceptual model, as shown in Figure 1. Though these mechanisms control generation and release of metals in sulfidic tailings in all TSFs, the site-specific controls influencing these mechanisms are unique to an individual mine site. Specifically, the water saturation, water table, and capillary fringe height, as well as oxygen diffusion rates into the tailings, are controlled by the water balance and geochemistry of the material, which are dictated by regional considerations (i.e., climate, hydrogeology, deposit type, and mineralogy) and TSF design.

Methodology

To evaluate the conceptual model described above, a series of one-dimensional (1D) reactive transport models in MIN3P (Mayer et al., 2002) were used to simulate pyrite oxidation through a 20 m thick TSF block model (20 m × 1 m × 1 m). Physical material properties were assumed to remain consistent in all scenarios (Table 2), assuming steady state flow for simplification. Influences of climate, TSF design, and sulfide kinetic variability (Table 2) were simulated to enhance conceptual understanding of mechanistic processes controlling the release of metals from TSFs under different scenarios, described below. For each tailings storage design, two climate scenarios and two pyrite reactivity scenarios were modeled, resulting in 12 simulations in the sensitivity analysis.

Table 1: Physical parameters defining the tailings materials in the sensitivity analysis

Parameter	Value
Free phase diffusion coefficient in water (D_a) [$m^2\ s^{-1}$]	$2.4x10^{-9}$
Free phase diffusion coefficient in soil gas (D_g) [$m^2\ s^{-1}$]	$2.1x10^{-5}$
Porosity [$cm^3\ cm^{-3}$]	0.35
Hydraulic conductivity [$m\ s^{-1}$]	$1x10^{-6}$
Residual saturation [-]	0.05
van Genuchten - α [m−1]	3.5
van Genuchten - n [-]	3.2

Table 2: Parameters tested in 1D TSF models

Parameter	Variable tested		
Tailings storage design	Uncovered filtered (h = 0 m)	Uncovered conventional (h = 18 m)	Covered tailings (h = 19.5 m)
Net surface infiltration	Temperate (T) (250 mm year^{-1})	Drier (D) (70 mm year^{-1})	
Sulfidic tailings	Faster pyrite (k_{eff} = 1x10^{-9} mol L^{-1} bulk s^{-1})	Slower pyrite (k_{eff} = 1x10^{-10} mol L^{-1} bulk s^{-1})	

h is hydraulic head boundary or water table height and k_{eff} is the effective average rate constant for pyrite (mol L^{-1} bulk s^{-1}) (see Table 3)

Tailings storage design methods (specifically, conventional tailings versus filtered tailings) were captured as differences in water table height in the 1D models. A simulated water table 2 m below the surface was assumed for conventional tailings design and a basal head boundary of 0 m (simulating gravity drainage at the base) was assigned for the filtered tailings (Figure 2). These models represent uncovered TSFs. A third design was incorporated to simulate a covered TSF that simulates tailings below a hypothetical cover system that limits oxygen depth to the top 50 cm by assigning a water table boundary at 19.5 m. While simulated here by raising the water table height (such as a water cover in a conventional TSF), this covered TSF could also be considered to represent a low oxygen barrier cover (INAP, 2017; Bussière and Guittonny, 2021).

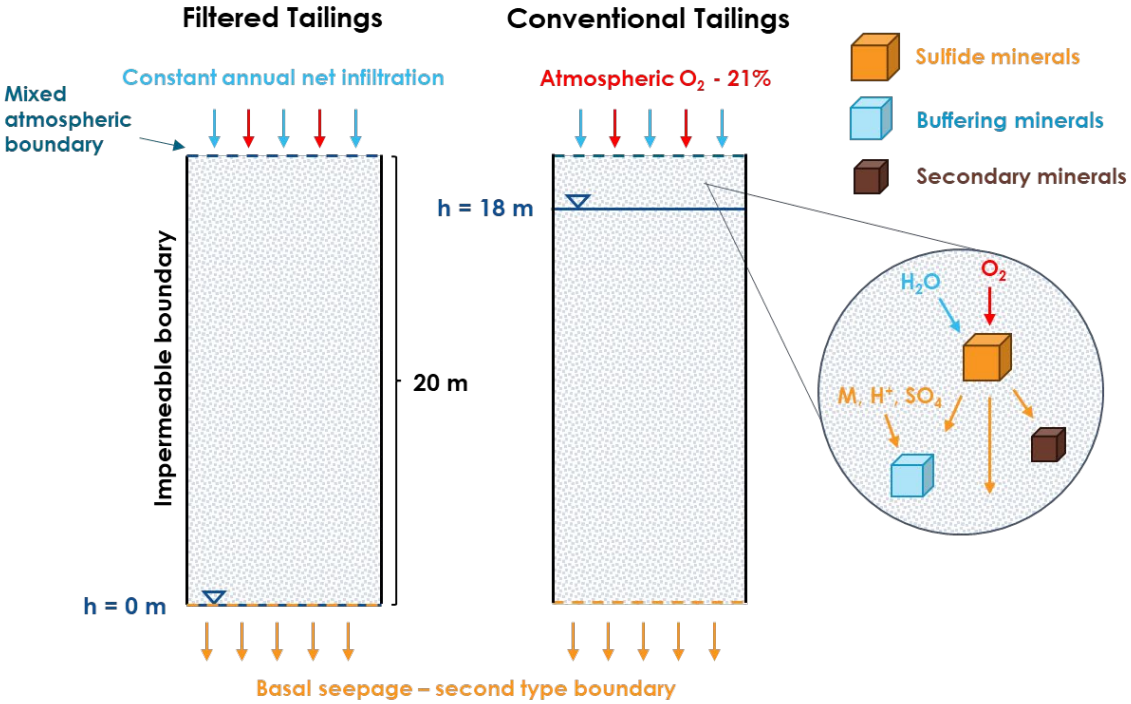


Figure 2: Conceptual model for the uncovered 1D reactive transport models

Differences between climate conditions were considered as changes in net surface infiltration, simulated as a constant infiltration rate applied on the surface of the 1D models under steady-state flow (Figure 2). Scenarios considered include a temperate climate with a net surface infiltration of 250 mm year^{-1} and a drier climate with 70 mm year^{-1} net infiltration.

Reactivity of sulfidic tailings was captured through differences in the assigned effective rate constant for pyrite. Primary minerals simulated include pyrite (7.0 wt. %), calcite (2.5 wt.%), and K-feldspar (5.4 wt. %), where pyrite oxidation is captured by the oxygen-pathway described by Williamson and Rimstidt (1994) and releases metals, SO_4^{2-}, and H^+ ions that are consumed by dissolution of calcite and silicate minerals (Figure 2; Table 3). Effective rate constants from other models were adjusted slightly to generate mineral dissolution rates within range, based on previous experience. The neutralization potential ratio (NPR) of the conceptual tailings material is 0.2, classifying the material as potentially acid-generating (PAG) (Price, 2009). While gypsum, ferrihydrite, gibbsite, and jarosite were not initially present, they were allowed to precipitate out as secondary minerals in the model. Gases were simulated at atmospheric conditions (an $O_{2(g)}$ concentration of 21 vol.% and $CO_{2(g)}$ concentration of 420 ppm), entering through the surface mixed boundary condition (and in the case of CO_2, released after carbonate dissolution).

Table 3: Minerals and reaction rates considered for the conceptual tailings models

Mineral	Reaction rate expression	logK$_i$	$k_i^{m,eff}$
Pyrite	$-\left(\frac{\varphi_i}{\varphi_i^0}\right)^{\frac{2}{3}} k_{i,1}^{m,eff} \frac{\{O_2\}^{0.5}}{\{H^+\}^{0.11}}\left[1-\frac{\{Fe^{2+}\}\{SO_4^{2-}\}^2\{H^+\}^2\{H_2O\}^{-1}\{O_2\}^{-3.5}}{K_i}\right]$	-215.3	Faster: 20 Slower: 2
Calcite	$-\left(\frac{\varphi_i}{\varphi_i^0}\right)^{\frac{2}{3}} k_i^{m,eff}(10^{-6.19}+\{H_2CO_3\}^{-3.30}+\{H^+\}^{-0.05})\left[1-\frac{\{Ca^{2+}\}\{CO_3\}^2}{K_i}\right]$	8.48	5x10^{-5}
K-Feldspar	$-\left(\frac{\varphi_i}{\varphi_i^0}\right)^{\frac{2}{3}} k_i^{m,eff}\{H^+\}^{0.5}\left[1-\frac{\{K^+\}\{Al^{3+}\}\{H_4SiO_4\}^3\{H^+\}^{-4}\{H_2O\}^{-4}}{K_i}\right]$	-10.06	5
Gypsum	$-k_i^{m,eff}[1-\frac{\{H^+\}^{-3}\{Fe^{3+}\}\{H_2O\}^3}{K_i}]$	4.58	1x10^{-7}
Ferrihydrite	$-k_i^{m,eff}[1-\frac{\{Ca^{2+}\}\{SO_4^{2-}\}\{H_2O\}^2}{K_i}]$	-4.89	1x10^{-7}
Gibbsite	$-k_i^{m,eff}[1-\frac{\{H^+\}^{-3}\{Al^{3+}\}\{H_2O\}^3}{K_i}]$	-8.11	6x10^{-12}
Jarosite	$-k_i^{m,eff}[1-\frac{\{H^+\}^{-5}\{Fe^{3+}\}^3\{SO_4^{2-}\}^2\{H_2O\}^7}{K_i}]$	5.39	8x10^{-11}

$k_i^{m,eff}$ is the effective average rate constant (mol L^{-1} bulk s^{-1}), φ_i is the initial volume fraction; K_i is the equilibrium constant at 25°C.

Results

In the higher net infiltration climate scenario, water saturation is 33% above the water table compared to 25% in the drier climate scenario modeled. Aligned with the conceptual model, oxygen ingress is controlled by both water saturation and kinetic pyrite oxidation rates, where higher water saturation as well as faster pyrite oxidation rates limit oxygen ingress. These processes are reflected in the simulated oxygen profiles with time (Figure 3). As expected, the water table height of 18 m in the conventional tailings models limits oxygen ingress below that depth. In the filtered tailings models, oxygen is limited to shallower depths in the 33% water saturation scenarios relative to 25% (Figure 3).

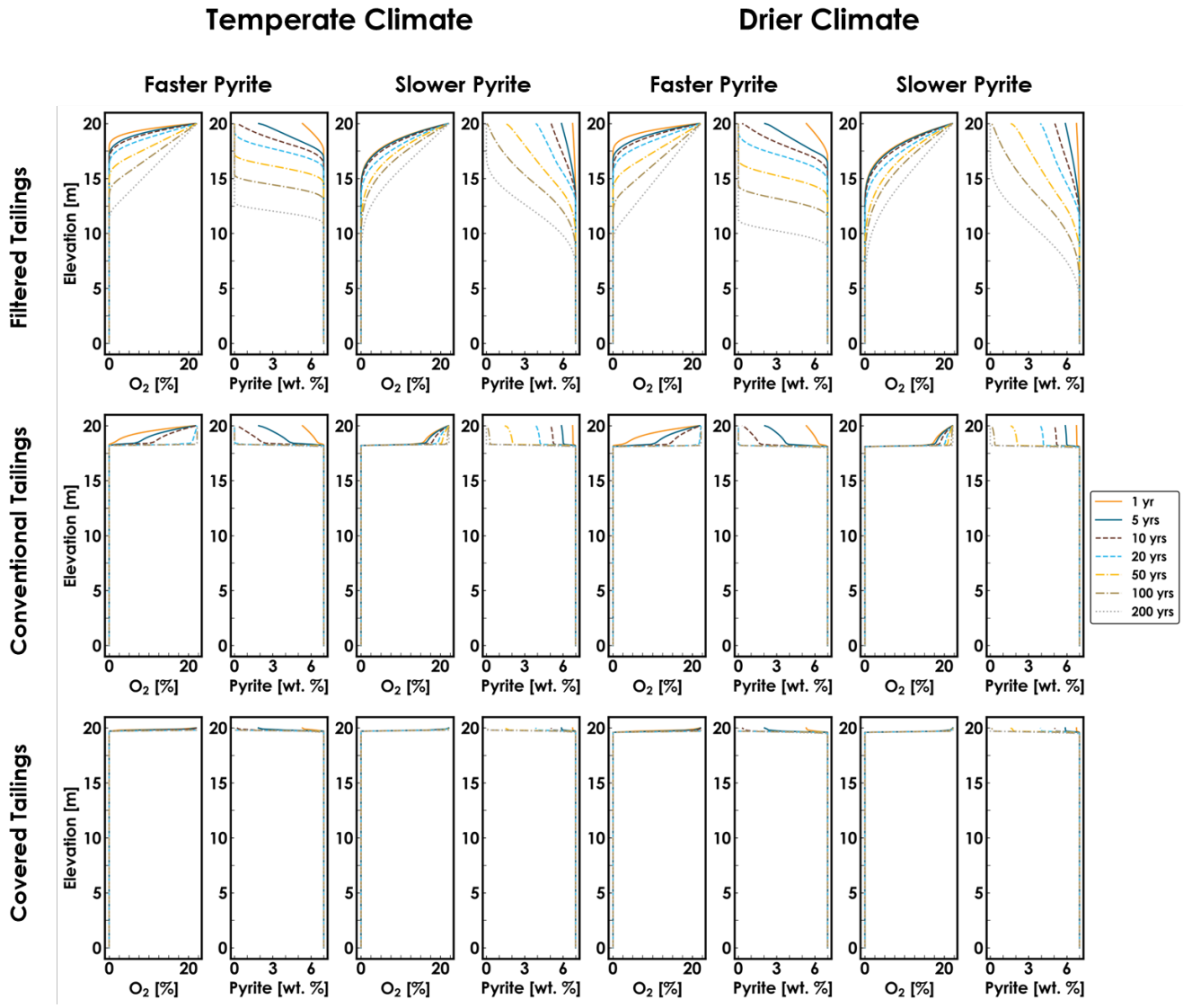


Figure 3: Depth profiles of oxygen ingress and pyrite consumption in TSF simulations from 1 to 200 years

Aligned with the conceptual model, oxygen ingress is influenced by pyrite oxidation kinetics. Models with faster pyrite oxidation limit oxygen ingress at depth more effectively than the slower pyrite oxidation models. In all filtered models, there is a gradual movement of oxygen to greater depths as pyrite is consumed (Figure 3). As a result, poor quality drainage is initially limited to the upper few meters (see Appendix) until transport processes (simulated here as downwards water flow) bring oxidation products towards the base. In all filtered tailings models, oxygen depth is eventually limited to a diffusion depth controlled by the simulated physical material properties and Fick's law.

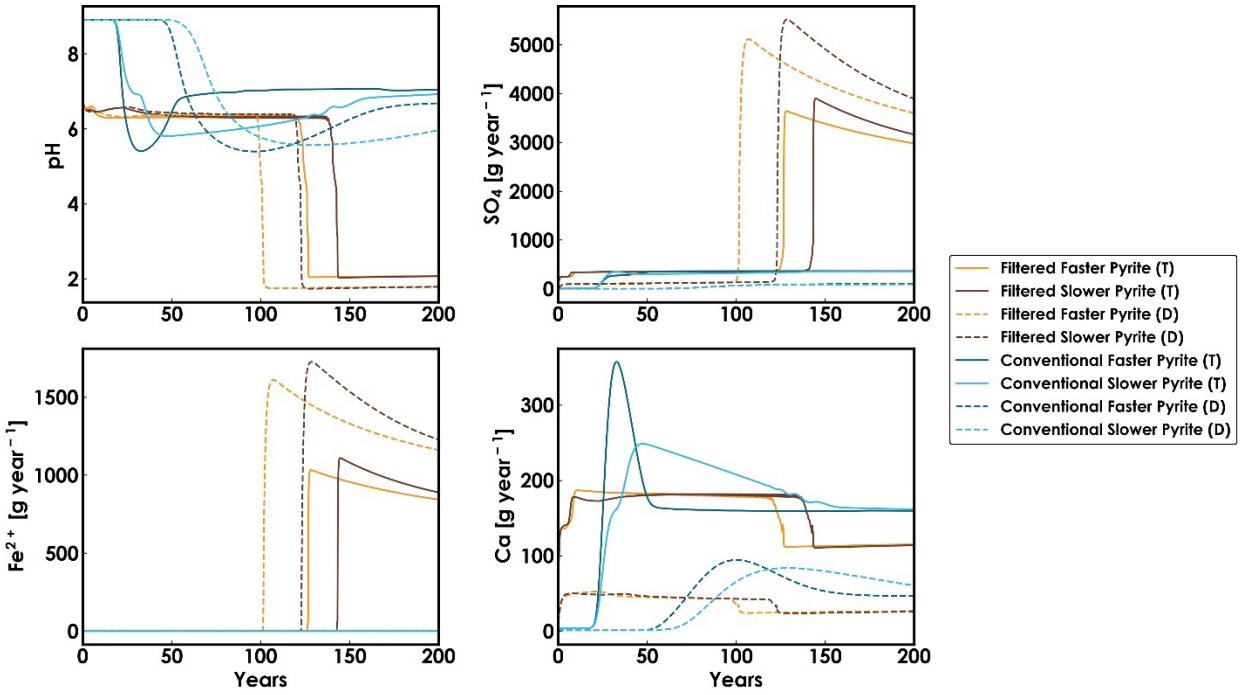


Figure 4: Comparison of basal pH and annual loads for TSF simulations

Comparing loads released from basal seepage (Figure 4), the higher net infiltration scenarios of 250 mm year-1 transport constituents released from mineral dissolution downwards at a faster rate than those scenarios with 70 mm year -1, which is observed through the delay in release curves by several decades. Loading rates show that pyrite oxidation products (like SO4 and Fe) released are comparable in the filtered and conventional TSF designs until ML/ARD impacted waters reach the base (Figure 4). Eventually, the higher water table in the conventional TSF design models results in decreased seepage loads compared to models with the same conditions under a filtered TSF design, since increasing the total water saturated volume of tailings decreases the total volume of oxidizing sulfidic tailings and the total amount of pyrite oxidized. In addition to the uncovered TSFs, a covered or oxygen limited scenario was simulated as a water table height of 19.5 m. As expected, in the covered tailings oxygen profiles and pyrite consumption profiles

(Figure 3) follow similar patterns to the conventionally placed tailings, but with a shallower depth of oxygen. This results in decreased basal loads and lower concentrations of constituents at depth (see Appendix).

Discussion

Mechanistic processes described in the conceptual model are reflected in the results of the simulated 1D tailings columns. The benefit of these simulations, while conceptual in nature, is that they provide an enhanced visualization of the spatial extent and timing of ML/ARD impacted waters through a TSF under different climate, design, and geochemical conditions. In most of the scenarios modeled in this paper, it may take several decades to see the release of constituents associated with ML/ARD in basal seepage. As highlighted in the conceptual model, during the earlier years of the TSF, poor quality water is constrained to the upper unsaturated portion of the tailings. Model simulations show that in the conventional TSF design, the water table limits oxygen ingress to a shallower depth than the filtered tailings (thus limiting the total "reactive" portion of tailings material); however, oxygen ingress is also limited by consumption through pyrite oxidation and diffusive flux, as dictated by Fick's law. Depending on the material properties, residual saturation, and sulfide reactivity, oxygen will be limited to different depths within a TSF. In some cases, such as the temperate climate with faster pyrite weathering rate, oxygen ingress is limited to similar depths in the first 20 years in both the conventional and filtered TSF designs (Figure 3). Even after a century, oxygen in filtered tailings may be limited to the top 5 m of the TSF.

In all the scenarios simulated, the tailings materials are classified as PAG, with an NPR of 0.2. Onset of acidic conditions occurs as calcite is depleted within the first five years at the surface, observed as pH decreases at depth (see Appendix). Due to the relatively low hydraulic conductivity and water saturation, acidic basal seepage conditions may not be observed until at least 100 years to beyond 200 years in the 20 m columns simulated (Figure 4).

The conceptual model, supported by simulation results, demonstrates that seepage water quality is unlikely to require management for decades to centuries in filtered tailings, whereas runoff water management is much more important prior to covering the tailings due to interaction with oxidized tailings at the surface. Furthermore, if runoff management decreases infiltration rates into the filtered tailings, this will increase the time frames for wetting up and onset of seepage. However, as shown by the higher loads associated with ML/ARD in the filtered tailings, this conceptual model also demonstrates the importance of implementing a cover system that limits poor quality runoff as well as infiltration (limiting transport of ML/ARD), or placement of a cover system with a layer of lower permeability to effectively limit oxygen ingress (limiting generation of ML/ARD) before ML/ARD seepage from a filtered TSF occurs. Cover

system options and suitability will also be site-specific (INAP, 2017; Bussière and Guittonny, 2021); TSF design techniques to manage ML/ARD will be dependent on factors like those explored in this paper.

Assumptions and limitations

For the purpose of generating sensitivity analyses of TSF designs under different climate, design, and geochemical conditions, several simplifications were made to the 1D columns simulated in this work. The materials selected for the tailings were based on physical tailings properties and mineralogical compositions that have been calibrated for other mine sites, but modified slightly to remain conceptual in nature. Additionally, 1D columns did not consider effects of sloped surfaces that may result in lateral flow in 2D simulations, and also excluded the buildup of tailings placement in the TSF construction over time (i.e., simulations began assuming fresh tailings placed in a 20 m profile). In reality, oxygen ingress occurs across exposed surfaces during deposition and in final tailings surfaces, where only the latter was simulated in this model. Future modeling work to integrate construction schedule and increasing height of TSFs is likely important to understanding the timing of onset of acidity and poor drainage quality being released, and is encouraged for site-specific TSF investigations.

Net infiltration boundaries and temperature conditions were held constant over time; heat generated due to pyrite oxidation was not considered. Temperature affects pyrite oxidation rates through the Arrhenius equation (Nicholson et al., 1988), where lower temperatures are associated with slower kinetics. As pyrite oxidation is an exothermic reaction, heat released from the oxidation process (particularly in the faster sulfide kinetics materials) should result in increasing temperatures around the oxidation sites, since tailings typically have low thermal conductivity (Harries and Ritchie, 1981; 1985; Lefebvre et al., 1997; Yanful et al., 1990). Higher internal temperatures have been known to result in death of microorganisms that facilitate pyrite oxidation reactions and limiting additional pyrite oxidation (Yanful et al., 1990). This is likely important to some climates, such as the drier scenario explored in this model, and should be considered in site-specific investigations.

Finally, the focus of this paper is on the behavior of tailings and their respective water saturation conditions; however, solute release associated with construction material of the TSF dam embankment were not considered. Dams are often constructed with mine rock or overburden material extracted in earlier years of mine life and may be a more significant source of solute loads than the tailings themselves coming from TSFs, due to high permeability of rock materials and mineral weathering through the same mechanistic processes explored in the conceptual model for tailings. Assessment of different TSF designs through sensitivity analysis should therefore consider the tonnage and loadings from materials used to construct dams in addition to the tailings materials themselves. Future work is recommended to test different models

that address the assumptions and limitations stated above, if site-specific data exists to validate model outputs.

Conclusion

It is well understood in the mining industry that release of constituents from mine waste storage facilities such as TSFs are site-specific. The purpose of the conceptual models simulated here is to provide enhanced conceptualization of these mechanistic processes to support decision-making during early project planning and modeling under different scenarios, and to demonstrate the importance of implementing calculations or models that consider the timing of release of constituents given specific design parameters and material properties that consider the diffusion limitations of filtered tailings. Results from models simulated in this work showed that filtered tailings did result in greater loads of sulfide oxidation products relative to the conventional slurry tailings over long time frames due to the greater oxygen ingress if left uncovered. The exact timing of their release will be dependent on TSF design parameters not considered in these 1D columns (namely, runoff and flow paths that control transport mechanisms constrained to the upper few meters of the TSF). If, however, it is anticipated that a conventional TSF design would include an oxic zone within the first few meters of the TSF, the quantity of metal loads produced under both conventional and filtered scenarios may be comparable within the first few decades to centuries, as the same volume of materials would be considered oxic due to diffusion limitations within the tailings profile. In both scenarios, a cover system is necessary to manage ML/ARD impacted waters from leaving as runoff and/or limit the oxygen depth into the sulfidic tailings.

The TSFs simulated in this paper are conceptual in nature, aimed to support the conceptual model; there is no “best” solution presented in this study. We suggest that sensitivity analyses in the design process can help lead practitioners to consider opportunities to construct and manage their TSF designs with closure in mind by incorporating mechanistic processes (e.g., including diffusion limitations and oxygen consumption by sulfide oxidation) to develop a “reasonable expectation” conceptual model for the thickness of reactive tailings through time, which can be used to enhance understanding of ML/ARD risk for reactive filtered TSFs on a site-specific basis. From here, practitioners can design cover systems to manage these filtered tailings with timing in mind to manage ML/ARD risk during operations and post-closure and meet regional closure objectives.

References

Aubertin, M., M. Aachib and K. Authier, 2000. Evaluation of diffusive gas flux through covers with a GCL. *Geotextiles and Geomembranes* 18: 1–19.

Barber L., D. Christensen and L. Tallon, 2015. Alberta oil sands cover system field trial – Development, construction, and results two years in. *ICARD-IMWA 10th International Conference on Acid Rock Drainage and International Mine Water Association Annual Conference*, Santiago, Chile, April 22, 2015.

Barritt R., S. McVeigh, B. Williams and R. Shurniak, 2022. Cover system trial at Earnest Henry Mine, proof of concept across the seasons. *ICARD 12th International Conference on Acid Rock Drainage*, Brisbane, Australia, September 22, 2022.

Bussière B. and M. Guittonny. 2021. *Hard Rock Mine Reclamation: From Prediction to Management of Acid Mine Drainage.* Boca Raton: CRC Press.

Harries, J.R. and A.I.M. Ritchie. 1981. The use of temperature profiles to estimate the pyritic oxidation rate in a waste rock dump from an opencut mine. *Water, Air, and Soil Pollution* 15: 405–423.

Harries, J.R. and A.I.M. Ritchie. 1985. Pore gas composition in waste rock dumps undergoing pyritic oxidation. *Water, Air, and Soil Pollution* 15: 405–423.

International Network for Acid Prevention (INAP). 2017. Global cover system design: Technical guidance document. November 2017.

Lefebvre, R., P. Gélinas and D. Isabel. 1997. Heat transfer during acid mine drainage production in a waste rock dump, La Mine Doyon (Québec). MEND Report 1.14.2c. August 1997.

Mayer, K.U., E.O. Frind and D.W. Blowes. 2002. Multicomponent reactive transport modeling in variably saturated porous media using a generalized formulation for kinetically controlled reactions. *Water Resour. Res.* 38(9): 13-1–13-21.

Mayer, K.U., P. Alt-Epping, D. Jacques, B. Arora and C.I. Steefel. 2015. Benchmark problems for reactive transport modeling of the generation and attenuation of acid rock drainage. *Comput. Geosci.* 19(3): 599–611.

Millington, R.J. 1959. Gas diffusion in porous media. *Science*. 130:100–102.

Mine Environment Neutral Drainage (MEND). 2017. Study of tailings management technologies. MEND Report 2.50.1. October 2017.

Mudd, G.M. 2010. The environmental sustainability of mining in Australia: Key megatrends and looming constraints. *Resources Policy* 35 (2): 98–115.

Nicolson, R.V., R.W. Gillham and E.J. Reardon. 1998. Pyrite oxidation in carbonate-buffered solution: 1. Experimental Kinetics. *Geochimica et Cosmochimica Acta* 52(5): 1077–1085.

Northey, S., S. Mohr, G.M. Mudd, Z. Weng and D. Guirco. 2014. Modelling future copper ore grade decline based on a detailed assessment of copper resources and mining. *Conservation and Recycling Resources.* 83: 190–201.

Price, W.A. 2009. Prediction manual for drainage chemistry from sulphidic geologic materials, MEND Report 1.20.1.

Williamson, M.A., Rimstidt, D. J. 1994. The kinetics and electrochemical rate-determining step of aqueous pyrite oxidation. *Geochimica et Cosmochimica Acta* 58 (24): 5443–5454.

Yanful, E.K., L. St-Arnaud and R. Prairie. 1990. Hydrogeochemical investigation of reactive tailings at the Waite-Amulet Tailings Site, Noranda, Québec, Generation and evolution of acidic pore waters at the Waite Amulet Tailings – Final Report. MEND Report 1.17.1d. April 1990.

Zhang, A., J.G. Bain, A. Schmall, C.J. Ptacek and D.W. Blowes. 2023. Geochemistry and mineralogy of legacy tailings under a composite cover. *App. Geochem.* 159: 105819.

Appendix

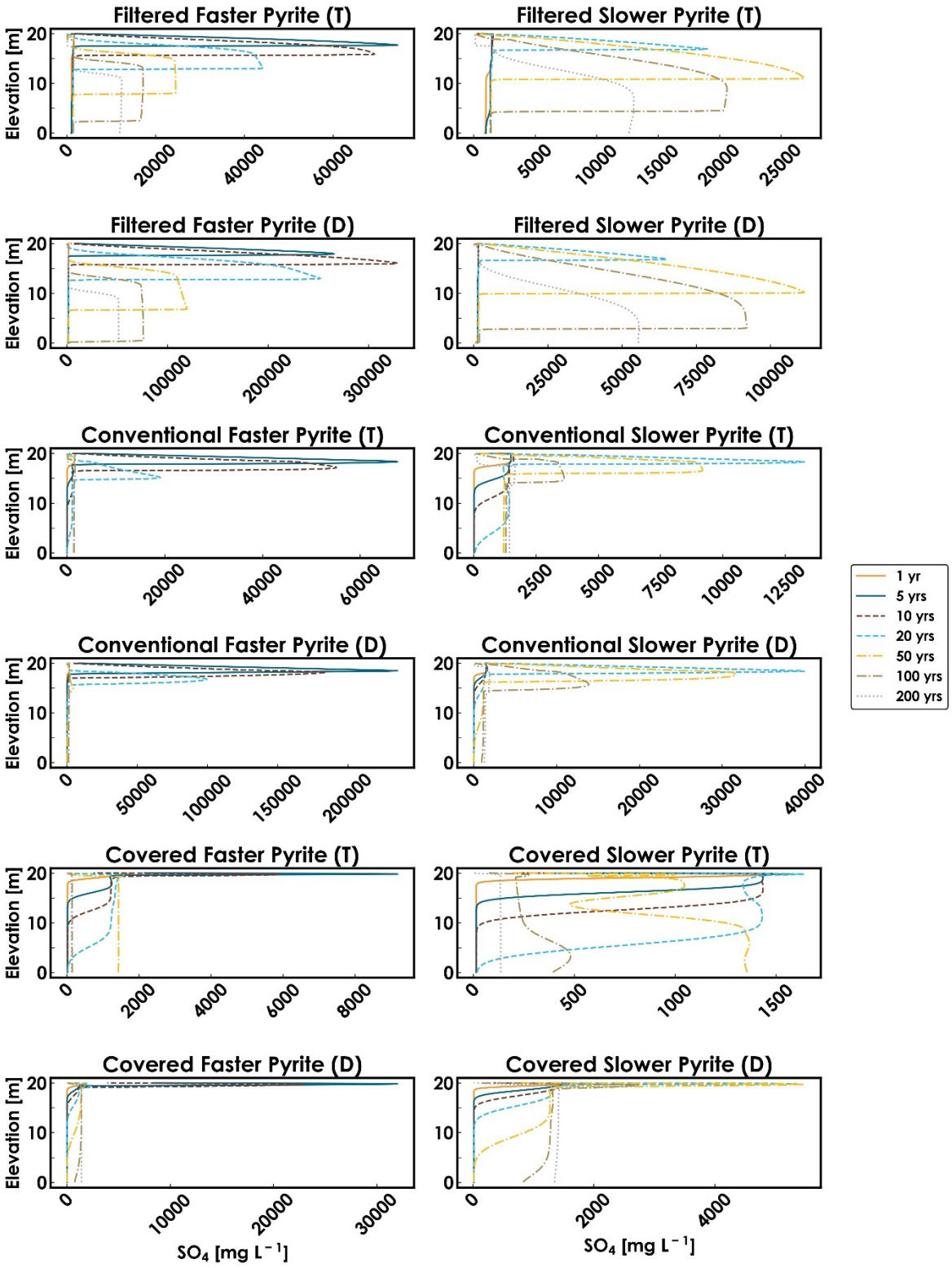


Figure A1: Depth profiles of SO_4 concentrations in TSF simulations from 1 to 200 years

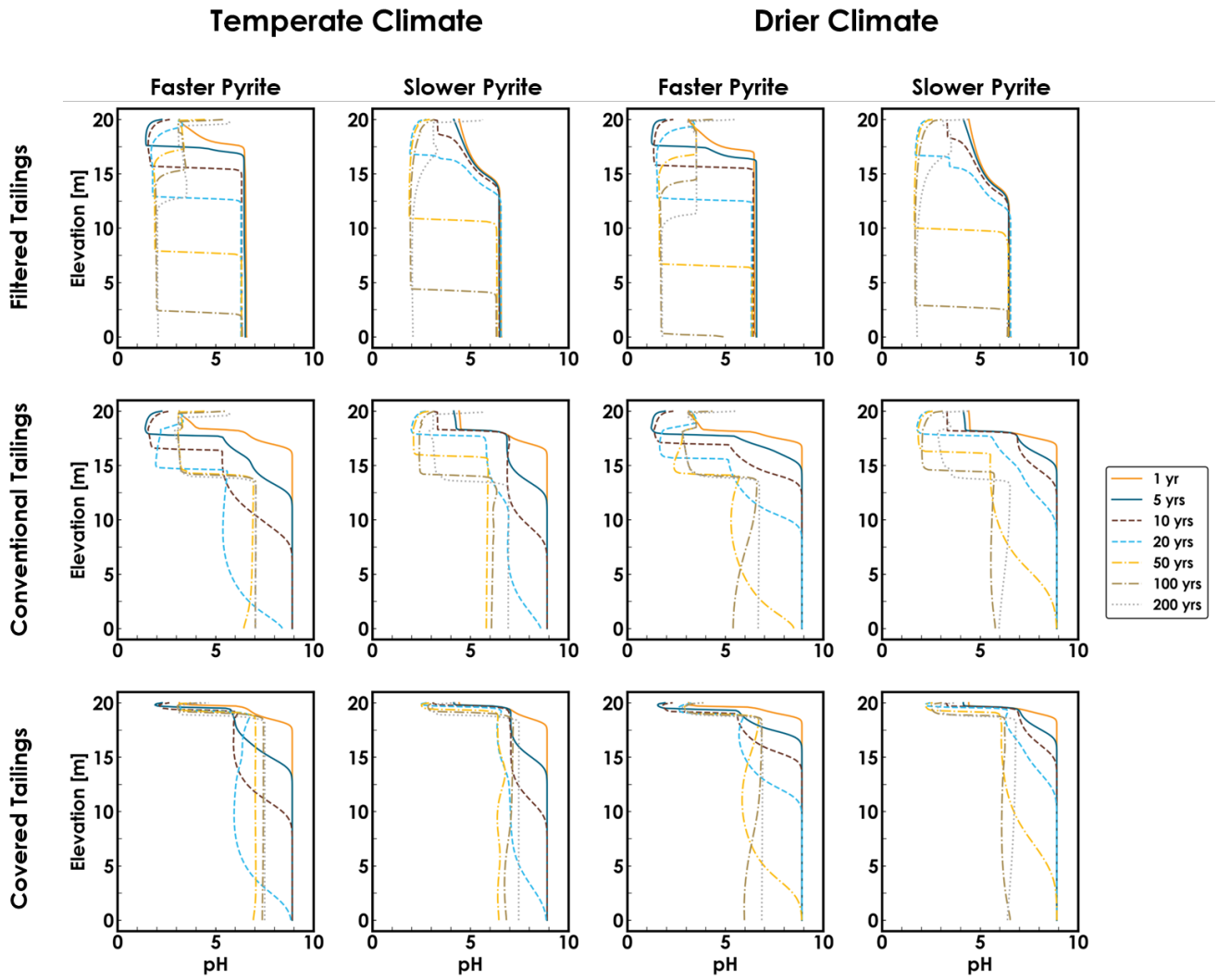


Figure A2: Depth profiles for pH in TSF simulations from 1 to 200 years

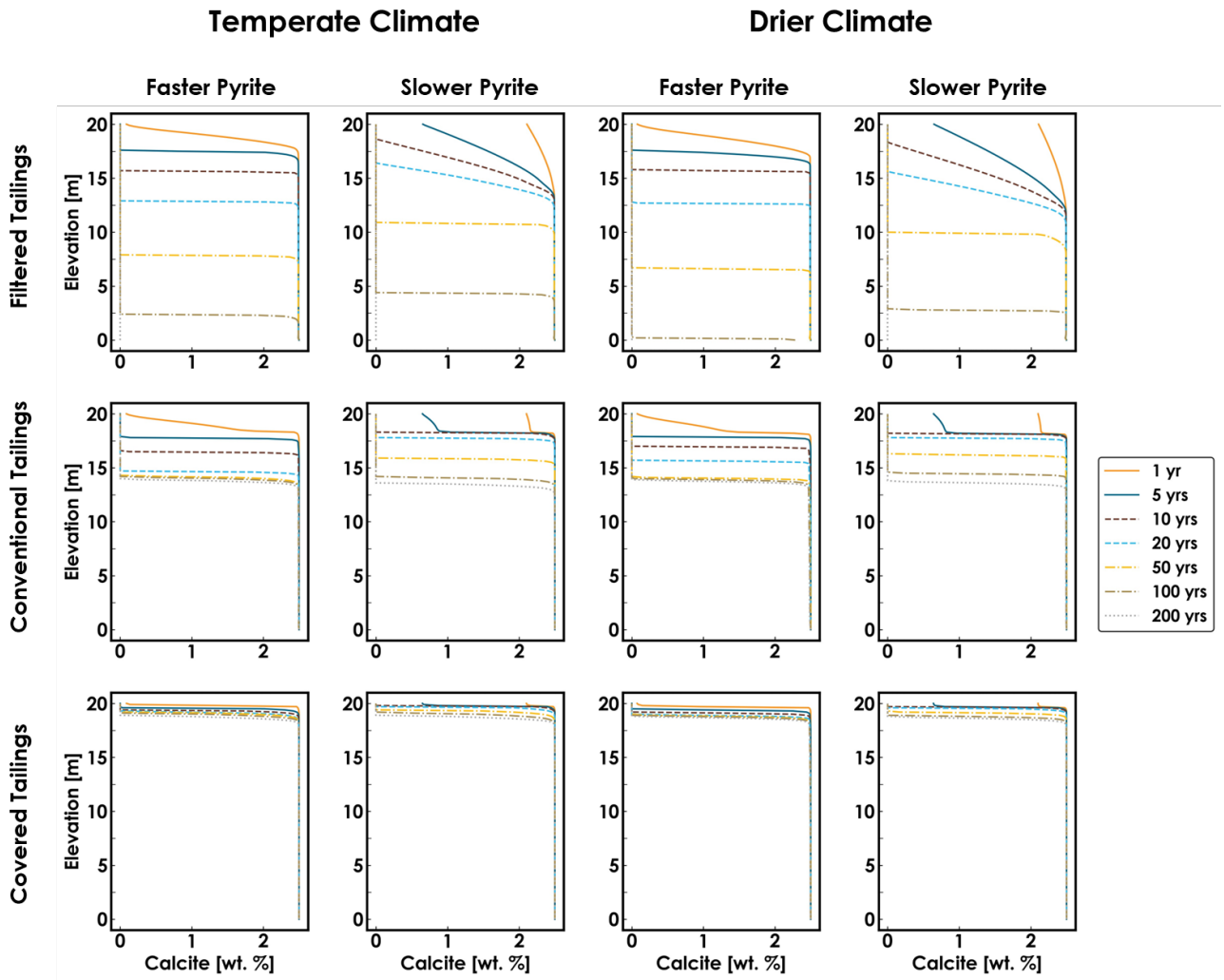


Figure A3: Depth profiles for calcite in TSF simulations from 1 to 200 years

Orphaned and Abandoned Mines in Manitoba: From Identifying Hazards to Achieving Closure

Mohammad Ahmeduzzaman, KGS Group, Canada
Dami Adedapo, KGS Group, Canada
Cory Graham, Government of Manitoba, Canada

Abstract

The government of Manitoba in Canada launched a program in 2006 to develop a database, identify and assess hazardous conditions, and estimate the cost of remediation of the orphaned and abandoned mine (OAM) sites located in Manitoba. OAM are the mine sites that have been returned to the Crown's ownership because the previous mining companies have either ceased to exist or lack the financial resources to undertake the necessary restoration efforts. As part of the program, background documents (government publications, maps, aerial photos, previous inspection reports) were reviewed, the sites were visited, and risk and liability assessments were undertaken. The OAM sites were categorized based on their level of hazards and closure costs were estimated. Stakeholder consultations were conducted as part of the closure plan design, and site-specific requirements were developed, to establish the closure objectives and success criteria for each OAM site.

Subsequently, from 2020 to 2024, risk and liability estimates were updated, final closure plans were developed, and the construction phase was initiated for several OAM sites. So far, the closure of more than thirty OAM mine sites has been completed, with others to follow. The closure works for OAM sites included capping mine openings using reinforced concrete caps, encapsulation of potentially acid-generating tailings and waste rock using HDPE geomembrane, stabilization of steep unstable slopes, demolition and disposal of debris, backfilling of test pits and trenches and restoration of disturbed areas back to pre-mining condition to eliminate evidence of anthropogenic activity as much as is practically possible. An overview of the OAM program is presented in this paper. The paper includes discussions of the closure plan development process and of construction activities that were undertaken for the sites. It also discusses key factors influencing the closure plan development including stakeholder feedback, closure costs, constructability, long-term monitoring needs, climate change, and site access.

Introduction

Orphaned and abandoned mines (OAM) are the mine sites that have been returned to the Crown's ownership because the previous mining companies have either ceased to exist or lack the financial resources to undertake the necessary restoration efforts. Canada is facing the legacy of more than 10,000 inactive, orphaned mines that were developed and closed throughout the long history of mining in Canada (Hogan and Tremblay, 2006). OAM sites generally encompass shafts, adits, raises, stopes, access points to underground workings, exploration trenches, open pit excavations, subsidence areas, unsafe derelict buildings and infrastructure, waste rock dumps, and tailings disposal sites. OAM sites often lack records or have very poor documentation of their development. Various types of mine openings, which may interconnect and reach significant depths, can be obstructed by random debris, ice plugs, vegetation overgrowth, or collapsed rock. Nearby mine workings might be flooded or filled with dangerous gases. Entering or approaching these hazardous openings can result in falling, drowning, or being buried by collapsed mine workings, leading to serious injury or death. Shallow underground openings can create crown pillars, which are thin layers of ground above the underground stopes. The collapse of these pillars can also be fatal. Beyond the physical and stability-related hazards of mine workings, additional dangers include toxic mine gases, derelict buildings and structures, mine drainage and seepage, mechanical and electrical equipment, and explosives. These hazards, both individually and collectively, pose significant risks to humans and wildlife. Unsecured mine openings are among the most serious physical hazards at abandoned mine sites. These openings were typically not designed to remain stable after closure and can fail for various reasons if not properly remediated (AANDC, 2011).

Moreover, OAM sites are often associated with environmental problems such as acid mine drainage (AMD), which can lead to severe water pollution and surface contamination. AMD occurs when sulfide minerals in exposed rock surfaces react with air and water, producing sulfuric acid and dissolved iron. This acidic runoff can leach heavy metals from surrounding rocks, contaminating nearby water bodies and soil. According to Johnson and Hallberg (2005), AMD is one of the most significant environmental challenges associated with abandoned mines, necessitating comprehensive remediation strategies to mitigate its effects.

The Manitoba Government became responsible for rehabilitation and funding remediation costs of orphaned and abandoned mine sites that were developed and ceased to exist prior to the implementation of closure plans and financial assurances under the Mine Closure Regulation in 1992. In 1999, the province introduced mine closure regulations that mandate financial security for environmental liabilities incurred during mining operations to cover future remediation costs. These regulations require that mine closure plans and financial security be submitted and approved before a new mine operation permit is issued.

In 2000, Manitoba launched the Orphaned and Abandoned Mine (OAM) Site Rehabilitation Program to address the public safety and environmental health issues related to orphaned and abandoned mine sites. Under the OAM rehabilitation program, location, ownership, previous inspections, availability of historical documents, and site condition for a total of 148 OAM sites (as shown in the overview in Figure 1) scattered throughout the province were identified.

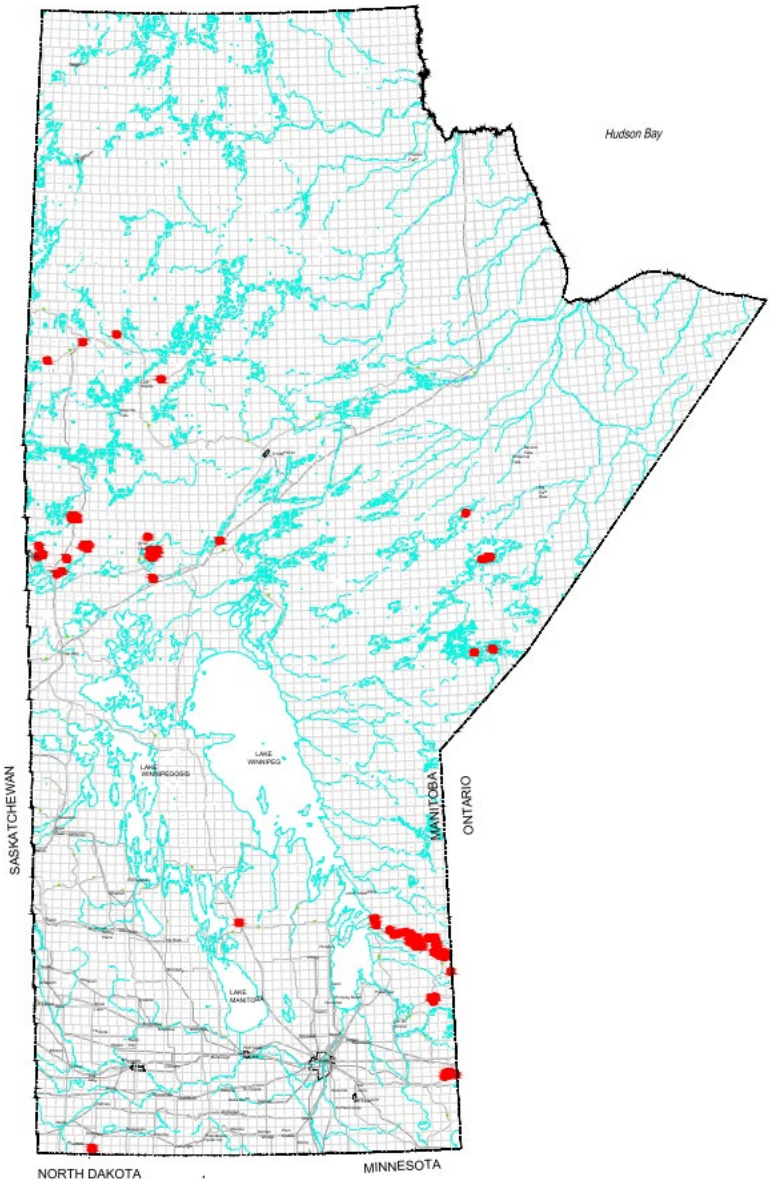


Figure 1: Overview of OAM sites in Manitoba

Most of the OAM sites operated between 1911 and the late 1970s (Richardson and Ostry, 1996). In 2006, Manitoba introduced a program to create a database, assess hazardous conditions, and estimate remediation costs for these sites. This involved reviewing government publications, maps, aerial photos, and previous inspection reports, visiting the sites, and conducting risk and liability assessments. During the

2006 program, a total of 131 sites were identified and evaluated. Sites were categorized by hazard level, and closure costs were estimated. Between 2007 and 2019, over thirty OAM sites were remediated, though some received limited attention due to various factors.

In November 2019, the OAM program was transferred to Manitoba Environment and Climate Change to align with its mandate for a cleaner Manitoba. Upon reviewing the Public Accounts, the OAM found insufficient evidence for the estimated liability. Consequently, from 2020 to 2024, risk and liability estimates were updated, closure plans were developed for over 25 additional sites, and the construction phase began for several OAM sites.

This paper provides an in-depth overview of the OAM program, highlighting the methodologies employed in identifying and assessing hazardous conditions, the estimation of remediation costs, and the execution of closure plans.

Hazard identification and closure plan development

Risk and liability assessments and closure cost estimates

A background review of available information such as review of government publications, topographic and geological maps, aerial photographs, and previous inspection reports was conducted prior to carrying out the risk and liability assessments. Upon completion of the background review, a site inspection was carried out to identify the OAM sites and confirm the present conditions. A detailed risk and liability assessment was performed for each OAM site. This assessment aimed to categorize the sites based on their potential hazards and the estimated costs of remediation. The criteria for this assessment included public safety risks (e.g., presence of open shafts, buildings and foundations, scrap metals and debris, terrain morphology, and stability and accessibility), and environmental risks (e.g., proximity to water bodies, water accumulations and discharges, presence of tailings and waste rock, ecological impacts, and human health impacts). Each site was then assigned a hazard level, ranging from low to high, to prioritize the sites for remediation. This categorization allowed the government to allocate resources efficiently and focus on the most critical sites first.

Based on the visual observations during the site inspection, closure cost with +40% to -20% accuracy was developed for the remediation of each OAM site. This cost estimate included the engineering, and project management costs, construction supervision and contract administration costs, and contractor's costs to rehabilitate the site including site mobilization and demobilization. The total cost of rehabilitating the identified 131 sites was estimated between $14.7 million and $24.9 million in 2006 $value.

Between 2007 and 2019, over 30 OAM sites were remediated, though some received limited attention due to various factors. Hence, in 2021, the province carried out another round of risk and liability assessment and closure cost estimates and subsequently commissioned the consultant (KGS Group) to

prepare closure plans, detailed design, tendering, and construction oversight of several OAM sites located at the eastern side of the province within the Canadian Shield. The hazard characterization and closure plan development process are discussed in the subsequent section.

Hazards identification

Mine openings

Out of the many hazards identified at the OAM sites, the presence of mine openings was the most significant type of hazard. During the site visits to the OAM sites, the mine shafts, vent raises, open adits, and stopes were found to be in different conditions as follows.

- Some mine openings were open without any covers, public safety fencing, warning signage, etc.
- Some mine openings were surrounded by public safety fencing with warning signs, both in worn-out shape.
- Some mine openings had relatively newer public safety fencing and warning signs but were vandalized by the public.
- Some mine openings were covered by concrete caps. At several sites, the caps failed due to inadequate structural capacity and due to foundation collapse. The caps did not have any vent pipes, and some did not have warning signs, and some caps were found to be partially to fully buried by fill materials making it extremely difficult to identify hazards.



Figure 2: Mine openings

Waste rock and tailings

In general, an abundance of waste rocks removed from the mine during its development to access the ore zones of economic value was found throughout the OAM sites. Waste rock may still contain a low concentration of ore, and over a long period, the metal content in the presence of water may generate acid

and leach out from the waste rock stockpile and affect the surrounding environment. In addition to the potential for acid generation, the waste rock had steep slopes, exhibited erosion, had unacceptable aesthetic conditions, undesirable topography by obstructing natural drainage, hazards for hikers by creating unsafe footing conditions, etc.

Mine tailings were also found at several OAM sites with the aerial extent varying from less than 500 m^2 to more than 100,000 m^2. Exposed tailings presented a risk of the generation of harmful leachate from overland flow which contacts the tailings. Tailings contained elevated concentrations of heavy metals such as arsenic, copper, or lead, which may be released into the environment. Tailings also exhibited a high potential for acid generation. Exposed tailings were easily erodible, leading to poor vegetation uptake and turbid overland flow.



Figure 3: Mine waste and tailings

Abandoned mine infrastructure and equipment

Remnants of the headframe, building foundations, mining equipment, scrap metal, and rubble from demolition were found throughout the OAM sites. The scrap metals posed hazards such as sharp edges coming into contact with skin or puncturing limbs of humans and wildlife, the collapse of the infrastructure and metal equipment over humans and wildlife, entrapment of humans and wildlife into the old machinery, and snowmobiles or off-road vehicles colliding with large machines or equipment were the risks associated with the abandoned mine infrastructure and equipment.



Figure 4: Abandoned mine infrastructure and equipment

Closure plan development

Closure vision

The government of Manitoba's closure vision for the OAM sites is to restore the site to a "satisfactory condition" with a practical, perpetual (i.e., little to no maintenance required but does not preclude regular inspection), and economically viable design that is acceptable to the stakeholders.

Stakeholder engagement

The importance of stakeholder engagement in the development and implementation of mine closure plans cannot be overstated. Successful remediation projects often involve extensive consultations with local communities, indigenous groups, environmental organizations, and other stakeholders. This participatory approach ensures that the concerns and expectations of all interested parties are considered, leading to more socially acceptable and sustainable outcomes. The work of Evans and Kemp (2009) emphasizes the role of stakeholder engagement in enhancing the legitimacy and effectiveness of environmental remediation efforts. Stakeholders such as various departments within the government of Manitoba such as Provincial Parks, Highways, Crown Lands, Historic Resources Branch, Forestry Branch, and the external stakeholders such as local aboriginal communities were engaged through meetings onsite and offsite during the mine closure plan development process and Manitoba's closure vision was coupled with the vision of various stakeholders to develop objectives of the closure work.

Closure objective and success criteria

The general closure objectives of the OAM sites were as follows.

- Eliminating unacceptable health hazards and ensuring public safety;
- Limiting the production and circulation of substances that could cause damage to the environment and, in the long-term, eliminating the need for maintenance and monitoring;
- Restoring the site to a condition in which it is visually acceptable to the community; and
- Reclaiming for future use of the areas where infrastructures are located.

In addition, additional site-specific objectives were also identified based on the feedback from the various key stakeholders.

The success criteria are specific, measurable, achievable, relevant, and timely criteria that are defined with input and agreement with appropriate stakeholders are key to completing closure works (ICMM, 2008). Examples of the success criteria developed to achieve closure of OAM sites are presented in Table 1 as follows.

Table 1: Example closure objective and success criteria for OAM sites

Hazards	Closure objective	Success criteria
Mine openings	Eliminating unacceptable health hazards and ensuring public safety;	Mine openings are to be sealed using an engineered cap with appropriate signage and venting
Acid-generating tailings	Limiting the production and circulation of substances that could cause damage to the environment and, in the long-term, eliminating the need for maintenance and monitoring;	Acid-generating tailings are to be encapsulated to isolate the tailings from air and water to eliminate acid generation
Poorly draining stockpiles of waste rock	Restoring the site to a condition in which it is visually acceptable to the community; and	The stockpiles are to be graded to eliminate water ponding and to ensure positive drainage
Scattered metal and infrastructure debris	Reclaiming for future use of the areas where infrastructures are located.	The scattered metal and infrastructure debris are to be collected and disposed of and the site is to be returned to a state that is suitable for future land use as acceptable by stakeholders

Closure plan options

A range of practical remediation alternatives were identified and assessed as part of the closure plan development for the OAM sites. Factors such as long-term performance, constructability, adherence to mine closure regulations, design life, level of risk, cost-benefit, and stakeholder feedback, were considered in selecting the preferred alternative.

For the closure of the mine openings, alternatives such as signage, fencing, steel grate, steel plate, concrete cap/bulkhead, polyurethane foam plug, backfilling, and closure through blasting were considered and based on the analysis of the abovementioned factors, concrete cap anchored into bedrock was the most preferred option.

Alternatives such as do nothing, leave as is with monitoring, regrading of stockpiles, revegetation, and encapsulation were considered for waste rock stockpiles and based on the analysis of the abovementioned factors, regrading of stockpiles and crushing and spreading of fallen trees to cover the regraded surface was the most preferred option. Encapsulation was the preferred option for all potentially acid-generating tailings due to its potential to significantly impact the environment. Caps such as clay caps, geomembrane liners, and granular fill caps were considered and a combination of geomembrane and granular was selected for encapsulation.

Demolition, cutting, burning, and burial were options for the remediation of scattered metal and infrastructure debris. Depending on the location of the site, constructability, and accessibility, demolition, cutting, and burial or disposal offsite were selected as remedial options. Based on a heritage resources impact assessment (HRIA) screening at the OAM sites, some infrastructure and machinery were considered to carry heritage value and were left in place without disturbing them.

Achieving closure of OAM sites

Contracting strategy

Remediation work for multiple sites that have geographical proximity and similar scope of work was lumped to form construction packages to increase the efficiency of the work. A single contractor was able to utilize the same sets of crew and equipment to move from one site to another and perform remedial activities.

Capping of mine openings

Reinforced concrete caps were built to cap the mine openings. The caps included a reinforced concrete slab and walls where the walls were doweled into bedrock. The foundation area of the cap was carefully examined for competence before selecting the exact location of the foundation. Vent pipes were installed at the cap for air passage and to allow the release of any pressure built up inside the openings. The caps were generally elevated from the ground with posts and signage with reflected markings (Figure 5) making them and the hazards readily recognizable to the public.



Figure 5: Capped mine shaft

Encapsulation of tailings

1.5 mm double-sided textured high-density polyethylene (HDPE) geomembrane was used to encapsulate the potentially acid-generating tailings. The details for the tailing's encapsulation varied from site to site and depending on the aerial extent, thickness, topography, and site-specific characteristics of the tailings. The geomembrane came in rolls and was unrolled on site and seamed together to build the encapsulation. The encapsulated area was covered using quarried non-acid-generating rock. The geomembrane layer was

protected from sharp objects and crushed waste rocks by sandwiching them between non-woven geotextiles. Figure 6 shows an example of tailings encapsulation using an HDPE geomembrane liner at one of the OAM (Central Mine Manitoba) sites.



Figure 6: Encapsulation of tailings using HDPE geomembrane

Regrading of waste rock stockpiles

Steep and undulating stockpiles of the waste rock were regraded to achieve a more stable slope, positive drainage, and aesthetically better condition. Waste rock was also used as a source of fill materials to backfill the test pits and trenches located at the OAM sites.

Demolition and disposal of debris

The metal and infrastructure debris that are not considered to carry any heritage value were collected, broken down, and disposed of into the openings before closure or offsite into landfills and recycling facilities.

Construction constraints

Access constraints

Some of the OAM sites were very remote and away from the provincial access roads, trails, and all-season roads. The access would often require crossing swampy areas, lakes, and rough hummocky terrains. Historically access to those sites required a combination of either or both helicopters, boats, canoes, ATVs, and snowmobiles, etc. Logistics and accessibility were critical considerations for efficiently transporting

materials and personnel to and from the OAM sites. This included the development of access roads and other infrastructure needed to support the construction activities. The challenging access sites were accessed during the winter months by building winter roads through difficult terrains and building ice roads across the lakes.

Presence of archaeologic resources

In general, most of the OAM sites contained heritage objects that are from the mining activities from the 1910s to 1930s dating back to the pre-contact indigenous period (Figure 7). The objects were also very close to where the remediation activities took place, and it was essential to ensure the objects were not disturbed due to construction activities. Hence, visual and physical buffers were established around the objects of significance before starting construction activities and the construction equipment had to be carefully maneuvered around those buffer zones.



Figure 7: Heritage objects found in OAM sites (left: pre-contact, right: 1910s)

Protection of the biological environment

Some OAM sites were in densely vegetated areas and were not readily accessible. Tree clearing was required to access those sites. The nesting period varies from species to species; however, it generally falls between April 1st to August 1st in Manitoba. Bird nest sweeps were completed by qualified ecologists to confirm the presence of bird nests in the proposed disturbance areas.

Conclusion

The Orphaned and Abandoned Mine (OAM) Site Rehabilitation Program in Manitoba has made significant progress since its inception in 2000. Through systematic hazard identification, risk and liability

assessments, and the development and execution of detailed closure plans, the program has successfully remediated over 30 OAM sites, with many more in progress. The multi-faceted approach, which includes stakeholder consultations, site-specific requirements, and practical remediation strategies, has proven effective in mitigating the environmental and public safety risks associated with these sites.

The methodologies employed, such as capping mine openings, encapsulating acid-generating tailings, regrading waste rock stockpiles, and managing abandoned infrastructure, have restored these sites to conditions that are safer for the public and less harmful to the environment. The program's emphasis on long-term sustainability and minimal maintenance requirements ensures that these remediated sites will remain secure and environmentally stable for the foreseeable future.

Challenges such as remote site access, the presence of archaeological resources, and the need to protect biological environments were addressed through innovative solutions and careful planning. The successful implementation of the OAM rehabilitation program serves as a model for similar initiatives in other regions facing the legacy of abandoned mines.

Overall, the program's achievements reflect the commitment of the Manitoba government and its partners to environmental stewardship and public safety. The continued focus on comprehensive remediation and sustainable closure practices will ensure that the benefits of this program extend well into the future, contributing to a cleaner and safer Manitoba.

References

Aboriginal Affairs and Northern Development Canada (AANDC). 2011. Remediation guidelines for abandoned mine openings in Northern Canada, June 29, 2011.

AMEC, 2007. Condition and hazard assessment of crown-owned inactive mine sites in Manitoba

Evans, R. and Kemp, D. 2009. Community issues in mining development. *Mining Journal* 9: 19–23.

Hogan, C.M. and Tremblay, G.A. 2006. Abandoned mines in Canada. *Proceedings of the 7th International Conference on Acid Rock Drainage (ICARD),* American Society of Mining and Reclamation (ASMR): 774–784).

International Council on Mining and Metals (ICMM). 2008. Planning for integrated mine closure: Toolkit.

Johnson, D.B. and Hallberg, K.B. 2005. Acid mine drainage remediation options: a review. *Science of the Total Environment* 338(1–2): 3–14.

Priscu, C., Aldea, C.M., Wong, W.K., Dunham, D. and Lumley, B. 2010. Minimizing environmental impacts in rehabilitating small remote abandoned mine sites in Manitoba.

Richardson, D.J., Ostry, G., Weber, W. and Fogwill, D. 1996. Gold deposits of Manitoba. Manitoba Energy and Mines.

Decharacterization of Tailings and Sediment Dams in Brazil – Hydrological and Hydraulic Aspects

Manuelle Prado Cardoso Pereira, AECOM, Brazil
Mônica Torres dos Santos de Almeida, AECOM, Brazil
Caique Simões Renna Costa, AECOM, Brazil
Helena Maria Campos Castro, AECOM, Brazil
Fernando Pereira Aguilar, AECOM, Brazil
Vicente Mello, AECOM, Brazil

Abstract

This paper presents the technical, legal, and normative aspects of hydraulic safety for the decharacterization of mining dams in Brazil. These aspects guide professionals involved in the design and execution of decharacterization works. Recommendations associated with good engineering design practices are also addressed, particularly in the absence of regulatory support. Additionally, the criteria, premises, and methodologies commonly adopted in hydrology and hydraulics for the decharacterization of dams are presented.

Introduction

The mining dam life cycle includes planning, design, construction, implementation, filling, operation, deactivation, decharacterization, and future uses. The significant dam failures in Brazil in recent years (the Fundão tailings dam in Minas Gerais in 2015 and the Córrego do Feijão dam in Brumadinho in 2019) have led to stricter safety measures for each phase, particularly the creation of laws for decharacterizing dams constructed by the upstream raising method. The new laws established deadlines for the completion of decharacterization projects.

The decharacterized dam is a structure that neither allows water accumulation nor receives or stores tailings/sediments, and it no longer exhibits the characteristics of a dam. This concept means that the decharacterization of a tailings dam can be carried out through different methods, ranging from the total removal of previously deposited material and valley restoration to the maintenance of an anthropized structure. Each methodology for dam decharacterization will directly impact the criteria and premises defined for the project.

Moreover, the decharacterization of a dam serves the purpose of safely reintegrating the anthropized region into nature. Thus, no significant interventions are expected in the region of the structure beyond adjustments identified during the monitoring stage after the completion of decharacterization works.

This paper delves into the primary technical, legal, and normative aspects related to hydraulic safety for the decharacterization of mining dams in Brazil. These aspects are vital for professionals involved in the design and execution of decharacterization works. The paper also addresses recommendations associated with good engineering design practices, particularly in the absence of regulatory support. Additionally, it presents the criteria, premises, and methodologies commonly adopted in hydrology and hydraulics for the decharacterization of dams, underscoring the significance of the topic.

Concept

The concept of a decharacterized dam has evolved since the creation of the National Dam Safety Policy, culminating in its current form with ANM (National Mining Agency) Resolution No. 95/2022. This resolution defines a decharacterized dam as one that no longer permanently receives tailings or sediments from its primary activity and ceases to have the characteristics or function of a dam, following a technical decharacterization project.

The technical decharacterization project must necessarily include, but is not limited to, the following completed stages:

- Termination of operations with the removal of associated infrastructure, such as spigots and pipelines, except those necessary for the safety of the structure.
- Adoption of effective measures to reduce or eliminate surface and groundwater inflow into the reservoir, as well as controlled reduction of the phreatic line within the reservoir.
- Implementation of measures to ensure the long-term physical and chemical stability of the remaining structures.
- Monitoring for a minimum period of two years after the completion of decharacterization works to assess the effectiveness of stabilization measures.

Legislations, norms, resolutions, and terms of references

Following recent tailings dam failures, legislative bodies at the national and state levels in Brazil developed several new laws and resolutions containing restrictions on construction methods and regulations concerning mining dam safety. The main ones are cited below.

- ANM Resolution No. 4 of February 15, 2019 – This resolution established precautionary regulatory measures to ensure the stability of mining dams raised by the upstream method or with unknown

methods. It also prohibited the use, construction, and raising of mining dams by the upstream method in Brazil, and it set a schedule for their decharacterization. This resolution was replaced by ANM Resolution No. 13 of 2019.

- Joint SEMAD/FEAM Resolution No. 2.784 of March 21, 2019 – Mandates the decharacterization of all upstream-raised tailings and waste containment dams from mining activities in Minas Gerais and provides other measures.
- ANM Resolution No. 13 of August 8, 2019 – Updates regulatory measures to ensure the stability of mining dams raised by the upstream method or with unknown methods.
- Federal Law 14.066 of 2020 – Amends previous laws related to the National Dam Safety Policy, creation of the National Environment Fund, establishment of the National Water Resources Policy, and mining code. Regarding decharacterization, the law includes more detailed provisions on the decharacterization process in the National Dam Safety Policy.
- ANM Resolution No. 95 of February 7, 2022 – Consolidates the normative acts on mining dam safety. This resolution also addresses minimum technical criteria for mining dam decharacterization, the minimum monitoring period after the completion of decharacterization works, and procedures for communicating decharacterization to the competent authorities.
- ANM Resolution No. 130 of February 24, 2023 – Amends part of ANM Resolution No. 95 of February 7, 2022, including phases of active and passive monitoring of dam decharacterization.

For the state of Minas Gerais in Brazil, FEAM (*Fundação Estadual de Meio Ambiente* – the State Environmental Foundation) created terms of reference listed below, in which some hydraulic technical aspects related to the decharacterization of upstream-raised dams were mentioned:

- FEAM's 2020 term of reference for decharacterizing upstream-raised dams – Establishes minimum technical criteria for preparing projects for decharacterizing upstream-raised dams in Minas Gerais state.

At the national level, the only technical standard addressing hydraulic aspects related to mining dam decharacterization projects is NBR 13028/2017, mentioned below, and its revision is underway to align with current legislation.

- NBR 13028/2017 – Standard related to the preparation and presentation of mining dam projects, including some criteria for decommissioning and decharacterization.

Criteria related to hydrology and hydraulics, specifically for decharacterized structures, are not addressed in the national legislation and resolutions, except for ANM Resolution No. 95/2022. Given the superficial nature of current Brazilian legislation and standards regarding criteria for decharacterization projects and considering recent mining dam disasters, it is increasingly necessary to evaluate good

engineering practices established by technical professionals and literature from renowned national and international authors.

Currently, some publications stand out, such as *Guidelines for the Preparation of Hydrological Studies and Hydraulic Designs in Mining Works* (Pinheiro, 2011) and various publications from the Canadian Dam Association (CDA), the International Commission on Large Dams (ICOLD), and the Brazilian Dam Committee (CBDB). These technical publications, combined with knowledge of existing legislation, provide criteria, methodologies, and premises to be adopted in dam decharacterization projects, to guide in ensuring the safety of decharacterized structures.

Methodologies for decharacterization of mining dams in Brazil

There are no detailed technical standards or guidelines that provide methodologies for the decharacterization of tailings and sediment dams in Brazil. As a result, projects are guided by the understanding and discretion of each engineer or company, if they meet the requirements outlined in ANM Resolution No. 95/2022. Among the alternatives adopted for decharacterizing mining dams, the following stand out.

Complete removal of the dam and reintegration of the area into the environment

The project involves the complete removal of the dam and ancillary infrastructure, disposal of the materials in the reservoir, followed by the restoration of the remaining valley using natural elements. This process typically includes the construction of a channel at the bottom of the valley with various types of lining, such as grasses, riprap, and other materials, depending on the local flow velocities (Figure 1).

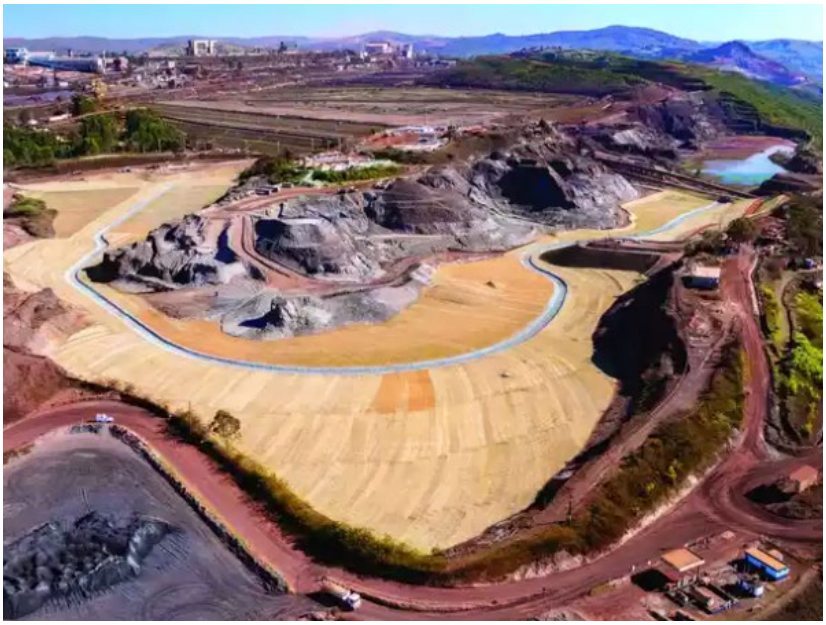


Figure 1: Dam completely removed (source: Estado De Minas, 2021)

Partial removal of the dam

The project includes maintaining part of the dam and the total or partial removal of the tailings/sediments from the reservoir. The reservoir surface is filled with low-permeability materials, and its slope is regularized and directed towards a drainage structure designed to carry all local contributions without forming a downstream lake (Figure 2). Open channels, such as "fishbone" channels, are typically planned for the remaining reservoir surface. These channels are designed without flow attenuation, minimizing water accumulation on the former reservoir surface. This structure should use appropriate linings for the flow velocities, avoiding sections that could create hydraulic flow restrictions, such as culverts or galleries. Some projects incorporate the existing spillway, which requires a hydraulic and structural evaluation.

After the reservoir backfilling, the exposed surfaces should be revegetated to prevent erosion and restore the landscape context. This solution has been identified for upstream-raised dams (with the upstream raises entirely removed down to the starter dike) and single-stage dams raised by centerline or downstream methods.



Figure 2: Dam partially removed (source: Valor Econômico, 2023)

Preservation of the dam

The project includes maintaining the structure (including the starter dike and any existing raises) and the tailings/sediments in the reservoir, filling the surface with low-permeability material, and vegetative restoration. The developer must assess the need to reinforce the dam's downstream side to increase the safety factor, in compliance with current legislation. For surface drainage, drainage channels are also

considered. These channels may or may not discharge into the existing spillways, provided their hydraulic and structural capacity to receive the flow without attenuation from the reservoir is proven.

Complete removal of the dams and the reintegration of the area into the environment is understood as the best alternative for their decharacterization, as there will be no risks related to the hydraulic and geotechnical safety of the structures, thus not requiring future maintenance. However, the complete removal of the structure may raise discussions regarding the definition of suitable locations for the disposal of materials removed from the decharacterization works, which may also involve environmental issues. Such discussions become more frequent in evaluations for the decharacterization of dams with large volumes stored. To avoid impacts from new areas, tailings can be disposed of in exhausted pits. The selection of the decharacterization alternative must always be carried out through a technical comparison, including the implementation risks, and an environmental impact assessment for each option.



Figure 3: Dam partially removed (source: Mansur, 2023)

Once the dam is entirely or partially removed, increasing the safety factor of the remaining structure, the possibilities of failures are minimized but not eliminated. Thus, the monitoring phase is crucial after the completion of decharacterization works. Developers are increasingly creating decharacterization projects that include solutions that do not entirely eliminate the dam embankment due to the absence of legal restrictions on its total or partial maintenance. They are also considering issues related to the disposal of removed materials, especially environmental impacts.

It is important to note that when the dam to be decharacterized has a sediment containment function, it must be demonstrated that the sediment generation rate upstream of the structure has reached a value similar to the natural rate. This assessment can be carried out based on field data surveys to monitor sediments downstream of the structure.

Regardless of the methodology adopted, solutions that partially or entirely maintain the dam must ensure surface water management according to rigorous hydraulic design criteria associated with low risks. This consideration is crucial for decharacterized structures, where maintenance should no longer be required.

The importance of assessing the impacts of dam decharacterization on the hydraulic safety of other structures within the same watershed is highlighted, in view of the elimination of flow attenuation in decharacterized structures. Other long-term environmental impacts and future use opportunities should also be considered.

Premises and criteria

Methodologies for dam decharacterization involve a series of interventions in the dam and reservoir to ensure long-term safety and stability. Therefore, defining premises and the criteria for hydrological and hydraulic parameters is essential.

Hydrological studies for decharacterization projects usually do not differ in terms of the chosen methodology for the complete removal of the dam or for partial/total maintenance.

The calculation of design flows, in general, is carried out by transforming rainfall into runoff, and the calculation method depends on the size of the catchment area.

For the characterization of the watershed, calculation methods for surface runoff coefficients (including the assessment of future land use and occupation) and the time of concentration are the same. However, the return periods adopted for calculating precipitation intensity differ for the alternative of complete dam removal and for the option of maintaining the structure. The terms of reference prepared by FEAM for the decharacterization of upstream-raised dams recommend a minimum return period (TR) of five hundred years for the re-establishment of the watercourse channel. The generally accepted practice is that this criterion should only be adopted in cases where the dam will be removed entirely. Resolution

95/2022 of ANM and Brazilian standard NBR 13.028 apply to partial removal or preservation of the dam, and indicate a TR of 10,000 years or Probable Maximum Precipitation as the criterion for the sizing of the spillway/drainage channel during the decharacterization/closure phase, as the dam structure will remain in the environment.

Usually, dam decharacterization projects include implementing drainage channels around the reservoir, known as “belt channels” or “contour channels,” whose function is to reduce water inflow from the watershed into the reservoir. These should be implemented even before the start of the decharacterization works. For their hydraulic design, the same criteria used for the spillway structure in operation are usually adopted. It is important to note that belt channels are often affected by siltation, resulting in a reduction of their capacity, and therefore, should not be considered for verifying the dam’s hydraulic safety.

To minimize water accumulation in the reservoir during decharacterization works, the operation of pumping systems enables the progress of the works and can contribute to reducing the water table and promoting the geotechnical safety of the structure. The criteria adopted for the design of these systems must be associated with the failure risk and usually a return period of one hundred years is adopted. It is important to note that the operation of pumping systems should not be considered in flood routing studies to assess dam hydraulic safety.

Regarding hydraulic aspects, the drainage/rehabilitation structures designed for river channels must evaluate not only engineering criteria for extreme flows (velocities and freeboard) but also verify the minimum water depth the designed structure will convey during dry periods. This verification is crucial to allow fauna (both terrestrial and aquatic) to survive throughout the year.

For a decommissioning project to achieve the environmental recovery goal of a dam area, the engineering team must collaborate closely with the environmental team, considering the habitat needs of the local fauna in the design. Therefore, the hydraulic design should avoid solutions such as large rock blocks on the channel bed with many voids, as this material allows complete infiltration of surface water through the blocks, preventing the formation of a perennial water layer over them. Along the banks, materials for covering should be evaluated to minimize erosion while allowing access to terrestrial fauna.

Monitoring

The monitoring and maintenance plan for a decharacterized dam must ensure that the structure maintains geotechnical and hydraulic safety conditions, while promoting environmental restoration to reduce risks to public health and safety.

ANM Resolution No. 130/2023 requires monitoring of the decharacterized structures for a minimum period of two years after the completion of decharacterization works, aiming to ensure the effectiveness of

stabilization measures. The resolution outlines two phases for the monitoring period: the first phase is active monitoring (mandatory for two years), which will then transition to a second phase defined as passive monitoring.

During active monitoring, actions should be planned to track the evolution and effectiveness of measures adopted in decommissioning the structure, focusing on geotechnical, hydraulic, and environmental aspects. Therefore, activities such as visual inspections and monitoring will be necessary to identify anomalies and determine the need for passive monitoring, which will be a continuation of active monitoring activities.

Typical post-closure activities include reducing the water table, operating drainage structures, preventing water accumulation during floods, stabilizing sediment generation and erosion points, promoting environmental restoration, and conducting water quality assessments. Monitoring and maintenance records help inform decisions regarding implementing additional corrective measures and/or mitigating impacts. It is also important to highlight the monitoring phase's significance in informing future decisions regarding new dam decommissioning projects.

Mining tailings dams, regardless of their construction method, are critical structures with catastrophic potential in case of failure. Therefore, the only abandonment alternative that no longer requires monitoring and oversight is the complete removal of 100% of the structure and its reservoir, along with the implementation of an environmental solution that restores the site to its natural condition prior to the existence of the dam.

Conclusion

The decharacterization of tailings and sediment dams in Brazil is a complex process that requires a multidisciplinary approach to promote long-term safety and stability. Adopting good engineering practices and adhering to legal and normative frameworks are essential for the success of decharacterization projects.

The methodologies, premises, and criteria presented in this article provide an overview of the hydrological and hydraulic aspects involved in dam decharacterization, guiding professionals in the design and execution of these projects.

The preferred decharacterization alternative will be chosen after considering the structure's specificities and technical, economic, social, and environmental aspects.

This paper notes an evolution in regulatory frameworks for the decommissioning of mining dams in recent years. However, the authors recognize the need for additional guidance to define actions and guide professionals, so as to ensure public safety and the recovery of degraded environments. Thus, there is a recognized need for the continuous evolution of these regulatory foundations to ensure the effective

decharacterization of dams, which will occur once the structure is reintegrated into nature, so that it no longer has a need for maintenance or monitoring.

References

Associação Brasileira de Normas Técnicas (ABNT). 2020. NBR 13.028 – *Preparation and Presentation of Projects for Dam Tailings Disposal, Sediment Containment, and Water Storage*. Belo Horizonte, Brazil.

Agência Nacional de Mineração (ANM). 2019. *Resolution No. 4, February 15, 2019*. Brasília, DF, Brazil.

Agência Nacional de Mineração (ANM). 2019. *Resolution No. 13, August 8, 2019*. Brasília, DF, Brazil.

Agência Nacional de Mineração (ANM). 2022. *Resolution No. 95, February 7, 2022*. Brasília, DF, Brazil.

Agência Nacional de Mineração (ANM). 2023. *Resolution No. 130, February 24, 2023*. Brasília, DF, Brazil.

Brasil. 2019. *Law No. 14,755, September 30, 2019*. Brasília, DF, Brazil.

Estado de Minas. 2021. *Technology for Eliminating Dams*. Accessed 6/26/2024 at https://www.em.com.br/app/noticia/patrocinado/ofuturoemconstrucao/2021/08/08/o-futuro-em-construcao,1293621/tecnologia-para-eliminacao-de-barragens.shtml

Fundação Estadual de Meio Ambiente (FEAM). 2020. *Reference Term for Dams Raised Using the Upstream Method Decharacterization*. Belo Horizonte, Brazil.

Mansur, R. 2023. *Samarco conclui descaracterização da cava do Germano em Mariana.* Accessed 6/26/2024 at https://g1.globo.com/mg/minas-gerais/noticia/2023/08/24/samarco-conclui-descaracterizacao-da-cava-do-germano-em-mariana.ghtml

Pinheiro, M.C. 2020. *Guidelines for the Preparation of Hydrological Studies and Hydraulic Designs in Mining Works*. Organized by ABRH. 1st ed., Porto Alegre, RS.

Secretaria de Estado de Meio Ambiente e Desenvolvimento Sustentável/Fundação Estadual de Meio Ambiente (SEMAD/FEAM). 2019. *Resolution SEMAD/FEAM No. 2,784*. Brasília, DF, Brazil.

Valor Econômico. 2023. *Vale begins work to eliminate 2 tailings dams in MG*. Accessed 6/26/2024 at https://valor.globo.com/empresas/noticia/2023/05/03/vale-inicia-obras-para-eliminar-2-barragens-de-rejeitos-em-mg.ghtml

Checklist for Decharacterization of Mining Dams: Engineering and Environmental Aspects

Rafael Caetano Cardoso Boaventura, AECOM, Brazil
Murilo Damato, AECOM, Brazil
Gislene F.S.R. Fournier, AECOM, Brazil
Manoela C.A. Neves, AECOM, Brazil

Abstract

Based on AECOM's experience auditing the decharacterization of over 20 mining dams in Brazil, the company developed a Checklist to assess the engineering and environmental aspects of dam decharacterization projects, the monitoring plans for the adopted solutions, and the respective impacts generated. AECOM also considered the Global Industry Standard on Tailings Management (GISTM) and the United Nations Sustainable Development Goals (SDGs) adopted as part of the 2030 Agenda.

The Checklist addresses engineering premises and the need to consider SDGs related to responsible natural resource management, including economic development and environmental protection. For its application, on-site evaluations and documentary analysis of geotechnical structures must be considered.

Regarding post-decommissioning monitoring, the Checklist addresses issues to be evaluated regarding geotechnical stability and environmental aspects, divided into physical, biological, and anthropic issues. Among the components of the physical environment are ecotoxicological indicators, water quality, soil quality, air quality, and sediment transport. Biological components include the protection of local fauna, ecotoxicological bioindicators, vegetation composition, and succession. Lastly, for anthropic components, actions and monitoring of fauna associated with human occupation and the presence of entomological vectors are evaluated. Thus, the aim is to obtain a set of environmental quality indicators for mining dam decharacterization projects.

Introduction

In Brazil, the state of Minas Gerais suffered two of the most significant socio-environmental disasters in mining history, with the ruptures of Fundão tailings dam (Municipality of Mariana, 2015) and B-I tailings dam in Córrego do Feijão mine (Municipality of Brumadinho, 2019). Between 2019 and 2021, structural problems in mining dams built using the upstream method led to the evacuation of communities, resulting

in serious socio-environmental impacts. As a result of these events, laws were created with stricter criteria regarding dam safety, defining the mandatory decharacterization of dams built using the upstream method. New federal and state legislation established standards and deadlines for the decharacterization of all dams constructed by the upstream method.

The decharacterization of a structure is a complex procedure involving numerous technical discussions due to the novelty of the legal and infra-legal determinations, the technical challenges, the risks inherent in the works, and the socio-environmental impacts that must be diagnosed and mitigated.

In Minas Gerais – a densely populated Brazilian state – large mining dams were raised upstream. These dams had nearby communities. Sometimes, the populations in the flood areas of these dams are exposed to significant risks arising from possible ruptures or leaks. These communities, located immediately downstream of the dams, depend on the proximity of water resources for their economic activities, such as agriculture and fishing, as well as homes and essential infrastructure. The safety of these populations requires effective emergency plans, awareness, and training programs for rapid evacuation, as well as constant monitoring of dam conditions.

Protecting these communities during the process of decharacterization of the dams is crucial, requiring an integrated approach involving authorities, companies responsible for the dams, and the local population itself. Thus, in addition to the need to mitigate safety risks to communities, such as preventive evacuations and construction of downstream containment structures (DCS), it is essential to pay attention to the impacts generated by decharacterization works.

The impacts caused by decharacterization are varied, ranging from the movement of trucks and equipment that generate air pollution, emission of noise and vibrations that harm the local populations and fauna to, in certain cases, the opening of new access roads and the suppression of native vegetation. The duration of the decharacterization of a tailings dam varies according to the complexity and size of each one, and the impacts generated may also vary according to the local landscape. For this reason, implementing environmental recovery plans and rehabilitating affected areas is essential to ensure long-term sustainability and minimize residual damage.

Additionally, in Minas Gerais, several tailing dams are in an emergency or alert situation due to the detection of structural anomalies, requiring increased speed and accurate techniques for decharacterization.

AECOM has developed an evaluation method based on a Checklist to effectively and comprehensively verify the engineering and environmental aspects of dam decharacterization projects, the monitoring plans of the solutions adopted, and the impacts generated.

This instrument is an essential tool for auditing all stages of the process, from initial planning to the completion of activities. This Checklist helps to identify and highlight the risks associated with the work, ensuring that all safety procedures are strictly followed. It also facilitates communication between

professionals, ensuring that no critical steps are overlooked. Using this Checklist, it is possible to monitor compliance with environmental and legal obligations, ensure the protection of adjacent populations and affected ecosystems, and ensure that the project is completed within the established deadlines and budgets.

Methodology

AECOM developed the Checklist to evaluate the engineering and environmental aspects of dam decharacterization projects, the monitoring plans for the solutions adopted, and the impacts generated.

The Checklist was developed in the following phases:

Phase 1: Identification of legal and normative requirements

The regulations and standards pertinent to the situation were identified, classified by theme, and included in a specific list for each mandatory topic in the dam decharacterization process. This included environmental regulations, engineering standards, safety guidelines, and more.

Phase 2: Analysis of risks and impacts

A list was made of the items to be observed prior to the decharacterization work that are related to the risks associated with the dam's decharacterization, and of the potential environmental impacts. Factors such as soil erosion, sediment release, and changes in rivers, have implications for fauna and flora, and surrounding communities.

Phase 3: Inclusion of items

The analysis had to include items related to environmental recovery projects, as well as monitoring plans for fauna and flora, and the impacts generated. Additionally, items related to structural stability, water quality, and biodiversity, among others, were included.

Phase 4: Inclusion of items related to GISTM and the UN SDG goals

Each phase of the decharacterization work had to be analyzed, and items had to be prepared to achieve the ultimate goal of avoiding any harm to people and the environment (zero damage), with zero tolerance for human fatalities. In addition, these criteria were interconnected with the SDGs, which address the main development challenges faced by people in Brazil and around the world.

Phase 5: Development of the Checklist

The Checklist items were grouped into five axes:

1. Decharacterization Engineering Projects;
2. Degraded Area Recovery Projects;

3. Socio-environmental Recovery Projects (adherence to the SDGs);

4. Monitoring Plans; and

5. the GISTM.

The items are evaluated as “met,” “not met,” and “not applicable.”

Phase 6: Cross-check

After the Checklist’s initial development, it was subjected to a cross-check process. Contributions were sought from other experts within the company to verify the approach in different contexts, structures, and for adherence to best practices.

Phase 7: Pilot test and final review

An initial version of the Checklist was applied to the decharacterization of a real dam to evaluate its effectiveness and identify possible improvements. After the pilot test, feedback was collected from those involved, and the document was revised for the final version.

Regarding post-decommissioning monitoring, the Checklist addresses issues to be evaluated regarding geotechnical stability and environmental aspects, divided into physical, biological, and anthropogenic means. Among the components of the physical environment are water quality, soil quality, air quality and sediment transport. Biological components include the protection of local fauna, ecotoxicological bioindicators, vegetation composition, and succession. Chemical components include toxicological indicators in water, soil, and air quality. Finally, for the anthropic components, actions and monitoring of the fauna associated with human occupation and the presence of entomological vectors are evaluated. Thus, it is intended to obtain a set of environmental quality indicators for decharacterization of mining dams projects.

Data and discussion

This Checklist was designed to be adaptable to different scenarios and should be applied so as to be most applicable to the items to be analyzed. As shown in Figure 1, and mentioned above, the Checklist was divided into 5 Axes: Decharacterization Engineering Project, Degraded Area Recovery Projects, Socio-environmental Recovery Projects (adherence to the SDGs), Monitoring Plans, and the GISTM.

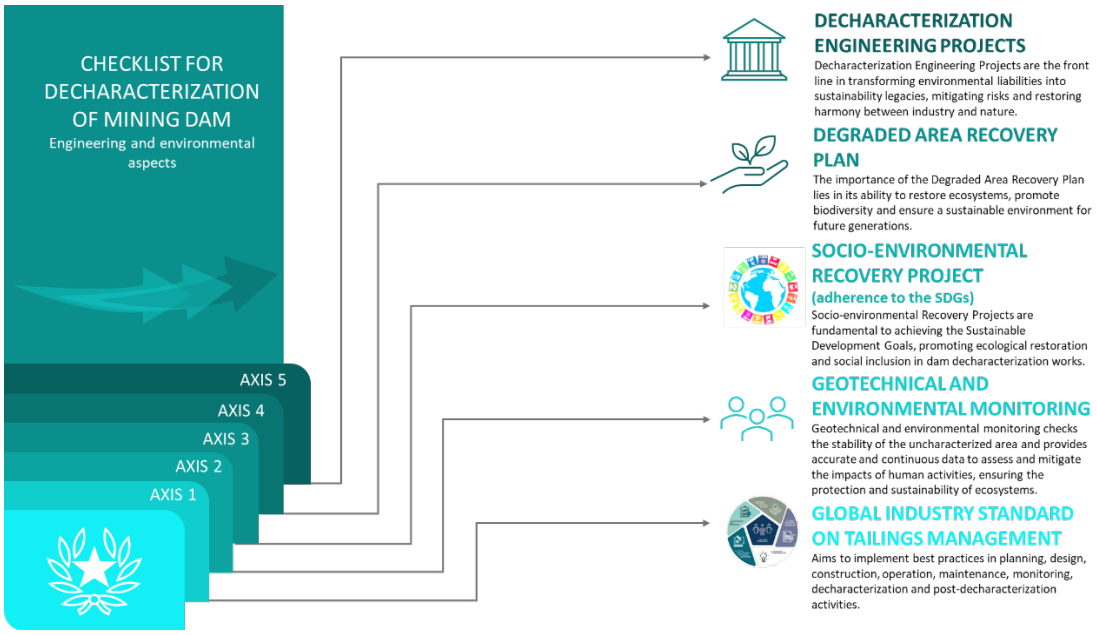


Figure 1: Main axes of the Checklist for decharacterization of mining dams

Decharacterization engineering projects

This axis was divided into three sets of requirements, adjusted to the legal and normative requirements of the State of Minas Gerais and Brazil. For application in other Brazilian states or countries, some requirements must be reviewed considering local characteristics. To fulfill the first requirement, the adequacy of the geological-geotechnical investigations, the instrumentation plans, the hydrological design criteria, and the safety factors, among others, are analyzed. This is based on the requirements of the Terms of Reference for the decharacterization of dams raised by the upstream method (prepared by the State Foundation for the Environment of Minas Gerais – FEAM).

The second analysis required is the Brazilian Standard NBR 13.028/2017, referring to the preparation and presentation of mining dam projects. In the last requirement of this set, criteria were defined to be met by the As Built Project.

Degraded area recovery plan

This axis refers to the aspects of environmental recovery of the area to be decharacterized. Its objective is to ensure the effectiveness of the proposal for the restoration of ecosystems to promote the conservation of biodiversity. First, the plan's goals should be defined, including the desired deadlines. Subsequently, the origin of the degradation, the regional and local characterization, the delimitation of the intervention area, the methodology, the maintenance plans, how the results will be evaluated, the schedule, and the ways to give visibility to these requirements must be analyzed.

Social-Environmental Recovery Project (adherence to the SDGs)

The Socio-Environmental Recovery Project combined with the UN Sustainable Development Goals (SDGs) are addressed for this axis. The SDGs provide a comprehensive framework that integrates environmental protection, social justice, and economic growth, guiding actions to address global challenges holistically. By aligning socio-environmental recovery projects with the SDGs, it is possible to create integrated solutions that meet environmental and social needs and promote the resilience of communities affected by dams.

Geotechnical and environmental monitoring plans

After the completion of the decharacterization works, geotechnical monitoring should be continued for the time necessary to verify the project hypotheses, such as the medium and long-term hydrogeological model and the final stability of the area.

Environmental aspects must be foreseen in the Recovery Plan for the Degraded Area. The pre-existing impacts and those caused by the decharacterization continue for longer than the execution of the work itself. Thus, environmental monitoring is necessary and should cover both the physical and biological environments. If any socioeconomic impacts of the decharacterizations have been diagnosed, the monitoring of these can also be contemplated. The primary objective is to provide a solid and informed basis for developing strategies and procedures that protect human lives, minimize property damage, and promote rapid environmental recovery.

Global Industry Standard on Tailings Management (GISTM)

The entire decharacterization process is evaluated in this last axis, considering the topics, principles, and GISTM requirements. This evaluation extends from identifying and documenting the changes observed and carried out on-site, to evaluating the implementation of best practices in the activities of planning, design, construction, operation, maintenance, monitoring, decharacterization, and post-decharacterization.

Results

In the end, the Checklist for the decharacterization of mining dams included the interactions between legislation, technical standards, good practices for recovery of a degraded area, GISTM, and the UN Sustainable Development Goals (SDGs). Through a document analysis, the company's technical expertise, environmental and social data, and interviews with stakeholders, we seek to understand how the decharacterization of dams can simultaneously achieve its safety objectives and contribute to sustainable development, mitigating its negative impacts. Table 1 shows the items evaluated by theme.

Table 1: Quantitative of items by axis for the Checklist for decharacterization of mining dams

Theme	Subtheme	Quantitative
Decharacterization Engineering Projects	Term of Reference for the decharacterization of Dams raised by the Upstream Method (FEAM)	12
	NBR 13.028/2017 – Elaboration of mining dam project	38
	As Built Project	15
Degraded Area Recovery Plan	General	56
Socio-environmental Recovery Project (Adherence to the SDGs)	General	23
Monitoring	Geotechnical	3
	Environmental	19
Global Industry Standard on Tailings Management (GISTM)	General	77
Total		243

In a decharacterization project audited by AECOM, the completed and commented upon Checklist was forwarded to the mining company after its application. In the completed Checklist, all items were classified as "met," "not met," or "not applicable" and commented on. With this document, the mining company can implement the necessary adjustments.

Conclusion

The decharacterization of dams generates technical and governance challenges, and long-term safety and environmental adaptability risks must be considered. To make clear the aspects that must be considered to ensure the effectiveness of decharacterization projects, AECOM Brazil's multidisciplinary team developed the Checklist to consider technical guidelines, covering the entire cycle of the work and the cumulative impacts of post-decharacterization. The process involved several stages of elaboration, validation, and revision, enhanced by the contribution of specialists from different areas (engineers, geologists, veterinarians, biologists, sociologists, and geographers, among others).

The adoption of the Checklist was crucial for identifying weaknesses and enabling actions to improve and mitigate the potential damage caused by the decharacterization of dams. In addition, fulfilling the items listed in each area highlighted in the Checklist allows mining companies to lead technological innovations that promote sustainability, invest in green mining technologies, and modernize works, while reducing environmental impacts.

AECOM Brazil has been directly involved in the audit of dams in the process of decharacterization. Intensive analyses and inspections in collaboration with the Brazilian authorities resulted in the creation of

this Checklist. The need to adhere to global standards to prevent future disasters, linked to the advent of the standards established by the UN through the SDGs, stimulated the strengthening of auditing actions beyond Brazilian legislation.

In addition to the technical and logistical challenges, the Checklist assists in the analysis of the socio-environmental impacts of decharacterization works. It should be noted that engineering projects must consider the medium and long-term objectives of the recovery plan for the degraded area. With the adoption of the Checklist, these correlations can be verified early in a practical way. In addition, the procedure makes essential contributions to monitoring plans after the decharacterization, including the monitoring of physical and environmental stability according to the objectives defined in the recovery plan. Thus, the Checklist generates significant opportunities to promote inclusive and sustainable economic growth. The Checklist provides a detailed overview of how mining can align its operations with the best sustainability and socio-environmental standards, creating practical recommendations for companies, policymakers, and civil society organizations.

Acknowledgments

We would like to thank all the experts at AECOM who worked hard to produce a comprehensive Checklist incorporating years of experience.

References

Associação Brasileira de Normas Técnicas (ABNT). 2017. NBR 13028. Mining — Preparation and Presentation of Dam Projects for Tailings Disposal, Sediment Containment and Water Reserve — Requirements. ICS ISBN 978-85-07.

State Institute of Forests (IEF), Directorate of Biodiversity, Minas Gerais. 2021. Joint Resolution SEMAD/FEAM/IEF/IGAM No. 3,049 of March 2, 2021. Terms of Reference for Connectivity Analysis Methodology – Emergency Action Plan (PAE). Government of the State of Minas Gerais.

State Institute of Forests (IEF), Directorate of Biodiversity, Minas Gerais. 2021. Joint Resolution SEMAD/FEAM/IEF/IGAM No. 3,049 of March 2, 2021. Terms of Reference for Baseline Characterization of Wildlife and Associated Ecosystem Services – Emergency Action Plan (PAE). Government of the State of Minas Gerais.

State Institute of Forests (IEF), Minas Gerais. 2021. Joint Resolution SEMAD/FEAM/IEF/IGAM No. 3,049 of March 2, 2021. Terms of Reference of the Project to Assess Environmental Impacts Resulting from a Disaster on Terrestrial Wildlife and Aquatic Biodiversity by the Comparative Monitoring of Affected Environments, Unaffected Environments, and Baseline – Emergency Action Plan (PAE). Government of the State of Minas Gerais.

State Institute of Forests (IEF), Minas Gerais. 2021. Joint Resolution SEMAD/FEAM/IEF/IGAM No. 3,049 of March 2, 2021. Terms of Reference of the Plan for Rescue, Rescue and Disposal of Wildlife and Identification of Mortality in Case of Disaster – Emergency Action Plan (PAE). Government of the State of Minas Gerais.

State Institute of Forests (IEF), Minas Gerais. 2021. Terms of Reference for the Baseline Characterization of Wildlife and Associated Ecosystem Services – Action Plan. Joint Resolution SEMAD/FEAM/IEF/IGAM No. 3,049 of March 2, 2021. Government of the State of Minas Gerais.

The Importance of Hydrogeological Models for Closure of Tailings Dams

Ana Carolina Neves, AECOM, Brazil
Waldemar Felitti, AECOM, Brazil

Abstract

The ultimate stage of a tailings storage facility's (TSF) life cycle encompasses the following steps: closure plan, closure operations, post-closure, and relinquishment. According to Brazilian legislation, all these stages, from the development of a closure plan, extending through the post-closure phase, are referred to as "tailings dam decharacterization."

Following the 2015 and 2019 tailings dam ruptures (Fundão and Córrego do Feijão), the decharacterization of upstream tailings dams has become a mandatory requirement under Brazilian legislation. This measure is crucial for enhancing safety conditions in the downstream areas of the dam and ensuring that these structures do not pose any hazards to the nearby communities and environment. The decharacterization process must adhere strictly to technical engineering and environmental aspects and standards, to allow the extensive areas occupied by the tailings to be properly restored for safe future use.

The decharacterization design, specifications, and works require detailed studies encompassing several disciplines, including hydrogeological studies.

Hydrogeological models (HM) are approximate representations of nature's conditions, elaborated for integrating and synthesizing all the available data and information, offering a systematic and comprehensive understanding of hydrogeological site conditions. A HM is technically necessary at all stages of the decharacterization process. A consistent conceptual hydrogeological model (CHM) is extremely important at the early stages of the conceptual decharacterization project to support the best decisions for the project alternative, strategy, and closure methodology. Once the level of data required to support the models increases, and the projects evolve through the conceptual and planning stages from basic to detailed projects, it becomes necessary to build a numerical hydrogeological model (NHM). This can provide fundamental information for detailed tailings dam decharacterization designs, specifications, and works. At decharacterization works, a NHM is indispensable to organize water-related monitoring data, to support dewatering/drawdown strategies, and to manage water table levels for a safe excavation or grounding. One important application of the NHM is to predict future groundwater conditions and hydrodynamics at

different construction or excavation phases. It estimates critical scenarios and potential geotechnical, engineering, and environmental risks.

At the post-closure stage, continuous monitoring is required, providing input data to the NHM and constant evaluation of the CHM. This enables the assessment of the hydrogeological and geotechnical aspects of the remaining structure, ensuring that its physical and chemical stability can be attested.

This paper examines the applications of the conceptual and numerical hydrogeological models as fundamental tools for the tailings dam decharacterization process. It argues that their application will ensure valuable support for decision-making concerning environmental and engineering aspects.

Introduction

Catastrophes involving the rupture of upstream tailings dams over the last decade in Brazil have caused unacceptable human losses and immeasurable environmental damage. Consequently, the governmental regulatory agency, the Brazilian National Mining Agency *(Agência Nacional de Mineração – ANM)* through Resolution ANM n° 4/2019, revised by ANM n° 13/2019, has prohibited the construction of upstream dams in Brazil. ANM set a deadline, determining that upstream dam owners are responsible for carrying out their decharacterization process.

Based on technical and scientific literature such as the *Waste Management – Good Practices Guide* (ICMM, 2021) and the *Tailings Management Handbook* (Morrison, 2022), this paper suggests that the protocols for tailings dam decharacterization align closely with the final stages of a TSF life cycle, as outlined below:

- Closure planning: this phase encompasses feasibility and alternative studies for closure, along with conceptual, basic, and detailed designs and plans.
- Closure operations: this stage includes TSF decommissioning, monitoring, and closure activities.
- Post-closure: routine inspections and monitoring of geotechnical, hydrological, hydrogeological, and environmental aspects are conducted.
- Relinquishment: the final stage involves the formal transfer of responsibilities associated with the TSF or, as established by the Brazilian National Mining Agency (ANM), the exclusion of the structure from the official list of tailings dams, so that the area can be available for future use.

The government determination for the upstream tailings dam decharacterization has required integrated studies across the various fields of expertise: geotechnics, geology, engineering, hydrology, hydrogeology, geophysics, and environmental sciences, among others.

A wide range of information should be considered in the tailings dam decharacterization, such as: risk assessment; physical, chemical, and mineralogical characteristics of the tailings; As Built and As Is facility

designs; regulatory and environmental requirements; engineering and mining industry standards and guidance; existing infrastructure maps; existing water management plan; topography data; climate; hydrology, hydrogeology and geotechnical monitoring; land restoration, revegetation; and studies of the availability of materials for use in the construction.

Hydrogeology makes an important interface with the mentioned disciplines, making it essential that hydrogeological models (HMs) are applied at all stages of the tailings dam decharacterization process.

The conceptual hydrogeological model (CHM) and the numerical hydrogeological model (NHM) require for their elaboration: tailings projects and As Is design; topographical data; existing infrastructure and tailings deposits (map and cross-sections); sectorization and characterization of the different types of tailings deposits; a water management plan; tailings chemical and physical characteristics; a hydrographic network; geomorphology; hydrology; climate (rainfall and evaporation data, including long-term climate change projections); hydrogeology of surficial and bedrock units; estimated hydraulic conductivity based on geological characteristics; soil characteristics; geotechnical monitoring; lithological and geological-structural information (including maps and cross-sections); water quality data; hydrogeochemical baseline; available monitoring data (well-monitoring data, groundwater level, and hydraulic head, flow and discharge rates, water level in reservoirs, etc.); spring maps and related data; and watershed delineation and flow patterns. Additional investigations may be necessary to add new information to the CHM and accuracy to the NHM, such as geophysical surveys, detailed geological-structural mapping, photointerpretation, log surveys, and hydrodynamic tests.

The model improvement and accuracy depend on data acquirements. It is expected that data will increase as the project evolves, so models demand regular updates as phases and work progress.

In general, a CHM is recommended from the closure project feasibility stage onwards. The CHN precedes the NHM and helps in the choice of the numerical code to be used to implement the numerical model. The most used codes are Finite Difference (MODFLOW) and Finite Elements (such as FEFLOW). The code choice is made mostly considering the complexity of the site and geology.

The tailings physical, chemical, and mineralogical characterization must be evaluated before deciding on tailings reclamation strategy, and the tailings acquired parameters should be included in the numerical model. It is crucial to consider the CNM and the NHM while making detailed designs for decharacterization and also while executing decharacterization operations and monitoring stages, and finally while evaluating the remaining structure's chemical and physical stability before its relinquishment.

Tailing dams decharacterization: Overview and concepts

Tailings are materials without economic interest, discarded from the processing of mined iron ore. They consist of uneconomic crushed rocks, metals, and effluent from the concentration processes used to extract

the desired elements from iron ore. Tailings are stored in a tailings storage facility (TSF); the most used in Brazil is the tailings dam. The upstream method consists of supporting the higher raised embankments on the tailings or sediments previously deposited in the dam reservoir.

Brazilian legislation defines a decharacterized dam as a structure without water accumulation and without tailings and sediments being received permanently. It no longer possesses the characteristics or performs the function of a dam. In accordance with the technical design, decharacterization comprises, but is not limited, several completed phases (ANM, 2022 and 2023).

The Brazilian National Mining Agency has established detailed regulatory legislation to ensure that the liable mining company performs the best practices and state-of-the-art technologies during the dam decharacterization process. According to ANM (Resolutions N° 95/2022, N° 130/2023) and the Environmental State Agency, the process must encompass several phases and procedures, summarized as:

1. decommissioning – ending operational work and removing related infrastructure;
2. hydrological and hydrogeological control – including procedures to reduce or eliminate the surface and groundwater supply to the reservoir and to control the water table;
3. ensuring the long-term physical and chemical stability of the remaining structures;
4. monitoring to ensure the effectiveness of hydrological and hydrogeological stabilization and control measures.

The monitoring stage must be divided into two distinct phases:

1. active monitoring: this comprises the minimum mandatory period of two years established in item "D," and may be extended as defined by the project designer;
2. flexible monitoring: an additional non-mandatory period of monitoring, unless formally required by the Brazilian National Mine Agency, or as defined by the project designer.

Implementing best practices and conducting continuous monitoring aims to meet the criteria prescribed in the technical and legal standards, ensuring long-term physical and chemical stability.

Environmental agencies of the Minas Gerais State (FEAM and SEMAD) also contributed to regulating environmental aspects by publishing the *Reference Document for the Decharacterization of Upstream Tailings Dams,* which establishes the minimum requirements for decharacterization projects and designs (Minas Gerais, 2019).

The Brazilian regulatory agencies consider a structure effectively decharacterized only upon fulfilling the minimum required stages stipulated by the mining and environmental authorities. Furthermore, the resolutions specify that completely removed mining dams and reservoirs are exempt from routine monitoring. As was mentioned, the regulatory guidelines from the Brazilian authorities concerning tailings dam decharacterization are aligned with international guidelines that define basically three stages: the

closure plan, closure, and post-closure. The closure stages begin when the tailings disposal ceases permanently, and the closure plan is implemented. This includes these activities:

- removal of infrastructures, such as tailings pipelines;
- changes in water management or treatment;
- construction of cover systems;
- a progressive reclamation plan;
- setup of reservoir, landfills, or other structural elements such as revegetation landform.

This broad range of measures aims to ensure the long-term physical and chemical stability of remaining structures, and to maintain the monitoring and surveillance plan during the post-closure period until effective site restoration.

Tailings dams can be classified according to their decharacterization works methodology (Neri et al., 2021), such as: complete or partial removal of tailings materials; the need for water level drawdown in the reservoir; and implementation of devices to reduce water input from surface and/or groundwater flow. Some designs propose the construction of downstream reinforcement buttresses to increase the safety factor.

Although there are many uncertainties related to dam conception phases regarding its final destination, there are useful tools to minimize the uncertainty, such as conceptual and numeric hydrogeological models, which can be applied to make predictions for different scenarios.

This paper presents examples of the application of hydrogeological models across different stages of a dam decharacterization project in the Iron Ore Quadrangle, Minas Gerais state. This work aims to contribute to the related subjects of hydrogeology and the decharacterization process, based on the authors' practical experiences of auditing TSF decharacterization works in the Minas Gerais Iron Ore Quadrangle. For the sake of confidentiality, the paper does not include site identification and company names.

Applying hydrogeology to tailings dam decharacterization process

Hydrogeological models are valuable tools that provide sufficient knowledge for planning tailings dams closure, on-going operation for closure and monitoring stages until its restoration (post-closure). As it was mentioned before, all these stages comprehend the process for tailings dam decharacterization, according to the Brazilian legislation and mining regulations.

Closure plan

Feasibility and plan: this consists of selecting the most appropriate combination of technology and the tailings facility location for a given site to reduce risks and minimize closure liability. From its conception, the tailings dam project for closure should be an important issue to be considered. Whatever the strategy is, the decharacterization project should be considered as part of the TSF life cycle. Planning the closure or

dam decharacterization from the point of conception is crucial, as the project's feasibility depends on costs, and the decharacterization process can be very costly, if not properly planned.

The selection of the best alternative for the dam decharacterization project must be based on information from local hydrogeology and must consider the tailings' chemical, physical, and mineralogical characteristics, aiming to achieve lower impacts and to ensure environmental safety.

It is an important concern that the decharacterization projects may require tailings dewatering and/or the drawdown of the water level of the foundation and embankments. Figure 1 illustrates a situation where the phreatic level must be lowered to achieve total tailings removal.

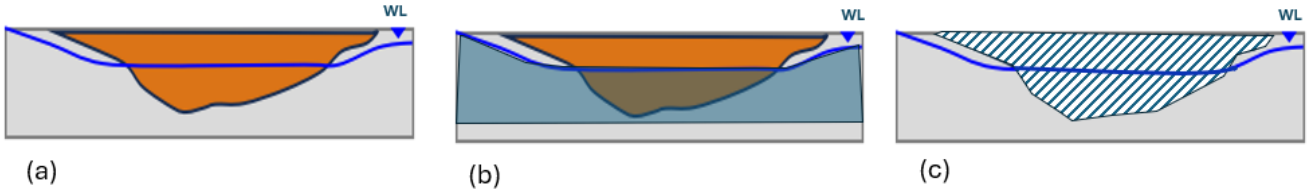


Figure 1: Amount of water needed to be extracted at excavated topography. (a) Initial condition, with intact tailings, (b) 2D representation of the amount of water needed to be removed, and (c) tailings deposits needed to be removed

Operational difficulties must be foreseen at the planning stage, and hydraulic conductivity of the waste cannot be disregarded, as it directly influences the time to draw down and the operational efforts.

The best design alternative for decharacterization must also integrate environmental and social aspects to the engineering pros and cons, and must be chosen over alternatives with greater social, biological, chemical, and physical impacts.

For a conceptual tailings decharacterization project, a CHM provides an understanding of whether the decharacterization solution must consider tailings dewatering and groundwater drawdown. An illustration is presented in the cross-sections in Figures 2 and 3, which represent an upstream dam that needed to be decharacterized, and three different engineering decharacterization approaches.

Figure 2b shows a decharacterization method in which no water drawdown is needed. This design solution is suitable for sites with unavailable disposal areas and no feasibility to drawdown the phreatic table due to hydrogeological, geotechnical, and/or environmental constraints. Figure 3 shows two different methods for a tailings dam decharacterization, both including tailings and embankments removal. The difference between them (Figures 3a and b) is the amount of tailings material removed and the existence or not of the remaining structure. There are pros and cons for each strategy, and the criteria to evaluate the best method must consider the time for dewatering, geotechnical parameters for the dam safety evaluation, and the availability of stock areas for the removed tailings.

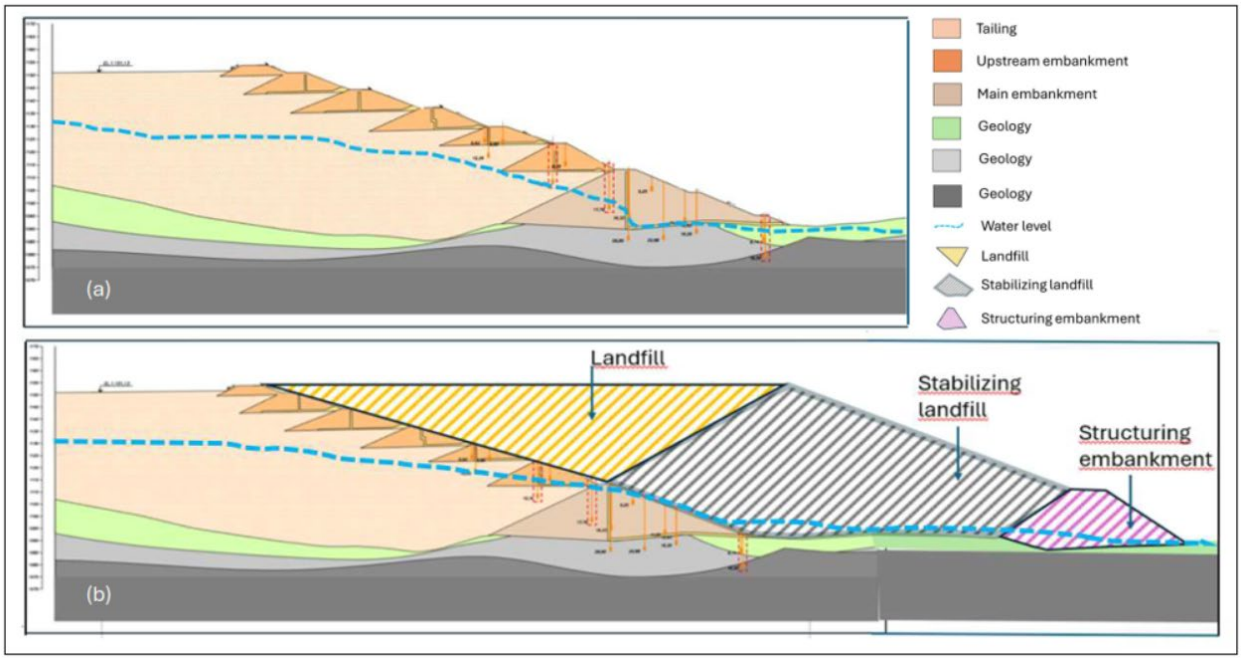


Figure 2: Schematic cross-sections for upstream tailings
(a) upstream dam section
(b) engineering strategy for stabilizing upstream tailings raise, using decharacterization fill and embankment buttresses

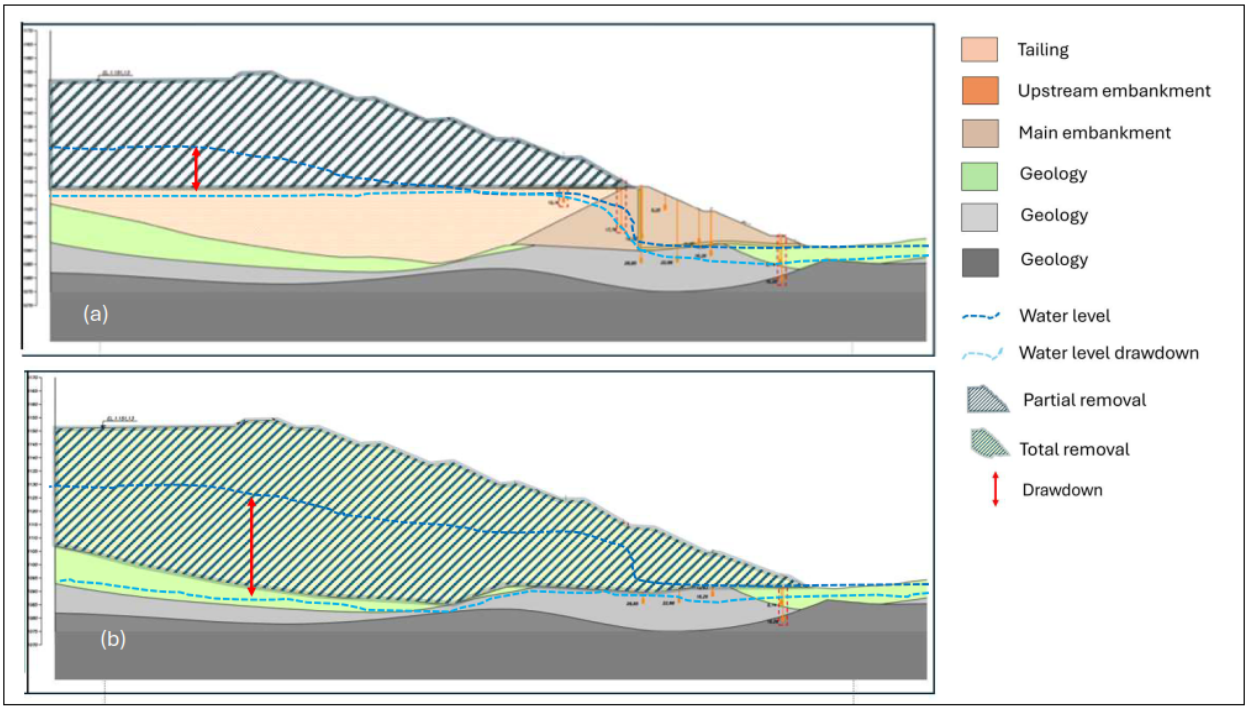


Figure 3: Schematic cross-sections for decharacterized upstream tailings dam
(a) partial tailings removal;
(b) total tailings removal

Environmental issues also need to be addressed: it is paramount to assess all the environmental and social impacts related to each project design and alternative.

Predictions can be made using a numerical model. These can simulate tailings and embankments drawdown using different techniques. Using these, the designers can evaluate the results to choose the best dewatering strategies for each case.

Both strategies, the decharacterization fill and embankment buttresses project (Figure 2b) and the partial tailing removal project (Figure 3a), require an internal drainage system. The numerical hydrogeological model (NHM) serves as an auxiliary tool to assess and compute the internal dam and buttress drainage systems capacity for the safe discharge of the water flows.

The designer must evaluate hypothetical groundwater levels during the construction stage for geotechnical stability assessments, and also for the remaining landfill embankments and natural terrain slopes. A suitable project design solution for each situation and condition must be carefully analyzed.

Concerning environmental aspects, during the planning stage, environmental professionals must consider the impacts of the water resources for each decharacterization strategy. The NHM provides predictive results for changes in hydrodynamics availability and quality; estimates the tailings transport constituents solubilized in groundwater; and provides time estimates for hydrodynamic stability. Depending on the decharacterization method, the time for stabilization could vary significantly. The choice of the types of covering and vegetation for restoration of the area should also take into account the implications for the ground and surface water resources, as they differ on recharge and infiltration precipitation percentages.

Closure operations

At the operational stage, a detailed NHM is useful for testing and implementing an effective strategy to reduce or eliminate the surface and groundwater supply for the tailings dam reservoir.

The numerical model provides information to evaluate the efficiency of the adopted procedures during operation and to manage the water table level during the excavation works. According to Brazilian legislation, the TSF owner must periodically report to environmental agencies about the procedures applied to reduce or eliminate the groundwater and surface water supply for the tailings dam reservoir during the operational stage.

Pumping wells for drawdown, excavation of sumps and drainage trenches are examples of procedures to implement water level control in the reservoir. The numerical models could indicate the best location for drainage systems, predicting the efficiency of each method.

An important aspect to be observed during the drawdown of the tailings water level is the rate of phreatic surface lowering. Numerical model simulations can provide the optimum discharge to avoid rapid water level variation, which can trigger static liquefaction of the tailings.

When a NHM is calibrated for a permanent situation, it can provide water level and discharge predictions for a specific moment (e.g., the discharge volume or water level for the end of an excavation phase). If it is calibrated for a transient situation, the predictions include the time parameter, providing essential answers for supporting engineering and decharacterization works; for example, time estimates for water level drawdown at desirable excavation levels. Figure 4 is an illustration of the water level at each excavation time, produced by numerical hydrogeological model software.

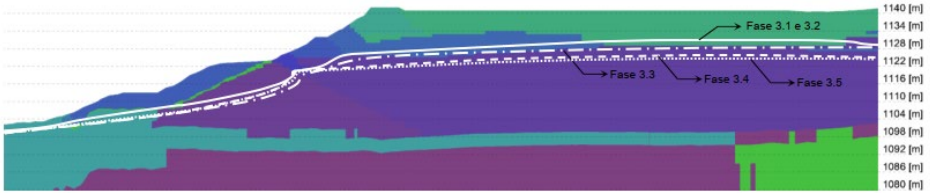


Figure 4: Illustration of water level drawdown computed for excavation stages

During decharacterization works, the NHM should be constantly updated. New data input can provide better calibration and simulations that may indicate a need to adjust the plan when unexpected conditions are encountered. As the model is updated, the implemented decharacterization design can be adjusted when water level and hydraulic head simulations over time do not achieve geotechnical safety parameters.

The NHM estimates the long-term groundwater level recovery conditions after decharacterization works, providing information for better planning of the decharacterization monitoring stages (passive and flexible).

Monitoring

The monitoring of the chemical and physical aspects of the water resources is essential throughout the entire tailings dam decharacterization process, from the initial closure design. The quali-quantitative parameters of the groundwater and surface water should be monitored. Measures of rainfall, evaporation, water level (phreatic, hydraulic heads, reservoir), and discharges (water catchment, water courses, pumping and dewatering wells, pumping in ponds), are essential data to be collected during the TSF life cycle. The existing monitoring plan should be maintained, as far as possible, for later evaluation. Historical data sets allow for the interpretation of the changes in water level, flow, and quality.

The diagnosis of physical and chemical aspects related to surface and groundwater resources, as well as the prognosis for impacts during the operational and post-decommissioning stages, are essential for the elaboration or adjustment of the monitoring decharacterization plan.

Impacts on water resources resulting from the implementation of the tailings dam decommissioning project may include changes in hydrodynamics, availability and quality. Forecasting these impacts using a

NHM will guide the optimal distribution of monitoring wells and surface points, parameters, and sampling frequency.

Water resources impact evaluations can better be assessed with the NHM, providing necessary information for mitigation and remediation procedures.

Physical stability is reached when hydrodynamic monitored parameters are in equilibrium with the surrounding environment. Similarly, chemical stability can be assessed based on monitored data, if the thermodynamics and chemical aspects are in balance with the surrounding environment. The NHM can predict when this stability should be achieved. An updated numerical model, through ongoing decharacterization works and a post-work monitoring period, is important to confirm design expectations and to forecast more realistic scenarios over time.

Conclusion

Hydrogeological models are valuable tools that can be applied and used in the tailings decharacterization process. The regulatory guidelines from the Brazilian authorities concerning tailings dam decharacterization are aligned with international guidelines that define the final stages of the life cycle of the TSF as closure plan, closure, and post-closure. The hydrogeological conceptual and numerical models must be integrated into other disciplines from the early stages of closure design: planning the tailings dam closure, ongoing operation for closure, monitoring stages, and the complete area restoration (post-closure).

A NHM helps to estimate the effects of the engineering and environmental procedures taken to ensure the long-term physical and chemical structures stability. Water level, discharges, and quality data through the flexible monitoring phase should be input data to be included in the model, with frequent updates, so that stability predictions can be improved.

As explained, transient models can predict the time required for site hydrodynamic stabilization; support geotechnical and environmental stability assessments, which are required for attesting its final stabilization; simulate critical situations; and support mitigating measures that could be implemented to avoid environmental and geotechnical losses or damage.

Acknowledgements

Acknowledgements to AECOM Brazil and the USA team who collaborated with the technical work and English review.

References

Associação Brasileira de Normas Técnicas (ABNT). 2017. ABNT – NBR 13028: *Mineração – Elaboração e Apresentação de Projeto de Barragens para Disposição de Rejeitos, Contenção de Sedimentos e Reservação de Água – Requisitos*. Rio de Janeiro, Brazil.

Brasil – Agência Nacional de Mineração. 2019. *Resolução ANM nº 13, de 8 de agosto de 2019. Estabelece medidas regulatórias objetivando assegurar a estabilidade de barragens de mineração, notadamente aquelas construídas ou alteadas pelo método denominado "a montante" ou por método declarado como desconhecido e dá outras providências*. Accessed 6/27/2024 at: https://www.snisb.gov.br/Entenda_Mais/legislacao-aplicada/anm-resolucao-13-2019.pdf.

Brasil – Agência Nacional de Mineração. 2019. *Resolução ANM nº 4, de 15 de fevereiro de 2019. Revogada pela Resolução ANM nº 13, de 8 de agosto de 2019. Estabelece medidas regulatórias objetivando assegurar a estabilidade de barragens de mineração, notadamente aquelas construídas ou alteadas pelo método denominado "a montante" ou por método declarado como desconhecido e dá outras providências*. Accessed 6/27/2024 at: https://www.snisb.gov.br/Entenda_Mais/legislacao-aplicada/anm-resolucao-13-2019.pdf.

Brasil – Agência Nacional de Mineração. 2022. *Resolução ANM nº 95, de 07 de fevereiro de 2022: Consolida os atos normativos que dispõem sobre segurança de barragens de mineração*. Accessed 6/27/2024 at: https://www.gov.br/anm/pt-br/assuntos/barragens/legislacao/resolucao-no-95-2022.pdf.

Brasil – Agência Nacional de Mineração. 2023. *Resolução ANM nº 130, de 24 de fevereiro de 2023: Altera a Resolução ANM nº 95, de 7 de fevereiro de 2022, e dá outras providências*. Accessed 6/27/2024 at: https://www.in.gov.br/en/web/dou/-/resolucao-anm-n-130-de-24-de-fevereiro-de-2023-466161726.

Environment Canada. 2012. *Metal Mining Technical Guidance for Environmental Effects Monitoring*. Accessed 6/26/2024 at: https://publications.gc.ca/collections/collection_2012/ec/En14-61-2012-eng.pdf.

International Council on Mining and Metals (ICMM). 2021. *Tailings Management: Good Practice Guide*. London: ICMM. Accessed 6/26/2024 at: https://www.icmm.com/en-gb/guidance/environmental-stewardship/tailings-management-good-practice.

Minas Gerais, Governo do Estado de. 2019. *Termo de Referência para Descaracterização de Barragens Alteadas pelo Método de Montante. Secretaria de Estado de Meio Ambiente e Desenvolvimento Sustentável (SEMAD) e Fundação Estadual do Meio Ambiente (FEAM)*. Accessed 6/26/2024 at: http://www.feam.br/gestao-de-barragens/descadastramento-e-descaracterizacao.

Morrison, K.F. 2022. *Tailings Management Handbook: A LifeCycle Approach*. Society for Mining, Metallurgy and Exploration (SME).

Neri, A.C., Sánchez, L.E., Alves, C.F.C., Dupin, P.C., Silva-Sánchez, S.S., Baeta, A.M., Modesto, A., Christofolletti, C., Cunha, C.B., Tanikawa, D.H., Piló, H., Yoshizaki, H., Bessa Júnior, J.E., Bezerra, J.S.B., Sanchez, J., Dias, L.G., Souza, L.T.M., Santos, M.R.G., Borghieri, M.G., Ferracini, M., Massignan, R.S., and

V.L. Monteiro. 2021. *Avaliação Ambiental Integrada das Obras de Descaracterização das Barragens de Rejeitos Alteadas pelo Método a Montante no Estado de Minas Gerais. Volume 1. São Paulo: Fundação para o Desenvolvimento Tecnológico da Engenharia (FDTE)*. Accessed 6/24/2024 at https://www.feam.br/avaliacao-ambiental-e-gestao-do-territorio/-avaliacao-ambiental-integrada-aai-das-obras-de-descaracterizacao-de-barragens-alteadas-pelo-metodo-a-montante-no-estado-de-minas.

Tailings Dam Decharacterization Projects: Proposal for Water Monitoring Plan

Ana Carolina Neves, AECOM, Brazil
Helen Simone Chiaranda, AECOM, Brazil
Bruno Resende Lopes, AECOM, Brazil
Rafael Gomes Oliveira, AECOM, Brazil

Abstract

The term "decharacterization" of a dam structure is a technical expression commonly used in Brazil to describe the final stages of a dam's lifecycle. The entire process encompasses studies for choosing the best decommissioning alternative and methods, planning and projects development, operations, monitoring, post-decommissioning management, and final assessments for attesting safety and environmental remaining structure stability, enabling the area to be fit for future uses.

The decharacterization of tailings dams demands engineering measures aimed to close mining structures, a mandatory requirement by Brazilian regulatory agencies for dams constructed using the upstream method. The guidelines regulating decharacterization projects encompass, in addition to engineering actions, measures to ensure the structure's physical, chemical, and biological stability. They also include monitoring the effectiveness of these measures through establishing a monitoring program for as long as necessary until these stabilities are achieved. Even though monitoring is fundamental, the normative instruments do not establish clear and comprehensive guidelines defining minimum requirements to ensure the sustainable stability of the remaining structures on site. Considering the influence of water presence on the stability of physical and chemical structures, this study proposes a water resource monitoring plan with the minimum requirements necessary to meet the objectives of a decharacterization project. The proposal addresses the sampling of surface water, groundwater, and effluents, including essential aspects for defining an efficient monitoring network, such as the parameters to be monitored, sampling frequency, criteria, and methodologies for data interpretation, and corrective actions. All points outlined in the plan were based on the authors' auditing experience of decharacterization projects in the state of Minas Gerais and the Brazilian governmental recommendations, legislation, and regulations.

Introduction

The decharacterization of upstream tailings dams has become mandatory in Brazil following the failures of such structures in Mariana (2015) and Brumadinho (2019), both in the state of Minas Gerais. This regulation aims to mitigate the inherent risks associated with this construction technique, which has proven to be susceptible to failure. Adopting this regulatory policy is a necessary response to safeguard the environmental safety of communities potentially affected by potential tailings dam ruptures.

In Brazil, the term "decharacterization" is a relatively recent concept that refers to a series of intervention actions aimed at rendering tailings dams non-functional. In general, these actions involve controlling surface and groundwater runoff into the reservoir, and prohibiting flood transit in the reservoir, which results in the transformation of the dam structure into an integrated part of the surrounding topography (Sánchez et al., 2013).

The regulatory legislation of the Brazilian state of Minas Gerais (Terms of Reference for Decharacterization of Dams Built using the Upstream Method [SEMAD and FEAM, 2019]) establishes the minimum requirements for a decharacterization project. In parallel, Federal Resolutions nº 95/2022, 130/2023, and 175/2024 of the National Mining Agency (ANM) consolidate the normative acts that govern the safety of mining dams. These regulatory guidelines establish that the technical decharacterization project must necessarily include effective measures aimed at minimizing or eliminating the input of surface and groundwater into the reservoir. Additionally, the project must incorporate measures that ensure the structure's physical, chemical, and biological stability, underscoring the requirement for continuous monitoring during and after the decharacterization process. According to regulatory legislation, this monitoring should persist for the necessary duration to validate the effectiveness of the adopted decharacterization measures.

According to Article 2 of ANM Resolution nº 130/2023, updates were made to the definition of decommissioned mining dams and their minimum decharacterization stages. Recent updates require a minimum of two years of monitoring after the completion of decharacterization works, during the active monitoring phase, and the possibility of passive or flexible monitoring after the mandatory period.

The environmental aspects of decharacterization are an important issue to be considered. Actions and programs to control, mitigate, recover, and compensate for the environmental impacts caused by dam decharacterization operations must be adopted and maintained for the same monitoring period after their completion.

All the data acquired during the active monitoring period, after the completion of the decharacterization works, will determine the fulfillment of all decharacterization objectives, especially those related to geotechnical and environmental stability. In this sense, it is important to emphasize that the

geotechnical and environmental stability of the remaining structure must be demonstrated, certified, and approved by government and mining agencies.

The presence of water governs geotechnical stability, hydraulic safety, and environmental aspects. The monitoring of groundwater, surface water, and tailings dam effluents during and after decharacterization works should encompass criteria that cover water quality, water levels, hydraulic head, and flows. Additionally, it is essential to adequately establish the baseline or background of surface water, groundwater, soil, and sediments in the areas affected by the structure, as well as the chemical and physical characterization of the tailing and remnant materials. Without this data, there is a risk of imposing unnecessary requirements to achieve water quality standards that may not align with the baseline or natural conditions observed initially.

Despite the importance of water monitoring during and after the execution of the decharacterization project, the lack of information on procedures and minimum requirements are a challenge to its effectiveness. To address this lack, this article aims to provide guidelines and a proposal for monitoring surface and groundwater resources and effluents in decommissioned dams and surrounding areas, based on the authors' auditing experience in the Quadrilátero Ferrífero region, state of Minas Gerais. Monitoring is crucial for obtaining data that can support the stability of the structure from an environmental and water resources perspective, supporting the declaration of the dam as effectively decommissioned.

Tailings dam decharacterization: overview and concepts

The upstream construction method is a dam-building methodology in which the embankment fills are supported on previously deposited tailings or sediment, including those built on tailings from existing reservoirs (ANM, 2024). According to the Terms of Reference for Decharacterization of Upstream Dams, developed by SEMAD and FEAM (2019), a decommissioned dam is one that no longer receives tailings from its core activity, ceases to function as a dam and meets adequate safety conditions according to the technical decharacterization project, which comprises the following stages:

1. cessation of operations with the removal of associated infrastructure (decommissioning);
2. adoption of effective measures to reduce or eliminate the input of surface and groundwater into the reservoir;
3. execution of measures aimed at ensuring the long-term physical, chemical, and biological stability of the structures remaining on-site; and
4. monitoring for the period necessary to verify the effectiveness of the measures adopted for decharacterization.

There is a correspondence between the stages established for the decharacterization of a tailings dam in SEMAD and FEAM (2019) and ANM (2022) and the stages of closure of tailings storage facilities (TSF) according to ICMM (2021) and Morrisson (2022). The closure phase begins when the disposal of tailings permanently ceases and the closure plan is implemented, including activities such as infrastructure removal, such as tailings pipelines, changes in water management or treatment, construction of covers, progressive recovery plan, and revegetation or reshaping of the tailing reservoir, landfills, or other structural elements.

The requirements of SEMAD and FEAM (2019) and ANM (2022) are similar to those of ICMM (2021) and Morrisson (2022) for ensuring the long-term physical and chemical stability of the tailing storage facilities and remaining materials as well as maintaining the monitoring and surveillance plans for the post-closure period until the effective restoration of the area (Post-Closure and Relinquishment).

The particularity of Brazilian legislation, compared to international technical guides, is outlined in Article 1 of ANM Resolution nº 130/2023, which establishes monitoring and follow-up stages for a minimum period of two years after the completion of decharacterization works (active monitoring) and an additional non-mandatory monitoring phase (passive monitoring), aiming to ensure the effectiveness of stabilization, hydrological, and hydrogeological control measures. According to the Terms of Reference, the dam will be considered decommissioned after the completion of decharacterization works, and the effectiveness of the measures will be evaluated through the monitoring of the maintenance and monitoring program (SEMAD and FEAM, 2019), as shown in Figure 1.

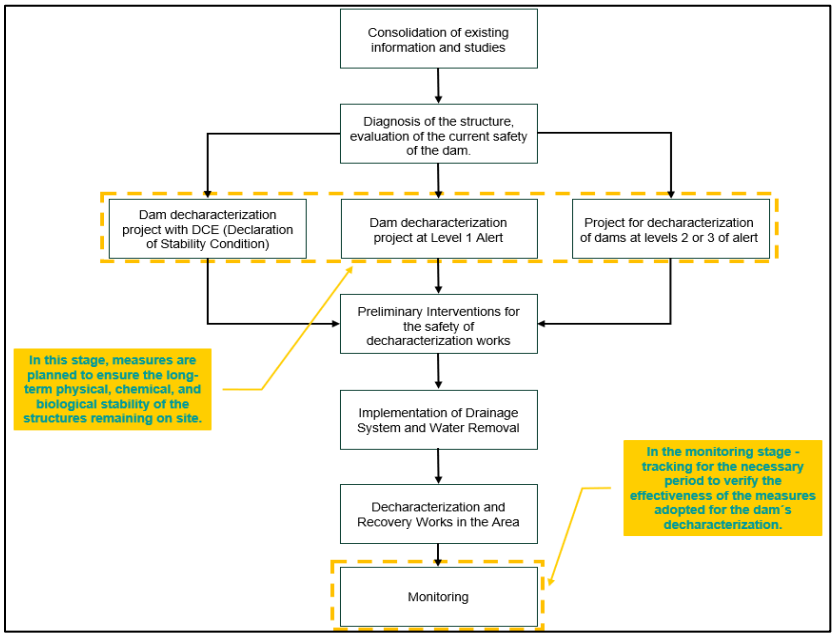


Figure 1: Synthesis of the decharacterization stages (modified from SEMAD and FEAM, 2019)

Tailings dam decharacterization project: water resources diagnostic and related impacts

Physical and chemical parameters should be monitored throughout all stages of a tailing dam decharacterization. A temporal representative data set would provide a better understanding of any changes in parameters, ensuring a good evaluation of the stability of the structure at the end of the process. The existing water monitoring network of the operating dam should be maintained and reviewed to encompass the modifications required in the decharacterization works stage and adapted for the active monitoring stage. A revision of the water resources monitoring plan is fundamental to incorporate all the probable or predicted impacts on surface and groundwater from the decharacterization works. Understanding hydrodynamic and chemical aspects concerning surface and groundwater resources, along with predicted impacts throughout operational and post-decharacterization phases, is crucial for developing or adapting the monitoring plan.

In Brazil, the Foundation for Technological Development of Engineering, State of Minas Gerais (Neri et al., 2021), conducted a study on the socio-environmental impacts associated with the decharacterization of tailings dams. The report presents a standardized list of activities involved in the decharacterization process, indicating potential socio-environmental impacts. Based on the practical examples in Neri et al. (2021) and the authors' expertise, the following potential impacts on water resources resulting from the implementation of tailings dam decharacterization projects are listed:

- Alteration of surface and/or groundwater dynamics.
- Increase or decrease in recharge areas.
- Landfilling of discharge areas and suppression of springs.
- Alteration (reduction or increase) of local or regional water availability.
- Reduction or increase in base flow rates of watercourses.
- Contamination of surface and groundwater resources.
- Alteration of surface and groundwater quality.
- Generation of acid drainage.
- Sedimentation of watercourses.

Regarding surface water resources, the impacts predicted during decharacterization works mainly affect the watercourses downstream of the worksites. Interventions imply the possibility of sediment input and other forms of degradation and pollution, intervention in areas of permanent preservation, diversion of watercourses, basin transposition, and construction of downstream containment dams. Given these possibilities, the surface water monitoring network during and after the decharacterization works should encompass the downstream watercourses where there will be direct interference with the project,

considering the impact as effective in these locations. However, there is also a need to monitor the watercourses in areas of indirect influence.

In numerous tailings dam decharacterization projects, lowering the groundwater level becomes necessary. This can be achieved by installing pumping wells or constructing structures like sumps and trenches within the tailing reservoirs. Such measures have the potential to significantly impact local hydrodynamic conditions.

It is important to conduct the diagnosis of the surface and groundwater resources, sediments, and soils within the area undergoing decharacterization efforts. Similarly, it is crucial to assess the potential impacts on these matrices. This ensures a comprehensive understanding and effective management of environmental impacts. This is a fundamental predecessor activity that will support an effective monitoring plan, guiding the optimal placement of monitoring points, parameters, and sampling frequencies. The monitoring plan should consider the specificities of each location. To support the development of a specific plan for the area subject to decharacterization interventions, this work proposes some minimum requirements necessary to assess changes in the monitored parameters. Implementation of a comprehensive monitoring program that collects both spatially and temporally representative data will effectively confirm the physical and chemical stability necessary for the decharacterization of a tailings dam.

Decharacterization baseline and background establishment

The decharacterization baseline refers to the condition and quality of the matrices (surface water, groundwater, soil, and sediments) prior to the implementation of the decharacterization works. The term background will be used to indicate the natural status of the matrices (hydrogeochemical and geochemical characterization) prior to the presence of the mining, without anthropic influence.

For baseline and background establishment these things are necessary:

- Representative locations for sampling each matrix considering the geological aspects and types of soil.
- Technical and statistical criteria for defining the number of observation points (location distribution).
- Sufficient and representative temporal data collection at each observation point.
- Technical and statistics methodology for data analysis.

Acquired monitoring data will provide support to evaluate and compare matrices characteristics in the pre-works stages, supporting measures to mitigate or remediate identified impacts. A robust historical data series of qualitative and quantitative data is necessary information for supporting the analysis of the hydrodynamic and chemical stability of the remaining structure.

Hydrogeological model

An effective surface and groundwater resources monitoring network should be supported by a conceptual hydrogeological model. Hydrogeological models are approximate representations of the natural environment. They are essential for the assessment and refinement of the water resources monitoring plan during decharacterization. Hydrogeological models integrate and synthesize all hydrogeological and relevant information, providing a systematic and comprehensive understanding of the site conditions. Although they are necessary for all stages of the decharacterization process, they are crucial for environmental purposes in the planning and post-works phases. During the planning phase, the hydrogeological model supports decisions on selecting the best methods for carrying out the decharacterization project and works, aiming to reduce impacts on water resources. At the post-works decharacterization stage, the models are fundamental to supporting the analysis of the physical and chemical stability of the remaining structure.

Numerical models can be applied to predict future groundwater and surface water qualitative and quantitative impacts. The continuous monitoring of hydrodynamic parameters (flow rate, groundwater level, hydraulic head, and water level in reservoirs) and water quality parameters provides new information to improve conceptual and numerical models. Consequently, a better representative model contributes to improving the monitoring network, facilitating a comprehensive assessment of the hydrodynamic and chemical stability site condition.

Water monitoring plan

The establishment of a water monitoring plan is intended to meet the decharacterization project's objective of verifying the maintenance of hydrodynamic and chemical stability by the structure undergoing decharacterization. Monitoring will allow for the evaluation of the effectiveness of the engineering actions employed in controlling the release of chemical load from the tailings to water resources. To this end, the plan must fulfill minimum requirements, such as:

- Monitoring network for surface water, groundwater, and effluents.
- Parameters monitored.
- Sampling frequency.
- Sampling and analysis methodologies.
- Data quality management procedures.
- Criteria and methodologies for data interpretation.
- Corrective actions.

Matrices analyzed

The selection of the matrices to be analyzed is intended for the evaluation of the effectiveness of the decharacterization measures adopted to reduce water input to the structure's reservoir and protect water resources. It is necessary to monitor:

- Effluents from surface water drainage captured by the dam's hydraulic structures and reservoir (including main and peripheral drainage channels and berm channels).
- Effluents originating from water percolating through the reservoir, captured by the structure's intermediate and deep internal drains.
- Effluents entering and exiting treatment systems.
- Surface waters potentially receiving drained effluents from intervened structures.
- Groundwaters potentially receiving drained effluents from the structure.

Monitoring network

To meet hydrodynamic and hydrological criteria, the monitoring plan should include strategically located monitoring points. These points will measure flow rates in watercourses and surface drainage systems, flow rates in bottom drains of dam or reinforcement structures, water levels in reservoirs, groundwater levels, hydraulic heads, flow rates in lowering wells, and flow rates in drainage systems such as trenches and sumps. Additionally, the plan should incorporate monitoring points for climatic conditions like precipitation and evaporation, although these will not be extensively covered in this work.

The monitoring network should be defined for surface water, groundwater and effluents, aiming to obtain data for the remaining structural stability assessments. It is important that the quality monitoring plan is accompanied by flow rate and water level monitoring, to provide data for an integrated analysis.

For effluents generated by the drainage of surface waters and waters that percolate through the tailings, the sampling grid should consider the discharge points of these drains, in locations where there is sufficient turbulence to ensure mixing and the consequent representativeness of the effluent to be sampled. Entry and discharge points of treatment systems, if they exist, should also be included in the effluent monitoring network (CETESB and ANA, 2023).

To define the sampling network for surface and groundwater, it is necessary to identify the watercourses and aquifer systems that may be impacted by the implementation of the decharacterization project. The basis for developing the monitoring plan and the sampling network for the different matrices should be the diagnosis of the physical environment (water, soil, morphology, hydrography, hydrogeology, and geology), the prognosis of impacts, and the hydrogeological model. Once the extent of the area to be monitored is defined, the sampling network should include points upstream and downstream of the structure undergoing decharacterization.

Regarding surface waters, the location of the points should also consider the presence of tributaries and the existence of liquid effluent discharges along the monitored water body, independent of whether they originate from the structure's drainage or not. The assessment of the variation in surface water quality should include points located before and after complete mixing with the discharged effluents and at the mouth of the tributaries. Sampling at different depths should also be considered (CETESB and ANA, 2023).

For groundwater, it is important that the monitoring network is supported by the hydrogeological model. The upstream and downstream points should be positioned according to the direction of groundwater flow. The monitoring wells must have their filter sections positioned to monitor the hydrogeological unit and the aquifer system under evaluation. Therefore, the number of points and their locations will depend on the characterization of the hydrogeological units and the aquifer systems (fractured, granular, or karstic) and the specificities of the site, such as the presence of faults and fractures, layer structuring, and topography, always using monitoring data to delineate the potentiometric map and the direction of the main groundwater flows. To comply with Brazilian technical standards, NBR 13896:1997, from the Brazilian Association of Technical Standards (ABNT), recommends that the monitoring well system must consist of at least four wells, one upstream and three downstream in the direction of preferential flow of the water table. The presence of springs and active wells for water extraction and groundwater lowering should also be considered.

Monitored parameters

The selection of the parameters to be monitored should consider the physical-chemical, chemical, and mineralogical characterization of the tailings contained within the structure, as well as the porewater present in the interstices of this material. In addition to the constituents identified in these matrices (tailing and pore water), the selection of parameters should also consider the analysis of:

- The same parameters in all monitored matrices in the site, such as sediments, tailings, soil, and water, to identify tracer elements.
- All major anions and cations, as well as relevant trace metals in both their total and dissolved fractions.
- Volatile and semi-volatile organic compounds.
- Substances covered by reference legislation.
- Chemical compounds used for blasting and during the mineral beneficiation process, as well as their byproducts and residual products.

Initially, a list of parameters that is broad and inclusive should be considered. However, this can be reduced after a year of monthly data has been collected, as it may be determined that some parameters are nonessential.

Sampling frequency

The sampling frequency should be defined based on the minimum amount of data and the time needed to evaluate the chemical stability of the structure undergoing decharacterization. Helsel et al. (2020) and APHA et al. (2023) present statistical calculations for defining the sample size, while Barnett (2022) presents a minimum estimate of 15 samples when using non-parametric methods for the statistical analysis of data and ten samples when using parametric methods. Regarding time, the Terms of Reference (SEMAD and FEAM, 2019) appropriately do not define a minimum period, allowing flexibility in response to specific project conditions, while ANM Resolution nº 130/2023 establishes a minimum period of two years after the completion of works to ensure the effectiveness of stabilization measures. Based on a minimum of 15 observations (since environmental variables are characterized by not having a normal distribution) and a minimum monitoring period of 2 years, it is recommended that surface water, groundwater, and effluent collection and analysis be conducted at least monthly frequency during the active monitoring period. Based on the evaluation of the results, the initially proposed frequency can be reviewed after a one-year data collection period.

Sampling and analysis methodologies

In Brazil, laboratories responsible for water and effluent sampling and chemical analysis must be accredited according to the Brazilian standard ABNT NBR ISO/IEC 17025:2005. Samplers and procedures for collecting, preserving, conditioning, transporting, and storing samples must be described in the monitoring plan and are based on the National Guide for Sample Collection and Preservation (CETESB and ANA, 2023). Analysis methods must also be specified in the plan and must follow the indications of the Standard Methods for the Examination of Water and Wastewater (SMWW) (APHA et al., 2023) and/or the U.S. Environmental Protection Agency (U.S. EPA). Specifically for the quantification limits of analytical methods, the ABNT NBR 16435:2015 standard establishes that these must be equal to or lower than the applicable legal values established by the environmental agencies, and, in the absence of national standards, international reference standards can be adopted.

Data quality management

To ensure data quality and reliability, the water resource monitoring plan should incorporate control samples. These samples are essential to maintain sampling procedure quality and trace any potential errors or contaminations. According to the National Guide for Sample Collection and Preservation (CETESB and ANA, 2023), recommended control samples include duplicates, field blanks, equipment blanks, transport blanks, reagent blanks, syringe and filter blanks, reagent water blanks, and temperature control during transport. These measures help maintain the integrity and accuracy of collected data.

The guide recommends that control samples represent between 5 and 10% of the total number of samples, except for transport temperature control, which should be used for all sample transport requiring refrigeration. For duplicate samples, the suggestion is to distribute the collections according to the diversity of sampling situations, such as the type of environment, matrix, collection strategy, and order of magnitude of the chemical substances of interest. Relative percentage differences (RPD) of up to 20% are acceptable between the results of duplicates and samples.

To guarantee the quality of analytical procedures in the laboratory, the implementation of method blanks, laboratory duplicates, spiked matrix, spiked matrix duplicate, and spiked blank should be planned (INMETRO, 2018; APHA et al., 2023). A control sample should be analyzed for every 20 samples.

All control procedures and data must be stored in a secure digital environment, and it is desirable to make use of cloud-based technologies.

Data interpretation

A methodological proposal for data analysis and interpretation should also be included in the water monitoring plan. For comparing the upstream data group with each of the downstream data groups, a minimum proposal should initially consider the evaluation of the normality of the variables distribution and the selection of parametric or non-parametric hypothesis tests, depending on the result of the normality tests. To evaluate the trend of variation in the concentrations of the analyzed compounds over time, a trend test and a linear regression model can be used (Helsel et al., 2020). It is also advisable to consider the use of advanced multivariate techniques, including advanced analytic methodologies such as machine learning.

Surface water results in relation to historical data can be evaluated using the hypothesis tests mentioned above. For groundwater, Barnett (2022) recommends defining a baseline through the calculation of the 95% Upper Confidence Level (UCL).

Corrective actions

Corrective actions and measures should be included in the monitoring plan to mitigate potential alterations in water and effluent quality related to the chemical instability of the structure. Measures to reduce the input of surface and groundwater to the landfill, systems for treating effluents from drainage and surface waters, and groundwater remediation actions should be described in the plan.

Conclusion

The decharacterization of tailings dams requires rigorous monitoring of surface water, groundwater, and effluents to ensure the physical and chemical stability of the structure and surroundings. The proposed water resources monitoring plan includes the following main topics: the representative distribution of sampling

points for chemical analysis and hydrodynamic data; monitoring of flows and water levels; the definition of the monitored parameters; the sampling frequency for assessing the chemical characteristics of water; data management procedures; and corrective actions. The monitoring plan also incorporated considerations regarding the methodologies for collecting and analyzing samples and data quality management, ensuring accurate and reliable results. The proposed items are supported by the definition of a baseline or background, the physical environment diagnosis, the assessment and prognosis of qualitative and quantitative impacts, and the hydrogeological model development.

It is noteworthy that the proposed water monitoring plan was based on the principle of meeting the decharacterization projects' objectives regarding the verification of hydrodynamic and chemical stability maintenance for the structures, adhering to the recommendations of Brazilian state and federal legislation and regulations.

The application of these minimum requirements in future tailings dam decharacterization projects is important to ensure environmental safety and public health in a structured and trackable way, reducing the risks of water contamination and guaranteeing the stability of the remaining structures.

References

Agência Nacional de Mineração (ANM). 2022. *Resolução Nº 95, de 07 de fevereiro de 2022*. Brasília, DF, Brazil.

Agência Nacional de Mineração (ANM). 2023. *Resolução Nº 130, de 24 de fevereiro de 2023*. Brasília, DF, Brazil.

Agência Nacional de Mineração (ANM). 2024. *Resolução Nº 175, de 01 de agosto de 2024*. Brasília, DF, Brazil.

American Public Health Association (APHA), American Water Works Association (AWWA), and Water Environment Federation (WEF). 2023. *Standard Methods for the Examination of Water and Wastewater*. 24th ed. Washington, D.C.: APHA Press.

Associação Brasileira de Normas Técnicas (ABNT). 1997. ABNT – NBR 13896: *Aterros de Resíduos Não Perigosos – Critérios para Projeto, Implantação e Operação*. Rio de Janeiro, Brazil.

Associação Brasileira de Normas Técnicas (ABNT). 2005. ABNT – NBR ISO/IEC 17025: *Requisitos Gerais para a Competência de Laboratórios de Ensaio e Calibração*. Rio de Janeiro, Brazil.

Associação Brasileira de Normas Técnicas (ABNT). 2015. ABNT – NBR 16435: *Controle da Qualidade na Amostragem para Fins de Investigação de Áreas Contaminadas – Procedimento*. Rio de Janeiro, Brazil.

Associação Brasileira de Normas Técnicas (ABNT). 2017. ABNT – NBR 13028: *Mineração – Elaboração e Apresentação de Projeto de Barragens para Disposição de Rejeitos, Contenção de Sedimentos e Reservação de Água – Requisitos*. Rio de Janeiro, Brazil.

Barnett, F. 2022. ProUCL Version 5.2.0 User Guide. *Statistical Software for Environmental Applications for Data Sets with and without Nondetect Observations*. Accessed 6/26/2024 at: https://cfpub.epa.gov/si/si_public_file_download.cfm?p_download_id=544823andLab=CESER.

Companhia Ambiental do Estado de São Paulo (CETESB) and Agência Nacional de Águas e Saneamento Básico (ANA). 2023. *Guia Nacional de Coleta e Preservação de Amostras: Água, Sedimento, Comunidades Aquáticas e Efluentes Líquidos.* 2nd ed. São Paulo: CETESB; Brasília: ANA.

Environment Canada. 2012. *Metal Mining Technical Guidance for Environmental Effects Monitoring*. Accessed 6/26/2024 at: https://publications.gc.ca/collections/collection_2012/ec/En14-61-2012-eng.pdf.

Helsel, D.R., Hirsch, R.M., Ryberg, K.R., Archfield, S.A. and Gilroy, E.J. 2020. *Statistical Methods in Water Resources*. In: U.S. Geological Survey Techniques and Methods, book 4, chap. A3. Reston, VA: USGS.

Instituto Nacional de Metrologia, Qualidade e Tecnologia (INMETRO). 2018. Norma Nº NIT-DICLA-057 Rev. 04: *Critérios para Acreditação da Amostragem para Ensaios de Águas e Matrizes Ambientais*. Rio de Janeiro, Brazil.

International Council on Mining and Metals (ICMM). 2021. *Tailings Management: Good Practice Guide*. London: ICMM. Accessed 6/26/2024 at: https://www.icmm.com/en-gb/guidance/environmental-stewardship/tailings-management-good-practice.

Morrison, K.F. 2022. *Tailings Management Handbook: A LifeCycle Approach*. Society for Mining, Metallurgy and Exploration (SME).

Neri, A.C., Sánchez, L.E., Alves, C.F.C., Dupin, P.C., Silva-Sánchez, S.S., Baeta, A.M., Modesto, A., Christofolletti, C., Cunha, C.B., Tanikawa, D.H., Piló, H., Yoshizaki, H., Bessa Júnior, J.E., Bezerra, J.S.B., Sanchez, J., Dias, L.G., Souza, L.T.M., Santos, M.R.G., Borghieri, M.G., Ferracini, M., Massignan, R.S. and V.L. Monteiro. 2021. *Avaliação Ambiental Integrada das Obras de Descaracterização das Barragens de Rejeitos Alteadas pelo Método a Montante no Estado de Minas Gerais*. Volume 1. São Paulo: Fundação para o Desenvolvimento Tecnológico da Engenharia (FDTE). Accessed 6/24/2024 at http://www.feam.br/avaliacao-ambiental-e-gestao-do-territorio/-avaliacao-ambiental-integrada-aai-das-obras-de-descaracterizacao-de-barragens-alteadas-pelo-metodo-a-montante-no-estado-de-minas-gerais.

Sánchez, L.E., Silva-Sánchez, S.S. and Neri, A.C. 2013. *Guia de Planejamento do Fechamento de Mina*. Brasília: Instituto Brasileiro de Mineração. Accessed 6/25/2024 at: https://ibram.org.br/wp-content/uploads/2021/02/00004091.pdf.

Secretaria de Estado de Meio Ambiente e Desenvolvimento Sustentável (SEMAD) and Fundação Estadual do Meio Ambiente (FEAM). 2019. *Resolução Conjunta Nº 2.784, de 21 de março de 2019*.

Boodarie Tailings Storage Facility – Our Journey to Closure

Nathalia Revelo Mendez, BHP, Australia
Daniel Meunier, BHP, Australia
Darren Springer, BHP, Australia
Bria Whiter, BHP, Australia
Simon Harris, BHP, Australia

Abstract

BHP is committed to working with the International Council on Mining and Metals (ICMM) and other organizations to pursue improvements in global tailings management practices, including the Global Industry Standard on Tailings Management (GISTM).

Keeping the people and communities where BHP operates safe is of the upmost importance, and it is for this reason that BHP is continuously looking for ways to reduce or eliminate hazards and adopt the best practice standards in our operations. For this reason, tailings dam failure has been classified as a material risk for the business, requiring the strictest governance, maintenance, risk management, and operational standards to be applied, with appropriate training of operators to understand the risks and how are we affecting or protecting the community and the world with our day-to-day operations.

BHP ceased operation of the Boodarie hot briquet iron (HBI) facility (located 8.5 kilometers south-west of Finucane Island in Port Headland, Western Australia) over 10 years ago, but the 200-hectare tailings facility was not rehabilitated at that time. In 2020 a project to convert the tailings facility to a free-draining landform was started. By early 2023 all credible dam failure modes have been removed and the residual storage impoundment (RSI) no longer constitutes a dam under the GISTM, meaning that the facility does not meet the GISTM definition of a dam anymore, but is still on its journey to closure. The facility is now on a pathway to declassification as a dam by the regulator of the Department of Mines, Industry Regulation and Safety of Western Australia (DMIRS).

The closure journey for the Boodarie tailings storage facility has taught us valuable lessons and ways to accelerate the reduction of dam-related risks, ensuring a safe, efficient, and value-adding exercise, while also achieving social value outcomes through the involvement of traditional-owner contracting companies in the execution of the rehabilitation work. This paper seeks to share engineering, governance, risk

management, environmental, and community engagement lessons for consideration by other mining companies planning to, or already on, the journey to rehabilitation of their tailing facilities.

Introduction

BHP has been on a continuous improvement journey within the tailings management space, much like the entire tailings industry, since the 2010s. While BHP has always governed and monitored tailings storage facilities (TSFs) in line with applicable international and local standards, tailings management was managed at a business level, so each individual asset independently managed identification, assessment, and management of risk for their tailing's storage facilities. However, after the release of the 2013 CDA guidelines and a series of industry failures in the early 2010s, BHP began to take a more holistic, business-wide approach to tailings.

The first step in this process was to undertake dam risk reviews for all known TSFs across the business. A BHP Global Tailings Practice Lead position was created, and Tailings Review Boards were introduced. Engineer of Record (EoR) and Responsible Dam Engineer roles were formalized and embedded for each facility. A tailings working group was also established so that all personnel involved in the management of tailings across BHP were given the opportunity to regularly share learnings and new developments.

In 2020, BHP established global, mandatory minimum performance requirements for tailings and water storage facilities through the development of Our Requirements (OR) for water and tailings storage facilities. The OR also established requirements around second-line assurance review requirements for high priority TSFs, which was later cascaded to all TSFs. More recently, BHP has committed to the implementation of GISTM across our assets, prioritizing very high and extreme facilities for first rollout.

For BHP's Western Australian Iron Ore (WAIO) operations, this improvement journey has allowed for iterative review of TSFs with each improvement. It was through this continuous review against the developing standards that it was identified that while most of the tailings stored within the facility had been removed for reprocessing, the inactive Boodarie residual storage impoundment (RSI) still met the definition of a TSF.

As a result of this classification the facility was extensively reviewed and re-assessed in accordance with Our Requirements, which led to the decision to rehabilitate the facility to reduce the ongoing risks associated with it. The intent of this paper is to share the learnings of BHP's journey towards closure and the subsequent reclassification of the Boodarie RSI from a TSF to a landscaped tailings profile.

Background

The Boodarie RSI was an inactive iron ore TSF located approximately 8.5 kilometers southwest of Port Headland (see Figure 1). The facility was constructed in 1995 to store waste from the now largely decommissioned and demolished Boodarie HBI facility.



Figure 1: Location of Boodarie RSI

The upstream raised TSF and associated infrastructure covered an area of approximately 200 hectares and operated from 1999 to 2004, with deposition of the non-acid forming iron ore tailings through a central discharge point. During its operational life it was raised twice, with a final embankment height of nine meters. The facility was not operated for the full design life due a significant plant fire that halted production; as a result, the tailings did not cover the full surface of the footprint.

Planning for decommissioning of the Boodarie hot briquet iron (HBI) site began in 2004. Capping of the TSF residue was completed in 2008, using reject material from the beneficiation plant to control fugitive

dust from the TSF surface. During further decommissioning planning, an opportunity was identified to sell the iron ore tailings as a commercial product. Over 4.3 million tonnes of iron ore tailings were excavated and hauled out of the facility for sale from 2010 to 2012. This significantly reduced the facility's risk of loss of tailings containment. However, approximately 330,000 m^3 of tailings were still stored within the impoundment.

Final plant decommissioning was completed shortly thereafter. The RSI was put into care and maintenance, managed by operational teams from BHP's Port Headland operations. As part of WAIO's continuous improvement tailing journey, the facility was risk reviewed several times against the tightening management criteria. During these reviews it was identified that there was a potential overtopping risk associated with rare extreme weather events, which might result in a water build-up leading to potential credible dam failure modes. This risk was outside of BHP's business risk appetite, even though no such significant events had been observed during the TSF's life.

As a result, a rehabilitation project was initiated in 2020 with the aim of converting the Boodarie RSI to a free-draining landform and removing all credible dam failure modes.

Defining clear objectives

To ensure the success of the project it was very important to have a clear understanding of what the regulators required, what the company required, and most of all, what would be the best outcome for the community in which BHP operates.

The key drivers for undertaking the Boodarie RSI Tailings Dam Rehabilitation Project were:

- Risk mitigation – removing outside of business appetite risks.
- Meeting our requirements – upholding BHP's regulatory obligations.
- Upskilling Indigenous communities.

As closure is a long process and has different interpretations across the globe and even within the Pilbara mining industry, depending on the facility and the most recent guideline, BHP decided that the primary objectives for the RSI closure would be removing all critical failure modes and building a useful landform for future use.

BHP acknowledges that removal of all failure modes is not possible for all facilities; however, reducing the number of failure modes, considering the operating environment, community, and regulatory requirements, and risk mitigation, should all be part of the decision-making process for defining the closure stage of the facility.

The closure solution

The preliminary concept for the closure solution was to encapsulate the existing in-situ tailings material within the existing embankment material, aiming to create a natural-looking, free-draining landform. After the project initiation in 2020, a study team reviewed alternative options considering the knowledge base, gap-closing activities, and regulatory, stakeholder, and corporate commitments. As part of these activities, stakeholder engagement was undertaken with the Western Australian regulators to understand their requirements. While there was support for the initial concept, further studies indicated that there were elevated erosion risks associated with the design.

The project was progressed through BHP's project phases and design optimization continued, which resulted in a final design solution that differed from the concept design. This solution would return the site to near original topography, while reducing the risk of erosion.

The execution works commenced in 2022, with a local Indigenous civil contractor engaged to complete the works. Onsite quality assurance and quality control (QA/QC) was completed by the engineering design consultants to ensure compliance with the design. Given the low volumes of tailings within the facility, the project was able to remove all embankments, and relocate the remaining tailings residue into existing low embankment borrow areas on the facility. The tailings were then capped with an engineered cover and the land was reshaped to near original topography. The site was able to be seeded within the 2023 wet season window, using a locally harvested seed mix supplied by a local Indigenous vendor.

Upon completion of the works, the EoR and the Senior Independent Technical Reviewer (SITR) conducted a review of the project construction. This included all construction records that verified that all credible flow failure modes had been removed, that the encapsulated residue was chemically benign, and that the facility could be considered a landscaped tailings profile in accordance with BHP's tailings guidance.

Boodarie RSI TSF is now moving into the post-closure monitoring phase of its life cycle. The monitoring being conducted over the coming years is to confirm that the facility has successfully achieved the closure objectives and the defined completion criteria. The post-closure monitoring phase is expected to be completed over the next twenty years.

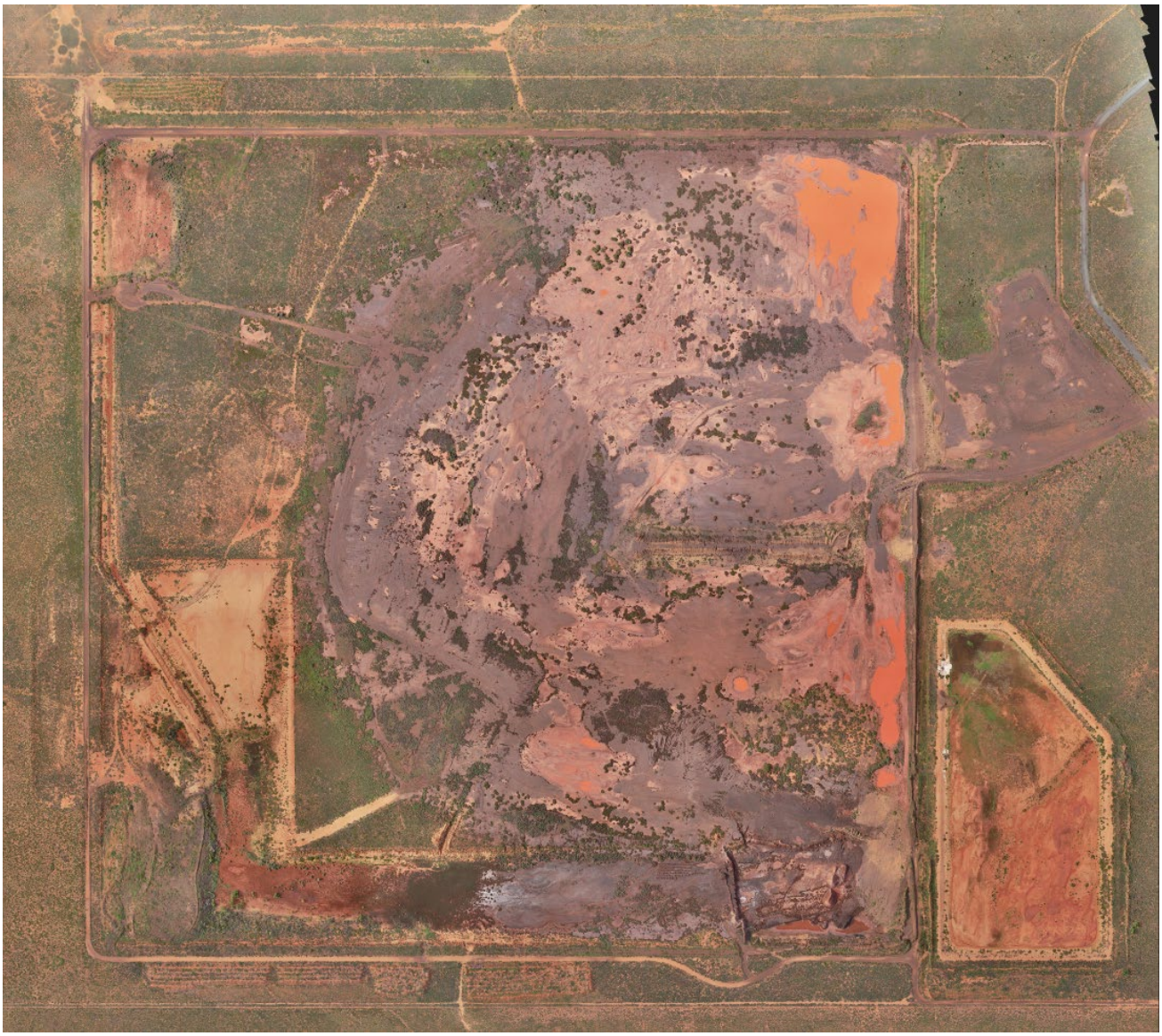


Figure 2: Boodarie RSI (aerial photo, 2019) – prior to final rehabilitation

Lessons learned

Governance matters

Through continuous improvement of BHP's tailings governance, we were able to utilize subject matter experts within the tailings industry to identify gaps or unappreciated risks associated with the Boodarie TSF. We consolidated a formal Tailings Centre of Excellence BHP-wide. This included technical subject matter experts (both internal and third party) and a Global BHP Tailings Practice Lead, as well as other TSF-related roles such as EoR, Responsible Tailings Dam engineer, dam owners, and various governance

roles. This allowed BHP to clearly define requirements for water and tailings storage facilities management to ensure that tailings management is prioritized at all levels through the business. These supports and frameworks allowed WAIO to successfully remove a TSF from our portfolio and reduce the risk to BHP's business.

Hidden opportunities

Changing the identification of a previously designated waste material to a saleable material added value to the business in a number of ways. There was a cost benefit as a result of the sale, and the removal of 4.3 million tonnes of tailings significantly reduced the facility's risk of loss of containment. Moreover, the reduction of material allowed for a modified design that reduced construction volumes and schedule times and also allowed for the successful removal of all credible geotechnical failure modes.

While the sale of tailings is not always feasible for other facilities, it is important to look for secondary use opportunities that can reduce the volumes of tailings material to be managed, in order to make closure easier.

Reclassification to a landscaped tailings profile

Through the removal of the RSI embankments and critical failure modes, BHP was able to successfully remove one TSF from the global portfolio. While there is still an erosion risk for the landscaped profile, it was important to define suitable tolerance levels to ensure that it does not constitute a critical failure mode. The project team successfully delivered the required engineering specifications (see Figure 3), which subsequently allowed for the reclassification of the facility from a TSF to a landscaped tailings profile (see Figure 4).

Community involvement

BHP saw the execution of the closure project as an opportunity to engage a traditional owner company, so as to benefit BHP and the community. The main execution activities were bulk earthworks. However, due to the complexity of being a TSF, higher levels of QA/QC than standard civil rehabilitation projects were required. During the tendering process, BHP aimed to find a suitable civil contracting company with the right expertise to partner with to deliver this technical closure project.

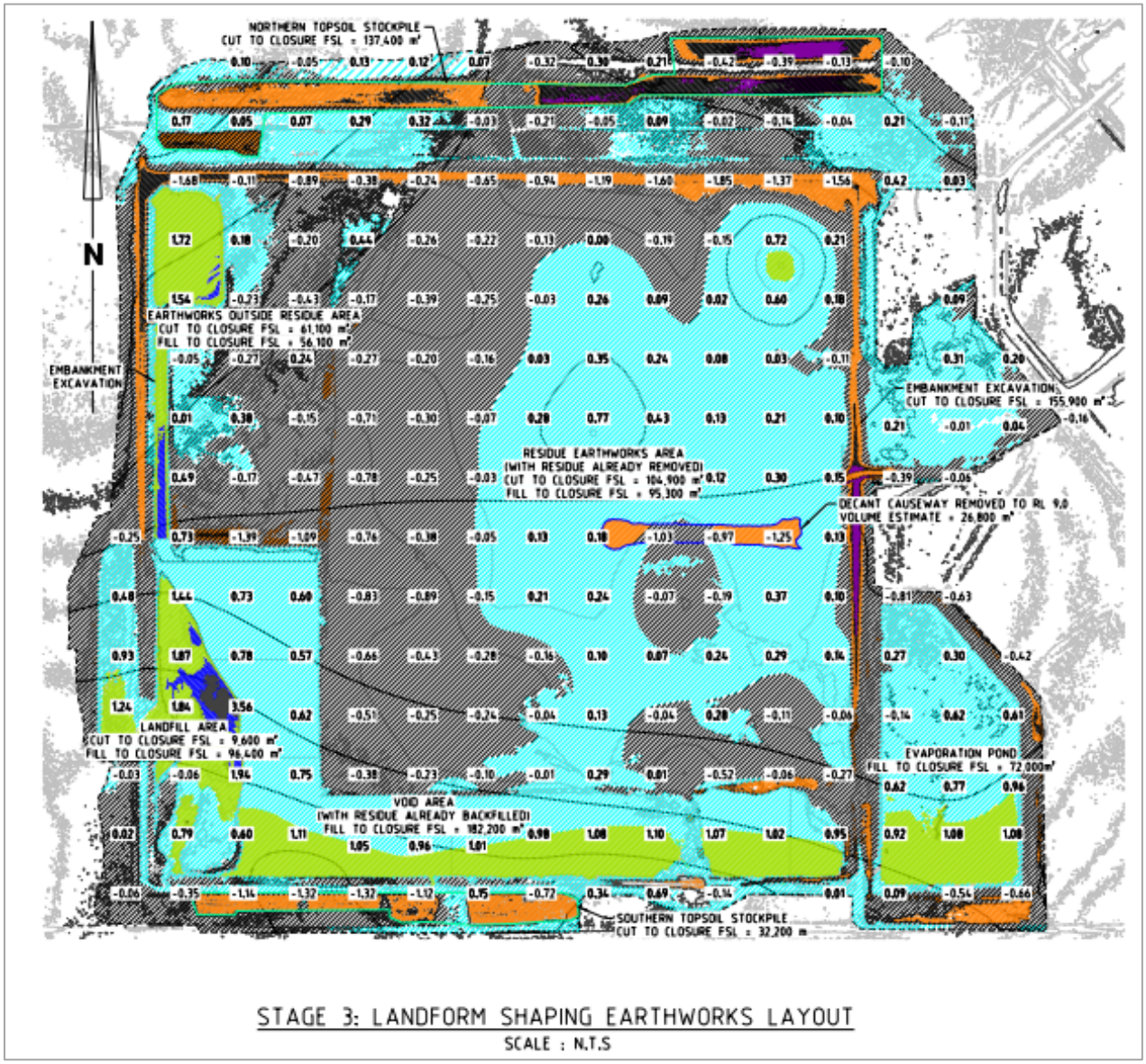


Figure 3: Closure design – landform shaping requirements

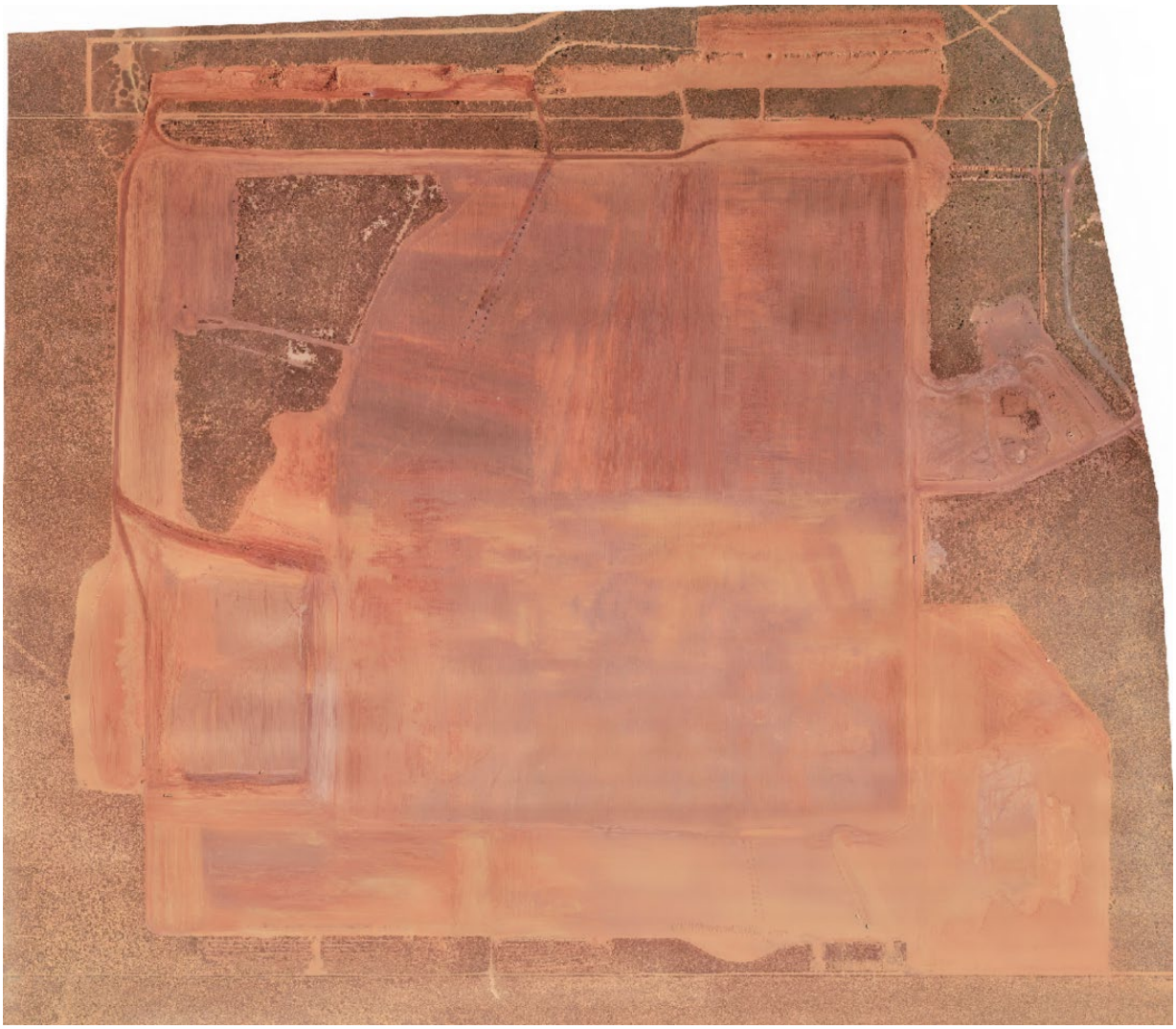


Figure 4: Aerial view of the completed closure works (2023)

The contract was awarded to a 100% Indigenous-owned company, with 48% Indigenous people participation in the project work force. For the BHP WA Asset Projects (WAAP) group, it was the largest direct engagement with a 100% Indigenous-owned company to date.



Figure 5: Indigenous company employees performing a field leadership activity

The contracting company was able to bring its experience to the project, optimizing execution plans and methods that resulted in delivery of the decommissioning and rehabilitation works ahead of both schedule and budget. This engagement and project performance showcased the collaborative work that can be achieved through the development of Indigenous partnerships. This will help to empower Indigenous contractors and communities to thrive under future economic and environmental conditions.

Conclusions and recommendations

We are stronger if we are together. By sharing the recommendations below, which worked for WAIO, BHP wishes to help to reduce the risks that TSFs pose to communities in their project areas.

- Take advantage of low-complexity projects, so that your company can engage, train, and create value for traditional owners and communities in your project areas.
- Ensure all TSFs are managed with the highest governance to ensure alignment to GISTM, so as to reduce risks.
- Evaluate tailings and assess if there is a potential use. Tailings can be reprocessed and used for many of the wonderful things that minerals do for the world.
- Determine whether there is an unidentified value stream that can reduce the closure impacts of a project.

- Aim to remove all critical failure modes, because by not having them, the facility will not pose a major risk to the community.
- Aim to declassify the facility, so that all TSF-related governance and GISTM requirements are removed, resulting in cost savings in operational expenses.
- Aim to have good relationships with closure experts, dam owners, governance teams, operators, and environmental departments. This will make everyone's lives easier and contribute to outstanding results.
- Aim to involve traditional owners. As well as removing the risk, a significant value for the community was achieved by the involvement of a traditional owner who owned a civil earth works company. The project had 48% Indigenous people representation in the workforce.
- Aim for a correct management of change process. This will help to remove all ongoing operational and group risk control requirements for the facility, which will result in great cost savings too.
- Share your experience and get in contact with anyone with your same objective. It is likely that someone in the industry has already done it and can guide you during your journey.

Acknowledgements

We wish to thank BHP and the project team for allowing us to publish these valuable lessons that can assist our industry as a whole. We also wish to thank the Indigenous contractor for allowing us to involve them in our project and for their willingness to learn and grow in the industry.

Chapter Seven

Design

TAILINGS AND
MINE WASTE 2024



Lessons Learnt by Applying a Risk-based Approach to Tailings Storage Facilities

Peter Chapman, WSP Australia Pty Ltd, Australia
Scott Gover, WSP Australia Pty Ltd, Australia
Jordan Ribbons, WSP Australia Pty Ltd, Australia

Abstract

The transition from standards-based design to risk-informed design has been discussed in industry for many years, but only implemented on a select basis, usually where more certainty is required to support capital investment for risk mitigation measures. However, the use of risk-based design has recently been accelerated as the industry undertook the initial round of reviews in the context of the Global Industry Standard on Tailings Management and incorporated Environmental, Social and Governance aspects in the journey towards responsible mining.

Many owners have been undertaking portfolio-based quantitative risk assessments to support assessments of whether the concept of "As Low as Reasonably Practicable" has been met. This process has highlighted both the benefits of risk-based approaches as well as the inherent flaws in standards-based engineering, particularly where there are high loss of life consequences.

This paper presents selected outcomes of quantitative risk assessments undertaken across 16 tailings storage facilities for multiple owners and multiple commodities. The assessments were undertaken across tailings storage facilities with constructions techniques, across a variety of countries and climatic zones, and considering both active and inactive (legacy) facilities. The key outcomes are presented in the form of risk-driving failure modes, considering both the probability of failure and the estimated consequences (usually potential loss of life), as well as the likelihood of the causes occurring (that is, excluding intervention and progression). By considering both views, the result can be used to identify the systematic deficiencies in design that indicate that standards-based approaches are not sufficient to manage high consequence TSFs, resulting in an over-reliance on identifying and rapidly addressing issues that evolve during operations.

Introduction

The transition from standards-based design to risk-informed design has been discussed in industry for many years, but only implemented on a select basis, usually where more certainty is required to support capital investment for risk mitigation measures. However, the use of risk-based design has recently been accelerated as the industry undertook the initial round of reviews in the context of the Global Industry Standard on Tailings Management (GISTM) and incorporated Environmental, Social and Governance aspects in the journey towards responsible mining.

This paper presents selected outcomes of quantitative risk assessments undertaken across 16 tailings storage facilities (TSFs) for multiple owners and multiple commodities. The assessments were undertaken across TSFs with varying constructions techniques, across a variety of countries and climatic zones, and considering both active and inactive (legacy) facilities. The key outcomes are presented in the form of risk-driving failure modes, considering both probability of failure (pF) and the estimated consequences (potential loss of life, PLL or N), as well as the pF of the causes occurring (that is, excluding intervention and progression). By considering both views, the result can be used to identify the systematic deficiencies in design that indicate that standards-based approaches are not sufficient to manage high consequence TSFs, resulting in an over-reliance on identifying and rapidly addressing issues that evolve during operations.

Risk-based design

As outlined in Chapman (2022), whilst the standards-based design approach appears to have been largely successful, it drives design behavior towards compliance rather than safety. Morgenstern, in his 2018 Victor De Mello lecture (Morgenstern, 2018), indicates that standards and guidelines are continuing to evolve. Chapman (2022) noted that the recent TSF failures, including Mt Polley, Samarco, Cadia and Feijão did not fail due to an extreme earthquake or rainfall event, but rather a series of undetected events that ultimately led to failure under "normal operating conditions." As noted in the relevant failure reports, the owners and operators of the facilities considered them to be compliant. This suggests that standards-based design, even with good governance, may have moved the industry significantly forward, but cannot support the next step in the TSF safety journey, towards zero catastrophic failures. It is in these circumstances that risk-informed design can provide a framework for additional risk management.

Morgenstern (2018) indicates that quantitative risk assessment (QRA) techniques have been shown to reduce risks over time, as demonstrated by the example of landslides in Hong Kong, provided there is sufficient information to support the assessment. Chapman and Williams (2019) show that a QRA can provide improved clarity and differentiation compared to more routinely adopted risk assessment approaches, particularly those that adopt a qualitative 5 × 5 matrix approach. The authors concluded that

the use of a QRA can demonstrate not only that the likelihood of catastrophic failure is lower (and also shows how low it is), but also provides the designer with information on the largest contributions to failure, allowing effective mitigation measures to be put in place. If a QRA approach is developed during the design stage, it can also be used as a decision-making tool during design and as a risk mitigation tool during operations.

The industry appears to be moving towards risk-informed design, and yet the process is not yet sufficiently accepted and implemented as a key tenet in TSF design. This paper provides a summary of a series of risk assessments completed across multiple owners and commodities on a variety of TSF construction types. The results highlight the marked difference between compliance and safety.

Approach to risk assessments

There are various ways to approach a QRA, with various levels of detail being applied in industry. The two most common approaches are fault trees and event trees.

Fault trees are logic diagrams based on the principle of multi-causality. They are used as a tool to analyze the potential for failure of an item or system using a top-down approach by tracing all branches of potential events that could contribute towards failure (or any undesirable top event). Fault trees use a series of "AND" gates (all contributing events need to occur) and "OR" gates (only one of the contributing events needs to occur) to graphically and mathematically estimate the probability of the top event occurring. A simple fault tree example, developed by the authors, is provided in Figure 1.

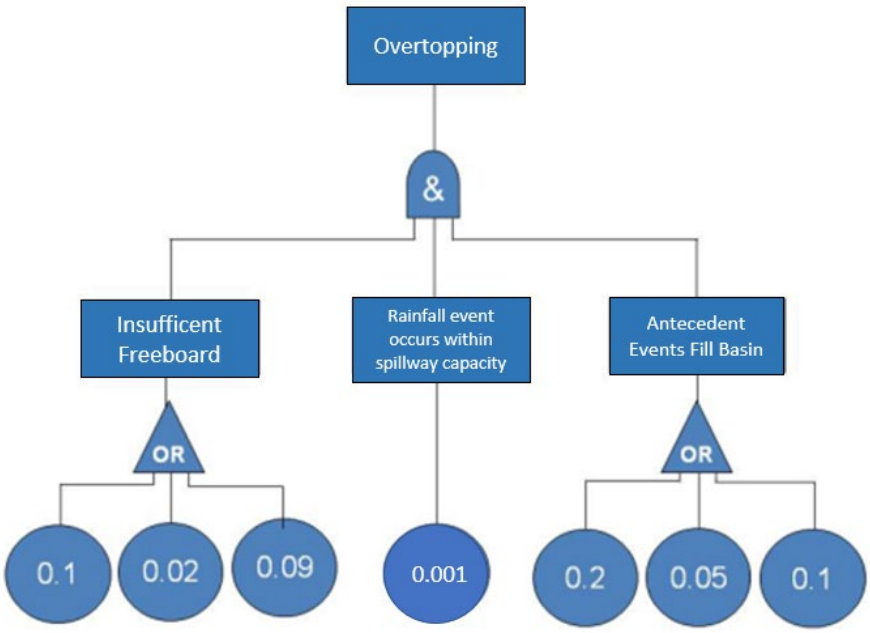


Figure 1: Fault tree example

Figure 1 demonstrates that insufficient freeboard AND a rainfall event occurring AND an antecedent event to fill the basin are required to contribute towards the top event of overtopping. At the next level down in the fault tree, the probability of a rainfall event occurring within the spillway capacity has been assigned a probability of 0.001 (1 in 1000), but insufficient freeboard and an antecedent event filling the basin could be made up of three different possible contributors that could occur independently of each other (OR gates), each with a different assigned probability.

An event tree analysis uses the same logic and mathematical techniques as a fault tree analysis. However, a fault tree considers how an undesirable top event may occur, whereas an event tree considers the impact of an event or failure occurring in a system, and subsequently works out the effect that such an event will have on the overall system risk or reliability. Event trees consist of an "initiating event" (and associated probability or frequency assigned to it), and a series of subsequent events with binary statements (yes/no, true/false etc.), each of which can be assigned a probability. A series of final outcomes can therefore be derived, each with a resulting probability of the particular outcome occurring. A hypothetical event tree example is presented as Figure 2.

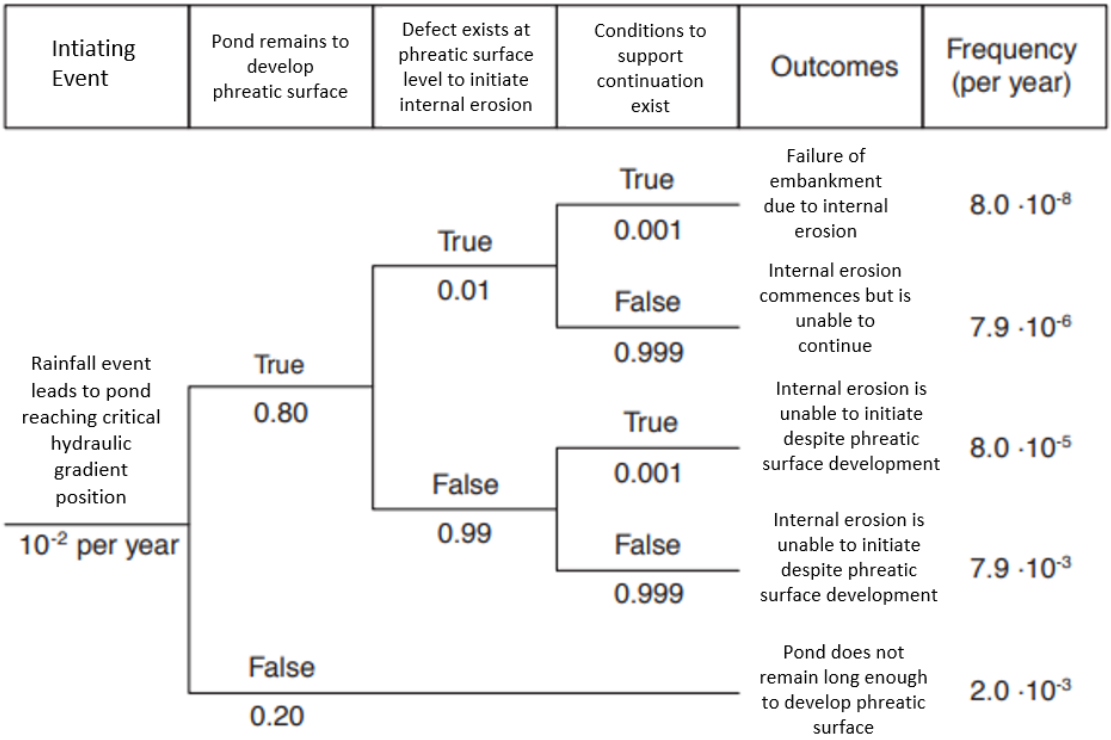


Figure 2: Event tree example

Figure 2 demonstrates that there is a 1×10^{-2} chance that an initiating event of rainfall event leading to the pond reaching the critical hydraulic gradient occurs per year. If the initiating event occurs, 80% of the time this will result the pond remaining long enough to develop a phreatic surface, of which there are

further conditions that need to be met in order for internal erosion leading to embankment failure to occur. These conditions are assigned a probability, which branch into a series of possible outcomes. The probability of each individual outcome can then be calculated (frequency/probability of initiating event × probability of each of the subsequent events).

As part of the preparation process for the QRAs undertaken, consideration was given to the approach to be adopted. A Microsoft Excel spreadsheet, primarily using an event tree logic approach adopting the "true" pathway, was adopted. A spreadsheet approach allows the Client ready access to the tool, in order to support future sensitivity analyses and updates if required, noting of course that the veracity of formulae and calculations within a spreadsheet needs to be continuously checked. The spreadsheet also contains notes and justifications, for future reference by the Client and others. For the purposes of the program, the veracity of the spreadsheet were verified using a commercially available fault tree software code (in this case, TopEvent FTA).

Summary of approach

The risk assessment process undertaken relies on appropriately identifying a non-duplicative set of potential failure modes (PFMs), followed by progressively subdividing them into their contributory components ("causes") through "AND" and "OR" logic gates, until it is possible to assign a probability to an individual "cause" with reasonable confidence. A brief summary of the approach adopted is described below:

System hazards (mechanisms that have potential to do harm, i.e., could potentially result in failure) were identified for which the consequence of failure could lead to a significant release of tailings and/or water (hazards include seepage, high precipitation, earthquakes, uncontrolled decant pond, etc.).

a) The "causes" of the potential release of material from the facilities were derived from the identified hazards, as well as drawing upon our understanding of the operation, gained through review of existing information and discussions with the Engineer of Record (EoR) or designer, along with other similar examples elsewhere ("causes" include slope failure, large-scale erosion, overtopping, piping, etc.).
b) The causes were logically combined through a series of "AND" gates and "OR" gates, depending upon whether the causes are statistically dependent (all had to occur), or independent of each other (any one or more would need to occur), respectively. The causes were progressively subdivided into their contributory components through the "AND" gates and "OR" gates, until it was considered possible to assign a probability to an individual cause with (what we consider to be) reasonable confidence, in this case through a workshop environment, supported by modelling/analyses undertaken by the EoR and a QRA framework prepared in advance by WSP.

c) Probabilities were assigned to the appropriate causes to yield a "fault tree." The probability of occurrence of the "top fault" (failure of the facilities leading to a release of a significant volume of tailings and/or water) were calculated by the fault tree according to the following formulae:
   i) for OR gates: Pt = 1 – (1-P1) × (1-P2) × ... × (1-Pn).
   ii) for AND gates: Pt = P1 × P2 × .... × Pn.
   iii) where P1, P2, etc., are contributory components to Pt.

d) The event analysis comprised a "failure location assessment" (in which the probability of occurrence for a given failure location was established), and an "exposure assessment" (in which the number of people exposed to a flow failure were identified based on dam break studies completed by the EoR/designer and supplemented by information from site personnel). The analysis was used to estimate the probability of loss of life or serious injury arising from the various failure mechanisms, for various failure locations.

The causes were based on the PFMs discussed in the workshop, with reference to a Failure Modes and Effects Assessment (FMEA) where available for a facility, as well as our wider industry experience related to risk assessments.

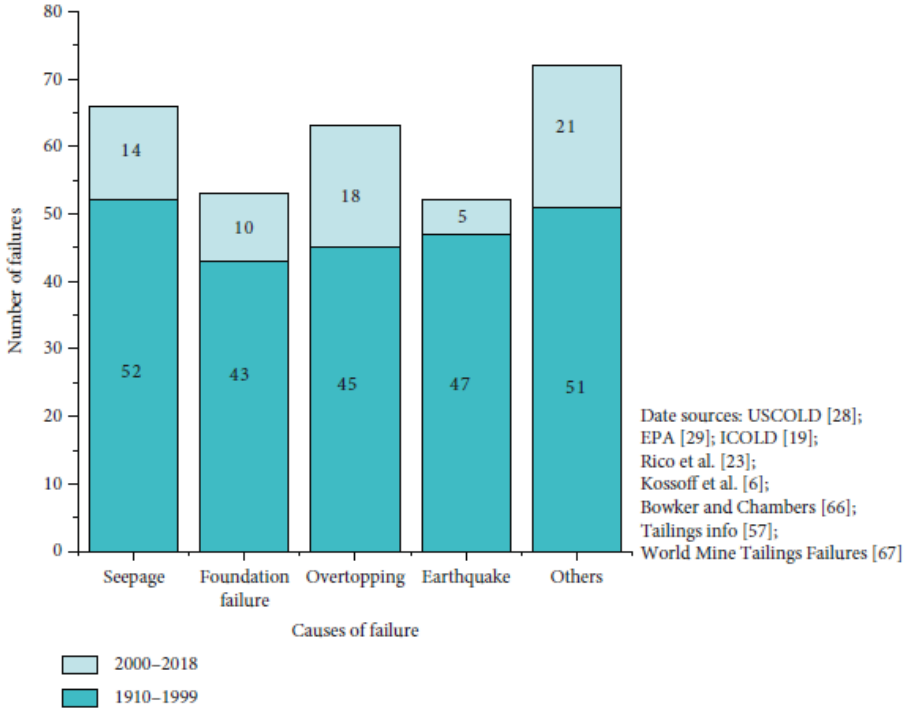


Figure 3: TSF failure distribution by cause (provided by Lyu et al., 2019)

Various documents have summarized "causes" of TSF failure. The data summarized in Bulletin 121 – Tailings Dams, Risk of Dangerous Occurrences, Lessons learnt from practical experiences (ICOLD, 2001) indicate that the bulk of catastrophic TSF failures are attributed to slope instability (including

foundation and earthquake in this category), overtopping, or piping erosion/seepage. This is supported by Lyu et. al (2019) who has characterized the leading cause for documented TSF failures from 1910 to 2018 (refer to Figure 3). The causes identified from investigations into more recent TSF failures (post-2018) have supported this dataset.

Prior to the workshop, the failure modes that could be relevant were pre-populated into the spreadsheet, with reference to the typical failure modes and building on the authors' experience with similar facilities. Each failure mode was given a description that included the "initiating event" or "damage mechanism." The damage mechanism is the impact or effect that could cause internal or external damage to, or failure of, the part of the TSF that resists failure. This is distinct from the cause of failure, which describes the source of the change. For example, slope instability could result from a rising phreatic surface (the damage mechanism), but the cause could be an increased pond size, or blocked drainage, resulting in the rising phreatic surface.

Table 1: Summary of failure modes considered in each QRA

Failure mode	Damage mechanism / initiator
Instability	Failure due to seismicity
Instability	Liquefaction/strain softening due to rapid loading from material entering the facility (e.g. avalanche or landslide)
Instability	Liquefaction/strain softening due to rapid loading from material placement
Instability	Removal of resisting forces (downstream slope) due to cracking/erosion of slopes
Instability	Removal of resisting forces (downstream slope) due to excavation at toe
Instability	Rising pore pressure resulting from large rainfall event
Instability	Rising pore pressure resulting from seasonal groundwater fluctuations
Instability	Slope failure due to non-conservative parameters/layering adopted for foundation
Instability	Slope failure due to non-conservative parameters/layering adopted for tailings
Instability	Slope failure following erosion due to poor surface water management at toe
Instability	Slope failure following erosion due to poor surface water management on slope
Instability	Slope failure due to local oversteepening
Instability	Slope failure under static conditions (normal conditions)
Internal Erosion	Differential settlement at abutment
Internal Erosion	Increased hydraulic gradient and initiation of piping erosion along conduit
Internal Erosion	Increased hydraulic gradient and initiation of piping erosion through embankment
Internal Erosion	Increased hydraulic gradient and initiation of piping erosion through foundation
Overtopping	Insufficient capacity to contain/manage the design rainfall event
Overtopping	Insufficient capacity to contain/manage a rainfall event – freeboard compromised
Overtopping	Insufficient capacity to contain/manage a rainfall event – outlet blocked
Instability	Liquefaction/strain softening due to rapid loading from waste rock

A summary of the failure modes considered for a typical QRA is presented in Table 1. The event tree for each was adjusted to suit local conditions, retaining the overall failure mode category for consistency between QRAs. The failure modes were discussed in each workshop and were updated/adjusted as required.

Key tenets of approach

The approach adopted, while generally consistent with the guidance available globally, was aimed at providing a summary of the risk-driving failure modes for TSFs, not water dams. The authors acknowledge the importance of partitions and system responses curves in detailed QRAs, but also note that the level of data available for a TSF, in general, is far less than a typical water dam. As such, the following limitations were acknowledged in the process:

- The EoR and/or designer was involved in the process and provided information critical to the failure modes assessed. The information provided anchored the assignment of probabilities in line with the item below. Where sufficient information was available to indicate that a failure mode could not occur, it was excluded given unanimous agreement from the QRA workshop attendees.
- The outcomes of the assessments included input from all the workshop attendees, which included personnel from a range of backgrounds including geotechnical engineering, hydrology, and operations. The potential for inaccuracy arising from the subjective opinion of a single individual was reduced by adopting the technique of "Expert Engineering Judgement" (ANCOLD, 2003), in which a group of knowledgeable persons discusses and assesses the likelihood of occurrence of an event, with reference to available information. The judgement of the group was supported with information from published literature (e.g., Silva et al. (2008) and Gover [2018]). Under this process, once agreement was reached, the assigned probability was the "agreed" probability of an event occurring. Where there is some uncertainty, these items were marked for potential future assessment, should they be a key contributor to the overall risk.
- Fully developed system response models are not typically readily available for TSFs, as they are designed to design criteria linked to the consequence category for the facility. For example, the facility may be designed to store an extreme rainfall or resist an extreme seismic event, but the response to smaller events may not have been explicitly considered. This results in the need for interpolation between known points as part of the risk assessment process. For this reason, partitions for events were not undertaken, but care was taken to identify the "key" event that would result in a step-change in the pF. For example, the expected return period of an earthquake that would result in liquefaction was identified, with more frequent events excluded on the basis that liquefaction would not occur, and less frequent events excluded on the basis that once liquefaction

occurs, the facility has already reached a state of failure[1].

- TSFs are evolving structures and hence the risk assessments were undertaken assuming the agreed baseline configuration. It should be recognized that ongoing operation of the TSF may result in a change to the risk assessment conditions. Where appropriate, this was discussed with the Client and included in the assessment, particularly in relation to alternative scenarios, but those results are not reported in this paper.
- Generally, detailed assessments of internal erosion using the techniques outlined in the "piping toolbox" (USBR, 2008) were not undertaken during the process. The intent of these approaches has been incorporated into the risk assessment, considering the potential for a hydraulic gradient to exist, the presence of defects within the embankment and/or foundation, the presence of conduits through embankments and the material characteristics being considered. Where internal erosion was noted as a risk-driving failure mode, more detailed assessments were recommended and the results of which were incorporated into the QRA once the detailed assessments were completed.

Data representation

Limits of tolerability are provided in both (ANCOLD, 2022) and (CDA, 2013). These are essentially guidelines for societal tolerability and are established based on the frequency of a particular hazard and the number of casualties if the hazard is realized. Tolerable risks should ideally be determined by society, with the risk of dam failure compared against all other societal risks, but no mechanism currently exists for this. It is typically only outrage at previous rare disasters that inform these limits.

Both references incorporate ALARP into their limits of tolerability, which prevents the interpretation of these limits as the boundary of "do something or do nothing." These limits can therefore be interpreted as a guide towards prioritization of risk management, i.e., where to focus investment and resources, and do not preclude implementing mitigation measures for risks below the tolerability limits (if it is reasonable to do so). (CDA, 2013) goes on to note that "society does not have infinite resources to spend on managing risks and often the resource spent in one area is the same resource that is missing in another area where investment could be more beneficial."

Noting that tolerability limits are developed for the cumulative pF of a facility (i.e., F-N), for the purpose of this paper, these are reproduced on f-N plots as "Reference Lines" to facilitate discussions related to individual failure modes. This has been shown to be acceptable by FERC (2016) which states "The analysis and evaluation of the individual potential failure modes can lead to an improved understanding of the potential failure modes that affect the combined annual probability of failure of the

[1] In this example, if large-scale liquefaction of the tailings did not result in failure of the facility, the failure mode could be excluded.

dam. It can also provide insights that can lead to the identification of both structural and non-structural risk reduction measures, including interim measures."

Summarized outcomes of assessments

In order to provide a comparison between the 16 TSFs, the full QRA dataset has been filtered to failure mode (i.e., stability, overtopping and internal erosion), facility type (i.e., upstream, downstream and centerline) and location. This is summarized in Table 2. The data are presented on f-N charts in Figure 4, Figure 5 and Figure 6 respectively. Finally, Figure 7 presents a filtered dataset of static versus seismic stability failure modes. The conclusions drawn from each view of the dataset are then discussed.

Table 2: Summary of dataset considered

Aspect	Value
Instability points	894
Overtopping points	244
Internal erosion points	113
Upstream TSFs	6
Downstream TSFs	9
Centerline TSFs	1
Asia	1
Australia	9
Europe	3
North America	3

The following observations are noted when the dataset is considered from a failure mode perspective:

- While all three failure modes include points plotting above Reference Line 1, instability was identified as plotting in the intolerable zone most often, regardless of PLL.
- When the points below Reference Line 1 are considered, there is no typical trend visible that suggests one failure mode is lower risk (i.e., plotting lower) than the rest.
- There is no typical trend indicating that a particular failure mode is better managed when there is a high PLL. In fact, the data appear to indicate that there is no trend between pF and N (PLL). In other words, the failure modes do not appear to take into account the PLL, despite higher consequence categories, and hence higher event loadings, being adopted for TSFs with higher PLL values. For instability under static conditions, this is consistent with standards-based engineering, where the same factor of safety minimum value is applied regardless of the consequence category. This is discussed further in relation to Figure 7.

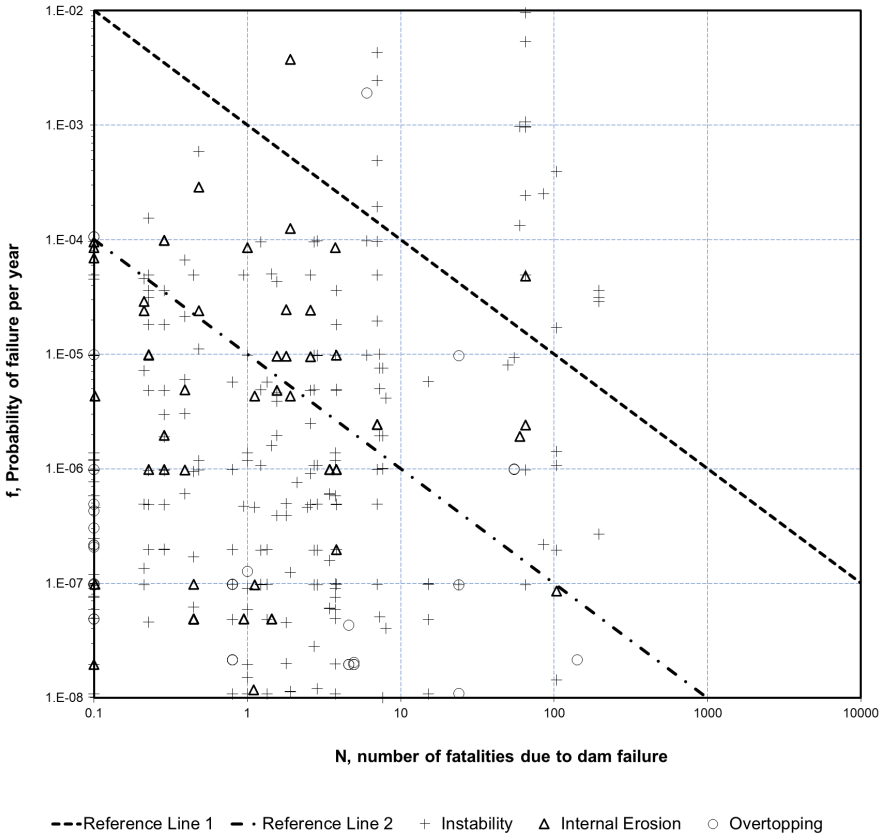


Figure 4: QRA dataset filtered to failure mode

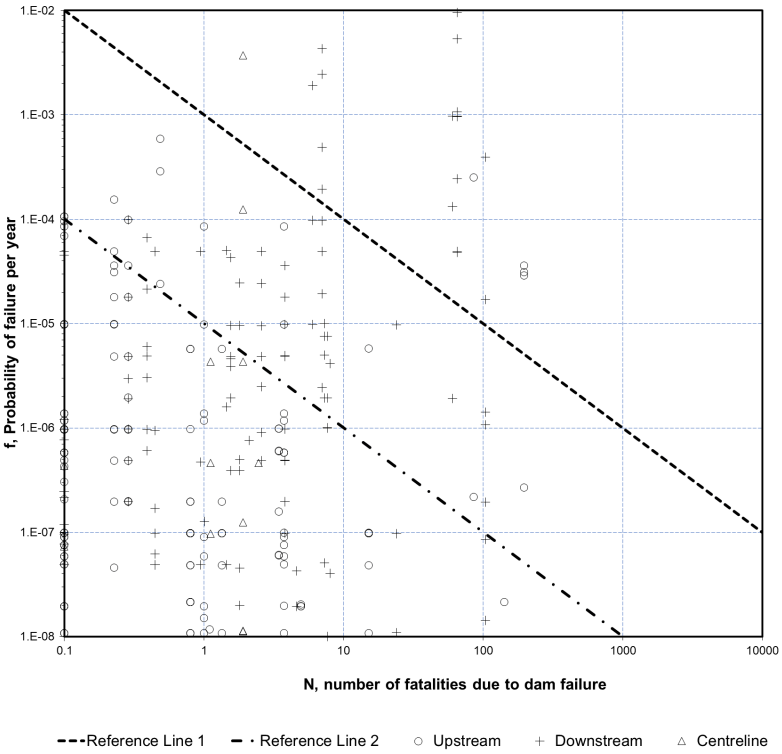


Figure 5: QRA dataset filtered to facility type

The following observations are noted when the dataset is considered based on construction type:

- Contrary to typical expectations, downstream-raised TSFs have more points in the intolerable zone (above Reference Line 1) than upstream facilities. As noted in Table 2, there were significantly less centerline facilities included in the dataset.
- There is no typical trend visible that suggests one facility type is safer (i.e., plotting lower) than the rest, with both upstream and downstream TSFs indicating variable pF values for the range of PLLs.
- With reference to Figure 4, instability was the key failure mode for both downstream and upstream facilities that plotted above Reference Line 1.

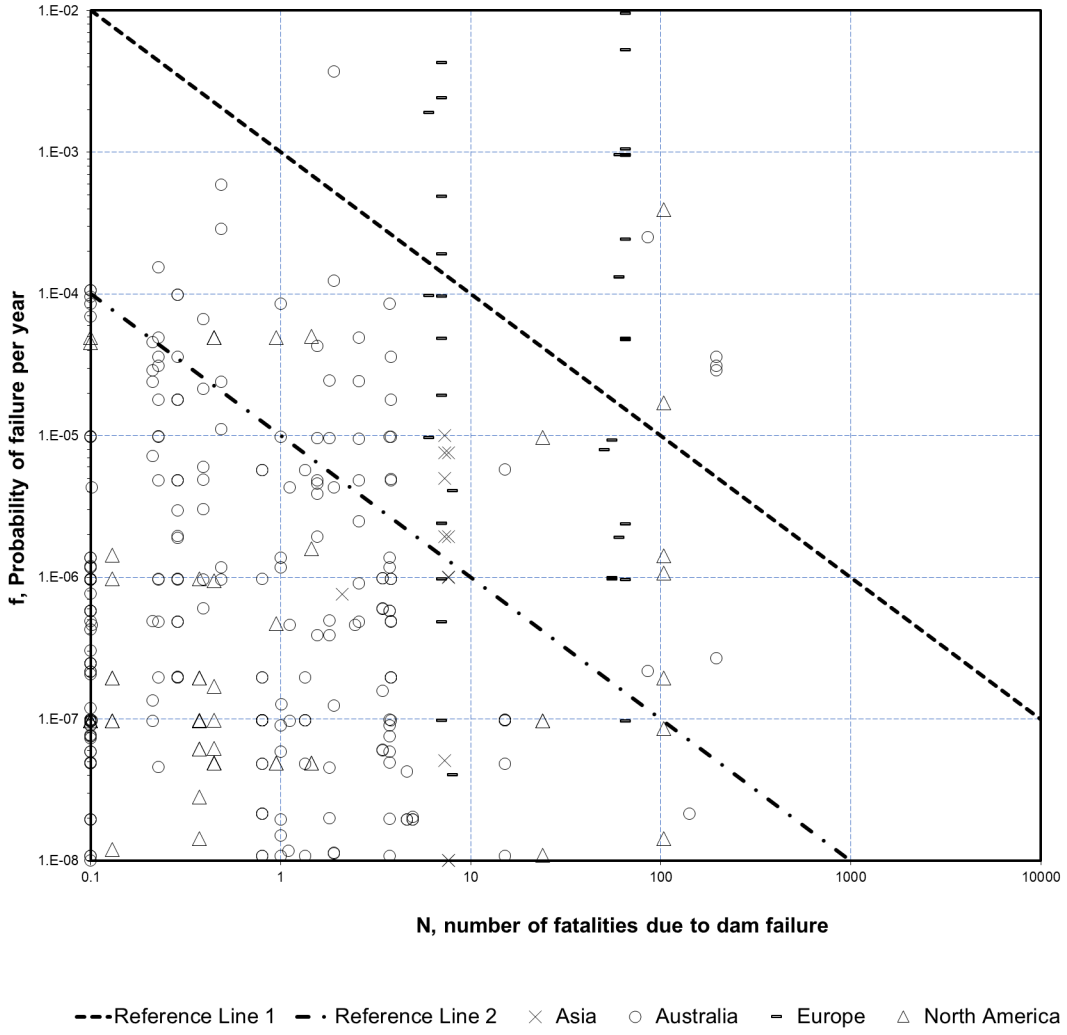


Figure 6: QRA dataset filtered by location

The following observations are noted when the dataset is considered based on location:

- There is no clear trend between location, with facilities above and below Reference Line 1, with high and low PLLs, in every location, with the exception of Asia. Due to only one assessment being

undertaken in Asia, the dataset is limited.

- The TSF design guidance for each region has the same factor of safety minimum value, although it is noted that the European sites were inactive and there was uncertainty about the data at the time of the assessment.

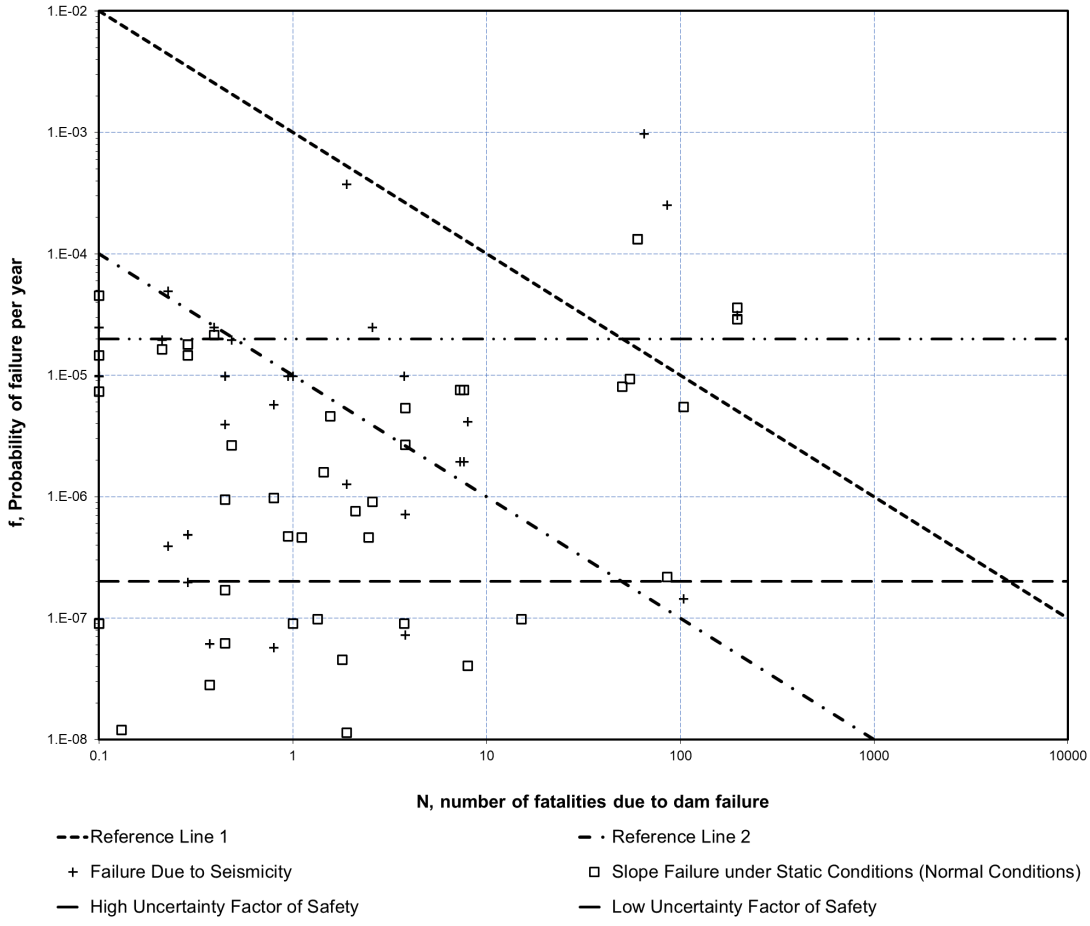


Figure 7: QRA dataset filtered by static versus seismic stability

Figure 7 shows the dataset for instability under static conditions (no upset conditions applied) and seismic conditions. The following observations are noted:

- There are points above Reference Line 1 for both static and seismic conditions.
- Under seismic conditions, there is a trend indicating an increased pF with increasing PLL, despite the requirement for a high design loading when the consequence category increases. For TSFs with high PLLs, meeting the design loading indicated by the relevant standard/guidelines did not indicate a tolerable risk position, despite being compliant.
- Under static conditions, whilst all the facilities were thought to be "compliant" (i.e., a factor of safety ≥1.5), prior to the assessment, significant uncertainty was noted in the parameter sets

adopted, resulting in a range of pF values being agreed in the workshops.

Two groups are evident from the results presented in Figure 7– those with high uncertainty in the assessment and those with low uncertainty. This is consistent with the data presented by Silva et al. (2008) and Gover (2018), where low confidence in the parameters supporting the stability assessment results in in a higher potential probability of failure. It follows that designs of new TSFs, along with taking into account best practices and new technologies, should also target high confidence datasets, in order to support a design that can be demonstrated to be ALARP. This would also include a better understanding of the natural variability of the materials (foundation and embankment) and implementing controls to suit, as part of managing the inevitable uncertainty that will exist.

Conclusion

QRAs undertaken on 16 TSFs have highlighted both the benefits of risk-based approaches as well as the inherent flaws in standards-based engineering, particularly where there are high loss of life consequences. When plotted in different datasets, the data indicate that there is no typical trend indicating that a particular failure mode is better managed, particularly when there is a high PLL. In fact, the data appear to indicate that there is no trend between pF and N (PLL). In other words, the failure modes do not appear to take into account the PLL, despite higher consequence categories, and hence higher event loadings, being adopted for TSFs with higher PLL values. The data also indicate that downstream facilities had significant points in the intolerable zone, despite being considered more robust than upstream facilities. For instability under static conditions, this is consistent with standards-based engineering, where the same factor of safety minimum value is applied regardless of the consequence category.

By considering both facility type and static versus seismic instability, the results can be used to identify the systematic deficiencies in design that indicate that standards-based approaches are not sufficient to manage high consequence TSFs. This is indicated by the facilities being considered “compliant” prior to the assessment, but significant parameter uncertainty led to intolerable values under static conditions and, where high PLL values were estimated, meeting the design loading indicated by the relevant standard/guidelines did not indicate a tolerable risk position, despite being compliant.

Based on the data presented, is it imperative that a risk-based approach be considered, in addition to standards-based design if required, to have an improved understanding of potential failure mechanisms, particularly when there is a significant population at risk and PLL. An increased focus on reducing uncertainty through investigations, testing and analysis for TSFs with high PLLs is strongly supported by the authors.

Acknowledgements

The authors would like to thank Leila Ang, Brendan Cummins, Andy Liu, and Nigel Moon for their contributions to the risk assessments, as well as the Clients who provided us the opportunity. The authors would also like to specifically acknowledge Andy Liu for his significant contribution to the data interpretation to support this paper.

References

Australian National Committee on Large Dams. 2019. *Guidelines on Tailings Dams, Planning, Design Construction, Operation and Closure*. Addendum published July 2019.

Australian National Committee on Large Dams. 2022. *Guidelines on Risk Assessment*. July 2022.

Canadian Dam Association. 2013. Dam Safety Guidelines 2007 (Revised 2013).

Chapman and Williams. 2019. The benefits of a quantitative risk assessment approach to assess the risk of catastrophic TSF Failure. *Proceedings of Tailings and Mine Waste, 2019.* Vancouver, Canada.

Chapman, P.J. 2022. Applying the concept of ALARP during the design process. *Proceedings of Tailings and Mine Waste, 2022*. Colorado, USA.

Global Tailings Review. 2020. *Global Industry Standard on Tailings Management*. August 2020.

Gover, S.M. 2018. Linking safety factor to probability of failure. *Proceedings of Mine Waste and Tailings, 2018.* Brisbane, Australia.

ICOLD, 2001. *Bulletin 121 – Tailings Dams, Risk of Dangerous Occurrences, Lessons learnt from practical experiences*.

Lyu, Z., Chai, J., Xu, Z., Qin, Y. and Cao, J. 2019. A comprehensive review on reasons for tailings dam failures based on case history. *Advances in Civil Engineering* 2019(9):1-18.

Morgenstern, N.R. 2018. Geotechnical risk, regulation, and public policy. The Sixth Victor de Mello Lecture. *Soils and Rocks, São Paulo* 41(2): 107–129, May–August, 2018.

Silva, F., Lambe, T.W. and Marr, W.A. 2008. Probability and risk of slope failure. Journal of geotechnical and geoenvironmental engineering 134(12): 1691–1699.

United States Bureau of Reclamation, United States Corps of Engineers, URS (now AECOM), and UNSW (Australia). 2008. *A Unified Method for Estimating Probabilities of Failure of Embankment Dams by Internal Erosion and Piping*, Version: Delta, Issue 2. August 2008.

Evaluating the Stability of Upstream and Brittle Facilities – Case History Validation of the "Rules"

Michael Davies, Davies Mining Consulting Ltd, Canada
John Lupo, Mayhem Creek LLC., USA

Abstract

Roughly twenty-five years ago, one of the current authors and a colleague provided the industry with "Upstream Constructed Tailings Dams – A Review of the Basics." That publication provided ten "Rules" for the design, construction, and operation of upstream tailings facilities, based upon soil mechanics principles that were then calibrated with case histories. These Rules have been cited many times since, and when followed, have universally led to sound outcomes. However, at times the Rules have seemingly been ignored – and in some of those cases, catastrophic outcomes have resulted.

The authors are two former mining company executives who were also global tailings practice leads and, prior to that, designers. From the owner perspective later in their careers, the challenge that seems to most often exist is discerning how "grey" the Rules are, and which are the most critical. From a designer standpoint, how conservative does the design have to be to avoid the triggers that lead to the checkered past of upstream facilities? This update reviews each of the previous Rules in the context of case examples that have occurred both prior to and, most importantly, since the original publication. The review leads to several focused conclusions about the Rules that are directly aimed at key failure prevention issues, and which should assist owners, designers, and regulators. Although originally envisaged as Rules just for upstream constructed facilities, the rules are applicable to other tailings construction methods for which brittle failure may be of concern.

The paper clearly identifies a list of non-optional attributes for designers, owners, operators and reviewers to fully embrace for both themselves and any upstream facility or facility with a similar brittle failure concern. The update is of particular value for legacy (operating or closed) facilities where the details regarding the previous design and/or development history can be murky at best, and therefore guidance on a paradigm based upon both sound soil mechanics fundaments *and* case history outcomes is needed to enable confidence in evaluations.

Upstream/brittle facilities – the basics

Davies and Martin (2000) provided a set of 10 "Rules" for upstream constructed tailings dams based on both their commonality across the industry and also on their considerable presence in the global tailings failure database. The Rules included a combination of issues ranging from nomenclature confusion to technical considerations to governance aspects. After more than two decades, some of the less technical items can now likely be retired, as very few practitioners are still trying to convince others that by simply calling an upstream facility something else it will abide by a different level of physical laws. Further, the vilification of the very concept of using upstream construction has become very popular, to the point that many facilities that have had an incident (from a close call all the way to catastrophic) that are *not* upstream facilities have been given that label by those with a mission of banning the practice altogether.

We will arrive at all of the above later in this paper, but the basics still apply: an upstream facility is one in which the dam crest, including the upstream edge of the crest, moves over beached tailings at any point in its sequential raising. This is unambiguous. The best test for an upstream constructed facility is whether a vertical line extended to the foundation of the facility from the upstream edge of the crest ever touches beached tailings. If the answer is yes, regardless of how much it touches, the facility is an upstream constructed facility. To argue along the lines of "only x% is upstream" is to argue not to worry about one or two weak continuous layers in a large slope; however, this is not an argument that will stand any test of logic.

The aspect that seems to escape many is that merely being an upstream facility does not constitute a black mark on the facility. On the contrary, many of the largest facilities in the mining industry are both upstream constructed and some of its safest. A theme throughout this paper is that a properly conceived and operated upstream facility will potentially have failure modes that other geometries may not; however, they can be constructed, operated, and closed/reclaimed with no higher risk profile than non-upstream facilities. Of all the documented tailings failure case studies, there is not one that has met all of the Ten Rules laid out in 2000. By contrast, those facilities that have followed the Rules have continued to function without incident.

The Ten Rules revisited

Table 1 provides a summary of the Ten Rules from Davies and Martin (2000), along with a note about the current thinking on each. As was evident to the authors, it is likely acceptable to consolidate the Rules down a bit into a tighter set of items. Assisted by the case history, the remainder of this paper is focused on precisely that attempt at developing a tighter set of Rules.

Table 1: The ten upstream tailings facility Rules (after Davies and Martin, 2000)

No.	Rule	Comment(s)
1	If there are any beached tailings beneath the upstream crest of the tailings dam, then the structure has been developed using upstream construction.	Far more obvious in 2024 than in 2000, as few are now trying to use alternative terms like "modified centerline."
2	Maximizing the beach above water (BAW) zone is good practice when developing an upstream tailings dam.	As it pertains to creating a sufficient shell of drained and dilatant material, this remains very relevant.
3	Upstream constructed tailings dams are not necessarily bad engineering practice.	This remains very topical, but is more political than technical in 2024.
4	Upstream dams require a good foundation – preferably well-drained and of adequate constitutive behavior.	This remains relevant.
5	Correct tailings bulk densities and in-situ stress conditions need to be used when estimating in-situ state.	The authors are seeing less confusion in practice on this issue. It can perhaps be combined with a more overall design requirement.
6	If the impoundment has an upstream constructed dam, and the dam slopes are steeper than about 4H:1V, the facility has a greater susceptibility to static liquefaction with minimal trigger application.	This can be even more strongly stated in 2024 through confirmatory soil mechanics practice/theory.
7	Undrained strength analysis (USA) should be used for upstream dams where the tailings are uncompacted and largely to wholly saturated.	Again, this is all fundament training in soil mechanics, and remains perhaps the most relevant design requirement. Unfortunately, it was missed with several failures.
8	Design geotechnical requirements and actual operating criteria must be compatible.	This remains relevant.
9	Laboratory-scale and literature-predicted beach slopes tend to be incorrect. We should not rely upon steep beach slopes to meet operating criteria.	This seems to have been an issue that has been well addressed over the past 25 years with few, if any, unrealistically steep beaches being designed and then not realized.
10	Designers should avoid designing upstream tailings dams where the designer will not be able to maintain a high level of involvement in the monitoring and evaluation of the facility.	This aspect was well addressed in the 2020 GISTM.*

* Global Industry Standard on Tailings Management

The comments in Table 1 are based upon the authors' combined experience for each of the Ten Rules developed in 2000. All of the Rules still apply, but there is no question that emphasis can be altered, and some reworking of the items is possible. Moreover, items like Rule 10 that address an overall governance issue have been addressed across the industry, assuming adherence to one of the Mining Association of Canada Tailings Guidance series (e.g., MAC, 1998) or the largely duplicative Global Industry Standard on Tailings Management (GISTM, 2020). It is also the expectation of the authors that anyone working with tailings facilities in 2024 is a student of the core teachings of Peck (1980) and considers sound judgment to be essential for any role in this field. With this initial evaluation of the 2000 work, the paper now turns to the twenty-five years since the paper was published. Over that period of time, in terms of upstream

constructed tailings facilities, what has been observed in terms of both the practice of tailings management and the actual performance of facilities?

The elephant in the room – should upstream tailings facilities exist?

Some key mining jurisdictions (e.g., Chile and Brazil) have banned the use of upstream tailings facilities, and many outside of the industry continually call for a cessation of the practice. To not address the basic question of "why upstream at all?" would be grossly disingenuous when developing a summary position paper on the topic. The claim by some that upstream facilities are disproportionately represented in the failure database ignores the fact that they are also historically the most common type of tailings facility. There is also considerable variation in the nature of upstream facilities in terms of structural competency, as the construction methodology can vary considerably. There is also a claim by many that the industry only uses upstream construction as it is the least expensive option. This was likely valid in many cases prior to the 2000 paper, but the authors' experiences do not reveal that as the sole or even the main driver twenty-five years later. The modern tailings facility has to consider many key points beyond just the economic viability that upstream constructed facilities can provide. These include the following:

- Considering whether the upstream facilities allow progressive reclamation and erosion/dust protection on the shell to occur during operation.
- Setting the ultimate footprint for the facility at the outset to allow certainty for infrastructure placement and community boundaries.
- Depending upon location and topography, the planners can dramatically reduce the footprint of the project by requiring far less construction material (and hence less energy expended, etc.).
- Developing closure surface drainage systems at the outset and maintaining these throughout operations.
- Putting in long-term instrumentation on slope sections – and as the toe and slope remain constant after being placed, it is possible to monitor comparative surface movements over time via technology like InSAR, drones, and other remote sensing options, whereas this is not necessarily the case with other methods.

In Chile, the March 1965 failure of the El Cobre tailings facility (which caused more than 200 deaths) prompted widespread discussion in Chile and public pressure for stricter control over tailings facilities. The Chilean authorities issued Decree No. 86 in 1970 to regulate the design, construction, and operation of these facilities, and included one special clause, which was the prohibition of the tailings facility upstream construction method. Over the sixty years since that tragic event, similar calls for restrictions on upstream construction have stemmed from events such as Samarco/Mariana (2015) and Brumadinho/Feijão (2019).

Most notably, the 25 January 2019 upstream tailings facility that collapsed at the Córrego do Feijão iron ore mine (9 kilometers east of Brumadinho, in the state of Minas Gerais, Brazil) released a mudflow that engulfed the mine's headquarters and its downstream surroundings and caused the death of 270 workers.

This paper does not attempt to be a full case study evaluative review of any one failure and does not provide commentary on the many publications (inclusive of expert reports from such failures). However, it is very clear that many more than one of the Ten Rules provided in 2000 were ignored in all of these failure events. Some argument as to the degree of contribution of any one Rule over another is inevitable, but this is often like arguing about what broken bone was more severe for a patient who was decapitated; the point being that the failure happened because Rules were broken. The Rules, as stated in 2000, are not a "use as many as you can" situation. We cannot hope that "following 7 is better than following 3." Then or now, *none* of the Rules should be considered optional. There is no "better" based upon any degree of partial compliance. Of course, basing the entirety of the structural integrity evaluation on a flawed premised (e.g., drained strength), which seems almost universal in all of the upstream case histories, almost always ensures becoming a failure case history. However, the other nine Rules can each in their own way create a pathway to a catastrophic outcome.

This all sounds pretty bleak. However, one also must remember that many of these Rules fully apply to any other geometry as well; particularly if there are any credible brittle (strain-softening) failure mechanisms present and/or susceptibility to failure by facility overtopping or suffusion. If we get past Rules 2 and 7 (and these are both directly related to Rule 6), all of these other items apply to everything from dry stacked tailings facilities through the most robust downstream rockfill shell facility. Even Rules 2 and 7 can play a role in a "drystack" filtered facility if operational controls are not both appropriate for site conditions and followed within very tight boundaries.

So, why do the authors then come out firmly on the side that upstream facilities should be part of options for tailings facilities both today and into the future? The answer is simple; it is because sometimes they *are* the best option when all things are considered. Moreover, and perhaps most importantly, there are no case histories of an upstream facility having ever failed if it was following the Ten Rules. This perhaps is the best evidence that the Rules work. It follows from this that is you obey the Rules then using upstream constructed tailings facilities can be an option for you. However, the one essential component that was not stressed as much in 2000 as today, and that is addressed in the next section, has become evident over the past twenty-five years and needs highlighting.

The hard truth – competence matters

Perhaps a positive step for global regulation of tailings facilities is to get beyond the often meaningless fixation with "one size fits all" items like limit-equilibrium factors of safety and move towards regulating

the competency of those involved in owning, designing, and reviewing tailings facilities. Being a qualified owner perhaps needs to go beyond present-day practice and evolve towards having to use pre-qualified designers and reviewers. To do this, regulatory practice should evolve past the present levels. For example, the current fixation with computed "factors of safety" is not a sound regulatory basis. The reality is that, dependent upon material behavior types, some facilities with computed values near unity will be safer and less able to – if at all – fail catastrophically than facilities with far higher computed values. While the seductive simplicity of striving for target values is obvious, the practice oversimplifies the situation to the point where disastrous outcomes are possible. This perspective is substantiated based upon forensic evaluations of facility failures where the designers of these facilities had almost universally demonstrated high factors of safety prior to their demise. Instead, we need to have a regulatory process that only allows upstream facilities (or any for that matter – but that is another topic) to be constructed by:

- Owners who clearly demonstrate commitment to a governance model like MAC or GISTM, inclusive of having internal personnel with vetted experience with similar structures and who demonstrate application of sound, risk-informed decision making.
- Owners who retain Designers/Engineers-of-Record who have demonstrated experience with similar facilities in similar climatic/tectonic settings and most certainly have vetted competency in undrained strength evaluation, the fundamentals of static liquefaction, and in the practical application of these principles in sand embankment construction. If these personnel are to be changed at any point, strong succession plans and change management processes must be in place.
- Owners who commit to having fully Independent Reviewers who meet all the tests of the Designer/Engineer-of-Record, with the additional buffer of more experience, varied experience, and a thorough understanding of failures that have occurred across the history of the industry.

The above would address what Morgenstern (2018) termed "weak engineering." The analogy the authors suggest is that of the medical profession, although many other equally valid comparisons across other human activities potentially impacting human health and safety can be applied here. Using the "ban upstream facilities" approach in medicine would mean that some types of surgery could not be used any longer as not all surgeons are capable of the procedures. For example, perhaps almost every licensed cranial surgeon practicing today can effectively remove a concerning mass from a brain with typical risk outcomes. However, for the most leading-edge surgery on the more involved brain tumors, only a smaller number of surgeons are qualified for such procedures. If having such a surgery is the best option for the patient, why deny it? We realize that those opposed to upstream facilities will cry foul as such an analogy, but before they do, what about airline pilots? Is there not a pecking order in competence with certain sizes and complexities of aircraft? Do airlines not offer certain plane options that are perfectly safe if the Rules are

followed by the appropriately trained pilots? Well, why can't the same logic be applied to upstream tailings facilities? For those owners in jurisdictions where the practice is common, and many of the facilities are very large and demonstrated to be safe and have followed the Rules – why is it not a valid option both today and moving forward?

Perhaps the confidence society needs to have to remove a blanket fear of the practice is some assurance that those involved are competent, and vetted as such, coupled with the unblemished record of those facilities that follow the Rules. If we combine the above noted competence requirements for the key roles with the essential technical elements offered near the end of this paper, then that confidence should be attainable. If we were to embed these requirements into professional licensing (e.g., P.Eng./P.E.) and employ externally verified (through independent review boards) processes for vetting the designer, then most, or even all, of the concerns can likely be addressed.

Case history learnings

Table 2: Notable upstream tailings facility case histories

Case	Rules Not Followed	Comments	Key Reference
Stava, Italy, 1985	2, 6, 7 and 10	Very steep slopes, no one is quite sure who was responsible for the design, no beach guidance and the only stability work was drained evaluation. Failed in static liquefaction.	Davies and McRoberts (2002)
Brumadinho/ Feijão, Brazil, 2019	2, 6, 7 and 10	Saturated relatively steep slopes with high pore pressures evaluated with drained strengths. Failed in static liquefaction and likely occlusion of high pore pressures.	De Melo et al. (2019)
Mariana/Samarco, Brazil, 2015	2, 6 and 7	Undrained failure with contributions from abutments that was seemingly ignored in laying out design and construction sequencing. Failed in liquefaction.	Embargoed
Sullivan, Canada, 1990	2, 6 and 7	Rapid construction without the ability for pore pressures to dissipate. Designs only considered drained strengths. Failed in static liquefaction.	Davies et al. (1988)
Confidential, North America, since 2000	2, 6 and 7	Drained evaluation only considered, very little beaching occurred subaerially and previous "near failures" were not used as bellwether. Failed in static liquefaction.	Authors' files
Porco Mine, Bolivia, 1996	2, 6, 7 and 8	Lack of alignment between design beach requirements and operating pond realities led to large zone of loose saturated tailings that failed in static liquefaction.	Martin et al. (2002)

Table 2 provides a list of notable upstream tailings facility failures where there is sufficient knowledge to be able to compare the contributing factors to the failure event with the Ten Rules established in 2000 and

summarized in Table 1. Each case is identified with those top few Rules broken based upon public domain information (in all cases except a confidential case on which the authors have detailed information). The only Rule not included is Rule 1. There is no question that each and every case involved an upstream constructed facility. These findings are then used to allow the paper to wrap up with some technical essentials that all such facilities require to avoid becoming a case history candidate.

The interesting conclusion from Table 2 when looking at the broken Rules deemed to have contributed the most is that Rules 2, 6 and 7 are present for each and every failure event. Table 2 includes the two most tragic events in the industry's documented history (Stava and Feijão combined led to more than 500 fatalities), along with textbook examples of sudden "collapse" failures of upstream facilities that have been independently reviewed and documented. From the consistently broken Rules 2, 6 and 7, clarity on what the technical essentials are for upstream construction becomes evident.

The technical essentials

Case histories, such as those in Table 2 and the many others, inclusive of "close calls," are very helpful. The latter can be very helpful by defining the edge of imminent collapse, which can assist greatly in modeling future behavior. Ignoring the set of Rules from 2000 and simply looking at "what good looks like" from the collective experience of the industry with upstream facilities, inclusive of the failure case histories, the following appear to be essential for a successful upstream constructed tailings facility:

1. A stable foundation without a brittle failure mode is present along with any other included elements following standard practice (such as filter zones, erosion protection, sizing of drainage features, surface water management etc.). This would be essential for all geometries (upstream, centerline, or downstream) and is included for completeness.
2. An active surveillance program and commitment to a sound quality assurance program that regularly manages beach width, embankment pore pressures, and deformation characteristics of critical embankment sections in as close to real-time as practical. This program should have strategic key performance indicators (KPIs) that are underpinned by conservative trigger action response plans (TARPS) for all instruments that are inclusive of at least two levels of response/evaluation prior to levels reaching a facility safety concern level.
3. An adequate zone, both in width and from the base of beached tailings to the top of the embankment, of either sufficiently unsaturated or dilatant tailings. In terms of saturation, if solely relying upon that characteristic, it appears that staying below about 70% is required. For the achievement of a sufficient zone of dilatant tailings, the initial lifts are often the most challenging. Early in a facility's life, it is necessary to have a combination of the pond being

relatively close with insufficient geometry to create the strong downward gradients and resultant densities from subaerial beaching. For this period in the construction cycle, mechanical compaction/cell construction is likely required from start-up and then for some portion of the construction dictated by measured performance (e.g. cone penetration testing for in-situ state).

4. For any materials that can potentially become saturated, use undrained analyses with appropriately obtained strength (e.g. lower bound for the stress state) and constitutive relationships and appropriate triggering stability analyses/deformation modeling based upon these relationships. Properties should be routinely confirmed, as required, through investigations and updated analyses that embrace any advances/learnings on material sampling, in-situ testing, constitutive characterization, and methods of analyses.
5. For any materials in the tailings facility or the foundation that may be susceptible to seismically induced liquefaction due to their saturation and/or density state, carry out such evaluations using the maximum credible (or the 1 in 10,000-year event, whichever is most appropriate) applicable ground motions for the site in evaluating the potential for post-liquefied strengths to impact structural integrity.

Should the above essentials, which embrace the Ten Rules, be followed and maintained within a governance structure of ownership, engineering and independent review as described in this paper and implied by publications like MAC Guides and the GISTM, upstream constructed tailings facilities can have a risk profile on par with any other type of tailings facility.

Finally, Rule 6 from 2000 can further simplify things. If the foundation and other elements for the facility are stable and/or designed and constructed with appropriate design criteria per established practice, an upstream facility constructed with an overall slope of 4 horizontal to 1 vertical or flatter only need demonstrate seismic stability. Static brittle response at slopes flatter than 4H to 1V are not possible in any loading path and a "collapse" failure is not available. Where the material balance and site footprint allow, the adoption of these flatter slopes can be an excellent way to avoid almost all credible failure related to instability.

Where the rubber hits the road – operations

All the Rules, with the exception of 8, are focused on design. Rule 8 focuses on the compatibility between the design and operational criteria. What is implied here is that the facility must be operated in a way that is compatible with the design. A sound change management system should be in place, but even then, a lack of compatibility can still arise. While avoiding this incompatibility between design and operation may seem

obvious, experience unfortunately shows that implementation can be very challenging leading to less than desirable consequences in some cases. For example, in the early years of the facility and/or right after a raise, pond management can become difficult, resulting in an inability to achieve the minimum beach length or freeboard requirements. Difficulty in pond management may have follow-on effects with deposition (e.g., poor sand production or non-uniform beaching), which can worsen the situation. Effective layer density state (e.g., non-contractant) is less likely to be achieved. These are some of the reasons the authors recommend above formal mechanical beaching/cell construction with compaction for such situations and in particular for the start-up of new upstream facilities, unless it is absolute and independently verified by qualified people that it will not be required.

Changes in staffing within the operations team can result in the loss of institutional knowledge, leading to practices that are counter to the original design intent. Succession planning in the operations team is as important as succession planning within the EOR's team. If a consistent experienced team that has demonstrated an ability to meet the technical essentials noted above for the constructed facility is changed or replaced, then most certainly method specification is not to be used and complete adoption of a performance specification with a comprehensive control and assurance program will be required. All of this can be assisted greatly by the aforementioned use of surveillance program KPIs and TARPs that can be augmented with practical operation procedures. All of these materials should be concisely and readily available through a facility's Operations, Maintenance and Surveillance Manual (OMS).

For long-life facilities (e.g., a number of decades), the original design criteria/intent will likely change due to modifications in raise configuration to account for land constraints, ore mineralogy, mill throughput, sand production/quality, etc. In these cases, the design and design basis will likely need to change, requiring a corresponding change in the operational criteria and practices. The operations team needs to be working closely with the designer to fully understand the implications of these changes. Incremental changes need to be looked at in their cumulative entirety compared to the current design in terms of the design's operational requirements to avoid complacency.

Finally, the owner needs to have made and demonstrated a clear statement of a safety culture that underpins all aspects of tailings management. This culture embraces the concept of all site personnel and community members having no impacts on their health or safety from the tailings facility. The culture also recognizes the benefits of regularly updated risk analyses so that risk-informed decisions are made based on current information.

Conclusion

The Ten Rules established in 2000 remain valid nearly twenty-five years later. At the same time, the list can be reduced thanks to other initiatives being adopted by the industry (e.g., better governance through

strong programs like MAC or GISTM) and a reduction in "playing games" with nomenclature and other issues regarding upstream facilities (what is or what is not such a facility). To that end, the authors believe that keeping the Ten Rules handy is useful, but emphasize five essential technical components, along with a sixth (flatter than 4H to 1V), that can render many of them very robust facilities in terms of instability concerns.

The failure case histories available, the current understanding of undrained response of tailings to shear loading, and the demonstrated successes of many major upstream facilities all align with keeping this geometry as a viable option for the industry. As the authors note, only appropriately qualified owners, operators, designers, and reviewers should be involved with such facilities. They encourage those who regulate and permit such facilities to, instead of bowing to calls to ban the practice, instead concentrate on getting assurance as to the teams involved in each case.

References

Davies, M.P., B.G. Chin and B.B. Dawson. 1998. Static liquefaction slump of mine tailings – a case history. Proceedings of 51st Canadian Geotechnical Conference, Edmonton.

Davies, M.P. and T.E. Martin. 2000. Upstream constructed tailings dams – a review of the basics. *Tailings and Mine Waste 2000*. CRC Press: 3–15.

Davies, M.P. and E.C. McRoberts. 2002. Static Liquefaction of Mine Tailings – Fundamentals and Case Histories, Association of State Dam Safety Officials, Las Vegas.

De Melo, L., P.K. Robertson, D.J. Williams and G. Ward Wilson. 2019. Report of the Expert Panel on the Technical Causes of the Failure of Feijão Dam I.

Global Tailings Review. 2020. Global Industry Standard on Tailings Management. Accessed at https://www.icmm.com/en-gb/our-principles/tailings/global-industry-standard-on-tailings-management

International Council on Mining and Metals. 2021. ICMM – Tailings Management: Good Practice Guide. May 2021. Accessed at https://www.icmm.com/en-gb/guidance/innovation/2021/tailings-management-good-practice

Martin, T.E. and E. McRoberts. 1998. Some considerations in the stability analysis of upstream tailings dams.

Martin, T.E., E. McRoberts and M.P. Davies. 2002. A tale of four upstream tailings dams. *Proceedings of Tailings Dams 2002,* ASDSO.

Mining Association of Canada (MAC). 1998. *A Guide to the Management of Tailings Facilities*. First edition. The Mining Association of Canada. Pp: 54

Morgenstern, N.R. 2018. Geotechnical risk, regulation, and public policy. The Sixth Victor de Mello Lecture. *Soils and Rocks, São Paulo* 41(2): 107–129, May–August, 2018.

Peck, R. 1980. Where has all the judgement gone? The fifth Laurits Bjerrum memorial lecture. *Canadian Geotechnical Journal* 17: 584–590.

UNEP. 1996. United Nations Environment Programme. Tailings Dam Incidents 1980–1996. A report by Mining Journal Research Services, UK, May.

USCOLD. 1994. Tailings dam incidents. U.S. Committee on Large Dams.

How to Design a Tailing's Dam Full Removal? Lessons Learned from a Case Study in Brazil

Benicio Junior, Klohn Crippen Berger, Brazil
Claudio Rodrigues, Vale S.A., Brazil
Neil Singh, Klohn Crippen Berger, Canada
Luciano Souza, Klohn Crippen Berger, York

Abstract

Following the catastrophic mining dam failures in Mariana (2015) and Brumadinho (2019), Brazil enforced stricter legislation on mining dams, including the prohibition of upstream raising construction methods and the mandatory decommissioning and decharacterization of existing upstream-raised dams as stipulated in ANM Resolution No. 13/2019. This case study presents the decharacterization project of a high-priority dam featuring two pits and a reservoir, initially holding approximately 2,000,000 m³ of tailings. The project involved extensive trade-off studies, geotechnical and hydrogeological assessments, and pilot testing to identify the optimal decharacterization approach.

The selected solution, involving the complete removal of upstream tailings and the creation of a uniform flat slope with a central channel over the starter dam, was chosen for its reduced consequence classification and potential for tailings reuse. The project was divided into multiple phases, with each phase addressing specific challenges and leveraging remote excavation technology. Detailed investigations and pilot tests provided critical insights, leading to phased excavation and continuous model refinement. During the design and governance review process, the final design outcome was modified from a decommissioned starter dam to complete removal of the embankment and tailings, and restoration of the original valley.

Key challenges included remote investigation and excavation, tailings variability, 3D modeling complexity, stakeholder engagement, and stringent water management requirements. The project's iterative design approach, underpinned by robust stakeholder engagement and advanced modeling techniques, facilitated successful decharacterization while ensuring safety and compliance with regulatory standards. Lessons learned emphasize the importance of early and continuous stakeholder involvement, iterative design processes, the observational method, and the critical role of hydrogeological and deformation models in managing complex decharacterization projects.

Introduction

After the disasters in Mariana in 2015 and Brumadinho in 2019, Brazilian legislation became stricter regarding mining dams. These incidents led to the prohibition of the upstream raising construction method through National Mining Agency (ANM) Resolution No. 4/2019, which was later replaced by ANM Resolution No. 13/2019. Besides banning the construction of new upstream dams, Article 8 of the mentioned resolution required the decommissioning and decharacterization of existing upstream structures. ANM Resolution No. 95/2022 consolidates the normative acts that provide for the safety of mining dams, later amended by ANM Resolution No. 130/2023, defining a decharacterized structure as a structure that does not permanently receive inputs of tailings and/or sediments from its core activity, and which no longer possesses characteristics or performs the function of a dam, in accordance with the technical project. The project goal was for the TSF to be decharacterized.

According to ANM Resolution No. 13/2019 and the Terms of Reference for the decharacterization of upstream-raised dams by the State Environmental Foundation of the state of Minas Gerais, decommissioning is defined as the cessation of operations and the removal of associated infrastructure, such as spillways and pipelines, except those necessary to ensure the structure's safety. Whereas decharacterization is defined as decommissioning plus the implementation of effective measures to reduce or eliminate the influx of surface and groundwater into the reservoir. This includes preventing flood routing in the reservoir during the design of the spillway system, ensuring the long-term physical, chemical, and biological stability of the remaining structures, and monitoring the effectiveness of these measures for as long as necessary.

Typically, decharacterization projects in Brazil involve either one of the following alternatives: full removal of upstream embankments, partial removal of upstream embankments, or sufficient buttress to allow the dam to no longer be classified as an upstream raise.

Facility description

The total area of the facility that will be presented in this case study is composed of two pits (Pit A and Pit B) and the Reservoir, as shown in Figure 1. At the start of the decharacterization project, the dam stored around 2,000,000 m³ of tailings within the three areas of disposal. The tailings were well above the rim of the two pits, forming a continuous deposit from the dam.

The starter dam, built in the 1970s, has undergone four upstream raisings and a buttress reinforcement, at various stages during operation until the 1980s. The dam stands at a maximum height of 42 meters, with a crest width of approximately 10 meters and a length of 246 meters. The reservoir area at crest elevation

covers around 235,000 square meters, covering the reservoir area and pits A and B, which were filled during the 2010s.

There are two downstream reinforcements berms with maximum heights of 10 meters and 9 meters, and widths of 3 meters and 19 meters, respectively. The dam upstream slopes are not specified, as the beach meets the crest, while the downstream slopes have gradients ranging from 2H:1V to 1.64H:1V. The dam fill is comprised of a homogenous compacted saprolitic soil sourced locally.

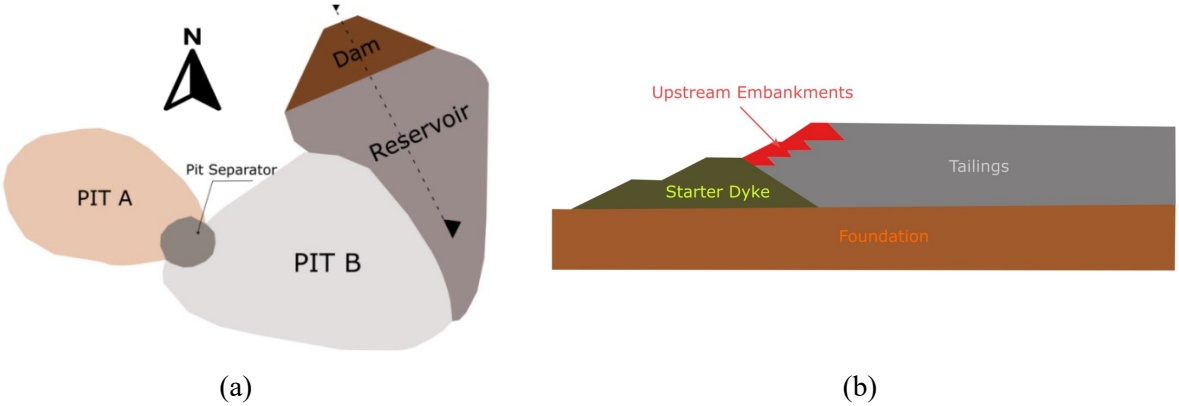


Figure 1: Schematic view – (a) plan view (b) cross-section

A granular internal drainage system runs beneath through the starter dam as basal drain. Foundation soils are residual phyllite soil, averaging 5.0 to 6.0 meters thick, overlying phyllite saprolite of similar thickness. The residual soil at the dam's base is thinner than at the abutments due to partial excavation. Beneath the saprolite, the material transitions to moderately resistant phyllites with increasing depth.

The dam is classified as high priority (DPA) with a high-risk category at the federal level and a low-risk category at the state level. According to CDA and GISTM standards, the dam is designated as Very High consequence.

Trade-off studies and conceptual engineering

Based on the initial goal to decharacterize this upstream raised dam, seven alternatives were analyzed in a trade-off study. This study included a qualitative analysis of all alternatives and a detailed evaluation of the three most viable options: upstream portion removal, rockfill buttressing, and complete removal with a downstream check dam.

For each alternative, risks associated with geotechnical, hydrological, and hydrogeological conditions were assessed. A Potential Failure Modes Analysis (PFMA) was conducted to identify potential failure modes, involving discussions with all stakeholders, including engineering and operational teams, the Engineer of Record, the Design Reviewer, and the corporate geotechnical team.

A technical gate was then held to determine the best alternative for further detailed engineering. After thorough analysis, the stakeholders decided that the removal of the upstream raised portions of the dam was the optimal solution, considering technical, environmental, and social aspects. The technical gate process was used at each major design and decision stage of the project.

After this initial technical gate, the chosen solution was to remove all upstream tailings, creating a uniform flat slope with a central channel to connect the reservoir with two pits. This alternative was selected for several reasons:

- With no upstream raises left, the dam would no longer be characterized as an upstream raise, and the remaining dam (Starter Dam only) would have a reduced consequence classification.
- The alternative buttressing solution would have required advanced technologies for proper QA/QC and extensive investigation at the dam's toe, necessitating remote equipment.
- The high iron content of the excavated tailings (> 60% hematite, Gs ~ 4.5) offered opportunities for re-processing, which would offset the cost of the decharacterization works.

A conceptual design was developed for the selected alternative, which included a gap assessment, initial data consolidation, and technical specifications for the next engineering stage. The concept involved hydraulically connecting Pit A, Pit B, and the reservoir with a channel excavated in the tailings with outflow to a concrete channel on the left abutment of the dam.

A conceptual deformation model developed in FLAC 2D indicated that the excavation process was technically feasible, with a low probability of initiating static liquefaction during excavation. However, due to the limited availability of data to characterize the tailings and limited construction records, the initial FLAC model used critical state parameters from the Fundão dam as representative of the tailings. This gap in critical state laboratory testing was to be addressed through site investigation and lab testing of the tailings in subsequent engineering phases.

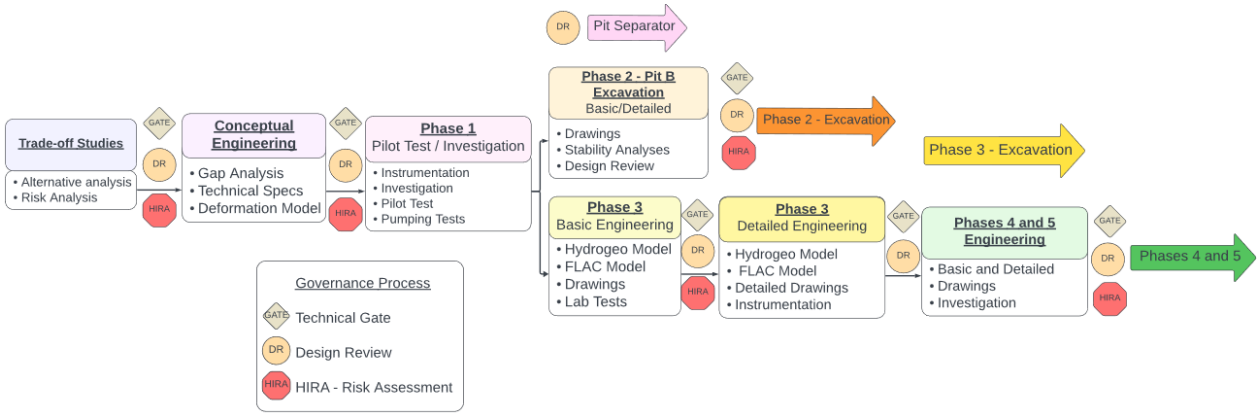


Figure 2: Project flowchart with initial phases in detail

During the conceptual engineering phase, the project was conceived of as proceeding with excavation of long continuous layers beginning from Pit A and extending across Pit B and the Reservoir. Phase 1 however, began as a pilot test in the most upstream portion of the excavation in Pit A. The pilot test was intended to assist in determining water management, and thickness of each continuously excavated layer down to the Starter Dam. Instead, the pilot test revealed a completely different approach that separated the work into five phases. Figure 2 illustrates the project phases, emphasizing the initial stages.

Phase 1 – project development and Pit A excavation

Phase 1 advanced the project from a conceptual engineering gap assessment and preparation of initial technical specifications into a pilot excavation test program, coupled with site investigations, pump tests and instrumentation installation to better characterize the tailings, dam fills, and foundation materials.

Pilot test and pit separator

The primary objective of the pilot test was to explore excavation criteria under controlled conditions, away from the dam crest, using unmanned equipment which would then lead to a plan for the full tailings removal. Initially, it was assumed that the tailings in Pit A would exhibit similar saturation levels as those in the reservoir, making the excavation trial representative for the remainder of the excavation, closer to the dam. However, during the installation of push-in piezometers and CPTu tests in Pit A, it was discovered that the water table was lower than anticipated for the pilot test's maximum excavation depth. This finding provided an opportunity to adjust the initial plan.

The CPTu tests also revealed that the region between Pit A and Pit B, initially thought to be larger and deeper, was shallower and narrower (Figure 3). The approximate depth to the old pit crest between Pit A and Pit B, was confirmed to be at a maximum depth of 6 meters, sloping upwards towards the abutments. This discovery enabled the physical separation of both pits, by excavating a "Pit Separator" down to native ground, excavating the dry tailings in Pit A to a shallow slope and reinforcing the Pit A tailings surface with rockfill. This separation not only significantly reduced the risk of tailings from Pit A contributing to a larger tailings' failure, but it also allowed Pit A to be re-designated so that manned equipment instead of remotely operated equipment could be used. Moreover, it created a substantial area for temporary tailings disposal during subsequent phases of excavation. This innovation notably enhanced the efficiency of excavation by minimizing the distance that remote-controlled equipment needed to transport tailings.

Additionally, the temporary disposal area in Pit A served as a stockpile zone where remote trucks deposited tailings from other areas. Manned equipment then transferred these tailings to their permanent disposal location, optimizing operational productivity across several projects.

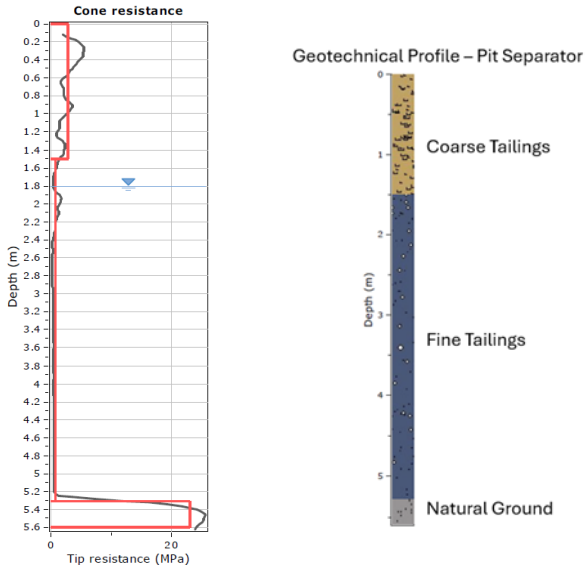


Figure 3: CPTu results in the pit separator region

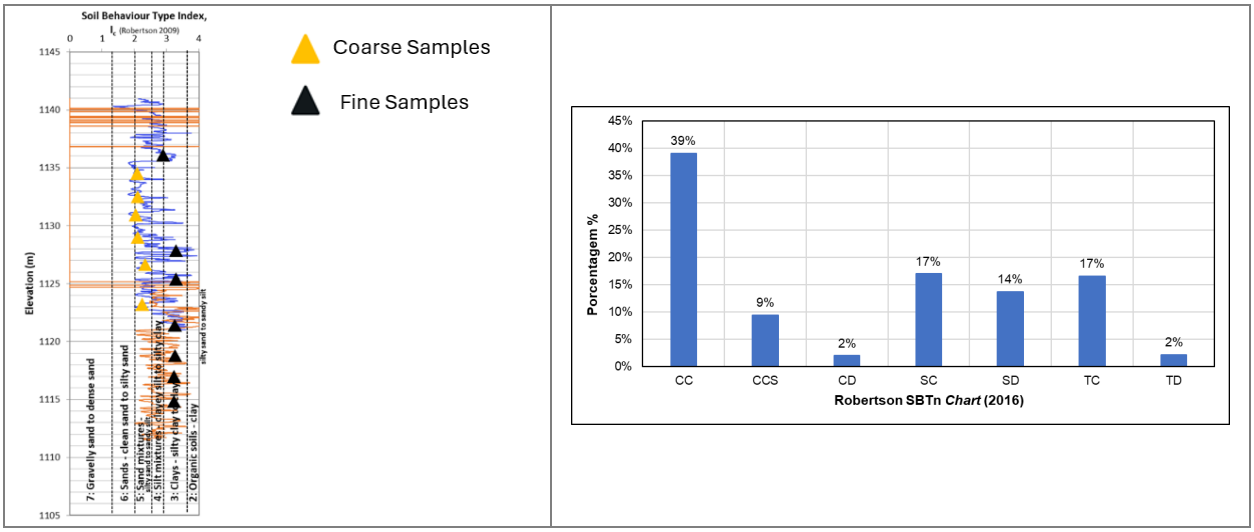
The Pilot Test phase also marked contractors' first experience with state-of-the-art remote excavation technology, a critical step in early project mobilization. This phase facilitated operator training, identified opportunities for improving remote excavation technology, and provided valuable insights to the design team regarding the limitations of remote operated excavation.

Phase 2 – investigation campaign and Pit B excavation

With the completion of the pilot test, initial investigation and pit separator, the next phase had originally been intended to be the main excavation of the upstream raises and tailings from Pit A to the Reservoir, but instead, with the separation of Pit A from the system, focus turned to excavation of Pit B. An investigation campaign and pumping tests were conducted to inform the basic and detailed engineering phases. Regulatory constraints required all activities within the tailing reservoir, including inspections and investigations, to be performed remotely or with lifelines (Andrade et al, 2022). Lifeline systems were installed at the crest and between Pit B and the Reservoir, effectively limiting investigation to the areas below the lifelines, excluding berms and upstream embankments. Furthermore, following the Brumadinho incident, drilling in tailings dams could not involve water or fluids, necessitating the use of hollow auger systems with restricted depth capabilities. Additionally, vibrations tests were run to estimate the level of vibration associated with investigation and excavation activities.

Over 60 CPTu and SCPTu tests and 15 push-in piezometer installations were conducted using Deep Drive® (Wood et al., 2023) remote equipment, which allowed for instrumentation outside lifeline areas. MASW surveys were also conducted across multiple sections of the dam and reservoir.

CPTu results, which included behavior and permeability assessments, were used to categorize tailings into fine, intermediate, and coarse in the reservoir and Pit B. Figure 4(a) demonstrated a correlation between soil behavior and grain size distribution, and a laboratory testing program was prepared to assess each of the three tailings categories.



(a) (b)

Figure 4: CPTu results – (a) Comparison with samples grain size; (b) Distribution of tailings based on soil type behavior

Laboratory testing was conducted primarily on remolded specimens due to difficulties in obtaining undisturbed samples. The laboratory testing campaign focused on determining critical state parameters for the tailings, crucial for deformation modeling. Figure 4(b) shows that over 80% of the tailings exhibited contractive behavior. However, due to restrictions on using only remotely operated machinery and the inability to collect manual samples, efforts to characterize foundation and embankment materials were limited. Some key challenges of this process were:

- Sample Collection: Despite planning to use disturbed samples from the beginning, field operations faced significant challenges in obtaining representative fractions for the three types of tailings. Depth limitations and inadequate representation of coarse and intermediate tailings needed multiple collection attempts, causing schedule delays.
- Communication: Coordination with a third-party commercial laboratory for critical state testing posed communication challenges initially. As the campaign progressed, closer collaboration improved feedback on test conditions.
- Behavior Variability: Despite classification into three types, the tailings exhibited inconsistent behavior during laboratory tests. Tests under similar remolding conditions and grain size distributions showed variability in stress paths, particularly in contractive tests, extending the duration of the laboratory campaign.

Figure 5 illustrates the Critical State Lines for the three tailing types and compares them with the Brumadinho tailings used in the conceptual phase. Despite differences in grain size distribution, the three types exhibited similar critical state lines, suggesting that these differences were not significant. Interestingly, the assumption of using Brumadinho CSL parameters proved conservative compared to actual test results.

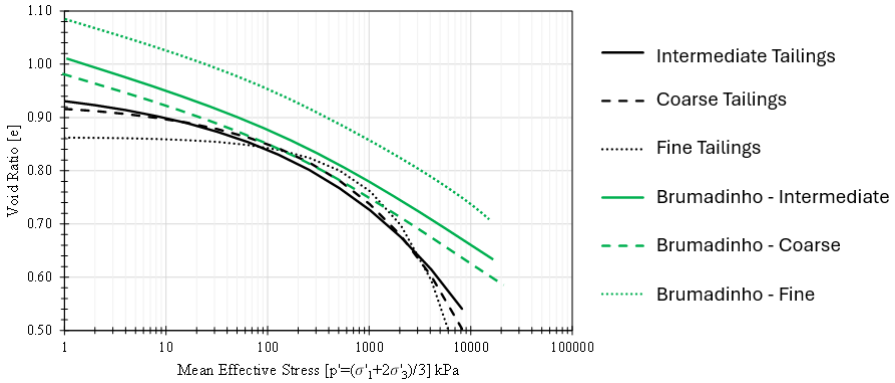


Figure 5: Critical State Line results and comparison with Brumadinho tailings results

Pit B excavation

Because of the construction of the pit separator between Pits A and B, and with the confidence gained during the Phase 1 excavation and the site investigation campaign, the next design step applied the results of Phase 1 (Pit A pilot test and pit separator excavation) and the site investigation test results on excavating Pit B.

Following the project governance structure, the decision to divide the excavation into segments (Pit A, Pit B and Reservoir) was reviewed by all stakeholders following a risk assessment (HIRA) and a technical gate. It was concluded that based on the distance between Pit B and the main dam, and the success of Pit A excavation, that excavation of Pit B could be allowed to proceed (as Phase 2 of the works) separating the excavation of the Reservoir into a new Phase 3. The governance structure allowed clear and open communication between the engineering team, the designer, and constructors to approve this meaningful change.

Similar to Phase 1, the excavation during Phase 2 provided additional validation of project design criteria, and application of the observational method allowed modifications to construction requirements which then fed into the Phase 3 design. Phase 3 was the most critical excavation phase which would begin excavation of the dam upstream raises and the main reservoir and so Pit B excavation results provided the basis for parameters such as speed and depth of excavation, dewatering requirements, and vibration limits.

Phase 3 – reservoir excavation

The goal of (both basic and detailed) engineering for Phase 3 was to better understand the geotechnical and hydrogeological characteristics of the Reservoir and the upstream dam raises. The separation of Phase 2 Pit B excavation from the Reservoir excavation reduced the pressure on moving forward with the engineering for Phase 3, giving the team more time to work on modelling to characterize the Reservoir and, in particular, the upstream dam raises.

Initially, because of restrictions to access the Reservoir and dam downstream areas, geological mapping was not possible. After Phase 1 (Pit A excavation) and the start of Phase 2 (Pit B excavation) the restriction on access was partially lifted, allowing new mapping activities and personnel access to the Reservoir and dam areas (with new warning and tracking systems). The new mapping advances the preparation of a detailed hydrogeological model. Piezometric data, flow data and field observations fed the model and led to the conclusion that the east portion of the reservoir received most of the groundwater contribution, but due to the regional structural bedrock dip, this contribution was less than what was predicted initially. With this updated information on the geological features of the area and a complete hydrological history for all piezometers, the numerical model presented excellent results with a nRMS < 6%.

The calibrated hydrogeological model was used to provide piezometric conditions to be used in the 3D deformation model, providing an excellent calibration that represented the piezometric conditions for each step of excavation. Since the hydrogeological model was calibrated in the transient condition, it was possible to have an estimate of the piezometric surface for each stage of excavation considering the annual variation of rainfall and the amount of water being intercepted at each stage.

Due to the limited information regarding the construction history of dam construction and tailings deposition, it was not possible to model the construction sequence satisfactorily. The calibration of the model focused on matching the current state parameter, K0 and G0 condition in the reservoir based on CPTu estimates, and then modeled the excavation in layers, with the hydrogeologic model providing estimates of the phreatic surface at the beginning and end of each step. The deformation model results showed that the areas with susceptibility to liquefaction during the proposed excavation sequence were limited to small portions at the top of each layer.

Phases 4 and 5 – starter dam excavation and final channel

The revised project goal was to complete excavation of the Reservoir and all upstream raises down to the Starter Dam level, leaving the Starter Dam in place in three phases.

However, once again, the robust governance structure and procedures provided a new opportunity to completely restore the valley to pre-mining conditions. The owner indicated an interest in remining some

specific portions of Pit B that would deepen the excavation on Pit B and the Reservoir. This led to a new trade-off study to assess the best option for this new remining opportunity. The option to fully remove the Starter Dam was the chosen option. This new direction closed the iterative process of design that both started and ended with trade-off studies.

From the beginning, no-risk closure was a primary focus for all stakeholders. The project transformed from a two Phase (pilot test – main excavation) to a three Phase (Pit A, Pit B, and Reservoir Excavation) to a five-stage final solution that will now include a full removal of all tailings and the dam, not just the upstream raises. This was made possible by a team that was always looking for opportunities for improvement. At the end of the project, the once tailings-filled-valley will be fully restored. Design of Phases 4 and 5 are ongoing and the works are expected to be completed by the end of 2026. The main challenges for these new project phases will be similar to the previous phases: minimal information on topography, construction history and uncertainties in piezometric information and in foundation characterization. The same iterative process and project governance structure is anticipated to bring the final works to a successful conclusion.

Discussion

Challenges

The project history highlights important challenges faced by the engineering teams during the development of the engineering for all five phases of engineering. Key challenges include:

- **Remote works for investigation and excavation –** Restrictive regulations set in place in Brazil after the recent incidents limited accessibility of manned equipment, forcing most early works to be conducted by remote equipment or innovations such as an overhead lifeline, and a remote-controlled CPTu rig.
- **Tailings variability –** Although CPTu testing indicated three distinct tailing types, fine, medium, and coarse, the tailings did not show significant behavioral differences. The exception was the permeability of the coarse tailings' layers.
- **3D modelling (deformation and hydrogeological) –** Even though three-dimensional models present great advantage while dealing with complex problems, they have challenges associated with their complexity. The development of a single geological model that should be able to represent the same hydrogeological and geotechnical conditions increased the time necessary to finish the models especially with the difficulties in determining both hydrogeological and geotechnical soil parameters, but both models proved to be vital for a full understanding of the behavior of the tailings during the excavation.

- **Stakeholder engagement –** With multiple interests in the table and with strict internal and external governance, dealing with all the stakeholders was a big challenge to the project. In general, the design team had to interact with the client's internal line of defense and exterior stakeholders including the EoR, the Design Reviewer, the HIRA Facilitator, the Federal Prosecutor audit team, and national and state legislators.
- **Water management –** State law requires that the minimum return period for a spillway system during the excavation works should be higher than 1,000 years. This impacted the planning of each phase and required creative solutions to maintain adequate spillway and water channels for each phase.

Lessons learned

The development of engineering provides lessons learned in both governance and technical areas that could be helpful for similar projects in the future.

In terms of governance, stakeholder engagement and management communication were critical to the success of the project. The process of continual review is vital to a high-risk engineering project; a high-profile project such as a tailings dam removal also involves engagement of national and state officials, audit teams and external reviewers. By establishing a process of open communication, and regular, detailed technical gates, the overall process became easier as transparency led to trust between stakeholders. All stakeholders were included in the process – all concerns and comments were taken seriously and dealt with openly. Weekly in-person field meetings and monthly auditing meetings were held to keep team members apprised.

This strategy seems simple, but it was time consuming and at times slowed the progress of the work. However, in the end, it proved successful in establishing an iterative design process and resulted in several modifications that enhanced the overall project. Through multiple trade-off studies, technical gates, risk assessment discussions, rounds of reviews and regular meetings, the project advanced with fewer obstacles. This strategy led to the implementation of a phased excavation sequence that allowed the contractors to establish methodology for excavation and train workers in a less risky environment, reducing the learning curve while addressing the data gaps for the most critical phase of the project. With this approach, the observational method was applied during Phase 1 and Phase 2 that enhanced the design and excavation of Phase 3 (and the ongoing Phase 4 and 5).

There were challenges in characterizing the soils and tailings hydrogeologic and geotechnical parameters, but the results of the hydrogeological model have proven to be crucial for understanding the groundwater behavior and led to an improved 3D deformation model. A simpler 2D seepage model would

not have captured the geological complexity of the area. Calibration of the model against actual piezometric readings improved the confidence in the model results.

Finally, the 3D deformation model became a critical tool for predicting the behavior of the excavation and the potential for liquefaction during the works using a calibrated hydrogeologic model, site investigations and laboratory testing even though there was limited construction history for the site. Critical state laboratory tests were used to define the model constitutive relationships and predict the site performance during excavation. This was critical to successful completion of the works.

Conclusion

The decharacterization project of the high-priority upstream-raised dam presented in this case study demonstrates the effectiveness of a phased engineering approach. Key conclusions from this project include:

- The integration of technical innovation and rigorous modeling is essential for addressing the complexities of high-risk mining dams.
- A holistic and adaptive engineering and governance strategy, incorporating initiative-taking stakeholder management, is critical for successful project outcomes.
- Continuous evaluation and updates to the hydrogeological and deformation models are necessary to reflect the evolving conditions during the excavation.

Overall, this project underscores the importance of a comprehensive and flexible engineering methodology to achieve compliant and effective decharacterization of high-risk mining dams.

Acknowledgements

The authors would like to acknowledge the help of other colleagues involved in this project. From Vale: Jhonatam Bortolanza, Adriana Ribeiro, Guilherme Mattedi, Frank Perreira e Marcia Palhares. From KCB: Benicio Junior, Bruno Bicalho, Bruno Rodrigues, Chris Strachotta, Cristian Henrique, Daniel Faria, Enzo Dias, Felipe Abbas, Felipe Santos, Frank Espinoza, Hugo Ninanya, Isabella Costa, Jackeline Huertas, Joe Quinn, Jordan Vaz, Len Murray, Maryam Saaly, Monica Silva, Rayanne Bicalho, Sabrina Cardoso, Thales Santos, Vicky Nguyen, Vinicius Lanza, Walace Gonçalves.

References

Andrade, R.M.S.A., Andrade, C.R., Micheluzzi, V.F.C., Kelly, E.R. and Mendonça, T.M. 2022. Sistema de Resgate de Emergência em Barragens. *COBRAMSEG 2022. Proceedings of the 20th Brazilian Congress on Soil Mechanics and Geotechnical Engineering*. Campinas (SP).

ANM 2019. Resolution No. 13, of August 8th, 2019. Establishes regulatory measures aimed at ensuring the stability of mining dams. Brazil.

ANM 2019. Resolution No. 4, of February 15th, 2019. Establishes precautionary regulatory measures aimed at ensuring the stability of mining dams. Brazil.

SEMAD 2019. Terms of Reference for the decharacterization of upstream-raised dams. Brazil. 2019.

Design of a Co-disposal Facility for Thickened Tailings and Potentially Acid-generating Waste Rock

Patrick Williamson, INTERA Inc., USA
Wilson Muir, Knight Piésold Ltd, Canada

Abstract

Environmental and geotechnical risks and impacts from surface disposal of mine waste are increasingly becoming a source of concern for regulators, investors, operators, and communities within the potential area of influence of mining operations. Waste disposal strategies should implement the Best Available Technology and Best Available Practice for waste management, while considering specifics of the local topography, climate, foundation conditions, construction materials, and waste characteristics. The Alacrán Cu-Au-Ag Mine Project (the Project) in northwestern Colombia will need to manage potentially acid-generating waste rock during mining. The steep, rolling terrain limits disposal site options, and water management is challenging, with approximately 3 m of rain annually. Minimizing water in tailings storage facilities and reducing waste rock exposure to atmospheric oxygen and precipitation are common challenges at many mine projects. One emerging technology addressing both issues is co-disposal, which combines tailings and waste rock in a single engineered storage facility.

Co-disposal was selected as the preferred waste management strategy for the Project after multiple investigations. This waste management strategy will create a low-permeability waste deposit, reduce foundation seepage, and centralize the storage of all mining and processing waste. Co-disposal, in places where suitable, may reduce environmental risks and impacts, improve public perception, and lower costs and timelines for mining projects. Multiple lines of investigation are necessary for the effective design of a co-disposal waste management facility.

Introduction

Environmental and geotechnical risks and impacts from surface mine waste disposal are increasingly becoming a source of concern to regulators, investors, operators, and the communities within the potential area of influence of mining operations. Operational, financial, ecological, and reputational risks arise from drainage of mine-impacted water from waste rock storage facilities, reactive surfaces exposed by mining, and tailings storage facilities (TSFs). Recent TSF failures, resulting in the sudden release of large volumes

of tailings and solutions, include the Williamson Mine (Tanzania, 12.8 M m^3), Brumadinho (Brazil, 12 M m^3), and the Germano mine (Brazil, 32 M m^3) (WISE, 2024). These challenges have led the mining industry to develop Best Available Practices for waste disposal by minimizing water in tailings storage facilities and reducing the exposure of waste rock to atmospheric oxygen and precipitation. An emerging technology that addresses both issues is co-disposal, which is the placement of tailings and waste rock together in an engineered storage facility. Co-disposal, also known as co-placement, co-deposition, co-mingling, co-layering, or PasteRock®, ranges from heterogeneous co-placement of tailings with waste rock to very homogeneous blends (Figure 1). The proposed co-disposal strategy for this Project involves layered co-mingling as the best balance between effectiveness and feasibility. Due to the space limitations for this publication, only an overview of the details will be provided here. The complete Feasibility Study is available at Cordoba Minerals (Corboba Minerals, 2023).

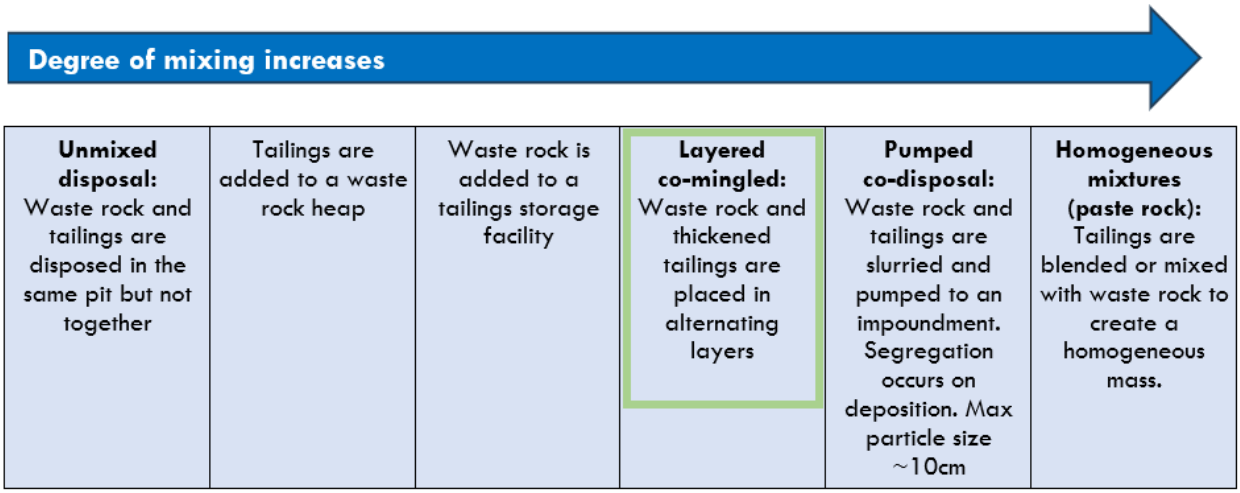


Figure 1: Co-disposal methods (after Pukkinen et al., 2019)

Research and mine site applications have demonstrated that co-disposal has the following benefits (Gowan et al., 2010; Habte and Bocking, 2012; Ulrich and Coffin, 2015; Wickland et al., 2006):

- Reduces oxygen flux and infiltration through mine rock (i.e., to control sulfide oxidation, acidic drainage, and metal leaching).
- Improves stability (static and dynamic) of a disposal facility and decreases probability of liquefaction.
- Reduces the footprint required for the disposal of two waste streams.
- Simplifies water management, monitoring, and closure.
- Accelerates tailings consolidation, improves permitting timeline, and facilitates earlier closure.
- Reduces the erodibility of tailings by either water or wind.

Critical factors for effective co-disposal include the moisture content of the tailings and waste rock placement practices. Oxygen diffusivity in a fine-grained porous media decreases sharply with increasing moisture content. Tailings at approximately 85% saturation form an effective barrier to oxygen diffusion (INAP, 2018), minimizing sulfide oxidation. In a homogeneous blend, the optimal ratio of rock to tailings required to fill the pore space in waste rock is 5:1 or less (Wickland et al., 2006). In co-mingling, the objective is not to fill the waste rock pore space, but to minimize oxygen diffusion and infiltration into the layers of waste rock using contiguous layers of tailings to isolate the waste rock from the atmosphere.

The selection of a specific co-disposal method depends on several factors, including:

- Site topography and ease of construction and operation.
- Climatic conditions (e.g., cold, extremely dry, extremely wet).
- Tailings characteristics (e.g., geochemistry, viscosity, grain size distribution, mineralogy).
- Mine rock characteristics (e.g., geochemistry, grain size distribution, mineralogy).
- The volume ratio of mine rock to tailings.
- Life cycle costs of the co-disposal facility.
- Risk potential (e.g., wind and water erosion, slope stability, liquefaction, closure).

Currently, several mines employ co-disposal, including Marmato (Colombia), Navachab (Namibia), Nunavik (Canada), Greens Creek (USA), Snap Lake (Canada), Caraíba (Brazil), Neves Corvo (Portugal), Mount Thorley (Australia), and Argyle (Australia) (Verburg, 2024; Gowan et al., 2010). All these mines have a daily production of less than 20,000 tonnes per day.

Site background

The Project is in the Department of Cordoba, Colombia, 390 km northwest of Bogotá and 160 km north of Medellín. The mine site lies in the northern foothills of the Western Cordillera of the Andes mountains, with elevations ranging between 100 m and 350 m above sea level.

The Project is in an accreted oceanic terrane of the Western Andean Cordillera. The El Alacrán deposit's mineralization is hosted by a west-dipping Cretaceous succession comprising mafic volcanic rocks overlain by a calcareous volcaniclastic sequence, capped by pre- to syn-mineralization sill-like diorite and felsic sub-volcanic bodies. Cu-Au-Ag mineralization occurs throughout the volcaniclastic package. Research by Manco (2020), in combination with previous work, suggests that the genetic model for the El Alacrán deposit is a hybrid between Iron Oxide Copper-Gold and Carbonate Replacement deposits associated with a porphyry source. The climate in the region is humid and warm, with average monthly temperatures ranging from 24.5°C and 27°C. The Project receives approximately 3,000 mm of rainfall annually, with rain occurring year-round and a wet season between April and November. The

evapotranspiration rate is approximately 1,500 mm/year. Due to the high rainfall and warm climate, the igneous and volcaniclastic rocks in the region have undergone extensive weathering, characterized by up to 11 m of saprolite (composed principally of quartz, chlorite and aluminous and lateritic clays), a transition zone (weathered bedrock), and then unaltered bedrock.

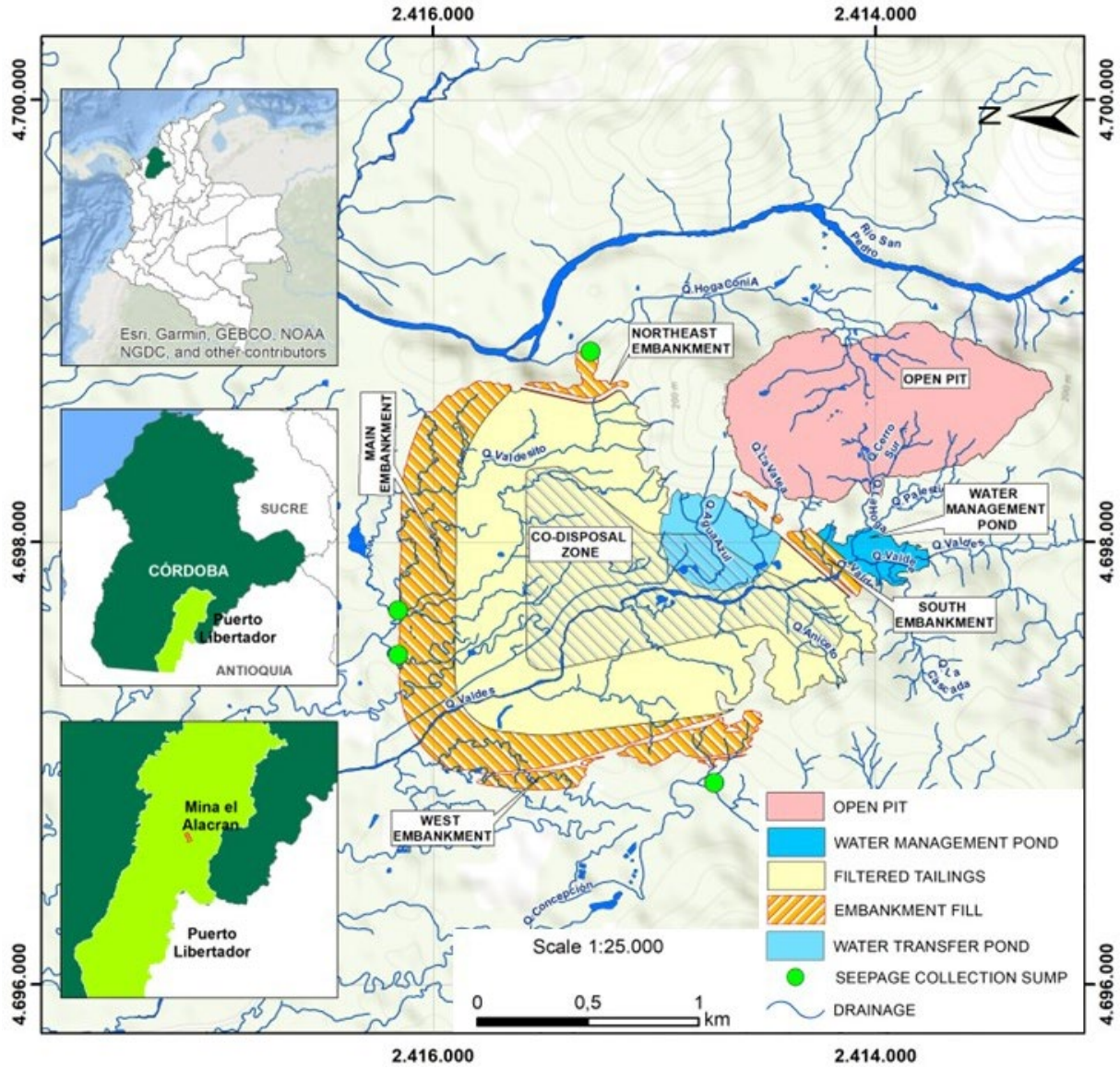


Figure 2: Site location and waste management facility features

Conventional open-pit mining methods will be used to extract ore from the El Alacrán deposit, with an anticipated production period of 14 years. The ore will be processed through crushing and a four-stage flotation circuit, which includes rougher, cleaner scalper, cleaner scavenger, and recleaner stages. Concentrate from the cleaner scalper and recleaner stages will be thickened and filtered to produce the final

concentrate. Tailings produced in the rougher and cleaner scavenger stage flotation (after passing through the gravity concentrator) will be sent to the tailings thickener, and subsequently to the waste management facility (WMF) at approximately 55% solids by mass. The mill throughput rate is set at 17,600 tonnes per day. It is anticipated that 34 million tonnes (Mt) of potentially acid-generating (PAG) waste rock and 102 Mt of thickened tailings will be stored in the WMF basin during mining and milling operations over the 14-year mine life.

Investigations

Studies supporting the design and operation of the WMF included foundation assessments, geochemical characterization of waste rock, tailings, and tailings decant within the proposed WMF area (described in more detail below), along with various hydrogeological and water chemistry studies of the valley where the WMF will be located.

Foundation characterization

The foundation characteristics at the WMF reinforce the suitability of co-disposal at the Project. Topsoil covers the entire WMF area, underlain primarily by saprolite, with isolated pockets of fine or coarse alluvium. The fine alluvium has very similar engineering properties to the saprolite. Beneath the soil units, weathered bedrock and bedrock are present. The saprolite will form the basin for tailings deposition and reduce seepage from the WMF. The saprolite typically consists of silt and clay with varying sand content and is classified as CH (inorganic clays of high plasticity) to MH (inorganic silts of high plasticity) according to the United Soil Classification System (ASTM D2487). Five permeability tests indicate that the permeability ranges from 4.2E-10 to 5.6E-08 m/s, which is at the low end of typical values for saprolite, effectively minimizing seepage (Blight, 1997).

Waste geochemical characterization

Geochemical characterization of the waste streams generated by a mine is an essential element of a Feasibility Study. Samples of mine waste to be deposited in the WMF included tailings (n=4), tailings decant (n=1), waste rock (n=80), and saprolite (n=20). These materials were characterized using a standard suite of geochemical static and kinetic analyses, including mineralogy, total elements (52 elements), shake flask extraction and leachate analysis, net acid generation, and acid-base accounting (ABA). Kinetic tests included site barrel (n=10) and humidity cell tests (n=14). A geochemical sampling and analysis program was developed and implemented to inform the Pre-Feasibility and Feasibility studies, as well as the Environmental Impact Assessment required to obtain a Colombian environmental permit. The program was based on a site-specific conceptual geochemical model, considering the range of anticipated waste rock

lithotypes (including lithology, alteration, and degree of weathering), expected volumes of each potential waste rock lithotype, and operational factors. Results from this geochemical program were correlated to the much larger exploration data set (n=47,231 for waste rock), which was used to generate a block model for the waste rock.

Results of the program indicate that the range of waste rock lithotypes from the mining operation at the Project are a mixture of PAG, uncertain acid generation, and non-acid-generating (NPAG). Most of the waste rock to be generated by the Project falls into the uncertain range (Figure 3) based on static tests.

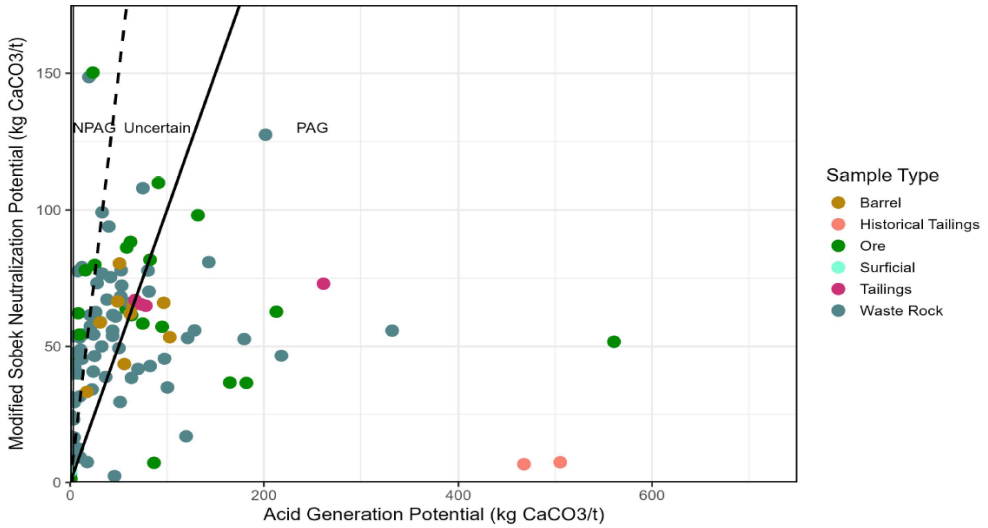


Figure 3: Acid-generation potential vs. acid-neutralization potential for Project waste.

Field barrel test results from 10 waste rock composites after 17 months suggest that mixed waste rock could produce drainage with pH < 6 drainage and elevated metal concentrations, indicating that it could have uncertain acid-generation potential in the long-term. Results for saprolite within the proposed WMF footprint had very low sulfide concentrations and were classified as NPAG. Decant samples were analyzed for the full list of organic compounds, metals, major ions, and potential mining by-products listed in the Resolution 0631 limits for mine discharge (MINAMBIENTE, 2015). The only parameter that exceeded the Resolution 0631 limits was pH at 9.5 (limit is 9). Sulfate concentrations in the decant were 300 mg/L.

Tailings geotechnical characterization

Laboratory physical characterization testing was completed on thickened tailings samples to estimate their Atterberg limits (index test), settling, consolidation, and permeability properties. The index test results suggest that the tailings are non-plastic, consist of 32% sand, 55% silt, and 13% clay, and have a specific gravity of 2.87. The P80 of the tailings is 150 micrometers (i.e., 80% of the particles are finer than 150 micrometers). The tailings are classified as an inorganic silt of slight plasticity.

Undrained, drained, and drained plus air-drying settling tests were completed on tailings slurry samples at 60% and 65% solids content by mass. The results indicate that the estimated settled density ranges from 1.34 to 1.36 t/m^3 under undrained conditions and from 1.45 to 1.50 t/m^3 under drained conditions. Air-dried settling test results at 60% solids content indicate that the solids content increased to 71% (11% increase) in 2 days and were fully dry after approximately 4 weeks.

Consolidation tests were conducted using a Rowe cell, allowing the tailings to settle and consolidate under their own weight. Confining stresses ranging from very low (10 kilopascals [kPa]) to high (800 kPa) were applied in incremental loading stages, while maintaining two-way drainage conditions. The measured Coefficient of Consolidation (Cv) values ranged from 31 m^2/year at low effective stress (10 kPa) to 5 m^2/year at high effective stress (800 kPa). The Cv values are considered to be at the low end of the range of typical values for copper mine tailings (Vick, 1990).

Permeability test results indicate that the hydraulic conductivity of the tailings decreases from 4.9x10^{-9} m/s at 200 kPa to 2.2x10^{-10} m/s at 800 kPa. This suggests that the hydraulic conductivity of the tailings will likely decrease with increased tailings depth and effective stress. Permeability tests on compacted saprolite yielded hydraulic conductivities ranging from 4×10^{-10} to 6×10^{-8} m/s, with a geometric mean of 4×10^{-9} m/s. These values are comparable to the permeability of high plasticity tailings silts and clays (Vick, 1990).

WMF design overview

The WMF will consist of a valley-type impoundment to provide permanent storage for PAG tailings and PAG/uncertain waste rock. A schematic of the proposed WMF is provided in Figure 4.

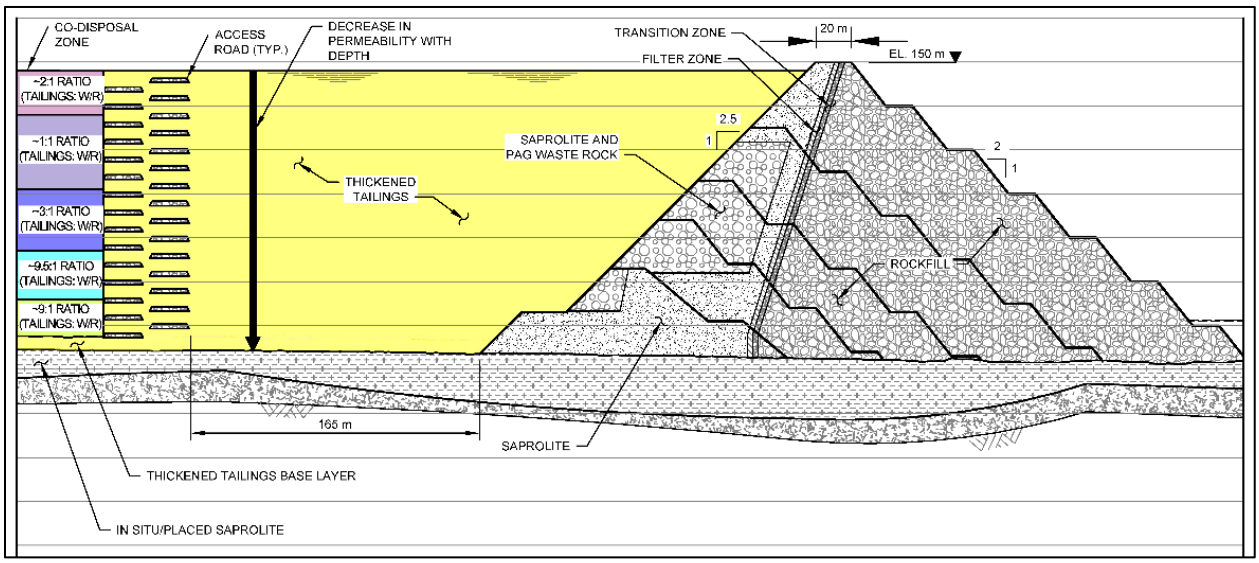


Figure 4: Typical WMF embankment and basin section (Cordoba Minerals, 2023)

Key components of the design of the WMF include perimeter embankments, a basin liner, and drainage.

Perimeter embankments

Perimeter embankments will be constructed using waste saprolite and waste rock from open-pit development to safely store the thickened tailings and PAG/uncertain waste rock. The impoundment will be developed by constructing embankments around the perimeter of the valley (Figure 2). The West, Main, and Northeast Embankments will be raised using the downstream construction method. The South Embankment will be constructed as a full-width divider embankment to establish a water management pond (WMP) in the southern portion of the valley. The embankments will be raised in five stages (Figure 4) to a maximum height of 68 m. The typical embankment cross-section from upstream to downstream includes saprolite to provide a low-permeability zone, filter and transition zones to provide drainage within the embankment fill, and a downstream rockfill shell zone.

Basin liner

The basin liner will consist of at least 3 m of saprolite within the WMF basin to reduce potential seepage from the facility. Saprolite, along with isolated areas of fine to coarse alluvium are present within the WMF basin. The WMF basin will be cleared and grubbed, and topsoil will be removed to expose the saprolite. In most areas, the foundation will consist of in-situ saprolite that is greater than 3 m in thickness, which will be grubbed, compacted and proof rolled. Additional saprolite will be placed and compacted following stripping and grubbing in areas of the WMF footprint with less than 3 m of in-situ saprolite.

Drainage

To manage water and maintain a low phreatic surface within the embankments, the design includes internal filter and transition zones, and a series of finger drains at approximate 200 m intervals in the Main, West, and Northeast Embankment foundations. The finger drains will connect to a conveyance drain along the ultimate downstream toe of the Main and West Embankments (parallel to the embankments) or directly to a collection sump (Figure 2). Multiple collection sumps will be located along the conveyance drain. The finger and conveyance drains will consist of gravel with a slotted CPT pipe wrapped in a filter sock and fully wrapped in non-woven geotextile.

WMF operation

Key aspects of the WMF operation will include water management, tailings deposition, PAG/uncertain waste rock placement, and basin filling.

Water management

The water management strategy for the WMF involves collecting supernatant and runoff for transfer to the WMP and maintaining a small water pond along the southeast side of the WMF basin (Figure 2). This will maximize the WMF basin surface area for drying and consolidation of the tailings and provide a suitable area to haul, place, and spread PAG waste rock.

Tailings deposition

The tailings will be pumped from the thickener at approximately 55% solids by mass to a series of centrifugal pumps and conveyed to the WMF via pressurized HDPE pipelines. Tailings discharge during operation will be rotated around the perimeter of the embankments and basin to achieve a tailings beach slope of approximately 2%. Multiple spigots will be used to maintain a low deposition velocity and the homogeneity and non-segregating properties of the tailings during deposition. Tailings deposition will be managed to route the supernatant liberated from the tailings and runoff towards the Water Transfer Pond located in the southern portion of the basin. This approach will facilitate the efficient transfer of supernatant and runoff to the WMP.

The tailings will consolidate over time due to the weight of overlying layers of tailings and waste rock. The dry density of the tailings will range from 1.3 tonnes per cubic meter (t/m^3) to 1.6 t/m^3, with a corresponding vertical hydraulic conductivity of 8.5×10^{-8} meters per second (m/s) to 1.1×10^{-10} m/s.

Waste rock placement and basin filling

The tailings deposition and waste rock placement strategy are illustrated in Figure 4. Prior to placement of PAG and uncertain waste rock within the WMF basin, tailings will be deposited in layers to develop a low-permeability deposit approximately 3 m thick immediately above the compacted foundation. The initial deposition of tailings will lower the hydraulic conductivity of the foundation and reduce potential seepage from the WMF basin into the underlying material.

Waste rock will be strategically placed at least 165 m from the Main, West, and Northeast Embankments and co-disposed with the thickened tailings. The waste rock will be placed in alternating layers and in such a manner as to avoid the formation of higher-permeability zones through the deposit. The waste rock will be continuously buried by subsequent tailings deposition to encapsulate the waste rock and minimize the potential for the onset of acid-rock drainage (ARD) and/or metal leaching (ML) conditions. The tailings in the co-disposal zone will partially fill the waste rock voids (estimated at 30%) and increase the overall dry density of the stored materials to an estimated dry density of 1.64 t/m^3 by the end of operations.

The ratio of tailings to waste rock placed in the co-disposal zone will vary over the five stages of WMF development. Initially, during Stage 1 operations, the ratio is estimated to be approximately 9:1. This ratio is expected to decrease to approximately 1:1 during Stage 4 operations and to approximately 2:1 during Stage 5 operations. Access roads constructed with waste rock will be incorporated into the WMF impoundment to facilitate waste rock placement. As each road is inundated with thickened tailings, a subsequent access road will be constructed, offset from the previous roads. This approach will prevent the formation of higher permeability zones in the WMF and help maintain the overall 2% tailings beach slope.

Closure

At closure, the WMF will be covered, and a spillway will be constructed to direct runoff from the WMF to the open pit. The WMF closure cover will consist of a 2 m thick, compacted saprolite layer covering the entire WMF basin, graded at 2% towards the closure spillway. Over this saprolite cover, a 0.25 m thick layer of topsoil will be applied and hydroseeded. This will minimize water and air infiltration into the tailings mass and provide controlled drainage from the surface of the WMF. This strategy will also help create a landform that will blend into the local topography, prevent standing water on the closed WMF and eliminate the possibility of uncontrolled embankment overtopping.

The infiltration of meteoric water through the WMF cover, mass of interlayered tailings and waste rock, and into the underlying saturated layer were estimated using a HELP model (USEPA, 2020). The model, developed for the final WMF arrangement, incorporated complex climate and land boundary conditions. The HELP model included parameters such as the saprolite cover layer, six fully saturated layers of tailings and waste rock, a final cover slope of 2%, local climate data, and evapotranspiration estimates, along with characteristics of the saprolite and tailings. The model was simulated for a period of 6 years. The results from the model suggest that the average infiltration rate through the bottom of the thickened tailings will be less than 100 m^3 per year. Based on the modelled flux through the WMF and groundwater flux under the WMF, the pore solution in the WMF will be diluted by a factor of approximately 12,000 by groundwater. Assuming the WMF source term chemistry reflects the pore water chemistry in the WMF that might eventually migrate into the underlying groundwater, mixing with groundwater will have a minimal effect on groundwater quality.

Conclusion

The combination of the compacted saprolite liner, the initial layer of consolidated tailings on the saprolite liner, and the tailings against the embankments will create a low-permeability waste deposit that minimizes oxygen diffusion and water infiltration within the waste. This waste management strategy is designed to reduce the oxidant and transport mechanisms that create ARD conditions. The following key additional

conclusions can be made based on the waste co-disposal strategies discussed above.

- The tailings and PAG/uncertain waste rock can be effectively co-disposed in a single facility over the life of the mine, with the waste rock fully encapsulated within the tailings.
- Partial ingress of tailings into the waste rock voids will increase the overall density of the waste deposit over time and reduce the overall height of the perimeter embankments.
- The WMF can become a landform at closure, while minimizing potential seepage to the environment post-closure.

Acknowledgements

The authors would like to acknowledge the following people in relation to this paper:

- Ms. Sarah Armstrong-Montoya (President and Chief Executive Officer) and Mark Gibson (Chief Operating Officer) of Cordoba Minerals Corporation, as well as Glen Kuntz (Senior Vice President, Mine Development) of Ivanhoe Electric Inc., who kindly gave the authors permission to present this paper.
- María Isabel Ramírez and Isaura Qunitero Ortega at Servicios Hidrogeologicos Integrales S.A.S. in Colombia who assisted with field studies and figure development.
- Joanna Stakutis and Elanor Heil for technical editing.

References

ASTM D2487. 2020. Standard Practice for Classification of Soils for Engineering Purposes (Unified Soil Classification System). ASTM International. West Conshohocken, PA.

Blight, G.E. 1997. *Mechanics of Residual Soils.* International Society for Soil Mechanics and Foundation Engineering. Technical Committee 25 on the Properties of Tropical and Residual Soils. Brookfield, VT: Rotterdam.

Cordoba Minerals. 2023. NI 43-101 Technical report – Feasibility Study, Alacrán Project in Colombia. Written by G.P. Barco, P. Cepuritis, A. Duggan, D. Frost, L. Jone, T. McDracken, W. Muir, J. Robinson and P. Williamson. Issue date February 1, 2024. https://cordobaminerals.com/projects/feasibility-study

Gowan, M., M. Lee and D.J. Williams. 2010. Co-disposal techniques that may mitigate risks associated with storage and management of potentially acid generating wastes. *Proceedings of Mine Waste 2010.* Australian Centre for Geomechanics.

Habte, K and K. Bocking. 2012. Co-Disposal Practices in Mine Waste Management. Technical Memorandum for Fortune Minerals Ltd. February 8, 2012.

International Network for Acid Prevention (INAP). 2018. *Global Acid Rock Drainage (GARD) Guide.* Accessed June 5, 2024, at: www.gardguide.com.

Manco, J.D. 2020. Geology, Geochronology and Geochemistry of the El Alacran Deposit, San Matias District, Cordoba, Colombia. Thesis research, Geological Sciences, College of Earth Sciences, University of British Columbia, Vancouver.

Ministerio de Ambiente y Desarrollo Sostenible (MINAMBIENTE), Gobierno de Colombia. 2015. *Resolución 0631: Parámetros y los valores limites máximos en vertimientos punctuales a cuerpos de aguas superficiales y a los sistemas de alcantirillado.*

Pukkinen, H., M. Juvankoski, T. Kaartinen, J. Laine-Ylijoki, E. Merta, U.M. Mroueh, J. Mäkinen, E. Niemeläinen and M. Wahlström. 2019. Co-disposal of waste rock with tailings. Mine Closure GTK. Accessed at https://mineclosure.gtk.fi/co-disposal-of-waste-rock-with-tailings/

Ulrich, B. and J. Coffin. 2015. Combined tailings and mine waste. *Proceedings of Tailings and Mine Waste 2015.* Vancouver, BC. October 26–28. 2015.

United States Environmental Protection Agency (USEPA). 2020. Hydrologic Evaluation of Landfill Performance: HELP 4.0 User Manual. EPA/600/B-20/219 | January 2020.

Verburg, R. 2024. Personal communication regarding mines using co-disposal.

Vick, S.G. 1990. *Planning, Design and Analysis of Tailings Dams.* BiTech Publishers Limited. Vancouver, BC.

Wickland, B.E., G. Ward Wilson, D. Wijewickreme and B. Klein. 2006. Design and evaluation of mixtures of mine waste rock and tailings. *Can. Geotech. J.* 43: 928–945.

World Information Service on Energy (WISE). 2024. Chronology of major tailings dam failures. Accessed 6/5/2024 at https://www.wise-uranium.org/mdaf.html

A Study on the Possibilities, Constraints, and Motivation for Transitioning a Conventionally Designed TSF into a Full-scale Hydraulically Dewatered Stack Facility for Fine Residue Disposal in South Africa

N.W. Nxumalo, Jones & Wagener (Pty) Ltd, South Africa
P. Newman, Anglo American, UK
A. López, Anglo American, Chile

Abstract

Tailings dewatering and optimized water recovery are desirable objectives for owners and operators of tailings storage facilities (TSFs) in the mining industry. A large international mining firm has undertaken several studies and field-scale trials on the feasibility of hydraulically dewatered stacking (HDS) to improve water recovery from fine residue facilities. A concept study has been undertaken to transition a TSF designed to operate with conventional deposition and water recovery methods (ring feed pipe, spigots, penstock intake, and outfall system) into an HDS facility. This paper discusses the possibilities, constraints, and risks identified for full-scale implementation of the HDS methodology on a TSF. Findings on the preliminary preferred configurations from a high-level water balance and conceptual 3D numerical modeling are also presented.

Introduction

Conventional methods of recovering water from a tailings storage facility (TSF) comprise (i) a gravity penstock intake and outfall pipe,; (ii) a pumped decant system; and (iii) a network of basal drains. Gravity penstock and pumped decant systems drain supernatant water only. Basal drains collect water, which infiltrates through the settled tailings and reports to the bottom of the facility. This water must infiltrate through the very fine and cohesive silty material, through which water flow is impeded due to very low permeabilities. The process of draining water from the settled tailings occurs over extended durations and results in large volumes of water that are not recovered from the settled tailings. This water is undesirable, as it reduces the strength of the settled tailings material, increasing risks to mining operations, the environment, and surrounding communities.

The hydraulically dewatered stacking (HDS) deposition methodology enables recovery of both supernatant and interstitial water. Successful implementation of HDS is a significant deviation from current water recovery strategies and will substantially increase water reuse quantities in mining operations.

CPR and HDS process and definition

Anglo American (AA) has successfully implemented coarse particle recovery (CPR) at several of its assets. The technology generates a coarse reject material and creates a bulk concentrate for further processing (Filmer and Alexander, 2016; Filmer and Alexander, 2017, Filmer et al.., 2020). CPR uses a fluidized bed to enable valuable minerals, with as little as 1% mineral surface exposure, to be separated from gangue, a commercially valueless ore (Arburo et al., 2022). This process increases ore recovery rates, improves plant energy efficiency rates and reduces water consumption by recovering minerals at a particle size 2 to 3 times coarser than conventional flotation processes (Arburo et al., 2022). In the CPR process, underflow from the cyclones within the plant is recycled and reprocessed, increasing product recovery, while the overflow, a coarse graded reject sand referred to as CPR sand, is pumped directly to the TSF.

The CPR sands are characterized by low fines content (less than 5% particles <75μm) (Newman et al., 2022) resulting in relatively high permeability (Bustamante et al., 2024). The CPR sands are co-disposed with conventional tailings to form preferential and connected three-dimensional (3D) drainage paths within the tailings. When engineered correctly, such a configuration has the potential to change dewatering of freshly deposited tailings slurry (abstracting pool water via infiltration into pre-configured berms vs. penstock recovery), increases consolidation, and improves recovery of water from the in-situ settled tailings, thereby leaving a waste residue that is desaturated.

HDS trials and studies by Anglo American

Previous studies were undertaken by AA and WSP-Golder in Chile and by AA and SRK Consulting in South Africa. Both studies focused on: (i) material characterization through geotechnical testing programs in the laboratory; (ii) simulation of expected drainage behavior in the laboratory; and (iii) implementation of field-scale trials to characterize drainage behavior and verify laboratory test results.

El Soldado trial, Chile

Newman et al. (2022) highlighted that the El Soldado trial formed part of the laboratory test work carried out as part of the proof-of-concept study. The proof-of concept study was premised on the hypothesis that *"… placing interbedded layers of tailings with free draining sands (being a by-product produced by coarse particle recovery techniques from within the process flow sheet) will accelerate consolidation and increase the reduction in degree of saturation of the tailings mass. The purpose of this being to increase the tailings*

resistance to liquefaction." The El Soldado study therefore considered two main objectives: (i) laboratory characterization of tailings and CPR sand samples; and (ii) the design and implementation of a field-scale trial.

Mogalakwena trial, South Africa

A concept design for the BW2 TSF was undertaken by AA and Jones & Wagener (Pty) Ltd (J&W) in 2022, and a key finding of the study was that the options for implementing HDS on the BW2 TSF were dependent on the capabilities of the deposition equipment. This resulted in AA commissioning the Blinkwater 1 TSF trial (Murray et al., 2023). The primary objective was to assess the effectiveness of the sand placement unit. The focus of the field-scale trial was thus on advancing the knowledge base relating to operating a Self-Propelled Cyclone Unit (SPCU) and its performance in relation to: (i) sand thickness required to form a stable working platform; (ii) ease of preforming controlled deposition to form drainage channels; (iii) formation of blanket drains; and (iv) the potential erosion of CPR sand.

Contributions of present paper

The objectives and learnings of previous studies do not extend to the design of a full-scale facility for the HDS deposition method. The scope did not include assessment of appropriate spacing for CPR sand berms and the constraints that must be considered when the HDS method is implemented. This paper seeks to expand the knowledge base gained from previous studies and field-scale trials. The focus and objectives include: (i) documenting risks associated with design and full-scale implementation of the HDS methodology; (ii) identifying constraints associated with full-scale implementation of the HDS methodology; and (iii) evaluating water recovery performance of the platinum CPR sand berm configurations under high inflow rates.

Transitioning a conventional TSF design to HDS deposition

AA commissioned J&W to undertake the feasibility and detailed engineering for BW2 at the Mogalakwena Mine in Limpopo, South Africa. BW2 has a consequence classification of Extreme (ICMM, 2020) and is a waste rock impounded facility with a peak tailings throughput of 14.2 Mtpa, an annual rate of rise of 6.0 m, and a total capacity of 114 Mt. The conventional design, referred to as the "base case," comprises an embankment constructed in the downstream direction to a maximum height of 60 m, a Class C barrier, with an above and below liner drainage system as well as temporary and permanent penstocks. The penstock systems (temporary and permanent) are designed to accommodate the planned commissioning of the TSF in two phases.

Prior to commencement of the detailed engineering for the base case, AA commissioned the study to investigate transitioning BW2 from the conventional base case design into an HDS facility.

Three-dimensional numerical model

The influence of CPR sand berms on dewatering of tailings and the flow regime is omni-directional in nature and occurs in the 3D space. To understand the omni-directional flow properties and quantity of water reporting into the CPR sand columns, several 3D flow and seepage models were constructed in FEFLOW software.

FEFLOW uses finite element analysis to solve the groundwater flow equation for saturated and unsaturated conditions, which are critical for accurate modeling of the movement of water through tailings. All materials in the present study were modeled as saturated. Furthermore, consolidation of the tailings during deposition and cycling were not modeled. As a result, variability in saturation levels and the effect on permeabilities are not built into the model, resulting in conservative estimates of water reporting to the CPR sand berms. Permeabilities of the tailings slurry and CPR sand berm/outer embankment were specified as 0.0035 m/d and 1.7 m/d, respectively. The vertical permeability to horizontal permeability ratio of all materials present was specified as 0.1.

The FEFLOW models were used to evaluate ideal spacing (40 m, 60 m, 80 m, and 100 m) for the proposed CPR sand berm columns, evaluate inclusion of horizontal sand layers connected to the vertical sand columns, and to assess the impact of the hydraulic gradient on abstraction capacity of the drains. The models considered cyclic deposition through a series of paddocks.

This enabled simulation of the omni-directional flow regime and hydraulic interaction between the tailings and the CPR sand columns, both in the short term (i.e., during deposition), and in the long term (i.e., during consolidation) phases. Figure 1 illustrates a simplified TSF model with paddocks spaced at 40 m, 60 m, 80 m, and 100 m.

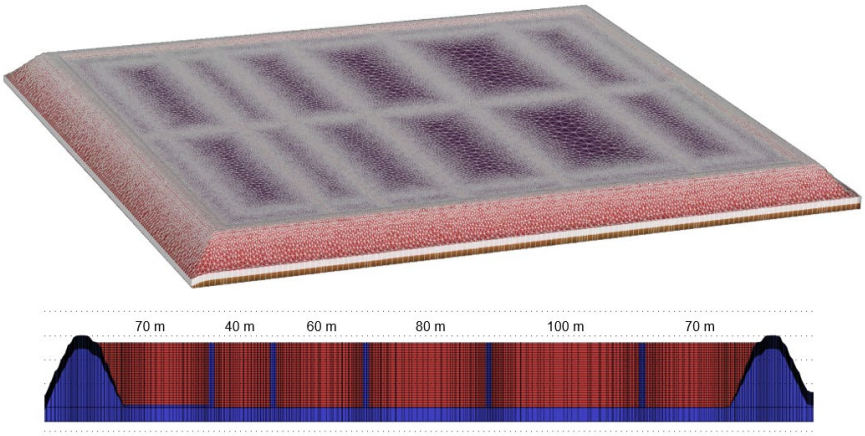


Figure 1: Simplified FEFLOW model with paddock spacings of 40 m to 100 m

Cases evaluated included CPR sand configuration for: (i) tailings only (base case); (ii) tailings with vertical sand drains only; and (iii) tailings with vertical sand drains and horizontal sand layers. Figure 2 presents schematic cross-sections of vertical sand columns only and columns with horizontal sand layers.

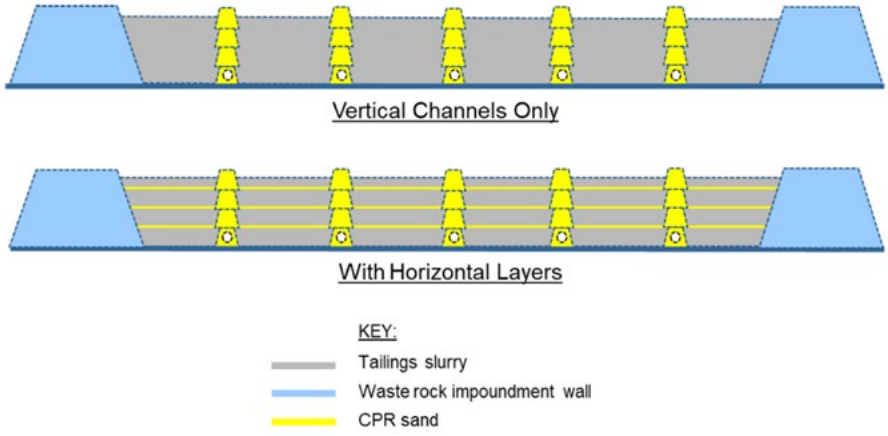


Figure 2: CPR sand configuration with horizontal and without horizontal layers

Typical results are presented in Figure 3 and demonstrate the influence of the of horizontal sand layers and CPR sand column spacing. The phreatic surface for Case 1 is located on the surface, indicating a pool, and for Case 2 and Case 3, the phreatic surface varied depending on the sand column spacing.

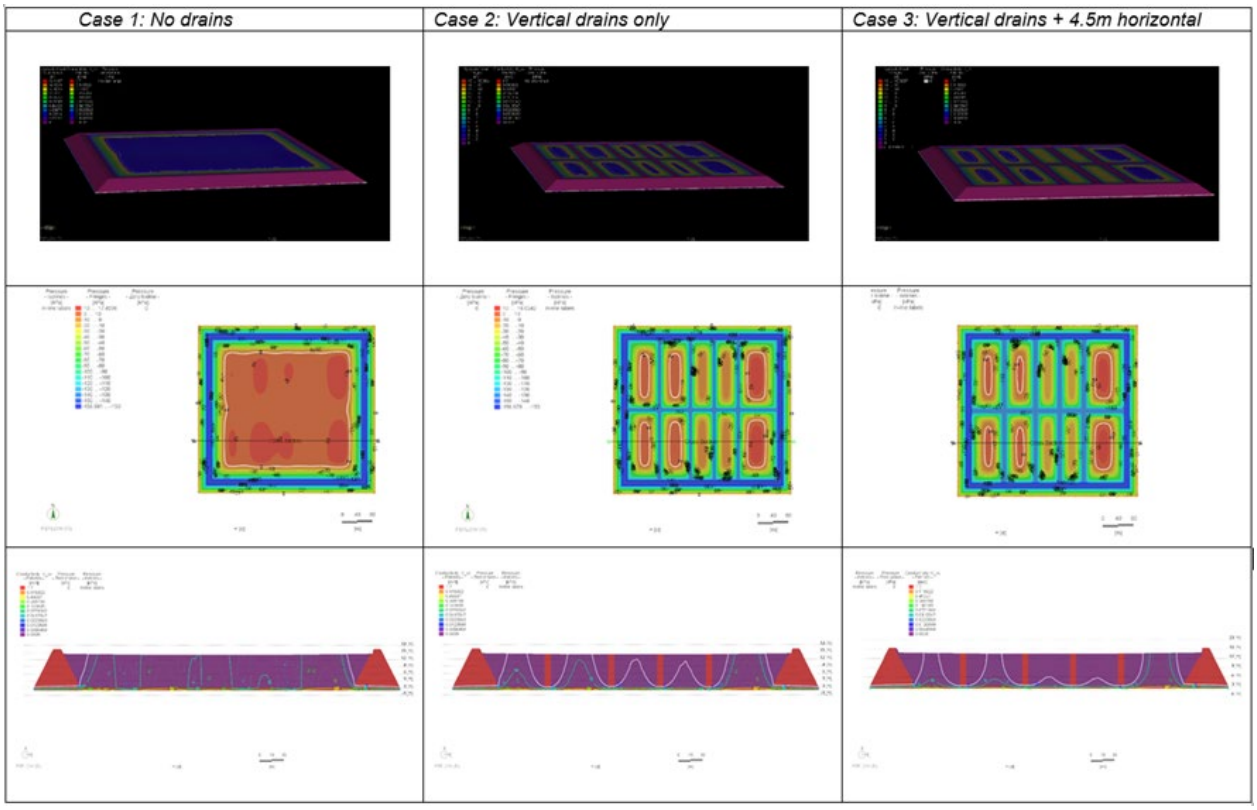


Figure 3: FEFLOW geometry and model results

Inclusion of horizontal sand drainage layers is ideal and improves recovery of water. The phreatic surface in Case 3 is lower compared to that of Case 1 and Case 2 as more water is intercepted and conveyed out of the facility. However, such a geometry increases the required volume of CPR sand, which is limited, and was regarded as a prohibitive constraint to implementing the horizontal drains.

The paddocks with 40 m spacing had lower phreatic surfaces and it was concluded that depending on availability of CPR sand berm spacing ranging between 40 m to 60 m is ideal.

Furthermore, abstraction of pool water via CPR sand berms depends on the hydraulic gradient, and it was found that in the early stages of deposition the hydraulic gradient is not adequate for recovery of pool water and results in a low outflow rate of the system. This results in larger supernatant water pools with a risk of overflow between paddocks. Inclusion of a penstock intake and outfall pipe must therefore be implemented to provide decant capacity in the initial stages of an HDS facility and for stormwater management.

High level water balance

Several options were identified for the CPR sand configuration and with iterative workshops and ratings, two options were selected, for which water balances were developed in order to undertake a comparative evaluation and selection of the preferred go-forward solution. The water balance was carried out at a monthly timestep, using stochastically generated rainfall data for the LoM duration (2028 to 2038), and is not intended as a detailed/final water balance. Figure 4 (on the next page) illustrates the schematic inputs, storage and output components considered in the water balance.

The comparative water recovery results are presented in Table 1. For Option 1, 70% of the total inflow water volume is recovered. Option 2 recovers 82% of the total inflow water volume.

Table 1: Comparative water recovery results

Scenario	Total water stored	Total water loss (evaporation)	Total water recovered	Recovery rate (m^3/t)
Option 1	24%	6%	70%	0.87
Option 2	16%	2%	82%	0.96
Base case	29%	11%	60%	0.57

The makeup of the recovered water volume in Option 1 is (i) 19,588 m^3/d (53%) from pool abstraction; (ii) 2,703 m^3/d (7%) from the settled tailings; (iii) 1,238 m^3/d (3%) through the above and below liner drains; and (iv) 2,577 m^3/d (7 %) through the waste rock (W/R) wall drains. The makeup of the recovered water volume in Option 2 is (i) 20,991 m^3/d (56%) from pool abstraction; (ii) 6,311 m^3/d (17%) from the settled tailings; (iii) 697 m^3/d (2%) through the above and below liner drains; and (iv) 2,577 m^3/d (7%)

through the W/R wall drains. The recovery via pool abstraction and from settled tailings is substantially higher in Option 2 compared to that achieved in Option 1.

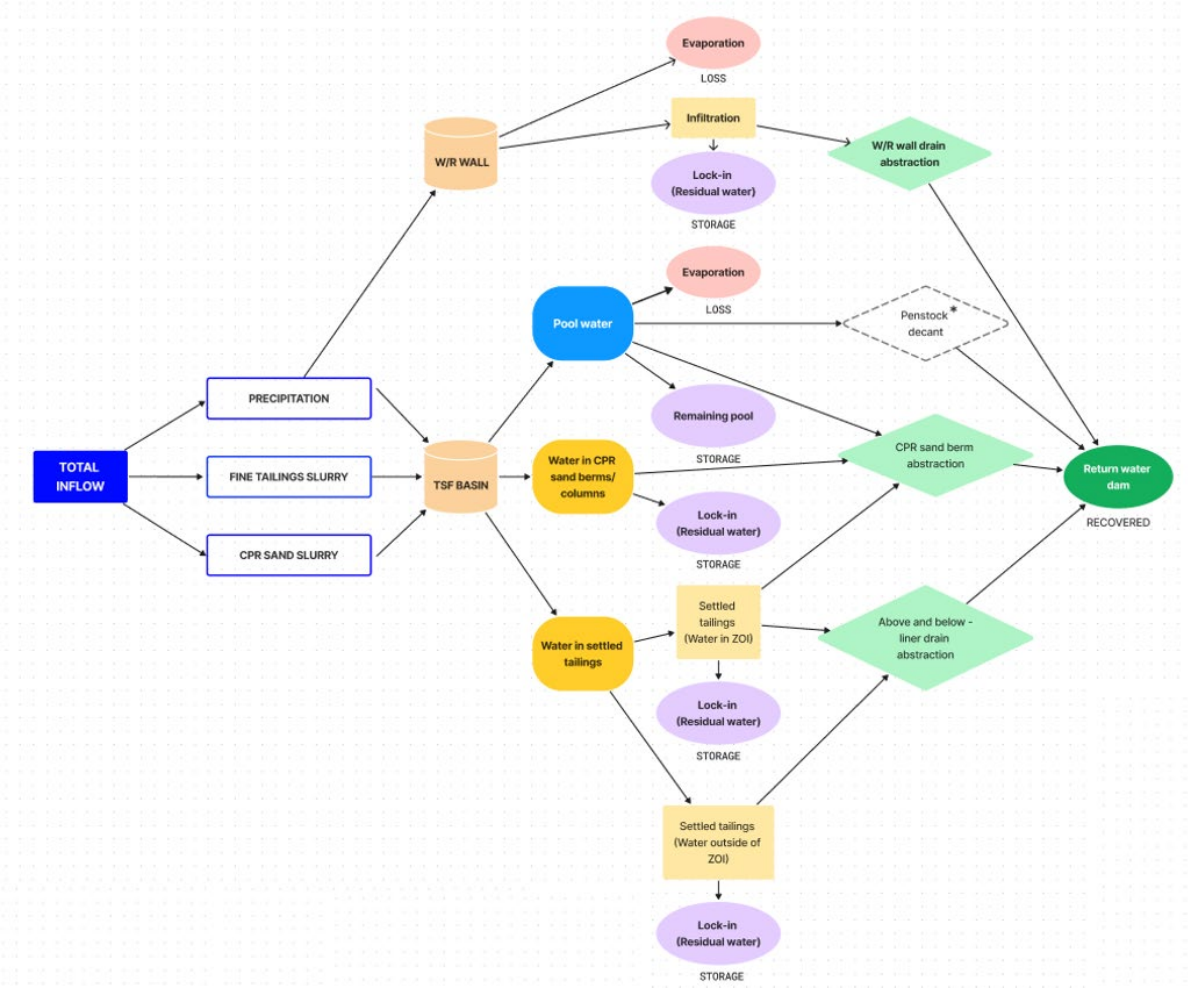


Figure 4: Water balance schematic diagram

These recoveries were also compared to the water balance undertaken for the base case. The comparison confirms that while both Option 1 and Option 2 will improve water recovery compared to the base case configuration, Option 2 is significantly better than Option 1.

Options identification and go-forward solution

Option 1 (Figure 5) comprises 8 compartments divided by CPR sand berms that intersect at the centroid of the TSF. A single penstock intake is located at this centroid position and all CPR sand berms are constructed radially from the outer embankment towards this centroid. Each compartment has additional inter-compartment CPR sand berms that are constructed to leave a minimum gap of ± 60 m to enable operational and storm water to flow unimpeded towards the centroid position where the pool will form. Potential erosion of the CPR sand berms during deposition is a risk due to narrowing of the flow paths. A second

drawback is that the CPR sand berms are concentrated on the outer footprint of the basin away from the pool area where saturation, and hence potential for abstracting interstitial water, is expected to be highest. Set-up and mobilizing of SPCUs to construct CPR sand berms is expected to require more effort during deposition since the berms are constructed from the outer basin perimeter and equipment must be moved continuously, over long distances, around the entire TSF perimeter to keep ahead of deposition.

Option 2 (Figure 6) comprises two penstock intakes located along a north-to-west divider road that will be constructed from waste rock material. The divider road will be raised continuously with deposition lifts as the facility rises. The basin footprint is divided into 6 compartments by CPR sand berms that intersect at the 2 penstock intake positions and extend to the outer perimeter of the basin. Each compartment contains CPR sand berms that do not extend to the perimeter and are constructed outwards from the divider road and penstock intake structure locations. The geometry is such that all CPR sand berms are not constructed from the outer perimeter of the basin and construction and set-up are therefore expected to be less onerous. This configuration is advantageous as CPR sand berms are concentrated centrally within the basin footprint and therefore are expected to be more efficient with higher water recovery from both the pool and interstitial water.

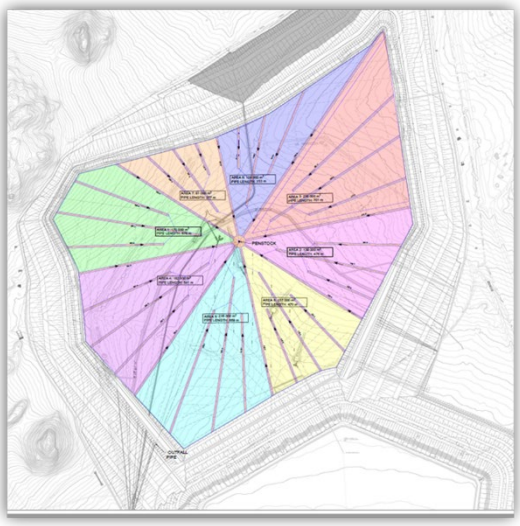


Figure 5: Option 1 configuration

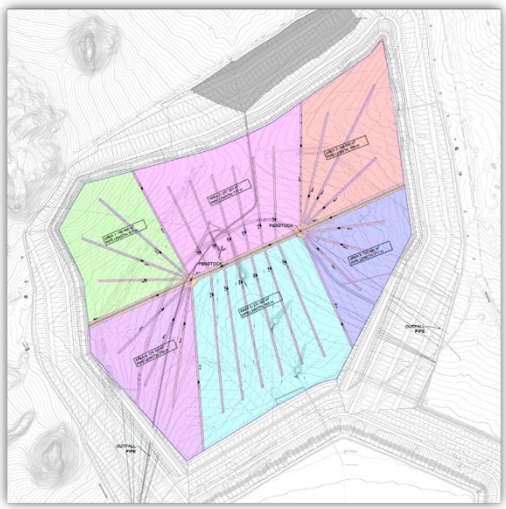


Figure 6: Option 2 configuration

A workshop was held during which advantages and disadvantages associated with each option were evaluated. Option 2 scored the highest with a weighted score of 115, compared to Option 1, which scored 77. Option 2 achieved the higher score due to: (i) advantageous berm location to optimize wicking and abstraction; (ii) easier operation with all berms constructed from the central divider road instead of along the TSF perimeter; (iii) higher operational safety; and (iv) the higher water recovery.

Infrastructure requirements

Compared to the base case, HDS is expected to increase costs substantially. In order to transition BW2 to an HDS facility an additional pipeline and pump station are required. Furthermore, since the base case engineering had been completed to feasibility level, modifications to the penstock, drainage system, and phase 1 containment infrastructure were required. Although the HDS solution delivers significant additional water, mitigates against the most likely failure mechanism (seepage driven) and enables a far lower closure cost, the business case for HDS is not yet positive.

Closure

The base case closure profile for BW2 comprises constructing a convex surface with waste rock on top of the TSF basin to allow surface runoff to drain towards the side slopes. The convex topography will have a final slope of 1:200, with the highest point being above the proposed base case penstock location. The constructability of the waste rock dome shape at end of life is improved significantly due to the "drier" tailings and additional access provided by the divider road. The CPR sand berms (with associated collector pipes) and divider road must therefore not be demolished at closure. A major risk associated with the base case closure solution is the potential ponding of water above the tailings level inside the waste rock dome after sealing the penstock. The ponded water due to infiltration will collect on top of the tailings and eventually infiltrate the tailings, feeding the phreatic surface within the TSF, thus delaying its desired drawdown.

Mitigation considered in the base case scenario comprised either a capping layer (barrier system with a liner), which must be placed over the dome to prevent infiltration, or the penstock should not be sealed, allowing ponded water to drain through it. The latter has safety risks related to an accessible penstock post closure due to potential access by unauthorized persons. The HDS system provides an advantageous alternative solution that is operable as a safe passive drainage system. This will reduce the risk of ponding above the tailings level inside the waste rock body, thereby allowing both penstocks to be sealed and negating the need for a capping layer.

Conclusion

The HDS deposition methodology is a significant deviation to current water recovery strategies and enables recovery of both supernatant and interstitial water. The CPR sand berms significantly improve the recovery, by shortening the drainage paths for seepage water and creating preferential drainage paths through which water including the interstitial water (which is not accessible in conventional deposition methods) is recovered. This leads to a TSF that is comparatively drier than a conventional facility. This paper documents salient considerations for the design and for transitioning a conventionally designed facility into an HDS

facility. Availability of CPR sand is a prohibitive constraint when considering the use of the more effective horizontal sand layer configuration. It was concluded that typical spacing of 40 m to 60 m is ideal for CPR sand berm configuration at BW2. Furthermore, implementation of HDS and recovery of pool water does not immediately replace the use of traditional penstock or pump recovery systems. Outflow through the CPR sand berms is driven by the hydraulic gradient, which is not adequate in the early stages of development, and this motivates for the inclusion of a secondary penstock or pump outflow system.

Acknowledgements

This paper is a summary of a study undertaken by Jones & Wagener and funded by Anglo America. The authors wish to thank Anglo American for the continued support and financial backing towards HDS studies.

References

Arburo, K., Zuniga, J., McDonald, A., Valdes, F., Concha, J. and Wasmund, E. 2022. Commissioning hydro-float in a copper concentrator application. *Copper 22, Copper International Conference*, Santiago, Chile.

Bustamante, N., Newman, P., López, A. and Suazo, G. 2024. Hydraulic dewatered stacking (HDS): Effects of fines content in the drainage performance of the sands. *10th International Conference on Tailings Management*.

Filmer, A.O. and Alexander, D.J. 2016. Patent No. WO 2016/170437.

Filmer, A.O. and Alexander, D.J. 2017. Patent No. WO 2017/195008.

Filmer, A.O., Newman, P.D., Alexander, D.J. and Soles, J.J. 2020. Patent No. WO 2020/183309.

Furnell E., Bilaniuk, K. and Goldbaum, M. 2022. Dewatered and stacked mine tailings: a review. *American Chemical Society*. Accessed at https://doi.org/10.1021/acsestengg.1c00480

ICMM. 2020. Global industry Standard on Tailings Management. International Council on Mining and Metals, London.

Murry, M., Newman, P. and López, A. 2023. Hydraulic Dewatered Stacking – Developing Strategies for Brownfield application at Mogalakwena, South Africa. *Proceedings of Tailings and Mine Waste 2023*.

Newman P., Bruton, M., Burgos, J. and Purington, J. 2022. Innovations in tailings management – hydraulic "dry" stacking. *Proceedings of Tailings and Mine Waste 2022*.

The Relevance of Particle Crushing for the Design of Compacted Filtered Iron Ore Tailings Storage Facilities

João Paulo de Sousa Silva, Vale S.A., Brazil
Bruno Guimarães Delgado, Vale S.A., Brazil
Alexia Cindy Wagner, Universidade Federal do Rio Grande do Sul, Brazil
João Vítor de Azambuja Carvalho, Universidade Federal do Rio Grande do Sul, Brazil
Nilo Cesar Consoli, Universidade Federal do Rio Grande do Sul, Brazil

Abstract

Brazil is one of the largest iron ore producers in the world, and its major producing region mainly explores downgrade iron deposits. Thus, large volumes of tailings have to be stored daily. Although compacted filtered tailings disposal has long been used in arid areas, their use in tropical climate regions is still reduced and demands a deeper understanding of tailings behavior. Moreover, compacted filtered tailings storage can reach hundreds of meters in height, which introduces more complexities to the design of these structures, such as particle breakage.

Geotechnical engineering applications usually are restricted to pressures of 1 MPa, where particle crushing may have a less significant influence than for conventional materials. However, higher pressures may arise for high-rise tailings stackings. Particle breakage is known to affect the behavior of granular materials, regarding their volumetric response, critical state parameters, and stiffness. Therefore, this paper aims to investigate the relevance of grain crushing to the behavior of tailings in the usual range of pressures they might achieve in compacted filtered tailings stacking. Triaxial compression tests were conducted in distinct tailings specimens sheared at 1.2 MPa and 12 MPa, and the tailings' particle size distribution was evaluated after testing. It was found that particle breakage depends on the grading distribution of the tailings tested. Breakage increases the fines content and can change the coefficients of curvature and uniformity. The material with more breakage presented a greater reduction in M value. Also, particle breakage changes the stiffness trends with increasing pressures. Nonetheless, the observation of particle breakage in the tests highlights the relevance of crushing to the behavior of tailings and mandates further understanding of this clastic and anthropic material.

Introduction

Mineral exploitation is an essential economic activity. Yet, the large volume of tailings produced during the ore beneficiation requires finding options for their safe and appropriate storage (Hu et al., 2017). Regulatory limitations on the disposal of saturated tailings in upstream dams and advancements in dewatering technologies have encouraged the disposal of these materials in stacks (Crystal et al., 2018; Schaper et al., 2020). The tailings are then filtered and compacted to form a dry stack structure. Compaction reduces the risk of liquefaction and increases the stability of the stacks, allowing them to achieve elevated heights, even hundreds of meters (Davies, 2011; Wagner et al., 2023). During the stacking raising, the tailings may be exposed to much higher pressures than those experienced in typical geotechnical engineering applications, which can affect the tailings particles and their mechanical response (Consoli et al., 2024a).

Particle breakage is the most important mechanism observed in soils subjected to compression or shearing at high pressures. As pressure increases, the amount of particle breakage also increases. Simulations indicate that most of the particle breakage is due to the breakage of the fragments produced, resulting in the development of various particle sizes during loading (De Bono and McDowell, 2014). Then, particle breakage changes the material's grading, affecting its mechanical behavior and fundamental constitutive properties. The packing of particles can become more efficient when breakage occurs, leading to changes in the states achieved in a stress-density space observed in the position of the critical state locus (Muir Wood and Maeda, 2008). The strength and stress-strain behavior of soil are influenced by the degree of particle crushing during loading and deformation: particle breakage increases the volume reduction during compression and decreases the dilation rate during shearing (Hardin, 1985; Yamamuro and Lade, 1996). Beyond the stress state, the degree of particle crushing is influenced by other factors such as the grains' size, shape, and mineralogy (Mitchell and Soga, 2005). The lower the particle strength, the lower the pressure at which particle crushing starts to influence the material's response.

The breakage potential of an individual particle generally increases with its size, as larger particles tend to have more internal defects, resulting in lower tensile strength (Hardin, 1985). However, studies have shown that larger particles tend to survive during loadings (McDowell and Bolton, 1998; McDowell and Harireche, 2002), which indicates that the coordination number greatly influences particle failure. Particles with a higher coordination number (more surrounding particles = more contacts) experience better stress distribution and are less susceptible to break by tensile splitting (Muir Wood and Maeda, 2008). As stress increases, smaller particles created by breakage tend to surround the larger ones, increasing their coordination number and preserving them from breakage. The breakage is then predominant in the smaller particles with lower coordination numbers. In addition, soils that have higher fines content and are more well-graded will result in better grain arrangements and more contacts between particles, which increases the coordination number and reduces the breakage potential (Altuhafi and Coop, 2011).

The characteristics of iron ore tailings vary depending on the ore's nature and the beneficiation processes (Fourie et al., 2022). As a result, materials from the same mine may have different grading and mineral compositions (Consoli et al., 2024). Therefore, understanding the impact of grain breakage on tailings' behavior is crucial for safely designing compacted tailings stacks. Accordingly, the present work evaluates the breakage occurrence on two iron ore tailings with distinct characteristics obtained in different mines. The influence of particle breakage on stress-strain response, stiffness, and volume change is evaluated through triaxial compression tests conducted over two confining pressures representing typical stress levels (1.2 MPa) and higher stress that is possible to be achieved in dry stacks structures (12 MPa).

Methodology

Materials

Two iron ore tailings obtained from different mines in the Quadrilátero Ferrífero, located at Minas Gerais, Brazil, were studied herein. Figure 1 shows their particle size distribution (PSD) obtained via sieve and sedimentation analysis, considering the ASTM D7928 (ASTM, 2021). The materials present distinct geotechnical characteristics associated with their different origins, as summarized in Table 1.

Table 1: Characterization of the tailings

Parameters	Tailings A	Tailings B
D_{50} (mm)	0.17	0.08
Fines content (< 0.075 mm)	14.07	47.98
Uniformity coefficient- C_u	2.75	9.97
Curvature coefficient - C_c	0.87	1.89
ASTM-USCS Classification	SM	SM
Plastic index - PI	non-plastic	
Specific gravity – G_s	3.1	3.05
Quartz content (%)	78.69	78.44
Fe oxides content (%)	19.23	17.21

Tailings A is more uniformly graded (Cu = 2.75 and Cc =0.87) and has more coarse particles, while Tailings B is well-graded (Cu = 9.97 and Cc =1.89) and presents higher fines content. Despite the differences in tailings grading, their mineralogy is very similar, and both materials are predominantly composed of quartz (around 78%) and iron oxides (17 to 19%), resulting in similar specific gravity (Gs) values (3.10 for Tailings A and 3.05 for Tailings B). The mineralogical characterization was obtained using the Quantitative Evaluation of Minerals by Scanning Electron Microscopy (QEMSCAN®) system, and the specific gravity was evaluated using ASTM D7928 (ASTM, 2014). The differences in grain size

distribution and mineralogy of particles can be observed in Figure 2 for Tailings A and B. Also, the tailings are non-plastic and classified as silty sand (SM) by ASTM-USCS Classification (ASTM, 2017).

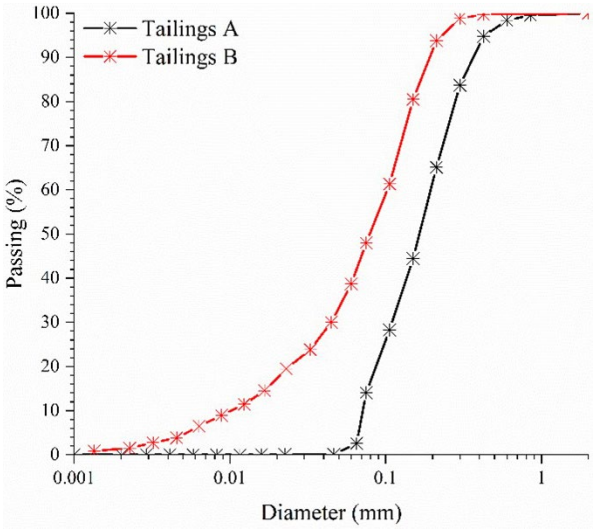


Figure 1: Particle size distribution of the tailings

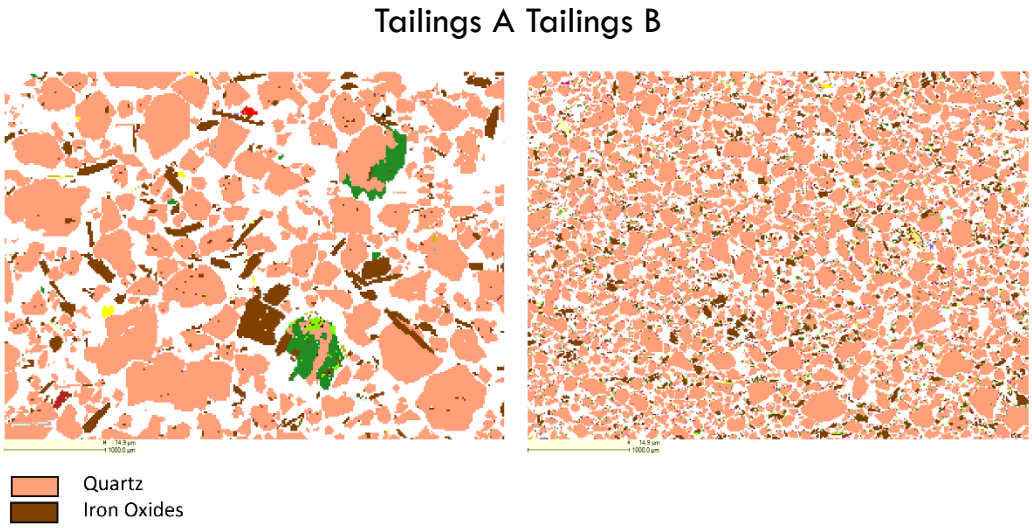


Figure 2: Mineralogy of tailings particles

Testing

The tests were performed using a high-pressure triaxial device typically used in rock mechanics' practice. Dry samples were used to avoid suction effects, and the volumetric change was calculated using internal measurements and the variation in the triaxial cell chamber confining fluid volume. Cylindrical specimens (50 mm in diameter and 100 mm in height) were molded using the dry funnel deposition method (Shi et al., 2021; Silva et al., 2024; Yamamuro and Lade, 1996), aiming to obtain dense specimens with similar states of compacted tailings stacks. The confining pressure was incremented to the target value (1.2 or 12 MPa)

during the isotropic compression stage. Then, the shearing phase was strain-controlled and performed at 1.5 mm/h. Consoli et al. (2024) described the triaxial equipment and procedures adopted herein. Table 2 summarizes the performed tests.

Table 2: Triaxial testing

Material	Confining pressure (MPa)	After shearing	End of test		
		v_c	v_f	q/p'	ϕ'_{cs} (°)
Tailings A	1.2	1.57	1.43	1.43	35.3
Tailings A	12	1.53	1.33	1.33	33.0
Tailings B	1.2	1.52	1.57	1.45	35.7
Tailings B	12	1.46	1.36	1.43	35.4

Results

Particle breakage and grading changes

Representative samples were retrieved at the end of each test from specimens sheared at distinct confining pressures to assess the occurrence of grain breakage. The PSD curves obtained are shown in Figure 3 and can be compared with the respective untested tailings. As expected, the amount of breakage increases with the confining pressure, and the PSD curves offset upwards from the untested material.

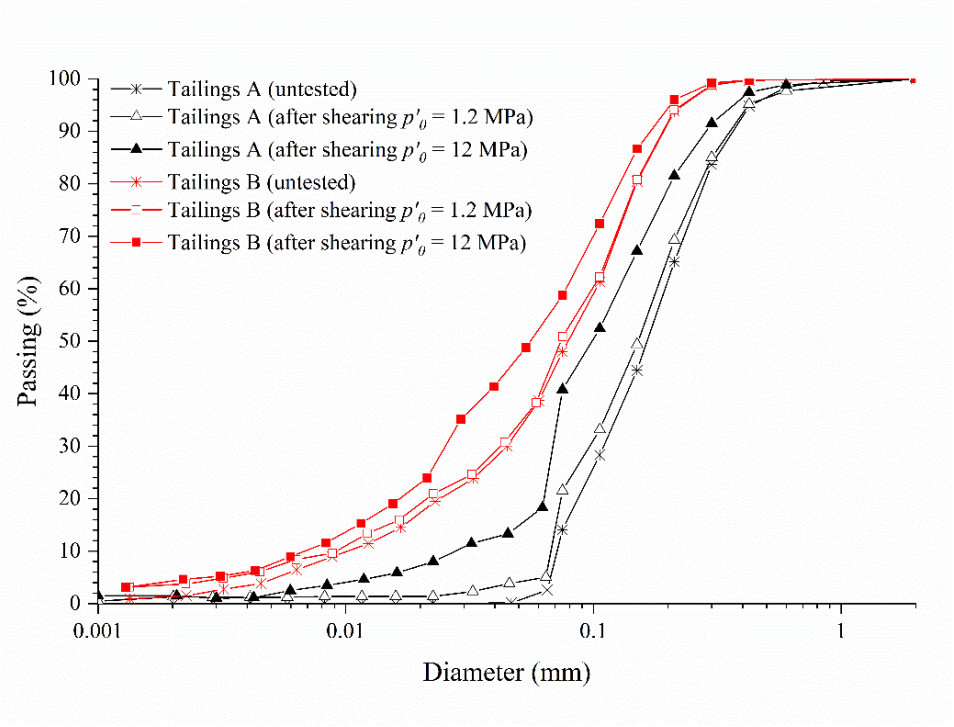
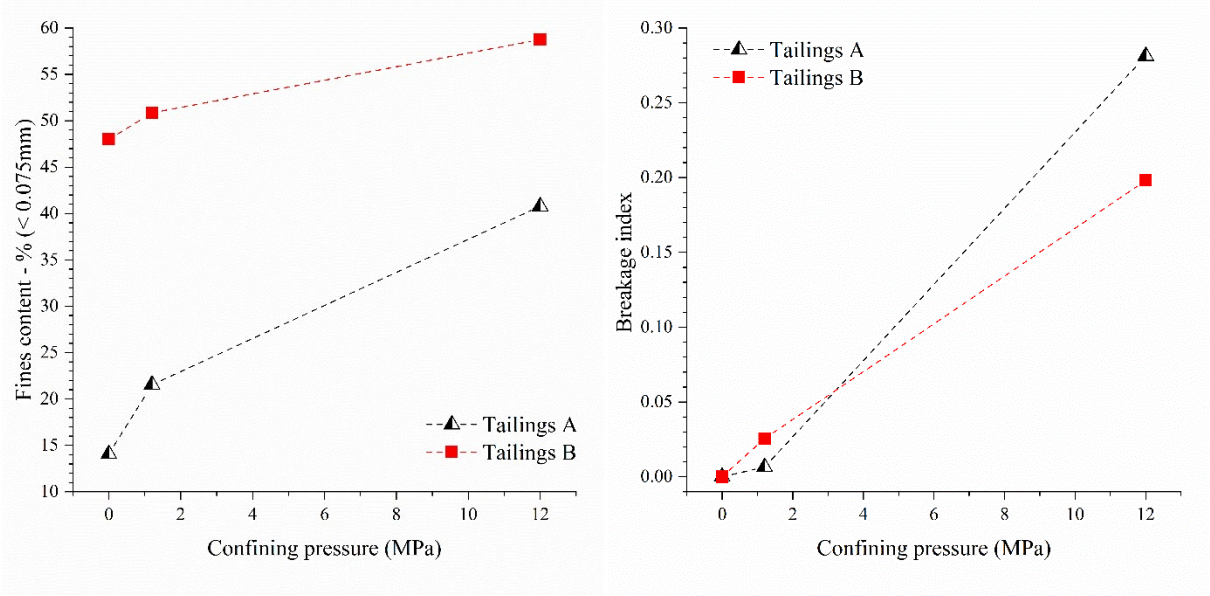


Figure 3: Particle size distribution after testing

Figure 4a shows that the fines content increases with confining pressures, and the changes become more pronounced for the specimens shearing with 12 MPa. Additionally, it is observed that the rate of increase in fines content is higher for tailings A, suggesting that there is more particle breakage for tailings with a coarser initial particle size.

The relative breakage parameter proposed by Hardin (1985) was employed to quantify the particle breakage. However, all grain sizes of the PSD curves were used in the calculation, differently from the Hardin index, which set a lower limit for grain size at 0.074 mm. Figure 4b shows the breakage indexes obtained for each confining pressure. The particle breakage of the two tailings was very similar up to 1.2 MPa, with Tailings B being slightly superior. However, at 12 MPa, the breakage of Tailings A was significantly greater than Tailings B. This result demonstrates how the grain size distribution affects the tailings breakage: well-graded tailings with higher fines content (Tailings B) result in better arrangements with higher coordination number, reducing the average stress in the contact points and particle breakage.

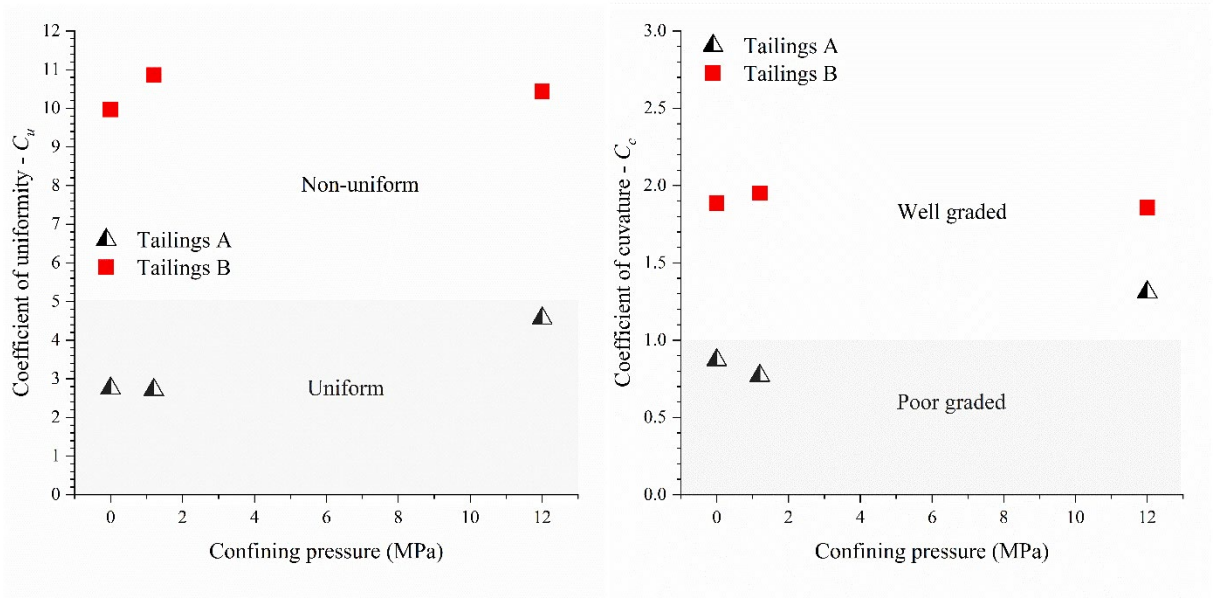


(a) (b)

Figure 4: Particle breakage measure (a) fines content (b) breakage index

Particle breakage creates smaller particles that tend to alter the original PSD. For this reason, Figure 5 evaluates the change in C_u and C_c of the PSDs obtained. Tailings A, which was initially well-graded, does not exhibit much difference in grain distribution. The coefficients are similar to those of the untested material, suggesting only a shift in the PSD and a slight change in its format. Conversely, the coefficients of Tailings B changed significantly after the shearing under 12 MPa, and the addition of fine particles

reduced its uniformity, making the PSD more well-graded. These changes in grading certainly impact the grain arrangements and may affect the mechanical behavior of the tailings.



(a) (b)

Figure 5: Influence of particle breakage on (a) coefficient of uniformity (b) coefficient of curvature

Stress-strain behavior

Figure 6 exhibits the normalized stress-strain behavior and the volume change response for the tailings sheared at distinct confining pressures. Table 2 summarizes the data about the tests. The specimens sheared at 1.2 MPa confinement showed an initial compression followed by dilation, accompanied by a brittle behavior with a defined peak strength (Tailings B) or no defined peak strength (Tailings A). On the other hand, both specimens sheared at 12 MPa presented a ductile response accompanied by a fully contractive behavior.

The higher peak value observed for Tailings B can be attributed to the lower void ratio and the better grain packing formed during molding for the well-graded material, resulting in a higher contribution from interlocking. The more compressive behavior observed at 12 MPa is due to significant particle breakage, which allows for a new grain arrangement and greater volume reduction compared to 1.2 MPa.

The specimens presented practically constant volumetric strain rate values and deviatoric stresses at the end of the tests, indicating they were close to reaching the critical state. For Tailings A, the stress ratio at critical state (M) achieved at two different confining pressures is very similar (1.45 for 1.2 MPa and 1.43

for 12 MPa), suggesting that grain breakage may have slightly influenced *M* value. In the case of Tailings B, the *M* value varies from 1.43 at 1.2 MPa (similar to Tailings A) to 1.33 at 12 MPa. This result indicates a stronger influence of higher pressure for Tailings B, which can lead to more particle breakage, possible particle shape alterations, and changes in particle size distribution towards a more well-graded condition.

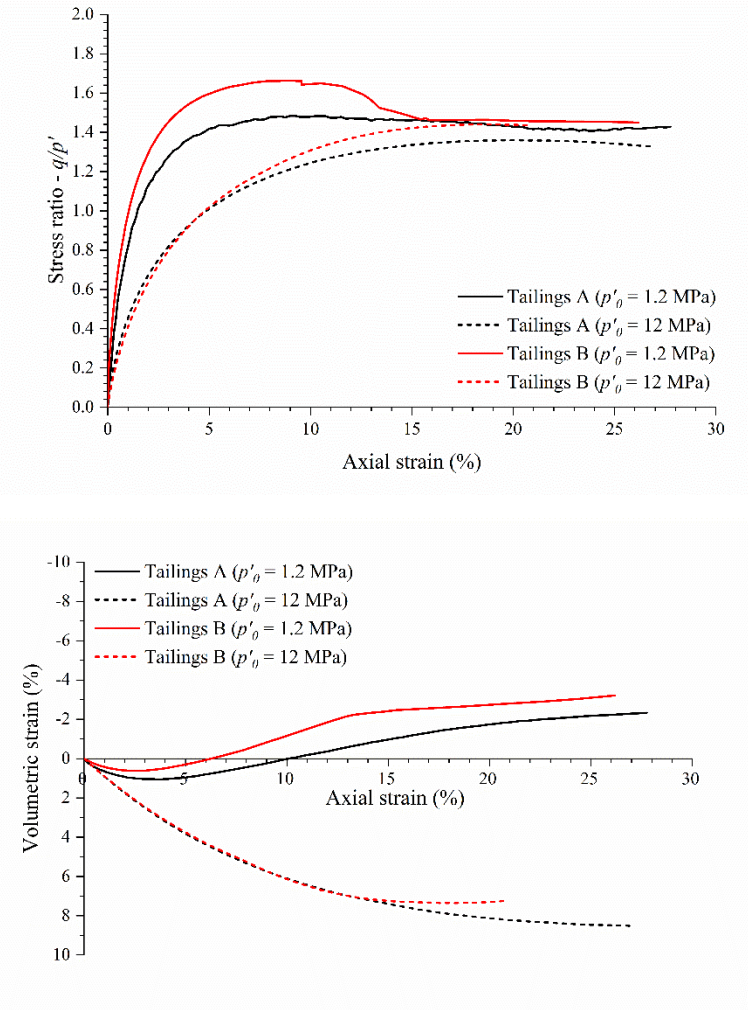


Figure 6: Stress-strain response of tailings

Figure 6 shows a change in stiffness trend for lower and higher stresses, and Figure 7 presents the Secant Young modulus degradation for each test during the axial strain development. At a lower confining pressure (1.2 MPa), Tailings B shows higher stiffness compared to Tailings A. This is expected due to the lower void ratio and well-graded state of Tailings B, leading to a higher particle contact number and better stress distribution. However, when the pressure is increased to 12 MPa, Tailings A became stiffer than Tailings B. This difference can be explained by the increased breakage in Tailings A, resulting in finer particles that alter the grain contacts and improve stress transmission. Moreover, at higher strains, the stiffness of both Tailings A and Tailings B is quite similar under the two stress conditions.

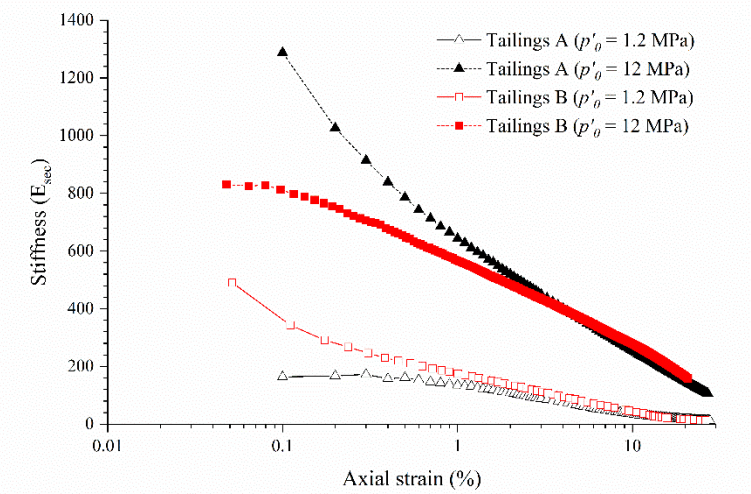


Figure 7: Stiffness degradation curves of tailings

Conclusion

This paper examined the mechanical behavior associated with the particle crushing occurrence of two iron ore tailings under two different confining pressures (1.2 and 12 MPa) through triaxial tests. Considering the boundaries of this work, the following conclusions can be drawn.

Particle breakage is most significant in tailings sheared with a confining pressure of 12 MPa. This stress level can be achieved in very high stacks (up to 600 m, for example).

Tailings with coarser grain size distribution and more uniform grading tend to present more particle breakage due to the lower coordination number and greater stresses in the particle contacts.

Particle breakage generates new small particles that can alter the original PSD, changing the fines' content, coefficient of uniformity, and coefficient of curvature.

The change in PSD due to particle breakage can impact the mechanical response of the tailings. The present study showed that particle breakage can increase compression, reduce the *M* value, and increase the stiffness.

Finally, the results demonstrate the importance of considering the correct stress level in laboratory analysis corresponding to the expected height of the structure. This is essential for assessing particle breakage and its influence on the PSD, as well as the strength and stiffness properties of the tailings, which can impact the design of storage facilities.

Acknowledgements

The authors thank Vale S.A., MEC-CAPES, and the Brazilian Conselho Nacional de Desenvolvimento Científico e Tecnológico (CNPq) for supporting the research group.

References

Altuhafi, F.N. and M.R. Coop. 2011. Changes to particle characteristics associated with the compression of sands. *Géotechnique* (6): 459–471. https://doi.org/10.1680/geot.9.P.114

ASTM. 2021. Standard test method for particle-size distribution (gradation) of fine-grained soils using the sedimentation (hydrometer) analysis. West Conshohocken, PA.

ASTM. 2017. Standard practice for classification of soils for engineering purposes (unified soil classification system). West Conshohocken, PA.

ASTM. 2014. Standard test methods for specific gravity of soil solids by water pycnometer. West Conshohocken, PA.

Consoli, N.C., J.V.D. Azambuja Carvalho, A.C. Wagner, H.C. Scheuermann Filho, I. Carvalho, P.P. Cacciari and J.P.D Sousa Silva. 2024a. Determination of critical state line (CSL) for silty-sandy iron ore tailings subjected to low-high confining pressures. *Journal of Rock Mechanics and Geotechnical Engineering* 16(5): 1684–1695. https://doi.org/10.1016/j.jrmge.2023.06.014

Consoli, N.C., J.P.S. Silva, A.C. Wagner, J.V.D.A. Carvalho, B.A. Baudet, M.R. Coop, H.C. Scheuermann Filho, I. Carvalho, G.M. De Sousa and P.P. Cacciari. 2024b. Critical state analysis of two compacted filtered iron ore tailings with different gradings and mineralogy at different stages of treatment. *Acta Geotechnica* 19(2): 881–898. https://doi.org/10.1007/s11440-023-01963-9

Crystal, C., C. Hore and I. Ezama. 2018. Filter-pressed dry stacking: Design considerations based on practical experience. *Proceedings of Tailings and Mine Waste 2018.* Keystone, Colorado, USA: 209–220.

Davies, M. 2011. Filtered dry stacked tailings: The fundamentals. *Proceedings of Tailings and Mine Waste Conference 2011*. The University of British Columbia, Vancouver, Canada. Accessed at https://doi.org/10.14288/1.0107683

De Bono, J.P. and G.R McDowell. 2014. DEM of triaxial tests on crushable sand. *Granular Matter* 16: 551–562. Accessed at https://doi.org/10.1007/s10035-014-0500-x

Fourie, A.B., R. Verdugo, A. Bjelkevik, L.A. Torres-Cruz and D. Znidarcic. 2022. Geotechnics of mine tailings: A 2022 State of the Art. In *Proceedings of the 20th ICSMGE*. Presented at the 20th International Conference on Soil Mechanics and Geotechnical Engineering, Sydney, Australia.

Hardin, B.O. 1985. Crushing of soil particles. *J. Geotech. Eng.* 111(10):1177–1192. Accessed at https://doi.org/10.1061/(ASCE)0733-9410(1985)111:10(1177)

Hu, L., H. Wu, L. Zhang, P. Zhang and Q. Wen. 2017. Geotechnical properties of mine tailings. *J. Mater. Civ. Eng.* 29(2): 04016220. Accessed at https://doi.org/10.1061/(ASCE)MT.1943-5533.0001736

McDowell, G.R. and M.D. Bolton. 1998. On the micromechanics of crushable aggregates. *Géotechnique* 48: 667–679. Accessed at https://doi.org/10.1680/geot.1998.48.5.667

McDowell, G.R. and O. Harireche. 2002. Discrete element modelling of yielding and normal compression of sand. *Géotechnique* 52: 299–304. Accessed at https://doi.org/10.1680/geot.2002.52.4.299

Mitchell, J.K. and K. Soga. 2005. *Fundamentals of Soil Behavior*. 3rd edition. John Wiley & Sons.

Muir Wood, D. and K. Maeda. 2008. Changing grading of soil: Effect on critical states. *Acta Geotech.* 3(1): 3–14. Accessed at https://doi.org/10.1007/s11440-007-0041-0

Schaper, D., R. Lessa, A. Freitas and B. Weeks. 2020. De-characterization and closure of TSF: concepts of the Brazilian legislation and international criteria. *Proceedings of Planning for Closure 2020, 3rd International Congress on Planning for Closure of Mining Operations* (Chapter 6). Presented at the 3rd International Congress on Planning for Closure of Mining Operations. Gecamin Digital Publications.

Shi, J., W. Haegeman and V. Cnudde. 2021. Anisotropic small-strain stiffness of calcareous sand affected by sample preparation, particle characteristic and gradation. *Géotechnique* 71: 305–319. Accessed at https://doi.org/10.1680/jgeot.18.P.348

Silva, J.P.D.S., J.V.D.A. Carvalho, A.C., Wagner, P.P. Cacciari and N.C. Consoli. 2024. On the mechanics of filtered compacted consolidated and overconsolidated iron ore tailings at high pressures. *Can. Geotech. J.* 61: 575–581. Accessed at https://doi.org/10.1139/cgj-2023-0056

Wagner, A.C., J.P. de Sousa Silva, J.V. de Azambuja Carvalho, A.L. Cezar Rissoli, P.P. Cacciari, H.M. Chaves, H.C. Scheuermann Filho and N.C. Consoli. 2023. Mechanical behavior of iron ore tailings under standard compression and extension triaxial stress paths. *Journal of Rock Mechanics and Geotechnical Engineering* S1674775522002396. Accessed at https://doi.org/10.1016/j.jrmge.2022.11.013

Yamamuro, J.A. and P.V. Lade. 1996. Drained sand behavior in axisymmetric tests at high pressures. *J. Geotech. Eng.* 122: 109–119. Accessed at https://doi.org/10.1061/(ASCE)0733-9410(1996)122:2(109)

Iron Ore Tailings Dam De-Characterization: Evaluation of Key Parameters for Future Dry Stacking

Hugo Carlos Scheuermann Filho, Universidade Federal do Rio Grande do Sul, Brazil
Thatyane Martins Gonçalves, Vale S.A., Brazil
Nilo Cesar Consoli, Universidade Federal do Rio Grande do Sul, Brazil
Gino Vizcarra, Vale S.A., Brazil
Frank Pereira, Vale S.A., Brazil
Nilthson Noreña, Vale S.A., Brazil

Abstract

Brazil has been one of the top world iron ore suppliers, generating vast amounts of tailings which are usually stored in upstream heightened dams. These rising embankments are supported on the deposited tailings, often saturated and loose. This, combined with the uncertainties associated with the tailings' characterization within the reservoir, leads to unsafe structures. Thus, Brazilian regulatory agencies have introduced novel legislation requiring the closure of the upstream heightened tailings storage facilities (TSFs) by decommissioning or de-characterization. Such procedures demand the removal and reallocation of a significant volume of tailings that must be characterized to provide necessary data for its upcoming use. An option is piling up the removed tailings in stacks to prescribed design specifications. Nevertheless, laboratory testing is mandatory to characterize the material. Accordingly, the present research's main goal was to assess the small-strain stiffness (G_0) and the stress-strain behavior of four samples of iron ore tailings retrieved from distinct locations of a dam that was about to be de-characterized. Before mechanical testing, each material was thoroughly characterized, revealing gradation, mineralogical, and morphological differences. The mechanical testing consisted of consolidated drained triaxial tests, in which G_0 was evaluated using bender elements during the consolidation phase. These tests were conducted on specimens of the four materials compacted at two relative density values (D_r = 20% and 100%). In general, the stiffness results have shown that, by adopting a proper void ratio function $f(e)$, the same power-type relationship can express the G_0 of the same material, regardless of molding D_r value. It was also demonstrated that $f(e)$ depends on the material's gradation and can be expressed as a function of the effective particle size (d_{10}). Moreover, despite the differences between the four materials, they tended towards the same stress ratio at larger strain values.

Introduction

In the past decades, upstream heightened dams have prevailed in storing iron ore tailings in Brazil. The stability of such structures relies on embankments raised above the hydraulically disposed tailings, which are often saturated and loosely disposed of; that is, the material is prone to liquefy (Bedin et al., 2012; Silva et al., 2024). The recent episodes concerning upstream heightened tailings storage facilities (TSF) have starkly highlighted the risks and potential damage associated with their collapse, compelling the governing agencies to introduce a set of new rules regarding tailings storage to mitigate these risks and increase safety in the mining sector (Islam and Murakami, 2021; Rodrigues Leão and dos Santos Santiago, 2022).

Essentially, those rules forbid the construction of new upstream heightened tailings dams and demand the shutdown of existing ones via decommissioning and/or de-characterization (Schaper et al., 2020). Decommissioning includes the closure of the TSF and denotes the beginning of the de-characterization process, in which the structure completely loses its dam characteristics and is safely reincorporated into the landscape.

These actions involve the withdrawal and reallocation of significant amounts of tailings, whose geotechnical characteristics are essential data for ensuing use, which may include tailings dewatering with subsequent compaction into piles with specified design requirements (Lupo and Hall, 2010; Wagner et al., 2023). Understanding the compacted tailings response under distinct boundary conditions is essential in this context, particularly when considering the variability of the tailings within the same reservoir (Velten et al., 2024).

In this context, the present work evaluates the small-strain stiffness (G_0) of four iron ore tailings samples collected from different areas within a reservoir that was to be de-characterized. The tailings were previously dewatered, and the tests were conducted using two relative density (D_r) values for each sample: G_0 was evaluated during the isotropic consolidation stage of a triaxial test using bender elements. The intrinsic variability of the tailings, associated with the uneven tailings distribution during the dam's operation time, resulted in samples differing in gradation and mineralogy. As a result, this study helps to enlarge understanding of the effects of gradation and mineralogy on the small strain stiffness of compacted iron ore tailings for dry stacking purposes.

Experimental program

The experimental program comprises the geotechnical and mineralogical characterization of the four iron ore tailings samples (termed materials 1, 2, 3, and 4) and the conduction of eight drained triaxial tests with coupled bender element analysis during the isotropic consolidation stage. Tests were performed on specimens compacted at two relative density values (D_r = 20 and 100%) using the moist tamping technique

(Quinteros and Carraro, 2023), with a moisture content of 10% for materials 1, 3, and 4, and a moisture content of 14% for material 2.

Materials

The samples were collected in an undisturbed state from a dam located at the Iron Quadrangle (Minas Gerais, Brazil). Table 1 summarizes the main physical characteristics of each tailings. All the materials are non-plastic silts, except material 2, a non-plastic silty sand. Also, only material 3 is well-graded (CU > 5); the others are uniformly graded. Mineralogically, QEMSCAM® tests revealed that tailings 1, 2, and 4 are mainly composed of quartz (~47%) and iron oxide (~49%), with minor amounts of minerals such as chlorite, biotite, and gibbsite. In contrast, tailings 3 presents a smaller quantity of quartz (~24%) and more significant amounts of feldspar (1.5%), chlorite (11.3%), and iron oxide (~58%). Table 1 also displays four particle shape parameters calculated based on SEM micrographs. Despite the differences in gradation and mineralogy, the morphology of the four tailings is similar because of the beneficiation processes they underwent. These resulted in angular to subangular particles with intermediate sphericity and elevated surface roughness.

Table 1: Physical characteristics of the tailings

Parameters	1	2	3	4
Specific gravity – G_s	3.70	3.52	3.71	3.64
Medium sand: 0.425 mm < d < 2.00 mm (%)	0.10	3.70	0.10	0.20
Fine sand: 0.075 mm < d < 0.425 mm (%)	34.00	71.20	1.60	34.20
Silt: 0.002 mm < d < 0.075 mm (%)	64.40	23.70	86.90	63.20
Clay: d < 0.002 mm	1.50	1.40	11.40	2.40
d_{10} (mm)	0.025	0.05	0.002	0.03
Coefficient of uniformity – CU	2.6	2.4	9.0	2.2
Coefficient of curvature – CC	0.98	1.10	1.36	0.82
USCS Classification	ML	SM	ML	ML
Maximum void ratio – e_{max}	1.03	0.99	1.34	0.99
Minimum void ratio – e_{min}	0.52	0.60	1.12	0.54
Aspect ratio	0.60	0.50	0.60	0.60
Sphericity	0.60	0.45	0.61	0.57
Convexity	0.82	0.75	0.77	0.78
Overall regularity	0.67	0.56	0.66	0.65

Triaxial testing

The ASTM D7181 (ASTM, 2020) underlined the procedures of the consolidated drained (CID) triaxial tests carried out on fully automated triaxial equipment using saturated specimens. These were previously flushed

with de-aired water and saturated under backpressure until a B-value greater than 0.95 was obtained. The isotropic consolidation took place in stages; at the end of each stage, bender elements tests were carried out to assess the shear wave velocity (V_s) by ASTM D8295 (ASTM, 2019). The small strain stiffness (G_0) is the product of the square of V_s and the bulk density of the specimen (ρ). The shearing was strain-controlled (1% per hour) and conducted under an effective confining pressure (σ'_3) of around 805 kPa for the loose specimens (D_r = 20%) and 610 kPa for the dense ones (D_r = 100%). Table 2 contains the characteristics of the tested specimens: molding void ratio (e_0), void ratio after consolidation (e_c), and void ratio after shearing (e_{final}).

Table 2: Characteristics of the tested specimens

Material	σ'_3 (kPa)	e_0	e_c	e_{final}
1	808	0.93	0.80	0.70
1	610	0.52	0.52	0.59
2	809	0.93	0.86	0.74
2	606	0.61	0.54	0.63
3	804	1.37	0.96	0.77
3	603	0.98	0.83	0.73
4	808	0.90	0.80	0.71
4	605	0.58	0.56	0.62

Results

Bender elements

Figure 1 displays the evolution of the small strain stiffness (G_0) during the consolidation stage of each tested specimen (each plot contains the data of the loose and dense samples of the same material). The increase in the confining pressure compresses the sample, diminishing the void ratio and augmenting the interparticle contact area, which causes the G_0 to increase (Santamarina et al., 2001). The same mechanism accounts for the higher stiffness values amongst the dense samples within each material. Equation 1 captures the relationship between G_0 and the mean effective stress (p') through a power-type format.

$$G_0 = A \cdot \left(\frac{p'}{p'_{ref}}\right)^{\beta} \quad \text{(Equation 1)}$$

Where A is a scalar (expressed in MPa) depending on the grain characteristics and the packing properties, β is the adjustment exponent dependent upon the material's compressibility, and p'_{ref} is a reference pressure taken as 1 kPa.

Parameters A and β are inversely proportional because denser packing implies stiffer (and less compressible) material. The fabric differences decurrent from compacting the same tailings at different D_r

values justify a unique relationship for each tested specimen. Yet, it is possible to express A by the product of two terms: a scalar α (expressed in MPa) and a void ratio function $f(e)$ that captures the features of particle packing (He et al., 2019). Therefore, Equation 1 becomes:

$$G_0 = f(e) \cdot \alpha \cdot \left(\frac{p'}{p'_{ref}}\right)^{\beta} \quad \text{(Equation 2)}$$

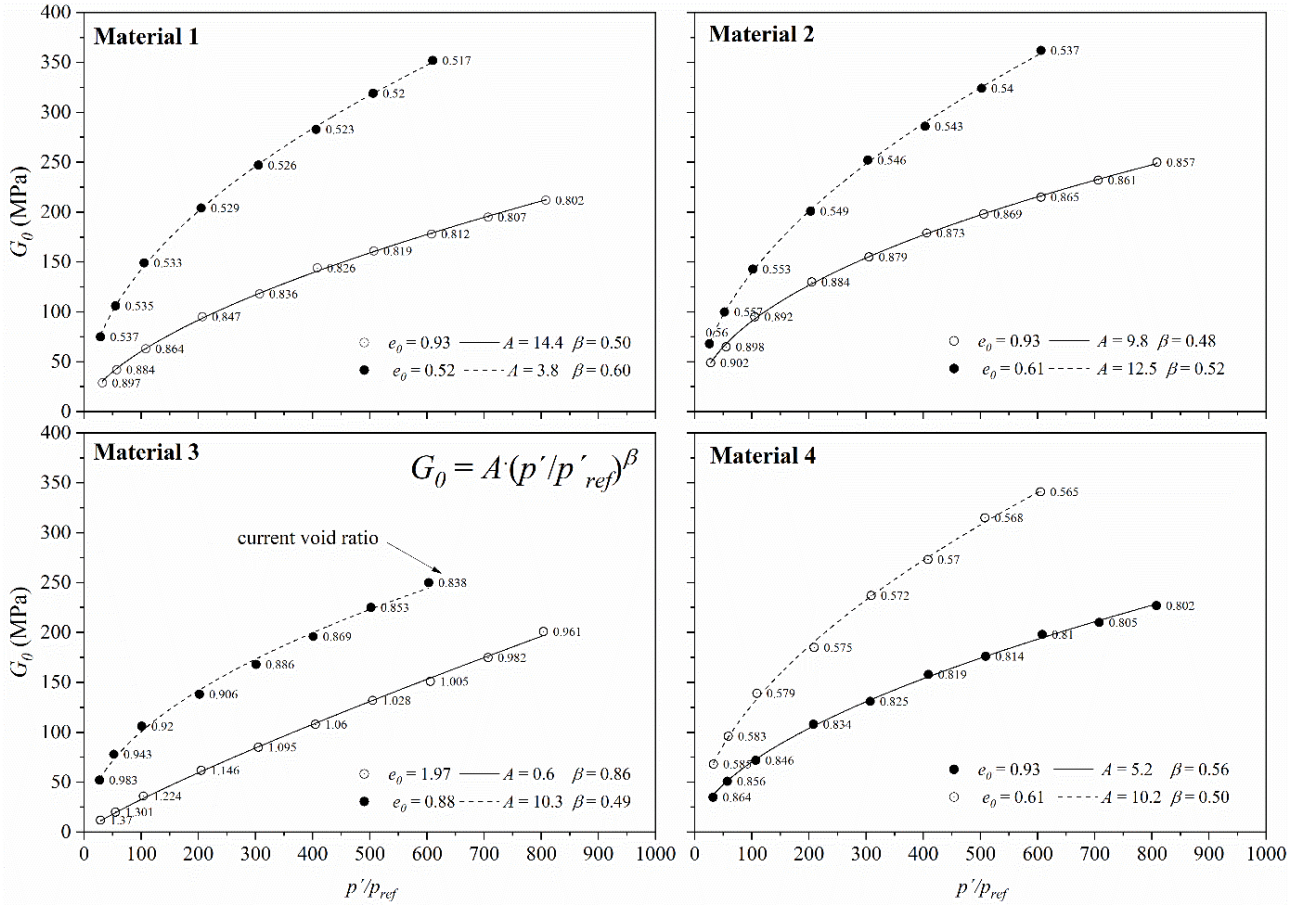


Figure 1: G_0 variation during the consolidation phase

Despite the existence of several forms of the function $f(e)$ (Goudarzy et al., 2016; Lo Presti et al., 1997), a simplified form of $f(e)$ was used to adjust the stiffness results within each material. It is given as follows:

$$f(e) = e^{-a} \quad \text{(Equation 3)}$$

Where a is an exponent depending upon the particle's characteristics.

Figure 2 shows the normalized small strain stiffness data $G_0/f(e)$ versus p'/p'_{ref} for all the tested specimens. When using the adequate a value, the specimens molded at different D_r collapsed onto the same

trend (Equation 2) within each material. In other words, this permits the mathematical description of the G_0 for a series of void ratios and pressure combinations.

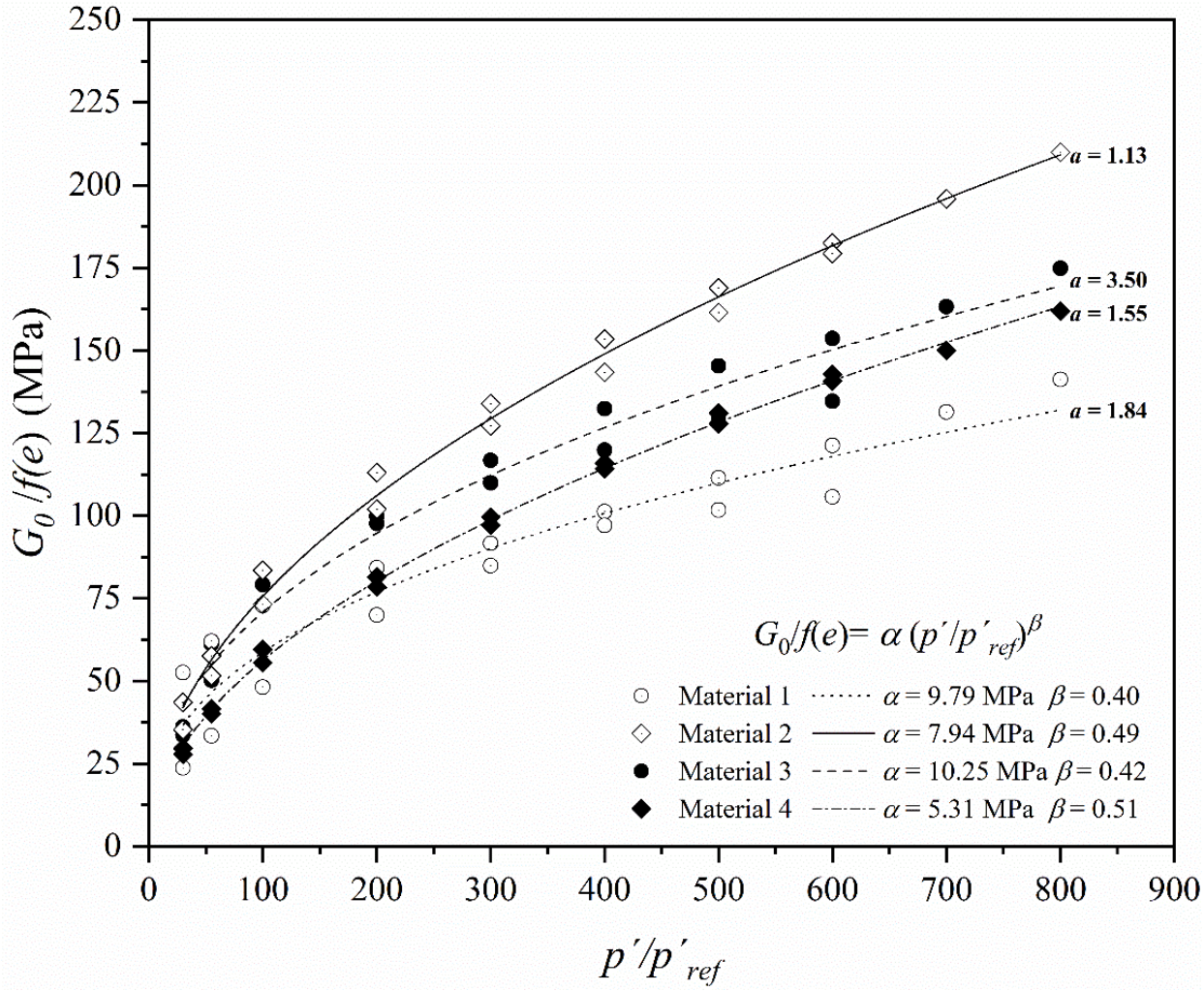


Figure 2: Normalized G_0 data

The four materials are generally similar but differ slightly in grading, mineralogy, and particle morphology, especially material 3. Those distinctions affect the particle packing-related characteristics (i.e. fabric), influencing the stiffness at the interparticle contact (Fernandez and Santamarina, 2001; Shi et al., 2021), which explains individual equations for each material.

Nonetheless, a relationship between exponent a and the effective particle size (d_{10}) appears to exist, accounting for the influence of the particle size on the value of a. Figure 3 displays such a relationship, fitting a power-type equation that portrays an inverse trend between the value of a and the effective particle diameter – higher a values occur for finer tailings. A coefficient of determination (R^2) of 0.97 was obtained.

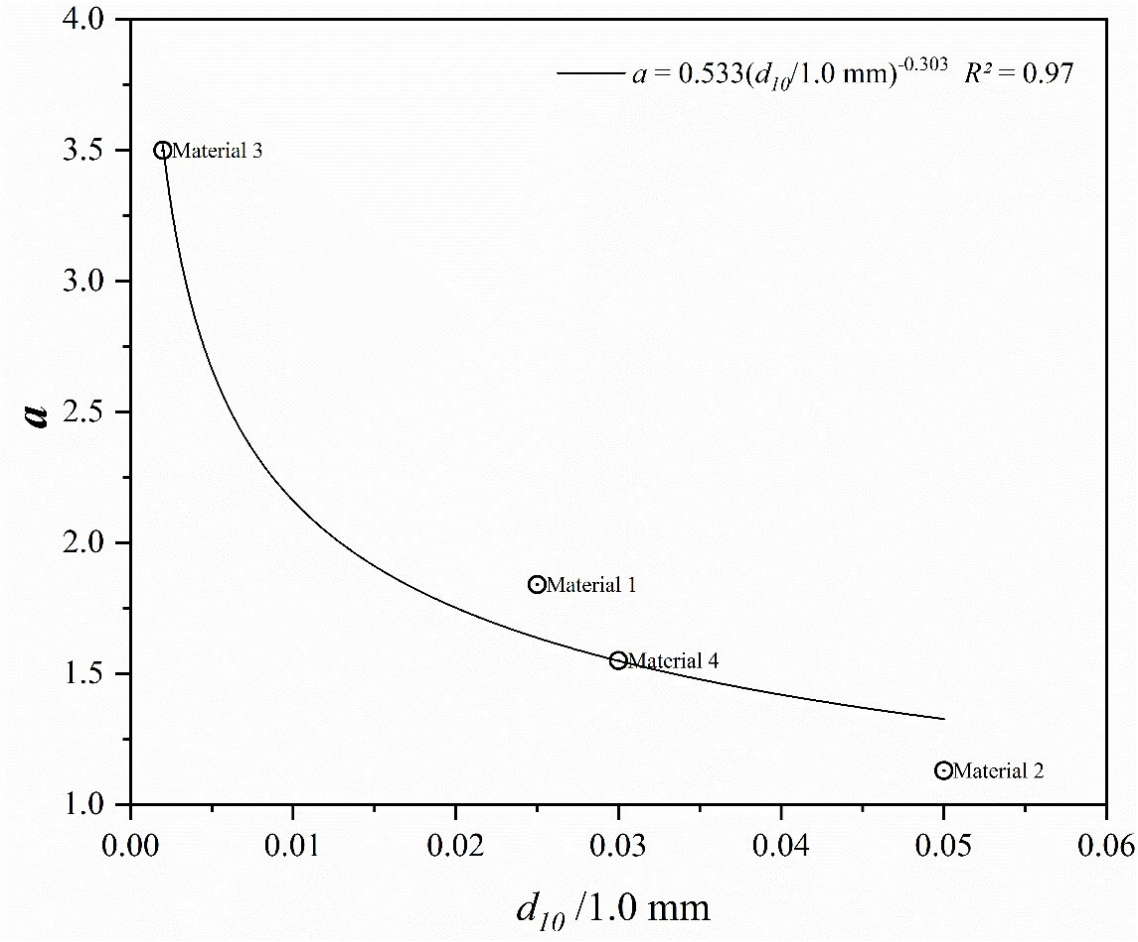


Figure 3: Coefficient of void ratio function

Triaxial testing

Figure 4 displays the normalized stress-strain behavior and the volume change response of the loose and dense samples of the four materials. All the loose specimens presented a ductile behavior and a fully compressive response in which the amount of compression was proportional to the void ratio at the beginning of the shearing (e_c value). All the dense specimens but the material's A exhibited a slightly fragile response: defined peak strength, post-peak strain softening, and initial compression followed by dilation. At the later stages of shearing, the specimens that have solely compressed stabilized in volumetric strain and directed towards the same stress ratio value ($q/p' = 1.33$), indicating that the fabric differences arising from gradation, mineralogy, and D_r values erased because of shearing.

In other words, the differences that influence the interparticle stiffness at small strain values are erased; the same critical state line can fit the data in the effective stress plane $q{:}p'$, denoting a critical state friction angle (ϕ'_{cs}) of 33°.

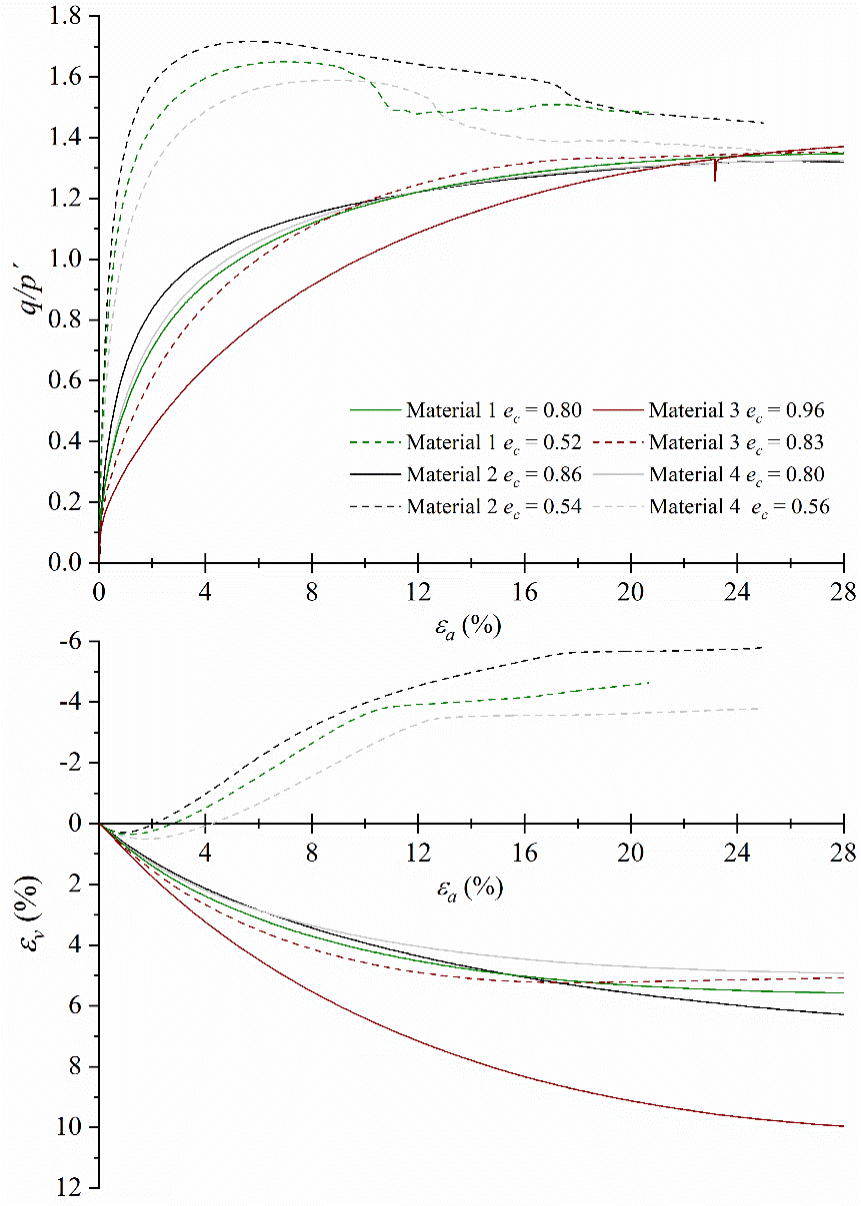


Figure 4: Shearing response

Conclusion

This study assessed the small-strain stiffness of four iron ore tailings through bender elements tests carried out during the isotropic consolidation phase of triaxial compression tests. The tailings were tested considering two initial relative density values (D_r = 20 and 100%). Therefore, considering the boundaries of the present work, the following conclusions can be drawn:

- The small strain-stiffness was shown to be proportional to the effective confining pressure and to the void ratio, which influences the interparticle contact stiffness.

- A power-type equation, depending on parameters A and β, can express the relationship between G_0 and the mean effective stress for each tested specimen. Yet, within each material, the data of the loose and dense specimens solely fall towards the same relationship by splitting A into two parameters and adopting a proper void ratio function $f(e)$.
- The grading and mineralogy characteristics influence the fabric, and thus the interparticle contact stiffness, explaining the existence of individual normalized relationships for each material.
- The value of the parameter a, related to the adopted $f(e)$, was shown to be dependent on the grain size characteristics of the tailings; it could be correlated with d_{10} of each material.
- Shearing appears to remove the fabric differences related to initial density, gradation, and mineralogy, as all the samples reached the same critical state stress ratio at the later stages of shearing.

This study has provided valuable insights into predicting small strain stiffness, considering aspects depending on the tailings gradation and state (void ratio and mean effective stress), which are relatively easy to measure within the context of dry stacking facilities.

Acknowledgements

The authors are grateful for the financial support provided by Vale S.A. and by the Brazilian Conselho Nacional de Desenvolvimento Científico e Tecnológico (CNPq).

References

ASTM. 2019. Standard Test Method for Determination of Shear Wave Velocity and Initial Shear Modulus in Soil Specimens using Bender Elements – ASTM D8295. ASTM International. https://doi.org/10.1520/D8295-19

ASTM. 2020. Test Method for Consolidated Drained Triaxial Compression Test for Soils – ASTM D7181. ASTM International. https://doi.org/10.1520/D7181-20

Bedin, J., Schnaid, F., Da Fonseca, A.V. and Costa Filho, L.D.M., 2012. Gold tailings liquefaction under critical state soil mechanics. *Géotechnique* 62: 263–267. https://doi.org/10.1680/geot.10.P.037

Fernandez, A.L., Santamarina, J.C., 2001. Effect of cementation on the small-strain parameters of sands. *Can. Geotech. J.* 38: 191–199. https://doi.org/10.1139/t00-081

Goudarzy, M., König, D. and Schanz, T. 2016. Small strain stiffness of granular materials containing fines. *Soils Found.* 56: 756–764. https://doi.org/10.1016/j.sandf.2016.08.002

He, H., Li, W. and Senetakis, K. 2019. Small strain dynamic behaviour of two types of carbonate sands. *Soils and Foundations* 59: 571–585. https://doi.org/10.1016/j.sandf.2018.11.003

Islam, K., and Murakami, S. 2021. Global-scale impact analysis of mine tailings dam failures: 1915–2020. Glob. Environ. Change 70, 102361. https://doi.org/10.1016/j.gloenvcha.2021.102361

Lo Presti, D.C.F., Jamiolkowski, M., Pallara, O., Cavallaro, A. and Pedroni, S. 1997. Shear modulus and damping of soils. *Géotechnique* 47: 603–617. https://doi.org/10.1680/geot.1997.47.3.603

Lupo, J.F. and Hall, J.E. 2010. *Dry Stack Tailings – Design Considerations.*

Quinteros, V.S. and Carraro, J.A.H. 2023. The initial fabric of undisturbed and reconstituted fluvial sand. *Géotechnique* 73 : 1–15. https://doi.org/10.1680/jgeot.20.P.121

Rodrigues Leão, S.R. and Dos Santos Santiago, A.M. 2022. Tailings dam scenario: Knowing how to avoid new catastrophes. *Ambiente Soc.* 25: e00661. https://doi.org/10.1590/1809-4422asoc20210066r1vu2022l2oa

Rodrigues Leão, S.R., Santiago and Dos Santos Santiago, A.M. 2022. Tailings dam scenario: Knowing how to avoid new catastrophes. *Ambiente Soc.* 25, e00661. https://doi.org/10.1590/1809-4422asoc20210066r1vu2022l2oa

Santamarina, J.C., Klein, K.A. and Fam, M.A. 2001. *Soils and Waves*. Chichester , New York: J. Wiley & Sons.

Schaper, D., Lessa, R., Freitas, A. and Weeks, B. 2020. De-characterization and closure of TSF: Concepts of the Brazilian legislation and international criteria. *Proceedings of Planning for Closure 2020,* Gecamin Digital Publications, virtual format.

Shi, J., Haegeman, W. and Cnudde, V. 2021. Anisotropic small-strain stiffness of calcareous sand affected by sample preparation, particle characteristic and gradation. *Géotechnique* 71: 305–319. https://doi.org/10.1680/jgeot.18.P.348

Silva, J.P.S., Rissoli, A.L.C., Cacciari, P.P., Viana Da Fonseca, A.J.P., Scheuermann Filho, H.C., Wagner, A.C., Carvalho, J.V.A., Festugato, L. and Consoli, N.C. 2024. Triaxial testing response of compacted iron ore tailings considering a broad spectrum of confining pressures. *Soils and Foundations* 64: 101438. https://doi.org/10.1016/j.sandf.2024.101438

Velten, R.Z., Consoli, N.C., Scheuermann Filho, H.C., Wagner, A.C., Schnaid, F. and Da Costa, J.P.R. 2024. Influence of grading and fabric arising from the initial compaction on the geomechanical characterization of compacted copper tailings. *Géotechnique* 74(5): 461–472. https://doi.org/10.1680/jgeot.22.00087

Wagner, A.C., De Azambuia Carvalho, J.V., Sousa Silva, J.P., Scheuermann Filho, H.C. and Consoli, N.C. 2023. Dry stacking of iron ore tailings: Possible particle breakage during compaction. *Proceedings of the Institution of Civil Engineers* 1–9. https://doi.org/10.1680/jgeen.22.00216

Lessons Learned in Applying the Observational Method to a Tailings Facility Constructed on a Soft Clay Foundation

Bryce Marcotte, SRK Consulting, Canada
Kyle Scale, SRK Consulting, Canada
Calvin Boese, SRK Consulting, Canada
Michael Andree, SRK Consulting, Canada
Travis Pastachak, New Gold Inc., Canada
Brent McFarlane, New Gold Inc., Canada
Jason Bell, New Gold Inc., Canada

Abstract

The Rainy River tailings management area (TMA) in Northern Ontario is situated above highly plastic, normally consolidated glacial clay soils of variable thickness. The TMA consists of clay core dams, with chimney and blanket filters, constructed upwards of ~30m in height. The clay foundation soils govern the design and construction of the dams. The design of the TMA requires large upstream and downstream rockfill buttressing combined with extensive monitoring to ensure continued performance is maintained.

The design and construction procedures attempt to best employ the observational method (Peck, 1969) to complete each raise safely. Construction raises are completed yearly to facilitate additional storage capacity and deposition. Dissipation of excess pore water pressure allows for the optimization of rockfill buttress placement after each construction season prior to the next raise. The design of the dams is completed using conventional methods to meet or exceed the minimum Canadian design standards.

Over 400 piezometers, 30 slope inclinometers, numerous settlement plates, and magnetic extensometers are used to monitor the site. Displacements (both lateral and vertical) and excess pore water pressures are observed throughout the year in response to additional loading. Monitoring of the instrumentation is ongoing by both the owner and the Engineer of Record (EOR).

The successful construction and operation of the site has benefited from continuous improvements to the monitoring and reporting system, yearly field investigations, interrogation of the most-probable and unfavorable conditions through numerical modelling, and open communication between the EOR and owner/site operations. This case-study paper describes the continued improvement and challenges of applying of the observational method. Specific emphasis is on the lessons learned with respect to the

importance of the governance structure, continuous improvements to the instrumentation monitoring and reporting system, and communication between stakeholders.

Background

The Rainy River mine site is located ~160 km south of Kenora, in the Lake of the Woods area of Northern Ontario, Canada, as shown in Figure 1. The site is operated by New Gold Inc., an intermediate Canadian-based mining company with core assets based in Canada. The mine is estimated to have an average annual processing rate of approximately 25,000 tonnes per day (tpd) and the TMA currently stores approximately 38 Mm^3 of tailings, with projected life of mine estimates around ~80 Mm^3. Tailings containment is currently provided by natural topography to the north and three perimeter dams to the northwest, southwest, and southeast.

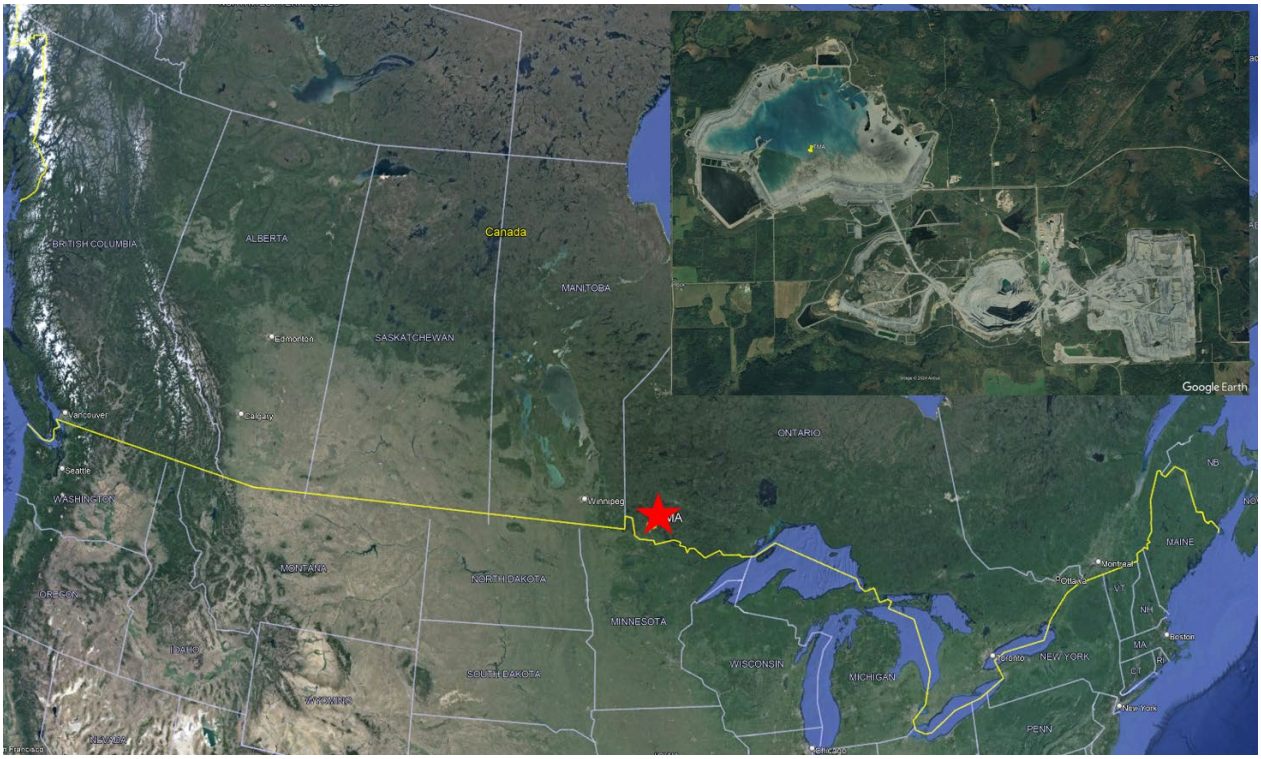


Figure 1: Location of the Rainy River Mine

Geological setting

The quaternary geology of the area is based on glacial deposition from the Laurentide ice sheet. Starting from the lowest unit, undulating bedrock of the Canadian Shield is present on site and visible from surface outcrops (390 m), or as low as ~310 m below overburden soils within the tailings management area (TMA). Soils within the TMA were deposited because of two main glacial advances: the Labradorean and Keewatin

sectors of the Laurentide ice sheet (Ontario Geological Survey, 2001; BGC, 2021). Sequencing of the geological units is provided in Figure 2, as shown in SRK's 3D geological model.

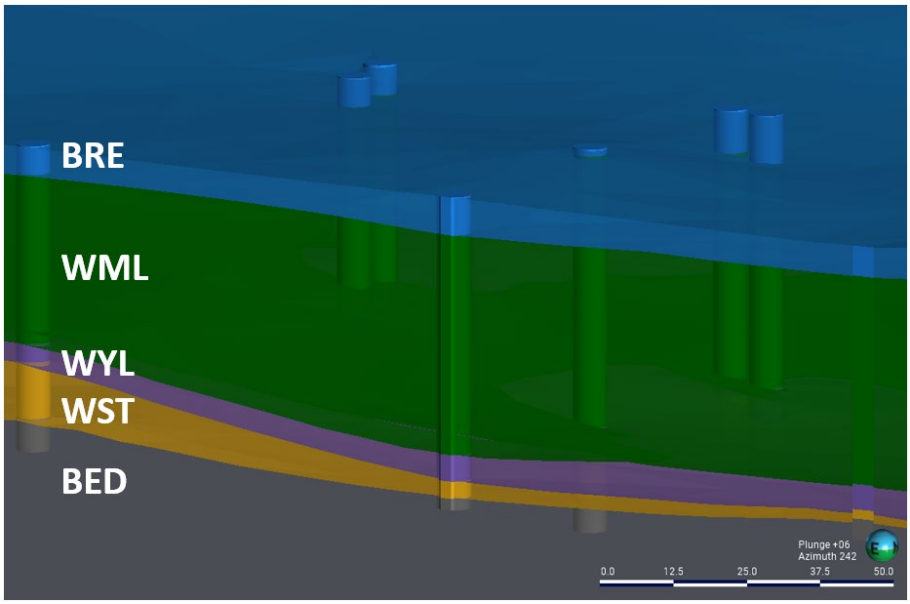


Figure 2: Generalized geotechnical geology of the tailings management area at the Rainy River Mine

The geological history of the TMA area on site is as follows (from bedrock to surface):

WST: The Labradorean ice sheet advanced towards the southwest, depositing coarse Whiteshell Till (WST) along the bedrock. The WST is variable in thickness and is found in bedrock troughs or depressions crosswise and on the leeward side of the bedrock highs. Thicknesses within the site area typically range from 0 to ~15 m. The WST can be observed to daylight at bedrock highs around the site and acts as a confined aquifer – artesian conditions are observed in some locations.

WYL: The retreat of the Labradorean ice sheet likely resulted in a pro-glacial lake over the site area in the period prior to the Keewatin ice advancement. The unit, coined the Wylie formation (WYL) is rhythmically layered sediments, progressing from sands and silts near the bottom (Labradorean sourced) to increasingly more Keewatin ice-derived clays near the surface, reflected by a change in mineralogy (Keewatin clays contain a high volume of expansive clay minerals).

WML: Movement of the Keewatin glacier from west to east resulted in the deposit of Whitemouth Lake Till (WML) across the site in a buoyant environment. The clay is a highly plastic montmorillitic soil and is typically overconsolidated (OC) from depths of 4–10 m, likely due to desiccation/weathering or grounded glacial advance, and normally to lightly overconsolidated at greater depths.

BRE: The Brenna layer, deposited within the retreat of the Kewaatin ice and emergence of the Lockhart Phase Glacial Lake Agassiz, has variable grain size and characteristics due to its dynamic

depositional environment. It has generally been observed to be spatially continuous below elevation 375 m, with thickness ranging from 0.5 m to 6 m. The depositional environment varied both temporally and spatially, resulting in different types of BRE – classified as low or high plasticity clay.

Organics: Thick fibrous peat deposits and topsoil can be observed around site.

At the Rainy River mine site, organics and BRE are removed to construct the dam core. The WML is used for dam core construction due to its consistency and low hydraulic conductivity. Meanwhile, the WST acts as a confined aquifer, recharged from areas with bedrock highs and daylighting WST. Groundwater is present at or near the surface as observed in piezometers, boreholes, and many local lakes and streams evident in the area. Although the WST has been observed to be artesian in some areas disconnected from the open pit, the transmissivity has generally been observed to be low.

Cross-section and design basics

The TMA is constructed as a centerline raise clay core dam with chimney and blanket filters, as shown in Figure 3. Due to the weak, compressible foundation soils, large rockfill buttresses and tailings are placed on both the upstream and downstream sides. As the foundation varies over the length of the dam (~7.6 km), the dam is segmented into 18 critical cross-sections. Each cross-section buttress is optimized to meet CDA (2019) requirements based on the interpreted foundation conditions.

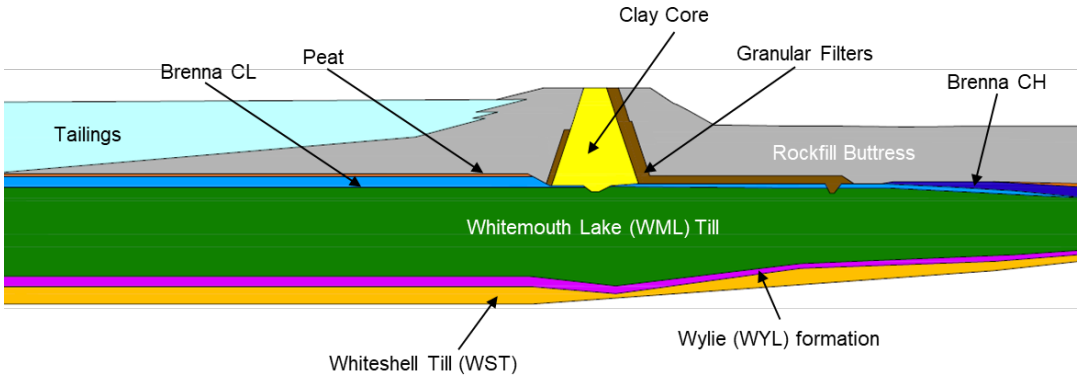


Figure 3: Typical cross-section of a tailings management area dam

The dam height varies from tying into the bedrock outcrops to a maximum dam height of ~27 m (as of 2024). The downstream buttress varies in width depending on the foundation conditions (described below) but can range from ~8H:1V to ~20H:1V, resulting in buttresses exceeding 400 m offset from the centerline of the crest.

Foundation conditions

The plastic clay foundation soils at Rainy River result in low strength clays that generate high excess porewater pressures upon loading. Extensive work has been performed characterizing both the BRE and

WML units as they relate to TMA performance (BGC 2019, 2021; SRK, 2023). New Gold has supported several site investigations, which have been conducted for both the TMA, waste rock, and overburden stockpiles. Additionally, test embankments and numerical modelling has been undertaken on site (Etezad et al., 2019, 2022). Examples of triaxial testing on the WML and BRE CH as shown in Figure 4, with a sample with a pre-sheared slickenside failure given in the photo. Design strengths lines of 15° and 12° are provided for reference.

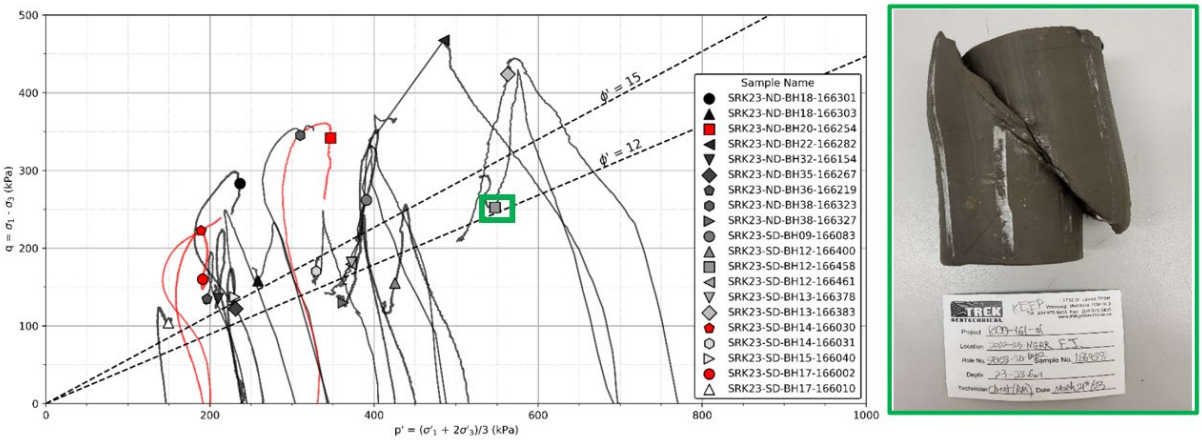


Figure 4: Triaxial test results on WML (grey) and BRE CH (red) samples

The Whitemouth Lake Till has been identified to contain discontinuous shear zones "slickensides" present across the site. The slickensides vary in size from ~10 mm to ~10,000 mm in size. They are assumed to be discontinuous and occur at several angles, as shown in Figure 5.



Figure 5: Examples of slickensides surfaces observed in borrow pit development

The pre-sheared slickensides are a function of the depositional history of the lodgement till (BGC, 2019). The shear strength along the slickenside is assumed to be at or near residual, although the bulk strength is assumed to be a combination of the peak-post-peak-residual value (i.e., "operational")

(Skempton, 1985; Lo, 1972). Observations and numerical modelling of the clay borrow pits indicate the clay reduces in strength with increasing strain (Marcotte et al., 2023).

Observational method in design and construction

To keep the buttresses a reasonable size (and not overdesign), the observational method is employed. Many historical tailings facilities are not well suited to the observational method due to the potential for brittle strain-weakening behavior of loose tailings deposits. However, the limit equilibrium critical downstream stability sections during design do not predict failure through the tailings mass even when fully liquefied tailings are assumed to occur.

The buttress requirements at Rainy River were initially based on stability assessments developed from preliminary site investigations. A higher operational strength for the WML and a lower minimum required factor of safety (FOS) (1.3) were adopted during construction and were used during the initial construction, but unfavorable displacements led to additional buttressing as the dams grew in height.

After further data collection and review, the geological and geotechnical models were updated, adopting a lower operational shear strength (φ'=12°) and a higher FOS requirement (1.5) for the following dam raise (2020). The additional rockfill buttressing that was required to satisfy the new parameters led to reduced lateral displacements and controlled movement rates during construction.

A comprehensive site investigation during winter 2021 refined the geological model (BGC, 2021), enhancing site understanding. Improved performance and increased confidence in the geotechnical model provided confidence for a 3° increase in operational strength of the WML, reducing buttressing requirements for select design segments. Using Peck's observational method, the lower-bound operational strength was applied if unfavorable movements occurred.

If unfavorable instrumentation readings indicate that additional rockfill buttressing may be required, the mine has a fleet of construction equipment that can be immediately mobilized. Additional rockfill is stored at the toe of the TMA for both convenience during construction and expediency should it be required.

The third raise (2022) with the increased clay strength demonstrated satisfactory performance, improving understanding of clay behavior. Consequently, a φ'=15° was adopted for the 4th, 5th, and 6th raises across all design segments.

The design assumptions, instrumentation, and construction are reviewed on an ongoing basis, and adjusted to reflect the actual site conditions. Modifications are made yearly to the stability assessments and detailed design for the next raise to best reflect the current interpretation of the dams. Stability assessments on an adverse foundation using the observational method require the engineer to continually measure and observe conditions, and test them against the current design assumptions.

Monitoring

To successfully apply the "observational method" to the Rainy River site, an extensive suite of monitoring instrumentation is employed by the mine, as shown in Figure 6. This includes:

- 486 active VWPs at the TMA and associated water management structures;
- 36 installed slope inclinometers;
- 2 Shape Array accelerometers;
- 13 settlement plates;
- 29 magnetic extensometers;
- 19 standpipe piezometers;
- regular InSAR surveys and reporting;
- regular photogrammetric drone flights;
- regular LiDAR surveys; and
- regular dam inspections.

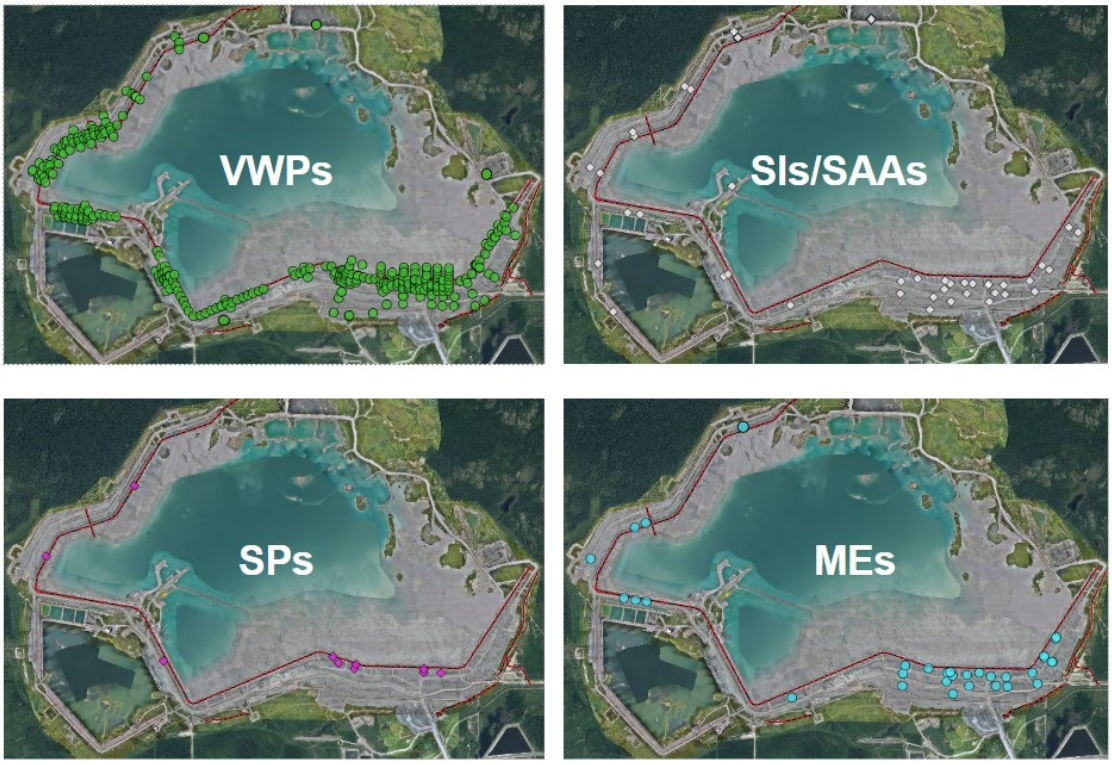


Figure 6: Instrumentation at the Rainy River tailings management area

To accommodate the significant data collected, New Gold has developed in-house geographic information systems (GIS) and stores all data within a SQL server. As communication between the EOR and client is a critical component of the monitoring system, the SQL server is provided directly to the EOR.

From the SQL database, the EOR can download specific data, develop custom interpretation visualizations, and keep up to date with the latest readings. The developed system can track and timestamp changes made, to aid in any future troubleshooting and help address any discrepancies that may arise. The GIS system developed by New Gold collects and stores the following key information used by the EOR for interpretation and performance monitoring:

- VWP metadata, readings, health (battery, signal) and any changes that occur;
- slope inclinometer readings, azimuth directions, configurations, and any changes that occur;
- tailings spigots that are active, elevation of tailings at spigot;
- weather; and
- pond water levels.

The ability to have unrestricted access to real-time site data has allowed the EOR team to create visuals to expedite data review and performance monitoring. For example, a capture of the monitoring data output is given in Figure 7.

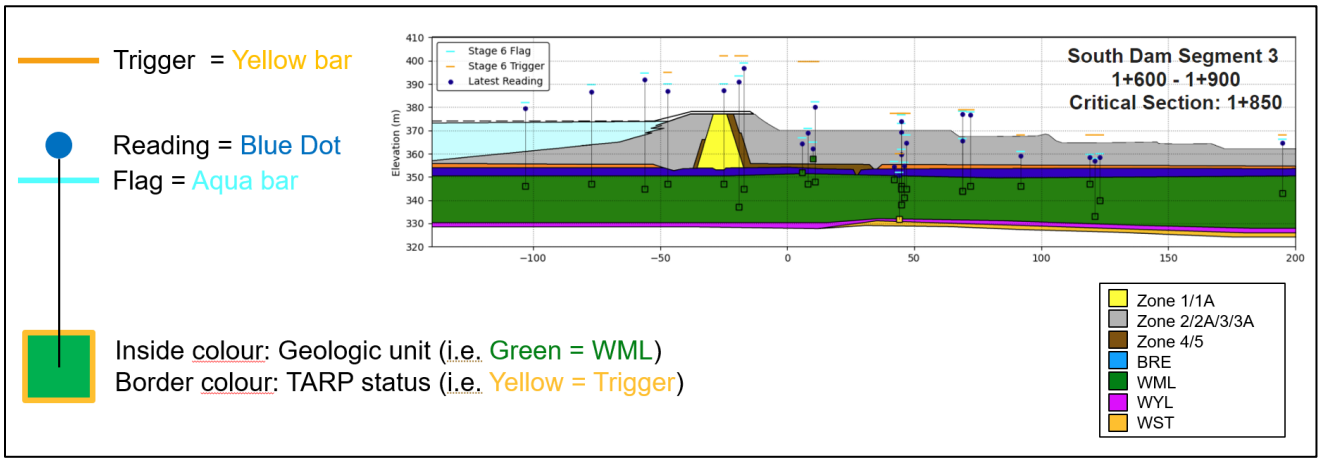


Figure 7: Real-time plots of total head superimposed on critical cross-section

The visual quickly communicates information to the engineer inspecting the data about the current total heads within the foundation, any "Trigger" or "Flag" alerts that are noted, as well as time-series data that can be inspected further.

TARPS and governance

SRK revised the sitewide trigger action response plans (TARP) in 2024 to be more in line with the Mining Association of Canada (MAC) tailings guide TARPS (MAC, 2021, 2022). As outlined in the example by MAC, a clearly defined risk-management plan for specific indicators is required. Although just an example,

MAC provides a four-level risk-framework. A similar framework was developed to fit the site conditions, as shown in Figure 8.

Segment Status	Potential Actions	Notified Personnel
Green	Standard surveillance activities and frequencies.	-
Yellow	Halting construction; Additional buttressing; Reduce pond volume; Increased instrumentation reading frequency; Increased survey and inspection frequency; Adjustments to instrumentation thresholds.	EOR Team; Tailings Dam Engineer; Responsible Person.
Orange	All applicable activities in Yellow; Preparation for unfavorable conditions; EOR site visit; Reassess thresholds and conditions that may result in a high-risk situation.	SRK internal review panel; NGRR ITRB; Emergency Response Personnel; Accountable Executive.
Red	All applicable activities in Orange; Mandatory EOR site visit; Prepare to activate the Emergency Response Plan; Evacuate areas of concern and notify Communities of Interest.	All stakeholders. Communities of Interest; Regulators.

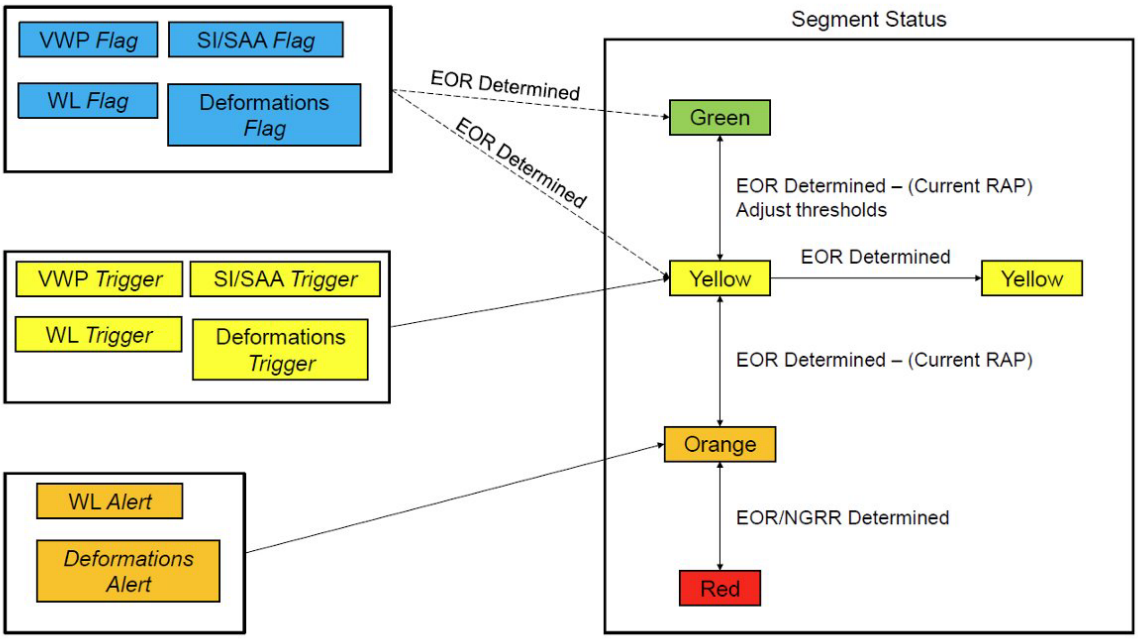


Figure 8: TARPs framework for the Rainy River Mine site

For each of the 18 individual dam segments, an operational status is assigned based on current observations or instrument readings. If the segment moves into a new operational status predetermined actions are initiated, as depicted in Figure 8.

As described previously, the Rainy River site employs the observational method to construct the dams in stages. The dams are expected to move, with upwards of 1–2 m of total vertical settlement expected over

the decades, primarily due to consolidation. Lateral displacements and high excess porewater pressures are anticipated due to the nature of the foundation and consolidation of the materials. The instruments inform the engineer of the movement/responses of the structure, but in isolation, may not directly correlate with a "Yellow" or "Orange" status.

Importantly, based on the spirit of the observational method as described by Peck (1969) a "Flag" level was adopted for data with quantitative values, such as SIs and VWPs, representing the anticipated response of the instrument. This varies instrument to instrument, based on previous history and expected fill placement near the instrument. A flag in isolation may not be indicative of a problem, but rather notifies the engineer that an instrument should be reviewed. If the EOR determines that a flag (or several flags/observations) is a symptom of a larger or developing problem, the engineer may increase the segment status and initiate actions to be taken. Flag values are evaluated on a weekly basis.

Trigger values represent observations that require a formal EOR response to the mine. For example, if a VWP total head exceeds the total heads used during the design, the EOR must reevaluate stability using the current conditions and geometry. Once this is complete, the EOR may determine that the segment can return to "green" or an acceptable status if the stability is acceptable (along with consideration for other observation instrumentation at that section). If other instrumentation indicated a potentially worsening problem, the EOR may determine that the segment should remain at the "yellow" status, or be moved to the "orange" status, and begin actions associated with that stage. The outcome of these actions is summarized and communicated with NGRR.

Conclusion and recommendations

The Rainy River TMA is located on thick, high plasticity, soft clay foundation soils that make construction and monitoring challenging. To keep the buttresses a reasonable size (and not overdesign), the observational method is employed. This involves developing a plan based on the expected conditions, having action plans developed if unfavorable conditions arise, and implementing continuous monitoring to assess the actual behavior during construction.

To support the observational method approach, extensive instrumentation has been deployed at the site to measure displacements, porewater pressures, settlement, and any movements that have occurred. The significant effort taken by the mine to fully digitize and automate the data collection and distribution has reduced the time spent troubleshooting errors, allowing the EOR to spend more time analyzing and interpreting the data.

The TARPs system was developed strategically to capture the spirit of the observational method. The site employs "Flag" and "Trigger" threshold levels to indicate responses to instrumentation. Notably, in

2024, the initial threshold level was renamed "Flag" to properly reflect the response of any flag threshold levels that may occur.

Unusual behavior and movement are expected when foundations are founded on clays with an undrained shear strength of ~30 kPa. It is expected that "Flag" thresholds will occur throughout the year. For this particular site, it is important to set the initial threshold low enough that deviations from expectations can be observed prior to them progressing to a more significant problem, allowing time to properly assess and react.

Lessons are learned each year by the EOR. The instrumentation thresholds and expectations are revised annually, and these lessons are incorporated into the new thresholds. During the 2024 construction season, SRK has observed less "Flag" threshold responses as the site understanding was increased and adjusted after the 2023 season.

There can be a tendency in engineering to set thresholds high enough that they are only triggered in cases of serious concern, reducing the overall workload. However, if the observational method is truly being used, the thresholds should be set to alert the engineer when something outside of expectations occurs, so that further learnings of the foundation and subsequent fill can be assessed. Care must also be taken to ensure that false alarms are not set off frequently, as this can lead to complacency. Often (at this site), false alarms may be as simple as a temporary stockpile being located above a handful of piezometers.

Acknowledgements

The authors would like to acknowledge the continued support of New Gold Rainy River (NGRR) mine for the support in development of this paper. NGRR has been highly supportive in initiatives such as this paper, and previous papers (Etezad et al., 2019, 2022; Marcotte et al., 2023).The greater geotechnical committee benefits from their transparency and willingness to participate in more academic activities.

References

BGC. 2019. Surficial Geological Model Development (internal).

BGC. 2021. TMA Foundation Characterization and Geotechnical Parameters. Report Rev. 1 (Internal)

Canadian Dam Association (CDA). 2019a. Technical Bulletin: Application of Dam Safety Guidelines to Mining Dams (2019 edition).

Canadian Dam Association (CDA). 2019b. Revision to Section 3.5.4.1 of the Technical Bulletin: Application of Dam Safety Guidelines to Mining Dams. April 7, 2019.

Etezad, M., Riddell, B., Bocking, K., Becker, D., Hamdani, A., Buchana, P. and DaSilva, F. 2019. Interpretation and analysis of a test embankment on soft clay. *Geo St. John's*.

Etezad, M., Riddell, B., Bocking, K., Becker, D., Steve, B. Pastachak, T., Bell, J. and Wimmelbacher, E. 2022. Three-dimensional effect on a large stockpile slope stability analysis. *Proceedings of GeoCalgary 2022.*

Lo, K.Y. 1972. An approach to the problem of progressive failure. *Canadian Geotechnical Journal* 9(4):407–429.

Marcotte, B.A., Leik, A., Boese, C., Elwood, D., Pastachak, T., McFarlane, B. and Bell, J. 2023. Insights into medium term borrow pit stability for slopes cut in high plastic clay. *GeoSaskatoon 2003. Proceedings of the 76th Canadian Geotechnical Society Conference*. Saskatoon.

Mining Association of Canada (MAC). 2021. Developing an Operation, Maintenance, and Surveillance Manual for Tailings and Water Management Facilities. Version 2.1, dated March 2021.

Mining Association of Canada (MAC). 2022. Tailings Management Protocol. Version dated June 2022.

Ontario Geological Survey. 2001. Quaternary Geology Fort-Frances-Rainy River Area. Report 286

Peck, R.B. 1969. Advantages and limitations of the observational method in applied soil mechanics. *Géotechnique* 19(2): 171–187.

Skempton, A.W. 1985. Residual strength of clays in landslides, folded strata and the laboratory. *Géotechnique* 35(1): 3–18.

Compaction Sensitivity in Tailings Stack Infiltration Modeling: Unsaturated Properties Uncertainty Analysis

Letícia B. L. Garcia, Knight Piésold Consulting, Brazil
Marcos A. Lemos Júnior, Companhia Brasileira de Metalurgia e Mineração (CBMM), Brazil
Guilherme J. C. Gomes, Universidade Federal de Ouro Preto (UFOP), Brazil

Abstract

Filtered tailings stacks have become increasingly prevalent in the mining industry since the 1990s, particularly in regions with arid climates. However, the adoption of filtered tailings technology has expanded globally, regardless of climatic conditions, as mining operations seek to reduce water in tailings to improve safety. Nonetheless, the implementation of tailings stacks in high-rainfall areas contradicts conventional practices, as filtered tailings operations are typically associated with regions of low precipitation due to compaction challenges during rainy periods. This poses significant challenges for tailings stacking in high-rainfall conditions, including their unsaturated characteristics and the absence of specific guidelines tailored to such environments.

Consequently, numerical modeling of infiltration under the principles of Unsaturated Soil Mechanics offers a promising approach to optimize recharge calculations, enabling more precise assessment of various factors such as moisture content, compaction, and drain sizing for these stacks. While optimized values are expected through modeling, inherent uncertainties exist in calibrating soil water retention curves (SWCC) and permeability functions, which involve Van Genuchten parameters, thereby affecting both parameter definition and model results. This study utilized tailings properties from a Brazilian mine, along with site climatic data, and employed a Bayesian approach to address calibration uncertainties. A hypothetical two-dimensional (2D) section of a test pad was considered for the study, and a software that simulates the movement of water and solutes in variably saturated media, for obtaining infiltration rates by solving the Richards Equation, was employed. In addition to calibration uncertainties, the simulation assessed the compaction sensitivity (different void ratios) on the SWCC, revealing that both factors influenced infiltration rates and pressure head fluctuations. These findings underscore the critical importance of proper compaction control and suitable drainage system design.

Introduction

The mining industry is a cornerstone of many economies, significantly contributing to employment, income generation, and the supply of raw materials to various industrial sectors. Understanding the entire mining production process is crucial to ensure the adoption of the best technologies and operational practices for more sustainable mining. As part of this effort, companies are continuously seeking innovative solutions to improve their ore treatment processes, enhance recovery rates, and extract minerals that were previously regarded as waste.

Waste and tailings management is a vital aspect of mining operations, and extensive research is being conducted to find better uses for these materials. However, these applications are often limited by the physical and chemical properties of the materials and the high costs associated with their logistical deployment. Given the technical and economic limitations of repurposing a large portion of mining tailings, it becomes imperative to dispose of these materials in geotechnical structures such as dams and stacks. Traditionally, tailings dams have been the preferred method in high-rainfall regions due to established engineering practices, regional topography, and climate conditions. However, recent changes in legislation and licensing processes, particularly after several catastrophic tailings dam failures in Brazil, have led to a growing interest in alternative methods, such as tailings filtration and stack disposal.

In some mining operations, filtered tailings stacks have gained prominence due to their potential for safer and more efficient waste management. As mentioned by Davies (2011), the installation of tailings stacks has grown significantly since the 1990s, particularly in countries such as Australia, Zambia, Chile, Mexico, and the United States (Ulrich and Coffin, 2013). However, areas with substantial annual rainfall require careful evaluation of this method. Considering operational criteria during the rainy season is essential, and understanding how these stacks behave given the variability in geotechnical parameters influenced by the moisture content of the filtered tailings from industrial processes is crucial. According to Patterson et al. (2016), the success of filtered tailings stacks depends on site conditions, operation scale, and the geotechnical and geochemical properties of the tailings.

Therefore, the implementation of tailings stacks in high-rainfall areas poses significant challenges, including their unsaturated characteristics and the absence of specific guidelines tailored to such environments. Key factors influencing this scenario include: (i) the moisture content of dewatered tailings, influenced by processing plants and precipitation; (ii) high infiltration and transient anisotropic seepage associated with precipitation, compaction, and tailings properties; and (iii) evaporation rate. Moreover, the constant need for tailings disposal exacerbates operational difficulties in compaction during rainy seasons.

Consequently, numerical modeling of infiltration under the principles of unsaturated soil mechanics offers a promising approach to optimize recharge calculations (Watson et al., 1995), enabling more precise assessment of various factors such as moisture content and drain sizing for these stacks. While optimized

values are expected through modeling, inherent uncertainties exist in calibrating soil water retention curves (SWCC) and permeability functions, which involve van Genuchten (1980) parameters, thereby affecting both parameter definitions and model results.

This paper proposes to address calibration uncertainties using a Bayesian approach and discuss their implications for the results of numerical infiltration modeling in tailings stacks based on sensitivity analyses of the compaction void ratio. Tailings properties from a mine in a high-rainfall area in Brazil were used as a case study, along with site climatic data. A fictional 2D section of a test pad was considered for the study, and a software that simulates the two-dimensional movement of water and solutes in variably saturated media, for obtaining infiltration rates by solving the Richards Equation (1931), was employed.

Methodology

This research focuses on a hypothetical filtered tailings stack located in a high-rainfall region. Data for the tailings were obtained from a mining company. Although tailings stacks are typically raised progressively, this study considers a three months long simulation in a test pad with a single raise.

While classical soil mechanics assumes that saturated pores between soil grains are completely filled with liquid below the water table and with gas above it – simplistically filled with water or air, respectively – unsaturated soil mechanics studies the simultaneous presence of water and air in different proportions between soil grains. Thus, a soil can present three distinct zones of saturation above the water table: the capillary zone, the two-phase zone, and the dry zone (Fredlund, 2017). The potential variation in the degree of saturation in the "two-phase" zone highlights the need to define the properties of unsaturated soil through functions.

The determination of the soil-water characteristic curve (SWCC) is the fundamental distinction between the behavior of saturated and unsaturated soils (Morgenstern, 2012). The SWCC is a curve that represents the nonlinear relationship between moisture content and pressure head in a given soil under a specific compaction state. In laboratory settings, the SWCC is obtained by measuring the soil suction at different moisture contents. A mathematical fit is then used to calibrate the curve. The following van Genuchten (1980) equation is one of the most widely used models for the SWCC (Gitirana et al., 2023) and it was adopted for the current study calibration.

$$\theta_w(\psi) = \theta_r + (\theta_s - \theta_r)\frac{(1 + (\alpha \cdot \psi)^n)^{\frac{1}{n}}}{1 + (\alpha \cdot \psi)^n}$$

Where: θ_w is the volumetric moisture content; θ_r is the residual volumetric moisture content; θ_s is the saturated volumetric moisture content; ψ is pressure head; α is the air-entry value; and n is a fitting parameter of the model that determines the curve inclination.

The van Genuchten parameters are calibrated using a Bayesian approach via the Markov Chain Monte Carlo (MCMC) method with the DREAM algorithm (Gomes et al., 2017). Calibration involves data collection through hanging column tests on different void ratio compactions. The MCMC calibration is implemented in MATLAB, involving the generation of one hundred combinations of possible van Genuchten parameters for each one of the three void ratio specimens that will be analyzed. With the volumetric moisture content function, the hydraulic conductivity function can be obtained as per the following equation (van Genuchten, 1980).

$$K(\theta) = K_s \cdot S_e(\psi)^L \left\{1 - \left[1 - S_e(\psi)^{\frac{1}{m}}\right]^m\right\}^2$$

Where: K_s is saturated hydraulic conductivity; S_e is effective saturation; ψ is pressure head; m is 1 – 1/n; and L is a pore-connectivity parameter (commonly equal to 0.5).

In possession of the parameters input, the flow can be simulated with Richards Equation (1931). Based on Darcy's Law (1856), Buckingham (1907) developed an equation for flow in unsaturated porous media, also known as the Darcy-Buckingham Equation, which relates hydraulic conductivity, suction, and moisture content. Later, Richards (1931) developed a differential equation that describes water movement in unsaturated soil using the Darcy-Buckingham Equation and Bernoulli's Equation. Due to its complexity, the Richards Equation (1931), presented below, is typically solved through numerical modeling.

$$\frac{\delta\theta}{\delta t} = \frac{\delta}{\delta z}\left[K(\theta) \cdot \left(\frac{\delta\psi}{\delta z} + 1\right)\right]$$

Where: θ is the volumetric soil moisture content (m/m); t is time (s); z is gravitational potential (m); ψ is pressure head (m); and K(θ) is the hydraulic conductivity (m/s) function based on soil moisture content.

The numerical modeling of infiltration presented here is conducted using Hydrus-2D software (Šimůnek et al., 2008), which simulates the bidimensional movement of water and solutes in variably saturated media by solving the Richards Equation. Input data for the model include the one hundred sets of van Genuchten parameters derived from soil-water retention curves (SWCC) calibration for each void ratio compaction, saturated hydraulic conductivity, relevant meteorological data, and the physical dimensions of the tailings stack.

The sets of one hundred infiltration results from these simulations are analyzed to assess the impact of parameter uncertainty arising from the calibration of the non-linear SWCC. This analysis involves comparing infiltration rates, moisture contents, and pressure heads while evaluating the variability introduced by the different combinations of possible van Genuchten parameters for each one of the three void ratio specimens that are being analyzed. Average values and 95% confidence intervals were calculated

for each set of one hundred simulations, facilitating meaningful comparisons of the impact of different void ratios. A 95% confidence interval is widely used in statistical analysis because it offers a balance between precision and reliability. This interval means that if many samples were taken and an interval estimate were built from each, 95% of these intervals would contain the true population parameter. A 95% confidence level is considered a standard in many fields because it provides reasonable certainty without excessively wide intervals, which can occur with higher confidence levels (Moore et al., 2017). This comprehensive methodology aims to account for inherent uncertainties in soil properties in infiltration modeling, providing optimized results for recharge calculations within the framework of unsaturated soil mechanics.

Data and discussion

Tailings characterization

The tailings investigated in this study are produced from niobium beneficiation, resulting from a flotation process. The particle size distribution testing, provided by the mining company, indicates that the tailings are primarily sand (~60%), with the remainder consisting of fines that pass through a No. 200 sieve. According to the Unified Soil Classification System (USCS), the authors classified the material as silty sand (SM), as the Atterberg limits testing indicates that the material exhibits non-plastic behavior. The selected sample for this study yielded a specific gravity of 4.44 g/cm³. Flexible wall permeability tests were conducted, according to ASTM D 5084, on the tailings sample at various stress levels and void ratios, and the results are presented in Table 1.

Table 1: Saturated hydraulic conductivity test results

Confining stress (kPa)	Void ratio (e)	K_{20} (cm/s)
400	0.89	9.15E-05
800	0.88	6.42E-05
100	0.73	1.91E-04
400	0.73	8.61E-05
800	0.73	5.33E-05
	Average:	1.22E-04

As a simplification of the treated uncertainties, and considering the available data and significant variability often encountered in hydraulic conductivity values, a saturated permeability input of 10^{-4} cm/s was uniformly defined for all simulations. Therefore, calibration of different hydraulic conductivity functions was not performed and the uncertainty was evaluated based on the SWCC parameters (θ_r, θ_s, α and n).

Parameters calibration

Three specimens from the same filtered tailings sample were compacted to achieve saturated void ratios (e) of 0.85, 0.71, and 0.69. The hanging column test, specified by ASTM D6836, was conducted for each specimen, and the results are presented as data in the SWCC calibration shown in Figure 1.

Since volumetric moisture content is the volume of water divided by the total volume, in a saturated condition, the volume of water is equivalent to the volume of voids. Therefore, since soil porosity is defined as the volume of voids divided by the total volume, θ_s is equivalent to the porosity of saturated soil. In this context, truncating saturated moisture content could be considered for the calibration presented here, given that porosity is determined by a straightforward indexing formula using void ratio as input. However, the curves showed the best fit when no truncation was applied to the SWCC parameters, as shown in the calibration results presented in Figure 1. Therefore, from the obtained uncertainty limits, one hundred sets of parameters (θ_r, θ_s, α and n) were generated to perform 100 simulations for each analyzed void ratio.

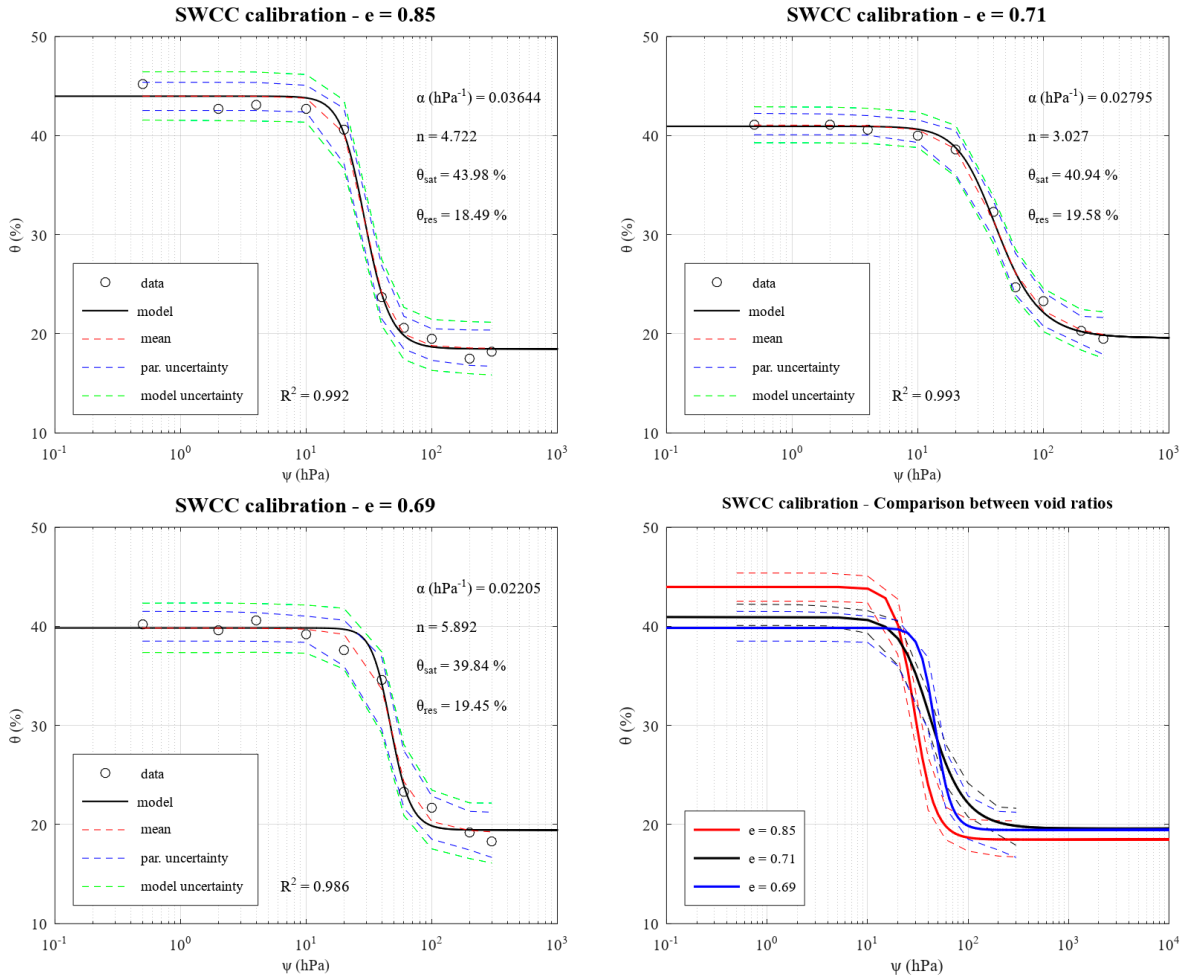


Figure 1: Calibration of van Genuchten parameters

As can be observed from the calibration results, in which each curve corresponds to a specimen with a specific void ratio, there is a noticeable relationship between the decrease in void ratio and the reduction in saturated volumetric moisture content. This relationship is attributed to the correlation between void ratio and porosity, which, as mentioned, corresponds to θ_s. Furthermore, the decrease in the parameter α when there is a decrease in void ratio can be explained by its role as the air-entry value. In saturated conditions, a smaller volume of voids hinders air entry, thereby influencing the observed decrease in α. However, the obtained parameter n does not clearly exhibit a direct relationship with void ratio. Since this parameter represents the curve's inclination, it suggests that, from an unsaturated perspective, moisture content may not necessarily increase with larger void ratios as typically observed in saturated conditions, indicating that it depends on the suction conditions at the time.

Hypothetical filtered stack and climatic conditions

The hypothetical filtered stack section shown in Figure 2 was developed to support the current study. The boundary conditions include an atmospheric boundary, where rainfall and evaporation are applied, and a seepage face at the stack bottom, indicating the location for drain installation. Observation nodes were placed at the bottom, top, and middle of the stacks. These nodes are specific points in the mesh marked to evaluate variations in moisture content and pressure head. To simulate the compaction process, an optimum moisture content of 33% was selected and used as the initial condition for all simulations.

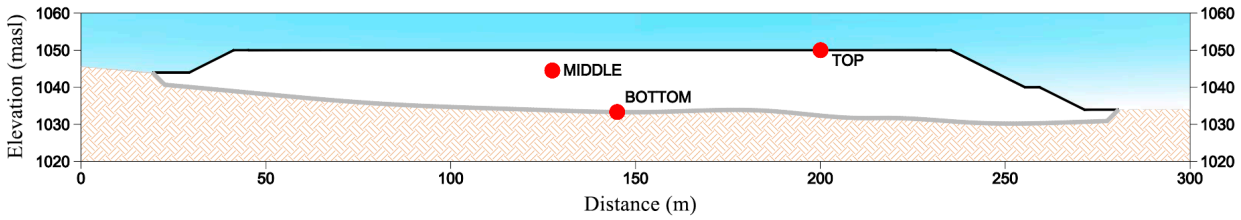


Figure 2: Hypothetical filtered stack

The climatic conditions used as input data included rainfall and evaporation, sourced from a specific location in Triângulo Mineiro (the Minas Triangle), Minas Gerais, Brazil. Evaporation was standardized to a daily value of 3.7 mm/day due to data availability. Actual daily rainfall data from the rainy season (January through March) of a particularly wet year (2013) in Minas Gerais were provided by the mining company's own weather station. This data was utilized in the simulations and is presented alongside the results in the following section.

Results

A total of 100 sets of parameters were simulated for each void ratio (0.85, 0.71, and 0.69). Some numerical

models did not converge and were excluded as outliers. The flux across the seepage face and the average head pressure at the seepage face were obtained for each simulation. From the results, the average and 95% confidence interval were calculated for each set of void ratio results, as presented in Figure 3.

The results indicate that uncertainties exert a greater influence on the bottom of the stack during the initial stages, immediately after the simulation begins, prior to saturation. Additionally, the differences in void ratio are evident from the beginning, as each calibrated SWCC exhibits unique behavior, leading to variability in the three sets of simulations before reaching saturation. The numerical model results align with the obtained SWCC, particularly highlighting the variability of the parameter n mentioned previously. This variability indicates that, depending on the head pressure, different void ratio inputs can result in significantly different moisture content. Notably, saturation at the base of the stack under high rainfall is anticipated by the model, emphasizing the need for a suitable drainage system installation. As the initial peak of flux diminishes when saturation is achieved at the bottom, the variability between the results of different void ratios and uncertainties limits also decreases, resulting in similar outcomes. This indicates that over time, after operational phases, the variability resulting from compaction and parameter uncertainties for infiltration levels becomes less significant.

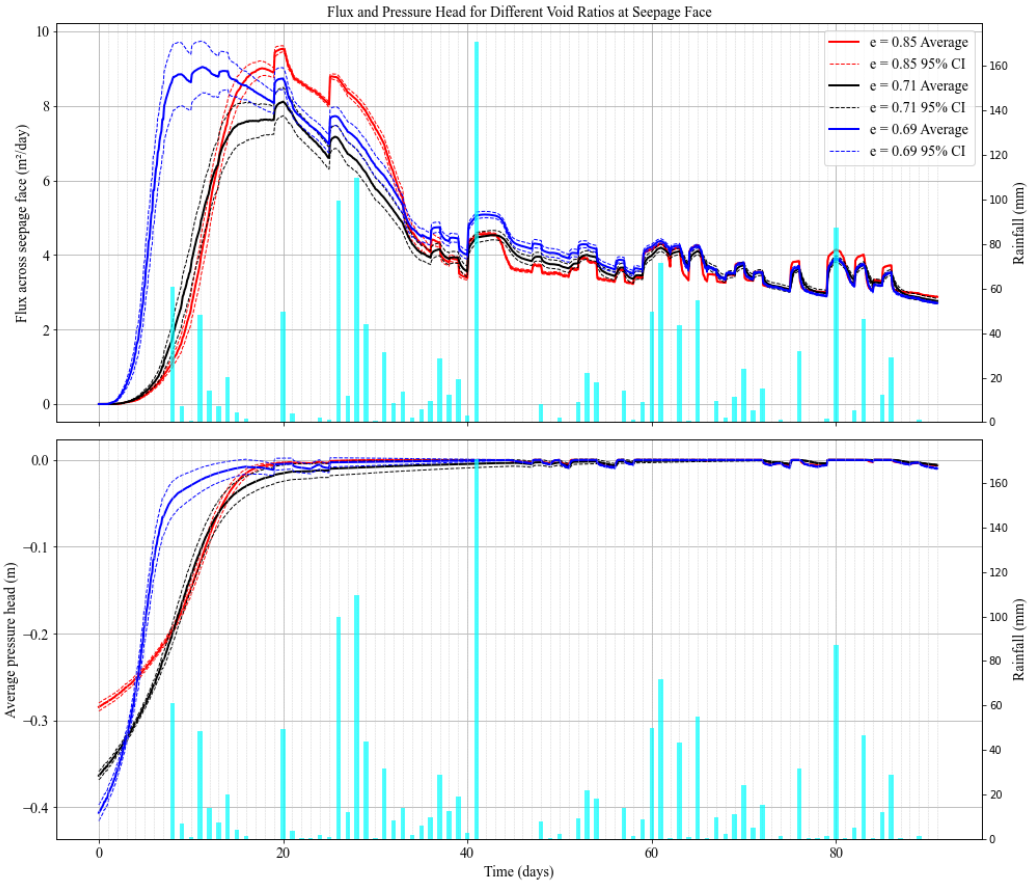


Figure 3: Seepage face results

The same data treatment applied to the results of the seepage face was also applied to the results of the observation nodes from each of the 100 simulation sets. Based on the results, presented in Figures 4, 5, and 6, it is noticeable that nodes at higher elevations are more significantly affected by climatic conditions than expected.

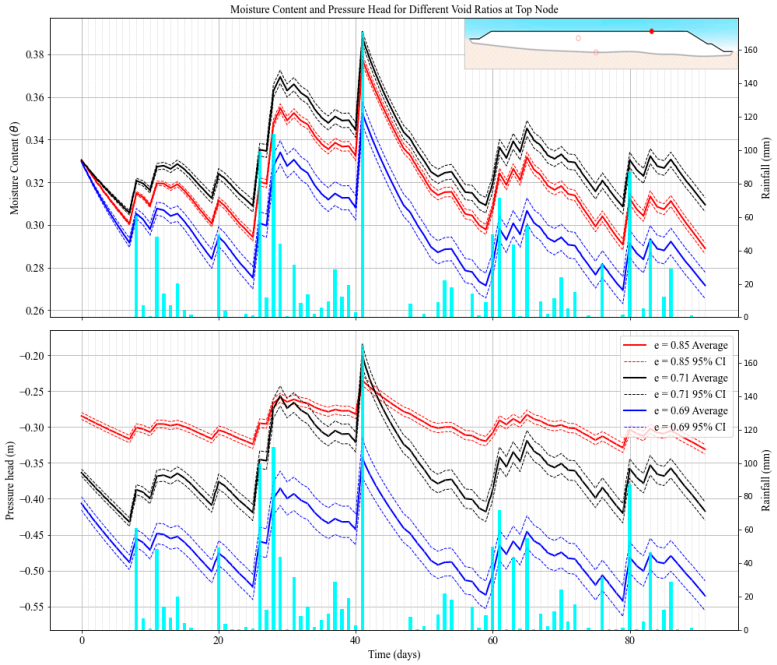


Figure 4: Top node results

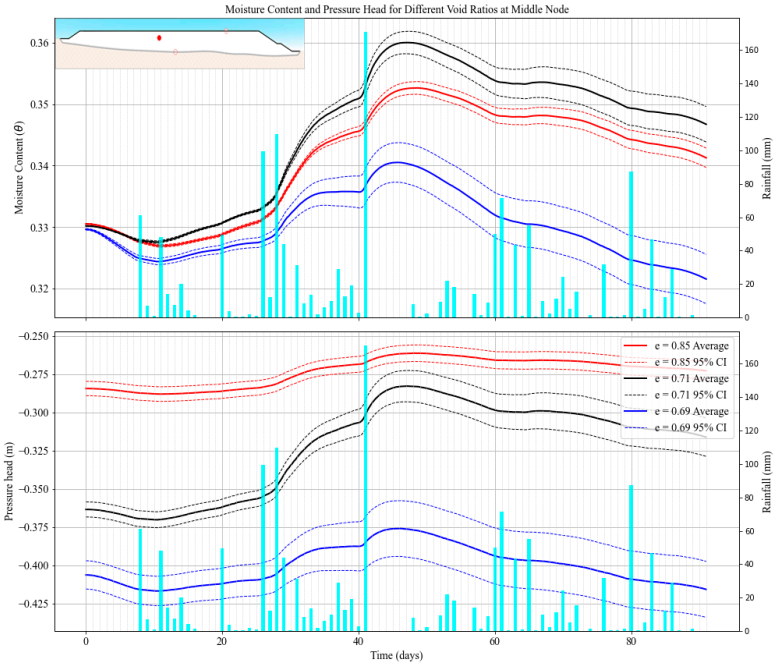


Figure 5: Middle node results

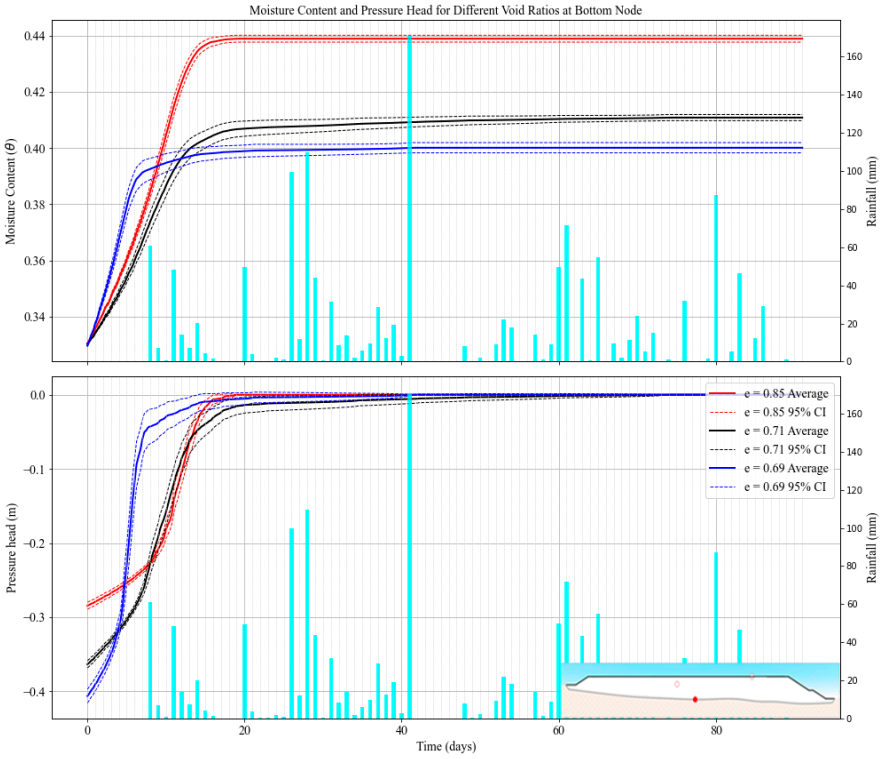


Figure 6: Bottom node results

The top node begins drying almost immediately, likely due to evaporation and drainage of the moisture used for compaction, and never reaches saturation, fluctuating with rainfall events. This lack of saturation results in greater variability influenced by both the initial void ratio and uncertainties from the calibration process, which are observable throughout the analyzed period.

The middle node exhibits an intermediate behavior, showing a delayed peak and smoother fluctuations with rainfall events. Like the top node, it also does not achieve saturation, presenting similar variability in behavior. Considering this variability and the possibility that a slip surface could pass through a similar middle area, it is important to further evaluate the potential impact of these uncertainties on Factor of Safety evaluations. As for the lower node, installed at the seepage face, its behavior closely resembles that of the seepage face, as anticipated, and it was monitored for validation purposes.

In this case study, due to the complexity of the simulation, it was assumed that a single lift would be constructed. However, in reality, the stack undergoes continuous raising during its operational phase. Therefore, the modeling highlights the critical importance of the operational phase, emphasizing the necessity for accurately sizing drainage with a suitable factor of safety and ensuring proper compaction control. This approach addresses both the inherent uncertainties in the model's design aspects and the variability encountered in field conditions, ensuring a more robust and reliable outcome.

Conclusion

In conclusion, this study emphasizes the significant challenges and complexities associated with implementing filtered tailings stacks in high-rainfall regions. The research employed advanced numerical modeling techniques underpinned by unsaturated soil mechanics principles to evaluate the infiltration behavior of tailings stacks, particularly focusing on the calibration of van Genuchten parameters using a Bayesian approach. The results underscored the significant influence of uncertainties in parameter calibration on infiltration rates and moisture content fluctuations during initial compaction stages. However, over time, these impacts diminished considerably. This comprehensive approach not only highlighted the variability introduced by different void ratios but also demonstrated the critical role of appropriate drainage design in managing saturation risks, particularly at the bottom of the stack during intense rainfall events.

Moving forward, further advancements in understanding the interactions between tailings properties, climatic conditions, and drainage systems will be essential for enhancing the reliability and efficiency of filtered tailings stacks in such challenging environments. This includes refining the impact of continuous raising on simulations and incorporating real-time data feedback mechanisms to improve predictive accuracy. Additionally, evaluating the impacts of uncertainties on stability analyses will be crucial. By addressing these complexities, future research can contribute to more sustainable mining practices that mitigate environmental risks and optimize operational outcomes in regions prone to high rainfall.

In summary, while the implementation of filtered tailings stacks in high-rainfall areas presents formidable engineering hurdles, integrating sophisticated modeling approaches and empirical data offers promising avenues for advancing the field of tailings management towards greater sustainability and resilience in diverse geographic contexts.

Acknowledgements

The authors would like to express their sincere gratitude to Companhia Brasileira de Metalurgia e Mineração, Knight Piésold, Universidade Federal de Ouro Preto and the Pontifical Catholic University of Rio de Janeiro for their support, and to all colleagues involved for their invaluable guidance and contributions to this project.

References

ASTM D 5084 – Standard Test Methods for Measurement of Hydraulic Conductivity of Saturated Porous Materials Using Flexible Wall Permeameter.

ASTM D 6836 – Standard Test Methods for Determination of the Soil Water Characteristic Curve for Desorption Using Hanging Column, Pressure Extractor, Chilled Mirror Hygrometer, or Centrifuge.

Buckingham, E. 1907. *Studies on the Movement of Soil Moisture*. US Department of Agriculture, Bureau of Soils: Washington, DC, USA.

Davies, M. 2011. Filtered dry stacked tailings: the fundamentals. *Proceedings of Tailings and Mine Waste 2011*. Vancouver.

Fredlund, D. 2017. Role of the soil-water characteristic curve in unsaturated soil mechanics. *Proceedings of the 19th International Conference on Soil Mechanics and Geotechnical Engineering* (the Blight Lecture, Honour lecture). Seoul.

Gitirana, G. de F.N., Marinho, F.A.M. and Soto, M.A.A. 2023. A curva de retenção de água de materiais porosos. In *Solos não saturados no contexto geotécnico*. ABMS, São Paulo, SP, Brazil: 295–323.

Gomes, G.J.C., Vrugt, J.A., Vargas Jr., E.A., Camargo, J.T., Velloso, R.Q. and van Genuchten, M.Th. 2017. The role of uncertainty in bedrock depth and hydraulic properties on the stability of a variably-saturated slope. *Computers and Geotechnics* 88: 222–241.

Moore, D.S., McCabe, G.P. and Craig, B.A. 2017. *Introduction to the Practice of Statistics*. W.H. Freeman.

Morgenstern, N.R. 2012. Foreword of *Unsaturated Soil Mechanics in Engineering Practice*. Edited by D.G. Fredlund, H. Rahardjo and M.D. Fredlund. Hoboken: John Wiley & Sons, p. xiii.

Patterson, K., McLeod, H., Hegaroden, D., Parkinson, G., Williams, P. and Murphy, B. 2016. Are filter tailings practical for a high production mine in a cold, wet climate? *Proceedings of the 20th International Conference on Tailings and Mine Waste*. Colorado State University, Keystone, Colorado: 359–371.

Richards, L.A. 1931. Capillary conduction of liquids through porous mediums. *Physics* 1(5): 318–333.

Šimůnek, J., van Genuchten, M.Th. and Šejna, M. 2008. Development and applications of the HYDRUS and STANMOD software packages and related codes. *Vadose Zone Journal* 7(2): 587–600. https://doi.org/10.2136/vzj2007.0077

Ulrich, B. and J. Coffin. 2013. Considerations for tailings facility design and operation using filtered tailings. In R.J. Jewell, A.B. Fourie, J. Caldwell and J. Pimenta (editors), *Paste 2013: Proceedings of the 16th International Seminar on Paste and Thickened Tailings,* Australian Centre for Geomechanics, Perth, pp. 201–210, https://doi.org/10.36487/ACG_rep/1363_15_Ulrich

van Genuchten, M.Th. 1980. A closed-form equation for predicting the hydraulic conductivity of unsaturated soils. *Soil Science Society of America Journal* 44(5): 892–898.

Watson, K.K., Sardana, V.A. and Sander, G.C. 1995. Comparison of analytical and numerical results for constant flux infiltration. *Journal of Hydrology* 165: 101–112.

Stay and Fight, or Flee? Assessing the Risks of Intervention Leading up to a Catastrophic Failure

Justin Willis, BHP, Australia

Abstract

How much time exists between the signs of potential failure of a TSF, and full catastrophic release? Should the focus during this time be on remedial works to prevent the failure, or on ensuring the safety of workers and public? This paper assesses this decision by reviewing past failures where timelines of the events leading up to failure are available. The timelines are assessed for the signs of impending failure, providing an estimate of the time available between these signs and failure during which an evacuation or intervention response could be initiated. An estimate of the likelihood of a successful evacuation or intervention is provided based on this assessment.

This paper also looks at examples and practices in other settings and industries, where the choice between intervening to prevent a catastrophic failure versus the risk to workers' lives exists. Consideration is also made of the advice for managing fires, including residential/commercial and wildfires, where the guidance between staying and fighting and evacuating has evolved over time.

Introduction

According to the Good Practice Guide (ICMM, 2021), the key document for managing an emergency at a Tailings Storage Facility (TSF) is the Emergency Preparedness and Response Plan (EPRP). The goal of an EPRP is to prevent, or mitigate, or reduce impacts in the event of an emergency, and the Good Practice Guide notes the EPRP should describe procedures or actions to be taken to prevent an upset or unusual condition from becoming an emergency. These aims can be in conflict, as addressing upset and unusual conditions and preventing failure may involve actions and activities around the tailings storage facility (TSF) that can expose personnel to hazards or place them in the line of fire. It is possible that at some point a decision will need to be made to send personnel into an escalating situation to prevent failure or remove personnel to prevent loss of life, acknowledging that failure of the TSF may result, with this decision likely to be made based on the judgment of the management and technical staff at the site.

This paper seeks to support that decision by providing data on timeframes at TSFs and water dams that did result in failure and providing estimates on the likelihood of success of evacuation or intervention

to prevent failure. This paper can also be used to support assigning likelihood of a successful intervention to prevent failure used in risk assessments such as event fault trees or FMECA (Failure Mode Effects Criticality Assessment) (ANCOLD, 2022).

Method

Approach

This paper assesses how much time exists between the early signs of potential failure and when the failure occurs by reviewing available failure reports and records and noting the elapsed time between the signs of potential failure and when the failure occurred. This elapsed time is the period in which a decision can be made on intervention or evacuation. The failure timings have been grouped based on failure mode, and the different signs within those failure modes. The timings associated with each failure mode/observed signs were assessed to assign a likelihood of successful evacuation or intervention, considering examples of evacuations and intervention attempts sourced from the failure reports and available literature, along with reflections on the likely timeframes of evacuation and intervention.

Notes on the approach

This paper does not seek to comment on the decisions made in past failures, nor on whether a successful intervention could have prevented failure. This paper also does not seek to comment on the recognition or otherwise of the signs of failure noted in the reports, or the actions taken in response to those signs of failure. Upset conditions and emergencies are complex, high-pressure situations, and all assessment in this paper is made with the benefit of hindsight that the TSF did progress to failure.

Discerning whether the signs of an upset or unusual condition will lead to failure is difficult, and even more difficult is understanding the time frame available, or when the point of no return is reached. This paper does not indicate that failure should have been obvious from the signs adopted as the indicators of potential failure. TSFs and water dams often exhibit seepage, cracking, movement etc., and not all signs of this nature lead to failure; in fact, some level of cracking, movement, and seepage can expected. It is for this reason that signs recorded in the failure reports that could be considered normal behavior by TSFs and water dams have not been considered as a sign of potential failure.

Regulatory and industry guidance

Tailings Industry Guidance is largely silent on the choice between evacuating and intervening to prevent failure, with the tailings guidance from ANCOLD, CDA, ICMM, and ICOLD making no comments on the choice. For water dams, FEMA (Federal Emergency Management Agency) funded the development of a Dam Owner Emergency Intervention Toolbox (Gannett Flemming, 2016). This toolbox suggests

intervention to prevent or delay failure should be taken after notification to regulatory agencies, local authorities and emergency personnel, and only if working conditions are safe. Public safety should be the primary concern, followed by downstream property, with the dam itself being the lowest priority. The toolbox notes that the upset condition may have progressed too far to prevent failure, in which case the intervention could be to delay the breach and provide additional time for evacuation. A controlled breach may be the safest intervention in some situations.

Within Australia, the Commonwealth Work Health and Safety Regulations (2011) for major hazard facilities require procedures to be developed for the safe evacuation of and accounting for all people on site. It is expected that other jurisdictions will have similar requirements. Matters relating to the prevention of events are to be covered in the preparation of a Safety Case for the major hazard facility.

Dataset

Table 1 presents the TSF failures assessed, based on failures where a published failure report or paper providing details on the timing and circumstances of the failure was available.

Table 1: TSF failures assessed in this paper

TSF name	Date	Location	Failure type
El Cobre Old and New Dams	28 March 1965	Valparaiso, Chile	Seismic liquefaction
Middle Fork Dam 3	26 February 1972	West Virginia, USA	Liquefaction/overtopping
Mochikoshi Dikes 1 and 2	14 January 1978	Izu, Japan	Seismic liquefaction
Prestavel upper and lower basin	19 July 1985	Trentino-Alto Adige, Italy	Static liquefaction
Tapo Canyon	17 January 1994	California, USA	Seismic liquefaction
Merriespruit TSF	22 February 1994	Virginia, South Africa	Overtopping
Omai TSF	19 August 1995	Cuyuni-Mazaruni, Guyana	Internal erosion
Aznalcóllar	25 April 1998	Seville, Spain	Foundation failure
Baia Mare	30 January 2000	Maramures County, Romania	Overtopping
Baia Borsa	10 March 2000	Maramures County, Romania	Overtopping
Big Branch Refuse Impoundment	11 October 2000	Kentucky, USA	Internal erosion
Reservoir 10 Ajka Alum	4 October 2010	Veszprem County, Hungary	Foundation failure
Mount Polley TSF	4 August 2014	British Columbia, Canada	Foundation failure
Fundão Tailings Dam	5 November 2015	Minas Gerais, Brazil	Static liquefaction
Harmony Waste Pond	3 June 2016	Mississippi, USA	Foundation failure*
NTSF Cadia Operations	9 March 2018	NSW, Australia	Foundation failure
Dam 1 Córrego do Feijão	25 January 2019	Minas Gerais, Brazil	Static liquefaction

* Failure was due to excavation at the toe of the embankment

In addition to the TSF failures in Table 1, a select number of water dam failures were reviewed (Table 2), where a detailed record of the failure is available. These were chosen to include internal erosion and overtopping failure timings, as these are failure modes with a clear progression to failure without intervention.

Table 2: Water dam failures assessed in this paper

Dam name	Date	Location	Failure type
Baldwin Hills	14 December 1963	California, USA	Internal erosion
Teton	5 June 1976	Idaho, USA	Internal erosion
Big Bay	12 March 2004	Mississippi, USA	Internal erosion
Taum Sauk	14 December 2005	Missouri USA	Overtopping
Edenville	19 May 2020	Michigan USA	Liquefaction/Overtopping

Indications of potential failure

The signs of potential failure listed below were used to identify the timing to failure. These were chosen based on a typical operator accepting these as unusual or upset conditions or an escalating situation, or events that may trigger a response as part of a trigger action response plan (TARP).

- Fresh seepage that developed rapidly, or rapid increases in seepage.
- Cloudy or discolored seepage, or seepage carrying sediment.
- Rapid saturation of the embankment or toe.
- Initial overtopping of embankment (wave action or other).
- Large or intense rain event.
- Inflow into the TSF/Dam greater than the spillway capacity.
- Earthquake.

The timing has been taken as the moment of observation or recording of the metric, as this is when the opportunity for intervention would have commenced. For a number of TSFs the failure was unexpected, and there is little or no detail on the signs of potential failure. In these instances, the timing is based on the last inspection or observation of the TSF where conditions were noted as normal.

The indication of potential failure does not consider any underlying assessment of TSF or water dam integrity, including out of target factors of safety, inadequate design, inadequate characterization or investigation, excessive pond size or inadequate spillway capacity. This paper is not commenting on the conditions that led up to the failure, rather it is focused on signs that indicated an upset or escalating situation.

Intervention

Successful intervention

The datasets in Tables 1 and 2 only include TSFs that have progressed to failure, and as such only represent a portion of the TSFs and water dams that have experienced signs of potential failure. Examples where the signs of potential failure were recognized and the response successfully avoided failure, or where conditions changed such that the TSF did not progress to failure (e.g. overtopping that ultimately did not lead to failure as the rainfall ceased), are largely absent from the public record.

Only one paper could be located that contained detail on an intervention that was believed to have prevented a larger failure; this was for a platinum TSF in the (then) Transvaal Province of South Africa (Fourie and McPhail, 1993). In this instance the TSF embankment failed but did not result in a loss of containment, and a dewatering program using vertical wells stabilized the TSF sufficiently that it was able to be used until a new TSF was constructed. The exact timing of the dewatering program was not specified, however it was inferred to be 6 months to a year, and the TSF was operated during this time with additional controls in place.

According to the Samarco failure report, on 27 August 2014 extensive cracking at the crest and toe of the left setback was observed, accompanied by saturation at the setback toe (Morgenstern et al, 2016). An equilibrium berm was constructed at the toe within two weeks of the cracks being observed. This appears to be a second example of a successful intervention to prevent failure.

It is difficult to judge if an intervention prevented a failure, as even in cases where a clear failure progression could be expected, there are often too many variables (rainfall, uncertainties in material properties and geometry, uncertainties in phreatic condition, etc.) to say with confidence a catastrophe was averted. None the less, it is considered highly likely that there have been multiple occasions where early signs of potential failure were noted, and intervention successfully prevented a catastrophic failure. The lack of examples in the literature is attributed to a reluctance to share details of potential failures for fear of how this would be perceived by stakeholders.

Unsuccessful intervention

During the development of the internal erosion failure at Teton Dam, two bulldozers were dispatched to push material into the downstream expression of the erosion pipe (Wallace et al., 1976). Both bulldozers were lost in the rapidly growing outflow, with the operators abandoning their machines and escaping on foot (Johnson and Flynn, 1977). An attempt was also made to place large material into the upstream inflow of the developing erosion pipe; however, this was also unsuccessful. No machines were lost in the attempt to block the upstream expression of the pipe.

The Baldwin Hills failure report details an unsuccessful intervention to prevent failure (Jansen et al, 1964). When the upstream expression of the erosion pipe was observed it was small in size and onsite personnel believed that placing sandbags into the hole would slow or block the flow. A worker was lowered by rope above the hole, and sandbags were placed. This was quickly realized to be futile and abandoned, as the hole was significantly larger than first believed.

At Middle Fork Dam 3, a plan was developed to install additional spill capacity at the TSF as the water level rose. Surplus pipe was available nearby and bulldozers were being mobilized, however the TSF failed before the additional capacity could be installed.

While not resulting in a failure, an intervention was attempted at Oroville Dam, USA in 2017. Water overtopping the emergency spillway rapidly eroded the hillside, threatening the integrity of the spillway (France et al, 2018). Helicopters were mobilized and dropped bags of rock into the erosion gullies to reduce the rate of erosion (Associated Press, 2017). An evacuation order was issued concurrently and remained in place until the water level reduced and the threat to embankment stability had passed.

Increased fatalities from attempted intervention

Notably none of the failures assessed (TSF or water) included fatalities of workers sent into the line of fire in an attempt to prevent the failure. This extends to less well documented failures not included in Tables 1 or 2, as while there are a number of failures where workers have lost their lives, none have been identified where the loss of life was directly attributable to an attempt to prevent the failure.

Response timing

Evacuation

The time for successful evacuation can vary greatly depending on factors such as the size and geographical distribution of the population at risk, the means of notifying the population at risk, and the maturity of the evacuation procedures. Minesite personnel may be able to be evacuated in under an hour, while larger public populations may take several hours or longer. The reduction in population at risk during an evacuation is typically progressive, so even a brief warning time may save lives.

Within the assessed dataset there are several examples of public evacuation. A formal evacuation order was requested approximately two hours before the Baldwin Hills failure (Jansen et al., 1964), with approximately 1,600 people evacuated before the failure occurred (Barnes, 1992). At Teton Dam, the evacuation order was placed approximately 1½ hours before the dam failed (Johnson and Flynn, 1977). As the Cadia TSF failure developed, a decision was made to evacuate workers in the vicinity of the TSF two to three hours ahead of the failure.

Intervention

The time required to successfully intervene and prevent a failure is equally highly variable. Once an upset or deteriorating situation has been escalated within the chain of command, there are a further number of steps that would likely occur before a decision to intervene is made. These include understanding the current status of the TSF and how the situation is evolving, understanding the failure mode, and designing a suitable response. Responses may be described in the EPRP, along with details on resources and equipment, which may reduce the time required to intervene. Not all interventions may be technically feasible, and instead may exacerbate an escalating situation, such as involving additional loading.

Typical interventions are a reaction weight buttress, additional spill capacity, additional embankment height, or a reverse filter. These are difficult without placing personnel in danger, even if remote equipment is used. If the intervention requires placing personnel in the line of fire, additional approvals and controls may be required. While some of these activities may be completed concurrently, the estimated timeframe from escalation of the situation to implementation of the remedial measures is likely days, and based on the two examples of intervention in the assessed dataset that may have prevented failure, may take weeks .

Results

Failure timings

Tables 3 and 4 present the timings to failure for TSFs, separated based on whether there were recorded signs of upset conditions or an escalating situation noted ahead of the failure. Table 5 presents the failure timings for the water dams assessed.

Table 3: TSF failure timings based on observed signs

TSF name	Sign of potential failure	Time to failure from sign
El Cobre Old and New dams	Earthquake	< 90 seconds
Middle Fork Dam 3	Flow into TSF greater than spill capacity	40 hours
	Cracks on embankment, saturation of embankment	2–9 hours*
Mochikoshi Dike 1	Earthquake	≈10 seconds
Mochikoshi Dike 2	Earthquake	24.5 hours
	Cracking on TSF (following earthquake and aftershocks)	4.5 hours
Tapo Canyon	Earthquake	≈ 10 in es
Merriespruit TSF	Water overtopping embankment	2 hours
Reservoir 10 Ajka Alum	Large volume of flow through cracks in embankment	≈ 1 in es
Fundão Tailings Dam	Dirty water discharge from drains	≈ in es
Cadia TSF	Extensive developing cracking	9–11 hours**

* Conflicting eyewitness accounts

** Exact moment of failure not observed

Table 4: TSF Failure timings where signs were not observed ahead of failure

TSF name	Timing point	Time to failure from timing point
Prestavel upper and lower basin	Movement recorded on seismograph	< 1 minute
Omai TSF	No sign of failure at last inspection of TSF (southern end)	< 9 hours
	No sign of failure at last inspection of TSF (northern end)	< 10 hours
Aznalcóllar	No sign of failure at last inspection of TSF	< 12 hours
Baia Mare	Rapid increase in temperature leading to snowmelt	< 72 hours
	40 mm of rain	< 24 hours
Baia Borsa	Extreme rainfall and failure of pumping system	< 60 hours
Big Branch Refuse Impoundment	No sign of failure at last inspection of area	< 15 minutes
Mount Polley	No sign of failure at last inspection of TSF	< 1.5 hours
Harmony Waste Pond	Excavation at toe of embankment	< 1 minute
Dam 1 Córrego do Feijão	No sign of failure visible in video	< 1 minute

Table 5: Timing of water dam failures

Dam name	Sign of potential failure	Time to failure from sign
Baldwin Hills	Large seepage through underdrains	4.5 hrs
	Rapidly developing seep on embankment	2.5 hrs
Teton	Large seepages at embankment toe	19 hours
	Rapidly developing seep on embankment	2.5 hrs
Big Bay	Muddy seepage from drainpipe	21 hours
Taum Sauk	Overtopping of embankment	≈ 0 minutes*
Edenville Dam	Flow into reservoir greater than spillway capacity	26 hrs
	Slump and depression in embankment	≈ 0 minutes

* Failure sign was not observed, and back calculated from pumping data

Failure modes

Table 6 presents the failure timings grouped based on failure mode and for both TSF and water failures.

Table 6: Timings based on failures modes

Failure mode	Observed sign	Min. time to failure	Max. time to failure
Foundation failure	–	< 1 minute	9-12 hours
Static liquefaction	–	<1 minute	30 mins
Overtopping	Large inflows commenced	26 hours	72 hours
	Flow over embankment commenced	30 minutes	2 hours
Internal Erosion	Unusual seepage observed	4.5 hours	21 hours
	Pipe observed	2.5 hours	2.5 hours
Seismic Liquefaction	–	10 secs	24.5 hours

Likelihood of successful response

Table 7 presents the estimated likelihood of a successful response for each of the failure modes, based on the timings in Table 6 and the considerations for evacuation and intervention discussed previously.

Table 7: Estimated likelihood of successful response based on failure mode

Failure mode	Observed sign	Successful Evacuation	Successful Intervention
Foundation failure	–	Possible	Unlikely
Static liquefaction	–	Unlikely	Highly unlikely
Overtopping	Large inflows commenced	Likely	Possible
	Flow over embankment commenced	Possible	Highly unlikely
Internal Erosion	Unusual seepage observed	Likely	Unlikely
	Pipe observed	Likely	Highly unlikely
Seismic Liquefaction	-	Unlikely	Highly unlikely

Examples from other industries and situations

TSFs and water dams are not the only instances where a failure could have serious consequences, and a decision between intervention to prevent failure and evacuation to prevent loss of life may be required. Landslides and pit slopes share a common reliance on geotechnics and hydrogeology with their associated uncertainties and can be materially affected by rainfall. However, for these situations, once the signs of an unusual or escalating situation are observed, the options to prevent failure are limited and evacuation is the preferred action, such as at Bingham Canyon Mine (FEMA, 2018; Pankow et al., 2014).

Major hazard facilities such as oil refineries, oil rigs and nuclear facilities also face serious consequences in the event of a failure, leading to a conflict between preventing an escalating situation from developing into failure and ensuring the safety of the personnel. A search of available literature revealed

no information on incidents where failure had been averted, while major failures such as the 2005 explosion at BP's Texas City refinery happened without warning (CSB, 2007). The Piper Alpha disaster in 1988 warrants mentions, as after the initial explosion the remaining workers moved to the accommodation area furthest from the fire and waited for instructions that never came. It is believed that lives could have been saved with an attempt to evacuate (Human Factors 101, 2024).

The guidance for fires in public buildings is based on prioritizing evacuation to minimize the potential for fire-related injuries (OSHA, 2024). While there are a variety of sources of guidance around fires with slight differences, a broad consensus can be summarized as raise the alarm/evacuate before attempting to fight the fire (MFS, 2024; Fire and Rescue NSW, 2024; Weekly Safety, 2024). Once the evacuation is underway or complete, the guidance recommends fighting the fire if the type of fire is understood and can be tackled with confidence, including having the correct fire extinguisher, making sure the atmosphere is safe, gauging the size and how quickly the fire is spreading, and ensuring you have a safe evacuation route.

Of interest is the evolution of messaging relating to fighting wildfires. In 2006 the AFAC (Australasian Fire and Emergency Services Authorities Council) position was people should either stay and defend their property or leave early (AFAC, 2006). Following the 2009 "Black Saturday" fires in Victoria, Australia, when 173 people lost their lives, the position was revised with more weight given to leaving early (McLennan et al., 2014). The current position is that leaving early is always the safest action and may be the only safe option when wildfires are burning on days when weather conditions are extreme, or the topography or fuel load may create intense fire behavior (AFAC, 2019). The Camp fire (2018) and Lahaina fire (2023) tragedies in USA and the Valparaiso fire (2024) in Chile all resulted in mass fatalities, in part attributed to a failure to evacuate early (Koop, 2024; Zebratski, 2023).

Discussion

All the failures assessed had a relatively short duration of elapsed time between the signs noted or last observed stable condition, with 43% of failures occurring in under an hour, 35% between 1 hour and 1 day, and 22% greater than a day. This is a rapid progression from signs of an escalating situation to failure, with little opportunity for intervention and requiring a quick evacuation response to prevent or reduce loss of life. This dataset is comprised of TSFs and water dams that did ultimately progress to failure, and if that progression had not been as rapid it is likely that a successful intervention would have been made that might have prevented failure. It is likely there are examples where similar signs were recorded and catastrophic failure did not result, either without intervention, or as a result of intervention. This leads to the inference that if the TSF is progressing to failure, this progression can be expected to occur quickly, and if conditions stabilize after a period of time, then failure is less likely.

The lack of an example in the dataset of a failure that has resulted in the fatalities of workers attempting an intervention does not necessarily mean that this will not occur in the future. Considering the bushfire example, it may simply be that the combination of conditions has not been encountered yet and such a circumstance may be encountered in the future.

Evacuation and intervention do not need to be mutually exclusive, and as per the intervention toolbox for water dams it is possible to pursue an evacuation of non-essential workers and public while concurrently attempting to delay or prevent the failure. This is similar to the guidance for fires in buildings, ensuring the alarm is raised and evacuation has commenced before tackling the fire.

Conclusion

A review of the timings associated with past TSF and water dam failures indicates that a rapid progression to failure is possible. This makes evacuation possible in such scenarios, but makes intervention less likely to be successful. This information can be assessed with professional judgment, considering the circumstances when deciding whether to intervene in the situation or keep personnel out of the line of fire. Considering the guidance provided for water dams and fighting fires, the most prudent approach is likely to be prioritizing evacuation, and considering intervention once the evacuation is underway or substantially complete.

References

Associated Press. 2017. Evacuees might not go home until Oroville Dam spillway is repaired. Los Angeles Daily News. 13 February 2017. Accessed 26/6/2024 at https://www.dailynews.com/2017/02/13/evacuees-might-not-go-home-until-oroville-dam-spillway-is-repaired/

Australasian Fire and Emergency Services Authorities Council (AFAC). 2019. Bushfires and Community Safety Position. AFAC Publication No. 2028. Melbourne, Australia.

Australian Fire Authorities Council (AFAC) and Bushfire Cooperative Research Centre (Bushfire CRC). 2006. Fire Note – The stay and defend your property or go early policy. Issue 7 October 2006.

Australian National Committee on Large Dams (ANCOLD). 2022. Guidelines on Risk Assessment July 2022.

Barnes, M. 1992. Famous failures: Revisiting major dam catastrophes. ASDSO, September 13–16, 1992. *Proceedings of the 9th Association of State Dam Safety Officials Annual Conference,* Baltimore: 363–368.

Chemical Safety and Hazard Investigation Board (CSB). 2007. Investigation Report Refinery Explosion and Fire. Report No.2005-04-I-TX March 2007.

Commonwealth Government of Australia. 2011. Work Health and Safety Regulations 2011. Select Legislative Instrument No.262, 2011. Compilation No. 19. Office of Parliamentary Counsel, Canberra.

Federal Emergency Management Agency (FEMA). 2018. Landslide hazard Info Sheet V-1007 May 2018. Accessed 20/6/2024 at https://www.ready.gov/sites/default/files/2024-03/ready.gov_landslide_hazard-info-sheet.pdf

Fire and Rescue NSW. 2024. In Case of Fire. Accessed 20/6/2024 at https://www.fire.nsw.gov.au/page.php?id=74

Fourie, A.B and McPhail, G.I. 1993. Stabilization of a tailings dam by de-watering. *Proceedings of the Third International Conference on Case Histories in Geotechnical Engineering*. St Louis, Missouri. June 1–4.

France, J.W. Alvi, A.I. Dickson, P.A. Falvey, H.T. Rigbey and S.J. Trojanowski, J. 2018. Independent Forensic Team Report Oroville Dam Spillway Incident. 5 January 2018.

Gannett Fleming, Inc. 2016. Dam Owner Emergency Intervention Toolbox. Project No. 059950, July 2016.

Human Factors 101. 2024. Piper Alpha. Accessed 20/6/2024 at https://humanfactors101.com/incidents/piper-alpha/

International Council on Mining and Metallurgy (ICMM). 2021. Tailings Management Good Practice Guide, May 2021.

Jansen et al. 1964. Investigation of Failure Baldwin Hills Reservoir. State of California Department of Water Resources, April 1964.

Johnson, O.K. and Flynn, D. 1977. *Idaho State Journal* Sunday 5th June 1977. Accessed 19/6/2024 at https://www.newspapers.com/article/idaho-state-journal-no-finger-in-the-dik/23922672/

Koop, F. 2024. Chile Forest fires: Five factors that led to devastating impacts. *Dialogue Earth* February 14, 2024. Accessed 26/6/2024 at https://dialogue.earth/en/climate/389148-chile-forest-fires-five-factors-that-led-to-devastating-impacts/

McLennan, J. Elliot, G. and Wright, L. 2014. Bushfire survival preparations by householders in at-risk areas of south-eastern Australia. *Australian Journal of Emergency Management* 29(2).

Metropolitan Fire Service (MFS). 2024. Extinguishing a fire. Accessed 20/6/2024 at https://www.mfs.sa.gov.au/community/safety-and-education/fact-sheets-and-brochures/fact-sheet-pages/extinguishing-a-fire

Morgenstern, N.R., Vick, S.G., Viotti, C.B. and Watts, B.D. 2016. Report on the immediate causes of the failure of the Fundão Dam. Fundão Tailings Dam Review Panel. August 25, 2016.

Occupational Safety and Health Administration (OSHA). 2024. Evacuation Plans and Procedures eTool. Accessed 20/6/2024 at https://www.osha.gov/etools/evacuation-plans-procedures/eap/fight-or-flee

Pankow, K.L Moore, J.R Hale, J.M. Koper, K.D. Kubacki, T. Whidden, K.M. and McCarter, M.K. 2014. Massive landslide at Utah copper mine generates wealth of geophysical data. *GSA Today* 24(1): 4–9.

Wallace et al. 1976. Report to the US Department of the Interior and State of Idaho on failure of the Teton Dam by Independent Panel to review cause of Teton Dam Failure. Idaho Falls, Idaho. December 1976.

Weekly Safety. 2024. Fight the Fire or Evacuate, Know How to make the call. Accessed 20/6/2024 at https://weeklysafety.com/blog/fight-or-evacuate

Zebratski, K. 2023. Lessons Learned from Lahaina and Other Similar Wildfires. AMWINS Client Advisory. 25 September 2023. Accessed 26/6/2024 at https://www.amwins.com/resources-insights/article/lessons-learned-from-lahaina-and-other-similar-wildfires

Bayesian Networks Application and Analysis of Failure Mechanism and Triggers in Tailings Dams: A Case Study

Keith Mandisodza, The University of Queensland, Australia
David J. Williams, The University of Queensland, Australia
Chenming Zhang, The University of Queensland, Australia

Abstract

Learning from past dam failures can help us to understand failure mechanisms, which can be instrumental in future tailings storage facility designs or improvement of existing operational and management processes through a better understanding of input parameters, failure triggers and contributing factors, and inherent uncertainties. Historically, when tailings dam failures occur, concerted efforts, time, and resources are channeled into understanding the failure mechanisms and triggers, sometimes more than what is input during initial geotechnical site investigations for designing and constructing a tailings storage facility. Such efforts aim to deduce failure mechanisms and triggers through forensic investigations conducted through expert panel reviews. Industry experts exhaustively analyze the system's and sub-system's events and decisions that potentially lead to failure. The failure event sequence analysis is often qualitatively or quantitively conducted through static logic methods such as event tree analysis (ETA) and fault tree analysis (FTA), or other less frequently used techniques such as fuzzy analysis or artificial intelligence neural networks (ANN), which have limitations in dynamic risk evaluations. Tailings dams are complex and dynamic systems that go through phases from design, construction, operation and transitions to closure and post-closure into perpetuity. The inherent system complexities in tailings dams depend on system variables, which can be exposed when the weakest variable link leads to failure. In this paper, we:

- Discuss some of the significant past tailings dam failures.
- Introduce Bayesian networks (BNs).
- Show how BNs can be applied to review the failure mechanism as reported in past expert panel reports by reproducing and analyzing the applied FTA and conversion to BNs.
- Show how this information can be used to examine variables that influence tailings dam failures comprehensively.
- Determine variable dependencies.

- Formulate a model for risk assessment.
- Conduct inference updating of the prior probability of events on obtaining new information under uncertainty, and application as an accident or predictive analysis for system processes.

Introduction

Mineral recovery improvement, commodity demands, and technological advances enable the processing of low-grade orebodies as they become economically lucrative, generating more waste processing and storage requirements. The demands of the global economic and energy transition are the main drivers for the market (Cacciuttolo and Atencio, 2022; Kossoff et al., 2014). Most of this mine waste is stored in tailings dams whose construction and depositional processes are a function of geographical location, topography, climatic conditions, seismicity, and jurisdictional and regulatory requirements, most of which are influenced by uncertainties. In addition to these uncertainties are the design, construction, and operational uncertainties that compound the complexities in the analysis of tailing dams (ICOLD, 1989; Klohn, 1972; McLeod et al., 2003; Ramon and Hinks, 2023). The result of such complexity, primarily from the applied conditional stability, a function of blended analyses for geotechnical, hydrology, hydraulics and seismic loading conditions, and associated uncertainties, are not considered explicitly in practice and hence the associated risk is not considered explicitly (Phoon et al., 2022; Phoon and Ching, 2018). This gap induces time-dependent structural issues in the embankment shell and the overall behavior and response of the contained tailings due to aging effects, causing significant failures.

Considering that the probability of failure and resulting consequences (i.e., estimates of loss of life or environmental damages) are used for risk quantification (Feinberg et al., 2016) as an empirical approach based on failure case histories, the differences in the case history's geographic location, topography, climate, and seismic conditions mean that the consequence approach might not suit other regions that do not have conditions similar to those in the applied case histories. However, since this approach is widely accepted in the dam design industry, it implies that the risk analysis and quantification for tailings dams might be compromised on these premises of the probability of the information used to determine the risk (Borovcnik, 2015).

Based on professional expertise and subjective judgements, expert panel reviews are undertaken when tailings failures occur (Jefferies et al., 2019; Morgenstern et al., 2014; Morgenstern et al., 2016; Robertson et al., 2019) to "exhaustively" analyze the system and sub-systems' events and decisions that might have caused the failure. The hierarchical and sequential causation of the failure is determined forensically and through qualitative and quantitative analyses, through static logic methods such as failure modes and effects analysis (FMEA), fault tree analysis (FTA), event tree analysis (ETA), bowtie risk analysis (BTA) and other methods such as fuzzy analysis (FA) and artificial intelligence neural networks (ANN), though less

applicable. Case history records for tailings dam failures indicate an increased failure rate in the last two decades, partly attributed to the abovementioned issues regarding improved processing methods due to technological advancement allowing for lesser grade ore to be processed. Hence, more waste is mined for ore recovery, as well as time-dependent storage growth and aging effects of tailings dam structures as more volume is mined and processed. Figure 1 shows recorded global tailings dam failures and some of the significant failures that have led to significant changes in the governance and management of tailings dams.

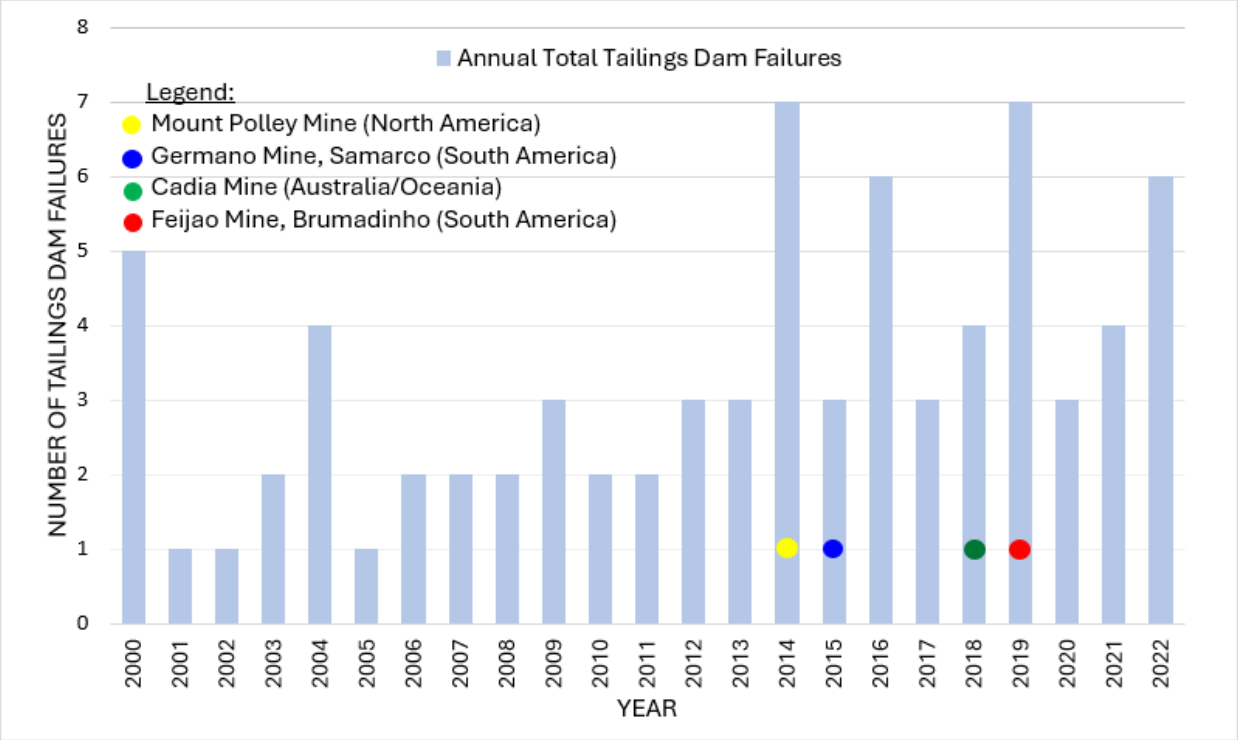


Figure 1: Tailings dam failures in the last two decades, with four significant failures that have contributed to significant governance changes in the tailings management

The static logic risk analysis methods mentioned above have limitations in analyzing the dynamic and complex nature of tailings dam failures and inherent dependencies of failure triggers. Hence, another paradigm is needed to analyze many continuous random variables without discretizing their probability. Bayesian networks (BNs) have slowly gained popularity in different industries through their capability to incorporate uncertainty analysis and conditional probabilities in the analysis models (Bobbio et al., 2001) and their ability to update model distributions following observations (inference modeling) and have been successfully applied in dam risk analysis (Delgado-Hernández et al., 2014). Risk analysis is characterized by natural variability, knowledge, and decision-model uncertainty (Baecher and Christian, 2005). These are characteristic of generic dam risk analysis and are more specific to tailings dams.

Literature review

Bayesian networks

BNs represent high-dimensional modeling using graph theory to model uncertainties and random variable dependencies. They are characterized by a directed acyclic graph (DAG) with conditional probability distributions, with nodes representing the random variable and the arcs the dependence relationship between nodes. Hence, they express a simplified representation of joint distributions and their dependencies (Hanea et al., 2015; Morales-Nápoles et al., 2013).

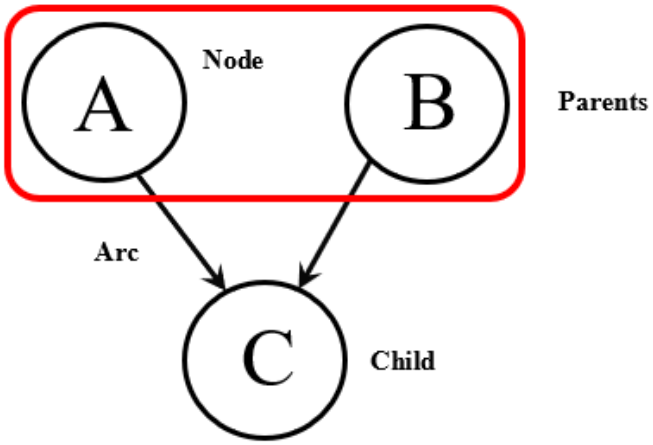


Figure 2: A Bayesian network with three random variables

Each node represents a random variable (qualitative aspect), also called the parent, and the arcs represent the dependency relation between the random variables (quantitative aspect), also called the child, through conditional probabilities. A marginal distribution is specified for each node with no parents, and a conditional distribution is associated with each child node. It can be obtained from data without full dependency relationships between nodes (parent and child), representing the most critical information for models (Hanea et al., 2006). Assuming a set of random variables $(X_1, \cdots, X_n)$ with high dimensional uncertainty encoded with conditional independence statements in the form of a DAG, shown in Figure 2, and probabilistic functions, the factorization of the joint density can be written as shown in Equation (1), according to probability theory.

$$f(x_1, x_2, \cdots, x_n) = f(x_1) \prod_{i=2}^{n} f(x_i | x_1, \cdots, x_{i-1}) \quad \text{(Equation 1)}$$

Equation (1) can be simplified to Equation (2) as a joint probability, each variable with a conditional probability function given $f(X_1 | X_{Pa(i)}, i = 1, \ldots, n$, where $Pa(i)$ represents the parents.

$$f(x_1, x_2, \cdots, x_n) = f(x_1) \prod_{i=2}^{n} f(x_i | x_{Pa(i)}) \quad \text{(Equation 2)}$$

The BN structure defined above can be simplified as $BN = f(D, C)$ where the D represents the parent nodes and directed edges (arcs) as represented in Figure 2 and C is the conditional probability distribution (CPD) of each node and propagation of uncertainty sources. Applying the chain rule to the right side of Equation (1), we can represent the CPD as shown in Equation (3), assuming the parent node random variable. $x_{Pa(i)}$ at any period in time (T) is $i = t_j$ ($\forall_{t_j \in T}$), follows a temporal sequence, and the parent node x_i is the set of prior variables $x_{i-1}, \ldots \ldots, x_1$, as shown in Equation (1) (Pan et al., 2019).

$$f(x_i | x_1, \cdots, x_{i-1}) = \frac{f(x_1, x_2, \cdots, x_n)}{f(x_1, x_2, \cdots, x_{n-1})} \quad \text{(Equation 3)}$$

Copulas

Copulas define the dependence between random variables by simplifying complex relationships into a marginal distribution, which enables the construction of multivariate distributions that satisfy non-parametric measures of dependence and prescribed marginal distributions. No restriction is placed on marginal distributions for multivariate models when copulas are applied. Thus, any bivariate distribution can be constructed by assigning any two assessed marginals subjectively (Clemen and Reilly, 1999; Phoon and Ching, 2018), such as $u = F(x)$ or $v = G(y)$, where $F(x)$ and $G(y)$ are the marginals. If X and Y are random variables with cumulative distribution functions $F_X(x)$ and $F_Y(y)$, respectively, the rank correlation ($r_{X,Y}$) of the random variables, which defines the product-moment correlation,

$$r_{X,Y} = \frac{E((F_X(X)F_X(X)) - E\big(F_X(X)\big)E(F_X(X))}{\sqrt{var\big(F_X(X)\big)var(F_X(X))}} \quad \text{(Equation 4)}$$

Where E is the finite expectation of the random variables (Morales et al., 2008). Thus, bivariate copula C defines the multivariate cumulative distribution function $[0,1]^2$ in which the marginal distribution of the variables is uniform on the interval $[0,1]$. Hence, the random variables, X and Y, can be joined by the copula, as shown below:

$$F_{X,Y}(x, y) = C(F_X(x), F_Y(y)) \quad \text{(Equation 5)}$$

Based on Equation (5), any copula for a continuous joint distribution can be determined. According to Sklar's Theorem (1959) (Clemen and Reilly, 1999; Zhang and Singh, 2019), the bivariate cumulative distribution function (CDF) of two random variables can be written as

$$F_{X,Y}(x,y) = C(F_X(x), F_Y(y)) = C(u_X, u_Y; \theta) \quad \text{(Equation 6)}$$

where, $C(u_X, u_Y; \theta)$, is the bivariate copula function in which θ is a copula measure of dependence between random variables X and Y.

Coupling marginals in a model into a joint distribution requires assigning a distribution function to define model parameters, which can be accomplished by analyzing case histories and subjective opinions from experts through statistical, probabilistic, or conditional quantile approaches. Once suitable marginal distributions have been assigned to fit the data range of the random variables, dependencies of the random variables can be determined. The Pearson product-moment correlation coefficient, δ_{ij}, defines the dependence between variables, quantifying the degree of linearity between them. It is defined as

$$\delta_{ij} = \frac{COV(X_i, X_j)}{\sigma_i \cdot \sigma_j} \quad \text{(Equation 7)}$$

Where COV is the covariance of two standard bivariate normal distributions, X_i and X_j, with standard deviations σ_i and σ_j, respectively. Perfect positive linear correlations have δ_{ij} = 1, negative linear correlations have δ_{ij} = -1, and if there is no correlation δ_{ij} = 0. Several methods can be used to estimate δ_{ij}. Some of the methods include methods of moments, maximum likelihood, and rank correlation methods (Phoon and Ching, 2018). Some popular measures of dependence and association of random variables are Spearman's ρ, a measure of linearity, and Kendall's τ, a measure of concordance.

Fault tree analysis

Fault tree analysis (FTA) is a widely used and accepted method for both qualitative and quantitative risk evaluation in the dam industry. It was initially developed to evaluate reliability and complex (Phoon and Ching, 2018). Fault trees (FTs) are members of the influence diagrams that exclusively express probabilistic relationships among system states without explicit consideration of decisions and values (Henrion et al., 1991). This leads to deducing the conjunction of events leading to the top event. Hence, it is a deductive failure-based approach. FTA relies on a top-down static logical deduction of a critical system event and its causes. As a static risk analysis method, FTA has limitations in dynamic risk analysis associated with

complex systems such as tailings dams. However, these limitations can be alleviated through BNs (Bobbio et al., 2001), as described in the preceding sections above.

The logical application of Boolean algebra to represent the top event allows the deduction of the "failure modes," also known as the minimal cut set, to define how the events cause the top event (Vesely et al., 1981). The cut set defines the basic events in a fault tree that ensure the eventuation of the top event. Hence, a minimum cut set combines the events (system failures) that, by coincidence, cause the top event. The quantitative analysis of FTs has two parts: quantifying the top event's probability and measuring the event's importance to that probability.

Fault trees are mostly tailored to the top event (TE), corresponding to a system failure mode, with the FT only including events that contribute to the TE, meaning the events might not be exhaustive and only cover those events that the expert panels consider as credible events leading to the failure. The structures of the FT are composed of a hierarchical setup of gates where high-placed events in the FT are the outputs of the gates, and the lower events (also called basic events) are the inputs to the gates. In constructing FTs, the basic concepts of fault effects, failure mode and failure mechanisms are important in determining interrelationships between events (Vesely et al., 1981). Thus, failure mechanisms produce failure modes that affect the system operation.

Methodology

Uncertainty analysis is a critical element when analyzing failures for complex structures, such as tailings dams, whether in the design phase to assess the behavior of the structure during the operational phases, or post-failure to determine the inherent parameters and uncertainties that led to failure and how they can be mitigated in future construction, and to learn lessons for future designs. Generally, two sources of uncertainty should be considered: natural or randomness and epistemic uncertainty, which are important in quantitative risk analysis in complex structures, according to Baraldi and Zeo (2008) (Phoon and Ching, 2018).

The applied effort in risk analysis for tailings dams to determine the consequences should be structured to be helpful to the risk control process. A graphical representation of frequencies and consequences is also useful (Hartford and Baecher, 2004). Risk assessment in tailings dams is usually done through the failure modes and effects analysis (FMEA), an inductive analysis method where initiating conditions (basic events) are postulated, and their effects are iterated to get to the top event. It is a method best suited for system failures, where logical frameworks are developed through case histories and expert knowledge to frame risk sources in a system. However, the system has disadvantages in modeling redundancy in dam safety, as dam systems do not behave in a binary manner from functional to non-functional since they exhibit dependencies between failure paths. These issues can be solved by applying

influence diagrams (Bayesian networks), which capture the dependencies between nodes, whether deterministic or probabilistic.

Mapping a fault tree analysis into a Bayesian network

Mapping of a fault tree into a Bayesian network (BN) has been conducted in several studies (Bobbio et al., 2001; George and Renjith, 2021; Khakzad et al., 2011). Most of the studies focus on risk assessment, system dependability, and the capability of BNs to make inferences on the fault tree (FT) and assess the reliability of the top event. This conversion capability from FT to BN enables static information from the FT to be used to examine variables that influence tailings dam failures comprehensively, determine variable dependencies, formulate a model for risk assessment, and conduct inference updating of the prior probability of events on obtaining new information under uncertainty, and application as an accident or predictive analysis for system processes.

Converting an FT into a BN requires converting its binary nature into a marginal probability that can be assigned to each node based on the translation of the basic gate rules. Construction of the BN from an FT is done through an equivalent node transfer from the FT, with parent nodes assigned the marginal probability from the nodes and the arcs assigned the conditional probabilities to indicate the dependencies between nodes. Figure 3 shows a mapping block diagram from FT to BN.

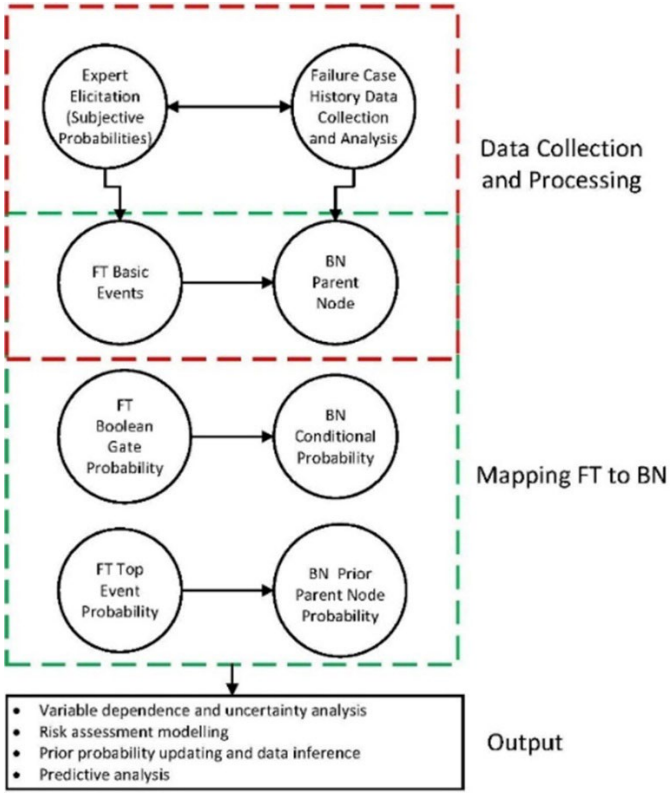


Figure 3: Mapping a fault tree (FT) to a Bayesian network (BN)

The contribution of each event to the top event can be estimated by calculating the probability of the top event and repeating the FT analysis with and without the event, and then transforming the contribution of each event into an improvement index (Khakzad et al., 2011).

Case study – Fundão tailings dam failure

The Fundão tailings dam failure occurred on November 5, 2015. The dam location is Minas Gerais, Brazil. According to the expert panel review report, several people were working on or near the dam at the time of the failure (Morgenstern et al., 2016). An excerpt from the expert panel review report (EPRR) describing the "trigger" events that led to the failure mechanism reads:

"Hence, the failure of the Fundão Tailings Dam by liquefaction flowsliding was the consequence of a chain of events and conditions. A change in design brought about an increase in saturation, which introduced the potential for liquefaction. As a result of various developments, soft slimes encroached into unintended areas on the left abutment of the dam, and the embankment alignment was setback from its originally planned location. As a result of this setback, slimes existed beneath the embankment and were subjected to the loading its raising imposed. This initiated a mechanism of extrusion of the slimes and pulling apart of the sands as the embankment height increased. With only a small additional increment of loading produced by the earthquakes, the triggering of liquefaction was accelerated and the flow slide initiated." – EPRR Executive Summary.

The above excerpt highlights various failure modes and dependencies that could have triggered the flow failure (top event). Expert statements extracted from the EPRR regarding the failure occurrence and timing of events that triggered the flow failure were modeled in the TEFTA software (Reliotec, 2024). Tables 1 to 3 highlight how the probability functions were derived in TEFTA. The respective events used in the model are labeled E1 to E17.

Table 1: Probability functions in the fault tree analysis

Failure probability model	Model	Definition of terms
Constant failure model		The model specifies unavailability and failure frequencies that do not vary with time.
Unrepairable failure model	$q(t) = 1 - (1 - q)e^{-\lambda t}$	Where $q(t)$ is component unavailability, q is component unavailability at $t = 0$, and λ is the component failure rate
Repairable failure model	$q(t) = qe^{-(\lambda+\mu)t} + \frac{\lambda}{\lambda+\mu}(1 - e^{-(\lambda+\mu)t})$	Where $q(t)$ is component unavailability, q is component unavailability at $t = 0$, λ is the component failure rate, and μ is the component repair rate

Failure probability model	Model	Definition of terms
MTBF failure model	$q(t) = \frac{\lambda}{\lambda+\mu}\left(1 - e^{-(\lambda+\mu)t}\right)$ where $\lambda = \frac{1}{MTBF}$ and $\mu = \frac{1}{MTTR}$	Where $q(t)$ is component unavailability, λ is the component failure rate, μ is the component repair rate, $MTBF$ is the mean time between failures, and $MTTR$ is the mean time to repair
MTTF failure model	$q(t) = 1 - e^{-(\lambda+\mu)t}$ where $\lambda = \frac{1}{MTTF}$	Where $q(t)$ is component unavailability, λ is the component failure rate, μ is the component repair rate, and $MTTF$ is the mean time to failure
Weibull failure model	$q(t) = 1 - exp\left[-\left(\frac{t-\gamma}{\eta}\right)^{\beta}\right]$	Where $q(t)$ is component unavailability, η is the component characteristic life, β is the shape, and γ is the location

Table 2: Fundão dam failure fault tree – probability function derivation for modeling

Name	Description	Function	Unit
Bench encroachment	The sand and slimes were no longer physically separated (EPRR Pg. 10) – 2007 – 2012	MTTF(MTTF=5)	Year
Gallery collapse	In July 2010, a vortex appears. Cracking and structural damage were observed during the inspection. In January 2011, a jet grouting program was initiated. July 2012 gallery was unrepairable, and November 2012 repair efforts were abandoned (EPRR Pg. 11)	Unrepairable(q=0, λ=2.333)	Year
Gallery overload	Because of the height of the tailings, the left abutment exceeded the load capacity (EPRR Pg. 11)	Repairable(q=0, λ=0.1666, μ=1)	Year
Blanket drain construction		MTBF(MTBF=1, MTTR=1)	Year
Modified design 826	Concept to raise to El. 920 m in 2011, updated in 2012 (EPRR Pg. 9)	MTBF(MTBF=0.5, MTTR=2)	Year
Starter dam drain failure	Dike 1 starter dam completed in October 2008. On April 13, 2009, large seepage flows occurred (EPRR Pg. 7)	MTBF(MTBF=0.5, MTTR=1.5)	Year
Drain stack concept	Conception between 2004-2007 (EPRR Pg. 4)	MTBF(MTBF=5, MTTR=5)	Year
Static pore pressure increase	Based on blasting and earthquakes	MTTF(MTTF=1)	Day
Excess pore pressure in slimes	Based on blasting and earthquakes	MTTF(MTTF=1)	Day
Solution feature collapse	Based on the gallery collapse	Repairable(q=0, λ=0.1666, μ=1)	Year

Name	Description	Function	Unit
Earthquake	Three small magnitude earthquakes occurred over a period of four minutes, preceding the failure by some 90 minutes (EPRR Pg. 16)	MTTF(MTTF=1.63)	Hour
Saturation of sand	The sand below the dam remained saturated from 2007 to 2012 (EPRR Pg. 10)	MTTF(MTTF=5)	Year
Equipment vibration	On November 15, 2015, most activity was on or near the right abutment where drains were being constructed (EPRR Pg. 16)	Constant(q=0, w=0)	Year
Mine blast	Two blasts occurred at a nearby mine within seconds of each other, three hours before failure (EPRR Pg. 16)	Constant(q=0, w=0)	Year
Without earthquake		Constant(q=0, w=0)	Year

Table 3: Basic event description

Event	Type	Description
E1	Basic	Saturation of sand
E2	Basic	Bench encroachment and slimes deposition
E3	Basic	Secondary gallery collapse (sinkhole)
E4	Basic	Secondary gallery overload
E5	Basic	Blanket drain construction for 940 raise
E6	Basic	Modified design with 826 blanket drain
E7	Basic	Starter dam base drain failure
E8	Basic	“Drained stack design concept”
E9	Basic	Static pore pressure increase
E10	Basic	Excess pore pressure in slimes
E11	Basic	Secondary gallery collapse
E12	Basic	Solution feature collapse
E13	Basic	with earthquake
E14	Basic	without earthquake
E15	Basic	Equipment vibration
E16	Basic	Mine blast
E17	Basic	Seismic event
X1	Intermediate	Static liquefaction
X2	Intermediate	Cyclic liquefaction

Fault tree results analysis

The results from the fault tree analysis in Tables 4 and 5, based on the methodology described above, indicate that the minimal cut set for the flow liquefaction of the Fundão failure was primarily triggered by

the cumulative loading of the three earthquakes, which mobilized dependent events, and static loading through (static) pore pressure increase, causing excess pore pressure build-up in the slimes. However, it is interesting to note that there was also the impact of cyclic liquefaction's contribution to the flow liquefaction mechanism. The results indicated that the seismic event resulting from the earthquake(s) also contributed to the failure mechanism. However, at a lower contribution in comparison to static liquefaction contribution. Based on the above, the probability of flow liquefaction was calculated using Equation 8,
$TE\ (flow\ liquefaction) = X_1 \cup X_2 = 0.9999$.

Table 4: Static liquefaction minimal cut set and contribution to flow liquefaction failure mechanism

Minimal cut set	Probability	Importance index (%)
E13	0.458545874	84.706
E9	0.040810543	7.539
E10	0.040810543	7.539
E3	0.000266289	0.049
E6	0.000228278	0.042
E11	0.000228278	0.042
E7	0.000228276	0.042
E5	0.000114142	0.021
E1	2.28E-05	0.004
E2	2.28E-05	0.004
E8	2.28E-05	0.004
E4	1.90E-05	0.004
E12	1.90E-05	0.004
E14	0	0.000

Table 5: Cyclic liquefaction minimal cut set and contribution to flow liquefaction failure mechanism

Minimal cut set	Probability	Importance index (%)
E17	0.458546	100
E15	0	0
E16	0	0

After processing the fault tree, the data was converted to a Bayesian Network (Bayesnet) using the Uninet Software (Ababei, 2008) as described in the methodology section. The Bayesian network was constructed assuming a uniform marginal distribution for the events and arc directionality as suggested in the EPRR.

The conditional probabilities linking the nodes were obtained by calculating the probability of the top event and repeating the FT analysis with and without the event. For static liquefaction, E1 was 0.569353. The results obtained from this process are shown in Table 6.

Table 6: The probability of each event contributing to the failure

Event	Probability
E1	0.569353
E2	0.999862
E3	0.999618
E4	0.999866
E5	0.99977
E6	0.999428
E7	0.999656
E8	0.999862
E9	0.959074
E10	0.959074
E11	0.999428
E12	0.999866
E13	0.08279
E14	0.999885
E15	0.999885
E16	0.999885
E17	0.08279

A directed acyclic graph (DAG) created from this process is shown in Figure 4. The flow failure was represented as a functional node, which is a union of the static and cyclic liquefaction events ($X_1 \cup X_2$). The Bayesian network could be processed once the DAG and conditional probabilities were assigned to the arcs. Results obtained from this model indicated similar results to those discussed in the previous FT, as shown in Figure 5.

However, in the analytical conditioning of the BN model, the model did not produce similar results as the FT as per the minimal cut set analysis, where E13, E9, and E10 events had the highest importance index in causing the failure. The results indicated a correlation between E1, E2, and E15, leading to X1.

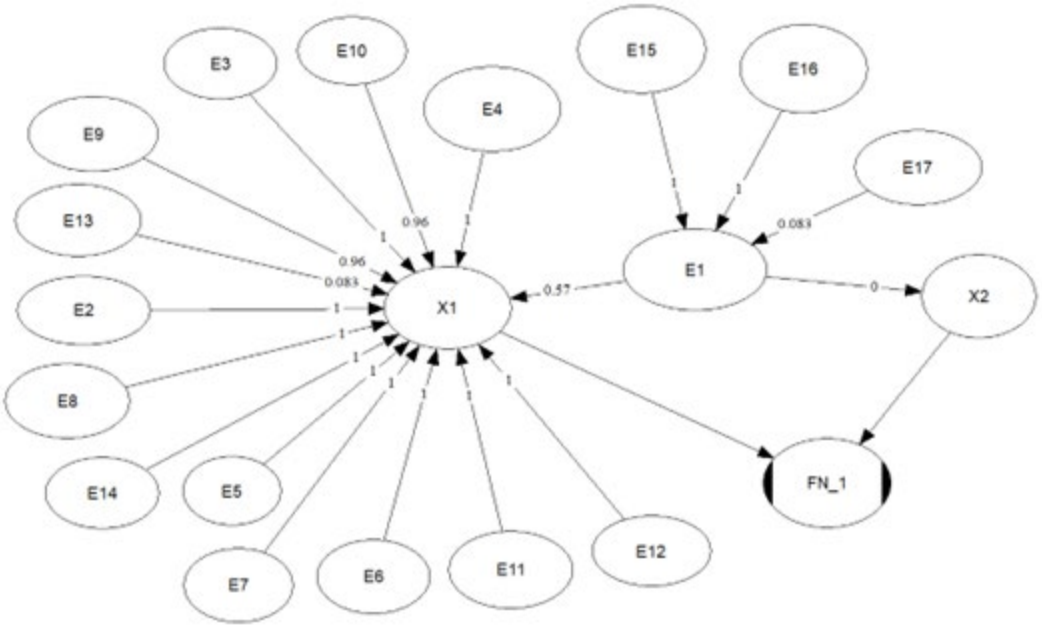


Figure 4: DAG showing nodes and arcs that led to the Fundão failure

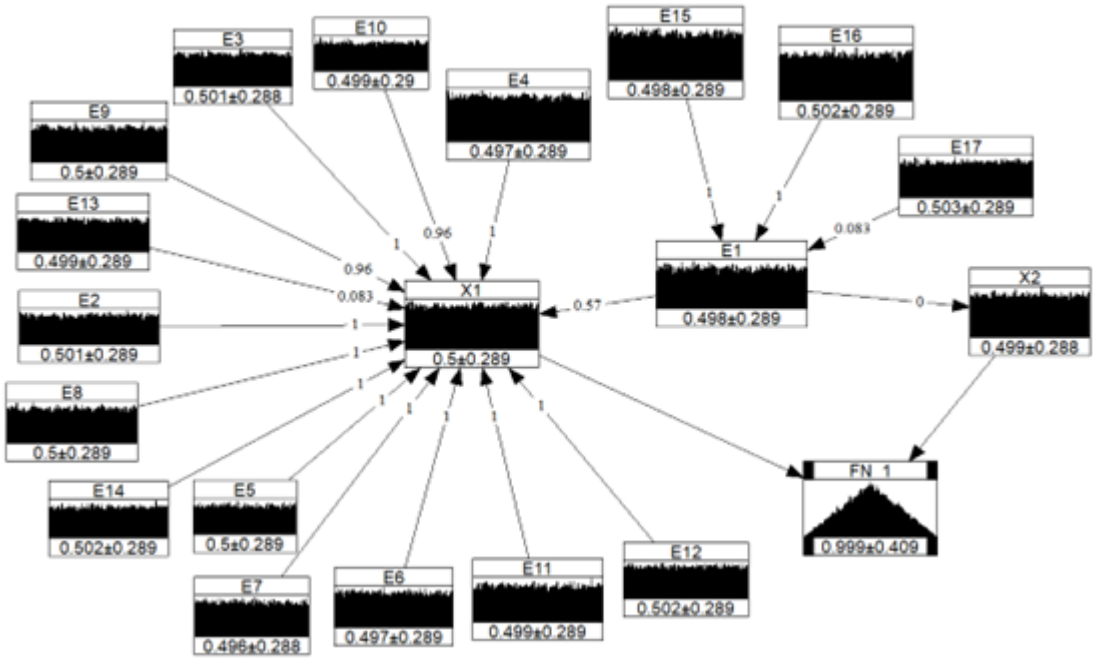
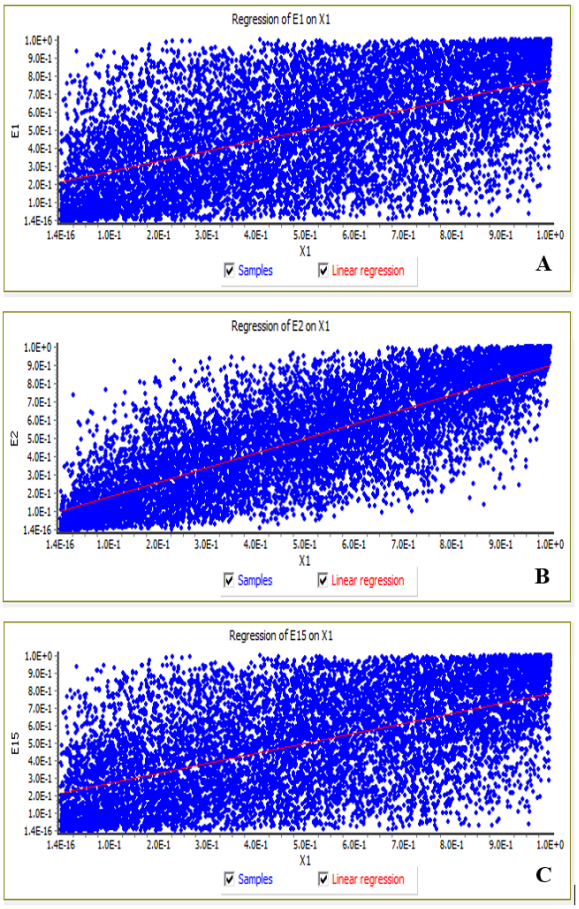


Figure 5: Bayesian network for the Fundão failure

A quantitative analysis of the results highlighted the correlation between the input variables. Quantitative analysis of the Person product moment, Spearman's rank correlation and the regression analysis of the base variables E1, E2 and E15 to predict X1 are shown in Table 7. It can be observed that there is a high correlation between the variables. Another correlation was between E9 and E1, E2, and E15 base variables.

Table 7: Correlation coefficients to predict static liquefaction (X1)

Base variables	E1	E2	E15
Pearson product-moment correlation	0.5698	0.7945	0.5697
Spearman's correlation	0.5696	0.7942	0.5695
Regression coefficient	0.5703	0.7938	0.5702



	X1	E17	E1	E10	E11	E12	E13	E14	E15	E16	E2	E3	E4	E5	E6	E7	E8	E9	X1	X2	FN_1
FN_1	1	-0.0035	0.5698	0.0113	-0.0035	0.0036	-0.0045	0.002	0.5697	0.0108	0.7945	0.011	-0.0029	0.0025	0.0039	0.0005	0.0068	-0.0004	1	-0.0059	0.7038
FN_1	-0.0035	1	-0.002	-0.0075	0.0066	-0.0045	0.0033	0.0042	-0.0019	-0.0029	-0.0024	0.0014	0.0046	-0.0044	0.0006	-0.0002	0.0011	0.0057	-0.0035	0.0006	-0.002
E1	0.5698	-0.002	1	0.0087	-0.0039	0.0025	-0.007	0.0073	0.9999	0.0161	-0.0011	-0.0006	-0.0005	-0.0009	0.0041	0.0012	0.0036	-0.0043	0.5698	0.0008	0.404
E10	0.0113	-0.0075	0.0087	1	-0.0044	-0.0011	-0.0071	0.0076	0.0087	0	0.0053	-0.0003	-0.0018	0.0023	0.0048	0.0053	-0.0021	0.0016	0.0113	0.0018	0.0093
E11	-0.0035	0.0066	-0.0039	-0.0044	1	-0.0056	0.0007	-0.0048	-0.0039	0.0018	-0.0039	0.0031	0.0015	-0.0007	0.004	0.0011	0.0038	0.003	-0.0035	0.0069	0.0024
E12	0.0036	-0.0045	0.0025	-0.0011	-0.0056	1	-0.0045	-0.0007	0.0026	-0.0034	0.0034	0.0075	-0.0049	-0.0084	0.0008	0.0091	-0.0035	-0.0014	0.0036	-0.002	0.0011
E13	-0.0045	0.0033	-0.007	-0.0071	0.0007	-0.0045	1	-0.0026	-0.0068	-0.012	-0.0012	0.0009	0.0024	0.0002	0.0078	0.002	0.0045	-0.0022	-0.0045	0.001	-0.0025
E14	0.002	0.0042	0.0073	0.0076	-0.0048	-0.0007	-0.0026	1	0.0072	0.0009	-0.0022	0.0009	0.0027	0.0024	0.0001	0.0053	0.0031	-0.005	0.002	0.0069	0.0063
E15	0.5697	-0.0019	0.9999	0.0087	-0.0039	0.0026	-0.0068	0.0072	1	0.0023	-0.0011	-0.0005	-0.0005	-0.001	0.0041	0.0012	0.0036	-0.0043	0.5697	0.0009	0.404
E16	0.0108	-0.0029	0.0161	0	0.0018	-0.0034	-0.012	0.0009	0.0023	1	0.0008	-0.006	0.0021	0.0062	0	0.0013	0.0053	0.0054	0.0108	-0.003	0.0055
E17	0.7945	-0.0024	-0.0011	0.0053	-0.0039	0.0034	-0.0012	-0.0022	-0.0011	0.0008	1	-0.0015	-0.0036	0.0065	0.0025	0.0016	0.0053	0.0024	0.7945	-0.0059	0.5583
E2	0.011	0.0014	-0.0006	-0.0003	0.0031	0.0075	0.0009	0.0009	-0.0005	-0.006	-0.0015	1	0	0.0007	0.0036	0.0093	0.0026	-0.0034	0.011	-0.0012	0.007
E3	-0.0029	0.0046	-0.0005	-0.0018	0.0015	-0.0049	0.0024	0.0027	-0.0005	0.0021	-0.0036	0	1	0.0023	-0.0031	0.0055	0.006	0.0068	-0.0029	-0.0022	-0.0036
E4	0.0025	-0.0044	-0.0009	0.0023	-0.0007	-0.0084	0.0002	0.0024	-0.001	0.0062	0.0065	0.0007	0.0023	1	0.0008	0.0039	-0.0043	0	0.0025	-0.0015	0.0007
E5	0.0039	0.0006	0.0041	0.0048	0.004	0.0008	0.0078	0.0001	0.0041	0	0.0025	0.0036	-0.0031	0.0008	1	0.0061	0.0007	-0.001	0.0039	0.0047	0.0061
E6	0.0005	-0.0002	0.0012	0.0053	0.0011	0.0091	0.002	0.0053	0.0012	0.0013	0.0016	0.0093	0.0055	0.0039	0.0061	1	-0.0005	0.0032	0.0005	0.0049	0.0039
E7	0.0068	0.0011	0.0036	-0.0021	0.0038	-0.0035	0.0045	0.0031	0.0036	0.0053	0.0053	0.0026	0.006	-0.0043	0.0007	-0.0005	1	0.0017	0.0068	0.0022	0.0064
E8	-0.0004	0.0057	-0.0043	0.0016	0.003	-0.0014	-0.0022	-0.005	-0.0043	0.0054	0.0024	-0.0034	0.0068	0	-0.001	0.0032	0.0017	1	-0.0004	-0.0007	-0.0008
E9	1	-0.0035	0.5698	0.0113	-0.0035	0.0036	-0.0045	0.002	0.5697	0.0108	0.7945	0.011	-0.0029	0.0025	0.0039	0.0005	0.0068	-0.0004	1	-0.0059	0.7038
X1	-0.0059	0.0006	0.0008	0.0018	0.0069	-0.002	0.001	0.0069	0.0009	-0.003	-0.0059	-0.0012	-0.0022	-0.0015	0.0047	0.0049	0.0022	-0.0007	-0.0059	1	0.7062
X2	0.7038	-0.002	0.404	0.0093	0.0024	0.0011	-0.0025	0.0063	0.404	0.0055	0.5583	0.007	-0.0036	0.0007	0.0061	0.0039	0.0064	-0.0008	0.7038	0.7062	1

Figure 6: Scatter plots of regression coefficients and product moment correlation table

Conclusion

An alternative approach using Bayesian networks in the analysis of tailings dam risks was addressed in this paper. The shortfalls of the current approach of using static approaches like the fault tree were discussed. An application case study was analyzed, with results indicating that although the BN model had the same result of predicting the flow failure probability, the correlation of the variables to static liquefaction was different to the importance index of the fault tree that had E13, E9, and E10 as the minimal cut set. The BN results indicated that E1, E2, and E15 base variables correlate better with predicting X1 in the case study.

The model could be used to conditionalize the variables by constraining the uncertainty range in the marginal distribution to estimate dependence correlations on other variables. For example, by constraining the probability of the equipment vibration between the interval [0.01,0.03], the dependence effect of this change can be seen on the other variables, such as static liquefaction and overall probability of flow failure, as shown in Figure 7. These results clearly show the advantages of using Bayesian networks over static risk assessment approaches. This inherent capability can be adopted in risk assessments, failure modes analysis, and failure trigger inference for robust tailings dam design and engineering.

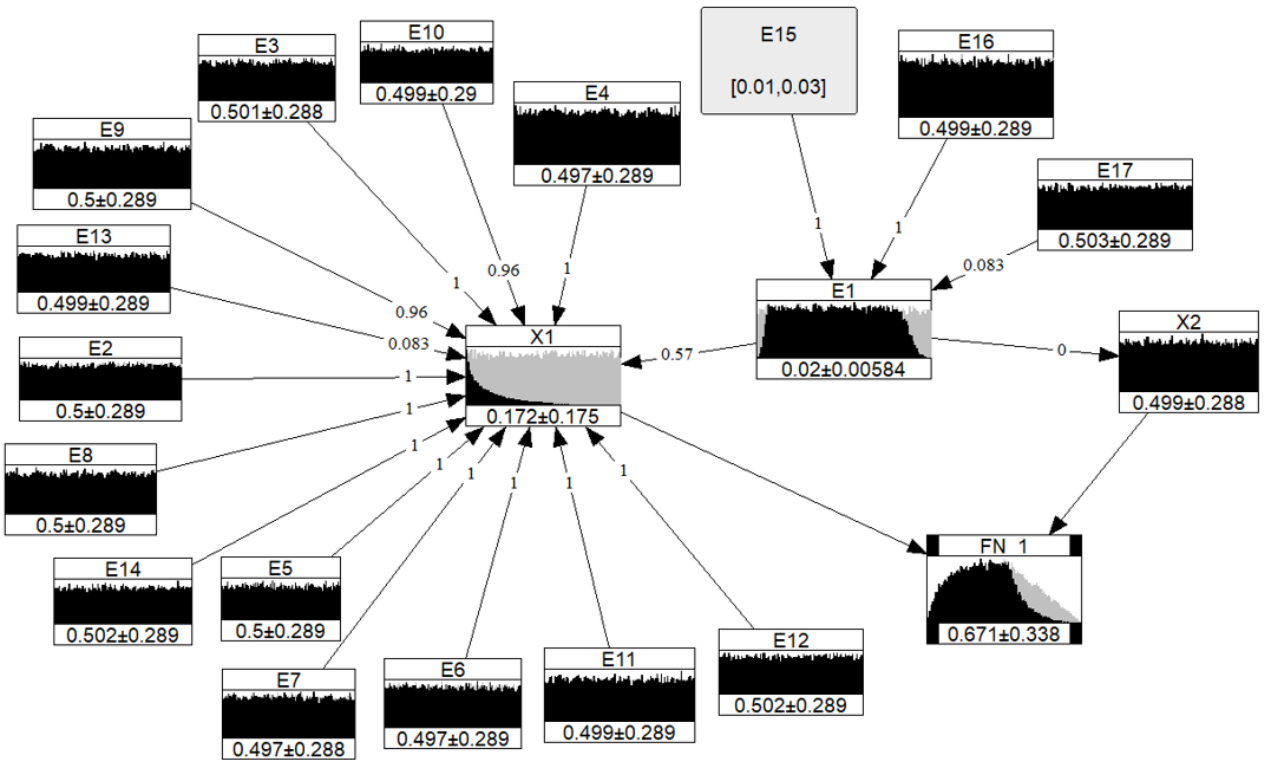


Figure 7: Conditionalizing variable E15 and its dependence relationship with other variables, a function that can be used for inference and predictive analysis

Acknowledgements

The lead author wishes to thank the Geotechnical Engineering Centre (GEC) at the University of Queensland for the opportunity to research an exciting topic and for supporting and directing his research. He would also like to thank LightTwist Inc. for providing an academic license for UNINET software for uncertainty analysis.

References

Ababei, D. 2008. Uninet, Version 3.2. Accessed at https://www.lighttwist.net/wp/uninet/

Baecher, G. B. and Christian, J. T. 2005. *Reliability and Statistics in Geotechnical Engineering*. John Wiley & Sons.

Baraldi, P. and Zio, E. 2008. A combined Monte Carlo and possibilistic approach to uncertainty propagation in event tree analysis. *Risk Analysis: An International Journal* 28(5): 1309–1326.

Bobbio, A., Portinale, L., Minichino, M. and Ciancamerla, E. 2001. Improving the analysis of dependable systems by mapping fault trees into Bayesian networks. *Reliability Engineering and System Safety* 71(3): 249–260.

Borovcnik, M. 2015. Risk and decision making: The logic of probability. *The Mathematics Enthusiast* 12(1): 113–139.

Cacciuttolo, C. and Atencio, E. 2022. Past, present, and future of copper mine tailings governance in Chile (1905; 2022): A review in one of the leading mining countries in the world. *International Journal of Environmental Research and Public Health* 19(20): 13060. Accessed at https://www.mdpi.com/1660-4601/19/20/13060

Clemen, R. T. and Reilly, T. 1999. Correlations and copulas for decision and risk analysis. *Management Science* 45(2): 208–224.

Delgado-Hernández, D.-J., Morales-Nápoles, O., De-León-Escobedo, D. and Arteaga-Arcos, J.-C. 2014. A continuous Bayesian network for earth dams' risk assessment: an application. *Structure and Infrastructure Engineering* 10(2): 225–238.

Feinberg, B., Engemoen, W., Fiedler, W. and Osmun, D. 2016. Reclamation's empirical method for estimating life loss due to dam failure. E3S Web of Conferences,

George, P. G. and Renjith, V. 2021. Evolution of safety and security risk assessment methodologies towards the use of Bayesian networks in process industries. *Process Safety and Environmental Protection* 149: 758–775.

Hanea, A. M., Kurowicka, D. and Cooke, R. M. 2006. Hybrid method for quantifying and analyzing Bayesian belief nets. *Quality and Reliability Engineering International* 22(6): 709–729.

Hanea, A., Napoles, O. M. and Ababei, D. 2015. Non-parametric Bayesian networks: Improving theory and reviewing applications. *Reliability Engineering and System Safety* 144: 265–284.

Hartford, D. N. and Baecher, G. B. 2004. *Risk and Uncertainty in Dam Safety*. Thomas Telford.

Henrion, M., Breese, J. S. and Horvitz, E. J. 1991. Decision analysis and expert systems. *AI magazine* 12(4): 64–64.

ICOLD. 1989. Tailings Dam Safety Guideline Bulletin 074.

Jefferies, M., Morgenstern, N.R., Van Zyl, D. and Wates, J. 2019. Report of ITRB on NTSF Embankment Failure, Cadia Valley Operations for Ashurst Australia. Accessed at https://www.newcrest.com/sites/default/files/2019-10/190417_Report%20on%20NTSF%20Embankment%20Failure%20at%20Cadia%20for%20Ashurst.pdf

Khakzad, N., Khan, F. and Amyotte, P. 2011. Safety analysis in process facilities: Comparison of fault tree and Bayesian network approaches. *Reliability Engineering and System Safety* 96(8): 925–932.

Klohn, E.J. 1972. Design and construction of tailings dams. *CIM Transactions* 75: 50–66.

Kossoff, D., Dubbin, W., Alfredsson, M., Edwards, S., Macklin, M. and Hudson-Edwards, K. A. 2014. Mine tailings dams: characteristics, failure, environmental impacts, and remediation. *Applied Geochemistry* 51: 229–245.

McLeod, H., Murray, L. and Berger, K.C. 2003. Tailings dam versus a water dam, what is the design difference. *Proceedings of ICOLD Symposium on Major Challenges in Tailings Dams.*

Morales, O., Kurowicka, D. and Roelen, A. 2008. Eliciting conditional and unconditional rank correlations from conditional probabilities. *Reliability Engineering and System Safety* 93(5): 699–710.

Morales-Nápoles, O., Delgado-Hernández, D.J., De-León-Escobedo, D. and Arteaga-Arcos, J.C. 2013. A continuous Bayesian network for earth dams' risk assessment: methodology and quantification. *Structure and Infrastructure Engineering* 10(5): 589–603. https://doi.org/10.1080/15732479.2012.757789

Morgenstern, N.R., Vick, S.G., Viotti, C. and Watts, B. 2016. Fundão tailings dam review panel report on the immediate causes of the failure of the Fundão dam. Cleary Gottlieb Steen and Hamilton LLP, New York.

Morgenstern, N.R.,Vick, S.G and Van Zyl, D. 2014. Mount Polley independent expert investigation and review report. https://www.mountpolleyreviewpanel.ca/

Pan, Y., Ou, S., Zhang, L., Zhang, W., Wu, X. and Li, H. 2019. Modeling risks in dependent systems: A Copula-Bayesian approach. *Reliability Engineering and System Safety* 188: 416–431.

Phoon, K.-K. and Ching, J. 2018. *Risk and Reliability in Geotechnical Engineering*. CRC Press.

Phoon, K.-K., Cao, Z-J and Ji, J. 2022. Uncertainty-informed decision-making in Burland Triangle. In *Uncertainty, Modeling, and Decision Making in Geotechnics:* 1–36. CRC Press.

Ramon, V. and Hinks, J. 2023. Tailings dams. Accessed at https://doi.org/10.1680/eedr.66151.243

Reliotec. 2024. TopEvent FTA. Retrieved 28/06/2024 from https://www.fault-tree-analysis.com/

Robertson, P.K., de Melo, L., Williams, D.J. and Wilson, G.W. 2019. *Report of the expert panel on the technical causes of the failure of Feijão Dam I.*

Vesely, W.E., Goldberg, F.F., Roberts, N.H. and Haasl, D.F. 1981. Fault tree handbook. Systems and Reliability Research, Office of Nuclear Regulatory Research, USA.

Zhang, L. and Singh, V. P. 2019. *Copulas and their Applications in Water Resources Engineering*. Cambridge University Press.

A Feed Forward Approach to Optimizing Oilsands Tailings Centrifuge Operation

Paul Mikula, Kalium Research, Alberta, Canada
Adeola Bello-Hamilton, Syncrude Research, Alberta, Canada
Nan Wang, Syncrude Research, Alberta, Canada
Jim Lorentz, Syncrude Research, Alberta, Canada
Randy Mikula, Kalium Research, Alberta, Canada

Abstract

Managing fluid fine tailings accumulation in surface mined oil sands is a challenge, and centrifugation is one of the dewatering technologies developed and commercialized by Syncrude Canada at their Mildred Lake surface mined oil sands operation located near Fort McMurray in northern Alberta. Development started with pilot testing in 2007, culminating in the operation of eight Alfa Laval Lynx 1000 centrifuges from 2011 to 2013 in what was known as the centrifuge demonstration plant. From 2013 to 2024, Syncrude's full-scale commercial plant was in operation with 18 Lynx 1000 centrifuges and played a major role in Syncrude's commitment to meeting regulatory requirements for treating fluid fine tailings. The target throughput of 72 tonnes of fines per machine was difficult to consistently achieve because of feed density variations that caused a variety of operational problems including washouts. A study undertaken in 2017 to identify centrifuge plant operational bottlenecks identified a shortcoming in the torque control that is conventionally used to adjust cake discharge rates as feed rate changes. The results of that study lead directly to development of the improved operational approach described in this paper.

The operation of the Syncrude centrifuge plant from 2017 to 2022 relied on controlling the torque on the cake scroll to change the rate at which cake is pushed out of the centrifuge and thereby automatically respond to changes in feed density or flow rate. In practice this is only true if feed properties change slowly. When feed density varies rapidly the torque control cannot respond quickly enough to prevent centrifuge washouts. By examining centrifuge plant data over several years, an equation was developed to determine the ideal scroll speed based on MFT feed density and flow rate. Controlling the centrifuge operation proactively based on feed properties leads to smoother differential speed adjustments and requires less operator intervention. The equation provides a physically motivated first-order relationship between the MFT density, flow rate, and the differential speed, which can be expanded on with a more in-depth analysis

of the data using machine learning. Using a neural net, the optimal differential speed can be predicted based on all the centrifuge parameters, including polymer dosage and bowl speed. In general, the neural net results agree with the equation, but can also account for large changes in centrifuge bowl speed. Currently the operators determine the torque setting to optimize fines capture, and that setting might vary depending upon feed density, clay content, bowl speed, or polymer dosage. Similarly, the equation has a bias term that would be used to account for those parameters that are typically fixed or slowly changing. With either a simple equation or a neural net, adjusting the centrifuge operation in response to changes in the MFT feed measured before it enters the centrifuge will proactively adjust to feed changes before they lead to disruption of the centrifuge operation. Preliminary results of the implementation of these feed forward principles are presented from the Syncrude full-scale centrifuge operation.

Introduction

The centrifuge plant consists of 18 Alfa Laval Lynx-1000 centrifuges split into two trains, which ran from 2017 to 2022. Figure 1 shows a basic diagram of a centrifuge, indicating the operating parameters and important operational details.

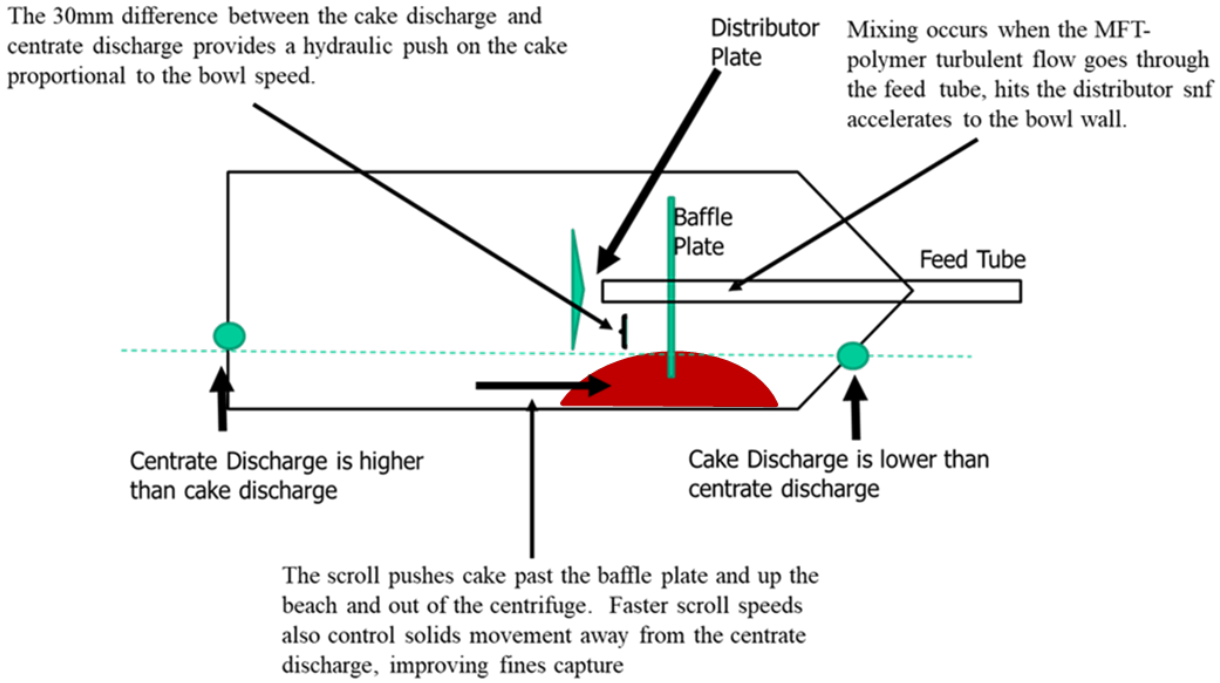


Figure 1: Schematic of the centrifuge with highlights of relevant operating considerations

It is important to note that the centrifuges are designed to operate with a negative pool, which means the centrate discharge is higher than the cake discharge. Operationally, this means that a minimum feed rate and cake formation is required in order to form a cake plug that separates the centrate from the cake

discharge. If the feed rate (MFT density and flow rate) is not high enough this plug can wash out, resulting in significant loss of production.

In order to prevent wash outs and otherwise control the cake discharge rate, torque control is used. The operator sets a scroll discharge torque that the control algorithm attempts to keep constant. The torque on the scroll discharge will be a function of the solids loading, bowl speed, the polymer flocculant mixing and dosage, and the scroll discharge rate itself. With rapidly changing MFT density or flow rate (solids loading) the torque control approach has difficulty responding rapidly enough to prevent cake washouts.

Data from each of the 9 centrifuges in train 1 and 2 (18 total) was taken in 6-hour intervals for three years, from January 2017 to December 2019, and in two-hour intervals from January 2020 to December 2020. Since physical centrate solids and cake solids measurements are taken at three-hour intervals, the increased data sampling frequency for the 2020 data was done to determine if a shorter time interval would change the data quality. It did not. In addition to the date/time of the measurements and the production status of each centrifuge, this study looks at the following key measurements:

1. torque on the cake scroll (kNm)
2. torque setpoint (kNm)
3. differential (cake scroll) speed (rpm)
4. bowl speed (rpm)
5. polymer dosage (g/tonne)
6. polymer flow (m^3/h)
7. MFT flow (m^3/h)
8. MFT density (kg/m^3)
9. cake solids (%weight)
10. centrate solids (%weight).

The first eight of these quantities are indicators of the input into the centrifuge, and the cake solids and centrate solids are indicators of the centrifuge performance. The efficiency of a centrifuge is measured by the solids capture, which is defined as the ratio of solids in the cake to the solids input.

Controlling the torque is not an ideal method for controlling the centrifuges for two reasons. The scroll cake discharge torque is kept constant by adjusting the scroll (differential) speed or cake discharge rate. The algorithm cannot respond quickly enough to maintain torque and the integrity of the cake plug when feed density changes rapidly. Additionally, when the operator recognizes that the torque has changed quickly an intervention is required, which is generally too late to prevent a washout. A feed forward method for controlling the scroll speed in the centrifuges based on MFT density and flow rate before entering the

centrifuge can solve these problems. Since the MFT density gauge is several minutes upstream of the centrifuges, controlling differential speed using that information allows for a more controlled response to potential washouts.

The goal of this analysis is to determine the optimal differential speed for a given MFT density and flow rate, in order to maximize the solids capture and prevent wash outs. Unlike most mineral processing applications, the oilsands tailings MFT density is not controlled in the centrifuge operation. This study uses three years of operational data to determine the relationship between differential speed and MFT flow rate and density for a given bowl speed and polymer dosage that also results in a high (>95%) solids capture. The MFT flow can be controlled somewhat, but should be maximized, if possible, to increase the amount of MFT processed by the centrifuge and help maintain the cake plug.

The polymer is required for the formation of cake, and an optimal value has already been determined in an ADW (accelerated dewatering) process where the mixing has been optimized (Bara, 2020). Increased polymer dose can compensate for imperfect mixing, but overdosing can lead to problems in the cake transport, and in particular with the torque the cake will produce for a given differential speed. Too much polymer can create a slippery cake that is difficult to auger out of the centrifuge. The bowl speed and the MFT flow rate both contribute to the mixing of polymer and MFT. In addition, the bowl speed creates a hydraulic pressure to help transport cake out of the centrifuge (Bara et al., 2011; Mikula et al., 2017; Mikula et al., 2021). In the final analysis, however, the differential speed is the most important factor in transporting the cake out of the centrifuge and therefore in determining the steady state operating conditions for a given MFT flow rate and density.

Results and discussion

Developing an equation for differential speed

The data collected over four years from 2017 to 2020 contains a wide range of operating conditions, far more than could be collected in a sampling program. Unfortunately, this also includes a significant amount of data where centrifuge operation is not optimal. Additionally, since not all the quantities are measured at the same locations or times, there are some cases that lead to unphysical data such as solids captures in excess of 100%. The first step in determining the optimal differential speed for given feed properties is reducing the dataset to only times where centrifuges are running in a steady state and efficiently. The centrifuge can be considered to be running in a steady state if operator intervention is not required, the operator intervenes by changing the torque setpoint, and an algorithm adjusts the differential speed until that torque is reached. If the torque is within 5% of the torque setpoint, it is not likely there has been any recent operator intervention, and the centrifuge is running in a steady state. The efficiency of the centrifuges is measured by the solids capture; a centrifuge is running efficiently with solids capture above 97.5%.

Once the data has been reduced to centrifuges with a high solids capture (above 97.5%) in a steady state (torque within 5% of the torque setpoint), it is then grouped according to feed density by rounding to the nearest 10 kg/m^3. Initially the data is separated into train 1 and train 2, in case there is a significant systematic difference between the trains, but this does not appear to be the case. For a fixed density, we expect a linear relationship between the differential speed and the MFT flow rate, since the differential speed controls the rate at which solids leave the centrifuge, and the MFT flow rate is the rate solids enter the centrifuge. Although there is significant scatter in the data, there is a strong linear relationship between differential speed and MFT flow rate. The slopes and intercepts of these lines for each density grouping are given with their standard errors in Table 1.

Table 1: The slopes and intercepts for the linear fit of differential speed to MFT flow rate, grouped by density range

MFT density	Train 1 slope	Train 1 intercept	Train 2 slope	Train 2 intercept
1,160	0.15 ± 0.012	−2.22 ± 2.15	0.14 ± 0.02	−1.68 ± 2.03
1,170	0.13 ± 0.001	3.05 ± 1.65	0.15 ± 0.01	6.13 ± 1.66
1,180	0.13 ± 0.009	3.60 ± 1.55	0.11 ± 0.01	1.13 ± 1.43
1,190	0.15 ± 0.010	0.97 ± 1.75	0.14 ± 0.01	10.35 ± 1.52
1,200	0.11 ± 0.010	7.46 ± 1.74	0.09 ± 0.01	7.43 ± 1.79
1,210	0.13 ± 0.010	4.84 ± 1.70	0.12 ± 0.01	4.16 ± 1.85
1,220	0.18 ± 0.011	−4.11 ± 1.94	0.14 ± 0.01	6.26 ± 1.74
1,230	0.14 ± 0.011	3.66 ± 1.79	0.13 ± 0.01	8.80 ± 1.89
1,240	0.15 ± 0.011	4.21 ± 1.81	0.18 ± 0.01	−0.47 ± 2.10
1,250	0.12 ± 0.012	8.95 ± 1.90	0.15 ± 0.01	4.79 ± 2.02

The intercepts have large errors, and are near 0, with no strong evidence of a trend as density increases. As a boundary condition, if there is no flow of MFT into the centrifuge, there is no need for the differential to push cake out. It is therefore reasonable to take the intercept to be 0 in all cases and use this to refit the linear equations. The resulting slopes of the new linear fits are given in Table 2. Requiring the y-intercept to be 0 has several advantages. It makes the changes in the slope between density groups more obvious, since the goal is to obtain a value for the differential speed. It also means the slope is simply the ratio between differential speed and MFT flow for a given density group. This will greatly simplify the resulting determination of differential speed.

Table 2: The slopes from the linear fit for differential speed to MFT flow rate, with the y-intercept set to 0

Density	Train 1	Train 2
kg/m³	Estimated slope	Estimated slope
1,140	0.118 ± 0.003	0.126 ± 0.003
1,150	0.133 ± 0.002	0.125 ± 0.002
1,160	0.137 ± 0.002	0.144 ± 0.002
1,170	0.144 ± 0.001	0.142 ± 0.002
1,180	0.147 ± 0.001	0.148 ± 0.001
1,190	0.151 ± 0.001	0.153 ± 0.001
1,200	0.156 ± 0.002	0.162 ± 0.002
1,210	0.160 ± 0.002	0.163 ± 0.002
1,220	0.156 ± 0.002	0.165 ± 0.002
1,230	0.164 ± 0.002	0.171 ± 0.002
1,240	0.172 ± 0.002	0.173 ± 0.002
1,250	0.170 ± 0.002	0.174 ± 0.002

To determine the final equation for differential speed as a function of MFT density and flow rate, the slopes in Table 3 are plotted as a function of the density group, and a linear fit is found to average the data and provide values for any MFT density. Since trains 1 and 2 both give similar results, they can be combined to create a single master equation to determine the differential speed for a given MFT density and flow rate. The combined data is shown in Figure 2.

The equation for the linear fit in Figure 2 is

$$y = 0.4418x - 0.3757 \qquad \text{(Equation 1)}$$

where y is the ratio of differential speed to MFT flow rate and x is the MFT density. This leads to our equation for the differential speed as a function of the MFT density and flow rate:

$$\text{Differential Speed} = (0.4418 * \text{MFT Density} - 0.3757) * \text{MFT FlowRate}. \qquad \text{(Equation 2)}$$

Some differential speed (in rpm) values calculated with this equation are shown in Table 3.

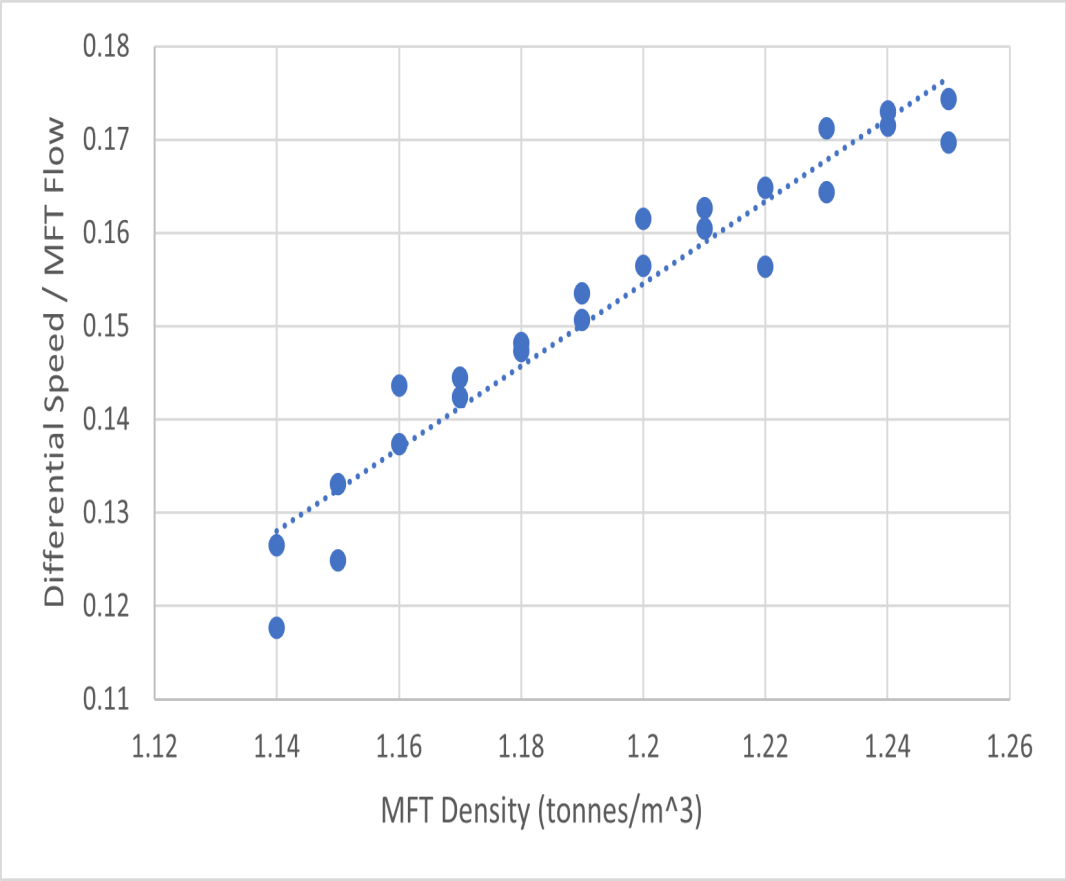


Figure 2: The combined data from Trains 1 and 2

Table 3: The differential speeds (rpm) calculated for some values of MFT density and flow rate

Density (tonnes/m^3)	MFT flow rate (m^3/hour)						
	75	**100**	**125**	**150**	**175**	**200**	**225**
1.14	9.6	12.8	16.0	19.2	22.4	25.6	28.8
1.15	9.9	13.2	16.5	19.9	23.2	26.5	29.8
1.16	10.3	13.7	17.1	20.5	23.9	27.4	30.8
1.17	10.6	14.1	17.7	21.2	24.7	28.2	31.8
1.18	10.9	14.6	18.2	21.8	25.5	29.1	32.8
1.19	11.3	15.0	18.8	22.5	26.3	30.0	33.8
1.20	11.6	15.4	19.3	23.2	27.0	30.9	34.8
1.21	11.9	15.9	19.9	23.8	27.8	31.8	35.7
1.22	12.2	16.3	20.4	24.5	28.6	32.7	36.7
1.23	12.6	16.8	21.0	25.2	29.3	33.5	37.7
1.24	12.9	17.2	21.5	25.8	30.1	34.4	38.7
1.25	13.2	17.7	22.1	26.5	30.9	35.3	39.7

Equation 2 was created using only densities from 1,135 kg/m^3 to 1,255 kg/m^3, grouped by rounding to the nearest 10 kg/m^3. It is possible to consider either a wider range of total densities or a smaller density group size. The main limitation in choosing group size is the amount of data.

Equation 2 assumes an approximate linear relationship between the differential speed and the MFT flow for a given MFT density, and then further assumes a linear relationship between the ratio of differential speed to flow rate and the MFT density. The exact relationships between these quantities may be more complicated, but for many of the applicable values of MFT flow and density, the linear relationship is a good approximation. To account for some of this uncertainty, and to better deal with more extreme values of MFT flow and density, an operator bias can be introduced to the equation to allow for some adjusting of the differential speed.

$$\text{Differential Speed} = \textit{Bias} \times ((0.4418 * \text{MFT Density} - 0.3757) * \text{MFT FlowRate}) \quad \text{(Equation 3)}$$

Deployment of the equation compared to torque control

Centrifuge operation over the four years of operation has been controlled through the torque measured on the scroll. Using the torque to control the differential speed compensates for drift in feed properties. The operator will set the torque value and the control system adjusts the differential speed to maintain that value. The operator will choose the torque setpoint depending on bowl speed, polymer dose, and fines in the MFT in order to maximize the fines capture and maintain high cake solids. As noted earlier the torque control approach has difficulty responding to rapid changes in feed density. The equation that relates feed flow and density to the differential speed is better able to respond to changes in feed density because the density meter is significantly upstream of the centrifuges. The bias factor in the equation is set by the operator to account for bowl speed, polymer dose, and fines content. There was an opportunity on April 13, 2021, to compare the two control systems on nearby centrifuges.

The new control system was commissioned successfully from April 12 to 14, 2021. Preliminary evaluations of an “operator bias” function showed that there is a wide operating window for the system, and that operators could quickly become accustomed to the new system relative to the existing torque control method.

Figure 3 shows data from April 13, when the differential speed of the test centrifuge 1G is shown responding to changes in feed rate. During this five-hour period, the operator bias was adjusted only twice for testing purposes (between .85 to .95). The blue arrows show a lag between the MFT feed rate to 1G and the differential speed response. This response time can be adjusted by appropriate changes to the control system. Figure 4 shows the same time period for centrifuge 1E, using the operator torque setting to define the differential speed. The upper plot of torque setting represents an operator intervention to set the torque, and the lower plot shows the resulting differential speed response. The advantages of the new control system

based on the equation are obvious considering that more than 10 operator changes to the torque setpoint were required during the five-hour test period.

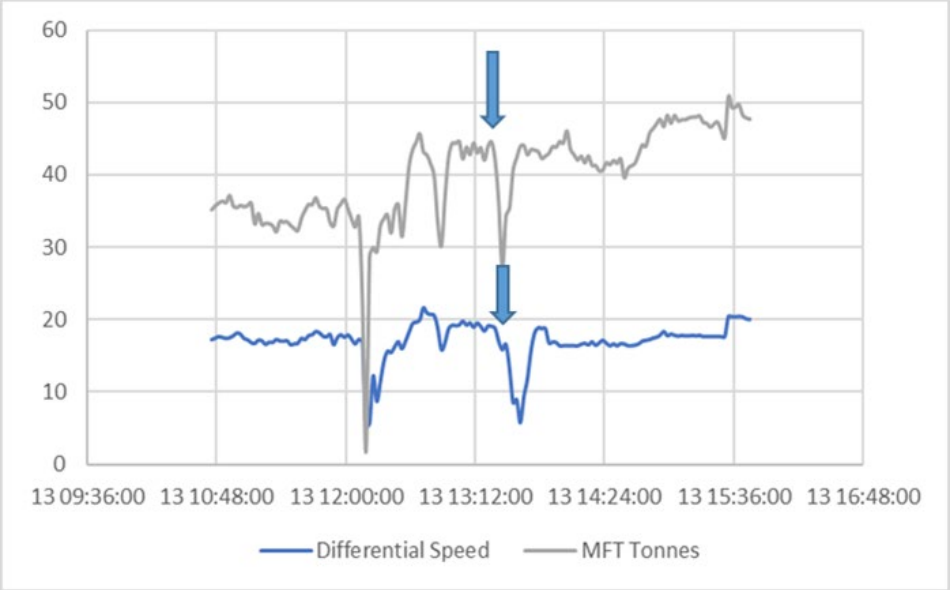


Figure 3: A five-hour test period on April 13, Centrifuge 1G, showing the Equation 3 control of differential based on MFT feed rate shown in tonnes per hour.
During this time period, the operator bias was only changed twice for test purposes

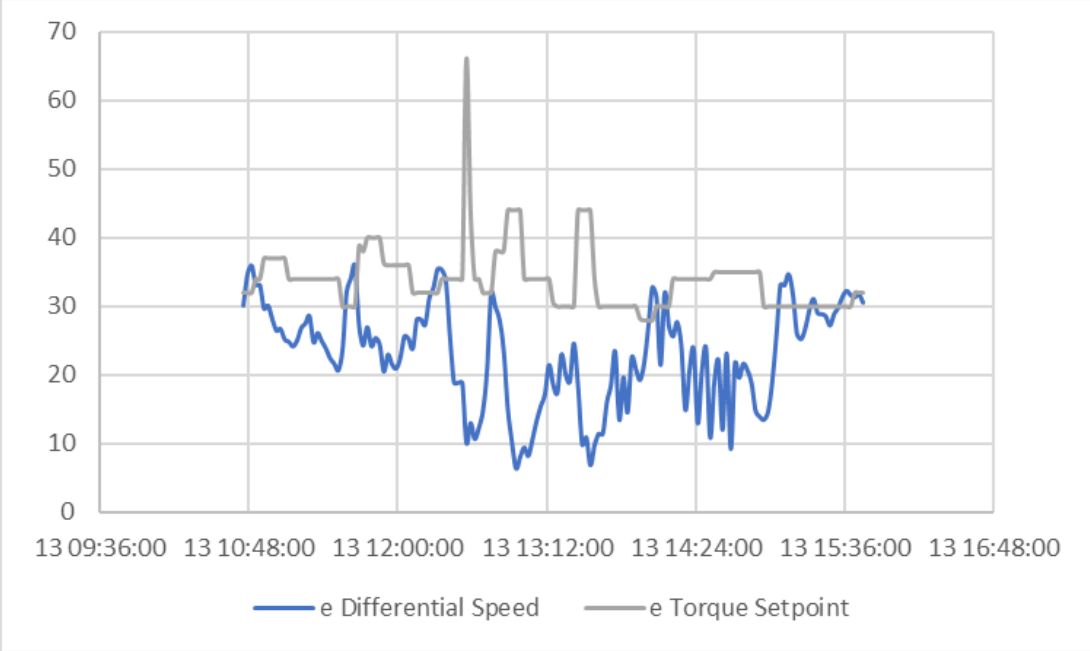


Figure 4: The same five-hour test period as Figure 3, showing centrifuge 1E under the conventional torque control system.
The upper graph shows every time the operator changed the torque setpoint. The lower plot shows the differential response to that change. The indirect control of differential speed (cake removal) by torque settings is clearly inefficient relative to control based on MFT feed rate

In practice the torque control did not lead to a steady differential speed or smooth centrifuge operation. Figure 4 shows how differential speed changes in response to changes in the torque setpoint. Note that in some cases when the torque setpoint is constant, the differential speed oscillates to try to reach a steady torque value.

Machine learning approaches using neural nets

Machine learning can potentially be used as an alternative feed forward approach for controlling differential speed, allowing for the differential speed equation to explicitly take into account bowl speed and polymer dosage, as well as potentially non-linear relationships with the feed properties. Currently those factors are accounted for with the operator choice of bias in the equation.

Neural nets take input variables and pass them through several "hidden layers" of computation to determine an output variable. Each layer consists of a linear combination of the variables in the previous layer. The weights of each combination are determined by minimizing the difference between the predicted output and the actual output from the provided data.

Using the NumPy and Sklearn packages in Python, neural nets are trained on the entire dataset to predict the differential speed based on bowl speed, polymer dose, solids capture, MFT flow rate and MFT density. Figure 5 shows the optimum differential speed predicted from the equation and the neural net for the densities and flow rates.

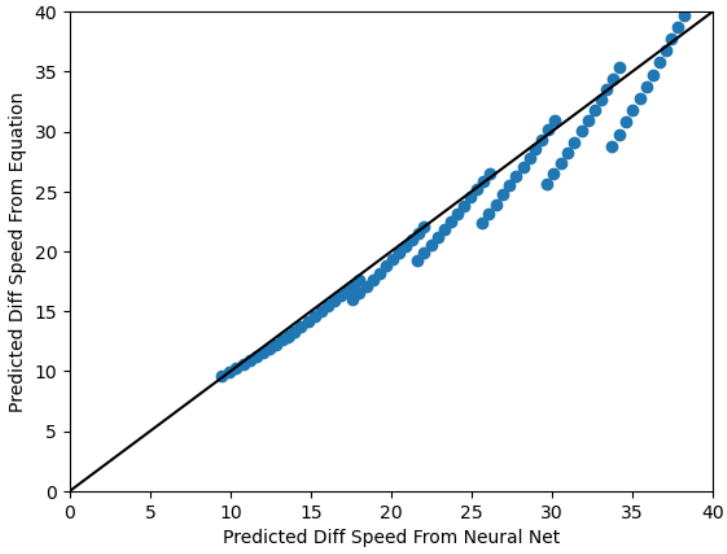


Figure 5: The differential speed from the equation compared with the neural net assuming 1,300 G/tonne polymer dose, 98% solids capture and 1,500 rpm bowl speed for a range of flow rates and densities

Figure 5 assumes a polymer dose of 1,300 g/tonnes, solids capture of 98% and a bowl speed of 1,500 rpm. Figure 6 assumes a polymer dose of 1,300 g/tonnes, solids capture of 98% and a bowl speed of 1,200

rpm. For the higher bowl speed, the neural net predicts higher optimal differential speeds. This is consistent with the physics of the centrifuge: higher bowl speeds create a higher settling rate, allowing for more rapid cake formation and removal without reduced cake solids or risk of washout. With the equation alone, the centrifuge performance differences due to the higher bowl speed need to be accounted for by adjusting the operator bias.

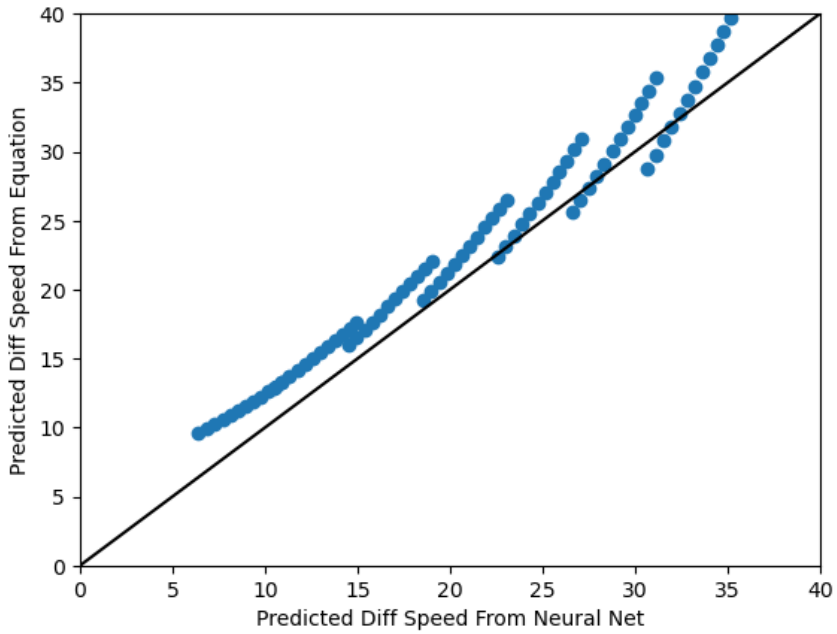


Figure 6: The differential speed from the equation compared with the neural net assuming a 1,300 G/tonne polymer dose, 98% solids capture, and 1,200 rpm bowl speed for a range of flow rates and densities

Conclusion

Operating experience suggests that using the torque to control centrifuge operation is not an optimal approach when feed density varies. With wide swings in feed density the torque control often cannot respond fast enough to prevent washouts. Operator interventions attempting to correct the differential speed by changing the torque setting are also often too little too late. The use of density and flow information from meters ahead of the centrifuges allows the equation determined in this study to adjust the differential speed proactively. This proactive approach will prevent centrifuge washouts when feed density and/or flow rate change rapidly.

This alternative method to the torque control can change differential speed in order to rapidly respond to changes in the MFT feed rate or density. Altering the differential speed in response to changes in the

feed will proactively prevent potential washout problems before they lead to disruption of the centrifuge operation. The equation

$$\text{Differential Speed} = \textit{Bias} \times ((0.4418 * \text{MFT Density} - 0.3757) * \text{MFT FlowRate}) \quad \text{(Equation 4)}$$

includes a bias correction to account for or correct for differences in feed clay content, bowl speed or polymer dosage. This first-order physical approach proved successful in controlling one centrifuge in a limited five-hour test.

Machine learning techniques can more easily consider the other centrifuge operating parameters and could provide control over the differential speed that also takes into account bowl speed and polymer dose. However, since much of the data collected over the four-year period does not reflect optimal centrifuge control, care must be taken in the application of machine learning methods. The results obtained in this study using neural nets to predict the optimal differential speed for given feed conditions agree with the result of the physical approach, but also consider bowl speed and polymer dosage explicitly. While the neural net results may perform better if bowl speed is inconsistent, the main advantage of the equation is that it is easily implemented on any system and requires no additional software. Note also that the bowl speed and polymer dosage are controlled and would not require an automated response.

In most mineral processing systems, the feed properties to a centrifuge or other equipment are carefully controlled. This is not possible with the variability and high-volume throughputs in oil sands tailings operations. The use of upstream data to proactively control equipment could be applied to a wide variety of industrial optimization processes where feed properties can vary considerably. In this case, the use of data mining techniques saved the considerable cost of a sampling campaign and provided a significantly better end product. It is unlikely that even an extensive sampling effort would have seen the wide variety of feed densities that informed this study.

References

Bara, B. 2020. 2017–2018 Accelerated dewatering field program – Cell #3 deposit. Syncrude research progress report 49 (01): 2020.

Bara, B., R. Mikula, S. Yuan and R. Siman. 2012. Fluid fine tailings centrifuge prototype: Part 3 – Mixing polymer and gypsum with FFT. Syncrude Canada Ltd. Research and Development Progress Report, July 2012.

Mikula, R., A. Bello and J. Lorentz. 2021. Centrifuge fundamentals, development of an operations guide. Syncrude research progress report 50 (03), 2021.

Mikula, R., J. Spence and S. Boilard. 2017. Full-scale centrifuge plant commissioning and optimization: first steps. Kalium Research Data Memo 17-08, 2017.

An Often-Overlooked Approach for Slope Stability of Tailings Dams Built Using Centerline and Downstream Construction

Jed D. Greenwood, Barr Engineering Co., USA
Iván A. Contreras, Barr Engineering Co., USA
Junhong Li, Barr Engineering Co., USA

Abstract

Many tailings dams are founded on overconsolidated clays of stiff to very stiff consistency, which in general tend to provide a relatively suitable foundation for these earthen structures. The authors have found in multiple dam safety reviews that there is a tendency in practice to overlook the nature and impact that the stress changes have on the characteristics of these clays. On the one hand, there are cases in which the stiff clays are solely characterized with drained shear strength because they are seen as "stiff clays" and thus the drained shear strength should govern stability. On the other hand, there are cases in which the possibility of mobilizing the undrained shear strength is acknowledged, but it is assumed that the undrained shear strength ratio initially determined remains constant over time and does not change with increasing effective stresses as the dams are raised. This paper presents lessons learned on the characterization of foundations on clays of stiff to very stiff consistency through several dam safety reviews, as well as practical examples and steps associated with the SHANSEP (Stress History and Normalized Soil Engineering Properties) technique to be utilized in the design of tailings dams using the centerline and downstream construction methods.

Introduction

When tailings dams are founded on overconsolidated clays of stiff to very stiff consistency, these clays tend to provide a relatively suitable foundation for these earthen structures. However, as tailings dams are raised to provide additional storage capacity, the stress history of these foundation clays changes and so does their behavior and undrained shear strength. The authors have found that in practice there is a tendency to overlook the nature and the impact that the stress changes have on the characteristics of these clays. On one hand, there are cases in which the stiff clays are solely characterized with drained shear strength because they are seen as "stiff clays" and thus the drained shear strength should govern stability. This is initially true but upon loading and subsequent consolidation, this behavior changes. On the other hand, there are

cases in which the possibility of mobilizing the undrained shear strength is acknowledged but it is assumed that the undrained shear strength ratio (s_u/σ'_{vc}, or USSR) initially determined on the overconsolidated specimens remains constant over time and does not change with increasing effective stresses as the dams are raised. In reality, the USSR of the clay foundation will change as a function of the stresses imposed by the dam (i.e., overconsolidation ratio, or OCR), which are variable under the dam in terms of stress history, pore pressures, applied loads, and consolidation. This is particularly relevant for centerline and downstream construction, which are becoming more typical in the industry for slurried tailings storage. There is a relatively simple but powerful technique to incorporate these stress history and strength effects in slope stability analyses, which is often overlooked in practice.

The authors have found through multiple dam safety reviews that in practice there is a tendency to overlook the nature and impact that the stress changes have on the characteristics of these clays. This complex impact of stress history on undrained shear strength is best captured by the SHANSEP approach. SHANSEP stands for Stress History and Normalized Soil Engineering Properties. The SHANSEP approach is briefly described subsequently and followed with an applicable example to illustrate its benefits and implications.

SHANSEP concept

SHANSEP is a concept introduced by Ladd and Foott (1974), with follow-up research by Ladd (1991). This approach is based on the experimental observation that the shear strength of many soils can be normalized with respect to the vertical consolidation stress. In other words, the method is based on the concept that, for a given failure mode such as triaxial compression (TC) or direct simple shear (DSS), the undrained stress-strain-strength behavior of most "ordinary" clays is governed by the stress history of the clay. The method assumes that these soils exhibit normalized behavior. Accounting for stress history in the laboratory is done by using mechanical overconsolidation to represent all preconsolidation mechanisms; thus, the procedure explicitly requires the stress history profile for the clay to be evaluated.

The increase in undrained shear strength ratio s_u/σ'_{vc} of clays with increasing OCR can be modeled by the following equation:

$$s_u/\sigma'_{vc} = S(OCR)^m$$

where:

s_u = undrained shear strength

σ'_{vc} = effective vertical consolidation stress

$S = s_u/\sigma'_{vc}$ at OCR = 1

OCR = overconsolidation ratio

m = empirical factor

Obtaining this relationship in the laboratory first involves determining the stress history of the soil in the form of the preconsolidation stress σ'_p , which can be obtained from laboratory consolidation tests or through field methods such as dilatometer or CPT. Specimens are then often isotropically consolidated to 1.5, 2.5, and 4.0 times σ'_p so they can be sheared in the normally consolidated range at OCR = 1, while other specimens are often isotropically consolidated to 2.5 times σ'_p and then unloaded to nominal OCR values of 2, 4, and 6, so they can be sheared in the overconsolidated range (Ladd and DeGroot, 2003). The resulting USSR values can then be plotted against the OCR on a log scale to obtain the empirical factor *m*.

Numerical modeling

A generic, two-dimensional numerical modeling exercise was carried out in FLAC2D to demonstrate the effect of a change in stress history for a "very stiff" foundation clay under staged construction of a downstream tailings dam. The modeling is intended to show that the foundation clay gains undrained shear strength due to material loading and subsequent consolidation during and after each dam raise, but also that the OCR and the corresponding USSR decrease as the dam is raised. The OCR can decrease to the point where the material transitions from a very stiff, dilative clay to a lightly overconsolidated, or even normally consolidated, brittle clay.

Model geometry

The model geometry comprises a downstream tailings dam constructed in six phases on a simple clay foundation, as shown in Figure 1.

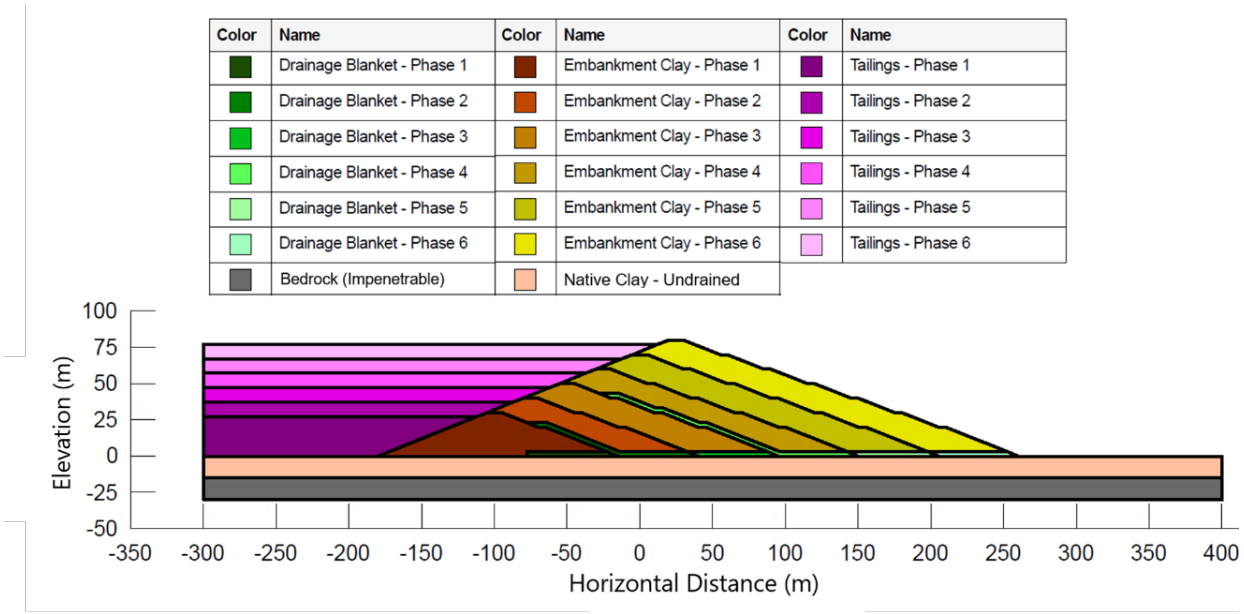


Figure 1: Model geometry of generic downstream tailings dam

The foundation clay is 15 meters thick with a horizontal native ground surface. The clay is underlain by 15-meter-thick bedrock, which is considered to be impenetrable, with a horizontal contact between them.

The embankment comprises a 30-meter-high starter dam called Phase 1, which includes a 3-meter-thick drainage blanket extending 60 meters under the starter dam from the dam toe. The starter dam includes upstream and downstream slopes of 2.5H:1V, with 5-meter-wide benches every 10 meters vertically on the downstream face. Note that the bottom 20 meters on the downstream face do not include a bench. The crest width is 10 meters.

The five additional phases, referred to as Phases 2 through 6, are each 10-meter raises with the same slope and crest geometry as Phase 1. The ultimate dam height is 80 meters with an overall downstream slope of 2.875H:1V.

The drainage blanket is 3 meters thick for Phases 2 through 6 to reduce contrast in zone size and thus reduce model run time. The drainage blanket continuously underlies the embankment, with chimney drains covering the downstream faces of Phases 1 and 3 (extended to the first bench below the crest) to intercept seepage.

The tailings on the upstream side were modeled with a freeboard of 3 meters below the dam crest of each respective phase. The upstream pond is assumed to be at the tailings surface.

Methodology

After the Phase 1 starter dam was placed, the model was run to end-of-primary consolidation such that all excess pore pressures were dissipated. For each phase subsequent raise, the model was run coupled, meaning that mechanical and flow calculations were performed simultaneously to simulate stress increase during embankment filling and consolidation during and after embankment filling. Each phase was gradually raised over a period of one year by ramping up the embankment density in 10 percent increments. After construction was completed for the individual phase, the model was run for an additional two years to allow for consolidation and dissipation of excess porewater pressures. Tailings deposition and the upstream pond were then placed against the upstream face of the dam, with the model brought to end-of-primary conditions. These steps were then repeated for subsequent raises.

Material parameters

The material parameters are shown in Table 1. The undrained shear strength s_u was estimated at the bottom of the clay foundation layer. The pre-consolidation stress was assumed to be about 890 kPa, which corresponds to an OCR of approximately 6 at the bottom of the clay layer, assuming a water table at the native ground surface with hydrostatic pore pressures.

Table 1: Material properties

Property	Bedrock	Native clay	Drainage blanket	Embankment clay	Tailings
Dry Unit Weight, γ_{dry} (kN/m^3)	25.0	17.5	18.0	17.5	14.5
Sat. Unit Weight, γ_{sat} (kN/m^3)	26.0	21.0	21.0	21.0	19.5
Young's Modulus, E (MPa)	100	20	30	20	1
Poisson's Ratio, ν'	0.20	0.30	0.30	0.30	0.25
Horizontal Perm., k_H (m/s)	1.0×10^{-6}	1.0×10^{-8}	2.5×10^{-5}	1.0×10^{-8}	1.0×10^{-6}
Anisotropy, k_H/k_V	1.0	1.0	1.0	1.0	1.0
Cohesion, c' (MPa)	1.5	0	0	0	0
Friction Angle, ϕ' (deg.)	38.0	28.0	35.0	28.0	25.0
USSR[1]	–	$0.22\times OCR^{0.8}$	–	–	0.18

[1] USSR is the yield undrained shear strength ratio; USSR = s_u/σ'_{vc}. Note that some researchers (e.g., Brown and Gillani, 2016) advocate capping the undrained envelope with the drained envelope at low confining stresses because negative porewater pressures can dissipate quickly in the field. This capping was not done in this exercise because the rate at which negative porewater pressures might dissipate, relative to positive porewater pressures, is unknown

Software

The phased construction of the downstream tailings dam presented herein was performed using the FLAC2D (Fast Lagrangian Analysis of Continua) version 8.1 software program developed by Itasca Consulting Group, Inc., which uses the finite difference method to solve nonlinear stress-strain systems. In this method, materials are represented by zones that form a grid to fit the geometry of the cross-section being analyzed. Each element behaves according to the user-prescribed linear or nonlinear stress-strain-strength model (i.e., constitutive model) in response to the applied forces and boundary conditions.

FLAC simulates the consolidation process (i.e., deformation and dissipation of the excess porewater pressures being generated from the embankment fill placement) in a realistic time frame by coupling the mechanical response and the porewater flow regime. As such, the model allows for the analysis of dam stability during construction, when excess porewater pressures are present in the native soils and consolidation is underway.

Results and discussion

During modeling, six monitoring points were established, as shown in Figure 2. Three were set near the bottom of the foundation clay layer, while three were in the middle of the clay layer. The x-coordinates were as follows: -105 m (under Phase 1 dam crest); -25 m (near Phase 1 dam toe); and 25 m (near Phase 2 dam toe, or under the ultimate Phase 6 dam crest).

Figure 3 shows the porewater pressure development during and after construction of Phase 2. The increase in porewater pressure during each 10 percent increment can be seen, with subsequent consolidation

before the next increment is placed. This discretization is a modeling simplification, but the overall general increase in pore pressures throughout the one year of Phase 2 construction can be seen.

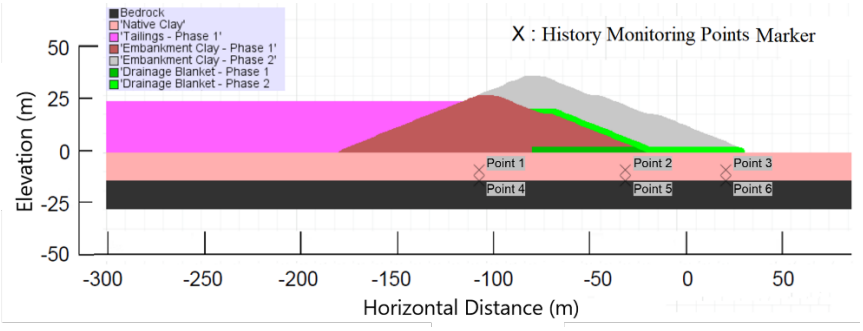


Figure 2: Monitoring point locations (with Phase 2 dam geometry)

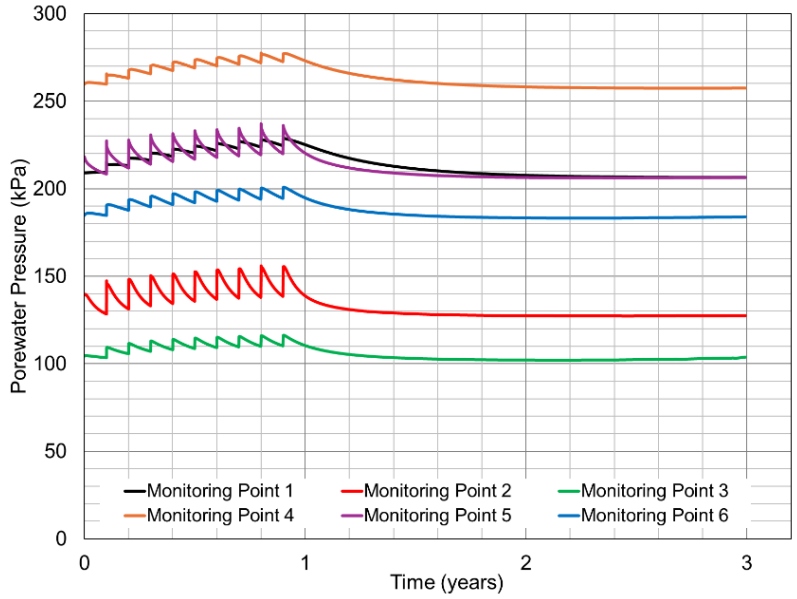


Figure 3: Porewater pressure histories in foundation clay during and after Phase 2 construction

Figure 4 is very similar to Figure 3, but it shows porewater pressure development for Phases 2 through 6. The same discretization can be seen during embankment filling for each phase, along with the two years of consolidation between each raise. It should be noted that an overall increase in porewater pressure can be seen even though end-of-primary conditions are generally reached after each raise. This is because the hydraulic boundary condition is increasing on the upstream face of the dam as the tailings and pond increase with the dam crest. In other words, excess pore pressure dissipation and accompanying effective stress increases are occurring during and after construction of the various raises, even though steady-state pore pressures are increasing throughout the embankment construction as the pond rises.

Figure 5 shows the OCR history at the same six monitoring points for Phases 2 through 6. It can be seen that initial OCR values after Phase 1 range from about 2 to 15. The OCR values of 2 are at Monitoring Points 1 and 4, which are located directly under the crest of the starter dam (Phase 1), such that they have already undergone some loading due to the end-of-primary conditions prior to Phase 2 loading. The OCR values of 15 and 8.5 at Monitoring Points 3 and 6, respectively, are consistent with a "very stiff" clay and represent the foundation clay in its native, pre-construction state. The OCR values then decrease with additional raises until all six fall below 2.0 during Phase 3, and reach 1.0 during Phase 5. During Phase 3, the material likely became contractive at all six monitoring locations and during Phase 5, the material became completely normally consolidated.

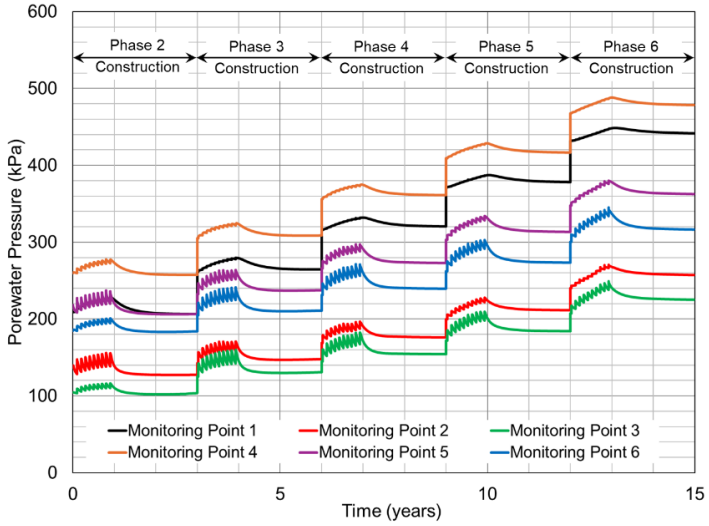


Figure 4: Porewater pressure histories in foundation clay throughout construction (Phases 2 – 6)

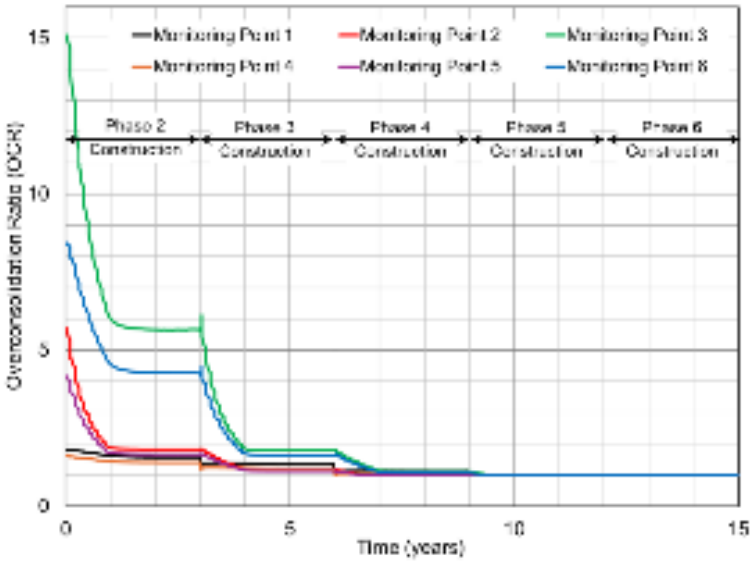


Figure 5: History of OCR at monitoring points throughout the phased construction

Given that the OCR is known throughout the construction process (Phases 2 through 6), the USSR can also be plotted as a function of the SHANSEP relationship, as shown in Figure 6. The initial USSR values at the end of Phase 1 range from about 0.3 to 1.9, with the low USSR values being under the starter dam (Phase 1) crest and the high USSR values being well downstream of the Phase 1 toe. During continued construction, the OCR values then decrease with additional raises until all six monitoring points fall below 0.40 during Phase 3 and reach 0.22 during Phase 5, which is consistent with the USSR of a completely normally consolidated clay.

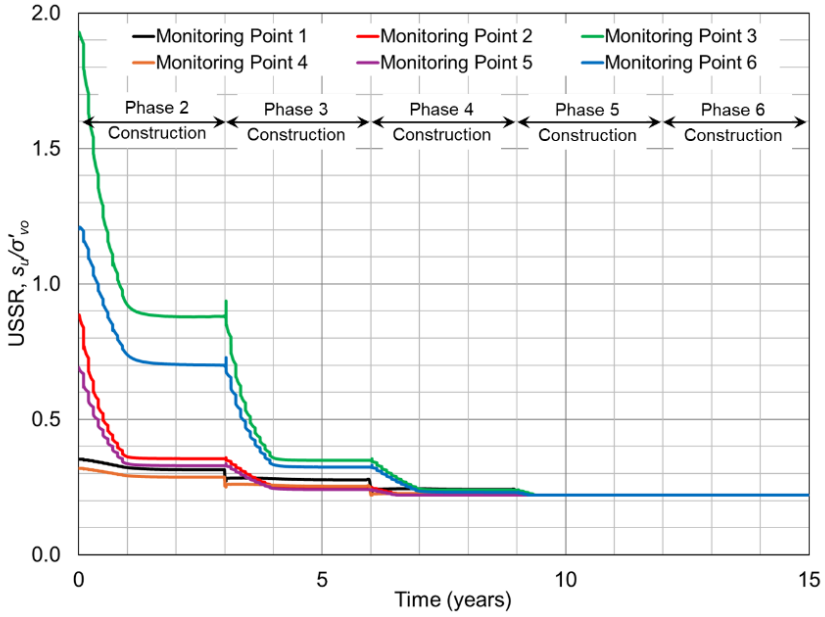


Figure 6: History of USSR at monitoring points throughout the phased construction

Figure 7 shows the evolution of s_u for all six phases of construction. It can be seen that s_u starts at 137 kPa at the bottom of the foundation clay downstream of the starter dam (Phase 1), which classifies the material as "very stiff" according to Terzaghi and Peck (1967). With subsequent raises, the s_u only increases with additional embankment filling and associated consolidation until it reaches about 325 kPa under the upstream portion of the ultimate embankment, with the load from the tailings contributing to this maximum s_u. However, as seen in Figures 5 and 6, the OCR and the normalized undrained shear strength ratio, or USSR, are decreasing, which leads to contractive, brittle behavior in which the undrained shear strength of the clay rather than the drained shear strength will likely be mobilized.

For each phase of construction, the factor of safety was computed for three cases: ESSA, USSA (EOP), and USSA (EOC), as shown in Table 2. ESSA stands for Effective Stress Stability Analysis; USSA stands for Undrained Strength Stability Analysis; EOP stands for End-of-Primary in which excess load-induced porewater pressures from the current raise are dissipated; EOC stands for End-of-Construction, in which

excess load-induced porewater pressures from the current raise are fully engaged. It should be noted that the ESSA factors of safety remain relatively constant throughout all phases of construction, as expected. The USSA cases, on the other hand, show a consistent drop in the computed factor of safety as the USSR in the foundation clay continues to decrease with increasing load from successive embankment filling.

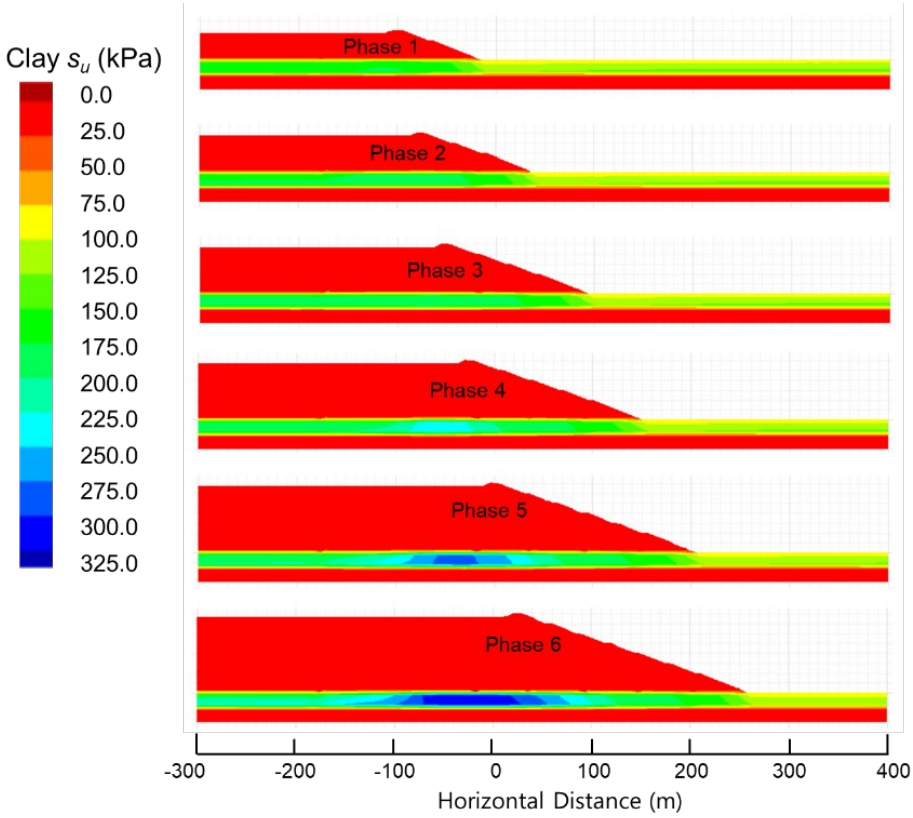


Figure 7: Evolution of s_u in foundation clay throughout the phased construction

Table 2: Factor of safety summary

Phase	ESSA	USSA-EOP	USSA-EOC
Phase 1 (Initial)	1.37	1.58	–
Phase 2	1.36	1.44	1.35
Phase 3	1.37	1.37	1.24
Phase 4	1.37	1.32	1.15
Phase 5	1.37	1.23	1.11
Phase 6	1.36	1.20	1.07

Figure 8 shows the critical slip surface for USSA-EOP conditions at Phase 5, with a computed factor of safety of 1.23. A very large composite, or block, potential failure surface can be seen extending to the

bottom of the foundation clay, indicating that the clay that is becoming normally consolidated at the base of the foundation clay is governing stability.

Figure 9 shows the critical slip surface for USSA-EOC conditions at Phase 6. The computed factor of safety is 1.07, and this represents the most critical undrained case at the ultimate dam height. Obviously, a factor of safety of 1.07 would not be considered acceptable for a tailings dam, especially when a brittle failure mode would be predicted.

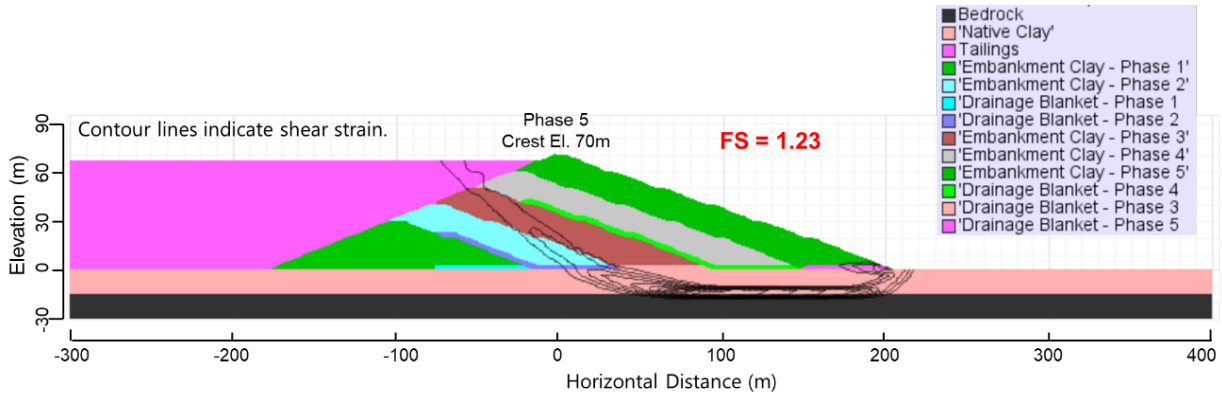


Figure 8: Typical critical slip surface for USSA-EOP conditions (Phase 5 shown)

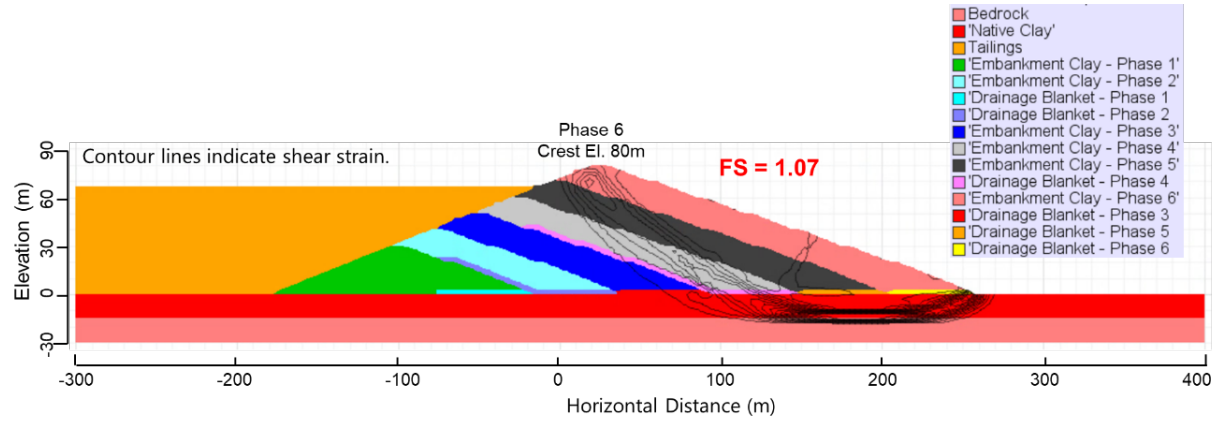


Figure 9: Critical slip surface for USSA-EOC conditions of Phase 6 dam raise

As a point of contrast to the USSA figures related to the SHANSEP phenomenon included above, Figure 10 shows the critical slip surface for the ESSA case at Phase 6, with a computed factor of safety of 1.36. As stated previously, this factor of safety remains relatively constant throughout dam construction, likely due to the shallow potential failure surface at the toe that remains constant throughout construction, in addition to low pore pressures in this area as a result of the drainage blanket. Also, the drained shear strength of the embankment and foundation materials, in the form of the friction angle, remains relatively constant throughout construction, in contrast to the USSR, which decreases as a function of increasing load according to the SHANSEP formulation.

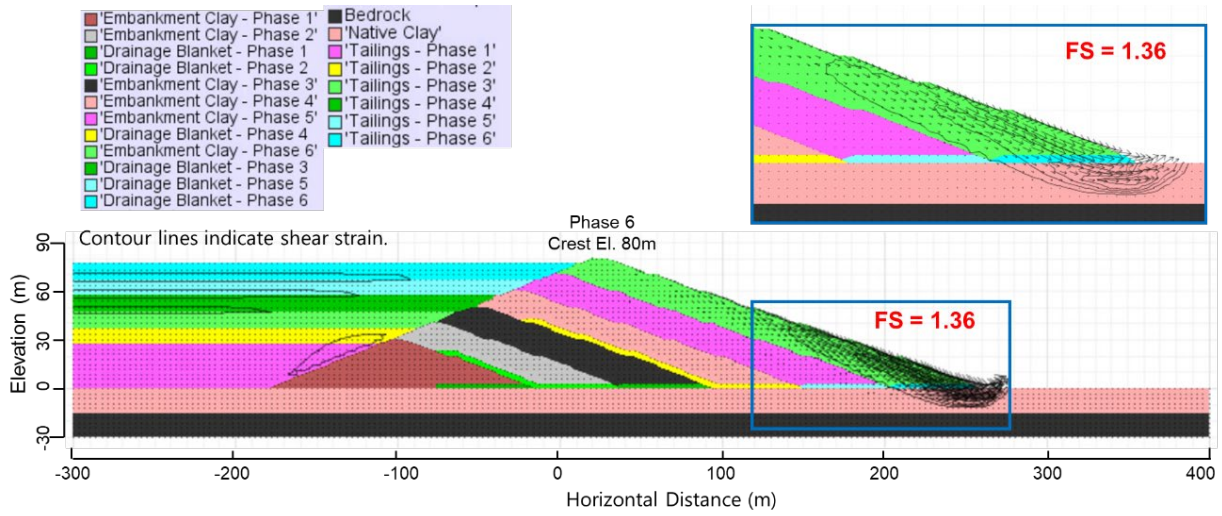


Figure 10: General critical slip surface for ESSA conditions (Phase 6 shown)

Conclusion

The discussion in this paper has led to the following conclusions:

- Overconsolidated clays of stiff to very stiff consistency can provide, in general, a relatively suitable foundation for tailings storage facilities when properly designed, considering the impact of stress history on strength.
- It is found that in practice these foundations are often mischaracterized during design, and this can lead to and has resulted in catastrophic failures.
- In some cases, the stiff clay foundations are solely characterized using the drained shear strength because they are considered “stiff clays” and thus they will mobilize the drained shear strength. While this is initially true, the stress history may change as the effective stress increases and the OCR decreases, resulting in slightly overconsolidated or normally consolidated clays, which tend to mobilize the undrained shear strength.
- In other cases, the possibility of mobilizing the undrained shear strength is acknowledged, but it is assumed that the undrained shear strength ratio initially determined on overconsolidated specimens remains constant over time and does not change with increasing effective stresses as the dams are raised. In reality, the initially high undrained shear strength ratio will tend to decrease with increasing effective stress.
- The SHANSEP procedure represents a practical technique that readily captures the change in undrained shear strength ratio and shear strength based on stress history. An example simulating construction of a downstream tailings dam founded on an overconsolidated clay using SHANSEP has been presented to illustrate its application.

- Figure 5 clearly shows how the OCR at the monitoring points within the foundation clay decreases as the dam crest increases with different construction phases. At Phase 5, the foundation clay becomes normally consolidated with an OCR=1.0.
- Similarly, Figure 6 clearly illustrates how the USSR at the monitoring points within the foundation clay decreases as the dam crest increases with different construction phases. At Phase 5, the foundation clay exhibits an undrained shear strength ratio of 0.22, which is associated with a normally consolidated undrained shear strength.
- In its native, pre-construction state, the bottom of the foundation clay was classified as "very stiff" and exhibited an undrained shear strength of 137 kPa with an OCR of about 8.5. With additional embankment loading, the undrained shear strength increased from 137 to 325 kPa while the OCR decreased from about 8.5 to 1, resulting in the USSR falling from about 1.2 to 0.22.
- Even though the undrained shear strength increased substantially due to embankment filling, the behavior would likely change from dilative, in which the drained shear strength would govern, to contractive in which the undrained shear strength would govern. This change in behavior is significant in that undrained failures of normally consolidated clay foundations can be brittle and sudden.
- The impact of these stress history effects on slope stability is indicated in Table 2, which summarizes the computed factor of safety. Table 2 shows that at Phase 6 the computed factors of safety are lower than the minimum recommended values.

References

Brown, B. and Gillani, I. 2016. Common errors in the slope stability analyses of tailings dams. In P.M. Dight (ed.), *APSSIM, 2016. Proceedings of the First Asia Pacific Slope Stability in Mining* Conference: 545–556. Australian Centre for Geomechanics, Perth. https://doi.org/10.36487/ACG_rep/1604_36_Brown

Ladd, C.C and DeGroot, D.J. 2003. Recommended practice for soft ground site characterization: Arthur Casagrande lecture. *Proceedings of the 12th Panamerican Conference on Soil Mechanics and Geotechnical Engineering,* Cambridge.

Ladd, C.C. 1991. Stability evaluation during staged construction. 22nd Terzaghi Lecture. *J. Geotech. Eng.* 117(4): 540–615.

Ladd, C.C. and Foott, R. 1974. New design procedure for stability of soft clays. *J. Geotech. Eng.* 100(GT7): 763–786.

Terzaghi, K. and Peck, R. 1967. *Soil Mechanics in Engineering Practice*. 2nd edition. John Wiley, New York.

Buttressing of Tailings Storage Facilities

Raquibul Alam, AtkinsRéalis, Canada
Ljiljana Josic, AtkinsRéalis, Canada

Abstract

Tailings dams, which store the tailings (usually in the form of slurry), a byproduct of mining operations, have a global impact. With over 18,000 such dams worldwide (the actual number may be higher), and about 3,500 currently active, the potential for catastrophic failure is not just a concern but a looming threat. The past few decades have seen numerous such failures, each releasing significant quantities of tailings into the natural environment. The resulting damage, including loss of life, environmental degradation, and economic disruption, underscores the urgent need for effective solutions. The instability of many existing tailing dams has become a significant concern in the mining industry. Mining companies are taking different measures in collaboration with engineering consulting companies to address the instability issues of existing tailings dams so as to avoid any casualties. Constructing buttresses at the dam toe is one practical solution, as it can effectively provide a resisting moment against slope failure by providing enough dead load near the toe of the dam. Buttresses are being designed and constructed to stabilize the existing tailings dams worldwide, including in high seismic areas. Adherence to international standards and guidelines is critical to their success and reliability. However, the authors have found that the buttressing of tailings dams has yet to be independently reviewed with an emphasis on fundamentals and design considerations. This paper presents how buttresses reinforce unstable tailings dams. Two case studies have also been summarized and discussed, in which buttresses stabilize the tailings dam by increasing the Factor of Safety (FoS) to safeguard and mitigate dam failures.

Introduction

Tailings are a by-product of the mining operations after extracting and recovering valuable minerals from ore. A tailings dam is typically an earth-fill or rock-fill embankment dam used to create tailings storage facilities (TSF) that store the tailings. The process of transporting these tailings involves using a pipeline to transport the tailings as a slurry to the TSF. This slurry, a mixture of water and soil particles, including medium sand, silt, and clay, is then discharged into the TSF using different techniques, including sub-aerial discharge, sub-aqueous discharge, and thickened discharge (Jewell, 1998). The coarse particles of tailings

(i.e., sand) settle close to discharging points while the fine particles (i.e., silt and clay) move down the beach into the tailings pond (Vick, 1990). Tailings dams are generally constructed by upstream, downstream, or center-line methods (Vick, 1990). Upstream tailings dams often show slope stability problems when the dam raising rate is too fast, generates excess pore water pressure and tailings with low hydraulic conductivity undergo slow consolidation (Zardari, 2011). Slope instability occurs when overturning moments exceed resisting moments, resulting in a slip failure.

On a global scale, the issue of tailings dam failure is not just a concern but a significant and pressing problem. There are more than 18,000 tailings dams, of which about 3,500 are active. Lyu et al. (2019) reported that in the past 100 years, about 1.2% of the total tailings dam failed or breached compared to the 0.01% failure rate of the traditional water storage dam. This alarming statistic, underscoring the global magnitude of the problem, should serve as a wake-up call to the industry. For instance, the 2019 Brumadinho dam disaster in Brazil resulted in the release of 12 million cubic meters of tailings, causing the loss of 270 lives and significant environmental damage. There are numerous causes for tailings dams' failures, including dam slope instability, inadequate foundation support, improper design without following any international guideline or standard, overtopping of tailings, seepage, erosion, earthquake, lack of monitoring and surveillance, etc. (Lyu et al., 2019; Rico et al., 2008). A failure of a tailings dam releases substantial quantities of tailings into the natural environment, causing severe casualties, including loss of life and the deterioration of environmental and cultural values, infrastructure, and economy.

Mining companies are collaborating with engineering consulting companies to address the instability issues of existing tailings dams and prevent potential casualties. This collaborative approach is a testament to the industry's commitment to safety and environmental responsibility. Buttresses, a proven method, are being designed and constructed to stabilize existing tailings dams worldwide, even in high seismic areas. It is important to note that the buttressing of the tailings dam has yet to be independently reviewed with an emphasis on fundamentals and design considerations. This paper aims to fill that gap by presenting how buttresses reinforce unstable tailings dams. Two case studies have also been summarized and discussed, where buttresses have not just increased the Factor of Safety (FoS) but have done so effectively, instilling confidence in their ability to safeguard and mitigate dam failures.

Factors affecting the stability of tailings dam

The literature has extensively cataloged a comprehensive list (e.g., Lyu et al., 2019) of dam failures. These failures, primarily attributed to earthquakes, seepage, foundation failure, and over-topping, are reminders of the critical need for robust design and maintenance of tailings dam construction. The following subsections present an overview of factors affecting dam stabilization.

Seepage/liquefaction

Many historical tailings dams were breached due to the rise in water level. Reasons for the water level (phreatic surface) to rise in the TSF include rains, floods, and the tailings dam's limited drainage capacity. The tailings below the phreatic surface have a slow consolidation process; saturated tailings increase the weight and reduce the shear strength and modulus of deformation, initiating piping effects, and liquefaction of granular materials or strain softening of the cohesive materials and ending up with tailings dam failure. Lyu et al. (2019) reported that about 21.6% of the total dam failures are due to seepage.

Each dam failure has a unique story. For example, the Huangmeishan tailings dam failed in 1986 after continuous rain for several days (Davies et al., 2000). The Omai dam failed in 1994 due to the tailings dam's limited filtration capacity, poor drainage performance, and high phreatic surface (Davies et al., 2000). In Aurul tailings dam, the phreatic line rose in 2000 due to heavy snow and snowmelt, which affected the stability of the tailings dam (Lyu et al., 2019).

Earthquakes

Lyu et al. (2019) reported that a significant portion, about 17.0%, of dam failures can be attributed to the destructive force of earthquakes. The consequences of these failures are stark, as evidenced by the El Cobre copper mine in Chile, which collapsed in 1965 due to earthquake liquefaction, releasing 2.3 Mm^3 of tailings and causing the loss of more than 200 lives (Dobry and Alvarez, 1967). Similarly, the Kayakari dam at the Ohya mine in Japan failed due to liquefaction in 2011, leading to significant damage to the downstream environment, following an earthquake (Lyu et al., 2019).

Foundation failure

Lyu et al. (2019) reported that about 17.3% of dam failures were caused by foundation failure. A notable instance of such a failure is the Mount Polley tailings dam failure in 2014, which released about 25 million m^3 of tailings and tailings water into the downstream lake basin (Petticrew et al., 2015). Lyu et al. (2019) explained that the load from the dam was more than the bearing capacity of the dam foundation material, resulting in shear damage to the dam foundation material. This technical detail is crucial for understanding the root cause of such failures.

Overtopping

Overtopping is one of the major causes of tailings dam failure. Lyu et al. (2019) reported that about 20.6% of dam failures were caused by overtopping. Many tailings ponds are located close to the dam crest. During heavy rainfall events, the water level in the TSF rises quickly. In addition, if the dam's permeability is poor, rainwater is discharged at a prolonged rate, resulting in the overtopping phenomenon, drastically affecting the dam's stability. Lyu et al. (2019) listed the three steps of a dam failure by overtopping: destabilization

under adverse conditions (e.g., flooding), followed by the interaction of tailings sand with water, forming a debris flow with high energy, and ending up with debris flow with high potential energy moving downstream. Merriespruit tailings dam, with less free board and less reservoir area, released 600,000 m^3 of tailings after a few hours of thundershowers in 1994 (Blight, 1997). Zijin tailings pond dam in Guangdong, China, also failed by overtopping after heavy rain, killing 22 people and destroying 6,370 houses (Lyu et al., 2019).

Others

Lyu et al. (2019) reported that about 23.5% of dam failures are caused by other reasons or combinations of two or more causes. One of the most devastating tailings dam failures in recent years happened in Córrego do Feijão Iron Ore Mine ("Dam I"), located 9 km northeast of Brumadinho, in Minas Gerais, Brazil. It suffered a sudden failure, resulting in a catastrophic mudflow that travelled rapidly downstream. The experts found several reasons behind this catastrophe (Peter et al., 2019):

1. a tailings pond closer to the crest resulted in weak tailings near the crest;
2. poor design;
3. insufficient internal drainage resulted in high water levels in the dam, particularly in the toe region;
4. high iron content, that made it susceptible to a brittle to undrained condition; and
5. high and intense regional rainfall reduced the strength of the unsaturated materials above the water level.

Based on the above discussion, it is evident that addressing the instability issues of existing tailings dams is one of the top priorities for mining companies to avoid casualties. The following section has outlined different options for stabilizing tailings dams, providing a roadmap for a safer and more sustainable future.

Stabilization of tailings dam

There are many ways to improve the stabilization of a tailings dam, such as ground improvement and creating unsaturated conditions in tailings to prevent liquefaction and flowability. In the context of tailings dams, unsaturated conditions refer to a state where the voids in the tailings are not entirely filled with water, which can help prevent the tailings from behaving like a liquid. Other methods include treating dam materials to increase their shear strength, using geogrids, constructing a buttress at the toe of a tailings dam, etc.

Several specific methods have been investigated for ground improvement to enhance slope stability and allow an existing dam to rise. For instance, Poulos (1995) found that installing piles on unstable slopes can effectively counteract driving forces and stabilize existing dams, a testament to the success of this method. Samuel and Jordan (2018) presented a case study on the nickel tailings dam in Thompson, Manitoba, where they found that rapid impact compaction of existing dam materials provided a solution by densifying the loose state of the dam material and improving its overall stability. Jet grouting, another ground improvement technique, has also been documented to stabilize the dam slope (e.g., Nikbakhtan et al., 2007), further reinforcing the effectiveness of these methods.

It is well established that the sensitivity of the dam stability depends on the increase in pore water pressure along a potential failure surface. Dewatering, a process of removing water from the tailings, might be an effective way of stabilizing the tailings dam where the phreatic level is high. Fourie and McPhail (1993) have shown that pumping and vertical de-watering wells successfully improved stability by lowering the phreatic surface and decommissioning the tailings dam in the (then) Transvaal province of South Africa. After successful dewatering, Fourie and McPhail (1993) noticed no surface sloughing on the outer slope. Electrokinetic and other dewatering techniques can also be considered for stabilizing tailings dams where excess pore water is an issue for stability (Shang and Xu, 2019).

Chemical treatment can be another solution for tailings dam stabilization by increasing the shear strength of the dam materials. Alsharedah (2023) simulated the treated tailings as construction materials for Sweden's Aitik upstream mine tailings dam. They used emulsified polymer, a cement kiln dust (CKD) mixture and recycled Gypsum (B) as the chemical agents. They concluded that the factor of safety (FoS) with the treated tailings was 20 to 25% higher than that of untreated tailings. Their proposed treatment also reduced the maximum settlement by 40%. Other mixing techniques, such as mixing with biopolymer (Chen et al., 2013), have also been documented to increase dam stability.

The slope stabilization of a tailings dam can also be achieved by using geogrids, due to their high tensile strength and resistance to chemical degradation (Mudenge and Kalumba, 2023). Geogrid reinforcement is a technique where a geogrid, a geosynthetic material with a grid-like structure, is introduced to provide additional strength to the dam structure. This reinforcement introduces a second resisting moment to the conventional moment equilibrium, enhancing the dam's stability. In a study by Mudenge and Kalumba (2023), the geogrid reinforcement system approximately doubled the FoS. However, they pointed out that the efficiency of geogrid reinforcement will vary depending on the geogrid type and other factors, including the tailings' geochemical and geotechnical characteristics and the dam geometry.

Adding a toe buttress is one of the most common and widely used practices in dam retrofitting. A toe buttress is a structure that provides sufficient dead load near the dam's toe and effectively provides a

resisting moment against slope failure. In other words, it counterbalances the driving forces that could cause the dam to fail. Ormann et al. (2013) found that the Aitik tailings dam in northern Sweden was stable up to the eleventh raising if the rockfill buttress was constructed at the downstream toe. Guilherme et al. (2023) concluded that the construction of a reinforcement buttress was needed to stabilize a tailings dam in Brazil. More details on buttressing, including fundamentals, design basis and case studies, are discussed in the following sections.

Fundamentals of stabilizing tailings dams with buttresses

Among the various options, as discussed in the previous section, this paper underscores the effectiveness of stabilizing tailings dams through buttress construction. Adding a buttress at the downstream toe proves to be a robust measure in resisting a tailings dam's slope failure. Figure 1 illustrates a typical circular slope failure, which can be more complex. However, for the sake of clarity, a circular failure surface is considered in this explanation. On a dam slope, two moments typically act on the failure mass: the resisting moment stabilizing the slope and the driving moment destabilizing it. Introducing a buttress at the dam toe significantly reduces the driving moment while simultaneously increasing the resisting moment, effectively stabilizing the dam. The resisting moment and driving moments are defined as follows:

$$\text{Resisting Moment} = T * R \qquad \text{(Equation 1)}$$

$$\text{Driving moment} = W * L \qquad \text{(Equation 2)}$$

Where T = Shear Force; R= Radius (also the moment arm of the shear force); W= weight of the soil (in failure mass), and L= moment arm of the weight

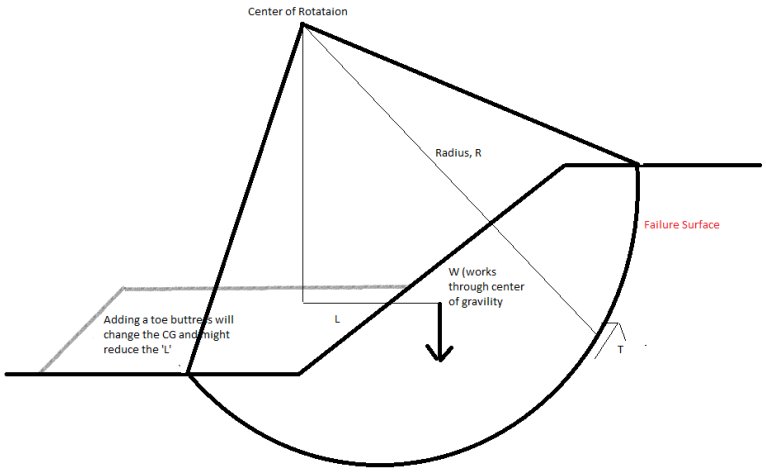


Figure 1: Failure surface on the slope without buttress

Adding a toe buttress modifies the dam's center of gravity. In most cases, it lowers the moment arms, L. As a result, it increases the overall slope stability by reducing the driving moment, as shown in Equation

2. Adding a buttress extends the failure surface through the buttress materials. Shear Force, T, is intricately linked to the soil's cohesion and friction. Therefore, using high-strength buttress materials (with higher cohesion and friction angle) plays a pivotal role in enhancing the resisting moment (Equation 1), thereby bolstering the overall strength and stability of the dam. However, it is crucial to note that optimizing buttress materials is a critical step. While it can increase the weight, W, and the driving moment, as shown in Equation 2, careful planning can prevent these issues. The buttress volume/quantity needs to be optimized to avoid a scenario where the overweight of the rockfill buttress may increase the sliding force and reduce the stability. Optimum design of buttressing ensures slope stability and reduces the construction cost by utilizing the minimum volume of a rockfill, a key consideration in any project.

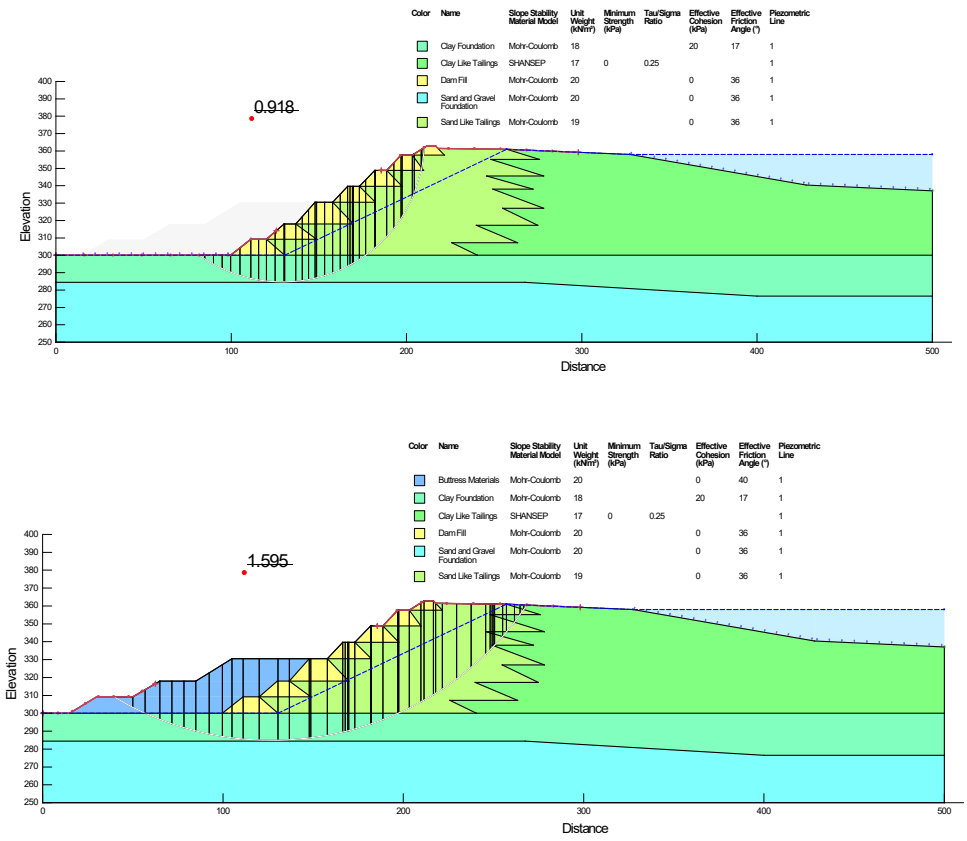


Figure 2: Slope stability analysis results before (upper) and after buttress (lower) construction

The authors have designed a typical tailings storage facility using GeoStudio 2021.4 (Slope/W) for demonstration purposes unrelated to specific projects, which is likely less complicated than an actual tailings storage facility. The strength of the materials used in this design is that they are typical values and are not based on any field or laboratory data. To evaluate the FoS, the authors used the limit equilibrium method (LEM). As seen in Figure 2, the FoS is only 0.918 without the buttress, whereas after adding the buttress, the FoS increases to 1.595. As shown in the illustration, the buttress extends the failure surface

through the buttress materials, which is a typical scenario. However, the failure surface might change based on material properties, geometry, etc. This typical design not only showcases the potential of a buttress to enhance the stability of an existing upstream tailings dam, but also opens up a world of possibilities for further research and innovation in the field.

The design basis of buttressing

There is no universal way of designing tailings dam buttresses, as every dam is unique in terms of tailings properties (such as particle size distribution, density, and chemical composition), mine site conditions (including topography, soil type, and climate), the storage capacity of the dam, and the available construction materials (such as rockfill, or compacted soil). There are national, state, or local governmental statutes, laws, regulations, ordinances, or other government directives for tailings dams and buttresses design, operation, and safety. The Global Industry Standard on Tailings Management (GISTM), a comprehensive framework developed by a coalition of industry leaders, plays a crucial role in providing a safe tailings facility management framework. It sets clear standards when designing dams and buttresses, ensuring that all aspects of design and construction are considered. The Canadian Dam Association (CDA), the Australian National Committee on Large Dams (ANCOLD), and the International Commission on Large Dams (ICOLD) can be used as guidelines. Many mining companies, such as Glencore, have developed standards and guidelines for their mining sites, reflecting each site's unique challenges and conditions.

The initial step in tailings dam or buttress design is the crucial process of dam classification, which involves assessing factors like population at risk and incremental losses. The details of the dam classification, which can be found in references like CDA (2019), ANCOLD (2012), or GISTM (2020), provide a comprehensive understanding of the dam's potential risks and vulnerabilities. The dam classification, determined through a dam break analysis and compared with the guidelines and standards mentioned above, guides the selection of earthquake loading and inflow design flood (IDF) loading conditions for the design analysis.

For example, Table 1 presents the recommended earthquake loading for designing based on dam classification. The authors refer to the CDA (2019) and ANCOLD (2012) for IDF loading, the most severe inflow flood to be considered in the design. Conducting a site-specific seismic hazard assessment is crucial for adapting the peak ground acceleration (PGA) corresponding to the annual exceedance probability (AEP) for liquefaction potential and stability analysis.

Buttressing is a pivotal step in the design process, significantly enhancing the safety of an existing tailings dam. The primary objective is to directly increase the dam's FoS, a critical ratio representing the available shear resistance along the potential failure plane, to the activating shear forces along the same plane. This understanding of FoS is vital in the design process, as it ensures that the dam is strong enough

to withstand potential stress. CDA (2019) and ANCOLD (2012) have recommended that the FoS values be considered under different loading conditions, as presented as examples in Table 2.

Table 1: Recommended design earthquake loading

Dam Category	CDA (2019)	ANCOLD (2012)			GISTM (2020)	
	AEP	OBE	MDE	Post Closure	Operations and Closure (Active care)	Passive-Closure (Passive Care)
Low	1/100 AEP	1:50	1:100	MCE	1/200	1/10,000
Significant	Between 1/100 and 1/1000	1:100	1:1000	MCE	1/1,000	1/10,000
High	1/2475	NA	NA	NA	1/2,475	1/10,000
Very high	Between 1/2475 and 1/10,000 or MCE	NA	NA	NA	1/5,000	1/10,000
Extreme	1/10,000 or MCE	NA	NA	NA	1/10,000	1/10,000
High/Extreme	NA	1:1000	1:10000	MCE		

Note: AEP: Annual Exceedance Probability-Earthquake; OBE: Operational Basis Earthquake; MDE: Maximum Design Earthquake; MCE: Maximum Credible Earthquake NA: Not Applicable

Table 2: Recommended factors of safety

CDA (2019)			ANCOLD (2012)		
Loading Condition	Minimum factor of safety	Slope	Loading Condition	Minimum for Tailings Dams	Shear strength to be used for evaluation
During or at the end of construction	>1.3 Depending on risk assessment during construction	Typically, downstream	Short-term undrained	1.5	Effective Strength
Long-term	1.5	Downstream	Long Term Drained	1.5	Consolidated Undrained Strength
Full or partial rapid drawdown	1.2-1.3	Upstream	Short-term undrained (no potential loss of containment)	1.3	Consolidated Undrained Strength
Pseudo-static	1.0		Post-seismic	1.0 -1.2	Post Seismic Shear Strength
Post-earthquake	1.2				

Stability analysis, a complex process that involves assessing the dam's ability to resist sliding and overturning under various conditions, is a crucial stage in buttress design. The goal is to find a buttress geometry that requires the lowest material volume and simultaneously provides the target FoS under different loading conditions to stabilize the dam. The loading condition will depend on several factors, including liquefaction potential, phase of operation, etc. The input data for slope stability analysis can be adopted from geotechnical investigations, laboratory analysis and instrumentation data. Different

commercial software, such as GeoStudio (geo slope), is available for performing stability analysis. Numerical Analysis (using Flac or Plexis) can also be performed for deformation analysis under earthquake loading to support the design if needed. The Engineer of Record (EoR) should verify the design, and any comments from the Independent Technical Review Board (ITRB) should be incorporated.

Case studies

In the following sub-sections, two case studies have been selected from two different continents, where designing phases show that a buttress at the downstream toe of the dams can effectively solve the stability issue of a tailings dam.

Case study #1

The Aitik tailings dam, primarily constructed using the upstream method, is near Gällivare in northern Sweden. The dam experienced a significant failure in 2000, spanning over 120 m of its length. This event, which underscored the importance of dam stability, prompted numerous subsequent studies on the Aitik tailings dam (e.g., Ormann et al., 2013; Alsharedah, 2023). One such study by Ormann et al. (2013) focused on fortifying the dam's slope by incorporating rockfill berms on the downstream toe. This approach was deemed effective as a substantial volume of rockfill was readily available at a short distance from the TSF. The study also detailed the optimization of the buttress design, with a typical section featuring a rockfill buttress shown in Figure 3.

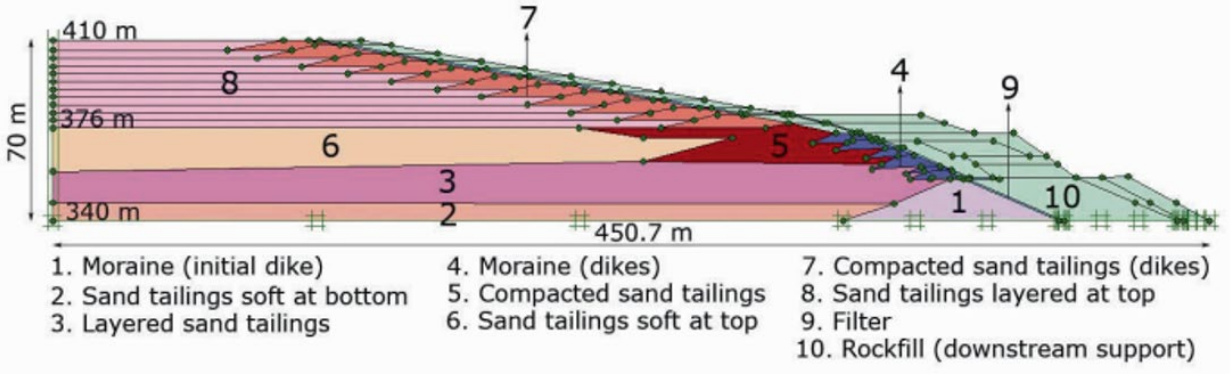


Figure 3: Cross-section of dam E-F (Ormann et al., 2013)

The authors undertook a meticulous finite element analysis using PLAXIS 2D to model the dam's staged construction and optimize the buttress's volume. The model parameters were derived from either laboratory testing or the available literature, ensuring a comprehensive and reliable foundation for the analysis. The phreatic level of the dam was determined using data obtained from piezometers installed at the dam. The dam was assumed to be constructed in eleven stages (from level 376 m to 410 m), with each stage thoroughly accounted for in the analysis.

The consolidation analyses were performed for staged construction to determine strength gain due to the dissipation of excess pore pressures. The Mohr-Coulomb (MC) model was chosen for all the dam's materials (tailings, rockfill and filter), ensuring a comprehensive and accurate representation of the dam's materials. A rockfill buttress was strategically placed on the downstream side, a key factor in improving the slope stability. The volume of the rockfill bank P (Figure 4) was optimized by changing the width and height of the buttress until a FoS of 1.5 was achieved according to the Swedish safety guidelines.

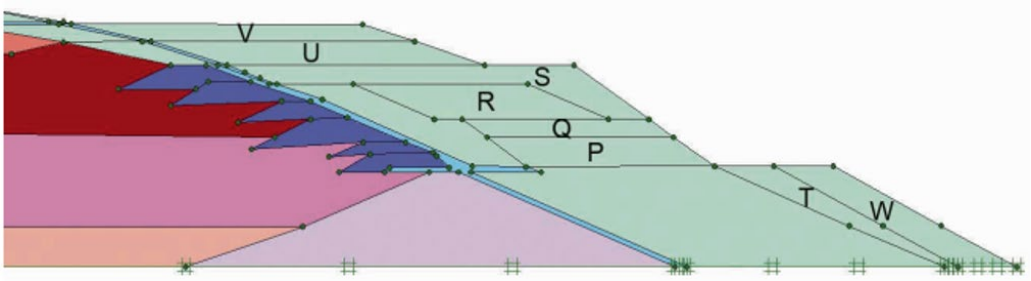


Figure 4: Placement of the rockfill banks on the downstream side to increase slope stability during construction (Ormann et al., 2013)

Following a similar procedure, the rockfill buttress Q, R, S, T, U, V, and W were assessed and designed for the fourth to tenth raisings, respectively (Figure 4). The slope stability was sufficient during the eleventh raising, so no rockfill buttress was added from this raise. This careful study demonstrated that the dam is stable up to the eleventh raising (level 410 m) only if the rockfill buttress was deliberately added to the downstream slope.

Case study #2

Guilherme et al. (2023) presented a study to simulate the stability of a dam in Brazil after reinforcement with a buttress at the downstream toe. The starter dike was designed with a 1H:2V slope. The dam was raised with a 1H:4V slope and constructed with tailings underflow. All the overflow was deposited on the TSF, creating a tailings beach. The structure has a 1 m thick drainage system of sand and gravel. The authors assessed the stability of the dam in two stages.

Firstly, they evaluated the FoS under the dam's current condition, using different failure surfaces, and compared it with CDA and Brazilian regulators' recommendations. Secondly, they assessed the buttress construction at the downstream toe to reinforce the structure, analyzing the excess porewater pressure generated and the deformation in the foundation soil during and after construction. To evaluate the FoS, they used the LEM in the initial condition (without buttress); a coupled analysis was performed using SLOPE/W and SEEP/W. The Morgenstern-Price method was applied. SIGMA/W was used to simulate the buttress construction, considering linear elastic parameters. Figure 5 shows a typical section of the dam and buttress used in the study.

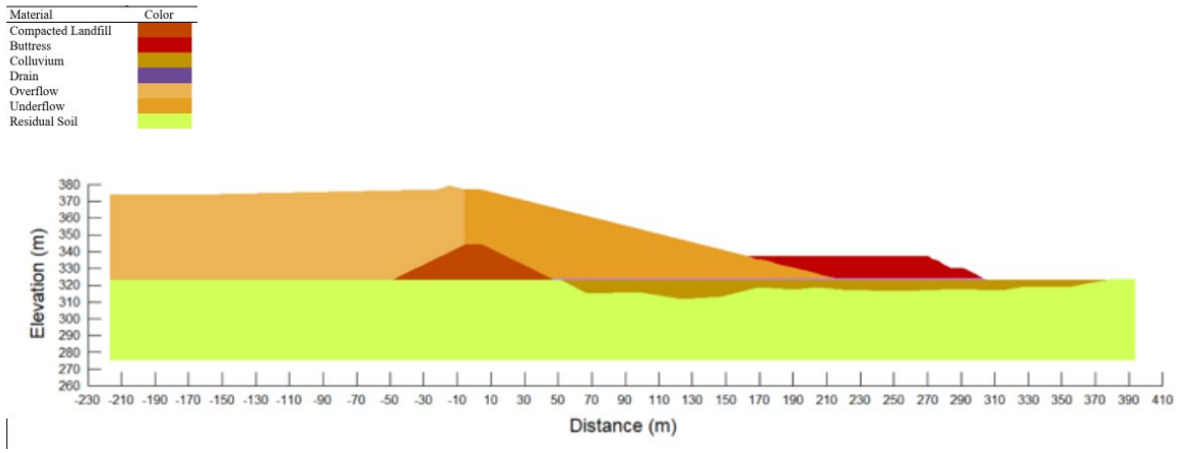


Figure 5: Dam cross-section with the preliminary buttress (in dark red) (Guilherme et al., 2023)

The authors found the structure did not meet the minimum FoS without a buttress at the downstream toe under non-circular, optimized circular, and non-circular surface failure. However, after reinforcing with a buttress, the dam met the requirements of CDA and Brazilian regulators' recommendations (ABNT NBR 13028), achieving an FoS higher than 1.50 as the criterion adopted in their study. The excess pore water pressure generation during and after the construction was evaluated using SIGMA/W. Figure 7 shows the variation of $\overline{B}$ over at a single point, tagged as a "Monitoring point" in the figure. The highest $\overline{B}$ found at the beginning of the buttress construction was 0.67, which decreases over time and becomes zero after approximately 60 days of construction. $\overline{B}$ equals 0, indicating the final dissipation of the generated pore pressure.

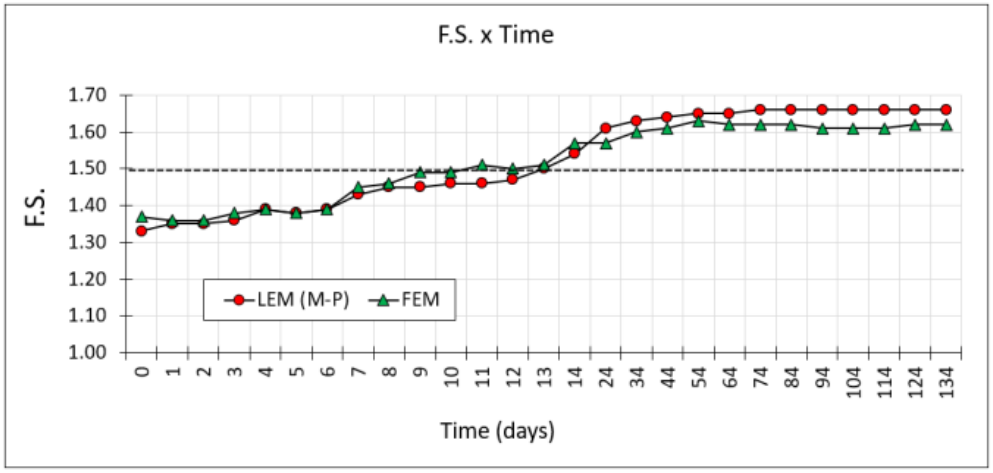


Figure 6: FoS over time (Guilherme et al., 2023)

Figure 6 shows that the calculated FoS (F.S) is lower than 1.50 at the beginning of the construction due to the high generation of porewater pressure. At the end of the construction, on the 14th day, the

porewater pressure dissipates. The calculated FoS (F.S in the figure) becomes higher than 1.50 and reaches the maximum of around 1.65 after 55 days. The study concludes that the construction of a reinforcement buttress was needed to stabilize the dam. However, it might take some time to dissipate the pore water pressure and achieve the target FoS.

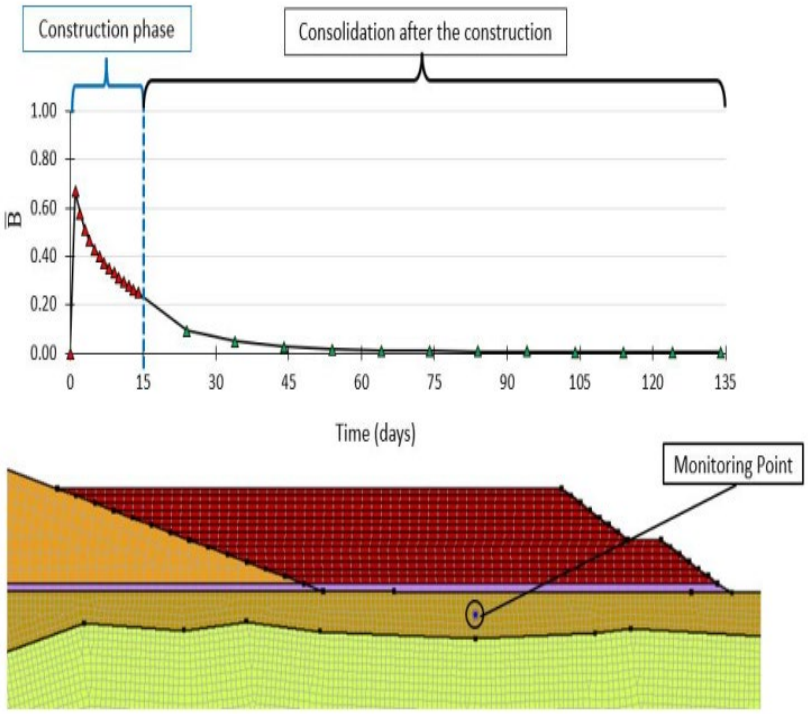


Figure 7 $\bar{B}$ summary over time (Guilherme et al., 2023)

Conclusion

This paper focuses on fundamentals, design basis, and three case studies in which buttressing has been demonstrated as a viable option for stabilizing tailing dams. The following conclusions can be drawn from the discussion:

- A tailings dam can fail for different causes, including but not limited to earthquakes, seepage, foundation failure, and over-topping, underscoring the critical need for robust design and maintenance in dam construction.
- There are many options to stabilize tailings dams, including ground improvement, treating dam materials, buttressing at the downstream toe, dewatering, geogrid application, etc.
- Buttressing is one of the effective solutions for stabilizing tailings dams. The optimum buttress configuration increases the overall slope stability by reducing the driving moment and improving the resisting moment.

- Appropriate guidelines or standard requirements must be followed while designing the buttress, without conflicting with local laws and regulations.
- This paper presents two compelling case studies from open literature. Case study 1 showcases the successful optimization of buttress geometry to stabilize a tailings dam. Case study 2, despite the time it took to achieve the target FoS, illustrates the effectiveness of buttressing in stabilizing a tailings dam once the pore water pressure has disappeared. These successes should instill confidence in the potential of buttressing as a solution.

References

Alsharedah, Y., Alsharedah, Y. and Aly, A. 2023. Improving tailings dam safety via soil treatment. *Sustainability* 15(21): 15276.

ANCOLD. 2012. Guidelines on Tailings Dams. Australian National Committee on Large Dams.

Bhadriraju, V., Puppala, A.J., Madhyannapu, R.S. and Williammee, R. 2008. Laboratory procedure to obtain well-mixed soil binder samples of medium stiff to stiff expansive clayey soil for deep soil mixing simulation. *Geotech. Test. J.* 31: 225–238.

Blight, G.E.1997. Destructive mudflows as a consequence of tailings dyke failures. *Proceedings of the Institution of Civil Engineers-Geotechnical Engineering* 125(1): 9–18.

Canadian Dam Association (CDA). 2019. Application of Dam Safety Guidelines to Mining Dams.

Chen, R., Zhang, L. and Budhu, M. 2013. Biopolymer stabilization of mine tailings**.** *J. Geotech. Geoenviron. Eng.* 139(1802).

Davies, M.P., Martin, T. and Lighthall, P. 2000. Mine tailings dams: when things go wrong. *Proceedings of Tailings Dams 2000:* 261–273. Association of State Dam Safety Officials.

Dobry, R. and Alvarez, L.1967. Seismic failures of Chilean tailings dams. *Journal of the Soil Mechanics and Foundations Division* 93: 237–260.

Draves, J.F. and Fox, M.G. 1998. Effects of a mine tailings spill on feeding and metal concentrations in yellow perch *(Perca flavescens). Environmental Toxicology and Chemistry* 17(8): 1626–1632.

Fourie, A.B. and McPhail, G.I. 1993. Stabilization of a tailings dam by de-watering. *Proceedings of International Conference on Case Histories in Geotechnical Engineering* 29.

GISTM. 2020. Global Industry Standard on Tailings Management.

Guilherme, H.S. Pinto, Rocha, P.M., Brandão, H.A. and de Oliveira, R.R.V. 2023. Numerical analysis of a downstream dam reinforcement. Numerical-analysis-of-a-downstream-dam-reinforcement.pdf (pimentadeavila.com.br)

Harper, T.G., McLeod, H.N. and Davies, M.P.1992. Seismic assessment of tailings dams. Civil Engineering 62(12): 64.

ICOLD. 1996. A Guide to Tailings and Impoundments. Bulletin 106.

Jewell, J.R. 1998. An introduction to tailings. *Case Studies on Tailings Management*. United Nations publications. ISBN 1-895720-29-x.

Lyu, Z., Chai, J., Xu, Z., Qin, Y. and Jing, C. 2019. A comprehensive review on reasons for tailings dam failures based on case history. *Advances in Civil Engineering* 2019, 4159306. doi.org/10.1155/2019/4159306

Lyu, Z., Jaturapitakkul, C., Xu, Z., Qin, Y. and Cao, J. 2019. A comprehensive review on reasons for tailings dam failures based on case history. *Advances in Civil Engineering* 2019(9):1–18.

Mudenge, S.T. and Kalumba D. 2023. Application of geogrids in the slope stabilization of tailings storage facilities: A case study of an upstream tailings dam. *Proceedings of the 9ICEG 9th International Congress on Environmental Geotechnics* 25–28 June 2023, Chania, Greece.

Nikbakhtan, B., Pourrahimian, Y. and Aghababaei, H. 2007. The effects of jet grouting on slope stability at Shahriar Dam, Iran (pp. 1075–1081).

Ormann, L., Zardari, M.A., Bjelkevik, A., Mattsson, H. and Knutson, S. 2013. Numerical analysis of strengthening by rockfill embankments on an upstream tailings dam. *Canadian Geotechnical Journal* 50(4).

Petticrew, E.L., Albers, S.J., Baldwin, S.A. et al. 2015. The impact of a catastrophic mine tailings impoundment spill into one of North America's largest fjord lakes: Quesnel Lake, British Columbia, Canada. *Geophysical Research Letters* 42(9): 3347–3355.

Poulos, H.G. 1995. Design of reinforcing piles to increase slope stability. *Can. Geotech. J.* 32: 808–818.

Rico, M., Benito, G., Salgueiro, A.R., Dìez-Herrero, A. and Pereira, H.G. 2008. Reported tailings dam failures: A review of the European incidents in the worldwide context. *Journal of Hazardous Materials* 152(2): 846–852.

Samuel B. and Jordan. 2018. Upgrade of a tailings dam using ground improvement. *Proceedings of GeoEdmonton.*

Shang, J.Q. and Xu, Y. 2019. Electrokinetic dewatering of mine tailings from hydrometallurgical processes. In A.J.C. Paterson, A.B. Fourie and D. Reid (eds), Paste 2019: Proceedings of the 22nd International Conference on Paste, Thickened and Filtered Tailings, Australian Centre for Geomechanics, Perth: 275–283.

Sun, S.-W., Zhu, B.-Z. and Wang, J.-C. 2013. Design method for stabilization of earth slopes with micropiles. *Soils and Foundation* 53: 487–497.

Vick, S.G. 1990. *Planning, Design, and Analysis of Tailings Dams*. Second edition. BiTech Publishers Ltd, Canada. ISBN 0-921095-12-0.

Williams, D.J., Ward Wilson, G., de Melo, L. and Robertson, P.K. 2019. Report of the Expert Panel on the Technical Causes of the Failure of Feijão Dam I.

Zardari, M.A. 2011. Stability of tailings dams. PhD thesis, Luleå University of Technology, SE-97187 Luleå, Sweden.

Transportable Moisture Limit vs. Conveyability Testing

Christopher Olsen, FLSmidth, USA
Kenneth Rahal, FLSmidth, USA
Chris Braun, FLSmidth, USA
Skyler Pinnick, FLSmidth, USA

Abstract

As mining operations move towards adopting dry stack tailings, striking a delicate balance between the costs of dewatering systems and the transportability and stackability of the dewatered tailings becomes paramount. Typically, the expenses linked with dewatering tailings rise proportionally with the volume of water extracted from them. Conversely, the hazards associated with conveying and stacking dewatered tailings decrease significantly with the reduction in water content within the tailings. Achieving an optimal equilibrium between these factors is crucial for ensuring efficient and cost-effective implementation of dry stack tailings systems.

The Flow Moisture Point (FMP) and Transportable Moisture Limit (TML) serve as crucial indicators concerning the moisture content of bulk materials. The FMP signifies the moisture level at which a bulk material initiates flowability issues, transitioning from a cohesive and stagnant state to a free-flowing state. The TML is derived as 90% of the FMP value and represents the maximum allowable moisture content for bulk cargo to be deemed safe for transport. Specifically tied to maritime safety, the TML indicates the moisture content beyond which the material is susceptible to liquefaction.

Similarly, the utilization of a conveyor simulator apparatus for material testing is significant in optimizing operational and economic efficiencies in conveyor design. This level of simulation helps engineers and designers gain valuable insights into how different materials interact with the conveyor components under diverse material conditions. The data acquired from materials tested on the conveyor simulator apparatus serves as input values during the engineering phase of conveyor design, reducing the likelihood of failures and enhancing overall system safety.

As belt conveyor systems for transporting tailings are uncommon, industry standards for tailings conveyor handling are lacking. Consequently, TML testing data has been commonly adopted as a reference for establishing acceptable moisture levels for conveying dewatered tailings via belt conveyors.

This paper will illustrate the comparison of contrasting methods and their respective test data results through a case study focusing on flow table testing for TML and conveyor testing for material conveyability.

Each tailings sample will undergo testing for FMP, TML, conveyability, Proctor compaction, Atterberg limits, and plastic limits. The testing methods will be detailed, with particular attention given to the difference in the energy applied to the sample materials. Subsequently, the paper will analyze and compare the outcomes of these case study tests.

Introduction

The efficient transportation of bulk materials is a cornerstone of industrial operations, necessitating precise engineering and design to ensure both safety and operational effectiveness. The use of a conveyor testing apparatus has emerged as a crucial tool in optimizing these parameters. This apparatus provides engineers and designers with valuable insights into the behavior of different materials, including their varying moisture levels and characteristics, as they are transported along a conveyor belt. The data obtained from these tests are critical during the engineering phase of conveyor design, helping to reduce the likelihood of failures and enhance overall system performance. Notably, while the CEMA (2007) publication "Belt Conveyors for Bulk Materials" offers extensive guidance on conveyor operations and design calculations, it provides limited information on transporting mine tailings. The conveyor tester addresses this gap by simulating conveyor-like energy in the testing sample without the need for a full-size conveyor, allowing laboratory technicians to gather data at any point during the test.

In a parallel context, the Flow Moisture Point (FMP) and Transportable Moisture Limit (TML) are vital indicators of the moisture content in bulk materials, particularly for maritime transport. The FMP signifies the moisture level at which a bulk material begins to encounter flowability issues, shifting from a cohesive and stagnant state to a free-flowing one. This is crucial for managing material flow during loading, unloading, and storage, effectively addressing challenges such as caking and bridging. Conversely, the TML, set at 90% of the FMP, represents the maximum moisture content at which bulk cargo can be safely transported by sea. This limit is specifically tied to maritime safety, indicating the moisture content beyond which the material is susceptible to liquefaction – a phenomenon where solid bulk cargo behaves like a liquid under certain conditions, potentially compromising the ship's stability. In many cases, FMP and TML data from flow table testing have been integrated into material handling via conveyance systems to determine the maximum moisture at which materials, particularly tailings, can be safely transported.

This paper explores the similarities and differences between these two tailings material testing procedures and methods. It compares the intended applications of the test results, material preparation, and energy input into the sample material during testing, and the material data collected from these tests. By examining these aspects, the study aims to provide a comprehensive understanding of how these testing tools contribute to the design of an efficient conveyor system for the transport of bulk materials, addressing gaps found in other conveyor publications.

The tailings samples for the case study

The tailings samples were collected from a pilot study with a focus on evaluating the tailings in various flowsheet dewatering processes. The pilot dewatering equipment included a cyclone, a thickener, and an automatic filterpress (AFP). The three samples collected were from the same tailings stream from the plant.

The Whole Tails (WT) sample bypassed the cyclone separation and was first thickened with the thickener with a XX flocculant, and then pumped to the filter feed tank and then to the AFP, producing a filter cake of 16%/wt moisture[1].

The Cyclone Overflow (COF) sample comes first from the overflow outlet of the cyclone, then is thickened with the thickener with a XX flocculant, and then is pumped to the filter feed tank and then to the AFP, producing a filter cake of 21%/wt moisture.

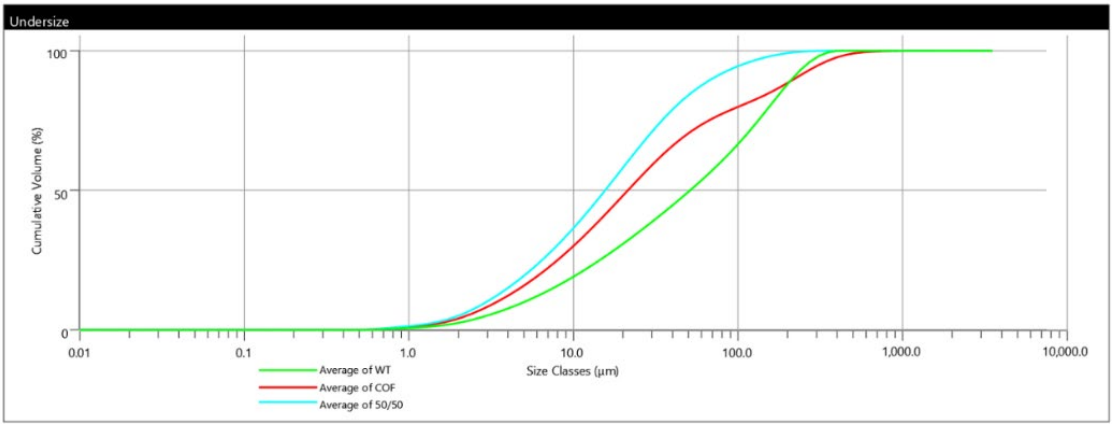
The 50/50 is a 50% WT and 50% COF sample blended in the filter feed and then pumped to the AFP, producing a filter cake of 18%/wt moisture.

The particle size distribution (PSD) and specific gravity (SG) of the samples are detailed in Table 1 and Table 2, respectively. The SG was measured using a Micromeritics AccuPyc II 1340 v2.01 pycnometer, while the PSD was evaluated with a Malvern Mastersizer v3.50 laser size analyzer. Additionally, an X-ray diffraction (XRD) analyzer was employed to determine the sample material's structure, mineral composition, and physical properties (Table 3).

Table 1: Sample specific gravity and PSD

Sample	SG	PSD		
Units:	g/cm³	P80 passing (µm)	P50 passing (µm)	P10 passing (µm)
WT	2.7018	155	51	5.0
COF	2.6755	101	21	3.4
50/50	2.7018	42	16	3.0

Table 2: Tailings sample particle size distribution (PSD) chart



[1] All material moistures are derived from dry mass divided by wet mass calculations.

Table 3: Tailings sample mineralogy

Sample (ppm)	Ag 328.068	Al 396	As 193.696	Ba 455	Bi 223.061	Ca 422.673	Cd 226	Co 230	Cr 267	Cu 324	Fe 239.562	K 766	Li 670	Mg 285.213	Mn 257
50/50	<5	53,460	<5	1,732	32.5	18,072	5.9	15.5	93.6	632	21,507	50,313	12.8	17,753	199
WT	<5	54,007	<5	2,059	37.5	24,960	7.1	15.4	67.4	459	27,425	42,244	10.3	16,442	222
COF	<5	58,050	<5	1,842	33.7	17,861	6.3	15.3	98.6	536	23,712	49,606	13.6	20,057	208

Sample (ppm)	Mo	Na 588.995	Ni 231	P 213	Pb 220.353	S 181	Sb 217	Si 251	Sn 189	Sr 407	Ti 334	V 310.230	W 207	Zn 206.200	Zr 343
50/50	23.4	6,192	33.1	23.9	<5	5,029	<5	293,013	<5	341	2,940	145	13.8	53.8	12.9
WT	76.8	5,636	22.8	17.5	21.3	8,201	5.2	310,362	<5	431	2,274	110	17.3	56.4	13.5
COF	23.3	6,209	35.8	20.5	<5	5,232	6.8	295,555	<5	369	3,009	157	17.2	66.8	13.8

Flow moisture point testing

Laboratory testing for the flow moisture point (FMP) involves a systematic procedure to determine the moisture content at which a bulk material changes its flowability characteristics, particularly becoming prone to liquefaction. This testing is crucial for understanding how moisture affects the material's cohesion and flow.

"To prevent the risk of liquefaction, International Maritime Organization (IMO) has specified tests to be carried out as per BC Code to determine upper bound acceptable of moisture content of cargo, which is defined by the Flow Moisture Point (FMP). The Transportable Moisture Limit (TML) is derived from the FMP… The Flow Table test is widely adopted for carrying out the test of FMP and TML" (Pinto et al., 2011).

The testing procedures carried out for this case study are based on the standard for flow table testing and adapted for testing tailings materials. Representative samples are collected to accurately reflect the moisture distribution of the material to be transported. The initial moisture content of the samples is measured to establish a baseline, ensuring that the material is initially in a dry state before controlled moisture is introduced. See Figures 2 through 4 for the before and after images for the flow table testing on the material samples.

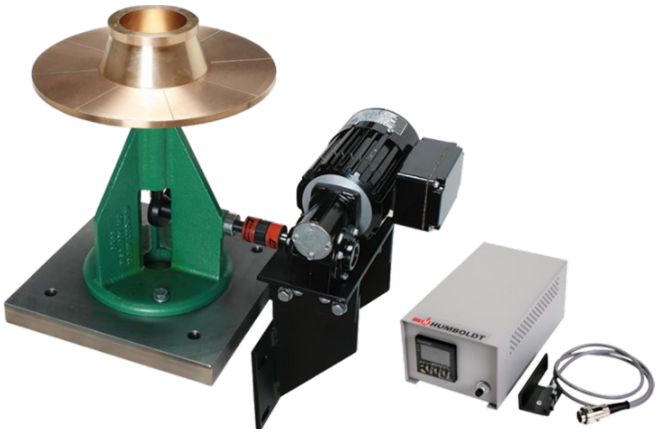


Figure 1: Flow table test unit

The flow table testing apparatus (see Figure 1) agitates the material to mimic handling conditions, assessing its flow characteristics at different moisture contents. The tailings samples were compacted into a truncated cone mold with a base diameter of 100 mm in three compacted levels. The flow table is initiated to apply 25 cycles of 12 mm drops. The testing identifies the moisture level at which the material begins to exhibit fluid-like behavior. Measurements and observations are taken to note changes in cohesion, clumping, and resistance to flow (see Figures 2 through 4).

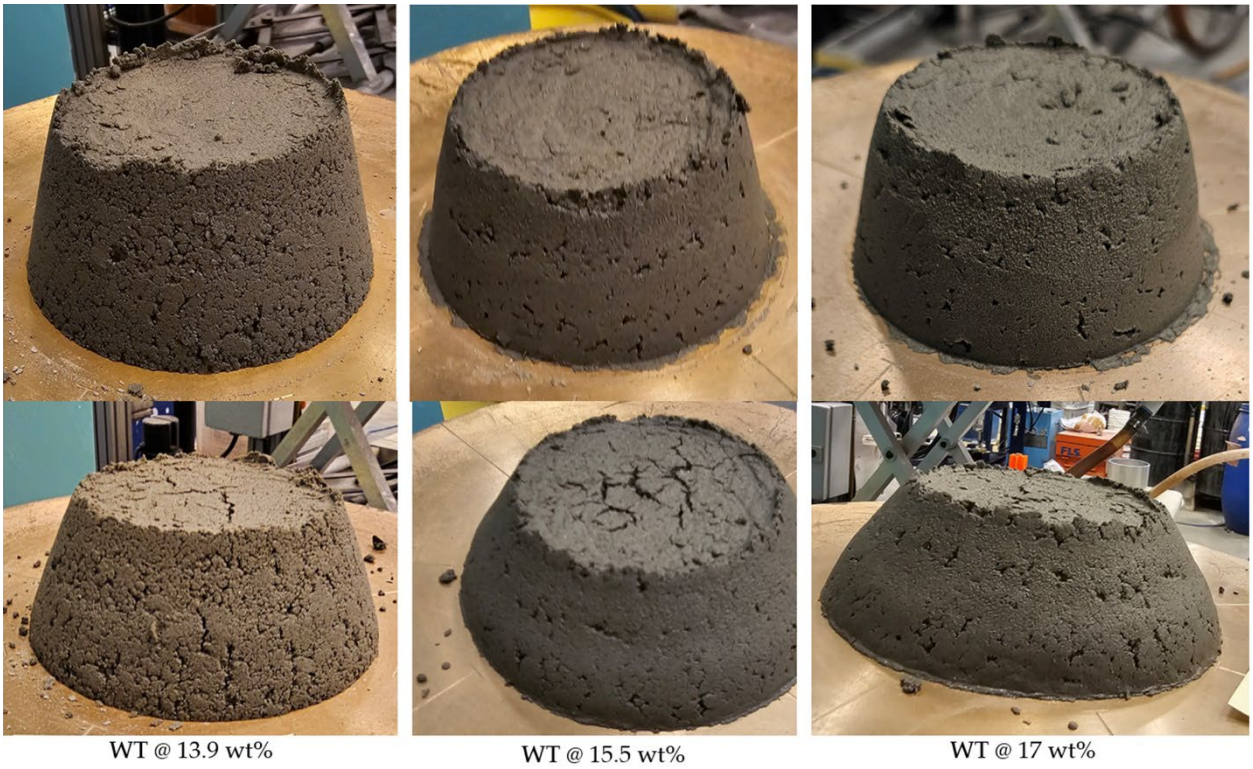


Figure 2: WT samples before and after

The data collected is used to determine the critical moisture content for TML, which is calculated as 90% of the FMP (see Tables 4 through 6). This analysis interprets the material's response to varying moisture levels and identifies the specific point of significant change in flowability.

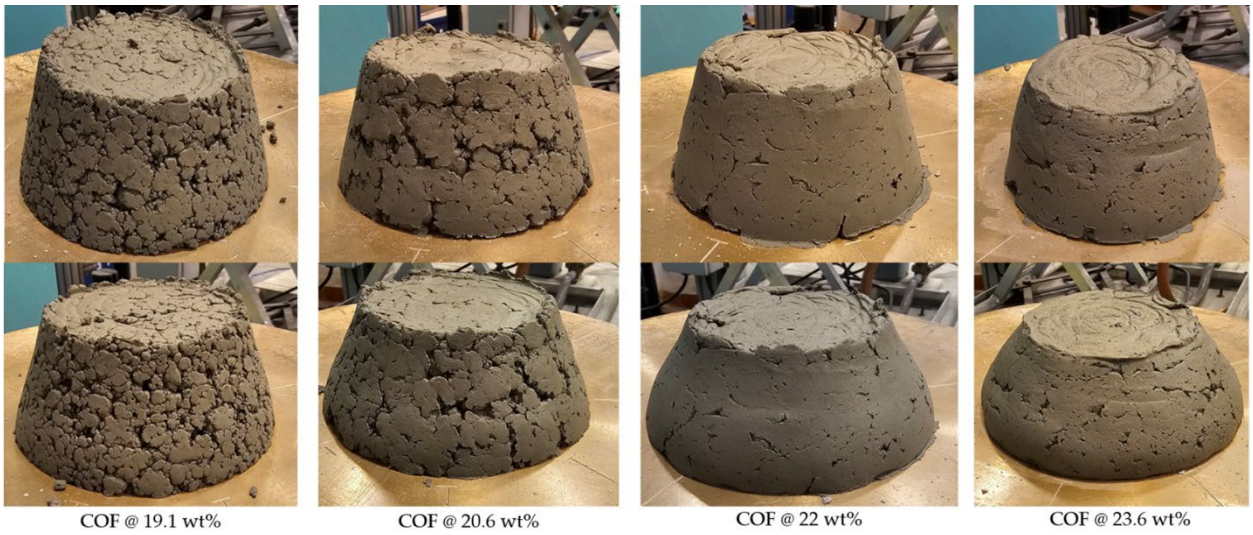


Figure 3: COF samples before and after

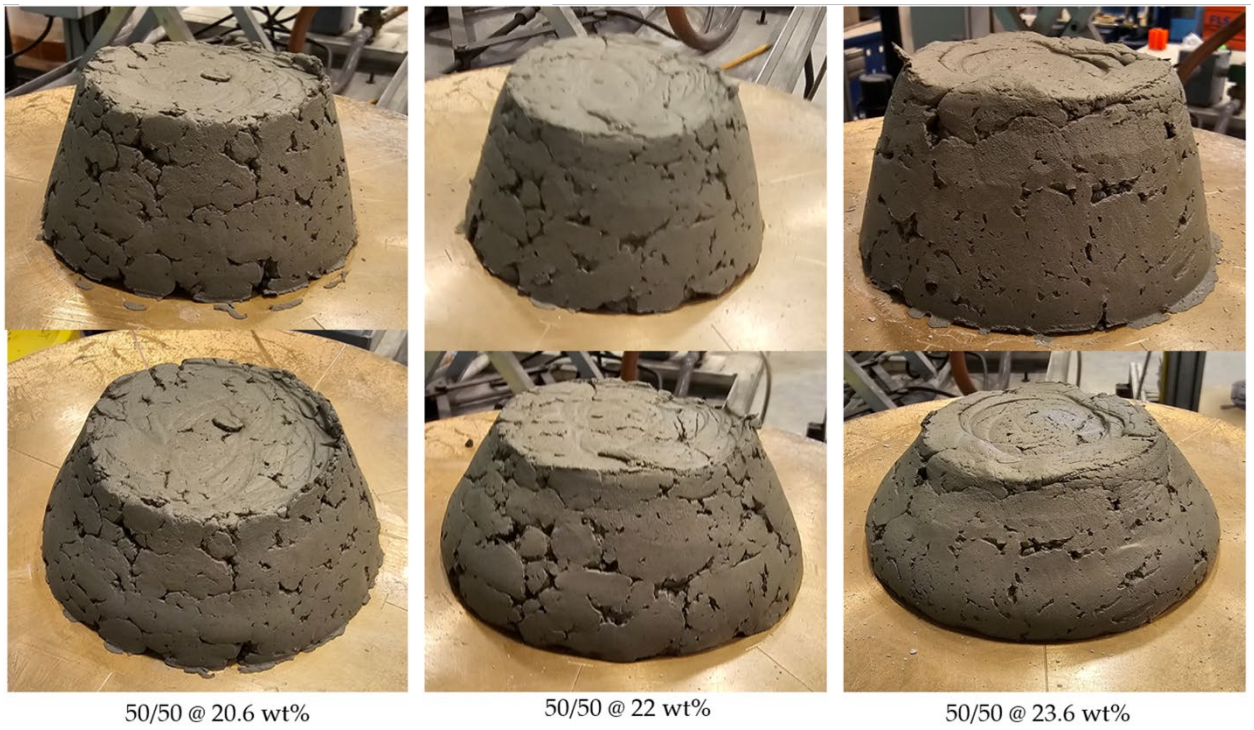


Figure 4: 50/50 Samples before and after

Table 4: WT sample flow moisture point

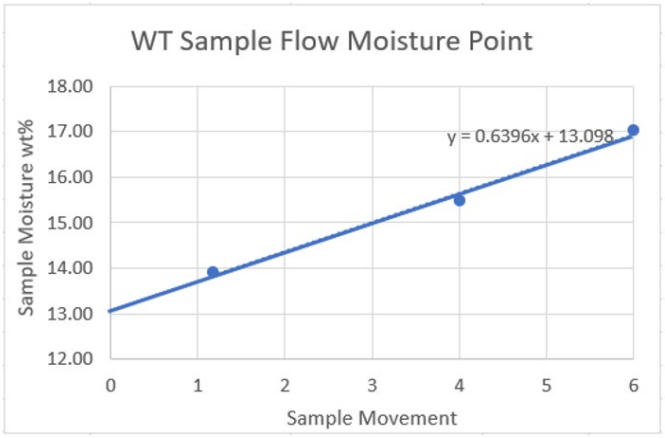


Table 5: COF sample flow moisture point

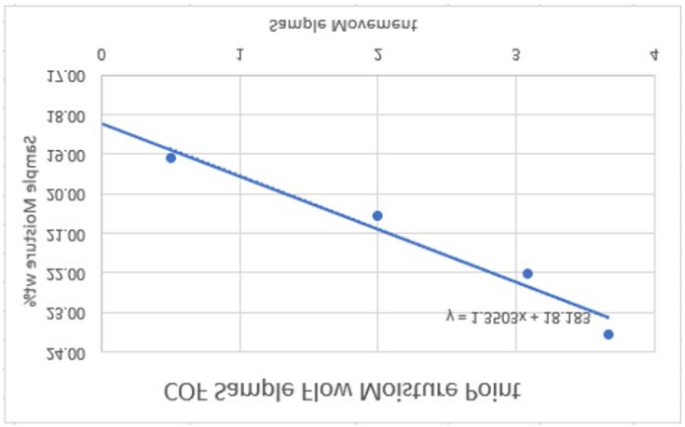
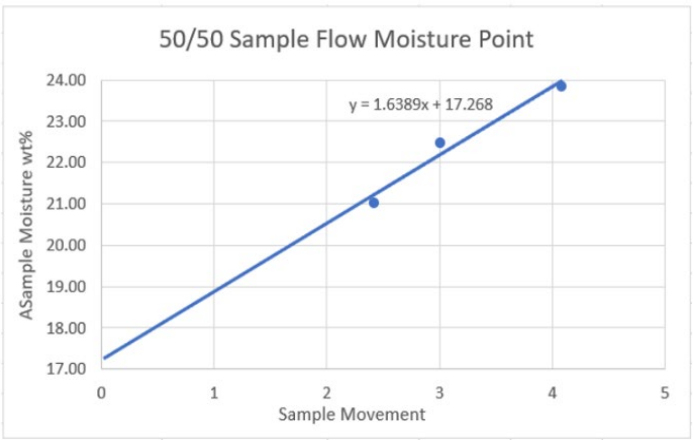


Table 6: COF sample flow moisture point



Conveyability testing

The FLS conveyor testing simulators, illustrated in Figure 5, are designed to simulate how bulk materials behave during conveyor transportation. These simulators feature a static belt with revolving idler rollers, whose speed is controlled by a Variable Frequency Drive (VFD). Additionally, the belt's tension is adjustable to match the belt sag parameters established by conveyor sizing calculations. The simulators can also be inclined to represent different conveyor slopes. *"The proper design and operation of the MH portion of the tailing solution requires thorough testing of the conveying properties of the material at the laboratory and pilot scale. This testing will ensure that the material handling system meets the important availability and capacity needs of the mine, even during periods of variability in the upstream processes and mine plan. This testing must include investigation of the impact of moisture content on the MH system"* (Rahal et al., 2018).



Figure 5: Left: conveyor tester 1.0. Right: conveyor tester 2.0

The conveyability testing apparatus simulates real-world conditions to evaluate the behavior of tailings on a conveyor system. Since no standard procedures exist for this unique equipment, FLSmidth has developed specific testing methods. Tests use filter cake samples representing various flowsheet options like whole mill tails, cyclone underflow, and overflow, with different tailings blends, particle sizes, and moisture contents. The goal is to assess the conveyability parameters of these samples.

Each test starts with calibrating the belt speed and tension. Tailings samples, prepared with various blends and moisture levels, are loaded onto the conveyor to simulate realistic conditions. The tests simulate incremental conveyed distances to evaluate material behavior at incremental conveyed distances (see figures 6 through 8). For slope tests, the conveyor runs horizontally for a duration for the material to start to self-compact, then runs for a shorter duration at an incline and then at a decline, observing factors like liquefaction potential, material flow-back, surcharge angle changes (see Table 7), material self-compacting, material loss to belt friction, and deviations from expected behavior. Monitoring these factors helps identify potential issues affecting conveyor system efficiency and design.

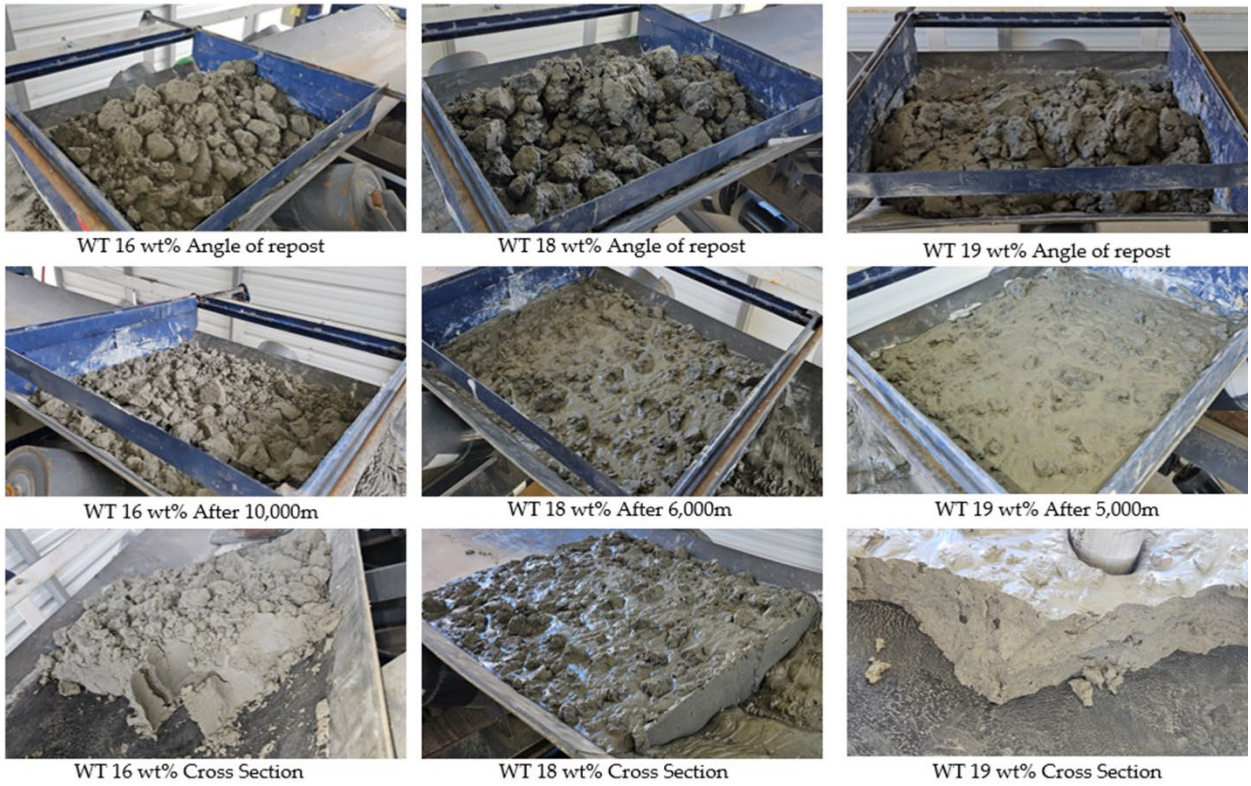


Figure 6: Whole tails (WT) sample conveyor testing

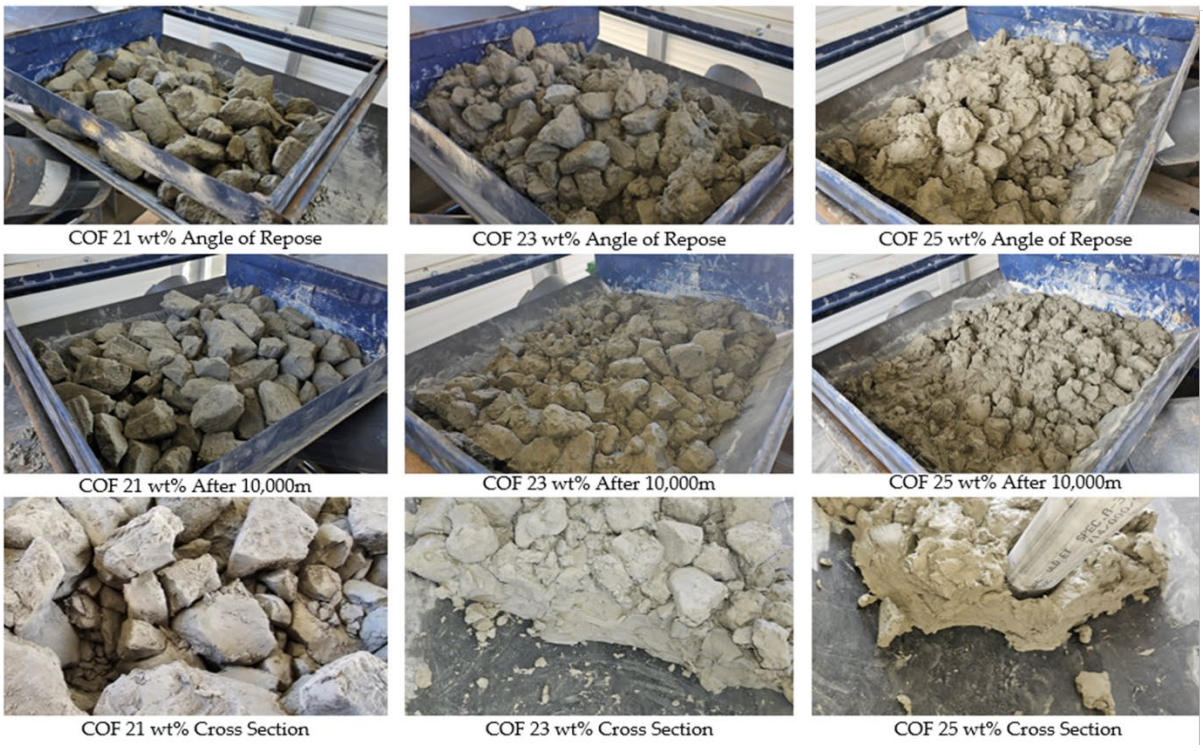


Figure 7: Cyclone overflow (COF) sample conveyor testing

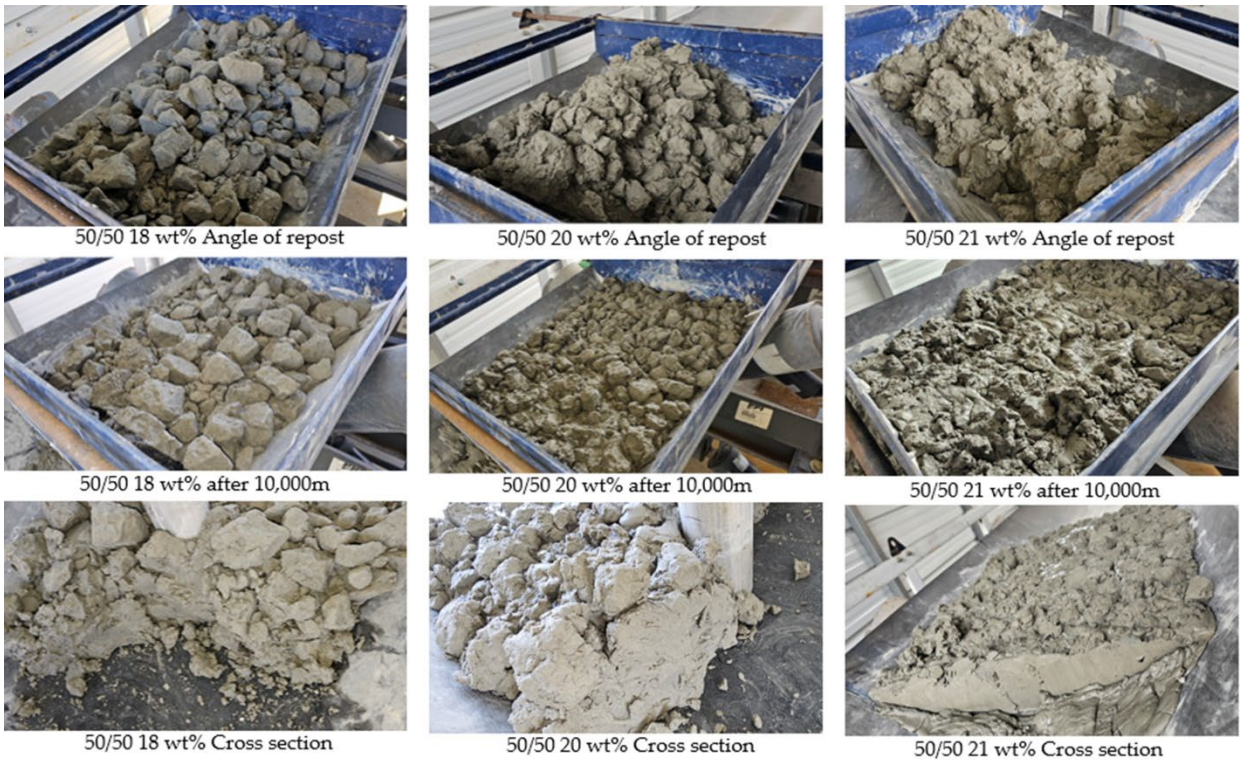
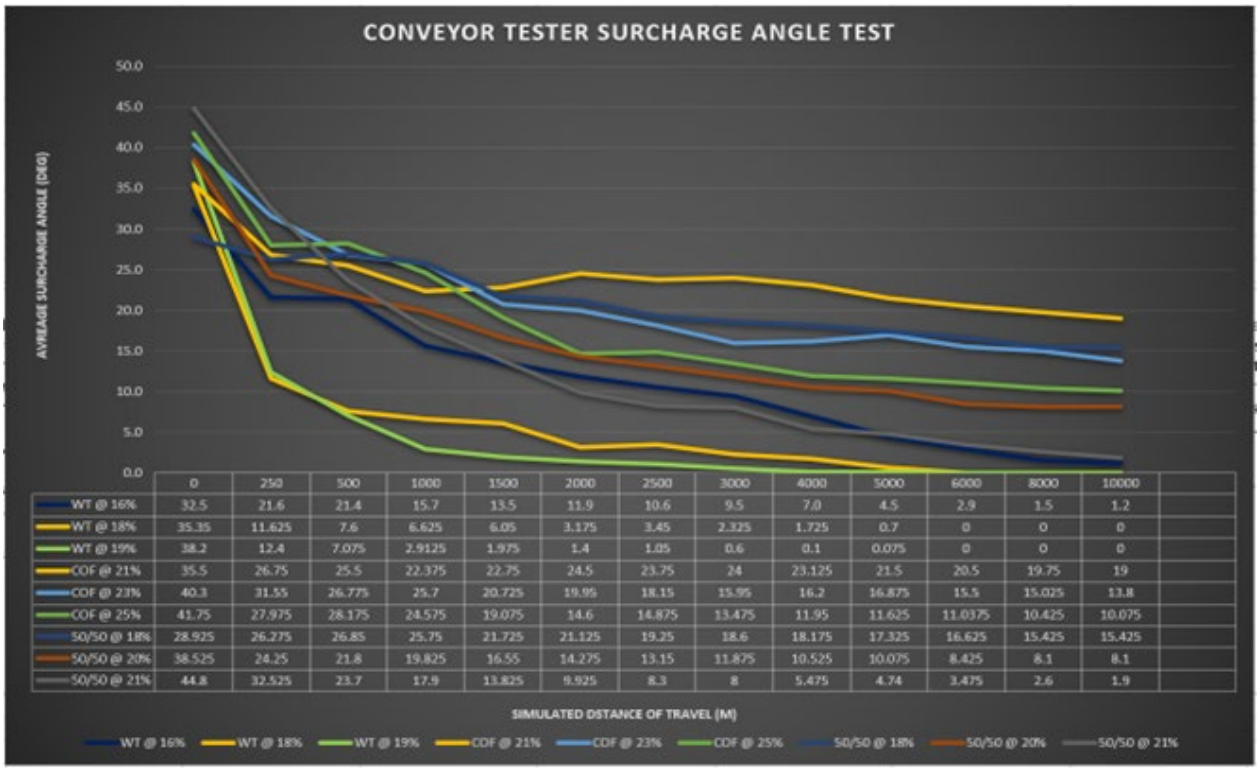


Figure 8: 50/50 Split sample conveyor testing

Table 7: Conveyor testing change in surcharge angle chart



	0	250	500	1000	1500	2000	2500	3000	4000	5000	6000	8000	10000
WT @ 16%	32.5	21.6	21.4	15.7	13.5	11.9	10.6	9.5	7.0	4.5	2.9	1.5	1.2
WT @ 18%	35.35	11.625	7.6	6.625	6.05	3.175	3.45	2.325	1.725	0.7	0	0	0
WT @ 19%	38.2	12.4	7.075	2.9125	1.975	1.4	1.05	0.6	0.1	0.075	0	0	0
COF @ 21%	35.5	26.75	25.5	22.375	22.75	24.5	23.75	24	23.125	21.5	20.5	19.75	19
COF @ 23%	40.3	31.55	26.775	25.7	20.725	19.95	18.15	15.95	16.2	16.875	15.5	15.025	13.8
COF @ 25%	41.75	27.975	28.175	24.575	19.075	14.6	14.875	13.475	11.95	11.625	11.0375	10.425	10.075
50/50 @ 18%	28.925	26.275	26.85	25.75	21.725	21.125	19.25	18.6	18.175	17.325	16.625	15.425	15.425
50/50 @ 20%	38.525	24.25	21.8	19.825	16.55	14.275	13.15	11.875	10.525	10.075	8.425	8.1	8.1
50/50 @ 21%	44.8	32.525	23.7	17.9	13.825	9.925	8.3	8	5.475	4.74	3.475	2.6	1.9

Testing comparison

The intent of the results from the material testing

FMP testing establishes a material's moisture content limit, serving as the basis for determining the Transportable Moisture Limit (TML). The TML test identifies the moisture content at which a bulk cargo begins to behave like a liquid. Set 10% below the FMP, the TML represents the maximum moisture content for safely transporting bulk cargo without risking liquefaction, ensuring a safety margin for dynamic conditions during transport.

"A solid bulk cargo consists of three main components: a solid component; a moisture component; and an amount of air (void space) in between. Vibration and the motion of a vessel will cause the cargo stowed in the holds to compact the moisture and small particles contained in the cargo. In certain conditions, a cargo can compact to such an extent that there is no more void space (air) between solid and water particles. When there is more water inside the cargo than there is space between the particles, and the water has nowhere to go, then the water pressure between the particles may rise and press the particles apart. This will either result in a sliding failure or the wet base of the cargo will transition from a solid state to a viscous fluid." (London P&I Club, 2017)

Shipping companies use the TML to comply with international maritime safety regulations, especially those set by the International Maritime Organization (IMO).

"It has been found that moist, loosely deposited fine-grain ore stockpiles can liquify during transportation by barges. This liquefaction occurs when the vibrations caused by the motion of the barges causes the wet ore to densify (compact). The body weight of the ore is transferred to the water existing in the voids between the ore particles and shear resistance is loss. The ore becomes a very dense liquid and this jeopardizes the stability of the vessel." (Gallagher et al., 2005)

These measurement values are crucial for the safe loading and transport of bulk materials by shipping vessels. In some cases, the TML has been adopted as a measurement variable to define the moisture level for tailings transportation on conveyor applications.

The conveyor tester was specifically developed to test materials transported via conveyor belts. "*Both thickened and paste tailings are saturated with water. Filter cake can be saturated or not saturated depending on whether air is used to dewater the cake. Some filters like belt presses and centrifuges cannot blow air through the cake. Saturated and unsaturated filter cake can usually be conveyed but may have a low surcharge angle which is important to understand so the conveyor can be correctly sized. FLSmidth has developed a proprietary test to determine the conveyability of filter tailings… that must be understood to ensure proper conveyor and design."* (Wisdom, 2020). The data collected from the conveyability tests go directly into the engineering design calculations for each conveyor within the system, from plant conveyors to overland conveyors.

Material preparation for the testing apprentices

The preparation of tailings blends and moisture content for both types of testing follow the same procedure. Material blends were sourced from the filter press pilot study, using the three specified sample types. Moisture preparation was carried out according to the specified testing procedures.

In flow table testing, the sample material is compacted into the mold at three levels to fill it completely. This process introduces inconsistencies due to manual compaction. While devices exist to apply consistent pressure, many tests use a spring-loaded tamper for manual compaction. This results in variability between tests and different laboratory technicians. Additionally, this method does not account for the self-compaction of tailings during conveyor agitation, focusing instead on a pre-compacted state before any external energy is applied.

For conveyability testing, the tailings material is dumped into the testing bed, simulating a conveyor-to-conveyor transfer point with realistic drop height, skirtboard boundaries, and cross-sectional fill. The material is in an as-loaded condition, partially compacted with a measurable angle of repose. Ensuring the correct quantity of material is critical for consistency, as under-filled or over-filled conveyor sections can affect the energy input differently than intended by the test procedures.

The energy input into the sample material during testing

In flow table testing, the energy input is associated with the potential energy transferred to the material when the table is raised and subsequently released. This allows the table to fall from a predetermined height, creating a full-impact, inelastic collision. The energy input vector is strictly vertical, meaning the force is directed straight downward. As a result, the tailings material absorbs a significant portion of the collision energy, leading to noticeable effects on the molded sample.

Each time the table falls, the impact causes the molded tailings sample to either bounce and fragment or deform progressively from the base upward. This deformation occurs as the material responds to the force, with the lower layers compacting first and the upper layers following suit. The repeated impacts simulate dynamic impact conditions, providing insights into how the tailings material behaves under stress at varying moisture levels. The vertical impact force not only compacts the material but also causes it to spread radially, mimicking the way tailings would spread when subjected to similar conditions in practical applications.

During the conveyability testing the movement of the tailings material is much more like a wave than a vertical rise and fall inelastic collision. The wave that the tailings material constantly travels on has a low amplitude-to-wavelength ratio, with the wavelength being the points where the conveyor belt contacts the idlers and the amplitude being one-half of the belt sag distance. With the material traveling like a wave, the energy and the force vectors become very different. The tailings material does not absorb nearly the same

amount of energy from the up-and-down movement because it does not experience an inelastic collision. An example comparison between the vertical forces applied in the two test methods is like driving down a bumpy road in a car without any suspension versus the same bumpy road in a car with suspension. See Figure 9 for a side-by-side comparison of the two tests performed on the same samples with the same moisture content. Comparing the highest tested moisture content of the sample types shows the most movement, self-compaction, and deformation from the testing.

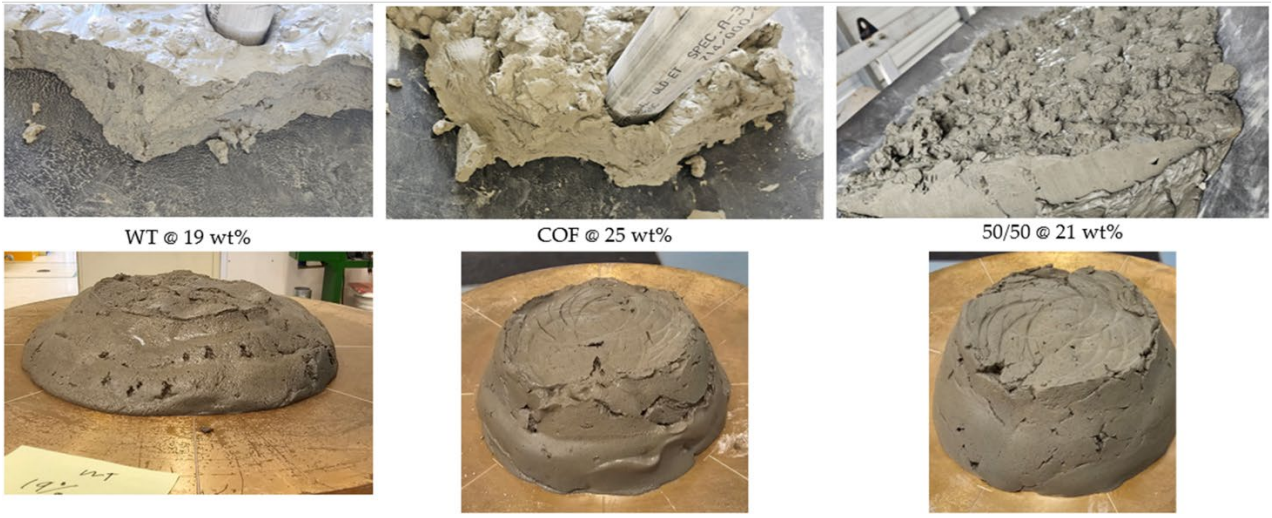


Figure 9: Side-by-side testing comparison of the samples tested at the highest moisture content

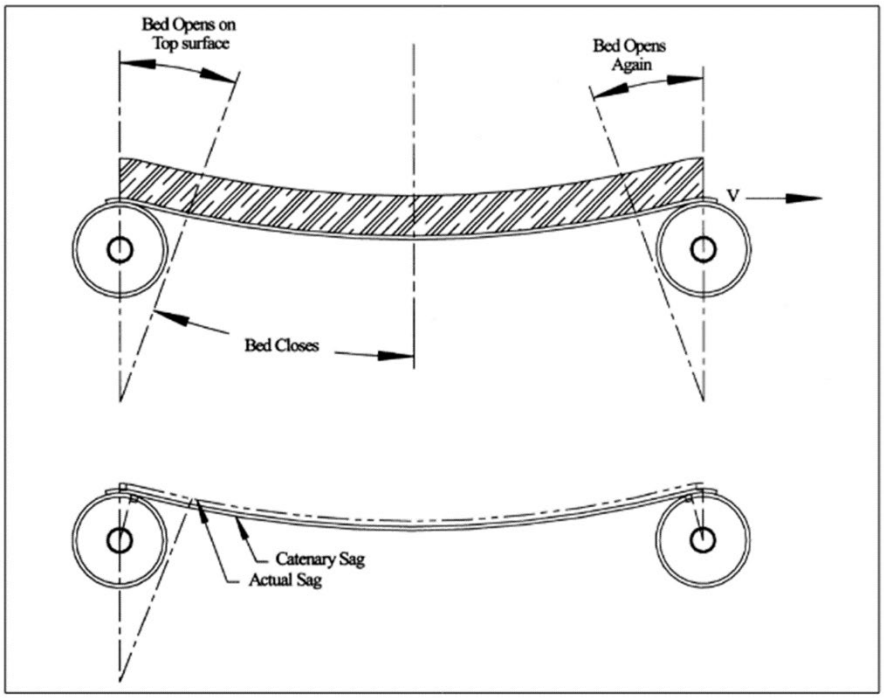


Figure 10: CEMA material deformation caused by belt sag (CEMA, 2007)

The energy input observed with the conveyor tester involves the tailings material continuously undergoing tension and compression forces. The material experiences slight separation as it reaches the apex of the wave amplitude while traveling over the idler, and slight compression at the trough's apex when passing through the belt sag's low point between idlers (see Figure 10). This wave travel energy causes the tailings material to self-compact, promoting internal movement that fills voids and transitions the material bed from its initial angle of repose to the dynamic surcharge angle. This energy transfer from the conveyor belt into the material bed is referred to in CEMA standards as Material Trampling Loss.

"The belt sag causes the individual particles of bulk material to repeatedly move against each other as they progress from one idler to the next, with consequent energy loss due to internal friction. Energy must be added through the material depth to overcome the internal friction forces as the material closes on itself between an idler and the point of maximum sag at the center of the idler spacing. A portion of this energy is recovered as the bed depth opens up again in the section from mid span to the idler. Note that there is no net elevation change and therefore no potential energy change between idlers" (CEMA, 2007).

The CEMA standards outline the calculations for determining material trample loss, which is one of the many factors considered when sizing the power requirements for a conveyor.

The CEMA publications provide a comprehensive list of material and belt factors that contribute to energy loss during conveyor operations. They include the necessary equations to calculate and quantify these losses accurately. The primary purpose of these guidelines is to account for as many energy losses as possible, aiding engineers in correctly determining the energy requirements of a conveyor system.

In the context of conveyor operations, we consider both the energy loss in the conveyor system and the energy gain for the transported material. The material gains energy through material-on-material movement and friction. These interactions, driven by the conveyor's motion, contribute to the material's self-compaction. As the material moves along the conveyor belt, it experiences various forces that cause internal movement, filling voids, and increasing density. If sufficient moisture is present, there may be a fleeting occurrence of material liquefaction. This self-compaction is a critical factor for engineers to consider, as it affects the overall efficiency and design of the conveyor system.

In addition to material trampling in the parallel plane of the conveyor belt, a small amount of material deformation also occurs in a plane perpendicular to the conveyor belt's length. Although not mentioned in CEMA publications, this secondary material trampling is observed during the conveyor tester's testing. It happens when the tension on the conveyor belt causes it to flatten slightly between the idlers and then return to a full trough as the belt moves directly over the carry idler. This "belt flapping" causes the tailings material on the belt to experience tension and compression cycles perpendicular to the belt length.

The compression and tension forces from the belt trampling parallel to the belt and the belt flapping perpendicular to the belt directly oppose each other. When the belt is at the bottom of the sag, trampling is

in compression, and flapping is in tension. Conversely, when the belt is at its peak, directly over the conveyor idler, trampling is in tension, and flapping is in compression.



Figure 11: Top left: the tailings start to "camel hump." Top right: the camel hump continues to form. Bottom: the camel humps at the end of the testing

There have been instances where tailings and other tested materials formed into a "camel hump" on the cross-section of the belt (see Figure 11)[2]. This rare occurrence is considered a combination of belt flapping and material characteristics. In tests performed on this tailings sample, only the sample with lower moisture content exhibited camel humps during testing, indicating that moisture levels might play a role in this phenomenon. Three conveyor tests were conducted, and this anomaly was observed solely in the lowest moisture sample, suggesting that specific conditions are necessary for the camel hump effect to manifest.

Data that is collected from the tests

The flow table test generates highly specific data, focusing on identifying the FMP where material experiences liquefaction under specific energy loading. Understanding the FMP helps industries determine the TML, crucial for implementing preventive measures against material flow issues. These measures include adjusting storage conditions, using moisture control strategies, or selecting suitable handling equipment to maintain optimal material flow. Adhering to TML regulations ensures the moisture content of transported material stays within acceptable limits, vital for international shipping compliance. The primary

[2] Note: the sample referenced in Figure 5 is not among the three test samples from this case study.

goal of using TML for conveyor transport of tailings is to prevent the material from liquefying during conveyance.

Secondary data from the flow table test includes bulk density and visual analysis of material deformation, complementing the primary goal of determining the FMP.

Conveyor testing yields two main data points: the change in the surcharge angle throughout the conveyor's travel length and the maximum slope angle at which material can be conveyed at a tested moisture level. A graph is created based on the tailings sample and its moisture content. For example, if an engineer expects the tailings on the conveyor to have a 16 wt% moisture content and is designing conveyors of 550 m, 2,067 m, and 560 m in length, they can use the graph to determine the appropriate surcharge angle for each conveyor calculation. Additionally, the maximum slope angle data aids in the design and layout of the conveyor system.

Secondary data for the conveyor tests include the initial and ending bulk densities of the tailings material, the initial angle of repose of the material loaded onto the conveyor, and visual observations of the material's behavior during conveyance. These secondary data points provide additional insights into the material's handling characteristics, supporting the optimization of conveyor system design and operation.

Conclusion

The transportation of bulk materials, especially mine tailings, is crucial to industrial operations, requiring precise engineering and design. Specialized testing apparatuses, such as the conveyor tester and FMP testing, provide essential insights into these materials' behavior under various conditions. This paper details the methodologies and outcomes of these tests, highlighting their importance in optimizing conveyor systems and ensuring safe material transport.

The conveyor tester offers a practical solution to the challenges of tailings transportation. By simulating real-world conveyor conditions, it assesses conveyability parameters, including moisture content and material composition. This data directly informs the engineering design of conveyor systems, ensuring they can handle the dynamic nature of bulk materials in mining operations.

FMP testing determines the safe moisture limits for bulk materials during maritime transport. The FMP and derived TML are vital for preventing liquefaction, a hazardous condition where materials behave like liquids under certain conditions. This testing ensures compliance with international maritime safety standards and provides guidelines for managing moisture content in conveyor systems to prevent flowability issues.

Using the TML as a limit for conveyor transport offers only a partial understanding of a broader issue. Conveyor testing of tailings has shown that while these materials can liquefy during transport, they can still be conveyed. Comparing these two testing methodologies highlights their roles in tailings conveyor system

design. FMP testing focuses on moisture-induced flow characteristics, while conveyor testing emphasizes physical handling and dynamics. Both sets of data are useful for determining conveyability, but conveyor testing offers deeper insights and is essential for designing efficient and safe tailings handling systems.

These tests provide comprehensive data supporting the development of robust conveyor systems capable of maintaining operational efficiency and safety. By addressing gaps left by standard conveyor design publications, particularly for mine tailings, these testing methods advance material handling technologies and practices.

References

CEMA. 2007. Belt Conveyors for Bulk Material. In *Belt Conveyors for Bulk Material* 6th edition (p. 122). Naples, Florida: Conveyor Equipment Manufacturers Association.

Gallagher, B., Stogsdill, S. and Stephenson, R.W. 2005. Influence of Ore Physical Properties on the Transportable Moisture Limit. Rolla, MO: Center for Infrastructure Engineering Studies/UTC program.

London P&I Club. 2017. Reducing the risk of liquefaction – operational guidance for vessels that carry cargoes which may liquefy. Retrieved from londonpandi.com: https://www.londonpandi.com/media/2142/reducing-the-risk-of-liquefaction-operational-guidance-for-vessels-that-carry-cargoes-which-may-liquefy.pdf

Pinto, F.K., Ghosh, A. and Pal, D. 2011. MitraSK Blog. Retrieved from https://mskworldwide.wordpress.com/2011/03/25/tml-by-flow-table-test-method/

Rahal, K., Nicholson, A., Stefansen, R. and Wisdom, T. 2018. Material handling testing and control system requirements for dry stack tailings. *Proceedings of Mine Waste and Tailings 2018.* Brisbane, Queensland.

Wisdom, T. 2020. Filtering down. P. Moore, Interviewer.

Learning from Experience – Let's Get Real

Malcolm Barker, GHD, Australia

Abstract

Having been in the design, safety and risk analysis of dams for nearly fifty years, what have I learned and what does it mean for the younger generation of engineers? Can we learn from other people's experiences or do we just carry on making the same mistakes or errors?

Many of the safety procedures that have been put in place over recent years have significantly reduced the potential for life loss and injury, but these have come at a cost, and have we reduced the risks as low as reasonably practicable in our design and construction for tailings facilities?

In this paper, I will share some of my experiences in the hope that other engineers will learn from my failures and successes.

Introduction

There are good and bad human behaviors that define the way we approach problems of design, construction, operation, maintenance, and finally decommissioning of structures or closure of tailings storage facilities. Life's journey is up and down or round and around, as shown in Figure 1.



Figure 1: Life's journey is up and down or round and about

"Insanity is doing the same thing over and over and expecting a different result." This is a quote often attributed to Albert Einstein, although it is likely he never said this.

"Learning is a matter of gathering knowledge; wisdom is applying that knowledge." Unknown.

So, what about human behavior and how this can lead to failures and successes?

Human behavior

In his article "Dam incidents and failures can fundamentally be attributed to human factors" Irfan (undated) states the following:

"The field of "human factors" considers how and why systems meet or don't meet performance expectations, with an emphasis on understanding and prevention of incidents and failures. The systems considered in human factors work, such as dams, typically include both human and physical aspects, and are sometimes referred to as "sociotechnical" systems. To prevent future dam failures, it is essential that dam safety professionals understand both physical factors and human factors, and how they contribute to failures or safety.

Physical processes deterministically follow physical laws, with no possibility of physical 'mistakes.' Failures are, therefore, fundamentally due to human factors and a story of why a failure happened therefore cannot be complete without reference to contributing human factors."

According to the UK Health and Safety Guidance document "Reducing Error and Influencing Behaviour" (HSG48, 1999), human failures can be categorized as either errors or violations, as shown in Figure 2. In the context of dam safety, "mistakes" are the most common type of human error which contribute to failures. "Violations" generally involve situations in which there is deliberate non-compliance with rules and procedures, usually because the rules or procedures are viewed as unworkable in practice.

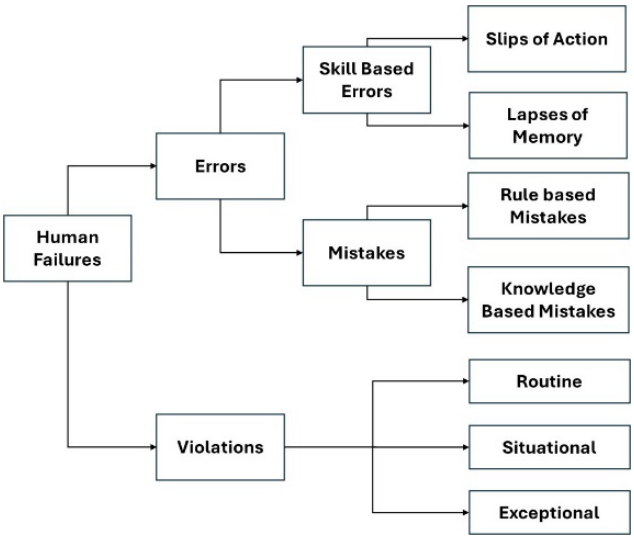


Figure 2: Types of human failure (HSG48, 1999)

Systems such as dams, including the people involved in designing, building, operating, and managing them, tend to conservatively have numerous "barriers" that must be breached for failures to occur. Failures will occur owing to physical and human factors "lining up" in an adverse way that overcomes all barriers. The Swiss cheese model of accident causation, originally proposed by Reason (1997), likens human system

defenses to a series of slices of randomly holed Swiss cheese arranged vertically and parallel to each other with gaps in-between each slice. Figure 3 is a typical Swiss cheese model that shows that engineering is one of the controls for an unwanted event. All of the controls, however, are essentially human-based with the propensity for failures.

What are the barriers in life or organizations that are effective in reducing the risks As Low as Reasonably Practicable (ALARP) when it comes to dam design, construction, operation, and maintenance?

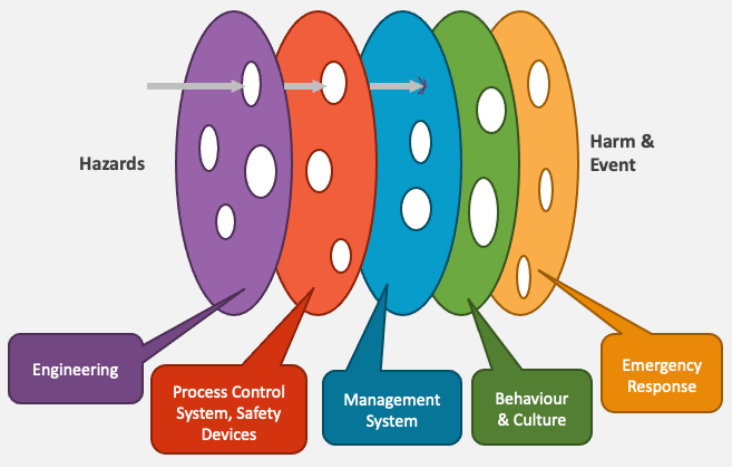


Figure 3: Typical Swiss cheese model of accident causation (https://www.collidu.com/presentation-swiss-cheese-model)

My early learning from other experiences

The following experiences were significant in my early career and provided me with an understanding of how human errors and violations can lead to infrastructure failures, particularly in relation to dams.

St. Francis Dam failure (1928) – Foundation failure (432 fatalities)



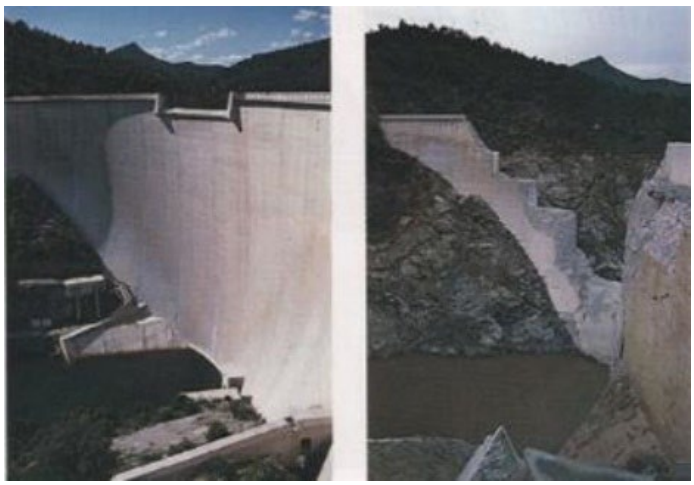
Sources: Left – https://lessthan3ley.wordpress.com/2016/12/28/the-st-francis-dam-disaster-of-1928/
Right – https://damfailures.org/case-study/st-francis-dam-california-1928/ASDSO Case Study

Tacoma Narrows bridge (1940) – Wind and resonance of a structure with modes of vibration



Source: https://adsimutec.com/en/fem-cfd-simulation-pinboard/application-examples/multiphysics-coupling-interaction/tacoma-narrows-bridge

Malpasset (1959) – Foundation failure due to geological feature and uplift (412 casualties)



Source: George, 2010.

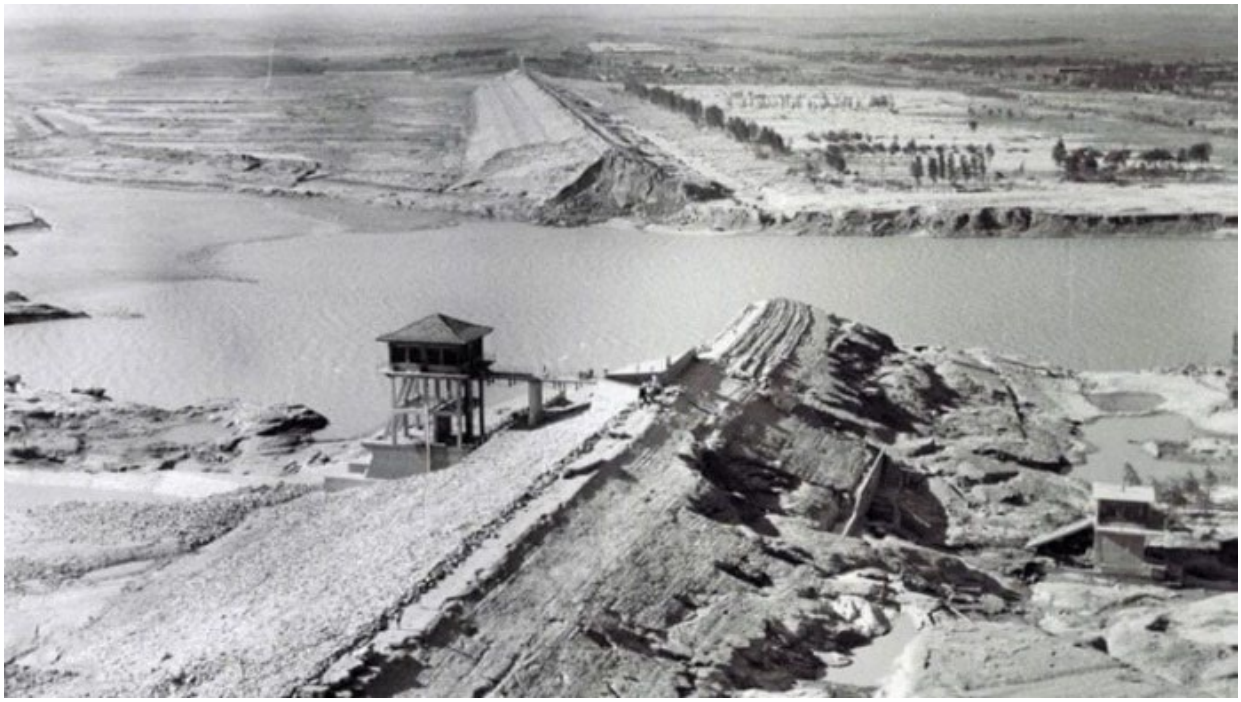
Vaiont Dam Failure (1963) – Landslide overtopping of the arch dam by 250 m (2,000 fatalities)



Source: https://www.geotech.hr/en/vajont-a-tragedy-that-killed-more-than-2000-people/

Banqiao dam failure (1975)

Design flood 1 in 1,000 Annual Exceedance Probability (AEP). Overtopping failure during a 1 in 10,000 AEP flood with cascade failure of downstream dams (10 hours breach) (230,000 fatalities).



Source: https://u.osu.edu/mclc/2019/02/18/dam-collapse-that-china-kept-secret/

Teton dam failure (1976)

The dam failed due to hydraulic fracturing as a result of failure to thoroughly investigate and account for defects in the abutment and foundation (14 casualties).





Source: https://damfailures.org/case-study/teton-dam-idaho-1976/

Table 1 summarizes where things had gone wrong and highlights what human behaviors could have contributed to these failures that I could apply in my dam design career.

Table 1: Human behavior that contributed to failures

Where failures have occurred	Why did the failures occur?	Human behaviors that contributed to these failures
Banqiao Dam	Inadequate spillway capacity in design to cater for the consequence of failure leading to overtopping of dams.	Knowledge based and rules-based mistake in applying flood design parameters
St. Francis Dam	Design and construction flaws that can be made by very experienced people.	Overconfidence knowledge-based mistake – be humble and willing to listen to others
St. Francis Dam Malpasset Dam	Lack of clear understanding of the foundation and failure modes associated with kinematically feasible failure modes – Understand the geological conditions and kinematics of failure modes.	Knowledge based mistake
Malpasset Dam	The importance of understanding foundation uplift and pressure relief or lack of pressure relief in the foundation, even for an arch dam. Precedent is not always good practice.	Knowledge and rules-based mistake
Vaiont Dam	Significance of landslide reservoir rim failures – Look beyond the dam site to understand the historical evidence of slope instability and the effect of impulse-generated waves.	Knowledge based mistake
Vaiont Dam St. Francis Dam	Investigation limitations – we can never have enough, but what is required for a good, robust sustainable design?	Knowledge based mistake and possibly routine violation
Teton Dam	Piping through the embankment core zone into the foundation – lack of filter control and foundation preparation cannot be overlooked or compromised.	Situational violation and knowledge-based mistake
	Lack of communication between design team and the construction team – Ensure regular construction site inspections by the design team and ask for advice.	Systemic routine violation
Teton Dam	Budget constraints – Limited funding cannot be an excuse for not implementing good practice (ALARP).	Situational violation
Tacoma Narrows Bridge	The importance of understanding wind load. For dams, wind causing waves and surge.	Knowledge based mistake

What about my experiences?

I will share some of the experiences from which I learned a great deal, that have relevance to achieving goals and engineering "good practice" and recognizing where human failures occurred, or where opportunities arose that have had a significant bearing on my career pathway.

Zimbabwe

Analysis accuracy

My first job was designing an effluent disposal scheme comprising five maturation ponds with a maximum 2 m depth leading to the outlet works and a canal where two offtakes were used for spray irrigation with pump stations. My manager shared his experience with outlet works design where he did not fully account for the energy dissipation through the outlet works, and because of that the flow through a downstream V

notch weir used for flow measurement on his project was supercritical. All of the discharge measurements were wrong until additional energy dissipation works were installed in the outlet chamber.

This taught me the importance of energy dissipation and tailwater effects for design of outlets, as well as what a lack of knowledge with a very experienced engineer can look like in design. Actually, this scared me into an awareness of how to achieve the levels of accuracy needed for a good operational design.

Safety in design and construction

I was the chief resident engineer for the construction of Mazvikadei Dam, which is a 63.5 m high zoned earthfill embankment dam with a drop inlet spillway. During the construction in 1997, a very experienced contractor was excavating the lower part of the right abutment, which comprised large granite boulders in a soil matrix. The contractor used blasting to break up one very large boulder. During the excavation of the material using benches, which were carefully placed, one of my inspectors was standing on a rock on one of the benches, which collapsed under him and killed him. This was a shocking accident and one which I have lived with for the rest of my career.

This was a result of process control safety, management, and cultural behavior control failures and showed me the importance of safe work methods and understanding the risks associated with construction of something that was meant to be relatively straightforward.



Figure 4: Mazvikadei Dam right abutment core trench excavation (author's photograph)

As shown in Figure 4, the excavation of the cut-off trench clearly revealed the openness and extent of the exfoliation in the granite foundation. Following on from the Teton experience, we were very careful to

seal the downstream joints with mortar and provide a full sand filter against the downstream face as well as foundation slurry and dental concrete to avoid steps and open joints in the cut-off trench.

Compromise in materials for construction:

The diversion works for the Mazvikadei dam comprised construction of a homogeneous highly plastic earthfill embankment coffer dam to divert the river flows through the outlet tunnel. The coffer dam was to allow overtopping to an undefined depth. During the construction, I was trying to optimize use of material and placed less plastic material in some areas. During a large flood, while I was on leave, the coffer dam stood for 14 hours with a depth of flow of about 300 mm over the crest. The assistant resident engineer went to make a call to head office in the night and when he returned after about 10 minutes, the coffer dam had breached, as shown in Figure 5.



Figure 5: Mazvikadei Dam breached coffer dam (author's photograph)

This was a situational violation of the design requirements and taught me not to compromise on material usage in the zones for which it is required, in particular for subsequent construction in the use of properly graded sand filters.

Blast zone

During the construction of the Mazvikadei dam, my office was located in a perfect location on a hill feature between the main dam and the saddle dam about 100 m from the drop inlet spillway entrance channel, as shown in Figure 6. One morning I arrived at my office to find a rock fragment lying on my table that had come through the roof. That could have been a major incident, including potential life loss in the event that a rock had hit anyone around or in the offices.

Clearly this was a knowledge-based mistake related to safe blasting distances, but perhaps also the blasting contractor being overzealous in charging the blast.



Figure 6: Mazvikadei Dam layout and office location

The importance of good testing and alternative use of soil testing equipment

I had the privilege of being assigned to the soils laboratory, where we were using state of the art electronic digital equipment for the triaxial testing, including measurements of pore air pressure. This was seldom done owing to the difficulty of ensuring a good seal with the porous disc measuring the air pressure. Nearly all the tests were done using saturated undrained tests with pore water pressure measurement. I learned the importance of saturation at high pressures to ensure at least 98% saturation to obtain good pore water pressure data, as well as the need for good soils testing equipment, procedures, and well-trained personnel completing the testing.

We were in the process of improving the safety of a buttress dam where we were concrete infilling between the buttresses. I made use of our oedometers to test the various density grades and thicknesses of Polystyrene. This was required to determine which grade would allow construction of the first concrete lift without crushing the Polystyrene, but would then allow crushing on further loading by the buttress dam to ensure that the mass gravity infill concrete load was not reduced.

South Africa

Moving to South Africa – introduction to risk assessment

When I returned to head office after Mazvikadei dam construction in Zimbabwe, I was given the opportunity for promotion above my level of experience of 14 years. I was not confident to take this role.

We moved to South Africa where I was employed in the Department of Water Affairs. I thought I was going to get more design experience in the design branch but I went to work with Dr Chris Oosthuizen in the Dam Safety Sub-Directorate of the design branch. This was one of the most significant changes in my career as I was launched into the world of Dam Safety and Risk Assessment for six wonderful years. This was also an opportunity for moving out of my comfort zone.

Piping along the outlet conduit on first filling owing to lack of filter material

As shown in Figure 7, this was a classic case of piping along the conduit of Zoeknog dam conduit on first filling owing to lack of filter protection around the conduit. The filter zone with geofabric extended to just above the conduit and I was one of the team from Water Affairs to inspect the dam. There was some uncertainty about whether the conduit had structurally deformed allowing the pipe to initiate, as shown by the failed conduit on the right of Figure 7. Following receipt of the photo on the left, it was clear that the conduit had failed owing to the unbalanced load after the piping failure had occurred.

This was a knowledge-based mistake, possibly a situational violation of the design requirements, if the Contractor failed to take the filters to the design level.



Figure 7: Zoeknog Dam piping failure (left: anonymous source; right: author's photograph)

Canada

Risk assessment challenges

While in Canada, I was given the great opportunity to complete a risk analysis for a hydropower concrete gravity dam with vertical lift gates. Given the situation where a load rejection and failure of the gates to operate could occur during a seismic event, resulting in failure of the dam within hours, the challenge was to complete the risk assessment for all failure modes and hazards including seismic, floods, ice, and debris. Following extensive modelling for all of the failure modes, physical model testing for debris loading and a detailed 156-page fault tree analysis for the spillway gate reliability and drainage system failure as well as numerous folders of calculations, we were not able to provide the client with a robust mathematical outcome

for the risk assessment. This resulted in a lot of stress for the team and the client rejecting the risk assessment to complete remedial works to ensure that the gates would open in the event of loss of power to ensure the dam could handle load rejection.

This was a clear result of inadequate knowledge and experience in the field of risk assessment to obtain robust mathematical modeling required for input to probabilistic modeling of the failure modes. Subsequent risk analyses that I have been involved with have placed reliance on judgmental probabilities, aided by modeling of failure modes without the absolute rigor of mathematical analyses to obtain probabilistic input.

Australia

Normalizing site inspection observations and minimizing testing

During routine annual inspections of the embankment at the west side of the tailings storage facility (TSF), I noticed longitudinal cracking. Operators advised that there was an old river channel in this area that was the cause of the cracking and I normalized this as an occurrence without significance as far as embankment safety. After all, the surface of the deposited tailings was firm with no issues for vehicular traffic.

During design for a 4 m upstream raise, we did dynamic cone penetrometer (DCP) testing at 100 m centers around the perimeter to prove the foundation. This raise height was more than the usual 2 to 3 m raise, but we were keen to maximize storage and the client did not want to do closer spacing testing. We were all convinced that the foundation material was relatively uniform with layers of weak material interspersed in the stronger material in a typical manner for tailings. Factors of safety for slope instability were acceptable.

The construction was in progress when I received a call that the embankment was moving. I thought that this was normal for rotational movement but this was translational movement with an opening of about 150 mm. Work was stopped while the design was reviewed and new alignment was used to prevent further failure.

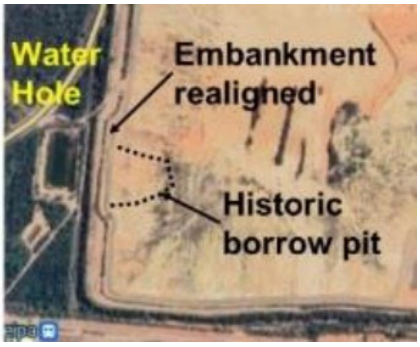


Figure 8: TSF example of normalizing observations and limiting testing for design (Google 2024)

The obvious question "What was the root cause?" was answered by the client design manager, who showed us an obscure figure with the outline of an old borrow area in the area of the failure, as shown in Figure 8. We had not seen this figure before. The first stage of the TSF cell went around this hole to the west and the tailings deposition into the borrow area hole was effectively subaqueous with no drainage owing to the high-water table. Note that water hole on the west of the cell. The investigations found the material had a strength of between 5 to 10 kPa at a depth below 9 m and the translation occurred in this material.

Clearly this was a knowledge-based mistake, as well as a situational violation by assuming the material was similar over the entire foundation area and construction of a larger than normal raise owing to over confidence in the foundation based on visual interpretation.

HSE – steps

This sounds trivial, but three points of contact are always specified when using stairs. However, how many times are the staircases too wide to prevent this happening, or people just don't use the handrail owing to overconfidence? I fell down a flight of nine steps when helping my daughter move as I was carrying my cup of coffee in one hand and my tools in the other. The picture below shows a very narrow step at the corner where I lost my footing and went tumbling down the steps with no way of stopping myself and hit my head on my drill case, which softened the blow.



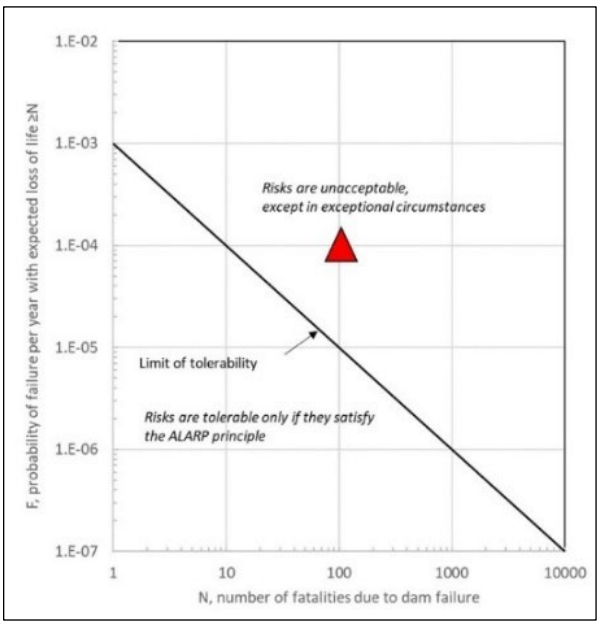
Figure 9: Spiral staircase (author's photograph)

I was all right, but this was clearly a situational violation for not using the handrail, as well as a design problem because there was no landing where the staircase turned the corner rather than narrowing the treads.

Cascade failure and design for fuse plug operation – do's and don'ts of residual risk:

A fuse plug spillway is a collapsible structure installed on spillways, or as a separate section on dams, in

order to increase the dam's flood capacity during remote events. Designing fuse plug spillways can often lead to incremental risk when compared with a flood of the same magnitude, without the rapid change in flow and water level resulting from the fuse plug operation. This is part of the normal operational residual risk, not the dam failure risk. The potential life loss (PLL) associated with some fuse plugs has been estimated to be in the hundreds. With an operational annual probability of 1 in 10,000 and PLL of 100, this would result in the societal risk exceeding the tolerable limit, as shown schematically in Figure 10.



n

Figure 10: ANCOLD societal risk with fuse plug operation example (author's figure)

This figure does not include the other residual flooding risks that would exacerbate the unacceptable risk. In order to achieve an acceptable risk with fuse plug operation at this AEP, the PLL would need to be less than 10 for "normal" operation. Ignoring the residual risks associated with fuse plug normal operation could be a knowledge-based mistake, but once understood becomes a clear situational violation human error.

Biases that affect how we evaluate risk for tailings facilities

We all have biases as a result of our background and engineering experience. In my experience of risk analyses for tailings storage facilities and water dams, some of the more significant biases I have seen are shown in Table 2 (Dwyer, 2018), where I have shown the potential human failure that may result when evaluating data for risk analyses.

Table 2: Biases and human failure

Bias	Description	Resulting human failure
Motivational bias	Having a vested interest in wanting to prove something	Situational Violation
Confirmation bias	Favor ideas that confirm their existing beliefs, ignoring contradictory evidence	Knowledge based mistakes
Optimism bias	When in a good mood, individuals overestimate the likelihood of positive outcomes	Slips of Action
Declinism bias	Favor of the past due to resistance to change	Knowledge based mistakes
Dunning-Kruger Effect	Individuals with low knowledge mistakenly assess their ability as greater than it is, while experts may underestimate their own knowledge	Knowledge based mistakes
Anchoring bias	Relying too heavily on the first piece of information encountered when making decisions	Rule based Mistake
Affect Heuristic	Decisions influenced by emotions or feelings rather than rational analysis	Situational Violation
Outcome bias	Judging decisions based on the outcome rather than the process	Rule based Mistakes
Illusory Superiority	Overestimating one's abilities or qualities relative to others. A belief that your work is correct/accurate	Situational violation
Availability Heuristic	Overestimating the importance of information readily available in memory	Knowledge based mistakes

Being accountable

We all have biases, but we need to be accountable. When dealing with accountability, the triangle of Means, Motivation and Meaning is useful, as shown in Figure 11 and summarized in the following points:

- Means – Make sure that you have the skills and experience for the work. Acknowledge your own fallibility and ask for help where needed.
- Motivation – Are you motivated to do this work and are you curious?
- Meaning – Understand the importance of the work that you are tasked to complete in the project.

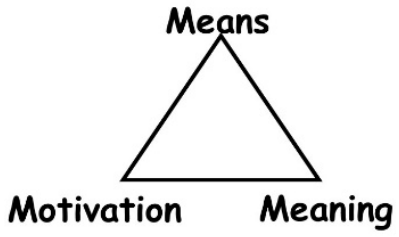


Figure 11: The triangle of Means, Motivation and Meaning (attributed to Trevor Roberts)

When asking people to be accountable, the most important thing is really knowing the people and understanding their limitations and your own limitations for the task in hand.

When dealing with a team, it is important to know the people and understand their limitations, while assisting them to develop their skills. It is also important to communicate on a personal basis whenever possible and to take time to understand what may be causing difficulties in learning and preventing people in the team from applying their experiences, with the aim of preventing mistakes from reoccurring.

Can we as an engineering body ensure that we are accountable and make every effort to get real about what the data is telling us and how to get the ongoing message to professionals as to what failures and experiences are telling us with respect to reducing risks to ALARP?

Let's get real about experiences

In Canada, when becoming a professional engineer you have the privilege (responsibility) of wearing an iron ring as a symbol of professional duty and obligation. The tradition began in 1922. The ring has long been rumored to have been created in response to the collapse of the Quebec Bridge that crosses the Saint Lawrence River. It collapsed twice and claimed 88 lives.

Every major religion in the world has remembrance rituals or celebrations of significant events or experiences. Is there a way for the engineering community to be reminded of historical events that have shaped our engineering design, construction operation, and maintenance? The historical events of interest will differ for water and tailings dams owing to the differing significance of failure modes.

Should international bodies such as ICOLD, ANCOLD, USSD, ASDSO, British Dam Association, and ICMM, to name a few, develop an annual reminder of failures and their significance? This will help to ensure that engineers, technicians, and drafters of all ages and experience are aware of failure modes and how to deal with them in design, construction, operation, and maintenance, in an effort to reduce risk to people and the environment to as low as reasonably practicable (ALARP) in accordance with GISTM requirements.

Conclusion

In the author's opinion, getting real about learning from experiences on a personal level is about understanding why I make mistakes, recognizing my own biases to learning from experiences, and being humble in my approach to all aspects of design, construction, operation and maintenance, risk evaluation and finally closure of tailings facilities.

References

Dwyer, Christopher. 2018. *Psychology Today.* Sourced from https://www.psychologytoday.com/us/blog/thoughts-on-thinking/201809/12-common-biases-that-affect-how-we-make-everyday-decisions

George, D.L. 2010. Adaptive finite volume methods with well-balanced Riemann solvers for modeling floods in rugged terrain: Application to the Malpasset dam-break flood (France, 1959). *International Journal for Numerical Methods in Fluids* 66(8):1000–1018. https://doi.org/10.1002/fld.2298

HSG48. 1999. *Reducing Error and Influencing Behaviour.* Health and Safety Executive (HSE) Second edition, TSO (The Stationary Office).

Irfan, A. Undated. Dam incidents and failures can fundamentally be attributed to human factors, ASDSO Lesson learned.

Reason, J. 1997. *Managing Risks of Organizational Accidents*. Ashgate Publishing Limited, Aldershot, UK.

Sinclair, A. 2024. People who never learn from their mistakes usually display these 9 patterns of behavior. HackSpirit. Accessed at https://hackspirit.com/people-who-never-learn-from-their-mistakes-usually-display-these-patterns-of-behavior/

Talent Insider. 2023. Why people don’t learn from failure: The psychology behind it. LinkedIn. Sourced from https://www.linkedin.com/pulse/why-people-dont-learn-from-failure-psychology-behind-talentinsider/

Southeast Rock Site Tailings Co-disposal Facility

Ben Wickland, WSP Canada Inc., Canada
Don Parsons, Imperial Metals Corporation, Canada
Anthony van Engelen, WSP Canada Inc., Canada
Scott Coombs, NewFields, Canada

Abstract

This paper presents a case study of co-disposal of tailings and waste rock at the Mount Polley Mine, British Columbia, Canada. Approximately 2.2 M m^3 tailings were excavated from Springer Pit over 12 months and stored in the Southeast Rock Disposal Site (SERDS) tailings co-disposal facility. The design concept was to place tailings on the crest of an existing 60 m high rock storage facility. Berms were constructed with rock around to form cells for the tailings and used as haul roads. The berms were raised by the upstream method in 5 m lifts to a total height of 20 m. The design includes overall outer slopes of 2H:1V and a 5 m cover of rock; stores only non-acid generating materials; and has no liners, filters, compaction, instrumentation, or permanent water pond. The facility was operated successfully following standard procedures for rock storage facilities at Mount Polley, with no issues related to instability, liquefaction, seepage, erosion, or water management. The facility provides a case study of tailings co-disposal in a surface facility without a permanent water pond.

Introduction

This paper presents a case study of co-disposal of tailings and rock at the Mount Polley Mine, British Columbia, Canada. Approximately 2.2 M m^3 tailings were excavated from Springer Pit over 12 months and stored in the Southeast Rock Disposal Site (SERDS) tailings co-disposal facility. The site background, facility design, construction, and operation sequence, and a summary of issues and lessons learned, are presented in this paper.

Background

The Mount Polley Mine is a copper and gold mine operated by Mount Polley Mining Corporation (MPMC), a subsidiary of Imperial Metals Corporation. The mine is located on a ridge between Polley Lake and

Bootjack Lake. Major features include the Cariboo and Springer pits, the mill complex, rock disposal sites including the SERDS, and the tailings storage facility (TSF). The mine began production in 1997 and operated until 2001, when operations were suspended for economic reasons. In 2005, the mine restarted and was in operation up to the time of the TSF breach in August 2014. During 2015 and 2016, tailings were discharged as slurry into Springer Pit from the south pit wall (Figures 1 and 2). In June 2016, the mine returned to full operations. Approximately one-third of the tailings were dredged from Springer Pit and pumped as slurry to the TSF between March 2016 and October 2019. Mining operations were suspended again in May 2019 for economic reasons and the site remained in care and maintenance until late 2021. Approximately 2.2 M m^3 of tailings remained in Springer Pit at the end of 2021.



Source: MPMC, 21 June 2021 Satellite Orthophoto.

Figure 1: Mount Polley Mine site in 2021
(the TSF is to the south, and is not the subject of this paper)



Source: L. Nikl.

Figure 2: Springer Pit (left), and Cariboo Pit (right) in 2021, looking north

The free water was pumped out of Springer Pit in 2022. The tailings were dewatered from September 2022 to May 2023 by pumping from three wells installed in the tailings from rockfill causeways. Tailings were excavated from May 2023 until May 2024 in 12 m high benches plated with 1 to 2 m of rock (Figure 3). The tailings held near-vertical faces that sometimes toppled during excavation, calving in 1 to 3 m thick slabs, and did not flow or liquefy. No seepage from the bench faces in tailings was observed during excavation.



Figure 3: Excavation of tailings from Cariboo-Springer Pit (top – looking west; bottom – looking southeast)

SERDS tailings co-disposal facility design

The design concept was to place tailings excavated from Springer Pit in cells constructed with rock on the crest of an existing rock disposal site – the SERDS (see Figures 1 and 4). The design concept is shown in Figure 5.



Figure 4: Southeast rock disposal site in 2021 prior to tailings placement (view of crest looking north)

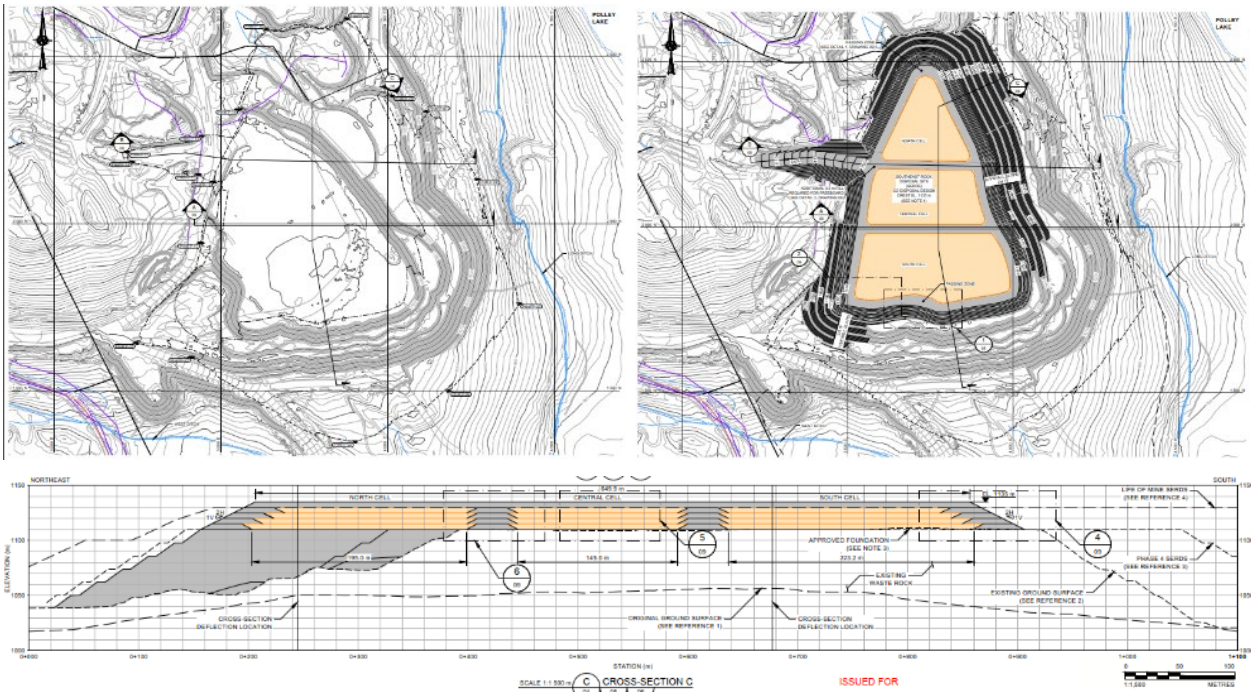


Figure 5: Southeast rock disposal site tailings co-disposal facility design

The design construction sequence considered:

- Widening of the existing crest platform using rock excavated from the Cariboo-Springer Pit.
- Construction of berms on the crest to form cells for tailings storage.
    - Berm construction was staged in 5 m lifts, constructed by the upstream raise method to a total height of 20 m.
    - The rock berms were intended to be used as haul roads to limit traffic over tailings. The design berm crest width was 27 m.
- Storage of tailings and rock excavated from Springer Pit in the cells.
    - The design storage capacity was 3.8 M m^3, which was conservatively overestimated to allow for increase in volume on excavation and for storage of rock with the tailings. The loads reporting to the SERDS could be tailings only, a combination of rock and tailings, and/or rock only. The tailings were anticipated to require surfacing with rock in the pit and in the cells at the SERDS for trafficability and access.
    - Tailings placement by dumping short and pushing into the cells with a bulldozer. The berm alignments limited bulldozer push distance to approximately 100 m.
    - Water management in the cells by collection in sumps and pumping to a downstream surface water management system.
    - Capping the cells after tailings placement with 5 m of rock to control erosion.
- Rock could be placed concurrently in the portions of the SERDS outside the cells and around the toe, which buttresses the outer slopes (not shown in Figure 5).
- Operation follows standard operating procedures for rock disposal sites at Mount Polley.

The facility does not have a permanent water pond, instrumentation, filters, liners or impermeable elements, does not require compaction, and does not rely on the tailings for stability. Rock and tailings placed in the SERDS are non-acid generating (NAG) and are only sourced from Cariboo-Springer pit.

The foundation was characterized by drilling and test pit investigations around the toe of the existing facility. The foundation generally consists of 60 to 70 m of rockfill over up to 20 m of till. No continuous glacial lacustrine units (GLU) were identified in the foundation. The design requires limiting staff presence in the runout zone of the SERDS in case of instability. Little geotechnical information was available on the tailings deposit to inform the design.

Construction and operation

Construction activities generally included:

- Platform construction. The platform of the existing rock storage facility was widened by rock placement.
- Foundation preparation. Crest areas that allowed ponding of water were ripped by bulldozer to promote infiltration. Toe areas were stripped of topsoil to found rockfill on till.
- Berm construction. Rock was hauled by truck, dumped on the berm crests, then pushed and shaped by bulldozer. Typically, end dumps were placed as a first lift, then a ramp was constructed to the 5 m lift height then dump-short and push methods were used to advance the berms over the end dumps. The outer slopes were then trimmed, and safety berms constructed along the crests.
- Cell filling. Tailings and rock were hauled by truck into the cells, end dumped on the floor of the cell, then pushed and shaped by bulldozer. Following covering of the floor of the cell with end dumps, placement was by dump short and push from the berm crests or from causeways constructed across the cells to limit bulldozer push distance. The upper 0.5 m of each 5 m lift was generally rock, to create a trafficable surface for the next lift of end dumps. Tailings placement started in May 2023 and was completed in May 2024.
- Prior to construction of the next lift, the berm crests were ripped to break up traffic surfaces. In some instances, tailings and finer grained materials on the crests were bladed into the cells.

Equipment included a P&H 2300 shovel and Komatsu PC2000 and PC4000 excavators in Cariboo-Springer Pit, CAT 789 & 785 haul trucks and Komatsu 375 bulldozers at the SERDS.

The cell geometry was modified during construction – only two of three cells were constructed to reduce foundation preparation requirements and the quantity of rock required for platform and berm construction. The design carried excess storage capacity, so only two cells were required for the tailings.

Materials included non-acid generating rock used for berm construction, loads of tailings mixed with rock loaded from the tailings benches in Springer Pit, and rock placed in the cells as causeways and running surfaces, summarized in Table 1 as of end of May 2024. The majority of the rockfill cover remained to be placed.

Table 1: Materials placed on the crest of the SERDS based on load counts (source: Mount Polley Mining Corporation – MPMC)

Tailings and rock placed in cells (tonnes)	Rock placed in cells as causeways and surfacing (tonnes)	Rock placed for berm construction (tonnes)
5,129,500	556,200	5,453,500

The tailings consistency varied from sand to silty clay (Figure 6), and placed water contents generally varied between 2% and 30% (Figure 7). The loads of "tailings" reporting to the SERDS generally included 10% to 15% rock. The sandy tailings had 3 to 4% water contents and were immediately trafficable (Figure 8). The wettest tailings slumped after placement, with water expressed at surface that collected in minor ponds then infiltrated within a few days. The tailings did not flow on excavation or placement and did not generate excess water that was required to be managed (Figures 10 and 11). Rock generally consisted of sound, hard, durable rock particles free from organic matter and other unsuitable materials.

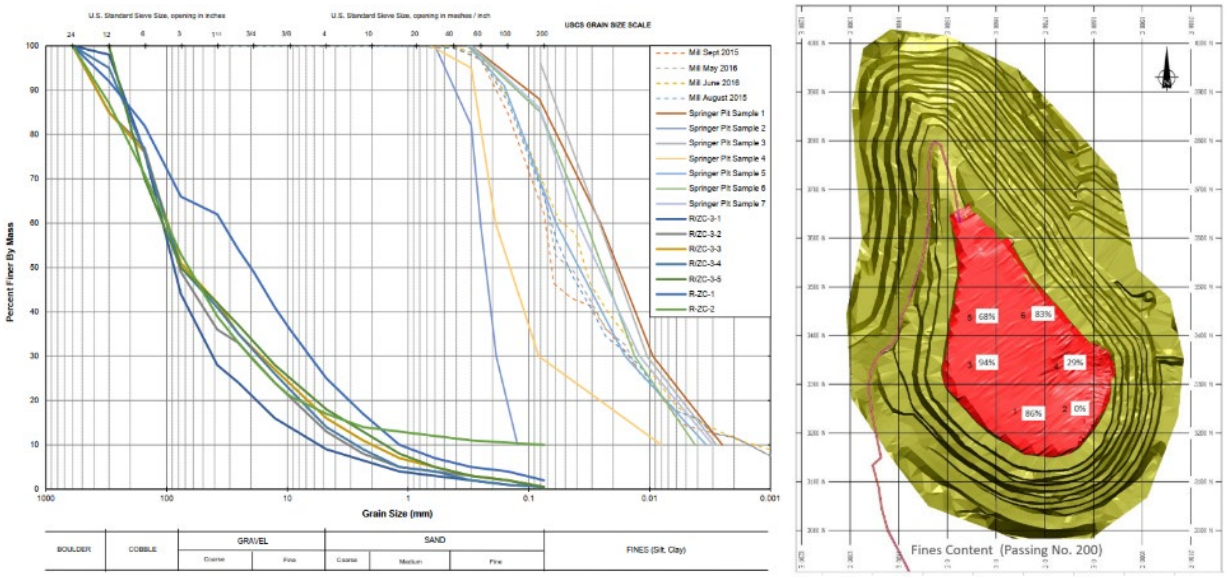


Figure 6: Gradations of tailings from Springer Pit, and historic rock gradations from TSF construction

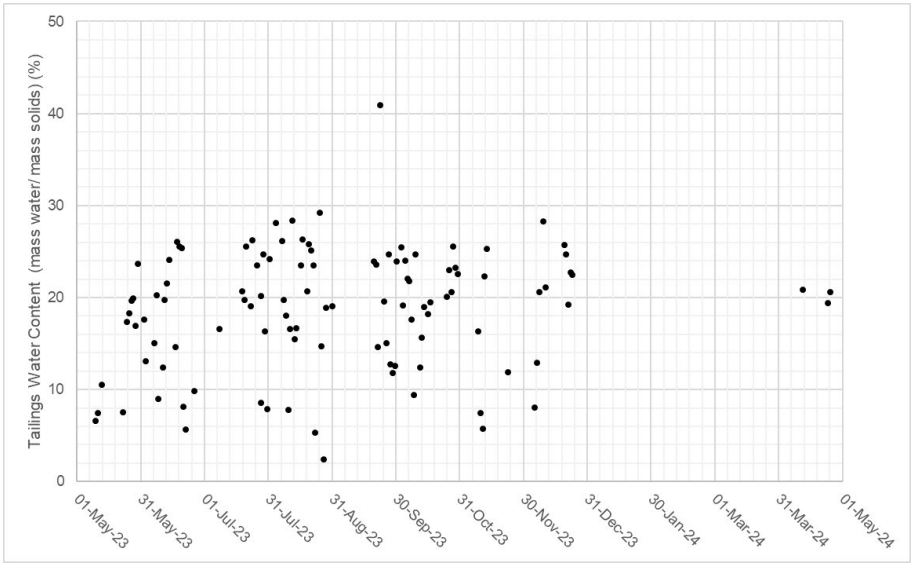


Figure 7: Water content of tailings placed in the SERDS (source: MPMC)



Figure 8: Sandy tailings (source: MPMC)



Figure 9: Finer, wetter tailings



Figure 10: Tailings surface after filling



Figure 11: Tailings In place, capping advancing from north, looking south, 14 May 2024 (source: MPMC)

Conclusion: Challenges and lessons learned

The facility was operated without any geotechnical or water management issues in the first year. No signs of instability or loss of tailings were observed. The primary operational challenge was sequencing berm construction in advance of tailings placement because less rock was available during operation than the design basis mine plan.

The primary area of uncertainty during the design process was the lack of geotechnical information on the tailings deposit in Springer Pit – only six gradations and the specific gravity were available. The design therefore included excess storage capacity, strict requirements to manage water accumulating in the cells, and large perimeter berms. During operation, the tailings performed better than expected and the facility was operated as a dry stack (with robust erosion protection). The tailings did not liquefy on excavation or placement, only two cells were required to store the tailings, and the active management of water envisioned during design was never required because insufficient water accumulated in the cells to require pumping.

Feasibility of Repurposing Wood Processing Waste as an Industrial Liner Material

Robyn Gaebel, Geosyntec Consultants, Canada
Heidi Cossey, Geosyntec Consultants, Canada
Ali Nasseri-Moghaddam, Geosyntec Consultants, Canada
Kristin Salzsauler, Geosyntec Consultants, Canada

Abstract

Owners and operators of tailings storage facilities often have to rely on manufactured liners for their facilities due to the limited availability of clay materials. An alternative and economical option is to use waste by-products, such as wood processing waste, as liner material. This study evaluated the feasibility of repurposing wood processing waste as liner material for tailings storage facilities. Sludge from wood processing facilities has high organic and moisture contents and is expected to behave similar to clay or organic soils. Previous research has shown that pulp and paper sludges have advantageous characteristics, including low hydraulic conductivity, making them suitable for use as hydraulic barriers. As a result, this material has successfully been used in geotechnical applications including landfill cover systems. We propose using wood processing waste as liner material which allows site owners and operators to take advantage of the beneficial properties of this material while addressing the limited availability of natural liner materials.

Sludge samples were received from a Canadian wood processing facility and underwent geotechnical and geochemical testing to i) quantify the process the material would have to undergo to be functional liner material and ii) evaluate the geochemical stability of the waste as liner material. Primary sludge (wood fiber) and raw water treatment plant sludge were included in this testing program. The findings suggest that the wood processing wastes assessed in this study would require handling, specifically compactive effort, but may be suitable for use as a liner material; alternatives to clay and manufactured liners.

Introduction

Availability of suitable liner materials (typically clay) for industrial applications, such as tailings storage facilities (TSFs), is often limited. Consequently, site owners and operators rely on manufactured liners to maintain facility design, which can be cost prohibitive. An alternative economical and readily available

option is the use of waste by-products as liner materials, which is discussed in detail in Gaebel (2019). Wood processing facilities generate residue (wastes) that may be processed into suitable liner materials, given their material properties. Using wood processing waste as liner material is an attractive option because of the abundance of waste available and the proximity of many wood processing facilities to mining projects. This study is one of the first to evaluate the repurposing of wood processing waste as liner material for TSFs. Previous studies on wood processing waste have been conducted but their focus was on use as a cover material rather than a subsurface liner.

The objective of this study is to evaluate the feasibility of repurposing wood processing waste as liner material for TSFs. Two materials from a Canadian wood processing facility were assessed: primary sludge (wood fiber, Material A) and raw water treatment plant sludge (Material B). To assess the suitability of Materials A and B as liner material for TSFs, this study identified a series of geotechnical and geochemical tests. The testing regime was designed to i) quantify the process the materials would have to undergo to be functional liner material; and ii) evaluate the geochemical stability of using repurposed waste as liner material. The testing program evaluated the feasibility of use of these materials by measuring their compactive effort and leachate quality.

Literature review

Beneficial use of wood processing waste

Recent studies have demonstrated successful repurposing of paper recycling and pulp and paper wastes that have characteristics similar to wood processing waste (i.e., sludge with high organic and moisture contents). These materials typically behave similarly to clay or organic soil (Slim et al., 2016). One of the main advantages of repurposing wood processing waste in geotechnical applications is its capabilities as a hydraulic barrier. For example, Van Ham et al. (2009) successfully compacted pulp and paper sludge into a suitable barrier layer in a landfill cover system in British Columbia (BC), Canada. The compacted sludge performed comparably to conventional barrier materials such as geomembranes, compacted clay liners, or geosynthetic clay liners.

Moo-Young and Zimmie (1996) found that paper mill sludge with high water content and compressibility behaved like highly organic soil. The hydraulic conductivity of the sludge was sufficient for use in a landfill cover (10^{-7} cm/s) and could be further decreased with additional consolidation and decomposition of organics (Moo-Young and Zimmie, 1996). Similarly, Alrashed et al. (2016) achieved hydraulic conductivities as low as 6×10^{-8} cm/s using pulp and paper sludge mixed with lime, polymers, or bentonite.

Studies also found that paper sludges may have compressive and shear strengths suitable for use in geotechnical applications, such as retaining walls, after sufficient compaction of the material

(Mavroulidou et al., 2019; Bizjack et al., 2021). Wood processing waste may have other favorable attributes as well, such as the ability to repair itself after being punctured or damaged ("self-healing") and acid-buffering capacity owing to its basic pH (Sylvis Environmental, 2019). Based on previous research and the specific properties of wood processing waste, it is anticipated that this material can be processed into a self-healing, geotechnically sound liner material with potential neutralizing capacity to facilitate the management of acid-generating tailings should any pore water constituents eventually pass through the liner via diffusion or (less likely) advection.

Cost savings are an additional benefit of using wood processing waste as liner material. A pre-feasibility study by Sylvis Environmental (2019) found that material and installation costs for using pulp and paper sludge as liner material would be roughly half that of a geosynthetic clay liner based on the handling requirements. As such, wood processing waste is an attractive option that warrants further evaluation regarding its suitability for use as liner material.

Potential limitations

One of the main concerns with using pulp and paper sludge in landfill cover systems in cold climates is its susceptibility to freeze-thaw cycles, which can increase hydraulic conductivity by one to two orders of magnitude (Moo-Young and Zimmie, 1996). Moo-Young and Zimmie (1996) suggested that increasing the effective stress on the material (thereby increasing consolidation) and protecting the material with a thick layer of overburden may reduce the effects of freeze-thaw on hydraulic conductivity. In the proposed application, using wood processing waste as liner material would better protect the material from freeze-thaw cycles.

The high organic content of pulp and paper waste materials could also be seen as a limitation to repurposing of this material for use in geotechnical applications. However, research has indicated that degradation of organics may improve geotechnical properties of the sludge, such as hydraulic conductivity (Moo-Young and Zimmie, 1996; Zule et al., 2007). Additional testing would be required to determine how biodegradation of organics might impact leachate quality from pulp and paper wastes; for example, decomposition of organics could result in reducing conditions, which could impact the stability of minerals like iron oxyhydroxide. Alternatively, chemical stabilizers, such as hydrated lime, may be added to the sludge to i) prevent biodegradation of organics by hindering the activity of microorganisms; and ii) enhance geotechnical properties and stability of the sludge (Alrashed et al., 2016; Mavroulidou et al., 2019; Slim et al., 2016).

Additionally, there is significant variability in wood processing between different sites. The wastes generated are likely different chemically from site to site, with the waste and sludge streams containing

potential contaminants beyond the metals, anions, and nutrients discussed in this study. This study was conducted at a prefeasibility level with two specific wastes and results could be considered facility specific.

Materials

For this study, two similar wood processing waste sludges were analyzed: primary wood fiber sludge (Material A) and raw water treatment plant sludge (Material B). Both materials are available at volumes that would theoretically be sufficient for construction use. Approximately 100 L of Material A (Figure 1) and 60 L of Material B (Figure 2) were collected from a Canadian wood processing facility in 2024 using an excavator and manual handling for storage and transportation in plastic five-gallon pails.



Figure 1: Material A at sampling

Material A was heterogeneous in terms of particle size (Figure 1) and demonstrated high compressibility with a high void ratio and low density, and a high capacity for water absorption. Material B (Figure 2) was similar to Material A, though it was generally finer grained and had a higher initial moisture content.



Figure 2: Material B in situ

Laboratory analyses

Materials A and B were shipped to ITL Testing in Port Coquitlam, BC, for geotechnical testing and ALS Global in Burnaby, BC, for geochemical testing. Geotechnical testing of the materials is crucial in understanding the compactive effort required to process the waste into suitable liner material, as well as the ease with which this processing could be completed in the field. Geotechnical testing can also indicate physical properties of the materials such as hydraulic conductivity and moisture attributes.

Materials A and B are considered non-hazardous and generally contain fine organics and inorganics, as well as food-grade polymer residual (J. Fowler, personal communication, July 10, 2024). However, geochemical assessment of the chemical properties was deemed critical in understanding the feasibility of use, specifically for any impacts to the environment and interaction with tailings or other waste material.

Geotechnical analyses included modified and standard Proctor tests (ASTM D1557, 2021a; ASTM D698, 2021b). Method C (150 mm diameter mold) was used for the standard Proctor test of Material A because the material was not homogenized before the, test and thus a larger mold was needed to accommodate the larger particle sizes. Method A (100 mm diameter mold) was used for the other Proctor tests. Four-point Proctor curves were generated for each set of Proctor tests. Samples were dried in the open air rather than in an oven, as placing the materials in an oven resulted in material deterioration, even at low temperatures. During the moisture content material conditioning, the samples were left for a longer amount of time than would have been used for clay materials to improve water absorption. The Proctor test points were developed from the saturated side, utilizing higher than optimum moisture content and then moving to points on the drier than optimum side due to the high-water absorbency expected and demonstrated by the material.

Material A needed processing prior to performing geotechnical testing to create a homogenous material for analyses. It underwent material conditioning (homogenization) using a hand blender to create smaller sized particles for better homogeneity of water content for the modified Proctor analyses. The homogenized Material A sample is presented in Figure 3.



Figure 3: Homogenized sample of Material A

This additional processing would have altered the initial particle size distribution of this material, equating to a need for additional handling or processing requirements for use in the field. Material B was more homogenized and had a smaller particle size than Material A. As such, Material B did not require material conditioning (homogenization) prior to geotechnical testing. Material B was also provided at a higher moisture content.

Geochemical testing involved analyzing the leachate quality of both Materials A and B. Leachate quality was evaluated by measuring pH, alkalinity, and concentrations of nitrogen, phosphorous, sulfate, and metals in shake flask extraction tests of Materials A and B (3:1 ratio with deionized water). The analyses performed followed modified versions of the methods outlined in MEND (2009), US EPA (1997, 2014), and APHA, AWWA, and WEF (2023).

Results and discussion

Results of the Proctor tests for Materials A and B are presented in Table 1. Material A underwent both modified (Method A) and standard (Method C) Proctor tests, whereas Material B was analyzed using the standard Proctor test (Method A). The initial moisture content for Material A was 120%, whereas the initial moisture content for Material B was over three times higher, at 400%. The optimum moisture content for each of the three tests was similar to or lower than the initial moisture content. This indicates that both materials would need to be dried prior to compaction in the field.

Material A underwent both standard and modified Proctor testing for comparison in processing and to identify the effect that processing could have. Because the method used for each of the Proctor tests varied, the compactive energy of each test was calculated using Equation 1 (Das, 2013). Given the higher compactive effort (larger hammer weight, higher drop height, and increased number of lifts) associated with the modified test (2,696 kN-m/m^3 for Method A), this test resulted in a higher maximum dry density (577 kg/m^3) and lower optimum moisture content (68%) for Material A relative to the standard test, which used a lower compactive energy (588 kN-m/m^3) and resulted in a maximum dry density of 412 kg/m^3 and an optimum moisture content of 121 wt%.

$$Compactive\ energy = \frac{(number\ of\ blows\ per\ layer)\ x\ (number\ of\ layers)\ x\ (weight\ of\ hammer)\ x\ (height\ of\ drop)}{volume\ of\ mold} \quad (1)$$

Table 1: Geotechnical Proctor results for Materials A and B

Sample Material	Proctor Test	Initial Moisture Content (%)*	Optimum Moisture Content (%)	Maximum Dry Density (kg/m³)	Compactive Energy (kN-m/m³)
Material A: Primary Sludge	Modified Proctor Method A (ASTM D1557, 2021a)	120	68	588	2696
Material A: Primary Sludge	Standard Proctor Method C (ASTM D698, 2021b)	120	121	412	588
Material B: Raw Water Treatment Plant Sludge	Standard Proctor Method A (ASTM D698, 2021b)	400	45	981	591

* Values are estimates rather than exact measurements

Material B had a higher maximum dry density (981 kg/m^3) and lower optimum moisture content (45%) than Material A when similar or lower compactive energy was used. This indicates that Material B would require less compactive effort in the field to be processed into a liner. Material B also required less physical conditioning to create a homogenous material to work with, and Material B bound together between subsequent lifts whereas Material A did not, as shown in Figure 4. This may be because Material A is more fibrous and has a larger particle size than Material B. Material A was also observed to have a lower water absorption capacity than Material B.

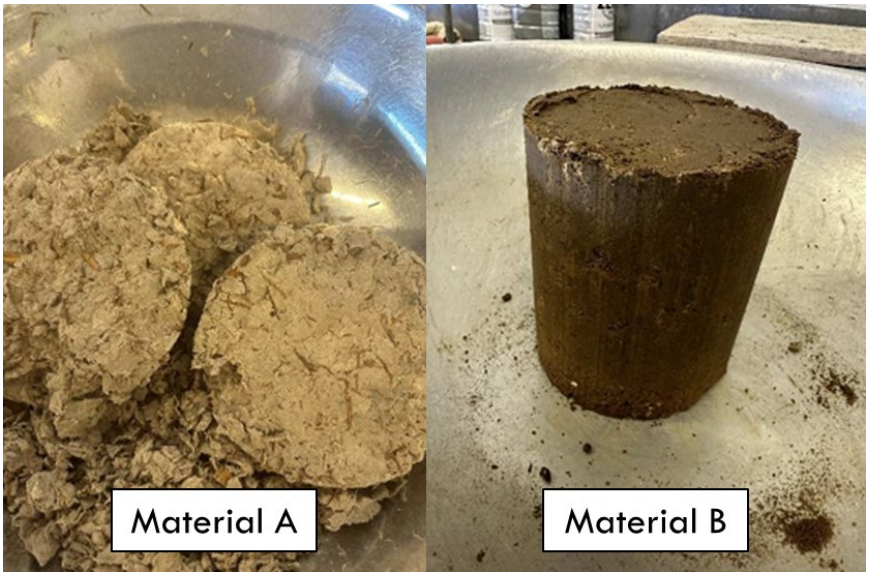


Figure 4: Materials A and B after Proctor testing

Particle size distribution tests were excluded from this study due to the nature of the materials and budget limitations. Estimates of the particle size were conducted as part of the material handling for the Proctor testing and indicated that Material A was similar to a well graded gravel before processing while Material B was a homogenous clay. It was noted once Material B was dried, the material handled identically to clay with a dry density of more than twice Material A.

Results of duplicate shake flask extraction tests for Materials A and B are presented in Table 2 (see next page). Shake flask extractions evaluate the soluble constituents that are most readily leached from material. Evaluating soluble constituents in the wood processing waste sludges is an important component of this study, as the soluble constituents could eventually be leached to the surrounding environment if the materials were repurposed for liner application.

The leachate from Material A was basic, with an average pH of 10.1. The average alkalinity was 379 mg/L as $CaCO_3$, which suggests that the material has a high buffering capacity. The leachate hardness was high for Material A, with an average of 208 mg/L, which can be attributed to relatively high concentrations of leachable magnesium. Concentrations of leachable nutrients and metals were generally low or below detection for Material A. Material B leachate had a circumneutral pH of 7.5 and a lower alkalinity (29.3 mg/L as $CaCO_3$) than Material A. This suggests that Material B could have a lower acid-buffering capacity compared to Material A. Leachable metals in Material B were generally similar to those of Material A, though select metals (aluminum, manganese, and strontium) had higher leachable concentrations in Material B. Compared to Material A, the nutrients ammonia and nitrate were elevated in Material B leachate, with average concentrations of 1.78 and 6.28 mg/L as N, respectively. Concentrations of other parameters were generally similar between the two materials, though Material A had higher concentrations of leachable salt (sodium, 170 mg/L) than Material B.

Taken together, these results suggest that leachate generated from Materials A and B would generally be of acceptable quality and leachate from Material A would have acid-buffering capacity. However, the shake flask extractions were performed using deionized water as the leaching solution, with a 3:1 solid to liquid ratio, and 24-hour residence time. In the field, the leachate quality of these materials may be different due to the chemistry of the water, the ratio of solids to liquids, and the contact time (MEND, 2009).

While concentrations of metals were generally low or below detection in the leachate for Materials A and B, as noted, wastes from other facilities may differ. Because of the variability in wood processing wastes, results are limited to the material that was assessed. Most of the literature evaluating geotechnical applications of pulp and paper wastes did not evaluate the geochemical characteristics of the waste, though Van Ham et al. (2009) found that pulp and paper sludge in a landfill barrier system had low levels of nutrients but elevated concentrations of salt. Additional studies of these types of materials should include geochemical testing as part of evaluating their suitability for repurposing in geotechnical applications.

Table 2: Geochemistry shake flask extraction results for Materials A and B. Results presented as average ± standard deviation

Analyte	Units	Material A	Material B
Alkalinity, total (as $CaCO_3$)	mg/L	379 ± 16	29.3 ± 1.3
Aluminum	µg/L	28.9 ± 19.7	120 ± 6
Ammonia, total (as N)	mg/L	0.03 ± 0.00	1.78 ± 0.02
Antimony	µg/L	0.85 ± 0.06	0.35 ± 0.00
Arsenic	µg/L	< 1.0	3.9 ± 0.0
Barium	µg/L	18.2 ± 1.1	29.2 ± 0.4
Beryllium	µg/L	< 0.50	< 0.50
Bismuth	µg/L	< 0.50	< 0.50
Boron	µg/L	20.5 ± 0.7	< 10.0
Cadmium	µg/L	< 0.050	< 0.050
Calcium	mg/L	1.7 ± 0.1	17.4 ± 0.0
Chromium	µg/L	1.46 ± 0.07	< 0.50
Cobalt	µg/L	0.11 ± 0.01	< 0.10
Copper	µg/L	9.2 ± 0.7	5.8 ± 0.0
Hardness (as $CaCO_3$)	mg/L	208 ± 0	65.5 ± 0.4
Iron	mg/L	< 0.030	< 0.030
Lead	µg/L	< 0.10	< 0.10
Lithium	µg/L	< 5.0	< 5.0
Magnesium	mg/L	49.6 ± 0.1	5.3 ± 0.1
Manganese	µg/L	2.0 ± 1.2	23.7 ± 0.2
Molybdenum	µg/L	4.2 ± 0.2	1.6 ± 0.0
Nickel	µg/L	1.6 ± 0.3	2.2 ± 0.0
Nitrate (as N)	mg/L	0.04 ± 0.01	6.28 ± 0.65
Nitrite (as N)	mg/L	0.32 ± 0.10	0.20 ± 0.01
pH	pH units	10.1 ± 0.0	7.5 ± 0.0
Phosphorus	mg/L	0.08 ± 0.01	0.03 ± 0.00
Potassium	mg/L	12.5 ± 1.0	4.2 ± 0.1
Selenium	µg/L	0.52 ± 0.03	0.83 ± 0.05
Silicon	mg/L	0.60 ± 0.03	0.83 ± 0.04
Silver	µg/L	< 0.050	< 0.050
Sodium	mg/L	170 ± 17	7.5 ± 0.3
Strontium	µg/L	15.3 ± 0.2	82.8 ± 0.6
Sulfate	mg/L	43.2 ± 5.7	7.7 ± 0.1
Sulfur	mg/L	39.1 ± 4.2	3.7 ± 0.0
Thallium	µg/L	< 0.10	< 0.10
Tin	µg/L	< 0.10	< 0.50
Titanium	mg/L	< 0.010	< 0.010
Uranium	µg/L	0.11 ± 0.01	0.02 ± 0.00
Vanadium	µg/L	1.3 ± 0.1	< 1.0
Zinc	mg/L	< 0.010	< 0.010

Conclusion

The availability of suitable natural liner materials for industrial applications such as TSFs is often limited, leading to reliance on manufactured liners, which can be cost prohibitive. This study explored an alternative solution by evaluating the potential use of wood processing waste as liner material. Given the abundance of wood processing residues and their proximity to many mining projects, this option is both economical and practical, though effort and handling may be required.

Through geotechnical and geochemical testing of primary wood fiber sludge (Material A) and raw water treatment plant sludge (Material B) from a Canadian wood processing facility, this study confirms that these materials could be repurposed. The performance of the materials, specifically Material B, was promising as these waste products were able to be processed and compacted using standard practices to produce results similar to geotechnical materials. As noted, Material B specifically exhibited properties similar to homogeneous clay, preliminarily indicating it would be a suitable hydraulic barrier and act as a liner material. Optionality also would exist to mix materials to offset the dry aggregate nature of Material A with the clay-like properties of Material B for a better performing material. Further, geochemical testing indicated that leachate generated from Materials A and B would generally be of acceptable quality.

The testing program was designed to better understand the processes required to transform these materials into functional liners and to evaluate their geochemical stability. The findings of this research indicate a promising potential for using wood processing waste as an effective and sustainable liner material for TSFs. This approach not only addresses the issue of limited natural liner materials but also offers an environmentally friendly method of waste management for wood processing facilities.

Future studies and further testing are recommended to optimize the processing techniques and fully understand the long-term performance of these repurposed materials. To confirm the behavior of the materials is consistent, the laboratory analyses discussed here, as well as other laboratory analyses including particle size distribution and hydraulic conductivity, should be conducted. Microcosm studies could also be conducted to better understand how organics degradation might impact both geotechnical and geochemical performance.

As this study provides a proof-of-concept, next steps are envisioned to include the laboratory investigations detailed above, as well as desktop studies identifying the available and required volumes of material needed for a liner. At the field scale, next steps include benchtop or field level development of cells which would allow for i) bench scale validation of concept and ii) an evaluation of the constructability and long-term geotechnical and geochemical performance of these materials.

Acknowledgements

The authors would like to thank the Canadian wood processing facility for their support and for providing materials for with this study. The authors acknowledge the support and assistance received from ITL Testing and ALS in completing the analytical portion of this study. The authors are also thankful for financial support provided by Geosyntec's Canadian Operations Research and Development (CORD) Committee in conducting this research.

References

Alrashed, A., J. Atkinson, N. Alotaibi and X. Tan. 2016. Alternative Landfill Liner – Final Report. SK Geotechnical Company.

American Public Health Association (APHA), American Water Works Association (AWWA), and Water Environment Federation (WEF). 2023. Standard Methods for the Examination of Water and Wastewater, 24th ed. Eds W.C. Lipps, E.B. Braun-Howland, T.E. Baxter.

American Standard for Testing Materials (ASTM). 2021a. Standard Test Methods for Laboratory Compaction Characteristics of Soil Using Modified Effort (56,000 ft-lbf/ft^3 (2,700 kN-m/m^3)) D1557-12. West Conshohocken, US.

American Standard for Testing Materials (ASTM). 2021b. Standard Test Methods for Laboratory Compaction Characteristics of Soil Using Standard Effort (12,400 ft-lbf/ft^3 (600 kN-m/m^3)) D698-12. West Conshohocken, US.

Bizjack, K.F., B. Likar, A. Mladenovic and V.Z. Serjun. 2021. Valorized deinking paper residue as fill material foe geotechnical structures. *Sci. Rep.* 11: 22636.

Das, B.M. 2013. *Fundamentals of Geotechnical Engineering*. 4th ed. Stamford: Cengage.

Gaebel, R. 2019. Rethinking waste. *Proceedings of Tailings and Mine Waste 2019*, Vancouver, CA, November 2019.

Mavroulidou, M., S. Hassan, C. Gray, M.J. Gunn, A. Youssef and J. Garelick. 2019. Geotechnical properties of paper recycling waste streams. *Proceedings of the XVII European Conference on Soil Mechanics and Geotechnical Engineering,* Reykjavik, IS, September 2019.

MEND. 2009. Prediction Manual for Drainage Chemistry from Sulphidic Geologic Materials. MEND Report 1.20.1. Smithers, CA.

Moo-Young, H.K. and T.F. Zimmie. 1996. Geotechnical properties of paper mill sludges for use in landfill covers. *J. Geotech. Eng.* 122(9):768–775.

Slim, G.I., M. Morales, L. Alrumaidhin, P. Bridgman, J. Gloor, S.T. Hoff and W.I. Odem. 2016. Optimization of polymer-amended fly ash and paper pulp millings mixture for alternative landfill liner. *Procedia Eng.* 145: 312–318.

Sylvis Environmental. 2019. Pre-Feasibility and Costing Options Assessment for the Use of Organic Residuals in Mining Operations. Treasury Metals Inc.

United States Environmental Protection Agency (US EPA). 1997. Method 300.1: Determination of Inorganic Anions in Drinking Water by Ion Chromatography. Revision 1.0. Cincinnati, US.

United States Environmental Protection Agency (US EPA). 2014. Method 6020B (SW-846): Inductively Coupled Plasma-Mass Spectrometry. Revision 2. Washington, US.

Van Ham, M., L. Dampier, K. Morton and S. Mullen. 2009. Pulp and paper sludge as a barrier layer in landfill closure: A new opportunity. Pulp and Paper Canada.

Zule, J., F. Černec and M. Likon. 2007. Chemical properties and biodegradability of waste paper mill sludges to be used for landfill covering. *Waste Manage. Res.* 25:538–546.

Operational Processes for Stacking Filtered Tailings – Itabira Case Study

Rodney Silva, Vale S.A., Brazil
Felipe Bonucci, Vale S.A., Brazil
Danilo Eloi, Vale S.A., Brazil
Miguel Paganin, Vale S.A., Brazil
Weslley Maciel, Vale S.A., Brazil
Jonas Guedes, Vale S.A., Brazil
Maira Drumond, Vale S.A., Brazil
Mateus Leite, BVP Geotecnia Hidrotecnia, Brazil

Abstract

The process of stacking filtered tailings has several stages that are directly correlated and therefore interdependent. This process is divided into operational and geotechnical control stages, which are: the granulometric control stage of the tailings produced at the plant, the tailings transportation stage using trucks, the tailings disposal stage in the areas, the tailings spreading stage, the treatment stage using harrow tractors to reduce moisture, the testing stage to determine the moisture of the material for compaction, the topographic survey stage to determine the thickness of the layers, the area leveling and compaction stage, and the void ratio testing stage to approve the layer. In specific cases during rainy periods, additional stages of disposal in areas for moisture reduction and moisture testing may be necessary.

The operational capacity of the stack is directly related to area and to the amount of equipment available, including bulldozers, tractors with plow harrows, graders, compaction rollers, trucks, and the area available for disposing the material, since due to the difference between the moisture at which the tailings leave the plant and the moisture at which they must be compacted in order to guarantee the control parameters determined in the project, there is an average of four days of work on the spread material.

The entire process is controlled by systems that determine in which areas the material should be disposed of, showing how long the material has been undergoing treatment to reduce moisture, with a demonstration of working time and the results of moisture tests carried out for control reasons. In this same system, the entire topographic process, and the final release of the area with the void ratio is launched, speeding up the flow of information and ensuring safety in stacking operations.

Finally, control of the design geometries is essential for the structural stability of the operational stages. All this control is carried out by a topographical team, accompanied by a team of designers and registration engineers (EoR), following all the geometric assumptions necessary for the minimum safety factors, complemented by analysis of the controls and treatment of the results of the instrumentation in the operational phase.

Introduction

In the iron ore concentration process, physical-chemical processes are used to concentrate the ore and reach the levels necessary to meet the commercial specifications of the product. In this separation, the gangue minerals are separated from the minerals of interest and are generated: the concentrated product with the highest content of the mineral of interest; and the tailings with the lowest content of the mineral of interest and the highest content of gangue minerals (Wills and Finch, 2015). This tailing, as it is not of economic interest, is discarded, being historically disposed of in structures such as dams.

After the tragedies that occurred with tailings dams in Mariana and Brumadinho, the Brazilian mineral industry began to look for alternative ways of disposing of tailings. For this purpose, stacking of filtered tailings has been developed simultaneously by several mining companies, being an operationally viable form of disposal and with associated potential damage lower than that of a hydraulic tailings dam (Cacciuttolo and Atencio, 2023).

In iron mining, the most common concentration process is wet flotation, generating a concentrate pulp and a tailings pulp (Houot, 1983). To make these tailings manageable, it is necessary to dewater them, which can be achieved efficiently through filtration. After filtering, the tailings can be loaded and transported using traditional mining loading and transport equipment.

Finally, this material arrives at the disposal site and must go through the stacking process, which includes a series of unit operations such as spreading, leveling, topographic checking, homogenization, moisture treatment, compaction, and geotechnical tests that must guarantee project specifications. necessary for the safety of the stack (Guimarães, 2011).

In 2019, the Itabiruçu Dam in the Itabira mining complex was shut down. This dam was where most of the hydraulic tailings generated in the concentration plants were directed. In the short term, these tailings were provisionally disposed of in unexhausted pits. However, the volume available in these pits was restricted, giving rise to the challenge of quickly implementing the innovative processes of filtering and dry stacking tailings to mitigate impacts on ore production.

The filtration at the Conceição I plant began operating in 2020, but its capacity was insufficient to accommodate 100% of the tailings generated at the plants. Between 2020 and 2021, experimental landfills were carried out that subsidized the Itabira stacking filtered tailings projects. In 2022, the operation of the

Conceição II filtration began, which was built with capacity to serve the two concentration plants of the Conceição mine. In the same year, the dry stacking of filtered tailings began at the waste and tailings disposal stack (WTDS or PDER in Portuguese), Ipoema Borrachudo (Figure 1). And at the end of 2023, the Cauê filtration plant was started up, completing the construction of filtration plants to serve all of Itabira's tailings with a total capacity of 42 Mt per year. This is one of Itabira's biggest challenges – compacting approximately 115,000 tons per day.

The objective of this paper is to carry out a case study of filtered tailing piling in Itabira, describe its operational processes, and discuss improvements and difficulties associated with it.

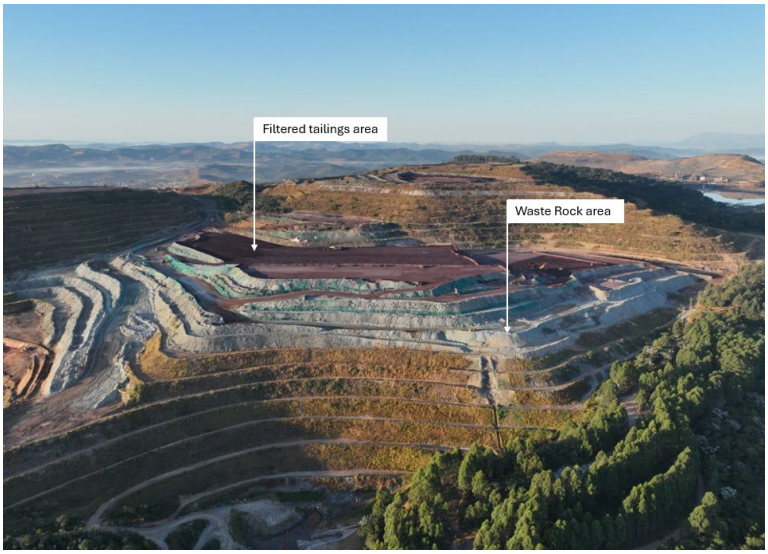


Figure 1: Filtered tailings and tailing rock pile – Ipoema Borrachudo

Methodology

The activity of compacting landfills in conventional civil works was operationally consolidated and rigorously studied throughout the 20th century, with large projects of dams, bridges, airports and roads that were a necessity for human development at the time (Lokkas et al., 2021). From all this demand came the peak of the development of soil mechanics, with significant publications such as *Soil Mechanics in Engineering Practice* by Karl Terzaghi and Ralph B. Peck, to support the development and implementation of large projects around the world. The work carried out by the entire global engineering body was focused on effective controls on soil compaction. At that time, the compaction of filtered tailings was not necessary in Brazil nor around the world, given the availability of dams for the disposal of hydraulic tailings and the high cost of operation (Cacciuttolo and Atencio, 2023).

The first step in operationalizing the filtered tailing disposal project in Itabira was to seek to adequately understand all the characteristics of the filtered tailing, based on characterization studies and

experimental landfills to evaluate the material's response to the compaction process. The main basis for starting operations was associated with compaction practices already applied to soils, but always observing and understanding the divergences arising from the difference between soils and tailing, making adaptations to the process to enable the compaction of the large volume of filtered tailing in a single day.

The second step in operationalization was to understand all the criteria listed in the structure's operating manual and associate them with the necessary resources to be able to execute all the steps, fulfilling the operating rate necessary to compact the entire mass of tailing produced in the period. Based on this assessment, we were able to divide the process into large teams: Production and destination; Stacking operation; Auxiliary teams; and Quality control.

The production and disposal group is associated with the tailing filtration plant, where we need to guarantee the physical and chemical characteristics of the material, which informs decisions as to which destination will be given to the tailing, depending on the filtration output moisture. The compaction operation group has all the equipment for transporting, loading, spreading, homogenizing, treating and compacting the filtered tailing. Auxiliary teams play a fundamental role in the entire operation cycle and are home to all the topography and laboratory personnel. The quality control team is responsible for construction inspection; their main objective is to ensure compliance with the structure's operating manual and to approve the layers.

This was the first stage of structuring the process. From there, the quantity of equipment and people in the operation of the structure was developed, in addition to the structuring of the operational cycle and management systems.

Results and discussion

This section will be subdivided into the macroprocesses that make up the filtered tailings disposal chain: filtration, loading and hauling, and dry stacking.

Filtration

In Brazil, the traditional process of concentrating itabiritic iron ores involves the stages of crushing, sieving, grinding, desliming, classification, flotation, and filtering of the product, in addition to auxiliary stages such as belt transport or pumping (Araujo and Peres, 2006). Tailings filtration is a new operation within processing plants, and seeks to transform the waste arising from desliming and flotation, which is in a pulp condition, with a low percentage of solids, into a material with relatively low moisture that can be handled by loading and hauling equipment.

In Itabira, separate buildings were built for filtration. The hydraulic waste from the concentration plants is pumped to these buildings, reaching an agitator tank where the filtration plant process begins, as

seen in Figure 2. Since the tailings have a significant percentage of fines (between 10 and 20% of materials passing through the 10 μm sieve), after leaving the agitator tank, it passes through a battery of cyclones that separate the finer material that will undergo thickening from the coarser material that will go directly to the tanks that feed the filters.

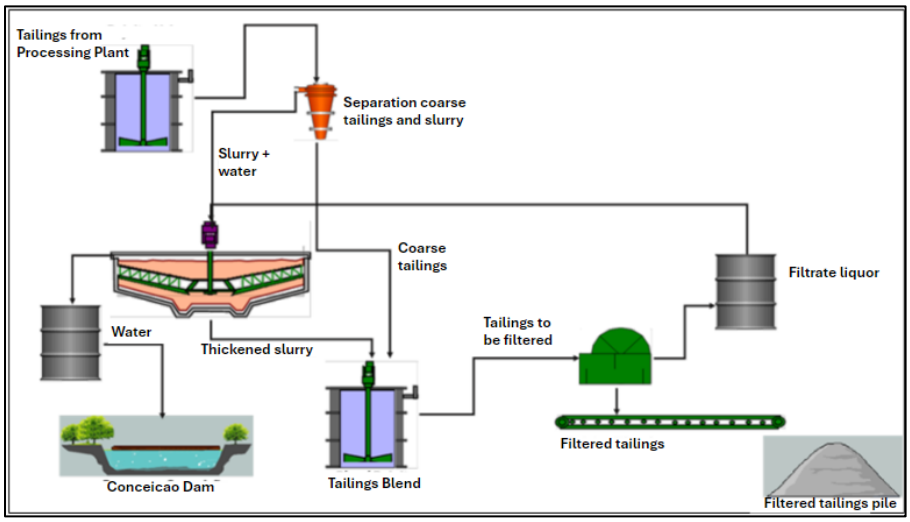


Figure 2: Simplified flowchart of a tailings filtration plant

The thickener densifies the finer portion of the material, recovering water, and optimizing the performance of the filters to allow filtration to achieve a lower final moisture content of the material than if the tailings went straight into the filters. After thickening, the fines exit through the thickener underflow and go to the tank that will feed the filters. The water obtained from the thickener is directed to a dam that no longer receives tailings, only water that is reused in the concentration plant.

The filters at the Itabira filtration plants are vertical filters, which use a technology that achieves an adequate reduction of material moisture. Less maintenance is required for them. Consequently, they have greater physical availability than flat filters or press filters (Dahlstron and Silverblatt, 1977). The filtrate liquor that leaves the filters returns to the thickener, to keep the solids in the circuit and send only clean water to the dam. The filtered tailings fall onto belt conveyors, which take them to the buffer pile where the material will be loaded and transported.

On the belt conveyor, through an automatic sampler, aliquots are collected every 15 minutes, to make up a sample that is collected and sent every hour for physical-chemical laboratory tests. These tests assess moisture, chemical composition ,and grain size distribution of the material, which serves as a basis for evaluating the quality of the material.

There are limits specified in the project for the grain size distribution of the material that can be stacked, as seen in Figure 3. If there is any disturbance in the process that generates material that falls

outside these limits, it will be rejected. It cannot be stacked and has to be discarded in another disposal location.

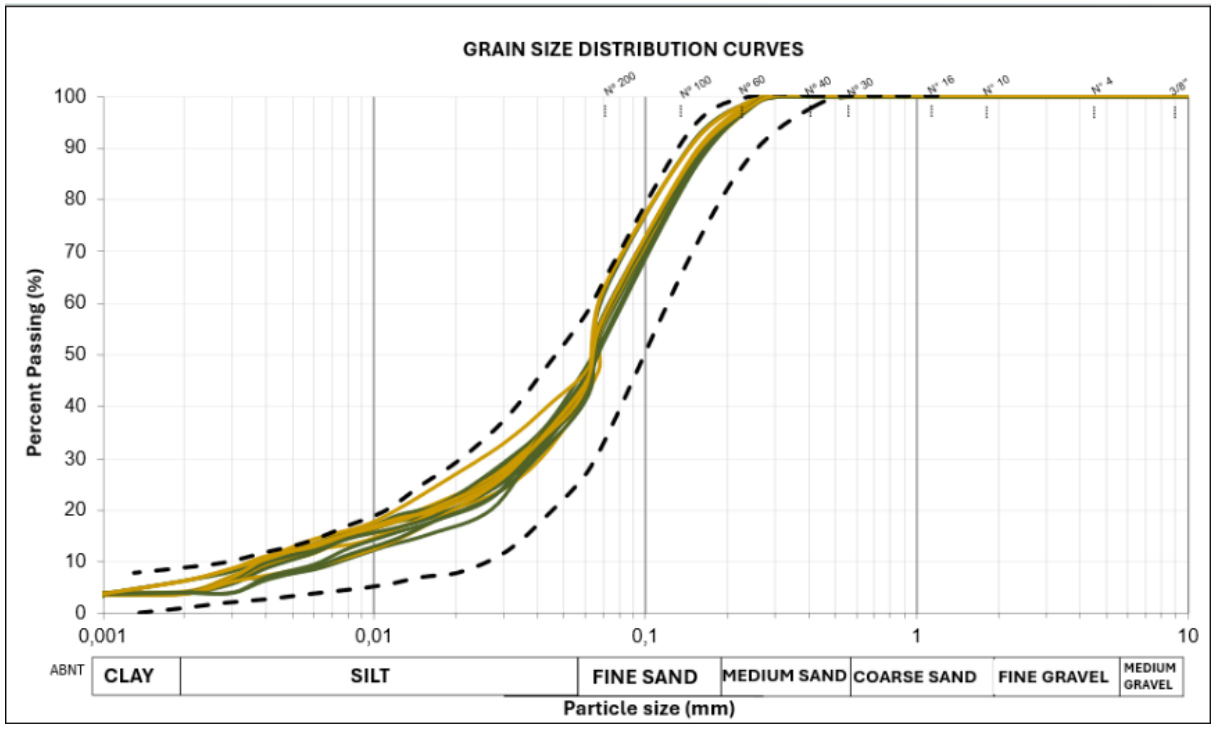


Figure 3: Grain size curves of the filtered tailings

Moisture, on the other hand, does not disqualify the material. However, if it exceeds a certain limit, it will lengthen the time for treatment and final drying of the waste in the stacking area, reducing the productivity of the available area. In this case, the material is sent to storage areas for drying, but will later be recovered and dry stacked. On the other hand, when the material is within the particle size and humidity limits, it is sent directly to the stacking area.

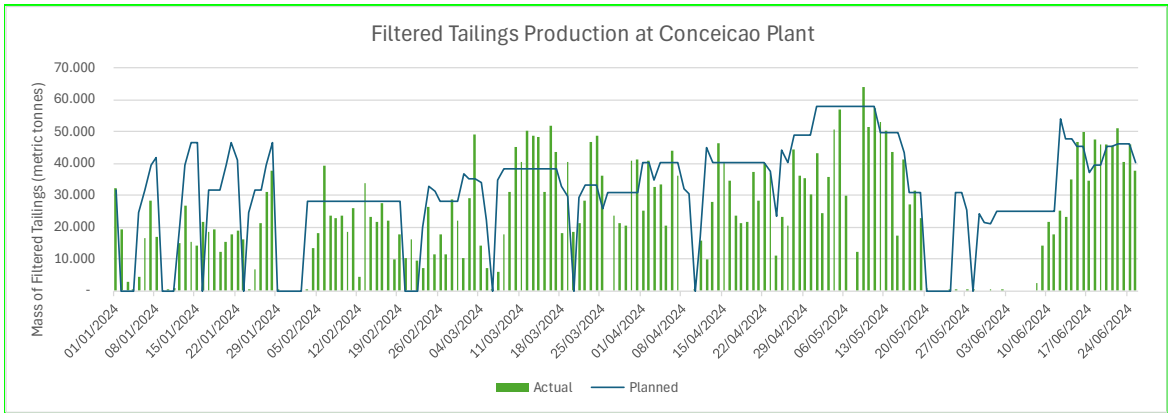


Figure 4: Daily production of the filtered tailings

Loading and hauling

After filtering, belt conveyors take the already filtered waste to a mobile boom that will form the tailing buffer pile for loading. This spear rotates with a constant radius, forming a pile with a circular arc shape, with a geometry similar to a "bean." For this reason, this stack is called the bean stack.

In this area the boom rotates, controlled by automatic systems, forming a pile on one side only, to guarantee the safety of the loading operation. In other words, while the pile on the right side is being formed, material is not falling into the pile on the left side. This allows the loading machine to operate without the risk of material falling onto itself. In addition to the safety of the equipment, this division into two piles facilitates control of the quality of the material. As soon as a pile completes its formation, the laboratory results of the analyses of the samples collected on the belt is recorded, and the control room checks the quality of the material in terms of particle size and humidity, to define the destination of the material.

With a defined destination, the material is loaded by LeTourneau L-2350 large loading equipment (as shown in Figure 5) and transported by CAT 793F off-road trucks. The same equipment is used to load ore and waste, bringing flexibility to mine operations in the use of resources.



Figure 5: Loading and hauling of filtered tailings at the "bean" stock pile

Dry stacking

PDER Ipoema Borrachudo was designed to carry out the controlled disposal of filtered tailings and rock waste, originating from the process of processing iron ore from the Conceição Mine and Minas do Meio

mine. The characteristics of the materials to be stacked are low iron content and low moisture content.

PDER Ipoema Borrachudo is subdivided into smaller sections, in order to facilitate the control of activities and the technological control of stacking. These zones are called banks, sections and lanes, which evolve vertically in layers.

- Bank: elevated subdivisions of PDER, with names that are related to their quota (e.g. 1010, 1020, 1030, 1040). It is made up of a set of bays, which rise in layers and joint heights.
- Sections: superficial subdivisions of the bank, named after variations of the phonetic alphabet (e.g. Alfa, Bravo, Charlie, and others). This is made up of a set of 2 or 3 tracks.
- Lanes: the lowest degree of superficial subdivision of the section, its name is the composition of the section name and number (e.g. Alpha F1, Alpha F2, Alpha F3). The area and volume are pre-defined, usually 2,300 tons of filtered tailing per lane. Note: the operating manual limits the volume of lanes to 1,000 m³. Therefore, for filtered tailing with a density of 2.3 t/m³, the capacity is 2,300 t.
- Layer: the vertical subdivision of the bench, with a thickness that can vary from 35 to 55 cm.

Visual identification of the subdivisions of the tracks is carried out using white spikes, which are seen only when in the field. All spatial and geographic control of the stack is supported by a bay management system and other geolocation technologies (terrain, grid control, and others).



Figure 6: Spatial subdivisions of the stacking area as seen in the operational control software

The filtered tailing stacking operation is cyclical, with the PDER bands evolving sequentially in layers of defined thickness. All cycles are standardized, with pre-defined steps and objective criteria for quality

approval. The operational team must conduct activities so that the tracks evolve quickly, but at all times must also guarantee compliance with geotechnical quality criteria and safety rules and good practices.

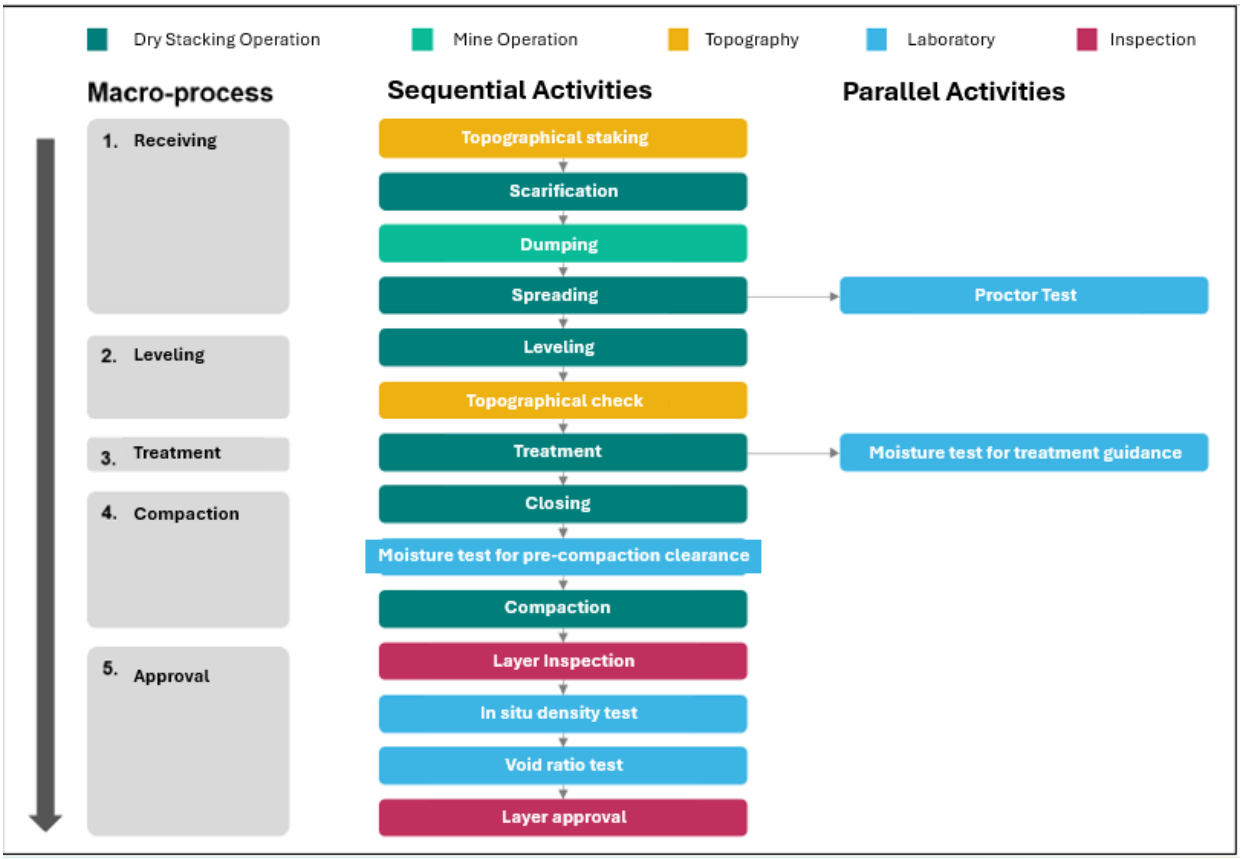


Figure 7: Operational cycle of the tailings dry stacking in Itabira

Receiving macroprocess

The receiving macroprocess consists of topographic marking, scarification, tipping, and spreading.

The topographic marking process is carried out by the topography team. The objective is to provide visual references of the limits of the bands to be received and the layer thickness for technicians and operators, facilitating spatial navigation in the field. The operation technician is responsible for understanding which markings are necessary and requesting them from the topography team.

Before receiving material for a new layer, the surface of the previous layer must be scratched via the scarification process, increasing adhesion between layers. To do this, operators can use the plow harrow or the motor grader's scarifier. The scarification must not be greater than 5 cm, and in periods of rain, exposing scarified strips to rain must be avoided, as this can generate a preferential flow of water, increasing the risk of puddles or ravines in approved layers. Therefore, in periods of rain, only strips that will receive material in the following hours should be scarified.

Once prepared, the strips can receive approved filtered tailing, delivered with off-road trucks that tip material into the PDER. The receiving strategy will be defined by the receiving technician, maximizing productivity, but respecting all safety rules for equipment operation. The origin of the material can be directly from the bean pile (after the quality of the pile has been approved in the design criteria) or from the material stock in the PRUs.

To avoid contamination, off-road truck operators must check the weighbridge in a suitable location before loading, especially for trucks whose last trip was for ore or waste. If there is any material in the weighbridge, cleaning must be requested. The presence of contamination can damage piling equipment and impact the results of geotechnical tests.

Tilting should preferably be carried out in advance, in the longitudinal direction of the seat. Off-road trucks must always travel under the loose, recently spread layers, respecting the maximum speed of 20 km/hour. The transit of these under approved layers must be avoided. However, if necessary, it must be carried out under supervision and at reduced speed. The objective is to avoid damage to previous layers.

The piles of material tipped by off-road trucks are broken using medium- and large-tracked tractors (for example, CAT D8 or D10), in the spreading stage. The crawler tractors are equipped with Terrain software, and must spread the layer, respecting the layer thickness. At this point, it is not necessary to meet the thickness specification with an accuracy of 5 cm, as there is a subsequent leveling step, but care must be taken to avoid the need for excessive cuts or fills.

As soon as the bay region is received and the area is safe for people to enter (i.e., no large equipment is moving), a sample must be collected per bay to perform the Proctor test. This test provides the optimal humidity and target density of the material, which can be compared with humidity and density tests carried out in the field in subsequent stages.



Figure 8: Receiving process

Leveling macro process

The leveling step consists of shaping the layer thickness so that it meets the established criteria (+-5 cm error from the defined layer thickness). The receiving technician must guide the motor grader operator within the limits of the lane to be leveled and in the direction of leveling, preferably in a longitudinal direction.

The process is carried out with motor graders equipped with high-precision technology called Terrain, to identify whether there are cuts or fills in relation to the topographic project. The receiving technician must check the terrain accuracy at least once every four work shifts, with the help of GPS. It is important to pay special attention when there are discrepancies in relation to other equipment and at night, when the occurrence of ionospheric scintillation is greater, or in case of doubts or discrepancies in the software findings.

Treatment macroprocess

The treatment stage consists of preparing the material disposed in the field for the compaction process. The two main issues to be resolved at this point are the regulation of humidity and the reduction of material heterogeneity.

The material sent to PDER Ipoema Borrachudo usually has an optimum moisture ranging from 9% to 13%, with small exceptions, with the physical and chemical characteristics of the material determining the variation within this range.

Once the layer is leveled and the thickness is checked, the next stage is the treatment stage, which begins with a tactile-visual assessment of the layer.

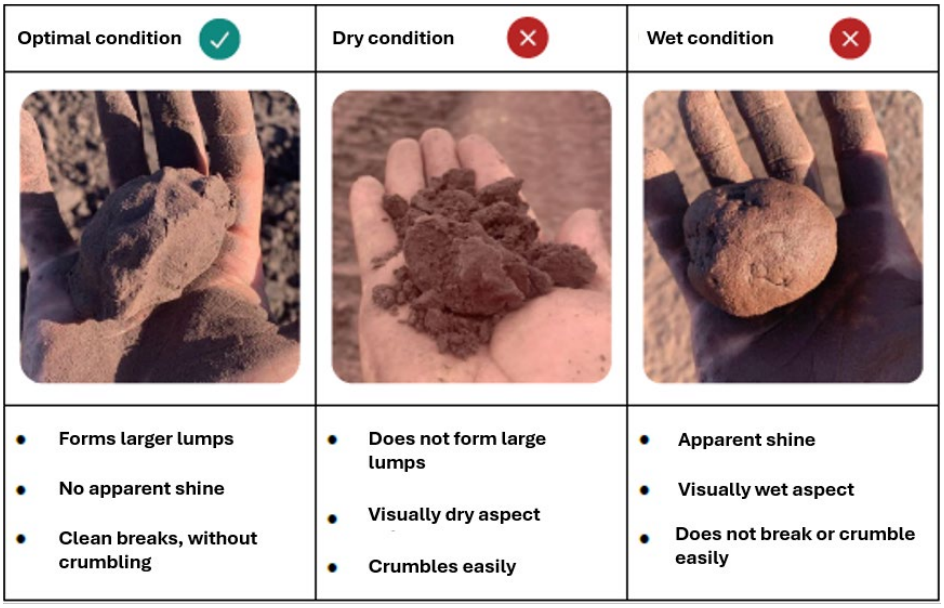


Figure 9: Visual and tactile inspection done by the treatment technician

This assessment is important to decide on appropriate treatment for the material. This method consists of using touch and vision, aligned with the maturity and experience of the treatment technician, to classify the material. There are some characteristics to evaluate during this investigation. A test that can be carried out consists of removing the soil in field conditions with bare hands, and squeezing it well until it forms a "cake." Once formed, the soil can be shaken in the hands to evaluate characteristics such as color, shine, consistency, and formation of clods.

Based on this assessment, the treatment technician can identify cases that require immediate treatment: when the layer has moisture far above the ideal level or far below it. If the layer has humidity close to ideal, it is only necessary to carry out homogenization with two passes with a plowing harrow, and then the technician will ask the laboratory to collect three sample points per lane to validate that the moisture is within the specified range for compression.

When the technician assesses that the material is damp, and/or presents a deviation greater than 1 p.p. for wet branch, drying must be carried out in the field. The drying process consists of opening the layer and exposing it to the daytime sun, homogenizing from time to time. It is estimated that the tailing filtered in PDER loses between 1 and 2 p.p. on average sunny days, with an open layer, between 06:00 and 20:00.

When the material is visually dry, and/or has a moisture deviation greater than 2 p.p. for the dry branch, the treatment is to add water. This operation is carried out by opening the layer with a plow and adding water with a water truck. This must be gradual to avoid flooding the strip. During the operation of the water truck, priority should be given to using the "shower" implement, which applies water in smaller quantities, and mitigates the risk of black flies appearing. Homogenizing the material after adding water is important to ensure successful compaction.



Figure 10: Treatment process

Compaction macroprocess

After treatment, whether it was homogenization, addition of water or drying in the sun, the layer will be open and disturbed. Therefore, it must first be closed again using a motor grader, ensuring that the thickness returns to the specified range.

Next, moisture test samples will be collected to validate that it is indeed within the specified range, which must meet two criteria: the geotechnical moisture must be within the range of 9% to 13% (design criteria), and the operational recommendation is that the moisture deviation (obtained by subtracting the field moisture from the optimal moisture of the material obtained in the Proctor test) must be within the range of -3 to +1.0 p.p.

Moisture levels drier than -3 tend to not be able to adequately densify the material, and so cannot achieve good compaction. On the other hand, deviations wetter than +1 tend to generate excess water between the voids in the material and the compaction energy of the roller cannot completely densify the material due to the excess water, generating a "rubbery" quality.

Once there is adequate moisture and the layer is closed, the next step is to compact the lane, which is carried out by the compaction roller. The treatment technician must request the passage of the compaction roller and clarify the boundaries of the strip that will be compacted and the number of passes. Two passes (two back and forth) of the compaction roller are used to carry out complete compaction. The compaction roller must always follow the same direction in which the layer is closed with the motor grader, which is normally longitudinal.

By default, compression is performed at high amplitude and low frequency. Other parameters can be used in exceptional cases (e.g., additional energy in the band). The ideal speed of the equipment is 4.5 to 5.0 km/h (similar to a person walking) – any discrepancy could harm the compaction result. The roller must pass (30 to 50 cm) between compaction lanes, avoiding spaces without receiving energy.

Approval macroprocess

After compaction, in order for it to be approved, the layer must be inspected by the operations, topography and inspection team. This inspection may find features such as rubberiness; lack of compaction in any section, with material still loose; inadequate thickness; or any occurrence that visually indicates that the compaction of the lane was not successful. If any non-compliance is identified, the lane must be reworked in the non-conforming section until it is in good condition.

Once the material passes inspection, the laboratory will collect a sample for density and void index tests. The approval criterion is only the void index; however, the field density is a good operational indication that the densification was successful. The result of the void index test using the vacuum pump method to obtain the real density of the grains takes around 14 hours. To speed up the process, the operation

can use the density as a reference to decide whether the compaction of the layer needs to be redone, or if it can proceed to the final test.

The history of the material worked shows that when the field density reaches values above 2,150 g/cm³, the probability of passing the void index is high, above 95%. On the other hand, below 2,000 g/cm³, the approval rate is low, below 10%. If the density is in the intermediate range, between 2,000 and 2,150 g/cm³, the field technician will use the target density value obtained in the Proctor test for reference.

If it is above the reference of 2,150 g/cm³, or if it is between 2,000 and 2,150, it presents a density greater than the target density obtained in Proctor, and the lane sample must await the void index test. If the density does not reach these references, the layer must be reworked, whether this is just additional compaction or a new moisture treatment. This decision will be made by the field technician who will evaluate the conditions of the track at the time and choose the most appropriate approach.

Having passed inspection, with good density, the void index test is awaited, with a criterion of a maximum of 0.6. If the void index is above 0.6, the layer must be reworked until the established criteria are reached. Once within the limit, the layer will be approved and the cycle starts again.

Geotechnical process control

Geotechnical control of the structure takes place throughout the entire operation, monitored by a team dedicated to supervising the tailing piling stages. Layer release tests are carried out systematically by the laboratory team. In addition to this control, undisturbed samples are collected every 8 layers of compacted tailing. From these collections, tests are carried out to confirm the mechanical behavior of the material.



Figure 11: Collection of undisturbed samples



Figure 12: Collection of in-situ compacted soil cylinder sample

Conclusion

The filtered tailings disposal process is a major challenge due to the difficulty in achieving synergy of the various unit operations associated with the compaction process, which until now was not part of the operational stages in a mine. The particularities of each tailing will encourage variations in the stacking process, but the compaction dynamics remain the same as in soil embankment processes. Much of the disposal strategy is associated with the area available for compaction and the availability of equipment for compacting large volumes. The control of activities involves equipment automation and systematization based on the development of control software, fleet management, and production stages.

Acknowledgements

The authors thank Vale S.A. for supporting the development of the work.

References

Araújo, A.C. and Peres, A.E.C. 2006. *Flotação de minérios de ferro*. In Chaves, A.P. *Teoria e prática do tratamento de minérios. Flotação – o estado da arte no Brasil São Paulo.* Signus.

Cacciuttolo, C. and Atencio, E. 2023. Dry stacking of filtered tailings for large-scale production rates over 100,000 metric tons per day: Envisioning the sustainable future of mine tailings storage facilities. *Minerals* 13: 1445. https://doi.org/10.3390/min13111445

Dahlstron, D.A., Silverblatt, C.E. 1977. Continuous vacuum and pressure filtration. In Purchas, D.B. (ed). *Solid/Liquid Separation and Scale Up*. Croydon Uplands Press: 445–491.

Guimarães, N.C. 2011. *Filtragem de rejeitos de minério de ferro visando a sua disposição em pilhas*. Thesis research, Universidade Federal de Minas Gerais.

Houot, R. 1983. Beneficiation of iron ore by flotation — Review of industrial and potential applications. *International Journal of Mineral Processing* (10): 183–204.

Lokkas, P. Ioannis, C. Theodoros, C., Dimitrios, C. Emmanouil, P. Evangelos, P. 2021 Historical background and evolution of soil mechanics. *WSEAS Transactions on Advances in Engineering Education*: 96–113.

Wills, B.A. and Finch, J. 2015. Wills' *Mineral Processing Technology: An Introduction to the Practical Aspects of Ore Treatment and Mineral Recovery*. Butterworth-Heinemann, Oxford.

Performance Assessment of a Filtered Tailings Storage Facility Partially Built with Uncompacted Tailings

Edwin Sanchez, Anddes, Peru
Denys Parra, Anddes, Peru

Abstract

The common practice of dry stacking for filtered tailings disposal includes stacking, spreading, aeration to reduce moisture provided by the filtration plant, and compaction with smooth vibratory rollers. All of this is done to create a material with dilative behavior, adequate strength, and very low liquefaction potential, contributing to the stability of the facility without the need for large retention dams. These processes involve significant operating costs for the disposal of filtered tailings, which is one of the main restrictions for the use of this technology. This work has focused on analyzing the static behavior of a filtered tailings storage facility, which will be built by dividing the facility into two zones: 1) a structural zone made up of compacted tailings to ensure the overall stability of the facility; and 2) a non-structural zone made up of filtered tailings disposed as received, that is, without compaction. The inherent risk of this solution is that the relatively low initial degree of saturation of the uncompacted tailings in loose conditions may be increased by the static loads of the tailings disposal up to the saturation, making it susceptible to static or seismic liquefaction. The geotechnical parameters of the foundation soils and the filtered tailings were estimated based on field, literature, and laboratory geotechnical investigations. The tailings disposal operation was simulated through numerical modelling using Sigma/W, in which the uncompacted filtered tailings were analyzed by the NorSand model. The simulation results indicated that it is possible to place uncompacted filtered tailings, thereby reducing operating costs, but this requires reducing the moisture content of these materials to at least the optimum to prevent liquefaction and ensure the overall stability of the facility.

Introduction

Currently, not much research is conducted on filtered tailings. Additionally, in recent years, the number of tailings dams built using this technology has been increasing due to its safety advantages compared to more traditional tailings disposal procedures (Copeland et al., 2023; Cacciuttolo and Pérez Campomanes, 2022; Pizarro and Olivares, 2018; Davies and Rice, 2001; Hambley and Verbeek, 2020).

Filtered tailings are usually placed in the storage facility and spread to promote moisture loss until reaching the optimum moisture content, after which they are compacted to increase their strength and generate a self-supporting structure. This process requires a high operating cost, which is one of the main restrictions on the use of this technology. Therefore, with the aim of reducing costs, the following questions arise: is it necessary to reduce the moisture of the filtered tailings below the values obtained in the filtration plant? Is it possible to place the filtered tailings, or at least part of them, uncompacted without compromising the structural integrity of the facility? This research aims to answer these questions.

Filtered tailings basic characteristics

The filtered tailings are classified as non-plastic sandy silt, ML; the fines content varies from 63 to 71%; the liquid limit is between 17 and 19; and the plasticity is very low to non-plastic. The uncompacted filtered tailings have a hydraulic conductivity of 1.3×10^{-6} to 7.3×10^{-7} cm/s.

Initial configuration of the FTSF

Structural and non-structural zones

To guarantee the correct stability condition of the projected filtered tailings storage facility (FTSF), a shell or structural zone needs to be built consisting of structural fill, that is, filtered tailings compacted to 95% of its maximum dry density according to the Standard Proctor Test, in layers of up to 50 cm. Behind this shell, uncompacted tailings will be placed by dumping with trucks. A limit equilibrium analysis was performed with the objective of an initial determination of the structural zone extension.

Stability analysis of the initial configuration

Stability assessments were carried out through limit equilibrium analyses of the section (shown in Figure 1), using the Slope/W module from Geostudio software (2023), using Spencer's procedure (1967) alongside the cuckoo search algorithm by Yang and Deb (2010). These analyses were carried out by modifying the extension of the structural zone (Tailings C) and considering the most critical behavior of the uncompacted tailings (Tailings NC), that is, an undrained response, static or seismic liquefaction of these materials and their characterization through their residual strength. Pore water pressure was not considered in this preliminary analysis. Based on triaxial testing results, Tailings C material was modeled with a density of 20 kN/m^3, zero cohesion and an angle of friction of 35 degrees, while Tailings NC was modeled with a density of 14 kN/m^3 and undrained residual strength ratio of S_{ur}/σ'_0=0.11 obtained conservatively from a monotonic simple shear test after liquefaction by cyclic loading. The required post-liquefaction factor of safety (FoS) for this analysis mut be equal to or greater than 1.2, which is considered acceptable for a post-liquefaction condition according to the Canadian Dam Association (CDA, 2019).

Figure 1 shows the most critical failure surface based on the limit equilibrium analysis. It was concluded that the extension of the structural zone (Tailings C) must be at least 250 meters to guarantee the stability of the FTSF for a critical condition represented by the liquefaction of the uncompacted tailings.

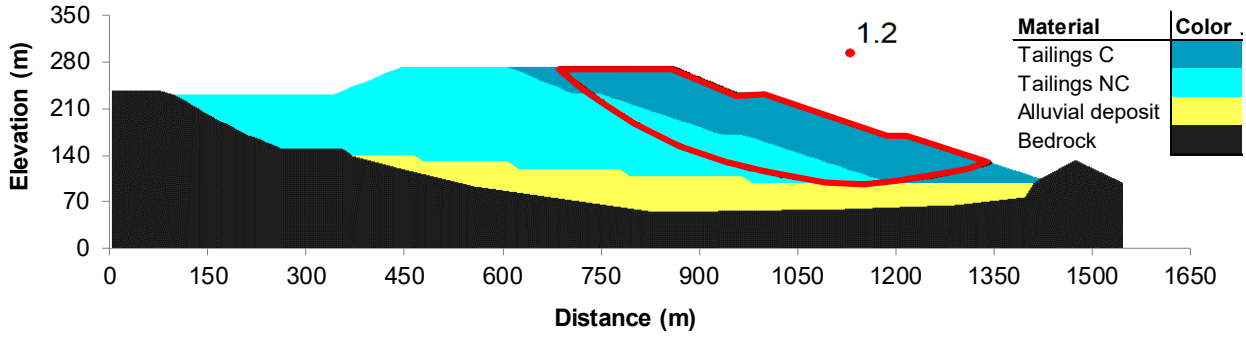


Figure 1: Section analyzed for definition of the structural zone

Cases analyzed

Two cases were analyzed. In both of them the moisture content of Tailings C material was reduced from 20% (as received from the filtration plant) to the optimum, which is 16%, achieved after in-situ drying by aerating, and compacted at 95% of their maximum dry density of 17.3 kN/m³ based on the Standard Proctor Test, to try to produce a material with essentially dilative behavior. Uncompacted filtered tailings NC were disposed of by stacking, exhibiting contractive behavior. The foundation consists of a sand alluvial deposit classified as SM overlying an andesite bedrock (see Figure 1).

Oedometer test results

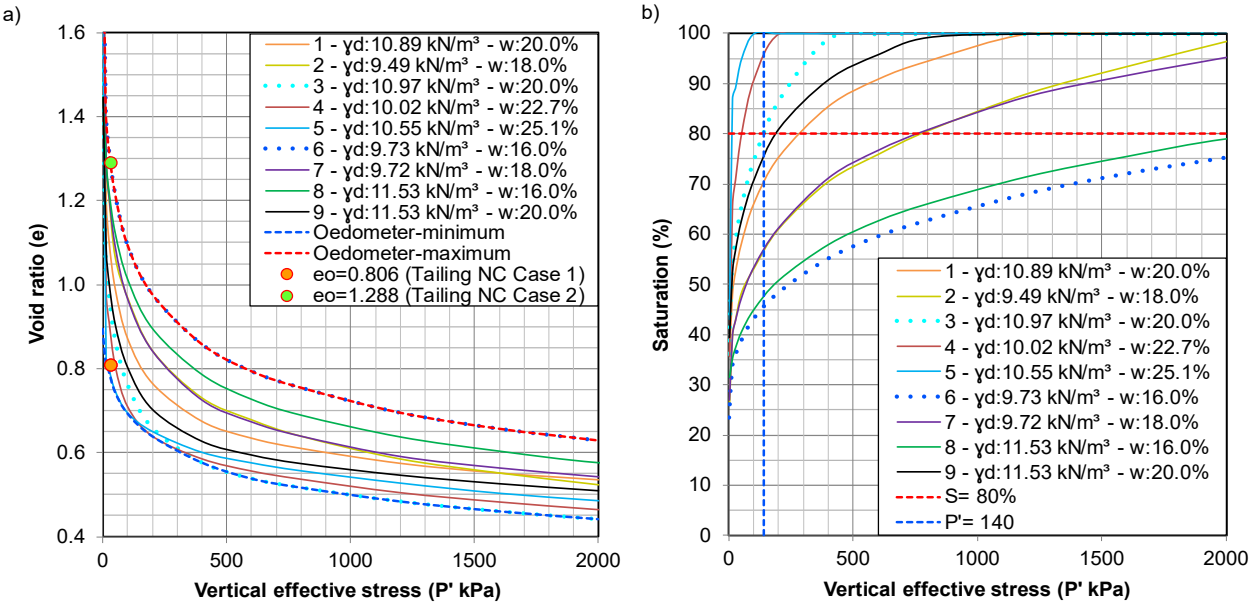


Figure 2: Oedometer curves of a) vertical stress vs. void ratio and b) vertical stress vs. saturation

Figure 2 shows the results of an oedometer test conducted on Tailings NC, where a variability in void ratios and degree of saturation was observed, primarily influenced by their density and initial moisture content. Based on the oedometer testing, the maximum and minimum envelopes were evaluated to establish the initial void ratio for each lift of the Tailings NC, assuming an average lift of 5 meters thick that provides a vertical stress of 70 kPa, and considering that the control nodes are located in the middle of each lift.

According to Aghazamani et al. (2021), soils with equal to or greater than 80% saturation and with a contractive behavior, are prone to liquefaction; thus, an undrained behavior was chosen for such conditions.

Case 1

This represents the conditions of the uncompacted filtered tailings with an average moisture content of 20% obtained from the filtration plant. The initial void ratio was assumed to represent the lower envelope of the oedometer curves (see Figure 2a), corresponding to tailings filtered at a vertical stress of 35 kPa (half a lift), resulting in an initial void ratio of 0.806 and a corresponding degree of saturation of 60% (Figure 2b), which is a relatively high initial value. According to Figure 2b, 80% saturation (threshold value below which conditions are essentially drained,) is reached with a vertical stress of 140 kPa, which corresponds to loads transmitted by two lifts (Tailings NC-D1 in Figure 3). Layers from the bottom to the top generate greater stresses, and therefore, saturation degrees greater than 80%, so Tailings NC-U in Figure 3 were analyzed in an undrained condition.

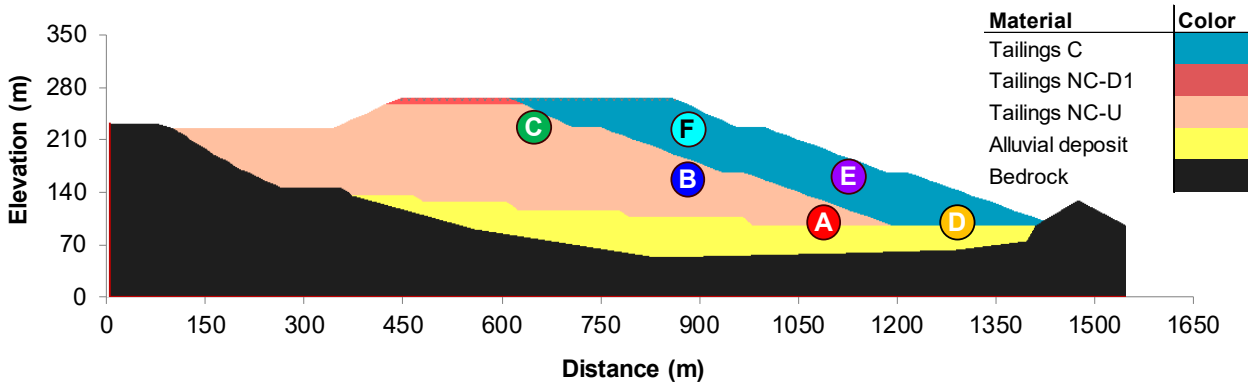


Figure 3: Section analyzed for Case 1

Case 2

This represents the conditions of uncompacted filtered tailings with the optimum moisture content of 16%, which is achieved in the same way as Tailings C, i.e., it is spread in small layers and undergoes in-situ drying by aerating, which increases the operating cost of the FTSF. Based on the oedometer test curves, the upper boundary representing the behavior of uncompacted filtered tailings with 16% moisture content and a vertical stress of 35 kPa, corresponds to an initial void ratio of 1.288 (Figure 2a); the corresponding degree of saturation is 37% (Figure 2b). As can be seen in Figure 2b, the degree of saturation of the selected curve

is less than 80% up to 2,000 kPa of vertical stress, i.e., it is higher than the maximum height of the FTSF. Therefore, Tailings NC-D2 in Figure 4 were analyzed considering drained behavior.

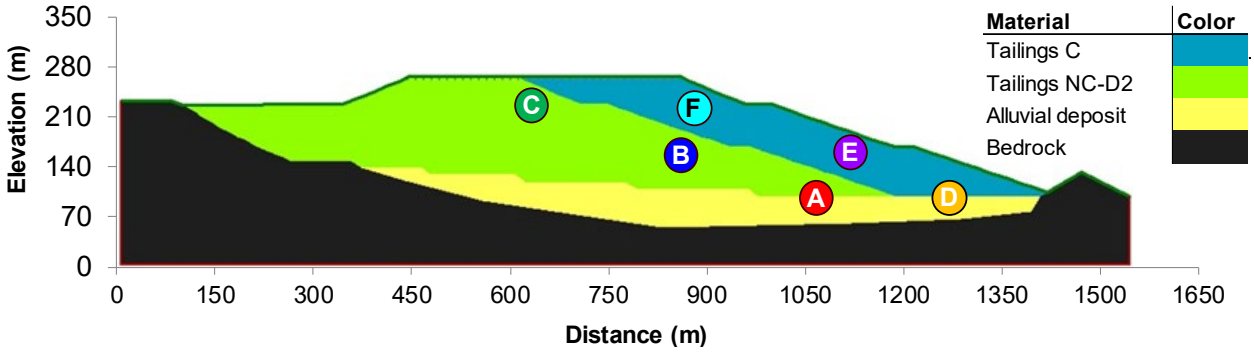


Figure 4: Section analyzed for Case 2

It is important to note that the initial condition (void ratio) for the Tailings C in Case 1 and Case 2, was obtained at the maximum dry density of the Standard Proctor, with a dry density of 17.3 kN/m³, and a moisture content of 16%. Six representative control points from the initial, intermediate, and final stages of the Tailings NC (A, B and C) and Tailings C (D, E and F) shown in Figures 3 and 4, were considered to compare the contractive and dilative behavior of the filtered tailings.

Performance assessment of FTSF

Constitutive models

In geotechnical numerical modeling, selecting the right constitutive models is crucial for accurate simulations. The NorSand (NS) model, introduced by Jefferies and Been (2016), is based on critical state soil mechanics, and is adept at simulating static liquefaction and dilatancy in granular materials. Its parameters allow for modeling of complex behavior in tailings, demonstrating its effectiveness in predicting the responses of different tailing types under stress, and was used for modeling the uncompacted filtered tailings. The Hardening Soil (HS) model, developed by Schanz et al. in 1999, is advanced and non-linear, designed for detailed soil behavior simulation. It incorporates stress limit states with confinement-dependent strength and stiffness parameters, which is essential for realistic soil behavior modeling under high loads, such as in tailings storage facilities. This model was used for the compacted filtered tailings and the alluvial foundation soil. The generalized Hoek-Brown (GHB) model, an evolution of the original Hoek-Brown failure criterion, is widely used for modeling rock masses in geotechnical engineering (Hoek et al., 2002) and was used for bedrock modeling. These models, each with distinct advantages, are integral to geotechnical engineering, especially in numerical modeling, for a comprehensive analysis of soil and rock behavior under various conditions.

Numerical modeling

To assess the serviceability of the structure based on deformation, a finite element numerical modeling was conducted for Case 1 and Case 2. A plastic analysis was performed, considering lifts of 5 meters, using the Sigma/W module of the Geostudio software (2022). These analyses were performed to identify liquefaction zones of the Tailings NC (Case 1), magnitude of displacements in the whole structure, and stress path in the control points within the FTSF, among other factors. In Case 1, the criteria for conducting this analysis was based on the drained behavior of the Tailings NC for the first 10 meters raise (2 lifts), followed by an undrained behavior of this material for deeper layers. In contrast, for Case 2, all layers were modeled with drained behavior, as determined from oedometer tests.

Geotechnical characterization

Table 1: Summary parameters for the FEM, tailings (NS)

	Tailing NC-U (Case 1)	Tailing NC-D1 (Case 1)	Tailing NC-D2 (Case 2)	Tailing C (Case 1 and 2)
Color				
Response	Undrained	Drained	Drained	Drained
e_0	0.806	0.806	1.288	0.59
H_0	72.3	72.3	72.3	100
H_y	72.1	72.1	72.1	0
γ (kN/m^3)	14	14	14	20
G_0 (MPa)	30	30	30	151
m	0.2	0.2	0.2	0.05
OCR	1.3	1.3	1.3	1.3
v	0.2	0.2	0.2	0.2
Pref	100	100	100	100
M_{tc}	1.6	1.6	1.6	1.6
N	0.1	0.1	0.1	0.3
X_c	2.9	2.9	2.9	4.0
C_a	2.35	2.35	2.35	2.35
C_b	1.72	1.72	1.72	1.72
C_c	0.03	0.03	0.03	0.03
Γ	0.88	0.88	0.88	0.88
λ	0.0538	0.0538	0.0538	0.0538
S	0.5	0.5	0.5	0.5

For this study, a field investigation and laboratory testing program were conducted for the characterization of the foundation soil, including drillholes, test pits, and geophysical surveying. The geotechnical characterization of the filtered tailings was performed based on laboratory testing including oedometer and drained and undrained isotropically consolidated triaxial tests to characterize material strength. Also,

information from the literature (Robertson et al., 2017), and from Anddes' project database was used to characterize the geotechnical properties of the foundation and tailings. For the finite element method (FEM), the Norsand constitutive model was calibrated according to Jefferies and Been (2016), while Hardening Soil and Generalized Hoek-Brown models were calibrated based on Geostudio (2022) (see Tables 1 and 2). Figure 5 shows the calibration for the uncompacted tailings with the triaxial tests performed.

Table 2: Summary parameters for the FEM, foundation

	Alluvial deposit (HS)	Bedrock (GHB)
Color		
Response	Drained	Drained
ϕ (°)	35	(–)
ν	0.2	0.2
γ (kN/m³)	20	26
E (kN/m²)	(–)	60E6
E_{50} (kN/m²)	10.5E3	(–)
E_{oed} (kN/m²)	10.5E3	(–)
E_{ur} (kN/m²)	31.5E3	(–)
m	0.87	(–)
Rf	0.94	(–)
UCS (kPa)	(–)	190
mb	(–)	0.36
s	(–)	0
a	(–)	0.51

Finite element analysis

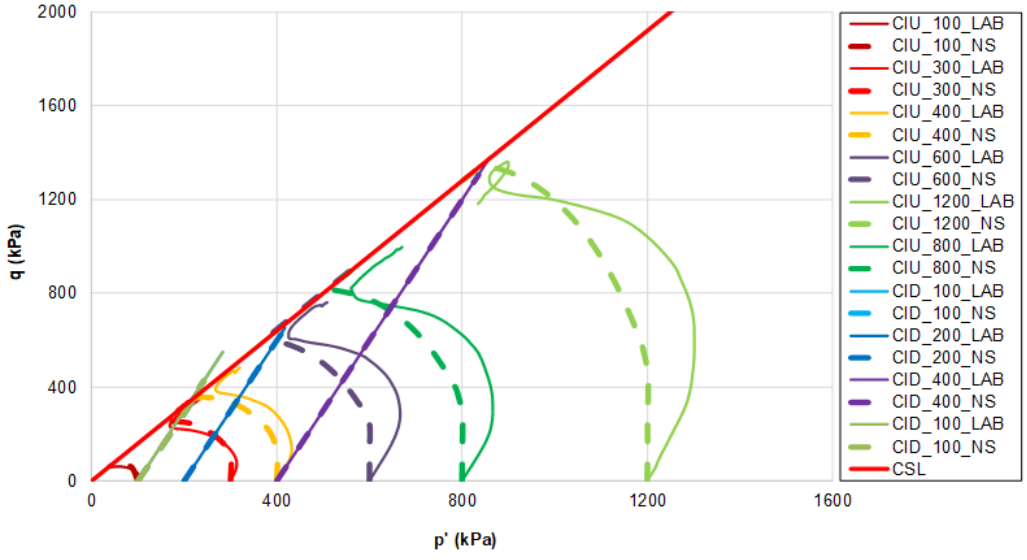


Figure 5: Model calibration based on triaxial tests. p'-q diagram

Figure 6 shows the finite element mesh of the numerical analysis of Case 1 with the discretization for each material; similar mesh was prepared for the analysis of Case 2. For both cases, the FTSF raise was simulated by 34 lifts of 5 meters thickness. For Case 1 where the conditions are undrained, the dissipation of pore water pressure generated during disposal has not been considered, due to the very low permeability of the filtered tailings, even when not compacted, which significantly reduces the water flow.

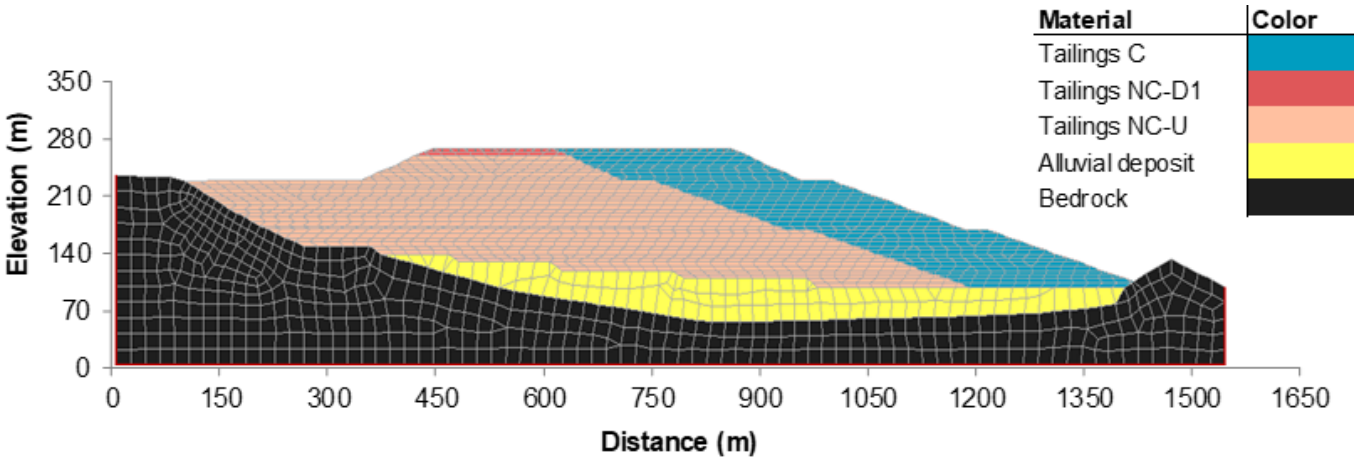


Figure 6: Finite element mesh for analysis of Case 1

Figures 7a and 7b show the p' vs. q and p' vs. void ratio (e) graphs during the filtered tailings disposal. In Figure 7a, for Case 1 and Case 2, where M is the critical state stress ratio defined based on drained and undrained triaxial tests performed to determine the critical state line (CSL), and IL is the instability line defined as the maximum q value after which the critical state is reached. As can be seen in Figure 7a, the stress paths of control points A, B and C (Tailings NC-U) for Case 1 show a clear contractive trend, reaching the instability line at $\eta=q/p'=0.74$, and then liquefaction at the critical state, while points D, E, and F (Tailings C) show a dilative behavior.

For Case 2, the stress paths in all cases do not show a contractive trend or decrease in effective stress. That is because the saturation degree is less than 80% with no generation of excess pore pressures. Figure 7b shows that points A, B, and C for Case 1, reach the CSL and static liquefaction occurs, while points D, E, and F are far from the CSL. The same analysis was performed for the entire finite element model.

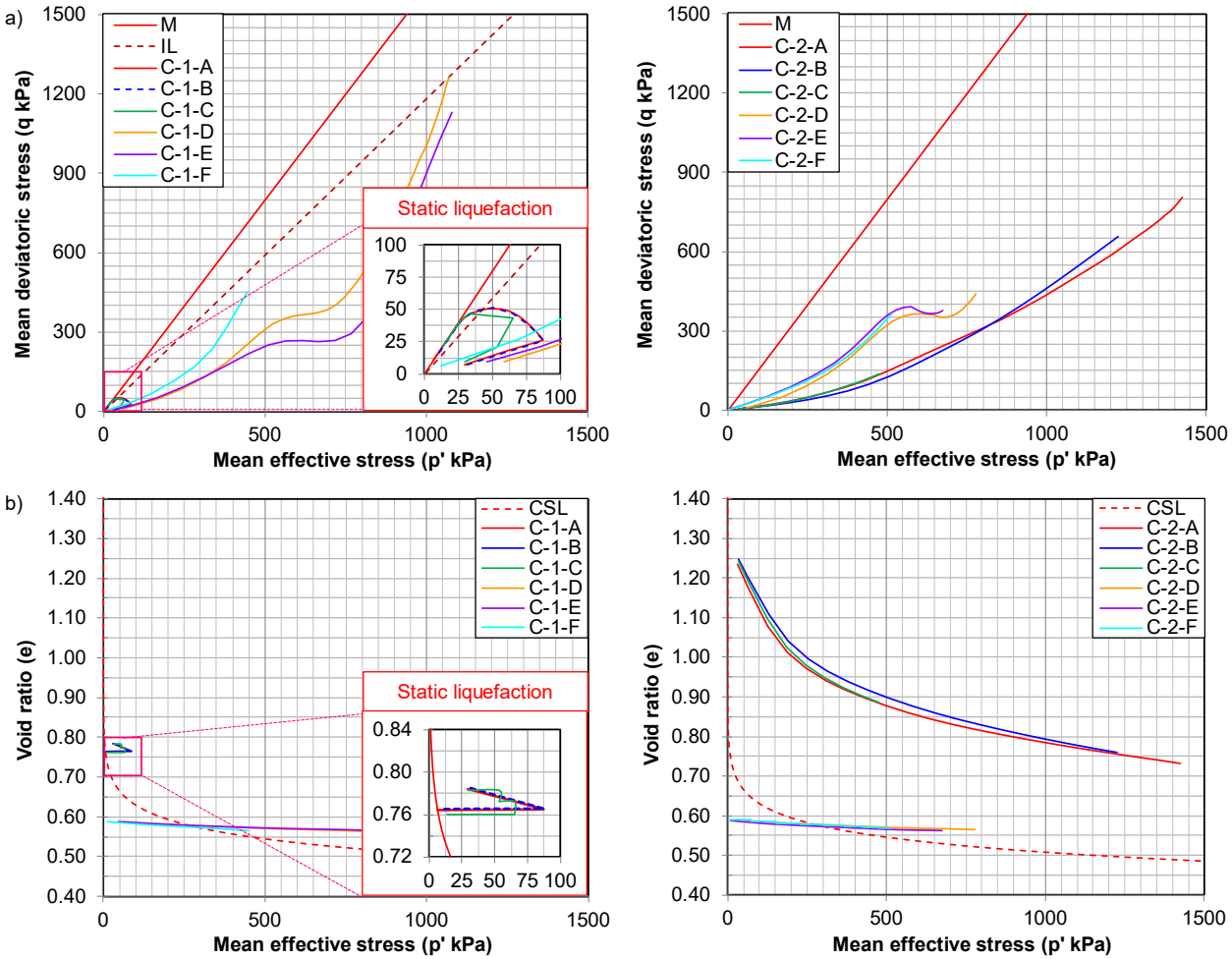


Figure 7: a) p'-q and b) p vs. e, during filtered tailings disposal for Case 1 and Case 2

Other criteria for identifying zones of static liquefaction were based on the failure criteria proposed by Geostudio (2022), as presented in equations 1 and 2.

$$|\psi| < 0.001 \quad (1)$$

$$|\eta\text{-}M_i| < 0.1 \quad (2)$$

Where ψ is the state parameter.

Figures 8a and 8b show the evolution of the above failure criteria per lift during the FTSF raise. Figure 8a shows that points A and B (Tailings NC-U) reach a $|\psi| < 0.001$ condition for lifts 22 and 32, respectively, predictably achieving the critical state (liquefaction) and fluctuating within a range from 0 to -0.05, while point C does not reach this condition. However, points A, B, and C adhere to the second criteria ($|\eta\text{-}M_i| < 0.1$) for lifts 16, 22 and 29, respectively, indicating liquefaction at that specific raise.

Figure 8c shows the FTSF raise versus η/M, displaying a rapidly escalating mobilized strength in the Tailings NC-U, particularly after reaching the instability line (η/M=0.74), approaching 1.0 (critical state) indicating liquefaction. Figure 8d shows the rapid increase of the pore water pressure during the FTSF raise.

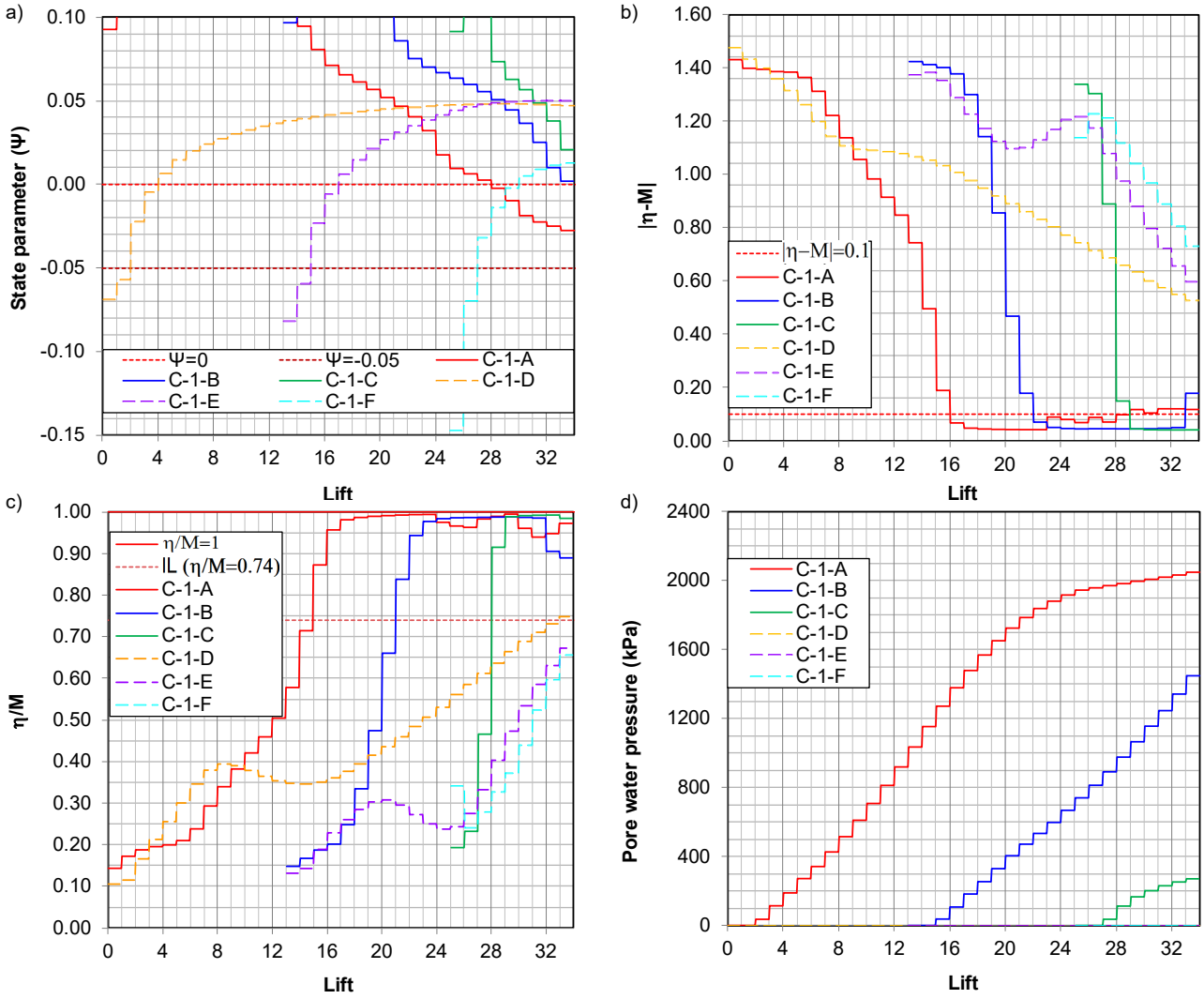


Figure 8: Variation of a) Ψ, b) |η-M|, d) η/M and c) pore pressure, during Case 1 FTSF raise

Figure 9 shows that the NC-U tailings have reached a mobilized strength, η-M, greater than 0.74, surpassing the instability line, indicative of static liquefaction and approaching the critical state.

Horizontal and vertical displacements were calculated at each raise. Figures 10 and 11 illustrate the displacements at the maximum height of the FTSF for Case 1 and Case 2, respectively. For Case 1, maximum horizontal and vertical displacements of 10.3 and 4.3 m, respectively, were obtained, which occurred in the middle and upper part, respectively, of the FTSF at Tailings C. For Case 2, maximum

horizontal and vertical displacements of 2.0 and 8.8 m, respectively, were calculated. As expected, horizontal displacements in Case 1 are larger than in Case 2, due to an undrained condition that generates predominantly shear strains and liquefaction of uncompacted tailings, while the drained conditions of the uncompacted tailings in Case 2 predominantly generate volumetric strains and vertical displacements (settlements).

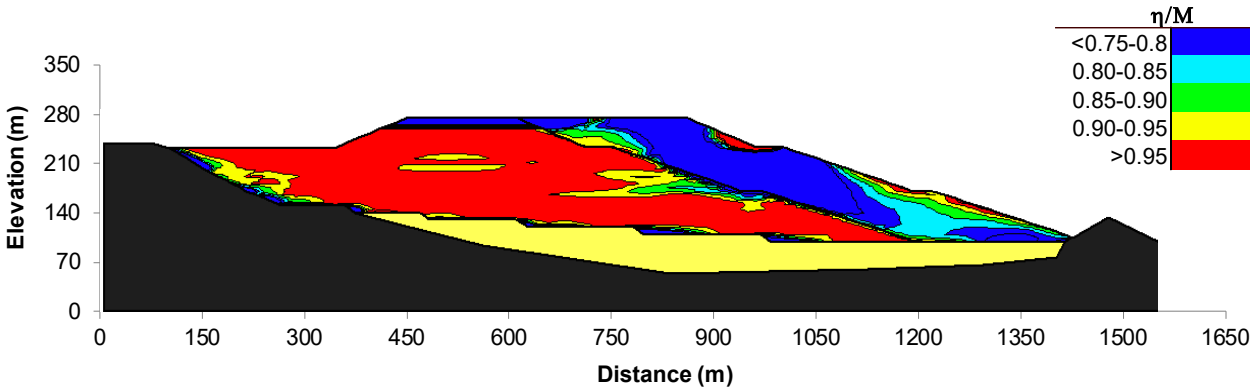


Figure 9: Mobilized strength, η/M. Case 1

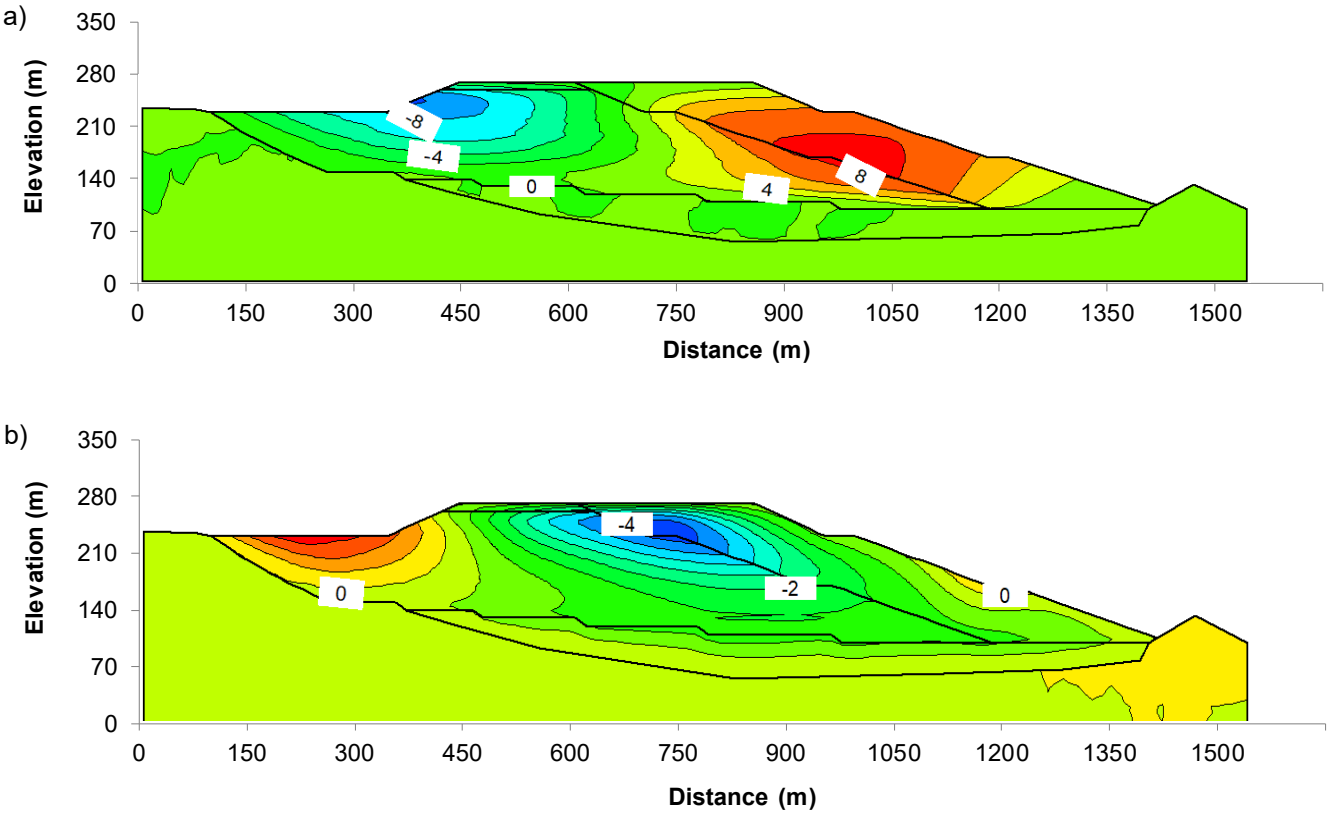


Figure 10: a) horizontal displacements and b) vertical displacements. Case 1

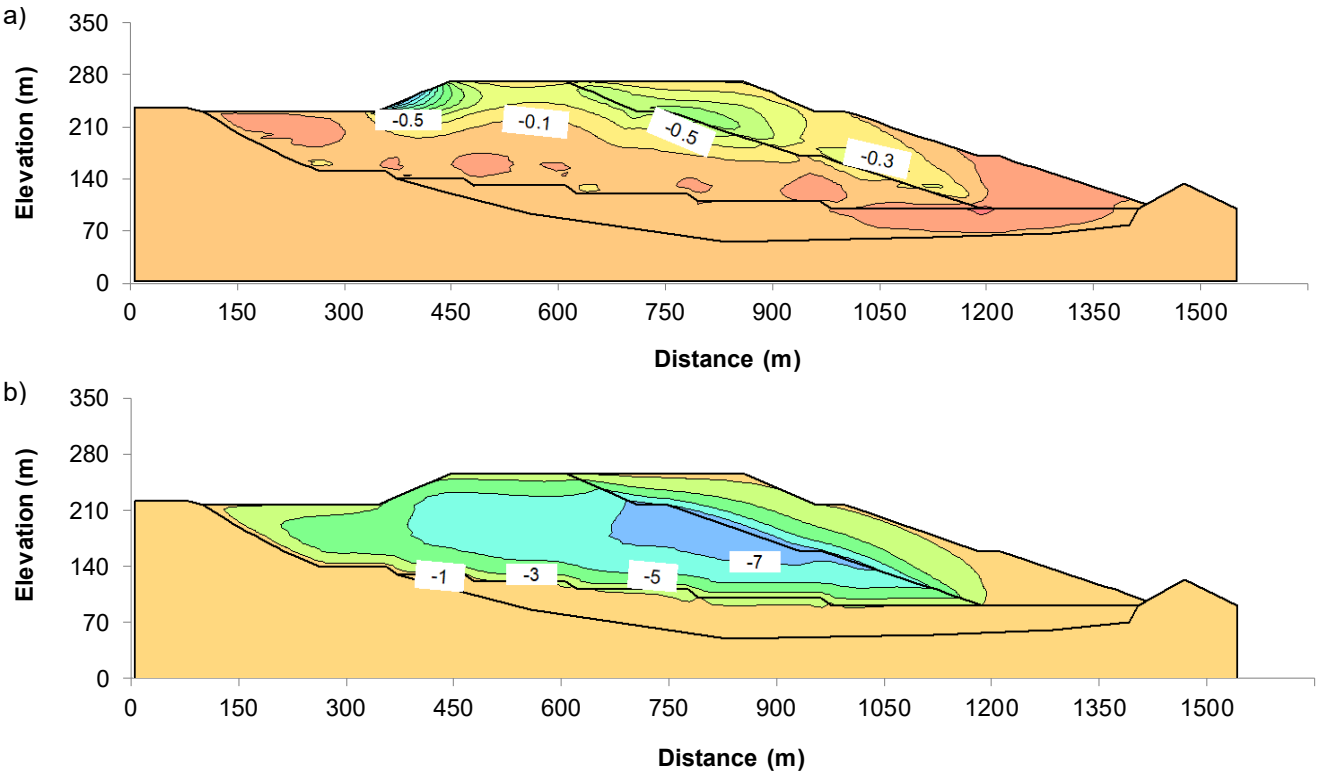


Figure 11: a) horizontal displacements and b) vertical displacements. Case 2

Final limit equilibrium analysis

As a final step, a stability analysis was carried out using the limit equilibrium method (LEM) to complement the performance evaluation previously performed through the numerical analysis. The stability analysis considers the geotechnical parameters shown in Table 3. The post-liquefaction strength of Case 1 Tailings NC-U were estimated from Equation 3 derived from the Norsand model (Jefferies and Been, 2016) when contractive material meets critical state conditions, and based on best practices recommended by Jefferies and Been (2016) considering historical cases. It should be noted that any particle crushing effect due to the maximum loading of the ultimate FTSF configuration, that may influence the shear strength of the uncompacted tailings, has not been considered.

$$\frac{Su_{liq}}{\sigma'_v} = \frac{1+2*K_0}{3} * \frac{M}{2} e^{\frac{-\Psi}{\lambda}} \quad (3)$$

Table 3: LEM summary parameters

Case	Material	ɣ (kN/m³)	c (kPa)	ϕ (°)	Sur/σ'	Color
1	Tailings NC-D1	14	0	30	–	
1	Tailings NC-U	14	–	–	Equation 3 and best practice	
2	Tailings NC-D2	14	0	30	–	
All	Tailings C	20	0	35	–	
All	Alluvial deposit	20	0	35	–	
All	Bedrock	26	230	28	–	

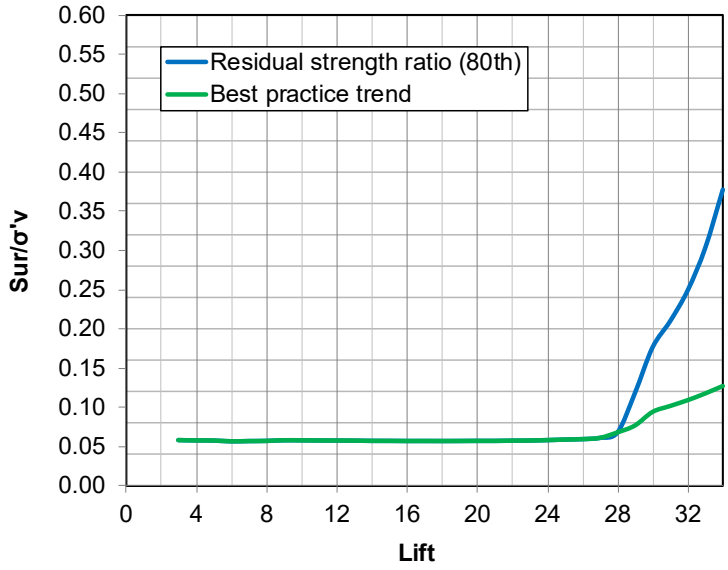


Figure 12: Post-liquefaction strength ratio for contractive uncompacted tailings for Case 1

Figure 12 shows the variation of the post-liquefaction strength, which represents the evolution of the 80th percentile of the state parameter at each lift and is based on best practices recommended by Jefferies and Been (2016) considering historical cases. It is interesting to note that the two post-liquefaction strength adjustments indicated above are equal up to lift 28, from which point the post-liquefaction strength from historical cases is noticeably lower. The increase in pore water pressure during the FTSF raise was incorporated from the numerical analysis (FEM) for the estimation of the effective vertical stress. For Case 1, a minimum FoS of 1.2 is assumed. For Case 2, the minimum FoS should be 1.5.

Figure 13 shows the limit equilibrium analysis results. As can be observed for Case 1 and Case 2, the FoS are similar up to approximately lift 16 (approximately 80 m high). This is because the failure surface develops only in Tailings C. For Case 1, with the following lifts the failure surface extends towards Tailings NC-U, which mostly presents a liquefaction condition, which significantly reduces the FoS, reaching the

minimum required (FoS=1.2) for lift 24. A further raise causes FoS below the minimum required. For Case 2, the static FoS reaches a value of 2.54 for the maximum height of the FTSF.

It is important to mention that to reach at least a FoS=1.2 for Case 1 for the maximum height of the FTSF, it would be required to enlarge the structural zone (Tailings C) to more than 250 m in length, resulting in a more robust configuration. Furthermore, the high values of FoS shown in the stability analyses of Case 2 indicate that the structural zone may eventually be reduced.

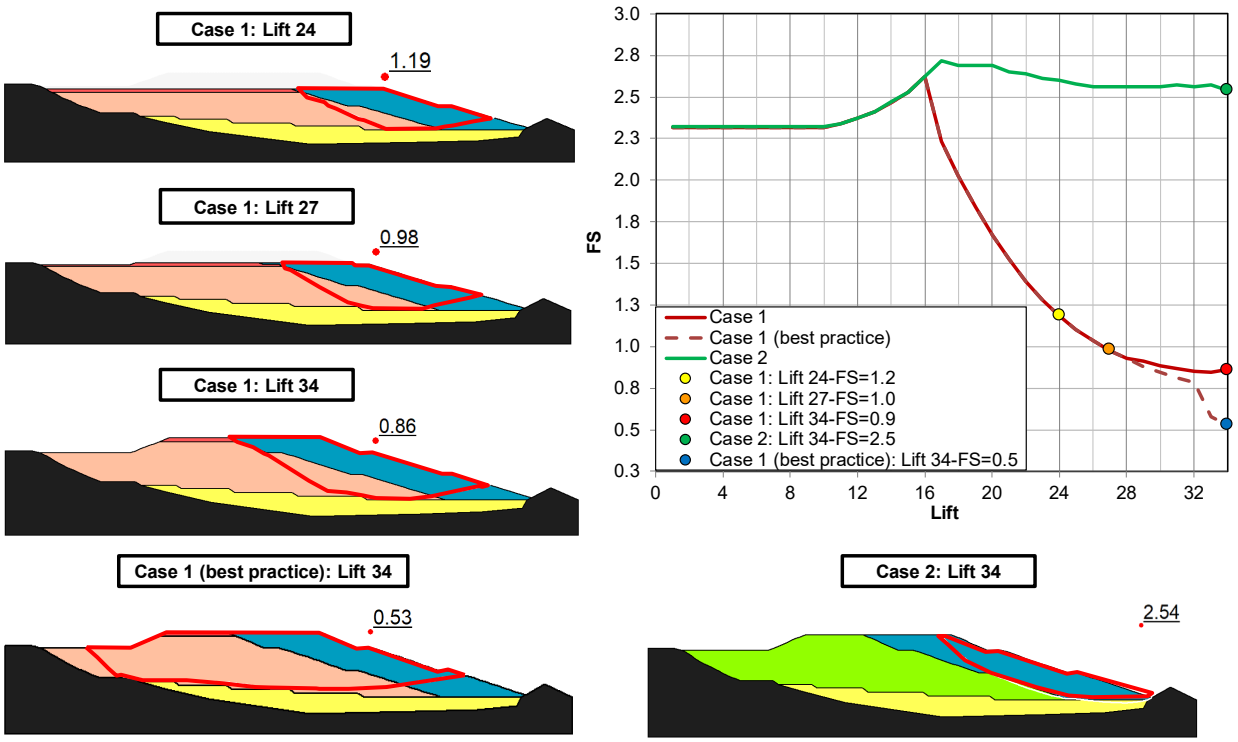


Figure 13: Limit equilibrium analysis results

Conclusion

Oedometer tests on uncompacted tailings showed that the filtered tailings exhibit a clear trend to more contractive behavior at high moisture content. Therefore, reducing the moisture content either at the filtration plant or by in-situ aeration will improve the strength of the filtered tailings.

In a FTSF project, the construction of a shell or a structural zone composed of compacted filtered tailings is required, which guarantees the stability of the entire facility, since uncompacted tailings will be placed behind this zone. The structural zone may be sized based on a limit equilibrium analysis considering the most critical conditions of the uncompacted tailings.

Numerical simulation using the Norsand model indicates that for Case 1, the uncompacted filtered tailings with the filtration plant moisture (20%) quickly reach a degree of saturation of 80% for a load equivalent to two lifts (10 m), exhibiting a contractive behavior, generating excess pore pressure and

liquefaction from lift 16. However, for Case 2 when the moisture content is equal to the optimum (16%), the initial degree of saturation is very low, not reaching 80% saturation for the maximum height of the FTSF, so there are no excess pore water pressures and therefore, no liquefaction. In both cases, the compacted tailings exhibit a dilative behavior, as expected.

Case 1 corresponds to an undrained scenario where shear strains predominate, while Case 2 represents drained conditions where volumetric conditions will be predominant, which is why horizontal displacements are greater for Case 1 than for Case 2 due to the liquefaction of the uncompacted tailings observed in Case 1, while vertical displacements in Case 2 are greater than in Case 1.

For Case 1, the limit equilibrium analyses show a FoS=1.2 (minimum required) at lift 24, reducing to approximately FoS=0.9 and FoS=0.5 considering Norsand formulation (equation 3) and best practices post-liquefaction strength ratio, respectively, for the maximum height of the FTSF (lift 34). To achieve at least a minimum FoS, the structural zone must be enlarged. For Case 2, the FoS always remains above 2.3, indicating adequate stability conditions.

The results obtained indicate that the procedure presented is suitable for evaluating the performance of a FTSF partially constructed with uncompacted tailings.

References

Aghazamani, N., Scalia IV, J. and Bareither, C.A. 2021. Assessing the generation of positive excess pore pressure during undrained compression of unsaturated filtered tailings. *Proceedings of Tailings Mine and Waste 2021:* 55–59.

Cacciuttolo Vargas, C. and Pérez Campomanes, G. 2022. Practical experience of filtered tailings technology in Chile and Peru: an environmentally friendly solution. *Minerals* 12(7): 889. https://doi.org/10.3390/min12070889

Canadian Dam Association (CDA). 2019. Application of Dam Safety Guidelines to Mining Dams.

Copeland, A., Daigle, V. and Strauss, A. 2023. Is the implementation of dry stacking for tailings storage increasing? A Southern African perspective. In G.W. Wilson, N.A. Beier, D.C. Sego, A.B. Fourie and D. Reid (eds), Paste 2023: Proceedings of the 25th International Conference on Paste, Thickened and Filtered Tailings, University of Alberta, Edmonton, and Australian Centre for Geomechanics, Perth: 611–619.

Davies, M. and S. Rice. 2001. Tailings management: Dry stacking of tailings. *Proceedings of the International Seminar on Mine Closure, Tailings and Mine Waste 2001,* Vancouver, Canada.

Geostudio. 2022. GEOSLOPE International Ltd. Static Stress-Strain Modeling with GeoStudio; GEOSLOPE International Ltd.: Calgary, Alberta, Canada.

Geostudio. 2023. GEOSLOPE International Ltd. Stability Modeling with GeoStudio; GEOSLOPE International Ltd.: Calgary, Alberta, Canada.

Hambley, D. and T. Verbeek. 2020. Dry stacking for sustainable mining. *Proceedings of the Tailings and Mine Waste Conference 2020,* University of British Columbia, Vancouver, Canada.

Hoek, E., Carranza-Torres, C. and Corkum, B. 2002. Hoek-Brown failure criterion-2002 edition. *Proceedings of the Fifth North American Symposium, NARMS-TAC*, Toronto, Ontario, Canada.

Jefferies, M. and K. Been. 2016. *Soil Liquefaction: A Critical State Approach*. Second Edition. Taylor and Francis Group LLC, Boca Raton, FL.

Pizarro, J.F. and R. Olivares. 2018. Filtered tailings: state of the practice. *Proceedings of the Tailings and Mine Waste Conference 2018,* Vancouver, BC, Canada.

Robertson, P.K., A. Viana da Fonseca, B. Ulrich and J. Coffin. 2017. Characterization of unsaturated mine waste: A case history. *Canadian Geotechnical Journal* 54: 1752–1761.

Schanz, T., P.A. Vermeer and B.G. Bonnier. 1999. The hardening soil model: Formulation and verification. *Beyond 2000 in Computational Geotechnics – 10 Years of PLAXIS.* Balkema.

Spencer, E. 1967. A method of analysis of the stability of embankments assuming parallel interslice forces. *Géotechnique* 17: 11–26.

Yang, X.S. and S. Deb. 2010. Engineering optimisation by cuckoo search. PhD thesis. *International Journal of Mathematical Modelling and Numerical Optimisation* 1: 330–343.

Next-Gen Tailings Waste Management: Transforming Life-Cycle Strategies

Lakshmin Bachu, Tetra Tech Inc., Canada

Abstract

Ensuring the integrity of tailings waste (TW) facilities is crucial for public safety, environmental conservation, and socio-economic growth. The complexities stemming from operational demands, data management, socio-economic factors, and climate variability require innovative solutions. Generative Artificial Intelligence (GenAI) offers vast potential in this domain. With capabilities in text, vision, audio, video, programming, and numerical analysis, GenAI can revolutionize data management, provide data-driven predictions, and improve decision-making. This paper explores GenAI's transformative applications in tailings waste management, emphasizing its ability to process extensive data sets, integrate diverse data formats, and offer insights beyond conventional methods. Effective deployment requires high-quality data, bias mitigation, data security, and specialized expertise. The paper discusses GenAI's opportunities and limitations, providing an implementation roadmap and valuable insights for professionals, regulators, and researchers to enhance safety management and empower the future of tailings waste facilities globally.

Introduction

Effective management of tailings waste is crucial for safeguarding communities, protecting ecosystems, and ensuring the mining industry's continued acceptance by society. Figure 1, obtained from MEND (2001) and Snow (2022), shows a schematic of tailings waste facilities. Due to the complexity of processes such as hydrology and geoenvironment, infrastructure requirements, stakeholder involvement, and other variables, these sites encounter unique challenges.

LePoudre and Morrison (2022) proposed a framework for tailings management systems (TMSs), as shown in Figure 2. The framework emphasizes a comprehensive and integrated approach, covering corporate policy, resources, failure mode analysis, and a tailings management system. Key critical control areas include tailings storage facility integrity, operations, maintenance and surveillance, emergency preparedness and response, and governance and assurance. The framework operates within a continuous improvement cycle of planning, doing, checking, and acting, ensuring compliance with regulations and addressing the entire life of the mine, including closure planning, risk and change management.

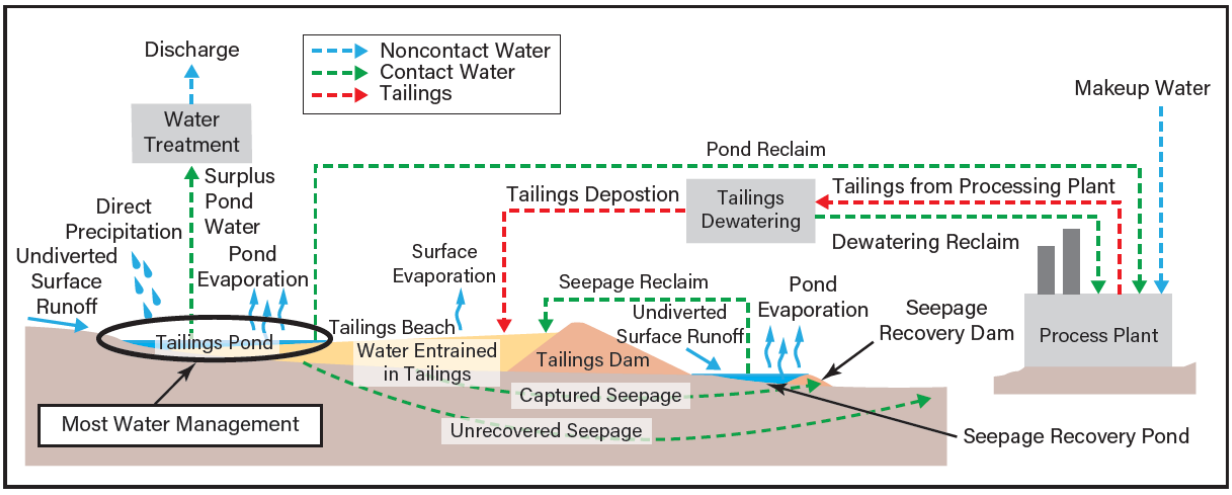


Figure 1: An illustration of tailings waste facilities (source: MEND, 2001 and Snow, 2022)

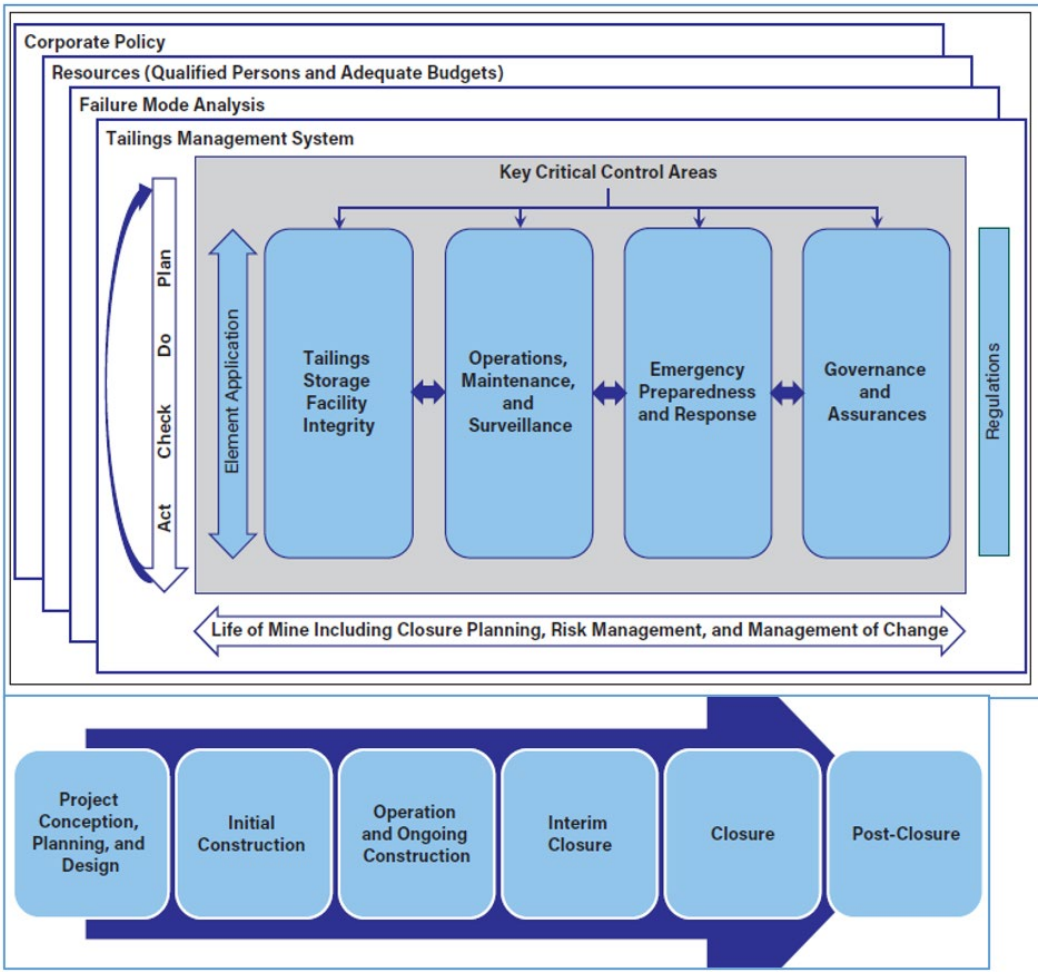


Figure 2: Tailings management system framework as proposed by LePoudre and Morrison (2022)

Hariri-Ardebili et al. (2023) highlight various technologies enhancing safety and operations of dam infrastructure, including digital twins, drones, Internet of Things (IoT), satellite remote sensing, and Building Information Modeling (BIM). However, to further alleviate the challenges in tailings management, advanced technologies are required. Key challenges in tailings waste management include: data management: vast amounts of siloed information that is difficult to integrate; operational demands: labor-intensive routine inspections and maintenance; climate variability: increasing risks from extreme weather events; and human error: complexity heightening risks during data interpretation and inspections. Traditional management methods are labor-intensive and prone to human error, highlighting the need for advanced technologies to streamline operations and improve predictive capabilities.

Generative Artificial Intelligence (GenAI), a branch of artificial intelligence, offers a transformative solution by analyzing vast amounts of data both off-line and in real time, collating various sources of data (e.g., text, images, numbers, audio), detecting patterns and anomalies, enhancing predictions and forecasting, and improving decision-making processes. GenAI has the potential to elevate tailings waste management to new levels of efficiency and reliability. Implementing GenAI requires a strategic approach, including stakeholder involvement, compliance with regulations, and addressing ethical considerations. By embracing these advancements responsibly, the tailings waste community can usher in a new era of infrastructure resilience, ready to face the challenges of operations, extreme weather events, and aging facilities.

The objectives of this paper are to:

1. Provide an overview of GenAI.
2. Detail how GenAI can be applied to tailings waste (TW) management.
3. Identify the challenges and future opportunities using GenAI.
4. Summarize the conclusions with best practices.

Generative Artificial Intelligence

GenAI is a versatile technology capable of producing various types of content, such as text, images, numbers, audio, and video, including segmenting objects in videos. It can also generate programming code and interact with users. These models, known as large language models (LLMs), are trained on vast datasets, including both private and publicly available information from the internet. The training process involves passing input data through multiple layers of neurons in a neural network, where each neuron's weight is adjusted using complex mathematical algorithms to minimize errors and enhance accuracy. These LLMs predict the next word in a sentence based on probabilistic estimates and other sophisticated processes.

GenAI models are designed for understanding and generating human-like text, particularly useful for processing large text data and providing contextually accurate responses. Models like GPT-4o (Omni) by

OpenAI (2024), Llama 3.1 by Meta, and Gemini by Google are increasingly becoming popular. These models excel in processing extensive datasets, identifying patterns, and generating actionable insights. The field of GenAI is rapidly evolving, with new architectures and hybrid approaches continually being developed to address specific challenges and improve performance across various domains. Leveraging GenAI may allow TW management to transition from reactive to proactive strategies, improving the resilience and reliability of tailings infrastructure.

Tailings waste management applications

GenAI distinguishes itself not only by its ability to create, simulate, and predict, thereby surpassing the capabilities of traditional data analysis, but also by encompassing a wide range of features including text, vision, listening, voice recognition, programming, graphs, and numerical acumen. The multifaceted nature allows it to interact and interpret various forms of data, enhancing its applicability and effectiveness across diverse data sources and scenarios. This technology may enable a paradigm shift from reactive to proactive strategies, which would be crucial for ensuring long-term safety and efficiency of tailings waste infrastructure.

The power of GenAI lies in its ability to process vast datasets, collating information, and deriving insights that could elude conventional methods. In the context of TW management, where numerous and intricate variables interact, this is particularly valuable. GenAI can analyze data from multiple sources, including previous reports, historical data, sophisticated sensor networks monitoring critical conditions and AI-augmented drone inspections, to offer predictive insights and decision-making support in uncertain scenarios. GenAI LLM capabilities are categorized into basic, emerging, and augmented levels as shown in Figure 3, each of which can be crucial for proactive TW management.

Basic capabilities include comprehension, multilingual processing, world knowledge, and coding. These foundational skills enable LLMs to perform tasks such as summarization, translation, and function calling, which are essential for managing diverse data sources in tailings management. Emerging capabilities encompass instruction following, reasoning, and in-context learning. Instruction following allows LLMs to execute complex tasks based on specific guidelines, enhancing the precision of operational procedures. Reasoning capabilities, including symbolic and logical reasoning, enable the models to solve problems step-by-step and make informed decisions. In-context learning allows LLMs to adapt to new information quickly, making them valuable for dynamic environments like mine waste management. Augmented capabilities involve interacting with users, self-improvement, and tool utilization. These advanced features enable LLMs to engage in physical and virtual interactions, continuously refine their performance, and effectively utilize various tools. For instance, in tailings management, LLMs can assist

in real-time monitoring, predictive maintenance, and emergency response planning, thereby improving overall efficiency and safety.

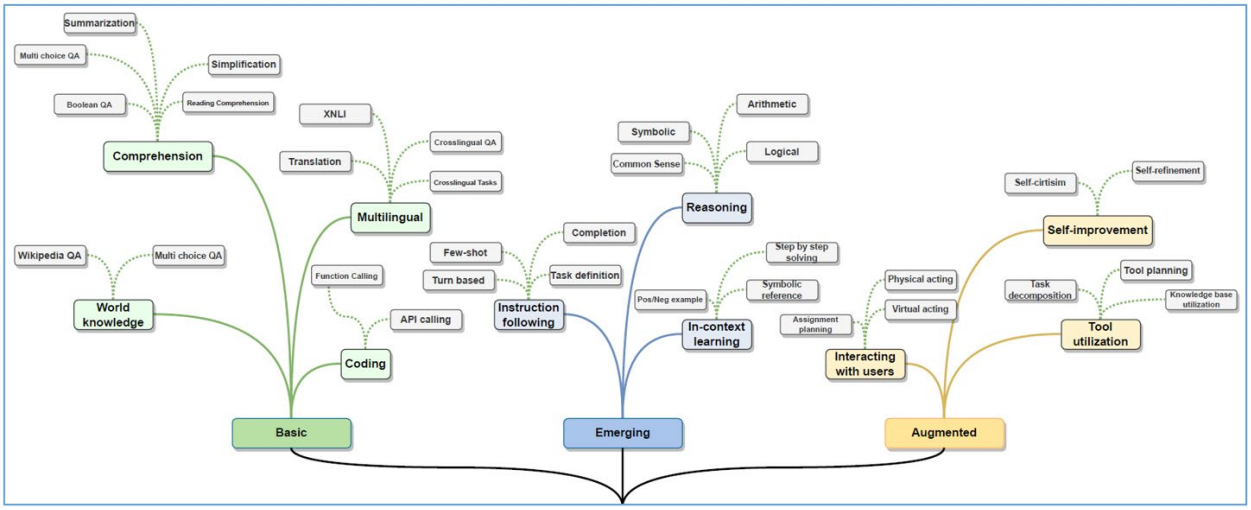


Figure 3: GenAI LLM capabilities (source: Minaee et al., 2024)

Developing and fine-tuning GenAI models enhances TW management. As shown in Figure 4, the process starts with data documentation and governance, collecting historical performance data, inspection reports, and real-time monitoring data from IoT sensors and drones.

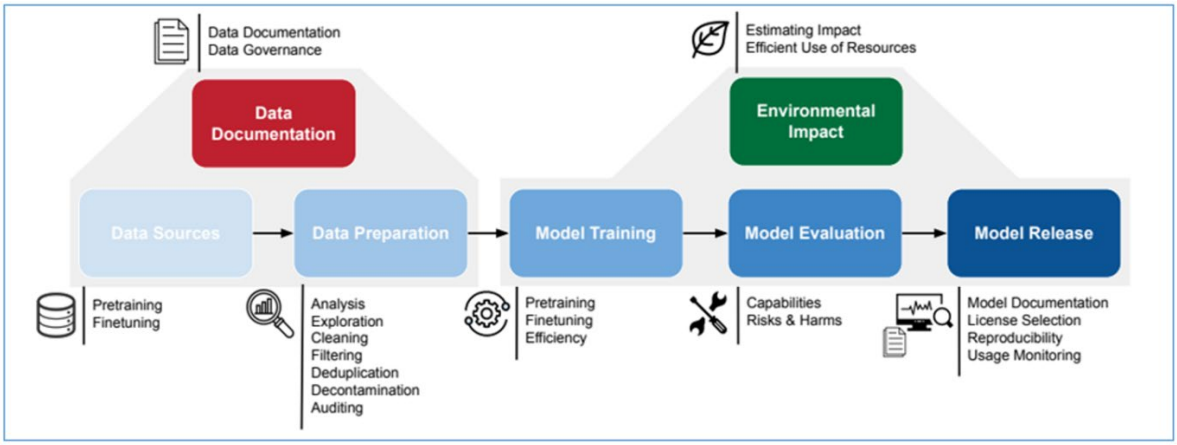


Figure 4: An overview of GenAI development (Source: Foundation Model Cheatsheet, 2024)

Next, data preparation involves cleaning, filtering, deduplication, and auditing to ensure quality and relevance. The data preparation phase of GenAI model development also aligns with the Integrated Knowledge Base concept in the Global Industry Standard on Tailings Management (GISTM) (GTR 2020) as it emphasizes the importance of data quality, relevance, and continuous updating, which are essential for both effective tailings management and the development of robust AI models. The prepared data is used

for model training, including pretraining and fine-tuning, to handle individual TW management tasks like dam safety reviews (DSRs), predicting structural issues, optimizing maintenance schedules, and simulating scenarios. Tasks are compartmentalized into modules for independent development and optimization.

Model evaluation assesses capabilities, risks, and potential harms, ensuring the model supports proactive tailings safety management. The final phase includes thorough documentation, regulatory compliance, reproducibility checks, and usage monitoring to ensure reliability. Environmental impact and resource efficiency are considered throughout. This modular approach enhances precision, reliability, and continuous innovation in tailings waste management. Integrating conventional approaches and advanced technology with GenAI offers transformative potential for enhancing completion of tailings DSRs. This integration can make the process more efficient, accurate, and comprehensive with proper risk management in place. For example, GenAI can be integrated into the tailings DSR processes (i.e., integral part of tailings management) that are outlined in the CDA Dam Safety Guidelines (CDA, 2013), and noted as a requirement of the GISTM, and the integration potential is described in the following.

Data and records review, and data book update

Integrating GenAI with traditional procedures may significantly enhance the data and records review process. Traditionally, this task involves manually reviewing historical data, inspection reports, and maintenance logs, which can be time-consuming and prone to human error. GenAI can streamline this process by summarizing large datasets, extracting key insights, and identifying patterns of concern. For instance, GPT-4o can quickly analyze and summarize documents containing historical data, while GenAI spatial tools like the ChatGPT plugin for Quantum Geographic Information System (QGIS) can visually present data, making it easier to identify patterns and areas of concern. Fine-tuning GenAI models with specific tailings DSR reports and data could improve the quality and accuracy of outputs tailored to each dam's unique characteristics, significantly reducing review time and overall tailings DSR completion time.

Site inspection and staff interviews

Site inspections and staff interviews traditionally require extensive manual effort and can result in delays and potential human errors. GenAI can automate the creation of comprehensive inspection checklists based on historical data. During inspections, AI-enhanced drones and sensors capture high-quality images and data, which are processed by Generative Adversarial Networks (GANs) to detect structural defects. GenAI spatial tools provide real-time geospatial visualization, enabling prompt assessment of issues. Additionally, GPT-4o models can transcribe and analyze verbal interviews with staff, efficiently extracting key information. Images from site inspections can be automatically processed (Figure 5) for potential TW management concerns. Fine-tuning these models with data from previous inspections and interviews provides more accurate and relevant outputs. This integration can significantly reduce the time required for

site inspections and staff interviews, enhancing the efficiency of TW management engineers without replacing their expertise.



Based on the attached image of the tailings dam, here are some technical observations:

1. **Dam Type and Condition**: The dam appears to be an earthen embankment, likely designed for tailings storage. The embankment slope is relatively steep, and the surface appears to be primarily composed of rock fill, which provides stability but might be prone to erosion without proper maintenance.
2. **Erosion and Stability**: No visible erosion control measures, such as riprap or vegetation, were observed. Regular inspections and maintenance are necessary to prevent erosion, particularly during heavy rainfall.
3. **Water Management**: The ponded water level seems relatively low, which is favorable for reducing hydraulic pressure on the dam. However, ongoing water management is crucial to prevent overtopping, especially during storm events.
4. **Safety Concerns**: It's essential to monitor for any signs of seepage, slumping, or erosion, especially near the dam crest and toe, as these could indicate potential failure mechanisms.

Figure 5: Demonstration of ChatGPT interaction using a tailings dam picture (source: Logan, 2022)

Tailings dam safety review and analysis

GenAI can enhance tailings dam safety analysis and review by analyzing large datasets from historical data, inspection reports, and real-time sensor inputs to identify potential issues. Engineers can use GPT-4o for querying specific aspects of dam performance and summarizing key findings. GenAI spatial tools provide advanced geospatial visualizations, helping simulate flood scenarios and assist in geotechnical assessments, improving TW management accuracy and efficiency. The Hydat-FlowGPT program shown in Figure 6, developed using GPT-4o, acquires hydrometric flow data and performs flow-frequency analysis to help estimate inflow design floods (IDFs).

```
import sqlite3
import numpy as np
import matplotlib.pyplot as plt
from scipy.stats import genextreme, gumbel_r, lognorm, weibull_min, genpareto
import sys
# Connect to HYDAT database
hydat_db_path = "C:\Program Files (x86)\ECCC\ECDataExplorer\Database\Hydat.sqlite3"
conn = sqlite3.connect(hydat_db_path)

cur = conn.cursor()

# Add the following functions to fit and predict using the mentioned distributions
def fit_gumbel(data):

    return gumbel_r.fit(data)

def fit_lognormal(data):

    return lognorm.fit(data)

def fit_weibull(data):

    return weibull_min.fit(data)

def fit_genextreme(data):

    return genextreme.fit(data)

def fit_genpareto(data):

    return genpareto.fit(data)

# Function to predict flow values for each distribution
def predict_flow(distribution, params, return_periods):
```

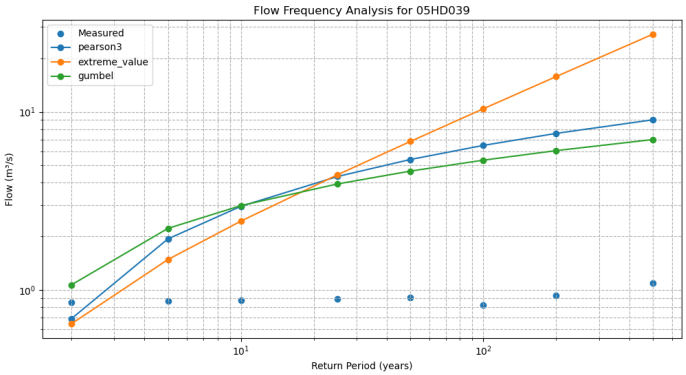


Figure 6: A snapshot of the code developed using GPT-4o and design flow frequency plot

GenAI may be used to automate the processes of calculation of dam classification parameters such as population at risk, environmental and cultural values, and infrastructure and economic impacts and provide the user with results in a Microsoft (MS) Word document (Figure 7) and can assist the professionals with developing workshop slides (Figure 8) and visuals for review.

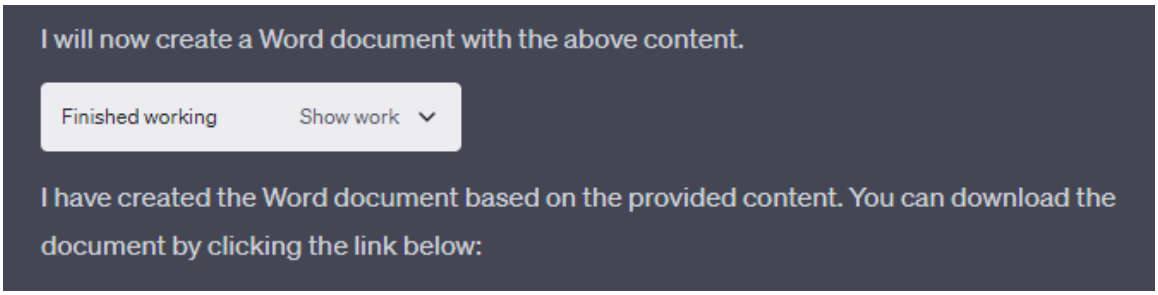


Figure 7: An overview of GPT4o's ability to create MS Word file with tailings DSR report template

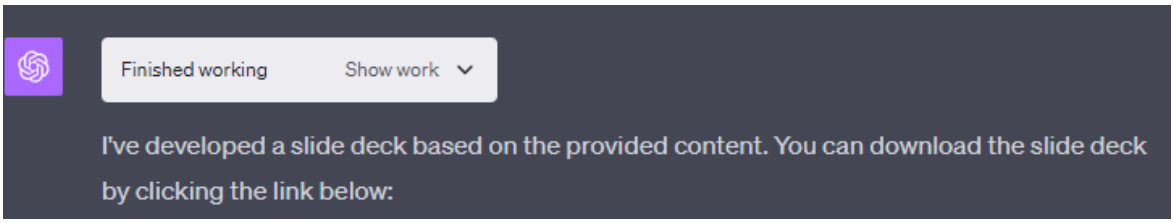


Figure 8: An overview of GPT4o's ability to create MS PowerPoint slides with tailings DSR workshop template

Challenges and opportunities

The effectiveness of GenAI in TW management relies on high-quality datasets. Poor data quality and biases in AI models can lead to inaccurate predictions. Mitigating biases requires detection algorithms, diverse training datasets, and continuous evaluation. Robust cybersecurity measures, including encryption, access controls, and regular audits, are essential to protect sensitive data. Compliance with data privacy regulations is crucial to safeguard personal and sensitive data, ensuring legal compliance and stakeholder trust. Implementing GenAI systems demands specialized skills in AI, data science, and TW management engineering. Collaboration between AI specialists and TW engineers is necessary for accurate application and interpretation of AI models.

GenAI enhances tailings management efficiency but cannot replace human judgment and experience. Over-reliance on AI risks missing critical issues detectable only through on-the-ground inspections. Human oversight remains essential to interpret AI outputs and maintain safety standards. Continuous training and support for personnel are essential to stay updated with AI advancements. Despite these challenges, GenAI holds significant promise for transforming TW management practices (but not limited to):

- Enhanced Prediction and Analysis – Improved predictive models can be used to better forecast structural issues, maintenance needs, and environmental impacts. Real-time analysis of data from IoT sensors and drones could enable rapid detection of anomalies and potential problems.
- Customized AI Models – Developing and fine-tuning AI models with dam-specific historical data and inspection reports may provide more accurate and relevant recommendations.
- Advanced Monitoring and Maintenance – Integration with IoT devices creates a more interconnected monitoring approach, feeding continuous real-time data to AI systems. AI-driven robotics can be used to conduct detailed inspections and perform minor repairs in hard-to-reach or hazardous areas, enhancing safety and efficiency.
- Proactive Management – Continuous data streams could enable AI to provide timely alerts and recommendations for maintenance and emergency response. AI can be used to help optimize water usage, energy consumption, and environmental impact, supporting more sustainable tailings waste management.
- Climate Resilience – AI can be used to provide predictive insights into extreme weather events and long-term environmental changes, helping develop adaptive strategies for dam infrastructure.

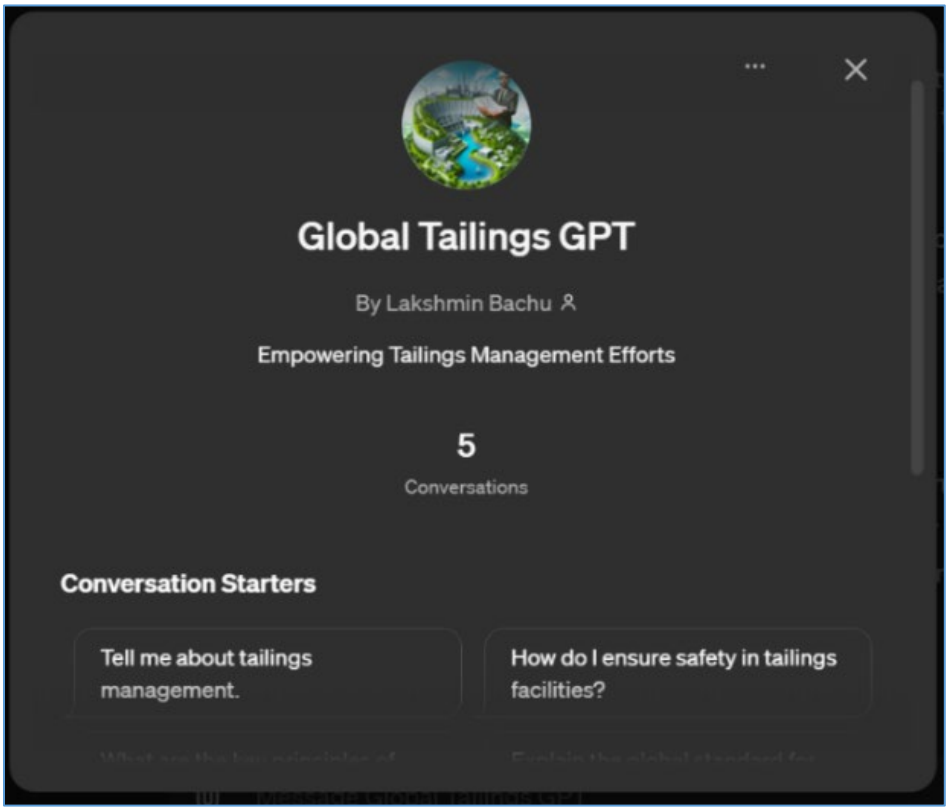


Figure 9: Global tailings GPT developed in ChatGPT for the public to learn about GISTM guidelines

- A multimodal LLM, ChatGPT enables users to create specialized GPTs using custom knowledge bases and instructions, particularly useful for reviewing tailings DSR reports and related information. Users can compare tailings DSRs with regulatory guidelines like CDA, the Mining Association of Canada (MAC), and the GISTM for comprehensive evaluations (e.g., Figure 9). Multiple team members can interact with GPTs simultaneously, streamlining information exchange and DSR completion. These GPTs can identify potential deviations or compliance issues based on TW management guidelines, allowing engineers to evaluate them more efficiently. GPTs also serve educational purposes for dam professionals, and organizations like CDA can deploy them for advisory purposes.
- AI Agents – These are autonomous software entities designed to perform tasks, make decisions, and interact with their environment with minimal human intervention (Figure 10). Leveraging GenAI, these agents may one day transform TW management by automating data reviews, analysis, document preparations, continuously monitoring conditions, analyzing structural integrity, and predicting potential failures with reasonable accuracy. For instance, AI-enhanced drones equipped with high-resolution cameras can capture detailed images of tailings dam and other structures, while IoT devices provide real-time data on environmental and structural parameters.
- Small Language Models (SLMs) – These are specialized AI systems trained on focused datasets with fewer than one billion parameters, unlike LLMs which exceed 100 billion parameters. In TW management, SLMs offer distinct advantages where targeted training allows them to excel in TW engineering and safety protocols, potentially outperforming larger models in this niche. SLMs require less computational power, making them suitable for on-site deployment, even in remote areas. They process data and generate insights rapidly, enabling near real-time monitoring crucial for TW management. SLMs are effective with smaller datasets, beneficial for mine sites with limited data.
- Retrieval-Augmented Generation (RAG) – RAG models combine retrieval-based and generation-based AI to enhance decision-making by integrating diverse data sources like structural health and environmental information, generating alerts, simulating emergency scenarios, and assessing risks, as well as automating report generation for thorough documentation and compliance. By improving efficiency, accuracy, and proactive maintenance, these AI technologies may lead to better safety outcomes and decision-making, ultimately protecting public safety and the environment. RAGs are also integrated with Agents for improved efficiency, often referring to AgentRAGs.

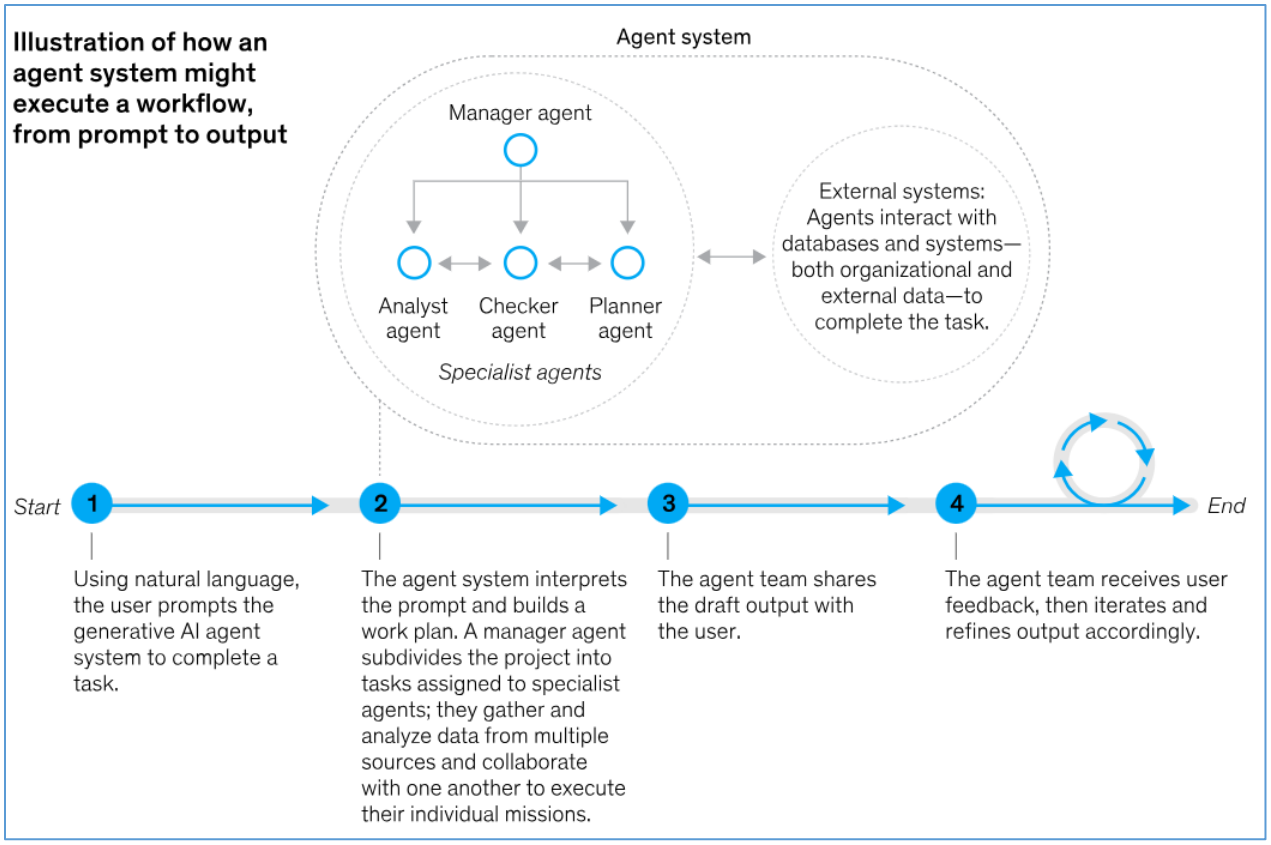


Figure 10: GenAI multi-agent system illustration (McKinsey and Company, 2024)

Implementing GenAI in TW management involves several strategic steps. A high-level roadmap is shown in Figure 11 and will encompass developing task specific SLMs and TW specific LLMs, revitalizing the models by using GenAI methods such as RAGs, ensuring robust cybersecurity to protect sensitive data, addressing potential biases in AI models, involving stakeholders and ensuring compliance with relevant regulations and standards. By following this roadmap, organizations can integrate GenAI into TW management, enhancing safety, reliability, and sustainability.

Conclusion

This paper explores GenAI for enhancing tailings waste management. Integrating GenAI can leverage safety, project management, reliability, and sustainability of tailings waste facilities. Advanced GenAI methods like GPT-4o, SLMs, RAG, Multi-AgentRAG systems developed based on a life-cycle approach have the potential to transform all the life-cycle strategies for sustainable TW management. GenAI augments human efforts and enhances efficiency in tailings management, complementing rather than replacing human expertise.

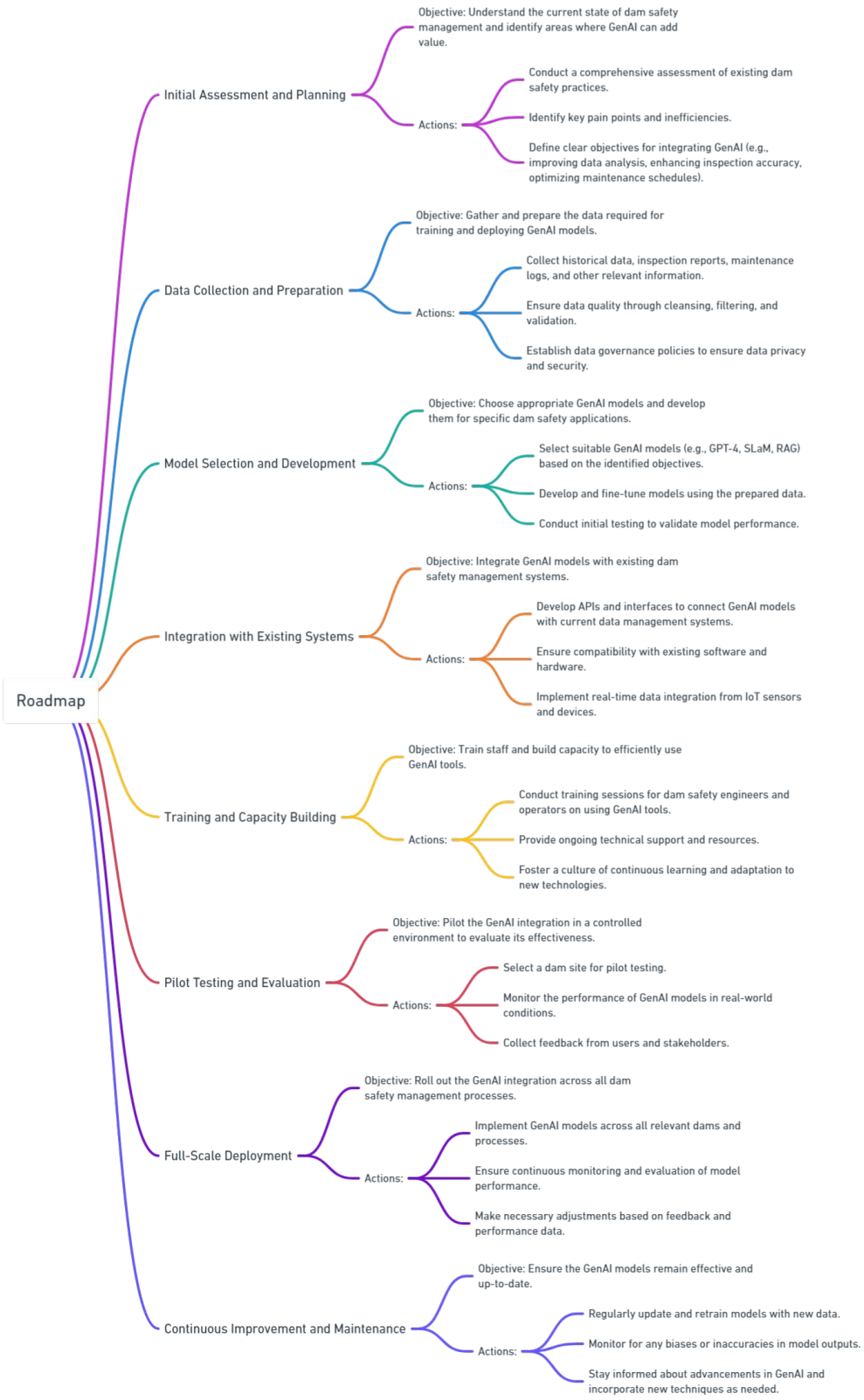


Figure 11: A high level roadmap of developing TW Management GenAI tools for life cycle phases

Responsible GenAI implementation requires attention to data quality, bias mitigation, cybersecurity, and specialized expertise. Collaboration between AI specialists, tailings waste engineers, and regulatory bodies is essential. The potential for TW management transformation through GenAI lies in integrating it with human expertise and physics-based models, empowering professionals to enhance management while maintaining ultimate responsibility. By responsibly embracing these advancements, the mining industry can address challenges like extreme weather and aging infrastructure. This paper provides insights and roadmap for integrating GenAI to enhance tailings waste management, and has potential use globally.

References

CDA (Canadian Dam Association). 2013. 2007 Dam Safety Guidelines, 2013 edition.

ECCC (Environment and Climate Change Canada). 2018. National Water Data Archive: HYDAT.

Foundation Model Cheatsheet. 2024. Foundation Model Training Overview. Retrieved from https://fmcheatsheet.org/; accessed July, 2024.

Hariri-Ardebili, M. Amin, Mahdavi, Golsa, Nuss, Larry K. and Lall, Upmanu. 2023. The role of artificial intelligence and digital technologies in dam engineering: Narrative review and outlook. *Engineering Applications of Artificial Intelligence* 126(A). https://doi.org/10.1016/j.engappai.2023.106813

LePoudre, C. and Morrison, K.F. 2022. Tailings management systems. In KF Morrison (ed.)*, Tailings Management Handbook: A Life-Cycle Approach,* Society for Mining, Metallurgy and Exploration, Englewood.

Logan, C. 2022. Critics worry more tailings pond waste at gold mine could mean disaster for Nova Scotia. Retrieved from https://www.nationalobserver.com/2022/07/29/news/critics-worry-more-tailings-pond-waste-gold-mine-NS

McKinsey and Company. 2024. The promise and the reality of Gen AI agents, accessed in July 2024.

MEND. 2001. MEND 5.4.2d. MEND Manual, Volume 4 – Prevention and Control, ed. G.A. Tremblay and C.H. Hogan, February.

Minaee, S., Mikolov, T., Nikzad, N., Chenaghlu, M., Socher, R., Amatriain, X. and Gao, J. 2024. Large Language Models: A Survey. arXiv preprint arXiv:2401.00001.

OpenAI. 2024. Announcing GPT-4o in the API! Retrieved from https://www.openai.com; accessed in May,2024.

Snow, R. 2022. Overview of tailings management, in K.F. Morrison (ed.), *Tailings Management Handbook: A Life-Cycle Approach,* Society for Mining, Metallurgy and Exploration, Englewood.

Chapter Eight

Environment and Water

TAILINGS AND
MINE WASTE 2024



Evaluation of Biogeochemical Processes for Weak Acid Dissociable Cyanide

Larissa Smith, SiREM, Canada
Sandra Dworatzek, SiREM, Canada
Jeff Roberts, SiREM, Canada
Valerie Bertrand, WSP, Canada
Elizabeth Walsh, WSP, Canada

Abstract

Cyanide (CN^-) is a small, highly reactive, inorganic compound that readily forms metal-cyanide complexes and organic compounds. It is commonly used in the mining industry as a lixiviant to extract precious metals, including gold. The composition of cyanide in the environment can be affected by factors such as pH, temperature, and trace metal content. Free cyanide (HCN or CN^-) is extremely toxic to organisms due to its ability to bind metalloproteins. Weak acid dissociable (WAD) cyanide refers to metal-cyanide complexes that dissociate under weakly acidic conditions (pH 4.5-6) and release free cyanide. Remedial methods for cyanide include adsorption, oxidation, and bioremediation. The most common byproducts of cyanide biodegradation are ammonia, formic acid, carbon dioxide, cyanate, and thiocyanate. Abiotic reactions such as hydrolysis or oxidation can also occur naturally, forming ammonia, cyanate, or thiocyanate.

This paper discusses the assessment of natural biodegradation processes controlling the fate of WAD cyanide in tailings to be deposited in an open pit above backfilled stopes, where process water could potentially migrate through these infrastructures into the local groundwater. A laboratory study was designed to monitor changes in aqueous concentrations of key parameters, including aqueous concentrations of cyanide, cyanate, thiocyanate, and ammonia in laboratory microcosms that simulated tailing pore water contacting cement, tailings, and waste rock backfill. Tests over nine months were performed under aerobic and anaerobic conditions at 4°C and at progressively longer time intervals. The results showed that the total bacteria increased while the WAD and free cyanide concentrations initially varied, but ultimately decreased in the reactors. Thiocyanate was observed to increase in both the aerobic and anaerobic microcosms. The addition of cement to the microcosms increased the pH and slowed the rate of CN degradation. This suggested that a microbially mediated process was degrading the cyanide. Lessons learned will be discussed.

Introduction

Cyanide (CN^-) has been used by the mining industry for over a century as a powerful lixiviant during the gold extraction process. Due to its small molecular size and negative charge, cyanide is one of the strongest ligands in organometallic chemistry (Chadwick and Sharp, 1966). In the presence of gold and oxygen, it forms a soluble coordination complex that can be separated from other minerals. As lower grade gold ores are mined in order to meet increasing global gold demand, it has become increasingly important to improve the extraction yield. The cyanidation process has become a key method to efficiently extract and process gold.

However, the same chemical properties that make cyanide useful for gold extraction, also allow it to form strong bonds with other metals, including those incorporated in metalloproteins. This biotoxicity leads to even small concentrations of cyanide being dangerous to human health and damaging to the environment (Eisler and Wiemeyer, 2004). By keeping the pH of mining extraction solutions high, the risk of cyanide poisoning during the extraction process is low, as hydrogen cyanide (HCN), a gas, is not formed. Once the extraction process is complete, excess amounts of cyanide can be oxidized to a less toxic form: cyanate or thiocyanate. This oxidation can be done using treatment methods such as sulfur dioxide and air oxidation, alkaline chlorination, or electrochemical oxidation (Botz, 2001). Even with an oxidation process, however, small amounts of cyanide can still be released into tailings, which, in turn, can cause persistent release of other metals, such as mercury (Boyle and Smith, 1994) into groundwater. Additionally, some notable dam collapses, including that at Baia Mare in 2000, have caused large environmental impacts as cyanide was also released (Soldán et al., 2001).

Environmental cyanide can occur as free cyanide (CN^- or HCN), or in metal coordination compounds. Weak acid dissociable (WAD) cyanide compounds are metal-cyanide coordination compounds that release free cyanide under slightly acidic conditions (pH 4.5 – 6). Stronger metal-cyanide compounds, especially iron-cyanide complexes, are not usually environmentally degraded until the free and WAD cyanide compounds have been degraded, but these complexes may release free cyanide under strong UV light (Smith and Mudder, 1997). Once released into the environment, cyanide degradation can occur through abiotic or biotic mechanisms. Abiotic mechanisms include hydrolysis, which produces carbonate and ammonia, and oxidation, which produces cyanate that can be further broken down into carbonate and ammonia (Novak et al., 2013). Multiple different microbial species have been identified that can biodegrade cyanide, especially in aerobic environments. These biodegradation mechanisms are usually oxidative, reductive, hydrolytic, or substitution/transfer mechanisms that produce byproducts such as cyanate, formic acid, ammonia, carbon dioxide, and/or thiocyanate (Luque-Almagro et al., 2018). Anaerobic cyanide biodegradation has been observed under methanogenic conditions, although it is notably slower and often occurs alongside abiotic hydrolysis reactions (Novak et al., 2013).

Tailings from a mine using the gold cyanidation process were planned for deposition in an open pit above backfilled stopes, where process water could potentially migrate through these infrastructures and into the local groundwater. To determine if the cyanide in the tailings and process water could be naturally attenuated and monitored natural attenuation (MNA) could be considered for the site tailings area, a laboratory study was designed to monitor changes in aqueous concentrations of key parameters including cyanide, cyanate, thiocyanate, and ammonia in laboratory microcosms that simulated tailing pore water contacting cement, tailings, and waste rock backfill. The regulator specified that the total cyanide release limit was 5 micrograms per liter (µg/L). Tests over nine months were performed under aerobic and anaerobic conditions at 4ºC and at progressively longer time intervals, as determined in consultation with the Site consultant. This paper will discuss the methodology, results, and conclusions of the laboratory study.

Methodology

Reactors to evaluate the treatments were constructed by filling sterile 250 milliliter (mL) screw cap Boston round clear glass bottles with 100 g of tailings material and 200 mL of Site process water. The microcosms were then capped with 1" × 1" foam plugs (aerobic treatments) or Mininert™ caps (anaerobic treatments) to promote or prevent gas exchange and allow for repeated amendments or sampling throughout the incubation period. All controls and treatments were constructed in duplicate. Figure 1 shows the construction of the anaerobic microcosms under a nitrogen atmosphere.



Figure 1: Anaerobic microcosms were constructed in a glove bag under a nitrogen atmosphere

In order to provide sufficient sample volumes for analysis, additional sacrificial microcosms were constructed for each analysis timepoint throughout the study. Table 1 summarizes the details of microcosm construction for both treatment conditions.

Table 1: Summary of controls, treatments, and amendments

Control/Treatment	Amendments
Aerobic Control	Only Site process water
Aerobic Tailings	Site process water and tailings
Aerobic Tailings and Cement	Site process water, tailings, and 1% w/w cement
Anaerobic Control	Only Site process water
Anaerobic Tailings	Site process water and tailings
Anaerobic Tailings and Cement	Site process water, tailings, and 1% w/w cement
Anaerobic Waste Rock	Site process water and waste rock

All microcosms were incubated in an air-filled (or nitrogen-filled) autoclavable bag that was sealed. The air (or nitrogen) in the bag was refreshed every time sacrificial reactors were removed for sampling. During incubation, all microcosms were stored in a refrigerator at 4°C in the dark to prevent photodegradation. Microcosms were incubated for a period of up to 280 days.

Microcosms were sampled more frequently at the beginning of the study and less frequently near the end of the study. At each sampling event, the microcosms were analyzed for: pH, oxidation-reduction potential (ORP), dissolved oxygen (DO), ammonia, total, free, and WAD cyanide, thiocyanate, cyanate, and dissolved metals. Analysis of cyanides, thiocyanate, cyanate, and dissolved metals were performed at an external analytical laboratory using standard methods. Additionally, at Time 0 and at the endpoint of the study, the microcosms were sampled for analysis of total bacteria.

Results and discussion

Microcosms were incubated for up to 280 days. Due to the large sampling volumes required for analysis at each time point, sacrificial microcosms were constructed and sampled. The use of sacrificial microcosms increases the variability in the data compared to continuously samples microcosms, which is especially observed during the early sampling points in the study. However, clear trends existed in the cyanide, cyanate, thiocyanate, ammonia, and total bacteria results over the course of the study incubation period.

Cyanide trends

Similar cyanide degradation trends were observed in both the aerobic and anaerobic microcosms. Figure 2 shows the concentration of free, WAD, and total cyanide at each time point in the microcosms.

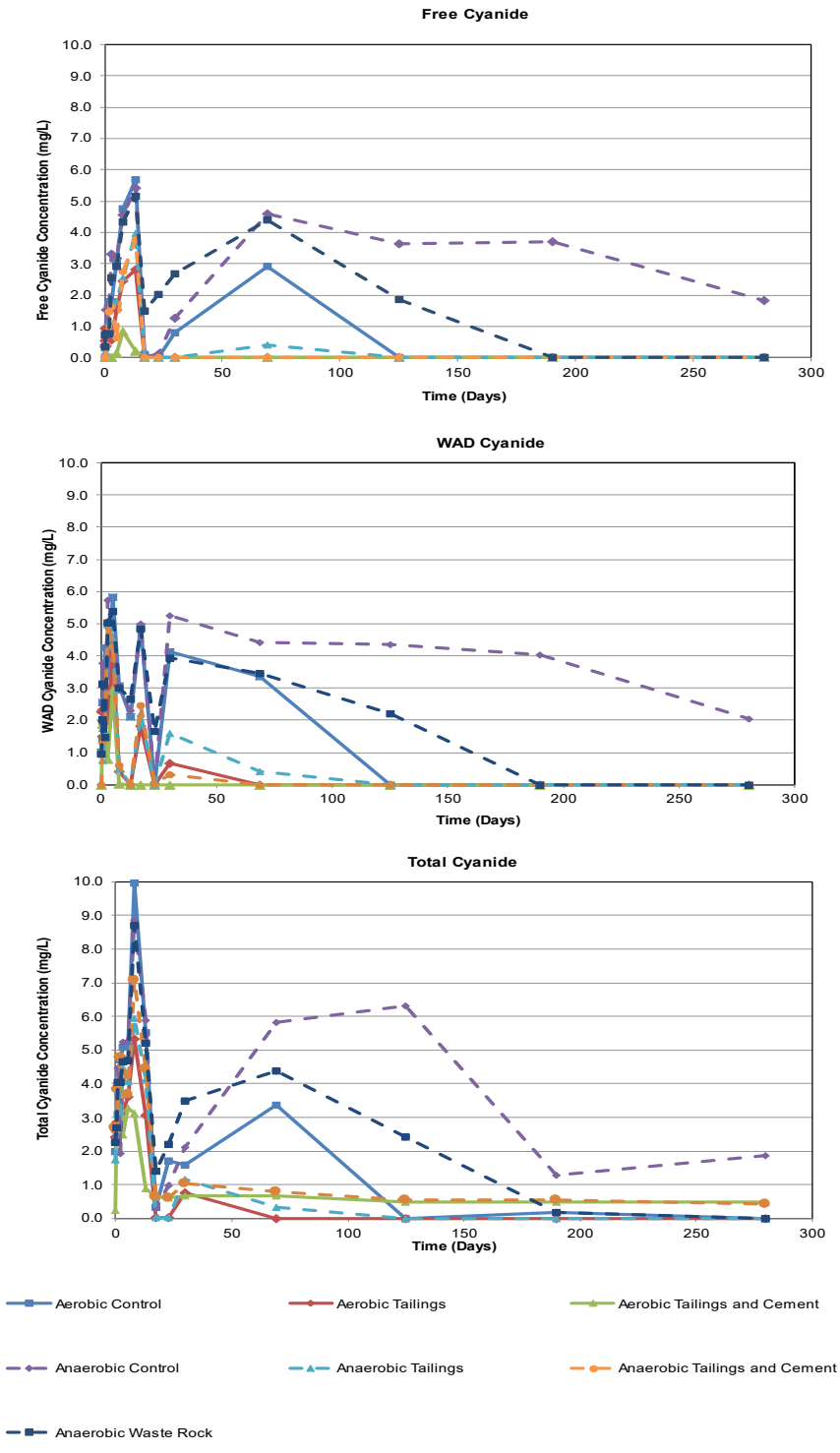


Figure 2: The concentration of free, WAD, and total cyanide in control and treatment microcosms

In general, cyanide in the control microcosms, with no tailings present, took the longest time to degrade and by Day 280, free, WAD, and total cyanide concentrations were still observed in the anaerobic control microcosms only. Aerobic and anerobic treatment microcosms with tailings present both showed similar trends: free cyanide was present until Day 13 and WAD cyanide was present until Day 30 in the aerobic treatment and Day 69 in the anaerobic treatment, while total cyanide was present until Day 69 in both treatments.

Microcosms amended with both tailings and cement had also removed all of the free cyanide by Day 13 and the WAD cyanide by Day 30. However, these treatments were not able to completely degrade all of the total cyanide and the concentration of total cyanide was relatively stable from Day 125 until the end of the study. It is possible the addition of cement, which increased the pH in the treatment microcosms, caused less favorable conditions for cyanide biodegradation. The addition of waste rock instead of tailings did not appear to improve the degradation conditions and free, WAD, and total cyanide were present in this treatment until Day 125. This may have been due to less microbial biomass associated with the waste rock.

Degradation byproducts

Degradation products of cyanide include cyanate, thiocyanate, and ammonia. Figure 3 shows the concentration trends of these products at each timepoint. The concentration of cyanate in the microcosms was already elevated at Time 0, but over the course of the study the concentration decreased in each control and treatment. Cyanate degradation can yield ammonia, which also increased in the microcosms during the study period. Thiocyanate was also present at Time 0 and slightly increased in the control and treatment microcosms over the duration of the study.

In the Aerobic Control microcosms, cyanate decreased slowly over the course of 280 days, while ammonia slowly increased. Conversely, cyanate had completely degraded by Day 125 in the Aerobic Tailings treatment, with corresponding increases in ammonia. This suggests that the presence of tailings material may be enhancing the rate of degradation, either by supporting a microbially mediated process or an abiotic hydrolyzing process. In the Aerobic Tailings and Cement treatment, cyanate only slightly decreased and ammonia did not significantly increase, suggesting that the increased pH was inhibiting the microbial growth or biological degradation process. A similar trend was observed in the anaerobic treatment microcosms, although the degradation rates were slower. In the Aerobic Tailings and Cement treatment, cyanate only slightly decreased and ammonia did not significantly increase, suggesting that the increased pH was inhibiting the microbial growth or biological degradation process. A similar trend was observed in the anaerobic treatment microcosms, although the degradation rates were slower.

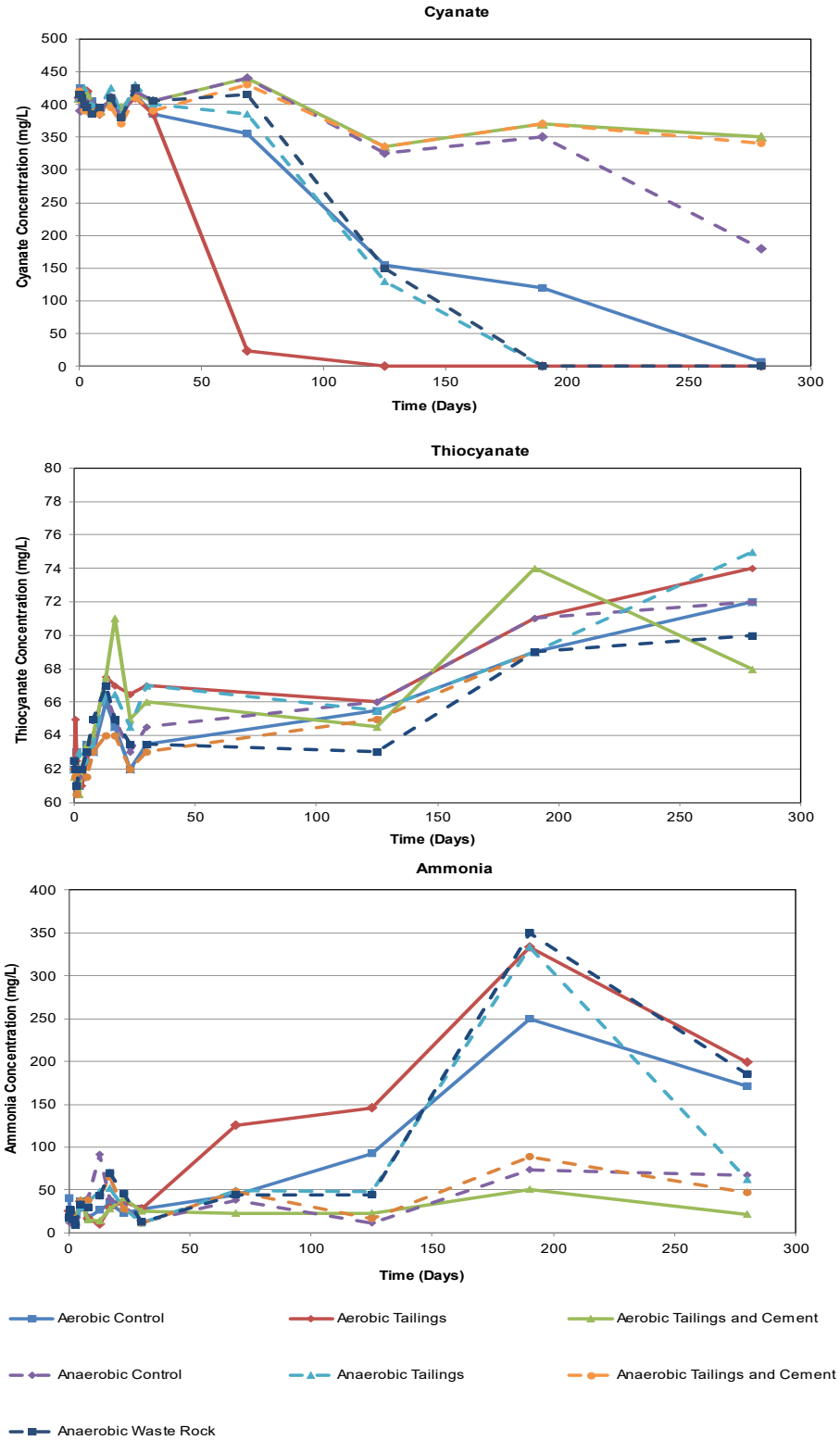


Figure 3: Concentration trends of cyanate, thiocyanate and ammonia in the control and treatment microcosms

Total bacteria

Analysis of total bacteria was performed at Time 0 (baseline) and at the endpoint of the study to determine the amount of total bacteria present in a sample. Table 2 shows the gene copies per liter (gene copies/L) present at both time points.

Table 2: Summary of total bacteria results

Control/Treatment	Gene Copies/L
Baseline	1×10^4
Aerobic Control	2×10^{11}
Aerobic Tailings	7×10^6
Aerobic Tailings and Cement	2×10^6
Anaerobic Control	2×10^{10}
Anaerobic Tailings	6×10^7
Anaerobic Tailings and Cement	1×10^5
Anaerobic Waste Rock	5×10^8

These results suggest that microbial growth occurred in all the controls and treatments, especially in the control reactors. The relatively smaller microbial growth that occurred in the tailings and cement treatments may be explained by the presence of cement, which increased the pH. Higher pH levels can impact the growth of non-extremophile microbial communities that cannot tolerate those pH levels. The anaerobic waste rock also showed significant microbial growth, although the cyanide degradation in that treatment was slower in comparison to the tailings treatments. The total bacteria results, in conjunction with the cyanide and degradation products results, suggest that the cyanide degradation occurring in the microcosm may have been microbially mediated.

Conclusion

A laboratory treatability test was conducted to determine if MNA of cyanide was possible using process water, tailings, and waste rock from a mine site. All the results combined indicated that cyanide degradation was occurring under aerobic and anaerobic conditions, likely due to a biological degradation. The byproducts of cyanide degradation, especially cyanate, were also being degraded. The total bacteria concentration increased over the course of the study, indicating that microbial populations were able to survive and potentially biodegrade cyanide and/or its degradation byproducts. The results also indicated that degradation would be slower in the presence of cement if it was used as a stabilizing agent. The Site consultant was able to use this data to complete their Site evaluation to support a natural attenuation recommendation.

References

Botz, M.M. 2001. Overview of cyanide treatment methods. In *Mining Environmental Management*. Mining Journal Ltd. London, pp 28–30.

Boyle, D.R. and C.N. Smith. 1994. Mobilization of mercury from a gossan tailings pile, Murray Brook precious metal vat leaching operation, New Brunswick, Canada. United States Department of the Interior, Bureau of Mines, Special Publication, SP 06B-94, 234-241.

Chadwick, B.M. and A.G. Sharpe. 1966. Transition metal cyanides and their complexes. *Adv. Inorg. Chem. Radiochem.* 8: 83–176.

Eisler, R. and S.N. Wiemeyer. 2004. Cyanide hazards to plants and animals from gold mining and related water issues. *Rev. Environ. Contam. Toxicol.* 183: 21–54.

Luque-Almagro, V.M., P. Cabello, L. P. Sáez, A. Olaya-Abril, C. Monero-Vivián and M.D. Roldán. 2018. Exploring anaerobic environments for cyanide and cyano-derivatives microbial degradation. *Appl. Microbiol. Biotechnol.* 102: 1067–1074.

Novak, D., I. H. Franke-Whittle, E. Tratar Pirc, V. Jerman, H. Insam, R. Marinšek Loger, B. Stres. 2013. Biotic and abiotic processes contribute to successful anaerobic degradation of cyanide by UASB reactor biomass treating brewery waste water. *Water Res.* 47(11): 3644–3653.

Smith, A.C.S. and T.I. Mudder. 1997. The environmental geochemistry of cyanide. In *The Environmental Geochemistry of Mineral Deposits*. *Reviews in Economic Geology:* 229–248.

Soldán, P., M. Pavonič, J. Bouček and J. Kokeš. 2001. Baia Mare accident – brief ecotoxicological report of Czech Experts. *Ecotoxicol. Environ. Saf.* 49: 255–261.

Combining Approaches for Environmental Assessment of Tailings Ponds and Waste Piles in the Eastern Amazon

Silvio Ramos, Vale Institute of Technology, Brazil
Paula Ribeiro, Vale Institute of Technology, Brazil
Cecilio Caldeira, Vale Institute of Technology, Brazil
Wendel Pereira, Vale Institute of Technology, Brazil
Markus Gastauer, Vale Institute of Technology, Brazil
Pedro Souza-Filho, Vale Institute of Technology, Brazil

Abstract

At the Igarapé Bahia Gold Mine, situated within the Carajás Mineral Province in Brazil, environmental rehabilitation initiatives have been implemented in waste piles (WPs) and tailings pounds (TPs) since the cessation of gold extraction in 2002. Monitoring soil and vegetative attributes within these areas is crucial to ensure the efficacy of the implemented intervention techniques, which can be done by integrating different approaches. Thus, the aims of this study were to (i) assess soil contamination and the associated ecological risks posed by potentially toxic elements (PTE); (ii) obtain a soil quality index based on soil chemical attributes; (iii) calculate Normalized Difference Vegetation Index (NDVI); (iv) show rehabilitation status based on vegetation parameters; and (v) combine these measures into a single index. For this, four TPs, two WPs, and an area of native forest from Igarapé Bahia mine in the Brazilian Amazon were assessed. The results of the single index indicate that the environmental conditions of the WPs are superior to those of the TPs. The WPs areas show positive signs that the activities developed for their rehabilitation were favorable, contributing to the development of vegetation and soil quality. On the other hand, the TPs exhibit low fertility and vegetation cover, in addition to elevated levels of PTE, signaling that their current attributes are far from ideal conditions. The ecological risk index indicates a low risk for all studied areas. The incorporation of soil conditioners and the planting of species tolerant to adverse conditions could enhance soil attributes and vegetation development in TPs areas. Finally, the integrative approach of the different indices proved to be a valuable tool for evaluating the rehabilitation status of the tailing ponds and waste piles.

Introduction

In the Amazon region, gold (Au) is mined in artisanal mining areas without environmental concern and supervision, resulting in significant environmental impacts (Teixeira et al., 2021). Conversely, mining corporations conduct industrial exploration with environmental and social responsibility, mitigating the impacts associated with mining activities and promoting the environmental rehabilitation of impacted areas (Gastauer et al., 2019).

The research on industrial gold mining is limited, but it can inform as to the benefits of environmentally responsible mining in terms of ecosystem quality and human health protection. In this context, several indices have been applied to monitor mining areas, including spectral indices, the soil quality index (SQI) (Ribeiro et al., 2022), and the ecological risk index. In order to provide a comprehensive representation of the overall soil and environmental status, these indices have been also compiled into a single, comprehensive index (Gastauer et al., 2020; Wang et al., 2018).

One example of an industrial mining complex is the Igarapé Bahia (IGB) located in Carajás Mineral Province (CMP), which is situated in the Eastern Amazon. The exploration activities in IGB stopped in 2002, when a rehabilitation process began in the tailings deposition ponds (TPs) and waste piles (WPs). The rehabilitation measures included geotechnical conformation, liming, fertilizer treatment (organic compost, NPK, and micronutrients) and planting a mix of exotic and native species seeds. After 20 years, to assess the effectiveness of the rehabilitation interventions, soil and vegetation attributes were collected in permanent plots (10 × 20 m), installed in two WPs (WP-1 and WP-2), four TPs (TP1-6, TP7, TP8, and TP9) (Figure 1), and a native forest area with a low degree of anthropic influence in the IGB mining complex.

This study examines the environmental rehabilitation activities in the IGB mining complex, assessing:

1. soil contamination and the associated ecological risks posed by potentially toxic elements (PTE);
2. SQI based on soil chemical attributes;
3. the Normalized Difference Vegetation Index – NDVI;
4. the rehabilitation status based on vegetation parameters; and
5. combining these measures into a single index.

The hypothesis of this study is that this single index can differentiate between TPs, WPs, and native forests.

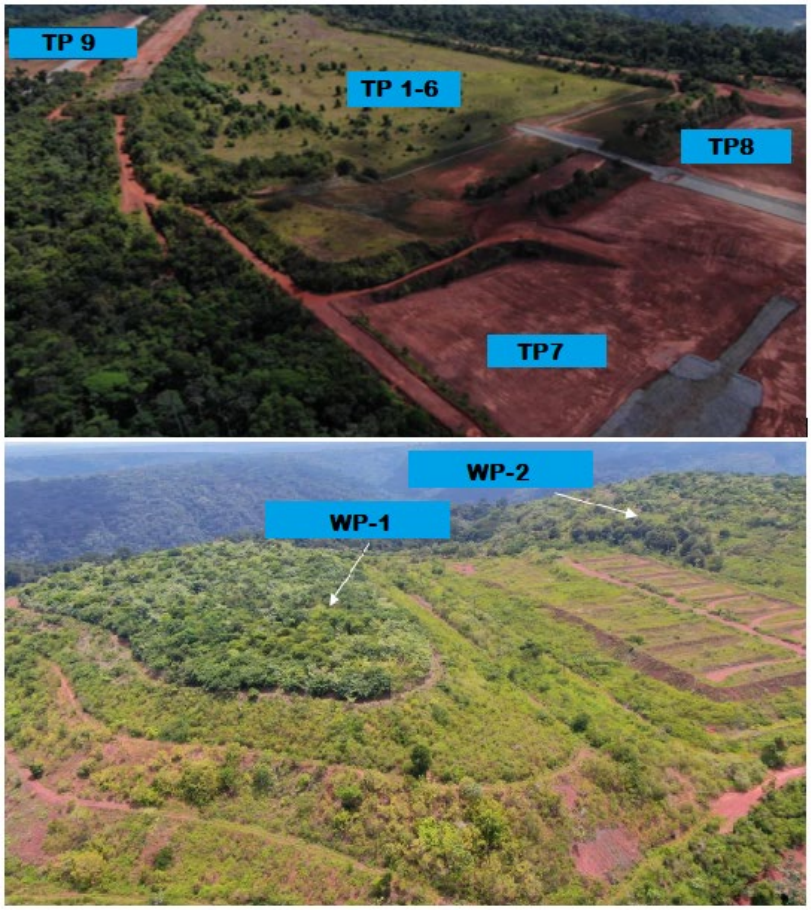


Figure 1: Tailings deposition ponds (TPs) and waste piles (WPs) in the IGB mining complex. Adapted from Oliveira et al. (2023)

Methodology

Soil characterization and SQI

Soil samples (0–10 cm) were collected from five points distributed within permanent plots. These samples were air-dried, sieved to the 2 mm fraction, and analyzed for chemical attributes following Teixeira et al. (2017): pH, soil organic matter (OM), sulfur (S), exchangeable calcium (Ca^{2+}), magnesium (Mg^{2+}), and aluminum (Al^{3+}), phosphorus (P), potassium (K^{+}), copper (Cu), iron (Fe), manganese (Mn), and zinc (Zn) and boron (B), sum of bases (SB), cation exchange capacity (CEC), and base saturation (V%).

The levels of arsenic (As), barium (Ba), cadmium (Cd), cobalt (Co), chromium (Cr), copper (Cu), iron (Fe), manganese (Mn), molybdenum (Mo), nickel (Ni), lead (Pb), selenium (Se), and zinc (Zn) were evaluated in soil samples sieved in the 80-mesh fraction and digested in *aqua regia* solution. The concentrations of PTE were determined by inductively coupled plasma–optical emission spectrometry

(ICP-OES) and Inductively Coupled Plasma – Mass Spectrometry (ICP-MS) or Cold Vapor Atomic Absorption Spectrometry (CV-AAS) for Hg.

An SQI was employed to assess the impact of revegetation progress on soil fertility. The soil properties included in the index were selected based on a principal component analysis (Mukhopadhyay et al., 2014). Soil parameters were converted into scores (S) ranging from 0 to 1 using the Wymore equation (Freitas et al., 2012) and methodology described in Ribeiro et al. (2022). The mean values observed in the reference areas were considered to be the optimal for each soil attribute. After determining the score, the SQI was calculated by multiplying the score value with the weight according to Equation 1.

$$SQI = \sum_{i=1}^{n} W_i S_i \quad \text{(Equation 1)}$$

where W is the weighting factor and S is the score for each variable. The SQI means were scaled by dividing the obtained values by the mean value of the forest area.

NDVI

Images of the WorldView2 satellite (July 2020) with a spatial resolution of 2 m (pixel size) and four spectral bands (blue, green, red, and near infrared) were acquired and used for the determination of the NDVI. This was made using the raster calculator of the QGis 3.10 software and the equation described by Rouse et al. (1974).

Environmental recovery status

The calculation of the environmental recovery status (ERS) followed methodology described by Gastauer et al. (2020, 2021). For this, in the installed plots, all trees with a diameter at breast height larger than 3 cm were tagged and identified. The following variables were considered in the index: species richness and tree density; basal area; above-ground biomass and functional diversity.

A principal coordinate analysis (PCoA) based on Gower distances was performed with scaled and centered variables. This approach accounts for possible autocorrelations between the measured variables and transfers the variation between plots to a Euclidean space. Based on that, the Euclidean distances between all rehabilitating plots and native forest plots were retrieved. The obtained distances were scaled between 0 and 1, where 0 corresponds to the average distance from all plots in areas with exposed soil to the reference plots, and 1 is the average distance between all reference plots. After, the average values for the different areas were calculated (Gastauer et al., 2020, 2021).

Contamination index and ecological risk assessment

The contamination factors of As, Ba, Cd, Co, Cr, Cu, Hg, Mn, Mo, Ni, Pb, Se, V, and Zn for the studied areas were calculated as the ratio between PTE concentration (mg kg^{-1}) in the soil and the PTE background value (mg kg^{-1}) established for the studied region using method mMAD (Sahoo et al., 2020). Then, the modified degree of contamination index (mCd) was calculated according to Equation 2 (Abrahim and Parker, 2007).

$$mC_d = \frac{\sum_{i=1}^{n} CF}{n} \quad \text{(Equation 2)}$$

where n is the number of analyzed pollutants and CF is the contamination factor.

The potential ecological risk index (ERI) was calculated according to Equation 3:

$$ERI = (CF_1 \times T_1) + (CF_2 \times T_2) + (CF_3 \times T_3) + \ldots + (CF_n \times T_n) \quad \text{(Equation 3)}$$

where CF is the contamination factor, T is the toxic response factor of As, Cd, Cr, Cu, Hg, Ni, Pb, and Zn (Hakanson, 1980), Ba (Yang et al., 2015) and Co (Zhang et al., 2017) and n is the number of PTE. The RI results were interpreted as follows: RI ≤ 150 suggests low risk, 150 < RI ≤ 300 suggests moderate risk, 300 < RI ≤ 600 suggests considerable risk, and RI > 600 suggests high risk (Hakanson, 1980).

Single index evaluation

The data from the five selected indices (SQI, NDVI, mCd, ERI, and ERS) were multiplied by a similar weight (0.2) and then summed. Prior to this, the ERI and mCd indices were converted through simple mathematical procedures to a scale ranging from 0-1, as they have different units and scales. The higher the single index, the better the results of the environmental index of the studied areas.

Statistical analyses

All analyses were carried out using the software R (R Core Team, 2023). The means of the SQI and mCd for the studied areas were compared by the Tukey test ($p < 0.05$).

Data and discussion

Soil quality and contamination by PTE

The SQI values ranged from 0.06 to 1 (Table 1). All studied areas had lower SQI values compared to the native area, indicating that the soil attributes included in the index (i.e., pH, OM, B, CEC, SB, Cu, and Mn)

are still far from the edaphic conditions of the forest area. The TP9 and TP8 had the smallest values of SQI among the evaluated areas, mainly due to the lower levels of OM and nutrients such as B and Mn (see Table A1 in Appendix).

Table 1: Soil quality, contamination, and ecological risk indices of the different sampled areas of tailing ponds: TP1-6, TP7-9; waste piles: WP-1 and WP-2, and forest areas.
Data obtained from Ramos et al. (2024). The classification of mCd values of the studied areas is as ollo s d 1. indi a es nil o e lo on a ina ion, 1. d indi a es lo on a ina ion, d 4 indi a es ode a e on a ina ion and 4 d 8 indicates moderate-heavily contamination (Abrahim and Parker, 2007)

Site	SQI	mCd	ERI
WP-1	0.46 (0.15)b*	1.99 (0.64)b	79.6
WP-2	0.42 (0.12)b	0.81 (0.41)cd	81.9
TP7	0.39 (0.05)b	4.51 (0.86)a	103
TP8	0.25 (0.13)bc	5.93 (2.14)a	123
TP9	0.06 (0.03)c	1.28 (0.15)bc	67.3
TP1-6	0.32 (0.17)b	4.26 (0.39)a	122
Forest	1.00 (0.02)a	0.16 (0.07)d	–

*Means followed by the same letter do not differ from each other according to the post hoc Tukey's HSD test
0.0 . eans and s anda d de ia ion

Concerning mCd, the TP1-6, TP7, and TP8 indicated a high degree of contamination (Table 1), which was mainly attributed to Cu and Mo levels (Table A2 from Appendix). The greatest contribution of these elements can be associated with the type of ore deposits (Fe oxide-Cu-Au type) and the presence of molybdenite (De Melo et al., 2019). Conversely, the WP-1 presented a low degree of contamination and WP-2, TP9, and forest had a very low degree of contamination. The WPs had low mCd values, probably because they received low-grade ores and materials from pickling, which present lower PTE contents. The low degree of contamination in TP9 may be related to the heterogeneity of processed ores, which is a common characteristic in mining areas. Despite the low level of contamination, this material is one of the most challenging to revegetate, which may be associated with its low OM content and other factors. Considering the ERI values, all analyzed samples represent a low environmental risk (Table 1).

Vegetation parameters and NDVI

The NDVI values extracted from the sampled area ranged from 0.10 to 0.92 (Table 2). Between the areas in recovery process, the highest NDVI values were found in the WP-1 and WP-2, while TPs showed low NDVI values. The lower NDVI values in TPs can be explained by the almost null vegetation cover in these areas. TPs come from various processes adopted in mineral beneficiation, and present low levels of OM and nutrients, impairing the regeneration of plant species. In addition, the TPs are covered by a waterproof

blanket below the waste. Some portions of TP8, for example, experience flooding during certain periods of the year, which favors the long-term retention of contaminants and can negatively impact plant growth.

Table 2: Environmental recovery status (ERS) and NDVI of the different sampled areas of tailing ponds: TP1-6, TP7-9; waste piles: WP-1 and WP-2, and native reference forest: Forest. Data obtained from Ramos et al. (2024)

Site	ERS	NDVI
WP-1	46	0.70
WP-2	38	0.59
TP7	0	0.10
TP8	0	0.10
TP9	0	0.12
TP1-6	12	0.40
Forest	100	0.92

When comparing with NDVI values, the findings from ERS showed a significantly low index for the TPs (Table 2), indicating the poor quality of these materials due to severe soil chemical limitations. These restrictions limit plant development and the restoration of ecosystem services. Therefore, it is recommended to consider alternate methods for reestablishing vegetation using plant species that are ideal to these specific conditions, such as with phytoremediation potential and the use of soil conditioners to improve the quality of the soil. This can enhance the soil's structure and fertility, enabling it to develop into a more resilient ecosystem. Conversely, it is possible to notice the recovery of WPs. However, efforts are still needed to achieve ideal rehabilitation status values due to the contrasting edaphic conditions observed in the examined areas compared to forested areas, which have an impact on the ideal targets of ecosystem services, carbon stocks, and forest communities.

Single index evaluation

The forest area had higher values for all the studied indices, resulting in the highest single index value (Figure 2). Moreover, forest area has ideal soil quality and vegetation cover. Conversely, the TPs exhibited the lowest single index, which was primarily attributed to the low values for SQI, NDVI, and ERS. This suggests that soil fertility characteristics in TPs diverge from those observed in forest areas, plant cover is scarce or absent, and the rehabilitation status remains poor.

The WPs exhibited intermediate single index values when compared to the TPs and the natural forest, indicating that the activities developed for their rehabilitation were helpful and are following the desired pathway. Finally, the variations between WP and TP results raise questions for future research. It is possible that the same restoration/rehabilitation targets may not apply to both locations.

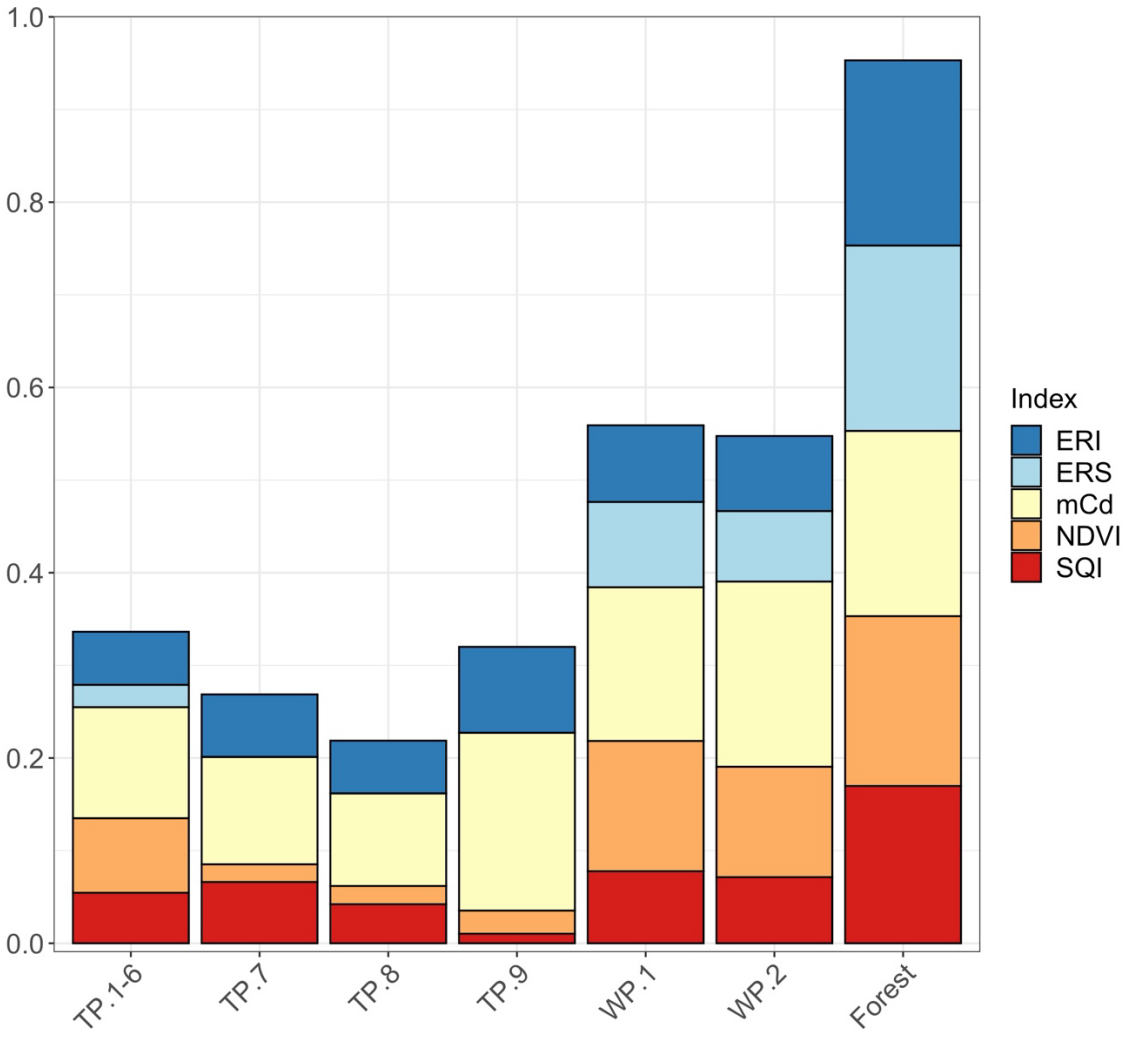


Figure 2: Single index for sampled areas of tailing ponds: TP1-6, TP7-9; waste piles: WP-1 and WP-2, and native reference forest: Forest at the Igarapé Bahia mining complex, Brazil.
SQI – Soil quality index; NDVI – Normalized difference vegetation index; ERS – Estimated rehabilitation status; ERI – Ecological risk index; mCd – modified degree of contamination. Data obtained from Ramos et al. (2024)

Conclusion

The integrated approach of the five indices has proven to be an effective tool for assessing the rehabilitation status of the sites. After twenty years of rehabilitation actions, the single index shows that these activities were beneficial in terms of vegetation development (higher NDVI values) and soil quality in WPs areas. On the other hand, TPs performed most poorly for the examined indices, indicating that their status was far from ideal and that steps must be taken to improve the quality of these materials, such as the application of soil conditioners and plant species. Finally, all analyzed areas presented low ecological risk indices.

Acknowledgements

The authors thank the Brazilian Coordination for the Improvement of Higher Education Personnel (CAPES), the Brazilian National Council for Scientific and Technological Development (CNPq), and the Instituto Tecnológico Vale and Vale for their financial support.

References

Abrahim, G.M.S. and R.J. Parker. 2007. Assessment of heavy metal enrichment factors and the degree of contamination in marine sediments from Tamaki Estuary, Auckland, New Zealand. *Environmental Monitoring and Assessment* 136(1–3): 227–238.

De Melo, G.H.C., L.V.S. Monteiro, R.P. Xavier, C.P.N. Moreto and E. Santiago. 2019. Tracing fluid sources for the Salobo and Igarapé Bahia Deposits: Implications for the genesis of the iron oxide copper-gold deposits in the Carajás Province, Brazil. *Economic Geology* 114(4): 697–718.

Freitas, D.A.F.D., M.L.N. Silva, E.L. Cardoso and N. Curi. 2012. Índices de Qualidade Do Solo Sob Diferentes Sistemas de Uso e Manejo Florestal e Cerrado Nativo Adjacente. *Revista Ciência Agronômica* 43(3): 417–428.

Gastauer, M., C.F. Caldeira, S.J. Ramos, L.C. Trevelin, R. Jaffé, G. Oliveira, M.P.O. Vera, E. Pires, F.L.A Santiago, M.A.C Carneiro, F.T.A Coelho, R. Silva, P.W.M. Souza-Filho and J.O. Siqueira. 2020. Integrating environmental variables by multivariate ordination enables the reliable estimation of mineland rehabilitation status. *Journal of Environmental Management* 256: 109894.

Gastauer, M., P.S.D.M. Sarmento, C.F. Caldeira, A.F. Castro, S.J. Ramos, L.C. Trevelin, R. Jaffé, G.A Rosa, M.A.C. Carneiro, R.B.S Valadares, G. Oliveira and P.W.M. Souza Filho. 2021. shannon tree diversity is a surrogate for mineland rehabilitation status. *Ecological Indicators* 130: 108100.

Gastauer, M., P.W.M. Souza Filho, S.J. Ramos, C.F. Caldeira, J.R. Silva, J.O. Siqueira and A.E. Furtini Neto. 2019. Mine land rehabilitation in Brazil: Goals and *Techniques in the Context of Legal Requirements*. *Ambio* 48(1): 74–88.

Hakanson, L. 1980. An ecological risk index for aquatic pollution control: A sedimentological approach. *Water Research* 14(8): 975–1001.

Mukhopadhyay, S., S.K. Maiti and R.E. Masto. 2014. Development of Mine Soil Quality Index (MSQI) for evaluation of reclamation success: A chronosequence study. *Ecological Engineering* 71:10–20.

Oliveira, S.S.H. 2022. Fechamento progressivo de mina: Qualidade do solo em áreas afetadas pela mineração de ouro sob processo de reabilitação ambiental. Master's thesis research. Instituto Tecnológico Vale.

R Development Core Team. 2023. R: A language and environment for statistical computing. R Foundation for Statistical Computing. Retrieved from https://www.r-project.org/

Ramos, S.J., S.S.H. de Oliveira, P.G. Ribeiro, G.C. Martins, E.C. Da Silva Junior, M. Gastauer, C.F. Caldeira, W.V.S. Pereira, D.C. Santos, P.S.M. Sarmento, W.R. Nascimento Júnior and P.W.M Souza-Filho. 2024. Combining approaches for environmental assessment of rehabilitated gold-mining areas in the Eastern Amazon. *Land Degradation and Development* 35: 2313–2325.

Ribeiro, P.G., G.C. Martins, M. Gastauer, E.C. Da Silva Junior, D.C. Santos, C. Frois Caldeira Júnior, R.B.L. Cavalcante, D.S. dos Santos, M.A.C. Carneiro, R.B.S Valadares, W.R. Nascimento Junior, G. Oliveira, P.W.M. Souza-Filho and S.J. Ramos. 2022. Spectral and soil quality index for monitoring environmental rehabilitation and soil carbon stock in an Amazonian sandstone mine. *Sustainability* 14(2): 597.

Rouse, J.W., R.H. Haas, J.A. Schell and D.W. Deering. 1974. Monitoring vegetation systems in the Great Plains with ERTS. In S.C. Freden, E.P. Mercanti and M.A. Becker (eds.), *Proceedings of the Third ERTS Symposium,* Washington, DC, USA, 10–14 December 1973. NASA.

Sahoo, P.K., R. Dall'Agnol, G.N. Salomão, J.D.S.F. Junior, M.S. Silva, P.W.M. Souza Filho, M.L. da Costa, R.S. Angélica, C.A. Medeiros Filho, M.F da Costa, L.R.G Guilherme and J.O. Siqueira. 2020. Regional-scale mapping for determining geochemical background values in soils of the Itacaiúnas river basin, Brazil: The use of compositional data analysis (CoDA). *Geoderma* 376: 114504.

Teixeira, P.C., G.K. Donagemma, A. Fontana and W.G. Teixeira. 2017. Manual de Métodos de Análise de Solo. 3. ed. rev. Accessed at http://www.cse.edu.uy/sites/www.cse.edu.uy/files/documentos/Liccom_Camejo_2011-07-28.pdf.

Teixeira, R.A., W.V.D.S. Pereira, E.S.D. Souza, S.J. Ramos, Y.N. Dias, M.W.D. Lima, H.F. De Souza Neto, E.S.D. Oliveira and A.R. Fernandes. 2021. Artisanal gold mining in the Eastern Amazon: Environmental and human health risks of mercury from different mining methods. *Chemosphere* 284: 131220.

Wang, W., Y. Sun and J. Wu. 2018. Environmental warning system based on the DPSIR Model: A practical and concise method for environmental assessment. *Sustainability* 10(6): 1728.

Yang, J., W. Wang, M. Zhao, B. Chen, O.A. Dada and Z. Chu. 2015. Spatial distribution and historical trends of heavy metals in the sediments of petroleum producing regions of the Beibu Gulf, China. *Marine Pollution Bulletin* 91(1): 87–95.

Zhang, H., Y.H. Jiang, M.J. Ding, Z.L. Xie. 2017. Level, source identification, and risk analysis of heavy metal in surface sediments from river-lake ecosystems in the Poyang Lake, China. *Environ. Sci. Pollut. Res.* 24: 21902–21916.

Appendix

Table A1: Chemical attributes in samples collected in tailings ponds, waste piles, and forest areas in Igarapé-Bahia mining areas. Data obtained from Ramos et al. (2024)

Site	Forest	TP1-6	TP7	TP8	TP9	WP-1	WP-2
pH	4.51 ± 0.10	7.16 ± 0.18	7.63 ± 0.22	7.55 ± 0.09	6.95 ± 0.21	5.54 ± 0.14	5.73 ± 0.15
P (mg dm^{-3})	1.96 ± 0.19	15.4 ± 1.96	0.17 ± 0.03	6.99 ± 2.12	2.22 ± 0.57	14.4 ± 5.68	11.8 ± 5.83
K (mg dm^{-3})	63.5 ± 5.79	27.4 ± 3.94	20.3 ± 1.19	24.5 ± 1.62	15.8 ± 0.70	36.3 ± 7.13	45.9 ± 4.40
S (mg dm^{-3})	18.1 ± 3.02	12.3 ± 6.17	47.5 ± 8.78	57.0 ± 19.8	180 ± 25.0	6.35 ± 1.34	12.4 ± 2.58
Ca ($cmol_c$ dm^{-3})	1.38 ± 0.27	2.10 ± 0.25	1.56 ± 0.27	2.63 ± 0.36	0.04 ± 0.00	2.30 ± 0.58	3.22 ± 0.30
Mg ($cmol_c$ dm^{-3})	0.33 ± 0.04	0.16 ± 0.02	0.10 ± 0.01	0.09 ± 0.02	0.11 ± 0.02	0.32 ± 0.05	0.48 ± 0.06
Al ($cmol_c$ dm^{-3})	0.61 ± 0.10	0.00 ± 0.00	0.00 ± 0.00	0.00 ± 0.00	0.00 ± 0.00	0.06 ± 0.02	0.03 ± 0.01
OM (%)	4.17 ± 0.41	1.03 ± 0.21	0.53 ± 0.13	0.48 ± 0.08	0.48 ± 0.05	3.87 ± 0.71	4.86 ± 0.56
B (mg kg^{-1})	0.65 ± 0.11	0.05 ± 0.01	0.06 ± 0.01	0.05 ± 0.01	0.03 ± 0.00	0.06 ± 0.01	0.15 ± 0.03
Cu (mg dm^{-3})	0.29 ± 0.03	76.6 ± 13.2	182 ± 64.18	212 ± 57.7	1.65 ± 0.52	101 ± 52.5	29.5 ± 12.9
Fe (mg dm^{-3})	191 ± 18.9	17.8 ± 4.50	2.67 ± 0.33	2.50 ± 0.42	3.25 ± 0.25	83.9 ± 46.5	66.9 ± 20.9
Mn (mg dm^{-3})	27.5 ± 4.43	71.8 ± 18.2	9.00 ± 2.22	4.36 ± 1.10	2.62 ± 1.00	104 ± 20.4	51.0 ± 12.4
Zn (mg dm^{-3})	0.61 ± 0.08	0.57 ± 0.06	1.20 ± 0.38	1.40 ± 0.35	0.22 ± 0.02	1.21 ± 0.37	0.94 ± 0.19
SB ($cmol_c$ dm^{-3})	1.87 ± 0.31	2.72 ± 0.28	1.81 ± 0.3	2.87 ± 0.37	0.24 ± 0.02	2.76 ± 0.63	3.86 ± 0.34
CEC ($cmol_c$ dm^{-3})	9.29 ± 0.74	3.84 ± 0.25	2.74 ± 0.23	3.82 ± 0.34	1.81 ± 0.11	4.67 ± 0.60	6.20 ± 0.40
V (%)	19.7 ± 2.02	68.5 ± 3.28	65.1 ± 5.00	73.3 ± 3.19	13.1 ± 0.73	54.7 ± 6.39	62.5 ± 4.32

OM = organic matter; SB = Sum of bases; CEC = cation exchange capacity; V = base saturation

Table A2: Contamination factors of PTEs in the studied areas. Data obtained from Ramos et al. (2024)

Area	TP1-6	TP7	TP8	TP9	WP-1	WP-2	Forest
Hg	0.20	0.16	0.16	0.16	0.16	0.34	0.30
As	0.54	0.62	0.57	0.57	0.57	0.53	0.15
Ba	0.53	0.44	0.70	0.18	0.23	0.05	0.03
Cd	1.13	1.19	1.25	0.29	0.44	0.25	0.21
Co	1.68	0.72	1.25	0.36	0.51	0.14	0.02
Cr	0.41	0.44	0.47	0.50	0.63	0.58	0.36
Cu	20.5	18.3	31.1	9.25	13.2	3.47	0.08
Mn	2.14	1.55	2.12	0.75	0.88	0.25	0.12
Mo	27.8	35.6	27.9	3.77	8.61	3.96	0.38
Ni	2.08	1.71	1.85	0.61	0.90	0.33	0.10
Pb	1.31	1.28	1.51	0.26	0.45	0.25	0.07
Se	0.32	0.32	0.32	0.32	0.32	0.32	0.09
V	0.62	0.55	0.62	0.72	0.77	0.67	0.14
Zn	0.45	0.17	0.27	0.18	0.19	0.19	0.12

Freeze-thaw Durability of Cemented Paste Backfill Containing Arsenic Trioxide Roaster Waste Dust

Caroline Alexon, University of Alberta, Canada
Nicholas Beier, University of Alberta, Canada
Amirhossein Mohammadi, University of Quebec in Abitibi-Temiscamingue, Canada
Isabelle Demers, University of Quebec in Abitibi-Temiscamingue, Canada

Abstract

During Giant Mine's operation, 237,000 tonnes of arsenic trioxide (As_2O_3) roaster waste (ATRW) dust were generated. The current remediation plan for Giant Mine is the frozen block method to prevent migration of the dust, although the long-term performance of this method is a concern. An alternative approach to the long-term management of ATRW is incorporating the dust into cemented paste backfill (CPB) which may be capable of physically and/or chemically stabilizing the arsenic. Seasonal weather variations, permafrost and ground freezing for the frozen block method at the site could induce freezing and thawing of CPB deposited in near-surface underground workings or stopes, which has been known to decrease the strength of other cemented soils. Unconfined compressive strength (UCS) tests on small samples determined that using 10% ATRW and general use (GU) cement binder will optimize strength and dust content. To evaluate whether the CPB containing As_2O_3 dust can maintain strength after freezing, cylinders of CPB containing Giant Mine As_2O_3 dust were exposed to cyclic freezing and thawing conditions at -5°C and 20°C for 0, 1, and 5 cycles and a variety of long-term curing conditions. Samples from each test condition were tested for strength using UCS tests. The results show that one freeze-thaw cycle may decrease the strength by 26%; however, increasing to five cycles does not decrease the strength further. They also indicate that long-term storage decreases the strength regardless of time and temperature and has a lower effect than freeze-thaw cycles.

Introduction

Giant Mine is a former gold mine located 5 km north of Yellowknife, NWT, Canada. The gold was produced by roasting arsenopyrite (FeAsS) and arsenian pyrite (FeS_2) that hosted the gold. This process produced not only SO_2 emissions, but also precipitated arsenic trioxide (As_2O_3)-rich dust (Bromstad et al., 2017). During its 50 years of operation, the site produced 237,000 tonnes of this dust which contained 60

wt% arsenic (Arcadis, 2017; Bromstad et al., 2017). The dust mixture was collected in baghouses and stored on-site in chambers and mined-out stopes beginning in 1951 (Arcadis, 2017). Being one of the most toxic and bioaccessible forms of arsenic, As_2O_3, the dust poses high risks to the environment and human health (Bromstad et al., 2017). Also concerning, As_2O_3 can dissolve in water, so there is potential risk to human health and the environment by transport to surrounding water bodies (Arcadis, 2017).

Due to the quantity of dust, dust-like physical characteristics, and current storage in subsurface stopes and chambers, the long-term management of the dust is complex. Many methods or technologies have been investigated to assess the effectiveness of treatment. The chosen method to manage the dust involves using passive thermosyphons to freeze the ground surrounding the dust, which is currently stored in underground chambers. This will freeze the surrounding bedrock and fill around the chambers to prevent the release of arsenic. However, this is not a long-term solution as it requires ongoing maintenance and is suspected to last up to 100 years (Arcadis, 2017). Therefore, a long-term management approach is necessary to successfully manage the ATRW dust.

Backfilling is a process in mining of placing hazardous waste in underground mine cavities referred to as "stopes." Underground mining produces large quantities of waste material from excavating and processing the ore. The underground mine cavities are also susceptible to failure if not properly supported. Backfilling is used to reduce surface storage waste, reduce surface subsidence, and improve stability, which reduces the environmental and economic impacts of a mine site (Zhang et al., 2020; Zhou and Fall, 2023a, 2023b). There are three types of backfilling: hydraulic fill, rockfill, and cemented paste backfill (CPB) (Mohammadi et al., 2023). CPB is a heterogeneous, non-Newtonian mixture of dewatered tailings, cement binding agents, water, and sometimes admixtures (Sivakugan et al., 2006). In the mixture, the cement binder stabilizes tailings in place once it is hardened (Fall et al., 2008). Tailings account for 70% to 85% of the total mass of the CPB with a fines content (<20 μm) greater than 20% (Belem, 2023; Chang and Fall, 2022; Oke et al., 2021; Zhang et al., 2020; Zhou and Fall, 2023a). Whereas the binder usually accounts for 3% to 7% of the total mass of the CPB (Cheng and Fall, 2022). Binding agents allow for chemical stabilization and physical solidification, thereby contributing to much of the strength of the CPB (Tariq and Yanful, 2013).

CPB has been used in the past to physically and chemically stabilize pollutants and reduce the reactivity potential of sulfides. CPB has been proven to successfully stabilize other arsenic-bearing materials, but little has been researched on stabilizing arsenic trioxide with CPB (Mohammadi et al., 2023). Mechanical strength can be used as an indicator of cementation reactions that favor the stabilization of arsenic trioxide (Mohammadi et al., 2023). UCS tests are the most common method of testing the strength of CPB in the laboratory (Chen et al., 2017). Although the addition of arsenic trioxide into CPB has been

determined to decrease the strength, with the right mix design of the CPB based on solids content, binder content, and dust content, the strength decrease of the CPB can be minimized (Mohammadi et al., 2023).

The Frozen Block method will involve freezing the underground chambers, stopes, and surrounding rock to a temperature of -5˚C or lower, which will isolate the ATRW dust from the environment (CIRNAC, 2018). This ground freezing, coupled with discontinuous permafrost around Yellowknife at around -5 ˚C and seasonal temperature variations, could induce freeze-thaw cycles for CPB deposited near the surface or freezing for CPB in existing stopes (Kokelj and Wolfe, 2018). Previous research on the mechanical response of CPB, cemented paste tailings, or cemented soils suggest that with increasing freeze-thaw cycles, the unconfined compressive strength will decrease (Ding et al., 2018; Liu et al. 2022; Liu et al., 2023; Xu et al 2020). However, it is unknown how the addition of arsenic trioxide will impact the mechanical response of CPB after freezing and thawing.

Materials and methods

Materials

The materials used in this study for the cemented paste backfill include a binding agent, mine tailings, ATRW dust, and deionized water. Tailings originate from the north pond at the Giant Mine site, outside of Yellowknife, Northwest Territories. The tailings have previously been dried at 40˚C for 48 hours (Mohammadi et al., 2023). Four binding agents were used; general use (GU) Portland cement supplied by Bomix (Quebec, Canada), fly ash (FA) supplied by Lehigh Cement (Alberta, Canada), lime (LI) and lime kiln dust (LKD) both supplied by Graymont (Quebec, Canada). The ATRW dust originated from different stopes and chambers at the Giant Mine. This dust was sent in eight samples and homogenized to create a representative sample for use in characterization and the CPB samples (Mohammadi et al., 2023). To minimize the effects of water chemistry on the strength of CPB, deionized water was used. These materials have been previously characterized in Mohammadi et al. (2023).

Methods

Determination of ATRW dust content and binder selection

To define the appropriate ATRW dust content as well as the potential binders, some small initial cemented paste backfill samples prepared at various ATRW dust contents (4%, 6%, 8%, 10%, 12%, and 14% wt.) at solid content of 74% wt. using four different binders (GU cement and a mixture of GU cement with fly ash (GU/FA), lime (GU/LI) and lime kiln dust, (GU/LKD) all in the proportion of 50/50) and Giant Mine tailings. All binder contents for these tests were fixed at 5% wt. These samples were prepared in the molds with a diameter of 3.4 cm and height of 6.2 cm and cured up to 28 days (Figure 1). After curing, UCS tests were done on these samples to determine the optimal dust content and binder selection for strength.



Figure 1: A photo of the prepared CPB samples using various types of binders and ATRW dust contents

Preparation of cemented paste backfill samples

According to Mohammadi et al. (2023) and the preliminary assessment for ATRW dust and binder content, using a mix of 6% GU cement, 10% arsenic trioxide and 76% solids is best to maximize the strength of CPB. Knowing these mix proportions, the specific gravity of the tailings, binder, and ATRW dust, and the required total volume, the mass of each material required for a given batch can be calculated according to equations in Mohammadi et al. (2023). For each variation in testing, 3 cylindrical samples were prepared using 2 × 4-inch (diameter × height, 50.8 × 101.6 mm) molds with an extra 20% of material to accommodate for the potential losses during preparation and molding.

To prepare the samples, the mass of each material was measured. Dry materials including the tailings, binder, and ATRW dust were mixed on a large piece of paper by folding the corners into the middle 80 times. The dry materials were added to the bowl of a 4.8L Hobart mixer. The water was gradually added while the mixer was on low. After about 1 min, the mixer was stopped so the sides could be scraped into the bowl, then turned back on for 2-3 minutes until a homogenous paste was formed. Using a ½ tablespoon, the paste was scooped into the molds. To rid the paste of air pockets in the mold, a 3/8-inch (9.53 mm) rod was used to hammer the paste 25 times, then the same rod was used to tap around the sides of the mold. The samples were then labelled, sealed with a lid, and stored at 20˚C and 90% relative humidity in a humidity chamber to cure for 14 days, which has been previously determined to be adequate for strength development (Mohammdi et al., 2023).

Freeze-thaw testing and long-term storage

Next, samples were separated into groups based on the curing condition they would undergo, or the number of freeze-thaw cycles they would be exposed to. For each group, three samples were prepared so that triplicates could be tested during the UCS tests. Table 1 shows the variation in curing temperature, curing time, or freeze-thaw cycles.

Table 1: Groups of CPB samples based on storage time, storage temperature, and/or number of freeze-thaw cycles

Group #	Storage Time (days)	Batch #	Long-term Temperature (˚C)	Number of Freeze-Thaw Cycles
1	42	1	20	0
2	40	2	20	0
3	268	1	20	0
4	203	2	5	0
5	42	1	20	1
6	268	1	-10	1
7	40	2	20	5

Samples maintained at approximately 20˚C were cured using a temperature bath to maintain humidity of approximately 90%. Following the initial 14 days of curing, samples from group 6 were placed in a freezer to maintain a frozen temperature at or below -10˚C and samples from group 4 were placed in a humidity-controlled room with a relative humidity of 80% and a temperature of 5˚C. Before long-term storage, all samples were sealed in two Ziplock bags to ensure moisture did not influence the curing.

For the freeze-thaw testing of groups 5 and 6, samples were sealed in two Ziplock bags before being placed into the reservoir of a Fisher Scientific Isotemp 1028S chiller. All three samples from each group were placed in the reservoir at the same time. Each group was exposed to a temperature of -5˚C for 24 hours, to simulate the anticipated frozen conditions on site, then allowed to thaw at 20˚C for 24 hours (CIRNAC, 2018). This method is based on previous freeze-thaw testing of other cemented soils (Liu et al., 2022; 2023). For group 6, samples were frozen for 266 days, to simulate a long-term frozen period, then thawed in the same Isotemp 1028S chiller reservoir for 48 hours.

Unconfined compressive strength tests

Samples from each test condition were tested for strength using UCS tests based on ASTM C39 standard. These tests were performed using a mechanical press with a loading capacity of 50 kN and a rate of 1 mm/min. After each curing period was completed, samples were taken out of their molds, and the top and bottoms of each sample were flattened parallel to the mechanical press plates. The UCS was measured as

the maximum stress value that was reached before failure during the UCS tests. The average of each triplicate was taken as the final strength for a given group. The ultimate strength of each set of samples will help determine how multiple freeze-thaw cycles affect the CPB mixture compared to none.

CT scanning

Micro-Computerized Tomography (μ-CT) scanning was used to assess the 3D internal structure of long-term curing samples before and after freeze-thaw cycles, and before UCS testing. This method extracts a set of 2D X-ray radiographs of an object at multiple angles (typically 180˚ or 360˚), then reconstructs the 2D slices using a mathematical algorithm. A 3D image can be created by stacking the 2D slices and allows the viewer to analyze the internal structure of the samples. One sample from group 6 was scanned before and after thawing, and one sample from each of group 3 and 4 were scanned at 20℃.

Scanning was performed on a Nikon XTH 225 ST industrial CT scanner with an exposure time of four frames per second for the frozen sample and two frames per second for all samples at 20℃. All samples had a voxel size of 33 micrometers (size of the pixel resolution and slice thickness of a 3D volume element). The reconstruction was done using Nikon CT pro 3D software and analyzed using Dragonfly 2022 software.

Results and discussions

ATRW dust content and binder selection

Figure 2 presents the results of UCS tests on the small CPB samples prepared using four various binding agents to define maximum probable ATRW dust in the main samples as well as the desirable binding agents after 7 and 28 days of curing. Generally, the samples prepared using the GU cement showed the highest strength followed by the GU/LI, GU/LKD, and GU/FA samples. Increasing the curing time did not greatly increase the strength of the samples, except for the samples prepared using GU/LKD binder and most of the samples gained their strength in the initial days of curing. The strength behavior of the samples was different after 7 and 28 days. After 7 days, the strength of GU samples increased up to 10% ATRW dust and then decreased; however, after 28 days, a decreasing trend was observed by increasing the ATRW dust content. For the other binding agent, a complex trend was observed. Based on these results, it was decided to prepare the main CPB samples using GU cement and 10% dust since these conditions revealed the highest strength with the maximum applicable ATRW content.

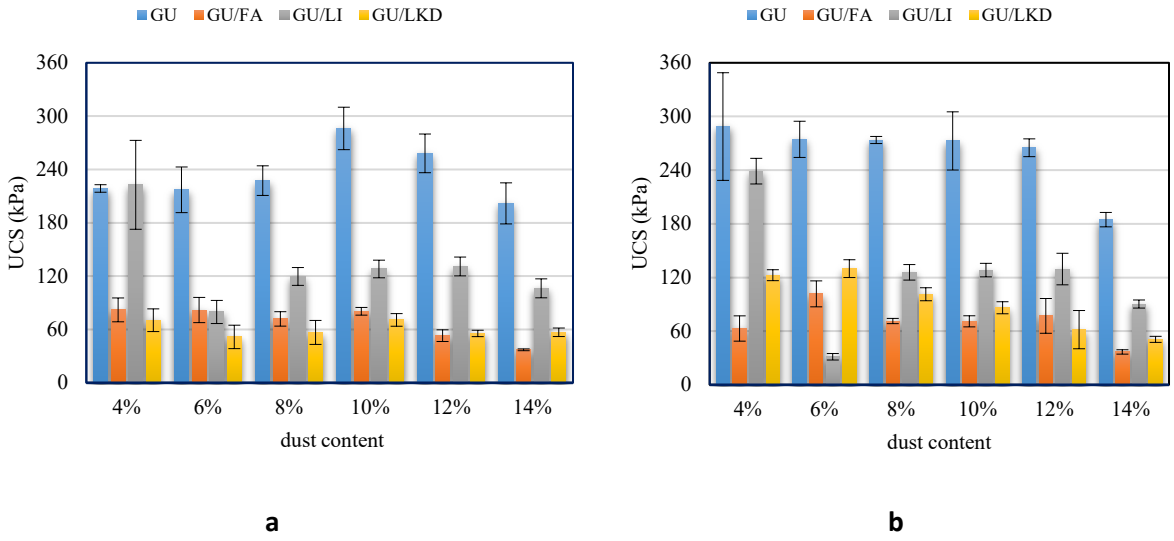


Figure 2: The UCS of small CPB samples prepared using General Use (GU) cement and a mixture of GU cement with fly ash (GU/FA), lime (GU/LI) and lime kiln dust, (GU/LKD) after a) 7 days and b) 28 days of curing

Mechanical strength results

Figure 3 presents peak average strength results from triplicate UCS tests for each group of samples used to test the effects of freeze-thaw cycles and long-term storage temperature. Generally, with increased storage time there is a decrease in strength. When comparing the same batches, group 3 shows an average decrease of 21% compared to group 1. Decreasing the storage temperature long-term shows a slight decrease in average peak UCS values when comparing group 2 and 4, however this is a smaller decrease than increased storage time. This suggests the strength will continue to decrease with increased storage time, regardless of temperature.

These results also show that regardless of storage time or storage temperature there will be a decrease in strength with freeze-thaw cycles. One freeze-thaw cycle after short term storage decreases the strength on average by 26%, however increasing the number of freeze-thaw cycles does not show a further decrease in strength. This suggests that the first freeze-thaw cycle has the largest impact on damage of the samples, subsequent freeze-thaw cycles do not further decrease the strength. Group 6 shows that long-term freezing and one thaw cycle shows an average decrease in strength of 20%, similar to long-term, unfrozen storage. This suggests that the storage time has a greater influence on the strength than the storage temperature. Overall, freeze-thaw cycles after short term storage decreases the strength the most, compared to other variables.

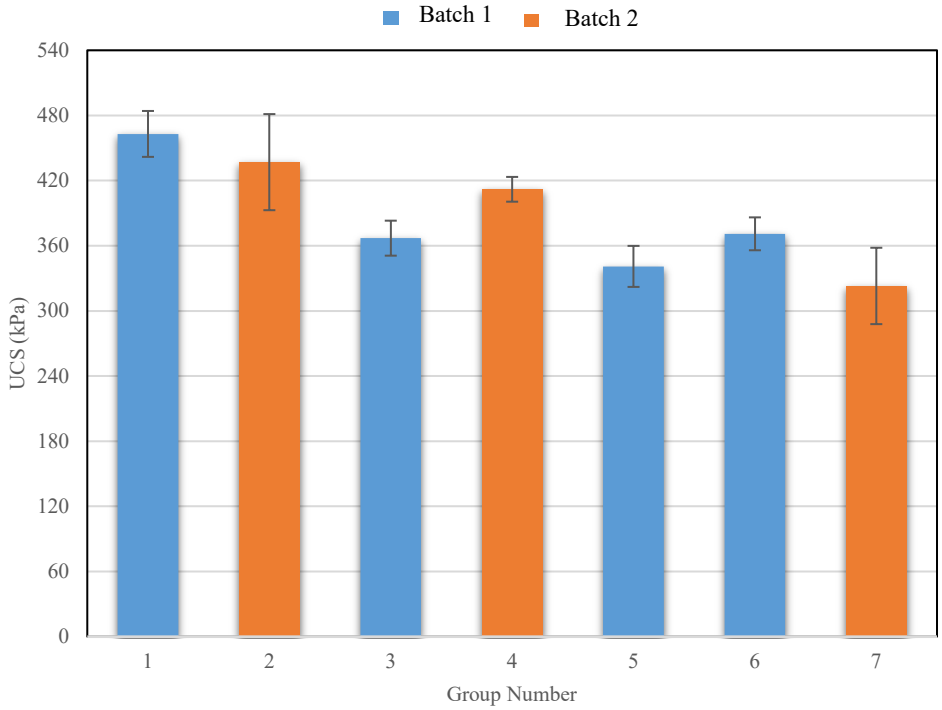


Figure 3: The UCS of samples based on storage temperature, storage time, and/or number of freeze-thaw (F/T) cycles. Test conditions for each group can be found in Table 1

Qualitative CT scan observations

A qualitative analysis was conducted on images rendered from the CT scanning of four samples (Group 3, 4, 6 frozen and 6 thawed, as shown in Figure 4). The longitudinal slice taken in the middle of the sample from the aerial view was examined for each sample. All four samples show similar shape and size of pores, and no visual differences between the internal structure of the samples. The only visual difference between these samples is a slight density contrast in Figure 4d, the frozen sample. Surrounding the edges, there are lower density areas shown by slightly darker sections. This does not appear in the other samples and suggests that perhaps the sample's core did not freeze completely, or moisture entered the edges of the sample from the environment. As shown in Figure 4c and d, freezing and thawing did not induce fracturing in the sample from group 6. A lack of fracturing indicates that leaching of the arsenic dust may not increase after freezing and thawing. Quantitative analysis is being undertaken to confirm that temperature and freeze-thaw did not influence the porosity of these samples.

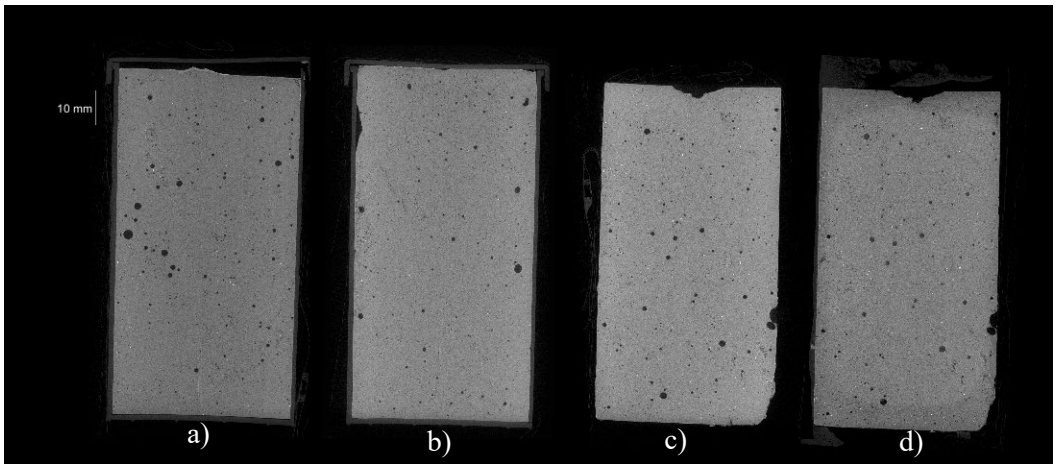


Figure 4: Images of the longitudinal middle slice from CT scans of a) Group 3, b) Group 4, c) Group 6 thawed, d) Group 6 frozen

Conclusion

The results of this study showed that samples prepared with GU cement maintain the highest strength compared to those with a mix of GU cement and other binders. Most samples will gain their strength in the initial 7 days of curing, and increasing the curing time did not increase the strength, except for GU/LKD samples. For samples with up to 10% arsenic dust and GU cement, increasing the curing time increased the strength slightly, but for samples with greater than 10% arsenic dust, increasing the curing time decreased the strength. Based on these results it is recommended to prepare samples with GU cement and 10% ATRW dust.

For long-term storage, increasing the storage time before UCS testing leads to a decrease in strength. However, this is not dependent on storage temperature, and storage time may have a greater influence on strength than temperature does. For short-term stored samples, one and five freeze-thaw cycles show a similar decrease in strength, suggesting that the first freeze-thaw cycle has the greatest influence on strength of the sample and does the most amount of damage. Overall, freezing and thawing have the greatest influence on strength compared to other variables tested.

Based on qualitative analysis of CT scan images, there is no visual difference between the pore size or shape of samples stored long-term at 20°C, 5°C, or -10°C. Also, freezing and thawing did not induce fractures or other visual differences, except for density changes in the frozen sample. Quantitative analysis is being undertaken and will confirm whether the changes in temperature and freeze-thaw have an impact on the porosity of these samples.

Acknowledgements

The authors would like to thank the Giant Mine Oversight Board (GMOB) and NSERC Alliance program for their financial support throughout this project. The authors would also like to thank the Permafrost ArChives Science Laboratory (PACS) at the University of Alberta for conducting the CT scans and helping with interpretations.

References

Arcadis. 2017. Giant Mine State of Knowledge Review: Arsenic Dust Management Strategies. *Giant Mine Oversight Board (GMOB).* Accessed 05/06/2024 at: https://gmob.ca/wp-content/uploads/2017/09/2017-08-Giant-Mine-State-of-Knowledge-Review_FINAL.pdf

Belem, T. 2023. Mining with backfill: predicting backfill strength requirements, long-term behaviour, and placement. In G.W. Wilson, N.A. Beier, D.C. Sego, A.B. Fourie and D. Reid (editors), *Paste 2023: Proceedings of the 25th International Conference on Paste, Thickened and Filtered Tailings*. University of Alberta, Edmonton, and Australian Centre for Geomechanics, Perth: 19–22

Bromstad, MJ, L.A. Wrye and H.E. Jamieson. 2017. The characterization, mobility, and persistence of roaster-derived arsenic in soils at Giant Mine, NWT. *Applied Geochemistry* 82: 102–118.

Chang, S. and M. Fall. 2022. Strength, microstructure, and deformation behavior of frozen cemented tailing material. *J. Cold Reg. Eng*. 37(2): 04021017.

Chen, Q, Q.L. Zhang, A. Fourie, X. Chen and C. Qi. 2017. Experimental investigation on the strength characteristics of cement paste backfill in a similar stope model and its mechanism. *Construction and Building Materials*. 154: 34–43.

Crown-Indigenous Relations and Northern Affairs Canada (CIRNAC). 2018. The remediation project's frozen block method. *Government of Canada.* Accessed 05/06/2024 at https://www.rcaanc-cirnac.gc.ca/eng/1100100027422/1617999507283

Ding, M., F. Zhang, X. Ling and B. Lin. 2018. Effects of freeze-thaw cycles on mechanical properties of polypropylene Fiber and cement stabilized clay. *Cold Regions Science and Technology* 154: 155–165.

Kokelj, S.V. and S. A. Wolfe. 2018. Northwest Territories Geological Survey – Permafrost 101. *Northwest Territories Geological Survey*. Accessed 05/06/2024 at https://climatechange.toolkitnwtac.com/wp-content/uploads/sites/21/2019/01/Permafrost-101-NWT-Geological-Survey.pdf

Liu, C., C. Berard and L. Deng. 2022. Review of the effects of freezing/thawing cycles on the engineering properties of soilcrete. *Geotechnics* 2(4): 1003–1026.

Liu, C., C. Berard and L. Deng. 2023. Engineering behavior of cement-treated stiff clay subjected to freezing/thawing cycles. *Cold Regions Science and Technology* 2(4): 1003–1026.

Mohammadi, A., Demers, I., Beier, N.A. and Benzaazoua, M. 2023. Study of the effects of ATRW dusts on the mechanical behaviour of cemented paste backfills. In G.W. Wilson, N.A. Beier, D.C. Sego, A.B. Fourie and D. Reid (editors), *Paste 2023. Proceedings of the 25th International Conference on Paste, Thickened and Filtered Tailings*, University of Alberta, Edmonton, and Australian Centre for Geomechanics, Perth: 71–81.

Oke, J., K. Hawley, T. Belem and A. Hashemi. 2021. Paste backfill thermal contraction: Red Lake operations case study. In A.B. Fourie and D. Reid (editors), *Paste 2021. Proceedings of the 24th International Conference on Paste, Thickened and Filtered Tailings*. Australian Centre for Geomechanics, Perth: 425–438.

Sivakugan, N., R. M. Rankine, K.J. Rankine and K.S. Rankine. 2006. Geotechnical considerations in mine backfilling in Australia. *J. Clean. Prod.* 14(12–13): 1168–1175

Tariq, A. and E.K. Yanful. 2013. A review of binders used in cemented paste tailings for underground and surface disposal practices. *J. Environ. Manage.* 131: 138–149.

Zhou, Y. and M. Fall. 2023a. Strength, deformation behavior, and microstructure of cement paste backfill with calcium chloride in subzero environments. *J. Cold Reg. Eng.* 37: 04023005.

Zhou, Y. and M. Fall. 2023b. Mechanical and microstructural properties of cemented paste backfill with chloride-free antifreeze additives in subzero environments. *J. Mater. Civ. Eng.* 35:04023148.

Water Balance and Water Quality Predictions for the Cariboo Gold Project Filtered Tailings Facility

Adrian Moreau, Klohn Crippen Berger, Canada
Jiajia Zheng, Klohn Crippen Berger, Australia
Michelle Liew, Klohn Crippen Berger, Canada
Alex Fitzpatrick, Klohn Crippen Berger, Australia

Abstract

Klohn Crippen Berger Ltd. (KCB) developed an integrated water balance and water quality model ("the model") in GoldSimfor the provincial Environmental Assessment of the proposed Cariboo Gold Project ("the Project") at the Quesnel River (QR) Mill site near Quesnel, British Columbia, Canada.

Previous operations at the QR Mill site from 1994 to 2022 processed and stored conventional tailings under a water cover designed for geochemical control in the Tailings Storage Facility (TSF) and Main Zone Pit. For the proposed Project, the existing TSF pond water will be drained down, treated, and discharged. New tailings generated from the Project will be filtered and placed in lifts over the existing TSF tailings. However, the Project's filtered tailings will be highly sulfidic and potentially acid generating. As a result, proactive water management is required during the Project to achieve environmental discharge criteria.

KCB used the model to assess required water management and treatment, control measures, and facility design for each project phase, including closure. Discharge flow and water quality predictions for the Project footprint and receiving environment were used to support the Project effects assessments for the Environmental Assessment. This process evaluates how the proposed strategies will meet regulatory criteria and provincial guidelines. The Project Environmental Assessment started shortly after the 2018 revision to the British Columbia Environmental Assessment Act. The timing of the assessment provided unique challenges for the owner, regulatory agencies, stakeholders, and consultants navigating the updated Act.

To assess a range of potential conditions, KCB conducted sensitivity scenarios on the control measures, climate conditions, and geochemical conditions. Water treatment, geomembrane covers, and seepage interception were identified as important control measures to meet water quality requirements.

Key takeaways from the application of the model for the Project include the importance of proactive risk management, early consideration of best available technologies, communicating with regulators and other consultants, and planning for closure in a changing climate.

Introduction

Osisko Development Corp. (ODV) is currently proposing to develop and operate the Cariboo Gold Project ("the Project"), located in the Cariboo Regional District of British Columbia (BC), Canada (ODV, 2022a). This paper describes the development and application of the Quesnel River (QR) Mill water balance and water quality model ("the model") to support the Project application for an Environmental Assessment Certificate under the BC Environmental Assessment Act. The Project was the first project entirely assessed under the new 2018 Environmental Assessment Act (EAA, 2018) and was granted an Environmental Assessment Certificate in 2023 (EAO, 2023). The model has since been updated to support permit applications and will be improved and utilized as the Project continues to construction and operations.

For the EA, the model was used to assess the water treatment requirements, seepage control measures, water demand requirements, discharge flows, and water quality concentrations within the QR Mill project footprint and at the receiving environment during Project startup, operations, closure, and post-closure. The model output is intended to inform water treatment and management strategies and evaluate whether regulatory criteria and provincial guidelines will be met under these strategies.

Existing site conditions

The QR Mill site is located approximately 58 km southeast of Quesnel, British Columbia, above the north side of the Quesnel River valley at an elevation of about 1000 meters above sea level. Temperatures are typically around 15°C to 25°C in the summer and 0°C to -10°C in the winter, with extremes ranging from over 30°C in the summer to below -30°C in the winter. The estimated mean annual precipitation and mean annual lake evaporation at the QR Mill site are 670 mm and 440 mm, respectively (KCB, 2022a). The QR Mill site straddles a watershed boundary: runoff to the north eventually joins Rudy Creek, and runoff to the south joins the Quesnel River, via Creek No. 3. The QR Mill site is currently in a care and maintenance phase. Existing site conditions are shown in Figure 1 (modified from KCB, 2022b) and described below.

- Past operations at the QR Mill site from 1994 to 2022 processed and stored conventional tailings under a water cover in two tailings storage facilities, which are the Tailings Storage Facility (TSF) and Main Zone Pit (MZP). The TSF is unlined and has a net negative average water balance. It is confined by the Tailings Dam to the north and the Cross Dyke to the south. The MZP is a depleted open pit with its southern wall located near the Quesnel River valley.
- The two seepage collection ponds, the North Seepage Collection Pond (NSCP) and South Seepage Collection Pond (SSCP), are at the toes of the Tailings Dam and Cross Dyke, respectively. The NSCP and SSCP are unlined. Weir 2 is the discharge point for the NSCP. The SSCP discharges via Weir 9 (to the MZP) or Weir 8 (to Creek No. 3).

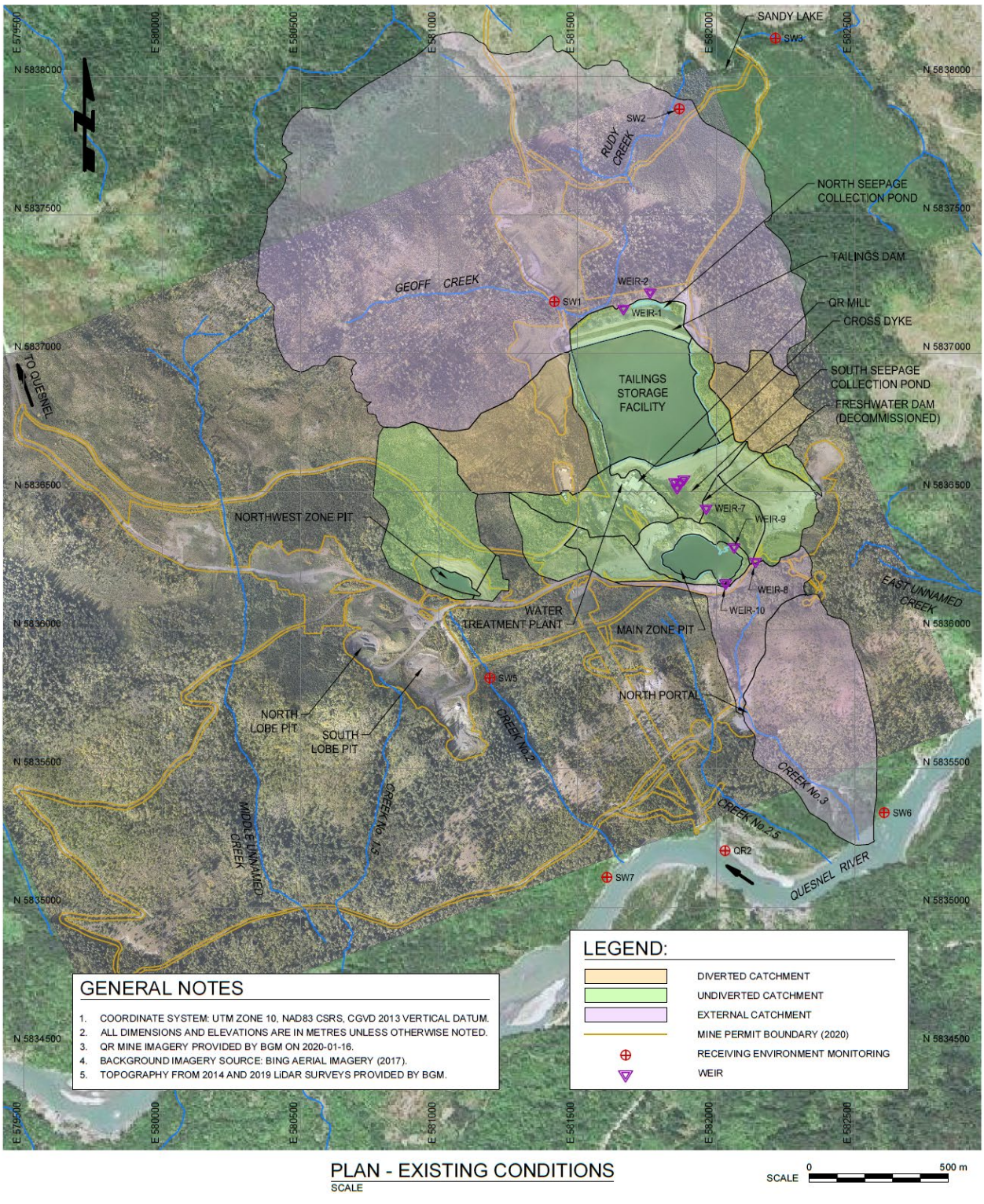


Figure 1: Existing site conditions with modelled catchment areas

- With a net-positive site water balance, contact water is actively managed in the TSF, MZP, and seepage collection ponds. Excess contact water is treated at the water treatment plant (WTP) and discharged into Rudy Creek. The WTP retentate is returned to the MZP.
- There are other legacy mine components on site, including waste rock piles (WRPs), the Northwest Zone Pit, North Lobe Pit, and South Lobe Pit; and inactive underground workings (via the Mid-West Portal, West Zone Portal, and North Portal). Excess water from these legacy mine components meets the permit limits and discharges into the Quesnel River.

A simplified schematic of the existing sources, pathways and receptors is included in Figure 2 (modified from KCB, 2022a). The model boundary is shown as a red dashed line.

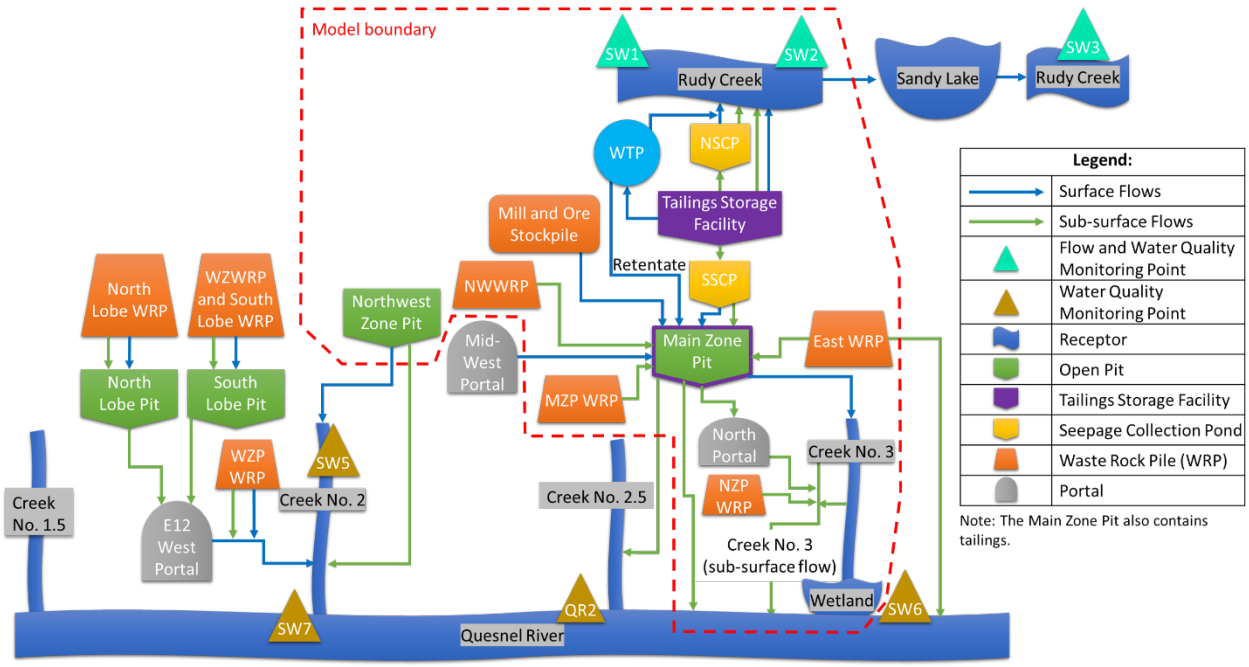


Figure 2: Schematic of the QR Mill existing sources and pathways to receptors

Proposed project description

The Project is located in the traditional territories of the Lhtako Dené Nation, Xatśūll First Nation (Xat ūll), and Williams Lake First Nation. The Project includes the development of the Mine Site Complex near the District of Wells, BC, and the QR Mill. Ore produced at the Mine Site Complex will undergo crushing, ore sorting, milling, flotation, and dewatering before the concentrate is trucked to the QR Mill for the final stage of processing. The mine has an estimated operational mine life of 16 years (ODV, 2022a).

Most of the Project tailings will be stored underground at the Mine Site Complex as paste backfill (ODV, 2022b). The final Project tailings produced from the concentrated ore at the QR Mill site will be

filtered to 90% solids content by weight. The Project tailings will then be placed over the existing TSF tailings following TSF pond drawdown, forming the Filtered Stack Tailings Storage Facility (FSTSF) (ODV, 2022b). Applying filtered tailings technology in this configuration achieves ODV, Indigenous and other stakeholder end land use objectives with the following strengths (KCB, 2021 and Golder, 2022):

- The FSTSF will form a geotechnically stable landform with a low risk of failure. The fully reclaimed FSTSF will result in a landform akin to the pre-mining land use, which is the primary end land use goal for the Project.
- Tailings are stored in the existing TSF, which minimizes new disturbance areas.
- Seepage and loading from the TSF to Rudy Creek are reduced due to removal of the TSF pond.
- Progressive reclamation can occur during the Project by building parts of the FSTSF to their ultimate configuration early in the mine life.

The QR Mill Project tailings are highly sulfidic and have high potential for acid generation (neutralization potential ratio of 0.26) and metal leaching (KCB, 2022b). Storing these tailings in a filtered state can lead to oxidation and generation of poor water quality without adequate controls. The evaluation of control measures is discussed in later sections of this paper.

Model approach

Model structure

KCB developed the model using GoldSim software (Version 14), which is a dynamic simulation software frequently used in the mining industry for water balance and water quality modelling. The model is an integrated water balance and water quality model based on a daily time step, allowing for assessments of daily maximum flows and concentrations. The model was developed based on the conceptualization in Figure 2. To represent the complex relationships, the model was developed as a network of independent subsystems, as follows (KCB, 2022a):

- The hydro-climatology subsystem processes weather data (measured on-site or adjusted from nearby climate stations) to generate rainfall, snowmelt, runoff, and evaporation rates. These rates are multiplied by the catchment and pond areas to estimate catchment flows and losses.
- Water bodies such as the TSF and MZP are modelled as reservoirs with their storage represented by their stage-storage curves obtained from bathymetric surveys and 3D modelling. Pump capacity and pond level triggers are included in the model to reflect operational conditions.

- Subsurface flow information incorporated in the model, such as seepage rates and pathways from source to receptors, is from 2D and 3D hydrogeological modelling. This includes seepage rates through the Project tailings and existing TSF tailings.
- The void spaces within the Project tailings and the existing TSF tailings are modelled as reservoirs. Seepage outflows occur when the predicted moisture content exceeds the materials' residual voids saturation. If the saturation exceeds the maximum reservoir size, based on the material porosity, additional water will not infiltrate and is directed to surface flow.
- The water quality of the surface and subsurface flows is linked to the chemistry simulation systems:
    - Load generation is modelled for the tailings, waste rock and milling operation products using site-specific source terms and scaling factors calibrated with site monitoring data.
    - Chemical mechanisms that reflect the thermodynamics of likely geochemical processes are incorporated into the site reservoirs (ponds and tailings pore space). These include calculations of ionic strength and activity coefficients, pH and alkalinity/carbonate buffering, and the chemical equilibrium state resulting in precipitation or dissolution of minerals.

The subsystems are calibrated using site monitoring data and are subsequently used for future predictions.

Model calibration

The model was calibrated using site monitoring data from 2020 to 2022, including weather data, deposited tailings, flow rates, water levels, and water qualities. In general, the model water balance and water quality predictions are intended to provide conservative estimates for water management requirements in on-site reservoirs (e.g., treatment). The site water balance calibration was completed by adjusting the watershed runoff assumptions so the modelled site reservoir water levels and discharge rates resembled measured data (Figure 3). The average overall site water balance error was 4%.

The water quality was calibrated by assessing the load sources, source terms, chemistry mechanisms, groundwater attenuation factors, and other scaling factors. The proportion of load generating material was the main calibration variable for water quality (e.g., generating load from the top 2 m of waste rock piles, instead of the full pile).

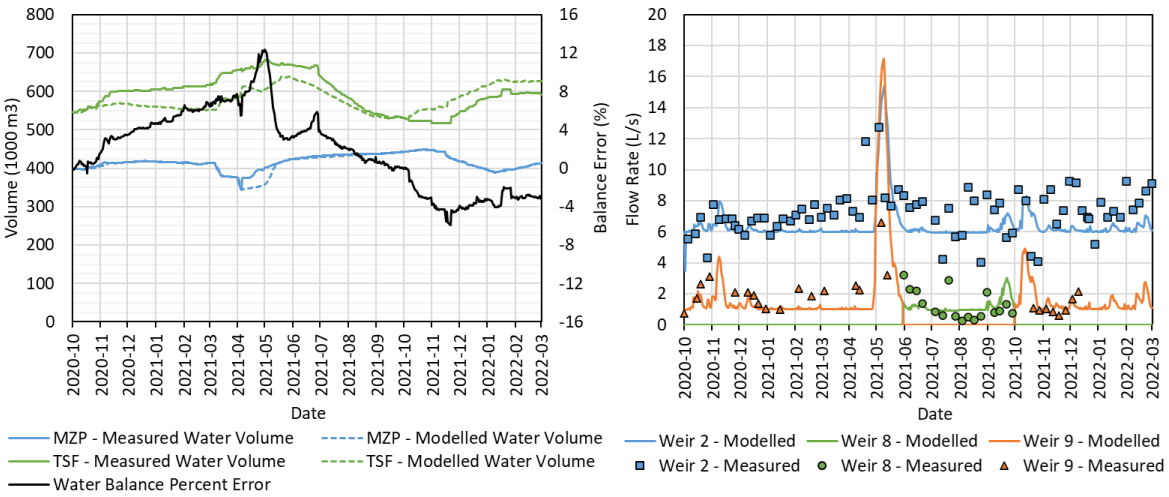


Figure 3: Water balance calibration plots for the MZP, TSF, and discharge weirs

Model inputs and assumptions

For the EA, the modelled period was July 1, 2023, to December 31, 2060. KCB developed a long-term daily climate sequence by transposing 105 years of daily precipitation and temperature data recorded at the Environment Canada Barkerville climate station (1889 to 2006) to the QR Mill (KCB, 2022b). This approach allows for realistic fluctuations in weather conditions, such as alternating dry and wet years, which occurred prior to commissioning the QR Mill weather station in 2018. Table 1 lists the model scenarios included in the final EA report. The selected climate change scenario was based on the Centre National de Recherches Météorologiques Climate Model version 5; using the Representative Concentration Pathway (RCP) of 8.5. This was the most extreme scenario in the Golder climate assessment (Golder, 2021c).

Table 1: Environmental assessment model scenarios

Scenario name	Description
Base Case	Typical climate conditions during Project operations, ranging from 10-year dry to 30-year wet years
Wet	Contains a 500-year wet year during Project operations
Dry	Contains a range of 20-year dry to 10-year wet years during Project operations
Base Case with Climate Change	Same climate sequence as base case, but with linearly applied increases of precipitation by 24% and temperature by 4.2°C between 2010 and 2085
Base Case Climate with No Chemistry	Same climate sequence as base case, with model chemistry mechanisms disabled to assess chemistry modelling impacts on results

The source terms for geochemical load sources were not varied between scenarios because the model is intended to produce conservative water quality results for assessing required controls. The source terms for existing load sources which would not be impacted by the proposed Project, such as pit walls, waste

rock piles and existing tailings in the MZP, were assessed using the calibration model period and retained for the Project predictive modelling.

KCB applied conservative assumptions for load generation from the existing TSF tailings. The top 2 m of the existing tailings are assumed to generate load using loading rates based on saturated and unsaturated kinetic column testing results. For the existing tailings, the saturated testing load rates are applied prior to TSF drawdown, and the unsaturated rates are applied following TSF drawdown. The existing tailings generate load until the existing tailings are covered by 2 m of filtered Project tailings.

The first three cycles of the kinetic column testing for the Project tailings showed acid generation consistent with static test results (KCB, 2022a). However, subsequent cycles showed increasing pH due to neutralization from the available neutralizing minerals. Prior geochemical assessments indicated that the Project tailings are expected to generate acidity once the neutralizing capacity is depleted (KCB, 2022a). Results from the first three cycles were applied to represent a conservative model scenario for operations.

Model applications

Many iterations of the model were developed throughout the EA process to support the development of the Project. During the EA process, regulatory and Indigenous review groups emphasized the importance of producing conservative model results to assess that the Project "will not have a significant adverse environmental, economic, social, cultural or health effect" (EAA, 2018). Indigenous engagement was a central part of the EA and model refinement, but this is not the focus of this paper. The following sections discuss the application of the model for effects assessment, control measure development, facility design, and closure planning as part of the EA process.

Effects assessment

The model was used during the EA process to inform the effects assessment, documented in the human health and ecological risk assessment (Golder, 2021a), and the surface water chapter of the EA application report (ODV, 2022c). During this process, KCB assessed the model results for each Project phase against the applicable regulatory requirements, such as discharge permit criteria, Metal and Diamond Mining Effluent Regulations (MDMER, 2002), and the receiving environment water quality guidelines for the protection of aquatic life (KCB, 2022a). Due to the conservative nature of the model, some exceedances of these requirements were flagged for the effects assessment team to further investigate. If the exceedances were expected to negatively impact the environment, the facility design was revised with control measures discussed in the following section. This iterative process was conducted until the design for the Project achieved the objectives for the protection of human and ecological health.

Control measures

Earlier versions of the model predicted that without water quality controls, there would be chronic water quality guideline exceedances at the receiving environment nodes from uncaptured site seepage, with sources attributed to milling activities and Project tailings reactivity. KCB assessed different combinations of water quality control measures as part of the EA process and Project development. The control measures selected to meet water quality criteria at the discharge points and receiving environment include:

1. Various water treatment components to target contaminants of potential concern. These include the WTP, retentate management system, FSTSF runoff liming system, and treating excess mill process water with iron co-precipitation and a moving bed biofilm reactor.
2. Temporary geomembrane covers over the Project tailings during operations to reduce contact water runoff from Project tailings surface, reduce uncaptured seepage to the environment, and minimize water treatment effort.
3. Permanent closure cover to reduce long-term infiltration and seepage through the FSTSF.
4. Groundwater interception wells downstream of the NSCP to intercept TSF/FSTSF seepage that bypasses the NSCP before it reaches Rudy Creek (SW2).

Water treatment design

Active water treatment controls identified during the EA process include the WTP, liming of the FSTSF runoff, and the iron co-precipitation and moving bed biofilm reactor treatment units for excess process water to the MZP (Golder, 2021b). The water treatment design process involved iterations between KCB, ODV, and the water treatment design team (Golder), to align the water treatment design effectiveness with the model predictions. The model predictions provide the operational flow rate and water quality ranges, which inform the design requirements for the treatment system. The treatment system revisions change the subsequent model predictions because most of the waste removed by the treatment system is returned to the MZP/FSTSF, forming a feedback loop. To break this loop, we (KCB, ODV and Golder) decided on a simplified approach: the water treatment system in the model would calculate and apply the required effectiveness to meet the discharge requirements, rather than applying the design treatment effectiveness which may not be sufficient. The model outputs were then provided to Golder to review and adjust the water treatment design as required. This greatly reduced the model iterations required to achieve a suitable treatment design and made it easier to identify other controls required. The water treatment strategy proposed in the EA will be further optimized in subsequent design stages.

Project temporary and permanent tailings covers

Water contacting the Project tailings is expected to result in poor quality runoff and seepage due to the

Project tailings' high potential for acid generation and metal leaching. To reduce this risk, temporary geomembrane covers will be placed daily over the Project tailings. The primary purpose of the covers is to reduce infiltration into the Project tailings. This reduces the quantity of seepage exiting the TSF, which is more difficult to capture and treat than surface runoff. The covers will also improve the water quality of the FSTSF surface runoff by reducing contact between the tailings and precipitation. The model was used to assess the impact of the temporary cover system on the receiving environment predictions. This assessment informs the cover selection (e.g. material type and permeability) and procedures during operations (e.g., staging and sequencing of the FSTSF construction, and the surface area coverage requirements).

The permanent closure cover was assessed in the model like the temporary geomembrane covers. The modelling of the permanent cover considered progressive reclamation of the FSTSF, and the associated impacts to the water management strategy. If the temporary and permanent covers perform poorly, additional seepage loading from the TSF to the receiving environment at SW2 will occur. To mitigate this risk, a seepage interception system will be implemented between the TSF and SW2.

Seepage interception system

The Tailings Dam containing the north side of the TSF is a rockfill dam with a till core founded on till overburden and weathered bedrock (KCB, 2022a). Most of the north TSF seepage reports to the NSCP near the Tailings Dam toe. However, a portion of the seepage through the Tailings Dam foundation bypasses the NSCP and reports to Rudy Creek downstream. Although the Project involves removing the TSF pond and implementing temporary covers, which will greatly reduce the magnitude of seepage, there is potential for this seepage pathway to impact the receiving environment, particularly during dry summer months. As part of the EA process, ODV conducted feasibility level studies and site investigation work for a seepage interception system (SIS) just downstream of the NSCP. This will consist of a network of pumping and monitoring wells that capture seepage and return it to the MZP for treatment. The model outputs were used to inform the SIS required pumping rates, capture efficiency to meet environmental criteria, and operational duration. The current model assumes a capture efficiency of 70%, which is sufficient to achieve environmental requirements and is expected to be realistically achievable with the SIS.

Water management design

In addition to the control measures, the model also informed other aspects of the water management design for the Project. For example, the mill process water requirements are generally consistent throughout the year, however, the availability of water is impacted by seasonal climate variations. The dynamic nature of the model was useful for assessing mill process water quantities available from the Northwest Zone Pit and SSCP, particularly for extremely dry years.

The TSF and MZP ponds are currently both required to provide flood storage for the site's environmental design flood (EDF), which is "the hydrological event that is to be managed without release of untreated water to the environment" (EMLI, 2022). When the TSF pond is removed during the Project to build the FSTSF, the SSCP and MZP will need sufficient capacity to store the site's EDF. The model was used to size the SSCP to provide adequate operating pond volume (for mill operations) and flood storage. To provide additional flexibility managing the EDF, a one-meter-high concrete sill was designed for the existing MZP spillway invert to provide an additional 33,000 m^3 of EDF storage. The EDF event was modelled with the revised SSCP and MZP capacity to confirm the EDF could be managed without discharge to the environment. For events exceeding the EDF, the model was used to assess the quantity and water quality of discharges from the site. This information was provided to the effects assessment teams.

Closure planning

Closure planning was an important consideration for the regulatory and Indigenous reviewers during the EA process. The long-term liability of the site is governed by the duration of the post-closure active care phase. The post-closure active care phase involves active water treatment, water management (including operation of the SIS), maintenance of the site, and environmental monitoring. When reclamation is complete and active management is no longer required to meet receiving environment criteria, the site will transition to the post-closure passive care phase (Golder, 2022).

The model was utilized to inform the expected duration of the post-closure active care phase and potential residual effects from the Project. By applying the proactive control measures during the Project operations phase, the site is expected to be able to transition to passive care relatively quickly. The closure plan and timeline will continue to be assessed as the Project design stages progress.

Key takeaways

Key takeaways from the application of the model for the Project include the importance of proactive risk management, early consideration of best available technologies, communicating with regulators and other consultants, and planning for closure in a changing climate.

The risk management system applied for the Project aligns with the Risk Management Framework for Mining in BC, which states, "Risk management is the practice of reducing uncertainty wherever possible, and evaluating the effectiveness of mitigating actions on either preventing the risk or reducing the impacts if the risk were to occur to an acceptable, or tolerable, level" (EMPR et al., 2018). As discussed in this paper, proactive risk management measures were assessed throughout the Project, such as implementing temporary covering over the Project tailings daily. Iterating through the control development and modelling results provided valuable risk management experience to apply to other projects and technologies.

Risk management for the Project also includes the application of best available technologies, particularly the use of filtered tailings and water treatment. From a modelling perspective, it is easy to see the benefits of filtered tailings by comparing the existing TSF seepage outflows to the predicted FSTSF seepage outflows. Considering the use of best available technologies early in the Project, such as the tailings alternative assessment in KCB (2021), can reduce design and modelling effort by avoiding reassessments during the design process. This can reduce cost and time for engineering work during the EA application process, and ideally for the Project itself.

Due to the interdisciplinary nature of mining projects, they are susceptible to conflicts (and potentially delays) arising from coordination with other consultants and regulatory reviewers. As the first project to be assessed under the new 2018 Environmental Assessment Act (EAA, 2018), this Project was no exception. The 2018 EAA is more extensive and stringent than previous regulations, which resulted in more iterations between consultants, ODV, and the regulatory reviewers to confirm the Project application meets the regulatory requirements. ODV's planning and coordination helped sustain positive relationships between consultants and regulatory reviewers during the EA process. Modelling for the Project required consistent, timely communications between the design teams, which was achievable in most instances. Clear planning and documentation of scope boundaries/responsibilities, design bases/criteria, and dependencies between scopes was critical to meet the Project application schedule. With the model results being used by the treatment and effects assessment teams, it was especially important to prioritize model checks and minimizing revisions to the issued results.

When receiving regulatory comments, it was useful to address the comments with individual scenarios compared to the original baseline, rather than attempting to quantify the impact of many changes in one set of model results. The regulatory reviewer comments focused on the development and application of loading source terms, scaling factors, control measures, and the potential impacts to the receiving environment. The EA process also highlighted the importance of planning for closure in a changing climate. Planning for closure requires a thoughtful approach considering Indigenous end land use objectives and realizing a resilient and robust plan to continue achieving these objectives for future generations.

Conclusion

The QR Mill water balance and water quality model successfully supported the application for an Environmental Assessment Certificate for the Project under the BC Environmental Assessment Act. The model will continue to be updated and utilized in future design stages, and as the Project moves into operations. The model includes the existing site conditions and infrastructure, as well as the proposed configuration for the Project. The model has been calibrated using site monitoring data, including climate data, flow measurements, and water quality testing. Kinetic column test data was used for the Project

geochemical load sources, which are intended to produce "worst-case" water quality predictions for the EA process. The model was an integral component of the design process for water management infrastructure and associated control measures during the Project. Results from the model were reviewed during the effects assessment to identify and minimize risks to human and ecological receptors related to the Project. The key takeaways from the EA process are related to early planning to account for risks for all stages of a project, from design, to operations, and onwards into post-closure.

Acknowledgements

We would like to thank ODV for their support in the development of the many iterations of this model and for allowing us to share our experience in this paper. We would also like to acknowledge the efforts of the Indigenous groups, regulatory agencies, and other stakeholders who provided invaluable feedback during the EA process. Lastly, a big thank you to our colleagues at KCB who made this work possible.

References

Unless otherwise noted, the references are from the Cariboo Gold Project Environmental Assessment Application, accessed May 18, 2024, at: https://projects.eao.gov.bc.ca/p/5d40cc5b4cb2c7001b1336b8/documents

British Columbia Environmental Assessment Offices (EAO). 2023. Assessment Report: Cariboo Gold Project with Respect to the Application by Osisko Development Corp. for an Environmental Assessment Certificate.

British Columbia Ministry of Energy, Mines and Low Carbon Innovation (EMLI). 2022. Health, Safety and Reclamation Code for Mines in British Columbia. Accessed June 11, 2024, at: https://www2.gov.bc.ca/assets/gov/farming-natural-resources-and-industry/mineral-exploration-mining/documents/health-and-safety/code-review/health_safety_and_reclamation_code_nov2022.pdf

British Columbia Ministry of Energy, Mines and Petroleum Resources (EMPR), British Columbia Ministry of Environment and Climate Change Strategy, and the Environmental Assessment Office. 2018. Risk Management Framework for Mining in BC. Accessed June 11, 2024, at: https://www2.gov.bc.ca/assets/gov/farming-natural-resources-and-industry/mineral-exploration-mining/documents/compliance-and-enforcement/miningbc_risk_management_framework_july2018.pdf

Environmental Assessment Act (EAA). Statutes of British Columbia 2018, c.51. Accessed May 20, 2024, at: https://www.bclaws.gov.bc.ca/civix/document/id/complete/statreg/18051

Golder Associates Ltd. (Golder). 2021a. Cariboo Gold Project – Human Health and Ecological Risk Assessment.

Golder Associates Ltd. (Golder). 2021b. Cariboo Gold Project – Water Treatment at Quesnel River Site – Environmental Assessment Support Engineering Study.

Golder Associates Ltd. (Golder). 2021c. Cariboo Gold Project – QR Mill – Climate Existing Conditions Report.

Golder Associates Ltd. (Golder). 2022. Cariboo Gold Project – Reclamation and Closure Plan Summary.

Klohn Crippen Berger Ltd. (KCB). 2021. Cariboo Gold Project – Alternatives Assessment for Tailings Management at QR Mine.

Klohn Crippen Berger Ltd. (KCB). 2022a. Cariboo Gold Project – QR Mill Water Balance Water Quality Model Report for Environmental Assessment – Rev. 2.

Klohn Crippen Berger Ltd. (KCB). 2022b. Cariboo Gold Project – Design of Tailings and Water Management Infrastructure at QR Mill – Rev. 4.

Metal and Diamond Mining Effluent Regulations (MDMER). 2002. SOR/2002-222. Accessed June 11, 2024, at: https://laws-lois.justice.gc.ca/eng/regulations/sor-2002-222/FullText.html

Osisko Development Corp. (ODV). 2022a. Cariboo Gold Project – Application Summary.

Osisko Development Corp. (ODV). 2022b. Cariboo Gold Project – Chapter 1.0: Project Overview.

Osisko Development Corp. (ODV). 2022c. Cariboo Gold Project – Chapter 7.4: Surface Water.

Development of a Calibrated Seepage Model to Predict Pore Pressure Reduction to Inform Tailings Storage Facility Closure Planning

W.E. Rouncivell, SRK Consulting, South Africa
R.L.C. James, SRK Consulting, South Africa
S.A. Lorentz, SRK Consulting, South Africa

Abstract

The long-term stability of tailings storage facilities (TSFs) is largely dependent on the pore pressure regime. If the tailings are contractive, and thus susceptible to liquefaction, knowledge of the phreatic surface and extent of the partially saturated zone of tailings above this are particularly critical to inform the slope stability of the TSF. The reduction of this saturated and partially saturated zone over time will reduce the risk from the TSF to the environment, both from a slope stability and seepage to groundwater perspective. Numerical seepage drain-down analyses predict the reduction of pore pressures and saturation over time. In this case study, monitoring data from a recently closed upstream platinum TSF are used to calibrate 2D transient models in the Hydrus software. Tailings particle size distributions, a Cone Penetration Test with pore pressure measurement (CPTu) dissipation field test results, standpipe piezometers, and drain flows are utilized.

Zoning is incorporated in the model based on the CPTu and grading data. The predictive scenario results are dependent on numerous key variables, including the hydraulic conductivity of the foundation and tailings material the horizontal versus vertical hydraulic conductivity anisotropy ratio of the tailings material, as well as surface infiltration on the tailings beach. The Soil Water Characteristic Curve (SWCC) of the tailings and its variability across a TSF are also important in such analyses. The SWCC is estimated based on the tailings particle size distribution. A model calibration framework is developed to improve the confidence of the parameters used for predicting the drain-down profile. It is shown that the tailings SWCC and foundation hydraulic conductivity are central to the drain-down modeling, which is critical for TSF closure planning.

Introduction

A case study of a platinum upstream tailings storage facility (TSF) is presented in this paper. Deposition

has ceased for 2two years on the TSF, which is currently in a care and maintenance phase while closure options are evaluated. In addition to slope stability, surface water management is a key focus in the long term. Currently, no water is released from the top surface except via penstocks to the return water dam (if required), which is part of the contaminated water circuit. The penstocks are planned to be sealed in the medium term; therefore. a sustainable surface stormwater management solution is required. The options include a "store and evaporate" and/or "removal via spillway" strategy. If storage results in recharge to the saturated tailings, then the phreatic surface rise will increase the stability risk of the TSF.

The publication of the Global Industry Standard on Tailings Management (GISTM) standard brought all TSFs, particularly upstream constructed facilities, under the microscope. In some cases, improved analysis and design methods are required to validate their performance. Pore pressures play a significant role in slope stability analyses, therefore understanding of the seepage regime over the life of a facility is imperative. Numerical seepage analyses have been undertaken to model the effect of potential stormwater storage on the TSF as well as the anticipated timeframe in which drain flows can be expected, which will require a form of treatment. GISTM highlights the importance of closure and post-closure in many of its principles, including developing an interdisciplinary knowledge base, having a robust design, and proactively managing risk. Advanced seepage modeling and integration of ongoing monitoring data for regular model calibration refinements will improve the confidence of the predictive capability.

The goals of this study were threefold. Firstly, to estimate the drain-down period for water treatment planning purposes; secondly, to determine whether storing stormwater on the TSF in evaporation paddocks in the short term, with no cover design or vegetation plan, is feasible without compromising long-term closure objectives. Lastly, if water can be stored, the study aims to identify the location in the basin that poses the lowest risk to recharging the saturated zone.

TSF description

The TSF was operated for 18.5 years with an average deposition of 140,000 tonnes per month and a maximum rate of rise of 2.5 m per year. The average outer slope is 1V(vertical):4H(horizontal) and the average Natural Ground Level (NGL) slope is 1V:45H. At final height, the TSF is 42 m high at the main embankment; this includes a starter wall of 13 m. Figure 1 and Figure 2 show the plan layout and downstream portion of the transect, respectively, including the monitoring and sampling locations.

Spigot deposition promotes significant segregation along the beach, resulting in approximately 80% of sand near the crest to near zero percent sand at the centralized pool low spot. The pool has reduced significantly over the period since deposition stopped. The phreatic surface, measured by standpipe piezometers, has dropped by approximately 0.5 m along the perimeter.

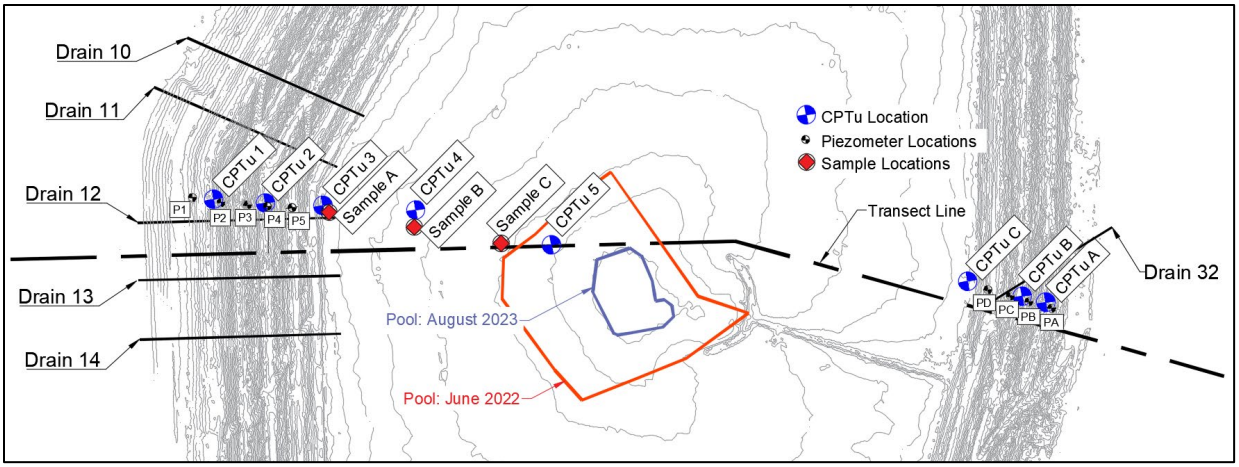


Figure 1: TSF layout

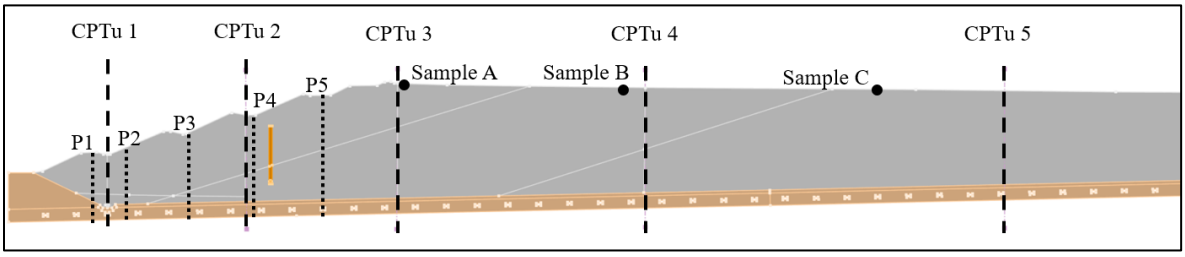


Figure 2: Transect (downstream portion) with monitoring data locations

The site is situated in South Africa in the highveld region with a mean annual precipitation (MAP) of 436 mm, 1:50 yr storm depth of 120 mm and average annual evaporation of 1,316 mm. Site rainfall data was available for the previous 16 years from the mine site (Figure 3).

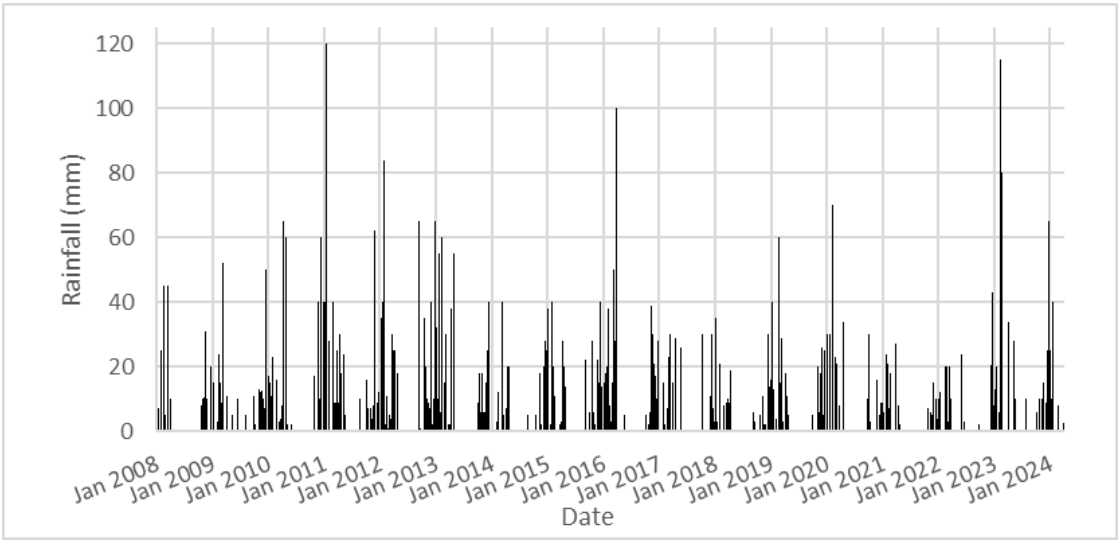


Figure 3: Site rainfall record (recorded at the mine's weather station, gaps filled using CHIRPS data)

Gaps were filled using the Climate Hazards Group Infrared Precipitation with Station data (CHIRPS). Evapotranspiration rates were estimated based on two years of A-pan data, which ranged from 4 mm/day in the summer to 2.5 mm/day in the winter.

Calibration data

Standpipe piezometer levels and drain flows are measured monthly. The toe drain and curtain drain flows per meter along the transect were determined from the monitoring data. Drain 12 flows decreased from 0.22 m^3/day/m and 0.49 m^3/day/m for the toe and curtain drain respectively to 0.08 m^3/day/m and 0.44 m^3/day/m over the transient calibration period. Drain 13 toe drain flows decreased from 0.85 m^3/day/m to 0.60 m^3/day/m over the transient calibration period. The standpipe piezometric levels dropped, on average, by 1.5 m. A CPTu campaign was undertaken 14 months after deposition stopped, which provided confirmation of the phreatic surface as well as vertical pore pressure gradients. Tailings samples were obtained near the surface to determine the particle size distribution information from the crest to the pool.

The pool on the TSF varies in size based on rainfall and evaporation. The stage capacity characteristics of the basin were determined from the freeboard survey and the pool area from monthly satellite imagery. Since deposition ceased, the pool volume has ranged between 0 to 10,000 m^3 (with an average of 4,420 m^3), and the pool area ranged between 0 to 29,980 m^2. The horizontal extent of the pool across the transect was modeled as a head condition in 4 size steps over the transient calibration period.

Methodology

A 2D transect across the TSF, including footprint and starter wall geometry, was imported into HYDRUS-2D and appropriate mesh and boundary conditions were applied. Steady state conditions (at the time deposition ceased) were established by adjusting certain boundary conditions and foundation hydraulic properties to align the phreatic surface and drain flows with monitoring data.

The transient simulation in Hydrus was undertaken using four distinct constant head conditions to mimic the changing pool size over the transient period. These pool sizes were determined by averaging similar-sized pools over a specific timeframe, as direct implementation of varying pool sizes in the model was not feasible. To maintain the continuity between phases, the pore pressure regime from the final day of each pool size/constant head simulation was imported into the next pool size model, using it as the initial condition to commence the subsequent transient phase. An atmospheric boundary condition was applied to the remaining surface nodes of the TSF to apply the rainfall and evaporation for the specific time period being modeled.

The feasibility of an evaporative paddock was investigated using a HYDRUS-1D analysis initialized with the head condition from the transient calibration model.

Tailings characterization

Hydraulic properties

Particle size distribution results of the tailings (Table 1) show clear segregation along the beach. Samples were taken at locations A, B, and C at 7 m, 110 m, and 210 m from the outer crest, respectively. The tailings material classifies in the range between SM to ML (sand with silty fines to fine-grained sands), according to the Unified Soil Classification System (USCS).

No water retention laboratory testing was undertaken on the tailings. The Soil Water Characteristic Curve (SWCC) is estimated based on the tailings particle size distribution using the Hydrus neural network prediction tool, which uses pedotransfer functions (Schaap et al., 2001) to predict van Genuchten (Van Genuchten, 1980) water retention parameters and hydraulic conductivity. Data from a nearby platinum TSF (Site B) where water retention testing was conducted on cycloned tailings material were plotted as reference curves (Figure 4). The overflow and underflow sample (coarse and fine material) results compare reasonably to the Zone A and Zone C material, respectively. The model transect was zoned horizontally based on this grading variation into Zone A, B, and C.

The hydraulic conductivity characteristic curves were derived using the Van Genuchten/Mualem model (Table 2). Qr and Qs denote the residual and saturated water contents respectively, Alpha (1/m) and n are empirical coefficients affecting the shape of the hydraulic functions. Ks is the saturated hydraulic conductivity (m/day). *l* is a pore connectivity parameter; a value of 0.5 was used. The water content and hydraulic conductivity versus suction pressure are shown in Figures 4 and 5 respectively. The hydraulic conductivity determined for tailings ranged from $1.5e^{-5}$ m/s to $1.9e^{-6}$ m/s.

Table 1: Material properties

Zone	% Sand	% Silt	% Clay	USCS Classification	Bulk Density (g/cm³)	Dry Density (g/cm³)
Tailings Zone A	78.6	19.4	2.0	SM/SC	2.1	1.9
Tailings Zone B	25.8	71.3	3.0	ML	2.1	1.7
Tailings Zone C	0.4	89.6	10.0	ML	2.0	1.6
Foundation 1	14.6	21.4	64	CH	1.6	1.3

Table 2: Hydraulic parameters

Material	Name	Qr (-)	Qs (-)	Alpha (1/m)	n (-)	Ks(m/day)
1	Tailings Zone A	0.04	0.38	4.59	1.76	1.30
2	Tailings Zone B	0.04	0.34	0.93	1.55	0.35
3	Tailings Zone C	0.06	0.43	0.68	1.61	0.16
4	Foundation 1	0.06	0.43	0.68	1.61	0.02

The curtain and toe drains were modeled with an opening in the mesh surrounded by a seepage face. During calibration the number of faces activated around the opening was adjusted to limit or increase flux to the drain. Although the drains are surrounded by filter aggregate, this was not included in the model setup.

Foundation 2 has similar parameters to Foundation 1, except that the hydraulic conductivity is half that of Foundation 1. The Zone C material was assigned as a layer over the toe drain to simulate a lower hydraulic conductivity material during the early stages of deposition when segregation is limited due to a short beach and high rate of rise. This impacts the flattening of the phreatic surface near the starter wall.

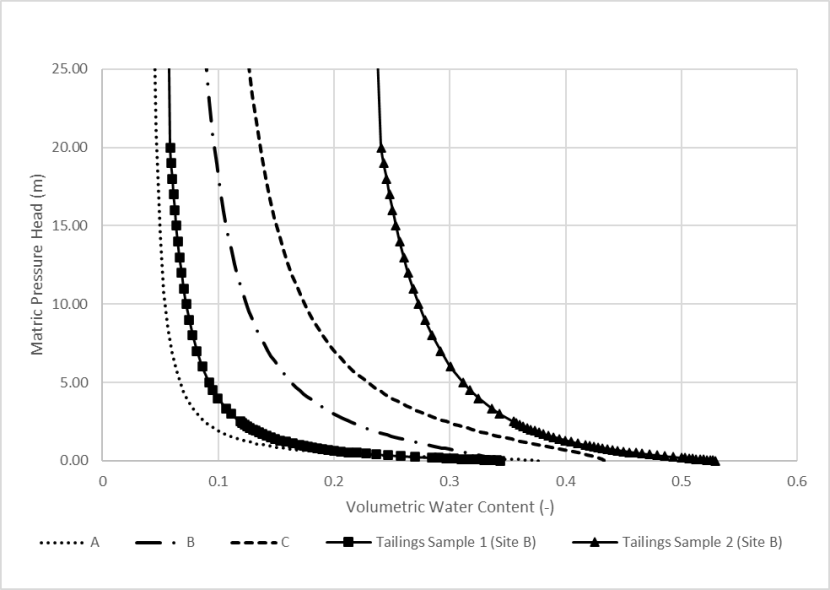


Figure 4: Tailings hydraulic properties: pressure head vs. volumetric water content

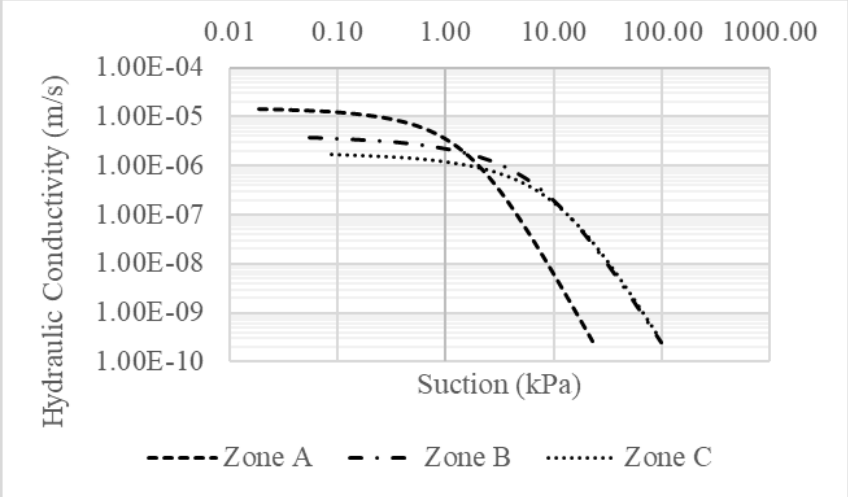


Figure 5: Tailings hydraulic properties: hydraulic conductivity vs. suction

Model setup and calibration

Each model was formulated in the 2D finite element software package, HYDRUS 5.03.0290, to simulate water movement and numerically solve the Richard's Equation for variably saturated flow. The model contained 5,824 nodes with a total of 10,800 triangular elements. Material zoning and boundary conditions are shown in Figure 6.

Model calibration

Model calibration is required to account for unmeasured, unknown, or unrepresented conditions or processes and for uncertainty in measured input data. To calibrate the model, hydraulic conductivity and certain boundary conditions were adjusted until the calibration criteria was met and the model was deemed "fit for purpose" and for use as a predictive tool. Two stages of calibration were undertaken:

- A steady state calibration to simulate the state of the TSF pore pressure regime at the end of deposition. A head boundary condition was applied across the pool area and a flux applied across the beach. This "infiltration" represents the net effect of deposition, rainfall, and evaporation. The flux boundary value was adjusted iteratively until observed phreatic surface, vertical pore pressure gradient, and drain flows were closely matched.
- A transient model calibration from the end of deposition till the CPTu testing date (456 days) was undertaken, initialized by the results of the calibrated steady state model. The flux boundary was replaced with an atmospheric boundary condition while the pool size was gradually reduced in line with the satellite imagery. The reduction of the phreatic surface and drain flows were used as criteria.

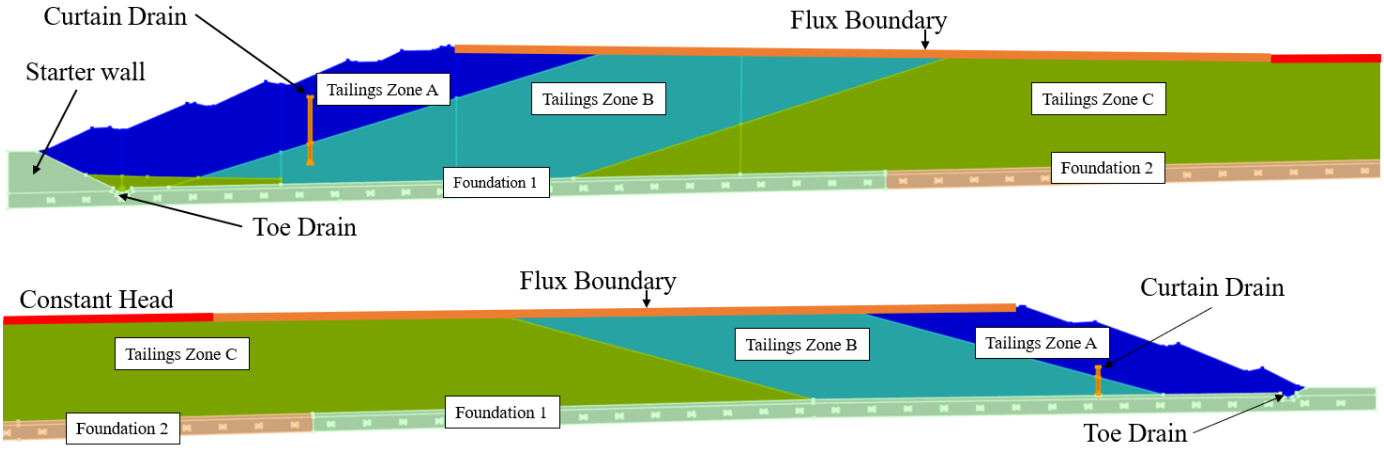


Figure 6: 2D Hydrus Model setup

Results and discussion

The results of the steady state and transient calibration period aligned well with observed CPTu and monitoring data. The model phreatic surface location (Figure 7) aligned very closely with the observed location at each time period since this was a calibration criterion. The vertical hydraulic gradient comparison (Table 3) shows the same trend of overall decreasing gradients towards the center of the TSF. The drain flows (Table 4) show reasonable alignment, particularly for the curtain drain flows, which include drain 32 flows (no toe drain flows observed at drain 32). The correlation improves if the average flow of drains 12 – 14 are used for comparison, considering the model as representative of that flank of the TSF. The average flow of these drains was 0.54 m^3/day/m and 0.40 m^3/day/m for the start and end of the calibration period, respectively. Some cross flow from Drain 12 towards drain 13 is believed to occur, which is not captured in the 2D model.

Storage in the original pool area recharges the saturated zone directly, therefore stormwater should be decanted promptly via the penstocks.

Table 3: Vertical hydraulic gradient comparison

	CPTu 1	CPTu 2	CPTu 3	CPTu 4	CPTu 5
Model Vertical Hydraulic Gradient (m/m)	0.7	0.91	0.81	0.68	0.49
CPTu Vertical Gradient (m/m)	0.67	0.74	0.43	0.5	0.3

Table 4: Drain flow comparison

	Toe drains: End of deposition	Toe drains: End of transient period	Curtain drains: End of deposition	Curtain drains: End of transient period
Actual (Drain 12 and 32) (m^3/day/m)	0.22	0.08	1.50	0.96
Model (Drain 12 and 32) (m^3/day/m)	1.22	0.42	1.21	0.71

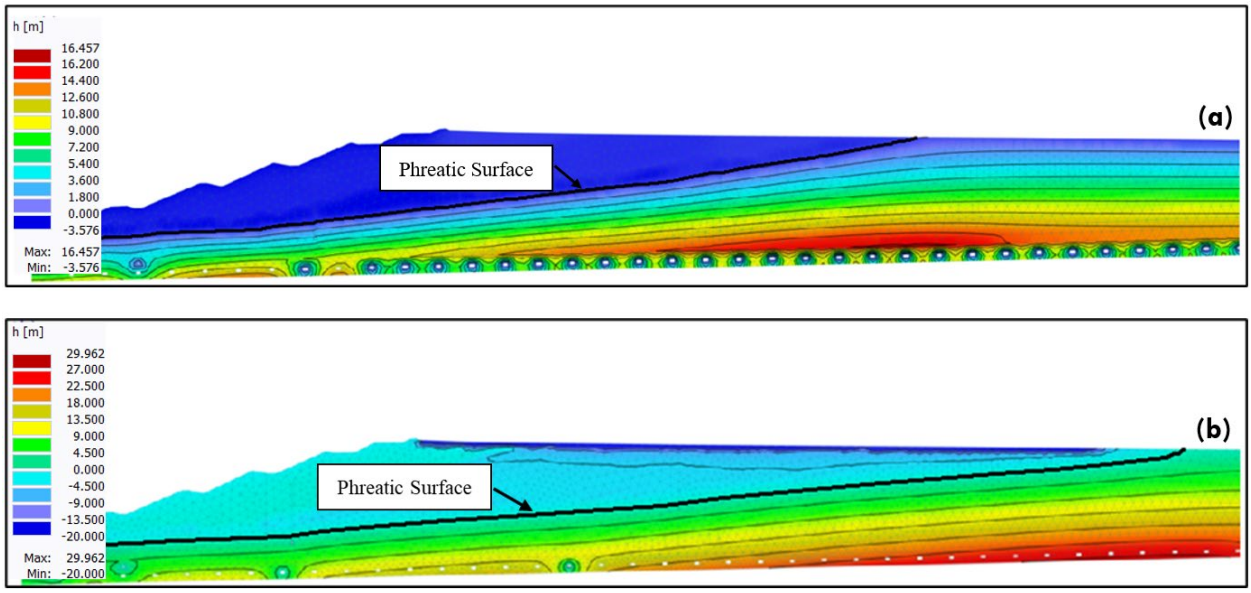


Figure 7: Pressure heads (a) steady state (start of transient calibration period) (b) end of transient calibration period

Drain-down profile

The calibrated model was used to run a scenario in which the pool has reduced significantly and then been removed, based on the assumption that stormwater reporting to the pool area will be decanted via the penstock in the future. The model was then run with an atmospheric boundary condition until drain flows reduced significantly. In addition to the zoned TSF model, a scenario where Zone C material was applied throughout the tailings body was run. This was motivated by the fact that the porosity and hydraulic conductivity of this material more closely matched the porosity and hydraulic conductivity of the tailings observed on similar TSFs. The drain-down profile of both scenarios is shown in Figure 8, each near five years. The use of a single material did not make a significant difference to the result.

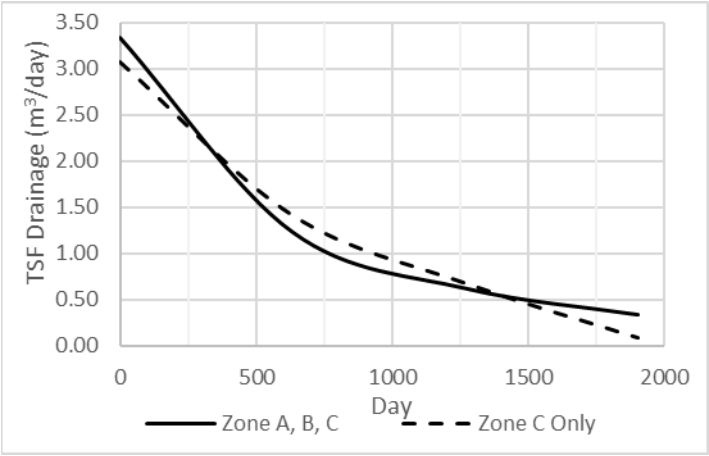


Figure 8: Drain-down profile

This predicted drain-down period is considered an underestimate. Since the transient calibration period was relatively short, a longer period is recommended to improve the confidence of the model parameters, particularly the foundation hydraulic conductivity and drainage conditions.

Evaporation paddocks

To reduce the volume of discharge via the penstocks, storage of stormwater in evaporation paddocks away from the pool area was investigated. Location B was interrogated via a 1D simulation over a 16-year rainfall period. The model was initialized from the pore pressure profile from the 2D transient model (Figure 9). The bottom boundary head condition was kept constant, i.e., the phreatic surface was not permitted to reduce. This is considered conservative since the phreatic surface is expected to drain-down according to the 2D transient model. Over the simulation period the water content of the unsaturated zone increased, and the phreatic surface increased by 2 m. Therefore, a trial over a short period will not rapidly impact the saturated zone. However, this should be closely monitored.

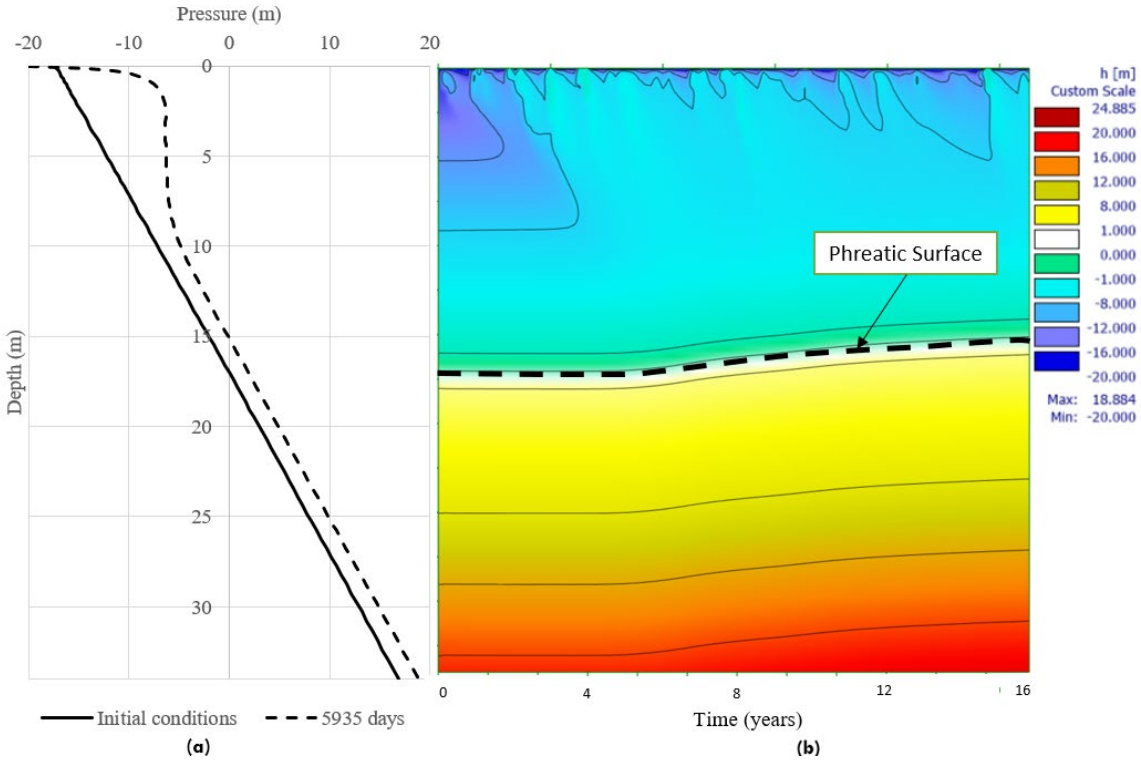


Figure 9: (a) Pressure head changes over 16 years of rainfall and evaporation. (b) Initial and final pore pressure distributions at sample B location

Conclusion and recommendations

TSF 2D Hydrus seepage models were calibrated using monitoring and CPTu data. The SWCC, derived from tailings particle size distribution data (pedotransfer functions) provided a reasonable prediction of

hydraulic parameters that resulted in drain flows and pore pressure gradients matching reasonably the monitoring data for the calibration periods, both steady state and transient.

The outcomes included the estimation of the drain-down period and the feasibility of storing stormwater in evaporative paddocks during the TSF care and maintenance phase. Evaporation paddocks away from the pool area are recommended, but can potentially re-saturate the unsaturated zone and recharge the phreatic surface. A trial over a relatively small area of the TSF, at different distances from the crest, is recommended to test their performance. Cover design and vegetation options could be incorporated into the trial.

A CPTu campaign is recommended in future to enable calibrating the transient model over at least 4 years to improve the confidence of the predicted drain-down period. Drain flows, standpipe piezometers and pool size data should be collected monthly to support this analysis.

References

GISTM (Global Industry Standard on Tailings Management).2020. Co-convened by the International Council on Mining and Metals (ICMM), United Nations Environment Programme (UNEP) and Principles for Responsible Investment (PRI). Accessed 05/01/2024 at https://globaltailingsreview.org/

Schaap, M.G., Leij, F.J. and van Genuchten, M.Th. 2001. Rosetta: A computer program for estimating soil hydraulic parameters with hierarchical pedotransfer functions. *Journal of Hydrology* 251: 163–176.

van Genuchten, M.T. 1980. A closed-form equation for predicting the hydraulic conductivity of unsaturated soils. *Soil Science Society of America Journal* 44(5): 892–898.

Rapid Water Table Response to Transient Pressure Wave Generation in the Unsaturated Zone of Tailings Dams

Charné Theron, Hanze University of Applied Sciences, Netherlands
Simon A. Lorentz, SRK Consulting, South Africa

Abstract

Recent years have seen a global rise in the failure of tailings dams. Studies investigating the causes of slope failure often recognize that high intensity rainfall events significantly contribute to liquefaction, erosion, and overtopping. This study aims to investigate the influence of alternative physical and geohydrological processes that, under tension saturation conditions, contribute to slope instability in tailings dams. It has been suggested that the generation of transient pressure wave mechanisms by high intensity rainfall events, surface ponding, and wetting front advancement result in the formation of an induced pressure head that triggers the mobilization of pre-event water. In order to quantify these physical processes, this study included the analysis of rapid transmission conditions in a silica fines mix, with similar physical and hydraulic characteristics as platinum tailings. A tall leak-proof soil column, containing the soil sample compacted to in-situ dry bulk density, was fitted with seven observation ports. Each port consisted of a pore air pressure probe, a mini tensiometer, and a time domain reflectometry probe. After set-up and initial stabilization, three separate artificial high intensity rainfall events were applied to the surface. Monitoring of hydraulic state variables was recorded at 30-second intervals by automatic logging, thereby enabling the analysis of measured outcomes. Observations showed instant spikes in pore air pressure ahead of the wetting front, as well as a number of delayed responses. The interpretation of laboratory results led to the conclusion that pressure diffusion mechanisms throughout the porous medium could result in the rapid release and mobilization of previously stagnant antecedent moisture, thereby enabling phreatic levels to rise rapidly and in excess to the amount of surface infiltration. Also, since an increase in pore water pressure is likely to cause a reduction in shear strength, it is suggested that these physical and geohydrological processes could have an adverse impact on the stability of tailings dams.

Introduction

Ng and Shi (1998) proposed that slope stability of tailings dams is not only affected by high intensity rainfall events, but that pre-event water makes a significant contribution to a reduction in the factor of safety. Based

on this premise, it is suggested that preceding rainfall events contribute significantly to the establishment of the tension saturated continuous pore water phase, which enables rapid transmission of the induced pressure head to a potential failure plane. This study intends to demonstrate pressure diffusion mechanisms throughout the porous medium. It was previously suggested that these physical processes, known as Groundwater Ridging (GWR) and the Lisse Effect (LE), are largely responsible for the rapid release and mobilization of previously stagnant antecedent moisture, thereby enabling groundwater levels to rise in excess compared to the amount of water infiltrating the soil profile (Theron et al., 2022). The increase in pore water pressure contributes to stresses that reduce shear strength and lower the factor of safety. It could therefore have an adverse impact on the stability of tailings dams (Theron, 2023).

Ground water ridging

Abdul and Gillham (1984) describe the physical process of GWR as occurring near a stream, and allowing for the rapid rise of the water table to the surface. The rise occurs due to the conversion of pre-event water held in tension in the unsaturated zone to water contained within the phreatic zone. According to Cloke et al. (2006) the addition of rainwater and a small amount of infiltration relieves tension in the tension saturated capillary zone and instantly converts the negative pressure head to a positive pressure head (Theron and Lorentz, 2023). The release of antecedent water occurs due to the development of a steep hydraulic gradient that is directed towards the stream. According to Zang et al. (2018) the rise in the water table is dependent on the amount of pre-event water already held in the capillary zone, and not on how much water is infiltrating the soil profile during or shortly after the rainfall event. The rise in the water table is therefore inconsistent with the amount of infiltrated water (Theron et al., 2022). According to Waswa and Lorentz (2016) the rapid and exaggerated rise in the phreatic surface occurs since such a small amount of water is required, through infiltration, to fill the capillary menisci. The process of GWR is shown in Figure 1 and is recognized by the rapid uneven rise in the water table after the occurrence of a high intensity rainfall event (Theron, 2023).

It is further recognized that diminished GWR responses are closely related to rainfall events of low intensity. This is also suggested by Zang et al. (2018), who found that low intensity rainfall events result in lower pore air pressure in the vadose zone and diminished transient pressure waves. According to Abdul and Gillham (1984) GWR is entirely dependent on rainfall intensity, adjacent surface slope, and soil hydraulic conductivity. Adding to this, Ng and Shi (1998) mention that the presence of antecedent water within the soil profile and the position of the initial water table before occurrence of a rainfall event, would also be required for GWR to occur. This is confirmed by Cloke et al. (2006) who found a strong relationship between riparian characteristics and GWR and suggested that the development of a positive ridge would also be dependent on soil type.

Coarse soils allow for higher levels of infiltration, while fine-grained soils, such as tailings, enable the extension of the capillary fringe (CF) and therefore provide conditions required for GWR to occur (Theron, 2023). As pore size, and inversely particle size of soil, will determine the height of the capillary fringe above the water table, it is suggested that the fine nature of tailings would contribute to higher rising water levels in the capillary zone. However, Zang et al. (2018) mention that the capillary fringe is only an influence factor, and not a controlling factor in the generation of GWR.

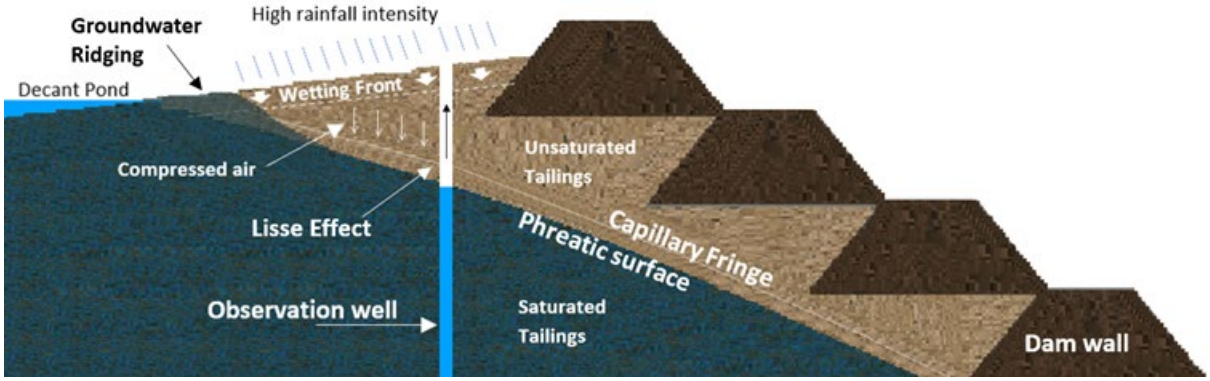


Figure 1: Schematic depiction of GWR and the LE (Theron, 2023)

Lisse Effect

The LE, illustrated together with GWR in Figure 1, happens as a result of the accumulation of air pressure between the approaching wetting front and the water table (Guo et al., 2008). After infiltration of rainfall at the soil surface, the downward moving wetting front functions as an impermeable cap that limits the outflow of air, thereby causing an increase in pore air pressure (Meyboom, 1967). According to Weeks (2005) pressure at the top of the capillary fringe will continue to rise until entrapped air pressure is higher than the pressure head of the infiltration profile above. The process is likely more pronounced if soil air content is high in the unsaturated zone above the capillary fringe and the phreatic surface is located at a sufficient depth. Fayer and Hillel (1986) suggest that some entrapped air will eventually escape, and some will remain in the soil profile, reducing saturation moisture content. However, it is possible that the brief increase in saturated zone pressure may be of sufficient magnitude to induce slope instabilities. Cloke et al. (2006) hypothesize that the increase in pore air pressure generates a downward transient air pressure wave that causes an increase in pore water pressure, which enables the formation of a continuous water phase in the capillary fringe (Theron and Lorentz, 2023). This event is discernible because there is an almost instant rise of the water level in an observation well, indicating the rapid transmission of antecedent water. Similar to GWR, this mechanism is dependent on certain variables, including whether rainfall intensity exceeds infiltration capacity (leading to ponding), ponding depth that prevents air from escaping and results in

compression in the unsaturated zone, pore size distribution, permeability that inhibits infiltration rates and pre-event water conditions (Theron, 2023).

Laboratory experiments

Similar to Waswa (2013), this study's experimental design included infiltration experiments in a tall sand column under controlled boundary conditions. After the application of artificial rainfall events, responses were recorded by automatic logging, and analyzed to determine the physical response of hydraulic state variables. The analysis of this data was used as an indication of the physical generation of transient pressure waves associated with water flow in an unsaturated soil medium (Theron, 2023).

Laboratory apparatus

Apart from the much larger scale of the laboratory experimentation, the 2.85 m high tall soil column, with an internal diameter of 600 mm, was set up similarly to studies conducted by Waswa (2013) and Salas-García et al. (2017). It was filled up to 2.65 m with a tailings substitute of similar physical properties and bulk density. Due to the intricate nature of physical and hydrological processes in the unsaturated zone, the column was fitted with sensing devices at seven data ports spaced 500, 600, 700, 800, 1,100, 1,400, and 1,700 mm from the bottom of the column. Each of the seven ports consisted of three different instruments that included a time domain reflectometry (TDR), a 1 bar mini-tensiometer (MT) and a 0.1 bar pore air pressure probe (PAPP) to measure pore air pressure (Theron, 2023). A drainage tube and piezometer were installed at a distance of 200 mm from the base of the pipe to discharge water and monitor the phreatic surface (Theron and Lorentz, 2023).

Sensor development

Volumetric water content (VWC) was measured by a custom-made time-domain reflectometry (TDR), shown in Figure 2. The probes consisted of three (5 mm ø) 200 mm long stainless-steel rods (50 mm c/c). A CR1000 Campbell Scientific data logger was used to store data through an SDMX50 Multiplexer and Campbell Scientific TDR100 wave generator. Matric suction was measured by means of purpose-made mini tensiometers that were fitted with 25 mm-long porous ceramic-cups (15 mm exposed) with an outer diameter of 6 mm (see Figure 3). The high-air-entry ceramic cup was joined to a rigid non-corrosive fiberglass tube (100 mm long, 6 mm outer ø, 3 mm inside ø). The other end was connected to a 1 bar Honeywell differential pressure transducer. The entire instrument was carefully filled with deaired water using a syringe, before insertion into the soil column. This was done to ensure equilibrium with the soil moisture content (Salas-Garcia et al., 2017). Once equilibrium was reached, the water in the mini-tensiometer was therefore also under negative pressure, similar to the porewater in the soil medium.

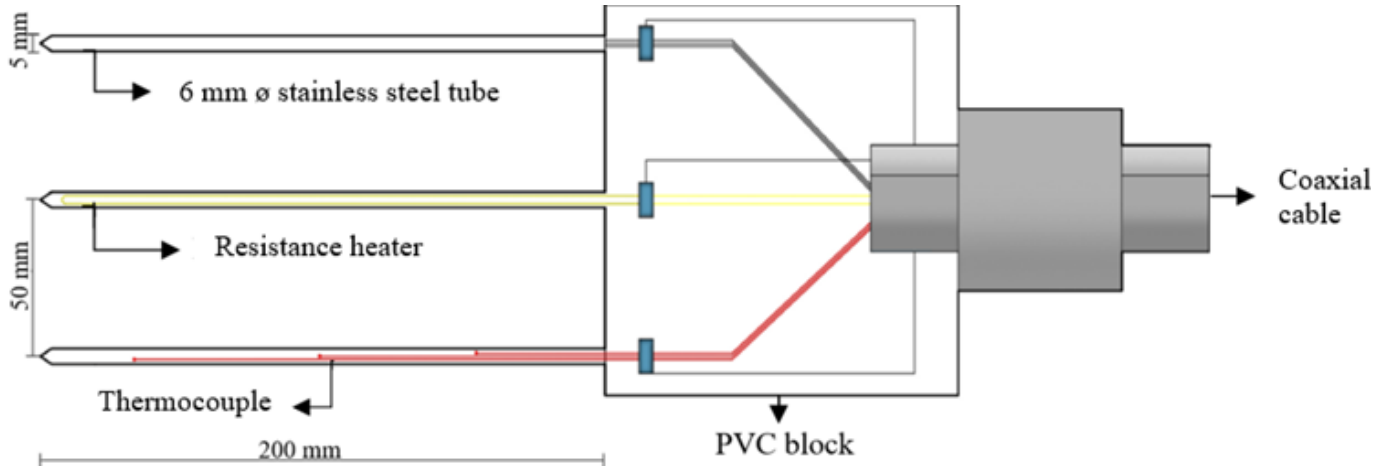


Figure 2: Custom-made TDR used to measure volumetric water content

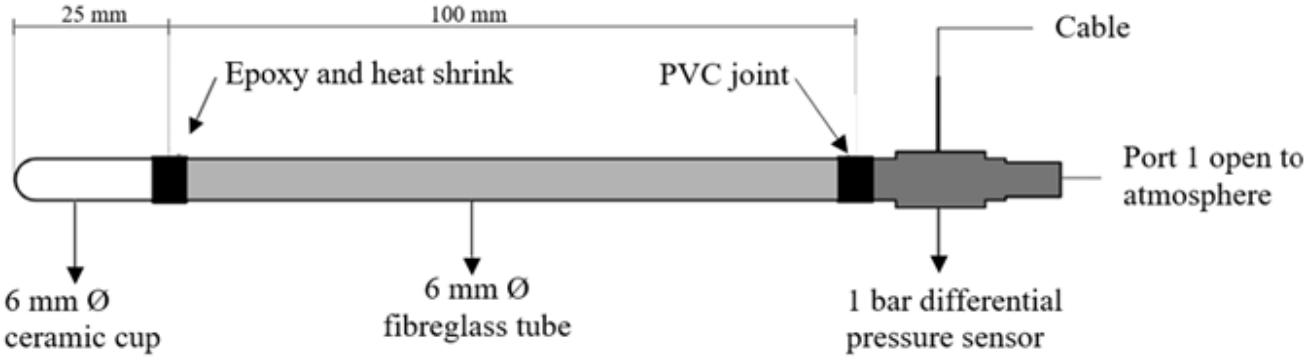


Figure 3: Custom-made mini tensiometer

Pore air pressure probes (PAPP) were used to measure pore air pressure. See Figure 4.

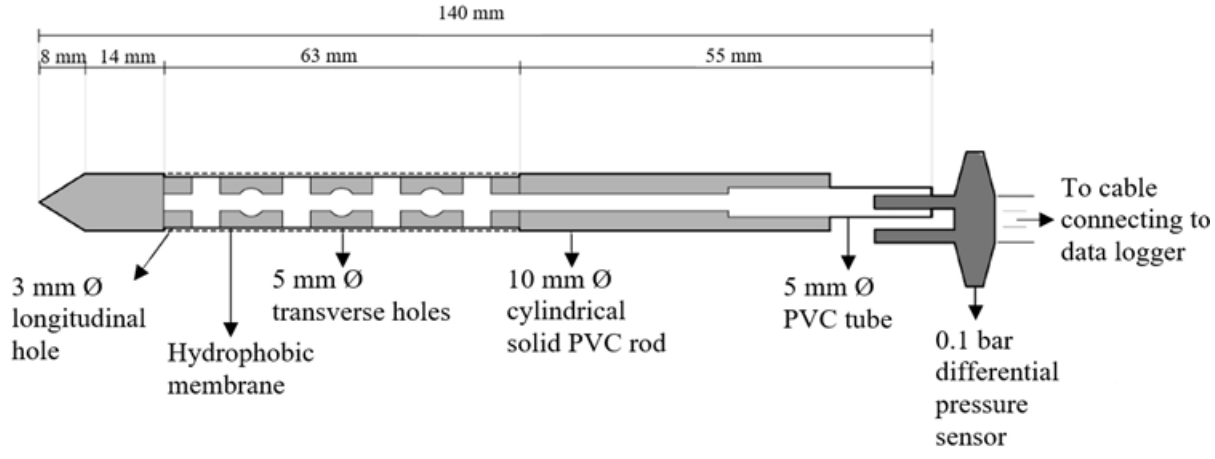


Figure 4: Custom made pore air pressure probe (modified from Waswa, 2013)

Experimental procedure

In order to draw comparisons with results obtained by Waswa (2013), a similar experimental procedure was followed. The sample was packed in a tall soil column in layers of 300 mm. Each layer was compacted at uniform bulk density to replicate that of tailings (Theron and Lorentz, 2023). Instrumentation was inserted through openings into the soil and sealed to prevent leakage and influence from external factors. After completion of the entire setup, water was introduced from the bottom of the column via the inlet valve, to avoid the entrapment of pore air (Waswa, 2013). Every care was taken to establish a constant water level at about 400 mm above the base where it remained constant, as indicated by the piezometer, for approximately 4 hours preceding each experiment. From the recorded data, the CF extended to about 200 to 300 mm above the water table. It was however not possible to determine the exact position of the water table, likely due to the soils' fineness and resulting high capillarity resulting in exaggerated levels of matric suction. Waswa (2013) also noted this concern and ascribed it to the fact that the zero-pressure line could rise above the CF.

The installation was left to reach equilibrium before application of three artificial rainfall events, each representing different return periods. Storm events 1:200, 1:100, and 1:50 years were selected to represent high intensity rainfall events that are likely to increase under future climate change conditions. Table 1 shows the calculation of ponding depth based on design storm data provided by Smithers and Schulze (2002). The setup allowed for continuous recording of data in 20-second intervals, allowing for the detailed analysis of both instantaneous and delayed responses.

Table 1: Description of incremental addition of water to tall soil column (Theron, 2023)

Event	Return period	Rainfall depth/h	Volume/h	Addition of water to tall soil column
1	1:200	84.1 mm	24 *l*	9 *l* over 30 min, 14 *l* over 15 min, 1 *l* over last 15 min
2	1:100	74.9 mm	21.2 *l*	8 *l* over 15 min and 13.2 *l* over 45 min
3	1:50	66.1 mm	18.7 *l*	7 *l* over 15 min and 11.7 *l* over 45 min

Although similar to Waswa's 2013 design, some alterations were made. The solid 140 mm long PVC rod (10 mm ø) was manufactured with a 3 mm ø hole drilled in the longitudinal center, together with seven 5 mm crosswise holes, drilled over 50 mm across the length. The length of the probe along which crosswise holes were made, was recessed and covered in a hydrophobic membrane that only enabled moisture to pass a high pressure while the flow of air is at low pressure (Waswa, 2013). The PAPP was connected to a differential pressure transducer, by means of a PVC tube, which in turn was eventually connected to a CR1000 Campbell Scientific Data Logger through a SDMX50 multiplexer.

Physical soil properties

With the purpose of producing an artificial substitute of tailings, physical characteristics were reproduced through the analysis of previous laboratory tests conducted by MacRobert and Blight (2013). The experimental material consisted of a concise mix of silica sand and silica dust and the particles were uniform in shape, clean and free of organic matter. The material is classified as a silty loam. Soil hydraulic parameters, such as hydraulic conductivity and water retention characteristics, were determined in the laboratory and were found to be similar to a known platinum tailings (Theron, 2023).

Observations

Each of the three artificial rainfall events exceeded the soil's infiltration capacity, which resulted in ponding, preventing the escape of air. This resulted in several rapid responses being recorded, but there were also a number of delayed responses. Ponding event 1 resulted in somewhat insignificant instant increases in pore air pressure at the four deep probes and was evident after the first two applications of event 1. The third application consisted of only one liter of water, which did not register any response. This finding highlights the significance of the intensity of rainfall events. With the exception of MT5, some minor changes (not shown) in pore water pressure were recorded 45 minutes after the start of the experiment. Since these changes were not caused by the arrival of the wetting front, tensiometric pore water pressure is likely to have responded to compressed pore air pressure.

Approximately seventy-three hours after the start of the experiment, the shallow TDRs recorded a slight response (see Figure 5). At the same time the deep PAPPs also registered significant changes, indicating the potential increase in pore air pressure, likely due to infiltration. In response, a simultaneous response in pore water pressure was measured in the unsaturated zone above the phreatic surface. From these results, it could be concluded that the magnitude of compressed pore air pressure has a direct impact on the extent to which groundwater levels will respond.

Similar observations were made by Waswa (2013) after analyzing responses during and after a high intensity rainfall event, that included a peak intensity of 228 mm/h that lasted 60 seconds. It resulted in the rapid response of tensiometric pore water pressure probes at different soil depths and a disproportionate rise of groundwater by 10.395 kPa (106 cmH_2O), not related to the arrival of the saturated front. Both these studies found a connection between the extent of compressed pore air pressure and the total change in pressure potential near the phreatic surface. According to Waswa (2013) the occurrence of compressed air ahead of the wetting front is indicative of the LE. It is suggested that the response of pore water pressure to compressed pore pressure is indicative of the presence of a pressure wave (Theron, 2023).

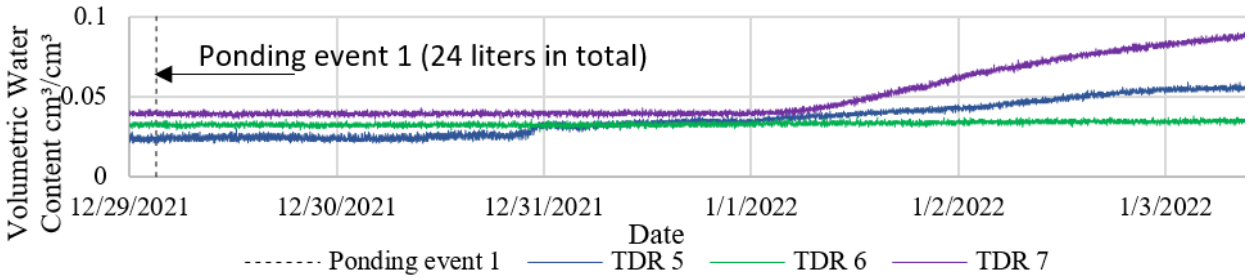


Figure 5: VWC observation before, during and after ponding event 1 (Theron, 2023)

The second infiltration test was carried out in the tall soil column after about nine weeks. The piezometric water level during the pre-simulation period of event 2 was again observed at about 400 to 500 mm from the base. The deepest TDRs indicated near saturated conditions, while TDR 4 was situated in the upper boundary of the capillary zone. After application of the second ponding event, there was an immediate change recorded at the three shallow probes. Responses at the four deep probes were measured shortly after but at less magnitude. Figure 6 shows the behavior before and after application with constant higher levels after application, resulting in VWC values that are substantially above the residual value.

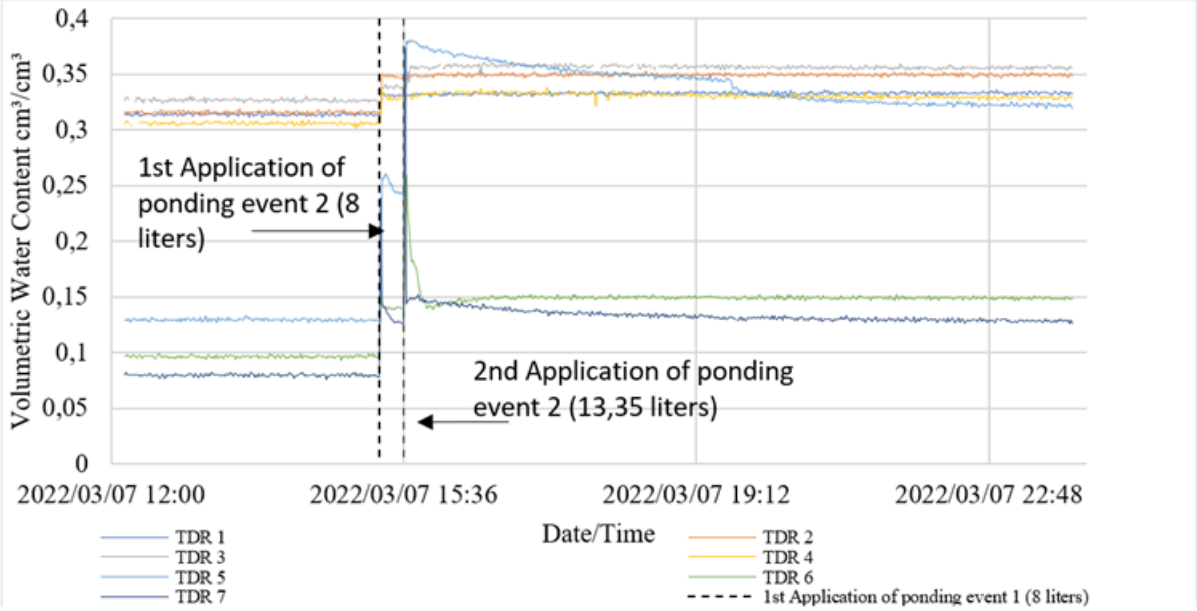


Figure 6: VWC observation before, during and after 1st and 2nd application of artificial rainfall event 2 (Theron, 2023)

Immediately following each application of ponding event 2, pore air pressure increased in relation to ponding depth. Application 1 of event 2 resulted in less ponding and pore air pressure increases at a maximum of 1.8 kPa. This is similar to Waswa's (2013) study that observed a 1.961 kPa change in pressure potential in fine soil within ten minutes of infiltration at the soil surface. The second application of 13.2 liters resulted in pore air pressure increasing instantly to a maximum of 10 kPa. In response, deep pore

water pressure sensors recorded several rapid as well as gradual declines. MT1 for instance showed an inverted spike at application 2 resulting in a 0.5 kPa change in tensiometric water pressure. MT4 also decreased rapidly from 70 kPa to 60 kPa. Both MT2 and MT3 declined gradually between 10 to 50 kPa.

Ponding event 3 consisted of the lowest simulated rainfall intensity. Even though there were no significant pressure changes observed in the unsaturated zone (therefore results are not shown), the three shallow TDRs showed similar results to event 2.

Interpretation of results

Shortly after the artificial rainfall event was administered to the soil surface, the majority of PAPPs, MTs, and TDRs responded. During event 1, the initial rapid response of pore air pressure probes is likely due to loading conditions after applications 1 and 2 (Theron, 2023). Although this resulted in small variations in pore water pressure, changes were insignificant. Observations further indicate that the significant (delayed) responses of deep pore air pressure probes were met with similar responses in deep pore water pressure probes. It is therefore suggested that the response recorded in the tensiometric pore water pressure was due to the change in compressed pore air pressure, as the saturation front advanced downwards into the soil profile. From the observations it was also evident that, as infiltration advanced, the magnitude of change in compressed pore air pressure also increased. This change transferred directly to the magnitude of change in pore water pressure. This is similar to the observed results interpreted by Waswa (2013), in which corresponding changes in pore water pressure were relative to compressed pore air pressure. The initial slow infiltration rates are attributed to the fine nature of the soil (not previously wetted) and the fact that eventual responses in pore water pressure were brought about by the advancing wetting front, compressed air pressure and the subsequent generation of transient pressure waves (Theron, 2023).

Both application 1 and 2 of ponding event 2 yielded rapid responses from most sensors. Of particular interest is the instantaneous increase in deep TDRs, indicating the rapid mobilization of pre-event water. Although Waswa (2013) confirmed VWC at the shallowest sensor to respond before arrival of the wetting front, this was only after 44 minutes from the start of the experiment, and therefore in contrast to the current study's findings. It should however be reiterated that these two studies have conducted analysis on different scales, which may have an influence on measured responses. Results do however coincide with infiltration tests conducted by Salas-Garcia et al. (2017), which found a sharp increase in water content at the shallow sensors within a few minutes after application. Similarly to the current study, VWC also decreased shortly after ponded infiltration stopped. Both studies found deep sensors to respond slower than top sensors and these responses were also at a lesser magnitude than changes recorded at shallow probes.

The magnitude of pore air pressure responses differed considerably between application 1 and 2 of ponding event 2. PAPP 2 for instance increased by almost 2 kPa after the application of 8 liters of water to

the soil surface, whereas the same sensor recorded an increase of almost 10 kPa after application of 13.3 liters. This illustrates the sensitivity of induced pressure head to rainfall intensity. Similarly to event 1, pore water responses at deep probes responded to the induction of compressed pore air pressure.

The last ponding event had the lowest rainfall intensity. It resulted in disparate yet insignificant fluctuations in pressure responses. Even though all TDRs recorded an instant increase, these were more rapid and of far greater magnitude at the shallow TDRs. Based on this, it is assumed that some degree of transient pressure wave generation caused responses at the deep probes, but that ponding depth was insufficient to trigger stable responses. These insignificant results in themselves support the premise of this study, i.e., that lower intensity rainfall events have less of an impact on the compression of pore air in the region of the CF, and thus are less inclined to impose pressure that results the diffusion of the injected energy through soil water.

Discussion

Although the wetting front did not reach the deep sensors, its downward approach brought about pressurized pore air in the unsaturated zone, which in turn resulted in a change in pore water pressure. It is recognized that the dynamic load applied to the soil surface could result in the tailings porous medium contracting, thereby generating excessive pore pressure. However, the delayed response of ponding event 1, demonstrated before arrival of the wetting front, suggests that transient air pressure waves contribute significantly to the generation of pore air propagation and a subsequent change in pore water pressure. It is therefore postulated that the gradual rise in pore air pressure at the deep probes is an indication of entrapped air and, as the wetting front approached, it compressed. The corresponding change in tensiometric pore water pressure, measured at the three deepest sensors, may be indicative of the formation of a distinct CF and rising phreatic surface, fed by groundwater and not due to infiltration. It is suggested that this may point towards the formation of an upward water pressure wave causing the water table to rise in response to a downward air pressure wave brought about by the descending wetting front.

It was also interesting to note that the magnitude of groundwater level responses showed a strong relationship with the magnitude of the compressed pore air pressure. In turn, it was found that the extent of pore air propagation was determined by the intensity of the rainfall event and points to the significance of energy injected into the tension saturation zone as the downward air pressure wave propagates towards the water table (WT). As it reached the WT, groundwater started to ascend as an upward water pressure wave. In contrast to Waswa (2013), and since the laboratory set up did not allow for the extension of the CF throughout the tall soil column, a continuous pore water phase was not found to be a prerequisite for GWR to occur. According to Waswa (2013), GWR is more likely to occur due to the energy of the rainfall event, whereas the LE is more likely to occur due to compressed pore air. It is suggested that responses observed

in the above laboratory experiments provide sufficient indicators pointing towards the presence of both these mechanisms.

Conclusion

The most noteworthy observation of the analysis is the change in pore water pressure above the water table brought about by the release of water held in tension to the phreatic surface. Since it occurs before arrival of the wetting front, this study has demonstrated the rapid mobilization of groundwater after the advancing wetting front compresses pore air in the vicinity of the CF, thereby increasing pressure between the wetting front and the phreatic surface. This finding is consistent with Waswa (2013), who showed these responses to manifest themselves in the form of either GWR or the LE.

Based on the results of laboratory analysis, it is suggested that transient pressure waves are generated by the intensity of a rainfall event as well as by the advancement of an approaching wetting front after infiltration. These pressure diffusion mechanisms cause an increase in the WT that changes groundwater pressure heads and matric suction, thereby reducing slope stability in partially saturated conditions. Waswa (2013) described comparable findings and suggested that pore air propagation and transient pressure wave generation contribute to slope instability in natural hillslopes. As a consequence, it is therefore probable that high intensity rainfall events also contribute to slope instability in tailings dams.

References

Abdul, A.S. and Gillham, R.W. 1984. Laboratory studies of the effects of the capillary fringe on streamflow generation. *Water Resources Research* 20(6): 691–698.

Cloke, H.L., Anderson, M. G., McDonnell, J. J. and Renaud, J. P. 2006. Using numerical modelling to evaluate the capillary fringe groundwater ridging hypothesis of streamflow generation. *Journal of Hydrology* 316(1–4): 141–162.

Fayer, M.J. and Hillel, D. 1986. Air encapsulation: I. Measurement in a field soil. *Soil Sci. Soc. Am.* 50(3): 568–572.

Guo, H., Jiao, J.J. and Weeks, E.P. 2008. Rain-induced subsurface airflow and Lisse effect. *Water Resources Research* 44(7): 1–9.

MacRobert, C.J. and Blight, G.E. 2013. A field study of the in-situ moisture regime during active hydraulic tailings deposition. *Journal of the South African Institution of Civil Engineering* 55(3): 57–68.

Meyboom, P. 1967. Groundwater studies in the Assiniboine river drainage basin: Hydraulic characteristics of phreatophytic vegetation in the south-central Saskatchewan. *Geological Survey Bulletin* 139.

Ng, C.W.W. and Shi, Q. 1998. Influence of rainfall intensity and duration on slope stability in unsaturated soils. *Quarterly Journal of Engineering Geology* 31(2): 105–113. https://doi.org/10.1144/GSL.QJEG.1998.031.P2.04

Salas-García, J., Garfias, J., Martel, R. and Bibiano-Cruz, L. 2017. A low-cost automated test column to estimate soil hydraulic characteristics in unsaturated porous medium. *Geofluids* 2017: 1–13.

Smithers, J.C. and Schulze, R.E. 2002. Design rainfall and flood estimation in South Africa. December, 1–180. Water Resource Commission, Pretoria, RSA, WRC Project No: K5/1060.

Theron, C., Lorentz, S.A. and Xu, Y. 2022. Rainfall-induced groundwater ridging and the Lisse effect on tailings storage facilities: A literature review. *Journal of the Southern African Institute of Mining and Metallurgy* 122(2): 37–44.

Theron, C. 2023. Rainfall induced transient pressure wave mechanisms and pore water pressure dynamics in tailings. Thesis research, Department of Natural Sciences. University of the Western Cape.

Theron, C. and Lorentz, S. 2023. Rainfall induced transient pressure wave mechanisms in tailings dams. In P. Stanley, C. Wolkersdorfer and K. Wolkersdorfer (eds.), *The Future: Proceedings of the International Mine Water Association Conference.* International Mine Water Association: 497–503.

Waswa, G.W. 2013. Transient pressure waves in hillslopes. Thesis research, Department of Civil Engineering, University of Kwa-Zulu Natal.

Waswa, G.W. and Lorentz, S. A. 2016. Transmission of pressure head through the zone of tension saturation in the Lisse effect phenomenon. *Hydrological Sciences Journal* 61(10): 1770–1777.

Weeks, E.P. 2005. The Lisse effect revisited. *Ground Water* 40(6): 652–656.

Zang, G., Sun, D.M., Feng, P. and Semprich, S. 2018. Numerical analysis of groundwater ridging processes considering water-air flow in a hillslope. *Groundwater* 56(4): 5.

Geochemical Investigations toward a Groundwater Compliance Action Plan at the Moab UMTRA Project Site

Lisa Burgess, Geosyntec Consultants, USA
Keaton Belli, Geosyntec Consultants, USA
Chelsea Bokman, Geosyntec Consultants, USA
Jennifer Nyman, Geosyntec Consultants, USA
Liz Moran, Department of Energy Office of Environmental Management, USA
Ken Pill, North Wind Portage, USA

Abstract

A geochemical investigation was performed to support the development of a Groundwater Compliance Action Plan and the selection of a groundwater remedy for the United States Department of Energy Moab Uranium Mill Tailings Remedial Action (UMTRA) Project Site (Site). The objectives of the investigation were to identify sources of ammonia and uranium to groundwater and associated biogeochemical processes that contribute to natural attenuation of these contaminants. The investigation included soil and groundwater sampling and analysis, geochemical modeling, and laboratory column and batch reactor testing.

Groundwater redox conditions across the Site were found to be heterogenous and ranged from oxidizing to strongly reducing, resulting in attenuation of uranium via adsorption, association with iron and manganese (oxy)hydroxides, and precipitation of reduced mineral phases. Batch reactors provided evidence of biological ammonia oxidation (nitrification), rates of which are likely variable across the ammonia plume. A batch pore flushing model was used to estimate the time to achieve groundwater standards using column test data. Batch pore flushing model results indicated that the concentration target for the ammonia plume may be reached within one hundred years of natural flushing, while the uranium plume may require greater than one hundred years to reach concentration targets. Results of this investigation will support the development of a three-dimensional numerical groundwater fate and transport model that accounts for these geochemical processes and will improve the accuracy of remedial timeframe estimates.

Introduction

The Moab Uranium Mill Tailings Remedial Action (UMTRA) Project Site (Site), located in Moab, Utah, is a former uranium-ore processing facility where production ended in 1984. The United States Department of Energy Office of Environmental Management (DOE-EM) is responsible for remediating the site to meet 40 Code of Federal Regulations (CFR) 192 standards promulgated by the United States Environmental Protection Agency under the authority of the Nuclear Regulatory Commission (NRC). Tailings from the former mill were stored in an unlined impoundment (tailings pile), totaling 16 million tons of waste material. Surface cleanup has been ongoing since 2009 and consists of removal and transport of tailings via rail to an off-site disposal facility, with an estimated completion date around 2029.

Gravity-driven migration of tailings fluids and recharge through the tailings pile and former on-site ore storage areas in the northeastern part of the site led to contamination of site soil and groundwater. The primary contaminants of concern are ammonia, which was present in fluids used in the milling process (DOE, 2003), and uranium. An interim groundwater remedy is currently in place that utilizes a system of extraction and injection wells to prevent discharge of contaminated groundwater into the nearby Colorado River. Once surface cleanup concludes and the tailings pile is removed, a formal groundwater remedy must be selected and documented in a Groundwater Compliance Action Plan (GCAP). Under Title 1 of the Uranium Mill Tailings Radiation Control Act, natural flushing (i.e., monitored natural attenuation), may be selected as the groundwater remedy if it can be demonstrated that the remedy will achieve groundwater standards within one hundred years. The 40 CFR 192 groundwater standard for uranium is 44 micrograms per liter (µg/L), and the target groundwater concentration of ammonia based on adverse effects on local fish species is 3 milligrams per liter (mg/L).

A collaboration with Geosyntec Consultants, Inc. (Geosyntec), the Moab UMTRA Project team, the DOE Office of Legacy Management, the DOE-EM, and the Network of National Laboratories for Environmental Management and Stewardship was held in 2022 with the goal of generating actionable recommendations to develop a GCAP for the Site. The primary recommendation was development of a groundwater fate and transport model to predict the remedial timeframe under various groundwater remedies. This paper presents the results of soil and groundwater sampling, geochemical modeling, and laboratory column and batch reactor testing that will be used to parameterize a numerical model for estimating the remedial timeframe under various scenarios, including natural flushing.

Soil and groundwater collection

Soil and groundwater samples were collected from six temporary boreholes that were advanced using a track-mounted sonic rig. Borehole locations were identified based on existing data to target areas with

variable uranium and ammonia concentrations (Figure 1). Freshwater in the unconfined alluvial aquifer is underlain by a brine zone that varies seasonally in elevation but is often encountered at approximately 55 feet below ground surface (bgs) (DOE, 2003). Soil and groundwater collection targeted the vadose and freshwater saturated zones. At the Site, total dissolved solids (TDS) concentrations below 35,000 mg/L are considered to be in the freshwater zone.

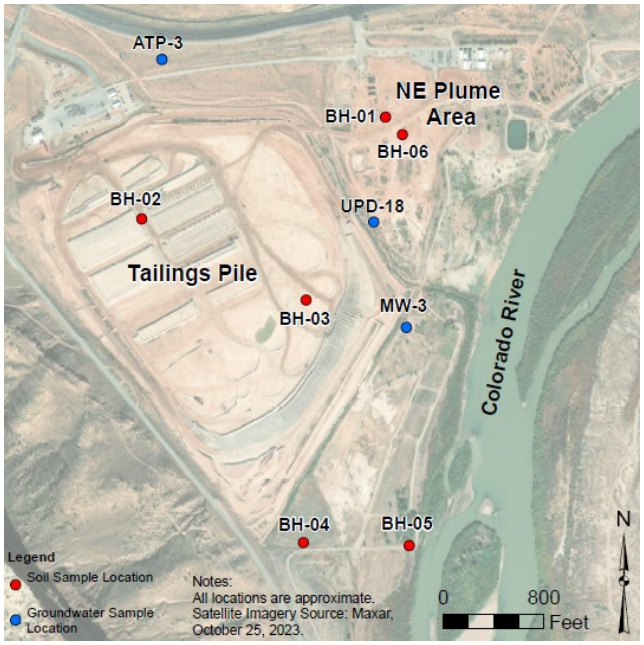


Figure 1: Site layout and soil and groundwater sampling locations

Soil collection and analysis

Soil was inspected, logged, and sampled as boreholes were advanced to a maximum of 60 feet bgs. Soil samples were collected at four depths within each boring to target the top and bottom of the vadose and freshwater saturated zones. Soil samples were shipped to GEL Laboratories of Charleston, South Carolina, for analytical characterization and Hazen Research of Golden, Colorado, for solid-phase extraction analysis and column testing.

Solid-phase extractions were performed on vadose and saturated zone soil samples to quantify the fraction of solid-phase uranium that has the potential to mobilize to groundwater. The solid-phase extractions consisted of sequentially exposing soil samples to four extraction solutions, each of which targeted a specific fraction of solid-associated uranium. The four-step sequential extraction procedure was based on the Tessier extraction method for trace metals (Tessier et al., 1979) and modified to target solid-associated uranium species based on the geochemical behavior of uranium (Salome et al., 2017). Step 1 targeted weakly sorbed/exchanged uranium; Step 2 targeted strongly sorbed/weak acid extractable uranium associated with carbonate minerals; Step 3 targeted uranium associated with iron and manganese

(oxy)hydroxide minerals; and Step 4 targeted uranium phosphate minerals and recalcitrant fractions. Reduced uranium minerals were likely extracted during Step 1 because the solution was oxic.

Groundwater collection and analysis

One grab groundwater sample was collected from the upper freshwater saturated zone at each borehole for analytical characterization. Additional bulk groundwater samples were collected from three existing monitoring wells for column and batch reactor testing (Figure 1). Bulk groundwater collected from ATP-3, located upgradient of the tailings pile, was used as influent for the column tests. Bulk groundwater samples from UPD-18 and MW-3, located downgradient of the tailings pile, were used for batch reactor testing. Groundwater samples were collected using a bladder pump or disposable bailer and shipped to GEL Laboratories of Charleston, South Carolina, for analytical characterization and Hazen Research of Golden, Colorado, for batch reactor testing.

Soil analytical results

Soil uranium concentrations ranged from 0.580 milligrams per kilogram (mg/kg) to 9.80 mg/kg and were moderately to strongly correlated with iron and manganese at some locations (r^2=0.57 to 0.93 and 0.52 to 0.79, respectively) when soil results were analyzed at individual borings, consistent with sequestration of uranium via adsorption to, or co-precipitation within, iron and manganese (oxy)hydroxide minerals. Uranium concentrations in soil samples were also strongly correlated to soil phosphorus concentrations at some borings (r^2=0.66 to 0.98). Geochemical modeling results indicate that uranyl phosphate minerals are undersaturated in Site groundwater (discussed below), and therefore, strong correlations between uranium and phosphorus are more likely to reflect the affinity of the phosphate and uranyl ions for adsorption onto iron (oxy)hydroxide minerals rather than evidence of precipitation of uranyl phosphate minerals.

Solid-phase sequential extraction results indicate that approximately 30% of solid-phase uranium was weakly adsorbed or reduced (Step 1); 30% of uranium was strongly adsorbed (Step 2); 25% of uranium was associated with iron and manganese (oxy)hydroxides (Step 3); and 15% of uranium was recalcitrant (Step 4). The percentage of uranium in the adsorbed fraction (approximately 60% in Steps 1 and 2 combined) was similar between the vadose and saturated zones. This fraction of uranium could mobilize via desorption during recharge through the vadose zone or inflow of background groundwater through the saturated zone. Iron- and manganese-associated uranium (Step 3) is less likely to mobilize to groundwater than adsorbed uranium because it would require dissolution of iron and manganese (oxy)hydroxides, which typically occurs under reducing conditions. Uranium is typically less mobile under reducing conditions because it tends to precipitate as insoluble reduced uranium minerals, such as uraninite. The fraction of uranium extracted during Step 4 (recalcitrant) is unlikely to mobilize to groundwater under current and

future site conditions. The average percentage of potentially mobile uranium (Steps 1 through 3) across all samples was 86%, with averages for individual boreholes ranging from 44% to 100%.

Soil ammonia concentrations at the Site ranged from approximately 1 mg/kg to 300 mg/kg. On average, the highest soil ammonia concentrations were beneath and downgradient of the tailings pile (BH-03, -04, and -05), consistent with the tailings pile as the primary source of ammonia to soil and groundwater.

Groundwater analytical results

TDS concentrations of groundwater samples ranged from approximately 1,000 to 31,200 mg/L and were less than 35,000 mg/L, confirming that samples were collected from the freshwater zone. Sodium and chloride were the most abundant cation and anion, respectively. Groundwater pH was circumneutral, ranging from 7.03 to 7.96. Dissolved oxygen (DO), oxidation-reduction potential (ORP), and redox indicator species, including nitrate/nitrite, dissolved iron, dissolved manganese, and sulfate, indicated that redox conditions varied across the Site from oxidizing to strongly reducing. Oxidizing conditions were observed at BH-04, ATP-3, UPD-18, and MW-3. Reducing conditions were observed in the northeastern plume area of the Site (BH-01 and BH-06) and at BH-03 and BH-05. Low concentrations of dissolved iron and sulfate at BH-01 and BH-06, combined with the other indicators of reducing conditions, suggest that sulfate reduction and formation of iron sulfide minerals were likely occurring at these locations.

Phosphate was measured in groundwater samples due to its importance for sequestering uranium as uranium-phosphate minerals. Phosphate concentrations were not detected in groundwater samples above the reporting limits (0.400 to 10.0 mg/L). Total organic carbon concentrations ranged from 1.85 to 17.9 mg/L, suggesting that sufficient organic carbon is available to support microbial transformations of uranium and ammonia (e.g., nitrification of ammonia, bioreduction of uranium) where redox conditions are suitable for those processes to occur. Groundwater uranium concentrations ranged from 3.57 to 3,480 µg/L and were not proportional to soil uranium concentrations, consistent with results of past site investigations (DOE, 2012) and indicating that geochemical processes besides adsorption are likely contributing to uranium sequestration in soil. Boring locations with the highest groundwater uranium concentrations also had the most oxidizing conditions. In contrast, borings with the lowest groundwater uranium concentrations had the most reducing geochemical conditions.

Precipitation of uranium and ammonia minerals

The Geochemist's Workbench® (GWB®) software package with the Minteq thermodynamic database (thermo_minteq.dat) was used to evaluate the likelihood of uranium and ammonia mineral precipitation in the freshwater saturated zone. Uranium and ammonia minerals were undersaturated in the groundwater samples, suggesting their formation is unlikely. To further evaluate the precipitation of uranium and

ammonia minerals, solubility diagrams were generated in GWB®. Groundwater uranium concentrations were less than the solubility of rutherfordine, UO_2OH_2 (beta), and schoepite, the least soluble uranyl minerals under Site conditions, indicating that formation of these phases is unlikely. The high ionic strength of Site groundwater increases mineral solubility and likely prevents precipitation of these phases. Although phosphate was not detected above the laboratory reporting limit in the groundwater samples, the impact of phosphate on uranium mineral saturation was evaluated. Groundwater uranium concentrations were less than the solubility of uramphite, Na-autunite, and K-autunite, the most insoluble uranyl phosphate minerals under site conditions, when phosphate concentrations were equal to the laboratory reporting limits (0.4 to 10 mg/L), indicating the formation of these phases in Site soil is unlikely.

Groundwater samples were plotted on a Pourbaix diagram (redox potential versus pH) of uranium speciation generated in GWB® using the groundwater composition at BH-02 to evaluate the potential for precipitation of reduced uranium minerals (Figure 2). Locations with strongly reducing conditions (BH-01, BH-03, BH-05, and BH-06) plotted within or near the stability field of uraninite, indicating that geochemical conditions at these locations are sufficiently reducing to support uraninite formation.

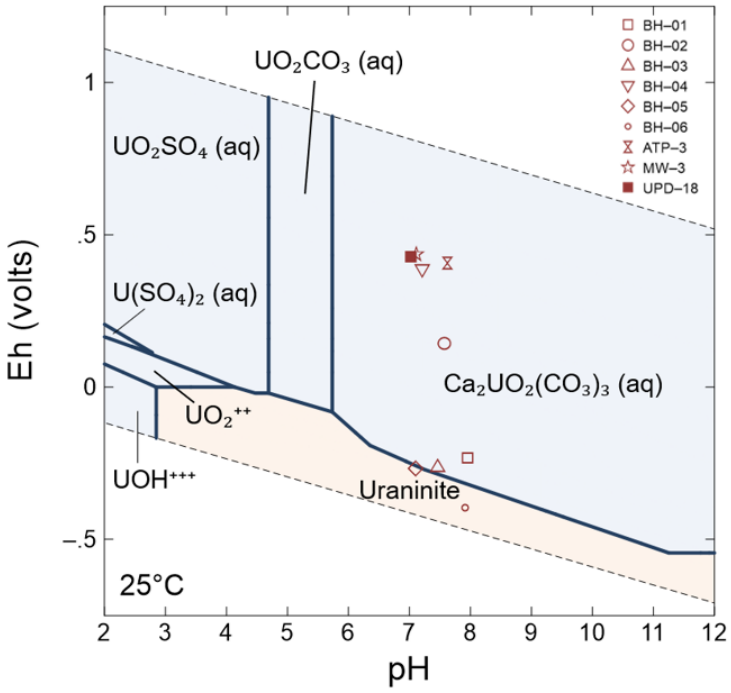


Figure 2: Uranium Pourbaix diagram calculated in GWB® using the groundwater composition at BH-02. Symbols represent groundwater samples collected during this investigation

Column testing setup and results

The primary objectives of column testing were to (1) estimate the number of pore volumes of groundwater to be flushed through Site soil to reach target groundwater concentrations of uranium and ammonia and (2)

quantify cation exchange/absorption processes for uranium and ammonia for use in a future groundwater fate and transport model. The column test included operation of 12 columns—one column for each saturated zone soil sample collected from each boring. The columns were constructed from polyvinylchloride (PVC) with dimensions of 3 inches in diameter and 20 inches in length. PVC endcaps held the soil in place within the column. Tubing was connected to each end of the column through a hole drilled in each end cap. Tubing delivered influent to the bottom of the column and collected effluent from the top end of the column.

Saturated zone soil collected from the Site served as the media within the columns. Bulk saturated soil samples were homogenized prior to loading the columns with soil. Approximately one inch of clean sand was emplaced below and above the soil within the column to ensure even distribution of the influent across the diameter of the column and to prevent soil particles from exiting the column. Columns were tapped and swirled during loading to minimize formation of void spaces and preferential pathways.

The columns were operated for at least 28 days, representing approximately 165 years of groundwater flow through the Site based on the groundwater flow rate (approximately 0.17 pore volumes per year) and the flow rate through the columns (approximately 1 pore volume per day [PV/day]). Background groundwater from ATP-3 with a low uranium concentration (3.57 µg/L uranium) served as the column influent. Influent was pumped through each column in an up-flow direction with an average flow rate of 1.4 PV/day. Column influent and effluent were periodically sampled during the column test and analyzed for pH, DO, ORP, conductivity, and dissolved (0.45 µm filtered) uranium, ammonia, and alkalinity. For five days during the test, column influent was amended with bromide (41 mg/L), and bromide was measured in the column effluent. Bromide breakthrough curves were fitted with the Domenico analytical model (Domenico 1987) to calculate the flow rate and effective pore volume of each column. Effluent from each column was collected for the duration of the column test, weighed to determine the volume, and analyzed for uranium and ammonia to calculate the mass of each that was leached from column soil.

The column influent composition remained stable throughout the duration of the column tests and was representative of background Site groundwater. Column influent pH was circumneutral, with values ranging from 7.76 to 7.94. Influent groundwater was oxidizing, indicated by high ORP (>200 mV) and DO concentrations (>9 mg/L).

Effluent pH generally ranged from 7.6 to 8.6, and effluent DO concentrations were lower than the influent concentration. Effluent ORP values were initially lower than the influent value, then increased to the influent value over the course of the column test. These results indicate that the soil within the columns is more reducing than the influent groundwater, consistent with reducing conditions observed in some areas of Site groundwater. Effluent uranium concentrations exceeded the influent concentrations at all 12 columns, consistent with leaching of solid-phase uranium from Site soil as background groundwater flushes through uranium-impacted soil. Maximum uranium effluent concentrations ranged from 13 to 340 µg/L

and were strongly correlated with concentrations of total uranium ($r^2 = 0.84$) and adsorbed (sum of Steps 1 and 2 of the sequential extraction, $r^2 = 0.73$) uranium in column soil.

Maximum effluent uranium concentrations for each column were often measured in the second or third effluent sample, suggesting the rate of uranium desorption from Site soil is kinetically limited or other geochemical processes besides desorption are involved in uranium mobilization. Column effluent uranium concentrations were less than recent groundwater uranium concentrations measured at the site (up to 7 mg/L, DOE 2023), indicating that solid-associated uranium is not the only source of uranium to groundwater. Additional sources of uranium to groundwater include tailing fluids and solid-associated uranium in the vadose zone that can mobilize during groundwater table fluctuations or precipitation events. Once the maximum effluent uranium concentration was achieved, concentrations generally declined to a steady state or below the reporting limit (1 µg/L), consistent with an initial flushing of uranium from the column soil and attenuation of uranium over time. Effluent uranium concentrations did not exceed the groundwater standard at the deeper BH-01, BH-03, and BH-06 columns and the shallow BH-04 column. Effluent uranium concentrations exceeded the 40 CFR 192 groundwater standard of 44 µg/L in the remaining 8, and effluent concentrations in 7 of those columns were below the groundwater standard by the end of the test. The effluent uranium concentration of the shallow BH-05 column remained below the groundwater standard until 21.1 pore volumes, when it increased in the final effluent sample. The delayed increase in uranium coincided with a gradual increase of ORP in the column. The number of pore volumes pumped through the columns to achieve the groundwater standard ranged from 6.3 to 34.5.

The percentage of total uranium leached from the soil within each column ranged from 4.6% to 51%, and the percentage of adsorbed uranium leached from the soil within each column (sum of Steps 1 and 2 of the sequential extraction test), ranged from 7.6% to 71%. These results are consistent with the solid-phase extraction results which demonstrated that some solid-phase uranium is unlikely to mobilize to groundwater during flushing of background groundwater through the saturated zone.

Effluent ammonia concentrations were relatively stable during the column test; however, the majority of effluent ammonia concentrations were not detected above the laboratory reporting limit (1 to 10 mg/L). Column effluent ammonia concentrations were far below recent concentrations in Site groundwater (up to around 450 mg/L, DOE 2023), indicating that tailing fluids likely contribute to elevated ammonia concentrations recently observed in Site groundwater.

Batch reactor testing setup and results

The primary objective of batch reactor testing was to evaluate whether biological degradation of ammonia (nitrification) is occurring in groundwater at the Site. The batch reactor test used groundwater collected from two monitoring wells (MW-3 and UPD-18) and included operating duplicate live reactors and one

control reactor per location. Glass bottles served as the batch reactors, and Site groundwater served as the batch reactor medium. Batch reactors were periodically sparged with air during operation so the reactors remained oxic, a requirement for nitrification. Prior to beginning the batch test, the control reactors were sterilized in a 90 °C hot water bath for 2 hours. The reactors operated for 3 weeks and were agitated throughout the test using a shaker table. Batch reactors were sampled weekly and analyzed for pH, ORP, DO, conductivity, ammonia, nitrate, and nitrite.

Strong evidence of nitrification was observed in the UPD-18 live reactors. Over the course of the test, ammonia concentrations decreased, while nitrate concentrations simultaneously increased (Figure 3). Concentrations of nitrite, a transient nitrification intermediate, fluctuated and ultimately decreased by the end of the test. Ammonia concentrations in the control reactors remained relatively stable at the initial concentration. Changes in the average nitrogen species concentrations over the course of the test confirmed stoichiometric consumption of ammonia and nitrite and production of nitrate, indicative of nitrification. Evidence of nitrification was not observed in the MW-3 live reactors; ammonia concentrations decreased slightly during the test, but nitrate concentrations remained relatively constant at the initial concentration.

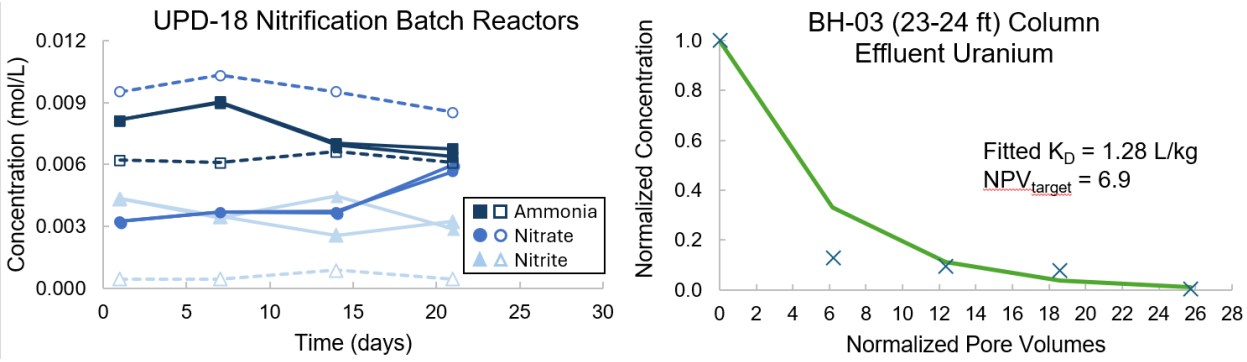


Figure 3: Left: time series of nitrogen species in duplicate live reactors (solid lines) and abiotic control reactors (dashed lines) containing groundwater from UPD-18. Right: time series of normalized effluent uranium concentrations in the BH-03 (23-24 feet bgs) column. The batch pore flushing model (green line) was fitted to the data by adjusting the value of K_d in Equation 1

Results of the batch reactor test are consistent with higher concentrations of oxidized nitrogen species (nitrate and nitrite) in the groundwater sample collected at UPD-18 (57.5 mg/L) compared to MW-3 (21.5 mg/L). These results also indicate that the degree of nitrification may vary across the ammonia plume. Although groundwater at UPD-18 and MW-3 is geochemically oxidizing with circumneutral pH and detectable concentrations of DO, nitrification was only observed at UPD-18 during the batch reactor test. Variable rates of nitrification across the Site could be due to the distribution of nitrifying bacteria in groundwater, which was not evaluated in this study.

Batch pore flushing modeling

The batch pore flushing model is an analytical model used to estimate the remediation timeframe for flushing clean water through a defined volume (Antelmi et al., 2020). Contaminant transport is assumed to be dominated by advection and linear sorption processes with negligible dispersion. For this analysis, the batch pore flushing model was first fit to the column test effluent uranium data to estimate the soil partitioning coefficient (K_d) and to calculate the number of pore volumes flushed to reach the 40 CFR 192 groundwater standard of 44 µg/L (Figure 3). Insufficient detections of ammonia in the column effluent data prevented calculation of K_d for ammonia. Next, a plume-scale batch pore flushing model was used with the average K_d for uranium derived from the column tests and a previous estimate of the K_d for ammonia (0.5 L/kg, DOE 2003) to estimate the remediation timeframe for natural flushing of uranium and ammonia.

The batch pore flushing model concentrations were calculated using Equation 1, where C is contaminant concentration at time, t; C_0 is the initial concentration, NPV is the number of pore volumes at time, t; R is the retardation factor; Q is the flowrate through the column; PV is the pore volume of column, derived from bromide tracer test; ρ_b is the bulk density of soil in column, calculated as the dry mass of soil divided by the volume of soil in the column; n_e is the effective porosity, derived from bromide tracer test; and K_d is the soil partitioning coefficient.

$$\frac{C}{C_0} = e^{\frac{-NPV}{R}} = e^{\frac{-Q*t/PV}{1+(\rho_b \times K_d/n_e)}} \quad \text{(Equation 1)}$$

C, C_0, Q, and ρ_b were measured for each column, and n_e and PV were derived from the bromide tracer test for each column. K_d is the only unknown and was varied to fit the model to the normalized measured effluent concentration data. The Excel solver tool was used to minimize the sum of the squared residuals between the measured and calculated normalized uranium concentrations by varying the values for K_d.

For columns with effluent concentrations exceeding the 40 CFR 192 groundwater uranium standard of 44 µg/L, the number of pore volumes flushed to reach the groundwater standard (NPV_{target}) was calculated using Equation 2, where R is the retardation factor, $R = 1 + \frac{\rho_b + K_d}{n_e}$, C_f is the target concentration, and C_0 is the initial concentration.

$$NPV_{target} = -R \times ln\left(\frac{C_f}{C_0}\right) \quad \text{(Equation 2)}$$

The fitted K_d values for each column ranged from 0.99 to 7.45 liters per kilogram (L/kg), with an average of 3.62 L/kg. The range for the six columns with effluent concentrations greater than the uranium groundwater standard is from 0.99 to 2.75 L/kg, with an average K_d of 1.71 L/kg. The average K_d for the columns with lower effluent concentrations is 6.14 L/kg. This suggests that sorption is nonlinear over the entire concentration range at the Site, and at lower concentrations (below the 40 CFR 192 groundwater standard) uranium may be more tightly sorbed to solids. This observation also indicates that the estimated

K_d of 1.71 L/kg may be representative of the low concentration plume area (average concentration of 0.29 mg/L), but the column test results may not be representative of the sorption coefficient for the high concentration plume area (average concentration of 1.8 mg/L). Based on the batch pore flushing model, the calculated number of pore volumes to achieve the 40 CFR 192 groundwater standard in each column ranged from 5.2 to 19.8 with an average of 14.3 pore volumes.

The plume-scale batch pore flushing model used the same equations as described above, but the parameters were based on the groundwater plume. For example, one pore volume is defined by the plume extent, and the flow rate is the estimated natural flushing rate through the plume (Antelmi et al., 2020). The plume-scale model results using parameters derived from the column tests show that proposed groundwater standards may be reached under natural flushing conditions within one hundred years for the ammonia plume, but longer than one hundred years may be required for the uranium plume. The plume-scale model indicates the proposed groundwater standard of 3 mg/L for ammonia may be reached in 50 years for expected natural flushing flow rates (140 gallons per minute [gpm]) and 58 years for the lowest estimated natural flushing flow rate (70 gpm). These estimates assume that ammonia biodegradation is occurring uniformly across the plume at a consistent average rate. The plume-scale batch pore flushing model indicates that achieving the target cleanup concentration for uranium may require more than one hundred years under natural flushing conditions. For expected natural flushing flow rates (190 gpm) through the high concentration portion of the plume, the estimated predicted remediation timeframe is 180 years. The estimated predicted remediation timeframe for the low concentration portion of the plume is at least 110 years. However, because of the complex processes associated with uranium transport, there is high uncertainty in the plume-scale batch pore flushing model estimates for uranium. The batch pore flushing model does not account for other relevant geochemical processes that have been identified in this investigation, including variable redox conditions, mineral precipitation, and nonlinear sorption. The model also does not account for heterogeneous hydrogeological conditions at the Site.

Conclusion

Groundwater redox conditions across the Site were heterogenous and ranged from oxidizing to strongly reducing. The primary mechanism of uranium sequestration at sampling locations with oxidizing geochemical conditions was adsorption to iron and manganese (oxy)hydroxides. Co-precipitation of uranium with metal (oxy)hydroxides was a secondary mechanism of sequestration. Precipitation of oxidized uranium minerals (e.g., uranyl phosphates) at the sampling locations is unlikely due to the high ionic strength and low phosphate concentrations of Site groundwater. At sampling locations with reducing geochemical conditions, the dominant mechanisms of uranium sequestration included adsorption of uranium to iron and manganese (oxy)hydroxides, co-precipitation of uranium with metal (oxy)hydroxides,

and precipitation of reduced uranium minerals (e.g., uraninite). On average, 63% of solid-phase uranium was adsorbed or reduced, 23% of solid-phase uranium was associated with iron and manganese (oxy)hydroxides, and 14% of solid-phase uranium was recalcitrant and unlikely to mobilize to groundwater under naturally occurring geochemical conditions. The primary mechanism of ammonia sequestration at sampling locations with oxidizing and reducing geochemical conditions was adsorption/cation exchange. Evidence of nitrification was observed in one reactor, and therefore, nitrification may be contributing to attenuation of ammonia in groundwater, but at variable rates within the groundwater ammonia plume.

Based on the batch pore flushing model fits of the column testing results, the calculated number of pore volumes to achieve the groundwater uranium standard was between 5 and 20 pore volumes (with an average of 14 pore volumes). The updated plume-scale batch pore flushing model results show that groundwater standards may be achieved under natural flushing conditions within one hundred years for the ammonia plume, but longer than one hundred years may be needed for the uranium plume. The plume-scale batch pore flushing model does not account for the complex uranium geochemical processes identified during this investigation or for heterogeneous hydrogeological conditions. Results of this investigation support development of a three-dimensional numerical groundwater fate and transport model that accounts for these geochemical processes in order to improve the accuracy of remedial timeframe estimates.

References

Antelmi, M., Renoldi, F. and Alberti, L. 2020. Analytical and numerical methods for a preliminary assessment of the remediation time of pump and treat systems. *Water* 12(10): 2850.

DOE. 2012. *Moab UMTRA Project Northeastern Uranium Plume Investigation Report*. DOE-EM/GJTAC2020. January.

DOE. 2023. *Moab UMTRA Groundwater and Surface Water Monitoring Report January through June 2023*, Revision 0. DOE-EM/GJRAC3106. October.

Domenico, P.A. 1987. An analytical model for multidimensional transport of decaying contaminant species. *Journal of Hydrology* 91: 49–58.

Salome, K.R., Beazley, M.J., Webb, S.M., Sobecky, P.A. and Taillefert, M. 2017. Biomineralization of U(VI) phosphate promoted by microbially-mediated phytate hydrolysis in contaminated soils. *Geochim. et Cosmochim. Acta*. 197: 27–42.

Tessier, A., Campbell, P.G.C. and Bisson, M. 1979. Sequential extraction procedure for the speciation of particulate trace metals. *Anal. Chem*. 51: 844–851.

United States Department of Energy (DOE). 2003. *Site observational work plan for the Moab, Utah, Site*. GJO-2003-424-TAC. December.

Critical Seepage Analyses for Stability of Tailings Dams

Dobroslav Znidarcic, University of Colorado, USA
Gordan Gjerapic, University of Colorado, USA
David Rees Gillette, Independent Consultant, USA

Abstract

The instability and catastrophic failures of tailings dams are caused by the presence of water, irrespective of the triggering mechanism. The most significant sources of water in tailings impoundments are water inflows brought into the impoundment during the deposition process and precipitation inflows (rain and snowmelt). Other sources of water such as inflows from different mine facilities, run-on, and potential inflows from antecedent seeps are typically less significant during standard operating conditions but may play a significant role during extreme events. Upon deposition, the pore water seeps through the impoundment and the tailings dam under the hydraulic gradients induced by gravity and any additional loading. While seepage analyses are often conducted for the purpose of calculating water balance, especially during filling operations, the seepage impact on the stability of tailings dams is frequently evaluated using only simplified methods, and without paying adequate attention to details of the underlying flow mechanisms.

This paper explores the effects of anisotropy and the presence of unsaturated zones on the stability of a tailings dam. It demonstrates that the commonly employed assumption of a linear piezometric line may lead to underestimated pore pressures on critical failure surfaces, especially in the zone near the downstream slope of the dam, which is essential for maintaining dam stability. In addition to the steady state analyses, the transient process of pore water infiltration into the previously unsaturated ("dry") regions of the tailings dam is modeled to evaluate the time required for the seepage from the pool area of the impoundment to reach the downstream slope of the dam.

The results highlight the need for realistic, problem-specific seepage analyses to be carried out throughout different stages of the impoundment life, including deposition, and closure and post-closure, to provide a realistic estimate of the tailings dam performance.

Introduction

Catastrophic failures of tailings dams are almost always facilitated or caused by the presence of water within

the tailings. The water is brought to the impoundment during deposition, with rainfall and snowmelt, and from run-on and any seeps existing in and around the impoundment. The recent paper by Reid and Fourie (2024) summarizes the results of a tailings slope stability comparative design ("round robin") exercise that focused on changes in the slope stability as the linear phreatic surface moves from its initial location (with the gradient/inclination of 9.2H:1V) to the ultimate inclination of 3H:1V parallel to the downstream slope. For simplicity, the "phreatic line" and the "piezometric line" are used synonymously in this paper. In geotechnical literature, it is customary to use the "phreatic line" as a "top" flow line and/or boundary between saturated and unsaturated zones, while the "piezometric line" is commonly used to denote the pressure head on the failure surface. The focus of the round robin exercise by Reid and Fourie (2024) was the selection of shear strength parameters for the tailings and the method of stability analysis. The selected linear piezometric lines in the exercise were consistent with the commonly employed approach in engineering practice; however, this linearization approach often fails to capture impacts of various seepage scenarios that are critical for the stability of tailings dams (see for example Gjerapic and Znidarcic, 2020 and Gjerapic et al., 2022). Hence, the focus of this paper is to demonstrate the importance of seepage analyses and the associated hydraulic conditions in evaluating critical scenarios for the stability of tailings dams.

Tailings densities and strength parameters used in this paper were selected based on the range reported by Reid and Fourie (2024) in their round robin stability exercise, while considering tailings properties reported for the recent failures of tailings storage facilities, see Morgenstern et al. (2016), Jefferies et al. (2019) and Robertson et al. (2019). The hypothetical tailings dam geometry from Reid and Fourie (2024) and the adopted parameters were chosen to correspond to the factor of safety (FoS) of 1.5 for the initial conditions in Figure 1. In addition to this baseline scenario, a set of seepage scenarios was chosen to demonstrate that the risks to tailings stability need to be evaluated by considering both geomechanical and hydraulic conditions, while bearing in mind that a careful consideration of seepage conditions may prove to be sufficient to indicate potential instability of the tailings dam, sometimes even without the need to conduct the corresponding stability analyses.

Figure 1 presents the selected hypothetical geometry for the analyses with three potential failure surfaces that are selected in this paper to evaluate the change in the FoS as the seepage conditions change. The deep-seated failure surface S1 in Figure 1 is the critical failure surface for the initial piezometric line when the shear strength below the piezometric line is given by $s_u/\sigma'_v=0.25$ and the shear strength above the line is given by $\phi'=36°$. The FoS of 1.5 for these baseline conditions indicates that the tailings dam is considered stable based on standards in current engineering practice. The other two shallower failure surfaces are selected to evaluate seepage effects on the general stability of the tailings dam (S2) and the toe stability (S3) as the seepage approaches the downstream slope of the dam.

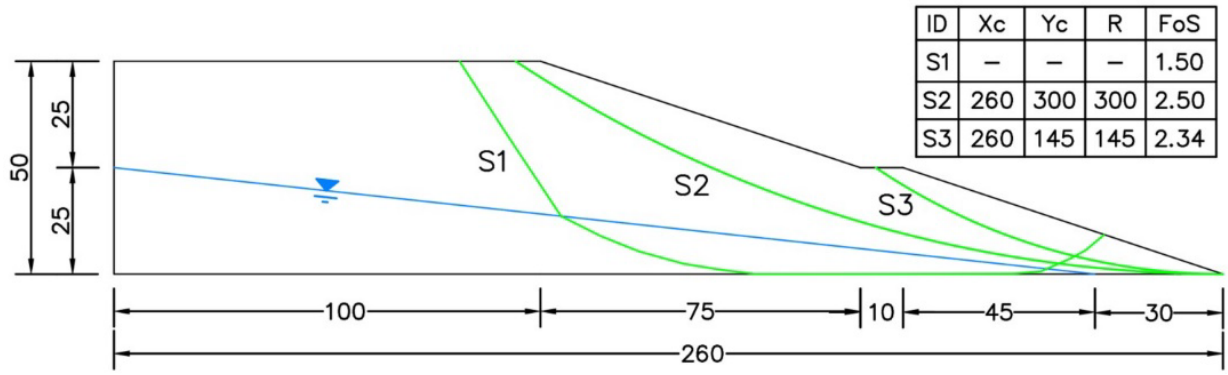


Figure 1: Geometry selected for the analyses with the initial linear piezometric line and the potential failure surfaces (based on Reid and Fourie, 2024)

A selected set of seepage scenarios in this paper was chosen to demonstrate flow conditions that could lead to compromised stability of tailings dams while neglecting a variety of other factors (e.g., the effects of earthquakes or depositional loading). The selected seepage scenarios explore stability impacts of the hydraulic conductivity anisotropy and the effects of re-saturation of tailings material along the wetting path under transient flow conditions. The effects of external seeps (e.g., perennial or seasonal inflows from antecedent sources) and rainwater/snow melt infiltration are not considered explicitly; however, these effects always warrant careful consideration when evaluating the stability of tailings dams.

Seepage scenarios

The seepage analyses in this paper were conducted using Slide2 (Rocscience, 2024) software because its groundwater module allows for the treatment of both saturated and unsaturated conditions, as well as the treatment of steady state and transient flow (e.g., the finite element groundwater module in Slide 2 can be used to model infiltration into initially unsaturated tailings zones). For all seepage analyses, it is assumed that the hypothetical tailings dam is resting on an impervious base, with the exception of the last 30 m at the downstream toe where a drainage layer is assumed, and that the pressure head is set to zero along that part of the bottom boundary (see Figure 1). On the left-hand side, 260 m behind the toe, a constant head boundary is assumed with two water levels and the hydrostatic pressure head distributions below the water levels. The top and downstream slope are assumed to be impervious (no water infiltration) except when the phreatic line reaches the boundaries, a zero-pressure head is imposed to allow for the seeping water to exit the domain.

Figures 2 presents the total head distributions and the associated phreatic surface for isotropic conditions (K_h=K_v) assuming the maximum water elevation of 25 m at the left-hand boundary.

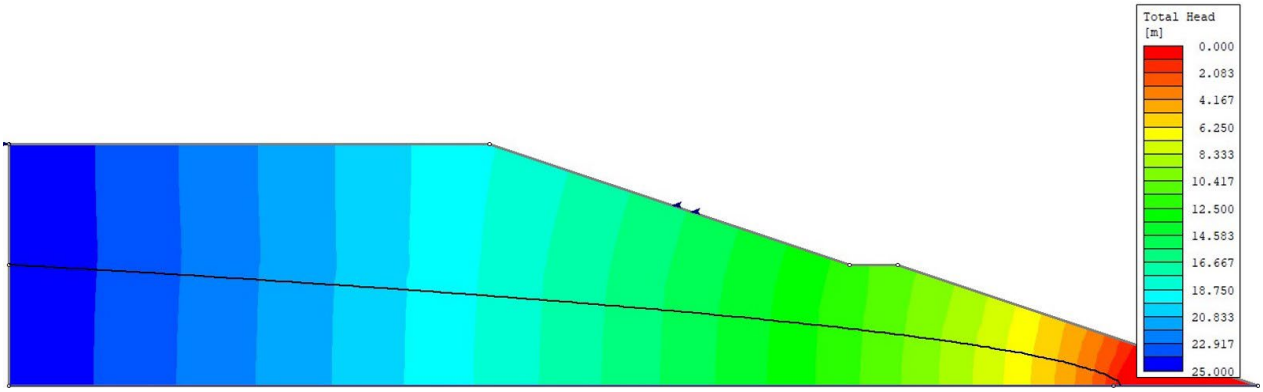


Figure 2: Total head distribution for isotropic conditions and maximum water elevation of 25 m at left boundary (base of tailings at elevation of 0.0 m)

It is noted that the phreatic lines (top flow line) in Figure 2 are substantially higher than the assumed liner piezometric line shown in Figure 1 at locations towards the embankment toe. For the upstream water level at 50 m shown in Figure 3, the seeping water reaches the downstream slope at an elevation of 25 m. This condition is considered critical in terms of factors of safety and the associated stability of the tailings dam.

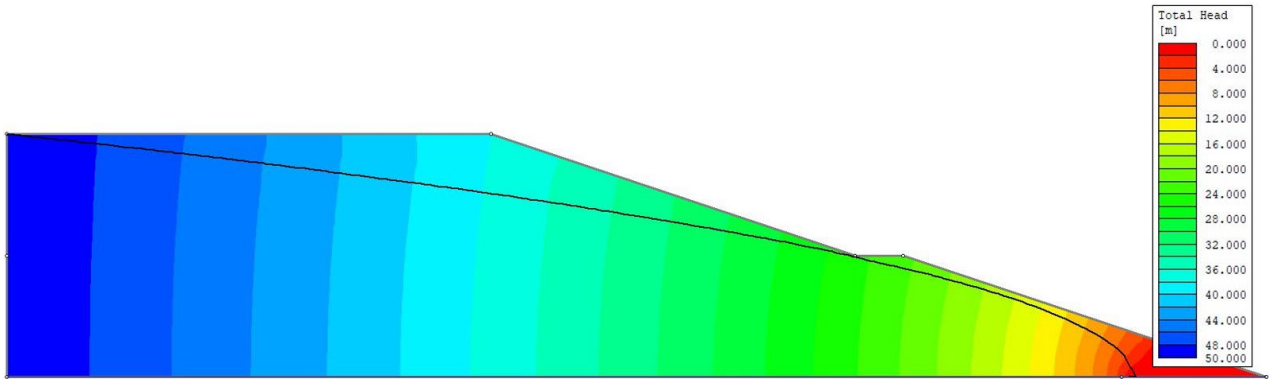


Figure 3: Total head distribution for isotropic conditions and maximum water elevation of 50 m at left boundary (base of tailings at elevation of 0.0 m)

Figures 4 and 5 present the results for the analyses where the hydraulic conductivity anisotropy ratio is considered (i.e., K_h/K_v denotes the ratio between horizonal and vertical hydraulic conductivities). Three cases are considered: 1) isotropic conditions with $K_h/K_v = 1$; 2) $K_h/K_v = 10$; and 3) $K_h/K_v = 100$. Note that the adopted anisotropy ratios do not necessarily represent the inherent anisotropy for a given tailings material (at a scale of millimeters or centimeters), but reflect the possible layering in the system due to segregation and other effects of material sorting during deposition (at a scale of meters).

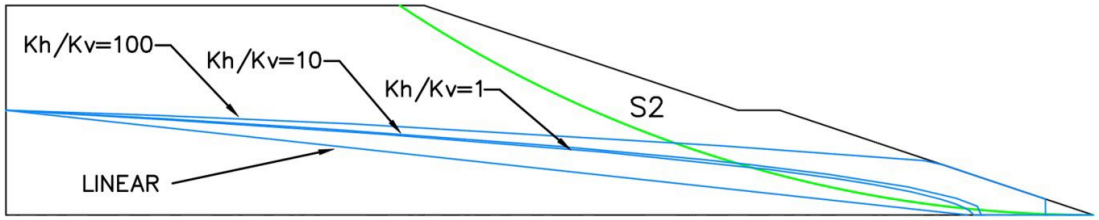


Figure 4: Comparison of steady-state phreatic lines for Kh/Kv = 1, 10 and 100 and maximum water elevation (total head) of 25 m at left boundary

For clarity, only the phreatic lines determined in these analyses are presented in Figure 4 and 5. Each of these lines is then used as a piezometric line for the FoS calculations. Figures 4 and 5 demonstrate that the tailings field-scale anisotropy may lead to increased elevation of the phreatic line, cause the seepage to saturate downstream zone of the dam, and eventually exit the toe of the dam. Any uncontrolled seepage out of the slope at the toe of the dam compromises its stability and may be an indicator of an imminent (large-scale) catastrophic failure, or may lead to gradual deterioration of stability conditions, e.g., a progressive failure due to washing out of the material caused by the high exit gradients.

Results in Figure 4 and Figure 5 indicate that, as the anisotropy ratio increases from 1 (isotropic) to 100, the seepage pattern becomes dominated by the horizontal flow. In such cases the presence of any horizontal drainage layers may become ineffective because these layers cannot protect the downstream slope from destabilizing effects of the seeping water exiting the slope. In such cases a positive vertical cutoff, in the form of a chimney drain or a massive, drained buttress at the down-stream slope, could prevent the seepage induced failure of a dam.

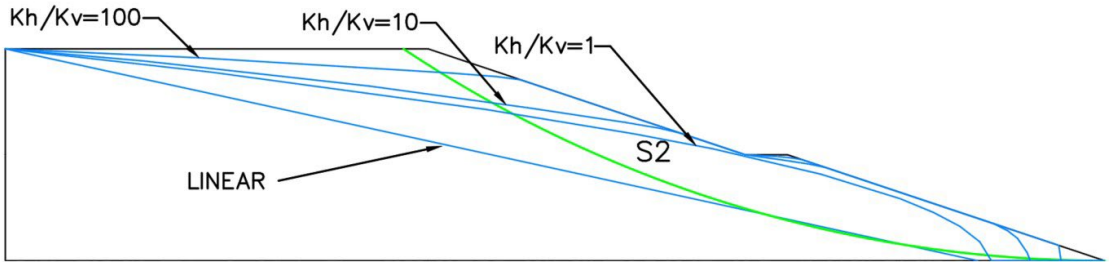


Figure 5: Comparison of steady-state phreatic lines for Kh/Kv = 1, 10 and 100 and maximum water elevation (total head) of 50 m at left boundary

Figure 6 presents the results of transient infiltration analysis, assuming an increase in the water levels at the upstream (left-hand) boundary from 25 to 50 m (the tailings base elevation is 0.0 m). In this analysis, we assumed that a steady state seepage condition has been established for the maximum water level at 25 m and then the water level is rapidly increased to a new elevation of 50 m. Initially, the area above the phreatic line at 25 m is unsaturated with pore pressures corresponding to suctions consistent with the initial steady state conditions.

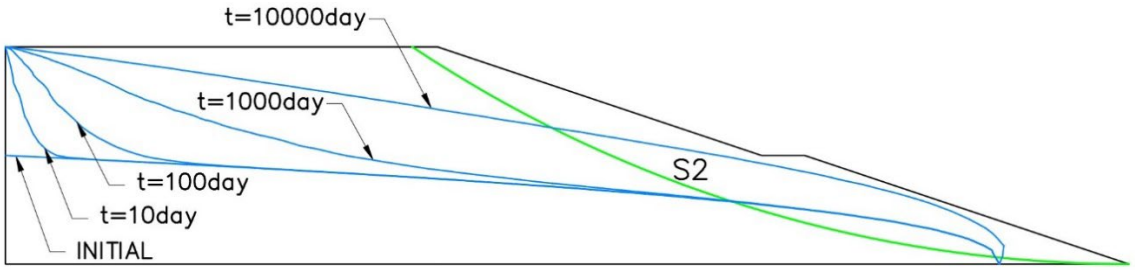


Figure 6: Transient seepage for the total head change from 25 to 50 m at left boundary

The governing unsaturated flow relationships used for the transient flow calculations are presented in Figures 7 and 8. These relationships from Hwang (1999) are typical for the fine-grained non-plastic or low plasticity soils with a clay content of less than about 15 percent. The soil water characteristic curves (SWCCs) for both drying and wetting conditions are displayed in Figure 7.

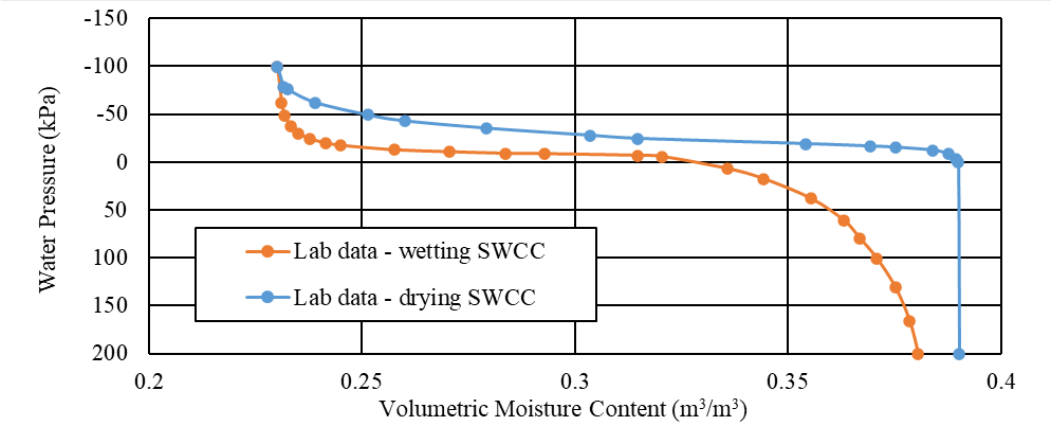


Figure 7: SWCC assumed for seepage analyses (after Hwang, 1999)

The unsaturated hydraulic conductivity relationships are shown in Figure 8.

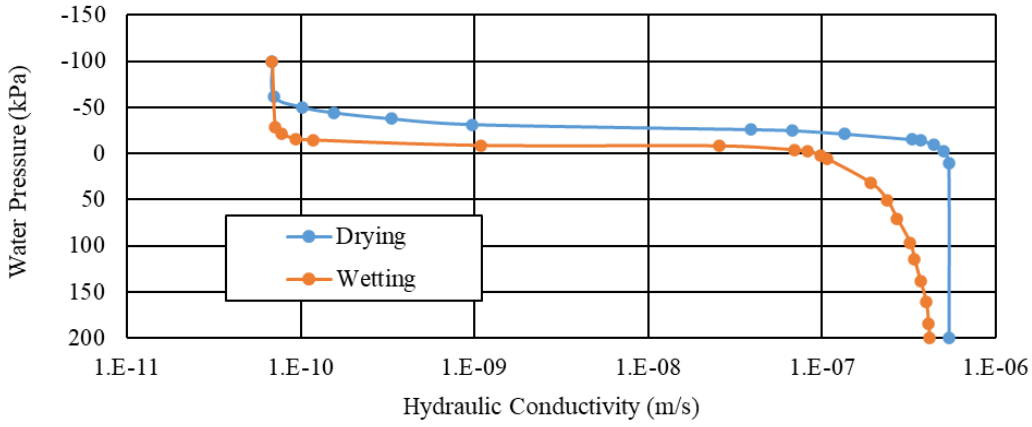


Figure 8: Unsaturated hydraulic conductivity for transient seepage analyses (after Hwang, 1999)

The results in Figure 6 illustrate the migration of the phreatic line towards the downstream slope which, initially, does not affect the tailings dam stability. However, as time progresses, the infiltrating front reaches the potential failure surface, reducing the dam stability to critical levels. The results in Figure 6 were determined for the wetting conditions with the hydraulic properties presented in Figures 7 and 8, that is, assuming that the tailings are initially dry. The actual propagation of the infiltration front, however, depends on the antecedent moisture conditions. If the pre-existing conditions are characterized by moisture contents higher than the initially dry state for the wetting curves, the hydraulic properties for the transient simulations may be in between the wetting and the drying relationships presented in Figures 7 and 8. In order to approximately account for the varying initial conditions, the transient analysis is repeated using the drying relationships presented in Figures 7 and 8. Thus, the two sets of properties will bracket the possible solutions and give a better sense of how quickly the saturation front might reach the downstream slope of the dam.

In addition, a change in water management practices or climate conditions is also likely to affect the migration of the infiltration front towards the downstream slope. Figure 9 presents the results for the same conditions as in Figure 6, but assuming that the top boundary is inundated from rain infiltration from the left boundary (x=0) to the crest of downstream slope (x=100 m). Substantially shorter saturation time is noted by comparing the phreatic lines at equal times in Figures 6 and 9.

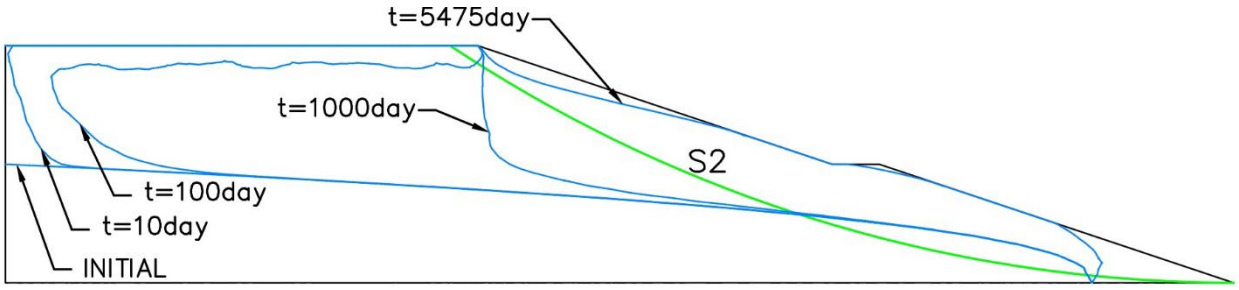


Figure 9: Transient seepage for the total head change from 25 to 50 m at left boundary and water infiltration on the top boundary from x=0 to x=100 m

The time for the infiltration front to reach the downstream slope, i.e., the time to initiate TSF failure, was determined for a subset of seepage calculations, with the results summarized in Table 1. These calculations were conducted to investigate the effects of initial moisture conditions and potential stability impacts due to changes in climate conditions or water management practices. Conducted seepage analyses utilize “Unknown” boundaries, where Slide2 seeks the elevation of the phreatic surface (location of zero pore-water pressure), and are referred to as “Open Head” boundaries or “Review Nodes” in some other programs (these nodes are subjected to seepage face condition where the total head is not able to exceed the elevation head). For case scenarios 12.1 and 12.2, the entire length of the surface boundary is defined

in this way. For case scenarios 12.3 and 12.4, only the portion between x=100 and x=260 m is defined that way, with zero pressure imposed at the top of the tailings from x=0 to x=100 m.

Table 1: Transient scenarios and estimated time to initiate TSF failure

Case ID	Surface boundary	Hydraulic parameters	Time to initiate TSF failure (year)
12.1	Unknown/seepage face (x=0-260)	Wetting	27
12.2	Unknown/seepage face (x=0-260)	Drying	12
12.3	Zero pressure (x=0-100), unknown (x=100-260)	Wetting	15
12.4	Zero pressure (x=0-100), unknown (x=100-260)	Drying	1.6

The results in Table 1 indicate that the scenarios exhibiting higher initial moisture contents and larger infiltration along surface boundaries will exhibit less favorable seepage conditions and shorter times before triggering failure conditions. For Cases 12.3 and 12.4, wetting by rainfall is assumed to result in zero pore-water pressures at the top of the TSF, resulting in the loss of suction with depth. For these scenarios, the upper parts of the TSF, which were previously characterized by negative pore pressures and low permeabilities, are now more permeable and are increasing the rate of infiltration towards the embankment toe. Therefore, depending on the antecedent moisture and boundary conditions, the TSF failure may be triggered after less than a couple of years (Case 12.4) or after several decades (Case 12.1) assuming that similar changes in the seepage conditions are imposed.

It should be noted that all steady-state (non-transient) seepage scenarios assume no external source of water, such as rainfall or snow melt, along the surface (top) boundaries. The presence of such external sources of water will lead to further increase in pore water pressure and will further compromise the dam stability. In any seepage and stability analyses for an actual project, such effects must be included based on the site-specific conditions.

Slope stability analyses

The change in the factor of safety for the various seepage scenarios and for the two selected potential failure surfaces (the first one considering a large-scale/global failure and the second one considering the toe stability) is evaluated by two strength approaches. The first approach, often referred to as the total stress or undrained shear strength analysis, assumes that the material below the phreatic lines is saturated and the shear strength for this material is given by $s_u/\sigma'_v=0.25$. In the second approach, often referred to as the effective stress analysis, the effective friction angle of 36 degrees is assigned to both saturated and unsaturated tailings. The porewater pressures are calculated along the failure surface by multiplying the vertical distance to the phreatic line by the unit weight of water. It should be noted that the piezometric line

for each potential failure surface is different, and strictly speaking it should be obtained from the flow net by calculating the pressure head at each point along the potential failure surface. The approximation of using the phreatic line as the piezometric line for all potential failure surfaces is acceptable as long as the seepage pattern is primarily horizontal, and the equipotential lines can be approximated with vertical lines. The assumed geotechnical properties for limiting equilibrium analyses are summarized in Table 2.

Table 2: Geotechnical properties for stability analyses

Peak undrained strength ratio, s_u/σ'_v	Effective friction angle, ϕ'	Unit weight above phreatic surface	Unit weight below phreatic surface
0.25	36°	18 kN/m^3	20 kN/m^3

The two strength approaches in this study differ depending on which sources of water pressures are considered for the stability analyses. For the undrained shear strength analyses it is assumed that the developed shear induced pore pressures are consistent with stresses and deformations at or before reaching the assumed peak undrained strength conditions, i.e., the residual (steady-state) undrained strengths and the potential effects of brittleness were not considered. In the effective stress analyses any shear induced pore pressures are neglected and the calculated pore pressures along the potential failure surfaces are calculated from seepage analyses only, i.e., without considering pressures induced by the deformation of tailings. Such an approach could be justified only for cases where tailings exhibit dilative behavior and/or tailings deformations cannot result in the development of positive pore pressures.

Table 3 summarizes the results of slope stability analyses for two selected potential failure surfaces, S2 and S3 in Figure 1, using both the undrained shear strength and effective stress approaches. As expected, the undrained shear strength approach yields lower factors of safety than the effective stress approach for all analyzed scenarios because it assumes that the additional pore pressures are generated due to either anticipated or actual deformation of tailings. These shear (strain) induced pressures are added to pore pressures resulting from the existing/undeformed seepage conditions. Considering that the focus of this study is a realistic portrayal of seepage conditions, it should be noted that both approaches lead to a significant reduction in the factor of safety as the water level increases from the initial value of 25 m to 50 m and/or when taking into account the effects of anisotropy.

For general stability (S2) and the undrained shear strength analysis approach, the factor of safety reduces from the initial value of 2.5 to 1.08 as the water level increases to 50 m and the piezometric lines are assumed linear. When a more realistic seepage pattern is assumed, even under isotropic conditions, the factor of safety is reduced to FoS=1.79 for the 25 m level and to FoS=0.87 for the 50 m level. The anisotropy ratio of 100 further reduces these values to FoS=1.27 at the 25 m level and FoS=0.52 at the 50 m level. For

the same failure surface (S2), the effective stress analysis (drained) approach results in significantly higher FoS values, however, these values are dramatically reduced from the initial value of FoS=2.5 for the initial conditions, with the linear phreatic line to FoS=1.11 for the elevated water level of 50 m at the left-hand boundary and the anisotropy ratio of 100.

Table 3: Calculated factors of safety for various seepage scenarios

Case ID	Description	General Stability Failure Surface S2		Toe Stability Failure Surface S3	
		s_u/σ'_v= 0.25	ϕ'=36°	s_u/σ'_v= 0.25	ϕ'=36°
1	Linear piezo-line, hmax=25 m	2.5	2.51	2.34	2.34
2	Linear piezo-line, hmax=50 m	1.08	2.13	2.34	2.34
3	FEM phreatic line, hmax=25 m, Kh/Kv=1	1.79	2.42	2.34	2.34
4	FEM phreatic line, hmax=25 m, Kh/Kv=10	1.7	2.38	2.1	2.34
5	FEM phreatic line, hmax=25 m, Kh/Kv=100	1.27	1.97	0.84	1.5
6	FEM phreatic line, hmax=50 m, Kh/Kv=1	0.87	1.59	1.08	1.67
7	FEM phreatic line, hmax=50 m, Kh/Kv=10	0.66	1.32	0.72	1.19
8	FEM phreatic line, hmax=50 m, Kh/Kv=100	0.52	1.11	0.52	1.02
9.1	FEM phreatic line, hmax=50 m, t=10 days	1.79	2.42	2.34	2.34
10.1	FEM phreatic line, hmax=50 m, t=100 days	1.79	2.42	2.34	2.34
11.1	FEM phreatic line, hmax=50 m, t=1000 days	1.79	2.42	2.34	2.34
12.1	FEM phreatic line, hmax=50 m, t=10000 days	0.87	1.59	1.08	1.67

Similar trends are seen for the transient infiltration analysis as the water level increases from 25 m to 50 m. For the initial 1,000 days of infiltration, there is no change in the FoS for S2 or S3 failure surface because the infiltrating front has not yet reached either of the failure surface locations nor caused changes in the initial pore pressures. However, when the wetting front reaches the global failure surface (S2) the factor of safety is reduced to 0.87 for the undrained shear strength approach and to 1.59 for the effective stress approach. Had this infiltration analysis been combined with the assumed anisotropy, the FoS reductions would have been more drastic, and the changes would have happened in a much shorter period of time.

For the toe stability potential failure surface (S3), similar trends in the FoS reduction are observed. The FoS is reduced from the initial value of 2.34 (no seepage effect at all) to the low value of 0.52 when considering the undrained shear strength approach and to 1.02 for the effective stress approach. Such a low value of FoS for the effective stress approach clearly indicates a high likelihood for the embankment toe to

become unstable when the seepage reaches the downstream slope and indicates a high likelihood of global or progressive failure being triggered in an undrained fashion.

Conclusion

The presented seepage and stability analyses demonstrate that the stability of a tailings dam can be compromised by internal seepage even in the absence of any other external triggers, such as earthquake or static loading, infiltration from rainfall or snow melt, increased antecedent flows, and other natural or man-induced triggers. Unless a substantial downstream zone of the dam can be protected from saturation by a properly designed drain or a toe buttress made of highly permeable material, the uncontrolled seepage at the downstream face of the dam will almost certainly result in tailing dam instability.

The commonly employed assumption of a linear piezometric line can significantly underestimate the pore pressures on the potential failure surfaces. When the results of properly executed seepage analyses are compared to the linear piezometric line, the factor of safety reduces by 25%, 30%, or even 50%. Accounting for the inevitable presence of tailings anisotropy may result in a further reduction in the FoS to 50% or even 20% of the original value.

For the vast majority of TSFs, conducting slope stability analyses using the undrained shear strength will lead to more conservative FoS values than using effective stress analyses or drained conditions. This is not surprising because the undrained shear strength approach accounts for the shear (deformation) induced pore pressures, while the effective stress approach accounts only for the pore pressures calculated in the seepage analysis (assuming dilative tailings and/or conditions that are not conducive to generation of positive pore water pressures). Hence, effective stress analyses would be justified only for cases where all tailings exhibit dilative behavior ("But who could guarantee that for a conventional tailings deposition?"), or where tailings are at a low level of saturation throughout the life of the impoundment so that any generated pore pressures during loading are negligible ("And who could guarantee that either?").

The presented transient seepage analyses demonstrate that, even when a portion of the tailings dam is initially unsaturated, the presence of water in the upstream body of the impoundment may inevitably lead to saturation of the downstream slope and reach the toe of the dam, unless adequate drainage and groundwater control measures are implemented in the design to manage these flows. The time required for triggering of these unstable downstream conditions depends on the material characteristics, climate, and general water management conditions, but it is expected to vary from several decades to several years (e.g., the Feijão dam failure) or even less.

The analyses in this study were conducted for a hypothetical tailings dam, but they illustrate the need for similar analyses to be conducted for any tailings dam design where the material properties and long-term changes in seepage conditions present a stability concern. In particular, the range of in-situ anisotropy,

unsaturated soil properties, time-dependency of material parameters, and any sources of water (e.g., rainfall, snowmelt, existing seeps, surface streams, and potential inflows due to water management at the mine site) must be considered. The absence of these critical seepage analyses is one of the factors that leads to underestimation of the severity of potential failure modes and, more importantly, the increased likelihood of catastrophic failures.

References

Gjerapic, G. and Znidarcic, D. 2020. Assessment of liquefaction triggering for upstream tailings dams using limiting equilibrium methods. *Proceedings of Tailings and Mine Waste 2020*, November 15–18, University of British Columbia, Vancouver BC, 413–424.

Gjerapic, G., Gillette, D. and Znidarcic, D. 2022. Addressing saturation and seepage issues to improve the safety assessment of mining facilities. *Proceedings of Tailings and Mine Waste 2022*, November 6–9, University of British Columbia, Vancouver BC, 127–138.

Hwang, C. 1999. Flow processes in unsaturated soils. Master of Science thesis, University of Colorado at Boulder.

Jefferies, M., Morgenstern, N.R., Van Zyl, D.V. and Wates, J. 2019. Report on NTSF embankment failure, Cadia Valley Operations, Ashurst Australia.

Morgenstern, N.R., Vick, S.G., Viotti, C.B. and Watts, B.D. 2016. Report on the immediate causes of the failure of the Fundão Dam. Fundão Tailings Dam Review Panel. August 25, 2016.

Reid, D. and Fourie, A. 2024. Development and outcomes of a tailings slope stability comparative design exercise, *Canadian Geotechnical Journal* 61(8): 1683–1704.

Robertson, P.K., de Melo, L., Williams, D.J. and Wilson, G.W. 2019. Report of the Expert Panel on the Technical Causes of the Failure of Feijão Dam I. Retrieved from http://www.b1technicalinvestigation.com/report.html

Rocscience, Inc. (Rocscience). 2024. Tutorials Overview. (https://www.rocscience.com/help/slide2/tutorials) Accessed on June 25, 2024.

Assessment of Silicate- and Catecholate-based Surface Treatment Performances to Limit the Mobilization of As from Low Sulfide Filtered Tailings

E. Lagae Capelle, University of Quebec in Abitibi-Temiscamingue, Canada
L. Coudert, University of Quebec in Abitibi-Temiscamingue, Canada
I. Demers, University of Quebec in Abitibi-Temiscamingue, Canada
C. M. Neculita, University of Quebec in Abitibi-Temiscamingue, Canada
G. Pépin, Newmont Eleonore, Canada

Abstract

The generation of contaminated neutral drainage (CND) is an important environmental issue for the mining industry, especially from filtered tailings whose reactivity may be enhanced. The gold mining industry is particularly challenged by the co-occurrence of Au and As-bearing minerals, including arsenopyrite and loellingite, leading to the generation of As-CND. Surface treatments using inorganic and organometallic passivation layers are increasingly recognized as promising strategies to limit oxygen access and the generation of As-CND. This study aims to evaluate and compare the performances of silicate- and catecholate-based coatings to limit As mobilization from low sulfide filtered tailings (0.07% As, 0.05% S). Four treatment solutions were studied: 1) Si/H_2O_2, 2) Si/Fe, 3) Si/catechol, and 4) Fe/catechol. The effect of reagents concentration (10 – 100 mM), drying time (1 – 5 days) and pre-washing cycles was investigated using batch tests. The mobility of As from reprocessed tailings was evaluated through static leaching tests. Results showed that the use of Si in inorganic and organometallic coatings had a negative effect, as it induced twice as much As mobilization (up to 1.5 mg/L vs. 0.6 ± 0.2 mg/L for untreated tailings), highlighting the prevalent role of anionic competitiveness on passivation mechanisms. On the contrary, the use of Fe in inorganic and organometallic coatings was beneficial. It enhanced the immobilization of As, which increased at greater concentrations of reagents (up to 95% of immobilization) and allowed the tailings to reach Canadian federal legislative limits (<0.3 mg/L) in final post-treatment effluents and leachates. The drying time had a moderate influence on As mobilization from reprocessed tailings, suggesting that environmental conditions of the management of low sulfide filtered tailings will impact treatment efficiencies. Further studies are required to evaluate the long-term performances of the surface treatments in oxidative and reductive conditions.

Introduction

Contaminated neutral drainage (CND) occurs through the oxidation of mine wastes in which neutralizing minerals are in abundance compared to acidifying minerals (i.e., sulfides), as in the case of low sulfide tailings. Although desulfurization was proved to be efficient as an integrated management option for mine drainage prevention, recent studies have shown that desulfurized tailings can still induce CND (Barago et al., 2023; Rey et al., 2020). CND has become a major environmental issue for the mining industry, but its treatment is challenged by the low contents of contaminants, the low stability of treatment residues, and the need for chemical reagents, energy, and infrastructure (Prepilková et al., 2022). These challenges, associated with stricter regulations (e.g., Metal and Diamond Mining Effluent Regulations – MDMER), has led to an interest in prevention strategies, especially for filtered tailings whose reactivity is enhanced by their low degree of saturation (Lara et al., 2013; Davies, 2011).

Prevention strategies for CND include, among others, surface treatments. Several coating agents are available for the surface treatment of mine tailings, such as oxide layers (Tabelin et al., 2016), organic or inorganic compounds (e.g., calcite, silicates, silanes) (Feng et al., 2023; Fan et al., 2021; Roy et al., 2020), organometallic complexes (Park et al., 2021), and even biological coatings (He et al., 2022; Gerson et al., 2022). They control the type of coating mechanisms at stake: i) organic or inorganic passivation, ii) carrier-microencapsulation (CME), iii) biocalcification or iv) biopassivation, respectively. Biological surface treatment will not be discussed in further detail in this paper.

Immobilization mechanisms and, therefore, the physicochemical properties of coating layers are strongly dependent on the nature of the coating agent used. Inorganic coating reagents generally create sorption sites through Fe-nonmetal-O bonds (Fan et al., 2017). Phosphates, silicates, and carbonates are all options for the surface treatment of main sulfides (Roy et al., 2020; Kollias et al., 2019), but the competitive effects of As and similar anions regarding Fe affinity could represent a challenge for As-rich tailings (Kollias et al., 2022; Cheng et al., 2009). Catechol is an isomeric benzenediol ($C_6H_6O_2$) capable of forming mono-, bis-, or tris- coordination complex with diverse metals and anions. Catecholate-based coatings are increasingly studied as viable organometallic complexes for surface treatment. They can be synthetized using different metals (e.g., Fe, Al), as well as different anions (e.g., PO_4^{3-}, SiO_4^{3-}) (Li et al., 2021; Park et al., 2020). The decrease of sulfide oxidation by CME is based on three different mechanisms: i) the degradation of catechol at the surface of the minerals, ii) the production and adsorption of intermediates catecholate, and iii) the liberation of metals or anions that can precipitate and form a protective layer at the surface of the sulfide minerals (Satur et al., 2007).

Previous studies on surface treatments carried out in the mining context mainly targeted the oxidation of pyrite, and to a lesser extent arsenopyrite, but did not cover their effect on non-sulfidic As-bearing minerals (i.e., loellingite) that can be found in low sulfide tailings (Lagae Capelle et al., 2024) and present

divergent chemical behaviors due to different bulk structures and electronegativity (Harmer and Nesbitt, 2004). For example, lower yields of natural coatings formation through oxidation dissolution were observed on loellingite vs. arsenopyrite (Stolze et al., 2022). Besides, the efficiency of such treatments depends on many operating conditions, such as tailings mineralogy and particle size, the nature of the coating agent and its concentration, as well as drying time (Tu et al., 2022). Temperature, pH, and reaction time also play an essential role in the formation of coating layers (Kollias et al., 2022; Li et al., 2021).

In this context, the main objective of this study was to assess and compare the efficiency of different surface treatments, including Si-based inorganic passivation, Fe- and Si-bearing catecholates (CME), to decrease the mobility of As from low sulfide filtered tailings. Immobilization mechanisms were investigated to understand the challenges associated with the use of inorganic silicates. The influence of the nature of coating agents and their concentrations as well as the drying time on the immobilization of As was evaluated using a static leaching test on untreated vs. reprocessed tailings.

Materials and methods

Physico-chemical and mineralogical characterization of tailings

Low sulfide filtered tailings were sampled at the Éléonore mine site, an active gold mine located in the James Bay region (Quebec, Canada) in 2021. They were stored in 500 L barrels, sampled through drilling, dried, and homogenized using the 80-stroke technique prior to physico-chemical and mineralogical characterization as well as surface treatment experiments. Initial characterization included water content, particle size distribution, and chemical and mineralogical composition. Water content was estimated by drying samples at 60°C for 48 hours (ASTM, 2010). Particle size distribution was determined using a laser diffraction grain size analyzer (Malvern Mastersizer S). The chemical composition was reconciled using: i) inductively coupled plasma-atomic emission spectroscopy (ICP-AES – Perkin Elmer Optima 3100-RL) after 4-acid standard digestion (HNO_3/HBr/HF/HCl); ii) whole rock analysis; and iii) X-ray fluorescence spectroscopy (XRF – Bruker S2 Ranger) on homogeneous and deagglomerated samples. Sulfur and carbon contents were determined using an induction furnace at 1,360°C (ELTRA CS-20) equipped with an infrared analyzer. Main gangue, sulfides, and As-bearing minerals were identified using an X-ray diffractometer (XRD) (Bruker A.S. Advance D8) and a scanning electron microscope (SEM) (Zeiss Sigma 300 VP) equipped with an energy-dispersive X-ray spectrometer (EDS) (Oxford Instrument, Ultim-Max 170 mm^2).

Preparation of surface treatment solutions

Surface treatment solutions included two inorganic solutions (Si/H_2O_2 – I-Si, $Si/Fe/H_2O_2$ – I-Fe-Si) and two organometallic solutions, also referred to as CME solutions (Fe/catechol – CME-Fe and Si/catechol – CME-Si). Inorganic solutions were produced by mixing a source of silicate ions (5-25 mM Na_2SiO_3, Alfa

Aesar) with an oxidizing agent (2% H_2O_2, Anachemia VWR), with (I-Fe-Si) or without (I-Si) a source of Fe ions (5-25 mM $FeSO_4$, Sigma Aldrich) during 5 minutes at 200 rpm and room temperature. The choice of reagent concentrations was based on previous work performed on a Ni-rich waste rock (Roy et al., 2020). CME solutions were synthesized according to experimental procedures described by Li et al. (2021) for CME-Fe and Yuniati et al. (2015) for CME-Si, using a source of catechol (2-15 mM pyrocatechol 99%, ThermoScientific) and either a source of Fe (4-20 mM $FeNO_3$, Anachemia VWR) or Si (10-100 mM Na_2SiO_3, Alfa Aesar). Their synthesis was realized by titration to reach pH 7-8, using NaOH (0.1 M, Mat Laboratory) or H_2SO_4 (95-98%, VWR Chemicals), to produce bis-catecholate that is chemically stable in the targeted pH range (Park et al., 2018).

Surface treatment

Surface treatments were carried out on 10 g of tailings in 100 mL Erlenmeyer flasks. Inorganic and CME solutions were added to tailings to reach a solid/liquid ratio of 1/10 (v/v) and the slurry was mixed for 4 hours at 200 rpm and room temperature. Post-treatment effluents were recovered by Buchner filtration (0.45 µm porosity) and analyzed for metallic and anionic contents using ICP-AES and ionic chromatography (IC, Methrom 940 Professional IC Vario), respectively. The final content of catechol after CME treatments was quantified using UV-vis spectroscopy (Ultrospec 2100 Pro). Solids, referred to as reprocessed tailings, were recovered, and dried at 60°C for 1 to 5 days. The mobility of As and S in initial and reprocessed tailings was assessed using modified Field Leaching Tests (FLT – Hageman, 2007). The bulk chemical composition of reprocessed tailings was determined by XRF.

Evaluation of contaminants mobilization: field leaching tests

The mobility of As and S from tailings (untreated vs. reprocessed with inorganic and CME solutions) was estimated using a FLT based on the method developed by Hageman (2007). Samples were mixed with deionized water at 250 rpm and room temperature, using a solid/liquid ratio of 1/20 (w/w), for 5 minutes. Leachates were recovered after a Buchner filtration (0.45 µm porosity) and analyzed for metallic, anionic, and organic contents using ICP-AES, IC, and UV-vis spectroscopy, respectively. The results were used to evaluate the surface treatment efficiency for limiting the mobilization of As.

The efficiency calculation (E_{tr} – Equation 1) was based on the comparison of the amounts of contaminants released during FLT performed on reprocessed tailings ($Q_{FLT\text{-}tr}$ – Equation 2) and on initial tailings ($Q_{FLT\text{-}ini}$ – Equation 3). Negative E_{tr} values indicate that the mobility of the contaminant of interest increased after passivation treatment, while positive values indicate a diminution of the mobility of the targeted contaminant after the passivation treatment.

$$E_{tr}\ (\%) = (Q_{FLT\text{-}ini} - Q_{FLT\text{-}tr}) / Q_{FLT\text{-}ini} \times 100 \qquad \text{(Equation 1)}$$

$$Q_{FLT\text{-}tr}\ (mg_{As}) = (C_{FLT\text{-}tr}.V_{FLT})/(C_{ini}.m_{ini} - C_{leached}.V_{leached}) \quad \text{(Equation 2)}$$

$$Q_{FLT\text{-}ini}\ (mg_{As}) = (C_{FLT\text{-}ini}.V_{FLT})/(C_{ini}.m_{ini}) \quad \text{(Equation 3)}$$

Where $C_{FLT\text{-}tr}$ and $C_{FLT\text{-}ini}$ are the concentrations of contaminants released during FLT carried out on reprocessed and untreated tailings (mg/L), respectively, V_{FLT} is the volume of FLT solution (L), C_{ini} is the concentration of contaminants initially present in the tailings (mg/kg), m_{ini} is the mass of tailings used for FLT (0.01 kg), $C_{leached}$ and $V_{leached}$ are the concentrations of contaminants leached (mg/L) and the volume (L) of the solution used during the passivation treatment, respectively.

Results and discussion

Physico-chemical and mineralogical characterization of tailings

Low sulfide filtered tailings were uniformly graded (Cu < 3) and fine-grained (D_{10}: 3.5 µm, D_{60}: 41.7 µm and D_{80}: 77.0 µm) materials with a low water content (15.8% – v/v). They were mainly composed of Si (30%), followed by Fe (2.5%), Al (2.5%), and Mg (2.1%). The concentrations of As and S were low (848 and 1,216 mg/kg, respectively), which is consistent with previous studies (Rakotonimaro et al., 2021). Main gangue minerals were quartz (38%), plagioclase (20%), biotite (12%), and K-feldspar (9.0%), while identified sulfides and As-bearing minerals were loellingite (0.04%), pyrrhotite (0.006%), and arsenopyrite (0.004%).

The concentration of As and Fe in the leachates obtained from FLT on untreated tailings were 0.62 ± 0.14 mg/L and 0.12 ± 0.04 mg/L, respectively. These values were used to compare the mobility of contaminants from untreated and reprocessed tailings and therefore to quantify the efficiency of the different surface treatments tested.

Influence of the nature and concentration of reagents

Evolution of As and Fe concentration in final post-treatment effluents

The effect of the nature and the concentration of different inorganic (I-Si, I-Fe-Si) and organometallic (CME-Fe, CME-Si) coating agents on the passivation of As-bearing minerals to limit the mobilization of As from tailings was assessed. Figure 1 presents, for each tested initial concentration of reagents (x), the final concentration of As and Fe in the post-treatment effluents (y_1) (i.e., the concentration of As leached [$C_{leached}$, Eq. 2] during the surface treatment), as well as the content of coating agent immobilized onto the tailings surface (y_2) (i.e., the difference between final and initial concentrations of coating indicators).

For I-Si and CME-Si, high contents of As, generally above legislative limits in Canada (0.3 mg/L – MDMER, Minister of Environment and Climate Change), were leached during the treatment step, indicating that post-treatment effluents will require further appropriate treatment before their discharge due

to their low quality. Increasing the initial concentration of Si improved the immobilization rate of Si, which reached above 80% for both I-Si and CME-Si, but it did not impact (for I-Si) and even increased (for CME-Si) the leaching of As during the treatment step (Figures 1a, 1c). However, for I-Fe-Si, higher immobilization rates of Si at higher initial Si concentrations (> 90% at [Si] > 15mM) were combined with an immobilization rate of Fe near 100%, inducing 10 to 50 times less As leaching than I-Si and CME-Si respectively. The results suggest the formation of Fe-Si complexes or Si-doped Fe-(hydr)oxides (Fan et al., 2017) onto the tailings surface when Fe ions were added to the coating solution. Concentrations of As leached during I-Fe-Si treatment were below 0.1 mg/L and were not influenced by initial [Si] and [Fe], which indicates that ferrosilites can limit tailings oxidation and As mobilization despite the possible competitive effects between Si and As anions that were previously reported (Kollias et al., 2022).

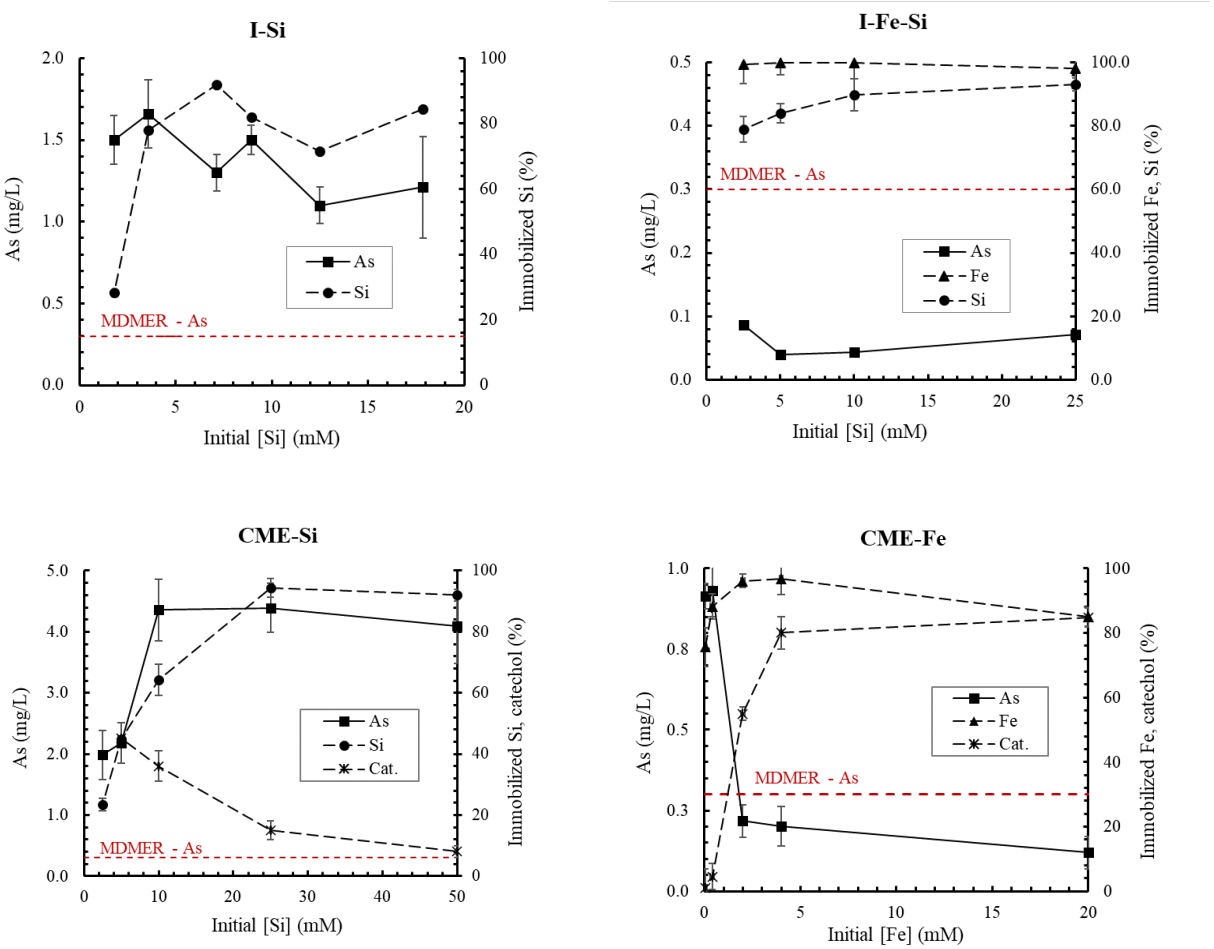


Figure 1: Influence of initial concentration of Si for I-Si, I-Fe-Si, CME-Si, and Fe for CME-Fe on the concentration of As (square) leached during the treatment step and the immobilization of coating indicators (dotted line) like Si (circle), Fe (delta), and catechol (cross) (treatment time: 4 h, drying time: 24 h)

The levels of As leached during treatment are higher for CME-Si than I-Si (up to 5.6 mg/L for CME-Si vs. up to 1.7 mg/L for I-Si) despite relatively similar Si immobilization rates, indicating that the use of an oxidizing agent (H_2O_2) during I-Si treatment may have enhanced the formation of Fe-(hydr)oxides at the tailings surface, a natural coating layer (Tabelin et al., 2016), which was more concluding than catechol immobilized at rates below 40%. The comparison of CME treatments showed that the concentrations of As released during CME-Fe treatment were much lower than during CME-Si for the same initial [catechol] of 2 to 3 mM (0.21 ± 0.09 mg/L for CME-Fe vs. 3.2 ± 0.44 mg/L for CME-Si) (Figures 1b, 1d). The decrease in As mobility during CME-Fe can be associated with the simultaneous immobilization of Fe and catechol at rates above 80%.

I-Fe-Si and CME-Fe would present higher efficiency for limiting As mobilization from reprocessed tailings, confirming the important role played by Fe ions in the immobilization of As (Park et al., 2021; Cheng et al., 2009).

Efficiency of prevention: mobilization of As and Fe from reprocessed tailings

The mobility of As (and Fe for I-Si and CME-Si) from reprocessed tailings was compared to their mobility from untreated tailings to evaluate the efficiency of the surface treatment presented in Figure 2. Negative efficiencies represent As and Fe levels in FLT leachates from reprocessed tailings higher than in untreated tailings (i.e., 0.62 mg/L of As and 0.12 mg/L of Fe). They indicate that the surface treatments were not only inefficient but increased the mobility of As and/or Fe from tailings. The remobilization of coating indicators (i.e., Si, Fe, catechol) is also presented in Figure 2 to correlate As mobility to the stability of coating layers.

Despite low remobilization rates of Si (and catechol) (0-15%), negative efficiencies for As mobilization were calculated for I-Si regardless of the initial Si concentration and for CME-Si at more than 25 mM of Si (Figures 2a, 2c). Whereas the mobility of Fe was decreased by 60-100% in both cases. Results are consistent with previous work on sulfurized tailings and confirm the low effectiveness of Si-based tailings for As-rich tailings (Kollias et al., 2022). The use of catechol in CME-Si treatment improved efficiency (E_{tr} of -30% for I-Si vs. +30% for CME-Si at 10 mM of Si), possibly because of the higher stability of Si-based coating layers (<2% of remobilization for CME-Si vs. up to 5% for I-Si) as well as the occurrence of a low catecholate layer.

The efficiencies of I-Fe-Si and CME-Fe treatments were positive regardless of the initial Si and Fe contents, reaching up to 95% of As immobilization (Figures 2b, 2d), decreasing the concentration of As in FLT leachates below legislative limits (0.3 mg/L) for [Si] > 2.5 mM and [Fe] > 4 mM, respectively. The results showed the positive influence of using Fe ions as part of a coating agent for the retreatment of As-rich tailings. For instance, the use of I-Fe-Si (vs. I-Si) increased the passivation efficiency from -33%

to 89% at an initial [Si] of 10 mM, while the use of CME-Fe (vs. CME-Si) increased it from 33 to 55% for As at an initial [catechol] of 3 mM. A slight improvement of As immobilization in I-Fe-Si reprocessed tailings was observed at greater initial Si concentrations, which can be associated with lower Si and Fe remobilization rates (Figure 2b). For CME-Fe, the passivation efficiency went up from 55% to 95% and can also be associated with lower catechol and Fe remobilization (Figure 2d). Increasing the initial content of coating agents was beneficial for producing more stable passivation layers.

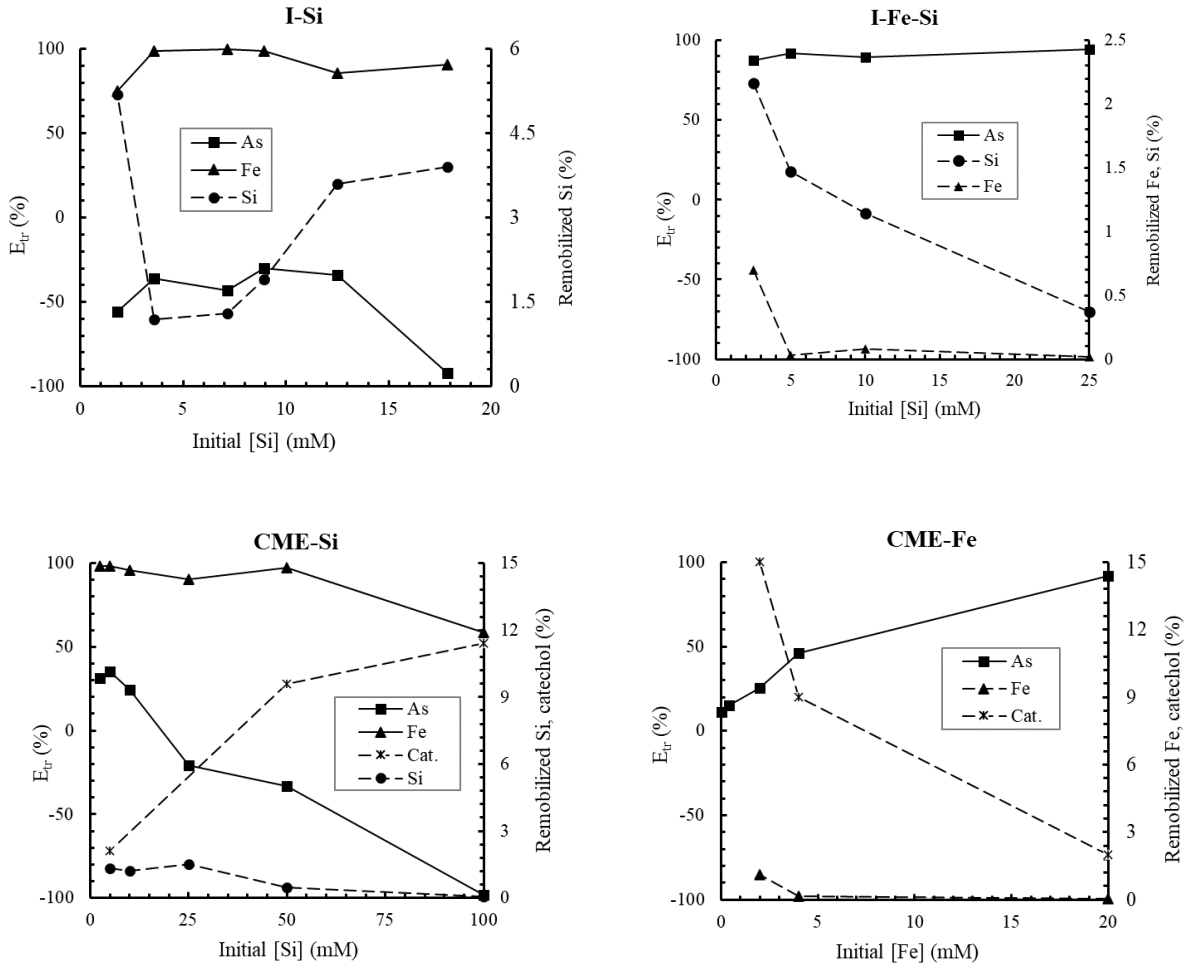


Figure 2: Influence of initial concentration of Si for I-Si, I-Fe-Si, and CME-Si, and Fe for CME-Fe, on the treatment efficiency to limit the mobility of As (square), Fe (delta), and the remobilization (dotted line) of Si (circle) and catechol (cross) (treatment time: 4 h, drying time: 24 h)

Influence of drying time

The influence of drying time (time between passivation treatment and FLT) on the performances of surface treatments applied to mine wastes or sulfide minerals is not well documented. Additional experiments have been carried out to evaluate the effect of drying time on inorganic and organometallic passivation efficiency

regarding As mobilization. Based on the results of the FLT performed on untreated vs. reprocessed tailings that are shown in Figure 3, the drying process had a strong (R^2: 0.953, R^2: 0.922, R^2: 0.855 for CME-Fe, I-FeSi, CME-Si, respectively) and positive influence on the efficiency of CME-Fe, I-Fe-Si and CME-Si treatments. According to the linear correlation identified between As passivation efficiency and drying time, the immobilization of As increased by 6.8, 7.9, and 7.5 point of percentage per day of drying respectively for CME-Fe, I-Fe-Si, and CME-Si. While, for I-Si, the results showed no significant effect of the drying time on the efficiency of the coating layers. These preliminary results suggest that the drying process influences the stability of catecholate layers, as well as of ferrosilite complexes. On site, the drying process of filtered tailings is controlled by environmental conditions of disposal. Further work is required to evaluate the influence of drying temperature, a factor that is especially important for mining activities in Nordic climates.

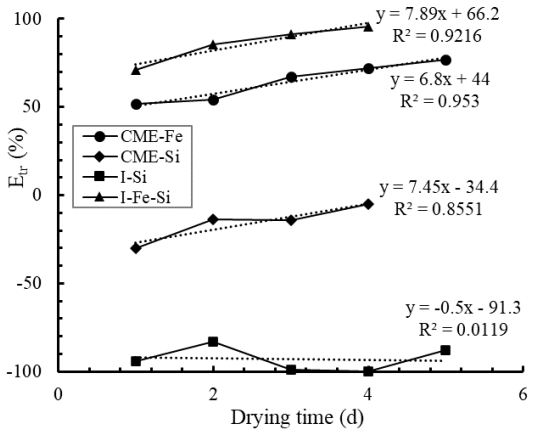


Figure 3: Influence of drying time () on the immobilization of As for CME-Fe (circle), CME-Si (diamond), I-Si (square) and I-Fe-Si (delta) treatments (respective initial concentrations: [Fe]: 4 mM, [Si]: 50 mM, [Si]: 18 mM, treatment time: 4 h)

Conclusion

The oxidation of As-rich low sulfide filtered tailings plays a role in the major environmental challenges faced by the Au mining industry. This study investigated the efficiency of surface treatment to limit loellingite and arsenopyrite oxidation and reduce As mobility using inorganic or organometallic agents: Si/H_2O_2, Si/Fe/H_2O_2, Si/catechol, Fe/catechol. Among the four types of surface treatment, I-Fe-Si (i.e., Si/Fe/H_2O_2) and CME-Fe (i.e., Fe/catechol) seemed to be the best options. They both induced lower As solubilization during the treatment step, while producing stable coating layers that limited up to 90% of As mobility during leaching tests. The concentration of As in post-treatment effluents and FLT leachates for CME-Fe and I-Fe-Si were generally below the Canadian federal regulations (0.3 mg/L – MDMER).

The influence of the operating conditions was inconsistent from one coating agent to another. Increasing Fe and catechol initial contents allowed the improvement of the passivation efficiency and decreased As solubilization during the treatment step, whereas increasing Si initial content had a negative impact on the treatment, indicating the prevalence of anionic competition onto the coating mechanisms. The drying process was observed to be influent on the passivation efficiency of catecholate-based treatments (i.e., CME-Fe and CME-Si), possibly because of the production of more stable organic coating, and of the production of more stable ferrosilite complexes for I-Fe-Si, while having no effect on I-Si treatment. The findings of this study suggest that the use of silicates, without the addition of Fe ions, is not appropriate for the surface treatment of As-rich low sulfide tailings due to their high anionic competition. The use of Fe ions, in combination with silicates or catecholates, is a promising option to reduce As-CND.

Ongoing and upcoming work includes:

1. the estimation of optimal operating conditions for CME-Fe and I-Fe-Si using a Box-Benhken experimental design,
2. the investigation of biological coatings,
3. the evaluation of the long-term stability of reprocessed tailings in oxidative and reductive conditions (both found in filtered tailings storage facilities).

Acknowledgements

This research was funded by the Natural Sciences and Engineering Research Council (NSERC), the Canada Research Chairs Program and the industrial partners of the Research Institute on Mines and Environment (RIME) – University of Quebec in Abitibi-Temiscamingue – Polytechnique Montreal, including Newmont Eleonore, Agnico Eagles Mines, Iamgold, Canadian Malartic Mine, Raglan Mine – a Glencore Company, and Rio Tinto Iron and Titanium. The authors thank the URSTM staff for their support with chemical analysis, as well as Jonathan Tremblay from IOS Services Geoscientific Inc., for their help in achieving SEM-EDS analysis.

References

Barago, N., E. Pavoni, F. Floreani, M. Crosera, G. Adami, D. Lenaz and S. Vovelli. 2023. Hydrogeochemistry of thallium and other potentially toxic elements in neutral mine drainage at the decommissioned Pb-Zn Raibl mine (Eastern Alps, Italy). *J. Geochem. Explor.* 245: 107129.

Cheng, H., Y. Hu, J. Luo, B. Xu and J. Zhao. 2009. Geochemical processes controlling fate and transport of arsenic in acid mine drainage (AMD) and natural systems. *J. Hazard. Mater.* 165(1): 13–26.

Davies, M. 2011. Filtered dry stacked tailings – the fundamentals. *Proceedings of Tailings and Mine Waste 2011.* Vancouver. 1–9.

Fan, R., G. Qian, M.D. Short, R.C. Schumann, S. Brienne, R.S.C. Smart and A.R. Gerson. 2021. Passivation of pyrite for reduced rates of acid and metalliferous drainage using readily available mineralogic and organic carbon resources: A laboratory mine waste study. *Chemosphere.* 258:131330.

Fan, R., M.D. Short, S.J. Zeng, G. Qian, J. Li, R.C. Schumann, N. Kawahima, R.S.C. Smart and A.R. Gerson. 2017. The formation of silicate-stabilized passivating layers on pyrite for reduced acid rock drainage. *Environ. Sci. Technol.* 51(19):11317–11325.

Feng, J., C. Zhou, Q. Yang, Z. Dang and L. Zhang. 2023. Performance and mechanisms of PropS-SH/Ce(dbp)3 coatings in the inhibition of pyrite oxidationtion for acid mine drainage control. *Environ. Pollut.* 322: 121162.

Gerson, A.R., R. Fan, G. Qian, R.C. Schumann, P. Olin, D.L. Howard and R.S.C. Smart. 2022. Examination of multiple sources of selenium release from coal wastes and strategies for remediation. *J. Hazard. Mater.* 422: 126924.

Hageman, P. L. 2007. U.S. Geological Survey field leach test for assessing water reactivity and leaching potential of mine-wastes, soils, and other geologic and environmental materials. *U.S. Geological Survey Techniques and Methods*, book 5, chapter D3. Available online at http://pubs.usgs.gov/tm/2007/05D03/.

He, Z., Y. Xu, X. Yang, J. Shi, X. Wang, Z. Jin, D. Zhang and X. Pan. 2022. Passivation of heavy metals in copper–nickel tailings by in-situ bio-mineralization: A pilot trial and mechanistic analysis. *Sci. Total Environ.* 838: 156504.

Kollias, K., E. Mylona, K. Adam, M. Chrysochoou, N. Papassiopi and A. Xenidis. 2019. Characterization of phosphate coating formed on pyrite surface to prevent oxidation. *Appl. Geochem.* 110: 104435.

Kollias, K., E. Mylona, N. Papassiopi and M. Thymi. 2022. Application of silicate-based coating on pyrite and arsenopyrite to inhibit acid mine drainage. *Bull. Environ. Contam. Toxicol.* 108*(*3): 532–540.

Lagae Capelle, E., L. Coudert, I. Demers and C. M. Neculita. 2024. Influence of particle size on arsenic mobility from low-sulfide and filtered tailings and investigation of gravimetric separation to prevent contaminated neutral mine drainage. *Proceedings of the 13th International Conference on Acid Rock Drainage.* Halifax.

Lara, J., E.U. Pornillos and H. Muñoz. 2013. Geotechnical-geochemical and operational considerations for the application of dry stacking tailings deposits – state-of-the-art. in R. Jewell, A.B. Fourie, J. Caldwell and J. Pimenta (eds), *Paste 2013: Proceedings of the 16th International Seminar on Paste and Thickened Tailings,* Australian Centre for Geomechanics, Perth: 249–260, https://doi.org/10.36487/ACG_rep/1363_19_Munoz

Li, X., I. Park, C.B. Tabelin, K. Naruwa, T. Goda, C. Harada, S. Jeon, M. Ito and N. Hiroyoshi. 2021. Enhanced pyrite passivation by carrier-microencapsulation using Fe-catechol and Ti-catechol complexes. *J. Hazard. Mater.* 416: 126089.

Minister of Environment and Climate Change. 2023. Metal and diamond mining effluent regulations (MDMER) SOR/2002-22. Canada, 82 p. Accessed 2024-03-23 at https://laws.justice.gc.ca/eng/regulations/SOR-2002-222/FullText.html

Park, I., C.B. Tabelin, K. Magaribuchi, K. Seno, M. Ito and N. Hiroyoshi. 2018. Suppression of the release of arsenic from arsenopyrite by carrier-microencapsulation using Ti-catechol complex. *J. Hazard. Mater.* 344: 322–332.

Park, I., C.B. Tabelin, K. Seno, S. Jeon, H. Inano, M. Ito and N. Hiroyoshi. 2020. Carrier-microencapsulation of arsenopyrite using Al-catecholate complex: nature of oxidation products, effects on anodic and cathodic reactions, and coating stability under simulated weathering conditions. *Heliyon.* 6(1).

Park, I., K. Higuchi, C.B. Tabelin, S. Jeon, M. Ito and N. Hiroyoshi. 2021. Suppression of arsenopyrite oxidation by microencapsulation using ferric-catecholate complexes and phosphate. *Chemosphere.* 269: 129413.

Prepilková, V., J. Poništ, M. Schwarz and D. Samešová. 2022. Possibilities of remediation of neutral mine drainage-removal and recovery of potentially hazardous elements. *Soil Water Res.* 17(4): 251–267.

Rakotonimaro, T.V., M. Guittony and C.M. Neculita. 2021. Compaction of peat cover over desulfurized gold mine tailings changes: Arsenic speciation and mobility. *Appl. Geochem.* 128: 104923.

Rey, N.J., I. Demers, B. Bussière, M. Mbonimpa and M. Gagnon. 2020. A geochemical evaluation of a monolayer cover with an elevated water table for the reclamation of the Doyon-Westwood tailings ponds, Canada. *Environ. Earth Sci.* 79(2): 58.

Roy, V., I. Demers, B. Plante and M. Thériault. 2020. Kinetic testing for oxidation acceleration and passivation of sulfides in waste rock piles to reduce contaminated neutral drainage generation potential. *Mine Water Environ.* 39(2): 242–255.

Satur, J., N. Hiroyoshi, M. Tsunekawa, M. Ito and H. Okamoto. 2007. Carrier-microencapsulation for preventing pyrite oxidation. *Int. J. Miner. Process.* 83(3): 116–124.

Stolze, L., M. Battistel and M. Rolle. 2022. Oxidative dissolution of arsenic-bearing sulfide minerals in groundwater: Impact of hydrochemical and hydrodynamic conditions on arsenic release and surface evolution. *Environ. Sci. Technol.* 56(8): 5049–5061.

Tabelin, C.B., R.D. Corpuz, S. Veerawattananun, M. Ito, N. Hiroyoshi and T. Igarashi. 2016. Formation of schwertmannite-like and scorodite-like coatings on pyrite and its implications in acid mine drainage control. *Proceedings of IMPC 2016. 28th International Mineral Processing Congress.* Quebec City, 101–112.

Tu, Z., Q. Wu, H. He, S. Zhou, J. Liu, H. He, C. Liu, Z. Dang and J.R. Reinfelder. 2022. Reduction of acid mine drainage by passivation of pyrite surfaces: A review. *Sci. Total Environ.* 832: 155116.

Yuniati, M.D., K. Kitagawa, T. Hirajima, H. Miki, N. Okibe and K. Sasaki. 2015. Suppression of pyrite oxidation in acid mine drainage by carrier microencapsulation using liquid product of hydrothermal treatment of low-rank coal, and electrochemical behavior of resultant encapsulating coatings. *Hydrometallurgy* 158(158): 83–93. https://doi.org/10.1016/j.hydromet.2015.09.028.

The Internal and Interface Shear Strength of Geosynthetic Clay Liners for Mining Application

Andrew Jung, Western GeoSystems, USA
Reza Gorakhki, CETCO, USA

Abstract

Geosynthetic clay liners (GCLs) have been used widely as an alternative for compacted clay liners and covers in mine waste applications. The high swelling of bentonite particles in the GCL creates a uniform barrier layer that results in low permeability of water and mine waste leachate. GCLs must provide sufficient internal and interface shear strength stability, especially if GCLs are used in steep slopes under high normal loads. Peel strength is a common parameter that is typically correlated to internal shear strength properties of GCLs. The relationship between internal shear strength and peel strength of GCL at normal stresses of 287, 575, 862, and 1,724 kPa is evaluated in this study. The data in this study was compared with the peel strength-internal shear strength relationships found in the literature. The interface shear strength of GCL and two textured geomembranes under normal stresses ranging from 240 kPa to 2,310 kPa is presented in this study. The study concludes that the relationship between peel strength and internal shear strength is unique based on manufacturing, needle-punching density and the method with and without heat treatment of the geotextile end fiber bundles. Additionally, in a composite liner system with a separate geomembrane above the GCL, the high peel strength GCL can force the failure mechanism from internal GCL failure to the interface between the GCL and the geomembrane.

Introduction

Geosynthetic clay liners (GCLs) are widely used as a hydraulic barrier in mine waste containment systems due to their superior hydraulic performance, self-healing properties, ease of installation, economic advantages, and easier quality control process (Robbins et al., 1995; Babu et al., 2001, Guyonnet et al., 2009; Fox and Stark, 2015; Rowe et al., 2019; Rowe, 2020). GCLs consist of a low permeability layer encapsulated between two geotextile layers. The low permeability layer typically contains natural sodium or a mixture of bentonite and polymer that primarily controls the hydraulic properties of the GCL. Many studies have evaluated the hydraulic properties, advantages, and limitations of the low permeability layer in GCLs (Meer and Benson 2007; Scalia and Benson, 2011; Bradshaw et al., 2013; Chen et al., 2019).

Internal and interface shear strength of GCLs and adjacent layers are typically measured via displacement-controlled direct shear testing. Internal and interface shear strength of GCLs is primarily controlled by the geotextile types, the method used to bond the geotextile and low permeability layer together (e.g., needle punching, heat treating after needle punching, stich bonding), bentonite extrusion, and the properties of adjacent material (geomembrane or soil). In the side slope and bottom liner applications, GCLs should provide appropriate internal and interface shear strength (Ghazizadeh and Bareither, 2021). In most heap leach pad applications, a high normal stress ranging between 1,000 to 2,000 kPa is applied on the liner system. The liner not only should have a high enough peak shear strength, but also the failure mechanism (i.e., interface failure or internal GCL shear strength failure) is also important since it governs the long displacement shear strength. The GCL should have high enough internal shear strength that it forces the failure to the interface layer between GCL and geomembrane.

Bareither and Ghazizadeh (2021) evaluated the failure mechanism of GCLs and textured geomembrane in normal stress ranging between 100 kPa to 2,000 kPa. They reported that as normal stress or geomembrane texture intensity (i.e., asperity height or spike density) increases, the failure mechanism moves from the interface between the GCL and the geomembrane to the GCL internal failure mode. GCL internal failure in design is undesirable since the long displacement shear strength of GCL is equivalent to the shear strength of unreinforced bentonite.

To evaluate the needle-punching extent on GCLs, industry uses a parameter known as peel strength. Peel strength is defined as the tensile force per specimen width that is required to separate the top and bottom geotextile (ASTM, 2015; Ghazizadeh and Bareither, 2018). Zornberg et al. (2005) evaluated the relationship between GCL peel strength and internal shear strength in normal stress of 35, 138, and 310 kPa and showed that a relationship between the GCL peel strength and internal shear strength appeared at the 310 kPa normal stress, but not at the lower normal stress of 35 and 138 kPa (Zornberg et al., 2005). Athanassopoulos and Yuan (2011) evaluated the GCL peel strength-shear strength relationship at normal stresses of 240 kPa, 479 kPa, and 718 kPa and suggested the following relationships for peel strength ranging between 740 to 2,666 N/m:

$$\tau_p=9.73\cdot(Ps)\text{^}0.4101 \quad \sigma_n=240 \text{ kPa} \qquad \text{(Equation 1)}$$

$$\tau_p=24.55\cdot(Ps)\text{^}0.3463 \quad \sigma_n=479 \text{ kPa} \qquad \text{(Equation 2)}$$

$$\tau_p=33.16\cdot(Ps)\text{^}0.3364 \quad \sigma_n=718 \text{ kPa} \qquad \text{(Equation 3)}$$

where τ_p is peak internal shear strength of GCL, Ps is the peel strength, and σ_n is normal stress applied during shear test.

Ghazizadeh and Bareither (2021) evaluated Equation 2 for Ps ranging between 740 to 2,180 N/m for heat and non-heat treated GCLs. They confirmed the general trend suggested in Athanassopoulos and Yuan (2011); however, they found disparities in shear strength results between products with relatively similar peel strength values.

The objective of this study was to: (i) evaluate the Athanassopoulos and Yuan (2011) relationship for higher Ps ranges up to 4,500 N/m; (ii) evaluate the effect of the needle-punching method (i.e., heat treated versus non-heat treated) on the internal shear strength of GCL; and (iii) evaluate the interface shear strength between GCL and geomembrane in high normal stress for heap leach pad applications.

Methods and materials

Characteristics of the eight GCLs used in this study are listed in Table 1. The materials were all commercially available needle-punched GCLs in North America. GCLs in this study were varied between geotextile mass per unit area, peel strength, and needle-punching methods. Two interface shear strength tests between soil and GCL were conducted as part of this study. The soil used in this study was a silty sand compacted to approximately 95% of maximum dry density at optimum moisture content according to standard compaction effort. The maximum dry unit weight of soil was 15.4 kN/m^2 and optimum water content was 20%. Two geomembranes were used in this study to perform the interface shear strength between GCL and geomembrane. Both geomembranes were HDPE and commonly used for heap leach pad application, one geomembrane had a thickness of 60 and the other had a thickness of 80 mm.

Table 1: Characteristics of the geosynthetic clay liners

Characteristic	GCL1	GCL2	GCL3	GCL4	GCL5	GCL6	GCL7	GCL8
Peel Strength , P_s (N/m)	1,874	2,417	2,539	2,434	3,275	3,362	4,448	4,203
Needle Punching Method	NHT[1]	NHT	NHT	HT[2]	HT	NHT	NHT	NHT
Carrier geotextile mass/area (g/m^2)	200	200	200	200	200	200	200	200
Cover geotextile mass/area (g/m^2)	200	200	200	200	200	300	300	300

[1]NHT = non heat treated needle-punching method, [2]HT = heat treated needle-punching method

The laboratory study includes: (i) 21 GCL internal shear strength tests under normal stresses of 287 kPa, 575 kPa, 862 kPa, and 1,724 kPa; (ii) 2 interface shear strength tests between GCL7 and silty sand soil under normal stress of 862 kPa and 1,724 kPa; and (iii) 7 GCL and geomembrane interface shear strength tests. The testing was performed according to ASTM D 6243.

GCL samples were prepared in 300 mm by 300 mm specimens for normal loads up to 861 kPa. Specimens with 150 mm by 150 mm dimensions were prepared for normal stress higher than 861 kPa. Prior to testing, GCLs were hydrated in deionized water for 24 hours under low normal stress of 9.6 kPa. Hydration was followed by a consolidation stage and increased load on top of GCL was doubled every 2 hours until the target normal load was achieved. Then the GCL was consolidated under the target normal load for 24 hours prior to shearing. Shearing was performed using a displacement-controlled method at a shear rate of 1 mm/min.

Results

GCL internal shear strength

A summary of the GCL internal shear tests is listed in Table 2. Data in Table 2 includes normal stress, peak and residual shear strength, secant and peak shear strength, and failure mode. Two general trends were observed for the internal shear strength of GCLs. The peak internal secant friction angle of a given GCL decreased with an increase in normal stress. Additionally, the internal shear strength of GCL increased as peel strength increased for a given normal load. Both of these trends agree with previous findings in the literature (Athanassopoulos and Yuan, 2011; Ghazizadeh and Bareither, 2021).

None of the GCL samples failed internally at a normal load of 287 kPa. The internal shear strength of GCL at a normal load of 287 kPa was higher than the interface strength between GCL's geotextiles and the steel grip of direct shear machine. The same behavior was recorded for high peel GCLs at higher normal stresses. GCL2 did not fail internally at normal stress of 575 kPa and GCL7 did not fail internally at a normal stress of 862 kPa.

A summary of the peak secant friction angle against GCL peel strength for a normal load of 575 kPa is shown in Figure 1. Figure 1 also shows the Athanassopoulos and Yuan (2011) model for a normal load of 718 kPa as well as the maximum peel strength that they used to establish Equations 1 to 3 (peel strength < 2,666 N/m). The secant peak friction angle of non-heat treated GCLs matched with the Athanassopoulos and Yuan (2011) model.

The secant friction angle of non-heat treated GCL was higher than the secant friction angle of heat treated GCL at comparable peel strength. This could be due to the difference in failure mechanism in the peel strength test and direct shear strength test. The secant friction angle of GCL4 was approximately 4.00 lower than GCL 2 despite having very close peel strength (peel strength for GCL2 and GCL4 were 2,417 N/m and 2,434 N/m, respectively). GCL2 and GCL3 resulted in approximately similar peak secant friction angle as GCL5 despite having a lower peel strength. The peel strength of GCL2 and GCL3 were 2,417 and 2,539 N/m, respectively, and GCL5 had a peel strength of 3,275 N/m. This result suggests that the

correlation curves suggested by Athanassopoulos and Yuan (2011) are not applicable for different needle-punching methods. This behavior suggests that the correlation between shear strength and peel strength is different for heat treated compared to non-heat treated GCLs. The higher secant friction angles are achievable with both methods; however, the non-heat treated GCLs can achieve the target shear strength at lower peel strength values.

Table 2: Summary of internal direct shear tests on 150-mm and 300-mm GCL specimens

Product	Normal Load (kPa)	Peak Shear Strength (kPa)	Secant Peak Friction Angle (°)	Long displacement Shear Strength (kPa)	Long displacement Friction Angle (°)	Failure Mode
GCL1	287	276	43	125	23	No Internal
	575	344	31	74	7	Internal
	862	399	25	89	6	Internal
	1,724	646	21	106	4	Internal
GCL2	287	216	37	124	23	No Internal
	575	366	32	184	18	No Internal
	862	477	29	95	6	Internal
GCL3	287	322	48.2	103	19.7	No Internal
	575	370.2	32.8	63	6.3	Internal
	862	469.7	28.6	86	5.7	Internal
GCL4	287	279	44	60	12	No Internal
	575	311	28	63	6	Internal
	862	402	25	82	5	Internal
	1,724	569	18	106	4	Internal
GCL5	287	317	48	96	18.5	No Internal
	575	361	32	60	6	Internal
	862	475	29	77	5.1	Internal
GCL6	862	503	30	79	5	Internal
	1,724	811	25	154	5	Internal
GCL7	862	573	34	572	32	No Internal
	1,724	944	29	159	5	Internal

A summary of the peak internal secant friction angle and peel strength of GCL for normal stress of 861 kPa is shown in Figure 2. The Athanassopoulos and Yuan (2011) model was not plotted for this normal stress since the normal stress of 861 kPa was larger than the normal stress range used in Athanassopoulos and Yuan (2011) study.

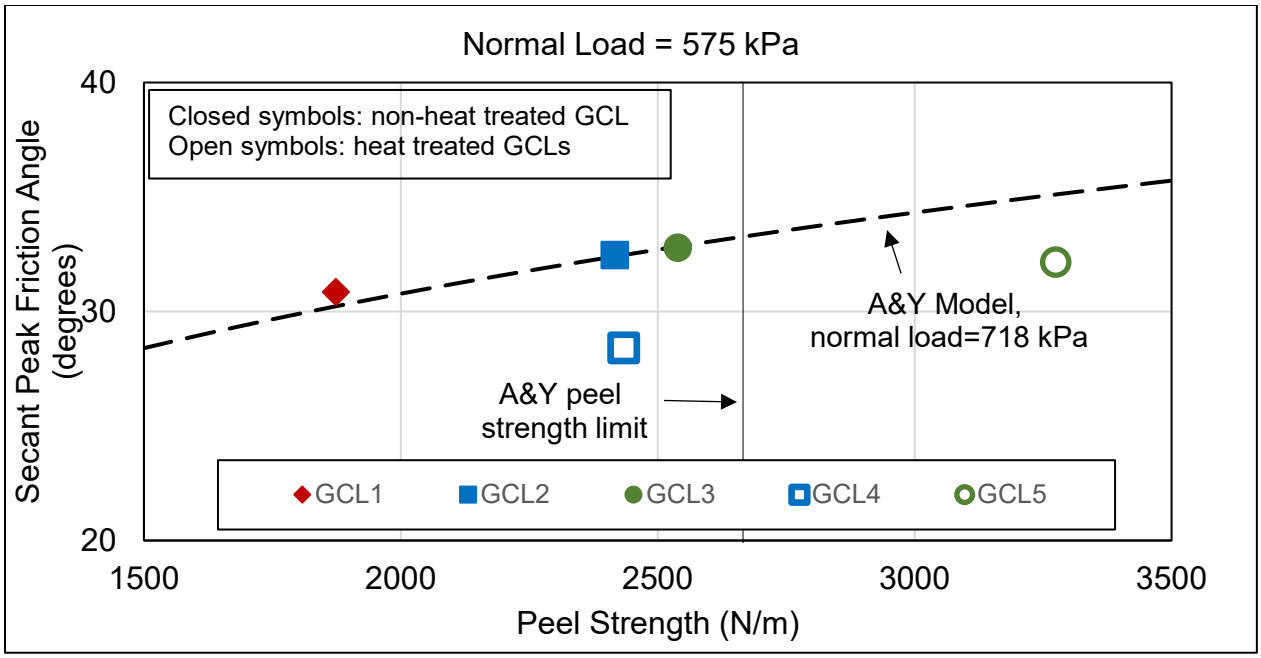


Figure 1: Relationship between internal peak secant friction angle with peel strength of GCL at normal stress of 575 kPa

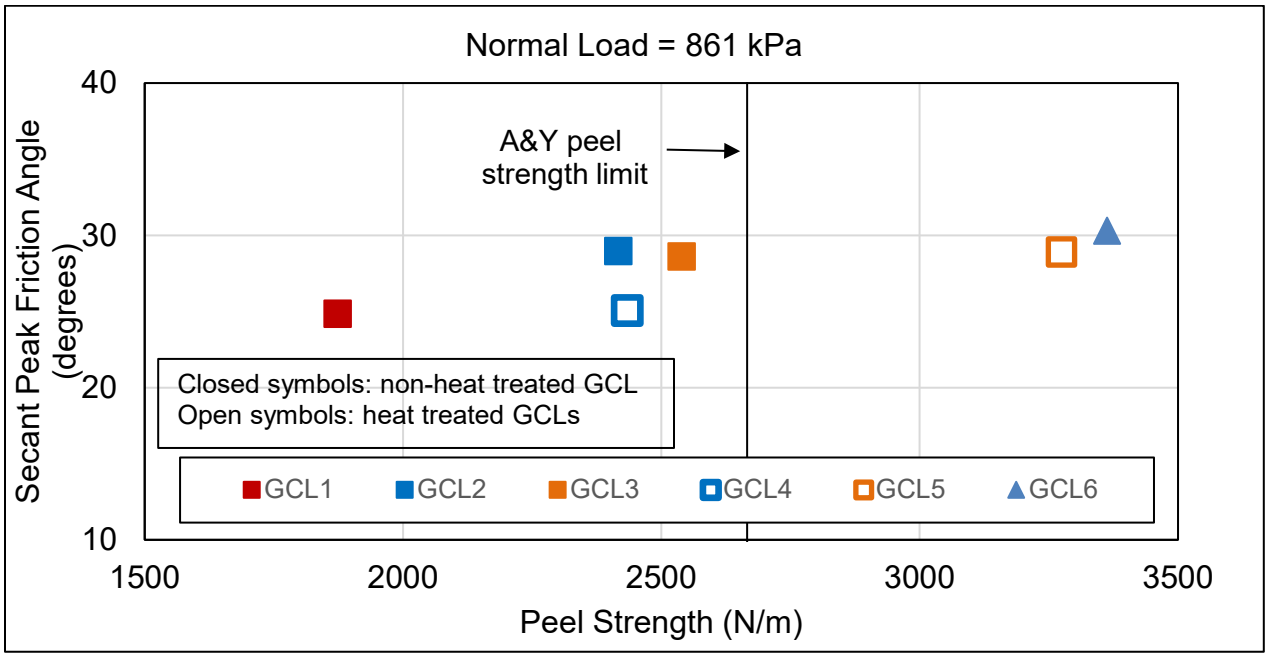


Figure 2: Relationship between internal peak secant friction angle with peel strength of GCL at normal stress of 861 kPa

In general, the secant friction angle increased with an increase in peel strength of GCL when data was evaluated independently (GCL4 and GCL5 as heat treated and GCL1, GCL2, GCL3, and GCL6 as non-heat treated).

Similarly to lower normal stress, the peak secant friction angle of the non-heat treated GCLs were higher than the heat treated GCLs with similar peel strength. Comparison of GCL2 and GCL3 with GCL4 suggests that the secant peak friction angle of non-heat treated GCL is approximately 3.7° higher than the heat treated GCL. Similarly, GCL6 had approximately 1.4° higher peak secant friction angle than GCL5 at approximately similar peel strength. This behavior suggests that high internal shear strength of GCL is achievable with both methods; however, peel strength and needle-punching methods should be considered in combination to evaluate the internal shear strength of a GCL.

A summary of internal peak friction angle of GCLs at a normal load of 1,724 kPa on 150 mm by 150 mm specimens is shown in Figure 3. Similarly, secant friction of GCL increased via an increase in peel strength of GCL in non-heat treated specimens. No conclusion can be drawn for heat-treated GCL since only one heat treated GCL specimen was tested for this normal stress.

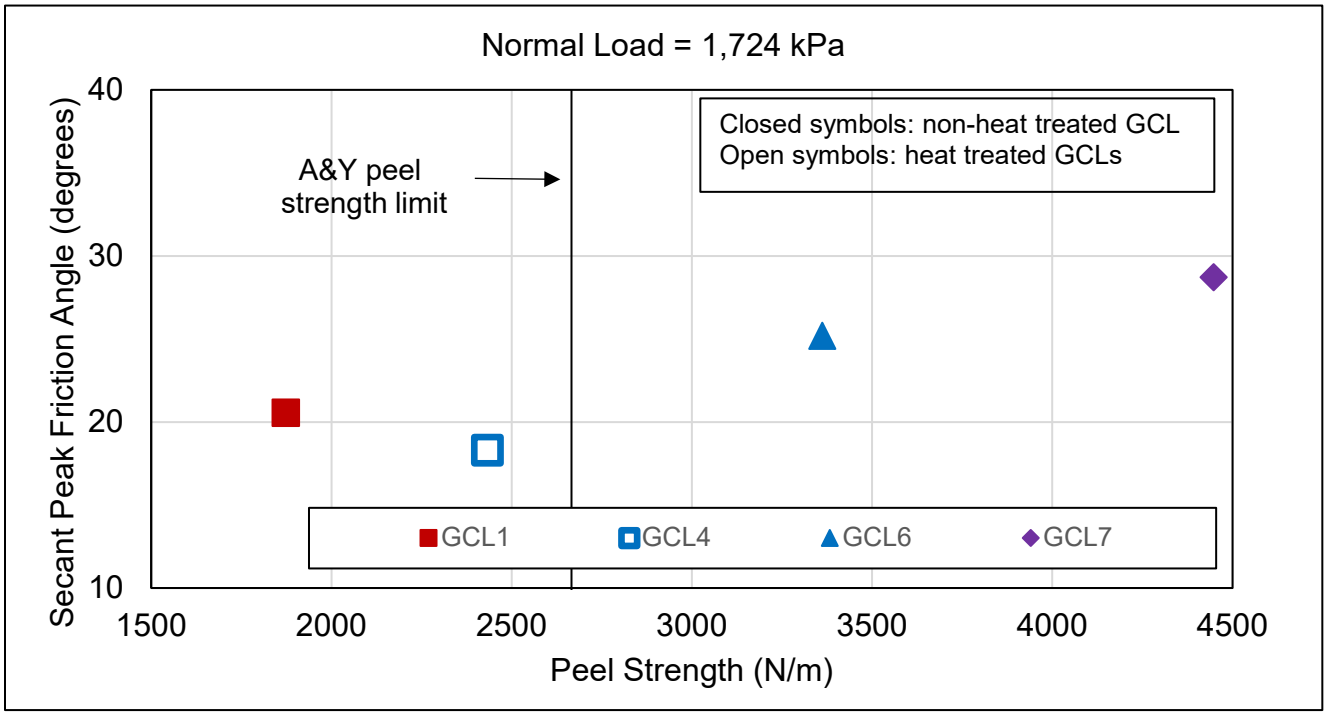


Figure 3: Relationship between internal peak secant friction angle with peel strength of GCL at normal stress of 1,724 kPa

Compacted soil and GCL interface shear strength

Two interface tests were performed between GCL and a compacted silty sand at 95% of maximum dry unit weight at optimum moisture content (dry unit weight = 15.4 kN/m^2 and water content = 20%) to further investigate the shear behavior of the GCL with the highest peel strength (i.e., GCL7). A summary of results is shown in Table 3. GCL7 did not fail internally in normal loads of 862 kPa and 1,724 kPa. The secant

friction angle of interface between silty sand and GCL was 27° and 25°. The long displacement friction angle of 24° and 23° confirms that the failure mechanism did not involve the internal GCL failure.

Table 3: Summary of interface shear strength between GCL7 (peel strength = 4,448 N/m) and compacted silty sand

Normal Load (kPa)	Peak Shear Strength (kPa)	Secant Peak Friction Angle (°)	Long-displacement Shear Strength (kPa)	Long displacement Friction Angle (°)	Failure Mode
862	443	27	377	24	Interface
1,724	817	25	741	23	Interface

Geomembrane and GCL interface shear strength

The results of interface shear strength between GCL8 and two geomembranes are shown in Table 4. Similarly to the observations of Bareither and Ghazizadeh (2021), the peak shear strength and residual shear strength decreased with an increase in normal stress.

Table 4: Summary of interface shear strength between GCL8 and two textured geomembranes

GM thickness (mm)	Normal Load (kPa)	Peak Shear Strength (kPa)	Secant Peak Friction Angle (°)	Long-displacement Shear Strength (kPa)	Long displacement Friction Angle (°)	Failure Mode
60	239	119	26	76	18	Interface
60	718	320	24	195	15	Interface
60	1,436	623	24	310	12	Interface
60	1,915	810	23	399	12	Interface
80	479	242	27	175	20	Interface
80	958	464	26	279	16	Interface
80	3,208	1,350	23	759	13	Interface/Partial GCL failure

However, the complete internal shear strength in GCL was not observed in any of the tests. This is due to the very high peel strength of GCL8, which provided enough internal shear strength to force failure mechanism to the interface between GCL and geomembrane. The only exception is the interface between GCL8 and the 80 mm geomembrane at 3,208 kPa normal stress, which resulted in partial GCL internal failure. This phenomenon happens when some of the GCL needle bonds fail but the two geotextiles do not completely get separated. As a result of the high peel strength of GCL8, the long displacement secant

friction angles range between 12 degrees (for very high normal stress) to 20 degrees (for medium normal stress).

Conclusion

The objectives of this study were to assess the internal and interface shear strength of high peel strength GCL for high normal loads in mining applications (e.g., heap leach pads) and understand the role of needle-punching method on the internal shear strength of GCL under high normal stress. The following conclusions have been drawn based on the results of this study:

- An increase in the peel strength of GCLs resulted in an increase in the internal shear strength of GCLs at a given normal stress, regardless of the needle-punching method (i.e., heat treated or non-heat treated). However, the relationship between peel strength and GCL internal shear strength was unique based on the needle-punching method.
- High secant friction angles were achieved in both heat treated and non-heat treated GCLs. However, the non-heat treated GCLs reached the target shear strength at a lower peel strength.
- Both the internal shear strength and interface shear strength of GCL decreased with an increase in normal stress.
- An increase in the peel strength of GCLs can change the failure mechanisms from the internal failure of the GCL (low long displacement shear strength) to geomembrane-GCL interface (high long displacement shear strength).

Acknowledgements

All of the peel strength and direct shear tests were performed at iSGI Testing Services, LLC. The authors would like to thank Dr Yuan for his useful input in this study.

References

ASTM. 2015. Standard test method for determining average bonding peel strength between top and bottom layers of needle-punched geosynthetic clay liners. ASTM D6496/6496M. West Conshohocken, PA: ASTM.

Athanassopoulos, C. and Yuan, Z. 2011. Correlation between needle punch-reinforced geosynthetic clay liner peel strength and internal shear strength. In *Geo-Frontiers 2011: Advances in Geotechnical Engineering*, edited by J. Han and D.E. Alzamora: 1922–1930.

Babu, Sivakumar G.L., Sporer, H., Zanzinger, H. and Gartung, E. 2001. Self-healing properties of geosynthetic clay liners. *Geosynth. Int.* 8(5): 461–470.

Bradshaw, S.L., Benson, C.H. and Scalia IV, J. 2013. Hydration and cation exchange during subgrade hydration and effect on hydraulic conductivity of geosynthetic clay liners. *J. Geotech. Geoenviron. Eng.* 139(4): 526–538.

Chen, J., Salihoglu, H., Benson, C.H., Likos, W.J. and Edil, T.B. 2019. Hydraulic conductivity of bentonite–polymer composite geosynthetic clay liners permeated with coal combustion product leachates. *J. Geotech. Geoenviron. Eng.* 145(9): 04019038.

Fox, P.J. and Stark, T.D. 2015. State-of-the-art report: GCL shear strength and its measurement – ten-year update. *Geosynth. Int*. 22(1): 3–47.

Ghazizadeh, S. and Bareither, C.A. 2018. Critical strength of high peel strength geosynthetic clay liners at low normal stresses. *Proceedings of Tailing and Mine Waste 2018*.

Ghazizadeh, S. and Bareither, C.A. 2021. Failure mechanisms of geosynthetic clay liner and textured geomembrane composite systems. *Geotext. and Geomembr.* 49(3): 789–803.

Ghazizadeh, S. and Bareither, C.A. 2021. Variability of fiber reinforcement, peel strength, and internal shear strength in needle-punched GCLs. *J. Geotech. Geoenviron. Eng.* 147(3): 04020181.

Guyonnet, D., Touze-Foltz, N., Norotte, V., Pothier, C., Didier, G., Gailhanou, H. and Warmont, F. 2009. Performance-based indicators for controlling geosynthetic clay liners in landfill applications. *Geotext. Geomembr*. 27(5): 321–331.

Meer, S.R. and Benson, C.H. 2007. Hydraulic conductivity of geosynthetic clay liners exhumed from landfill final covers. *J. Geotech. Geoenviron. Eng.* 133(5): 550–563.

Robbins, M.C. and Lu, H. 1995. Investigation of the suitability of a geosynthetic clay liner system for the El Paso solar pond (No. CONF-950725-). *American Solar Energy Society*, Boulder, CO, USA.

Rowe, R.K. 2020. Geosynthetic clay liners: perceptions and misconceptions. *Geotext. Geomembr*. 48(2): 137–156.

Rowe, R.K., Garcia, J.D.D., Brachman, R.W.I. and Hosney, M.S. 2019. Chemical interaction and hydraulic performance of geosynthetic clay liners isothermally hydrated from silty sand subgrade. *Geotext. Geomembr*. 47(6): 740–754.

Scalia IV, J. and Benson, C.H. 2011. Hydraulic conductivity of geosynthetic clay liners exhumed from landfill final covers with composite barriers. *J. Geotech. Geoenviron. Eng.* 137(1): 1–13.

Zornberg, J.G., McCartney, J.S. and Swan Jr., R.H. 2005. Analysis of a large database of GCL internal shear strength results. *J. Geotech. Geoenviron. Eng.* 131(3): 367–380.

Prediction of Pore Air and Water Pressure Propagation Induced by Extreme Rainfall in Tailings Dams

Simon A. Lorentz, SRK Consulting, South Africa
Charné Theron, Hanze University of Applied Sciences, Groningen, Netherlands

Abstract

The stability of upstream deposited tailings dams is dependent on maintaining a drawn down phreatic surface and unsaturated profile in its outer edge. However, it has been speculated that intense rainfall events could induce unexpected translation of pore air and water pressures into the tailings profile and thus compromise the effective stress in the unsaturated zone, or result in a sudden rise in the phreatic surface. This phenomenon, known as the Lisse effect, has been observed and studied in hydrological sciences to explain the rapid delivery of antecedent hillslope groundwater during storm events. However, the phenomenon has not been comprehensively applied to evaluating tailings dam slope stability. In this paper, the outcomes of controlled observations of the phenomenon in column and analytical experiments are assembled and evaluated in terms of the surface water application volumes and rate, the properties of the porous media, and the resultant nature of pore pressure and phreatic surface responses. In addition, application of applied theories to evaluate the rapid transmission of pore pressures through a profile in response to an advancing wetting front, leads to the development of a methodology that could be applied to tailings materials with a range of hydraulic conductivities and water retention characteristics. The theory is applied to a series of profiles of different tailings porous media, using varied water application rates. Resultant perturbations in phreatic surface elevation and changes to pore pressures in the unsaturated zone are used to evaluate changes in effective stress distribution in the unsaturated outer wedge and subsequent stability criteria. A possible evaluation algorithm for assessing stability criteria is suggested.

Introduction

The effects of pore air pressure increase due to advancing wetting fronts during extreme rainfall events have been the subject of considerable study (Guo et al., 2008; Sun et al., 2015; Waswa and Lorentz, 2019). Nevertheless, experimental observations are rare, particularly for soil materials of a range of textures. As a first attempt at observing pore air pressure, unsaturated water content, and suction dynamics during an advancing wetting front, tall columns (3 m) were filled with porous media and instrumented. Observations

were used to derive the dynamics of the transfer of pore air pressure to the capillary fringe (saturated porous media above the phreatic surface) and deductions were made on the effects on the effective stress.

These dynamics are illustrated for a sand, a tailings mix, and a platinum tailings material.

Methodology

Two columns that were 3,000 mm tall by 600 mm diameter were filled with porous media and instrumented with sensors to monitor the volumetric water content (TDR), pore water suction (tensiometers) and pore air pressure (especially constructed hollow probes [10 mm diameter] with breather holes and wrapped with a hydrophobic membrane). Pore air pressure was measured relative to atmospheric pressure using a differential pressure transducer attached to the hollow probe (Waswa, 2013). The column layout is illustrated in Figure 1.

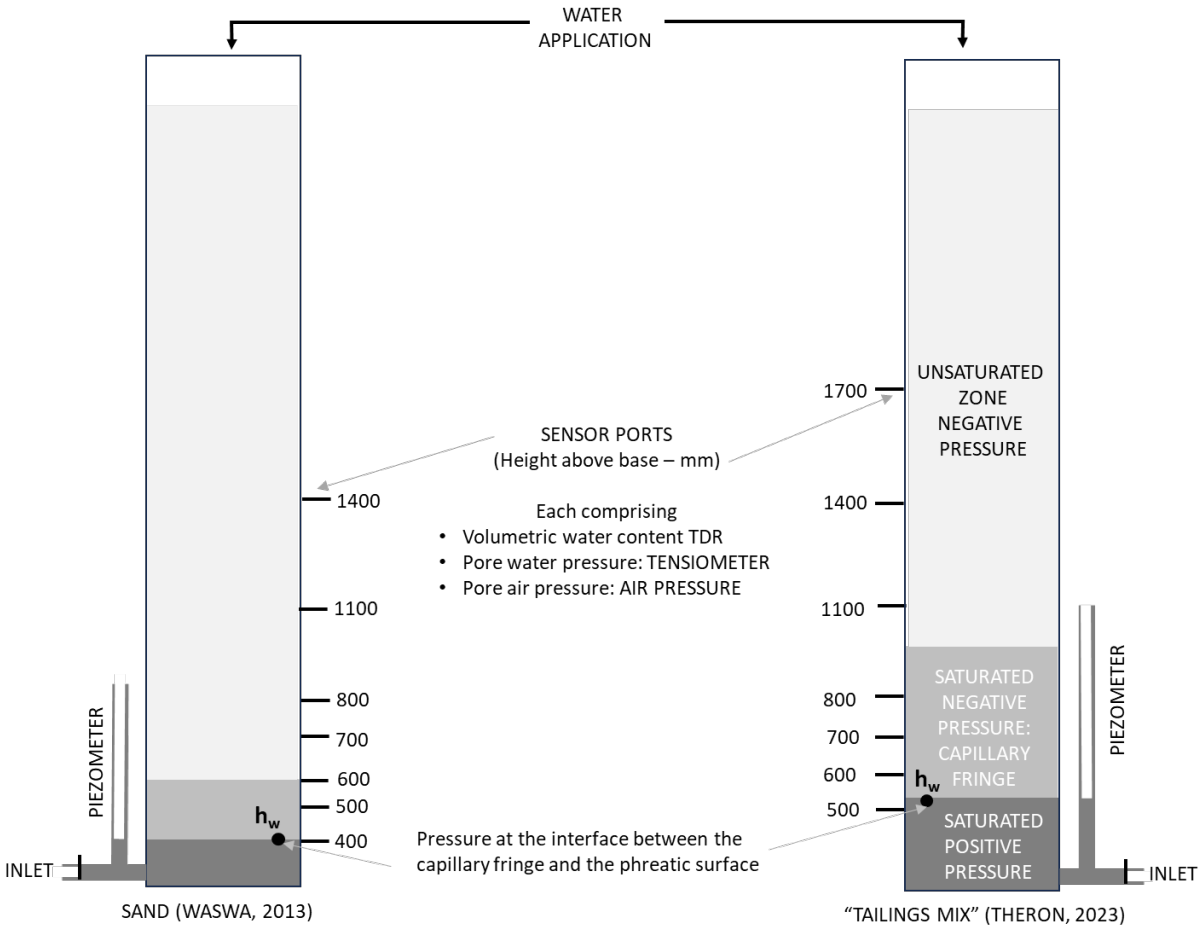


Figure 1: Column tests on sand (left) and tailings equivalent (right)

The first column (Waswa, 2013) was filled with a fine sand and the second with a "tailings mix," made up by combining two fine silica sands with two silica dust fractions so that the final texture was

similar to a known platinum tailings (Theron, 2023). The textural characteristics of the two materials are shown in Figure 2. The saturated hydraulic conductivity of the sand material was 8.7×10^{-5} m/s and that of the "tailings mix" was 7.5×10^{-8} m/s. Water retention characteristics of the materials were derived by air pressure desorption. The resultant van Genuchten parameters for these retention characteristics are listed in Table 1 and the curves are illustrated in Figure 3.

Table 1: van Genuchten hydraulic characteristics of the sand and "tailings mix"

	θ_s	θ_r	α (1/m)	n
Sand (Waswa, 2013)	0.36	0.05	3.15	2.54
Tailings Mix (Theron, 2023)	0.46	0.04	0.12	1.58

The instrumentation was inserted through the column walls and sealed. All the sensors were linked to a logger for recording at 20-second intervals. Water was introduced near the base of the column to establish a phreatic surface near the base (400 mm above the base in the sand and 500 mm above the base in the "tailings mix"). Once equilibrium was reached an extreme rainfall event was simulated by rapidly applying water to the top of the column.

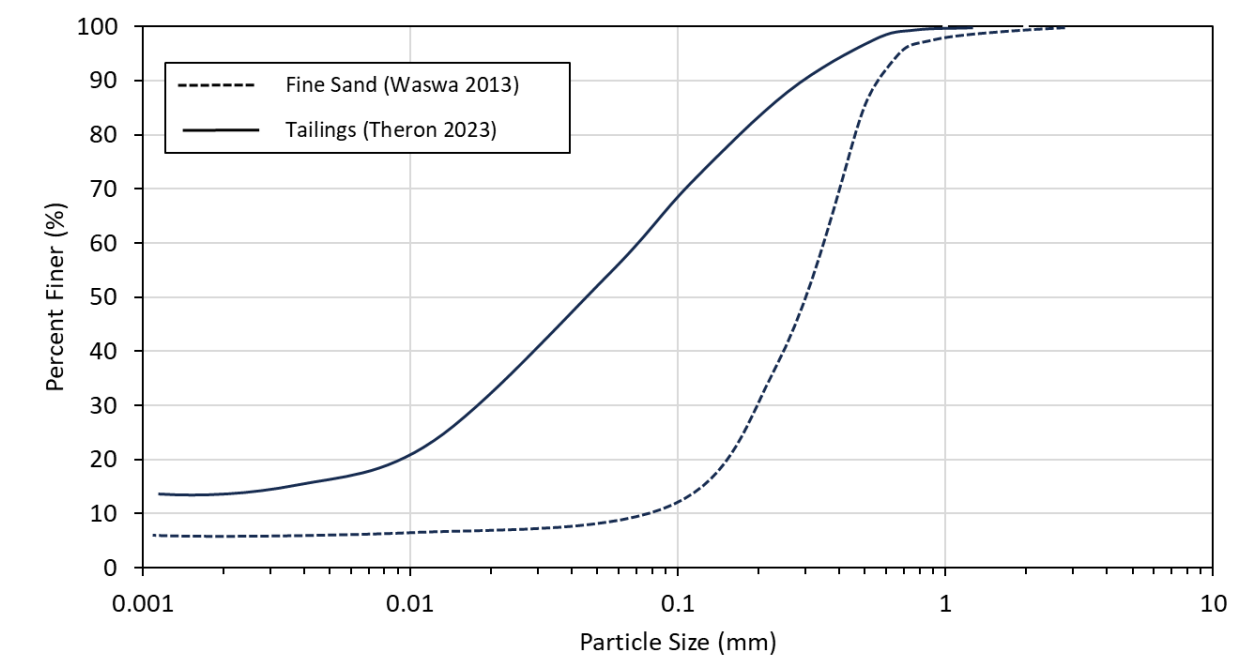


Figure 2: Texture of the sand and "tailings mix" materials

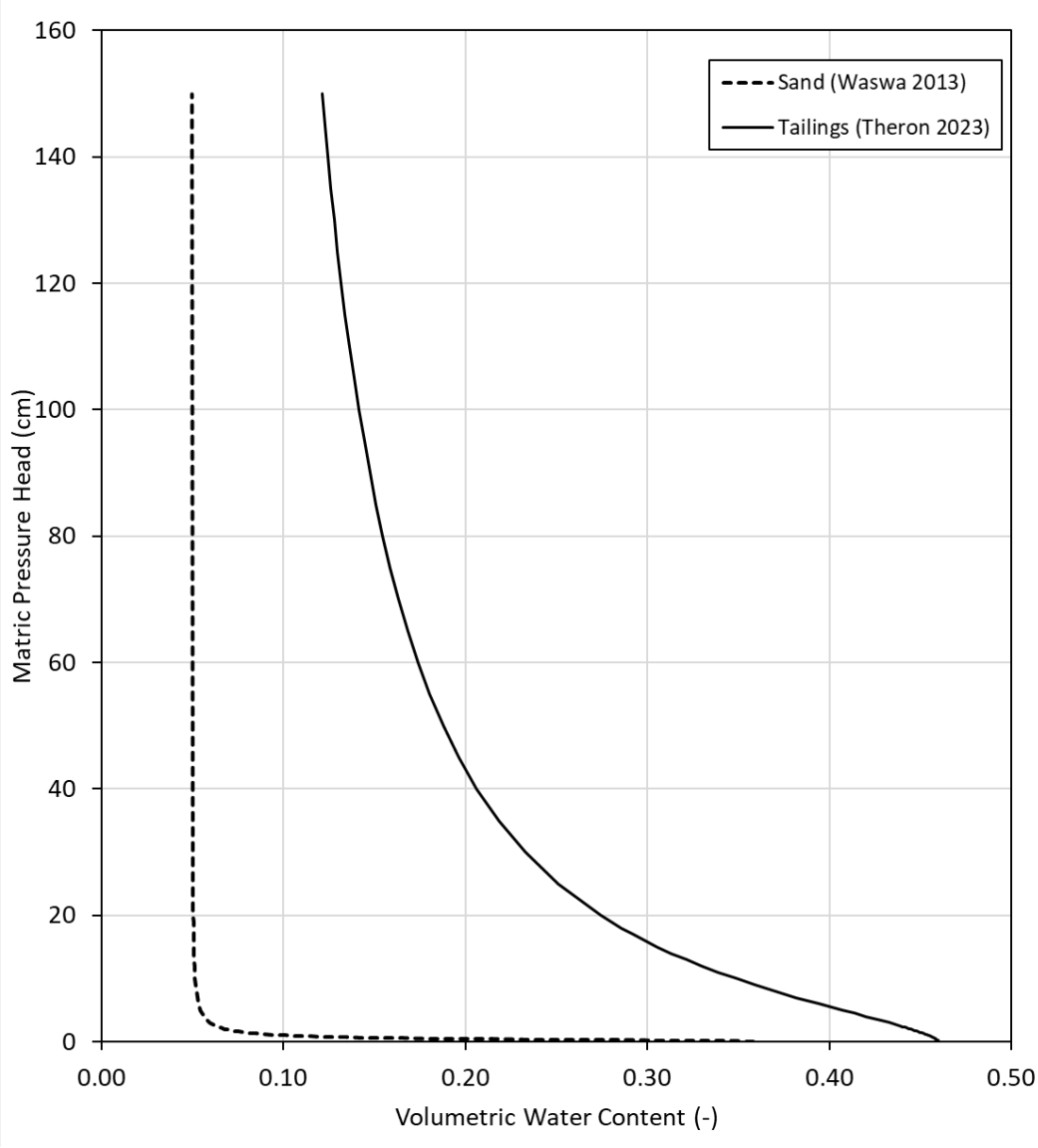


Figure 3: Water retention characteristics of the sand and "tailings mix" materials

Results

Although additional grades of sand were tested and multiple applications of simulated rain were made during the two experiments, the results of the first application for the fine sand and the "tailings mix" are used in an assessment of the dynamics.

Following Waswa (2013), a simple diffusion equation was used to simulate the transfer of pressure from air to water. The pore water pressure at the interface between the phreatic surface and the capillary fringe (h_w illustrated in Figure 1), was predicted using the diffusion equation solution as:

$$h_w = erfc\left(\frac{y_d}{\sqrt{4d_e t}}\right)$$

Where y_d is the depth of the capillary zone, d_e is an effective diffusion coefficient and t is the time. The diffusion coefficient was derived by fitting the equation to the observed pore water pressure data at the phreatic surface. The sand phreatic surface responded fully in 1 hour, with the applied pore air pressure completely transferred to the capillary fringe (h_w). The "tailings mix" however, took over 65 hours for the transfer of pressure to the capillary zone. These responses resulted in diffusion coefficients of 3.7×10^{-1} m^2/hour for the sand material and 3.0×10^{-2} m^2/hour for the "tailings mix." The responses are shown in Figure 4, together with a simulated response for a platinum tailings impoundment profile, which predicts a phreatic surface rise of almost 2 m.

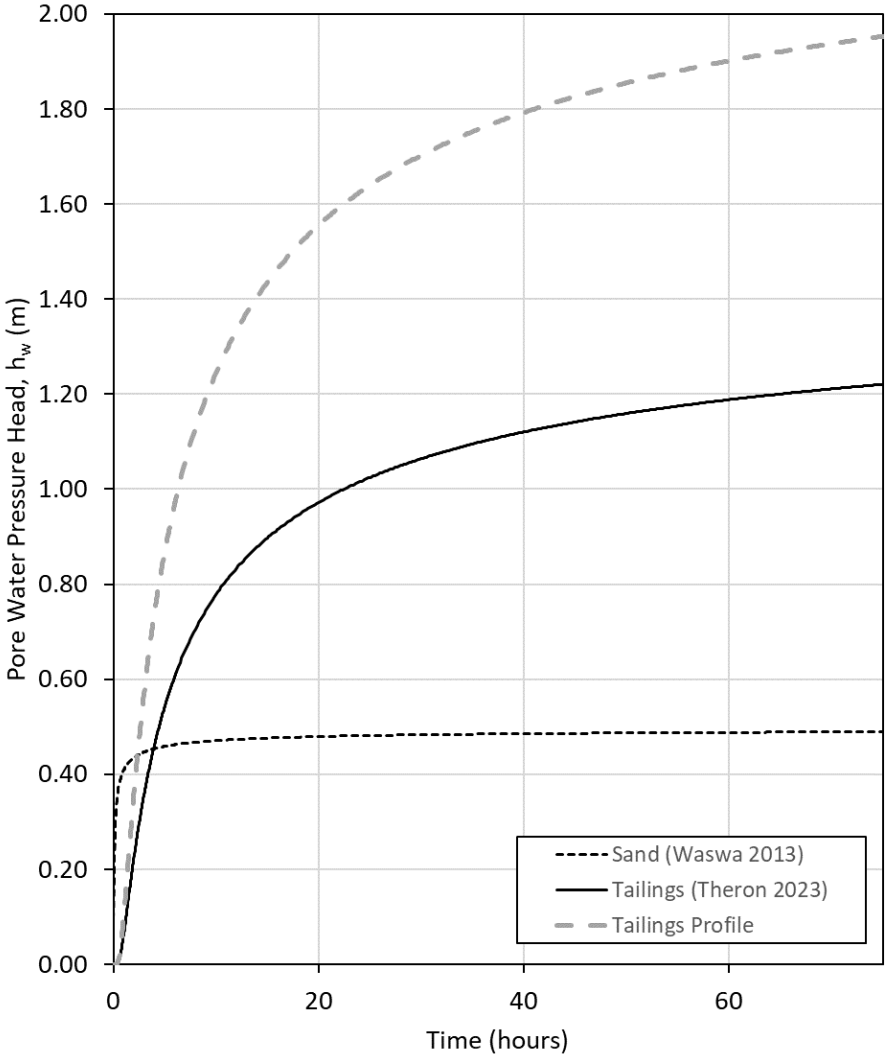


Figure 4: Interface pressure (h_w) response of the sand, "tailings equivalent" tests and platinum tailings profile

Discussion

Although the column experiments are somewhat shallow, compared to a profile in a tailings impoundment, the results indicate a significant difference in responses between the sand and the tailings materials. The tailings material took 10 times as long as the sand to respond to the pore air pressure propagation in the capillary fringe. In addition, these responses are far more rapid than the response of a wetting front predicted by Darcy's law. At a unit hydraulic gradient, it is predicted by Darcy's law that a wetting front would take a year to move through 2.5 m, whereas the pore air pressure induced a positive pressure rise in the phreatic surface within 65 hours. Experimental and analytical assessment of the phenomenon have been attempted in hillslope hydrology (Zhao et al., 2017; Waswa, et al., 2013), but attempts to link these responses to slope stability seem to be lacking.

While the rapid rise of the phreatic surface in the capillary fringe has been easily deduced from these experiments, the significance to stability criteria of an increased pore air pressure in the unsaturated part of the profile is less obvious. Relationships have been derived between the suction stress and unsaturated porous media characteristics (Fredlund and Morgenstern, 1977; Sun et al., 2015). The effective stress, (σ') is defined as the difference between the total stress, (σ) and the pore water pressure (μ_w), and the pore water pressure has been defined as the difference between the wetting phase pressure and a suction stress (σ^s), (Sun et al., 2015), so:

$$\sigma' = \sigma - u_a - \sigma^s$$

Where the suction stress is defined in terms of the water retention characteristic parameters as:

$$\sigma^s = -\frac{S_e}{\alpha}\left(S_e^{\frac{n}{1-n}} - 1\right)^{\frac{1}{n}}$$

So, it is evident that an increase in air pressure, without immediate, complete transference to the water phase pressure, may well affect the effective stress in the unsaturated profile of a tailings impoundment and lead to unstable conditions.

Conclusion

Tall column experiments have demonstrated a rapid response to pore air pressure increasing ahead of a significant wetting front. The pore air pressure increase responds immediately to the top surface of the capillary fringe and results in a rise in the phreatic surface. These responses, whether in sandy soils or fine tailings materials, occur far more rapidly than the predicted arrival of the wetting front through Darcy flux. This sudden rise in the phreatic surface could result in unstable slope conditions.

Pore air pressure increases in the unsaturated zone of a tailings profile may also impact the effective stress. Further experimentation and in-situ observation are required to determine how the pore air pressure

increase would influence stability conditions in the unsaturated profile as well as the phreatic surface. It is also recommended that documented tailings slope failures are examined using hydraulic characteristics, initial conditions, and rainfall sequences (up to 21 days antecedent rain) in the light of the mechanisms described here. In-situ, or larger scale tests, using porous media with a range of textures and varying antecedent application rates, are also recommended.

References

Fredlund, D.G. and N.R. Morgenstern. 1977. Stress state variables for unsaturated soils. *J. Geotech. Eng. Div.* 103(5): 447–466.

Guo, H., J.J. Jiao and E.P. Weeks. 2008. Rain-induced subsurface airflow and Lisse effect. *Water Resources Research* 44(7): 1–9. doi:10.1029/2007WR006294

Lu, N., M. Kaya and J.W. Godt, 2014. Interrelations among the soil-water retention, hydraulic conductivity, and suction-stress characteristic curves. *Journal of Geotechnical and Geoenvironmental Engineering* 140(5): 04014007: 1–10.

Sun, D.-M., Y-G. Zang and S. Semprich. 2015. Effects of airflow induced by rainfall infiltration on unsaturated soil slope stability. *Transp. Porous Med.* 107: 821–841.

Theron, C. 2023. Rainfall induced transient pressure wave mechanisms and pore water pressure dynamics in tailings. PhD thesis research, Department of Natural Sciences, University of the Western Cape, South Africa.

Waswa, G. and S.A. Lorentz. 2019. Dynamics of groundwater flow and upwelling pressure heads at a wetland zone in a headwater catchment. *SN Applied Sciences* 1: 1069 doi.org/10.1007/s42452-019-1052-9

Waswa, G.W. 2013. Transient pressure waves in hillslopes. PhD thesis research, Department of Civil Engineering, University of Kwa-Zulu Natal, South Africa.

Waswa, GW., A.D. Clulow, C. Freese, C., P.A.L. Le Roux. and S.A. Lorentz. 2103. Transient pressure waves in the vadose zone and the rapid water table response. *Vadose Zone Journal* 12(1): 1–18. doi:10.2136/vzj2012.0054.

Zhao, Peng, Pei Zhao, Chuan Liang, Li Tianyang and Zhou Baojia. 2017. Understanding the rapidity of subsurface storm flow response from a fracture-oriented shallow vadose through a new perspective. *Journal of Hydrology* 544: 628–639. DOI:10.1016/j.jhydrol.2016.12.007

Deportments of Magnesium and Silicon in a Two-part HCl-NaOH Leaching of Asbestos Tailings

Terry C. Cheng, CanmetMINING, Natural Resources Canada, Canada
Claude L. Morissette, COALIA, Thetford Mines (Quebec), Canada

Abstract

Asbestos tailings in the historical asbestos mines in Quebec were known to contain significant amounts of magnesium, nickel, iron, and silicon. The tailings sample used in the study contained 24.5% Mg, 0.268% Ni, 5.70% Fe, 17.4% Si. A two-part HCl-NaOH leach process was used to extract magnesium (Mg) from the tailings, while reducing the environmental footprints by valorization of the silicon (Si) content in the tailings to a sodium silicate solution, a precursor for amorphous silica production. The leaching of the asbestos tailings in a 10 M HCl solution at 60ºC for 60 minutes followed by the leaching of the acid leach residue in a 5 M NaOH solution at 60ºC for 60 minutes resulted in over 90% Mg extraction in the acid leachate, and nearly 90% Si extraction in the alkaline leachate. The overall mass reduction of the asbestos tailings was over 90%. The deportment results showed that 91.5% of the Mg was in the acid leachate, 1.03% was in the alkaline leachate and 7.44% was in the final residue. On the other hand, 3.43% of the Si was in the acid leachate, 85.7% in the alkaline leachate, and 10.9% in the final residue. Higher HCl strength (10 M) was found to be crucial not only to achieve high extraction yield for magnesium (> 90% Mg) in the acid leach, but also for higher silicon extraction (~ 90%) in the subsequent alkaline leach. Increasing the leaching time in the acid leach had little effect on the extraction yield of Mg, but undesirably more Si was dissolved in the acid leachate.

Introduction

The mining of chrysotile fibers (asbestos) began in the Eastern Townships of Quebec between 1877 and 1879 (BAPE, 2020). The annual production of asbestos reached its peak at 1.3 million tonnes in the 1980s, before restrictions of its use were in place in numerous countries (Vigneux and Roy, 2010). Asbestos tailings were generated after chrysotile was mined. At least 22 heaps of tailings and waste rocks are situated in three areas (Thetford Mines, East Broughton and Val des Sources, formerly Asbestos) with the total tonnage and area estimated to be over 2.0 Gt and 2240 ha, respectively (Beaudoin et al., 2008; Vigneux and Roy, 2010). According to mineralogical studies of the tailings samples obtained in the areas (Chen et al., 2000; Beaudoin

et al., 2008; Thibault, 2011), over 90% of the materials are serpentine, present mainly as lizardite, $Mg_3Si_2O_5(OH)_4$, with minor antigorite $(Mg,Fe)_3Si_2O_5(OH)_4$, but occasionally chrysotile free fibers are spotted ranging from less than 1% to 38% by volume. Minor amounts of brucite $Mg(OH)_2$, magnetite Fe_3O_4, and awaruite Ni_8Fe_3 are also present. The typical compositions of these asbestos tailings is as follows: 20 – 25% Mg, 0.2 – 0.3% Ni, 5 – 6% Fe and 18 – 20% Si (Ficara et al., 1998; Chen et al., 2000; Holcroft et al., 2018).

The most common remediation strategy for asbestos tailings is to leave them as they are in heaps, as the formation of hard cemented crust on the surface helps to limit the release of fibers into the air. However, other field remediation options, including revegetation and CO_2 sequestration by serpentine carbonation, have been tried (Lechat et al., 2016; Beaudoin et al., 2018). The shortfalls of these options are their inability to reduce the footprints of these tailings, as well as the permanent lock-up of valuable mineral resources present in them. Another well-developed strategy is to reprocess the asbestos tailings, because they are a vast potential magnesium resource, available at little or no cost (Celik et al., 1992; Ficara et al., 1998; Watson et al., 2000).

For over a decade, the Magnola project has directed research and development efforts towards resolving the technical issues in filtration and solution purification associated with the leaching of silicate minerals as well as iron and impurities controls. Technologies for extracting Mg from the asbestos tailings to produce ultra-pure $MgCl_2$ brine suitable for the electrolytic production of high-quality magnesium metal was commercialized and operationalized in Danville, Quebec, between 2000 and 2003. Unfortunately, the Magnola plant was shut down due to the significant drop in the magnesium price at the time (Burstow, 2002; Creber et al., 2011; Habashi, 2017). Nevertheless, the electrolytic production of Mg powered by hydroelectricity (as is the case in Quebec) is considered to produce lower GHG emissions (5 kg CO_2 per kg Mg produced) when compared to the thermal reduction process, the so-called Pidgeon Process (12 kg CO_2 per kg Mg produced), which currently produces around 85% of the world's primary magnesium (Ehrenberger, 2020). Another advantage of extracting Mg from serpentine tailings using concentrated HCl acid is its potential of valorization of the Si content in the tailings as silicates are converted to amorphous silica during the leaching process (Chen et al., 2000; Dutrizac et al., 2000):

$$Mg_3Si_2O_5(OH)_{4(s)} + 6HCl_{(aq)} \rightarrow 3\,MgCl_{2(aq)} + 2SiO_{2(amorphous)} + 5H_2O_{(l)} \qquad \text{Reaction 1}$$

The amorphous silica in the resulting acid leach residue can be dissolved in a concentrated NaOH solution, thus producing a concentrated sodium silicate solution:

$$SiO_{2(amorphous)} + 2NaOH_{(aq)} \rightarrow Na_2SiO_{3(aq)} + H_2O_{(l)} \qquad \text{Reaction 2}$$

The latter can be further purified and used as a feed stock to produce high-quality amorphous silica suitable for a wide range of commercial uses, for example in rubber and chemical sensor applications (Fedoročková et al., 2014 and 2015).

The present study examines the potential of reprocessing the asbestos tailings with a two-part HCl-NaOH leaching process. The objective is to reveal the operating conditions under which the extraction of Mg and Si from asbestos tailings can be optimized. Five series of two-part leaching experiments, involving the leaching of asbestos tailings sample in concentrated HCl solutions in part A, and the leaching of the resulting acid leach residue in concentrated NaOH solutions in part B, were conducted. The extraction yields of the elements of interest (Mg, Ni, Fe, and Si) in both the acid and alkaline leachates were determined based on the compositions of the feed and the product streams. The deportment of the elements, as a result of the two-part HCl-NaOH leaching, were partitioned into three fractions; that is, (i) in the acid leachate; (ii) in the alkaline leachate; and (iii) in the final leach residue. The mass reduction achieved in each leaching step and the overall mass reduction were also reported.

Methods

Materials

An asbestos tailings sample (ABT) was collected in a tailings storage facility in the historical Thetford Mines areas in Quebec. The tailings sample was sent to COALIA, a research laboratory specialized in the safe processing of asbestos materials, where sample preparation, characterization, and leaching experiments were conducted.

Procedure

Five series of two-part HCl-NaOH leach experiments were conducted. Each series of experiments consisted of part A (acid leach) and part B (alkaline leach). The experimental conditions included the initial concentrations of the leachates ($[HCl]_i$ and $[NaOH]_i$), the respective leaching temperatures, T_A and T_B, and retention times, τ_A and τ_B, for each series of experiments are given in Table 1. In part A, a pre-determined amount of tailings sample ABT (250.00 ± 0.12 g) was placed in a known volume of concentrated HCl solution such that the initial pulp density was kept at 45.0 wt.%, which was equivalent to a solid-to-liquid (S/L) ratio of about 2:5. At the end of each acid leach test, the final acid leachate and leach residue were separated and collected. The acid leach residue was washed with a copious amount of deionized water before drying in an oven at 60°C until there was no further change in weight. A portion of the acid leach residue was returned to be used as a feed to part B (alkaline leach tests). A fixed amount (100.00 ± 0.01 g) of the acid leach residue was placed in a known volume of concentrated NaOH solution such that the initial pulp density was kept at 17.0 wt.%, which was equivalent to a S/L ratio of 1:6. The final alkaline leachate

and leach residue were collected following the same procedure used in the acid leach tests. The dried solid and filtrate samples obtained in the leach tests were analyzed for the element of interests using XRF and ICP-OES, respectively. The calculations of the percent extraction and deportment of the elements of interest (Mg, Ni, Fe and Si) are given in the Appendix.

Table 1: Experimental conditions for the two-stage acid and alkaline leach experiments

	Part A (Acid Leach)			Part B (Alkaline Leach)		
Series	$[HCl]_i$ (M)	T_A (°C)	τ_A (min)	$[NaOH]_i$ (M)	T_B (°C)	τ_B (min)
1	5.0.	60.	60.	5.0	60.	60.
2	10.	60.	60.	5.0	60.	60.
3	10.	60.	300.	5.0	60.	60.
4	10.	60.	360.	5.0	60.	360.
5	10.	60.	360.	5.0	90.	360.

Results and discussion

The composition of the tailings sample ABT is given in Table 2. The tailings sample contained 24.5% Mg, 0.268% Ni, 5.70% Fe, and 17.4% Si, and had a LOI of 14.2%. The sample was well homogenized as indicated by the low standard deviations for the elements of interest. The X-ray diffraction pattern of the sample indicates lizardite $Mg_3(Si_2O_5)(OH)_4$ as the major serpentine phase and antigorite (Mg, $Fe)_3Si_2O_5(OH)_4$, as the minor serpentine phase, with a fair amount of magnesium and nickel presented as brucite $Mg(OH)_2$, and awaruite Ni_8Fe_3, respectively. Other iron phases such as magnetite Fe_3O_4 are also present. The mineralogy of the tailings sample ABT is comparable to those previously obtained in the Thetford Mines areas (Chen et al., 2000; Thibault, 2011). The tailings sample was ground and used in the two-part HCl-NaOH leach tests. The bulk particle size distribution (PSD) of the tailings sample is given in Figure 1, whereas the apparent particle size P_{80} was determined to be around 114 μm.

Table 2: Composition of the asbestos tailings samples used in the acid leach (stage A) experiments

sample	Mg (%)	Ni (%)	Fe (%)	Ca (%)	Al (%)	Si (%)	LOI (%)
ABT	24.5	0.268	5.70	0.289	0.807	17.4	14.2
$\sigma \times 10^1$	± 2.18	± 0.279	± 0.784	±0.0412	± 1.29	± 5.34	± 5.01
n	4	4	4	4	4	4	4

There were five series of two-part leaching experiments, involving the leaching of asbestos tailings sample (ABT) in concentrated HCl solutions in part A, followed by the leaching of the resulting acid leach

residue in concentrated NaOH solutions in part B. The compositions of the resulting leach residues and leachates obtained in part A and part B leach tests are shown in Tables A1 to A4 in the Appendix.

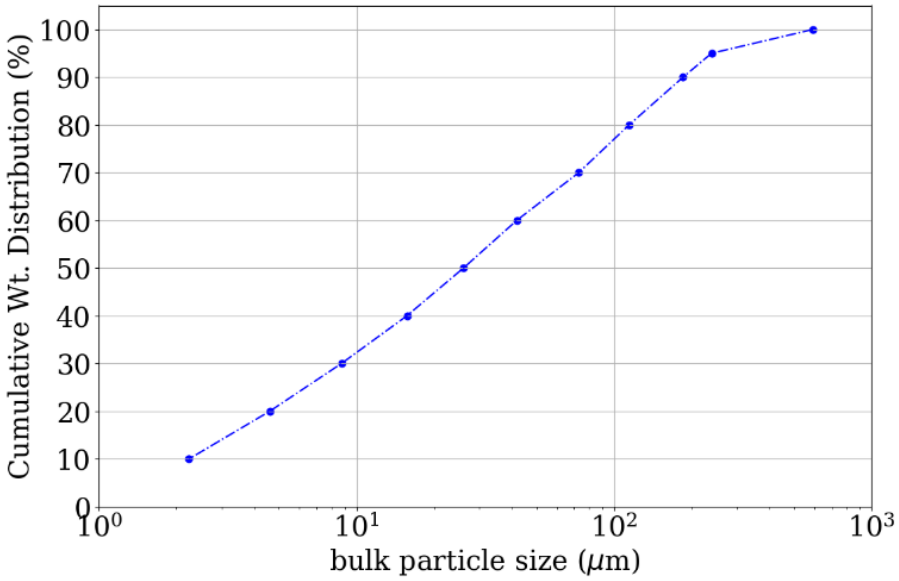


Figure 1: The bulk particle size of the asbestos tailings sample (ABT) with P_{80} of 114 µm

Effects of HCl strength

In Series 1 of the two-part HCl-NaOH leach experiments, the tailings sample was leached in a 5 M HCl solution at 60ºC for 60 minutes in part A, followed by part B, leaching of the leach residue obtained from part A in a 5 M NaOH solution at 60ºC for 60 min. The extraction yields of the elements of interest (Mg, Ni, Fe and Si) in each part are presented as a bar chart in Figure 2. The results of Series 1, denoted as (A1: 5M HCl) and (B1: 5 M NaOH), showed that over 90% of Ni but less than 60% of Mg and around 45% of Fe were extracted in the acid leachate, while around 50% of Si was extracted in the alkaline leachate. In Series 2, the HCl strength in part A (acid leach) was increased from 5 M to 10 M. As a result, both the extraction yields of Mg and Fe increased to over 90% (see bars denoted as A2: 10 M HCl). Importantly, the extraction yield of Si in the subsequent alkaline leach (B2: 5 M NaOH) increased significantly to almost 90% despite all conditions being identical to that used in Series 1, except for the increase in HCl strength. The HCl strength not only increased the extraction yield of Mg in the acid leach stage but also enhanced the dissolution of Si in the subsequent alkaline leach stage.

However, at a higher HCl strength, the co-extraction of Fe also increased from 45 to 90%. This suggested that at least one of the Mg- and Fe-bearing silicate minerals present in the tailings sample was leached only at higher HCl strength, resulting in more silicate minerals converted to amorphous silica as in Reaction 1. The use of higher HCl strength was necessary in the acid leach stage for a higher extraction

yield of Si in the subsequent alkaline leach stage. Higher HCl strength resulted in higher mass reduction in the acid leach step (Series 1: 31.7% vs. Series 2: 39.3%), and significantly higher mass reduction in the subsequent alkaline leach step (Series 1: 38.1% vs. Series 2: 85.2%), as shown in Figure 2.

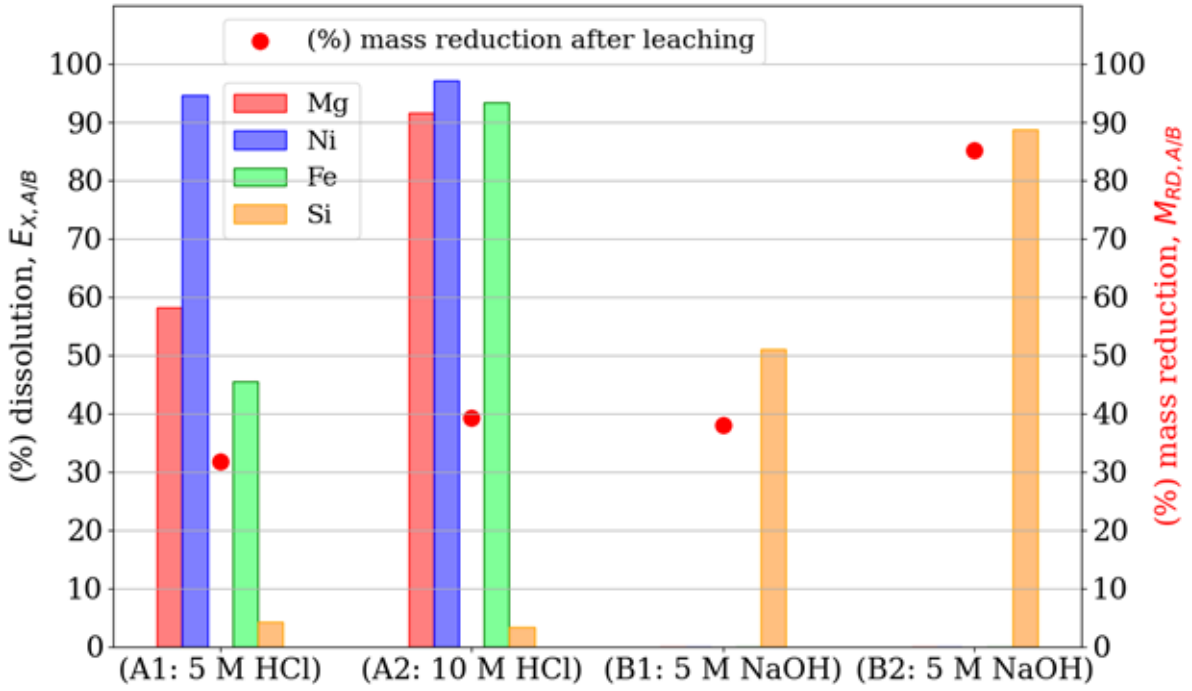


Figure 2: The comparison of the percent extraction, $\%E_{X,A/B}$, of the elements of interest (Mg, Ni, Fe and Si) and the percent mass reduction, $\%M_{RD,A/B}$, in the two-part (A) HCl - (B) NaOH leach process conducted with 5 M and 10 M HCl strength (Series 1 vs. Series 2)

Effects of retention time and temperature

The retention time of the acid leach (part A) was increased from 60 minutes in Series 2 to 300 minutes in Series 3. When comparing the results of Series 3 to Series 2, there was no considerable difference in terms of Mg, Ni and Fe extraction, except a higher Si extraction (6.15% vs. 3.43%) in the acid leach. The retention time of the acid leach (part A) was further increased to 360 minutes in Series 4. Again, no considerable difference was observed when the results of Series 4 were compared to those obtained in Series 2 and 3. However extended retention time in the acid leach resulted in more Si extracted in the acid leachate (i.e., 16.4% in Series 4), but it had little effect on the extraction of Si in the alkaline leachate. An increase in the temperature of the alkaline leach from 60 to 90°C in Series 5 also had little effect on the extraction of Si.

Deportments of Mg, Ni, Fe and Si

Based on the compositions of the acid and alkaline leachates as well as the final residues obtained in the five series of two-part HCl-NaOH leach tests (see Tables A1 to A4 in the Appendix), the deportments of the

elements of interest under various leaching conditions are mapped out in Figure 3. The deportment results showed that the leaching of the asbestos tailings in a 10 M HCl at 60°C, followed by the leaching of the acid leach residue in a 5 M NaOH solution, resulted in the maximum extractions of Mg, Ni, Fe and Si in the leachates (refer to Series 2). The amount of Mg, Ni, Fe, and Si remaining in the final residue obtained from Series 2 were 7.44%, 1.30%, 5.22%, and 10.9%, respectively. The deportments of Mg, Ni, and Si in the acid leachate were 91.5%, 97.1%, 93.4%, and 3.43%, respectively. The deportments of Mg, Ni, and Si in the alkaline leachate were 1.03%, 1.55%, 1.41%, and 85.7%, respectively. The overall mass reduction after the two-part HCl-NaOH leaching was around 90%.

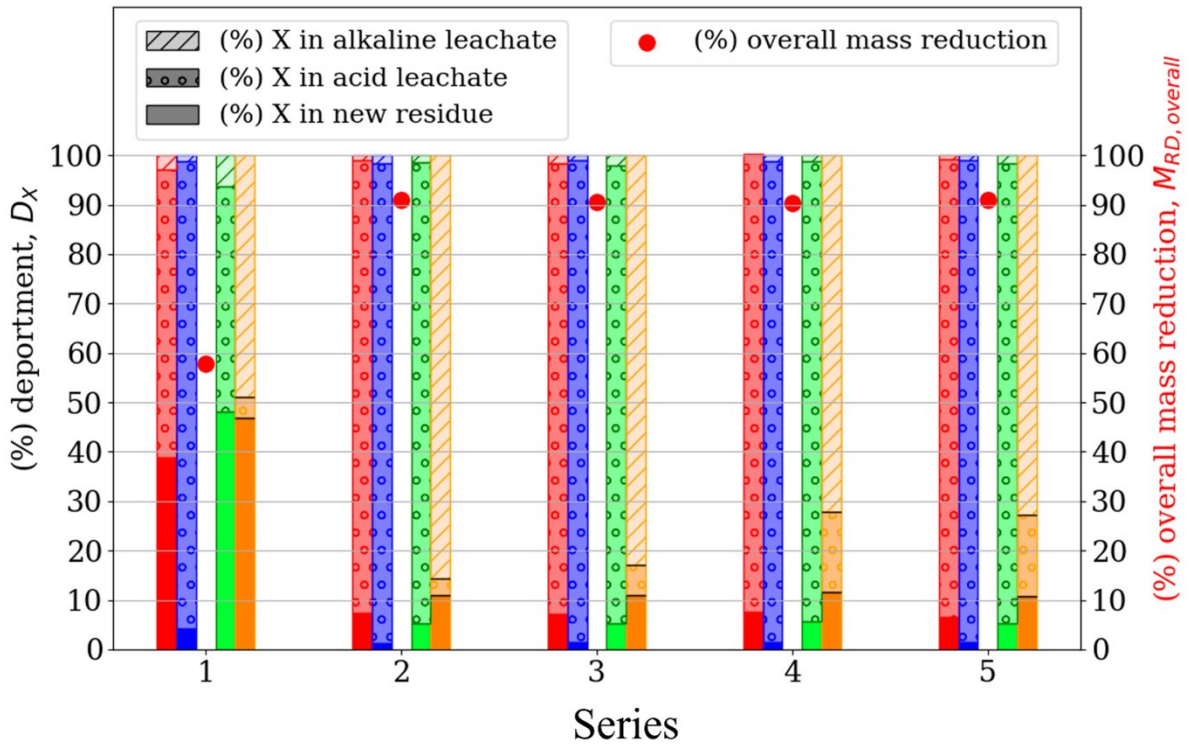


Figure 3: The deportments of the elements of interest, $\%D_X$, where X: Mg (red), Ni (blue), Fe (green) and Si (orange), and the percent overall mass reduction, $\%M_{RD, overall}$, in the five series of two-part HCl-NaOH leach process

Conclusion

1. The leaching of asbestos tailings sample ABT in a 10 M HCl solution at 60oC in 60 minutes, followed by the leaching of the resulting acid leach residue in a 5 M NaOH solution, resulted in over 90% extractions of Mg and Ni in the acid leachate and nearly 90% Si extraction in the alkaline leachate.
2. The use of higher HCl strength (10 M vs. 5 M) was found to be crucial not only in achieving higher Mg extraction in the acid leach but also in reaching higher Si extraction in the subsequent alkaline leach step.

3. The increase in the acid leach retention time had not improved the extraction of Mg and Ni but undesirably increased the dissolution of Si in the acid leachate.
4. The increase in the alkaline leach temperature and/retention time had not improved the extraction of Si in the alkaline leachate.

Acknowledgements

Funding for the work was provided by Natural Resources Canada's Critical Minerals Research, Development and Demonstration Program.

References

BAPE. 2020. *L'état des lieux et la gestion de l'amiante et des résidus miniers amiantés: rapport d'enquête et d'audience publique. Rapport 351.* Québec: Bureau d'audiences publiques sur l'environnement Québec.

Beaudoin, G., Hébert, R., Constantin, M., Duchesne, J., Cecchi, E., Huot, F., Vigneau, S. and Fiola, R. 2008. Spontaneous carbonation of serpentine in milling and mining waste, southern Québec and Italy. *Proceedings of Accelerated Carbonation for Environmental and Materials Engineering (ACEME2008),* Rome, Italy: 73–82.

Burstow, C. 2002. Magnesium: the impact of projected new supply on prices over the next five years. *Mineral Processing and Extractive Metallurgy* 111(2): 62–64.

Celik, C., Ghastas, N.E., Lenz, J., Létourneau, C. and Santiago, R. 1992. Magnola – an innovative approach for magnesium production. *Proceedings of the International Symposium on Advances in Production and Fabrication of Light Metals Matrix Composites* (eds: M.M. Avedesian, L.J. Larouche and J. Masounave). 31st Annual Conference of Metallurgists of CIM. Edmonton, Canada, August 23–27: 3–22.

Chen, T.T., Dutrizac, J.E. and White, C.W. 2000. Serpentine ore microtextures occurring in the magnola magnesium process. *JOM* 52 (4): 20–22.

Creber, D., Davis, B. and Kashani-Nejad, S. 2011. Magnesium metal production in Canada. In *The Canadian Metallurgical and Materials Landscape:* 1960–2011.

Dutrizac, J.E., Chen, T.T. and White, C.W. 2000. Fundamentals of serpentine leaching in hydrochloric acid media. *Proceedings of Magnesium Technology 2000* (eds: H.I. Kaplan, J.N. Hryn and B.B. Clow), TMS, Warrendale, U.S.A.: 41–50.

Ehrenberger, S. 2020. Carbon footprint of magnesium production and its use in transport applications – Update of IMA Report Life cycle assessment of magnesium components in vehicle construction (2013). International Magnesium Association (IMA), Minneapolis, U.S.A., 41 pages.

Fedoročková, A., Plešingerová, B., Sučik, G., Raschman, P. and Doráková, A. 2014. Characteristics of amorphous silica prepared from serpentinite using various acidifying agents. *International Journal of Mineral Processing* 130: 42–47.

Fedoročková, A., Raschman, P., Sučik, G., Plešingerová, B., Popovič, Ľ. and Briančin, J. 2015. Processing of serpentinite tailings to pure amorphous silica. *Ceramics – Silikáty* 59(4): 275–282.

Ficara, P., Chin, E., Walker, T., Laroche, D., Palumbo, E. and Celik, C. 1998. Magnola: A novel commercial process for the primary production of magnesium. *CIM Bulletin* 75–80.

Habashi, F. 2017. Success and failure of the Canadian metallurgical industry. *SciFed Journal of Metallurgical Science* (2017).

Holcroft, G., Whitton, T., Skalbania, N.M., Dreisinger, D. and Zuliani, D. 2018. Novel modular process to produce magnesium metal from serpentine tailings. *Proceedings of the 75th Annual World Magnesium Conference, International Magnesium Association.*

Lechat, K., Lemieux, J.-M., Molson, J., Beaudoin, G. and Hébert, R. 2016. Field evidence of CO_2 sequestration by mineral carbonation in ultramafic milling wastes, Thetford Mines, Canada. *International Journal of Greenhouse Gas Control* 47, 110–121.

Thibault, Y. 2011. Mineralogical characterization of near-surface tailings materials produced from chrysotile mining in the Thetford Mines area, Quebec. Division Report MMSL 11-008(TR), CanmetMINING and Mineral Science Laboratories, Ottawa, Canada, 78 pages.

Vigneux, J. and Roy, S. 2010. Revegetation and reforestation techniques of asbestos mine waste piles in Québec. *Canadian Reclamation* 1: 8–11.

Watson, K., Ficara, O., Charron, M., Peacey, J., Chin, E., Bishop, G. 2000. The magnola demonstration plant: a valuable investment in technology development and improvement. *Proceedings of Magnesium Technology 2000* (eds: H.I. Kaplan, J.N. Hryn and B.B. Clow), TMS, Warrendale, U.S.A.: 27–30.

Appendix

Calculations

The percent extraction of the elements of interest (X: Mg, Ni, Fe, and Si) in part A (acid leach), $\%E_{X,A}$, and part B (alkaline leach), $\%E_{X,B}$, can be determined with this equation:

$$\%E_{X,A/B} = (1 - \frac{\%X_P \times m_P}{\%X_f \times m_f}) \times 100\% \quad \text{(A1)}$$

where m and $\%X$ are the mass and the percent content of element X in the solid sample. The subscripts, f and p, correspond to the terms for the feed and the leach residue, respectively. The deportments of the respective elements are partitioned into three fractions: those reported to (i) acid leachate, (ii) alkaline leachate and (iii) final leach residue. The percent deportment of element X in the acid leachate, $\%D_{X,A}$ is the amount of element X extracted from the tailings sample ABT in part A (acid leach) and can be equated as:

$$\%D_{X,A} = \%E_{X,A} \quad \text{(A2)}$$

The deportment of element X in the alkaline leachate, $\%D_{X,B}$ is the amount of element X extracted from the acid leach residue in part B (alkaline leach) and can be written as:

$$\%D_{X,B} = (100 - \%E_{X,A}) \times \%E_{X,B} \quad \text{(A3)}$$

Then, the deportment of element X in the final alkaline leach residue, $\%D_{X,S}$ is determined by differences; that is:

$$\%D_{X,S} = 100 - \%E_{X,A} - \%E_{X,B} \quad \text{(A4)}$$

The percent mass reduction, $\%M_{RD,A/B}$ as a result of acid leaching in part A or alkaline leaching in part B is determined by this equation:

$$\%M_{RD,A/B} = (1 - \frac{m_P}{m_f}) \times 100\% \quad \text{(A5)}$$

whereas the overall percent mass reduction, $\%M_{RD,overall}$ is equated as:

$$\%M_{RD,overall} = \%M_{RD,A} + \%M_{RD,B} - \frac{\%M_{RD,A} \times \%M_{RD,B}}{100} \quad \text{(A6)}$$

Tables

Table A1: Compositions of the acid leach residues from the part A acid leach experiments

Test no.	Mg (%)	Ni (%)	Fe (%)	Ca (%)	Al (%)	Si (%)	LOI (%)
1A	15.0	0.0212	4.54	0.222	0.877	24.5	16.8
2A	3.43	0.0126	0.622	0.272	0.663	27.8	33.4
3A	4.67	0.0144	0.920	0.300	0.866	35.5	14.5
4A/5A	4.14	0.0157	0.902	0.264	0.776	33.2	20.5

Table A2: Compositions of the acid leachates from part A acid leach experiments

Test no.	Mg (g/kg)	Ni (g/kg)	Fe (g/kg)	Ca (g/kg)	Al (g/kg)	Si (g/kg)
1A	42.1	0.642	9.27	0.419	0.268	0.295
2A	55.1	0.604	16.0	0.400	0.397	0.0705
3A	59.0	0.586	16.2	0.378	0.437	0.0262
4A/5A	60.9	0.634	16.6	0.449	0.472	0.0212

Table A3: Compositions of the alkaline leach residues from part B alkaline leach experiments

Test no.	Mg (%)	Ni (%)	Fe (%)	Ca (%)	Al (%)	Si (%)	LOI (%)
1B	22.6	0.0267	6.47	0.314	1.18	19.3	12.0
2B	20.3	0.0385	3.30	1.22	3.60	21.2	10.1
3B	18.6	0.0390	3.19	1.19	3.40	20.1	14.5
4B	19.2	0.0385	3.32	1.21	3.29	20.8	12.0
5B	17.7	0.0448	3.39	1.02	2.84	20.9	13.4

Table A4: Compositions of the alkaline leachates from part B alkaline leach experiments

Test no.	Si (g/kg)
1B	15.6
2B	30.1
3B	39.8
4B	39.8
5B	40.9

Evaluation of Best Available Technologies and Practices for Tailings Seepage Detection and Monitoring at Cobre Panamá

John H. Fortuna, FloSolutions, Ecuador
Carlos Hubner Torres, First Quantum Minerals, Cobre Panamá, Panamá

Abstract

The Cobre Panamá porphyry copper project is in the District of Donoso, Colon, 120 kilometers west of Panamá City. Mining is open pit; processing includes in-pit primary crushers, overland conveyors to secondary crushers, SAG mills, and ball mills. A flotation circuit produces copper sulfide concentrates, delivered by slurry pipeline to a filter plant co-located at a purpose-built port facility. Tailings are stored in a downstream-construction tailings management facility (TMF), and water is reclaimed for operations. Commercial production started in 2019.

At all TMFs, proper control of seepage and gradients in the tailings embankment and foundation is fundamental for successful facility performance, physical stability, and environmental protection. Cobre Panamá has methods in place to measure seepage from the embankments and foundation that reports to onsite collection systems, and a robust surface water and groundwater monitoring program. Given the tropical monsoon climate and the associated challenges of detecting dilute seepage, Cobre Panamá initiated a study to evaluate collection system efficiency and potential for seepage bypass. This study also sought to develop and comprehensively assess practical solutions to measure and estimate seepage rates, informed by field monitoring, best available technologies (BATs), and best available practices (BAPs). About 20 technologies and alternatives were assessed systematically and ranked in terms of capital and operational cost, time for implementation, complexity, accuracy, and precision of results. A process for technology identification, screening, scoring, and selection, including incorporation of site-specific selection and ranking criteria, is described. Selected technologies and best practices include instrumentation upgrades, new detection technologies, incorporation of telemetry and data management practices, and preparation of a mitigation action plan that describes the steps and actions that will be taken to evaluate and mitigate any seepage release.

Introduction

First Quantum Minerals Limited (FQM) is the 90% owner of Minera Panamá S.A. (MPSA), the Panamanian company that holds the Cobre Panamá concession, and is the operator of the Cobre Panamá Mine. This study was undertaken to evaluate alternatives to improve seepage monitoring from the tailings management facility (TMF) of the Cobre Panamá mining project.

At the time of this study (2022), Cobre Panamá had in place a robust TMF monitoring strategy, including a downgradient surface water and groundwater monitoring network, and was in full compliance with all regulatory requirements for environmental monitoring and reporting. However, Cobre Panamá was concerned that due to the high rainfall environment, there might still be a potential for dilute seepage to bypass collection and monitoring systems. This study was undertaken to assess if there were better ways to assess and monitor seepage, so as to prevent any release to the environment.

Background

The TMF is located next to the main pit and the process plant. The impoundment footprint is 20 square km, with sides roughly 4 km by 5 km. There are two large embankments of 4 and 3.5 kilometers at the east and north limits (East and North dams). The starter dams of both embankments were constructed up to a dam crest at 76 meters above sea level (masl). Their design included an adequate foundation, core, rockfill, and filters blanket and chimney. The continuous construction of the embankment uses cyclone sand obtained from tailings up to the ultimate dam crest elevation of 146 masl (Figure 1).



Figure 1: Cyclone sand embankment construction at Cobre Panamá

The TMF started to receive tailings in late February 2019. Two initial downstream lifts have been completed with a dam crest elevation of 85 masl, including a downstream buttress. Future lifts of the embankment may move to a modified centerline method.

Project objectives

The Mine is in a wet tropical environment on the Caribbean coast of Panama and receives up to 3.5 m of rain per year. The TMF construction method – hydraulic sand slurry discharged to the construction area – combined with the wet climate, lead to difficulty in isolating the seepage rate from other sources of water that mix with it and report to the same location.

At all TMFs, proper control of seepage and seepage gradients in the tailings embankment and foundation is fundamental for successful facility performance, physical stability, and protection against internal erosion (Byler and Morrison, 2022). At present, Cobre Panamá has methods in place to control and measure seepage from the embankments and foundation that reports to onsite collection systems. However, the potential for seepage to bypass collection systems has not been evaluated systematically.

This study was undertaken to identify and evaluate practical solutions to measure and estimate seepage rates, informed by field monitoring, best available technologies (BATs), and best available practices (BAPs).

Evaluation approach

Relevant guidance

Development and ranking of alternatives considered the framework of the GlobalTailingsReview.org / International Council on Mining and Metals (ICMM) "Global Industry Standard on Tailings Management" (ICMM, 2020). Topic III: "Design, Construction, Operation, and Monitoring of the Tailings Facility" and Topic IV "Management and Governance" contain key principles related to design and implementation of monitoring systems to manage risk at all phases of the facility lifecycle. This assessment also considers the integration of tailings and water management, including hydrology and hydrogeology data, into water management plans and practices as advocated by the ICMM "Tailings Management Good Practice Guide" (ICMM, 2021).

Consideration of site conceptual model

Assessments of seepage and collection system bypass must start with a robust understanding of the site conceptual model, degree of hydrogeologic complexity, natural hydraulic containment, expected interactions between the TMF and groundwater, and the potential for seepage risk. The level of certainty in the site characterization and site conceptual model must also be considered.

Engineered structures, including seepage collection and containment systems, can have unintended consequences on the tailings-groundwater system, with several examples documented at major copper TMFs globally (Fortuna et al., 2021). At Cobre Panamá, rockfill starter dams have a saprolitic core anchored in the foundation up to the design height of the crest (76 masl), with an additional 9 m of saprolitic face (76 to 85 masl) to mitigate seepage.

Review of best available technologies and practices

In general, BATs are technologies that help identify and assess risk, and BAPs are practices, strategies, and ideas that help manage risk or reduce the probability of occurrence (Boswell and Sobkowicz, 2015). A more detailed description of BATs and BAPs is available from the Mining Association of Canada (MAC) (MAC, 2021).

While there is a recent history of application of BATs/BAPs to TMFs (e.g., Boswell and Sobkowicz, 2015), studies on BATs and BAPs for control of seepage problems are lacking. Recent guidance documents that include BATs/BAPs assessments (MEND, 2017) are focused primarily on tailings storage type (e.g., conventional vs. filtered vs. paste) and do not consider seepage control and potential environmental impacts. MAC (2021) briefly discusses seepage management and control technologies, but only in terms of the original design and engineering elements emplaced during construction (i.e., use of liners, underdrains, and water retaining dams).

Screening of BATs against technology selection criteria should result in selection of the solution that most effectively reduces the physical, geochemical, ecological, social, and economic risks associated with seepage during the entire tailings storage life cycle. Upon selection, these technologies can be integrated more broadly into BAPs for seepage detection of monitoring. A schematic illustrating this overall process is shown in Figure 2.

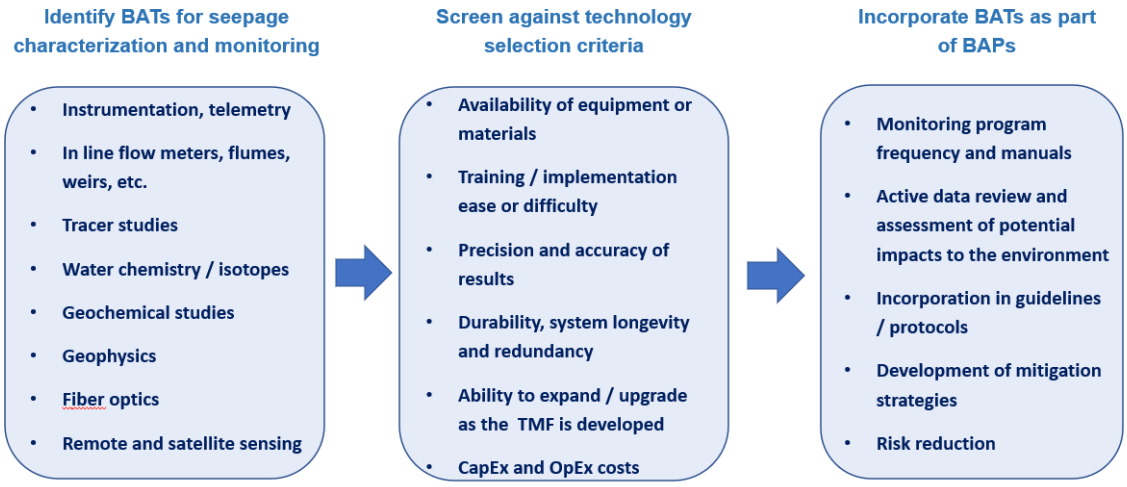


Figure 2: Schematic illustration of the application of BATs/BAPs to seepage characterization

There is often a heavy emphasis on technology selection and instrumentation at TMFs, but in our experience BAPs are equally if not more important in the monitoring of overall TMF performance. Development of appropriate management systems, monitoring plans, and operational procedures are fundamental to getting the most out of the selected technologies.

Technology identification and screening

Technology identification considers all readily available technologies that may be suitable for meeting project objectives, including new and emerging technologies. In addition to literature searches and reviews, we held numerous teleconferences to discuss applications and case studies with suppliers and vendors, including CGG SA, EWS Australia, SkyGeo, Silixa Ltd, and others. The process we used for identification and selection of technologies for incorporation into BAPs is illustrated graphically in Figure 3.

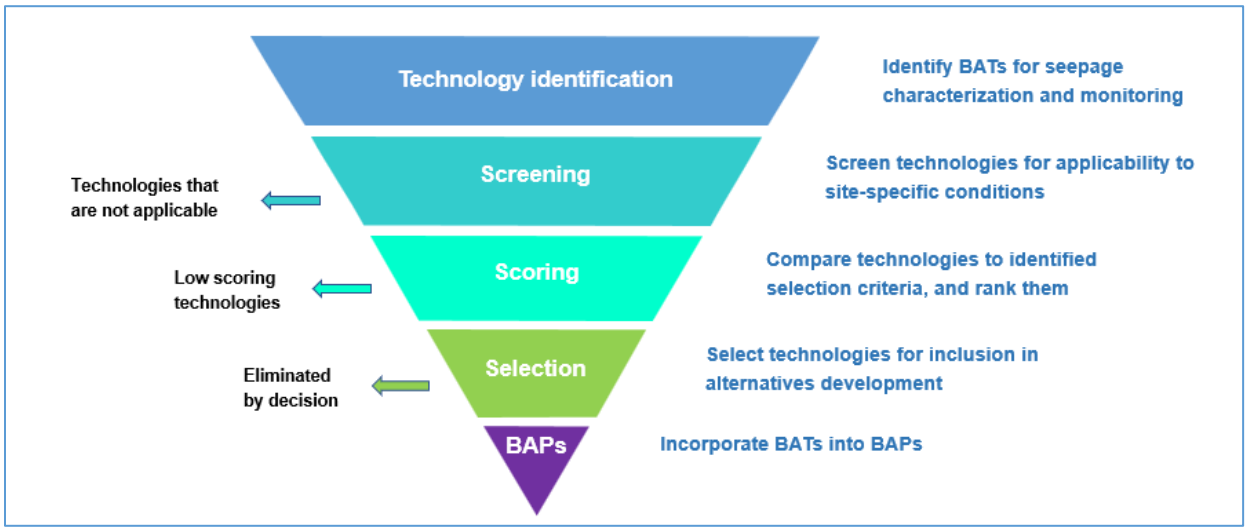


Figure 3: Technology identification and screening process

Technologies available for the monitoring of TMFs and seepage processes are constantly evolving and advancing. Monitoring systems generally fall into two categories of systems: i) terrestrial-based; and ii) remote systems (Hatton and Chapman, 2022). Monitoring frequency, data recovery, and data management practices need to be considered as part of monitoring systems. Automated data collection systems allow for enhancements in these areas. For example, use of electronic sensors linked to satellite-based telemetry systems combined with secure web-based data portals provide real-time access for viewing instrument measurements, data trends, and exceedances of water quality criteria.

The technology screening process considers the applicability of these different technologies to the site-specific conditions and project objectives at Cobre Panamá that may limit their use, or materially affect their potential performance. Technologies that do not meet project objectives are unlikely to function properly based on site conditions that have been eliminated during the screening process. All technologies

that pass to the technology screening phase are considered potentially able to meet project objectives and aid in compliance with the Environmental and Social Impact Assessment (ESIA) and permit conditions for seepage detection and monitoring.

Technology selection and scoring

The approach to technology selection uses a criteria-based decision matrix with criteria scoring. Key steps in this process are as follows:

1. Identify relevant user requirements or criteria.
2. Develop weights for each of the requirements.
3. Generate several viable technologies for a solution.
4. Select one of the technologies as a baseline to establish the current state.
5. Evaluate each alternative technology against the baseline, scoring it as positive, negative, or equal in meeting the criteria.
6. Total the values from each option, multiplying each value by its weight if the optional scoring mechanism was used.
7. Combine the best elements of each technology to create an optimal hybrid solution.

There are many potential criteria that can be used for technology selection, as illustrated graphically in Figure 4. Criteria may include commercial risk, technical feasibility, team skills and confidence, system redundancy, and other factors. Best practice dictates that a limited number of key criteria be used to streamline the ranking and selection process. Use of too many criteria may slow down the process or result in several technologies scoring within a narrow range, making selection more difficult.

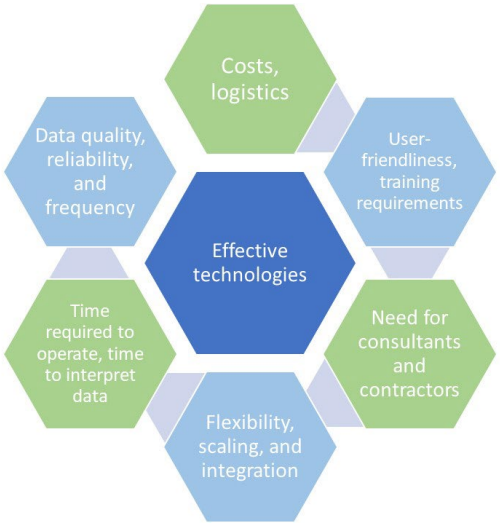


Figure 4: Example of technology screening criteria

Criteria should be selected from each of the general categories important to corporate approval and technology implementation: "technical," "people," "economic," and "operational" categories. This will ensure proper balance in scoring. Evaluation criteria are rarely of equal importance, and the selected criteria should be weighted based on how important they are to final technology selection. Numerical scales are used for criteria weighting (typically from 1 to 5 or 1 to 10), with input from the operational team on the relative importance of each criterion. The baseline for comparison is typically the "current state," in this case, the ongoing water level measurements and water quality monitoring program.

Alternatives development

Following the technology scoring and selection, we developed alternatives and recommendations to incorporate BATs into BAPs for the Cobre Panamá site. Each alternative is a combination of one or more technologies that follow a common implementation theme, e.g., installation of vibrating wire piezometers (VWPs) and groundwater wells with manual water level measurements – where the activities undertaken as part of the alternative are complimentary.

Based on experience at similar sites, seepage detection and monitoring technologies may be different for detection of embankment seepage than they are for downgradient seepage bypassing collection systems. We have developed alternatives with consideration of implementation difficulty, complexity, accuracy of measurements, training required to implement, expected monitoring frequency, capital and operational costs, and other site-specific factors.

Technology identification and screening

Technology identification describes all technologies considered as part of our assessment and preliminary screening to assess applicability to the project site. The screening includes both terrestrial and remote monitoring systems, as well as a variety of instrumentation, measurements, and study techniques.

Terrestrial monitoring systems and instrumentation

Piezometers and water level measurements

Piezometers and vibrating wire piezometers (VWPs) are important instruments at most TMFs. Measurement of changes in water levels and gradients are one of the primary ways to detect changes in TMF-groundwater system behavior, including changes related to seepage discharge.

Groundwater wells and water quality data

Groundwater wells allow for collection of water quality samples. Water quality parameters elevated in tailings pond water relative to groundwater can serve as natural tracers for seepage flow. Use of exploratory

data analyses and machine learning (EDA/ML) techniques applied to the entire water quality data set can be effective at identifying unique water signatures and seepage impacts (Ezzy and Fortuna, 2020).

At Cobre Panamá, primary and secondary seepage indicator parameters and levels have previously been identified. Water quality monitoring is highly effective for seepage detection at this site. Additional water quality parameters, such as stable isotopes of oxygen and hydrogen, may provide insights into surface water-groundwater interactions and flow pathways.

Drain flow monitoring

Flow monitoring in drain systems helps understand changing system dynamics in the TMF. Changes in drain flow may indicate changes to seepage rates from the TMF, or phreatic surface levels in the embankments. A complete monitoring system must include drain flow rates, drain water quality, and water levels in piezometers in embankments.

Seepage collection facility monitoring

There are 7 sand/seepage collection facilities (SCFs) distributed in the north (3 SCFs) and east dams (4 SCFs). The SCFs consist of seepage collection ponds and trenches linked to pumps, pumping stations, and piping to route water back to the TMF pond. The SCFs may be useful for monitoring or estimating seepage if the relative contributions from various water sources can be distinguished. Water collected at SCFs may include multiple sources, including water from slurry sand construction of embankments, rainfall runoff, seepage from the TMF, and shallow groundwater discharge to SCF trenches, where they intersect the water table. Discharge/pumping volumes in SCFs can be related to these various components using a water balance approach.

Tracer studies

To date applied tracer studies have seen little application to TMF sites, perhaps because travel times through tailings are excessively long and monitoring for “natural” tracers like elevated sulphate in TMF pond water serve almost the same purpose. Tracer testing applications at TMFs are typically concerned with travel times and flow pathways (British Geological Survey, 2007), but they have also been used for a variety of other purposes including quantification of tailings properties and characterization of fluid flow behavior (Divine et al., 2013).

Perimeter fiber optics

Great advances have been made in the development and application of distributed fiber-optic sensing systems over the last decade. There are two basic classes of these systems that can be employed at TMFs. Distributed acoustic/vibration sensing systems (DAS or DVS), and distributed temperature sensing systems

(DTS). DAS technologies detect vibrations and capture acoustic energy along optical fibers. Classification algorithms are used to detect and located acoustic "events" such as leaks, cable faults, or strain deformation (AP Sensing, 2022). DTS technologies function as linear temperature sensors, which can be used to generate a continuous temperature profile along the entire sensor cable.

Fiber optical sensing offers the advantage of cost-effective, high spatial monitoring coverage (Mondanos and Johansson, 2020). Seepage can be tracked through seasonal temperature variations common in surface water. Key advantages over traditional sensing systems include precision, durability, reliability, density of information, and economic aspects (Inaudi and Blin, 2016). In Sweden, more than 100 dams have been outfitted with fiber optic cables for detection of seepage using DTS (HydroResearch; Silixa; Sisprobe, 2020). Most installations are made by installing cables in the dam toe, upstream of the drainage system, or just downstream of the dam (Mondanos and Johansson, 2020). Recent study results show that temperature monitoring in the upstream filter gives information about seepage inflow areas, while measurements in the dam toe provide information about small leakage flows (HydroResearch; Silixa; Sisprobe, 2020

Ground geophysics

Various ground geophysics techniques have been explored for use in seepage detection monitoring over the last 20+ years. Combinations of self-potential (SP), direct current (DC) resistivity, induce polarization (IP) and transient electromagnetic (TEM) methods have been applied to mine sites to develop a clearer understanding of seepage problems (Buselli and Lu, 2001). Focused research into this topic have identified electrical resistivity (ERT) and SP as potentially applicable to seepage detection, but background changes to dam conditions (e.g., embankment raises) affect responses, and it takes a long time for equilibrium conditions to reestablish (Mainali, 2007).

Seepage paths have also been mapped using Electric-based technology, where a low voltage, low amperage alternating electrical current is used to energize water by electrodes placed in tailings and another in contact water below the tailings dam. Successful case studies have been published (Urlich and Garnder, 2017) demonstrating the use of this technology for mapping seepage pathways and increasing understanding of flow pathways between sources and discharge areas.

Seismic interferometry

Ambient seismic noise interferometry is a relatively new technique to identify subsurface changes associated with strain or saturation, potentially including seepage (Hatton and Chapman, 2022).

In one study, the authors recorded three weeks of continues data during a period of heavy rainfall using 10 short-period geophones at a tailings dam in Tasmania (Olivier et al., 2017). Although this study was not specific to seepage, the implication is clear: if seepage losses result in additional saturation (i.e., of

a previously unsaturated zone), then it could be detected using this method. Currently, this technology is being trialed at several other facilities; however, it may be more appropriate for monitoring seepage build-up in embankments rather than detecting seepage losses downstream.

Remote monitoring technologies

Remote monitoring includes aerial photography/unmanned aerial systems, and satellite-based systems. Remote monitoring systems may be passive – utilizing naturally occurring radiated or reflected energy screened based on discrete wavelength or spectrum, or active – where the sensor system emits energy such as laser or radio waves and measures the reflected condition (Hatton and Chapman, 2022).

UAV/drone surveys

The sheer size of most TMFs combined with the potential for environmental or stability risks inherently make appropriate surveying and monitoring costly and difficult. Surveys using unmanned aerial vehicles ("UAVs" or "drones") have gained widespread acceptance for tailings applications due to the low cost and potential to survey large areas quickly and easily. Drone surveys can provide a variety of different types of information depending on sensor configuration but are commonly used to survey topography and monitor changes in embankment deformation or displacement, tailings volumes/material placement, pond size, tailings subsidence and consolidation (Rauhala et al., 2017). In terms of seepage detection and monitoring at TMFs, at least one provider advocates for use of drone surveys with a thermal camera + HD imaging (Skymine AUV, 2022).

The ability of a UAV survey to detect seepage depends on two principal factors: 1) the expected change in the environment that the seepage will create and 2) the ability of the sensor to detect that change. A UAV survey may be useful in identifying any preferential flow pathways through embankments or the shallow subsurface – particularly in environments where the surface water (tailings pond) temperature is significantly different than groundwater temperature.

Satellite sensing

Early applications of satellite sensing for TMF seepage monitoring focused on vegetation health surrounding the facilities, as determined by satellite-based monitoring indices using combinations of surface reflectance at two or more wavelengths (Chetty, 2013). More recent "Earth Observation" ("EO") techniques include optical-based satellite data, Global Navigation Satellite System, Global Weather forecasting models and Interferometric Synthetic Aperture Radar (InSAR).

Recent research across a range of these techniques have concluded that while these technologies can be used to improve dam monitoring and reduce risk posed by failure, particularly in remote environments, they are not a substitute for onsite measurements (Lumbroso et al., 2021).

LiDAR

Advanced light detection and ranging (LiDAR) sensors are gaining widespread acceptance for monitoring of tailings facilities, principally for monitoring of dam highwalls to detect movement or deformation. LiDAR deployment by manned aviation is common, but often cost-prohibitive. In the past, the poor weight-bearing capacity of traditional drones has limited their ability to carry LiDAR technology. Larger modern multi-rotor drones and fixed wing unmanned aerial systems are suitable for this purpose (Rocket Mine, 2022), and can be more accurate than those due to the higher point density obtained by flying at lower altitudes (WingtraOne, 2022). A key advantage of LiDAR is the ability to sense in areas of moderate to dense forest canopy.

The applications of LiDAR to seepage detection and monitoring are limited. Although some providers claim they can detect zones of saturation with this technology, and by proxy changes to the elevation of the groundwater table, seepage detection use cases at TMFs are not well established.

InSAR

Interferometric Synthetic Aperture Radar (INSAR) is a remote, satellite-based technology for measurement of millimeter-scale displacement in the ground surface. INSAR relies on interferometry – the collection and interpretation of two SAR images acquired at different times over the same area. Interferometry and interpretation of these measurements are used to estimate displacement.

Due to the frequency with which potential displacements can be monitored, many mine sites are adapting this technology for routine TMF monitoring. The use case for seepage monitoring is less established; however, there are documented cases where visual signs of seepage have been correlated to localized horizontal displacement or "bulging" near the seepage location (personal communication with SkyGeo, 1 March 2022).

In February 2022, an "InSAR Feasibility Report" for monitoring of the TMF embankment was prepared by CGG for the Cobre Panama Mine. The report indicates some InSAR limitations at this site including dense vegetation, which SAR struggles to penetrate, and active mine operations which change the ground cover too rapidly to remain coherent. Based on the reported results during the trial, this technology is not considered sufficient for seepage detection and monitoring at this site.

SkyTEM

SkyTEM is an airborne electromagnetic method (AEM) originally developed at Aarhus University in Denmark. SkyTEM systems can map the near surface in high resolution concurrently with accurate high-resolution measurements to depths over 500 meters (Skytem, 2022). The technology has been effectively demonstrated for accurately mapping water levels and salinity in complex environments (Kirkegaard, et al., 2011).

SkyTEM has seen numerous applications to TMFs. Tailings are typically highly conductive due to the presence of high salt, acid, or base contents in dam waters. Typical objectives of these surveys are detection of conductive seepage plumes downstream of embankments, mapping of permeable geologic features like faults, mapping depth to bedrock, and assessment of groundwater interception systems (Reid, Christensen, and Godber, 2012). Substantial advances in the development of both hardware and inversion software since 2005 have resulted in data and results from an airborne (helicopter) platform from time domain methods that are comparable to ground-based geophysical systems (Auken et al., 2015).

Automated data collection and telemetry

In addition to instrumentation, monitoring frequency, data recovery, and data management practices need to be considered as part of monitoring systems. Automated systems allow for enhancements in these areas. Use of electronic data collection and satellite-based telemetry systems combined with secure web-based data portals provide real-time access for viewing instrument measurements, data trends, and exceedances of water quality criteria.

Telemetry systems

Automatic data acquisition of geotechnical and hydrogeologic instrumentation is usually done by connecting instruments via cabling or wirelessly to a central gateway or instrumentation housing. The gateway may transmit data by cellular signal, satellite modem, or directly using the mine Wi-Fi. There are also low power, stand-alone single instrument satellite transmitters that have been developed for remote sites, including for VWPs and "well caps" for groundwater monitoring wells (EWS Monitoring, 2022). Companies like Sensemetrics offer complete end-to-end solutions including sensors, connectivity, a cloud platform, and dashboards and analytics.

When combined with instrumentation, telemetry systems can provide data on water levels, secondary parameters like chloride (if ion-specific probes are deployed in wells), and temperature that may be useful in detecting seepage. At the time of this study (2022), Cobre Panamá was already undertaking installation of a telemetry system for existing instrumentation.

Data visualization and dashboards

Dashboards are data visualization tool that track, analyze, and display key information, metrics, and data points. A variety of tools are available for the building of dashboards, including PowerBI, Tableau, and others. Site-specific custom dashboards can be developed to provide easy review of relevant site parameters and set with "flags" or "alerts" when parameters exceed trigger levels or other criteria. At Cobre Panamá, a custom dashboard could be constructed with alerts when primary and secondary seepage indicator

parameters (from water quality monitoring data) exceed threshold or trigger values, or for temperature (for dataloggers or VWPS with telemetry or fiber optic data).

Analytical approaches

This category includes calculations and models that can be used to assess the potential for seepage discharge through embankments and the foundation and bypass of collection systems. This category is unique in that they can be used to make forward or future predictions, and for this reason have great utility for planning purposes. For example, models can be used to assess the impact of future embankment raises on seepage discharge patterns, and to plan for improvements in seepage detection and monitoring programs to accommodate these changes. Models can also be used to evaluate mitigation strategies when seepage is detected – such as increased pumping rates at SCFs to capture seepage bypass. The reliability of these approaches can be continually improved through recalibration to operational monitoring data.

Water balances

If a detailed TMF water balance exists, flow measurements from drains and seepage collection systems can be compared to expected discharge identified in the water balance to estimate the quantity of seepage being lost (bypassing the collection system). However, water balances may be circular, i.e., measured seepage rates from seepage collection structures are sometimes used as inputs to the water balance – and use of flow measurements may not work unless there are significant changes in observed rates reporting to the SCFs.

TMF water balances often start as estimates that are refined over time during the life of operations as additional data become available. Use of a water balance and flow estimates to estimate seepage losses at an early-stage TMF can be problematic. There is a site wide-water balance developed primarily as an operational support tool, with particular focus on the prediction of the discharge water quality compliance risks (Piteau Associates, 2022). However, this site-wide model is not specific to the TMF and does not appear to be calibrated to SCF drain flows.

Seepage modeling

Analytical and numerical models can be useful tools for evaluating hydrogeological risks associated with TMFs, including migration of seepage through the embankments and foundation. The value in these approaches is influenced by the amount of supporting data and the quality of the site conceptual hydrogeologic model. Modeling approaches are not direct tools for detecting and monitoring seepage but can provide estimates of expected seepage for use in water balances or for comparison to other site observations. Simple two-dimensional (2D) section models using software like SEEP/W (GeoStudio) are relatively easy to set up and run and can provide preliminary estimates of seepage quantities and travel times to downgradient monitoring points. However, due to geometric limitations, these models cannot

provide information on likely flow pathways and studies have shown that if the flow patterns internal to the TMF are 3-dimensional (e.g., flow into and out of the design section), there can be significantly different predictions of the phreatic surface and pore pressures in 2D models relative to 3-dimensional models (Rouncivell et al., 2020).

Groundwater modeling

A well-constructed, properly calibrated local-scale 3D numerical groundwater flow model can provide many advantages for an operational TMF. When sufficient information is available to build and calibrate this type of model, it can be used for a variety of predictive purposes including estimation of seepage from the impoundment to the foundation, prediction of seepage through embankments, evaluation of mounding in embankments and foundation pore pressures, and evaluation of seepage flow paths. In addition, this type of model can be used to evaluate expected changes in future seepage rates during embankment raises and TMF development, to design and assess monitoring systems, and to assess the effects of changes to seepage capture systems (i.e., pumping rates). There is no tool that is better or more useful for understanding the impact of TMF construction on interactions in the TMF-groundwater environment.

TMFs are inherently complex. TMG-groundwater models can also be complex, and care must be taken not to overcomplicate them, i.e. by including too fine of a mesh resolution around drainage structures or too much detail in tailings deposition time steps, or they become unwieldly.

Technology scoring and selection

Selection criteria

To define the selection criteria and appropriate weighting factors, FloSolutions and Cobre Panamá operational personnel participated in a technology selection criteria workshop. More than 20 possible criteria in three broad categories were considered: economic and logistics criteria, technical criteria, and people and operations criteria. During the workshop, a total of ten criteria were selected for the technology scoring process.

The reduction aimed to avoid an over-parameterization of criteria that could complicate the selection process. Too many criteria can overlap, causing some aspects to be double-valued and thus over-weighted in the final score. Alternatively, some criteria might have had the same score across all technologies to be evaluated and, therefore, would not have made any difference. The criteria reduction process considers the specific context of the mining operation under evaluation, which may differ if applied to another operation, resulting in a different set of criteria than those ultimately used in this study.

Technologies are assigned a qualitative score on a scale of 1 to 5 for each criterion, with 1 being least favorable and 5 being the most favorable. Each criterion was assigned a weighting factor ranging from 1-

3, with 1 being the least important and 3 being the most important. Selected criteria and weighting are summarized in Table 1.

Selection scoring matrix

For selection purposes, the "base case" is the current seepage detection and monitoring system at Cobre Panamá, which consists of a series of 7 SCFs and a network of perimeter monitoring bores and piezometers surrounding the TMF to the north and east sides. The technology scoring matrix is presented in Table 2. The matrix includes both nominal (raw) and weighted scores. There are ten evaluation criteria, resulting in maximum nominal and weighted scores of 50 and 95, respectively.

Table 1: Selection criteria descriptions and weighting

Criteria	Description	Weight
Economic and logistics criteria		
Capital expenditure (CapEx)	Includes the cost of procurement and deployment or installation	3
Operational expenditure (OpEx)	Ongoing (annual) system operations fees, upgrades, and replacement costs. This criterion considers that the TMF will be continually raised over time, and whether technology deployment will need continuous updates to accommodate these changes	1
Consultants and contractors	The need for onsite contractors and consultants to install instrumentation or program or deploy systems or train staff. Important due to the challenges of obtaining visas and other site logistics. Instrumentation that can be installed by local contractors receives high scores; when international and out-of-country contractors are required scores are low.	2
Technical criteria		
Data	Data reliability, quality, frequency, precision, accuracy, and spatial and temporal density	2
Flexibility	Technology flexibility, adaptability to different site conditions, and ease of scaling as the TMF is raised and developed	2
Integration	Ability to integrate with existing or future onsite monitoring technologies, such as slope stability monitoring systems. Includes "co-benefits" – technology for one purpose that provides benefits in another area	3
Time Lag	The time required to identify or detect seepage risks or impacts after they occur.	1
People and operations criteria		
Ease of use	User-friendliness of technology, including time required by onsite staff to use / monitor	1
Automation	Automation vs. need for inspection. For example, the need for manual review of laboratory analytical data vs. a dashboard that uploads data and instantly flags water quality exceedances.	2
Skills and training	The level of staff technical skills or training required to implement or operate technology or process and interpret data	2

Table 2: Technology scoring matrix

		Evaluation Criteria Scores										Total Score	
	Technology	CapEx	OpEx	Consultants/ contractors	Data	Flexibility	Integration	Time Lag	Ease of Use	Automation	Skills and Training	Nominal	Weighted
No.	*Weighting factor*	3	1	2	2	2	3	1	1	2	2		
0	Base case	5	3	1	2	3	2	1	5	1	5	28	54
1	Piezometers	2	3	4	4	5	5	1	5	1	5	35	68
2	Wells / Water quality	2	3	4	4	5	5	1	5	1	5	35	68
3	Drain monitoring	4	4	5	4	3	5	2	5	1	5	38	74
4	Seepage Control Facilities	5	4	4	3	2	1	2	3	2	4	30	57
5	Tracer studies	4	4	3	4	4	3	3	3	2	3	33	63
6	Fiber optics	1	5	4	5	5	5	5	3	5	2	40	73
7	Ground geophysics	3	5	1	4	3	3	3	3	2	2	29	53
8	Seismic interferometry	1	4	1	5	5	5	5	2	5	1	34	63
9	UAV/Drone Surveys	4	5	5	2	5	3	4	4	2	3	37	68
10	Satellite Sensing	3	3	4	2	4	2	1	2	3	3	27	53
11	LiDAR	3	4	2	3	5	4	3	2	3	2	31	60
12	InSAR	3	3	1	2	3	2	3	2	2	3	24	45
13	SkyTEM	2	5	1	5	5	5	5	4	3	3	38	69
14	Telemetry systems	3	5	3	5	5	5	5	2	5	2	40	76
15	Dashboards	4	3	4	5	5	5	5	3	5	3	42	82
16	Water balances	3	4	4	1	2	4	2	3	3	3	29	56
17	Seepage modeling	5	4	4	3	4	3	4	3	2	3	35	67
18	Groundwater modeling	3	3	4	5	5	4	5	3	4	2	38	72

Selected technologies

Detection and monitoring of seepage through embankments and foundation

In terms of instrumentation, continuous fiber optic systems may be an effective technology for identifying seepage releases. Perimeter fiber optics score highly due to their ability to provide continuous, real-time data of high precision and accuracy, integration with existing technologies, and flexibility as the dam configuration changes (only a basal perimeter system is required). As a co-benefit, modern systems include ULTRA HD quality distributed temperature, strain, and acoustic measurements in real-time using the same optical fiber cable (Silixa, 2022). They can be used to monitor slope stability, map seepage below the drainage system, and identify density changes in subsurface geology with distributed acoustic sensing using both passive and active seismic surveys (Mondanos and Johansson, 2020). This technology has high capital costs for deployment of a perimeter fiber optic cable over several kilometers, which reduces the weighted score.

Flow monitoring in drain systems helps understand changing system dynamics in the TMF and should be considered a critical part of a comprehensive seepage detection and monitoring program. A complete monitoring system should include drain flow rates, drain water quality, and water levels in piezometers in embankments. More information is needed on the drain configuration and available monitoring points at Cobre Panamá to provide specific recommendations for implementation of this technology.

SkyTEM has seen numerous successful applications to TMFs and should be considered for establishing baseline conditions at Cobre Panamá. The mapping of the foundation conditions prior to further tailings deposition, combined with mapping of depth to bedrock and conductive and permeable geologic features like faults in and around the TMF would establish a powerful baseline data set for use in seepage detection and monitoring, as well as for foundation parameterization during future predictive groundwater modeling.

Detection and monitoring of downstream seepage that bypasses the SCFs

Traditional monitoring techniques like piezometers, groundwater monitoring wells, and water quality data have moderate scores due to the need to collect manual measurements and samples and resulting data infrequency. Nevertheless, these systems are familiar, easy to use, do not require training, and are adaptable. Water quality sampling is the sole method to detect sulfate, the primary seepage indicator parameter, downstream of the SCFs. When these traditional systems are combined with automated instrumentation and telemetry (discussed below), scores increase significantly. For the foreseeable future, these systems will continue to provide the core of instrumentation and seepage monitoring programs at most TMFs, including Cobre Panamá.

UAV/drone surveys score well in the ranking criteria but score low in the data category because it is not clear how effective they may be in detecting seepage. They should function well when seepage coincides with "bulging" in embankments, results in temperature changes, or when seepage visibly daylights through embankments. The downstream migration of seepage in groundwater (beyond SCFs) would not be detected. UAV surveys may be more useful in detecting seepage in embankments and in the shallow subsurface upstream of SCFs. Periodic embankment surveys are the most appropriate application of this technology.

Incorporation of selected technologies into best available practices

BAPs include management systems, operation procedures, techniques, and methodologies that have proven to reliably manage risk and achieve performance objectives (MAC, 2021). While a BAP is an operating philosophy, proper technology selection and incorporation is a cornerstone of BAP development. This section presents a brief overview of how the selected technologies (BATs) can be incorporated into operational best practices.

The technology selection process described above confirm that some our identified BATs had already been incorporated into BAPs at Cobre Panamá, including the use of a robust seepage detection and monitoring network. At the time of this study, the TMF team had already upgraded much of the

instrumentation network with telemetry and was ordering new flow meters for the SCF systems as part of the commitment to continuous improvement. Some of the recommendations reflect ongoing practice.

Enhanced downgradient monitoring network with telemetry

The current monitoring network could be improved to provide a more robust seepage detection, particularly if combined with telemetry and dashboards. Specific improvements that could be considered include:

- Develop an instrumentation plan describing location, construction, and rationale for new VWPs, piezometers, and monitoring wells to augment the existing downgradient monitoring network.
- Installation of additional downgradient monitoring points at select locations
- Continuation of routine water quality sampling and analyses at the expanded network
- Equipping most/all monitoring points with automatic measurement instrumentation and Wi-Fi or satellite-based telemetry

Data management practices and dashboards

In addition to an enhanced instrumentation and monitoring program, automated data upload and data screening using dashboards are particularly useful for rapid identification of seepage at monitoring points after water quality monitoring events. Specific improvements that could be considered include:

- Linking telemetry systems to a central database
- Enabling automatic upload of laboratory analyses into the central database
- Development of user-friendly dashboards with automatic screening of seepage indicator parameters with dashboard notices/alerts
- Integrate with Trigger Action Response Plans (TARPs) or other established alert levels and Emergency Response Plans (ERPs)

Perimeter fiber optics

Installation of perimeter fiber optic cables represents state-of-the art seepage detection technology, but at high capital cost. It can be installed around the TMF to measure temperature, strain, and acoustic measurements in real-time. Under this option, fewer additional VWPs and monitoring points would be needed, potentially offsetting some of the capital costs associated with this option.

Periodic/supplemental studies

Based on the review of available technologies, it would be difficult to detect seepage transport through embankments or the shallow subsurface upstream of SCFs using traditional techniques if the perimeter fiber optic sensors are not installed. In this case, periodic embankment-specific surveys would be useful. These

surveys may include:

- UAV/drone photography with thermal + HD cameras
- Data evaluation for embankment geometry changes and zones of temperature anomalies
- If seepage is detected downstream of embankments, and preferential seepage pathways are suspected or identified during UAV survey, applied tracer studies may assist with identification and mapping of seepage flow patterns.

Mitigation action plan

A mitigation action plan describes the steps and actions that will be taken within a defined timeframe to further evaluate and mitigate the release. Example actions that could be included in a mitigation plan:

- Confirm concentrations with repeat/duplicate sampling
- Confirm trigger level exceedances are a result of seepage impacts through more detailed geochemical assessment of water quality data (potential including EDA/ML techniques)
- Confirm seepage releases and flow pathways using supplemental studies
- Summarize results of assessments and submit a mitigation work plan within a defined timeline of seepage detection and confirmation.

As part of mitigation plan development, site should consider whether baseline studies are required. For example, if fiber optic lines are not installed, baseline geophysics or SkyTEM along key areas such as embankment toes may provide useful starting information. When a seepage release is detected downgradient, these lines can be repeated to identify preferential flow paths.

Periodic review and revision of seepage monitoring strategy

After BATs have been implemented and monitoring and mitigation plans have been updated, the overall monitoring program should undergo periodic review as part of BAPs, to make sure that it meets changing demands of the TMF.

- Conduct internal annual reviews and periodic external reviews of the seepage monitoring strategy
- As the TMF height increases, consider the suitability of the monitoring network the meet stated goals and objectives
- Evaluate new /evolving technologies where appropriate. When evaluating new technologies, they should be compared to the matrix selection criteria and weighting to see how they compare to existing options

Consideration of analytical and numerical modeling approaches

There are significant operational advantages to having a robust TMF water balance, seepage models, and

numerical groundwater flow models. The value in these approaches is influenced by the amount of available supporting data and the quality of the site conceptual hydrogeologic model. During site operations, the amount of available data is continually increasing, and sites interested in implementing BAPs should periodically update and improve the site water balances and numerical models.

A well-constructed, properly calibrated local-scale 3D numerical groundwater flow model can provide many advantages for an operational TMF, and this is one of the highest scoring technologies in the scoring matrix (Table 2), in part due to the predictive capabilities. Development of a 3D numerical groundwater flow model will not only assist with seepage detection and monitoring, but it will help to understand the potential impacts of future construction activities and expected discharge to various drainage components, and it will enable the identification of flow paths, velocities, and seepage fluxes within the foundation and beyond. Many operational TMFs maintain a robust model for this purpose.

Conclusion

This paper contains a comprehensive review of the best available technologies for seepage detection and monitoring at tailings facilities, and a proposed approach to assess them – with an example application at the Cobre Panamá TMF.

The most applicable technologies at any site will be dependent on several factors, including site conditions (geology, hydrogeology, tailings configuration, etc.), operational considerations, and the available team to implement them. When selecting and ranking BATs, selection criteria should only be established with input from the onsite operational team, who have working knowledge of day-to-day conditions and implementation constraints. It is not constructive to recommend "state-of-the-art" technologies if they are impractical to implement or if the necessary capital cannot be allocated.

Technologies that did not score well at Cobre Panamá may have greater applicability at other sites, and a low score in our assessment should not be a discouragement to considering these technologies at other sites where conditions may be different.

The current systems employed to monitor TMF seepage at Cobre Panamá are equivalent to or surpass common practices observed at many tailings facilities globally. Undertaking regular studies to update conceptual hydrogeological models, combined with the commissioning of this study – in the absence of any regulatory requirement or external motivating factor – indicates a commitment to continuous improvement. In short, BAP implementation was already well underway at the time of this assessment.

Finally, although this study focuses on BATs, we believe that BAPs are equally if not more important in establishing and maintaining robust detection, monitoring, and mitigation programs. Our discussion of BAPs is limited for the sake of brevity, and because they are even more site-specific than selection of BATs due to greater reliability on organizational factors.

Acknowledgements

The authors wish to thank First Quantum Minerals (FQM) and FloSolutions for funding this work.

References

AP Sensing. 2022. Website accessed July 2022 at https://www.apsensing.com/

Boswell, J. and Sobkowicz, J. 2015. International tailings failures and best available technology. *Proceedings of Tailings and Mine Waste 2015:* 57–74. Vancouver, BC.

British Geological Survey. 2007. Tracer test feasibility assessment: Frongoch Mine Tailings Lagoon, Open Report OR/12/035. Keyworth, Nottingham, UK: British Geological Survey.

Buselli, G. and Lu, K. 2001. Groundwater contamination monitoring with multichannel electrical and electromagnetic methods. *Journal of Applied Geophysics* 48(1): 11–23.

Byler, B. and Morrison, K.F. 2022. Filters, drains, and pipes. In K.F. Morrison, *Tailings Management Handbook, a Life-Cycle Approach* (pp. 639–657). Englewood, Colorado: Society for Mining, Metallurgy and Exploration (SME).

Chetty, P. 2013. Monitoring of mine tailings using satellite and lidar data. *PositionIT,* 22–28.

Divine, C., Griffen, A., Christoffersen, L., Gillow, J., Preston, K. and DeDycker, P. 2013. Tracer testing to evaluate tailing pile hydrogeologic characteristics to support closure and reclamation. *Reliable Mine Water Technology* (pp. 967–972). Golden, Colorado: International Mine Water Association.

EWS Monitoring. 2022. Accessed July 2022 at https://www.ewsmonitoring.com/

Ezzy, T. R. and Fortuna, J. 2020. Using data science and machine learning to improve site hydrogeological conceptual models. *Mine Water Solutions* (pp. 206–212). Christchurch: International Mine Water Association.

Fortuna, J., Waterhouse, J., Gowan, M. and Chapman, P. 2021. Applying practical hydrogeology to tailings storage facility design and management. *Mine Water and the Environment*.

Hatton, C. N. and Chapman, P. 2022. Monitoring systems and instrumentation. In K.F. Morrison, *Tailings Management Handbook, A Life-Cycle Approach:* 835–858. Englewood, Colorado: Society for Mining, Metallurgy, and Exploration (SME).

ICMM. 2020. Global Industry Standards on Tailings Management. Accessed at GlobalTailingsReview.org.

ICMM. 2021. *Tailings Management Good Practice Guide*. London, UK.

Inaudi, D. E. and Blin, R. 2016. Monitoring dams with distributed fiber optic sensing. Manno, Switzerland. Accessed at semanticscholar.org.

Kirkegaard, C., Sonnenborg, T. and Auken, E.J. 2011, 10). Salinity distribution in heterogeneous coastal aquifers mapped by airborne electromagnetics. *Vadose Zone Journal* 10(1): 125–135.

Lumbroso, D., Davison, M., Boyd, R. and Petkovsek, G. 2021. Modelling the Brumadinho tailings dam failure, the subsequent loss of life and how it could have been reduced. *Nat. Hazards Earth Syst. Sci*. 21: 21–37.

MAC (The Mining Association of Canada). 2021. *A Guide to the Management of Tailings Facilities,* version 3.2.

Mainali, G. 2007. Monitoring of tailings dams with geophysical methods. Lulea, Sweden: Lulea University of Technology, Department of Chemical Engineering and Geosciences.

MEND. 2017. Study of tailings management technologies, MEND Report 2.50.1. Mine Environmental Neutral Drainage.

Mondanos, M. and Johansson, S. 2020. Fibre optic sensing for dam monitoring. *International Water Power,* accessed at www.waterpowermagazine.com.

Olivier, G., Brenguier, F., de Wit, T. and Lynch, R. 2017. Monitoring the stability of tailings dams walls with ambient seismic noise. *The Leading Edge* 36(4): 282–368.

Piteau Associates. 2022. Cobre Panama, 2021 update and calibration of site-wide physical water and chemical mass balance model. Johannesburg: Piteau Associates South Africa (Pty) Ltd.

Rauhala, A., Tuomela, A., Davids, C. and Rossi, P.M. 2017. UAV Remote sensing surveillance of a mine tailings impoundment in sub-artic conditions. *Remote Sensing* 9(12): 1318, 1–14.

Rocket Mine. 2022. Website accessed August 2022 at www.rocketmine.com.

Rouncivell, W., Imrie, S., Howell, G. and Meintjes, H. 2020. 3D seepage modelling in tailings storage facility analysis and design for low permeability lined basins. *Proceedings of Tailings Storage Conference 2020*: 15–27. Johannesburg: The South African Institute of Mining and Metallurgy.

Silixa. 2022. Website accessed August 2022 at https://silixa.com/

Skymine UAV. 2022. Website accessed August 2022 at https://www.skymineuav.com/

Skytem. 2022. Website accessed August 2022 at https://skytem.com/

Urlich, C., Hughes, A. and Garnder, V. 2017. Tailings Seepage paths mapped using electric-based technology. Mine *Water and the Circular Economy:* 64–72. Lappeenranta, Finland: International Mine Water Association (IMWA).

WingtraOne. 2022. Website accessed August 2022 at https://wingtra.com/

Standardizing Sediment Porewater Passive Samplers to Measure Metal Availability at Mine Sites

Florent Risacher, Geosyntec Consultants International Inc., Canada
Jason Conder, Geosyntec Consultants Inc., USA
Brent Pautler, SiREM, Canada
Alex Sweett, SiREM, Canada
Andrew Jackson, Texas Tech University, USA

Abstract

Dialysis passive samplers, also called peepers, have been used to measure the availability of metals at contaminated sites for decades, but have remained largely underused at mine sites. Peepers are a type of passive sampler that function by allowing metals to diffuse from the sampled media, through a membrane, into laboratory-provided water. After an equilibration period, the peepers are retrieved, and the solution is analyzed for metal(oids) and reported as a concentration in water that can be easily compared to water criteria or used in fate modelling. Despite more than forty years of research, passive sampling lacks a set of standardized protocols, which has led to greatly varied methodologies, thus hindering the use of peepers for regulatory and decision-making purposes at mine sites.

To advance peeper technology, Geosyntec conducted a three-year study comprised of a review of the literature to document past successes/limitations, a series of laboratory experiments aimed at refining a set of standard methods, and a field deployment to demonstrate the developed best practices. This work culminated in the development of a guidance document that provides a comprehensive reference for industry practitioners and regulators and answers key questions for the successful application of the technology for decision making.

To facilitate the dissemination of the technology and provide additional tools for water quality and tailings management, this paper will synthesize a brief overview of the technology and the importance of measuring metal(oids) availability. Additional information about the relevance of the technology for the mining industry, such as the use of peepers to measure metal speciation and organo-metal complexes, will also be discussed. This work is conducted as part of an Environmental Security Technology Certification Program (ESTCP) project funded by the U.S. Department of Defense.

Measuring metal availability

Sub-aqueous sediments, wet tailings and various saturated media (herein referred to as sediments) containing high concentrations of inorganic constituents, primarily metals and metalloids, present significant challenges at many mine sites. Biologically available constituents in sediments can be characterized by measurements that seek to quantify the concentration of freely dissolved contaminants (Cfree) in sediments and sediment porewater (Conder et al., 2015; Cleveland et al., 2017). This approach presents an advantage over measuring the total extractable concentration of inorganics in bulk sediment (USEPA, 2005), which can overestimate the fraction of inorganics that are mobile and biologically available (Peijnenburg et al., 2014). Cfree measurements can provide a superior quantitative understanding of metals in sediment (compared to bulk analysis of metals in sediment) that is particularly useful in filling a variety of data gaps typical of environmental site investigations, such as environmental fate, availability, nature and extent, ecological risks, speciation, source control, and remedial performance.

A multitude of methods have been developed to measure the availability of metal(oids) in sediments such as mechanical extractions and acid volatile sulfide. Mechanical sediment porewater analysis usually consists of collecting bulk sediments, which are mechanically squeezed, or centrifuged, to produce a supernatant liquid (porewater) that is then filtered to extract the water for analysis (Gruzalski et al., 2016). The mechanical extraction process poses challenges due to the heterogeneity of sediments, the high reactivity of some inorganic analytes, and chemical and physical disturbances of the sediments. These factors can cause the concentration of dissolved inorganics obtained from analyzing a mechanically extracted sample to deviate from the concentration of available metals in sediment porewater (Peijnenburg et al., 2014). For example, it is recognized that sampling disturbances can affect redox conditions (Teasdale et al., 1995; Schroeder et al., 2020), thus leading to an under- or over-representation of inorganic chemical concentrations relative to the true dissolved phase concentration in the sediment porewater (Wise, 2009; Gruzalski et al., 2016).

Analysis of acid volatile sulfide and simultaneously extracted metals (AVS/SEM) in bulk sediment is often used to evaluate metal availability in sediment (USEPA, 2005). This measurement evaluates bioavailability of divalent metals (cadmium, copper, lead, nickel, and zinc) via a weak acid extraction of a bulk sediment sample (i.e., SEM measurement). Along with measuring and normalizing a chelating agent (AVS), the approach can provide a quantitative value of available divalent metals. Sample-specific AVS/SEM values can be compared to a conservative threshold that, if exceeded, may indicate the need for additional toxicity testing or evaluation due to the potential for toxicity (USEPA, 2005). This approach has the advantage of using simple procedures in the field (e.g., collecting a bulk sediment sample), relatively simple data evaluation (USEPA, 2005; DeForest et al., 2022), and a relatively high acceptance and familiarity among regulatory stakeholders. However, the AVS/SEM approach is primarily limited to

cadmium, copper, lead, nickel, and zinc, and the quantitative estimate produced by the analysis is primarily limited to evaluating the need for aquatic toxicity testing, rather than more broad data uses in nature and extent evaluation or fate and transport.

Sediment porewater dialysis passive samplers

Sediment porewater dialysis passive samplers, also known as "peepers," were developed more than 45 years ago (Hesslein, 1976) as a potential approach to circumvent challenges associated with other methods of sampling inorganic chemicals in sediment. Peepers are inert containers with a small volume of purified water ("peeper water") capped with a semipermeable membrane. Peepers usually feature a protective cap or structure that secures the membrane to the peeper chamber. Peepers are typically prepared under clean laboratory conditions and can be shipped directly to the field site. Various commercial providers exist, and some universities may also have the equipment to construct their own samplers. Deploying a peeper consists of inserting it into the sediment, where it is left for a period of a few days to a few weeks. During this time, passive sampling is achieved via the principle of diffusion, as the enclosed volume of peeper water equilibrates with the surrounding aquatic matrix via transport of inorganics through the peeper's semipermeable membrane (Figure 1; Risacher et al., 2023a). After an equilibration period, the peeper is retrieved, and the peeper water is transferred to a storage container and analyzed for inorganics in the same manner as a typical surface water sample. The results from the analysis are then reported as a concentration in water (i.e., milligram per liter of water [mg/L]).

Peepers have numerous advantages over other sampling approaches, including:

1. Minimal sediment disturbance during sampling which allows to preserve existing sediment structure.
2. Limited exposure of the sample to the atmosphere which prevents highly sensitive redox compounds to react.
3. Minimal risk of the peeper reflecting surface water overlying the sediment that can accidentally contaminates porewater during collection via suction methods.
4. Peepers can provide availability data on any metal, not just divalent metals measured in the AVS/SEM approach.
5. Data from peepers are on a mass per volume basis (i.e., mg/L or µg/L), which facilitates use of the data in fate models, and comparisons to risk-based criteria for water.
6. Peepers integrate Cfree over the deployment period, averaging any changes of the concentration.
7. Peeper chambers can be stacked in a frame to provide porewater concentrations over a vertical sediment profile at higher resolution than conventional extraction methods; and
8. Some passive samplers also contain a Performance Reference Compound, or reverse tracer, which

can help ensure equilibrium has been reached after sampling.

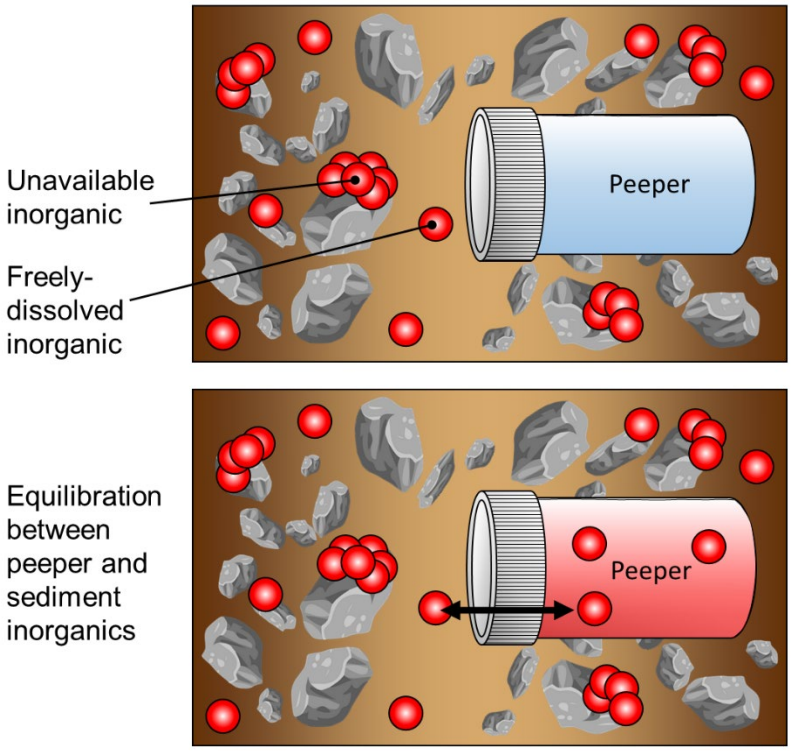


Figure 1: Conceptual illustration of peeper passive sampling in a sediment matrix, showing peeper immediately after deployment (top) and after equilibration between the porewater and peeper chamber water (bottom)

Using peeper data

Peeper data can be used to enable site-specific decision-making in a variety of ways throughout the mine life cycle. Peepers can provide information on 1) nature and extent; 2) sources and fate; 3) the potential direct toxicity to aquatic life; 4) the potential bioaccumulation of metals in aquatic life; 5) the efficacy of remediation and source control; and 6) assessing speciation.

Nature and Extent: Peepers can be helpful in characterizing the presence and availability of metals and inorganics in aqueous media at mine sites. Multiple peeper deployments in sediments can help delineate areas of increased metal availability in the same manner as traditional bulk sediment sampling. Peepers are especially helpful for sites that may not be conducive to traditional bulk sediment sampling. For example, substrates that are comprised of coarse, relatively inert materials, such as gravel or fine fluid materials that may be difficult to sample with sediment grab or coring techniques. Collecting and analyzing such material can be challenging as much of the inorganics present in the sample may be more associated with the porewater phase rather than the solid phase. Explicit measurement of Cfree in the porewater of coarse or fine fluid substrate samples can provide a more robust and precise measurement in these cases.

Additionally, at sites where hydrological disturbances (pumping, groundwater flux) may be influencing the nature and extent of inorganics, peepers have a distinct advantage to bulk sediment sampling or other point-in-time measurements, as peepers can provide an average measurement that integrates the variability in the hydrodynamic and chemical conditions over time.

Sources and Fate: A considerable advantage to using peepers is that the numerical product of a peeper measurement is Cfree, a concentration that is expressed in units of mass per volume (e.g., mg/L or µg/L). Cfree provides a common unit of measurement for evaluating the presence of inorganics across multiple aquatic media such as sediment, tailings, surface water, stormwater, and groundwater. For example, synchronous measurements of Cfree using peepers deployed in tailings and the surface water above can elucidate the potential flux of inorganics from tailings to surface water (or vice versa). Paired measurements of Cfree and bulk metals in sediment can also allow site-specific sediment-porewater partition coefficients to be calculated. These values can be useful in understanding and predicting fate, especially in situations where the potential dissolution of metals from a substrate are critical to predict, such as when sediment is dredged or when tailings are deposited sub aqueously.

Direct Toxicity to Aquatic Life: Peepers are frequently used to understand the potential direct toxicity to aquatic life, such as benthic invertebrates and fish. A Cfree measurement obtained from a passive sampler, such as a peeper deployed in sediment or surface water, can be compared to toxicological benchmarks for aquatic life to understand the potential toxicity to aquatic life and to set remediation goals (USEPA, 2017). Benchmarks are concentrations of chemicals that are associated with adverse effects (or a lack of adverse effects) to aquatic life and are usually obtained from peer-reviewed laboratory toxicity studies in which aquatic life are exposed to known concentrations in water. Formal regulatory benchmark values are available in the form of aquatic life criteria promulgated by environmental agencies such as the USEPA and various states. These benchmark or screening values can be directly used with Cfree measurements and incorporated with more sophisticated approaches, such as the Biotic Ligand Model (Santore et al., 2022) to understand the potential for toxicity and need to conduct additional toxicological testing or ecological evaluations. Cfree measurements and benchmark values can also be applied in aquatic toxicity studies performed in the laboratory with samples of sediment or water, specifically using peepers to understand links between elevated inorganic Cfree measurements and toxicity.

Bioaccumulation of Inorganics by Aquatic Life: Peepers can also be used to understand site-specific relationships between Cfree and concentrations of inorganics in aquatic life. For example, measuring Cfree in surface sediment from which organisms are obtained and analyzed can enable the estimation of a site-specific uptake factor or predictive model relationship. This Cfree-to-organism uptake factor (or model) could then be applied for a variety of uses, including predicting the concentration of inorganics in aquatic life if measurements in organisms are unavailable, or estimating a Cfree value at a

concentration in aquatic life that would be safe for consumption by fish, wildlife, or humans. Because several decades of research have found that the correlation between Cfree measurements and bioavailability is usually better than the correlation between measurements of chemicals in bulk sediment and bioavailability, Cfree-to-organism uptake factors (or models) are likely to be more accurate and precise than uptake factors based on bulk sediment (e.g., Biota Sediment Accumulation Factors).

Evaluating Remediation and Source Control Efficacy: Passive sampling has been used widely to evaluate the efficacy of remediation and source control treatments such as active amendments, thin layer placements, and capping to reduce the availability of chemicals at sediment sites. A particularly powerful data use is a simple comparison of baseline (pre-remedy) Cfree in aqueous media to Cfree in aqueous media after the remedy has been applied. Peepers can be used in this context for inorganics, allowing the remedy's success to be evaluated and monitored in laboratory benchtop remedy evaluations, pilot scale remedy evaluations, and full-scale remediation monitoring.

Assessing Speciation: Metal speciation, especially for organo-complexes, has been given more attention in the past few years due to the increased toxicity and environmental impact compared to their inorganic forms. Peepers can be used to assess the speciation of multiple metal(oids) species in aqueous media, such as arsenic, mercury and selenium, thus providing better understanding of the availability and the potential risk to aquatic organisms. Sulfur speciation can similarly be conducted which can help identify early signs of acidification of pit lakes (Whaley-Martin et al., 2023).

Conclusion and additional resources

Despite more than forty years of research, passive sampling for inorganics has had limited uses in the mining industry as a decision-making tool. This paper aimed to provide a brief overview of passive sampling for inorganics and its potential uses at mine sites, in the hope of providing industry practitioners with another tool for site assessment. Additional resources such as a guidance document, standard operating procedure, and video demonstrations can be found on the SERDP/ESTCP website.

Acknowledgements

This work was funded by the Environmental Security Technology Certification Program (ESTCP) as project ER20-5261.

References

Cleveland, D., Brumbaugh, W.G. and MacDonald, D. 2017. A comparison of four porewater sampling methods for metal mixtures and dissolved organic carbon and the implications of toxicity evaluations. *Environ. Toxicol. Chem.* 36(11): 2909–2915. https://doi.org/10.1002/etc.3884

Conder, J. M., Fuchsman, P.C., Grover, M.M., Magar, V.S. and Henning, M.H. 2015. Critical review of mercury SQVs for the protection of benthic invertebrates. *Environ. Toxicol. Chem.* 34: 6–21. https://doi.org/10.1002/etc.2769

DeForest D., Toll, J., Judd, N., Shaw, A., McPeek, K., Tobiason, K. and Santore, R. 2022. Sediment toxicity data and excess simultaneously extracted metals from field-collected samples: Comparison to United States Environmental Protection Agency benchmarks. *Integr. Environ. Assess. Manag.* 18: 174–186. https://setac.onlinelibrary.wiley.com/doi/epdf/10.1002/ieam.4462

Gruzalski, J.G., Markwiese, J.T., Carriker, N.E., Rogers, W.J., Vitale, R.J. and Thal, D.I. 2016. Pore water collection, analysis, and evolution: the need for standardization. *Reviews of Environmental Contamination and Toxicology* 237: 37–51. Springer New York LLC. https://doi.org/10.1007/978-3-319-23573-8_2

Hesslein, R.H. 1976. An in-situ sampler for close interval pore water studies. *Limnology and Oceanography* 21 (6): 912–914. https://doi.org/10.4319/lo.1976.21.6.0912

Peijnenburg, W.J.G M., Teasdale, P.R., Reible, D., Mondon, J., Bennett, W.W. and P.G.C. Campbell. 2014. Passive sampling methods for contaminated sediments: State of the science for metals. *Integr. Environ. Assess. Manag.* 10(2): 179–196. https://doi.org/10.1002/ieam.1502

Risacher, F.F., Schneider, H., Drygiannaki, I., Conder, J., Pautler, B.G. and Jackson, A.W. 2023. A review of peeper passive sampling approaches to measure the availability of inorganics in sediment porewater. *Environ. Pollut.* 328: 121581.

Santore C.R., Toll, E.J., DeForest, K.D., Croteau, K., Baldwin, A., Bergquist, B., McPeek, K., Tobiason, K. and Judd, L.N. 2022. Refining our understanding of metal bioavailability in sediments using information from porewater: Application of a multi-metal BLM as an extension of the Equilibrium Partitioning Sediment Benchmarks. *Integr. Environ. Assess. Manag.* 18 (5): 1335–1347. https://doi.org/10.1002/ieam.4572

Schroeder, H., Duester, L., Fabricius, A.L., Ecker, D., Breitung, V. and Ternes, T.A. 2020. Sediment water (interface) mobility of metal(loid)s and nutrients under undisturbed conditions and during resuspension. *Journal of Hazardous Materials* 394: 122543. https://doi.org/10.1016/j.jhazmat.2020.122543

Teasdale, P.R., Batley, G.E., Apte, S.C. and Webster, I.T. 1995. Pore water sampling with sediment peepers. *Trends in Analytical Chemistry* 14 (6): 250–256. https://doi.org/10.1016/0165-9936(95)91617-2

USEPA (US Environmental Protection Agency). 2005. Procedures for the derivation of equilibrium partitioning sediment benchmarks (ESBs) for the protection of benthic organisms: Metal mixtures (cadmium, copper, lead, nickel, silver and zinc) (EPA/600/R-02-011). Washington, DC: Office of Research and Development, US Environmental Protection Agency.

USEPA (US Environmental Protection Agency). 2017. Developing Sediment Remediation Goals at Superfund Sites Based on Pore Water for the Protection of Benthic Organisms from Direct Toxicity to Nonionic Organic Contaminants. EPA/600/R 15/289. October.

Whaley-Martin, K.J., Chen, LX., Nelson, T.C. et al. 2023. O_2 partitioning of sulfur oxidizing bacteria drives acidity and thiosulfate distributions in mining waters. *Nature Communications* 14 2006(2023). https://doi.org/10.1038/s41467-023-37426-8

Wise, D.E. 2009. Sampling techniques for sediment pore water in evaluation of reactive capping efficacy. ProQuest Dissertations and Theses. Retrieved from https://scholars.unh.edu/thesis/502

Preliminary Assessment of the Environmental Impacts of Artisanal Gold Mining: The Case of the Kashozi Mining Site, South Kivu, DRC

Akonkwa Mudekuza Kepler, Université Officielle de Bukavu, DRC
Alex Kalonji-Kabambi, Université Officielle de Bukavu, DRC
Bwemere Ciribuka Grâce, Université Catholique de Bukavu, DRC/Université Officielle de Bukavu, DRC

Abstract

Artisanal gold mining is one of the sources of income for the population of the eastern Democratic Republic of Congo (DRC). But this activity still fails to consider tailings management and environmental protection measures for the entire life cycle of an artisanal mine.

In this study, research was carried out for the preliminary assessment of heavy metal contamination levels in the waters and sediments of the Luzinzi River, which borders the Kashozi gold mining site in Walungu, South Kivu province, DRC.

To achieve this objective, the methodology was to conduct field observations to get information about the gold mining and processing circuit at the site. Samples of water and sediment from the Luzinzi River were taken, and laboratory analyses were conducted to determine the physico-chemical parameters and chemical and geochemical composition of the samples.

The results showed that the pH of the waters studied was acidic to neutral (between 5.09 and 6.09), and that these waters were also poorly conductive (between 37.6 to 43.9 µS/cm). Analysis of heavy metals in water and sediments revealed largely elevated levels of heavy metals such as As, Cd, Cr, Cu, Fe, Mn, Ni, Pb, Se, and Zn, compared with the DRC mining regulations and the World Health Organization (WHO) standard for drinking water.

Analysis of these results led to the conclusion that surface waters and sediments in the study area were polluted with heavy metals, notably As, Cd, Cr, Cu, Fe, Mn, Ni, Pb, Se, and Zn, and that this pollution was due to gold panning activities in the area.

Finally, the last objective of this ongoing study was to formulate recommendations concerning alternatives to the use of mercury and the rehabilitation of the polluted environment.

Introduction

Artisanal mining is any small-scale operation involving the extraction and concentration of mineral substances from primary outcropping or underground and/or secondary deposits and the recovery of valuable minerals and metals using manual or traditional methods and processes (Dembele, 2021). Artisanal and small-scale mining (ASSM) involves individual miners or small enterprises with limited capital and production. It is generally a decentralized production system. ASSM is seen as an operation with a diverse range of mining activities, little mechanization, and labor-intensive (Bikubanya and Radley, 2021).

In South Kivu, as in other provinces of the DRC, artisanal mining originated to meet the survival needs of the population. It has attracted several thousand individuals, including young people, and employs a considerable number of people on a precarious basis. It is well known that there are currently more artisanal gold mining sites than industrial ones in the province of Grand Kivu. Small-scale gold mining using traditional techniques, now uses chemicals (cyanide, mercury, etc.) that pollute the environment, particularly river water, air, and soil. As a result, populations living in areas with artisanal mining operations are exposed to several forms of health risk.

Artisanal miners are responsible for extracting the ore from the mine (in the case of underground galleries), which they clean at the edge of streams (after crushing and grinding if necessary) to carry out an initial concentration (Bauma, 2017), and then mercury is mixed in. The mercury binds with the gold in the ore, creating a gold-mercury amalgam that excludes other elements. The miners then heat this amalgam over an open-air flame. The mercury then evaporates and escapes into the air, while the pure gold is isolated for sale on the market (Human Rights Watch, 2010). Gold mining is a source of considerable environmental and health impacts and challenges. These include landscape, health, ecology, and hydrogeology. The risks most often cited are the “uncontrolled release of acid mine effluents,” heavy metal discharges that are dangerous for the long term, and suspended matter discharged into watercourses and thus degrading aquatic ecosystems (Bauma, 2017).

Heavy metals are considered serious pollutants of the aquatic environment, due to their persistence and tendency to bioaccumulate in aquatic organisms. They have toxic effects when organisms are exposed to concentration levels higher than those which they normally require, causing harmful effects on fish and humans through the food chain (Oumar et al., 2014). Poor management of mine tailings is a source of pollution for the environment (surface water and groundwater) and it is essential to control what is released into the environment so as not to exceed a certain threshold, in order to ensure the protection of ecosystems and human health.

In the DRC, the mining code and regulations govern the quality of water and mining effluents to be discharged into the environment. These regulations prohibit the discharge of wastewater, mine drainage, mine tailings, waste or any other contaminant into surface waters or within one hundred meters of a source

of drinking water or food for humans or livestock. All contaminants must be stored and treated in such a way as to eliminate any risk of water pollution. No stream, lake, or river may be used for partial or total wastewater treatment purposes. Also, no dilution of wastewater is permitted (Règlement minier RDC, 2018). Unfortunately, these regulations and mining code are not always respected due to weak official enforcement structures and lack of awareness (Nkuba et al., 2019).

This paper presents a preliminary assessment of the environmental impacts of artisanal gold mining: the case of the Kashozi mining site in South Kivu province, DRC. The objective is to evaluate the level of heavy metal contamination in the waters and sediments of the Luzinzi River, which borders the Kashozi gold mining site. The following sections present the study area and the methodology, and then presents, interprets and discusses the preliminary results.

Methodology

Description of the study area, climatic, mineralization, and geological context

The Kashozi *groupement* (grouping), where the gold mining site is located, is one of the fifteen administrative groupings of the Kaziba chieftaincy in the DRC (Figure 1). It is located at 02.50'18.8" south latitude and 028°49'26.2" east longitude, approximately 60 km southeast of the town of Bukavu in South Kivu province (Rumama, 2017).

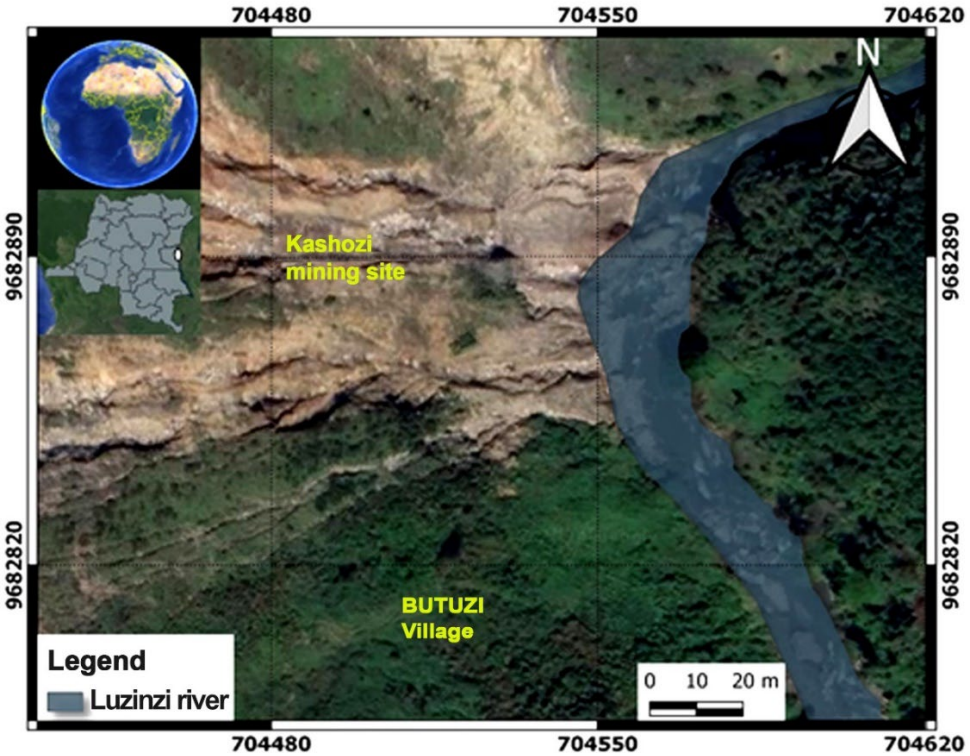


Figure 1: Location of the Kashozi mining site in South Kivu, DRC

With altitudes ranging from 1,800 to 3,200 m, the Kashozi grouping reaches to the Mubuga highlands. Its hydrography consists solely of rivers, including the Kalango, Kaderhe, Nachibundu, Muguka, Lulindja, and Luzinzi rivers. Kashozi has an equatorial climate modified by altitude (Ndeko et al., 2018).



Figure 2: Topography overview around the Kashozi mining site

Rainfall is abundant, with an average annual rainfall of 1,500 mm. Average annual temperatures range from 17 to 18°C and daily temperatures average from 12 to 22°C (Buhendwa and Bwira, 2019). There are two seasons, a long rainy season lasting 9 to 10 months, from September to June, and a short a short dry season lasting 2 to 3 months (from June to September).

In terms of local geology, Kashozi lies in the Upper Kibaran of Kivu, in the Nyangezi *"Synclinorium d'Itombwe"* sector. This sector is approximately 3,000 to 3,500 m thick and consists of conglomerates with quartzite elements at the base. This is followed by conglomerates topped by phyllades. Then a mixed formation (glacial formation of unknown origin), a schistosandstone formation and tillite with various pebbles at the top (Kalalizi, 2014).

At Kashozi, gold mineralization occurs in the form of intrusions in the rocky mass of the hillside and alluvial deposits in the Lunzizi riverbed. There is alluvial mining in the Lunzizi river and underground mining in drifts on the hillside. Artisanal miners use sluices and pan for washing and concentration. Gold miners add a little mercury to the concentrate to make the amalgam, which they then heat. In the case of primary and secondary deposits, there is no method for managing tailings, which are discharged directly into the environment (Figure 3).

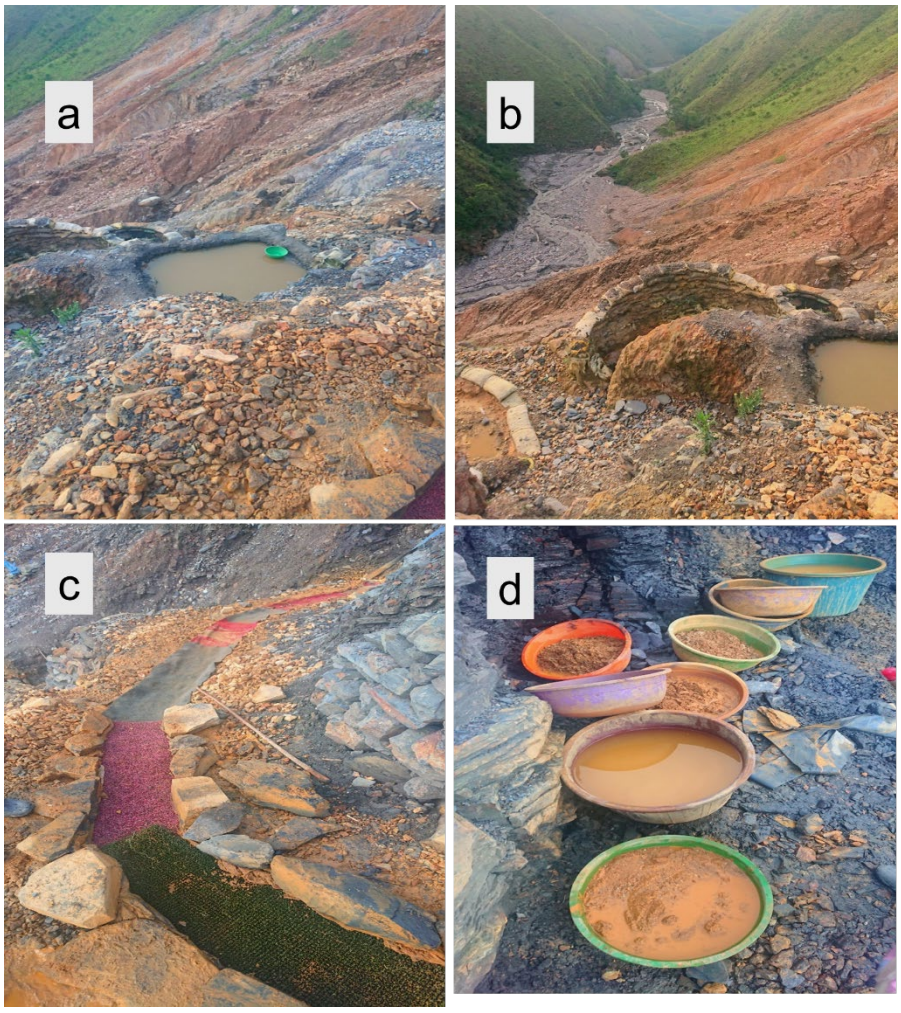


Figure 3: Artisanal mining workspaces and material at the Kashozi mining site: wash basin (a), Luzinzi River (b), slice (c) and pan (d)

Sampling and materials preparation

The following components were necessary to achieve the objectives of this study:

1. Field work, which involved field observations and studying the gold mining and processing circuit at the site, as well as taking water and sediment samples.
2. Chemical and geochemical analysis of samples at the laboratory to determine metal concentrations in surface water and sediments around the Kashozi site.
3. Discussion and interpretation of the results in relation to similar work carried out in the area or elsewhere, the directives of the DRC mining regulation, and the criteria for drinking water according to the World Health Organization (WHO) standard.

Sampling was carried out while the artisanal workers were washing the ore on the hill. After drawing up a sampling plan and getting the equipment ready, the first water sample was taken from the wash water

coming from the washing of ores on the hill. The second water sample was taken from the water upstream of the river, as it was before it encountered the water discharged from the mine. The third water sample was taken at the point where the mine and river waters meet. Seven other samples were taken downstream of the meeting point, spaced 5 m apart (the last sample was therefore taken 35 m from the meeting point of the river and mine waters). At each water sampling point, the pH was measured.

For sediment samples, the first sediment sample was taken on the hillside in the washing basin (to obtain information on the mineralogy of the materials carried to the river by runoff during rainfall or by washing water during ore processing). The second sediment sample was taken upstream in the river in an area less impacted by artisanal mining operations. The third sediment sample was taken at the point where the mine waters meet those of the river. The fourth sediment sample was taken 5 m downstream of the meeting point. Three further sediment samples were taken in areas of low influence downstream of the meeting point. In all, ten water samples and seven sediment samples were taken to enable us to assess the environmental impacts of gold mining and processing at the Kashozi mine site (Figure 4).

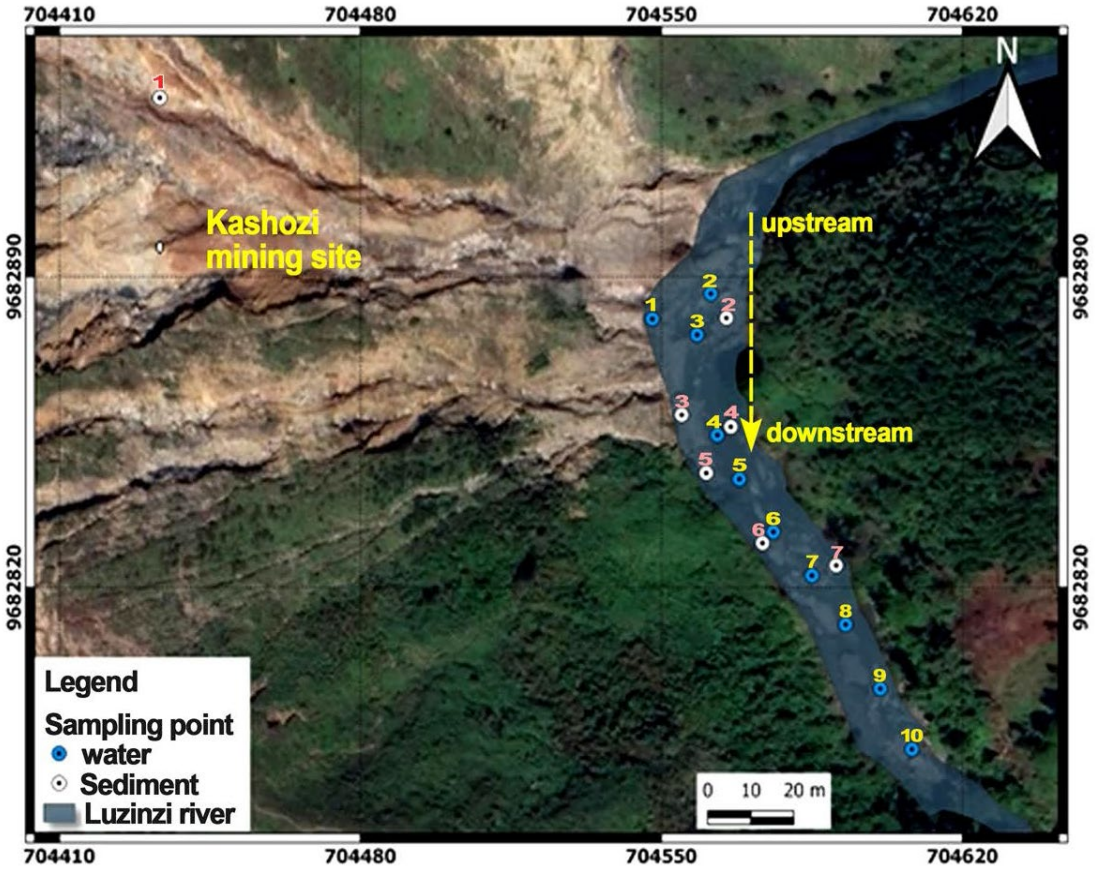


Figure 4: Sampling map of water and stream sediment at the Kashozi mining site

Liquid samples were stored in accordance with the guidelines of the Centre d'expertise en analyse environnementale du Québec (CEAEQ), which recommends 6 months' cold storage in well-closed plastic

containers (CEAEQ, 2012). To comply with this recommendation, all liquid samples were kept in a freezer (at around 0°C) until the day of laboratory analysis, which was done within less than two months.

The following equipment was used: an auger to drill into the sediment, a pH meter to measure the pH of the water at the site, 500 ml plastic bottles to collect the water samples, plastic bags to collect the sediment samples, Arc Gis and Google Earth software to map the site and locate the sampled areas, and Excel software to produce the graphs. The analyses, which were carried out at the Office Congolaise de Contrôle (OCC) laboratory over a three-day period, focused on determining the concentration levels of metals in the sediments and waters samples using two spectrometers: the Quantum RX spectrometer and the Tal instrument X spectrometer; and also on measurement of the pH and conductivity in water samples using an electric pH meter and an electronic conductivity meter, respectively (Figure 5).

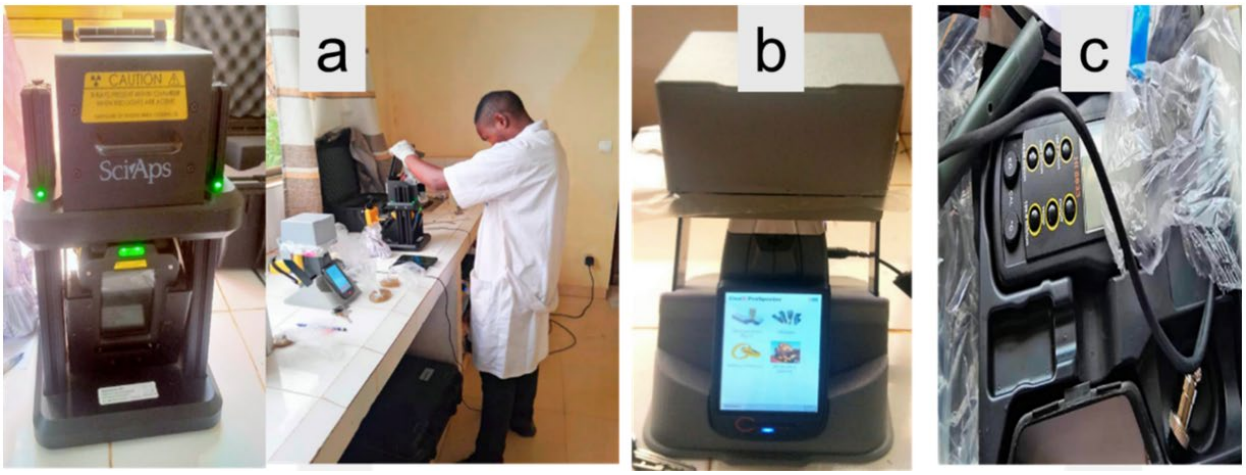


Figure 5: Laboratory analysis: Quantum RX spectrometers(a), Tal instrument (b) and conductivity meter (c)

Preliminary results

Physical characteristics of water samples

The pH values varied between 4.95 and 6.25 (site value) and between 5.09 and 6.09 (laboratory value). It should be noted that the pH varied from acidic to neutral, with mine water being more acidic than river water, and that after the confluence zone, there was regulation between mine and river water, with the pH increasing slightly further away from the confluence zone.

The pH values measured are below the WHO's optimum drinking water range (6.5 and 9.5) (OMS, 2017). This may be due to the local geological context, which is characterized by the presence of sulfide minerals, such as pyrite in association with gold. The sulfide minerals contained in the waste rock and tailings, stored in the open air, are gradually oxidized, contributing to a decrease of pH value in the environment.

In terms of conductivity, the water analyzed had values below 250 µS/cm (WHO limit). These waters are low in mineral salts and therefore poor conductors (between 37.6 and 43.9 µS/cm) (Table 1).

Table 1: Main physical characteristics of water simples

Sample number	Sample location*	pH measured on site	pH measured in laboratory	Conductivity measured in the laboratory (µS/cm)
1	Mine water before mixing with river water	4.95	5.09	42.8
2	Upstream river water before mixing with mine water	6.23	5.45	43.9
3	Meeting point of mine and river waters	5.08	5.28	37.6
4	5 m downstream of the meeting point	5.56	5.31	40.0
5	10 m downstream of the meeting point	5.6	6.09	42.2
6	15 m downstream of the meeting point	5.8	5.58	43.8
7	20 m downstream of the meeting point	6.05	5.56	43.1
8	25 m downstream of the meeting point	6.15	5.55	42.6
9	30 m downstream of the meeting point	6.25	5.62	41.0
10	35 m downstream of the meeting point	5.91	5.35	43.7

* See also Figure 4 for samples location

Chemical results of water samples

The results in Figure 6 show an increase in concentration of the majority of chemical elements in the water. As can be seen from the graph, the elements with the highest concentrations, exceeding 30,000 mg/l and reaching 100,000 mg/l for some elements, are: Aluminum (Al), Iron (Fe), Potassium (K), Silicon (Si), and Titanium (Ti).

Given the difference in concentrations, we can assert that the Luzinzi river water was polluted long before it was impacted by Kashozi mining activities. This may be due to mining at other sites upstream of the Kashozi mining site (e.g., the Mufumbé site, etc.), and also to the local geology through the processes and mechanisms of weathering, erosion, leaching, and sedimentation.

High concentrations of heavy metals such as As, Cd, Cr, Cu, Fe, Mn, Ni, Pb, Se, and Zn are noticeable in water samples, and these concentrations are well above DRC mining regulations and WHO standards.

Figure 7 shows the difference in concentration between the upstream maximum and minimum measured concentrations and the concentration requirements in the DRC mining regulations at the final effluent point and the drinking water quality proposed by the WHO.

Although it is used in the gold recovery process (by amalgamation), Hg does not appear in the water and sediments sampled and analyzed at the Kashozi site. This can be explained by the fact that the amalgam is burnt outside the mine site.

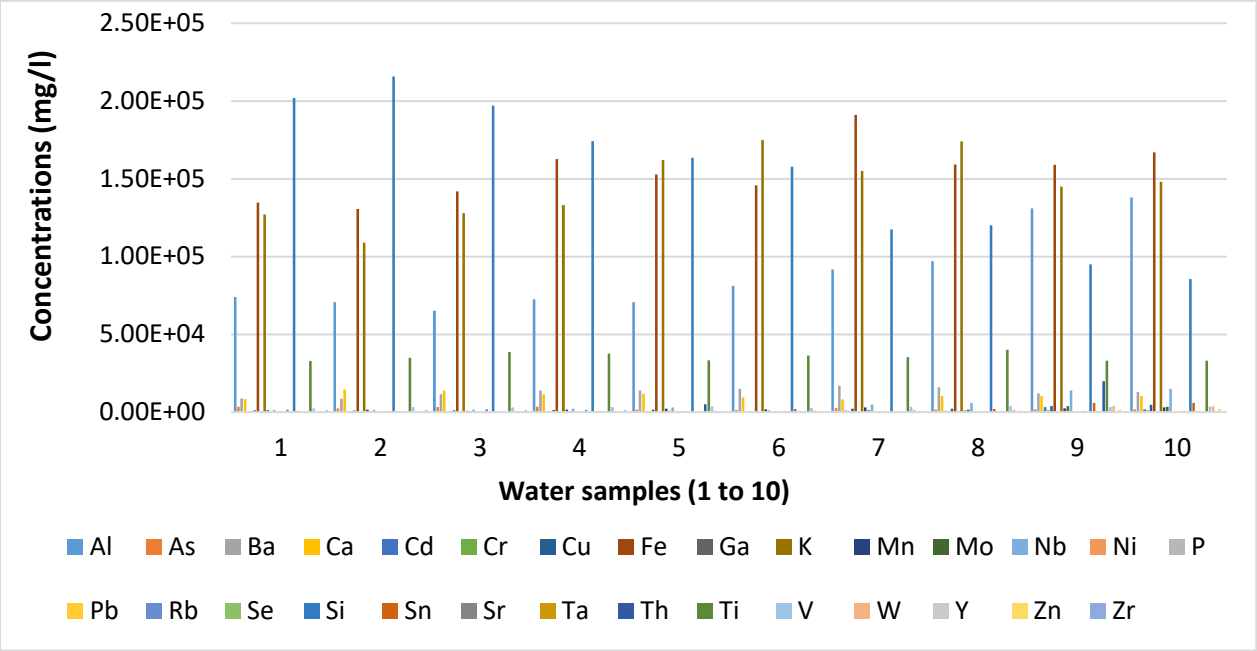


Figure 6: Chemical results of water samples
(see also Figure 4 and Table 1 for location of samples)

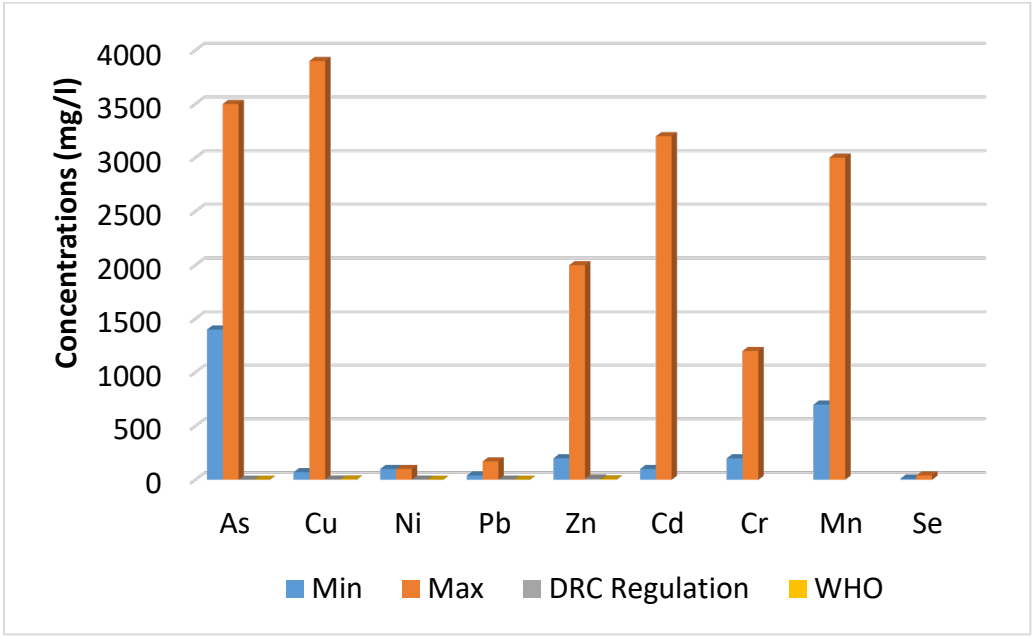


Figure 7: Upstream measured concentrations, compared to the DRC mining regulation and WHO standards

Geochemical results of river sediment samples

As with the water samples, the graph in Figure 8 shows that, the elements with the highest concentrations, exceeding 15,000 mg/l and reaching 100,000 mg/l for some elements, are: Aluminum (Al), Iron (Fe), Potassium (K) Silicon (Si), and Calcium (Ca).

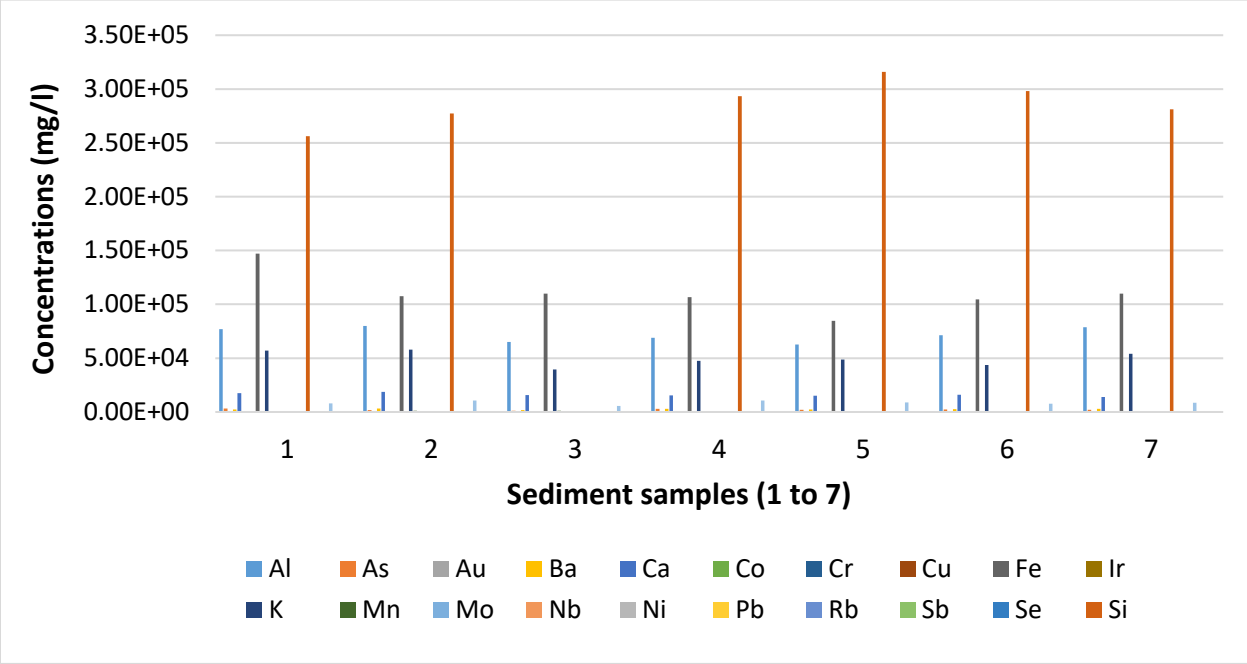


Figure 8: Geochemical results of river sediments samples

The high concentrations of silicon (> 200,000 mg/l and iron > 100,000 mg/l) may be due to the fact that silicon is more abundant in the earth's crust, and also because pyrite is among the main minerals making up the rocks at the mining site.

Chemical element concentrations in the washing basin are almost identical to sediment concentrations in the zone of low influence upstream of the river. There is a drop in concentration at the percolation zone, followed by a slight increase in concentration as the river flows downstream of the percolation zone.

Heavy metals such as arsenic (As), chromium (Cr), copper (Cu), iron (Fe), lead (Pb), and tin (Sn) are also present in high concentrations in the washing basin, while vanadium (V) and zinc (Zn) are present in high concentrations in the sediments upstream of the river (Figure 8).

Given these results we can say that the mine has little influence on the sediments of river. This can be explained by the fact that the river crosses the site in the form of a torrent with a low sedimentation rate, which means that the particles in the river from the mine or from run-off do not have time to settle.

Probable origin of high metal concentrations

The metals are of natural origin. The Nyenyezi deposit in Kaziba supplies the Kashozi processing site with ore. It is of the vein type, with schists (phyllades) and quartzophyllades as the host rocks. These rocks alternate with quartzites. Mineralization is essentially gold-bearing, with iron oxides as accompanying elements. The high concentration of iron can be explained by weathering and erosion phenomena, but even more so by the activities that lead to its exposure on the surface. From a mineralogical point of view, this could be explained by the fact that iron is found in pyrite, copper in chalcopyrite, and calcium in calcite and ankerite. These minerals constitute the mineral paragenesis of orogenic gold deposits (Nkere, 2022).

Selenium may come from suspended clay minerals. Copper could come from the alteration of quartzites but also, in accordance with the regional geology, from malachite and/or azurite (Rumama, 2017).

The results of this study show high levels of heavy metals in water samples, such as As (1,400 – 3,500), Cd (100 – 3,200 mg/l), Cr (200 – 1,200 mg/l), Cu (70 – 3,900 mg/l), Iron (13,500 – 166,900mg/l), Mn (700 – 3,000 mg/l), Ni (100 mg/l), Pb (40 – 170 mg/l), Se (10 – 40 mg/l), and Zn (200 – 2,000 mg/l). Most of these grades are higher than those found by other authors in studies carried out at other sites in the South Kivu province (e.g., Wenga, 2022; Bazikange, 2022). We can therefore confirm that the Luzinzi River is indeed polluted with heavy metals as a result of the leaching of mine tailings from the gold mining and processing circuit.

Conclusion

The aim of this study was to assess the level of heavy metal contamination in the waters and sediments of the Luzinzi River, potentially due to artisanal gold mining at the Kashozi mine site.

To achieve this, the methodology consisted of carrying out on-site observations of the treatment circuit; and taking water and sediment samples and analyzing them (in situ and in the laboratory) to determine physical parameters (water conductivity and pH) and geochemical composition of stream sediments and the chemical composition of water samples.

With regard to physical parameters, the analyses show that the pH of the waters is acidic to neutral (between 5.09 and 6.09) and therefore below WHO standards for drinking water (between 6.5 and 9.5), but these waters are also low-conducting (between 37.6 to 43.8 µS/cm) and therefore perfectly within WHO standards (EC < 250 µS/cm).

Analysis of heavy metals in water showed high levels of As (1,400 – 3,500 mg/l), Cd (100 – 3,200 mg/l), Cr (200 – 1,200 mg/l), Cu (70 – 3,900 mg/l), Iron (13,500 – 166,900 mg/l), Mn (700 – 3,000 mg/l), Ni (100 mg/l), Pb (40 – 170 mg/l), Se (10 – 40 mg/l), and Zn (200 – 2,000 mg/l), compared with mining regulations and WHO standards for drinking water.

Analysis of these results led to the preliminary conclusion that surface waters in the study area are polluted with heavy metals, in particular As, Cd, Cr, Cu, Fe, Mn, Ni, Pb, Se, and Zn. The pollution observed is largely due to mining activities in the area. The results of this study suggest that this is long-standing pollution, dating back to the start of artisanal mining activities in the sector.

In view of the partial results of this study, which confirm the pollution of the study area by heavy metals, the following recommendations can be made:

1. Implement existing legislation (deemed sufficient but generally not applied).
2. Establish an institutionalized system for monitoring pollution of the hydrographic network in active artisanal mining areas.
3. Ban the use of mercury when concentrating gold.
4. Raise awareness among populations about the potential risks involved in consuming polluted river water without prior treatment.
5. Build a lagoon purification system with hyper-accumulating species of heavy metals in order to treat mining effluents before their release into the natural environment.

Acknowledgements

The authors would like to acknowledge Mr. Ciza Murhabazi Emmanuel, candidate engineer at the Mining School of the Université Officielle de Bukavu, for his help with the fieldwork, and the staff of the Mining School and the Office Congolaise de Contrôle laboratory for their collaboration.

References

Bauma, K.F. 2017. Etude sur l'utilisation du mercure et du cyanure dans l'exploitation artisanale. Save Act Mine, 18 pp.

Bazikange. 2022. *Evaluation de l'impact du circuit de traitement des minerais artisanal sur l'environnement: cas du site de traitement Kajabwe au sud-Kivu en RDC. Travail de fin de cycle*. Université Officielle de Bukavu.

Bikubanya, D-L and Radley, B. 2021. *Productivité et profitabilité: une analyse comparative basée sur l'impact de la mécanisation dans l'EMAPE de l'or en RDC.* Université Catholique de Bukavu.

Buhendwa and Bwira. 2019. *Contribution à l'étude pétrographique et géochimique des formations géologiques de Mulambi Chefferie de Kaziba, province du Sud-Kivu en RDC. Mémoire de fin d'étude en géologie.* Université Officielle de Bukavu.

Centre d'expertise en analyse environnementale du Québec (CEAEQ). 2012. *Modes de conservation pour l'échantillonnage des rejets liquides (eaux usées), DR-09-04, Ministère du Développement durable, de l'Environnement et des Parcs,* 6 pp.

Dembele, A. 2021. *L'orpaillage, la population et l'environnement dans la commune de Fourou. Mémoire de master.* Centre de Formation et d'Apuis Conseil pour le Developpement Local-DELTA-C. Bamako.

Human Rights Watch. 2010. *Le mercure: une question de santé et de droits humains. Un traité mondial à l'horizon.* Brent Stirton/Reportage pour Human Rights Watch. Mercury A Global Health Treaty FRENCH (hrw.org).

Kalalizi, E.M. 2014. *Les stratégies de développement des entités territoriales décentralisées du Sud-Kivu. Cas de la chefferie de Kaziba en territoire de Walungu. Travail de fin de cycle*. Université Officielle de Bukavu.

Ndeko Mubembe, S.D., Murhula Cizungu, A., Balagizi Karhagomba, I., Bararunyeretse, P., Bisimwa Ntagereka, P., Ntiharirizwa, S. and Buhungu, S. 2018. *Analyse bactériologique et physico-chimique des eaux des sources publiques. Bulletin Scientifique sur l'Environnement et la Biodiversité* 5 (a): 1 – 11.

Nkere, J. 2022. *Cours de complement de géologie.* Université Officielle de Bukavu.

Nkuba, B., Zahinda, F., Chakirwa, P., Murhi, I., De Haan, J. and Bashwira, M.-R. 2019. *Rapport du projet Minamata Initial Assessment (MIA) pour la préparation du Plan d'Action National (NAP) pour la réduction de l'utilisation du mercure en RDC, par le Centre d'Expertise en Gestion du secteur Minier de l'Université Catholique de Bukavu.*

Organisation Mondiale de la Santé (OMS). 2017. *Directives de qualité pour l'eau de boisson*. 4th edition including the first addendum.

Oumar, B., Ekengele, N.L. and Balla, O.A.D. 2014. *Évaluation du niveau de pollution par les métaux lourds des lacs Bini et Dang, Région de l'Adamaoua, journal/Afrique Science: Revue Internationale des Sciences et Technologie* 10(2). Cameroun.

Règlement minier de la République Démocratique du Congo. 2018. *Décret N° 038/2003 du 26 Mars 2003 portant sur le règlement minier tel que modifié et completé par le décret N° 18/024 du 08 Juin 2018.*

Rumama. 2017. *Rapport de stage de professionnalisation effectue à Kaziba.* Université Officielle de Bukavu.

Wenga, F. 2022. *Evaluation de la pollution des eaux par les activités d'exploitation minière artisanale: Cas du site minier de Mobale à Kamituga dans le territoire de Mwenga. Travail de fin de cycle.* Université Officielle de Bukavu.

Implementation of Saturated and Unsaturated Seepage Analysis in a Polymetallic Tailings Storage Facility: A Case Study

Jose Alfredo Promotor, Flopac Geotecnia, Mexico
Sergio Hernández, Flopac Geotecnia, Mexico
Osvaldo Flores, Instituto de Ingeniería – UNAM, Mexico
Cesar Gallegos, Corporativo Peñoles, Mexico

Abstract

Tailings dam failures around the world have brought tailings storage facilities (TSFs) under intensive evaluation by experts in the field of engineering. Several working groups and government agencies have emphasized the importance of risk management associated with TSFs. Therefore, numerical analyses to aid in decision-making are often appropriate support tools. The implementation of numerical models can have advantages associated with the design, planning, operation, and closure of a TSF. However, to reduce the uncertainties associated with numerical analysis, these must be accompanied by the application of the observational method. Thus, this paper presents a case study in which a saturated and unsaturated flow numerical model was implemented, which has helped in decision-making to reduce the associated risks before, during, and after the operational periods of a TSF. The case study highlights the analysis methodology, which included stages of calibration, verification, and prediction of the drainage conditions of the TSF. The results show the benefits of numerical seepage modeling, which, under appropriate evaluation criteria, can be a supportive tool for decision-making in the management and control of a TSF. Finally, some experiences gained over the three years of observation of the case study are highlighted.

Introduction

Water flow analyses are a specific evaluation of the design, planning, operation, and closure stages of a tailings storage facility (TSF) (Mittal and Morgenstern, 1976). From a geotechnical perspective, these analyses focus on estimating saturation, pore pressures, and seepage that can influence the short- and long-term stability of the TSF (Finke Morrison, 2022; Beier et. al., 2023). Historically, there are records of several collapses directly or indirectly related to water flow through these structures (Alexander, 1986; Macklin et

al., 2006). Although water flow is not the sole contributing factor, it is one of the primary ones (Azam and Li, 2010; Lyu et al., 2019).

Several morphological, hydrogeological, and operational factors influence water flow behavior in a TSF (Fredlund and Dakshanamurthy, 1981). Identifying each of these factors is essential for a clear understanding of its hydraulic characteristics. Given this condition, the geotechnical engineer must actively collaborate with hydrology and hydrogeology specialists to develop the conceptual and numerical simulation of water flow within the TSF. However, the development of both elements must be conducted under the principles of saturated and unsaturated flow concepts (Lam et al., 1987; Cooley, 1983).

Based on the above, the objective of this paper is to demonstrate the methodology for implementing a saturated and unsaturated seepage numerical model for monitoring, planning, and decision-making in a tailings storage facility. The general results of the case study, collected over a three-year observation period, are highlighted. It is hoped that this publication will encourage the development of specialists with a hydro-geotechnical focus capable of conceptualizing hydraulic behavior and its implications for the stability conditions of tailings dams.

Case study

The case study is a representative cross-section of an upstream tailings dam with a height of 45 m and an average slope of 2H:1V (Figure 1). The TSF operation is based on cycles of excavation and deposition of tailings using the conventional spigots method.

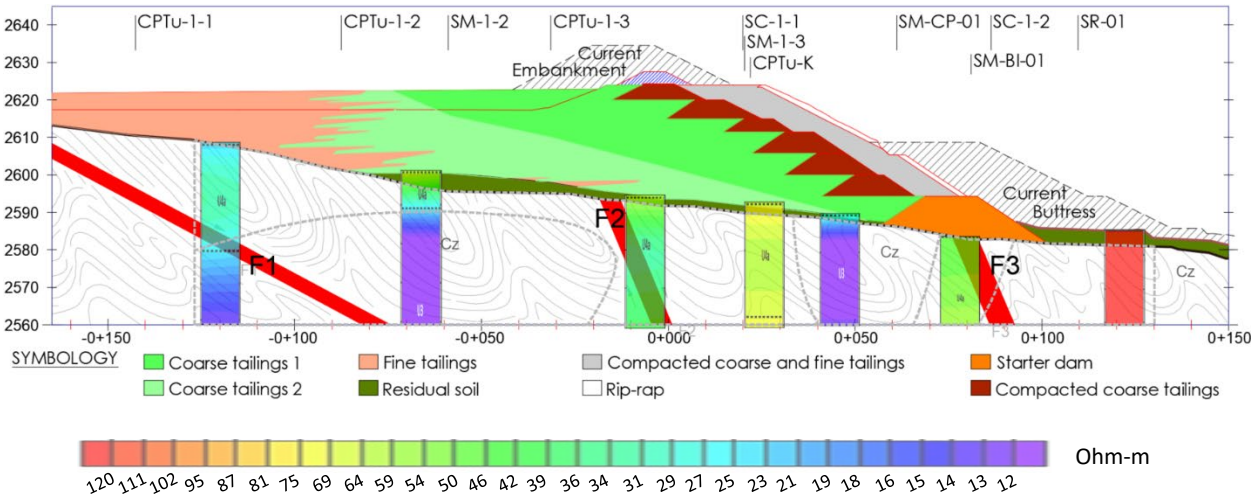


Figure 1: Cross-section view of the TSF

The material characterization of the TSF was based on geophysical, geotechnical, and geological investigations. The geological study characterized the foundation as limestone rock with shale intercalations. Three inactive and permeable geological faults, designated as F1, F2, and F3, were also

identified. Geophysics identified low resistivity zones (0-20 Ohm-m) associated with potential saturation areas related to the location of the geological faults. The interpretation of geotechnical exploration helped in the classification of tailings according to the fine content (%F) and the normalized soil behavior type index from the CPTu (Ic-SBTn): coarse tailings 1 (%Fines ≤ 25 and Ic-SBTn ≤ 2.0); coarse tailings 2 (25 < %Fines ≤ 50 and Ic-SBTn≤2.6); and fine tailings (%Fines ≥ 50 and Ic-SBTn ≥ 2.6). A cross-section of the TSF is shown in Figure 1.

Saturated and unsaturated tailings properties

The coefficient of permeability ($k_{Measured}$) was determined based on laboratory tests, in-situ tests, and empirical relationships. The analysis distinguished the hydraulic conductivities in the horizontal and vertical directions, expressed as k_x/k_y ratio (Table 1). It should be noted that the hydraulic conductivities are expressed using the geometric mean and the standard deviation as a decimal logarithm.

Table 1: Saturated hydraulic conductivity and fitting parameters for the SWCC

Material	$k_{y\ Measured}$ (m/s)			$k_{y\ Calibrated}$ (m/s)		Fredlund and Xing (1994)				
	σ_{std}	k_{mk}	k_x/k_y	k_y	k_x/k_y	$\theta_{w\ sat}$	a_f (kPa)	n_f (-)	m_f (–)	h_r (kPa)
Coarse tailings 1	0.2	2.16E-06	~2	1.55E-06	15	0.49	10.1	1.9	1.5	40.0
Coarse tailings 2	0.4	3.86E-07	~2	5.33E-07	15	0.46	11.7	2.2	1.0	55.0
Fine tailings	0.6	1.52E-08	~2	3.29E-08	15	0.40	765.1	0.9	1.7	7500
Compacted coarse tailings	0.5	4.18E-06	–	5.0e-07	1	0.30	13.0	1.0	0.7	1500
Starter dam	–	3.34E-06	–	2.39e-06	1	0.30	0.9	4.7	0.6	6.0
Residual soil	–	1.42E-06	–	1.72e-08	1	0.50	0.6	4.6	0.6	2.5
Faults	–	1.53E-04	–	2.50e-05	1	–	–	–	–	–

The unsaturated tailings property functions (Soil Water Characteristic Curve – SWCC and Hydraulic Conductivity Function – HCF) were defined through estimation procedures based on four stages: 1) Fitting the tailings grain-size distribution curves with the Fredlund et al. (2000) equation; 2) Estimating the SWCC from grain-size data using the Arya and Paris (1981) or Aubertin et al. (2003) method; 3) Fitting the estimated SWCC with the Fredlund and Xing (1994) equation; and 4) Estimating the HCF using the Fredlund et al. (1994) equation. Table 1 summarizes the fitting parameters for the SWCC and the saturated hydraulic conductivity for the HCF.

Conceptual model

The conceptual model for the case study is illustrated in Figure 2. The essential features of the conceptual model are highlighted below Figure 2.

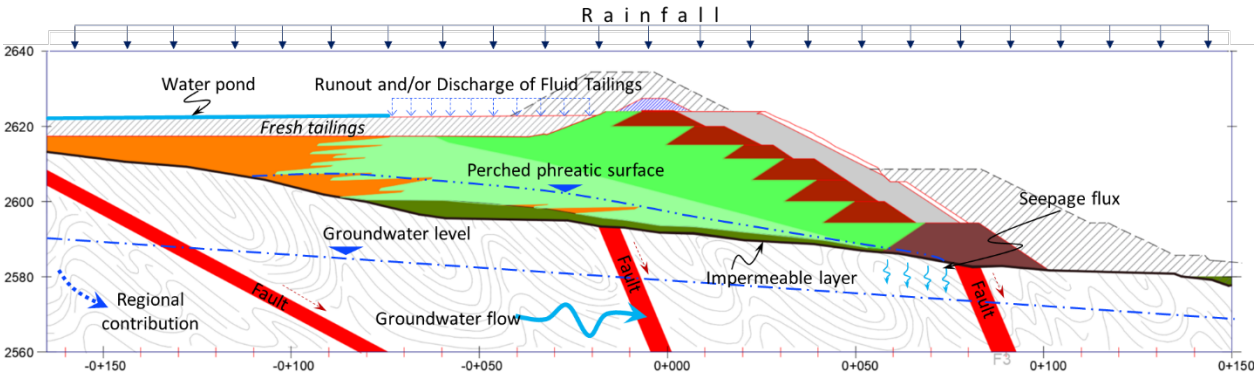


Figure 2: Conceptual model for the case study

- Regional contributions and groundwater flows are associated with runoff that infiltrates through the slopes and contributions from the upper part of the basin.
- Faults act as preferential flow paths that influence the saturation and desaturation of the foundation.
- An impermeable layer partially extends through the footprint of the TSF, limiting seepage toward the foundation and creating a perched phreatic surface. The discharge of the perched phreatic surface occurs at the base of the starter dam, where the impermeable layer was removed during its construction.
- The main seepage to the perched phreatic surface comes from the operational periods of the TSF.
- Surface infiltrations through the beach area depend on the water pond, tailings deposition, and rainfall. These input variables contribute to the saturation of the TSF.

Numerical modeling

The seepage analysis was conducted for a two-dimensional section representing the maximum cross-section of the TSF. The analysis was performed under a transient regime that involved both saturated and unsaturated flow conditions. Evaluation was performed using the commercial software Seep/W (Geoslope, 1991-2021), which solves the Richards equation (1931) with the finite element method (FEM). The mesh was adjusted based on geometric changes in the section, comprising over ~10,000 triangular elements and 5,250 nodes (Figure 3).

Boundary conditions were based on the conceptual model described in the previous section (Figure 2). Details of each boundary condition are described in the following points (see also Figure 3):

- Rainfall ($q_{Rainfall}$): represented by a function given by the average of annual daily rainfall over a 40-year period. It was verified to prevent unrealistic pressure heads on the model surface.
- Groundwater flow (HGW): idealized as constant hydraulic heads assigned at the boundaries of the numerical model, inducing gradients for the interaction of the TSF with the foundation.

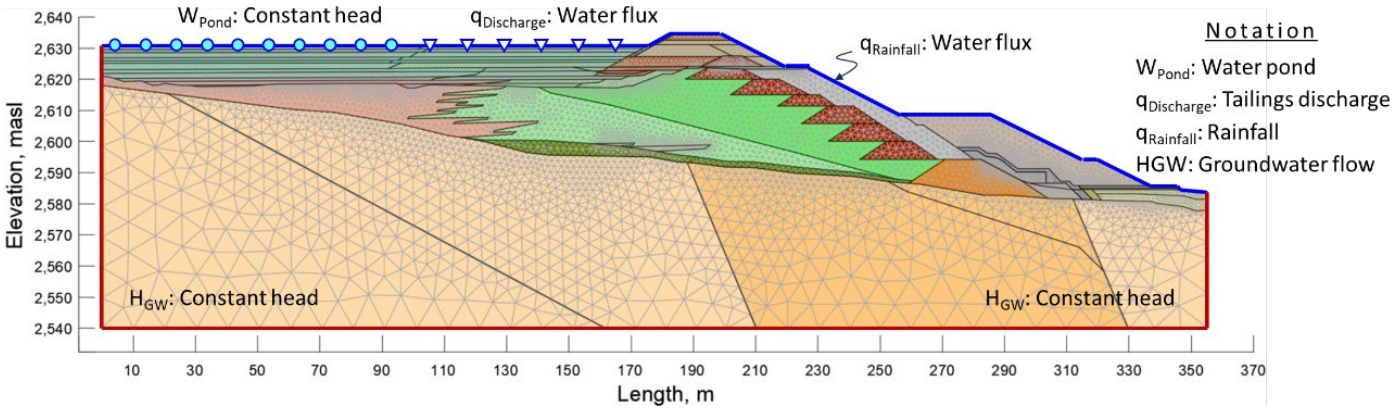


Figure 3: Numerical model and boundary conditions

- Water pond (W_{Pond}): given by a constant head associated with the water levels related to the slope of tailings deposition.
- Beach length: defined as the average monthly value of the monitoring data.
- Fluid tailings discharge ($q_{Discharge}$): incorporated as a unit flux considering the number of spigots, discharge rates, solids content in the tailings mixture, the average tailings runout from the spigots to the water pond, and a width equivalent to the separation between two adjacent spigots. The unit flux was applied as a function simulating the spigot cycle, maintaining the discharge rate for a 24-hour period at 10-day intervals, representing the 11 operational spigots. Throughout all stages of the numerical modeling, the unit flux was made dependent on the infiltration rate to prevent the development of unrealistic pressure heads on the model surface.
- Fresh tailings: associated with the storage curve of the TSF and tailings with high permeability.

The methodology and criteria adopted in the numerical modeling are summarized in Table 2.

Discussion

The calibration stage focused on simulating the water level readings in observation wells (PO) and electric piezometers (PZE) (Figure 4). The calibration period was set from July 2020 to March 2021. Since water level readings began with the tailings deposition, calibrations were updated based on field observations. The outcome of this stage was a numerical model with calibrated conductivities ($k_{Calibrated}$) (Table 1) capable of simulating the water level changes at PO and PZE. Although a temporal lag in the response of the model was identified, the absolute changes in pore pressures matched well with field records.

Table 2: Procedure and stages of analysis

No.	Stage	Description
1	CALIBRATION[1]	(Figure 4)
1.1	Calibration technique	Manual trial-and-error
1.2	Calibration parameter[2]	Saturated hydraulic conductivity
1.3	Calibration target	Hydraulic head pressure
1.4	Calibration acceptance criteria	Qualitative and statistical (R>0.95, RMSE<10m y nRMSE<10%)
2	VERIFICATION	(Figure 5)
2.1	Piezometric data	Comparison of calculated and measured water levels
2.2	Cone penetration test (CPTu) (First stage)[3]	Comparison of in-situ and numerical pore pressures (u_w) (Row A)
2.3	Cone penetration test (CPTu) (Second stage)[3], [4]	Comparison of dynamic pore pressures (u_2) with numerical saturation profiles (Row B)
2.4	Water content profile (SPT)[3], [5]	Comparison of in-situ and numerical saturation profiles (Row C)
2.5	Seepage or groundwater fluxes	Comparison of in-situ seepage or groundwater flux with modeled values
3	SENSITIVITY	(Figure 6)
3.1	Operational cases	Analysis related to operational conditions of the TSF: Operation period, beach length, deposition method, etc.
3.2	Environmental cases[6]	Analysis related to climatological variables.
4	PREDICTION	(Figure 7)
4.1	True predictive case	Evaluation of the most representative operational conditions reconciled with the TSF operator

Notes:
[1] This stage includes the analysis of an "initial condition" that defines a phreatic surface linked to a specific date of the TSF. The "initial condition" precedes the operational simulation of the TSF, representing the starting condition of the numerical model.
[2] To minimize non-uniqueness issues, a single calibration parameter was adopted.
[3] Qualitative verifications.
[4] Assumes a relationship between the pore pressure (u_2) of the CPTu and tailings saturation. It is inferred that an increase in u_2 may be associated with a high water content or saturation.
[5] Assumes the estimation of saturations based on water content profiles from SPT.
[6] Due to space limitations, these are not included in this publication.

The validity of the calibration model was assessed during the verification stage. This phase relied on qualitative correlation of modeled saturation and pore pressure profiles with those obtained from geotechnical exploration campaign (CPTu and SPT) (Figure 5). Profile comparisons were made for a time equivalent to the date of each sounding. The results in Figure 5 (Row A) showed an adequate match between both pressure profiles, particularly in zones below the water table. For pore pressure (u2) and modeled saturation profiles (Figure 5, Row B), both variables exhibited a direct relationship. Each pressure increase was associated with perched saturation zones (Sw ≥ 80%). Regarding saturation profiles (Figure 5, Row

C), the match between estimated and modeled values showed a suitable correlation, with modeled trends remaining within measured limits.

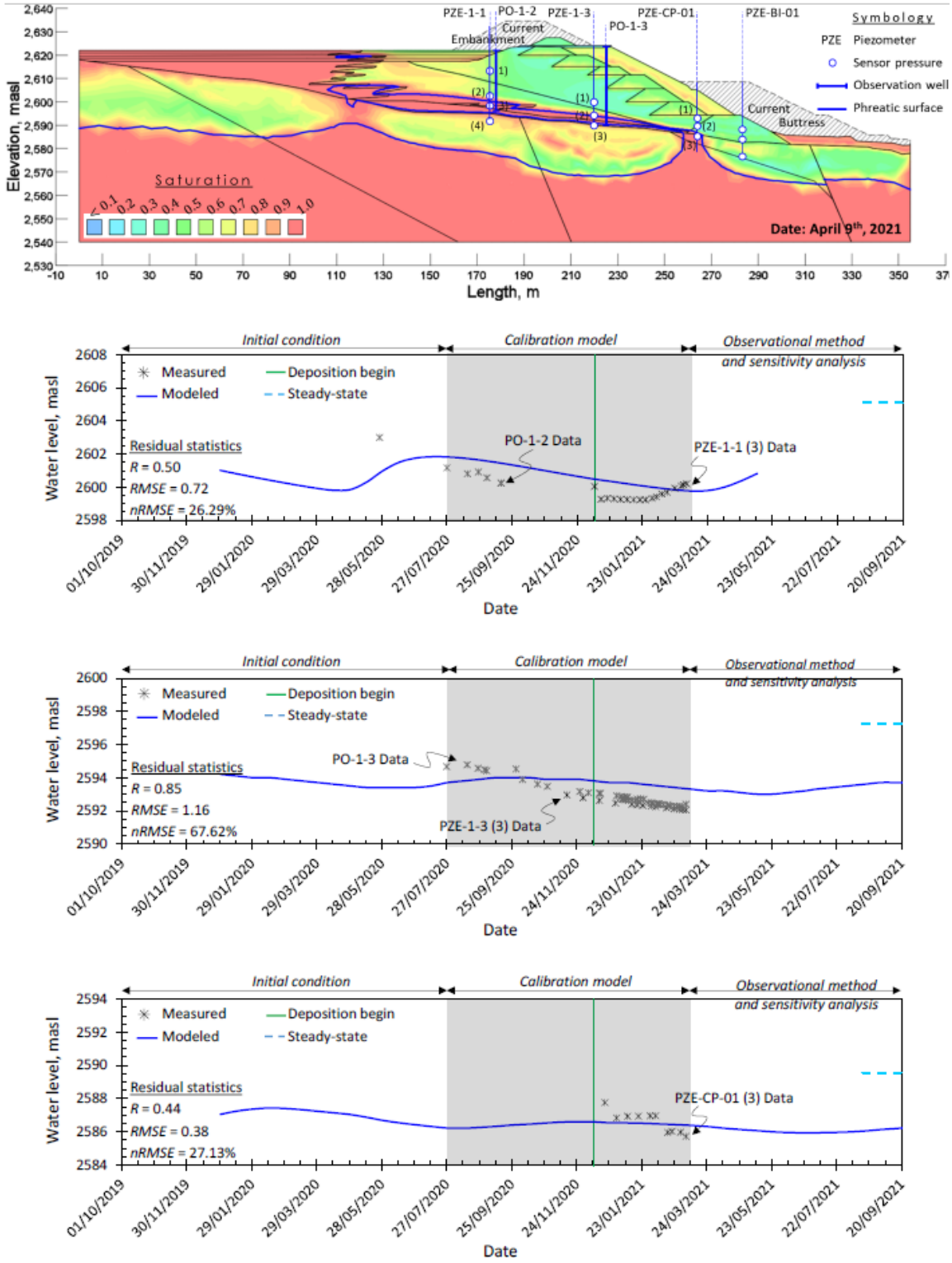
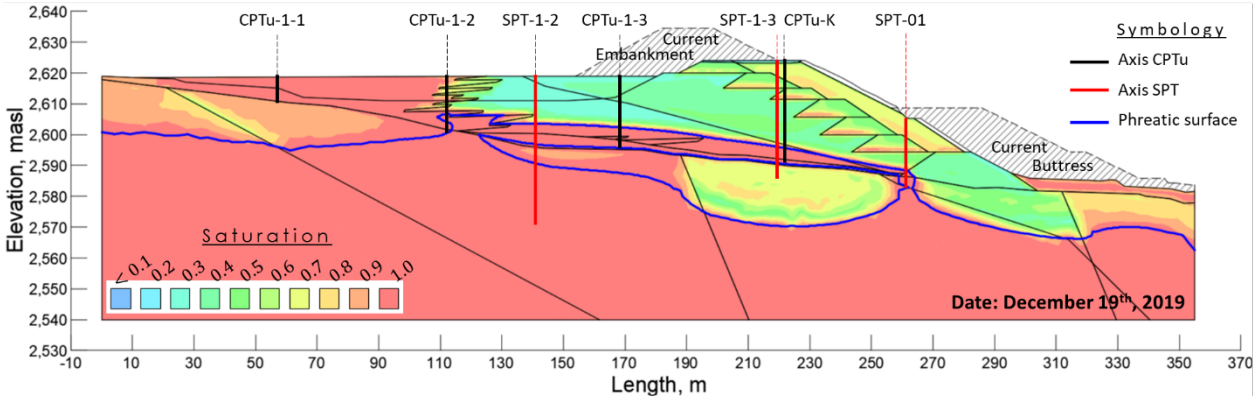
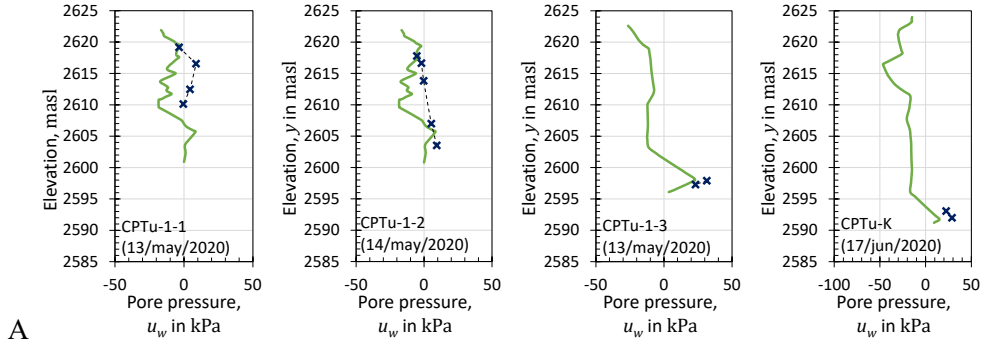
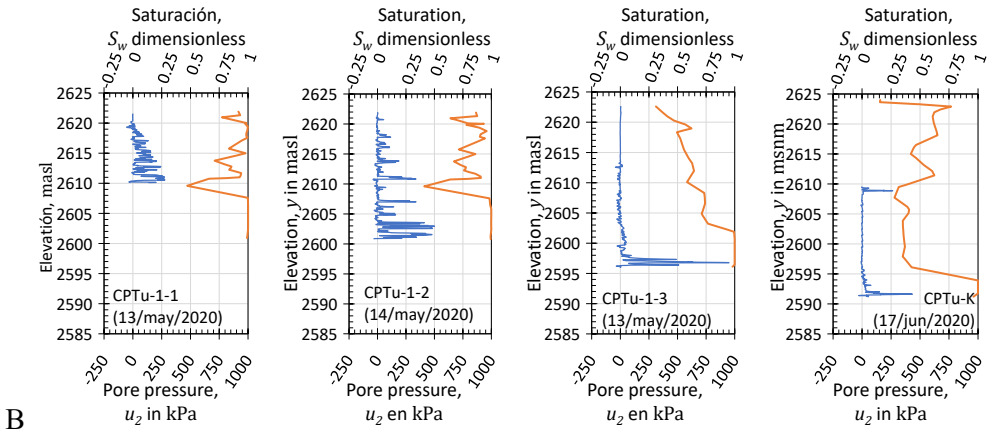


Figure 4: Calibrated model results







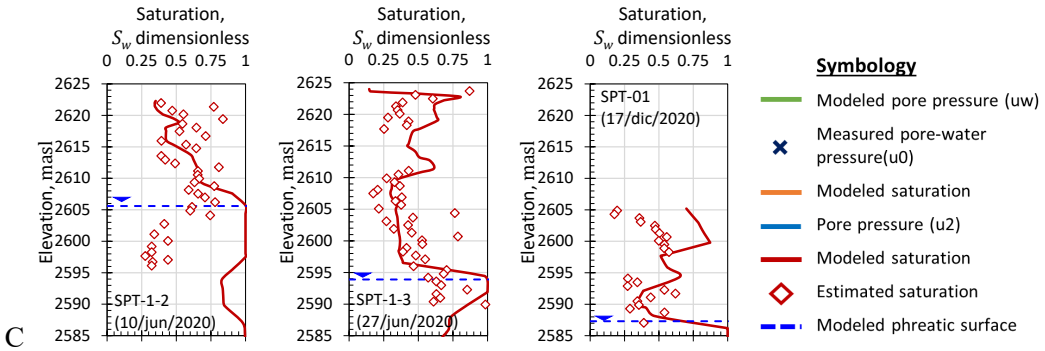


Figure 5: Verification model results

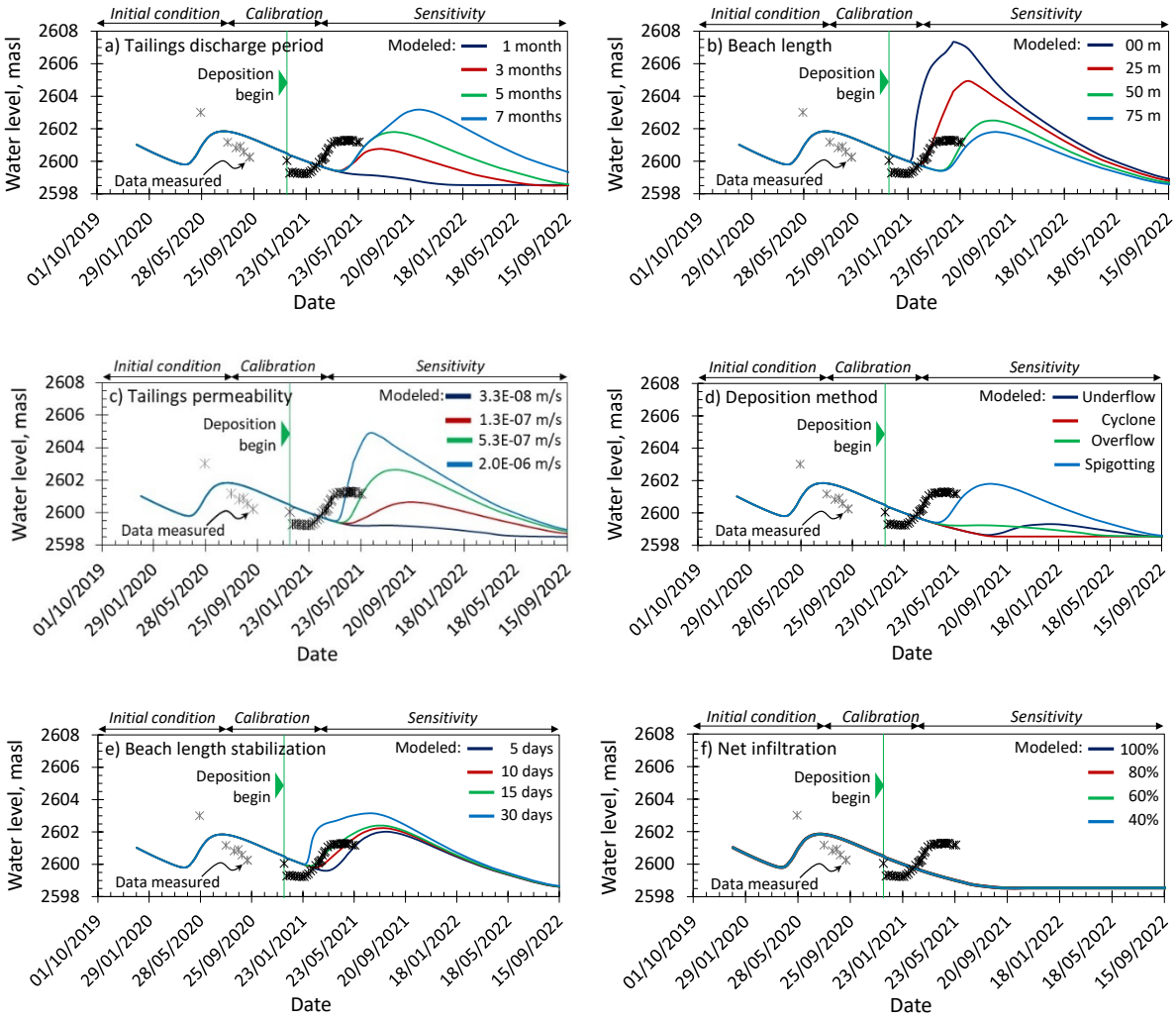


Figure 6: Sensitivity results

The outcome of the calibration and verification stages enabled the development of a sensitivity analysis to establish the operational plan, with careful consideration of potential increases in water levels and saturations that could impact the stability conditions of the TSF. The results from each scenario contributed to the establishment of operational controls and risk levels during and after the operational period of the TSF. Figure 6 illustrates some results, highlighting the variation in water levels for piezometer PZE-1-1 (3).

Each stage of the analysis has led to the implementation of a numerical model capable of capturing the hydraulic conditions of the TSF. Although the numerical model has been complemented by the observational method, it has proven to be an effective tool in the decision-making process during operational periods and extraordinary events at the TSF. Figure 7 shows the historical record of three years of observations and numerical modeling related to the case study.

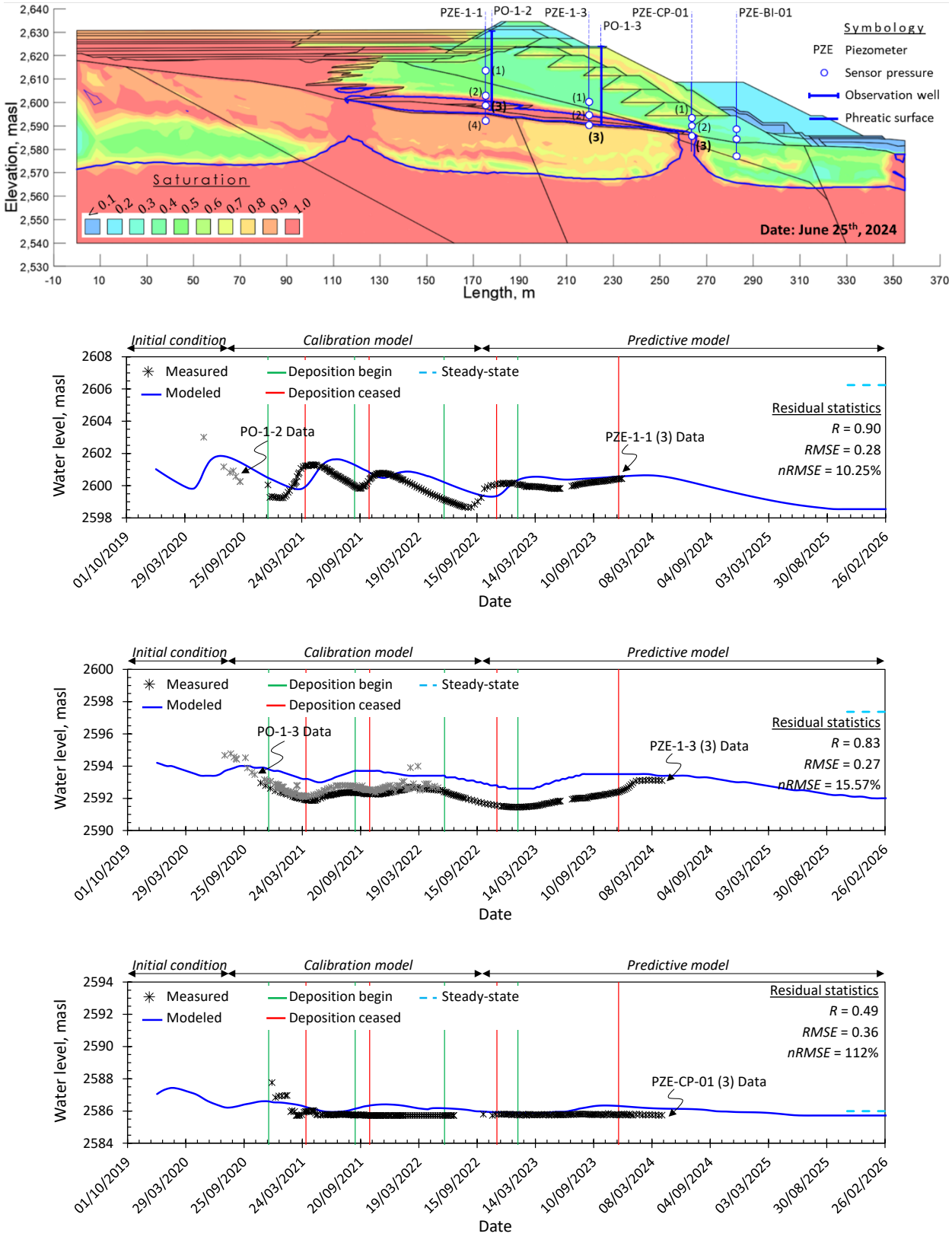


Figure 7: Predictive model and data measured

Conclusion

This article presents a case study where numerical seepage analysis is implemented as a tool for monitoring and estimating the drainage conditions in the TSF water management. The results obtained over three years of monitoring allow for the following conclusions:

- The analysis of hydraulic conductivities showed that anisotropic flow does not depend on the tailings microstructure but rather on the layering of coarse and fine tailings associated with discharge points (such as segregation, spigot location, operation method, etc.).
- Numerical modeling is a tool that should be complemented by the observational method. Deviations between measured and modeled conditions lead to the verification of either the numerical model or field conditions. In both cases, the agents that modify the expected behavior of the TSF must be identified. Collaboration between the designer and the TSF manager is essential to identify each agent.

This study presented a successful case of a two-dimensional (2D) seepage analysis. However, it is important to note that three-dimensional (3D) effects influence the water flow behavior within a TSF. While these effects can be partially simplified in the main drainage section, appropriate simplifications of the boundary conditions and a clear conceptualization of the numerical model are required.

Saturations can be a topic of discussion in geotechnical engineering, primarily due to challenges with sample recovery during the exploration campaign. Therefore, considering additional verification variables is justified as a process to enhance the certainty of the numerical model by incorporating direct field measurements that can correlate with the analysis results.

Seepage analysis should not be limited to water level estimations alone. Saturation zones or perched phreatic surface should be of interest, especially as these factors can influence the stability of the TSF.

The assessment of the type of material stored in the TSF should be conducted as a specific analysis. Coarse tailings, with higher infiltration rates, promote increased water levels and may be seen as unfavorable for the TSF. Conversely, fine tailings, with limited infiltration rates, tend to result in lower water level increases within the TSF, thereby considered a favorable condition. However, it should be noted that the low hydraulic conductivity and water retention capacity of fine tailings can lead to the development of saturations or perched phreatic surfaces, which may represent preferential failure planes affecting both local and global stability of the TSF.

Numerical modeling of saturated and unsaturated flow is a tool that can support the development of monitoring, operational, and closure plans for a TSF. However, the analyses and results should always be complemented by the observational method for effective decision-making. Regardless of the predictive capability of the numerical model, there will always be uncertainties.

The response in water levels may show a delay in relation to the start and end of TSF operations. The response time will depend on the wetting front, which can be influenced by agents such as hydraulic conductivity, water retention capacity, and the degree of saturation of the materials. Sensitivity assessments can provide key elements for decision-making, allowing for effective operational control of the TSF.

The degree of correspondence between measured and modeled data is often subject to the judgment of the modeler. Temporal or elevation lags may be evident and can impact the calculation of residual errors. However, the response of numerical model to operational periods and absolute increases in water levels can be representative of the actual condition. Therefore, the numerical model may be considered acceptable.

Acknowledgements

The authors thank the team at Flopac Geotecnia and Corporativo Peñoles, who directly or indirectly contributed to the development of the work described in this paper.

References

Alexander, D. 1986. Northern Italian dam failure and mudflow, July 1985. *Disasters* 10(1): 3–7.

Arya, L.M. and Paris, J.F. 1981. *Physicoempirical model to predict the soil moisture characteristic from particle-size distribution and bulk density. Soil Sci. Soc. Am. J.* 45: 1023–1030.

Aubertin, M., Mbonimpa, M., Bussière, B. and Chapuis, R.P. 2003. *A model to predict the water retention curve from basic geotechnical properties. Canadian Geotechnical Journal* 40(6): 1104–1122.

Azam, S. and Li, Q. 2010. Tailings dam failures: A review of the last one hundred years. *Geotechnical News* 28(4): 50–54.

Beier, N.A., Schafer, H.L. and Macciotta, R. 2023. Long-term evolution of the phreatic surface in a tailings dam following closure. *Proceedings of Tailings and Mine Waste 2023*. Vancouver, BC, Canada.

Bentley. 2023. Seep/W. GeoStudio 2023.1.2, Version 23.1.2.11. Bentley Systems – Seequeent.

Cooley, R.L. 1983. *Some new procedures for numerical solution of variably saturated flow problems. Water Resour. Res.* 19(5): 1271–1285.

Finke Morrison, K. 2022. *Tailings Management Handbook: A LifeCycle Approach*. Society for Mining, Metallurgy and Exploration (SME).

Fredlund, D.G., Xing, A. and Huang S.Y. 1994. *Predicting the permeability function for unsaturated soils using the soil-water characteristic curve. Canadian Geotechnical Journal* 31(3): 533–546.

Fredlund, D.G. and Dakshanamurthy, V. 1981. Transient flow theory for geotechnical engineering. *EOS Transactions American Geophysical Union* 62(45): 860. American Geophysical Union Conference, Hydrology Section, San Francisco, CA, USA.

Fredlund, D.G. and Xing, A. 1994. Equations for the soil-water characteristic curve. *Canadian Geotechnical Journal* 31(4): 521–532.

Fredlund, M.D., Fredlund, D.G. and Wilson, W. 2000. An equation to represent grain size distribution. *Canadian Geotechnical Journal* 37: 817–827.

Lam, L., Fredlund, D.G. and Barbour, S.L. 1987. Transient seepage model for saturated-unsaturated soil systems: A geotechnical engineering approach. *Canadian Geotechnical Journal* 24(4): 565–580.

Lyu, Z., Chai, J., Xu, Z., Qin, Y. and Cao, J. 2019. A comprehensive review on reasons for tailings dam failures based on case history. *Advances in Civil Engineering* 2019(1): 4159306.

Macklin, M.G., Payne, I., Preston, D. and Sedgwick, C. 1996. *Review of the Porco mine tailings dam burst and associated mining waste problems, Pilcomayo Basin, Bolivia.* Report to the UK Overseas Development Agency.

Mittal, H.K. and Morgenstern, N.R. 1976. Seepage control in tailings dams. *Canadian Geotechnical Journal* 13(3): 277–293.

Richards, L. A. 1931. Capillary conduction of liquids through porous medium. *J. Physics.* 1: 318–333.

Challenges Faced in Developing Plans for Emergency Drinking Water Supply in the Context of Mining Dam Collapses

Josiani Esteves Cordova, Vale S.A., Brazil
Lucas França Carvalho Silveira, Vale S.A., Brazil
Yuri Abner Rocha Lebron, Vale S.A., Brazil
Gabriela Rodrigues Barroso, Vale S.A., Brazil
Fernanda Luiza Costa Lisboa, Vale S.A., Brazil
Vicente Alimento Júnior, Vale S.A., Brazil

Abstract

The installation of mining dams is a common method to store mining tailings due to their technical and economic benefits. Nonetheless, they can pose serious socio-environmental effects in case of failures, especially in water bodies, threatening water security and drinking water supply, and undermining Sustainable Development Goals (SDGs). Thus, considering the recent mining dam collapses – especially in Minas Gerais, Brazil (Mariana, 2015; Brumadinho, 2019) – laws and regulations have been either published or amended to ensure stricter rules around the operation and safety of mining dams. In those regulations, ensuring that an Emergency Preparedness and Response Plan (EPRP) for mining dams is in place in case of an adverse event is required, including an Emergency Action Plan for Drinking Water Supply (EAP-DWS). However, there are numerous challenges in preparing an EAP-DWS, including: the difficulty of gathering reliable data; the construction of the plan in conjunction with stakeholders; the deployment of structuring actions in complex scenarios; and the constant updating of current legislation. Moreover, in order to ensure that the EAP-DWS is operational, emergency drills need to be carried out to check the efficiency of the action plans and to train and engage all the participants. The aim of this paper is to share the experiences, challenges, and lessons learned in drawing up EAP-DWSs in the context of mining dam collapses. This sharing of experiences is fundamental to increasing municipalities' water security and strengthening emergency response plans to guarantee access to drinking water in crisis scenarios.

Introduction

Mining activity has been growing globally due to various factors, among which population growth,

economic advances, and consequently the increased demand for minerals, stand out. Associated with the rise in mining activity is the increase in the production of mining waste, and thus, tailings storage facilities (TSFs).

Among the different types of technologies and methods for storing these tailings, the construction of dams is commonly applied due to its technical and economic advantages. However, in the event of a rupture, they can have deleterious social and environmental effects, especially concerning the water-environment nexus – altering the quality of water bodies and consequently making their catchment, treatment, and use impossible, at least temporarily.

In this context, historically, a number of dam rupture events have occurred, and in Brazil, the collapses of structures in Mariana (2015) and Brumadinho (2019) were significant in terms of social, environmental, and even legislative aspects (Guimarães et al., 2022). Given the risk of dam collapses, regulations have been published or amended to ensure stricter rules on the operation and safety of dams in Brazil. Among these regulations, the guarantee of an Emergency Preparedness and Response Plan (EPRP) for mining dams in case of an adverse event is a prerequisite for environmental licensing. Among the sections that make up this plan, specific actions to ensure the supply of drinking water to potentially impacted populations stand out.

Not only in Brazil, but internationally as well, changes have occurred in response to these events. In 2020, the Global Industry Standard on Tailings Management (GISTM) was published, aiming to prevent similar failures in the future and provide transparency in the management and executive oversight of TSFs. This global standard was developed by a multidisciplinary panel of experts, including the International Council on Mining and Metals (ICMM), the United Nations Environment Programme (UNEP), and the Principles for Responsible Investment (PRI). In addition, an advisory group conducted extensive public consultation with affected communities, government representatives, investors, organizations, and mining industry stakeholders, analyzing best existing practices along with experiences from previous tailings disposal structure failures (Dladla and Ramsamy, 2022).

The GISTM is organized around six thematic areas, encompasses 15 principles, and has 77 auditable requirements. However, its adoption is challenging, requiring significant changes in various aspects, including ensuring water security. Meeting specific requirements, such as Requirement 2.2, which covers water resources, demands continuous effort to map and assess water quality in potentially affected areas. Furthermore, Requirement 1.1 – ensuring human rights, for which a basic or fundamental right is access to safe drinking water – implies the need for a range of activities to guarantee access to water, ranging from developing emergency drinking water supply plans to implementing structural actions to ensure water security in potentially impacted areas.

Given these points, it is evident that the journey towards structures compliant with the GISTM standard requires persistence, integration, and a multifaceted approach to ensure safety and protection at all stages of the project. Thus, the development of emergency water supply plans is more than a legal requirement; it is also compliance with and adherence to international standards that aim to guarantee a fundamental human right.

Water supply in the scope of EPRPs for mining dams

Ensuring the availability of safe drinking water has become an increasingly significant challenge. On a global scale, water security, in terms of both quantity and quality, has been identified as one of the primary challenges in water management (ANA, 2021; MacAlister et al., 2023). The task is more complex in multi-use watersheds, with probable spatial and temporal imbalances between water supply and demand (Chen et al., 2020). This is further exacerbated by extreme and more frequent climatic changes and the limited resilience of public water supply systems (de Melo et al., 2021), as recently recorded in the state of Rio Grande do Sul, Brazil.

The issue of water security is on the agenda of various organizations, notably the United Nations and the Organization for Economic Co-operation and Development. In this context, the need to prevent crises in the drinking water supply sector is emphasized to ensure compliance with the sixth Sustainable Development Goal (SDG-6), establishing a new paradigm in water resource management (United Nations in Brazil, 2024). SDG-6 focuses on ensuring the availability and sustainable management of safe drinking water and sanitation for all by 2030, recognizing these as fundamental human rights and vital components for sustainable development. Globally, billions of people still lack access to drinking water, and inadequate sanitation poses serious health risks. Thus, SDG-6 aims to address these challenges through the promotion of water conservation, sustainable water resource management, and the development of efficient sanitation infrastructure (Ogunbode et al., 2024).

It is important to highlight that cooperation between countries, international organizations, and industrial sectors is essential to achieving the SDGs, especially SDG-6. For example, the mining sector can contribute by:

- adopting responsible practices to reduce social and environmental risks;
- investing in technologies that promote efficient water use in their operations;
- collaborating with other countries and organizations to share knowledge and experience in water and sanitation-related activities; and
- developing emergency water supply plans to ensure access to this universal right in emergency situations (Saenz, 2023).

This context includes the development of Emergency Action Plans for Drinking Water Supply (EAP-DWSs) in the event of mining dam collapses, which could potentially impact drinking water supply systems. The emergency actions proposed in such plans must consider providing a minimum per capita volume of drinking water sufficient for basic needs and maintaining the health of potentially affected populations. Relevant literature indicates a minimum per capita value ranging from 15 to 30 L/person per day, sufficient to meet basic hygiene and food needs. Considering that in emergency situations it is not possible to satisfy all water needs and demands of the affected population, the initial focus should be on survival. However, as the situation and human, logistical, operational, and other resources permit, the water supply should be increased for other uses, considering the scaling up of drinking water volumes to be supplied in the developed plans (FUNASA, 2018; WHO, 2013).

In an emergency, beyond the need to guarantee fundamental rights – aligned with the SDGs and adherence to the global standard (GISTM) – the provision of drinking water to the population poses significant challenges for the developers (mining companies) and competent authorities, even in high-income countries with high security in the water supply sector (Bross et al., 2019).

Therefore, this paper aims to present how EAP-DWSs are developed in the context of potential impacts on water supply systems resulting from mining dam collapses, as well as the challenges faced in the development of these plans.

Development of emergency action plans for drinking water supply and challenges faced

In developing EAP-DWSs, various important issues must be considered, such as the amount of water needed and available for supply, transportation logistics, available resources, and responsible parties involved. Thus, some central questions must be explored when developing the plans: (i) Who needs to be supplied? (ii) How much water is needed? (iii) From where will the water be sourced? (iv) How will the water be distributed? (v) For how long is the emergency supply planned? and (vi) Who will provide the water supply?

In this context, Figure 1 presents a summary of the main steps for developing EAP-DWSs. The first action involves the developer's (mining companies) contact with the stakeholders involved (water supply service providers, municipal emergency response agencies, and other responsible parties) to introduce the topic, discuss applicable legislation, present flood maps, and request primary data from the public water supply system. After receiving the data, as well as collecting relevant information available in public databases, the impacts concerning the flood map are consolidated and characterized. Based on the characterized impacts, solutions for emergency services to the affected population are proposed through action protocols scaled at emergency levels (defined according to the geotechnical conditions of the

structure). Once the plan is constructed, the developer forwards the document to public agencies and stakeholders responsible for acknowledgment and validation. Finally, the plans are filed with the competent authorities, made available to stakeholders, and, if possible, published digitally.

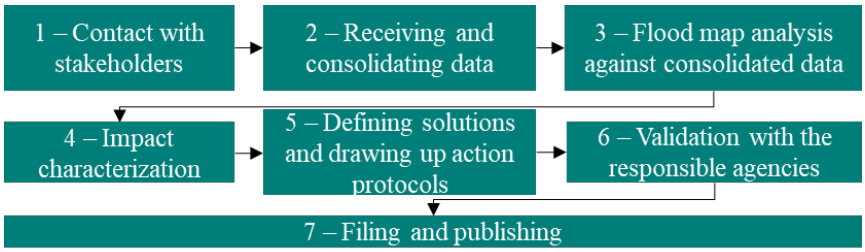


Figure 1: Summary of the steps for developing EAP-DWSs

Conducting these stages, and consequently consolidating an operational and effective emergency action plan for drinking water supply, encounters various specific challenges, which will be addressed below in this paper.

Data collection from the drinking water supply system

For the development of the plan, it is essential to have detailed knowledge of the municipal water supply systems to accurately characterize the potential impacts and to propose assertive solutions. One way to achieve this characterization is through secondary data, which are publicly available information sources. Although this is an easily accessible option, it has several challenges and weaknesses, such as: (i) the data may be outdated and may not reflect the current conditions of the municipality; (ii) there may be multiple sources for the same information, often conflicting, making it difficult to identify the correct data; (iii) some data may be erroneous, possibly due to typographical errors; and (iv) data is generally only available for water catchment and water treatment plants (WTPs), making it impossible to assess impacts on other system components (water mains, reservoirs, pumping stations).

Therefore, the ideal is to obtain primary information directly from the drinking water supply system, provided by the municipality or the service provider. However, this approach also presents obstacles, such as: (i) smaller municipalities may not have this information and may need to conduct surveys, requiring specialized labor that is often unavailable in these areas; and (ii) there may be a lack of engagement from service providers, leading to delayed, incomplete, or even no responses.

Thus, obtaining both primary and secondary information on the municipal water supply system faces adversities and impasses. While primary data are generally more accurate, the aforementioned difficulties – such as the lack of information in smaller municipalities and low engagement from service providers – make the use of secondary data an alternative for developing the EAP-DWSs. If the EAP-DWSs are developed with secondary data, it is necessary for the developer, together with public agencies, to strive to

obtain the primary data and incorporate them in a subsequent plan revision. Moreover, even when the document includes primary data, updates, at appropriate times – or when the legislation requires (each 3 years for the current legislation) – are essential to incorporate changes in city infrastructure and their water supply systems.

Stakeholder engagement

Engaging stakeholders in the plan development process is crucial and challenging. As such, it is essential that the agency responsible for regulating the development of these plans clearly defines the roles and responsibilities of those involved. Generally, the main parties involved are the developer, the water supply service provider, and the municipal emergency response agency.

Developer, water supply service provider, and municipal emergency response agency

It is crucial that these parties maintain efficient communication, based on the responsibilities established by legislation. Otherwise, engagement may be hindered from the start due to the lack of a solid legal basis. Additionally, it is recommended that the timeframe for plan development involves not only the developer but also the other stakeholders involved, according to their responsibilities. A current challenge in Brazil, especially in Minas Gerais, is that the developer has defined deadlines for plan development, while the service provider and the municipal emergency response agency, although part of the process, do not. This can result in a lack of collaboration or in timelines incompatible with legal requirements. Therefore, it is crucial that the regulatory agency clearly establishes roles, responsibilities, and deadlines in the process for all stakeholders.

Beyond these issues, some challenges for good stakeholder engagement can be observed. When it comes to water supply service providers, their involvement is crucial since they possess detailed knowledge of the municipal water supply systems they serve, allowing for a more accurate characterization of potential impacts. Additionally, these providers have the expertise to define solutions that could be implemented in emergencies. However, in some cases, providers refuse to participate in this process, especially in joint plan development and data provision, arguing that this data is sensitive and cannot be disclosed. In other situations, the water supply service provider has such a small team and simple infrastructure that it struggles to share these demands with developers in addition to their daily responsibilities.

Mutual aid plan – synergy between developers

In addition to engagement between the developer, the water supply service provider, and the municipal emergency response agency, a relevant challenge is fostering synergy between developers (other mining companies) in the development of plans and, if possible, in creating Mutual Aid Plans. These plans promote collaboration between companies, public agencies, and the community. But why is this exchange of

experiences, resources, and cooperation between companies important during the creation of EAP-DWSs?

The answer becomes clear when identifying the main problem that arises without this cooperation: many developers share similar flood areas that may result in the same impacts on the water supply systems of specific municipalities. If each developer works alone, there will be distinct solutions, resources, and plans for the same problems. The municipality, in turn, will have to deal with multiple solutions for a single problem, creating redundancies and unnecessary complications. Furthermore, the plans, once finalized, need to be simulated to ensure their applicability and correct potential errors. Imagine a municipality simulating five different plans for the same impact on its water supply system? This overburdens municipal resources and generates inefficiencies. In the long term, this lack of synergy can significantly slow down the process. Therefore, collaboration between developers (other mining companies) not only optimizes resources but also accelerates the implementation of effective and cohesive solutions.

On the other hand, the time for conducting dam break studies and the deadlines for submitting them to the agencies vary for each developer, making plan compatibility challenging. If it is not possible to provide this synergy from the beginning of the studies due to individual deadlines, it is recommended to adopt approaches that allow continuous adjustments as the process matures. Technical working groups among developers can be formed with frequent agendas to discuss the topic and join efforts in plan development. Another point to consider is that if developers have already developed different plans for the same impacts, municipalities could indicate the most suitable plan, adopting a single option for the municipality.

Addressing complex scenarios

In assessing potential impacts on the drinking water supply system, it is essential to consider complex scenarios where the consequences extend beyond the scope of emergency response, sometimes requiring prior structural actions and more robust solutions to ensure a minimum drinking water volume required by legislation during the emergency and return to the normal public water supply. These scenarios are characterized by several factors that amplify challenges and require more detailed technical and strategic approaches, as discussed below for three scenarios dealing with high flow impacts, isolated areas and low water availability. Furthermore, these cases highlight the necessity of mutual collaboration between the parties (drinking water service provider and the municipal emergency response agency).

High flow impacts

In situations where the number of affected people in a municipality exceeds 100,000 inhabitants – usually scenarios impacting high flows in the supply system (i.e., > 300 L/s) – proposing an efficient emergency response is challenging. This is because the calculated resource quantities in the plan can be so high that some points of attention arise: (i) If water trucks or other vehicles are adopted, do the roads support this

high quantity? (ii) Has the developer mapped suppliers capable of meeting this high demand? (iii) Does the developer have the capacity to allocate many support teams for these situations?

In some cases, operationalizing these plans requires prior planning and execution of structural actions. This can include reinforcing water treatment plant (WTP), physically protecting water catchments and WTPs, opening access routes, installing reservoirs, implementing alternative water mains, drilling wells, among other measures.

It is recommended that these actions be linked to the dam's emergency levels (based upon the TSF geotechnical conditions), allowing them to be executed in a scaled, programmed manner, prior to a rupture event. With the implementation of these measures, the impacts on the water supply system resulting from a potential rupture are minimized, making an efficient emergency response feasible or, in some cases, eliminating the need for emergency intervention.

Isolated areas

Another complex scenario occurs when the impact is associated with road obstruction by the flood map, creating isolated areas. This blockage hinders water distribution logistics and delays repairs to potentially affected supply structures. In these cases, if possible, alternative land access routes must be planned. If this is not feasible, the use of aircrafts should be evaluated as a last resort. This resource is not relatively easy to obtain in large quantities during an emergency and requires complex logistics.

A recent example of using aircrafts in emergency water supply response occurred due to the floods in Rio Grande do Sul, Brazil, starting in April 2024. This was one of Brazil's largest climate tragedies, affecting approximately 900,000 people across 400 municipalities, with an estimated mobilization of 2500 vehicles and 42 aircraft for emergency response in various isolated access areas (Agência GOV, 2024). In this context, Brazilian Air Force (FAB) helicopters played a significant role in emergency drinking water supply. In addition to distributing bottled water to the isolated population, the aircraft were responsible for transporting a power generator to a water treatment plant, restoring the water supply to some neighborhoods that had been without water for three days, and transporting a nearly 2.5-ton water pump capable of pumping 500 L/s (EB, 2024; FAB, 2024).

Therefore, in plans identifying multiple isolated areas, it is advisable to include structural actions related to the dam's emergency levels. Relevant measures for this scenario include opening alternative accesses and implementing water catchment and reservoir systems for emergency situations.

Low water availability

Impacts in regions with low water availability represent an additional challenge, as the response capacity is limited by local water resource scarcity. In such areas, any interruption in the supply system can have severe consequences due to the difficulty in finding alternative water sources.

In these circumstances, it is also recommended to conduct studies and implement structural measures prior to a potential collapse, associated with the dam's emergency levels. Developing integrated water resource management strategies and promoting technological alternatives for water treatment are imperative. This includes evaluating the feasibility of implementing rainwater catchment and treatment systems. Additionally, the construction of infrastructure to supply water from neighboring regions, adopting rotational supply systems, and creating emergency reservoirs can be viable solutions to ensure supply resilience in crisis situations.

In conclusion, addressing complex impacts on the drinking water supply system requires a combination of detailed planning, infrastructure investments, adopting integrated management, and scheduling studies and structural actions linked to the dam's emergency levels. This ensures the system's resilience in the face of different crisis scenarios, securing continuous and safe water supply for the population.

Serving buildings of public interest

Buildings of public interest refer to those that provide essential services to society, such as daycare centers and public educational institutions, hospitals and units for public health care, and collective housing facilities. Ensuring an emergency drinking water supply to these locations is a complex challenge that requires careful planning and coordination.

Data availability

To ensure effective emergency water supply, it is essential that data on these establishments is available and up to date. However, as previously mentioned concerning the acquisition of municipal water supply system data, the same issues apply to data on buildings of public interest. In many cases, municipalities do not have a centralized or updated registry of this information. Therefore, one of the primary challenges is creating a centralized system for collecting and updating information on such buildings and essential services, involving collaboration among different levels of government, institutions, and service providers.

Prioritizing emergency response

The water supply of buildings of public interest must be treated with the utmost priority both in planning and in emergency response. During emergencies, it is crucial to allocate larger volumes of water to these buildings to ensure that essential services are not interrupted. Additionally, the logistics of distributing water to buildings of public interest can be complex and must be considered separately from the rest of the population. Factors such as distance, accessibility, storage capacity, and demand must be carefully evaluated. In densely populated urban areas, effective coordination among different agencies and service providers is essential for an effective plan.

In summary, prioritizing the emergency response to these buildings requires a specific approach, considering their particularities and the collaboration of all involved. The community's resilience depends on the continuous functioning of these essential services.

Adherence to constantly changing legislation

The constant changes in legislation regulating the topic of water supply within EPRPs represent a significant challenge for the development and implementation of these plans. Although these regulations are published with the aim of improving the subject, each new legislative change requires revisions of the already prepared documents, directly impacting the maturity of the process.

The continuous need for review also demands efficient communication among stakeholders. Each legislative change must be promptly communicated and understood by all involved, including municipalities, service providers, and regulatory agencies, to ensure that all parties are aligned and can adequately contribute to the necessary revisions.

For example, in Minas Gerais, Brazil, in the past five years, approximately eight standards, including resolutions, decrees, terms of reference, and technical instructions, have been published regarding EPRPs for Mining Dams with an interface in water supply (Minas Gerais, 2019, 2020, 2021a, 2021b, 2022, 2024a, 2024b; Brazil, 2022, 2024). These publications required the re-evaluation of the prepared documents or introduced new guidelines to the process.

It is crucial that the regulatory bodies improve the legislation, but at a frequency that is consistent with the process and with due care to ensure that different agencies do not issue conflicting standards or guidelines on the same subject.

Implementation of plans

The implementation of EAP-DWSs aims to ensure that the affected population has access to drinking water in emergency situations. To ensure that these plans are effective in such situations, the implementation can be divided into three main phases: (i) engagement of all agents involved in the emergency; (ii) assessment of the necessary resources; and (iii) simulation of the plans.

Engagement of those involved in the emergency

The engagement of agents involved in the emergency refers to the active participation of all sectors or individuals with actions and responsibilities described in the plans, which is fundamental to ensuring the success of their implementation. Examples of agents or sectors with responsibilities in the plans, based on the Incident Command System (ICS) – a US methodology for Command and Control of emergencies – include: the EPRP coordinator; the logistics section, responsible for all services (e.g., supply of people,

equipment, transportation, supplies) and logistical support needs within the plan; the planning section, which manages information and encompasses the environment and resource management units.

Engaging people in the implementation of these plans can be challenging for various reasons, particularly those related to communication; understanding of responsibilities, i.e., making them feel part of and responsible for the plan; and monitoring their responsibilities and actions throughout the plan's effective term.

Therefore, overcoming these challenges requires a strategic approach that includes effective communication among all involved, assignment of specific and objective roles, accountability for processes and results, and training of those involved through courses and drills. The need for engagement extends not only to the internal teams of the developer but also to the water service provider and emergency response agencies. These agencies are essential to ensure public safety while emergency drinking water is supplied.

Resource assessment

The assessment of resources for the implementation of plans involves the stages of identification, analysis, and management of these assets to ensure effectiveness in actual emergencies. These resources can include human resources, which consider the labor, skills, and knowledge required; and logistical resources, which consider the use of materials and equipment, such as water transport vehicles, bottled water, mobile treatment stations, aircrafts, among others.

The challenges related to these resources in implementation are mainly due to the difficulty of allocating the necessary quantity in an efficient manner. Therefore, thorough advanced planning is of the utmost importance, including verification of the availability of internal resources and the establishment of umbrella contracts with suppliers to prevent the unavailability of these items from becoming a limitation in emergency response.

Given the above, it is concluded that for the implementation of EAP-DWSs, it is necessary to have properly sized and trained teams, ensuring that the agents involved in the plans are aware of their actions and responsibilities. It is also crucial to have access to qualified internal specialists and external service providers, as well as appropriate logistical resources and equipment.

Plan simulation

Simulations play an important role in evaluating and exploring impact scenarios arising from dam failures, as they are a way to predict the behavior and outcomes of a plan before activation. These drills not only help identify improvements in the plans but also promote greater engagement of the agents involved and keep resources and teams prepared to face an emergency. However, challenges are encountered in this area, especially when it comes to complex scenarios.

The challenges related to simulations in general, and particularly in more complex scenarios, as discussed earlier, arise due to the logistical effort needed to obtain resources, as these plans may encompass many water transport vehicles, various supply routes, the need for mobile treatment stations, among other resources that increase the cost and time required to execute these drills. In addition to the resource aspect, one of the main challenges is performing maneuvers in the supply systems in plans that foresee rotational supply to the community. Finally, there are also the challenges of information management and ensuring the engagement of all the players involved.

Overcoming these challenges requires a planned approach and a commitment to continuous improvement. Regarding EAP-DWSs, an approach found to face these challenges is the scalability of simulations. The scalability of these drills helps reinforce theoretical knowledge about the plans, promote the engagement of all agents involved, allocate resources efficiently, and ultimately simplify the simulation stages. This scalability involves creating a program of exercises, training, and drills: (i) Exercises aim to provide a theoretical and comprehensive understanding of what the plan is and the fundamental points of knowledge. (ii) Training aims to guide the activation flow and the actions of each responsible person in the emergency, in addition to addressing any questions. (iii) Drills aim to test participants in the practical execution of their roles and responsibilities in an emergency, while in a controlled and risk-free environment. Finally, it is important to find a balance between reality and simulation, especially in complex scenarios. Excessive simplification may neglect important aspects, while a simulation too close to reality can become impractical. Therefore, it is crucial to identify the critical points of the plan that need to be trained and kept true to reality, while others can be simplified.

Conclusion

The experience presented in the development of emergency action plans for drinking water supply in the context of impacts on supply due to mining dam failures can be a valuable source of information for developing guidelines for emergency drinking water supplies. Such guidelines need to be uniform, detailed, and transnational, aiming to meet the targets of the SDGs as well as the GISTM standards, in line with sustainable development. However, given the various challenges presented, when developing such plans, local specificities must be taken into account, considering demographic, territorial, socioeconomic, and cultural aspects, as well as the different phases of emergencies and the players involved, aiming for the effective implementation of the plan at the time of an emergency.

References

Agência GOV. 2024. *Número de resgatados no Rio Grande do Sul sobe para 46 mil*. Accessed 06/05/2024 at: https://agenciagov.ebc.com.br/noticias/202405/numero-de-resgatados-no-rio-grande-do-sul-sobe-para-46-mil

ANA. 2021. *Atlas águas: segurança hídrica do abastecimento urbano*. Accessed 06/05/2024 at: https://biblioteca.ana.gov.br/sophia_web/asp/download.asp?codigo=151307andtipo_midia=2andiIndexSrv=1andiUsuario=0andobra=90683andtipo=1andiBanner=0andiIdioma=0

Brazil. Agência Nacional de Mineração. 2022. *Resolução 95/2022: Consolida os atos normativos que dispõem sobre segurança de barragens de mineração.* Accessed 05/08/2024 at: resolucao-no-95-2022.pdf (www.gov.br)

Brazil. Agência Nacional de Mineração. 2024. *Resolução 175/2024: Altera a Resolução ANM nº 95, de 7 de fevereiro de 2022, que consolida os atos normativos que dispõem sobre segurança de barragens de mineração.* Accessed 05/08/2024 at: RESOLUÇÃO ANM Nº 175, DE 1º DE AGOSTO DE 2024 – ANMlegis (datalegis.net)

Brazil. Ministério da Saúde. Fundação Nacional da Saúde. 2018. *Protocolo de atuação da Funasa em situações de desastres / Fundação Nacional de Saúde.* Brasília: Funasa.

Bross, Lisa. Krause, Steffen, Wannewitz, Mia, Stock, Eva, Sandholz, Simone and Wienand, Ina. 2019. Insecure security: Emergency water supply and minimum standards in countries with a high supply reliability. *Water.* 11(4): 732.

Chen, Xinchuang, Li, Feng, Li, Xiaoqian, Hu,Yinhong and Hu, Panpan. 2020. Evaluating and mapping water supply and demand for sustainable urban ecosystem management in Shenzhen, China. *Journal of Cleaner Production* 251.

de Melo, M.C., Formiga-Johnsson, R.M., de Azevedo, J.P.S., de Oliveira Nascimento, N., Machado, F.L.V., Pacheco, F.A.L. and Fernandes, L.F.S. 2021. A raw water security risk model for urban supply based on failure mode analysis. *Journal of Hydrology* 593: 125843.

Dladla, S.D. and Ramsamy, S. 2022. Practical steps to Global Industry Standard on Tailings Management (GISTM) compliance for operational tailings storage facilities in South Africa. *J.S. Afr. Inst. Min. Metall.* 122(6): 283–290

EB. 2024. *Aviação do Exército apoia o abastecimento de água, oxigênio e medicamentos*. Accessed 06/05/2024 at https://www.eb.mil.br/web/noticias/w/aviacao-do-exercito-auxilia-o-restabelecimento-de-agua-em-canoas-rs-

FAB. 2024. *FAB transfere gerador e restabelece fornecimento de água no interior do RS – Força Aérea Brasileira.* Accessed 06/05/2024 at https://www.fab.mil.br/noticias/mostra/42577/TODOS%20PELO%20SUL%20-%20FAB%20transfere%20gerador%20e%20restabelece%20fornecimento%20de%20%C3%A1gua%20no%20interior%20do%20RS

Guimarães, Roberta, Moreira, Victor, Cruz, Joyce, Saliba, Aloysio and Amaral, Míriam. 2022. History of tailings dam failure: Impacts on access to safe water and influence on the legislative framework. *Science of the Total Environment* 852: 158536.

MacAlister, C., Baggio, G., Perera, D., Qadir, M., Taing, L. and Smakhtin, V. 2023. *Global Water Security 2023 Assessment.* University Institute for Water, Environment and Health, United Nations University.

Minas Gerais. Assembléia Legislativa de Minas Gerais. 2019. Lei nº 23.291/2019*: Institui a política estadual de segurança de barragens*. Accessed 05/08/2024 at Lei nº 23.291, de 25/02/2019 – Texto Original – Assembleia Legislativa de Minas Gerais (almg.gov.br).

Minas Gerais. Assembléia Legislativa de Minas Gerais. 2020. *Decreto nº 48.078/2020: Regulamenta os procedimentos para análise e aprovação do Plano de Ação de Emergência – PAE, estabelecido no art. 9º da Lei nº 23.291, de 25 de fevereiro de 2019, que instituiu a Política Estadual de Segurança de Barragens.* Decreto nº 48.078, de 05/11/2020 – Texto Atualizado – Assembleia Legislativa de Minas Gerais (almg.gov.br).

Minas Gerais. Coordenadoria Estadual de Defesa Civil. 2021b. *Instrução Técnica 01/2021: Estabelecer os requisitos mínimos necessários para elaboração e aprovação do Plano de Ação de Emergência – PAE concernentes à competência do órgão estadual de Proteção e Defesa Civil, expressa no Decreto Estadual 48.078, de 05 de novembro de 2020.* Acessed at 2021_Instrucao Técnica_versão_publicada.pdf (defesacivil.mg.gov.br)

Minas Gerais. Coordenadoria Estadual de Defesa Civil. 2024. *Resolução 83/2024: Estabelece os requisitos mínimos necessários para elaboração, análise e aprovação da Segunda Seção do Plano de Ação de Emergência, concernentes à competência do órgão Estadual de Proteção e Defesa Civil, expressa no Decreto Estadual n. 48.078, de 05 de novembro de 2020.* Acessed at ResolucaoGMG_Nr83-2024.pdf (gabinetemilitar.mg.gov.br)

Minas Gerais. Diário do executivo Minas Gerais. 2021a. *Resolução Conjunta Semad/IEF/Igam/Feam 3.049/2021: Estabelece diretrizes para a apresentação do Plano de Ação de Emergência, para as barragens abrangidas pela Lei nº 23.291, de 25 de janeiro de 2019, no âmbito das competências do Sistema Estadual de Meio Ambiente e Recursos Hídricos definidas pelo Decreto nº 48.078, de 5 de novembro de 2020, e determina procedimentos a serem adotados pelos responsáveis destas barragens quando estiverem em situação de emergência.* Acessed at: siam.mg.gov.br/sla/download.pdf?idNorma=53502

Minas Gerais. Diário do executivo Minas Gerais. 2022. *Resolução conjunta SEMAD/FEAM/IEF/IGAM Nº 3.181/2022: Estabelece diretrizes para a apresentação do Plano de Ação de Emergência das barragens abrangidas pela Lei nº 23.291, de 25 de janeiro de 2019, no âmbito das competências do Sistema Estadual de Meio Ambiente e Recursos Hídricos definidas pelo Decreto nº 48.078, de 5 de novembro de 2020; determina os procedimentos a serem adotados pelos responsáveis destas barragens quando estiverem em situação de emergência e as providências a serem tomadas na hipótese de incidente, acidente ou ruptura, e dá outras providências.* Acessed at: siam.mg.gov.br/sla/download.pdf?idNorma=56489

Nações Unidas Do Brasil. 2024. *Objetivo de Desenvolvimento Sustentável 6: Água potável e saneamento*. Acessed at https://brasil.un.org/pt-br/sdgs/6

Ogunbode, T. O., Esan, V. I., Oyebamiji, V. O. and Akande, J. A. 2024. Sustainable development goal 6 and the challenge of pipe-borne water connectivity in a growing tropical city: a case study. *Discover Sustainability* 5(1): 53.

Saenz, C. 2023. Creating shared value strategies to reach the United Nations sustainable development goals: Evidence from the mining industry. *The Extractive Industries and Society* 14(2): 101255.

World Health Organization. 2013. Technical notes on drinking-water, sanitation and hygiene in emergencies updated: July.

Chapter Nine

Geotechnical Issues

TAILINGS AND
MINE WASTE 2024



Exploration of Passive Desaturation of In-place Tailings Using Wicking Geosynthetics

Kendall Monley, WSP, USA
Joseph Scalia IV, Colorado State University, USA

Abstract

As global demand for metals and critical minerals increases, so too does the production of tailings and tailings storage facilities (TSF). A common assumption is that the water initially contained in a TSF will drain down to an unsaturated condition after deposition of new tailings ceases. However, a review of literature on geotechnical and hydrotechnical conditions of legacy TSFs (TSFs that have stopped receiving tailings) in arid environments illustrates that achievement of unsaturated conditions in internal fine-grained layers may not always occur. As the tailings are deposited, layers of finer and coarser particles are interbedded causing the formation of capillary barriers. This may ultimately result in finer-grained layers held at near saturation after draining down. The fine-grained layers are more susceptible to liquefaction concerns and can necessitate costly remedial actions to ensure geotechnical stability. In this study, I explore in-situ dewatering via use of capillary (wicking) geotextiles, and the effectiveness of the wicking geotextiles. The employed wicking geotextiles have been used successfully in roadway applications to prevent migration of water into the subgrade, but implementation for tailings dewatering is novel. Column experiments were created to emulate stratigraphy seen in legacy TSFs. Column testing reveals the wicking geotextiles accelerated saturated and unsaturated dewatering by 2.8 times the rate of natural drying processes. This promising approach to passively dewatering tailings warranted additional study.

Introduction

There are more than 17,000 tailings storage facilities (TSFs) globally, with ~40% (~6,800 TSFs) active or currently operational (Spencer et al., 2022). The remaining 60% exist in some form of inactive (mining paused), closure, or post-closure status, deemed legacy TSFs. Due to a lack of available site data, the geotechnical conditions of legacy sites are often generalized. One frequent assumption is that relatively uniform tailings deposits have undergone, or are in the process of undergoing, drain down of stored water under gravity and are now unsaturated. However, based on reports from legacy tailings facilities in arid (Hardy et al., 2003; Casey et al., 2022) and non-arid environments (Godley and Quaglia, 2023) this

assumption may not be reflective of the state of many legacy TSFs.

Figure 1 is a schematic of the development of saturated fine-grained layers from initial deposition to the final configuration of the TSF. Continuous heterogenous tailings deposition results in segregation of particle sizes. Deposition of newly segregated tailings above previously deposited material results in interbedded layers of fine and coarse tailings. Over time, the tailings will drain excess pore water under gravity; however, as the tailings transition to an unsaturated state, drain down of the confined fine grain layers will be impeded, thus producing permanent interbedded near-saturated fine grain layers with liquefaction potential.

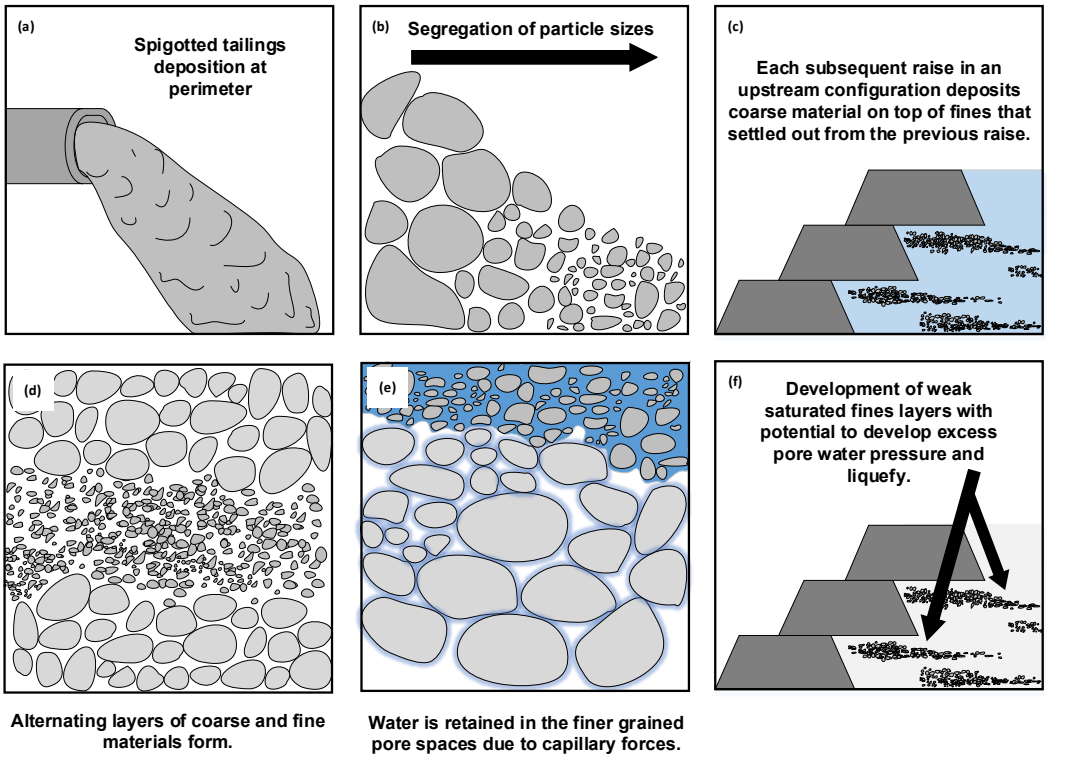


Figure 1: Schematic progression of TSF construction, drain down, and retention of saturations

The soil water characteristic curve (SWCC) and the hydraulic conductivity function (HCF) are illustrated in Figure 2 (Fredlund et al., 2012) and provide insight into the development of these permanent near-saturated layers. The upper bound of hydraulic conductivity (Figure 2b) represents the saturated condition. Initial gravity drain down occurs due to saturation throughout the tailings. As both layers begin to desaturate, the suction at the two-media interface is effectively equal. The coarser tailings pores drain more rapidly than the finer tailings pores, and as a result the coarse tailings hydraulic conductivity drops lower than that of the finer tailings. The point at which the coarser soil will stop admitting water can be

approximated as the height of capillary rise (H_c) within the soil. H_c can be translated onto the SWCC (Figure 2a), and the associated suction is denoted Ψ_H. Hydraulic conductivity decreases rapidly after reaching the inflection point value as suction increases due to increased tortuosity and reduced area for flow.

Capillary barriers form at the interface of the two homogenous soils of contrasting pore size (i.e., coarse- and fine-grained tailings) and limit the movement of water through the system under unsaturated conditions (Stormont and Anderson, 1999). The result is interspersed near permanently saturated fine-grain layers confined by coarse layers with extremely low hydraulic conductivities.

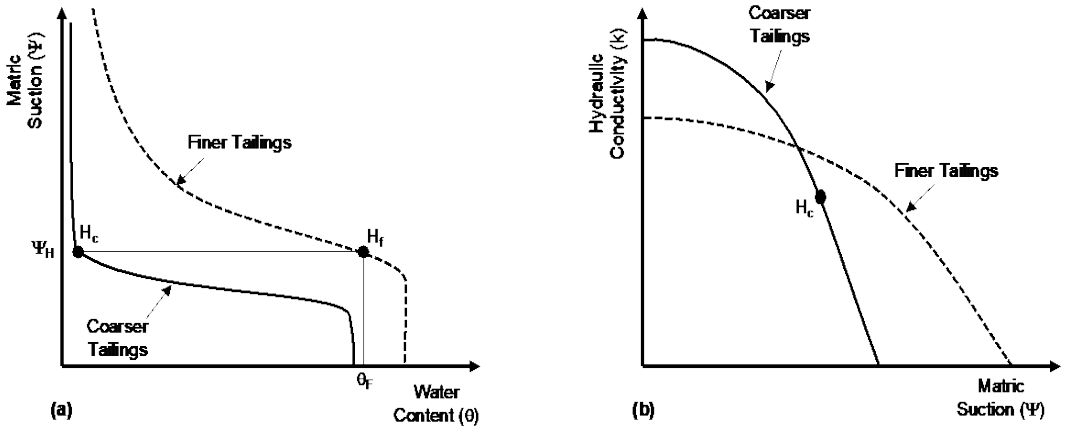


Figure 2: (a) Soil water characteristic curve (SWCC) and (b) hydraulic conductivity function (HCF) for finer- and coarser-grained tailings (derived from Khire et al., 1999)

Retention of saturated, or near-saturated, conditions often elevate geotechnical stability concerns for TSFs, particularly seismic stability and susceptibility to flow liquification. Long-term retention of near-saturated conditions yields conservative assumptions of full saturation and may drive financially costly and environmentally disruptive mitigation efforts. Common industry practice is to assume that tailings are fully saturated until a value of less than 60% saturation is reached.

Global initiatives to enhance water stewardship in mining are a significant driver for tailings dewatering. However, this option makes material handling (i.e., transport and placement) more difficult and expensive in comparison to pumping slurry tailings (Carneiro et al., 2018). Additionally, dewatering practices that occur prior to deposition are not a solution for existing (active and legacy) TSFs, without significant capital investments or implementation of remining practices. Dewatering existing tailings in-situ (i.e., after tailings have been deposited) offers numerous benefits, the most significant being the ability to densify the deposit, thereby reducing the likelihood of generating positive pore water pressures during seismic or similar events.

There are two main categories into which in-situ dewatering methods are divided: active and passive. Active dewatering requires continuous energy or reagent inputs. While passive dewatering operates using

low intensity or minimal energy inputs beyond initial installation, such as prefabricated vertical wick drains (Adams et al., 2017). Both methods are primarily designed around the removal of pore water that is under positive pressures or draining permeable strata. Thus, additional tools are needed for the removal of water retained in fine strata by capillary barriers in TSFs.

Wicking geotextiles

Wicking geotextiles are a recent advancement designed to remove moisture from roadway embankments or subbases (Lin and Zhang, 2018). The cross-section of the fiber is shown in Figure 3. This geotextile, created from weaving high-tenacity polypropylene filaments and deep-grooved nylon-wicking fibers, produces a coherent drain by effectively wicking water from soil pores. The diameters of the wicking fibers range from 30 to 50 μm and the width of each groove is between 5 and 12 μm (Zhang and Connor, 2015).

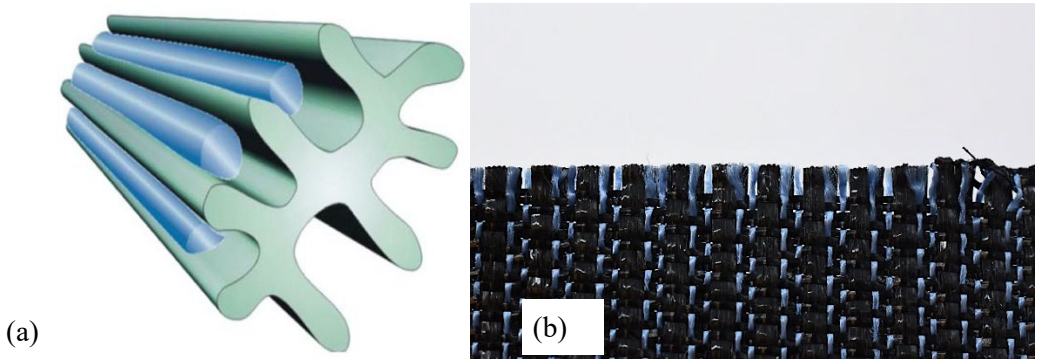


Figure 3: (a) Wicking fiber cross-section (Lin and Zhang, 2018) and (b) close-up of wicking (blue) fibers

There are several unique properties of the wicking geotextile. The wicking fibers have hydrophilic and hygroscopic properties that provide enhanced lateral drainage along the plane of the geosynthetic, meaning that the nylon will pull water from the surrounding soil pores and then provide a conduit for the water to the surface along the inner channels (TenCate, 2022). In addition, wicking geotextiles have greater air-entry values, compared to non-wicking geotextiles, allowing for the development of capillary force or suction to remove moisture from soils in unsaturated conditions (Lin et al., 2016).

The geotechnical advantages of wicking geotextiles have been proven in transportation and roadway studies. Guo et al. (2019) summarized the available studies and projects that demonstrated the effectiveness of the wicking geotextile as a drainage material. Zhang et al. (2014) and Lin and Zhang (2018) estimated that due to the suction difference induced by the relative humidity between the unsaturated soil, geotextile, and air, a large hydraulic gradient is formed; thus, the geotextile can absorb water from the surrounding soil and transport to the exposed/atmospheric end. Zornberg et al. (2017) reported field studies in which the daily water content reduction was evaluated in the soil column from a nearly saturated condition. This study

determined that the wicking geotextile was more effective in reducing the water content than the non-wicking geotextile under the same conditions. Additionally, the drainage function of the wicking geotextile continued at a lower water content than the non-wicking geotextile.

The success observed by the geotextile in the field of transportation indicates a promising ability that may be transferable to other engineering applications such as tailings dewatering. Assessing the capability to dewater tailings fines is a novel application explored in this research.

Methodology

Column experiments, in which tailings were confined between layers of fine and coarse sand, were constructed and conducted to assess the in-situ capillary water dewatering capabilities of the wicking geotextiles. Filtered tailings from a confidential precious metal mine, herein referred to as Mine P, as well as a fine and a coarse sand, were used for testing. Filtered tailings were dewatered at the mine during pilot-scale tests before shipment to Colorado State University.

Two capillary geosynthetics were used in this study. Wicking geotextile 1 is a prototype material and wicking geotextile 2 is sold commercially under the name H2Ri by TenCate Geosynthetics. The characteristics of wicking geotextiles 1 and 2 are the same and summarized in Table 1.

Table 1: Mechanical properties of wicking geotextile 1 and 2

Mechanical Properties	Test Method	Unit	Minimum Average Value
Wide Width Tensile Modulus (CD)	ASTM D4595	kN/m	77.0
Tensile Modulus @ 2% Strain (CD)		kN/m	15.8
Permittivity	ASTM D4491	s^{-1}	0.4
Flow Rate		L/min/m2	0.1222
Pore Size (050)	ASTM D6767	µm	85
Pore Size (095)		µm	195
			Maximum Opening Size
Apparent Opening Size	ASTM D4751	U.S. Sieve (mm)	40 (0.425)

Column construction

Column experiments were created to emulate the previously described stratigraphy observed in legacy TSFs. The final set-ups are shown in Figure 4. The tailings used in the column experiments were created at 50% solids contents. The columns were created by depositing layers of varying granular sizes into clear PVC columns to force the development of capillary barriers. One end of the column was plastic welded to a square base plate and the column was sealed with silicone caulk to prevent water loss through the bottom

of the system. Columns were weighed at regular intervals to observe water mass loss and to determine the change in solids contents corresponding to the new total masses.

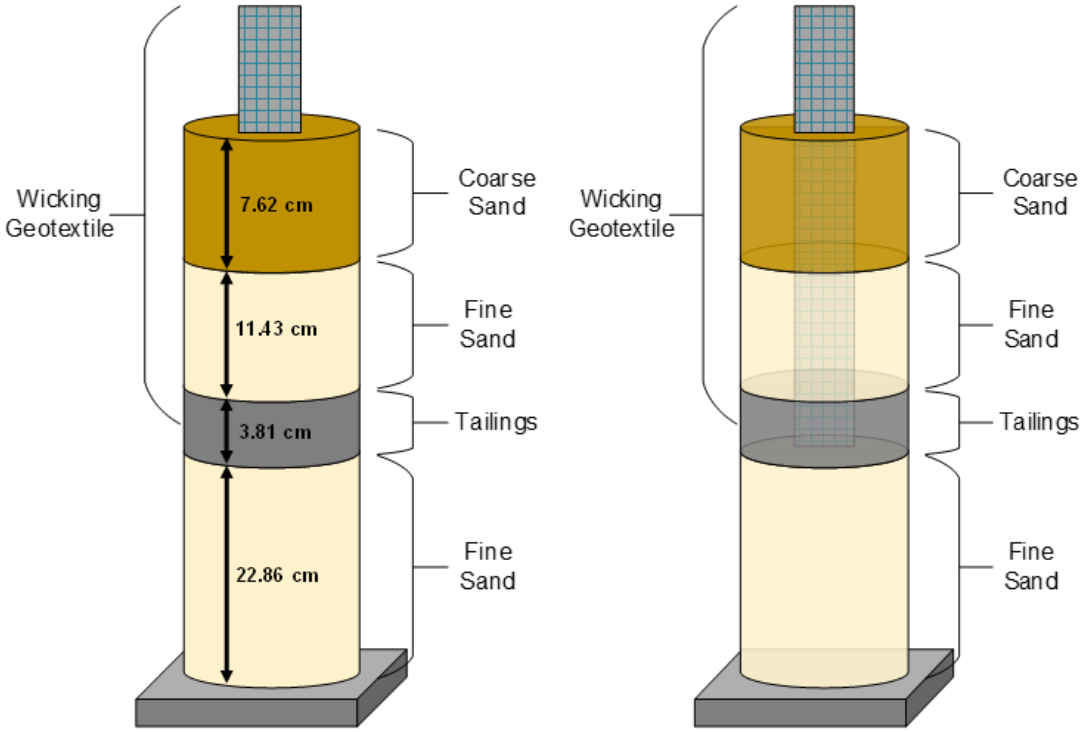


Figure 4: Tailings columns created at 50% solids contents: digital renderings

Results

The van Genuchten (1980) equation was used to calculate the volumetric water contents of the fine sand and tailings:

$$\theta = \theta_r + (\theta_s - \theta_r)\left[\frac{1}{1+(\alpha\psi)^n}\right]^m \quad \text{(Equation 1)}$$

where θ_r is the residual volumetric water content, θ_s is the saturated volumetric water content, α is inversely related to the air entry value, n controls the slope of the SWCC, $m = 1 - n^{-1}$. The van Genuchten (1980) equation was used to calculate the unsaturated hydraulic conductivities of the fine sand and tailings:

$$K_r = \left(\frac{\theta-\theta_r}{\theta_s-\theta_r}\right)^P \left[1 - \left(1 - \left(\frac{\theta-\theta_r}{\theta_s-\theta_r}\right)^{\frac{1}{m}}\right)^m\right]^2, \; P = -2 \quad \text{(Equation 2)}$$

where K_r is the relative hydraulic conductivity, and P is a fitting parameter, usually considered -2 for fine soils. Fitting parameters to Equations 2 and 3 are provided in Table 2.

Table 2: SWCC parameters for the tailings and fine sand (tailings parameters provided by Aghazamani, 2022)

Parameter	Value	
	Fine Sand	Tailings at 95% $\gamma_{d,\,max}$
θ_r	0.01	0.004
θ_s	0.206	0.339
α (kPa^{-1})	0.833	0.013
n	3.449	1.421
m	0.710	0.296
k_{sat} (m/s)	1.2x10^{-3}	2.3x10^{-9}

The SWCCs and HCFs of the wicking geotextile 2, provided by Lin et al. (2016), the tailings, and fine sand are displayed in Figure 5.

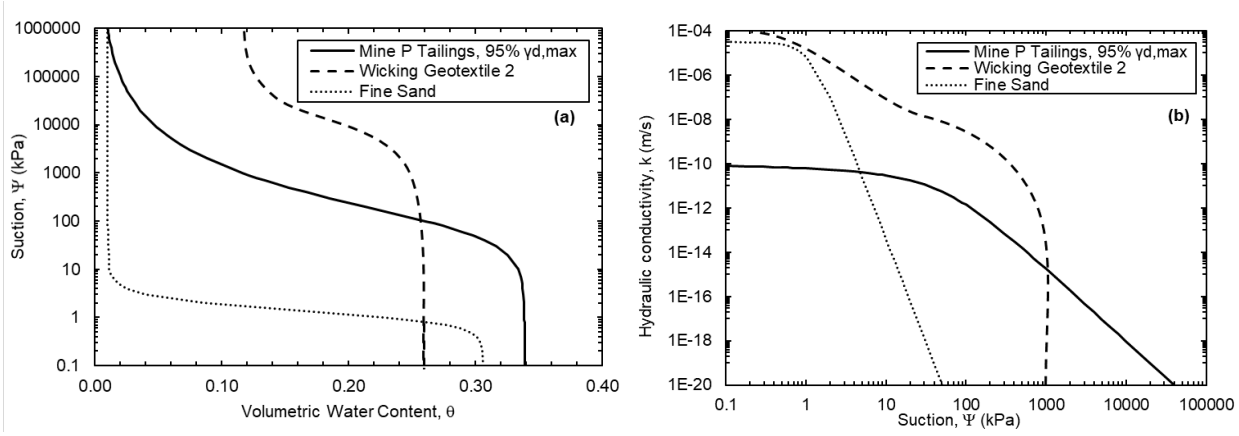


Figure 5: (a) Drying SWCC and (b) HCF curves for the fine sand, tailings, and wicking geotextile 2

The suction potential of the geotextile can be viewed in two parts: the geotextile surface, and the inter-yarn drainage path (the deep grooves that have an average spacing of 5 microns to 12 microns). Air and soil particles cannot easily infiltrate the drainage path due to the small openings. When the suction is less than 200 kPa, water movement from the surrounding soil into the geotextile multichannel is assumed due to greater unsaturated hydraulic conductivity of the geotextile. The transmissivity of the geotextile surface decreases significantly within the suction range of 45 kPa to 200 kPa, but the deep grooves remain saturated and continuously wick water into the atmosphere due to the gradient pressure difference (Lin et al., 2016). As the tailings dewater the unsaturated hydraulic conductivity of the wicking geotextile 2 is greater than that of the tailings up to a suction of around 1,000 kPa.

Beyond this point, the hydraulic conductivity of the wicking geotextile drops off significantly, and the drainage efficiency is dramatically reduced. The suction potential of the wicking geotextiles was not reassessed in this study, but based on previous findings, the estimated working range of the geotextile is up to 1,000 kPa of suction. For Mine P tailings, a suction of 1,000 kPa translates to a saturation of 28%. This is a saturation reduction of 70% beyond the capillary barrier effect of the fine sand, which resulted in retention of a saturation of 98% within the tailings layer.

Magnitude of drying and dewatering

The percent total water mass removed of the total initial water mass for each column at experiment deconstruction are presented in Figure 6a. The wicking geotextiles removed water from the tailings layer to a greater extent by test conclusion (80 days) than natural evaporation or gravity processes as shown by the control column. At the conclusion and deconstruction of the columns, the wicking geotextile 2 had removed 48% of the column water, while the control column had only lost 19% water. To support the water loss values calculated throughout the testing period, water content samples were taken from the columns at the end of testing. The final water contents observed in Figure 6b were collected from the midpoint of the tailings layer and averaged across three points at the same depth.

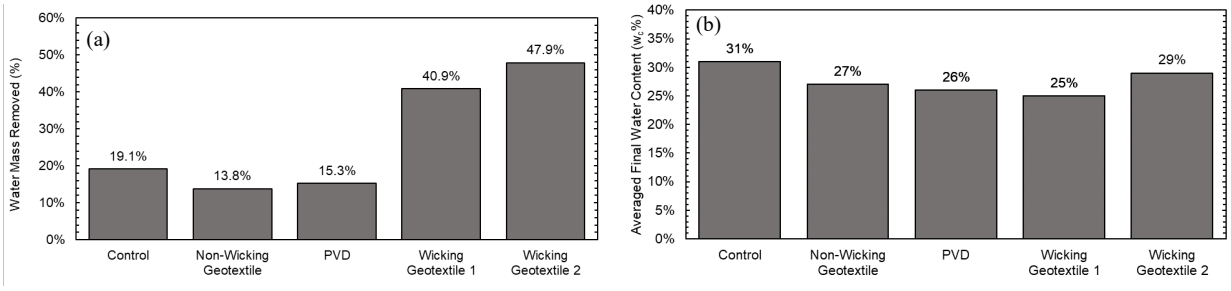


Figure 6: (a) Percent water mass removed in column tests and (b) water content samples taken from the midpoint of the columns' tailings layers

While the final water contents for each mid layer were similar, the wicking geotextile columns were observed losing more mass than the other columns during testing. Therefore, additional water content samples were taken in the layers above and below the tailings. Figure 7 presents a graphical representation of the water contents seen throughout the layering of the columns. Gravimetric water content samples taken from the lower fine sand layer in the wicking geotextiles column contained 0% moisture. While in the control and non-wicking columns water contents varied between 5% - 9%. Minimal movement of moisture into the fine sand layer above the tailings can be observed in all the columns, but further movement was impeded by the coarser grained sand. Beyond dewatering the tailings, the wicking geotextiles are effectively creating a vacuum that pulls up the water that previously drained into the lower fine sand layer during column construction (as supported by the w_c% samples = 0%).

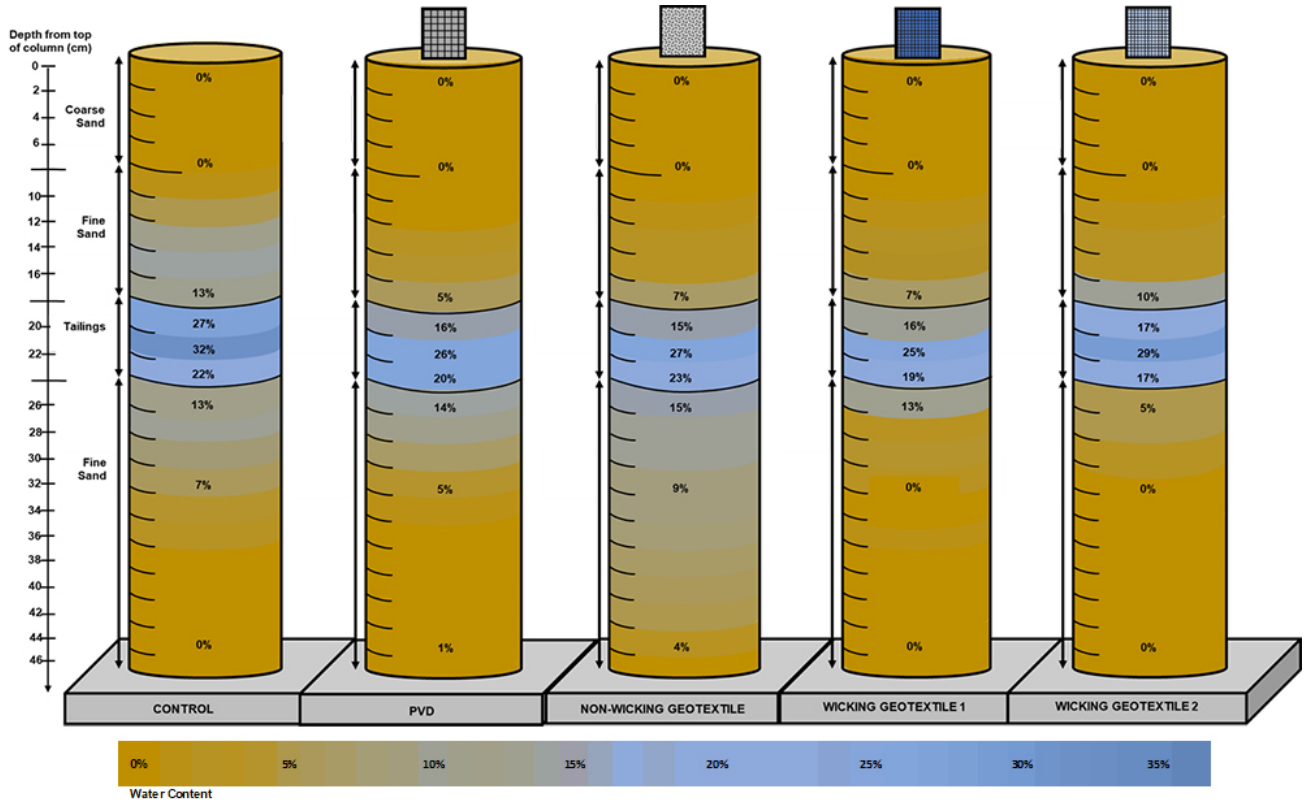


Figure 7: Column experiments schematics representing water content samples versus depth

Rate of drying and dewatering

After 80 days of allowing the columns to rest under the fume hood and weighing at regular intervals, the average rate of water removal per day for each of the columns was assessed, these values are illustrated in Figure 8. The water mass removed in grams per day of the wicking geotextile 2 was 2.1 g/day, while the control was 0.8 g/day, less than half of the rate of the wicking geotextile.

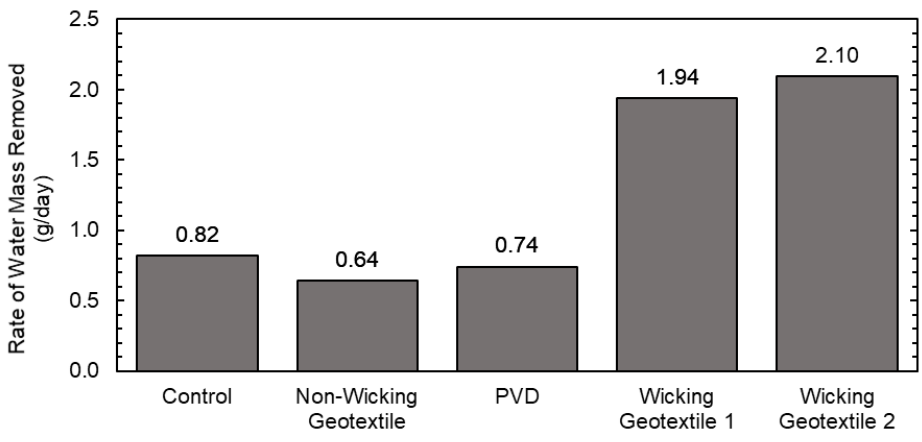


Figure 8: Rate of water mass removed from the tailings columns per day

The change in solids contents of the columns were calculated at regular intervals and these values are plotted in Figure 9. Although some water was initially observed percolating into the lowest fine sand layer upon initial construction, the amount of water was not determined. The change in solids content of the columns was therefore made with the assumption that water loss was occurring directly in the tailings beginning with an initial solids content of 50%. At the conclusion of testing, the wicking geotextiles had removed more than twice as much water than the control columns. The wicking geotextile 1 reached a solids content of 61.4% and the wicking geotextile 2 reached a solids content of 68.5%. This indicates that the wicking geotextile 2 tailings had transitioned to the paste form of the dewatering continuum. The control columns reached a solids content of 55.4%; extrapolated data predict an additional 120 days of drying would be required to reach the lower end of the paste boundary, due to the < 1 g of water mass loss per day.

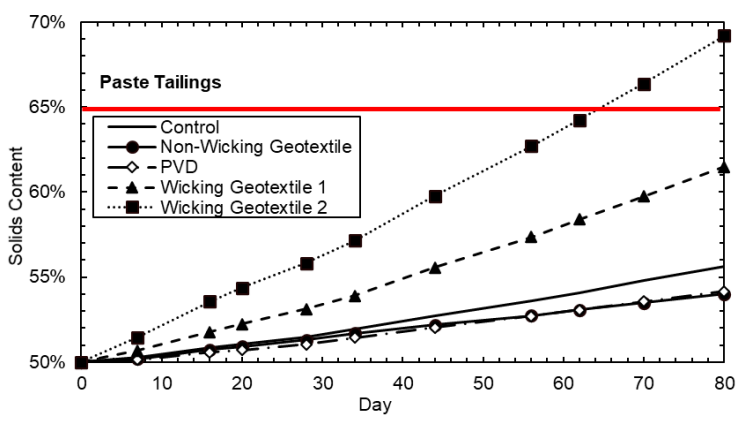


Figure 9: Dewatered paste boundary surpassed by wicking geotextile 2

Discussion

Magnitude of drying and dewatering

Dewatering beyond the 60% conservative threshold, practiced by industry, would indicate achievement of transitioning the tailings from an undrained to drained state. In the case of the column experiments, by day 80, between 41 – 48% of the initial water mass had been removed by the wicking geotextiles. The removal of this magnitude of water and the achievement of a solids content above 80% has moved the tailings into a filtered tailings dewatering state. These interim results were contradictory to the actual magnitude of dewatering of which the wicking geotextiles were capable. Due to the rapid dewatering occurring in the wicking geotextile columns, the assumption was that the tailings were at lower water contents than the tailings in the other columns. However, final water content samples presented relative uniformity for all the columns.

Rate of drying and dewatering

The ability of the wicking geotextile to accelerate dewatering and therefore reduce the consolidation period was assessed. Envisioned implementation of wicking geotextiles in a TSF were hypothesized. The two hypothetical scenarios included: a) dewatering occurring while the mine is operational and therefore both surface and pore water dewatering will be accelerated by the wicking geotextiles; and b) dewatering in a legacy TSF in which the geotextiles would need to be installed following TSF closure. In both scenarios, the wicking geotextiles theoretically aided in unsaturated dewatering and increased the consolidation rate of the tailings deposit. Accelerated drying during placement emulates filtered tailings deposition and densifies the freshly deposited tailings. Accelerated drying in-situ implies the ability to overcome capillary barriers. The column experimental results support envisioned implementations and the conclusion that increased tailings consolidation rates are expediated by the introduction of wicking geotextiles.

Overcoming capillary barriers

The wicking geotextile creates a capillary continuum from the fine-grained tailings layer to the atmosphere. Figure 7 displayed the wicking geotextiles removing water directly from the tailings layer and transferring the water to the atmosphere, overriding the capillary barriers formed by the fine grain and coarse grain sand. However, since this series of columns was deconstructed prior to an asymptote being reached, a definitive statement on the capillary dewatering success of the wicking geotextile cannot be made. Additional long-duration testing has been started concurrent to the finalization of this document. The ability of wicking geotextiles to remove both excess and non-excess pore water out of tailings is a novel characteristic. Dewatering excess pore water pressure would decrease the pressure existing within the system; then transitioning to non-excess, or hydrostatic, dewatering may aid in desaturating to a degree where overly conservative estimates of strength are not needed. At the time of writing this, no known passive methods of dewatering are available to remove capillary non-excess pore water beyond gravity drainage. This renders the capabilities of existing passive methods, such as PVDs, relatively futile for legacy TSFs in which water is already retained by capillary barriers.

Conclusion

As a potential solution to dewatering beyond excess porewater pressure, use of a wicking geotextile is proposed. Throughout the testing period, the wicking geotextiles were observed dewatering at a rate 1.5 – 2 times faster than the control. At the end of the 80-day testing period, the columns were deconstructed, and gravimetric water content samples were collected. The water content samples taken from the midpoint of the tailings layer ranged between 25 to 31% for all columns, with the control having the highest moisture content and the wicking geotextile 1 having the lowest moisture content. The following conclusions are

extracted from this study:

- Reviewed legacy TSF characterization data show that interbedded layers of near saturated fines exist within the tailings. These fine layers desaturate on the magnitude of hundreds to thousands of years, and therefore as they currently exist may pose liquefaction concerns.
- Wicking geotextiles can accelerate water removal from the tailings up to 2.8 times the rate of natural dewatering processes as illustrated by the column tests. These results highlight that incorporation of capillary geosynthetics is a potential method to enhance the rate of evaporative drying of exposed tailings.
- The wicking geotextiles have potential to overcoming in-situ capillary barriers via the inner-yarn drainage path of the wicking geotextile.

References

Adams, A., Friedman, D., Brouwer, K. and Davidson, S. 2017. Tailings Impoundment Stabilization to Mitigate Mudrush Rise. *Proceedings of the 85th Annual Meeting of International Commission on Large Dams*.

Aghazamani, N. 2022. *Unsaturated fluid flow and volume change behavior of filtered tailings*. PhD thesis, Colorado State University. https://hdl.handle.net/10217/235334

Carneiro, A., Fourie, A., Jewell, R. and Fourie, B. 2018. A conceptual cost comparison of alternative tailings disposal strategies in Western Australia. *Australian Centre for Geomechanics:* 439–454. https://doi.org/10.36487/ACG_rep/1805_36_Carneiro

Casey, J., Chambers, R. and Eng, P. 2022. Characterizing Tailings behavior at the San Manuel copper TSFs Part 1: In-situ and laboratory geotechnical techniques. *Proceedings of the 26th International Conference on Tailings and Mine Waste*, 652–653.

Fredlund, D.G., Rahardjo, H. and Fredlund, M.D. 2012. *Unsaturated Soil Mechanics in Engineering Practice*. John Wiley & Sons.

Godley, D. and Quaglia, G. 2023. Deconstruction of an upstream raised tailings storage facility: Project design and execution. *Proceedings of Tailings and Mine Waste 2023.* Vancouver, BC.

Guo, J., Han, J., Zhang, X. and Li, Z. 2019. Evaluation of moisture reduction in aggregate base by wicking geotextile using soil column tests. *Geotextiles and Geomembranes* 47(3): 306–314. https://doi.org/10.1016/j.geotexmem.2019.01.014

Hardy, J., Lindstrom, R., Bingham, L., Fuller, A. and Krohn, C. 2003. Characterization and design of the old dominion remedial action plan. *National Meeting of the American Society of Mining and Reclamation and the 9th Billings Land Reclamation Symposium:* 329–352.

Khire, M., Benson, C. and Bosscher, P. 1999. Field data from a capillary barrier and model predictions with UNSAT-H. *Journal of Geotechnical and Geoenvironmental Engineering* 125(6): 518–527. https://doi.org/10.1061/(ASCE)1090-0241(1999)125:6(518)

Lin, C. and Zhang, X. 2018. Laboratory Drainage Performance of a New Geotextile with Wicking Fabric. *Journal of Materials in Civil Engineering* 30(11): 04018293.

Lin, C., Zhang, X. and Han, J. 2016. Development of a Design Method for H2Ri Wicking Fabric in Pavement Structures. *Center for Environmentally Sustainable Transportation in Cold Climates*. https://scholarworks.alaska.edu/handle/11122/10398

Spencer, D., Bareither, C., Scalia IV, J., Hatton, C. and Ward, K. 2022. Characterizing tailings professional labor demand. *Mining Engineering* 74(277): 16–16.

Stormont, J. and Anderson, C. 1999. Capillary barrier effect from underlying coarser soil layer. *Journal of Geotechnical and Geoenvironmental Engineering* 125(8): 641–648. https://doi.org/10.1061/(ASCE)1090-0241(1999)125:8(641)

TenCate. 2022. Mirafi® H2Ri Woven Geosynthetic. PDF.

Zhang, X. and Connor, B. 2015. Evaluate H2RI wicking fabric for pavement application – Year 2. *Pacific Northwest Transportation Consortium.* https://scholarworks.alaska.edu/handle/11122/10380

Zhang, X., Presler, W., Li, L., Jones, D. and Odgers, B. 2014. Use of wicking fabric to help prevent frost boils in Alaskan pavements. *ASCE J. Mater. Civil Eng.* 26(4): 728–740.

Zornberg, J., Azevedo, M., Sikkema, M. and Odgers, B. 2017. Geosynthetics with enhanced lateral drainage capabilities in roadway systems. *Transportat. Geotech.* 12: 85–100.

Rate Effects in In-situ Testing in Hard Rock Mine Tailings and their Impact on the Estimation of Shear Strength Parameters

Mohammad Zarrabi, WSP Canada Inc., Canada
Estelle Nkamegue, WSP Canada Inc., Canada
Michael Demers-Bonin, (formerly with WSP Canada Inc., Canada), Canada
Mohammad Kermani, WSP Canada Inc., Canada
Kendell Cator, BHP Billiton Canada Inc., Canada

Abstract

Selbaie is a closed mine site in the Joutel-Matagami region near James Bay and the town of Rouyn-Noranda, both located in the Province of Quebec, Canada. WSP performed a geotechnical investigation at the Tailings Storage Facilities (TSF) which included seismic cone penetration tests (SCPTs) and field vane tests (FVTs), as well as advanced laboratory testing including direct simple shear (DSS) tests, among others. These tests were completed to characterize hard rock mine tailings as well as foundation soils.

Contrary to clays and sands, transient materials such as tailings can undergo partially drained conditions during in-situ SCPTs performed at the standard penetration rate of 2 cm/s. For this reason, at one location in the Selbaie mine TSF, duplicate (A/B) SCPTs were performed within a 3-meter distance of each other at different penetration rates to evaluate its effects on the in-situ state and shear strength parameters of tailings, and drainage conditions. The first SCPT (A) was performed at a standard penetration rate of 2 cm/s while the second one (B) was advanced at a penetration rate of 10 cm/s.

The shearing rate is also known to influence FVT results. Therefore, FVTs were performed using an electronic vane at several locations in parallel with SCPTs. To assess rate effects on the inferred shear strength and drainage conditions, at one location, FVTs in tailings were performed at different rotation speeds including the standard rate (0.1°/s) as well as two higher vane rotation rates ranging between 0.8°/s and, 10°/s.

This paper provides results of the in-situ SCPTs and FVTs in tailings. SCPT and FVT results were analyzed using existing frameworks from the literature, including Chandler (1988), Blight (1962), and Dejong et al. (2013). It appears that higher rotation rates of FVTs could lead to undrained shearing response

according to Chandler (1988) and Blight (1962) criteria, but do not systematically lead to lower peak shear strength. As for SCPTs, the standard advancement rate was not high enough to guarantee undrained response during piezocone penetration. However, higher penetration rates led to higher sleeve friction measurements, and higher liquefied strength ratios estimated using screening-level methods.

Review of the in-situ testing program

A geotechnical investigation, including in-situ seismic cone penetrations (SCPTs) and electronic shear field vane tests (FVTs), was carried out by WSP in 2021 at the Selbaie mine site Tailings Storage Facility (TSF) located in the Province of Quebec, Canada. The TSF investigation program included 9 geotechnical boreholes, 11 SCPTs, and 9 FVT profiles. In situ soundings were accompanied by index and advanced laboratory tests for tailings characterization.

Electronic shear vane testing in tailings was carried out in boreholes within 5 m of selected SCPTs to assess the in-situ peak, post-peak, and remolded undrained shear strength. Testing was performed in accordance with ASTM D2573 (2018b). All FVTs utilized 50 × 100 mm blades to eliminate blade size effects.

Peak and post-peak undrained shear strengths were measured by rotating the vane until failure and by further rotating the vane up to 360°. The remolded strength was obtained by repeating the test after 20 turns of the vane rods. Peak and post-peak strength testing was generally performed at intervals of 0.5 m or 1.0 m, depending on the thickness of tailings. Remolded shear strength testing was generally conducted once every two (peak and/or post-peak) tests conducted.

A standard electronic vane apparatus with the standard shearing rate of 0.1°/s was used at all testing locations to align with ASTM requirements (2018b). This rate usually leads to undrained shearing in clayey materials, thus providing undrained shear strength estimates. However, in intermediate soils such as tailings, silt, and low-plasticity clay, partially drained or drained conditions usually prevail, leading to overestimated undrained shear strength measurements (Reid, 2016). This was notably observed in previous investigations at the Selbaie mine site.

To attempt to measure the undrained shear strength in tailings and evaluate shearing rate effects, a series of tests at varying shearing rates of 0.1 °/s, 0.8 °/s, and 7.5 to 10 °/s were performed with a standard and fast vane apparatus in FVT-21-02A and FVT-21-02B. These two tests, along with SCPT-21-02A/B, were performed in close proximity. Drainage conditions during FVTs were determined using a method developed by Blight (1962) and updated in Chandler (1988).

Eleven SCPTs were also carried out and deployed using a 20-tonne ramset drilling sonic rig. Testing was conducted in general accordance with ASTM D5778 (2020a). In addition to the cone tip resistance, sleeve friction and dynamic porewater pressure readings, three to five porewater pressure dissipation (PPD)

tests were performed per SCPT. These tests were used to define the equilibrium pore water pressure profile of each SCPT, which served to estimate the groundwater table level, effective stress profile, and vertical hydraulic gradients. Testing results were also used to estimate the horizontal coefficient of consolidation and hydraulic conductivity of the unit tested.

Similarly to FVTs, an analysis should be conducted to determine what drainage conditions (undrained, partially drained, or drained) prevail during SCPTs performed in intermediate soils such as tailings, silt, and low-plasticity clay. If partial drainage prevails, estimation of shear parameters should account for partial drainage effects to avoid shear strength overestimation. Partial drainage in SCPTs is inferred from parameters such as the pore pressure ratio (B_q), and the time rate of decay during pore pressure dissipation tests (time to reach 50% dissipation, t_{50}) using an approach proposed by Dejong et al. (2013).

The standard SCPT advancement rate of 2 cm/s was used at all locations in the TSF. Given that the penetration is expected to be partially drained when the standard rate is used in intermediate soils such as tailings, a duplicate test (SCPT-21-02B) was performed at a higher penetration rate of 100 mm/s next to SCPT-21-02A. SCPT-21-02B sought to assess penetration rate effects on the inferred in-situ state and tailings undrained shear strength parameters, and on drainage conditions.

Tailings characteristics based on laboratory testing

Basic tailings characteristics

Table 1 presents the results of a water content test, specific gravity measurement, and particle size distribution analyses conducted on a specimen to which tailings encountered in SCPT-21-02A/B and FVT-21-02A/B are correlated. The water content measurement was used to estimate the in-situ void ratio and saturated unit weight. The sample was classified as a silt (ML) with trace sand.

Table 1: Tailings management area tailings index test results in the vicinity of the SCPTs and FVTs in situ tests

Material Type	Sample Average Depth (m)	Water Content (%)	Fines Content (%)	Sand and Gravel Content (%)	Specific Gravity	Inferred Void Ratio[a]	Inferred Unit Weight[a] (kN/m³)
Tailings	22.10	34.8	98.5	S: 1.5 G: 0.0	2.82	0.98	18.8

(a) The void ratio and unit weight of the tailings specimen were inferred from the water content and specific gravity measurements under the assumption that the sample was fully saturated and that no disturbance occurred.

kN/m³ = kilonewtons per cubic meter; S = sand; G = gravel.

In-situ state parameter and shearing response

The characteristic in-situ state parameters (ψ_k) of the TSF tailings estimated from the Been and

Jefferies (1992) and the Plewes et al. (1992) methods are shown in Figure 1. The 80th percentile of estimated state parameters is considered for tailings. Tailings display contractive behavior as the 80th percentile of ψ_k ranged from 0.06 to 0.13 in SCPT-21-02A and SCPT-21-02B.

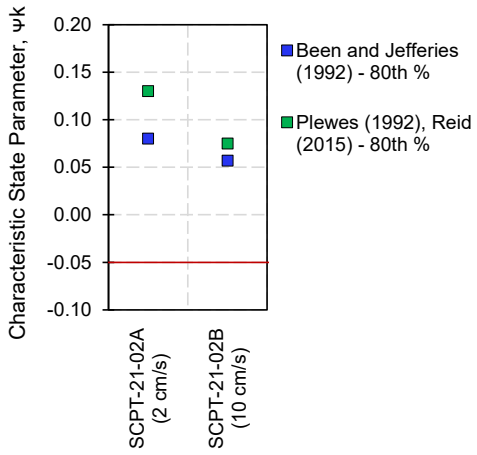


Figure 1: Characteristic state parameter using Been and Jefferies (1992) and Plewes et al. (1992) methods

In-situ testing results and interpretations

Effect of partial drainage on field vane tests

When performing FVTs at the standard rotation rate (0.1 °/s) in intermediate soils such as tailings, partial drainage may occur which can then lead to overestimating the undrained shear strength. This was observed in FVTs performed in Selbaie TSF tailings in 2018 and 2019. To assess drainage conditions of the 2021 FVTs, the dimensionless time factor, T, serving as an indication of the degree of drainage (Reid, 2016; Reid et al., 2023) was calculated for each test using an equation presented in Blight (1962) and updated in Chandler (1988). As outlined in the studies, undrained conditions would occur when the time factor is smaller than 0.05.

Figure 2 presents peak undrained shear strength ratios plotted against the estimated time factor. The data suggests that for a single rotation rate, lower shear strength ratios generally correspond to lower time factors.

In addition to the FVTs with the standard rotation rate (0.1 °/s) in FVT-21-02A, a series of tests with varying rotation rates was carried out in FVT-21-02B, located near FVT-21-02A. The shearing rates in FVT-21-02B varied between higher rates of 0.8 °/s and 7.5 to 10 °/s. Figure 2 shows that 1 out of 32 tests performed at the standard rate exhibited undrained conditions, compared to 5 out of 15 valid intermediate tests with a 0.8 °/s rotation rate and 12 out of 15 tests with the highest rates ranging from 7.5 to 10 °/s.

However, undrained shearing conditions did not necessarily result in lower strength measurements, as evidenced by the shear strength profiles presented in Figure 3. In most cases, lower measurements were obtained with the standard rotation rate, which would suggest that other phenomena such as viscous effects may affect shear strength measurement at higher shearing rates. Peak strength ratios in FVT-21-02A performed at the standard rate averaged at 0.61 and were similar in FVT-21-02B, averaging at 0.77 irrespective of the rate. It appears that due to the TSF tailings rheology, none of the rotation rates utilized could have resulted in lower shear strength values and undrained shearing conditions. Additional factors such as the principal stresses orientation and/or the shear band size and shape developing around vanes may have played a role in the interpreted results (Gylland, 2013).

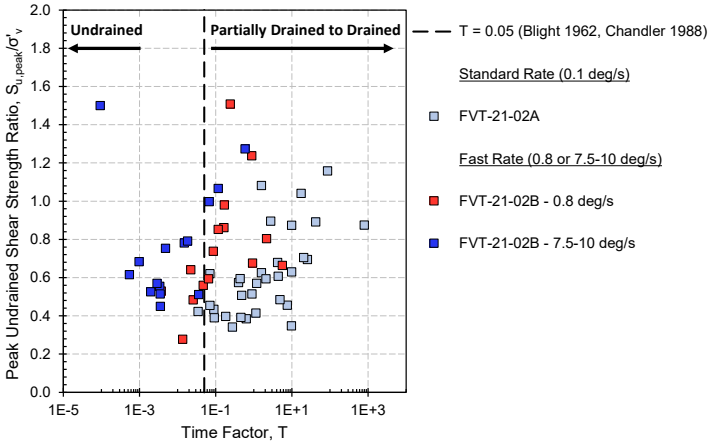


Figure 2: Peak undrained shear strength ratios measured in tailings management area tailings versus time factor

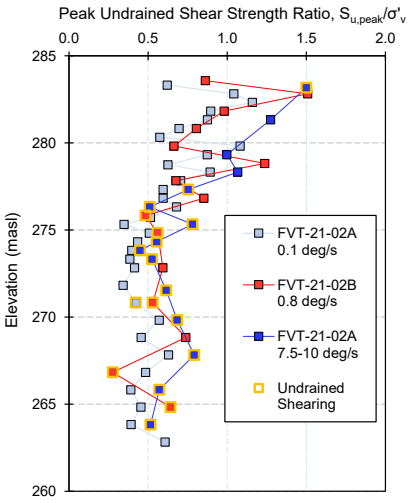


Figure 3: Peak undrained shear strength ratio profiles obtained in tailings management area tailings in FVT-21-02A/B at rotation rates of 0.1, 0.8, and 7.5 to 10 °/s

Effects of partial drainage on cone penetration tests

Results of PPD tests are presented in Table 2. Equilibrium porewater pressures inferred from the PPD tests results generally indicate hydrostatic or near hydrostatic conditions in tailings, and a downward hydraulic gradient in the underlying native soils. The following discusses results of the PPD tests conducted in tailings (Table 2):

The average time required to reach 50% dissipation of penetration-induced porewater pressures (t_{50}) was always smaller than 100 s, suggesting partially drained cone penetration according to DeJong et al. (2013).

The normalized velocity was calculated from SCPT data to assess drainage conditions during cone penetration using a method developed by Dejong et al. (2013). Table 2 shows that partially drained conditions generally prevailed whereas undrained penetration only occurred in SCPT-21-02B. The latter was performed at a higher advancement rate of 10 cm/s to assess advancement rate effects on drainage conditions and SCPT parameters. Despite the higher penetration rate used in SCPT-21-02B, it was not possible to achieve fully undrained penetration at this sounding through the entire tailings deposit. However, these findings cannot be broadly applied to the entire site since this faster rate sounding was only performed in one location and other SCPTs carried out in the TSF tailings revealed spatial variability in SCPT response.

Partially drained penetration leads to underestimation of t_{50} values, which in turn results in overestimated horizontal coefficients of consolidation and hydraulic conductivity. This is apparent upon examination of Figure 4, which compares coefficients of consolidation obtained in SCPT-21-02A and SCPT-21-02B at equivalent test depths. SCPT-21-02B yielded higher normalized velocity values, suggesting less partial drainage, which resulted in lower coefficients of consolidation. Partial drainage during SCPT implies that empirical equations could potentially underestimate shear strength (Ayala et al., 2024; Boschi et al., 2023). Therefore, attention must be paid to this aspect when results of this campaign are used to assess the stability of TSF dams.

Table 2: Summary of porewater pressure dissipation test results in tailings

Material Type	Number of Tests	Time to Reach 50% Dissipation, t_{50} (s) Min-Max-Mean	Drainage Conditions During SCPT Penetration[a] (Dejong et al., 2013) at Dissipation Test Depths Fully Drained-Partially Drained-Undrained
SCPT-21-02A (2 cm/s)	4	8-20-13	0-4-0
SCPT-21-02B (10 cm/s)	4	13-19-16	0-2-2

(a) Drainage conditions can be evaluated as fully drained, partially drained or undrained using dissipation test results according to the Dejong et al. (2013) method. Analysis of SCPT-21-02A and SCPT-21-02B dissipation tests indicated that either partially drained or undrained conditions prevailed (full conditions never achieved).

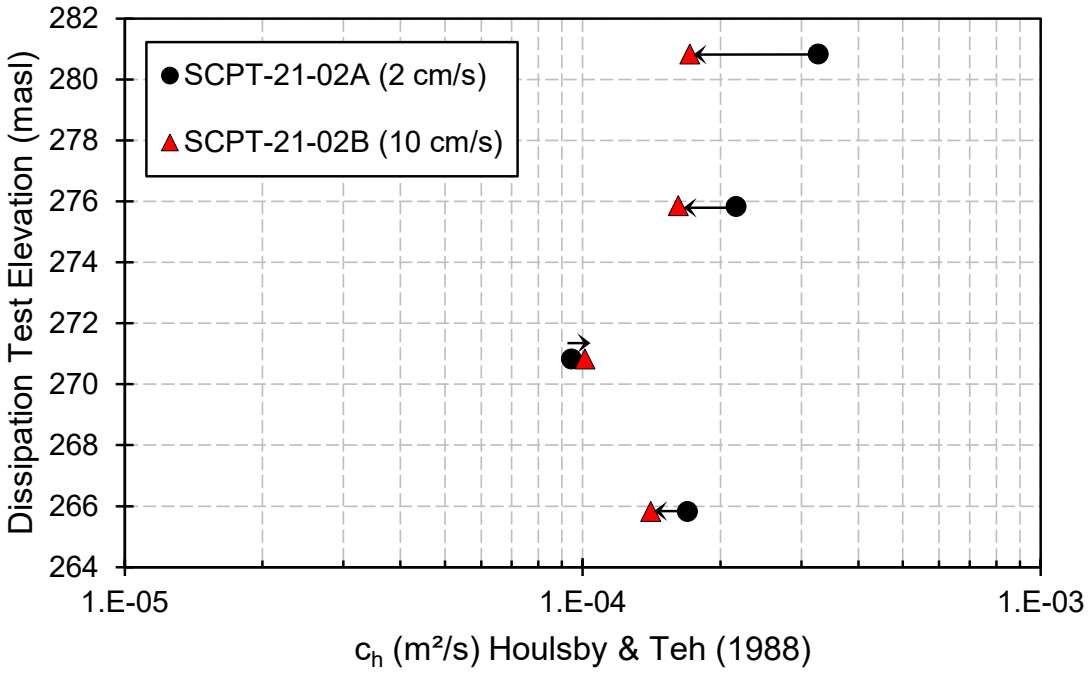
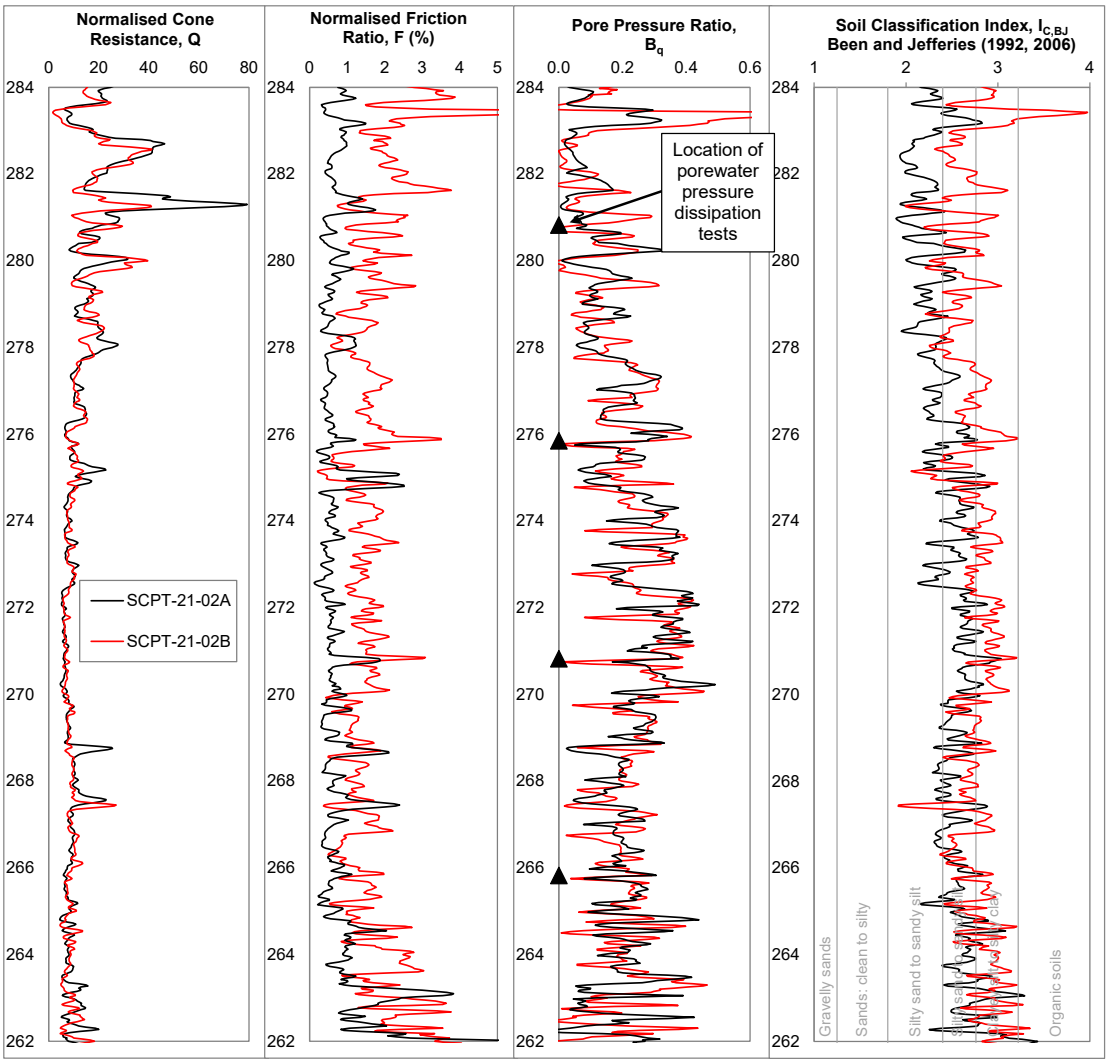


Figure 4: Comparison of tailings horizontal coefficients of consolidation estimated from SCPT- 21-02A (2 cm/s) and SCPT-21-02B (10 cm/s) porewater pressure dissipation tests data

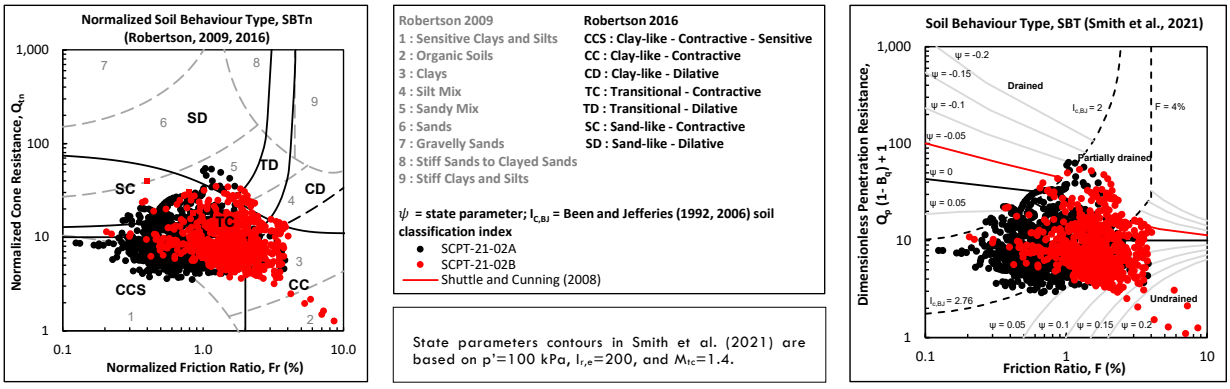
Penetration rate effects

The standard SCPT advancement rate of 2 cm/s was used at all locations except for SCPT-21-02B where a 10 cm/s penetration rate was used to assess advancement rate effects on strength parameters and drainage conditions. Figure 5 (a) presents the normalized SCPT parameters measured in SCPT-21-02A and SCPT-21-02B, performed in close proximity. It also shows the soil classification index ($I_{c,BJ}$) calculated from the Been and Jefferies methods (Been and Jefferies, 1992; Jefferies and Been, 2006). Results are also compared using Robertson (2016) and Smith et al. (2021) screening charts in Figure 5 (b) and (c), respectively. Only the friction sleeve response seemed to be affected by the higher advancement rate, with SCPT-21-02B showing distinctly higher sleeve friction measurements.

Observing changes only in the measured sleeve friction due to a higher penetration rate was reported by Smith et al. (2021) and could be attributed to SCPT sleeve measurements being potentially unreliable, particularly in intermediate loose soils such as tailings (Torres-Cruz 2021). The higher sleeve friction led to slightly higher values of $I_{c,BJ}$. For the SCPTs with an adjacent borehole, the $I_{c,BJ}$ values determined using the standard rate showed a good match with the adjacent borehole description.



a)



b) c)

Figure 5: Comparison of (a) normalized CPT parameters and soil behavior type in tailings in SCPT-21-02A (2 cm/s) and SCPT-21-02B (10 cm/s), and data plotted on the (b) Robertson (2009, 2016) and Smith et al. (2021) screening charts

When comparing SCPT-21-02A carried out at the standard advancement rate of 2 cm/s to SCPT-21-02B advanced at 10 cm/s, SCPT-21-02B consistently resulted in higher liquefied ratios irrespective of the assessment method used: Sadrekarimi (2014), Robertson (2010, 2022), and Jefferies and Been (2016) using the ψ_k estimated with the Been and Jefferies (1992) method and the Plewes et al. (1992) method (Figure 6). This would be largely attributed to the higher friction sleeve measurements in SCPT-21-02B resulting in a slightly higher behavior type index (Figure 5), higher compressibility, lower ψ_k, and higher liquefied strength. The difference observed in Robertson (2022) could be attributed to the employed correction factor parameter (K_c) that is derived from the soil behavior type index which relies on friction sleeve measurements.

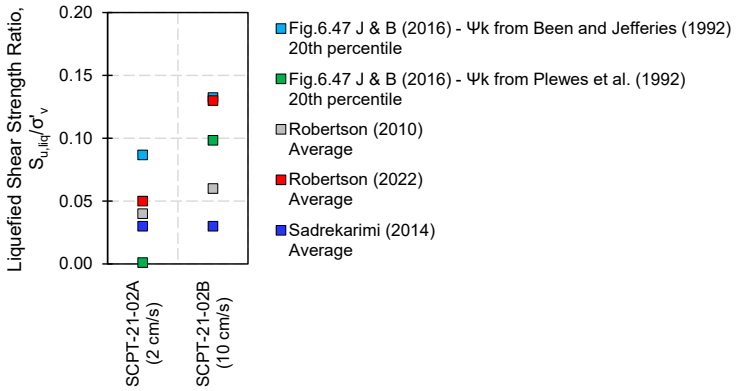


Figure 6: Liquified shear strength ratio using different methods (Jefferies and Been, 2016; Plewes et al., 1992; Robertson, 2010; Robertson, 2022, Sadrekarimi, 2014)

Summary and conclusion

A geotechnical investigation was carried out at the Selbaie TSF and included 9 geotechnical boreholes, 11 SCPTs, 9 FVT profiles, as well as index and advanced laboratory tests to obtain a better comprehension of tailings deposits characteristics.

To attempt measuring the undrained shear strength in tailings and evaluate shearing rate effects, a series of tests at varying shearing rates of 0.1 °/s, 0.8 °/s, and 7.5 °/s to 10 °/s were performed with a standard and fast vane apparatus in FVT-21-02A and FVT-21-02B. These two tests, along with SCPT- 21-02A/B, were performed in close proximity. It was observed that higher rotation rates of FVTs could satisfy undrained shearing criteria, but did not systematically lead to lower peak shear strength.

To evaluate penetration rate effects in SCPTs, SCPT-21-02A was pushed at the standard penetration rate of 2 cm/s next to a duplicate test (SCPT-21-02B) advanced at a higher penetration rate of 10 cm/s. These SCPTs sought to assess penetration rate effects on the inferred in-situ state and undrained shear strength parameters of tailings, and drainage conditions. It was observed that the rate of shearing was not

high enough to guarantee undrained shearing. However, higher penetration rates led to measurement of higher sleeve friction, and higher liquefied strength ratio estimated using screening-level methods.

In conclusion, it is recommended that penetration and/or rotation rate effects on drainage conditions, peak and post-peak shear resistance of tailings be evaluated in site investigations. These effects should be considered when selecting engineering parameters for design and/or stability analyses.

References

ASTM. 2018b. Standard test method for field vane shear test in saturated fine-grained soils. Designation ASTM D2573/D2573M-18.

ASTM. 2020a. Standard test method for electronic friction cone and piezocone penetration testing of soils. Designation ASTM D5778-20.

Ayala, J., Fourie, A.B., Reid, D. and Jefferies, M. 2024. Inferring the state parameter from partially drained cone penetration test data using the soil behaviour-type index to adjust drained/undrained correlations. In A.B. Fourie and D. Reid (eds), *Paste 2024: Proceedings of the 26th International Conference on Paste, Thickened and Filtered Tailings*, Australian Centre for Geomechanics, Perth: 335–348.

Been, K. and Jefferies, M.G. 1992. Towards systematic CPT interpretation. *Proceedings of the Wroth Memorial Symposium,* 27–29 July 1992; Oxford U.K. London U.K.: 121–134.

Blight, G.E. 1962. A note on field testing of silty soils. *Canadian Geotechnical Journal* 3: 142–149.

Boschi, K., Monforte, L., Arroyo, M., Carbonell, J.M. and Gens, A. 2023. Effects of drainage conditions on state parameter inversion from CPTu. *Proceedings of the 10th European Conference on Numerical Methods in Geotechnical Engineering (NUMGE 2023)* London.

Chandler, R.J. 1988. The in-situ measurement of the undrained shear strength of clays using the field vane. In A.F. Richards, editor. *Vane Shear Strength Testing in Soils: Field and Laboratory Studies*.

DeJong, J.T., Jaeger, R.A., Boulanger, R.W., Randolph, M.F. and Wahl, D.A.J. 2013. Variable penetration rate cone testing for characterization of intermediate soils. *Proceedings of the 4th International Site Characterization Conference:* 25–42.

Gylland, A.S., Jostad, H.P., Nordal, S. and Emdal, A. 2013. Micro-level investigation of the in-situ shear vane failure geometry in sensitive clay. *Géotechnique* 63(14): 1264–1270.

Jefferies, M. and Been, K. 2006. *Soil Liquefaction: A Critical State Approach*. First edition. London: CRC Press.

Jefferies, M. and Been., K. 2016. *Soil Liquefaction: A Critical State Approach*. Second edition. Boca Raton: CRC Press, Taylor and Francis, Boca Raton, FL, USA.

Plewes, H.D., Davies, M.P. and Jefferies, M.G. 1992. CPT based screening procedure for evaluating liquefaction susceptibility. *Proceedings of the 45th Canadian Geotechnical Conference* 4: 1–9.

Reid, D. 2016. Effect of rotation rate on shear vane results in a silty tailing. *Proceedings of Geotechnical and Geophysical Site Characterization 5.* Sydney: Australian Geomechanics Society.

Reid, D., Rodriguez, C., Fourie, A. and Tiwari, B. 2023. Partial drainage effects during vane shear tests, with an emphasis on the measurement of remoulded strengths. *Proceedings of Tailings and Mine Waste 2023*, Vancouver, Canada.

Robertson, P.K. 2010. Evaluation of flow liquefaction and liquefied strength using the cone penetration test. *Journal of Geotechnical and Geoenvironmental Engineering* 136 (6): 842–853.

Robertson, P.K. 2016. Cone penetration test (CPT)-based soil behaviour type (SBT) classification system – an update. *Canadian Geotechnical Journal* 53(12): 1910–1927.

Robertson, P.K. 2022. Evaluation of flow liquefaction and liquefied strength using the cone penetration test: An update. *Canadian Geotechnical Journal* 59: 620–624.

Sadrekarimi, A. 2014. Effect of the mode of shear on static liquefaction analysis. *Journal of Geotechnical and Geoenvironmental Engineering* 140(12).

Smith, K., Reid, D. and Fanni, R. 2021. A generalized CPTu state parameter inversion method based on the NorSand widget. *Proceedings of DAMS: Perceptions of the Realties of Risk*, 24 November to 15 December 2021; online. Australian National Committee on Large Dams.

Torres-Cruz, L.A. 2021. The Plewes method: A word of caution. *Mining, Metallurgy and Exploration* 38(3): 1329–1338.

Geotechnical Challenges of Tailings Storage Facilities in Cold Regions

Morteza Esfehani, WSP, Canada

Abstract

Cold regions experience significant fluctuations in temperature, leading to freezing and thawing cycles of exposed soils. This can cause the tailings to expand and contract, leading to structural instability and potential failure of containment structures. The repeated freezing and thawing can also disrupt the integrity of the containment systems designed to hold the tailings, increasing the risk of leaks or spills. Trapped frozen tailings can have significant effects on stability as well. When tailings are deposited in an area where freezing occurs, the water within the tailings can freeze, leading to the formation of ice lenses and ice-rich layers. These frozen components can alter the physical and mechanical properties of the tailings, impacting stability in several ways. The presence of trapped frozen tailings can have long-term implications for stability. Frozen ground tends to reduce the permeability and affect the groundwater flow patterns, which can influence the stability of earthworks structures. Frozen zones can act as barriers to groundwater movement, leading to localized saturation and increased pore pressures. Preventing the formation of trapped frozen tailings in storage facilities in cold regions requires careful planning, design, and implementation of engineering measures. If deep frozen zones are detected in a tailing facility, a thorough assessment is required to determine the extent and characteristics of the affected zones. The potential risks should be identified in order to develop and implement engineering mitigative solutions. Then, comprehensive monitoring and management plans are required to track the effectiveness of mitigation measures and respond to changing conditions. Proper characterization and management of tailings are essential to prevent or mitigate potential stability risks and ensure the long-term integrity of tailings storage facilities in cold regions. The paper addresses some of these challenges, for which tailored engineering design and management strategies are necessary.

Introduction

Managing hydraulic tailing deposition in cold weather requires a comprehensive approach that integrates design, operational practices, monitoring, environmental protection, and safety considerations. Trapped frozen tailings can significantly affect stability by altering the mechanical, thermal, and hydraulic properties

of the surrounding ground. The formation of embedded layers of frozen tailings should be avoided, especially close to tailing dams, to prevent impermeable barriers, which may cause an increase in pore water pressure during thaw, and to reduce effective stress.

By implementing site-specific strategies, mining operations can effectively manage tailings in cold regions, ensuring the stability of containment structures and minimizing environmental impact. If trapped frozen tailings happens, zones are identified in a storage facility, and proper characterization and management of frozen tailings are essential to mitigate potential stability risks. This may include implementing specialized engineering designs, monitoring systems, and maintenance protocols.

Tailings depositional rate and arrangement and water management are activities that must be handled with concern in cold weather conditions. If a facility is managed poorly in sub-zero temperatures, it may degrade tailing mechanical properties and drainage efficiency by creating embedded frozen tailings layers.

The volume increase of the soil due to freezing generally results in uplift or frost heave, and the excess of pore water developing during thaw results in a loss of strength and substantial deformations. Therefore, these soils are classified as frost susceptible and thaw weakening (Arenson et al., 2007). The classification methods developed for natural soils are often valid for evaluation of the frost susceptibility of tailings. However, the influence of added reagents should be considered (Tuomela et al., 2021).

Shear strength of frozen soils

Understanding the shear strength characteristics of frozen soils helps engineers develop more accurate models and design safer and more reliable structures. Arenson and Springman (2005) have conducted extensive research on the shear strength of frozen soils. Their work also contributes to the comprehensive understanding of seasonal freeze-thaw cycles and their impact on soil stability and infrastructure performance. Here is a summary of key findings from their research.

It was shown that frozen soil resistance is temperature-dependent since the shear strength of frozen soil increases as the temperature decreases. This is due to the strengthening of ice bonds within the soil matrix at lower temperatures.

Ice content, related to the initial water content, influences the shear strength as well. Higher ice content generally increases the shear strength of frozen soils. Ice acts as a cementing agent, binding soil particles together and enhancing overall strength. However, very high ice content can lead to a brittle failure mode, where the material may crack and fail suddenly under stress.

The shear strength of frozen soils is also influenced by the rate of loading or strain rate. Higher strain rates typically result in higher measured shear strength due to the rate-dependent behavior of the ice.

Arenson and Springman (2005) conducted triaxial compression tests on frozen soil samples to determine their shear strength under various confining pressures and temperatures. The results showed a

clear increase in shear strength with decreasing temperature and increasing confining pressure. They also performed direct shear tests to measure the shear strength along predefined planes. These tests confirmed the temperature dependence and highlighted the role of ice content and strain rate in influencing shear strength. Based on their experimental data, Arenson and Springman (2005) developed empirical correlations to predict the shear strength of frozen soils. Figure 1 shows the correlations as a function of temperature, ice content, and strain rate. It was concluded that, at low ice content, the shear resistance is developed by solid grains within a frozen matrix mobilizing frictional resistance. In other words, the shear strength depends more on normal stress as more interlocking is mobilized within the low ice content frozen soil. Cohesion is present in a granular soil only if there is sufficient ice in the voids between the particles to hold them together. Because the ice matrix is responsible for this cohesion, all factors that control the strength of pure ice, such as temperature or strain rate, influence the cohesive term for the strength of frozen soils.

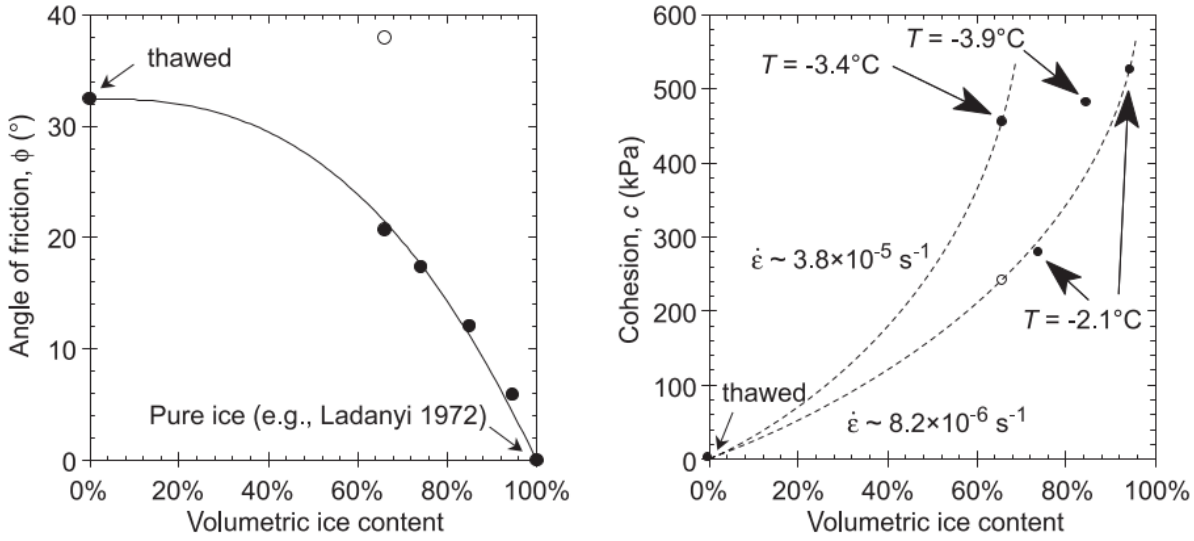


Figure 1: Shear strength parameters of frozen soils as a function of volumetric ice content and temperature (from Arenson and Springman, 2005)

Effect of freeze-thaw cycles on shear strength of tailings

Freeze–thaw cycles have a strong influence on the mechanical properties of tailings. Several researchers have investigated this subject through experimental and theoretical studies. The effects of freeze–thaw cycles on the mechanical properties and pore structure of granular tailings were investigated by Li et al. (2022). The results showed that the shear strength of the tailings decreases after freeze–thaw cycles, as shown in Figure 2. Considerable pore deformation between particles of tailings was observed after 40 freeze-thaw cycles through photointerpretation of samples.

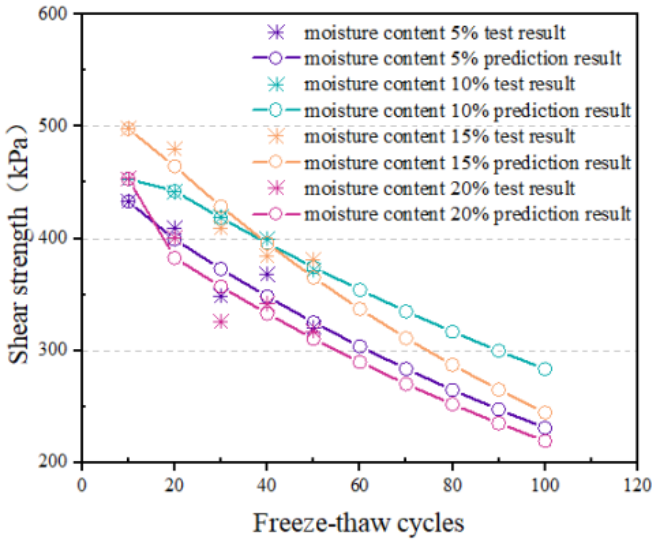


Figure 2: Peak shear strength as a function of freeze-thaw cycles (from Li et al., 2022)

Fu et al. (2021) carried out experiments to examine the role of thawing on the mechanical properties of melting glacial tills. Direct shear tests were performed on till specimens with three different dry densities and three different initial water contents after each cycle of thaw for 18 freeze-thaw cycles. Tests were carried out in undrained condition at a shear rate of about 2.4 mm/min. Figure 3 shows some of the test results. It was concluded that the cemented ice can improve the cohesive component of the shear strength of frozen soils. However, shear strength decreases considerably after the initial thawing time. The decrease is greater in soils with higher initial water content. Moreover, the shear softening decreases with increasing thawing time.

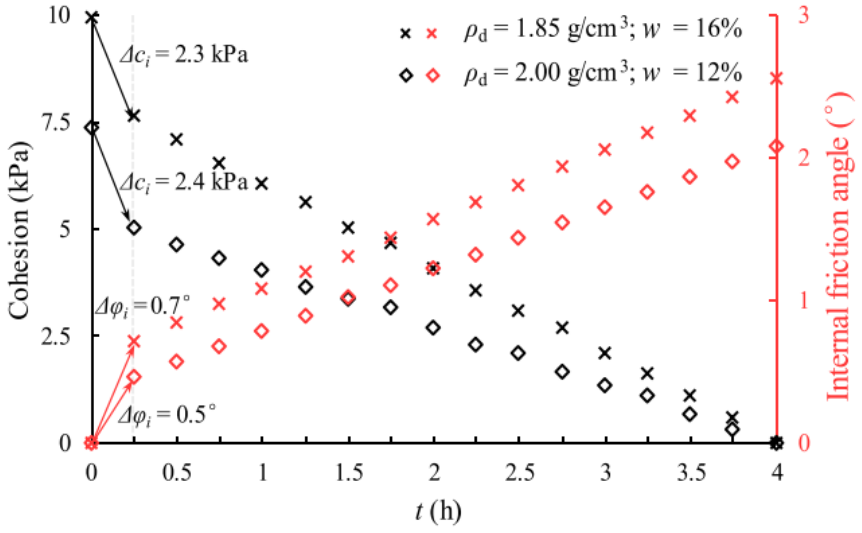


Figure 3: Test results for cohesion and internal friction angle as a function of thawing time in undrained condition (from Fu et al., 2021)

Geothermal simulation of tailing deposition rate (case study from literature)

Knutsson (2018) developed a one-dimensional geothermal model using the finite difference method. The model simulates the temperature profile in tailings where the surface elevation is increased due to deposition. The results showed that the deposition rate is the most influential factor in the generation of frozen zones. The temperature of new tailings deposited on the surface has a very small influence on the results. The type of simulations shown in Figure 4 can help to set up deposition schedules to prevent trapped frozen layers. For the case with tailings deposition, embedded layers of frozen tailings were generated with about 1.0 m of thickness. These layers remain frozen in the following seasons and are therefore regarded as permafrost. For the case with no tailing deposition (not shown here), all frozen tailings were thawed during the summer.

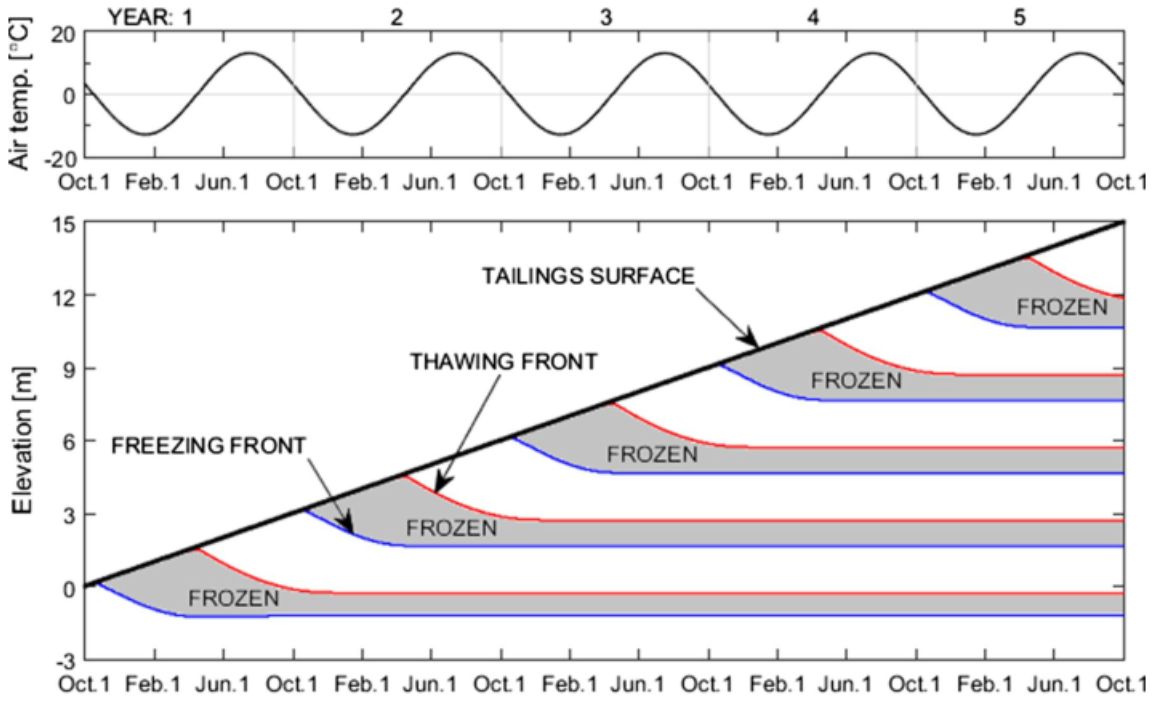


Figure 4: Freezing and thawing fronts with tailings deposition of 3 m/year (from Knutsson, 2018)

Creep deformation of frozen tailings (case-study from literature)

Limoges et al. (2022) investigated an upstream raised tailings storage facility (TSF) that showed lateral displacements indicative of a potential shearing plane. The differential lateral displacement was located at the interface with the frozen layer as shown in figure 5c. The paper discussed the design and implementation of mitigation measures, such as stability berms, to reduce the rate of lateral movement. The study identified two potential mechanisms that could impact the stability of the tailing storage facility: thaw-consolidation

and on-going creep deformation of the frozen layer. An initial strain rate of about 2% per month was recorded prior to any mitigation measures. The recorded strain rate became around 0.2% per month one year after the construction of a stability berm.

Figure 5b shows the profile of thermistor data as a function of elevation, confirming the presence of a frozen layer at a TSF. Figure 5a shows the water content profile at the same location. Interestingly, the identified frozen layer exhibits the highest water content. Figure 5c shows the recorded lateral displacement from inclinometers installed in the same sector. The highest lateral displacements were recorded at the interface of the identified frozen layer, where the highest water contents and lowest temperatures were registered.

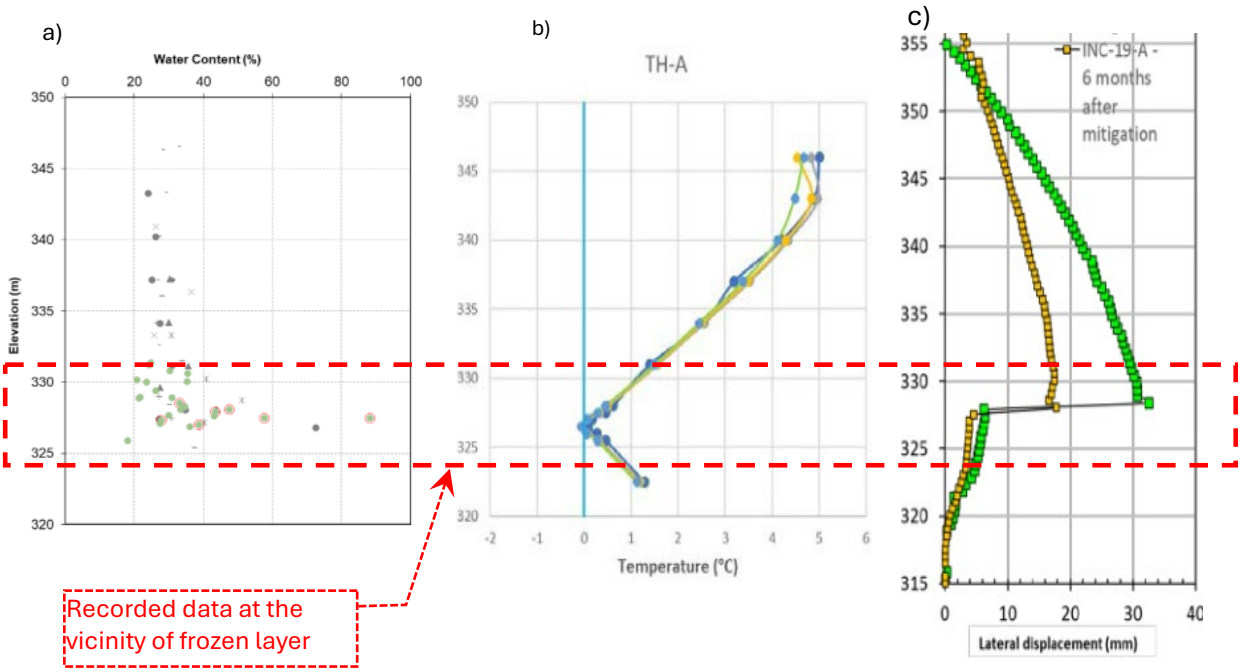


Figure 5: Recorded data in the vicinity of a frozen layer: a) water content; b) temperature profile; c) inclinometer data profile (from Limoges et al., 2022)

Prevention of trapped frozen tailings in the storage facility

Preventing the formation of trapped frozen tailings in storage facilities in cold regions requires careful planning, design, and implementation of engineering measures. Test results from Knutsson (2018) showed that the thickness of permafrost layers increases with an increased deposition rate and with increased water content. It was also shown that wet tailings must be deposited in short periods during summer to avoid permafrost generation. These precautions can help mining operations to set up deposition schedules. Thermodynamic models can identify periods of the year when tailings can be deposited in critical areas of

a deposit in order to avoid permafrost formation. They can also identify the required quantity of tailings deposition to achieve this aim.

Early site investigations, including geological and hydrological assessments, should be carried out to identify areas with a lower risk of freezing. Insulation layers beneath and around the storage facility can minimize heat transfer between the tailings and the underlying ground. Effective drainage systems within the storage facility are required to control groundwater flow and prevent water accumulation. Proper drainage helps minimize the presence of free water, which can contribute to freezing. Comprehensive monitoring programs are required to assess the effectiveness of preventive measures and detect potential issues early. Parameters such as temperature, moisture content, groundwater levels, and ground settlement should be monitored to identify signs of freezing and inform adaptive management strategies.

Mitigative actions when deep frozen zones are detected

If deep frozen zones are detected in a tailing facility, it is crucial to take prompt and effective action to mitigate potential risks and ensure the long-term integrity of the facility. Here are steps to consider:

- Assessment and monitoring: conduct a thorough assessment to determine the extent and characteristics of the frozen zones. This may involve geophysical surveys and thermal monitoring.
- Risk analysis: evaluate the potential risks associated with the presence of frozen zones, including impacts on stability, hydraulic conductivity, and environmental performance.
- Engineering solutions: develop and implement engineering solutions to mitigate the risks posed by deep frozen zones. Depending on the specific circumstances, potential solutions may include:
    - Active heating: implement heat tracing systems or other active heating methods to thaw frozen zones and prevent the formation of further ice lenses and ice-rich layers.
    - Drainage improvements: enhance drainage systems within the facility to control groundwater flow and reduce the accumulation of free water, which can contribute to further ice build.
    - Structural reinforcement: strengthen containment structures, such as dams and embankments, to withstand the additional loads and stresses imposed by frozen ground conditions.
- Adaptive management: develop a comprehensive monitoring and management plan to track the effectiveness of mitigation measures and respond to changing conditions. Implement regular monitoring of temperature profiles, moisture content, ground settlement, and other relevant parameters to detect signs of freezing and evaluate the performance of remedial actions.

- Stakeholder engagement: engage with relevant stakeholders to communicate transparently about the presence of frozen zones and the planned remediation efforts.
- Emergency Response Plan: develop an emergency response plan outlining procedures and protocols for responding to unforeseen events or emergencies related to frozen zone issues. Identify key personnel, resources, and communication channels needed to coordinate emergency response efforts to minimize potential impacts on human health, safety, and the environment.

Management of tailings hydraulic deposition in cold weather

Managing hydraulic tailing deposition in cold weather requires special considerations to ensure operational efficiency, environmental protection, and structural stability. Knutsson (2018) carried out extensive research work on the current practice in tailings management in cold regions. The following paragraphs provide some strategies and practices to effectively manage hydraulic tailing deposition in such conditions.

Risk assessment

The freezing risk can be quantified by using probabilistic methods at the design stage. The failure likelihood consequences as well as potential preventive and mitigative measures should be evaluated. To inform the design process, historical climate data should be collected for the project site, including temperature variations, freeze-thaw cycles, and seasonal trends. Hydrogeological analyses are required to evaluate groundwater flow patterns and potential seepage paths. The freezing risk increases when water infiltrates tailings and subsequently freezes.

Design considerations

At the design stage, the tailing facility should be placed in a site with minimal exposure to severe cold. Strategies should be adopted to control the ground heat loss by insulation to prevent freeze-thaw cycles. Geotechnical properties of the tailing facility components should be investigated. The physical and mechanical properties of tailings, including their thermal conductivity, moisture content, and grain size distribution govern freezing behavior. The containment structures should be designed to withstand freezing and thawing cycles, incorporating materials that retain structural integrity. Numerical models are recommended to simulate heat transfer within the tailings. These models allow for the estimation of the effect of factors like insulation, cover materials, and heat loss. Effective drainage systems should be implemented to manage water flow and prevent the accumulation of water prone to surface ice build.

Operational practices

Tailings deposition management plans should include the control of the deposition rate and layering of tailings to prevent the formation of ice lenses and frozen zones. The use of thickened tailings deposition is

recommended in the construction of containment structures to reduce water content, minimizing the risk of freezing. Active heating systems, such as heat tracing cables or thermal blankets, may be considered to maintain temperatures above freezing in critical areas. Thermal insulation to cover containment structures is another method of thermal control. The water management plan should include efficient protection of supernatant water from freezing by using heating systems or by removing it promptly.

Monitoring and maintenance

Temperature sensors should be installed throughout the tailings facility to monitor and manage thermal conditions. Remote sensing technology for real-time data collection and monitoring is recommended. Regular inspections should be conducted to identify and address any signs of freezing, thawing, or structural instability. A maintenance schedule should be implemented to ensure the functionality of drainage systems, heating systems, and other infrastructure. Strategies should be developed to properly manage any potential ice formation by mechanical removal or controlled melting. The ice removal operation should not cause any damage to containment structures or disrupt the integrity of the tailings.

Adaptation of best practices

Continuously adapt and improve practices based on the latest research and technological advancements in cold region engineering. Study successful case studies of tailings management in similar climatic conditions to apply proven strategies.

Case of paste or filtered tailing deposition

As mentioned by Neuffer (2015), filtered tailings can offer specific opportunities for cold regions tailings management relative to other approaches, including increased tolerance for differential thaw settlement associated with a degrading permafrost foundation, increased physical and chemical stability from permafrost within the stack, and reduced difficulties with water management in the winter. If exposed to sub-zero conditions, filtered tailings can freeze before being compacted. If frozen, tailings may not reach the target compaction despite the compaction effort. Filtered tailings should be kept from freezing during stockpiling and transit, and must be dumped and spread within minutes to hours. Once the lift is compacted to specification, the design may allow it to freeze (McKenna, 2023).

Beneficial case of frozen tailing barriers

The preservation of frozen tailing layers is important if oxidation of acid-generating tailings is to be minimized. As in the case study by Steffens et al. (1995), the ice and frozen tailing layers are a hydraulic barrier that controls the groundwater seepage and tends to minimize the oxidation of pyritic tailings.

Favorable perma-frost conditions were maintained to control conductive and convective heat flux. The frozen layer was preserved to ensure cold penetration during wintertime, and insulation during summer.

Conclusion

Implementing preventive measures and adopting a proactive approach to tailings management minimize the formation of trapped frozen tailings in storage facilities in cold regions. Trapped frozen tailings can have significant effects on stability. When tailings are deposited in an area with permafrost or where freezing occurs, the water within the tailings can freeze, leading to the formation of ice lenses and ice-rich layers. It can alter the physical properties of the tailings and the surrounding ground, impacting stability in several ways. Frozen ground tends to be stiffer and less permeable than unfrozen ground, which can affect the distribution of stresses and groundwater flow patterns. This can influence the stability of slopes, embankments, and other earthworks structures.

Trapped frozen tailings can disrupt the natural thermal regime of the ground, making it prone to thawing and subsidence issues. The presence of frozen tailings can also insulate the underlying permafrost, preventing it from thawing during warmer periods, which can result in differential thaw settlement.

The formation of ice lenses and ice-rich layers can act as barriers to groundwater movement, leading to localized saturation and increased pore pressures. This can weaken the stability of slopes and embankments and increase the risk of slope failure.

By taking a proactive approach to addressing deep frozen zones in tailings facilities, it is possible to mitigate risks and ensure responsible and sustainable tailings management practices. Regular reviews and updates to practices based on new research and technological advancements will enhance the management of tailing facilities in challenging cold weather conditions.

References

Arenson, L.U. and Springman, S.M. 2005. Mathematical descriptions for the behaviour of ice-rich frozen soils at temperatures close to 0°C. *Can. Geotech. J.* 42: 431–442 (2005). doi: 10.1139/T04-109

Arenson, L.U., Springman, S.M and Sego, D.C. 2007. The rheology of frozen soils. *Applied Rheology* 17(1): 12147-1 – 12147-14.

Chovan, K.M., Julien, M.R., Ingabire, É.-P., Masengo, E., Lépine, T., James, M. and Lavoie, P. 2021. Risk assessment for tailings management. *CIM Journal* 12(1): 9–24. DOI: 10.1080/19236026.2020.1866336

Fu, Y., Jiang, Y., Wang, J., Liu, Z. and Lu, X. 2021. Mechanical properties of frozen glacial tills due to short periods of thawing. *Front. Earth Sci.* 9: 799467. doi:10.3389/feart.2021.799467

Knutsson, R. 2018c. On the behaviour of tailings dams – Management in cold regions. Doctoral thesis. Printed by Luleå University of Technology, Graphic Production, 2018. ISBN 978-91-7790-030-6.

Knutsson, R., Tuomela, A., Rauhala, A., Knutsson, S. and Laue, J. 2021. Geothermal study of a tailings deposit: frost line modelling and comparison to field data. *Journal of Earth Sciences and Geotechnical Engineering*. 11(3) 15–32. https://urn.fi/URN:NBN:fi-fe202103298701

Knutsson, R., Viklander, P., Knutsson, S. and Laue, J. 2018a. Geothermal study to explain man-made permafrost in tailings with raised surface. *Environmental Earth Sciences* 77: 288. https://doi.org/10.1007/s12665-018-7465-8

Knutsson, R., Viklander, P., Knutsson, S. and Laue, J. 2018b. How to avoid permafrost while depositing tailings in cold climate. *Cold Regions Science and Technology* 153. DOI:10.1016/j.coldregions.2018.05.009

Lessard, F., Bussière, B., Côté, J., Benzaazoua, M., Boulanger-Martel, V. and Marcoux, L. 2018. Integrated environmental management of pyrrhotite tailings at Raglan Mine: Part 2 desulphurized tailings as cover material. *J. Clean. Prod.* 186: 883–893.

Li, C., Jin J., Wu P., Xu B. 2022. Effect of freeze-thaw cycles on shear strength of tailings and prediction by grey model. *Minerals* 12 : 1125. https://doi.org/10.3390/min12091125

Limoges-Shaigetz, M., Brenner, M., Becker, D., Krezewinski, T. and Masengo, E. 2022. Case study: impact of a frozen tailing layer in the design of a tailings storage facility. *Proceedings of Tailings and Mine Waste 2022,* Denver, Colorado, USA, November 2022.

McKenna, G. 2023. How to compact filtered tailings. in G.W. Wilson, N.A. Beier, D.C. Sego, A.B. Fourie and D. Reid (eds), *Paste 2023: Proceedings of the 25th International Conference on Paste, Thickened and Filtered Tailings,* University of Alberta, Edmonton, and Australian Centre for Geomechanics, Perth, pp. 440-454, https://doi.org/10.36487/ACG_repo/2355_33

Neuffer, D. 2015. Dry stack tailings in cold regions: Opportunities and constraints. *AMA 2015.*

Steffens, S.D., Lewis-Russ, A., Jones, J. and Rech, W. 1995. The effects of permafrost on the geochemistry and hydrology of a metal-sulfide tailing impoundment 20 years later. *Proceedings of the America Society of Mining and Reclamation:* 547–559. DOI: 10.21000/JASMR95010547.

Tuomela, A., Pekkala, V., Rauhala, A., Torabi Haghighi, A. and Leviäkangas, P. 2021. Frost susceptibility of Nordic metal mine tailings. *Cold Regions Science and Technology* 192: 103394, ISSN 0165-232X. https://doi.org/10.1016/j.coldregions.2021.103394.

Assessment of Flow Liquefaction Susceptibility of a Tailings Dry Stack Pile Using the State Parameter and Yield Stress Ratio Approach

Marcus Vinícius Lima Dias, Vale S.A., Brazil
Dieggo Santos, Vale S.A., Brazil
Mariela Silva, Vale S.A., Brazil
Gustavo Marçal de Sousa, Vale S.A., Brazil
Marília Freire, Vale S.A., Brazil

Abstract

Flow liquefaction is a behavior observed in saturated or nearly saturated geomaterials that show a strain softening response during undrained shear, mostly observed in very loose sands and silts as well as very sensitive clays. The Cone Penetration Test with pore-pressure measurements (CPTu) has been gaining in popularity among the geotechnical community to evaluate the state of a soil profile, due to its good repeatability, detailed information of the soil stratigraphy, and extensive detailed scientific studies to guide the application of the test results. Susceptibility to flow liquefaction is typically evaluated by estimating the in-situ state parameter (ψ), since it directly correlates to the soil behaviour at large strain, as shown by Jefferies and Been (2016). Mayne and Sharp (2019) suggested the use of the yield-stress-ratio (YSR = σp'/σv0') to estimate the soil state using a threshold of YSR ≈ 3.

This paper presents an evaluation of the susceptibility to flow liquefaction of a tailings dry stack pile using the following recently published approaches: i) Mayne and Sharp (2019), using the yield stress ratio (YSR) approach; ii) Smith et al. (2021), using a generalized CPTu state parameter inversion method based on the NorSand Widget; and iii) Robertson (2021), with the updated Kc. The results obtained from the evaluation of the susceptibility to flow liquefaction indicated a good convergence between the three methodologies in the region from filtered tailings and divergence in the region from excavated tailings from a reservoir of a TSF, using the Mayne and Sharp methodology.

Introduction

Recent tailings dam failures in Brazil, such as B-I Dam (2019) and Fundão Dam (2015), highlighted the importance of evaluating susceptibility to flow liquefaction, especially for structures constructed with sand-

like materials. Many field and laboratory procedures can be used to evaluate flow liquefaction susceptibility, such as: i) grain-size distribution curves; ii) Atterberg Limits; iii) CPTu tests; iv) the Vane Shear Test; and v) the Triaxial Compression Test. Due to its good repeatability and the detailed information it yields about the soil stratigraphy, the objective of this paper is to use the Seismic Cone Penetration (SCPTu) test to assess the susceptibility to flow liquefaction of a stacking of filtered iron ore tailings. Additionally, this paper aims to show the characterization of the two types of tailings deposited in the pile.

In the mining industry there are many studies to assess flow liquefaction using methodologies proposed by Plewes et al. (1992), Olson (2001), Shuttle and Cunning (2008), and Robertson (2016). In this context, this paper presents an evaluation of the susceptibility of a stacking dry tailings to flow liquefaction using the following recently published approaches: i) Mayne and Sharp (2019), using the yield stress ratio (YSR) approach; ii) Smith et al. (2021), using a generalized CPTu state parameter inversion method based on the NorSand Widget; and iii) Robertson (2021), with the updated Kc to evaluate the in-situ state parameter. It is noteworthy that these methodologies are initial screening tools to evaluate the phenomenon, and they alone are not enough to determine whether the tailings present strain-softening and brittle behavior in undrained shear.

Methodologies – susceptibility to flow liquefaction

State parameter definition

A possible reference to be used to define the state of sandy materials is the distance between the current void ratio of the material (*e)* and the critical state void ratio (Been and Jefferies, 1985). Therefore, this distance, or state path, indicates a direct representation of the tendency for volumetric variation of the soil under shear, which defines the state parameter (ψ), according to Equation 1.

$$\psi = e - e_c \qquad \text{(Equation 1)}$$

Been and Jefferies (1985) stated that the use of the state parameter to evaluate the material behavior is fundamental, since the evaluation of the expected behavior based on parameters such as void ratio and relative density does not provide the necessary rigor. Jefferies and Been (2016) showed that samples at the same relative density showed widely different stress paths because of changed stress levels. In contrast, samples at the same ψ but different densities and stress levels showed similar behaviour. Experimental studies performed by Jefferies and Been (2016) suggested that materials with $\psi > -0.05$ indicate contractive behavior (state looser than the critical state), whereas $\psi < -0.05$ indicate ductile behavior (state denser than the critical state).

Mayne and Sharp (2019)

Mayne et al. (2023) show that the preconsolidation stress can be presented in dimensionless terms using a normalized form called the overconsolidation ratio (OCR), or equivalent yield stress ratio (YSR), which is defined by Equation 2. According to the authors, the term YSR is becoming more prevalent because the traditional OCR is associated with mechanical unloading effects, while other geologic and environmental changes can also cause an apparent preconsolidation (i.e., desiccation, compaction, cyclic loading, repeated wetting-drying and other effects).

$$OCR = \frac{\sigma'_p}{\sigma'_{v0}} = YSR \quad \text{(Equation 2)}$$

In this context, Mayne at al. (2009) propose that the yield stress (σ'_p) of soils can be evaluated from cone net resistance (q_{net}), whereas Mayne (2017) indicates that the exponent m' is a function of CPT material index (I_c), according to Equation 3 and Equation 4, respectively.

$$\sigma'_p = 0.33(q_{net})^{m'}\left(\frac{\sigma_{atm}}{100}\right)^{1-m'} \quad \text{(Equation 3)}$$

$$m' = 1 - \frac{0.28}{1+\left(\frac{I_c}{2.65}\right)^{25}} \quad \text{(Equation 4)}$$

Where σ_{atm} is the atmospheric pressure ($\sigma_{atm} = 100\ kPa$).

As the threshold defined by the state parameter (ψ = -0.05) delimits the contractive-dilative behaviour (Jefferies and Been, 2016), alternatively, a critical threshold is defined in terms of yield stress ratio. Mayne (2017) explains that the YSR_{CSL} becomes the boundary separating contractive and dilative soil behavior, according to Equation 5 and Equation 6.

$$YSR_{CSL} = \left(\frac{2}{\cos\phi'}\right)^{\frac{1}{\Lambda}} \quad \text{(Equation 5)}$$

$$\Lambda = 1 - \frac{k}{\lambda} = 1 - \frac{C_s}{C_c} \quad \text{(Equation 6)}$$

Where ϕ' is the critical friction angle, k is the slope of the recompression/expansion line, and λ is the slope of CSL on $e - p'$ plane. Given the absence of oedometer tests for the present paper, λ_{10} was defined according to Plewes et al. (1992) and the condition $\lambda = \frac{\lambda_{10}}{2.303}$ was used. Additionally, the correlation $k = 0.1\lambda$ was assumed.

Considering the purposes of calculating the yield stress ratio at the critical state, Equation 7 and Equation 8 can be recommended for the effective friction angle (Mayne, 2007).

When $I_c < 2.6$:

$$\phi' = 17.6° + 11.0°\log(Q_{tn}) \quad \text{(Equation 7)}$$

When $I_c > 2.6$:

$$\phi' = 29.5°B_q{}^{0.121}\left[0.256 + 0.336B_q + \log(Q_{tn})\right] \quad \text{(Equation 8)}$$

Where Q_{tn} is the normalized tip resistance.

Mayne and Sharp (2019) indicated that considering a range of friction angles of sands between $30° \leq \phi' \leq 45°$ and a representative value $\Lambda = 0.8$, the corresponding range of YSR_{CSL} is $2 < YSR_{CSL} < 4$, with a typical value of $YSR_{CSL} \approx 3$.

Smith et al. (2021)

Smith et al. (2021) presented a generalized method to estimate ψ from either drained or undrained CPTu tests, based upon CPTu calibrations modeled using the Widget for a wide range of NorSand calibrated soils presented in the literature.

Using Critical State Soil Mechanics (CSSM) as a theoretical foundation, the NorSand model was developed during the 1980s and 1990s, based on experience with the construction of structures on loose sands. The analysis of the occurrence of static liquefaction during the construction of these structures contributed to the development of the model, initially proposed by Jefferies (1993) and later by Jefferies and Been (2016).

Therefore, as the names suggest, the intent of the model is to describe the behavior of loose and dense sands, in both drained and undrained conditions. The NorSand model was the first model to consider the state parameter based on the CCSM approach.

Considering the NorSand model and the cavity expansion modeling, Smith et al. (2021) proposed the correction of the k' and m' values proposed by Plewes et al. (1992).

Adopting the CPTu inversion parameter framework, Smith et al. (2021) indicated that some screening level methods suffer from stress level bias, which can result in overestimation of ψ with increasing depth. According to the authors, such bias can be removed through normalization by the elastic soil rigidity index $I_{r,e}$, as well as the use of drainage condition-specific functions, as indicated by Equation 9 to Equation 16.

Drained penetration:

$$\frac{k'}{M_{tc}} = a + b\ ln(\frac{1}{\lambda_{10}}) \quad \text{(Equation 9)}$$

$$a = 13.58 - 0.52\ln(I_{r,e}) \quad \text{(Equation 10)}$$

$$b = 0.87\ln(I_{r,e}) - 0.19 \quad \text{(Equation 11)}$$

$$m' = 3.83(\lambda_{10})^{-0.31} \quad \text{(Equation 12)}$$

Undrained penetration:

$$\frac{k'}{M_{tc}} = c + \frac{d}{\lambda_{10}} \quad \text{(Equation 13)}$$

$$c = 7.36 - 4.61G_0 \quad \text{(Equation 14)}$$

$$d = 0.06 + 0.02G_0 \quad \text{(Equation 15)}$$

$$m' = \frac{\ln(10)}{\lambda_{10}} \quad \text{(Equation 16)}$$

Where for the present paper M_{tc} was assumed as the mean value of 1.45 as indicated by Jefferies and Been (2016), given the absence of tests to define the CSL.

It is noteworthy that the proposed method does not provide inversion equations for partially drained CPTu. Based on this, Smith et al. (2021) suggest the use of drained inversion equations if $|B_q| < 0.02$ and $|\Delta u| < 20$ kPa. For the undrained inversion equations, it is important to consider the dissipation test $t_{50} >$ 60 s; otherwise, the use of an alternative screening level method (e.g. Plewes et al., 1992) is indicated. Additionally, the method is not applicable to soils with atypical soil fabric or bonding.

In terms of recorded CPTu data, the proposed method relies upon the accuracy of the $F_r - \lambda$ correlation proposed by Plewes et al. (1992), and therefore also relies upon accurate measurement of f_s. McConnell and Wassenaar (2022) indicate that the F_r values can be affected by the precision of the CPTu to measure the sleeve friction in very soft geomaterials, which require special attention of data obtained from hydraulically disposed tailings.

Robertson (2021)

To estimate ψ from CPTu tests, different methods are available. In sand-like soils, with $I_c < 2.6$, Robertson (2010) suggested that the normalized cone resistance (Q_{tn}) can be associated with the state parameter using a clean sand equivalent normalized cone resistance ($Q_{tn,cs}$), according to Equation 17.

$$Q_{tn,cs} = Q_{tn}K_c \quad \text{(Equation 17)}$$

Where K_c is a correction factor to account for changing behavior with increasing fines content. In this context, Roberston (2010) suggested a link between $Q_{tn,cs}$ and ψ for sand-like soils, as indicated by Equation 18.

$$\psi = 0.56 - 0.133\, log\,(Q_{tn,cs}) \quad \text{(Equation 18)}$$

To account for partial drainage, Robertson (2021) indicated an update in the equation to calculate K_c suggested by Robertson and Wride (1998), as shown in a simplified version by Equation 19 for $I_c \leq 3.0$.

$$K_c \approx 15 - \frac{14}{1+\left(\frac{I_c}{2.95}\right)^{11}} \quad \text{(Equation 19)}$$

Finally, Robertson (2021) indicates that the modified K_c relationship should not be extended beyond $I_c = 3.0$, where undrained penetration occurs.

Tailings characterization

Geotechnical characterization

The geotechnical characterization of the iron ore tailings was conducted by examining: i) the grain size distribution curve, ii) the water content, iii) the specific gravity of soils solids (G_s), iv) the liquid limit (LL), and v) the plastic limit (PL). The location of the samples collected to perform the tests and the SCPTu analyzed are indicated in Figure 1.



Figure 1: Location of the SCPTU and samples collected in the tailings dry stack pile

Considering the disposal methods and the origin of the stacking, it can be concluded that there are two types of tailings: i) filtered tailings between the depths of 0.00 m to 8.00 m; and ii) excavated tailings from a reservoir of a TSF and air-dried between the depths of 8.00 m to 25.25 m. Two samples (AM-201 and AM-105) were collected in each of the tailing's disposed in the pile.

The grain size distribution curves (ASTM D422-63) obtained from disturbed samples collected near the SCPTu are summarized in Table 1.

Table 1: Grain size distribution curves from disturbed samples

Filtered Tailings (0.00 – 8.00 m)	Excavation Tailings from TSF (8.00 – 25.25 m)
Clay: 0%	Clay: 15%
Silt: 61%	Silt: 75%
Sand: 39%	Sand: 10%
Classification ASTM D422: Sandy Silt	Classification ASTM D422: Clayey Silt

The Atterberg Limits were also evaluated, according to ABNT NBR 6459 and ABNT NBR 7180. Both samples collected in the two types of tailings were non-plastic.

According to ABNT NBR 6457, the filtered tailings has a natural moisture content of 12.3%, while the excavated tailings from a TSF natural moisture content of 13,5%. Additionally, the average of the specific gravity of soil solids (G_s) is 3.2. Using the grain size distribution curves and the Atterberg Limits the samples were classified according to the Unified Soil Classification System (USCS – ASTM D2487). The sample of filtered tailings was classified as silt with sand (Group Symbol ML) and the sample of excavated tailings was classified as silt (Group Symbol ML).

ICOLD Bulletin 181 (ICOLD, 2021) presents a system for classifying tailings into five broad categories based on grain size distribution curve and the Atterberg Limits. Using this system, the samples of filtered tailings were classified as Hard Rock Tailings (HRT), and the samples of excavated tailings were classified as Altered Rock Tailings (ART).

Evaluation of sCPTu test

An SCPTu was performed in the iron ore tailings with a total depth of 25.25 m. Figure 2 shows the normalized parameters. Based on this, it was possible to define two regions in depth in the filtered tailings (0.00 m – 4.00 m) and (4.00 m – 8.00 m), with clear patterns of Q_t and F_r variation. It was possible to note a uniform behavior of the normalized parameters from excavated tailings. In relationship to B_q, the result showed that the material does not generate considerable porewater pressure excess. A predominant drained behavior during cone penetration was observed, since the values did not reach the interval of 0.30 to 0.50 as suggested by Schnaid (2009) for undrained behavior.

Based on the soil behavior type indexes used and on the grain size distribution of the tailings, two different regions were identified (Figure 3). Region I (0.0 – 8.0 m) is composed predominantly of sand-like tailings, with IB > 32 and Ic(R&W) < 2.60; in this region the filtered tailings were deposited. Region II (8.0 – 25.25 m) was composed predominantly of transitional behavior, with 22< IB <32 and 2.05< Ic(R&W) <

2.60, with the presence of layers of Ic(R&W) > 2.60, in this region the tailings excavated from a reservoir of a TSF were deposited.

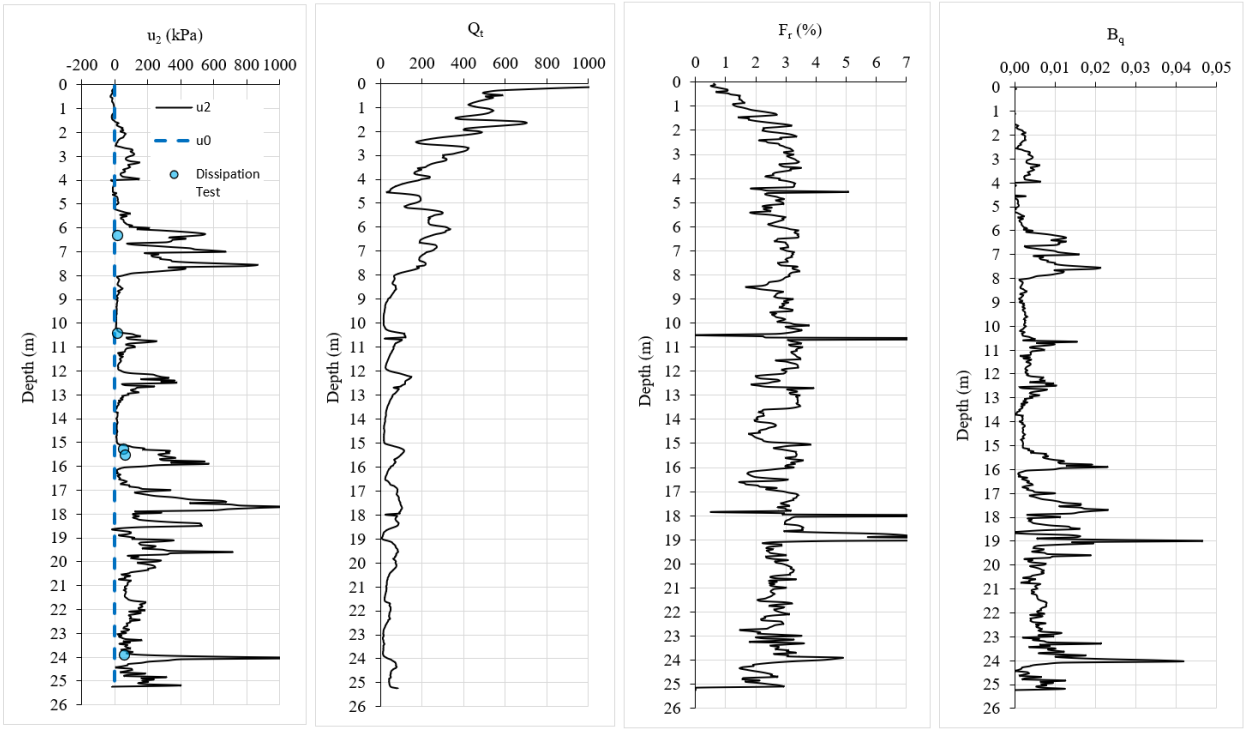


Figure 2: Results of normalized SCPTu parameters

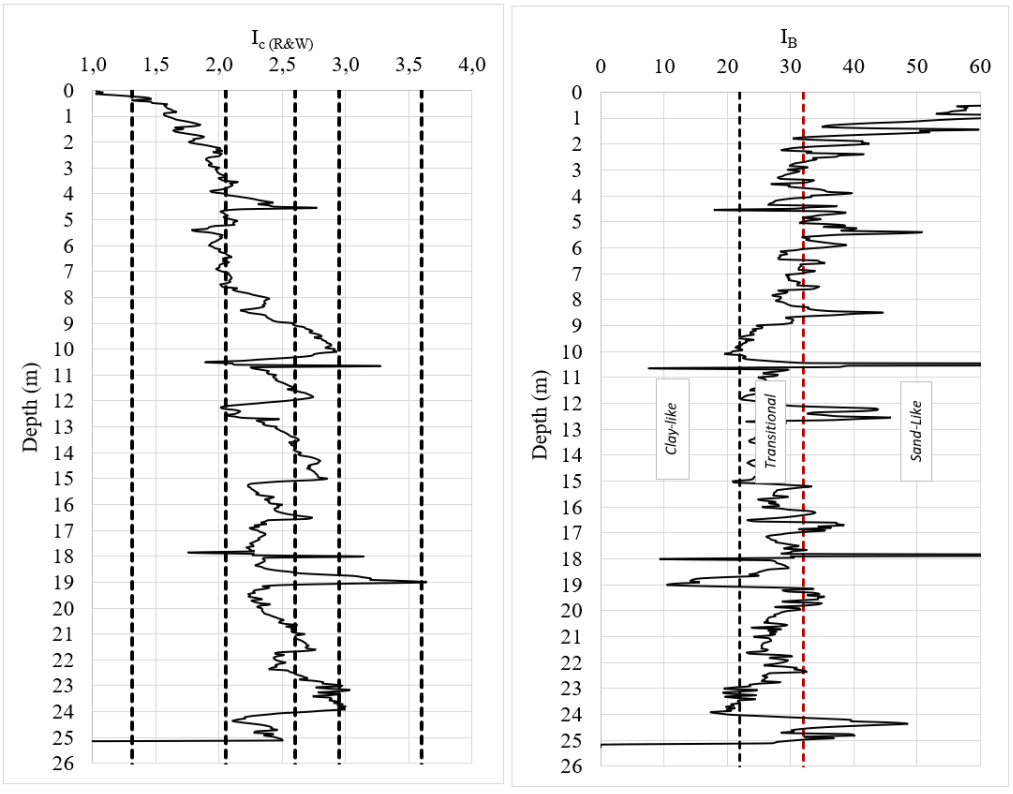


Figure 3: Soil behavior type suggested by Robertson and Wride (1998), modified soil behavior type index (I_B) suggested by Robertson (2016)

Table 2 shows the results of the five dissipation tests (DPP) performed in depth. As can be seen, all tests resulted in a $t_{50} < 45$ s, which indicates a drained penetration condition, since the values did not reach the interval of $t_{50} > 60$ s as suggested by DeJong and Randolph (2012) for undrained behavior.

Table 2: t_{50} in the dissipation tests performed in depth

Dissipation Depth (m)	t_{50} (s)
6.35	35
10.45	30
15.30	35
15.55	45
23.95	10

Microstructure

The evaluation of the microstructure in the iron ore tailings was performed using the shear wave velocity from the SCPTu. Almost all depths were tested, using the methodology suggested by Robertson (2016).

As shown in Figure 4, the results showed that the tailings classify as an ideal material (no microstructure) for most of the evaluations, with seven elevations in the structure region.

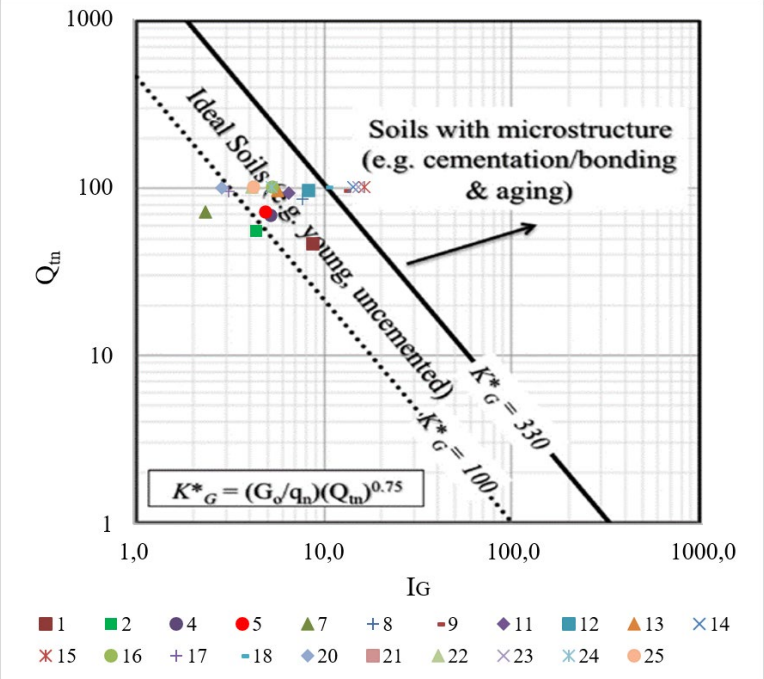


Figure 4: Microstructure evaluation (Robertson, 2016)

Results – susceptibility to flow liquefaction

The evaluation of the susceptibility to flow liquefaction of the tailings using the screening level methods of Mayne and Sharp (2019), Smith et al. (2021) and Robertson (2021) are shown in Figure 5.

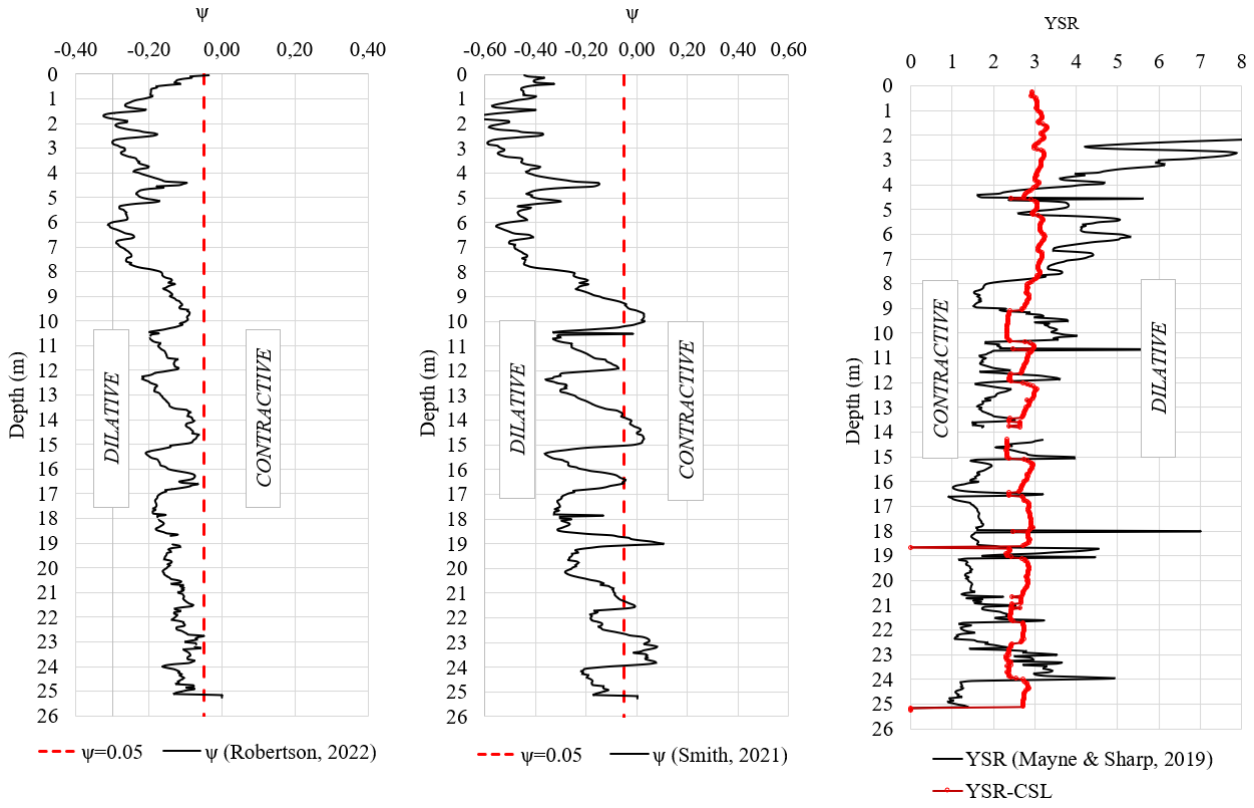


Figure 5: Evaluation of flow susceptibility based on (a) Robertson (2021), (b) Smith (2021) and (c) Mayne and Sharp (2019)

The drained inversion equations of Smith et al. (2021) were applied, because all the regions along the borehole resulted at $|B_q| < 0.02$ and $t_{50} < 60$.

Analyzing Figure 5 and considering the three methodologies, Region I (0.00 – 8.00 m) presented dilative behavior in the filtered tailings. This behavior indicates that the tailings deposited in this region were highly compacted and stacked at the optimum moisture content, according to the design. Also, we can observe a very small layer of contractive behavior at a depth of 4.00 m depth using the Mayne and Sharp method. At depth, Region II (8.00 – 25.25 m) presented a predominantly dilative behavior according to the Robertson (2021) and Smith (2021) methodologies. Also, we observed some small layers of contractive behavior at depths of 9.00 m, 14.00 m, 19.00 m and 23.00 m, using the Smith (2021) methodology. However, the yield stress ratio (YSR) used for the Mayne and Sharp method (2019) showed predominantly contractive behavior in this material, with YSR < 3.

Considering the three methods evaluated, there is a good convergence of tailings behavior in the methods that considered the evaluation of state parameter, Robertson (2021) and Smith (2021), with the dilative behavior along the borehole. For the methodology that considers the evaluation of YSR, Mayne and Sharp (2019), it is possible to confirm the contractive behavior of the excavated tailings from a reservoir of a TSF between 8.00 and 25.25 m, diverging from the other two methodologies.

Conclusion

This paper presented a case study of the susceptibility of IOTs to flow liquefaction using the screening level methods of i) Mayne and Sharp; (2019), ii) Smith et al. (2021); and iii) Robertson (2021).

The geotechnical characterization of the IOTs was conducted by performing: i) the grain size distribution curve, ii) the water content, iii) the specific gravity of soils solids (G_s), iv) the liquid limit (LL), and v) the plastic limit (PL). The classification of the tailings using the Unified Soil Classification System (ASTM D2487) showed that the IOTs are predominantly classified as silt (group symbol ML) with no plasticity.

A SCPTu with five dissipation tests was performed inside stacked dry tailings to evaluate the susceptibility of the tailings to flow liquefaction. Based on the behavioral characteristics, and on the geotechnical characterization and on the origin of tailings, two distinct regions were identified in depth. A predominant drained behavior during cone penetration was observed, and the results from the shear wave velocity indicated that in general the tailings classify as an ideal material (no microstructure).

The results obtained from the evaluation of the susceptibility to flow liquefaction indicated a good convergence between the three methodologies used in Region I between 0.00 and 8.00 m. In this region the filtered tailings presented a predominantly dilative behavior. With the methodology that evaluates the YSR (Mayne and Sharp, 2019), it is possible to confirm the contractive behavior of the excavated tailings from a reservoir of a TSF (Region II) between 8.00 a 25.25 m, diverging from Robertson (2021) and Smith (2021) methodologies in this region, that indicates dilative behavior. This behavior can be related to the compaction thickness realized in the Region II and air-drying process of this material.

It is noted that the methodologies used in this paper are initial screening tools to evaluate the susceptibility to flow liquefaction, and that they alone are insufficient to determine whether the tailings under evaluation present strain-softening and brittle behavior in undrained shear.

References

Mayne, P.W., and J. Sharp. 2019. CPT Approach to Evaluating Flow Liquefaction Using Yield Stress Ratio. *Proceedings of Tailings and Mine Waste 2019,* Vancouver, Canada: 655–670.

McConnell, A.J. and Wassenaar, E.J. 2022. An innovative new 3MPa CPT – to detect and measure very small fs values, *Proceedings of Cone Penetration Testing 2022*, Bologna, Italy, 2022: 198–203. https://doi.org/10.1201/9781003308829-22

Olson, S.M. 2001. Liquefaction analysis of level and sloping ground using field case histories and penetration resistance, PhD thesis, University of Illinois at Urbana-Champaign.

Plewes, H.D., Davies, M.P. and Jefferies, M.G. 1992. CPT based screening procedure for evaluating liquefaction susceptibility. *Proceedings of 45th Canadian Geotechnical Conference,* Toronto, Canada.

Poulos, S.J. 1981. The steady state of deformation. *Journal of the Geotechnical Engineering Division* 107(5): 553–562. http://dx.doi.org/10.1061/AJGEB6.0001129

Robertson, P.K. 2010. Evaluation of flow liquefaction and liquefied strength using the cone penetration test. *Journal of Geotechnical and Geoenvironmental Engineering* 136 (6): 842–853. https://doi.org/10.1061/(ASCE)GT.1943-5606.0000286

Robertson, P.K. 2016. Cone penetration test (CPT)-based soil behaviour type (SBT) classification system — An update. *Canadian Geotechnical Journal* 53(12): 1910–1927. https://doi.org/10.1139/cgj-2016-0044

Robertson, P.K. 2017. Evaluation of flow liquefaction: influence of high stresses. *Proceedings of the 3rd International Conference on Performance Based Design.* Vancouver, Canada, 2017: 16–19.

Robertson, P.K. 2021. Evaluation of flow liquefaction and liquefied strength using the cone penetration test: an update. *Canadian Geotechnical Journal* 00: 1–5.

Robertson, P.K. and Wride, C.E. 1998. Evaluating cyclic liquefaction potential using the cone penetration test. Canadian Geotechnical Journal 35(3): 442–459. https://doi.org/10.1139/t99-102

Schnaid, F. 2009. *In Situ Testing in Geomechanics: The Main Tests,* 1st ed. Abingdon, England: Taylor and Francis.

Shuttle, D.A. and Cunning, J. 2007. Liquefaction potential of silts from CPTu. *Canadian Geotechnical Journal* 44(1): 1–19. https://doi.org/10.1139/T06-086)

Shuttle, D.A. and Cunning, J. 2008. Reply to the discussion by Robertson on Liquefaction potential of silts from CPTu. *Canadian Geotechnical Journal* 45 (1): 142–145. https://doi.org/10.1139/T07-119

Smith, K., D. Reid and R. Fanni. 2021. A generalized CPTu state parameter inversion method based on the NorSand Widget. *Proceedings of ANCOLD 2021 Conference,* Gladstone, Australia,: 1–10.

Taylor, D.W. 1948. *Fundamentals of Soil Mechanics*. New York, USA: John Wiley & Sons.

Enhancing Soil and Tailings Characterization: Integration of Photonics Technology with Cone Penetration Testing

Iman Entezari, ConeTec Group, Canada
Dallas McGowan, ConeTec Group, Canada
Joseph Bindner, ConeTec Group, Canada
Joseph Glavina, ConeTec Group, Canada
Jason DeJong, University of California, Davis, USA

Abstract

The integration of photonics technology, particularly hyperspectral sensing and high-resolution imaging, with piezocone penetration tests (CPTu) offers a transformative approach to soil and tailings characterization. This paper presents preliminary work on the assessment of hyperspectral data combined with CPTu data for tailings characterization through analyzing a large dataset of paired hyperspectral, CPTu, and laboratory results using machine learning models. Additionally, it presents discussion on initial findings on particle size estimation employing a machine learning based approach to analyze high-resolution imaging acquired from reference samples and in-situ tests. The results demonstrate that incorporating hyperspectral and CPTu data significantly enhances tailings characterization, and the particle size determination using high-resolution images is promising.

Introduction

In geotechnical and geoenvironmental site investigations, characterization of soil and soil-like properties is essential. This often requires a combination of in-situ testing and sampling methods. Traditionally, laboratory testing and piezocone penetration testing (CPTu) have been the common techniques for soil characterization. While laboratory testing offers a comprehensive analysis of various soil properties, from constitutive, to geotechnical, to chemical, it involves drilling, sampling, and subsequent transportation, which is costly, carbon-intensive (Purdy et al., 2021), and more hazardous than CPTu operations. In-situ collection of soil hyperspectral data and high-resolution images coupled with CPTu or Seismic CPTu (SCPTu) offers promise for reducing cost, time, and environmental impacts associated with sampling and laboratory testing.

Building upon the foundation of CPTu technology, advancements are being made in incorporating hyperspectral sensors and high-resolution cameras into modules that can be placed in-line with the CPTu. The hyperspectral module enables real-time and continuous spectral data collection across an extended wavelength spectrum during CPTu operations. The vision module, designed for RGB imaging, facilitates the acquisition of high-resolution photographs in real-time during the CPTu push.

The hyperspectral module provides valuable insights into the chemical composition and crystal structure of geomaterials by measuring reflected light across different wavelengths. This capability allows for the identification and quantification of minerals (Clark, 1999; Entezari et al., 2017; Debaene et al., 2023), estimation of water content (Fabre et al, 2015; Entezari et al., 2016), detection and quantification of contaminants (Schwartz et al., 2011; Shi et al., 2014), and assessment of chemical composition (Cozzolino and Moron, 2003; McBride, 2022). The vision module provides detailed texture and color information about the geomaterial, aiding in the estimation of particle size distribution and identification of soil types (Hryciw et al., 2009 and 2015; Ventola and Hryciw, 2023).

This paper presents preliminary work on the analysis and interpretation of hyperspectral data coupled with CPTu data for tailings characterization. This assessment is conducted through the analysis of a dataset of paired hyperspectral and CPTu data, alongside tailings properties from laboratory testing. In our previous studies, we have developed machine learning models for the estimation of tailings constituents using hyperspectral data (Entezari et al., 2022a) and using Gamma-CPTu (GCPTu) data (Entezari et al., 2022b). In this paper, we evaluate the potential of combining hyperspectral and CPTu data for improved tailings characterization. Additionally, we present initial pilot results on particle size estimation using high-resolution benchtop and in-situ images analyzed with a machine learning based algorithm.

Background

Hyperspectral module

The hyperspectral module (patent pending) is configured with spectrometers capable of collecting reflectance spectra in the spectral ranges of 400-850 nm and 950-1700 nm. Alternate configurations can be used to collect different spectral ranges. To collect the reflectance spectra during CPTu operations, the hyperspectral module contains a light source to illuminate the soil through a window. The reflected light is then transferred to a spectrometer(s) that transmits a digitized signal to the CPTu data acquisition system (DAS). Figure 1 illustrates sample data obtained from a wet and a dry tailings sample using a benchtop setup of the hyperspectral module.

By measuring reflected light across different wavelengths, spectral sensors provide information about chemical composition and crystal structure (Clark, 1999). This versatile method enables both qualitative and quantitative assessments of various materials and substances.

Reflectance spectroscopy facilitates quantitative assessments of soil properties by correlating spectral signatures with specific parameters of interest. Through empirical relationships established between spectral features and target properties, quantitative estimations with high accuracy can be derived. By calibrating spectral data against reference measurements obtained from laboratory analyses, robust quantitative models can be constructed for diverse soil properties, including mineral content, organic carbon content, and contamination levels.

In qualitative analysis, reflectance spectroscopy can help identify and characterize different components present in the soil. By analyzing the spectral signature (the unique pattern of light absorption and reflection across various wavelengths) the presence of minerals, organic matter, and contaminants can be identified (Clark, 1999; Schwartz et al., 2011). Each component exhibits distinct spectral features, allowing for their identification without the need for physical extraction or laboratory testing.

The integration of hyperspectral sensors into CPTu modules allows for real-time, continuous hyperspectral reflectance data collection during CPTu or SCPTu operations. The synergistic integration of hyperspectral data with CPTu data (or SCPTu), correlated and analyzed by machine learning algorithms, can produce new methods to estimate soil properties such as plasticity, fines content, water content, degree of saturation, mineralogy, and contaminants.

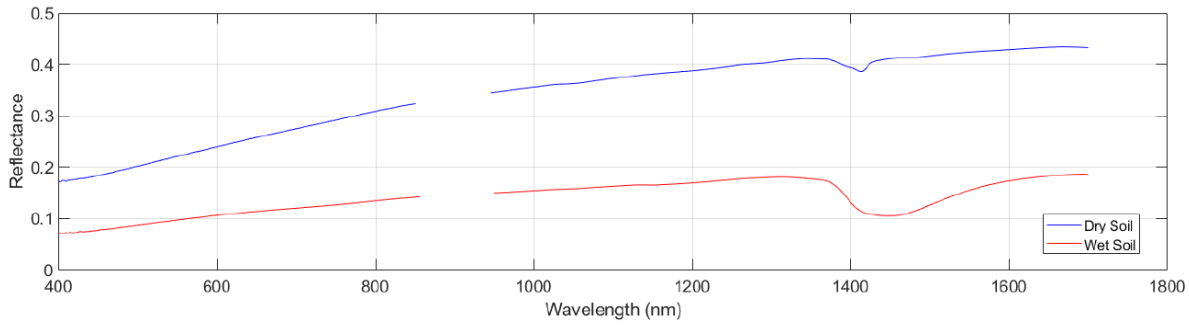


Figure 1: Example hyperspectral data from hyperspectral module

Vision module

The vision module is equipped with an 18 MP high-resolution image sensor which captures photographs through a 16 mm diameter window. With the present configuration, each pixel of the image corresponds to an area of approximately 4µm × 4µm. Figures 2a and 2b show example images acquired from two soil samples with particle diameters ranging from150-250 µm and 105-150 µm, respectively.

Vision module offers numerous advantages for geotechnical and geo-environmental site characterization. The ability to perform visual inspections using in-situ images reduces the need for visual assessment by physical soil sampling and complements soil behaviour type (SBT) derived soil stratigraphy. Additionally, it facilitates a thorough quality check of CPTu data by pairing images with the data, allowing for the identification of anomalies through supplementary visual evidence. This technology can also enable

the estimation of particle size distribution through textural analyses or machine learning modelling (Buscombe, 2019; Ventola and Hryciw, 2023). Furthermore, the detailed insights gained from analyzing particle size and colors enhance soil classification and characterization, making vision CPTu a valuable tool in site assessment and analysis.

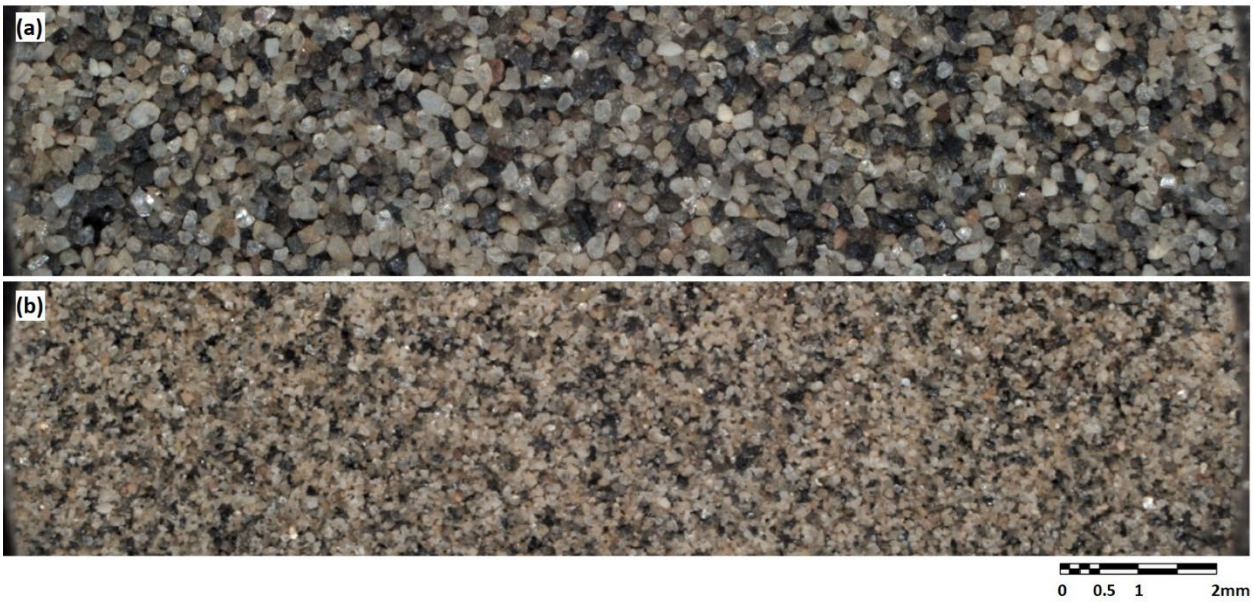


Figure 2: Example vision module data from samples with particle size of (a) 150-250 µm and (b) 105-150 µm

Data and methods

Hyperspectral GCPTu dataset

To explore the potential synergy between hyperspectral and CPTu data, a dataset combining hyperspectral and GCPTu data from the oil sands region in Canada was compiled. ConeTec's oil sands tailings dataset (Entezari et al., 2022a), originally collected in the 350-2500 nm range from ex-situ samples, was limited to the spectral ranges of 400-850 nm and 950-1700 nm, corresponding to the spectral ranges of the hyperspectral module.

To pair hyperspectral data with GCPTu data, our geospatial database was queried to identify GCPT soundings in proximity (within 10 m radially, 3 months temporally) of the hyperspectral data samples. The GCPT parameters, including gamma counts, undrained shear strength, and the slope and linearity of porewater pressure (Entezari et al., 2022b), were averaged over the sample length and paired with hyperspectral data. This process resulted in a dataset comprised of hyperspectral data, GCPTu data, and corresponding laboratory results. The final dataset included 4723 data pairs, providing a large dataset for analyzing the combined utility of hyperspectral and CPTu data in tailings characterization. The dataset was split into training and test sets, through random selection of ~10% of the data points as the test set. Four

models were trained using four different sets of input features including: (1) hyperspectral and GCPTu parameters, (2) hyperspectral and CPTu parameters (no gamma), (3) only hyperspectral parameters, and (4) only GCPTu parameters. Consistent with previous work (Entezari et al. 2022a and 2022b), the models of this study were trained using the training set and an ensemble of neural networks using bootstrap aggregation (Bagging) technique (Sollich and Krogh 1996, Breiman 1996). The models were trained to predict the contents of bitumen, solids, water, total fines, fines/(fines+water) (FFW) as well as methylene blue index (MBI). The performance of the models was evaluated using the cumulative distribution function (CDF) of errors on the test set (Error = Lab -predicted). The bias of the prediction was determined at the 50th percentile in the CDF. Assuming normal distribution of errors, the CDF values at 15.9% and 84.1% correspond to ±1 standard deviation and the average of these CDF values was adopted as the comprehensive error measure for the model.

High resolution images

To assess the use of vision module images to determine particle size distribution in coarse grained soils, the Segment Every Grain machine learning procedure (Sylvester, 2023) was applied to two images: one from a benchtop study, and one from in-situ imaging. The Segment Every Grain algorithm detects particles in images and provides estimates of particle diameter by identifying boundaries and determining the major and minor axis length of particles. The algorithm first identifies particles, then allows the user to delete improperly detected particles and add new particles. This combined machine-user approach allows for quick refinement of modeled results.

Imagery was first captured on the reference sample with particles ranging from 105 -150 μm (Figure 2b). The algorithm was then applied to the image and results were refined by the user. A field demonstration was also conducted using the vision CPTu to collect imagery and CPTu data up to a depth of 12 meters in oil sands tailings. During the CPTu test, the probe was stopped at 10 cm increments to capture images. Data collected from in-situ tests were compiled and a sample image of a predominantly sandy material was selected to assess the performance of the Segment Every Grain algorithm for the particle size estimation of the in-situ images.

Results

Tailings characterization using hyperspectral and CPTu data

The results of the trained models developed using different sets of input features are presented in Figures 3-6. These figures include scatter plots that depict the relationship between lab measured constituents and the predicted results for the test set. The model architecture and training parameters were consistent across all four models to facilitate a comparative analysis. As shown, models incorporating both hyperspectral and

GCPTu/CPTu parameters as input features outperformed those trained solely with hyperspectral parameters or solely with GCPTu parameters across all tailings characterizations. The summary of the error analysis is provided in Table 1.

The application of the developed models on in-situ data faces two challenges. First, collecting hyperspectral data in oil sands fluid tailings is impractical due to bitumen smearing and the lack of a self-cleaning mechanism, limiting the application of the model to soil-like materials in the oil sands where data collection is feasible. However, this limitation does not apply to non-hydrocarbon deposits. An error analysis was therefore conducted exclusively on soil-like material where in-situ hyperspectral data collection would be feasible (Table 1). The soil-like material was identified based on a pore pressure linearity of less than 0.8.

Second, variations between the spectrometers used during model development and those in the hyperspectral module may require calibration transfer to ensure accurate data interpretation. Future efforts will evaluate the need for calibration transfer methods to align data from different spectrometers, thereby enhancing the model's reliability and applicability to in-situ data.

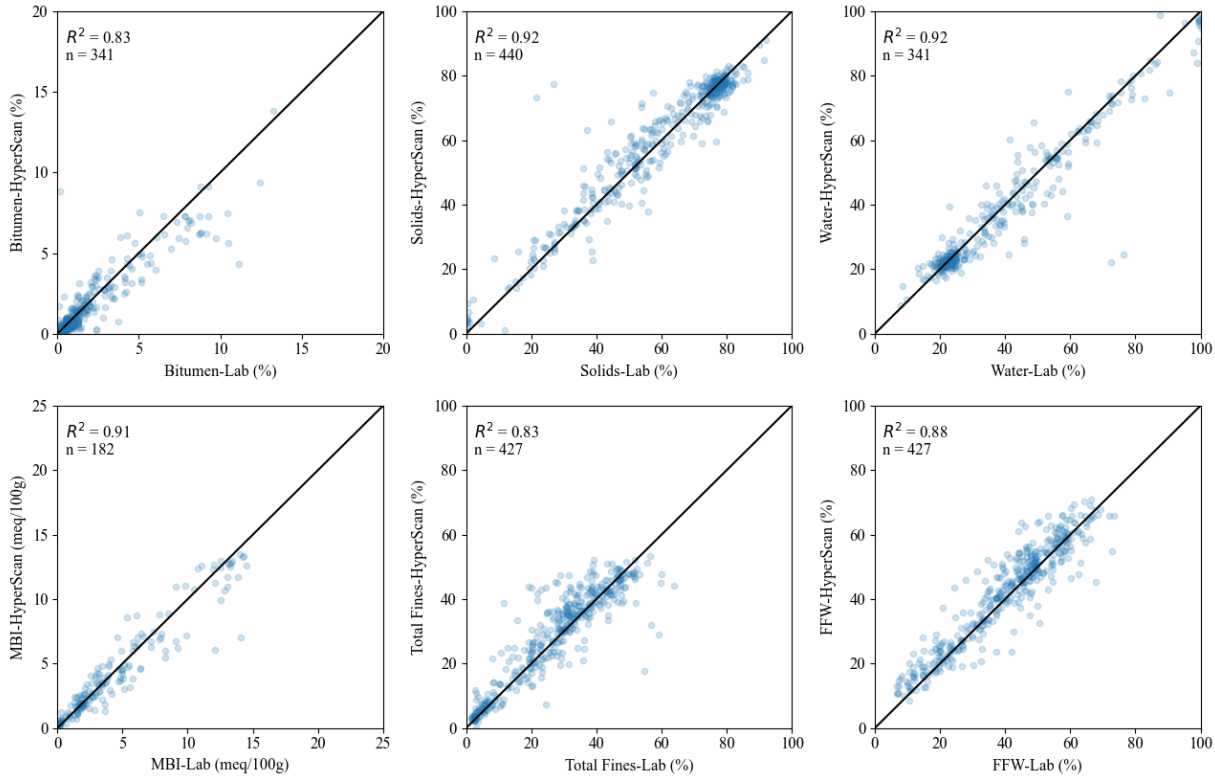


Figure 3: Performance assessment on the test set using the model trained with both hyperspectral and GCPTu parameters as input features

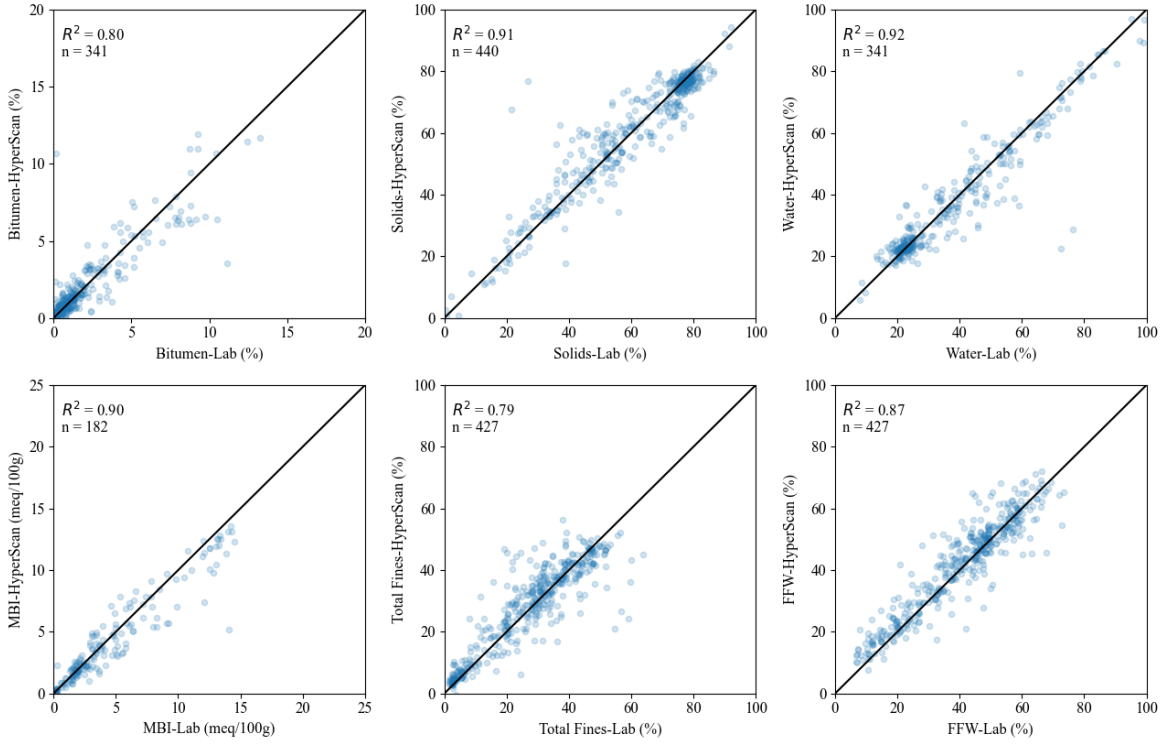


Figure 4: Performance assessment on the test set using the model trained with both hyperspectral and CPTu parameters as input features

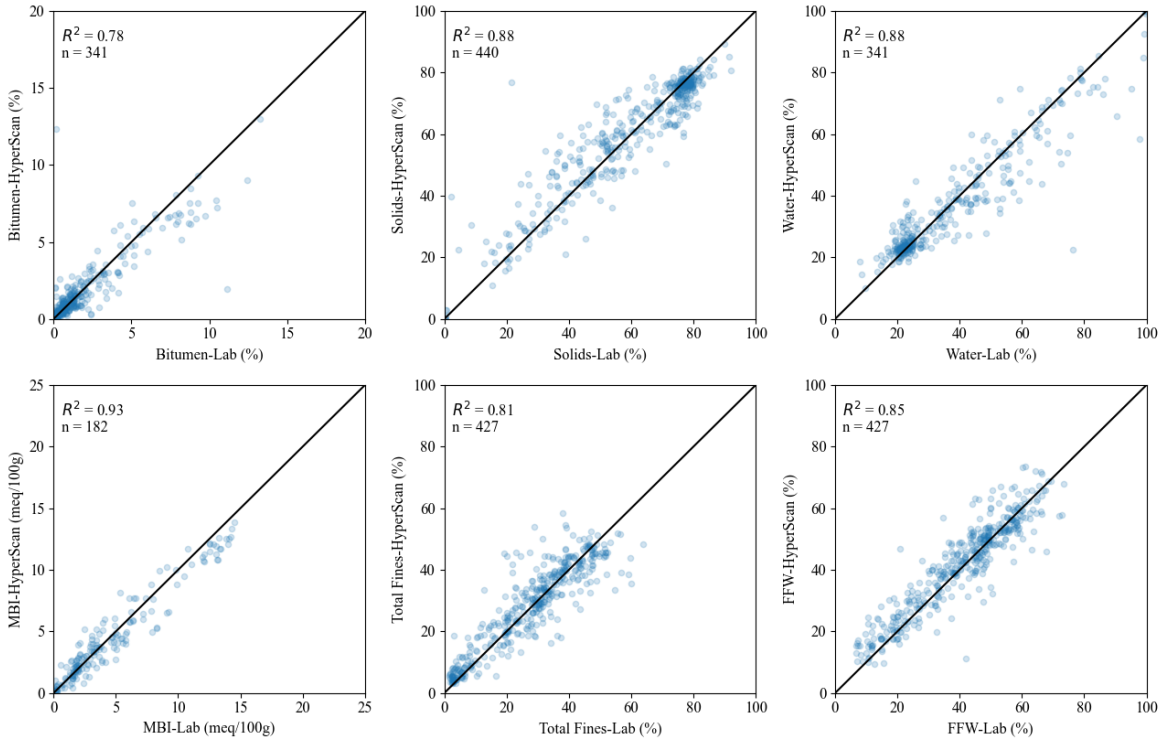


Figure 5: Performance assessment on the test set using the model trained with only hyperspectral data as input features

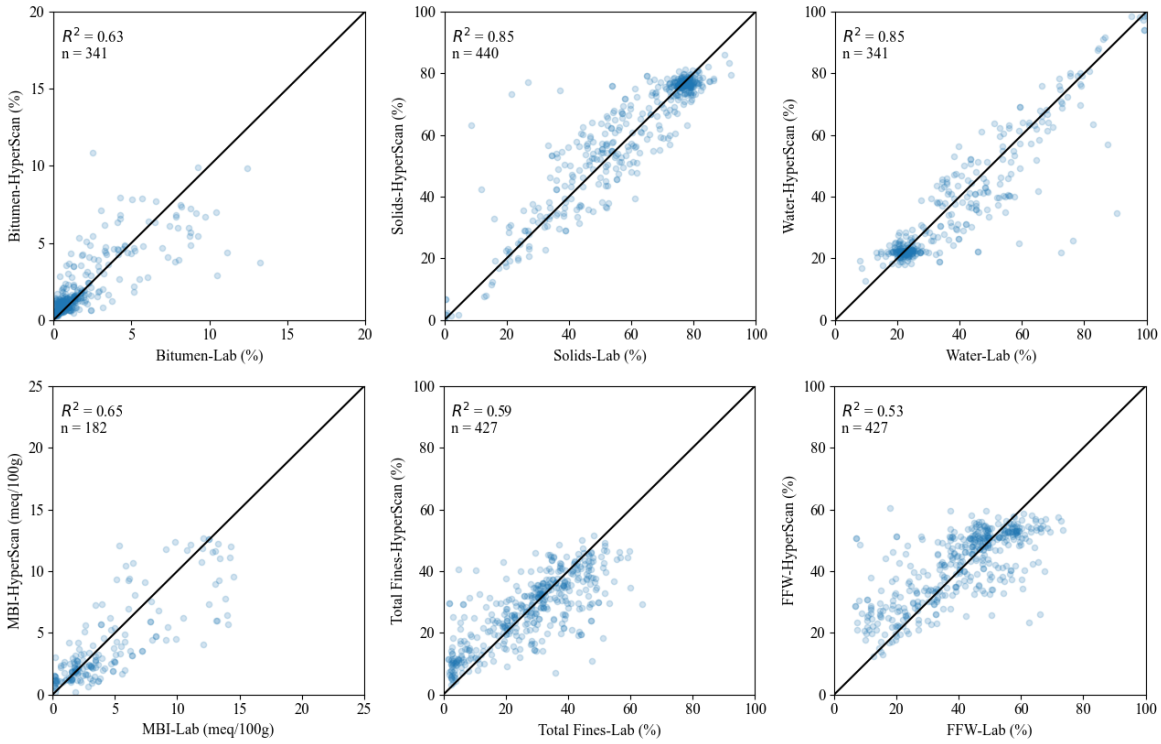


Figure 6: Performance assessment on the test set using the model trained with only GCPTu data as input features

Table 1: Summary of error analysis (bias ± error)

	Hyperspectral+GCPTu	Hyperspectral+CPTu	Hyperspectral Only	GCPTu Only
	Entire Test Set			
Bitumen (wt%)	0.05 ± 0.49	-0.08 ± 0.49	-0.03 ± 0.5	-0.25 ± 0.69
Solids (wt%)	-0.53 ± 4.18	0.15 ± 4.43	0.27 ± 5.59	0.01 ± 5.88
Water (wt%)	0.45 ± 3.2	0.1 ± 3.7	-0.26 ± 5.15	0.73 ± 5.8
MBI (meq/100g)	0.01 ± 0.88	0.11 ± 0.92	0.09 ± 1.02	0.2 ± 1.91
Total 44 µm Fines (wt%)	-0.99 ± 4.51	-0.98 ± 4.8	-1.0 ± 4.84	-0.98 ± 8.17
FFW (wt%)	-1.67 ± 4.29	-1.19 ± 4.4	-1.41 ± 5.04	-1.53 ± 8.86
	Soil-Like Tailings fraction of Test Set (linearity of pore pressure < 0.8)			
Bitumen (wt%)	0.02 ± 0.34	-0.07 ± 0.33	-0.07 ± 0.31	-0.26 ± 0.47
Solids (wt%)	-0.09 ± 2.85	0.43 ± 2.98	1.37 ± 3.21	0.13 ± 4.19
Water (wt%)	0.04 ± 2.71	-0.18 ± 2.82	-1.27 ± 3.2	0.69 ± 4.3
MBI (meq/100g)	-0.06 ± 0.43	0.04 ± 0.61	-0.1 ± 0.66	-0.09 ± 1.33
Total 44 µm Fines (wt%)	-0.73 ± 4.79	-1.07 ± 5.75	-1.37 ± 5.84	-1.78 ± 11.33
FFW (wt%)	-1.54 ± 4.94	-1.55 ± 4.93	-1.19 ± 6.29	-0.54 ± 13.11

PSD analysis using images

Figure 7a presents a benchtop image of a reference sample captured by the vision module, with the highlighted area enlarged in Figure 7b. The particle detection results are shown in Figure 7c, where the algorithm successfully detected most particles. The PSD results from machine learning are displayed in Figure 7d. Most particles fall within the 105-150 µm range (#100-140 sieve), though sizes below 105 µm and above 150 µm are also observed (Figure 7d). A close examination of Figure 7c, compared with the grains in Figure 7b, indicates that some adjacent grains were detected as larger agglomerated particles, leading to sizes over 150 µm. Additionally, overlapping particles sometimes resulted in only the uncovered part of a particle being detected, accounting for sizes under 105 µm.

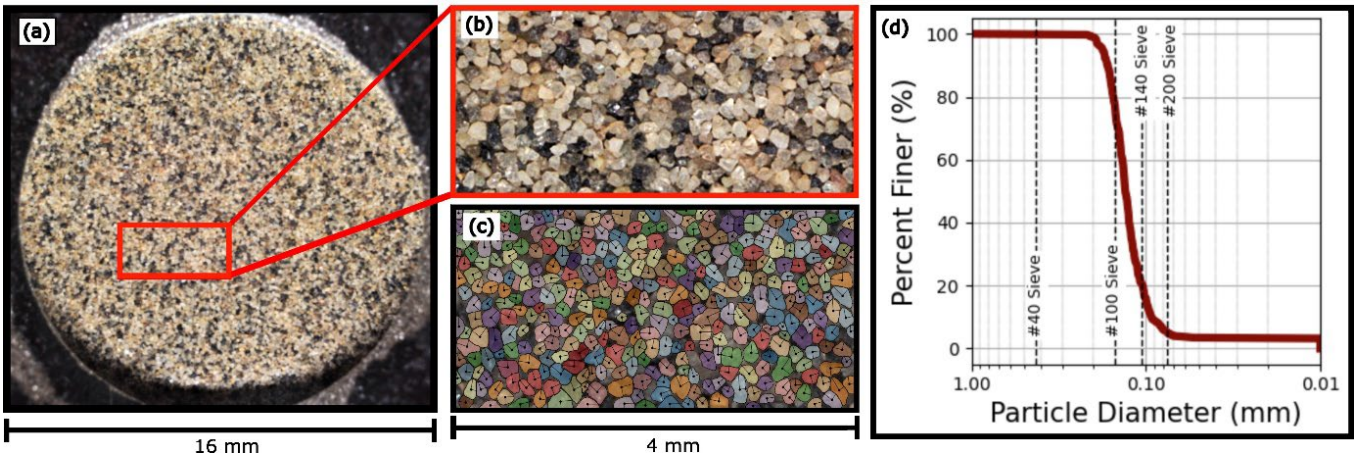


Figure 7: Results from benchtop imaging including (a) the image of the reference sample, (b) the cropped section used in analysis, (c) results from machine learning segmentation, and (d) the particle size distribution curve for detected particles

Figure 8 presents the results from in-situ field testing using the vision module, showcasing cone tip resistance (qt), sleeve friction (fs), stacked incremental images compiled from cropped thin sections from the imagery, and enlarged image sections at selected depths. As shown in Figure 8, a transition in qt is observed near a depth of 7 m, which corresponds to a transition from predominantly sandy material to fine grained mixtures. When cross referencing this information with in-situ images, a color change in the tailings profile is observed. Additionally, a visual change in moisture condition above and below the water table at 0.6 m depth is observed based on the enlarged images.

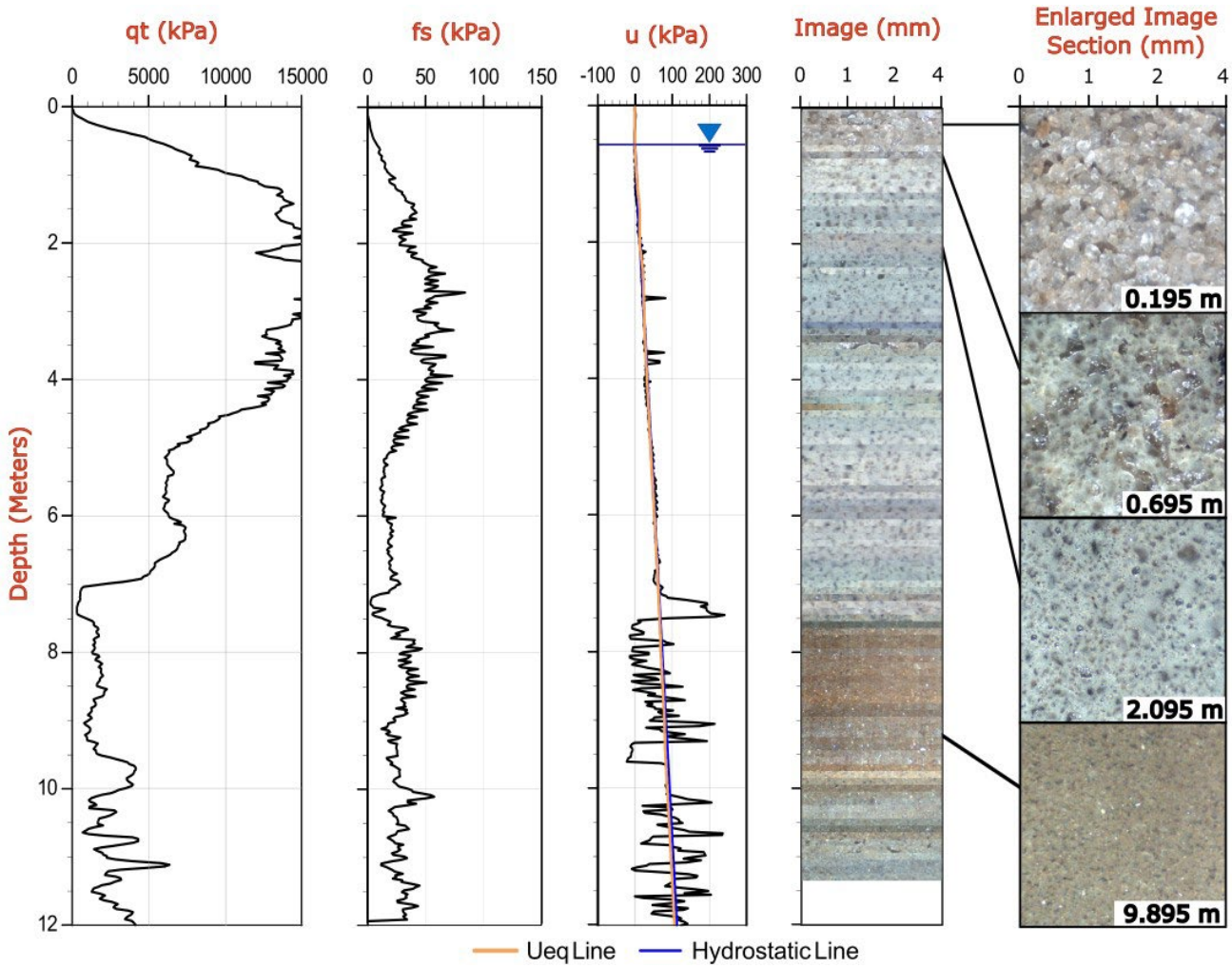


Figure 8: CPTu data and associated images including the cone tip resistance (qt), sleeve friction (fs), dynamic pore pressure (u), cropped image at each imaging depth, and enlarged image sections at selected depths

Figure 9 illustrates the results of the Segment Every Grain algorithm applied to an in-situ image from sand-dominated tailings. Visual interpretation suggests that the algorithm successfully identified the majority of particles in the image. However, due to the similar color of the particles, its performance is limited. While laboratory data are required to thoroughly evaluate the accuracy of the results, the preliminary PSD analysis indicates that most particles are larger than 75 µm, which is typical for such tailings. This initial assessment shows promise for predicting particle size distribution from in-situ images.

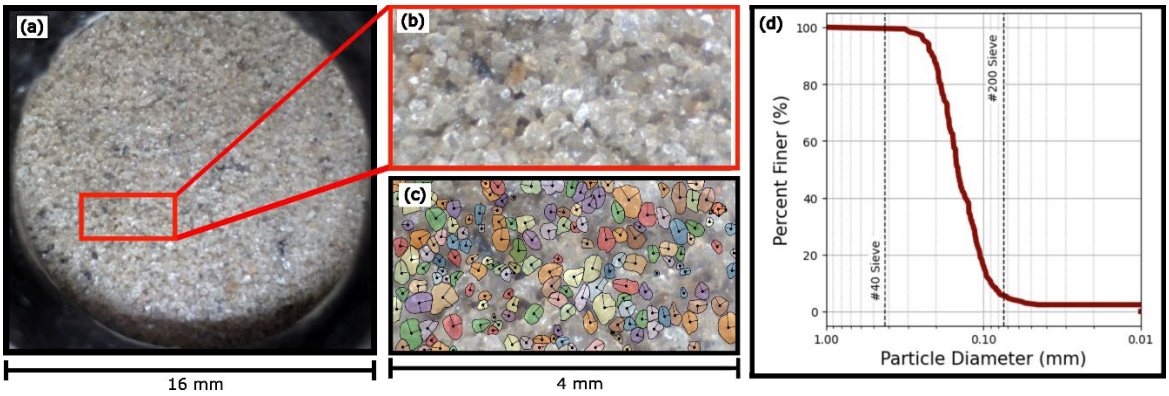


Figure 9: Results from in-situ imaging including (a) the image of the sand-dominated tailings, (b) the cropped section used in analysis, (c) results from machine learning segmentation, and (d) the particle size distribution curve for detected particles

Conclusion

This paper introduced initial research on the integration of advanced photonics technologies, including hyperspectral sensing and high-resolution imaging, into CPTu modules. Results show that the synergistic fusion of hyperspectral data with CPTu data, empowered by machine learning algorithms, improves the accuracy and reliability of predicting tailings properties. Analysis of a dataset containing hyperspectral, CPTu, and laboratory data demonstrates that modeling procedures that incorporate both hyperspectral and GCPTu/CPTu data outperform models that only use hyperspectral or CPTu data. Additionally, the use of the high-resolution images and machine learning-based analysis shows promise for the estimation of particle size distribution for coarse grained materials. Although the application of optical technologies and machine learning for soil and tailings characterization is still a developing field, this study, among others, highlights the potential of these technologies to enhance the speed, cost-efficiency, and resolution of site characterization.

References

Breiman, L. 1996. Bagging predictors. *Machine Learning* 24(2): 123–140.

Buscombe, D. 2019. SediNet: a configurable deep learning model for mixed qualitative and quantitative optical granulometry. *Earth Surface Processes and Landforms* 45(3): 638–651.

Clark, R.N. 1999. Spectroscopy of rocks and minerals, and principles of spectroscopy. *Manual of Remote Sensing* 3: 3–58.

Cozzolino, D. and A. Moron. 2003. The potential of near-infrared reflectance spectroscopy to analyse soil chemical and physical characteristics. *J. Agric. Sci.* 140(1): 65–71.

Debaene, G., P. Bartmiński and M. Siłuch. 2023. In situ VIS-NIR spectroscopy for a basic and rapid soil investigation. *Sensors* 23: 5495.

Entezari, I., D. McGowan, J. Glavina and J. Sharp. 2022b. Tailings behaviour type to predict oil sands tailings constituents from the gamma cone penetration test. *Proceedings of the International Oil Sands Tailings Conference (IOSTC)*, Edmonton, AB: 6–15.

Entezari, I., D. McGowan and J. Glavina. 2022a. Hyperspectral imaging technology for oil sand tailings characterization: practical aspects. *Proceedings of Tailings and Mine Waste 2022*, Denver, CO, USA.

Entezari, I., B. Rivard, M. Geramian and M.G. Lipsett. 2017. Predicting the abundance of clays and quartz in oil sands using hyperspectral measurements. *Int. J. Appl. Earth Obs. Geoinf.* 59:1–8.

Entezari, I., B. Rivard, M.G. Lipsett and G.W. Wilson. 2016. Prediction of water content and normalized evaporation from oil sands soft tailings surface using hyperspectral observations. *Canadian Geotech. J.* 53(10): 1742–1750.

Fabre, S., X. Briottet and A. Lesaignoux. 2015. Estimation of soil moisture content from the spectral reflectance of bare soils in the 0.4–2.5 µm domain. *Sensors* 15(2): 3262–3281.

Hryciw, R.D., H.-S. Ohm and J. Zhou. 2015. Theoretical basis for optical granulometry by wavelet transformation. *J. Comput. Civ. Eng.* 29(3): 04014050.

Hryciw, R.D., Y. Jung, E. Susila and A. Ibrahim. 2009. Thin soil layer detection by VisCPT and FEM simulations. *Proceedings of the 17th International Conference on Soil Mechanics and Geotechnical Engineering (ICSMGE)*, IOS, Amsterdam, Netherlands: 1052–1055.

McBride, M.B. 2022. Estimating soil chemical properties by diffuse reflectance spectroscopy: Promise versus reality. *Eur. J. Soil Sci.* 73: e13192.

Purdy, C.M., A.J. Raymond, J.T. DeJong, A. Kendall, C. Krage and J. Sharp. 2021. Life cycle sustainability assessment of geotechnical site investigation. *Canadian Geotech. J.* 59 (6).

Schwartz G., G. Eshel and E. Ben-Dor. 2011. Reflectance spectroscopy as a tool for monitoring contaminated soils. In: Pascucci S., editor. *Soil Contamination.* New York: InTech: 67–90.

Shi, T., Y. Chen, Y. Liu and G. Wu. 2014. Visible and near-infrared reflectance spectroscopy – An alternative for monitoring soil contamination by heavy metals. *J. Hazard. Mater.* 265: 166–176.

Sollich, P. and A. Krogh. 1996. Learning with ensembles: how over-fitting can be useful. In *Advances in Neural Information Processing Systems 8*, MIT Press, Cambridge, MA: 190–196.

Sylvester, Z. 2023. Segmenteverygrain. Accessed at https://github.com/zsylvester/segmenteverygrain

Ventola, A. and R.D. Hryciw. 2023. An autoadaptive Haar wavelet transform method for particle size analysis of sands. *Acta Geotech.* 18: 5341–5358.

Hydraulic Dewatered Stacking Demonstration – Approaching Operational Completion

Phil Newman, Anglo American, UK
Mark Bruton, WSP, UK
James Purrington, WSP, UK
Alireza Nickman, WSP, UK
Andrea López, Anglo American, Chile

Abstract

Hydraulic dewatered stacking (HDS) is an engineered co-disposal approach that uses a fines-free sand, derived from the tailings themselves, to deliver robust and effective omnipresent drainage channels throughout the tailings facility, accelerating consolidation and dewatering.

Since its inception in 2019, Anglo American have rapidly developed the science behind the new tailings system and designed, built, and commissioned a bespoke 150,000 m^3 capacity greenfield tailings facility at the El Soldado Mine in Chile.

This paper presents the results to date of the trial, encompassing two of the planned three stages of tailings and sand drainage layer deposition and the construction of drainage channels. A review of the efficacy of the technology will be presented and a comparison between two different methods of co-disposal and placement of sands will be considered.

Key parameters associated with the desaturation and resaturation of the facility will be presented based on the review of in-situ data collected from an extensive array of instrumentation and, where available, follow-on intrusive investigations and laboratory testing.

The industry appears ready to embrace the benefits of the technology, which include:

- enhanced water recovery delivering real value and increasing the resilience of operations in water-scarce regions;
- limited capital expenditure while delivering many of the performance benefits of filtered tailings stacking;
- a final tailings facility footprint suitable for re-purposing, reducing long-term liabilities; and
- an instrumentation solution that can deliver on enhanced transparency for stakeholders, helping owners to move towards GISTM compliance.

Introduction

Hydraulic dewatered stacking (HDS) is a novel tailings management approach developed by Anglo American that utilizes fines-free, rapidly draining sand to create a 3-dimensional drainage structure to deliver a predominantly desaturated tailings storage facility (TSF).

The sand is derived from the tailings themselves, which in most cases, assures compatibility as a robust and long-lasting filter medium (Terzaghi and Peck, 1948). Suction pressures are developed rapidly in the tailings, which drain both vertically and horizontally thanks to spigotted tailings possessing a K_h that is 10x K_v. This anisotropy in permeability is exploited well by the engineering design of HDS and although results remain preliminary, the data generated from the 150,000 m^3 demonstration facility at the El Soldado Mine in Chile supports the initial hypothesis. The dewatering and consolidation performance measured to date has been excellent and an extensive site investigation planned for Q4 2024 will provide the final calibration of the data collected to date.

The trial was constructed in 2021 after initial laboratory testing (Newman et al., 2022) indicated that a desaturated stack was feasible. As with all pilots, operational learnings and data generated has led to design changes during the trial. Significant data has been generated, and lessons learned regarding in-situ instrumentation to monitor tailings facilities. Data is presented below, with interpretation and reference to the ongoing concurrent modeling of the facility. The work completed has fed directly into studies for full-scale implementation of HDS both within and outside of Anglo American's assets. Cost estimates have confirmed that HDS is more expensive to operate than conventional wet tailings disposal, but highly water generative (with associated safety, expansion optionality, and closure benefits). When assessed using a Net Present Cost (NPC) approach, the results are dependent on i) water costs/constraints; ii) time to closure; and iii) estimated closure costs. When compared to filtered tailings, both capital and operating cost savings are significant and the approach can deliver an unsaturated stack where the net present cost of implementation is between one third and one half (Newman et al., 2024).

Demonstration design and operation

Concurrent modeling of the proposed trial led to a variation in design with the trial facility split into two cells testing two different approaches to HDS execution (see Figure 1).

The design in Cell A was varied to exclude sand blankets and only sand channels were utilized; modeling had shown that thin layers of tailings separated by sand blankets could increase the rate of consolidation. However, the development of suction pressures would be hindered such that air entry might not be achieved. Cell B was left with sand blankets so that a comparison could be made between the two approaches.

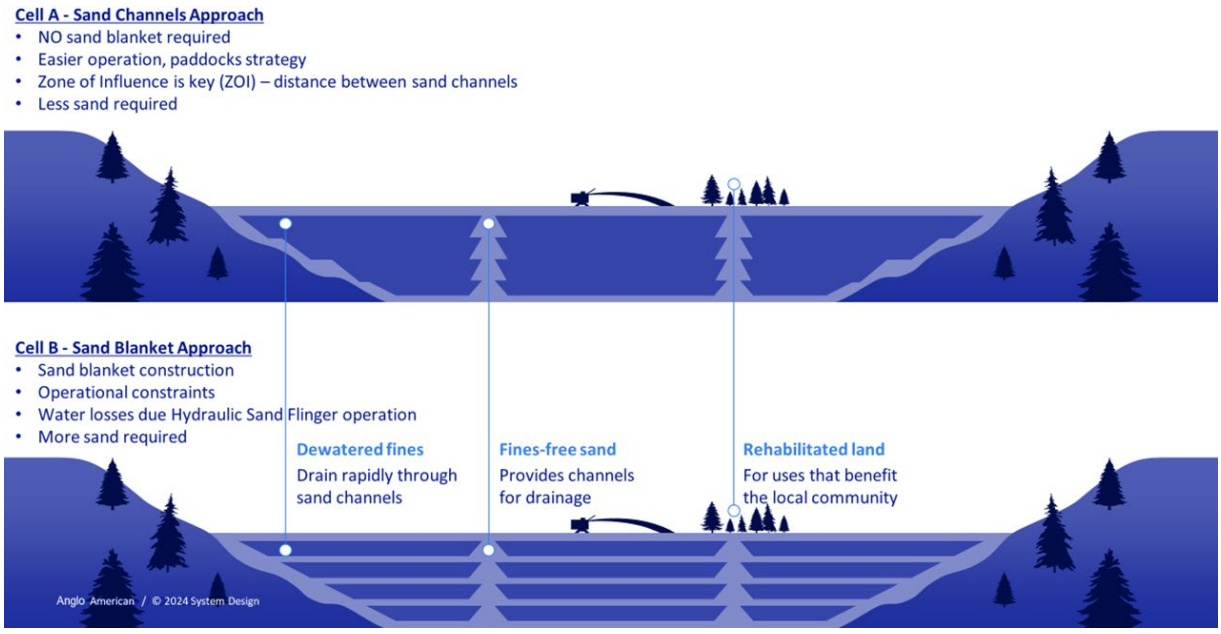


Figure 1: Sand blankets (Cell B) vs. sand channels (Cell A)

An important artefact of this change in design (of cell A) is that the sand channels are not physically continuous with the basal drain layer since a 2 m thick layer of tailings had already been placed in the cell. It was considered that this would limit the ability of the sand channel approach to drain and hence would have a conservative impact on the performance. A greenfield application of the HDS system would include such a connection – modeling of the two approaches is proposed and will be reported on in due course.

Lessons learned and impact on future commercial applications

The change in placement approach also has operational implications; the placement of the sand blankets was considered problematic. Working with the contractor, a Hydraulic Sand Flinger (HSF) was developed to place the sand blanket; the approach worked although getting an even layer was difficult, resulting in higher consumption of sand than expected. However, at larger scale applications (wherein most of the value for HDS exists for the mining industry) the placement of these blankets would likely involve the machine moving across recently placed tailings – adding another degree of operational uncertainty. In addition, the loss of water through evaporation also reduced the attractiveness of the sand blanket approach. Alternative sand blanket options investigated included open pipe placement, creating large cones of deposited sand about 600 to 800 mm high and 20 m in diameter; simple and effective.

The drainage channels have been built hydraulically with an SPCU (Self Propelled Cyclone Unit), which has performed well at approximately 80-90 tph. Higher placement capacity is feasible but the demonstration was limited by the size of the fluidizer plant. The SPCU was originally developed to classify

a conventional slurry. Hence, optimization of the system is required when the duty is changed to dewatering a fines-free sand.

Design work is ongoing with an Original Equipment Manufacturer (OEM) looking at other sand placement techniques, with a target of achieving >250 tph sand placement. At these placement rates, larger scale operations become easier to implement with a small number of "berm-builders." The constraint going forward will be the pipeline management for the delivery of the sand slurry given that the discharge point is continuously moving. Innovations developed on large scale conveying and stacking (i.e., the tripper conveyor) do not exist at this time for slurry transport. Hence, further innovation is required to fully automate the sand placement process.

Water recovery has been strong, and of good quality. Under steady state conditions, the water quality in terms of suspended solids is the same or better than conventional tailings return water. Geochemically, the water quality was similar.

Instrumentation

Designing a demonstration tailings facility provides an unparalleled opportunity to generate data on the settlement and consolidation behavior of tailings. Lining the facility was not a permitting requirement but was a decision taken to facilitate water balance calculations and monitoring.

The HDS contains an array of geotechnical instrumentation to allow designers and operators to monitor the desaturation of the facility through operations and into closure. Vibrating Wire Piezometers (VWPs), Moisture Content (MC) probes, Suction Transducers (ST) and Fiber Optic cabling have all been installed within the facility raises. Lidar surveys are conducted daily to monitor consolidation.

Following the development of two alternative construction approaches (Cell A and Cell B), the two approaches can be quantitatively compared. At the time of writing this paper the facility has been operated through Phase 1 and 2 of the trial. For the placement of the first 2 m layer of tailings in Phase 1 both cells were operated in the same approach, subsequent to this, two alternative approaches were implemented.

MC probes record Volumetric Water Content (Volume of water compared to volume of solid); laboratory calibration has been used to convert this to a gravimetric moisture content, but this is a function of the density of the tailings, so these values provide a relative gauge rather than absolute value. This can be seen in the data set when presenting the degree of saturation (Sr) based on a constant assumed voids ratio (Figure 2), where the consistently flat sections of the data correspond to the tailings in the location of the instrument being fully submerged by the supernatant pond.

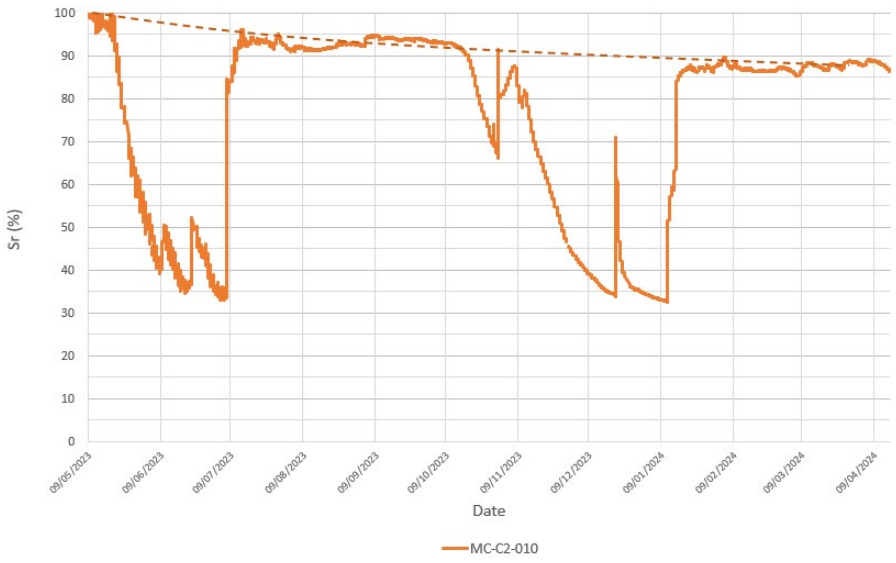


Figure 2: Change in voids ratio

The data acquisition system (DAS) at the demonstration has worked well. The permitted facility was built on top of an existing tailings facility and piezometers measure the development of excess pore pressure within the supporting tailings mass, and inclinometers in slopes that surround the facility monitor deformation that could adversely affect the safety of the staff working on the trial. The integrated satellite DAS connects directly to a user-friendly dashboard accessible globally through an internet connection. Alerts as required can be generated, resulting in direct communication with relevant personnel and linked to the Operations and Surveillance Manual (OMS) and trigger action response plan (TARP).

On-line site cameras covering the trial allows daily interaction with the facility from designers and stakeholders located thousands of miles from the site and it has provided unexpected insight. For example, a 1:10 year rain event experienced on site in June 2024 was an unscheduled (but valuable) test on the sand channels' capacity to remove excess water. Time lapse photography shows that as fast as water was entering the facility, it was being removed through the drainage system. Operational data shows that water removal through the drains rose steadily delivering clean water to the concentrator from unhindered flow through the sand channels at the demonstration site.

Lessons learned from instrumentation experience

The instrumentation installed in the facility has provided valuable insight into the performance of the facility. However, the discrete nature of the data points offer only part of the picture and it is evident that coupling moisture content and suction transducers at each location would offer greater insight. The attempt to create a broader spatial understanding of the facility using self-heating (active) fiber optics has proven elusive, with no significant data capture due to numerous failings in the system.

Discrete instruments have, in general, delivered a robust solution. Selecting suction transducers, not ideally suited to the intended use, has led to a few data gaps. In Phase 3 the addition of a different type of soil water potential sensor at each of the suction transducer locations has been included.

In addition to the instrumentation data the trial will be supplemented from a dense array of intrusive investigation holes, in-situ test work and laboratory testing, to increase the overall understanding of the performance of the facility.

Data and discussion

Some insights from the data obtained during Phase 1 and 2 of the trial are presented below. It is noted that instrumentation measures performance of the facility at discrete locations and the data is indicative of trends rather than absolute values. This is particularly important where data is interpreted using assumed constants (e.g. voids ratio assumptions used to interpret gravimetric moisture content or degree of saturation). Artifacts of the trial such as the large pond size relative to the tailings storage cell volume must be carefully considered when assessing and reporting on performance of the stack.

Phase 1

Results from Phase 1 of the trial have shown that through the construction of a substantial basal drain across the facility the tailings achieved an estimated degrees of saturation (Sr) of approximately 75-80 %. See Figure 3.

During Phase 1 high suction pressures were recorded in the instruments installed 1 m above the basal drain resulting in an initially low degree of saturation (Sr) from 75 to 80 %. However, with repeated wetting fronts from tailings and sand channel deposition, the tailings immediately above the basal drain became effectively fully saturated. It is likely that the initial high suction pressures were a result of desiccation at the surface of the tailings rather than downward flow into the basal drain, and as further layers of material are placed above, the influence of suction generated by desiccation, and the resultant finger flow evaporation, is lost. Figure 3 shows this general trend of reducing suction pressure development in the lower layer as more tailings are deposited. The data also indicates that air entry of the tailings occurs at around -11 kPa.

It is again noted that the apparent reduction in the degree of saturation is a function of an assumed constant voids ratio where in fact the materials have continued to consolidate. Where the suction transducer ST-C1-001 shows positive pore pressure (or even suctions less than the air entry value), it would suggest fully saturated conditions and as such Sr should be 100 %. Cell A and B showed a similar trend in the results through Phase 1. Since the instruments are in discrete locations from one another and are influenced

by operational factors such as pond migration, tailings deposition and wetting fronts, correlations between suction and moisture need to be considered with a degree of judgement.

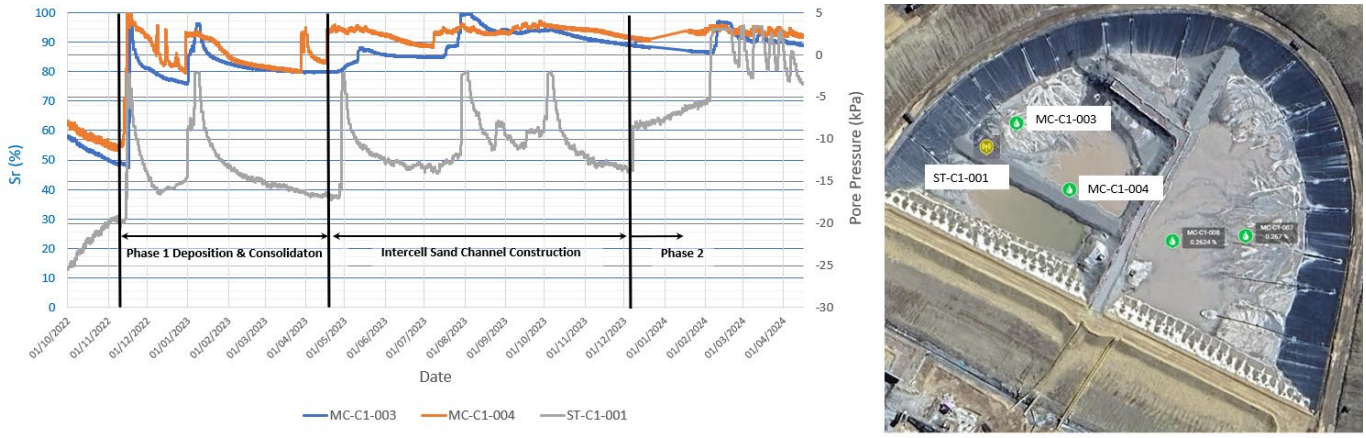


Figure 3: Phase 1 saturation of lower tailings layers (Cell A)

Phase 2

The Phase 2 tailings deposition occurs in Cell A as a continuation of tailings deposited on top of the already placed Phase 1 tailings. However, the cell is now subdivided into three sections with intercell sand channels that connect directly to the central sand channel separating the two cells (Cell A and Cell B), Figure 4. Cell B had a circa. 1 m thick sand blanket layer placed on the tailings surface prior to the next 2 m layer of tailings being deposited into the cell.

In Cell A the lower instruments clearly observed wetting fronts passing through the bottom layer of tailings and into the basal drain, as observed from instruments MC-C1-003 and MC-C1-004 shown in Figure 3. Instruments MC-C2-009 and MC-C2-010 installed 1 m into the next layer of tailings, circa 3 m above the basal drain. In this layer suction pressures were maintained even with 2 m of tailings placed above the instruments, Figure 5. In this instance the data has been plotted as the raw volumetric moisture content values reported by the instrument to avoid further ambiguity relating to computed Sr values, but the trends are obvious, and clearly result in very low Sr values which are estimated in the range from about 50 % in MC-C2-009 to 80 % in MC-C2-010 at the end of the data set presented. Further desaturation is expected after deposition ceases since suction pressures were beginning to approach the apparent air entry point of around -11 kPa as the supernatant pond receded.

The results for the second layer of tailings in Cell B show similar results to the lower layer. Since the instruments are approximately 1 m above the placed sand blanket, development of suction pressure is initially high due to desiccation that occurs due to rapid drainage of supernatant water as the tailings consolidate quickly. However, as seen in the lower layer, successive material deposition and wetting fronts reduce the ability for the tailings layers to generate suction in this way, thus trending towards high degrees of saturation.

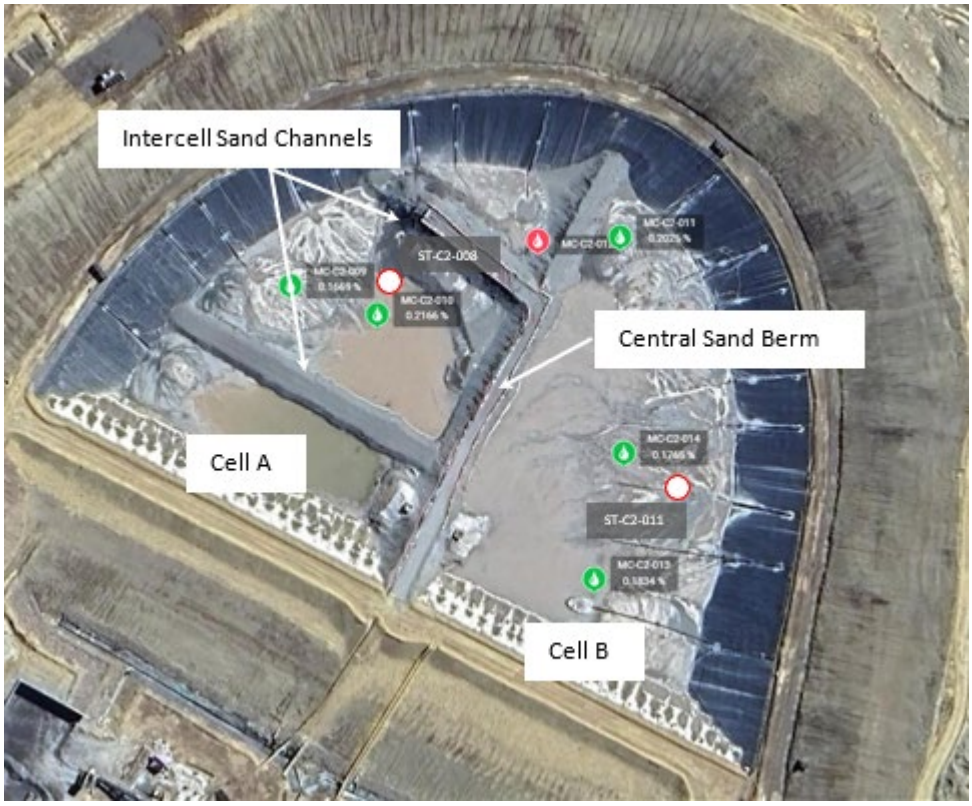


Figure 4: Phase 2 cell layout

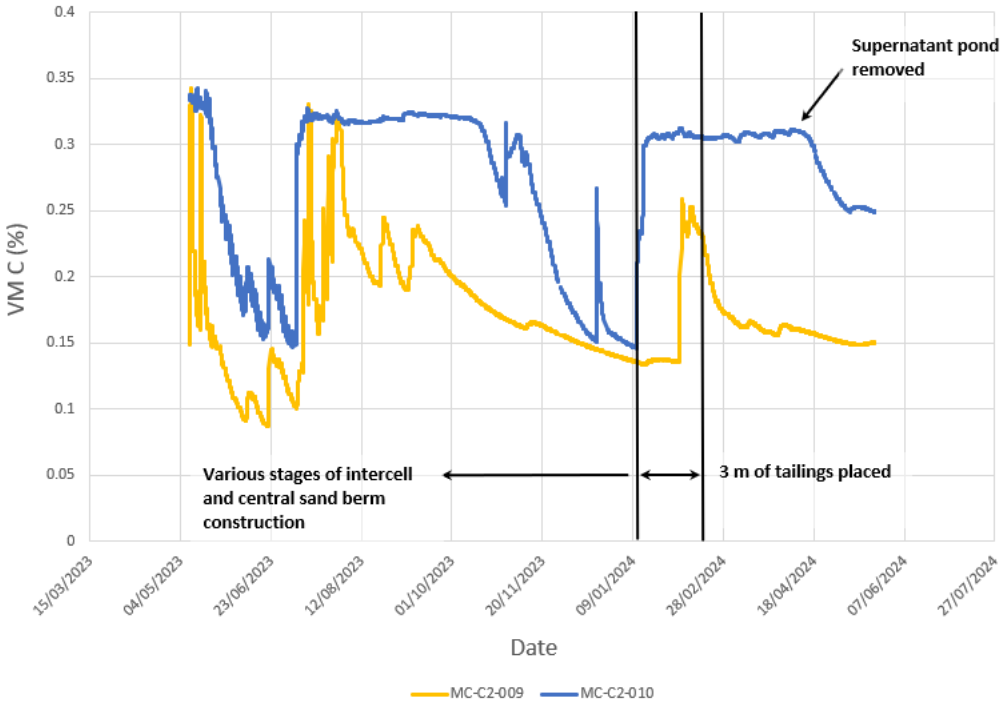


Figure 5: Moisture trends in Phase 2 tailings layers (Cell A)

Results suggest that interbedding layers of tailings with sands aids consolidation but also reduces the ability to generate ongoing gravitational desaturation (i.e., development of matric suction). This is only true where the range of suction pressures generated fall below the air entry value; hence, thicker layers of tailings between sand blankets may ultimately deliver both desaturation and accelerated consolidation. Further analyses would be required to ascertain the optimum conditions for a given tailings material and could ultimately be modeled in proprietary software.

The extent to which the sand channels are aiding the desaturation of the tailings is hard to assess based on the limited discrete instrument data points we have. However, extensive geotechnical investigations are planned to take place upon completion of the trial including 42 no. CPTs, 6 boreholes, and extensive sampling for laboratory analyses.

Moving from trials to simulations

Alongside the real time data collection and in preparation for the extensive geotechnical investigation, the demonstration facility is being modeled using Seep/W. The team have conducted an initial model for Phase 1 of the trial in Cell B. This will be extended to Phase 2 and will cover both Cell A and Cell B. Furthermore, the development of a 3D model is intended.

Soil water content characteristics

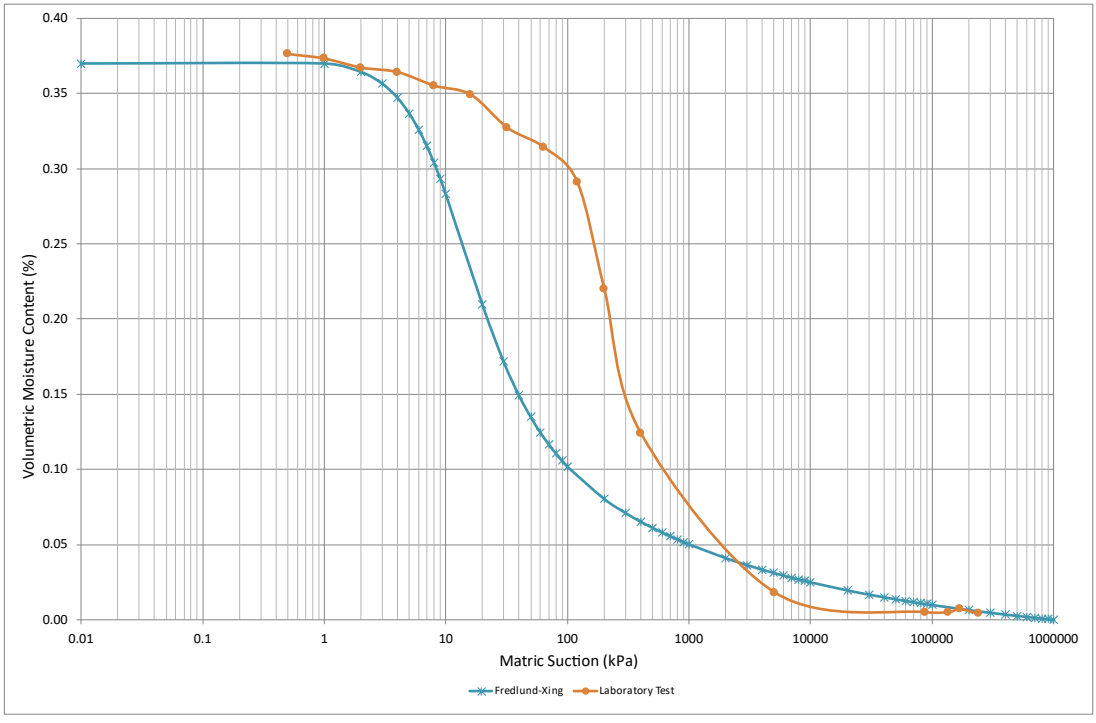


Figure 6: Comparison of matric suctions against volumetric water content for in-situ measurements (blue line) against laboratory measurements (orange line)

The soil water content parameters including the soil water content curves (SWCC) were initially established based on the results of the laboratory test results. The predicted air entry value of circa 40 kPa was not observed in the field. The approach by Fredlund and Xing (1994) was adopted, which is available as a built-in function within the modeling software used (Seep/W).

The comparison between the two resultant SWCC plots is shown in Figure 6. Fredlund and Xing (1994) provides a better correlation of the air entry value to that observed in the field. The specific reasons for the variance are being explored further as part of the ongoing work to build confidence in these modeling tools.

Boundary conditions

Boundary conditions were derived from field data using real-time on-site photos. Images from the cameras indicated the periods of expansion and contraction of the temporary ponds, and site records of tailings and sand deposition were also used. These are crucial factors in numerical modeling, as they influence the available moisture in the tailings. Additionally, the rate of rise of the gradually increasing tailings levels and the thickness of each modeled layer was found to be critical in achieving comparable results between the models and the field observations.

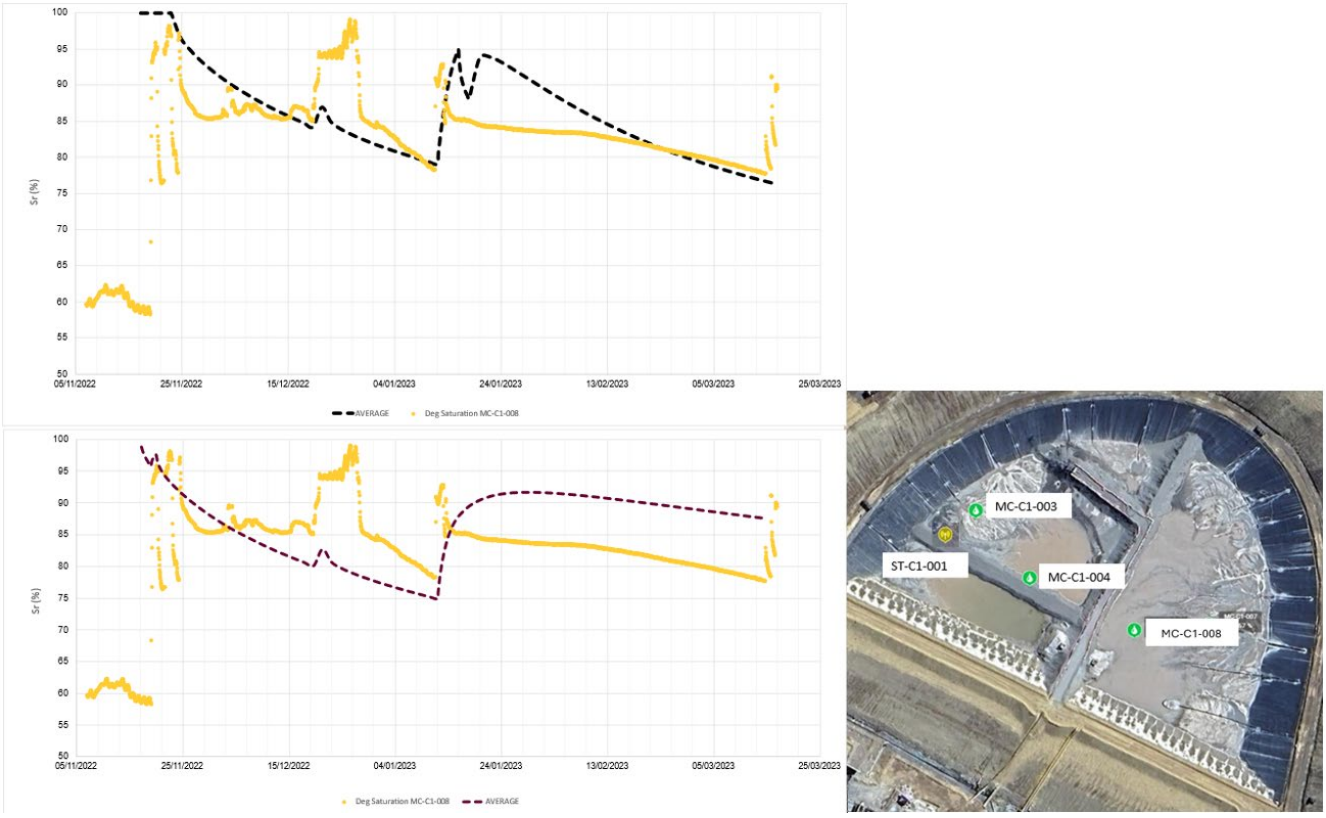


Figure 7: Variation in model calibration due to boundary conditions

The variation in the results, and particularly the steady-state conditions, between models and field results, for varying modeled layer thickness can be seen in Figure 7. For Cell B, this is considered likely associated with the desaturation due to desiccation, and as such may be less critical to the approach being taken in Cell A. This will be explored further as modeling works continue.

Calibration process

During the calibration process, various parameters were evaluated to identify the most relevant for optimizing the numerical model's performance. A few parameters were found to significantly impact the calibration, and they are detailed in the following sub-sections.

Saturated hydraulic conductivity

The saturated hydraulic conductivity of the tailings was analyzed to identify the optimal performance ranges. The study considered two relevant phases of the tailings in relation to field conditions: fully saturated tailings during deposition and partially saturated tailings during consolidation. The modifications to the saturated hydraulic conductivities are detailed in Table 1.

Table 1: Calibrated saturated hydraulic conductivity parameters

Saturated Hydraulic Conductivity	Original Values	Calibrated Values
Wet Tailings	5e-09 (m/s)	1e-08 (m/s)
Consolidated Tailings	1e-09 (m/s)	5e-08 (m/s)

Saturated hydraulic conductivity anisotropy

A review of images from the field cameras revealed that dewatered tailings desiccate and form cracks. This phenomenon enhances vertical flow in the form of finger flow. Therefore, the anisotropy of saturated conductivity was adjusted to find the optimal range, and a value of 1.1 was found to work better than 1. It is noted that this phenomenon is transient and appears to be more significant than the horizontal drainage for Cell B since the drainage paths to lateral drains are much greater than the vertical drainage paths. It is anticipated that anisotropy will have a more significant impact on the calibration process for Cell A, where anisotropy may be closer to a factor of 10.

Phase 1 Cell A seep model results

Simulation results were extracted, compared with the measured data, and are presented in Figure 8.

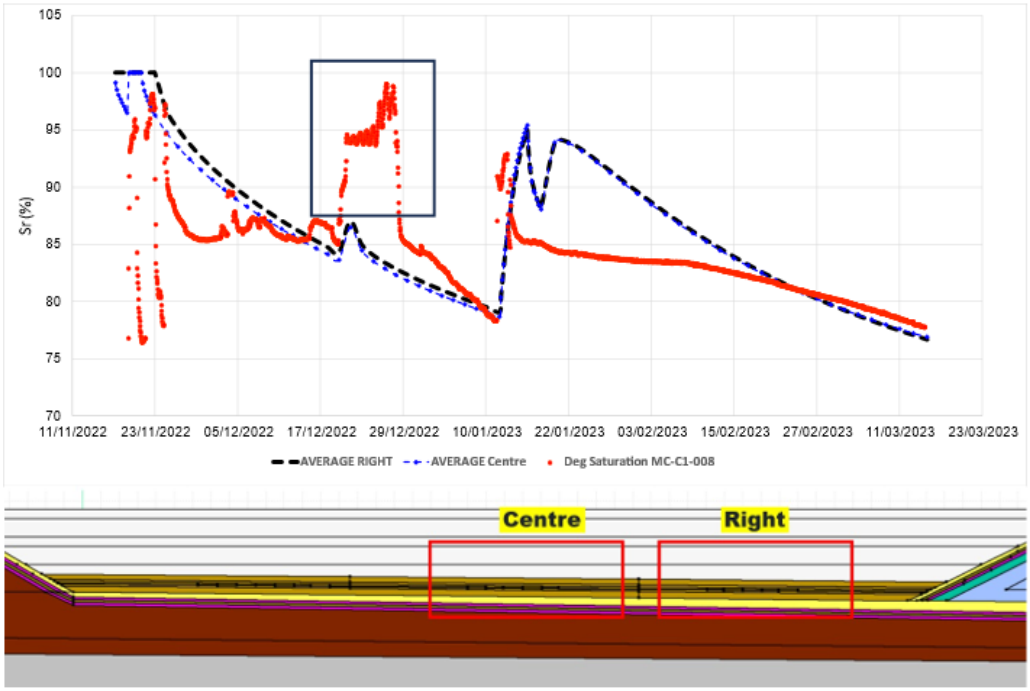


Figure 8: Phase 1 Cell B calibration results

The results indicate a good fit for the calibrated model, both in terms of trends and the steady-state condition of tailings during the consolidation period. During a specific period in December 2022, a high degree of saturation was observed, related to cyclone operation, with the overflow creating a significant pond area on Cell B. This was ignored in the modeling. During this period there is a significant deviation between the model results and field observation. This is highlighted with boxes in Figure 8. The calibrated model does not fully represent the measured data during deposition phases and wetting phases, and this discrepancy is attributed to the limitations of the numerical model in simulating finger flow due to surface desiccation and the transient nature of these characteristics. Importantly, steady-state conditions show a reasonable degree of alignment.

Conclusion

The HDS trial has exceeded expectations and much of the data has supported the hypothesis that a robust basal drainage layer, coupled with horizontal drainage channels, accelerates consolidation and delivers desaturated tailings.

As the demonstration extends vertically, the impacts of the horizontal drainage channels vs. sand blankets are becoming more apparent. The generation of matric suction is noted and the impact of discrepancies between laboratory-tested SWCC parameters and field data needs to be understood further.

The prevalence of drainage paths within a tailings facility will, intuitively, reduce the saturation levels in the co-disposed tailings. Finding the optimum engineering approach is the primary goal of the HDS demonstration team going forward, and modeling results show good correlation to date.

Tailings facilities are not currently designed for closure – the ability for HDS to offer a low-cost route to prevalent drainage offers a pathway to a hydraulically placed, yet rapidly desaturated tailings facility. Phase 2 and 3 modeling will allow prediction of in-situ tailings properties that can then be tested during the proposed extensive site investigation planned for Q4 2024. Water will be continually removed through operational stages of the facility. With the development of a robust cover and upon closure, drawdown to steady state seepage flows will be rapid and long-term water management will be significantly reduced. As operational experience continues to develop and additional laboratory and proof of concept testing generates more data, it is hoped that the HDS Working Group (a community of practice for geotechnical consultants) will facilitate data sharing and accelerate the implementation opportunities for this exciting tailings storage approach.

Acknowledgements

The authors wish to thank Anglo American Sur and the El Soldado Mine for their support. All contractors are also acknowledged for their excellent safety commitment in delivering an LTI-free project (3.5 years in April 2024).

References

Fredlund, D.G. and Xing, A. 1994. Equations for the soil-water characteristic curve. *Canadian Geotechnical Journal* 31 (4): 521–532.

Newman, P., Bruton, M., Burgos, J. and Purrington, J. 2022. Innovations in tailings management – hydraulic “dry” stacking. *Proceedings of Tailings and Mine Waste,* Denver, USA.

Newman, P., Lopez, A., Bruton, M. and Kulmagambetova, A. 2024. Hydraulic dewatered stacking – delivering desaturated tailings management without the capital cost of filtration. *International Conference on Tailings Management*, Santiago, Chile.

Terzaghi, K. and Peck, R.B. 1948. *Soil Mechanics in Engineering Practice*. New York: Wiley.

In-pond Mixing of Fine and Coarse Tailings – Results from a Commercial-scale Pilot in Canada's Oil Sands

Evan Davison, Canadian Natural Resources Ltd, Canada
Lucas Hu, Canadian Natural Resources Ltd, Canada
Bobby Hutchinson, Canadian Natural Resources Ltd, Canada
Peter House, Canadian Natural Resources Ltd, Canada

Abstract

Fluid fine tailings are a low-strength suspension of silts and clays formed during the extraction of bitumen in Canada's minable oil sands. These fluid fine tailings require treatment to support reclamation in a terrestrial landscape. In-pond mixing of treated fluid fine tailings with hydraulically deposited coarse sand tailings has proven to be an effective means of sequestering treated fluid fine tailings and creating a mixed or interlayered deposit with geotechnical properties conducive to terrestrial reclamation. Canadian Natural Resources Limited (Canadian Natural) is evaluating the potential use of in-line flocculation (ILF) as a means of creating a treated tailings material with approximately 45 to 50 wt.% solids content, capable of mixing with coarse sand tailings in an active tailings facility. This work supports Canadian Natural's "end-in-mind" tailings management strategy, in which closure considerations are integrated into mine and tailings planning processes.

Canadian Natural has conducted a multi-year pilot program studying the mixing of ILF-treated fluid fine tailings with hydraulically deposited coarse sand tailings. Building on ILF experience gained from atmospheric fines drying operations, the pilot program consisted of bench-scale proof of concept testing, development of a conceptual model for in-pond mixing, and execution of a commercial-scale mixing pilot over two successive summer seasons with different depositional configurations. Site investigations were conducted throughout the program to characterize the tailings deposits. This paper presents results from the pilot program. The presented results include the index properties and strength of the dewatered fluid tailings prior to sand addition, as well as the geometry, composition, strength, and consolidation properties of the resulting mixed deposit.

Introduction

Stabilization of fluid fine tailings (FT) produced during the aqueous extraction of bitumen is a key

consideration for mine reclamation and closure in the Athabasca oil sands in Alberta, Canada. Mine operators in the region aim to reclaim disturbed areas to form self-sustaining boreal forest ecosystems following mine closure, incorporating both terrestrial and aquatic elements into the closure landscape.

Challenges associated with reclamation of FT in a terrestrial landscape are well documented (COSIA, 2012 and 2014) and extensive research has been developed in this area over the past two decades. The addition of sand to FT to form a fines enriched sand or mixed deposit is a concept with the potential to improve the geotechnical performance of FT, resulting in deposits with strength conducive to capping and consolidation properties that can be accommodated in practical landform designs. Canadian Natural is evaluating the use of in-line flocculation (ILF) to form a treated FT product that can be mixed with coarse sand tailings (CST) to form a fines-enriched sand deposit. This paper presents the results from laboratory testing and field-scale piloting of various ILF FT/CST mixing techniques.

Background

Canadian Natural has observed the mixing and bedding of centrifuged FT (CFFT) and CST in the Jackpine Mine (JPM) External Tailings Facility (ETF), creating deposits that satisfy regulatory and technical performance criteria (Canadian Natural, 2022). Building on the observed CFFT/CST mixing behavior, it was hypothesized that ILF could be used to create a product similar to CFFT, which could be subsequently mixed with CST to achieve similar deposit performance.

Flocculation is a well-established means of treating and dewatering tailings slurries; however, flocculants are usually added into relatively dilute slurries. Recently a number of processes were developed for flocculation of relatively dense slurries, including Canadian Natural's Atmospheric Fines Drying (AFD) process. In the AFD process, high molecular weight anionic polyacrylamide (aPAM) is added as a bridging flocculant via jet mixing to FT at greater than 12 vol.% solids. A highly turbulent environment creates good conditions for rapid mixing of the polyacrylamide solution with FT; however, poor conditions for building large flocs are critical to the AFD process. So, exposure to high turbulence is brief (< 1 s), and the momentum of the stream is rapidly dissipated to transition to an environment more ideal for flocculation (low shear rate).

The resulting product is typically high yield stress (> 200 Pa) and/or very high permeability – capillary suction times are essentially unmeasurable as the rate of water release is too fast. The high yield stress is indicative of the formation of very large flocs (un-flocculated FT will typically have a yield stress 100× lower than AFD product). When this is achieved, FT will typically dewater from circa. 30 wt.% solids to 45 to 50 wt.% solids within a 24-hour period – comparable to CFFT, but stronger due to a high extent of residual flocculation. This similarity to centrifuge properties was the driver to attempt the ILF FT/CST

mixing process, in which the AFD flocculation process was used to form large sub-aqueous deposits of ILF FT for subsequent mixing with CST.

Pilot development

Conceptual model

Based on the observed CFFT/CST mixing behaviors, and incorporating learnings from commercial AFD operations, pilot work was developed with a focus on in-pond mixing of ILF FT and CST. In support of this objective, a laboratory-scale tailings mixing research project was carried out to characterize the mixing behavior of CST deposited into ILF FT in-pond. The work involved a desktop study, a series of jet (jar) tests, and physical model tests (flumes with length, width, and height of 240, 10, and 40 mm, respectively).

Eight jar tests were conducted to qualitatively assess the mixing behavior for different tailings types and CST addition methods. Approximately 2 L of treated FT was placed in 12×12×40 cm (length, width, and height) jars before fluidized CST was added by dropping from height. Three types of treated FT samples were tested, including ILF FT, CFFT, and shear-thinned CFFT. Each sample was tested with two CST velocities, controlled by drop heights of 0.1 and 1 m. An additional two tests were conducted on the shear-thinned CFFT using a constant drop height of 0.5 m and with the CST added in 20% (vol.) increments. It was observed that the ILF FT had the least sand penetration, followed by CFFT and shear-thinned CFFT. The higher drop height and higher CST addition frequency resulted in more penetration of CST into the treated FT.

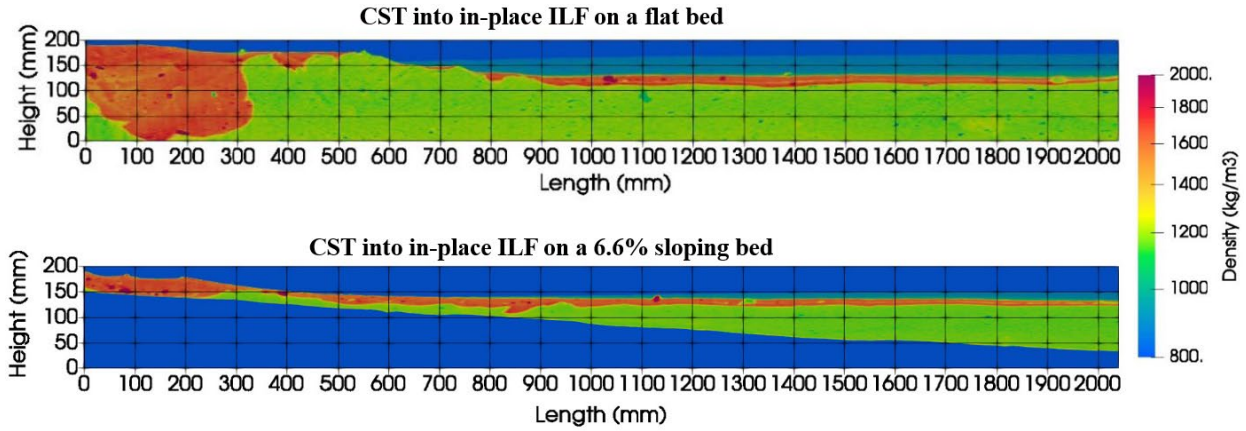


Figure 1: Density profiles of flume test deposits

The flume tests used ILF FT samples collected during the 2022 pilot. The geometry of the flume was based on a 1:100 scale of the expected field conditions and the tests were conducted with and without a 6.6% base slope. The ILF FT material was poured at the deposition end of the flumes and the top surfaces were levelled using a plastic plate. Prior to CST addition, ILF FT in the sloped-bed flume was present 20 mm thick on the first half of the slope, increasing in thickness up to 90 mm at the distal end of the flume.

ILF FT thickness in the flat-bed flume was 100 mm prior to CST addition. Fluidized CST with 55 wt.% solids content was discharged from height into the ILF FT. The resulting deposit was scanned using a computed tomography scanner. The density profiles of the deposits from the flat bed and sloped-bed flume tests are shown in Figure 1.

In both flume tests, CST formed a block near the discharge point and started to form a thin layer on top of the ILF FT. It was noted that more ILF FT was displaced by CST in the flat-bed flume. Figure 2 provides a conceptual model for the CST and ILF FT mixing behavior based on the observations and data collected during the jar and flume tests. At various points along the profile of a deposit, the ILF FT could be subject to erosion, entrapment, entrainment, and/or displacement, with behavior dependent on a number of variables. In the conceptual model, erosion occurs as CST slurry flows in parallel with the ILF FT deposit on the slope. Eroded ILF FT are incorporated into the CST slurry and degree or depth of erosion may be numerically represented by the entrainment ratio presented by Cenedese and Adduce (2010), which increases with Froude and Reynolds numbers.

Specifically, erosion increases with velocity and density of the CST slurry and decreases with density of the ILF FT. Entrapment occurs when the ILF FT or ILF FT/CST mixed material have sufficient strength to support the load of CST. Newton's second law in the vertical direction was used to describe the entrainment and displacement behaviors. Parameters governing entrainment and displacement behavior include mass rate and velocity of CST slurry and density and yield stress of ILF FT. Additional work is ongoing to investigate the relationship between ILF FT yield stress, shear rate, and consolidation pressure in order to further characterize in-pond mixing of ILF FT and CST.

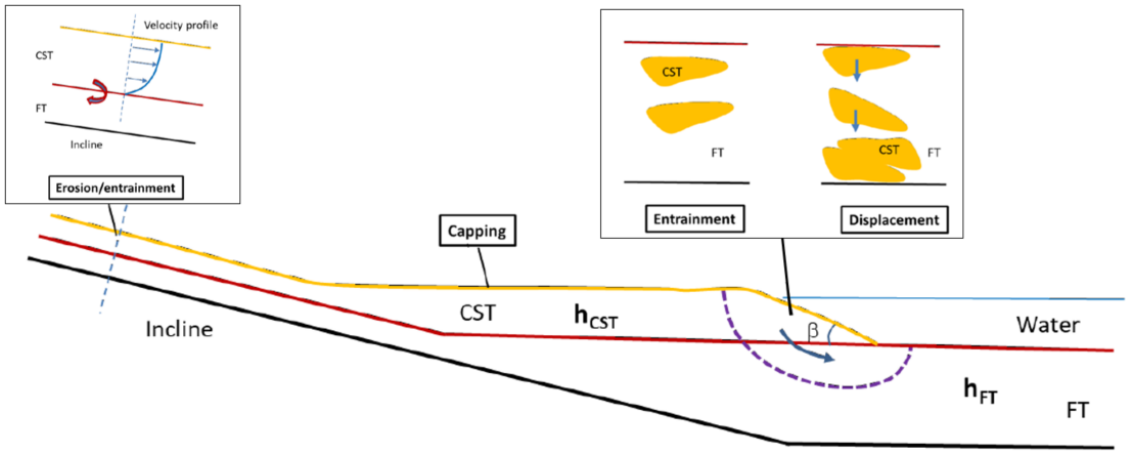


Figure 2: Illustration of CST and ILF FT mixing mechanisms

Trial location and setup

Fluid Cell 1 (FC 1) at JPM was chosen as the location for the field trial based on several factors including access to both CST and raw FT feed lines, relatively little previous deposition, and the ability to divert

production-related tailings to other cells during the trial period. This configuration ensured acquisition of the most accurate and clean data possible by minimizing variables that could impact the study outcomes.

The polymer used to treat the raw FT was received dry at site and required hydration prior to in-line injection for FT treatment. A skid-based hydration system and associated infrastructure were installed in an existing laydown roughly 500 m from the trial area in FC 1. The raw FT and hydrated polymer pipelines were piped to the deposition location on the south shoreline of FC 1 where the hydrated polymer was injected into the raw FT pipeline 3 m from the end of the pipe, forming ILF FT.

The injection header was setup to generate turbulent conditions immediately upon injection of the polymer solution to maximize contact between the polymer and the fines within the FT and then reduce turbulence shortly thereafter to minimize shearing of the flocculated FT. Turbulent conditions were generated by a reduction in piping diameter at the injection location and the subsequent dissipation of energy was accomplished by submerging the discharge of the ILF FT line in the treated tailings plunge pool. Figure 3 shows the configuration of the polymer injection header and discharge during ILF FT production.



Figure 3: Photograph showing ILF FT flocculant injection spool and submerged discharge line

Piping was installed to facilitate the deposition of CST on the north and south sides of the existing CST beach in FC 1. During the 2022 pilot, CST was deposited from both locations to confine the ILF FT in the southern half of FC 1 and promote mixing. During the 2023 pilot, the north CST deposition location was not used and CST was only deposited from the south deposition location. During both pilot seasons,

ILF FT was deposited from the south deposition location. Figure 4 shows the general layout and setup for the 2022 and 2023 pilots in JPM FC 1.

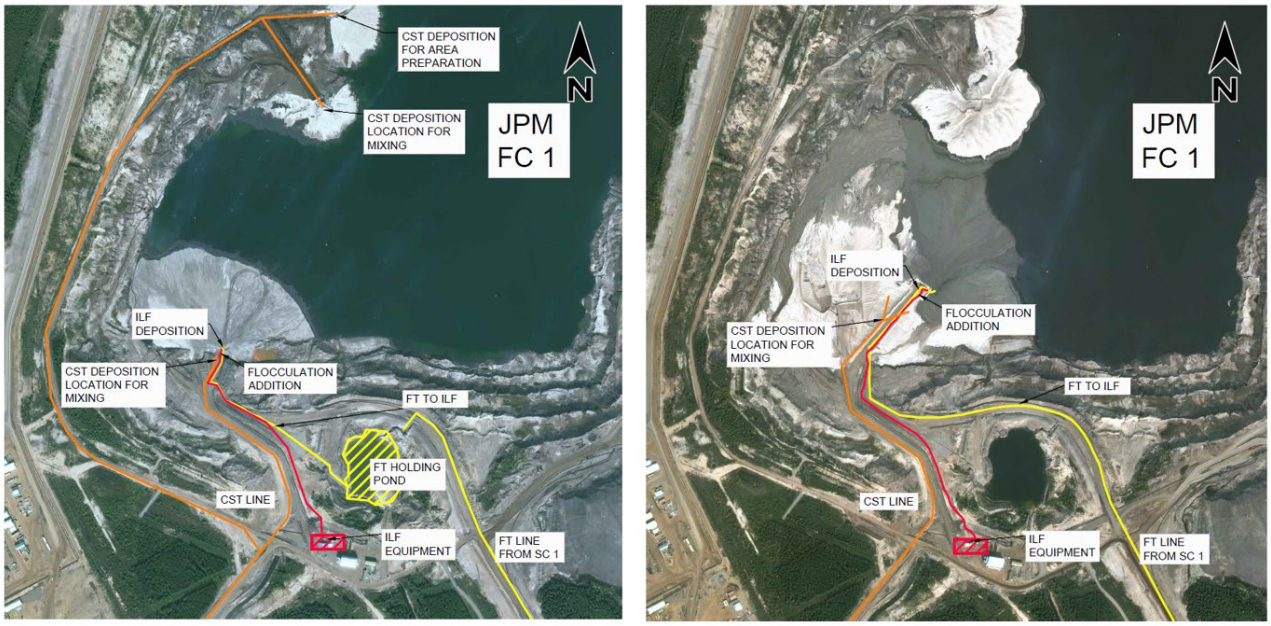


Figure 4: Infrastructure layout for 2022 (left) and 2023 (right) ILF FT/CST mixing pilots

Material properties

Raw FT was supplied to the pilot from a dredge located on the JPM external tailings facility at a design flow rate ranging between 800 to 1,000 m^3/hr. The average solids content of the raw FT was 26 wt.%, the fines content (<44 µm) was typically greater than 90 wt.%, and the residual bitumen was approximately 1.5 wt.%. Properties of the ILF FT prior to CST addition were variable due to the progressive dewatering of the material over time in the pond. The solids content of the ILF FT ranged from 40 to 50 wt.%, the dry density ranged from 1,300 to 1,450 kg/m^3, and the average yield stress was approximately 200 Pa. The CST stream deposited into the ILF FT had an average flow rate of approximately 7,500 m^3/hr and an average dry density of 1,510 kg/m^3. Mineral solids in the CST slurry are comprised of predominantly sand-sized particles.

In-pond mixing pilot program

The following sections summarize the activities undertaken during the two-year ILF FT/CST in-pond mixing pilot program. The 2022 and 2023 pilot results represent mixing performance following in-situ dewatering of ILF and deposition of CST under confined and unconfined beach below water (BBW) conditions, respectively.

Deposition activities

2022 Pilot – confined mixing conditions

The ILF FT produced during the 2022 pilot was deposited in the southwest corner of FC 1 and accumulated adjacent to the discharge on the beach above water (BAW) and on the slope of the pre-existing CST BBW. Over the course of the Phase 1 pilot, 1.4 Mm^3 of raw FT was treated, forming 0.65 Mm^3 of dewatered ILF FT in the trial area. 2.95 Mm^3 of CST was deposited into the ILF FT from the two locations shown in Figure 4, with 1.6 Mm^3 deposited into the ILF FT from the north deposition location and 1.35 Mm^3 deposited from the south location. This deposition resulted in the formation of 1.3 Mm^3 of ILF FT/CST mixed deposits during the 2022 pilot.

Sand deposition from 2022–2023

Following completion of the final 2022 pilot site investigation, and prior to the start of the 2023 pilot, approximately 0.95 Mm^3 of CST was deposited into FC 1 during normal operations of the tailings cell. This CST deposition resulted in the formation of an additional 0.6 Mm^3 of mixed ILF FT/CST deposit as residual ILF FT leftover from the Phase 1 pilot was captured. The deposit formed during this period was sandier than the deposit formed during the Phase 1 pilot due to the reduced volume of ILF FT available for mixing.

2023 Pilot – unconfined mixing conditions

The 2023 ILF FT/CST mixing pilot was set up to test mixing performance with limited downstream confinement at the toe of the BBW. ILF FT was deposited across the beach formed during the phase 1 pilot from the south deposition location. During the Phase 2 pilot, 1.4 Mm^3 of raw FT was treated, forming 0.68 Mm^3 of dewatered ILF FT in the trial area. The produced ILF FT accumulated on the BAW and BBW slopes downstream of the discharge location and was allowed to flow through a central unconfined central channel into the pond. Confinement of the ILF FT during the 2023 pilot was limited to the southeast corner of the BBW where a submerged dyke slope was present. Following the completion of ILF FT production, 1.7 Mm^3 of CST was deposited into the ILF FT from the south deposition location, in the same direction as ILF FT deposition. This deposition resulted in the formation of 0.9 Mm^3 of ILF FT/CST mixed deposit during the 2023 pilot.

Results

Site investigations were completed at various points throughout pilot program to validate performance of the ILF FT treatment system, measure properties and geometry of the ILF FT prior to sand addition, and to characterize the ILF FT/CST mixed deposits. In total, over 100 in-situ tests (cone penetration test (CPT), ball penetration test, electric vane shear test) were completed and over 1,500 tailings samples were collected

and tested to support the assessment of ILF FT/CST mixing performance over the two-year period.

Observations

The post-CST deposition site investigations highlighted regions within the trial area that demonstrated the behaviors of erosion, entrapment, entrainment, and displacement, similar to those hypothesized in the conceptual model. Figure 5 shows the observed regions within the 2022 (left) and 2023 (right) trial deposits.

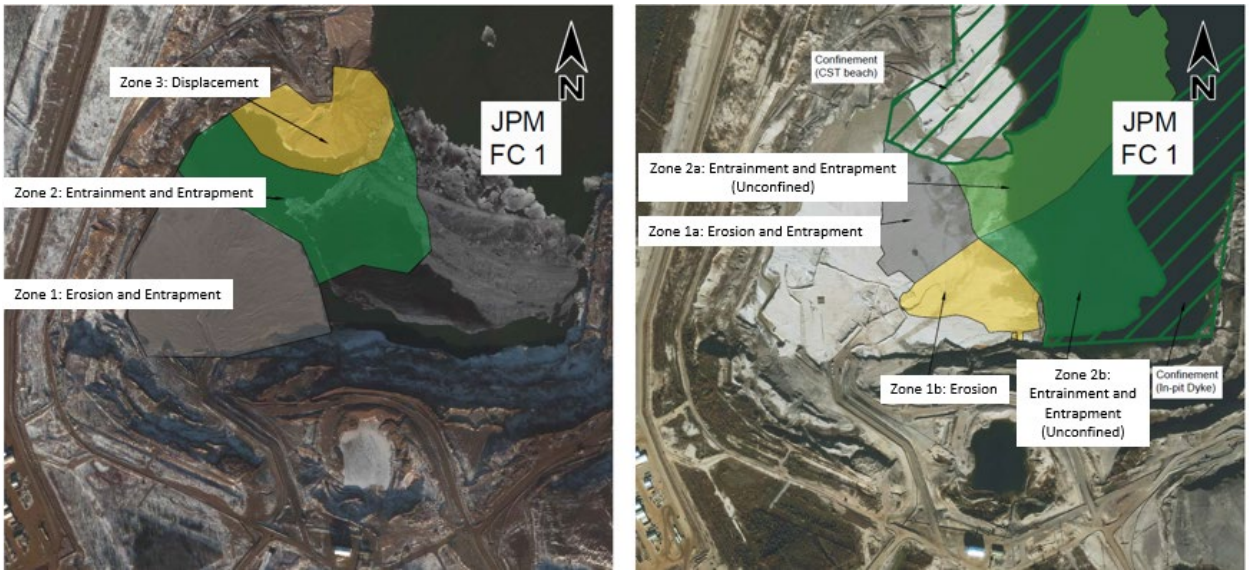


Figure 5: Behavioral regions observed following 2022 (left) and 2023 (right) ILF FT/CST mixing pilots

During the 2022 pilot, the in-pond ILF adjacent to the pit wall was generally displaced by the high-energy CST stream from the north deposition location. In the region located on the BAW immediately downstream of the south CST deposition location, a portion of the ILF FT present on the BAW was eroded by the CST and a portion of the ILF FT was capped (or entrapped) in place. In this region a CST-capped bed of ILF FT, generally 0.5 m thick, was observed at several BAW testing locations at the base of the deposit. The third region, located in-pond on the BBW slope downstream of the south CST deposition location, was characterized by entrainment and entrapment of the ILF FT into the trial beach. Fines incorporated into the beach in this region were comprised of eroded ILF FT from the BAW upstream as well as the in-pond ILF FT present on the BBW slope at the time of CST deposition. At the conclusion of the Phase 1 pilot, out of the 0.65 Mm^3 dewatered ILF FT, approximately 0.2 Mm^3 remained unmixed in the pond. This residual ILF FT was captured by CST deposition that occurred between the two pilot seasons.

During the 2023 pilot, the ILF FT present on the BAW prior to CST deposition was predominantly eroded, with only limited observations of a capped ILF FT bed on the BAW. This behavior differed from the frequent observations of capped ILF FT observed during the 2022 pilot, and was attributed to the

reduced aging time of the BAW ILF FT prior to CST addition. The observed behaviors on the BBW slopes differed depending on the degree of confinement at the toe, with more entrainment and entrapment observed in the confined region of the deposit than in the unconfined region. At the conclusion of the 2022 pilot, approximately 0.35 Mm^3 of unmixed ILF FT remained in the pond out of the 0.68 Mm^3 that was available for mixing. Based on observations following the 2022 pilot, this residual ILF FT is expected to be captured with additional CST deposition into FC 1.

Mixed deposit composition

The sampling data were used to generate a 3D block model of the ILF FT/CST mixed deposit. Figure 6 shows the modeled geometry and sand fines ratio (SFR, wt% of mineral solids larger than 44 µm over the wt% of mineral solids smaller than 44 µm) of the deposits formed during the 2022 and 2023 ILF FT/CST mixing pilots. In both pilot seasons, ILF FT/CST mixed deposits were successfully formed in the trial area. Incorporation of fines in the BAW and BBW was limited in areas where high-energy CST contacted unconfined ILF FT, evidenced by high SFR regions within the deposit. ILF FT which was eroded upstream, tended to be entrained or entrapped within the beach at lower elevations along the BBW slope as deposition energy decreased. In areas where the deposit was confined, increased entrainment and entrapment of ILF FT within the beach was observed.

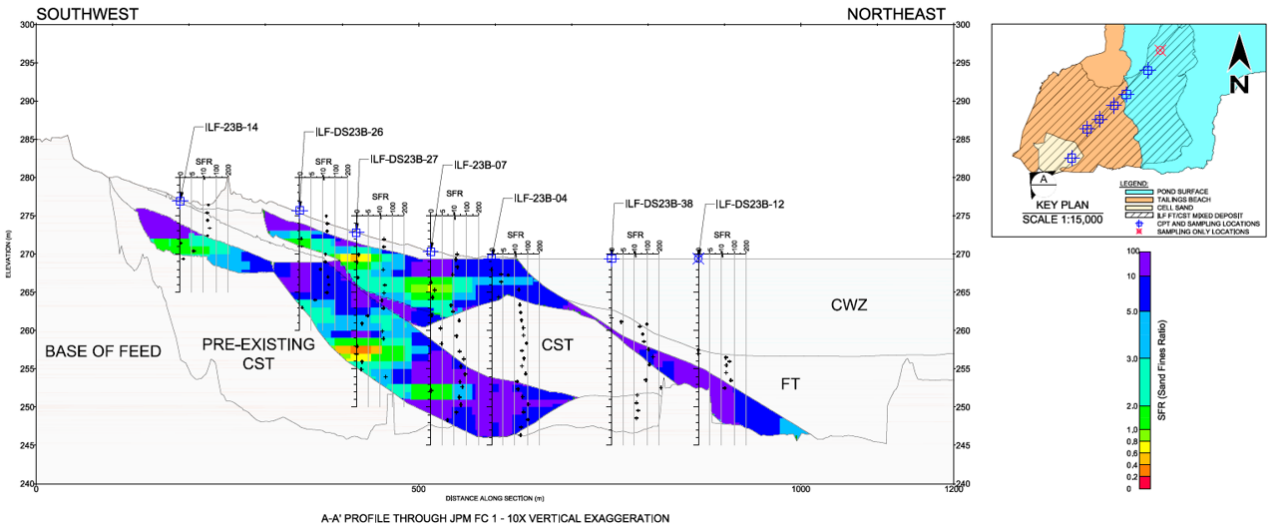


Figure 6: Geometry and composition of ILF FT/CST mixed deposits (adapted from Canadian Natural, 2024)

The block modeled properties of the deposit formed during the pilot program are presented in Table 1. The total estimated volume of the mixed deposit produced during the trial was 2.8 Mm^3, including the sandier mixed material formed via sand deposition between the 2022 and 2023 pilots, and not including

clean CST cap present on top of the mixed deposit. The modelled average solids content of the ILF FT/CST mixed deposit was 73.3 wt.%, ranging from 53 to 88 wt.%. The modeled average SFR was 3.9.

Table 1: ILF FT/CST mixed deposit properties

Deposit Zones	Estimated Deposit Volume (Mm³)	Modeled Solids Content and Range (wt.%)	Modeled SFR
2022 ILF FT/CST mixed deposit	1.3	75.2 (66–88)	3.2
2022-2023 ILF FT/CST mixed deposit	0.6	73.9 (53–78)	5.5
2023 ILF FT/CST mixed deposit	0.9	72.3 (54–87)	4.3

Laboratory testing data for ILF FT/CST mixed deposit samples used to populate the block model are shown on a ternary diagram (Figure 6). Regions illustrating the potential range of CST and ILF FT slurry and deposit properties are provided for reference. The data on the figure represent tailings samples collected following the 2023 pilot season and classified as ILF FT/CST mixed deposit. Note that the geometry of the pre-CST ILF FT deposit was considered when defining the extents of the mixed deposit in FC 1 in order to assess the efficiency of fines capture during the pilot program. As such, regions dominated by displacement are included in the data set in some cases. These sand-dominated regions are apparent in Figures 6 and 7.

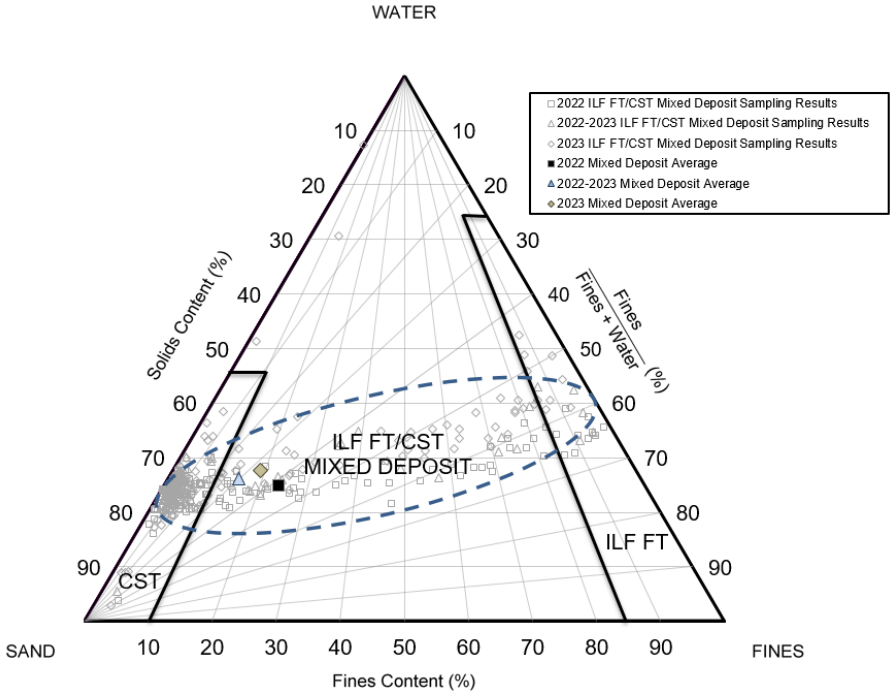


Figure 7: ILF FT/CST mixed deposit properties

Mixed deposit strength and heterogeneity

The in-situ testing programs completed at various points during the 2022 and 2023 pilots helped to inform the results and analyses presented above and provide insights into the characteristics of the ILF FT/CST mixed deposit. Given the multi-stage deposition approach and the nature of the fluvial deposition environment, the ILF FT/CST mixed deposit formed as a heterogeneous blend of entrapped high-fines beds, regions of entrained fines, and coarser low-fines zones. The development of this interlayered deposit in a commercial-scale field pilot supports the concept of enhanced fines capture through comingling of fine and coarse tailings streams hypothesized by BGC Engineering (2017).

Figure 8 shows a representative profile through the ILF FT/CST mixed deposit, including both sampling and CPT data, illustrating the complex inter-bedding of coarse and fine tailings throughout the profile. The measured undrained shear strengths consistently exceed 10 kPa. High-fines beds are typically less than 5 m thick, and are regularly overlain, or entrapped, by coarse tailings as the deposit is formed. This configuration is expected to result in more rapid consolidation of the fine tailings when compared with a homogeneous high-fines deposit because of the relatively short drainage paths and overall increase in coarse material present within the interlayered deposit. At this location, the deposit has been successfully capped with up to 4 m of CST at surface and any fine tailings present below the cap are expected to remain sequestered in place.

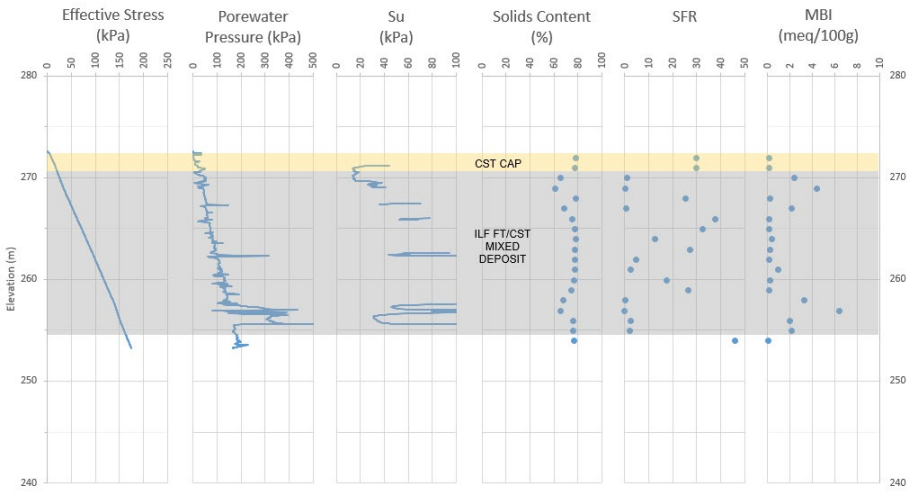


Figure 8: Example of heterogeneous ILF FT/CST mixed deposit profile

Mixed deposit consolidation properties

A series of consolidation tests were completed on samples collected following the 2022 pilot, selected to reflect a range of properties within the ILF FT/CST mixed deposit. Results from selected consolidation tests on samples with SFRs near the average of the ILF FT/CST mixed deposit are provided in Figure 9. Previously published consolidation testing data from CFFT/CST mixed deposits at similar SFRs are

included for comparison. The results show that ILF FT/CST mixed deposits and CFFT/CST mixed deposits have similar compressibility, evidenced by the convergence of the void ratio vs effective stress curves at anticipated in-situ effective stresses > 100 kPa. This suggests that ILF FT/CST and CFFT/CST mixed deposits are expected to undergo a similar magnitude of ultimate settlement if a similar initial void ratio (or solids content) is developed within the deposit. At comparable void ratios and SFRs, the hydraulic conductivity of ILF FT/CST material was found to be typically 0.5 orders of magnitude greater than that of CFFT/CST, indicating that consolidation of ILF FT/CST mixed deposits is expected to progress faster than consolidation of CFFT/CST deposits.

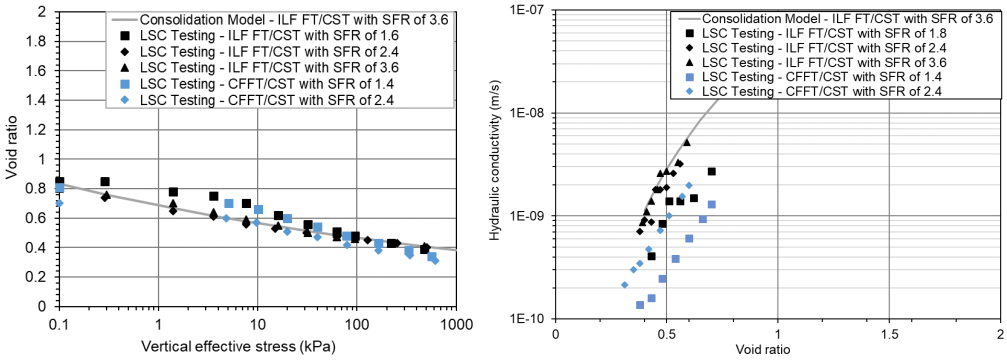


Figure 9: Large strain consolidation test results for ILF FT/CST and CFFT/CST mixed deposits

Conclusion

Results from the ILF FT/CST mixed deposit testing demonstrated the behaviors of erosion, entrainment, entrapment, and displacement identified in the conceptual model. The complex depositional environment resulted in a heterogeneous deposit with erosion and displacement tending to be more prevalent on the BAW and upper BBW slopes, entrainment and entrapment tending to be more prevalent on the lower BBW slopes, and displacement occurring in areas where high-energy CST was deposited into unconfined ILF FT. Based on the results from the pilot, the dominant drivers influencing fines-coarse mixing are hypothesized to be the density and strength of the ILF FT prior to CST addition, which increase with dewatering of the ILF FT in-situ, and the energy of the incoming CST, which decreases with distance from the discharge location.

Confinement at the toe of the ILF FT deposit also served to increase the entrainment/entrapment of fines into the trial beach. The ILF FT/CST mixed deposits were found to have strengths sufficient to support the development of a hydraulically placed sand cap both within the deposits, entrapping bedded high-fines layers, and at the surface. Consolidation testing results suggest that the magnitude of ILF FT/CST mixed deposit settlement will be similar to published values for CFFT/CST mixed deposits and that the rate of consolidation will be faster.

Overall, the pilot program demonstrated that in-pond mixing of ILF FT with CST is a viable means of producing a mixed sandy-fine deposit under the conditions tested. Potential next steps for the research program include:

- continued laboratory study to develop quantitative metrics that govern mixing behavior;
- development of 1D consolidation models based on the consolidation testing data and validation against field-measured settlement; and
- continued piloting to optimize and balance the metrics governing mixing behavior with operational constraints in an active tailings cell.

Acknowledgements

The authors would like to highlight the significant contributions made by Gavin Freeman, Paul Korba, Ian Mountain, Kate Bullis, Karsten Rudolf, Hayden Mills, Walter Prawdzik, and Mark Larade during the development, construction, and execution of the pilot program. Additionally, the authors would like to recognize Yadong Zhang, Longyang Shi, and Professor Ron Wong who were responsible for conducting the laboratory-scale jet and flume tests and developing the conceptual ILF FT/CST mixing model at the University of Calgary.

References

BGC. 2017. Prospects for enhancing fines capture in conventional tailings facilities. Consultant's report prepared for COSIA (Canada's Oil Sands Innovation Alliance) by BGC Engineering Inc, Edmonton. Report 1116-002, December 13, 2017.

Canadian Natural. 2022. Jackpine Mine Fluid Tailings Management Plan Amendment.

Canadian Natural. 2024. 2023 Jackpine Mine Fluid Tailings Management Report.

Cenedese C. and C. Adduce. 2010. A new parameterization for entrainment in overflows. *J. Physical Oceanography* 40: 1835–1850.

COSIA. 2012. Technical Guide for Fluid Fine Tailings Management. Canada's Oil Sands Innovation Alliance Report

COSIA. 2014. Guidelines for Performance Management of Oil Sands Fluid Fine Tailings Deposits to Meet Closure Commitments. Canada's Oil Sands Innovation Alliance. Calgary. Feb 2014.

Evaluating Iron Ore Tailings' Variability in an Upstream Dam For Dam Closure

Thatyane Martins Gonçalves, Vale S.A., Brazil
Alexia Cindy Wagner, Universidade Federal do Rio Grande do Sul, Brazil
João Vítor de Azambuja Carvalho, Universidade Federal do Rio Grande do Sul, Brazil
Frank Pereira, Vale S.A., Brazil
Nilo Cesar Consoli, Universidade Federal do Rio Grande do Sul, Brazil

Abstract

Tailings dams are among the biggest structures ever constructed. Managing and operating these structures is an arduous task that demands a deep understanding of tailings and mining processes. The lifecycle of tailings dams includes conception, construction, operation, and closure. Especially in Brazil, new legislation has demanded the closure of upstream raised tailings dams and prohibited the construction of dams by this method after recent incidents. Closing a tailings dam requires decommissioning the structure (it no longer receives material nor operates as a dam) and then rehabilitation of the dam area. However, closure operations pose several challenges – e.g., tailings variability, lack of records for the structure, changes occurring in the material over the deposition period, and insufficient safety for closure work. The tailings' variability can come from their natural variability, effects of uneven sedimentation and deposition, and changes in the beneficiation processes during the years (e.g., increasing mineral recovery with new technology).

This paper aims to evaluate the tailings variability in a dam that will be decommissioned soon. Hence, piezocone penetration tests were evaluated, and samples were collected at different points of the dam. The results were evaluated, and the response of different tailings was verified through in-situ testing and laboratory testing. The results demonstrated a stratified profile of tailings with variable particle size distribution. Regarding the laboratory tests, the finer tailings generally were more compressive than coarser tailings. Nonetheless, the strength mobilization for distinct tailings was similar, probably due to the common nature of the tailings in the dam.

Introduction

Sustainable mining principles require planning and designing all facilities in ore exploitation to deal with the distinct phases of this industrial operation. Regarding tailings storage facilities, it is necessary to evaluate several aspects during their lifecycle, such as the conception, construction, operation, and closure (Spitz and Trudinger, 2019). Among the viable options for tailings disposal, dams are the most common and cost-effective, although they are also the most challenging structures to operate (Santamarina et al., 2019; Yin et al., 2011). In upstream-raised dams, the dam storage capacity is expanded by raising the starting dyke over the previously stored material. Hence, the new dykes are supported by tailings themselves, usually in a loose and saturated state.

In Brazil, recent disasters motivated changes in legislation, requiring the closure of existing upstream raised tailings dams and prohibiting their construction. At the time, around sixty upstream raised tailings dams existed in Brazil, of which 3 were classified as stage 3 risk obligating immediate closure (ANM, 2023). However, tailings dam closure operations are challenging environmentally, economically, and in terms of safety, besides being very site-specific and despite there being few reports of successful cases. One aspect that makes closure operations intricate is the tailings' spatial variability inside the structure. Variability can come from uneven sedimentation and deposition effects, evolution in beneficiation processes over the years aiming for greater ore recovery, and the natural variability of the ore's deposit.

Tailings' characteristics can vary significantly inside a dam depending on their position. For example, tailings nearer to the deposition point usually are coarser, while those further from the deposition point are usually finer since finer particles take more time to sediment and thus are carried further (Consoli and Sills, 2000). Furthermore, tailings are generally mixed mineralogy geomaterials, and can be composed of minerals with very different specific gravities, resulting in complex sedimentation patterns. Li and Coop (2019) investigated the behavior of tailings from different locations of an impoundment and reported differences arising since particle size distribution (PSD) to constitutive parameters. The effects of grading and mineralogy on the behavior of tailings have been thoroughly investigated and demonstrated to highly influence their mechanical response (e.g., Consoli et al., 2024; Wagner et al., 2023).

The effects of fabric on tailings have also drawn the attention of researchers (Carrera et al., 2011; Carvalho et al., 2024; Chang et al., 2011). However, sampling undisturbed tailings at dam sites is still unresolved (Shuttle and Jefferies, 2016). Obtaining representative samples of tailings from impoundments is rather challenging due to their cohesionless nature and the usually loose state in which they are found. Although developments are currently being pursued in this sense (e.g., Dominguez-Quintans et al., 2023; Reid and Fanni, 2022), the use of in-situ tests remains the viable option to characterize tailings in dams and investigate their variability. The cone penetration test (CPTu) has long been used to determine the

geotechnical profile of tailings impoundments, as well as to estimate tailings properties and their state at the dam (Ayala et al., 2022; Shuttle and Jefferies, 2016; Shuttle and Cunning, 2007).

Therefore, this paper aims to investigate tailings variability inside a dam to be closed through in-situ and laboratory tests. The profile of tailings at two distinct points was determined by CPTu and representative tailings samples were selected for laboratory testing. Triaxial tests on reconstituted samples were conducted to investigate the differences arising from the distinct PSD and mineralogy of tailings on constitutive parameters necessary for properly designing closure operations.

Methodology

In-situ testing

The field investigation comprised piezocone tests executed according to ASTM 5778 (ASTM, 2020). The tests were performed with 10 cm² piezocones, a penetration velocity of 2 cm/s, and data acquisition with a resolution of 2 cm. The tests were performed at two locations in the same structure: one point is closer to the original tailings' deposition point, and the other is further away. Also, the typical profiles obtained from CPTu were used to identify the tailings characteristics along the depth.

Laboratory characterization

Based on the field tests, three samples of different materials were collected for laboratory characterization. The tailings were subjected to physical and mineralogical characterization tests. Also, consolidated drained triaxial (CID) tests were performed on a fully automated triaxial apparatus, in three main stages: saturation, consolidation, and shearing. The saturation stage consisted of CO_2 percolation, de-aired water flushing, and incrementing the backpressure until a B-value greater than 0.95 was obtained. After saturation, specimens were consolidated under hydrostatic conditions and then were sheared in a strain-controlled condition at 1 mm/hr. The specimens for triaxial tests were molded using the moist tamping method, and the confining pressures used were 100, 200, and 400 kPa. The experimental program focused on determining the extent of the variability of tailings properties, rather than simulating their in-situ fabric. Therefore, moist tamping was selected as the standard procedure because it enables obtaining mostly uniform specimens over a broad range of void ratios. Dense specimens were targeted (around 80% of relative density) to enable the evaluation of strength and dilatancy parameters usually adopted in conventional constitutive models.

Results

In-situ testing

Two piezocone tests were conducted at different locations inside the dam. CPTu-01 was conducted further from the deposition point, while CPTu-02 was nearer. Figure 1 presents the results of these tests. Both

CPTu profiles are stratified and present large portions with small tip resistance. Moreover, marked pore pressure generation occurred during piezocone penetration, indicating possible effects of partial drainage or completely undrained behavior. The main difference in the CPTu profiles is that CPTu-02 had a thick sandy layer below 6 m depth, clearly shown by the increase in tip strength q_t and the drop in pore pressure generation, remaining close to the equilibrium pore pressure.

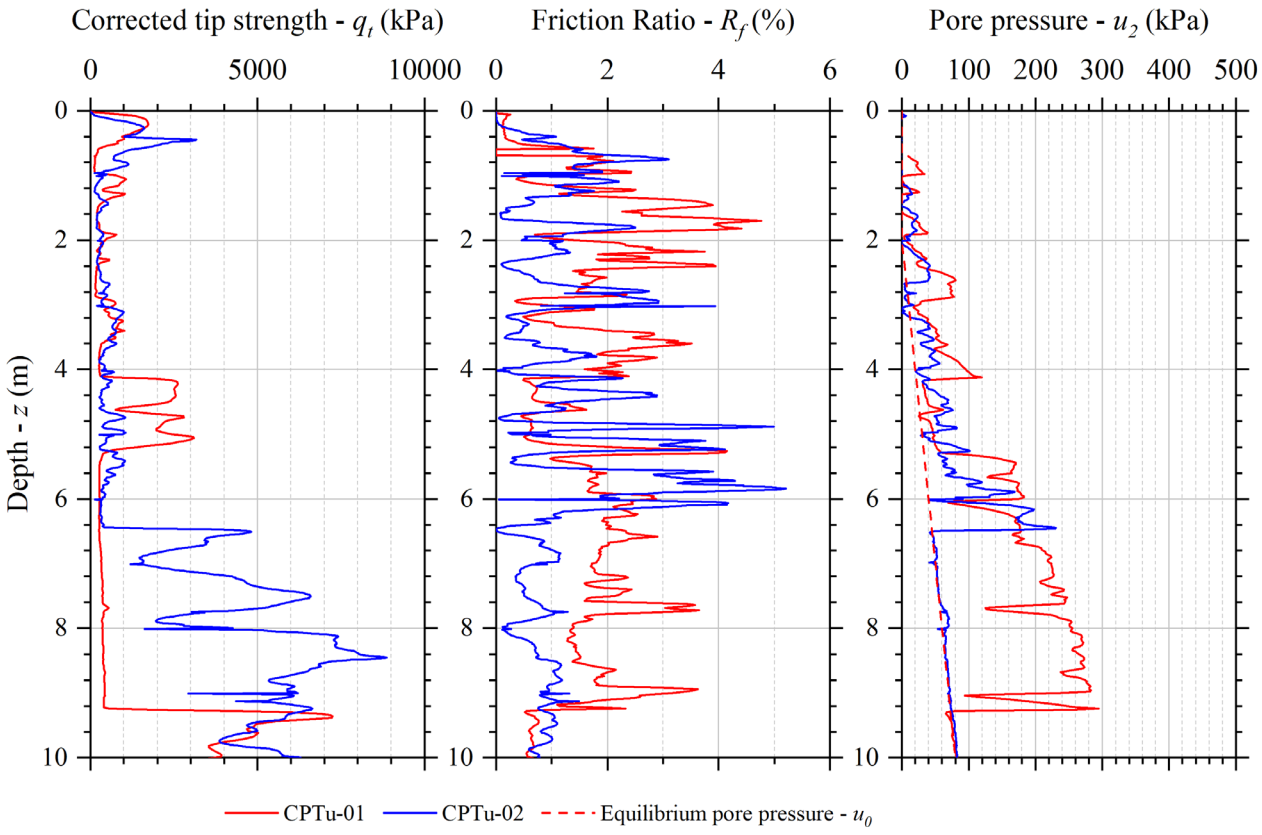


Figure 1: Results of piezocone testing

The results were also analyzed using the normalized tip strength and friction ratio framework. Figure 2 plots the CPTu data in a space where three large groups of tailings could be identified: one was finer tailings, another was a silty one referred to as intermediate tailings, and the third demonstrated sandy-like behavior. Although somewhat diverse, these groups were identified based on expected behavior from CPTu results. The data was classified over the depth and organized into clusters where the most data on this depth range lie on the graph. This procedure enabled the identification of similar tailings and the determination of the stratigraphy of tailings in the dam.

Figure 3 presents the CPTu profiles plotted according to the corresponding Soil Classification Index (I_c) (Jefferies and Davies, 1993). Figures 2 and 3 show that, although three large subgroups could be identified, the profiles are highly stratified with alternate layers of tailings, especially CPTu-01. Thus, the

stratigraphy of tailings was interpreted as composed of tailings from these three groups, as shown in Figure 3. The main difference between the two piezocone tests lies in the presence of a thick layer of finer tailings in CPTu-01 at greater depths and a layer of fine tailings at shallower depths. Figure 2 also indicates the state of the tailings in the field. The intermediate and fine tailings are predominantly contractive, while the coarse tailings are more dilative. This condition is related to the tailings' grain size distribution and depth. The dilative tailings were present mostly at shallower depths, which may be related to the seasonal variation of the water level. In addition, as the water level was found to be around 2 m, the tailings are considered fully saturated below this.

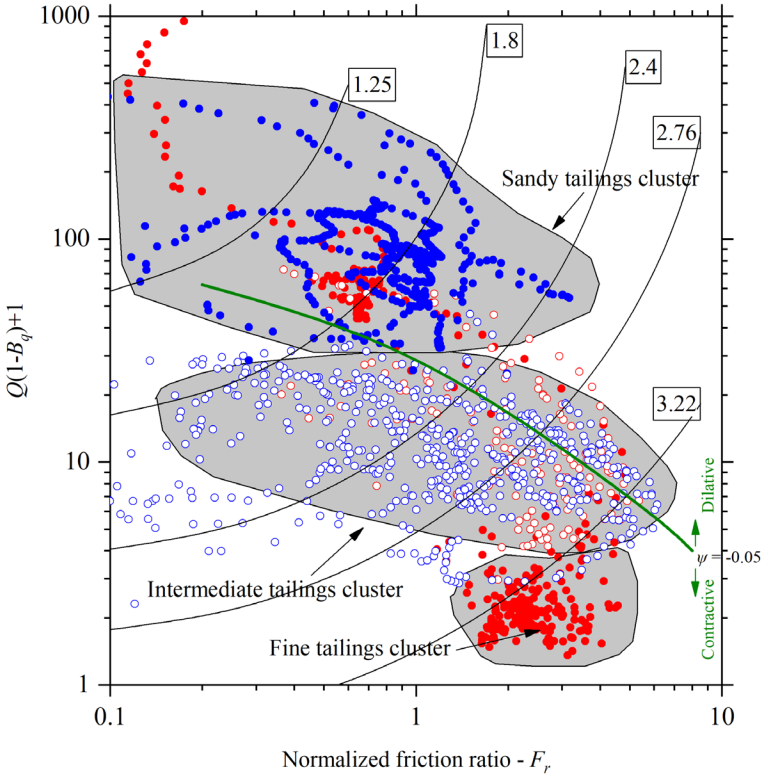


Figure 2: Normalized results of piezocone testing

Geotechnical characterization

Three characteristic groups of tailings were identified from the in-situ testing campaign. Then, representative samples of these groups were identified and collected for laboratory testing. It is important to note that the piezocone tests considered in this research are a portion of a much larger set of tests, conducted for characterizing the whole dam for closure planning, which enabled the identification of locations for collecting the representative samples of fine, intermediate, and sandy tailings. Figures 4 to 6 present the characteristics of tailings considered in the laboratory testing.

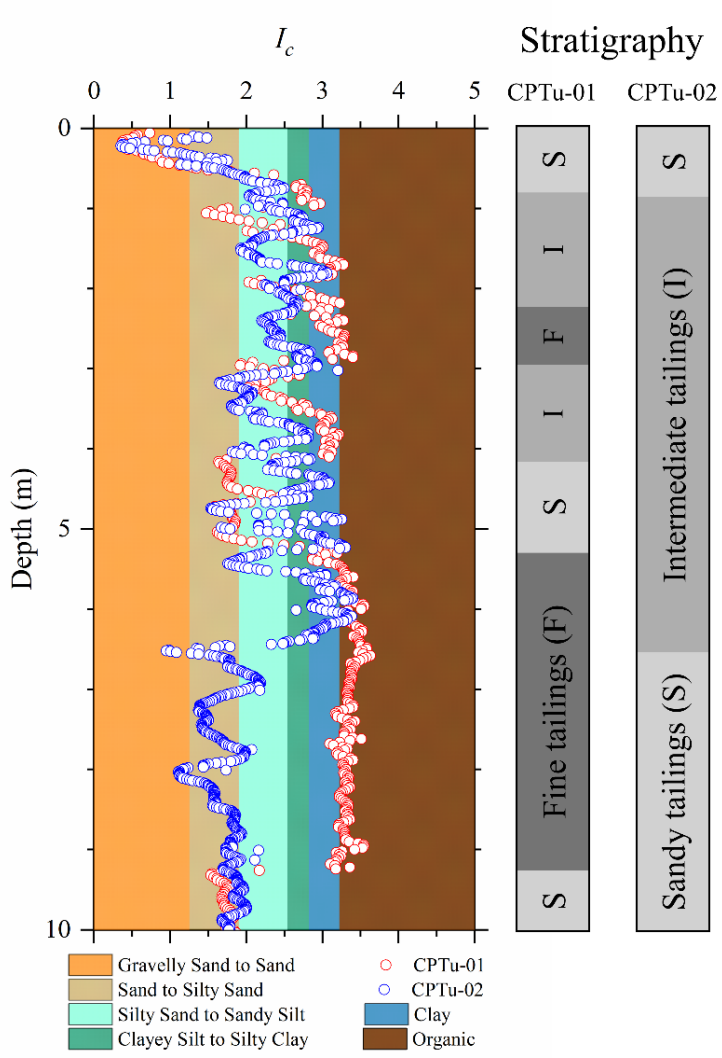


Figure 3: Tailings profile interpreted from CPTu

The PSD shown in Figure 4 and the calculated indices in Figure 5 demonstrate that the three collected tailings have distinct grading characteristics. The higher the fines content, the more well-graded are the tailings (higher values of C_u). Beyond the differences in fines content, the distribution and arrangements change throughout the tailings structure.

Hence, the tailings collected present distinct PSDs and mineralogy. The finer tailings present higher iron oxides content (Figure 6a) compared to sandy and intermediate tailings. Regarding the quartz content (Figure 6b), intermediate and sandy tailings have similar amounts. However, intermediate tailings appear to have another mineral in their composition, while sandy tailings are mainly composed of iron oxides and quartz. Regarding the specific gravity of tailings, they do not differ significantly (3.58-3.71) because all tailings present considerable amounts of iron oxides, which usually are heavier than other minerals in their composition (Souza et al., 2021).

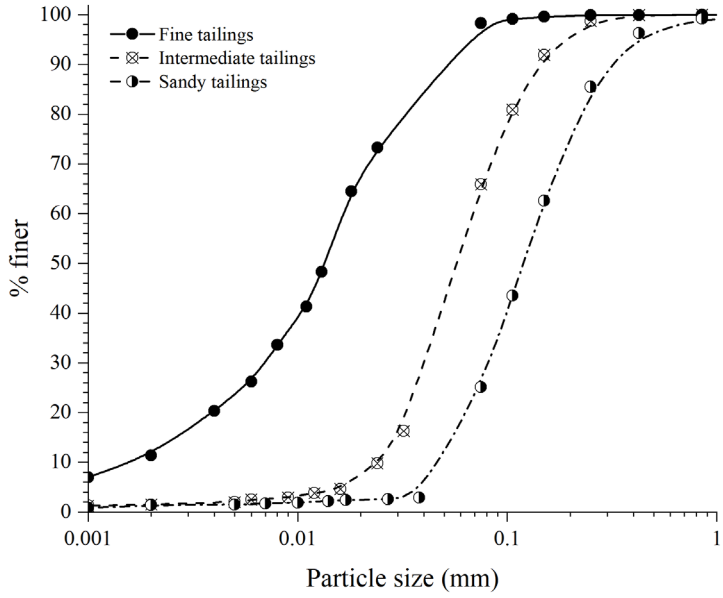


Figure 4: Particle size distribution of representative tailings samples

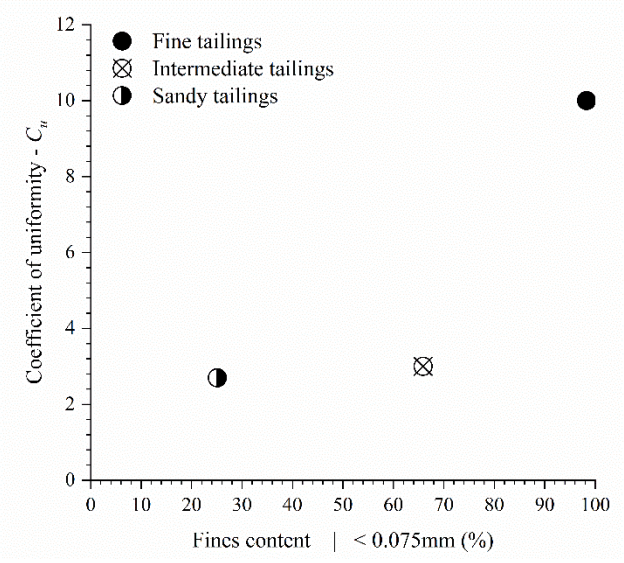


Figure 5: Distribution characteristics of tailings according to their fines content

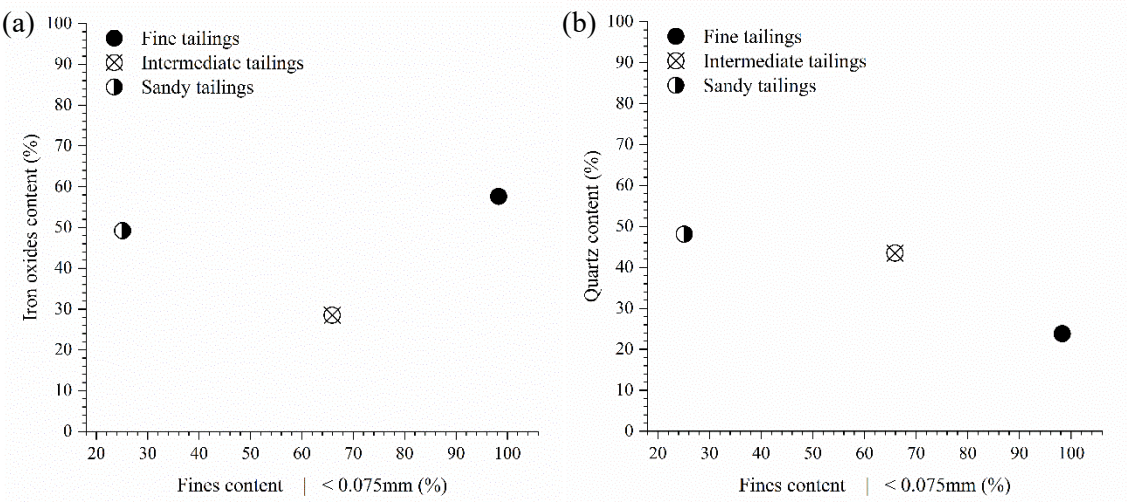


Figure 6: (a) Iron oxides content and (B) quartz content of tailings according to the fines content

Triaxial testing

Figure 7 depicts the stress-strain results of conventional triaxial tests conducted on tailings. Overall, sandy and intermediate tailings presented similar responses with brittle behavior indicated by marked peak strength followed by a loss of strength. The volumetric response was also similar, with slight compression followed by a dilative trend. On the other hand, fine tailings presented a ductile behavior up to large strains without loss of strength. The volumetric response of fine tailings was much more compressive than the other two, with a slight tendency to dilation at larger strains.

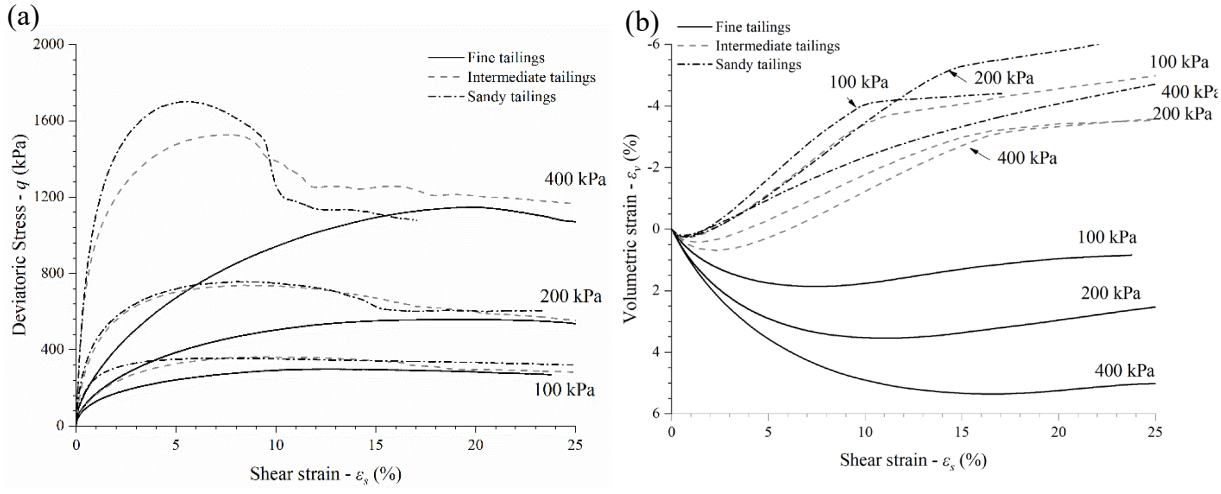


Figure 7: (a) Stress-strain results and (b) volumetric response of conventional triaxial testing

Since all specimens presented dilative behavior associated with dense states, it is difficult to estimate the critical state strength of the materials. This is because dense specimens generally suffer from localization effects, which can be detected in Figure 7 by the plateaus in the volumetric response of

intermediate and sandy tailings, as well as in the loss of strength after peak. However, dense specimens were selected to determine important parameters of tailings behavior, regardless of their actual condition in the field. Then, the triaxial results were analyzed under a stress-dilatancy framework (Figures 8 to 9), aiming to estimate critical state strength with higher confidence and to investigate other constitutive parameters relevant to the design of tailings structures.

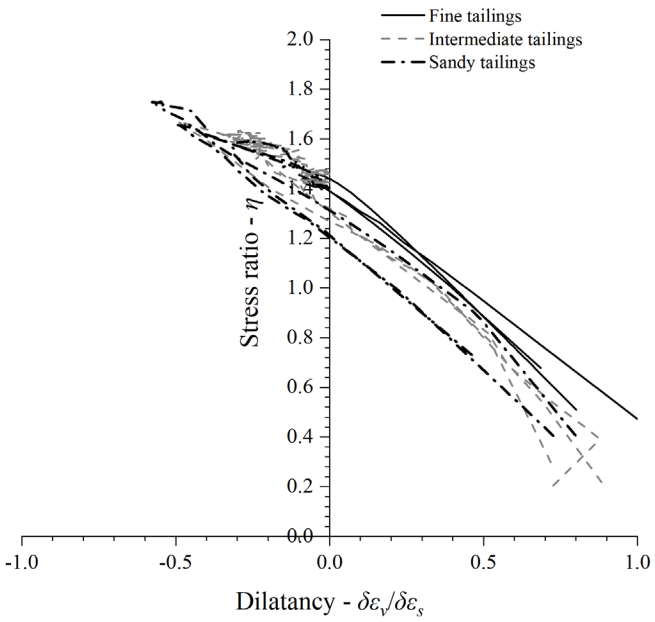


Figure 8: Stress-dilatancy of tailings

The results in Figure 8 demonstrate a trend of all tailings achieving a unique final stress ratio ($\eta = q/p'$) of approximately 1.4 ($\varphi = 34.6°$). Furthermore, the more dilative response of intermediate and sandy tailings can be clearly observed. Thus, although clear differences in volumetric response during shearing are observed, the differences in PSD and mineralogy of tailings do not influence their strength mobilization much. However, dilatancy depends on both the stress level and the density at which the samples were sheared (Been and Jefferies, 1985; Muir Wood and Belkheir, 1994; Silva et al., 2024; Wagner et al., 2023). The relationship between dilatancy and peak strength comes from the energy dissipation principles and defines a fundamental relationship from which other constitutive relations can be derived.

Figure 9 shows that a unique relationship between peak strength and minimum dilatancy could be obtained for all tailings, although they have distinct geological and geotechnical characteristics. This is an important finding since it can simplify the analysis by allowing us to adopt a single set of parameters regarding the stress-dilatancy behavior, for the distinct tailings present in the same structure.

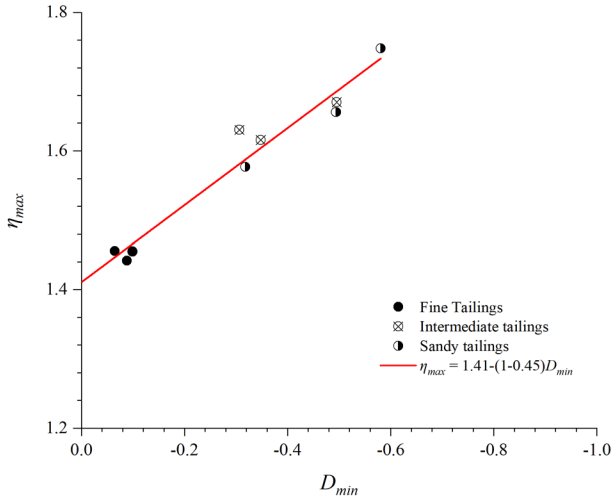


Figure 9: Peak states analysis of tailings

Conclusion

This paper investigated the variability of tailings in a dam to be closed using a set of in-situ and laboratory tests. Dam closure, especially that of upstream raised dams, is an operation that usually involves high-risk operations demanding appropriate design and planning, which can only be achieved through a deep understanding of tailings' behavior. One aspect to be considered in planning and designing for safe closure is the tailings' variability inside the impoundment and how engineers and practitioners can deal with it. The results obtained here demonstrated the existence of highly stratified tailings profiles inside a dam, composed of tailings with distinct geotechnical characteristics. However, although the volumetric response of the tailings differed greatly, the strength mobilization was similar, probably due to the common nature of the tailings in the dam. This characteristic can simplify design aspects by allowing the use of a single set of strength parameters for the tailings, reducing the effects of spatial variability.

Acknowledgements

The authors thank the MEC-CAPES (PROEX), CNPq (INCT and Produtividade em pesquisa), and Vale S.A. for their support of the research group.

References

ANM, 2023. Quarterly Report – Upstream dams decommissioning. National Mining Agency, Brasília, DF, Brazil.

ASTM, 2020. Standard Test Method for Electronic Friction Cone and Piezocone Penetration Testing of Soils, ASTM D5778. ASTM D5778, West Conshohocken, PA.

Ayala, J., Fourie, A. and Reid, D., 2022. Improved cone penetration test predictions of the state parameter of loose mine tailings. *Can. Geotech. J.* 59, 1969–1980.

Been, K. and Jefferies, M.G. 1985. A state parameter for sands. *Géotechnique* 35(2): 99–112.

Carrera, A., Coop, M.R. and Lancellotta, R. 2011. Influence of grading on the mechanical behaviour of Stava tailings. *Géotechnique* 61: 935–946.

Carvalho, J.V.D.A., Wagner, A.C., Scheuermann Filho, H.C. and Consoli, N.C. 2024. The role of fabric, stress history, mineralogy, and particle morphology on the triaxial behavior of nontextbook geomaterials. *J. Geotech. Geoenviron. Eng.* 150: 04024055.

Chang, N., Heymann, G. and Clayton, C. 2011. The effect of fabric on the behaviour of gold tailings. *Géotechnique* 61: 187–197.

Consoli, N.C. and Sills, G.C. 2000. Soil formation from tailings: comparison of predictions and field measurements. *Géotechnique* 50> 25–33.

Consoli, N.C., Silva, J.P.S., Wagner, A.C., Carvalho, J.V. de A., Baudet, B.A., Coop, M.R., Scheuermann Filho, H.C., Carvalho, I., De Sousa, G.M. and Cacciari, P.P. 2024. Critical state analysis of two compacted filtered iron ore tailings with different gradings and mineralogy at different stages of treatment. *Acta Geotech.* 19, 881–898.

Dominguez-Quintans, C., Carraro, J.A.H. and Zdravkovic, L. 2023. A critical assessment of the effect of initial fabric on key small-strain design parameters of slurry-deposited silts and sands. *J. Geotech. Geoenviron. Eng.* 149: 04023047.

Jefferies, M. and Davies, M. 1993. Use of CPTu to estimate equivalent SPT N 60. *Geotechnical Testing Journal* 16: 458–468.

Li, W., and Coop, M.R. 2019. The Mechanical behaviour of Panzhihua iron tailings. *Can. Geotech. J.* 56, 420–435.

Muir Wood, D. and Belkheir, K. 1994. Strain softening and state parameter for sand modelling. *Géotechnique* 44: 335–339.

Reid, D. and Fanni, R. 2022. A comparison of intact and reconstituted samples of a silt tailings. *Géotechnique* 72: 176–188.

Santamarina, J.C., Torres-Cruz, L.A. and Bachus, R.C. 2019. Why coal ash and tailings dam disasters occur. *Science* 364: 526–528.

Shuttle, D.A. and Cunning, J. 2007. Liquefaction potential of silts from CPTu. *Canadian Geotechnical Journal* 44(1): 1–19.

Shuttle, D.A. and Jefferies, M.G. 2016. Determining silt state from CPTu. *Geotechnical Research* 3(2): 90–118.

Silva, J.P.S., Rissoli, A.L.C., Cacciari, P.P., Viana Da Fonseca, A.J.P., Scheuermann Filho, H.C., Wagner, A.C., Carvalho, J.V. de A., Festugato, L. and Consoli, N.C. 2024. Triaxial testing response of compacted iron ore tailings considering a broad spectrum of confining pressures. *Soils and Foundations* 64: 101438.

Souza, A.H. de, Krüger, F.L. von, Araújo, F.G. da S. And Mendes, J.J. 2021. mineralogical characterization applied to iron ore tailings from the desliming stage with emphasis on quantitative electron microscopy (Qem). *Mat. Res.* 24: e20190677.

Spitz, K. and Trudinger, J. 2019. *Mining and the Environment: From Ore to Metal,* 2nd edition. London: CRC Press.

Wagner, A.C., Silva, J.P. de S., Carvalho, J.V. de A., Rissoli, A.L.C., Cacciari, P.P., Chaves, H.M., Scheuermann Filho, H.C. and Consoli, N.C. 2023. Mechanical behavior of iron ore tailings under standard compression and extension triaxial stress paths. *Journal of Rock Mechanics and Geotechnical Engineering* 15: 1883–1894.

Yin, G., Li, G., Wei, Z., Wan, L., Shui, G. and Jing, X. 2011. Stability analysis of a copper tailings dam via laboratory model tests: A Chinese case study. *Minerals Engineering* 24, 122–130.

Solar-powered Electrokinetic Tailings Dewatering

Ed Hanna, ElectroKinetic Solutions Inc., Canada
John Vandersleen, ElectroKinetic Solutions Inc., Canada

Abstract

The global inventory of tailings is currently >50 billion m^3 and continues to grow. Costs associated with these tailings include construction and maintenance of tailings storage facilities (TSFs), liability of catastrophic releases of tailings, and erosion of social license. Much effort has been spent innovating new, and improving existing, tailings management practices. The use of electrokinetics (EK) has been extensively researched for tailings dewatering. However, multiple efforts to commercialize EK technologies have failed. One of the major obstacles is high energy consumption. The EKS Dewatering Tailings (DT) Technology dewaters tailings in situ. The development of the DT Technology has spanned 14 years, overcoming past obstacles to EK commercialization, including the high energy consumption. A 19-month commercial demonstration was successfully completed in 2021, proving the performance of the technology. The energy consumption of the commercial demonstration was 15 kWh/m^3 of water released.

EKS is continuing to improve the DT Technology. A recent innovation is the exclusive use of solar energy to power commercial installations. Floating solar panels rest on the surface with the electrodes suspended below. DC power is sent directly from the solar panels to the underlying electrodes. Solar power has proven feasible even in areas with high levels of cloud cover and low incident solar radiation. Using solar power offers significant economic and environmental benefits. The use of solar power can reduce the energy consumption of the DT Technology by >50%. Solar power effectively eliminates operating costs. The technology involves no moving parts, no additives, and no onsite operator. At the end of dewatering operations, the solar panels can continue to produce energy for mining operations. This paper will describe the results of the commercial demonstration and the supporting data and analysis, demonstrating the feasibility and benefits of solar-powered electrokinetic dewatering.

Introduction

The mining industry is facing significant pressure from investors, governments, and the public to address the environmental liability associated with the large inventories of unstable tailings and the continuing increase in this inventory. The costs incurred by the mining industry for tailings management, including

tailings storage facility (TSF) construction, material transport, and tailings dewatering, are significant (Baker et al., 2020). In addition, the water trapped in the tailings is unable to be used for ore processing, requiring more freshwater to be imported into the mining process. This water demand can be difficult to source and costly in arid regions (Ghorbani and Kuan, 2017; Nasirov and Agostini, 2018). Another major safety and environmental liability is the risk of dam failure and resulting catastrophic release of fluid tailings. This liability can be reduced by strengthening the tailings dams, but is only removed when the tailings are dewatered and made geotechnically stable (Owen et al., 2020; Roche et al., 2017).

The EKS Tailings Dewatering Technology, developed by ElectroKinetic Solutions Inc. (EKS), can rapidly dewater the tailings in a TSF, addressing the liability posed by the tailings. The DT Technology consists of many parallel pairs of electrodes deployed inside a TSF. For TSFs with a water cap or fluid tailings surface layer, the electrodes are horizontal. Each installation consists of one or more independent modules, each occupying an area of ~50 × 25 m. The maximum size of a horizontal electrode EKS installation is limited by the number of modules that can be deployed in the fluid tailings portion of a TSF. Where the tailings' surface is covered by a solid "crust," vertical electrodes can be used.

Figure 1 is an end view schematic of horizontal EKS electrodes below the tailings' surface in a TSF. Direct current (DC) is passed between the electrodes. The electrochemical reaction at the cathodes is hydrogen evolution. At the anodes, the two primary electrochemical reactions are oxygen evolution and/or anode corrosion.

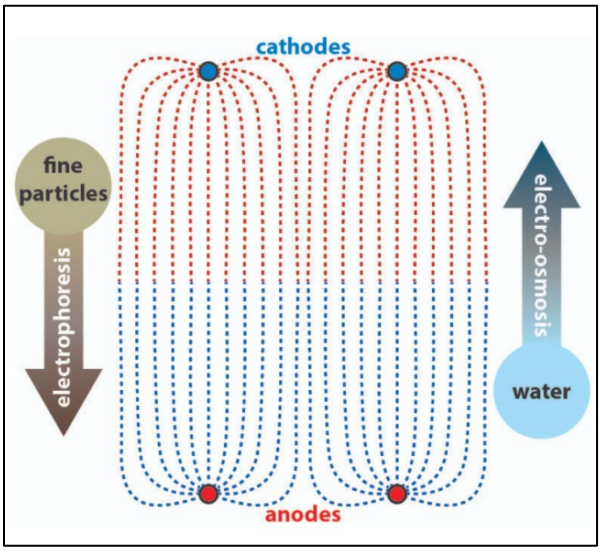


Figure 1: End view schematic of two DT electrode pairs, below the tailings' surface in a TSF

As current passes through the tailings, an electric field is created, resulting in rapid tailings dewatering via electroosmosis and electrophoresis. These electrokinetic (EK) processes have been studied extensively for decades (Casagrande, 1949; Dixit et al., 1975; Islam, 2014; Lockhart, 1983; Shang, 1997). EKS

previously presented a desktop case study quantifying the cost savings that can be achieved with the EKS Technology compared to current tailings management practices. The forecast net present value was $274 million, corresponding to an annual rate of return >90% on the EKS capital costs. The cost of water recovered by the EKS installation was forecast to be $1.11 per m^3 (Vandersleen and Hanna, 2023). In comparison, costs of $1.62 per m^3 of recovered water have been reported for tailings dry stacking (Zamorano et al., 2020).

The DT Technology has been progressively and reliably scaled up through laboratory and field research. EKS has recently proven the technology through a commercial demonstration in Alberta, Canada. This demonstration successfully operated continuously, year-round, from November 2019 to May 2021. The first purpose of this paper is to describe the dewatering performance achieved during the demonstration.

The commercial demonstration of the technology was powered by grid electricity. A recent innovation is the use of solar panels, floating on the surface of a TSF to power the technology. Laboratory experiments have been completed to quantify the impact of the use of solar power on the technology's dewatering performance. The second purpose of this paper is to describe these results.

Methodology

Commercial demonstration

A commercial demonstration of the DT Technology was carried out to prove that the technology scales as expected and that EKS can accurately forecast the performance of the technology. To determine whether these objectives were achieved, several key performance indicators (KPIs) were set for the commercial demonstration of the DT Technology. The target KPIs and the results are shown in Table 1. The results for these KPIs are described in more detail elsewhere (Vandersleen and Hanna, 2023).

Table 1: Key Performance Indicators for the DT commercial demonstration

Metric	Target	Result	Achieved?
Water released	1,000 m^3	1,100 m^3	✓
Released water quality	Suitable for reuse	Achieved goal!	✓
Increased tailings storage capacity	+58%	+63%	✓
Maximum solids content between electrodes	>60% (kg/kg)	>60% (kg/kg)	✓
Energy consumption	<30 kWh/m^3 water released	15 kWh/ m^3 water released	✓
Year-round operation	Successful winter operation	Achieved goal!	✓

The commercial demonstration occurred at InnoTech Alberta's research facility at Vegreville, Alberta, Canada. An inactive sewage lagoon was excavated to create a test cell. The dimensions of the top

of the test cell were 20 m × 25 m and its depth was 6 m; the walls of the test cell had a 1:1 slope. An impermeable liner was installed and over 1,700 m^3 of oil sands tailings were pumped into the test cell.

The average solids content of the tailings was 18% by weight. The tailings solids were primarily fine particles; the particle size distribution is shown in Figure 2. The average particle size is about 6 microns and over 25% is <2 microns. These fine-grained tailings are very difficult to dewater with current tailings management practices (McKenna and van Zyl, 2020).

The electrode array consisted of 16 electrode pairs, each 10 m long. A custom retrofitted sea container was designed to house the power supply and the central control system. Communication with the control system was via the internet. The primary purpose of the commercial test was to understand how the technology functions at scale and under field conditions. To support this objective, in situ sensors were installed in the test cell (e.g., sensors to measure the electric field pattern in the tailings).

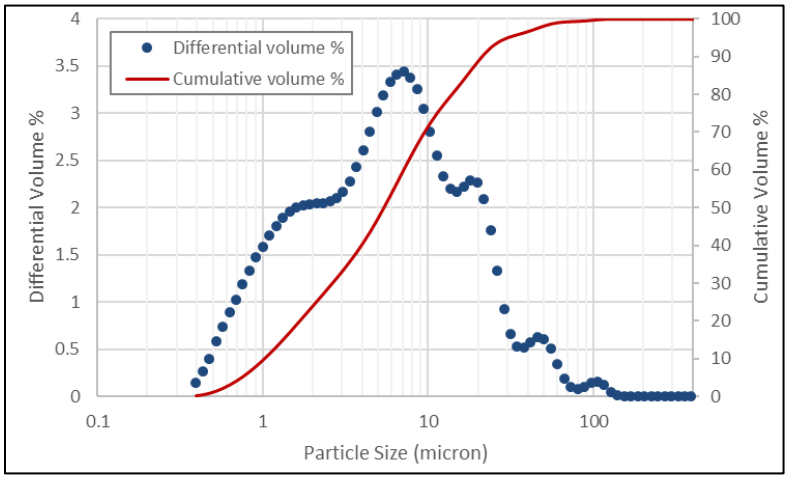


Figure 2: Particle size distribution (PSD) for the tailings dewatered during the DT commercial demonstration

Once the electrodes, sensors, and power supply and control systems were deployed, the operation of the commercial demonstration was initiated. During operations, the control system communicated with the rectifier which applied power continuously to the electrodes. The voltage and current applied to each individual electrode were monitored and recorded by the control system. Based on the measured dewatering performance, the control system adjusted the power applied to individual electrodes.

In addition to the continuous data recorded, physical sampling occurred approximately every six weeks. On each sample date, the water level within the test cell and the mudline depth at multiple locations within the test cell were measured. Core samples of tailings were also collected from multiple locations within the test cell using a custom-fabricated sampling device.

Each core was divided into sections and samples of each section were collected. For each section, including the sections that were above the mudline, the pH, electrolytic conductivity and solids content

were measured. Other analyses, including particle size distribution and ionic concentrations were measured for select sample sections.

The continuous data recorded by the sensors as well as the physical samples collected from the test cell were used to quantify the performance of the technology and to compare that performance to the KPIs set for the commercial demonstration (Table 1). In addition, the performance of the commercial demonstration was forecast using the EKS Model, proprietary software developed by EKS. This model has been developed through extensive laboratory research and is a critical tool used by EKS to design and optimize commercial EKS installations. The commercial demonstration results were also used to demonstrate the accuracy of the EKS Model and that EKS can accurately forecast the technology's performance.

Solar-powered dewatering

A recent EKS innovation, introducing another design variable, is the use of solar panels, floating on a TSF to power an EKS installation. There is significant synergy that can be achieved by powering the DT Technology with solar power. The DC power produced by the solar panels can be provided directly to the electrodes, without conversion to AC power. The DT Technology does not require a constant or reliable power source; the dewatering rate simply increases or decreases according to the power available. Finally, dewatering "pauses" at night (i.e., when no solar energy is available), and resumes in the morning without any operator intervention. As a result, no energy storage is required.

Large-scale laboratory tests were conducted to prove the performance of the DT Technology when powered by solar energy. Each experiment was conducted using a custom fabricated apparatus (Figure 3). 12 vertical electrodes were installed in a 500-L polycarbonate tank. The distance between each anode-cathode pair was 28 cm. The distance between adjacent cathodes was 14 cm. At the start of each experiment, 300 L of oil sands tailings were added to the tank. The initial solids content of the tailings was 42% by weight and the particle size distribution (PSD) is shown in Figure 2.

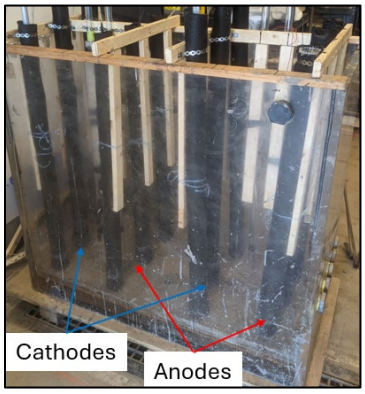


Figure 3: Experimental apparatus for GP and SP experiments

The electrodes were connected to a DC power supply which provided a specific power signature to the electrodes. The use of pulsed power (i.e., alternating periods of constant voltage and zero voltage) has been shown to maximize the efficiency of EK dewatering. (Kim et al., 2020) The automated control system for the DT Technology adjusts the power signature based on the measured properties of the tailings and the installation's objectives. The first experiment simulated the use of grid power (GP) for dewatering. As a result, a continuous power signature was applied (i.e., the voltage did not vary throughout the day). The second experiment simulated the use of solar power (SP). The applied voltage was varied over each 24-hour period according to the available solar radiation.

Each test was operated for five months. As the tailings were dewatered, the voltage applied for each experiment was increased. The recovered water was removed from the surface of the tailings. The volume of water recovered was measured by recording the height of tailings remaining in the tank. Core samples of tailings were also extracted periodically. The solids content was measured for each core and used to confirm the volume of water recovered.

Results and discussion

Commercial demonstration

The following sections summarize the key results achieved by the EKS commercial demonstration. In summary, the commercial demonstration met or exceeded each of the KPIs specified in Table 1, demonstrating that the technology functions well in the field, at scale.

Water release

The DT Technology released water from the tailings during the commercial demonstration. The released water was left in place as a "water cap" on top of the tailings. As water was released, the tailings depth decreased, and the water cap depth increased over time. By periodically measuring the depth of the mudline, the volume of water released from the tailings was determined. In addition, core samples were periodically collected from the test cell. The volume of water released from the tailings was also determined based on the solids contents of the core samples. The water released over time, expressed as a fraction of the initial tailings volume is shown in Figure 4.

The mudline-derived and the sample-derived water release estimates are similar. In addition, the water release estimated by the EKS Model was consistent with the measured water release, demonstrating its ability to accurately forecast the performance of the DT Technology. By the end of the commercial demonstration, the volume of water released was >60% of the initial tailings volume. This exceeded the KPI set for water release (58% of the initial tailings volume) shown in Table 1. The commercial demonstration was stopped due to schedule and budget constraints, not due to technical reasons. If the

demonstration had been extended, more water would have been released. Figure 5 shows the surface of the tailings at the end of the commercial demonstration, after the recovered water had been removed.

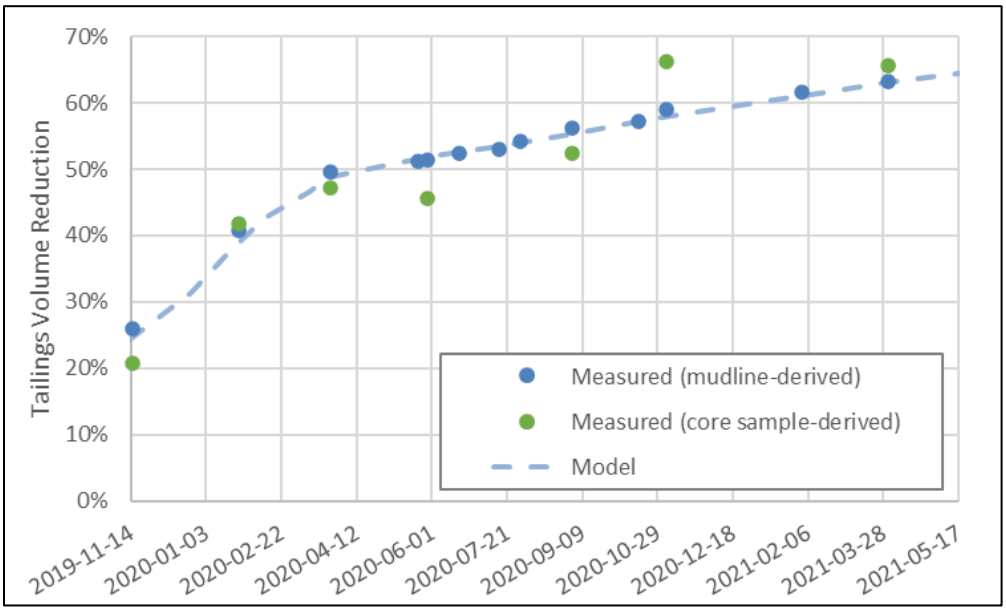


Figure 4: Forecast and measured tailings volume reduction during the commercial demonstration

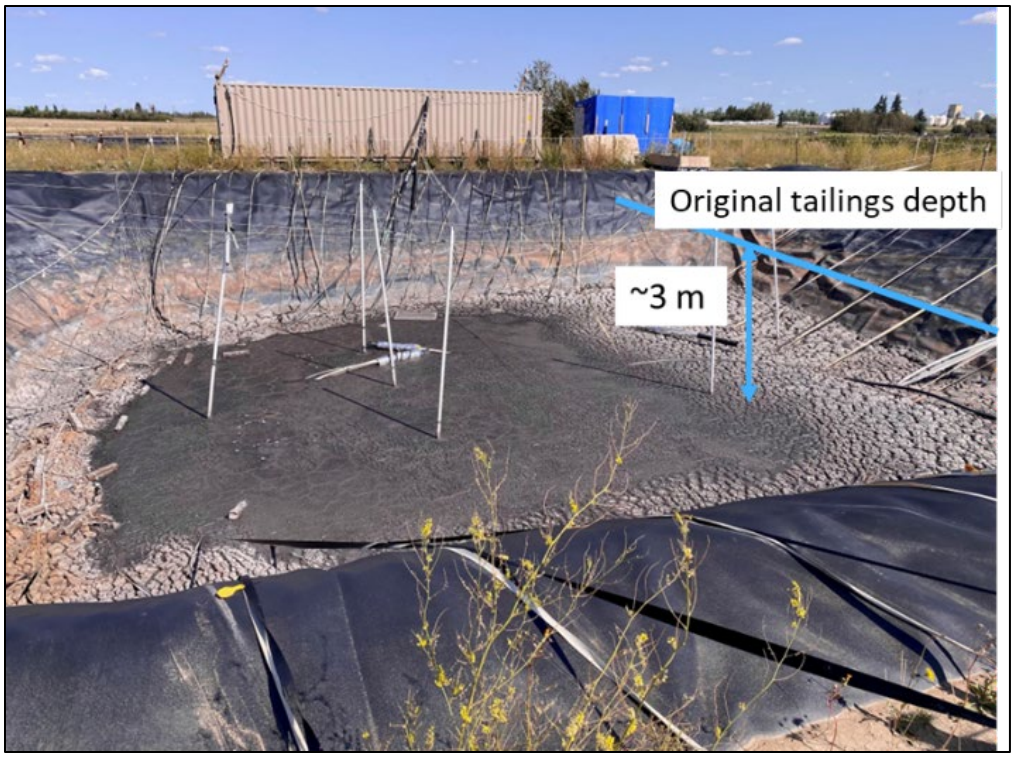


Figure 5: Surface of the tailings after the water cap was removed at the end of the commercial demonstration

For an active TSF, the released water would provide two significant benefits to the mine operator. Firstly, after the released water is recovered from the TSF, the TSF capacity would be increased by an equivalent volume. The commercial demonstration increased the capacity of the test cell by >60%. In addition, the water released from the tailings by the DT Technology is available for reuse in the mineral extraction process, reducing the amount of freshwater that is required from local waterbodies. The value of this released water varies between operations but can be quite significant in arid regions.

Solids content

The solids content at different depths and lateral locations within the test cell were determined from the core sample sections periodically collected during the commercial demonstration. This data was used to track the tailings solids content in the test cell over time, a trend shown in Figure 6. The anode solids content predicted by the EKS Model is also shown.

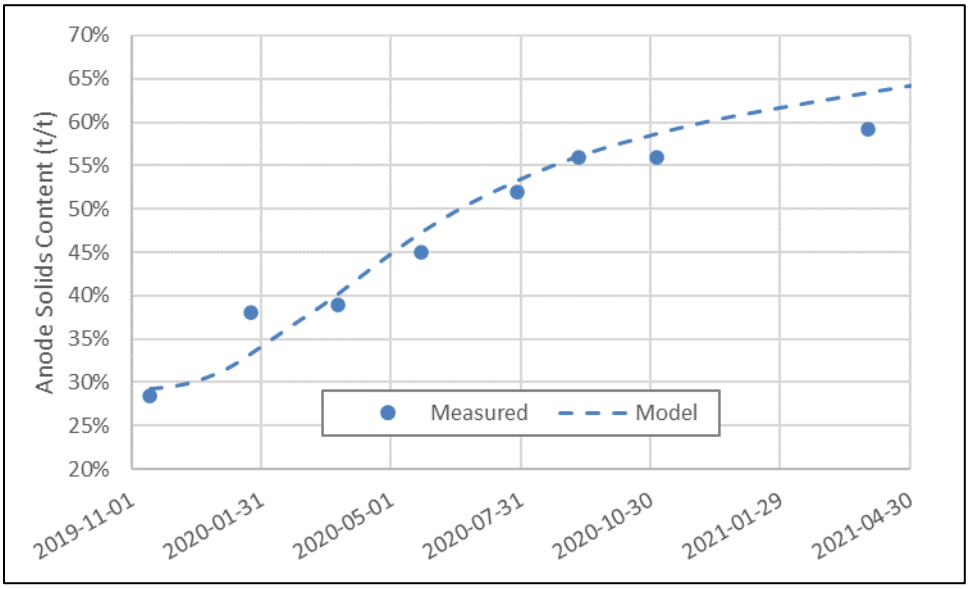


Figure 6: Forecast and measured tailings solids content near the anodes during the EKS commercial demonstration

Initially, the solids content was approximately 30% by weight near the anodes. This value increased over time and was ~60% at the end of the commercial demonstration, meeting the KPI set for solids content (Table 1). This trend was accurately forecast by the EKS Model.

Table 2 shows estimated properties for oil sands tailings at 60% solids. When the DT Technology is applied to an actual TSF and operated to produce tailings with similar properties as those shown in Table 2, the geotechnical stability of the material would be greatly increased, significantly reducing the risk of

catastrophic liquefaction of the tailings. Furthermore, the DT Technology could be used to create a stable layer on the surface of a TSF, enabling the TSF to be reclaimed sooner.

Table 2: Properties of oil sands tailings at 60% solids by weight

Property	Value	Reference
Density	1.57	Measured by EKS
Effective stress	7.7 kPa	(Jeeravipoolvarn et al. 2009)
Hydraulic conductivity	5.48 x 10^{-10} m/s	(Jeeravipoolvarn et al. 2009)

Energy consumption

The voltage and current applied to the electrodes were continuously recorded during the commercial demonstration. As the tailings were dewatered, the EKS control system was used to adjust the power signature applied to the electrodes to maximize the energy efficiency of the operation. The measured energy consumption of 14.8 kWh per m^3 of water released during the commercial demonstration was consistent with the prediction of the model of 16.2 kWh/m^3 of released water. Both values were significantly lower than the KPI of 30 kWh/m^3 set for the commercial demonstration.

Minimizing energy consumption is an important consideration for optimizing electrokinetic (EK) dewatering systems. Energy consumption is a function of the electric field pattern, the current density, the electrolytic conductivity of the pore water, and the porosity of the material being dewatered (Lo et al., 1990; Shang and Dunlap, 1996). Setting an optimal "applied voltage schedule" during the operation of an EK installation, considering the above factors, is essential to minimize energy consumption while maximizing the dewatering rate. Through its technology development program, EKS has optimized the applied voltage schedule used by the DT Technology. The low energy consumption achieved during the commercial demonstration demonstrates the result of this power signature optimization at scale.

Solar-powered dewatering

The following sections summarize the key results of EKS' large-scale experimental investigation of solar-powered EK dewatering. In summary, the use of solar power dramatically reduces the energy required for dewatering.

Energy efficiency for water recovery

Figure 7 shows the cumulative water recovery for the GP and SP experiments. The measured water release, as well as the water release forecast by the EKS Model is shown. The EKS Model was also used to forecast the water release with SWC alone.

The experiments recovered 240 to 280% more water than was forecast for SWC alone. As reported by many others (Casagrande, 1949; Islam, 2014; Lockhart, 1983; Shang, 1997), electrokinetic dewatering

is much faster than SWC, particularly for fine grained materials. In a commercial TSF, this recovered water could be reused in the mineral extraction process, reducing the need for fresh water from other sources (e.g., desalination). In addition, the recovered water increases the TSF storage capacity. The results of the GP and SP experiments correspond to 28% and 24%, respectively, increases in TSF capacity compared to SWC. This added capacity can provide significant cost savings (Vandersleen and Hanna, 2023)

The solar power experiment recovered 11% less water than with grid power. This was due to the lower levels of applied power used for the solar power experiment. Less solar power is available in the morning and evening compared to at noon, and no power is available at night (i.e., for 12 hours per day). As a result, the average applied power and resulting dewatering rate were less than for the grid power experiment.

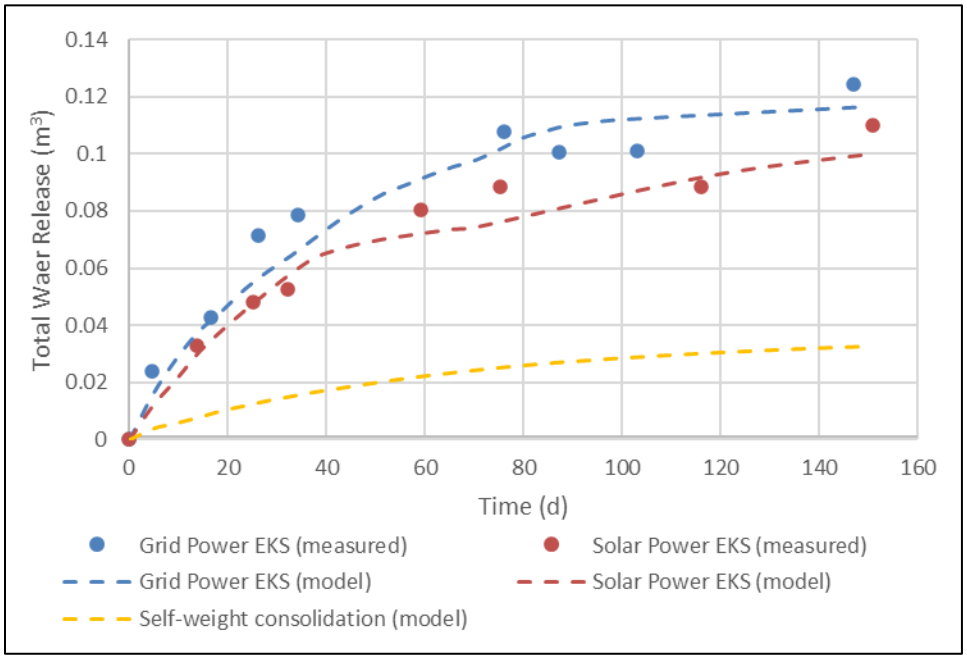


Figure 7: Volume of water released from the GP and SP experiments

Figure 8 shows the cumulative energy consumption required to dewater tailings from the initial 42% solids by weight to approximately 60% solids. The unit energy consumption per tonne of tailings solids is shown. Dewatering the tailings to 45% solids by weight required 47% less power with solar power than with grid power. To dewater the tailings to 58% solids by weight, the energy consumption of the solar power system was 77% less than for grid power.

The application of DC power signatures that vary voltage over time result in reduced energy consumption for EK dewatering. (Kim et al., 2020) The observed solar power experiment results are another example of how power signature variation can significantly improve energy efficiency.

A major barrier to the widespread commercialization of electrokinetic dewatering has been the high energy consumption associated with the technology (Fourie and Jones, 2010). The commercial

demonstration energy consumption of 14.8 kWh/m^3 shows that EKS' innovations have overcome this barrier. The SP test consumed over 47% less energy compared to the GP test. Applying this reduction to the commercial demonstration results would result in commercial-scale energy use <7.8 kWh/m^3. Further optimization of the applied power signature to minimize energy consumption continues to be a focus of EKS research.

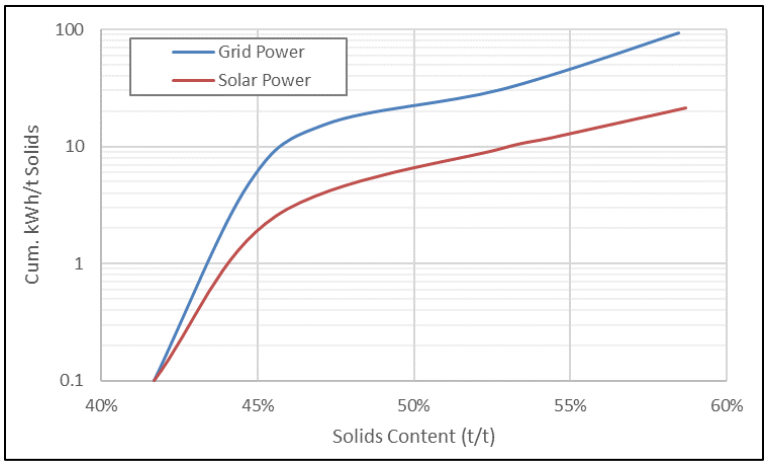


Figure 8: Unit energy consumption of the GP and SP experiments

Solids content

The initial tailings solids content for both experiments was 42% by weight. Figure 9 shows the lateral and vertical variations in solids content at the end of the experiments. These results show that the DT Technology avoids the low-density surface layer characteristic of SWC. The "soft spots" that result from the use of prefabricated vertical drains (PVDs) (Indraratna, 2009; Rixner et al., 1986) are also avoided. The greater density observed for the grid power experiment was due to the greater volume of water recovered. The density profile attainable with the DT Technology reduces reclamation costs and enables reclamation operations to commence immediately following tailings dewatering.

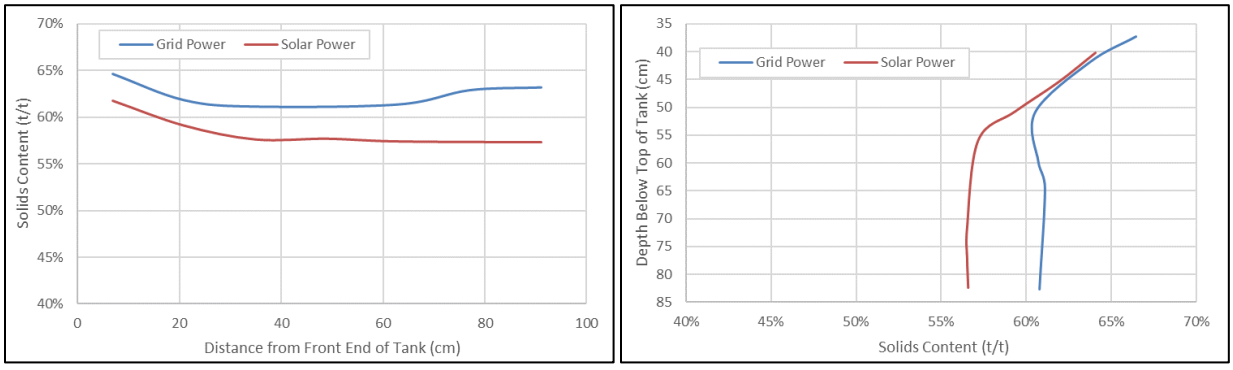


Figure 9: Final tailings density profiles for the GP and SP experiments

Conclusion

The EKS Tailings Dewatering Technology has been developed by EKS over the past 14 years to enable the mining industry to practically and economically address the liability posed by unconsolidated tailings. EKS' technology offers many opportunities to TSF operators, including increased TSF storage capacity, increased water conservation, and a reduced risk of tailings liquefaction.

A 1,700 m^3 commercial demonstration of the technology was completed in 2021 in Alberta, Canada. During the commercial demonstration, the tailings volume was reduced by >60% and the solids content near the anodes was dewatered to 60% solids by weight. The average energy consumption was <15 kWh/m^3 of water released. These results were all consistent with the estimates produced by the EKS Model, demonstrating that EKS can accurately forecast the dewatering performance of the technology. In addition, the commercial demonstration results met or exceeded all KPIs that were set for the technology, proving that the technology scales up as designed and is commercially viable.

There is significant synergy that can be achieved by powering the DT Technology with solar power. The DC power produced by the solar panels can be provided directly to the electrodes, without conversion to AC power. The DT Technology does not require a constant or reliable power source; the dewatering rate simply increases or decreases according to the power available. Dewatering "pauses" at night (i.e., when no solar energy is available), and resumes in the morning without any operator intervention. As a result, no energy storage is required.

Large-scale laboratory tests were completed to confirm the effectiveness of powering the DT Technology with solar power. Regardless of power source, the DT Technology dewaters tailings uniformly, minimizing variation in tailings' density both vertically and laterally. The tests demonstrated that the use of solar power can reduce energy consumption by over 50%, further increasing the efficiency of the technology. The DT Technology, powered by solar energy, is an attractive option for tailings operators to increase the capacity of TSFs and recover significant volumes of water for reuse.

Acknowledgements

The DT commercial demonstration was supported by Sustainable Development Technology Canada (SDTC), Alberta Innovates (AI), Natural Resources Canada (NRCan), Canadian Natural Resources Ltd. (CNRL), InnoTech Alberta and Suncor Energy.

References

Azam, S., S. Jeeravipoolvarn and J.D. Scott. 2009. Numerical modeling of tailings thickening for improved mine waste management. *Journal of Environmental Informatics* 13: 111–118.

Baker, E., M. Davies, A., Fourie, G., Mudd and K. Thygesen. 2020. Mine tailings facilities: Overview and industry trends. In B. Oberle, D. Brereton and A. Mihaylova (eds), *Towards Zero Harm – A Compendium of Papers Prepared for the Global Tailings Review*, pp.14–24. St Gallen, Switzerland.

Casagrande, L. 1949. Electro-osmosis in soils. *Géotechnique* 1(3): 159–177.

Caughill, D.L., N.R. Morgenstern and J.D. Scott. 1993. Geotechnics of nonsegregating oil sand tailings. *Can. Geotech. J.* 30(5): 801–811.

Dixit, S.P., R. Gombeer, and J. D'hoore. 1975. The electrophoretic mobility of natural clays and their potential mobility within the Pedon. *Geoderma* 13(4): 325–330.

Fourie, A.B. and C.J.F.P. Jones. 2010. Improved estimates of power consumption during dewatering of mine tailings using electrokinetic geosynthetics (EKGs). *Geotextiles and Geomembranes* 28(2): 181–190.

Ghorbani, Y. and S.H. Kuan. 2017. A review of sustainable development in the Chilean mining sector: Past, present and future. *International Journal of Mining, Reclamation and Environment* 31(2): 137–165.

Indraratna, B. 2009. Recent advances in the application of vertical drains and vacuum preloading in soft soil stabilisation. *2009 EH Davis Memorial Lecture – Australian Geomechanics Society* 45(2).

Islam, S. 2014. Thickening of mature fine oil sands tailings. *University of Western Ontario: Electronic Thesis and Dissertation Repository*. 2566.

Jeeravipoolvarn, S., J.D. Scott and R.J. Chalaturnyk. 2009. 10 m standpipe tests on oil sands tailings: Longterm experimental results and prediction. *Canadian Geotechnical Journal* 46(8): 875–888.

Kim, J., J. Lee and I.-M. Chung. 2020. Electro-osmotic dewatering under electro-osmotic pulse technology. T*he Journal of Engineering Geology* 30(4): 423–433.

Lo, K.Y., I.I. Inculet and K.S. Ho. 1990. Electroosmotic strengthening of soft sensitive clays. *Canadian Geotechnical Journal* 28: 62–73.

Lockhart, N.C. 1983. Electroosmotic dewatering of clays. 1. Influence of voltage. *Cotloids and Surfaces* 6: 229–238.

McKenna, G. and D. van Zyl. 2020. Closure and reclamation. In *Towards Zero Harm – A Compendium of Papers Prepared for the Global Tailings Review 109*. Martin, V. (ed), pp. 109–127.

Nasirov, S. and C.A. Agostini. 2018. Mining experts' perspectives on the determinants of solar technologies adoption in the Chilean mining industry. *Renewable and Sustainable Energy Reviews* 95(7): 194–202.

Owen, J.R., D. Kemp, E. Lèbre, K. Svobodova and G. Pérez Murillo. 2020. Catastrophic tailings dam failures and disaster risk disclosure. *International Journal of Disaster Risk Reduction* 42(12): 101361.

Rixner, J. J., S. R. Kraemer, A. D. Smith and Haley & Aldrich. 1986. *Prefabricated vertical drains, Vol. I: engineering guidelines*. FHWA/RD-86/168.

Roche, C., K. Thygesen and E. Baker. 2017. *Mine Tailings Storage: Safety Is no Accident*. ISBN: 978-82-7701-170-7.

Shang, J. and W. Dunlap. 1996. Improvement of soft clay by high voltage electronics. *Journal of geotechnical and geoenvironmental engineering*122(4):274–280.

Shang, J. and Y. Xu. 2019. Electrokinetic dewatering of mine tailings from hydrometallurgical processes. In A.J.C .Paterson, A.B. Fourie and D. Reid (eds), *Paste 2019: Proceedings of the 22nd International Conference on Paste, Thickened and Filtered Tailings,* Australian Centre for Geomechanics, Perth, pp. 275–283, https://doi.org/10.36487/ACG_rep/1910_18_Shang

Shang, J.Q. 1997. Electrokinetic sedimentation: a theoretical and experimental study. *Canadian Geotechnical Journal* 34: 305–314.

Vandersleen, J.K. and J.E. Hanna. 2023, Tailings dewatering with the EKS-DT process. In G.W. Wilson, N.A. Beier, D.C. Sego, A.B. Fourie and D. Reid (eds), *Paste 2023: Proceedings of the 25th International Conference on Paste, Thickened and Filtered Tailings*, University of Alberta, Edmonton, and Australian Centre for Geomechanics, Perth, pp. 414–428, https://doi.org/10.36487/ACG_repo/2355_31

Zamorano, C., S. Ramírez, I. Sánchez, and C. Garrido. 2020. Technical and economic evaluation of tailings dewatering circuits in the largest copper mines, in H. Quelopana (ed.), *Paste 2020: 23rd International Conference on Paste, Thickened and Filtered Tailings*, Gecamin Publications, Santiago, https://doi.org/10.36487/ACG_repo/2052_19

Effect of In-situ Dewatering and Compaction of Copper Tailings Using Accelerated Mechanical Consolidation

Oscar Santiago, Phibion Pty Ltd, Australia
William McAdam, Phibion Pty Ltd, Australia
Rafael Menezes, Phibion SpA, Chile

Abstract

The International Council on Mining and Metals (ICMM) and member organizations have set ambitious targets for advancing tailings management practices, including the removal of moisture and enhancement of tailings strength through the adoption of cost-effective, scalable technologies capable of processing tailings and, ideally, reducing or eliminating tailings generation altogether. The implementation of Best Available Technology (BAT) in tailings management systems (TMS) is paramount for ensuring the cost-effective creation of safe, stable, and environmentally sound landforms during both operational and post-closure phases. Mechanical consolidation is an available technology that aligns with conventional tailings storage facility design and operation, emphasizing the key principles of maximization of tailings density and minimization of water retention – a paradigm consistent with the requirements outlined in the Global Industry Standard on Tailings Management (GISTM).

Accelerated mechanical consolidation involves the application of specialized equipment to impose controlled loads on surface deposited tailings, significantly exceeding anticipated in-situ loads and accelerating the consolidation process. This approach reduces the time required for tailings consolidation, enhancing operational efficiency and reducing operational risks, while compacting and drying material stored in the facility.

A large-scale trial conducted at a copper tailings storage facility in Chile's central region aimed to demonstrate the applicability and effectiveness of mechanical aid in consolidating and compacting copper tailings. Various geotechnical monitoring parameters – including density (both dry and bulk), undrained shear vane, moisture content, in-situ infiltration, and cone penetration resistance – were meticulously assessed on both unaltered and mechanically treated tailings. Results indicated an overall improvement in all monitored parameters for areas subjected to in-situ mechanical consolidation and compaction, while unaltered sections exhibited either minimal change or marginal improvement over the trial duration. These quantifiable benefits suggest significant potential for enhancing tailings management practices through the

application of mechanical dewatering, consolidation and compaction techniques. The findings underscore the transformative potential of accelerated mechanical consolidation as a technology in addressing key challenges associated with copper tailings management.

Introduction

The global mining industry has faced numerous tragic incidents involving tailings storage facilities (TSFs). These failures have led to significant environmental damage, loss of human life, and financial repercussions, underscoring the urgent need for improved tailings management practices. In response, the International Council on Mining and Metals, in collaboration with the United Nations Environment Program and the Principles for Responsible Investment, convened the Global Tailings Review in 2019. The objective of this initiative was to establish a comprehensive international standard for tailings management, aiming to mitigate TSF failures and prevent future environmental and humanitarian crises. The resulting Global Tailings Standard, published in August 2020, mandates that operators explore emerging and alternative options (Best Available Technology, BAT) for conventional wet TSFs.

The industry has seen substantial investment in research and development focused on alternative tailings surface storage solutions. This includes the development and refinement of paste, filtered and thickened tailings technologies, which offer promising alternatives to traditional wet TSFs. However, green-field, legacy, and operational TSFs switching to one of these alternatives as a tailings management solution are burdened with high capital and operational costs as well as operational complexity and technology limitations (Crystal et al., 2018). Accelerated Mechanical Consolidation (AMC) presents an efficient and cost-effective solution to mechanically dewater, consolidate, and compact in-situ tailings with comparable and, in some cases, superior results to filtered and stacked tailings facilities (Woolston and DiDonna, 2020; Santiago et al., 2024). The theory of AMC implies that in-situ mechanical perturbation of a deposited material accelerates its consolidation process.

In the case of suspensions, this technique overcomes the effects of hindered settlement and facilitates the exit of water from the tailings profile. When applied to highly flocculated or porous materials, it collapses the pores and rapidly increases density to levels equivalent to those achieved by filtration or centrifugation (Munro and Smirk, 2018). Reduction of interstitial pore spaces and water is by far the most important consideration for the design and operation of TSFs. Significant efforts are made to maximize the water recovered from tailings to allow continued tailings transportation and process water.

Methodology

Accelerated mechanical consolidation trial

In the interest of advancing environmental management and optimizing operational efficiency, Phibion Pty Ltd undertook a large-scale trial on an active copper mine TSF between October 2022 and March 2023. The copper mine is operated by one of the largest copper producers in the world and is located in Chile, in the Santiago Metropolitan region. A trial area was established in the south-west part of the facility in close proximity to a tailings discharge point. It was segregated into ten individual work areas covering a total area of approximately 98.5 ha (Figure 1). The work area was isolated during the trial period to minimize uncontrolled deposition on fresh tailings within the area; any fresh tailings not needed for the trial were deposited elsewhere within the facility.

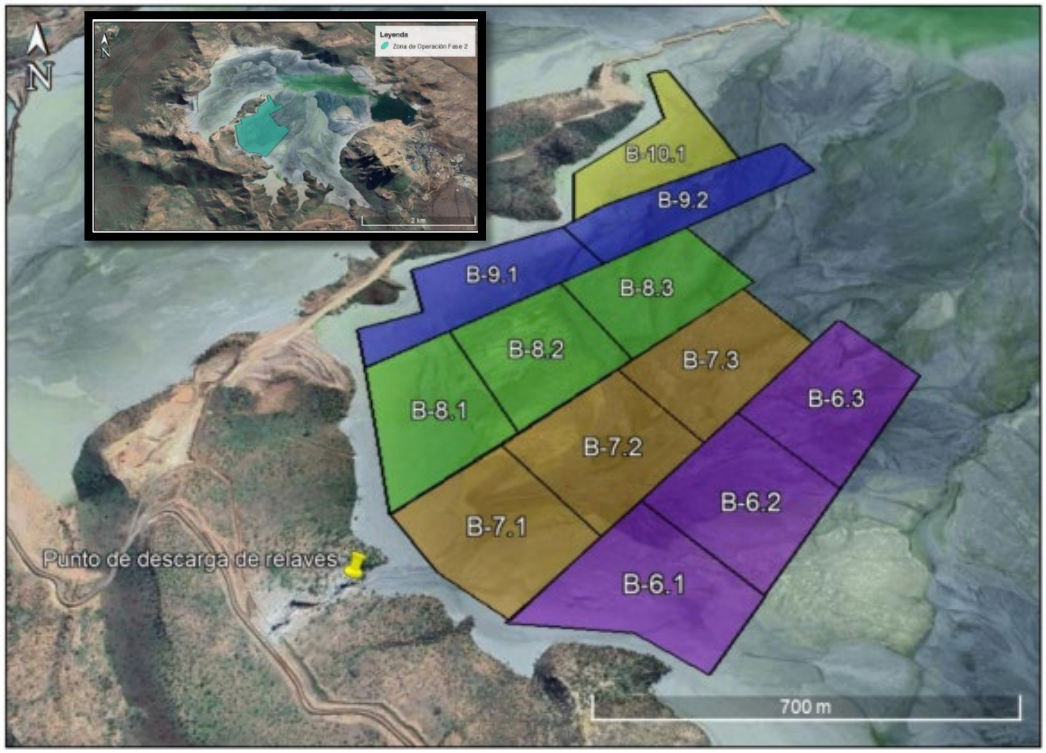


Figure 1: General location of the trial and full extent of the copper TSF

The TSF stores a mixture of copper and molybdenum tailings with a maximum tailings production storage of 180 kt per day covering an overall area of 20 km^2. Tailings generated at the outlet of the concentrator plant target a concentration of solids by weight of 54%, which is ultimately discharged at a series of outlets in upstream valleys that flow downstream towards the decant pond and return structure located in the north-east of the TSF. Prior to discharge the tailings pass through a series of hydro-cyclones on saddle dam embankments, removing the coarse fraction, which is utilized for progressive raising of

saddle dam embankments. Fresh tailings are discharged at a range of densities depending on the processing plant configuration and ore inputs; these bulk densities range from 1.23 to 1.56 t/m^3.

Over the course of the trial period Phibion operated a fleet of two MudMasters,® which are advanced amphibious machines that utilize Archimedes screws to traverse the tailings surface due to their low ground-bearing pressure. These machines employ a process known as Accelerated Mechanical Consolidation (AMC) to drive improvements in density within the tailings material, regain entrained tailings water, and consolidate and compact tailings in-situ.

The machine weight applies a concentrated load on the tailings surface, increasing surface pore pressure and effectively packing the material. Over a series of consecutive traverses this progressively increases the tailings strength through increased density and dewatering (South32, 2023; McPhail et al., 2021). Prior to deployment Phibion undertook modeling to establish the optimal machine weight (17.5 T), optimal scroll length (4.8 m), and maximum fresh tailings to achieve buoyancy requirements (1.3 m).



Figure 2: General location of the trial copper TSF and MudMaster® in action

The AMC process involves an initial period of "recovery," in which interstitial tailings water is compressed from the tailings to a point where the amphibious machine has consolidated the tailings into a dense material upon which the machine's weight is bearing. This stage is critical for operational effectiveness as machines then gain adequate traction in the consolidated tailings to traverse at greater speeds. It also creates a dense base upon which fresh tailings can be deposited and compressed against. Following the recovery phase, the operation moves into the production phase, where consolidation and dewatering are optimized. A specialized AMC plan was developed to optimally compact tailings while allowing surface water to drain freely towards the decant structure in the east of the TSF.

Critical to the AMC process is control of the deposition depth and timing of fresh tailings discharge. Throughout the trial period discharges were intermittent and not well controlled. The intent of the trial was to work the fresh tailings to understand the impact potential, rather than work within deposition sequencing. The details of subsequent deposition periods were as follows:

- Initial discharge (October 2022): fresh layer of tailings discharged across the entire surface of the trail area.
- Second discharge (end of December 2022 – beginning of January 2023): fresh discharge of tailings covering all work bays with controlled depth between 0.5 and 1.0 m maintained.
- Third discharge (end of February 2023): fresh tailings discharged over bays 6, 7, 8.1, and 8.2.

Between each discharge machines worked across the tailings surface, applying the tailored AMC operation plan.

Trial validation geotechnical testing

To investigate the effectiveness of AMC in the trial area, the TSF operator engaged an independent geotechnical testing contractor to test the tailings both in-situ and in the laboratory with representative sampling (Table 1).

Table 1: Summary of geotechnical testing

Test Type	Applied Testing Standard	Parameter	No. of Tests
Sand Cone Test	NCh 1516 (1979) ASTM D-1556-15	Dry density	15
Shear Vane Test	ASTM D 2573-15	Undrained shear strength	256
Granulometry	MC-V8 8.102.1 (Dec 2003)	Granulometric distribution – percentage fines	49
Atterberg limits	NCh 1517/1 (1979) & NCh 1517/2 (1979)	Liquid limit (LL), plastic limit (PL) and plasticity index (PI)	49
USCS Classification	–	–	38
Modified Proctor	NCh 1534/2 (1979)	Dry maximum compacted density (DMCS) and optimum moisture	1
Humidity	NCh 1515 (1979)	Percent humidity	158
Particle Density	NCh 1532 (1980)	Particle density solids – specific gravity (Gs)	49
Porchet Test	NCh 3610 (2020)	Infiltration rate	5
PANDA Test	NCh 3261 (2012)	Tip resistance	5
Unit weight	–	Dry density	3

The contractor endeavored to take representative tests at a series of intervals throughout the trial period from October 2022 to March 2023. Samples were taken to reflect the unaltered tailings (no treated material with AMC) as well as altered (treated with AMC) tailings at varying intervals (2, 4, and 6 passes and final stage). Refer to Appendix Table A1 for more detailed test information and Appendix Figure A1 for sample locations. In some instances, unaltered testing was taken at the final stage of altered tailings activity to compare self-consolidation results with AMC results. Other unaltered tests were taken as baseline tests to understand the impact of AMC activity with time. The majority of testing was undertaken in situ.

Data and discussion

Tailings classification

The results of Atterberg Limits testing determined the tailings to be classified as Non-Plastic (NP) with USCS classifications mainly as low plasticity silt (ML) with variations to silty sand (SM). The high proportion of silt reflects the effective hydro-cyclone of sands for embankment raising prior to discharge within the facility.

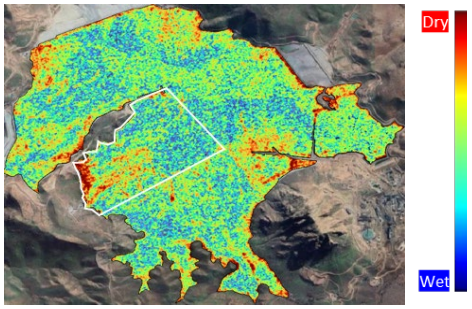
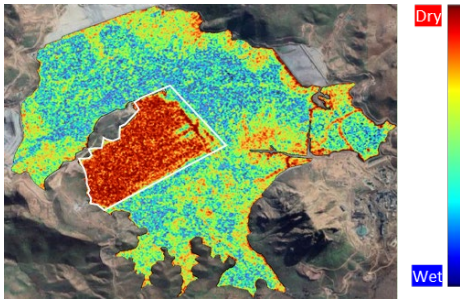
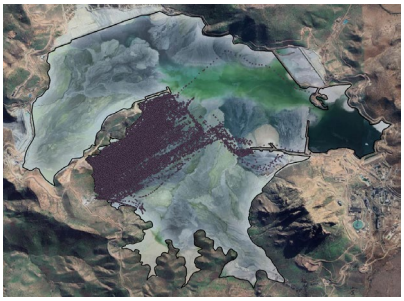
Visual observations

The visible tailings condition is an anecdotal indicator of the effectiveness of AMC. During the trial period there was marked improvement in the tailings surface condition, as shown in Figure 3. Fresh tailings deposited throughout the trial area in October 2022 appear wet and loose, contrasting with the post-trial image that presents a relatively dry, high strength surface. To achieve such a result required over six passes of the machines. However, there were substantial improvements in the tailings characteristics with less passes.



Figure 3: Tailings condition of the trial area prior to trial commencement 24/10/2022 (left) and approaching the completion of the trail 28/02/2023 (right)

Table 2: Variation in tailings surface moisture throughout AMC trial period, Sentinel 1 Radar Polar VV on the left in comparison to the MudMaster® tracking coverage

Date	Tailings Moisture (Radar Polar VV)	MudMaster Tracking
29/11/2022		
30/03/2023		

Tailings surface moisture is also observable through Sentinel 1 Radar Polar Moisture. This data throughout the trial period is displayed in Table 2 alongside MudMaster® GPS tracks. The rate of drying appears substantially better than unaltered areas of the TSF.

Strength and density observations

The undrained shear strength (S_u) of the tailings presents an increasing relationship with the number of passes of the equipment, due to the rapid densification and compaction of the tailings. This relationship stabilizes after four passes, reaching, for 0.5 m depth, S_u values of between 30 – 70 kPa, with an average of 48 kPa. This is ten times greater than the average S_u achieved naturally by the consolidation of the tailings in the same period of time and depth, as shown in Figure 4.

Furthermore, the decrease in S_u with depth is clear, so it is understandable to postulate that the effect of the MudMaster® and the AMC process decreases with depth, hence the need to maintain pour tailings layers to a set depth that can be worked effectively as the first 0.5 m deep. Data presented within Figures 4 to 9 represents the averaged data from all testing areas. Typically, AMC operations are analyzed in terms of number of passes of the machine as this is a quantifiable operation metric. In an active operation the number of passes to target desired performance objectives would be established.

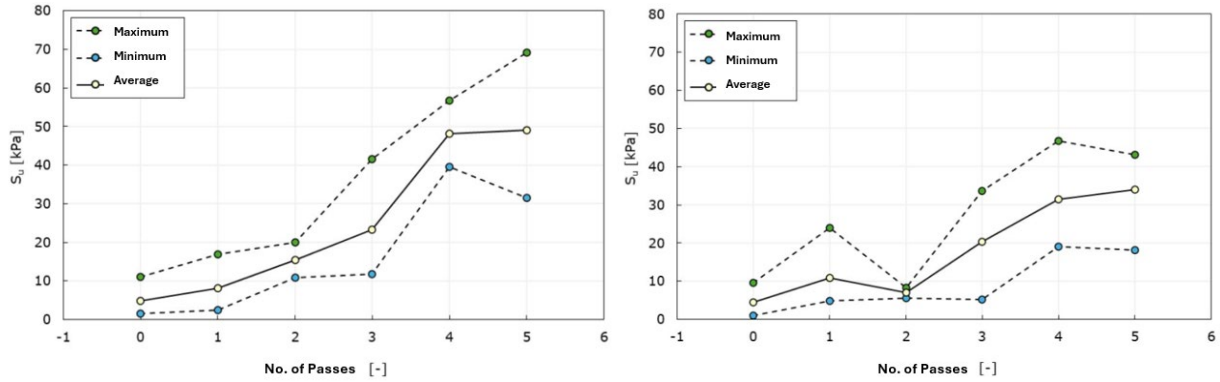


Figure 4: Undrained shear strength vs. number of passes, all data acquired October 2022 to March 2023. Left plot shows testing at 0.5 m deep and right plot shows at 1.0 m deep; data represents results across all test areas

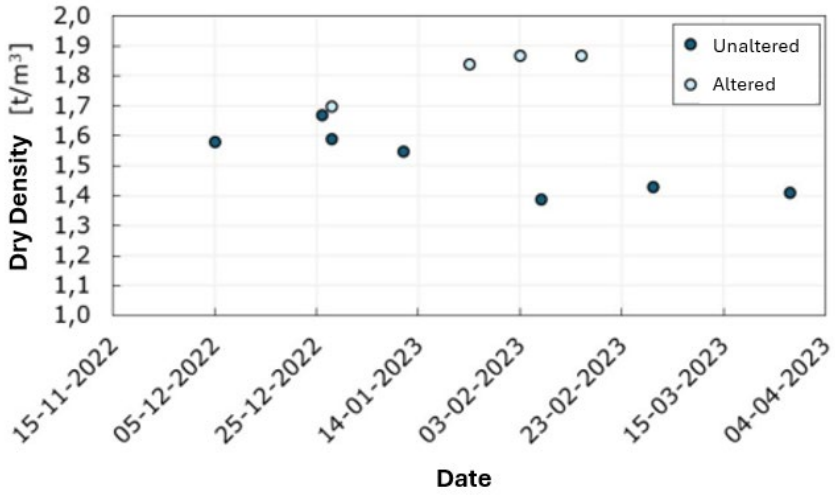


Figure 5: Dry density in unaltered and altered condition of tailings; lack of altered results within trial period due to invalid test results in February and March

A significant increase in the dry density of the tailings is evident, as shown in Figure 5, due to the action of the amphibious equipment, increasing from an average value of 1.52 t/m^3 in unchanged condition to 1.86 t/m^3 after four passes of the equipment. This has a great effect on the shear resistance parameters in drained conditions, since they are increased, especially the friction angle as there is greater interlocking between particles in a state of higher density.

An inversely proportional relationship is observed between S_u and the surface humidity of the tailings, as shown in Figure 6. This relationship arises because, by decreasing the humidity in the tailings, the amount of water stored in the interstices is reduced, which results in an increase in the effective tension between the particles, and therefore in a greater resistance to shear strength.

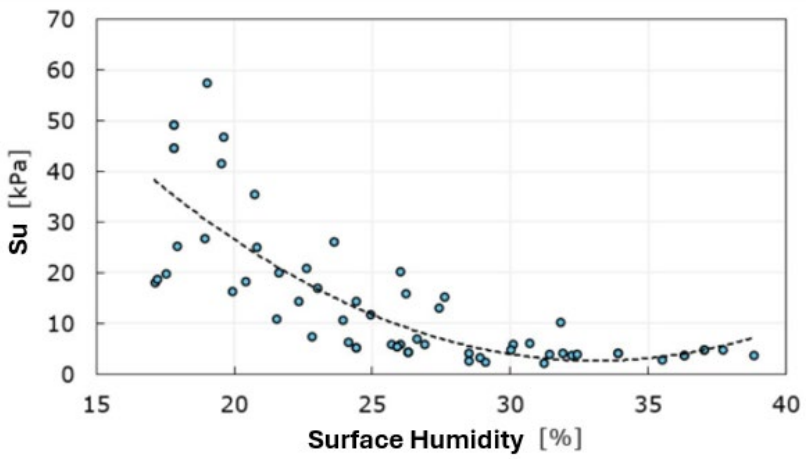


Figure 6: Correlation of undrained shear strength and surface humidity

Tailings moisture and seepage observations

A notable decrease in surface humidity is evident as the number of passes increases, until reaching a minimum value of 16% after three passes (Figure 7). To reach humidity lower than that value, the tailings should experience a suction value greater than 100 kPa (Figure 8). Additionally, the lower the humidity in the deposited tailings, the higher the yield stress and dynamic viscosity, which means the risk associated with dam failure is lower.

The reduction of the infiltration rate of the tailings deposited after the operation of the amphibious equipment is evident and contributes to the reduction of the infiltration of contacted waters in depth and towards the foundation soil, which helps reduce the risk of potential contamination of underground layers, weakening of foundation and seepage issues. Additionally, this reduction would increase the amount of water available for recovery from every wet deposition and precipitation events, which would be directed mainly toward the decant pond, except for the amount that is evaporated.

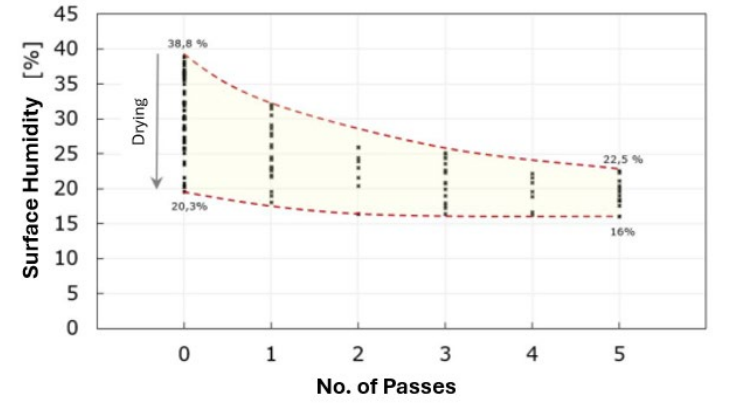


Figure 7: Surface humidity vs. number of passes

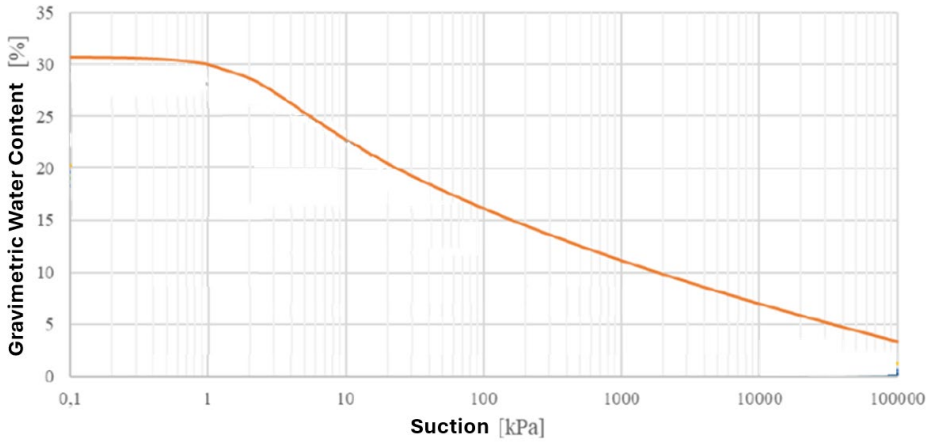


Figure 8: Tailings water retention curve

The density and compaction levels reached after four passes of the amphibious equipment indicate that the tailings experience diminishing returns in terms of infiltration rate with additional passes. This decreases the susceptibility of the tailings to static liquefaction and seepage. Furthermore, the tailings dewatering process reinforces this benefit, since the absence or scarcity of water in the interstices prevents the generation of the pore pressures necessary for liquefaction.

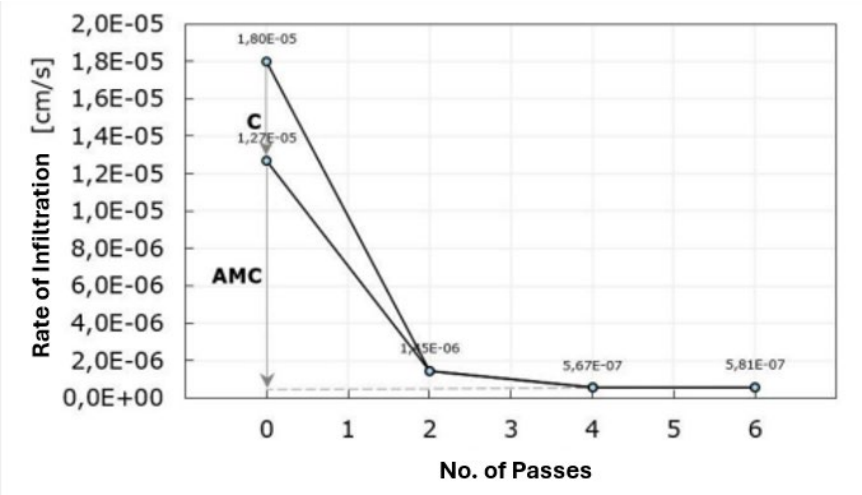


Figure 9: Infiltration rate decrease with increased number of passes of AMC in contrast to natural consolidation "C"

Impact of results on tailings operations

The operation completed effectively 66 days with two amphibious equipment and, consequently, the AMC process, to generate a net gain in the stored volume by displacing water and, therefore, in useful storage life in the TSF. In this particular case, the trial generated an estimated 3.4 days' worth of tailings deposited in the facility (4,918 m^3/day). This useful life gain, when extrapolated to the final total area of the TSF

(2,000 ha), and considering linearity and full implementation of AMC, translates into a useful life gain of over 40,000,000 m^3, which represents a total gain of 415 days' worth of storage.

The rapid reduction of the surface slopes of the basin in the areas operated by the amphibious equipment is a reflection of the rapid consolidation produced in the recently disposed tailings in the surroundings of the discharge point. Furthermore, the channels generated by the equipment's screws (scrolls) contribute to the conduction of the released water and the distribution of the tailings that are subsequently deposited.

Conclusion

The global mining industry must urgently adopt improved tailings management practices to prevent catastrophic failures of TSFs. The Global Tailings Standard, established in response to past failures, mandates the exploration of BAT alternatives to conventional wet TSFs. This study demonstrates the potential of AMC as a cost-effective and efficient method, scalable to high production rates, for enhancing tailings management compared to other methods.

The trial conducted by Phibion on an active copper mine TSF in Chile underscores the practical benefits of AMC. Over a five-month period, the use of MudMaster® machines resulted in significant improvements in tailings density and strength, reducing surface moisture and enhancing the structural integrity of the tailings. Geotechnical testing confirmed that AMC could achieve comparable, if not superior, results to traditional dewatering methods such as filtration and centrifugation.

Key findings from the trial include:

- A substantial increase in dry density and undrained shear strength (S_u) of the tailings, reaching values that significantly reduce the risk of liquefaction.
- Effective dewatering, resulting in lower surface moisture content and enhanced water recovery for processing operations.
- A reduction in infiltration rates, mitigating the potential for seepage related stability issues and contamination of underground water layers.

The AMC process not only improves the operational efficiency of TSFs but also extends their useful life, providing economic and environmental benefits. The trial's success highlights the importance of continued investment in innovative tailings management technologies. By adopting AMC and similar advanced techniques, the mining industry can better safeguard against environmental and humanitarian crises, ensuring a more sustainable future for mining operations worldwide.

Acknowledgements

Phibion would like to express our sincere gratitude to GA Consultores – Geotecnia Ambiental for their invaluable support and expertise in conducting the third-party review of this work. Their thorough analysis and insightful feedback greatly contributed to the rigor and integrity of this project.

References

Crystal, C., Hore, C. and Ezama, I. 2018. Filter press dry stacking: design considerations based on practical experience. *Proceedings of Tailings and Mine Waste 2018*. Colorado State University. Keystone.

McPhail, G.I., DiDonna, P. and Ugaz, R. 2021. Dam break analysis for BRDA 5 at Worsley Alumina Refinery. In A.B. Fourie & D. Reid (eds), *Paste 2021: Proceedings of the 24th International Conference on Paste, Thickened and Filtered Tailings*, Australian Centre for Geomechanics, Perth, pp. 177–200, https://doi.org/10.36487/ACG_repo/2115_16

Munro, L. and D. Smirk, 2018. How thick is thick enough? In R.J. Jewell and A.B. Fourie (editors). *Paste 2018: Proceedings of the 21st International Conference on Paste, Thickened and Filtered Tailings,* Australian Centre for Geomechanics. Perth. doi:10.36487/ACG_rep/1805_01_Munro

Santiago, O., Menezes, R., McAdam, W. and Smirk, D. 2024. Why accelerated mechanical consolidation delivers equal or greater benefits to other tailings management solutions. In A.B. Fourie and D. Reid (editors), *Paste 2024: Proceedings of the 26th International Conference on Paste, Thickened and Filtered Tailings*. Australian Centre for Geomechanics. Perth. pp. 349–360. https://doi.org/10.36487/ACG_repo/2455_28

South32. 2023. GISTM Requirement 15.1 Public Disclosure Worsley Alumina.

Woolston, J.S. and DiDonna, P. 2020. A case study comparison of best available technology (BAT) for the stacking of bauxite residue: Accelerated Mechanical Consolidation (AMC) and filtration and stacking (F&S). In A.B. Fourie and D. Reid (editors), *Paste 2020. Proceedings of the 23rd International Conference on Paste, Thickened and Filtered Tailings.* Australian Centre for Geomechanics. Perth.

Appendix

Table A1: Summary of tailings testing status and testing period

Test Type	Tailings Status at Test	Test Quantity in Test Period		
		Initial Discharge (Oct – Dec '22)	Second Discharge (Late Dec '22 – Jan '23)	Third Discharge (Late Feb – March '23)
Sand Cone Test	Unaltered	3	1	3
	Altered	2	3	3
Shear Vane Test	Unaltered	29	26	30
	Altered	61	85	30
Granulometry	Unaltered	12	1	20
	Altered	–	–	12
Atterberg limits	Unaltered	12	1	20
	Altered	–	–	12
Modified Proctor	Unaltered	1	–	–
	Altered	–	–	–
Humidity	Unaltered	18	26	29
	Altered	27	40	18
Specific Gravity	Unaltered	12	1	22
	Altered	–	2	12
Unit weight	Unaltered	–	–	3
	Altered	–	-	

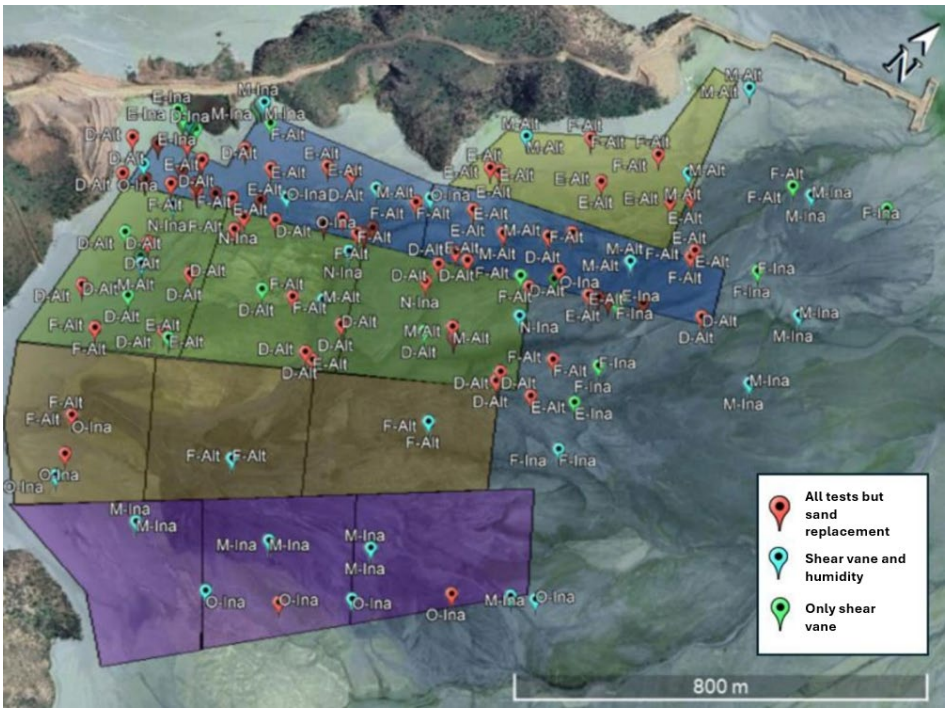


Figure A1: Trial geotechnical testing locations, symbology reflects the tests month and the tailings condition. Test months O-October, N-November, D-December, E-January, F-February, M-March. Tailings condition Alt-Altered, Ina-Unaltered

Influence of In-situ Soil Fabric on the Critical State of a Laminated Glaciolacustrine Silty Soil

Morteza Mohamadi, BGC Engineering Inc., Canada
Simon Dickinson, BGC Engineering Inc., Canada
Chang-Gyun Jeong, BGC Engineering Inc., Canada
Erinn Raison, BGC Engineering Inc., Canada
Adrian Wightman, BGC Engineering Inc., Canada

Abstract

The current state of practice for evaluating the flow liquefaction potential of a soil deposit is based on comparing its estimated in-situ state parameter (ψ_o) with a threshold value. To estimate ψ_o of a soil deposit and determine its critical state line (CSL), detailed analyses use triaxial test results on reconstituted specimens rather than undisturbed specimens. This approach implies that at critical state the influence of in-situ soil fabric on void ratios and stresses is minimal. Although this hypothesis may be generally acceptable for homogeneous fills and tailings, verification is required for naturally deposited soils that are deemed susceptible to flow liquefaction.

A series of drained and undrained triaxial compression tests were conducted on reconstituted specimens of a fine-grained glaciolacustrine soil to determine its CSL. Triaxial tests were also performed on high quality Shelby tube samples, and the results were compared to the CSL of reconstituted specimens. The testing of reconstituted specimens of glaciolacustrine soil indicated that a family of reasonably parallel CSLs rather than one single CSL existed. The tested Shelby tube specimens had initial states loose of the reconstituted specimens CSLs, and yet all tests on Shelby tube samples showed dilative behavior and moved away from the reconstituted specimens CSL. Several factors that are believed to have contributed to this observation are further investigated and discussed in this paper. The sensitivity of estimated ψ_o to a vertical shift in CSL position on the e-log p′ plane was also examined in the light of a series of spherical cavity expansion numerical simulations.

Introduction

Assessing the possibility of flow liquefaction in the foundation and construction materials of tailings dams has been an increased focus of importance within the mining sector following the failures of the Fundão

tailings dam (2015), Cadia tailings dam (2018), and Feijão tailings dam (2019). In general, geotechnical engineering practice currently relies on estimating the in-situ state parameter (ψ_o) of a soil to assess its susceptibility to flow liquefaction. The state parameter is defined as the difference between the in-situ void ratio and the void ratio at critical state for a given confining pressure (Jefferies and Been, 2016). Soils with a positive state parameter ($\psi_o > 0$) are contractive and soils with a negative state parameter ($\psi_o < 0$) are dilative. In lieu of the theoretical threshold $\psi_o = 0$, Jefferies and Been (2016) recommended adopting a practical value $\psi_o = -0.05$, where soils with $\psi_o > -0.05$ are considered contractive and prone to flow liquefaction.

Methods used to estimate ψ_o range from screening-level empirically based methods, such as those by Plewes et al. (1992) and Robertson (2010), to detailed material-specific methods like that of Jefferies and Been (2016). In the latter approach, a series of triaxial laboratory tests is conducted on a soil to define its critical state line (CSL) and calibrate the NorSand constitutive model. The NorSand model is a plasticity model developed within the critical state soil mechanics (CSSM) framework and is particularly useful for assessing the static liquefaction potential of loose strain softening cohesionless soils (Jefferies and Been, 2016). The calibrated NorSand model is then used to conduct a series of numerical cavity expansion simulations to determine CPTu inversion coefficients, which are subsequently used to calculate the ψ_o (Shuttle and Jefferies, 1998; Shuttle and Cunning, 2007).

The Jefferies and Been (2016) method uses triaxial testing of reconstituted specimens, implying that at critical state the influence of in-situ soil fabric on void ratios and stresses is minimal. Although this hypothesis may be generally acceptable for homogeneous soils and tailings, verification is required for naturally deposited materials that exhibit laminated structure. This paper presents the interpretation of the CSL for a natural laminated glaciolacustrine silt/clay based on triaxial compression tests completed on intact and reconstituted specimens. The effects of these variations on the interpretation of ψ_o are also discussed via a series of cavity expansion numerical simulations.

Tested materials

Testing was carried out on samples of a laminated glaciolacustrine (GLU) silt/clay deposit sourced from Ontario, Canada. The soils within the GLU deposit had varying amounts of silt and clay, consistencies ranging from non-plastic to low plasticity, and structure ranging from visually homogeneous to (micro) laminated, to varved. Figure 1 shows photographs of variable structures found within the GLU deposit.

Both reconstituted and intact samples of the GLU were tested. The reconstituted samples represent the average properties of the visually homogeneous non-plastic and low plastic silty parts of the GLU deposit and are referred to GLU1 and GLU2, respectively. GLU1 and GLU2 samples were created by blending and mixing Sonic core samples of similar materials to create batches of visually homogeneous

soils, from which the advanced test specimens were formed. Figure 2 compares the grain size distribution curves of GLU1 and GLU2 with those of other samples collected from the GLU deposit. GLU1 represents GLU materials with low clay content (< ~15%) and is categorized as non-plastic silt (ML) in the unified soil classification system (USCS). GLU2 represents glaciolacustrine materials with higher clay content (~25 – 40%) and is categorized as low plastic silt and clay (ML-CL) in USCS.

Intact Shelby tube samples collected from the GLU deposit were also tested to compare and assess the influence of in-situ soil fabric. The Shelby tube samples were collected from intervals within the GLU deposit where clay and silt laminations were observed. The Shelby tube samples were composed of predominantly fine-grained soils, ranging from low plastic silt and clay (ML-CL) mixtures to low plastic clay (CL).

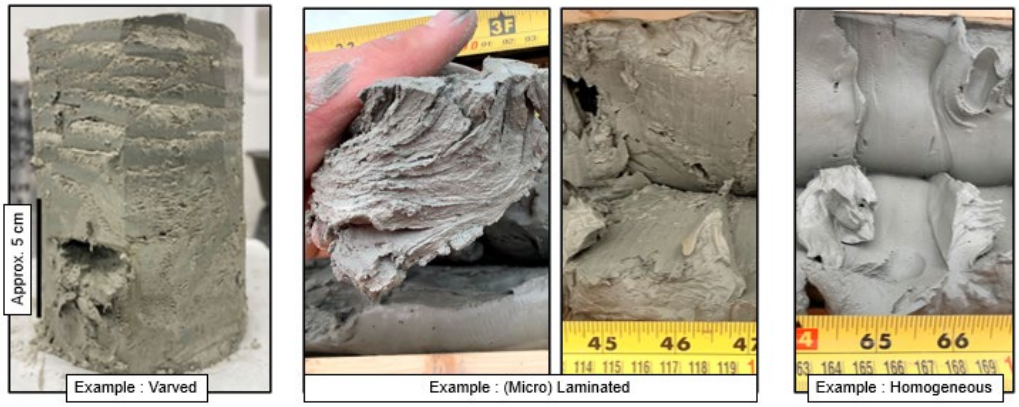


Figure 1: Photographs of variable structures found within the GLU deposit

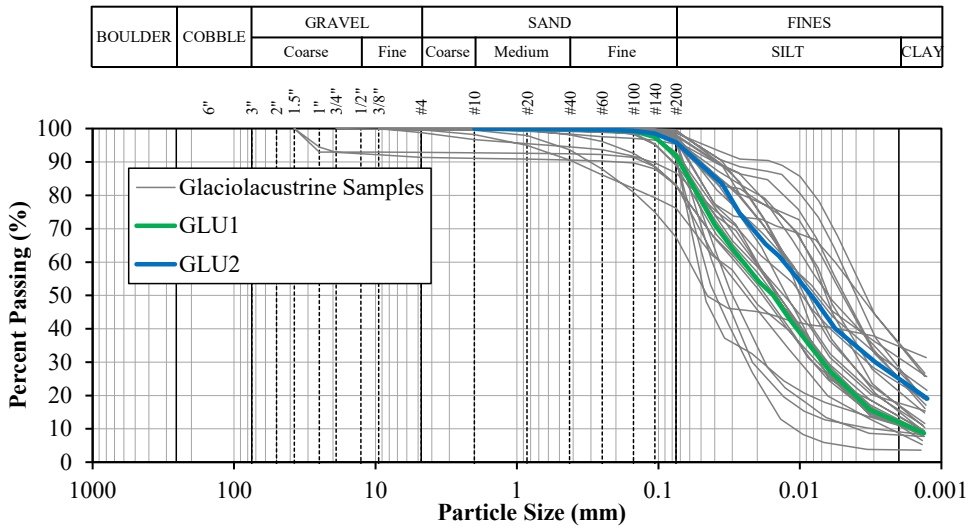


Figure 2: Gradation curves for glaciolacustrine (GLU) and blended GLU1 and GLU2 samples

Triaxial testing and NorSand calibration of GLU1 and GLU2

Triaxial tests were performed on GLU1 and GLU2 specimens to determine their CSLs and other necessary inputs for the calibration of the NorSand constitutive model. The results of these triaxial tests with emphasis on CSLs for GLU1 and GLU2 are presented first, followed by the NorSand calibration.

Triaxial testing and critical state lines

Triaxial tests were performed on GLU1 and GLU2 specimens. The triaxial specimens were prepared by reconstituting samples using the moist tamping method. The triaxial tests were completed on specimens 70mm in diameter by 140mm high with lubricated free ends, using an automated system manufactured by GDS. This servo-controlled system allows direct control of the cell pressure, testing rate, and data acquisition. The system uses an internal load cell that is placed within the cell at the end of the loading piston which eliminates the potential for piston friction. The cell pressure was controlled using GDS pressure/volume controllers. These controllers allow regulation and measurement of fluid pressures and volume changes.

A series of five isotropically consolidated drained (CID) and two isotropically consolidated undrained (CIU) tests were performed on each of GLU1 and GLU2 specimens, respectively. Of the five CID tests completed on each material, two specimens were prepared in a loose state and three were prepared in a dense state. Both CIU specimens were prepared in a loose state. The state paths of CID and CIU triaxial tests, showing variations of void ratio (e) with mean effective stress (p'), are summarized alongside CSLs for GLU1 and GLU2 in Figure 3a and Figure 3b, respectively. Figure 3c shows the comparison of CSLs for GLU1 and GLU2. Both CSLs can be defined by a semi-logarithmic equation: $e = \Gamma - \lambda \log(p')$ where Γ is the CSL intercept (altitude) at $p' = 1$ kPa and λ is the slope of the CSL. λ is associated with compressibility of soil during shear (Shuttle and Jefferies, 1996). Values of Γ and λ for GLU1 and GLU2 are summarized in Table 1, based on which GLU2 has greater compressibility and altitude than GLU1.

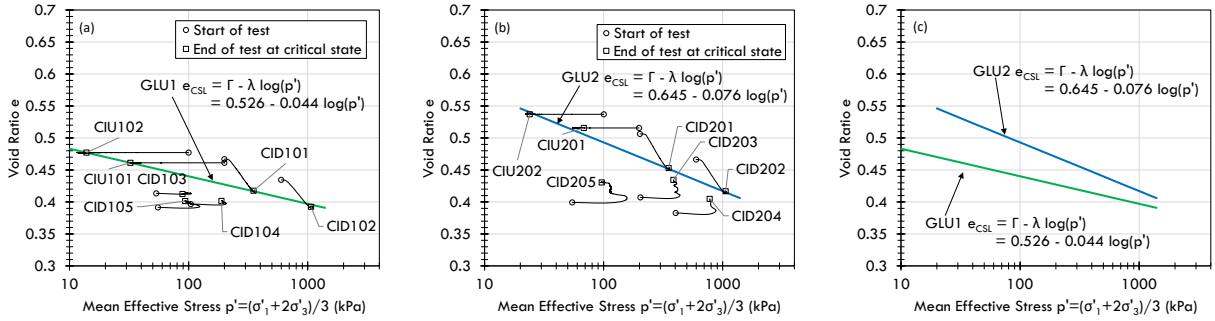


Figure 3: Triaxial test results and CSLs for (a) GLU1, (b) GLU2, and (c) both GLU1 and GLU2

Table 1: CSL parameters in e-p' plane for GLU1 and GLU2

Material	Γ	λ
GLU1	0.526	0.044
GLU2	0.645	0.076

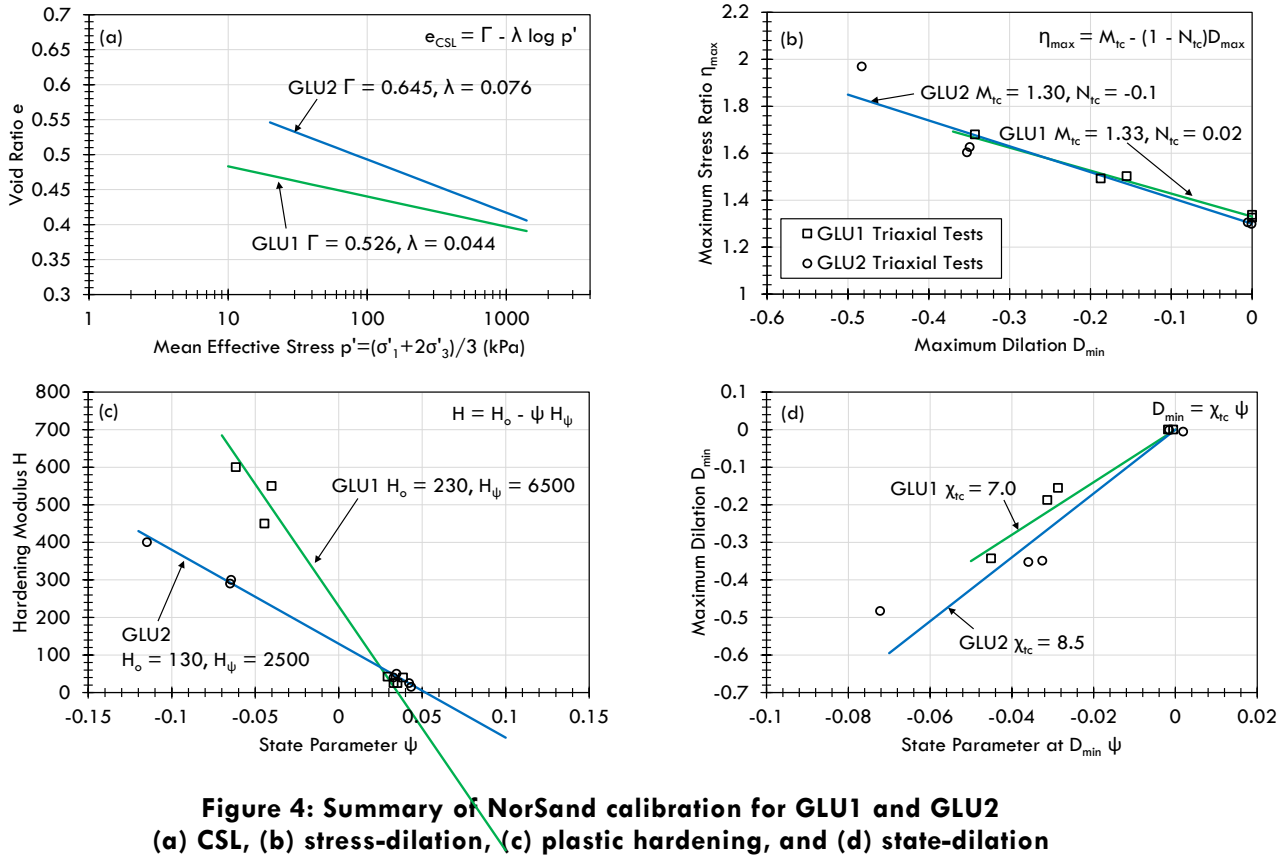


Figure 4: Summary of NorSand calibration for GLU1 and GLU2
(a) CSL, (b) stress-dilation, (c) plastic hardening, and (d) state-dilation

NorSand calibration

The triaxial tests results on GLU1 and GLU2 were used to calibrate the NorSand constitutive model (Jefferies and Shuttle, 2005; Jefferies and Been, 2016). Figure 4 shows the plots summarizing NorSand calibration for GLU1 and GLU2 as follows: Figure 4a shows CSLs in e – log p' plane; Figure 4b shows the stress-dilation relationship, which is the maximum dilation (D_{min}) versus the corresponding maximum stress ratio ($\eta_{max} = (q/p')_{max}$) fitted with $\eta_{max} = M_{tc} - (1 - N_{tc})\, D_{min}$, where M_{tc} and N_{tc} are the critical friction ratio and the volumetric coupling coefficient, respectively; Figure 4c shows plastic hardening parameter calibration, modulus (H) versus the corresponding values of state parameter (ψ) fitted with $H = H_o - H_\psi\, \psi$, where H_o and H_ψ are the intercept and slope of the plastic hardening modulus trendline; Figure 4d shows the stress-state relationship, D_{min} and its corresponding ψ values fitted with $D_{min} = \chi_{tc}\, \psi$, where χ_{tc} is the dilatancy parameter.

Typical CIU and CID test results alongside the corresponding NorSand simulations for GLU1 and GLU2 are shown on Figure 5. The model simulations fit test data reasonably well. The misfit of volumetric strains in CID105 (Figure 5g) and CID203 (Figure 5o) is attributed to the formation of a shear band, which onsets at an axial strain of approximately 1% to 2% in both tests.

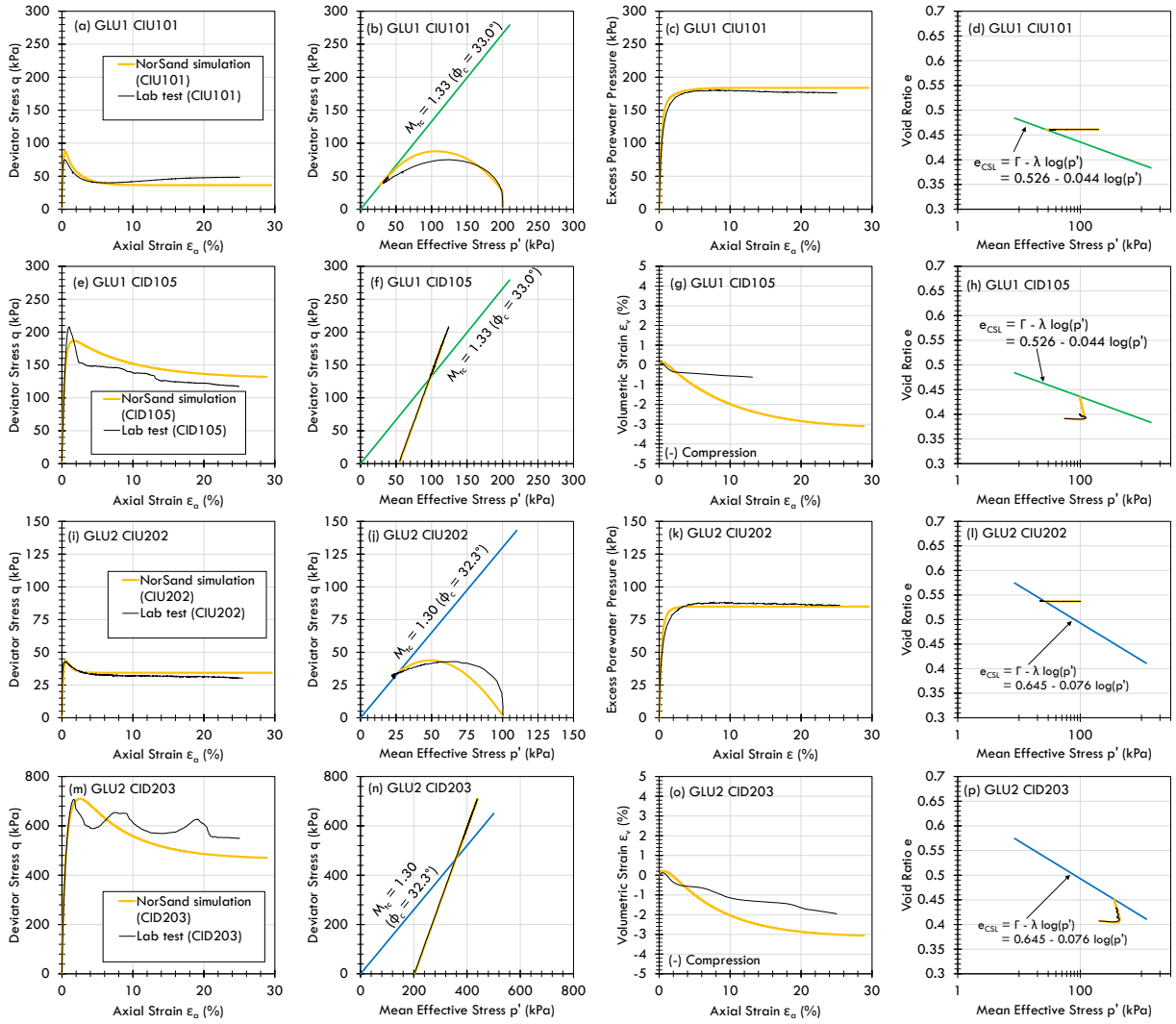


Figure 5: Comparison of NorSand simulations and typical CIU and CID test data for GLU1 (top two rows) and GLU2 (bottom two rows): (a), (e), (i), (m) stress-strain; (b), (f), (j), (n) p' – q; (c), (k) excess porewater pressure; (g), (o) volumetric strain; (d), (h), (l), (p) e – log p'

Influence of in-situ soil fabric on CSL interpretation

Several CIU triaxial tests were conducted on intact specimens recovered from Shelby tubes to assess the influence of in-situ laminated soil fabric on the CSL interpretations. These intact specimens were loose of GLU1 and GLU2 CSLs, and as such, it was expected that these samples would be contractive upon shearing, due to positive shear induced pore pressure development. However, test results on intact Shelby tube

samples generally showed dilative behavior. It was unclear whether the difference in behavior was the result of specimen variability or whether the destruction of laminated fabric during sample reconstitution was the cause.

To investigate this further, additional testing was completed on a third material referred to as GLU3. Following the same methodology used to prepare GLU1 and GLU2 samples, a Sonic core sample of GLU3 was thoroughly blended and mixed to create a batch of visually homogeneous soil. Figure 6 compares the gradation of GLU3 with those of GLU1 and GLU2. Similarly to GLU1, GLU3 was also categorized as non-plastic silt (ML) in the USCS.

One CID (CID301) and one CIU (CIU301) test were performed on loose reconstituted GLU3 specimens, each at a confining pressure of 200 kPa, as shown in Figure 7a. Both samples were contractive and converged on a CSL of similar slope to that of GLU1, albeit offset upwards by a void ratio of approximately 0.11. This "non-uniqueness" of the CSL is attributed to subtle variations in grain size distribution (and more specifically grain packing) and potentially initial void ratios of loose samples used to define CSLs for GLU1, GLU2, and GLU3. The "non-uniqueness" of CSL in e-logp' plane has been reported in the literature for several types of soils, e.g. Verdugo et. al (1995), Naesgaard and Byrne (2005), Martins et al. (2001), Nocilla et al. (2006), Shipton and Coop (2012), and Todisco and Coop (2019).

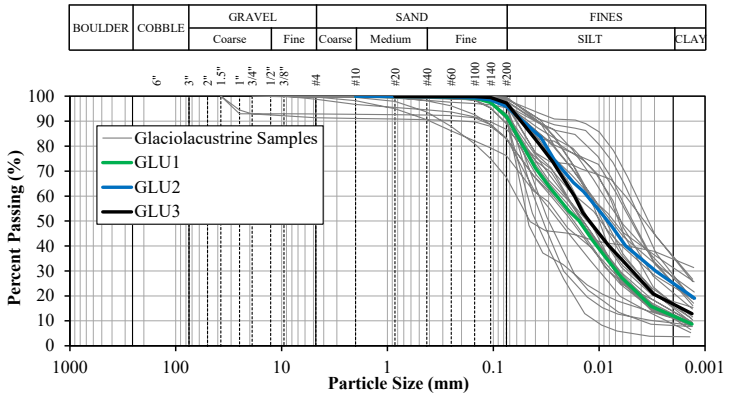


Figure 6: Comparison of GLU3 gradation with those of GLU1 and GLU2

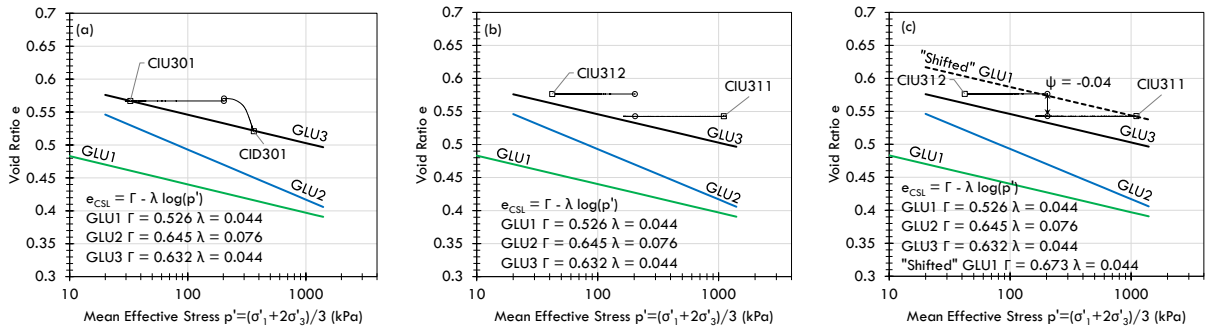


Figure 7: CIU triaxial tests on (a) reconstituted GLU3 samples, (b) intact Shelby and reused GLU3 samples, and (c) "Shifted" GLU1 CSL

Figure 7b shows the results of a CIU test (CIU311) on an intact Shelby tube sample of GLU3, recovered from directly below the Sonic core sample within the same borehole. CIU311 had an initial void ratio slightly above the CSL for GLU3, so it was expected that this specimen would be contractive or neutral in terms of pore pressure generation. Instead, the specimen was dilative with the state path moving away from the CSL, as shown in Figure 7b.

Following CIU311, the specimen was broken apart, thoroughly mixed, and reconstituted (moist tamped) to a similar, albeit slightly looser, initial void ratio. This allowed a direct comparison of behavior with the only difference being that the intact sample in CIU311 had the in-situ laminated fabric preserved, whereas the sample in CIU312 was completely homogeneous, with the acknowledgement that some minor gradational changes may have occurred as the material was retested. As shown in Figure 7b, the sample in CIU312 was now contractive and trended towards the reconstituted CSL of GLU3.

The comparison of CIU test results on intact Shelby tube and reconstituted samples of GLU3 clearly demonstrate the effects of soil fabric on the position of the CSL for this material. The difference in behavior is attributed to the fine laminated and heterogeneous structure of the in-situ material when compared to the uniform homogeneous reconstituted specimens. Similar observations of the effects of microlaminations on the position of the CSL for a tailings material were reported by Reid et al. (2021). Interestingly, the introduction of laminated structure appears to affect the vertical position of the CSL (specifically the term Γ) but does not appear to significantly change the slope (λ) of the CSL. This may be because λ is controlled by soil mineralogy as opposed to structure or minor gradational differences.

The NorSand constitutive model, which was previously developed for GLU1, was used to simulate the results from the intact GLU3 specimen in CIU311. In this case, the same NorSand parameters developed for GLU1 were used, with the exception being that the CSL was "shifted" upwards so that it coincided with the end point of CIU311 (refer to Figure 7c). The results of the NorSand simulation for CIU311 are shown in Figure 8. In general, the test data fit very well which demonstrates that the effects of in-situ laminated structure for this material are captured by changing the vertical position of the CSL (i.e. Γ), without change to λ, or to the other NorSand parameters.

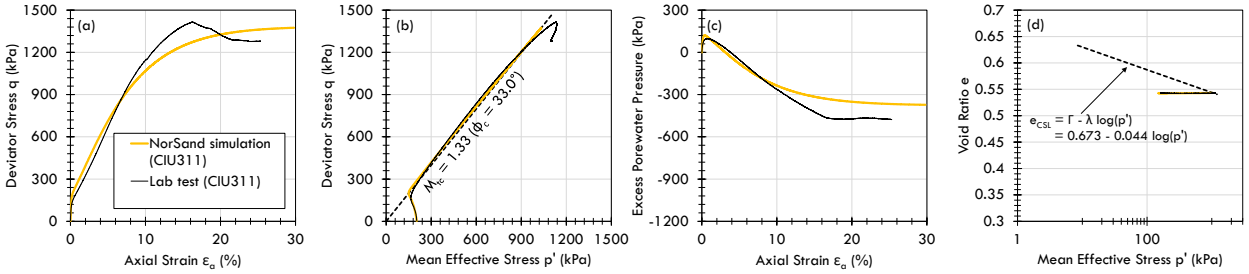


Figure 8: Comparison of NorSand simulation and test data for CIU311 (a) stress-strain, (b) p' – q, (c) excess porewater pressure, and (d) e – log p'

Influence of CSL variations on in-situ state parameter interpretation

The influence of CSL position on the ψ_o interpretations of GLU soils were investigated via cavity expansion numerical simulations. These simulations were completed under both drained and undrained conditions, using a Fortran based executable code referred to as "CPTwidget V3.1" (Shuttle 2018a; Shuttle, 2018b; Shuttle, 2018c). CPTwidget simulations were used to determine CPTu inversion coefficients, which were subsequently used to calculate ψ_o from measured CPTu data using equations recommended by Jefferies and Been (2016).

The work herein suggests that a laminated soil deposit is likely represented by a wide range of CSLs, all of similar slope (λ) but variable elevation (Γ), depending on subtle variations in laminated structure and gradation. It would also appear that the CSL of reconstituted "homogenous" materials are positioned at lower elevation on the e-log p′ plane, when compared to those of intact laminated specimens.

Figure 9 shows a comparison of interpreted ψ_o for a representative CPTu probe at the site. The analysis was first carried out by inversion using the CPTwidget and implementing the NorSand parameters established for GLU1. The process was then repeated with the only change being that Γ was increased to be consistent with the in-situ GLU3 CSL (refer to Figure 7c). From Figure 9, it is observed that changing Γ did not change the interpretation of ψ_o by inversion using the CPTwidget. This is because the cavity expansion methods used to interpret in-situ state from the dilative/contractive response of the CPTu are based on in-situ ψ_o as an offset from CSL as opposed to a direct measure of in-situ void ratio (e_0), and as such are not affected by variation of Γ.

This is an important finding because it suggests that provided the λ is unchanged during the reconstitution process (as appears to have been the case for the GLU material tested herein), the interpreted ψ_o from cavity expansion simulations in laminated soils can be considered as reliable even when the testing has been completed on reconstituted specimens where the laminated structure has been obliterated. This was confirmed by comparing the ψ_o of the CIU311 specimen from the laboratory testing data and using the interpreted intact CSL for GLU3 (refer to Figure 7c) with the in-situ ψ_o from the CPTWidget at the same depth (refer to Figure 10). In both cases the interpreted ψ_o was the same (-0.04) which appears to validate the approach.

When estimating the in-situ ψ_o of laminated soils, it is important to compare "absolute" void ratio measurements, such as those obtained from bulk density or natural water content of saturated samples, with critical state void ratios obtained from CSLs based on laboratory tests of intact laminated soil specimens. Using CSLs from reconstituted specimens to estimate in-situ void ratios may be inaccurate due to the vertical shift in the CSL for reconstituted versus intact samples.

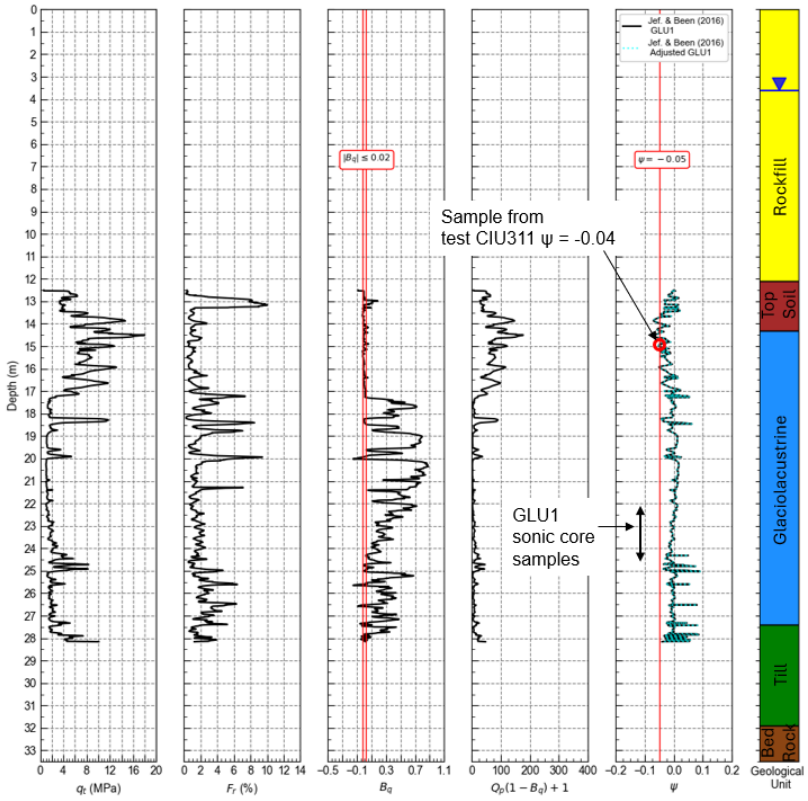


Figure 9: Interpreted in-situ state parameters for GLU1

Conclusion

A series of drained and undrained triaxial compression tests were conducted on reconstituted specimens of a fine-grained glaciolacustrine (GLU) soil to determine its CSL. Triaxial tests were also performed on intact Shelby tube samples and the results were compared to the CSL of reconstituted specimens. The following conclusions arose from this study:

1. A laminated glaciolacustrine deposit is characterized by a variety of similarly shaped (i.e., parallel) CSLs which vary in elevation (i.e., Γ) depending on differences in structure and gradation.
2. The CSL of reconstituted specimens were generally lower in elevation (i.e., Γ) when compared to those of the intact laminated specimens.
3. Provided the slope (λ) of the CSL does not change as a result of sample reconstitution (as was the case for the material tested herein), the loss of laminated structure induced by sample reconstitution does not adversely influence the reliability of ψ_o interpretated using CTP inversion (i.e., CPTWidget).
4. Caution must be used in laminated soils when comparing estimates of in-situ state based on "absolute" measurement of void ratio with interpreted critical state void ratios obtained from CSL's derived from laboratory testing of reconstituted specimens. In that case, the vertical shift in

reconstituted CSL arising from sample reconstitution may have a significant impact on the estimated in-situ ψ_o, which may lead to gross misunderstanding.

Acknowledgements

The authors would like to acknowledge the support of BGC Engineering Inc. and its internal reviewers and others who were involved throughout this process.

References

Been, K., Jefferies, M.G., Crooks, J.H.A. and Rothenburg, L. 1987. The cone penetration test in sands: part II, general inference of state. *Géotechnique* 37(3): 285–299. DOI: 10.1680/geot.1987.37.3.285

Jefferies, M. and Been., K. 2016. *Soil Liquefaction: A Critical State Approach*. Boca Raton: CRC Press.

Jefferies, M. and Shuttle., D.A. 2005. NorSand: features, calibration and use. In *Proceedings of the Geo-Frontiers 2005 Congress.* Austin, TX, USA, January 24–26, 2005. Geotechnical Special Publication. DOI: 10.1061/40771(169)9.

Martins, F. B., Bressani, L. A., Coop, M. R. and Bica, A. V. D. 2001. Some aspects of the compressibility behaviour of a clayey sand. *Canadian Geotechnical Journal*, 38(6): 1177–1186.

Morgenstern, N.R., Vick, S.G. and Van Zyl, D. 2016. Report on the Immediate Causes of the Failure of the Fundão Dam. Fundão Tailings Dam Review Panel.

Naesgaard, E. and Byrne, P.M. 2005. The flow liquefaction due to mixing of layered deposits. *Proceedings of ICSMGE TC4 Satellite Conference on Recent Developments in Earthquake Engineering:* 1031–08.

Nocilla, A., Coop, M.R. and Colleselli, F. 2006. The mechanics of an Italian silt: An example of 'transitional' behaviour. *Géotechnique* 56(4): 261–271.

Plewes, H.D., Davies, M.P. and Jefferies, M.G. 1992. CPT based screening procedure for evaluating liquefaction susceptibility. *Proceedings of the 45th Canadian Geotechnical Conference* 4: 1–9.

Reid, D., Fanni, R. and Fourie, A.B. 2021. Layering – the missing factor in fabric studies? *Proceedings of the International Conference on Soil Mechanics and Geotechnical Engineering 2021.* Sydney, Australia.

Robertson, P.K. 2010. Estimating in-situ state parameter and friction angle in sandy soils from CPT. *Proceedings of the 2nd International Symposium on Cone Penetration Testing,* Huntington Beach, CA, USA, May 2010.

Robertson, P.K., de Melo, L., Williams, D.J. and Wilson, G.W. 2019. *Report of the Expert Panel on the Technical Causes of the Failure of Feijão Dam I.*

Shipton, B. and Coop, M.R. 2012. On the compression behaviour of reconstituted soils. *Soils and Foundations* 52(4): 668–681.

Shuttle, D.A. 2018a. CPTWidget V3.1 Computer program. Data prepared for BGC Engineering Inc.

Shuttle, D.A. 2018b. CPTWidget V3.1 – Operation of the code. Data prepared for BGC Engineering Inc.

Shuttle, D.A. 2018c. Release notes for CPTWidget V3.1. Data prepared for BGC Engineering Inc.

Shuttle, D.A. and Cunning, J. 2007. Liquefaction potential of silts from CPTu. *Canadian Geotechnical Journal* 44(1): 1–19.

Shuttle, D.A. and Jefferies, M.G. 1996. Reliable parameters from imperfect SBP *Tests in Clays, Advances in Site Investigation Practice*. *Proceedings of the International Conference* held in London 30–31 March 1995. C. Craig (ed.). Published January 1996 by Thomas Telford, ISBN 0727725130: 571–585.

Shuttle, D.A. and Jefferies, M.G. 1998. Dimensionless and unbiased CPT interpretation in sand. *International Journal for Numerical and Analytical Methods in Geomechanics* 22(5): 351–391.

Todisco, M.C. and Coop, M.R. 2019. Quantifying transitional soil behaviour. *Soils and Foundations* 59: 2070–2082.

Verdugo, R., Castillo, P. and Briceno, L. 1995. Initial soil structure and steady state strength. *Earthquake Geotechnical Engineering,* Ishihara Edition, Balkema, Rotterdam, ISBN 90 5410578 X.

Mechanical Behavior of Gold Mine Tailings Dried by Natural Dewatering

Mayara Ferreira Rodrigues, Federal University of Rio de Janeiro – UFRJ, Brazil
Paula de Mello Martins, Ex-AngloGold Ashanti, Brazil
Jaime Pinheiro, AngloGold Ashanti, United States of America

Abstract

The various dam failures that have happened globally have resulted in changes in Brazilian legislation. As a result, the disposal of dry tailings in piles or stacks has become a widely used alternative, giving rise to a need to better understand the behavior of these tailings when dried and mechanically compacted in layers. Therefore, it is necessary to carry out experiments on a smaller scale with field and laboratory tests to evaluate the best construction methodology and geotechnical parameters to be adopted. This paper originated from the results of experimental landfills, and presents the field and laboratory results of the mechanical behavior of the naturally dewatered gold ore tailings, submitted to compaction with a road roller compactor and with a bulldozer. To this end, disturbed samples were used for characterization, compaction, and resistance tests and undisturbed samples were collected for resistance and permeability tests, in addition to the results of tests carried out in experimental landfills to verify the compaction conditions of the tailings.

The analyzed tailings come from the calcination process, part of the metallurgical process of gold ore beneficiation, classified as sandy silt with clay, with a specific gravity between 3.435 g/cm³ and 3.790 g/cm³, a maximum dry density between 1.384 g/cm³ and 1.516 g/cm³ and an average optimum moisture content of 33.5%. The resistance tests performed by undrained triaxial compression in the saturated condition showed null effective cohesion and a mean effective friction angle of 26°.

Although the experimental embankments did not aim to evaluate the dilating or contractile behavior of the tailings under the compaction conditions imposed by the experiment, or even its liquefaction potential, the analysis of the results allowed for this evaluation in an initial way, and it is now necessary to carry out specific tests to enable better data regarding such behaviors.

Introduction

The global history of accidents with dams, including notorious events in Brazil, has initiated the trend of disposal of tailings in piles or stacks, making it necessary to expand geotechnical studies related to tailings,

which can have considerable variations in geotechnical behavior.

Fourie et al. (2022), highlight that mining is growing, with production increasing every year. At the same time, ore bodies tend to have less and less ore content, which makes the increase in tailings generation into tailings disposal structures even larger. This reinforces the need to improve mining tailings disposal management processes, rethink design criteria, existing monitoring technologies, processes used, and several other issues.

For the construction of large geotechnical structures using materials whose behavior is not well known, it is necessary to carry out experiments on a smaller scale, using field and laboratory tests to evaluate the best construction systems and geotechnical parameters to be adopted in the project.

The main motivator of the experiment presented here was the need for a dam that receives the pulp tailings from the pyrometallurgy calcination process, one of the stages of gold ore processing. In this way, the tailings hydraulically deposited would go through a natural dewatering process and be deposited in piles.

It is noteworthy that this article is restricted to the results of the experimental landfill performed, considering tests carried out in situ and in the laboratory, and from these tests the characterization of the tailings, hydraulic conductivity and resistance parameters were determined. Evaluations of the contractile or dilating behavior of this tailings, as well as the potential for liquefaction, are initially based on the available results and were not the objective of the experimental landfills.

The study considered the execution of two experimental landfills, one with material compacted through a road roller compactor without vibration, called Experimental Landfill I, and the other compacted by a bulldozer, called Experimental Landfill II.

Materials and methods

Origin and processing of gold ore

The tailings analyzed come from the processing of gold ore mined from two underground mines located in the Iron Quadrangle of the state of Minas Gerais in Brazil.

Ore is extracted from underground mines and goes through the following processing stages: primary crushing, grinding, gravimetric separation, and flotation. In flotation, the separation takes place in two distinct processes, also separated into two parts, composed of 10% of the volume and 90% of the volume. The material that makes up 10% of the volume that comes out of the flotation is directed to metallurgy, where it goes through the processes of repulping, roasting, leaching, solid/liquid separation, CIP (Carbon in Pulp) processing, elution, precipitation with zinc and, finally, casting. In this metallurgical process, the tailings studied here are generated.

These tailings were directed to the reservoir of the dam, hydraulically disposed of by spiking along the reservoir, from where it was excavated and transported in weighbridge trucks to the site of the experimental landfills.

Characteristics of experimental landfills

In order to understand the behavior of the tailings when subjected to compaction, two different landfills were carried out, one with compaction of the tailings through a road compaction roller without vibration, called Experimental Landfill I, and the other with compaction of the tailings through the passage of a bulldozer, called Experimental Landfill II.

To prepare the foundation of the experimental landfills, a liner was laid in layers of waste material totaling a thickness of 80 cm. Then, above this liner, 3 layers were laid with the tailings itself with a thickness of 30 cm each and compacted to a degree of compaction equivalent to 95% Proctor and a moisture content in the range of ±2% in relation to the optimal moisture content. These layers served as the basis for the beginning of the experimental embankments and were defined to minimize the influence of the difference between materials and the stiffness of the soil in relation to the compacted landfill.

The tailings used in the experimental landfills were excavated with excavators and transported to the area close to the piles with dump trucks. At the time of excavation, the average moisture content of the tailings was approximately 52.4% and the optimum moisture content obtained through the standard Proctor compaction test was 33.5%. Treatment was needed to reduce the moisture. This treatment was carried out with a tractor with tires and rotating blades, and when the tailings reached the optimum moisture content, they were again transported to the area defined for the experimental landfills.

At the ends of both experimental area ramps, an acceleration and maneuvering area was maintained, approximately 20 m long and 20 m wide, so that the movement of machinery and equipment did not interfere with the control of the layers.

In Experimental Landfill I, tests were carried out to verify the degree of compaction after every two passes carried out by the compactor. This procedure was followed until 8 passes of the equipment were completed for the compaction of the layer. In the Experimental Landfill II, the degree of compaction was verified with 2, 4, and 6 passes of the compaction achieved by the bulldozer.

Table 1 presents the general characteristics of the experimental landfills.

Table 1: Characteristics of experimental landfills

Item	Landfill I	Landfill II
Compaction method	Road roller compactor without vibration	Bulldozer
Layer thickness (cm)	30	30
Width (m)	25	20
Height (m)	1.20	0.90
Volume (m³)	5.600	3.600
Moisture content for compaction	W_{opt} ±2%	W_{opt} ±2%

Sampling and laboratory and field tests

Samples were collected and assays were performed according to the standards shown in Table 2.

Table 2: Standards used as reference

Norm	Assay
ABNT NBR 6457:2016	Soil – Preparation of samples for compaction tests, characterization and determination of moisture content
ABNT NBR 6459:2017	Soil – determination of the liquidity limit
ABNT NBR 6508:2016	Cobblestone grains retained in the opening sieve 4.8 mm – Determination of specific mass, apparent specific mass and water absorption
ABNT NBR 7180:2016	Soil – determination of the plasticity limit
ABNT NBR 7181:2016	Soil – particle size analysis
ABNT NBR 7182:2016	Soil – compaction test
ABNT NBR 9813:2016	Soil – determination of the apparent specific mass in situ, using a driving cylinder
ABNT NBR 12102:2020	Soil – compaction control by the Hilf method
ABNT NBR 13292:2021	Soil – determination of the permeability coefficient of granular soils at constant load
ASTM D4767-11:2020	Standard test method for consolidated undrained triaxial compression test for cohesive soils
ASTM D7181-11:2015	Standard test method for consolidated drained triaxial compression test for soils

Compaction control tests were performed in all layers using the Hilf methodology to verify the density and moisture content in situ. In addition to the in-situ tests, disturbed samples were collected from both experimental landfills for laboratory tests, for characterization and compaction. Undisturbed samples of the block type from the Experimental I embankment were collected for resistance and permeability tests. These results are presented in the following section.

The triaxial compression tests in the drained condition were performed in specimens prepared from the undisturbed samples, saturated by percolation and back pressure and at confining stresses of 100 kPa, 200 kPa, 400 kPa, and 800 kPa, both for the drained and undrained tests.

Results

The tailings are classified as sandy silt with little clay, have a specific gravity between 3.435 g/cm³ and 3.790 g/cm³, a maximum dry density between 1.384 g/cm³ and 1.516 g/cm³, and an optimum moisture content ranging from 31.9% to 38.2%. The results of the characterization and compaction tests performed on the samples collected in the experimental landfill are summarized in Table 3.

Table 3: Summary of characterization and compaction tests

Sample	Particle size distribution				Specific gravity (g/cm³)	Liquidity and plasticity limits			Standard Proctor compaction	
	Clay (%)	Silt (%)	Sand (%)	Gravel (%)		Liquid Limit (%)	Plastic Limit (%)	Plasticity Index (%)	Maximum dry density (g/cm³)	Optimal moisture content (%)
1	13	67	19	1	3.649	Non-liquid	Non-plastic	Non-plastic	1.384	34.0
2	10	76	14	0	3.664				1.451	31.9
3	11	63	21	5	3.790				1.470	37.9
4	10	65	23	2	3.716				1.459	38.2
5	10	67	21	2	3.435				1.521	34.1
6	10	68	21	1	3.786				1.480	34.3
7	12	63	22	3	3.722				1.516	34.8
8	6	75	15	4	3.665				1.478	37.0
9	12	69	18	1	3.718				1.473	29.2
10	12	78	10	0	3.821				1.347	42.8

Two undisturbed samples of the block type were collected at Experimental Landfill I, identified as AI-01 and AI02, and were submitted for isotropic triaxial compression tests of the drained and saturated type (CIDsat) and the saturated undrained type (CIUsat), at the confining stresses of 100 kPa, 200 kPa, 400 kPa, and 800 kPa. Permeability tests at constant load were also carried out on specimens molded in the blocks, vertically and horizontally to the compaction plane. On a disturbed sample, identified as AD-01, an isotropic triaxial compression test of the drained and saturated type (CIDsat) was performed at the confining stresses of 200 kPa and 400 kPa and of the saturated undrained type (CIUsat), at the confining stresses of 100 kPa, 200 kPa, 400 kPa and 800 kPa, all specimens molded under two conditions. One with a degree of compaction of 90% and optimum moisture content and the other with a degree of compaction of 98% and

optimum moisture content, in relation to the standard Proctor compaction test. The results are presented in Table 4 below.

Table 4: Summary of strength and permeability tests

Sample	CIUsat				CIDsat		Permeability at constant load	
	Cohesion (c)	Friction Angle (ϕ)	Cohesion (c')	Friction Angle (ϕ')	Cohesion (c')	Friction Angle (ϕ')	Vertical (cm/s)	Horizontal (cm/s)
AD-01 – GC=90 %	0	12	0	22	10	31	–	–
AD-01 – GC=98 %	0	16	0	28	–	–	–	–
AI-01	0	14	0	23	12	22	9.75E-05	2.04E-04
AI-02	0	17	0	33	12	22	9.75E-05	2.10E-04

In Experimental Landfills I and II, tests were carried out to verify the density and moisture content in situ as the number of passes of compactor equipment increased. The summaries of the results of each experimental landfill are presented in Table 5 and Table 6 below.

Table 5: Results of the verification of density and moisture content in situ carried out at Experimental Landfill I

Assay	In-situ density verification				Number of passes of the equipment over the layer
	Density (g/cm³)	Moisture content (%)	Degree of compaction (%)	Moisture deviation (%)	
1	1.374	36	94.6	-1.8	2
2	1.35	38.1	95.5	1.4	2
3	1.398	37.8	96.3	0.0	2
4	1.345	34.8	92.6	-3.0	2
5	1.414	37.6	97.3	-0.2	3
6	1.38	35	97.5	-1.7	3
7	1.408	38.3	97	0.5	3
8	1.414	35.1	97.4	-1.3	4
9	1.450	37.6	99.9	1.2	4
10	1.366	37.6	95.8	1.6	4
11	1.402	35.4	98.3	-0.6	4
12	1.394	34.3	97.7	-1.7	4
13	1.463	36.0	100.2	-1.2	4
14	1.464	35.2	101.3	-1.5	4

Assay	In-situ density verification				Number of passes of the equipment over the layer
	Density (g/cm³)	Moisture content (%)	Degree of compaction (%)	Moisture deviation (%)	
15	1.462	35.4	101.1	-1.3	4
16	1.389	35.6	96	-1.1	4
17	1.426	36.8	98.6	0.1	4
18	1.424	35.6	98.5	-1.1	4
19	1.449	37.5	100.2	0.8	4
20	1.425	38.1	98.1	0.3	4
21	1.441	37.4	99.2	-0.4	4
22	1.402	36.4	96.5	-1.4	4
23	1.430	36	98.5	-1.8	4
24	1.436	38.8	101.3	-2.3	6
25	1.444	34.4	104.3	4.0	8
26	1.486	38	104.9	-0.8	8
27	1.496	37.1	105.6	-1.7	8

Table 6: Results of the verification of density and moisture content in situ carried out at Experimental Landfill II

Essay	In-situ density verification				Number of passes of the equipment over the layer
	Density (g/cm³)	Moisture content (%)	Degree of Compaction (%)	Moisture deviation (%)	
1	1.383	38.5	95.3	0.7	2
2	1.382	39.3	95.2	1.5	2
3	1.389	38.4	95.2	2.0	2
4	1.396	38.1	95.2	1.7	2
5	1.439	38.4	98.2	1.8	4
6	1.449	37.5	98.8	0.9	4
7	1.437	38.6	98	2.0	4
8	1.439	38.6	98.2	2.0	4
9	1.443	36.2	98.6	1.3	4
10	1.431	38.4	98.1	1.7	4
11	1.386	39.2	98.1	2.5	4
12	1.475	38.7	100.6	2.1	6
13	1.465	37.3	100	0.7	6
14	1.462	38.6	99.7	2.0	6
15	1.435	38.4	98.8	0.6	6

Discussion of the results

As previously shown in Table 3, the particle size analyses showed a sandy silt matrix material, with about 75% silt and 20% fine sand, with specific gravity ranging from 3.435 g/cm³ to 3.821 g/cm³, non-plastic. These values of the actual specific gravity fit within the variability of the specific gravity of mining tailings (from 1.5 g/cm³ to 3.8 g/cm³) proposed by Fourie et. al. (2022). Figure 1 shows the particle size range obtained from the particle size curves of the tests performed.

In this same figure, the ranges of materials susceptible to liquefaction and of materials with greater susceptibility to liquefaction are indicated, determined by the limits for analysis of liquefaction potential suggested by Terzaghi, et. al. (1996) (*apud* Tsuchida, 1970). The liquefaction process can be defined as the abrupt reduction of the effective tension as a function of an undrained loading in a saturated granular soil. It can be seen that part of the particle size range of the analyzed tailings is within the lower limit of the particle size distribution of the materials susceptible to liquefaction suggested by the authors for an initial evaluation of the liquefaction potential. Therefore, geotechnical studies aimed at the mechanics of soils in a critical state are necessary.

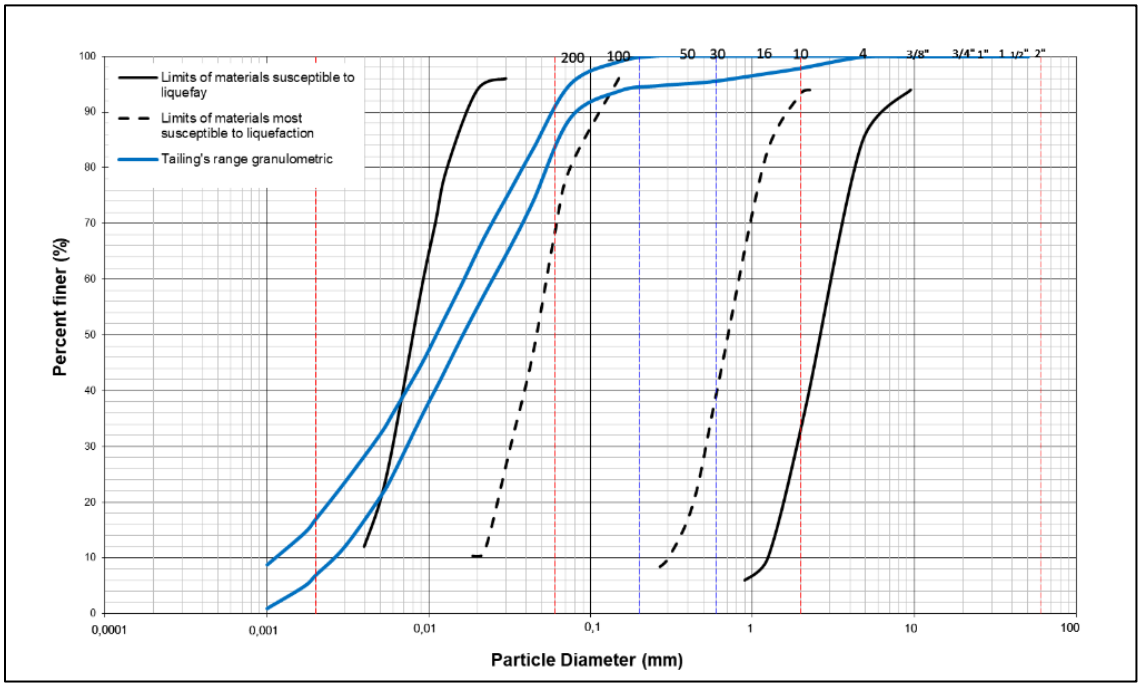


Figure 1: Particle size range of the tailings

The standard Proctor compaction tests showed an average maximum dry density of 1.469 g/cm³ and an average optimum moisture content of 33.5%. To determine the mean values, the result of sample 10 was disregarded because it was outside the sample standard deviation. The consolidation of the curves of the

standard Proctor compaction tests performed is shown in Figure 2, where it is also possible to highlight the mean curve obtained.

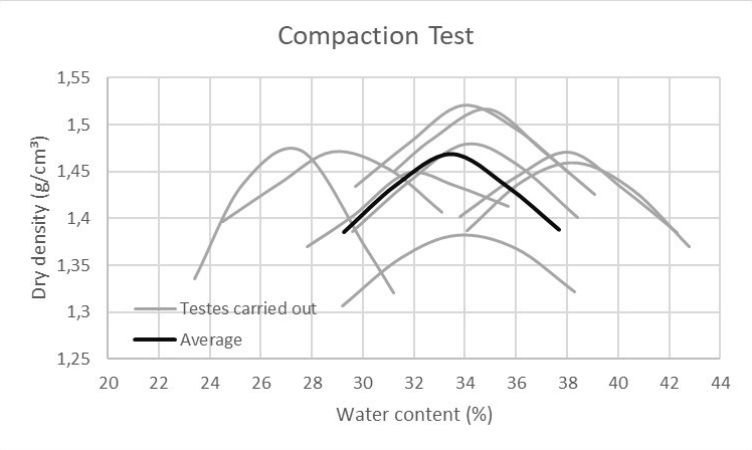


Figure 2: Consolidation of the standard Proctor compaction curves of the tests performed

When analyzing the degree of in-situ compaction from the two different conditions employed in the two experimental landfills, it can be seen that the tailings can be well compacted both using a road roller compactor or a bulldozer. Also, as expected for soil compaction, whether natural or not, there is a gain in the degree of compaction as the number of passes of compactor equipment increases. Another observation from the analysis of the tests is that, for this tailings, 4 passes of compaction equipment are sufficient to achieve a degree of compaction equal to or greater than 98%. These observations can be seen in the graph shown in Figure 3.

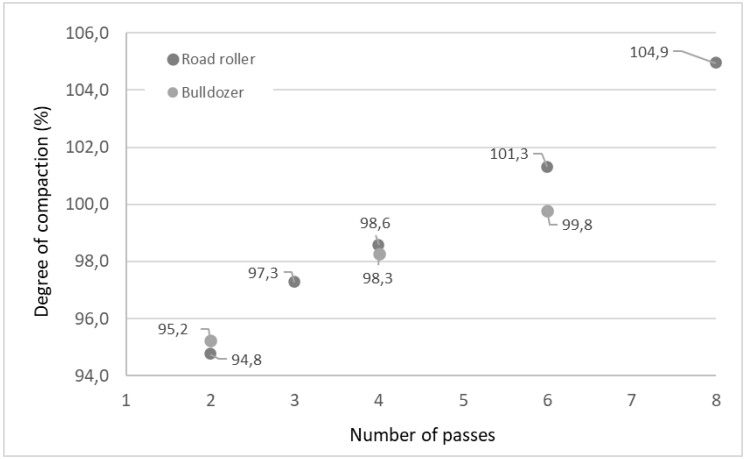


Figure 3: Graph of the degree of compaction as a function of the number of passes and type of equipment used for compaction

According to the results presented, the resistance tests performed on undisturbed samples indicate that the material has zero cohesion and an average effective friction angle of 28º for a degree of compaction of

approximately 98%. While the test performed on specimens molded at a degree of compaction of approximately 90% also indicates zero cohesion and an effective friction angle of 22º, in this test condition the tailings showed contractile behavior, as shown in Figure 4. It is noteworthy that for the tests performed on undisturbed samples whose degree of compaction was approximately 98%, this behavior was not observed.

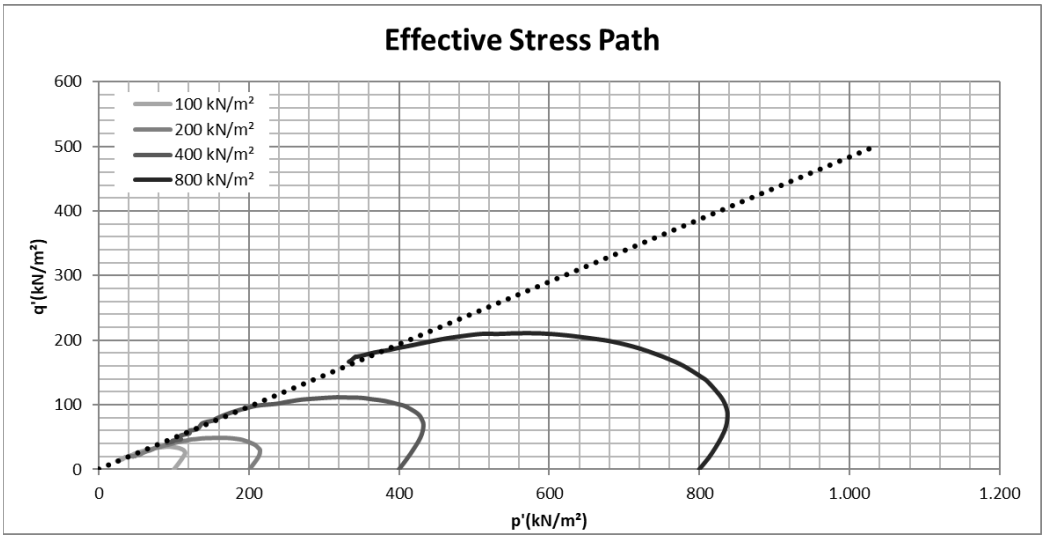


Figure 4: Effective stress trajectory of the CIUsat test performed on molded specimens at GC=90%

Based on the behavior of the tailings previously observed in Figure 4, it is necessary to develop more in-depth studies to establish the critical state line of this tailings and the trend of behavior as the degree of compaction increases.

To study the critical state line, Viana da Fonseca et al. (2021) highlighted that the most appropriate procedures for triaxial compression tests include the use of enlarged and lubricated extremities and recommend that the specimens be frozen at the end of the test to verify the total saturation condition and obtain the final moisture content. The authors explain that these procedures reduce the friction effect at the top and bottom of the specimens, allowing the deformations during the shear step to be more uniform. These procedures were not performed for the triaxial compression tests presented here. In addition, a test campaign was not carried out with laboratory-molded specimens in different degrees of compaction.

Conclusion

The results show that it is possible to carry out the compaction of these tailings in layers of 30 cm thickness both with a smooth roller and with bulldozer equipment. It is noteworthy that bulldozer equipment for the compaction of soils or tailings must be used with caution and supervision, to ensure that there is no

heterogeneity in the compaction of the layers, in strips or zones that the tracks of the bulldozer have not covered, creating fluffy or more fragile zones.

Regarding the evaluation of the liquefaction potential of the tailings, the tests carried out were insufficient to define the line of the critical state of the tailings. A complementary study is necessary for a better understanding of the behavior of the material.

There is a fundamental need to further the studies, and to widely share the results and experiences with the various types of tailings. There is also a fundamental need to review previously existing concepts in order to improve the disposal of dry tailings in piles or stacks, thus contributing to the quality of the processes and the structures, and developing a better technical basis for projects.

Finally, it cannot be said that the same parameters obtained in these tailings will be achieved in other materials, since the mechanical behavior of the tailings depends on several factors, especially the industrial processes used from mining to processing, the regional geology, and the mineralogical composition.

References

ABNT NBR 12102:2020. Soil – Compaction control by the Hilf method. Brazil: Rio de Janeiro.

ABNT NBR 13292:2021. Soil – Determination of the permeability coefficient of granular soils at constant load. Brazil: Rio de Janeiro.

ABNT NBR 6457:2016. Soils – Preparation of samples for compaction tests, characterization and determination of moisture content. Brazil: Rio de Janeiro.

ABNT NBR 6458:2016. Cobblestone grains retained in the opening sieve 4.8 mm – Determination of specific mass, apparent specific mass and water absorption. Brazil: Rio de Janeiro.

ABNT NBR 6459:2017. Solo – Determination of the liquidity limit. Brazil: Rio de Janeiro.

ABNT NBR 7180:2016. Soil – Determination of the plasticity limit. Brazil: Rio de Janeiro.

ABNT NBR 7181:2016. Soil – Particle size analysis. Brazil: Rio de Janeiro.

ABNT NBR 7182:2016. Soil – Compaction test. Brazil: Rio de Janeiro.

ABNT NBR 9813:2016. Soil – Determination of the apparent specific mass in situ, using a driving cylinder. Brazil: Rio de Janeiro.

Fourie, A., Verdugo, R., Bjelkevik, M., Torres-Cruz, L.A. and Znidarcic, D. 2022. Geotechnics of mine tailings: a 2022 state of the art. In M. Rahman and M. Jaksa (eds), *ICSMGE 2022. Proceedings of the 20th ICSMGE International Conference on Soil Mechanics and Geotechnical Engineering.* Australia. Sydney: 121–183.

Terzaghi, K., Peck, R.B. and Mesri, G. 1996. *Soil Mechanics in Engineering Practice*. New York: John Wiley & Sons, Inc.

Tsuchida, H. 1970. Evaluation of liquefaction potential of sandy deposits and measures against liquefaction induced damage. In Proceedings of the Annual Seminar of the Port and Harbour Research Institute: 3–33. Yokosuka, Japan. In Japanese.

Viana da Fonseca, A., et. al. 2021. Recommended procedures to assess critical state locus from triaxial tests in cohesionless remoulded samples. *Geotechnics* 1(1): 95–127.

Analysis of Video Images Obtained during Cone Penetration Testing

Gerald Verbeek, Eijkelkamp North America, USA
Gustavo Hamu, Royal Eijkelkamp, The Netherlands
Oksana Khomiak, TU Bergakademie Freiberg, Germany

Abstract

One of the ways to enhance the efficiency of the cone penetration testing process is to mount modules behind the cone. In this way the test will not only generate the standard CPT data (i.e., cone tip resistance, sleeve friction, and dynamic pore water pressure) but also the data obtained by the module pushed into the soil together with the cone. While for certain modules it is common practice to analyze the acquired data extensively (e.g., the seismic module) for other modules this is not necessarily the case. A good example of the latter is the video module when it is deployed with visible light, in which case the analysis is typically limited to viewing the recording and adding observation notes. During the recent TRIM4 research project the video module was deployed and initial attempts were made to identify the soil type and to determine the grain size distribution using the video images. This approach mitigates the effect of the CPT data, reflecting changes in soil strength behavior before a layer is actually penetrated by the cone. In this paper the authors will describe the analysis options they have identified for the video recordings.

Introduction

Cone Penetration Testing (CPT) is a widely accepted and applied soil investigation technique and the data generated during the testing (the cone tip resistance, the sleeve friction and the dynamic pore pressure) are used as inputs in numerous geotechnical and geohydrological engineering processes (e.g., the design of deep foundations, the assessment of the hydraulic conductivity of the soil, and the assessment of the condition of tailings storage facilities). To supplement the data acquisition one or more modules can be installed behind the cone and depending on the type of sensors mounted in the module, information can be obtained; for example, on seismic wave speed through the soil (when using a seismic module) or on the electric conductivity of the soil (when using a dieelectric module).

A module type that is not frequently used is the video module, which contains a camera that records data as the cone is pushed into the ground. This module is often used in combination with UV light sources

to record the visible light emitted by certain contaminants as they absorb UV light. Analysis of that visible light (intensity and frequency) can provide useful information on the type and extent of the contamination, which is very useful in geoenvironmental investigations.

However, the video module can also be used in combination with visible light to simply record imagery of the soil passing by the lens as the cone penetrates the soil. The analysis of that data is typically limited to viewing the recording and adding observation notes, but during the recent TRIM4 research project the video module was deployed and initial attempts were made to identify the soil type and to determine the grain size distribution using the video images.

TRIM4 Research Project

The TRIM4Post-Mining Research Project was a project funded by the European Union that brought together a consortium of European experts from industry and academia to develop an integrated information modelling system, designed to support decision making and planning during the transition from coal exploitation to a revitalized post-mining landscape, enabling infrastructure development for agricultural and industrial utilization, and contributing to the recovery of energy and materials from coal mining dumps. The basis of this system is a high-resolution spatiotemporal database, utilizing state-of-the-art multi-scale and multi-sensor monitoring technologies, which allow characterization of dynamic processes in mining waste dumps related to timely, dependent deformation and geochemical processes. As such it integrates efficient methods for operational and post-mining monitoring, comprehensive spatiotemporal data analytics, feature extraction, and predictive modelling; this then allows for the identification of potential contamination areas and the forecasting of geotechnical risks and ground conditions.

For the interactive exploration of alternative land-use planning scenarios – in terms of residual risks, technical feasibility, environmental and social impact, and affordability – up-to-date data and models are embedded in an interactive planning system, forming a TRIM – a Transition Information Modelling System. This system is designed to support decision making and planning during the transition from mine exploitation to a re-vitalized post-mining landscape enabling infrastructure development for agricultural and industrial utilization, and also to contribute to recover energy and materials from coal mining dumps.

Cone penetration testing (CPT)

For the TRIM4 Post Mining Project cone penetration testing was performed at two locations using a 10 cm^2 subtraction cone. The main objective of the CPT was to determine whether this soil investigation technique is useful to support decision making and planning during the transition from mine exploitation to a re-vitalized post-mining landscape enabling infrastructure development for agricultural and industrial utilization.

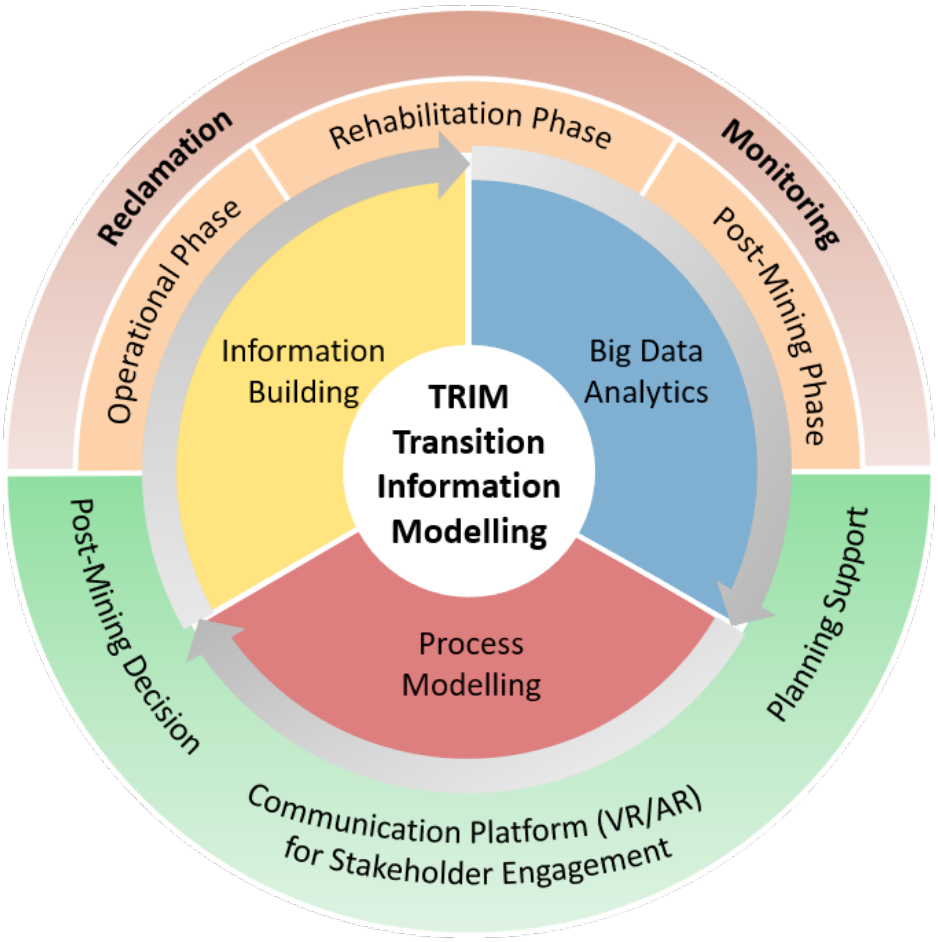


Figure 1: The structure of the TRIM

CPT – Location 1

At the first location CPT was performed to a depth of approximately 31 m when the tip resistance implied refusal. As shown in Figure 2 below, the data indicated that between a depth of 2 m and 18 m the cone tip resistance was generally low, with a sleeve friction that equated to a friction ratio of 2 % or higher, implying soil with a cohesive soil type behavior. Below 18 m the tip resistance increased, resulting in a lower friction ratio, implying the presence of soil with a granular soil type behavior. This was also clearly seen in the pore pressure readings. Due to the dynamic action associated with the testing, the recorded pore pressure increased, but then dropped to 0 kPa as soon as the cone entered the soil with a granular behavior, which allowed the excess pore pressure to dissipate immediately.

At the same location a soil boring was performed, and samples were obtained at various depths. The soil types for those samples were reported as shown in Figure 3 below, and they show a reasonable correlation with the soil type behavior derived from the CPT. While the two results don't match entirely, the results confirm the common understanding that CPT data can be used to obtain a realistic soil profile.

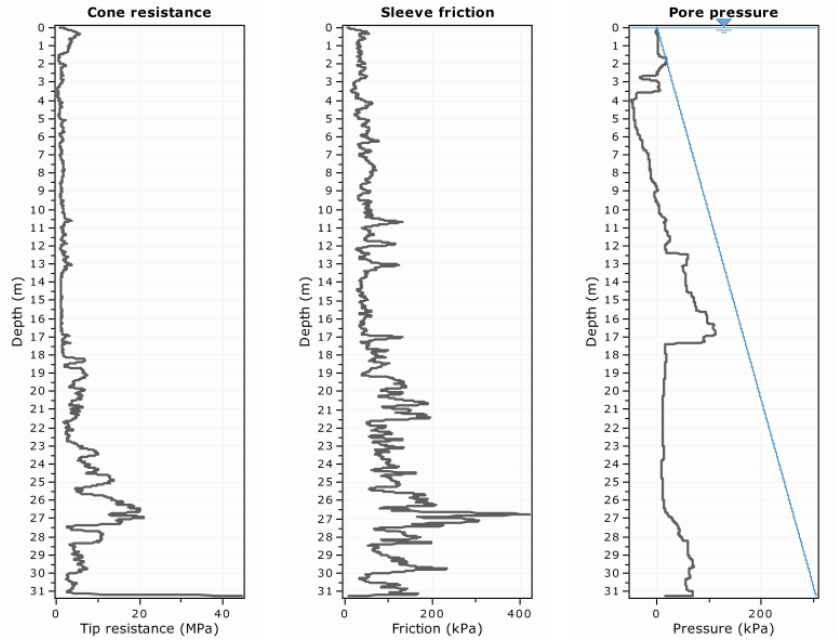


Figure 2: CPT data Location 1

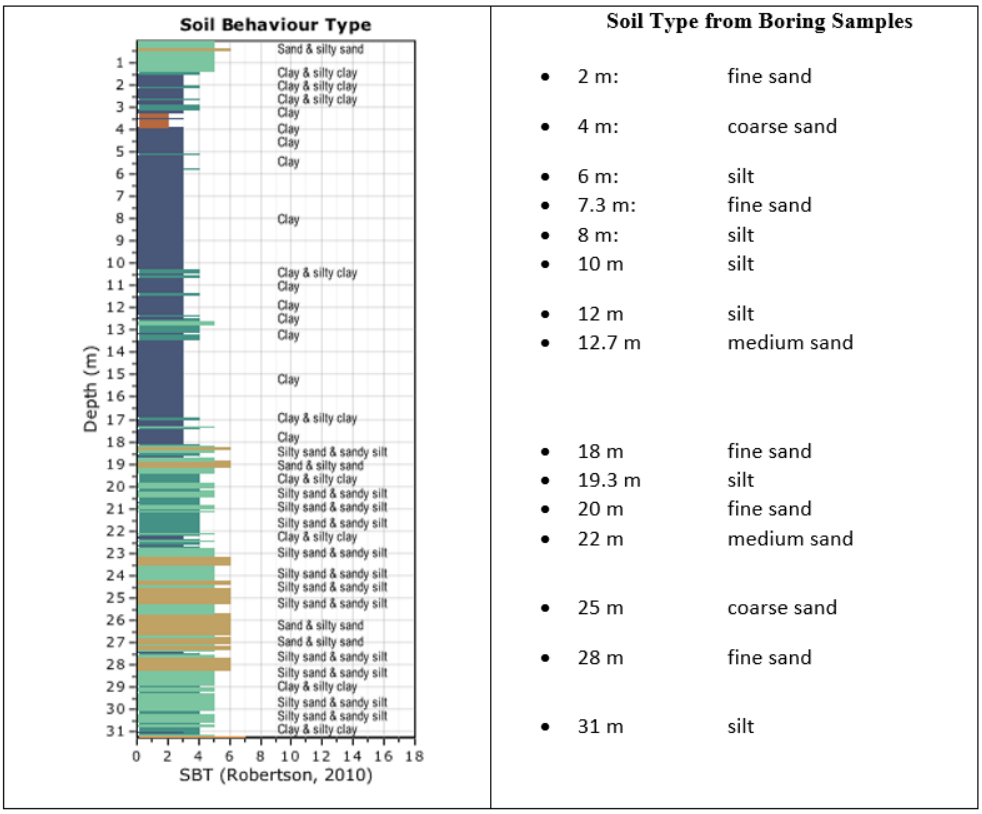


Figure 3: Soil profile characterization Location 1

CPT – Location 2

The CPT data for location 2 (see Figure 4) showed a different soil profile with mainly cohesive type soils down to approximately 44 m, albeit broken up by an intermediate granular soil type layer between 13 m and 21 m, with granular soil type underneath. Once again the dynamic pore pressure curve clearly showed the transition to the granular soil type at approximately 13 m. And while in a tailings facility there may be multiple hydrostatic regimes, it seems that the groundwater table was at a depth of approximately 40 m. This can be derived by simply extending the pressure reading once they follow the hydraulic gradient (as indicated in the light blue line) at say 45 m upwards until they cross the 0 kPa line.

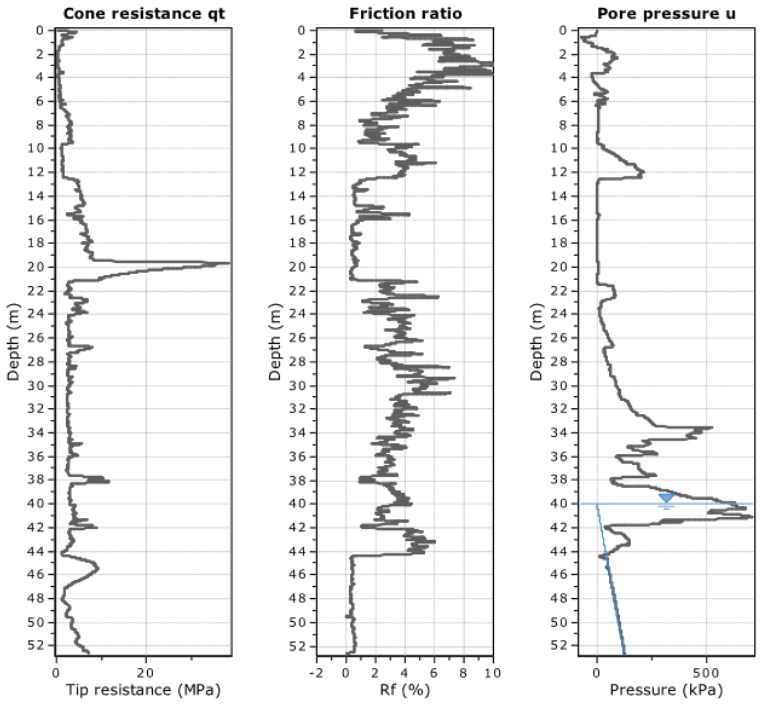


Figure 4: CPT Data Location 2

At this location a soil boring was performed as well with samples obtained at various depths. The soil types for those samples were reported as shown in Figure 5 below, and they show very good correlation with the soil type behavior derived from the CPT. Once again, while the two results don't match entirely, the results confirm the common understanding that CPT data can be used to obtain a reliable soil profile.

Video module

The video module used for the TRIM4 research project consists of a Standard Definition camera and 8 visible light LEDs housed inside a dedicated module and protected by a double layered sapphire window with a 10 mm x 10 mm view (see Figure 6). The module recorded images that showed the soil texture, color, and grain size as the soil passed the camera.

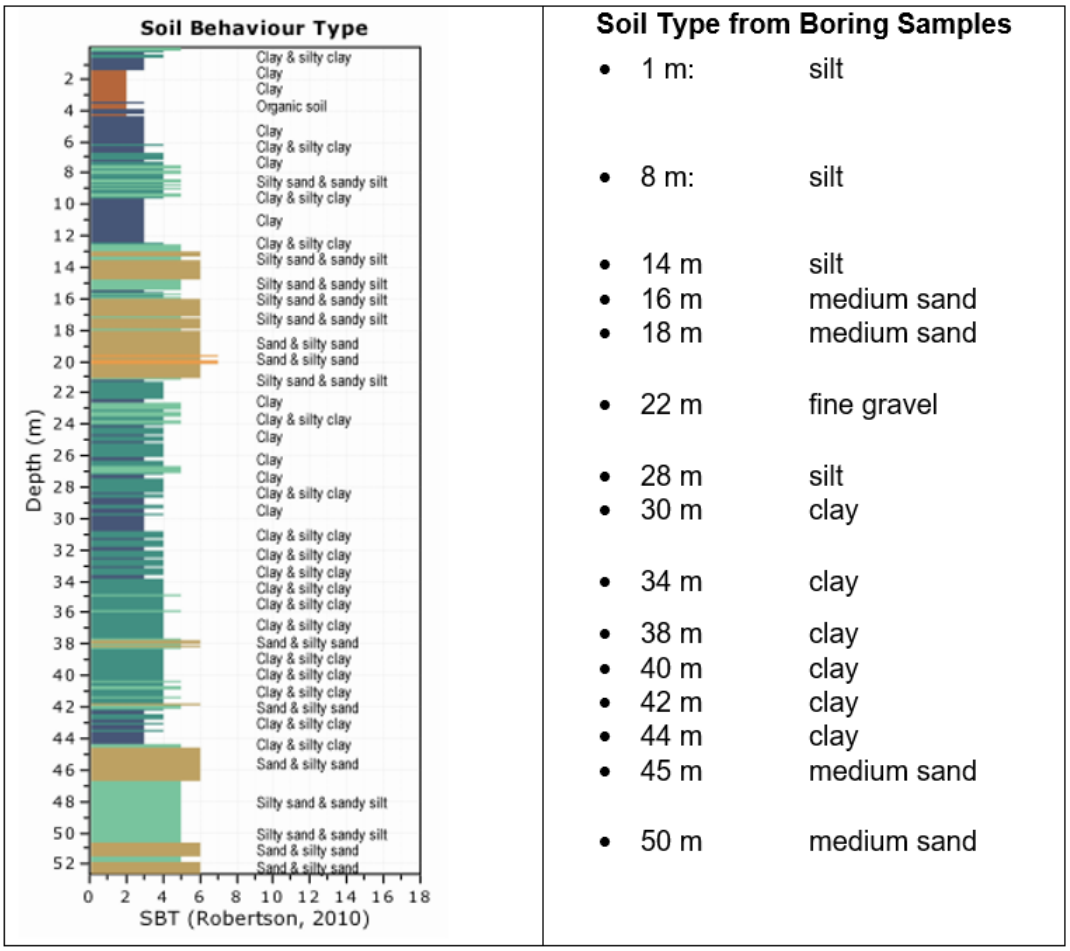


Figure 5: Soil profile characterization Location 2

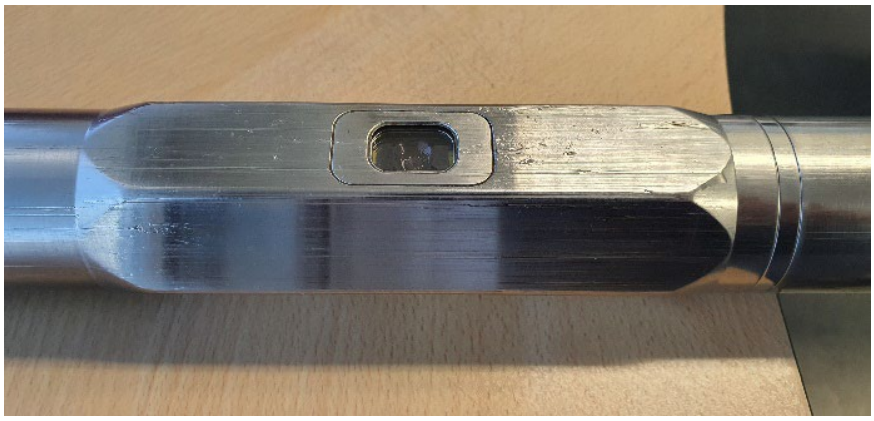


Figure 6: Video module

The initial intention was to try to derive a particle distribution from the recorded images by applying an automatic RBG interpretation to outline the particle in a particular image.as shown in Figure 7. During the project it became obvious that the resolution of the video images was not high enough to generate reliable results and it also raised the question whether fine particles were pushed into the soil away from

the cone, which would distort any particle distribution based on the soil immediately in front of the window. Based on this it was concluded that the test would have to be repeated with a high-definition camera.

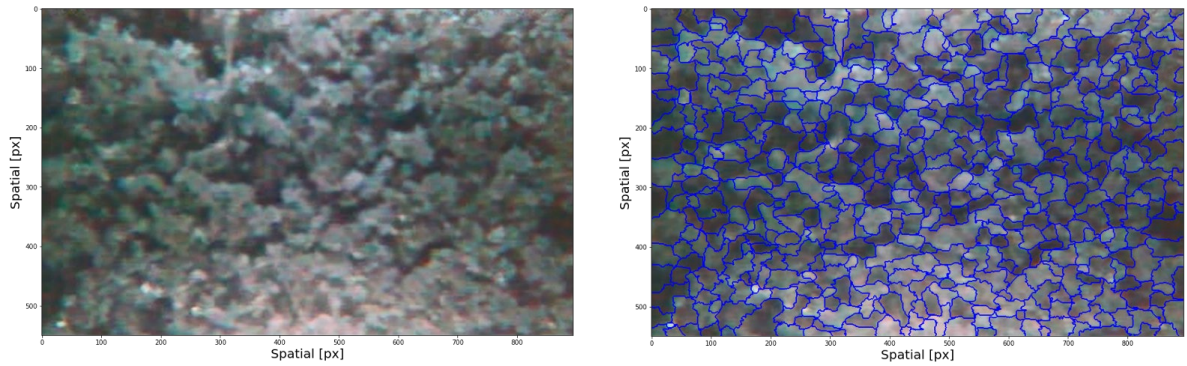


Figure 7: RGB interpretation of the video image shown at the left to delineate the soil particles (shown at the right) to derive a particle size distribution

Soil type transition identification based on video images

While the efforts to derive a particle distribution did not generate the desired results, the images did demonstrate that they can clearly identify transitions in the soil profile. To illustrate this, Figure 8 shows the image at 13.75 m, 13.99 m and 14.01 m, which clearly shows such a transition from granular to cohesive soils. And since they show the situation at a very specific depth, the images can define the transitions much better than the CPT data as both the tip resistance and the sleeve resistance are an average value for a certain (and different) depth interval.



Figure 8: Soil type transition based on video images at 13.75 m, 13.99 m and 14.01 m depth

The images were then analyzed as described in detail by Oksana et al. (2024). In summary the analysis involved a so-called *Grey level co-occurrence matrix (GLCM),* a statistical method to derive texture features considering the relationship between groups of two pixels in the image at certain distance and at certain angle. The distance parameter can range from 1 pixel to the entire image size, while for the angles 4 directions are used: horizontal (0°), diagonally upwards (45°), vertical (90°) and diagonally downwards (135°).

To describe the outcome there are two parameters:

- The GLCM Correlation, a measure of grey levels linear dependencies of neighboring pixels on an image.

$$\sum_{i,j=0}^{N-1} P_{i,j} \left[\frac{(i-\mu_i)(i-\mu_j)}{\sqrt{(\sigma_i^2)(\sigma_j^2)}} \right] \quad \text{(Equation 1)}$$

where μ_i and μ_j are mean values of GLCM and σ_i^2, σ_j^2 its variance. This correlation between neighboring pixels indicates their predictable and linear relationship and ranges -1 to 1.

- The GLCM Dissimilarity, which reflects the contrast of texture features using weights related to the distance from the GLCM diagonal.

$$\sum_{i,j=0}^{N-1} P_{i,j} |i-j| \quad \text{(Equation 2)}$$

To assess the use of this method 8 images were initially selected: 4 of soil that was cohesive and 4 others that depicted granular soil (see Figure 9). Each of these images was then analyzed in 3 directions: horizontally, diagonally and vertically and the results are shown in Figure 10.

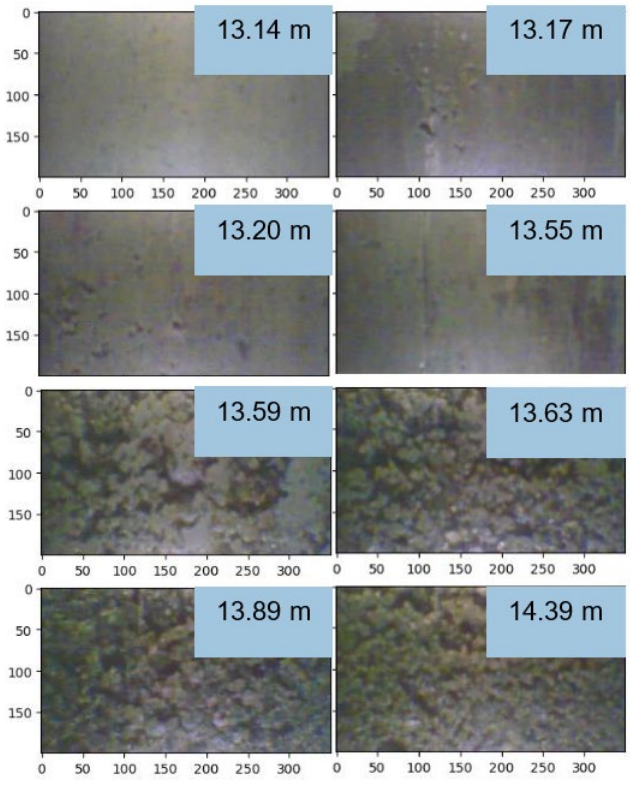


Figure 9: Video images to characterize soil type

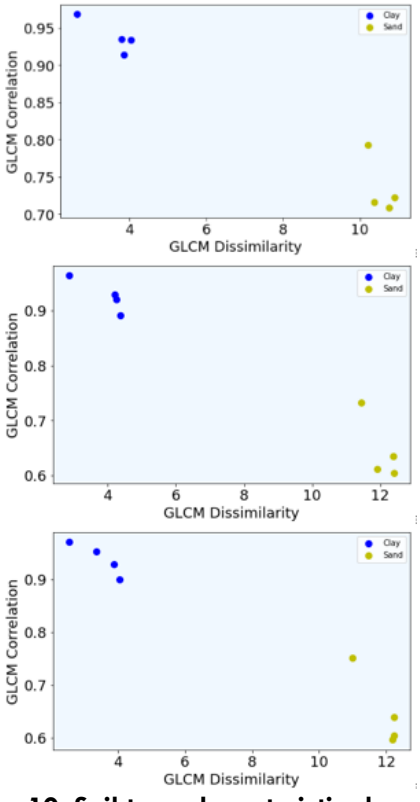


Figure 10: Soil type characteristics based on interpretation of video images (horizontally, diagonally and vertically from top to bottom)

The results showed clearly different values for both the correlation and dissimilarity for clay and sand, and very similar results for the 3 analysis directions. Given that outcome 13 minutes of video data was analyzed, again in 3 directions, with several distinct transitions between granular and cohesive soil. This time period covered the recordings of the depth interval between 11.52 m and 14.58 m related to the camera position (which equates to 11.95 m and 15.01 m based on the cone tip position). Once again for both parameters the results for the three different analysis directions (horizontal, diagonal and vertical) were very similar as is seen in Figure 11.

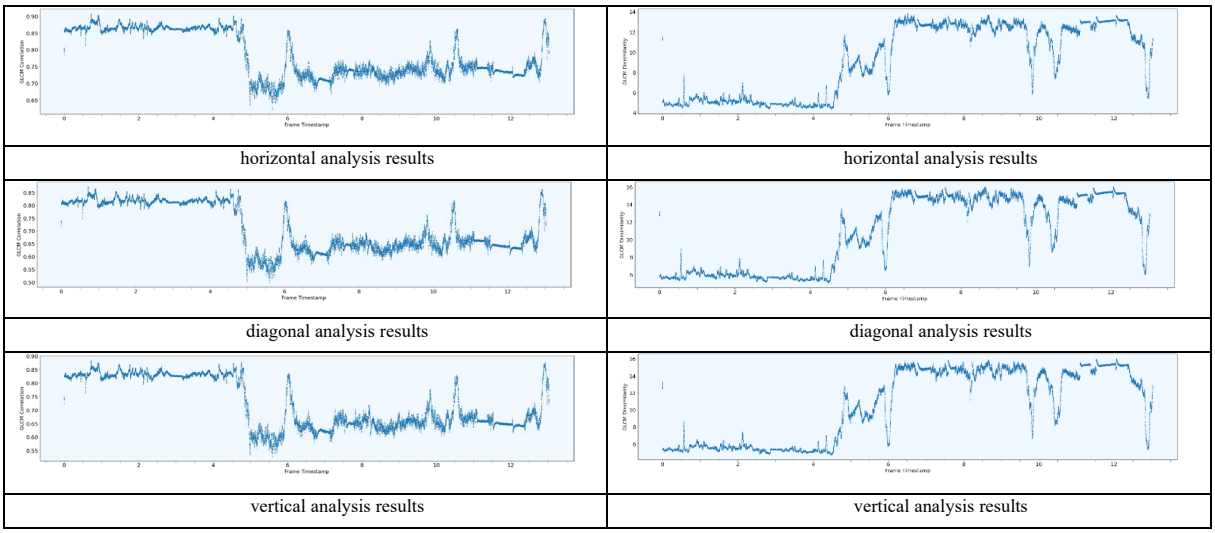


Figure 11: Soil type characteristics based on interpretation of video images (horizontally, diagonally and vertically from top to bottom); correlation values for 13 minutes of video images shown on the left and dissimilarity values for these images on the right

As the range of the dissimilarity values is larger (5 – 16 vs. 0.55 – 0.87 for dissimilarity and correlation values respectively), the dissimilarity results were then compared to the Soil Behavior Type (SBT) generated by the CPT data to try to correlate the results. It should be noted that these soil behavior types were confirmed as the actual soil types by soil borings that were performed in the direct vicinity of the CPT soundings. The outcome of the comparison of the SBTs and the dissimilarity values is shown in Figure 12, whereby in the graph for the dissimilarity results an initial attempt was made to classify the soils using the colors shown in Table 1.

Table 1: Color coding dissimilarity results

Soil type	SBT color	Video analysis color
Clay		
Clay & silty clay		
Silty sand & sandy silt		

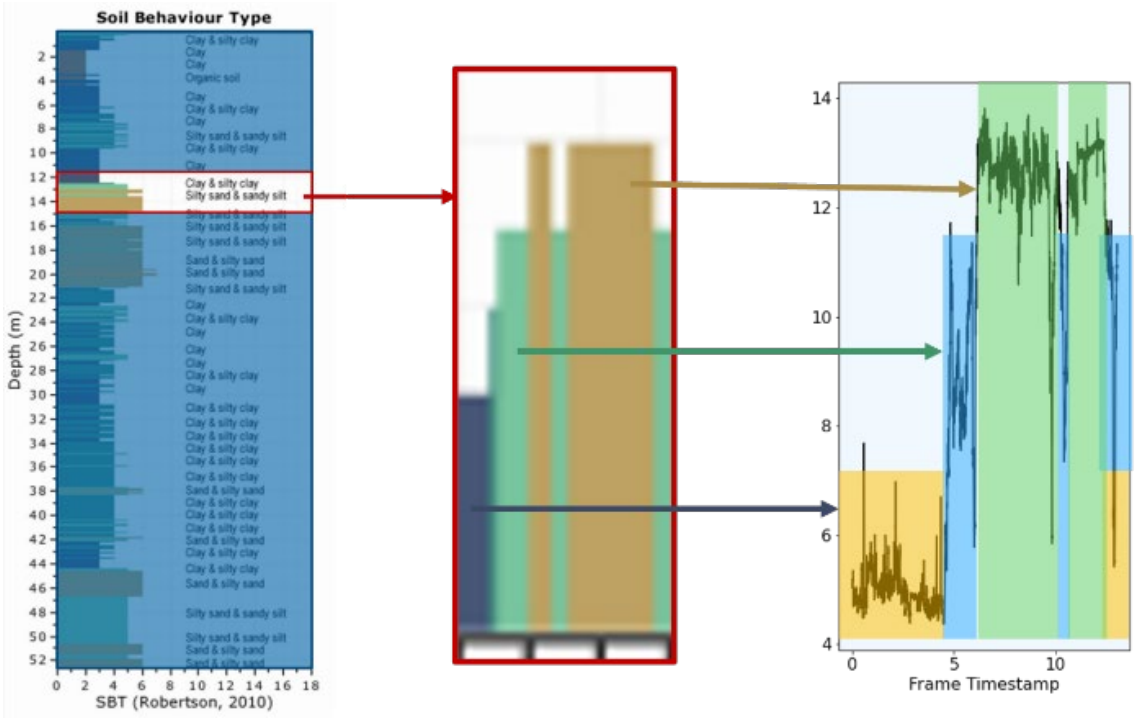


Figure 12: Dissimilarity values correlated with Soil Behavior Type with the graph in the center showing the Soil Behavior Types in the depth interval for which the comparison was made, and the graph on the right the dissimilarity results and interpretation

Since these seemed to be a good correlation the dissimilarity values for the same depth interval were also correlated with the actual SBT index values as shown in Figure 13. It should be noted that the sections in the graph where the cone was note moving (to add a CPT rod at the surface) are designated by the comment "camera/drill stop". Therefore, the camera depth values are listed with the associated cone tip depth. This cone tip depth values are then shown on the horizontal axis of the bottom graph that displays the SBC index values (I_c values). It is interesting to note that both characterizations show a distinct change from clay to more granular soils, but the I_c values (i.e., the CPT data) show this much sooner than the video data, reflecting once again the impact that the soil below the cone tip has on the readings.

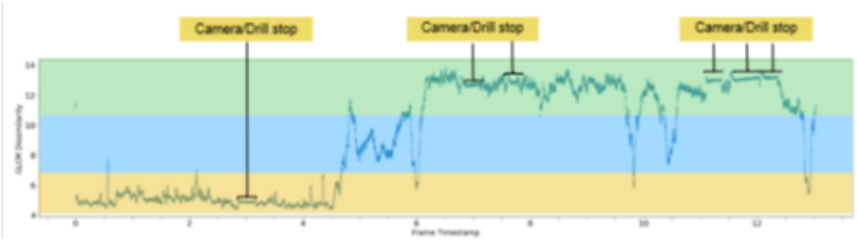
Conclusion

The video images obtained with visible light during a standard CPT seem to show great potential for in-depth analysis instead of a perfunctory visible review of the recorded images. However, before this can become a standard practice more testing is required:

1. Future testing should be done using a High-Definition camera to obtain images that will provide more suitably imagery to delineate soil particles, from which a soil particle distribution can be derived.

2. The soil particle distributions generated during future testing should be validated with actual sieve analysis results.
3. Analysis of additional video data should be performed to determine the dissimilarity values and comparison with the Ic values to confirm the correlation.

The authors will continue to explore the analysis of visible data and hope to present more results at the Tailings and Mine Waste conference in 2025.



Camera depth												
11.52 m	11.82 m	12.09 m	12.35 m	12.55 m	12.87 m	13.13 m	13.32 m	13.52 m	13.78 m	14.06 m	14.32 m	14.39 m	14.58 m
Cone tip depth													
11.95 m	12.25m	12.52 m	12.77 m	12.98 m	13.30 m	13.56 m	13.75 m	13.95 m	14.21 m	14.49 m	14.75 m	14.82 m	15.01 m

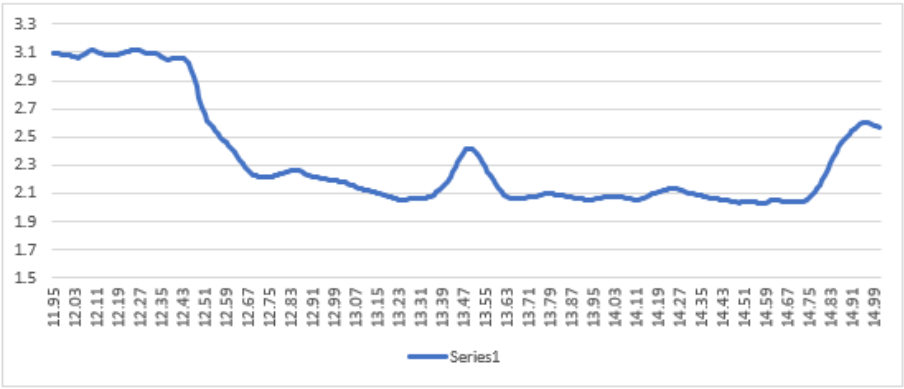


Figure 13: Dissimilarity values correlated with soil behavior classification index

References

Hall-Beyer, M. 2017. GLCM texture: A tutorial v. 3.0 March 2017

Khomiak, O., Benndorf, J. and Verbeek, G. 2024. Sub-Surface soil characterization using image analysis: material recognition using the grey level co-occurrence matrix applied to a Video-CPT-Cone *Mining* 4(1): 91–105. https://doi.org/10.3390/mining4010007

Oksana, K., Benndorf, J. and Verbeek, G. Sub-surface soil characterization using image analysis: material recognition using the grey level co-occurrence matrix applied to a video-CPT-cone. *Mining* 4(1): 91–195.

Robertson, P.K. Cone penetration test (CPT)-based soil behaviour type (SBT) classification system-an update. *Canadian Geotechnical Journal* 53(12): 1910–1927. https://doi.org/10.1139/cgj-2016-0044.

Shijin Kumar P.S #1, Dharun V.S., 2016. Extraction of texture features using GLCM and shape features using connected regions. *International Journal of Engineering and Technology* 8(6): 2926–2930. https://doi.org/10.21817/ijet/2016/v8i6/160806254

Singh, S., Srivastava, D. and Agarwal, S. 2017. GLCM and its application in pattern recognition. *Proceedings of the 5th International Symposium on Computational and Business Intelligence (ISCBI):* 20–25. IEEE. https://doi.org/10.1109/ISCBI.2017.8053537

TRIM4Post Mining website. 2024. Accessed at https://trim4postming.com

Predicting Tailings Properties Using Hyperspectral Sensing and Machine Learning

Joseph Bindner, ConeTec Group, Canada
Joseph Scalia IV, Colorado State University, USA
Christopher Bareither, Colorado State University, USA
Iman Entezari, ConeTec Group, Canada
Dallas McGowan, ConeTec Group, Canada

Abstract

Understanding tailings properties at high spatial resolutions is critical for geotechnical and geochemical analyses. While tailings properties can be characterized using undisturbed samples and in-situ tests, the current methods have limitations. Tailings properties determined from undisturbed samples represent a point measurement and obtaining enough samples to characterize tailings at high spatial resolutions may not be feasible. The characterization of tailings in situ, using methods such as the cone penetration test (CPT), can provide high resolution data, but does not provide information related to all relevant tailings properties. This study explores the use of hyperspectral sensing and convolutional neural networks (CNN) for the prediction of tailings properties, including percent sand, silt, clay, solids content, moisture content, and degree of saturation. Tailings from a gold, silver, lead, and zinc producing mine were used to create samples with diverse properties and hyperspectral scans of each sample were captured. The tailings-hyperspectral dataset was then split into training and testing subsets and a CNN was optimized and trained. Model performance was assessed using the testing data and the results demonstrate strong promise for the use of hyperspectral data and CNNs for the prediction of tailings properties.

Introduction

Tailings properties can inform geotechnical and geochemical analyses and include particle size distribution (PSD), solids content, moisture content, and degree of saturation. The PSD of tailings influences shear strength, hydraulic conductivity, consolidation, dry density, and beach angle, and can inform geochemical and rheological characterization of the material. The moisture content of tailings influences hydraulic conductivity, bearing capacity, compaction behavior, and acid-generation potential. At saturations below approximately 80%, geotechnical stability is improved (Rodriguez et al., 2021) and at saturations above

approximately 85%, oxygen diffusion exponentially decreases, indicating reduced acid generation in sulfide tailings (Aachib et al., 2004).

Tailings can be characterized by sampling and laboratory testing. However, the results only represent a point measurement and obtaining enough samples for high resolution characterization of tailings throughout a tailings facility is impractical. In-situ methods can be a cost-effective alternative for high resolution characterization and include the cone penetration test (CPT). Data from the CPT can be used to better understand tailings behavior; however, current methods for CPT interpretation may not apply universally and the CPT does not provide information on all geotechnically relevant tailings properties. Alternatively, hyperspectral sensing has shown promise for the characterization of soil and tailings properties.

Figure 1 illustrates a simplified conception of hyperspectral sensing, which involves illuminating a sample and measuring the intensity of reflected radiation from the material surface. Hyperspectral reflectance can be measured with a spectrometer and varies with tailings properties including water content, PSD, and mineralogy. Hyperspectral sensing is typically used to measure reflectance in the visible, near infrared, and short-wave infrared portions of the electromagnetic spectrum and can be conducted on disturbed or undisturbed samples in either laboratory or field settings.

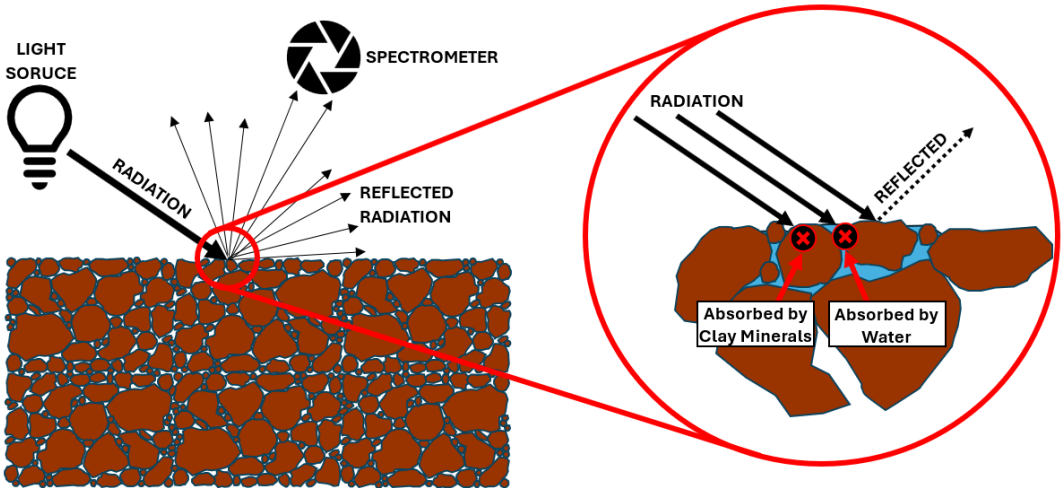


Figure 1: Simplified illustration of hyperspectral sensing for tailings

Machine learning models have been successfully used to predict soil texture from laboratory measured hyperspectral reflectance (Riese and Keller, 2019; Tsakiridis et al., 2020). In agriculture, studies have demonstrated the use of probe-based hyperspectral sensing for the estimation of in-situ soil texture and moisture content for near surface soils (Cho et al., 2017; Pei et al., 2018). Additionally, ex-situ hyperspectral sensing has been used for the prediction of tailings solids content, fines content, and water content for oil-sands tailings (Entezari et al., 2022). While machine learning models, such as convolutional neural networks (CNNs), and hyperspectral reflectance can be used to predict some tailings properties, less is

understood regarding the use of hyperspectral sensing for the prediction of tailings percent sand, silt, clay, and degree of saturation.

The objective of this study is to measure hyperspectral reflectance for tailings with diverse properties and assess how hyperspectral reflectance and CNNs can be used to predict geotechnically relevant tailings properties. Tailings from a gold, silver, lead, and zinc producing mine were processed to obtain 300 test specimens with unique PSDs, moisture contents, and densities. Hyperspectral reflectance was captured using a spectrometer and test specimen properties were measured using standard laboratory procedures. The tailings-hyperspectral dataset was separated into training and testing subsets and a CNN was constructed to assess the use of hyperspectral reflectance for the prediction of tailings properties including percent sand, percent silt, percent clay, solids content, gravimetric moisture content, and degree of saturation. The CNN was trained and tested using (1) the full range of measured wavelengths and (2) a limited range of wavelengths, to better understand how short-wave infrared data impacts the model's performance, as a potential cost-reducing measure.

Methodology

Test specimens

Table 1 outlines the engineering characteristics for a bulk tailings sample from a gold, silver, lead, and zinc producing mine (whole tailings). The tailings were processed to artificially prepare tailings specimens with diverse properties including PSD, moisture content, and density (test specimens). The whole tailings properties were determined according to ASTM standards and sensor testing manuals (see Table 1).

The whole tailings underwent a series of sieving and sedimentation procedures to separate out fractions of the whole tailings that were dominated by (1) sand, (2) silt, and (3) clay. Unique mass ratios of each tailings fraction were combined to prepare 100 test specimens with different PSDs (PSD specimens). Figure 2 displays the percentile ranges for the 100 PSD specimens and the typical range for tailings PSD from the literature.

Table 1: Whole tailings properties

Method	Property	Sample Value
ASTM D4318	Liquid Limit, LL (%)	21
	Plasticity Index, PI (%)	1
ASTM D6913	Percent Gravel (4.75 mm – 76.2 mm)	0
	Percent Sand (75 µm – 4.75 mm)	46
	Percent Fines (< 75 µm)	54
ASTM D2487	USCS Classification	ML
METER PARIO Plus	Percent Silt (75 µm – 2 µm)	47
	Percent Clay (< 2 µm)	8
ASTM D698	Optimum Water Content, w_{opt} (%)	12
	Maximum Dry Density, ρ_d (Mg/m^3)	1.85

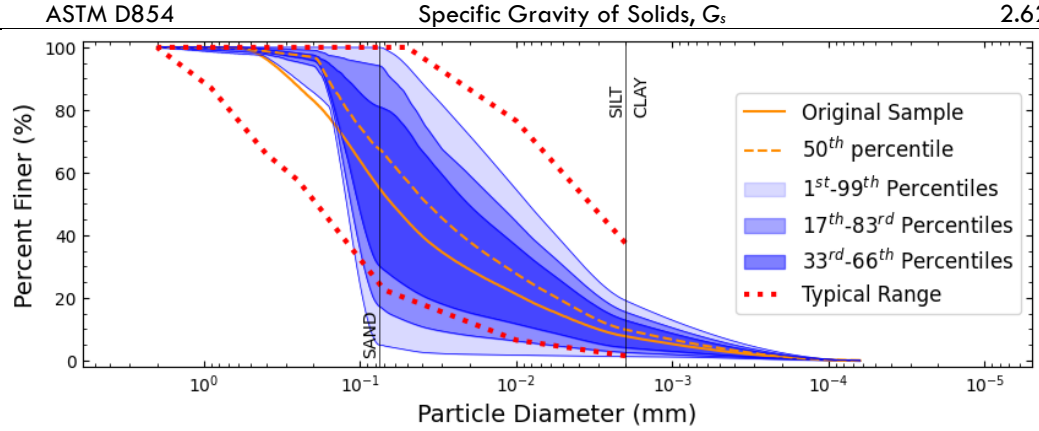


Figure 2: Particle size distribution of the whole tailings and the percentile ranges for all PSD specimens. Solid vertical lines differentiate sand, silt, and clay sized particles. Red dashed lines represent the average lower and upper bounds of PSD for typical mine tailings from the literature (after Gorakhki et al., 2019, adapted from Hamade, 2017)

Each PSD specimen was prepared to three moisture and density conditions, totaling 300 test specimens. Each test specimen was moisture conditioned using de-ionized water, sealed, and allowed to moisture equilibrate for 12 hours. Test specimens were then compacted in a 50 mm inner diameter, 15 mm height, petri dish to target a density, which was randomly determined and between 0.9 and 1.7 Mg/m³. Each specimen's total mass, volume, and gravimetric moisture content was measured and used to calculate solids content and saturation based on phase relationships.

Figure 3 illustrates the frequency distributions for the test specimens' properties. The sand, silt, and clay content ranged between 0–99%, 2–84%, and 1–20%, respectively (Figure 3a-c). Solids content spanned 65–100%, capturing a portion of the tailings continuum including thickened, paste, and filtered tailings (Figure 3d). Gravimetric moisture content ranged from 0–55% and saturation varied from 0–100% (Figure 3e-f).

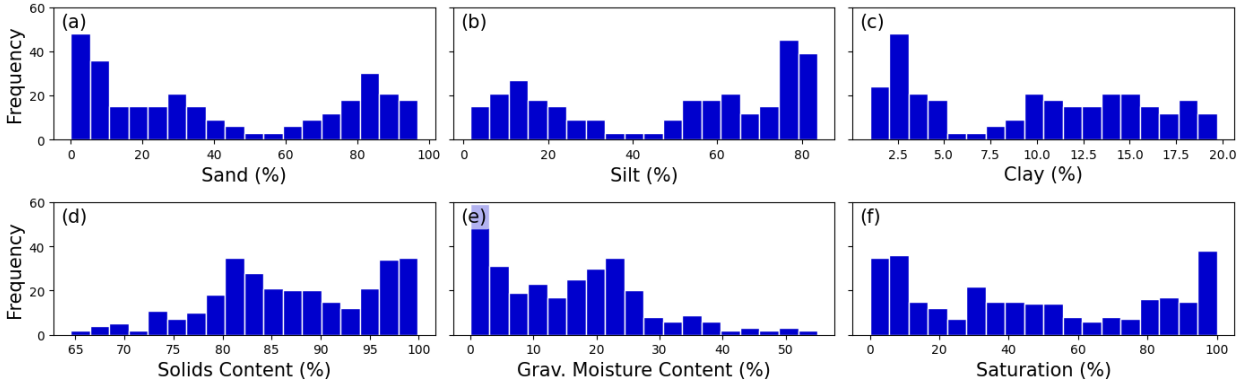


Figure 3: Distribution of test specimen properties including (a) percent sand, (b) percent silt, (c) percent clay, (d) solids content, (e) gravimetric moisture content, and (f) degree of saturation

Hyperspectral sensing

Figure 4 illustrates the preparation of test specimens and the spectrometer used to capture hyperspectral reflectance. Immediately following test specimen preparation, the specimen's reflectance intensity was measured at wavelengths ranging from 350 – 2500 nm. The spectrometer contains: (1) a visible-near-infrared sensor (VNIR) (350–1,000 nm); (2) two short-wave infrared sensors, referred to as SWIR-1 (1001–1,800 nm) and SWIR-2 (1,801–25,00 nm); and (3) an internal halogen light for sample illumination. The spectrometer's viewing window was placed in direct contact with the test specimen and hyperspectral reflectance was measured at two locations for each test specimen. The data from these two locations were averaged to generate a single hyperspectral signal for each test specimen.

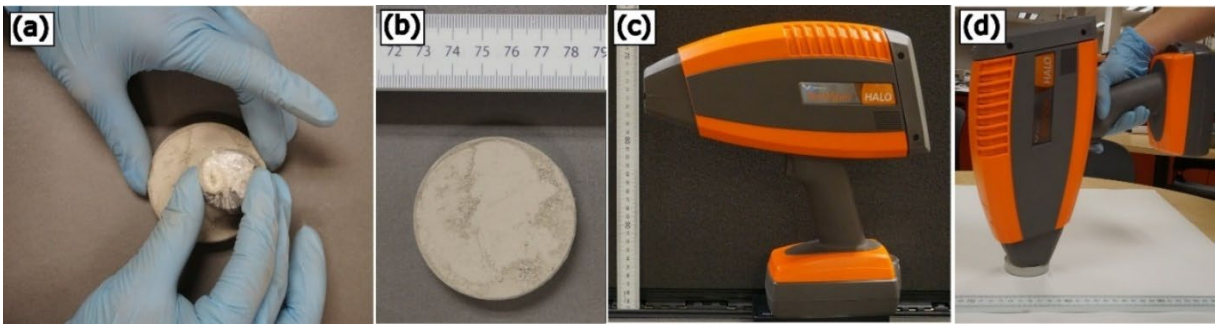


Figure 4: Photographs illustrating (a) test specimen compaction, (b) prepared test specimen, (c) spectrometer, and (d) spectrometer measuring hyperspectral reflectance of a test specimen

Data processing

Various preprocessing procedures were applied to the hyperspectral data including the discrete wavelet transform (Anand et al., 2021; Bruce et al., 2022) and the standard scaler transform (Pedregosa et al., 2011) to reduce data dimensionality and standardize data, which has been associated with improved model performance (Pedregosa et al., 2011; Anand et al., 2021; Bruce et al., 2022). The tailings-hyperspectral dataset was then split into training and testing sub-datasets using conditioned Latin Hypercube Sampling (cLHS) (Minasny and McBratney, 2006). The cLHS algorithm was used to create training and testing datasets that have similar distributions of hyperspectral data, which has been linked to improved model performance (Althnian et al., 2021). The testing data contains 20% of all samples (n=60) and the training data contains 80% (n=240).

Figure 5 illustrates the distribution of properties among test specimens in the training and testing datasets derived from cLHS. Results from cLHS demonstrate that the testing data has a similar distribution and range of properties as that seen in the training data.

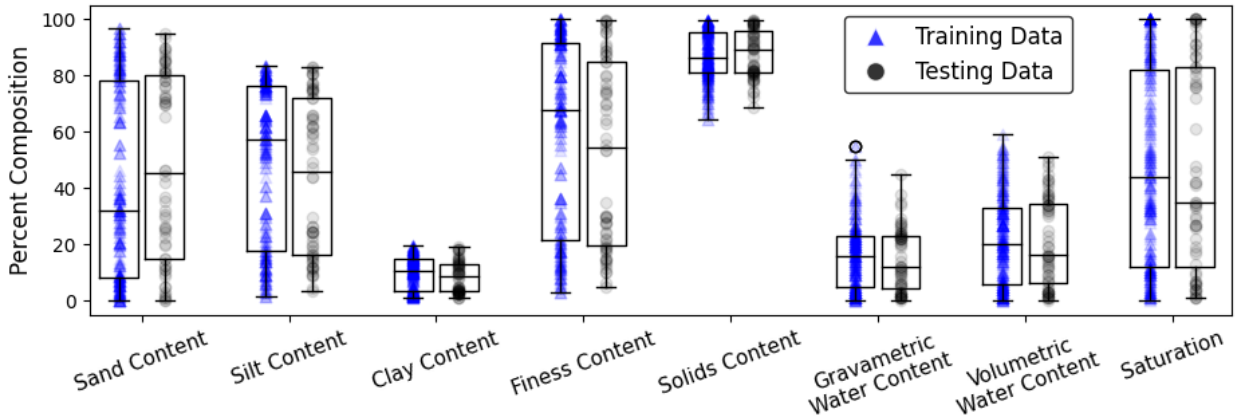


Figure 5: Distribution of tailings properties in the training and testing datasets

Machine learning

Convolutional neural networks have been shown to outperform other common algorithms in soil spectroscopy (Tsakiridis et al., 2020) and were used to predict tailings properties from hyperspectral data in this study. K-fold cross validation helps to generalize models for predictions on unseen data (i.e., the testing data) and was used to select the CNN architecture. The Keras deep learning application program interface was used for machine learning procedures (Chollet, 2015). The model was first trained and tested using the entire hyperspectral dataset, including VNIR, SWIR-1, and SWIR-2 data (V-S2 model). Then, to assess how the SWIR-2 data influences model performance, the model was trained and tested using only VNIR and SWIR-1 data (V-S1 model).

Results

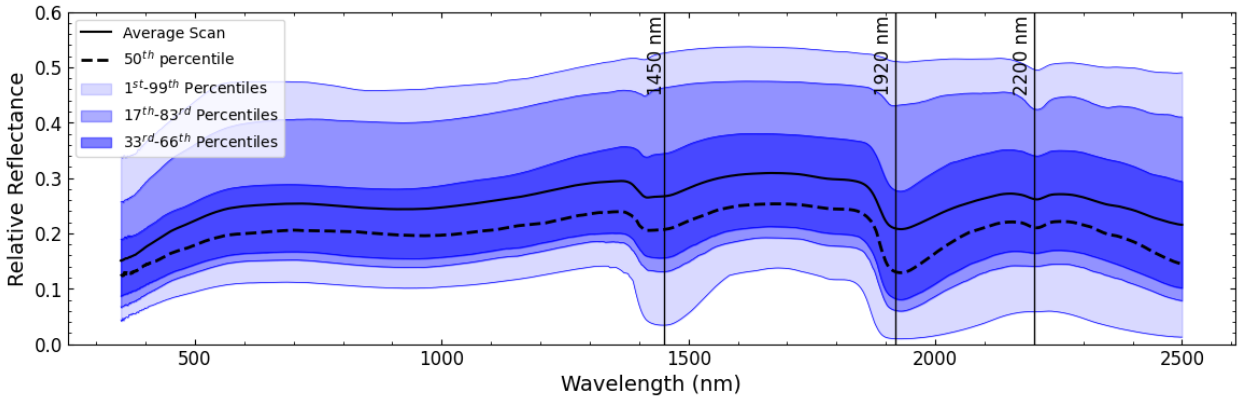


Figure 6: Hyperspectral signal percentile ranges including percentiles 1–99, 17–83, and 33–66. Vertical lines are shown at major absorptive features

Figure 6 illustrates the range of hyperspectral signals for test specimens. Relative reflectance denotes the spectrometer's measurement of radiation reflected from the surface of the test specimen and ranges from 0 to 1. A value of 0 indicates complete absorption, while 1 signifies total reflectance. Distinct absorptive

features are observed in the hyperspectral signals at wavelengths near 1,450 nm and 1,920 nm, indicating the presence of water (van der Meer, 2004). Additionally, the absorptive feature at 2,200 nm is attributed to clay minerals containing hydroxyl groups such as illite, chlorite, and kaolinite (Laukamp et al., 2021), which were present in the whole tailings based on X-ray diffraction analysis.

Figure 7 displays the results from the V-S1 and V-S2 models along with the root mean squared error (RMSE), mean bias error (MBE), and coefficient of determination (R^2) of predictions. For predictions of percent sand and silt, the V-S2 model has RMSEs of 5.9% and 5.1% respectively, which are approximately 2.5% lower than the V-S1 model (8.5% and 7.5% respectively). Additionally, the R^2 values are approximately 0.04 higher for the V-S2 model compared to the V-S1 model. Both models have MBEs near 0% for sand and silt predictions. Performance metrics for percent clay and solids content are comparable between both models with RMSEs less than 2%, MBE near 0%, and R^2 greater than 0.94. The V-S2 model performed slightly better than the V-S1 model for prediction of gravimetric moisture content (RMSE of 2.2% and 2.7% respectively). Conversely, for the prediction of degree of saturation, the V-S1 model outperforms the V-S2 model with RMSEs of 7.5% and 8.3% respectively and MBEs of 0.6% and 2.1% respectively.

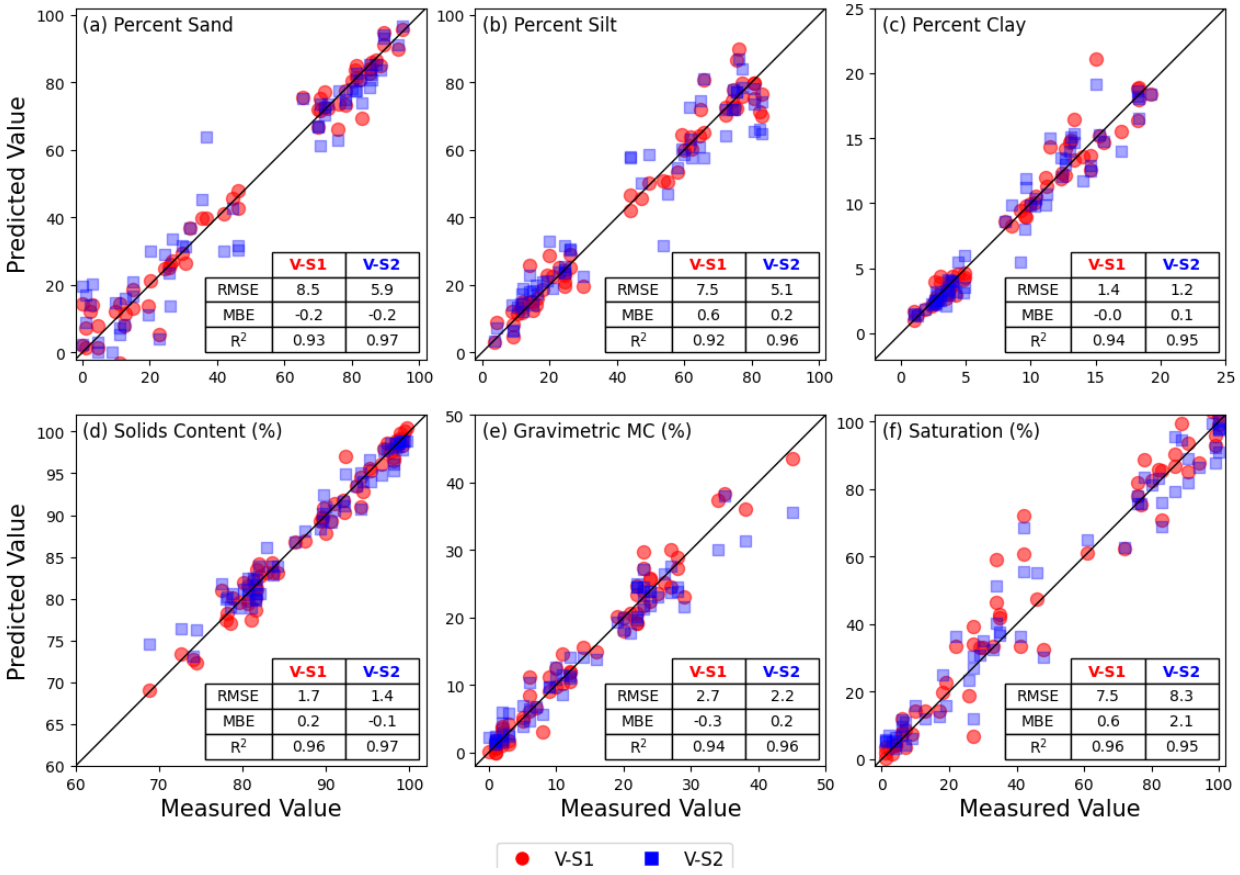


Figure 7: Results from V-S1 and V-S2 models for (a) percent sand, (b) percent silt, (c) percent clay, (d) solids content, (e) gravimetric moisture content, and (f) degree of saturation

Figure 8 shows results from the Shapley Additive Explanations (SHAP) analysis, which uses game theory to explain the importance of various input features in machine learning models (Lundberg and Lee, 2017). The SHAP analysis was used to understand wavelength importance for the V-S2 model, where greater SHAP values correspond to greater influence on the model output for a given wavelength. Results show the predictions of percent sand and silt are strongly influenced by wavelengths from 2,100 – 2,400 nm. For the prediction of percent clay, solids content, gravimetric moisture content, and degree of saturation, most wavelengths appear to have moderate influence on the prediction of these properties.

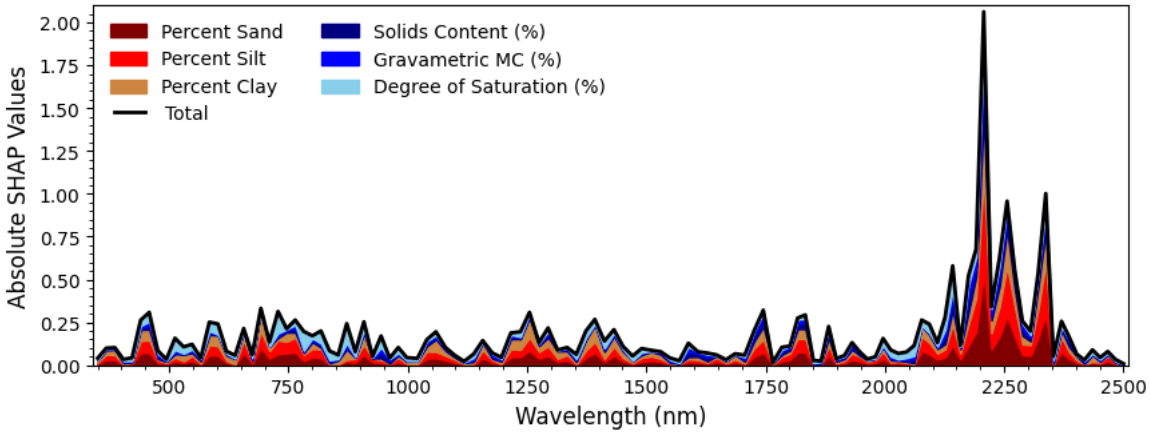


Figure 8: Absolute SHAP values for the V-S2 model where greater values correspond to greater influence of a wavelength on the model outputs. Cumulative absolute SHAP values are shown by the solid back line

Discussion

The model performance demonstrates that hyperspectral sensing can be used to estimate tailings properties including percent sand, silt, clay, solids content, moisture content, and saturation. Tsakiridis et al. (2020) used machine learning and laboratory hyperspectral reflectance to predict percent sand, silt and clay from hyperspectral data on 18,000 natural soil samples and achieved RMSEs of 12.0%, 9.3%, and 4.8% respectively. In comparison, the V-S1 and V-S2 models predictions of tailings sand, silt, and clay have lower RMSEs than Tsakiridis et al. (2020), possibly due to the simplified mineralogical composition of the tailings test specimens, which were derived from a single bulk sample. The coefficients of determination for predicted sand, silt, and clay percentages for the V-S1 and V-S2 models exceed 0.92, highlighting the capacity of hyperspectral reflectance to capture variability in particle size distribution.

For the prediction of tailings moisture content, the model demonstrates high accuracy, which is supported by the strong correlation between soil moisture and hyperspectral reflectance (van der Meer, 2004). Entezari et al. (2022) used hyperspectral sensing and machine learning to predict solids content and gravimetric moisture content of oil-sands tailings, yielding results comparable to those from the V-S1 and V-S2 models. While prior research has not explored the use of hyperspectral sensing for predicting tailings

saturation, the model results highlight the potential of hyperspectral sensing for the rapid characterization of tailings saturation.

The strong influence of wavelengths in the SWIR-2 sensor range on the predictions of percent sand and silt support the improved performance of the V-S2 model compared to the V-S1 model for these properties. However, for predictions of percent clay, solids content, moisture content, and degree of saturation, predictive accuracy between the two models did not vary substantially. Omission of the SWIR-2 sensor may result in cost savings for some applications. However, the potential implications of this on predictive accuracy should be considered.

Hyperspectral sensing shows promise for the rapid assessment of tailings properties in field settings. Recent research has used visible light cameras on CPT probes for enhanced soil profile characterization (Ventola et al., 2020). Additionally, hyperspectral sensing has been used in subsurface probes to analyze agricultural soil properties (Cho et al., 2017; Pei et al., 2018). Combining data from multiple sensors, such as hyperspectral sensing, current generation sensors, and the CPT, is anticipated to enhance the accuracy of predictive models for tailings properties (Pei et al., 2018; Riese and Keller, 2019). Future research should investigate the application of probe-based hyperspectral sensing for real-time characterization of in-situ tailings properties.

Conclusion

The objective of this study was to assess the use of hyperspectral sensing for the prediction of various tailings properties. Tailings from a bulk sample were processed to create a diverse tailings-hyperspectral dataset with 300 unique test specimens. Hyperspectral reflectance was captured for each test specimen and geotechnical properties were measured. The dataset was used to construct, train, and test a convolutional neural network for the prediction of percent sand, silt, clay, solids content, gravimetric moisture content, and degree of saturation. The model was evaluated using two scenarios: (1) using only VNIR and SWIR-1 sensor data (V-S1 model), and (2) using VNIR, SWIR-1, and SWIR-2 sensor data (V-S2 model). Based on the findings, the following conclusions were reached:

1. Hyperspectral sensing and machine learning show promise for the prediction of tailings percent sand, silt, and clay. Based on SHAP analysis, the V-S2 model is strongly influenced by SWIR-2 data for the prediction of percent sand and silt, which aligns with the reduced error in the V-S2 model results, compared to the V-S1 model for the properties. Both models have RMSEs less than 9% and R^2 values greater than 0.92 for the prediction of sand, silt, and clay.
2. Predictions of solids content, gravimetric moisture content, and degree of saturation using hyperspectral reflectance shows promise. The V-S1 and V-S2 models performed similarly for the predictions of these properties and have RMSEs less than 9% and R^2 values greater than 0.94.

Hyperspectral sensing can rapidly produce data related to tailings properties and demonstrates the potential for the high-speed characterization of tailings properties for various applications. Including data from hyperspectral sensing and other sensors in machine learning procedures is expected to improve tailings property predictions. Future studies should consider applying similar methodologies in situ for the characterization of tailings and explore how this methodology applies to tailings from other sites.

References

Aachib, M., Mbonimpa, M., Aubertin, M. 2004. Measurement and prediction of the oxygen diffusion coefficient in unsaturated media, with applications to soil covers. *Water, Air, and Soil Pollution*. 156: 163–193. http://doi.org/10.1023/B:WATE.0000036803.84061.e5

Althnian, A., AlSaeed, D., Al-Baity, H., Samha, A., Bin Dris, A., Alzakari, N., Elwafa., A.A. and Kurdi, H. 2021. Impact of dataset size on classification performance: an empirical evaluation in the medical domain. *Applied Sciences* 11(2). https://doi.org/10.3390/app11020796.

Anand, R., Veni, S. and Aravinth, J. 2021. Robust classification technique for hyperspectral images based on 3D-discrete wavelet transform. *Remote Sensing* (13)7. https://doi.org/10.3390/rs13071255.

Bruce, L.M., Koger, C.H. and Li, J. 2022. Dimensionality reduction of hyperspectral data using discrete wavelet transform feature extraction. *IEEE Transactions on Geoscience and Remote Sensing*. 40(10). http://doi.org/10.1109/TGRS.2002.804721.

Cho, Y., Sudduth, K.A. and Drummond, S.T. 2017. Profile soil property estimation using a Vis-NIR-EC-force probe. *Transactions of the ASABE*. http://doi.org/10.13031/trans.12049

Chollet, F. 2015. Keras. GitHub. Accessed at https://github.com/fchollet/keras

Entezari, I., McGowan, D. and Glavina, J. 2022. Hyperspectral imaging technology for oil sands tailings characterization: practical aspects. *Proceedings of Tailings and Mine Waste* 26: 1243–1252.

Gorakhki, M.R.H., Bareither, C.A., Scalia, J. and Jacobs, M. 2019. Hydraulic conductivity and soil water retention of waste rock and tailings mixtures. *Proceedings of the Eighth International Conference on Case Histories in Geotechnical Engineering.* Accessed at https://doi.org/10.1061/9780784482148.005.

Hamade, M.M. 2017. Undrained shear behavior of mixed mine waste rock and tailings. MS thesis, Civil and Environmental Engineering. Colorado State University, Fort Collins, Colorado.

Laukamp, C., Rodger, A., LeGras, M., Lampinen, H., Lau, I., Pejcic, B., Stromberg, J., Francis, N. and Ramanaidou, E. 2021. Mineral physiochemistry underlying feature-based extraction of mineral abundance and composition from shortwave, mid and thermal infrared reflectance spectra. *Minerals* 11(4). https://doi.org/10.3390/min11040347.

Lundberg, S., Lee, S. 2017. A unified approach to interpreting model predictions. *Advances in Neural Information Processing Systems* 30. Accessed at https://proceedings.neurips.cc/paper_files/paper/2017

Minasny, B. and McBratney, A.B. 2006. A conditioned Latin hypercube method for sampling in the presence of ancillary information. *Computer Geoscience* 32:1 378–1388. https:// doi.org/10.1016/j.cageo.2005.12.009

Pedregosa, F., Varoquaux, G., Gramfort, A., Michel, V., Thirion, B., Grisel, O., Blondel, M., Prettenhofer, P., Weiss, R., Dubourg, V., Vanderplas, J., Passo, A., Cournapeau, D., Brucher, M., Perrot, M. and Duchesnay, É. 2011. Scikit-learn: Machine learning in Python. *Journal of Machine Learning Research* 12(85): 2825–2830. Accessed at https://jmlr.csail.mit.edu/papers/v12/pedregosa11a.html.

Pei, X., Sudduth, K., Veum, K. and Minzan, L. 2018. Improving in-situ estimation of soil profile properties using a multi-sensor probe. *Sensors* 19(1011). http://doi.org/10.3390/s19051011.

Riese, F.M. and Keller, S. 2019. Soil texture classification with 1D convolutional neural networks based on hyperspectral data. *ISPRS Annals of the Photogrammetry, Remote Sensing and Spatial Information Sciences*. IV-2 (W5). https://doi.org/10.5194/isprs-annals-IV-2-W5-615-2019.

Rodríguez, R., Muñoz-Moreno, A., Caparrós, A., García-García, C., Brime-Barrios, A., Arranz-González, J., Rodríguez-Gómez, V., Fernández-Naranjo, F. and Alcolea, A. 2021. How to prevent flow failures in tailings dams. *Mine Water and Environment*. 40: 83–112. http://doi.org/10.1007/s10230-021-00752-8

Tsakiridis, N.L., Keramaris, K., Theocharis, J. and Zalidis, G. 2020. Simultaneous prediction of soil properties for VNIR-SWIR Spectra using a localized multi-channel 1-D convolutional neural network. *Geoderma* 367: 114208. https://doi.org/10.1016/j.geoderma.2020.114208.

van der Meer, F. 2004. Analysis of spectral absorption features in hyperspectral imagery. *International Journal of Applied Earth Observation and Geoinformation*. 5(1): 55–68. https://doi.org/10.1016/j.jag.2003.09.001

Ventola, A., Dolling and R., Hryciw, R. 2020. Image analysis and hardware development for the vision cone penetrometer (VisCPT). *Proceedings of Geo-Congress 2020*. https://doi.org/10.1061/9780784482803.068.

Fundamental Properties of Filtered Tailings on Density-Moisture Curves

Uddav Ghimire, University of Arizona, USA
Jackson S. Norbutas, University of Arizona, USA
Tejo V. Bheemasetti, University of Arizona, USA

Abstract

Mine tailings' disposal, maintenance, and rehabilitation measures present substantial challenges within the mining sector, encompassing environmental and geotechnical stability. Dry stacking of filtered tailings has emerged as a promising alternative to conventional slurry disposal methods. Ensuring the overall stability of dry stacks necessitates a thorough understanding of the physical and mechanical properties of unsaturated filtered tailings at different moisture levels over the compaction curve. Classical soil mechanics principles have established various properties of soils over the compaction curve. However, due to their distinct formation processes, these principles may not necessarily apply to tailings materials. This study investigates the properties of copper mine tailings across various moisture contents relative to the Optimum Moisture Content (OMC). Tests include Unconfined Compressive Strength (UCS), stress-strain behavior, failure patterns, permeability, and scanning electron microscopy (SEM) analysis. The samples were prepared at five different moisture contents at OMC, ± 10 % of OMC, and ± 20 % of OMC, which represents the moisture content variation of filtered tailings in the field. All the tests were performed in triplicate to establish the reliability of the properties. The results highlighted the performance of dry stack tailings at different moisture levels, with tailings fabric changing from flocculated to dispersed, leading to changes in their physical and mechanical properties.

Introduction

The management and disposal of mine tailings present significant environmental and geotechnical challenges within the mining industry. Traditional slurry disposal methods, which often involve the construction of large tailings dams, have been widely adopted. However, these dams can be prone to catastrophic failures and environmental contamination. Since 1915, there have been 257 major tailings dam failures, including the notable incidents of the Bento Rodrigues Dam (Samarco) in Brazil in 2015 and the Brumadinho Dam in 2019 (Piciullo et al., 2022). As an alternative, dry stacking of filtered tailings has

emerged, providing a more stable and sustainable solution (Gomes et al., 2016; Cacciuttolo and Atencio, 2023).

Dry stacking of tailings involves mechanically dewatering tailings to form a filter cake, allowing for stackable storage without the need for a dam, thereby enhancing safety and reducing environmental impacts. It offers multiple advantages over slurry disposal: reducing failure risks, conserving water by recycling dewatering process water, using less space, thus minimizing environmental disturbance, and supporting progressive reclamation and dust control for improved environmental management during and after mining operations (Davies and Rice, 2022). However, the conditions of filtered tailings at deposition can vary significantly due to differences in the parent ore, mineral gradation, and the processes they undergo. Additionally, the post-filtration moisture content varies because of different filtration plant processes. Consequently, understanding the properties of filtered tailings is crucial for the safe design and construction of dry stacks.

Tailings generated from ore extraction and beneficiation processes, ranging from crushing and screening are clastic in nature (Carvalho, 2024). Unlike natural soils, tailings exhibit distinct characteristics such as pronounced angularity, high surface roughness, and the presence of plastic or non-plastic fines (Yang et al., 2019; Carvalho, 2024). The primary difference between soils and tailings lies in their formation. The soils are derivative of rocks that undergo several physical and chemical weathering processes with seasonal cycles, whereas the mine tailings are derivative of industrial processes. This implies that the clay-size particles in tailings do not necessarily have similar physio-chemical characteristics as the weathered clay minerals (Schnaid, 2021). Classical soil mechanics demonstrates that clay structures are flocculated and dispersed when compacted on the dry and wet sides of the OMC, respectively. However, these principles may not necessarily apply to tailings materials due to their distinct formation processes. Thus, understanding their fundamental behavior over a range of moisture contents across the compaction curve is crucial. This knowledge is essential for designing and constructing safe and stable filtered tailings dry stacks.

Recently, numerous studies have expanded an understanding of the behavior of filtered tailings, shedding light on fundamental geotechnical characteristics such as Atterberg limits, density-moisture relationships, and specific gravity (Lara et al., 2013; Amoah et al., 2018). The compaction characteristics of filtered tailings are influenced by their particle size distribution and mineralogy. Fine-grained tailings with high clay content tend to exhibit higher water retention and lower permeability, making compaction more challenging (Qiu and Sego, 2001). Research indicates that the mechanical properties of filtered tailings are highly variable, depending on their source and processing methods (Blight, 2009). Filtered tailings typically show lower compressibility compared to slurry tailings, leading to reduced settlement over time, which is beneficial for maintaining the structural integrity of tailings stacks (Vick, 1990).

Additionally, the mechanical properties of tailings can be improved through soil enhancement techniques, such as using cement to increase strength and stiffness, or fibers to enhance strength and ductility and prevent liquefaction (Consoli et al., 2022, 2023).

This research study examined the fundamental physical properties of copper mine tailings including Unconfined Compressive Strength (UCS), stress-strain relationship, failure patterns, permeability, and fabrics at different moisture contents across the compaction curves. The samples were prepared at five different moisture contents at OMC, ± 10 % of OMC, and ± 20 % of OMC, which represents the moisture content variation that may exist in filtered tailings. The permeability of the samples was determined using a constant head permeameter and the fabric of the tailings using a Scanning Electron Microscope (SEM). All the tests were performed in triplicate to establish the reliability of the properties.

Materials and methods

Materials

In this study, copper mine tailings were collected from a mine in Arizona, USA, and subjected to basic geotechnical characterization studies. Basic characterization studies including sieve analysis, specific gravity, Atterberg limits, and compaction properties were determined in accordance with relevant ASTM standards (D422-63; D854-14; D4318; D698). Table 1 presents the physical indexes of copper tailings used. X-Ray Diffraction (XRD) analysis was performed to understand the mineralogical composition of tailings used for study. The results showed that copper mine tailings consisted of Muscovite (40.5 %), Quartz (18 %), Microcline (24 %), and others (Figure 1).

Table 1: Physical indexes of copper tailings used for the study

Index properties	Value
Specific gravity, Gs	2.6
Plasticity index, %	Non-plastic
Coarse Fraction (0.075 mm<diameter<4.75 mm), %	91
Fine Fraction (diameter<0.075 mm), %	9
Optimum moisture content (OMC), %	15
Maximum dry density (kN/m^3)	16.9

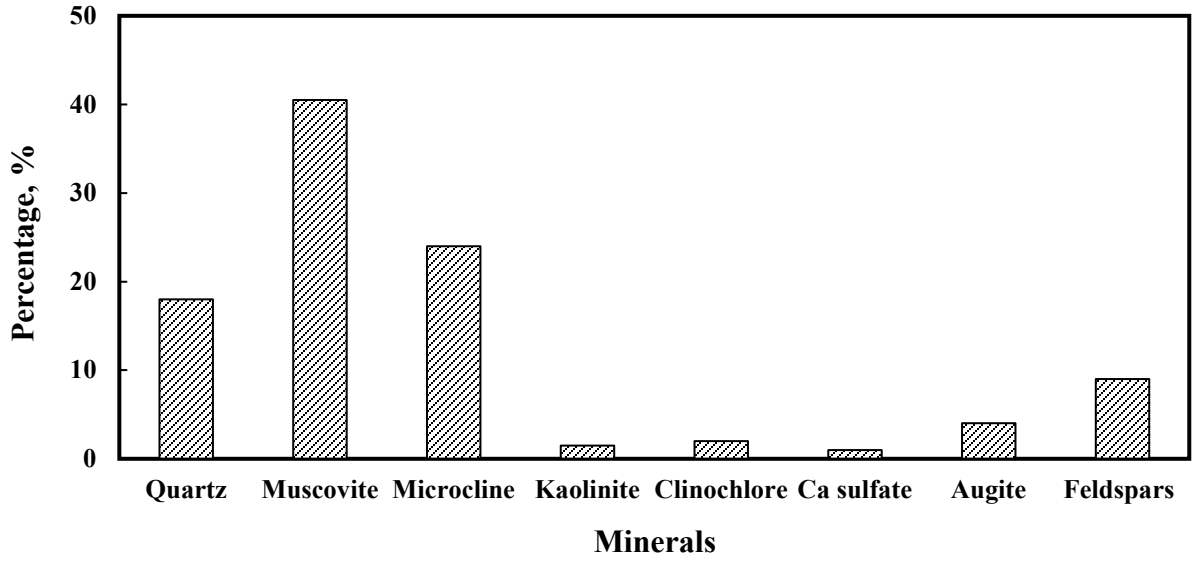


Figure 1: XRD test results of copper tailings used for this study

Experimental plan

The experimental plan for this study involves examining the fundamental physical properties of copper tailings at various moisture contents relative to the OMC. These moisture levels are set at OMC, ±10% of OMC, and ±20% of OMC, as illustrated in Figure 2. Specifically, point 1 represents -20% of OMC, point 2 represents -10% of OMC, point 3 represents OMC, point 4 represents +10% of OMC, and point 5 represents +20% of OMC. The molding points properties are tabulated in Table 2. Points 1 and 2 represent the dry side of the OMC, while Points 4 and 5 represent the wet side of the OMC. Samples were prepared at each of these points (1-5) and subjected to respective tests for analysis.

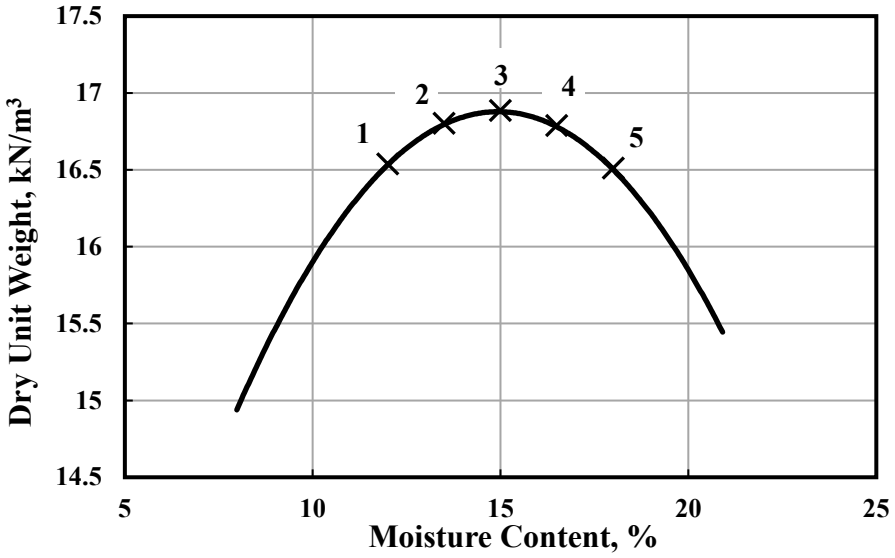


Figure 2: Standard energy compaction curve: density-moisture curve

Table 2: Molding points properties

Molding Points	Properties	
	Moisture content, %	Dry unit weight, kN/m³
1	12	16.55
2	13.5	16.8
3	15	16.9
4	16.5	16.75
5	18	16.5

Unconfined Compressive Strength (UCS) Tests

The static method of compaction was used to prepare cylindrical specimens, which were compacted in three layers. The top of each layer was slightly scarified before adding the next. Each specimen measured 72 mm in height and 33 mm in diameter. To prevent moisture loss, the prepared samples were wrapped in plastic and cured in a room at a temperature of 25°C ± 1°C for 48 hours, allowing moisture to move within the specimens. The strength of the specimens was measured using the unconfined compressive test apparatus, following the ASTM D2166 standard (ASTM, 2016). The load was applied to produce an axial strain at a rate of 1% per minute, continuing until failure bands formed and the stress dropped to 30% of the peak stress. After testing, the failure bands were photographed for further analysis. Tests were conducted in triplicate.

Permeability tests

The permeability of copper tailings was measured using the constant head permeability method following ASTM D2434-19. The specimens were prepared in the standard Proctor mold using standard energy efforts at respective molding points. Tests were conducted in triplicate and the average value was adopted for analysis.

SEM tests

SEM imaging was conducted to examine how the microstructure evolved within copper tailings compacted at different molding points. This analysis focused on observing the fabrics of copper tailings particles. The imaging was carried out using the SEM equipped with a tungsten filament, a secondary electron detector for standard imaging, a backscattered electron detector, Thermo Noran System Six X-ray microanalysis system (EDS), and a J.C. Nabity Nanometer Pattern Generation System (NPGS) for electron beam patterning and lithography and was operated in an environmental mode.

Results and discussion

Unconfined compressive strength

Figure 3 shows the UCS values of copper tailings at different molding points. The UCS value at OMC (point 3) is 178 kPa, which is the highest among all the points tested. This indicates that the copper tailings achieve their maximum strength when compacted at the optimum moisture content. It is clear from the plot that the copper tailings have higher strengths on the dry side as compared to the wet side of the compaction curve. Since the strength decreases significantly on the wet side of the OMC, care must be taken to avoid over-wetting the tailings during compaction.

On the other hand, compaction on the dry side can still yield relatively high strength, as observed at points 1 and 2. This understanding is critical when compacting filtered tailings for construction. Ensuring that the moisture content is close to the OMC will lead to more durable and stable structures.

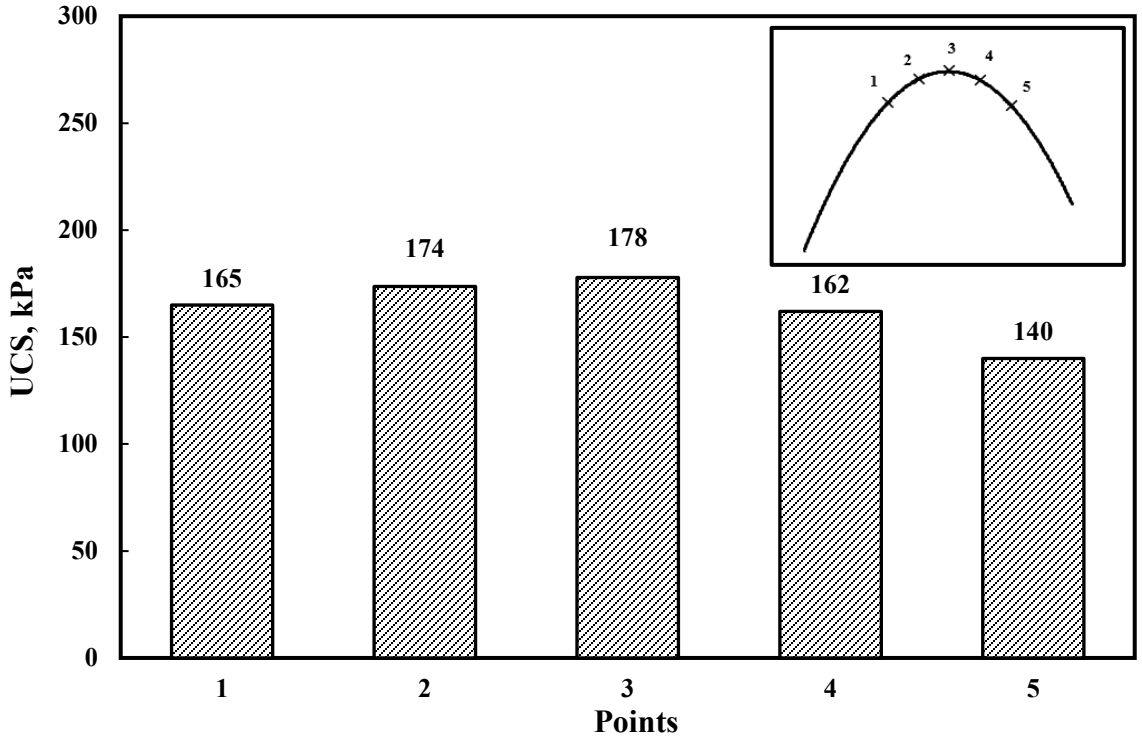


Figure 3: UCS values of copper tailings used for this study at different molding points

Stress-Strain Response

Figure 4 illustrates the typical stress-strain behavior of compacted copper tailings at various molding points. The stress-strain curves reveal that specimens compacted on the dry side (points 1 and 2) exhibit a steep initial slope, indicating higher initial stiffness, and fail at lower strains (0.7% and 1%, respectively). These specimens achieve higher peak stresses but demonstrate a rapid post-peak stress decline, signifying brittle

failure. In contrast, specimens compacted on the wet side (points 4 and 5) show a more gradual increase in stress with strain, reflecting lower initial stiffness, and fail at higher strains (1.39% and 1.41%, respectively). These specimens reach lower peak stresses and display a more gradual post-peak stress reduction, indicating ductile behavior. Point 3, located near the OMC, exhibits intermediate characteristics with a balanced combination of stiffness and ductility, failing at around 1.2% strain and reaching a maximum peak stress. This variability in mechanical response based on moisture content underscores the importance of precise moisture control in the compaction process to achieve desired stability and strength characteristics in tailings storage facilities.

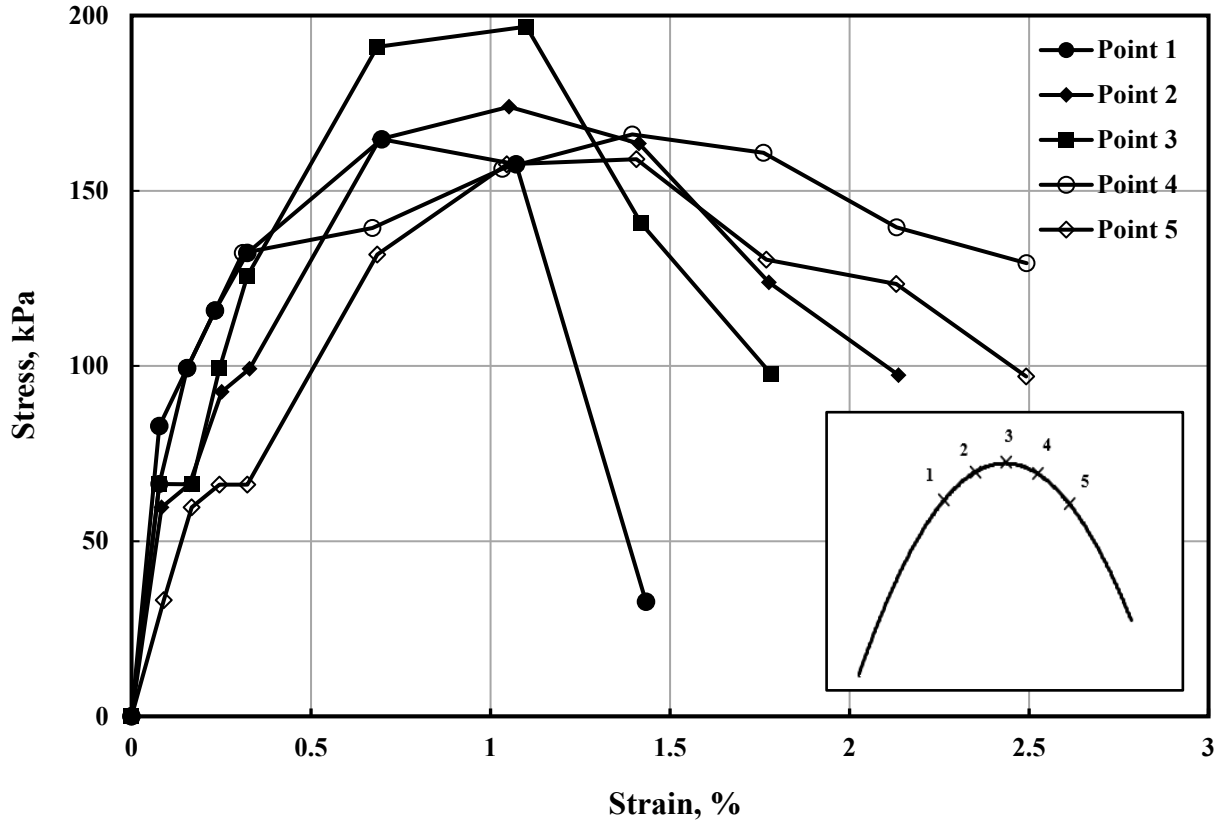


Figure 4: Stress-strain curves for compacted copper tailings at different molding points

Failure patterns

Figures 5(a-e) illustrate the failure patterns of compacted copper tailings at five different molding points, corresponding to the stress-strain behavior shown in Figure 4. Figures 5(a and b) display the failure patterns of specimens compacted on the dry side of the OMC (points 1 and 2, respectively). These specimens exhibit distinct shear bands with minimal bulging or microcracks, indicating brittle behavior characterized by abrupt failure along a shear plane. Figure 5(c) shows the failure pattern of the specimen compacted near the OMC (Point 3), which reveals a combination of a shear band, microcrack formation, and the initiation of

bulging, suggesting a more ductile failure mode compared to the dry side. Figures 5(d) and 5(e) depict the failure patterns of specimens compacted on the wet side of the OMC (points 4 and 5, respectively). These specimens show a combination of random microcracks and significant bulging, indicative of ductile failure.

These visual observations correlate with the stress-strain curves (Figure 4), where specimens on the dry side fail at lower strains with sharp stress drops, reflecting brittleness, while those on the wet side endure larger strains before failure, with gradual stress declines and extensive cracking and bulging, demonstrating ductile behavior. The specimen near the OMC exhibits mixed characteristics, indicating a transition from brittle to ductile failure. These findings underscore the critical influence of moisture content on the mechanical behavior and failure modes of compacted tailings.

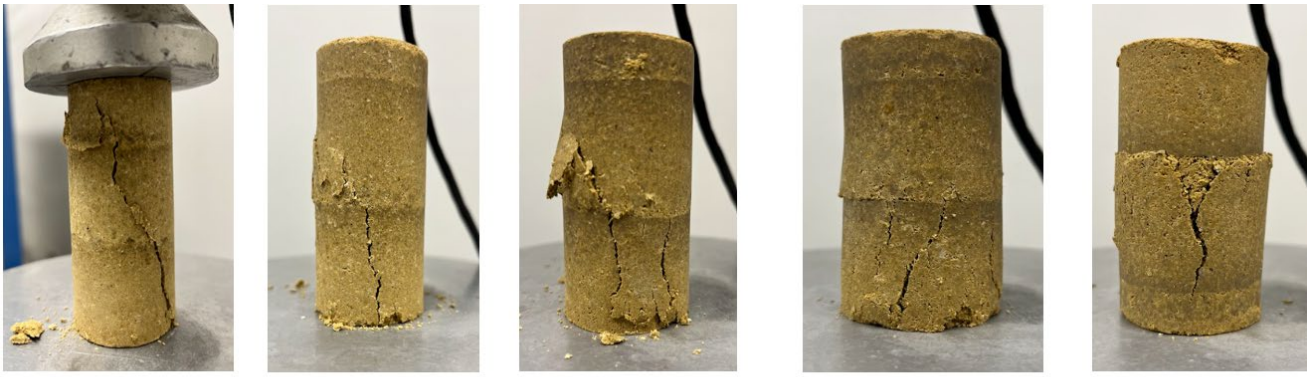


Figure 5: Failure patterns of specimens compacted at points: (a) 1; (b) 2; (c) 3; (d) 4; (e) 5

Permeability test results

Figure 6 illustrates the permeability values of copper tailings specimens compacted at various molding points. The highest permeability is observed at point 1, which gradually decreases until reaching its lowest value at point 3, before slightly increasing up to point 5. On the wet side, the permeability values are consistently lower compared to the dry side. This can be attributed to the larger pore spaces on the dry side due to less moisture and looser packing. In contrast, the wet side has more moisture, resulting in initially tighter packing, followed by slight separation due to excess water. At point 3, the particles are most densely packed, leading to fewer voids and the lowest permeability.

The collaborative evidence of these findings is presented in section 3.5 through SEM images. Permeability observations of copper tailings specimens offer crucial information for optimizing the compaction process of filtered tailings. By carefully adjusting the compaction level and moisture content, engineers can effectively control the permeability of the tailings.

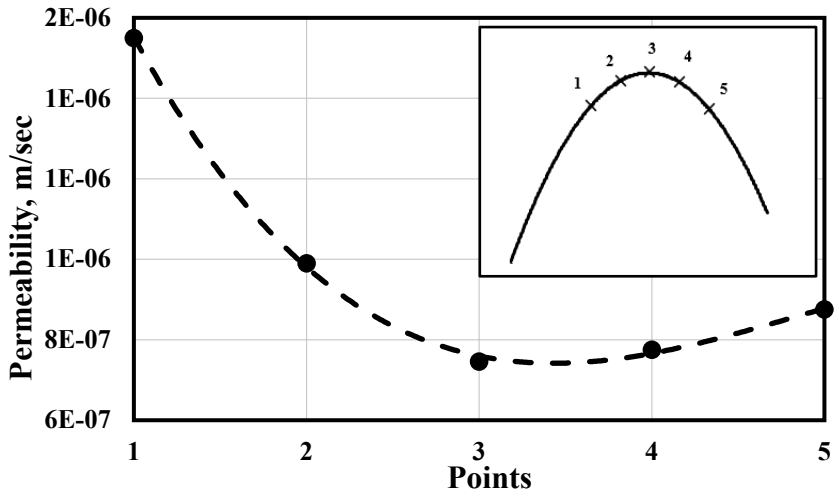


Figure 6: Permeability of compacted copper tailings at different molding points

SEM results

This section presents the results of SEM tests conducted on compacted copper tailings, as shown in Figures 7(a-c). Figure 7(a) depicts the particle distribution and fabric of copper tailings compacted at -20% OMC (point 1). In this condition, particles appear flocculated or randomly oriented within clusters, creating larger pore spaces. Figure 7(c) shows the SEM result of the specimen compacted at +20% OMC (point 5). It can be observed that the particles are dispersed and exhibit a more oriented and laminated structure, leading to smaller pore sizes. This arrangement is characterized by particles aligning more uniformly, which reduces the interconnected pore spaces. Figure 7(b) illustrates the densely packed particles at OMC (point 3), where minimal interconnected pore spaces are present, leading to the lowest permeability, consistent with earlier findings. The higher strength observed on the dry side can be attributed to the closely packed angular particles (Figure 7(a)) and increased interparticle friction. Conversely, the increased moisture on the wet side reduces interparticle friction, generally leading to lower strength.

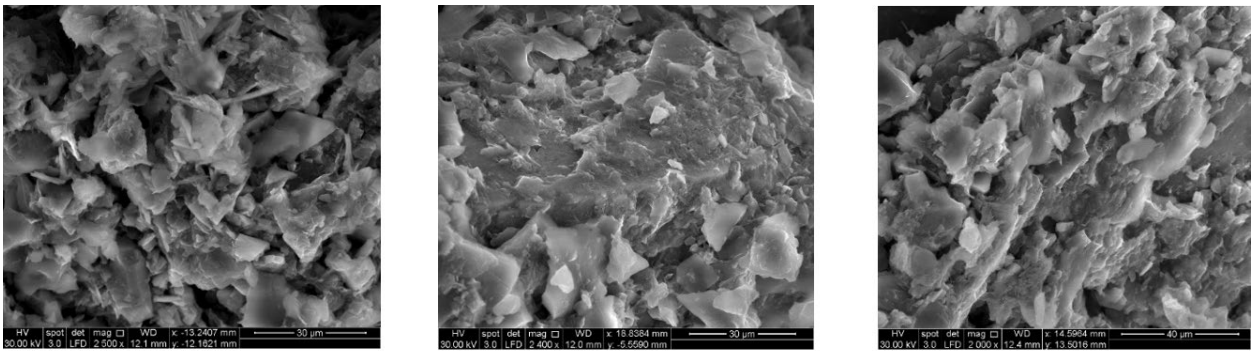


Figure 7: SEM images of copper tailings compacted at points: 1; 3; 5

Conclusion

This study highlights the critical importance of understanding filtered copper tailings' physical and mechanical properties across various moisture contents relative to the OMC. The findings emphasize that properly preparing filtered tailings at appropriate moisture levels is vital for ensuring the stability and performance of dry stack tailings facilities. With moisture contents less than optimum, the tailings can exhibit higher unconfined compressive strength and initial stiffness, but are prone to brittle failure with abrupt shear bands and minimal bulging. These tailings are vulnerable to sudden failure and increased permeability, potentially compromising the stability of the tailings stack. Whereas the tailings compacted on the wet side demonstrate lower strength and ductile failure patterns, with significant bulging and microcracking. The permeability is generally lower due to tighter initial packing, although excess moisture can cause a slight separation of particles. If filtered tailings are over-wetted, the resulting structure may lack strength and be prone to excessive deformation, undermining the structural integrity and stability of the tailings stack. Achieving the OMC during compaction is crucial for maximizing strength and minimizing permeability. Tailings compacted at OMC display balanced properties with the highest strength and lowest permeability, ensuring a stable and durable structure.

Overall, the study highlights the importance of precise moisture control during tailings compaction for optimal performance in dry stack applications. If there is successful extraction of water to the desired moisture contents, dry stack tailings can potentially advance sustainable tailings management practices and mitigate the environmental risks associated with conventional disposal methods.

Acknowledgments

All SEM images and data were collected in the W.M. Keck Center for Nano-Scale Imaging in the Department of Chemistry and Biochemistry at the University of Arizona, RRID: SCR_022884, with funding from the W.M. Keck Foundation Grant. The authors wish to convey their gratitude to the W.M. Keck Center for granting them access to the SEM.

References

Amoah, N., Dressel, W. and Fourie, A.B. 2018. Characterisation of unsaturated geotechnical properties of filtered magnetite tailings in a dry stack facility, in R.J. Jewell and A.B. Fourie (eds), *Paste 2018: Proceedings of the 21st International Seminar on Paste and Thickened Tailings,* Australian Centre for Geomechanics, Perth: 375–388, https://doi.org/10.36487/ACG_rep/1805_31_Amoah

ASTM, D. 2007. Standard test method for particle-size analysis of soils.

ASTM, D. 2014. 854-14. Standard Test Methods for Specific Gravity of Soil Solids by Water Pycnometer.

ASTM, D. 2016. 2166; Standard Test Method for Unconfined Compressive Strength of Cohesive Soil. *West Conshoshocken, PA, United States*.

ASTM, 2007. ASTM D698: Standard Test Methods for Laboratory Compaction Characteristics of Soil Using Standard Effort (12 400 ft lb/ft^3 [600 kN m/m^3]).

Blight, G.E. 2009. *Geotechnical Engineering for Mine Waste Storage Facilities*. CRC press.

Cacciuttolo, C. and Atencio, E. 2023. Dry Stacking of filtered tailings for large-scale production rates over 100,000 metric tons per day: Envisioning the sustainable future of mine tailings storage facilities. *Minerals* 13(11): 1445.

Carvalho, J.V.D.A., Wagner, A.C., Scheuermann Filho, H.C. and Consoli, N.C. 2024. The role of fabric, stress history, mineralogy, and particle morphology on the triaxial behavior of nontextbook geomaterials. *Journal of Geotechnical and Geoenvironmental Engineering* 150(8): 04024055.

Consoli, N.C., Vogt, J.C., Silva, J.P.S., Chaves, H.M., Scheuermann Filho, H.C., Moreira, E.B. and Lotero, A. 2022. Behaviour of compacted filtered iron ore tailings–Portland cement blends: New Brazilian trend for tailings disposal by stacking. *Applied Sciences* 12(2): 836.

Consoli, N.C., Tomasi, L.F. and Veloso Marques, S.F. 2023. Cement-enhancing mechanical behavior of tailings behind upstream tailings dam for safe decommissioning. *Journal of Materials in Civil Engineering* 35(5): 06023001.

Davies, M.P. and Rice, S. 2022. An alternative to conventional tailing management–dry stack filtered tailings. In *Tailings and Mine Waste 2001* (pp. 411–420). CRC Press.

Gomes, R.B., De Tomi, G. and Assis, P.S. 2016. Iron ore tailings dry stacking in Pau Branco mine, Brazil. *Journal of Materials Research and Technology* 5(4): 339–344.

Johansson, L. 1990. Geomechanical properties of tailings: a study of backfill materials for mines. Doctoral dissertation, Luleå tekniska universitet.

Lara, J.L., Pornillos, E.U. and Muñoz, H.E. 2013. Geotechnical-geochemical and operational considerations for the application of dry stacking tailings deposits–state-of-the-art. In R. Jewell, A.B. Fourie, J. Caldwell and J. Pimenta (eds), *Paste 2013: Proceedings of the 16th International Seminar on Paste and Thickened Tailings*, Australian Centre for Geomechanics, Perth, pp. 249–260, https://doi.org/10.36487/ACG_rep/1363_19_Munoz

Piciullo, L., Storrøsten, E.B., Liu, Z., Nadim, F. and Lacasse, S. 2022. A new look at the statistics of tailings dam failures. *Engineering Geology* 303: 106657.

Qiu, Y. and Sego, D.C. 2001. Laboratory properties of mine tailings. *Canadian Geotechnical Journal* 38(1): 183–190.

Schnaid, F. 2021. The ninth James K. Mitchell lecture: On the geomechanics and geocharacterization of tailings. *Proceedings of 6th International Conference on Geotechnical and Geophysical Site Characterization*.

Vick, S.G. 1990. Planning, Design, and Analysis of Tailings Dams. BiTech Publishers Ltd..

Yang, Y., Wei, Z., Fourie, A., Chen, Y., Zheng, B., Wang, W. and Zhuang, S. 2019. Particle shape analysis of tailings using digital image processing. *Environmental Science and Pollution Research* 26: 26397–26403.

Multi-Test Approach to Determining Consolidation Parameters in Flocculated Tailings and Soft Soils

Ehsan Eidi, Carleton University, Canada
Ken Dickson, Regional SNF Technical Centre, Canada
Arazooben Patel, Carleton University, Canada
Louise Whitham, Regional SNF Technical Centre, Canada
Morgan Tizzotti, SNF Headquarter, France
Paul Simms, Carleton University, Canada

Abstract

The consolidation characteristics of young soft geomaterials, such as dredged soils or clayey tailings, is important to their management, particularly to estimating the magnitude of settlement as well as the density and strength profiles with depth. Consolidation properties, however, are challenging to measure in these materials, specifically, determination of the hydraulic conductivity (or *k-e*) function can be time consuming (months for some clayey soils using standard methods), and the compressibility curve shifts with time due to ageing effects. This paper outlines a multi-test approach that can assess different parts of the *k-e* function relatively rapidly, as well as quantifying the magnitude of shifting of the compressibility curve. Tests to rapidly estimate the *k-e* curve in this paper use the settlement curve in settling columns as well as the final density profile with elevation.

Introduction

The oil sands industry has been producing for over five decades in Canada. The majority of Canada's oil sands are located in northeastern Alberta, specifically in the Athabasca region. There are also significant heavy oil deposits in northwestern Alberta (Peace River) and the Cold Lake/Lloydminster region, which spans Alberta and Saskatchewan. The oil sands deposits are a mixture of sand, water, clays, and bitumen (Fine Tailings Fundamentals Consortium, 1995). The primary production process includes open-pit mining, subsequent separation of bitumen from the ore using hot water and chemicals such as caustic soda (Masliyah et al., 2004), and subsequent refinement of the bitumen.

The residuals from the extraction process, including the sands and clays of the natural ore body, are deposited as tailings. Oil sands tailings naturally segregate into sand dominated and fines (silt and clay)

dominated fractions. The fines dominated tailings, called fluid fine tailings (FFT), typically form deposits that stabilize at ~ 200% gravimetric water content (30 to 40% solids content), much higher than their liquid limit (which is typically between 50% to 80%). FFT high natural water content is due to the high dispersion of the clays induced by the chemistry of the extraction process. In this state, FFT possess low strength and low permeability, rendering reclamation challenging (Abdulnabi et al., 2022).

Oil sands operations currently treat FFT with the goal of improving the dewatering properties. Treatments employ different combinations of flocculants and coagulants, the general objective being to reverse the dispersion of clays and generate larger flocs of an optimal size to improve dewatering. Generally, the success of a particular treatment is first evaluated in the laboratory, using specific key performance indicators (KPIs) such as settlement in a graduated cylinder over a set period, or CST (capillary suction time) tests. Selected treatments may be evaluated for consolidation properties using large-strain consolidation or seepage-induced consolidation tests; however, these usually take months for a single sample, even for treated FFT. The goal of this paper is to demonstrate the application of new methods to quickly estimate the consolidation properties of different treatments of FFT, and to show how such methods can be used as a screen for comparing the performance of different treatments. These methods are demonstrated by application to particular coagulant-polymer combinations, investigating substitution of alum with polymer-based coagulants.

Methodology

In the field the coagulation and flocculation processes occur in succession during the transportation of tailings to the tailings pond. Each amendment is introduced to the pipeline, where mixing may occur due to turbulent conditions, and/or may be enhanced by static mixers. After flocculation, the tailings will travel some distance in the pipeline (meters to hundreds of meters, depending on the operation). The influence of shear during transport on floc characteristics and subsequent performance is a critical consideration.

Various operators have come up with laboratory protocols that will create “field equivalent” samples, as verified by field campaigns to determine KPI (Key Performance Indicators) of field samples. These protocols allow for evaluating changes to tailings treatment before any changes are attempted at pilot or full scale. This study employs one of these protocols conforming to a particular mine in the oil sands, which is described in the following section. This protocol is developed to simulate treatment of legacy FFT.

The physical characteristics of the FFT utilized in this study were determined in accordance with ASTM standards, as detailed in Table 1 :

Table 1: Physical characteristics of the tailings

Properties	Unit	ASTM standard	Value
Solids content	%	D2216	34
Water content	%	D221	195
Liquid limit	%	D4318	65
Plastic limit	%	D4318	39
Bitumen content	%	D95	3.34
Specific gravity	Unitless	D854	2.13

Oil sands tailings are known to exhibit low specific gravity, due to the residual bitumen and other hydrocarbons tightly associated with the solids.

Sample generation

Samples are prepared by mixing flocculant and coagulant into 300 grams of FFT (at its initial solids content of 34%) using a metal cylinder cup equipped with four baffles. The cylinder cup has a diameter of 11 cm and a height of 8 cm, with each baffle measuring 1 cm in width. An overhead stirrer is employed to ensure thorough mixing. The stirrer has a single rectangular blade 7.6 cm wide and 2.5 cm deep. The flocculant and coagulant solutions are introduced using syringes.

The same flocculant, NRG 1000 (SNF), was used to prepare all polymer-amended FFT samples. First, 2.25 grams of NRG 1000 polymer was accurately weighed in a plastic weighing dish. The polymer was then transferred into a 1,000 ml glass beaker, and the volume was adjusted to 498 ml with bleed water. The solution was stirred using a jar tester at 300 revolutions per minute (rpm) for 30 minutes to ensure thorough mixing. After stirring, the polymer solution was allowed to mature for 15 minutes, enabling full hydration and activation.

Coagulation: Coagulant solutions are prepared by mixing concentrated coagulant with process water, to target the doses (In terms of mass of coagulant per mass of solid tailings) shown in Table 2. Coagulant solution is added to the mixing chamber when the mixer is set to 300 rpm. Mixing at 300 rpm occurs for 1 minute and 10 seconds and the speed is reduced 80 rpm for 12 minutes. The decrease in torque emulates the resistance to shear observed in a pipeline as the raw FFT becomes more viscous.

Flocculation: In the second step, the flocculant solution is injected while the mixer speed is 300 rpm. The duration of mixing is controlled in this step through monitoring the torque of the mixer. The mixing is

stopped after a peak torque is reached and the torque begins to noticeably decline, which can be generally detected within 2 seconds of the peak being reached.

Shearing Step: The third step simulates pipeline transport of the tailings. The mixing speed is set to 320 rpm and tailings are sheared for 10 minutes.

The shearing step may seem counter-intuitive in the sense that the floc size is being increased by flocculation and then subsequently decreased; however, the flocculation process is important to maximize readily released water and to minimize uncaptured fine particles- these phenomena will have a positive effect on dewatering and consolidation despite the subsequent reduction in floc size by simulated pipeline transport.

In this study, the type and dosage of coagulants are varied. The base treatment, named ADW, using metal-based coagulant (Alum) with the polymer FLOPAM™ NRG 1000 as a flocculant. Two other polymer-based coagulants were employed, termed FLOQUAT™ FL 4150 and FLOQUAT™ FL 2949. Table 2 presents the different doses of each coagulant examined. Optimum refers to optimum dose based on CST only.

Table 2: The different dose of the coagulant and flocculant used in the experiment

Flocculant Dose	Type of the Flocculant	Coagulant Dose	Type of coagulant
1,700 ppm (or g/t)	NRG 1000	1,000 ppm	Metal Base Alum
1,600 ppm	NRG 1000	1,000 ppm	Metal Base Alum
1,800 ppm	NRG 1000	1,000 ppm	Metal Base Alum
1,200 ppm	NRG 1000	1,250 ppm	Polymer FL 4150
1,260 ppm	NRG 1000	1,250 ppm	Polymer FL 4150
1,320 ppm	NRG 1000	1,250 ppm	Polymer FL 4150
1,140 ppm	NRG 1000	1,250 ppm	Polymer FL 4150
1,200 ppm	NRG 1000	2,265 ppm	Polymer FL 2949

CST tests

CST, or Capillary Suction Time (ASTM 2170 G), is a test used for short-term observation and quality control of flocculated tailings. It provides a simple and precise measure of the rate at which water is released from a treated tailing. It is based on the rate at which water is absorbed from the tailings sample by a particular filter paper (Whatman 4). Both the hydraulic conductivity of the tailings, and the viscosity of the release water (which will be affected by residual non-captured fines) controls this rate. In this set of experiments, the objective is to achieve a dewatering time about 40 seconds or less – this criteria is based on operator feedback on full-scale performance of tailings in the field.

Settlement tests

600 ml of treated tailings are deposited into a graduated cylinder of diameter 67 mm and left undisturbed for a period of 100 days. Settlement is monitored using a video camera. After 100 days, the sample is destructively tested, by removing the bleed water slowly, and then the tailings cm by cm. After each removal of ~1 cm of tailings, the whole column is weighed, while the gravimetric water content of the removed small sample is determined by oven drying. This double method of estimating the water content at specific elevations generally shows good agreement between the two estimates, indicating little mass is left behind on the cylinder walls. Assuming 100% degree of saturation, this allows for calculation of a final void ratio profile with elevation. Qi and Simms (2020) show a previous application of this methodology.

Oscillatory rheometry

Oscillatory rheometry tests were performed on samples after flocculation and pipeline shear modeling. These tests aimed to study the rheological properties, specifically the elastic modulus (G') and viscous modulus (G"), which were measured at a controlled, increasing shear stress amplitude (Aldaeef et al., 2022). G’ measurement at the very low shear stresses below the true elastic limit of the material enable by this instrument, allows for tracking of thixotropy in a sample with minimal disturbance.

The oscillatory time sweep involved applying a gradually increasing oscillation stress at a consistent angular frequency of 10 rad/s (equivalent to 1.6 Hz) (Mizani et al., 2017). This test characterizes the thixotropic /ageing behaviour of the tailings, which can have implications for long term dewatering (Salam et al., 2023). In particular, there is a given coefficient of rigidity (the ratio between G’ and the undrained shear strength), and a constant ratio between G’ and the pre-consolidation pressure for a given treatment of FFT.

Other tests part of this study but not reported in the paper include the oedometer tests and other consolidation tests. In this paper, the reported consolidation properties are those estimated from the settlement test data – these estimates will be compared with other measurements of compressibility (oedometer test) and hydraulic conductivity that our currently ongoing.

Results

CST

The CST results, are depicted in Figure 1. It is evident that polymer-based coagulants allow to somewhat lower CST and therefore lead to better dewatering performance in the short term. The time in the CST test indicates the time water takes to be transported through the filter paper; therefore, a low CST indicates some combination of the capacity of the sample to release water, but also is affected by the viscosity of the water released, which depends on the efficiency of the capture of small particles during flocculation-coagulation. Both these factors indicate desirable properties; therefore, lower CST is positive. "Overdoses" are shown that indicate no significant gain in CST despite additional chemical additions.

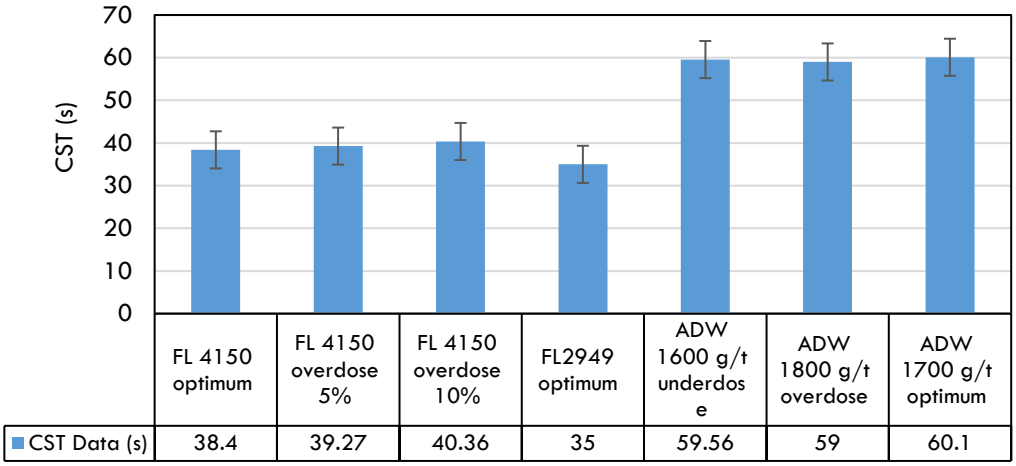


Figure 1: CST of each treatment

Settlement data

Figures 2 through 4 show the settlement data observed in the graduated cylinders. Figure 4 shows the data for all doses. Figures 3 and 4 show only data from three samples: ADW and FL 4150 optimum, and an overdosed FL 4150 sample.

Figure 3 shows the data in log time, which illustrates some differences between the FL4150 and the ADW treatments. The optimum FL 4150 has some initially faster settlement than the ADW, suggesting an initially higher hydraulic conductivity at its initial void ratio compared to the ADW treatment, but reaches a plateau and a definite final settlement by about 30 days. In contrast, the ADW samples show an almost log-linear behavior from 20 to 100 days. This suggests that the ADW treatments experience substantially more creep than the FL 4150 treatments. Pore-water pressure measurements show completion of primary consolidation before 20 days for all samples.

Figure 4 shows the settlement behavior during the first week, in linear time. Here it is clear that the settlement rate and consequently the hydraulic conductivity at high void ratios is higher in the FL 4150 optimum sample. This is confirmed quantitatively in the analysis presented in the next section.

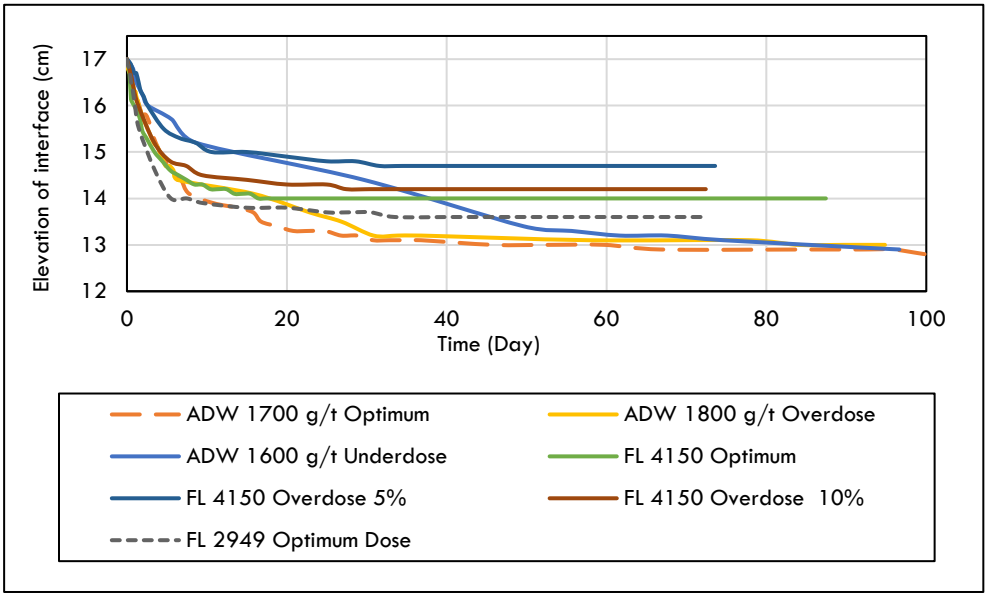


Figure 2: Settlement data for polymer-based coagulants and metal-based coagulant

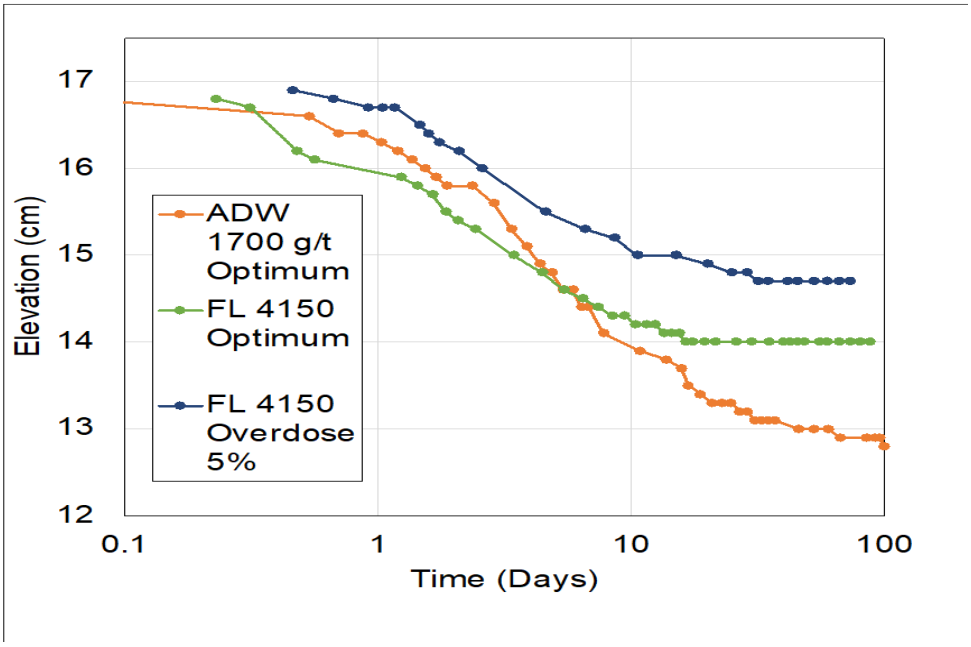


Figure 3: Settlement data for ADW optimum and two doses of FL4150

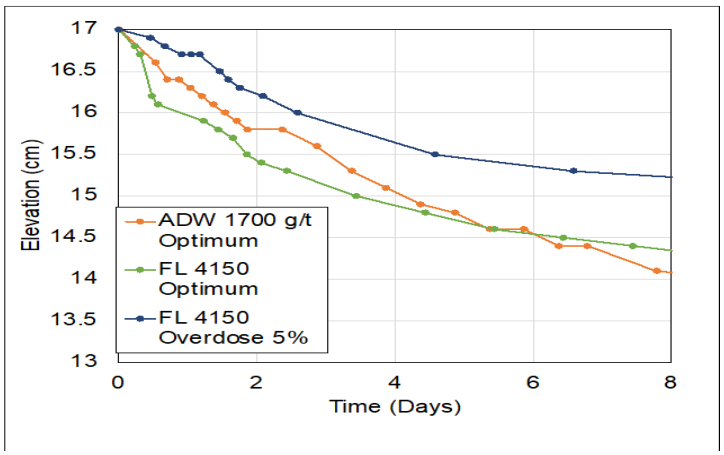


Figure 4: Early settlement data for ADW optimum and FL4150

Importantly, these data in Figures 2 through 4 should be interpreted considering difference in water content post-treatment when the FFT is deposited into the cylinder. For example, the FL 4150 samples post treatment water contents are at 230% whereas the ADW samples are at 240%.

Oscillatory rheometry

Figure 5 shows the measurement of G' over 100 days for the ADW and FL 4150 optimum doses and for the overdosed sample. The increase in G' in the first 7 days or so is attributed to consolidation, which is tracked by pore-water pressure measurements in duplicate samples. The remaining increase is due to thixotropy, reaching a plateau by about 100 days – this behavior is the same as reported for FFT by Salam et al. (2023) and by Patel et al. (2021).

It is very apparent that the FL 4150 shows a much higher value of G' from the end of consolidation and at later times, despite being at a higher void ratio than the ADW post-consolidation. The flocs or floc network produced by the FL 4150 process are thus stronger and stiffer. This is correlated with the decreased settlement in the long term observed for these samples (Figures 2 through 4).

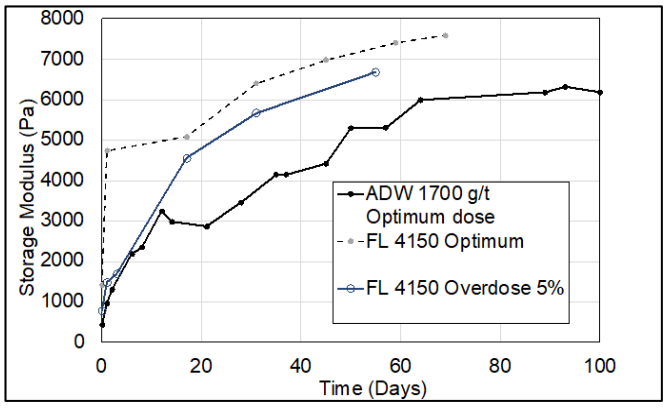


Figure 5: G' values of ADW optimum and FL4150 optimum, and overdose

Estimating the consolidation properties

Compressibility

The compressibility curve may be estimated by fitting the following equation to the measured distribution of void ratio with depth from the graduated cylinders (Qi and Simms 2020).

$$\xi = \frac{1}{\Upsilon}\left[\left(\frac{e}{a}\right)^{\frac{1}{b}}\left(\frac{e}{b+1}+1\right) - c\left(\frac{ac^b}{b+1}+1\right)\right] \quad \text{(Equation 1)}$$

Where the symbol ξ is elevation (m); a, b, c, are the parameters of the compressibility equation in modified power form ($e = a(\sigma'_v+c)^b$), such that the void ratio at zero vertical effective stress (e_c) is given by $e_c = ac^b$. The symbol Y is the submerged unit weight.

Figure 6 illustrates the measured and estimated void ratios of the tailings treated with 1700 g/t and the Alum and Polymer based coagulant FL 4150 at optimum doses and the FL 4150 overdose.

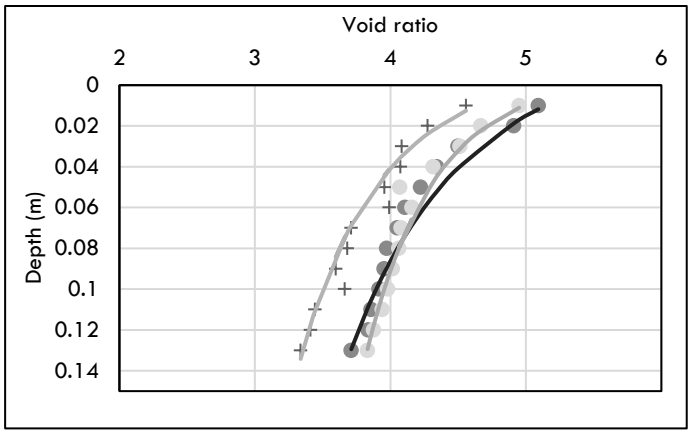


Figure 6: The measured and estimated void ratio after 100 days from the graduate cylinder of the optimum dose of alum-based (+) and FL4150 optimum(dark circle) and overdose (light circle)

Hydraulic conductivity (k-e)

Assuming the power form of the dependency of the hydraulic conductivity function on void ratio:

$$k = Ce^D \quad \text{(Equation 2)}$$

The hydraulic conductivity at the initial void ratio can be calculated using the method of Pane and Schiffman (1997):

$$K = \frac{(1+e)v_s}{G_s-1} \quad \text{(Equation 3)}$$

Where G_s is the specific gravity, e is the initial void ratio and v_s is the initial settling velocity of the solids. The parameter "C" can then be determined using different assumed values of D. For this type of material

(flocculated fluid fine tailings), it is reasonable to assume the D parameter is restricted to between 5 and 8 (reported results on clayey tailings and soft clays summarized in Babaoglu and Simms 2020). The optimal D and paired C parameter can then be determined by checking which set of parameters best match the full settlement data when employing both consolidation properties in a large-strain consolidation model. Here the UNSATCON model is employed (Gheisari et al., 2023, Abdulnabi et al., 2022, Qi and Simms, 2020), though any 1D large-strain model would work.

The simulations of settlement and post-consolidation depth profile of void ratio are compared with the measured data in Figures 7 and 8. The optimal sets consolidation parameters are shown in Table 4.

Table 3: The consolidation properties of each treatment

Tests	A	B	C	C	D
ADW 1,700 ppm	2.8	-0.16	0.02	5.02E-12	7
FI 4150 Optimum	3	-0.2	0.04	1.8E-10	6
FI 4150 5% overdose	3.3	-0.12	0.01	1.8E-11	6

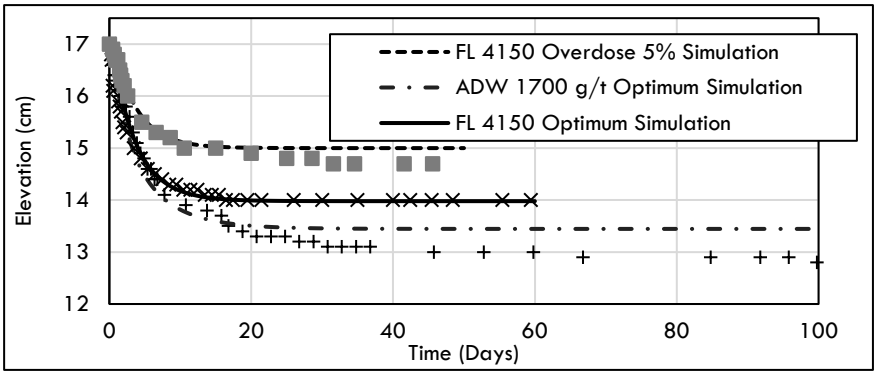


Figure 7: The simulation and the experimental data of the settlement test for 1,700 g/t optimum dose, FL 4150 optimum dose and FL 4150 5% overdose

The agreement between the modelled settlement curves and measured data is good, except for a noticeable deviation between the measured and predicted settlement after 20 days for ADW treatment. It is important to note that the end of primary consolidation predicted by the model, and the observed dissipation of pore-water pressure is good, and the remaining settlement is likely due to creep, and therefore not accounted for in the model results. It is clear that the stiffer (as indicated by G' measurements) FL4150 treatments exhibit less creep, at least for the low range of effective stresses developed in the graduated cylinders.

Hypothetical extrapolation to deposit performance

Acknowledging that future measurements will provide additional data at higher effective stresses for both

compressibility and *k-e*, nevertheless, comparative consolidation analyses are presented on a hypothetical 50 m deposit using the consolidation properties determined in the previous sections. The settlements over 50 years are presented in Figure 8.

Most remarkable is that the FL 4150 optimum and the ADW optimum show little difference in their performance, showing almost identical settlement behavior, and similar post-consolidation void ratio-elevation profiles. In reality, the magnitude of the predicted total settlement for the ADW would be larger due to creep, but the rate of settlement would be less. Looking at more in-depth analysis involving creep (Gheisari et al., 2023), the delay in consolidation due to creep is negative in the sense that there is a delay before reclamation can commence. Therefore, it is expected, though not yet confirmed, that the FL 4150 treatment would achieve a stable deposit more quickly than the standard ADW treatment, and still with a reasonable net reduction in deposit volume. Based on the stiffness (G') data, it would seem that the FL 4150 samples would also be stronger for a given void ratio.

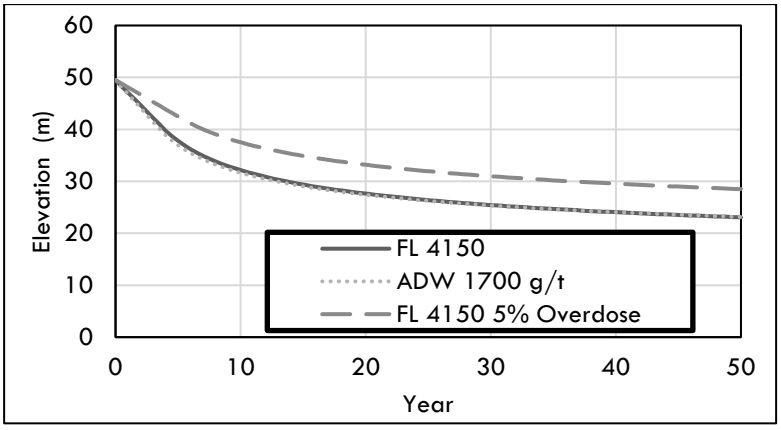


Figure 8: The settlement of a hypothetical tailings deposit over 50 years using the consolidation properties for the ADW and FL 4150 optimum dose and FL 4150 5% overdose treatments

Conclusion

1. FLOQUAT™ FL 4150 treatments provide superior and more consistent short-term dewatering than the base treatment, which is also evident from the early part of the settlement curve, indicating higher hydraulic conductivity in the 4150 optimum sample at its initial void ratio.
2. FLOQUAT™ FL 4150 treatments show a larger degree of ageing post consolidation than the base-treatment, as evidenced by the G' data; this is commensurate with the much lower degree of creep evidenced in the settlement curves.
3. Based on preliminary estimation of the compressibility properties, and employing these properties in simulation of large-strain consolidation in a 50 m deep hypothetical deposit, the FLOQUAT™ FL 4150 and base treatments provide very similar performance. However, given the larger tendency to

creep in the base treatment, which may substantially delay consolidation, the FLOQUAT™ FL 4150 may provide an advantage by achieving a sufficiently stable (minimal settlement) deposit more quickly than the base treatment.

Conclusion 3 is preliminary and must be re-evaluated once data on behaviour at higher effective stresses (the ongoing oedometer and instantaneous profile tests) becomes available.

Acknowledgements

This research is generously supported by SNF Oil & Gas division.

References

Abdulnabi, A., Amoako, K., Moran, D., Vanadara, K., Aldaeef, A.A., Esmaeilzadeh, A., Beier, N., Soares, J. and Simms, P. 2022. Evaluation of candidate polymers to maximize geotechnical performance of oil sands tailings. *Canadian Geotechnical Journal* 59(3): 359–371. doi:10.1139/cgj-2020-0714.

Aldaeef, A.A., Simms, P.H. and Soares, J.B.P. 2022. Torque-based evaluation of mixing optimization and shear sensitivity during transport of flocculated tailings. *Minerals Engineering* 181: 107541. doi:10.1016/j.mineng.2022.107541.

Babaoglu, Y. and Simms, P. 2020. Improving hydraulic conductivity estimation for soft clayey soils, sediments, or tailings using predictors measured at high-void ratio. *Journal of Geotechnical and Geoenvironmental Engineering* 146(10). https://doi.org/10.1061/(ASCE)GT.1943-5606.0002344

FTFC (Fine Tailings Fundamentals Consortium). 1995. Advances in Oil Sands Tailings Research.

Gheisari, N., Qi, S. and Simms, P. 2023. Incorporation of three different creep models into large-strain consolidation analysis of a clayey tailings deposit. *Computers and Geotechnics* 161: 105533. doi:10.1016/j.compgeo.2023.105533

Masliyah, J., Zhou, Z., Xu, Z., Czarnecki, J. and Hamza, H. 2004. Understanding water-based bitumen extraction from Athabasca oil sands. *Canadian Journal of Chemical Engineering* 82(4): 628–654. doi:10.1002/cjce.5450820403.

Mizani, S., Simms, P. and Wilson, W. 2017. Rheology for deposition control of polymer-amended oil sands tailings. *Rheologica Acta* 56(7–8): 623–634. *Rheologica Acta.* doi:10.1007/s00397-017-1015-2.

Pane, V. and Schiffman, R.L. 1997. The permeability of clay suspensions. *Géotechnique* 47(2): 273–288. doi.org/10.1680/geot.1997.47.2.273

Patel, A., Aldaeef, A. and Simms, P. 2021. Ageing in soft soils and clayey tailings. *Proceedings of Tailings and Mine Waste 2021,* Lake Louise, Alberta, Canada.

Qi, S. and Simms, P. 2020. Robust methods to estimate large-strain consolidation parameters from column experiments. *Canadian Geotechnical Journal* 57(5): 683–705. doi:10.1139/cgj-2018-0870.

Salam, M, Simms, P. And Örmeci, B. 2023. Ageing/thixotropy effects on strength and compressibility in Leda clay and polymer-amended clayey tailings. *Engineering Geology* 317: 107088. doi.org/10.1016/j.enggeo.2023.107088

Optimization of Operations Based on Monitoring and Construction Quality Assurance at Minera Peñasquito

Christian Armstrong, WSP, USA
Kenneth Rood, WSP, USA
Eduardo Jose Garcia Romero, Newmont Peñasquito, Mexico
Patrick Mwamba, WSP, USA

Abstract

Tailings storage facilities (TSFs) are dynamic environments that require active operational controls in order to meet the goals of physical stability, storage capacity, and other key design goals. Therefore, to operate a facility, robust construction quality assurance (CQA) and recurring field investigation programs must be performed to validate current conditions against the design. The TSF is operated as a cyclone sand, centerline raise facility with an outer shell of rockfill, with overflow tailings and whole tailings discharged into the TSF impoundment. The as-measured, in-situ properties should then inform lessons learned and be incorporated into future design and operations. The performance of the TSF at Minera Peñasquito was evaluated via a series of three significant Cone Penetration Test (CPT) programs, performed in 2014, 2019, and 2023 and two field sampling and geotechnical laboratory testing programs in 2014 and 2023, in combination with data and observations from the rolling CQA program. Results from the 2014 investigation were used to evaluate the materials properties, including changes of its characteristics due to optimization of operational and construction processes. Changes in the placement of the cyclone sand (e.g., improved water management, improved construction techniques) were evaluated by subsequent CPT programs and indicate that the cyclone sand and tailings materials are being placed in a more dense, more dilative state than previous stages of construction. The overflow and whole tailings behavior was evaluated and includes outcomes such as (a) the starter phase tailings placement resulted in a weak, fine tailings layer at depth and (b) changes in depositional management (e.g., rotating spigot deposition within the pond and removal of water near the edges of the facility) have resulted in denser/stronger materials.

Introduction

Tailings storage facilities (TSF) are inherently complex structures due to the continuous construction, scale, variability in ore characteristics, and other characteristics. Design for these structures is also based off pilot-

scale tailings generation, resulting in conditions that may vary from the in-place conditions due to variability in the ore body, operations during the initial starter and early years of deposition, and other factors. These factors are generally evaluated during the design phase by evaluating potential risks and variability and identifying potential contingencies that may be necessary. Due to this potential variability, field investigations and instrumentation are usually used to evaluate the performance of the facilities. Therefore, these tools should be used to support changes in the operations or design, which is inherently tied to the observational methodology.

The observational method has been employed throughout history by engineers and their precursors. For example, construction of the western façade of Notre Dame was halted for approximately a decade after builders observed the structure was leaning forward. They waited for settlement to reach a point where additional loading could be supported. A formalized version of the observational method was introduced to soils engineering by Karl Terzaghi and later refined and published in the seminal paper "Advantages and limitations of the observational method in applied soil mechanics" by Peck (1969). Peck argues that the observational method can be used to saved time or money by limiting overdesign of a complex structure prior to field observations that can be made during construction. Using field observations and data collected during and after construction can allow for continuous improvements to be made to the design.

The paper evaluates the use of the observational method based on information collected by the field investigations and instrumentation within the TSF at Minera Peñasquito, including the optimization of operations following the first significant field investigations.

Site background

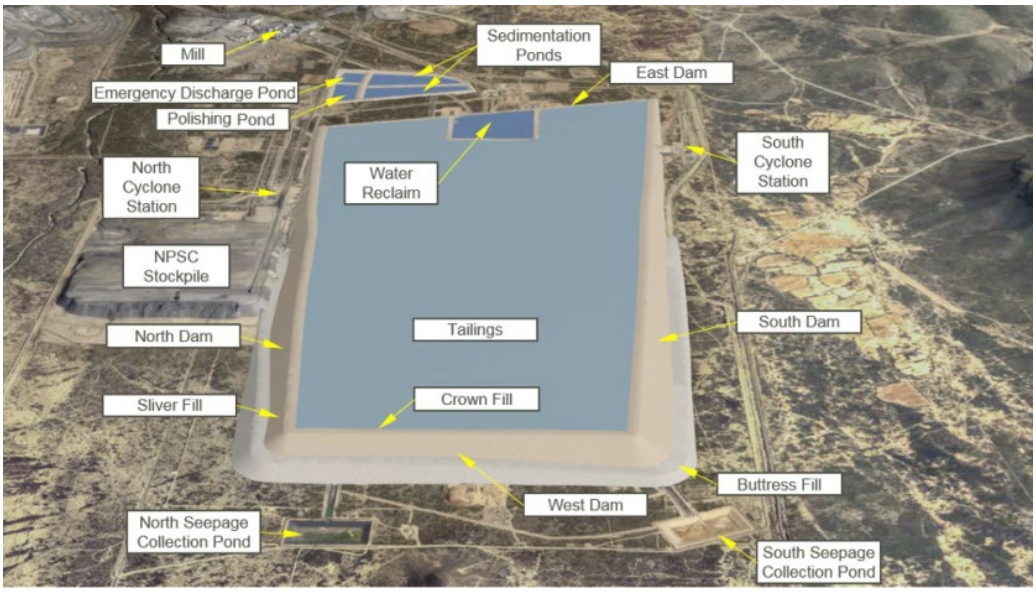


Figure 1: Key components of the TSF at Minera Peñasquito

The TSF at Minera Peñasquito tailings storage facility (TSF) is a four-sided structure with an 11 km perimeter and a current maximum height of approximately 117 m at the west embankment. The TSF receives 100,000 tons of tailings per day and has been in operation since 2009. The current design for the TSF includes a staged centerline raised to a maximum height of 134 m. Key components of the facility are presented in Figure 1.

The construction history for the Peñasquito TSF started with a 20-m-high starter dam constructed of borrowed alluvial fill with 2H:1V outer slopes (Golder, 2008, 2019). A rockfill buttress was constructed in 2011, and the dam has been raised continuously using the centerline methodology, with rockfill as the outer shell and cyclone sand as a compacted core separating the deposited tailings from the rockfill. Tailings are conveyed by gravity to cyclone stations located along the north and south dams. Cyclone underflow sand is separated from the whole tailings and used for dam construction, and cyclone overflow is deposited uniformly from the perimeter of the north, west, and south dams.

According to Golder (2019), the design and construction of the TSF has been dynamic in order to respond to changes in the availability of materials, operational experience, and shortages in quality sand production.

Construction of the TSF is separated into three activities defined as buttress fills, sliver fills, and crown fills. Buttress fills are required to stabilize the TSF dams as the facility is raised. Sliver fills are constructed over top of the buttress fills on the downstream of the centerline to allow for a widening of the dam crest, which facilitates the center line raise. Crown fills are constructed on the sliver fills to raise the elevation of the dam crest and support tailings deposition.

Operations of the facility

Construction of the TSF began in 2008 with a zoned earthfill starter dam, underdrain system, seepage collection system, starter impoundment system, and a start-up water reservoir impoundment. A technical review of the structure in 2011 found that due to insufficient quality sand production, a run of mine (ROM) rockfill buttress would be required to raise the embankment to 1,832.7 m. This construction would provide an additional two years of storage capacity, after which construction could continue as a centerline raise cyclone sand dam.

Following a 2014 technical review of the operations and TSF embankment stability, Minera Peñasquito concluded that it was not feasible to construct the facility with an embankment composed of only cyclone sand. The design was modified to make up the cyclone sand production deficit with ROM rockfill. A target crest elevation of 1862.7 m was selected as this corresponded with the maximum elevation where gravity discharge from the mill was possible. During this change in construction methods, full-time on-site engineering and construction quality assurance (CQA) services have been provided by Golder. The

CQA services included: material testing, construction oversight, dam inspections, oversight of tailings deposition, and oversight of seepage management.

Water management since 2014 has aimed to maintain a 200 m tailings beach from the centerline. Prior to this change in water management, minimum freeboard was not maintained in 2013, necessitating the construction of a temporary pipe berm. Following this event, significant improvements in construction methods and tailings deposition planning has led to a 200 m tailings beach being maintained, with only minor variances occurring. The effects of this water management can be seen in Figure 5, where the phreatic surface, observed via CPT soundings and VWP monitoring, has lowered and moved upstream in 2019 as compared to 2014.

Pipe berm construction is currently performed with the construction of temporary sand paddocks upstream of the dam centerline. As shown in Figure 2, a temporary sand paddock is constructed using existing cyclone sand, the paddocks are then filled hydraulically with underflow sand and water is allowed onto the tailings beach via a drain trench through the pipe berm. Once the sands have sufficiently drained, they are then excavated and used for quality sands at the centerline and for pipe berm raises. The quality sands are compacted using vibratory rolling to meet the design compaction specification. This construction methodology has led to an improvement in sand characteristics following 2014, with discrete variations in source materials occurring in 2020 where whole tailings and cyclone overflow sands were deposited into the paddocks.

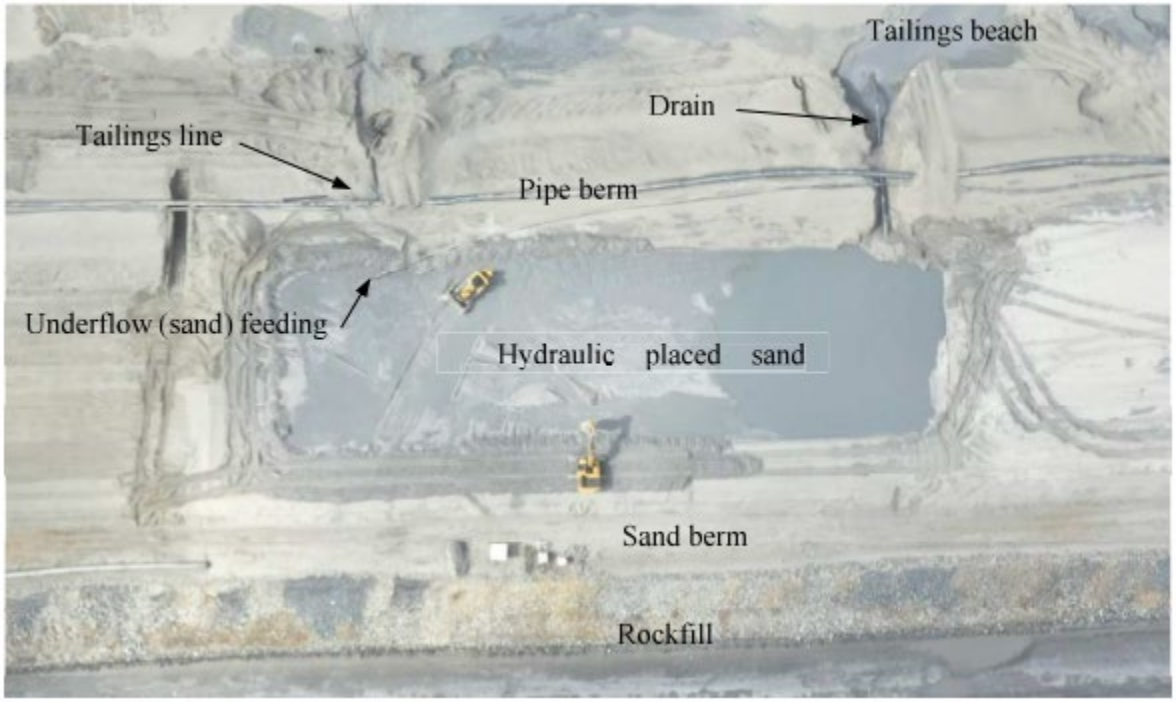


Figure 2: Aerial view of typical sand paddock construction (García and Sosa Dávila, 2020)

Analyses of seepage, stability, and consolidation have been performed to support the design changes and inform operational modifications. The 2016 buttress test fill program was instrumented and monitored to inform the maximum rate of rise achievable within the expected response of the subgrade. Since this investigation, construction of the buttress, sliver fill, and crest fill has been rotated around the perimeter of the facility to allow excess pore pressures generated by construction to dissipate before subsequent construction is performed. Additionally, tailings deposition is rotated through the spigots to maintain an even beach without the generation of localized depressions that would allow reclaim water to approach the pipe berm. The deposition is informed by visual observations, bi-weekly drone surveys, and subsurface phreatic surface monitoring. All these aspects inform a daily plan carried out by the Technical Services Planning team.

Field investigations and geotechnical testing

Field investigations were performed to evaluate the in-situ condition of the tailings versus the conditions anticipated from the detailed design analysis. In particular, the field investigations evaluated (1) the consolidation and density for a capacity analysis of the facility; (2) layering and interbedding of the tailings within the tailings beach/pond and pipe berm; (3) phreatic conditions and seepage to evaluate what flow routes are occurring within the field; (4) shear strength of the materials for modeling; and (5) critical state testing to evaluate the cyclone sand. The field investigations generally consisted of Cone Penetration Test (CPT) soundings following ASTM D5778, with additional borings performed in some investigations to support the correlated parameters. The more significant field investigations focused on the cyclone sand materials and tailings near the centerline, as these locations control the behavior of the facility, and were performed in 2014, 2019, and 2023.

The 2014 field investigation evaluated the performance of the facility following initial construction and operations using a combination of CPT soundings and seismic measurements, with a limited amount of seismic measurements, and boreholes correlated with selected locations. Results from the investigation supported the future capacity and design of the facility, including an evaluation of the phreatic conditions near the centerline of the facility, as these locations generally control stability and deformation. The vertical hydraulic gradients resulted in less than hydrostatic conditions within the cyclone sand, with a thinner saturated zone identified above the starter dam, and below hydrostatic conditions within the tailings beach materials, with closer to hydrostatic conditions further within the impoundment (see Figure 3).

However, portions of the phreatic surfaces are closer to hydrostatic in the tailings beach materials near the centerline along the west dam, indicating that the initial deposition had some variability in performance, particularly along the higher portions of the TSF near the starter facility. Perched pore pressure layers were observed within both the cyclone sand and the tailings beach. The cyclone sand is generally classified as

sand-like, with some silt-like layers, and the tailings varied from silt-like to clay-like, with heavily interbedded layers observed within the historic zone of the tailings placed behind the starter dam. These interbedded tailings generally were relatively loose and had low tip resistances.

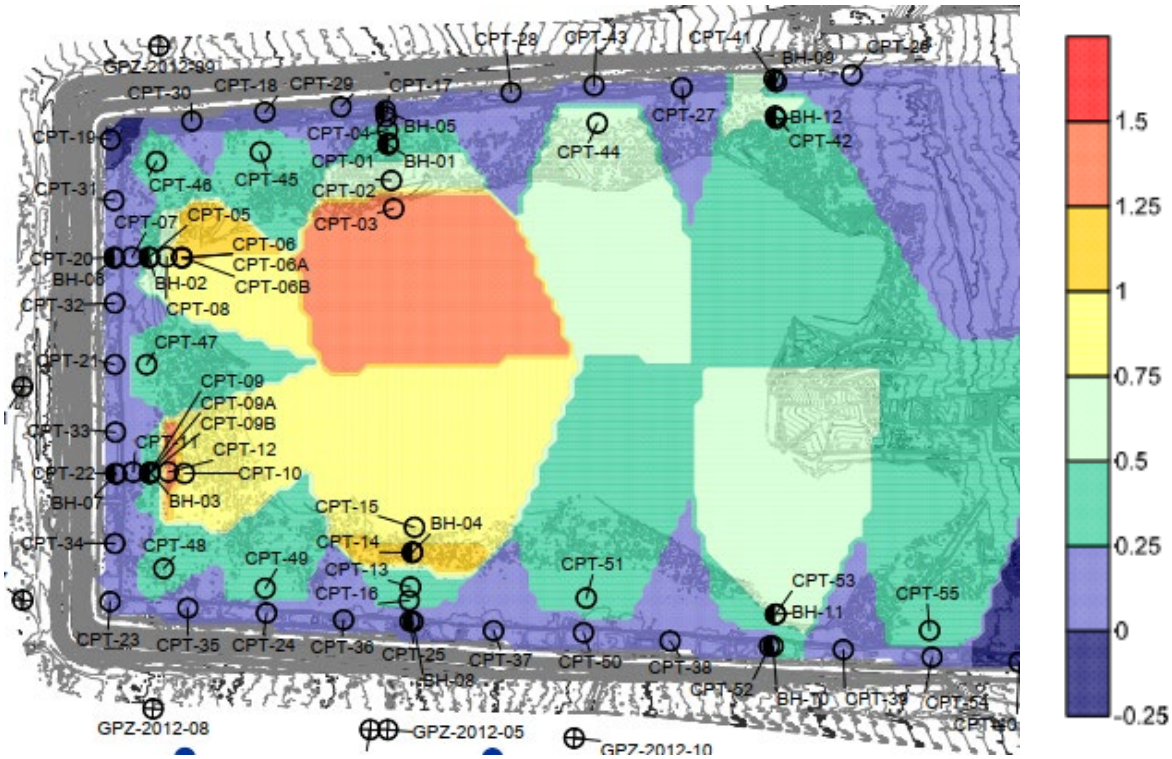


Figure 3: Vertical hydraulic gradients (unitless) within the TSF during the 2014 investigation (Golder, 2016)

The 2019 investigation was performed with CPTs and seismic measurements to evaluate how changes in operations affected the tailings, particularly the tailings beach. These changes in operations included the use of cyclone sand for the pipe berms as opposed to the reclaimed near tailings materials, and better control of the location of the decant pond. These operational changes resulted in a partially saturated cyclone sand section that was denser, with a higher shear strength, and with a more dilative correlated state parameter than observations from 2014, resulting in a performance improvement of the facility.

The better operational controls also resulted in denser tailings, as shown in Figure 4, using bulk unit weights (Robertson and Cabal, 2010) correlated from CPT data, presumably due to a higher effective stress during placement and reduced distances for consolidation pore pressures to dissipate. The change in operations also resulted in lower pore pressures near the interface between the cyclone sands and tailings beach, and in the phreatic surface moving further within the facility (Figure 5), due to discontinuing using excavated tailings beach materials to construct pipe berms. In general, the 2019 field investigations

validated the changes in operations performed following the 2014 investigation, and resulted in denser cyclone sand and tailings.

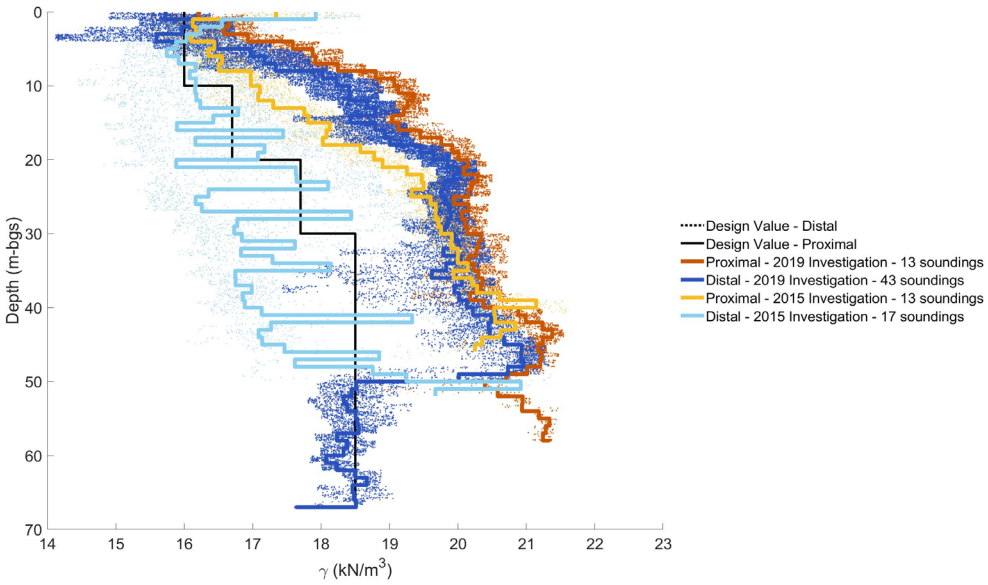


Figure 4: Correlated bulk unit weights from CPT soundings between 2015 and 2019 investigations (Golder, 2019)

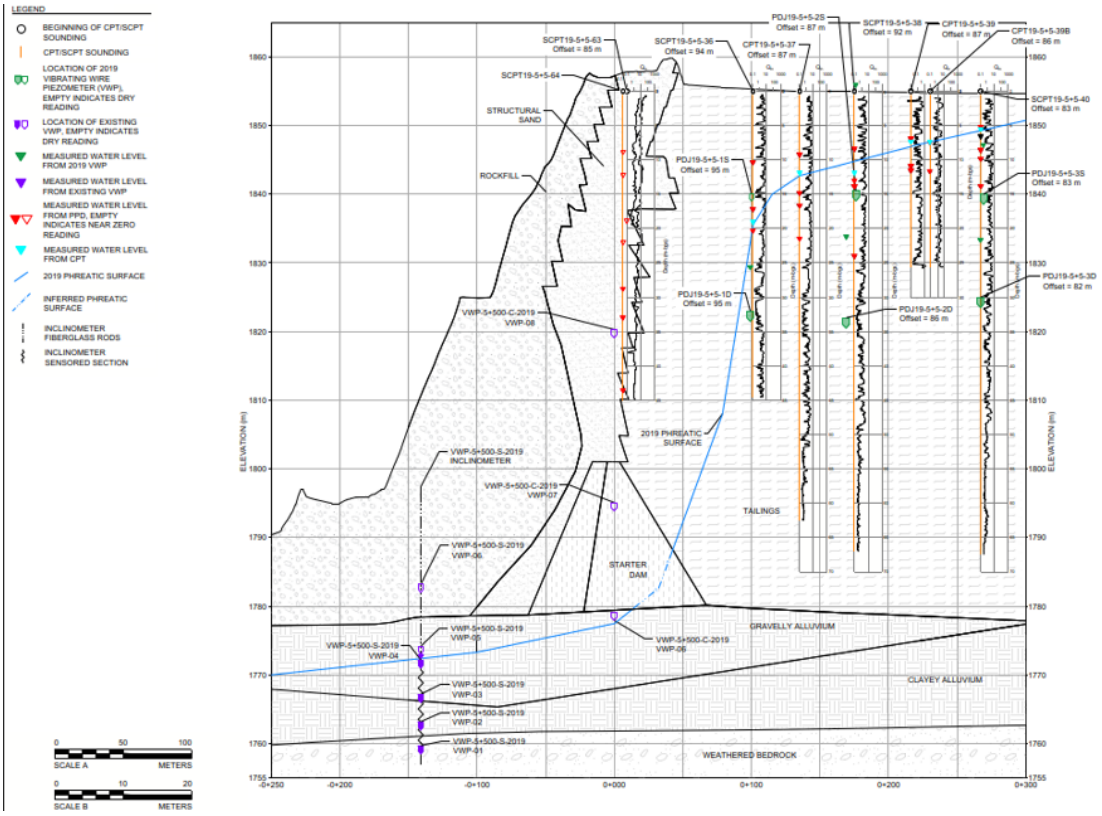


Figure 5: Generalized cross-section from 2019 field investigation (Golder, 2019)

The 2023 field investigation consisted of CPTs with seismic measurements and resistivity measurements to evaluate the saturation of materials above the inferred phreatic surface. Several soundings were co-located within the basin to evaluate changes in the material behavior over time. An example of the differences in observed behavior is presented in Figure 6 for a location within the tailings beach near the maximum cross-section. In general, the 2014 conditions were in materials classified as silt mixtures to sensitive fines, with a consistent significant excess pore water pressure generation and highly layered tailings.

The 2023 investigation indicated that these materials generally have had little densification, with similar normalized tip resistance, but materials placed in subsequent years have resulted in more sand-like to silt-like tailings behavior and reduced interbedded layers. While the initial program indicated generally near hydrostatic conditions, the operations following the 2014 investigation indicate that the phreatic conditions have shifted further within the impoundment and with lower than hydrostatic pore pressures. These changes result in tailings beach materials that are generally denser with higher shear strengths and more dilative conditions, resulting in better geotechnical performance of the facility due to the change in operations.

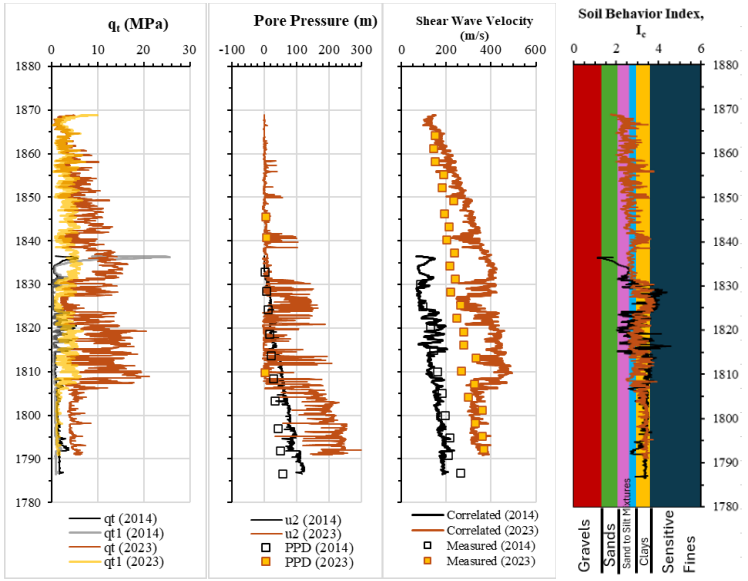


Figure 6: CPT Sounding measurements and interpretations for beach tailings from 2014 to 2023

In addition to the field investigations, robust instrumentation programs were performed, including installation of direct-push piezometers within the tailings and cyclone sands. These field instruments are an important tool to support the evaluation of the construction methodology and changes in operations. CPT soundings and corresponding Pore Pressure Dissipation (PPD) tests provide valuable information at the moment of the investigation; however, continuous monitoring provide information related to how normal operations and changes in observations can change the hydraulic performance of the materials. An array of

nested direct push vibrating wire piezometers is used to estimate the phreatic surface, to analyze the potential vertical and hydraulic gradients along with the corresponding flow paths during operations, and to generate and dissipate excess pore water pressures resulting in densification of materials via changes in response. Observations from these instruments generally are consistent with the results from the CPT investigations, indicating that the changes in operations have improved the performance of the facility by shifting the phreatic surface further within the impoundment via lowering the phreatic surface to below the elevation of the starter dam (Garcia and Sosa Dávila, 2020).

The field investigations also included various geotechnical laboratory tests on intact and bulk specimens recovered from the field. These tests were then used to evaluate the in-situ material properties and to evaluate whether assumptions made prior to design were consistent with the in-situ performance. Some examples of this testing used to support operations include testing on the cyclone sands prior to and during the 2014 investigation, evaluation of the large-strain consolidation characteristics, evaluation of saturated permeabilities, and critical state testing to evaluate and support the CPT investigations. Results from the geotechnical laboratory testing and field CQA testing of the cyclone sand prior to 2014 indicated that the material did have a higher fines content than anticipated during start-up and during the initial years of operations.

This observation was subsequently used to evaluate the placement of the cyclone sand and to determine how to adjust the operations to meet the specifications and design intent. The geotechnical laboratory program was also used to support volumetric analyses using in-place unit weight testing from intact specimens, bulk volumetric analyses from CQA records, and observations from piezometers to calibrate large-strain and normal consolidation results to models that better represented the field conditions by creating composite material properties. Composited parameters better represented the overall storage of the facility, as excessively fine resolution models may result in simulations that are heavily calibrated to a moment in time, as opposed to capturing variability observed during deposition due to changes or fluctuations in the ore body, operations, and other factors. Hydraulic testing in the field was used to estimate changes in the permeability for varying densities and confinement, and were also compared to interpreted PPD results to support hydraulic modeling. Testing evaluated the geotechnical characteristics and, to improve the accuracy of the interpreted state parameters, a critical state program was performed to evaluate the critical state behavior for coarser and finer cyclone sand and to use the CPTWidget to better interpret the in-situ state of the tailings.

Conclusion

TSFs are complex structures that inherently require the use of observational methodology, which involves designing facilities based on provided information and assessing risk prior to construction to design

contingencies. During operations, rigorous CQA monitoring, geotechnical instrumentation and monitoring, and field and laboratory investigations are needed to support the evaluation of these facilities. Observations and interpretations from these tools should be used together with operations to evaluate whether the TSF is currently meeting the design intention and whether any additional contingencies are necessary to design or implement. The field data should be evaluated using the state of the practice methodology, and previous analyses should be re-evaluated based on further advancement in the field, such as the development of additional or novel methodologies to estimate the residual shear strength and in-situ strength. Additionally, instrumentation provides a strong basis to reassess the conditions and performance of a facility and should be used to evaluate between field investigations, which may take upwards of a year to design, implement, and interpret results from. The focus of this paper has been on the geotechnical aspects, but geochemical, hydraulic, and other considerations are necessary as well.

From Minera Peñasquito, the operational changes to the materials used to construct pipe berms and maintain proper control of the operational pond indicate the inherent link between design and operations and how these groups should be in constant communication. Operators in the field provide valuable guidance into the actual behavior of the facility, while the design and planning teams can help support the evaluation and implementation of any additional contingencies. Good communication between these parties can result in significantly improved performance of the facilities, which reduces risks and helps to meet or exceed the design intent.

The flexible design of the TSF has allowed for the observational method to be employed effectively since 2014. This has proved beneficial, as design changes in the materials used to construct the dam embankment (moving from exclusively cyclone sand to a hybrid of rockfill and sand) allowed for construction to continue as the material production assumptions made during the initial design proved to be false. The use of the observational method in this project is limited, as Peck (1969) writes, to "The essential ingredient … the visualization of all possible eventualities and the preparation in advance of courses of action to whatever situation develops." It is only possible to observe for material responses to construction if a clear and comprehensive model of the facility and the surrounding geology is understood. Operational lessons include targeting field investigations and material analyses at credible failure mechanisms; clear understanding of regional geology and of the genesis of subsurface materials; periodic updates to material models (specifically tailings) as source materials change (pit host rock changing with depth, milling processes, etc.); and maintaining a design that is adaptable to these changes.

References

García, E.J. and Sosa Dávila, V.V. 2020. Recent geotechnical monitoring results reflect operational improvements at the Newmont Peñasquito. *Proceedings of Tailings and Mine Waste, 2020*. Vancouver, Canada: University of British Columbia.

Golder Associates. 2008. Detailed Engineering Design Report, Tailings Storage Starter Facility, Peñasquito Project.

Golder Associates. 2016. Geotechnical Data Report on Cyclone Sand and Tailings Beach.

Golder Associates. 2019. Geotechnical Analysis Report, Center Line Raise Project Stage 2 Update.

Golder Associates. 2020. 2019 CPT Tailings Geotechnical Factual Report.

Peck, R.B. 1969. Advantages and limitations of the observational method in applied soil mechanics. *Géotechnique* 19(2): 171–187.

Robertson, P.K. and Cabal, K.L. 2010. Estimating soil unit weight from CPT. *Proceedings of the 2nd International Symposium on Cone Penetration Testing*. Huntington Beach, CA, USA.

Robertson, P.K. and Cabal, K.L. 2015. *Guide to Cone Penetration Testing for Geotechnical Engineering*. Sixth edition, Signal Hill, CA: Gregg Drilling and Testing.

How Many Triaxial Tests Do You Actually Need to Get a Critical State Line?

Marcos Arroyo, CIMNE-UPC, Spain
Lluis Monforte, CIMNE-UPC, Spain
Stefano Collico, DMT, Germany

Abstract

Geotechnical analyses of tailing storage facilities (TSF) are nowadays very frequently based on critical state soil mechanics concepts. Obtaining a critical state line (CSL) for the different materials identified in the TSF is thus a necessary task. Given the large variability of materials commonly found in TSFs, that task may become onerous as several good quality triaxial tests are usually employed for each CSL, identifying the critical state condition attained in each triaxial test.

In this paper we explore an alternative approach, in which the effect of critical state properties on all the measured triaxial response of the soil is leveraged to minimize the amount of tests necessary to calibrate the CSL. For this purpose, we frame CSL calibration as a Bayesian updating problem, in which a generic "a priori" distribution of CSL parameters is updated with the results of a single triaxial test. Using examples from a well-known case history (Brumadinho) we show that, in some cases, the information embedded in a single test may provide close CSL calibrations to those obtained with the traditional procedure.

Introduction

Most tailings are deposited in a relatively loose condition and full saturation of the material is either present from the beginning or possible in the future. As a result, liquefaction is frequently a major consideration in the geotechnical analysis of TSFs. In the last decades a new paradigm has emerged (Jefferies and Been, 2006) in which analysis and management of liquefaction risks is informed by models and tools grounded on critical state soil mechanics. For instance, models incorporating critical state concepts have been used as tools in forensic analyses addressing the immediate cause of several landmark tailings storage facility (TSF) failures such as Fundão (Morgenstern et al., 2016), Cadia (Morgenstern et al., 2019) or Brumadinho (Arroyo and Gens, 2021). Similar models are increasingly employed in practice as predictive tools to help face a variety of design problems (e.g., Barrero et al., 2015; Halliday et al., 2022; Torres et al., 2023; Vargas-Moreno et al., 2023). All those models need as basic input a description of the critical state properties of

tailings. At a more fundamental level, many procedures currently employed to assess liquefaction susceptibility of a particular deposit from CPTu tests are reliant on critical state concepts and require an evaluation of critical state properties if they are to perform well (Torres Cruz, 2021; Shuttle and Jefferies, 2016). As a result, the determination of critical state properties for tailings has now become central in many geotechnical characterization campaigns for TSFs (e.g., Hone, 2023; Masengo et al., 2023; Toyra et al., 2023; Vieira Carneiro et al., 2023).

In the framework of critical state soil mechanics, critical state properties are described using a critical state line (CSL), i.e., the locus of void ratio-mean effective stress-deviatoric stress at which the soil shears at constant effective stress and void ratio. The relative position of the current state of the soil with respect to the CSL in the compression plane fully determines whether the soil will be contractive or dilative.

Current guidelines (Been and Olivera, 2016) recommend determining the CSL by means of drained and undrained triaxial tests on loose samples at different confining stresses. Triaxial testing on dense samples is discouraged, as these samples tend to develop localization planes during shearing, resulting in inhomogeneous stresses and strains in the sample (Desrues et al., 1996). The number of tests employed to define the CSL is influenced by budgetary and schedule restrictions in addition to the importance of the project. Been and Olivera (2016) propose a minimum of 4 tests to characterize the CSL within the range of 10-700 kPa, using undrained tests to characterize the low stress range and drained tests for the upper range. However, more than 4 tests are likely to be needed in most circumstances. In a recent round-robin exercise aimed at gauging the repeatability of CSL across geotechnical laboratories (Reid et al., 2021), the laboratories that achieved repeatable results performed 5.7 tests on average to determine the CSL.

While the number of triaxial tests required for a single CSL may not seem excessive, the problem is that a single CSL is frequently not enough. Materials deposited in TSFs are far from homogeneous, typically covering a wide range of gradations and frequently presenting also significant variability in terms of other fundamental properties, such as unit weight or plasticity. CSLs are known to vary significantly with material gradation or plasticity (Macedo and Vergaray, 2021) so the CSL characterization problem is likely to increase rapidly in size, if a realistic description of the deposit is sought. As the required testing procedures are not trivial (Reid et al., 2021) and the number of well-trained personnel and well-equipped laboratories available for CSL determination is never superabundant, critical state characterization may become a choke-point for some projects.

In this work we describe one approach to reduce or manage this problem by means of Bayesian statistics. The fundamental idea that is explored here is that information about critical state properties is present (but hidden) in all the datapoints that may be obtained from a triaxial test and not just on a few selected points. Exploiting that hidden information should allow us to obtain reliable estimates of CSL parameters using fewer tests.

Methodology

Critical state line formulation and determination in current practice

The most frequently employed formulation for CSL in current practice has a straight line in the triaxial compression plane, with slope given by the parameter M

$$q_c = M\ p'_c \qquad \text{(Equation 1)}$$

In the compression plane a straight line is also employed in the semilogarithmic compression plane, so that the CSL is given by

$$e_c = \Gamma_{100} - \lambda \ln \frac{p'}{p'_{ref}} \qquad \text{(Equation 2)}$$

where the parameters introduced to describe the CSL are λ, the plastic compressibility and Γ_{100}, the value of the void ratio in the CSL when the mean effective stress p' is equal to a reference value, p'_{ref}. In this work the reference mean stress value is taken as 100 kPa (Torres-Cruz and Santamarina, 2020).

It is widely accepted that this CSL straight line formulation in the semilogarithmic compression plane is an approximation, only valid in a restricted stress-range. More general curved CSL formulations are also available (Fourie et al., 2020). Their use would not change the argument presented here, although it would add some complication, unnecessary at this stage.

To determine parameters M, λ, and Γ_{100} current practice generally relies on identifying critical state conditions in different triaxial tests and fitting those points in the two reference planes. Because attaining critical state conditions requires the imposition of large strains and that may be challenging in practice, alternative methods that facilitate extrapolation to critical state conditions are also in use, like the use of stress-dilatancy plots (Ghafghazi and Shuttle, 2009).

CASM

CSL parameters are employed in constitutive models that, when correctly formulated, should be able to predict the whole response of the soil observed during the test. For a triaxial compression test in which axial deformation is imposed under constant confining stress, that response includes the deviatoric stress and the volume or pore pressure changes, respectively, if drained or undrained. There are several constitutive models that are able to replicate the triaxial response of triaxial tests employed to measure CSL. In this work we will use a modified version of the Clay and Sand Model (CASM; Yu, 1998). Note, however, that the methodology presented is not necessarily reliant on CASM; any other constitutive model with similar predictive capabilities may be employed.

CASM is an elasto-plastic isotropic critical state-based model, conceived to represent a wide range of soil behaviour, including the undrained softening characteristic of flow liquefaction. CASM has been

applied, with success, to analyze liquefaction failure in TSFs (Arroyo and Gens, 2021; Mánica et al, 2022) and to simulate CPTu in liquefiable soils (Monforte et al., 2019; Boschi et al., 2024). A detailed description of the CASM version used here can be found in those references. For the purposes of this work, it is enough to recall that, apart from the three CSL parameters, M, λ, and Γ_{100}, CASM features five more. Two of them, the Poisson ratio υ, and swelling index, κ, describe elastic response in the same terms as classical Cam-clay models. The remaining parameters are original to CASM. Two of them, n and r, appear on the yield surface formulation

$$f = \left(\frac{q}{Mp'}\right)^n + \left(\frac{\psi}{\psi_R} - 1\right) = \left(\frac{q}{Mp'}\right)^n + \left(\frac{\psi}{(\lambda - \kappa)\ln r} - 1\right) \qquad \text{(Equation 3)}$$

where ψ_R is the reference state parameter, value of the state parameter on the isotropic compression line (ICL), which is assumed parallel to the CSL. Because of this parallelism, determining the CSL value Γ_{100} is equivalent to determining e_{100}, the void ratio at the reference pressure in the ICL.

A final parameter m appears in the stress-dilatancy formulation derived from the plastic potential,

$$d^p = \frac{(m-1)}{m}\frac{\left(M^m - \eta^m\right)}{\eta^{m-1}} \qquad \text{(Equation 4)}$$

Manica et al. (2022) present several relations that simplify CASM calibration. They show that m is directly linked to the at-rest coefficient of earth pressure, K_0, and that, for normally consolidates materials, undrained peak and residual strengths are also directly linked to n and r.

Bayesian identification of constitutive parameters

Bayesian analysis has become increasingly popular in geotechnical engineering. From a Bayesian perspective, probability expresses a degree of belief on the outcome of an event or truth of a proposition, given some related evidence (Vick 2002). Bayesian analysis is thus able to integrate, in a systematic and rational manner, existing prior information, sometimes subjective, with observed data. It is also easily adaptable to sequential procedures, incorporating the result of new observations as they become available. For instance, Llano-Serna et al. (2022) used Bayesian inference to calibrate models of tailings compressibility combining oedometer results and field observations.

The Bayesian perspective on probability is different from the more traditional frequentist one. As explained by Contreras et al. (2018), frequentists treat statistical parameters (e.g., mean and standard deviation of error incurred by a geotechnical predictive model) as unknown fixed quantities, whereas observations are treated as realizations of random variables. On the contrary, from a Bayesian perspective, parameters of statistical models are unknown random variables, and observations are fixed known quantities.

In our case the observations are those obtained during one -or more- triaxial tests. For each axial deformation value recorded during the test, $\epsilon^i_{a\ obs}$, we have a set of observations $\boldsymbol{D}_i = [p^{i'}_{obs}, q^i_{obs}, e^i_{obs}]$; that is, the mean effective stress, the deviatoric stress and the void ratio. As unknown random variables we consider a set of CASM constitutive parameters $\boldsymbol{\alpha} = [\lambda, e_{100}, \phi, n, r, \nu, m\ ]$. For any possible value of those parameters a triaxial response may be simulated and the error incurred at any point in the triaxial path computed. We assumed that the model predictions are unbiased, so that those prediction errors are random, normally distributed variables, with zero mean. This is expressed as

$$\frac{p^{i'}_{obs} - p^{i'}_{sim}}{\max(p_{obs})} \sim N(0, \sigma_\sigma) \tag{5}$$

$$\frac{q^i_{obs} - q^i_{sim}}{\max(q_{obs})} \sim N(0, \sigma_\sigma) \tag{6}$$

$$e^i_{obs} - e^i_{sim} \sim N(0, \sigma_e) \tag{7}$$

where $p^{i'}_{sim}$, q^i_{sim} and e^i_{sim} are the model predictions of mean effective stress, deviatoric stress and void ratio computed with parameters $\boldsymbol{\alpha}$ and σ^2_σ and σ^2_e are the random model error variances for stress and void ratio measurements. These error variances are also considered as random variables.

A Bayesian inference scheme can thus be set-up. Calling $\boldsymbol{\theta} = [\boldsymbol{\alpha}, \sigma_\sigma, \sigma_e]$ the whole vector of random variables, we are interested in obtaining the statistical distribution of those random variables that best honors the test observations. Such distribution is known as the posterior distribution $P(\Theta|D)$, obtained by means of Bayes theorem as

$$P(\ \boldsymbol{\theta}\ |\boldsymbol{D}\ ) \sim L(\boldsymbol{D}|\boldsymbol{\theta})\ p(\boldsymbol{\theta}) \tag{8}$$

where $p(\boldsymbol{\theta})$ is the prior probability distribution of the inference variables, expressing previous knowledge or beliefs about them, and $L(\boldsymbol{D}|\boldsymbol{\theta})$ is the likelihood distribution: the probability of observing $\boldsymbol{D}$ given some model parameters. We define the likelihood function assuming that the errors incurred in the three triaxial predicted variables are independent, so that the joint probability of erroneous observation is:

$$L(\boldsymbol{D}|\boldsymbol{\theta}) = \prod_{i=1}^{N} \phi\left(\frac{p^{i'}_{obs} - p^{i'}_{sim}}{\max(p_{obs})\ \sigma_\sigma}\right) \phi\left(\frac{q^i_{obs} - q^i_{sim}}{\max(q_{obs})\ \sigma_\sigma}\right) \phi\left(\frac{e^i_{obs} - e^i_{sim}}{\sigma_e}\right) \tag{9}$$

where ϕ is the standard normal distribution.

To evaluate the posterior distributions numerical integration is required. In this work, a parallel version of the Transitional Markov Chain Monte Carlo method (TMCMC) (Ching and Chen, 2007) is employed to draw samples of the posterior distribution. TMCMC iteratively constructs a sequence of samples that transition from the prior to the posterior distribution by combining a sequential particle filter

method and Markov Chain Monte Carlo sampling (Ching and Chen, 2007; Betz et al, 2016). TMCMC has been used in many applications, including site geotechnical characterization based on CPTu (Ching and Wang 2016; Collico et al. 2022). The choice of prior distributions for the different random variables is explained in the next section.

Application example

Example dataset

A series of triaxial tests on reconstituted samples from an iron tailing recovered from Brumadinho B1 dam (Arroyo and Gens, 2021) are selected for application. The material corresponds to that described as "Type 2" tailings by Viana de Fonseca et al, (2022). The tests analyzed include five isotropically consolidated triaxial tests on loose specimens, four sheared drained and one undrained, as well as one isotropic, drained triaxial test on a dense specimen.

Figure 1 reports the main outputs of these triaxial tests. On first inspection, the end points of all loose specimens seem to define a straight CSL roughly parallel to the ICL - defined from the end-of consolidation points- on the compression plane. The exception is the dense specimen whose trajectory in the compression plane is not congruent with those obtained with the loose specimens. This discrepancy can be attributed to strain inhomogeneity as shear localization planes developed in the specimen prior to failure.

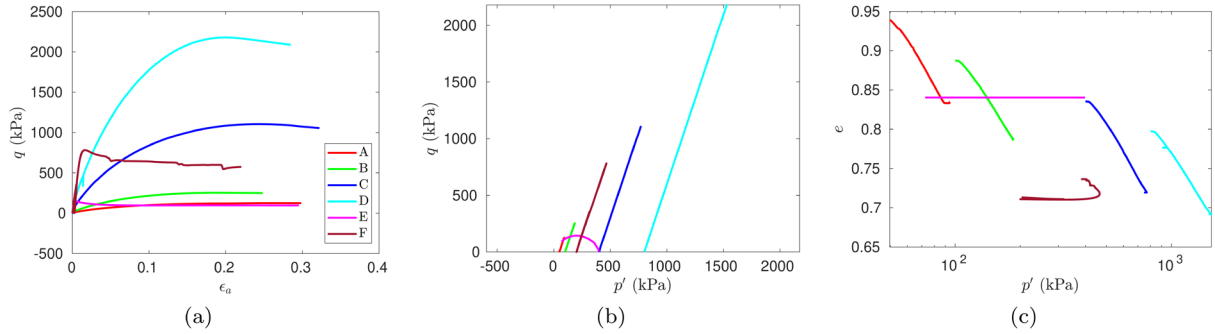


Figure 1: Triaxial compression test results for the example dataset (a) deviator stress vs axial strain (b) stress paths (c) compression paths

Figure 2 illustrates the traditional or "manual" calibration, in which the initial and final points of the 5 triaxial tests on loose specimens have been considered as points on the ICL and CSL respectively. The values $e_{100} = 0.901$ $\Gamma_{100} = 0.824$ and $\lambda = 0.049$ were estimated by minimizing the error on the predicted void ratio using Equations (1) and (2). The slope of the CSL on the triaxial plane M was estimated using a stress-dilatancy plot. A critical state friction angle $\phi = 35^{o}$ is obtained from the stress ratio at critical state using the relation $M = 6\sin(\phi)/(3 - \sin(\phi))$.

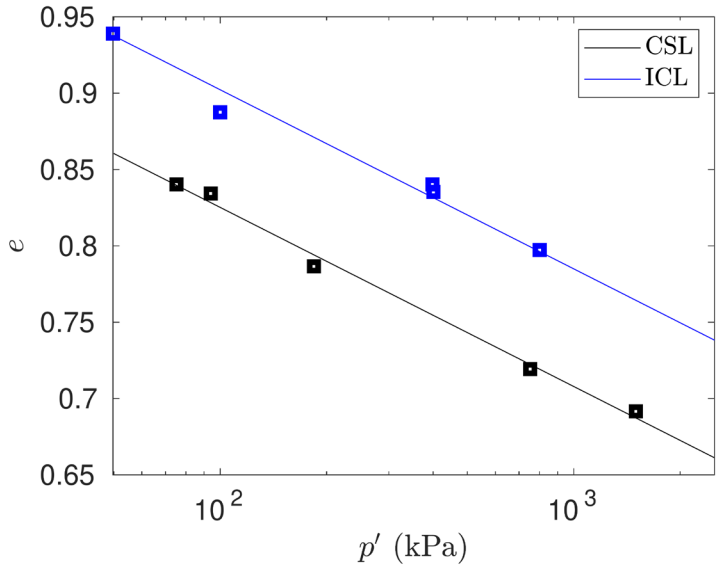


Figure 2: Manual fitting of the CSL and ICL on the compression plane

Prior distributions

All constitutive parameters of the model are calibrated except for the swelling slope, for which a value of 0.008 was adopted based on isotropic unloading tests (Viana de Fonseca, 2022). The prior distributions are always continuous uniform distributions. The limits of these distributions, shown in Table 1, have been chosen partly based on the database of Macedo and Vergaray (2022) and partly on visual inspection of the experimental data. For instance, the limits of the uniform distribution of the friction angle are equal to that inferred from the end of the test stress state ± 3º; likewise, the vertical position of the ICL at the mean effective stress corresponding to the test start is equal the experimental data ±0.03; on the other hand, the prior of λ is based on the consolidation phase performed before triaxial shearing (Figure 3). For other variables, such as n and r, large, uninformative priors are employed.

Table 1: Limits of distributions

	ϕ	λ	ν	n	r	m	e_{p_i}	σ_σ	σ_ϵ
Lower bound	ϕ_{EOF} −3°	0.04	0.2	1.1	2	1.7	e_i − 0.03	0	0
Upper bound	ϕ_{EOF}+3°	0.075	0.35	4	185	2.5	e_i + 0.03	0.05	0.01

Simulated triaxial test response

The Bayesian inference scheme was run independently using each one of the six available triaxial tests. CASM model prediction of triaxial response were computed using a constitutive driver based on Sloan et al (2001). Figure 4 and Figure 5 report the outputs of each model calibration alongside the experimental

data. For the simulated outputs we report the expected value in addition to the 95% credible interval (CI). Those CI are obtained combining, for a certain value of axial deformation ϵ_a^i , the variance of the predicted test outputs and the estimated model prediction error (through the calibrated variances σ_σ^2 and σ_e^2).

In all cases a very good match between the mean of the predictions and the laboratory test result was found, both in the compression plane and in the axial deformation-deviatoric stress plot. For the loose specimens, the error bands given by the CI are rather small, but they are significantly wider for the dense dilatant specimen. For this test, the model was adjusted including also the value of the initial overconsolidation ratio amongst the predicted variables. A value around 14.2, with a low variance, was estimated.

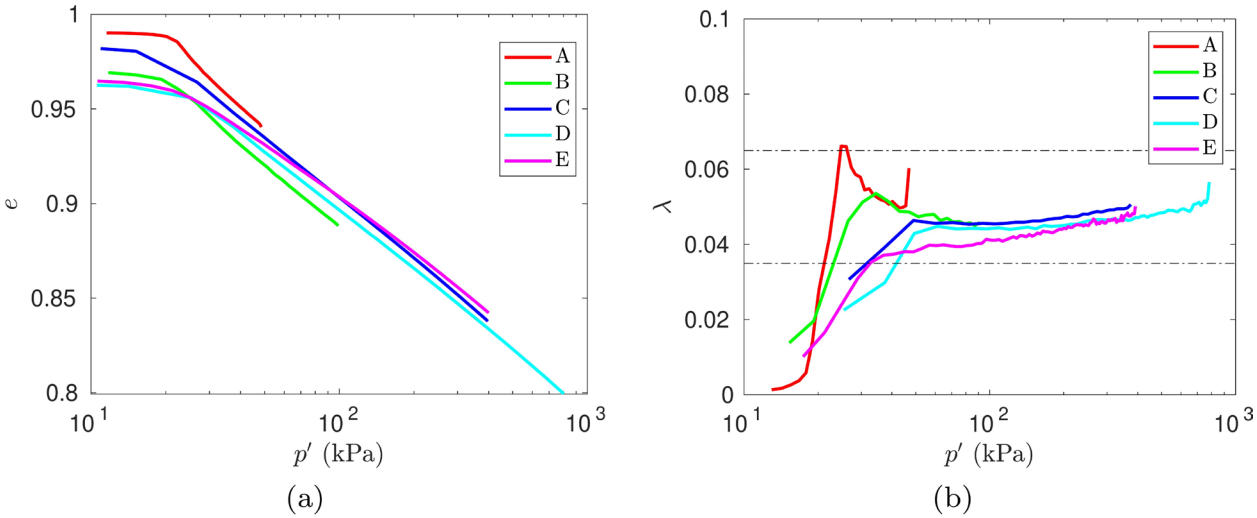


Figure 3: Isotropic compression paths and tangent approximation of plastic compressibility along the path

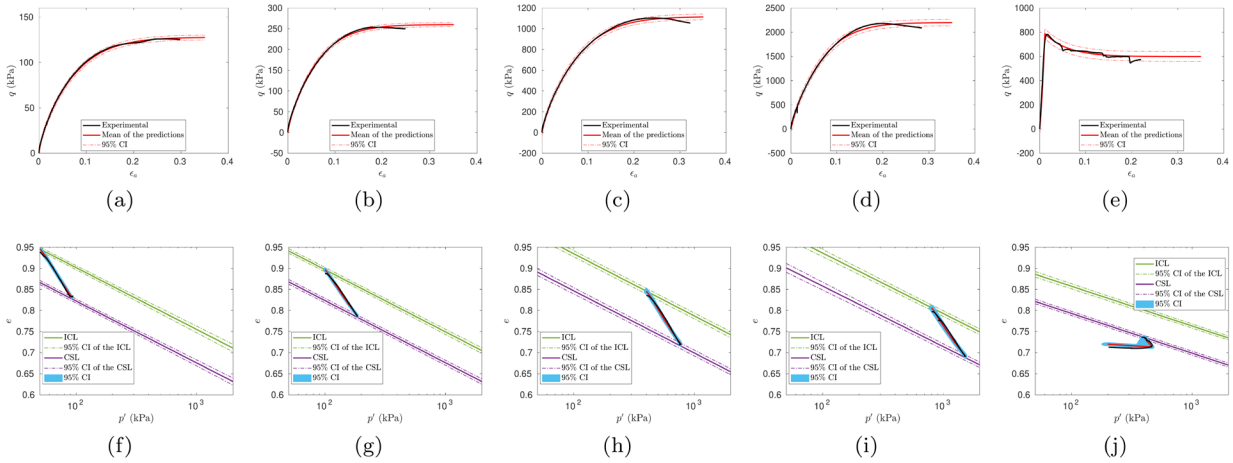


Figure 4: Outputs of model calibrations based on each separate drained triaxial test

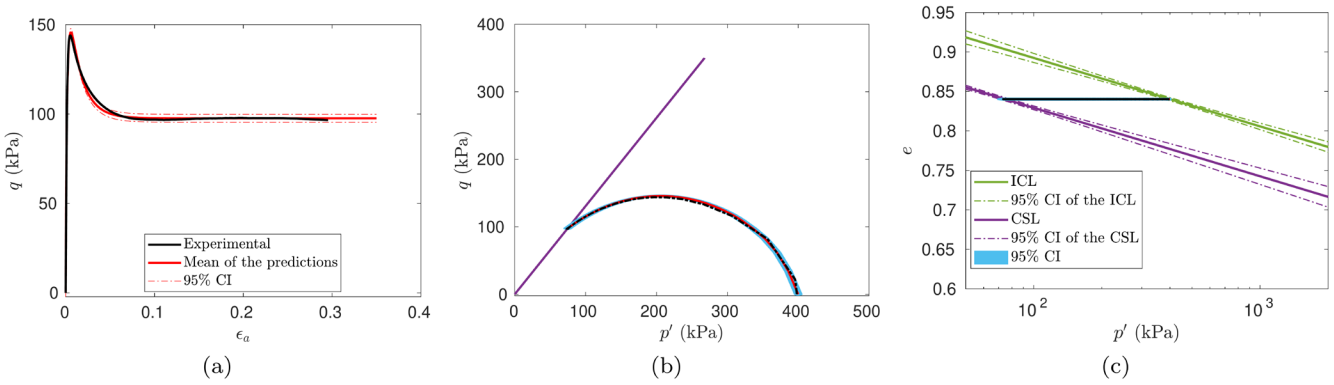


Figure 5: Outputs of model calibration based on the undrained triaxial test

CSL estimations

The Bayesian scheme produces a full probabilistic calibration of all the model parameters. Focusing only on CSL parameters, the posterior distributions obtained from each triaxial test through the Bayesian inference scheme are presented in Figure 6. The central (mean) estimates of CSL in the compression plane are presented in Figure 7. Examining these results, it can be observed that

- the central estimates obtained using a single test are never very distant from for the manual estimate obtained with all the loose tests (A to E). For the position of the critical state line Γ_{100} the differences with the manual estimate are within 0.03; for the slope of the critical state line within 0.012; for the critical state friction angle within 2.5°
- results obtained with the drained dilatant test (F) are clearly different from those obtained with the loose tests: it estimates a lower and flatter CSL and higher friction. Still, for a test that localized and where boundary stress and strain are not necessarily representative the results are surprisingly close.
- results obtained for the undrained test (E) are also distinctive in some respects: it estimates a flatter CSL and the lowest critical state friction angle.

Conclusion

Although more systematic exploration of the method is necessary, the exploratory results here obtained appear promising. Bayesian inference may be usefully employed to leverage the hidden constitutive information contained in every triaxial tests and thus facilitate the task of CSL determination. The methodology presented has the added advantage of being easily automated, thus reducing the scope for subjective estimation of CSL parameters.

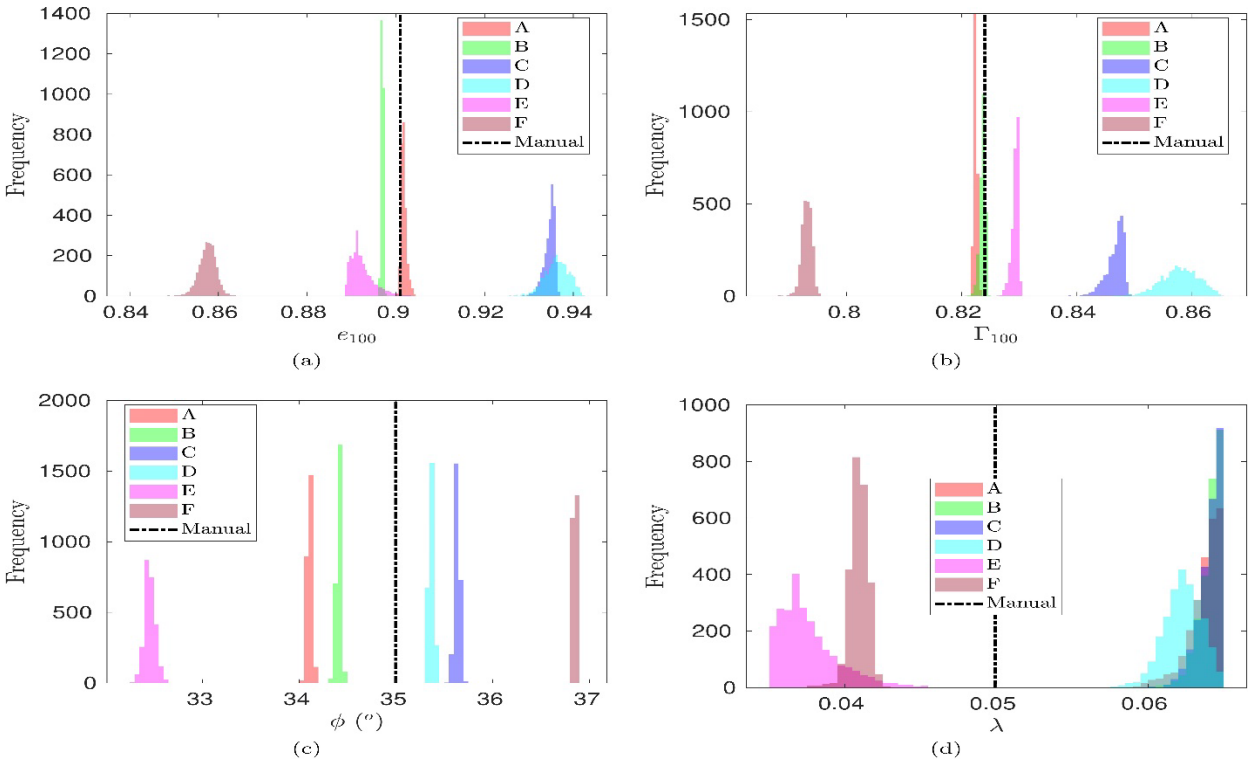


Figure 6: Posterior distributions of CSL parameters obtained from each triaxial test (a) void ratio at reference stress on ICL (b) void ratio at reference stress on CSL (b) friction angle on triaxial compression (d) plastic compressibility

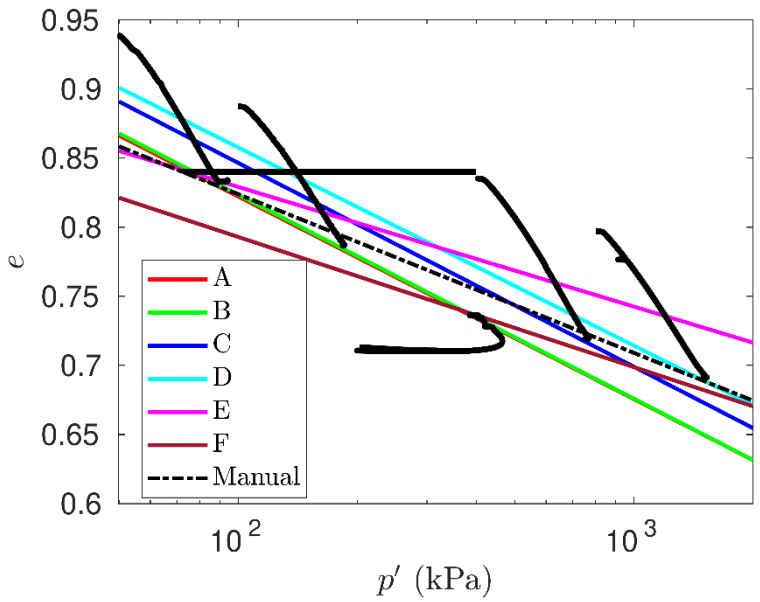


Figure 7: Inferred CSL from each triaxial test, alongside the manual fit based on all the tests

References

Arroyo, M. and Gens, A. 2021. Computational Analyses of Dam I Failure at the Córrego de Feijão Mine in Brumadinho: Final Report for Vale S.A.

Barrero, A.R., Taiebat, M. and Lizcano, A. 2015. Application of an advanced constitutive model in nonlinear dynamic analysis of tailings dam. *Proceedings of the 68th Canadian Geotechnical Conference*, Sept. (pp. 20–23).

Been, K. and Olivera, R. 2016. *Soil Liquefaction. A Critical State Approach*. Appendix B: Laboratory testing to determine the critical state of sands

Betz, W., Papaioannou, I. and Straub, D. 2016. Transitional Markov Chain Monte Carlo: Observations and improvements. *Journal of Engineering Mechanics* 142(5): 04016016

Boschi, K., Arroyo, M., Monforte, L., Carbonell, J.M. and Gens, A. 2024. Coupled hydromechanical modelling of cone penetration in layered liquefiable soils. *Géotechnique* 1–15.

Ching, J. and Wang, J.S. 2016. Application of the transitional Markov chain Monte Carlo algorithm to probabilistic site characterization. *Engineering Geology* 203: 151–167.

Ching, J., Chen, Y.-C. 2007. Transitional Markov chain Monte Carlo method for Bayesian model updating, model class selection, and model averaging. *Journal of Engineering Mechanics* 133 (7): 816–832.

Collico, S., Arroyo, M., Kopf, A. and Devincenzi, M. 2022. A probabilistic Bayesian methodology for the strain-rate correction of dynamic CPTu data. *Canadian Geotechnical Journal* 60(5): 669–686.

Contreras, L.F., Brown, E.T. and Ruest, M. 2018. Bayesian data analysis to quantify the uncertainty of intact rock strength. *Journal of Rock Mechanics and Geotechnical Engineering* 10(1): 11–31.

Desrues, J., Andò, E., Mevoli, F.A., Debove, L. and Viggiani, G. 2018. *How Does Strain Localise in Standard Triaxial Tests on Sand: Revisiting the Mechanism 20 Years On.*

Ghafghazi, M. and Shuttle, D. 2009. Confidence and accuracy in determination of the critical state friction angle. *Soils and Foundations* 49(3): 391–395.

Halliday, A., Vulpe, C., Fourie, A. and Arenas, A. 2022. Applications of classic and advanced constitutive models in tailings practice. *Proceedings of Tailings and Mine Waste 2022*. Colorado State University.

Hone, D. 2023. Operational liquor management, drainage improvements and influence on buttress design. In Goodwill, J. (ed.) *Proceedings of Tailings and Mine Waste 2023*, 715–725.

Jefferies, M. and Been, K. 2006. *Soil Liquefaction: A Critical State Approach*. First edition. Taylor and Francis.

Llano-Serna, M., Lines, S.H. and Contreras, L.F. 2022. Calibration of numerical models to improve tailings management through Bayesian methods. *Proceedings of Tailings and Mine Waste 2022,* Denver Colorado.

Mánica, M.A., Arroyo, M., Gens, A. and Monforte, L. 2022. Application of a critical state model to the Merriespruit tailings dam failure. *Proceedings of the Institution of Civil Engineers-Geotechnical Engineering*, 175(2): 151–165.

Masengo, E., Ingabire, E.P., Boily, S., Létourneau, Y., Laporte, P., Guay, F., ... and Julien, M.R. 2023. Transition to filtered tailings at LaRonde Gold Mine. In Goodwill, J. (ed.) *Proceedings of Tailings and Mine Waste 2023*, 413–425.

Monforte, L., Gens, A., Arroyo, M., Mánica, M. and Carbonell, J.M. 2021. Analysis of cone penetration in brittle liquefiable soils. *Computers and Geotechnics* 134, 104123.

Morgenstern, N.R., Jefferies, M., Van Zyl, D. and Wates, J. 2019. Report on NTSF embankment failure. Investigation report commissioned by Cadia Valley Operations for Ashurst Australia.

Morgenstern, N.R., Vick, S.G., Viotti, C.B. and Watts, B.D. 2016. Report on the immediate causes of the failure of the Fundão Dam. *Fundão Tailings Dam Review Panel*.

Reid, D., Fourie, A., Ayala, J.L., Dickinson, S., Ochoa-Cornejo, F., Fanni, R., ... and Suazo, G. 2021. Results of a critical state line testing round robin programme. *Géotechnique* 71(7): 616–630.

Shuttle, D.A. and Jefferies, M.G. 2016. Determining silt state from CPTu. *Geotechnical Research* 3(2): 90–118.

Sloan, S. W., Abbo, A.J. and Sheng, D. 2001. Refined explicit integration of elastoplastic models with automatic error control. *Engineering Computations* 18(1/2): 121–194.

Torres, P., Macedo, J. and Paihua, S. 2023. Earthquake-induced deformation analysis of a TSF undergoing tailings reprocessing. *Proceedings of Tailings and Mine Waste 2023*, 947–958.

Torres-Cruz, L.A. 2021. The Plewes Method: a word of caution. *Mining, Metallurgy and Exploration* 38(3): 1329–1338.

Torres-Cruz, L.A. and Santamarina, J.C. 2020. The critical state line of nonplastic tailings. *Canadian Geotechnical Journal* 57(10): 1508–1517.

Toyra, S., Lundell, D., Knutsson, R. and Bohlin, T. 2023. The development of LKAB's tailings facilities, from the beginning and into the future. In Goodwill, J. (ed.) *Proceedings of Tailings and Mine Waste 2023*, 427–438.

Vargas-Moreno, C.O., Bricio Guillen, J., Ramírez-Chávez, R., Preciado, H.F, Ang, E. and Servigna, D. 2023. Numerical analysis for the stress-strain evaluation of the conversion of a conventional slurry tailings storage facility to filtered tailings storage facility, considering different scenarios. In Goodwill, J. (ed.) *Proceedings of Tailings and Mine Waste 2023*, 29–41.

Vick, S.G. 2002. *Degrees of Belief: Subjective Probability and Engineering Judgment*. ASCE Publications.

Vieira Carneriro, J.J., Oliveira Faria, A. and dos Santos Jr., M.P. 2023. Calibration of modified cam-clay parameters for red mud tailings – a case study. In Goodwill, J. (ed.) *Proceedings of Tailings and Mine Waste 2023*, 69–8.

Holden Mine Post Closure Monitoring – a Statistical Method for Developing Trigger Action Levels

Summer Y. Sun, Stantec Consulting Service, USA
Ray Dorow, Stantec Consulting Service, USA
Paul Pellicer, Stantec Consulting Service, USA
Mohammad Rashidi, Stantec Consulting Service, USA
Phillip Crouse, Stantec Consulting Service, USA

Abstract

How do we know the effectiveness of closure implementation in meeting the closure objectives and success criteria? This paper provides a case study on a deterministic and statistical method for establishing trigger action levels for monitoring the physical stability of the Holden Mine tailings piles. Determining these thresholds is a multifaceted challenge, influenced by factors such as site-specific conditions, instrument characteristics, and potential failure modes. This paper will present a methodology using programming software tools such as Python or R, developing trigger action levels to determine triggers and appropriate actions so that the tailings piles maintain the physical stability criteria and document the physical behavior of the tailings piles to achieve the success criteria of safe closure.

Our methodology integrates deterministic and statistical analyses to establish thresholds. Initially, deterministic analysis identifies acceptable conditions, assesses associated risks, and informs the relative importance of geotechnical instruments across various locations within the tailings piles. Subsequently, statistical analysis tracks readings over time, identifying anomalies and evaluating data distribution. Leveraging programming tools, particularly Python or R, automates data processing tasks, facilitating rapid iteration and sensitivity analysis. This integration of deterministic and statistical approaches, augmented by programming software, enables engineers to explore a wide range of threshold scenarios efficiently, leading to informed decision-making.

To demonstrate the practical application of our methodology, we present a detailed case study focusing on a TSF. In this case, slope inclinometers and piezometers are deployed to monitor ground movements and pore water pressures. Through the application of our methodology and programming software, optimal Trigger Action Response Plan (TARP) thresholds are determined for the site. Notably,

we introduce sub-TARP levels tailored to the specific characteristics of the TSF, enabling stakeholders to detect changes at smaller increments and providing early warnings of potential issues before they escalate.

This case study underscores the importance of tailored threshold determination strategies, accounting for the unique characteristics of each project. By leveraging programming software, engineers can streamline the threshold determination process, saving time and resources while enhancing the overall effectiveness of geotechnical instrumentation and monitoring projects. Our findings contribute to the advancement of methodologies for establishing TARP thresholds, particularly in the context of mine waste facility closure, and highlight the significance of integrating geotechnical instruments with programming software for improved monitoring and risk management.

Introduction

The closure of a mine requires meticulous planning and execution to meet closure objectives and success criteria. A crucial aspect of this process is the establishment of trigger action levels (TALs) for monitoring closure performance. Trigger thresholds are essential for early detection of trends in the performance of the mine closure components for initiating timely remedial actions. Closed tailings storage facilities are a component of a mine closure that can require monitoring for physical stability years after the mine has closed. Past studies were performed to use deterministic and statistical approaches to evaluate the TAL for tailings facilities (Clarkson et al., 2020; Carvalho Nunes et al., 2023).

This paper presents a case study on the Holden Mine tailings piles, illustrating a combined deterministic and statistical approach to establishing TALs. The methodology utilizes programming tools such as Python or R to streamline the process, allowing for efficient and comprehensive analysis. The methodology can also be provided for developing TALs for other mine components such as waste rock piles, pit slopes, etc. This method is not only applicable to closure mine sites but also for active facilities.

Site background information

The Holden Mine site is situated in Chelan County, within the remote Cascade Mountains of the Wenatchee National Forest in North Central Washington. The initial mining claim was made in 1896–1897, identifying a significant copper resource. Mining operations began 20 years after the death of the man who staked a claim. It produced copper from 1937 to 1957 and generated around eight and a half million tons of tailings, which were stored in three tailings piles, TP-1, TP-2, and TP-3, as shown in Figure 1. After its closure, the mine's interests were transferred in 1961 to the Lutheran Bible Institute, which now operates the site as Holden Village, a nonprofit ministry. Holden Village, located on the north side of the project site, maintains about 20 structures and hosts approximately 40 to 60 year-round residents.

Since 2008–2009, significant reclamation and reshaping efforts have been undertaken. A fully penetrating groundwater containment barrier wall and collection system were constructed around TP-1, Lower West Area, and a portion of TP-2. The collected water is conveyed to a mine water treatment plant (MWTP) for treatment and release back to Railroad Creek.

In 2023, Rio Tinto installed piezometers and inclinometers with telemetry to facilitate automated data collection. These systems include vibrating wire piezometers and slope indicators, with data transmitted to the mine water treatment plant and accessible remotely via the Internet. The system is designed for expandability to integrate additional instruments into the remote monitoring system, enhancing safety and data collection at the site.

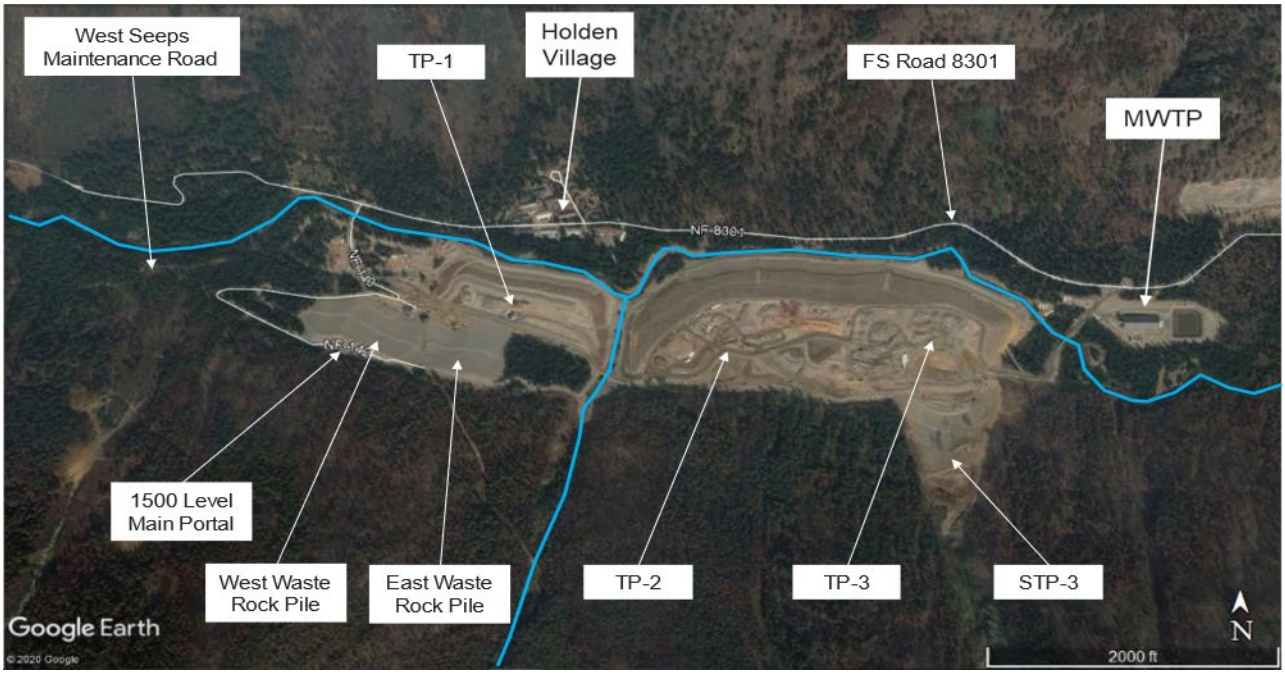


Figure 1: Site map of Holden Mine

Telemetry system

The telemetry system installed at Holden Mine consists of 63 vibrating wire piezometers (VWP) and 7 in-place slope inclinometers (SI). Figure 2 shows one of the monitoring stations, with a central datalogger mounted on a pole and connected to one or multiple VWP or SI sensors. The yellow bollards surrounding the station provide protection against accidental damage. The vibrating wire piezometers measure pore water pressures within the tailings and foundation soils. These sensors are strategically placed to cover various depths and locations across the site, ensuring thorough coverage and accurate data collection.

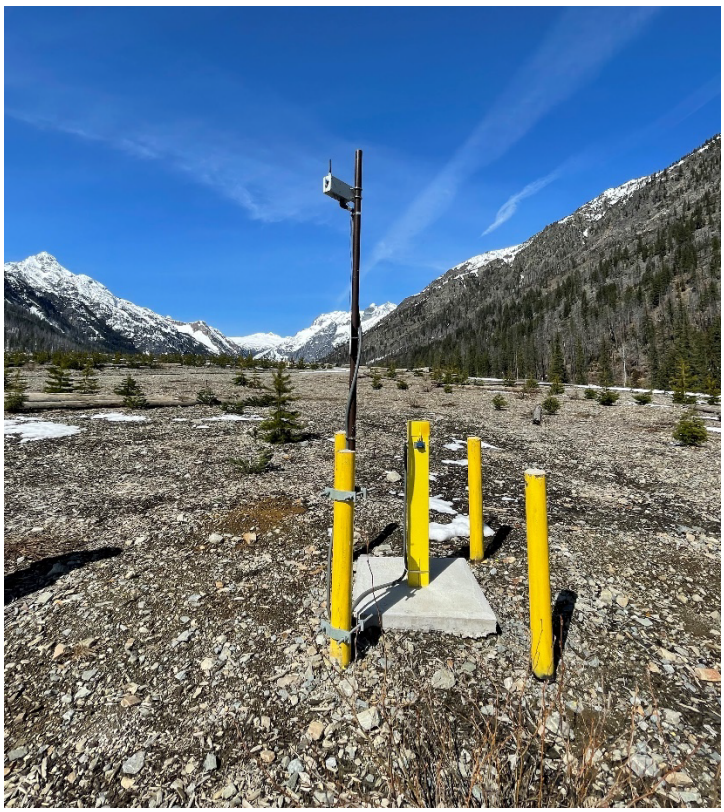


Figure 2: Monitoring station with Datalogger

Figure 3 presents a diagram of the telemetry system at Holden Mine. It shows the flow of data from the sensors (VWP or SI) through the Wireless Data Loggers to the central Gateway, and then to the Router, which connects to the internet via Starlink. The telemetry is configured this way because the site is outside of cellular coverage. By using Starlink connection, the telemetry system can transmit data via satellite internet. This allows for continuous, real-time monitoring and remote data access, even in remote locations where cellular service is unavailable.

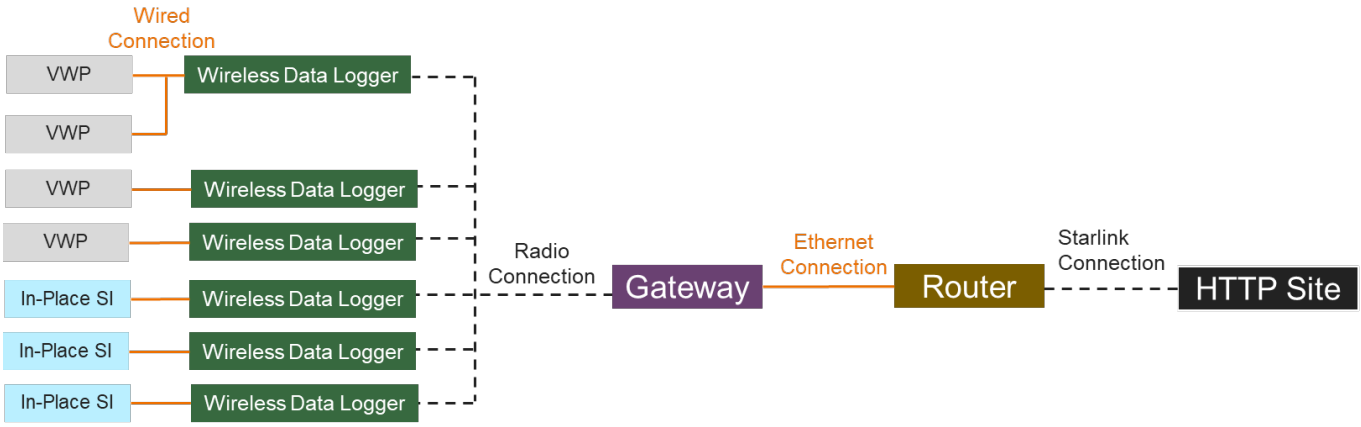


Figure 3: Holden Mine telemetry diagram

Methodologies

Establishing TARP thresholds using a deterministic analysis approach involves identifying normal conditions for the tailings pile closure performance parameters based on site-specific conditions and potential failure modes. The statistical analysis approach complements the deterministic analysis by tracking instrument readings over time to identify trends, anomalies, and deviations from expected behavior. Programming aids both approaches by:

- Data integration: combining data from multiple instruments and sources for comprehensive analysis.
- Data processing: streamlining the analysis workflow to efficiently handle large datasets.
- Anomaly detection: using statistical methods to identify outliers and unexpected trends in the data.
- Threshold refinement: adjusting TALs based on observed data distributions and statistical analysis.

The following subsections discuss the process of defining the trigger level thresholds for the VWPs as well as the SIs.

Defining trigger level thresholds for VWPs

Figure 4 provides the locations of selected existing monitoring wells and newly installed monitoring instruments within a tailings management facility. The upper part of Figure 4 shows the historical monitoring well locations, marked with purple dots, which indicate the positions of the existing piezometers. The lower part of Figure 4 highlights the newly installed vibrating wire piezometers and slope inclinometers, divided into four distinct zones: Area 1 (Mountain Side), Area 2 (Middle), Area 3 (Crest), and Area 4 (Intermediate Bench). Each type of instrument is color-coded for clarity, with new vibrating wire piezometers represented by blue dots and new slope inclinometers by green dots.

The readings from the existing piezometers play a crucial role in predicting TARP thresholds for the new piezometers. By analyzing historical data from these existing instruments, we calculated baseline conditions, the maximum and minimum readings in the past. This historical data helps establish initial TARP thresholds for the new piezometers, ensuring they are tailored to site-specific conditions. Future integration of real-time data from the new piezometers with historical data will enable refinement of these thresholds, enhancing the overall safety and effectiveness of the tailings management system.

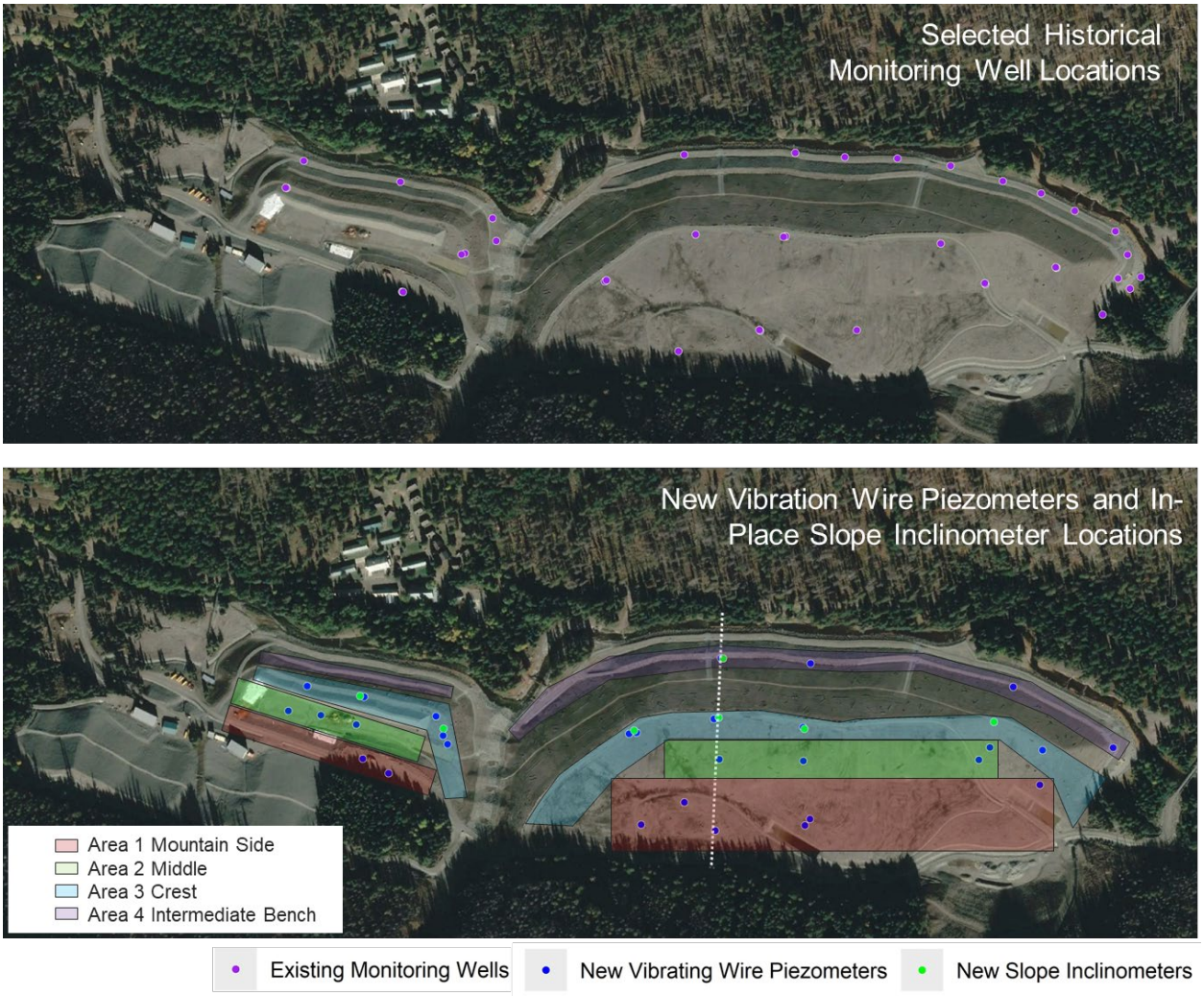


Figure 4: Vibration wire piezometer location maps

Figure 5 presents a detailed cross-sectional view of the tailings facility, corresponding to the dotted line location indicated in Figure 4. It illustrates the nested configuration of piezometers and the placement of slope inclinometers within various stratified materials. At each designated location, piezometers are nested, meaning there are either two or three piezometers installed at different depths, specifically targeting alluvium and fine-grained tailings (Group E), and intermediate fine-grained and coarse-grained tailings (Groups C and D). Coarse-grained tailings (Groups A and B) are considered faster drained and therefore are not targeted by the VWPs. This stratified approach allows for comprehensive monitoring of pore pressures across different material layers within the tailings structure.

Additionally, slope inclinometers are strategically placed at the crest and intermediate bench to monitor both overall stability of the entire slope and local toe slope stability. The blue lines in the figure represent historical monitoring data from previous piezometers, indicating historical maximum, average,

and minimum readings of pore pressure or water levels. These historical benchmarks provide a crucial reference for comparing current readings from the new piezometers, allowing engineers to assess current conditions against historical norms and identify any anomalies. The slope inclinometers contribute by detecting shifts or movements within the slope, offering early warnings for potential stability issues.

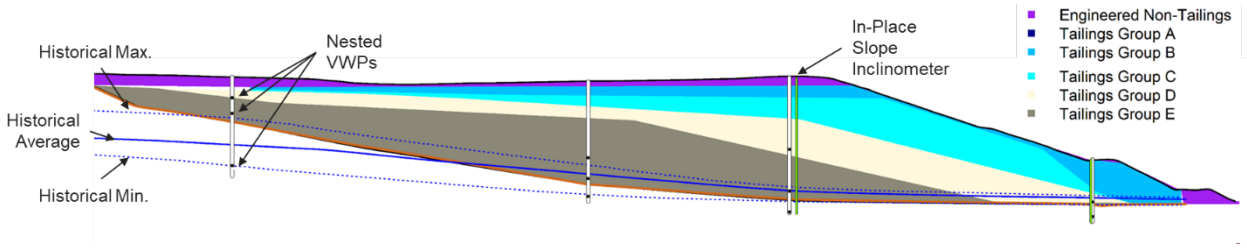


Figure 5: Example cross-section of Holden tailings pile and instruments

Figure 6 illustrates the rational for setting the VWP thresholds. The TARP for Holden Mine includes Normal, Alert, Watch, and Warning levels, each with associated response plans. The deterministic approach involves iteratively evaluating the factor of safety by raising the water table. Slope stability analyses were performed to verify if raising the water table alone would result in a factor of safety lower than the design criteria during both drained and undrained loading conditions. For the stability cross-sections analyzed, we were unable to reduce the factor of safety to a point where it did not meet the design criteria (FOS = 1.5) for slope stability of the global slope at a ratio of 3H:1V. Therefore, we adopted a statistical approach, where the alert trigger corresponds to readings that exceed the historical maximum readings. For VWPs within the intermediate bench area that is within the toe slope stability slip surface, the stability of the toe slope of 2H:1V determines the trigger for the Watch threshold.

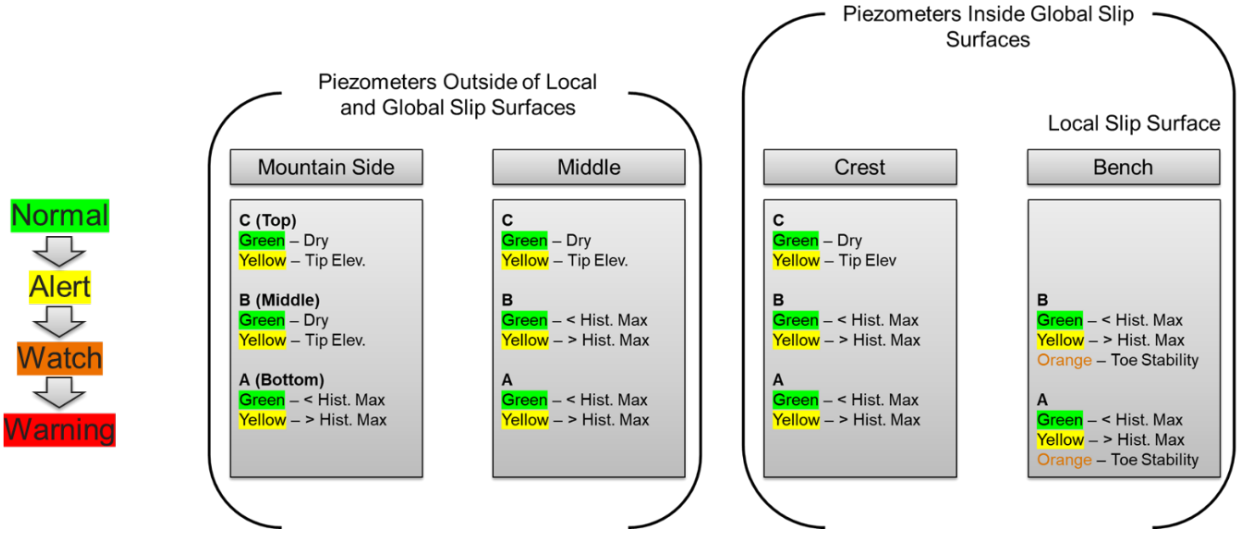


Figure 6: Rationale for setting vibrating wire piezometer thresholds

Defining trigger level thresholds for in-place slope inclinometers

To define the thresholds of the slope inclinometers, our first exercise was to collect readings over the first six months and analyze the trends. We used programming languages to process the data collected every hour. Figure 7 presents the readings from Holden's slope inclinometers along one of the axes during these six months. Defining "time zero" is crucial for interpreting inclinometer readings because it establishes a baseline reference point for all subsequent measurements. Without a clear baseline, initial readings can be influenced by various factors that might cause shifts, making the data unreliable. These factors include installation disturbances, and initial soil consolidation, or settling, which can cause erroneous movements not indicative of actual slope conditions. External factors such as weather changes, vibrations from nearby construction, or even the natural adjustment of the instrument in its casing can also affect initial readings. By setting a precise time zero, these initial variances are accounted for, ensuring that subsequent measurements reflect true changes in slope stability rather than installation-related anomalies or environmental influences. Based on Figure 7, the time zero for the inclinometers were set at January 1st.

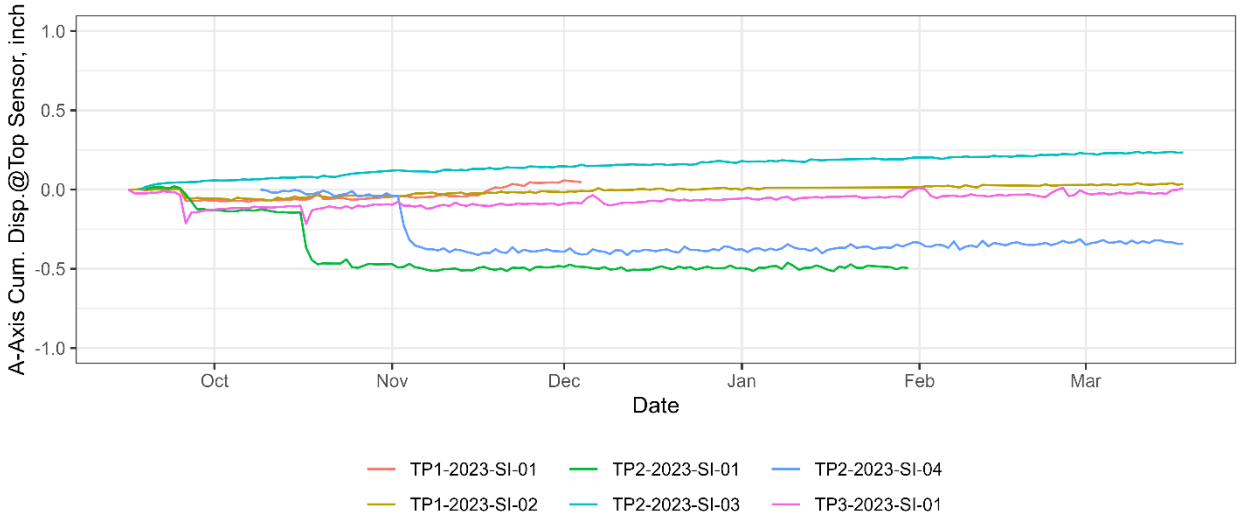


Figure 7: Initial readings of first six months from slope inclinometers

The alert trigger levels for the inclinometers were determined based on the predicted shear deformation from seismic deformation analysis over the shear bands and the peak strain observed in laboratory tests. We defined two key metrics: incremental displacement (displacement between two adjacent sensors) and cumulative displacement (displacement between the bottom fixity and the top sensor). Figure 8 illustrates the direct shear test results for Group E tailings, where most deformation is predicted to occur, according to seismic deformation analysis. The shear strain at peak stress is approximately 2%. Based on this, we set the threshold for incremental displacement between two sensors to 0.2 inches per foot.

Figure 9 presents the shear band color maps for a 1/10,000 year earthquake scenario. The shear band, which aligns with the fine-grained (Group E) tailings, is defined as the region where materials reach a 2% strain. The thickness of this shear band is about 15 feet. Consequently, the cumulative displacement threshold from the bottom fixity to the top of the SI (Slope Inclinometer) is determined to be 3 inches.

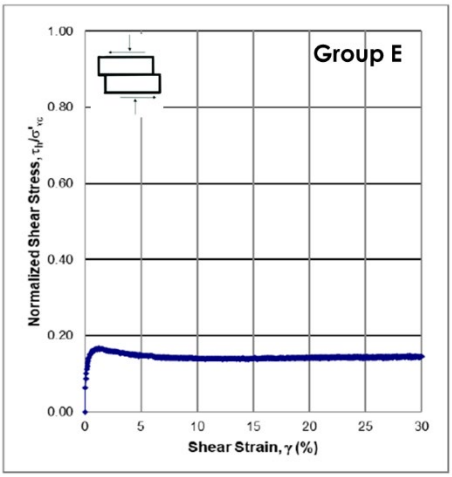


Figure 8: Direct simple shear test of group E tailings

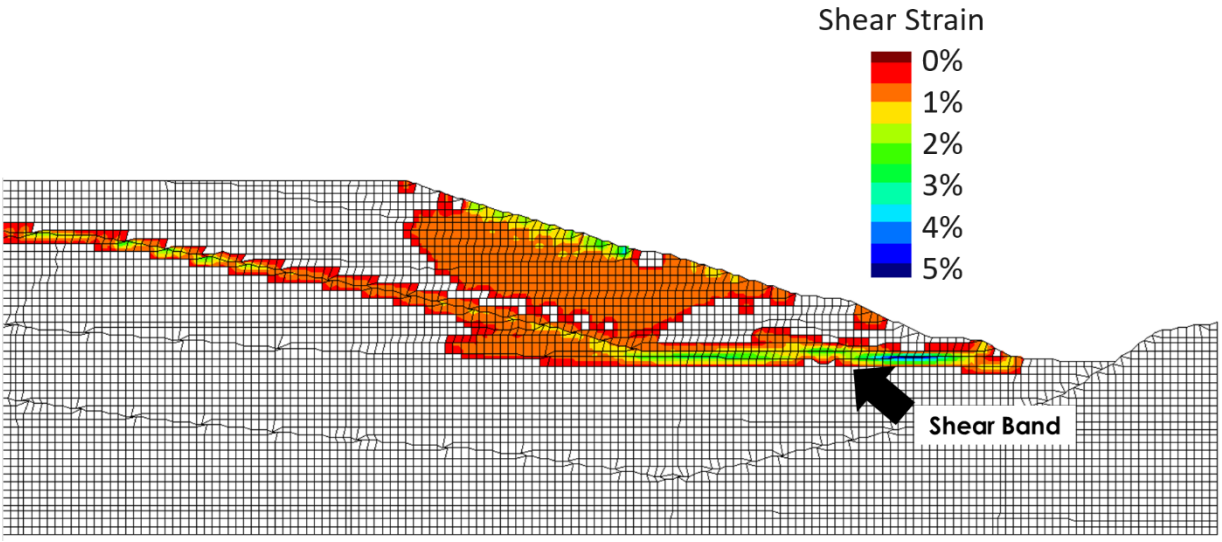


Figure 9: Shear band in seismic deformation analysis

Benefits of data automation and batch processing

Figures 10 through 13 show some examples.

Deciphering flow characteristics in tailings using a nested piezometer system

Figure 10 illustrates the effectiveness of a nested piezometer system in distinguishing between surface

infiltration and groundwater upwelling as sources of tailings saturation. The system involves installing multiple piezometers at various depths within the same borehole, enabling the measurement of pore water pressures across different strata within the tailings and underlying materials.

- Bottom piezometer: the bottom piezometer showed no significant rise in water pressure, indicating that groundwater from beneath did not upwell into the tailings.
- Top piezometer: the top piezometer transitioned from dry to saturated at the beginning of April, following snowmelt at the site, suggesting surface infiltration as the cause of saturation.
- Middle piezometer: the middle piezometer became saturated after the top piezometer, further indicating a top-to-bottom direction of water flow.

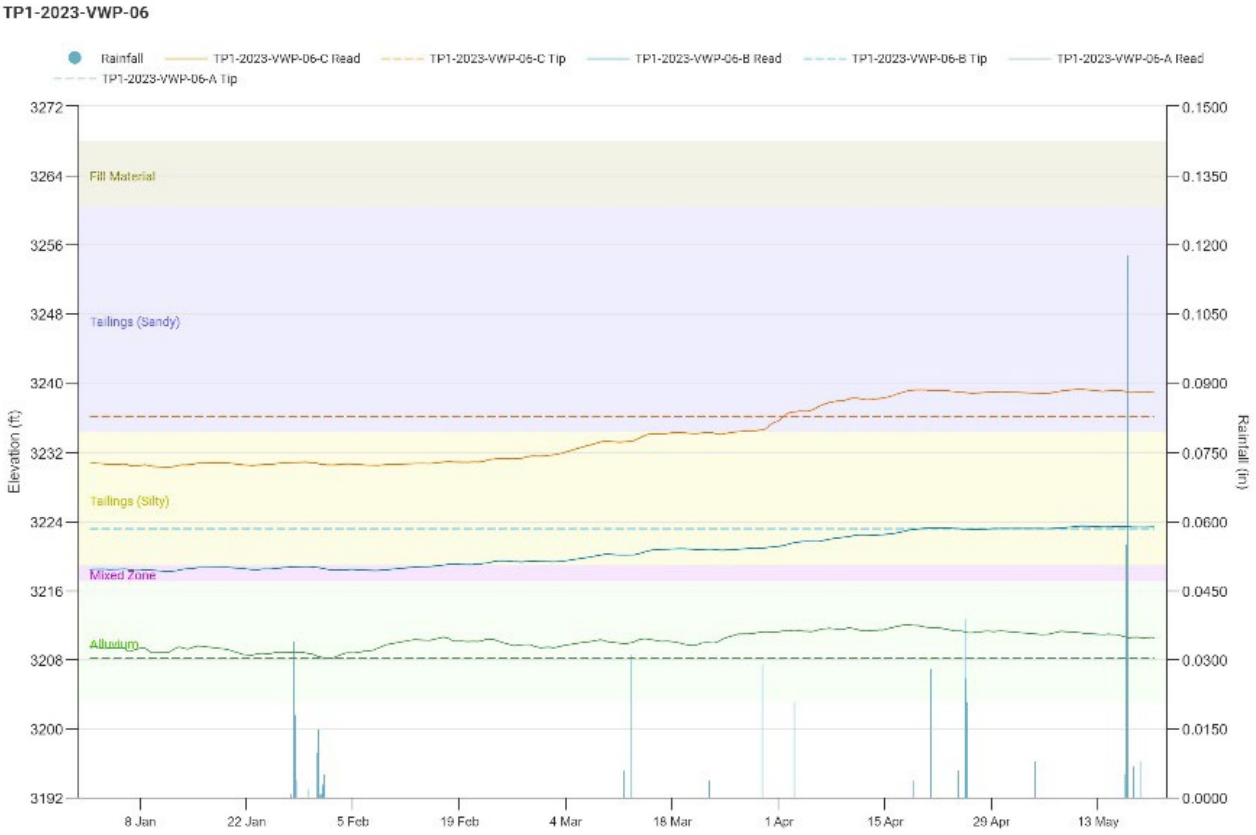


Figure 10: Readings of nested piezometers in the context of lithography

Assessing material conductivity and drainage characteristics through continuous piezometer readings

Figure 11 is an example that shows that continuous readings from piezometers provide valuable insights into how materials respond to changes in hydraulic conditions, distinguishing between fast-draining and slow-draining materials. Fast-draining materials exhibit rapid fluctuations in water pressure, while slow-

draining materials show more gradual responses. These continuous measurements are essential for assessing material conductivity and drainage characteristics, aiding in effective site management and risk assessment. Specifically, the lower piezometer responds more quickly to changes in the groundwater table, indicating fast-draining properties, whereas the upper piezometers respond more slowly, reflecting the behavior of slow-draining materials.

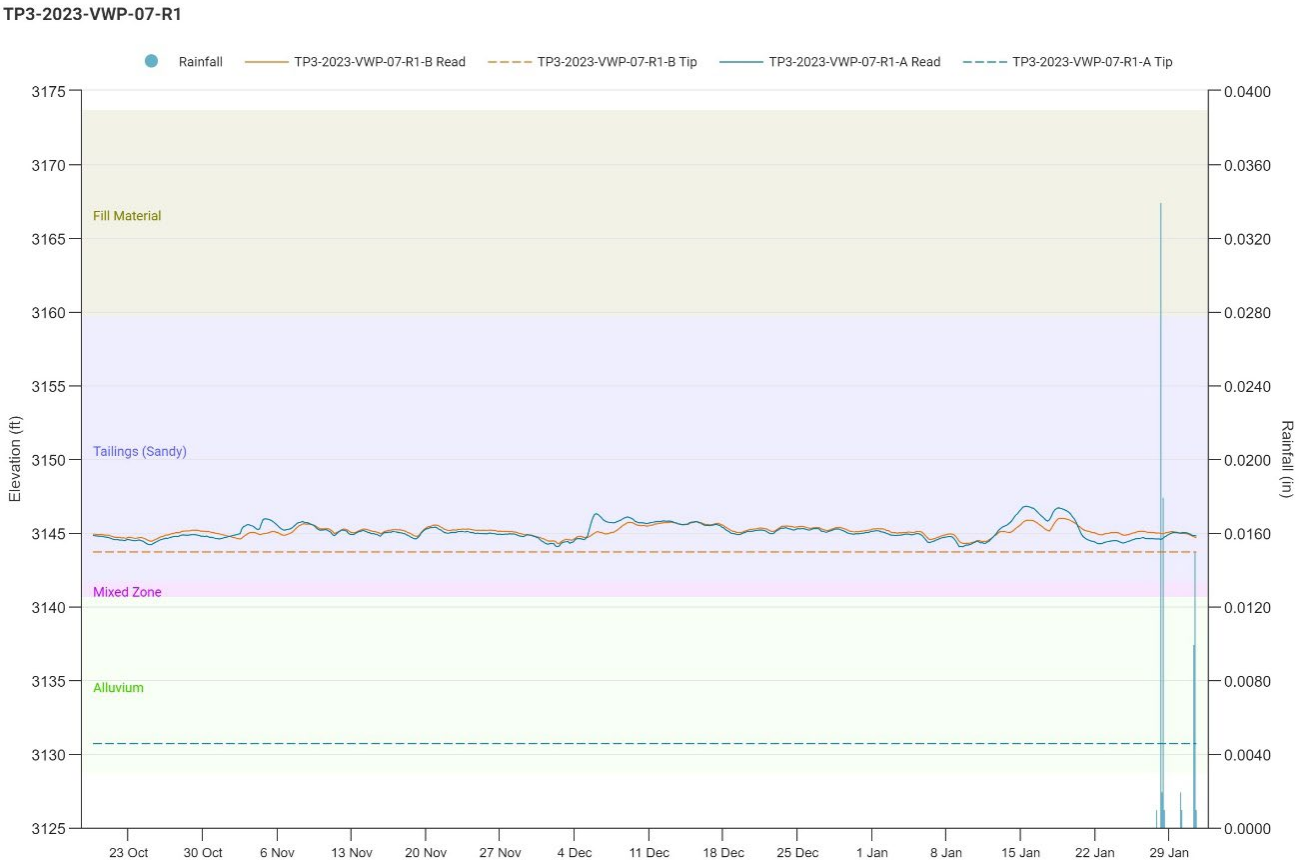


Figure 11: Different responses of piezometer sensor within different material types

Developing sub-TARP trigger levels for early warning and risk mitigation

Sub-TARP trigger levels are essential for providing early warning signs of potential issues or deviations from expected conditions within the facility. These trigger levels act as thresholds that, when reached or exceeded, prompt further investigation or action to prevent or mitigate risks such as slope instability, overtopping, or seepage. By establishing sub-TARP trigger levels, operators can proactively monitor specific parameters, such as pore water pressures or settlement rates, to detect trends or anomalies that may indicate emerging problems. This proactive approach allows for timely interventions and adjustments, ensuring the safety and integrity of the facilities and reducing the likelihood of accidents or environmental impacts.

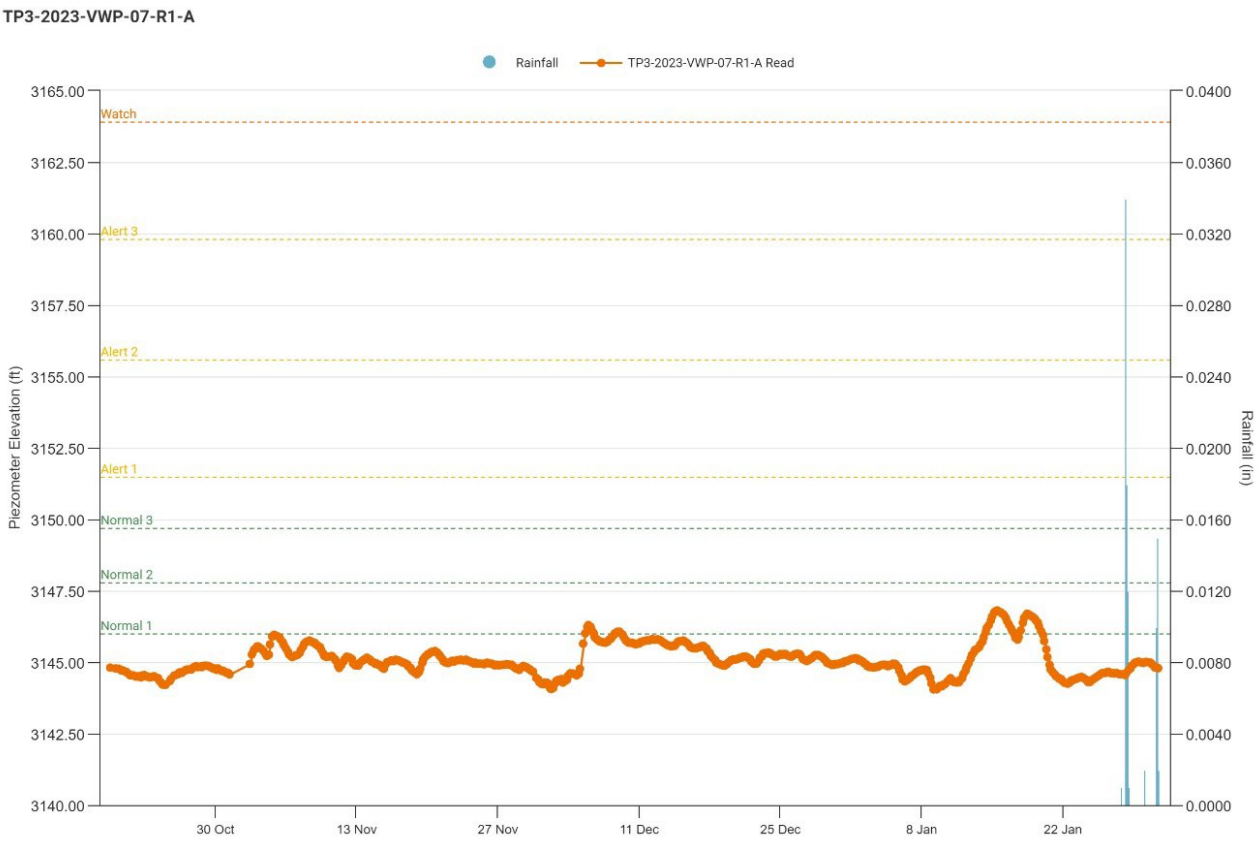


Figure 12: Sub-TARP trigger levels for piezometer readings

Advantages of continuous groundwater table monitoring over sporadic manual data collection

Piezometers are essential tools for identifying fluctuations in groundwater tables. By continuously measuring water pressure at various depths, piezometers provide real-time data on changes in groundwater levels. This continuous data collection is crucial as it captures the dynamic nature of groundwater systems, reflecting both short-term variations due to events like rainfall or snowmelt and long-term trends resulting from seasonal changes or human activities.

Unlike sporadic manual data collection, which might miss critical fluctuations and provide only a fragmented view, continuous monitoring ensures a comprehensive and accurate record of groundwater behavior. This continuous data is vital for understanding the complex interactions within the subsurface environment, enabling more precise predictions and better-informed management decisions regarding water resources and environmental protection.

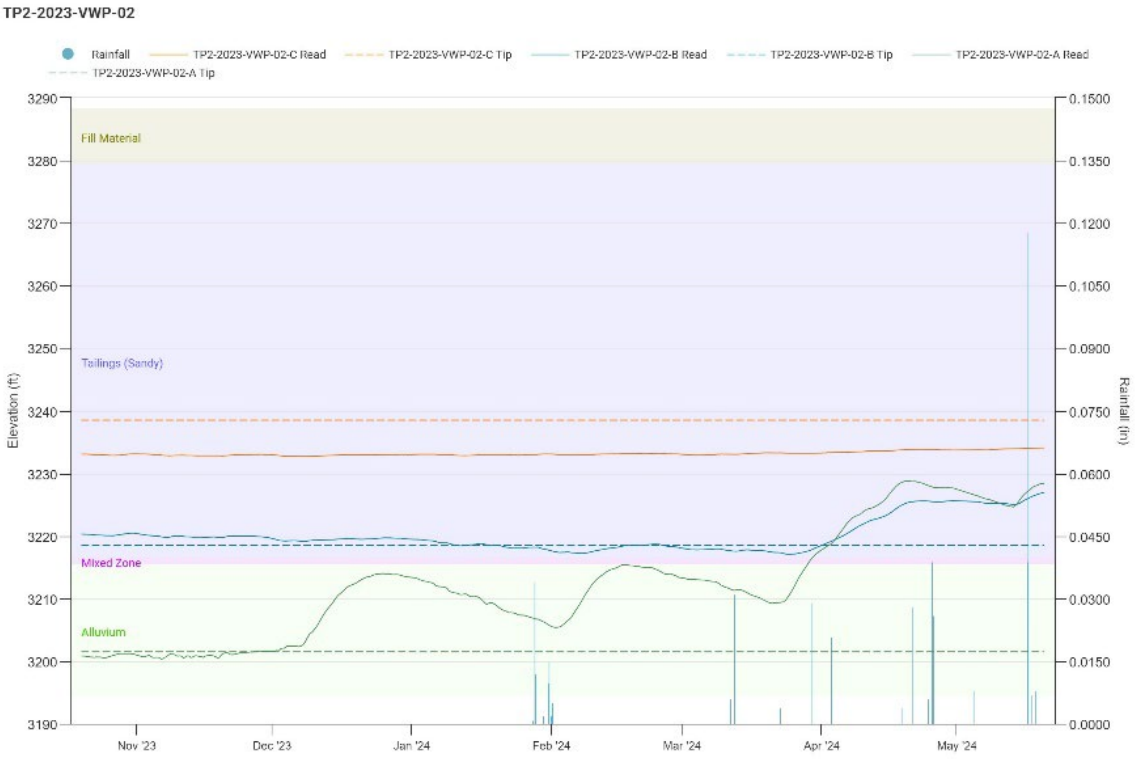


Figure 13: Fluctuating groundwater table as a result of changing conditions

Conclusion

The methodology detailed in this study combines deterministic and statistical analyses to establish TARP thresholds for monitoring mine tailings piles. Deterministic analysis identifies acceptable conditions and informs the significance of geotechnical instruments based on site-specific conditions, while statistical analysis tracks instrument readings over time to detect anomalies and trends. Programming tools like Python or R facilitate efficient data processing and real-time monitoring, ensuring precise thresholds and enhancing mine closure safety and effectiveness.

This approach can be broadly applied to other facilities and instruments requiring meticulous monitoring, such as waste rock piles, pit slopes, and various geotechnical and environmental applications. Industries beyond mining, including construction, dam safety, and environmental engineering, can adopt these techniques to improve infrastructure monitoring and maintenance. By leveraging programming tools and statistical methods, organizations can streamline data processing, quickly identify potential issues, and implement timely corrective actions, thereby improving overall operational safety and efficiency.

Acknowledgements

We extend our sincere gratitude to Rio Tinto for their invaluable support and approval to publish the data

presented in this study. Their collaboration and willingness to share information have made a significant contribution to the advancement of knowledge in the mining industry. This work not only enhances our understanding of tailings monitoring but also sets a precedent for future research and innovation in geotechnical and environmental instrumentation. We believe that the insights gained from this study will play a crucial role in improving safety, efficiency, and sustainability within the mining sector.

References

Carvalho Nunes, A.J., Cavalieri, F., Lopes, H., Lima, A.P. and Rodrigues, R.S. 2023. Deterministic and statistical analysis in the definition of triggered action response plans in tailings dams. *Tailings and Mine Waste Conference.* November 30.

Clarkson, L., Williams, D.J. and Seppälä, J. 2020. Real-time monitoring of tailings dams. *Georisk Assessment and Management of Risk for Engineered Systems and Geohazards* 15(2):113–127.

Shear Strength Characteristics and Joint Envelopes of Compacted Unsaturated Fine-grained Bauxite Residue

Hua Tian, The University of Queensland, Australia
David J. Williams, The University of Queensland, Australia
Keith Mandisodza, The University of Queensland, Australia

Abstract

Shear strength parameters of unsaturated compacted bauxite residue are critical for the construction and operation of upstream tailing dams. The shear strengths of unsaturated soils are commonly determined through suction-controlled direct shear or triaxial tests. However, this traditional experimental approach is apparatus-demanding, time-consuming, and relatively expensive to test in the laboratory. There have been reasonable successes in estimating shear strength parameters for the unsaturated soils when using the soil-water characteristic curve and conventional shear tests. In this study, the shear strength characteristics of the unsaturated compacted bauxite residue were investigated by carrying out a series of conventional multistage direct shear tests and flattened Brazilian tests over a broad range of water content. The water contents were interpreted to matric suction via the soil-water characteristic curve (SWCC), so the experimental results could be analyzed under the two stress state variables theory. The friction angle, ϕ', varied on different water contents due to the microstructure formed during compaction under low water contents and increased as the decrease of normal stress. The friction angle due to suction, ϕ^b, was less than the friction angle, ϕ', when the soil was nearly saturated and decreased to the negative regime before rebounding to zero as the matric suction approached the residual state. The nonlinear shear strength characteristics were described by a modified power law type joint strength envelope.

Introduction

Each year, a large amount of bauxite residue (also called red mud) is produced during the extraction of alumina from bauxite and commonly discharged in slurry pipes to an impoundment in a thin layer. Subsequently, it consolidates under its self-weight and compacts to form a tailing dam. Under climatic influences, water segregated from the slurry infiltrates into the previously deposited tailings or flows as surface runoff down to the decant pond or evaporates into the atmosphere. As a result, the surface of the tailings desiccates, creating an unsaturated zone above the phreatic surface. Therefore, using unsaturated

shear parameters is more appropriate for the actual site conditions.

Due to the smaller volume of the embankment, the upstream tailings dam is the most popular in the mining industry. In this type of dam, rising embankments are constructed directly on the dumped tailings. Given the importance of determining bearing capacity and evaluating tailing dam stability, the shear strength characteristics of bauxite residue have received extensive research attention (Jitsangiam and Nikraz, 2013; Rubinos et al., 2015; Alam et al., 2017; Reddy et al., 2021). However, most of these studies focused on saturated conditions. Until now, there has been little research regarding unsaturated conditions.

The mutual changes between tensile stress and compressive stress states occur during the soil failure process (Kong et al., 2022). Consequently, shear failure may occur under either compressive or tensile normal stress. To ensure the stability of constructed tailings dams, there is a need to comprehensively incorporate tensile strength into shear characteristics and establish a joint strength envelope considering both tensile and compressive normal stresses. Several pioneering studies (Toyota et al., 2003, 2004; Vesga 2009; Namikawa et al., 2017) have attempted to establish such a joint strength envelope for unsaturated soils. However, much of the existing research has been limited to narrow water content ranges and has not considered the nonlinearity in shear strength resulting from matric suction and normal stress.

To address the limitations in the current research, this study aimed to determine the soil-water characteristic curve (SWCC) to establish the relationship between water content and soil suction for subsequent analyses. Following this, multistage direct shear tests were conducted to understand the variation of shear strength characteristics across a broad range of water content and soil suction. Subsequently, to comprehensively and reasonably describe the shear strength characteristics of unsaturated bauxite residue, a nonlinear joint shear strength envelope for unsaturated soils was proposed by coupling the tensile strength obtained from flattened Brazilian tests.

Literature review

Fredlund et al. (1978) extended the Mohr-Coulomb theory to unsaturated soils by two independent stress state variables:

$$\tau = c' + (\sigma_n - u_a)\, tan\, \phi' + (u_a - u_w)\, tan\, \phi^b \qquad 1$$

Where, $(\sigma_n - u_a)$ is the effective normal stress; $(\sigma_a - u_w)$ is the matric suction; c' is the effective apparent cohesion; $\phi'$and ϕ^b are the friction angles indicating the rate of increase in shear strength relative to effective normal stress and matric suction respectively.

Suction-controlled direct shear and triaxial tests, in which matric suction is controlled by applying the axis-translation or osmotic technique, are two commonly used laboratory techniques for measuring the shear strength parameters of the extended Mohr-Coulomb theory (Ng et al., 2007). However, the traditional approaches mentioned above require sophisticated apparatus and are time-consuming, especially for clayey

soil due to its low permeability (Escario and Sáez, 1986; Gan et al., 1988; Khalili and Khabbaz, 1998). Alternatively, the variation in effective stress due to soil suction can be interpreted from and quantified in terms of water content through the SWCC. Therefore, conventional shear testing techniques developed within the framework of saturated soils mechanics remain effective in unsaturated soils.

Furthermore, it is widely accepted that the constant water content test is more suitable for engineering practice (Walton-Macaulay, 2015). This is because excess pore water pressure is expected to dissipate slowly, especially for clays that tend to retain water under loading, while excess pore air pressure is anticipated to dissipate almost instantaneously (Ma et al., 2013). The persistent nature of excess pore water pressure is a crucial aspect of geotechnical engineering problems, as it could be the cause of slope failure and long-term settlements (Thu et al., 2006). Therefore, the alternative approach using conventional shear tests and SWCC to determine the shear parameters of unsaturated soils is more practical in engineering practice. Its acceptability has been demonstrated through theoretical analysis (Oloo and Fredlund, 1996) and extensive experimental practices (Oloo and Fredlund, 1996; Bai and Liu, 2012; Chowdhury and Azam, 2016; Xing et al., 2016).

Cohesionless soils, such as sand (Kim and Sture, 2008; Lu et al., 2009; Yin and Vanapalli, 2018); hard rock tailings (Narvaez et al., 2015) exhibit significant tensile strength under unsaturated conditions due to negative pore water pressure and surface tension (Yin and Vanapalli, 2018). There are two types of methods applied to measure the tensile strength of unsaturated soils, namely direct and indirect methods.

In the direct method, the tensile strength of the soil is usually directly measured under uniaxial tensile strength conditions, in which the soil specimen is tested under tensile load directly applied normally to one principal plane, with zero loads applied to corresponding orthogonal planes (Lu et al., 2009). For the indirect method, mainly including the Brazilian test (ASTM, 2016a) and flexure beam test (ASTM, 2019), the specimen is split under compression loads, which are measured and then calculated into tensile strength through various functions developed based on specific testing conditions and assumptions. Originally developed for rocks, the Brazilian test was found to be able to determine the tensile strength of soils (Krishnayya and Eisenstein, 1974; Dexter and Kroesbergen, 1985; Beckett et al., 2015). Its low cost and convenience make it ideal for bulk testing of cover material (Beckett et al., 2015).

It is worth mentioning that the intersection of the shear strength envelope to the normal stress axis is the theoretical isotropic tensile strength derived from inherent material variables and independent of loading conditions (Lu et al., 2009). However, it should be recognized that the tensile strength obtained by most contemporary laboratory testing techniques was closer to the uniaxial condition rather than the isotropic condition (Lu et al., 2009). Li and Wong (2013) demonstrated that the measured tensile strength in the Brazilian tests is equal to the uniaxial tensile strength. Thus, in this research, the uniaxial tensile strength from the flattened Brazilian tests was used to approximate the tensile strength in the shear strength envelope.

The current paper applied the theory and test techniques of unsaturated soil mechanics to compacted unsaturated bauxite residue and developed a physical understanding regarding the shear strength characteristics and the shear strength envelope ranging from tensile to compressive normal stress of such fine-grained tailings.

Material and preparation

The bauxite residue investigated in this study was collected from a local tailings storage facility located in north Queensland, Australia. A series of laboratory tests were conducted to characterize the bauxite residue. According to the results of particle size distribution analysis, the bauxite residue consisted of a significant presence of clay-sized particles (54.43%), followed by silt-sized particles (43.25%), with the remainder (2.32%) in the sand range. The maximum dry density was 1.26 g/cm3 with an optimum water content of 34.5%. The investigated bauxite residue was classified as lean clay (CL) according to the Unified Soil Classification System (ASTM 2020), based on the testing results of plastic limit (33.5%), liquid limit (47.9%), and plasticity index (14.4).

The quantitative mineralogy (relative abundance) was estimated by X-ray diffraction (XRD) analyses. The bauxite residue was featured with the presence of significant quantities of hematite (Fe_2O_3) (36%) and nosean ($Na_8Al_6Si_6O_{24}(SO_4)$) (14%), with small quantities (2%) of clay mineral presenting as kaolinite ($Al_2Si_2O_5(OH)_4$).

To prepare the testing specimens, the collected bauxite residue was completely oven-dried at 60°C. After that, the aggregations of large particles were pulverized by a rubber mallet and sieved through an 850 BS sieve. Then, the predetermined amount of distilled water was added to the dried bauxite residue to reach a broad range of target moisture contents (4, 8, 12, 16, 20, 24, 28, and 32%). Next, the mixtures were sieved using an 1180 BS sieve to thoroughly mix the soil and prevent any conglomeration. After being placed in sealed jars for 2 days to reach water equilibrium, the well-moistened soils were ready for use.

Testing program

The testing program consisted of (i) SWCC test to establish the relationship between the water content and matric suction, (ii) multistage constant-water-content direct shear tests on unsaturated specimens, and (iii) flattened Brazilian tests on unsaturated specimens to determine the tensile strength.

SWCC

The water characteristic curves for bauxite residue under drying conditions were established using the GCTS pressure plate apparatus according to ASTM standard D6836-16 (ASTM, 2016b). The bauxite residue was compacted to a predetermined dry density of 1.23 g/cm^3 in the sample ring and then saturated

by soaking water from the bottom. Fully saturated specimens were then placed directly on the porous plates in the pressure chamber. To obtain a smooth curve, several pressure intervals (5, 10, 20, 40, 80, 160, 320, and 500 kPa) were tested.

Flattened Brazilian testing

A series of flattened Brazilian tests under a broad range of water contents (4%, 8%, 12%, 16%, 20%, 24%, 28%, and 32%) were conducted in the load frame manufactured by INSTRON. The specimens used in this research were 100 mm in diameter and 50 mm in length, as suggested by Beckett et al. (2015).

Initially, the predetermined moistened bauxite residue was placed in a split mold of 100 mm in diameter and compacted to a height of 50 mm in one layer. After compaction, the specimen was carefully removed from the split mold and sealed in plastic bags for 4 days for moisture equilibration. Subsequently, the specimen was tested by applying compressive forces with a constant loading rate of 0.02 mm/min, as suggested by Stirling et al. (2015), until failure. The tensile strength (σ_{tu}) was determined by the equation:

$$\boldsymbol{\sigma_{tu} = \frac{P}{\pi R L}} \qquad 2$$

where P, R, and L are the peak applied vertical load, the specimen radius, and length, respectively.

Multistage direct shear testing

A series of multi-stage direct shear tests under different water contents ranging from 4% to nearly saturated was carried out on a large-scale direct shear apparatus manufactured by WILLE to obtain the shear strength parameters under compressive normal stresses. The top and bottom porous stones were replaced with plastic plates, so the specimens were under constant water-content conditions during shearing.

The dimensions of the specimens used in this research were 150 mm × 150 mm × 150 mm (length × width × height). Firstly, the predetermined well-mixed moistened bauxite residue was compacted in the shear box to the target dry density of 1.23 g/cm³ in five layers, allowing a uniform distribution of density and moisture throughout the specimen.

Subsequently, the specimens were tested by applying shearing forces with a constant loading rate of 0.02 mm/min, as suggested by Suzuki et al.,(2001) , until failure. The applied effective normal stresses were chosen to be 5 kPa, 25 kPa, 50 kPa, and 100 kPa, representing the shallow depths of unsaturated zones in the tailings dam of approximately 0.3 m, 1.6 m, 3.1 m, and 6.3 m, respectively (assuming an in-situ unit weight of 16 kN/m³). A maximum shear displacement of 7.5 mm (10% shear strains) was controlled for every stage.

During the shearing tests, displacements and forces were measured and recorded at time intervals of 15s. After testing, water contents of the failure surface were checked to ensure the differential was less than 0.25%.

Presentation of test results

Measurements obtained from the stress plate apparatus are shown in Figure 1. The widely used empirical equation proposed by van Genuchten (1980) was used to approximate the SWCC in this study. The relation between the degree of saturation and suction is:

$$\frac{S - S_r}{1 - S_r} = \frac{1}{\{1 + [a(u_a - u_w)]^n\}^m} \quad 3$$

where S is the degree of saturation, a is approximately the air entry value (AEV), m and n control the slope at the inflection point on the SWCC. Fitting parameters a, m, and n values were given in Figure 1. The residual degree of saturation (S_r) corresponding to the residual suction and the capillary degree of saturation (S_c) corresponding to the AEV, which is the low bound of saturation to the boundary effect zone, was also obtained from the SWCC.

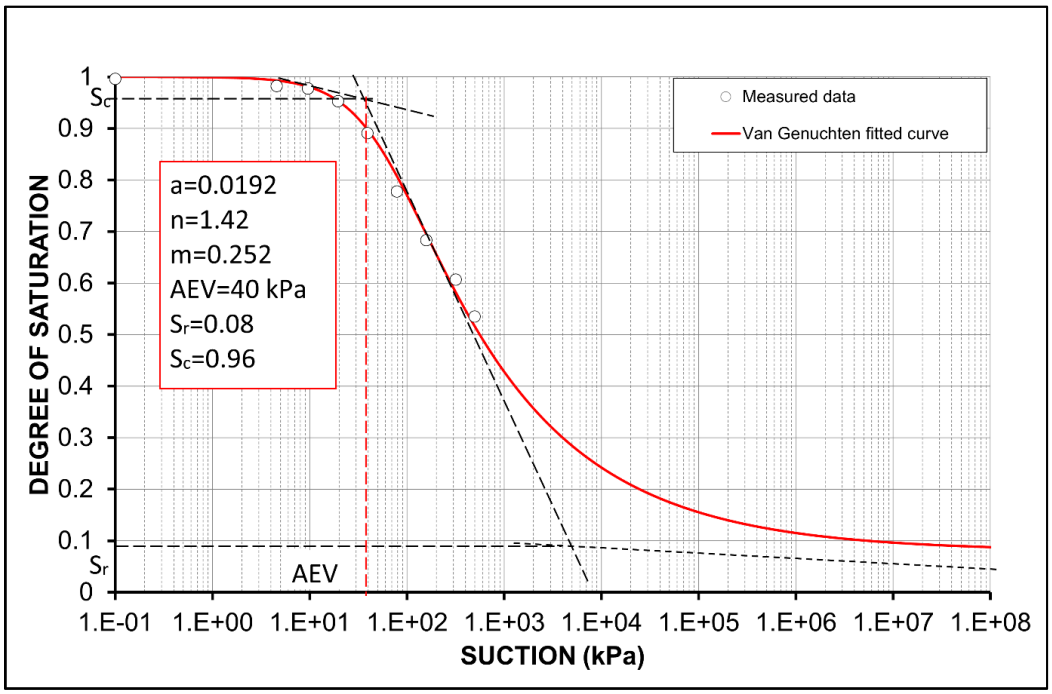


Figure 1: The best fitting SWCC and the experimental data of bauxite residue

The SWCC is defined as the relationship between water content and suction for the soil (Williams, 1982), through which the water contents defining the amount of water contained within the voids of the soil could be interpreted into soil suctions (Fredlund and Xing, 1994). The water contents and the corresponding suction in this research were presented in Table 1, based on which the measured shear strength was represented as points with different signs in Figure 2, together with the strength-suction curves.

Table 1: Results of suctions and strength

Water content (%)	Degree of saturation	Matric suction (kPa)	Tensile strength (kPa)	Shear strength (kPa)			
				5 kPa	25 kPa	50 kPa	100 kPa
4%	0.0838	242732015	-13.70	18.66	29.51	48.54	88.44
8%	0.166	37259	-15.73	20.38	29.78	49.79	91.56
12%	0.251	5703	-17.91	22.20	34.89	53.99	95.38
16%	0.335	1868	-19.96	25.17	38.63	56.89	97.92
20%	0.419	837	-28.63	29.86	49.28	67.98	104.67
24%	0.503	443	-28.28	28.22	46.94	66.52	102.30
28%	0.586	258	-23.38	20.20	36.37	54.32	85.85
32%	0.670	158	-13.06	13.85	26.79	42.88	70.63
nearly saturated	1.0	40*	–	6.07	15.11	28.43	51.68

*The AEV was used for the suction of nearly saturated condition

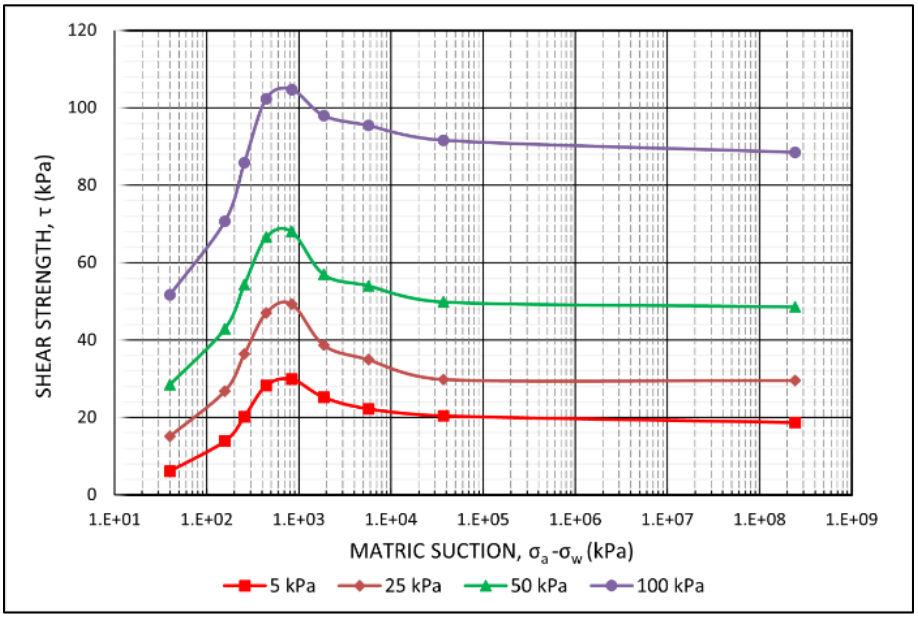


Figure 2: Shear strength plotted against the matric suction

As seen, the agreement was very satisfactory in general, despite the differences in applied normal stress. The strength-suction curves indicated that the shear strength depended significantly on suction. As the suction increased, the shear strength increased quickly before a critical suction was reached, which corresponds to the peak value of shear strength. From there on, the shear strength gradually decreased to the residual value with further increases in suction. The nonlinearity of the strength-suction curves was attributed to the diminishing contribution of matric suction to the shear strength, as the water content of the soil approached its residual value (Oloo and Fredlund, 1996).

The preceding observation shows an important conceptual change to the previous theories or findings wherein the effective shear strength of coarse-grained soils started to decrease beyond residual suction value (Donald 1957; Vanapalli 2009). However, a significant decrease in shear strength was not observed for fine-grained soils when tested over a broad range of suctions (Escario et al., 1989; Khalili and Khabbaz, 1998; Vanapalli et al., 2000; Huat et al., 2005; Vanapalli, 2009; Schnellmann et al., 2013) or water contents (Bai and Liu, 2012; Chowdhury and Azam, 2016; Xing et al., 2016), as shown in Figure 3.

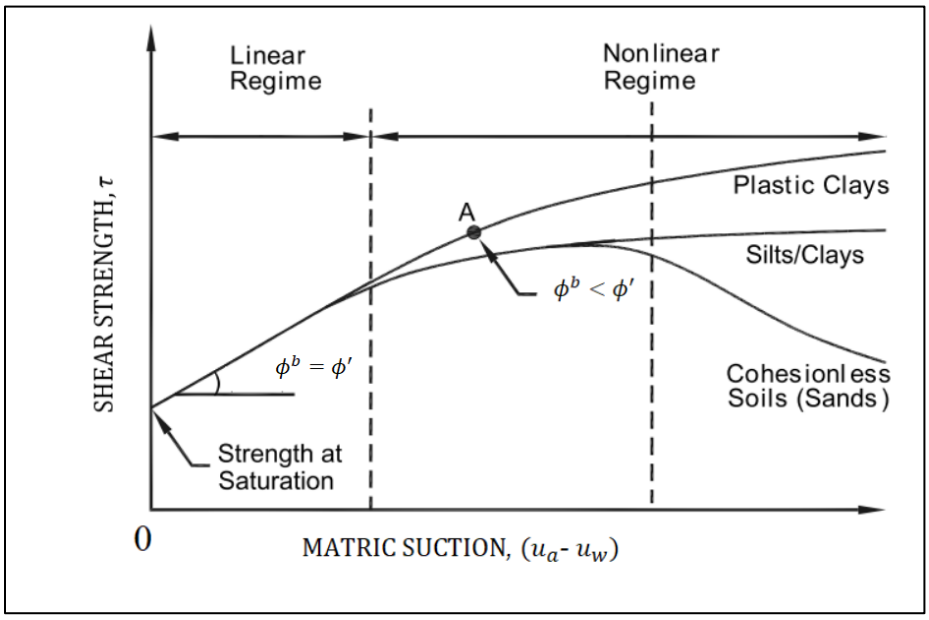


Figure 3: Typical unsaturated shear strength envelopes for different soil types, modified from (Vanapalli, 2009)

The high residual shear strength of fine-grained soils under excessively dry conditions could be attributed to the greater frictional resistance of soil aggregates resulting from cementation and/or shrinkage of the clayey mass, thus enhancing shear strength (Matsushi and Matsukura, 2006). In fine tailings such as bauxite residue, although particle size distribution analysis indicated a large presence of clay-sized or silt-sized particles, XRD patterns verified only a slight appearance of clay minerals. Consequently, slight cementation and/or shrinkage bonding provided by these clay minerals may contribute to shear strength.

The close agreement in the tendency of shear strength under residual suction between fine-grained bauxite residue and coarse-grained sand indicates that both particle size and mineralogy contribute to the shear strength of unsaturated soils. The absence of dominant clay minerals influenced the residual shear strength characteristics of fine-grained tailings (bauxite residue) in this research.

The load-displacement curves of flattened Brazilian tests under different water contents were shown in Figure 4a. The tensile strength was determined through Eq. (2) and presented in 4b.

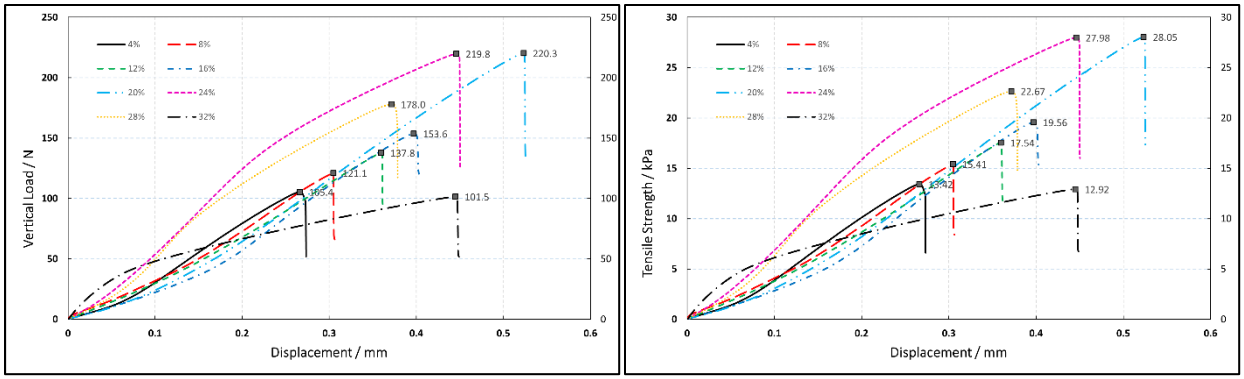


Figure 4: a) Vertical loads and b) tensile strength plotted against displacement

Discussion of test results

Shear strength characteristics under compressive normal stresses

In this research, the matric suction, $(\sigma_a - u_w)$ had been deduced from the SWCC of the bauxite residue, so the results of shear strength of unsaturated bauxite residue obtained from the conventional multistage direct shear tests could be analyzed in two planes (i.e., the τ versus $(\sigma_n - u_a)$ plane, and the τ versus $(u_a - u_w)$ plane) separately under the frame of the two independent stress state variables theory, as stated in Eq. (1). By assuming the pore-air pressure at failure was equal to the atmospheric pressure, the effective normal stress, $(\sigma_n - u_a)$, could be approximated to the applied normal stress, σ_n, due to its effectiveness nature. Thus, Eq. (1) could be revised as:

$$\tau = c' + \sigma_n \tan\phi' + (\sigma_a - u_w)\tan\phi^b \qquad 4$$

The shear strengths from the multistage direct shear tests were presented in Table 1, in which the water contents of the specimens at failure and the corresponding matric suctions estimated from the SWCC shown in Figure 1 were also provided.

The contribution of matric suction to the shear strength ($(\sigma_a - u_w)\tan\phi^b$) could be viewed in terms of being either part of the frictional component of shear strength or part of the cohesional component of shear strength (Gan et al., 1988). As part of the cohesional component, the failure surface could be projected to the shear strength versus normal stress plane ($\tau: \sigma_n$) at zero matric suction, and the internal friction angle ϕ' could be evaluated from the slope of the shear strength envelope. In the current research, the measured shear strengths were plotted against the applied effective normal stresses in Figure 4. The variation of the measured shear strengths with the applied normal stresses (i.e., the shear strength envelope) could be approximated by a linear Mohr-Coulomb strength envelope for each water content. The friction angle, ϕ', of strength envelope and the apparent cohesions, c', determined by extrapolating the strength envelope to the shear strength axis associated with different water contents were also present in Table 2.

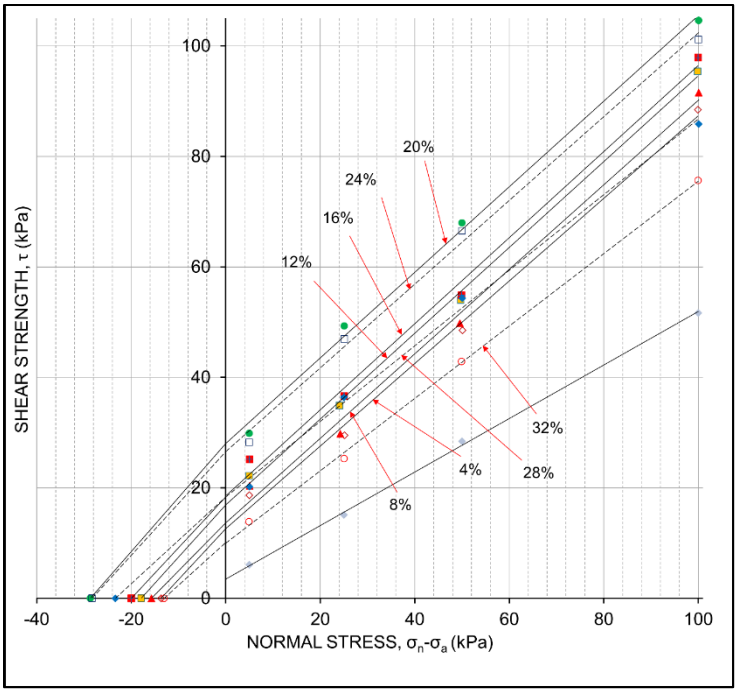


Figure 5: Shear strength plotted against the applied normal stress

It can be observed from Figure 5 that there is a tendency for divergence at increasing normal stresses in the shear strength envelope. As presented in Table 2, the apparent friction angle slightly increased from 36.80° at a water content of 4% to a plateau of 37.93° at a water content of 16%, with increasing water content. It then remained at a high level (greater than 37.0°) at water contents ranging from 20% to 24%. Beyond this point, a significant decreasing trend to a value of 25.86° in ϕ' was observed with further increases in water content (decreases in suction). It can be concluded that the friction angle, ϕ', under relatively low water content (high suction) was significantly higher than that at high water content (nearly saturated).

Earlier research (Fredlund et al., 1978; Krahn et al., 1989; Rahardjo et al., 2004; Thu et al., 2006), in an attempt to simplify the conditions, assumed that the strength envelopes for different water contents (or suctions) were parallel and that the friction angle was constant. However, extensive published works (Escario and Sáez, 1986; Cokca et al., 2004; Huat et al., 2005; Bai and Liu, 2012; Schnellmann et al., 2013; Chowdhury and Azam, 2016; Xing et al., 2016) correlated well with the divergent envelopes observed in this research. For example, Chowdhury and Azam (2016) reported that the friction angle for compacted expansive clay decreased from 44° to 27% for a water content range from 18% to 30%. The divergence became less significant in clayey/silty sand (Escario and Sáez, 1986; Schnellmann et al., 2013), where the observed variation in the friction angle due to suction (water content) change was considerably smaller. The particle size distribution (PSD) analysis verified high clay-sized contents in the bauxite residue used

in this research; thus, the variation of strength envelopes over water contents may highlight a close relationship between the bauxite residue and clayey soils in terms of frictional characteristics during shearing.

The scanning electron microscopy (SEM) and mercury intrusion porosimetry (MIP) techniques revealed that fine-grained soils compacted at low water content display a well-developed microstructure characterized by larger clusters formed by the gathering of small particles and dispersed grains surrounding them, while soils compacted at high water content exhibit dispersed grains with fewer or no clusters (Delage et al., 1996; Romero and Simms, 2008; Romero, 2013; Zabielska-Adamska et al., 2019). The clusters were agglomerated from small particles through the summation of interparticle actions. The interparticle actions contributing to the internal cohesion in unsaturated soil include (1) capillary force, (2) van der Waals attraction at the particle contacts, (3) electrical double layer force near the particle contacts, and (4) cementation bonding from chemical compounds. Cementation bonding is considered constant and negligible in cohesionless soils. Advances have been made in recent decades on the semiquantitative understanding of the magnitudes of the first three interparticle actions in unsaturated granular media (Lu and Likos 2006). Under the same degree of saturation, the first three interparticle actions are generally inversely proportional to particle size and separation distance.

For example, the capillary force could increase from several kilopascals among 0.075 mm particles to be as high as several hundred kilopascals among 0.002 mm particles. Therefore, internal cohesion within the clusters originating from the interparticle actions among fine particles with a short separation distance, which is the case within the clusters, is considerably stronger than that among the relatively large clusters. During loading, the clusters can withstand external loads as a whole instead of completely breaking down due to the strong internal cohesion. At low water content, the overall external loads are mainly resisted by the interaction transmitted from cluster to cluster. The internal frictional resistance of compacted bauxite residue at relatively low water content is derived from the interaction between clusters, which can be approximated by the internal friction of an equivalent granular material consisting of particles of the same size and shape as the clusters (Tang et al., 2015).

Normally, in granular material, the internal friction, made up of the resistance to sliding on the surface of the soil particles and the interlock between the soil particles, increases with particle size (Vangla and Latha, 2015). Because the interlock is proportional to particle size to some degree, the clusters formed under low water contents give rise to a higher interlock than dispersed particles, which is the case with high water contents. Consequently, the friction angle under low water contents is higher than that under high water contents.

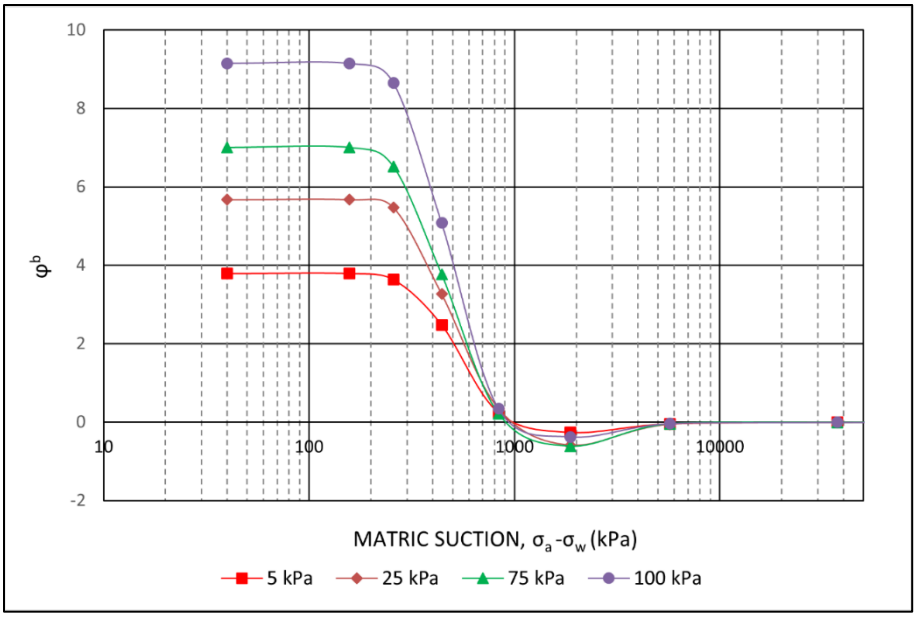


Figure 6: The friction angle due to suction, ϕ^b, against the matric suction

The material variable, ϕ^b, introduced by Fredlund et al. (1978) to capture the increase in shear strength with increasing matric suction, was defined as the slope describing the shear strength versus matric suction curve. The friction angle due to suction, ϕ^b, followed an S-shaped curve when plotted with respect to matric suction in Figure 7. The maximum value occurred at the commencement of the curve (nearly saturated), then ϕ^bdropped sharply from the initial peak value to a negative value as matric suction increased. From there, it gradually rebounded to zero as suction approached the residual saturation state. A good agreement was observed between the shapes of ϕ^b curves under different normal stresses. A similar shape had also been observed in clays by several previous researchers (Vanapalli, 2009; Bai and Liu, 2012; Chowdhury and Azam, 2016). The ϕ^b values were less than the ϕ' values, which was consistent with the shear strength parameters in most previous research.

Nonlinear joint shear strength envelope

The strength envelope that can describe the shear failure in both the compressive and tensile regimes is generally called the joint shear strength envelope. To establish the joint shear strength envelope, the measured tensile strengths were plotted together with the maximum shear stresses under the same water content in the shear strength versus normal stress (τ: σ_n) plane in Figure 5. For analysis purposes, the Mohr-coulomb envelope was handled by dividing into two linear portions, the first extending from the point of tensile strength to the apparent cohesion with a slope of ϕ_t, and the second extending beyond the apparent cohesion with a slope equal to ϕ'. By comparing the value of ϕ_t and ϕ' presented in Table 2, a significant discrepancy was observed, indicating a single linear Mohr-coulomb envelope couldn't accurately represent

the joint shear strength envelope of bauxite residue under partially saturated conditions, nor did the Fredlund envelope extended from the Mohr-coulomb envelope. This observation was consistent with experimental evidence of cohesionless saturated sands for small magnitudes of compressive stress (e.g., Sture et al., 1998; Kim, 2001) where the ratio of shear stress to normal stress typically increased significantly when the normal stress was approaching the far left point of shear strength envelope.

Due to the symmetry of Mohr circles and envelopes with respect to the normal stress axis, the derivative of the shear strength envelope is continuous at the intersection of the strength envelope to the normal stress axis, thus, the tangential friction angle interpreted from the derivative of the shear strength envelope should equal 90° at this point. However, the Mohr-Columb strength envelope implies the derivative is discontinuous here, therefore, many publications utilized the power law relation (Charles and Soares, 1984b, a; Jiang et al., 2003; Baker, 2004; Eid, 2014) to describe an increase in friction angle with decreasing normal stress. The generalization of this power law relationship can be expressed in the form:

$$\tau = P_a A \left(\frac{\sigma_n}{P_a}\right)^B, \left(\frac{1}{2} < B < 1\right) \quad 5$$

Where, P_a is boundary normal stress of low and normal compression, and usually taken as the atmosphere pressure; A and B are constants. A is a scale parameter controlling the magnitude of shear strength, and B controls the curvature of the envelope.

The situation became more complex in the unsaturated granular materials, which was the case in this research, where the van der Waals attractions, electrical double layer forces, and capillarity provided an additional component of interparticle bonding strength (Lu et al., 2007) giving rise to the tensile strength defined as the intercept of the strength envelope to the normal stress axis in the shear stress versus normal stress ($\tau: \sigma_n$) plane. This feature could be incorporated by considering the additional tensile strength (negative) as part of the effective normal stress, as:

$$\sigma' = \sigma_n - \sigma_t \quad 6$$

where σ_t is the tensile strength, σ_n is the normal stress, the difference between them is the unified effective normal stress.

Legitimate values of normal stress were restricted to range from the tensile strength rather than zero. The shear strength envelope for compacted unsaturated soils went through the tensile strength point and could be rewritten as:

$$\tau = P_a A \left(\frac{\sigma_n - \sigma_t}{P_a}\right)^B, \left(\frac{1}{2} < B < 1\right) \quad 7$$

The tangential friction angle was defined by the relation:

$$tan\, \phi_t = AB \left(\frac{\sigma_n - \sigma_t}{P_a}\right)^{B-1} \quad 8$$

As suggested in previous research (Lu and Likos 2006; Yin and Vanapalli 2018), the tensile strength in the unsaturated cohesionless soils could be considered as a function of matric suction:

$$\sigma_t = f(u_a - u_w) \quad 9$$

Thus, Eq. (7) could be written as:

$$\tau = P_a A \left(\frac{\sigma_n - f(u_a - u_w)}{P_a}\right)^B, \left(\frac{1}{2} < B < 1\right) \quad 10$$

The parameters A and B in the proposed strength envelope could be estimated by fitting the experimental results from tensile tests and shear tests. The fitting results of the proposed strength envelope for experimental results in this research were presented in Table 2. The comparison between a few typical experimental results and the corresponding fitted nonlinear envelopes was shown on the diagram in Figure 7, indicating the proposed strength envelope in Eq. (10) provided a reasonable approximation for the experimental results of unsaturated bauxite residue within the experimental normal stress range.

Table 2: Fitting parameters of nonlinear envelope

Water content (%)	Parameters of nonlinear envelope		Parameters of Fredlund envelope		
	A	B	Friction angle φ_t (tensive zone)	Apparent cohesion	Friction angle φ' (compressive zone)
4%	0.756	0.906	42.67	12.62	36.80
8%	0.773	0.906	40.97	14.65	37.45
12%	0.805	0.906	43.37	16.91	37.84
16%	0.814	0.906	42.64	18.96	37.92
20%	0.836	0.906	44.29	28.04	37.76
24%	0.812	0.906	43.24	26.57	37.17
28%	0.717	0.906	38.18	18.37	34.39
32%	0.663	0.906	37.73	10.48	33.25
nearly saturated	–	–	–	3.48	25.86

Figure 7 also displayed the alternative Fredlund shear strength envelopes fitted from the direct shear tests data. As may be seen, the proposed strength envelope provided more conservative strength estimations than those provided by the Fredlund envelope under small magnitudes of normal stress, particularly in the tensile stress regime. It is axiomatic that engineering models are best if accurate, acceptable if conservative, and unacceptable if neither (Travis et al., 2010). The conservative nature of the proposed strength envelope made it practically suitable for shallow slope failures occurring within the vadose zone under partially saturated soil conditions with significant tensile strength.

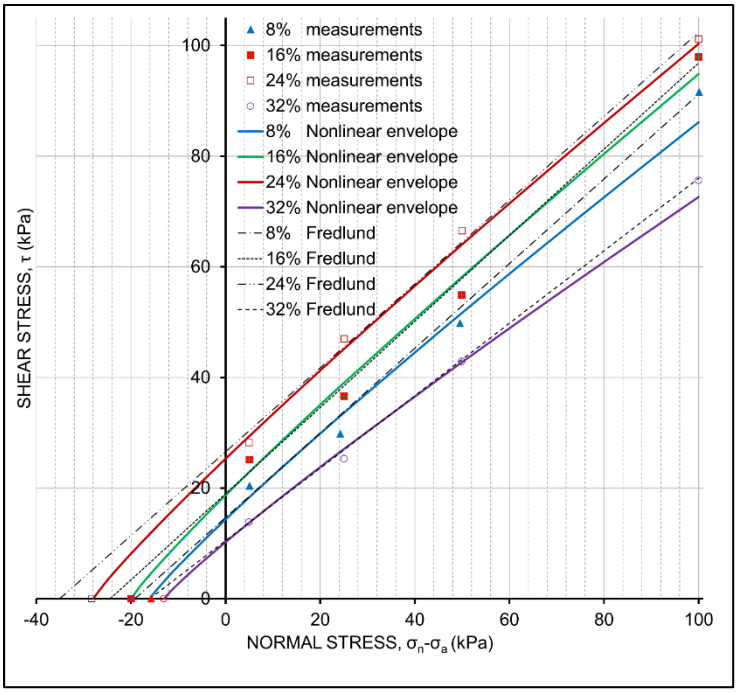


Figure 7: Comparisons of the measured shear strength and fitted envelope

Conclusion

Understanding the shear strength characteristics of compacted bauxite residue is essential for the construction and operation of upstream tailings dams due to their relationships to lateral earth pressure and bearing capacity for raised embankments. Based on the results of a comprehensive testing program on typical local bauxite residue presented and discussed in this paper, the following conclusions can be drawn:

- The shear strength characteristics of fine-grained bauxite residue neither agreed with those of coarse-grained sand nor with those of fine-grained silt/clay. This discrepancy could be attributed to the independent influences of both particle size and mineralogy on shear strength characteristics. The particle size led to divergence in shear strength envelopes due to the microstructure formed during compaction under low water content, while the mineralogy caused a significant drop in shear strength under residual suction due to the lack of clay minerals and the corresponding cementation and/or shrinkage bonding effect.
- The friction angle due to suction, ϕ^b, defined as the incremental shear strength on the incremental suction, peaked near the critical situation and then decreased to a negative value before rebounding to zero. The maximum value of the friction angle due to suction, ϕ^b, was less than the friction angle, ϕ', measured under saturation conditions, which did not comply with earlier unsaturated soil mechanics, but correlated well with extensive recent experimental results.

- The ratio of shear strength to normal stress increased as the normal stress approached the tensile strength, which was well captured by the modified power law type strength envelope established by considering the additional tensile strength of unsaturated cohesionless soils as part of effective normal stress. The proposed nonlinear envelope provided a more conservative strength estimation than that provided by the Fredlund envelope under small magnitudes of normal stress and particularly in the tensile stress regime, making it particularly suitable for geotechnical engineering practice in the shallow unsaturated zone.

References

Alam, S., Das S.K., Rao B.H. 2017. Characterization of coarse fraction of red mud as a civil engineering construction material. *Journal of Cleaner Production* 168: 679–691. https://doi.org/10.1016/j.jclepro.2017.08.210.

ASTM. 2016a. Standard test method for splitting tensile strength of intact rock core specimens. ASTM D3967-16, West Conshohocken, PA.

ASTM. 2016b. Standard test methods for determination of the soil water characteristic curve for desorption using hanging column, pressure extractor, chilled mirror hygrometer, or centrifuge. ASTM D6836-16, West Conshohocken, PA.

ASTM. 2019. Standard test method for flexural strength of soil-cement using simple beam with third-point loading. ASTM D1635, West Conshohocken, PA.

ASTM. 2020. Standard practice for classification of soils for engineering purposes (Unified Soil Classification System). ASTM D2487-17e1, West Conshohocken, PA.

Bai, F.Q. and Liu, S.H. 2012. Measurement of the shear strength of an expansive soil by combining a filter paper method and direct shear tests. *Geotech. Test. J.* 35: 451–459. https://doi.org/10.1520/GTJ103342

Baker, R. 2004. Nonlinear Mohr envelopes based on triaxial data. *Journal of Geotechnical and Geoenvironmental Engineering* 130: 498–506. https://doi.org/10.1061/(ASCE)1090-0241(2004)130:5(498)

Beckett, C.T.S., Smith, J.C., Ciancio, D. and Augarde, C.E. 2015. Tensile strengths of flocculated compacted unsaturated soils. *Géotechnique Letters* 5(4): 254–260. https://doi.org/10.1680/jgele.15.00087

Charles, J.A. and Soares, M.M. 1984a. Stability of compacted rockfill slopes. *Géotechnique* 34: 61–70. https://doi.org/10.1680/geot.1984.34.1.61

Charles, J.A. and Soares, M.M. 1984b. The stability slopes in soils with nonlinear failure envelopes. *Can. Geotech. J.* 21: 397–406. https://doi.org/10.1139/t84-044

Chowdhury, R.H. and Azam, S. 2016. Unsaturated shear strength properties of a compacted expansive soil from Regina, Canada. *Innovative Infrastructure Solutions* 1(47): 1–11. https://doi.org/10.1007/s41062-016-0047-2

Cokca, E., Erol, O. and Armangil, F. 2004. Effects of compaction moisture content on the shear strength of an unsaturated clay. *Geotechnical & Geological Engineering* 22: 285–297. https://doi.org/10.1023/B:GEGE.0000018349.40866.3e

Delage, P., Audiguier, M., Cui, Y.-J. and Howat, M.D. 1996. Microstructure of a compacted silt. *Can. Geotech. J.* 33: 150–158. https://doi.org/10.1139/t96-030

Dexter, A.R. and Kroesbergen, B. 1985. Methodology for determination of tensile strength of soil aggregates. *Journal of Agricultural Engineering Research* 31(2): 139–147. https://doi.org/10.1016/0021-8634(85)90066-6

Donald, I.B. 1957. Effective stresses in unsaturated non- cohesive soils with controlled negative pore pressure. M.Eng. Sc. thesis, University of Melbourne, Melbourne, Australia.

Eid, H.T. 2014. Stability charts for uniform slopes in soils with nonlinear failure envelopes. *Engineering Geology* 168: 38–45. https://doi.org/10.1016/j.enggeo.2013.10.021

Escario, V. and Sáez, J. 1986. The shear strength of partly saturated soils. *Géotechnique* 36: 453–456. https://doi.org/10.1680/geot.1986.36.3.453

Escario, V., Juca, J. and Coppe, M.S. 1989. Strength and deformation of partly saturated soils. *Proceedings of the12th International Conference on Soil Mechanics and Foundation Engineering:* 43–46.

Fredlund, D. and Xing, A. 1994. Equations for the soil-water characteristic curve. *Can. Geotech. J.* 31: 521–532. https://doi.org/10.1139/t94-061

Fredlund, D.G., Morgenstern, N.R. and Widger, R.A. 1978. The shear strength of unsaturated soils. *Can. Geotech. J.* 15: 313–321. https://doi.org/10.1139/t78-029

Gan, J.K.M., Fredlund, D.G. and Rahardjo, H. 1988. Determination of the shear strength parameters of an unsaturated soil using the direct shear test. *Can. Geotech. J.* 25: 500–510. https://doi.org/10.1139/t88-055

Ho, D.Y.F. and Fredlund, D.G. 1982. Increase in strength due to suction for two Hong Kong soils. *Proceedings of ASCE Geotechnical Conference on Engineering and Construction in Tropical and Residual Soils:* 263–295.

Huat, B.B.K., Ali, F.H. and Hashim, S. 2005. Modified shear box test apparatus for measuring shear strength of unsaturated residual soil. *American Journal of Applied Sciences* 2(9): 1283–1289. https://doi.org/10.3844/ajassp.2005.1283.1289

Jiang, J.C., Baker, R. and Yamagami, T. 2003. The effect of strength envelope nonlinearity on slope stability computations. *Can. Geotech. J.* 40: 308–325. https://doi.org/10.1139/t02-111

Jitsangiam, P. and Nikraz, H. 2013. Coarse bauxite residue for roadway construction materials. *International Journal of Pavement Engineering* 14(3): 265–273. https://doi.org/10.1080/10298436.2012.705843

Khalili, N. and Khabbaz, M.H. 1998. A unique relationship for χ for the determination of the shear strength of unsaturated soils. *Geotechnique* 48: 681–687. https://doi.org/10.1680/geot.1998.48.5.681

Kim T.-H. and Sture, S. 2008. Capillary-induced tensile strength in unsaturated sands. *Can. Geotech. J.* 45: 726–737. https://doi.org/10.1139/T08-017

Kim, T.-H. 2001. Moisture-induced tensile strength and cohesion in sand. University of Colorado, Boulder, Colo.

Kong, X., Cheng, Y. and Zhao, B., et al. 2022. The tension-shear and compression-shear joint strength model for unsaturated clay and its application to slopes. *Front. Earth Sci.* 10: 1–11. https://doi.org/10.3389/feart.2022.916805

Krahn, J., Fredlund, D.G. and Klassen, M.J. 1989. Effect of soil suction on slope stability at Notch Hill. *Can. Geotech. J.* 26: 269–278. https://doi.org/10.1139/t89-036

Krishnayya, A.V.G. and Eisenstein, Z. 1974. Brazilian tensile test for soils. *Can. Geotech. J.* 11: 632–642. https://doi.org/10.1139/t74-064

Li, D. and Wong, L.N.Y. 2013. The Brazilian disc test for rock mechanics applications: Review and new insights. *Rock Mechanics and Rock Engineering* 46: 269–287. https://doi.org/10.1007/s00603-012-0257-7

Lu, N. and Likos, W.J. 2006. Suction stress characteristic curve for unsaturated soil. *Journal of Geotechnical and Geoenvironmental Engineering* 132: 131–142. https://doi.org/10.1061/(ASCE)1090-0241(2006)132:2(131)

Lu, N., Kim, T.-H., Sture, S. and Likos, WJ. 2009. Tensile strength of unsaturated sand. *Journal of Engineering Mechanics* 135: 1410–1419. https://doi.org/10.1061/(asce)em.1943-7889.0000054

Lu, N., Wu, B. and Tan, C.P. 2007. Tensile strength characteristics of unsaturated sands. *Journal of Geotechnical and Geoenvironmental Engineering* 133: 144–154. https://doi.org/10.1061/(asce)1090-0241(2007)133:2(144)

Ma, K., Huang, M.S., Hu, P. and Yang, C. 2013. Soil-water characteristics and shear strength in constant water content triaxial tests on Yunnan red clay. *Journal of Central South University* 20: 1412–1419. https://doi.org/10.1007/s11771-013-1629-1

Matsushi, Y. and Matsukura, Y. 2006. Cohesion of unsaturated residual soils as a function of volumetric water content. *Bulletin of Engineering Geology and the Environment* 65: 449–455. https://doi.org/10.1007/s10064-005-0035-9

Nam, S., Gutierrez, M., Diplas, P. and Petrie, J. 2011. Determination of the shear strength of unsaturated soils using the multistage direct shear test. *Engineering Geology* 122(3–4): 272–280. https://doi.org/10.1016/j.enggeo.2011.06.003

Namikawa, T., Hiyama, S., Ando, Y. and Shibata, T. 2017. Failure behavior of cement-treated soil under triaxial tension conditions. *Soils and Foundations* 57: 815–827. https://doi.org/10.1016/j.sandf.2017.08.011

Narvaez, B., Aubertin, M. and Saleh-Mbemba, F. 2015. Determination of the tensile strength of unsaturated tailings using bending tests. *Can. Geotech. J.* 52: 1874–1885. https://doi.org/10.1139/cgj-2014-0156

Ng, C.W.W., Cui, Y., Chen, R. and Delage, P. 2007. The axis-translation and osmotic techniques in shear testing of unsaturated soils: A comparison. *Soils and Foundations* 47: 675–684. https://doi.org/10.3208/sandf.47.675

Oloo, S.Y. and Fredlund, DG. 1996. A method for determination of ϕ b for statically compacted soils. *Can. Geotech. J.* 33: 272–280. https://doi.org/10.1139/t96-006

Rahardjo, H., Heng, O.B. and Choon, L.E. 2004. Shear strength of a compacted residual soil from consolidated drained and constant water content triaxial tests. *Can. Geotech. J.* 41: 421–436. https://doi.org/10.1139/T03-093

Reddy, N.G., Nongmaithem, R.S., Basu, D. and Rao, B.H. 2021. Application of biopolymers for improving the strength characteristics of red mud waste. *Environmental Geotechnics* https://doi.org/10.1680/jenge.19.00018

Romero, E. 2013. A microstructural insight into compacted clayey soils and their hydraulic properties. *Engineering Geology* 165: 3–19. https://doi.org/10.1016/j.enggeo.2013.05.024

Romero, E. and Simms, P.H. 2008. Microstructure investigation in unsaturated soils: A review with special attention to contribution of mercury intrusion porosimetry and environmental scanning electron microscopy. *Geotechnical and Geological Engineering* 26: 705–727. https://doi.org/10.1007/s10706-008-9204-5

Rubinos, D., Spagnoli, G. and Barral, M.T. 2015. Assessment of bauxite refining residue (red mud) as a liner for waste disposal facilities. *International Journal of Mining, Reclamation and Environment* 29(6): 433–452. https://doi.org/10.1080/17480930.2013.830906

Schnellmann, R., Rahardjo, H. and Schneider, H.R. 2013. Unsaturated shear strength of a silty sand. Eng Geol 162: 88–96. https://doi.org/10.1016/j.enggeo.2013.05.011

Stirling, R.A., Hughes, P., Davie, C.T. and Glendinning, S. 2015. Tensile behaviour of unsaturated compacted clay soils — A direct assessment method. *Applied Clay Science* 112–113: 123–133. https://doi.org/10.1016/j.clay.2015.04.011

Sture, S., Costes, N.C., Batiste, S.N., et al. 1998. Mechanics of granular materials at low effective stresses. *Journal of Aerospace Engineering* 11: 67–72. https://doi.org/10.1061/(ASCE)0893-1321(1998)11(3): 67.

Suzuki, M., Yamamoto, T., Tanikawa, K., et al. 2001. Variation in residual strength of clay with shearing speed. Mem Fac Eng Yamagushi Univ 52: 45–49.

Tang, C.-S., Pei, X.-J., Wang, D.-Y., et al. 2015. Tensile Strength of Compacted Clayey Soil. *Journal of Geotechnical and Geoenvironmental Engineering* 141: 04014122. https://doi.org/10.1061/(ASCE)GT.1943-5606.0001267

Thu, T.M., Rahardjo, H. and Leong, E.-C. 2006. Shear strength and pore-water pressure characteristics during constant water content triaxial tests. *Journal of Geotechnical and Geoenvironmental Engineering* 132: 411–419. https://doi.org/10.1061/(asce)1090-0241(2006)132:3(411)

Toyota, H., Nakamura, K. and Sramoon, W. 2004. Failure criterion of unsaturated soil considering tensile stress under three-dimensional stress conditions. *Soils and Foundations* 44: 1–13. https://doi.org/10.3208/sandf.44.5_1

Toyota, H., Nakamura, K., Sakai, N. and Sramoon, W. 2003. Mechanical properties of unsaturated cohesive soil in consideration of tensile stress. *Soils and Foundations* 43(2): 115–122.

Travis, Q.B., Houston, S.L., Marinho, F.A.M. and Schmeeckle, M. 2010. Unsaturated infinite slope stability considering surface flux conditions. *Journal of Geotechnical and Geoenvironmental Engineering* 136: 963–974. https://doi.org/10.1061/(asce)gt.1943-5606.0000301

van Genuchten, M.T. 1980. A closed-form equation for predicting the hydraulic conductivity of unsaturated soils. *Soil Science Society of America Journal* 44: 892–898. https://doi.org/10.2136/sssaj1980.03615995004400050002x

Vanapalli, S.K. 2009. Shear strength of unsaturated soils and its applications in geotechnical engineering practice. *Proceedings of the 4th Asia Pacific Conference on Unsaturated Soils:* 579–598.

Vanapalli, S.K., Wright, A. and Fredlund, D.G. 2000. Shear strength behavior of a silty soil over the suction range from 0 to 1,000,000 kPa. *Proceedings of the 53rd Canadian Geotechnical Conference:* 1161–1168.

Vangla, P. and Latha, G.M. 2015. Influence of particle size on the friction and interfacial shear strength of sands of similar morphology. *International Journal of Geosynthetics and Ground Engineering* 1(6). https://doi.org/10.1007/s40891-014-0008-9

Vesga L.F. 2009. Direct Tensile-Shear Test (DTS) on unsaturated kaolinite clay. *Geotech. Test. J.* 32: 397–409. https://doi.org/10.1520/GTJ101563

Walton-Macaulay, C. 2015. Prediction of strength and shear modulus of compacted clays within an unsaturated critical state framework. PhD thesis.

Williams, P.J. 1982. *The Surface of the Earth: An Introduction to Geotechnical Science*. Longman Inc., New York.

Xing, X., Li ,T. and Fu, Y. 2016. Determination of the related strength parameters of unsaturated loess with conventional triaxial test. *Environmental Earth Sciences* 75(82): 1–11. https://doi.org/10.1007/s12665-015-4797-5

Yin, P. and Vanapalli, S.K. 2018. Model for predicting tensile strength of unsaturated cohesionless soils. *Can. Geotech. J.* 55: 1313–1333. https://doi.org/10.1139/cgj-2017-0376

Zabielska-Adamska, K., Małaszkiewicz, D. and Konopko, M. 2019. Microstructure of compacted fly ash. Proceedings of the 17th European Conference Soil Mechanics and Geotechnical Engineering ECSMGE-2019: 1–8. https://doi.org/10.32075/17ECSMGE-2019-0465

Measurement of Bingham Yield Stress and Plastic Viscosity of Tailings Slimes using an In-situ Viscometer

Dallas McGowan, ConeTec, Canada
Yasmin Byrne, ConeTec, UK
Y. Simon Sun, Northern Alberta Institute of Technology, Canada
Heather Kaminsky, Northern Alberta Institute of Technology, Canada
Jason DeJong, University of California Davis, USA

Abstract

Rheological properties of colloidal suspensions such as clay-based tailings are complex and can be difficult to measure due to their non-Newtonian state. Viscosity and yield stress are valuable to tailings operators as they are relied upon to inform dredging operations, model interactions between pond fluids and subsequently deposited sands, mixing characteristics, and dam breach modeling exercises to determine run out and impacts in emergency planning. Currently, rheological properties of tailings are measured ex situ in a laboratory environment. Errors are introduced through the sampling and transport processes, and real-time decision making based on results is not possible.

NAIT (the Northern Alberta Institute of Technology) and ConeTec developed two experimental vane shear testing protocols applied to a variable rate field vane shear testing apparatus (VR-eVST), patent pending. Field VR-eVST tests using each testing protocol were conducted at five testing locations and multiple depths at an operating mine near Fort McKay, Alberta, Canada. Following each test, a tailings sample was retrieved from the tested location and shipped to NAIT's laboratory in Edmonton for laboratory rheology measurements and index testing. Each VR-eVST test was paired with a Gamma Piezo-Cone Penetration Test (GCPTu). NAIT applied the Bingham fluid rheological model to calculate fluid properties from the field VR-eVST data. The plastic viscosity and Bingham yield stress parameters obtained from model fitting applied to the in-situ data are plausible for the type of tailings encountered in this study. Further study is required to determine the size and dynamics of the shear band during testing as well as the impacts of repeated shearing on laboratory analysis. Early work indicates that in-situ rheology measurements are promising and may add value to tailings management.

Introduction

The study of the flow and deformation of matter in response to applied shear forces is called rheology. Resistance to flow is defined as viscosity. Newtonian fluids, like water and oil, are homogenous single-phase fluids and have a constant viscosity at a constant temperature regardless of the applied stress. However, industrial slurries, and suspensions including fluid tailings, are more commonly non-Newtonian fluids. These fluids exhibit complex behaviors such as non-constant viscosity, yield stress and time- and shear- history dependent properties (Piette et al., 2022). Simultaneously, these properties are critical parameters for operators to understand, impact both operations and closure, including the efficiency of dredge operations, how tailings materials interact with sand mixing, and are required for modeling runout.

The Bingham plastic fluid model is commonly utilized to represent oil sands tailings behavior (Sanders et al., 2004; Litzenberger and Sumner, 2004). The Bingham plastic fluid is a simple rheological model that reasonably captures the behavior of tailings. It is characterized by a yield stress that must be overcome before flow is initiated and a plastic viscosity beyond that yield point. Additionally, a stepped rate approach has been applied. This involves stepping the VR-eVST rotation rate up and down; and holding at stepped speeds, to investigate the development of shear stress during variable rate testing in fluid materials. This approach has been partially inspired by the concept that a critical vane velocity exists for determining minimum undrained shear strength, as demonstrated in transitional mine tailings by Harvey et al. (2023) and originally developed by Blight (1968). This study examines whether excessively high shear stresses are observed at high rotation speeds and if they are associated with viscous effects.

Background

Currently, the best practice for measuring rheological parameters for industrial fluid tailings is to sample materials and transport them to an offsite laboratory for analysis. This process is not only costly and time-consuming, but it also has the potential to yield results that do not accurately reflect the true in-situ rheological properties (Bugg et. al., 2022). This discrepancy arises from the time- and shear history-dependent nature of non-Newtonian tailings materials. It is not uncommon for viscosity and yield stress values measured by offsite laboratories to be significantly lower than expected true in-situ values, an observation that could be explained by the thixotropic nature of tailings slurries.

The rheological properties of tailings slurries are highly susceptible to breakdown through shear history, especially if they have been previously flocculated. Previous studies, such as Sun (2018), have shown that although initially strong, clay aggregate flocs formed through polymer amendment become mechanically dissociated and revert to a near pre-flocculation state after exposure to significant shear energy. Once the polymer-amended clay aggregates are sheared apart in this manner, their strength

properties are not recoverable. The sampling, transport, and requirement to forcefully homogenize samples associated with laboratory testing induce significant shearing and potentially irreversible breakdown in rheological properties, causing the results to no longer be representative of the in-situ conditions. For these reasons, it is advantageous to measure the rheological properties in the field, in-situ, and in real time. This paper investigates the use of novel VR-eVST, like those typically used for undrained shear strength tests, with an operating protocol similar to those described by Fisher et al. (2007), to measure the viscosity of fluid tailings. Several existing studies explore modifying the operating protocol field vane shear testing to allow for variable rates (Harvey et al., 2023; Reid et al., 2023). Harvey et al. (2023) emphasize the significance of identifying optimal vane rotation rates to achieve accurate undrained shear strength measurements in mine tailings. While these studies focus on transitional soils, they show that higher rotation rates displayed increasing shear stress, which was assumed to be an effect of viscous rate effects. Stepped VR-eVST tests have been undertaken in fluid tailings to investigate the impact of variable vane rotation rates on the shear stress generated.

The testing locations (A, B, C, and D) were chosen to target materials within the fluid body with potentially complex rheological properties. All testing locations contained tailings subject to deliberate treatment, including the addition of anionic polyacrylamide flocculants to encourage dewatering. The fluid in location A was additionally subjected to significant post-flocculation shear stress, aging (likely in excess of a year), and potentially mixing with other fluid tailings streams. Location A gave the opportunity to characterize a highly variable fluid deposit under relatively challenging testing conditions. The other locations (B, C, and D) were chosen in a relatively homogenous flocculated fine tailings deposit. Flocculant was recently added at the point of deposition, with visual monitoring used to control and optimize polymer dosage. The fluid was then left to rest (< 6 months), subject only to sedimentation and self-weight consolidation, resulting in a thickened, uniform fluid. Locations B, C, and D afforded the opportunity to evaluate the test performance in a treated fluid tailings deposit where the tailings deposition plan is partially dependent on the undrained shear strength and viscous properties of the fluid to later entrain sand.

Objectives

The primary objective of this study is to develop a test protocol to accurately measure the rheological properties of fluid tailings in-situ through innovations to VR-eVST equipment and methodologies, to provide reliable, real-time data on the viscosity and yield stress, overcoming limitations associated with sample transport and laboratory testing. While vanes of this type are commonly used to measure undrained shear strength of fine-grained soils at a rotation rate of 6 degrees per second (ASTM D2573), this study investigates the industrial application of a more rapid rate of rotation in industrial slurries. To achieve this, the study tests the following hypotheses:

1. The rheological properties of fluid tailings can be effectively measured in situ using VR-eVST.
2. Modified variable, stepped rate tests will reveal a continuum in responses across different grain size materials, from transitional soils to fluid tailings, bridging the gap between geotechnical and rheological measurements.

Additionally, the study seeks to understand the in-situ measurements by comparing them with traditional laboratory results. A discrepancy between in-situ rheology and the laboratory measured rheology is expected as a result of the field conditions (Bugg et al., 2022).

Methodology

In situ

The in-situ testing was conducted using a VR-eVST developed by ConeTec and applying a testing protocol developed by NAIT. Testing was conducted at four distinct locations and five depths at two tailings storage facilities, within a single operating mine, near Ft. McKay, Alberta, Canada. A ConeTec amphibious platform and crew facilitated access to these testing sites. The detailed procedures are as follows:

1. **Gamma Piezo-Cone Penetration Test** (GCPTu) (Figure 2): At each testing site, a GCPTu was conducted for stratigraphy and selection of VR-eVST testing elevations.
2. **Initial VR-eVST**: At each elevation, an initial VR-eVST was performed ramping up from 0 to 15 RPM (90 degrees per second). The equipment subsequently ramped down to 0 RPM.
3. **Remolded VR-eVST:** Without repositioning the equipment, a second ramped VR-eVST test was conducted on the same in-situ specimen to the same RPM. This aimed to observe the behavior of the disturbed sample under the same testing conditions.
4. **Sample Collection and Analysis**: Following the VR-eVST tests, an 8-liter fluid sample of the tested tailings was collected. This sample was split into two pails:
    - The first pail was sent to a commercial laboratory for constituent analysis.
    - The second pail was delivered to NAIT for rheology testing.
5. **Stepped VR-eVST**: At approximately a 1m horizontal offset from the original test point, a third VR-eVST was performed using a step-up rate hold methodology at rotation rates between 0.3 and 90 degrees per second. This was conducted to investigate the rheological properties of the tailings under varying shear rates.

In total, the research work comprised fifteen VR-eVST tests (three of which are presented in Figure 1), the collection of five fluid samples, and three GCPTu (one of which is presented in Figure 2). It is important to acknowledge that the data set is relatively small and limited to a single operating mine.

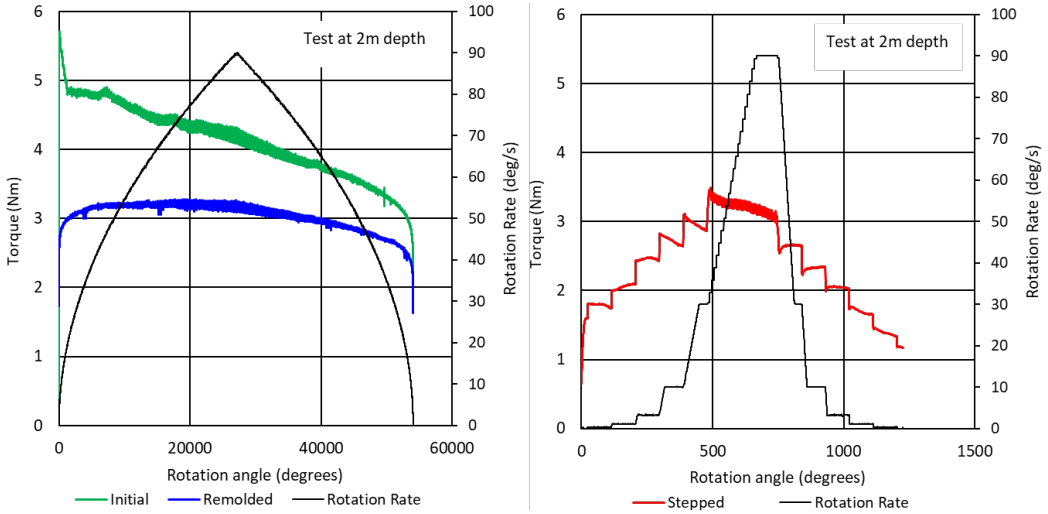


Figure 1: Example VR-eVST rotation curves from ramped test (left) and stepped test (right)

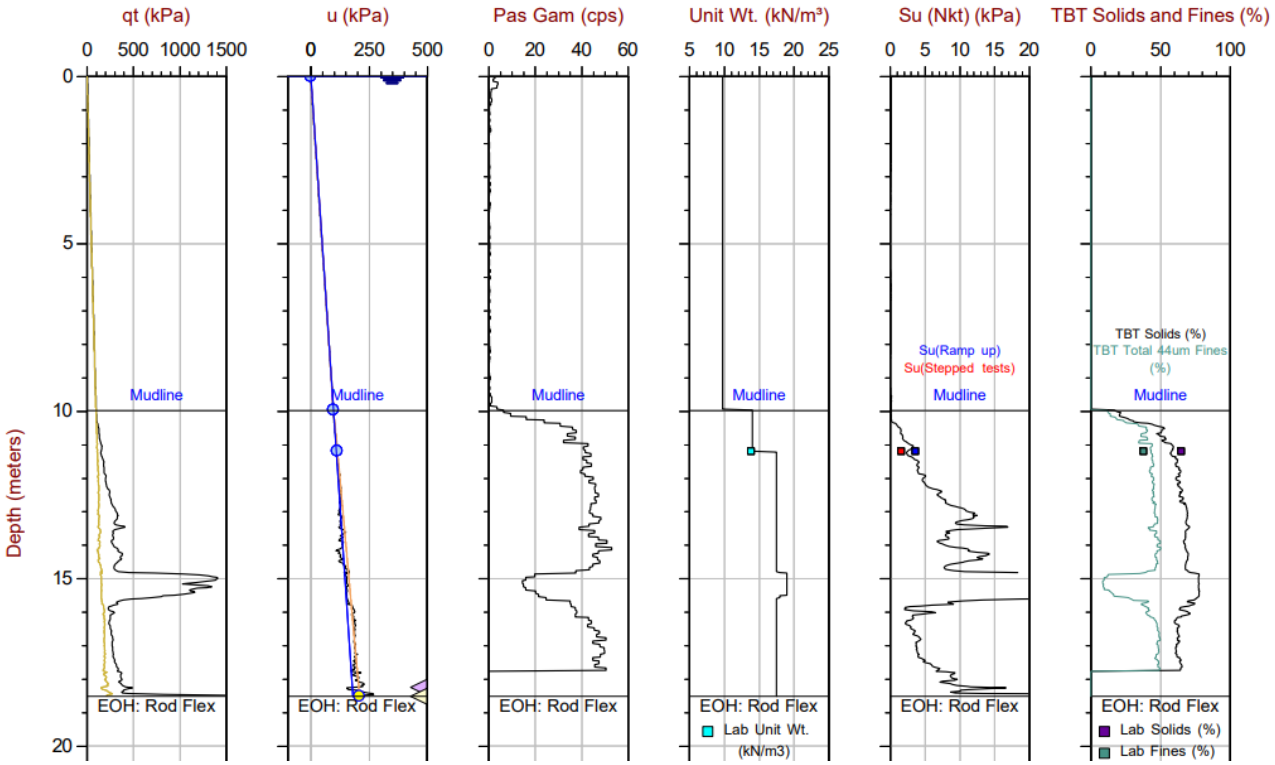


Figure 2: Example GCPTu Plot with annotated key features at location D.
Unit weights were determined using the equilibrium fluid pressure in fluid behaving materials, and soil behavior type (SBT) zones (Robertson et al., 2009) in non-fluid tailings, SBT zones 0-3 were assumed to have a unit weight of 17.5 kN/m³. Continuous profiles of solids and 44µm fines from tailings behavior type (TBT) (Entezari et al., 2023)

The VR-eVST torque load cells were calibrated ensuring a linear relationship between the load cell recorded torque and the applied torque at a rate of 1:1 (Figure 3). The lowest value on the torque calibration curve was 0.74 Nm and 0.76 Nm dependent on the instrument used, defining the sensitivity limits. The torque range for the field tests varied between 1 and 45 Nm, with the full range output of the VR-eVST being 100 Nm, indicating linearity of the torque load cell, and field measurements fell within the tool's operating range despite the low shear resistance of the fluid tailings (Figure 3).

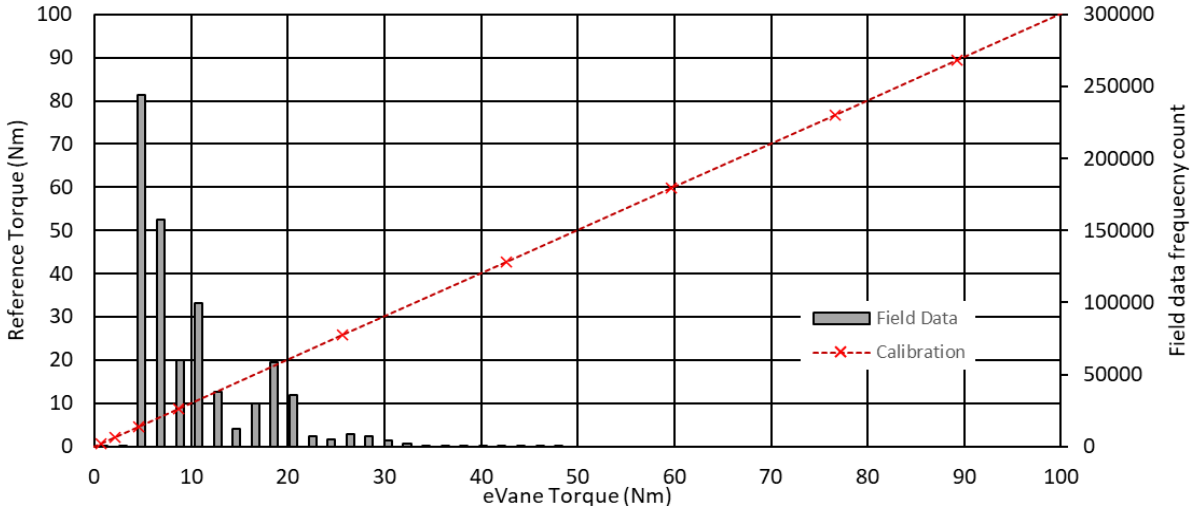


Figure 3: Vane calibration co-plotted with a histogram of the field measured torque showing the deployed ranges of the ramped VR-eVST, at all test sites

Laboratory control reference

Laboratory testing was undertaken as a control to validate the in-situ results. The samples gathered from the five test locations, were shipped and retested in a similar but scaled down shearing protocol on a Brookfield RST rheometer. The use of a slim profile blade rather than a concentric cylinder aims to minimize sample disturbance during instrument insertion reducing the impact on the shear-history dependent fluids properties. For polymer-treated materials, wall slips are a critical concern. Wall slip arises from a localized near-wall solids depletion effect, leading to artificially lowered measurements. When rotating in a fluid exhibiting a yield stress, the fluid within the vane blades rotates as a solid body. Consequently, yielding occurs within the fluid itself rather than at the boundary between the fluid and a smooth solid surface, significantly reducing the likelihood of wall slip errors (Nguyen and Boger, 1985). The majority of laboratory confirmation testing was conducted using a small vane (L = 40 mm, D = 20 mm), however a larger vane (L = 80mm, D = 70mm) was also used to conduct a portion of the tests to increase the full-scale torque (FST).

Analysis

Calculating viscosity and yield stress of non-Newtonian fluids depends heavily on measurement protocol,

geometry, and proper model fit. For this study, the Bingham Model analysis for the in-situ measurements was confined to the ramp-down data only. The thixotropic complexities of the tailings slurries had mostly been removed by a period of shearing, allowing the calculations to be performed on a relatively steady-state fluid. The data was plotted as torque response to imposed vane rotation speed and the Bingham plastic fluid model has been applied. The model is defined by Equation 1:

$$\tau = \mu_p \gamma + \tau_B \quad (1)$$

where τ= shear stress, μ_p = plastic viscosity, γ = shear rate and τ_B = Bingham yield stress.

For a rotational rheometer it is more useful to consider behavior in terms of rotational angular velocity and torque response. The equation describing Bingham plastic fluid behavior in concentric cylinder geometry is described Shook & Roco, (1991), and can be rearranged for a torque response as:

$$T=4\pi L[(R_1^2 R_2^2)/(R_2^2-R_1^2)]\mu_p\omega+4\pi L\ln(R_2/R_1)[(R_1^2 R_2^2)/(R_2^2-R_1^2)]\tau_B \quad (2)$$

where T= Torque, [N.m], L= cylinder length [m], ω = Angular velocity [rad/s], R_1= Radius of rotating inner cylinder [m] and R_2 = Radius of stationary cup [m].

By assessing the torque and angular velocity of the vane rotation at both field scale and laboratory scale, and determining the slope and y-intercept of the linear line, Equation 2 can be recognized as:

$$\text{Slope}= 4\pi L[(R_1^2 R_2^2)/(R_2^2-R_1^2)]\mu_p \quad (3)$$

$$\text{Intercept} = 4\pi L\ln(R_2/R_1)[(R_1^2 R_2^2)/(R_2^2-R_1^2)]\tau_B \quad (4)$$

Example results are presented in Figure 4, where the slope and intercept from the linear portion of have been identified. The "ramp-down" results from the "peak" rotation sweep were preferentially used in the calculations, as the initial ramp up results have inherent breakdown in tailings structure due to thixotropic effects not adequately covered by the Bingham fluid model used at this stage in research.

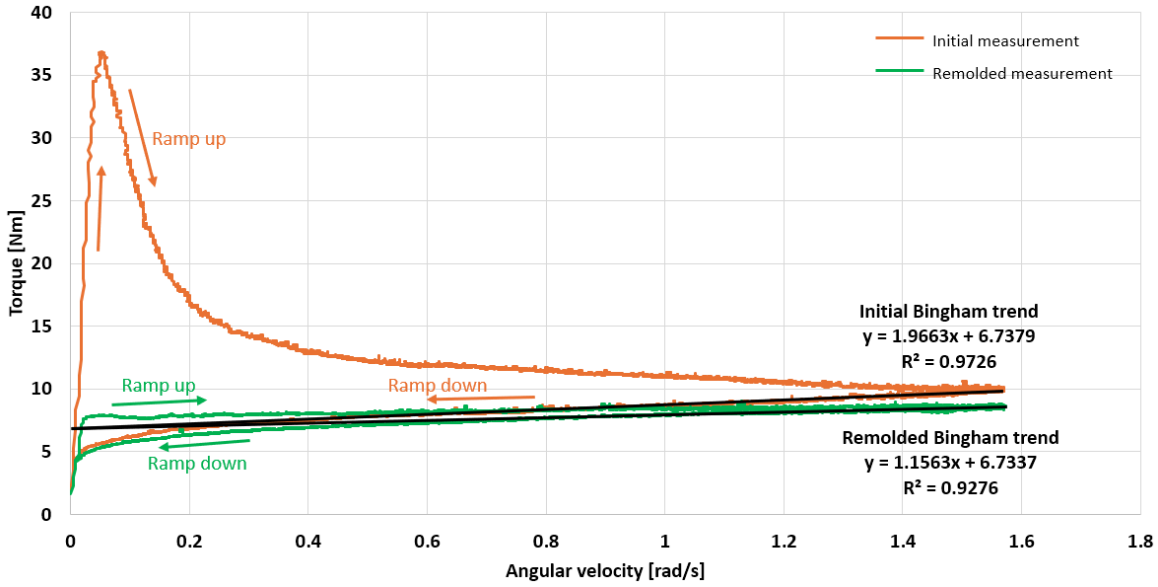


Figure 4: Interpretation of the initial VR-eVST and remolded VR-eVST at 8.3 m (Location B)

Both L and R_1 are known constants depending only on the geometry on the vane. For the laboratory case of a vane rotating within a large container, the shear at the edge of the rotating surface is a maximum, that decays exponentially outwards due to frictional losses. When the local shear stress decays past the yield stress of the fluid, the fluid at that radial position and beyond is considered to be unsheared, and essentially behaving as a solid. In the case of a vane rotating in a sufficiently large container (such as a tailings pond), where the container radius is sufficiently larger than R_2, the vane may be considered to be rotating in an infinite medium. Under these circumstances, R_2, representing the radius of the sheared area, is not clearly defined.

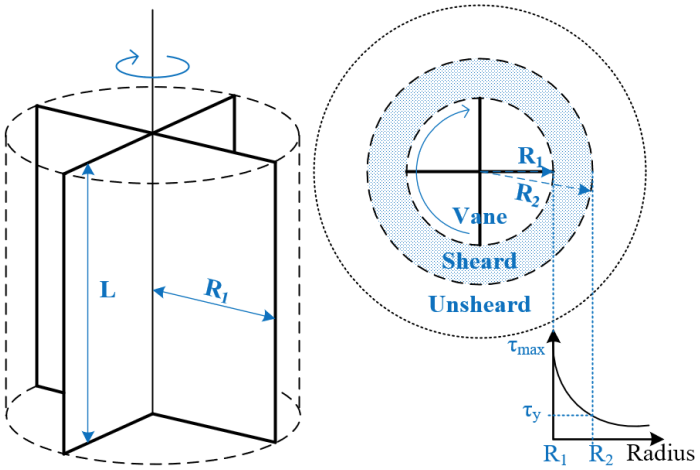


Figure 5: Representation of the vane geometry, illustrating the inner radius (R_1) and the radius of the sheared area (R_2).
Cylindrical shear profile is also shown (Fischer, 2007). Diagram is not to scale

To conduct the calculations at this preliminary stage of method development, R_2 was determined via iterative calculations to assess the relationship between an assumed value of R_2 and calculated plastic viscosity and Bingham yield stress. It was noted that both plastic viscosity and Bingham yield stress initially changed significantly for small values of R_2, but remained constant beyond a point. Assuming the calculated critical point to be R_2 allowed for the calculation of rheological properties for this early study. Using this methodology, for the field vane tests, R_2 was assumed to be 0.3 m, whereas R_2 at the laboratory scale using the small vane was assumed to be 0.02 m. A simplifying assumption was made that R_2 remained constant through the duration of testing. These assumptions for R_2 will be refined in ongoing studies.

In support of Objective 2, the stepped VR-eVST tests were analyzed to understand how shear stress develops at different rotation speeds (between 0.3 and 90 degrees per second) considering an average shear stress both increasing and decreasing rotation rates. For each rotation speed, shear stress was calculated in accordance with ASTM D2573/D2573M – 18.

Results

Viscosity and yield stress

The field VR-eVST tests conducted gave calculated values for plastic viscosity ranging between 40 Pa.s and 124 Pa.s, as presented in Table 1. These values are comparable to model suspensions of kaolinite and bentonite clay at similar compositions to the measured slurries, and other laboratory testing on true oil sands tailings (Piette et al., 2022; Shakeel et al., 2021). The calculated viscosity and yield stress aligns with plausible values with respect to the depth, location, solid content, and density of the tailings.

Table 1: Bingham plastic fluid properties calculated based on field data from initial VR-eVST

Location	Density Kg/L	Depth (m)	Initial VR-eVST field data results			Remolded VR-eVST field data results		
			Plastic Viscosity (Pa.s)	Bingham Yield Stress (Pa)	Peak Su from ramp up (kPa)	Plastic Viscosity (Pa.s)	Bingham Yield Stress (Pa)	Remolded Su from ramp up (kPa)
A	1.23	2.0	40.31	90.63	0.436	21.50	78.38	0.245
A	1.67	4.0	79.20	138.96	2.376	10.82	134.62	0.351
B	1.27	8.3	85.19	216.43	2.813	51.12	214.74	0.661
C	1.66	9.7	–	–	1.356	–	–	0.243
D	1.41	11.2	123.52	445.13	3.595	76.83	521.19	1.438

As shown by Figures 1 and 4, and Table 1, viscosity values for the tailings fluids continue to decrease after remolding shear until reaching a state of fully sheared structural equilibrium. At the current phase of study, the initial VR-eVST values were preferentially chosen as they are sufficiently stable to allow measurement, yet more representative of the in-situ characteristics of the tailings fluids. It should be noted that there was no observable trend in how much the calculated viscosity decreased following remolding. These thixotropic effects are likely sample dependent, and are influenced by solids content, clay content, flocculant content, and the water chemistry of the sample.

In contrast, the laboratory data, as presented in Table 2 seem to significantly underrepresent the viscosity and yield stress compared to the field values. The values appear erratic without trends occurring with respect to depth, location and density. The smaller vane used in laboratory testing may be partially at fault for the lower readings, as the rheometer was only able to reach 2.5% FST. For typical rheometer operations, 10-30% FST is recommended. However, viscosity values measured using the laboratory rheometer did not increase significantly after switching to the larger diameter vane, which was able to achieve 50% FST. The discrepancy between laboratory and in-situ data was expected due to the thixotropic nature of tailings slurries and shear break during the sampling, transport, and homogenization for required laboratory testing. At both field scale and laboratory scale, the sample collected from location D at 9.7m

consistently resisted measurement. This was likely due to high sand content in this sample leading to a settling, non-homogenous suspension over the duration of testing. Heterogeneous fluids are known to cause difficulties for rheological measurements due to the constantly changing solid content of the sample. In the case of a laboratory rheometer, where the vane spindle is positioned close to the vessel bottom, the formation of a sand bed may act as an additional brake to the vane rotation. It is currently undetermined at what sand-to-fines ratios rheological measurements become unstable due to settling suspensions and is an opportunity for future study.

Table 2: Bingham plastic fluid properties calculated based on laboratory data

Location	Depth (m)	Laboratory results from small vane		Laboratory results from large vane	
		Plastic Viscosity (Pa.s)	Bingham Yield Stress (Pa)	Plastic Viscosity (Pa.s)	Bingham Yield Stress (Pa)
A	2.0	1.09	55.98	0.147±0.044	72.86±1.238
A	4.0	0.52±0.009	51.69±0.366	0.431±0.020	52.21±0.086
B	8.3	1.155±0.02	24.85±1.551	–	–
C	9.7	–	–	–	–
D	11.2	2.464±0.036	149.99±2.771	–	–

When comparing the viscosity determined from VR-eVST field data from the adjacent CPTs, there is strong agreement between the cone resistance (q_t) (averaged over vane length) and viscosity values. This correlation, if supported by future studies, stands to add a valuable interpreted parameter to a CPTu test; it also suggests fluid tailings viscosity may be related to similar factors influencing penetration resistance in fluid tailings, such as stresses and fabric.

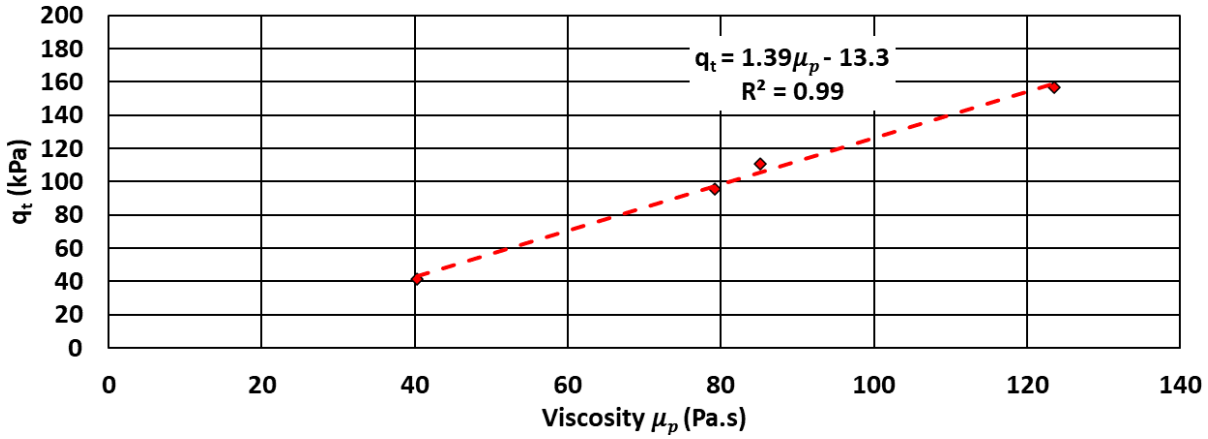


Figure 6: Relationship between viscosity from VR-eVST field data and cone resistance (qt) from adjacent CPT plots. Data is from the initial ramped VR-eVST at locations A, B, and D

Shear stress development

The results for the field VR-eVST tests, focusing on the shear stress calculated for each held vane speed have been presented in Figure 7 on a linear scale and Figure 8 on a log-log scale, both increasing speed and decreasing speed data has been considered. It is challenging to decern a trend on the linear-linear data, though some curvature towards a "U-shape" is apparent, occurring at low vane rotation speeds during the increasing speed part of the test. This trend is not apparent when the vane rotation speed is decreased.

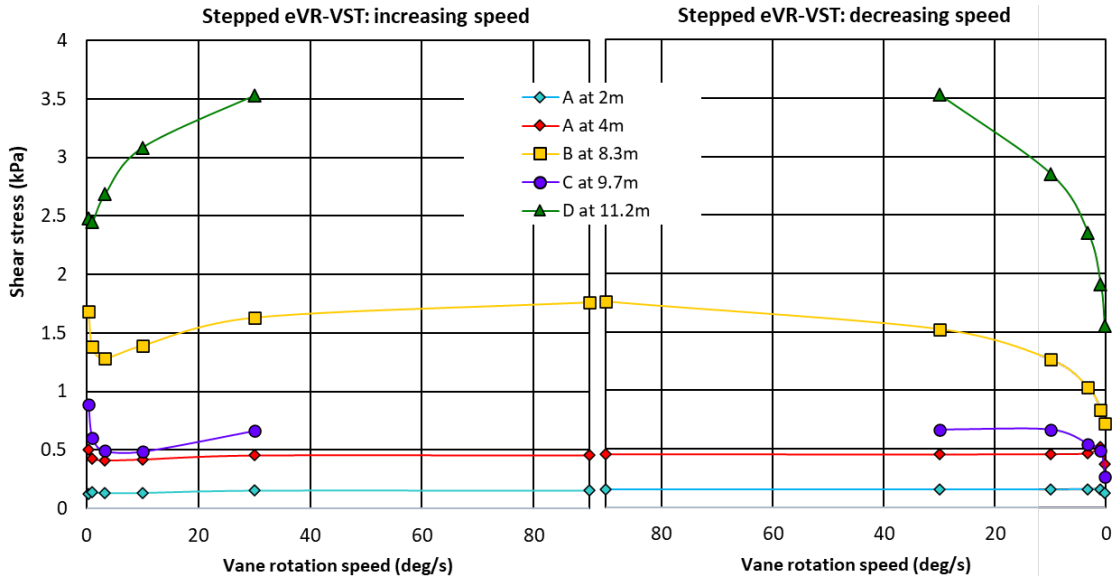


Figure 7: Comparison of the stepped eVR-VST increasing in speed and decreasing in speed

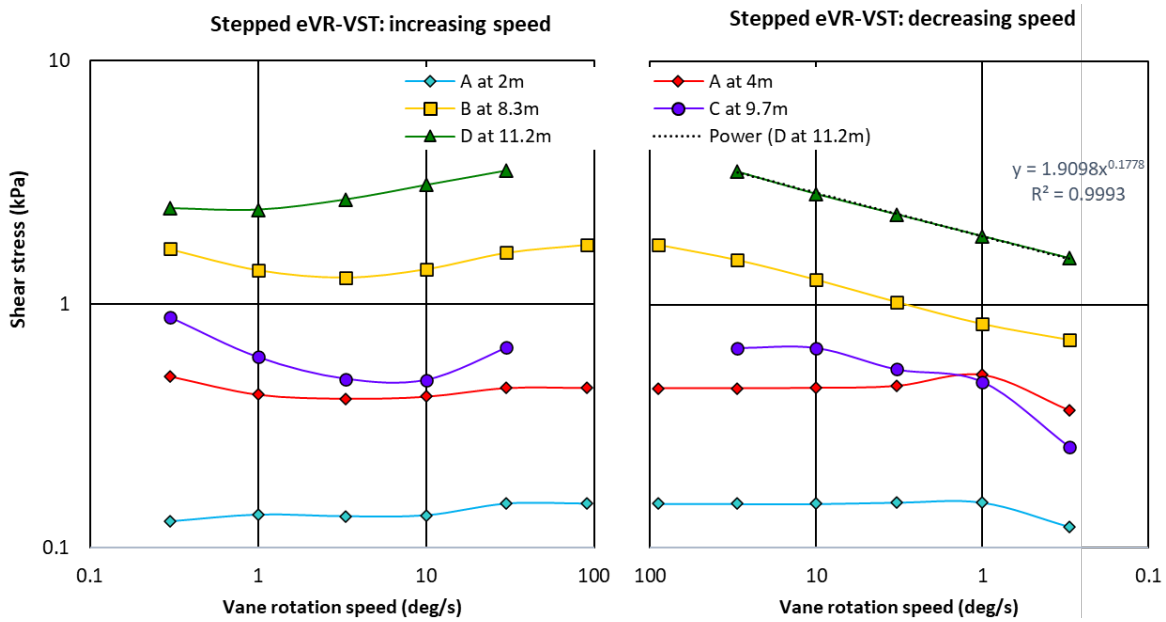


Figure 8: Comparison of the stepped eVR-VST Increasing in speed and decreasing in speed on a log-log scale. D shows the selection of the rate effect parameters

When plotted on a log-log scale, the U-shape trend becomes more apparent in tests B, C, and D during the increasing speed phase, while a linear trend is observed during the decreasing speed phase. For the two tests in location A no significant rate dependency appears to occur. This is likely due to the distinct treatment strategies between Location A and Locations B, C and D.

Work conducted by Yafrate et al., considers the rate-dependent effects on resistance for full flow penetrometers, fitting rate effect parameters to the measured data. The data obtained through decreasing the speed has been assessed in this manner. A power trendline was found most appropriate for the data that showed rate dependency. Results are presented in Table 3.

Table 3: Rate effect parameters from stepped eVR-VST considering minimum undrained shear strength

Location	Undrained Shear Strength (kPa)	Constant	Exponent	R^2
A	0.12	No significant rate dependency		
A	0.40			
B	0.71	0.85	0.16	0.99
C	*0.26 (high sand content)*	0.40	0.19	0.81
D	1.5	1.91	0.18	0.99

Discussion

Several hundred million cubic meters of oil sands tailings need to be removed from containment and treated, often with polymer flocculants, to meet existing regulatory guidelines. The rheological properties of fluid tailings have typically been assumed conservatively low. However, as an oil sands facility matures, significant proportions of coarse sand particles from beach deposition suspend within the fluid tailings, creating dense and viscous fluid tailings that can be challenging to mobilize. As per Bugg et al. (2022), understanding the flow properties of tailings can enable process engineers to plan dredge moves to support re-processing of fluid tailings from existing tailings deposits and erroneously low laboratory rheology measurements can lead to incorrect predictions of coning during dredge operations. Additionally, if not understood, rheological variability can impact flow of the fluid tailings to a single point dredge, resulting in time consuming and expensive “targeted dredging”. The dredging of tailings may also be of interest in hard rock mining where re-processing tailings is becoming increasingly attractive.

In the alternative case (in which much of the tailings can be left in place through infilling), viscous fluids have been observed to mix with infilling sand, impacting the geotechnical properties of the resultant beach. Tailings planners influence the degree of mixing by controlling the thickness of deposited thickened fluid tailings layer, allowing for ageing periods, controlling the decant water depth, and rate of coarse tailings placement. If uncontrolled, this mixing could produce low strength tailings in the beach. When

controlled, mixing has been observed to produce geotechnically competent, fines enriched mixed deposits. The in-situ rheological properties of the fluid are the primary mechanism for determining when and where mixing occurs. From a dam safety and emergency planning perspective, understanding the flow properties of the contained fluid is necessary to predict run out distances in a breach scenario.

The field trial using the VR-eVST to measure rheological properties of oil sands fluid tailings produced promising results and requires further development. Measuring viscosity in-situ using vane geometry with an infinite boundary condition may better reflect the true nature of the shear-sensitive tailings, minimally impacted by sampling, transport, and handling. The presence of polymer in all samples at least partially impacted the results, as polymer treated samples are known to show rheomalaxis (Schramm et al, 2018).

Despite plausible values for plastic viscosity and Bingham yield stress calculated from VR-eVST, laboratory verification test results were significantly lower than the field-measured values. Lower-than-expected laboratory rheological measurements of tailings fluids were previously observed in industry (Bugg et al., 2022), and is the primary motivation behind the present research. In both the study by Bugg et al. and the present research, the likely cause of low laboratory measurements is the shear-induced breakdown in rheology of tailings, exacerbated by requisite sampling, transport, storage, handling, and homogenization prior to laboratory testing. The authors are presently developing validation methods to evaluate VR-eVST performance in the laboratory.

The findings presented show a decline in plastic viscosity and yield stress with cumulative shear. Reductions in viscosity and yield stress were observed between all initial and remolded tests, which are due to the breakdown of the material structure (thixotropy) of the tailings. Shear-thinning behavior can be captured more accurately by advanced rheological models such as Herschel-Bulkley and Casson (Saasen and Ytrehus, 2020; Kelessidis and Maglione, 2006) which consider pseudoplastic behaviors. While the Bingham model is suitable for initial studies, more advanced models should be explored in future research.

The data from the stepped tests was hypothesized to show a u-shaped curve, enabling the identification of a critical velocity providing a minimum shear response above which viscous effects cause increasing shear stress response. This phenomenon was not observed, likely due to the interplay between thixotropic response (fabric destruction) and simultaneous onset of viscous effects. Further work in partially drained mine tailings or soils would be useful to further test this hypothesis. Conducting a stepped test from high to low rotation speed is likely to yield the most representative data and be most compatible with the Bingham Model, without the inclusion of complexities associated with thixotropy.

This initial proof-of-concept study has a limited sample size and further study is ongoing. This includes a second phase of testing scheduled to expand the data set in non-polymer treated tailings and consider the impact which an infinite boundary condition has on results, investigating the use of

confinement around the VR-eVST vane, therefore defining a constant R_2. When unconfined it is expected that the shear boundary around the vane (as R_2) is dynamic and likely changes with total rotation and rotation rate, and thus R_2-R_1 becomes smaller at higher speeds. Further studies will also be undertaken to assess the utility of piezometric sensors, inclinometers, and thermal compensation in the VR-eVST, with an emphasis on the critical velocity and viscous effects in tailings subject to partial drainage under standard rates of shear, such as those commonly found in hard rock mill tailings.

Conclusion

The use of novel VR-eVST with protocols to measure the rheological properties of fluid tailings in-situ shows early promise, and provided viscosity and yield stress values that were physically reasonable. This study's findings indicate that in-situ data may be more representative than laboratory measurements. Observations from the VR-eVST show viscosity and yield stress reduced with cumulative shear in the field from the initial peak to remolded properties, therefore it would be expected that laboratory results after sampling, shipping, homogenization, sub-sampling would provide the lowest bound measurement of rheological properties. Tailings are known to exhibit shear-sensitive rheological behaviors, highlighting a need for in-situ measurements which minimize error due to handling. The viscosities obtained in-situ may influence both runout modeling, mixing and dredging operations.

Although the sample size is small, VR-eVST equipment appears to have reliably and efficiently measured rheological properties in fluids with shear strengths ranging from 0.1 kPa to 3.5 kPa. Remolded strengths obtained from the stepped hold tests and remolded VR-eVST tests are comparable, suggesting either method is appropriate to determine a minimum undrained shear strength. Additionally, there appears to be a strong relationship between plastic viscosity and the CPTu q_t.

Future work should expand the data set and consider applying the method of adjacent VR-eVST, each with a unique constant speed (Harvey et al., 2023), rather than the stepped method. This approach will provide a better understanding of peak rather than remolded strength and the relationship with vane speed.

Acknowledgements

The authors would like to thank Wale Akanni, Jared Young, Trae Whorms, and Mahdi Askaripour for collecting and analyzing the data, and Alice Zheng, Vitali Sakalou, and Roque Obusan for their efforts developing the VR-eVST. Lastly, we would like to thank the mine operator involved for their support.

References

American Society for Testing and Materials (ASTM). 2018. S*tandard Test Method for Field Vane Shear Test in Cohesive Soil. ASTM D2573 / D2573M-18.* ASTM International, West Conshohocken, PA.

Blight, G. 1968. A note on field vane testing of silty soils. *Canadian Geotechnical Journal* 5(3): 142–149.

Bugg, T., Bittner, T. and Derakhshandeh, B. 2022. Cone formation dynamics during dredging of oil sands tailings ponds – field observations and comparison with prediction of computational models. *IOSTC 2022*, Edmonton.

Entezari, I., McGowan, D., Glavina, J. and Sharp, J. 2023. Comparison between in-situ techniques to measure undrained shear strength of oil sands tailings. In G.W. Wilson, N.A. Beier, D.C. Sego, A.B. Fourie & D. Reid (eds), *Paste 2023: Proceedings of the 25th International Conference on Paste, Thickened and Filtered Tailings*, University of Alberta, Edmonton, and Australian Centre for Geomechanics, Perth, pp. 787–797, https://doi.org/10.36487/ACG_repo/2355_62

Fisher, D., McClintock, T., Bartholomew, R. and Smith, J. 2007. The bucket rheometer for shear stress-shear rate measurement of industrial suspensions. *J. Rheol.* 51(3): 569–582.

Harvey, J. Hogan, A. Obeidat, D. Contreras, I. and Kelly, S. 2023. Establishing a site-specific standard of practice for field vane shear testing in mine tailings. *Proceedings of Tailings and Mine Waste 2023,* Vancouver.

Kelessidis, V. and Maglione, R. 2006. Modeling rheological behavior of bentonite suspensions as Casson and Robertson-Stiff fluids using Newtonian and true shear rates in Couette viscometry. *Powder Technology*, 168(3): 134–147.

Litzenberger, C. and Sumner, R. 2004. Flow behavior of kaolin clay slurries. *Proceedings of the 16th International Conferemce on Slurry Handling and Pipeline Transport: Hydrotransport* 16: 26–28.

Nguyen, Q. and Boger, D. 1985. Thixotropic behavior of concentrated bauxite residue suspensions. *Rheologica Acta* 24: 427–437.

Piette, J., Moud, A., Poisson, J., Derakhshandeh, B., Hudson, Z. and Hatzikiriakos, S. 2022. Rheology of mature fine tailings. *Physics of Fluids* 34(6).

Reid, D., Rodriguez, C., Fourie, A. and Tiwari, B. 2023. Partial drainage effects during vane shear tests with an emphasis on the measurement of remolded strengths. *Proceedings of Tailings and Mine Waste 2023,* Vancouver.

Robertson, P. 2009. Interpretation of cone penetration tests—a unified approach. *Canadian Geotechnical Journal* 46(11): 1337–1355.

Saasen, A. and Ytrehus, J. 2020. Viscosity models for drilling fluids – Herschel-Bulkley parameters and their use. *Energies* 13(20).

Sanders, R. S., Schaan, J., Hughes, R. and Shook, C. 2004. Performance of sand slurry pipelines in the oil sands industry. *The Canadian Journal of Chemical Engineering* 82(4): 850–857.

Schramm, L. 2018. Colloid Rheology. In *Emulsions, Foams, Suspensions, and Aerosols: Microscience and Applications*, 2nd ed.: 209–258. John Wiley & Sons, Inc.

Shakeel, A., Kirichek, A. and Chassagne, C. 2021. Rheology and yielding transitions in mixed kaolinite/bentonite suspensions. *Applied Clay Science* 211: 106206.

Shook, C. and Roco, M. 1991. *Slurry Flow: Principles and Practice*. Elsevier.

Sun, Y. 2018. Recovery of thickened kaolinite suspension properties through shear. Thesis, University of Alberta.

Mechanical Response of Plastic Fine Tailings under Constant Shear Drained Loading

Luis Vergaray-Astupina, Georgia Institute of Technology, USA
Jorge Macedo, Georgia Institute of Technology, USA

Abstract

Several case histories of tailings dam failures have highlighted that the instability onset in loose particulate materials can be triggered under prevailing drained conditions and stress paths that can be represented by constant shear drained loading. This study investigates the mechanical response of a plastic fine tailing, which has received limited research attention. The examined tailing has a fine content of 90% and a plasticity index of 14. Common coarse and intermediate materials exhibit distinct responses – either loose or dense – depending on their initial state. In contrast, this fine tailing exhibits predominantly a dense-type response, despite initial states above the critical state line (i.e., loose) due to their compressibility and states before the stress relief stage. This "mixed" response was interpreted using the critical state soil mechanics framework, and the underlying mechanism was postulated. This study advances the understanding of plastic fine tailings response, aligning with the Global Industry Standard on Tailings Management (GISTM) recommendations.

Introduction

Static liquefaction, often associated with the onset of instability in particulate materials under static loading, is commonly assessed under undrained conditions, highlighting the role of excess pore pressure development and the associated reduction in effective stresses (e.g., Jefferies and Been, 2015). However, static liquefaction can also occur under prevailing drained conditions. Previous case studies (e.g., Bishop, 1973; Zhu and Anderson, 1998; Olson et al., 2000; ICOLD, 2001; Morgenstern, 2001; Morgenstern et al., 2016, 2019) have highlighted the development of static liquefaction under prevailing drained conditions. For instance, the 1966 Sgurigrad TSF failure was caused by a pond level rise during three days of heavy rain (ICOLD, 2001). As the pond level increased, the mean effective stresses decreased, and the shear stresses changed marginally, triggering the liquefaction of the stored tailings. This process can be represented in the laboratory by considering a constant shear drained (CSD) stress path (e.g., Brand, 1981; Anderson and Sitar, 1995). The Baia Mare disaster in 2000 and the Buffalo Creek failure in 1972 are

examples of TSF failures caused by extreme weather conditions, similar to the Sgurigrad TSF failure. With global warming, extreme weather events are expected to become more frequent, increasing the risk of similar failures. Therefore, it is crucial to understand the mechanical response of mine tailings and other granular materials under unconventional loadings such as CSD stress paths.

Most previous efforts on assessing drained-type instabilities have been focused on natural sands with low or not fine contents (e.g., Skopek et al., 1994; Zhu and Anderson, 1998; Anderson and Sitar, 1995; Junaideen et al.. 2010; Wanatowski and Chu, 2010; Dong et al., 2015; Alipour and Lashkari, 2018; Rabbi et al., 2019). In contrast, previous studies considering mine tailings are scarce (e.g., Morgenstern et al., 2016; Morgenstern et al., 2019; Fotovvat et al., 2022), despite the importance of drained type instabilities in TSF case history failures. Initially, the efforts on mine tailings were limited to forensic studies after the recent failures with somewhat limited scope.

For example, Morgenstern et al. (2016) conducted three tests under CSD and LE (lateral extrusion – a variation of the CSD test where q is increased) stress paths in the assessment of the Fundão failure; Morgenstern et al. (2019) conducted 6 CSD tests in evaluating the Cadia failure. More recently, studies have increasingly assessed the response of mine tailings under CSD stress paths (e.g., Riveros and Sadrekarimi, 2021; Fotovvat et al., 2022; Fanni et al., 2022).

Riveros and Sadrekarimi (2021) evaluated the instability of gold tailings using a direct simple shear (DSS) device, finding similar instability mobilized friction angles between CSD and constant volume stress paths. Fotovvat et al. (2022) evaluated the response of two non-plastic mine tailings (fine contents of 17 and 84%) under triaxial CSD stress paths. Their study suggests that the instability stress ratios under CSD and triaxial undrained stress paths are consistent but are affected by the stress ratio (η) and state at consolidation. Fanni et al. (2022) approximated CSD conditions in a hollow cylinder to study anisotropic effects. The studies above are a step toward better understanding drained-type instabilities within the tailings community. However, given their relevance to recent TSF failures, more efforts focused on mine tailings are warranted, especially for materials with medium to high plasticity. This study contributes to this direction by studying the drained-type instability of a plastic fine tailing, by conducting experimental tests under CSD stress paths and interpreting the results under the critical state soil mechanics framework.

Investigated material

Figure 1 shows the particle size distribution of the mine tailing gradation investigated in this study. This material has a fine content (FC) of 91% and a plasticity index (PI) of 14. Using the Unified Soil Classification System (USCS), this material is classified as low to moderate plasticity clay (CL). Table 1 shows additional information on this material, including Atterberg limits, packing and particle size distribution indexes, and specific gravity. Figure 2 shows scanning electron microscope (SEM) images for

this material, showing that the fine particles dominate the matrix, with angular coarse particles floating around. X-ray diffraction analyses indicated that the material is mainly composed of quartz and chlorite, with traces of K-feldspar and other minerals (tin, copper, and molybdenum). The fine gradation has a significant amount of chlorite (a soft clay mineral), which likely caused the high PI of 14.

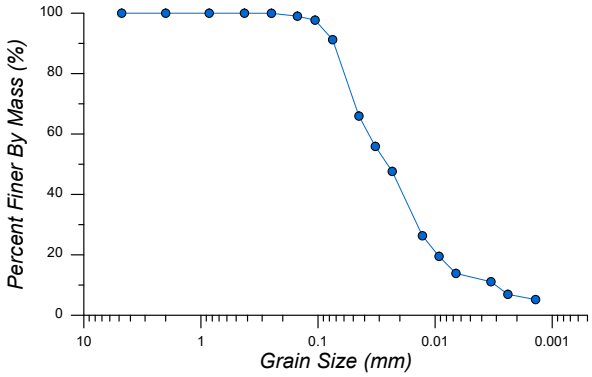
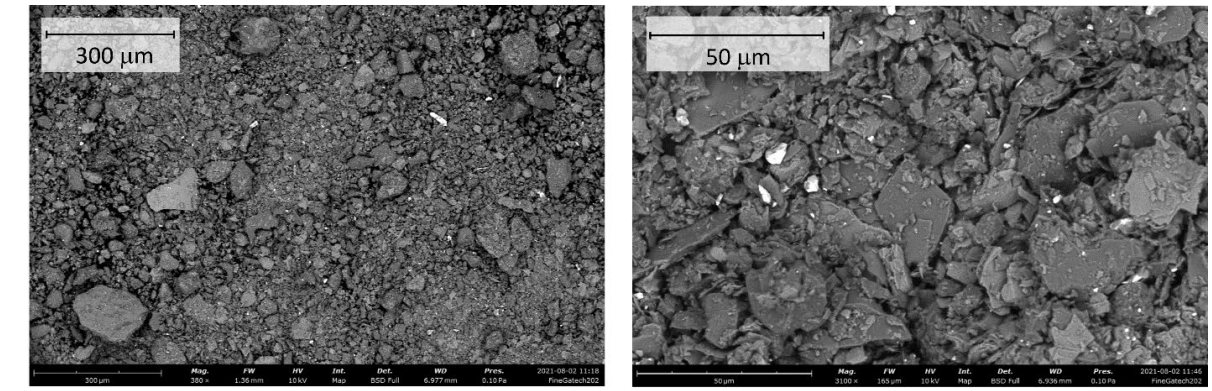


Figure 1: Particle size distribution



a) *b)*

Figure 2: SEM image of the fine tailings at two different magnifications

Table 1: Index properties of the mine tailing investigated in this study

Material		Fine tailing
Plasticity index	PI	14
Fine contents	FC	91
Specific gravity	G_s	2.90
Mean particle size	D_{50}	0.025
Coefficient of uniformity	C_u	14
Coefficient of curvature	C_{curv}	1.80
Mineralogy in %:(quartz, chlorite, and others)		57, 38, 4

Experimental setup

The equipment used in this study represents a state-of-the-art triaxial device. Two electromechanical water pumps are used to control the cell and back pressure; each of them has an electrical pressure transducer capable of controlling pressure and volume changes, with a precision of 0.2 kPa and 0.1 mm^3, respectively. The equipment also has an additional air pump to provide suction during water flushing before saturation. The data acquisition system allows automatic saturation, consolidation, and shearing for several stress paths under strain and stress-controlled conditions. The load control system is equipped with dynamic sensors, which are well suited to control stresses even at large rates of deformations. This is a desirable feature for CSD stress paths as the vertical and horizontal stresses need to be controlled, especially when approaching an instability condition where deformation rates are accelerated. This feature provides advantages relative to previous studies on CSD paths focused on sands with challenges in controlling stresses as the instability onset is approached (e.g., Rabbi et al., 2019).

Sample preparation

The samples were reconstituted using the moist tamping method (MT), with the end-of-test freezing procedure used to measure void ratios (e), as commonly used in tailings engineering (e.g., Reid et al., 2020). Specimens were prepared by mixing water to achieve a moisture content of approximately 20% , allowing the specimens to cure for about 12 hours. The specimens were then reconstituted in seven layers using the "under-compaction" method (Ladd, 1978) to achieve a uniform specimen with a targeted void ratio. The diameter of the samples is D=2.7 in, and the height-to-diameter ratio (H/D) was fixed at 2 to mitigate potential end platen effects (Lade et al., 1996). Following the recommendations of Viana da Fonseca et al. (2021), a small suction was applied to place the specimen into the triaxial cell, and a rubber suction cap was placed at the top of the specimen to avoid tilting due to misalignment. Once the specimen was placed, the cell was filled with water, and a small p' (<20 kPa) was applied. Then, the specimen was flushed with deaired water, before saturation using a back pressure ramp saturation method.

This saturation method steadily increases the cell and back pressures to avoid sample collapse while keeping a constant small p' value (<20 kPa). A back pressure of 750 kPa was used, and Skempton's B values higher than 0.98 were considered to represent saturated conditions. The saturated specimens were then consolidated, and once the desired confinement in the range of 50–350 kPa was achieved, the specimens were sheared under strain-controlled conditions in the standard triaxial tests and under stress-controlled conditions in the CSD tests. In the CSD tests, the samples were sheared in two stages. First, a triaxial loading was imposed until the desired shear stress (q) was achieved. Then, in the second stage (the

stress relief stage), the vertical and horizontal stresses were decreased by the same magnitude to decrease p' at a constant q. The samples were sheared at stress reduction rates (dp' / dt) of 0.25 kPa/min.

Response in triaxial tests and critical state line assessment

Figure 3 shows the material's stress-strain response (i.e., axial strain, ε_a, versus q) and stress paths (i.e., p' versus q and e versus p') under standard triaxial drained (TxC-CD) and undrained (TxC-CU) loadings. Macedo and Vergaray (2022) defined terminology to describe the response of mine tailings under TxC-CU loadings as i) full softening, where there is a drop from peak to residual conditions, and q is close to zero at large strains; ii) partial softening, which is similar to full softening, but q is not close to zero; iii) limited flow, when there is a transition from contractive to dilative response after the peak (i.e., q initially decreases after the peak, but then increases); and iv) non-flow when q tends to increase. The full/partial softening cases are particularly associated with static liquefaction in the literature (e.g., Jefferies and Been, 2015). In this context, the typical responses observed in the plastic fine tailing range from limited flow to non-flow, which is likely influenced by its large compressibility. The slope of the CSL (λ_e) and the PI can serve as proxies of compressibility (Macedo and Vergaray, 2022; Vergaray et al., 2023). The λ_e of this material is about two times the typical values of sands (e.g., λ_e ~ 0.02 to 0.04, see Jefferies and Been, 2015); hence, highlighting its significant compressibility.

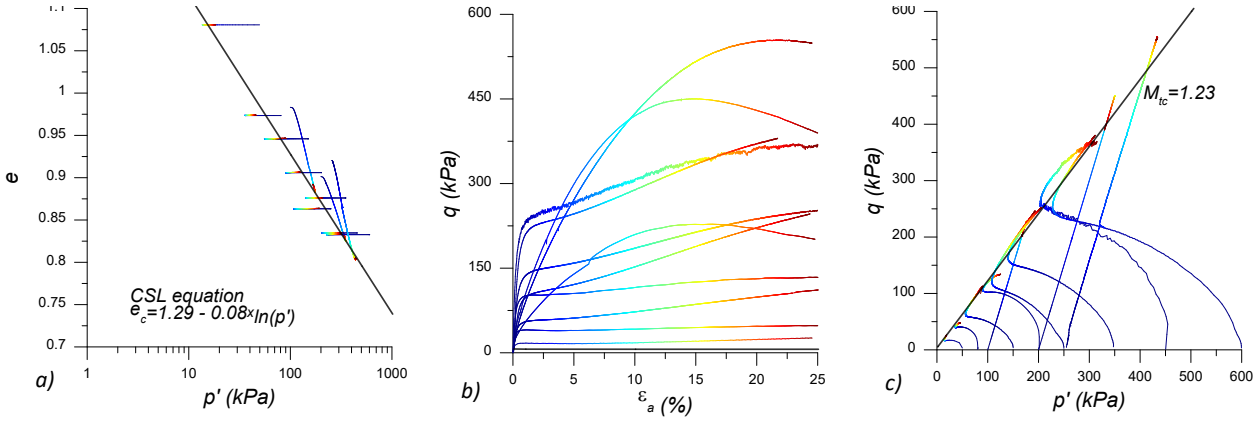


Figure 3: a) Critical state location, b) stress-strain response, and c) stress paths in the $p' - q$ space of the plastic fine tailing

Response under CSD stress paths

Figure 4 presents typical responses of CSD tests in the $e - p'$ (left column), $p' - q$ spaces (middle column), and the evolution of ε_a versus p' (right column) for the examined tailing, considering different initial states as defined by the initial state parameter (Been and Jefferies, 1985), which is expressed as $\psi_0 = e_0 - e_{cs}$, where e_0 and e_{cs} are the initial and critical state void ratios for the same p'. ψ_0 was estimated using the

CSLs defined in the previous section, which are also shown in Figure 4 for reference. Also, the instability points in Figure 4 (yellow starts) are obtained using a second-order work-based criterion (Hill, 1958) and, for now, are only presented for illustrative purposes.

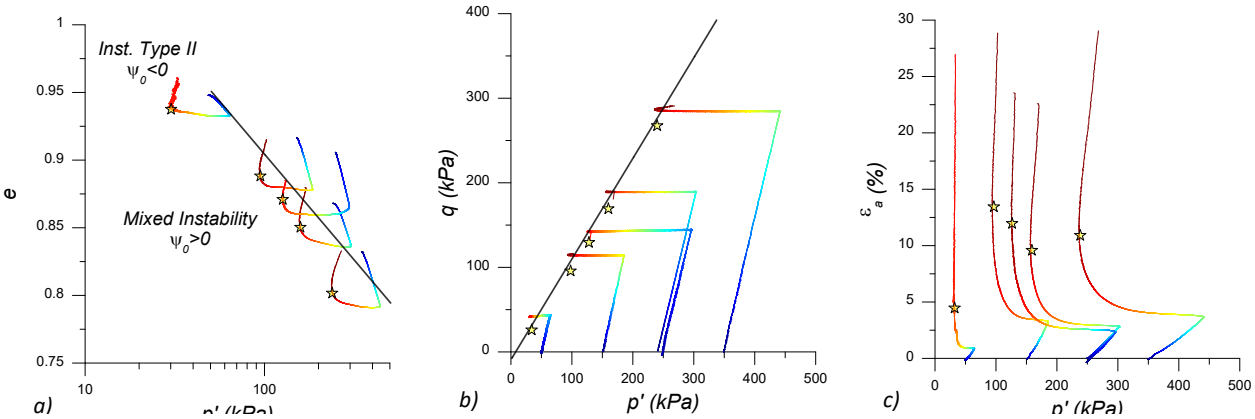


Figure 4: CSD response of the plastic fine tailing in the a) $e - p'$, b) $p' - q$, and p' versus ε_a plots

Typically, loose states (i.e., above the CSL – $\psi_0 > 0$) in sands make the initial part of the response (triaxial loading) contractive (Figure 5a). Then an initial volume increase in the stress relief stage is followed by a subsequent decrease after the instability onset, where large deformations occur. In addition, the stress path in the $e - p'$ space stays above the CSL and the instability stress ratio (η_{IL}) is lower than the critical stress ratio (M_{tc}). This type of instability has been defined as Type I by Alipour and Lashkari (2018). In initial dense samples (i.e., below the CSL – $\psi_0 < 0$) in sands, the volume mainly increases before and after the instability onset, with the stress paths in the $e - p$ space staying below the CSL and crossing the M_{tc} (Figure 5b) in the $p' - q$ space (i.e., $\eta_{IL} > M_{tc}$). As per Alipour and Lashkari (2018), this constitutes a Type II instability.

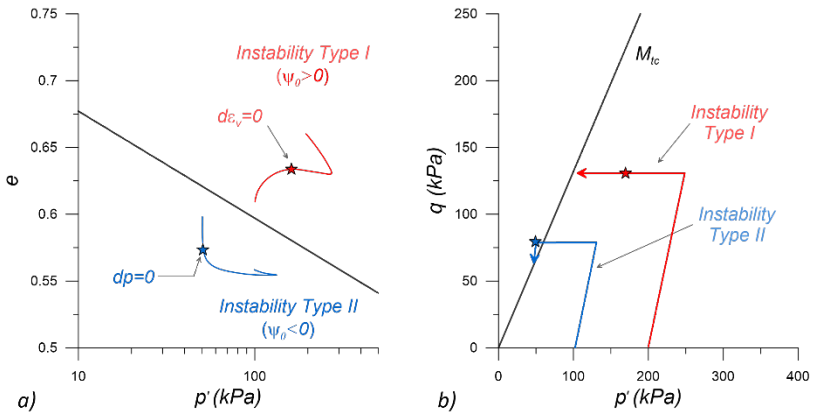


Figure 5: Instability responses (Type I and II) in CSD tests in the a) $e - p'$, and b) $p' - q$ spaces

However, the response observed on this plastic fine tailing differs from the typical response observed in clean sands (e.g., Junaideen et al., 2010; Wanatowski and Chu, 2010; Dong et al., 2015; Alipour and Lashkari, 2018; Rabbi et al., 2019), which are illustrated in Figure 5. In terms of the instability observed on the fine tailing, it is first relevant to highlight that the states after consolidation and before the CSD stress relief phase are close to the CSL, as shown in Figure 4. This is attributed to the significant compressibility reflected in a large Γ (1.29) and λ_e (0.08), which correspond to the 84th percentile of the ranges provided by Macedo and Vergaray (2022).

Thus, the "high altitude (i.e., high Γ)" of the CSL line in the $e - p'$ space and the significant compressibility result in initial states close to the CSL before the stress relief in the CSD loading, which, in turn, affects the tradeoff of $d\varepsilon_v^e$ and $d\varepsilon_v^p$. When $\psi > 0$, during initial stress relief, $d\varepsilon_v^e$ is negative (p' decreases), and $d\varepsilon_v^p$ is positive ($\psi > 0$). Since the state is close to the CSL, there is not enough room to build up the required $d\varepsilon_v^p$ to counteract $d\varepsilon_v^e$, a condition required for a Type I instability, as postulated in Bokkisa et al. (2023) and Vergaray and Macedo (2024). As the stress-relief stage advances, the stress path in the $e - p'$ space eventually crosses the CSL, and $d\varepsilon_v^p$ becomes negative. Consequently, $d\varepsilon_v = 0$ cannot be zero, and a Type II instability occurs. This study describes mixed instability as this instability type on initially loose specimens ($\psi > 0$) where a Type I instability would be expected, but a Type II instability occurs.

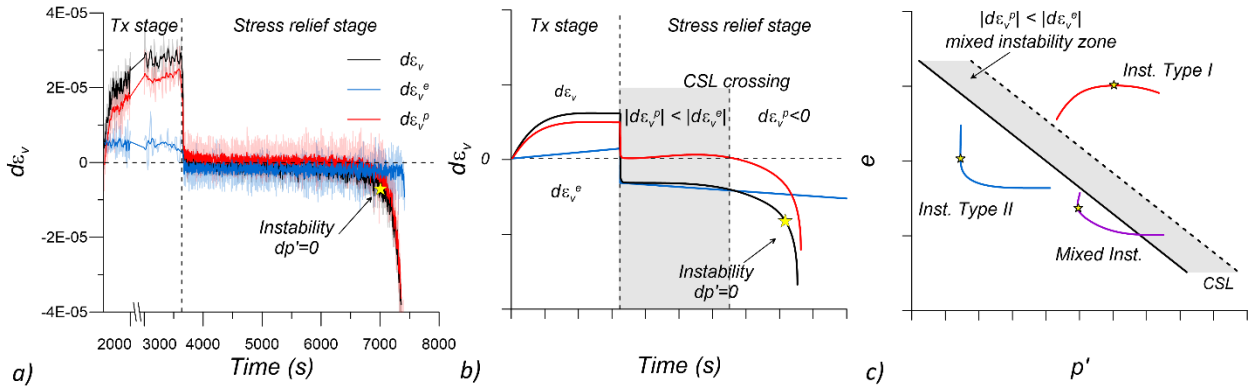


Figure 6: a) Experimental-based and b) schematic variation of ε_v components in a mixed instability. c) Schematic representation of the mixed instability zone in the $e - p'$ space

Figure 6 shows an example of the experimental variation ε_v for the instability just described, considering a test with a positive initial state (ψ~0.01). ε_v components were estimated as in the previous section. Figure 6b shows a schematic generalization. The observations just discussed indicate that there is a region above the CSL within which a mixed instability occurs, i.e., the initial ψ is positive, but instability manifests as Type II. If the state before stress relief is within this region or below the CSL, the response will be similar to that of an initially dense material. If the state is above that region, the response will be

similar to that of an initially loose material. Figure 6c illustrates the described concept schematically. The authors are unaware of previous efforts unraveling the mechanisms behind this instability type as conducted in this study. Previous efforts to assess CSD stress paths in materials with high FC and plasticity are limited and mostly focused on natural soils. For instance, the CSD tests from Anderson and Sitar (1995) on colluvial soils (FC~95%, PI=19), and Xu et al. (2011) on loess (FC=70-85% and PI=19) seem to suggest a mixed instability; however, definitive conclusions cannot be drawn as the CSL assessment is either not fully detailed (Anderson and Sitar, 1995) or not available (Xu et al., 2011).

Finally, it is also instructive to inspect the post-instability responses. Figure 7 shows typical responses after loss of control. In this case, Δu after instability is negative, increasing p', which results in an additional η drop. The $p' - q$ stress path tends to go to the critical state with a tendency to increase q, resembling the hardening behavior observed for this material in the Tx-CU tests. Parallels could be drawn between the response of this fine tailing and the response observed during the Cadia case history failure, where the deposited tailings had a comparable compressibility with relatively large PI (19-24) and λ_e values (~0.05). For instance, after instability and loading control loss in the laboratory, negative excess pore pressure and a tendency to increase q towards the CSL, resembling typical hardening responses in TxC-CU tests, were observed. In the Cadia failure, the runout was controlled (defined by the subsequent forensic study as a slump), which might be associated with the hardening-type response post-instability just discussed.

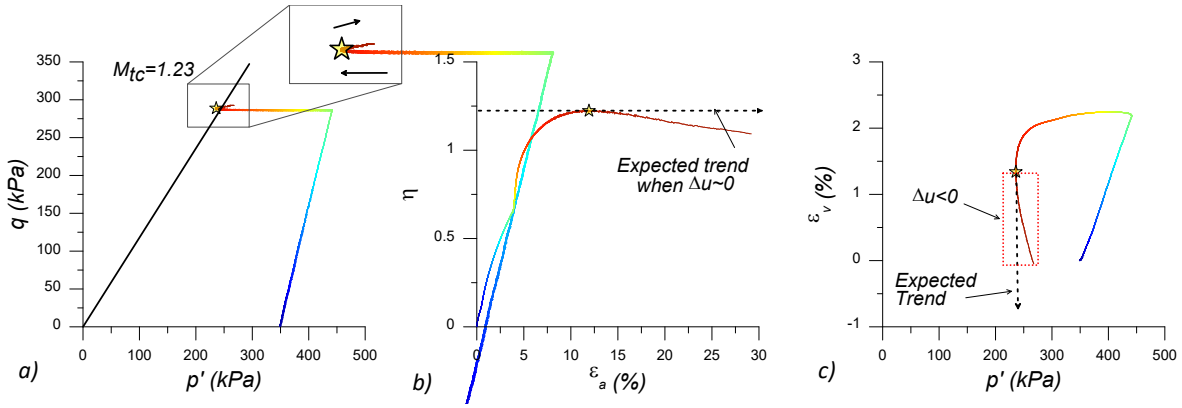


Figure 7: CSD test results in the a) $p' - q$, b) ε_a vs η, and c) p' vs ε_v

Conclusion

As discussed in the introduction, several TSF failures have occurred under prevailing drained conditions, highlighting the importance of drained stress paths. This is particularly important because any pre-failure indicators would be minimal, making it dangerous in terms of static liquefaction. This study assessed the mechanical response of a plastic fine tailing under CSD stress paths. Interestingly, in the examined material only Type II instability was observed, regardless of the initial state (i.e., loose, or dense). This response was described as mixed and attributed to the high compressibility of the fine tailing.

Acknowledgments

This study has been partially funded by the National Science Foundation (NSF) under the CMMI 2013947 project. The authors acknowledge the financial support provided by the PRONABEC program of the Peruvian government.

References

Alipour, M. and A. Lashkari. 2018. Sand instability under constant shear drained stress path. *International Journal of Solids and Structures* 150(10): 66–82.

Anderson, S.A. and N. Sitar. 1995. Analysis of rainfall-induced debris flows. *J. Geotech. Engng.* 121(7): 544–552.

Been, K. and M.G. Jefferies, 1985. A state parameter for sands. *Géotechnique* 35(2): 99–112.

Bishop, A.W. 1973. The stability of tips and spoil heaps. *Quarterly Journal of Engineering Geology* 6(3–4): 335–376.

Bokkisa, S.V., J. Macedo and A.L. Petalas. 2023. Fabric anisotropy effects on static liquefaction under constant shear drained loading. *Comput. Geotech.* 163: 105724.

Brand, E.W. 1981. Some thoughts on rain-induced slope failures. *Proceedings of the 10th International Conference on Soil Mechanics and Foundation Engineering:* 373–376.

Dong, Q., C. Xu, Y. Cai, H. Juang, J. Wang, Z. Yang and C. Gu. 2015. Drained instability in loose granular material. *International Journal of Geomechanics* 16(2): 04015043.

Fanni, R., D. Reid and A. Fourie. 2022. On reliability of inferring liquefied shear strengths from simple shear testing. *Soils and Foundations* 62(3): 101151.

Fotovvat, A., A. Sadrekarimi and M. Etezad. 2022. Instability of gold mine tailings subjected to undrained and drained unloading stress paths. *Géotechnique* 74(2): 174–192.

Hill, R. 1958. A general theory of uniqueness and stability in elastic-plastic solids. *J. Mech. Phys. Solids*. 6(3): 236–249.

ICOLD (International Commission on Large Dams). 2001. Tailings dams: Risk of dangerous occurrences: Lessons learnt from practical experiences. Paris: ICOLD.

Jefferies, M.G. and K. Been. 2015. *Soil Liquefaction: A Critical State Approach*. 2nd ed. Boca Raton, FL: CRC Press.

Junaideen, S.M., L.G. Tham, K.T. Law, F.C. Dai and C.F. 2010. Behaviour of recompacted residual soils in a constant shear stress path. *Canadian Geotechnical Journal* 47(6): 648–661.

Ladd, R. 1978. Preparing Test Specimens Using Undercompaction. *Geotechnical Testing Journal* 1(1): 16.

Lade, P., J. Yamamuro and B. Skyers. 1996. Effects of shear band formation in triaxial extension tests. *Geotechnical Testing Journal* 19: 398–410.

Macedo, J. and L. Vergaray. 2022. Properties of mine tailings for static liquefaction assessment. *Canadian Geotechnical Journal* 59(5): 667–687.

Morgenstern, N.R. 2001. Geotechnics and mine waste management – Update. *Proceedings of the Seminar on Safe Tailings Dam Constructions*, Gällivare, Sweden, 20–21 September 2001.

Morgenstern, N.R., M. Jefferies, D. Van Zyl and J. Wates. 2019. *Independent Technical Review Board*. Report on NTSF Embankment Failure. Ashurst Australia.

Morgenstern, N.R., S. Vick, C. Viotti and B. Watts. 2016. *Fundão tailings dam review panel*. Report in the immediate causes of the failure of the Fundão Dam. New York: Cleary Gottlieb Steen and Hamilton LLP. Available at: http://fundaoinvestigation.com/the-panel-report/

Olson, S.M., Stark, T.D., Walton, W.H. and Castro, G. 2000. 1907 Static liquefaction flow failure on the North Dike of Wachusett dam. *Journal of Geotechnical and Geoenvironmental Engineering* 126(12): 1184–1193.

Rabbi, A., M. Rahman and D. Cameron. 2019. Critical state study of natural silty sand instability under undrained and constant shear drained path. *International Journal of Geomechanics* 19(8): 04019083

Riveros, G.A. and A. Sadrekarimi. 2021. Static liquefaction behaviour of gold mine tailings. *Canadian Geotechnical Journal* 58(6): 889–901.

Skopek, P., N. Morgenstern, P.K. Robertson and D.C. Sego. 1994. Collapse of dry sand. *Canadian Geotechnical Journal* 31(6): 1008–1014.

Vergaray, L. and J. Macedo. 2024. Mechanical response of mine tailings under constant shear drained loading. *Journal of Geotechnical and Geoenvironmental engineering* 150(10): 04024082

Vergaray, L., J. Macedo and C. Arnold. 2023. Static and Cyclic Liquefaction of Copper Mine Tailings. *Journal of Geotechnical and Geoenvironmental Engineering* 149(5): 04023021.

Viana Da Fonseca, A., Cordeiro, D. and Molina Gómez, F. 2021. Recommended procedures to assess critical state locus from triaxial tests in cohesionless remoulded samples. *Geotechnics* 1(1): 95–127.

Wanatowski, D. and J. Chu. 2012. Factors affecting pre-failure instability of sand under plane-strain conditions. *Géotechnique* 62(2): 121–135.

Xu, L., F. Dai, L. Tham, X. Tu and Y. Jin. 2011. Landslides in the Transitional Slopes between a Loess Platform and River Terrace, Northwest China. *Environmental and Engineering Geoscience* 17: 267–279.

Zhu, J.H. and S.A. Anderson. 1998. Determination of shear strength of Hawaiian residual soil subjected to rainfall-induced landslides. *Géotechnique* 48(1): 73–82.

Development of Tailings-specific Correlations for Estimating Fines Content from CPT Data Using Artificial Intelligence Method for the Holden Mine

Mohammad Rashidi, Stantec, USA
Phillip E. Crouse, Stantec, USA
Summer Y. Sun, Stantec, USA

Abstract

Empirical correlations for estimating fines content from cone penetration test (CPT) data have traditionally been derived from various sites such as earth dams, road subgrades, and building foundations, encompassing a range of soil types. However, the applicability of these relationships to tailings facilities is limited due to the distinct mineralogy and behavior of slimes, fines, and coarse tailings compared to naturally deposited sandy, silty, and clayey soils found at typical sites. Consequently, there is a pressing need to develop tailored correlations specifically suited to the unique materials encountered in the tailings industry.

This paper addresses this gap by presenting a correlation developed from field data obtained through co-located CPTs and boreholes at a Holden tailings storage facility in Washington state. Artificial intelligence methods were employed to establish this correlation, utilizing laboratory-measured fines contents and CPT results. Specifically, genetic expression programming (GEP) techniques were employed to develop an equation based on data from 136 tested borehole samples.

The findings from our study underscore that the conventional empirical relationships tend to underestimate fines content, emphasizing the importance of tailoring correlations to the distinct characteristics of tailings dams. Comparison between the artificial intelligence method and traditional empirical relationships demonstrates that GEP yields more accurate estimations of fines content in tailings piles. The newly developed model offers a robust tool for predicting fines content from CPT data, facilitating improved characterization and management of tailings facilities.

Introduction

Traditionally, engineers use empirical correlations for estimating fines content from CPT data derived from various civil projects such as earth dams, road subgrades, and building foundations. These correlations,

which have been proposed by Davies (1999), Robertson and Wride (1998), and Suzuki et al. (1998), are well documented and encompass a wide range of soil types, such as sandy, silty, and clayey soils. However, the applicability of these correlations for tailings is limited due to the distinct mineralogy and behavior of slimes, fines, and coarse tailings, which differ significantly from naturally deposited soils (Russell et al., 2022).

Accurate estimation of fines content is necessary for deriving shear strength and liquefaction potential from standard CPT data, such as corrected equivalent penetration resistance in clean sand. Developing site-specific correlation can be very expensive for a project. It involves drilling numerous boreholes and conducting cone penetration tests (CPTs) in close proximity to establish a reliable relationship between laboratory test results from borehole samples and CPT data, such as cone resistance and friction ratio. This process can incur substantial costs due to the extensive fieldwork and analysis required. This paper presents a method to develop a site-specific correlation between CPT and fines content using genetic expression programming (GEP) techniques that is straightforward, reliable, and easily adapted to other sites. The GEP offers significant advantages over traditional statistical correlation methods. GEP excels at managing complex, high-dimensional data by automatically selecting and combining relevant features, which can uncover intricate, non-linear relationships that traditional methods might lack. This automatic feature selection and creation process simplifies the model-building effort and enhances predictive performance, especially in scenarios where interactions between variables are not straightforward (Koza, 1992).

The GEP technique was applied for a tailings pile characterization program for GISTM compliance at Rio Tinto's Holden legacy mine in Washington state. Artificial intelligence methods were employed to establish this correlation, utilizing laboratory-measured fines contents and CPT results. Specifically, genetic expression programming (GEP) techniques were employed to develop an equation based on data from 136 tested borehole samples. Using a traditional correlation underestimated the fines content in Holden tailings, which could result in unconservative shear strength and liquefaction potential.

The GEP technique provided a reliable site-specific correlation for Holden by leveraging laboratory-measured fines contents and CPT results to create a site-specific relationship between CPT and fines content. This paper provides a step-by-step process for using the GEP technique using data from 136 borehole samples at the Holden Mine site, in conjunction with co-located CPTs, employing Genetic Expression Programming (GEP) methods.

Site background and geotechnical data source

The Holden Mine is in north central Washington near Lake Chelan in the Cascade Mountain Range. The mine was owned and operated by the Howe Sound Company from 1937 until the cessation of mining activities in 1957. Processing of mine ores resulted in the construction of three tailings piles at the site's

TP-1, TP-2, and TP-3. These tailings piles were constructed using the upstream method with starter dams constructed with alluvial material, and are approximately 67, 120, and 84 feet high, respectively. The location of Holden Mine and the three tailings piles are shown in Figure 1.



Figure 1: Holden mine location and site general overview

Over the past 15 years, comprehensive geotechnical site investigations have been conducted on these three tailings piles to facilitate the closure of the tailings storage facilities, and more recently conformance to GISTM, as shown in Figure 2. Geotechnical investigation methods included cone penetration testing (CPT), sonic drilling, and mud rotary boreholes. The purpose of the recent investigations was to update tailings properties since reclamation was completed in 2016. Tailing properties were used for slope stability and deformation using critical state methods. An important component of critical state analyses is the accurate delineation of tailings layers with a narrow range of fine content since the critical state locus is sensitive to small changes in fines content (Jefferies and Been, 2016) for these layers.

The location of a total of 35 co-located CPTs and boreholes from the post-reclamation investigation is provided in Table 1. The average horizontal and vertical distances between these CPTs and boreholes were between 1 to 10 feet, providing data for developing the site-specific fines correlation. The particle size distribution for a total of 136 grab and in-situ samples from the bore holes and the soil behavior type index (Ic) parameter determined by the CPT were used to develop site-specific relationships for fine content estimation for CPT locations without borehole data.

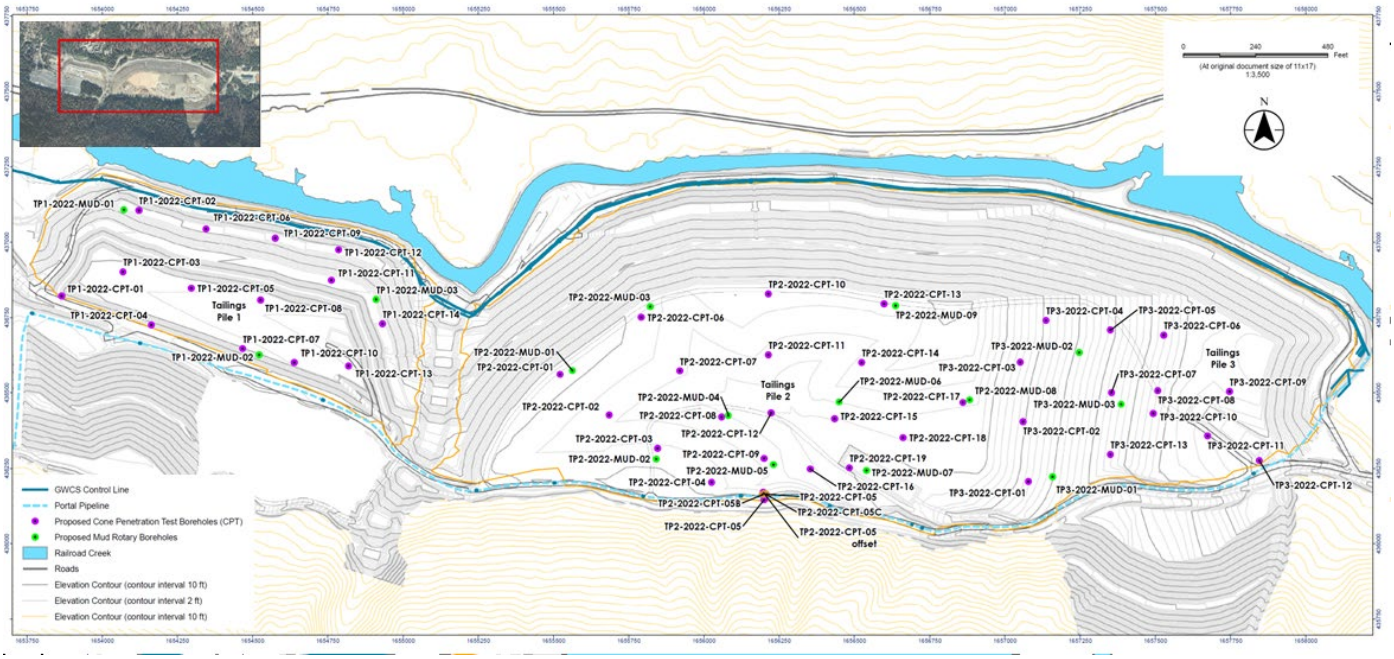
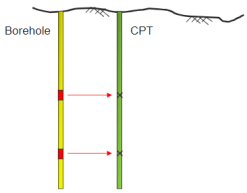


Figure 2: 2022 Geotechnical site investigation plan

Table 1: Coordinates and elevations for 35 co-located CPTs and boreholes

Borehole	Easting (ft)	Northing (ft)	Elevation (ft)	CPT	Easting (ft)	Northing (ft)	Elevation (ft)	Horizontal Distance Difference (ft)	Vertical Distance Difference (ft)
TP1-SD-04	1654153	436713.9	3266.7	TP1-CPT-04B	1654155	436717	3266.55	3.3	0.1
TP1-MUD-01	1654297	436836.9	3251.95	TP1-CPT-05	1654298	436843	3248.17	5.8	3.8
TP1-SD-07	1654467	436640.5	3267.88	TP1-CPT-07	1654472	436640	3267.9	5.4	0
TP1-SD-08	1654493	436810.8	3247.1	TP1-CPT-08	1654487	436806	3247.02	7.6	0.1
TP1-SD-10	1654647	436587.2	3268.04	TP1-CPT-10	1654639	436597	3267.91	12.3	0.1
TP1-SD-11	1654769	436864.8	3248.91	TP1-CPT-11	1654767	436869	3248.69	4.6	0.2
TP1-MUD-03	1654887	436738.5	3250.3	TP1-CPT-14	1654910	436732	3246.15	24	4.2
TP2-SD-02	1655683	436419.5	3286.67	TP2-CPT-02B	1655679	436412	3286.64	8.4	0
TP2-SD-06	1655785	436748.4	3289.66	TP2-CPT-06	1655791	436747	3289.4	7.1	0.3
TP2-MUD-03	1655786	436750.3	3289.77	TP2-CPT-06	1655791	436747	3289.4	6.9	0.4
TP2-SD-03	1655840	436303.2	3288.59	TP2-CPT-03	1655845	436312	3288.5	10.4	0.1
TP2-SD-07	1655962	436555.2	3285.7	TP2-CPT-07B	1655944	436555	3285.83	18	0.1
TP2-SD-04	1656028	436189.3	3290.75	TP2-CPT-04	1656029	436197	3290.58	7.8	0.2
TP2-MUD-04	1656051	436419.9	3289.9	TP2-CPT-08	1656058	436413	3286.41	10.1	3.5
TP2-SD-08	1656063	436413	3286.45	TP2-CPT-08	1656058	436413	3286.41	5.2	0
TP2-SD-11	1656204	436627.1	3286.02	TP2-CPT-11	1656215	436620	3285.52	13.2	0.5
TP2-SD-09	1656205	436286.5	3289.5	TP2-CPT-09	1656201	436279	3290.7	8.8	1.2
TP2-MUD-05	1656215	436282.7	3289.74	TP2-CPT-09	1656201	436279	3290.7	14.6	1
TP2-SD-12	1656227	436431.2	3282.15	TP2-CPT-12	1656228	436428	3282.4	3.8	0.2
TP2-SD-15	1656414	436408.7	3282.01	TP2-CPT-15	1656426	436409	3281.87	12	0.1
TP2-SD-14	1656497	436586.3	3286.5	TP2-CPT-14	1656507	436580	3286.6	11.8	0.1
TP2-SD-13	1656603	436782.3	3288.71	TP2-CPT-13	1656600	436789	3288.8	7.3	0.1
TP2-MUD-06	1656659	436336.8	3285.49	TP2-CPT-18	1656662	436345	3282.17	9	3.3
TP2-SD-18	1656665	436337.6	3281.95	TP2-CPT-18	1656662	436345	3282.17	8.3	0.2
TP2-SD-17	1656870	436464.1	3284.67	TP2-CPT-17	1656863	436462	3284.45	7.6	0.2
TP3-SD-01	1657091	436203.4	3265.38	TP3-CPT-01	1657080	436199	3266.37	11.6	1
TP3-SD-04	1657139	436733.1	3269.03	TP3-CPT-04	1657142	436730	3268.9	3.5	0.1

Borehole	Easting (ft)	Northing (ft)	Elevation (ft)	CPT	Easting (ft)	Northing (ft)	Elevation (ft)	Horizontal Distance Difference (ft)	Vertical Distance Difference (ft)
TP3-SD-13B	1657346	436276.5	3256.25	TP3-CPT-13B	1657353	436285	3255.85	10.6	0.4
TP3-SD-07	1657358	436489.2	3250.68	TP3-CPT-07	1657356	436481	3240.35	8.1	10.3
TP3-MUD-01	1657364	436277.1	3255.63	TP3-CPT-13B	1657353	436285	3255.85	14	0.2
TP3-MUD-02	1657526	436681.5	3240.42	TP3-CPT-06	1657529	436697	3236.5	15.9	3.9
TP3-SD-06	1657533	436699	3236.24	TP3-CPT-06	1657529	436697	3236.5	4.9	0.3
TP3-SD-11	1657663	436348.6	3225.3	TP3-CPT-11	1657669	436342	3225.08	9.6	0.2
TP3-SD-09	1657759	436500.2	3226.58	TP3-CPT-09	1657762	436484	3226.07	16.3	0.5
TP3-SD-12	1657842	436674.1	3229.07	TP3-CPT-12	1657857	436671	3228.87	15.3	0.2
				Average Distance 				9.8	1

Empirical relationships

Three common empirical relationships for estimating fine content from CPT data developed by Davies (1999), Robertson and Wride (1998), and Suzuki et al. (1998), predict the fines content based on the soil behavior type index (I_C) parameter in CPT, as shown in the equations below:

$$FC(\%) = 42.4179 \times I_C - 54.8574 \text{ (Davies, 1999)} \quad \text{(Equation 1)}$$

$$FC(\%) = 1.75 \times {I_C}^{3.25} - 3.7 \text{ (Robertson and Wride, 1998)} \quad \text{(Equation 2)}$$

$$FC(\%) = 2.8 \times {I_C}^{2.6} \text{ (Suzuki et al., 1998)} \quad \text{(Equation 3)}$$

Soil behavior type index (I_C) in CPT is estimated based on the normalized friction ratio (F_r) and normalized cone resistance (Q_t). To evaluate the applicability of these empirical relationships to tailings materials, we estimated the fine content from CPT data using these empirical relationships and compared them to laboratory data obtained from gradation tests, where the fine content was measured as the percentage passing the #200 sieve.

Figure 3 presents the estimated fine content based on the empirical relationships developed by Davies (1999), Robertson and Wride (1998), and Suzuki et al. (1998). The plots demonstrate that these well-known empirical correlations generally underestimate the fine content for these tailings materials.

Figure 4 shows the estimated fine content versus depth using the Robertson and Wride (1998) relationship. The plot reveals that underestimation of the fine content is more pronounced in the deeper portions of the tailings layers. Due to these discrepancies, it was necessary to develop a tailings-specific relationship based on the co-located CPT and borehole data to provide more accurate estimates for the fine content of the Holden tailings materials.

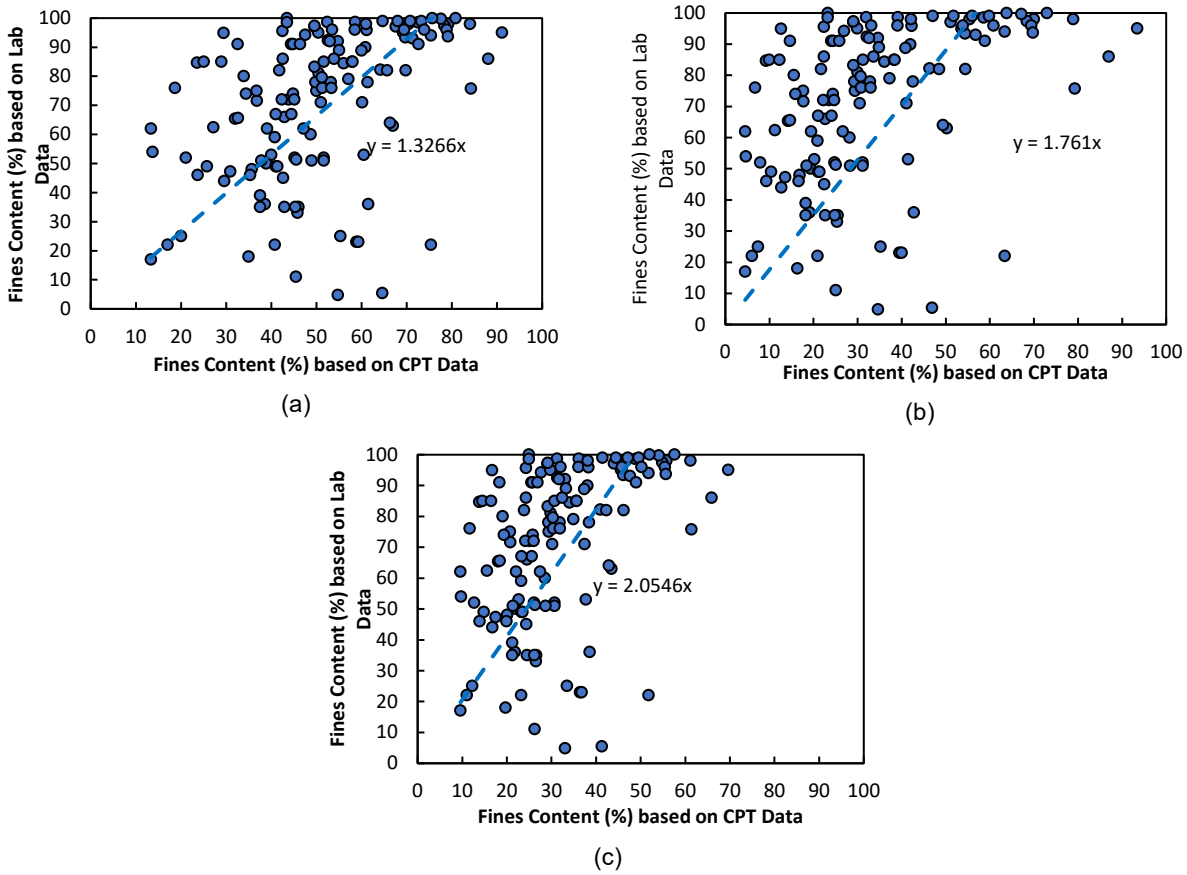


Figure 3: Estimated fines content based on the empirical relationships: (a) Davies (1999), (b) Robertson and Wride 1998, and (c) Suzuki et al. (1998)

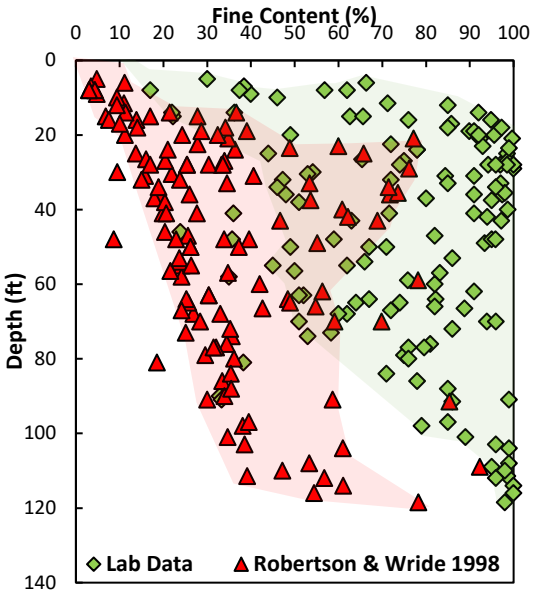


Figure 4: Comparison between laboratory data and estimated fines content from CPT data based on the Robertson and Wride (1998) relationship

Methodology

Genetic expression programming (GEP) techniques were employed to estimate fine content from CPT data based on data from the 136 borehole samples. GEP is a subfield of artificial intelligence that extends the principles of genetic algorithms (GAs) (Goldberg, 1989). GEP begins with an initial population consisting of randomly generated computer programs, represented as syntax trees, composed of functions and terminals suitable for the given problem domain. Functions encompass standard arithmetic operations, programming operations, mathematical functions, logical functions, and domain-specific functions. Terminals, on the other hand, represent constants or variables. Through a supervised trial and error process, the initial functions and terminals undergo adjustments to obtain refined functions and terminals that accurately estimate the desired output.

GEP, much like nature, is inherently a random process and cannot guarantee specific results. However, the stochastic nature of GEP enables it to escape traps that deterministic methods may encounter. This randomness has proven to be a key factor in the success of GEP, as it allows for the evolution of solutions to complex problems in a short amount of time.

In GEP, programs are commonly represented as syntax trees, as opposed to traditional lines of code. For instance, Figure 5 depicts a tree representation of the program "max(x + y, x - 6)," where x and y are independent variables, and 6 is a constant. In GEP, the leaves of the tree, such as variables and constants, are referred to as terminals, while the internal nodes, such as arithmetic operations and functions like "max," are called functions. The collective set of allowed functions and terminals forms the primitive set of a GEP system.

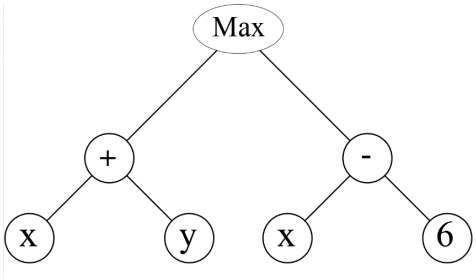


Figure 5: Representation of an expression tree in GEP ("Max" represents the maximum function)

Like other evolutionary algorithms, GEP involves the generation of an initial population of individuals, typically generated randomly. Various approaches exist for generating this initial population, including the full and grow methods, which are simpler and earlier techniques, as well as a widely used combination of the two, known as ramped half and half (Koza, 1992). Genetic operators in GEP, such as crossover and mutation, are applied to individuals who are probabilistically selected based on their fitness, as determined by the objective function.

GEP allows for the exploration of evolving novel solutions, and for addressing complex problems through adaptive and self-improving computational processes.

The advantage of GEP over other soft computing techniques (such as artificial neural networks and adaptive neuro fuzzy inference systems) is that GEP is not a black box and outputs are in the form of semi-complex mathematical solutions, which could be applied to the actual problems. The GEP approach is relatively new in the field of dam engineering, although some studies have been dedicated to their application recently (Rashidi et al, 2022; Yong et al, 2021). In this study the data set was divided into training (80%), and validation (20%) subsets to prevent overfitting. The performance of the testing set is an important step since it validates the accuracy and generalization capability of the model.

For the Holden tailing piles, two statistical evaluation criteria were used to assess the performance of the intelligent methods. These criteria are root mean square error (RMSE) and the determination coefficient (R^2), respectively, given by Equations 4 and 5.

$$RMSE = \sqrt{(\frac{1}{n}) \sum_{i=1}^{n} (a_i - p_i)^2} \quad \text{(Equation 4)}$$

$$R^2 = (\frac{\sum_{i=1}^{n} (p_i - \bar{p})(a_i - \bar{a})}{\sqrt{\sum_{i=1}^{n} (p_i - \bar{p})^2 (a_i - \bar{a})^2}})^2 \quad \text{(Equation 5)}$$

where a is the actual value and p is the predicted value, $\bar{a}$ and $\bar{p}$ are the mean of actual and predicted values, respectively. Evidently, a model with good performance (i.e., RMSE close to 0 or R^2 close to 1) will be the best model among several candidates.

Results and discussion

GEP was utilized to construct a prediction model for estimating the fines content from CPT data for tailings dams. The following equation (Equation 6) was developed using 136 data points based on two parameters of Q_t (normalized cone resistance) and F_r (normalized friction ratio) which are extracted from CPT data. We employed the parameters Q_t and F_r in developing this correlation due to their pivotal role in shaping the soil behavior type index. By incorporating these parameters, we were able to enhance the model's performance significantly for tailings materials, resulting in a robust and highly determinative coefficient of determination.

$$FC(\%) = 37.8 + \frac{2770}{51.5 + Q_t} + 5.62 \times \sin(2980 \times Q_t) + 16.5 \times \cos(0.0402 \times Q_t + \cos(2110 \times Q_t + \sin(F_r))) \quad \text{(Equation 6)}$$

For the estimation of fines content, out of the 136 sets of data, 109 sets of data (80%) were considered for training and the remaining 27 sets of the data (20%) were considered for validation. The training and

validation data sets were selected randomly from the database. Figure 6 shows the relationship between actual fines content and the predictions of GEP for Equation 6.

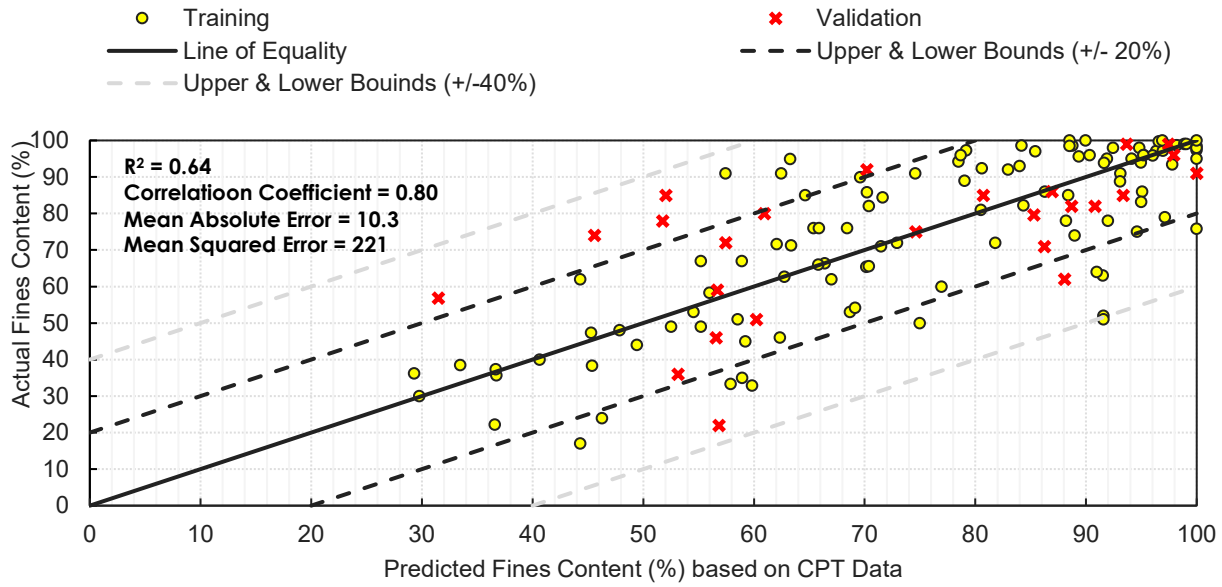


Figure 6: Coefficient of determination between the actual fines content and predictions of GEP model

After developing the GEP prediction model, the results were compared to the well-known empirical relationship noted by Robertson and Wride (1998) to examine the level of accuracy of the newly developed model compared to the traditional equations. Figures 7 and 8 illustrate the statistical results of the newly developed, tailings-specific model in comparison with the empirical relationship. This plot indicates the underestimation of fines content using the existing empirical relationship and its non-applicability for the prediction of fines content in the Holden mine site.

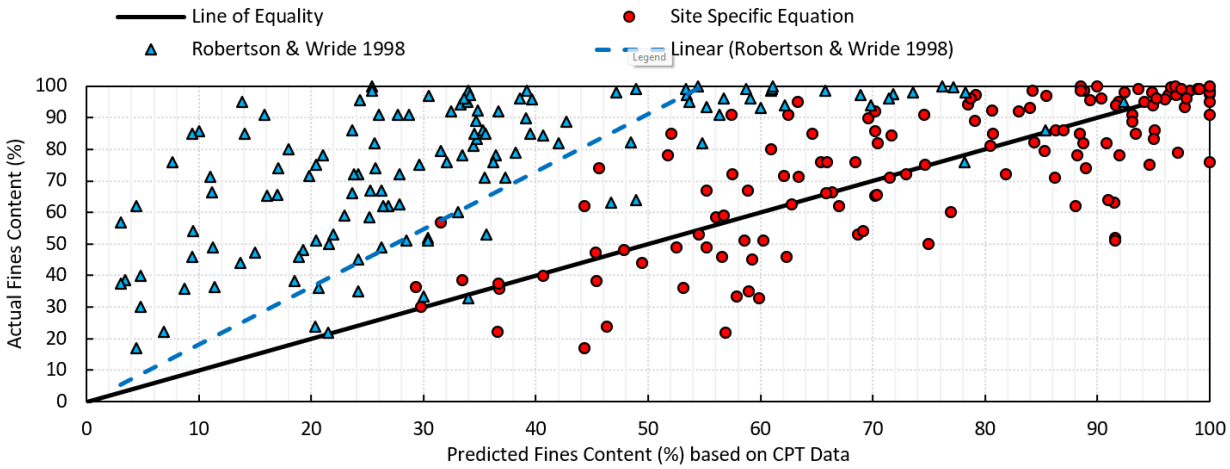


Figure 7: Comparing the actual fines content with tailings-specific model and experimental relationship

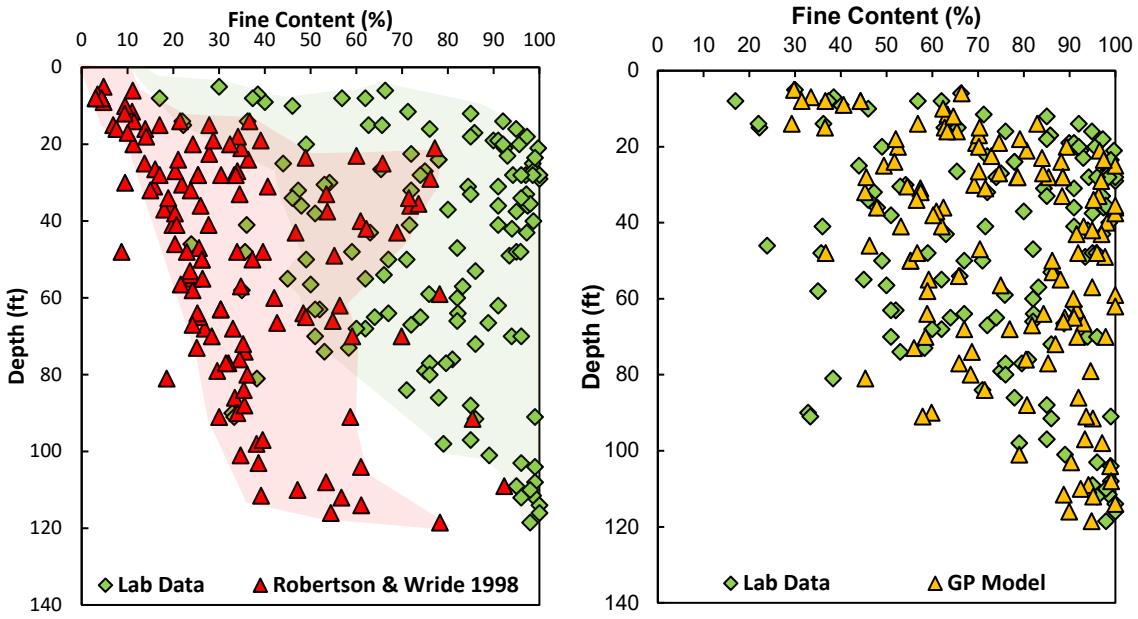


Figure 8: Comparison between laboratory data and estimated fines content from CPT data based on the Robertson and Wride (1998) relationship and the newly developed GEP model

Figure 9 illustrates a comparison of the prediction performance between the GEP models developed in this study and the empirical relationship proposed by Robertson and Wride (1998). The results obtained from comparing the artificial intelligent method and empirical relationships showed that GEP results appears to provide a more reasonable estimation of fines contents of tailings piles at Holden mine site. The newly developed model in this project is ready to be applied as a robust tool for prediction of fines content from CPT data for the Holden tailings piles.

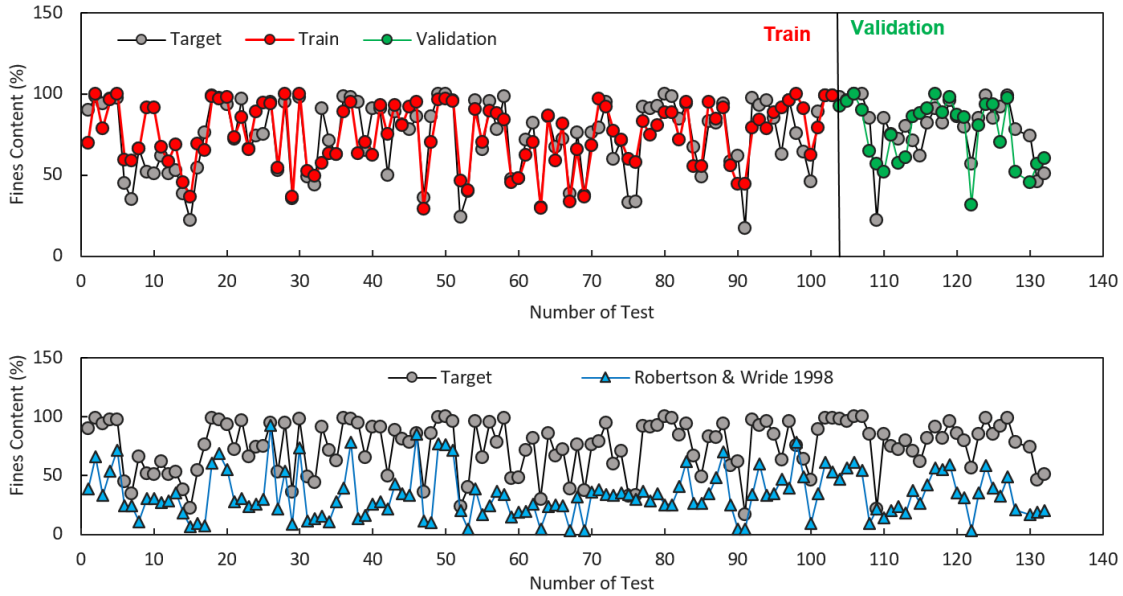


Figure 9: Comparing the actual fines content and predicted intelligent models

Figure 10 presents a cross-sectional view of the Holden tailings piles, illustrating the delineation of tailing layers based on estimated fines content from the GEP model. The plot reveals that tailings with higher fines content are located in the deeper sections of the piles (groups D and E, with fines contents exceeding 75%), whereas coarser tailings are found in the shallower zones (groups A, B, and C, with fine contents less than 75%). This distribution aligns with the historical deposition process at this site: fine tailings, discharged from the cyclone overflow, accumulate in the central parts of the piles, while coarse tailings from the cyclone underflow are deposited along the embankment face.

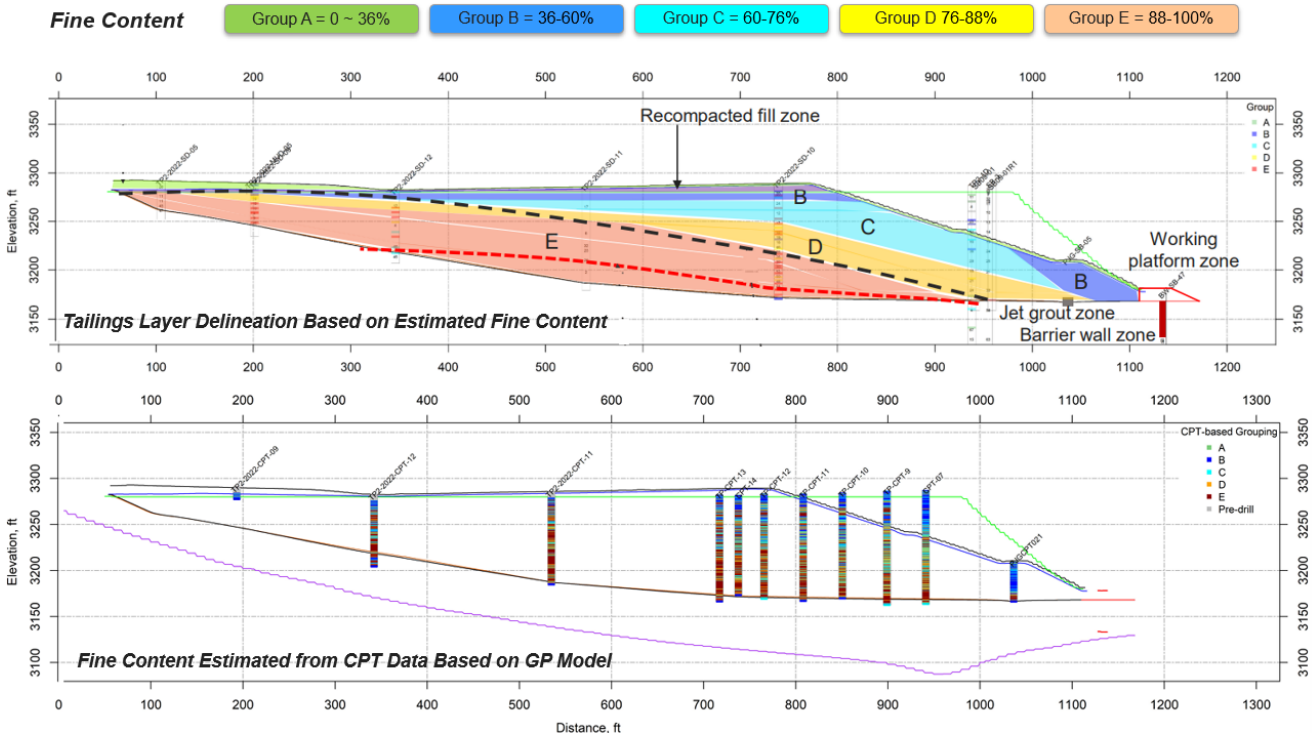


Figure 10: Tailings layer delineation using estimated fine content from GEP model

Conclusion

This study addressed the need for tailings-specific correlations to estimate fines content in tailings materials from CPT data. Conventional empirical correlations, derived from a range of soil types and conditions distinct from those found in tailings facilities, were shown to underestimate fines content at the Holden Mine tailings site. By employing GEP, a form of artificial intelligence, the study developed a robust correlation specifically for the Holden mine tailings. The newly developed model demonstrated superior accuracy in predicting fines content compared to traditional empirical relationships. Statistical evaluations showed the GEP model outperformed traditional methods, with lower RMSE and a higher coefficient of determination, indicating better accuracy and generalization capability.

The successful application of GEP in this context underscores the potential of artificial intelligence methods in geotechnical engineering, particularly for specialized materials like mine tailings. This paper paves the way for more precise and reliable geotechnical assessments, contributing to safer and more efficient tailings management practices and in achieving GISTM Compliance.

Acknowledgements

We extend our sincere gratitude to Rio Tinto for their invaluable support and approval to publish the data presented in this study. Their collaboration and willingness to share information have made a significant contribution to the advancement of knowledge in the mining industry.

References

Davies, M.P. 1999. Piezocone technology for the geoenvironmental characterization of mine tailings. PhD thesis.

Goldberg, D.E. 1989. Messy genetic algorithms: Motivation, analysis, and first results. *Complex Systems* 3(5): 493–530. (First published in 1989 as TCGA Report No. 89003.)

Jefferies, M. and Been, K. 2016. *Soil Liquefaction: A Critical State Approach.* Second Edition. Taylor and Francis Group LLC, Boca Raton, FL.

Koza, J.R. 1992. *Genetic Programming: on the Programming of Computers by Means of Natural Selection*. MIT Press, Cambridge, MA.

Rashidi, M., Ebrahimi, A. and Mosaiebian, A. 2022. Effectiveness of subsurface drainage for mitigation of landslides affecting pipelines. *Proceedings of International Pipeline Conference* 86564: V001T02A003. American Society of Mechanical Engineers.

Robertson, P.K. and Wride, C.E. 1998. Evaluating cyclic liquefaction potential using the cone penetration test. *Canadian Geotechnical Journal* 35(3): 442–459.

Russell, A.R., Vo, T., Ayala, J., Wang, Y., Reid, D. and Fourie, A.B. 2022. Cone penetration tests in saturated and unsaturated silty tailings. *Géotechnique* 74(3): 281–295.

Suzuki, Y., Sanematsu, T. and Tokimatsu, K. 1998. Correlation between SPT and seismic CPT. *Proceedings of Conference on Geotechnical Site Characterization.* Balkema, Rotterdam: 1375–1380.

Yong, W., Zhou, J., Jahed Armaghani, D., Tahir, M.M., Tarinejad, R., Pham, B.T. and Van Huynh, V. 2021. A new hybrid simulated annealing-based genetic expression programming technique to predict the ultimate bearing capacity of piles. *Engineering with Computers* 37(4): 2111–2127.

Stacked Deposits of Filtered Fluid Fine Tailings Using Geotextile Tubes – Updates on Enhancing Chemical Stability

Fernando Da Silva, WSP Australia Pty Limited, Australia

Abstract

Stacked deposits of thickened and filtered fine tailings using geotextile tubes have the potential to improve tailings management, reducing geotechnical risk and the complexity of closure compared with traditional methods. To this end, previous work has demonstrated that geotextile tubes combined with a novel physicochemical treatment recipe is a feasible alternative approach for filtration and fines capture, accelerated dewatering and consolidation, and reinforcing the shear strength of the fluid fine tailings (FFT) deposits, facilitating reclamation and post-closure long-term safety performance (physical and chemical stability). In this paper, solids and water mass balance and concentration of the major ions (anions and cations) of the analyzed treated FFT within the geotextile tubes show that most ions remain bound in the solid phases, which increases flocculation efficiency. The solids retained inside the geotextile tube are considered captured solids, and the release water is considered process water. This water is used either for the same FFT management or routed into the mining process, since its chemistry, the pH and especially the divalent ion content (i.e., calcium) is kept unchanged, avoiding impacts on bitumen recovery (i.e., oil sands tailings). The outcomes of this study can be used to define the success of the physicochemical treatment recipe as an alternative technology to accelerate dewatering and consolidation, improving the physical and chemical stability of the treated FFT closure land-forms to facilitate reclamation, while opening the potential for further investigating carbon capture, which is linked to solids phase and carbonates precipitation.

Introduction

An important objective of effective tailings management is to protect the environment. Because the main pathway for contaminants is by water, the water balance is a very important element in any tailings management strategy. Mining companies, industry bodies, consulting companies, and regulators have been continuously improving best practice guidelines for the design, construction, and management of tailings facilities and mine-waste.

Dam safety revised practice does not accept the concept of a tolerable failure rate for tailings dams. This resulted in recommending the implementation of the best available tailings technology (BAT) based on principles for physical stability (PS) and chemical stability (CS). Principles for PS consider eliminating surface water from the impoundment; promote unsaturated conditions in the tailings with drainage provisions; and achieve dilatant conditions throughout the tailings deposit by compaction.

A key component for the design of tailings stacks is the degree of water saturation within the tailings profile established over the long-term. For example, tailings profiles with water saturation levels less than 85% are considered resistant to liquefaction. Conversely, tailings profiles with water saturation levels greater than 85% are considered resistant to oxygen diffusion. By including both PS and CS failure mechanisms, likelihood and consequences, one is better able to optimize the trade-offs between PS and CS measures to minimize overall risk.

The objectives of this study are to provide an understanding of the fundamentals of the FFT dispersion and flocculation behaviors, and the enhanced chemical stability of the treated FFT. These objectives will be achieved if the following supporting objectives are completed: (a) investigate how the chemistry and pH of the process water and FFT porewater, inherent properties of the FFT constituents, and zeta potential affect the dispersion and flocculation behaviors of the FFT; (b) investigate why thickening FFT with flocculant only is not enough to provide efficient fines agglomeration and dewatering of the FFT, and determine the gaps to be filled; (c) develop a physicochemical treatment recipe for FFT to assist solids-water separation, fines agglomeration with maximized capture, enhanced dewatering, and accelerated consolidation; (d) develop an inline mixing process of the FFT with the chemical treatment recipe (coagulation and flocculation) for effective flocculation prior to the discharge into the geotextile tube; (e) develop a solids and water mass balance of the treated FFT discharged into the geotextile tube, including concentration and mass of major anions and cations, to understand the solids captured inside the geotextile tube, and release water as process water either for use in the same FFT management or routed into the mining process; and (f) investigate additional benefits of the enhanced chemical stability of the solids captured into the geotextile tube, such as the potential for carbon capture, which is linked to solids phase and carbonates precipitation.

Lessons learned

Oil sands background

Mineable “oil sands” deposits are located relatively close to the surface, typically no more than 50 m deep. Once mined, oil sands are mixed with water to produce a pumpable slurry that can be gravity separated. After bitumen separation from the solids and water, coarse sand tailings (CST) and FFT are formed. The CST are separated from FFT by the hydro-cyclone overflow and settle on deposition to form tailings dikes

and beaches. The hydro-cyclone underflow is much of the water, residual bitumen and approximately 85% of the fines that form FFT (silts and clays). FFT are typically thickened with flocculant only, pumped to storage facilities where process water is recovered, and to form future deposits of mature fine tailings. Therefore, the inherent properties of the oil sands constituents and the oil sands extraction process collectively dictate the characteristics and mechanical properties of the FFT.

Key problems with long-term reclamation performance of the FFT deposits are related to a low rate of shear strength gain and long consolidation timeframes that pose significant challenges in converting FFT into deposits that can facilitate reclamation.

Gaps in assessing the physicochemical properties of the FFT still exist, including their dispersion and flocculation behaviors with regards to mineralogy, pore water chemistry, pH, and the mine extraction processes impacting the characteristics and mechanical properties of the FFT. This study will explain the potential causes of the significant amounts of trapped water when thickening FFT with flocculation only and will provide a rationale for the physicochemical treatment recipe to increase fines agglomeration and dewatering of the FFT.

Previous studies have shown that geotextile tubes are an innovative solution in engineering projects because of their ability to modify mechanical and hydraulic properties in a controlled manner. Additionally, the geotextile tube deposits with treated FFT will act more as a filter pressure system, with most of the water recovery happening while the geotextile tubes are being filled.

Key testing, materials, and methods

The identification and quantification of FFT mineralogy is considered “critical” for the successful manipulation of clay and non-clay mineral behaviors, along with porewater chemistry and pH. Bulk X-Ray Diffraction (XRD) analysis, elemental analysis by X-Ray Energy Dispersive Spectrometry (EDS) and Scanning Electron Microscopy (SEM) were performed to characterize the mineralogy of the FFT used in this study. Quantitative elemental analysis was performed by an Oxford INCA microanalysis system attached to a JEOL JSM-6610 scanning electron microscope.

All particles in suspension exhibit a zeta potential, or surface charge. The measurement and knowledge of the zeta potential is critical for optimizing processes, predicting particle stability and interactions, and as a simple method of flocculation quality control. The zeta potential is crucial in determining the stability of a colloidal suspension. When all particles have a large negative or large positive charge, they will repel each other, and the suspension will be stable. The higher the value (positive or negative), the more stable the colloid dispersion is. If the zeta potential is low, the tendency for flocculation is higher. Another important consideration when discussing zeta potential is pH; in fact, quoting a zeta potential without considering pH is nearly meaningless. For suspensions of most materials, a plot of zeta

potential versus pH exhibits an isoelectric point, which is the pH where the net charge on the particles is zero. At this point, the suspension is highly unstable, and flocculation is most likely to occur.

The FFT slurry density, specific gravity, water content, and bulk and dry densities were determined to characterize the tailings and evaluate coagulant and flocculant dosages and concentrations.

Particle Size Distribution (PSD) was obtained by sieve and hydrometer method (SH), as per ASTM D422-63. The SH was carried out with the variant of "dirty" hydrometer dispersed (bitumen as-is).

Dilution was applied to control variations of the feed densities if the initial slurry density by mass was higher than 20%. FFT at initial slurry density by mass of 20% provided enhanced mixing and maximized flocculant adsorption at relatively low dosages.

Coagulation was applied prior to flocculation to efficiently neutralize the electrostatic charges of particles (mainly quartz and kaolinite) and reduce repulsion between them. The coagulant solution was prepared using Alum and process water. Flocculant solution was prepared using anionic polyacrylamide (PAM) flocculant and process water.

FFT was coagulated with Alum at concentration 0.1% and dosage 0.65% (by mass) of dry solids, prior to flocculation with 30% charge high molecular weight (HMW) anionic PAM flocculant at concentration 0.1% and dosage 0.1% (by mass) of dry solids.

Settling tests were carried out to evaluate the initial dewatering performance of the physicochemical treatment recipe applied to FFT inline prior to the discharge into the geotextile tube.

This study summarizes results of a parametric analysis of the FFT dispersion and flocculation behaviors, Da Silva (2022), to investigate the causes and manners of why significant amounts of trapped water remain in the flocculated FFT. The findings and recommendations, supported by facts observed in the laboratory are also included. A pure kaolinite powder (≤ 2 μm size) and pure quartz flour (≤75 μm size) were used for laboratory bench scale observations of their individual and combined behaviors. This observational method focused on the dispersion and flocculation behaviors of quartz and kaolinite suspensions as a function of pH, hydrolyzed salts (calcium and aluminum), and anionic PAM flocculant.

The chemical analyses performed in this study focused on the interaction between the mineral composition (i.e., FFT mineralogy) and pore water chemistry (i.e., pore solution electrolytes, ion concentrations, and pH) with the aim of understanding their significant influence on FFT dispersion and flocculation behaviors. Routine chemical analyses were necessary for characterization of the ion concentrations and pH of the FFT pore water, plant process water, and release water from the treated FFT that can be used as recycle water (FFT management and mining process). In addition to pH, the key component of the FFT pore water chemistry is the calcium content due to its significant impact on the flocculation behavior of the FFT.

Inherent properties, soil characterization, pore water chemistry and zeta potential

Mineralogy is the primary factor that controls the size, shape, and properties of soil particles. These same factors determine the possible ranges of physical and chemical properties of any given soil. A prior knowledge of what minerals are in a soil provides intuitive insight as to its behavior (Mitchell, 2005).

The XRD analysis of the original FFT shows the crystalline components of the sample consist of kaolinite, 52.35; quartz, 40.1%; illite, 4.6%; microcline, 1.3%; albite, 0.7%; siderite, 0.8%; and rutile; 0.2%.

Quartz is a non-clay mineral within the fine particle size fraction of the FFT in this study. At pH > 2, quartz particles possess negatively charged surface, show dispersive behavior and are more hydrophilic (van Lierde, 1980), (Hunter, 1981), (Hussain et al., 1996), and (Gan and Liu, 2008). The reason for this behavior is that the particle surface reacts with water, forming silicic acid, which in turn dissociates to form a silicic anion at the surface and a hydrogen (H^+) ion that diffuses off into the solution. This chain of events negatively charges the particle surface as the diffusing H^+ carries away a positive charge and leaves a negative charge behind.

Kaolinite is a clay mineral and has negatively charged surface at pH >2 (Goldberg et al., 1991). The illite is a non-swelling clay mineral in nature and has a lower cation exchange capacity than kaolinite.

The elemental analysis by EDS of the original FFT of this study shows Oxygen (O) and silicon (Si) dominate the elemental spectrograph, respectively forming approximately 54.92 wt.% and 23.05 wt.% of the sample. Aluminum (Al) is common, forming approximately 9.42 wt.%. Carbon (C) as non-crystalline oxygen-bearing compound was measured at 6.96 wt.%, as shown in Table 1 and Figure 1.

Table 1: Elemental composition by EDS of the original FFT of this study

Sample ID	H	C	N	O	Na	Mg	Al	Si	S	Cl	K	Ca	Ti	Mn	Fe	Cu
Original FFT	–	6.96	–	54.92	0.21	0.21	9.42	23.05	0.27	0.04	1.84	0.31	0.41	0.03	2.01	0.27

H – Hydrogen	Mg – Magnesium	K – Potassium	Cu – Copper
C – Carbon	Al – Aluminum	Ca – Calcium	
N – Nitrogen	Si – Silicon	Ti – Titanium	
O – Oxygen	S – Sulphur	Mn – Manganese	
Na – Sodium	Cl – Chlorine	Fe – Iron	

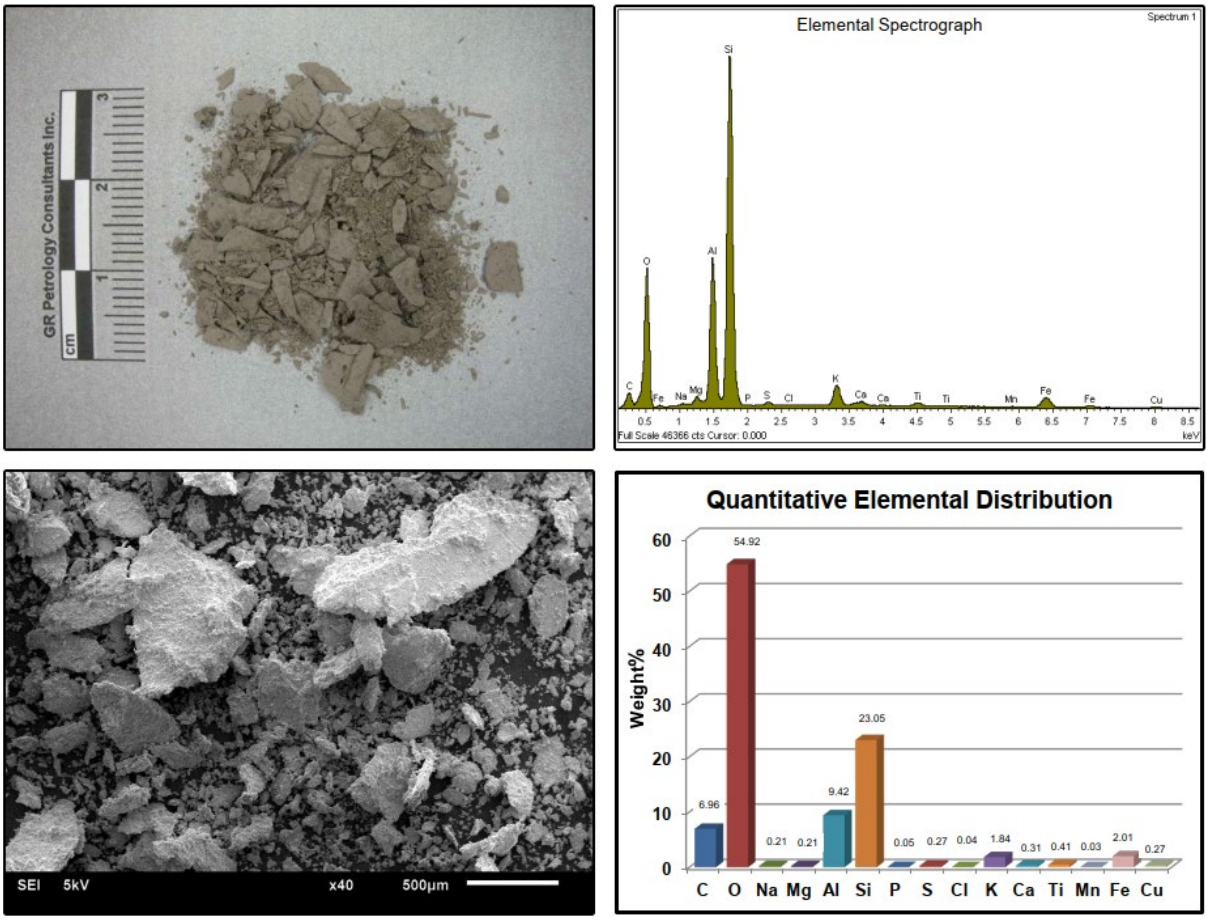


Figure 1: Quantitative elemental distribution, spectrograph and scanning electron microscopy analyses of the original FFT of this study

The PSD results of the analyzed original FFT is consistent with the results from the mineralogy analysis of this study. It should also be noted that the measured solids specific gravity is 2.5 and solids content by mass vary between 15 and 39%. The original FFT porewater chemistry contains 47 ppm calcium ions and process reclaim water contains 86 ppm calcium ions (high calcium concentration). The original FFT has a measured zeta potential -47 mV at porewater pH 8.

The XRD analysis of the treated FFT shows the crystalline components of the sample consist of kaolinite, 30.8%; quartz, 41.2%; illite, 9.6%; microcline, 2.1%; albite, 1.3%; siderite, 3.9%; greigite, 3.1%; pyrite, 1.2%; anatase, 1.7; rutile 0.8%; halite, 1.6%; tenorite, 1.2%; dolomite, 0.8%; and calcite, 0.7%.

The EDS results of the treated FFT show Oxygen (O) and silicon (Si) dominate the elemental spectrograph, respectively forming approximately 51.75 wt.% and 18.93 wt.% of the sample. Aluminum (Al) is common, forming approximately 10.61 wt.% of the sample. Carbon (C) as non-crystalline carbon oxygen-bearing compounds is approximately 12.60 wt.% which compared to the original FFT sample

suggests that 80% of the carbon oxygen-bearing compounds were transferred to the solid phase of the treated FFT, as shown in Figure 2 and Table 2.

These findings are very encouraging and suggest the potential for carbon capture, which is linked to solids phase and carbonates precipitation. Transition metal carbonate and bicarbonate complexes are coordination compounds containing carbonate (CO_3^{2-}) and bicarbonate (HCO_3^-) as ligands.

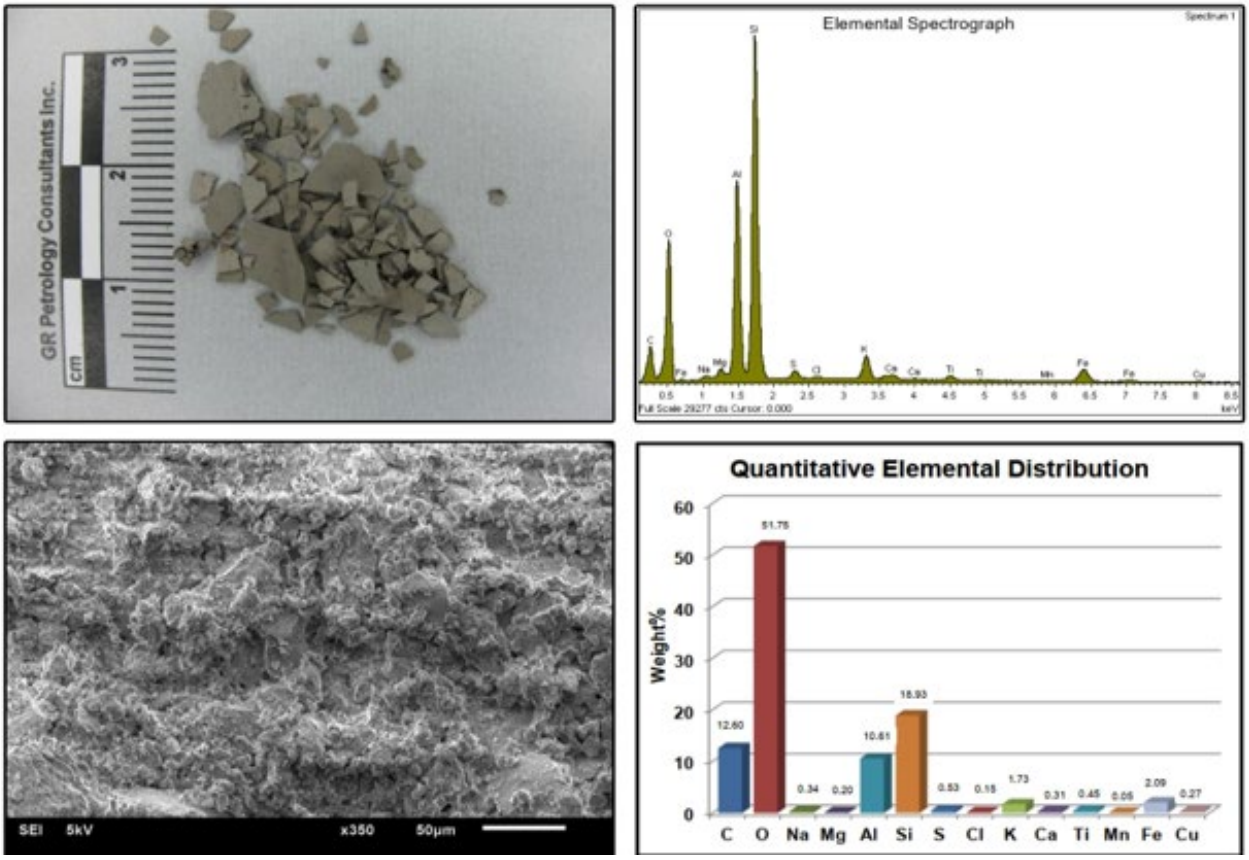


Figure 2: Quantitative elemental distribution, spectrograph and scanning electron microscopy analyses of the treated FFT of this study

The PSD of the analyzed treated FFT is consistent with the results from the mineralogy analysis of this study.

The treated FFT released water contains 86 ppm calcium ions which means the same concentration of the reclaimed water used for the process, showing no increase in calcium ions. The treated FFT measured zeta potential is -17 mV at porewater pH 8.

Table 2: Elemental composition by EDS of the treated FFT of this study

Sample ID	H	C	N	O	Na	Mg	Al	Si	S	Cl	K	Ca	Ti	Mn	Fe	Cu
Original FFT	–	12.6	–	51.75	0.34	0.20	10.61	18.93	0.53	0.15	1.73	0.31	0.45	0.05	2.09	0.27

H – Hydrogen	Mg – Magnesium	K – Potassium	Cu – Copper
C – Carbon	Al – Aluminum	Ca – Calcium	
N – Nitrogen	Si – Silicon	Ti – Titanium	
O – Oxygen	S – Sulphur	Mn – Manganese	
Na – Sodium	Cl – Chlorine	Fe – Iron	

Coagulation and flocculation behaviors of the FFT

The objective of the physicochemical treatment recipe is to maximize fines capture, enhance dewatering, accelerate consolidation, increase shear strength, and maintain the integrity of the aggregate to ensure that fines segregation does not occur.

Maintaining the initial slurry density of the original FFT at 20 wt.% solids was part of the methodology to control variations of the feed densities while maintaining unaltered coagulant and flocculant dosages.

The measured average properties of the original FFT of this study were solids specific gravity, 2.50; water content (geotechnical), 360.0%; solids content, 20 wt.% solids; total bulk density, 1.15 t/m^3; dry density, 0.25 t/m^3; and void ratio of 9. These initial properties are fundamental for the design of the physicochemical treatment recipe, including flocculant and coagulant dosages and concentrations and release water volumes.

The results of the treated FFT obtained immediately after the geotextile tubes were completed (filled up to the specified maximum height by the manufacturer), were solids specific gravity, 2.48; water content, 86.9%; solids content, 53.6 wt.% solids; total bulk density, 1.47 t/m^3; dry density, 0.79 t/m^3; and void ratio, 2.16. The laboratory and field test results indicated that the treated FFT was dewatered in the geotextile tubes during filling, providing significantly enhanced fines capture as indicated by its dry density and void ratio. Unified Soil Classification System (USCS) classification was CH, the liquid limit was 76.8%, the plastic limit was 29.0%, and the liquid index was 47.8%.

A rigorous control of the original FFT slurry density intake was part of the inline mixing process of the physicochemical treatment recipe to provide the required amount of dilution water (reclaim process water) for adjustment of the initial slurry density to 20 wt.% solids if it was higher than 20 wt.% solids.

Quartz particles at pH > 2 are dispersed by action of electrostatic repulsive forces. These forces are affected by the ionic strength of the soil-water-ionized system, which depends on the pore solution electrolyte concentration and ion types (Verwey and Overbeek, 1948). In the presence of high valence cations, such as aluminum, the repulsive forces of quartz particles are reduced, resulting in the coagulation of particles. The mechanism of coagulation effectively lowers the electrostatic repulsive forces between

particles causing charge neutralization and the formation of stable micro-flocs (slow-settling flocs). Charge neutralization is equivalent to compressing the diffuse double ionic layer energy barrier (i.e., reducing the double ionic layer charge to near zero). It was observed in this study that at pH 8, quartz particles showed poor flocculation performance in the presence of calcium at concentrations of 40 and 72 ppm and anionic PAM flocculant. This observation confirms that as Ca^{2+} ions are predominant they influence the behavior of the anionic PAM flocculant. Calcium ions can be adsorbed onto the COO− functional groups of the anionic PAM flocculant to form $(–COO)_2Ca$. $CaOH^+$ may also be adsorbed onto $–COO^-$ functional groups to form (–COO)Ca(OH). As the concentration of calcium increases, more Ca^{2+} ions are available to adsorb onto the anionic PAM flocculant; however, when in excess, these Ca^{2+} ions are partially attracted as counter-ions in the double layer of the adsorbed anionic flocculant chains, causing steric stabilization at the particle surface. Steric stabilization results from covering the particles with the anionic flocculant, preventing the particles from getting close to the range of attractive forces and thereby allowing quartz particles to be dispersed. It was also observed in this study that the impact of excess calcium at pH 8 on the flocculation of quartz can be reversed with the addition of metal salts of a higher valence than calcium, such as aluminum ions.

While kaolinite surfaces are negatively charged in media such as water, they exhibit positive surface charge characteristics at pH < 3 in the solution of calcium ions, and at pH 9.2 in the solution of aluminum ions, as shown in Figure 3 (Peng and Di., 1994). However, in solution of aluminum ions, the zeta potential decreases from +30 to -7 mV as the pH increases from 3 to 10 with a point-of-zero charge at pH 9.2. In contrast, kaolinite maintains close to a constant value of zeta potential -15 mV at pH 4 or higher in the presence of calcium ions; as pH decreases below 4, zeta potential increases passing by a point-of-zero-charge (PZC) at pH 3, approximately, as showing in Figure 3. Calcium alone has a small effect on kaolinite coagulation (Atesok et al., 1988).

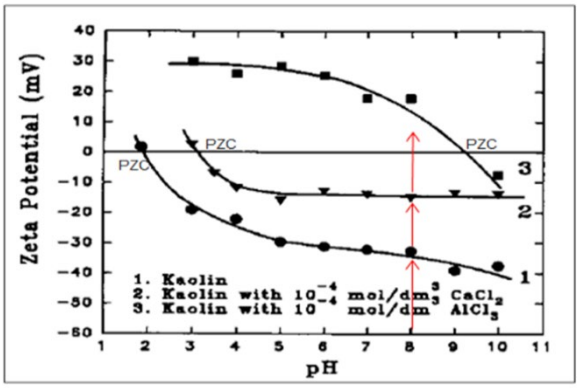


Figure3: Zeta potential of kaolinite particles vs. pH adopted from Peng and Di (1994)

An excess of hydrolyzed metal ions (i.e., aluminum) used to coagulate negative charged particles of kaolinite might cause the reversal of double layer charge and lead to a stable suspension with positive

double layer charge which could suppress the kaolinite flocculation process (Matijevic et al., 1966), as also showing in Figure 3. Increasing pH causes the hydroxyl ion to react with the kaolinite surface, which will make the zeta potential more negative. Sulfate and bicarbonate ions can also adsorb on the kaolinite surface and make zeta potential more negative. The suggested adsorption mechanism of anionic PAM flocculant on kaolinite is by hydrogen bonding. However, it is possible for anionic PAM flocculant to be attracted to the positively charged sites of kaolinite by electrostatic attraction (Peng and Di, 1994). Precipitation of calcium hydroxyl on the kaolinite surface covers up the active function groups, which prevent the formation of hydrogen bonding between kaolinite and anionic PAM flocculant.

Supported by facts observed in the laboratory a parametric analysis on of the coagulation and flocculation behaviors of the FFT was performed by Da Silva (2022). A pure kaolinite powder (≤ 2 µm size) and pure quartz flour (≤ 75 µm size) were used to observe the dispersion and flocculation behaviors of kaolinite and quartz suspensions as a function of pH, hydrolyzed salts (i.e., calcium and aluminum hydrolyzed metal ions), and anionic PAM flocculant.

The parametric analysis has shown that both quartz and kaolinite particles have similar issues regarding the adsorption of anionic PAM flocculant due to pH, and that the presence of an excess of Ca^{2+} ions could cause their poor flocculation at pH 8 with flocculant only. In addition, the parametric analysis has shown that the impact on the flocculation of quartz and kaolinite, caused by an excess of Ca^{2+} ions at pH 8, can be reversed by addition of metal salts of higher valence than calcium, such as aluminum ions.

Photograph 1 shows an efficient flocculation of the treated FFT (quartz and kaolinite) at initial slurry density 20 wt.% solids, coagulated with 0.1% aluminum ions concentration at a 0.65% dosage (by mass of dry solids), prior to flocculation with medium charge density HMW anionic PAM flocculant at concentration of 0.1% and dosage of 0.1% (by mass of dry solids).



Photograph 1: Settling test performed on the treated FFT

Solids, water and chemical mass balance calculations for dewatering the treated FFT within geotextile tubes

The simplified process flow diagram of an actual field trial, shown in Figure 4, refers to the original FFT treated inline by coagulation and flocculation prior to the discharge into geotextile tubes.

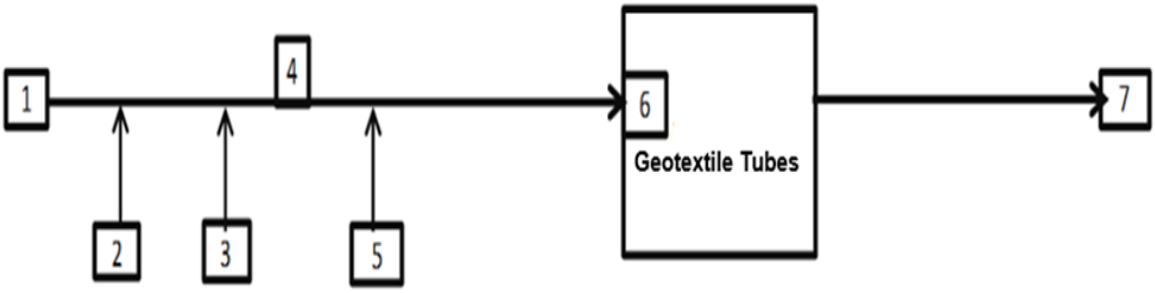


Figure 4: Simplified process flow diagram of the treated FFT inline, sampling, discharged into geotextile tubes and monitoring of the released water

Definitions of the streams and sampling points

- Stream #1 is the original FFT Stream.
- Stream #2 is the process water used to dilute FFT to 20 wt.% solids (as the original FFT is > 20 wt.% solids).
- Stream #3 is the coagulant addition using Alum to coagulate the diluted FFT inline.
- Node #4 is a sampling point where samples are taken periodically to measure the wt.% solids and to analyze the chemical components of the aqueous phase (including major cations and anions).
- Stream #5 is the flocculant addition using anionic PAM flocculant to flocculate the coagulated FFT inline.
- Node #6 is the sampling point right at the discharge of the treated FFT inline into geotextile tubes where samples are collected to measure the wt.% solids and to analyze the chemical components of the aqueous phase (including major cations and anions).
- Stream #7 is the release water from the geotextile tubes where samples are collected to analyze the chemical components of the release water (including major cations and anions).

Between Node #6 and Stream #7, solid core samples are retrieved from the geotextile tubes and analyzed for wt.% solids, pore water chemistry, and in-situ and laboratory shear strength of the deposit. The analyzed volume of each stream is presented in Table 3.

Table 3: Volume of each stream used in the field trial

Stream/ Node #	Stream/Node description	Slurry volume (m^3)	Wt.% solids
1	Original FFT Stream	12.0	28.0
2	Dilution water stream (process water)	5.0	0.00
3	Coagulant stream (Alum solution)	27.0	0.00
4	Coagulated FFT sampling (node # 4)	44.0	8.70
5	Flocculant stream (anionic PAM solution)	4.4	0.00
6	Flocculated FFT (stream/node = Treated FFT discharge into geotextile tubes and sampling)	48.0	8.00

Solid and water mass balance calculations

In this field trial, the easily measured parameter was to record the volume of each stream used to fill the geotextile tube and take grab samples at predefined points such as Node #4 (before flocculation addition) and Stream/Node #6 (at the discharge into geotextile tube). The first basic step in a mass balance is to calculate the volume of solids and fluids in the slurry following the process flow diagram of the Figure 4, and then convert these volumes into mass using the specific gravity of the solids and liquid in the streams.

- Solid mass fraction conversion.

Stream #1 was analyzed for wt.% solids, slurry bulk density, and solids specific gravity. The rest of the streams were measured for wt.% solids and water during the trial period. The average values of the measured parameters of the Stream #1 were:

- Bulk density = 1.2 t/m^3
- Solids content = 28 wt.% solids
- Specific gravity of solids = 2.5

To conduct a mass balance on the water and solids contents in the slurry in each stream, the first approach was to convert all the solids in the streams to a volumetric basis so that the volume of water (refer to as fluid phase volume) in the FFT slurry can be accurately calculated. The following correlation was used:

$$\emptyset_{sl,v} = \frac{1}{1 + SG_s\left(\frac{1}{\emptyset_{sl,m}} - 1\right)} \ldots\ldots (1)$$

where:

$ø_{s,l,v}$ = solids content of the FFT slurry on a volumetric basis

$ø_{sl,m}$ = solids content of the FFT slurry on a mass basis = 28 wt.% solids (for Stream #1)

SGs = specific gravity of solids of the FFT slurry = 2.5 (for solids in Stream #1)

From the correlation (1) the solids content of the FFT slurry on volumetric basis were 13.5%. This means 28 wt.% solids represent 13.5% of the slurry volume in the FFT slurry. Therefore, in 12 m^3 of FFT slurry, the solids volume based on the above correlation will be (13.5% × 12 m^3) = 1.62 m^3. Other input streams do not have solids; therefore, their volumetric representation will remain unchanged. Specific gravity of other streams (fluid phase) is considered as that of water. The mass of any phase (solid or fluid/water) in a stream is the product of specific gravity and volume of that phase. Percent mass representation of any phase (solid or fluid/water) in any stream is fraction of a phase in the total stream mass multiplied by 100. The fundamental principle in mass balance is conservation of mass if something is not measured or known.

Inline flocculation mass balance on solids

Table 4 represents a complete mass balance for solids when the original FFT was added inline and then discharged into the geotextile tube after the inline treatment with coagulation and flocculation. Once the flocculated FFT is released into geotextile tube, the mass in the tube will change with time through the release of the water; because of this change, a separate mass balance is presented in the following section.

Errors in the field-measured data can be back-checked with the calculated mass balance as shown in Table 4; for example, the sum of all the masses from Streams #1 to #3 must be equal to the mass measured at Node #4. In addition, the subtotal mass Node #4 + Stream #5 must be equal to the mass measured at Node #6. If this is not true, then there are errors in the field measurements or in the calculations. The mass balance results in Table 4 do not have any errors with respect to the field measurement at Nodes #4 and #6.

Table 4: Solid and water mass balance (inline)

Stream/ Node #	Stream/node description	Volume (m^3)			Specific gravity		Mass (T)		Wt.% Solid	Wt.% Fluid
		Slurry	Fluid	Solid	Solids	Fluid	Solids	Fluid		
1	Original FFT	12.0	10.38	1.62	2.5	1.0	4.04	10.38	28.0	72.0
2	Dilution with process water	5.0	5.00	0.00		1.0	0.00	5.00	20.8	79.2
3	Alum solution	27.0	27.00	0.00		1.0	0.00	27.00	8.7	91.3
Subtotal	**(1 +2 + 3)**	**44.0**	**42.38**	**1.62**			**4.04**	**42.38**	**8.7**	**91.3**
4	Coagulated FFT	44.0	42.38	1.62	2.5	1.0	4.04	42.38	8.7	91.3
5	Flocculant	4.0	4.0	0.00		1.0	0.00	4.00	8.0	92.0
Subtotal	**4 + 5**	**48.0**	**46.38**	**1.62**			**4.04**	**46.38**	**8.0**	**92.0**
6	Flocculated FFT	48.0	46.38	1.62	2.5	1.0	4.04	46.38	8.0	92.0
		Errors in mass balance					**0.00**	**0.00**	**–**	**–**

By carefully reviewing the mass balance, it can be concluded that at the start of this process, the solids fraction of the original FFT Stream #1 was 28 wt.% solids, which was diluted down to 8 wt.% solids at the stage of flocculant addition. This changes the volume of the fluid from 10.38 m^3 to 46.38 m^3, representing 4.5 times additional water that needs to be handled at the front and back-end of the process, in addition to the water in the original FFT.

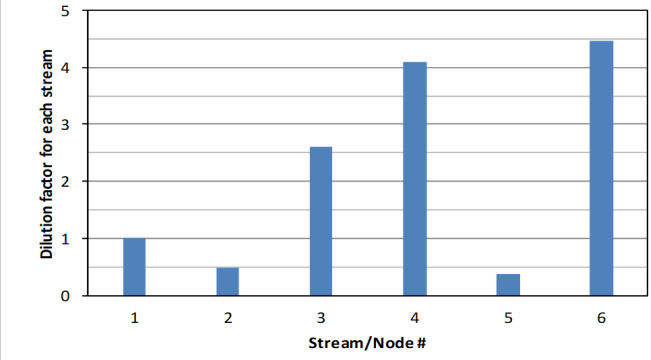


Figure 5: Relative water volume after every stream addition to the process

Figure 5 shows the cumulative water added during the process with respect to unit water volume in original FFT Stream #1. Stream #2, dilution of the original FFT with additional water, is only required if the original FFT solids content is higher than 20 wt.% solids. Streams 3 and 5 are waters from the coagulation and flocculant solutions. Nodes #4 and #6 are measurements (monitoring) points. This analysis is important because the proposed treatment in this study will be utilizing existing tailings lines and therefore, it is necessary to evaluate if there will be any issues with infrastructure regarding sizing of the water management systems.

Balance after deposition in the geotextile tubes

Once the treated FFT was poured into the geotextile tube, instantaneous dewatering was observed. However, it will be extremely difficult, although not impossible, to measure the exact volume of water released by collecting in a sump to avoid seepage losses. In this trial, the volume of the water released from the geotextile tube was not measured. During the pour, the water split into two parts: the volume of water retained inside the geotextile tube and water released from the geotextile tube. This split of water reported in Table 5 is an indirect measurement (back calculated).

In the trial program, core samples were collected from the geotextile tubes for solids and water analysis. Porewater chemistry was also analyzed from the core samples. Grab samples were collected from the release water and analyzed for chemistry. Four key data points were selected to evaluate the dewatering and solids consolidation into the geotextile tubes. The mass of release water was calculated using the difference between the starting mass of water and the residual from the core sample. Since the density of

water is unity, the mass for water reported can be interpreted as volume (m^3) of water. Table 5 shows the solid/water mass balance of the core samples collected from the geotextile tube at different time intervals.

Calculations in Table 5 reveal most of the dewatering from the geotextile tubes occurs during the first five hours after deposition, which may be attributed to the release of the dilution waters added to the original FFT feed. The solids content after the first five hours of deposition is approximately 27 wt.% solids, which is close to that of the original FFT used in the trial. Next, core samples were collected from the geotextile tube after 7 and 30 days, which had 50 wt.% and 55 wt.% solids, respectively. A comparison of the results from the end-of-pipe and after five hours with the 7-day samples shows that there is a significant initial increase in dewatering from 8 wt.% to 50 wt.% solids.

Table 5: Solid and water mass balance on the core samples from the geotextile tube

Stream/ Node #	Stream Node description	Mass (T)				% Mass in tubes		Cum. wt.% water release	Drying time (days)
		Solid	Water in /tube	Cum. Water release	Total	Solid	Water		
6	Flocculated FFT	4.04	46.38	0.00	50.42	8.0	92.0	0.00	0.0
Inside Tube	5 hours after tube filled	4.04	10.88	35.50	50.42	27.0	73.0	76.54	0.2
	7 days after tube filled	4.04	4.08	42.30	50.42	50.0	50.0	91.20	7.0
	30 days after tube filled	4.04	3.3	43.08	50.42	55.0	45.0	92.88	30.0

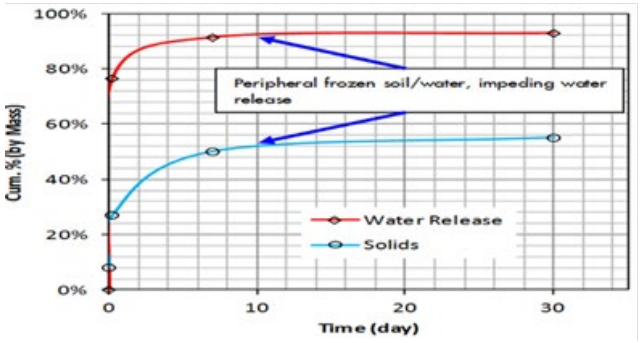


Figure 6: Variation in wt.% solids content and mass of water released within 30 days after deposition (Nov. 3rd = time zero)

Figure 6 shows a summary of the dewatering of the treated FFT poured into the geotextile tube as a function of time. After 30 days, the sample does not show a change in dewatering kinetics because of the physical limitation to dewatering caused by the peripheral frozen soil/pore water that impedes water release during wintertime (freeze condition).

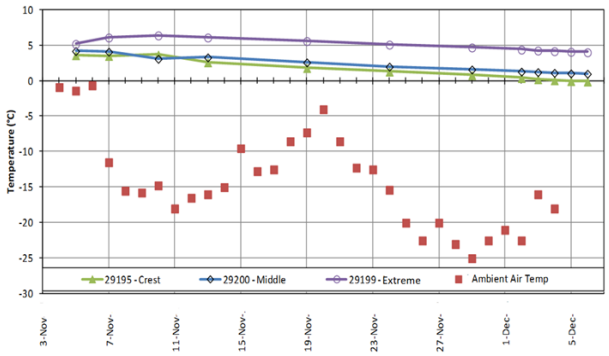


Figure 7: Temperature measurements inside the geotextile tube and outside (ambient)

Figure 7 shows the temperature measurements inside and outside (ambient temperature) the geotextile tube from November 3rd (the day when the geotextile tube was completed) to December 5th (± 30 days after the tube was filled completely with treated FFT). Additional water release will likely occur during the "thaw" cycle of the freeze-thaw process during the spring season as freeze/thaw is a well-known dewatering process for shallow fine tailings deposits.

Chemistry balance calculations

The original FFT consist of approximately 70% by mass water which is a major constituent. To ensure that the recovered water is suitable for reuse in the process as a process water, it is important to analyze the chemistry of the recovered water. It becomes more crucial when chemical treatment (coagulation and flocculation) is used to separate the solids and water in the FFT. Chemicals used in coagulation and flocculation may poses reactivity with the solid surface where different anions and cations are released from the solid minerals in the FFT. The best way to understand the chemistry of the released water is to perform an anions and cations balance analysis where sum of all cations mass should be equal to the sum of all anions mass to maintain a charge neutrality in the aqueous phase. This makes the entire chemistry balance analysis more complex. However, for indicative purposes concentration analysis and mass balance of major cations and anions will provide predictions on the reactive behaviors in the FFT when chemically treated and suitability of the released water as a process water.

The chemical analyses of the mixed inline streams and the release water from the geotextile tube show changes in the chemistry throughout the treatment process. Process water containing high concentrations of dissolved divalent cations (Ca^{2+} ions), was used to investigate their impacts on the flocculation of quartz and kaolinite at pH 8.

The mass balance and concentration analyses of the major ions in the water phases show that majority of the ions remained in the solid phase after deposition. The concentration of Ca^{2+} in the release water was the same as in the process water used for the field trial. The major source of Al^{3+} in the process is from

Alum (coagulant stream), which has a negligible concentration of 0.015 mg/L in the release water. Therefore, there is no indication of any excess divalent or multivalent cations in the release water. Generally, the concentration of anions and cations show encouraging results for the release water chemistry.

Based on the process flow diagram shown in Figure 4, all the process streams and samples collected at Nodes #4 and #6 were analyzed for major anions and cations to understand the chemistry of the release water. Table 6 shows the concentration (anions and cations) of individual process streams, Node #4, and Node #6.

Table 6: Concentration of major anions and cations in the process streams

Stream/ Node #	Stream node description	Concentration of major ions (mg/L)							
		HCO_3^-	SO_4^{2-}	Cl^-	Ca^{2+}	Mg^{2+}	Na^+	K^+	Al^{3+}
1	Original FFT	420	190	150	47	22	260	22	0.12
2	Dilution with process water	440	180	59	86	26	110	16	0.0091
3	Alum solution	40	550	72	92	28	160	10	110
		Subtotal (1 + 2 + 3)							
4	Coagulated FFT	310	430	74	97	35	170	59	0.012
5	Flocculant solution	540	190	180	43	13	140	51	0.037
6	Flocculated FFT	330	460	110	99	36	220	19	0.011
7		**Release/Retained of anions/cations**							
	Tube Run-off water	**280**	**470**	**99**	**86**	**31**	**180**	**15**	**0.015**

To calculate the mass balance of the anions and cations, the fluid phase volumes from Table 4 for the Streams #1, #2, #3, #5 and Nodes #4 and #6 were used.

Table 7 shows the results of the mass balance conducted on the process flow diagram shown in Figure 4. Carefully reviewing the results in Table 7, the cumulative mass for Streams #1, #2, and #3 should be equal to the mass at Node #4, which is calculated from the chemical analysis results of Node #4 (sampling point) collected during the deposition of materials in the process. If there is a difference in the masses, this suggests some sort of chemical reaction.

When the mass of Node #4 is subtracted from the sum of Streams #1, #2 and #3 and results in a negative number, this indicates that the mass has increased in the liquid phase by means of some reaction(s) in the original FFT. Conversely, a positive result means those cations or anions have been transferred from the liquid phase onto the solids, which is commonly referred to as cation exchange reactions taking place at the soil particle surfaces.

Comparing the coagulated FFT (Node #4) with the collective mass of the input streams #1 to #3, it can be concluded from the sign conventions for HCO_3^- , SO_4^{2-}, Ca^{2+}, Mg^{2+}, and K^+ that they are released

into the fluid (aqueous) phase of the coagulated FFT where Cl^-, Na^+ and Al^{3+} are retained into the solid phase. This change in chemical composition suggests that cation exchange reactions are happening on the solid surfaces.

Similarly, subtracting the chemistry of the flocculated stream (Node #6) from the subtotal upstream sites (Node #4 + Stream #5) a major shift in the overall chemistry is seen. In the flocculated FFT, only K^+ is released into the fluid (aqueous) phase while other major cations and anions are retained in the solid phase.

The difference in the ion mass of flocculated FFT (Node #6) and the release water (Stream #7) indicates that all the anions and cations have positive values. This means the anions and cations are retained into solid phase, including bicarbonate (HCO_3^-) after treatment (coagulation + flocculation) with the physicochemical recipe. This can provide miss guidance if not interpreted correctly. Therefore, the stream(s) mass needs to be compared on individual basis to see the impact of the input stream(s) on the product stream.

Table 7: Mass of major anions and cations in the process streams

Stream/ Node #	Stream/node description	Fluid vol.	Mass of major ions (kg)								Unit load T/m³
		(m³)	HCO_3^-	SO_4^{2-}	Cl^-	Ca^{2+}	Mg^{2+}	Na^+	K^+	Al^{3+}	
1	Original FFT	10.38	4.36	1.97	1.56	0.49	0.23	2.70	0.23	0.00	1.11
2	Dilution with process water	5.00	2.20	0.90	0.30	0.43	0.13	0.55	0.08	0.00	0.92
3	Alum solution	27.00	1.08	14.85	1.94	2.48	0.76	4.32	0.27	2.97	1.06
	Subtotal (1 + 2 + 3)	42.38	7.64	17.72	3.80	3.40	1.11	7.57	0.58	2.97	1.06
4	Coagulated FFT	42.38	13.10	18.23	3.14	4.11	1.48	7.21	2.50	0.001	1.18
	Release/Retained in coagulated FFT in the pipeline (1 + 2 + 3) – (4)	–	-5.5	-0.5	0.7	-0.7	-0.4	0.4	-1.9	3.0	
5	Flocculant solution	4.00	2.2	0.8	0.7	0.2	0.1	0.6	0.0	0.00	1.15
	Subtotal (Node 4 + 5)	46.38	15.3	19.0	3.9	4.3	1.5	7.8	2.5	0.00	1.17
6	Flocculated FFT	46.38	15.3	21.3	5.1	4.6	1.7	10.2	0.9	0.00	1.27
	Release/Retained in the flocculated FFT in the geotextile tube Node 6 – (4 + 5)	–	0.00	2.27	1.26	0.30	0.12	2.40	-1.6	0.00	
7	Tube Run-off water	45.00	12.6	21.2	4.5	3.9	1.4	8.1	0.7	0.00	1.16
Chemistry difference between 6 and 7			2.7	0.1	0.6	0.7	0.3	2.1	0.2	0.00	0.11
Chemistry difference between 1 and 7			-8.2	-19.2	-2.9	-3.4	-1.2	-5.4	-0.4	0.00	

Comparing Stream #1 to Stream #7, there is an increase in the mass of all the cations and anions in the aqueous phase. This is indicative that the other process streams added between Stream #1 and #7 contributed to this increase of anions and cations mass in the aqueous phase in addition to the surface reaction. Example, if we replace the Stream #2 (dilution water) with an alternative stream having no or low concentration of anions and cations the overall mass in Stream #7 will be lower.

Comparing all the streams individually for mass loading of cations and anions, the most complex is the coagulant Stream #3. The unit loading of anions and cations masses for all streams is approximately 1 kg/m^3, suggesting that all the stock solutions (coagulant Stream #3 and flocculant Stream #5) were prepared in similar type of water (the water used from Stream #2).

Comparing the volumes of fluid added into the process from different streams, the volume of the Alum solution Stream #3 is about three times that of the original FFT Stream #1 plus the dilution Stream #2 volume. See Figure 5 to understand the rationale behind the change in unit volume of water from the Alum solution Stream #3. This suggests that this stream alone is a major contributor to the change in the downstream process chemistry.

The geotextile tube run-off or release water Stream #7 was sampled at different intervals of time. The same concentrations of ions in the release water were reported each time the sample was collected. The concentrations of the anions and cations are presented in Table 6 (Stream #7). The 45 m^3 run-off volume shown in Table 7 from the geotextile tube is considered an approximation for complete drying when all water is released.

Table 8 shows the mass of major cations and anions in the release water from the geotextile tubes.

Table 8: Mass of major anions and cations in the released water from the geotextile tubes

Stream/ Node #	Stream/node description	Fluid volume	Mass of major ions (kg)								Unit load T/m^3
		(m^3)	HCO_3^-	SO_4^{2-}	Cl^-	Ca^{2+}	Mg^{2+}	Na^+	K^+	Al^{3+}	
6	Flocculated FFT	46.4	15.3	21.3	5.1	4.6	1.7	10.2	0.9	0.0	1.27
7	5 hours after tube filled	35.5	9.9	16.7	3.5	3.0	1.1	6.4	0.5	0.0	1.16
	7 days after tube filled	6.8	1.9	3.2	0.7	0.6	0.2	1.2	0.1	0.0	1.16
	30 days after tube filled	0.78	0.2	0.1	0.0	0.0	0.0	0.0	0.0	0.0	0.38

As mentioned above, the concentration of the major ions remains the same, but the mass loading varies depending on the volume of water released, and subsequently the unit mass loading is also reduced. In a nonreactive environment (solid surface), the sum of the individual species masses should be equal to the corresponding species in the treated (flocculated = flocculation of the coagulated FFT) FFT Stream (#6),

and the unit loading should continue decreasing. If this is not true, then the solid surface is reactive and cations are released during the dewatering process in the geotextile tube, causing the ion concentrations and overall mass to change.

Conclusion

This study has confirmed that the poor flocculation of quartz and kaolinite particles observed in the range of pH 8 is due to the adsorption of Ca^{2+} ions on anionic PAM flocculant, causing steric stabilization at the particles surface. Steric stabilization results from covering the particles with the anionic flocculant, preventing the particles from getting close to the range of attractive forces and thereby allowing the particles to be dispersed.

The physicochemical treatment recipe of the FFT is designed to achieve efficient flocculation performance by maximizing the agglomeration of fines to form large flocs while maximizing water release. To achieve this design criterion, the coagulated FFT slurry density at the flocculation step should be approximately 8 wt.% solids and, therefore, the dilution of the original FFT should be set for this condition while maintaining the concentration and dosage of the coagulant and flocculant constant.

The initial change in the solids content by mass of the flocculated FFT from 8% (end-of-pipe) to 27% in the geotextile tube after five hours of pour shows release of dilution water used in the process and an effective coagulation and flocculation in the pipeline prior to the discharge into the geotextile tube. Comparing the results at end-of-pipe and after five hours with the data after seven days of the completion of the geotextile tube filling, there is a significant initial increase in dewatering from 8 wt.% to 50 wt.% solids.

The concentration of Ca^{2+} ions in the release water is the same as the process water used for the trial (86 ppm). The Al^{3+} loading is mainly contributed from the coagulant (Alum) stream, which is transferred to the solid phase and remains in very low concentration in the release water. The results show that the physicochemical treatment recipe for FFT with coagulation and flocculation does not generate any excess divalent or multi-valent cations in the release water in the scenario of high divalent ion-content dilution water.

As a result, this study through the solid, ions and water mass balance analyses has identified that the negative impact of an excess of calcium ions on flocculation of the FFT can be reduced or even eliminated by aluminum ions in the range of pH 8.

The mineralogy identification and quantification by elemental distribution, spectrograph, and scanning electron microscopy analyses of this study show that 45% – 80% of carbon oxygen-bearing compounds, approximately, were transferred to the solid phase of the treated FFT with Da Silva's recipe. The mass balance and concentration of major anions and cations analyses performed in this study have

confirmed that about 2% – 33% of the major ions except Al (100%), including 22% bicarbonate (HCO_3^-), were transferred and remained in the solid phases of the treated FFT after deposition in the geotextile tube. These findings are very encouraging and suggest further investigation of the potential for carbon capture (more work is still needed to quantify accurately how much carbon can be sequestrated into the treated FFT from organic carbon and inorganic carbon dioxide from the atmosphere), which is linked to solids phase and carbonate compounds precipitation. However minuscule the amount may be, this bit of CO_2 pulled from the air, mineralized, and turned into part of the solid phase of the reclaimed geotextile tube tailings deposits is no longer heating up our planet.

Carbon sequestration by carbonation through FFT treatment is promising and has potential to benefit the environment, especially for oil sand tailings, where the residual organic carbon from extraction of oil and bicarbonate originating from the atmosphere are both mineralized into carbonate. Formation of carbonate can enhance the consolidation of the treated FFT and directly trap some metals into the crystal of carbonate. Because of coagulation and flocculation, almost all cations and anions in solution, dissolved or suspended, are trapped into solids, and therefore this process would allow an assessment of all contaminants trapped in the solids (up to 50 elements) using inductively coupled plasma mass spectrometry (ICP-MS).

Acknowledgments

Thanks to Dr Nicholas Beier (U of A) and Dr Hailin Deng (WSP Australia) for their support on the review of this paper.

References

Atesok, G., Somasundaran, P. and Morgan, L. 1988. Adsorption properties of Ca2+ on na-kaolinite and its effect on flocculation using polyacrylamides. *Colloids and Surfaces* 32: 127–138.

Da Silva, F. 2022. Geo-composite physicochemical treatment using synthetic fibers for enhanced dewatering, shear strength and consolidation of oil sands fluid fine tailings deposits – concepts and lessons learned. *Proceedings of Tailings and Mine Waste 2022,* Denver, Colorado, United States.

Gan, W. and Liu, Q. 2008. Coagulation of Bitumen with kaolinite in Aqueous Solutions containing Ca, Mg and Fe: Effect of citric acid. *Journal of Colloid and Interface Science* 324: 85–91.

Goldberg, S., Foster H.S. and Heick, E.L. 1991. Flocculation of illite/kaolinite and illite/montmorillonite mixtures as affected by sodium adsorption ratio and pH. *Clays and Clay Minerals* 39(4): 375–380.

Hunter, J. 1981. *Zeta Potential in Colloid Science: Principles and Applications*. Academic Press, London.

Hussain, A., Demirci, S. and Ozbayoglu, G. 1996. Zeta Potential measurements of three clays from Turkey and effects of clay on coal flotation. *Journal of Colloid and Interface Science* 184: 535–541.

Matijevic, E., Stryker, J. and Janauer, E. 1966. *Colloid Interface Science.*

Mitchell, J.K. 2005. *Fundamentals of Soil Behavior*, 3rd ed. New York: Wiley.

Peng, F. and Di, P. 1994. Effect of multivalent salts – calcium and aluminum on the flocculation of kaolin suspension with anionic polyacrylamide. *Journal of Colloid and Interface Science* 164: 229–237.

Van Lierde, A. 1980. *Behavior of Quartz Suspensions in the Presence of Calcium Ions and Acrylate Polymers.* Amsterdam: Elsevier.

Verwey, E.J.W. and Overbeek, J.T.G. 1948. *Theory of the Stability of Lyophobics Colloids*. Amsterdam: Elsevier.

Spatial Variability Assessment of Mine Tailings

Luis Vergaray-Astupina, Georgia Institute of Technology, USA
Jorge Macedo, Georgia Institute of Technology, USA

Abstract

The Global Industry Standard on Tailings Management (GISTM) promotes performance-based approaches in geotechnical assessments. Hence, characterizing the spatial variability of deposited tailings is expected to be a key input for some tailings storage facilities (TSFs); however, it has seldom been investigated. In this study, we assess the spatial variability of thickened and conventional tailings that have been deposited into the same TSF, providing a unique opportunity to investigate two tailings technologies. A dense array of 15 cone penetration tests (CPTus) has been conducted to collect data. The results were processed using traditional and machine learning-based methods for data detrending when deriving random fields. In terms of correlation lengths, we find similar ranges for the thickened and conventional tailings and similar distributions, likely influenced by the depositional processes. In contrast, the variance in the conventional tailings is higher, which we attribute to its segregating nature.

Introduction

Previous efforts on characterizing the spatial variability of soil deposits have been mainly focused on natural soils, often using the random field theory (RFT). In terms of man-made waste materials, the Bagińska et al. (2016) study characterized the vertical spatial variability of a mine waste dump in a coal mine using CPTu. However, they focused only on the vertical variability due to the large spacing between the CPTus. Regarding mine tailings, to the best of the author's knowledge, there have been no previous efforts to characterize the extent of their spatial variability at a local scale considering vertical and horizontal directions, which is one of the key contributions of our study.

Advancing the spatial variability characterization of mine tailings is a step forward to enable better treatment of uncertainties in performance-based assessments, a framework recommended in the Global Industry Standard on Tailings Management (Global Tailings Review, 2020). In addition, gaining insights into the spatial variability of mine tailings provides valuable information to improve the planning of site investigation programs for TSFs. The spatial variability assessments of this study rely on data collected on conventional and thickened tailings using a dense array of CPTus. In addition to the traditional use of

polynomial functions in the detrending process to assess the extent of spatial variability, we highlight the significant potential of modern machine learning-based procedures for trend removal, which is a major contribution from our study. Unlike traditional polynomial functions with limited flexibility due to their fixed forms, machine learning-based methods offer greater flexibility in capturing trends in CPTu data.

CPTu characterization

The investigated tailings were deposited using conventional deposition starting in the 1990s until 2010, when the deposition method was changed to high-density thickened tailings, providing a unique opportunity to investigate both conventional and thickened tailings in the same TSF. The solids contents for the conventional and high-density thickened tailings are about 50% and 62 to 70% (the variation is due to seasonal change), respectively. The field characterization was planned to collect data on both tailings and included 15 CPTus. The CPTu array was oriented parallel to the discharge points in the dam, as illustrated by Figure 1a. The CPTus were conducted at a standard penetration rate of 2 cm/s and were spaced at a distance of 1.5 m, as shown in Figure 1b. The separation was selected following the recommendations of Cary (2021) to minimize any potential disturbance between nearby CPTus. The dissipation tests confirmed a phreatic surface approximately 6.1 m below the surface. The CPTus were pushed to a depth of 16 m.

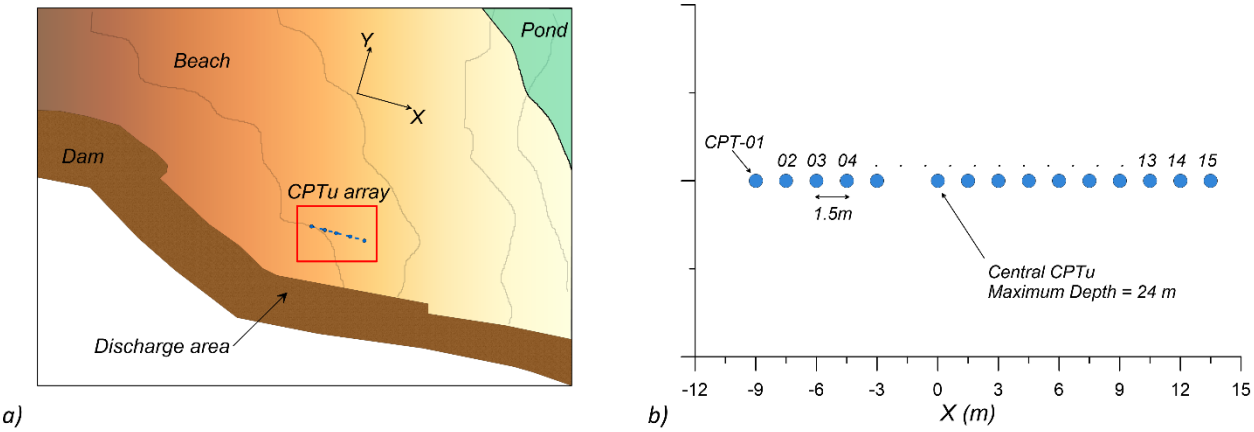


Figure 1: a) CPTu array location relative to the discharge area b) CPTu array zoom-in and labels

Figure 2a and 2b show q_t and f_s profiles, soil layering, and the phreatic surface inferred from the CPTu tests. The inferred soil profile can be divided into three layers. The layer from the surface to 2 m is a pad access built to access the site, which is not considered in the interpretations. The second layer, extending from 2.0 to about 8.5 m, corresponds to the thickened tailings showing relatively uniform q_t, f_s, and a linear trend in u_2. The conventional tailings underlay the thickened tailings and extend to the bottom of the profile, showing a more erratic variation of q_t, f_s and u_2 values. The separation of the conventional and thickened tailings at about 8.5 m is consistent with the tailing's deposition history.

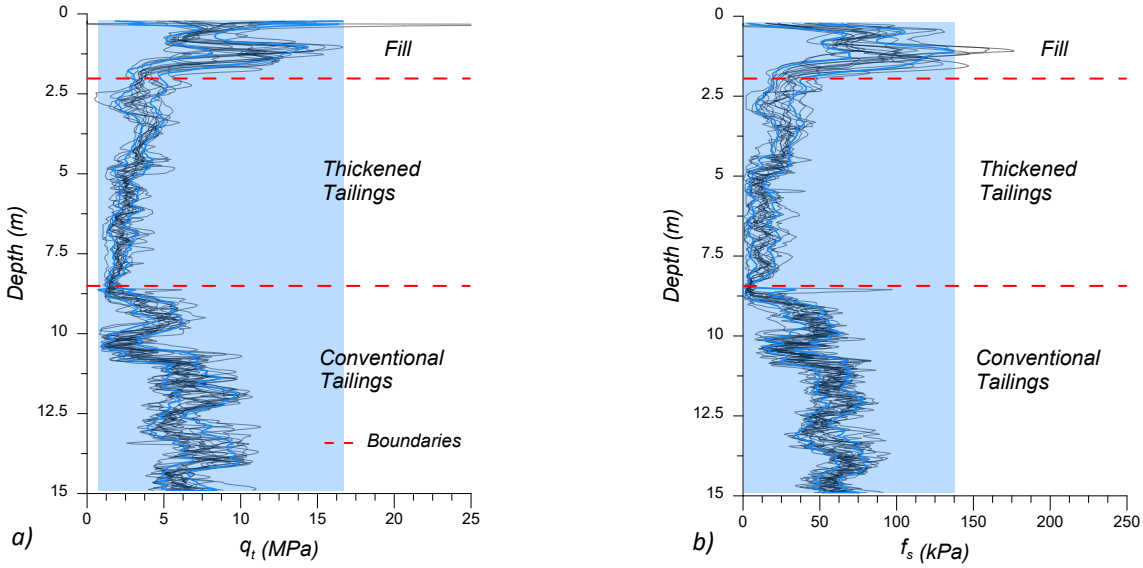


Figure 2: a) q_t, and b) f_s, profiles

Spatial variability assessment

The inherent spatial variability of soils can be modeled with the random field theory (RFT), which has been used in several previous studies mainly focused on natural soils. In the following, we provide a brief overview of the RFT framework and its use in assessing spatial soil variability. Interested readers can refer to Jaksa et al. (1999) and Bong and Stuedlein (2017) for additional details. Under the RFT framework, a measurement of some spatially varying soil property of interest $g(z)$ at a given depth z can be expressed as the sum of a deterministic trend $[t(z)]$ and a fluctuating component $[w(z)]$ as expressed by Equation 1. The spatially varying parameter of interest is then characterized by the correlation length (δ), and the coefficient of variation (COV) of $w(z)$. δ is a measure of the distance within which a particular measurement is correlated, and COV is the standard deviation (σ) of $w(z)$ normalized by the mean of $t(z)$.

$$g(z) = t(z) + w(z) \tag{1}$$

The δ can be calculated by different geostatistical procedures (e.g., Jaksa, 1995; Vanmarcke, 1977; DeGroot and Baecher, 1993). In particular, the use of autocorrelation models to fit the autocorrelation in the observed data is common in geotechnical applications. In this procedure, the sample autocorrelation function $\rho(\tau_j)$ – i.e., based on the observed data, which defines the spatial correlation for a given lag distance (τ_j) on the measurement of interest – is evaluated according to Equation 2.

$$\rho(\tau_j) = \frac{\sum_{i=1}^{n_d-j} w_i \times w_{i+j}}{\sum_{i=1}^{n_d-j} w_i^2} \tag{2}$$

As suggested by Box and Jenkins (1970), different lag distances τ_j can be considered by varying the sampling space (Δz) for $j = 1,2,3 \ldots n_d/4$, where n_d is the sample size. Once $\rho(\tau_j)$ is assessed, δ can be estimated by fitting different autocorrelation models (ACMs – Table 1) to $\rho(\tau_j)$. In using the RFT framework, it is highly beneficial to have stationarity in w, i.e., the covariance structure only depends on the distance between observations (τ). Thus, a key step in assessing spatial soil variability is detrending the data (i.e., removing $t(z)$), ideally leading to a stationary $w(z)$ random field.

This study used traditional polynomial and three non-parametric machine learning (ML) methods, namely, Random Forest (Breiman, 2001), Gradient Boosting Decision Tree (GBDT – Friedman, 2001), and the K-Nearest Neighbor (KNN – Peterson, 2009) for conducting the CPTu data detrending. The autocorrelation models were fitted to $\rho(\tau_j)$ above the Bartlett's limit $r_B = 1.96/\sqrt{n_d}$, where n_d is the number of samples, . The fitting is considered acceptable when the coefficient of determination R^2 is above 0.9 (Phoon et al., 2003).

The stationarity conditions of the detrended data were assessed using the stationarity score (S), which is based on the Bartlett's statistic test. S is a normalized scalar quantity (bounded from −1 to 1), where negative values indicate nonstationary and positive values indicate stationary. S combines the contributions from both R^2 and Bartlett's statistic and can be used as a single metric to evaluate the performance of different trend functions. Further details are provided in Macedo et al. (2024).

Table 1: Autocorrelation models and corresponding correlation length (Uzielli and Vanucchi, 2005)

Autocorrelation model	Functional form	Correlation length
Single exponential (SNX)	$\rho(\tau) = e^{-k\|\tau\|}$	$\delta = 2/k$
Cosine exponential (CSX)	$\rho(\tau) = e^{-k\|\tau\|}\cos k\tau$	$\delta = 1/k$
Second-order Markov (SMK)	$\rho(\tau) = (1 + k\|\tau\|)e^{-k\|\tau\|}$	$\delta = 4/k$
Square exponential (SQX)	$\rho(\tau) = e^{-(kt)^2}$	$\delta = \sqrt{\pi}/k$

Vertical correlation length

The vertical autocorrelation length (δ_{wv}) was calculated by fitting four different autocorrelation models (Table 1) to the sample autocorrelation functions. Figure 3 illustrates the process by showing the results obtained for the q_t profile of CPT-14 for the conventional tailings using the CSX autocorrelation model with polynomial and random forest detrending methods. The hyperparameters that produce the highest S for each method are noted in the figure titles. In this case, a polynomial function of order two was selected because it gives the highest S. However, S is negative, implying nonstationarity. In contrast, all ML-based

methods produce stationarity (Figure 3, right column). Hence, the CSX model would be discarded if only traditional polynomials were considered.

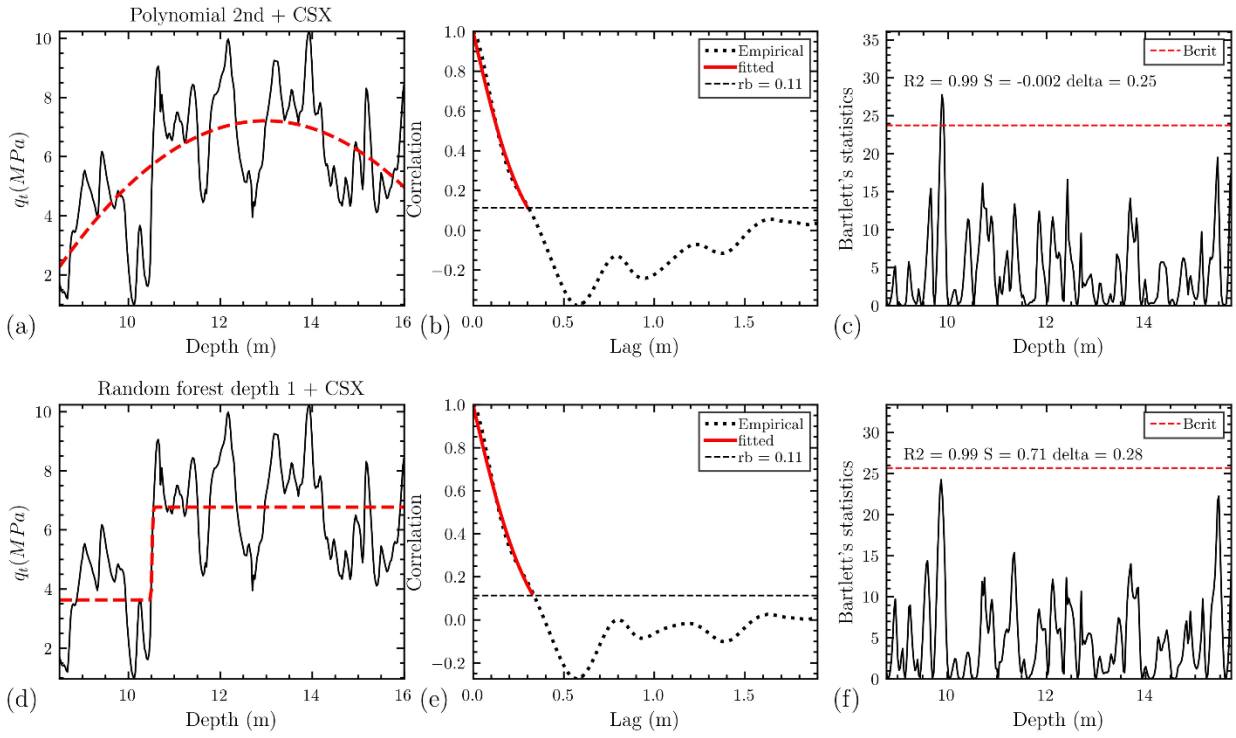


Figure 3: Results using polynomial and ML-based trend functions for a representative q_t profile, considering the conventional tailings

Figure 4 presents the cumulative distribution functions (CDFs) of δ_{wv} and COV_{wv} for q_t (Figure 4a and 4b) and f_s (Figure 4c and 4d), respectively. Interestingly, the estimated δ_{wv} and COV_{wv} values are in a relatively narrow range. In the case of the thickened tailings, the mean δ_{wv} estimated from q_t is 0.33 m, which is smaller, but still comparable with the δ_{wv} of 0.49 m based on f_s. In the conventional tailings, the mean δ_{wv} estimated from q_t is 0.35 m, quite close to the mean δ_{wv} of 0.31 m considering f_s. The q_t-based δ_{wv} CDFs for both tailings are also consistent. The f_s-based δ_{wv} CDFs for the thickened tailings are shifted to the right with respect to the CDFs for conventional tailings, but the δ_{wv} are still comparable.

The similar δ_{wv} values can be attributed to the combination of two aspects i) the deposition scheme for the conventional and thickened tailings; and ii) averaging effects in CPTu measurements. In terms of the deposition process, similar phenomena are involved in both the deposition of the conventional and thickened tailings. These phenomena include pauses in the tailings discharge (the deposition is conducted on layers), drying-wetting cycles, induced consolidation when new layers are deposited, and induced flow gradients. Moreover, even though the thickened tailings have a less segregating nature, it is still reasonable to expect some segregation under field conditions during the deposition process. In terms of the averaging

during CPTu penetration, it is well known that q_t is influenced by the response of the units that are at a distance of 1 to 3 cone diameters for soft soils and 20 to 30 cone diameters for stiffer soils (Lunne et al., 1997; Ahmadi and Robertson, 2005). Similarly, f_s also represents an averaged measurement. Thus, the relatively increased heterogeneity on the conventional tailings may have also been averaged out to some extent by the nature of the CPTu process.

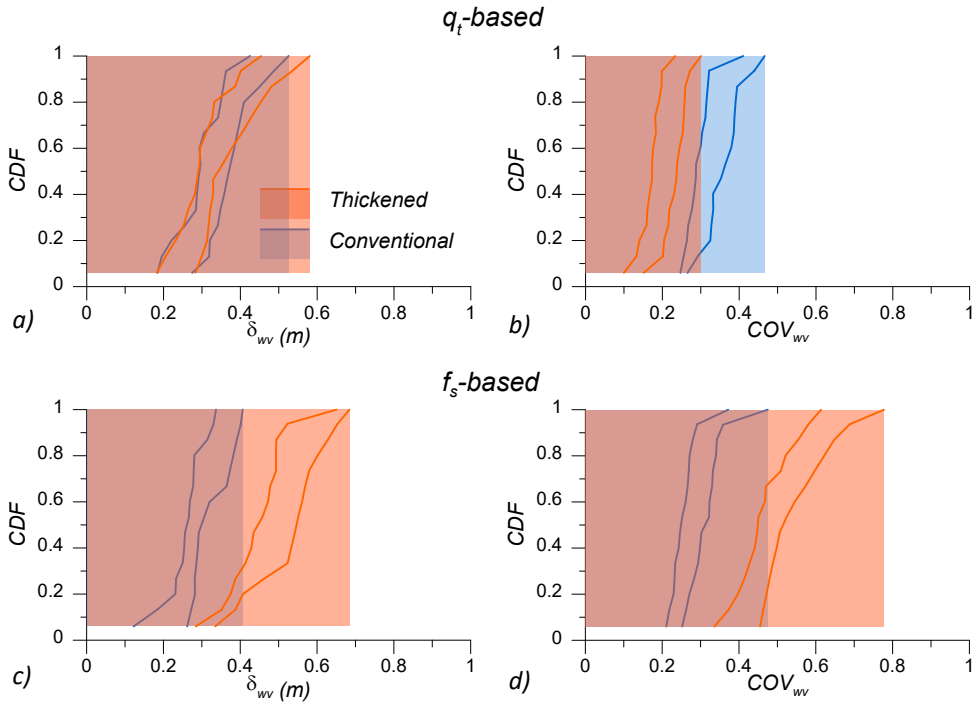


Figure 4: Ranges of a) δ_{wv} and b) COV_{wv} CDFs estimated from q_t data. Ranges of c) δ_{wv} and d) COV_{wv} CDFs estimated from f_s data

In terms of the COV_{wv} CDFs, it is important to put in context that COV_{wv} is a measurement of the fluctuation (i.e., σ) of $w(z)$ with respect to its order of magnitude (i.e., $t(z)$). The relatively larger COV_{wv} for q_t in the conventional tailings reflects the more significant fluctuation of q_t, potentially influenced by the more segregating nature of the conventional tailings. In contrast, the larger COV_{wv} for f_s in the thickened tailings reflects the significantly lower f_s in the thickened tailings compared to the conventional tailings (i.e., a factor of about 3), which counteracts the σ contribution.

Horizontal correlation length

Due to the relatively large sampling interval in the horizontal direction compared to the vertical, deriving on significantly fewer points at a given depth, the horizontal correlation length (δ_{wh}) is estimated following the expeditive method, which was originally proposed by Vanmarcke (1977) and has been used in previous studies for natural soils (e.g., Stuedlein et al., 2012; Bong and Stuedlein, 2017; Cary, 2021). The expeditive

method estimates δ_{wh} as $\sqrt{2/\pi}\,\bar{d}$, where $\bar{d}$ is the average length of the segments obtained at the crossings of $g(z)$ and its linear trend function $t(z)$, where $g(z)$ is the metric of interest (i.e., q_t or f_s). Following the recommendations of Stuedlein et al. (2012) and Bong and Stuedlein (2017), in applying the expeditive method, we considered a minimum of five crossings to get stable COV_{wh} and δ_{wh} estimates. Figure 5a illustrates the q_t-based δ_{wh} estimation in the thickened and conventional tailings at depths of 4 and 12 m, and Figure 5b illustrates the f_s-based δ_{wh} estimation at the same depths.

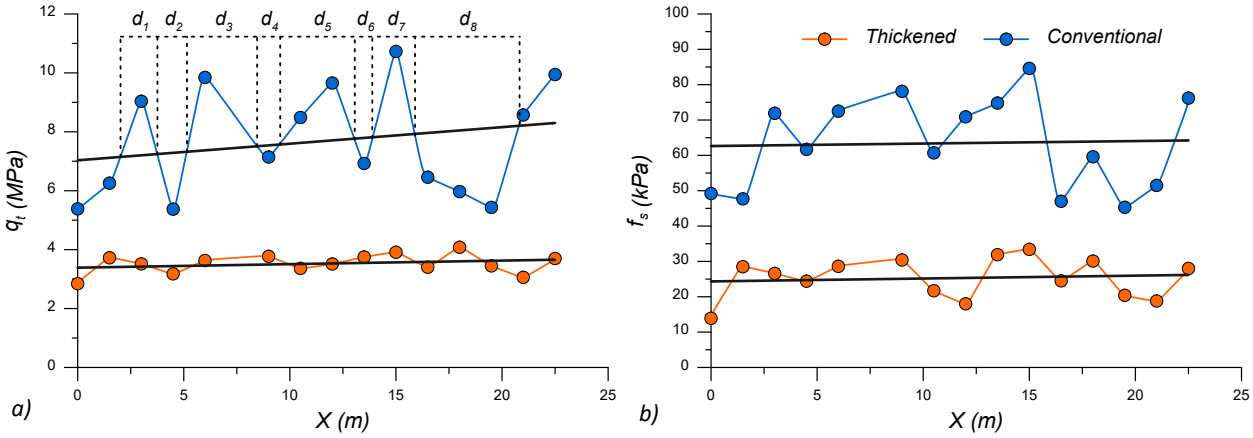


Figure 5: Application of Vanmarcke's expeditive method for estimating the horizontal autocorrelation l based on a) q_t and b) f_s, considering the thickened and conventional tailings at selected depths (4 m for the thickened tailings and 12 m for the conventional tailings)

Figure 6a shows the estimated δ_{wh} considering q_t and f_s for the entire deposit, and Figure 6b presents the associated horizontal coefficient of variations (COV_{wh}). It can be observed that the thickened and conventional tailings exhibit a similar δ_{wh}. For instance, the 16 – 84 percentiles for the q_t-based δ_{wh} is in the range of 2 to 3.5 m for the thickened tailings and in the range of 1.8 to 3.0 m for the conventional tailings. In the case of the f_s-based estimations, the 16 – 84 percentiles δ_h is in the range of 1.7 to 3.2 m for the thickened tailings and 1.9 to 2.9 m for the conventional tailings. The similar δ_{wh} in both tailings can be attributed to the deposition process and associated phenomena (e.g., pauses in the discharge, flow gradient, drying-wetting cycles, freezing, and consolidation) as discussed before for the δ_{wv}.

Moreover, it is reasonable to expect segregation to have less effect in the horizontal direction compared to the vertical, which is reflected in a similar δ_{wh}. The q_t-based COV_{wh}values tend to be slightly larger for the conventional tailings as the existing variance controls them, whereas the f_s-based COV_{wh} values are larger for the thickened tailings as they are controlled by the lower f_s values in the thickened tailings.

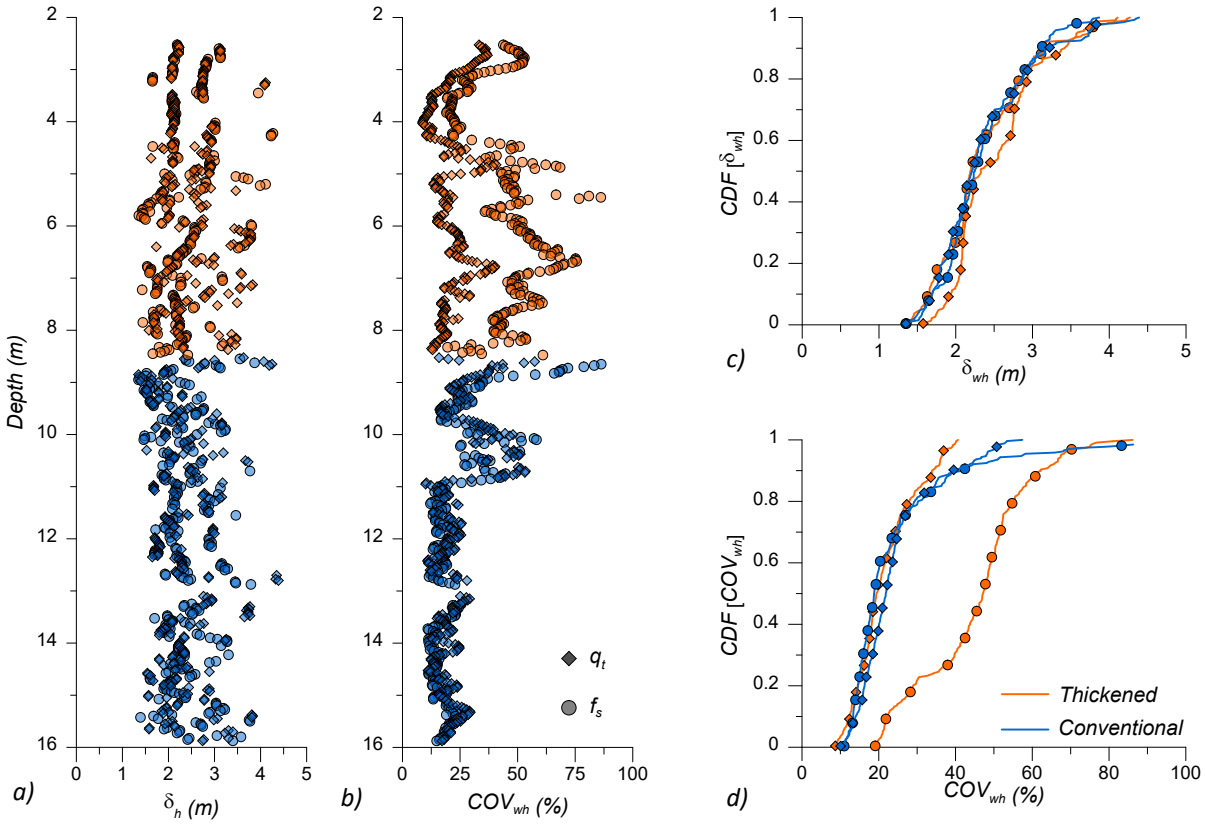


Figure 6: a) δ_{wh} and b) COV_{wh} profiles based on q_t and f_s, considering the thickened and conventional tailings. CDFs of q_t and f_s based c) δ_{wh} and d) COV_{wh} in the thickened and conventional tailings.

Figure 6c and 6d present q_t- and f_s-based CDFs for δ_{wh} and COV_{wh}; it can be observed that the δ_{wh} CDFs for q_t and f_s are consistent for both the thickened and conventional tailings. In addition, similar q_t-based COV_{wh} CDFs for the thickened and conventional tailings are also observed, being also consistent with the f_s-based COV_{wh} for the conventional tailings, whereas the f_s-based COV_{wh} CDF for the thickened tailings is shifted to the right, showing larger values for reasons already discussed.

Discussion

The generation of random fields depends on δ and COV (or variance, σ^2); hence, having similar δ, which is the case for the thickened and conventional tailings, does not necessarily imply similar random fields. This can be illustrated by generating random fields with the parameters evaluated for the thickened and conventional tailings using the GSTools package (Muller and Schüler, 2021). Figure 7a shows one of these realizations considering the SNX autocorrelation model and parameters estimated using the GBDT model for detrending. In this case, the q_t-based estimated parameters for the thickened tailings are $\sigma^2 = 0.3$ MPa, $\delta_{wv} = 0.37$ m, and $\delta_{wh} = 2.45$ m, whereas the parameters for the conventional tailings are $\sigma^2 = 2.6$ MPa,

$\delta_{wv} = 0.41$ m, and $\delta_{wh} = 2.29$ m. As can be inferred from these parameters, the main difference is in σ^2. It is interesting to note that the extent and shape of zones with similar $w(z)$ values are comparable for the two types of tailings due to the similar δ. However, the random field for the thickened tailings is significantly more stable (i.e., it presents less variability) due to the lower σ^2. Thus, despite the similar δ for both tailings, the simulated random field for the thickened tailings shows a more homogeneous structure than conventional tailings.

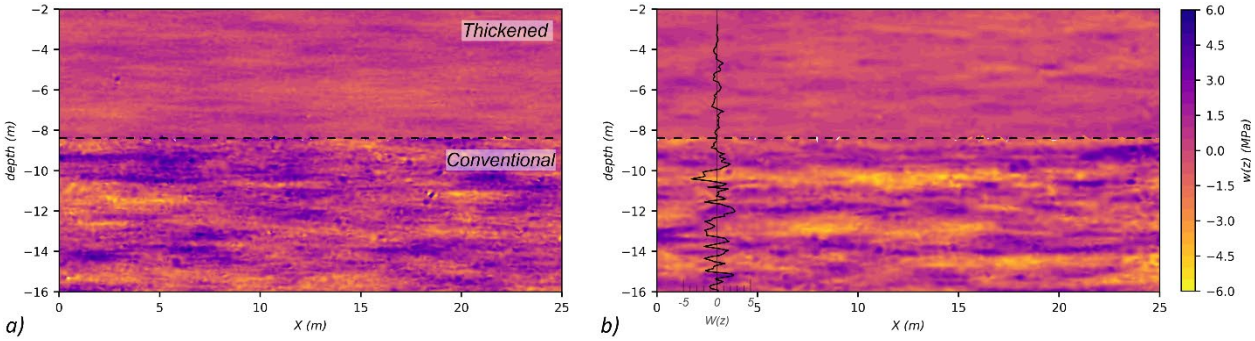


Figure 7: a) Unconditioned and b) conditioned q_t -based $w(z)$ random field realizations for the thickened and conventional tailings

Figure 7b presents a $w(z)$ random field realization conditioned at various depths across the 15 CPTu locations. This conditional random field (CRF) offers a more realistic representation of spatial variability by incorporating site-specific data. Consequently, CRF realizations enhance the understanding of the distribution of tailings properties and improve the stability analysis and modeling of TSFs, which often rely on simplified assumptions, such as uniform layers, isotropic and homogeneous properties, and deterministic characteristics. By enabling probabilistic assessments, CRFs provide a more accurate and comprehensive approach to evaluating TSF stability.

Conclusion

As the application of performance-based approaches to tailings management advances (Morgenstern, 2018), the quantification of variabilities (spatial and aleatory) is expected to become crucial, particularly for TSFs where the geotechnical characterization of mine tailings is key in assessing the overall response (e.g., the overall physical stability in upstream TSFs). In this context, we have collected data using a dense CPTu array to assess the spatial variability of two different types of tailings deposited in the same TSF. We also evaluated the potential of modern machine-learning methods for informing the estimation of random field parameters. The examined methods provided advantages, which we attribute to the interpolation nature of CPTu detrending (machine learning can act as a black box for extrapolation problems). This study's findings may prove valuable in geotechnical analyses that require adopting δ values to account for spatial

variability in mine tailings similar to those examined in this study, specifically thickened and conventional tailings produced from gold ore. Given the lack of spatial correlation information on mine tailings, we expect that it would also be helpful as a benchmark for future efforts. Of note, case studies exist documenting the importance of spatial variability parameters for water dams (Sanchez-Lizarraga and Lai, 2014; Boulanger and Montgomery, 2016; Guo et al., 2019). Thus, it is reasonable to expect similar spatial variability studies focused on TSFs to translate into engineering practice in the future.

Acknowledgments

This material is based upon work supported by the National Science Foundation (NSF) under Grant No. CMMI 2145092. Any opinions, findings, conclusions, or recommendations expressed in this material are those of the authors and do not necessarily reflect the views of the NSF. The PRONABEC program of the Peruvian government also provided complementary support. In addition, we would like to thank ConeTec, Newmont, and WSP-Golder for supporting the site characterization efforts. Finally, we thank Prof. Armin Stuedlein for sharing VBA codes that we used to validate our implementations and Prof. Jason Dejong for discussions when planning the CPTu campaign for the spatial variability characterization.

References

Ahmadi, M.M. and Robertson, P.K. 2005. Thin-layer effects on the CPT qc measurement. *Canadian Geotechnical Journal* 42(5): 1302–1317.

Bong, T. and Stuedlein, A.W. 2017. Spatial variability of CPT parameters and silty fines in liquefiable beach sands. *Journal of Geotechnical and Geoenvironmental Engineering* 143(12).

Boulanger, R.W. and Montgomery, J. 2016. Nonlinear deformation analyses of an embankment dam on a spatially variable liquefiable deposit. *Soil Dynamics and Earthquake Engineering* 91: 222–233.

Box, G. and Jenkins, G. 1970 *Time Series Analysis: Forecasting and Control.* Holden-Day, San Francisco.

Breiman, L. 2001. Random forests. *Machine Learning* 45: 5–32.

Breysse, D., Niandou, H., Elachachi, S. and Houy, L. 2007. A generic approach to soil–structure interaction considering the effects of soil heterogeneity. *Risk and Variability in Geotechnical Engineering* 117–124.

Cai, G., Lin, J., Liu, S. and Puppala, A.J., 2017. Characterization of spatial variability of CPTU data in a liquefaction site improved by vibro-compaction method. *KSCE Journal of Civil Engineering* 21(1): 209–219.

Cami, B., Javankhoshdel, S., Phoon, K.-K. and Ching, J. 2020. Scale of fluctuation for spatially varying soils: Estimation methods and values. *Journal of Risk and Uncertainty in Engineering Systems, Part A: Civil Engineering* 6(4).

Cary, J. 2021. An investigation into the role of spatial variability on liquefaction consequence severity. Master's thesis, Oregon State University.

Ching, J., Wu, T.-J., Stuedlein, A.W. and Bong, T. 2018. Estimating horizontal scale of fluctuation with limited CPT soundings. *Geoscience Frontiers* 9(6): 1597–1608.

DeGroot, D.J. and Baecher, G.B. 1993. Estimating autocovariance of in situ soil properties. *J. Geotech. Geoenviron. Eng*. 119(1): 147–166.

Fenton, G.A. and Griffiths, D.V. 2005. Three-dimensional probabilistic foundation settlement. *Journal of Geotechnical and Geoenvironmental Engineering* 131(2): 232–239.

Friedman, J. 2001. Greedy function approximation: A gradient boosting machine. *The Annals of Statistics* 29(5): 1189–1232.

GTR (Global Tailings Review). 2020. Global Industry Standard on Tailings Management. https://globaltailingsreview.org/wp-content/uploads/2020/08/global-industry-standard_EN.pdf

Griffiths, D.V., Fenton, G.A. and Manoharan, N. 2006. Undrained bearing capacity of two-strip footings on spatially random soil. *International Journal of Geomechanics* 6(6): 421–427.

Guo, X., Dias, D. and Pan, Q. 2019. Probabilistic stability analysis of an embankment dam considering soil spatial variability. *Computers and Geotechnics* 113: 103093.

Hu, Y.-G. and Ching, J. 2015. Impact of spatial variability in undrained shear strength on active lateral force in clay. *Structural Safety* 52: 121–131.

Jaksa, M.B. 1995. The influence of spatial variability on the geotechnical design properties of a stiff, overconsolidated clay. PhD thesis, Faculty of Engineering, University of Adelaide, Adelaide, SA.

Jaksa, M.B., Goldsworthy, J.S., Fenton, G.A., Kaggwa, W.S., Griffiths, D.V., Kuo, Y.L. and Poulos, H.G. 2005. Towards reliable and effective site investigations. *Géotechnique* 55(2): 109–121.

Jaksa, M.B., Kaggwa, W.S. and Brooker, P.I. 1999. Experimental evaluation of the scale of fluctuation of a stiff clay. *Proceedings of the 8th International Conference on Application of Statistics and Probability*, A.A. Balkema, Rotterdam, The Netherlands, 415–422.

Lunne, T., Robertson, P. and Powell, J. 1997. Cone penetration testing in geotechnical practice. *Soil Mechanics and Foundation Engineering* 46. 10.1007/s11204-010-9072-x.

Müller, S. and Schüler, L. 2021. GeoStat – Framework/GSTools: v1.3.5 "Pure Pink", Zenodo [code], https://doi.org/10.5281/zenodo.5883346

Vergaray, L. and J. Macedo. 2024. Mechanical response of mine tailings under constant shear drained loading. *Journal of Geotechnical and Geoenvironmental engineering* 150(10): 04024082

Peterson, L. 2009. K-nearest neighbor. *Scholarpedia* 4: 1883. 10.4249/scholarpedia.1883.

Phoon, K.K., Quek, S.-T. and An, P. Identification of statistically homogeneous soil layers using modified bartlett statistics. *Journal of Geotechnical and Geoenvironmental Engineering* 129(7): https://doi.org/10.1061/(ASCE)1090-0241(2003)129:7(649)

Sanchez Lizarraga, H. and Lai, C.G. 2014. Effects of spatial variability of soil properties on the seismic response of an embankment dam. *Soil Dynamics and Earthquake Engineering* 64: 113–128.

Stuedlein, A.W., Kramer, S.L., Arduino, P. and Holtz, R.D. 2012. Geotechnical characterization and random field modeling of desiccated clay. *J. Geotech. Geoenviron. Eng*. 1301–1313.

Uzielli, M. and Vanucchi, G. 2005. Investigation of correlation structures and weak stationarity using the CPT soil behavior classification index. *Proceedings of the 9th International Conference on Structural Safety and Reliability – ICOSSAR 2005,* Rome.

Vanmarcke, E.H. 1977. Probabilistic modeling of soil profiles. *Journal of the Geotechnical Engineering Division* 103(11): 1227–1246.

Tailings Characterization for Flow Liquefaction Evaluation at a Large Tailings Storage Facility by Advanced Laboratory Testing

Juan Carlos Ayes-Zamudio, WSP, USA
Akhter Hossain, WSP, USA
Tony Freiman, WSP, USA

Abstract

This paper presents the material characterization results of a large tailings storage facility (TSF) with an upstream-constructed tailings dam, currently exceeding 230 m in height. The tailings deposits beneath the outer coarse (sand) shell forming the dam generally consist of non-plastic to low-plasticity, mostly contractive, sandy silt and silty sand-type materials. The results of an advanced laboratory testing program designed to characterize these contractive tailings for flow liquefaction evaluation are presented. The program comprised 17 isotropically consolidated undrained (CIU) and 17 isotropically consolidated drained (CID) triaxial compression tests conducted on saturated reconstituted tailings specimens with 21 to 61% fines under effective confining pressures ranging from approximately 97 to 3,040 kPa. Critical state loci for the tailings, based on the results of the CIU and CID triaxial tests, are presented. The strength loss and brittleness behavior of the tailings, derived from the CIU tests, indicate the presence of highly brittle materials within the TSF. The program also included nine constant-volume cyclic direct simple shear (CDSS) tests with post-cyclic monotonic shear and reversals of loading to complete five shear loops. Liquefied (residual) undrained shear strengths of the tailings, obtained from the CIU triaxial tests and post-cyclic DSS prior to reversal, as well as the final shear loop, are plotted against normalized effective vertical stresses. The triaxial test-based results indicate an increasing trend consistent with other published laboratory test results. The post-cyclic DSS prior-to-reversal residual strength values appear to provide a more reasonable estimate for the tailings within the studied TSF.

Introduction

The studied TSF is currently active with regular tailings deposition. It is the largest active upstream-constructed tailings dam in North America, with a current height exceeding 230 m from crest to toe and a maximum tailings thickness of 175 m. Periodic geotechnical investigations, involving extensive field and

laboratory testing, have been conducted at the TSF to characterize the tailings deposits. These investigations have revealed that beneath the coarse (sand) shell forming the dam are deposits of generally non-plastic to low-plasticity, mostly contractive, sandy silt and silty sand-type tailings. This paper presents the results of a recent advanced laboratory testing program aimed at characterizing these contractive tailings for a flow (static) liquefaction evaluation.

Index property testing

All laboratory test results presented in this paper were performed at a specialized WSP geotechnical laboratory in Lakewood, Colorado. Index property testing, including particle size distribution, Atterberg limits, and specific gravity (G_s) tests, was conducted on three sonic drill core samples collected from depths of 15.5 to 28.5 m below ground surface and a bulk sample from a test pit excavated within the tailings impoundment. The core samples were tested in May 2020, and the bulk sample was tested in April 2023. Table 1 summarizes the index test results, showing that the tailings are non-plastic silty sand (SM) and sandy silt (ML) with fines content (*FC*) varying from 21 to 61% and G_s ranging from 2.66 to 2.72.

Table 1: Summary of index properties of tailings

Sample type and number	Sample depth below ground surface (m)	*FC* (%)	USCS group name [group symbol]	*LL*	*PL*	G_s	Tailings type as characterized in this study
Sonic Drill Core Sample 1	21.6 – 22.9	21	Silty sand [SM]	NP	NP	2.72	Coarse Tailings (CT)
Sonic Drill Core Sample 2	15.5 – 16.6	43	Silty sand [SM]	NP	NP	2.69	Intermediate Tailings (IT)
Sonic Drill Core Sample 3	28 – 28.5	61	Sandy silt [ML]	NP	NP	2.7	Fine Tailings (FT)
Test Pit Bulk Sample	< 1	49	Silty sand [SM]	NP	NP	2.66	Intermediate Tailings (IT)

Note: *FC* = fines content; USCS = unified soil classification system; *LL* = liquid limit; *PL* = plastic limit; G_s = specific gravity; NP = non-plastic

The particle size distribution (PSD) curves for the tailings samples are plotted alongside the indicative gradation curves by ICOLD (2022) in Figure 1. For the purpose of this study, tailings are characterized as coarse tailings (CT), intermediate tailings (IT), and fine tailings (FT) based on their *FC*: less than 30%, between 30 and 55%, and more than 55%, respectively. It is noteworthy that the PSD curves for both CT and IT samples tested in this study plot within the zone of CT as defined by ICOLD, whereas the PSD curve for the FT sample tested in this study plots within the zone defined by ICOLD as hard rock tailings (HRT).

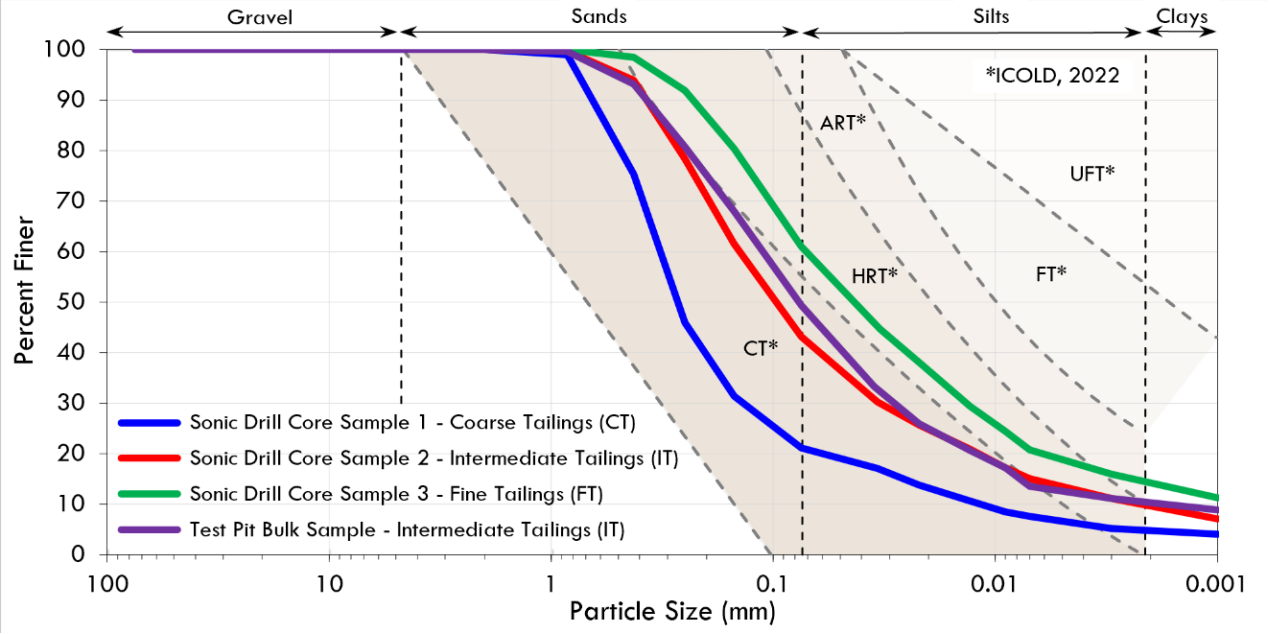


Figure 1: Tailings particle size distributions compared to ICOLD (2022) indicative gradation curves (HRT = hard rock tailings, ART = altered rock tailings, UFT = ultra fine tailings)

CIU and CID triaxial compression testing

A total of 17 isotropically consolidated undrained (CIU) and 17 isotropically consolidated drained (CID) triaxial compression tests were conducted between February 2021 and March 2023. These tests were performed in general accordance with the American Society for Testing and Materials (ASTM) Standard Specifications D4767 (ASTM, 2020a) for CIU tests and D7181 (ASTM, 2020b) for CID tests, incorporating the recommended modifications by Jefferies and Been (2016) on standard equipment. Summaries of the CIU and CID triaxial tests are presented in Tables 2 and 3, respectively. For the CIU tests, 6 were performed on CT samples, 3 on IT samples, and 8 on FT samples. Similarly, for the CID tests, 6 were conducted on CT samples, 5 on IT samples, and 6 on FT samples.

The tests were conducted on a combination of initially loose and dense tailings samples with a diameter of 71 mm and a height of 142 mm. Sample preparation was carried out using the water pluviation method, employing oversized lubricated end platens at the base of the specimens.

Values of e ranged from 0.66 to 0.99 prior to consolidation, and the confining pressures varied from 96.5 to 3,039.9 kPa (1 to 30 atm) in the CIU triaxial tests, as shown in Table 2. Consolidation resulted in a 4 to 50% reduction in e across the specimens. All specimens achieved 100% saturation at the end of the consolidation phase. Subsequently, undrained triaxial compression was applied in a strain-controlled manner at an axial strain (ε_a) rate of 0.083% per minute.

Table 2: Summary of CIU triaxial compression testing

Test ID	*FC* (%)	G_s	Confining pressure (kPa [atm])	e in consolidation stage		Y_d in consolidation stage (kN/m³)		s_r (kPa)	s_r ratio	Ψ
				Before	After	Before	After			
CIU-CT1	21	2.72	48.3 [0.5]	0.74	0.71	15.3	15.6	NA	NA	0.061
CIU-CT2			96.5 [1]	0.83	0.72	14.5	15.5	NA	NA	0.095
CIU-CT3			151.7 [1.5]	0.69	0.61	15.7	16.6	56	0.37	0
CIU-CT4			201.3 [2]	0.66	0.57	16	16.9	93	0.46	-0.023
CIU-CT5			337.8 [3.3]	0.69	0.62	15.7	16.5	62	0.18	0.042
CIU-CT6			430.9 [4.3]	0.75	0.63	15.2	16.4	41	0.1	0.071
CIU-IT1	43	2.69	120 [1.2]	0.74	0.52	15.1	17.4	21	0.17	0.035
CIU-IT2			191.7 [1.9]	0.82	0.51	14.5	17.5	26	0.13	0.039
CIU-IT3			335.1 [3.3]	0.8	0.48	14.6	17.8	67	0.2	0.036
CIU-FT1	61	2.71	101.4 [1]	0.99	0.63	13.3	16.3	19	0.19	0.053
CIU-FT2		2.7	120 [1.2]	0.72	0.57	15.3	16.8	32	0.27	0
CIU-FT3		2.7	191.7 [1.9]	0.9	0.52	13.9	17.4	71	0.37	-0.029
CIU-FT4		2.71	304.1 [3]	0.89	0.56	14	17.1	75	0.25	0.038
CIU-FT5		2.7	335.1 [3.3]	0.68	0.53	15.8	17.4	105	0.31	0.01
CIU-FT6		2.71	1013.5 [10]	0.89	0.49	14	17.8	285	0.28	0.046
CIU-FT7		2.71	1519.6 [15]	0.8	0.46	14.8	18.2	450	0.3	0.047
CIU-FT8		2.71	3039.9 [30]	0.8	0.4	14.8	18.9	955	0.31	0.046

Note: *FC* = fines content; G_s = specific gravity; e = void ratio; Y_d = dry unit weight; s_r = residual undrained shear strength; Ψ = state parameter; NA = not available.

For the CID tests, as presented in Table 3, values of *e* ranged from 0.51 to 0.9 before consolidation, with confining pressures varying from 81.4 to 500.6 kPa (0.8 to 4.9 atm). Consolidation led to a 10 to 46% reduction in *e* across the specimens, and all test specimens achieved 100% saturation at the end of this phase. Following consolidation, drained triaxial compression was applied in a strain-controlled manner with rates of ε_a ranging from 0.004 to 0.017% per minute.

Table 3: Summary of CID triaxial compression testing

Test ID	*FC* (%)	G_s	Confining pressure (kPa [atm])	e in consolidation stage		e after shear	Y_d (kN/m³)		Ψ
				Before	After		Before consolidation	After shear	
CID-CT1	21	2.72	144.8 [1.4]	0.79	0.7	0.59	14.8	16.7	0.089
CID-CT2			239.2 [2.4]	0.6	0.54	0.53	16.6	17.4	-0.049
CID-CT3			382.7 [3.8]	0.56	0.49	0.5	17.1	17.8	-0.076
CID-CT4			382.7 [3.8]	0.89	0.67	0.53	14.1	17.4	0.104
CID-CT5			475.7 [4.7]	0.58	0.46	0.48	14.4	17.7	-0.094
CID-CT6			478.5 [4.7]	0.85	0.64	0.51	17.5	18.1	0.086

Table 3: Summary of CID triaxial compression testing (continued)

CID-IT1	43	2.69	81.4 [0.8]	0.62	0.44	0.46	16.3	18	-0.057
CID-IT2			96.5 [1]	0.9	0.52	0.47	13.9	18	0.029
CID-IT3			143.4 [1.4]	0.89	0.5	0.46	13.9	18.1	0.022
CID-IT4			191.7 [1.9]	0.9	0.5	0.45	13.9	18.3	0.033
CID-IT5			303.4 [3]	0.6	0.39	0.41	16.5	18.7	-0.06
CID-FT1	61	2.7	81.4 [0.8]	0.56	0.46	0.48	16.9	17.9	-0.127
CID-FT2			199.9 [2]	0.51	0.41	0.44	17.5	18.4	-0.135
CID-FT3			287.5 [2.8]	0.84	0.5	0.45	14.4	18.3	-0.025
CID-FT4			382.7 [3.8]	0.9	0.49	0.44	13.9	18.4	-0.019
CID-FT5			478.5 [4.7]	0.86	0.48	0.43	14.2	18.5	-0.015
CID-FT6			500.6 [4.9]	0.57	0.39	0.39	16.8	19	-0.102

Note: *FC* = fines content; G_s = specific gravity; e = void ratio; Y_d = dry unit weight; Ψ = state parameter.

Critical state locus

Figures 2(a, c, and e) present the effective stress paths plotted in mean effective stress (p')-deviator stress (q) space for the CIU tests on the CT, FT, and IT samples, respectively. These figures also display the critical state friction ratio from triaxial compression (M_{tc}) for each tailings type.

The state (e-log p') plots for the triaxial tests on the CT, FT, and IT samples are presented in Figures 2(b, d, and f), respectively. These figures also show the straight-line critical state locus (CSL) fitted for each tailings type and the associated tailings properties (i.e., altitude of CSL at reference stress [p_{ref}] of 100 kPa, Γ, and slope of CSL, λ_{10}). Furthermore, the curved CSLs represented by power law equations (critical state void ratio (e_c)-p'/p_{ref} relationships) fitted for each tailings type are shown.

The CIU tests were primarily used to determine the CSL parameters, as they tend to reach critical state more reliably, while the CID tests provided additional data points to validate and refine the CSL definition. As evident from Figure 2, at higher stress levels, the CT samples exhibit significant divergence between the straight-line and curved CSLs, whereas for the IT and FT samples, the two CSLs essentially coincide.

Figure 2 shows that the λ_{10} values increase as the grain size decreases, following the order: CT < IT < FT. This trend indicates increasing compressibility with decreasing grain size. Values of M_{tc} generally exhibits an increasing trend with grain size from FT to CT. However, the IT samples deviate from this trend, showing anomalous behavior. Conversely, the Γ values decreases with increasing grain size from FT to CT. Again, the IT samples demonstrate behavior that deviates from this general trend.

The estimated values of state parameter (Ψ) with respect to the curved CSLs, presented in Figure 2(b, d, and f), are included in Table 2 and 3. As shown in Table 2, all CIU tests yield Ψ values greater than

-0.05, the commonly accepted contractive/dilative boundary. However, the CID test samples yield a combination of Ψ values both greater and less than -0.05.

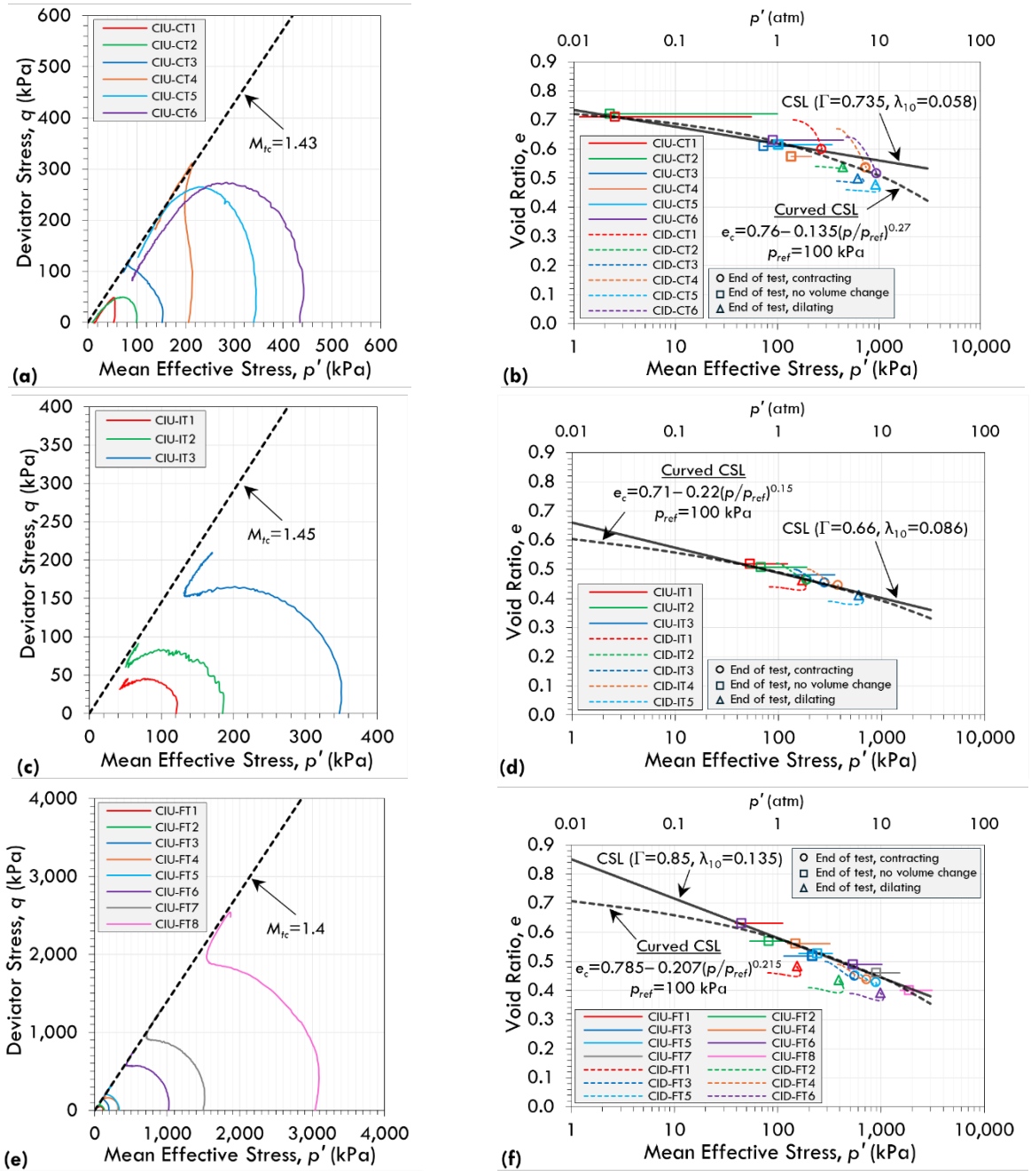


Figure 2: Effective stress paths and critical state loci for (a and b) coarse tailings, (c and d) intermediate tailings, and (e and f) fine tailings

The effective stress path for each CIU test, as presented in Figure 2, demonstrates that most samples did not reach liquefaction. Instead, they exhibited the typical S-shaped curve, characterized by initial contraction followed by dilation. Values of residual undrained shear strength (s_r) and s_r *ratio* (ratio of s_r to

effective vertical stress, σ'_{v0}) were determined based on either the points of phase transformation (from contractive to dilative behavior) or the points of minimum strength. These s_r and s_r *ratio* values are included in Table 2.

Strength loss and brittleness behavior

Results of the CIU tests were utilized to evaluate the potential ductile/brittle stress-strain behavior and to identify possible "highly brittle" tailings using the indicative criteria outlined by ICOLD (2022). Figure 3(a) presents the stress-strain curves (q versus ε_a) for the 17 CIU tests. All CT and IT samples exhibit strain-softening behavior, while five of the FT samples (CIU-FT3, CIU-FT5, CIU-FT6, CIU-FT7, and CIU-FT8) demonstrate strain-hardening behavior.

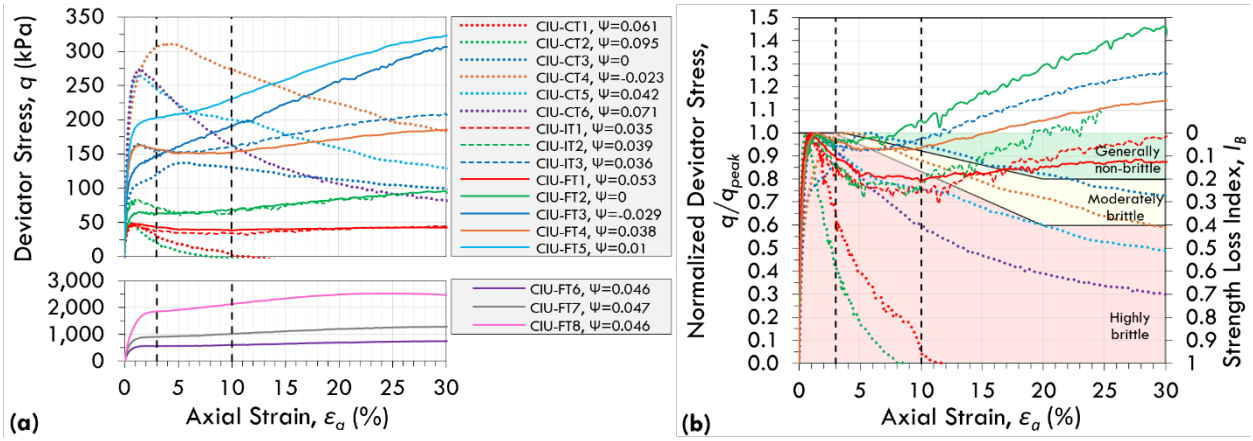


Figure 3: Strength loss behavior and brittleness assessment in CIU triaxial compression tests: (a) deviator stress vs. axial strain curves and (b) normalized deviator stress vs. axial strain curves on ICOLD (2022) brittleness chart

The majority of samples exhibiting strain-softening reach an initial peak value of q (q_{peak}) at a ε_a of 3% or less. Figure 3(b) presents the q/q_{peak} versus ε_a curves for these samples plotted on the brittleness assessment chart as defined by ICOLD. They lose more than 20% of their initial peak strength (i.e., strength loss index, $I_B > 0.2$) prior to reaching 10% strain and can therefore be characterized as "highly brittle" tailings according to the ICOLD criteria. However, it is noteworthy that six of these samples exhibit strain-hardening behavior at ε_a higher than 10%.

Cyclic and post-cyclic monotonic DSS testing

A total of nine constant-volume CDSS tests with post-cyclic monotonic shear were conducted between January 2021 and May 2024 in general accordance with the ASTM Standard Specification D8296 (ASTM, 2019). These tests were performed using a Norwegian Geotechnical Institute (NGI)-type simple shear

device. Table 4 summarizes the CDSS tests, indicating that 3 tests were performed on CT samples, 1 on IT samples, and 5 on FT samples.

Samples were prepared using the slurry deposition method, with solids content ranging from 72 to 73% and moisture content (w) between 36 and 37%. The specimens were formed in a shear ring measuring 71 mm in diameter and 30 mm in height.

Following the initial seating load, vertical stresses were applied at a load increment ratio of two until the target vertical stress was reached, which ranged from 24.5 to 497.5 kPa (0.24 to 4.9 atm) in the tests. Cyclic horizontal shear loads corresponding to cyclic stress ratio (CSR) values of 0.077 to 0.125 were applied at a frequency of 0.1 Hz until the samples reached a single-amplitude shear strain (γ) of 3.75%.

Strain-controlled monotonic shear loads were applied at the end of cyclic loading at a rate of 5% per hour until γ reached 20%. As shown in Table 4, three of the nine tests were completed at this point. For the other six tests, direction of the monotonic shear was reversed until a total of five shear loops were completed.

Table 4: Summary of CDSS testing with post-cyclic shear

Test ID	*FC* (%)	G_s	γ_d (kN/m³)	Vertical stress (kPa [atm])	*CSR*	No. of post-cyclic shear loop	s_r *ratio* from post-cyclic shear before reversal	s_r *ratio* from final shear loop	ψ
CDSS-CT1			12.8	99.8 [1]	0.083	5	0.1	0.02	0.012
CDSS-CT2	21	2.72	13.2	100 [1]	0.101	5	0.11	0.02	0.017
CDSS-CT3			13.3	100.1[1]	0.077	5	0.12	0.02	0.002
CDSS-IT1	49	2.66	13	497.5 [4.9]	0.11	5	0.07	0.02	0.061
CDSS-FT1			12.8	24.5 [0.24]	0.11	0 (no reversal)	0.23	NA	0.091
CDSS-FT2			13.1	49.5 [0.5]	0.1	0 (no reversal)	0.18	NA	0.059
CDSS-FT3	61	2.7	11.6	99.7 [1]	0.09	5	0.13	0.06	NA
CDSS-FT4			12.8	99.2 [1]	0.1	0 (no reversal)	0.16	NA	0.055
CDSS-FT5			12.6	100.3 [1]	0.125	5	0.13	0.05	0.06

Note: *FC* = fines content; G_s = specific gravity; *CSR* = cyclic stress ratio; s_r = residual undrained shear strength; Ψ = state parameter; NA = not available.

Since the stress state in a CDSS test is not fully defined, approximate values of Ψ were estimated and included in Table 4. The results of one post-cyclic DSS test per tailings type (CDSS-CT2, CDSS-IT1, and CDSS-FT5) are presented in Figure 4. Figure 4(a) presents the shear stress ratio (defined as the ratio of shear stress, τ, to σ'_{v0}) versus γ curves, while Figure 4(b) shows the excess pore pressure ratio (defined as the ratio of change in pore pressure, Δu, to σ'_{v0}) plotted against γ.

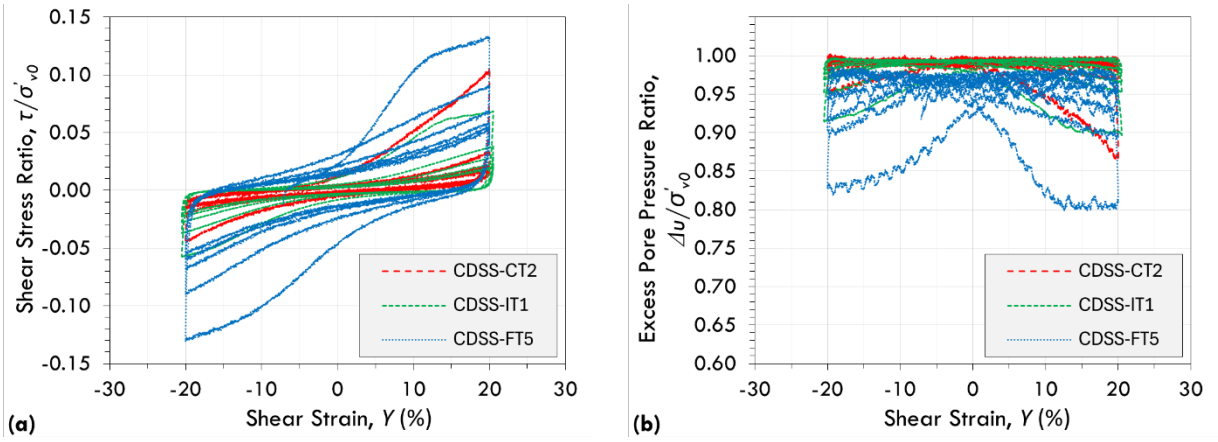


Figure 4: Post-cyclic shear response of tailings – (a) shear stress ratio vs. shear strain and (b) excess pore pressure ratio vs. shear strain

Figures 5(a and b) present the variation of s_r *ratio* and $\Delta u/\sigma'_{v0}$ with number of post-cyclic shear loops for all nine tests. As evident from Figure 5(a), s_r *ratio* values decrease rapidly, with approximately 30 to 70% reduction occurring during the first loop. The rate of decrease then slows during the second and third loops, ultimately stabilizing after the third loop. Conversely, the $\Delta u/\sigma'_{v0}$ values increase rapidly during the first loop and stabilizes after the third loop, as shown in Figure 5(b). Samples with lower $\Delta u/\sigma'_{v0}$ values throughout the tests yield higher values of s_r *ratio*.

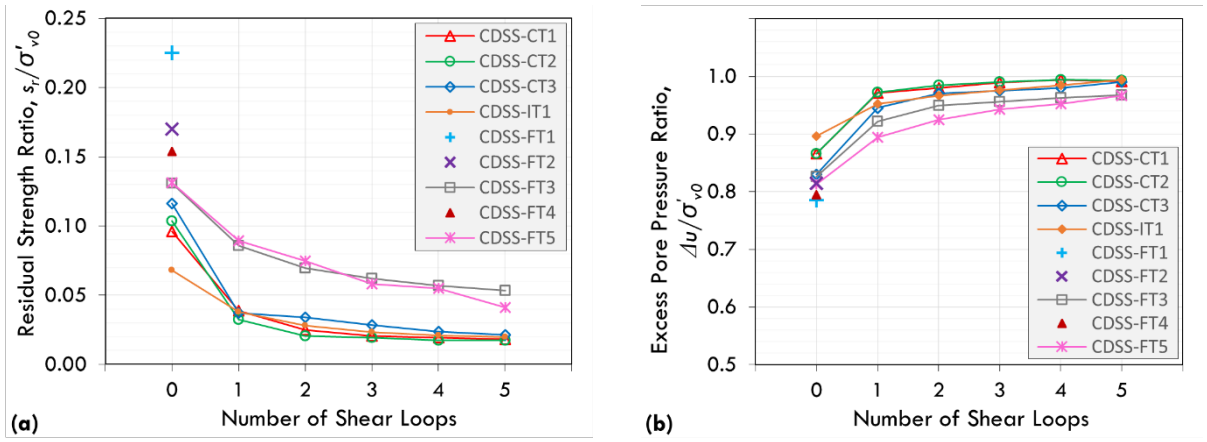


Figure 5: (a) Residual undrained shear strength vs. number of post-cyclic shear loop and (b) excess pore pressure ratio vs. number of post-cyclic shear loop

Residual strength ratio and effective vertical stress

Values of s_r *ratio* estimated from the CIU and post-cyclic DSS tests, as presented in Tables 2 and 4 respectively, are plotted against the normalized σ'_{v0} (σ'_{v0}/p_a, where p_a is the atmospheric pressure) in Figure 6. Published s_r *ratio* curves for other tailings by several researchers (Robertson et al., 2023; Schnaid et al., 2013; Jefferies and Been, 2016) are also included in Figure 6 for comparison. Generally, the s_r *ratio* values

increase with the *FC* of the tailings.

Figure 6 demonstrates that the triaxial tests yield higher s_r *ratio* values (represented by triangular markers) compared to the post-cyclic DSS tests for all tailings types, which is consistent with other published data. Although significant scatter in data exists, there is an observable increasing trend in the s_r *ratio* values, ranging from 0.1 to 0.46 as σ'_{v0}/p_a varied from 1 to 30. Note that the three data points with very high s_r *ratio* values at σ'_{v0}/p_a of 1.5 to 2 correspond to CIU tests in which the initial *e* values were very close to the CSLs, rather than being entirely in the contractive zone.

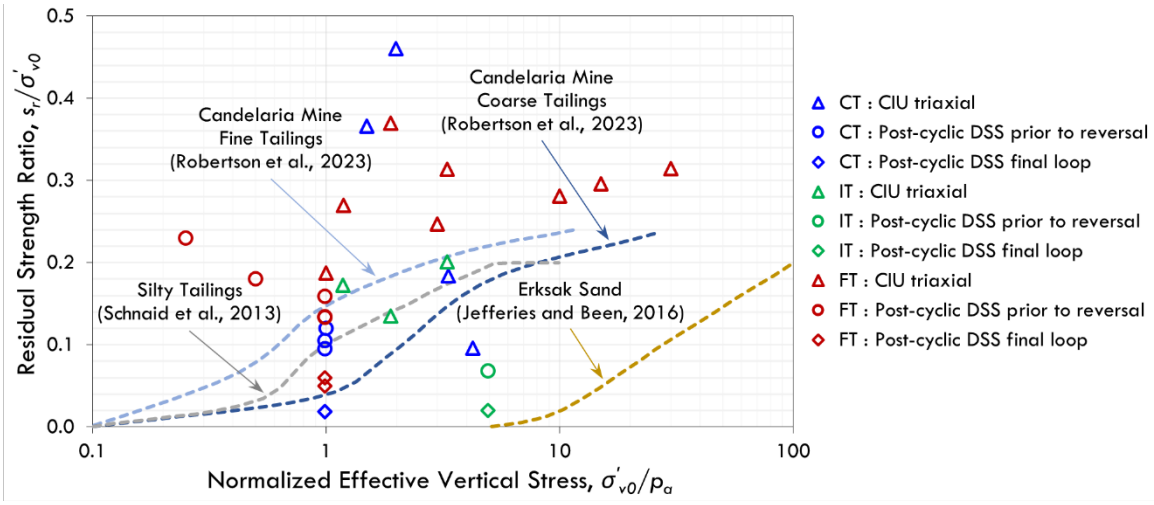


Figure 6: Variation of residual strength ratio of tailings with normalized effective vertical stress

The s_r *ratio* values from the post-cyclic DSS tests presented in Figure 6 include estimates based on the post-cyclic monotonic shear prior to load reversal for all nine tests. It also includes the post-cyclic final (fifth) shear loop results for the six tests where reversal loading was applied. The s_r *ratio* values from shear prior to reversal (represented by circular markers) range between 0.07 and 0.17, with σ'_{v0}/p_a varying from 1 to 5 for the three tailings types. The s_r *ratio* values from the post-cyclic final shear loop (represented by diamond markers) are significantly lower, ranging from 0.02 to 0.05. Due to the limited range of σ'_{v0} tested, no conclusive observations can be made in this study regarding the trend of s_r *ratio* with respect to σ'_{v0}/p_a from the post-cyclic DSS test data. A wider range of σ'_{v0} would be necessary to establish a definitive relationship.

Presented in Table 5 is a summary of four previous studies involving the estimation of s_r *ratio* values for various tailings from post-cyclic DSS testing. The reported s_r *ratio* values exhibit significant variation across these studies. The estimated s_r *ratio* values of the studied TSF tailings fall at the lower end of the published range, both in terms of prior-to-reversal and final loop results. However, the prior-to-reversal s_r *ratio* values (ranging from 0.07 to 0.17) appear to provide a more reasonable estimate. The authors intend

to compare these laboratory-estimated s_r *ratio* values of the studied TSF tailings with those derived using cone penetration test-based empirical correlations and the state parameter approach in a forthcoming paper.

Table 5: Summary of four previous studies involving post-cyclic DSS testing

Study	Tailings type	Sample type	No. of tests	*FC* (%)	*PI*	G_s	Vertical stress (kPa)	s_r *ratio* from post-cyclic DSS	s_r *ratio* from post-cyclic final shear loop
Wijewickreme et al., 2005	Laterite	U	9	93-100	12	4.1	100-200	0.41 to 0.6	No loop
	Copper-gold	U	4	97-99.6	NP	2.78	100	0.42 to 0.64	No loop
	Copper-gold-zinc	U	18	81.1-94.1	2	3.36-4.42	144-461	0.13 to 0.53	No loop
		R	3	97.6	1	3.67	100-250	0.27 to 0.33	No loop
Al-Tarhouni, 2008	Gold	R	23	> 70	2-3	2.89	100-400	0.1 to 0.36	No loop
James et al., 2011	Gold	R	5	55-80	NP	3.62-3.9	102-401	0.08 to 0.12	No loop
Nadarajah et al., 2019	Gold	U	4	95-100	NP	NA	100	0.3 to >1	Only 1 loop
		R	4			NA	100	0.14 to 0.37	0.04 to 0.06
	Copper-zinc	U	4	80-100	0-3	NA	100	0.48 to 0.75	0.16-0.23
		U	4			NA	100	0.25 to 0.36	0.09-0.13

Note: *FC* = fines content; *PL* = plasticity index; G_s = specific gravity; s_r = residual undrained shear strength; U = undisturbed; R= reconstituted; NP = non-plastic; NA = not available.

Conclusion

The results of an advanced laboratory testing program designed to characterize the tailings within a large TSF for flow liquefaction evaluation were presented. A series of tests were performed on reconstituted tailings samples, including CIU and CID triaxial compression tests, as well as constant-volume CDSS tests with post-cyclic monotonic shear and reversals of shear loading to complete five loops. These samples had fines content ranging from 21 to 61%, representing the full range of contractive tailings present within the TSF. Critical state loci were formulated, and the associated tailings properties were derived for the various tailings types. The strength loss and brittleness behavior were evaluated, indicating the presence of highly brittle materials within the TSF. Residual strengths of the tailings were estimated from the CIU and post-cyclic DSS tests. The CIU tests generally yielded higher residual strengths compared to post-cyclic shear. Residual strengths from post-cyclic shear prior to reversal were significantly higher than those from the post-cyclic final shear loop. The prior-to-reversal residual strength ratio values (ranging from 0.07 to 0.17) appeared to provide a more reasonable estimate. The impact of vertical stress on residual strength was examined, revealing a noticeable increasing trend in triaxial test-based estimates. However, due to limited post-cyclic DSS test data across a broad range of vertical stresses, definitive conclusions regarding this relationship could not be established.

Acknowledgements

The authors would like to express their sincere gratitude to the mine personnel involved in the TSF management for granting permission to publish the data.

References

Al-Tarhouni, M. 2008. Liquefaction and post-liquefaction behaviour of gold mine tailings under simple shear loading, Doctoral thesis, Carleton University, Ottawa, Canada.

American Society for Testing and Materials (ASTM). 2019. Standard test method for consolidated undrained cyclic direct simple shear test under constant volume with load control or displacement control. D8296, ASTM International, West Conshohocken, PA.

American Society for Testing and Materials (ASTM). 2020a. Standard test method for consolidated undrained triaxial compression test for cohesive soils. D4767, ASTM International, West Conshohocken, PA.

American Society for Testing and Materials (ASTM). 2020b. Standard test method for consolidated drained triaxial compression test for soils. D7181, ASTM International, West Conshohocken, PA.

International Commission on Large Dams (ICOLD). 2022. Tailings dam safety bulletin no. 194 (draft). ICOLD, Paris, France.

James, M., Aubertin, M., Wijewickreme D. and Wilson, G.W. 2011. A laboratory investigation of the dynamic properties of tailings. *Canadian Geotechnical Journal* 48(11): 1587–1600.

Jefferies, M. and Been, K. 2016. *Soil Liquefaction: A Critical State Approach*. 2nd edition, Boca Raton: CRC press.

Nadarajah, G., Bleiker, D. and Sivathayalan, S. 2019. Comparison of liquefied shear strength of tailings estimated using standard empirical methods and post-cyclic direct simple shear tests. *Proceedings of the Sustainable and Safe Dams around the World*. 1st edition, CRC press.

Robertson, P.K., Brouwer, K., Sully, T.E. and Gagnon, A. 2023. Influence of increased confining stress on undrained behavior of tailings: A case history at the Candelaria Mine. *International Journal of Geoengineering Case Histories* 7(3): 34–55.

Schnaid, F., Bedin, J., Viana da Fonseca, A.J.P. and de Moura Costa Filho, L. 2013. Stiffness and strength governing the static liquefaction of tailings. *J. Geotech. Geoenviron. Eng.* 138(12): 2136–2144.

Wijewickreme, D., Sanin, M.V. and Greenaway, G.R. 2005. Cyclic shear response of fine-grained mine tailings. *Can. Geotech. J.* 42(5): 1408–1421.

Chapter Ten

Monitoring and Risk Management

TAILINGS AND MINE WASTE 2024



Improving Tailings Deposition: A Drone and Satellite Survey Validation Framework for Enhanced Facility Management

John Thuysbaert, Klohn Crippen Berger, UK
Joe Piccolo-Lawrance, Klohn Crippen Berger, UK
Joseph Quinn, Klohn Crippen Berger, Canada
Romain Girard, Boliden AB, Sweden

Abstract

To enable continued deposition at the Aitik Tailings Management Facility (TMF) during a period of remediation works since 2022, it was necessary to reconfigure the tailings deposition plan to divert the deposited tailings and surface water to a different area of the facility. The Aitik TMF, owned by Boliden AB, is a sidehill impoundment formed by a contiguous sequence of dams. An unusual feature of this facility is that all the perimeter dams are constructed at different elevations, such that the dams at the bottom of the original valley are at a lower elevation than those at the top of the original valley.

Historically this simplified tailings operations, but it added complexity when it was necessary to reconfigure the deposition arrangement for this period of remediation works. A temporary exclusion zone for deposition near the downstream dams had to be demarcated on the surface of the tailings impoundment via the construction of rockfill "piers" to redirect annual deposition of tailings (43 Mtpa) and water towards a newly constructed spillway located south of the previous spillway.

Deposition modeling was performed using Muk3D Tailings+ Software by MineBridge to simulate short- and long-term deposition with the construction of rockfill piers to assess the effect on shaping the TMF tailings surface and water contours towards a new sedimentation pond and spillway. Due to the complexity of the deposition modeling and sequencing of the deposition with construction of additional piers, the deposition modeling has been updated on an ongoing basis and calibrated against field monitoring data.

To assess the validity of the models, regular as-built drone (weekly) and satellite (monthly) surveys (including high resolution photographs) were recorded and compared with models processed by Muk3D Tailings+ simulations monthly. The implementation of a validation framework for tailings deposition operations through the integration of drone and satellite survey data has allowed Boliden to continue normal deposition operations despite a temporarily exclusion of its Downstream Dams until April 2025.

Introduction

The Aitik Mine is an open-pit copper mine located approximately 15 km southeast of Gällivare in the Arctic region of northern Sweden. Waste tailings generated from mineral ore processing at the mine are deposited hydraulically within the Aitik tailings management facility (TMF) for storage, with approximately 1,000 Mt of tailings deposited to date. The current TMF footprint covers an area of ≈15 km^2, impounded by 10 km of continuous perimeter embankments around the eastern, northern, and western extents, and partially by natural ground and Dam V2 in the south (see Figure 1).



Figure 1: Satellite imagery/overview of the Aitik TMF, dated May 31, 2024

All the perimeter dams are constructed at different elevations that reflect the grade of the natural topography, such that the dams at the bottom of the original (i.e., pre-construction) valley are at a lower elevation than those at the top of the original valley. This has the benefit of allowing deposition to occur primarily from the dams at a higher elevation (referred to as the *Upstream Dams* and Dam H-S), denoted as Dams H-S, H-S2, A-B2, A-B, C-D and C-D2, using gravity to form an average beach slope of 0.4% towards the dams at lower elevation (referred to as the *Downstream Dams*). The original cross-valley or sidehill impoundment dams are up to approximately 70 m high, following periodic expansion to increase storage capacity. The existing tailings impoundment dams are currently being raised using the upstream construction method.

Boliden has committed to complying with the Global Industry Standard on Tailings Management (GISTM, 2020). Under GISTM, the TMF has a consequence classification of *"Very High,"* and a design flood with a 5,000-year return period is recommended. Under the Swedish Mining industry's (SVEmin)

dam safety guideline (GruvRIDAS, 2021), the TMF has a consequence classification of *"Klass B,"* and the Class 1 Flood is recommended. The Guidelines for Design Flood Determination for Dams states that the Class 1 Flood has an annual probability lower than 1:10,000, implying that the Class 1 Flood, calculated according to the Guidelines, is a more significant event either in volume, peak inflow, or both, than the GISTM recommendation.

Following geotechnical investigations, an extensive remediation program was put in place to improve the stability of the Downstream Dams (Boliden, 2023), denoted as Dam E-F/E-F2 and Dam G-H/G-H2 (refer Figure 1). As part of the remediation measures (Girard and Quinn, 2024), a temporary exclusion zone was demarcated in June 2022 from Dam G-H2 through Dam E-F2. The design objective of the exclusion zone was to redirect water and tailings towards the new *"U3 spillway,"* located south of the existing *"U2 spillway."* The aim was mitigating tailings and water from accumulating near the Downstream Dams (while the remediation measures were implemented).

To achieve this aim, a series of rockfill piers (Piers 1-2, 3-4 and 5-6) was designed and constructed on the tailings surface to retain tailings and re-shape the TMF surface contours towards the U3 spillway (see Figure 1). The typical pier design comprises a 20 m wide crest with a maximum height of 5 m from the tailings surface, with 2H:1V side slopes and the inclusion of a 25 m wide × 2 m high support buttress constructed immediately downstream (see Figure 2). All piers are constructed from non-frozen granular mine waste rockfill. Where required, Combigrid 40/40 GRK4 geogrid was laid directly on top of the tailings surface to improve the bearing capacity for plant/machinery during construction and to reduce settlement of the rockfill into the underlying tailings.

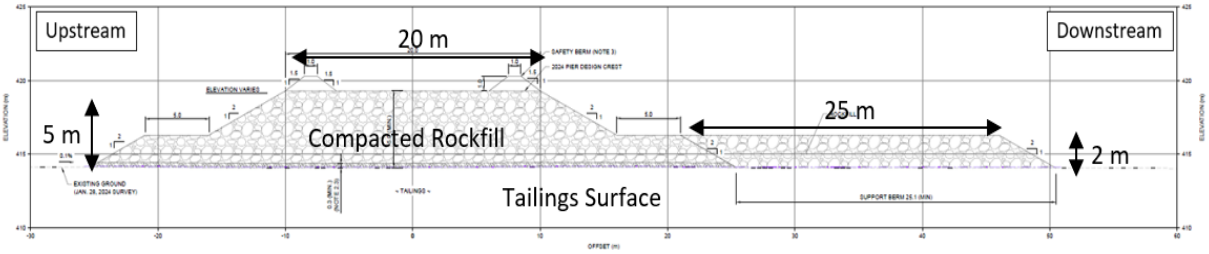


Figure 2: Typical cross-section of a TMF rockfill pier

Although water (including fine tailings) was expected to permeate through the piers, an interceptor drainage ditch was constructed downstream of the lowest pier (Pier 1 – see Figure 1) to redirect water southwards and away from the Downstream Dam exclusion zone. If a significant accumulation of fine tailings developed in the sedimentation pond downstream of Pier 2, this was removed using either mechanical excavation, dredging, or a combination of both.

The piers were constructed over time as a function of tailings deposition to maintain a maximum tailings longitudinal slope less than 2% between piers. The pier design, with a maximum height of 5 m and spaced 300 m apart upstream in the TMF (centerline to centerline), was intended to limit the potential for a runout failure into the Downstream Dams region, should failure of a pier occur. This is to maintain an overall slope that is flatter than the lower-bound post failure ground slope angle of liquefaction case histories (Martin et al., 2019).

A trapezoidal broad-crested weir was designed at Piers 2, 4 and 6 to safely pass the Class 1 Flood and allow it to flow to either the U2 or U3 spillway. The weir freeboard (weir invert to pier crest level) is set to 1 m, which allows for at least 4 m of operational tailings capacity retained for each set of piers.

Methodology

To forecast whether the constructed pier configuration would be successful in re-shaping the contours of the TMF surface until the restart of operations at Dam E-F/E-F2 and Dam G-H/G-H2, planned for April 2025, deposition simulations were initially performed in MUK3D Tailings+ by Minebridge (MUK3D). Once finalized, weekly and monthly drone and satellite surveys of deposition operation were subsequently undertaken to validate and regularly re-calibrate the short- and long-term MUK3D simulations (1 month to 3 years), respectively. Additionally, simulations were used to forecast the stage-capacity for each constructed pier to plan the construction of the subsequent set of piers.

This section initially describes the survey files referenced and the input parameters used in MUK3D prior to running deposition simulations. Subsequently, the methodology regarding the deposition analyses is outlined, with a description of how these were validated on site using drone and satellite technology.

Drone and satellite surveys

Weekly drone and monthly satellite (1 m) surveys, including high-resolution (50 cm) orthophotographs, were delivered to Klohn Crippen Berger (KCB) by Team EXACT (surveyors) and PhotoSat Survey Services, respectively. The Coordinate Reference System (CRS) used is *"Aitik Local,"* which is a local site-specific CRS based on SWEREF99 2015 – EPSG:3016. The height datum referenced is *"RH00,"* which involves a correction of 0.79 m from *"RH2000"* based on the Swedish national height system from 1900.

Satellite surveys (including high-resolution orthophotographs) were used as the primary ground reference tool, given the wide coverage of surface area available in a single record. The weekly drone surveys were used as a backup reference tool when inclement weather or winter conditions meant a clear satellite record was not possible (usually because of excess cloud cover). The disadvantage with using drone surveys was that only a quarter of the full extent of the deposition area could be covered weekly, meaning

that 4No. weekly surveys would be "stitched" together with Quantum Geographic Information System (QGIS) software to represent a monthly survey.

MUK3D parameters

The input parameters that were used when running simulations in MUK3D are as follows:

- **Tailings production** – Storage of a maximum of 43 Million tonnes per annum (Mtpa) of tailings upstream of the pier configuration based on Boliden plant requirements, equating to 3.58 Mt per month.
- **Tailings pipeline discharge locations –**Tailings pipeline discharge at the Aitik TMF occurs solely from the Upstream Dams (see Figure 1) during this period while the exclusion zone is in place. The Boliden deposition plan operates 3No. and 4No. pipelines during the summer (June to September) and winter (October to May) months, respectively. The total tailings production was divided by the number of pipelines depending on the seasonal requirements; e.g., 25% per pipeline for summer and 33% per pipeline for winter conditions. The multi-stream deposition function was applied in MUK3D to represent the above.
- **Dam raising** – Dam raising at the Aitik TMF is performed using the upstream dam methodology, which involves sourcing tailings from the deposited beach as construction material for the subsequent dam raise. Operations at the Downstream Dams were paused, hence no dam raising was modeled at Dam E-F/E-F2 and Dam G-H/G-H2. The Upstream Dams comprise a +3 m raise in dam crest per year, typically constructed during the summer months to the beginning of the winter months, depending on annual plans (typically June to October).
- **Pipeline discharge parameters –** Each pipeline comprises spigot discharge points spaced 40 m apart along its length, with a primary outlet at the end of the pipeline. Modeling assumptions considered that 70% of the total pipeline discharge would be spread across the number of individual spigots points, while 30% would report to the end of the pipeline. This was based on KCB estimations of pipeline flow rates based on relative accumulation depths observed on site.
- **Tailings density** – Tailings slurry dry density equal to 1.4 tonnes/m^3 based on material testing records received from Boliden.
- **Tailings beach slope (%)** – Overall TSF average longitudinal beach slope (equal to ≈ 0.4%) and compound beach slope parameters based on LIDAR surveys of the facility conducted prior to the construction of the piers (pre-2022). The input of compound slope parameters shapes the characteristic TMF beach over a defined incremental distance (see Table 1), while maintaining an average slope specified (0.4%) over the full length of the beach.

- **Water management (pond)** – Deposition simulations in MUK3D did not include the modeling of a water pond, as the pier system constructed from granular waste rock material was assumed to be free-draining towards the U3 Spillway.

Table 1: MUK3D Compound slope parameters

Incremental distance (m)	Beach slope (%)
191	1.73%
154	0.74%
901	0.49%
2,113	0.31%
824	0.26%

Analyses and validation

Monthly cumulative MUK3D deposition analyses were performed to forecast and simulate deposition operations up to April 2025 (from June 2022), with the most recent satellite surveys used as the topographical reference in the model. Because of the uncertainty in calibration of the modeling to actual operations, a validation framework was progressively introduced. Calibration of the MUK3D analyses was performed by comparing monthly MUK3D models with as-built surveys every month.

An example of a typical monthly deposition plan for input into MUK3D is shown in Figure 3. Figure 3 illustrates the December 2024 deposition plan, whereby 3No. pipelines, denoted as SL5, SL3 and SL4, are depositing from Dam A-B and C-D. SL1 and SL2 located on Dam H-S and near H-S2 are shown as inactive for this month, given previous months of deposition in this region.

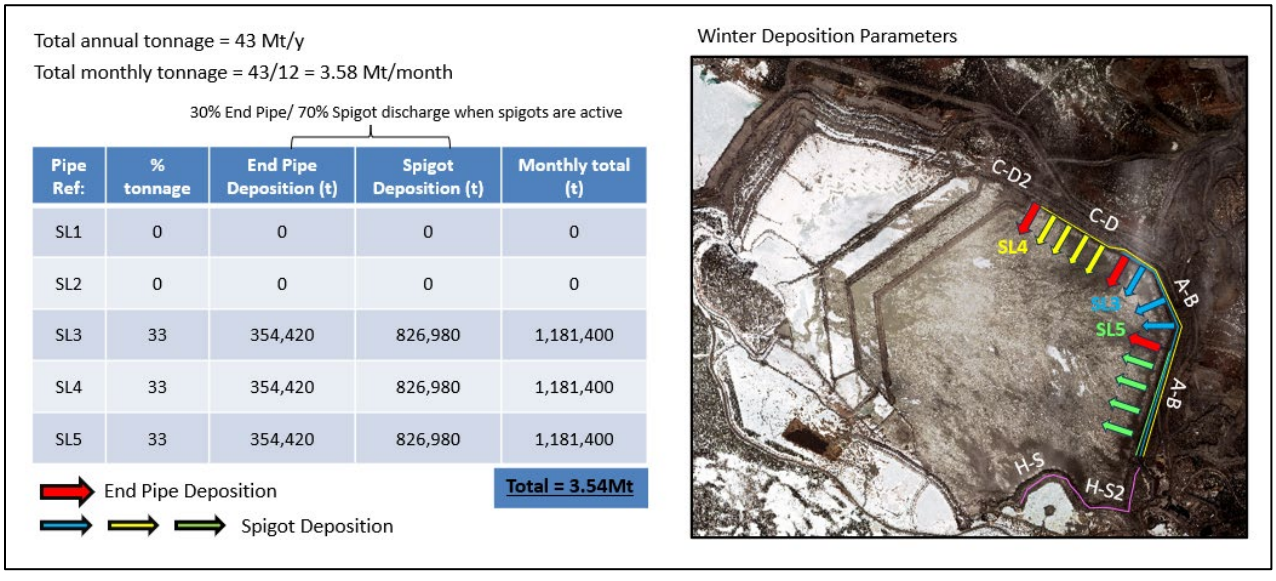


Figure 3: Example of monthly deposition plan – December, 2024

Short-term validation and iterative calibration are essential because they provide the mine with confidence that the long-term plan can be achieved. The dynamic nature associated with deposition means that a plan is subject to regular updates. For deposition modeling and validation to be successful, the following were performed on a regular basis:

- Comparing as-built tailings beach slope (%) and monthly Rate of Rise (RoR) data with the MUK3D models across the TMF deposition area (upstream of the piers).
- Assessing hourly tailings production and deposition data received from the Boliden Mine plant for each pipeline.
- Tracking the position and operational status of end pipes and spigots on the TMF via site inspections by KCB and Boliden personnel.
- Assessing the overall TMF contour surface shape to assess whether the deposition plan adopted is redirecting water towards the U3 Spillway as planned.
- Evaluating upstream beach capacity to inform pipeline deposition planning and construction of subsequent dam raises.
- Re-calibrating long-term deposition assumptions based on recent as-built survey data updates.
- Bi-weekly meetings with the Boliden operations team for scheduling of construction and deposition activities, with an emphasis on regular client-consultant communication.

Observed changes to MUK3D forecasts would necessitate iterative re-calibration of short and long-term deposition simulations, whether this be refining initial MUK3D parameters to suit, accommodating unexpected changes in pipeline production, or adjustments in planning for potential delays in construction activities (e.g., dam raising). While all the above items are good practice for regular deposition planning, there was a heightened focus on achieving reliable forecasts for the current scenario because of the need to avoid deposition in the exclusion zone and the need to sequence construction of subsequent piers at the right time.

Additionally, as the project progressed, previous surveys provided a site-specific historical database for identification of deposition trends within the TMF, which improved the accuracy of deposition projections. This also benefits early detection of potential deviations, which becomes a tool for proactive management of deposition operations on the TMF, whether that is sequencing construction for the next set of piers or planning annual Upstream Dam raises.

Results and discussion

This section outlines the results from the MUK3D simulations, including the validation undertaken to date. Deposition planning/MUK3D iterations indicated that preferential deposition along Dam C-D and the northern part of Dam A-B would assist in shaping TMF contours towards the U3 Spillway (see Figure 3).

The MUK3D models and as-built records both indicated that the RoR of the tailings surface adjacent to the pier would range between 0.3 m and 0.4 m per month (on average). By measuring the clear height between the pier crest and the abutting tailings surface, it was possible to forecast the remaining tailings capacity upstream for each set of piers.

Figure 4 illustrates the long-term cumulative deposition model, which indicates that Piers 5-6 would likely reach full capacity by April 2025. This is indicated by the Δ0.1m elevation difference between the tailings surface and the nearby invert level of the weir located on pier 6. Colors represent relative elevation with red-yellow shades being higher elevations, and green shades being lower elevations.

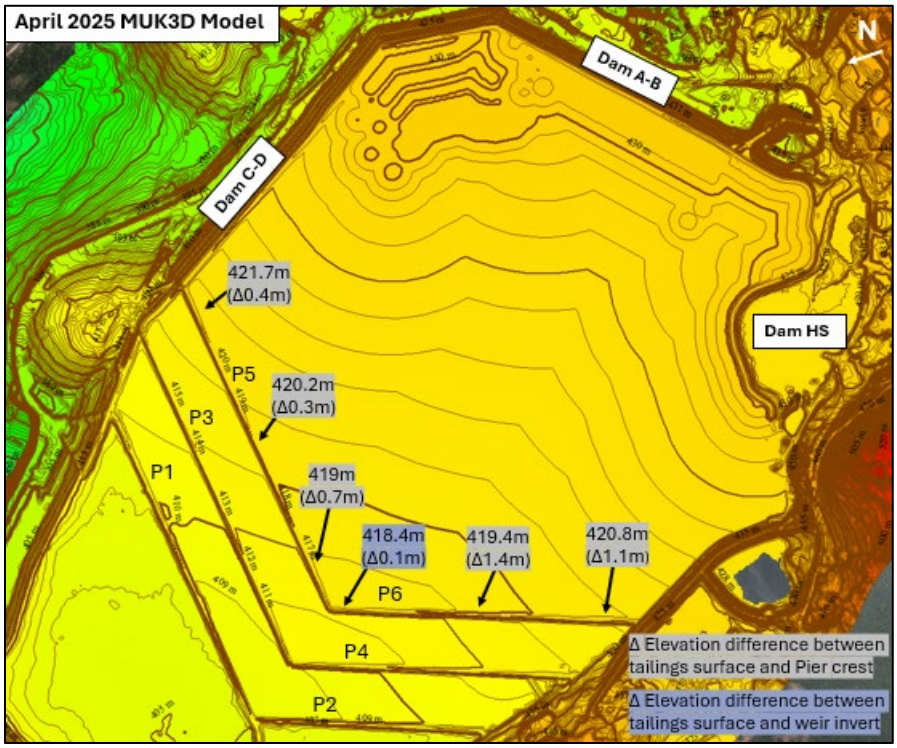


Figure 4: Cumulative MUK3D model projection for April 2025

Challenges encountered

Operational constraints meant that between September and December 2023 deposition of tailings was not possible from the northern Dams C-D and A-B. By January 2024, three months of central deposition from Dam A-B resulted in an altered TMF tailings surface contour shape that sloped predominantly towards the Downstream Dams – see Figure 5 (left). As a result, an increase of water flow conveyed to the U2 Spillway was reported on site.

A modified short-term deposition plan to re-shape the TMF tailings contour surface towards the U3 Spillway was required. The plan focused on placing pipelines and depositing primarily from the northern part of Dams C-D and A-B for an extended period (3 to 4 months) until May 2024. The execution can be

seen from satellite imagery recorded during the winter months, dated March 10, 2024 (see Figure 6). By May 2024, the survey record in Figure 5 (right) showed that the short-term objectives had been achieved.

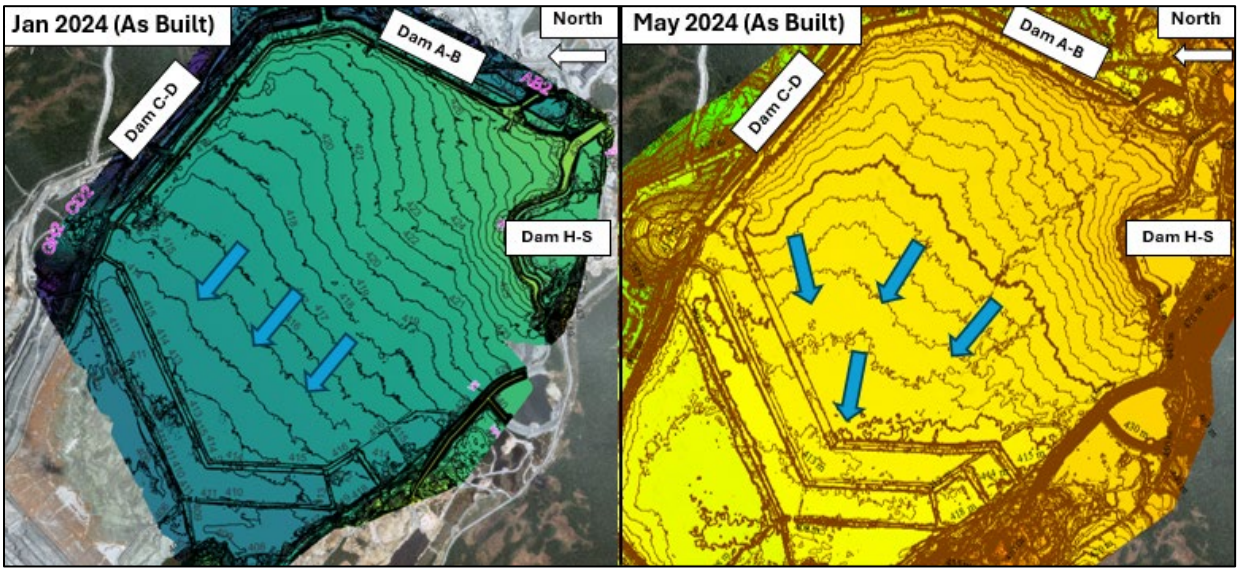


Figure 5: As-built comparison records between January 2024 (left) and May 2024 (right)

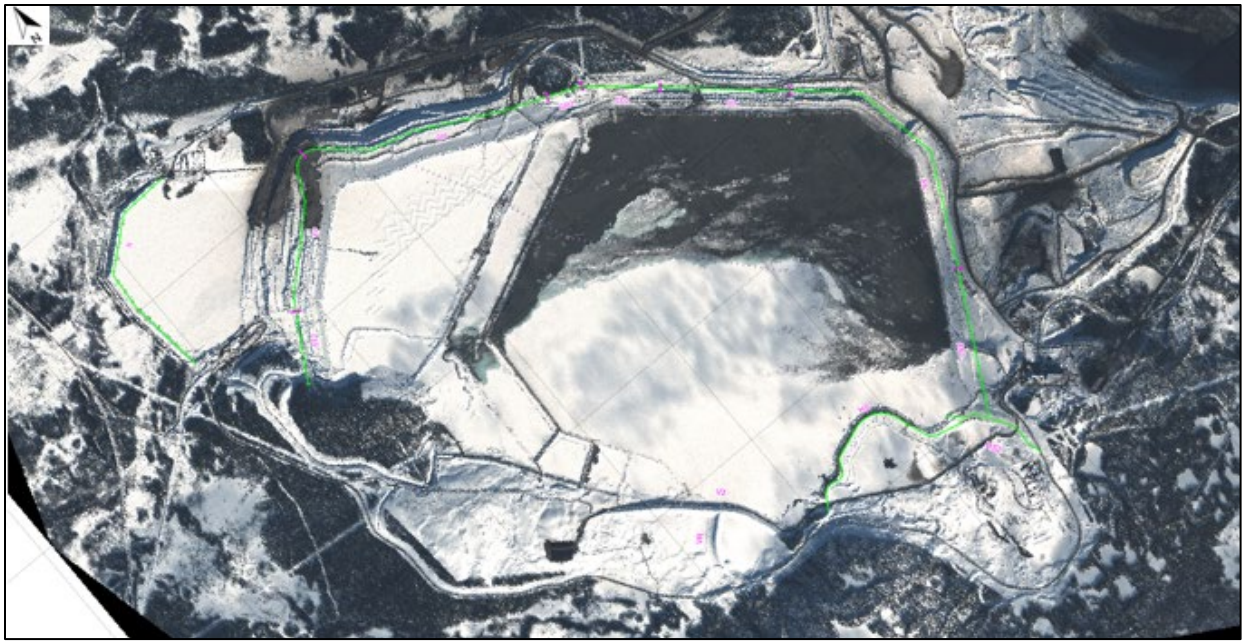


Figure 6: Satellite imagery of the Aitik TMF dated March 10, 2024

A comparison of the tailings surface in the section immediately upstream of Piers 3-4 in Figure 7 shows that approximately 2 to 3 m of tailings was placed in the northern portion of the TMF between January 6 and May 5, 2024. To maintain the longer-term deposition plan, it is essential that the shape of the

tailings surface remains parallel to the MUK3D long-term target for that month (demonstrated by the black dashed line in Figure 7).

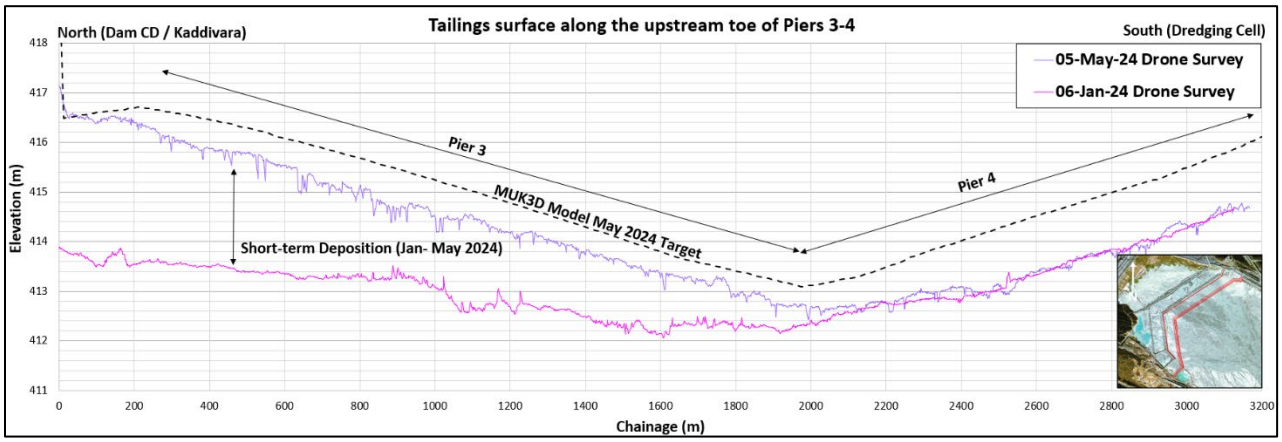


Figure 7: Elevation of the tailings surface along the upstream toe of Piers 3 and 4

Figure 7 shows that in January 2024, it was identified that the tailings surface was too flat. However, by May 2024, the TMF tailings surface was successfully re-shaped relative to the long-term target as expected. Although the shape of the May 2024 survey is parallel to the May 2024 MUK3D target, it is observed below expected targets – this indicates that less tailings were placed into the TMF by May 2024 than initially expected. Upon further investigation of plant production data, it was noted that the tailings deposition rate had temporarily decreased from 43 to 41 Mtpa during this time. Upon discussion with Boliden, this was not considered as an input parameter change in the future and did not necessitate a full re-calibration of the long-term model to April 2025 (Figure 4).

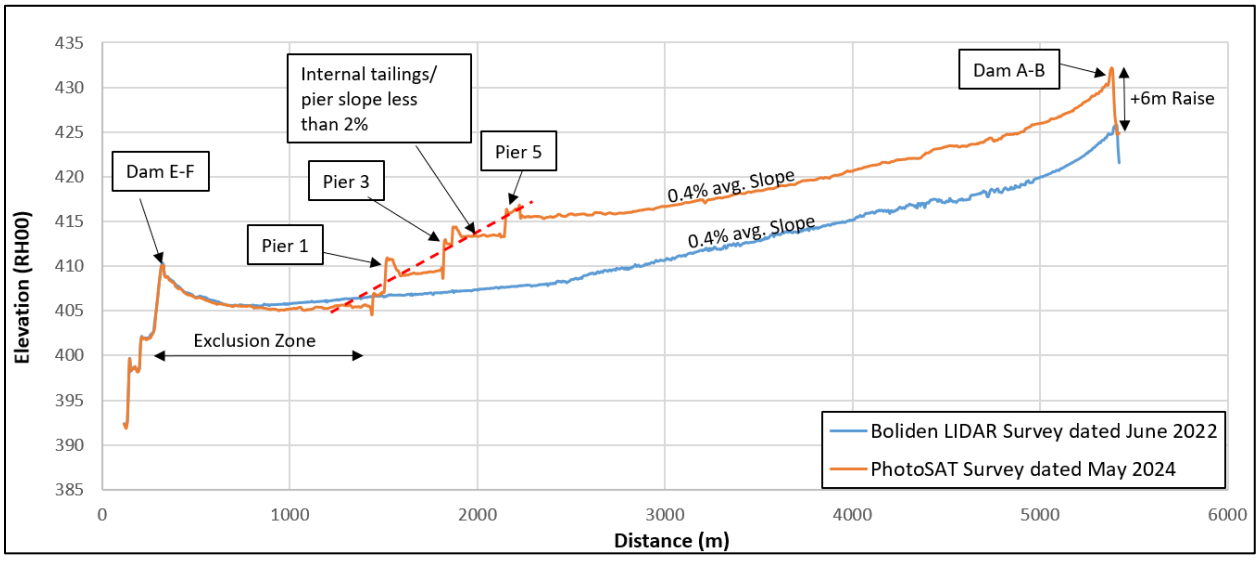


Figure 8: Longitudinal TMF survey comparison

To conclude for operations to date, a comparison of TMF surface surveys between June 2022 and May 2024 (see Figure 8) shows that the pier system has allowed Boliden to continue normal deposition operations as planned to date; thereby facilitating continued operations at the TMF during this period while the exclusion zone is in place at the Downstream Dams.

Figure 8 shows that the pier system has maintained a slope of less than 2%, while the exclusion zone has not accumulated additional tailings since June 2022. Conversely, observations in the exclusion zone show that the tailings surface has decreased in height by up to one meter, likely due to consolidation of the tailings mass beneath.

Conclusion

As demonstrated in this paper, three sets of piers (Piers 1-2, 3-4, and 5-6) were constructed on the TMF surface by May 2024, each providing tailings capacity for a maximum of one year of operations (as initially forecasted in MUK3D). With Piers 5-6 recently constructed in April 2024, it was expected that a total of approximately 122 Mt of tailings would be deposited in the Aitik TMF from June 2022 to April 2025 whilst preventing additional loading and pore pressure at Dams E-F and G-H.

The implementation of a validation framework for tailings deposition operations through the integration of drone and satellite survey data has allowed Boliden to continue normal deposition operations despite a temporarily exclusion of its Downstream Dams until April 2025.

The dynamic nature associated with deposition means a plan is subject to regular updates. As demonstrated, deposition forecasting is only as reliable as the accuracy of the input parameters, which must be maintained regularly. When unexpected operational scenarios occur, MUK3D modeling in combination with the established validation framework can reliably forecast alternative options to mitigate the effect of operational deviations through effective client-consultant communication.

References

Boliden, A.B. 2023. Public disclosure regarding Aitik tailings facility. Aitik Mine, Gällivare, Northern Sweden.

Girard, R. and Quinn, J. 2024. Dam safety remediation of the Aitik Tailings Storage Facility, Northern Sweden. *Proceedings of Tailings and Mine Waste, 2024*. Colorado. USA.

GISTM. 2020. Global Industry Standard on Tailings Management, International Council on Mining United Nations Environment (UNEP) and Principles for Responsible Investment.

GruvRIDAS. 2021. *GruvRIDAS – Gruvbranschens riktlinjer för dammsäkerhet*, Guideline for Tailings Dam Safety. Svensk Energi AB / SVEmin.

Martin, V., Al-Mamun, M. and Small, A. 2019. CDA technical bulletin on tailings dam breach analyses. Sustainable and Safe Dams Around the World/*Un Monde de barrages durables et sécuritaires*. CRC Press: 3484–3498.

Risk Management for Access to Dams at Emergency Level Control: Control Levels (OMS Manual) and Safety Plan

Virginie Queiroz Rezende Pinto, Vale S.A., Brazil
Daniel Bernardes Raposo, Vale S.A., Brazil
Milena Fernandes Xavier Matos, Vale S.A., Brazil
Elias Silva de Sousa, Vale S.A., Brazil
Alexandre Cristino Correa dos Santos, Vale S.A., Brazil

Abstract

Following recent accidents at tailings dams, countless efforts have been made to implement and improve governance models capable of effectively managing the risks involved. The main governance model is the Global Industry Standard for Tailings Management (GISTM), comprising 15 Principles that integrate various disciplines to prioritize the management and safety of tailings structure facilities. Among these, Principle 6 emphasizes the importance of implementing Operation, Maintenance, and Surveillance (OMS) Manuals, which serve to provide critical controls for safe operations. While the implementation of these principles does not guarantee dam stability, they can form crucial barriers for efficient risk management.

A project was therefore developed to enable conventional access for workers to tailings dams with restricted access due to an emergency condition having been established. The objective of the "Emergency Level Dam's Access Plan" is to establish monitoring measures, their corresponding control levels, and criteria for activating TARPs – Trigger Action Response Plans, to be adopted during the execution of essential activities aimed at enhancing the structural integrity that may be compromised during periods of restricted access to the dams. This information was integrated into the OMS Manual to ensure safe operations and facilitate communication and evacuation plans during maintenance, inspection, and monitoring activities, especially in the event of any change indicating a potential rupture.

The implementation of integrated controls and communication flows has enabled the safe execution of necessary monitoring, inspection, and maintenance activities, through conventional access by workers to the structures' Self-Rescue Zone. The efficacy of implementing the Access Plan is validated by the considerable improvement in the dams' state of conservation, including the removal of emergency level

from one of the structures covered, as well as by a notable reduction in the number of outstanding anomalies in these tailings storage facilities.

Introduction

Dam safety management is of paramount importance to prevent disasters and environmental damage and protect lives. Dam failures can cause devastating impacts and correct management requires a multidisciplinary approach, combined with current legislation and best engineering practices.

In 2010, the National Dam Safety Policy (PNSB) was established in Brazil through Law 12.334, and since then, several national and state regulations have been published focusing on dam safety. In 2020, Law 14.066 amended the PNSB with respect to various safety aspects, mainly focusing on dams raised upstream. This included the prohibition of this methodology for building new dams, further reinforcing the need to eliminate existing upstream dams in the country.

In addition to federal laws, two other regulations are worth highlighting: Law No. 23.291, which establishes the State Dam Safety Policy that defines safety aspects, self-rescue zones, emergency response plans, and environmental issues, and Resolution No. 95/2022 of the National Mining Agency (ANM), which details various aspects of mining dam safety management. Regarding compliance with legislation, mining companies must register their dams in the official government system, keep the information up to date and submit, among other documents, declarations of stability conditions (semi-annually), as well as provide details of any anomalies and changes to the dams that have been detected with regular and special inspections.

These regulations also define matters related to the potential damage associated with the structure and its risk category, both related to possible failures. Depending on the risks mapped in the classification matrices, a dam is associated with a certain emergency level, indicating that it failed to meet the criteria of current legislation and/or safety factors for normal stability conditions.

It is important to highlight that any dam project, in the design, operation and closure phases, must prioritize the integrity of the geotechnical structure and, above all, guarantee the safety of workers involved in all stages of the dam's useful life.

This project called the "Emergency Level Dam's Access Plan" fits into this context of dam management with a focus on prior planning of activities, worker safety, and an efficient solution for dealing with anomalies, pursuing continuous improvement of the structure. This methodology has been applied for almost two years in six Brazilian dams, including three raised upstream, at different emergency levels in accordance with current Brazilian legislation, one raised by center line and one dam built in a single stage. The results obtained are positive and made it possible to reduce risks, improve the state of conservation of structures, and improve safety controls for the workers involved.

Methodology

The premise of the Access Plan is to guarantee the safety of workers when carrying out essential monitoring, inspection, and maintenance-related activities of dam structures, without increasing the geotechnical risk to the structure.

This Plan is a document prepared and then revised by the company's technical team (Geotechnics and Occupational Safety) whenever improvement points are identified, coordinated by the dam's Technical Specialist in Tailings Management (RTFE) and validated by the Engineer of Record (EoR). It consists of a safety protocol made up of three main documents:

1. Safety Plan: a document that defines the basic occupational health and safety guidelines for the workers, establishing responsibilities, procedures, training, and actions that must be adopted to carry out previously approved essential activities.
2. Activity Planning: a document that clearly and objectively summarizes the survey of all necessary maintenance and repairs in compliance with current regulations.
3. Geotechnical Monitoring Plan: a document that establishes the set of existing monitoring instruments, their respective levels of control, and the associated Trigger Action Response Plans (TARPs) to be considered during the execution of essential activities to maintain the conservation condition of the structures, these being defined within the OMS Manual for each dam.

These three documents form a safety protocol that details what must be done, how it must be carried out, the deadline for each activity, the number of people involved, specific training, the monitoring systems that must be working, and the TARPs.

The basis of the Access Plan are the TARPs, as they reflect the dam's performance based on the control levels of the different monitoring instruments (such as piezometers, radars, ETR and microseismic), indicating whether these are within the pre-defined limits considered safe, which can allow people to access them in a conventional way. Therefore, if any instrument considered critical for granting access is not functioning properly, activities are suspended until it returns to operation.

The control levels of the instruments and their respective TARPs are defined in the Operation, Maintenance and Surveillance Manuals (OMS Manuals) and are specific to each dam, based on its individual technical characteristics. Based on the control levels defined for each instrument (attention, alert and emergency), four TARPs were associated that indicate variations in monitoring data or anomalous conditions observed in field inspections, identifying the need to start the action protocols in response to deviations.

The TARPs defined are:

- TARP 1 – Green TARP or normal operating condition;
- TARP 2 – Yellow TARP or low risk alert condition;
- TARP 3 – Orange TARP or moderate risk condition;
- TARP 4 – Red TARP or high-risk condition.

Brazilian legislation defines the emergency levels of dams through the association with safety factors obtained through flow and stability analyses considering drained and undrained conditions of the structures. Commonly, the definition of instrumentation control levels (attention, alert, and emergency) is also linked to the safety factors obtained in stability analyses, as shown in Table 1.

Table 1: Levels of controls, TARPS and associated safety factors

MANAGEMENT LEVEL	TARP/ Color	Peak Undrained Safety Factor		Correspondence with the Emergency Levels provided for in ANM Resolution No. 95 (2022) for Peak Undrained Safety Factor. (Art. 41) [1]
Normal	TARP 1	1. 0		–
Warning	TARP 2	1. 0	1. 0	Emergency Level 1
Alert	A P	1.00	1. 0	Emergency Level 2
Emergency	TARP 4	1.00		e en e el

[1] The correspondence between TARPS and the Emergency Levels provided for in ANM Resolution No. 95 (2022) is strictly related to safety factors. Other aspects that can classify the structure according to the Emergency Levels provided for in this legislation are not included in the Table.

An example control level for instruments that measure interferometry, such as ground-based radars or Robotic Total Stations (ETRs), is shown in Figure 1.

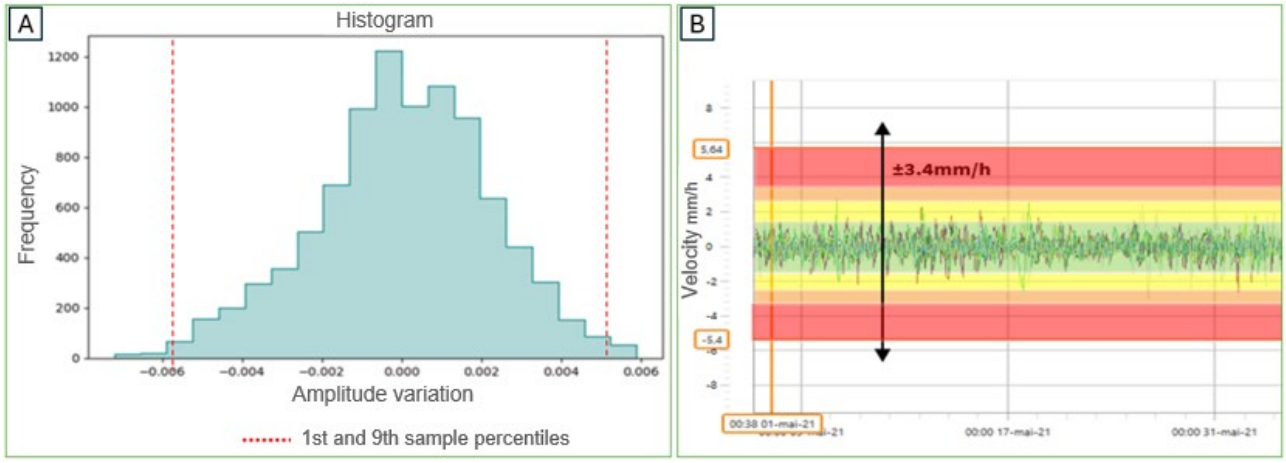


Figure 1: Example of control level for an interferometric radar. (A) Analysis of the distribution of displacement speed (B) Methodology for defining control levels

The definition of individual control levels for each piezometry instrument was based on percolation/ seepage analyses carried out in a 3D model using the Rocscience RS3 software. This model considered the finite element method and saturated and unsaturated flow conditions in a steady state. Based on individual control levels, it was possible to divide the dam into sectors, considering the behavior of piezometers and water level indicators through an individual calculation of the hydraulic loads observed in each sector, and associating the position and level of importance of the instrument with the respective minimum safety factors obtained in the analysis. The result is the maximum TARP for each region of the dam. It is important to highlight that the overall TARP of the structure represents the highest TARP (worst condition) observed in the assessments of the individual sectors.

For this assessment to occur in real time, it is important that readings from manual instruments are automated. Instruments considered critical were automated and the monitoring system sends data 24 hours a day, which is a premise for the access protocol. Figure 2 shows how the level of control is applied to each region of the dam.

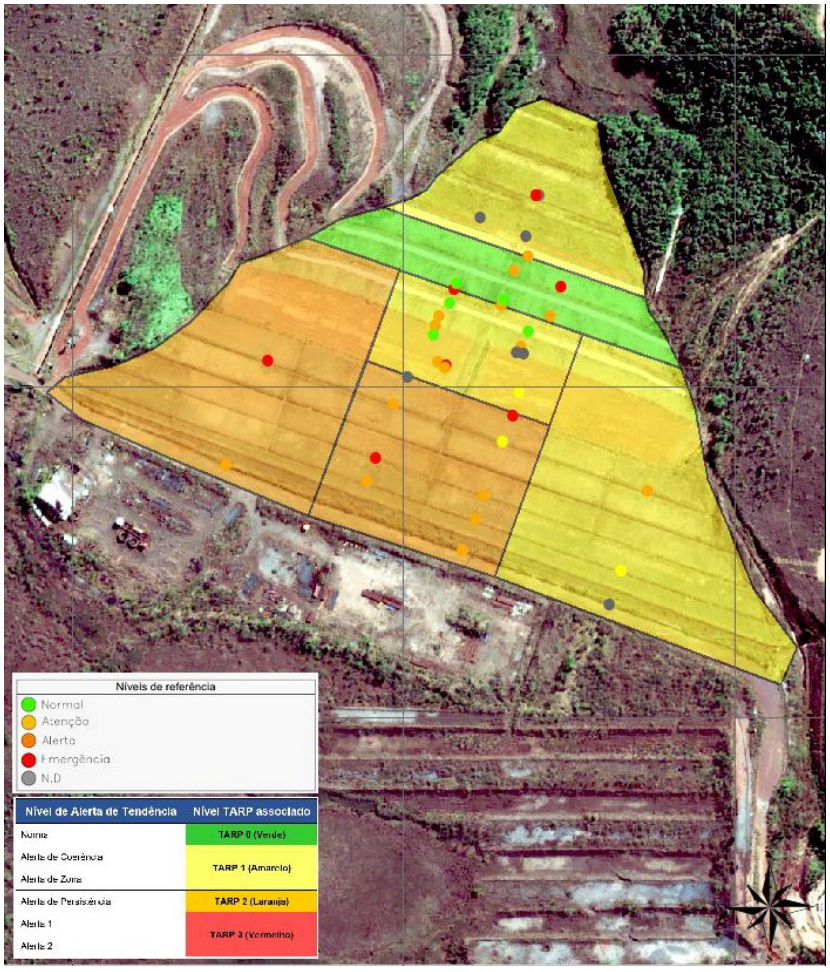


Figure 2: Control levels and TARPs applied to piezometers

It should be noted that in addition to the control levels established for embankment's piezometry and water level indicators, control levels were also established for displacements, water level in the reservoir, and allowable vibrations.

As mentioned, Deviation Response Action Protocols are tools designed to assist in risk management, according to performance criteria based on risk controls and critical controls of the tailing facility. The activation of each TARP is associated with a particular communication flow depending on its severity, and its main objective is to mitigate consequences, which must be checked periodically or on demand.

Automated graphs and tables were created, and every morning a one page report is sent describing the system's operation throughout the night. It includes any anomalous situations observed. This report is analyzed by the geotechnical team, which authorizes access to the dam and area of influence defined in a Dam Break analysis. This cycle of evaluating the conditions of each dam is repeated every new day. The automation of systems and reports previously formatted in software is essential to avoid human error.

An emergency TARP is not expected to require evacuation or access restrictions. In TARP 2, monitoring of the entire structure is intensified. When changing from TARP 2 to TARP 3, it is preventatively requested that activities be interrupted, and employees be evacuated. Activities are resumed after a detailed assessment by the structure's RTFE and EoR, detailing the reasons and likely consequences for activating the TARP, in addition to the assessment of the risks vs. benefits of the activities being continued. TARP 4 activation blocks routine access of people to the dam until a more favorable condition is restored.

Access plan operationalization

The cycle starts with the Activity Planning of essential elements, contained in maintenance planning. This document contains all the anomalies, audit recommendations, monitoring plan, and works necessary to guarantee the safety of the dam. From this, the activities are detailed in terms of execution productivity, number of people, and specific services, such as the use of tools or equipment. Also, in the Planning phase, the work procedures and safety requirements that must be met are evaluated.

The workers involved in the activities must undergo specific training on access, focusing on compliance with safety evacuation rules, and detailing escape routes, access control procedures and communication plans. All these requirements are found in the Safety Plan.

On the day that the activities begin, the conditions of the dam are evaluated through a one page report, which considers the TARPs (explained in the previous item) and is used to determine whether a certain activity is called for or not. This is detailed in the Geotechnical Monitoring Plan. When necessary and authorized, professionals fill out specific documents, such as a Preliminary Task Analysis, and request a

Work Permit. At this time, each team carries out a Health and Safety Dialogue, so as to be aligned with the risks of the task and the requirements for performance of the activity.

A weekly safety meeting is held with the geotechnical team, occupational safety team, and auditors team. Points for improvement are raised and the access plan is updated. Figure 3 shows the flow of the previously detailed activities.

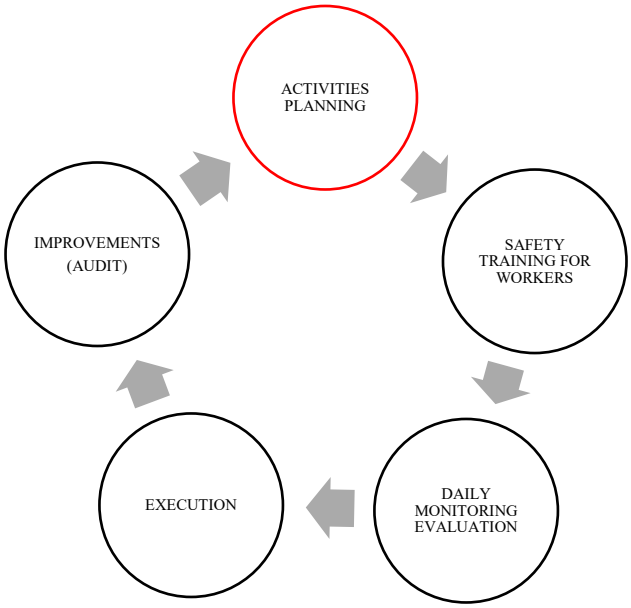


Figure 3: Activity flow within the access plan routine

Results

One of the parameters that measures maintenance efficiency is Adherence to Activity Programming, which is a direct relationship between what was planned and what was accomplished.

Before implementing the Plan, deviations of 300% were observed in relation to what was programmed. Since the beginning of this project, implemented in September 2022, compliance has reached 98% of what was planned. Figure 4 shows the situation from before implementation to present day.

Another improvement observed is in a parameter called Conservation Status Note, defined by current legislation, and evaluated every fortnight by the geotechnical team within the official government system. The Conservation Status Note is the sum of the criteria presented in Table 2 (ANM, 2017). All anomalies receive a score from 2 to 10, depending on severity, with 10 being the most serious. Therefore, the higher the sum, the worse the condition of the dams. This methodology is formalized in the biannual EoR audits.

Figure 5 shows that after implementing this methodology, the conservation of dams improved by 79% compared to their initial condition.

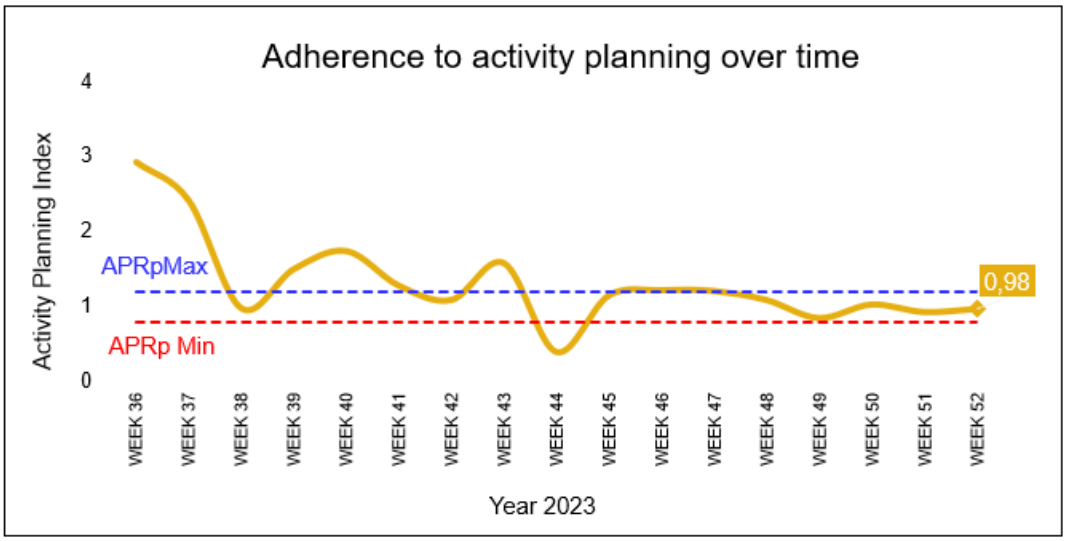


Figure 4: Maintenance adherence over time (total for 6 dams)

Table 2: Risk category classification matrix – Conservation Status (ANM, 2017)

Conservation status (EC)			
Spillway (f)	**Seepage (g)**	**Settlements (h)**	**Deterioration of Slopes (i)**
Well-maintained civil facilities operating normally / dam does not need outflow structures (0)	Seepage is fully controlled by the drainage system (0)	There are no disturbances and settlements that can potentially compromise the safety of the facility (0)	Slopes and parameters have deteriorated (0)
Facilities with identified problems and remedial measures are being implemented	Moisture or uncontrolled seepage in downstream areas, stable and monitored facings, slopes and abutments	Remedial measures for existing cracks and slumps are being implemented (2)	Slope and facing protection faults, presence of shrub vegetation (2)
Facilities with identified problems and no required remedial measures are in place (6)	Moisture or uncontrolled seepage in downstream areas, facings, slopes or abutments without required remedial measures in place (6)	There are cracks and slumps with no required remedial measures in place (6)	Surface erosion, exposed reinforcements, presence of trees, no required remedial measures in place (6)
Facilities with identified problems, with reduced spilling capacity and no remedial measures are in place (10)	Seepages in downstream areas with material transport, growing flow or contained material infiltration, with potential to compromise safety of the facility (10)	There are cracks, slumps or slides that can potentially compromise the safety of the facility (10)	Steep depressions in slops, slides, deep erosion grooves that can potentially compromise the safety of the facility (10)
0	0	0	0
EC sum: (∑ EC = XX)			

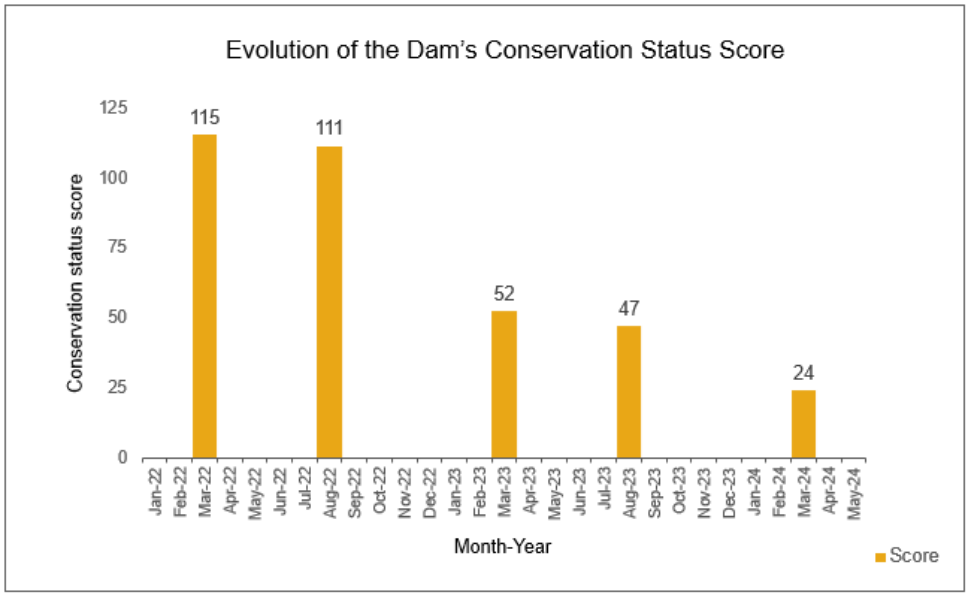


Figure 5: Evolution of the dam's Conservation Status score (total for 6 dams)

Conclusion

The dam management model presented in this paper, entitled "Emergency Level Dam's Access Plan," has enabled Vale to improve the conservation status of tailings storage facilities with access restrictions according to the Brazilian regulations.

Since applying this model, at this specific site, 79% improvement has been achieved in the assessment of dam conservation status, increasing safety conditions in the structures. Additionally, based on a standardized and systematic risk assessment method enabled to increase the access time to those dams, adherence to maintenance planning has improved by 98%. This shows how planned activities are safer and more efficient for workers.

Furthermore, after attending to some maintenance and correction activities, one of the six dams covered by the Access Plan had its emergency level removed, bringing its status back to normal condition.

Acknowledgements

The authors would like to thank Vale for the opportunity to publish this paper.

References

ANM. 2017. National Mining Agency. Law N. 70.389.2017. Consolidates the normative acts that provide for the safety of mining dams. Accessed 2/07/2022 at: https://www.gov.br/anm/pt-br/assuntos/barragens/portaria-dnpm-no-70-389-de-17-de-maio-de-2017

Global Tailings Review. 2020. Global Industry Standard on Tailings Management (GISTM). Accessed 1/15/2022 at: https://globaltailingsreview.org/wp-content/uploads/2020/08/global-industry-standard_EN.pdf

International Council on Mining and Metals (ICMM). 2020. *Conformance Protocols: Global Industry Standard on Tailings Management (GISTM)*. Accessed 1/15/2022 at: https://www.icmm.com/website/publications/pdfs/environmental-stewardship/2021/tailings_conformance-protocols.pdf?cb=21097

Law N. 12.334. 2010. Establishes the National Safety Policy for Dams intended for the accumulation of water for any use, the final or temporary disposal of tailings and the accumulation of industrial waste, creates the National Information System on Dam Safety and changes the wording of art. 35 of Law No. 9,433, of January 8, 1997, and art. 4th of Law No. 9,984, of July 17, 2000. Accessed at https://www.planalto.gov.br/ccivil_03/_ato2007-2010/2010/lei/l12334.htm

Law N. 14.066. 2020. Establishes the National Dam Safety Policy (PNSB), of Law No. 7,797, of July 10, 1989, which creates the National Environmental Fund (FNMA), of Law No. 9,433, of January 8, 1997, which establishes the National Water Resources Policy, and Decree-Law No. 227, of February 28, 1967 (Mining Code). Accessed at https://www.planalto.gov.br/ccivil_03/_ato2019-2022/2020/lei/l14066.htm

Law N. 23.291. 2019. Established the state dam safety policy, to be implemented in conjunction with the National Dam Safety Policy – PNSB –, established by Federal Law No. 12,334, of September 20, 2010, and with the National and State Environmental Policies Environment and Civil Protection and Defense. Accessed at https://www.almg.gov.br/legislacao-mineira/texto/LEI/23291/2019/

Resolution N. 95 ANM. 2022. Consolidates the normative acts that provide for the safety of mining dams. Accessed 2/07/2022 at: https://www.gov.br/anm/pt-br/assuntos/barragens/legislacao/resolucao-no-95-2022.pdf

Resolution N. 95 ANM. 2022. Consolidates the normative acts that provide for the safety of mining dams. Accessed 2/07/2022 at https://www.gov.br/anm/pt-br/assuntos/barragens/legislacao/resolucao-no-95-2022.pdf

Passive Seismic and Interferometry Techniques in Dam Decharacterization Monitoring

Camilla Rodrigues, Nanometrics, Canada
Marc Lambert, Nanometrics, USA
Ben Witten, Nanometrics, Canada

Abstract

Decharacterization of monitoring dams is crucial to ensure structural stability and mitigate environmental risks. It enables the early detection of potential issues, thereby safeguarding nearby communities and ecosystems. In this study, a complete overview of the installation procedures for seismic systems deployed in dams undergoing the decharacterization process is provided. Moreover, the application of passive seismic and seismic interferometry in the monitoring of ground motions and medium changes is discussed. Our findings demonstrate that the ground motion level induced by operations can be one hundred times greater than the background level, and that peaks of ground motion are usually induced by operations near seismic stations, detonations in the mine site, or natural events. The authors demonstrate that with noise-based monitoring, it is possible to detect velocity changes related to operations and determine the occurrence of structural changes in the dam's body.

Introduction

The decharacterization process marks a significant stage in reintegrating a dam into its natural surroundings, releasing it from its primary function of containing tailings. This transition ensures minimal environmental risks and safeguards nearby communities. The decharacterization process typically involves several key stages (ANM, 2017; Schaper et al., 2020):

- Decommissioning: closing operations and removing associated infrastructure, such as spigots and pipelines, except those intended to ensure the safety of the structure.
- Hydrological and hydrogeological control: adopting effective measures to reduce or eliminate the inflow of surface and groundwater into the reservoir.
- Stabilization: implementing measures to ensure the long-term physical and chemical stability of the structures that remain in place.

- Monitoring: observing for the necessary period to verify the effectiveness of the stabilization measures.

Geotechnical instrumentation has traditionally played a key role in monitoring this process; however, its limitations lie in spatial coverage, presenting discrete data points over time and space.

To overcome this constraint, Passive Seismic (PS) and Seismic Interferometry (SI) techniques have emerged as promising tools for assessing the medium during decharacterization. PS methods evaluate high-amplitude ground motions induced at the dam in terms of velocity and acceleration, while SI uses ambient noise (background noise) to monitor velocity changes related to alterations in the medium's stiffness. SI offers cumulative monitoring, detecting the evolution of the dam's response from the initial state at the array deployment moment, making it a valuable tool for understanding how the dam reacts to the decharacterization process. In other words, if the system has been deployed before the start of the decharacterization process, the SI response will highlight changes in the dam during the entire decharacterization process.

In this study, the application of both techniques for tailings dams undergoing the decharacterization process is discussed. Initially, a complete overview of the installation and network deployment is provided, highlighting the best practices adopted during the decharacterization. The processing workflow applied in these two monitoring approaches is described. Next, ground motion levels and the main sources of strong ground motion that can be characterized are presented. Furthermore, velocity changes are correlated with operations performed during the decharacterization process.

Installation and network deployment

A fully operational network, where waveforms are acquired by all receivers and streamed to a server for processing and analysis, is essential for the continuous acquisition of ambient noise. The hardware components, e.g. receivers, data acquisition and communications equipment, are built to collect and digitize information with high sensitivity and send it to a seismic server, where the data should be processed.

The seismic array is typically deployed near the surface in a non-invasive manner. In this installation procedure, the soil is excavated and compacted into a cylindrical shape with a diameter larger than the sensors. Then a posthole receiver, designed for shallow depths, is inserted into this hole, aligned with North and horizontally and vertically leveled. In the case of wired sensors, the cables are run from the hole towards a trench with a depth of 20 – 50 cm. For increasing depths, as shown by De Paula (2020), a borehole receiver can be fixed using grouting material that corresponds to a water-cement mixture with an acoustic impedance similar to the surrounding material. To place the receiver, the hole must have an adequate diameter to accommodate the sensor and the tubes that inject the grouting solution.

The spacing between sensors depends on the sensitivity required. For PS monitoring, an initial sensitivity analysis must be performed to estimate the magnitude of completeness (minimum magnitude detectable) and location uncertainty. Usually, a microseismicity level with a magnitude greater than -2 (ML, local magnitude) is recommended, while a small epicentral uncertainty of a few tens of meters is recommended. For SI, the inter-station distance should be less than one wavelength (λ). For example, with an S-wave velocity (v_S) of approximately 200 m/s in tailings and a frequency (f) of 1 Hz, the maximum inter-station distance should be roughly 200 meters ($< \lambda = v_S / f$).

The usual seismic configuration deployed in mining dams is shown in Figure 1.

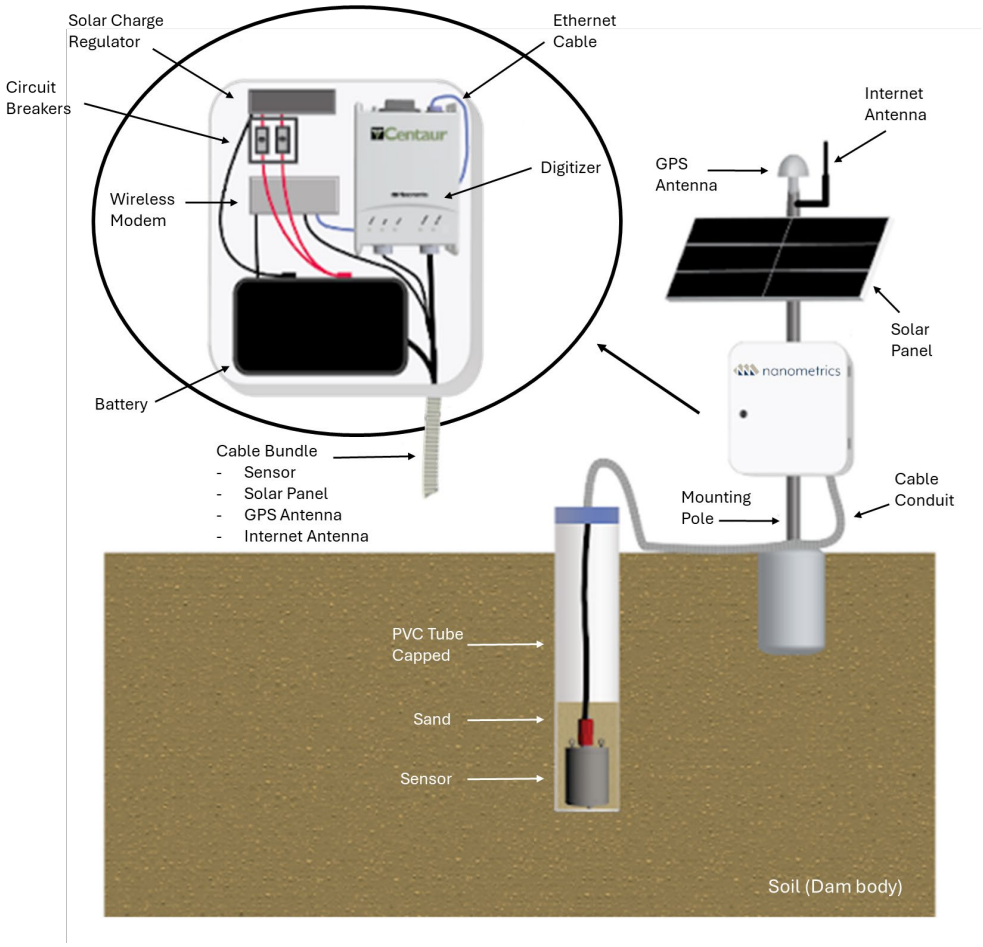


Figure 1: Seismic system architecture

Besides the receivers, all devices are stored inside a seismic station, powered by solar energy. The seismic station is affixed to a pole that serves as a mast for solar panels and communication antennas. This should be as close as possible to the seismic array, in an area of easy access, to allow maintenance. This distance is influenced by the signal strength loss (attenuation) caused by the transmission process. As

suggested by Xiao et al. (2016), the distance between receivers and seismic stations "should be less than the maximum distance that signal reduction affects the monitoring data," which is usually less than 300 meters. The pole height can be designed and customized for each monitored area. For instance, in areas with any incidence of vandalism, a tall pole can be designed to discourage unauthorized access.

The continuous analog signal registered by the receivers needs to be converted into a discrete digital signal before the data collection and processing on a seismic server (Xiao et al., 2016; Mendecki, 1996). This conversion process is performed by equipment known as a digitizer or analogue-to-digital converter.

This converter equipment has a finite number of channels for digitization. The uniaxial receiver requires one channel, while a triaxial requires three channels. Thus, depending on the seismic array, the number of required digitizer devices inside the seismic station varies.

All the aforementioned equipment is connected to a GPS, which provides time information via satellite to ensure synchronization within milliseconds. A poor time synchronization can lead to a poor location and create instability in the SI measurements. Thus, if an instrument is not synchronized, its data is generally unusable. Hence, the GPS is a crucial device for seismic monitoring.

To guarantee continuous monitoring and prevent power outages, an independent energy source can be implemented. Usually, for one seismic station, two photovoltaic modules, two stationary batteries, and a charger controller are installed. The charger controller is responsible for managing the batteries, and the supply of energy in the seismic station devices and network equipment.

The communication between the seismic station and the server can be made via internet. The wireless communication network needs to be stable, as the amount of data collected can be high. Eventually, it is recommended to work with redundancy to ensure the system will always be online. Still, if the transmission network fails, a data storage device (USB flash drive) can be connected to the station to store data during this period. Once the communication has been restored, the storage data is sent to the server. However, should the disruption last long, the newest data could overwrite the oldest, and then the data is lost.

Furthermore, for cases where the seismic system uses the same web network communication as other systems, a Virtual Private Network (VPN) can be employed to isolate all networks. The processed data can be visualized using online tools for quick assessment and interpretation.

For dams undergoing the decharacterization process, careful installation of monitoring equipment is crucial. This involves the precise demarcation of station and network equipment locations. As continuous operations are conducted on the dam body, the operational team must be vigilant about the locations of stations and cables. This awareness is essential to avoid interference with these areas, which could lead to issues such as cable breakage and subsequent interruption of monitoring.

Passive seismic monitoring

The objective of seismic monitoring is to quantify exposure to seismic activity, providing critical inputs for risk management strategies and protocols. Acquired and processed data can be utilized by geotechnical engineers for preventive measures, alert determination, Trigger Response Action Plans (TARP), and predictive analysis.

Ideally, the seismic array should be deployed before the decharacterization process begins to establish a baseline of background vibrations and event history – i.e., the vibrations and number of events the dam experienced prior to the start of the process.

The seismic waveforms recorded by the system can amount to around 50 to 100 GB per month. This data undergoes a processing scheme designed to estimate source parameters (e.g., magnitude and location) and classify the source mechanism (Figure 2).

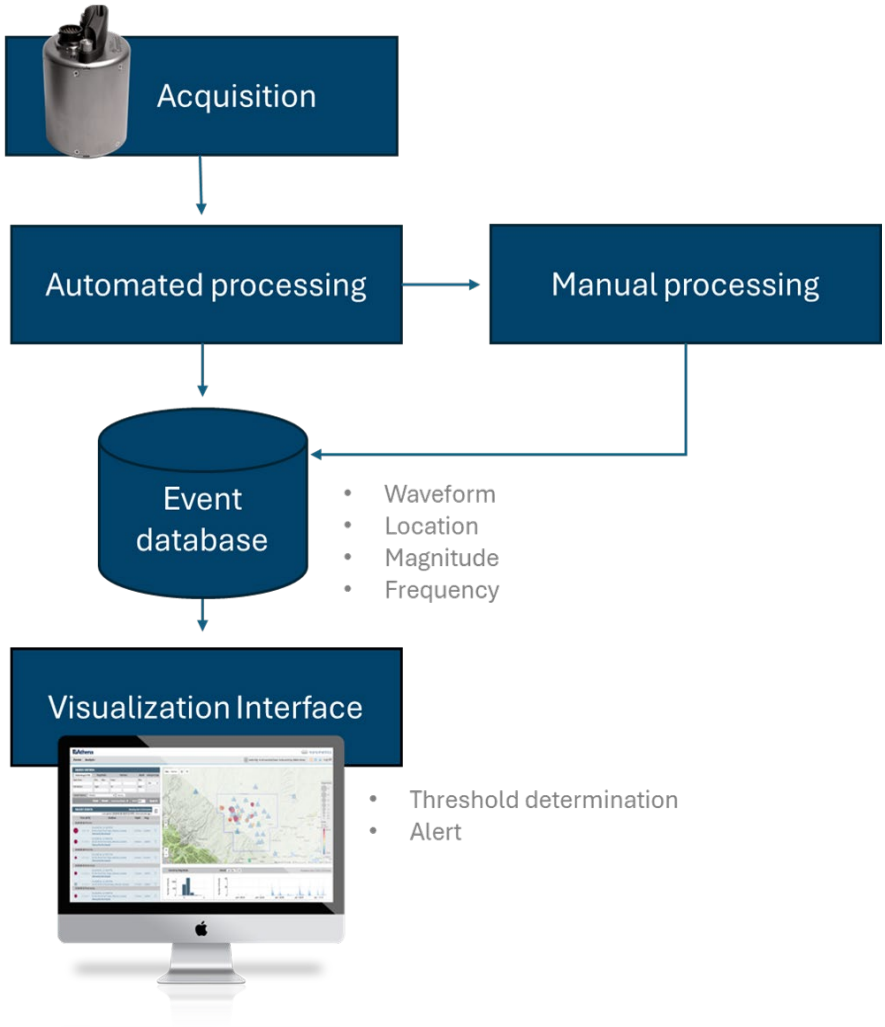


Figure 2: Simplified processing workflow

Two approaches can be applied: automated and/or manual processing. When both approaches are used, differing results may arise not only due to the subjectivity inherent in manual processing but also because of the varying quality of the automated algorithms. Consequently, the quality of the data is influenced by the seismologist's expertise.

As a best practice, automatic processing is typically applied to all databases, while manual processing is reserved for specific data samples, such as events that exceed a certain threshold. In the case of dams undergoing a decharacterization process, routine analysis is essential for identifying outliers, particularly in terms of unusual strong ground motions, and for characterizing their sources. This requires active communication between the mining operators and the monitoring team. A thorough analysis should include the event waveform, spectral content, source parameters, magnitude, and source location.

Seismic Interferometry monitoring

The Seismic Interferometry (SI) technique originated from the potential to extract valuable information from ambient noise data. SI comprises two distinct processing techniques: Seismic Ambient Noise Interferometry (SANI) and Coda-Wave Interferometry (CWI). The SANI concept was introduced in the 1960s by Claerbout (1968), who suggested the feasibility of cross-correlating noise signals recorded between a pair of receivers. This approach allows for the reconstruction of the signal that would be recorded at one receiver when a source is positioned at the other. Thus, considering two stations located at x_A and x_B and a noise source at x_S, the response at one receiver A can be described as $G(x_A, x_S, t_A)$, where G corresponds to the Green's Function, and its arguments represent the receiver, source and travel time, respectively. As described by Wapenaar et al. (2010), the process of convolving two-time reversal responses acquired by two stations ($u(x_B, x_S, t)$ and $u(x_A, x_S, -t)$) turns into a correlation. This correlation yields the Green's function between stations, which represents the response at one receiver if a source was placed at the other ($G(x_B, x_A, t)$), convolved with the noise wavelet $N(t)$ autocorrelation ($S_N(t) = N(t) * N(-t)$) :

$$G(x_B, x_A, t) * S_N(t) = u(x_B, x_S, t) * u(x_A, x_S, -t). \quad \text{(Eq. 1)}$$

$$u(x_A, x_S, t) = G(x_A, x_S, t) * N(t) \quad \text{(Eq. 2)}$$

$$u(x_B, x_S, t) = G(x_B, x_S, t) * N(t) \quad \text{(Eq. 3)}$$

$$G(x_B, x_A, t) = G(x_B, x_S, t) * G(x_A, x_S, -t) \quad \text{(Eq. 4)}$$

These wavefields are estimated at regular time intervals and serve as a representation of the medium between pairs of stations (Figure 3). The CWI technique uses this data as input, measuring changes in phase

and amplitude by comparing these wavefields. This comparison is conducted in the scattered waves within the tail of the Cross-Correlation Functions (CCF) obtained by the SANI technique. These scattered waves, known as coda-waves, are more sensitive to small perturbation in the monitored structure, as they spend more time propagating through the medium. Thus, changes that are not visible in the direct arrival can be seen in the coda portion (Figure 3).

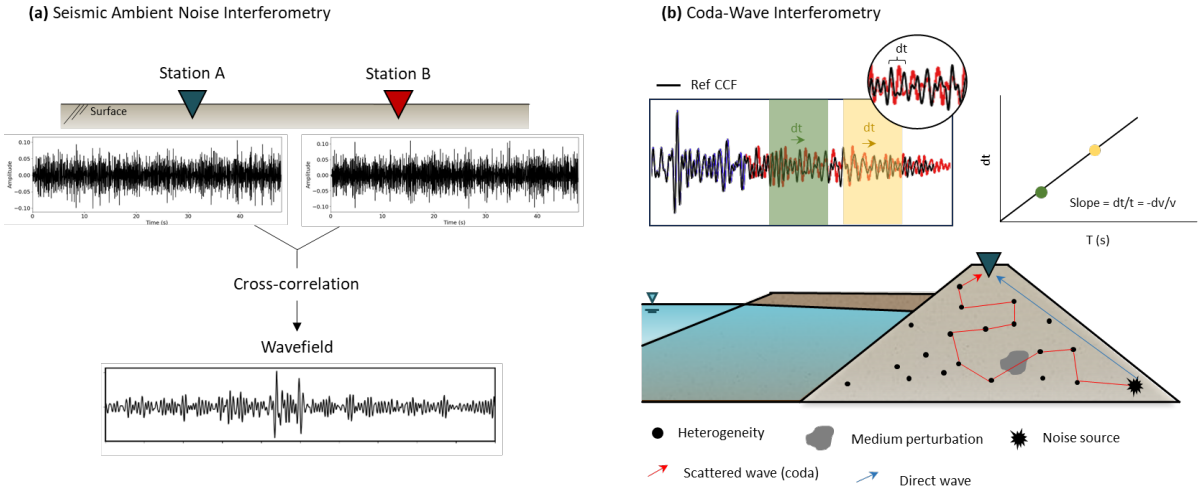


Figure 3: Seismic interferometry. (a) Seismic ambient noise interferometry: cross-correlation of signal recorded at two fixed locations, yielding a wavefield that represents the medium between these points; (b) Coda-wave Interferometry: time perturbations measured in scattered waves provide velocity changes (modified from Rodrigues et al., 2024)

To estimate the velocity changes, the Moving-Window Cross-Spectral (MWCS) method, also known as the doublet method, was applied. As explained by Le Breton et al. (2021), the MWCS method consists of measuring the time shifts (dt) between two CCF over a narrow moving window. This procedure can be executed in either the time or frequency domain. By extracting the slope ($dt/t = -dv/v$), changes in velocity can be estimated.

In the context of monitoring dams, it is crucial to emphasize that velocity changes are cumulative, serving as a reflection of the dam's evolving behavior in relation to the initial monitoring point (the first CCF measured). In practical terms, this implies that, for example, if a dam exhibited the presence of water, cracks, or any structural complications prior to the deployment of the system, the monitoring would assess whether there has been an increase or not from these pre-existing conditions.

Seismic data of a decharacterization process

To illustrate the response of a decharacterization process, this study will analyze data from real tailings dams located at active mine sites. These dams were monitored using an array of posthole stations installed near the surface. The array was deployed after the beginning of the decharacterization process, not allowing

the establishment of a baseline level of ground motion. In this case, for the PS monitoring, an alternative process adopted was the confrontation between the ground motion data registered during periods with active and without active operations. As some operations may be continuously performed (e.g., pumping), major operations responsible for strong ground motions will usually be conducted during business hours, such as detonations on the mine site, drilling, excavation, etc.

Figure 4 shows the Peak Ground Velocity (PGV, in m/s), where daily variations are observed with peaks during working hours and lower vibrations at night. Considering the low ground motions, it is possible to establish a baseline, in this case 0.00004 m/s. Decharacterization operations and detonations induced a maximum of 0.007 m/s, 100 times greater than the background level.

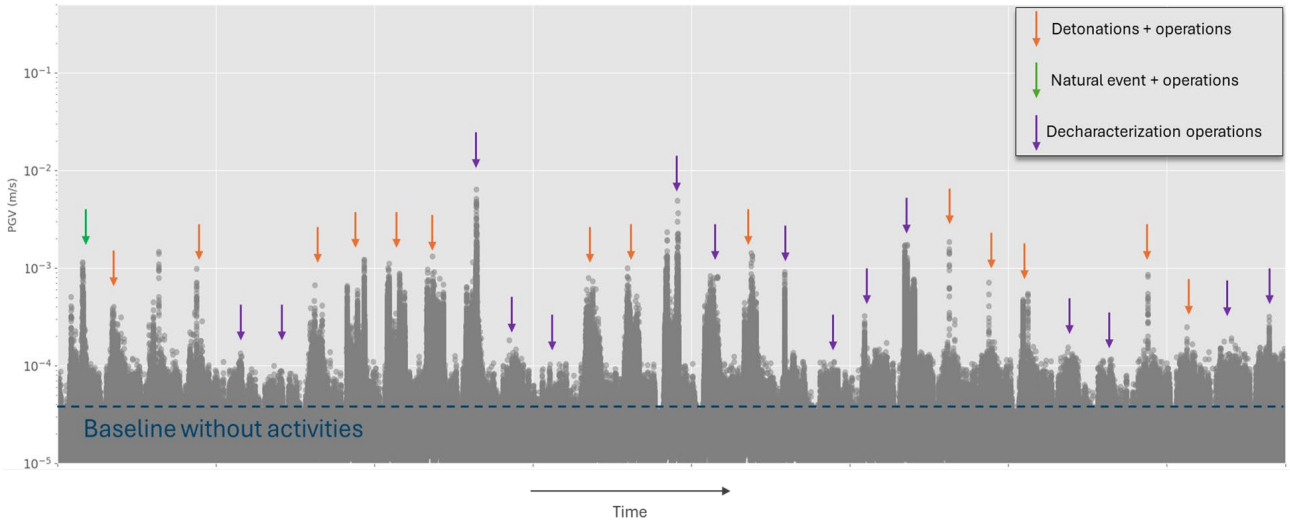


Figure 4: Vibration levels variation – peaks induced by operations

The peak ground motion observed in the data was carefully analyzed during a manual processing stage. Three types of sources were identified as responsible for this level of ground motion: operations near the stations, detonations, and natural seismic events. Figure 5 presents examples of waveforms. For the ground motion data generated by operations, the location was not determined, as the data is mainly noise and did not exhibit clear arrivals necessary for the picking process (Figure 5a).

However, in the context of a decharacterization process, this data is the most important, as it provides the level of ground motion propagated in the dam body induced by decharacterization activities. Nonetheless, for a more accurate source type characterization, collaboration from the operational team is essential. Their access to mine plans allows them to share critical information on the timing and location of activities.

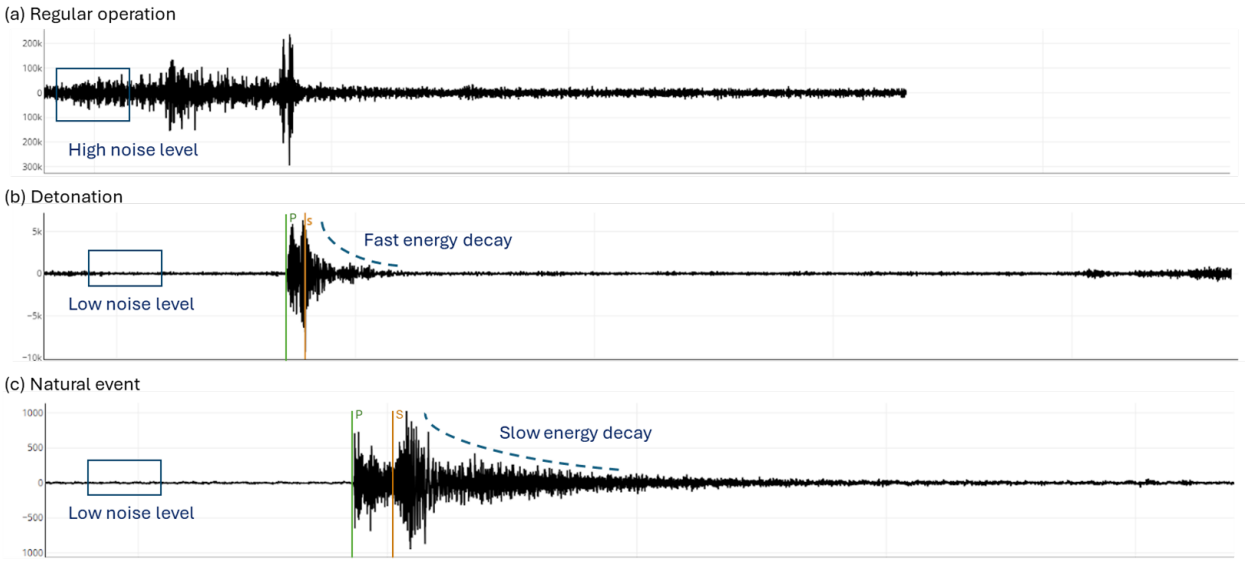


Figure 5: Seismic waveforms (a) decharacterization operation conducted near stations; (b) detonations performed in the mine site; (c) natural events

Despite the ongoing decharacterization process, normal activities at the mine site continued, resulting in significant ground motions due to detonations (Figure 5b). Additionally, natural seismic events (i.e., earthquakes) were also detected at the site (Figure 5c). During their characterization, a common feature used to identify natural events was the slow energy decay. This characteristic is notable because natural events typically exhibit a high content of S-waves, which are more energetic, resulting in a slower energy decay compared to mine detonations, which have a lower content of S-waves (Figure 5).

These events, characterized by a favorable signal-to-noise ratio, were initially located using automatic picking and were re-evaluated during manual processing for final characterization and comparison with the mine blast plan and the local public seismographic network.

In parallel with ground motion monitoring, velocity changes were estimated. Due to the system not being deployed prior to the decharacterization process, a baseline of typical changes observed in the dams before decharacterization could not be established. However, the SI method was utilized to detect new perturbations within the dam body.

Figure 6 provides examples of responses due to typical operations during the decharacterization process, as well as potential issues arising from these operations.

- The removal of tailings from the reservoir resulted in decrease of velocity changes due to the loss of material compared to the reference (Figure 6a).
- Local operations led to a small landslide in the dam slope, which led to a loss of stiffness in the area and consequently a decrease in velocity changes (Figure 6b).

- During the rainy season, the water content in the dam's body increases, which results in a decrease of velocity changes (Figure 6c).

Due to the high sensitivity of SI measurements, even minor perturbations can induce small velocity changes, typically oscillating around a specific threshold. However, when significant alterations in dam behavior occur, a new plateau may emerge. This can indicate a physical change in the medium, reflecting potential structural modifications within the monitored area.

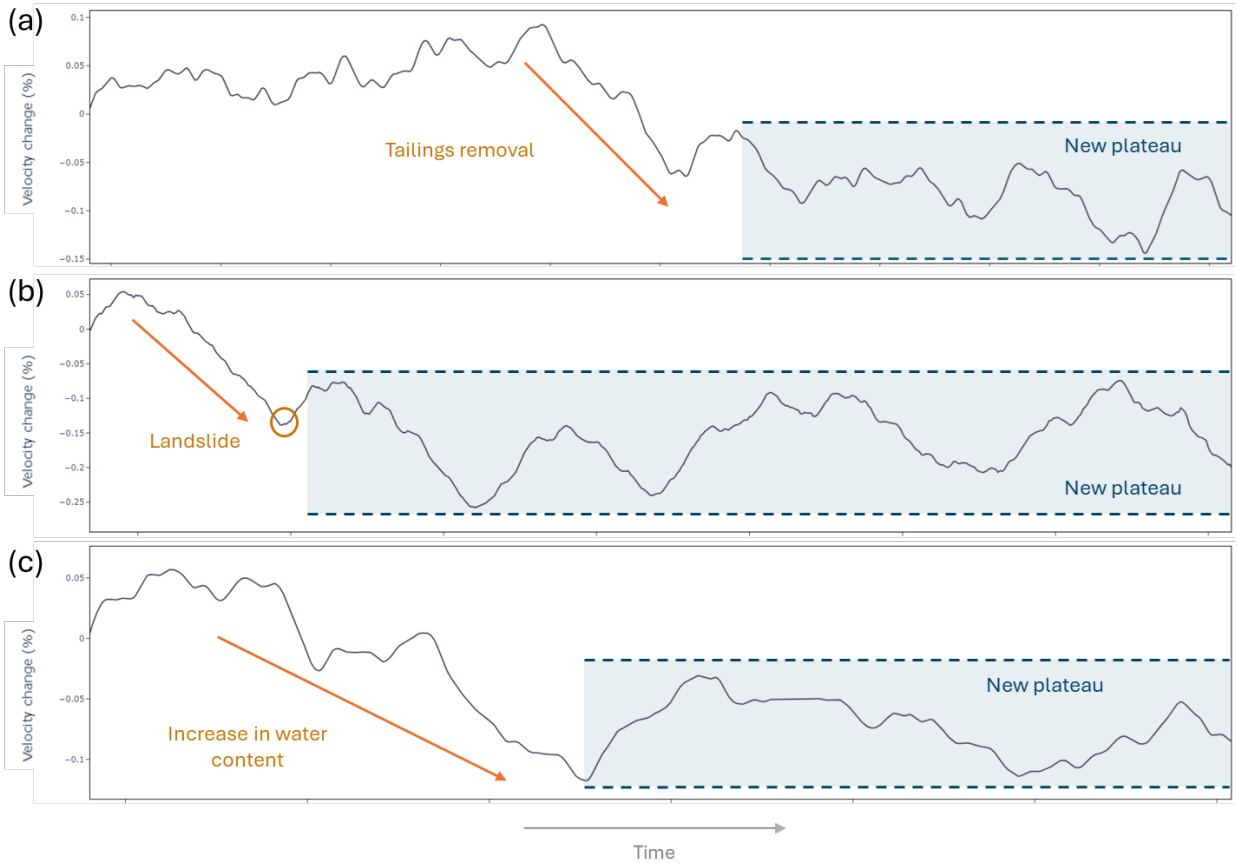


Figure 6: Example of velocity changes response (a) tailings removal during decharacterization; (b) landslide caused by decharacterization operations; (c) increase in water content during the rainy season

Conclusion

Passive seismic monitoring and seismic interferometry can be valuable tools for monitoring dams, especially those undergoing the decharacterization process. By deploying a non-invasive seismic array covering the dam's body, it is possible to measure ground motion induced not only by decharacterization operations but also by regular mining activities and natural events. This approach enhances the ability to detect and analyze changes within the dam structure, providing critical data for ensuring the stability and

safety of the dam during and after decharacterization.

In this study, best practices for seismic system deployments were discussed, emphasizing the importance of active communication between the operational and monitoring teams. The passive data demonstrate that ground motions induced by decharacterization processes and regular mine operations can surpass background levels. Finally, it was demonstrated that with a high-sensitivity SI approach, effective monitoring of the physical changes in dams induced by decharacterization processes (e.g., tailings removal) can occur, as well as during local incidents and the rainy season.

Acknowledgements

The authors would like to express our gratitude to the Nanometrics team for their support and dedication in developing these technologies. Their valuable contributions and insightful discussions were instrumental in the development of this study.

References

ANM. 2017. Portaria nº 70.389, de 17 de Maio de 2017. Accessed 8/21/2024 at https://www.gov.br/anm/pt-br/assuntos/barragens/portaria-dnpm-no-70-389-de-17-de-maio-de-2017

Claerbout, J.F. 1968. Synthesis of a layered medium from its acoustic transmission response. *Geophysics* 33(2): 264–269.

De Paula, A. 2020. *Retroanálise do registro de um sistema de monitoramento microssísmico de uma ruptura de talude de mina.* Thesis research, Master's degree, Universidade Federal de Ouro Preto.

Le Breton, M., N. Bontemps, A. Guillemot, L. Baillet and É. Larose. 2021. Landslide monitoring using seismic ambient noise correlation: challenges and applications. *Earth-Science Reviews* 216: 103518.

Mendecki, A.J. 1996. *Seismic monitoring in mines*. Springer Science and Business Media.

Rodrigues, C.T., G. Fabien-Ouellet and M. Braga. 2024. Seismic Interferometry for mining dams – a noise distribution assessment. *Proceedings of GeoMontreal 2024*. Canada.

Schaper, D., R. Lessa, A. Freitas and B. Weeks. 2020. De-characterization and closure of TSF: concepts of the Brazilian legislation and international criteria. *Planning for Closure 2020. 3rd International Congress on Planning for Closure of Mining Operations.*

Wapenaar, K., Draganov, D., Snieder, R. and Campman, X. 2010. Tutorial on seismic interferometry. Part I: Basic principles and applications. *Geophysics* 75(5): 75A195-75209. DOI:10.1190/1.3457445

Xiao, Y. X., X.T. Feng, J.A. Hudson, B.R. Chen, G.L. Feng and J.P. Liu. 2016. ISRM suggested method for in situ microseismic monitoring of the fracturing process in rock masses. *Rock Mechanics and Rock Engineering* 49: 343–369.

New Wireless Technology for Tailings Monitoring

Leonnardo Probst Simoes, GroundProbe, Australia
Braulio Rodrigues, Vale, Brazil
Sean Allen, Elexon Mining, Australia
Jake Lloyd, Elexon Mining, Australia
Vitor Almeida, GroundProbe, Brazil
Jhonimar Santos, Progen SA, Brazil
Denis Rafael Valentim, Progen SA, Brazil

Abstract

One of the major challenges in the modern mining industry is the disposal and management of its tailings. Following significant accidents in the last decade, the mining industry has been pursuing viable and safer alternatives for tailings disposal, aiming to make mining a more sustainable activity. One alternative is drained stacking of tailings, which involves creating a dry stack pile with waste that has been drained through filtration processes or other dewatering methods. The material is transported to the storage location by trucks or conveyors, then disposed of and compacted with suitable equipment. One of the major concerns about this type of storage is its geotechnical performance throughout the structure's lifetime, from construction to closure. Parameters such as material consolidation, deformation, saturation, and density are crucial for understanding performance and ensuring geotechnical safety. Effective management of this type of structure necessitates a robust geotechnical monitoring program from the implementation phases onwards to understand all aspects of performance and safety.

Given that these structures are still uncommon in the mining industry and their behavior is not well known, monitoring from the initial stages of project implementation – including the foundation and tailing layers as they are deposited and compacted – is extremely important.

The most common technologies in geotechnical monitoring currently face challenges related to the infrastructure needed for reading and supplying power to the sensors. Most sensors require cables connecting the monitoring point to a power source and/or equipment for data reading, making installation difficult in areas with constant equipment movement for material deposition. Additionally, there is a risk of damaging these cables, potentially compromising the monitoring system. In response, a new technology comprising wireless sensors with high-durability batteries, capable of collecting information on the water table level and deformation over approximately 10 years, has been tested for monitoring such geotechnical

structures. This greatly facilitates installation and real-time data collection during the execution of drained stacking, thus providing vital information for geotechnical understanding.

Introduction

This work presents the initial monitoring results of a trial project of a dry stack deposited over hydraulic tailings material inside a non-operational open pit. The monitoring system aims to evaluate the behavior of the foundation of the dry stack in response to the loading generated by the construction of the dry stack on top of the hydraulically deposited tailing material. The focus here is not to evaluate the performance of the structures, but to assess the functionality of the monitoring system for this application.

Traditional geotechnical monitoring systems (e.g., piezometers, inclinometers, shape arrays) typically need to be connected to a datalogger and power source using cables. One of the biggest challenges in this application is to have a system that can be installed in an operational area without the risk of damaging the communication and power cables, and without requiring complex operational procedures to protect those cables.

Geotechnical engineers cannot risk losing relevant information about the performance of the structure due to infrastructure problems (Aguirre and Lloyd, 2020). Therefore, the Geo4Sight Platform was selected – a wireless in-ground monitoring system developed for underground mines, especially block caving mines, capable of monitoring tilt and water pore pressures.

Monitoring system overview

According to Aguirre and Lloyd (2020), the Geo4Sight Platform is a wireless system for monitoring tilt and water pressure in challenging geotechnical environments, where cables have a significant potential to be damaged by operational work or by moving ground.

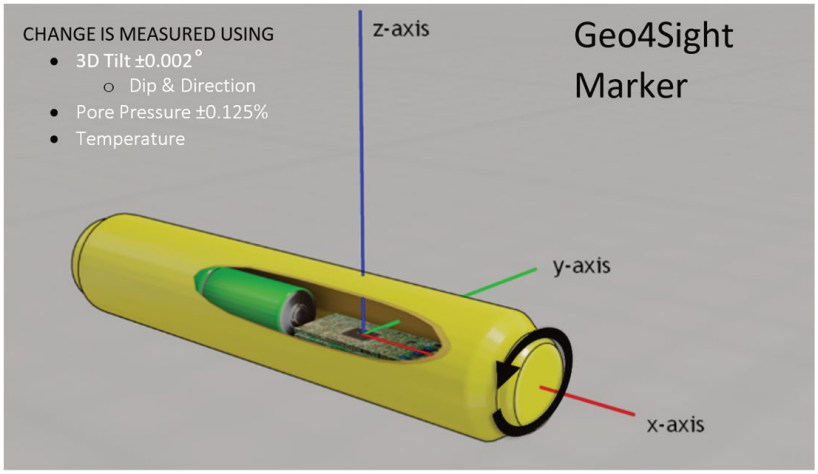


Figure 1: Geo4Sight sensor

The sensor (Figure 1) is a rugged, waterproof, blast-proof, battery-powered system with on-board accelerometers, magnetometers, thermocouples, and pressure transducers used to determine device 3D tilt and water pore pressure. An on-board radio transceiver transmits measurement data to the surface in a daisy-chain fashion.

The Geo4Sight can monitor movement, ground deformation, and groundwater. Changes are measured by 3D tilt with an accuracy of ±0.002˚, dip and direction, pore pressure with an accuracy of ±0.125%, and temperature with an accuracy of ±1%.

System topology

The system operates in an ultra-low-power in-ground radio mesh network of Markers. The Markers have a radio communication range of ~5 meters through the ground. However, for redundancy and to account for ground movement, they are installed much closer to each other, typically at 2-meter intervals (Kamp et al., 2020).

Communication from the surface datalogger to any underground Marker is conducted by sending "queries" down the chain, passing from one to the next until reaching the destination Marker. When the query command is received, the destination Marker takes measurements and sends the data back up the chain to be recorded and transmitted to a database for analysis (Figure 2).

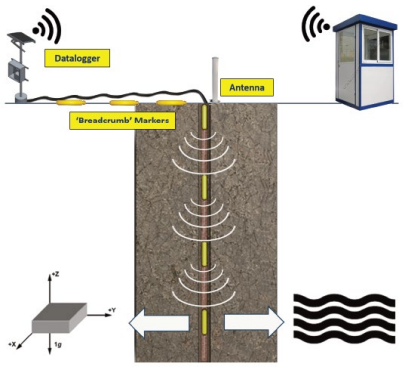


Figure 2: Typical system topology

Installation

As mentioned, the installation was carried out in the foundation of a dry stack under construction. The foundation primarily consists of tailing materials hydraulically deposited in an old pit. A layer of coarse material was deposited between the tailings of the foundation and the dry stack, acting as a filter. The sensors were installed at this interface before the coarse material was positioned (Figure 3). The geotechnical team identified the installation location as one of the critical sections for analyzing the future stability of the pile.

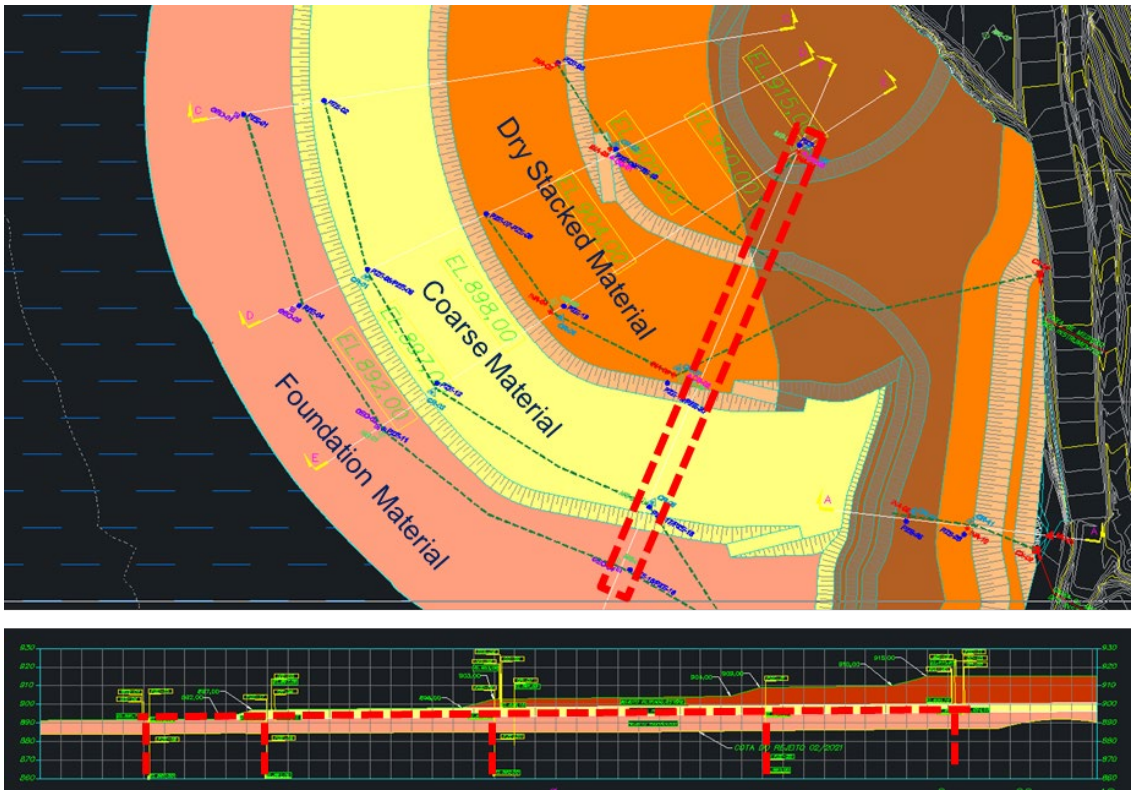


Figure 3: Schematic map and cross-section of the sensors location

A total of 260 sensors were installed with a 2-meter spacing in a trench 400 meters long and in 5 boreholes with a total length of 120 meters. Of these, 240 sensors measure tilt only and 20 measure both tilt and pore pressure. The sensors in the boreholes (Figure 4) were installed using a traditional drilling rig. First, the holes were drilled, and then the sensors were placed inside with the help of a fiberglass rod to prevent them from collapsing to the bottom. Once in place, the holes were filled with the same tailing material from the drilling process, thereby grouting the sensors in position.



Figure 4: Sequence of images showing the installation process in a vertical borehole

For the horizontal installation (Figure 5), a 400-meter-long by 0.5-meter-deep trench was opened with a small digger. The sensors were attached to a coaxial cable with 2-meter spacing and then laid inside the trench. The coaxial cable serves two purposes: it ensures ideal spacing during installation and enhances the sensor signal, facilitating safe wireless communication between the sensors. The trench was then closed with the excavated material.



Figure 5: Horizontal trench with the sensors in place

To collect sensor data, a mobile data logger was installed at one end of the trench. This data logger was mounted on a solar generator trailer (Figure 6), responsible for data collection and processing.



Figure 6: Datalogger mounted in a solar generator trailer

The solar trailer provides power and communications (4G), making the system robust and negating the need for additional infrastructure. It also allows for easy relocation if operational activities require intervention in the area.

After the installation, the system began collecting data once a day, processing it locally. This frequency was selected to maximize the sensor battery life, estimated at 8 to 10 years depending on conditions. The data collection interval can be adjusted as needed.

First results

Two types of sensors were installed: 240 with tilt sensors only and 20 with both tilt and water pore pressure sensors. The analysis is divided into two sections: tilt results and pore pressure results. The data analysis period is from January to May 2024.

Tilt analysis

During the analysis period, the system registered several instances of deformation in different locations. The cumulative tilt variation is shown in Figure 7, where the dots represent sensor locations, with their size and color indicating the amount of variation during the period.

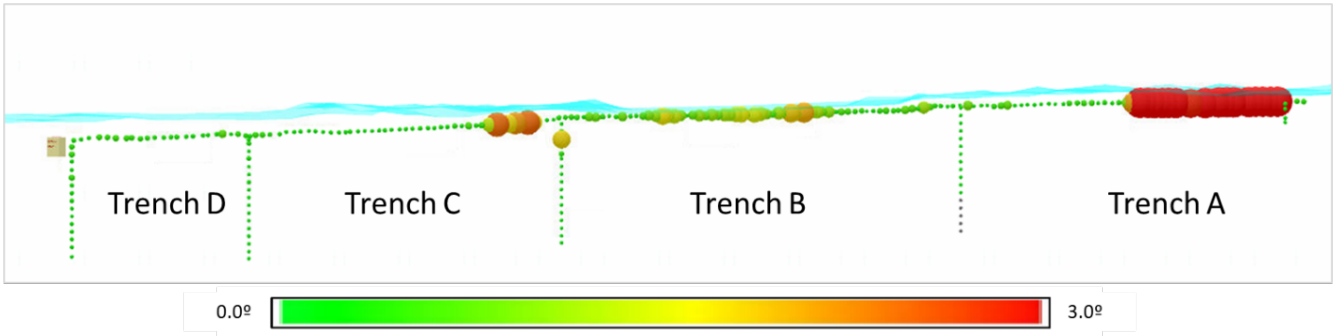


Figure 7: Cumulated tilt variation of the sensors.
For practical reason the trench was divided into 4 sectors (A to D)

Time-based data analysis reveals that deformation occurs at different times depending on sensor position, correlating with the operational moments of the structure. One sector shows deformation early in the period, while others show it later (Figure 8).

A spatial analysis correlating sensor deformation with local topography changes shows a direct relationship (Figure 9). The areas with material volume changes align with sensors showing higher deformation. Notably, the blue area with negative volume variation is related to the main access where trucks deposit material. In this case, deformation is associated with truck loads on unconsolidated material.

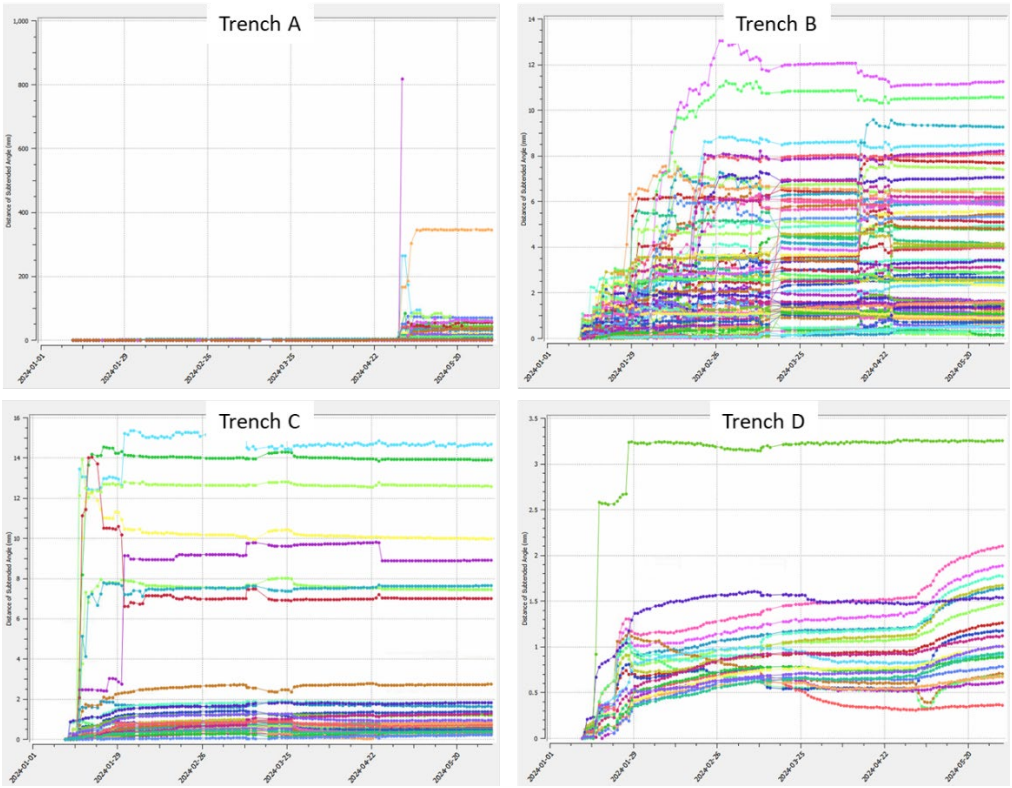


Figure 8: Tilt variation along time in the different sectors of the trench

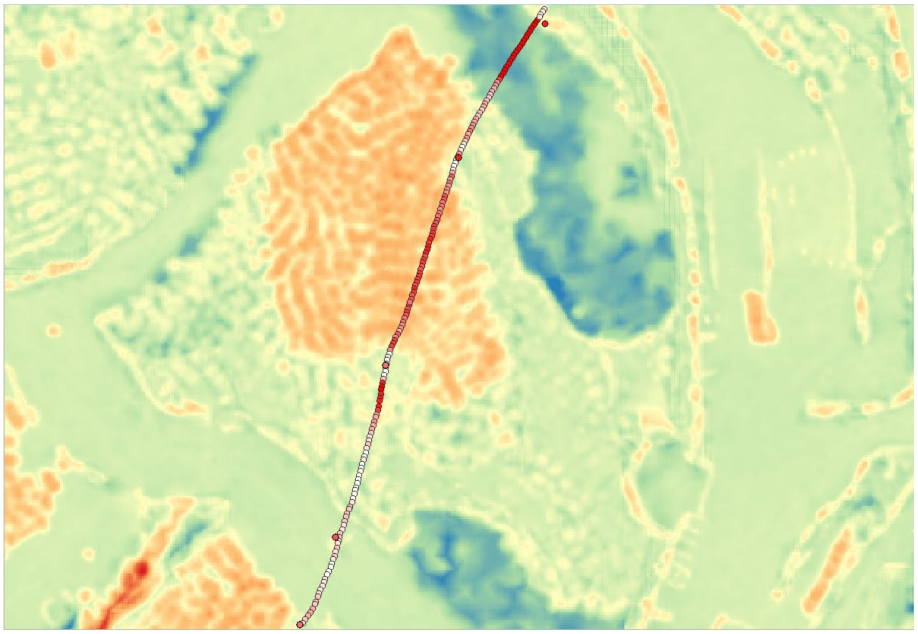


Figure 9: Map showing the correlation of the tilt results with the change in the local topography. The points represent the location of the sensors in the trench, the colors of the dots represent the cumulative tilt change over the period (white to red). The color of the map shows the areas where the thickness of the material over the sensors changed, hot colors mean increase of material and cold colors reduction of thickness

Pore pressure analysis

In the pore pressure charts (Figure 10), two data sets are visible: one with values higher than 250 Kpa and another averaging close to 100 Kpa. The higher values correspond to sensors in boreholes within a saturated zone with a water column over 15 meters, while the lower values correspond to sensors near the surface in non-saturated areas or local high aquifers.

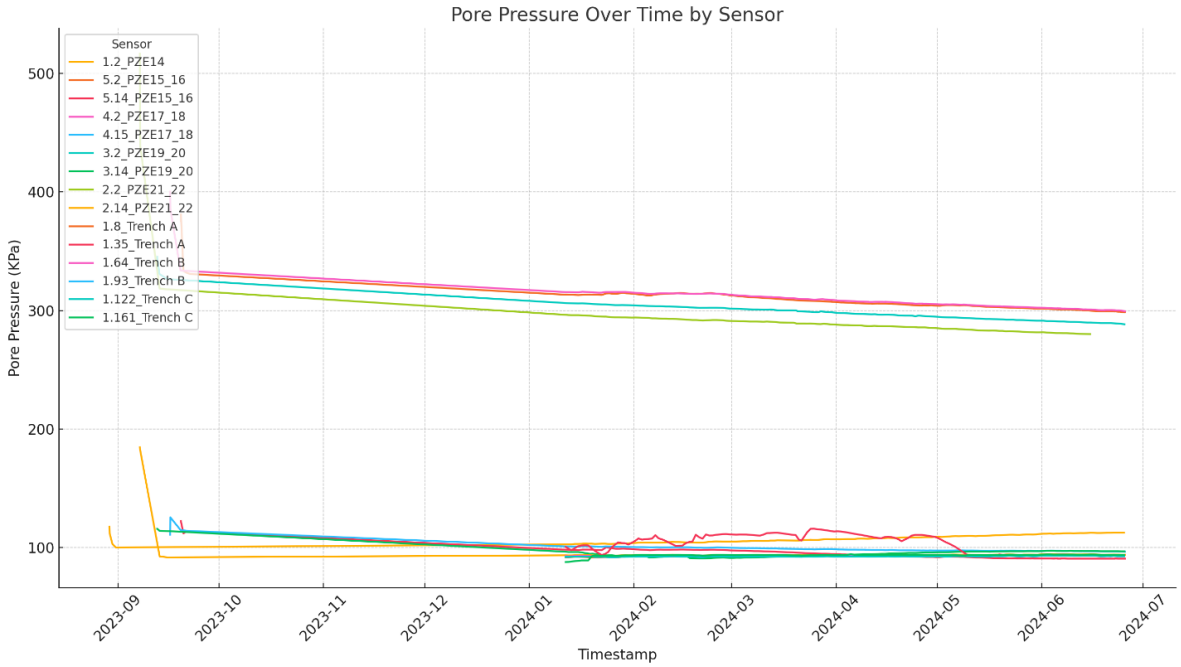


Figure 10: Pore pressure variation chart

Saturated zone sensors show a clear trend of reducing pore pressure values over time, indicating an overall water level reduction in the foundation. Near-surface sensors mainly show variations related to atmospheric changes and local suspended water levels. One sensor near the surface correlates water level increase with rain (Figure 11).

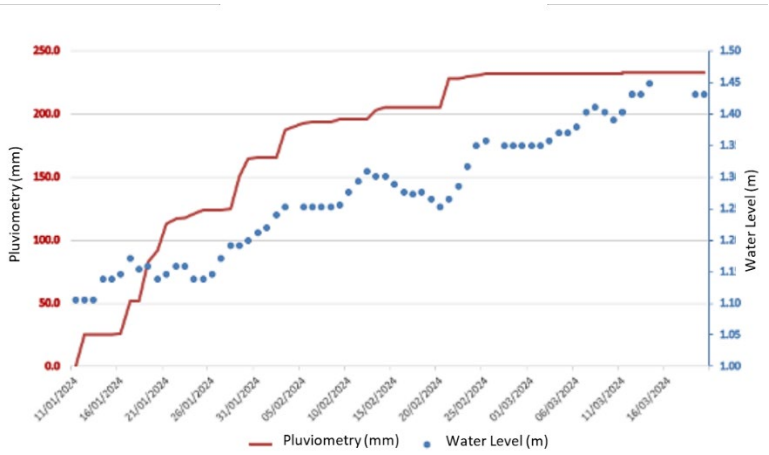


Figure 11: Water level correlation in time with local rain cumulation

Conclusion

The system demonstrates significant value in monitoring geotechnical structures from the initial construction stages. It offers an easy installation solution with the robustness of wireless technology, reducing the risk of damage compared to traditional cabled solutions. This makes structure construction more efficient by eliminating the need to manage, protect, or extend cables.

In terms of results, the system provides reliable data output, showing excellent correlation between collected data and field activities. The tilt sensors respond directly to material disposal and soil settlement in operational areas. The pore pressure sensors show a direct response to rain near the surface, and for deeper sensors, a clear trend of water level reduction is evident.

References

Aguirre, A. and Lloyd, J. 2020. Fundamentals for cave back and in-ground monitoring using wireless technology. In J. Wesseloo (ed.), *UMT 2020: Proceedings of the Second International Conference on Underground Mining Technology,* Australian Centre for Geomechanics, Perth, pp. 261–272. https://doi.org/10.36487/ACG_repo/2035_11

Kamp, C., Thomas, A., Hamilton, D. and Davies, A. 2020. Smart technology for monitoring caving subsidence. In R. Castro, F. Báez and K. Suzuki (eds), *MassMin 2020: Proceedings of the Eighth International Conference & Exhibition on Mass Mining,* University of Chile, Santiago, pp. 289–298. https://doi.org/10.36487/ACG_repo/2063_16

UPLOAD – ANALYSE – ACT: Artificial Intelligence-assisted Faster, Seamless, and Almost Real-time Tailings Dam Construction Quality Assurance is Knocking at our Doorstep

Anjan Kundu, GHD Pty Ltd, Australia

Abstract

Tailings dam construction involves managing vast data volumes over extended periods, presenting challenges in data handling and quality assurance. This paper introduces an artificial intelligence (AI)-assisted approach that streamlines material quality control data analysis, significantly reducing human effort. The method intelligently identifies, extracts, analyzes, and visually presents data, flagging inconsistencies for further investigation. Our trial shows a reduction in effort from 45 minutes to 3 minutes. This innovation enhances real-time communication between remote teams, improves construction compliance visibility, and elevates quality assurance standards. Furthermore, the broader applications of AI in tailings dam management are explored, highlighting its potential in operational planning and safety assessments through predictive analytics and real-time monitoring.

Introduction

The construction of tailings dams is a complex process involving numerous lots in line with technical specifications. Managing data from various formats, such as those from contractor organizations and testing laboratories, has been a continuous challenge, especially where legal certification is required. Ensuring data consistency and quality in such a multifaceted environment is crucial but remains difficult with traditional methods.

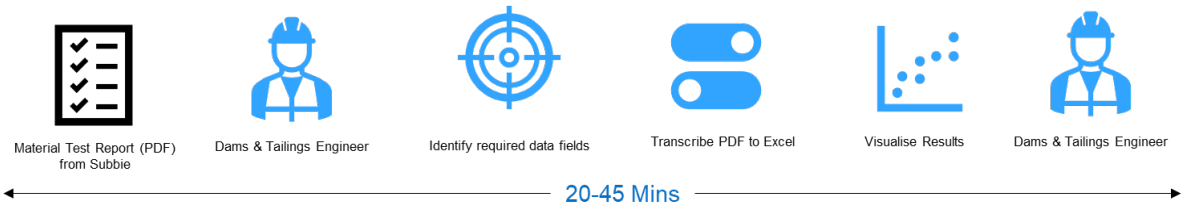
In recent years, the emergence of artificial intelligence (AI) has revolutionized various industries by automating complex tasks, enhancing data analysis capabilities, and improving decision-making processes. Despite its proven benefits in fields such as healthcare, finance, and manufacturing, the application of AI in tailings dam management remains relatively unexplored.

This paper aims to bridge this gap by introducing an AI-assisted approach designed to streamline the analysis of material quality control data in tailings dam construction. By leveraging AI's ability to intelligently identify, extract, analyze, and visually present data, our method significantly reduces the time

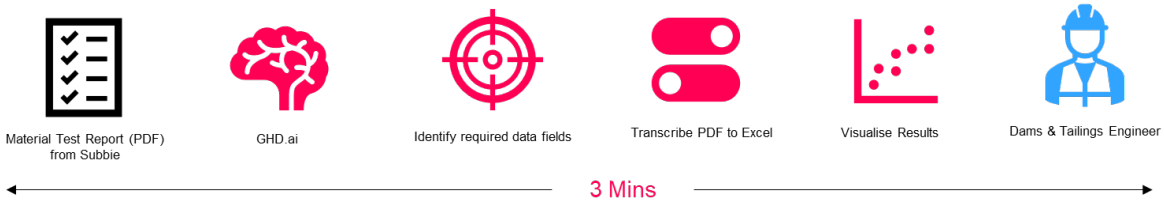
and effort required for data handling, from an average of 45 minutes to just 3 minutes. This not only enhances real-time communication between remote teams but also improves visibility into construction compliance and elevates quality assurance standards.

The current process involves a Dams and Tailings engineer to extract the required information from the PDF file to an Excel file and perform visual analysis that is shared with the wider teams to perform necessary actions.

- Current approach



- AI-assisted approach



Furthermore, we explore the broader potential of AI in tailings dam management, highlighting its applications in operational planning and safety assessments through predictive analytics, and real-time monitoring. Our findings suggest that the integration of AI technologies can lead to more efficient and safer tailings dam operations, setting a new standard for data management in the mining industry.

In the following sections, we detail our methodology, present our findings, and discuss the implications of AI adoption in tailings dam management, offering insights into the future of this critical field.

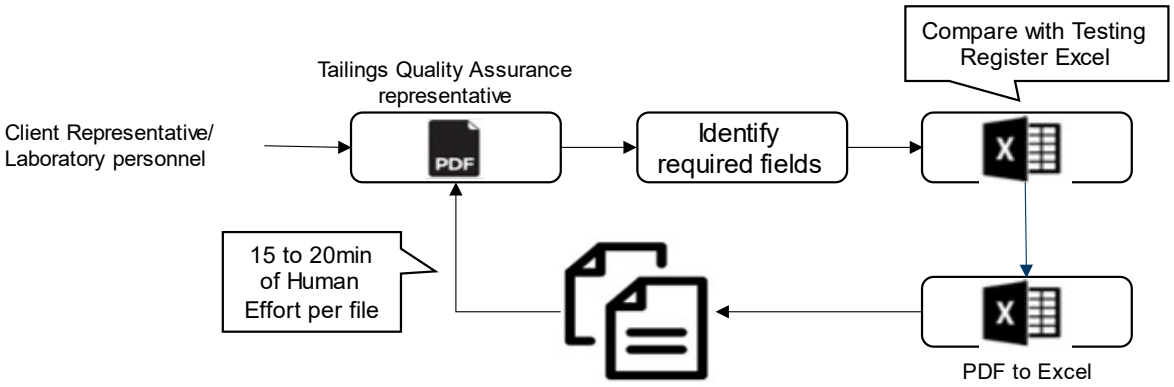
Methodology

Current process

The current process for managing quality control data involves several manual steps. Initially, data is extracted from PDF files, which requires significant human effort. Once the data is extracted, the next step involves identifying the required fields within the extracted data. This step is also performed manually and requires careful attention to detail to ensure that all necessary information is accurately captured.

After identifying the required fields, the data is manually compared with a Testing Register Excel file. This comparison is crucial for ensuring that the data meets the specified quality standards and technical

specifications. However, this manual process is time-consuming, typically taking between 15 to 20 minutes per file. The reliance on human effort introduces the potential for errors and inconsistencies, which can affect the overall quality assurance process.

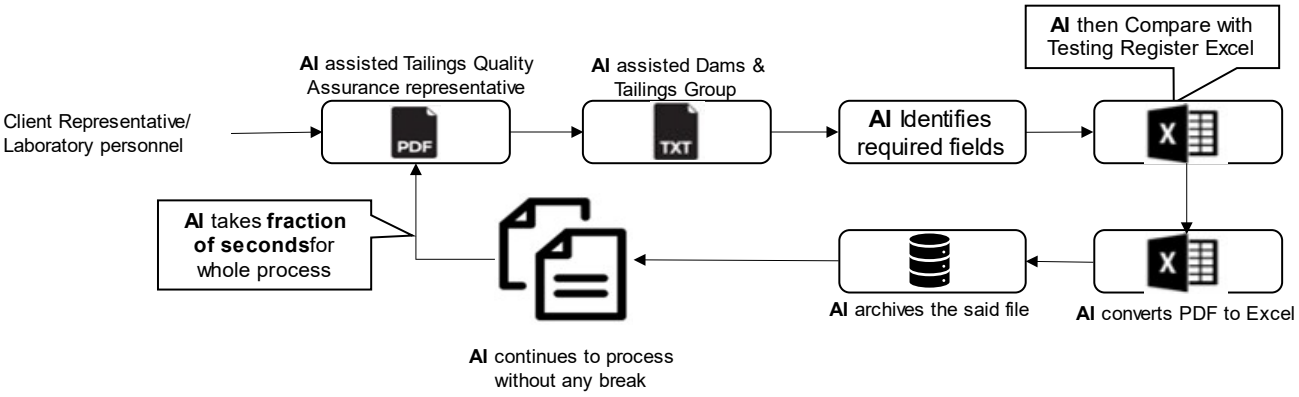


AI-assisted process

By contrast, the AI-assisted process significantly streamlines these tasks, leveraging advanced technologies to enhance efficiency and accuracy. The process still begins with handling PDF files, but from this point onward, AI takes over the tasks that were previously done manually.

AI automates the extraction and identification of required fields from the PDF data. This automation not only speeds up the process but also ensures a higher level of accuracy by minimizing the potential for human error. Following the identification of the required fields, AI then automatically compares these fields with the Testing Register Excel file. This comparison is done swiftly and accurately, further enhancing the reliability of the quality control process.

One of the most significant advantages of the AI-assisted process is the drastic reduction in time required. What used to take 15 to 20 minutes per file is now accomplished in a fraction of a second. This immense improvement in efficiency not only saves time but also allows for real-time communication and better compliance visibility. The enhanced speed and accuracy of data handling contribute to improved quality assurance standards, ensuring that construction compliance is maintained consistently.



The proposed AI-assisted system also integrates several key technologies to manage and analyze quality control data:

- **Data Collection and Integration:** Automated systems for data collection from various sources (electronic documents, paper scans) and in various formats (PDFs, Word documents, Excel sheets).
- **Data Processing and Analysis:** Machine learning algorithms to extract relevant data points, identify patterns, and detect anomalies. We used Computer Vision and an Optical Character Recognition approach to identify the relevant data to extract, analyze, and generate insights that would have been a manual task otherwise.
- **Visualization:** Advanced data visualization tools to present analyzed data in user-friendly formats, aiding in quick decision-making.

The system's efficacy was tested on multiple projects and multiple document formats, showing a drastic reduction in human effort from 45 minutes to 3 minutes per lot analysis.

Data and discussion

Our analysis involved a comprehensive evaluation of multiple tailings dam construction projects to assess the effectiveness of an AI-assisted approach in data management. By implementing AI technology in these projects, we were able to gather substantial data and insights that highlight several key findings:

- **Efficiency Gains:** One of the most remarkable outcomes of our study is the significant time savings achieved using AI in data processing and analysis. Traditional methods of handling quality control data in tailings dam construction are labor-intensive and time-consuming, often requiring 15 to 20 minutes per file. However, the AI-assisted process reduces this time to mere seconds. This dramatic reduction in processing time not only enhances operational efficiency but also frees up valuable human resources, allowing staff to focus on more strategic and complex tasks. The increased efficiency contributes to faster decision-making and project progression, ultimately leading to cost savings and improved project timelines.
- **Accuracy Improvement:** Accuracy in data management is crucial for maintaining high standards of quality control in tailings dam construction. Manual data entry and analysis are prone to human errors, which can compromise the reliability of the data and lead to potential compliance issues. Our analysis revealed that the AI-assisted approach significantly reduces errors in data entry and analysis. By automating these processes, AI ensures that data is consistently and accurately extracted, identified, and compared with the Testing Register files. This reduction in errors enhances the overall integrity of the data, leading to more reliable quality control outcomes and reducing the risk of non-compliance with technical specifications and regulatory requirements.
- **Real-Time Monitoring:** The implementation of AI also brings substantial improvements in real-

time data monitoring and anomaly detection capabilities. Traditional data management methods often involve delays in data processing and reporting, hindering the ability to detect and respond to anomalies promptly. With AI, data from various sources can be processed and analyzed in real time, providing immediate insights and alerts. This enhanced capability allows for active monitoring of tailings dam construction activities, enabling teams to identify and address potential issues before they escalate. Real-time monitoring not only improves the responsiveness to anomalies but also enhances overall project management and risk mitigation strategies.

The integration of AI into the data management processes of tailings dam construction projects demonstrates significant potential for transforming the industry. The efficiency gains achieved through AI-driven models led to faster and more streamlined operations, reducing the burden on human resources and improving project timelines. The marked improvement in data accuracy enhances the reliability and consistency of quality control, ensuring that all data meets stringent technical and regulatory standards.

The findings from our analysis emphasize various benefits of adopting AI technology in tailings dam construction. It is even more favorable where the mine waste is used as construction material. The significant improvements in efficiency, accuracy, and real-time monitoring capabilities highlight the transformative potential of AI in enhancing quality control and operational excellence. As the industry continues to evolve, the integration of AI-driven solutions will play a pivotal role in driving projects and ensuring the sustainable development of tailings dam infrastructure.

Results

The implementation of the AI-assisted approach yielded substantial improvements:

- **Time Efficiency:** Reduced processing times by over 90%.
- **Error Reduction:** Lowered the incidence of data entry errors by 80%.
- **Enhanced Communication:** Facilitated better communication among geographically dispersed teams through real-time data sharing.

Applications of AI in tailings dam management

Beyond quality control, AI has broad applications in tailings dam management, including:

- **Predictive Analytics:** Using historical data to predict potential issues and optimize resource allocation, AI will be able to determine the root cause of any non-compliance and trigger precautionary measures.
- **Safety Assessments:** Real-time monitoring and analysis to enhance safety protocols. For a fast-track construction, it will have the power to remove any detected deficiency for future work.

- **Proactive Decision-Making:** AI-driven insights to support strategic planning and risk mitigation.

These are some examples only. The opportunities to make tailings dams safer are unlimited.

Conclusion

The AI-assisted approach for tailings dam construction quality assurance offers significant advantages in efficiency, accuracy, and real-time monitoring. The broader application of AI in tailings dam management holds promise for transformative improvements in operational planning, safety, and decision-making. Future research should focus on expanding these capabilities and integrating them into standard practice.

Vale Base Metals Modernization of Instrumentation Monitoring System for Dam Safety at Canada Tailings Storage Facilities

Wing-Keat (Wayne) Wong, Tetra Tech, Canada
Greg Puro, Vale Base Metals, Canada
Lucas Lobato Ribeiro, Vale Base Metals, Canada

Abstract

The failure of the B1 Dam in the Córrego do Feijão Mine, in Brumadinho, Brazil, has underscored the need for Vale to further enhance dam safety through the modernization of instrumentation monitoring systems at tailings storage facilities. This endeavor resulted in the creation of an automatic real-time telemetry monitoring system, facilitating the connection and installation of approximately 400 existing and new instruments, alongside the design and installation of over 110 monitoring stations across seven Vale Base Metals (Vale) sites in Canada. This paper offers a case study showing the establishment of the real-time telemetry system, illustrating how the field dam monitoring instruments transmit the data to an online software platform. It discusses considerations pertinent to instrumentation data management, result output displays, and alert notifications aimed at monitoring both instrument health and dam stability to enhance safety. The project entailed collaboration with various stakeholders, including Vale Base Metals' dam safety management, IT security, communication teams, instrumentation vendors, installation contractors, dam Engineers of Records (EoRs), Responsible Tailings Facilities Engineers (RTFEs), and engineering consultants across Canada.

Each site's real-time monitoring system was engineered with radio and cellular wireless signals, enabling monitoring stations to intercommunicate and transmit monitoring data from remote tailings storage facilities to the central hub at the local site, before disseminating it beyond the mine site. An array of alert notifications for instrumentation and monitoring station health has been established to inform RTFEs of any disruptions, prompting on-site assessments. Collected field instrument data has been integrated into Vale's mine operation system utilizing OSISoft's PI System (PI), with instrumentation locations depicted on site aerial layouts and dam structure cross-sections within the PI program. Real-time monitoring data, in conjunction with historical data, is presented through graphical plots and values of site instrumentations.

Introduction

Modern technology has advanced recently with unprecedented speed, with the invention of smart phones, and cloud computing, and the advancements on fast computing microchips. Technological advances over the past 20 years have improved instrumentation capability and reduced costs. Therefore, most the mine operators worldwide have installed more advanced monitoring instruments system to improve dam safety as part of their Operation, Maintenance and Surveillance (OMS) programs. Despite technological advancements, most mine operators still manually execute their dam instrumentation monitoring programs. The adoption of real-time instrumentation data collection systems with wireless data transmission for a remote telemetry dam monitoring has been relatively slow.

The failure of the B1 Dam in Brumadinho, Brazil, has underscored the imperative for Vale to further enhance dam safety programs through modernization of instrumentation monitoring systems at Tailings Storage Facilities (TSF). This initiative was applied globally by Vale and included all of Vale Base Metals' TSFs in Canada. The key objectives of the initiatives that were established by the Vale Base Metals' Dam Safety Group were to improve dam monitoring data collection practices, to enhance the visibility of dam status, and to implement an early warning system; while at the same time, modernizing and standardizing the monitoring system.

Modernization of instrumentation monitoring system

The modernization of the instrumentation monitoring system commenced in 2019 with the establishment of a framework for a preferred dam monitoring system and the formulation of design criteria. A comprehensive technology review and market study were conducted to evaluate potential systems and product options aimed at selecting a more reliable and robust system applicable across all mine sites in Canada. Another project goal was to standardize and unify the instrumentation monitoring platform for the dam safety program. Following the study's completion, a fully automated and self-sustaining data collection system was developed, designed to accommodate additional instruments easily and capable of operating on existing electrical power and communication networks.

The monitoring system was required to have lightning protection to protect the integrity of the instruments and its dataloggers. Due to the critical nature of dam instrumentation monitoring for dam safety, each component and function involved in instrumentation data collection, storage, communication paths, and data outputs includes redundancy measures. These measures ensure backup options, both primary and secondary, in case of failures at the primary option. Figure 1 illustrates the concept of field data collection and its wired and wireless communications from the field to the network server, further delivering instrumentation data to end users.

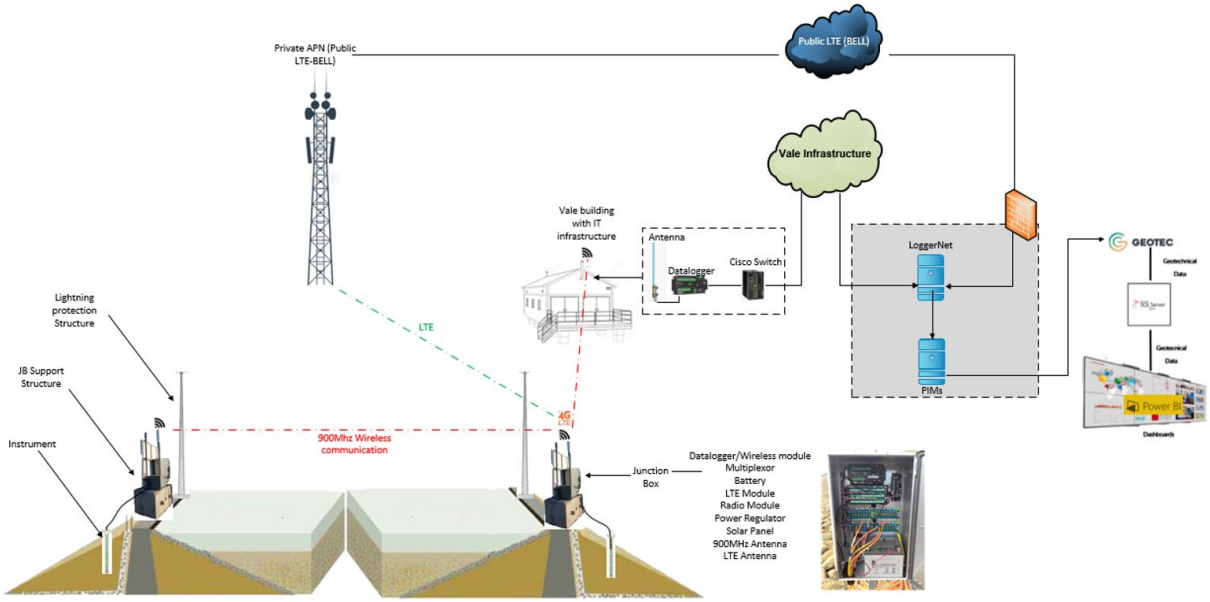


Figure 1: Conceptual diagram of the instrumentation data communication network

Based on the communication and design concepts selected by Vale, the instrumentation telemetry system was developed to consist of field monitoring stations connecting nearby instruments embedded in the dams. Each monitoring station location includes approximately 5-meter-high Junction Box Structures (JBS) and approximately 8-meter-high Lightning Protection Structures (LPS), as shown in Figure 2. These structures were erected on granular foundation pads to ensure stability and visibility.

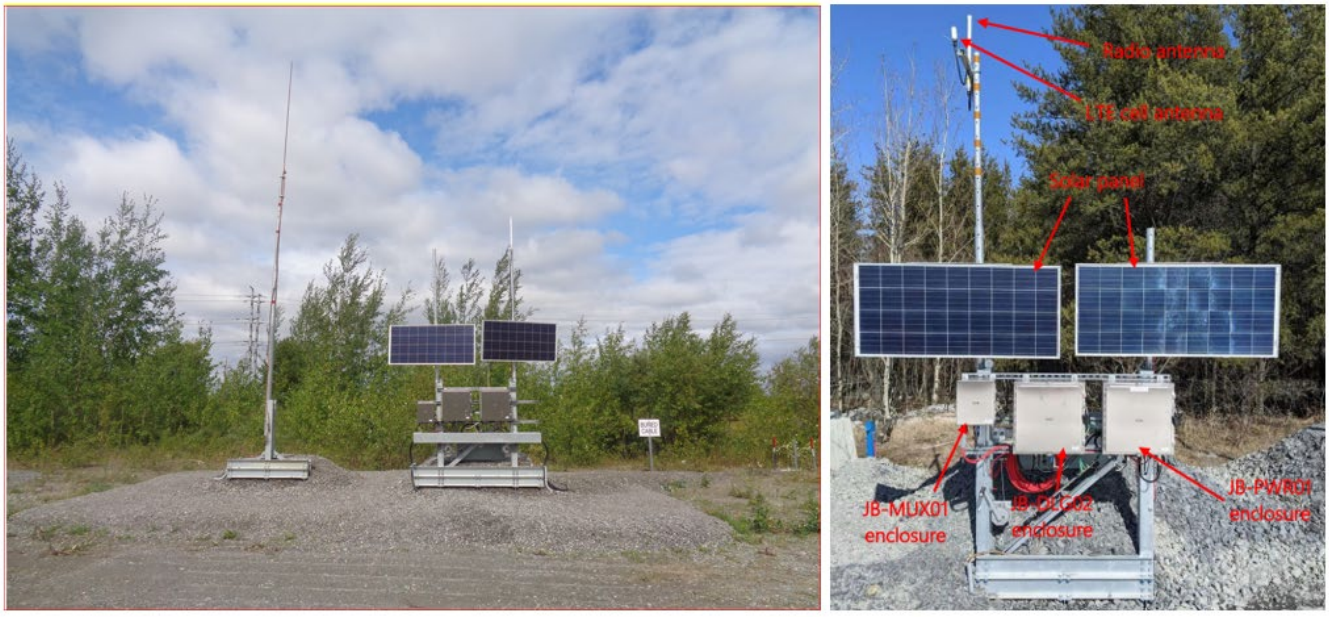


Figure 2: Typical instrumentation monitoring station with Lightning Protection Structure (LPS) on the left and Junction Box Structure (JBS) on the right

The JBS typically includes a radio antenna to establish a wireless communication network with nearby monitoring stations, featuring designated primary and secondary communication paths. Selected monitoring stations within each dam area group also house an LTE cell antenna at the top of the JBS pole. This setup enables transmission of instrumentation data from the field to the mine plant server via LTE cellular towers, as depicted in Figure 1. In case of communication challenges at the primary station, the system automatically switches to a secondary monitoring station to transmit field monitoring data. The front rack of the JBS accommodates two to four enclosures for instrumentation cable connections, power control and distribution, data storage, and wireless communication components.

The LPS is a galvanized metal structure with extendable tele-masts, topped with a 1.5-meter-high copper lightning rod, creating a total height of 8 meters. The LPS height is designed to provide an umbrella of protection against lightning strikes, safeguarding connected instruments across the station. The project established minimum safe distances from the LPS to the JBS, buried routed cables, instruments, associated grounding rods, and established maximum distances to ensure effective lightning protection. Ground resistivity requirements for the number of grounding rods were specified and confirmed on site post-installation.

Implementation of the modernization system on site

Implementing the telemetry system to connect all field instruments necessitated a comprehensive understanding of the quantity, quality, type, location, and identity of existing site instruments. Additionally, various new instruments were designed and installed on site. By project completion, over 400 dam monitoring instruments were interconnected, with 110 monitoring stations erected across all seven mine sites in Canada.

The feasibility and constraints of cable trenching, routes, burial methods on dam crests and slopes, and the positioning of monitoring stations, including the load on granular foundation pads, were evaluated on site in collaboration with local stakeholders. These findings were subsequently submitted to the EoR of each tailings storage facility for approval. During site visits, assessments were also made regarding the availability of power sources, such as nearby 120 VAC electrical cable lines, or the necessity for solar panels to power monitoring stations in remote locations.

Preliminary tests were conducted to assess the availability and LTE signal strength at each dam structure. This is crucial for establishing wireless communication and data transmission paths at each dam location. Figure 3 illustrates a sample of cable routing and monitoring station locations at one of the tailings storage facilities.

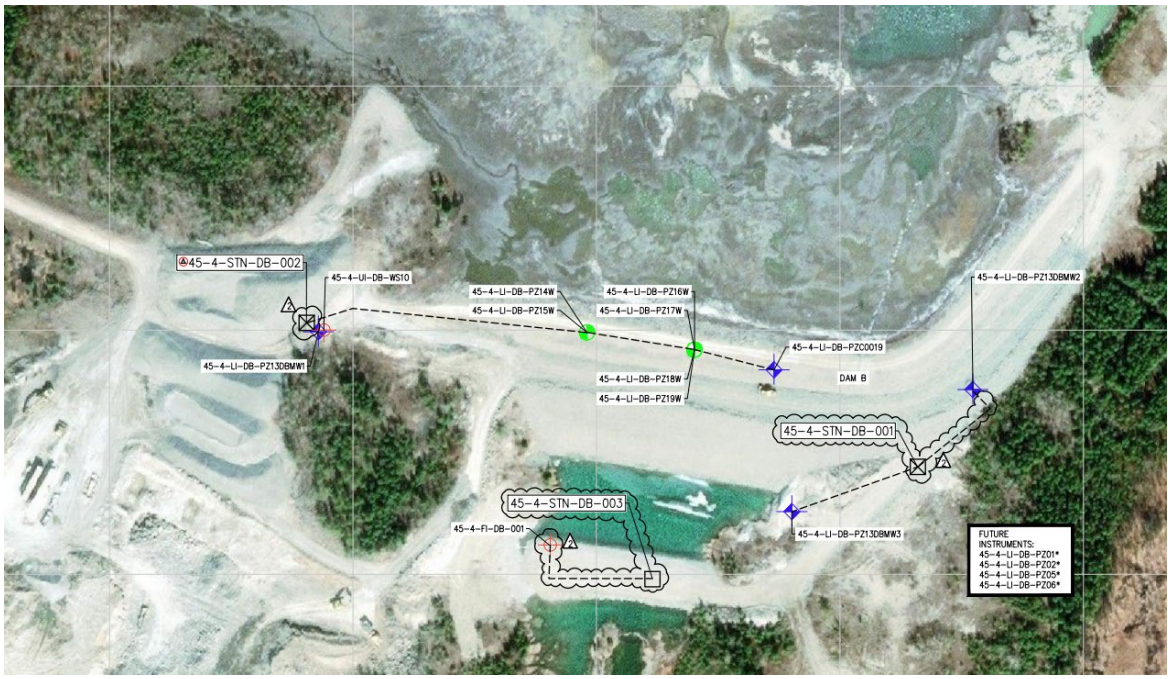


Figure 3: Sample instrumentation cable routing and monitoring station (STN) locations at a tailings storage facility

Types of dam monitoring instruments

As previously mentioned, over 400 dam monitoring instruments have been integrated into the monitoring stations. These instruments comprise both existing ones from the sites and new installations during the construction of the monitoring stations. The types of instruments deployed include:

1. Vibrating wire piezometers
2. Radar water level sensors
3. Laser water level sensors
4. Vented pressure level sensor
5. Shape Arrays (SAA)
6. Vibration sensors (geophones)
7. Weather stations
8. Temperature and humidity sensors

Site instruments vary in shape and condition. Therefore, instrument condition assessment and calibration are essential to confirm instrumentation measurement accuracy for the project. Calibration of the instruments was conducted on-site, encompassing existing accessible instruments (not grouted) as well as all newly installed instruments for the project. Figure 4 illustrates typical site instruments.



Figure 4: Sample site instruments

Instrumentation data management using OSISoft PI System

Instrumentation data management and dashboard monitoring displays are crucial components for the new automated monitoring system. All raw data from field instruments is collected within a centralized program platform. This raw data undergoes extraction by the OSIsoft PI (PI) program for further processing and calculations. Processed data is then stored and presented in PI, enabling end users to remotely review real-time measurements collected on-site, thus facilitating assessment of dam structure conditions.

Early in the project, all instrument data underwent comprehensive review and calibration to validate calculation accuracy. Throughout the project lifecycle, Vale Base Metals' IT team collaborated with local RTFEs and EoRs, as well as the Dam Safety Group and other stakeholders, to develop user-friendly output

interfaces within the PI program. These interfaces include features such as presenting aerial plan views of dam structures and the relative positions of instruments, illustrated in Figure 5.

The system continuously monitors instrumentation data collection and communication health conditions. Various health categories are rated to provide stakeholders with insights into the continuous and uninterrupted collection and reporting of data from each specific instrument. In cases of interruptions, the system evaluates the duration and frequency, thereby assessing the reliability of site instruments and overall monitoring station performance. Figure 6 displays a cross-section view detailing the depths and positions of installed instrumentation sensors, along with real-time site measurement values.

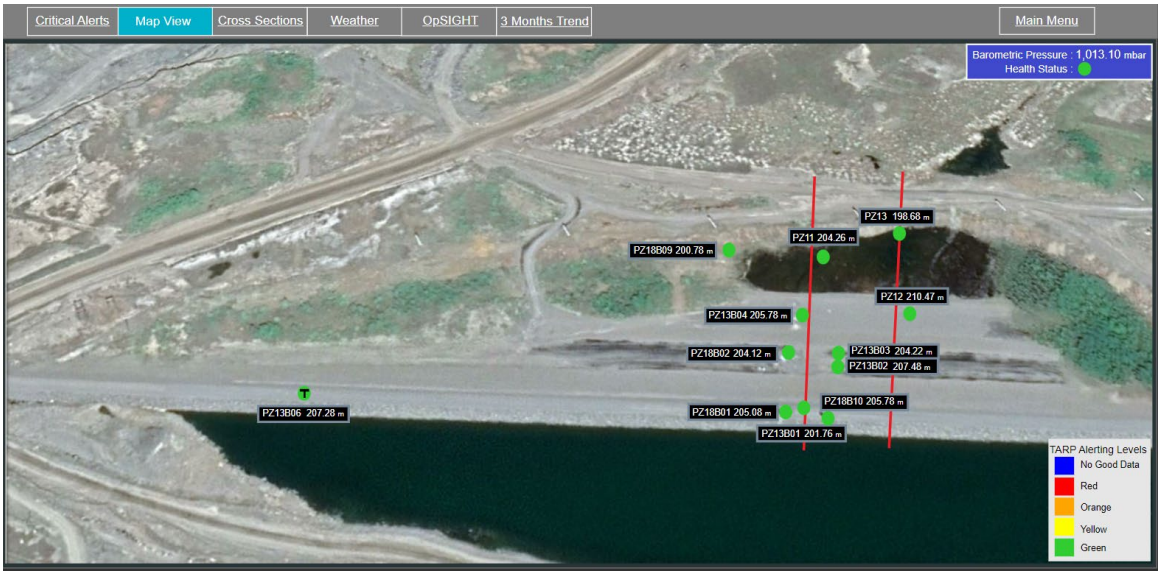


Figure 5: Plan view of site instruments on dam structure in PI

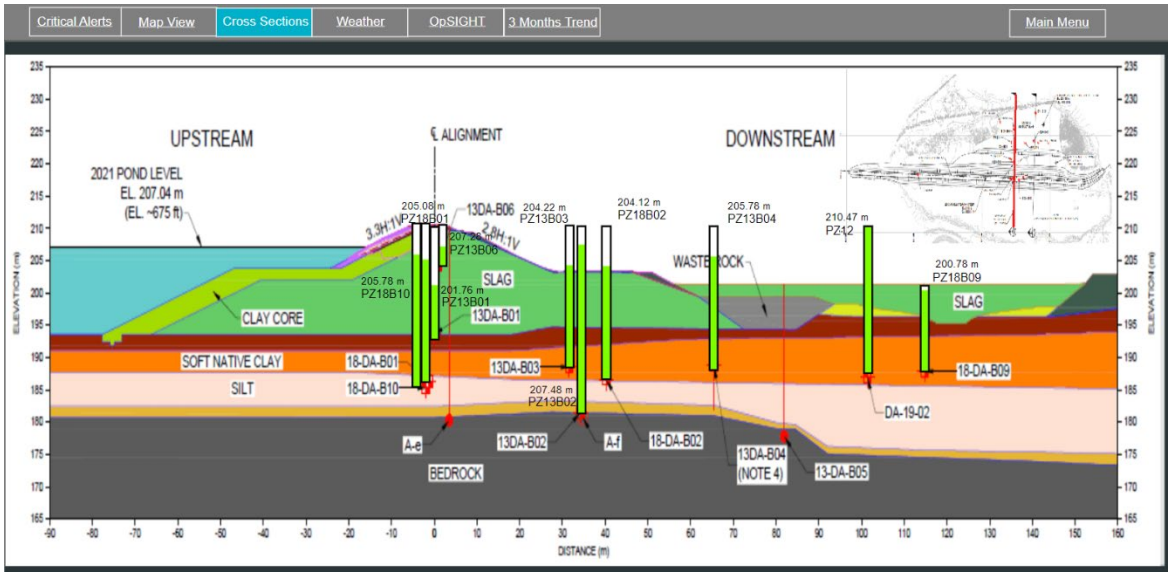


Figure 6: Cross-section view of the site instruments in PI

Monitoring the health conditions of instruments and monitoring stations provides a unique and valuable feature enabling stakeholders to promptly identify potential issues. Health alert notifications have been established to cover various instrument conditions, including:

- Instruments not reporting data or experiencing stale data issues.
- Monitoring station conditions such as temperature and humidity measurements within enclosures, wireless communication signal strength, solar panel charges, and battery voltage levels.

Details of the health measurement interface are shown in Figure 7.

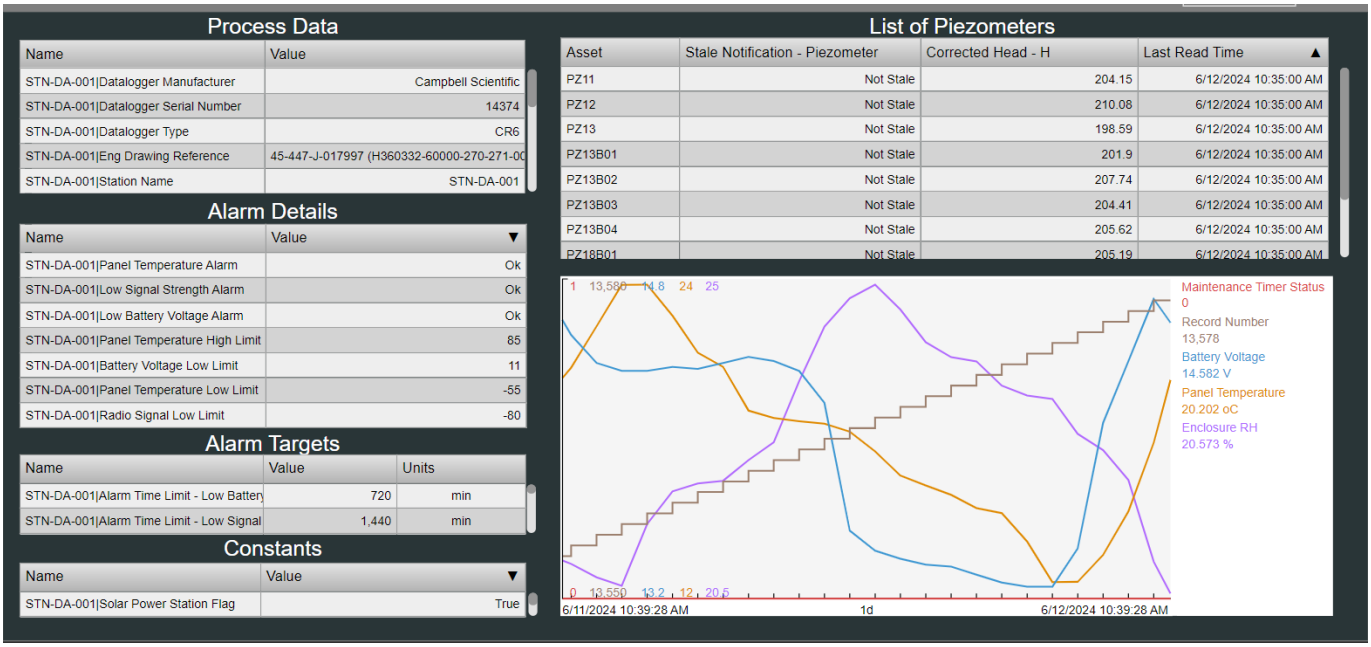


Figure 7: Instruments and monitoring station health condition measurement interface

In addition to health condition monitoring and associated alert notifications, thresholds for allowable instrumentation measurement values have been set for each dam structure. When field measurements approach these thresholds, email notifications are triggered to inform RTFEs and other critical stakeholders. Sample instrumentation measurements and their threshold alert or alarm configurations are presented in Figure 8.

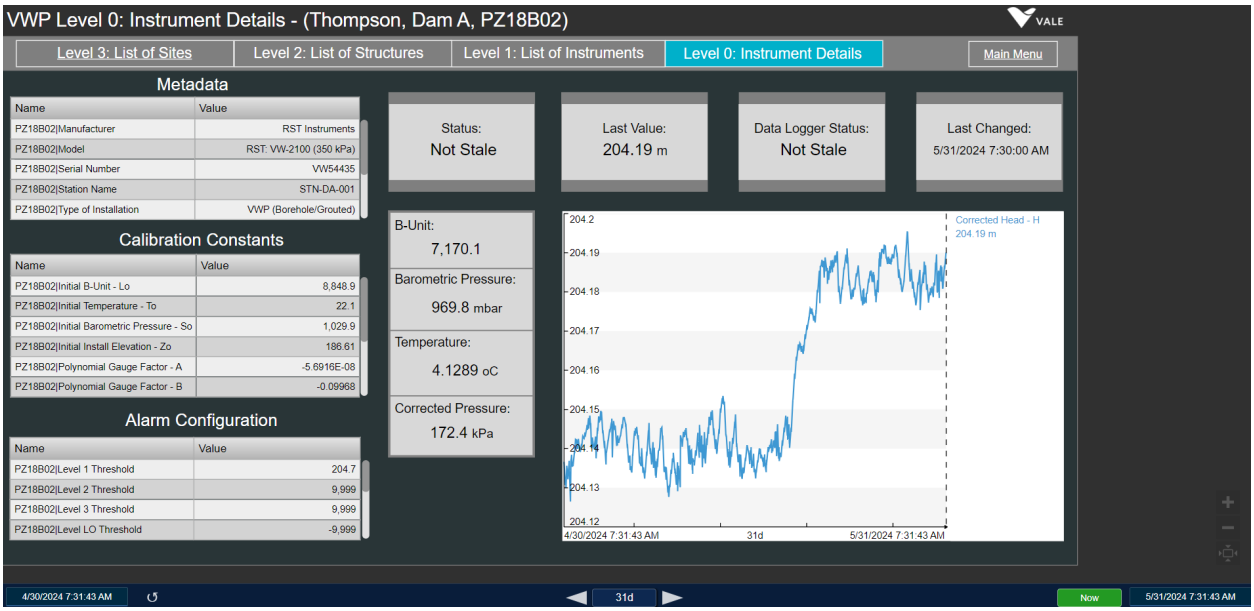


Figure 8: Instrument measurement details and alarm configuration

Conclusion

The Tailings Storage Facilities Monitoring Systems (TSFMS) Project aimed to establish a fully automated data collection system for geotechnical sensors in remote environments. Upon completion of this project, several significant benefits had been realized through enhanced data collection practices:

- Digitization of data: the project successfully transitioned to digital data collection, improving accessibility and data management efficiency.
- Increased resolution and frequency of data samples: by automating data collection, the system achieved higher data resolution and frequency, providing more detailed insights into dam conditions.
- Standardization across Vale Base Metals: the implementation standardized monitoring practices across all business units, enhancing consistency and reliability in dam safety monitoring.
- Visibility and situational awareness: stakeholders gained improved visibility and situational awareness of dam conditions, facilitating proactive decision-making and risk management.

The project successfully achieved its objective of automating instrumentation data collection, enabling authorized users to remotely access dam monitoring data. As a result, the instrumentation monitoring system for dam safety has been modernized across all seven sites in Canada.

Acknowledgements

We extend our sincere thanks to all Vale Base Metals stakeholders who worked tirelessly to ensure the

success of the project aimed at enhancing the dam safety program. The substantial investment made by Vale Base Metals to achieve the project goals is greatly appreciated and deserves recognition within the mining industry.

Assessing SAR, InSAR and Multispectral Optical Data for Mapping Supernatant Pond Evolution

Élyse Gaudreau, TRE Altamira Inc., Canada
Ajinkya Koleshwar, TRE Altamira Inc., Canada
Kenny Yue, TRE Altamira Inc., Canada
Pablo Blanco, TRE Altamira Inc., Spain
Riccardo Tortini, TRE Altamira Inc., Canada
Giacomo Falorni, TRE Altamira Inc., Canada

Abstract

The effective management of mine Tailings Storage Facilities (TSF) is a high priority for mine operators, communities, and governments to mitigate the risks associated with water contamination, pollution, and dam failures. The Global Industry Standard on Tailings Management (GISTM) guidelines identify TSF water management as a key requirement for the safety of mining operations. Commonly used methods for monitoring the location and spatial extent of surficial moisture and supernatant ponding within TSFs include the use of multispectral optical satellite imagery. This application requires high accuracy in identifying small water bodies and frequent updates due to the high dynamicity of mining operations; however, freely accessible imagery from Sentinel-2 and Landsat satellites have a pixel resolution of 10 to 20 m and 30 m, respectively, and the temporal coverage can be affected by the presence of cloud cover, illumination differences, and terrain shadow. These limitations can be overcome using high-resolution Synthetic Aperture Radar (SAR) amplitude satellite data, as SAR signals can penetrate cloud cover.

In this study, machine learning techniques are used to characterize TSF saturation changes by combining both Sentinel-2 optical images and high-resolution (3 m) TerraSAR-X SAR data. This study investigates (i) the differences between the supernatant pond areas classified using multiple satellite data sources (SAR amplitude and multispectral optical imagery), (ii) the factors driving the accuracy of SAR water maps in TSF impoundments, and (iii) developing guidelines for the combined use of optical, SAR, and InSAR data for TSF water mapping.

Mapping TSF supernatant water bodies solely with Synthetic Aperture Radar (SAR) data presents major challenges since fully saturated sediments or slurry often appear indistinguishable from water bodies in SAR amplitude data. However, we find that optical, SAR, and InSAR data complement each other well for water body mapping and provide a substantial improvement over the use of each input individually.

High-resolution SAR can provide detailed water body maps over time and space, and when available, cloud- and shadow-free multispectral water indices are reliable indicators of surface water to use as refinement and validation.

Introduction

Mine tailings are the finely ground residuals, including heavy metals and toxins, that remain after the mill process has removed the valuable metals from the ore. Tailings are typically stored permanently in tailings storage facilities (TSFs), ground impoundments retained by dams. The effective management of TSF supernatant ponds (that form due to process and pumped water and natural precipitation) is critical for mine operators, the environment, and communities that would be affected by a dam failure. Different tailings dam databases (ICOLD, WISE, World Mine Tailings Failures, CSP) indicate that, since 1915, a total of 257 failures have been recorded with circa 2,650 fatalities and 250 Mm^3 of contaminated residues released to the environment (Piciullo et al., 2022). As attested to by the different analyses and investigations, the control of water stored inside the TSF reservoir area is a critical issue (Cacciuttolo and Cano, 2023). The Global Industry Standard on Tailings Management (GISTM) guidelines, published in August 2020, also identifies TSF water management as one of the main requirements for the safety of mining operations. In this framework, TSF supernatant pond maps can be effective operational tools for mine operators to identify unexpected or unpredicted behaviors that may contribute to embankment failure.

Remote sensing methods provide cost-effective ways of monitoring water bodies and the saturation levels of tailings facilities over large areas (e.g., Koleshwar et al., 2023), particularly with freely available datasets such as the European Space Agency's Sentinel-1 Synthetic Aperture Radar (SAR) satellite and the Sentinel-2 satellites' multispectral (MS) sensors, as well as the National Aeronautics and Space Administration and United States Geological Survey's MS Landsat sensor. These platforms image most of the surface of the Earth at regular intervals, providing up-to-date data without the need for in-situ measurements or instrumentation.

SAR satellites are active, meaning they emit radar pulses and detect the energy backscattered off the ground. The amplitude of the measured signal represents the fraction of the emitted signal that is reflected in the direction of the satellite and can be used to identify features on the ground. The phase of the returning signal is a function of the distance travelled, and by combining the phase data of successive acquisitions, Interferometric SAR (InSAR) can be used to map ground displacements at a precision on the order of millimeters (Ferretti et al., 2011; Ferretti, 2014). In contrast, MS sensors are passive, and measure the radiation emitted by the sun that reflects off the Earth's surface in the direction of the satellite. While SAR platforms emit and detect a specific wavelength of the electromagnetic spectrum, MS sensors detect a stack

of images with each acquisition, each representing the total reflected energy within a specific band of the electromagnetic spectrum.

The most well-established remote sensing methods of mapping of water bodies and saturation levels use MS data, as different bands of the electromagnetic spectrum have different reflective properties over various types of material such as water, dry soil and vegetation, allowing for land cover classification (e.g., Townshend et al., 1991). These methods include the use of water and moisture indices such as normalized difference water index (NDWI), modified normalized difference water index (MNDWI) and normalized difference moisture index (NDMI) (e.g., Gao, 1996; Xu, 2006; Acharya et al., 2018). For example, the NDWI exploits the contrast in reflectance values of green (500 – 600 nm wavelength) and near-infrared (700 – 1,400 nm wavelength) radiation over water bodies and dry material. One of the main limitations of MS sensors is that electromagnetic radiation at these wavelengths does not penetrate through cloud cover, which can result in lengthy and/or regular temporal data gaps in certain parts of the world. However, SAR satellites operate at wavelengths that are capable of imaging the Earth's surface in any weather, as well as at night.

In this study, we explore the feasibility of using SAR amplitude data to monitor the extent of supernatant ponds using a machine learning (ML; using k-means clustering) and Deep Learning (DL; with a convolutional neural network; CNN) approaches, as this greatly expands the number of datasets available for remotely monitoring supernatant ponds within TSFs. We apply these algorithms to four anonymized TSFs located in a drought-prone area. Two TSFs (referred to as TSF1 and TSF2) are constructed with an upstream raised method, and two are integrated waste landforms (IWL1 and IWL2). The primary TSFs are purposed for storing waste material produced during mining operations, whereas the IWLs are used for both waste storage and controlled seepage recovery of return water from the primary TSFs to reduce the amount of fresh water required from external sources.

The results obtained using a preliminary CNN algorithm show that SAR imagery can successfully identify combined wet beach and ponding areas. The results also reveal different SAR reflectance behaviors over different TSF materials, providing clear directions for further refinement of the algorithm. Additionally, we demonstrate the compatibility of TSF ponding and saturation mapping and InSAR displacement measurements for monitoring and understanding the relationship between TSF activity and embankment stability.

Data and methods

SAR water body mapping

In this study, supernatant ponds within TSFs are mapped using SAR data from different satellite missions with different polarizations, wavelengths, spatial and temporal resolutions. The polarization refers to the

plane in which the electromagnetic wave of the SAR sensor oscillates (vertical or horizontal). Targets imaged on the ground can have different polarimetric properties which may affect the results of a SAR-based water mapping approach (Brisco et al., 2011). The first dataset is the freely available C-band (5.6-cm wavelength) Sentinel-1 data in the VV polarization (i.e., both emitted and return signal are vertically polarized) from the European Space Agency. Its ground resolution is 20 m × 5 m, and the revisit period is 12 days. The second dataset was also acquired by the Sentinel-1 satellite, but in the VH polarization (i.e., the emitted signal is vertically polarized, and the return signal is horizontally polarized). The third dataset is obtained from the TerraSAR-X satellite constellation in the HH polarization (i.e., both emitted and return signal are horizontally polarized). These are commercial X-band data (3.1-cm wavelength), have a ground resolution of 3 m × 3 m and a revisit period of 11 days. The acquisition period for each dataset is listed in Table 1.

Table 1: Datasets used in this study. ML label refers to dataset used for machine learning-based water mapping. InSAR label refers to dataset used for multi-temporal InSAR analysis

Constellation	Sensor	Wavelength	Resolution (m)	Revisit Period (days)	Geometry	Analysis Period
Sentinel-1	SAR	5.6 cm	20 × 5	12	Descending	2018-12-15 to 2024-02-18 (ML) 2021-01-09 to 2024-02-23 (InSAR)
TerraSAR-X	SAR	3.1 cm	3 × 3	11	Ascending	2018-10-30 to 2023-10-19 (ML) 2021-01-10 to 2024-02-28 (InSAR)
Sentinel-2	MS	543 – 578 nm, 785 – 900 nm, 1,565 – 1,655 nm	10 × 10, 10 × 10, 20 × 20	5	Descending	2018-12-14 to 2024-02-16

The SAR data are first pre-processed (i.e., co-registered, amplitude calibrated/normalized), and a Deep Learning speckle filter is applied to reduce noise (*cfr.* Lattari et al., 2019). Two ML water classification algorithms are then used: (i) a statistical approach using K-means clustering and the Sobel operator (Kanopoulos et al., 1988) to define the location and outline of the pond areas, and (ii) a Convolutional Neural Network (CNN) trained on waterbodies such as lakes and rivers using Sentinel-1 data in the VV polarization and MS images. The CNN uses unfiltered SAR data to increase the spatial resolution of the water classification result. While the differences between the backscattering properties of lakes and TSFs are substantial, the results of the CNN algorithm are expected to provide preliminary insights on the use of SAR for TSF water body mapping and help determine directions to refine a CNN specifically tailored to TSFs. A block diagram of the water classification algorithms is shown in Figure 1A. The output is a

raster map of the probability that a pixel is water. A binary map is then created, in which pixels with a probability greater than 0.9 are classified as water.

The results of the SAR water mapping algorithms are validated using the NDWI derived from the green and near-infrared bands of the Sentinel-2 constellation (Table 1). Therefore, we only process SAR images acquired within 1 day of a cloud-free Sentinel-2 acquisition. The NDWI can range from -1 (i.e., dry ground) to 1 (i.e., water) where there is a short transition between dry ground and supernatant ponding near 0 (Gao, 1996). NDWI water classification was performed using two methods: one with a dynamic threshold selected using k-means clustering, and the other where all pixels with an index value greater than 0.3 are selected (Figure 1B). The latter threshold was selected using the statistical distribution of indices in this dataset and a visual check of true color imagery derived from Sentinel-2 data.

Since SAR amplitude data can have similar backscatter behavior over shallow water and saturated material, we classify pixels corresponding to saturated tailings (moisture levels between dry and standing water) using MNDWI, which uses the green and shortwave infrared bands (central wavelength: 1,610 nm) and also ranges from -1 to 1 for dry ground and water, respectively. Its transition zone from dry ground through wet material to water is wider than with NDWI, therefore its water threshold is typically higher and it can better detect beach wetness. We classify MNDWI index values between 0.1 and 0.6 as saturated material and values greater than 0.6 as supernatant pond based on the statistical distribution of indices in this dataset and a qualitative visual assessment of Sentinel-2 true color imagery).

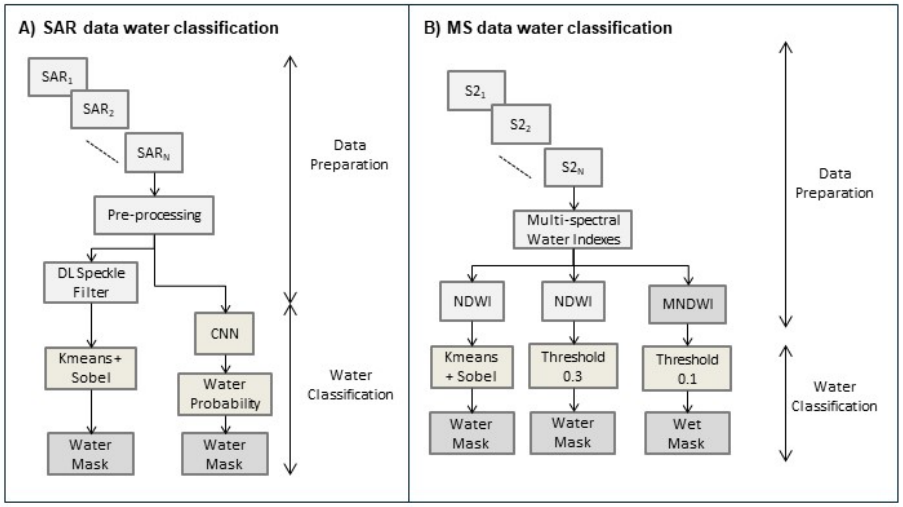


Figure 1: Water classification block diagrams. DL = Deep Learning

Multi-temporal InSAR

Multi-temporal InSAR is a commonly used method for monitoring the stability of TSF embankments. It involves processing dozens to hundreds of SAR phase data acquisitions to extract time series of gradual, millimeter-scale displacements. We use TRE Altamira's proprietary SqueeSAR algorithm to find and follow

natural reflectors on the ground that are statistically reliable throughout the analysis period (Ferretti et al., 2011; Ferretti, 2014). InSAR detects displacements along the satellite line-of-sight (LOS) vector, which "looks" to the right of the satellite's roughly north-south-oriented path. When travelling from south to north (referred to as the "ascending" geometry), the satellite is east-looking. Conversely, when travelling from north to south ("descending" geometry) the satellite is west-looking. We estimate the vertical and east-west components of displacement by decomposing the ascending and descending vectors of displacement occurring at approximately the same time and location.

Results and discussion

Tailings storage facility supernatant pond mapping with synthetic aperture radar

In this section we use the pixels classified as water using NDWI as the reference for the ponding areas. Figures 2a, 2c, 2e and 2g show the time series of the area that was classified as standing water using area within TSF1 and TSF2. The % area within the TSF that has a MNDWI greater than 0.1 (including saturated tailings and ponding areas) is also shown. Figures 3a, 3c, 3e and 3g show the time series of the % area that was classified as standing water using NDWI, saturated material using MNDWI, and the ML statistical (k-means/Sobel) and CNN SAR algorithms, as a percentage of the total TSF and water (ponding) using MNDWI, and the ML statistical (k-means/Sobel) and CNN SAR algorithms, within IWL1 and IWL2, respectively. Some observations are common to all four TSFs: firstly, hardly any pixels of the Sentinel-1 VH-polarized data were classified by the CNN as having a probability of being water greater than 0.9 leading to the % area being 0 or near 0 throughout. We therefore show, for the VH-polarized data only, the % area of pixels with a probability of being water greater than 0.7, and we refer to this dataset for the remainder of the section.

In general, the area classified as water using SAR tends to be greater than the pond area mapped using NDWI. The statistical Sentinel-1 results in the VV polarization are slightly lower and similar to the combined area of saturated material and ponds as mapped by MNDWI, compared to the results from the Sentinel-1 VH polarization and the TerraSAR-X results (HH polarization; Figures 2a, 2e, Figures 3a, 3e). The difference between the VV polarization results and the other two datasets is greater when using the CNN. Furthermore, there are many data acquisitions where the CNN failed to identify any water or saturated material in the VH polarization only. Within TSF1 and TSF2, the statistical and CNN approaches were successful in identifying dry material in the absence of moisture using the VV and HH polarizations (Figure 2a, 2c, 2e, 2g). Starting in September 2022, many dry pixels in TSF1 and TSF2 were identified as water by the statistical and CNN approaches using the VH-polarized data. This is not the case for IWL1 and IWL2, where all datasets were successful at identifying dry pixels in the absence of moisture throughout the

analysis period (Figure 3a, 3c, 3e, 3g). Figure 4 shows an example of the areas classified as water by the different algorithms.

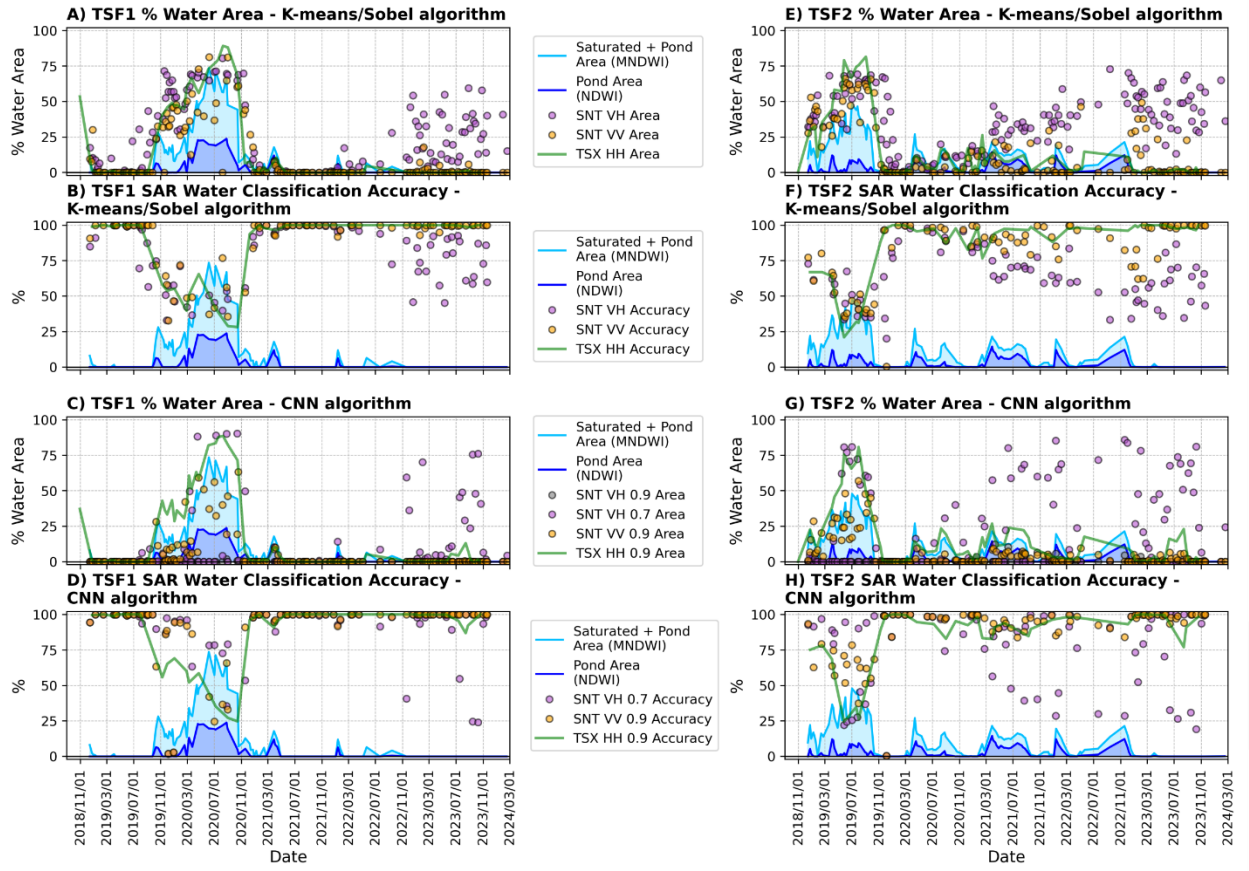


Figure 2: Time series of percentage of tailings storage facility (TSF) area mapped as water using SAR machine learning algorithms and their accuracy. Percentage area of pond and saturated material as measured using normalized difference water indices are shown in each plot as a reference. A-D: TSF1 results. E-H: TSF2 results

The accuracy of the ML algorithms is calculated using a pixel-by-pixel comparison of the SAR and NDWI water masks, with the latter used as the reference for water vs. dry material. Binary SAR water masks are resampled to the same grid as the NDWI masks, and pixels are classified as (i) true positives (TP): SAR and corresponding NDWI pixel are classified as water; (ii) true negatives (TN): SAR and corresponding NDWI pixel are classified as dry; (iii) false positives (FP): SAR pixel classified as water and corresponding NDWI pixel classified as dry; (iv) false negatives (FN): SAR pixel classified as dry and NDWI pixel classified as water. Accuracy is calculated using the following equation:

$$\frac{TP + TN}{TP + TN + FP + FN}$$

Time series of the accuracy of the statistical and CNN SAR water masks for TSF1 and TSF2 are shown in Figures 2b, 2d, 2f and 2h. The accuracy of the statistical water mask is comparable between input

datasets, with high accuracy during dry periods and lower accuracy when there is significant coverage of saturated material, except starting in September 2022 when the Sentinel-1 VH data starts identifying many false positives. The statistical and CNN results are comparable, however in some instances the CNN performs better (e.g. between 11/2019 and 03/2020; Figures 2b and 2d). Note that the higher accuracy of Sentinel-1 VH data during periods with extensive saturation is misleading and is due to the algorithm failing to classify any (or hardly any) pixels as water, resulting in no true positives but still numerous true negatives.

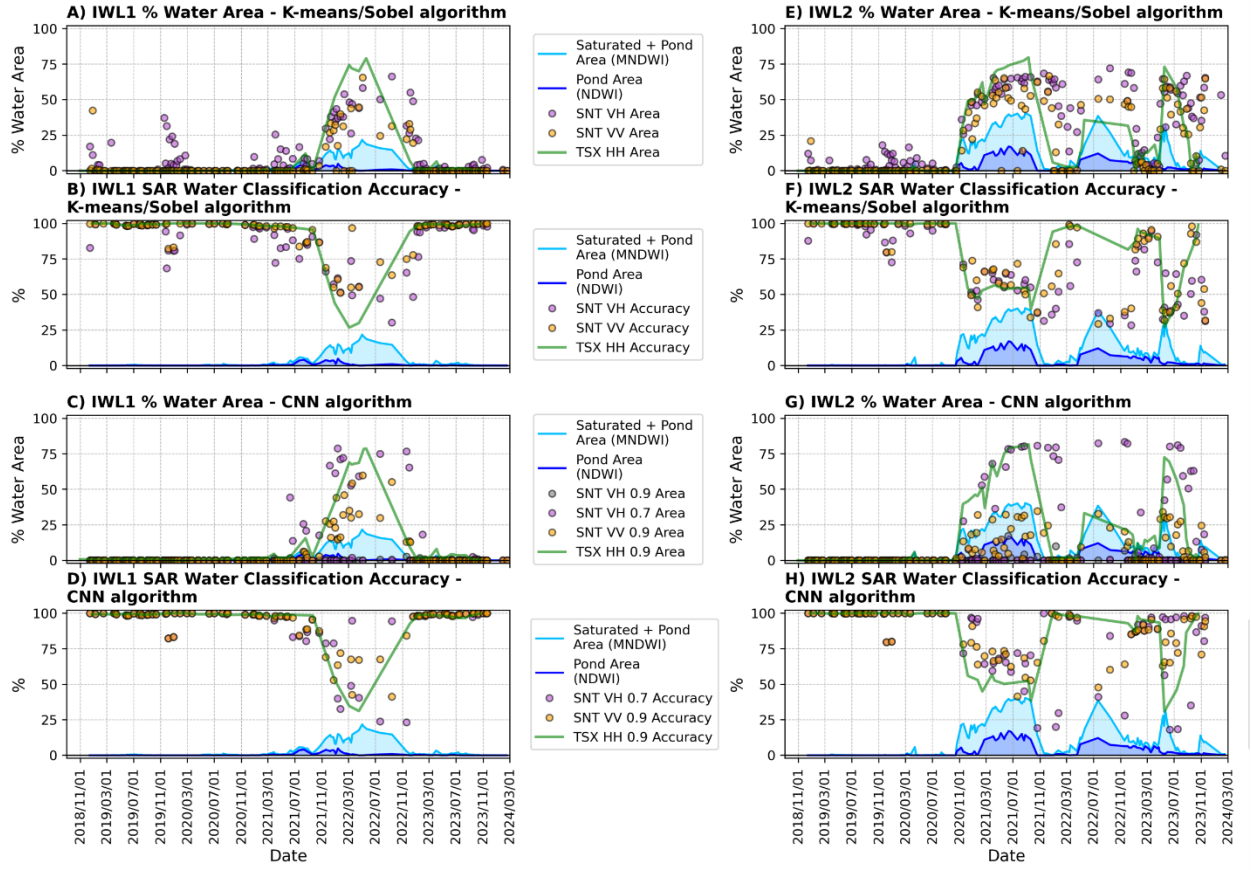


Figure 3: Time series of percentage of integrated waste landform (IWL) area mapped as water using SAR machine learning algorithms and their accuracy. Percentage area of pond and saturated material as measured using normalized difference water indices are shown in each plot as a reference. A-D: IWL1 results. E-H: IWL2 results

Time series of the accuracy of the statistical and CNN SAR water masks for IWL1 and IWL2 are shown in Figures 3b, 3d, 3f and 3h. In general, Sentinel-1 VV results (0.9 probability threshold) are slightly more accurate than Sentinel-1 VH polarization results (0.7 probability threshold), which in turn are slightly more accurate than TerraSAR-X HH polarization results (0.9 probability threshold). Similarly to TSF1 and TSF2, there is a higher accuracy for all datasets during dry periods and lower accuracy when there is a significant amount of ponding and/or saturated material as identified by NDWI and MNDWI.

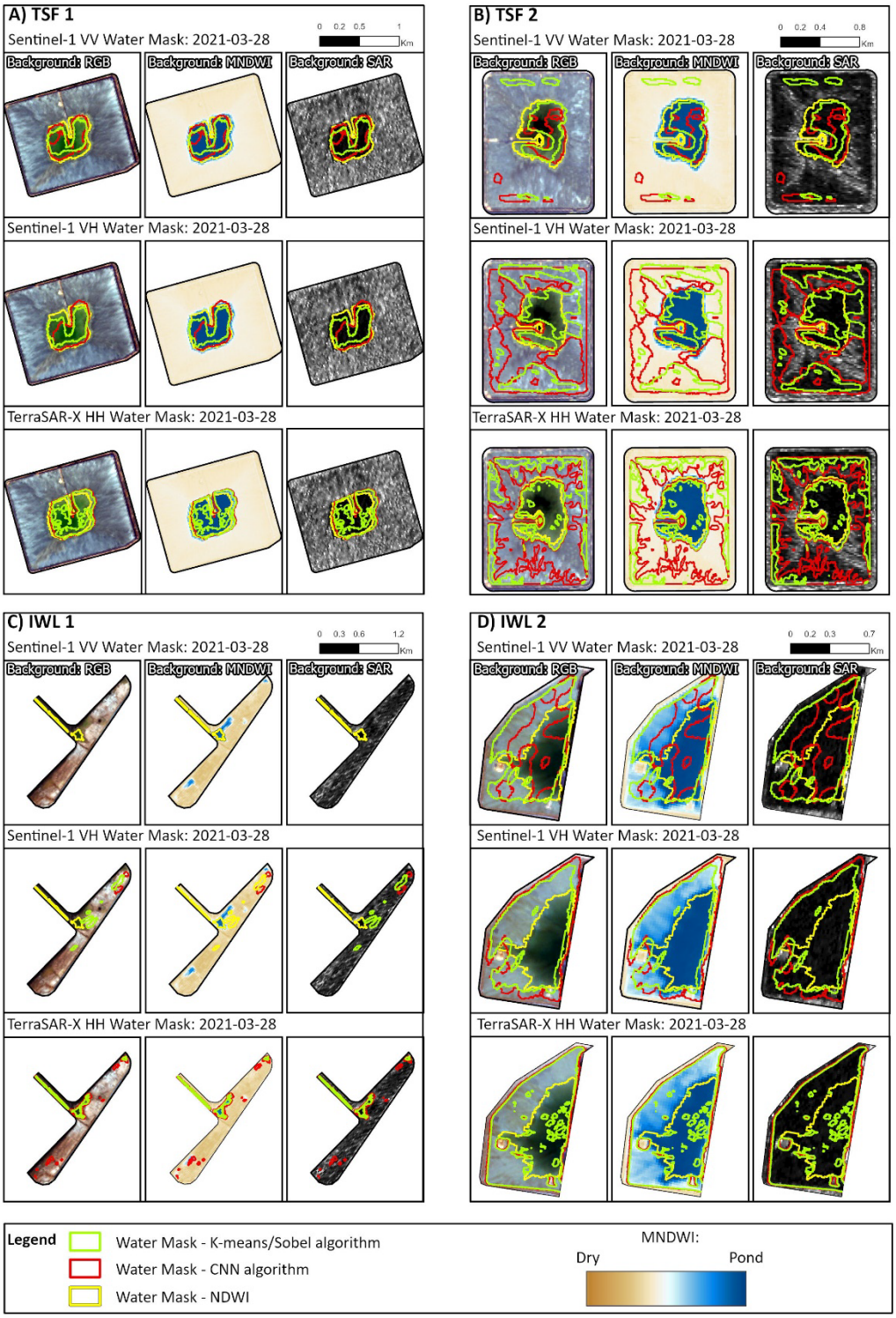


Figure 4: Water mask extent polygons produced using the k-means/Sobel and CNN algorithms (SAR data) and k-means/Sobel (NDWI) overlaid over true color (labelled RGB), MNDWI and SAR amplitude rasters for A) TSF1; B) TSF2; C) IWL1; D) IWL2

The low accuracy of the SAR water masks during periods of high-water content is explained by the algorithm often classifying wet beach areas as water, therefore there are many false positives since the reference water masks correspond only to supernatant ponds as classified by NDWI. This is likely due to the lack of contrast between wet material and pond areas in the SAR amplitude data for some acquisitions (e.g., SAR amplitude panel in Figure 4d). The notable discrepancies between the Sentinel-1 VH results and the other polarizations are limited to one of two TSF categories presented in this study (i.e., TSF1 and TSF2) and occur within a specific period (Figures 2a, 2c, 2e and 2g). This may suggest that specific types of material deposited within these TSFs may be indistinguishable from moisture in the VH polarization with the statistical and CNN algorithms used.

This preliminary CNN algorithm proved to be successful at detecting TSF moisture despite being trained on very different water bodies such as lakes and with data limited to Sentinel-1 in the VV polarization. Differences in the backscatter properties of SAR are expected to be significant between natural water bodies and tailings due to sediment content and water depth, as are differences in the spatial distribution and the saturation gradient around standing water. Based on the results of this analysis, a CNN trained on TSFs may be able to better discriminate between wet beach and supernatant ponds.

Integration of water mapping and InSAR monitoring results

In this section, InSAR is used in conjunction with supernatant pond and saturation mapping to demonstrate the relationship between TSF activity and embankment stability, with a focus on the integrated waste landforms. Embankment stability can be affected by variations in moisture content. Moisture from the material deposited in the TSFs can saturate the embankment, increasing pore pressure and therefore the stresses acting on the embankment. Increased moisture content also increases the weight of the tailings, which can negatively impact embankment stability, as well as settling of the material (Han et al., 2012; Dimitrova and Yanful, 2011). Finally, dry conditions leading to desiccation, cracking and erosion, can also undermine the stability of the embankment (e.g., Vardon, 2015).

The SqueeSAR algorithm provides measurements over areas where the natural radar targets on the ground surface have not changed significantly over time – areas with significant surface changes will contain gaps in data coverage. IWL1 was constructed during the first 6 months of the analysis period, therefore the SqueeSAR analysis resulted in displacement measurements only on the undisturbed portions of the embankments. IWL2 was constructed prior to the start of the SqueeSAR analysis. At IWL1, two areas of subsidence are identified (Figure 5a). The displacement history is similar for both, with three main phases of subsidence as follows: (A) slow average displacement velocity (-9 mm/yr) from approximately January 2021 to January 2022; (B) increased displacement velocity (-24 mm/yr) from approximately January 2022 to July 2023; (C) decreased displacement velocity (-12 mm/yr) from approximately July 2023

to the end of the analysis in February 2024 (Figure 5c). Fifty-three mm of cumulative subsidence are measured over the analysis period.

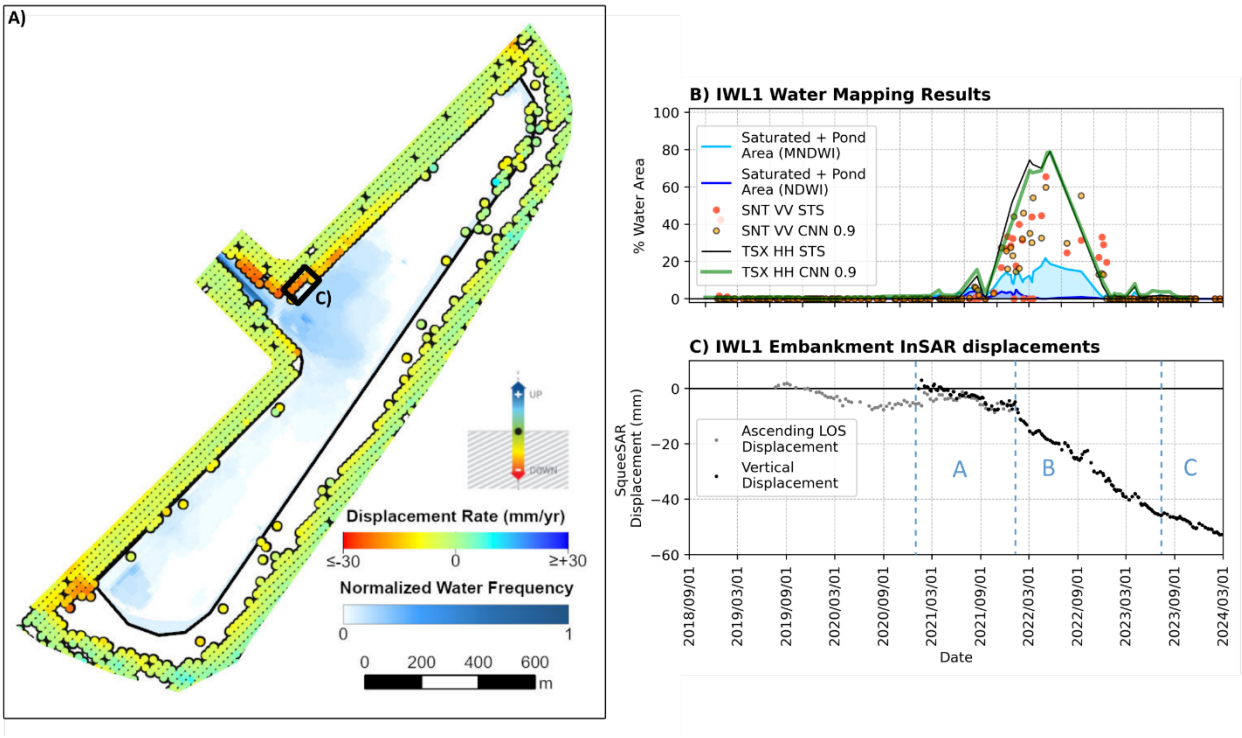


Figure 5: A) Points represent the average velocity of the multi-temporal InSAR analysis on the embankments of IWL1. Colors within the TSF represent the normalized frequency at which each pixel was classified as water during the analysis period using NDWI (1 being the most frequent). B) Percentage water area mapped within this TSF using MS and SAR data. C) Average time series of displacement at the location denoted by thick black polygon in A)

For IWL1, while the main ponding areas shown in Figure 5a correspond to the higher displacement areas, the relationship between the prolonged period of higher InSAR velocity (phase B) and the relatively short period of supernatant ponding is not straightforward. However, the period of increased % area of combined saturated and water pixels (based on MNDWI pixels > 0.1 and SAR-derived water classification) has a similar time scale (Figure 5b), only the phase B InSAR velocity increase is delayed by approximately 6 months. The supplementary monitoring of saturated material rather than ponding only may therefore provide valuable information on the interplay between TSF activity and embankment instability.

An area of subsidence was also identified at IWL2, as shown in Figure 6a. The main phases of displacement are as follows: (A) relatively low average velocity (-13 mm/yr) from the beginning of the analysis (January 2021) to approximately August 2021; (B) higher average velocity (-40 mm/yr) from approximately August 2021 to March 2022; (C) lower velocity (-18 mm/yr) from approximately March 2022 to August 2022; (D) higher velocity (-51 mm/yr) from approximately August 2022 to January 2023;

and (E) lower average velocity (-17 mm/yr) and gradual deceleration from approximately January 2023 to the end of the analysis period (Figure 6c). Eighty mm of subsidence occurred throughout the analysis period.

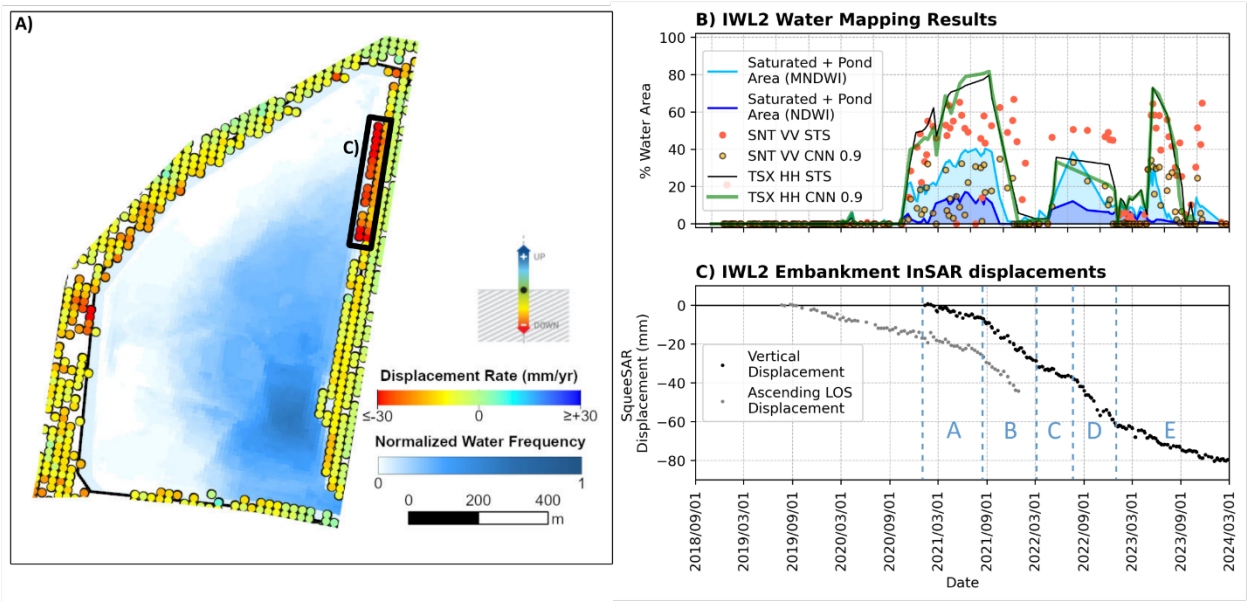


Figure 6: A) Points represent the average velocity of the multi-temporal InSAR analysis on the embankments of IWL2. Shades of blue within the TSF represent the normalized frequency at which each pixel was classified as water during the analysis period using NDWI (1 being the most frequent). B) Percentage water area mapped within this TSF using MS and SAR data. C) Average time series of displacement at the location denoted by thick black polygon in A)

Similarly to IWL1, the less stable portion of the IWL2 embankment is in proximity of an area frequently classified as water (Figure 6a). Furthermore, there are higher InSAR velocity periods starting a few months after periods with large areas covered by ponds and saturated material (Figure 6b). The delay may be related to the gradual change in the stress field due to the saturation and increase of pore pressure of the embankment reducing its shear strength, and other factors such as the weight of the settled tailings, seepage leading to embankment erosion, or the draining of water away from the IWL (Clarkson and Williams, 2021; Saad and Mitri, 2011).

These results illustrate the complementarity of surface water indices, SAR amplitude data and multi-temporal InSAR in monitoring and assessing the impact of the TSF operations on embankment instability. While remote sensing methods can provide long-term history of data over large areas, determining the exact deformation mechanisms in play in the locations identified by InSAR and their causes will require input from the mine operator on their operational schedules and in-situ measurements such as pore pressure, tilting and settlement data, and signs of cracking and tension.

Conclusion

This study demonstrates the ability of two ML algorithms (i.e., a k-means/Sobel operator approach and a preliminary CNN trained on lakes and rivers with VV-polarized SAR data) to identify saturated material within TSFs using SAR amplitude imagery alone. The outcomes are impactful, as well-established methods of detecting TSF moisture and ponding rely on MS imagery that can be heavily impacted by cloud cover.

The results outline specific recommendations for the use of these algorithms in monitoring TSF moisture. Firstly, although further refinement is required to accurately discriminate between fully saturated tailings and standing water, the ML algorithms using SAR data were able to detect large areas corresponding to the combined saturated and pond areas detected by MNDWI. Secondly, the choice of SAR data polarization, and potentially the wavelength (and therefore spatial resolution), significantly affect the results. Of the datasets used in this analysis, Sentinel-1 VV and TerraSAR-X HH-polarized data were generally more successful at mapping TSF moisture than Sentinel-1 VH polarized data. The spatial and temporal trends of saturated material detected using Sentinel-1 VV and TerraSAR-X HH data are also shown to be useful in interpreting TSF embankment displacements measured by InSAR, with periods of extensive saturated material followed by periods of faster embankment subsidence.

The accuracy of the CNN in mapping supernatant ponds is expected to improve with a network trained on TSFs and a variety of SAR polarizations and resolutions. Additionally, information on the operational schedules and specific tailings material deposited is required to fully characterize the polarimetric properties of the TSFs.

References

Acharya, T.D., Subedi, A. and Lee, D.H. 2018. Evaluation of Water Indices for Surface Water Extraction in a Landsat 8 Scene of Nepal. *Sensors* 18: 2580.

Brisco, B., Kapfer, M., Hirose, T., Tedford, B. and J. Liu. 2011. Evaluation of C-band polarization diversity and polarimetry for wetland mapping. *Canadian Journal of Remote Sensing* 37: 82–92.

Cacciuttolo, C. and Cano, D. 2023. Spatial and temporal study of supernatant process water pond in tailings storage facilities: Use of remote sensing techniques for preventing mine tailings dam failures. *Sustainability* 15(6): 4984.

Clarkson, L. and Williams, D. 2021. An overview of conventional tailings dam geotechnical failure mechanisms. *Mining, Metallurgy and Exploration* 38(3): 1305–1328.

Dimitrova, R.S. and Yanful, E.K. 2011. Undrained strength of deposited mine tailings beds: Effect of water content, effective stress and time of consolidation. *Geotechnical and Geological Engineering* 29: 935–951.

Ferretti, A. 2014. *Satellite InSAR Data: Reservoir Monitoring from Space*. EAGE.

Ferretti, A., Fumagalli, A., Novali, F., Prati, C., Rocca, F. and Rucci, A. 2011. A new algorithm for processing interferometric data-stacks: SqueeSAR. *IEEE Transactions on Geoscience and Remote Sensing* 49(9): 3460–3470.

Gao, B.C., 1996. NDWI—A normalized difference water index for remote sensing of vegetation liquid water from space. *Remote Sensing of Environment* 58(3): 257–266.

Han, J., Bhandari, A. and Wang, F. 2012. DEM analysis of stresses and deformations of geogrid-reinforced embankments over piles. *International Journal of geomechanics* 12(4): 340–350.

Jiang, J., Sun, H., Wang, Y., Cacciuttolo, C. and Cano, D. 2023. Spatial and temporal study of supernatant process water pond in tailings storage facilities: use of remote sensing techniques for preventing mine tailings dam failures. *Sustainability* 15(6): 4984.

Kanopoulos, N., Vasanthavada, N. and Baker, R. L. 1988. Design of an image edge detection filter using the Sobel operator. *IEEE Journal of Solid-State Circuits* 23(2):358–367.

Koleshwar, A., Tortini, R. and Falorni, G. 2023. Assessing tailings consolidation and changes in supernatant pond area using InSAR and the normalised difference moisture index. In G.W. Wilson, N.A. Beier, D.C. Sego, A.B. Fourie and D. Reid (editors), *Paste 2023. Proceedings of the 25th International Conference on Paste, Thickened and Filtered Tailings.* University of Alberta, Edmonton, and Australian Centre for Geomechanics, Perth: 765–775.

Lattari, F., Gonzalez Leon, B., Asaro, F., Rucci, A., Prati, C. and Matteucci, M. 2019. Deep learning for SAR image despeckling. *Remote Sensing* 11(13): 1532.

Piciullo, L., Storrøsten, E.B., Liu, Z., Nadim, F. and Lacasse, S. 2022. A new look at the statistics of tailings dam failures. *Engineering Geology* 303: 106657.

Robinove, C.J. 1981. The logic of multispectral classification and mapping of land. *Remote Sensing of Environment* 11(C): 231–244.

Saad, B. and Mitri, H. 2011. Hydromechanical analysis of upstream tailings disposal facilities. *Journal of Geotechnical and Geoenvironmental Engineering* 137(1) :27–42.

Townshend, J., Justice, C., Li, W., Gurney, C. and McManus, J. 1991. Global land cover classification by remote sensing: present capabilities and future possibilities. *Remote Sensing of Environment* 35(2–3): 243–255.

Vardon, P.J., 2015. Climatic influence on geotechnical infrastructure: A review. *Environmental Geotechnics* 2(3): 166–174.

Xu, H. 2006. Modification of normalised difference water index (NDWI) to enhance open water features in remotely sensed imagery. *Int. J. Remote Sens*. 27: 3025–3033.

The Application of a 3D Inclinometer in Monitoring the Performance of a TSF near an Active Mine Pit

Zhen Ran Yung, Red Earth Engineering: A Geosyntec Company, Australia
Qing Zhan, Red Earth Engineering: A Geosyntec Company, Australia
Stephen Darmawan, Geotesta, Australia
Rudy Moniaga, Geotesta, Australia

Abstract

Tailings storage facilities (TSFs) present significant safety and environmental challenges in the mining industry due to the potential for catastrophic failure. TSF operators and engineers have for many years relied on monitoring instruments to assess the performance of a TSF against the design intent and to facilitate early detection of potential hazards, which in turn enables a timely response in the form of a Trigger Action and Response Plan (TARP). The monitoring program for a TSF may include the use of extensometers, survey monuments, and inclinometers to detect embankment movements. However, these instruments typically provide unidirectional (single axis) measurements, which alone may not provide sufficient data for an engineer to make an informed decision that may inadvertently affect TSF stability.

This study introduces the use of an in-place 3D inclinometer settlement system (IPIS), an advanced tool capable of monitoring lateral (horizontal) movement and settlement (vertical) in slopes, embankments, retaining structures, and dams. An IPIS was installed on a TSF embankment at a depth of 40 m, extending into the foundation, founded on a loosely compacted mine spoil material. The implementation of the IPIS was to monitor the stability of the TSF while active open pit mining was occurring downstream of the facility.

Unlike conventional inclinometers and other systems, the IPIS excels in its ability to record both real-time vertical and horizontal deformations at various depths, which are subsequently linked to a cloud-based telemetry system. The movement tolerance or exceedances are programmed into the telemetry, which when exceeded triggers an automated alert (i.e., TARP) to the TSF engineer or dam owner. This monitoring technology and approach is therefore considered to be well suited for high-risk geotechnical structures such as tailings dams, and within the context of this study.

This paper presents an overview of the IPIS with actual site monitoring data to demonstrate the applicability of the equipment to improve stability monitoring of a TSF located adjacent to a 30 m deep

open pit mine. It is envisaged that adopting the IPIS, in conjunction with existing instrumentation monitoring tools such as survey monuments and vibrating wire piezometers (VWPs), will add to the robustness of the monitoring program and allow designers and dam operators a wider range of monitoring options to suit site-specific conditions.

Introduction

TSF monitoring is a critical component within the tailings management framework as it allows engineers to assess the performance of a TSF against the original design parameters, predictions, and overall behavior of the facility. The Global Industry Standard on Tailings Management (GISTM) (ICMM, 2020) requires many of its members to implement a comprehensive and integrated TSF monitoring program for the purpose of verifying design assumptions and monitoring potential failure modes under Requirements 7.1 and 7.2. This must be applied to all phases of the facility lifecycle, including the Closure and Post-Closure phases.

There are a vast variety of commercially available monitoring technologies, and many new and improved instruments are rapidly emerging, or are at various stages of development. Recent advances in the development of new sensors, analytics, and remote monitoring techniques have provided the mining industry with more opportunities and tools to access real-time monitoring information, allowing for a more rapid detection of potential issues, which in turn enables a more proactive response. However, most of these conventional instruments are purpose-built to measure a single source of data, which when used in isolation may not be sufficient for an engineer to make an informed decision affecting the stability of a TSF.

This gap in monitoring was realized at a mine site located in Northern Australia, where open pit mining was carried out to extract valuable minerals within 50 m of an active TSF. This paper discusses the implementation of a “new” 3D in-place inclinometer settlement system (IPIS) that was installed on a TSF to monitor both lateral and vertical displacement of the embankment and foundation soil. This provided dam owners and mining operators increased coverage and confidence to assess the condition of the facility while active mining was occurring downstream.

Facility description

The TSF was constructed circa 2019 as a downstream raise facility comprising a perimeter embankment with a maximum height of 14 m, founded predominantly on loosely compacted overburden mine spoil up to 25 m thick. The TSF is designed to store a total of 14.1 Mm^3 of fine slimes tailings generated from processing mined ore, with the distribution of tailings shared with adjacent TSFs through cyclic deposition to promote consolidation and overall increase in the in-situ settled dry density of the tailings. In 2021, mining was proposed west of the facility, which initiated additional geotechnical investigation through cone

penetrometer testing (CPT) with the intent of reducing geotechnical uncertainty regarding the mine spoil foundation material. Figure 1 shows the location of the existing TSF and the mine pit. Although there are existing monitoring instruments installed on the facility, the risk of embankment failure resulting from the adjacent mining activities was determined to be critical to downstream receptors. Therefore, further dam safety initiatives with a more robust monitoring system were considered necessary.

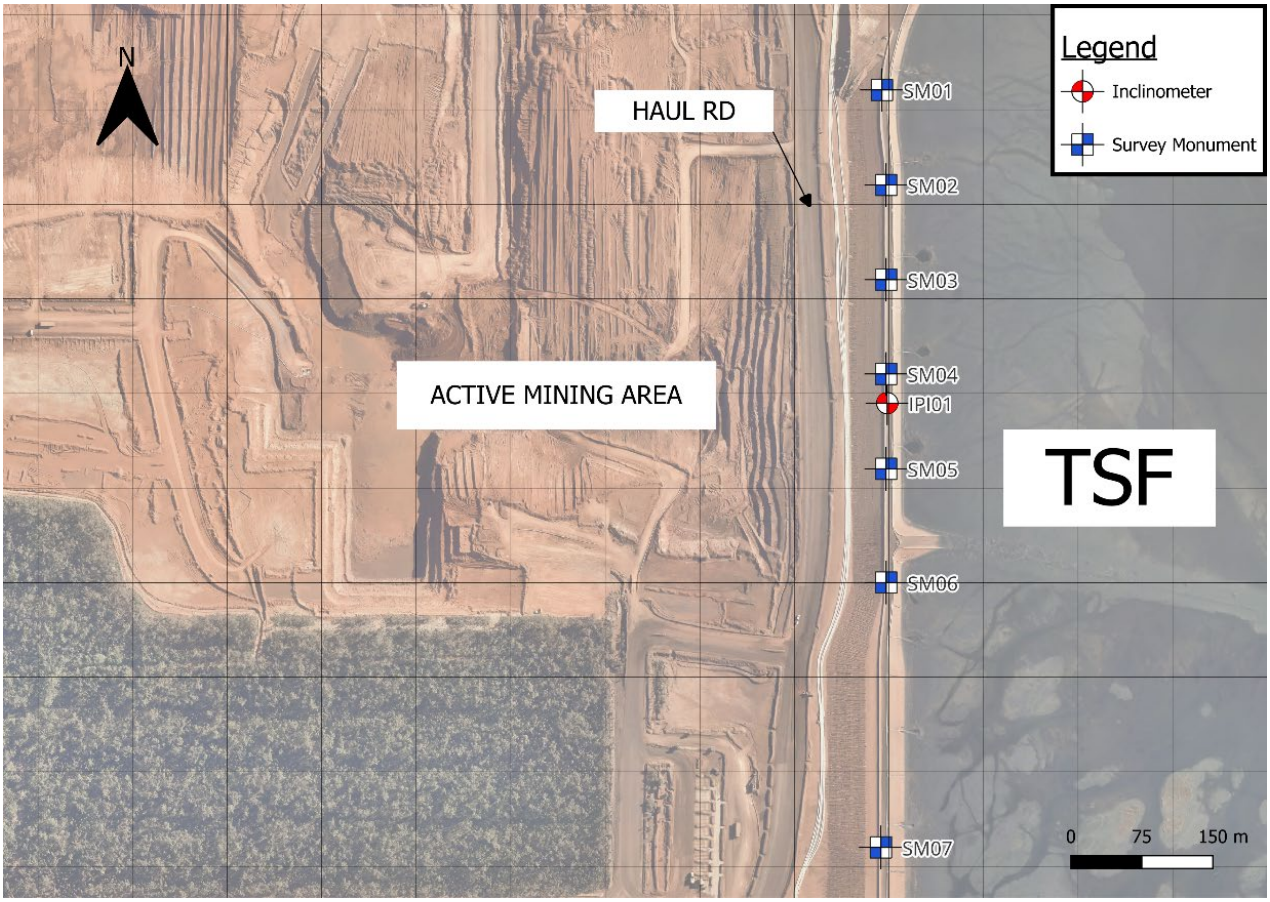


Figure 1: Overview of TSF and adjacent mine pit

Current monitoring practices and challenges

The mine site is situated in a tropical savanna climate that produces two distinct seasons (tropical wet and dry seasons). During the wet period, increased rainfall intensity and frequency result in enlarged ponds and reduces drying time of the tailings surface, which is managed carefully as per the facility operations, monitoring, and surveillance manuals. Currently, the facility utilizes a range of monitoring tools consisting of survey monuments (SMs) and vibrating wire piezometers (VWPs) that are connected to a telemetry system that provides an automated response to the TSF Engineer should a TARP alarm be triggered. Interferometric Synthetic Aperture Radar (InSAR) technology is also employed to monitor the displacement of the TSFs on a bi-weekly basis.

A risk assessment was undertaken by key stakeholders to assess the impact on mining progression near the TSF. A key action arising from the review was to rationalize the existing monitoring program with a view to improving the quality and reliability of the data to detect potential slope instability, recognizing the limitations of current monitoring methods. For example, lateral movements below the embankment and foundation layers cannot be accurately monitored using SMs and InSAR, as these are surface-based monitoring tools (i.e., propagation of movements is delayed). During normal operation, the settlement would in some instances trigger yellow (>25 mm movements) and/or amber (>50 mm movements) TARPs, which were often found to be erroneous due to potential issues of "noise" and/or bias movement readings. These issues can be attributed to the limitations on the accuracy of survey instruments, satellite duration, and surveyor experience when undertaking SM readings. Additional filtering of the data, as investigated by Han et al. (2023), is required.

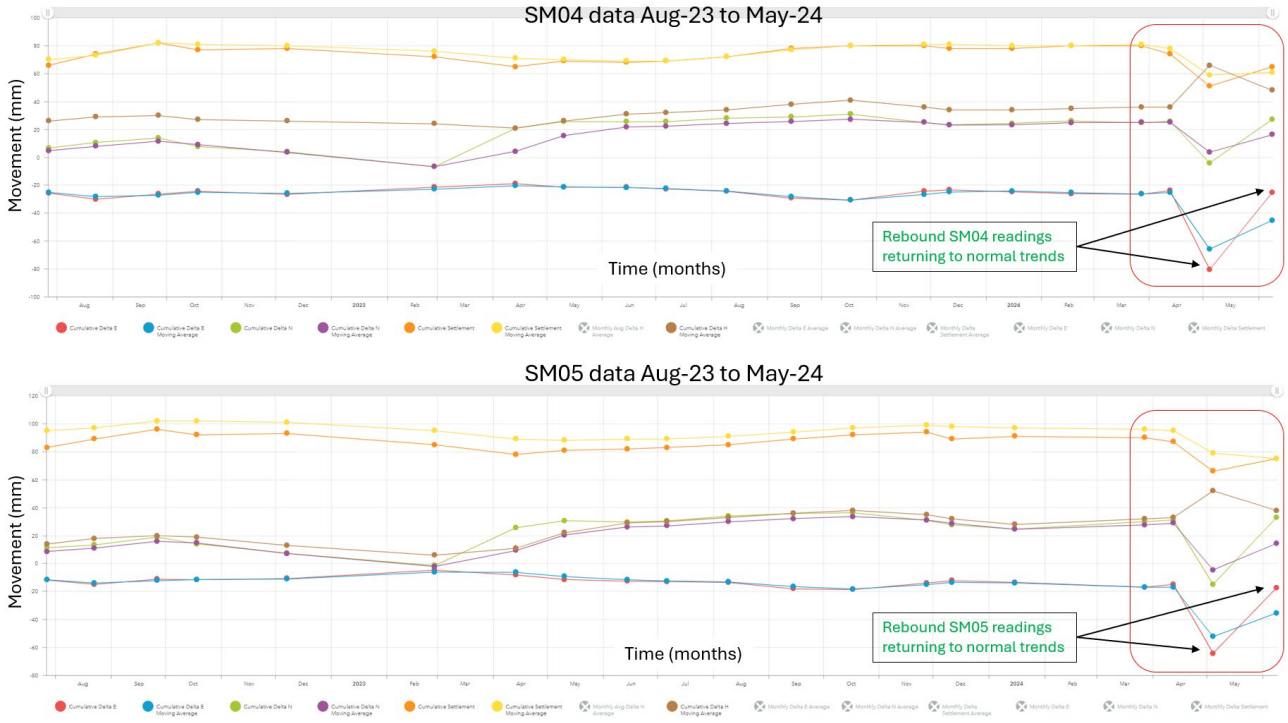


Figure 2: Survey monuments (SM04 and SM05) readings showing "false" embankment movements

An example of this reliability issue is presented in Figure 2, which shows the real SM data from the TSF presented in this study. The SM04 and SM05 have a set trigger tolerance of 25 mm for both horizontal and vertical displacement per month. The example in Figure 2 clearly shows the exceedance of this tolerance of up to approximately 60 mm movement in the month of May 2024. This is nearly triple the prescribed threshold, which would put the facility at a serious Amber trigger alert. However, the readings

received in the next month's data show a rebound of the movement, which is consistent with historical trends and is clearly an indication of data error. The reliability and consistency of the data thus become questionable – is the monitoring program robust and can we rely on this when carrying out high risk activities?

Application example of IPIS

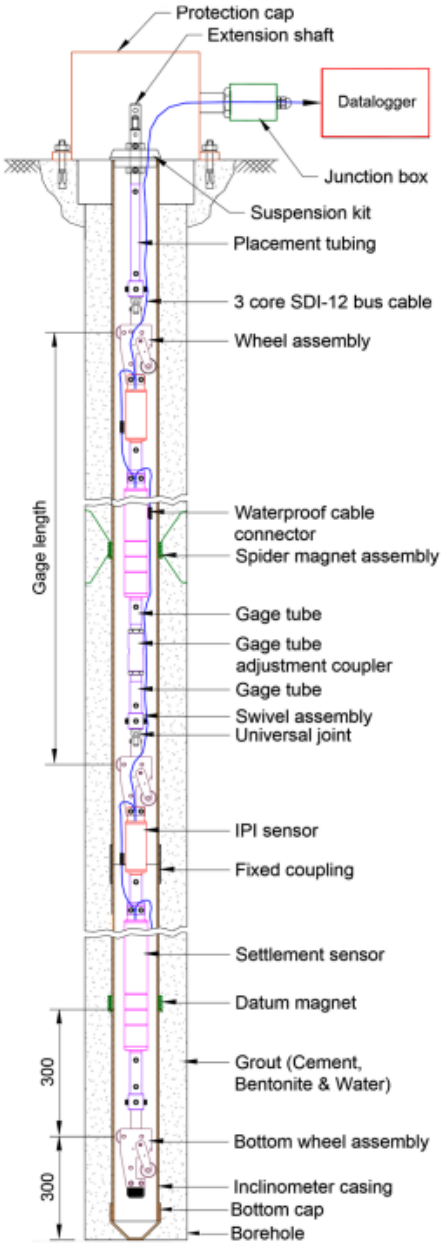


Figure 3: Schematic of the 3D IPIS and protective cover (Encardio Rite, 2020)

Overview

The 3D IPIS has wide applications where monitoring lateral movement and settlements in soils and embankments is required (i.e., potential faults and landslide zones) (Encardio Rite, 2020). It is used to provide quantitative data on the magnitude of settlement and inclination or tilt of a foundation and embankment (or slope) and its variations over time in a single borehole.

A typical schematic of the IPIS is illustrated in Figure 3, comprising an in-place inclinometer (IPI) and spider magnets (consisting of sensors and magnet rings).

When subsurface movements occur laterally, the IPIS detects the movement by showing a tile in the sensors. The same principle applies when settlement takes place that changes the vertical position of the outer magnet rings relative to the internal sensors. The range of the settlement sensors used at this site is up to 100 mm, within and below the estimated theoretical settlement prediction. The vertical displacement (settlement) is simply calculated by subtracting the total vertical differences from the point of reference (i.e., datum).

Installation and setup

The 3D IPIS model EAN-61MS was installed on the critical embankment section relative to the direction of the downstream mining area. The IPIS setup of the casing and positioning of the spider magnets is shown in Figure 4, which consists of sixteen inclinometer arrays and seventeen spider magnets installed at a nominal 2 m spacing.



Figure 4: Example of installation preparation of the 3D IPIS on embankment crest and the lowering of IPIS casing and spider magnets into the borehole

The IPIS was lowered into a 40 m deep borehole (cased) incrementally to target depth before being fully grouted in stages. At the top of the IPIS is the "Junction Box," which is connected to a datalogger on the TSF with remote monitoring capabilities, which feeds the data to a centralized monitoring database server (telemetry) where the data is automatically reviewed and compared against a site-specific trigger tolerance.

Discussion

The IPIS was installed before mining works commenced, providing an ideal scenario to establish a baseline reading for the instrument, which effectively allows for the monitoring of the progressive mining and excavation downstream works and their effects on the performance of the TSF. Approximately 18 months of monitoring data is presented in the figures below, showing minimal total vertical (<10 mm) and horizontal (<1 mm) displacements in Figure 5 and Figure 6 respectively.

The monitoring data indicates that the foundation, comprised of poorly compacted layers of mine spoil, has potentially fully consolidated under the embankment load. This is supported by the outputs from the survey monuments in Figure 2, despite the issues of intermittent trigger exceedance warnings.

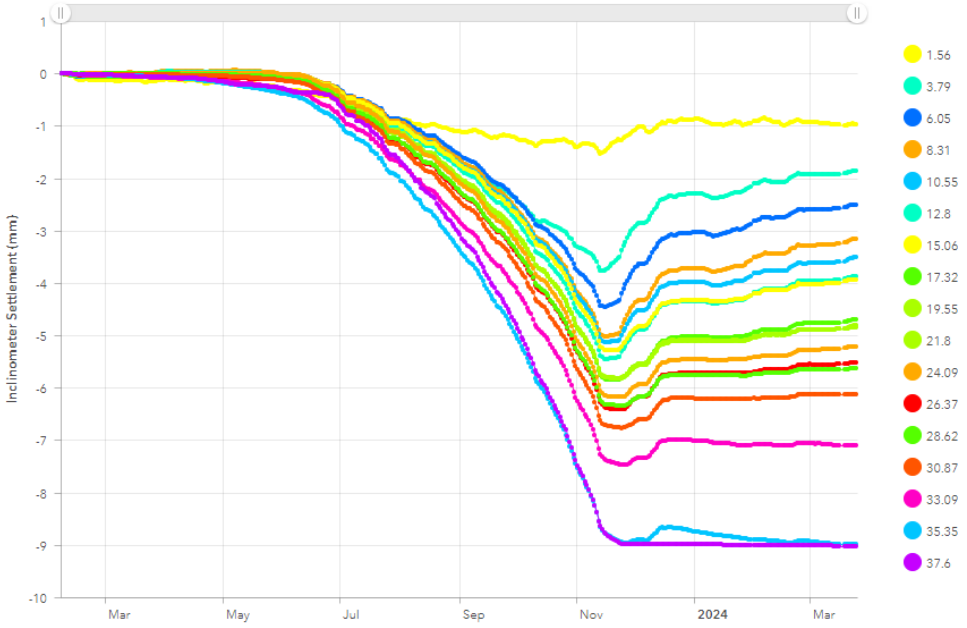


Figure 5: Monitoring IPIS showing cumulative settlement (vertical movement) readings

A key performance indicator of the performance of a facility is the analysis of trends and comparison with past data (i.e., moving averages), and it can be seen from the following figures that all the recorded readings have been consistent since its inception. Monitoring of the embankment is still ongoing in the

field; however, it is worth noting that the mining activities have since transitioned to backfilling of the pit void, which will improve overall TSF stability.

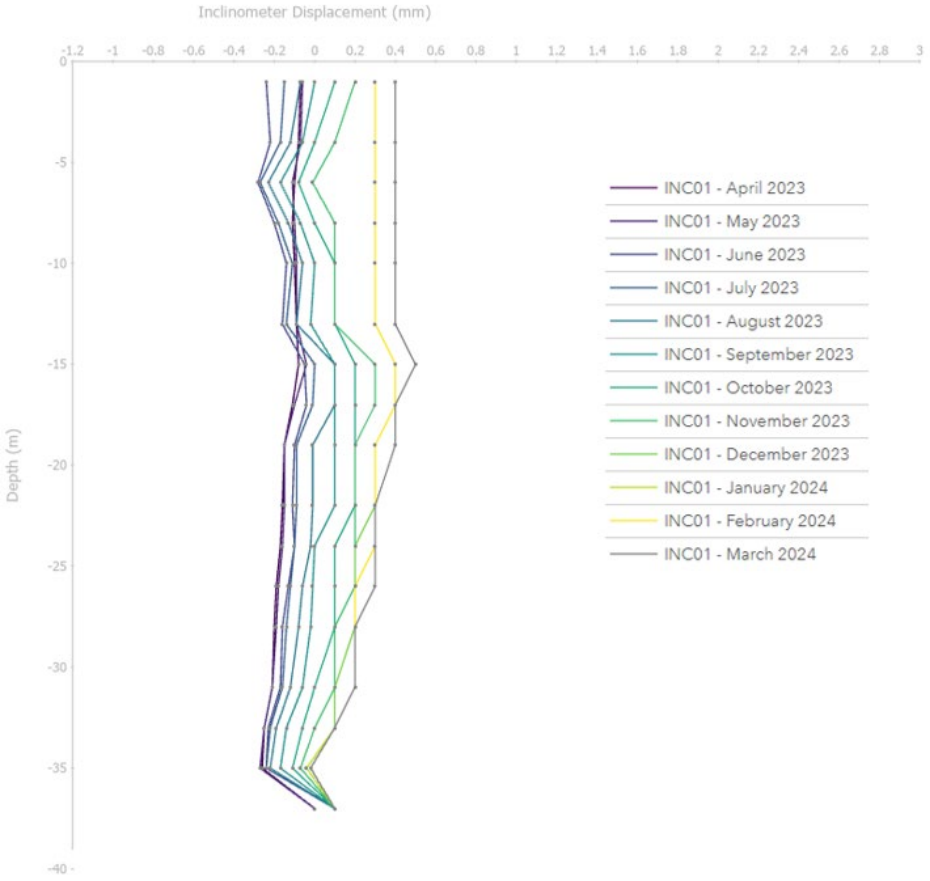


Figure 6: Monitoring IPIS showing lateral (horizontal) movement readings

The use of an IPIS thus avoids survey accuracy limitations that are pertinent in some of the current monitoring practices that rely on GPS receivers or satellites to monitor tailings dam movements. It also removes the need for complex noise reduction algorithms to filter survey noise ("the data is the data") and in retrospect, perhaps even bias interpretation from TSF engineers. The instrument is considered a useful tool to validate the geotechnical models or to demonstrate that the critical deformation behavior, as in the case of this TSF example, has already been exceeded, and what remains is just the residual settlement, which is relatively minor.

Conclusion

Implementation of a robust monitoring program is critical and is one of the key conformance protocols required by GISTM. The monitoring programs need to be designed, implemented, and operated to monitor facility performance and validate design assumptions for all phases of the facility lifecycle. Throughout this

paper we have highlighted the importance of understanding the limitations of monitoring instrumentations and the need to adopt alternative monitoring strategies to suit site-specific needs. Combining the inclination and settlement behavior of the monitored embankment is considered practical and provides spatial information at discrete points of observation in similar embankment materials.

This paper presents an alternative tool to monitor embankment movements using a 3D in-placement inclinometer and settlement system, which is considered to offer a robust and reliable way to monitor TSF movements, in conjunction with existing instrumentation tools such as survey monuments and piezometers.

References

Encardio Rite. 2020. In-place 3D inclinometer cum settlement system (IPIS) for monitoring lateral movement and settlement. *User's Manual.* Accessed 16/06/2024 at https://www.encardio.com/uploads/manual/EAN-61MS-3D%20In-place-inclinometer%20with%20settlement.pdf

Han, C., Wong, K.F., Ludlow, W. and Yung, Z.R. 2023. A noise reduction algorithm for automatic interpretation of periodical survey data for tailings dam performance monitoring. In *Proceedings of the Mine Waste and Tailings Conference 2023.* Brisbane, pp. 365-373.

International Council on Mining and Metals (ICMM). 2020. *Global Industry Standard on Tailings Management.* International Council on Mining and Metals (ICMM).

Integration of Multi-sensing Technologies for the Monitoring of Tailing Storage Facilities

Vincent Le Borgne, GKM Consultants, Canada
Adam Dulmage, GKM Consultants, Canada
Josh Sun, CNUL, Canada
Evan Davison, CNUL, Canada
Divya Sekha Vaka, GEOFEM, Cyprus
Skevi Perdikou, GEOFEM, Cyprus

Abstract

This paper presents the results of a synergistic application of three different but complementary monitoring technologies for a tailings storage facility (TSF) in Canada currently undergoing a transition from active operations to closure. The monitoring technologies discussed are Global Navigation Satellite Systems (GNSS), Interferometric Synthetic Aperture Radar (InSAR), and Light Detection and Ranging (Lidar). Monitoring has become a mandatory part of TSF management. Monitoring ensures TSFs meet their performance goals during construction, operations, and post-closure. A key method to prevent TSF failures is to monitor parameters such as ground displacement as part of early-warning systems. GNSS refers to the use of satellites for determining highly accurate, localized measurements of position. New satellite constellations and advancing technologies have contributed to the endorsement of satellite-based assessments for infrastructure assets. The use of InSAR as a means of monitoring ground displacements is also presented in this paper. Taking advantage of the wide area coverage within a single analysis, InSAR provides an efficient and effective way of identifying developing trends. LiDAR, on the other hand, can provide digital elevation models of a site.

Introduction

The TSF covers an area approximately 10 km^2 and has a maximum dyke height of approximately 60 m. Land clearing for the TSF began in approximately 1999, and starter dyke construction started in 2001. The structure reached its full design height in 2013 and is currently transitioning from operation as an active storage facility for fluid tailings into decommissioning and closure.

Within the TSF, various tailings streams have been deposited, including coarse sand tailings (CST), whole tailings (WT), fluid tailings (FT), thickened tailings (TT), and tailings solvent recovery unit (TSRU) tailings. FT and TT are classified as high-fines tailings, which are known to be compressible, having low hydraulic conductivity, and relatively long consolidation times that may extend into the closure time frame. Settlement analysis is crucial for the closure of TSF because it directly impacts the stability and sustainability of the reclaimed landform. Understanding the settlement behavior helps in predicting long-term land deformation, which is essential for designing effective closure strategies.

As part of a pilot project, this study compares several methods of settlement monitoring. Three existing settlement plates that were surveyed manually for the past 6 years were re-purposed with solar-powered Global Navigation Satellite Systems (GNSS) receivers (Basetime) in early 2024. Manual monitoring was maintained to compare the quality of the results with this novel method. Moreover, large-scale validation was conducted with satellite-based interferometric Synthetic Aperture Radar (InSAR) and satellite-based Light Detection and Ranging (LiDAR). These methods can be compared on a sliding-scale: GNSS are point measurements that are attached to a specific point in space but are completely automated. Manual survey is also point-monitoring but is very flexible, as monitoring points can be added or removed as needed without additional investments. At the other end of the scale, large-scale methods such as InSAR and LiDAR can monitor large areas but have a slow acquisition rate and can require specialized analysis to extract high-accuracy data. In this paper, we show that GNSS, InSAR, and manual surveying have similar repeatability and accuracy, while LiDAR appears to be less reliable. The methods are shown to be complementary, fulfilling different, but related, requirements.

Methods

GNSS

Monitoring with GNSS and global positioning systems (GPS) for ground movement has been used since the 1990s for landslide monitoring and structural health monitoring. It is currently being introduced to tailings and tailings dams to track slow long-term movements. The GNSS monitoring system used in this project was developed specifically to monitor large settlements over long periods of time. The position determination is based on calculated post-processed baselines using a reference station that utilizes a star-shaped pattern method. It is equipped with a multiband GNSS receiver and antenna (186 channels), collecting data from the following bands: GPS L1C/A and L2C, GLONASS L1OF and L2OF, Galileo E1B/C and E5b, and BeiDou B1I and B2I. For a standard reading the device will do an observation with 1 Hz for 5 minutes counting. Within 30 seconds, they should receive all possible and necessary satellite data within an elevation mask of 10 degrees, yielding 270 epochs that are available to compute positions. The designed accuracy of the system for long-term monitoring is 4 mm (1σ) for a base station located within

a 4 km radius of the monitoring points. The mobile stations were installed in settlement plates that had been surveyed for years prior. A typical installation is shown in Figure 1. The system is self-contained with a solar panel that keeps a supercapacitor charged, providing complete autonomy. It is designed to be attached to settlement plates with a tailor-made bracket.

Manual survey

A manual survey involves the measurement of the elevation of the settlement plate. This process employs Real-Time Kinematic (RTK) GPS technology, which includes a Trimble R8S GPS receiver and a Trimble TSC3 data collector. The GPS receiver is mounted on a fixed post of the settlement plate during surveying. The operator initiates the measurement on the data collector, which records the elevation data with an accuracy of 1 to 1.5 cm. Manual surveying of settlement plates poses challenges such as accessibility issues, worker exposure in active operating areas, high labor costs, time consumption, and potential human errors. Automated surveying addresses these problems by providing continuous, accurate, and consistent data with reduced labor costs and improved safety. This shift enhances efficiency, reliability, and comprehensive monitoring, making automated systems a valuable advancement over manual methods.

The respective positions of the three surveyed locations are shown in Figure 1.

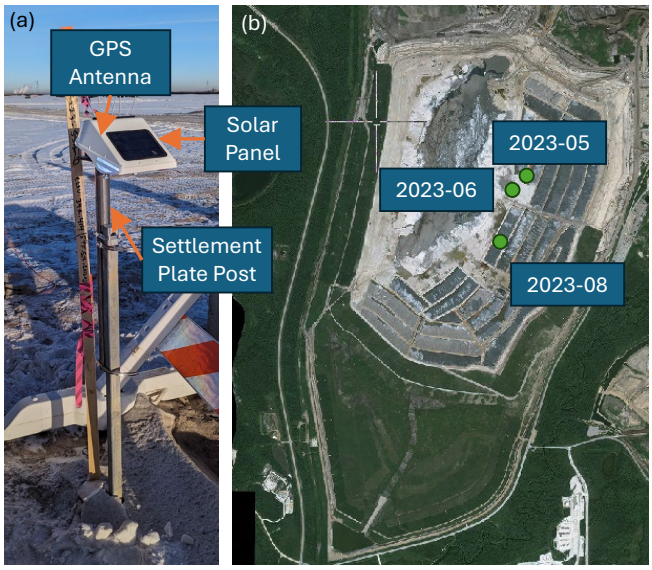


Figure 1(a): Typical automated GNSS installation
(b): locations of the three automated stations with respect to the structure

InSAR

Time series analysis of Interferometric Synthetic Aperture Radar (InSAR) has become increasingly significant in the mining industry due to its efficiency in measuring millimetric-scale displacements by employing multiple SAR images for displacement monitoring. Techniques such as Persistent Scatterer

Interferometry (PSI) and Small Baseline Subset (SBAS) are particularly effective for TSFs that exhibit slow, long-term deformations (Rana et al., 2024). Additionally, InSAR monitoring can detect precursor accelerations, providing valuable information for time-to-failure predictions. When available, results from ascending and descending tracks of the sensor can be used to decompose the line-of-sight (LOS) measurements into horizontal and vertical components.

The widespread availability of Synthetic Aperture Radar (SAR) data, both free and commercial, with global coverage, allows for regular, accurate, and simultaneous monitoring of TSFs using various InSAR techniques. For instance, InSAR is widely utilized for TSF monitoring in several countries, including Australia (Thomas et al., 2019), Brazil (Duro et al., 2020), Poland (Sciortino et al., 2021), South Africa (Perdikou and Lees, 2023), and Egypt (Mohamadi, 2024).

However, due to the ambiguous nature of phase difference between two acquisitions, time series InSAR can only estimate deformations up to a quarter of the wavelength between acquisitions. Any deformation exceeding this threshold is not detected in the time series. Considering this limitation, the maximum deformation that can be measured using Sentinel-1 is 42.6 cm/year (Crosetto et al., 2016).

For the analysis presented in this paper, sixty-four ascending pass Sentinel-1 SLC data in interferometric wide-swath (IW) mode from January 2022 to April 2024 were analyzed using the Small Baseline Subset (SBAS) technique. In the SBAS technique, the phase history of a pixel with respect to the first acquisition is reconstructed from a network of interferograms with small temporal and perpendicular baselines, ensuring maximum interferometric coherence (Berardino et al., 2002). Interferograms were formed by setting a temporal baseline threshold of 40 days. The topographic phase was removed using a Shuttle Radar Topography Mission (SRTM) Digital Elevation Model (DEM). The differential interferograms were filtered using a Goldstein filter and multi-looked to form an approximately 15 m pixel. An unwrapped coherence threshold of 0.1 was used to mask low coherence areas during phase unwrapping, which was performed using the Minimum Cost Flow (MCF) approach. The entire InSAR processing was carried out using ENVI SARscape software.

LiDAR

LiDAR (Light Detection and Ranging) is a remote sensing method that uses laser light to measure distances and create detailed 3D maps of surfaces. The survey was completed using a Riegl VQ-1560ii LiDAR system mounted on an aircraft, operating at a flying height of 1,500 meters and a speed of 160 knots. This system features a pulse repetition rate of 23,000 kHz, a scan frequency of 374 Hz, and a scan angle of 60 degrees. During the survey, the laser scanner emits rapid pulses of light, which bounce off objects and return to the sensor, capturing precise distance measurements. The GPS receiver determines the exact position of the scanner, while the Inertial Measurement Unit (IMU) records its orientation. The collected data is processed

to generate high-resolution, three-dimensional representations of the surveyed area, with an end result of a point density of approximately 10 points per square meter. The system achieves a horizontal accuracy of 30 cm (2σ) and a vertical accuracy of 10 cm (2σ).

LiDAR has been used to survey TSF primarily to estimate elevation changes. Its high precision and accuracy in capturing elevation data make it ideal for creating detailed topographic maps and models. These models are crucial for calculating volumes, which is essential for resource management, environmental monitoring, and infrastructure planning.

Results

The SBAS results are shown in Figure 2. The majority of the InSAR deformation points are located on the outside of the TSF, with very few points observed within the tailings. This lack of observation points within the tailings is attributed to coherence loss over time.

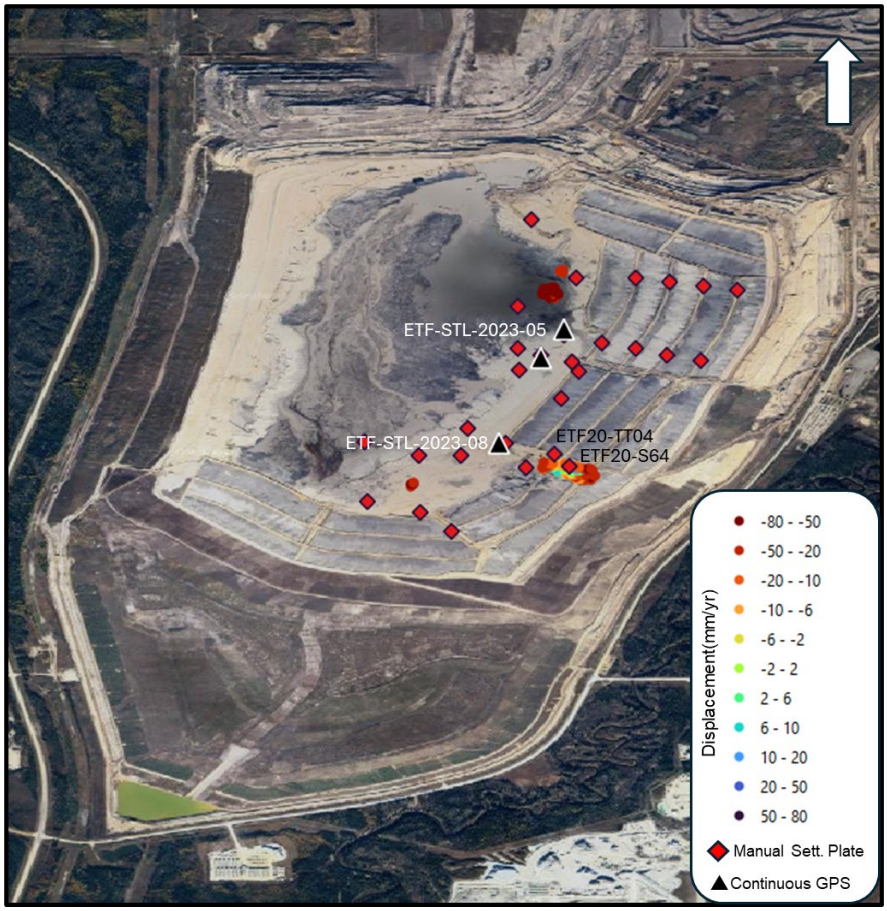


Figure 2: InSAR SBAS results (January 2022 to April 2024) overlaid on Google Earth imagery

The InSAR measurements within a 500-meter radius of the automatic GNSS stations (shown as black triangles in Figure 2) are averaged to facilitate comparison with the GNSS readings.

Figure 3 illustrates the comparison of InSAR, continuous GNSS, and manual GPS measurements of GPS locations as acquired. It can be seen that while InSAR shows the right trend, going much further back in time than the GNSS measurements, it appears to measure a much lower rate of displacement.

Manual survey and automatic GNSS show good agreement for the ETF-STL-2023-05 and ETF-STL-2023-08 locations. Coherence loss prevented performing the InSAR analysis for the ETF-STL-2023-06 monitoring point. For ETF-STL-2023-08, the match was good, but was better for the first part of the monitoring period (from December to February 2024). Due to logistical constraints, the reference station had to be moved from an initial location 1.1 km from the monitoring area to a new location approximately 4.2 km away. This led to a significant increase in noise in the system. The trends appear to hold, but it has made it impossible to compare daily readings directly. Returning the reference station to a location closer to the monitoring points has reduced noise to more acceptable levels. The reference station was in the less favorable location between the two dashed lines on the graphs of Figure 3.

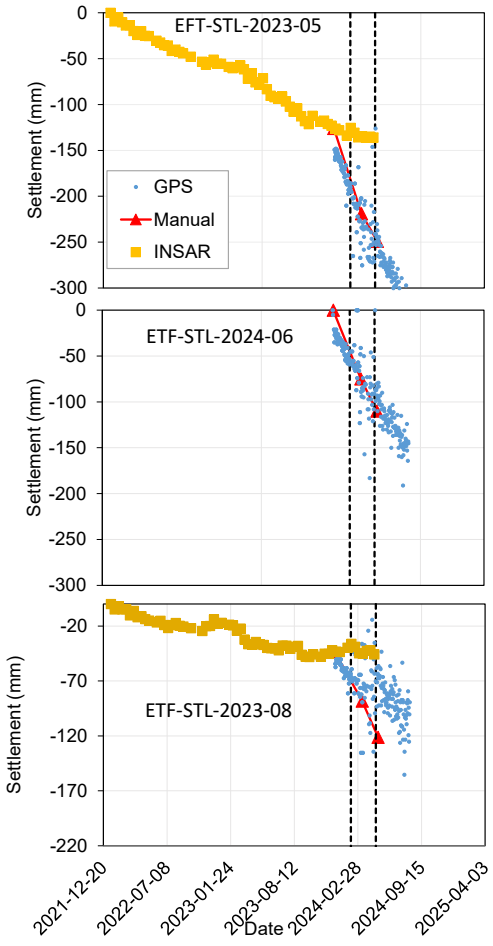


Figure 3: Comparison of InSAR, as-measured automatic GNSS, and as-measured manual survey displacements from January 2024 to June 2025 at select settlement plate locations

The InSAR analysis for these points was begun in January 2022. It was used to zero the measurements, with the GNSS measurements shifted so that their first point matches the corresponding point of the InSAR measurements. InSAR appears to have underestimated the deformation rates compared to the automatic GNSS and manual measurements.

This is partially explained by the angle of incidence and heading of the satellite, which cannot completely discriminate between horizontal and vertical movement. The up-down (Z), east-west (E), and north-south (N) components of the GNSS readings are projected onto the InSAR line-of-sight using Equation (1), where θ and α represent the incidence and heading angles of the Sentinel-1 satellite, respectively (Ng et al., 2011).

$$AutomaticGNSS_{LOS} = Z * \cos\theta - E * \sin\theta\cos\alpha + N * \sin\theta\sin\alpha \quad (1)$$

The GNSS readings are projected onto the InSAR line-of-sight (LOS) using Equation (2). It is important to note that horizontal measurements are not recorded at manual GPS locations. Consequently, the LOS conversion assumes that the observed movement is purely vertical. While this assumption may not precisely reflect the actual field conditions, it enables a reasonable comparison between different independent measurements.

$$ManualGNNS_{LOS} = Z * \cos\theta \quad (2)$$

The adjusted GNSS measurements are shown in Figure 4. While it has reduced the discrepancy between InSAR and GNSS by approximately 40 %, there remains a large difference between the rates of displacement between both sets of measurements, with for instance for 2023-05 InSAR reporting a rate of 5 mm/month and GNSS reporting a rate of 9 mm/month.

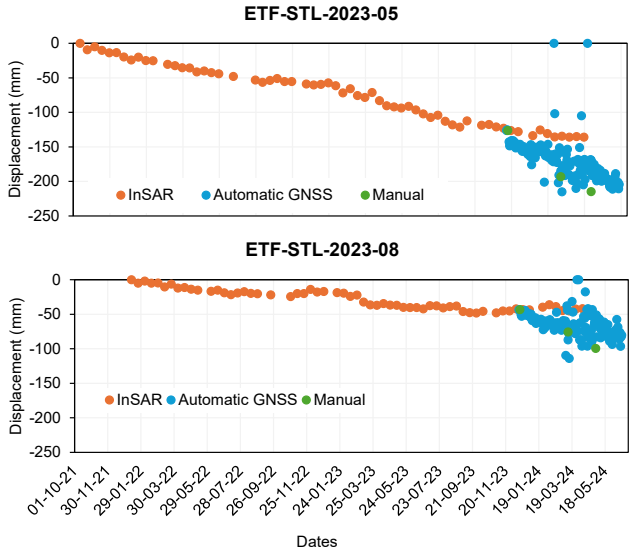


Figure 4: Comparison of adjusted automatic GNSS and Manual survey and InSAR

InSAR measurements within a 200 m radius of the manual settlement plates (shown as a red rhombus in Figure 2) are averaged to facilitate comparison with the manual settlement plate readings. The vertical displacement recorded at the manual settlement plates is projected onto the InSAR Line of Sight (LOS) using Equation (2).

InSAR measurements within a 200 m radius are available for ETF-STL-2023-03, ETF-STL-2023-04, ETF19-S2A-D, ETF20-S5A-B, ETF20-S64, and ETF20-TT04. However, manual survey data during the assessment period are only available for the latter 2. Figure 5 illustrates a comparison of InSAR and manual settlement plate readings for ETF20-S64 and ETF20-TT04. The results exhibit similar trends and values, particularly for ETF20-TT04. Conversely, the values at ETF20-S64 also indicated a similar trend, aligning with the InSAR displacement data.

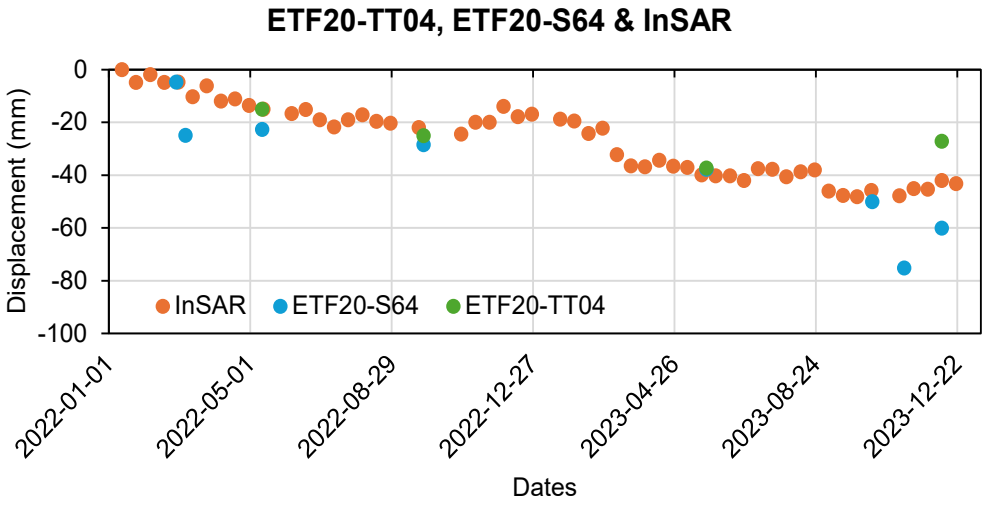


Figure 5: Comparison of InSAR and manual settlement plate readings for ETF20-S64 and ETF20-TT04

The wide area of the InSAR study also allows for comparisons with points that have been monitored with LiDAR. However, the validation of the two measurements against each other is difficult to do, due to the infrequent manual and LiDAR measurements. The plots in Figures 6 and 7 show the comparison between the manual settlement plates, LiDAR, and InSAR, using the closest InSAR acquisition as a reference.

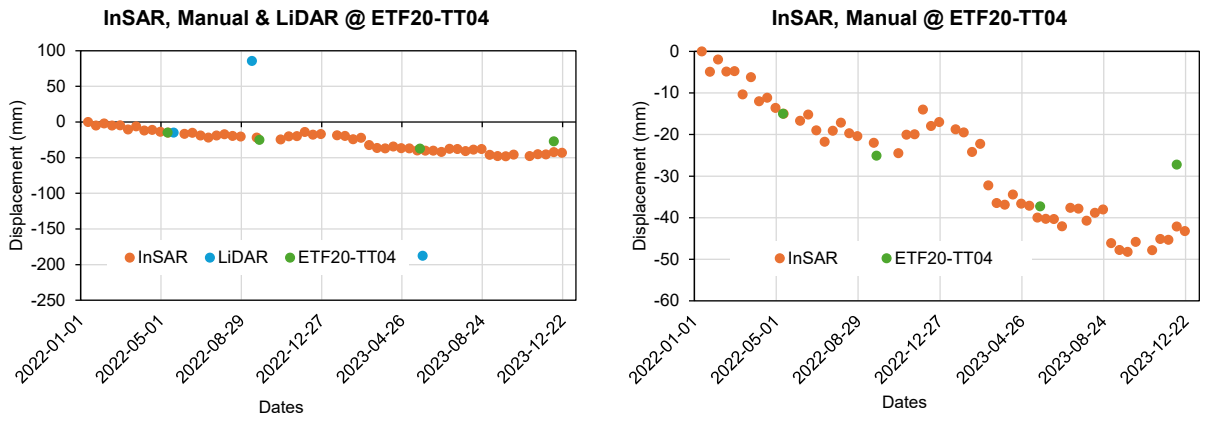


Figure 6: Comparison of a) InSAR, Manual settlement and LiDAR measurements and b) InSAR, manual settlement measurements at ETF20-TT04

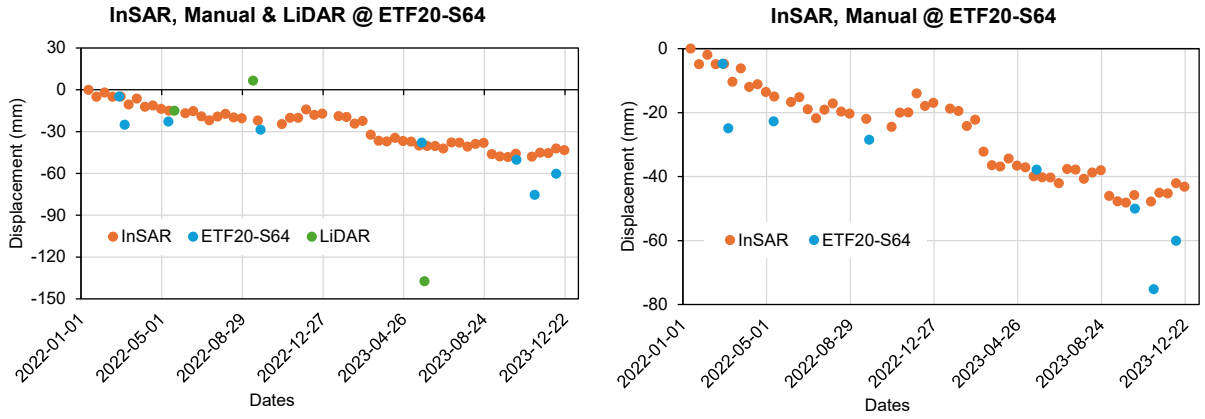


Figure 7: Comparison of a) InSAR, Manual settlement and LiDAR measurements and b) InSAR, manual settlement measurements at ETF20-S64

Automatic GNSS and manual surveys have provided similar results for the three points of interest, as shown by the red triangles of Figure 3. The error on the automatic GNSS increased beyond expected values during operations when moving the reference station to a 4.2 km distance for a period of over one month. This was addressed and the reference station was returned to a more suitable location, limiting noise to an acceptable level. Automatic GNSS allows for much more frequent measurements than manual survey, InSAR and LiDAR; by increasing the frequency of the readings, the noise can be smoothed by methods such as a gliding average to increase the accuracy of long-term monitoring of slow movements.

The agreement between GNSS and InSAR was lower than what was expected for the three points of interest. It was not possible to observe coherence for one of the three points. It appears that InSAR has underestimated vertical displacement by 30 to 50 %, even after applying LOS corrections. There are several possible causes to be investigated that may have led to this discrepancy: atmospheric phase screen,

movements faster than one quarter wavelength, radar speckle and phase unwrapping errors. This will be the subject of future research, which will include the addition of corner reflectors near automated GNSS stations.

We have seen that InSAR is in agreement with LiDAR measurements outside of the GNSS study area, measuring rates up to 30 mm/year. This observation will require further study; the LiDAR system is not designed for settlement monitoring and its repeatability may not be high enough for accurate monitoring. Comparison of the InSAR measurements with the existing LiDAR data was made difficult due to the small number of samples taken over the past years.

Conclusion

The goal of this pilot project was to compare automatic GNSS against manually surveyed settlement plates inside a TSF. In the first 6 months of 2024, settlements of up to 16 cm were measured both with manual surveys and automatic GNSS. The noise levels on the GNSS were higher than anticipated, but this issue will be addressed in future work. The study was extended to include InSAR to validate if this tool could be used to perform the same type monitoring on TSFs. The InSAR measurements demonstrate a generally consistent trend in observed displacements. While InSAR underestimated the deformation compared to the GNSS measurements, the overall subsidence trend was observed in all three independent measurement techniques. For the manual settlement plate locations, particularly ETF20-TT04 and ETF20-S64, InSAR data showed similar trends and values, indicating good agreement.

However, comparisons with LiDAR measurements were less reliable due to the lack of synchronization between data acquisition times. While InSAR is cost-effective and can cover larger spatial areas compared to conventional monitoring methods, GNSS measurements can capture higher rates of deformation that InSAR might miss due to its limitations on differential phase between two successive acquisitions.

Future work will investigate expanding the use of both GNSS and INSAR. Additional GNSS stations will provide a more robust network of measurements and new stations may be installed in locations with horizontal movement and what is assumed to be stable reference areas for InSAR. Pursuing InSAR analysis over the long term against GNSS measurements will provide more insight into the discrepancies observed between the two methods. Future studies will also include auxiliary measurements such as ground-level moisture content.

References

Berardino, P., Fornaro, G., Lanari, R., Sansosti, E., 2002. A new algorithm for surface deformation monitoring based on small baseline differential SAR interferograms. *IEEE Trans. Geosci. Remote Sens*. 40: 2375–2383.

Crosetto, M., Monserrat, O., Cuevas-González, M., Devanthéry, N. and Crippa, B. 2016. Persistent scatterer interferometry: A review. *ISPRS J. Photogramm. Remote Sens*. 115: 78–89.

Duro, J., Iglesias, R., Monells, D. and Calvo, R. 2020. Exploitation of InSAR techniques as a support of in situ sensors to improve safety and productivity in mining operations. *Proceedings of the 2020 International Symposium on Slope Stability in Open Pit Mining and Civil Engineering*. pp. 1531–1546.

Mohamadi, B. 2024. Utilizing InSAR for surface stability monitoring in mining sites: A case study of Sukari Gold Mine in Egypt. *Int. Arch. Photogramm. Remote Sens. Spat. Inf. Sci*. 48: 523–528.

Perdikou, S. and Lees, A. 2023. Could regular satellite InSAR monitoring have helped prevent the Jagersfontein tailings dam failure? *Proceedings of Geosaskatoon 2023*.

Rana, N.M., Delaney, K.B., Evans, S.G., Deane, E., Small, A., Adria, D.A.M., McDougall, S., Ghahramani, N. and Take, W.A. 2024. Application of Sentinel-1 InSAR to monitor tailings dams and predict geotechnical instability: practical considerations based on case study insights. *Bull. Eng. Geol. Environ.* 83: 204.

Sciortino, A., Antonielli, B., Scancella, S., Bozzano, F., Mazzanti, P. and Moretto, S. 2021. Satellite InSAR for assessing deformation processes at the Zelazny Most Tailings Dam (Poland). *Proceedings of 7th International Conference on Tailings Management.*

Thomas, A., Edwards, S.J., Engels, J., McCormack, H., Hopkins, V. and Holley, R. 2019. Earth observation data and satellite InSAR for the remote monitoring of tailings storage facilities: A case study of Cadia Mine, Australia. In A.J.C. Paterson, A.B. Fourie & D. Reid (eds), *Paste 2019: Proceedings of the 22nd International Conference on Paste, Thickened and Filtered Tailings*, Australian Centre for Geomechanics, Perth: 183–195, https://doi.org/10.36487/ACG_rep/1910_11_Thomas

Integrated Analysis of Dam Surface Displacement Monitoring

Felipe Bolívar Domingos, Vale S.A., Brazil
Alessandra Mazon, Vale S.A., Brazil
Jefferson Barbosa, Vale S.A., Brazil

Abstract

Following recent dam failures in Brazil (Mariana in 2015 and Brumadinho in 2019), mining companies have implemented extensive geotechnical monitoring plans, particularly for tailings dams. To enhance the safety of tailings management, various technologies have been widely adopted for geotechnical surveillance. Interpreting data and making informed decisions remain significant challenges for the mining sector. This paper presents a study of a tailings dam in Brazil, where InSAR (Interferometric Synthetic Aperture Radar), ground-based radar, and Robotic Total Station (RTS) technologies were used to monitor surface displacements. InSAR was initially used for broad assessment and long-term displacement monitoring, similar to RTS. Ground-based radar focused on critical, short-term analysis.

During the first stage of the monitoring strategy, InSAR data identified anomalous physical response zones in the dam. This analysis guided field inspections. The extent of the anomalous area was defined through fieldwork, allowing for improved RTS monitoring. Reflectors were installed around the deformation area to better track movements. In the final phase, data from InSAR and RTS were correlated, revealing a high correlation between the magnitudes of slow movements from both datasets. Meanwhile, ground-based radar showed no significant deformations, supporting its use for detecting rapid displacements due to its line-of-sight limitations. This study underscores the importance of integrating remote monitoring technologies, and the value of a robust monitoring program in deriving accurate conclusions about dam deformation and performance.

Introduction

In recent years, the mining industry in Brazil has faced significant challenges due to catastrophic dam failures, most notably in Mariana (2015) and Brumadinho (2019). These incidents underscored the critical need for robust geotechnical monitoring systems for tailings dams to prevent future disasters. Consequently, mining companies have increasingly implemented comprehensive monitoring plans, utilizing a variety of

advanced technologies. The primary objective of these monitoring efforts is to ensure the safety and stability of tailings dams, thereby protecting both human lives and the environment.

This paper focuses on the importance of integrating multiple monitoring techniques to obtain precise and complementary data for effective dam management. By employing Interferometric Synthetic Aperture Radar (InSAR), Ground-based Radar (GBR), and Robotic Total Station (RTS) technologies, this study aims to demonstrate how different methods can be used synergistically to monitor surface displacements and identify potential risks. InSAR provides broad and long-term displacement data, making it ideal for initial assessments and continuous monitoring. Ground-based radar provides essential short-term analysis, detecting rapid displacements that could indicate potential failure more promptly, contingent on the line of sight. RTS provides precise measurements of surface movements, which are essential for detailed analysis and verification of findings from other technologies.

The integration of these technologies allows for a comprehensive understanding of dam behavior, improving the accuracy of deformation assessments and enhancing decision-making processes. By correlating data from multiple sources, this approach not only identifies potential issues more reliably but also optimizes the overall monitoring strategy, ensuring a higher level of safety and operational efficiency in tailings dam management.

Equipment and technologies used

InSAR (Interferometric Synthetic Aperture Radar)

Satellite InSAR is generally used by mining operations for site-wide deformation monitoring, with acquisition footprints that cover a broad area of the Earth's surface allowing a bird's-eye view and full coverage of a mine site, making this technology ideally suited to deformation monitoring of large tailings facilities (Sharon and Eberhardt, 2020).

The Synthetic Aperture Radar (SAR) is based on the emission of electromagnetic energy in the microwave range (Moreira et al., 2013) during successive passes at different times and under various geometries (Ferretti et al., 2011). SAR systems operate within a wavelength range of 1 mm to 1 m, or a frequency range from 0.3 GHz to 300 GHz. These systems utilize a side-looking geometry, where a microwave beam is emitted at an angle orthogonal to the sensor's velocity vector, aligning with the satellite's path. This configuration allows for the creation of a two-dimensional imaging plane, defined by the dimensions of range and azimuth, which is achieved through the sensor's movement and the periodic transmission of pulses orthogonal to its trajectory (Paradella et al., 2021).

Figure 1 shows the standard geometry of SAR. In this configuration, the radar platform travels in the azimuth or along-track direction, while the slant range refers to the direction perpendicular to the radar's flight path. The swath width indicates the ground-range coverage of the radar scene, and its length is

determined by the duration of the data acquisition, which corresponds to the period the radar is active (Moreira et al., 2013).

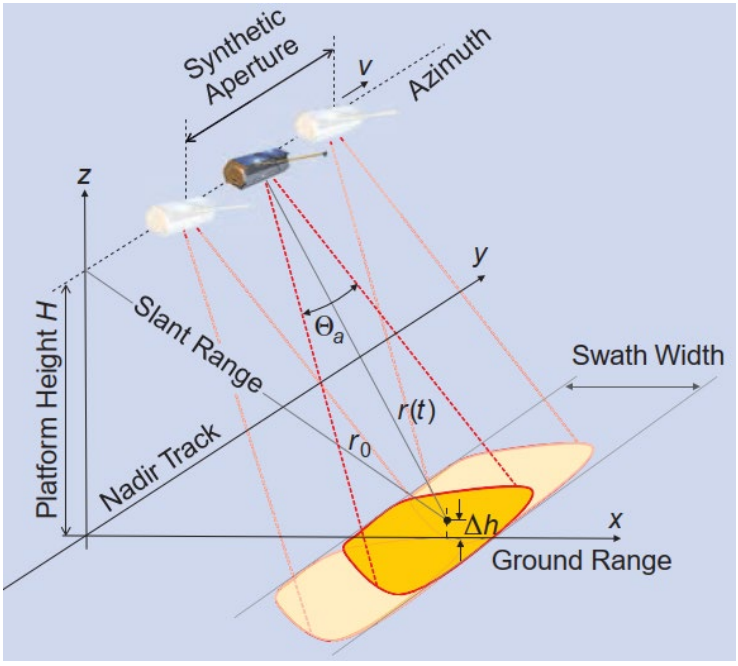


Figure 1: SAR imaging geometry. r_0 stands for the shortest approach distance, θ_a for the azimuth beam width and v for the sensor velocity (Moreira et al., 2013)

By identifying variations between the emitted and received wave phases, it is possible to obtain digital elevation models in the order of meters and deformation measurements in the order of millimeters (Ferretti et al., 2011).

Although using the spectral range corresponding to microwaves, the satellites (or constellations) may exhibit variations in the applied band. Table 1, adapted from Moreira et al. (2013), shows the relationship between wavelength, frequency, and the corresponding band, characteristics directly associated with monitoring precision. The radar used in this work is COSMO-SkyMed (X-band). For this work the radar used is COSMO-SkyMed (band X).

Table 1: Commonly used frequency bands for SAR systems and the corresponding frequency and wavelength ranges (Moreira et al., 2013)

Frequency Band	Ka	Ku	X	C	S	L	P
Frequency (GHz)	40-25	17.6 –12	12–7.5	7.5–3.75	3.75–2	2–1	0.5 – 0.25
Wavelength (cm)	0.75-1.2	1.7–2.5	2.5–4	4–8	8–15	15–30	60–120

GBR (ground-based radar)

The GBR is an instrument that allows the monitoring of mine slopes, hillsides, and dams. It has been designed to remotely scan a rock slope to continuously monitor the spatial deformation of the surface. Similar to the satellite-based technique, using differential radar interferometry the system can detect deformation movements of a rough wall with sub-millimeter accuracy and with high spatial and temporal resolution (Noon et al., 2001).

According to Atzeni et al. (2014), the first application of ground-based synthetic aperture radar interferometry for measuring surface tilt movements was carried out in the Italian Alps in the year 2000. Over time, due to the development of specific radar sensors and dedicated processing techniques, the technology evolved from an early prototype, which consisted of laboratory instrumentation temporarily used in the field, to an industrial product with the highest quality standards (Atzeni et al., 2014).

In summary, as shown in Figure 2, the system works (Sharon and Eberhardt, 2020):

- The system operates by generating a sinusoidal waveform with a precise frequency. This waveform is transmitted through an antenna as a narrow beam of electromagnetic waves.
- The beam is directed towards the monitored pit slope, where a small portion of the energy is reflected back to the radar (also known as backscattering). The backscattered wave, or echo, is intercepted by the antenna and converted into a signal.
- This signal is then processed and analyzed using interferometry to detect differences in the phase values of backscattered waves between consecutive measurements. If a phase change is detected, it indicates movement of the target between the two acquisitions.

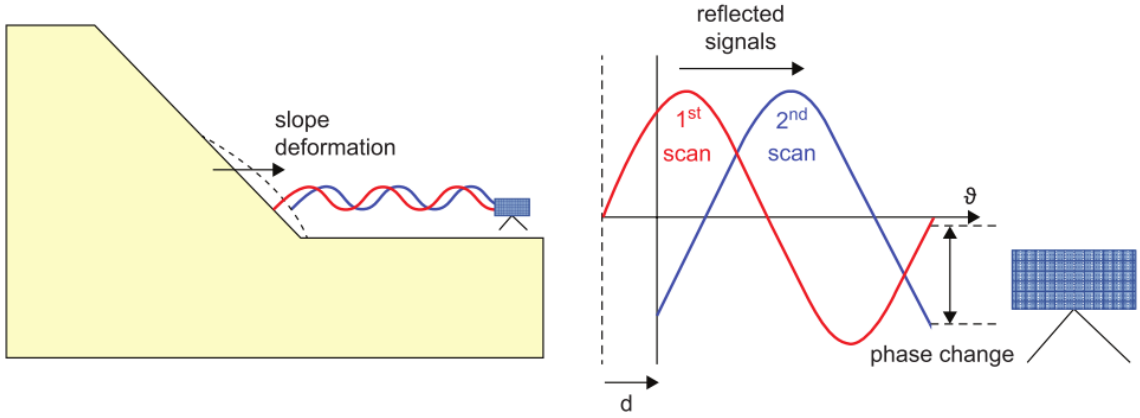


Figure 2: Measurement of displacement using radar interferometry calculated by comparing changes in phase of the reflected signals between two consecutive radar measurements (Sharon and Eberhardt, 2020)

Currently, there are two types of interferometric radars commonly used for slope monitoring: real aperture radar (RAR) and SAR (Figure 3). For this work, IDS's SAR IBIS-FM ground-based radar was used. The systems use a small moving antenna along a guide to simulate a larger aperture, enabling wide-area coverage without significantly varying scan times relative to the monitored area, unlike RAR systems (Sharon and Eberhardt, 2020).

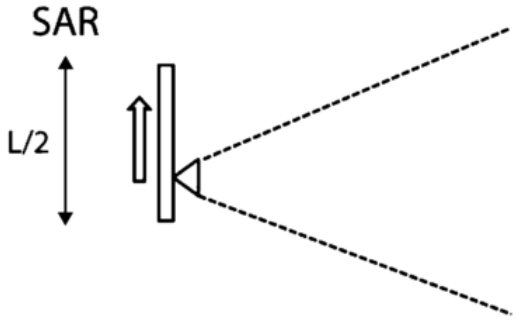


Figure 3: Synthetic-aperture radar (SAR) (adapted from Atzeni et al., 2014)

RTS (robotic total station)

The total station (TS) is an instrument that integrates an electronic theodolite with an electronic distance meter (electronic distance measurement – EDM). Modern robotic total stations (RTSs) are multi-sensor systems that combine distance and angle measurements and automatic aiming data to obtain three-dimensional coordinates.

There are some ways to measure distances by electronic means, among them, pulse method and phase difference method.

Pulse Method (Rueger, 1996)

A short, intensive signal is transmitted by an instrument. It travels to a target point and back, covering twice the distance d. By measuring the flight time between transmission and reception of the same pulse, the distance can be calculated.

$$2d = c\,\Delta t'$$

d = distance between instrument and target

c = velocity of light in the medium

$\Delta t'$= flight time of pulse

Phase Difference Method (Ghilani and Wolf, 2010):

The EDM device is positioned over station A using a plumb line or optical alignment device (Figure 4). The instrument emits a carrier signal of electromagnetic energy to station B. A reference frequency with a precisely regulated wavelength is superimposed or modulated onto the carrier. A reflector at B returns the

signal to the receiver, resulting in a travel path that is double the slope distance AB. In the Figure, the modulated electromagnetic energy is represented by a series of sine waves, each with a wavelength λ. The unit at A determines the number of wavelengths in the double path, multiplied by the wavelength in feet or meters, and divided by 2 to obtain distance AB.

$$L = (n\lambda + p)\frac{1}{2}$$

λ = wavelength;

n = number of full wavelengths;

p = length of the fractional part (some fractional part of a wavelength would in general be expected

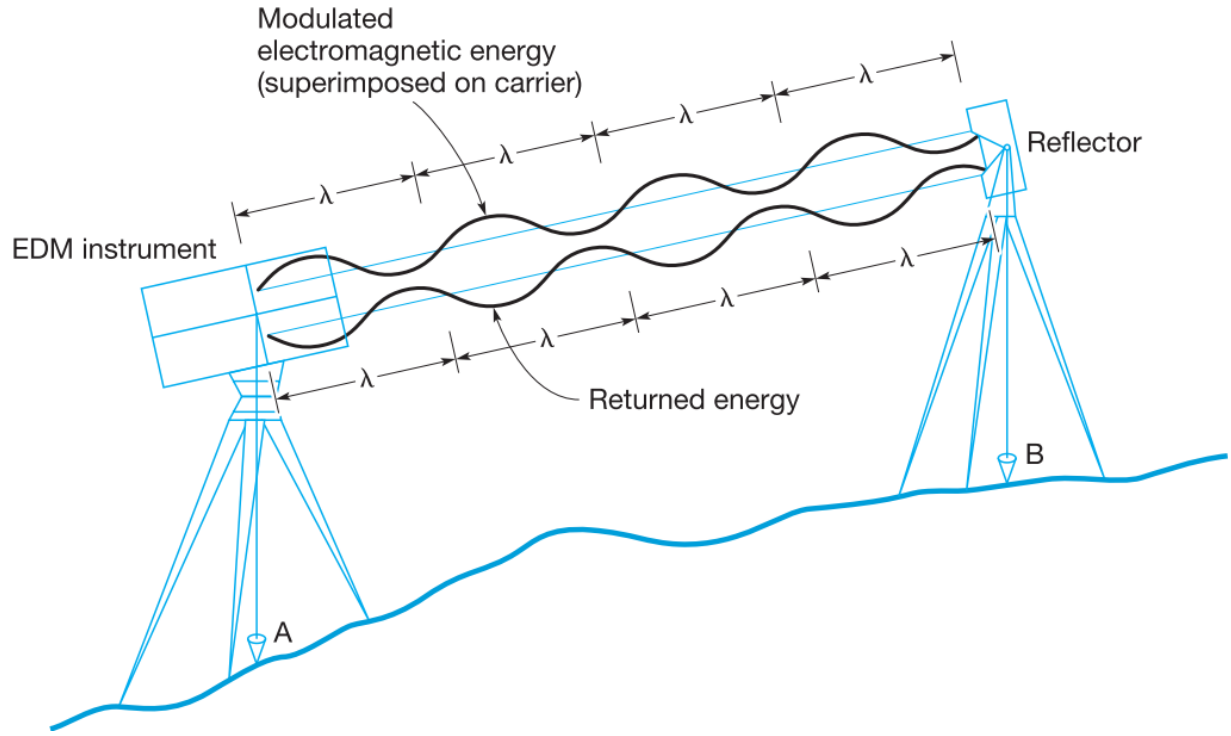


Figure 4: Generalized EDM procedure (Ghilani and Wolf, 2010)

Thus, based on the principles of EDM (Electronic Distance Measurement) and electronic theodolites capable of measuring horizontal and vertical angles (or zeniths), the RTS performs measurements automatically. To locate the prisms (targets), RTSs are equipped with an Automatic Target Recognition (ATR) device, which allows for identification, and a servomechanism that enables tracking of the target (Stiros and Psimoulis, 2012). After measuring distances and angles, it is geometrically possible to obtain the coordinates of the target.

Methodology

To assess the behavior of the surface displacement of the dam, the acquisition and analysis of monitoring data were divided into two main stages. The first stage involved the individual collection and analysis of surface displacement monitoring using the three technologies over a period of three months: InSAR, RTS and GBR subsequently, the monitoring data were integrated and jointly analyzed, which was essential to identify trends and standards of displacements and to better correlate the characteristics of the movements with the appropriate use of surface displacement monitoring tools.

InSAR data were derived from SAR images acquired by the CSK satellite constellation in ascending (ASC) and descending (DSC) orbits. This dual geometry approach allowed for vector decomposition of the line of sight (LoS) movement and analysis in the vertical and east-west directions, as shown in Figure 5. The data sample was obtained with an acquisition frequency of eight days.

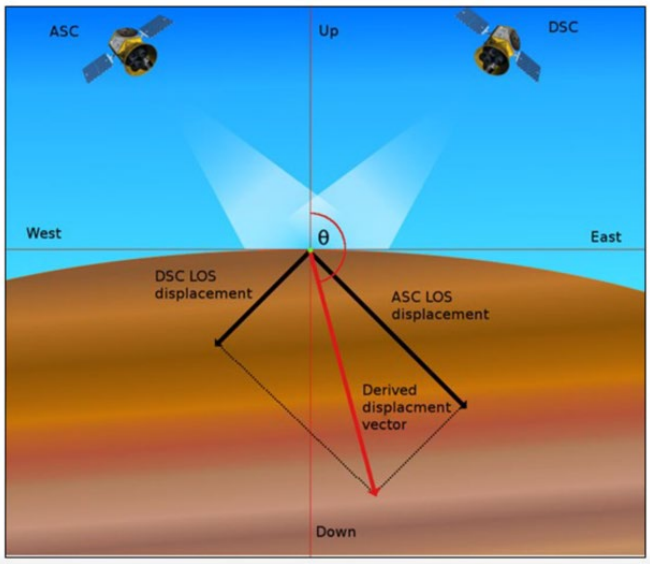


Figure 5: CSK acquisition geometry and LoS vector decomposition (modified from Leighton, 2020)

The use of RTS and monitoring through prisms installed on the surface allowed continuous monitoring of the downstream slope of the tailings dam. The reading cycle for each monitoring prism was approximately 15 minutes. Temperature and pressure data were collected through a weather station and processed using an algorithm to correct noise from atmospheric variations (humidity, temperature, and pressure), as recommended by the manufacturer. The RTS Leica TM-50 was used for this purpose.

GBR monitoring was conducted using the IBIS-FM equipment, configured for continuous monitoring with an approximate acquisition frequency of 2 minutes per cycle on the downstream slope surface of the dam. The GBR was installed as frontally as possible to the structure for better radar signal return. Since the radar measures displacements in the Line of Sight (LoS), the more frontal to the structure, the closer the

movement trends will be to the actual movement. Vegetation on the slopes can generate noise in the data, complicating the detection of slow movements. To mitigate this limitation, subsampling of the data was performed for the analysis of very slow movement, allowing for the analysis of slow deformations in the structures.

Data and discussion

InSAR data were analyzed using velocity maps on a GIS platform (Figure 6) using displacement rate time series, showing a pattern of slow displacement trends in a specific region near the left abutment of the upper portion of the dam. Consequently, this region where the pixels with the highest displacement ranges are concentrated, as indicated in Figure 6, was selected for integrated data analysis. The sample period considered for this analysis was from December 2019 to February 2020.

The data of the time series evaluation during this period demonstrated a very slow vertical displacement downward trend in this region of the structure, with maximum velocity on the order of 3 mm/month.

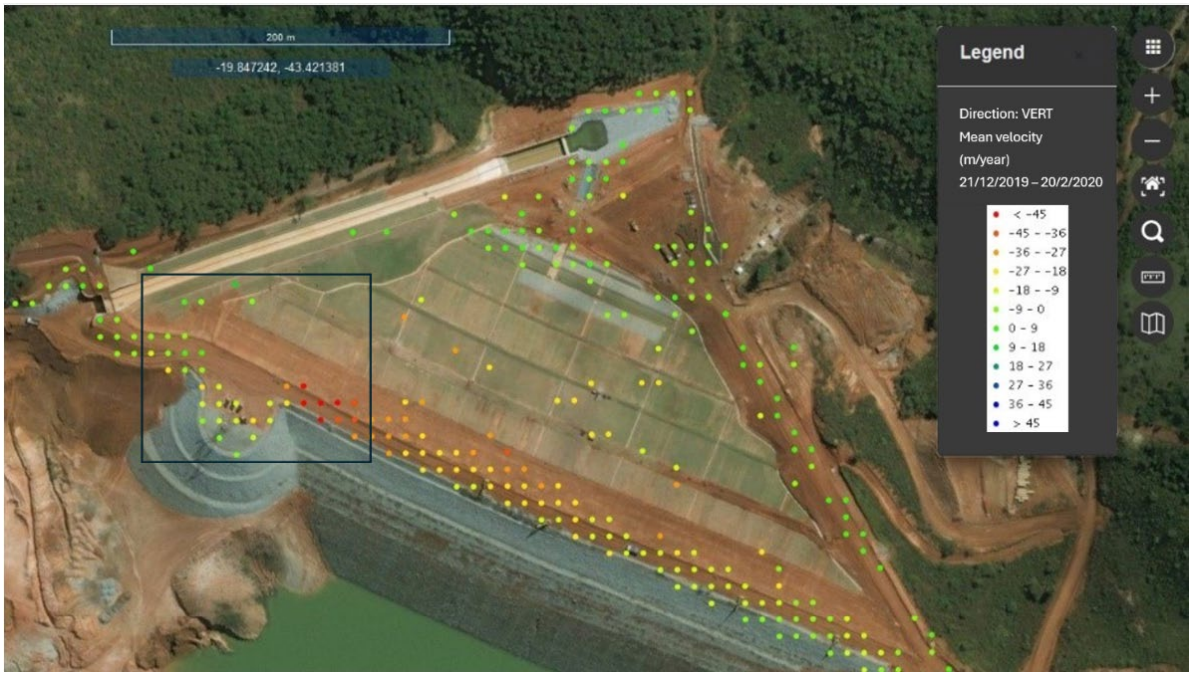


Figure 6: InSAR monitoring displacement rate data

In the region where the InSAR monitoring data showed pixels with the highest displacement ranges are concentrated, RTS-monitored prism data were evaluated (Figure 7). The monitoring prisms, through vertical and horizontal vector time series, showed vertical displacements on the order of 9 mm in 3 months downward. No trends of horizontal movement were observed in the monitoring data in the east-west direction.

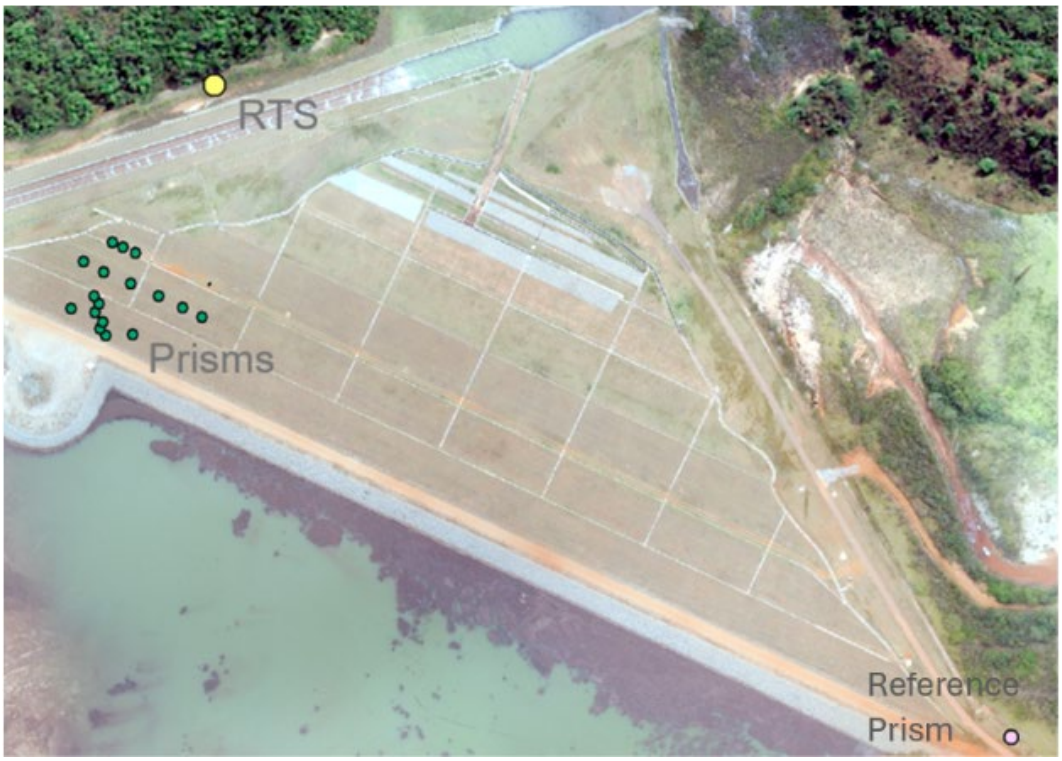


Figure 7: Prisms installed on the downstream slope of the dam for RTS monitoring

GBR data processing was used to detect slow displacement (Figure 8). This technique, called subsampling, processes data sampled over a longer period to reduce noise from the dam's vegetation cover, atmospheric noise, and other sources. These noises can mask slow displacements. For this subsampling process, data were sampled every 16 hours to reduce noise.

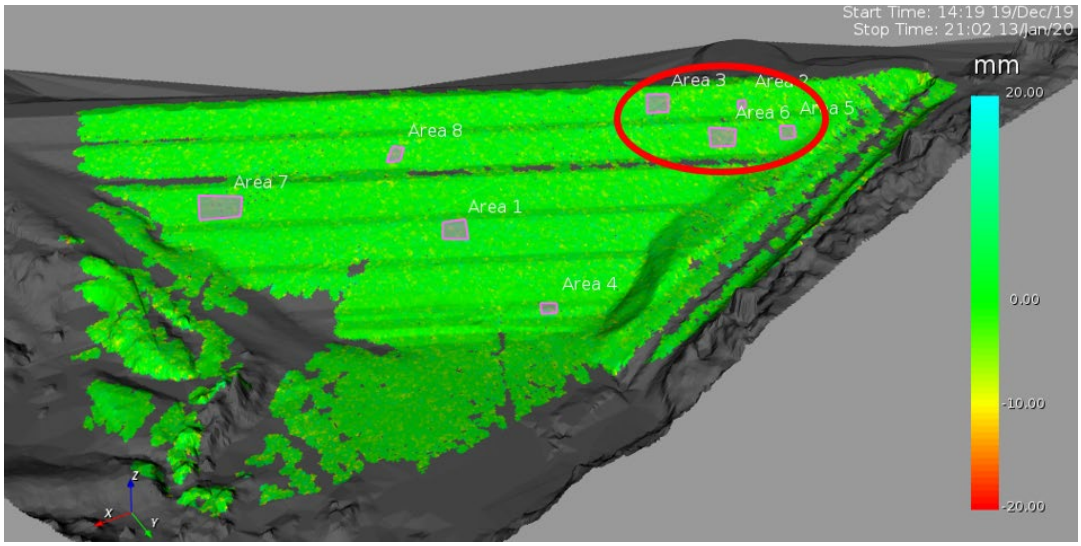


Figure 8: Radar displacement map in subsampling processing. The areas of interest in this study were 2, 3, 5, and 6

Results

Through the integrated evaluation of the monitoring data over the period analyzed in this study, the same patterns of vertical displacements downward were observed in both InSAR and RTS technologies. Both technologies detected slow settlement movements on the order of 3 mm/month (Figures 9 and 10).

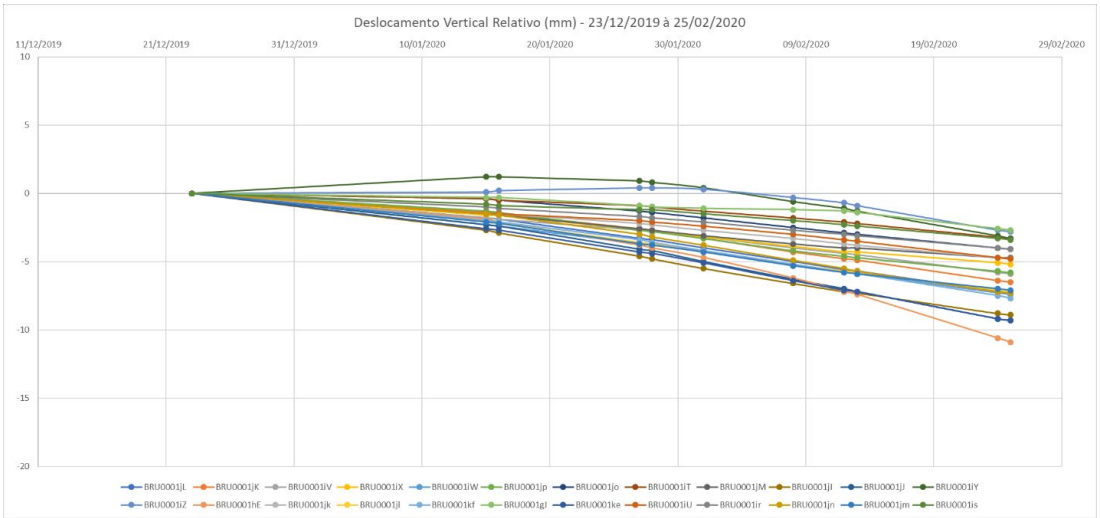


Figure 9: InSAR vertical displacement downward rate data

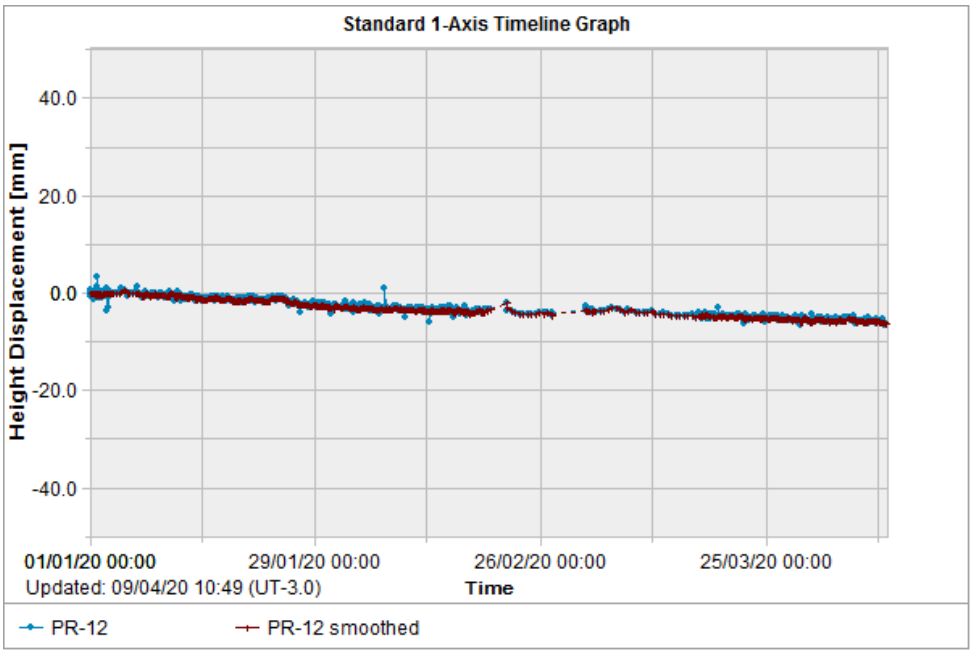


Figure 10: RTS vertical displacement downward data

In the GBR and RTS monitoring, no LoS movements were detected (Figure 11, 12). Since the LoS component is more horizontal than vertical, this is consistent with the other methodologies, as they did not show trends of horizontal movement either.

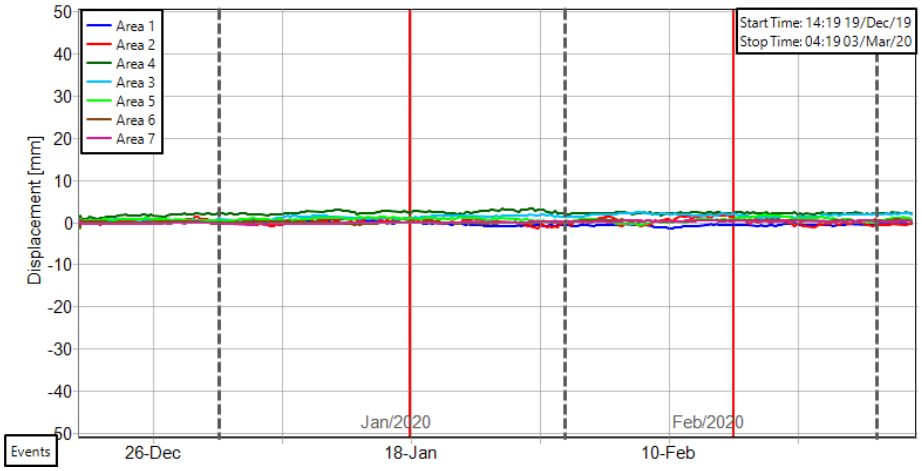


Figure 11: GBR line-of-sight displacement data. The areas of interest in this study were 2, 3, 5, and 6

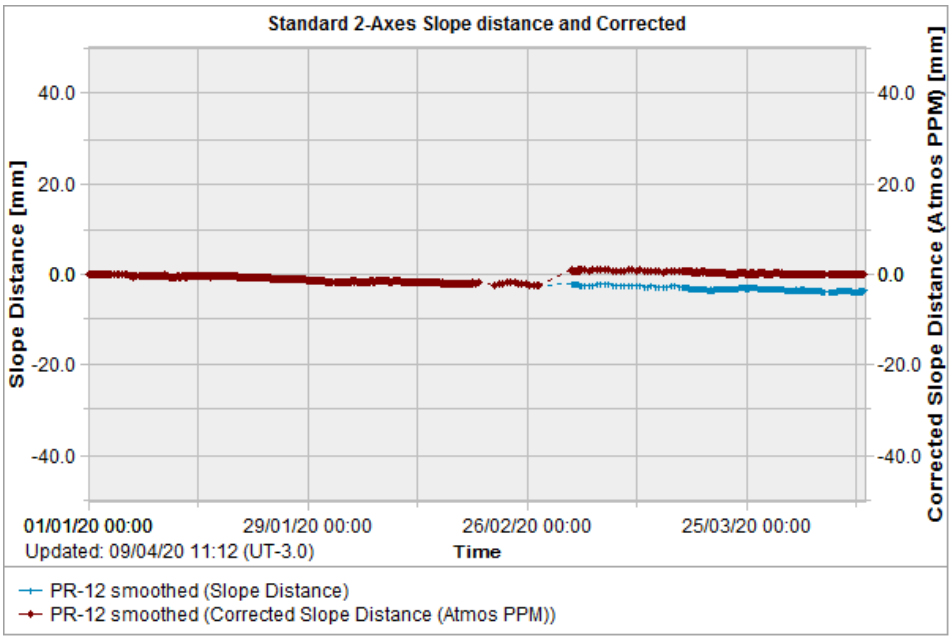


Figure 12: RTS slope displacement (LoS) data

Conclusion

This study showcased how the three displacement monitoring methodologies are applicable to tailings dams, provided their response objectives are well-understood, including the accuracies and limitations of each methodology and understanding what and where to monitor. In this study, a good correlation was observed between the vertical displacement monitoring data of the InSAR and RTS methodologies. Both methodologies, despite being different, showed the same trends and order of displacement in the time series over the same period. In the GBR monitoring data, no displacement trends were observed, likely because

the main movement was vertical, which could not be detected by the GBR, even with the subsampling processing.

Additionally, the methodologies were found to be complementary due to their limitations. Radar has the potential to detect fast movements in the structure, complemented by the robotic total station. However, InSAR is effective in detecting slower, more regional movements that can define regions for refinement and complementation by RTS monitoring. For slow horizontal movements, RTS is the best detection system in this case study and can be complemented by GBR slow movement monitoring using subsampling processing. No horizontal displacements were identified by any of the three technologies in this study.

References

Atzeni, C. et al. 2014. Early warning monitoring of natural and engineered slopes with ground-based synthetic-aperture radar. *Rock Mechanics and Rock Engineering* 48(1): 235–246.

Ferretti, A., A. Fumagalli, F.P. Novali, R.F.C. and A. Rucci. 2011. A new algorithm for processing interferometric datastacks: SqueeSAR: 3460–3470. *IEEE T. Geosci. Remote* 3460 – 3470.

Ghilani, C.D. and Wolf, P.R. 2010. *Elementary Surveying – An Introduction to Geomatics*. 13th edition, Pearson.

Gojcic, Z., Kalenjuk, S. and Lienhart, W. 2017. Synchronization routine for real-time synchronization of robotic total stations. *Proceedings of INGEO 2017 – 7th International Conference on Engineering Surveying*.

Leighton, J. 2020. Introduction to satellite-based SAR. In 2020 Radar Monitoring Short Course. Geotechnical Center of Excellence, University of Arizona.

Moreira, A. et al. 2013. A tutorial on synthetic aperture radar. *IEEE Ceosci. Remote Sens. Mag.* 1(1): 6–43.

Noon, D., Reeves, B., Stickley, G. and Longstaff, D. 2001. Slope stability radar for monitoring mine walls. *Proceedings of SPIE – The International Society for Optical Engineering:* 4491.

Paradella, W.R., Mura, J.C. and Gama, F.F. 2021. *Monitoramento Dinsar Para Mineração e Geotecnia*. Oficina de Textos.

Rueger, J.M. 1996. *Electronic Distance Measurement. An Introduction*. Fourth edition. Springer.

Sharon, R. and Eberhardt, E. 2020. *Guidelines for Slope Performance Monitoring.* CSIRO,.

Stiros, S.C. and Psimoulis, P.A. 2012. Response of a historical short-span railway bridge to passing trains: 3-D deflections and dominant frequencies derived from Robotic Total Station (RTS) measurements. *Engineering Structures:* 362–371.

Chapter Eleven

Site Investigation

TAILINGS AND
MINE WASTE 2024



Enhancing Safety and Reducing Environmental Impact through Development of a Robotic Hybrid CPT Rig

David Slack, ConeTec, Canada
Roque Obusan, ConeTec, Canada
Yasmin Byrne, ConeTec, UK
Dora de Melo, University of California Davis, USA
Jason DeJong, University of California Davis, USA

Abstract

The mining industry continually seeks advancements in technology to enhance operational safety and minimize environmental impact. This paper presents the development of a state-of-the-art Remote Robotic Hybrid Diesel-Electric Cone Penetration Testing Track Rig (Robotic Rig), designed to address the critical need for conducting geotechnical investigations in hazardous mine waste environments while ensuring the safety of personnel and reducing carbon emissions.

The innovation of remote robotic capabilities enables high quality geotechnical testing without the risks associated with personnel working in a hazardous environment. This functionality is crucial for investigating unstable or high-risk areas. The hybrid diesel-electric power system represents a significant step forward in reducing the carbon intensity of geotechnical investigations.

The paper will detail the objectives of the Robotic Rig, discuss its technical features including comparison against conventional ConeTec Penetration Testing (CPT) track rigs, and present the measurable health and safety and environmental impact. The paper will also present findings from field trials demonstrating the rig's operational effectiveness. Through this development, we propose a novel solution that addresses the dual challenges of safety and sustainability in mine waste management, offering a model for future innovations in the mining sector.

Introduction and motivation

The mining industry continuously seeks innovation in response to increasing demands to improve safety, environmental performance, and operational efficiency. Geotechnical investigation plays a key role in this by providing essential data and improving the understanding of the ground conditions, which permits the optimization of design for stability and sustainability. All work areas have inherent risks; however, the risk

in some mine tailings environments exceeds the tolerance under which it is acceptable for personnel to perform their work (Baker et al., 2018). In these cases, it is essential to reduce the risk to personnel by keeping them out of the hazardous environment. This paper discusses the development of robotic capabilities to allow for geotechnical testing from safer and remote work areas by remotely maneuvering the rig into the high-risk area and remotely operating the rig robotics to perform Seismic Cone Penetration Testing (SCPTu), piston sampling, or piezometer installations.

Conducting any ground investigation incurs a carbon cost. Life cycle analysis of geotechnical site investigations demonstrates that while direct push investigations such as Cone Penetration Testing (CPT) have substantially lower environmental impacts than drill-type investigation methods, by a factor of 3–5 (Purdy et al., 2022), there is still a significant emission of carbon dioxide and greenhouse gases. The Robotic Rig development aims to address this environmental issue through implementation of technologies that further reduce the carbon intensity of direct push investigations. Thus, the objectives are twofold:

1. Protect field personnel through remote robotic functionality of the rig, which allows for critical data collection on high-risk sites with a significant reduction in risk to personnel.
2. Reduce the environmental impact of direct push testing by optimizing the use of electric energy conversion, usage, and storage.

Background and standard diesel operation

Conventional CPT rigs are powered by diesel engines such as a Caterpillar C7.1 (Cat C7.1), which powers both rig locomotion and testing operations. The maximum theoretical brake-horsepower efficiency, defined as the efficiency at the output shaft of the engine and before any powertrain losses, of a Cat C7.1 is 41% (Caterpillar, 2024). Once powertrain and energy conversion losses are accounted for the efficiency of converting the chemical energy stored in diesel fuel into work is much lower. To derive the maximum efficiency of conversion of chemical energy into work, the diesel engine should be sized appropriately for the load. This is the case when a conventional CPT track rig is moving, especially in soft ground or on an incline where a significant portion of the 432 hp, the maximum power of the Cat C7.1, is needed. However, the peak power demand for CPT testing is typically between 13–67 hp depending on pushing conditions including tip resistance, friction on the rods, and penetration depth. This means that for CPT and direct push applications an engine such as the Cat C7.1 is greatly oversized and even at a low idle the engine will be producing excess power which is not needed and thus will be converted into heat rather than work. During CPT and direct push operations only around 20% of the power output is utilized, as shown in Figure 1.

In addition to the diesel engine in a conventional CPT track rig being oversized for advancing the cone, there is also significant time during a CPT test where no hydraulic power is needed such as during

pore pressure dissipations, seismic tests, or when adding and removing rods. The diesel engines in conventional CPT rigs are not designed to shut off during these periods when no hydraulic power is needed thus during these operations, all of the engine power output is converted to heat. The total idle time for the push presented in Figure 1 is 27 minutes (68%) where fuel is being consumed unnecessarily, resulting in higher operational costs and excess greenhouse gas emissions.

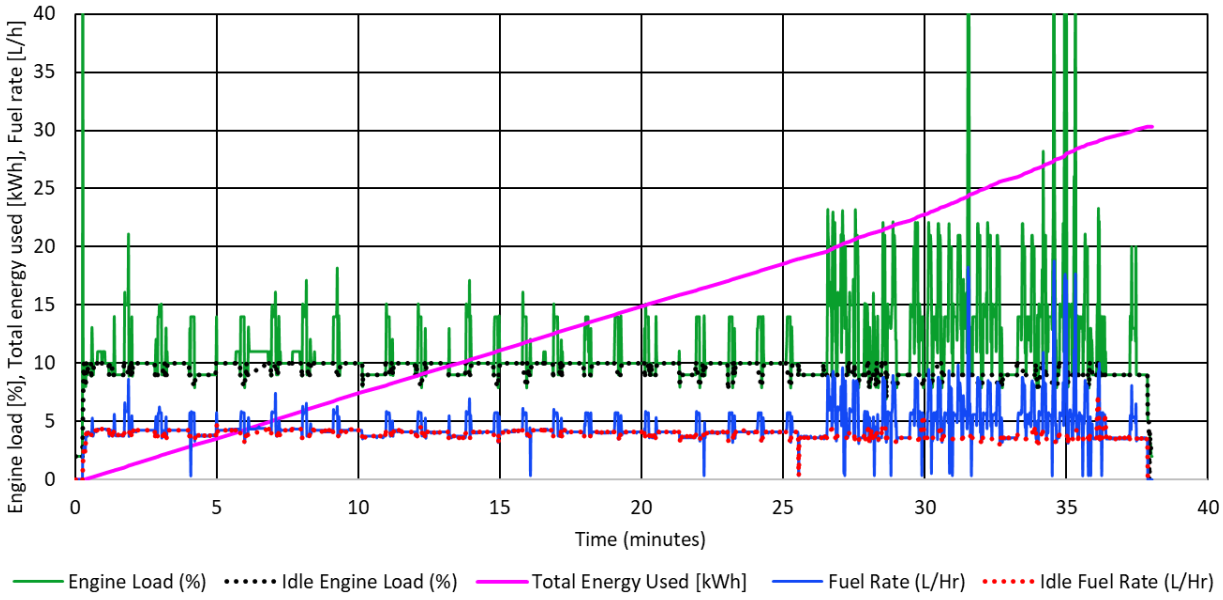


Figure 1: Example fuel usage rate (l/hr) and engine load for standard diesel operations at 1,200 RPM during a 20 m CPT push

Development of features and capabilities

Hybrid diesel electric system

Development of the hybrid diesel-electric system focused on decreasing fuel usage and lifecycle environmental impact while maintaining productivity. A key strategy to realize these objectives was to design a diesel electric system that would capture the excess power produced during idling as electrical energy which would be stored in an onboard battery. This power was optimized for CPT and direct push functions and allows for CPT operations to be powered either by the diesel engine or by the onboard battery system. When the CPT operations are powered by the diesel engine, excess power which is not needed for these operations is captured by the integrated generator and converted into electrical energy and stored in the battery. When CPT and direct push operations are powered by the electrical system, the diesel engine does not run and the electrical system only outputs power when there is a demand. This means that during the operations when hydraulic power is not needed such as pore pressure dissipations, seismic testing, and adding and removing rods, the batteries do not output any energy to the hydraulic system. This greatly reduces the energy wasted as compared to a conventional CPT track rig.

The electric batteries in the Robotic Rig are designed to charge anytime excess power is being output by the diesel engine including during locomotion and during testing when running off the diesel engine. The batteries can also be charged from the grid. When conducting CPT on battery power, as shown in Figure 2, the diesel engines are off and no fuel is being consumed.

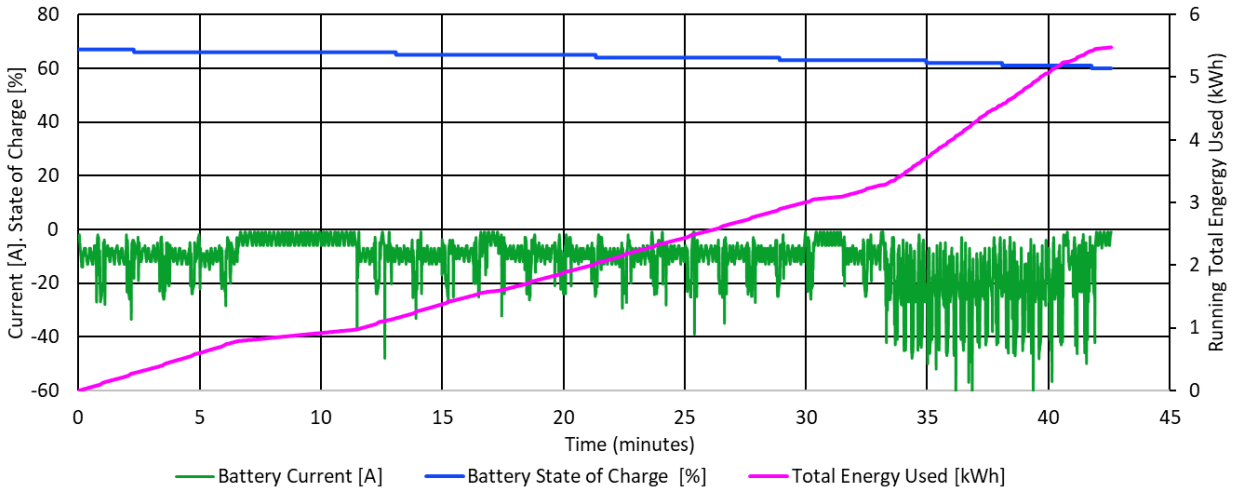


Figure 2: Example fully electric 20 m CPT push comparing work to energy usage. Push was conducted with no diesel usage

The total energy used by the diesel and electric systems for a 20 m CPT can be compared. Based on the data presented in Figures 1 and 2, the electric system when powering the CPT pump only is about five times more efficient than the conventional diesel system and requires only 20% of the energy to conduct a comparable amount of work.

Remote robotic functionality

The primary goal of the remote robotic function is to eliminate the need for operator presence within hazardous sites. This necessitates the ability to track the rig remotely to the testing location and conduct the CPT or other direct push operations remotely through the onboard robotics. The key operations of the robotic system of the Robotic Rig are:

- Add and remove a cone penetrometer, direct push sampler, or piezometer through the push clamp.
- Add and remove a 1-meter-long cone rod on to the end of a direct push tool or another cone rod.
- Tighten and loosen the cone rods from each other.
- Move the thrust cylinders with speed precision.
- Operate the seismic hammer.

The primary robotic equipment in the Robotic Rig is a commercially available industrial 6 degree of freedom robot. While this robot is highly versatile and allow for a great amount of flexibility in the system, some custom robotics apparatuses were also required. The custom robotics and apparatuses implemented for the Robotic Rig include a vertical rod rack, a hydraulically powered seismic beam, a rod tightening and loosening device and a cone rod that does not rely on a continuous cable from the cone to the data acquisition system (DAS). Commercially available cableless rod solutions, such as acoustic and fiber optic technologies, were evaluated and did not meet the geotechnical data requirements established for this project which included the requirement for shear and compression wave seismic testing a penetration depth up to 100 meters. Therefore, a new cableless rod system was developed to support low-latency seismic triggering, allowing the transmission of both standard CPT and seismic data. This system permits the sustained transfer rates of 100 Mb/s while allowing for seismic triggering.

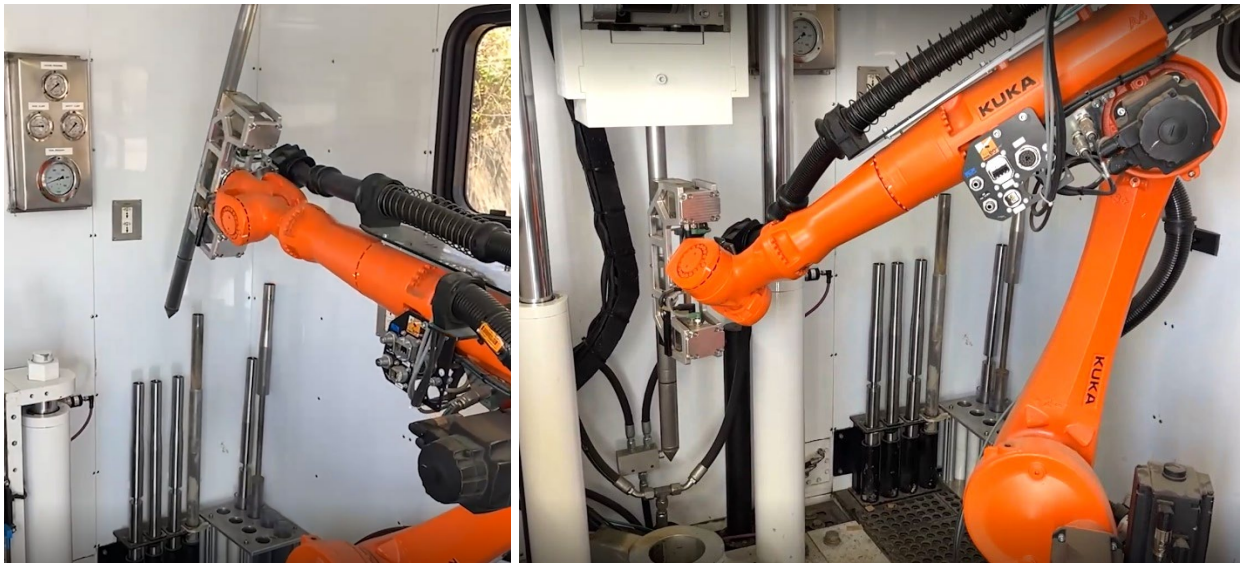


Figure 3: Robotic installation of cone penetrometer through the push clamp

To optimize efficiency, the Robotic Rig is designed to be able to perform a full day of testing in the field without operator intervention. This includes up to four seismic cone tests and the recovery of eight samples, but these limitations are only practical based on the space available in the rig and could be expanded if it became important. The operator intervention involves loading prepared piezocones and sample tubes into the rig before the rig leaves the safe area.

Data geotechnical quality checks

Ensuring the accuracy and reliability of geotechnical data obtained from site characterization is vital when any changes are made to an established technique. Throughout the development of the Robotic Rig, there

was an objective to use as much standard equipment as possible through the data transmission chain. In a conventional push, data would be transmitted from the piezocone, through the cone cable to the DAS. In the Robotic Rig, the data is transmitted from the piezocone through the cableless cone rod system and into the DAS where the data is saved and also re-transmitted to the cloud. It was essential to perform control testing to validate the performance of the cableless cone rod system. Figure 4 shows a comparison between CPT pushes deployed with the cableless rod system and neighboring CPT pushes with a standard cabled rod system. The data presented shows that though spatial variability exists on the test site, cableless rod system obtains comparable geotechnical data, matching the standard of conventional methods.

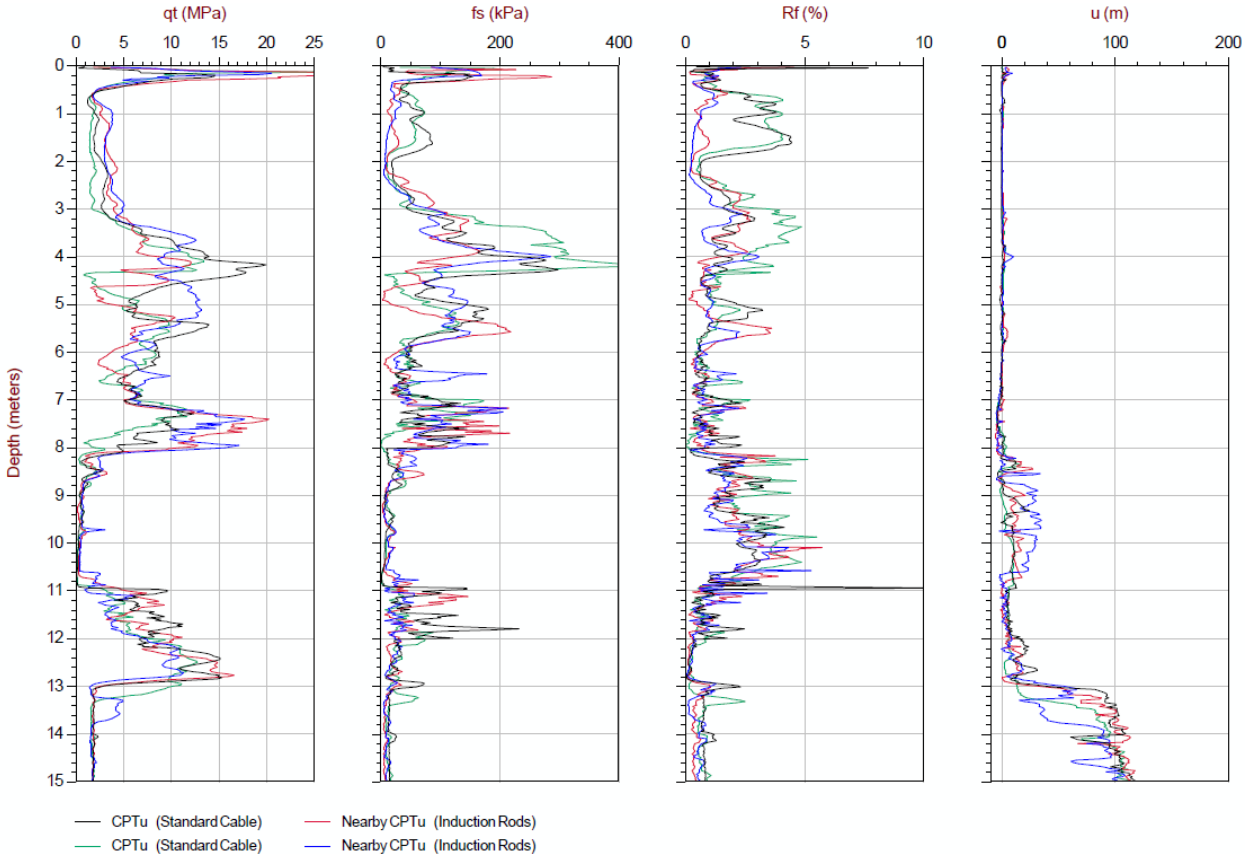


Figure 4: Example CPT pushes comparing in the cableless rod system with standard data

It was observed that when the Robotic Rig performed testing in electric mode, rig vibrations were reduced as the diesel engine was not running. This reduction in vibration has potential safety implications and could also lead to improved surface seismic responses.

Productivity and charging efficiency

There is no discernible difference in productivity between diesel and electric operations, both can provide sufficient power for CPT and direct push testing. Additionally, the system is designed to always fall back

to diesel in case of any issue with the electric system. In most cases, grid power has a lower carbon intensity than a diesel engine so charging the Robotic Rig through the grid would have a lower environmental impact, however in most of the identified use cases today this is not practical. Therefore, a key design element of the electric system is the ability to charge the batteries from the diesel engine. Charging the batteries does add an additional load on the system however it can be optimized to reduce the energy lost through idling. By capturing this otherwise wasted energy the system can charge the batteries for later use, reducing overall fuel consumption. As shown in Figure 2, the energy required for a 20 m CPT push is 5.8 kWh. Traction for 20–30 minutes (moving the rig across site for example) should generate enough electricity to conduct a 20 m push with zero fuel usage during the CPT.

To understand the system efficiency during charging the fuel usage for the Hybrid Diesel-Electric System during regen has been compared against a conventional diesel operation, as presented in Table 1. Though this data was collected during idling in order to minimize the variables on engine load, regen is targeted to occur during traction, while using start-stop functionality to reduce fuel usage when idling. Of the differential energy available 63% (at 1200 RPM) was successfully converted into stored energy for electrical operation.

Table 1: Comparison of fuel usage and efficiency considering regen mode when idling

	Conventional diesel operation			Hybrid operation with regen		
Engine Speed (rpm)	800	1200	1800	800	1,200	1,800
Total Diesel Used (L)	1.64	2.85	5.07	2.32	4.41	5.80
Total Time (Mins)	30.04	33.16	31.52	24.02	28.29	21.12
Average Fuel Rate (L/Hr)	3.27	5.15	9.66	5.80	9.37	16.47
Total Energy Gained (kWh)				1.69	5.49	6.37
Maximum Diesel engine efficiency (%)	41	41	41	41	41	41
Diesel Needed for Energy Gained (1L = 10.56kWh) (L/Hr)				0.97	2.68	4.14
Efficiency of Regen (Diesel Need / Diesel Used) (%)				38.34	63.43	60.75
Torque Load (%)	15.56	15.97	22.14	24.19	26.00	33.05
Torque Load (Nm)	221.14	226.95	314.60	343.72	369.47	469.57
L/hr per SoC%				0.24	0.36	0.50

Operational rates

The current operational rates of the Robotic Rig are comparable to standard non-automated operations, however there is a reduction in productivity when associated activities such as rod handling are considered. The capacity for faster operation exists with further development. Increasing autonomy and reducing

operator interaction is expected to lead to increased standardization of the CPT test, enhancing overall productivity. This is expected to be achieved through improving sensor capabilities, making the robotics system faster and simpler to control. The robotic system is specifically designed for safety-critical sites, where the priority is to make testing possible.

Health and safety impact

Conventional geotechnical testing in mine tailings environments poses many hazards to personnel. It is critical that the risks associated with these hazards are minimized through a robust health and safety program which incorporates the philosophy of a hierarchy of controls, a step-by-step approach to eliminating or reducing workplace hazards (CCOHS, 2024). This approach ranks controls from the most effective to the least effective levels of protection, ranking elimination as the most effective control and PPE as the least effective. According to a 2021 report from International Council on Mining and Metals (ICMM), fatality, except for 2019, and injury incidents are generally following a downward trend for member companies (ICMM, 2021) with a Fatality Frequency Rate (FFR) of 0.033 and a Total Recordable Injury Rate of 5.07 in 2012 compared with 0.018 and 2.94 in 2020. While the rate for fatalities and incidents is on the decline, the total number of fatalities and recordable incidents in 2020 was 44 and 6,977 respectively. Thus, despite the robust health and safety controls in place reducing the risk of working in mine tailings environments, significant risks still exist.

The development of the remote robotic functionality for CPT offers the opportunity to eliminate the need for personnel to work in hazardous environments, by moving the working environment from directly on a mine tailings structure to a safe location nearby. This allows for the elimination or substitution of many of the risks to which personnel are exposed when using conventional equipment, especially those that are typically not managed or are managed through administrative or PPE controls. This approach aligns with the hierarchy of controls, prioritizing elimination and substitution of hazards, and demonstrates a proactive commitment to improving safety and efficiency within the mining industry.

This advancement is most apparent when a job safety analysis (JSA) is applied, and a risk level is determined. In a JSA, risk levels are determined by evaluating the consequence and probability of potential hazards. First, hazards for each job step are identified. The consequence (severity of harm or damage) and probability (likelihood of occurrence) are assessed and combined using a risk matrix to quantify the risk by assigning a rating to both the consequence (1–5) and the probability (A–E). Safety controls are then applied to mitigate the identified risks resulting in an acceptable residual risk. Table 2 presents a selection of typical hazards associated with Cone Penetration Testing. In total, 35 typical hazards were identified and evaluated to calculate the risk before controls, with conventional controls, and with remote robotic controls.

Table 2: Example hazards found in a job safety analysis for cone penetration testing with related controls for both conventional and remote robotic equipment

Item	Step	Hazard
1.1	Inspect Work Area	Personnel encounter hostile wildlife
2.1	Position Equipment	Slips, trip, falls due to ground conditions
2.2	Position Equipment	Local traffic, pedestrians, or other workers in the area
2.3	Position Equipment	Overhead hazard with potential contact
2.4	Position Equipment	Soft or uneven terrain causing immobility or damage
3.1	Deploy Stabilizers and Pads	Crush hazard to body with ground contact
3.2	Deploy Stabilizers and Pads	Pinch points between jack pads, ground, and swivel points
3.3	Deploy Stabilizers and Pads	Property damage from pressure of stabilizers
4.1	Setup CPT probe and software	Moisture damage to equipment
4.2	Setup CPT probe and software	Small cuts on hand from equipment
5.1	Lower seismic beam	Pinch/crush points on ground.
5.2	Lower seismic beam	Heavy lifting causing back injury
6.1	Place cone in pushing system	Pinch point in chuck and rams causing hand injuries
7.1	Add first rod	Small cuts on hand from equipment
8.1	Push cone into ground	Pinch points on ground and around moon-pool area
8.2	Push cone into ground	Utility contact causing injury or damage

Consequence and probability do not increase linearly (Bao et al., 2022). To determine risk, a logarithmic scale has been applied to consequences and probabilities to appropriately represent the wide range of potential outcomes and their impacts, and the vast differences in the frequency of potential events. The approach reflects the exponential difference in impact from minor injuries to catastrophic events and that both high-probability, low-consequence events and low-probability, high-consequence events are appropriately quantified and managed as supported by research (Bao et al., 2022).

The consequence and probability rankings and scores are illustrated in Figures 5 and 6. The risk level is then calculated by: $Risk\ Level = \log_{10}(Consequence\ Score \times Probability\ Score)$

			Probability				
Consequence	Ranking		A	B	C	D	E
		Description	Improbable	Unlikely	Possible	Likely	Certain
	1	Slight Injury	L	L	L	L	L
	2	Minor Injury	L	L	L	M	M
	3	Severe Injury	L	L	M	M	H
	4	Death	L	M	M	H	H
	5	Multiple Deaths	M	M	H	H	H

Figure 5: Typical risk ranking table

			Probability				
Consequence	Score		1	10	100	1000	10000
		Description	Improbable	Unlikely	Possible	Likely	Certain
	1	Slight Injury	0	1	2	3	4
	10	Minor Injury	1	2	3	4	5
	100	Severe Injury	2	3	4	5	6
	1000	Death	3	4	5	6	7
	10000	Multiple Deaths	4	5	6	7	8

Figure 6: Risk score table

By comparing the risk scores associated with tasks identified in the hazard assessment, a risk score reduction can be calculated, before and after the application of safety controls, including both conventional and remote robotic controls (Figure 7). Initially, the cumulative risk score across all tasks identified was 149 before any controls were applied. This score was reduced to 94 after implementing conventional safety controls. The introduction of remote robotic controls further lowered the cumulative risk score to 54, showcasing the enhanced effectiveness of these advanced technologies in minimizing hazards and ensuring a safer working environment. This progression clearly illustrates the impact of employing innovative safety measures in high-risk operations.

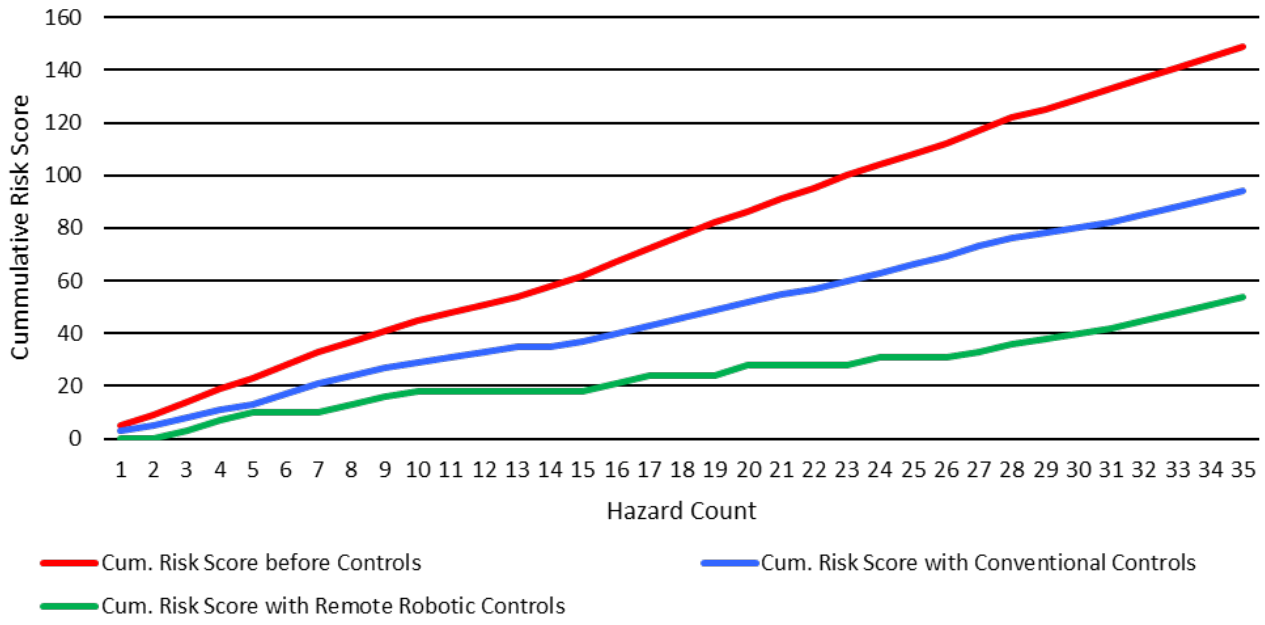


Figure 7: Cumulative risk scores without controls, with conventional controls, and with remote robotic controls

Life cycle assessment

Life cycle assessment (LCA) is a framework used to characterize, quantify, and interpret environmental impacts associated with a product or a system over its entire life cycle. In this study, LCA is used to evaluate the impacts of three site investigation programs that capture possible configurations of the CPT Hybrid Diesel-Electric System. The scope of this study includes impacts associated with raw material extraction, materials and energy processing, mobilization of vehicles and equipment to site, site maneuvering and idling, and penetration (i.e., CPT pushes) for a site in British Columbia, Canada. The methodology used for the LCA calculations, including the calculations in the life cycle inventory (LCI), transportation modeling, and life cycle impact assessment (LCIA), follows the procedure detailed in Purdy et al. (2022). Table 3 below shows the details of Scenarios 1 and 2. Scenario 3 adopts a traditional, fully diesel-powered program. For each scenario, the fuel usage is calculated based on the value during hybrid operation with regeneration at an engine speed of 1,200 RPM, as listed in Table 2 (9.37 L/hr). The roundtrip mobilization from yard to mine site is assumed to be 100 km.

Table 3: Specifications for each modeled scenario

Scenario	Activities	Pushes	Electricity consumption (kWh)	Diesel consumption (kg)
Scenario 1 - Arrive to Site Fully Charged	Charge battery to 100% from grid (from hydro power source)	–	+84	–
	Electric CPT	12	-69.8	–
	Diesel CPT	3	+22	15.62
	Site Maneuver/Idle (1 hr)	–	+20	7.81
	Electric CPT	7	-40.6	–
	Diesel CPT	3	+22	15.62
	Electric CPT	3	-17.4	–
Scenario 2 – Arrive to Site with Zero Charge	Diesel CPT	7	+51.3	36.4
	Electric CPT	8	-46.4	–
	Site Maneuver/Idle (1 hr)	–	+20	7.81
	Diesel CPT	6	+44	31.2
	Electric CPT	9	-52.2	–

The results are presented in a range of formats to provide normalized environmental impacts and representative impacts for each scenario. The normalized results for primary energy (PE) and global warming potential (GWP) can be seen in Table 4 for each life cycle phase, and associated functional unit. The total GWP for each scenario is shown in Figure 8. There is a 44.75% increase in total GWP from Scenario 1 to Scenario 2, and a 67.9% increase from Scenario 2 to Scenario 3.

Table 4: Normalized impacts of primary energy (PE) and global warming potential (GWP)

Life Cycle Phase	Mobilization	Fuel for Pushes	Site Maneuver/Idling	Electricity from Grid
Functional Unit	per 1 km	per 1 m	per 1 hr	per 1 kWh
PE (MJ)	1.28E+01	1.50E+01	2.25E+01	1.24E+00
GWP (kg CO_2-eq)	4.55E-01	2.96E-01	4.44E-01	4.44E-03

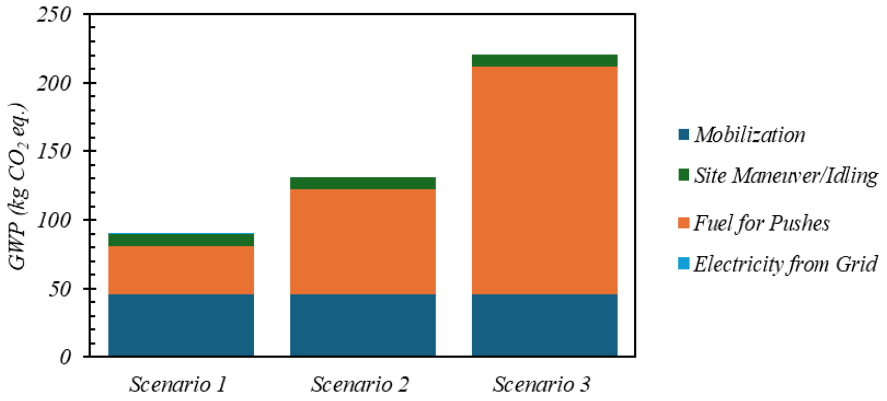


Figure 8: Total GWP (kg CO_2-eq) for each life cycle phase for each scenario

Fuel production and consumption for CPT pushes accounted for 39.3%, 58.6%, and 75.3% of impacts for Scenarios 1, 2, and 3, respectively. However, an opposite trend is observed for site maneuvering and idling. These activities account for 9.8%, 6.76%, and 4.03% of GWP for Scenarios 1, 2, and 3, respectively. This is because the total impacts of this life cycle phase remain the same across scenarios, thus constituting a larger percentage of Scenario 1, which has lower overall impacts compared to the others. A similar trend is observed for mobilization, which also remains constant across scenarios. The only scenario which has impacts from electricity from the grid is Scenario 1. Because the grid pulls electricity from renewable sources, namely hydropower, the impacts associated with this stage are proportionally minimal, making up only 0.55% of total impacts.

Conclusion

The development of the Remote Robotic Hybrid Diesel-Electric Cone Penetration Testing (CPT) Track Rig offers positive environmental and health and safety impacts, helping address the need for safer and more environmentally sustainable operations. The hybrid system, which combines diesel and electric power, offers the flexibility to switch modes based on operational demands, thereby optimizing efficiency and minimizing carbon emissions while maintaining the versatility necessary to cope with testing in rugged environments. Field trials have validated the rig's capability to perform precise geotechnical testing, using energy of the same quality as conventional testing, remotely and from stored electrical. These trials have

shown that the hybrid system has the potential to generate enough stored energy during typical traction operations over 20 to 30 minutes to conduct a 20 m CPT push, though charging through mains power from renewable energy is preferable.

The robotics developed now allow for ground investigation in safety critical tailings storage facilities where traditional methods may endanger human lives and are not considered permissible. By allowing for a deeper understanding of ground conditions, more informed design decisions can be made.

References

Bao, C., Li, J. and Wu, D. 2022. *Risk Matrix: Rating Scheme Design and Risk Aggregation*. Springer Nature Singapore Pte Ltd.

Baker, K.E., Zettl, J., Macciotta, R., Hendry, M. and Lefsrud, L. 2018. Protecting workers exposed to ground hazards through enhanced hazard identification and management tools. *Proceedings of GeoEdmonton 2018, 71st Canadian Geotechnical Conference*, Edmonton, AB, Canada, September 2018.

Canadian Center for Occupational Health and Safety (CCOHS). 2024. Hierarchy of Controls. Accessed June 10, 2024 at https://www.ccohs.ca.

Caterpillar. 2024. C7.1 Industrial Diesel Engines. Accessed June 10, 2024 at https://www.cat.com/en_US/products/new/power-systems/industrial/industrial-diesel-engines/1000029571.html.

International Council on Mining and Metals (ICMM). 2021. Safety and Health Performance. ICMM Annual Report 2021. Accessed June 10, 2024 at https://www.icmm.com.

Purdy, C.M., Raymond, A.J., DeJong, J.T., Kendall, A., Krage, C. and Sharp, J. 2022. Life-cycle sustainability assessment of geotechnical site investigation. *Canadian Geotechnical Journal* 59(6): 863–877.

Tailings Facility Surveying Leveraging Complementary Technologies

Veronique Nell, PhotoSat, Canada
Andrea Krupa, PhotoSat, Canada

Abstract

Ensuring the safety, compliance, and efficient management of tailings storage facilities (TSFs) demands robust surveying techniques. In this context, the integration of complementary technologies and data sources offers a holistic approach to TSF surveying. This paper explores the synergies between imagery and surveys from drones, high-resolution optical satellites, rapid revisit optical satellites, bathymetric sensors, and LiDAR for comprehensive TSF surveying.

While LiDAR excels at capturing elevation data, it faces constraints related to accessibility, expense, and revisit intervals. Drones, in comparison, can offer excellent flexibility and accessibility for capturing detailed video, imagery, and topography of TSFs. However, their limited collection area can lead to challenges in the merging of data from multiple flights, as well as the time to acquire and process data over an entire TSF.

High-resolution and rapid revisit optical satellites provide complementary data to drones and LiDAR by capturing a whole TSF in a single acquisition at revisit rates ranging from days to weeks. They offer a supplementary, cost-effective solution with rapid delivery times. In addition to on-going surveying, archived satellite imagery can retroactively provide time-stamped data to determine the deposition history of a TSF when as-built records are unavailable.

Finally, bathymetric surveys provide essential information about underwater topography. By combining bathymetric data with surface topography, operators can gain a comprehensive understanding of TSF geometry, construction, and deposition plan advancement.

Integrating data from these complementary sources allows the TSF operator to overcome the limitations of each technology and enhances the overall accuracy and completeness of TSF surveying.

This paper highlights the collaborative potential of diverse technologies, emphasizing their collective impact on TSF survey quality and accuracy. The integration of these complementary technologies provides operators with the data for safer and more efficient management of tailings facilities, aligning with industry standards and sustainability goals.

Introduction

Ensuring the safety, compliance, and efficient management of tailings storage facilities (TSFs) demands robust surveying techniques. In this context, the integration of complementary technologies and data sources offers a robust approach to TSF surveying.

No two sites are identical. Each location presents unique challenges, influenced by factors such as size, ease of access, operating requirements, and reporting requirements. TSF operators often face recurring challenges that affect the overall design and implementation of the survey program.

Frequency of data acquisition: different data is needed at different frequencies and for different tasks. Month end reporting, weekly operational updates, and integration with multiple sensors such as bathymetry collections, all require data collections at different frequencies, resolutions, accuracies, and over different areas. Another consideration in this category is how quickly data can be collected and how fast the topography can be delivered post collection, so that a site has the data they need when they need it.

Offset errors and data integration: once the data from multiple sources and sensors is collected, it is important to ensure that all the data sets are coherent for all teams to be working from the same baseline. Correcting any offset errors is a key step in achieving effective data integration.

Lack of data continuity: with many TSFs having been in operation for years, if not decades, changing regulations, staff turnover, and changes of ownership can lead to incomplete records and lack of topographic data continuity. With the implementation of new global standards for TSF management, these data gaps can hinder current operators managing their TSFs within the GISTM requirements and in accordance with the "As Low as Reasonably Possible" (ALARP) principles.

In this paper, we will look at the strengths and weaknesses of four surveying methods, or tools: ground surveyors, manned airborne LiDAR, drones, and satellites (high resolution optical and rapid revisit optical). We will compare their performance in six main categories:

1. Area coverage: how large of an area can this tool survey in a single pickup?
2. Accuracy: what is the absolute vertical accuracy of the survey?
3. Repeatability: how repeatable are the results from one survey to the next?
4. Flexibility: how quickly can data be captured from request?
5. Cost: what is the cost of the survey?
6. Processing time: how quickly after the raw data is captured can the survey be delivered?

The following sections will detail how these different tools can be used to address different surveying needs and how, by leveraging their complementary characteristics, their individual weaknesses can be offset.

Different tools for different needs

Ground surveying

Ground surveying is the original surveying method and ground surveyors provide unmatched accuracy on discrete areas of change – sub-centimeter horizontal and vertical accuracy in some cases. The cost of these surveyed points can also be low if work is being performed by existing site survey teams.

The presence of personnel on-site can present challenges, as the surveying work needs to be conducted in a way that does not interfere with operation, while ensuring the safety of all personnel. Also, with a limited number of on-site surveyors, the demands of multiple groups can lead to scheduling issues. When scheduling challenges can be avoided, ground surveyors provide a very flexible way to collect data points over small areas.

Survey points from ground surveyors provide valuable and accurate survey points. Their value can be increased exponentially when paired and merged with the other survey methods described below, where they can be used as ground control or to get a small number of highly accurate survey points over a critical area.

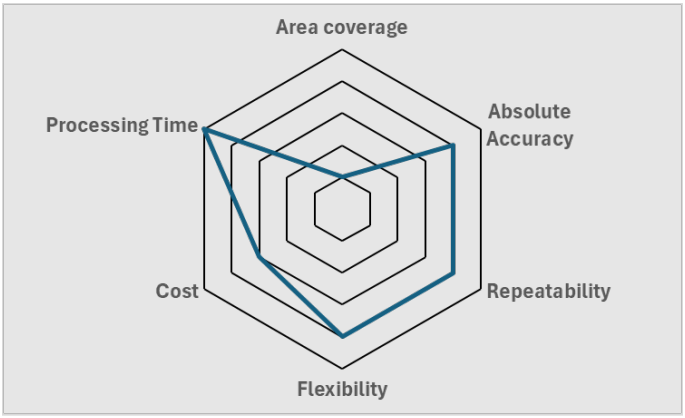


Figure 1: Strengths and weaknesses of ground surveying

Manned airborne LiDAR

Manned airborne LiDAR is the traditional benchmark for high accuracy surveys over mine site scale areas. With vertical accuracies as low as 5 cm with ground control and the ability to capture an entire TSF in a single flight, LiDAR surveys can be a great option for a baseline survey that all subsequent surveys are matched to. LiDAR's ability to penetrate vegetation means that the resulting surface is a bare ground surface – also referred to as a DTM, Digital Terrain Model – another key feature of a baseline survey.

LiDAR surveys are large data sets with very high data density. These can take a long time to process and they can be hard to manipulate. The need to dispatch a manned aircraft means this is a relatively high-

cost option and can also present challenges for more remote sites, or in parts of the world where this type of service may not be readily available.

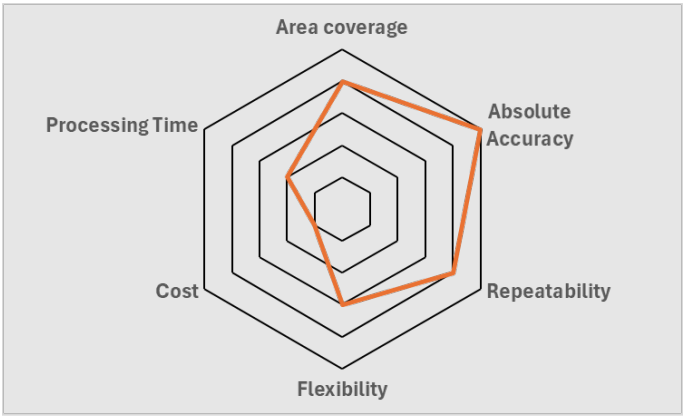


Figure 2: Strengths and weaknesses of manned airborne LiDAR

Drones

Drones have come a long way in the last five years, significantly increasing their payload capacity and autonomy. In the context of topography, the key sensors are optical (including multispectral) and LiDAR. Despite the improvements, the payload capacity is still limited, so high-end LiDAR and multispectral sensors may require larger, more expensive drones.

Since they fly at a lower elevation than traditional manned aircraft, drones can avoid some atmospheric conditions and capture clear data even when clouds are present. The lower flight altitude can also lead to higher resolution imagery and topography with vertical accuracy down to the centimeter level. They are nevertheless sensitive to weather conditions such as high winds, rain, fog, or extreme temperatures that can affect flight stability and data quality. Adverse weather may limit the operational window for surveys.

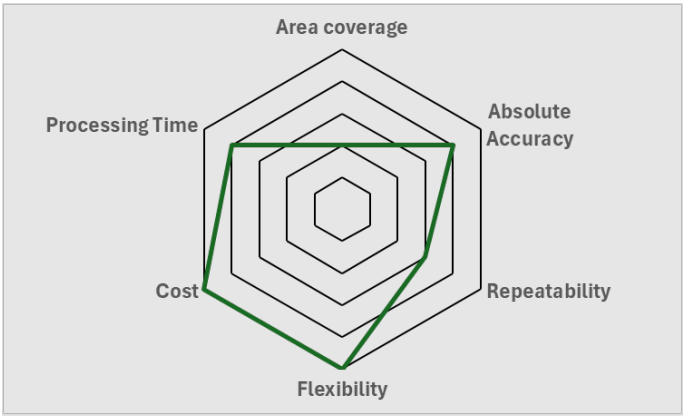


Figure 3: Strengths and weaknesses of drones

In-house drone programs provide incredible flexibility for regular pickups if scheduling requests from multiple teams on a site can be managed.

Limited flight times mean that one TSF can often not be captured in a single flight, which can lead to offsets between different pickups. Also, surfaces derived from drone data are typically Digital Surface Models (DSM), which still include features such as vegetation and buildings. These surfaces need to be post processed to remove these features and produce a bare ground survey.

Satellites

High-resolution satellites

Data from high resolution optical satellites has been commercially available since the early 2000s. Their ability to collect high resolution (30 cm to 50 cm pixel) imagery over very large areas (hundreds of square kilometers) in one shot is unparalleled. By collecting stereo imagery of an area of interest, that is two images of the same area at different angles, taken only seconds to minutes apart, topography can be derived from these stereo pairs. By using previous bare ground surveys, either from LiDAR or previous satellite surveys, as ground control, and tying into areas where no change occurred, this type of surveying can achieve absolute vertical accuracies better than 15 cm RMSE.

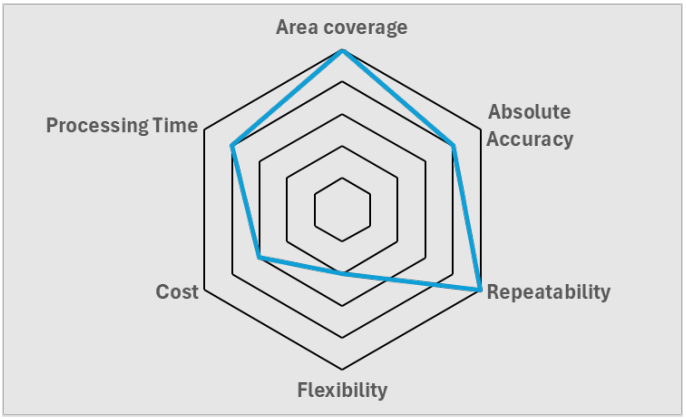


Figure 4: Strengths and weaknesses of high-resolution satellites

When applied to TSFs, this means a whole TSF, even a whole mine site, can be collected in a single, instantaneous snapshot. Since the topography is derived from a single acquisition, the consistency of the data over the whole area of interest is excellent. The challenges of correction for errors and offsets that can come when multiple collections need to be stitched together are avoided. The data is self-consistent, which leads to high precision topography. As subsequent collections are coming from the same sensor and going through the same processing systems, there is excellent repeatability between surveys over the same area and the results from surveys over different areas are easily comparable.

Rapid-revisit satellites

Rapid Revisit Satellite constellation, and specifically ones from which topography can be derived, are a new development in surveying. These growing constellation of 10 or more satellites can provide collection opportunities weekly or even daily anywhere in the world, with collection occurring as little as three hours after tasking.

Their collection area offers larger coverage than a single drone pickup but smaller than high-resolution satellites and manned airborne LiDAR. The imagery resolution and survey accuracy from these satellites is currently lower than what is achieved with the other tools described above, but the sensor technology and processing is rapidly improving.

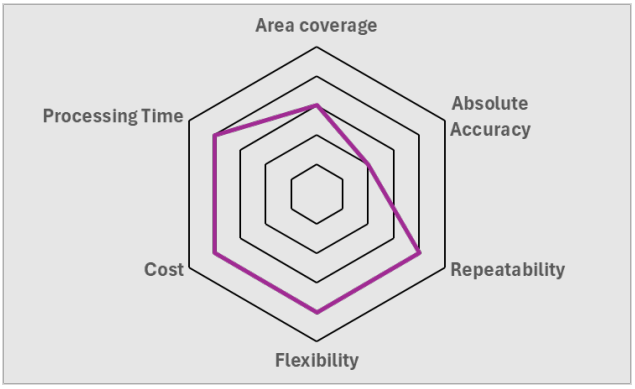


Figure 5: Strengths and weaknesses of rapid revisit satellites

Archived satellite imagery

There is a continuous archive of commercially available data dating back to the 1960s. Figure 6 gives a non-exhaustive list of satellites from which archive data is commercially available. Topography can be generated from most of the sensors on this list.

Accessing archived imagery means that current operators can fill potential data gaps created by change of ownership, personnel, and regulations, to better understand how a site was operated in the past, in order to plan for safer and more efficient operations moving forward.

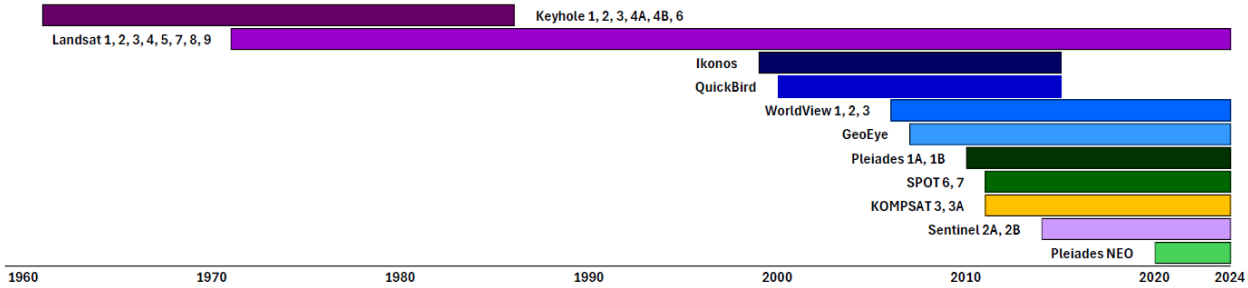


Figure 6: A timeline of satellite imagery

Leveraging synergies

Integrating data from multiple sources

The surveys derived from all the acquisition tools described above are valuable on their own, but to fully leverage their synergies, the various surfaces can be integrated with one another to provide a single, up-to-date surface for teams to work with. This is also true for other sensors such as bathymetric sensors, whose data can be integrated with the above water surface.

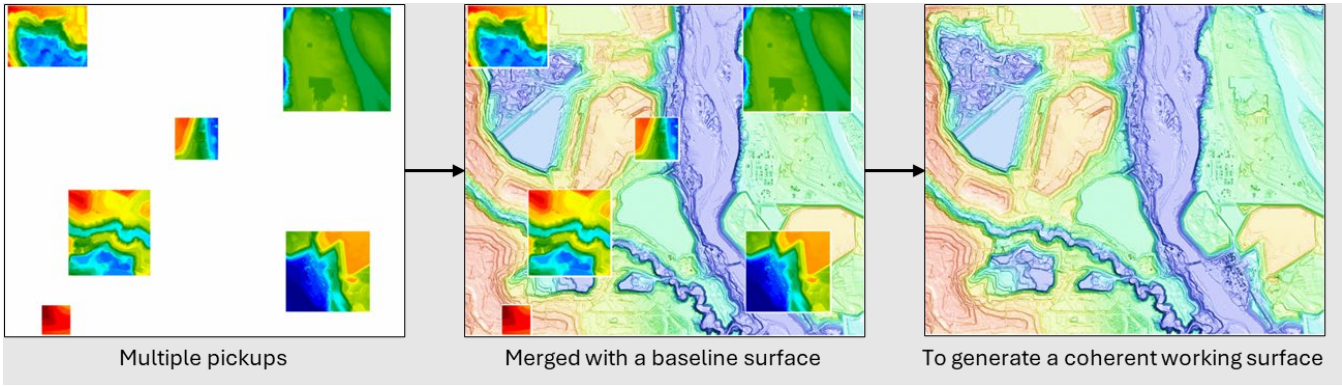


Figure 7: Merging data from multiple sources

A common challenge in integrating surfaces from multiple sources is handling offsets in data and, in some cases, managing surveys in different mine grids. Figure 8 shows how using a baseline surface of a whole TSF can help shed light on offsets between different drone pickups and thereby help to correct them. Comparing newly acquired surfaces to a baseline surface will help avoid any propagation of error over time and ensure teams are working with precise and reliable data.

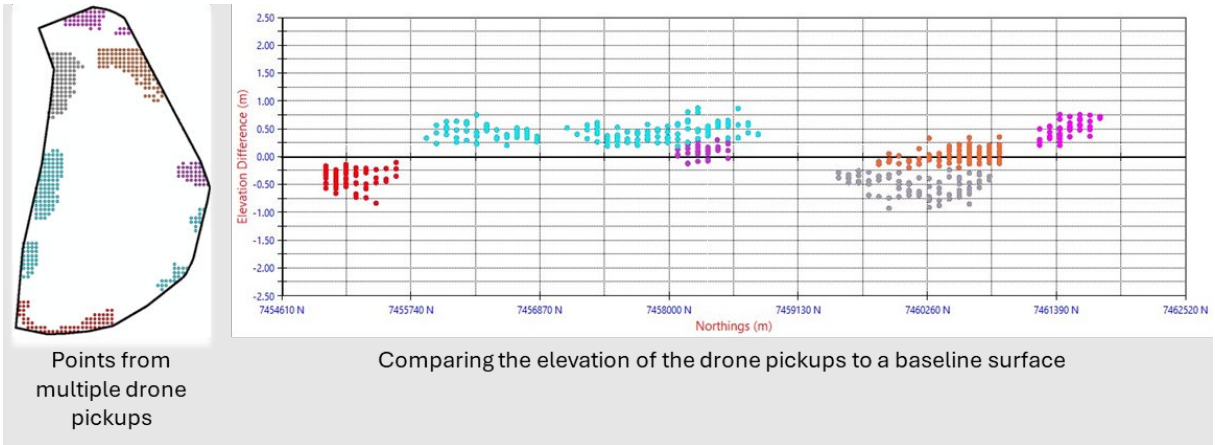


Figure 8: Correcting offsets with a baseline survey

Leveraging strengths to offset weaknesses

When comparing the strengths and weaknesses of all the tools discussed above, we see that by using a combination of them, we can offset the weaknesses of one with the strengths of another.

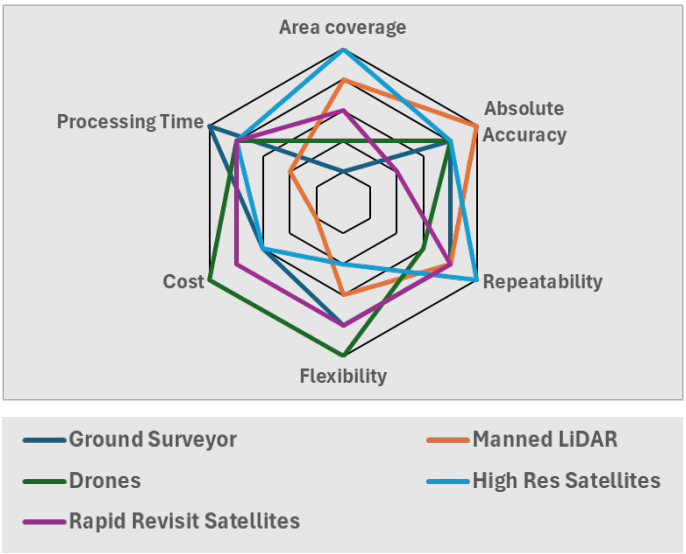


Figure 9: Leveraging strengths to offset weaknesses

Using multiple tools supporting each other can increase the value of each of those tools on their own. For example:

- Using a baseline high-resolution satellite or LiDAR survey as a baseline to QC drone data and correct any offsets makes the survey from drone data more precise and reliable.
- Using highly accurate points surveyed by a ground surveyor to tie any other kind of survey to, will greatly improve the absolute accuracy of that survey.
- By integrating an above water surface survey with a bathymetric survey, operators can generate a single TSF survey to work from, improving overall understanding of the TSF surface and supporting efficient operations.

The right data at the right frequency

Each tool described above is better suited to a different frequency of acquisition. By leaning into the strengths of each tool, TSF operators can ensure they have the right, reliable data when they need it. The cycle shown in Figure 10 is an example of a possible acquisition frequency for each tool.



Figure 10: The right data at the right frequency

Conclusion

Designing and implementing a complete survey program is less about getting more data and more about getting the right data at the right time and efficiently integrating survey data from multiple sources.

Trade-offs will always need to be made around safety of personnel onsite, collection logistics, cost over time, and accuracy. However, by optimizing collection frequency to capitalize on the strength of the tools at their disposal, TSF managers will be able to acquire the survey data necessary to make informed decisions for optimized operations.

Potential of X-ray Micro-CT Imaging for Mine Tailings Deposit Characterization

Dharma Wijewickreme, University of British Columbia, Canada
Ana Valverde, WSP, Canada

Abstract

Characterizing mine tailings from a geotechnical engineering perspective is critical to maintaining the stability and safety of mining facilities. The engineering parameters derived from these characterizations provide the keys to evaluate risks associated with slope stability, liquefaction, and seepage, as well as to develop mitigation measures against potential dam failures. Laboratory studies on tailings have indicated complex behavior patterns during shear. For example, direct simple shear testing carried out on reconstituted specimens of sand and silt tailings have shown that the behavior of the tailings is governed not only by the stress and density state, but also by the soil particle arrangement (fabric) attained during specimen preparation. The commonly used slurry-deposition method for preparing reconstituted specimens for laboratory testing, while arguably it should represent field deposition mechanisms, has not been very successful in enabling the reproduction of in-situ loose densities, and may explain some abrupt flow-failure-type responses observed in the field. Greater attention needs to be paid to details such as particle breakage and particle fabric rearrangement, etc., within the soil skeleton. X-ray Micro-Computed Tomography (X-ray micro-CT) is a non-destructive technique that enables imaging of internal structures in complex solid matrices, and the technique can be used to characterize and examine the soil particle fabric when coupled with advanced image processing. In this paper, building on the experience gained from the study of silt particle matrices at the University of British Columbia, Canada, the potential use of X-ray micro-CT in the characterization of mine tailings is demonstrated, focusing especially on its ability to reveal particle size distributions and internal structure.

Introduction

The stability and safety of mining facilities are paramount in geotechnical engineering, and accurate characterization of mine tailings plays a key role in this regard. Observations from past tailings dam failures have indicated that the mechanical behavior of tailings is influenced by more than just the confining stress and density. The fabric of the soil, or the spatial arrangement of particles, also plays a critical role. Research

conducted at the University of British Columbia (UBC), Canada, has demonstrated the significant impact of soil particle fabric on the mechanical response of silts. This research work has highlighted the differences in behavior between reconstituted and field specimens, young and aged conditions, and uniform and gap-graded particle matrices. These findings underscore the necessity of accounting for particle fabric alongside traditional factors such as void ratio and confining stress to fully describe soil behavior.

One significant challenge in laboratory testing is replicating the in-situ stress, density, and particle fabric states of tailings in test specimens. Commonly used methods, such as slurry deposition, often fail to reproduce the densities and fabrics observed in situ, leading to discrepancies between laboratory results and field behavior. This gap underscores the need for advanced techniques that can provide more accurate understanding of soil internal structure and properties. X-ray Micro-Computed Tomography (X-ray micro-CT) offers a potential approach to this challenge. As a non-destructive imaging technique, X-ray micro-CT enables detailed visualization of internal structures within complex solid matrices. By coupling this technique with advanced image processing, it is possible to characterize the soil particle fabric and obtain precise particle size distributions. Previous studies have primarily focused on the fabric of sandy materials (Al Mahbub and Haque, 2016; Hight and Leroueil, 2003; Fonseca et al., 2012). However, recent advancements have made it possible to investigate finer (silt size) particles (Wesolowski, 2020; Valverde et al., 2020; Valverde and Wijewickreme, 2021a; Valverde and Wijewickreme, 2021b; Valverde and Wijewickreme, 2024).

This study presents the application of X-ray micro-CT to three different gradations of mine tailings – fine, medium, and coarse grain sizes. While preliminary, the results demonstrate the potential of the technique to enhance our understanding of internal structures present in tailings. In particular, the details on the materials tested, specimen preparation methods, and equipment used, as well as how the X-ray micro-CT can reveal particle size distributions, are provided. Overall, the paper aims to contribute to the ongoing efforts to improve the characterization of mine tailings, providing a foundation for further research.

Experimental program

Material description

Three tailings were used for this research. The properties and index parameters of the materials are given in Table 1. PSD testing using hydrometer analysis and mechanical sieving (ASTM (2017) D7928-21 and ASTM (2021) D6913/D6913M-17), was performed on the tailings for comparisons with those from X-ray micro-CT.

Table 1: Soil properties and index parameters of tested tailings

Parameter/Material	Tailings 1	Tailings 2	Tailings 3
Specific gravity, G_s	2.81	3.50	2.74
Plasticity index, PI	CI (Silty Clay)	–	–
Sand	–	52%	96%
Fines (Silt and Clay)	100%	48%	4%

Specimen preparation

Loose tailings in dry form were deposited into 5-mm plastic tubes. A small funnel was employed to carefully pour the dry tailings into the tube. The arrival at a very specific arrangement of particles in these specimens was not considered a significant concern herein, as the current scope and purpose was mainly to determine particle sizes and shapes. After placing the tailings, the tubes were sealed using small rubber plugs at the ends to keep the tailings intact during transit to the X-ray micro-CT scanning facility and also during the imaging process.

Image acquisition, processing, and analysis

The X-ray micro-CT scanner available at the Pulp and Paper Research Center at the Vancouver campus of UBC was used to obtain 3-dimensional high-resolution non-destructive images of the specimens. The scanner available at this facility is a ZEISS Xradia 520 Versa manufactured by Zeiss International, Oberkochen, Germany, as shown in Figure 1. This scanner restricts the movement of the source and detector allowing for greater control and more precise scanning at higher resolutions (Ketcham and Carlson, 2001; Helliwell et al., 2013).



Figure 1: ZEISS Xradia 520 Versa by Zeiss International

The X-ray μ-CT scans essentially produce 2D images of the specimen (as a sequence of thin 2D slices of the 3D specimen) that record the variation of X-ray attenuation within objects, which is a parameter that relates closely to the density of material penetrated by the X-ray (see Figure 2). The 2D images are later stacked and reconstructed into a 3D image. The steadiness of the specimen during the scan is key to

achieving high-resolution images. A specimen holder was specifically designed and fabricated to provide a well-secured specimen during the scan (Valverde, 2023). Several parameters need to be controlled to achieve scans providing images with a satisfactory resolution. For example, the field of view (FoV) – which is one of the key parameters to obtain a minimum achievable voxel size. A FoV of ~1000 µm was used for these scans and resulted in 1 µm resolution.

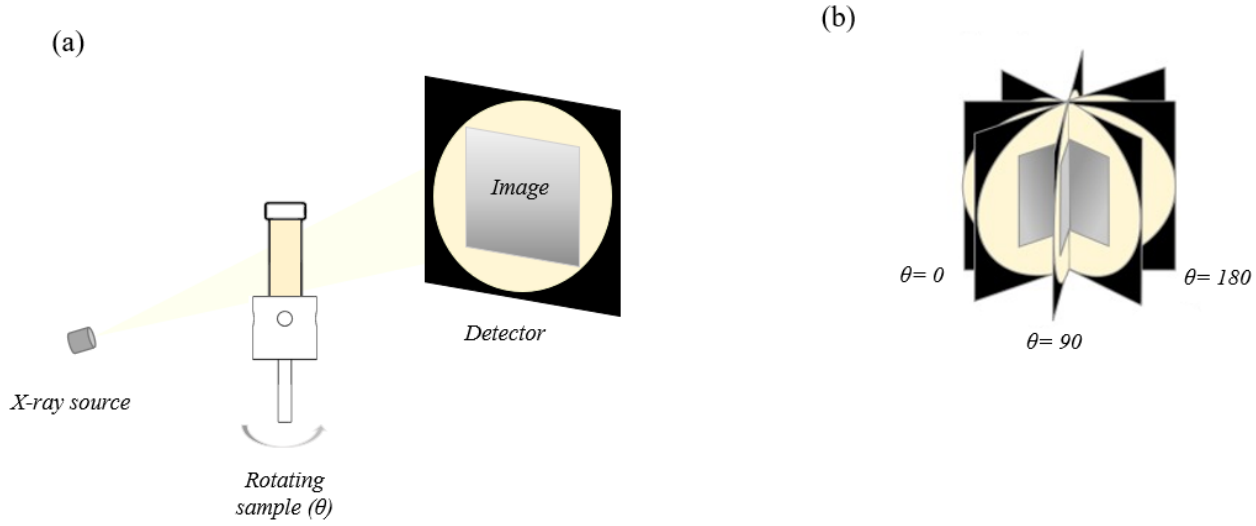


Figure 2: Image acquisition process in X-ray micro-CT scanning (a) image acquisition (b) 2D projections of a sample

The reconstruction and analysis of the digital images yielded was performed using the commercially available Avizo 9.7 software (Thermo Fisher Scientific, 2019). This software has been used by various researchers to successfully study particulate geomaterials (Fonseca, 2011; Markussen et al., 2019). Image processing and analysis were completed by already established workflows at UBC (Valverde, 2023), and they broadly consisted of two phases. First, the images were filtered and segmented to partition the individual grains; herein, the "watershed" algorithm was used to segment the particles. Second, quantitative measurements were obtained from the resulting image. The label analysis tool was used to retrieve the data required for establishing grain size distributions. The feasibility of this technique was calibrated using glass beads (Wesolowski, 2020) and silica powder (Valverde, 2023).

Initial findings

Visual assessment

The raw and processed images for a specific slice of each tailings particle size range (i.e., fine, medium, coarse) are presented in Figure 3 (top to bottom row, respectively) to illustrate typical images generated from micro-CT technology.

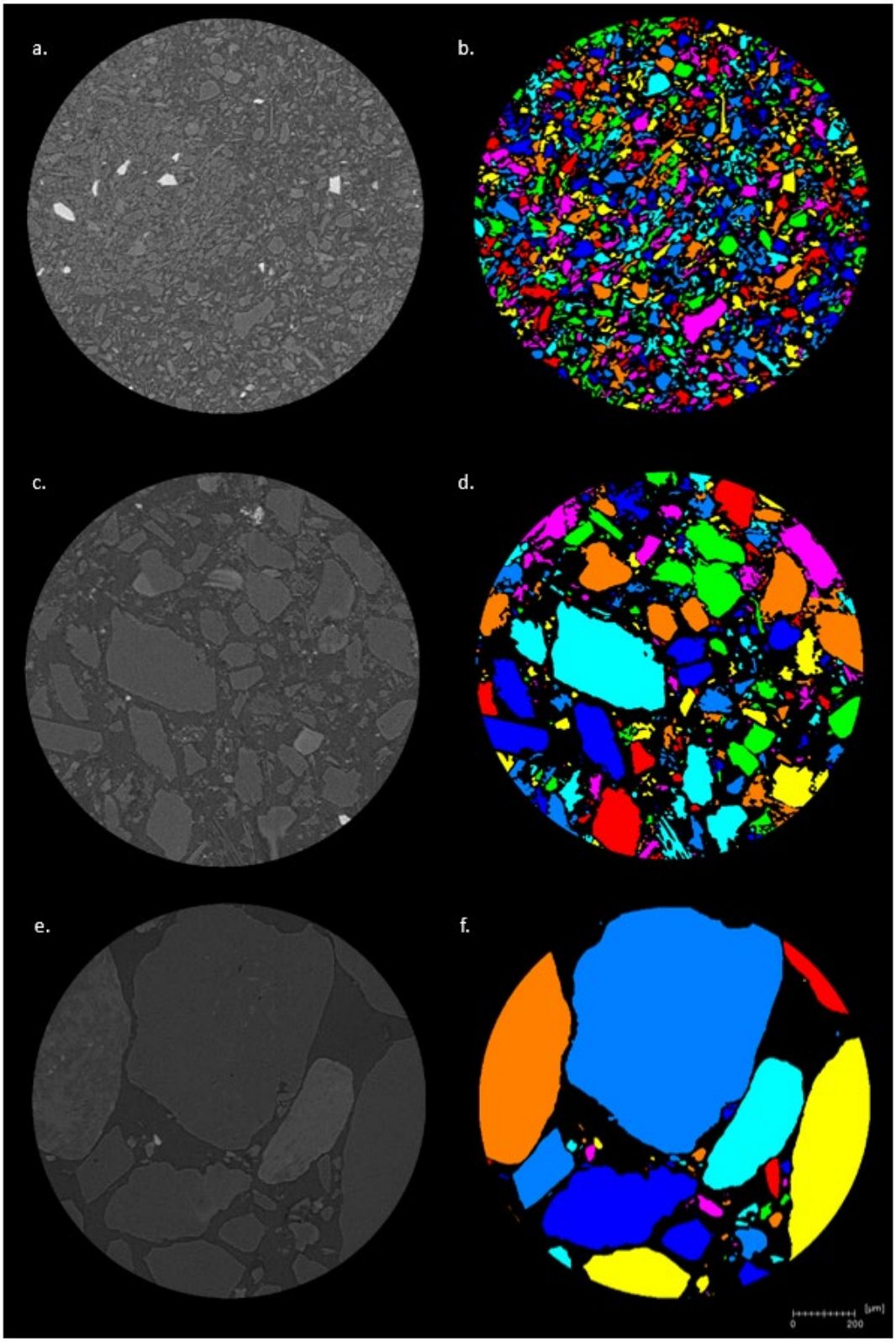


Figure 3: Raw and processed images for the samples used for this study.
Note: top level – fine tailings; second level – medium tailings; third level – coarse tailings

Approximately a thousand 2D images were stacked to reconstruct a given 3D image – as shown by the example in Figure 4 for the coarser tailings.

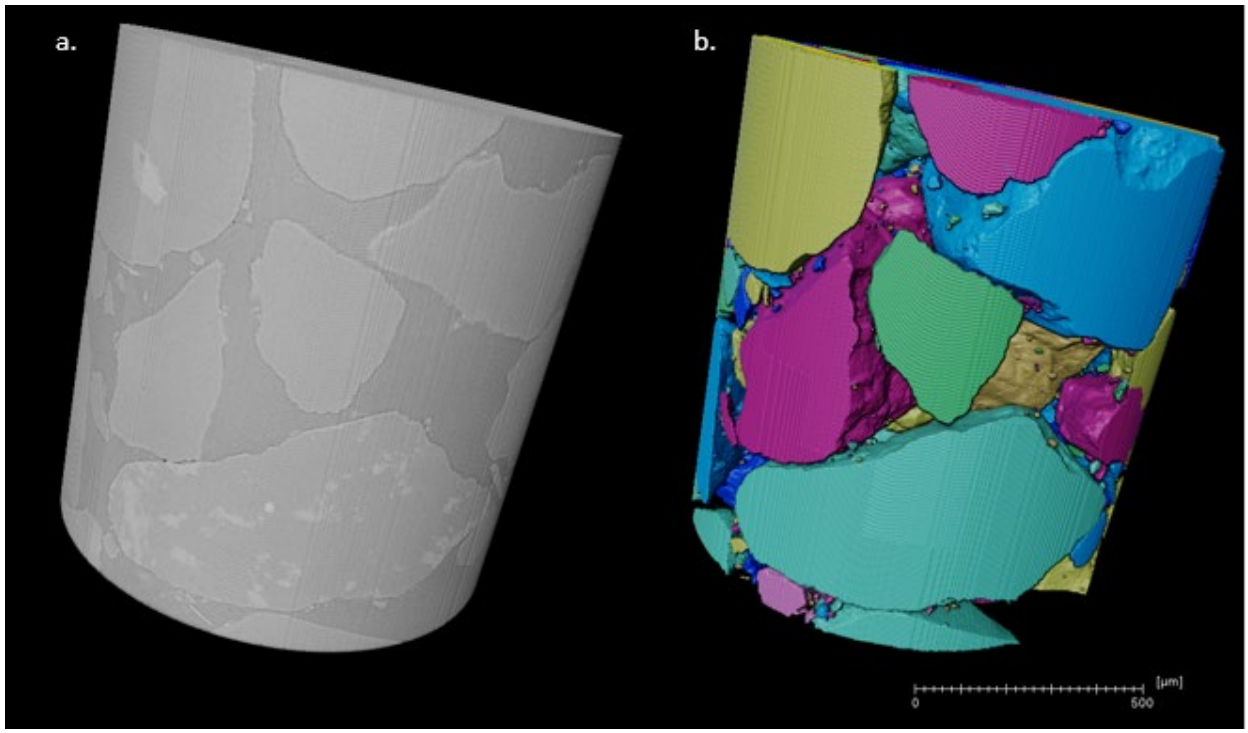


Figure 4: 3D view of a coarse tailings sample (Tailings 3)

In the raw images, it is possible to distinguish a wide variety of soil particles in different tones of grey color. This greyscale intensity reflects the density detected by the imaging device at a given location, and these values, form the key input data for the segmentation process (i.e., pure white = void and solid black = very dense material). The particles that have been segmented for each of the raw images in the left column of Figure 3, using Avizo software, are presented in the respective, counterpart right column. The purpose of segmentation is to individually identify/separate a given particle from the adjoining others.

After the segmentation process, the software allows retrieving the information related to a given individual particle (i.e., length, area, volume, orientation, etc.). If subsequent quantitative analyses were to be undertaken, this data would serve as the main input for all such work. The success of the segmentation process depends on several variable factors including the scanning process and the image processing. From visual inspection, it can be seen that the raw image of the coarser particle matrix (Figure 3.e) is more readily segmented (Figure 3.f.) compared to that for finer particles (see Figures 3.a and 3.b).

It is also of relevance to highlight some of the challenges in interpreting image data, as indicated below. Firstly, it is important to recognize that the imaging resolution controls the smallest particle size that could be meaningfully segmented. For example, some of the black gaps that can be seen between the

colored particles may be a direct result of the resolution. Secondly, it was found that the computer image processing approach tends to treat the smaller particles immediately adjacent to a bigger particle as part of the latter bigger particle. This effect, in turn, could cause the digital particle to have larger dimensions compared to the real particle. Thirdly, it was noted that some bigger particles could be segmented by the software as two smaller particles (i.e., "digital particle breakage"). From visual inspection of the outputs, this does not seem to become a persistent factor with respect to the images of medium and coarse tailings in comparison to those for fine tailings.

Particle size distribution

Knowledge of the particle size distribution (PSD) for a given soil (a plot of percentage weight passing a given particle size versus that grain size) is one of the key metrics used in classifying and characterizing soils (ASTM (2017) D7928-21 and ASTM (2021) D6913/D6913M-17). The information on individual particle information -including length, width, breath, thickness, volume, etc. – from Avizo image processing provided a direct basis to determine digital particle size distributions from a given 3D micro-CT scan. In this effort, for a given particle, the particle size for the x-axis of the PSD plot was assumed to be the smallest dimension derived from the image segmentation process. Since the y-axis of the PSD plot is based on the weight passing a given particle size, it was considered reasonable to assume a constant specific gravity and thereby use the volume of a given particle as the proxy for weight. On this basis, the volume "retained" on digital particle sizes corresponding to each sieve size, as per ASTM (2017) D7928-21, was calculated; afterward, the cumulative volume for each sieve size was divided by the total volume retained over all sieves leading to the percent passing by mass equivalent volume.

The PSD curves obtained for the different tailings from laboratory testing are overlain in Figure 5 for comparison with those obtained from the present analysis of digital data. It can be noted that, while there is a relatively good agreement for the coarser and medium tailings, the results from laboratory tests indicated a coarser fraction larger than that from the analysis of digital imaging data in both cases. On the other hand, for the finer tailings, the laboratory tests indicate a finer fraction than that from the analysis of the digital images.

This difference can be attributed to several factors, as per below. As per the visual observations discussed in the previous section, the resolution is a limiting factor for segmenting the smallest particles. In the present work, the scan resolution was 1 μm, therefore the particles smaller than 0.003 mm would not be considered in the digital grain size analysis. Furthermore, it was seen during visual inspection that the smaller particles immediately adjacent of the bigger particles were treated as part of the bigger particle during segmentation, and this would contribute to the digital curves being of a coarser grain size compared to the laboratory PSD.

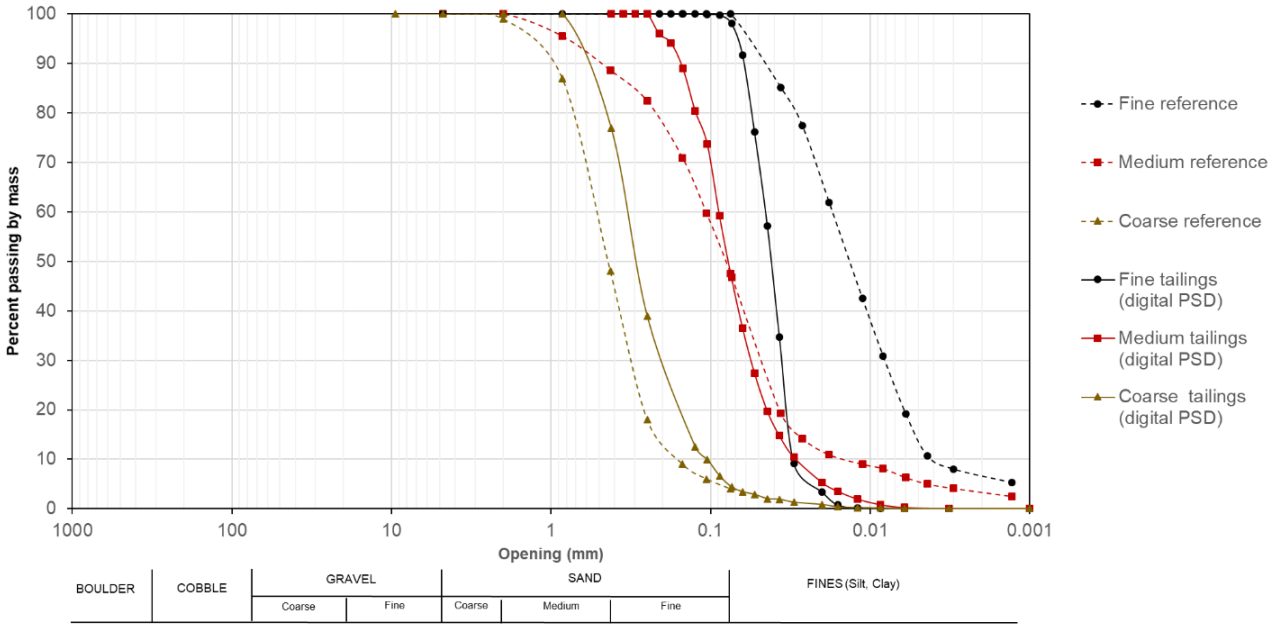


Figure 5: Comparison of digital and laboratory-obtained PSD for tailings

Another factor that affects digital segmentation is that some bigger particles could be segmented by the software as two smaller particles (i.e., "digital particle breakage" which results in a finer gradation compared to the laboratory PSD). It is also important to recognize that grain size distributions for fine-grained materials, obtained from mechanical/hydrometer sedimentation analysis methods could also have limitations, especially if the tailings contain platy fine soil particles. Overall, it is considered that the comparisons between the laboratory and digital PSD would benefit from improvements in the image processing steps.

It is of value to assess the PSDs in relation to their D_{10}, D_{50}, and D_{90} values. Note: D_n value is defined as the grain diameter that corresponds with the point where n% of the particles are finer by weight on a given PSD. For medium tailings the digital PSD has a D_{10} of 0.03 mm, while the reference PSD has a slightly smaller D_{10} of 0.017 mm. This indicates that the digital PSD predicts a slightly coarser material at the 10% finer mark compared to the reference PSD. Moreover, both the digital and reference PSDs have very similar D_{50} values (0.078 mm and 0.08 mm, respectively), suggesting that the median particle size is well approximated by the digital PSD. There is a significant difference in D_{90} values, with the digital PSD at 0.15 mm and the reference PSD at 0.5 mm. The C_u (Coefficient of uniformity = D_{60} / D_{10}) values are 3 for the digital PSD and 5.5 for the reference PSD. A higher C_u value in the reference PSD suggests a wider range of particle sizes, indicating that the digital PSD did not effectively capture the full variability of the particle sizes.

With respect to the coarse tailings, the digital PSD has a D_{10} of 0.105 mm, while the reference PSD has a D_{10} of 0.16 mm. This shows that the digital PSD estimates finer particles at the 10% finer mark compared to the reference PSD. The D_{50} values are 0.3 mm for the digital PSD and 0.45 mm for the reference PSD, indicating that the digital PSD predicts a finer median particle size. The D90 values are 0.58 mm for the digital PSD and 0.95 mm for the reference PSD, again showing that the digital PSD predicts finer particles at the 90% finer mark. The C_u values are close, with 3.3 for the digital PSD and 3.5 for the reference PSD, suggesting that the digital PSD provides a reasonable approximation of the range of particle sizes for this case with coarse tailings.

Conclusion

This paper presents some initial observations from an investigation undertaken to demonstrate the ability of micro-CT imaging to study the particle fabric of mine tailings. Three types of mine tailings were examined using images obtained from high-resolution 3D non-destructive micro-CT scanning. In spite of the limited scope of the study, the initial results from this imaging work illustrated the potential of X-ray micro-CT for the visualization of fabric and microstructure of tailings. Moreover, the importance of the analysis technique selected to process the images, the difficulties and constraints in arriving at reliable outcomes, and the need for further studies and improvements on this subject were highlighted.

In particular, the difficulties in imaging tailings containing both silt and sand size particles was revealed. The need for future work to refine and improve the image analysis process to better account for the true 3D volume of individual particles, and in turn, improvements in particle segmentation, was highlighted. It is recognized that the exploration of scalar and directional parameters (i.e., including particle orientation) will be the end goal in arriving at a complete description of fabric in tailings materials.

Acknowledgments

The authors would like to acknowledge the financial support of the Natural Science and Engineering Research Council of Canada (NSERC). Enthusiastic collaborative support provided by Dr Mark Martinez and James Drummond at the Pulp and Paper Centre at UBC Vancouver is appreciated. Thanks are due to Dr Mavi Sanin of WSP for facilitating the provision of the tailing materials for imaging work.

References

Al Mahbub, A. and Haque, A. 2016. X-ray computed tomography imaging of the microstructure of sand particles subjected to high pressure one-dimensional compression. *Materials* 9(11): 7–15.

ASTM, 2017, D6913/D6913M – 17. Standard test methods for particle-size distribution (gradation) of soils using sieve analysis. West Conshohocken, PA: Annual Book of ASTM Standards, ASTM International.

ASTM. 2021. D7928-21. Test method for particle-size distribution (gradation) of fine- grained soils using the sedimentation (hydrometer) analysis. West Conshohocken, PA: Annual Book of ASTM Standards, ASTM International; 2021.

Fonseca, J. 2011. The evolution of morphology and fabric of a sand during shearing. PhD thesis, Imperial College London.

Fonseca, J., O'Sullivan, C., Coop, M.R. and Lee, P.D. 2012. Non-invasive characterization of particle morphology of natural sands. *Soils and Foundations* 52: 712–722.

Helliwell, J.R., Sturrock, C.J., Grayling, K.M., Tracy, S.R., Flavel, R.J., Young, I. M., Whalley, W.R. and Mooney, S.J. 2013. Applications of X-ray computed tomography for examining biophysical interactions and structural development in soil systems: A review. *European Journal of Soil Science* 64(3): 279–297.

Hight, D. W. and Leroueil, S. 2003. Characterisation of soils for engineering purposes. *Natural Soils Conference* 255: 140.

Ketcham, R.A. and Carlson, W.D. 2001. Acquisition, optimization and interpretation of X-ray computed tomographic imagery: Applications to the geosciences. *Computers and Geosciences* 27: 381–400.

Markussen, Ø., Dypvik, H., Hammer, E., Long, H. and Hammer, Ø. 2019. 3D characterization of porosity and authigenic cementation in Triassic conglomerates/arenites in the Edvard Grieg field using 3D micro-CT imaging. *Marine and Petroleum Geology* 99: 265–281.

Thermo Fisher Scientific (TFS). 2019. Thermo Scientific Avizo Software 9 User's Guide. Berlin.

Valverde, A. 2023. Image-based characterization of low-plastic matrix for fabric quantification using X-ray micro-computed tomography. PhD Thesis, Department of Civil Engineering. The University of British Columbia, Canada.

Valverde, A. and Wijewickreme, D. 2021a. Towards understanding the particle fabric of silt – Assessment of laboratory specimen uniformity. *Proceedings of GeoNiagara*. Niagara, Canada.

Valverde, A. and Wijewickreme, D. 2021b. Image-processing to identify soil particles for fabric quantification using X-ray μ-CT scanning. *Proceedings of 20th International Conference on Soil Mechanics and Geotechnical Engineering.* Sydney, Australia.

Valverde, A. and Wijewickreme, D. 2024. Examination of silt-size particle matrices using X-ray micro-CT imaging: advancements, selected findings and challenges. *Proceedings of International Symposium on Geomechanics, from Micro to Macro.* Grenoble, France.

Valverde, A. Wesolowski, M. and Wijewickreme. D. 2020. Towards understanding the fabric and microstructure of silt – initial findings of soil fabric from X-ray μ-CT. *Proceedings of 17th World Conference on Earthquake Engineering, 17WCEE,* September 13 to 18, 2020, Sendai, Japan.

Wesolowski, M. 2020. Application of computed tomography for visualizing three- dimensional fabric and microstructure of Fraser River Delta silt. MSc Thesis, Department of Civil Engineering. The University of British Columbia, Canada.

Wijewickreme, D and Valverde Sancho, A.M. 2023. Particle fabric imaging for understanding the monotonic and cyclic shear response of silts. *Soil Dynamics and Earthquake Engineering* 171: 107931. https://doi.org/10.1016/j.soildyn.2023.107931.

Influence of Density on Predicting Saturation in Filtered Tailings using an Electromagnetic Sensor

Garret M. Martin, NewFields Mining Design and Technical Services, USA
Christopher A. Bareither, Colorado State University, USA
Joseph Scalia IV, Colorado State University, USA

Abstract

Filtered tailings stacks can experience changes in degree of saturation over time due to compression from subsequent tailings placement, climate interactions, and seepage. Understanding spatial and temporal changes in saturation within a filtered tailings stack is important when evaluating geotechnical and geochemical stability. The main objectives of this study were to characterize the effects of density on sensor output and create a density correction procedure that improves saturation and volumetric water content predictions. Laboratory-scale compression tests were conducted on filtered, hardrock mine tailings with an electromagnetic sensor embedded in the tailings specimens to measure volumetric water content and degree of saturation. Results indicate the predicted volumetric water content was generally within 8% of the measured value, and saturation was generally within 5% of the measured value during testing when the effects of density were not considered. However, correcting for density can improve the volumetric water content and saturation predictions to within 1% to 3% of measured values. A density correction method is outlined in this paper and is accompanied by discussions on field-scale implementation for measuring the volumetric water content and degree of saturation in filtered tailings stacks.

Introduction

Filtered tailings offer the benefits of water conservation as well as enhanced geotechnical stability via stacking tailings in an unsaturated state. However, filtered tailings stacks are not immune to risks associated with other tailings management strategies (e.g., slurry tailings). The degree of saturation in filtered tailings can increase due to compression induced by the growing height of the tailings stack. Additionally, during the lifetime of the facility the degree of saturation in filtered tailings can change due to desiccation and/or infiltration. Filtered tailings stacks must be properly designed, constructed, and managed throughout the facility lifecycle to minimize risk to people and the environment (Morrison, 2022).

The degree of saturation of filtered tailings plays an important role in the geotechnical and geochemical stability of filtered tailings facilities. Rodriguez et al. (2021) reported that maintaining saturation below 80% is the most influential factor to enhance geotechnical stability in tailings facilities. Opposingly, Aachib et al. (2004) report that the oxygen diffusion into unsaturated porous media (e.g., tailings) decreases exponentially at saturation above 85%, which implies that mitigation of acid generation in sulfide-containing tailings requires a high degree of saturation. However, geochemical stability also may be enhanced via low saturations and low unsaturated hydraulic conductivities, and thus low fluxes of percolating water. Regardless of the tailings management strategy, there is a need to reliably determine in-situ tailings saturation to assess stability.

Electromagnetic sensors have been implemented and researched within the agricultural community for many years (e.g., Topp et al., 1980; Noborio, 2001). These sensors are relatively inexpensive and can be designed to be durable, corrosion resistant, and compatible with different data loggers. Woyshner (1992) predicted the volumetric water content of a sulfide ore tailings facility with an average error of +1.1%, standard deviation of 2.2%, and a maximum error of 5.5%. However, Landim et al. (2023) identified substantial error (≈ 20%) when predicting volumetric water content in iron mine tailings using the manufacturer calibration, and indicated that sensor output was affected by tailings dry density. The test results and discussion included herein provide further insight into the effects of tailings dry density on sensor output.

Mine tailings within a tailings facility can experience spatial and temporal variation in dry density. Although the attributes of electromagnetic sensors support monitoring spatial and temporal variations in degree of saturation throughout a filtered tailings stack, the impacts of dry density on sensor performance must be considered during sensor implementation. The objectives of this study were to characterize the effects of density on sensor output and to create density correction procedures that improve volumetric water content and saturation predictions.

Materials and methods

Experimental program overview

The experimental scope of the project involved sensor calibration, measurement of sensor response to compression and infiltration, and characterization of density affects. All testing was conducted on a single hardrock mine tailings. Calibration testing was first completed to relate raw electromagnetic sensor output to measured values of volumetric water content and degree of saturation. The calibration equations were used in a simulated filtered tailings stack scenario to assess the timeliness and accuracy of sensor response to changes in volumetric water content and degree of saturation due to specimen compression and water infiltration. Moist-tamped specimens were used to characterize changes in sensor output as tailings dry

density varied, and the test results were used to develop an approach to correct sensor output for density affects.

Mine tailings

Hardrock mine tailings from a precious metal mine were used in this study. Particle size analysis yielded 14% fine sand and 86% fine-grained particles (i.e., silt and clay that pass the No. 200 sieve), by mass. The tailings had low plasticity with a liquid limit of 30 and a plasticity index of 9. The specific gravity of the tailings was 2.72. Standard Proctor compaction testing (ASTM D698) yielded a maximum dry density of 1.69 Mg/m^3 and optimum gravimetric water content of 15.8%. Particle size, plasticity, and compaction test results were extracted from Aghazamani (2022), and the specific gravity was determined as part of this study.

Teros 10 soil moisture sensor

The Teros 10 is an electromagnetic soil moisture sensor (METER Group, Inc., Pullman, WA, USA) that is sensitive to the dielectric permittivity of the surrounding medium. The raw sensor output in millivolts (mV) can be calibrated to volumetric water content and degree of saturation. Additional information regarding dielectric permittivity and soil moisture sensor principals of operation are discussed in previous studies (Topp et al., 1980; Peddinti et al., 2020).

An ESP32 Adafruit Feather micro-controller was used to operate Teros 10 sensors and record output values. The ESP32 was programmed using Arduino IDE software. The micro-controller was programmed to report the average of a specified number of measurements as a single output value to smooth noise in the raw sensor output.

Tailings specimens prepared to a target water content and dry density yielded a single, averaged millivolt sensor output, which was coupled with physical measurements of volumetric water content, degree of saturation, and dry density. All sensor output as a function of time was recoded for compression and infiltration tests. Additional details on sensor operation and data processing are in Martin (2023).

Test molds

Customized test molds were fabricated to accommodate the sensor volume of influence. Two test molds were used in this study: small-mold = 100-mm diameter; and large-mold = 300-mm diameter. Both molds were fabricated from PVC pipe and enclosed at one end with PVC end caps.

Specimen preparation and testing methodology

Specimen preparation methods were similar across the various tests performed. Tailings were oven-dried for ≥ 24 hours, manually broken up, and passed through a No. 40 sieve (0.425 mm). Subsequently, tailings were hydrated to target water contents.

The small mold was used to conduct calibration and characterization of density affects testing, and the large mold was used to conduct specimen compression and infiltration proof-of-concept tests. For moist-tamped specimens, moisture conditioned tailings were compacted in uniform lifts to achieve a desired volumetric water content and dry density. Several slurry-deposited specimens were prepared in the small mold during sensor calibration by pouring slurry into the mold to a target total volume. Mass-volume measurements were taken from the constructed specimens before and after testing to determine the actual volumetric water content, degree of saturation, and dry density of the specimen to the nearest 0.1% or 0.01 g/cm^3. Further discussion and details regarding specimen preparation are in Martin (2023).

Following specimen preparation in the small mold, sensor output was recorded for a desired period, and the data was processed as described in Martin (2023). After specimen preparation in the large mold, the specimen was prepared for compression testing. Vertical load was applied to the surface of the test specimen incrementally via an air-cylinder. Applied load and vertical deformation were recorded during testing. Output from an embedded Teros 10 sensor was continuously recorded. After completing Compression Test 2, water was added incrementally to the top of the specimen while under the final applied load to observe the sensor response as the wetting front infiltrated through the specimen. Specimen deformation was recorded throughout the water infiltration period to correct volumetric water content and saturation calculations for comparison with predictions made via the Teros 10 sensor. Further discussion and details on the laboratory testing procedures are in Martin (2023).

Sensor calibration and accuracy

Calibration testing of the Teros 10 was conducted by relating raw sensor output to physical measurements. Three Teros 10 sensors, each inserted into a unique tailings specimen, were used to account for potential variations between sensors. Relationships between volumetric water content and degree of saturation versus sensor output are shown in Figure 1. Calibration equations for volumetric water content and degree of saturation were fit to each data set and are included in Figure 1. A third-order polynomial was used for the volumetric water content calibration curve, which is consistent with the calibration curve developed by METER Group (i.e., the Teros 10 manufacturer) and other studies on electromagnetic sensors (Topp et al., 1980; Bhuyan et al., 2020; Narayanan and Sathian, 2021). The degree of saturation calibration is a linear relationship.

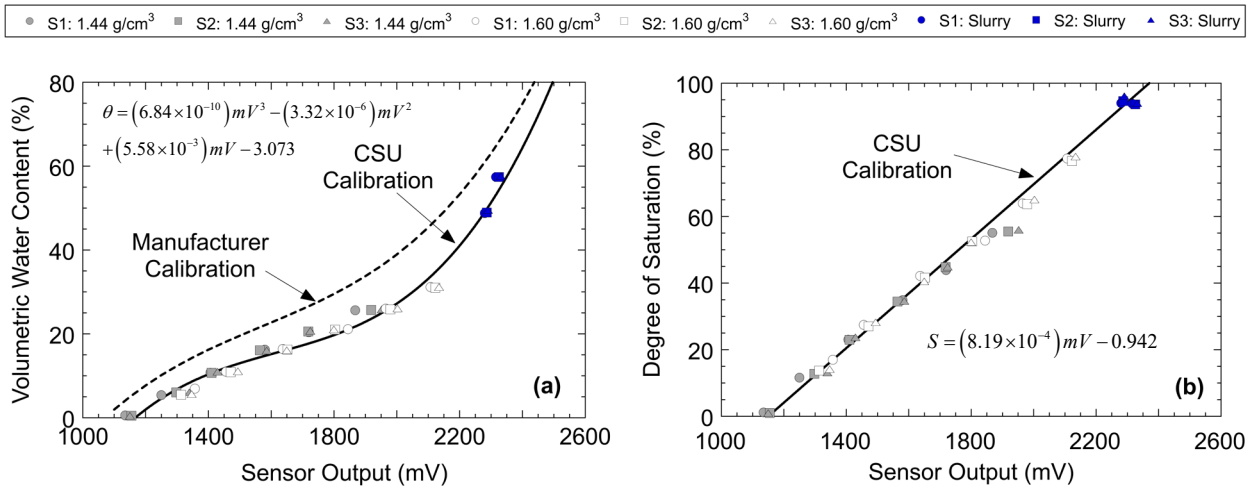


Figure 1: Results from calibration testing of (a) volumetric water content and (b) degree of saturation versus sensor output in millivolts (mV)

Compression and infiltration testing

Two compression experiments were conducted on moist-tamped specimens prepared in the large mold to a target dry density of 1.36 g/cm^3 (approximately 80% Standard Proctor maximum dry density) and target volumetric water content of 15%. A total of 10 uniform load increments were applied to the specimens and the final vertical stress was 668 kPa. Each applied load was maintained for approximately 5 to 7 minutes to allow for immediate deformation to reach apparent completion before the subsequent load was applied. The volumetric water content and degree of saturation predicted by the Teros 10 sensor via the calibration equations presented in Figure 1 (i.e., Predicted) were compared to actual values (i.e., Measured) determined from direct measurement of specimen volume based on continuously recorded deformation.

At the conclusion of Compression Test 2, water was poured on the specimen surface in four daily 600-mL increments; the specimen remained under the final applied stress during infiltration. Sensor output was recorded throughout the wetting process and the test concluded when the signal showed negligible change for 24 hours, which occurred about 4 days after the final water application. Due to uncertainty in the amount of water that infiltrated into the specimen, the accuracy of the sensor response to specimen infiltration was only evaluated by comparing sensor predictions to the measurements at the beginning and conclusion of the infiltration test.

Results and discussion

Characterization of density affects

Mine tailings within a tailings facility can experience spatial and temporal variation in dry density. Landim et al. (2023) noted an increase in raw sensor output for specimens prepared at higher dry densities, and

Narayanan and Sathian (2021) concluded that sensor accuracy when predicting volumetric water content is affected by dry density of the surrounding medium. A general understanding of the dielectric permittivity of porous media and sensor function can help explain the sensor behavior.

Porous media, such as filtered tailings, can generally be separated into air, water, and solid phases, whereby each has a unique dielectric permittivity. The Teros 10 sensor output is representative of the weighted average dielectric permittivity of the three phases occupying the total volume of influence of the sensor. Therefore, the sensor output is unique to a specific combination of air, water, and solid particles present within the sensor volume of influence. If the volumetric proportions of the three phases change, the weighted average dielectric permittivity will also change and yield a different sensor output. Thus, two specimens of tailings can have the same volumetric water content or degree of saturation, but variations in dry density between the two specimens would yield different sensor outputs.

The effect of varying dry density on sensor output was evaluated using moist-tamped specimens prepared in the small mold to a range of volumetric water contents and degrees of saturation for several dry densities. Relationships between sensor output and specimen dry density for target volumetric water contents of 15%, 20%, and 25% and degrees of saturation of 30%, 45%, and 60% are shown in Figure 2. For a given volumetric water content or degree of saturation, a linear response in sensor output was observed with variations in dry density. The slope between sensor output and dry density (shown as *"m"*) was generally consistent for the three volumetric water contents evaluated. However, as the degree of saturation increased, the slope of the linear relationship between sensor output and dry density, *m*, became increasingly negative.

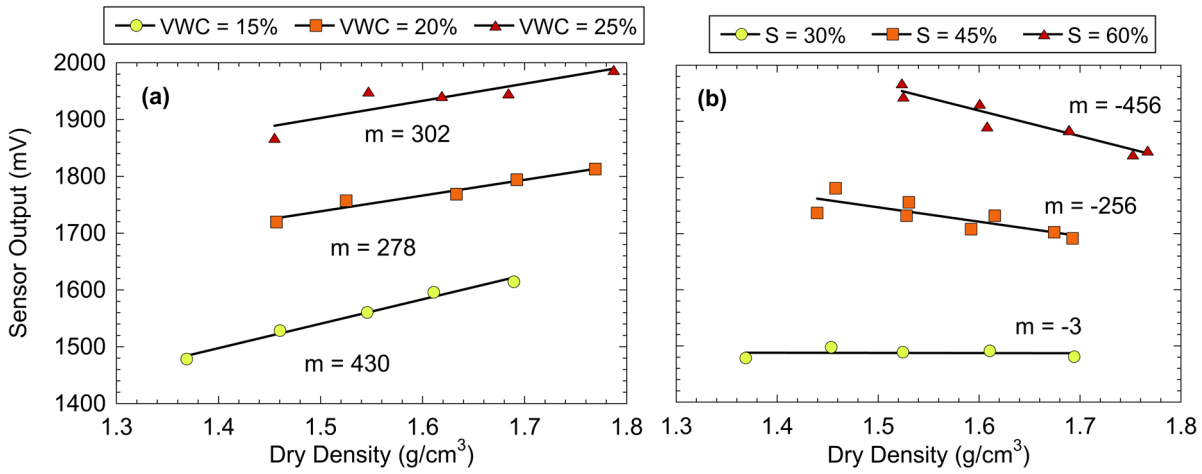


Figure 2: Relationships between sensor output and specimen dry density for (a) constant values of volumetric water content (VWC) and (b) constant values of degree of saturation (S). The parameter m is the slope of the linear regression

The results in Figure 2a suggest that *m* is generally constant and independent of volumetric water content. Therefore, the sensor-predicted volumetric water content should exhibit relatively consistent

sensitivity to dry density regardless of actual volumetric water content. The results in Figure 2b suggest that m is dependent on the degree of saturation. Specimens prepared at a degree of saturation of 30% exhibited negligible change in sensor output for the range of dry density. However, at higher degrees of saturation, variations in dry density had a more pronounced effect on sensor output, thus making sensor prediction of saturation more sensitive to changes in dry density at elevated saturation levels.

An approach for density correction

A correction for density effects was applied to the compression and infiltration test results to reduce the error in predicted volumetric water content and saturation (described subsequently). The following sections discuss the framework and process used to correct the compression and infiltration test data for density effects. Results of the correction process are presented accordingly.

Correction framework

Equation 1 serves as the core framework of the density correction process discussed herein:

$$mV_{corrected} = mV_{raw} - m(\rho_i - \rho_{ref}) \quad \text{(Equation 1)}$$

where $mV_{corrected}$ = sensor output corrected for dry density, mV_{raw} = raw (uncorrected) sensor output, m = relationship between sensor output and dry density, ρ_i = measured specimen dry density during testing, and ρ_{ref} = reference density deemed representative of sensor calibration. The corrected sensor output ($mV_{corrected}$) was then used to predict the volumetric water content and saturation based on the calibration equations developed during this study (Figure 1). If the specimen dry density at a given point in time during sensor operation is known, the specimen density relative to the reference density can be determined. The relationship between the change in specimen dry density and resulting change in sensor output, *m*, can be used in conjunction with the density of the specimen to approximate an increase or decrease in sensor millivolt output due to variations in dry density.

Selecting an "*m*" value

Results in Figure 2a suggest *m* is consistent regardless of volumetric water content, provided the specimen remains unsaturated. Therefore, the average value of *m* for the three volumetric water contents shown in Figure 2a was used when correcting sensor output for volumetric water content predictions (m_{vwc} = 336.5). In contrast, *m* varies depending on degree of saturation. A linear relationship was created between the slope *m* and degree of saturation data from Figure 2b to yield m = -1523.3(*S*) + 466.23. Thus, the slope *m* decreases linearly as the degree of saturation increases.

Determining an appropriate *m* value for density correction of sensor-predicted saturation required an iterative process. The iterative process developed to determine m_{sat} is shown in Figure 3. The iterative process was repeated until no appreciable change in predicted saturation was observed.

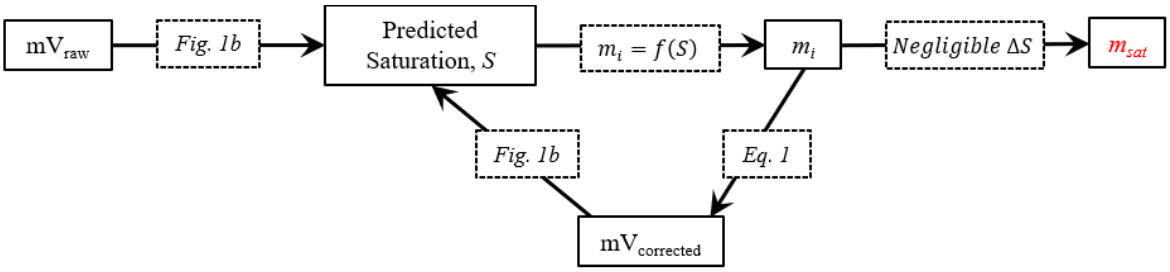


Figure 3: Depiction of iterative correction process saturation calibration

Data processing indicated the number of iterations required to reach a consistent saturation value was dependent on the magnitude of the $(\rho_i - \rho_{ref})$ term. Values of 0.36 g/cm^3 required at least 5 iterations while values of 0.59 g/cm^3 required as many as 14 iterations to reach a consistent saturation value. Care should be taken during the density correction process for predicted saturation to ensure sufficient iterations are performed to reach a stable m_{sat} value.

Selecting a reference density (ρ_{ref})

Determining an appropriate reference density (ρ_{ref}) representative of the sensor calibration is critical to the density correction process. Three different approaches for determining ρ_{ref} were considered for density correction. The first, and simplest, approach assumed the average dry density of moist-tamped specimens prepared during sensor calibration was generally representative of the calibration equations. Therefore, the average dry density of moist-tamped calibration specimens was considered for density correction ($\rho_{ref} = 1.55\ g/cm\text{^}3$). However, the results of the correction process indicate mixed success when assuming an average value for ρ_{ref}, and alternative approaches were considered.

The second and third approach for determining ρ_{ref} both sought to optimize the ρ_{ref} value based on available data sets obtained from directly measured specimens. A laboratory optimized reference density was determined based on moist-tamped specimen data from the Characterization of Density Affects testing. The density correction framework was applied to the laboratory data, and the value of ρ_{ref} was then adjusted using MS Excel's solver application to minimize the calculated mean squared error (MSE) between the corrected sensor prediction and the known volumetric water content or saturation. The same optimization approach was also performed using two discrete data points extracted from the compression and infiltration testing data sets. This approach essentially simulates the act of obtaining undisturbed samples at two discrete points in time during the field operation of a sensor network. Data points near the onset and midpoint of the compression tests were used for optimization. For the infiltration test, only the two measured data points at the start and end of the test were available for optimization. Table 1 summarizes the ρ_{ref} values determined from the three approaches tested.

Table 1: Reference density (ρ_{ref}) values determined for volumetric water content (VWC) and saturation (S) density correction procedures based three different approaches

Test Scenario	Calculated Reference Density, ρ_{ref} (g/cm^3)		
	Average Moist-Tamped Specimen Density	Laboratory Optimization	Field Optimization
Compression Test 1 (VWC)	1.55	1.71	1.62
Compression Test 1 (S)		1.66	1.70
Compression Test 2 (VWC)		1.71	1.49
Compression Test 2 (S)		1.66	1.98
Infiltration Test (VWC)		1.71	1.39
Infiltration Test (S)		1.66	1.80

Density correction results

The uncorrected temporal trends of the predicted volumetric water content and degree of saturation during compression and infiltration testing are shown in Figure 4 through Figure 8, along with the density-corrected predictions that incorporate the three approaches for determining ρ_{ref} discussed in the preceding section. Also included with the compression test results (Figures 4 to 7) are residual plots presenting the difference between the sensor-predicted and measured values throughout each test. In general, the sensors responded in a timely way to changes in volumetric water content and degree of saturation induced by compression and infiltration of the surrounding tailings. In the absence of a density correction, the volumetric water content and degree of saturation predicted by the sensor during compression generally remained within about 1.5% and 5% of the measured value, respectively. Results from infiltration testing indicate that, in the absence of a density correction, saturation predicted by the sensor remained within about 5%, whereas volumetric water content was over-predicted by about 8% at the completion of infiltration.

Table 2 summarizes the average error and maximum error for each test based on the density correction approach applied. The use of an average dry density value for ρ_{ref} generally yielded mixed success at improving sensor accuracy. Optimizing ρ_{ref} based on available laboratory data generally showed improved sensor accuracy across most scenarios, but still displayed some inconsistency. The use of a field optimized ρ_{ref} generally yielded improved sensor accuracy across all scenarios except for predicted volumetric water content during Compression Test 2. However, the field optimized ρ_{ref} consistently resulted in sensor predictions of volumetric water content within about 1% of the measured value, and predicted saturation remained within about 3% of the measured value.

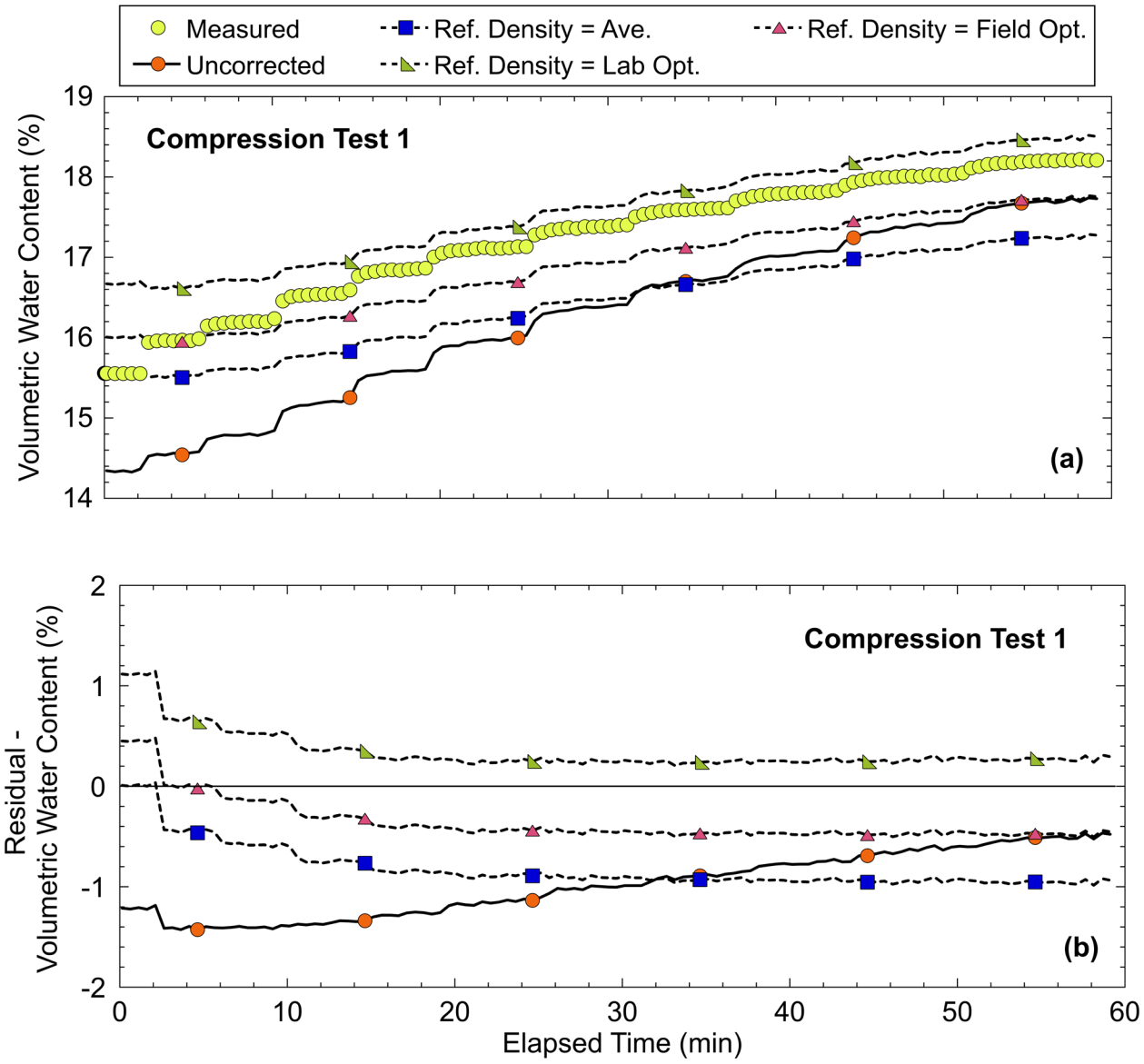


Figure 4: Compression Test 1 uncorrected and corrected results for volumetric water content (a) and residual (b; difference between measured and predicted volumetric water content)

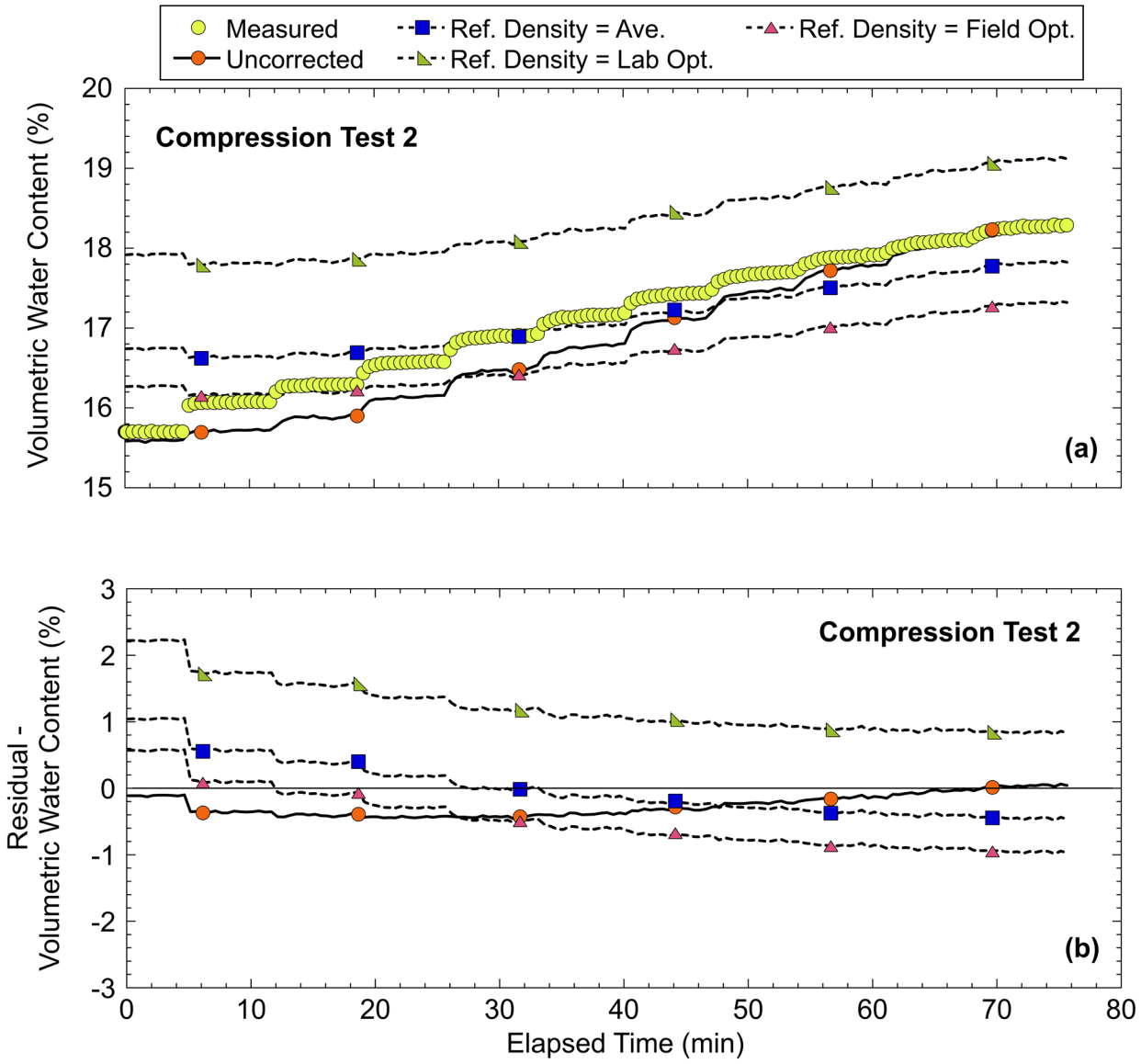


Figure 5: Compression Test 2 uncorrected and corrected results for volumetric water content (a) and residual (b; difference between measured and predicted volumetric water content)

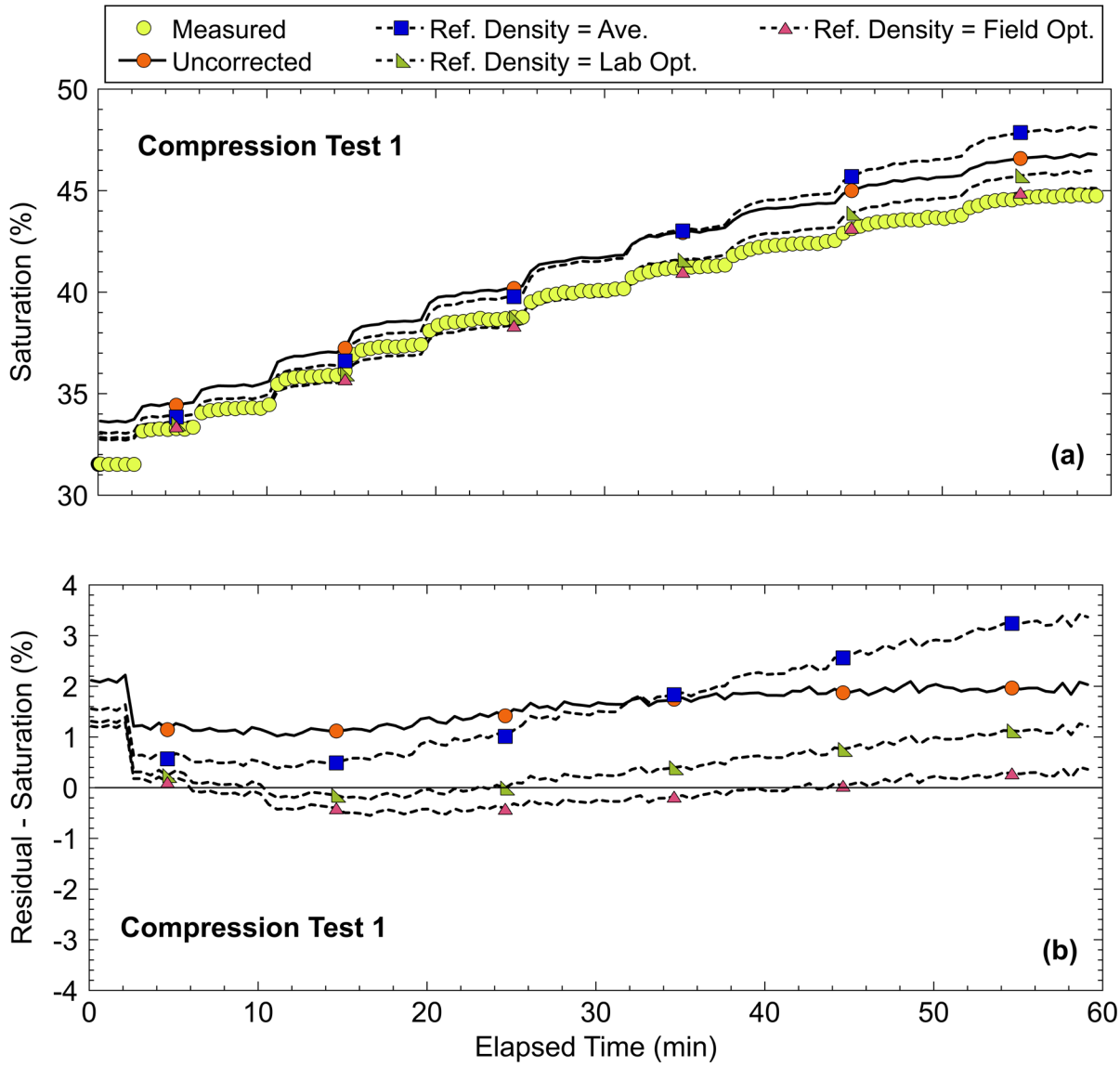


Figure 6: Compression Test 1 uncorrected and corrected results for saturation (a) and residual (b; difference between measured and predicted saturation)

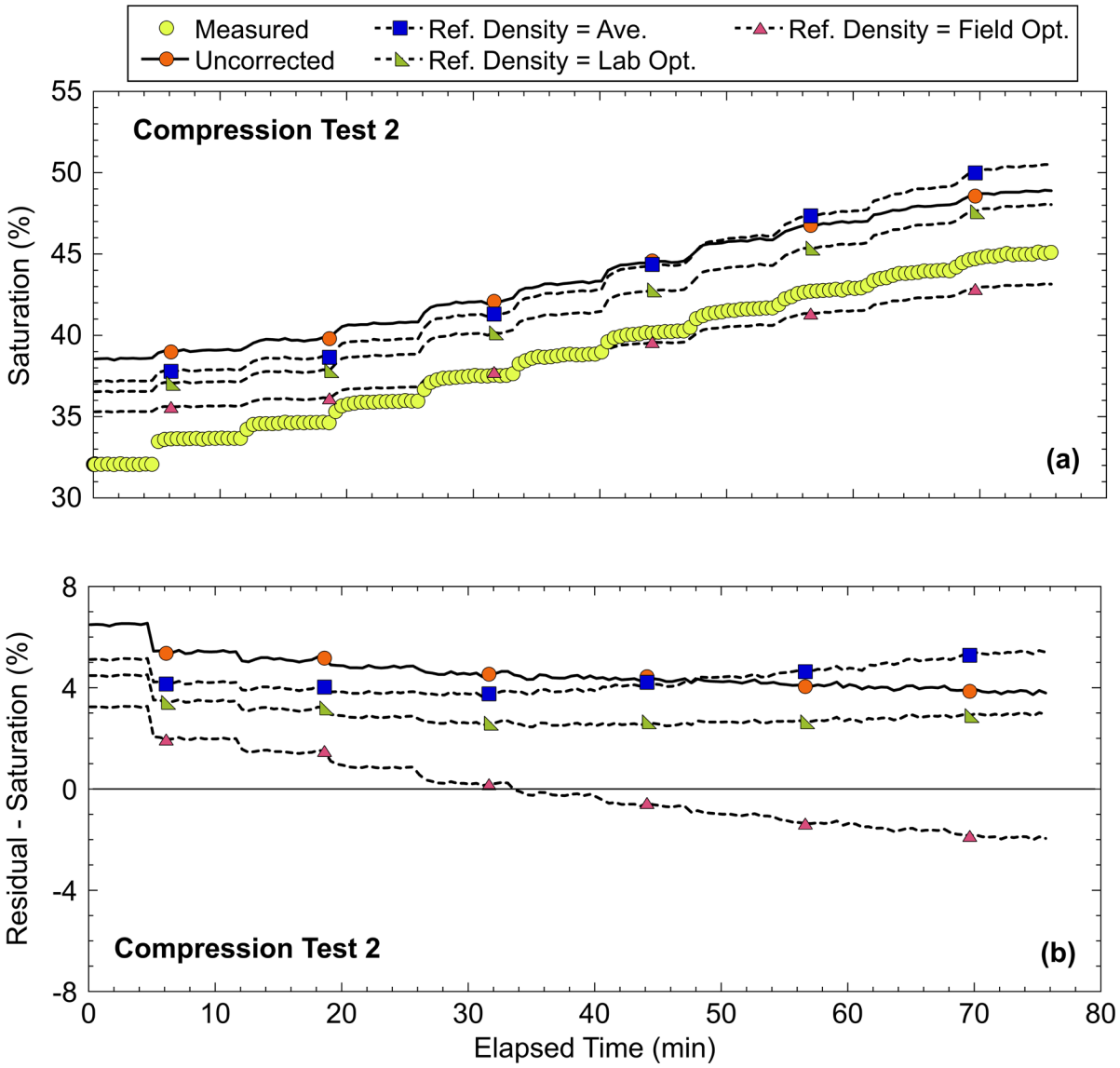


Figure 7: Compression Test 2 uncorrected and corrected results for saturation (a) and residual (b; difference between measured and predicted saturation)

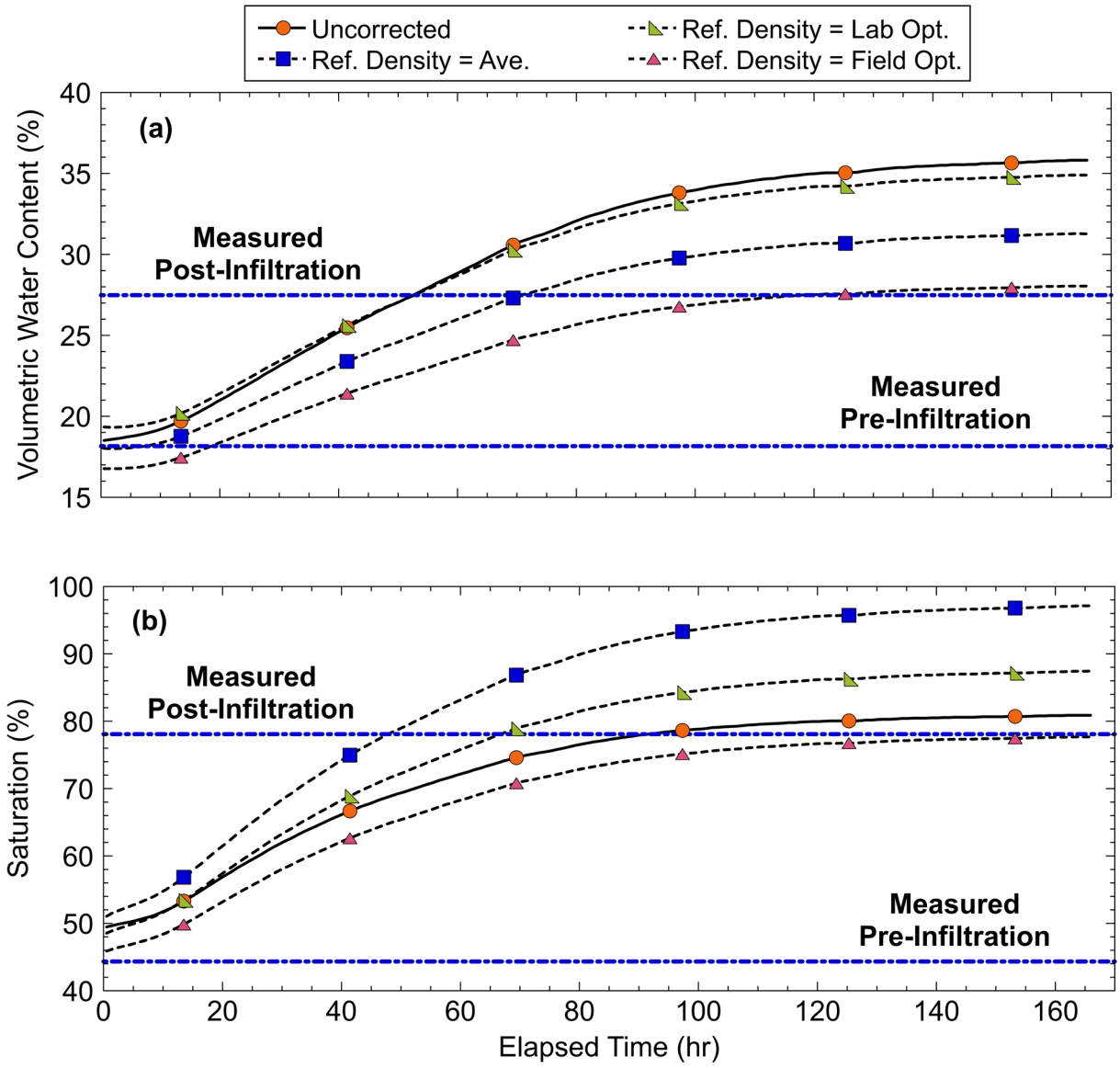


Figure 8: Infiltration Test uncorrected and corrected results for volumetric water content (a) and degree of saturation (b)

Table 2: Summary of average error and maximum error of uncorrected and corrected compression and infiltration test results

Test Scenario	Correction Approach							
	Uncorrected		Average		Lab. Optimized		Field Optimized	
	Avg. Error	Max. Error	Avg. Error	Max. Error	Avg. Error	Max. Error	Avg. Error	Max. Error
Compression Test 1 (VWC)	-1.0%	-1.4%	-0.8%	-1.0%	0.3%	1.1%	-0.4%	0.5%
Compression Test 2 (VWC)	-0.3%	-0.5%	-0.2%	1.1%	1.0%	2.2%	-0.7%	-1.0%
Compression Test 1 (S)	1.6%	2.2%	1.7%	3.4%	0.4%	1.4%	-0.1%	1.3%
Compression Test 2 (S)	4.3%	6.5%	4.4%	5.5%	2.7%	4.5%	-0.6%	3.3%
Infiltration Test (VWC)	4.3%	8.4%	1.8%	3.8%	4.3%	7.4%	-0.4%	-1.4%
Infiltration Test (S)	3.9%	4.9%	12.7%	19.2%	6.6%	9.4%	0.4%	1.2%

Practical implications of density correction approach

When deploying a network of electromagnetic sensors within a tailings facility, the sensor output and the accuracy of the sensor will be affected by variations in dry density. The potential error in predicted volumetric water content and degree of saturation due to variations in tailings dry density will depend, in part, on the range of dry density the sensor will be subjected to in a field application. The simulated filtered tailings scenario tested during this study indicates that the sensor was reasonably accurate when predicting saturation despite the variations in dry density imposed. Should greater accuracy be desired, a method to correct sensor output for the effects of dry density is described herein. The proposed correction process infers the following practical implications.

- The relationship between dry density and sensor output for a given tailings (i.e. m value) is related to the composition of the tailings and pore fluid being tested because the composition impacts the dielectric permittivity of the material. As such, a material-specific characterization of density affects will need to be performed to use the correction process. This would include a series of laboratory tests of remolded specimens similar to those used in this study. See Martin (2023) for additional details on laboratory testing.
- The success of the density correction process is directly impacted by the ability to successfully estimate the dry density of the tailings at any given point in time during sensor operation. Laboratory testing, modeling, and/or field monitoring to provide insight into volumetric strains within a filtered tailings stack over time could be used to aid in predicting in-situ dry density within the facility.
- The correction process provides a framework that can be used to "tune" the sensor calibration by adjusting the ρ_{ref} value based on available datasets of directly measured values.

Performing a field optimization of the ρ_{ref}, as described above, would require direct measurements of in-situ volumetric water content or saturation near an operating sensor (i.e., undisturbed samples). The results from this study suggest confidence in the sensor-predicted value can generally be improved with as few as two discrete field data points. A greater number of data points would allow for further improvement in confidence and/or accuracy. The benefit of improved accuracy/confidence should be weighed against the cost of performing the correction process as well as the odds of achieving success in a field environment.

Conclusion

The results of this study suggest that an electromagnetic soil moisture sensor can be used to predict variations in volumetric water content and degree of saturation within a filtered tailings stack with anticipated compression and surface water infiltration. Sensor output is affected by variation in dry density, and the effects of compression on sensor performance should be considered when evaluating the accuracy of sensor-predicted volumetric water content and saturation. Understanding of the effects of variations in dry density on sensor performance can be utilized to correct sensor output for density affects and to reduce potential error.

During specimen compression and infiltration, error in predicted volumetric water content varied from less than 1.5% to 8%, and error in predicted saturation was predominantly less than 5% when no correction for density affects was applied. A possible framework for correcting the effects of dry density on sensor output was presented in this study and could be considered if greater accuracy or confidence in sensor-predicted volumetric water content or saturation is desired. Several variants of the density correction approach were evaluated and produced varying degrees of success in improving sensor accuracy. The method of using in-situ field measurements of volumetric water content and saturation to "tune" the sensor calibration via an optimized reference density (ρ_{ref}) consistently yielded an error of less than 1% and 3% in predicted volumetric water content and saturation, respectively. The effects of dry density on sensor performance and possible approach for correcting density affects should be further explored and studied.

References

Aachib, M., Mbonimpa, M. and Aubertin, M. 2004. Measurement and prediction of the oxygen diffusion coefficient in unsaturated media, with applications to soil covers. *Water, Air, and Soil Pollution* 156(1): 163–193. https://doi.org/10.1023/B:WATE.0000036803.84061.e5

Aghazamani, N. 2022. Unsaturated fluid flow and volume change behavior of filtered tailings. Doctoral dissertation, Colorado State University.

Bhuyan, H., Scheuermann, A., Bodin, D. and Becker, R. 2020. Soil moisture and density monitoring methodology using TDR measurements. *International Journal of Pavement Engineering* 21(10): 1263–1274. https://doi.org/10.1080/10298436.2018.1537491

Landim, A.D.S., Corrêa, Y., Silva, J.P. and Marinho, A.M.F. 2023. Evaluation a volumetric water content sensor to be used for compacted filtered iron ore tailings. *E3S Web of Conferences*, *382*, 16003. https://doi.org/10.1051/e3sconf/202338216003

Martin, G. 2023. Predicting water content and saturation in mine tailings with an electromagnetic soil moisture sensor. Master's thesis, Colorado State University.

Morrison, K.F. 2022. *Tailings Management Handbook: A LifeCycle Approach*. Society for Mining, Metallurgy and Exploration (SME).

Narayanan, J. and Sathian, K.K. 2021. Laboratory calibration of capacitance-based soil moisture sensor to monitor subsurface soil moisture movement in laterite soil. *International Journal of Plant and Soil Science* 137–147. https://doi.org/10.9734/ijpss/2021/v33i1730558

Noborio, K. 2001. Measurement of soil water content and electrical conductivity by time domain reflectometry: A review. *Computers and Electronics in Agriculture* 31(3):213–237. https://doi.org/10.1016/S0168-1699(00)00184-8

Peddinti, S., Hopmans, J., Najm, M. and Kisekka, I. 2020. Assessing effects of salinity on the performance of a low-cost wireless soil water sensor. *Sensors* 20. https://doi.org/10.3390/s20247041

Rodríguez, R., Muñoz-Moreno, A., Vanessa Caparrós, A., García-García, C., Brime-Barrios, Á., César Arranz-González, J., Rodríguez-Gómez, V., Javier Fernández-Naranjo, F. and Alcolea, A. 2021. How to prevent flow failures in tailings dams. *Mine Water and the Environment* 40(1): 83–112. https://doi.org/10.1007/s10230-021-00752-8

Topp, G.C., Davis, J.L. and Annan, A.P. 1980. Electromagnetic determination of soil water content: Measurements in coaxial transmission lines. *Water Resources Research* 16(3): 574–582. https://doi.org/10.1029/WR016i003p00574

Woyshner, M.R. 1992. In-situ vadose-zone monitoring and hydrologic evaluation of sulfide-mine mill-tailings wastes at Waite Amulet, Quebec. Master's thesis, McGill University, Montreal, Quebec.

Testing of an Autonomous Rheometer for Optimized Tailings Thickeners Operation

Arno Talmon, Deltares/Delft University of Technology, The Netherlands
Wiebe Boomsma, IHC Mining, The Netherlands
Bas Nieuwboer, IHC Mining, The Netherlands
Samir Rustamov, Rhosonics Analytical B.V., The Netherlands
Menno Jaspers, Sweco, The Netherlands
Sven van Asperen, IHC Mining, The Netherlands
Miguel de Lucas Pardo, Deltares, The Netherlands

Abstract

Nowadays tailings thickening is monitored on the basis of underflow density. But with greater demands placed on minerals processing, the thickening is expected to be better controlled by continuous monitoring of underflow rheology. Responding to an industry request, an online pipe viscometer was developed for monitoring the underflow of tailings thickening for the industry's largest mines. The paper reports on recent testing of the autonomous apparatus. It consists of a multiple pipe viscometer unit housed in a transportable shipping container. By vertically orienting, the design safeguards against settling solids in the measuring section. In our application of a pressure differential membrane system, a temperature drift problem was encountered, adding to earlier experienced persistent problems with the downward pipes. Without such problems the unit also measures tailings density, but now an additional independent density meter is necessary. In the processing of data only the upward pipe is now utilized, and the strategy to convert from raw data to rheological Bingham parameter values was upgraded. Similar issues are emerging in wastewater transport and treatment. The paper concludes on the technological readiness level of the instrument.

Introduction

Royal IHC and Deltares co-created an Autonomous Rheometer (ARM) which continuously measures the rheology and density of tailings (Boomsma et al., 2022). The ARM was primarily developed for the mining industry but can be used in other sectors too. The mining industry, while delivering great value to our society and civilization, inadvertently produces waste, e.g., tailings. These tailings contain a significant amount of water and demand a huge amount of storage volume. Today, there are about 217 billion m^3 of tailings

accumulated in the world; this amount is enough to fill up a pipeline with a 30 m diameter connecting the Earth to the Moon. Roughly speaking, half of this volume is water. The irony is that about 50% of mines are located in arid and semi-arid areas, suffering severely from water scarcity (Meshkati et al., 2021).

The main question is: how can we ensure that less watery tailings end up in storage facilities? Without converting the processing chain to deliver thicker paste, mine industries use thickener units to achieve this goal, by adding and mixing flocculants and coagulants and allowing time for tailings to consolidate. Nonetheless, very watery tailings end up in storage facilities. The performance of a thickener unit can be optimized by rheological feedback (Chryss et al., 2019; Wang et al., 2020) from downstream of the thickener, e.g., improving the quality of its underflow tailings, as shown in Figure 1. The ARM was developed to serve that purpose, providing continuous measurement of rheology and density to the thickening operation.

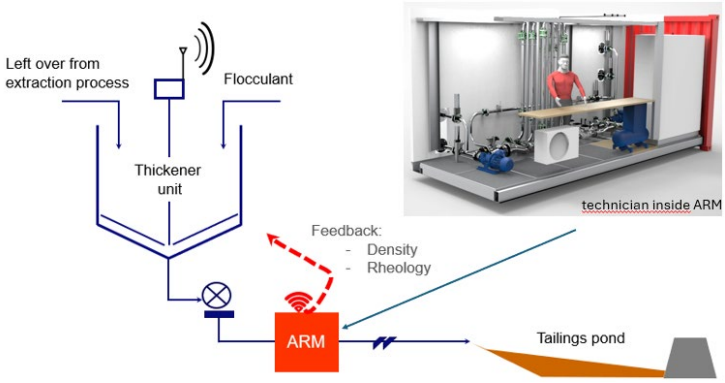


Figure 1: ARM in the underflow of the thickener providing feedback on rheology and density

The ARM is installed in an airconditioned container with a 6 m length, about 2.5 m wide and about 2.5 m high (e.g., a 20' high cubical standard shipping container). It is designed to output, 24/7, Bingham yield stress and dynamic viscosity plus density. It has 3 parallel simultaneously operating measuring units: three inverted U-loops (see Figure 2) for redundancy and for eventual compensation for wall slip of the tailings. The automatic measuring cycle is governed by a control valve in each pipe steering the discharge. It also contains a water flushing circuit for cleaning and verification of the instruments' performance. It is designed for large discharges (diverging a slip stream through the ARM), high solids content slurries and tailings with sand. The ARM may potentially help save up to 10 to 20% of water in thickeners.

In the initial phase (TRL1-3) it was decided to rely on known physical principles and combining experiences in manufacturing and hydraulic transport at IHC and experiences in non-Newtonian rheology and its hydraulic transport fundamentals at Deltares. Testing went through a couple of phases: prototype single U-loop testing and pump type testing (in the year 2019, TRL 4). Integral testing of the manufactured containerized ARM (in the year 2020), where it appeared sometimes difficult to obtain reliable results from

the largest descending pipe, specific testing for wall-slip and density measurement (in the year 2022), component testing (in the year 2023), and integral testing with an additional independent density meter, in the year 2024.

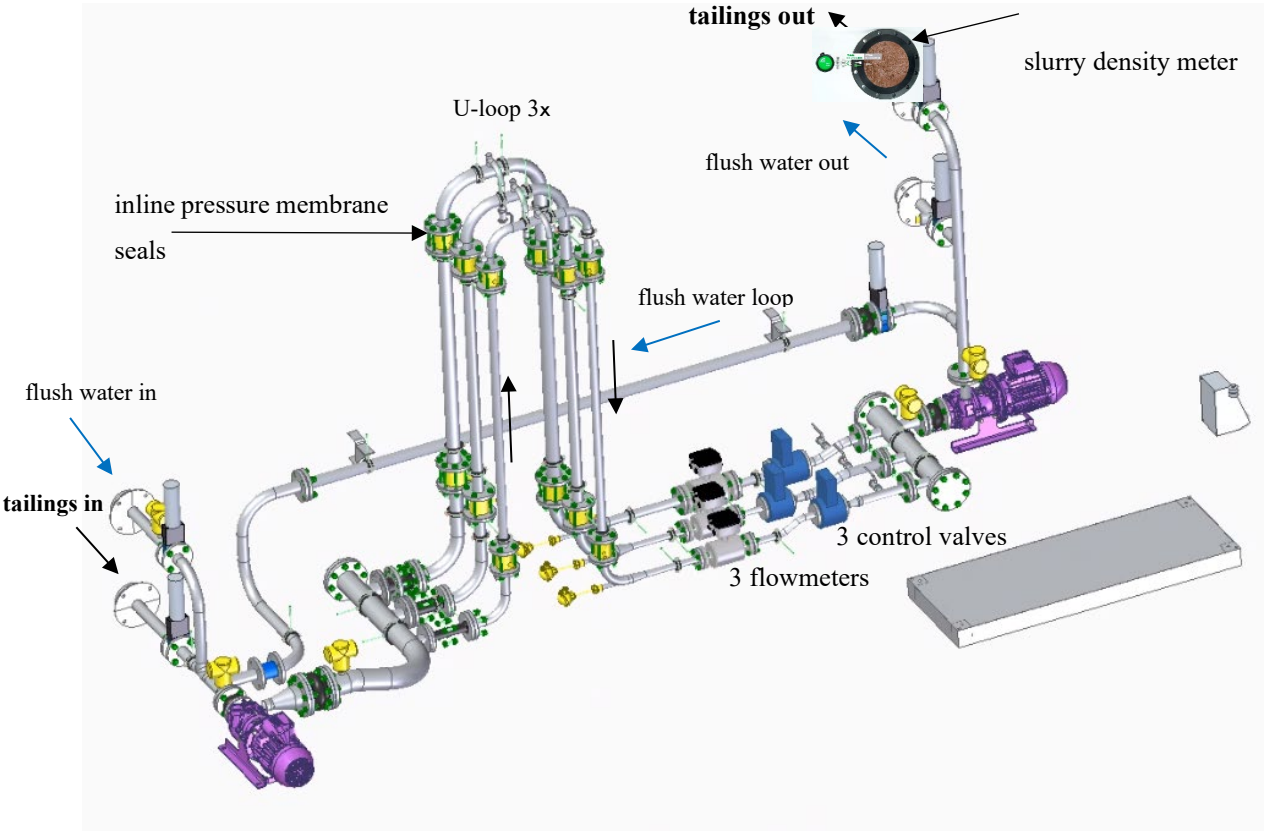


Figure 2: Internal view of an ARM and an external densitometer situated at an outlet

The TKI Water Technology research component (a Public-Private Partnership), which commenced in the year 2022, studies densitometering and wall slip. Wall slip may occur with mixtures at a high solids concentration. The 3 U-loops in the ARM are a provision to detect wall slip and are designed to provide information to correct for wall slip. As a spin-off of its vertical design, the ARM in principle also outputs density, enabling a verification of performance, and if differences occur between pipes, it is necessary to have an independent density measurement to assist in determining the hydraulic resistance from the U-loop measurements for rheological characterization.

The first measuring campaign in the TKI measured density and investigated wall slip using U-loop pipes only. Using clay-based model tailings without coarse material, the ARM produced data autonomously. While it was doing so, it associated rotoviscometry on these model tailings, but with added coarse plastic 1 mm spheres; this was done to investigate whether such a mixture could be used in a next phase to test wall slipping with the ARM. The results appear positive. More importantly, it was concluded

that the ARM gave unworkable results, and it was decided to commence investigating the performance of several components individually (which was done in 2023). It turned out that there was a temperature sensitivity problem, despite the air-conditioning of the ARM housing. The temperature of the circulated water varied, the testing fluid, which had consequences that we will discuss in this paper. The need for independent density metering hence appeared even stronger. The 2024 measuring campaign planned to include Rhosonics slurry density metering (SDM). Note that these temperature differences are less likely to occur when tailings are handled, since these come from a large thickener, which does not heat up very quickly, as compared to our model tailings, which circulate.

Pressure measuring system

The ARM is purposely equipped with pressure sensor membrane technology (Siemens SITRANS inline seals in a sandwich design), contrary to the usual pressure taps. This is done to prevent clogging of such pressure taps and associated impulse tubes leading to the differential pressure sensor. A sketch of the differential pressure measurement system utilizing membrane seals is shown in Figure 3. The membranes are not aligned entirely flush with the pipe's inside, but rather are recessed a little, to provide shelter from the abrasive influences of the tailings. In the vertical pipes, the distance between the membrane pairs is 1.3 to 1.7 m.

$$\left.\frac{\Delta p}{\Delta z}\right|_{up} = -(\rho - \rho_{oil})\,g - \frac{4\tau_w}{D}$$

$$\left.\frac{\Delta p}{\Delta z}\right|_{down} = -(\rho - \rho_{oil})\,g + \frac{4\tau_w}{D}$$

$$\left.\frac{\Delta p}{\Delta z}\right|_{up} + \left.\frac{\Delta p}{\Delta z}\right|_{down} = -2(\rho - \rho_{oil})\,g$$

$$\left.\frac{\Delta p}{\Delta z}\right|_{up} - \left.\frac{\Delta p}{\Delta z}\right|_{down} = -\frac{8\tau_w}{D}$$

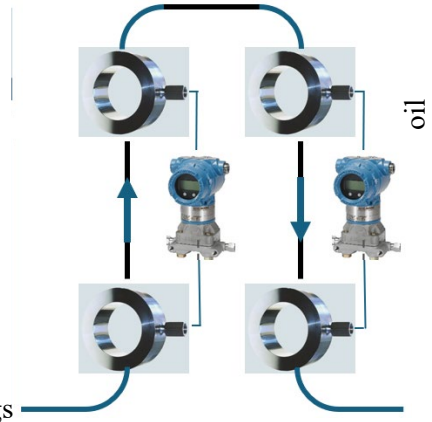


Figure 3: Membrane-based, differential pressure measuring system utilized in ARM's U-tubes

Additional density meter

The Rhosonics additional slurry density meter (SDM) functions on the basis of acoustic impedance (measuring the power of reflected acoustic waves). It measures outputted mixture densities accurately up to +/– 0.5% of the reading (Rhosonics SDM ECO, 2024), e.g. + –7 kg/m^3 for our conditions. In the trial, it is positioned at the outlet of the ARM, Figure 2, such that it can be flushed with water, for reference/validation purposes.

Method

The objective is to characterize the tailings rheology by the Bingham rheological model:

$$\tau = \tau_y + \eta_B \dot{\gamma} \quad (1)$$

where τ is the shear stress [Pa], τ_y is the yield stress [Pa], η_B is the plastic viscosity [Pa s] and $\dot{\gamma}$ is the shear rate [1/s].

To determine rheology, the ARM produces, during its measuring cycle, simultaneous data pairs of flow rate and pressure differences measured in the 3 U-loops, from which the rheological properties τ_y and η_B are determined. The pressure differences are processed, such that wall shear stress due to the flow's friction is calculated (see fourth equation in Figure 3). Basically, the static pressure due to tailings density ρ, principally measured in the U-loop configuration (Clift and Manning-Clift, 1981), is subtracted from the measured DP's (see first two equations in Figure 3), but also an external density meter can be used for ρ. There are two methods applied to determine the rheological properties: 1) The bulk shear rate (=8U/D) is transformed into wall shear rate (Rabinowich-Mooney transformation), and next the rheological parameters of the Bingham model are determined. 2) Fitting of the entire non-linear analytical solution to integral data sets of flow rate, pipe diameter and wall shear stress,(Magnon and Cayeux, 2021).

Previous implementation of determining rheological parameters by ARM

Initially the Rabinowich-Mooney transformation to determine wall-shear rate was utilized (Van Wijk et al. 2023), on the basis of which the Bingham parameters were determined next. The transformation proceeds via a piecewise power-law approach of the raw data (bulk shear rate and wall shear stress). The detection and correction principle for wall slip, based on the availability of 3 pipes, is described in Van Wijk et al. (2023), where the data is evaluated at the same wall shear stress. The transformation results in a limiting resolution, because of the rather flat rheometric flow curves.

Current non-linear implementation (upgrade)

The current implementation is an integral method. The Levenberg-Marquardt (LM) method is used to fit the Buckingham-Reiner equation (Buckingham, 1921), quantifying Bingham laminar flow in a pipe to the data, to find the Bingham yield stress (τ_y) and plastic viscosity (η_B). The Levenberg-Marquardt (LM) method is a non-linear method for fitting data to equations (Magnon and Cayeux, 2021), implemented via the python SciPy toolbox leastsq. The Buckingham-Reiner equation reads:

$$Q = \frac{\pi}{\eta_B} \frac{\left(\tau_w - \tau_y\right)^2}{\left(\frac{\tau_w}{R}\right)^3} \left[\frac{\left(\tau_w - \tau_y\right)^2}{4} + \frac{2\,\tau_y\left(\tau_w - \tau_y\right)}{3} + \frac{\tau_y^2}{2}\right] \quad (2)$$

where Q is flow rate [m^3/s], R is pipe radius [m] and τ_w is wall shear stress [Pa].

Fitting is done for each pipe separately and the average of the thus determined Bingham yield stress and plastic viscosity of the three pipes is given on output.

Measurement

The mixtures were created at IHC's Kinderdijk shipyard by mixing dry kaolinite-based clay powder (FTS1) and tap water. At the beginning of the current test program, the test set-up was filled with existing FTS1 slurry from a 200 liter storage vessel. FTS1 suspensions are thixotropic. For such fluids, only a Bingham characterization of the remolded conditions is meaningful, which is exactly what occurs in the intake and by shearing in the ARM.

Temperature influence

Measurements of the three pipes do not always converge well, like the result shown in Van Wijk et al. (2023). Hence, it was decided to verify the behavior of components, revealing a relevant temperature drift problem of the pressure sensors (see Figure 4). Note that the depicted pressure difference of DP=1,600 [Pa] corresponds to a measurement error of 16 [Pa] wall shear stress in the DN40 pipe. Experience with another U-loop system in a sand-water test set-up, where corrections/calibration were conducted with clear standstill water, led to the conclusion that the same must be done, but with the actual slurry in the pipes.

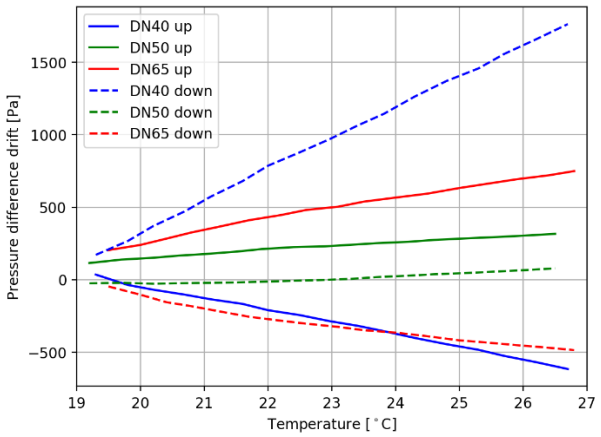


Figure 4: Temperature drift of differential pressure sensors in U-tubes, 8-6-2023, pumping water for 4 hours. The graph shows reference conditions with (almost) zero flow in ARM's normal cycle

Non-linear fitting of the Bingham model to the ARM data

In the days ahead of the next trial, one year later, the SDM was calibrated on water and three FTS1 slurry densities covering the measurement range in the coming trial and, because it revealed a velocity dependency, it was calibrated for the specific velocity range of the ARM's outlet. On the morning of the trial, the pressure sensors were nulled. Temperature variation during the trial is shown in Figure 5, e.g., the

same range as in Figure 4. The slurry's temperature is higher than the ambient air, indicating energy dissipation within the flowing slurry, raising its temperature.

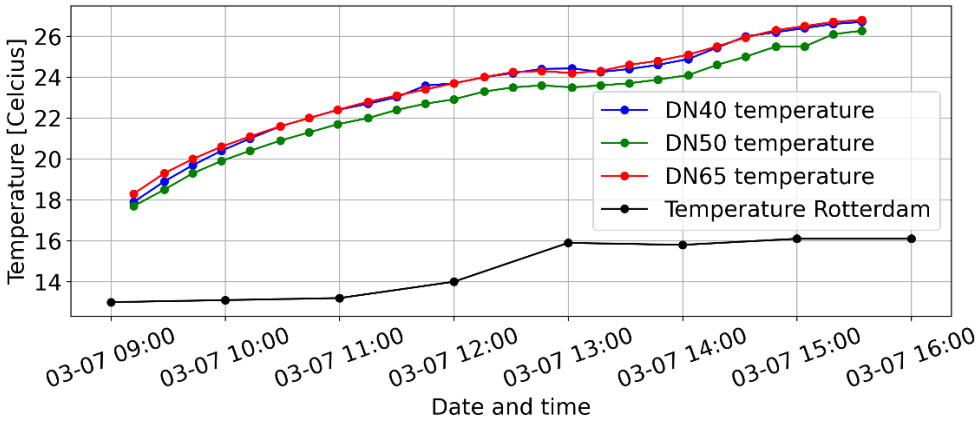


Figure 5: Temperature during the trial

The density outputted by the ARM according to the Uloop principle is shown in Figure 6. We see a lot of strong variation, although the same slurry was pumped around all the time. On the contrary, the SDM outputted a fairly constant density during the day: 1,310 to 1,320 kg/m^3. Sample densities were 1,296, 1,295 and 1,296 kg/m^3. Hence, we base rheological output of the ARM on density by SDM.

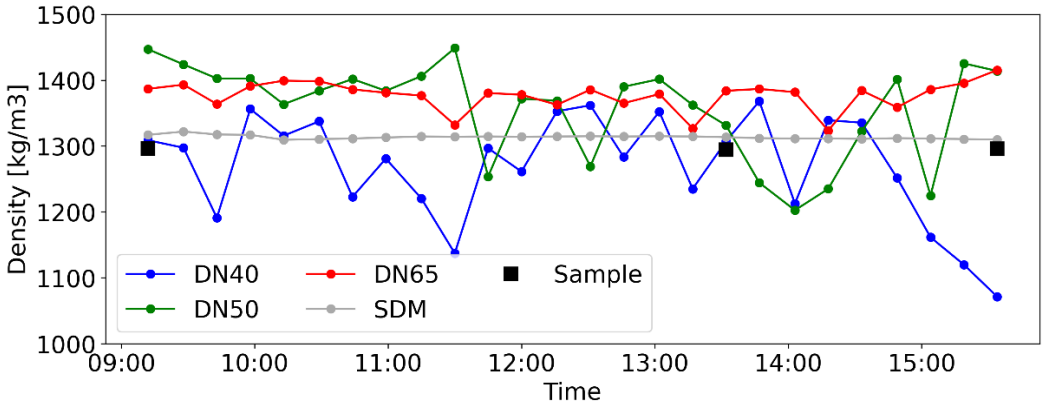


Figure 6: Density according to U-loop principle, SDM and laboratory sample during the trial

Figure 7 shows the synchronously produced data points from the three U-loops. Each data point represents 30 seconds of constant testing conditions recorded at 10 Hz (of which the first 15 seconds are discarded to ensure a steady situation). The displayed data points are 15 second averages. The day-average density of the SDM, used for computing the shear stress, is given in the legend as well as the Bingham parameters according to the LM fit. We see how the steady data of each pipe is fitted by the Bingham based Buckingham-Reiner equation, nicely following the data points. Given the available flow rates, the largest pipe diameter experiences a smaller range of shear stress variation. Naturally, the small diameter pipe

captures the higher shear stresses, while the greater diameter pipes may accentuate lower shear stresses conditions.

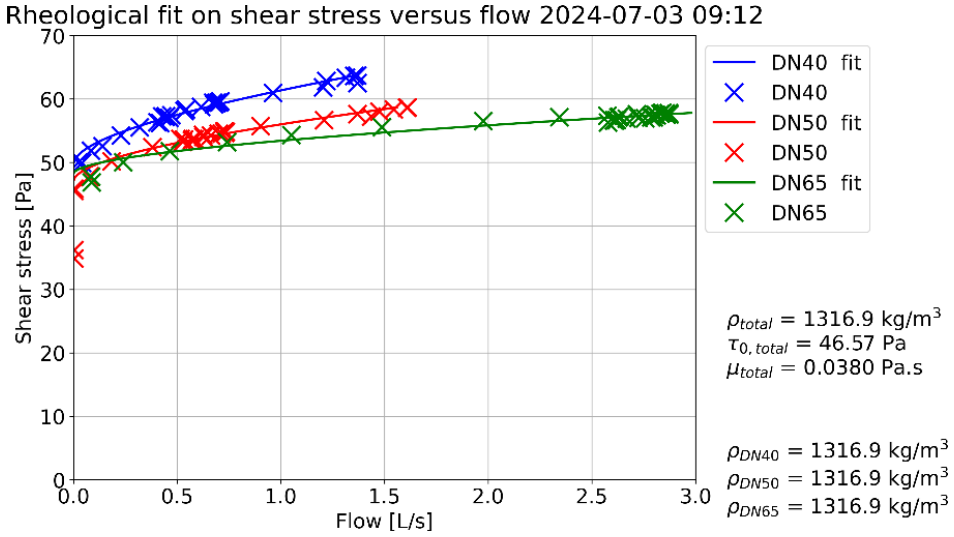


Figure 7: Results of Levenberg-Marquardt fitting of measurements

Figure 8 shows the same data organized as a rheogram, and we see the flow curve according to the ARM data, including the LM fit and the results of rotoviscometric testing (Haake Mars 1 DIN CC 25 coaxial element, remolded conditions) of sampled slurry at the same moment. An interesting paralleling of ARM and rotoviscometric flow curves is observed, with a difference of circa 10 to 15 Pa. This is of the same order as the shear stress at cessation of rotoviscometric measurement (notice the orange data point located on the y-axis at ~16 Pa). Similar readings were experienced in a Fann type rotoviscometer. It is hence likely that in the nulling procedure, the fluid was "hanging" partly in the vertical pipe, leading to this difference.

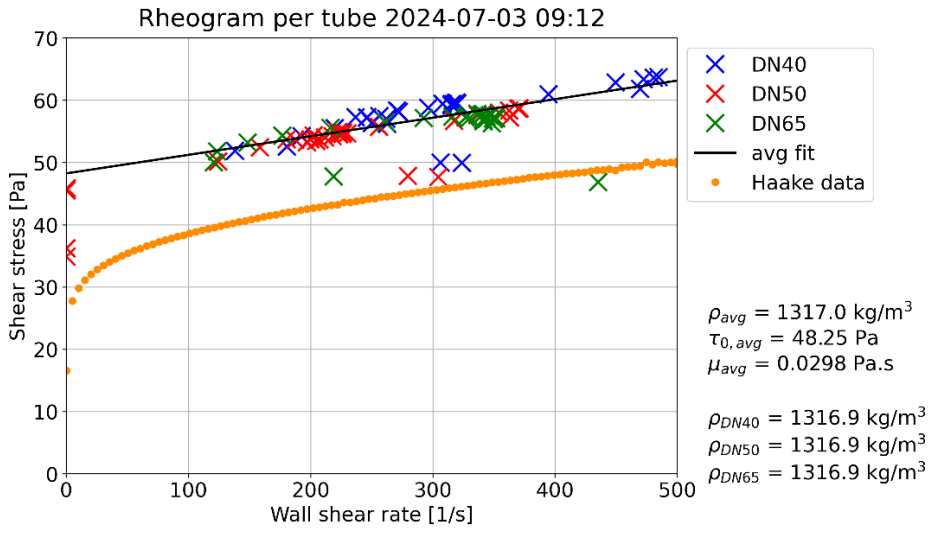


Figure 8: Just after nulling the DP-cells: ARM data processed into flow curve and rotoviscometric measurement; the legend shows ARM's Bingham model parameters and SDM density

Figure 9 shows the rheology six hours later, revealing divergence of data. The yield stress measured by the ARM increases 4.5 Pa and the plastic viscosity increases are similar. The rotoviscometric Haake flow curves increase by 3 Pa (tested at the same temperature as the slurry in the ARM).

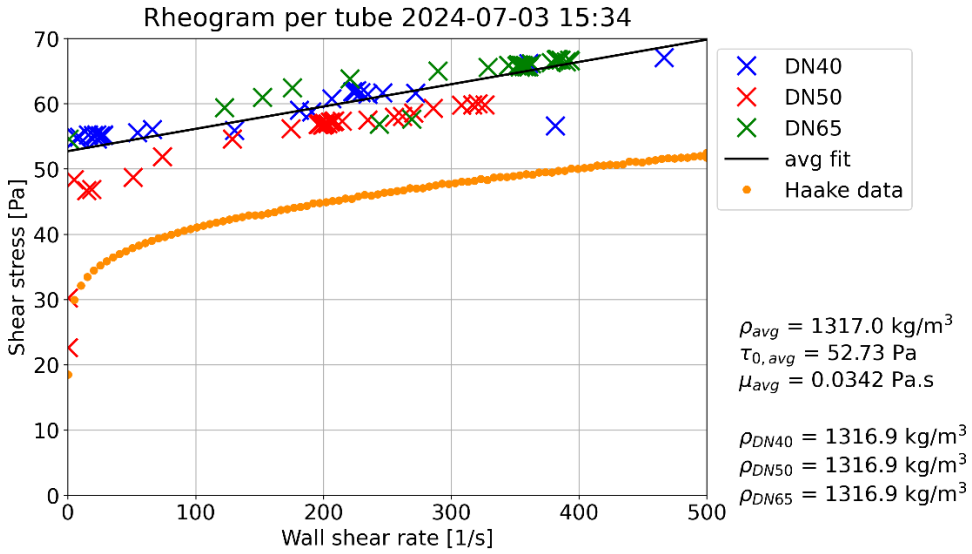


Figure 9: ARM data processed into flow curve and rotoviscometric flow curve

Evaluation

Temperature variation appeared to be a problem under the testing conditions. Under prototype conditions at the underflow of a mine's thickener, temperature variation is expected to be much less because the enormous volume of fluid does not heat up or cool down significantly during the day-night cycle. But since the influence of temperature on pressure measurements was so big, it was deemed better to be able to correct for it. In the prototype a divergence of flow curves or densities between pipes such as in Figure 9 or Figure 6 can be monitored, and when necessary, a flushing procedure can be activated for nulling the DPs, using water that does not exhibit a yield stress.

The cohesive clay slurry must have been partly hanging on the pipe wall during calibration. It is therefore better to calibrate with water from the flushing circuit. It does not need to be clean, since yield stresses decay exponentially with clay concentration decreasing and the actual density can be measured by an SDM.

Wall slip of mixtures is a concern and, if it occurs, it will affect readings. In the course of our research, not described here, we have come up with a formulation of a model tailings that, as expected, will give wall slip for > 30 Pa strength. ARM's identification software and correction software may be tested with this, if the fluid temperature is kept constant.

Rhosonics SDM measures at a distance of micrometers from the wall (Maas and Boerma, 2024). The slurry should therefore be homogeneous. A remaining question is: is this SDM suitable for measuring tailings that have wall slip? In case a thin fluid layer is present at the wall, the SDM might only measure the density of this layer. Rhosonics is aware of this potential risk and has developed a special spool with pockets, to remove the wall effect in front of the sensor (Maas and Boerma, 2024).

The Technological Readiness Levels that the ARM went through are shown in Figure 10: TRL 1 = literature/experience, TRL2 = the proposal, TRL3 = literature and creation of digital twin, TRL 4 = our first testing in the laboratory, TRL5 = tested at industrial yard, TRL 6 = Manufactured ARM is tested in industrial setting, TRL = 7 and 8 and 9 are to be gone through at the mine.

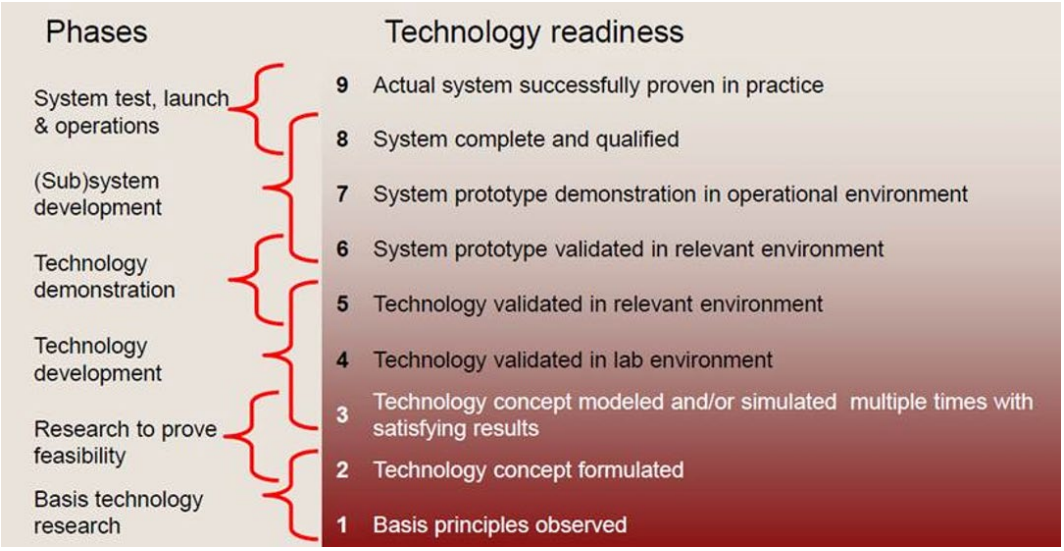


Figure 10: TRL definitions used in the development of the ARM

Waste water industries' transport and treatment may benefit from the current development and it may lead to a reduction of water usage and to innovations in waste water transport. The maximal strengths of Concentrated Domestic Slurries (Thota Radhakrishnan, 2019) can be of the same order as the tailings. In the development of the ARM a digital twin is developed, on the basis of which similar dedicated ARM units for waste water industry can be designed.

Conclusion

As a consequence of temperature drift in the membrane-based DP-measuring system, it is necessary to have an independent and accurate density meter.

The nulling procedure for the off-set of DP-cells needs to be reviewed, the fluid's adhesion probably interfered, and an alternative is necessary and is proposed.

It is recommended to:

- investigate the suitability of a nulling procedure of the DP-sensors based on intermittent flushing, to minimize discrepancies between ARM output and rotoviscometric measurements on drawn samples;
- repeat the described ARM test with model tailings containing coarse settling material to test wall-slip detection and correct for it; and
- transfer the ARM to the mine.

Acknowledgements

The authors would like to thank the concerned mining innovation program for granting Royal IHC and Deltares the principal project. Performance evaluation of the ARM is conducted by Royal IHC, Deltares, Rhosonics Analytical and Sweco Nederland within a Public-Private Partnership: TKI Water Technology, project 2022DEL002. We wish to thank the earlier researchers: J. van Wijk, M. In ‘t Veld, and J. van der Hoeven. We are grateful for the financial and organizational engineering of the TKI by E. Meshkati and C. McLeod, and our partners in initiation of the TKI: F. Vermeulen and V. Braz, and experimenters S. Huisman and M. Busink. Finally, we would like to thank J. Ohalloran for the work on de SDM and E. de Hoog for the final data analysis.

References

Boomsma W., van der Hoeven, J., in ’t Veld, M., van Wijk, J.M., Talmon, A.M. and Meshkati, E. 2022. Autonomous online pipeline rheometer: development and application to tailings slurry. In H. Quelopana (ed.), *Tailings 2022, Proceedings of the 8th International Conference on Tailings Management.* Gecamin, Santiago, Chile, 6–8 July.

Buckingham, E. 1921. On plastic flow through capillary tubes. *ASTM Proceedings* 21:1154–1156.

Chryss, A.G., Monch, A. and Constanti-Carey, K. 2019. Online rheology monitoring of a thickener underflow. In A.J.C. Paterson, A.B. Fourie and D. Reid (eds), *Proceedings of the 22nd International Conference on Paste, Thickened and Filtered Tailings*, Australian Centre for Geomechanics; 8–10 May 2019, Cape Town: 495–504.

Clift, R. and Manning-Clift, D.H. 1981. Continuous measurement of the density of flowing slurries. *International Journal of Multiphase Flow* 7(5):555–561.

Maas, R. and Boerma. 2024. M. Inline real-time process monitoring based on ultrasonic measurement and tomography. *Proceedings of CEDA Dredging Days.* Rotterdam.

Magnon, E. and Cayeux, E. 2021. Precise method to estimate the Herschel-Bulkley parameters from pipe rheometer measurements. *Fluids* 6(4):157.

Meshkati E., Boomsma, W., Talmon, A.M., van Wijk, J., van der Hoeven, J., de Jong, S., Hoebe, J. and In't Veld, M. 2021. Autonomous Pipe RheoMeter (ARM): Towards more efficient water and tailings management. Industry innovation presentation. *CEDA* Rotterdam Ahoy. 3-11-2021.

Rhosonics SDM ECO. 2024. Accessed 27/06/2024 at https://www.proconsystems.com/wp-content/uploads/2020/05/rhosonics_brochure_sdm_en_revi.pdf

Thota Radhakrishnan, A.K. 2019. Domestic slurry hydraulics in transport. PhD thesis. Delft University of Technology.

Van Wijk, J., Talmon, A.M., Meshkati, E., Boomsma, W., Van der Hoeven, J., de Jong, S., Hoebe, J. and In 't Veld, M. 2023. Development of a prototype Autonomous RheoMeter for optimized tailings thickeners operations. In S. Sanders, *IHA 21st Hydrotransport conference*. Edmonton, Canada (in press).

Wang, Y., Ai-xiang Wu, Zhu-en Ruan, Zhi-hui Wang, Zong-su Wei, Gang-feng Yang and Yi-ming Wang. 2020. Reconstructed rheometer for direct monitoring of dewatering performance and torque in tailings thickening process. *International Journal of Minerals, Metallurgy and Materials* 27(11):1430.

Chapter Twelve

Author Index

TAILINGS AND
MINE WASTE 2024



Author Index

Abbaszadeh, Sam 929
Accadia, David 251
Adedapo, Dami 1407
Adria, Daniel 911
Afriyie, George 745
Aguilar, Fernando Pereira 955, 1111, 1419
Ahmeduzzaman, Mohammad 1407
Alam, Raquibul 1645
Alexander, Stephanie 1189
Alexon, Caroline 1787
Alfredo Promotor, Jose 1947
Alimento Júnior, Vicente 1961
Allen, Sean 2357
Almeida, Vitor 2357
Alshafti, Louai 885
Alves Lima, Carlos Alex 1033
Andree, Michael 1565
Arenas, Alfredo 517
Armstrong, Christian 2179
Arnold, Cody 423
Arroyo, Marcos 2191
Artigas, Jacinto 845
Ayes-Zamudio, Juan Carlos 2309
Bachu, Lakshmin 1749

Bale, Bryan 621

Bale, Stephanie 897

Banerjee, Soham 173

Barbosa, Jefferson 2419

Barbosa, Marcelo Roberto 803

Bareither, Christopher 2143, 2467

Barham, Thomas 83, 1163

Barker, Malcolm 545, 1337, 1679

Barroso, Gabriela Rodrigues 1961

Barton, Meghan 661

Baruah, Ajit 967

Bechard, Karen 733

Behzadipour, Hamed 151

Beier, Nicholas 885, 1787

Bell, Jason 1565

Belli, Keaton 1837

Bello-Hamilton, Adeola 1083, 1621

Belotto, Gustavo 1033

Bernardes Raposo, Daniel 2335

Bernardo, Jose 977

Bertrand, Valerie 1765

Besso, Carlos 393

Bezuidenhout, Alvino 279

Bheemasetti, Tejo V. 2155

Bindner, Joseph 2027, 2143

Bjelkevik, Annika 3

Blanco, Pablo 2383

Boczek, Lis 711, 779

Boese, Calvin 1565
Bokkisa, Srinivas Vivek 473
Bokman, Chelsea 1837
Bolívar Domingos, Felipe 2419
Bonucci, Felipe 441, 1717
Boomsma, Wiebe 2485
Borges, Marina 803
Borja, Raquel 305
Bosomtwi, Ankomah 745
Boswell, Jeremy 661
Boulanger-Martel, Vincent 1269
Braun, Chris 1661
Braun, Terry 1019
Bray, Jonathan 363
Brouard, Eric 1353
Brown, Tenaya 675
Bruton, Mark 2039
Burgess, Lisa 1837
Burgin, Andrew 163, 977
Bussière, Bruno, ... 1269
Byrne, Yasmin 2237, 2433
Caldeira, Cecilio 1775
Caldwell, Sam 1175
Calero, Nick 845
Campolina, Felipe 1033
Campos Castro, Helena Maria 1419
Capanema, Denise 803
Capellão, Sergio 393

Capelle, E. Lagae 1861

Cardoso Boaventura, Rafael Caetano 1429

Cardoso Pereira, Manuelle Prado 955

Carey, Ed 1149

Carr, Lucas P. 567

Carvalho Silveira, Lucas França 1961

Castonguay, Vincent 1281

Castro, Alex 1111

Cator, Kendell 1991

Ccarita, Juan 1175

Ccotohuanca, José 379

Cedro, Letícia 441, 505

Cella, Paulo 323

Cerna Diaz, Alfonso 409, 453

Cesar Consoli, Nilo 1555, 2067

Channakian, Gricor 441, 505

Chapman, Peter 1479

Chen, Jason 223, 991

Chen, Jiarui 173

Cheng, Terry C. 1891

Chhetri, Jenisha 929

Chiaranda, Helen Simone 1451

Chiorando, Adam 621

Chung, Jade 1189

Clohan, Daley 897

Cloutier, Eric 1231

Coelho, José Henrique Wanderley Costa 1033

Coia, Vincenzo 897

Collico, Stefano 2191

Conder, Jason 1925

Consoli, Nilo Cesar 1543, 1555

Contreras, Iván A. 1633

Coombs, Scott 1695

Cordova, Josiani Esteves 1961

Correa dos Santos, Alexandre Cristino 45, 2335

Correa, Adolfo 845

Cossey, Heidi 1705

Costa Lisboa, Fernanda Luiza 1961

Costa, Caique Simões Renna 943

Coudert, L. 1861

Couto, Rui 1123

Coyle, Ezra 433

Cromey, Tiffiany 1163

Crouse, Phillip 531, 1241, 2203, 2263

Cruz Pereira, Flavia 803

Cruz, Felipe 137, 265

Cueto, Ignacio A. 609

Cumbers, Jason 293

Da Silva, Fernando 2275

Dagenais, Anne-Marie 223

Damasio, Fernando 791

Damato, Murilo 1429

Dang-Vu, Trong 209

Darmawan, Stephen 2397

Davidson, Richard 453

Davies, Michael 1495

Davison, Evan 2053, 2407

Dawson, Richard 163, 977

De Azambuja Carvalho, João Vítor 1543, 2067

de Castro, João Marcus S.A. 601

de Castro, Paulo Victor S.A. 601

de la Duarantaye, Paul 967

de Lucas Pardo, Miguel 2485

de Mello Martins, Paula 2119

de Melo, Dora 2433

de Membrillera Ortuño, Manuel 545

de Sousa Silva, João Paulo 1543

de Sousa, Gustavo Marçal 45, 1307

DeJong, Jason 2237, 2433

Demers, Isabelle 1005, 1353, 1787, 1861

Demers-Bonin, Michael 1991

Dewoolkar, Mandar M. 173

Dias, Marcus Vinícius Lima 393, 2015

Diaz, Alfonso Cerna 409, 453

Dickinson, Simon 2107

Dickson, Ken 2167

Doherty, Jonathon 1293

Dorow, Ray 2203

dos Santos de Almeida, Mônica Torres 943, 1419

dos Santos, Mauro 765

Doyle, Keiran 753

Drumond, Maira 1717

du Toit, Johan 791

Dubief, Yves 173

Dugie, Matt 1149

Dulmage, Adam 2407

Dunn, Erin 293

Dworatzek, Sandra 1765

Eidi, Ehsan 2167

El Mansouri, Soumia 1231

Eloi, Danilo 441, 505, 1717

Entezari, Iman 2027, 2143

Esfehani, Morteza 2003

Espinoza, David 95

Etezad, Michael 151

Éthier, Marie-Pier 1353

Falorni, Giacomo 2383

Fanni, Riccardo 57

Farhangi, Siavash 1123

Faulder, Anthony 991

Fávero Neto, Alomir 137, 265

Fecht, Steven F. 567

Felitti, Waldemar 1111, 1439

Ferreira Rodrigues, Mayara 2119

Ferreira, Marina 505

Fidel, Laura 779

Fisseha, Bereket 487

Fitzpatrick, Alex 1799

Flores, Osvaldo 1947

Ford, Tony 1337

Fortuna, John H. 1903

Fourie, Andy 1377

Fournier, Gislene F.S.R. 1429

Fredlund, Delwyn G. 487

Freiman, Tony 2309

Freire, Marília 2015

Gaebel, Robyn 1705

Gallegos, Cesar 1947

Garcia Romero, Eduardo Jose 2179

Garcia, Letícia B.L. 1577

Garcia, Reinaldo 845, 857

Garcia-Navarro, Pilar 845

Gastauer, Markus 1775

Gaudreau, Élyse 2383

Gaylard, Peter 1337

Genty, Thomas 1353

Gerritsen, Theo 453, 721, 779

Ghimire, Uddav 2155

Gideon Steyl 711

Gillette, David Rees 1849

Girard, Romain 1045, 2323

Gjerapic, Gordan 1849

Glavina, Joseph 2027

Glover, Nick 545

Gomes Oliveira, Rafael 1451

Gomes, Alessandra 137, 265

Gomes, Guilherme J.C. 1577

Gonçalves, Thatyane Martins 1073, 1555, 2067

Gorakhki, Reza 1873

Gover, Scott 1479

Grâce, Bwemere Ciribuka 1933
Graham, Cory 1407
Granja Guerzoni, Henrique Tropia 1033
Gravel, Shawn 621
Greenwood, Jed D. 1633
Guang, Raymond 209
Guedes, Jonas 1717
Guimarães Delgado, Bruno 137, 1543
Guindon, Marie-Andrée 1353
Gupta, Ranjiv 83, 1163
Hamade, Matteus 765
Hamu, Gustavo 1367, 2131
Han, Chao 585
Hanna, Ed 2079
Harris, Simon 1465
Hashemi, Shayan 433
Hatton, Chris 779
Haynes, Matthew 57
Hernández, Sergio 1947
Hilgers, Jason 409, 1163
Hojka, Kris 127, 633
Hossain, Akhter 2309
House, Peter 2053
Hsiao, Evan 185, 197
Hu, Lucas 2053
Hubner Torres, Carlos 1903
Hultstrand, Doug 689
Hussien, Mahmoud N. 1231

Hutchinson, Bobby 2053

Inparajah, Delakshan 991

Jackson, Andrew 1925

Jalce, Audrey 1353

James, Michael 237

James, R.L.C. 1813

James, Rachel 733

Jarriel, Julia 1163

Jaspers, Menno 2485

Jayasiri, Nilan 1377

Jeong, Chang-Gyun 2107

Johns, Chris 1255

Johnstone, William 829

Josic, Ljiljana 1217, 1645

Joyce, Susan 753

Jung, Andrew 1873

Junior, Benicio 1507

Kafash, Masood 83

Kaheshi, Peter 351

Kalonji-Kabambi, Alex 1933

Kaminsky, Heather 351, 2237

Kappel, Bill 689

Karcher, Geoff 1095

Kepler, Akonkwa Mudekuza 1933

Kermani, Mohammad 1991

Khomiak, Oksana 2131

Klassen, Daniel 379

Koleshwar, Ajinkya 2383

Kramka, Benjamin 293
Krupa, Andrea 2447
Kujawa, Thomas 661
Kundu, Anjan 2367
Kupper, Angela 645
Lambert, Marc 2345
Lanoix, Marie-Lin Breard 1323
Le Borgne, Vincent 2407
Ledesma, Osvaldo N. 609
Lee, Ahreum 991
Leite, Mateus 1717
Leite, Mateus 441
Lemos Júnior, Marcos A. 1577
LePoudre, Chad 675
Lessard, Fannie 1281
Levandowski, Will 1135
Li, Junhong 1633
Liew, Michelle 1799
Lima Dias, Marcus Vinícius 393, 2015
Lima Rasmussen, Leandro 137
Lloyd, Jake 2357
Lobato Ribeiro, Lucas 2373
López, Andrea 1533, 2039
Lorentz, Jim 1621
Lorentz, Simon A. 1813, 1825, 1883
Louws, Michael 1061
Ludlow, Wade 585
Lupo, John 1495

Lysay, Georgia 83

Macedo, Jorge 363, 423, 473, 2253, 2297

Maciel, Weslley 1717

Majdanishabestari, Kasra 1217

Mandisodza, Keith 1603, 2217

Manmatharajan, Mathan V. 151

Marçal de Sousa, Gustavo 1307, 2015

Marcotte, Bryce 1565

Marinaro, Rodrigo 393

Martens, Scott 645

Martin, Garret M. 2467

Martin, Violeta 911

Martinelli, Mario 873, 885

Martinez, Sergio 845

Mazon, Alessandra 2419

McAdam, William 2093

McFarlane, Brent 1565

McGowan, Dallas 2027, 2143, 2237

Medina, Miguel 1281

Melberg, Sarah 857

Mello, Vicente 943, 955, 1419

Menezes, Rafael 2093

Meunier, Daniel 1465

Meyer, Lauren 293

Mikula, Paul 1083, 1621

Mirzanejad, Majid 1135

Mohamadi, Morteza 2107

Mohammadi, Amirhossein 1787

Monforte, Lluis 2191
Moniaga, Rudy 2397
Monley, Kendall 1977
Moraes Russo, Felipe 1307
Moran, Liz 1837
Moreau, Adrian 1799
Morissette, Claude L. 1891
Morrill-Winter, Jesse 829
Morshed, Anan 661
Muir, Wilson 1521
Murillo, Javier 845
Mwamba, Patrick 2179
Naftchali, Fahimeh Mahdavi 151
Nahir, Michael 1095
Narvaez, Gonzalo Zambrano 885
Nasseri-Moghaddam, Ali 1705
Neculita, C.M. 1861
Neiva, Felipe 323
Nell, Veronique 2447
Neves, Ana Carolina 1439, 1451
Neves, Manoela C.A. 1429
Newman, Phil 1533, 2039
Nguyen, Nguyet (Wit Win) 567
Nickman, Alireza 2039
Nieuwboer, Bas 2485
Niyazi, Faegheh 1061
Nkamegue, Estelle 1991
Noël, Michel 339, 1293

Nogueira, Mateus 251

Norbutas, Jackson S. 2155

Noreña, Nilthson 1555

Nunoo, Sam 1061

Nxumalo, N.W. 1533

Nyman, Jennifer 1837

O'Kane, Mike 1391

Oboni, Franco 609

Obusan, Roque 2433

O'Connell, Dan 1135

Oliveira, Jefferson 1033

Olsen, Christopher 1661

Olson, Scott M. 173

Ortuño, Manuel de Membrillera 545

Ozeir, Elissar 1281

Pabst, Thomas 1005

Paes, Ian 137

Paganin, Miguel 441, 505, 1717

Pais, Paula 265

Palape, Miguel 601

Panda, Bibhuti 223

Parra, Denys 1733

Parsons, Don 1695

Pastachak, Travis 1565

Patel, Arazooben 2167

Pautler, Brent 1925

Pellicer, Paul 2203

Pépin, G. 1861

Perdikou, Skevi 1207, 2407

Pereira, Frank 1073, 1555, 2067

Pereira, Nicolas 517

Pereira, Wendel 1775

Pham, Daniel 107

Piccolo-Lawrance, Joe 2323

Pill, Ken 1837

Pinheiro, Jaime 2119

Pinheiro, Mauricio 163, 185, 197, 977

Pinnick, Skyler 1661

Plante, Benoît 1269, 1353

Pollock, Gordon W. 991

Praça, Luciana 765

Probst Simoes, Leonnardo 2357

Promotor, Jose Alfredo 1947

Puro, Greg 2373

Purrington, James 2039

Qoreishi, Mehdi 185, 197

Quaglia, Gastón 1293

Quinn, Joseph 1045, 2323

Rafael Valentim, Denis 2357

Rahal, Kenneth 1661

Raison, Erinn 2107

Ramirez, Devinne 1163

Ramirez, Jenny 95

Ramos, Silvio 1775

Rashidi, Mohammad 929, 1241, 2203, 2263

Rasouli, Rouzbeh 223

Raymond, Katherine 1391

Rego Silva, Roberto Cezar 601

Reid, David 57

Renna Costa, Caique Simões 943, 1419

Resende Lopes, Bruno 1451

Revelo Mendez, Nathalia 1465

Rezende Pinto, Virginie Queiroz 2335

Ribbons, Jordan 1479

Ribeiro, Paula 1775

Risacher, Florent 1925

Ritter, Kevin 409

Roberts, Jeff 1765

Robertson, Jared 1391

Rocco, Nick 857

Rocha Lanzieri, Daniel 137

Rocha Lebron, Yuri Abner 1961

Rodrigues Costa, João Paulo 1033

Rodrigues, Braulio 2357

Rodrigues, Camilla 2345

Rodrigues, Claudio 1507

Rodríguez, Laura 323

Rógenes, Erick 137, 265

Rood, Kenneth 2179

Rose, Angus 251

Ross, Trevor 1149

Rouncivell, W.E. 1813

Rousseau, Marie 1095

Russell, Brad 897, 1149

Rust, E. 69

Rust, M. 69, 857

Rustamov, Samir 2485

Saeedi, Armin 873, 885

Salzsauler, Kristin 1705

Samson, Andréane 1005

Sanchez, Edwin 1733

Santander, Ricardo 1175

Santiago, Oscar 2093

Santos Brasil, Lucas Samuel 803

Santos, Adrielle 441

Santos, Carlos 323

Santos, Dieggo 2015

Santos, Jhonimar 2357

Scale, Kyle 1565

Scalia IV, Joseph 1977, 2143, 2467

Schafer, Matthew 1149

Scheuermann Filho, Hugo Carlos 1555

Schiavon Yamamoto, Lucio 1307

Schiavon Yamamoto, Lucio 45

Seutin, Elaura 1269

Sgavioli, Fernando 1073

Sheykhloo, Pooya 453

Silva de Sousa, Elias 2335

Silva, Mariela 2015

Silva, Raika 765

Silva, Rayssa 505

Silva, Roberto Cezar Rego 601

Silva, Rodney 441, 505, 1717

Simms, Paul 873, 885, 2167

Simoes, Leonnardo Probst 2357

Singh, Neil 1507

Sisson, Richard 813

Slack, David 2433

Small, Andy 3, 689

Smith, Kyle 57

Smith, Larissa 1765

Snow, Robert 1163

Soares, Elaine 1111

Somensi, Cauê Stocchi 45

Sonntag, Chris 675

Souza, Luciano 1507

Souza, Luciano 765

Souza-Filho, Pedro 1775

Spence, Zach 1135

Springer, Darren 1465

Stapleton, Karina 1061

Steele, Lincoln 1135

Sun, Josh 2407

Sun, Summer Y. 531, 1241, 2203, 2263

Sun, Y. Simon 2237

Sweett, Alex 1925

Sylvain, Karine 1005, 1323

Talebi, Ela 127

Talmon, Arno 2485

Tehrani, Kathy 1073

Terlisky, Ariel 339, 1293
Theron, Charné 1825, 1883
Thuysbaert, John 2323
Tian, Hua 2217
Tizzotti, Morgan 2167
Topham, Chris 545
Torres, Ana 1307
Torres, Rogerio 977
Torres-Cruz, Luis A. 279
Tortini, Riccardo 2383
Tostes Firmo, Douglas Deoclécio 45
Townsend, Heather 733
Tran, Vu 1231
Turcotte, Sophie 1005, 1353
Umar, Rashida 745
Vaka, Divya Sekha 1207, 2407
Valverde, Ana 2457
van Asperen, Sven 2485
van Engelen, Anthony 1695
van Zyl, Dirk 813
Vandersleen, John 2079
Vasconcelos, Anelisa 163, 977
Vega, I.J. 339
Vega, Imanol 1293
Verbeek, Gerald 1367, 2131
Vergaray-Astupina, Luis 2253, 2297
Verge, Ashley 1217
Vilas Bôas, Luiz 1111

Villalobos Bravo, Miguel A. 29

Villalta, Geinfranco 305

Vizcarra, Gino 1073, 1555

Vulpe, Cristina 1377

Wacowich, Mathieu 977

Wagner, Alexia Cindy 1543, 2067

Walden, Mark 857

Walsh, Elizabeth 1765

Wanderley Costa, José Henrique Coelho 1033

Wang, Nan 1083, 1621

Whatnall, Oliver 1175

Whiter, Bria 1465

Whitham, Louise 2167

Wickland, Ben 1695

Wightman, Adrian 1189, 2107

Wijewickreme, Dharma 2457

Williams, David J. 1603, 2217

Williams, Jeremiah 745

Williamson, Patrick 1521

Willis, Justin 675, 1589

Wilson, G. Ward 351, 487

Wilson, Stuart 1175

Witasse, Richard 29

Witte, Andrew 3, 1061

Witten, Ben 2345

Wong, Heleman 911

Wong, Wing-Keat (Wayne) 2373

Xavier Matos, Milena Fernandes 2335

Xia, Xuexin 885

Yamamoto, Lucio Schiavon 1307

Yang, Pu 185, 197

Yavari, Fariba 127, 633

Yenne, Lisa 83, 453

Yue, Kenny 2383

Yung, Zhen Ran 2397

Zambrano Narvaez, Gonzalo 885

Zarrabi, Mohammad 1991

Zayler, Richard 711

Zettl, Julie 1391

Zhan, Qing 2397

Zhang, Anthony 1255

Zhang, Chenming 1603

Zheng, Jiajia 1799

Zhu, Yi 721

Znidarcic, Dobroslav 1849